OCS Study
BOEM 2017-060

Exploration and Research of Mid-Atlantic Deepwater Hard Bottom Habitats and Shipwrecks with Emphasis on Canyons and Coral Communities: Atlantic Deepwater Canyons Study

Volume I: Final Technical Report

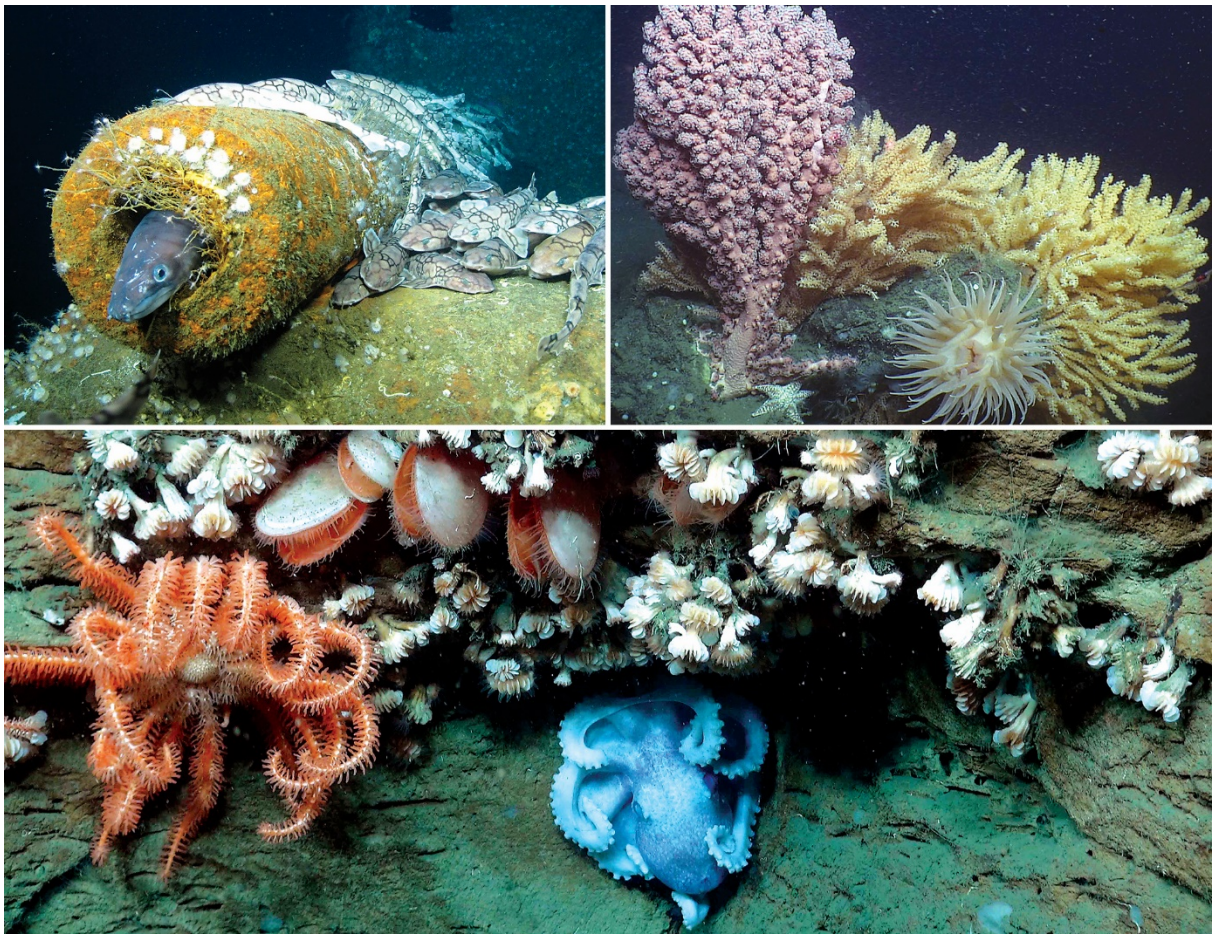

U.S. Department of the Interior
Bureau of Ocean Energy Management
Atlantic OCS Region

BOEM
Bureau of Ocean Energy Management

OCS Study
BOEM 2017-060

Exploration and Research of Mid-Atlantic Deepwater Hard Bottom Habitats and Shipwrecks with Emphasis on Canyons and Coral Communities: Atlantic Deepwater Canyons Study

Volume I: Final Technical Report

Authors (listed alphabetically by surname):

Elizabeth Baird
Jill Bourque
Sandra Brooke
Pamela Campbell-Swarzenski
Rachel Clostio
Katharine Coykendall
Andrew Davies
Amanda Demopoulos
Gerard Duineveld
Scott France
Austin Heil
Ashley Horton
Art Howard
John O. Jensen
Chris Kellogg
Stephanie Lawler
Rod Mather
Jennifer McClain-Counts
Kirsten Meyer
Furu Mienis
Cheryl Morrison
Martha Nizinski
Neal Phillips
Nancy Prouty
Mike Rhode
Brendan Roark
Craig Robertson
Steve Ross
Lakyn Sanders
Kelsey Shroades
Anthony Sogluizzo
Marcus Springmann
Stephen Viada
Rhian Waller
Maya Wolf-Watts
Craig Young

Prepared under BOEM Contract M10PC00100
by:

CSA Ocean Sciences Inc. (primary contractor)
8502 SW Kansas Avenue
Stuart, Florida 34997

U.S. Department of the Interior
Bureau of Ocean Energy Management
Atlantic OCS Region

BOEM
Bureau of Ocean Energy Management

This page intentionally left blank

DISCLAIMER

Study concept, oversight, and funding were provided by the U.S. Department of the Interior, Bureau of Ocean Energy Management, Environmental Studies Program, Washington, DC, under Contract Number M10PC00100. This report has been technically reviewed by BOEM and it has been approved for publication. The views and conclusions contained in this document are those of the authors and should not be interpreted as representing the opinions or policies of the U.S. Government, nor does mention of trade names or commercial products constitute endorsement or recommendation for use.

REPORT AVAILABILITY

To download a PDF file of this report, go to the US Department of the Interior, Bureau of Ocean Energy Management website at www.boem.gov/Environmental-Studies-EnvData/, click on the link for the Environmental Studies Program Information System (ESPIS), and search on 2017-060.

CITATION

1 CSA Ocean Sciences Inc. Ross S, Brooke S, Baird E, Coykendall E, Davies A, Demopoulos A, France S, Kellogg C, Mather R, Mienis F, Morrison C, Prouty N, Roark B, Robertson C. 2017. Exploration and Research of Mid-Atlantic Deepwater Hard Bottom Habitats and Shipwrecks with Emphasis on Canyons and Coral Communities: Atlantic Deepwater Canyons Study. Draft Report. Sterling (VA): U.S. Dept. of the Interior, Bureau of Ocean Energy Management, Atlantic OCS Region. OCS Study BOEM 2017-060. 1,000 p. + apps.

[1] The affiliation of the Principal Investigators is different than that listed for Project Manager. The order of principal investigators begins with the CSA team technical leads (Ross and Brooke), followed by other principal investigators from the CSA team and the U.S. Geological Service arranged in alphabetical order by surname.

This page intentionally left blank

ACKNOWLEDGMENTS

Funding for this project (sponsored by the National Oceanographic Partnership Program) was supplied by the Bureau of Ocean Energy Management (BOEM) (contracted to CSA Ocean Sciences Inc., contract number M10PC00100). We thank G. Boland (BOEM) for invaluable support during the overall project. Jack Irion (BOEM) provided assistance with archaeological investigations during the first field sampling cruise. We appreciate efforts by Jay Odell and Monty Hawkins for cruise location planning, and Barbara Hecker for proposal data and support at the onset of the project. The National Oceanic and Atmospheric Administration (NOAA) ships *Nancy Foster* and *Ronald H. Brown* and the ROVs *Kraken 2* and *Jason II* were provided by the NOAA Office of Ocean Exploration and Research. We thank vessel officers and crew, and ROV crews for their patience and skills during the field surveys. Thanks to Cape Henry Launch Service for safe and efficient transfer of personnel and equipment during the second field sampling cruise. G. Burgess, T. Iwamoto, D. Markle, J. McEachran, T. Munroe, J. Nielsen, D. Smith, and Lea-Anne Henry assisted with identifying collected fishes and invertebrates. A. Quattrini assisted with some statistical analysis. Thanks to U.S. Geological Survey personnel (Daniel Brothers, Jason Chaytor, Olivia Cheriton, Kurt Rosenberger, Carolyn Ruppel, Jared Kluesner, and Jonathan Borden), NOAA personnel (John Tomczuk, Frank Cantelas, Emily McDonald, and Kasey Cantwell) and Marc Lavaleye of the Royal Netherlands Institute for Sea Research (NIOZ). We appreciate the assistance of all the science and outreach personnel for their hard work during the cruises, including Art Howard, Eric Hanneman, Walt Gurley, and Karen Swain. Lastly, we wish to acknowledge the assistance of the project's scientific review group: Robert Carney, Ken Able, and Tim Runyon.

This page intentionally left blank

TABLE OF CONTENTS

Page

TABLE OF CONTENTS
(Continued) **Page**

TABLE OF CONTENTS
(Continued) **Page**

TABLE OF CONTENTS
(Continued) **Page**

TABLE OF CONTENTS
(Continued) **Page**

TABLE OF CONTENTS
(Continued) **Page**

TABLE OF CONTENTS
(Continued) **Page**

TABLE OF CONTENTS
(Continued) **Page**

TABLE OF CONTENTS
(Continued) **Page**

Volume II

This page intentionally left blank

LIST OF FIGURES

Figure **Page**

LIST OF FIGURES
(Continued) **Page**

LIST OF FIGURES
(Continued) **Page**

LIST OF FIGURES
(Continued) **Page**

LIST OF FIGURES
(Continued) **Page**

LIST OF FIGURES
(Continued) **Page**

LIST OF FIGURES
(Continued) **Page**

LIST OF FIGURES
(Continued) **Page**

LIST OF FIGURES
(Continued) **Page**

LIST OF FIGURES
(Continued) **Page**

LIST OF FIGURES
(Continued) **Page**

LIST OF FIGURES
(Continued) **Page**

LIST OF FIGURES
(Continued) **Page**

LIST OF FIGURES
(Continued) **Page**

LIST OF FIGURES
(Continued) **Page**

LIST OF FIGURES
(Continued) **Page**

LIST OF FIGURES
(Continued) **Page**

LIST OF FIGURES
(Continued) **Page**

LIST OF TABLES

LIST OF TABLES
(Continued) **Page**

LIST OF TABLES
(Continued) **Page**

LIST OF TABLES
(Continued) **Page**

LIST OF TABLES
(Continued) **Page**

LIST OF TABLES
(Continued) **Page**

LIST OF PHOTOS

This page intentionally left blank

LIST OF ACRONYMS AND ABBREVIATIONS

α	local biodiversity
ΔR	marine reservoir age
$\Delta^{14}C$ (‰)	DIC-radiocarbon
δC	stable isotope of carbon
$\delta^{13}C$	DIC-stable carbon
δD	deuterium depletion
δN	stable isotope of nitrogen
γ	regional biodiversity
η	number of mutations
ΣCO_2	radiocarbon content of seawater
Ω_{arag}	saturation state of aragonite
$\Omega_{Calcite}$	saturation state of calcite
aa	number of amino acids upon translation using the *Drosophila* translation table
ADCP	acoustic Doppler current profiler
AICc	Akaike information criterion
ALBEX	Autonomous Lander for Biological Experiments (NIOZ lander)
AMOVA	analysis of molecular variance
AMS	accelerator mass spectrometry
ANOSIM	analysis of similarities
ANOVA	analysis of variance
ANU	Australian National University
AOM	anaerobic oxidation of methane
Ap	private allelic richness
Ar	allelic richness
AUC	area under curve
AUV	autonomous underwater vehicle
AWIOS	Automated Wrecks and Obstructions Information System
$B(OH)_3$	boric acid
BC	bulk box core processed for macrofauna
BCS	Baltimore Canyon seep
BIC	Bayesian Information Criterion
BLM	Bureau of Land Management
BOBO	Bottom Boundary Layer (lander)
BOEM	U.SBureau of Ocean Energy Management
bp	number of base pairs of COI gene used in an analyses
BPI	bathymetric position index
^{14}C	carbon-14 (radiocarbon)
CCD	calcite compensation depth
CLO	Cape Lookout, North Carolina
cmd	cumulative mass depth
CO^{2-}_3	carbonate ion
COI barcoding	cytochrome c oxidase subunit I gene
COI	cytochrome oxidase subunit 1
CO-OPS (1x)	National Oceanic and Atmospheric Administration's National Ocean Service Center for Operational Oceanographic Products and Services
cpd	counts per day
CSA	CSA Ocean Sciences Inc.
CSIA	compound-specific isotope analysis

LIST OF ACRONYMS AND ABBREVIATIONS
(Continued)

CTD	conductivity-temperature-depth (profiler)
d	Margalef's species richness index
dbRDA	distance-based redundancy analysis
df	degrees of freedom
DIC	dissolved inorganic carbon
DISCOVRE	DIversity, Systematics, and COnnectivity of Vulnerable Reef Ecosystems
DistLM	distance-based linear modeling
DSC	deepsea coral
DVM	diel vertical migrators
EHS	emergent hard substrate
EMP	Earth Microbiome Project
EST	Eastern Standard Time
F	inbreeding coefficient, fixation index?
f	Weir and Cockerham (1984) estimator of FIS inbreeding coefficient
FIS	heterozygote deficits
FISH	fluorescent *in situ* hybridization
FM	fraction modern
F_{ST}	genetic differentiation among populations
FTU	formazin turbidity unit
GC-MS	gas chromatography-mass spectrometry
GFF	glass microfiber filter
GMT	Greenwich Mean Time
GoM	Gulf of Mexico
GRDN	General Records of the Department of the Navy
H	number of total, unique haplotypes in the data
H′(loge)	Shannon-Wiener diversity index
ha	hectare
HCO_3^-	biocarbonate ion
H_d	haplotype diversity
HD	high definition
HE	expected heterozygosity
$HgCl^2$	mercuric chloride
HMS	Hatteras Middle Slope
HO	observed heterozygosity
hp	horsepower
HPLC	high-pressure liquid chromatography (instrument)
HSD	(Tukey's) honestly significant difference
HWE	Hardy-Weinberg equilibrium
i7 and i5	adapter sequences
IAEA	International Atomic Energy Agency (standards)
IBD	isolation by distance (population genetic pattern)
IBDWS	Isolation by Distance Web Service (population genetics analysis software)
ICP-MS	inductively coupled-mass spectrometry
IFE	Institute for Exploration
ITS	internal transcribed spacer (region)
J′	Pielou's evenness
K value	population cluster
K	genetic cluster
k	number of pairwise differences between sequences

LIST OF ACRONYMS AND ABBREVIATIONS
(Continued)

ka	kiloannum
KW	Kruskal Wallis test
La	lanthanum
LA-ICP-MS	laser ablation inductively coupled plasmas mass spectrometry
LCDR	Lieutenant Commander
LD	linkage disequilibrium
LGM	Last Glacial Maximum
LPLC	low-pressure liquid chromatography (instrument)
LSW	Labrador Sea Water
LVO	late vitellogenic oocytes
M/L	Manus/Lau Basin
MAB	Mid-Atlantic Bight
MAC	mid-Atlantic canyon
MAFMC	Mid Atlantic Fisheries Management Council
MARINE13	Marine Reservoir Correction Database
MCMC	Markov Chain Monte Carlo simulation method
MDS	multidimensional scaling ordination
ME	subsampled push core processed for meiofaunal analysis
MF	subsampled push core processed for macrofaunal analysis
Mg/Ca	magnesium/calcium ratio
MLG	multilocus genotype
MMS	Minerals Management Service
Mo	molybdenum
mtMutS	mismatch repair gene homolog
MVDISP	multivariate dispersion
MWU	Mann-Whitney U test
mya	million years ago
N	number of unique multilocus genotypes
N1	Hill's Index
NA	mean number of alleles per locus
NADW	North Atlantic Deep Water
NCBI	National Center for Biotechnology Information, U.SNational Library of Medicine, National Institutes of Health
NCMNS	North Carolina Museum of Natural Sciences
NCS	Norfolk Canyon seep
$^{143}Nd/^{144}Nd$	neodymium isotopes
Nd	neodymium
NHHC	Naval History and Heritage Program
NIOZ	Royal Netherlands Institute for Sea Research
NIST	National Institute of Standards and Technology
NMFS	National Marine Fisheries Service
nmi	nautical mile
No	nucelolus
NOAA	National Oceanic and Atmospheric Administration
NOAA-OER	National Oceanic and Atmospheric Administration Office of Ocean of Exploration and Research
NOSAMS	National Ocean Sciences Accelerator Mass Spectrometer Facility
nSyn	number of nonsynonymous changes
NUWC	Navy Undersea Warfare Center

LIST OF ACRONYMS AND ABBREVIATIONS
(Continued)

OCS	Outer Continental Shelf
Og	pre-vitellogenic oocytes
OTUs	operational taxonomic units
P	probability value
PAH	polycyclic aromatic hydrocarbon
^{210}Pb	(lead-210) radioactive form of lead with an atomic weight of 210
Pb-Ra	lead-radium
PBS	phosphate-buffered saline
PCA	principal component analysis
PCO	principal coordinates ordination
pCO_2	atmospheric carbon dioxide
PCR	polymerase chain reaction
PID	unbiased probability of identity
pM	percent Modern
POM	particulate organic matter
ppb	parts per billion
ppm	parts per million
pss	practical salinity scale
PTFE	polytetrafluroethylene
PVC	polyvinyl chloride
PVO	pre-vitellogenic oocytes
R^2	proportion of explained variation attributable to each variable
RAAF	Records of the Army Air Forces
RCONRL	Records Collection of the Office of Naval Records and Library
REE	rare earth element
RG	Records Group
RIEP	Rhode Island Endeavor Program
ROC	receiver operating characteristic
ROV	remotely operated vehicle
S	number of variable sites
SBE	Sea-Bird Electronics, Inc.
SC	core processed for sediment geochemistry
SD	standard deviation
SE	standard error
SEAB	Bayesian standard ellipse area
SEM	secondary electron multiplier
SFC	structure-forming cnidarians
SIA	stable isotope analysis
SIAR	Stable Isotope Analysis in R (statistical package)
SIBER	Stable Isotope Bayesian Ellipses in R-Jackson et al2011
SIMPER	similarity of percentages
SL	standard length
SNK	Student–Newman–Keuls test
SNP	Single nucleotide polymorphism
	solubility product of aragonite
SP	spermatocysts
Sp	total number of taxa present in each core
Sr	strontium
SS	sum of squares

LIST OF ACRONYMS AND ABBREVIATIONS
(Continued)

StL	StLawrence, Canada
Syn	number of synonymous changes
Ta	tantalum
TA	total alkalinity
TB	terabyte
Th	thorium
$^{230}Th/^{238}U$	activity ratio of thorium-230 and uranium-238
TIMS	thermal ionization mass spectrometer
Tl	thallium
TL	total length or trophic level
U	uranium
UNCW	University of North Carolina, Wilmington
USBL	ultrashort baseline
USGS	U.SGeological Survey
UTC	Coordinated Universal Time
UTM	universal transverse Mercator
VCDT	Vienna Canon Diablo Troilite
VK826	Viosca Knoll Block 826
VO	vitellogenic oocytes
VPDB	Vienna Pee Dee Belemnite (international reference standard)
VRM	vector ruggedness measure
VSMOW	Vienna Standard Mean Ocean Water
WASIW	Western Atlantic Subarctic Intermediate Water
WHOI	Woods Hole Oceanographic Institution
WNACW	West North Atlantic Central Water
XbaI and *EcoR1*	restriction enzymes
XRD	X-ray diffraction
XRF	X-Ray fluorescence
YBP	year before present

This page intentionally left blank

CHAPTER 1. INTRODUCTION

The Atlantic Deepwater Canyons study was a multidisciplinary research project initiated in 2010 through the National Oceanographic Partnership Program (NOPP). The study was a collaborative effort among the Bureau of Ocean Energy Management (BOEM), the National Oceanic and Atmospheric Administration's Office of Ocean Exploration and Research (NOAA-OER), the U.S. Geological Survey (USGS), CSA Ocean Sciences Inc. (CSA, the prime contractor), 11 academic institutions, and other organizations. The federal agencies sponsoring the study will use the findings to help better understand ocean resources and to develop protection and conservation measures for sensitive seafloor habitats, biota, and cultural resources. Furthermore, the canyons investigated during this study have been considered in the past for National Marine Sanctuary designation, are also located in a region that supports intensive fisheries, and are under consideration for future oil and gas exploration.

The overall goal of the study was to explore hard bottom biological communities and shipwreck sites in the vicinity of Mid-Atlantic Bight (MAB) canyons using state-of-the-art sampling methods and technologies. The study included four research cruises between June 2011 and August 2013. Prior to the first cruise, historical data from MAB canyons were reviewed to aid in cruise planning, and preliminary predictive habitat models were generated. The first cruise mapped the seafloor of Baltimore, Norfolk, Washington canyons, and adjacent areas using multibeam echo sounders. All subsequent cruises focused on intensive surveying and sampling of Baltimore and Norfolk canyons (**Figure 1-1**) for multiple objectives using remotely operated vehicles (ROVs). Water column profiling and sampling were also conducted using conductivity-temperature-depth (CTD) profilers/Niskin carousels, and benthic samples were collected from soft sediment areas using box corers and otter trawls. Four benthic landers and two instrumented moorings were deployed in the two canyons to collect oceanographic data continuously for one year. The study also included an archaeological component directed at identifying and studying shipwrecks in the area. These historic sites were included for their cultural significance as well as to evaluate their function as artificial reefs, which can serve as hard substrate in areas where natural hard bottom is scarce. In addition to the scientific objectives, this project had a significant outreach component that communicated cruise findings through multiple media outlets and resulted in the production of a short documentary about the project and its significance to science and management.

This technical report describes all aspects of the Atlantic Deepwater Canyons study including objectives, methods, results, and discussion for each study component. A synthesis of key findings is presented at the end of the report (**Chapter 19**).

1.1 STUDY AREA

The initial study area, as specified in the Minerals Management Service Request for Proposal (Number M10PS00206) was based on the administrative area for a potential oil and gas lease sale in federal waters within the administrative lines for Virginia and enlarged to include Baltimore Canyon offshore Maryland. The resultant study area was approximately outlined by a triangle (**Figure 1-1**).

After analyzing historical data and reviewing the 2011 multibeam data collected during the initial mapping survey in 2011, Baltimore and Norfolk canyons (**Figure 1-2**) were chosen as the targets for this study.

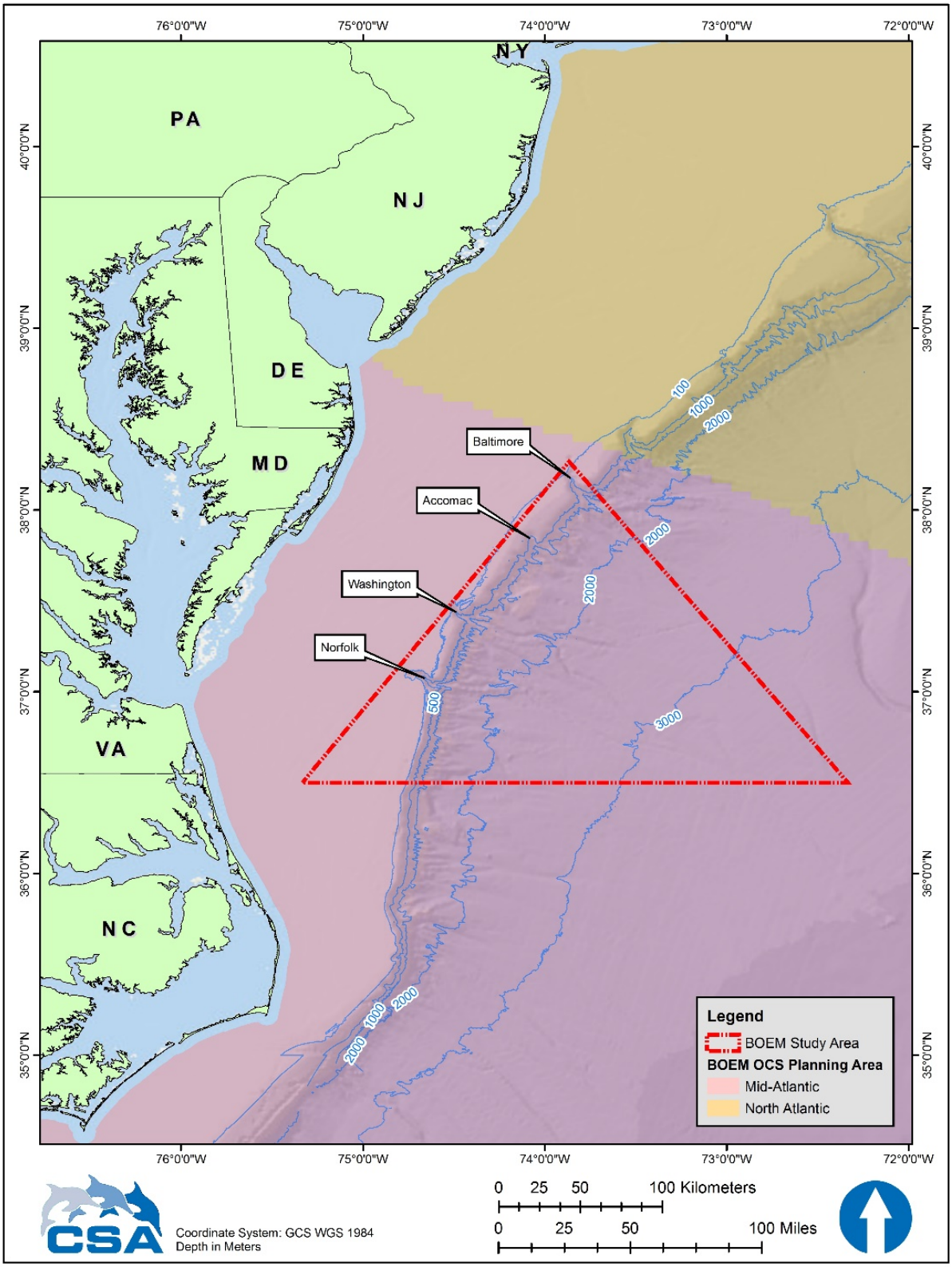

Figure 1-1. Original study area as specified in the Minerals Management Service Request for Proposal (No. M10PS00206).

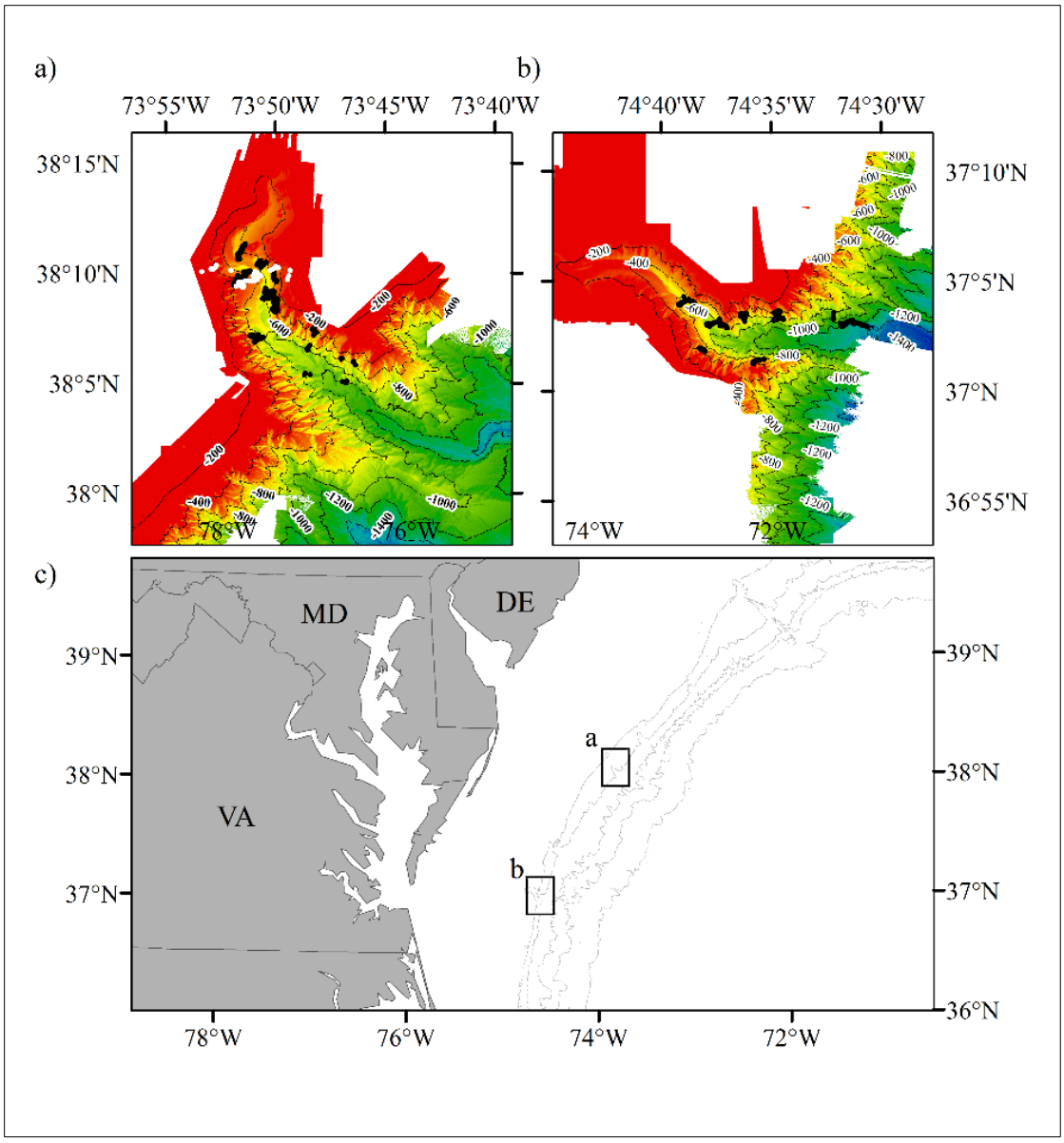

Figure 1-2. Locations of Baltimore (a) and Norfolk (b) canyons, which were the focus of most sampling efforts during the Atlantic Deepwater Canyons study.

1.2 BACKGROUND

1.2.1 Physical Oceanography

The oceanography of waters of the MAB of the northeastern United States (Cape Hatteras to Cape Cod) is one of the best studied in the world (Robinson and Brink 2006). Complex hydrographic structures of the MAB water column are the result of the interaction between major current circulation patterns (Csanady and Hamilton 1988), position of shelf-slope fronts (Voorhis et al. 1976, Houghton et al. 1986, Garvine et al. 1988), entrainment of shelf waters by Gulf Stream eddies (Churchill et al. 1989, Lillibridge et al. 1990), Gulf Stream meanders, water column stratification, and upwelling events (Houghton et al. 1982, Csanady and Hamilton 1988). In addition, sources of freshwater can substantially affect the oceanography of the region (Loder et al. 1998).

1.2.2 Geological Setting

Thirteen major canyons incise the continental shelf of the MAB. The canyons vary in size, shape, and morphological complexity; some have a riverine origin (e.g., Wilmington and Hudson canyons), but most formed via other erosional processes such as slides, debris flows, and turbidity currents (Uchupi 1968, Malahoff et al. 1980, Tucholke 1987). Canyon features of the MAB are conduits for transporting fine sediments (Bennett et al. 1985), with temporal variability in mass flux dominated by storm-driven resuspension, as was also noted in European canyons (de Stigter et al. 2007, Oliveira et al. 2007).

At the current elevated sea level, sediment transport activity at MAB canyons is reduced due to a diminished sediment supply (Gardner 1989a). Mainly modern-type sediments (pelagic and reworked shelf sediments) are transported, and fine-grained material is retained in the upper and middle parts of the canyons, which act as a temporary storage of sediment and organic carbon (de Stigter et al. 2007, Gardner 1989a). At present, erosion and sedimentation is mainly related to off-shelf spill in canyon heads, failure on steep canyon walls (Mitchell 2005), and resuspension by bottom currents (Forde et al. 1981, Gardner 1989b). Biological activity plays a major role in sediment reworking in canyons, which ranges from tubes, tracks, and depressions to large, complex structures excavated by larger fishes (e.g., tilefish) and invertebrates (Grimes et al. 1987, Tucholke 1987). Bioerosion may be the dominant process for moving sediments in many canyons (Warme et al. 1978). Exposed hard substrate is also present in most MAB canyons, including steep-sided walls, exposed ridges, talus fields, and isolated rocks and boulders (Tucholke 1987).

1.2.3 Biological Description

The continental shelf and upper slope biology and ecology off the MAB are particularly well known from extensive surveys conducted in this region by the National Marine Fisheries Service (27 to 366 m depths) and others (e.g., Theroux and Wigley, 1998). These research efforts were partly driven by the economically-important fisheries in the MAB and, to a lesser extent, concerns related to environmental impacts. The deeper (>300 m) MAB slope fauna and ecology are less well documented, with studies usually covering only small areas (e.g., Haedrich et al. 1980, Markle and Musick 1974, Cohen and Pawson, 1977, Musick 1979). Methods used in many benthic studies (e.g., trawls) provided little information on habitat associations or behaviors and almost no data on canyons, hard grounds, or shipwrecks, because these rough bottoms were usually avoided.

With few exceptions (Hudson and Haedrich 1984, King et al. 2008), submarine canyon communities are generally different in species composition from communities in similar depths outside the canyon influence. Megafauna in canyons are often more abundant at all depths, but an unusual feature of canyons is that faunal diversity increases with depth, whereas on the slope the reverse is generally true (Griggs et al. 1969, Rowe 1972, Vetter and Dayton 1998, Carney 2005, De Leo et al. 2010). Observations on overall benthic biomass indicated that canyons are deep sea areas of very high productivity (Stefanescu et al. 1994, De Leo et al. 2010).

The complex interplay of several physical and hydrographic factors contributes to patchiness in faunal assemblages within canyon ecosystems (McClain and Barry 2010). Areas of hard substrate often support dense and diverse communities of suspension and filter feeders such as gorgonians, antipatharians, stony corals, anemones, crinoids, sponges, and other sessile benthic species (Hecker et al. 1983). Deepsea corals and other complex substrates exhibit strong effects on both benthic and mid-water communities (e.g., Ross and Nizinski 2007, Roberts et al. 2009, Young 2009), but their influence appears to vary regionally. Some organisms require hard substrate or other specific environments such as methane seeps (areas of methane and sulfide expulsion from the seafloor) to survive (Levin 2005, Young 2009, Buhl-Mortensen et al. 2010). Although seep and vent communities are known throughout the North Atlantic Basin, including the Gulf of Mexico, they were thought to be rare off the eastern coast of the United States (Van Dover 2000, Cordes et al. 2007). Prior to the Atlantic Deepwater Canyons study, only

two chemosynthetic methane seep communities had been reported (off South Carolina), the Cape Fear Diapir (Brothers et al. 2013) and the Blake Ridge Diapir (Paull et al. 1995, Van Dover et al. 2003) in depths ranging from 2,155 to 2,600 m.

Biogenic habitats in soft or unconsolidated substrate are also present in MAB canyons. A variety of species, notably red crabs (*Chaceon quinqueden*) and tilefish (*Lopholatilus chamaeleonticeps*), construct complex biological excavations in many locations and depths in most MAB canyons (Cacchione et al. 1978, Hecker et al. 1980, Malahoff et al. 1982, Grimes et al. 1986). Dense aggregations of several invertebrate species also create structure in the relatively uniform soft substrates; large fields of pennatulid octocorals (sea pens) and burrowing species such as cerianthid anemones create habitat for other animals (Shepard et al. 1986). Burrowing animals also maintain sediment aeration and may increase habitability for other infauna (Shepard et al. 1986, Wilson 1991). Soft sediment habitats also support mobile fauna (e.g., crabs, lobsters, shrimps, echinoderms). As with the invertebrates, abundance of demersal fish species is often many times higher in canyons than on intercanyon slope areas of the same depth (Stefanescu et al. 1994, Sulak and Ross 1996, De Leo et al. 2010).

1.2.4 Regional Archaeology

The mid-Atlantic Outer Continental Shelf (OCS) includes some of the most historically significant waters in the United States. The area has a long and rich history associated with exploration, warfare, commerce, fishing, and recreation. It encompasses the approaches to Chesapeake Bay and Delaware Bay and, by extension, key mid-Atlantic ports such as Norfolk, Baltimore, Wilmington, and Philadelphia. The region also represents an ancient embayment, where the Susquehanna River that flowed across the coastal plain during the last Ice Age emptied into the Atlantic Ocean. During this time, sea level was approximately 100 m lower than it is today, and it is likely that Pleistocene megafauna and early human populations (Paleoindians) occupied the region. The unique shape and bathymetric structure of the ancient embayment occupied by the present-day Norfolk Canyon suggests that this area may have had very protected and habitable sites.

1.3 STUDY OBJECTIVES

The overall objective of this study was to conduct an intensive multidisciplinary investigation of deepwater hard and soft substrata communities and archaeological sites off Virginia and Maryland within and adjacent to submarine canyons. Specific objectives for the study (natural substrate, archaeological targets, and education and outreach) are listed below.

Specific Objectives for Natural Substrate

- Better understand the distribution of different habitat types (particularly natural hard substrate) within the target canyons and adjacent slopes;
- Understand the physical setting of the study area using samples collected during cruises and long-term, high-resolution data from benthic landers and moorings;
- Describe and characterize canyon communities (invertebrates and fishes) and their habitat associations, with particular emphasis on deepsea coral communities;
- Combine physical and environmental data with information on coral distribution to generate MAB deepsea coral predictive models;
- Understand patterns of connectivity between canyons for dominant species of stony corals and octocorals;
- Determine the age and growth rates of dominant coral species and use isotopic analysis to understand historical ocean conditions;
- Investigate the response of sediment infauna to different environmental and geological variables;

- Investigate trophic structure of canyon fauna using stable isotopes and diets; and
- Investigate microbial communities associated with deepsea corals.

Specific Objectives for Archaeological Targets

- Locate potentially important prehistoric habitation sites;
- Locate and document previously undiscovered shipwrecks within the study area,
- Determine potential eligibility of study sites and shipwrecks for the National Register of Historic Places and prepare a National Register nomination, if appropriate;
- Assess the physical stability of shipwrecks;
- Determine the ecological value of shipwrecks as artificial reefs; and
- Describe and assess diversity and spatial heterogeneity of epibiont invertebrate communities and fishes associated with shipwrecks.

Objectives for Education and Outreach

- Communicate project findings with the public through media outlets; and
- Create an educational documentary film on canyon ecosystems.

1.4 DATA MANAGEMENT

Data collected during this contract was submitted to the NOAA Office for Coastal Management (NOAA-OCM) (to be linked to the BOEM Environmental Studies Program Information System [ESPIS]). Some raw data collected during the various field data collection efforts were submitted to NOAA-OCM personnel at the end of each field effort, whereas other datasets were reviewed prior to the submittal, following the quality assurance/quality compliance (QA/QC) program developed by the Principal Investigators to ensure that all data submitted to ESPIS were correct.

Data were uploaded to a dedicated file transfer protocol (FTP) site at CSA and made available to BOEM, NOAA-OCM, and the CSA Team and USGS project investigators. Datasets within this location included:

- CTD data and Excel files;
- Mooring and Lander instrument and settlement plate data files;
- Multibeam bathymetry maps;
- Summary data for sampling stations and data collected during the contract;
- Multibeam bathymetry maps;
- Cruise plans and cruise reports;
- Fly-through Fledermaus videos of each canyon;
- Metadata documentation;
- Planning Meeting information for the Final Report; and
- PowerPoint Presentations.

All high-definition video data were (or will be) provided to NOAA-OCM by the end of the contract. Due to the size of the files, external digital hard drive units are used to ship these data to NOAA-OCM.

All data, photographs, and video collected during the contract have been copied (backed up) in multiple locations for safe storage and easy retrieval. All video data mailed to NOAA-OCM are copies of original data collected during the survey. As per contract specifications, all collected data will be retained for a period of 1 year from the contract completion date.

Biological samples will be transferred to the Smithsonian National Museum of Natural History to be permanently archived. CSA will contact the museum for updates to their current procedures. Specimens will be shipped to the museum according to Smithsonian directions.

All National Register of Historic Places Nomination Forms were submitted to both BOEM and NOAA-OER personnel.

1.5 STUDY CHRONOLOGY

A brief overview of study methods is presented in **Chapter 1**, and further details are described in **Chapter 3**. A review of historical data (**Chapter 2**) was conducted prior to the field research to identify potential areas of deepsea coral habitat. Four research cruises were conducted to address study objectives; these are briefly described below and are discussed in greater detail in cruise reports (Volume II, Appendices A, B, C, and D [instrument retrieval report]).

- 2011 Mapping Cruise (4 to 17 June 2011). This cruise included seafloor mapping, hydrographic profiling, and water sampling. The survey focused mainly on Baltimore, Norfolk, and Washington canyons. Six high-priority archaeological targets that were indicative of shipwrecks were detected in the Norfolk Canyon area. Among these were five previously unidentified sites suspected to be from the historic "Billy Mitchell Fleet."
- 2012 Sampling Cruise (15 August to 3 October 2012). This cruise included ROV surveys and collections in Baltimore and Norfolk canyons. Benthic landers and moorings were deployed in each canyon. The survey also included box core, monocore, and trawl sampling; hydrographic profiling; water sampling; and additional seafloor mapping. All shipwrecks from the Billy Mitchell Fleet were identified and confirmed along with one other shipwreck.
- 2013 Sampling Cruise (30 April to 27 May 2013). This cruise included ROV surveys and collections in Baltimore and Norfolk canyons. Two benthic landers in Baltimore Canyon were retrieved and redeployed to replace faulty acoustic release mechanisms. The survey also included box core, monocore, and trawl sampling; hydrographic profiling; water sampling; and additional seafloor mapping. ROV surveys were conducted at four of the shipwrecks.
- 2013 Instrument Retrieval Cruise (21 to 27 August 2013). Benthic landers and moorings were retrieved. The cruise also included monocore sampling, hydrographic profiling, and water sampling.

Education and outreach activities were part of all cruises. Two websites documented the progress and facilitated public awareness of the project. Background essays, daily logs, and photographs were posted to both sites prior to and during the cruises. Skype interviews with principal investigators were broadcast live during the 2012 and 2013 cruises. Other outreach efforts included an article in the *Washington Post* and *Herald Tribune*, among many others. Details of education and outreach activities are discussed in **Chapter 18**.

1.6 STUDY COMPONENTS AND PRINCIPAL INVESTIGATORS

Each of the three sponsoring agencies (BOEM, NOAA-OER, and USGS) played an important role in the Atlantic Deepwater Canyons study. BOEM, as the agency responsible for managing energy and mineral resource development on the OCS, defined the study region and scope and managed the contract. NOAA-OER provided operational support, funded research vessels and ROVs, and provided support for education and outreach objectives. USGS scientific expertise was incorporated into the study design, and USGS principal investigators conducted research that examined canyon geology, oceanography, ecology,

animal and microbial distribution, and genetics. CSA managed financial details of the subcontracts, helped coordinate the international team of scientists, assisted the science team during the field missions, and reviewed and edited this final report.

Table 1-1 lists the individual study components and investigators. Dr. Sandra Brooke (Florida State University) and Dr. Steve Ross (University of North Carolina-Wilmington) served as co-lead principal investigators. They were involved in all study components; coordinated the science objectives; served as co-chief scientists on the first three research cruises; wrote, reviewed, and edited chapters; and led the synthesis effort. Stephen Viada was the CSA project manager and served as co-chief scientist for portions of the 2012 and 2013 sampling cruises. Dr. Rod Mather (University of Rhode Island) led the archaeology effort and was co-chief scientist for portions of the 2012 and 2013 sampling cruises. Mike Rhode (University of North Carolina-Wilmington) was the lead technician on all cruises, led the night watches, and was chief scientist for the final cruise.

Table 1-1. Individual study components and investigators.

Chapter	Study Component	Investigators and Affiliations	Description
2	Analysis of historical data	Sandra Brooke (FSU) Steve Ross (UNCW) Maya Wolf-Watts (OIMB) Mike Rhode (UNCW)	**Chapter 2** contains descriptions of historical submersible and towed camera dives in the mid-Atlantic canyons between 1980 and 1993 (see **Volume II**, **Appendix E** for dive logs of historical video footage).
3	Study design and general methods	Sandra Brooke (FSU) Steve Ross (UNCW) Stephen Viada (CSA)	**Chapter 3** provides a general overview of field sampling efforts (research cruises) and methods, survey vessels and equipment, and a summary of sampling locations and data collected during the contract period.
4	Archaeological studies	Rod Mather (URI) John O. Jensen (URI)	**Chapter 4** describes the locations and descriptions of shipwrecks discovered during the project, including assessment of condition and historical status of each wreck.
5	Physical oceanographic processes	Andrew Davies (Bangor University) Craig Robertson (Bangor University) Furu Mienis (NIOZ) Gerard Duineveld (NIOZ) Nancy Prouty (USGS) Brendan Roark (TAMU) Steve Ross (UNCW) Sandra Brooke (FSU)	**Chapter 5** is a comprehensive overview of the oceanography of the Mid-Atlantic Bight (MAB) canyons and slope, from analysis of oceanographic data collected by conductivity-temperature-depth (CTD) casts and benthic lander instruments.
6	Geological studies	Furu Mienis (NIOZ) Gerard Duineveld (NIOZ) Brendan Roark (TAMU) Amanda Demopoulos (USGS) Nancy Prouty (USGS) Pamela Campbell-Swarzenski (USGS) Mike Rhode (UNCW) Sandra Brooke (FSU) Steve Ross (UNCW)	**Chapter 6** describes sediment transport and distribution of different sources of organic material within and outside the MAB canyons from sediment data of box core and push core samples.
7	Predictive habitat modeling	Andrew Davies (Bangor University) Craig Robertson (Bangor University) Mike Rhode (UNCW) Maya Wolff-Watts (OIMB) Steve Ross (UNCW) Sandra Brooke (FSU)	**Chapter 7** describes habitat suitability models that were created using physical and biological data generated during the project. Separate models were developed for octocorals and stony corals. Chapter 7 also compares model outputs using historical information vs. those using data from the Atlantic Deepwater Canyons study.

Table 1-1. (Continued).

Chapter	Study Component	Investigators and Affiliations	Description
8	Benthic invertebrate communities	Sandra Brooke (FSU) Maya Wolf-Watts (OIMB) Austin Heil (FSU) Kirsten Meyer (OIMB) Katharine Coykendall (USGS) Mike Rhode (UNCW) Craig Young (OIMB) Steve Ross (UNCW)	**Chapter 8** discusses various aspects of benthic community ecology, including factors driving coral distributions, description of cold seep communities and shipwreck fouling fauna, and preliminary observations on phylogenetics of selected invertebrates.
9	Benthic infaunal communities	Craig Robertson (Bangor University) Jill Bourque (USGS) Amanda Demopoulos (USGS) Sandra Brooke Steve Ross	**Chapter 9** discusses differences among soft sediment infaunal communities from different parts of each study canyon and the adjacent slope. Potential drivers of the observed differences are presented and discussed.
10	Molecular perspectives on anomuran biodiversity	Katharine Coykendall (USGS) Cheryl Morrison (USGS) Martha Nizinski (NMNH)	**Chapter 10** presents genetic analyses of anomuran crabs (squat lobsters) collected using ROVs and trawl sampling to evaluate diversity and connectivity within and beyond the MAB.
11	Invertebrate reproductive biology	Sandra Brooke (FSU) Anthony Sogluizzo (FSU)	**Chapter 11** is an overview of reproductive biology of selected invertebrates from hard bottom and cold seep habitats and discusses observed gametogenic patterns in the context of potential environmental drivers.
12	Microbiological studies	Chris Kellogg (USGS) Stephanie Lawler (University of South Florida) Sandra Brooke (FSU) Steve Ross (UNCW)	**Chapter 12** analyzed microbial communities associated with selected corals and long-term settlement plate arrays.
13	Coral taxonomy and connectivity	Rachel Clostio (University of Louisiana) Scott France (University of Louisiana)	**Chapter 13** analyzed genetic relationships, including the potential for population isolation and connectivity within selected octocoral and hexacoral species.
14	Patterns of intercanyon connectivity among four coral species	Cheryl Morrison (USGS) Katharine Coykendall (USGS) Marcus Springmann (USGS) Kelsey Shroades (USGS) Lakyn Sanders (USGS) Rhian Waller (University of Maine) Steve Ross (UNCW) Sandra Brooke (FSU)	**Chapter 14** analyzed genetic relationships among selected octocoral and scleractinian species including the potential for genetic isolation and connectivity.
15	Fish communities and diets	Steve Ross (UNCW) Mike Rhode (UNCW) Ashley Horton (UNCW)	**Chapter 15** describes fish communities, habitat associations, and diets using ROV video observations and trawl collections.
16	Food web structure revealed by stable isotopes	Amanda Demopoulos (USGS) Steve Ross (UNCW) Sandra Brooke (FSU) Mike Rhode (UNCW) Jennifer McClain-Counts (USGS)	**Chapter 16** describes stable isotopes in benthic fauna, fishes, sediments, and seawater to evaluate food web relationships among different faunal groups.
17	Paleoecology	Brendan Roark (TAMU) Nancy Prouty (USGS) Steve Ross (UNCW) Amanda Demopoulos (USGS)	**Chapter 17** used isotopic and elemental analysis of selected coral species and seawater to determine coral age and growth and to reconstruct historical variability of the marine environment.
18	Education & outreach	Elizabeth Baird (NCMNS) Art Howard (Artworks Inc.)	**Chapter 18** summarizes the public education and outreach activities on each cruise and for the study as a whole.
19	Synthesis	Sandra Brooke (FSU) Neal Phillips (CSA) Stephen Viada (CSA), et al.	**Chapter 19** synthesizes key findings from the individual study components into a multidisciplinary overview of the MAB canyon and slope ecosystems.

CSA = CSA Ocean Sciences Inc.; FSU = Florida State University Coastal and Marine Laboratory; NCMNS = North Carolina Museum of Natural Sciences; NIOZ = Royal Netherlands Institute for Sea Research; NMNH = Smithsonian National Museum of Natural History; OIMB = Oregon Institute of Marine Biology; TAMU = Texas A&M University; UNCW = University of North Carolina-Wilmington; URI = University of Rhode Island; USGS = U.S. Geological Survey.

1.7 REPORT ORGANIZATION

This report consists of 19 chapters organized as follows:

- **Chapter 1** presents a general overview of the study, including a description of the study area, background information on the regional physical and biological environment, archaeology, and study objectives and chronology.
- **Chapter 2** reviews historical data from submersible dives made between 1980 and 1993 in the mid-Atlantic canyons.
- **Chapter 3** describes general methods including cruise chronologies, research vessels, sampling equipment and methods, and station locations.
- **Chapters 4** through **17** present detailed methods, results, and discussion for individual study components.
- **Chapter 18** summarizes outreach and education efforts.
- **Chapter 19** presents a synthesis of the key findings from the various study components.

Additional supporting material is presented in individual chapters or in Volume II appendices that are referenced in these chapters.

1.8 LITERATURE CITED

Bennett RH, Lehman L, Hulbert MH, Harvey GR, Bush SA, Forde EB, Crews P, Sawyer WB. 1985. Interrelationships of organic carbon and submarine sediment geotechnical properties. Marine Geotechnology. 6:61–98.

Brothers LL, Van Dover CL, German CR, Kaiser CL, Yoerger DR, Ruppel CD, Lobecker E, Skarke AD, Wagner JKS. 2013. Evidence for extensive methane venting on the southeastern U.S. Atlantic margin. Geology. 41:807–810.

Buhl-Mortensen L, Vanreusel A, Gooday AJ, Levin LA, Priede IG, Buhl-Mortensen P, Gheerardyn H, King NJ, Raes M. 2010. Biological structures as a source of habitat heterogeneity and biodiversity on the deep ocean margins. Marine Ecology. 31:21–50.

Cacchione DA, Rowe GT, Malahoff A. 1978. Submersible investigation of outer Hudson submarine canyon. In: Stanley D, Kelling JG, editors. Sedimentation in submarine canyons, fans, and trenches. Stroudsburg (PA): Dowdon, Hutchings and Ross, Inc. p. 42–50.

Carney RS. 2005. Zonation of deep biota on continental margins. Oceanography and Marine Biology: An Annual Review. 43:211–278.S

Churchill JH, Cornillon PC, Hamilton P. 1989. Velocity and hydrographic structure of subsurface shelf water at the Gulf Stream's edge. Journal of Geophysical Research-Oceans. 94:10791–10800.

Cohen DM, Pawson DL. 1977. Observations from the DSRV ALVIN on populations of benthic fishes and selected larger invertebrates in and near DWD-106. NOAA Dumpsite Evaluation Report 77-1. p. 423–450. doi:10.1016/j.dsr.2007.01.001.

Cordes EE, Carney SL, Hourdez S, Carney RS, Brooks JM, Fisher CR. 2007. Cold seeps of the deep Gulf of Mexico: community structure and biogeographic comparisons to Atlantic equatorial belt seep communities. Deep Sea Research Part I: Oceanographic Research Papers. 54(4):637–653.

Csanady GT, Hamilton P. 1988. Circulation of slopewater. Continental Shelf Research. 8:565–624.

CHAPTER 2. ANALYSIS OF HISTORICAL DATA

Sandra Brooke, Steve Ross, Maya Wolf-Watts, and Mike Rhode

2.1 RATIONALE

The analysis of historical data from mid-Atlantic canyons was initiated to gather information on habitats and communities in the region and was conducted in the period between the mapping cruise (June 2011) and the first sampling cruise (August 2012). Several archived submersible videos and associated datasets were identified from within the region. These historical data were valuable for 1) expanding our understanding of mid-Atlantic canyons and surrounding ecosystems, 2) identifying important potential target areas for future research cruises in the larger study, 3) providing a baseline against which to evaluate new data from the Atlantic Deepwater Canyons study, and 4) placing the biological significance of the canyons in a larger regional context for evaluation of energy activities. The historical datasets overlapped with the Atlantic Deepwater Canyons study area, and the combined datasets provided coverage of the entire mid-Atlantic continental slope.

2.2 METHODS

2.2.1 Data Sources

Videos from 124 submersible dives made by the *Johnson Sea-Link* (Harbor Branch Oceanographic Institution) and the *Delta* (Delta Oceanics) between 1980 and 1993 were converted from their original format ([National Television System Committee] NTSC: U-matic, VHS, or Hi8) to digital format and stored on hard drives. The dives were made in Baltimore, Hudson, Norfolk, Tom's, Wilmington, Lydonia, Veatch, Atlantis, Hydrographer, Lasse, Block, Munson, No Name, and Lindenkohl canyons and the Middle Grounds. Principal investigators for these cruises (Barbara Hecker, Hecker Environmental Consulting; Kenneth Able, Rutgers University Institute of Marine and Coastal Science; and Ivar Babb, University of Connecticut, Avery Point) provided original videos and associated dive logs. **Table 2-1** lists the videos that were converted and stored on hard drives.

Table 2-1. List of all dives for which videos were copied for review of historical data.

Year	Vehicle	Dive No.	Location	Original Format
1984	*Johnson Sea-Link*	911, 912	Atlantis Canyon	U-matic
1989	*Johnson Sea-Link*	1574, 1575	Atlantis Canyon	VHS
1990	*Johnson Sea-Link*	1969, 1970	Baltimore Canyon	Hi8
1981	*Johnson Sea-Link*	1083–1085, 1087, 1089–1090	Baltimore Canyon	U-matic
1983	*Johnson Sea-Link*	1427, 1428	Baltimore Canyon	U-matic
1991	*Johnson Sea-Link*	2170	Block Canyon	Hi8
1990	*Johnson Sea-Link*	1998	Block Canyon	Hi8
1992	*Johnson Sea-Link*	2361	Block Canyon	Hi8
1993	*Johnson Sea-Link*	2550−2557	Block Canyon	Hi8
1990	*Johnson Sea-Link*	1973	Hudson Canyon	Hi8
1990	*Johnson Sea-Link*	1975−1982	Hudson Canyon	Hi8
1990	*Johnson Sea-Link*	1986−1991	Hudson Canyon	Hi8
1991	*Johnson Sea-Link*	2172, 2173	Hudson Canyon	Hi8
1991	*Johnson Sea-Link*	2175	Hudson Canyon	Hi8
1980	*Johnson Sea-Link*	889, 892	Hudson Canyon	U-matic
1981	*Johnson Sea-Link*	1079, 1080	Hudson Canyon	U-matic
1982	*Johnson Sea-Link*	1234−1239	Hudson Canyon	U-matic

Table 2-1. (Continued).

Year	Vehicle	Dive No.	Location	Original Format
1983	*Johnson Sea-Link*	1423−1425	Hudson Canyon	U-matic
1992	*Johnson Sea-Link*	2368−2370	Hudson Canyon	Hi8
1991	*Johnson Sea-Link*	2167	Hydrographer Canyon	Hi8
1990	*Johnson Sea-Link*	1996	Lasse Canyon	Hi8
1990	*Johnson Sea-Link*	1984, 1985	Lindenkohl Canyon	Hi8
1991	*Johnson Sea-Link*	2176	Lydonia Canyon	Hi8
1980	*Johnson Sea-Link*	874, 877–878, 880–881, 883	Lydonia Canyon	U-matic
1980	*Johnson Sea-Link*	1070, 1072	Lydonia Canyon	U-matic
1992	*Johnson Sea-Link*	2360	Lydonia Canyon	Hi8
1984	*Johnson Sea-Link*	901–902, 904–905, 906, 909	Middle Grounds	U-matic
1987	*Delta*	622−634	Middle Grounds	VHS
1991	*Johnson Sea-Link*	2165, 2166	Munson Canyon	Hi8
1992	*Johnson Sea-Link*	2359	Munson Canyon	Hi8
1991	*Johnson Sea-Link*	2161−2164	No Name Canyon	Hi8
1981	*Johnson Sea-Link*	1091−1096	Norfolk Canyon	U-matic
1983	*Johnson Sea-Link*	1429	Norfolk Canyon	U-matic
1990	*Johnson Sea-Link*	1972	Tom's Canyon	Hi8
1990	*Johnson Sea-Link*	1974	Tom's Canyon	Hi8
1991	*Johnson Sea-Link*	2174	Tom's Canyon	Hi8
1992	*Johnson Sea-Link*	2367	Tom's Canyon	Hi8
1988	*Johnson Sea-Link*	1664, 1666	Unknown	VHS
1980	*Johnson Sea-Link*	887	Veatch Canyon	U-matic
1990	*Johnson Sea-Link*	1992−1995	Veatch Canyon	Hi8
1991	*Johnson Sea-Link*	2168, 2169	Veatch Canyon	Hi8
1980	*Johnson Sea-Link*	888	Veatch Canyon	U-matic
1981	*Johnson Sea-Link*	1074, 1076	Veatch Canyon	U-matic
1984	*Johnson Sea-Link*	913	Veatch Canyon	U-matic
1990	*Johnson Sea-Link*	1971	Wilmington Canyon	Hi8
1990	*Johnson Sea-Link*	1983	Wilmington Canyon	Hi8

2.2.2 Video Conversion

In November 2011 and March 2012, post-doctoral fellow M. Wolf (Oregon Institute of Marine Biology) traveled to Rutgers Marine Station and the University of Connecticut Marine Station at Avery Point to retrieve and convert historical video data. Original audio and video for each dive were converted from U-matic, VHS, or Hi8 tapes into digital format using one of three digital converters (Canopus ADVC-300 DV media, Hollywood DV-Bridge, or an AJA HD Digital converter), and digitized video was stored in Audio Video Interleave (.AVI) format on external hard drives. Dive navigation data (time, depth, and coordinates for each navigational fix) were retrieved from dive logs and recorded in Microsoft Excel spreadsheets. Some cruise coordinates were recorded in Long Range Navigation-C (LORAN-C). These coordinates were converted to latitude and longitude with DOSBox version 0.74 conversion software.

2.2.3 Digitized Images

Digital images were collected during surveys in Baltimore Canyon (Hecker et al. 1980, 1983) with either a camera sled (named ‘Cheep Tow’) or cameras mounted on the submersibles. Cameras used on the

sled were a 35 mm EG&G or a 70 mm Hydroproducts camera. Hecker provided a subset of these images in .jpeg format. Digital copies of 35 mm slides (from R.A. Cooper, University of Connecticut) of habitat and fauna from Norfolk, Hydrographer, Veatch, Lydonia, and Corsair canyons were stored on external hard drives. Each image was saved in Joint Photographic Experts Group (.jpeg, low resolution) or tagged image file format (.tiff, high resolution) format. Images also were extracted (.jpeg format) from the video footage and embedded into the summary logs for each dive.

2.2.4 Video Analysis

Video was analyzed from the 46 dives and listed in **Table 2-2**. These include 44 dives by the *Johnson Sea-Link* submersible (Harbor Branch Oceanographic Institute) in Baltimore, Hudson, Norfolk, Tom's, and Wilmington canyons between 1981 and 1992 (Hecker et al. 1983, Grimes et al. 1987, Cooper et al. 1992, Able 2002). In addition, two dives were analyzed from *Delta* submersible (Delta Oceanics) dives in the Middle Grounds in 1987 (Able 2002) (**Figure 2-1**). The remaining dives that were copied were not analyzed for several reasons. The video quality was frequently too poor to resolve fauna or the audio was missing. In the absence of continuous navigation data, audio is essential to interpolate habitats between geographical waypoints. Other problems included fragmented transects, limited footage, missing metadata, or mislabeled tapes. Some of the dives were from areas outside the Mid-Atlantic Bight and were given a lower priority and therefore have not yet been analyzed.

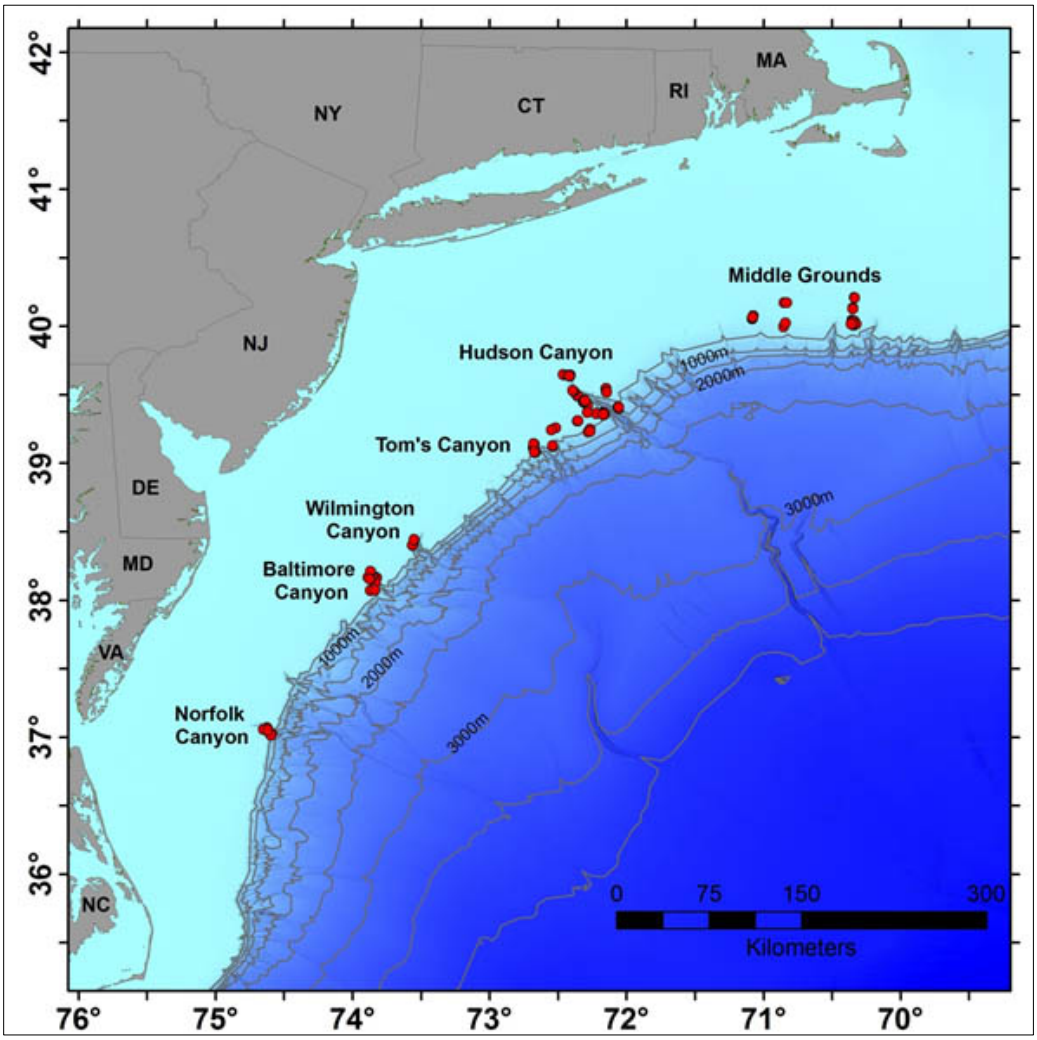

Figure 2-1. Locations of the historical dives analyzed for habitat and fauna.

Table 2-2. Metadata for all historical dives analyzed. Dives at Baltimore, Hudson, Norfolk, Tom's, and Wilmington canyons from 1981−1992 used the *Johnson Sea-Link* submersible; dives at the Middle Grounds in 1987 used the *Delta* submersible (*). n/a = no data available.

Date	Canyon	Dive No.	Dive Length (min)	Video Length (min)	Start Latitude (N)	Start Longitude (W)	End Latitude (N)	End Longitude (W)	Depth Range (m)	Source[1]
6 Aug 1981	Norfolk	1092	138	34	37°03′18.6000″	74°37′34.2000″	37°03'14.4000″	74°37′19.8000″	360−557	Hecker
7 Aug 1981	Norfolk	1093	216	90	37°02′45.6000″	74°37′13.8000″	37°03′37.2000″	74°37′08.4000″	162−580	Hecker
7 Aug 1981	Norfolk	1094	201	66	37°03′24.0000″	74°37′09.0000″	37°03′56.4000″	74°37′19.2000″	192−226	Hecker
8 Aug 1981	Norfolk	1095	186	76	37°01′30.0000″	74°35′30.6000″	37°01′01.8000″	74°35′54.0000″	255−597	Hecker
8 Aug 1981	Norfolk	1096	81	23	37°03′32.4000″	74°38′56.4000″	37°03′27.6000″	74°39′09.6000″	472−597	Hecker
18 Aug 1983	Norfolk	1429	164	88	37°03′10.2000″	74°37′08.4000″	37°03′12.0000″	74°37′10.8000″	155−292	Able
2 Aug 1981	Baltimore	1083	181	23	38°09′25.2000″	73°51′45.0000″	38°09′59.4000″	73°51′51.6000″	381−560	Hecker
2 Aug 1981	Baltimore	1084	132	51	38°09′30.0000″	73°51′00.0000″	38°10′03.0000″	73°53′21.6000″	127−330	Hecker
3 Aug 1981	Baltimore	1085	235	91	38°09′22.2000″	73°51′28.2000″	38°09′23.4000″	73°51′48.0000″	195−271	Hecker
4 Aug 1981	Baltimore	1087	180	54	38°10′07.2000″	73°50′13.2000″	38°09′46.2000″	73°49′27.6000″	213−542	Hecker
5 Aug 1981	Baltimore	1089	219	88	38°09′50.4000″	73°50′46.8000″	38°09′36.6000″	73°51′37.8000″	195−570	Hecker
5 Aug 1981	Baltimore	1090	118	76	38°10′04.2000″	73°50′51.6000″	38°09′54.6000″	73°50′58.8000″	403−583	Hecker
17 Aug 1983	Baltimore	1427	181	66	38°09′18.6000″	73°52′01.2000″	38°09′15.6000″	73°52′33.6000″	114−325	Able
17 Aug 1983	Baltimore	1428	n/a	20	38°09′18.0000″	73°52′01.2000″	38°09′14.4000″	73°52′33.6000″	n/a	Able
5 June 1990	Baltimore	1969	184	97	38°12′33.6000″	73°52′18.6000″	38°12′41.4000″	73°52′10.2000″	193−214	Babb
7 June 1990	Baltimore	1970	139	139	38°07′46.8000″	73°50′25.8000″	38°07′42.6000″	73°50′05.4000″	543−615	Babb
7 June 1990	Wilmington	1971	74	74	38°24′07.8000″	73°33′51.6000″	38°24′22.2000″	73°33′54.6000″	538−594	Babb
12 June 1990	Wilmington	1983	85	85	38°26′32.4000″	73°32′56.4000″	38°26′40.8000″	73°33′03.6000″	148−175	Babb
8 June 1990	Tom's	1972	135	135	39°06′41.4000″	72°40′34.8000″	39°06′45.6000″	72°40′45.0000″	664−683	Babb
8 June 1990	Tom's	1974	70	70	39°08′31.2000″	72°40′40.8000″	39°08′27.6000″	72°40′26.4000″	203−207	Babb
16 July 1991	Tom's	2174	117	95	39°04′58.8000″	72°40′22.8000″	39°05′06.0000″	72°39′57.6000″	579−605	Babb
23 July 1982	Hudson	1234	130	15	39°27′42.6000″	72°18′34.2000″	39°26′54.6000″	72°18′57.0000″	144−156	Able
23 July 1982	Hudson	1235	156	12	39°27′36.6000″	72°18′27.6000″	39°27′29.4000″	72°18′52.2000″	151−165	Able
25 July 1982	Hudson	1237	225	10	39°31′18.0000″	72°08′57.0000″	39°31′12.6000″	72°08′46.2000″	227−237	Able
25 July 1982	Hudson	1238	141	44	39°27′28.8000″	72°18′36.0000″	39°27′42.0000″	72°18′33.0000″	156−175	Able
26 July 1982	Hudson	1239	n/a	31	39°27′39.6000″	72°18′32.4000″	n/a	n/a	175	Able
15 Aug. 1983	Hudson	1423	168	31	39°15′27.6000″	72°31′08.4000″	39°14′35.4000″	72°33′03.6000″	143−144	Able
16 Aug. 1983	Hudson	1425	157	32	39°27′22.2000″	72°18′21.0000″	39°27′25.8000″	72°18′19.2000″	101−105	Able
8 June 1990	Hudson	1973	82	82	39°13′55.2000″	72°16′22.8000″	39°13′58.8000″	72°16′33.6000″	606	Babb

Table 2-2. (Continued).

Date	Canyon	Dive No.	Dive Length (min)	Video Length (min)	Start Latitude (N)	Start Longitude (W)	End Latitude (N)	End Longitude (W)	Depth Range (m)	Source[1]
9 June 1990	Hudson	1975	163	163	39°21′18.0000″	72°10′12.0000″	39°21′36.0000″	72°10′19.2000″	549−602	Babb
9 June 1990	Hudson	1976	91	91	39°24′36.0000″	72°03′46.8000″	39°24′21.6000″	72°03′21.6000″	642−691	Babb
10 June 1990	Hudson	1977	73	73	39°32′42.0000″	72°09′03.6000″	39°32′52.8000″	72°09′03.6000″	183−188	Babb
10 June 1990	Hudson	1978	109	109	39°25′12.0000″	72°16′58.8000″	39°25′22.8000″	72°16′58.8000″	179−181	Babb
10 June 1990	Hudson	1979	74	74	39°29′45.6000″	72°21′35.4000″	39°29′49.2000″	72°21′43.2000″	199−251	Babb
11 June 1990	Hudson	1980	59	59	39°31′37.2000″	72°23′09.6000″	39°31′40.8000″	72°23′27.6000″	620−622	Babb
11 June 1990	Hudson	1981	85	85	39°38′38.4000″	72°27′32.4000″	39°38′45.6000″	72°27′54.0000″	197−224	Babb
11 June 1990	Hudson	1982	59	59	39°38′31.2000″	72°24′57.6000″	39°38′43.2000″	72°24′36.0000″	193−221	Babb
16 June 1990	Hudson	1987	79	75	39°07′19.2000″	72°32′27.6000″	39°07′44.4000″	72°32′27.6000″	630	Babb
16 June 1990	Hudson	1988	40	40	39°18′32.4000″	72°21′29.4000″	39°18′33.0000″	72°21′43.2000″	175	Babb
16 June 1990	Hudson	1989	n/a	25	39°18′36.0000″	72°21′28.8000″	n/a	n/a	181	Babb
15 July 1991	Hudson	2172	125	122	39°21′42.6000″	72°09′51.0000″	39°22′21.0000″	72°10′08.4000″	n/a	Babb
16 July 1991	Hudson	2175	56	56	39°38′09.0000″	72°24′49.8000″	39°38′12.6000″	72°24′52.2000″	229	Babb
17 June 1992	Hudson	2368	125	96	39°13′39.6000″	72°16′49.8000″	39°13′54.6000″	72°16′01.2000″	594−613	Babb
18 June 1992	Hudson	2369	n/a	119	39°24′42.0000″	72°03′30.0000″	n/a	n/a	625−640	Babb
2 June 1987	Middle Grounds	*633	51	24	40°12′29.4000″	70°20′25.8000″	40°12′24.6000″	70°20′02.4000″	n/a	Able
2 June 1987	Middle Grounds	*634	32	26	40°08′11.4000″	70°21′02.4000″	40°07′44.4000″	70°20′54.6000″	117–119	Able

[1] Principal investigators who provided original videos and associated dive logs for these cruises were Barbara Hecker, Hecker Environmental Consulting; Kenneth Able, Rutgers University Institute of Marine and Coastal Science; and Ivar Babb, University of Connecticut, Avery Point.

Video from the dives was viewed in Apple Quicktime or Windows Movie-Maker. Video coverage for most dives was not continuous but often omitted portions of the dives. In such instances, audio cues were necessary to align video time and real time. If possible, the start and stop times for each video segment were recorded. While the length of dives ranged from 40 to 235 min, the video duration was often less, ranging from 10 to 163 min.

2.2.4.1 Habitat Types

Habitats encountered during each dive were classified into one of 15 habitat types as described below. All habitats, except two, were derived from the SEADESC project (Partyka et al. 2007), which is the habitat classification system used by NOAA to create dive logs. The two consolidated sediment classes (habitat types 14 and 15) were created specifically for analyzing deepwater canyons because these habitats were not present in the areas studied by Partyka et al. (2007).

1. **Soft substrate (S)**: Unconsolidated sands or muds, >50% unstructured with little to no vertical relief.
2. **Soft substrate/rubble/rock, barren (SRB)**: Soft substrate with <50% rubble and/or rock, lacking or sparse attached macrofauna, low relief.
3. **Soft substrate/rubble/rock with attached fauna (SRF)**: Soft substrate with <50% rubble and/or rock, with significant attached macrofauna (corals, anemones), low relief.
4. **Rubble (R)**: >50% rubble cover, no rocks or ledges, few or sparse attached macrofauna, low relief.
5. **Rock/ledges, barren (RLB)**: >50% rocks and/or ledges, lacking or sparse attached macrofauna, variable relief.
6. **Rock/ledges with attached fauna (RLF)**: >50% rocks and/or ledges, with significant attached macrofauna, variable relief.
7. **Pavement, barren (PB)**: Fairly flat rock pavement, lacking or sparse macrofauna.
8. **Pavement with attached fauna (PF)**: Flat rock pavement, with significant attached macrofauna.
9. **Mixed hard corals/soft corals/sponges (M)**: Mixtures of soft corals, sponges, and/or hard corals. Hard corals do not dominate this habitat. Bottom may have significant amounts of rubble and variable relief.
10. **Hard corals (HC)**: >50% live and/or dead stony coral cover. Corals are usually standing colonies. Moderate-to-high relief.
11. **Hard corals with attached fauna (HCF)**: >50% live and/or dead coral cover with abundant attached macrofauna. Corals are usually standing colonies. Moderate-to-high relief.
12. **Tilefish habitat (TH)**: Soft substrate with identifiable burrows. Tilefish may or may not be present.
13. **Artificial substrate (A)**: Artificial structure that provides habitat for invertebrates and/or fishes.
14. **Consolidated sediment, barren (CSB)**: >50% cover of compacted mud and clay substrate that forms moderate-to-high topographic relief, often with significant bioerosion. Sparse or absent attached fauna.
15. **Consolidated sediment with attached fauna (CSF)**: >50% cover of compacted mud and clay substrate that forms moderate-to-high topographic relief, often with significant bioerosion. Attached fauna, which can be abundant, generally consists of corals and sponges.

For each dive, the start and end times designating each habitat type were recorded as well as a description of the physical environment and a list of the macroinvertebrates and fishes observed during the entire dive. Representative video frame-grab images were taken of each habitat type encountered during a dive. The number of position fixes per dive ranged from 1 to 25, and these were used to make a track map for each dive in ArcMap 9.3.1. Each fix was mapped with its corresponding habitat classification (**Volume II**, **Appendix E**). If video was not recorded at a fix point, a 'no data' designation was assigned and an empty circle plotted on the map. Synopses of the faunal and physical characteristics of the dive were composed along with comments on dive activities and specimens collected. The track map, habitat pictures, comments, and dive metadata were entered into a Microsoft Access database and dive logs were produced to give a brief overview of each dive (**Volume II**, **Appendix E**).

The data from these historical sources do not have sufficient information to allow the analysis or comparisons of community structure from different habitat types. Most of the locations were on soft substrate, and the few that were on hard substrate were often too out of focus for accurate analysis. Summary logs were created (after Partyka et al. 2007) for all dives with locations of different habitats (as far as possible) and associated images embedded, together with site description, biological information, and source references. The low number of geographical reference points resulted in habitat maps that are not as complete as habitat maps derived from more recent.

2.2.4.2 Environmental Data

Limited environmental data available for these dives were either recorded during the dives or collected on board the ship during the cruise. All available data were extracted and entered into spreadsheets.

2.2.4.3 Habitat-Associated Invertebrates and Fishes

Because of the poor quality and incomplete data associated with some of the underwater footage, a detailed analysis of community structure and associations was not possible. However, a list of macroinvertebrates was compiled for each canyon, together with the habitat with which each taxa was associated. As no voucher specimens were available to examine for positive species identifications, invertebrates were identified to the lowest possible taxonomic level given the video quality. Fishes were noted and identified to the highest taxa possible for the dive, but again poor video quality precluded species level identification in most cases.

2.2.4.4 Database

Station data, dive start and finish, and dive tracks (as far as possible), together with habitat types and environmental data, were recorded into Excel spreadsheets. As part of the final deliverable, data from these spreadsheets were assimilated into a Microsoft Access database and provided to Continental Shelf Associates and will be archived by them. The database includes dive metadata specifying the project, principal investigators, underwater vehicles used, station, site, start and finish times and coordinates, observations, and comments on the habitat as well as the organisms observed during each dive. This database links to the site, dive track maps, and habitat images for each dive.

2.3 RESULTS

2.3.1 Video Analysis

A two-page log was produced for each dive. The first page comprised a station overview with site and dive metadata in addition to general and detailed maps of the dive site. The detailed map shows the location of the dive and habitat type along the track, overlaid on bathymetry, if available. The second page shows images of different habitat types and their location on the dive track in addition to a

description of the biological and physical environment of the dive. Any relevant supporting literature is cited for each dive. Some dives had incomplete navigation data, which prevented dive tracks from being created. In those cases, the start and end of the dive was plotted on the map, and examples of representative habitats and fauna were included as images, but their locations could not be included in the maps. The dive logs were compiled in the order of location from most southerly (Norfolk Canyon) to most northerly (Middle Grounds), then by date (**Volume II**, **Appendix E**).

Notable differences were observed among the canyons surveyed, although these differences were partly an artifact of the objectives of the various projects from which the videos were derived. The primary objective of the work done by Hecker et al. (1983) in Baltimore and Norfolk canyons was to compare habitats among mid-Atlantic canyons. This project covered water depths ranging from 127 to 597 m, whereas the dives made by Able (2002) in Baltimore, Norfolk, and Hudson canyons and the Middle Grounds targeted tilefish habitats and were in shallower water depths (101 to 327 m). Dives made by Cooper et al. (1992) in Baltimore, Wilmington, Hudson, and Tom's canyons were to assess the impact of dumping sewage in the canyons and covered a wide depth range (148 to 691 m) but were primarily conducted over soft sediment. Data extracted from the dive videos showed that dominant habitat type observed in Wilmington, Tom's, and Hudson canyons and the Middle Grounds was soft sediment with occasional consolidated mud. Baltimore and Norfolk canyons had a much greater representation of hard substrate habitats such as rocky ledges, rubble, and consolidated mud.

2.3.2 Environmental Data

Very limited environmental data were collected during these dives (**Table 2-3**). The sensors on the submersible included temperature and salinity, but data were recorded manually and had to be extracted from the dive logs and/or audio. There were no environmental data collected during the Hecker dives in Baltimore and Norfolk canyons, but sporadic temperature, conductivity, and current data were collected during five dives in Hudson Canyon and one dive each in Baltimore, Norfolk, and Tom's canyons.

Table 2-3. Environmental data collected during dives in Norfolk, Baltimore, Tom's, and Hudson canyons. (-- indicates no data available).

Dive No.	Canyon	Dive Date	Depth (ft)	Temp. (°C)	Conductivity (mS cm^{-1})	Current Speed and Direction knots (degrees)	Visibility (ft)
2172	Hudson	15 July 1991	1,917	5.2	34.37	0.1 (340)	--
2174	Tom's	16 July 1991	1,900	5.5	--	0	15−20
2175	Hudson	16 July 1991	750	9.3	--	--	12
2368	Hudson	17 June 1992	2,000	--	--	--	15−20
1423	Hudson	5 Aug 1983	20	23.3	--	--	--
			67	20.9	--	--	--
			100	13.5	--	--	--
			150	12.4	--	--	--
			200	11.5	--	--	--
			250	12.5	--	--	--
			300	12.8	--	--	--
			350	12.7	--	--	--
			400	12.7	--	--	--
			450	12.7	--	--	--
			468	12.1	--	0.1 (90)	--

Table 2-3. (Continued).

Dive No.	Canyon	Dive Date	Depth (ft)	Temp. (°C)	Conductivity (mS cm^{-1})	Current Speed and Direction knots (degrees)	Visibility (ft)
1425	Hudson	16 Aug 1983	50	23.4	39.8	--	--
			75	23.4	39.6	--	--
			100	17.4	44.2	--	--
			125	16.3	33.7	--	--
			150	13.6	41.8	--	--
			175	13.7	41.5	--	--
			200	12.5	40.5	--	--
			225	12.1	39.5	--	--
			250	12.1	39.5	--	--
			275	12.6	30.4	--	--
			325	12.5	30.2	--	--
			350	12.5	30.3	--	--
			375	12.5	40.2	--	--
			400	12.5	40.2	--	--
			425	12.4	30.2	--	--
			450	12.1	30.1	--	--
			475	12.2	30.1	--	--
			500	12.0	39.9	--	--
			526	11.9	39.9	--	--
			549	11.2	39.9	0.11	--
1427	Baltimore	17 Aug 1983	0	22.3	44.9	--	--
			30	22.3	36.0	--	--
			50	21.0	43.1	--	--
			75	10.9	36.5	--	--
			100	9.4	34.5	--	--
			125	9.5	33.7	--	--
			150	8.8	33.5	--	--
			175	8.7	33.4	--	--
			200	8.6	33.4	--	--
			225	8.8	33.5	--	--
			275	8.6	33.0	--	--
			300	8.6	33.6	--	--
			325	8.7	34.7	--	--
			350	9.9	35.7	--	--
			375	10.8	37.4	--	--
			400	11.0	38.4	--	--
			425	11.4	39.1	--	--
			450	11.8	39.4	--	--
			475	11.9	39.7	--	--
			500	11.5	39.7	--	--
			525	12.1	40.1	--	--
			550	12.2	40.2	--	--
			575	12.2	40.2	--	--
			600	12.3	40.3	--	--

Table 2-3. (Continued).

Dive No.	Canyon	Dive Date	Depth (ft)	Temp. (°C)	Conductivity (mS cm^{-1})	Current Speed and Direction knots (degrees)	Visibility (ft)
1427 (Cont'd)	Baltimore	17 Aug 1983	630	12.3	40.2	--	--
			650	12.2	40.1	--	--
			675	12.2	40.3	--	--
			700	12.2	40.3	--	--
			728	12.2	40.3	--	--
			750	12.2	40.3	--	--
			775	11.8	39.8	--	--
			800	11.7	39.2	--	--
			825	11.6	38.9	--	--
			850	11.5	38.9	--	--
			875	11.4	38.3	--	--
			900	10.6	38.7	--	--
			925	9.1	37.6	--	--
			964	9.9	37.1	--	--
			975	9.8	37.1	--	--
			1,000	9.6	37.0	--	--
			1,030	9.6	36.8	--	--
			1,050	9.2	--	--	--
			1,074	9.1	--	--	--
1429	Norfolk	18 Aug 1983	37	18.3	43.8	--	--
			100	18.9	33.8	--	--
			150	18.3	32.9	--	--
			200	18.2	33.0	--	--
			250	18.2	33.3	--	--
			300	18.3	33.6	--	--
			350	18.3	33.8	--	--
			400	9.8	36.1	--	--
			450	10.5	37.5	--	--
			500	11.0	38.9	--	--
			550	11.0	40.1	--	--
			600	10.9	--	--	--
			696	10.6	--	--	--
			800	10.5	38.2	--	--
			900	9.3	36.9	--	--
			958	9.1	37.0	--	--

2.3.3 Invertebrate Species Observed During Historical Dives

The poor quality of the video and the uncertainty of field identifications on dive logs resulted in an incomplete list of fauna with low taxonomic resolution. Despite these limitations, the data showed that the fauna observed in the different canyons reflects the dominant habitat type, with a greater representation of sessile benthic fauna such as sponges and octocorals in Norfolk and Baltimore canyons (~45% of all fauna observed), whereas mobile or soft sediment fauna such as crustaceans and echinoderms dominated the other canyons and the Middle Grounds (~80% of observations). A list of invertebrates observed during the dives was compiled from viewing the tapes and identifying the invertebrates from the dive audio and hard copy logs (**Table 2-4**).

Table 2-4. List of invertebrate taxa observed during analysis of historical submersible dives. Habitat types are defined in **Section 2.2.4.1**.

Canyon	Phylum	Taxa	Habitat Type
Norfolk	Porifera	Unidentified sponges	SRF, RLF, PF, CSF
Norfolk	Porifera	Yellow sponges	RLF, PF
Norfolk	Cnidaria	*Paragorgia arborea*	RLF
Norfolk	Cnidaria	*Acanthogorgia* sp.	RLF
Norfolk	Cnidaria	*Eunepthya florida**	RLF
Norfolk	Cnidaria	*Halcurias pilatus*	SRF, RLF, PF, CSF
Norfolk	Cnidaria	*Actinoscyphia* sp.	SRB, SRF, RLF, CSF
Norfolk	Cnidaria	*Bolocera* sp.	S, RLF
Norfolk	Cnidaria	Cerianthid anemone	SRF, RLF, CSF
Norfolk	Cnidaria	Mauve anemones	RLF
Norfolk	Cnidaria	Anemones	RLB, RLF, CSF
Norfolk	Mollusca	Squid	RLF
Norfolk	Anellida	Encrusting polychaetes	RLF
Norfolk	Arthropoda	*Chaceon quinquedens*	SRB, R, RLB, RLF, CSB
Norfolk	Arthropoda	*Bathynectes superba*	CSF
Norfolk	Arthropoda	*Cancer* sp. crab	RLF, CSF
Norfolk	Arthropoda	*Lithodes* sp. crab	RLF
Norfolk	Arthropoda	Small crabs	SRF
Norfolk	Arthropoda	*Homarus americanus*	S, RLF
Norfolk	Arthropoda	Galatheid crab	RLF, CSF
Norfolk	Arthropoda	Hermit crabs	SRB
Norfolk	Arthropoda	Shrimp	RLF
Norfolk	Echinodermata	*Gorgonocephalus* sp.	RLF
Norfolk	Echinodermata	Batstar	RLB, RLF
Norfolk	Echinodermata	Red seastar	SRF
Norfolk	Echinodermata	Seastars	SRB, SRF, RLF, CSF
Norfolk	Echinodermata	Sea urchin	RLF
Norfolk	Echinodermata	Crinoids	SRF, RLF
Baltimore	Porifera	Bright yellow sponge	RLF
Baltimore	Porifera	Bulbous sponge	SRF
Baltimore	Porifera	Encrusting sponge	RLF
Baltimore	Porifera	Potato chip sponge	RLF
Baltimore	Porifera	Unidentified sponge	SRB, SRF, RLF
Baltimore	Porifera	Yellow and white sponge	CSF
Baltimore	Porifera	Sponges	SRF, CSF
Baltimore	Porifera	Vase sponges	RLF
Baltimore	Porifera	White ball sponge	RLF
Baltimore	Porifera	White sponge	RLF
Baltimore	Porifera	Yellow sponge	RLF
Baltimore	Cnidaria	*Paragorgia arborea*	SRF, RLF, PF, CSF
Baltimore	Cnidaria	*Primnoa resedaeformis***	RLF
Baltimore	Cnidaria	*Anthothela* sp.	RLF
Baltimore	Cnidaria	Zooanthids	RLF
Baltimore	Cnidaria	*Eunepthya florida**	CSF

Table 2-4. (Continued).

Canyon	Phylum	Taxa	Habitat Type
Baltimore	Cnidaria	Sea pen	SRB, SRF, A
Baltimore	Cnidaria	Orange cup coral	RLF
Baltimore	Cnidaria	*Actinoscyphia* sp.	SRF, RLF, PF, CSF
Baltimore	Cnidaria	*Bolocera* sp.	SRF, R, RLF, PF, CSF
Baltimore	Cnidaria	*Cerianthus borealis*	R, RLF
Baltimore	Cnidaria	*Halcurias pilatus*	SRB, SRF, RLF, TH, CSF
Baltimore	Cnidaria	*Hormathia nodosa*	RLF
Baltimore	Cnidaria	Cerianthid anemone	S, SRB, SRF, RLF, PF, CSB, CSF
Baltimore	Cnidaria	Anemone	S
Baltimore	Cnidaria	Encrusting anemones	PF
Baltimore	Cnidaria	Mauve anemones	SRF, RLF
Baltimore	Cnidaria	White anemone	S, RLF
Baltimore	Cnidaria	Orange anemone	CSF
Baltimore	Cnidaria	Hydroids	SRF, RLF
Baltimore	Mollusca	Octopus	S, CSB, CSF
Baltimore	Mollusca	Squid	CSB, CSF
Baltimore	Annelida	Polychaete tubes	RLF
Baltimore	Annelida	Tubeworms	S, SRF
Baltimore	Arthropoda	*Bathynectes superba*	SRF, RLF, CSF
Baltimore	Arthropoda	*Bathynectes* sp.	S
Baltimore	Arthropoda	*Chaceon quinquedens*	S, SRB, SRF, RLF, PF
Baltimore	Arthropoda	*Cancer borealis*	SRB
Baltimore	Arthropoda	*Cancer* sp.	S, SRB, SRF, R, RLF, A, CSF
Baltimore	Arthropoda	*Lithodes* sp. crab	SRF, RLF, CSF
Baltimore	Arthropoda	Spider crab	S, A
Baltimore	Arthropoda	Crab	PF
Baltimore	Arthropoda	Galatheid crab	SRB, SRF, R, RLF, PF, CSF
Baltimore	Arthropoda	Hermit crab	S, SRB, SRF, RLF, TH
Baltimore	Arthropoda	*Homarus americanus*	SRF, R, RLF, CSB
Baltimore	Arthropoda	*Munida* sp. (galatheid)	SRB
Baltimore	Arthropoda	Large shrimp	S
Baltimore	Arthropoda	Shrimp	RLF
Baltimore	Arthropoda	Shrimp on Paragorgia	RLF
Baltimore	Echinodermata	Basketstar	RLF, CSF
Baltimore	Echinodermata	*Asterias* sp.	SRF
Baltimore	Echinodermata	*Astropecten* sp.	S, SRB
Baltimore	Echinodermata	*Henricia* sp.	SRB
Baltimore	Echinodermata	*Sclerasterias* sp.	SRB
Baltimore	Echinodermata	Batstar	RLF
Baltimore	Echinodermata	Brisingid seastars	R
Baltimore	Echinodermata	Light pink seastar	SRB
Baltimore	Echinodermata	Long-armed seastar	SRB
Baltimore	Echinodermata	Orange seastar	SRF
Baltimore	Echinodermata	Red and white seastars	RLF
Baltimore	Echinodermata	Red batstar	PF
Baltimore	Echinodermata	Thin-armed seastar	CSF

Table 2-4. (Continued).

Canyon	Phylum	Taxa	Habitat Type
Baltimore	Echinodermata	Seastar	SRB, SRF, R, RLF, A
Baltimore	Echinodermata	White and red seastar	RLF
Baltimore	Echinodermata	Yellow seastar	RLF
Baltimore	Echinodermata	Sea urchin	RLF
Baltimore	Echinodermata	Small white sea urchin	RLF
Baltimore	Echinodermata	Urchin	RLF, PF
Baltimore	Echinodermata	Small crinoid	SRF, RLF
Baltimore	Chordata	Large tunicates	RLF
Wilmington	Porifera	*Hyalonema* sp.	S
Wilmington	Cnidaria	*Bolocera* sp.	S
Wilmington	Arthropoda	*Chaceon quinquedens*	S
Wilmington	Arthropoda	Hermit crab	SRB, R
Wilmington	Arthropoda	Large red shrimp	S
Wilmington	Echinodermata	Red batstar	R
Wilmington	Echinodermata	Red long-armed seastar	SRB, R
Wilmington	Echinodermata	Seastar	SRB
Wilmington	Echinodermata	Small red urchin	R
Tom's	Cnidaria	*Actinoscyphia* sp.	S
Tom's	Cnidaria	*Cerianthid anemone*	S
Tom's	Cnidaria	Sea pen	S
Tom's	Annelida	*Hyalinoecia* sp	S
Tom's	Arthropoda	*Chaceon quinquedens*	S
Tom's	Arthropoda	*Cancer* sp.	S
Tom's	Arthropoda	Galatheid crabs	S
Tom's	Arthropoda	Hermit crab	S
Tom's	Echinodermata	*Sclerasterias* sp.	S
Tom's	Echinodermata	Brittlestars	S
Tom's	Echinodermata	Crinoid	S
Hudson	Cnidaria	*Actinoscyphia* sp.	S, SRB, RLF
Hudson	Cnidaria	Cerianthid anemone	S, TH
Hudson	Cnidaria	Octocoral	CSB
Hudson	Cnidaria	Sea pen	S
Hudson	Cnidaria	Small white anemones	SRB
Hudson	Cnidaria	Hydroids	S
Hudson	Mollusca	Snail	S
Hudson	Mollusca	Squid	S
Hudson	Annelida	*Hyalinoecia* sp	S
Hudson	Annelida	Small tube worms	S
Hudson	Arthropoda	*Chaceon quinquedens*	S, RLF, CSB
Hudson	Arthropoda	*Bathynectes* sp.	S
Hudson	Arthropoda	*Cancer* sp.	S, TH, A
Hudson	Arthropoda	*Homarus americanus*	S, TH
Hudson	Arthropoda	Galatheid crab	S, TH, A, CSB
Hudson	Arthropoda	Hermit crab	S, CSB
Hudson	Arthropoda	Large red shrimp	S, CSB
Hudson	Arthropoda	Shrimp	S

Table 2-4. (Continued).

Canyon	Phylum	Taxa	Habitat Type
Hudson	Echinodermata	*Sclerasterias* sp.	S
Hudson	Echinodermata	Orange seastar	S
Hudson	Echinodermata	Seastar	S
Hudson	Echinodermata	Ophiuroid	S
Hudson	Echinodermata	Large ophiuroid	S
Middle Grounds	Porifera	Hexactinellid sponge	S
Middle Grounds	Cnidaria	Anemone on *Cancer* sp.	S
Middle Grounds	Cnidaria	Cerianthid anemone	S
Middle Grounds	Cnidaria	Sea pens	S, TH
Middle Grounds	Mollusca	Topshell snails	S
Middle Grounds	Arthropoda	*Bathynectes superba*	S
Middle Grounds	Arthropoda	*Cancer* sp.	S, TH
Middle Grounds	Arthropoda	*Homarus americanus*	S
Middle Grounds	Arthropoda	Galatheid crab	TH
Middle Grounds	Echinodermata	Seastar	S

* *Eunepthya florida* was reclassified to *Duva florida* (Huzio 1961).
** Coral was identified on dive log as *Acanthogorgia* sp., but was actually *Primnoa resedaeformis*.
A = Artificial substrate; CSB = Consolidated sediment, barren; CSF = Consolidated sediment with attached fauna; HC = Hard corals; HCF = Hard corals with attached fauna; M = Mixed hard corals/soft corals/`sponges; PB = Pavement, barren; PF = Pavement with attached fauna; R = Rubble; RLB = Rock/ledges, barren; RLF = Rock/ledges with attached fauna; S = Soft substrate; SRB = Soft substrate/rubble/rock, barren; SRF = Soft substrate/rubble/rock with attached fauna; T = Tilefish habitat.

2.3.4 Fishes Observed During Historical Dives

The fishes observed were noted in the logs for each dive. The more common fish species included tilefish (*Lopholatilus chamaeleonticeps*), blackbelly rosefish (*Helicolenus dactylopterus*), synaphobranchid eels (*Synaphobranchus* sp.), conger eels (Congridae), hake (Phycidae and Merlucciidae), skates (Rajidae), hagfish (Myxinidae), rattails (*Nezumia* sp.), and roughies (*Hoplostethus* spp.). Large aggregations of chain dogfish (S*cyliorhinus retifer)* were observed in August 1981 during a shallow dive in Baltimore Canyon (JSLI-1085, 100 to 270 m) on broken rock pavement habitat, together with large numbers of hake. The chain dogfish was also observed in great numbers during the 2012 and 2013 shipwreck dives near the head of Norfolk Canyon, and trawl nets covering the wrecks had abundant shark or skate egg cases (**Chapter 15**). The large gatherings may be related to reproduction of this species. Dive JSLI-1085 shows that these aggregations also occur in natural habitats and are not a phenomenon associated only with artificial habitat.

2.4 DISCUSSION

The information derived from this analysis was valuable for generating potential dive targets for the 2012 and 2013 sampling cruises and was, therefore, a useful exercise. There were, however, challenges in analyzing these data and limitations in the data themselves. The video was often of poor quality; this was partly due to the age and storage conditions of the tapes, but the technology of the time was considerably less sophisticated than it is today. Video resolution was much lower than the high-definition digital imagery used by most modern underwater vehicles, which, in combination with the degraded quality, made identification of the fauna extremely challenging or impossible. Field identification by the submersible observers was used to help classify fauna, but these could not be verified. The taxonomic resolution produced was therefore low and possibly not always accurate. The navigation systems used during the dives was Loran-C (noted as time-delay numbers that were converted into latitude and longitude for the purposes of this report), but unlike today where submersible or remotely operated

vehicle (ROV) navigation tracks are recorded continuously, "fixes" or locations were recorded only when specifically requested by the submersible pilot. Consequently, generating dive tracks with accompanying habitat type was not possible, but points were plotted on the maps wherever fixes were available.

Environmental data were mostly absent from the dive logs, with a few exceptions (which are documented in **Table 2-3**). These data had to be entered manually by the submersible observers and was not done consistently. Given the poor quality of the data, it was not possible to conduct a statistically rigorous comparison of the benthic communities within the canyons.

The analysis of historical data on canyons in the mid-Atlantic region was intended to provide information on the distribution of different habitats and associated communities that occur in each canyon. These data were intended to assist in the selection of target canyons for the larger project objectives and identify potential dive locations for the ROV cruises. The hard substrate habitats that support sessile benthic communities were significantly more prevalent in Baltimore and Norfolk canyons as were the observations of octocorals (e.g., *Paragorgia, Primnoa,* and *Anthothela*), sponges, and large patches of anemones. The north and south walls of Norfolk Canyon and the east and west walls of Baltimore Canyon in moderate water depths of approximately 250 to 600 m showed the abundant hard substrate in the form of rocky ledges and pavement. The shallower depths were dominated by soft sediment with occasional hard substrate and therefore were of less interest as potential targets for the larger project. The depth limit of the *Johnson Sea-Link* submersible was 3,000 ft so the deeper sections of the canyons were not explored. In addition to the coral and sponge communities, a patch of mussels was observed during a camera tow in Baltimore Canyon during Hecker's cruise in 1981. This finding was particularly intriguing, because no cold seeps had ever been documented on the east coast at that time, and only two cold seeps were known prior to the first major research cruise of this project, both off the Blake Ridge, North Carolina. Finding "Hecker's seep" became one of the objectives of the first cruise (**Chapter 3**).

The historical data from this analysis, combined with the multibeam sonar obtained during the 2011 mapping cruise for this project, provided sufficient information to target the ROV dives on appropriate habitat for deepsea coral and other hard substrate communities. The site selection process is discussed in **Chapter 3**. Additional discussion of the historical data is provided in **Chapter 20** (Synthesis).

2.5 LITERATURE CITED

Able KW. 2002. An evaluation of the impact of mobile fishing gear on tilefish habitat: review of archived video images from submersible. Progress Report to the Mid-Atlantic Fishery Management Council. 6 p.

Cooper RA, Stewart LJ, Baker J, Babb I. 1992. Assessment of impact of sewage sludge dumping (106 mile dump site) on ocean habitats and megabenthic fauna, progress report. NOAA's National Undersea Research Center at the University of Connecticut at Avery Point. 41 p.

Grimes CB, Able KW, Jones RS, Twichell DC, Turner SC. 1987. Studies on tilefish fishery biology, ecology and bioerosion on the middle Atlantic and southern New England continental shelf. NOAA Symposium Series for Undersea Research. 2(2):49–69.

Hecker B, Blechschmidt G, Gibson P. 1980. Epifaunal zonation and community structure in three mid- and north Atlantic canyons. Final report for the canyon assessment study in the Mid-and North Atlantic Areas of the U.S. Outer Continental Shelf. Prepared for the U.S. Department of Interior, Bureau of Land Management under contract BLM AA5 51-CT8-49. Palisades (NY): Lamont-Doherty Geological Observatory.

Hecker B, Logan DT, Gandarillas FE, Gibson PR. 1983. Canyon and slope processes study, vol. III: biological processes. Report for the U.S. Department of the Interior, Minerals Management Service, under contract no. 14-12-0001-29178. Palisades (NY): Lamont-Doherty Geological Observatory. 212 p. [accessed 2016 June 1]. http://invertebrates.si.edu/boem/reports/CASPS_vol3.pdf.

Huzio U. 1961. A revision of the nomenclature of the family Nephtheidae (Octocorallia: Alcyonacea) II. The boreal genera G*ersemia, Duva, Drifa* and *Pseudodrifa*. Publications of the Seto Marine Biological Laboratory. 9(1):229–246.

Partyka ML, Ross SW, Quattrini AM, Sedberry GR, Birdsong TW, Potter J. 2007. Southeastern United States deep-sea corals (SEADESC) initiative: a collaborative effort to characterize areas of habitat-forming deep-sea corals. Silver Spring (MD). NOAA Technical Memorandum OER 1. 176 p.

De Leo FC, Smith CR, Rowden AA, Bowden DA, Clark MR. 2010. Submarine canyons: hotspots of benthic biomass and productivity in the deep sea. Proceedings of the Royal Society of London Series B, Biological Sciences. 277(1695):2783–2792. doi:10.1098/rspb.2010.0462.

de Stigter HC, Boer W, de Jesus Mendes PA, Jesus CC, Thomsen L, van den Bergh GD, van Weering TCE. 2007. Recent sediment transport and deposition in the Nazaré Canyon, Portuguese continental margin. Marine Geology. 246:144–164.

Forde EB, Stanley DJ, Sawyer WB, Slagle KJ. 1981. Sediment transport in Washington and Norfolk submarine canyons. Applied Ocean Research. 3:59–62.

Gardner WD. 1989a. Periodic resuspension in Baltimore Canyon by focusing of internal waves. Journal of Geophysical Research. 94:18,185–194.

Gardner WD. 1989b. Baltimore Canyon as a modern conduit of sediment to the deep sea. Deep-Sea Research Part A: Oceanographic Research Papers. 36:323–358.

Garvine RW, Wong KC, Gawarkiewicz GG, Mccarthy RK, Houghton RW, Aikman F. 1988. The morphology of shelfbreak eddies. Journal of Geophysical Research-Oceans. 93:15593–15607.

Griggs GB, Carey AG, Kulm LD. 1969. Deep-sea sedimentation and sediment-fauna interaction in Cascadia Channel and on Cascadia Abyssal Plain. Deep Sea Research and Oceanographic Abstracts. 16(2):157–170. doi:10.1016/0011-7471(69)90071-0.

Grimes CB, Able KW, Jones RS. 1986. Tilefish, *Lopholatilus chamaeleonticeps*, habitat, behavior and community structure in Mid-Atlantic and southern New England waters. Environmental Biology of Fishes. 15:273–292.

Grimes CB, Able KW, Jones RS, Twichell DC, Turner SC. 1987. Studies on tilefish fishery biology, ecology and bioerosion on the middle Atlantic and southern New England continental shelf. NOAA Symposium Series for Undersea Research. 2(2):49–69.

Haedrich RL, Rowe GT, Polloni PT. 1980. The megabenthic fauna in the deep sea south of New England, USA. Marine Biology. 57:165–179.

Hecker B, Blechschmidt G, Gibson P. 1980. Epifaunal zonation and community structure in three mid- and north Atlantic canyons. Final report for the canyon assessment study in the Mid-and North Atlantic Areas of the U.S. Outer Continental Shelf. Prepared for the U.S. Department of Interior, Bureau of Land Management under contract BLM AA5 51-CT8-49. Palisades (NY): Lamont-Doherty Geological Observatory.

Hecker B, Logan DT, Gandarillas FE, Gibson PR. 1983. Canyon and slope processes study, vol. III: biological processes. Report for the U.S. Department of the Interior, Minerals Management Service, under contract no. 14-12-0001-29178. Palisades (NY): Lamont-Doherty Geological Observatory. 212 p. [accessed 2016 June 1]. http://invertebrates.si.edu/boem/reports/CASPS_vol3.pdf.

Houghton RW, Schlitz R, Beardsley RC, Butman B, Chamberlin JL. 1982. The Middle Atlantic Bight cold pool−evolution of the temperature structure during summer 1979. Journal of Physical Oceanography. 12:1019–1029.

Houghton RW, Olson DB, Celone PJ. 1986. Observation of an anticyclonic eddy near the continental shelf break south of New-England. Journal of Physical Oceanography. 16:60–71.

Hudson KA, Haedrich RL. 1984. Abundance and biomass of macrobenthos in the vicinity of Carson Submarine Canyon, northwest Atlantic Ocean. Marine Biology. 82:301–305.

King NJ, Jamieson AJ, Bagley PM, Priede IG. 2008. Deep-sea scavenging demersal fish fauna of the Nazare Canyon system, Iberian coast, north-east Atlantic Ocean. Journal of Fish Biology. 72:1804-1814.

Levin LA. 2005. Ecology of cold seep sediments: interactions of fauna with flow, chemistry and microbes. Oceanography and Marine Biology Annual Review. 43:1–46.

Lillibridge JL, Hitchcock G, Rossby T, Lessard E, Mork M, Golmen L. 1990. Entrainment and mixing of shelf slope waters in the near-surface Gulf Stream. Journal of Geophysical Research−Oceans. 95(C8):13065–13087.

Loder JW, Petrie BG, Gawarkiewicz G. 1998. The coastal ocean off northeastern North America: a large-scale view. In: Robinson AR, Brink K, editors. The sea, volume 11: the global coastal ocean - regional studies and syntheses. John Wiley & Sons. p. 105–133.

Malahoff A, Embley RW, Perry RB, Fefe C. 1980. Submarine mass-wasting of sediments on the continental slope and upper rise south of Baltimore Canyon. Earth and Planetary Science Letters. 49:1–7.

Malahoff A, Embley RW, Fornari DJ. 1982. Geomorphology of Norfolk and Washington Canyons and the surrounding continental slope and upper rise as observed from DSRV Alvin. In: Scrutton RA, Talwani M., editors. The ocean floor. John Whiley & Sons. p. 97–114.

Markle DF, Musick JA. 1974. Benthic-slope fishes found at 900m depth along a transect in the western N. Atlantic Ocean. Marine Biology. 26:225–233.

McClain C R, Barry JP. 2010. Habitat heterogeneity, disturbance, and productivity work in concert to regulate biodiversity in deep submarine canyons. Ecology. 91(4):964–976.

Mitchell NC. 2005. Interpreting long-profiles of canyons in the USA Atlantic continental slope. Marine Geology. 214:75–99.

Musick JA. 1979. Community structure of fishes on the continental slope and rise off the middle Atlantic coast of the United States. Gloucester Point (VA): Virginia Institute of Marine Science. Special Scientific Report No. 96.

Oliveira A, Santos AI, Rodrigues A, Vitorino J. 2007. Sedimentary particle distribution and dynamics on the Nazaré canyon system and adjacent shelf (Portugal). Marine Geology. 246:105–122.

Paull CK, Ussler W, Borowski WS, Spiess FN. 1995. Methane-rich plumes on the Carolina continental rise: associations with gas hydrates. Geology. 23:89–92.

Roberts JM, Wheeler AJ, Freiwald A, Cairns S. 2009. Cold-water corals: the biology and geology of deep-sea coral habitats. Cambridge (UK): Cambridge University Press.

Robinson AR, Brink K. 2006. The sea, volume 14a: the global coastal ocean: interdisciplinary regional studies and syntheses. Boston (MA): Harvard University Press. 840 p.

Ross SW, Nizinski MS. 2007. State of deep coral ecosystems in the U.S. Southeast Region: Cape Hatteras to southeastern Florida. In: Lumsden SE, Hourigan TF, Bruckner AW, Dorr G, editors. The state of deep coral ecosystems of the United States. Silver Spring (MD): National Oceanic and Atmospheric Administration. NOAA Technical Memorandum CRCP-3. p. 233–270.

Rowe GT. 1972. The exploration of submarine canyons and their benthic faunal assemblages. Proceedings of the Royal Society of Edinburgh, Section B: Biology. 73(17):159–169.

Shepard AN, Theroux RB, Cooper RA, Uzmann JR. 1986. Ecology of *Ceriantharia* (Coelenterata, Anthozoa) of the northwest Atlantic from Cape Hatteras to Nova Scotia. Fisheries Bulletin. 84:625-646.

Stefanescu C, Morales-Nin B, Massutí E. 1994. Fish assemblages on the slope in the Catalan Sea (western Mediterranean): influence of a submarine canyon. Journal of Marine Biological Association of UK. 74:499–512.

Sulak KJ, Ross SW. 1996. Lilliputian bottom fish fauna of the Hatteras upper middle continental slope. Journal of Fish Biology. 49(Suppl. A):91–113.

Theroux RB, Wigley RL. 1998. Quantitative composition and distribution of the macrobenthic invertebrate fauna of the continental shelf ecosystems of the northeastern United States. Seattle (WA): U.S. Dept. of Commerce, National Oceanic and Atmospheric Administration, National Marine Fisheries Service, Scientific Publications Office. NOAA Technical Report NMFS 140. 240 p.

Tucholke BE. 1987. Submarine geology. In: Milliman JD, Wright WR, editors. The marine environment of the US Atlantic continental slope and rise. Boston (MA): Jones and Bartlett. p. 56–113.

Uchupi E. 1968. Seismic profiling survey of the east coast submarine canyons part 1. Wilmington, Baltimore, Washington and Norfolk canyons. Deep Sea Research and Oceanographic Abstracts. 15:613–616. doi:10.1016/0011-7471(68)90067-3.

Van Dover CL. 2000. The ecology of hydrothermal vents. Princeton (NJ): Princeton University Press. 448 p.

Van Dover CL, Aharon P, Bernhard JM, Caylor E, Doerries M, Flickinger W, Gilhooly W, Goffredi SK, Knick KE, Macko SA, et al. 2003. Blake Ridge methane seeps: characterization of a soft-sediment, chemosynthetically based ecosystem. Deep Sea Research Part I: Oceanographic Research Papers. 50(2):281–300. doi:10.1016/S0967-0637(02)00162-0.

Vetter EW, Dayton PK. 1998. Macrofaunal communities within and adjacent to a detritus-rich submarine canyon system. Deep Sea Research Part II: Topical Studies in Oceanography. 45:25–54.

Voorhis AD, Webb DC, Millard RC. 1976. Current structure and mixing in the shelf/slope water front south of New England. Journal of Geophysical Research. 81:3695–3708.

Warme JE, Slater RA, Cooper RA. 1978. Bioerosion in submarine canyons. In: Stanley DJ, Kelling G, editors. Sedimentations in submarine canyons, fans, and trenches. Stroudsburg, (PA): Dowden, Hutchinson and Ross. p. 65–70.

Wilson WHJ. 1991. Competition and predation in marine soft-sediment communities. Annual Review of Ecology and Systematics. 21:221–241.

Young CM. 2009. Communities on deep-sea hard bottom. In: Wahl M, editor. Marine hard bottom communities. New York (NY): Springer. p. 39–60.

This page intentionally left blank

CHAPTER 3. STUDY DESIGN AND GENERAL METHODS

3.1 RESEARCH CRUISES

3.1.1 Overview

Four research cruises were conducted during the Atlantic Deepwater Canyons study (**Table 3-1**). Environmental data on canyon habitats and fauna were collected on all four cruises, and three of the cruises also had an archaeological component. All cruises were collaborative efforts among the Bureau of Ocean Energy Management (BOEM), the National Oceanic and Atmospheric Administration (NOAA), the U.S. Geological Survey (USGS), and CSA Ocean Sciences Inc. (CSA) and its partners. Methods were standardized to the extent possible. Detailed cruise reports were submitted to BOEM and NOAA soon after each cruise. Summaries of each cruise are provided in this chapter, and the cruise reports can be found in **Volume II**, **Appendices A**, **B**, **C**, and **D**.

Table 3-1. Summary of cruises conducted during the Atlantic Deepwater Canyons study.

Cruise Name	Ship (and ROV)	Dates	Activities
2011 Mapping Cruise (NF-11-04)	*Nancy Foster*	4–17 June 2011	• Seafloor mapping (multibeam echo sounder) • Archaeological investigations • Hydrographic profiling and water sampling • Outreach activities
2012 Sampling Cruise (NF-12-07)	*Nancy Foster* (*Kraken 2*)	15 Aug. to 3 Oct. 2012	• ROV surveys and collections • Box core, monocore, and trawl sampling • Benthic lander and mooring deployment • Seafloor mapping (multibeam echo sounder) • Hydrographic profiling and water sampling • Archaeological investigations • Outreach activities
2013 Sampling Cruise (RB-13-03-HBH)	*Ronald H. Brown* (*Jason II*)	30 April to 27 May 2013	• ROV surveys and collections • Box core, monocore, and trawl sampling • Benthic lander redeployment • Seafloor mapping (multibeam echo sounder) • Hydrographic profiling and water sampling • Archaeological investigations • Outreach activities
2013 Instrument Retrieval Cruise (NF-13-09)	*Nancy Foster*	21–27 Aug. 2013	• Benthic lander and mooring retrieval • Hydrographic profiling and water sampling • Monocore sampling • Outreach activities

The 2011 mapping cruise (**Section 3.1.2**) provided high-resolution seafloor mapping of several Mid-Atlantic Bight (MAB) canyons to supplement previous coverage of these areas and aid in site selection for subsequent sampling cruises. Most of the seafloor mapping was done in and near Baltimore, Washington, and Norfolk canyons. After reviewing the 2011 mapping data along with historical data (**Chapter 2**), the principal investigators decided to focus on Baltimore and Norfolk canyons as the most promising sites for detailed study of canyon habitats and fauna. The decision was based on the rugged

topography of these two canyons, previous reports of deepwater corals there (Hecker et al. 1983), and the desire to best understand specific canyons.

The 2012 and 2013 sampling cruises (**Sections 3.1.3** and **3.1.4**) were the main sampling efforts that focused on Baltimore and Norfolk canyons. Both cruises included remotely operated vehicle (ROV) surveys of canyon habitats and fauna as well as box core and monocore sampling, trawl sampling, hydrographic profiling, and outreach activities.

Four benthic landers and two moorings were deployed during the 2012 sampling cruise. One benthic lander was placed near the head and the mouth of each canyon, and a mooring was placed in the middle of each canyon. The landers and moorings were intended to remain in place for 1 year. The two benthic landers in Baltimore Canyon were serviced and redeployed (at the same locations) during the 2013 sampling cruise to replace faulty release mechanisms.

The 2013 instrument retrieval cruise (**Section 3.1.5**) was conducted to recover the benthic landers and moorings deployed approximately 1 year earlier. One lander and one mooring could not be retrieved during the cruise, but the mooring was eventually recovered. Although the lander finally was discovered in the Bahamas, to date it and its data have not been retrieved (due to funding and logistical issues). The 2012 and 2013 cruises also included monocore sampling, hydrographic profiling, and outreach activities.

The first three cruises also included an archaeological component. The 2011 mapping cruise detected six high-priority targets in the Norfolk Canyon area indicative of shipwrecks. Among these were five previously unidentified sites suspected to be from the Billy Mitchell-Project B fleet. During the 2012 sampling cruise, all shipwrecks from the Billy Mitchell-Project B fleet, along with one other shipwreck, were identified and confirmed by ROV dives. During the 2013 sampling cruise, ROV surveys were conducted at four of the Billy Mitchell-Project B wrecks. The ROV collected invertebrate specimens and recorded video observations of fishes and epibiota associated with shipwrecks.

Outreach activities were part of all cruises. Two websites documented progress and facilitated public awareness of the project. One site (http://oceanexplorer.noaa.gov/explorations/12midatlantic/) was managed by the NOAA Office of Ocean Exploration as a Signature Expedition site. The North Carolina Museum of Natural Sciences set up a blog (http://deepwatercanyons.wordpress.com) to allow for easy posting of cruise activity logs. Background essays, daily logs, and various photographs were posted to both sites prior to and during the cruises. The blogs and daily logs were written by various scientific personnel while at sea. Skype interviews with principal investigators were broadcast live during the 2012 and 2013 sampling cruises. Other outreach efforts included an article in the *Washington Post* and *Herald Tribune*, among others. Details on education and outreach activities are discussed in **Chapter 18**.

3.1.2 2011 Mapping Cruise

The 2011 mapping cruise was conducted from 4 to 17 June aboard the NOAA ship *Nancy Foster*. Details are provided in the cruise report (**Volume II**, **Appendix A**). The main objective was to conduct high-resolution seafloor mapping of selected MAB canyons to aid in site selection. The multibeam bathymetric survey focused on Baltimore, Washington, and Norfolk canyons (**Figure 1** of **Appendix A**). During this cruise, 1,397.65 km^2 of seafloor were mapped, of which 997.63 km^2 (71%) were in and around these three canyons. Bathymetric data from the 2011 mapping cruise were combined with data from other USGS surveys to produce a detailed map of the MAB canyons (**Figure 2** of **Appendix A**).

In addition to the seafloor mapping, 32 conductivity-temperature-depth (CTD) stations were sampled during the cruise. Water column sampling was conducted using a Sea-Bird Electronics, Inc. (Sea-Bird) SBE 911*plus* recording probe mounted on a rosette sampler device fitted with Niskin bottles (**Section 3.2.6**). The probe measured turbidity, dissolved oxygen, altitude, depth, conductivity, temperature, salinity, and pH. In addition to these point samples, two hydrographic profile transects were

collected down the axes of Baltimore and Norfolk canyons. Water samples were collected in Niskin bottles from specific depths in the water column at selected stations.

Seafloor mapping in and to the north of Norfolk Canyon detected six high-priority targets that were interpreted as indicative of shipwrecks. These included five previously unidentified sites that were suspected (and later confirmed) to be the remains of the Billy Mitchell-Project B fleet. Those sites included the remains of the battleship *Ostfriesland*, the cruiser *Frankfurt*, and the destroyers *G-102*, *S132*, and *V-43*. An unidentified shipwreck was also discovered just south of Norfolk Canyon. In addition, high-resolution mapping of Norfolk, Baltimore, and Washington canyons revealed features that likely are paleo-shorelines dating back to the last glacial maximum.

3.1.3 2012 Sampling Cruise

The 2012 sampling cruise also used the NOAA ship *Nancy Foster*. Details are provided in the cruise report (**Volume II**, **Appendix B**). This cruise originated and ended in Charleston, South Carolina and was divided into three legs with port days in Norfolk, Virginia. Leg 1 (15 to 31 August 2012) and Leg 2 (3 to 14 September 2012) emphasized biological, geological, and oceanographic objectives, while Leg 3 (17 September to 2 October 2012) emphasized archaeological objectives. The detailed bathymetric maps generated during the 2011 mapping cruise were used to guide sampling activities.

Two benthic landers and one mooring were deployed in each of the two canyons (see **Section 3.2.3** for descriptions). Two landers (ALBEX [Autonomous Lander for Biological Experiments] and BOBO [bottom boundary layer]) were owned by the Royal Netherlands Institute for Sea Research (NIOZ) and were deployed in Norfolk Canyon. The other two landers were owned by the University of North Carolina, Wilmington (UNCW) and were deployed in Baltimore Canyon. The moorings were owned by USGS. One lander was placed near the head and the mouth of each canyon, and a mooring was placed in the middle of Baltimore and Norfolk canyons (**Figures 2** and **10**, respectively, of **Appendix B**). The sampling plan was designed to examine characteristics of the central axes of the canyons (e.g., movement of material up/down canyon, propagation of internal waves, water parameter variability, and sedimentation rates). The landers and moorings were equipped with instruments and samplers that collected long-term data and samples as described in **Section 3.2.3**.

ROV operations were conducted during all three cruise legs. During Legs 1 and 2, 20 ROV dives were conducted to survey canyon habitats and fauna and collect biological samples. Two dives were in Norfolk Canyon (**Figure 3** of **Appendix B**) and 18 were in Baltimore Canyon (**Figure 2** of **Appendix B**). During Leg 3, 10 dives were completed to investigate shipwreck sites near Norfolk Canyon (**Figure 13** of **Appendix B**). A substantial amount of canyon and shipwreck habitat was covered during the more than 220 hours of ROV bottom time, and a large number of samples (mostly corals and other invertebrates) were collected. Twenty-two bottom water samples were collected using Niskin bottles attached to the ROV, and CTD data were collected during each dive. Push cores were also collected for analysis of sediments and benthic infauna.

During Leg 3, an additional 85.38 km^2 of seafloor were mapped with multibeam echo sounders, all in the Norfolk Canyon area. As a result of the ten ROV dives during Leg 3, the identities of all eight Billy Mitchell-Project B wrecks were confirmed as well as one other vessel. A site of potential paleo-archaeological interest was investigated, as well as a potential archaeological site targeted, as a result of data from one of the box cores. A limited number of archaeological samples and artifacts were collected during ROV dives on Leg 3. Collections of benthic organisms were made from visited shipwrecks, box cores, and from an ROV dive to search for paleo-archaeological sites. Voucher samples of representative dominant benthic organisms from shipwreck locations were collected to facilitate their identifications in video data.

A total of 200 non-ROV stations were completed during this cruise, including 76 CTD stations, 84 box cores, 14 monocores, and 26 otter trawls. Non-ROV stations sampled during Legs 1 and 2 are

shown in **Figures 2** and **10** of **Appendix B** (Baltimore and Norfolk canyons, respectively). Non-ROV stations for Leg 3 (which focused on the Norfolk Canyon area) are shown in **Figures 17**, **18**, and **19** of **Appendix B**. Education and outreach activities were also conducted.

3.1.4 2013 Sampling Cruise

The 2013 sampling cruise was conducted in the spring of 2013 using the NOAA ship *Ronald H. Brown* and the ROV *Jason II*. Details are provided in the cruise report (**Volume II**, **Appendix C**). The cruise was split into two legs: Leg 1 (30 April to 19 May), which focused on natural substrates, and Leg 2 (19 to 27 May), which focused on shipwrecks. The cruise began and ended in Charleston, South Carolina.

During Leg 1, 11 ROV dives were completed, including 145 hours of dive time. Two of the dives were in Baltimore Canyon (Figure 8 of Appendix C) and nine were in Norfolk Canyon (**Figures 5**, **6**, and **7** of **Appendix C**). During the dives, a substantial amount of canyon habitat was covered, and a large number of invertebrates and some fishes were collected. Six water samples were collected using Niskin bottles attached to the ROV, and environmental data were collected during each dive using the CTD instrument. Replicate sediment cores (two to four) were taken on nine dives, and sediment/benthic fauna were also collected by the suction sampler and the Ekman box corer.

In addition to the ROV dives, 84 non-ROV stations were completed during Leg 1, including 31 CTD casts, 38 box core samples, 26 monocore samples, and 15 otter trawls. The UNCW benthic landers were recovered from Baltimore Canyon to replace faulty release mechanisms and were redeployed in the same location within 12 hours. The lander from the shallow site had been badly affected by sediment; the coral experimental chambers and sediment trap were full of mud, and only three sediment samples could be salvaged. All this equipment was therefore removed prior to redeployment.

During Leg 2 of the cruise, five ROV dives were completed (~50 hours of bottom time). The dives investigated four Billy Mitchell-Project B wrecks (*G102*, *Ostfriesland*, *Frankfurt*, and what is believed to be the *V43*). In addition, 4,922 km^2 of seafloor were mapped using multibeam, and three CTD casts and one otter trawl were conducted. During this leg, a series of technical and weather-related issues prevented the completion of several ROV dives and a planned multibeam sonar search for the wreck of *San Demetrio*.

3.1.5 2013 Instrument Retrieval Cruise

The 2013 instrument retrieval cruise used the NOAA ship *Nancy Foster* from 21 to 27 August 2013 and originated and ended in Charleston, South Carolina. Details are provided in the cruise report (**Volume II**, **Appendix D**). The main purpose of this cruise was to retrieve the four benthic landers and two moorings deployed in Baltimore and Norfolk canyons. Additional cruise activities included conducting CTD profiles, collecting water samples using Niskin bottles, and collecting monocores. Education and outreach activities were also incorporated into the cruise. The cruise plan included additional seafloor mapping near Norfolk Canyon, if time allowed. However, due to a problem with the ship's main engine, the cruise was shortened, and seafloor mapping was not conducted.

After the ship arrived at Norfolk Canyon, the BOBO lander was successfully retrieved at the canyon mouth, but the ALBEX lander and the USGS mooring were not recovered. Communications were established with both, but neither surfaced. We speculated that heavy sedimentation or turbidity flows may have damaged the lander and mooring or partially buried them. The ship transited to Baltimore Canyon and retrieved the two landers and the mooring that were deployed there. The ship transited back to Norfolk Canyon and spent the remainder of the time searching for the ALBEX, but the search was eventually aborted. During transit to a site for seafloor mapping operations, the ship discovered a severe problem with the main engine, and the decision was made to transit directly back to Charleston.

During the week of 8 September 2013, the USGS mooring surfaced and was recovered by the NOAA ship *Henry B. Bigelow*. The unrecovered ALBEX lander surfaced at some point and ultimately came ashore in the Bahamas in January 2015. The lander and its instruments await resolution of logistical issues (funding) before it can be recovered.

A total of 33 water and sediment stations were sampled during the cruise, including 22 CTD casts with 21 sets of water samples and 7 monocores (collected using a coring device attached to the bottom of the CTD carousel).

3.2 SURVEY VESSELS AND EQUIPMENT

The surveys were conducted using two NOAA oceanographic research vessels: *Nancy Foster* (2011 mapping cruise, 2012 sampling cruise, and 2013 instrument retrieval cruise) and *Ronald H. Brown* (2013 sampling cruise) (**Figure 3-1**). The home port for both oceanographic research vessels is Charleston, South Carolina. **Table 3-2** summarizes the main sampling equipment used during the study.

A

B

Figure 3-1. Research vessels used during the Atlantic Deepwater Canyons study: (A) NOAA ship *Nancy Foster* and (B) NOAA ship *Ronald H. Brown*.

Table 3-2. Sampling equipment used during the Atlantic Deepwater Canyons study.

Equipment Type	Model or Description	Cruises	Capabilities and Collections
Multibeam echo sounder	Kongsberg EM 1002 Reson 7125	2011 mapping cruise 2012 sampling cruise	• High-resolution seafloor mapping
	Kongsberg EM 122	2013 sampling cruise	
Remotely operated vehicles	*Kraken 2* (University of Connecticut)	2012 sampling cruise	• Video and still cameras • Manipulator arm to collect biological and sediment samples • Retractable sled with sample containers (bio-boxes, quivers) • Sediment samplers (push cores) • Suction sampler and 8 bucket carousel • CTD instrument (Sea-Bird SBE 19*plus*) • Niskin bottles (water sampling)
	Jason II (Woods Hole Oceanographic Institution)	2013 sampling cruise	• Video and still cameras • Two manipulator arms to collect biological and sediment samples • Retractable sled with sample containers (bio-boxes, quivers) • Sediment samplers (push cores, Eckman grab) • CTD instrument (Sea-Bird SBE 19*plus*) • Niskin bottles (water sampling)
Benthic landers	Two NIOZ landers, ALBEX and BOBO (both in Norfolk Canyon)	Deployed on 2012 sampling cruise; BOBO recovered on 2013 instrument retrieval cruise; ALBEX later washed ashore in Bahamas	• Sediment trap with rotating bottles • Salinity, temperature, turbidity, fluorescence • Current meter (one with ADCP) • Settlement plates
	Two UNCW landers (both in Baltimore Canyon)	Deployed on 2012 sampling cruise; serviced during 2013 sampling cruise; recovered on 2013 instrument retrieval cruise	• Sediment trap with rotating bottles • Salinity, temperature, turbidity, DO • Current meter • Live coral experiments in acrylic chambers (one lander) • Settlement plates (microbiology) • Additional settlement plates and two multisubstrate settlement units
Otter trawl	4.9 m headrope, 38.1 mm body mesh, 3 mm cod end liner mesh	2012 sampling cruise 2013 sampling cruise	• Collection of epibiota and fish in soft bottom areas near canyons
Moorings	Two USGS moorings (one in each canyon)	Deployed on 2012 sampling cruise; one recovered on 2013 instrument retrieval cruise; other recovered Sept. 2013	• Sediment trap with rotating bottles • Temperature and conductivity • Current meter (ADCP)
CTD-Niskin carousel (shipboard)	Sea-Bird SBE 911*plus* with Niskin bottle rosette	All cruises	• Profiling of conductivity, temperature, depth, turbidity, DO, pH, fluorescence • Collection of water samples for nutrients, trace metals, POM, aragonite saturation
Box core	NIOZ design, 30 cm diameter, 55 cm height	2012 sampling cruise 2013 sampling cruise	• Collection of sediment and benthic biological samples
Monocore	NIOZ design, 54 mm diameter	2012 sampling cruise 2013 sampling cruise 2013 retrieval cruise	• Single tube corer on CTD frame for collection of sediment samples

ADCP = acoustic Doppler current profiler; ALBEX = Autonomous Lander for Biological Experiments; BOBO = bottom boundary layer; CTD = conductivity-temperature-depth instrument; DO = dissolved oxygen; NIOZ = Royal Netherlands Institute for Sea Research; POM = particulate organic matter; SBE = Sea-Bird Electronics, Inc.; UNCW = University of North Carolina−Wilmington.

3.2.1 Multibeam Echo Sounder

Multibeam echo sounders were used for high-resolution mapping during all four cruises. The main effort was during the 2011 mapping cruise (June 2011) (**Section 3.1.2**). During this cruise, the NOAA ship *Nancy Foster* conducted multibeam echo sounder surveys along the shelf break, slope, and submarine canyons of the MAB. Potential shipwreck sites were also surveyed for archaeological objectives. Two multibeam echo sounders were used: the Kongsberg EM 1002 (95 kHz operating frequency and optimal operating depth range of 200 to 1,000 m) and the Reson 7125 (200 kHz or 400 kHz operating frequency and operational depth range of 5 to 250 m). The Kongsberg system was used for most of the surveys along the slope and canyons, but the Reson system was more effective for the shipwrecks located on the shelf. Sound velocity profiles were calculated from CTD data collected periodically during the surveys using a Sea-Bird SBE 911*plus* instrument, which was mounted on the shipboard carousel. Raw data were corrected for sound velocity and tidal variation and post-processed using CARIS HIPS and SIPS (version 7.0) to produce bathymetric and backscatter maps. Surveys of target features were conducted at ≤ 6 knots, but bathymetric data was also collected during transits between sites at normal cruising speed (~10 knots).

Additional sites (primarily shipwreck targets) were mapped during the 2012 sampling cruise (**Section 3.1.3**) and the 2013 sampling cruise (**Section 3.1.4**). The 2012 sampling cruise aboard the *Nancy Foster* used the same Kongsberg EM 1002 and Reson 7125 echo sounders. The 2013 sampling cruise was conducted aboard the NOAA ship *Ronald H. Brown*, which uses a Kongsberg EM 122 echo sounder (12 kHz operating frequency).

3.2.2 Remotely Operated Vehicles

Video surveys and sample collections during the 2012 and 2013 sampling cruises were accomplished using an ROV. Vehicles used for each cruise differed in their configurations and capabilities, but the scientific objectives for each vehicle and cruise were similar. Each ROV is described separately in the following subsections. The scientific objectives of the ROV dives are discussed in **Section 3.2.2.3**.

3.2.2.1 The ROV Kraken 2

The ROV *Kraken 2* (**Figure 3-2**) was used during the 2012 sampling cruise; ROV dive locations are summarized in **Section 3.1.3**. *Kraken 2* is a Max Rover science-configured ROV, owned and operated by the University of Connecticut, and is capable of operating to 1,000 m. *Kraken 2* was equipped with an ORE Trackpoint II ultra-short baseline tracking system combined with a Winfrog integrated navigation system. The system recorded and displayed the position of the vehicle every few seconds. Color-shaded bathymetric geotiff maps (products of the 2011 multibeam cruise) were provided for each dive as a georeferenced base map for the ROV tracking software. The pilots and scientists were therefore able to observe the ROV track in near real time overlaid on local bathymetry, which proved extremely valuable for guiding the dives and maximizing vehicle survey time. The *Kraken 2* science package included a high-definition (HD) video camera (Kongsberg OE14-502) and digital still camera (Kongsberg camera based on the Canon G11 Powershot) which were mounted on a pan and tilt unit. Two parallel lasers mounted 10 cm apart were visible in the video field of view and were used to calibrate distances. Data from the video camera were recorded in full resolution (from surface to surface during each dive) onto external hard drives. A six-function Hydro-Lek manipulator arm was used to collect geological and biological samples. The vehicle had an insulated polypropylene bio-box (30.5 × 91 × 25 cm) mounted in the center of the tool skid on the front of the vehicle. This box was divided into three sections to contain larger specimens and those that were to be kept alive after the dive. Surrounding the bio-box were seven PVC tubes (‘quivers’) that could hold small samples (when capped with rubber stoppers) or sediment core tubes (**Figure 3-2A**). Additional sampling capacity was provided by a suction sampler, which connected to eight separate sample buckets at the rear of the vehicle. Two 6 L Niskin bottles were used to collect

water samples; these were mounted vertically to the bow port side of the vehicle (**Figure 3-2B**) and were closed using a cable trigger activated by the manipulator arm. A Sea-Bird SBE 19*plus* CTD instrument, attached to the starboard side of the ROV, measured turbidity (Seapoint probe, formazin turbidity units), dissolved oxygen (mL L^{-1}), depth (m), conductivity (Siemens m^{-1}), temperature (^{o}C), salinity, and pH during each dive.

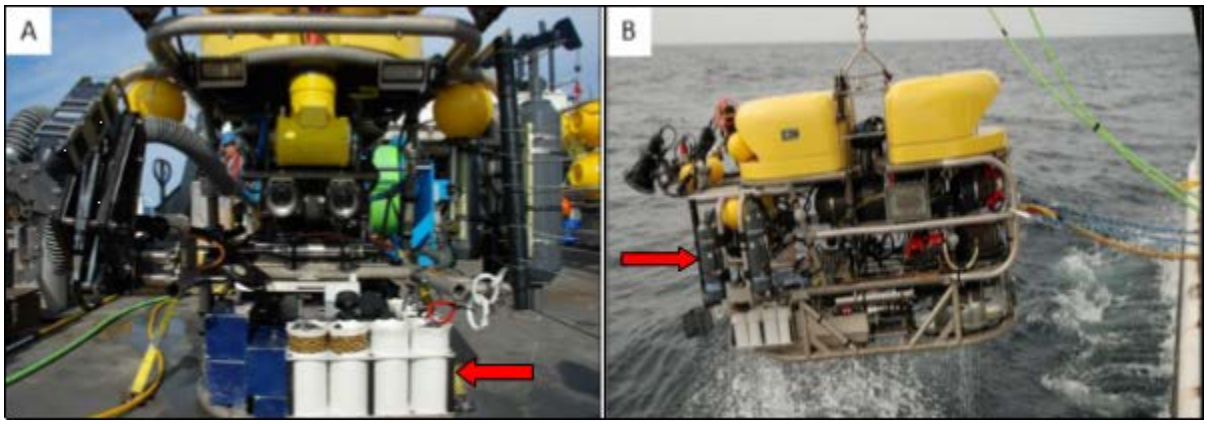

Figure 3-2. ROV *Kraken 2* showing (A) bow of *Kraken 2* showing tube sample containers ('quivers') and (B) two Niskin water collection bottles mounted vertically near the bow of the vehicle.

Each ROV dive was scheduled from 08:30 hours (launch) to 18:30 hours (recovery), subject to change as conditions and logistics dictated. During each ROV dive, a lead scientist (either Brooke or Ross during cruise legs for biological objectives, and Mather or Viada during cruise legs for archaeological and associated biological objectives) and a second observer were on watch with the ROV crew. The lead scientist directed the dive (course, speed, transect configuration, data collection, and sampling) and made audio annotations of dive activities. The second observer recorded events throughout the dive on hard copy and digital event logs. Position data were time-synchronized with all imagery and samples. The ROV instruments recorded all times as UTC (Coordinated Universal Time); however, local time (Eastern Standard Time [EST]) was recorded on all other data sheets and audio recordings.

3.2.2.2 The ROV Jason II

The ROV *Jason II* (**Figure 3-3A**) was used during the 2013 cruise aboard the NOAA Ship *Ronald H. Brown*; ROV dive locations are summarized in **Section 3.1.4**. This vehicle is owned and operated by the Deep Submergence Laboratory at Woods Hole Oceanographic Institution and is capable of diving to depths up to 6,500 m. The ROV system consists of two units: the ROV (*Jason*) and an active tethering unit (*Medea*) which reduces the load on the umbilical and helps buffer movement between the surface and the ROV. The ROV navigation system was a Sonardyne Ranger ultra-short baseline (USBL) and, as in the 2012 cruise, color-shaded bathymetric geotiff images were provided for each dive. The primary science camera on the ROV was an Insite Mini-Zeus HD video camera. Two parallel lasers mounted 10 cm apart projected onto the video image and provided a size reference for measuring objects on the seafloor. The video was recorded directly to external hard drives and DVDs during the dives. There were two digital still cameras: a Nikon CoolPix controlled by the science dive lead, and an Insite Super Scorpio that was operated by the ROV crew. Two seven-function hydraulic manipulator arms (a Schilling Titan 4 and a Kraft Predator II) were used to collect samples. A large retractable sled was mounted on the front of the ROV and was equipped with several different sampling devices including an insulated polypropylene bio-box, an array of 18 PVC quivers (7.6 cm diameter), a set of four to nine push cores, and an Ekman box corer. There were an additional two insulated bio-boxes mounted on retractable arms on either side of the sled and a five-bucket suction sampling system at the back of the

vehicle. A Sea-Bird SBE 19*plus* data logger (same configuration as the 2012 cruise) was attached to the ROV to record environmental data during the dives (**Figure 3-3B**).

Two 6 L Niskin bottles were mounted on the starboard side of the vehicle (**Figure 3-3C**) and were used to collect bottom water samples when triggered using one of the manipulator arms.

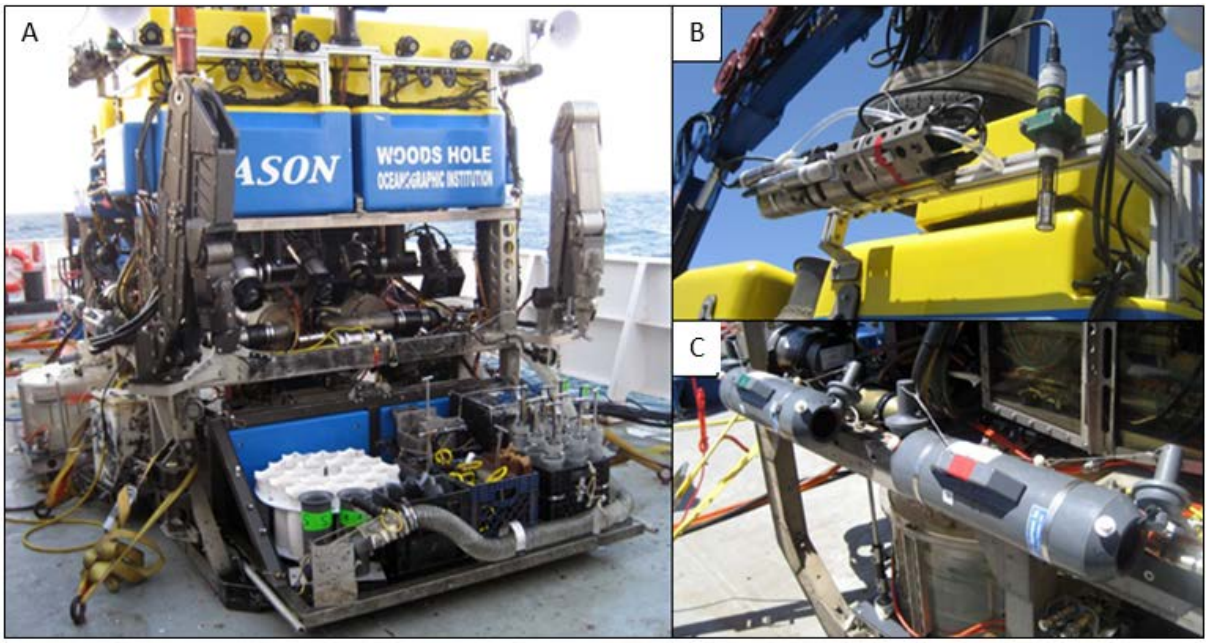

Figure 3-3. ROV *Jason II* (A) on deck before a dive with various sampling devices attached to the basket on the ROV; (B) Sea-Bird SBE 19*plus* profiler mounted on starboard side of the vehicle for collecting environmental data; and (C) two Niskin-type water collection bottles mounted horizontally on the starboard side of the vehicle.

The ROV dives were planned for launch at 06:00 hours and recovery at 19:00 hours, subject to change as conditions and logistics dictated. During each ROV dive, the lead scientist (Brooke or Ross, or Mather or Viada) and two other observers were on watch in the ROV van. The lead scientist directed the dive and made audio annotations of dive activities. The second observer recorded events throughout the dive on hard copy and logged events in the "Virtual Van." This system captured metadata and images for each operator-controlled entry and was used to document observations, samples, and other pertinent information during the dive. The third observer was responsible for keeping track of the media recordings, and switching and labeling the drives and disc. ROV navigation data were time-synchronized with all imagery and samples, and the Virtual Van was used to record data on observations and collections as well as images and environmental data throughout the dive. The ROV instruments recorded all times in UTC; however, station sheets and audio logs were recorded in local time.

3.2.2.3 ROV Objectives

Each dive had multiple objectives, with some tasks given priority on certain dives; however, most ROV dives followed a similar pattern: emphasizing benthic surveys to characterize different habitats and associated fauna; photographing features or fauna of particular interest; and collecting biological, geological, and archaeological samples. The ROV dive objectives for natural habitats are outlined below.

1. Conduct standardized video transects over different natural habitat types and their associated communities.
2. Conduct video transects and photoquadrats or photomosaics over selected shipwrecks and other archaeological features.

3. Collect invertebrates (particularly corals and coral-associated fauna) and fishes from different habitat types (natural and artificial) for multiple biological objectives (taxonomy and diversity assessments, reproductive biology, microbiology, population genetic analysis, trophic ecology, and paleoecology).
4. Collect digital still images of fauna or features of interest, including all samples collected.
5. Collect push cores and Ekman samples for analysis of sediments and infauna.
6. Conduct suction samples of target habitats to assess community diversity.
7. Collect environmental data (depth, oxygen, temperature, salinity, pH) using ROV-mounted instrumentation.
8. Collect near-bottom water samples using 6 L Niskin bottles mounted on the ROV.
9. Deploy site markers at locations of interest.

For natural habitats, ROV dives generally began at the deepest part of the target location and worked upslope. During descent and ascent (beginning and end of each dive), notes were taken on distributions and behaviors of mid-water fauna. When the ROV arrived on seafloor, the dive lead guided the pilots to areas of interest, stopping during transits to photograph or collect samples (fauna, sediment, water) as appropriate. During transit periods, the video camera was placed in a predetermined pan/tilt position, set on wide angle, and the ROV ran at slow speed (~0.25 knots) close to the seafloor with calibration lasers switched on. This method of collecting transect data was found to be the most efficient when working in an unexplored area where habitat locations and extents are unknown and samples must be collected opportunistically. ROV dives on artificial substrates focused on detailed video and photomosaic surveys of the target shipwreck to collect information on the status of the wreck and associated biological communities. Every collection (from natural or artificial substrates) was documented with video and digital images, and all transects, collections and other activities were documented, time-stamped and georeferenced. Sediments and water samples were collected for analysis of infaunal communities and water chemistry, and the Sea-Bird CTD instrument collected environmental data throughout each dive.

The ROVs were the primary survey and sampling equipment used during this project, and operations were conducted during the day. After the vehicle was recovered and secured, the science party removed and processed the samples and prepared the vehicle for the following day. During non-ROV hours (i.e., the night shift or when ROV operations were precluded due to weather or technical problems), other sampling was conducted such as collection of box core and monocore samples (**Section 3.2.4**), trawling (**Section 3.2.5**), or collection of CTD profiles and water samples (**Section 3.2.6**).

3.2.3 Benthic Landers and Moorings

During the 2012 sampling cruise, four benthic landers (**Figure 3-4**) and two moorings were deployed for long-term (1 year) data collection in Baltimore and Norfolk canyons. The landers and moorings were all equipped with instruments and samplers that collected long-term data and samples. Two landers were owned by NIOZ, the other two by UNCW, and the moorings were owned by USGS. A lander was placed near the head of each canyon and in deeper water down canyon with a mooring placed between them, near the center. The sampling plan was designed to examine characteristics of the central axes of the canyons (e.g., movement of material up/down canyon, propagation of internal waves, water parameter variability, sedimentation rates). Both landers and moorings were equipped with weights (to enable them to sink to the seafloor) that were secured to the lander/mooring by an acoustically activated release. On recovery, the release was triggered using an acoustic signal from the ship, which disengaged the weights from the lander/mooring. Floats attached to the upper part of each piece of equipment enabled the equipment to ascend.

A  B 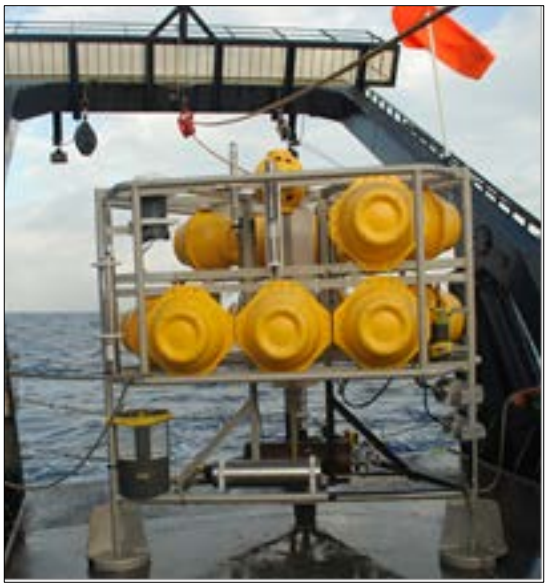

Figure 3-4. Benthic landers: (A) UNCW benthic lander and (B) NIOZ ALBEX lander.

Each lander was configured with a Sarl Technicap PPS 4/3 sediment trap (aperture of 0.05 m^2 mounted ~2 m above bottom) programmed to rotate a sample bottle (250 mL) at 30-day intervals, delivering a total of 12 samples during the 1-year deployment. Sediment trap bottles were dosed with a 200 µL solution of saturated HgCl fixative. The two NIOZ landers (ALBEX and BOBO) deployed in Norfolk Canyon used a Sea-Bird CTD instrument to record salinity and temperature and a WET Labs FLNTU sensor to measure turbidity and fluorescence every 15 minutes. To measure bottom currents, the BOBO lander had an upward-looking acoustic Doppler current profiler (ADCP) current meter mounted approximately 2 m off the bottom, and the ALBEX lander had a Nortek Aquadopp current meter mounted approximately 1.5 m off the bottom. Each of the two UNCW landers deployed in Baltimore Canyon had an Aanderaa RCM string logger with probes to measure temperature, conductivity, salinity, turbidity, dissolved oxygen, and bottom currents at 15-minute intervals. All RCM probes were approximately 1.5 m off bottom except the current meter, which was approximately 2 m off bottom. The UNCW lander placed in the head of Baltimore Canyon also carried live coral experiments housed within three acrylic chambers (designed by Brooke and Ross). All four landers carried settlement plate microbiology experiments. The two UNCW landers carried additional settlement plate arrays and two multisubstrate settlement units (**Figure 3-5**) as part of an international cooperation with the InDeep/Serpent Deep Ocean Colonization Project.

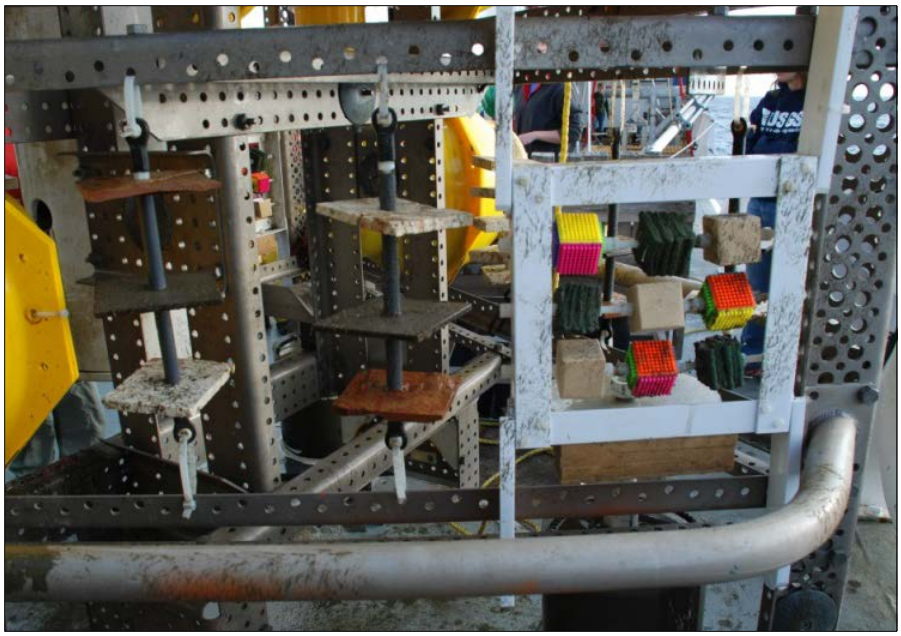

Figure 3-5. UNCW benthic lander after retrieval showing two settlement plate arrays (left and center) and an InDeep/Serpent settlement unit (right in white frame).

The two USGS moorings (**Figure 3-6**) were each 43 m long and were equipped with a Honjo Parflux sediment trap (mounted 4 m above bottom) with thirteen 500 mL bottles programmed to rotate at 30-day intervals. Each mooring also held a Sea-Bird Microcat 37 (mounted 9 m above bottom) that recorded temperature and conductivity at 5 minute intervals, and a 300 kHz ADCP current meter (mounted 10 m above bottom).

Lander and mooring deployments were similar, except that lowering the mooring was more time consuming. The gear was lifted over the stern (using the crane or A-frame and winch), floated briefly at the surface, and released via Sea-Catch release as the ship remained stationary over the drop site. After the lander or mooring reached the bottom, the ship moved to three positions in a triangle around the drop site. At each position, the range data for the lander/mooring were recorded via acoustic contact with the releases. The bottom location was calculated for each lander/mooring by triangulating the three positions. Lander or mooring recovery involved the ship remaining stationary near the site while a hydrophone was lowered over the side. Once contact was established, the acoustic releases attached to the lander/mooring were triggered, and the ascent was tracked using acoustic communication. Once on the surface, the ship moved into position to grapple the gear and lift it aboard either with the crane or through the aft A-frame.

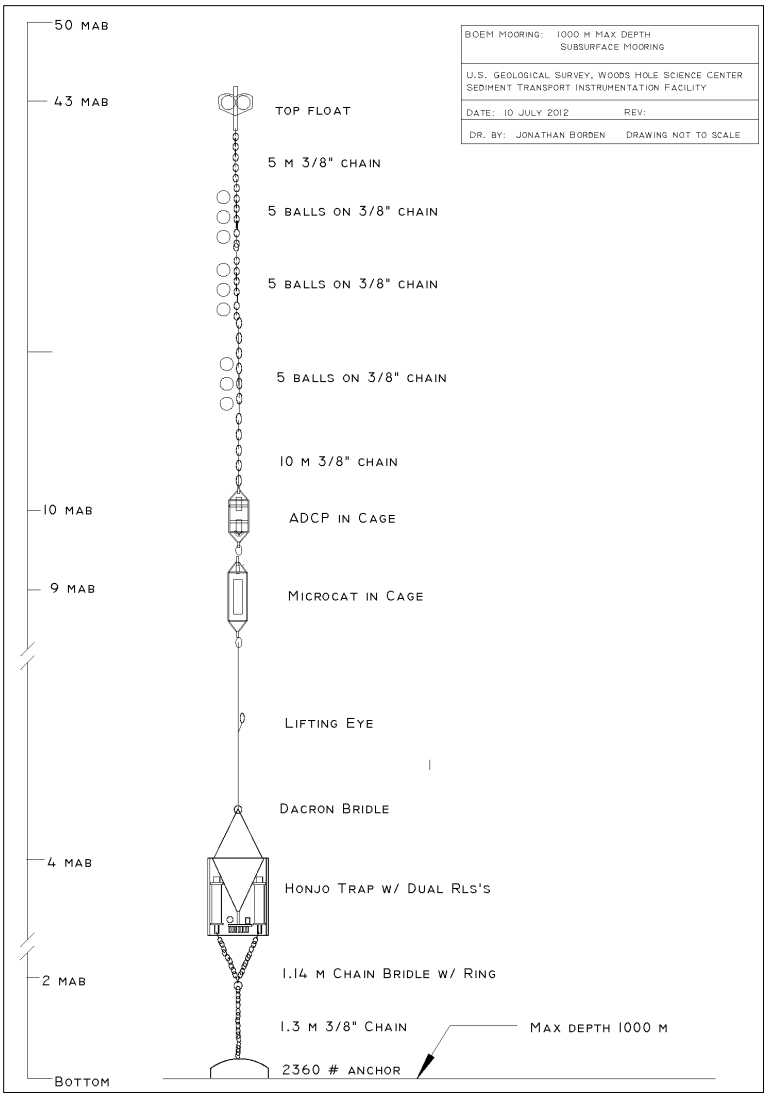

Figure 3-6. Configuration of USGS mooring used in Norfolk and Baltimore canyons.

3.2.4 Box Core and Monocore Sampling

During the 2012 and 2013 sampling cruises, sediment and infauna samples were collected using a cylindrical box corer (designed by NIOZ) equipped with a stainless steel core 30 cm in diameter and 55 cm in height and a trip valve sealing the top of the cylinder (**Figure 3-7A**). During sampling, the box corer was lowered vertically on a steel wire until it plunged into the sediment. At that point, the tension on the wire was released, and the knife of the box corer sealed the bottom of the core. When retrieving the box corer, the top of the core was closed by a lid, allowing the collection of undisturbed sediment and overlying bottom water. When the box corer arrived on deck, the valve was carefully opened and the corer was taken out of the box core frame. One box core sample collected at each station was used to take sedimentology subsamples, while the other cores were used for biodiversity sampling and microbiology.

The overall sampling approach using the box corer was to collect cores along a transect following the canyon axis and an adjacent slope transect. The sampling scheme was designed to allow determination of distinctive sedimentary characteristics (e.g., sedimentation rates, carbon content, grain size) in different zones of the canyon to provide insight into processes governing the particle transport and deposition in

the canyons. The different sedimentary zones in the canyon are also likely to be characterized by specific infaunal and potentially microbial communities. Sedimentary, microbial, and faunal characteristics of canyon sediments were compared with samples collected outside the canyon on the open slope.

Additional sediment samples were collected with a monocorer (**Figure 3-7B**). The monocore (internal diameter 54 mm) is a single tube version of a multicorer that can be suspended underneath the CTD frame. Monocore collections provided high-resolution sampling inside and outside the canyons at each CTD station. Cores that were retrieved successfully were immediately sliced in 1 cm depth intervals and stored frozen for pigment, organic carbon, and nitrogen analyses.

Figure 3-7. NIOZ sediment sampling equipment: (A) box corer and (B) monocorer.

3.2.5 Otter Trawl

Trawl samples were collected on both the 2012 and 2013 sampling cruises. Bottom trawling was conducted off the stern using the ship's main winch to deploy a 4.9 m head rope otter trawl (38.1 mm mesh wings and 3 mm mesh cod liner). Trawl deployments generally averaged about a 2.5:1 wire scope, although this was adjusted as needed. Upon reaching bottom, the trawl was towed for 30 minutes at a speed of 2 knots over ground, usually against the surface current, then the net was recovered. This operation was repeated as often as possible during the night watches. An attempt was made to sample as wide a depth range as possible in and around Baltimore and Norfolk canyons. After each trawl, animals were sorted from the catch depending on project objectives and were preserved as appropriate for the taxa and objectives. Selected specimens were photographed at sea. Details on preservation and specimen handling are in various other chapters of this report.

Multibeam bathymetry maps were used to identify uniform soft sediment areas within target areas and depth ranges. Much of the seafloor within the canyons exhibited such rugged topography that there was too great a risk of equipment loss to attempt trawl operations. Thus, most bottom trawl sampling was limited to areas along the outer sides of the canyons. Bottom trawl sampling was further obstructed from

the abundant fishing vessel traffic in the study areas, which required a wide avoidance margin. Although bottom trawling was successful and produced abundant valuable samples for many objectives, it was costly in terms of time and lost gear.

3.2.6 CTD-Niskin Rosette

During each cruise, a CTD instrument (Sea-Bird SBE 911*plus*) with a rosette of 12 Niskin bottles (10 L) was used to record water column environmental profiles and collect water samples (**Figure 3-8**). The CTD instrument measured turbidity (Seapoint probe, formazin turbidity units), dissolved oxygen (mL L^{-1}), depth (m), conductivity (Siemens m^{-1}), temperature (°C), pH, and fluorescence. The CTD data and water samples collected during this project were used for several different objectives such as: describing water column environmental conditions; calculating sound velocity for sonar data correction; and collecting water samples for carbonate chemistry, nutrient, radiocarbon, and other elemental analyses. Sampling locations are summarized in **Sections 3.1.2** through **3.1.4**.

Figure 3-8. Water collection rosette with 10 L Niskin bottles and CTD profiler used during the 2013 field sampling survey aboard the *Ronald H. Brown*.

3.3 SUMMARY OF SAMPLING LOCATIONS AND DATA COLLECTED

The four research cruises generated a vast amount of scientific data (>20 terabytes [TB]) and samples. A total of 48 ROV dives were completed, resulting in approximately 414 hours of underwater digital imagery and hundreds of scientific samples. A wide variety of sampling equipment was deployed at 420 stations within and around the two target canyons resulting in several thousand individual datasets and samples, and 6,406 km^2 were mapped using multibeam sonar.

Table 3-3 shows where the types of data and samples collected during the four cruises are presented and analyzed in other chapters of this report. Detailed methods for sample collection, processing, and analysis are presented in those chapters where appropriate. A complete list of stations sampled during each research cruise is presented in the cruise reports in Volume II (see **Table 2** of **Appendix A**; **Tables 2**, **4**, and **5** of **Appendix B**; **Tables A-1** and **A-2** of **Appendix C**; and **Table 1** of **Appendix D**).

Table 3-3. Chapters in the Atlantic Deepwater Canyons study where the various types of data and collected samples are discussed.

Chapter	Sources of Data and Samples						
	Topic	Seafloor Mapping (Bathymetry)	ROV Observations & Collections	Benthic Landers & Moorings	CTD & Water Samples	Box Core & Monocore Samples	Otter Trawls
4	Archaeological studies	✓	✓	--	--	--	--
5	Physical oceanographic processes	✓	✓	✓	✓	--	--
6	Geological studies	✓	✓	✓	✓	✓	--
7	Predictive habitat modeling	✓	✓	--	✓	--	--
8	Benthic invertebrate communities	--	✓	--	✓	✓	✓
9	Benthic infaunal communities	--	✓	--	--	✓	--
10	Molecular perspectives on anomuran biodiversity	--	✓	--	--	--	✓
11	Invertebrate reproductive biology	--	✓	--	--	--	✓
12	Microbiological studies	--	✓	--	--	✓	--
13	Coral taxonomy and connectivity	--	✓	--	--	--	✓
14	Patterns of inter-canyon connectivity among four coral species	--	✓	--	--	--	✓
15	Fish communities and diets	✓	✓	--	--	--	✓
16	Trophodynamics (stable isotopes)	--	✓	✓	✓	✓	✓
17	Paleocology	--	✓	--	✓	--	-
18	Education and outreach	✓	✓	✓	✓	✓	✓
19	Synthesis	✓	✓	✓	✓	✓	✓

CTD = conductivity-temperature-depth; ROV = remotely operated vehicle.

CHAPTER 4. HISTORICAL AND ARCHAEOLOGICAL STUDIES

Rod Mather and John O. Jensen

4.1 PREHISTORIC BACKGROUND

4.1.1 Overview

The mid-Atlantic canyons represent an important area for paleoarchaeological investigations. Norfolk Canyon, for example, is the southernmost canyon along the Mid-Atlantic Bight continental shelf, just north of the transition to the South Atlantic Bight/Blake Plateau region. This represents a major change in the geomorphology and general oceanographic character of the shelf. Archaeologically, the region represents an ancient embayment, where the ancient Susquehanna River that flowed across the coastal plain during the last Ice Age emptied into the ocean. During this time approximately 20,000 years ago, when the sea level was approximately 100 m lower than it is today, Pleistocene megafauna and early human populations (Paleoindians) likely occupied the region. The unique shape and bathymetric structure of the ancient embayment occupied by the present-day Norfolk Canyon suggest that this area may have had very protected and habitable sites. For these reasons, understanding Norfolk, Baltimore, and Washington canyons and their environmental settings is particularly important for the underwater archaeology of the mid-Atlantic Outer Continental Shelf (OCS). The potential for prehistoric sites on the OCS is the subject of ongoing investigations by academic archaeologists and federal agencies, including the Bureau of Ocean Energy Management (BOEM).[1]

To investigate the potential for prehistoric archaeological sites in the mid-Atlantic canyons region, it is necessary to understand the environmental setting of the area during the Last Glacial Maximum (LGM) and how it has changed since that time. The canyons lie far from shore and far from major sources of sedimentation. They are also south of the maximum extent of ice during the LGM. In addition, the land masses have not been subject to significant isostatic rebound, so they remain near the same elevation they were 20,000 years ago. Recent discoveries of projectile points (possibly related to Solutrean toolmaking types of southern Europe) at the head of Norfolk Canyon has added increased significance and urgency to understand the paleoarchaeological landscape of the mid-Atlantic canyon region.[2] Paleoarchaeological investigations for this study were limited to two reconnaissance dives using a remotely operated vehicle (ROV).

4.2 HISTORICAL STUDIES

4.2.1 General Overview

The mid-Atlantic OCS intersects with some of the most historically significant waters in the United States. The area has a long and rich history connected to exploration, warfare, commerce, fishing, and

[1] See for example TRC Environmental Corporation. 2012. *Inventory and Analysis of Archaeological Site Occurrence on the Atlantic Outer Continental Shelf.* (Prepared under BOEM Contract M08PD00024) New Orleans, LA. U.S. Department of the Interior, Washington, DC.

[2] Dennis J. Stanford and Bruce A. Bradley, *Across Atlantic Ice: The Origins of America's Clovis Culture* (Berkeley, CA: University of California Press, 2012); Stanford, Dennis, Darrin Lowery, Margaret Jodry, Bruce A. Bradley, Marvin Kay, Thomas W. Stafford, and Robert J. Speakman, "New Evidence for a Possible Paleolithic Occupation of the Eastern North American Continental Shelf at the Last Glacial Maximum." In: *Prehistoric Archaeology on the Continental Shelf*, A. M. Evans et al. (eds.) (New York, NY: Springer, 2014), pp. 73-93; for a recent rebuttal see Matthew T. Boulanger and Metin I. Erin "On the inferred age and origin of lithic bi-points on the Eastern Seaboard and their relevance to the Pleistocene peopling of North America," *American Antiquity* 80 (January 2015):134-145.

recreation. It encompasses the historic approaches to Chesapeake Bay and Delaware Bay and, by extension, key mid-Atlantic ports such as Norfolk, Baltimore, Wilmington, and Philadelphia. Four centuries of intense maritime use have left a rich, although poorly understood, repository of cultural material on the ocean floor on the edge of the shelf as well as in deeper waters to the east.

Europeans first began visiting the Chesapeake Bay and the associated approaches in the mid-16th century. In 1561, the bay was christened "Bahia de Santa Maria" by the Spanish explorer Pedro Menéndez de Avilés.[3] Two of the earliest English colonizing efforts in the New World took place in the region of Roanoke, North Carolina, in 1585 and Jamestown, Virginia, in 1607. Jamestown became the first permanent English settlement. Reports of shipwrecks were sparse at first, but became more frequent with time.

The introduction of tobacco cultivation to the region in 1612, along with forced slave labor shortly thereafter, stimulated the mid-Atlantic economies and increased shipping traversing the offshore waters. In 1728, William Byrd II commented that Norfolk alone had "near twenty brigantines and sloops riding at the wharves and often they have more."[4]

Virginia's offshore waters saw action during the American Revolution and the War of 1812, as the fledgling United States Navy took on Europe's most powerful sea power. At the same time, privateers also patrolled the seas looking for prizes. Between 1776 and 1783, Virginia issued more than 100 privateering licenses. The Civil War similarly impacted Virginia's offshore waters. On 17 April 1861, President Abraham Lincoln ordered a blockade of all southern ports. Because of the South's dependence on foreign commerce and intrastate shipping, the Confederate Navy was formed to challenge that blockade. In addition, commercial enterprises emerged with explicit intentions of running the blockade. As the blockade became stronger, the blockade-runners evolved into fast, sleek steamers with greater capacity and speed.[5]

In the late 19th and early 20th centuries, the Navy's presence in the waters off Virginia increased. Between 1889 and 1892, the country's first battleship was built at the Norfolk Navy Yard at Gosport, and between 1919 and 1922, the aircraft carrier USS *Langley* also was built there.[6] In 1917, the U.S. Navy established an operations and training base at Norfolk and, as a result, the waters off Virginia became some of the most intensely used training and the testing grounds in the world.[7] In the early 1920s, some of the most important military testing events in the history of the United States occurred in the waters off Virginia. During World War II, Norfolk became America's primary antisubmarine base, while off shore, American and Allied shipping attempted to run the gauntlet of German U-boat "Wolf Packs."[8] Today, Norfolk serves as one of the largest naval facilities in the world and is home to the North Atlantic Fleet.

Commercial shipping across and along the mid-Atlantic OCS also increased during the late 19th and early 20th centuries. Rapid industrialization in the United States, particularly the northeast, stimulated the

---

[3] William L Tazewell, *Norfolk's Waters: An Illustrated Maritime History of Hampton Roads* (Portland, ME: Windsor Publications, 1982).

[4] William W. Henning (ed.), *The Statutes at Large: Being a Collection of All the Laws of Virginia, From the First Session of the Legislature, in the year 1619*, vol. 6, rev. ed., (1819; repr., Charlottesville, VA: University Press of Virginia, 1969), 214.

[5] Donald G. Shomette, *Shipwrecks of the Civil War: The Encyclopedia of Union and Confederate Naval Losses* (Washington, DC: Donic, Ltd., 1973).

[6] Raus McDill Hanson, *Virginia Place Names: Derivations, Historical Uses* (Verona, VA: McClure Press, 1969).

[7] Mark Nesbitt, *Rebel Rivers: A Guide to Civil War Sites on the Potomac, Rappahannock, York, and James* (Mechanicsburg, PA: Stackpole Books, 1993); Richard P. Weinert, and Robert Arthur, *Defender of the Chesapeake: The Story of Fort Monroe* (Shippensburg, PA: White Mane, 1989).

[8] Louis D. Rubin, *Virginia: A Bicentennial History* (New York, NY: W.W. Norton & Company, 1977).

demand for coal, consumption of which increased 77 times between 1850 and 1918. Much of this coal was shipped out of Virginia, stimulating shipbuilding and shipping. During the early 20th century, upwards of 200 coal-carrying vessels per day cleared the Virginia Capes.[9] Today, Virginia entrepots continue to be some of the most important commercial shipping centers on the east coast.

The mid-Atlantic OCS saw a substantial increase in commercial fishing during the 20th century. During earlier times, Virginia had a commercial fishery (based primarily on sturgeon, herring, oysters, shad, and blue crabs), but it was of relatively minor importance to the region's economy. Landings, however, increased dramatically during the early 20th century, and by the 1930s, Virginia's seafood products were being shipped throughout the nation. At the time, croaker was the most important finfish, and oysters were the most important shellfish. In the second half of the 20th century, the major types of commercial fishing gear used in the mid-Atlantic offshore waters were scallop dredges, surf clams, ocean quahog dredges, trawls, purse seines, and long lines.[10]

This diversity and intensity of human activity along the mid-Atlantic OCS created an important submerged cultural landscape. The ocean floor is marked by fishing vessels, their gear, and dredge scars; warships, military experiments, and ammunition; and the remnants of commercial shipping dating back 400 years. Although the area is historically significant and archaeologically sensitive, it is also poorly understood. Gaps in our knowledge are extensive, and much of the reported information about shipwreck locations is incorrect or wildly inaccurate.

4.2.2 Potentially Significant Historic Resources

The findings in this section represent an assessment of potentially significant historic and archaeological resources in the project area identified from historic research. Although important archaeological sites may be associated with many aspects of the history of the OCS, three themes and time periods have particular significance—ships from early European exploration and settlement, the Billy Mitchell fleet and the "Project B" experiments, and ships from the Battle of the Atlantic.

4.2.2.1 Shipwrecks from Early European Exploration and Settlement

The discovery of a cannon by fishermen working off the coast of Virginia in 1983 provided the impetus for a University of Rhode Island investigation of the mid-Atlantic canyon region in 2006. The cannon was identified as an English falcon and a land piece that had been cast sometime between 1585--1598.[11] Although the cannon could have been used for several decades after its casting, four possible scenarios seemed likely explanations for its presence off the coast of Virginia. First, the cannon might have been associated with the so-called Lost Colony of Roanoke (1585). Second, it might have been associated with the voyage of Sir Francis Drake to the region in 1585–1586. Third, it might have related to the early history of Jamestown. Fourth, the cannon might have been an isolated find.
A shipwreck associated with this cannon representing any of the first three scenarios would likely be the earliest English shipwreck in the New World and would, therefore, represent a highly significant historical and archaeological resource.

4.2.2.2 Billy Mitchell Fleet and the Project B Experiments

In 30 days during the summer of 1921, the U.S. military establishment sunk eight German warships off the coast of Virginia. Among these eight vessels were three U-boats (U-*117*, U-*140*, and *UB-148*),

[9] Sam H. Schurr and Bruce C. Netschert, *Energy in the American Economy, 1850-1975: An Economic Study of its History and its Prospects* (Baltimore, MD: The Johns Hopkins Press, 1960).

[10] James Kirkley, *Virginia's Commercial Fishing Industry: Its Economic Performance and Contributions* (Williamsburg, VA: Virginia Institute of Marine Science, College of William & Mary, 1997).

[11] Roderick Mather, "Found: Clue to fate of vanished English colony," *The London Observer* 3 December 1989.

three destroyers (*G-102*, *S-132*, and *V-43*), a light cruiser (the *Frankfurt*), and a battleship (the *Ostfriesland*). The warships had been part of a larger collection of German vessels taken by the U.S. government as reparations at the end of World War I. All were subsequently commissioned into the U.S. Navy. The U-boats reached the United States in the spring of 1919 and spent the next few months traveling along the coast stopping at port cities where they were exhibited to the public as part of a U.S. government Victory Bond drive. The *Ostfriesland*, the *Frankfurt*, and the destroyers *G-102, S-132,* and *Y-43* arrived the following year.

It was no coincidence that these eight vessels were sunk in 1921. According to the conditions of the armistice that ended World War I, all German naval vessels were to be either scrapped or sunk irretrievably by 9 August 1921. The circumstances surrounding their sinking, however, were highly significant. In a series of controlled experiments and tests, four of the German warships were sunk by aerial bombardment and four were sunk by U.S. surface ships. This symbolized a rift and competition within the U.S. military establishment as to the nature and future of warfare. The highly controversial and charismatic U.S. Army General Billy Mitchell argued that the Great War demonstrated the impotence of naval power when faced with a new technological innovation—the airplane. Airpower, he argued, would wreak havoc on ponderous, slow-moving warships plying coastal waters. Naturally, this represented a serious threat to the U.S. Navy and paved the way for a showdown off the coast of Virginia as the eight German warships were sunk by a combination of aerial bombardment and surface ships. In 1923, the experiments continued, this time farther south off Cape Lookout, North Carolina. This time the target ships were the old American battleships USS *New Jersey* and USS *Virginia*. The discovery and location of these ships are highly significant, both historically and archaeologically. The material remains represent not only significant historic shipwrecks, but also direct evidence of the relative success of aerial bombardment and surface guns at a time when airpower was in its infancy.

Eight shipwrecks from the so-called "Billy Mitchell fleet" are known to be in the project area and have been confirmed during the Atlantic Deepwater Canyons study. These vessels that represent highly significant archaeological resources will be nominated to the National Register of Historic Places. A detailed historical assessment of the Billy Mitchell-Project B experiments is presented in this chapter.

4.2.2.3 The Battle of the Atlantic

Lasting from September 1939 to May 1945, the Battle of the Atlantic was the longest military campaign of World War II. The conflict pitted German U-boats against the Allied warships and merchant ships that transported essential military supplies across the Atlantic Ocean. Merchant ships, submarines, warships, and airplanes were sunk across the vast sea lanes of the North Atlantic as well as the South Atlantic, Caribbean, Gulf of Mexico, Gulf of St. Lawrence, Arctic Ocean, and North Sea. More than 30,000 British Merchant sailors were lost and possibly as many as 3,500 Allied and neutral merchant ships. Germany lost 765 submarines and approximately 28,000 submariners, most of which were lost during the last three years of the war. With death rates as high as 75%, service on board German submarines was probably the deadliest of any service during the war. Allied merchant ship losses reached their zenith in 1942. Thereafter, a combination of improved intelligence, increased British focus on protecting shipping lanes, an expansion of U.S. and Royal Canadian Navy defensive and offensive capabilities, and new depth charge technology shifted the balance in the Allies' favor.[12]

[12] The extensive literature on the Battle of the Atlantic includes: John Keegan, *The Second World War* (New York, NY: Penguin, 1989); Clay Blair, *Hitler's* U-*Boat War: the Hunters, 1939-1942* (New York, NY: Random House, 1996); Clay Blair, *Hitler's* U-*Boat War: the Hunted, 1942-1945* (New York, NY: Random House, 1998). Stephen Howarth and Derek Law (eds.), *The Battle of the Atlantic, 1939-1945: The 50th Anniversary International Naval Conference* (Annapolis, MD: Naval Institute Press, 1994); Terry Hughes and John Costello, *The Battle of the Atlantic* (New York, NY: Dial Press, 1977); David Syrett, *The Defeat of the German* U-*Boats: The Battle of the Atlantic* (Columbia, SC: University of South Carolina Press, 1994).

By 1941, German U-boats brought the conflict to the coastal waters of the United States.[13] The physical remains of the resulting attacks, skirmishes, and battles are imprinted on the submerged cultural landscape of the east coast of the United States, including the OCS off Virginia. Within the study area are the remains of the *Amerikland, Francis E. Powell, India Arrow, Olinda, Ocean Venture, Trepca, San Demetrio,* and *Rochester.* Most of these vessels were lost in the dark days of 1942, and they serve as a stark reminder of the death, destruction, and importance of the Battle of the Atlantic. Today, the wrecks of these merchant ships along with at least two World War II German submarines also in the study area (the U-*521* and U-*879*) form part of the rich repository of shipwrecks in the Mid- and South Atlantic Bights that many maritime historians and underwater archaeologists consider to be the "Graveyard of the Atlantic."[14]

4.2.2.4 Shipwrecks in the Project Area

A list of shipwrecks believed to be in the project area based on historical sources is provided in **Table 4-1**.

4.2.3 Detailed Historical Study of the Billy Mitchell Fleet and Project B Experiments

4.2.3.1 Summary

Project B was a series of military tests that took place off the coast of Virginia in June and July of 1921. When executed, this joint Navy-Army operation was considered the largest and most complicated naval arms test in the history of the United States. It was the first major U.S. test to include the underwater, surface, and aerial characteristic of modern naval warfare. The only such test to use former enemy warships as objects of study and as targets, Project B also included the first successful use of a remotely guided battleship as a test target. Historically significant as an innovative military test, Project B is also historically significant for its influence on the domestic, civilian, and military political landscape and the role of the United States as a leader in international Naval Arms Control. Project B is directly related to the calling of the Washington Conference of 1921 and the content and signing of the Washington (Five-Power) Treaty of February 1921. Through the intervention of Army Brigadier General William "Billy" Mitchell, Project B became the center of a national debate over the efficacy and efficiency of military aircraft and battleships. Mitchell was the most famous and broadly influential military aviator in the United States during the 1920s and is considered the father of the modern United States Air Force. The climax of Project B—the sinking of the German dreadnought battleship *Ostfriesland* by Army bombers under Mitchell's direct command—became the high point of his military career and public influence. Mitchell's willfully disobeying of Project B testing protocols and directors during the operations contributed to his later heroic status as a visionary and a maverick. Mitchell's final residence is a National Historic Landmark, and the Project B district (proposed as part of this study) has an even stronger association with his career and influence in the history of American military aviation.

[13] Michael Gannon, *Operation Drumbeat: The Dramatic True Story of Germany's First* U-*Boat Attacks along the American Coast in World War II* (New York, NY: Harper and Row, 1990).

[14] See for example Joseph Hoyt, James P. Delgado, Bradley Barr, Bruce Terrell, and Valerie Grussing, *"Graveyard of the Atlantic" An Overview of North Carolina's Maritime Cultural Landscape* (Silver Spring, MD: NOAA Office of National Marine Sanctuaries, 2014).

Table 4-1. Shipwrecks believed to be in the project area based on historical sources.

Vessel Name	Vessel Type (weight, tons)	Date of Loss	Depth (~m)	Location Accuracy	Comments
Amerikland	Swedish freighter (15,300 t)	2 Feb 1942	Unknown	Undetermined	Torpedoed by German submarine.
Benjamin A. Van Brunt	American schooner (1,191 t)	20 Sept 1925	85	Approximated	Coal schooner owned by Forde Construction Company of New York. Sunk after collision with U.S. Navy light cruiser *Milwaukee*.
Francis E. Powell	Tanker (7,096 t)	27 Jan 1942	30	Known and visited by tech divers	Sunk by torpedo from German submarine *U 130. V*essel broke apart leaving bow and stern sections some distance apart.
Frankfurt	German light cruiser	18 July 1921	130	Known by tech divers; location confirmed by this study	Part of the Billy Mitchell-Project B fleet. Sunk by aerial bombardment.
G-102	Torpedo-boat destroyer	13 July 1921	1,250	Known by tech divers; location confirmed by this study	Part of the Billy Mitchell-Project B fleet. Sunk by aerial bombardment.
India Arrow	Tanker (8,327 t)	4 Feb 1942	58	Known and visited by divers, but likely outside study area	Sunk by German submarine U-*103* while laden with oil and on route from Texas to New York. Twelve survived.
Isabella B. Parmenter	Four-masted schooner	1 Nov 1925	Unknown	Approximated	Sunk 40 miles off the coast. Her crew of six in addition to the captain, his wife, two children, sister-in-law, and two stowaways were rescued by the collier *Achilles*. The vessel was engaged in the coasting trade and hailed out of Boston. She sailed from the Turks and Caicos Islands with a cargo of salt and was bound for Philadelphia.
LikiTiki	Recreational schooner	Dec 1964	~36	Approximated	Coast Guard rescued six people from the *LikiTiki* on 1 Dec 1964; vessel was sailing north from the Florida Keys.
Merida	Passenger freighter	12 May 2011	65	Subject of several salvage attempts, but location unknown	Sunk after collision with SS *Admiral Farragut* while on route from New York to Cuba. The vessel may have been carrying a cargo of silver and copper. This, in turn, has stimulated a series of salvage attempts resulting in considerable damage to the wreck.
O.B. Jennings	American oil tanker (10,000 t)	4 Aug 1918	Unknown	Approximated	The tanker was running empty from Plymouth, UK, to Newport News when she was attacked by German submarine U-*140*.
Ocean Venture	Freighter (7,174 t)	8 Feb 1942	50	Possibly identified by multibeam during this project	Torpedoed by German U-boat U-*108*.

Table 4-1. (Continued).

Vessel Name	Vessel Type (weight, tons)	Date of Loss	Depth (~m)	Location Accuracy	Comments
Olinda (formerly Kennemerland)	Brazilian freighter	18 Feb 1942	180	Approximated (within 3 miles)	Sunk by German submarine U-*432* while on route from Pernambuco and St. Lucia to New York with a cargo of cocoa and castor beans.
Ostfriesland	German battleship	21 July 1921	125	Known by tech divers; location confirmed by this study	Part of the Billy Mitchell-Project B fleet. Sunk by aerial bombardment. This experiment of the effects of airpower on surface ships was by far the most important and was witnessed by a series of important dignitaries.
Rochester	American tanker (6,836 t)	30 Jan 1942	1,095	Approximated (within 5 miles); the subject of survey operations during this study, but not found or identified	Owned by Socony-Vacuum Oil of New York. Sunk by U-boat while on route from New York to Corpus Christi, Texas. The torpedo struck the propeller of the tanker.
S-132	Torpedo-boat destroyer	15 July 1921	125	Known by tech divers; location confirmed by this study	Part of the Billy Mitchell-Project B fleet. Sunk by fire from the USS *Delaware.*
San Demetrio	British tanker (8,073 t)	17 March 1942	2,450	Approximated (within 3 miles); the subject of survey operations during this study, but not found or identified	Sunk by German submarine U-*404* while on route from Baltimore to Halifax, Nova Scotia, with a cargo of alcohol and motor spirits. Earlier (1940) the *San Demetrio* had been attacked by the German warship *Admiral Scheer*. The crew took to lifeboats, but later returned to the ship, tried to put out the fires, and sailed her back across the Atlantic. The narrative attracted considerable public attention at the time and in 1943 a wartime film titled "San Demetrio London" starring Walter Fitzgerald and Robert Beatty was made about the incident. The vessel is also the subject of a book titled "The Saga of the San Demetrio."[15]
St. Augustine	Luxury yacht converted to Navy coastal patrol vessel	6 Jan 1944	75	Known and visited by divers	Sunk as a result of a collision with the tanker *Camas Meadows*.
Trepca	Yugoslavian freighter (5,042 t)	13 March 1942	Unknown	Approximated (within 5 miles)	Sunk by a German submarine (described as a larger cruiser type by the *Trepca*'s captain). The freighter had sailed from a Caribbean port. She was homeported in Dubrovnik and owned by Yogoslavenski-Lloyd.
U-*111*	German submarine	July 1921	413	Approximated	Scuttled. The vessel was supposed to be part of the Billy Mitchell-Project B experiments, but sank before those could take place. She was raised by the Navy, towed farther out to sea, and scuttled in 266 fathoms.

[15] F. Tennyson Jesse, *The Saga of the San Demetrio* (Toronto: The Ryerson Press, 1943).

Table 4-1. (Continued).

Vessel Name	Vessel Type (weight, tons)	Date of Loss	Depth (~m)	Location Accuracy	Comments
U-*117*	German U-boat (1,200 t)	22 June 1921	75	Known; identified by the University of Rhode Island in 2008; known by tech divers; location confirmed by this study	Part of the Billy Mitchell-Project B fleet. Sunk through aerial bombardment.
U-*140*	German U-boat (1,930 t)	22 June 1921	80	Known; identified by URI in 2008; known by tech divers; location confirmed by this study	Part of the Billy Mitchell-Project B fleet. Sunk by fire from the USS *Dickerson*.
UB-148	German U-boat (523 t)	22 June 1921	85	Known; identified by URI in 2008; known by tech divers; location confirmed by this study	Part of the Billy Mitchell-Project B fleet. Sunk by fire from the USS *Sicard*.
U-*521*	German submarine	2 June 1943	2,600	Approximated (within 5 miles)	Sunk by U.S. Navy convoy vessels *PC-565* and *PG-89*.
U-*879* (sometimes recorded incorrectly as U-*548*)	German U-boat	30 April 1945	2,450	Approximated (possibly within 5 miles)	Sunk by the USS *Natchez*, USS *Coffmann*, USS *Bostwick* and USS *Thomas* off northeast of Cape Hatteras.
V-43	Torpedo-boat destroyer	15 July 1921	120	Known; identified by URI in 2008; known by tech divers; location confirmed by this study	Part of the Billy Mitchell-Project B fleet. Sunk by fire from the USS *Florida*.
Vinland	Norwegian freighter (1,143 t)	5 May 1918	2,600	Approximated (possibly within 5 miles)	The remains of the *Vinland* may be close to the U-*879*.
W.L. Steed	American oil tanker (6,182 t)	2 Feb 1942	Unknown	Approximated, outside area	Built in Quincy, Massachusetts, in 1918. The tanker was owned by Standard Oil and homeported in Wilmington, Delaware. Torpedoed by U-boat.

Beyond their connection with the tests, the Project B wrecks are significant in the history of warship design. Although German built, the vessels were commissioned into the U.S. Navy and became objects of studies that substantially influenced the design of U.S. submarines and battleships built during the interwar period. Two submarines, the U-*117* and U-*140*, engaged in major offensives along the coast of the United States and sank many ships in the late summer and early fall of 1918. The Project B shipwrecks are significant for their association with the Treaty of Versailles and use as public trophies in events such as the Victory Bond drive of 1920. There are no other World War I–1920s era underwater historic landscapes of comparable significance in U.S. waters. Indeed, the Project B district is an internationally significant historic cultural landscape and is therefore the subject of considerable attention in this study.

4.2.3.2 World War I, the Treaty of Versailles, and Scapa Flow

On 11 November 1918, the Allied and Associated Powers and Germany signed an armistice to end fighting. In the same month, Germany surrendered its fleet to the Allied and Associated Powers. The warships were docked at various British ports.[16] This armistice included the surrender of 176 U-boats at Harwich on 19 November.[17] These U-boats were then redistributed to several British ports.[18] On 21 November, Admiral Ludwig von Reuter surrendered the German Imperial High Seas Fleet to the British Navy at Scapa Flow.[19] The German vessels were inspected offshore between 25 and 27 November.[20] The Allies had the breech blocks removed from the batteries of the German ships. Afterwards, the vessels were moved into Scapa Flow and a skeleton crew of German officers and men was tasked with cleaning and maintaining the vessels.[21]

Between November 1918 and June 1919, the small contingent of German sailors maintained the large German Imperial Fleet at Scapa Flow.[22] On 21 June 1919, in an act of defiance and resistance, Admiral Reuter gave the order to scuttle the ships.[23] German sailors opened the watertight doors on the ships and ten battleships, five cruisers, 46 torpedo boats, and five light cruisers sank.[24] While responding to the scuttling, British harbor patrols in Scapa Flow killed nine German sailors and wounded 21 others. An additional 1,860 men were taken as prisoners-of-war.[25] The German action at Scapa Flow sank 500,000 tons of naval shipping.[26] Great Britain successfully raised 52 of the 74 scuttled vessels.[27] As punishment, the Allied and Associated Powers required Germany to give them five additional light cruisers as well as 400,000 tons of docks, tugs, dredges, and cranes to aid in the salvage operations.[28]

In 1919, the governments of the Allied and Associated Powers signed the Treaty of Versailles. The Treaty's naval clauses required Germany to transfer all merchant vessels larger than 1,600 gross tons to the Allies as well as half of the vessels between 1,000 and 1,600 tons gross, and a quarter of the steam

[16] Holger H. Herwig, *"Luxury" Fleet: The Imperial German Navy 1888-1918* (New York, NY: Routledge, 2014), 254.

[17] Ibid.

[18] Ibid., 253.

[19] Ibid.

[20] Ibid., 255.

[21] Ibid., 254.

[22] Ibid., 256-257.

[23] Ibid.

[24] Ibid.

[25] Ibid., 257.

[26] Ibid.

[27] Ibid.

[28] Ibid., 256.

trawler and fishing fleets.[29] Article 181 of the Treaty capped the German Navy at six battleships, six light cruisers, 12 destroyers, and 12 torpedo boats. Germany was forbidden from retaining any submarines either for commercial or military purposes.

The Treaty also required Germany to turn over 8 battleships, 8 light cruisers, 42 destroyers, and 50 torpedo boats, with all their guns on board, to the Allied and Associated Powers.[30] As their share, the United States received the battleship *Ostfriesland*, light cruiser *Frankfort*, U-boats U-*111*, U-*117*, U-*140*, and *UB-148*, and destroyers *G-102*, *V-43*, and *S-132*. All German naval vessels were disarmed, but the guns remained with the ships.[31] Although they became the property of various Allied and Associated Powers, the Treaty put strict limits on the use of the captured vessels.[32] The *Frankfurt*, *V-43*, *G-102*, and *S-132* had been beached during the Scapa Flow scuttling.[33] After they were raised, the United States moved the vessels to Rosyth Yard in Scotland for inspection, repair, and commissioning before dispatching them across the Atlantic.[34] Under the terms of the Treaty of Versailles, the United States had to destroy or convert the former German warships to nonmilitary usage by 9 August 1921.[35]

4.2.3.3 Surface Ship Passage to the United States

On 20 April 1920, an American Board of Inspection convened on the USS *Falcon* at Port Edgar, Scotland, to examine the condition of the *Ostfriesland* and the other ex-German vessels transferred to the United States Navy and determine whether they were seaworthy enough to cross the Atlantic.[36] The Board of Inspection consisted of Captain Julius Hellweg, Commander Clarence Wood, Commander Stephen McKinney, Lieutenant Commander Francis Cogswell, Lieutenant George Herring, and Commander Denis Thibault.[37] The Board was tasked with "[informing] the Force Commander by telegraph, of the general condition of each vessel, and of her motive power at as early a date as practicable."[38]

The British Navy transferred the *Ostfriesland* to Rosyth Yard, Scotland, for inspection.[39] The American Board of Inspection found the battleship's steering, engines, ground tackle, boilers, electrical

---

[29] Major Reuben J. Clark Jr., *Data on German Peace Treaty: Data presented to the Committee on Foreign Relations, United States Senate, relating to the Treaty of peace with Germany* (Washington, DC, Government Printing Office, 1919), 18.

[30] Ibid., 79.

[31] Ibid., 32.

[32] Ibid.

[33] "List of Warships Scuttled at Scapa Flow," *World War 1 Naval Combat* (1998-2016). Website accessed 22 August 2016 at: http://worldwar1.co.uk/scapa-flow.html

[34] Vice Admiral Alfred W. Johnson, "The Naval Bombing Experiments off the Virginia Capes June and July 1921." Website accessed 22 August 2016 at: http://www.history.navy.mil/research/library/online-reading-room/title-list-alphabetically/n/the-naval-bombing-experiments.html

[35] Clark, *Data on German Peace Treaty*, 32.

[36] Record of Proceedings of a Board of Inspection Convened on Board the USS *Falcon*, at Port Edgar, Scotland, By Order of the Force Commander, U.S. Naval Forces Operating in European Waters to Inspect the Ex-German Ship *Ostfriesland*, Allocated to the United States, April 20, 1920; Box 2784, Folder 28785 (260) to (298). Secretary of the Navy General Correspondence (Sec. Navy Gen. Corr.) 1916-1926; General Records of the Department of the Navy (GRDN), Record Group 80 (RG 80); National Archives, College Park, MD.

[37] Letter from Force Commander to Captain Victor, commanding officer USS *Chattanooga*; Box 2784, Folder 28785 (260) to (298); Sec. Navy Gen. Corr.; GRDN, RG 80, National Archives, College Park, MD.

[38] Ibid.

[39] Letter to British Admiralty from Captain W.R. Stockton, U.S. Naval Attache in London; Box 2784, Folder 28785 (260) to (298); Sec. Navy Gen. Corr.; GRDN, RG 80; National Archives, College Park, MD.

installations, and watertight doors to be in good working order.[40] However, her navigational instruments, boilers, brickwork, fuses, bilges, quarters, galley, and auxiliary machinery had been stripped and would need to be replaced before passage across the Atlantic.[41] In addition to these repairs, the *Ostfriesland* was to carry four heavy guns, two 12 in and two 14 in, back to the United States for transfer to the Bureau of Ordnance.[42]

The USS *Hancock* arrived carrying most of the stores required to repair the ship for the voyage. The Board estimated that the repairs would cost approximately $26,500.[43] The Board indicated to Vice Admiral H.S. Knapp, Commander of U.S. Naval Forces operating in European Waters, that following repairs, the *Ostfriesland* could steam to the United States under her own power.[44]

In addition to examining the *Ostfriesland*, the Board of Inspectors assessed the condition and suitability of the *Frankfurt* and three destroyers to undertake trans-Atlantic passage. The inspectors concluded that the *Frankfurt* was in good structural condition but required some repairs to the steering gear, lights, and watertight doors. In addition, the light cruiser would need to be supplied with navigational instruments, pumps, furniture, water, and food supplies. Personnel from the USS *Panther* were to oversee the repairs on the *Frankfurt.*[45] On 28 March 1920, the inspectors concluded that the *Frankfurt* required one week in dry dock and $25,000 worth of repairs to be in condition to navigate across the Atlantic under her own power.[46] In the final analysis, this proved to be too ambitious and the *Frankfurt* was eventually towed across the Atlantic. The initial predictions by the Commandant of the Philadelphia Navy Yard for repairs to the destroyers were that the vessels would require 150 working days and $100,000. Even then, the ships also would have to be towed across the Atlantic. The personnel recommendations for the towing were 60 men for the *Frankfurt* and ten men for each destroyer.[47] Equipment added to each vessel for the crossing included a field radio and hand generator, navigational instruments and publications, lighting, signals, cooking utensils and gear, furniture, and toilets.[48]

At around the same time, the *G-102*, *S-132*, and *V-43* were moved to the Rosyth Dockyard for maintenance.[49] The USS *Hovey* oversaw the repairs on the *G-102*, with personnel from other vessels overseeing the repairs to the *V-43* and *S-132*.[50] The *G-102, S-132, V-43,* and *Frankfurt* had their

---

[40] Records of the Board of Inspectors, USS *Falcon* Port Edgar Scotland, 20 April 1920; Box 2784, Folder 28785 (260) to (298); Sec. Navy Gen. Corr.; GRDN, RG 80; National Archives, College Park, MD.

[41] Ibid.

[42] Letter from Staff Representative, London to Chief of Naval Operations, Washington; Box 2784, Folder 28785 (260) to (298); Sec. Navy Gen. Corr.; GRDN, RG 80; National Archives, College Park, MD. College Park, Natl Air and Space, and Downtown 3.12 and 3.13 188.

[43] Records of the Board of Inspectors, USS *Falcon* Port Edgar Scotland, 20 April 1920; Box 2784, Folder 28785 (260) to (298); Sec. Navy Gen. Corr.; GRDN, RG 80; National Archives, College Park, MD. College Park, Natl Air and Space, and Downtown 3.12 and 3.13 183.

[44] Ibid., 184.

[45] Ibid., 302.

[46] Dispatch from Board convening on *Frankfurt*; Box 2784, Folder 28785 (260) to (298); Sec. Navy Gen. Corr.; GRDN, RG 80; National Archives, College Park, MD.

[47] Letter from USS *Afean* to Naval Operations; Box 2784, Folder 28785 (260) to (298); Sec. Navy Gen. Corr.; GRDN, RG 80; National Archives, College Park, MD. College Park, Natl Air and Space, and Downtown 3.12 and 3.13 276.

[48] Ibid.

[49] Letter on USS *Frankfurt*, *G-102*, *S-132*, and *V-43* preparations; Box 2784, Folder 28785 (260) to (298); Sec. Navy Gen. Corr.; GRDN, RG 80; National Archives, College Park, MD.

[50] Records of the Board of Inspectors, USS *Falcon* Port Edgar Scotland, 13 March 1920; Box 2784, Folder 28785 (260) to (298); Sec. Navy Gen. Corr.; GRDN, RG 80; National Archives, College Park, MD.

propellers removed and stored on deck.[51] The *G-102* required additional repairs to seal underwater openings and to clean and coat the bottom of the vessel.[52] The *Frankfurt* required the installation of lighting inside the vessel.[53] Because the *Ostfriesland* was to proceed across the Atlantic under its own power, she required the most extensive work. The battleship needed cleaning and repair that included forging of new torpedo tube covers; tightening and cleaning the propellers; refitting and replacing underwater gratings; fixing pumps; clearing and overhauling the ash ejectors and discharge pipes; installing firebars and soiler plugs; replacing parts of pistons, pumps, compressors, and condensers; and supplying new engine wrenches.[54] The ship was commissioned as the USS *Ostfriesland* on 7 April 1920 in Rosyth, Scotland, and placed under the command of J.F. Hellweg.[55]

4.2.3.4 Arrival of the Ex-German Surface Ships in the United States

The Sunday edition of the *New-York Tribune* for 1 August 1920 announced the impending arrival of the captured German fleet. The article described the vessels as "five of the finest warships of the once great German navy." Although surprisingly respectful in its description of the warships, especially the *Ostfriesland*, the author included a bit of triumphant rhetoric.

> The Ostfriesland was launched in September, 1909. Little did the Germans think at that time that within ten years the ship which was then the pride of the German navy would be riding at anchor in the Hudson River, under the American Flag, a captive.

The article went into extraordinary technical detail about the *Ostfriesland*'s design and armament and recounted the battleship's actions in the Battle of Jutland. Similarly, it characterized the *Frankfurt* as "a hard fighter" and one of the hardest worked German fast cruisers."[56] The report was a bit premature, as the five ships did not arrive in New York until 10 August 1920.

On 22 August 1920 the Navy Department dashed the hopes of many along the eastern seaboard who had expected the ships to make a victory tour. The fault, according to Captain J.F. Hellweg who commanded the convoy, was entirely due to the German's "deliberate vandalism." "The gutted condition in which we found these vessels on taking them over cannot be exaggerated. What had not been stolen was wrecked. The vandalism indicated a very careful preparation and the usual thoroughness of the Huns in execution."[57] A month later, the *New-York Tribune* published a long account by Captain Hellweg. He scornfully described the remaining compliment of German sailors on the *Ostfriesland* as "an ill dressed, dirty, unshaven, sullen looking crowd." Hellweg seemed shocked at the concerted efforts of the German sailors to inconvenience the U.S. Navy: "the magnitude of their efforts astonished me . . . they had

---

[51] Work Carried out in Rosyth Yard, Records of the Board of Inspectors, USS *Falcon* Port Edgar Scotland, 13 March 1920; Box 2784, Folder 28785 (260) to (298); Sec. Navy Gen. Corr.; GRDN, RG 80; National Archives, College Park, MD.

[52] Ibid.

[53] Letter on USS *Frankfurt*, *G-102*, *S-132*, and *V-43* preparations; Box 2784, Folder 28785 (260) to (298); Sec. Navy Gen. Corr.; GRDN, RG 80; National Archives, College Park, MD.

[54] Work Carried out in Rosyth Yard, Records of the Board of Inspectors, USS Falcon Port Edgar Scotland, 13 March 1920; Box 2784, Folder 28785 (260) to (298); Sec. Navy Gen. Corr.; GRDN, RG 80; National Archives, College Park, MD; Chief Engineer Kent E. Smith, communication, USS *Ostfriesland*, Box 2784, Folder 28785 (260) to (298); Sec. Navy Gen. Corr.; GRDN, RG 80; National Archives, College Park, MD.

[55] Memorandum for Chief of Naval Operations, n.d.; Box 2784, Folder 28785 (260) to (298); Sec. Navy Gen. Corr.; GRDN, RG 80; National Archives, College Park, MD.

[56] *New-York Tribune*1 August 1920.

[57] *New-York Tribune*23 August 1920.

actually prepared to remove all the motor generators from the ship . . . I was surprised that they were not preparing to lift the main engines. There wasn't much else that they had not started to remove."[58]

4.2.3.5 Engineering Studies of the Ex-German Surface Ships

After arrival, the machinery and fittings on the vessels were tested before the ships were placed out of commission, dismantled, and towed out to sea to be destroyed by gunfire during target practice by the Atlantic Fleet.[59] U.S. personnel drained the boilers, machinery, and pipelines of water to prevent rupturing of these systems, which might have sunk the vessels.[60] Additionally, 1,000 tons of coal present on the *Ostfriesland* and 500 tons of coal on the *Frankfurt* were removed.[61] The USS *Ostfriesland*, USS *Frankfurt*, USS *V-43*, USS *S-132*, and USS *G-102* were decommissioned from the U.S. Navy on 25 August 1920 in the New York Navy Yard.[62]

On 28 August 1920, the Navy began receiving requests from educational institutions and other interested groups requesting material from the vessels.[63] After the ex-German vessels were brought to the United States and the intent to destroy them was announced, iron companies, including Henry A. Hitmer's Sons Co., inquired whether the iron from these ships would be sold to iron companies for repurposing.[64] The British Navy had recently melted down an obsolete dreadnought and Mr. Conyell from the company wrote to request a similar action by the U.S. Navy.[65] However, the U.S. Navy and Bureau of Ordnance refused all these requests, because the Treaty of Versailles prohibited the sale and repurposing of materials from vessels identified for destruction. There were minor exceptions; the ship bells from the *Ostfriesland* and *Frankfurt* went to the Naval Academy for public exhibition.[66]

The Commandant of the New York Navy Yard gave permission for a company out of Waterbury, Connecticut, to study the electronics and auxiliary machinery on the *Ostfriesland* and *Frankfurt*.[67] Similarly, the Redfield-Redfield Steel Company of Philadelphia, Pennsylvania; Main Electric Company of Portland, Maine; and the Bethlehem Building Corporation of Bethlehem, Pennsylvania, studied the auxiliary machinery installed on the same two ships.[68] Electrical components and other auxiliary

---

[58] *New-York Tribune*26 September 1920.

[59] Correspondence from Chief of Naval Operations to Chiefs of all Bureaus; Box 2784, Folder 28785 (260) to (298); Sec. Navy Gen. Corr.; GRDN, RG 80; National Archives, College Park, MD.

[60] Correspondence from Secretary of the Navy to the Commandant of the New York and Norfolk Navy Yards; Box 2784, Folder 28785 (260) to (298); Sec. Navy Gen. Corr.; GRDN, RG 80; National Archives, College Park, MD.

[61] Correspondence from Captain C.L. Arnold, U.S. Navy to Commandant Third Naval District; Box 2784, Folder 28785 (260) to (298); Sec. Navy Gen. Corr.; GRDN, RG 80; National Archives, College Park, MD.

[62] Correspondence from Chief of Naval Operations to the Commandants of the Third and Fifth Naval Districts, USS *Ostfriesland*, USS *Frankfurt*, USS *V-43*, USS *S-132*, USS *G-102*; Box 2784, Folder 28785 (260) to (298); Sec. Navy Gen. Corr.; GRDN, RG 80; National Archives, College Park, MD.

[63] Correspondence to William D. Upshaw; Box 2784, Folder 28785 (260) to (298); Sec. Navy Gen. Corr.; GRDN, RG 80; National Archives, College Park, MD.

[64] Correspondence from Professor M.E. Cooley to Chief of the Naval Bureau; Box 477, Folder 4153 (523) to (538); Records of the Army Air Forces (RAAF), RG 18; National Air and Space Museum Archives, Washington, DC.

[65] Ibid.

[66] Correspondence from the Secretary of the Navy to the Chief of the Bureau of Construction and Repair; Box 2784, Folder 28785 (260) to (298); Sec. Navy Gen. Corr.; GRDN, RG 80; National Archives, College Park, MD.

[67] Correspondence from the Department of the Navy to the Chief of the Bureau of Construction and Repair; Box 2784, Folder 28785 (260) to (298); Sec. Navy Gen. Corr.; GRDN, RG 80; National Archives, College Park, MD. College Park, Natl Air and Space, and Downtown 3.12 and 3.13 236.

[68] Correspondence from the Secretary of the Navy to the Chief of Bureau of Construction and Repair; Box 2784, Folder 28785 (260) to (298); Sec. Navy Gen. Corr.; GRDN, RG 80; National Archives, College Park, MD.

equipment including two 4.5 horsepower (hp) ventilation motors, a BHP shell handling actor, and one 0.25 hp motor used to ventilate the capstan were sent to Lehigh University.[69] The University of Pennsylvania was loaned a variety of electric motors and shell handling equipment including two searchlight motor generators and two step-down transformers [70] However, as per treaty requirements all electronic components and armament were returned to the vessels before their sinking.[71]

4.2.3.6 Project B Submarines as Artifacts of Victory and of Retribution 1919−1921

As artifacts, the German surface warships had strong meaning to American citizens in the immediate post-war period. Although some Americans had an opportunity to see the *Ostfriesland* and the other surface ships, the poor condition of the ships prevented them from being used in post-war patriotic tours. Representatives for communities and institutions from around the nation wrote to the Navy requesting pieces of the *Ostfriesland* as permanent war trophies. Navy leadership interpreted the terms of the Treaty for transferring the ships to the United States as requiring the disposal of the entire ship. Although this may not have been strictly true, a policy of parsing out the *Ostfriesland* would have quickly become a very expensive proposition and a political nightmare.

The story of submarines and their contemporary cultural meaning is more complicated than for the surface warships. Although the public associated the battleship arms race with the cause of the war in Europe, they did not see battleship warfare itself as against the laws of war and human decency. By contrast, most saw Germany's use of submarines as the reason why an otherwise neutral America had to fight in a European war. The use of submarines off America's shore, in combination with memories of the innocent lives lost on the RMS *Lusitania* and other passenger and merchant vessels, gave Americans an avenue to channel their hostility against Germany and demonstrate their patriotism and support for the war one last time. In that sense, the Project B U-boats became both war trophies and surrogates for the Germany that, through the agency of their armed forces, Americans could punish.

4.2.3.6.1 U-Boats as Artifacts of Victory

Although significant for their influence on the design of later American submarines, the U-boats used in Project B were first brought to the United States to help sell Victory War Bonds. In 1919, the official Navy stance against submarine warfare led to a refusal to take possession of the captured U-boats. Recognizing the folly of this stance, Navy submarine expert Captain Thomas Hart stepped outside of official channels, approached the civilian organizers of the Victory Bond drive, and persuaded them that the submarines would make "the best war trophy available." The Victory Bond drive organizers promptly convinced the Secretary of the Navy to bring the U-boats to the United States.[72] The Allies allocated six U-boats to the United States including the U-*111*, the U-*117*, the U-*140*, and the *UB-148*. A March 1919 Navy press release announced the impending voyage of the captured submarines to the United States:

> The five submarines [the U-111's departure was delayed] which are being brought over for the double purpose of giving the United States naval experts a chance to study them

[69] Correspondence regarding Lehigh University and electrical machinery from the Ostfriesland; Box 2784, Folder 28785 (260) to (298); Sec. Navy Gen. Corr.; GRDN, RG 80; National Archives, College Park, MD; Correspondence from Captain Friedenrich and the Bureau of Construction and Repair; Box 2784, Folder 28785 (260) to (298); Sec. Navy Gen. Corr.; GRDN, RG 80; National Archives, College Park, MD.

[70] Correspondence between the Chief of Naval Operations and the Commandant; Box 2784, Folder 28785 (260) to (298); Sec. Navy Gen. Corr.; GRDN, RG 80; National Archives, College Park, MD.

[71] Correspondence between Acting Secretary of the Navy Theodore Roosevelt and Dr. Emory General Box 2784, Folder 28785 (260) to (298); Sec. Navy Gen. Corr.; GRDN, RG 80; National Archives, College Park,

[72] Norman Friedman, *U.S. Submarines Through 1945: An Illustrated Design History* (Annapolis: Naval Institute Press, 1995).

and, principally, for exhibition in American ports during the Liberty loan drive, represent four different types of German undersea boats.

The ambitious goal of the Victory Bond drive was to raise $4.5 billion to fund the United States' war debts. Although criticized for its heavy-handed tactics, the Victory Bond drive successfully tapped into the waning reserves of America's wartime patriotism. German submarines brought a reluctant United States into the war, and German submarines brought the war to America's shores, deploying mines and attacking shipping in late summer and early fall of 1918. For the price of a safe government bond, a patriotic citizen could support the war effort one last time and personally gloat over the fate of a German submarine.

Newspapers tracked the progress of the submarine voyages. On 26 April 1919, the *Brooklyn Daily Eagl*e reported the arrival of the U-*117* and that one of her officers was Lieutenant Vincent Astor, who had the distinction of piloting the vessel up the harbor. "Jim, his wire-haired terrier, was also a passenger on the U-boat and seemed glad to hit terra firma again." Astor, heir to the famous family's fortune, reported, "the boat behaved remarkably well under the rough treatment it received."[73]

Four U-boats participated in the kick-off of the Victory Bond drive during "Battle Week" in April 1919. Newspaper stories during the tour emphasized the venal records of U-boats, especially the depredations of the U-*117* and U-*140* off America's shores. At Wilmington NC on 9 May 1919, "several thousand people saw the U-*117*, captured German submarine, ex-sea raider, pirate and destroyer of lives and Allied commerce."[74] The U-*117*'s tour included stops in Brooklyn, Philadelphia, Baltimore, Wilmington, Norfolk, and Washington, D.C. The *UB-148* tour included Brooklyn, Jersey City, Yonkers, and several cities along the Hudson River as well as Bridgeport, New Haven, and New London, Connecticut. Although a war-weary America proved reluctant to buy the bonds, the tour of the U-boats to ports along the eastern seaboard played a key role in inspiring cities and towns to meet their goals. The U-*117* and *UB-148* are historically significant for their importance in the final U.S. bond drive of the World War I era.

4.2.3.6.2 U-Boats as Artifacts of Retribution

While the anti-German rhetoric was rampant in the internal reports of naval officers charged with bringing the German surface vessels to the United States, the public coverage focused on their technical qualities and war records, especially those of the *Frankfurt* and *Ostfriesland* at the Battle of Jutland. By contrast, the public and press projected a deeply hostile attitude toward the U-boats of Project B. For Americans, no military artifact or acts of war more strongly represented the lawless character of the German Empire than the submarine and its use against "innocent" merchant vessels. For the American public, the destruction of the war prize U-boats in Project B became a final act of justice or vengeance for hundreds of ships and thousands of lives destroyed by Germany's undersea fleet during the war.

Describing the plan for Project B, the *Virginia Pilot* reported "the first vessel to be attacked will be the U-*117*, the largest of the German submarines allotted to the United States. She was among the larger types of German undersea craft, and has to her credit a black record of crimes on the high seas and violations of international laws of sea fighting." "Her first official appearance off American shores was August 10, 1918, when she sank eight small fishing schooners off Nantucket Shoals. Off Long Island, New York, two days later, according to information published by the Navy Intelligence Bureau, the U-*117* sank a steamer. She operated along the Atlantic coast until 9 September 1918, during this time sinking twenty ships, most of them flying the American flag and aggregating 19,918 tons. She also sank ten small fishing boats." The *Pilot* had no information on the other submarines, but stated "vessels are

[73] "Astor Arrives on German Submarine," *Brooklyn Daily Eagle* 26 April 1919.

[74] "Sea-Raider Leaves as Tank Arrives," *Wilmington Morning Star*10 May 1919.

said to have had black war records, although official accounts of their depredations during the war with Germany are lacking."[75]

Reporting on the impending destruction of the U-*140* and *UB-148*, the *Washington Times* exhorted, "the former German submarines U-*140* and *UB-148*, vessels which at one time cruised the North Sea raiding Allied commerce, are today lying at anchor sixty miles off Cape Charles as helpless as the prey which they formerly hunted, waiting for the guns of American destroyers to send them to the bottom."[76] Newspaper coverage in the aftermath which described German submarines in such terms as "Sea Monsters, Hun Devil Boats, Sea Thugs, Undersea Dastards, and Slayer of Innocents" shows that the public animus against the submarines continued well after their destruction.[77]

4.2.3.7 Ship Histories

4.2.3.7.1 The Battleship *Ostfriesland*

The *Helgoland* class battleship was designed between 1907 and 1908 to serve as a coastal defense vessel.[78] The *Ostfriesland*, one of four ships in the *Helgoland* class, was laid down on 19 October 1908 in the Wilhemshaven Imperial Navy Yard.[79] Launched on 30 September 1909 with a displacement of 22,800 tons, her maximum speed was 20 knots.[80] The ship was protected with Krupp plating on its deck, forward and aft roofs, turret roofs, and torpedo bulkheads.[81] The armor was a nickel-chrome steel plate that provided protection from torpedo and shell fire, but weighed less than earlier iron and steel plates, thus allowing the ships to carry more weight in guns.[82] On 1 August 1911, the ship was commissioned into the German Navy as SMS *Ostfriesland*.[83] The total cost for the SMS *Ostfriesland* was between 41.1 and 43.6 million marks.[84]

Of the approximately 42 million marks spent on the *Ostfriesland*, about 20.7 million marks were spent on the ship, while the armament accounted for the remaining costs.[85] The armament of the *Ostfriesland* consisted of a main, secondary, and tertiary battery of steel guns manufactured by Krupp.[86] Below the waterline, the *Ostfriesland* had six 20 in (50 cm) torpedo tubes with 16 rounds, positioned in a hexagonal arrangement similar to the 12 in (30.5 cm) guns, with one at the stern, one at the bow, and two on each lateral side of the hull.[87] The initial armament of the *Ostfriesland* was state-of-the-art when the vessel was commissioned in 1911. During her time in service, however, the armament of the *Ostfriesland* was updated to address new naval needs and weapons developments. From the torpedo tubes to the main

---

[75] Joseph A. Leslie, "History of Warships which will be Bombed by Navy and Army Aviators off Virginia Capes," *Virginian Pilot* 19 June 1921.

[76] *Washington Times* 22 June 1921.

[77] Chris Dubbs, *America's* U-*Boats: Terror Trophies of World War I* (Lincoln, NB: University of Nebraska Press, 2014), 93.

[78] Siegfried Breyer, *Battleships and Battle Cruisers* (New York, NY: Doubleday Publishing, 1974), 267.

[79] Ibid.

[80] Robert Gardiner (ed.), *The Eclipse of the Big Gun* (London: Conway Maritime Press, 1992), 18.

[81] Erich Gröner, *German Warships 1815-1945 Volume 1* (Annapolis, MD: Naval Institute Press, 1990), 24.

[82] David Stevenson, *Armaments and the Coming of War: Europe 1904-1914* (Oxford: Clarendon Press, 1996), 17.

[83] Breyer, *Battleships and Battlecruisers*, 267.

[84] Ian Hogg and John Batchelor, *Naval Gun* (Poole, Dorset: Blandford Press, 1978), 119; Gröner, *German Warships*, 24.

[85] Hogg and Batchelor, *Naval Gun*, 119.

[86] Stevenson, *Armaments and the Coming of War*, 22.

[87] Gröner, *German Warships*, 24.

battery on the deck of the *Ostfriesland*, the weapons show defensive adaptations to new weapons technologies and technological developments of guns, shells, turrets, and improved firing range.

Although torpedoes can be used by surface vessels, against surface vessels, the development of viable submarines and effective torpedoes were inextricably linked.[88] Although the idea of expanding warfare to underwater dates back to at least 332 BC, the first viable military submarine was not built until 1896.[89] Navies began adopting submarines in 1904, which made significant contributions to warfare at sea during World War I.[90] Early torpedo tubes were designed for 12 in (30.5 cm) charges, but the *Ostfriesland* was built with newer 20 in (50 cm) tubes.[91] The presence of torpedo tubes and Krupp armor at the ship's waterline demonstrate that the *Ostfriesland* was built to withstand the new military technologies.[92]

Although the torpedo tubes represent changes that were made to accommodate new technology during the design and construction of the ship, elements of the ship's armament were updated while the vessel was in service. The initial tertiary battery of the *Ostfriesland* was composed of fourteen 3.46 in (8.8 cm) guns.[93] These guns were 45 caliber quick-firing weapons with 2,800 rounds.[94] In 1914, two of the 3.46 in (8.8 cm) guns were replaced with anti-aircraft guns with a firing angle improved from approximately 20° to 85° of elevation.[95] In 1916, all 3.46 in (8.8 cm), except those that were changed to anti-aircraft guns, were removed from the ship.[96] Although airplanes did not play a major role in World War I, the changes made to the *Ostfriesland* during the course of the war indicate acceptance and accommodation of this new technology. By the 1930s, deck guns that were being used for anti-aircraft purposes had an angle of elevation of approximately 85° and water-cooling mechanisms to allow for faster rates of fire.[97]

The initial secondary battery of the *Ostfriesland* consisted of fourteen 5.9 in (15 cm) 45 caliber quick-firing guns with 2,100 rounds and a range of 13,500 m.[98] After 1915, the range of these guns was improved to 16,800 m.[99] Seven guns were arranged on either side of the hull, on the gun deck.[100] On each side, two 5.9 in (15 cm) guns were stored with the muzzle facing the stern and could rotate out while five 5.9 in (15 cm) guns were stored against the ship with the muzzle facing the bow and could swivel from the opposite direction.[101] Shells for the 5.9 in. (15 cm) guns were stored in compartments separate from those of the 12 in (30.5 cm) and 3.46 in (8.8 cm) guns and the powder magazines.[102]

---

[88] David Woodbury, *Submarine Warfare* (New York City, New York: W.W. Norton & Company, 1942), 38.

[89] Ibid., 17, 33-34.

[90] Ibid., 37.

[91] Herwig, "Luxury" Fleet, 64.

[92] Gröner, *German Warships*, 24.

[93] Ibid.

[94] Ibid.

[95] Ibid., 25.

[96] Navy News Bureau, Immediate Release, 19 July 1921; Records Collection of the Office of Naval Records and Library (RCONRL), RG-45; National Archives, College Park; Naval Spoils Coming to America Promise a Profitable Study, 1921.

[97] Hogg and Batchelor, *Naval Gun*, 125.

[98] Gröner, *German Warships*, 24.

[99] Gröner, *German Warships*, 25.

[100] Ex-German SS *Ostfriesland* Data on Bombings, Booklet of General Plans prepared in the Office of the Construction Officer, 9 May 1921, altered 22 August 1921, National Archives, College Park, MD.

[101] Ibid.

[102] Ibid.

The largest guns on the *Ostfriesland* were mounted in turrets on the main deck. This main battery consisted of twelve 12 in (30.5 cm), 50 caliber quick-firing guns with 1,020 rounds.[103] They were mounted in twin turrets in a hexagonal pattern on the deck of the ship.[104] These guns were breech-loading, with an angle of depression of -8°, an angle of elevation of 13.5°, and a range of 18,000 m.[105] Later, the angle of depression was changed to -5.5°, the angle of elevation was changed to 16°, and the gun range was improved to 20,400 m.[106] Although triple gun turrets had been developed, the German Navy decided to keep their twin turrets because the ammunition hoists in the triple turrets were still technologically problematic.[107]

The 12 in (30.5 cm) guns in the main battery fired 405 kg charges with heavy powder loads. The guns, therefore, could not be easily reloaded manually by the sailors.[108] The turrets on the *Ostfriesland* used combination electric and hydraulic systems to hoist ammunition and load the guns.[109] All parts of the reloading mechanism were made of steel and the powder and shells were kept in separate compartments to prevent fire in the turret.[110] This mechanized reload allowed for a quick firing rate of approximately one shot every 16 seconds.[111] The hexagonal set up of the gun turrets reduced the number of 12 in (30.5 cm) guns that could participate in the broadside fire. Only the bow, stern, and two lateral twin turrets could fire from the lateral side of the ship at one time. Because of this turret arrangement, the German naval policy was to include the smaller guns in the broadside.[112] Thus, the broadside fire of the *Ostfriesland* included eight 12 in (30.5 cm) guns and seven 5.9 in (15 cm) guns.[113]

The 12 in (30.5 cm) and 5.9 in (15 cm) guns on the *Ostfriesland* were quickly outsized by the guns on comparable British, American, and Japanese battleships.[114] By 1911, these three navies were firing 635 kg shells, or shells that were 40% heavier than German 12 in (30.5 cm) gun shells.[115] During the war, First Lord of the Admiralty, Winston Churchill, introduced 15 in guns that shot 870 kg shells over 30 km.[116] After the Battle of Jutland, even though the German navy performed well, the Germans believed that the British had the superior gunnery.[117] Although the Germans got more hits, they made no heavy-caliber hits against the British.[118] After the Battle of Jutland, the German navy gained interest in larger guns, and German battleships, laid down after the *Ostfriesland* had main batteries of 15 in (38 cm) guns to match the firepower of British ships.[119]

---

[103] Gröner, *German Warships*, 24.

[104] Herwig, "Luxury" Fleet, 64.

[105] Gröner, *German Warships*, 24.

[106] Ibid., 25.

[107] Norman Friedman, *Naval Firepower: Battleship Guns and Gunnery in the Dreadnought Era* (Yorkshire: Seaforth Publishing, 2008), 168.

[108] Germany 30.5 cm/50 (12") SK L/50. Website accessed 22 August 2016 at:http://www.navweaps.com/Weapons/WNGER_12-50_skc12.htm

[109] Ibid.

[110] Ex-German SS *Ostfriesland* Data 22 August 1921, National Archives, College Park, MD.

[111] Germany 30.5 cm/50 (12") SK L/50. Website accessed 22 August 2016 at: http://www.navweaps.com

[112] Herwig, "Luxury" Fleet, 64.

[113] Friedman, *Naval Firepower*, 163.

[114] Herwig, *"Luxury" Fleet*, 80.

[115] Ibid.

[116] Ibid., 82.

[117] Friedman, *Naval Firepower*, 166.

[118] Ibid.

[119] Herwig, *"Luxury" Fleet*, 82.

4.2.3.7.2 The Light Cruiser *Frankfurt*

The *Wiesbaden*-class light cruiser *Frankfurt* was built at the Imperial Dockyard in Kiel between 1913 and 1915.[120] It displaced 6,601 tons and had a maximum speed of 27.5 knots.[121] Because it was completed after the outbreak of the war, *Frankfurt* featured some of the newest naval technology. She was armed with eight 15 cm guns, four 3.46 in (8.8 cm) guns, and four 50 cm torpedo tubes.[122] She also had the capacity to lay 120 mines.[123] During the war, the secondary and tertiary batteries were replaced with guns that had a larger vertical range. This was preferable for anti-aircraft warfare.[124] Compared with other ships in the German fleet, light cruisers, including *Frankfurt*, had light armor. The Germans launched four to six light cruisers every year from 1913 until 1918.[125]

4.2.3.7.3 The Destroyers

Before World War I, Germany had 102 destroyers, and during the war an additional 95 were built. At the Battle of Jutland, 61 ships in the German fleet of 99 were destroyers.[126] These ships were the most numerous vessels in the navy and were used for various purposes including carrying troops, supporting other vessels, and minesweeping.[127] After the war, the United States was allotted several German destroyers that were anchored at Scapa Flow. However, after the scuttling attempt, the specific vessels that each of the Allied and Associated Powers was to receive changed.[128] The United States eventually took three vessels that had been beached during the scuttling attempt (*S-132, G-102,* and *V-43*) and transferred them across the Atlantic.[129] Although these vessels were built at different times, some aspects of their design were similar.

4.2.3.7.4 *G-102*

The destroyer *G-102* was built at the Germania Dockyard in Kiel between 1914 and 1915.[130][131] She displaced 1,734 tons, carried four 3.46 in (8.8 cm) guns, four 20 in (50 cm) torpedo tubes, and 24 mines.[132] In 1916, the four guns were replaced with larger 10.5 cm guns.[133] *G-102* was part of the Number Two Flotilla, led by *B-110* and comprising *G-101, G-103, V-100, B-109, B-111, B-112,* and *G-104*.[134] During World War I, *G-102* laid mines off the Atlantic coast of North America in areas ranging

---

[120] Friedman, *Naval Firepower*, 111.

[121] Ibid.

[122] Ibid.

[123] Ibid.

[124] Ibid.

[125] Breyer, *Battleships and Battlecruisers*, 256.

[126] James L. George, *History of Warships: From Ancient Times to the Twenty-First Century* (Annapolis, MD: Naval Institute Press, 1998), 140.

[127] Ibid.

[128] Clark, Data on German Peace Treaty.

[129] List of Warships Scuttled at Scapa Flow. Website accessed 22 August 2016 at: http://www.worldwar1.co.uk/scapa-flow.html

[130] Groner, *Battleships and Battlecruisers*, 188.

[131] Ibid.

[132] Ibid.

[133] Ibid.

[134] Dan van der Vat, *The Grand Scuttle: The Sinking of the German Fleet at Scapa Flow in 1919* (Edinburgh: Berlinn Limited, 1997), 224.

from Cape Hatteras to Newfoundland.[135] *G-102* was raised following the scuttling attempt at Scapa Flow. She was repaired at the Rosyth Yard in June 1920 and had her through-hull fittings sealed before making the trans-Atlantic voyage to the United States.[136]

4.2.3.7.5 *V-43*

The oldest of the three destroyers was *V-43*. *V-43* was built at the AG Vulcan Stettin Construction Yard between 1914 and 1915.[137] She displaced 1,106 tons and had a maximum speed of 36.2 knots.[138] *V-43* carried three 8.6 cm guns, six 20 in (50-cm) torpedo tubes, and 24 mines.[139] During the war, *V-43* was part of the Number Six Flotilla, which was split into the Eleven and Twelve Torpedo Half-Flotillas.[140] *V-43* was part of the Eleven Torpedo Half Flotilla led by *V-44*, which also included *V-45*, *V-46*, *S-49*, and *S-50*.[141] *V-43* was involved in minesweeping and patrolling operations in the North Sea.[142] She did not take part in the Battle of Jutland because she was undergoing repairs at Wilhelmshaven.[143]*V-43* was involved in some skirmishes during the war while patrolling the Heligoland Bight, but the ship was not damaged in these actions.[144] After the German scuttling attempt in June of 1919, *V-43* was raised and fixed and turned over to the United States at Rosyth, Scotland, in 1920.[145]

4.2.3.7.6 The *S-132*

Though *V-43* and *G-102* were active for most of the war, the newer *S-132* saw less action. She was built in the Schichau Yard in Danzig between 1916 and 1917.[146] She displaced 1,170 tons and had a maximum speed of 33.4 knots.[147] She carried three 10.5 cm guns, six 20 in (50 cm) torpedo tubes, and 24 mines.[148] This later destroyer had more torpedo tubes than *V-43* and *G-102*. During the war, *S-132* was part of the Number Six Torpedo Flotilla and the Number Twelve Half Flotilla along with *V-125*, *V-126*, *V-127*, *V-128*, and *S-131*.[149] *S-132* was launched in May of 1917 and was active for only 19 months before the armistice agreement ended the war.[150]

---

[135] "Bombing of the Submarine U-117 June 21, 1921"; Box 170, Folder 6; GU-U.S. Air Operations-Bombing Tests, Naval Aircraft Operations Flight, Air Stations; RCONRL, RG 45; National Archives, College Park, MD.

[136] Captain J.F. Hellweg, "Work Carried Out on "G. 102," Enclosure 3, communication No. 343 Admiral Superintendent, "Settling accounts for work done to ex-German ships allocated to the United States," June 15, 1920; Box 2784, Folder 28785 (260) to (298); Sec. Navy Gen. Corr.; GRDN, RG 80; National Archives, College Park, MD.

[137] Gröner, *Battleships and Battlecruisers*, 179.

[138] Gröner, *Battleships and Battlecruisers*, 179.

[139] Van der Vat, *The Grand Scuttle*, 224.

[140] Ibid., 223.

[141] Ibid.

[142] Naval History and Heritage Command (NHHC), *V-43*. Website published 20 October 2015, accessed 22 August 2016 at: https://www.history.navy.mil/research/histories/ship-histories/danfs/v/v-43.html

[143] Ibid.

[144] Ibid.

[145] Naval History and Heritage Command, *V-43*. Website published 20 October 2015, accessed 22 August 2016 at: https://www.history.navy.mil/research/histories/ship-histories/danfs/v/v-43.html

[146] Gröner, *Battleships and Battlecruisers*, 182.

[147] Ibid.

[148] Van der Vat, *The Grand Scuttle*, 181.

[149] Ibid., 223.

[150] NHHC, *S-132*. Website published 1 September 2015, accessed 22 August 2016 at: https://www.history.navy.mil/research/histories/ship-histories/danfs/s/s-132.html

Of the vessels that were later transferred to the United States, both *Frankfurt* and *Ostfriesland* were involved in the Battle of Jutland. *Frankfurt* was the flagship of the second scouting group at Jutland and provided protection and information for the line of battle cruisers.[151] During the battle, the *Ostfriesland* was the flagship of the first German squadron.[152] She played a significant role in sinking the HMS *Black Prince* without sustaining any serious damage herself.[153] However, on 1 June 1916, while returning from battle to the Wilhelmshaven Imperial Navy Yard, the *Ostfriesland* hit a mine and took damage to her hull. Several of her compartments below deck were flooded.[154] The ship was repaired by 26 July 1916 and acted as a coastal defense vessel until the end of the war. She was struck from the German Navy on 5 November 1919.[155] *Frankfurt* was involved and damaged in combat at Jutland when the group of German cruisers, which she was a part of, came under fire from HMS *Invincible* under the command of Rear Admiral Horace Hood.[156] By the end of the Battle of Jutland, Germany had lost 11 ships and 2,551 men.[157] Of the ten German ships lost, four were light cruisers.[158] At the end of the war, Germany had lost 26 capital ships, including five armored cruisers and 19 light cruisers.[159]

4.2.3.7.7 The Submarines

Three of the four German U-boats allocated to the United States at the close of the war and scheduled for use as targets during Project B took part in active combat cruises. The U-*111* made three combat cruises around the North Sea, Baltic Sea, Orkney Islands, and the western coast of Ireland. More significant in U.S. history were cruises of U-*117* and U-*140* along the eastern seaboard in the summer and fall of 1918.[160] In surface, torpedo, and mine-laying attacks, the two U-boats sunk thousands of tons of American and Allied merchant shipping, many fishing boats, and the *Diamond Shoals* lightship *LV-71*. The U-*117* and U-*140* hunted an area that included the Project B district.

4.2.3.7.8 *UB-148*

The *UB-148* was built at the A.G. Weser yard in Bremen, Germany, in 1918, but the end of the war came before she was commissioned. As a result, the submarine had no service history. The *UB-148* displaced 523 tons at the surface and 633 tons submerged. She measured 182 ft in length with a 19 ft beam and 12 ft draft. The *UB-148* was armed with one 3.46 in (8.8 cm) deck gun and five torpedo tubes; four in the bow and one in the stern. The vessel was surrendered to the Royal Navy on 26 November 1918 at Harwich, England. She was subsequently transferred to the U.S. Navy as part of the armistice negotiations and then transported to New York under the command of Harold T. Smith.[161]

---

[151] Richard Hough, *The Great War at Sea 1914-1918* (Oxford: Oxford University Press, 1983), 218.

[152] Thomas Frothingham, *A True Account of the Battle of Jutland May 31, 1916* (Cambridge, MA: Bacon and Brown, 1920), 7.

[153] Navy News Bureau, Immediate Release, 19 July 1921; RCONRL; National Archives, College Park; Naval Spoils Coming to America Promise a Profitable Study, 1921.

[154] Immediate Release, 19 July 1921; RCONRL, RG-45; National Archives, College Park, MD.

[155] Breyer, *Battleships and Battlecruisers*, 267.

[156] Hough, *The Great War at Sea*, 241-242

[157] Hansen, *German Fleets*, 153.

[158] George, *History of Warships*, 119.

[159] Ibid.

[160] For a detailed history of the submarine campaign and the activities of the U-140 and U-117, see Josephus Daniels (ed.), *German Submarine Activities on the Atlantic Coast of the United States and Canada* (Washington, DC: Government Printing Office, 1920).

[161] NHHC, *UB-148*. Website published 20 October 2015, accessed 22 August 2016 at: http://www.history.navy.mil/research/histories/ship-histories/danfs/u/ub-148.html

4.2.3.7.9 U-*140* (Kapitanleutnant Weddigen)

The large German submarine U-*140* was laid down and launched from the Germania Dockyard in Kiel during 1917 and commissioned early in 1918. She displaced 1,930 tons at the surface and 2,483 tons submerged. U-*140* measured 302 ft in length with a 29.5-ft beam and 17-ft draft. She was armed with two 5.9 in (15 cm) guns, two 3.4 in guns, and six 20 in (50 cm) torpedo tubes.[162] During World War I, U-*140* patrolled the western Atlantic and sunk many merchant vessels. On 14 July 1918, the USS *Harrisburg* spotted the U-*140* off the Atlantic coast of the United States.[163] Four days later, the Brazilian vessel SS *Atalia* spotted the submarine's periscope.[164] A few days later, the U-*140* had a similar encounter with British vessel *Melita,* resulting in an exchange of gunfire.[165] On 26 July 1918, the U-*140* fired on *HMS Major*.[166] In the subsequent weeks, U-*140* sunk the Japanese steamer *Tokuyama Maru* and then American steamer *O.B. Jennings.* On 5 August 1918, the U-*140* captured American schooner *Stanley M. Seaman* and the next day, fired on and sank American merchant ship *Merak.* Later that day, U-*140* sunk the *Diamond Shoal* Lightship, LV *71,* stationed 15 miles south of Cape Hatteras.[167] The crew of the lightship was able to escape and row ashore.[168] The crew of the American vessels *Mariner's Harbor* and *Cretan* witnessed the attack on the LV *71* and were able to move away before being attacked.[169] Later, the USS *Birmingham,* while responding to a distress call from Brazilian vessel *Uberaba,* spotted U-*140* and fired depth charges striking the vessel.[170] However, U-*140* continued patrolling the east coast, firing on American merchant vessel *Pleiades* and later sinking the British steamship SS *Diomed.* Following her encounter with the *Diomed,* U-*140* was forced to return to Germany for repairs stemming from leaking fuel tanks. After a brief stop in the Faroe Islands, she returned to Kiel having sunk 30,000 tons of Allied shipping. At the end of the War, in February 1919, she was taken from the Kiel Dockyard to the Royal Navy facility at Harwich. Allocated to the U.S. Navy, the U-*140* made her trans-Atlantic voyage to North America in April 1919.

4.2.3.7.10 U-*117*

Laid down in 1917 and commissioned in early 1918 at the Aktiengesellschaft Vulcan Dockyard, the mine-laying submarine U-*117* displaced 1164 tons at the surface and 1,512 tons submerged. At 267 ft in length, a 24 ft beam, and a 13 ft draft the U-*117* made 14.7 knots at the surface and 7.2 knots

---

[162] NHHC, U-*140*. Website published 20 October 2015, accessed 22 August 2016 at: http://www.history.navy.mil/research/histories/ship-histories/danfs/u/u-140.html

[163]"Ships Sunk or Attacked by U-140 Atl. Coast Raids of 1918"; Box 1, List of Sinkings and Other Incidents Involving U.S. Naval Craft, 1915-1919, 1921; RCONRL, 1897-1940, RG 45; National Archives, College Park, MD.

[164] "S.S. Joseph Cudahy U.S.A.C.T."; Box 1, List of Sinkings and Other Incidents Involving U.S. Naval Craft, 1915-1919, 1921; RCONRL, 1897-1940, RG 45; National Archives, College Park, MD.(Untitled event 4290.)

[165] "Melita br. 33,"Box 1, List of Sinkings and Other Incidents Involving U.S. Naval Craft, 1915-1919, 1921; RCONRL, 1897-1940; RG 45; National Archives, College Park, MD.(Untitled event 4292.)

[166] "British Major br. SS"; Box 1, List of Sinkings and Other Incidents Involving U.S. Naval Craft, 1915-1919, 1921; RCONRL, 1897-1940, RG 45; National Archives, College Park, MD.(Untitled event 4295.)

[167] "Stanley M. Seaman Am. Sch."; Box 1, List of Sinkings and Other Incidents Involving U.S. Naval Craft, 1915-1919, 1921; RCONRL, 1897-1940, RG 45; National Archives, College Park, MD; "Diamond Shoals Light Ship, "Box 1, List of Sinkings and Other Incidents Involving U.S. Naval Craft, 1915-1919, 1921; RCONRL, 1897-1940, RG 45; National Archives, College Park, MD. (Untitled event 4306, 4306, 4310.)

[168] "Diamond Shoals Light Ship"; Box 1, List of Sinkings and Other Incidents Involving U.S. Naval Craft, 1915-1919, 1921; RCONRL, 1897-1940, RG 45; National Archives, College Park, MD.(Untitled event 4310.)

[169] "S.S. Mariner's Harbor Am. S.S."; Box 1, List of Sinkings and Other Incidents Involving U.S. Naval Craft, 1915-1919, 1921; RCONRL, 1897-1940, RG 45; National Archives, College Park, MD.(Untitled event 4312.)

[170] "USS *Stringham,*"Box 1, List of Sinkings and Other Incidents Involving U.S. Naval Craft, 1915-1919, 1921; RCONRL, 1897-1940, RG 45; National Archives, College Park, MD. (Untitled event 4315.)

submerged.[171] In early July 1918, the U-*117* departed for the east coast of North America. She laid mines near Barnegat Light off New Jersey, Fenwick Island Lightship off Delaware, Winter Quarter Shoals Lightship off Virginia, and near Cape Hatteras, North Carolina. In between her mine-laying operations, she sunk several vessels including the Norwegian steamer *Sommerstadt*, the American tanker *Frederick R. Kellogg*, the American naval transport *Saetia*, the American sailing ship *Madrugada*, the British steamer *Mirlo*, the Norwegian sailing ship *Nordhav*, the American trawler *Rush*, the Norwegian freighter *Bergsdalen*, the British trawlers *Elsie Porter* and *Potentate*, and the British steamer *War Ranee*. In total, she sank 20 ships and damaged an additional four.[172] On 9 September 1918 during her voyage back to Europe, the U-*117* aided the damaged U-*140*. Following these military successes, U-*117* was laid up in Kiel, Germany, for the remainder of the war.

4.2.3.7.11 U-*111*

U-*111* was laid down, launched, and commissioned at the Germaniawerft Dockyard in Kiel in 1917. She displaced 830 tons at the surface and 1,030 tons submerged. She was 235 ft in length, with a 20.5-ft beam and 12.5 ft draft. U-*111* was armed with six 20 in (50 cm) torpedo tubes, a 4.1 in gun, and a 3.4 in gun.[173] She could make 16.4 knots at the surface and 8.4 knots submerged. During World War I, U-*111* undertook three combat cruises around the North Sea, Baltic Sea, Orkney Islands, and to the western coast of Ireland. During these cruises, she used her guns to attack British steamers SS *Bostcastle*, Danish SS *Dronning Margrethe*, and Norwegian SS *Rana*. In port at Emden at the time of the armistice, U-*111* was surrendered to the Royal Navy at Harwich in the United Kingdom.

4.2.3.8 Project B, Weapons Test and Experiments

By the 1920s, the U.S. Navy had a culture that had long valued testing and experimentation, and had a history of using tests and data to evaluate new technologies or refine existing ones.[174] On 28 February 1921, Secretary of the Navy Josephus Daniels announced "plans for the greatest naval and aerial gun and bombing test ever conducted."[175] Although remembered for the controversies created by Mitchell, Project B was also a nationally significant, highly ambitious, and intricately planned program of tests. Project B had three overarching technical objectives. These objectives were to determine:

1. The ability of the aircraft to locate vessels operating in the Coastal Zone and to concentrate on such vessels sufficient bombing of airplanes to launch an effective attack;
2. The probability of bombs from airplanes hitting a vessel on the water capable of maneuvering but incapable of anti-aircraft fire; and
3. The damage to vessels of comparatively recent design, which would result from hits with bombs of various types and weights. The vessels to be attacked by bombing were to be a battleship, light cruiser, destroyer, and submarine.[176]

---

[171] NHHC, U-*117*. Website published 20 October 2015, accessed 22 August 2016 at: http://www.history.navy.mil/research/histories/ship-histories/danfs/u/u-117.html

[172] Ibid.

[173] NHHC, "U-*111*." Accessed 9 September 2016 at: http://www.history.navy.mil/research/histories/ship-histories/danfs/u/u-111.html

[174] John Trost Kuehn, "The Influence of the Naval Arms Limitation on U.S. Naval Innovation during the Interwar Period, 1921-1937" (history dissertation, Kansas State, 2007), 70.

[175] "The Month in the United States Ended March 22, 1921," *Current History*, 1921.

[176] Thomas Wildenberg, *Billy Mitchell's War with the Navy: The Interwar Rivalry Over Air Power* (Annapolis MD: Naval Institute Press, 2013), 60.

The Navy would have only one opportunity to test weapons on a nearly complete collection of recently built enemy warships. Voluminous internal Navy correspondence and planning documents generated in the months leading up to the tests make clear that the overall objective was to generate the maximum data from the tests.

The Navy expended a great deal of time and resources in developing and refining their plans. For example, on 14 March 1921 the Navy Department Bureau of Construction and Repair issued orders to the Philadelphia and Portsmouth Navy Yards concerning the ex-German submarines:

> In connection with the recent bombing of the Ex-*Indiana*, some confusion arose in analyzing the reports and photographs, the confusion being due to the different nomenclature used by the various offices and photographers in making the reports and the photographs. In connection with the destruction of the Ex-German submarines, it is desired to prevent such confusion from arising and the Department has directed the Bureau of Construction and Repair to provide the necessary plans for the use of the Board. It is therefore directed that the Navy Yard, Philadelphia, prepare the necessary outline booklets of Submarines U-*117*, U-*140*, and *UB-148* and that the Navy Yard Portsmouth, prepare outline booklet of Submarine U-*111*, for use of the Board of Observers in making reports and photographs of the damage, hits, etc., to these submarines.
>
> In the preparation of the booklets, the purpose for which they are used shall be kept constantly in mind; namely, they are for the purpose of recording the damage sustained and the location of hits, so that the results of aerial bombing and gun fire may be studied. They will also be used by the observers in locating access to the various compartments.

On 25 May 1921, the U.S. Atlantic fleet received a detailed 14-page directive for the Project B exercises. Project B was to consist of seven separate phases:

1. The destruction of the submarine U-*117* by aerial bombardment
2. An air search for and dummy bombing of the radio-controlled vintage battleship *Iowa*
3. The destruction of the submarines U-*140* and *UB-148* by surface gunfire
4. The destruction of the destroyers *S-132* and *V-43* by surface gunfire
5. The destruction of the destroyer U-*102* by aerial bombardment
6. The destruction of the cruiser *Frankfurt* by aerial bombardment
7. The destruction of the battleship *Ostfriesland* by aerial bombardment

Surviving minutes of planning meetings reveal deep divisions between the naval officers in overall charge of Project B and General Mitchell. Despite public claims that his planes could attack vessels 200 miles offshore, Mitchell insisted that the Navy plan of holding the tests 60 miles offshore posed unnecessary risks to aircraft and pilots. Overruled, Mitchell agreed to the bombing location but refused to participate in the more difficult and less spectacular search and test bombing of the *Iowa*.

4.2.3.9 Project B, Technical Narrative

After months of preparation and planning, Project B aerial bombardment and gunnery testing started on 21 June 1921 under the command of Admiral A.H. Seales of the U.S. Navy battleship *Division*.[177] The first target was ex-German submarine U-*117*, and the final target was the battleship *Ostfriesland*, to be bombed on 21 July 1921. In between bombing attacks, a Board of Observers was appointed to study

[177] Correspondence, Commander in Chief of the Atlantic Fleet to the Fleet; Box 170; RCONRL, RG 45; National Archives, College Park, MD.

damage to the ships and take photographs. This board consisted of Captain J.R.Y. Blakely, Senior Member and Bureau of Ordnance; Captain J.T. Tompkins (USS *Delaware*); Commander G. McC. Courts (USS *Pennsylvania*); Commander W.G. Childs (USS *Shawmut*); Lieutenant Commander A.M. Penn (USS *Pennsylvania*); Lieutenant D.C. Laizure (USS *Florida*); a representative from the Bureau of Construction and Repair; a representative from the Bureau of Engineering; and to record, Lieutenant Commander F.B. Conger (USS *Delaware*).

On 21 June, U-*117* was anchored 50 miles east of Cape Charles when the first of seven divisions of planes scheduled to hit the submarine attacked.[178] Three Navy Curtiss F-5Ls flew at 1,200 ft and dropped salvos of three 164 lb Mark IV aerial bombs on the submarine in quick succession.[179] The bombs landed on either side of the submarine.[180] A second salvo delivered by the Navy's Curtiss flying boats resulted in two direct hits. The U-*117* sank before the inspectors could fully assess the damage, just seven minutes later.[181]

The second Project B test occurred on the following day with the destruction of the U-*140*.[182] On 22 June 1921 at 09:30, warships from Destroyer Division 36 led by USS *Dickerson* opened fire on the U-*140* with their 4 in (10−16 cm) 50 caliber guns from 3,300 yards. The destroyers continued firing for 8 ½ minutes expending 40 rounds and making 20 hits. An hour after firing commenced at 10:30, U-*140* began listing to port. At 11:05 she sank by the stern. As U-*140* sank, Destroyer Division 36 turned its attention to *UB-148.* At 11:06, USS *Sicard* opened fire on *UB-148* from 550 yards. After sustaining 19 hits (out of 40 shots) with 4 in (10–16 cm) 50 caliber guns, the *UB-148* began listing, first to port and then to starboard before finally sinking on an even keel at 11:44.

In addition to U-*140* and *UB-148*, Destroyer Division 36 also was scheduled to sink U-*111*. However, on 17 June 1921, following repairs and the journey from the Portsmouth, New Hampshire, Navy Yard to the Navy Yard in Norfolk, Virginia, the submarine sank in 29 ft of water in Lynnhaven Roads, Virginia,.[183] Before Project B testing began, a board was convened to investigate the sinking of the submarine; however, by late June, she still had not been raised and did not participate in testing. Her conning tower was marked with a navigational buoy and she was left at her sinking location in Lynnhaven Roads.[184]U-*111* was later moved to deeper water and has yet to be relocated.

On 29 June 1921, Project B testing continued with its most technologically challenging exercise—the search for and bombing of the vintage battleship *Iowa*. The *Iowa* experiment was intended to evaluate whether planes could first locate and then accurately bomb a moving battleship located somewhere off the American shore. Given General Mitchell's claim that airplanes could economically and effectively guard the nation's coasts from enemy warships, this was an important exercise.[185] After decommissioning on 31 March 1919 at the Philadelphia Navy Yard, the old battleship was equipped with radio-controlling

---

[178] Instructions for Exercises with ex-*Iowa* and ex-German ships; Box 170; RCONRL, RG 45; National Archives, College Park, MD.

[179] General H.H. Arnold, "The Naval Bombing Experiments: Bombing Operations on U-*117*, *Iowa*, *G-102*, *Frankfurt*, *Ostfriesland.*" In: *Global* Mission (Maxwell Airforce Base, AL: Air University Press, 1949), http://www.history.navy.mil/library/online/navybomb2.htm

[180] Wildenberg, *Billy Mitchell's War*, 70.

[181] Arnold, "The Naval Bombing Experiments."

[182] United States Atlantic Fleet USS *Pennsylvania*, Flagship; Box 170; RCONRL, RG 45; National Archives, College Park MD.

[183] Letter, Industrial Department, United States Navy, Norfolk, Virginia to Industrial Manager, Navy Yard, Portsmouth, New Hampshire; Box 69, "Sarah Clark" Correspondence Files; RG 342; National Archives, College Park, MD.

[184] Letter from Rear-Admiral E. Simpson, Commander USS *Train*; Box 69, "Sarah Clark" Correspondence Files; RG 342; National Archives, College Park, MD.

[185] Ibid.

equipment developed by John Hays Hamilton, Jr. Hamilton was towering figure in the history of remote guidance.[186] During Project B, the *Iowa* was controlled from a distance of 2 miles using a 5 kW spark transmitter and an automatic telephone system.[187] The experiment called for the *Iowa* to steam at 6 knots in a zig-zag pattern in a location somewhere between Cape Hatteras and Cape Henlopen 50 and 100 miles offshore.[188] Because of the expense incurred in converting the *Iowa* to a radio-controlled vessel, these tests were undertaken with dummy bombs rather than detonating charges.[189] Mitchell, citing the use of dummy bombs and the risks of operating offshore, refused to allow Army planes to participate in this phase of Project B. However, three Army blimps took part in the search.

At 8:00 on 29 June 1921, three Army blimps under the command of Captain John Pagelow began the search of the *Iowa*. Locating her at 10:45 am, the blimps guided 11 Navy F-5Ls, 2 Navy NCs, and five Marine DH4s from Yorktown, Virginia, to the *Iowa*.[190] At approximately 13:00, the 18 planes dropped 70 dummy bombs on the *Iowa* before returning to land. Only a handful of the 85 bombs dropped by the planes scored hits on the *Iowa*.[191] Observers on the USS *Henderson* included Joseph S. Ames, a physics professor from John Hopkins University; Roy G. Fitzgerald, a U.S. congressman from Ohio; and James F. Corrigan, a federal court reporter in New York City responsible for publicizing "Brian Boru" radio tower technologies.[192] Personnel from the USS *Henderson* sent information to the Associated Press, International News SVC, Universal News SVC, and United News in Washington, D.C.[193] The *Iowa* exercise was the first time that remote control was installed and successfully used on a major surface warship, further contributing to the national level of historical significance of the Project B test.

After a two-week pause, Project B continued 13 July 1921 with the aerial bombing of the destroyer *G-102*. The exercise was under the control of General Mitchell who ordered a three-phase attack on the destroyer.[194] During the first phase, 11 Army SE-5 planes each dropped four 25 lb copper fragmentation bombs. Diving from 1,500 to 200 ft, Mitchell's pilots scored 21 direct hits.[195] In the second phase, 16 DH-4s each dropped two 100 lb bombs from an altitude of 1,500 ft, but made no direct hits.[196] During the third and final phase, 15 Martin bombers dropped a total of forty-four 500 lb demolition bombs,

---

[186] Correspondence of the Navigation Navy Department Washington; Box 79, Folder 4153 (523) to (538); Sec. Navy Gen. Corr.; GRDN, RG 80; National Archives, College Park, MD.

[187] Ibid.

[188] "Daylight Search and Bombing of USS *Iowa*"; Box 170, RCONRL, 1897-1940, RG 45; National Archives, College Park, MD.

[189] Correspondence to the Chief of Naval Operations from Prof. M.E. Cooley; Box 79, Folder 4153 (523) to (538); Sec. Navy Gen. Corr.; GRDN, RG 80; National Archives, College Park, MD.

[190] "Daylight Search and Bombing of USS *Iowa*."

[191] "Correspondence between the Atlantic Fleet and Chief of Naval Operations."

[192] Correspondence from Joseph Ames to the Secretary of the Navy, Edwin Denby; Box 79, Folder 4153 (523) to (538) Sec. Navy Gen. Corr.; GRDN, RG 80; National Archives, College Park, MD; Correspondence from John Crouch to Josephus Daniels; Box 79, Folder 4153 (523) to (538) Sec. Navy Gen. Corr.; GRDN, RG 80; National Archives, College Park, MD; Frank H. Lancaster and Ernest F. Birmingham, *Fourth Estate: A Weekly Newspaper for Publishers, Advertisers, Advertising Agents and Allied Interests*. New York City (New York, NY: Fourth Estate Publishing Company, 14 May 1921).

[193] Correspondence from the USS Henderson to the Bureau of Naval Operations; Box 79, Folder 4153 (523) to (538) Sec. Navy Gen. Corr.; GRDN, RG 80; National Archives, College Park, MD.

[194]"Sinking of the Destroyer *G-102*"; Box 170; RCONRL, RG 45; National Archives, College Park, MD.

[195] Arnold, "The Naval Bombing Experiments."

[196] Ibid.

making three direct hits.[197] The *G-102* sunk by her bow after the third phase and before the Board of Observers could examine her.[198]

The other ex-German destroyers, *V-43* and *S-132,* were sunk by gunfire from the USS *Florida* and USS *Delaware* on 15 July 1921. At 13:30, one of the destroyers opened fire on *V-43,* with ten shots from each of three guns. Of the two successful shots, one damaged the pilothouse and the other tore a hole in the side of the hull 18 in below deck on the port side.[199] Due to inclement weather, observers were transferred from the USS *Shawmut* to the minelayer *Rail.*[200]The *Rail* pulled alongside *V-43* and the observers noted the damages. After these initial shots, the destroyers turned their attention to *S-132*. At 14:57, one of the destroyers opened fire on *S-132,* making five hits to her starboard side above the bridge, at the forward stack, near the waterline of the fire room and engine room, and above the waterline aft.[201]

After the destroyers failed to sink the *V-43* and *S-132,* the battleship USS *Florida* moved into position 5,000 yards away and, at 16:21, opened fire on *V-43*.[202] Between 16:21 and 16:34, *Florida* fired 140 shots from its 5 in battery and scored 11 hits on the starboard side.[203] The *V-43* began to settle forward and sank by the stern at 16:48. At 17:54, the battleship USS *Delaware* opened fire on *S-132* from 5,000 yards, firing 140 shots in seven minutes and scoring 13 hits causing significant damage to the starboard side.[204] By 18:50, *S-132* had noticeably settled at even keel. At 19:07 with the sea growing rough, the *S-132* rolled starboard and sank by the stern.[205]

The tests resumed on Monday 18 July 1921 with aerial bombing of the ex-German light cruiser *Frankfurt* by Army and Navy planes. At 09:30, three Navy F-5Ls dropped twelve 250 lb bombs from an altitude of 1,300 to 2,000 ft, making four direct hits—all duds.[206] Two other duds hit the water and six bombs detonated in the water near *Frankfurt*.[207] In the first Army attack, the planes carried 300 lb bombs. One of the Army Martin bombers made three flights over the *Frankfurt* dropping six bombs before a second Army Martin bomber made four flights over the *Frankfurt,* also dropping six bombs.[208] Finally, a third Army Martin bomber dropped six 300 lb bombs and three Navy F-5Ls flew and dropped two 250 lb bombs each in a single salvo.[209] At the end of these attacks, the Board of Observers boarded *Frankfurt* from the *Shawmut* to inspect the damage. The Navy scored four direct hits with their 250 lb bombs. Although none detonated, they penetrated the upper decks and damaged electrical components on the ship.[210] Two direct hits by Army 300 lb bombs successfully detonated, tearing 6 ft holes in the deck.[211]

---

[197] Ibid.

[198] Communication From USS Henderson to Bunav; Box 170; RCONRL, 1897-1940, RG 45; National Archives, College Park, MD.

[199] Report on the Sinking of Ex-German Destroyer *G-102* and *S-132*, Cruiser *Frankfurt* and Battleship *Ostfriesland*; Box 170, 3; RCONRL, 1897-1940, RG 45; National Archives, College Park, MD.

[200] Ibid.

[201] Ibid.

[202] Ibid.

[203] Ibid., 4.

[204] Ibid.

[205] Ibid., 5.

[206] Naval Historical Foundation, "Bombing Operations U-*117*, *Iowa*, *G-102*, *Frankfurt*, *Ostfriesland*"; Box 170; RCONRL, 1897-1940, RG 45; National Archives, College Park, MD, 16.

[207] Report on the Sinking of Ex-German Destroyer *G-102* and *S-132*, Cruiser *Frankfurt* and Battleship *Ostfriesland*; Box 170, 6; RCONRL, 1897-1940, RG 45; National Archives, College Park, MD.

[208] Ibid.

[209] Ibid.

[210] Ibid.

[211] Ibid.

The second phase of bombing commenced at 13:20 with three Navy F-5Ls dropping six 250 lb bombs in a single salvo.[212] None of the bombs detonated and only one made a direct hit.[213] Next, two Army Martin bombers flew with six 300 lb bombs each. In a total of seven flights, the Army pilots dropped 11 bombs, with no hits and three duds. Finally, three Navy Martin bombers made a total of six flights, dropping seven 520 lb bombs.[214] Two of these bombs made direct hits, three were duds, and two detonated in the water.[215] After these three attacks, the Board of Inspectors noted damages to the port torpedo tube aft and the mainmast.[216]

The final phase of bombing on the *Frankfurt* began with six Army Martin bombers attacking the ship one-by-one.[217] The first six bombs missed the vessel and detonated in the water. The next two bombs made direct hits at amidships, and the final six detonated in the water close to the *Frankfurt.*[218] At 16:37, she started settling in the water and the *Shawmut* pulled alongside to allow inspectors aboard. At 16:50, *Frankfurt* sank by the bow at a 45° angle, likely due to flooding in the torpedo and forward fire rooms, and other forward compartments.[219]

4.2.3.9.1 Bombing the Ostfriesland

Wildenberg provides the best published secondary account of the *Ostfriesland* bombing. The account that follows draws mainly from his work, but it has been verified and supplement by official military records consulted at the National Archives in Washington, D.C.

The Navy planned to bomb the *Ostfriesland* during a two-day period beginning on the morning of 20 July 1921. Going into the final round, the record of Navy and Army bombers seemed mixed at best. Airplanes had certainly not demonstrated the overwhelming destructive capacities touted by Mitchell. They had succeeded in sinking an unmanned submarine, destroyer, and cruiser. Direct hits by small- and medium-sized bombs (those that actually exploded) resulted in localized but not mortal damage. The mining effect of large bombs exploding close alongside of the surface warships proved far more damaging. The *Ostfriesland* presented a vastly more durable target above and below the waterline and had survived a mine explosion after the Battle of Jutland.

Despite the efforts of the Philadelphia Navy Yard, the *Ostfriesland* had arrived at the test site in poor condition. Souvenir hunters and scavengers had thoroughly looted the battleship, leaving most of the watertight doors unsecured and some completely off their hinges. During the voyage to the test site, plumbing systems designed to maintain the ship's stability had failed, flooding the coalbunkers adjacent to the steering engine room. Inspector Alexander Van Keuren observed the inward bowing of the coalbunkers from the flooding. Van Keuren and a Navy plumber re-secured the ship as much as possible before leaving, but the *Ostfriesland* lacked watertight integrity well before the first bomb was dropped.[220]

---

[212] Wildenberg, *Billy Mitchell's War*, 73.

[213] Report on the Sinking of Ex-German Destroyer *G-102* and *S-132*, Cruiser *Frankfurt* and Battleship *Ostfriesland*; Box 170, 8; RCONRL, 1897-1940, RG 45; National Archives, College Park, MD.

[214] Ibid.

[215] Ibid.

[216] Ibid.

[217] Ibid., 9.

[218] Ibid.

[219] Ibid.

[220] Wildenberg, *Billy Mitchell's War*, 77-78.

After a weather delay, the first attacks on the *Ostfriesland* began in the early afternoon of 20 July 1921.[221] Once the weather calmed, the four-phase attack on the *Ostfriesland* began. First, Marine DH4s and Navy F-5Ls attacked the battleship in five groups of three planes each. These planes carried a total of thirty-six 230 lb bombs. They dropped 33 of these charges, scoring nine hits.[222] Of those nine hits, two detonated and seven were duds.[223] The Board of Inspectors visited *Ostfriesland* and found that the seven duds each caused superficial damages to the deck of the *Ostfriesland* with one dud making a 10 in hole in the waterway.[224] The two bombs that detonated both hit between the third and fourth smokestacks.[225]

After the Board of Inspectors disembarked, the next phase of aerial attacks began at 15:42 with six Army Martin bombers carrying two 600 lb bombs each and six Navy F-5Ls carrying two 550 lb bombs each.[226] The Martin bombers flew first. In total, the planes scored five hits, of which three 550 lb charges were duds and one 600 lb bomb was a dud. One 600 lb bomb detonated close to the port side. After this attack, the Board of Inspectors boarded the *Ostfriesland* to make final observations before bombing was called off for the day. They found that the duds caused superficial damage, making 6 to 18 in holes in deck planking. The 600 lb bomb that detonated tore a 4 × 5 ft hole in the main deck, damaging the starboard bulkhead.[227] When the Board left, the ship was slowly taking on water through the coalbunker and already had a 5° list to port. Overall, the upper decks of the *Ostfriesland* had sustained minimal damage during the first day's attacks. However, below deck water was flowing in through an open seam in a forward boiler room. Without damage control, the leak would have eventually claimed the battleship, but in combat it would not have been a mortal or disabling blow.[228]

The next morning on 21 July 1921, testing resumed on *Ostfriesland.* The third wave involved aircraft carrying 1,000 lb bombs. The orders required that they be dropped one at a time with bombing to stop after each successful hit.[229] Mitchell's planes began their attacks at 8:23 am, dropping five bombs, but they failed to stop after scoring a direct hit with the third bomb. The first and second bombs missed the ship, but detonated while the third and fourth hits detonated on the *Ostfriesland* and the fifth bomb detonated in the water near the starboard side. The Board of Inspectors quickly boarded the vessel to observe damages and found that the hits made 4 to 8 ft holes in the upper deck with damage to the lower decks.[230] Despite these hits and her less than watertight condition going into the tests, the *Ostfriesland* was not taking on a substantial volume of water.

---

[221] Correspondence from Commanding Officer of the Provisional Air Brigade to Commander-in-Chief of the Atlantic Fleet; Box 79, Folder 4153 (523) to (538); Sec. Navy Gen. Corr.; GRDN, RG 80, National Archives, College Park, MD.

[222] Report on the Sinking of Ex-German Destroyer *G-102* and *S-132*, Cruiser *Frankfurt* and Battleship *Ostfriesland*; Box 170, 10; RCONRL, 1897-1940, RG 45; National Archives, College Park, MD.

[223] Ibid.

[224] Instructions for Exercises with ex-*Iowa* and ex-German ships; Box 170; RCONRL, RG 45; National Archives, College Park, MD

[225] Report on the Sinking of Ex-German Destroyer *G-102* and *S-132*, Cruiser *Frankfurt* and Battleship *Ostfriesland*; Box 170, 10; RCONRL, 1897-1940, RG 45; National Archives, College Park, MD.

[226] Ibid.

[227] Ibid. 12.

[228] Wildenberg, *Billy Mitchell's War*, 78.

[229] Correspondence from Commanding Officer of the Provisional Air Brigade to Commander-in-Chief of the Atlantic Fleet; Box 79, Folder 4153 (523) to (538); Secretary of the Navy General Correspondence 1916-1926, RG 80; National Archives, Washington, DC.

[230] "Instructions for Exercises with ex IOWA and ex-German ships," Box 170, 13; RCONRL, RG 45; National Archives, College Park, MD.

During the final phase, Mitchell again disregarded orders. The Army planes were limited to a total of three bombs or two hits after which they were to let Navy planes attack (if no hits had been scored) or stop and allow the inspectors a chance to evaluate the damage from their successful hit. Instead, Mitchell's planes dropped six bombs. The first three 2,000 lb bombs missed the vessel but the fourth detonated on the bow.[231] The next two bombs hit the water close to the *Ostfriesland*, shaking the ship and causing her to take on water. At 12:37, she listed port and at 12:40 she turned turtle before sinking by the stern.

An observer writing for the Scientific American provided a particularly lucid description of the event:

> The delayed action of the fuse must have worked admirably and have burst the bomb well down below the surface: for it lifted and dropped upon the ship an enormous quantity of water, which from our point of observation, completely hid the vessel from sight. As the finer mist disappeared we noticed that a perfect Niagara of solid water was pouring down from the bridge, the conning tower, the after turret and the quarter-deck. When this had fallen clear, there appeared all around the waterline at the stern of the vessel and well up toward amidships, a white line of foam boiling around the vessel, broken occasionally on both sides of the stern by burs of foaming water.
>
> There was but one interpretation of this phenomenon. It meant that not only the port side, but also much of the bottom of the ship must have been broken in and that this disturbance was caused by the escape of vast volumes of air from the wrecked underbody as the water rushed in. Immediately, the great ship began to list to port, turning steadily over as the after body of the ship submerged. When the bow of the vessel struck the bottom some 300 or 350 feet below the sinking was arrested, and the ship seemed to hang for a few moments before the stern took the final plunge and disappeared.[232]

4.2.3.9.2 Technical Results of Project B

4.2.3.9.2.1 Observer Reports and Recommendations

Navy and press photographers took hundreds, possibly thousands, of images documenting Project B. For the Navy, the test was more than about attacking a battleship. Bomb hits and damage observations were plotted, and official observers compiled highly detailed daily reports and straightforward observations and recommendations for improvements to warships.[233]

4.2.3.9.2.2 U-117 Bombing − Observer Conclusions

1. The submarine's best defense against aircraft is to maneuver submerged. If unable to submerge, the effect of bombing could be minimized by maneuvering on the surface with tanks fully blown, thereby avoiding transmission of pressure on the outer hull to the inner hull through the incompressible medium of water.
2. All submarines should have at least one gun capable of use against aircraft.[234]

---

[231] "Instructions for Exercises with ex IOWA and ex-German ships," Box 170 14; RCONRL, RG 45; National Archives, College Park, MD.

[232] "Depth-Bombing from the Air: Results and Lessons of the Sinking of the *Frankfurt* and *Ostfriesland* Off the Virginia Coast," *Scientific American*, 6 August 1921.

[233] Report of the Board of Observers, June – July 1921; ; Box 170; RCONRL, RG 45; National Archives, College Park, MD.

[234] Ibid.

4.2.3.9.2.3 U-140 and UB-148 Gunfire − Observer Conclusions

1. That submarines of any type intended to operate effectively on the surface should have at least one gun of the most powerful type that is practicable to carry.
2. The gun platforms of submarines should be installed sufficiently high above the deck to permit the pressure hull to receive substantial protection due to its distance below the waterline, as far as such stability will permit.
3. That all submarines carry a supply of suitable lash stoppers to minimize effect of enemy gunfire.[235]

4.2.3.9.2.4 V-43 and S-132 Gunfire − Observer Conclusions

1. For vessels already constructed and for new construction, it was recommended that the 5 in cartridge case gun be substituted for the 4 in (10−16 cm) gun, where the substitution could be made.[236]

4.2.3.9.2.5 G-102 Bombing − Observer Conclusions

1. All United States destroyers should be equipped with two 3 in, 50 caliber anti-aircraft guns. All future destroyers should have a battery of anti-aircraft guns.
2. As far as practical, all exposed personal should be protected from aircraft machine gun fire by means of overhead thin steel plating to stop a rifle bullet.
3. The anti-aircraft fire control equipment of all destroyers should be improved and made effective.[237]

4.2.3.9.2.6 Frankfurt Bombing − Observer Conclusions

1. One fairly heavy deck (⅞ to 1 in thick) at deck height below the deck receiving the original impact will completely stop a bombing explosion and damage in a downward direction, while the same result will probably be obtained by two lighter decks. Horizontal damage will probably be stopped the same way.
2. The mining effect of a 600 lb bomb detonated close aboard and a good distance below the surface of the water will be serious.
3. Ships of this type should have at least four anti-aircraft guns with proper ammunition supply and fire control systems and as many machine guns as practicable.
4. The mining effect of bombs should be minimized by the maximum number of watertight bulkheads.[238]

4.2.3.9.2.7 Ostfriesland Bombing − Observer Conclusions

1. At least eight anti-aircraft guns of the highest possible power must be provided with proper control systems, ammunition hoists, and a battery of heavy machine guns.
2. Submerged torpedo tubes and torpedo rooms on capital ships should be eliminated because these largely unprotected compartments rendered ships vulnerable.

---

[235] Ibid.

[236] Ibid.

[237] Ibid.

[238] Ibid.

3. Double watertight doors and manholes opening in opposite directions must be fitted where liable to blast from both directions.
4. Anti-aircraft guns must be so projected as to withstand the blast and fragments of the heaviest bomb exploding in the immediate vicinity.
5. All airport openings in the hull of the ship must be closed by battle ports as strong as the hull.[239]

The major public controversy surrounding the test results centered on the extent of the bomb damage and whether an operational *Ostfriesland* would have survived the attack. The observers concluded:[240]

> Summing up the whole attack, the damage in every case where bombs struck on deck was purely local. Bombs of 500 pounds and larger size blew through a deck of 1-⅞" thickness and caused considerable damage in the vicinity, in once case opening the side and in another putting the ammunition hoist of a secondary gun out of commission and badly smashing an uptake. In these cases damage of course was suffered to the general battle lighting and control systems, and in fact absolutely no damage was caused in any case behind the armor or below the protective deck. It is regrettable that no hits were secured on turret tops and the bombing of the Maine or Missouri with strengthened (modern) turret and conning tower tops, with animals and blast gauges inside, is suggested.
>
> With regard to the mining effect of bomb exploding under water the general below water structure of the ship, this, combined with the opening of equalizers and fire room doors and with possibly blowing in of glass in air ports was what eventually caused the sinking. This effect however was distinctly cumulative and it is believed that had there been personnel on board they could have handled the leakage due to all but the final attack by pumps so that the mining effect of these final attacks would have been greatly reduced and sinking might well not have resulted from the damage actually done the ship, by the bombs actually dropped as they were.

4.2.3.9.2.8 Conclusions of the Joint Army Navy Board

On 18 August 1921, the Joint Army Navy Board released a summary report on the results of Project B. Although Project B included tests of naval gunnery, the board's report focused on "the effectiveness of aircraft in offensive action against various types of naval vessel."[241] The Board framed their analysis based on three criteria.

> Within their radius of action which, relative to that of naval vessels, is extremely short the effectiveness of heavier-than-air craft carrying large capacity high explosive bombs, depends on:
> - Ability to locate the naval vessel;
> - Ability to hit the target vessel with the projectile carried; and
> - Ability of the projectile to damage to destroy the vessel.

While the *Iowa* experiment indicated the difficulty of directly hitting a moving ship, the mining effect of large aerial bombs on the *Frankfurt* and *Ostfriesland* made it clear that airplanes represented a genuine threat to surface ships, including battleships. In response, the Board emphasized "the rapid development

[239] Ibid.

[240] Ibid.

[241] Joint Board, "Report on results of aviation and ordnance test held ruing June and July 1921, and conclusions reached," August 18,1921; Box 170; RCONRL, RG 45; National Archives, College Park, MD

of anti-aircraft armament and for the provision of pursuit planes as part of the fleet."[242] The damage to the *Ostfriesland* convinced the board of the impossibility of building a battleship capable of withstanding the mining effects of the largest bombs. Although suggesting that, at present, aircraft offered only limited assistance to fleet gunnery reconnaissance, the airplane had "important strategical and tactical qualities in operations of coast defense."[243] Section 24 of the report offered a laundry list of observations about the future of Navy ships. Of these, four were the most controversial and important.[244]

- The battleship is still the backbone of the fleet and the bulwark of the nation's sea defense, and will so remain so long as the safe navigation of the sea for purposes of trade or transportation is vital to the success in war.
- The airplane like the submarine, destroyer and mine, has added to the dangers to which battleships are exposed but has not made the battleship obsolete.
- The battleship remains the greatest factor of naval strength.
- The development of aircraft instead of furnishing an economical instrument of war leading to the abolition of the battleship has but added to the complexity of naval war.

Generating less controversy, at the time but with abiding importance for the future was a concluding observation about the future of airpower in the Navy:[245]

> The aviation and ordnance experiments have proved that it has become imperative as a matter of national defense to provide for the maximum possible development of aviation in both the Army and the Navy. They have also proved the necessity for aircraft carriers of the maximum size and speed to supply our fleet with the offensive and defensive power which aircraft provide, within their radius of action, as an effective adjunct of the fleet. It is likewise essential that effective anti-aircraft armament be developed.

Outside of public view, at least one of the observers saw the test as the harbinger of a new era in warfare. In a secret report written 29 July 1921, Project B official observer Commander Alexander Van Keuren commented on *Ostfriesland*'s sinking from bombs that exploded underwater outside of the ship, "The shots that miss are the shots that count in this new form of warfare, we must see that the least possible number of shots are fired by hostile airplanes and that those that are fired go very wide of the mark." "This conclusion," according to historian John Kuehn, "was to have a dramatic influence on battleship modernization and design under the treaty system."[246]

4.2.3.10 Project B and General William "Billy" Mitchell

Brigadier General William "Billy" Mitchell (1879–1936) is well established as a person of national historical importance. His final home, Boxwood VA, is a National Historic Landmark. The Boxwood nomination describes Mitchell as the nation's "first great air war strategist" and the "dominant figure in American Aviation form 1919 to 1926." It credits him with taking "the lead in preparing the American people to accept the role of aeronautics in the Nation's military and diplomatic policies" and for being "an

[242] Ibid.

[243] Ibid.

[244] Ibid.

[245] Ibid.

[246] Kuehn, "The Influence of the Naval Arms Limitation,"139.

important agent in the growth of U.S. naval aviation and one of founding fathers of the U.S. Air Force."[247]

Project B, in 1921, was the largest and most elaborate naval arms test in U.S. history. The event itself and the individual target vessels have national historical significance. Brigadier General William "Billy" Mitchell was the central figure in this event. His framing of Project B as conflict between airplanes and battleships captured public attention and made air power a central element in the national debate over the role and shape of the military in a post-World War United States. Mitchell was the dominant figure in the Army Air Service between 1918 and 1926. His war record, followed by his relentless public campaign for an independent Air Force, made him a national celebrity.

Mitchell's own crusade was nonetheless unsuccessful. His military career was cut short by his famous court martial caused by his ill-judged criticism of President Calvin Coolidge's administration and his resignation from the Army in 1926. However, Mitchell's influence on the development of American military air doctrine continued through his own efforts until his death in 1936 and by the aviators who served under him. Posthumous confirmation of Mitchell's prediction of Japan's attack on Pearl Harbor on 7 December 1941 helped rehabilitate Mitchell's reputation and solidified his status as a martyr to air power. The establishment of the United States Air Force in 1947 was a realization of Mitchell's vision, and he is now considered the "father" of the service.

Although Mitchell's crusade for air power garnered enthusiasm among some Army airmen, he met stiff opposition from the public, military, and Congress. The isolationism that followed the armistice shaped this opposition, as did the belief of military strategists that aviation was nothing more than a supplement to ground forces. Failing to build his case for military aviation with the government, Mitchell mounted a "bold campaign of publicity and aerial accomplishments . . . In 1921, Mitchell conducted his most prominent campaign for an independent service when he decided to wrest control of the coastal defense mission from the Navy Air Services."[248] Through his electrifying statements before Congress and other public relations gambits, Mitchell inserted himself into the Navy's Project B, transforming it from a military test of unprecedented scale into a public spectacle, pitting the progressive airplane against the obsolete battleship, culminating in the bombing and sinking of the dreadnought battleship *Ostfriesland* on 22 July 1922. Under Mitchell's orders, the Army pilots ignored Project B's strict test protocols, dropping multiple 2,000 lb bombs alongside the *Ostfriesland* and causing her to sink.

Nearly four decades after the event, one of Mitchell's most outspoken and relentless critics Vice Admiral Alfred W. Johnson (Navy air commander for Project B) concluded:

> Looking back on it all, I don't see what else Mitchell could have done except keep on dropping bombs until the ship sank. If the ship had not sunk soon he would have been the object of ridicule because of the prebombing public pronouncements. The operation would make him or break him. It made him. In the public eye, he became the infallible prophet on aviation.[249]

The trajectory of Mitchell's later career and court marital is so closely associated with Project B that Otto Preminger chose to set the stage for the pro-Mitchell Hollywood film *The Court Martial of Billy Mitchell* with a David and Goliath account of the sinking of the *Ostfriesland.* Although Mitchell

---

[247] *General William "Billy" Mitchell House*, Statement of Significance, National Register of Historic Places Nomination From, 1976,

[248] Alexandra M. Lord, ed., *American Aviation Heritage: Identifying and Evaluation Nationally Significant Properties in U.S. Aviation History* (Washington, DC: The National Historic Landmarks Program, National Parks Service, U.S. Department of the Interior, 2011), 138.

[249] Vice Admiral Alfred W. Johnson, *The Naval Bombing Experiments off the Virginia Capes June and July 1921* (Washington, DC: Naval Historical Foundation, 1959), http://www.history.navy.mil/library/online/navybomb1.htm

participated in the test bombing the battleships *Indiana*, *Alabama*, and *Washington*, the Project B site is the one most strongly associated with his career as the "profit of air power."

No historic property in the United States has a stronger association with the career and influence of Mitchell than the Project B area. Mitchell did more than orchestrate controversy surrounding the sinking of the O*stfriesland;* he participated in the event itself. Commanding planes and observing the bombing from the cockpit of his plane, he experienced the entire landscape of Project B, from the runway at Langley Field to the individual bombing sites. Contemporary observers and historians all seem to agree that the climax of the Project B tests, the sinking of the ex-German battleship *Ostfriesland* by Mitchell's Army bombers, was the pivotal event in Mitchell's public career as the crusader for an independent air service. Mitchell biographer James Cook describes the sinking of *Ostfriesland* as "a highwater mark [and] pinnacle of Mitchell's career."[250] Roger Miller describes the event as "fulfillment and vindication" for Mitchell, and "in many ways the summit of his military career."[251]

Project B is important in the history of American military aviation history. This significance is explained in the National Historic Landmarks Theme Study titled *Identifying Nationally Significant Properties in U.S. Aviation History* and, in particular, the section of that study headed "Military Between the Wars, 1918–1939."

> Between the wars airmen set out to formulate policy and doctrine regarding airpower, create an organization, and establish a training system that laid the foundations of American air power in World War II. Throughout this period, two issues were hotly debated: the question of whether an air force, independent of the army and navy, was truly necessary and its corollary, whether airpower would continue to be supplemental to land and sea battles or whether it would be the dominant face of war.[252]

Project B became a watershed event in the development of national and international military policy for the interwar years. The event helped set the political and technological stage for the Washington Naval Conference of 1921 and the resulting Washington Naval Treaty of 1922 (Five-Power Treaty). Project B brought heightened attention to the importance of air power in both the Navy and the Army.

Indeed, while Mitchell failed to gain political support for a unified Air Force through Project B and the *Ostfriesland*, the public and political attention he brought to the event advanced the cause of air power in both the Navy and the Army. According to William Trimble, witnessing Mitchell's sinking of the *Ostfriesland*, "had a catalytic effect" on Navy Air Bureau Chief Admiral William J. Moffet and convinced "the architect of naval aviation" "that the best course for the Navy was to build a well-balanced fleet, with a mix of heavy and light ships, all of which are to be coordinated in their activities and protected by aircraft."[253] After witnessing the event, Moffett adopted the aircraft carrier as "the cornerstone of [his] grand plans for the development of fleet aviation." Calling for at least eight "big" aircraft carriers Moffett stated, "a Navy today without aircraft protection and the search-patrol, scouting patrol, and shot-spotting facilities which aviation provides, is fatally weak when it puts to sea."[254] Despite the harsh public criticism it brought to the Navy, the close scrutiny of Project B and the sinking of the *Ostfriesland* ultimately helped to preserve and strengthen naval aviation during the interwar period, including the establishment of the Bureau of Aeronautics on 11 August 1921. "Proposals for a separate aviation bureau in the Navy Department, which had been left unresolved for years, solidified following

---

[250] James J. Cook, *Billy Mitchell* (Boulder: Lynee Rienner, 2002), 126.

[251] Roger G. Miller, *Billy Mitchell "Stormy Petrel of the Air"* (Washington, DC: Office of Air Force History, 2004), 1.

[252] Lord, ed., *American Aviation Heritage*, 137.

[253] William Trimble, *Admiral William J. Moffat: Architect of Naval Aviation* (Annapolis, MD: Blue Jacket Books, 1994).

[254] Quoted in Ibid., 68.

General Mitchell's bombing trials in 1921. Alarmed Admirals banded together and supported legislation to create the Bureau of Aeronautics."[255]

Wagner and Braxton conclude in their studies of the development of strategic bombing that regardless of the surrounding politics and controversies, "the Project "B" test was highly influential at the time, causing budgets to be redrawn for further air development and forcing the Navy to look more closely at the possibilities of naval air power."[256] In a decade that saw military budgets slashed to pre-World War I levels, naval aviation had stable funding that grew substantially as a proportion of the overall Navy budget.

4.2.3.11 Project B and Airpower in Media History

Walter Boyne in *The Influence of Airpower Upon History* credits the "the co incidence of new media technologies with the dawn of aviation" gave airpower "measurably great influence . . . on public opinion, as compared with sea power." [257] The rising influence of the media and the power of new media technologies allowed air power evangelists to gain rapid fame and cultural influence. The motion picture, specifically newsreels, became a powerful shaping force in public perceptions of aviation.[258] Mitchell intuitively grasped the emerging power of print and visual media. The airplane vs. battleship controversy orchestrated by Mitchell made Project B a benchmark event in the history of American military media relations. Although the involvement of print media and still photography in military affairs was far from new in 1921, Mitchell went to exceptional efforts to shape the media message and promote the airplane vs. battleship controversy. Mitchell used every means at his disposal to exaggerate the strategic significance of the bombing tests as well as the strength of the *Ostfriesland.*

Both Mitchell and the Navy used film and still imagery in their respective public relations campaigns. However, Mitchell struck first and more effectively. In April 1921, he engaged a cameraman at Fox News to film and produce a deliberately misleading news reel featuring Army bombers attacking and (apparently) sinking the old battleship *Indiana*.[259] The film was interpreted by the Navy as another attempt by Mitchell to embarrass the naval air forces.[260] The Chief of the Army Information Group H.M. Hickman wrote a tart letter to the Fox News Company complaining that the film showed bombs dropping on the *Indiana* followed by a caption "which purported to show the result of such bombardment indicating that the battleship 'Indiana' was sunk there by." Voicing the commands of the outraged Secretary of the Navy, Hickman insisted that Fox executive E.H. Hancock "inform me immediately as to the individual or individuals who were responsible for this caption, particularly as to whether it was suggested by any Air Service officer."

> The Air Service and the Navy have been attempting to operate in the very valuable experiment of bombing battleships in order that both services might obtain necessary information. There have already been released a great deal of erroneous, misleading

[255] Robert O'Connell, *Sacred Vessels: The Cult of the Battleship and the Rise of the U.S. Navy* (Oxford University Press, 1991), 279.

[256] Arthur H. Wagner and Leon E. Braxton, *Birth of a Legend: The Bomber Mafia and the Y1B-17* (Bloomington, IN: Trafford, 2012), 92.

[257] Walter J. Boyne, *The Influence of Air Power Upon History* (Barnsley U.K.: Pen & Sword, 2005).

[258] Ibid. 14.

[259] Captions, Fox News, Langley Field Virginia; Box 2, 1920-1922; Records of the Predecessor Offices, 1911-1925, Records of the Offices of the Secretary of the Navy and the Chief of Naval Operations; Records of the Bureau of Aeronautics, RG 72; National Archives, College Park, MD.

[260] Memorandum, Chief of Naval Operations, Re: Data relative to Efforts of Army Air Service to discredit the service of Naval Aviation, 21 April 1921; Box 2, 1920-1922; Records of the Predecessor Offices, 1911-1925, Records of the Offices of the Secretary of the Navy and the Chief of Naval Operations; Records of the Bureau of Aeronautics, RG 72; National Archives, College Park, MD.

> statements which have caused a great deal of hard feeling between various Naval offices and the Army Air Services and the consequences of such releases as described above are very serious. It is requested that you expedite the report.[261]

Two days later, a chastened Fox executive E.H. Hancock reported that "we were entirely mislead by our cameraman in the south . . . he let us infer that the *Indiana* wreck was produced by Air bomb." In an effort to mollify the Navy, Hancock added, "Fox News ran twice as many features on the Atlantic Fleet as any other news reel and endeavored to rouse patriotism to the highest extent which is always our policy." Although Hancock did not implicate the Army in incident, the potential involvement was certainly implied.[262] Because records kept by the various Navy offices were thoroughly documented, such an action was completely in character for Mitchell.

The Navy learned hard lessons in public relations wars and developed an elaborate plan for including and controlling the press access to Project B. The tests were organized into four operations and newspapers had to specify, well in advance, which tests they wanted to witness. The Navy planned to include about 50 reporters and photographers among the largest parties of select congressmen and high-level government officials who would travel overnight from the Washington Navy Yard on the *Henderson*, or in the case of the *Frankfurt* test, on Navy ship from Norfolk. All correspondents and official guests were issued nontransferable boarding cards. A small press group would join the official test observers on their ships as they inspected the target vessels between the scheduled phases of bombing or shelling. During these intervals, the *Henderson* would approach to the target to provide the rest of the party opportunities for closer observation. The *Henderson* was fitted with a complete pressroom that included typewriters and working areas.

On the day before the first test, bombing of the U-*117*, newspapers commented on the unusual press access. "The results of such tests, involving data of the utmost importance to the nation's defense system, have usually been kept secret."[263]

The ship transmitted by wireless radio news bulletins concerning the tests to the Navy News Bureau, who then disseminated information to the national press. Each morning, the Navy supplied a destroyer to carrying press dispatches to Hampton Roads in time for the morning papers. When each test concluded, weather permitting, a Navy seaplane carried press dispatches for the afternoon newspapers. The Navy allowed the five national newsreel companies to film the tests from dirigibles, but insisted that all pictures (still and moving) be submitted for censorship[264]. Decades later, Vice Admiral Alfred W. Johnson, Ret., who commanded the naval air presence during Project B, concluded, ". . . our Navy learned as much about publicity from those experiments as it did about bombing battleships."[265]

---

[261] H.M. Hickman to E.E. Hancock, 20 April 1921; Box 2, 1920-1922; Records of the Predecessor Offices, 1911-1925, Records of the Offices of the Secretary of the Navy and the Chief of Naval Operations; Records of the Bureau of Aeronautics, RG 72; National Archives, College Park, MD.

[262] E.E. Hancock to H.M. Hickman, 22 April 1921; Box 2, 1920-1922; Records of the Predecessor Offices, 1911-1925, Records of the Offices of the Secretary of the Navy and the Chief of Naval Operations; Records of the Bureau of Aeronautics, RG 72; National Archives, College Park, MD.

[263] "German U-Boat To Be Target for Airplane Bomb Attack Tuesday," *Wilmington Morning Star* 20 June 1919.

[264] Memorandum for the Press: Press Arrangements for Bombing Tests, Box 170, 1911-1927; U.S. Air Operation-Bombing Tests; RCONRL, RG 45; National Archives, College Park, MD.

[265] Vice Admiral Alfred W. Johnson, The Naval Bombing Experiments off the Virginia Capes June and July 1921 (Washington, DC: Naval Historical Foundation, 1959), http://www.history.navy.mil/library/online/navybomb1.htm

4.2.3.12 The Washington Conference (1921) and the Washington (Five-Power) Treaty (1922)

At the beginning of World War I, the dreadnought battleship reigned unchallenged as "the uncontested measure of naval power."[266] Over the next four years, however, a combination of factors challenged the hegemony of the battleships in naval war and in the hearts and minds of the public and policy makers. During the war, the success of German submarines, the emergence of military air power, and the lack of its use in a decisive engagement undermined the battleship's aura of invincibility and potency as a symbol of national pride and global status. Furthermore, increasing size and technological complexity had driven up the estimated cost of a new U.S. battleship roughly $6 million in 1910 to over $40 million in 1921. Also damaging to the status of the battleship was the widespread popular belief that instead of winning wars, dreadnought battleships caused them by fostering ruinous arms building competition between great and would-be great powers. For these reasons, the years immediately after 1918 saw a growing popular and political reaction against battleships and big navies in the United States and abroad. Simply put, for many in the United States and Europe, a continuance of a battleship-based military threated the economic security as well as the peace of the world.

The German warships targeted during Project B were the only "war prizes" of the United States. Allocation of Project B vessels through the Treaty of Versailles illustrates the unprecedented international prestige of the United States in the immediate post-war period. The political dialogue surrounding Project B, especially the bombing of the *Ostfriesland*, represents a paradox in the status of the United States in the world community. Although Project B further galvanized political and popular support of American isolationism, the threat of the battleship to economic security and world peace led the United States to embrace global leadership once again. This manifested itself by calling the Washington Conference of 1921 and signing the Five-Power Naval disarmament treaty in February 1922.

The domestic political significance of Project B and its influence on international diplomacy and military policy is chiefly due to the machinations of General Billy Mitchell. He seized on the Navy's use of obsolete battleships in gunnery tests to wrest the control of American coastal defense away from the Navy and into the hands of the Army Air Service. In October and November of 1920, U.S. Navy used the old battleship *Indiana* as a target ship in a series of secret gunnery tests. Launched in 1895, the *Indiana* had been the first international-caliber steel battleship in the U.S. Navy fleet, but it had been obsolete since the beginning of the 20th century. Navy planes used dummy and live bombs to test the accuracy and potential effectiveness of aerial bombardment and detonated a series of larger bombs placed at specified points on the deck to assess the possible damages to warships from air attacks. Mitchell witnessed these tests and the damage he observed likely inspired his airplane vs. battleship campaign. On 4 January 1921, Mitchell appeared for the Army before a House appropriations subcommittee where, showing photographs of the damage to the *Indiana*, he asserted that with airplanes, "we can destroy or sink any ship in existence today." Against air power, the dreadnought battleship is "just as helpless as was the armored knight when the firearm was brought against him." Backing up this claim he told the committee, "All we want to do is to have you gentlemen watch us attack a battleship." The photographs were still secret when he revealed them in the public committee meeting. A few days later, photographs of the damaged *Indiana* appeared in the *New-York Tribune* causing tremendous public uproar. Although the allegations are unproven, historians believe Mitchell was responsible for leaking them to the press. He had been guilty of similar tactics while serving in Europe during World War I.[267]

Mitchell was the first American airman to articulate the use of aircraft in coastal defense—the military strategy always favored by isolationists since the early days of the United States.[268] Decrying the

[266] William M. McBride, *Technological Change and the United States Navy, 1865-1945* (Baltimore: The Johns Hopkins University Press, 2000), 137.

[267] Wildenberg, *Billy Mitchell's War*, 52-4.

[268] Ibid., 43.

continued spending on coastal fortifications and battleships, Mitchell asserted, ". . . our systems of coast defense today is wrong. The only way to really defend a coast is with aircraft and mobile troops and their accessories." In his testimony, Mitchell hailed the accuracy of aerial bombardment against ships, "we can hit very often, if we have to, if necessary, we will come down and lay the bomb on the deck." Promoting the airplanes in coastal defense, Mitchell exhorted, "distance is nothing to airplanes. Our ship has about a five and one-half hour supply of gas and she can work 200 miles off the coast. It is just as accurate at 200 miles as it is near shore."[269]

According to historian Mark Clodfelter, "Mitchell tried to transform the American populace into air power advocates by emphasizing the progressive notions of order and efficiency." "The wartime application of air power would," Mitchell contended, "result in a diminished loss of life, and treasure and will thus be a distinct benefit to civilization." If the public believed Mitchell's assertions about the combat capacity of airplanes, then it made no sense to invest national treasure in battleships. "You must remember that those battleships cost $45,000,000, and we can build a thousand airplanes for the cost of each battleship." Further, he claimed the current system of having air arms in both the Army and the Navy was wasting "at least thirty percent" of the money currently being appropriated and was retarding the strategic development of American airpower.[270] The brilliant Republican congressman from Virginia, Campbell Bascom Slemp, cut quickly to the main issue, "It seems to me that the principal problem is to demonstrate the certainty of your conclusions.... You will save millions of dollars if you can demonstrate it." Through sympathetic congressmen, Mitchell used these arguments and the photographs from the *Indiana* to pressure the Navy to turn over an obsolete battleship for his own use. The Navy unsuccessfully attempted to head off this request by inviting the Army to participate in Project B. They ultimately supplied the battleship *Alabama*, but stalled the transfer until after Project B.

The public scrutiny and inflammatory rhetoric Billy Mitchell brought to Project B and the bombing of the *Ostfriesland* helped build the popular case for disarmament and the eventual scrapping of United States' aggressive program of battleship construction.

Planning for Project B and the airplane vs. battleship controversy occurred during the time of growing political support for international naval arms reduction. By December 1920, Idaho Senator William Borah advanced a resolution calling on the newly elected President Warren G. Harding to negotiate a treaty with Great Britain and Japan. This precipitated months of political wrangling between the two branches of Congress and between Congress and President Harding concerning the boundaries between congressional and executive authority. Senator Borah worked tirelessly to link the naval appropriations bill with calls for the President to initiate disarmament talks with Britain and Japan. After finally signaling his approval of Borah's amendment in the naval appropriations bill calling for disarmament in June, President Harding took independent executive action on 10 July 1921 by issuing a preliminary invitation to Great Britain, France, Italy, and Japan to come to a formal conference in Washington. The official invitation came on 11 August, less than three weeks after the *Ostfriesland* went down under Mitchell's bombs. *Current History* reported:

> After many months of isolation, so far as Europe's efforts to establish the world's peace on a firm basis are concerned, the United States has acted on its own initiative in calling a conference of the principal naval powers for the purpose of discussing the limitation of armaments, as well as all vexed questions which obstruct the way to the attainment of this almost universal aspiration.[271]

---

[269] "Brig. General Mitchell's Startling Testimony," *Aviation and Aircraft Journal* 7 February 1921, 165.

[270] Mitchell as quoted in Mark Clodfelter, *Beneficial Bombing: The Progressive Foundations of American Air Power, 1917-1945* (Omaha: University of Nebraska Press, 2011).

[271] "The Disarmament Conference," *Current History*, 1921.

The Aeronautical Chamber of Commerce of America's *Aircraft Yearbook for 1922* opened with this definitive statement:

> In aviation, the year 1921 is marked by three outstanding events, one of universal and epochal importance.
>
> During June and July there were held, 100 miles off the Virginia Capes, a series of experiments in the course of which aircraft flown from land based, bombed and sank, one after the other, a submarine, destroyer, light cruiser and dreadnought, the most modern examples of warship construction.
>
> In the fall, the Conference on the Limitation of Armament was held in Washington, and it is asserted that the bombing tests cleared way, more than any other single event, for a possible solution of the international competition in capital ship construction. For the 2,000 pound TNT bomb which crushed in the steel walls of the "*Ostfriesland*" was, as the Army Chief of Ordnance remarked at the moment, "heard around the world."

The influence of the *Ostfriesland*'s destruction and Mitchell's campaign on public opinion remained strong during the Washington Conference. Oswald Villard, influential editor of *The Nation* wrote:

> Take the question of the battleship to the airplane. . . .the sinking of the old German battleship Ostfriesland off the Virginia Capes was accomplished by bombs that did not hit her but exploded in the water near her. But as we are going to scrap the newest and latest-planned ships first of all, we are plainly going to destroy those that are somewhat planned against aerial attack. Ergo, those that we shall keep afloat are the most vulnerable. Then why keep them afloat at all? If bombing machines continue to develop in the next two years as they have in the last two it will be folly to go to war with any battleships at all--perhaps it will even be sending men to sure death to let them go to war. Then why not scrap all the battleships?[272]

The Washington Naval Conference convened on 11 November 1921 and resulted in several bilateral agreements and three major treaties. The most important, "The Five-Power Treaty," also known as the "Washington Treaty" was signed on 6 February 1922.

> The Five-Power Treaty, signed by the United States, Great Britain, Japan, France and Italy was the cornerstone of the naval disarmament program. It called for each of the countries involved to maintain a set ratio of warship tonnage which allowed the United States and Britain 500,000 tons, Japan 300,000 tons and France and Italy each 175,000 tons. Though Japan preferred that tonnage be allotted at a 10:10:7 ratio, and the U.S. Navy preferred a 10:10:5 ratio, the conference ultimately adopted the 5:5:3 limits. The key reason why the United States and Britain required higher tonnage allowances was because both nations maintained two-ocean navies: they were active in both the Atlantic and the Pacific, with colonial territories scattered around the world. Finally, this agreement called on signatories to stop building capital ships and reduce the size of their navies by scrapping older ships.[273]

[272] Oswald Villard, "The Conference—The Second Phase," *The Nation*, 30 November 1921.

[273] Excerpt from U.S. Department of State, Office of the Historian, "The Washington Naval Conference, 1921-1922," n.d. Website accessed 9 September 2016 at: https://history.state.gov/milestones/1921-1936/naval-conference

According to historian John Jordon, the treaty became "the key reference point for all naval construction over the next fifteen years."[274] The Treaty obligated the United States to limit its fleet to under 525,000 tons, with no one ship larger than 35,000 tons.[275] The aircraft carrier fleet was limited to 135,000 tons with no ship larger than 27,000 tons.[276] The treaty prohibited guns of a caliber larger than 16 in and required that ships targeted for destruction under this treaty be sunk or broken up with their weapons such that they could not be used, or scrapped and sold, for future military service. Although the Treaty of Versailles had prohibited the use of submarines by Germany, the Washington Treaty limited the use of submarines by the signatories to protecting their economic security.

Under the Washington Treaty, the U.S. Navy carried on with the construction of three *Colorado*-class battleships, the *West Virginia*, *North Dakota*, and *Delaware*, but stopped construction on a fourth, the *Washington.*[277] This *Colorado*-class was considered a "super-dreadnought." New technological features of these vessels included turret and stern catapults.[278]*Colorado*-class vessels were armed with eight 16 in guns, twelve 5 in guns, eight 3 in guns, four 6 lb guns, and two 21 in torpedo tubes.[279] They represented an increased gun size and displacement from the earlier *Tennessee*-class.[280] In addition to the *Washington*, the U.S. Navy halted construction on 14 other capital ships.[281] In order to adhere to the limitations of the arms treaty, the *Washington* was destroyed in target practice in 1924 off the Virginia Capes.[282] While the Washington Treaty represented a challenge for the U.S. Navy, it generated new opportunity for supporters of air power.[283]

However persuasive to the public and congressmen intent on returning America to prewar "normalcy" in 1921, Mitchell's popularizing the bombing of the *Ostfriesland* and his post-bombing rhetoric had only limited influence among leaders of the Army and the Navy. Project B had been the largest naval testing exercise in U.S. history. The joint Army-Navy Aeronautical Board managed the tests, and its closely recorded results were carefully scrutinized by the Board and vetted by its senior member, America's leading military figure Army General John "Black Jack" Pershing. Project B did not lead the Joint Board to declare the battleship as obsolete. Anchored in perfect weather and without a crew to man anti-aircraft guns or contain damage, the *Ostfriesland* had resisted all but the most powerful bombs. The Joint Board and other influential observers within the Navy, however, formally recognized the airplane as a serious new threat to the safety of battleships.

---

[274] John Jordan, *Warships After Washington: The Development of the Five Major Fleets 1922-1930.* (Barnsley, UK: Pen & Sword, 2011), xi.

[275] Conference on the Limitation of Armament, Washington, 1922, Chapter I Article V, Chapter I Article IV; https://www.ibiblio.org/pha/pre-war/1922/nav_lim.html

[276] Conference on the Limitation of Armament, Washington, 1922, Chapter I Article VII, Chapter I Article IX; https://www.ibiblio.org/pha/pre-war/1922/nav_lim.html

[277] Conference on the Limitation of Armament, Washington, 1922, Chapter II Part 1, https://www.ibiblio.org/pha/pre-war/1922/nav_lim.html

[278] NHHC, "USS *Colorado* (BB-45), 1923-1959." Website accessed 9 September 2016 at: https://www.history.navy.mil/our-collections/photography/us-navy-ships/battleships/colorado-bb-45.html

[279] NHHC, "*West Virginia*," Website accessed 9 September 2016 at: https://www.history.navy.mil/our-collections/photography/us-navy-ships/battleships/west-virginia-bb-48.html

[280] NHHC, "*Colorado* Class (BB-45 through BB-48), 1917 Building Program," last modified March 26, 2001, http://www.history.navy.mil/photos/usnshtp/bb/bb45cl.htm

[281] "Halt Construction on 14 Capital Ships: Formal Orders Are Issued by Denby to Carry Out Provisions of the Naval Treaty," *New York Times* 9 February 1922.

[282] NHHC, "USS *Colorado*(BB-45), 1923-1959." Website accessed 9 September 2016 at: https://www.history.navy.mil/our-collections/photography/us-navy-ships/battleships/colorado-bb-45.html

[283] Special Board, General Board Room, Navy Department, November 10, 1924; Roll 20, p. 35; Secret and Confidential Correspondence of the Office of the Chief of Naval Operations (OPNAV) and the Office of the Secretary of the Navy, 1798-1947; RG 80, National Archives, College Park, MD.

While the Navy leadership successfully defended the military integrity of the modern battleship and its central place in naval strategy, the impact of Mitchell's sinking of the *Ostfriesland* and the spotlight he put on the extraordinary cost of new battleships put tremendous pressure on Congress to seek international arms control and to abandon the then current battleship building program. The Washington Conference, the treaty it helped inspire, and physical data from the testing all contributed toward Project B's influence on international diplomacy into the 1930s and advanced design of American warships (e.g., completion of the fast *South Dakota*-class battleships at the beginning of World War II).[284]

4.2.3.13 The Influence of Project B on the Design and Building of U.S. Submarines 1919−1940

During the period from 1914 to 1940, the U.S. Navy and the shipbuilding industry developed the technological expertise and the public-private institutional arrangement that "laid the foundation for the capability and quality of modern submarines." The studies of the captured German submarines brought to the United States after the war "precipitated a design and strategy debate that led to a complete redefinition of the submarine's place in a future war after 1928."[285] These studies focused on seven German submarines turned over to the United States as war prizes in 1919. Four of these seven submarines (U-*117*, U-*140*, *UB-148*, and U-*111*) were included in Project B. U-*111* sank on the way to the test site and is believed to lay undiscovered approximately 30 miles off the Virginia coast.

The Navy thoroughly documented all German submarines. The Navy Board of Inspection and Survey conducted extensive operational tests on U-*111* and *UB-148*. The U-*111* demonstrated a surface speed exceeding 17 knots. The *UB-148* made a crash dive in 27 seconds, less than one-quarter the time needed by a comparable U.S. submarine.[286] An examination of the hull of the large U-*140* revealed basic differences in German and American structural approaches. The Germans used lighter framing but heavier hull plating than American submarines, possibly imparting greater resistance to underwater explosions or enabling faster construction.[287] By any objective standard—propulsion, sea keeping, environmental control, and ballast systems—the German submarines proved far superior to American submarines.

The study of the German U-boats "enabled the technical bureaus and the submarine community to refine American submarine strategy, determine the best design to carry out the intended mission, and improve the services' technical capability. The Germans developed submarines that were beyond prewar expectations. Their substantial advances in U-boat design, construction, and combat systems dramatically illustrated how much the Navy still had to accomplish."[288]

---

[284] McBride, *Technological Change and the United States Navy, 1865-1945*, 201.

[285] Gary Weir, *Building American Submarines 1914-1940*, Contributions to Naval History No. 3 (Washington, DC: Naval Historical Center, 1991), 4, 23.

[286] Friedman, *U.S. Submarines Through 1945*, 160.

[287] Ibid.

[288] Weir, *Building American Submarines 1914-1940*, 114.

4.3 ARCHAEOLOGICAL STUDIES

4.3.1 Archaeological Knowledge and Previous Studies

The historical investigations conducted as part of the Atlantic Deepwater Canyons study suggest the presence of highly significant shipwrecks in the study area, possibly dating back to the 16th century. Our knowledge of archaeologically confirmed shipwreck locations, however, is largely incomplete and essentially limited to several known wrecks from the 20th century. Much of the information about these sites comes from recreational fishermen and technical divers.[289] Skilled technical divers have visited numerous historically significant sites in the study area, but the published and available data on those sites are limited and inaccurate.[290] Warships (including submarines) or freighters and tankers sunk by warships form the bulk of the identified and visited cultural resources on the mid-Atlantic OCS. The spatial distribution of those sites, however, is skewed toward the shallow waters (<200 m) and toward the vicinity of Norfolk Canyon. Very few wrecks have been identified in water depths between 200 and 1,500 m or near Baltimore and Washington canyons. Although this project generated significant archaeological information, financial, technical, and logistical limitations prevented the team from tackling the systemic biases in our archaeological knowledge. Even after this study, archaeological data in the vicinities of Washington and Baltimore canyons and in deep waters off the edge of the shelf remain limited.

Prior to this study, the only underwater archaeological research conducted directly in the vicinity of Norfolk Canyon was by the University of Rhode Island between 2006 and 2008. Data from those studies, including some shipwreck location data, were made available for the Atlantic Deepwater Canyons study. In addition to confirmed wreck locations, investigations by the University of Rhode Island provided an in-house cultural landscape assessment of a small (25 mi^2) area approximately 8 nmi west of the head of Norfolk Canyon. That assessment, based on high-resolution (acoustic) archaeological surveys and subsequent ground truthing, enabled the Atlantic Deepwater Canyons team to refine its methods and show the presence of diverse cultural features in the study area, including possible isolated shipwreck timbers, scour marks, shell concentrations, commercial fishing debris, and ammunition.

The previous archaeological investigations conducted by the University of Rhode Island, in collaboration with the Institute for International Maritime Research, comprised four separate cruises, which all focused on Norfolk Canyon and are briefly summarized in this section.

The first cruise by the University of Rhode Island in 2006 was sponsored by the National Oceanic and Atmospheric Administration Office of Exploration and Research (NOAA OER) on board the hydrographic survey ship *Thomas Jefferson.* This cruise resulted in 200% side-scan sonar and high-resolution multibeam bathymetry survey of a 25 mi^2 area centered on the reported location of a possible archaeological site. In addition, the ship's crew collected multibeam data in the vicinity of Automated Wrecks and Obstructions Information System (AWOIS) items #936, #955, and #2791. The collection of marine magnetometer data for select parts of the survey area was a secondary objective. Several shipwrecks were discovered, including three that would be subsequently identified from the Billy Mitchell-Project B experiments.

---

[289] Gary Gentile, *The Lusitania Controversies, Book Two: Dangerous Descents into Shipwrecks and Law* (Gary Gentile Productions, 1999); Gary Gentile, *Shipwreck Sagas* (Bellerophon Bookworks, 2008).

[290] Clif Darby, The Billy Mitchell Shipwrecks – Where are They? http://atlanticwreckdivers.net/Mitchell/Mitchell.html; Christina Young, "2002 *Ostfriesland* Photos I," http://christinayoung.com/pages/diving/misslindsey/ostfrieLif sland-02a.htm; Mike Boring "The Ultimate Gas Dive Weekend," http://atlanticwreckdivers.net/Mitchell/frankfrt-MB.html; see also http://www.capt-jt.com/photos_billym5.htm; websites accessed 9 September 2016.

The second cruise, also in 2006, was sponsored by the State of Rhode Island's Rhode Island Endeavor Program (RIEP). The archaeological team ground truthed the 20 highest priority acoustic and magnetic anomalies within the previously mapped 25 mi^2 survey area. The University of Rhode Island's 165-ft research vessel *Endeavor* served as the cruise platform with the Institute for Exploration's towed vehicle *Argus* and ROV *Little Hercules* functioning as the primary data acquisition tools. This cruise resulted in a cultural landscape assessment of the study area, but the absence of dynamic positioning on the RV *Endeavor* prevented detailed on-site documentation.

The third cruise took place in late July to early August 2007 and, as in the first cruise, was sponsored by NOAA OER and used the NOAA ship *Thomas Jefferson*. The team completed 100% side-scan and high-resolution multibeam coverage of the head of Norfolk Canyon and the seafloor immediately north of the canyon (approximately 30 mi^2). The team also conducted a high-resolution acoustic and magnetometer survey of a small area (1 mi^2) around the coordinates of what was thought to be a significant archaeological site. The team investigated AWOIS targets #954, #956, and #964, which were all inside the 100-fathom contour between Norfolk and Baltimore canyons. Side-scan sonar data revealed no surface expressions for these targets in the reported locations. That data had important implications in how our understanding of the Billy Mitchell-Project B wrecks were distributed and revealed inaccuracies in the data released by technical divers.

In August 2008, the archaeological team completed further survey operations and ground truthing in the vicinity of Norfolk Canyon. This cruise (again using the *Endeavor* as the platform) was jointly funded by NOAA OER and the State of Rhode Island through the Rhode Island Endeavor Program (RIEP). Equipment and personnel were contributed from the Navy Undersea Warfare Center (NUWC) in Newport, Rhode Island. The following four data acquisition systems were used:

1. Dual frequency towed side-scan sonar (400 and 100 kHz), named *Echo*, owned and operated by the Institute for Exploration (IFE);
2. Autonomous underwater vehicle (AUV) *Atalanta* (a Remus 1600) owned and operated by IFE;
3. AUV *MARV* built owned and operated by the Navy Undersea Warfare Center (NUWC); and
4. ROV *Hylas* (an Outland 1000) owned and operated by IFE.

The cruise identified at least two and possibly three vessels from the Billy Mitchell fleet and an additional 30 mi^2 of side-scan sonar survey and discovered what appeared to be a ship timber.

4.3.2 Archaeological Investigation Selection Criteria

Several sets of criteria were used to select primary shipwreck targets for investigation as part of the Atlantic Deepwater Canyons study. The most important criteria for assessing cultural resources in the United States are those established under the National Historic Preservation Act (1966) for evaluating the eligibility of historic properties to the National Register of Historic Places. Those criteria point to the potential associations between the nominated property and significant events, persons, types of property, and patterns in history. The National Register criteria shaped the site selection processes for this project.

Project archaeologists were cognizant of recent theoretical developments in underwater archaeology that emphasize the importance of cultural landscapes to understanding the nature and extent of the cultural resources in a particular area. Certain types of vessels (specifically warships, submarines, freighters, fishing boats, schooners, and tankers) and periods of history (specifically World War II, the early 1920s, and the year 1942) were known to have greatly influenced the submerged cultural landscape of the study area. To the extent that was practical and possible, sites that represented these vessel types and historic periods were targeted for investigation.

The location of the sites also was important in shaping the study. Archaeologists attempted to select sites that represented the spatial distribution of cultural resources that were located in different water depths and those that were near the three principal canyons. Unfortunately, logistical and technical (available equipment) limitations forced the archaeologists to focus on Norfolk Canyon. Finally, sites selected for study were based on their potential to contribute to the biological objectives identified as part of this study.

From these priorities and criteria, it was determined that the Billy Mitchell fleet and *San Demetrio* were of primary importance and warranted further historical investigation and archaeological assessment. The historical significance of these wrecks made detailed historical and archival research a central component of the study (**Section 4.2**, Historical Studies). The opportunities for on-site archaeological investigations came as a result of three cruises: the 2011 mapping cruise (aboard the NOAA ship *Nancy Foster*), the 2012 sampling cruise (aboard the *Nancy Foster*), and the 2013 sampling cruise (aboard the NOAA ship *Ronald H. Brown*).

4.3.3 2011 Mapping Cruise and 2012 Sampling Cruise

Significant archaeological objectives were achieved during the 2011 mapping cruise conducted 4 to 7 June aboard the *Nancy Foster*. This cruise was primarily a mapping expedition (**Chapter 3**) that enabled the team to generate high-resolution maps of Norfolk, Washington, and Baltimore canyons as well as areas of the OCS between those geological features. Because of this work, project archaeologists were able to identify ten potential shipwrecks and numerous features of the submerged landscape that could have conceivably provided suitable sites for human habitation approximately 10,000 years ago.

The 2012 sampling cruise also used the NOAA ship *Nancy Foster* along with the ROV *Kraken 2* operated by the University of Connecticut to investigate nine previously identified shipwreck sites. The team was able to confirm that eight of those vessels were World War I vintage German warships sunk during the Project B experiments (see **Section 4.2**, Historical Studies). The archaeologists were able to confirm the location of the German battleship *Ostfriesland;* the light cruiser *Frankfurt;* three destroyers, *G-102, S-132*, and *V-43;* and three U-boats, the U-*117,* U-*140,* and *UB-148.*

All shipwrecks that were investigated had suffered damage from heavy fishing gear, representing a significant impact on the historic sites and a heavy financial loss for regional fishermen. Nevertheless, it was clear that the wrecks still possessed significant archaeological integrity and were serving as essential habitats for extensive biological communities. A limited number of archaeological samples were raised during the 2012 sampling cruise, including a ballast brick from one of the destroyers.

4.3.3.1 Archaeological Objectives

Although the 2012 sampling cruise produced significant results in terms of site identification, the archaeological objectives for the cruise were much broader. The full extent of the archaeological objectives for the cruse can be summarized as follows:

Find and identify all eight shipwrecks from the Billy Mitchell-Project B fleet;

- Ground truth other potential shipwreck targets from multibeam sonar mapping data collected from Norfolk, Washington, and Baltimore canyons during the June 2011 mapping cruise (NF-11-04, 4-17);
- Conduct multibeam surveys of select areas south of Norfolk Canyon;
- Conduct video transects and photo quadrants or photomosaics over selected shipwrecks and other archaeological features;
- Document and image shipwrecks and other archaeological sites using high-definition (HD) video and still photography;

- Assess the condition, threats, and archaeological potential of submerged cultural heritage sites in the vicinity of Norfolk Canyon; and
- Assess the potential for paleoarchaeological sites in the vicinity of Norfolk Canyon and the potential for paleoarchaeological landscape reconstruction.

4.3.3.2 Methods

The primary tool used during archaeological operations in 2012 was the University of Connecticut's *Kraken 2*, a Max Rover-class ROV capable of operating in depths to 1,000 m (3,280 ft). Positioning was achieved using an ORE Trackpoint II ultra-short baseline (USBL) tracking system combined with a Winfrog integrated navigation system. The main science HD video camera on the ROV was a Kongsberg OE14-502. Two parallel lasers mounted 10 cm (4 in) apart were turned on most of the time when using the video camera. HD video was recorded to a hard drive during the dive, and two copies of the dive video were made onto two-terabyte hard drives every night after each dive. The main digital still camera was a Kongsberg camera using a Canon G11 Powershot system. This was mounted on the same pan and tilt as the video camera. A downward-looking digital still camera was also mounted on the ROV frame and was used in both continuous and intervalometer mode. Position data were time-synchronized with all imagery and samples. A six-function manipulator arm was used to collect biological and archaeological samples and store them in the vehicle's polypropylene biobox. Surrounding the biobox were seven PVC quivers capped with rubber stoppers that could hold small samples or sediment core tubes. Two (occasionally four) push corers were carried on many dives in the vicinity of the shipwrecks. A Sea-Bird Electronics, Inc. (Sea-Bird) SBE 911*plus* conductivity-temperature-depth (CTD) instrument (provided by the University of North Carolina-Wilmington) was attached to the ROV to record environmental data during the dive.

During archaeological investigations, most ROV dives followed a similar pattern emphasizing systematic video documentation and photography of shipwrecks and diagnostic features as well as the collection and photography of biological specimens on or near the shipwrecks. Tube cores were also taken on selected dives.

Archaeological sampling was undertaken very selectively. During each ROV dive, the lead scientist (Mather) and a second observer were on watch with the ROV crew. The lead scientist directed the dive (course, speed, transect configuration, data collection, and sampling) and made audio annotations of dive activities. The second observer recorded events throughout the dive on hard copy and digital event logs. In addition, at least one and usually two archaeologists (Watts or Irion) monitored the dives. All dives were systematic in coverage. Shipwrecks were usually imaged along both the port and starboard side before central longitudinal transects were attempted. In many cases, fishing gear and debris created significant challenges to ROV operations at shipwreck sites and impacted data acquisition. Biological specimen or sample collecting was generally reserved for the last part of each dive. As far as possible, every collection was documented with video. Video recording and digital still photography were conducted throughout each dive, and were suspended only during ROV ascent and decent.

4.3.3.3 Description of Work

The archaeological work took place during Leg 3 of the 2012 sampling cruise for that summer. The ship sailed from Norfolk, Virginia, on 17 September 2012 and returned to Charleston, South Carolina, on 2 October 2012. The ocean science and archaeology was impacted by a delay waiting for a replacement Kongsberg camera for the ROV at the beginning of the cruise, by bad weather and rough seas during the cruise, and by an accident that resulted in the loss of the ROV at the end of the voyage. Reacting to the delays at the beginning of the cruise, the archaeological team decided that the investigation of each actual or potential archaeological site would be shortened in favor of investigating multiple sites in a single day. This ensured that some data would be collected for each of the planned sites. As a result, the identities of all eight Billy Mitchell-Project B wrecks as well as one other vessel were confirmed during the cruise.

A site of potential paleoarchaeological interest was investigated as well as a site that emerged as a potential archaeological site as the result of data from one of the box cores. The ROV *Kraken 2* was lost at the end of the 10th dive due to a severed cable. It took more than 24 hours to recover the vehicle along with the onboard data. This accident compromised the final planned dives and, unfortunately, one of the shipwrecks identified during the multibeam survey in 2011 was not investigated. Overall, the archaeological investigations in 2012 were very productive.

All archaeological studies for the 2012 sampling cruise were in the vicinity of Norfolk Canyon. Ten ROV dives were completed (11 had been planned) (**Figure 4-1**; **Table 4-2**). The team captured 61 hours, 21 minutes, and 45 seconds of video footage; 8,646 still images with the downward camera; 3,546 still images with the pan and tilt camera; and 19 sonar images. In addition, 85.38 km^2 of seafloor were surveyed using the *Nancy Foster*'s Kongsberg EM1002 multibeam sonar. All station data sheets were scanned on board the ship and electronic PDFs were provided to project investigators. Data were also entered into an Access database, checked for errors, and archived at the University of North Carolina-Wilmington.

A limited number of archaeological samples and artifacts were collected during ROV dives on Leg 3 (**Table 4-3**). Researchers collected these as part of the archaeological identification and assessment process. All samples were photographed and cataloged and are currently being stored at the University of Rhode Island. Collections of benthic organisms were made from visited shipwrecks, box cores, and an ROV dive to search for paleoarchaeological sites. Voucher samples of representative dominant benthic organisms from shipwreck locations were collected to facilitate their identifications in video data.

4.3.3.4 Findings

The general findings from each ROV dive during Leg 3 of the 2012 sampling cruise are presented below. The analysis of each site is presented in **Section 4.3.5**. Site locations have been generalized or redacted.

- ROV-2012-NF-21 (20 September 2012) was completed at TGT-ROV_VA2008_1. This was a test dive on a speculative and potential archaeological site in shallower water. The potential site had been identified during the University of Rhode Island's investigations of Norfolk Canyon in 2006. During this dive, the team identified what appeared to be a ceramic bowl covered with marine growth. After recovery and analysis, the artifact was identified as being modern (late 20th century) and of no archaeological significance.
- ROV-2012-NF-22 (22 September 2012) was an archaeological reconnaissance investigation of two shipwrecks (TGT-MB VA2006_3 and TGT-MB VA2006_2). Dive operations confirmed that the shipwrecks were the remains of the submarines *UB-148* and U-*140*. The southern submarine was investigated first, the more northern was investigated second.
- ROV-2012-NF-23 (23 September 2012) was conducted on a shipwreck identified during the survey as TGT-MB VA2011_2. Dive operations at this site confirmed that it was the remains of the *Ostfriesland*. During the dive, archaeologists recovered a small sample of iron plate. That sample disintegrated during recovery.
- ROV-2012-NF-24 (24 September 2012) was conducted at TGT-MB VA2011_3. Dive operations at this site confirmed that it was the remains of the *Frankfurt*. A coal sample was taken during this dive, but it could not be analyzed.

- ROV-2012-NF-25 (25 September 2012) was conducted at the site of a box core along the southern edge of Norfolk Canyon taken on 24 September (Station 183 in 550 m), which resulted in the recovery of a smooth round river stone considered to have some archaeological potential. During the dive, a sample of what appeared to be chert (**Figure 4-2**) was recovered as was a piece of iron strapping, which was found to be debris on the seafloor.
- ROV-2012-NF-26 (26 September 2012) was conducted at TGT-MB VA2011_6. Dive operations at this site confirmed that it was the remains of the German destroyer *G-102*.
- ROV-2012-NF-27 (26 September 2012) comprised reconnaissance operations on two shipwrecks (TGT-MB VA2011_4 and TGT-MB VA2011_5) with an on-bottom transit between the two. The first part of the dive confirmed the presence a World War I German destroyer (later identified as the *V-43*). The second part of the dive confirmed the presence a second World War I German destroyer (later identified as the *S-132*). During this dive, archaeologists recovered an iron sample and ballast brick from the destroyer *S-132*. The ballast brick was desalinated and conserved at the University of Rhode Island (**Figure 4-3**).
- ROV-2012-NF-28 (27 September 2012) An ROV "archaeological prospecting" dive was conducted in Multibeam Area 3, which had showed interesting geological features possibly conducive for paleoarchaeological sites of human habitation. During this dive, the archaeologists recovered several samples of rock, glacial till, and shell. All were desalinated and conserved at the University of Rhode Island.
- ROV-2012-NF-29 (27 September 2012) was a second ROV dive for the day, conducted on a shipwreck identified as TGT-MB VA2011_1. Dive operations at this site confirmed it as the *Washington*.
- ROV-2012-NF-30 (28 to 29 September 2012) consisted of archaeological reconnaissance operations on shipwreck TGT-MB VA2006_1. During recovery, however, the ROV tether became entangled in the z-drive of the *Nancy Foster* and was severed. Unexpectedly, as the ROV drifted away from the vessel, it lost buoyancy and gradually sunk. Dive operations at this site confirmed that it was the U-*117*.

Table 4-2. Archaeological ROV dives in the Mid-Atlantic Bight off the east coast of the United States around and in Norfolk Canyon during Leg 3 of the 2012 sampling cruise (19 September to 2 October 2012). Locations have been generalized or redacted

Dive Number	Date	Location	Good	Gear	Latitude (N)	Longitude (W)	Day/Night
ROV-2012-NF-21	20 Sept 2012	Norfolk Canyon	Yes	ROV	37°10′	74°55′	Day
ROV-2012-NF-22	22 Sept 2012	Norfolk Canyon	Yes	ROV	37°10′	74°45′	Day
ROV-2012-NF-23	23 Sept 2012	Norfolk Canyon	Yes	ROV	37°10′	74°35′	Day
ROV-2012-NF-24	24 Sept 2012	Norfolk Canyon	Yes	ROV	37°15′	74°35′	Day
ROV-2012-NF-25	25 Sept 2012	Norfolk Canyon	Yes	ROV	37°00′	74°35′	Day
ROV-2012-NF-26	26 Sept 2012	Norfolk Canyon	Yes	ROV	37°10′	74°35′	Day
ROV-2012-NF-27	26 Sept 2012	Norfolk Canyon	Yes	ROV	37°15′	74°30′	Day
ROV-2012-NF-28	27 Sept 2012	Norfolk Canyon	Yes	ROV	37°00′	74°40′	Day
ROV-2012-NF-29	27 Sept 2012	Norfolk Canyon	Yes	ROV	36°55′	74°40′	Day
ROV-2012-NF-30	28 Sept 2012	Norfolk Canyon	Yes*	ROV	37°10′	74°45′	Day

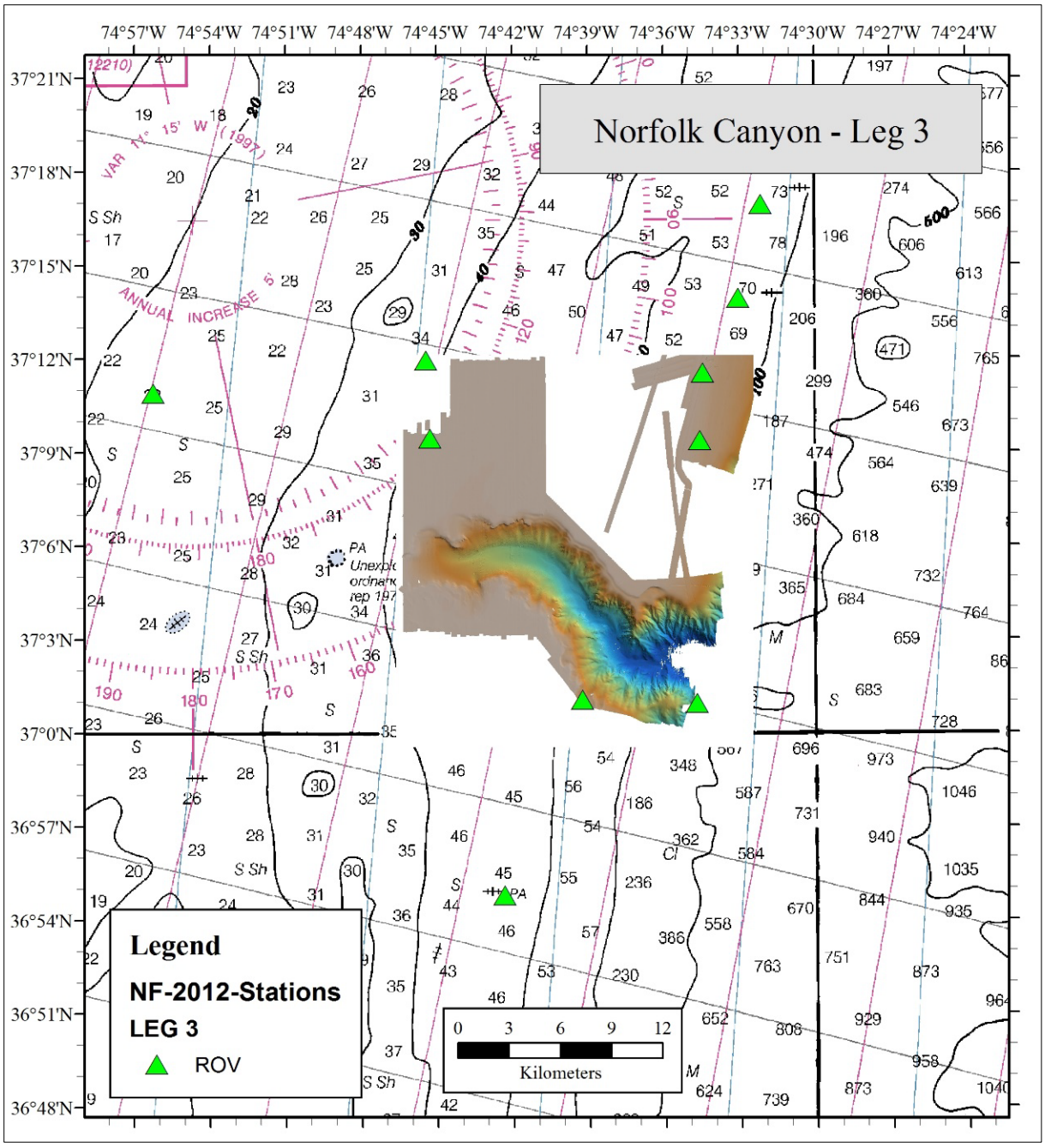

Figure 4-1. Remotely operated vehicle (ROV) dive locations for archaeological investigations during Leg 3 of the 2012 sampling cruise (19 September to 2 October 2012).

Table 4-3. Artifact catalog for archaeological sites sampled in Norfolk Canyon during Leg 3 of the 2012 sampling cruise (19 September to 2 October 2012).

Accession Number	Cruise	ROV Dive	Date	Site ID	Site Name	Description	Dimensions
NF2012_001	NF2012	ROV-2012-NF-21	20 Sept 2012	VA_2008_1	JOSMCW	Carlisle Dallas Ware bowl (modern)	13.9 cm (5.5 in) rim Diameter; 7.6 (3 in) base diameter
NF2012_002	NF2012	ROV-2012-NF-23	23 Sept 2012	MB VA2011_2	*Ostfriesland*	Iron plate sample	5 cm
NF2012_003	NF2012	ROV-2012-NF-24	24 Sept 2012	MB VA2011_3	*Frankfurt*	Coal	18 × 16 cm
NF2012_004	NF2012	ROV-2012-NF-25	25 Sept 2012	n/a*	Box Core F Site	Iron strapping (broken)	5 cm
NF2012_005	NF2012	ROV-2012-NF-25	25 Sept 2012	n/a*	Box Core F Site	Chert	7 × 4 cm
NF2012_006	NF2012	ROV-2012-NF-27	26 Sept 2012	MB VA2011_5	Destroyer3	Iron sample	Four pieces, 2−4 cm each
NF2012_007	NF2012	ROV-2012-NF-27	26 Sept 2012	MB VA2011_5	Destroyer3	Ballast brick	24.5 × 11.2 × 6.5 cm (9 ⅝ × 4 ⅝ × 2 ⅝ in)
NF2012_008	NF2012	ROV-2012-NF-28	27 Sept 2012	MB VA2012 Area3	Arch Prospecting	River cobble	19 × 14 cm
NF2012_009	NF2012	ROV-2012-NF-28	27 Sept 2012	MB VA2012 Area3	Arch Prospecting	River cobble	8 x 13 cm
NF2012_010	NF2012	ROV-2012-NF-28	27 Sept 2012	MB VA2012 Area3	Arch Prospecting	Glacial till sample	Six pieces, 3−5 cm each
NF2012_011	NF2012	ROV-2012-NF-28	27 Sept 2012	MB VA2012 Area3	Arch Prospecting	Glacial till rocks	Seven rocks: 1-, 1-, 2-, 4-, 5.5-, 8-, and 9 cm
NF2012_012	NF2012	ROV-2012-NF-28	27 Sept 2012	MB VA2012 Area3	Arch Prospecting	Shell	Seven shells: 1.5−2.5 cm
NF2012_013	NF2012	ROV-2012-NF-28	27 Sept 2012	MB VA2012 Area3	Arch Prospecting	Rock	12 × 9 cm
NF2012_014	NF2012	n/a*	−	n/a*	−	Fishing gear wheel	14 cm (outside diameter), 5 cm (inside diameter)

* Artifact was collected in a trawl sample.

Figure 4-2. Possible chert sample recovered on 25 September 2012.

Figure 4-3. Ballast brick recovered from the German destroyer *S-132* during the 2012 sampling cruise.

4.3.3.5 Multibeam Survey

The multibeam survey during Leg 3 of the 2012 sampling cruise was designed to further develop on the more extensive mapping mission from 2011. The archaeological team identified seven areas south and west of Norfolk Canyon numbered sequentially (**Figure 4-4**). Multibeam surveys were conducted during night operations or at times when ROV dives were not possible because of technical difficulties or weather. Multibeam surveys were conducted in the following areas according on the dates identified:

- 17 September 2012: Multibeam Area 1
- 18 September 2012: Multibeam Area 1
- 20 September 2012: Multibeam Area 3
- 21 September 2012: Multibeam Area 3 and Area 4
- 25 September 2012: Multibeam Area 2 and Area 4
- 26 September 2012: Multibeam Area 2

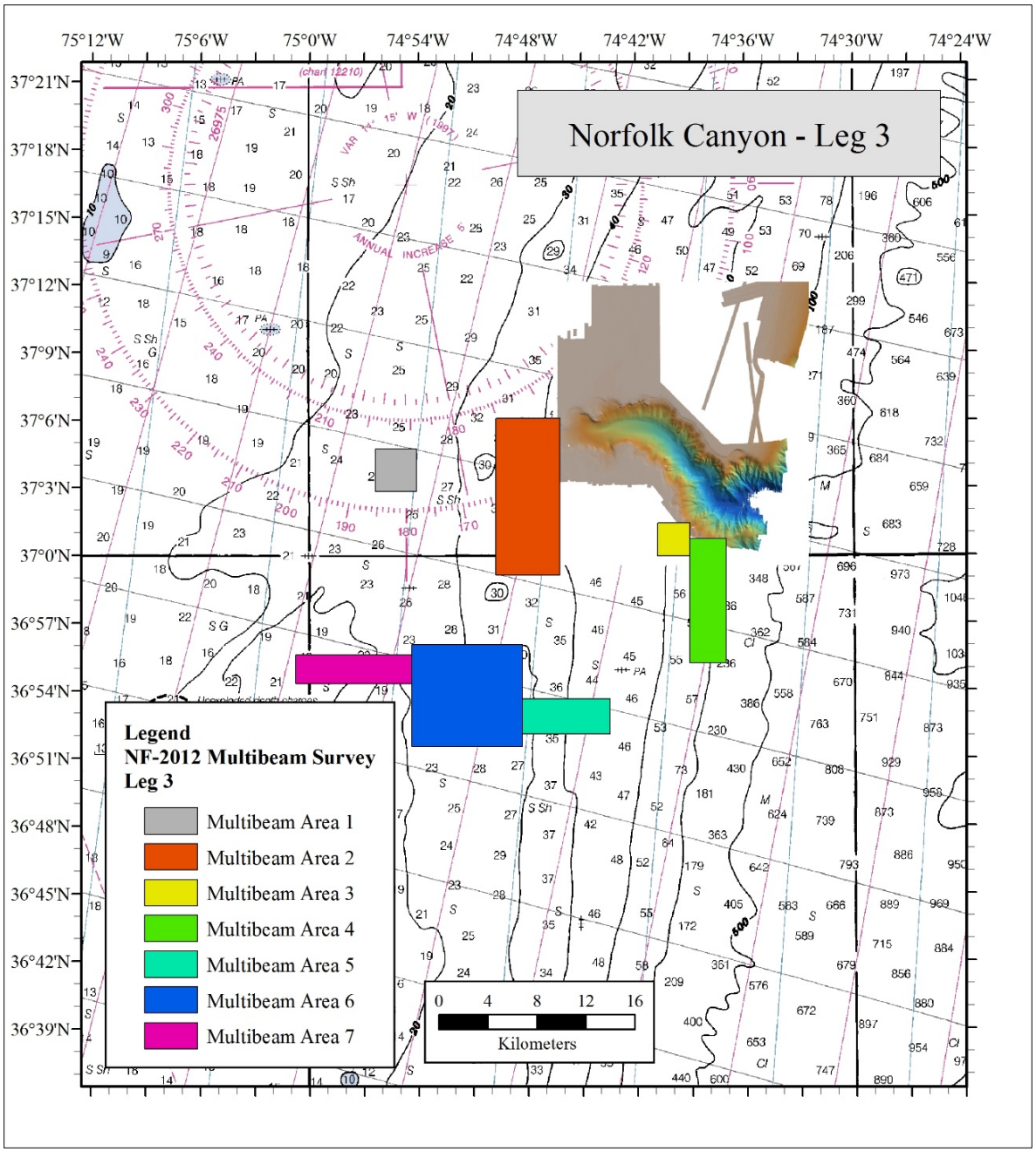

Figure 4-4. Multibeam survey areas mapped during Leg 3 of the 2012 sampling cruise (19 September to 2 October 2012).

4.3.3.6 Summary

Six of the eight vessels from the Billy Mitchell-Project B fleet were found and identified during the 2012 sampling cruise, namely the *Ostfriesland*, *Frankfurt*, *G-102*, *V-43*, *S-132*, and *UB-148*. The University of Rhode Island had previously visited the two remaining vessels, the U-*117* and U-*140*. As a result, all eight vessels of the Billy Mitchell-Project B fleet were identified and located to archaeological standards for the first time. In addition, the battleship *Washington* was also found and identified. All shipwrecks investigated in 2012 showed signs of significant damage from fishing gear, and in some cases the damage was extensive. Damage to shipwrecks from technical divers and souvenir hunting, however,

was minor in comparison. All shipwrecks were found to be sitting upright on the seafloor, except for the battleships *Ostfriesland* and *Washington*, which had capsized during the wrecking process.

Damage to the wrecks from the bombing missions in 1921 could be identified and, within reasonable parameters, separated from damage by other site formation processes, including impact with the seafloor and gradual deterioration. Deterioration, however, was not consistent. Shipwrecks in similar environments sunk at the same time had experienced different rates of degradation and site formation. The biologists and archaeologists on the team noted that all the wrecks investigated served as artificial reefs, hosting extensive biological communities, including major communities of chain dogfish. Elements of the submerged military landscape associated with the Southern Drill Grounds could also be identified during the 2012 season, including not only the ships themselves, but also ammunition. The archaeologists noted that paleoarchaeological landscape features (including ancient riverbeds) may be identifiable. Rounded river stones were observed and collected at one site. Those stones were subsequently stabilized and stored at the University of Rhode Island.

4.3.4 2013 Sampling Cruise

During the 2013 sampling cruise aboard the NOAA ship *Ronald H. Brown*, the archaeological team continued to investigate known sites and attempted to ground truth previously identified targets and find new sites. The team had at its disposal the sophisticated ROV *Jason II*, owned and operated by Woods Hole Oceanographic Institution. Some potential targets and sites, however, were judged to be either too shallow or in environments too dynamic to permit safe operations for the *Jason II*. In addition, the archaeological team was able to use the *Ronald H. Brown*'s Kongsberg Simrad EM 122 (12 kHz) swath bathymetric sonar system to conduct multibeam bathymetry work. The system is capable of imaging the seafloor in water depths ranging from 20 to 11,000 m, however, at depths greater than 1,000 m, the resolution of the data makes it difficult and sometimes impossible to identify archaeological sites. Multibeam survey work was directed toward imaging a 120 mi^2 area in deep water off the OCS in the vicinity of Norfolk Canyon. It was in this area that the *San Demetrio*, a British tanker with a fascinating history, was torpedoed and sunk by the U-*404* in March 1942.

The 2013 sampling cruise enabled archaeologists to collect data at the *Ostfriesland*, *Frankfurt*, *G-102*, and *V-43* sites. The site is believed to be the remains of the SS *Ocean Venture*, which was lost in 1942 and had not been investigated since it lay in water judged by the Woods Hole technical team to be too shallow for the ROV *Jason II* to operate safely. It had been one of the priorities for the cruise. The cruise confirmed that the Billy Mitchell-Project B wrecks were heavily impacted by fishing gear.

Although video and photographic data were collected, the extensive relief at the sites, combined with in-water obstructions, prevented full access to the sites and made consistent altitude for downward imaging difficult to obtain. As a result, the team did not achieve its desired objectives of full mosaicking data, but it was able to complete partial mosaics of the *Ostfriesland* and *Frankfurt*. Unfortunately, foul weather and poor sea states toward the end of the cruise forced the team to cancel several dives. As an alternative, the team attempted to conduct ROV dives on the remains of USS *New Jersey* and USS *Virginia* off the coast of North Carolina, but strong currents prevented these operations, and again the *Jason II* was unable to dive. Although out of the immediate study area, *New Jersey* and *Virginia* were sunk as part of Billy Mitchell's series of military experiments during the early 1920s. The multibeam survey of the 100 mi^2 area did not produce targets likely to be the remains of the *San Demetrio*.

4.3.4.1 Archaeological Objectives

The archaeological objectives for the 2013 sampling cruise were extensive and ambitious. Technical and weather-related difficulties meant that they were not all achieved. The objectives were as follows:

- Conduct daily ROV dives to document, record, and assess significant archaeological sites.

- Conduct multibeam surveys of a 100-mi^2 area approximately 35 mi east of Norfolk Canyon in an attempt to find the *San Demetrio.*
- If a target was discovered during a multibeam survey, the team envisioned an ROV dive on the potential location of the *San Demetrio*. The site was thought to be in water depths of approximately 2,500 m, 35 mi east of Norfolk Canyon.
- Return to at least four of the Billy Mitchell-Project B wrecks—*Ostfriesland, Frankfurt, G-102,* and U-*140,* and preferably a fifth—*Washington*. This would provide the team with information on a battleship, a cruiser, a destroyer, and a submarine. The purpose of these investigations was to collect data to generate high-quality photomosaics of wreck sites or part of wreck sites that would assist with the site assessments. All this work was within the vicinity of Norfolk Canyon.
- Conduct at least one and preferably two prehistoric site reconnaissance dives. Several locations were near Norfolk Canyon where this would be appropriate.
- Conduct an ROV dive on a shipwreck believed to be the *Ocean Venture*. This vessel was sunk by a German submarine in 1942. The potential site was found during the multibeam survey work on the 2012 sampling cruise, but the team did not have time to investigate the site with the *Kraken 2*. Had we not lost the ROV at the end of the 2012 cruise, we would have conducted a dive at this location.
- Several areas were identified as priorities for multibeam survey, but one was particularly important. The area was 15 mi^2 in size and located just west of Washington Canyon. The area was west of the head of Washington Canyon with water depth ranging from 80 to 120 m. Depending on the survey results, an expansion of operations to include an ROV dive would have completed the geographical range of the archaeological studies for the project. Unfortunately, time restrictions and weather delays prevented this survey and dive.
- The team also envisioned a possible ROV dive at the location of a Grumman *Hellcat F6F* airplane in Baltimore Canyon. Again, this was not possible.

The team did not think there was sufficient time to visit the *Bow Mariner,* a tanker carrying ethanol, diesel, and fuel oil that caught fire on 28 February 2004 and sank midway between Baltimore and Washington canyons (37°55′ N, 74°15′ E) – location generalized. The NOAA ship *Thomas Jefferson* surveyed the shipwreck with multibeam in 2009.

4.3.4.2 Methods

The ROV *Jason II* comprised two units: the ROV itself and a support sled and tethering unit (*Medea*), which reduced the load on the umbilical and helped buffer movement between the surface and the ROV. Navigation of the vehicle was achieved through a Sonardyne Ranger USBL, which recorded the position of the vehicle every few seconds. The primary science camera on the ROV was an Insite Mini-Zeus HD video camera. Two parallel lasers mounted 10 cm apart projected onto the video subject image and provided a size reference for measuring objects on the seafloor. The video was recorded directly to external hard drives and DVDs during the dive, and a copy of the dive was made at high resolution onto external hard drives as a backup for the original every night after each dive. Two digital still cameras were used: a Nikon CoolPix (3 Mb) controlled by the science dive lead, and an Insite Super Scorpio that was operated by the ROV crew. Two seven-function hydraulic manipulator arms (a Schilling Titan 4 and a Kraft Predator II) were used to collect samples. A large retractable sled was mounted on the front of the ROV and was equipped with several sampling devices. Two additional insulated bioboxes were mounted on retractable arms on either side of the sled and a five-bucket suction sampling system at the back of the vehicle. An SBE 911*plus* CTD instrument (provided by the University of North Carolina-Wilmington) was attached to the ROV to record environmental data during the dive (see CTD section below for details). During the first four archaeological ROV dives (J2-692, J2-693, J2-694 JS-695), the Nikon

CoolPix camera was orientated in a downward-looking configuration while the higher resolution Super Scorpio camera was configured as the ROV's pan and tilt. On May 25, we switched the positions of these cameras on the ROV so that the Super Scorpio was orientated in a downward-looking configuration. This change was aimed at improving data and imagery for photomosaics. Unfortunately, only one more dive could be completed; therefore, the only dive in which the Super Scorpio camera was in a downward-looking configuration was J2-696.

The cruise plan was scheduled to accommodate16 hour dives; however, this was reduced to 13 hours after the cruise began to accommodate rest and meal scheduling for the ROV crew. The ROV plan was to launch at 0600 hours and be back on deck at 1900 hours, but this was subject to change as conditions and logistics dictated.

ROV dives on shipwrecks followed a similar pattern, emphasizing systematic video documentation and photography of shipwrecks and diagnostic features, and the collection and photography of biological specimens on or near the shipwrecks. Tube cores were also taken on selected dives (see **Chapter 3**). Shipwrecks were usually imaged along both the port and starboard side before central longitudinal transects were attempted. In many cases, fishing gear and debris significantly challenged ROV operations at shipwreck sites.

ROV navigation data were time-synchronized with all imagery and samples, and the Virtual Van was used to record data on observations and collections as well as images and environmental data throughout the dive. *Jason II* instruments recorded all times in Greenwich Mean Time (GMT); however, station sheets and audio logs were recorded in Eastern Standard Time (EST). During each ROV dive, the lead scientist and two other observers were on watch in the ROV van. The lead scientist directed the dive and made audio annotations of dive activities. The second observer recorded events throughout the dive on hard copy and logged events in the Virtual Van. The third observer was responsible for keeping track of the media recordings, and switching and labeling the drives and discs.

4.3.4.3 Description of Work

The archaeological work during the 2013 sampling cruise took place between 20 and 27 May 2013 during Leg 2 in the summer. Archaeological investigations started with an at-sea transfer of personnel through the services of Cape Henry Launch and ended with docking of the *Ronald H. Brown* in Charleston, South Carolina, a week later.

The team completed five ROV dives for a total of 50 hours and 1 min bottom time as well as 120 mi^2 of multibeam mapping and three CTD casts. Initial multibeam data were post-processed on board the ship, and a list of targets was identified. None of the multibeam targets for the cruise proved sufficiently promising to warrant an ROV dive. All station data sheets were scanned on board the ship and electronic copies were provided to the principal investigators. Data were also entered into an Access database, checked for errors, and archived at the University of North Carolina-Wilmington, University of Rhode Island, and CSA Ocean Sciences Inc. in Stuart, Florida.

Despite the success of the cruise, a series of technical and weather-related issues prevented the team from completing all the objectives. Most of the known archaeological sites were only just deep enough for the *Jason II* ROV to operate safely, and some were too shallow. This meant that we were unable to dive on the suspected wreck of the *Ocean Venture*. In addition, water currents at three wreck sites were greater than 2 knots. The ROV team judged these conditions to be unsafe for *Jason II* operations. The *Ronald H. Brown*'s EM 122 multibeam system worked well, thanks in large part to a dedicated crew and the presence of a Kongsberg technician on board. However, the team did lose some time getting a replacement circuit board (generously provided at sea by the *Okeonos Explorer*), and the water depths in the deepwater survey area exceeded the capacity of the Kongsberg EM 122 to resolve objects the size of most shipwrecks. This may have contributed to the unsuccessful search for the *San Demetrio*, but it also could have been the case that historical evidence for the location of the wreck was inaccurate. The

weather conditions and sea state toward the end of the cruise significantly impacted operations. During the evening of 24 May, conditions were sufficiently adverse to prevent any science operations.

4.3.4.4 Findings

The archaeological leg of the NOAA ship *Ronald H. Brown* cruise completed five ROV dives (**Table 4-4**).

Table 4-4. Archaeological ROV dives in the Mid-Atlantic Bight off the east coast of the United States around Norfolk Canyon during Leg 2 of the 2013 sampling cruise (19 to 27 May 2013). Locations have been generalized or redacted

Dive No.	Date	Time	Total Time (min)	Start		End		Depth Range (m)
				Latitude (°N)	Longitude (°W)	Latitude (°N)	Longitude (°W)	
ROV-2013-RB-692	19 May 2013	N	295	37°10′	74°35′	37°10′	74°35′	91−105
ROV-2013-RB-693	20 May 2013	D	894	37°10′	74°35′	37°10′	74°35′	90−116
ROV-2013-RB-694	21 May 2013	D	861	37°15′	74°35′	37°15’	74°35′	101−126
ROV-2013-RB-695	22 May 2013	D	504	37°15′	74°30′	37°15′	74°30′	106−121
ROV-2013-RB-696	23 May 2013	D	197	37°10′	74°35′	37°10′	74°35′	90−114

D = daytime (0600 to 2000 hours Eastern Standard Time (EST), N = nighttime (2000 to 0600 hours EST). ROV = *Jason II*.

The findings from each ROV dive during the cruise are presented below. The analysis of each site is presented in **Section 4.3.5**.

- J2-692 was completed at target (MB VA2011_6), the site of the destroyer *G-102*. The site was found to be heavily impacted by fishing gear. The dive commenced with an approach to the wreck on the starboard side and then a transition to the stern. The port side to the wreck was then surveyed all the way to the bow. Video and photographic documentation of the bow showed that the vessel had been heavily damaged in that part of the superstructure. A series of athwartships and longitudinal transects failed to provide high-quality video or photographic data. This was due to the required altitude above the wreck for safe ROV operations. Documentation of the wreck was hampered by the presences of krill toward the end of the dive that made video and photography difficult.
- J2-693 was completed at target (MB VA2011_2), the site of the battleship *Ostfriesland.* The site was found to be moderately impacted by fishing gear.
- J2-694 was completed at target (MB VA2011_3), the site of the light cruiser *Frankfurt.* The site was found to be moderately impacted by fishing gear. Data acquisition started in the heavily degraded bow and moved aft via a series of athwartships transects. In several areas, fishing gear suspended by floats in the water column prevented downward imaging of the wreck. The stern was well preserved, but the muzzle of a 5.9 in (15 cm) gun, which had been resting on a half deck in the stern in 2012, had collapsed and was resting just inside the gunnel on the port side. It was clear that the stern of the *Frankfurt* was undergoing active deterioration and was highly vulnerable to further damage.
- J2-695 was completed at target (MB VA2001_4), the site of the destroyer *V-43*. The site was found to be heavily impacted by fishing gear.
- J2-696 was completed at target (MB VA2011_2), the site of the *Ostfriesland.* The purpose of the dive was to obtain additional images to photomosaic the site. While some data was obtained, the dive was aborted and the vehicle was recovered after 4 h 25 min due to worsening sea conditions.

4.3.4.5 Multibeam Survey

Multibeam survey operations during the 2013 sampling cruise focused on an area of deep water (~100 mi^2) off the continental shelf approximately 15 mi east of Norfolk Canyon (**Figure 4-5**). It was in this area that the remains of the *San Demetrio* were thought to be located. This survey did not identify any targets for shipwreck investigation. This result, however, was inconclusive since the hull-mounted multibeam system used during the survey generated only low-resolution data of the seafloor, on the order of approximately 30-m pixels. Multibeam surveys were conducted in the following areas according to the dates identified:

- 23 May 2013: Multibeam survey in deepwater area. No wrecks positively identified.
- 24 May 2013: Multibeam survey of deepwater area. No wrecks positively identified. Worsening sea conditions prompted a decision to head south to wreck sites off Hatteras.

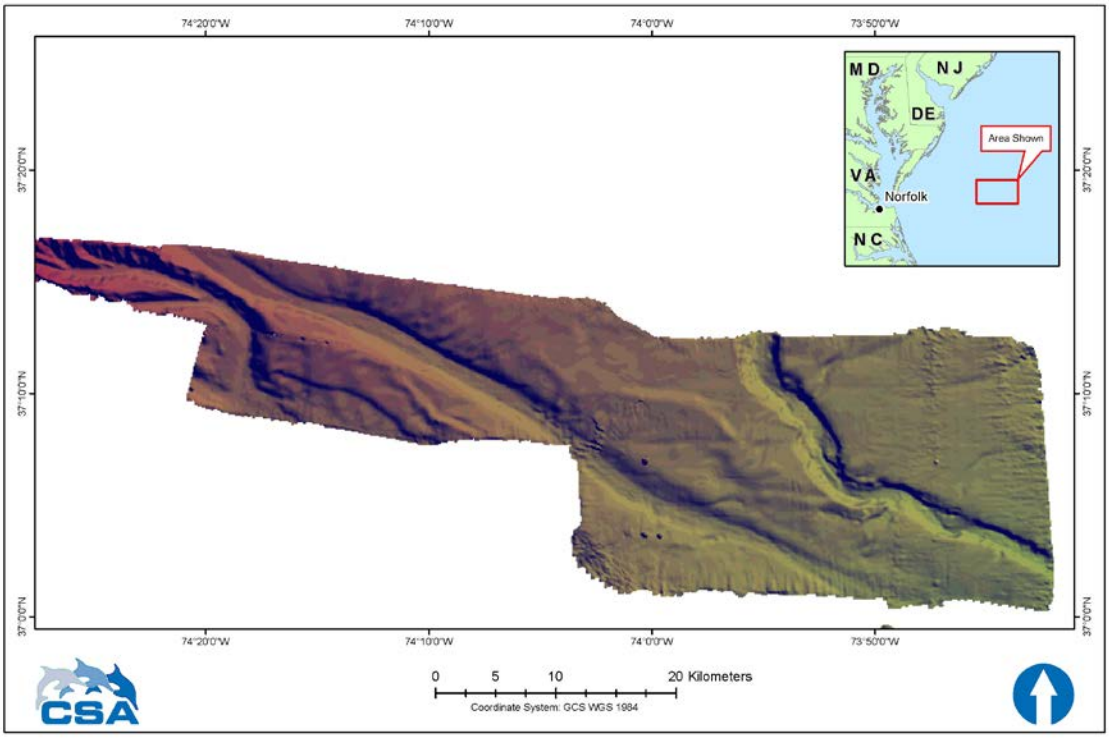

Figure 4-5. Multibeam map of deepwater area from the 2013 sampling cruise.

4.3.4.6 Investigations Not Completed

One objective of the 2013 sampling cruise was to investigate the remains of the steam ship *Ocean Venture*. Water depth at the site was judged to be too shallow for the ROV *Jason II*. In addition, the team was not able to investigate any of the submarines because of the shallowness of the water depth. The team attempted ROV dives on the remains of *New Jersey* and *Virginia* located off Cape Hatteras, North Carolina, on 25 May, but currents at the sites were greater than 2 and 2.8 knots, respectively, therefore ROV operations were cancelled. Poor weather and shortage of time prevented the team from investigating *Washington* and the Grumman *Hellcat F6F* airplane in Baltimore Canyon. Finally, as expected, the team was unable to visit the remains of the *Bow Mariner*, a tanker carrying ethanol, diesel, and fuel oil that caught fire on 28 February 2004 and sank midway between Baltimore and Washington canyons (37°55', 74°15') – location generalized. The NOAA ship *Thomas Jefferson* surveyed the shipwreck with multibeam in 2009.

4.3.4.7 Summary

During the Leg 2 of the 2013 sampling cruise (19 to 27 May), ROV dives were completed on the *Ostfriesland*, the *Frankfurt*, the *G-102*, and what is believed to be the *V-43*. All wrecks showed damage from fishing gear and possible damage from anchoring. Fishing gear was found to have impacted the larger ships, particularly the *Ostfriesland*, less than the smaller vessels with weaker original superstructure. The *Ostfriesland*, like with many other sunken battleships, turned turtle during the wrecking process leaving the vessel upside down on the seafloor. This disposition meant that the vessel's strong, well protected lower hull helped protect the site from fishing gear and associated damage. Recent impacts on all shipwrecks investigated from a combination of fishing gear and ground tackle were evidenced by extensive fresh patches of corrosion. The propellers were found to be missing from all wrecks examined. This finding is consistent with historical accounts of the removal of the propellers prior to sinking. Evidence of bomb damage during the Billy Mitchell-Project B experiments was discernable on all wrecks examined during this cruise. The bridge of the *G-102* is partially intact with compass binnacle and ship's telegraph still *in situ*. Very little of the bow of the *G-102* still exists, but the stern was found to be well preserved. There is a complete break running athwart ships toward the stern of the *Ostfriesland*. This was caused by the impact of the ship's stern with the seafloor.

A substantial entanglement of fishing gear was found located on the northern side of the *Ostfriesland* toward the stern. It extended approximately 13 m above the wreck.

The anchor chain was still in place in the port bow of *Ostfriesland.* It extends from the hawse pipe and runs east (there is one hawse pipe on the starboard bow of *Ostfriesland* and two on the port). The archaeological team found that *Frankfurt*'s stern was well preserved, but the bow had suffered extensive damage due to, in part, the impact of the ship's bow with the seafloor during sinking. The *V-43* was found to be heavily damaged and impacted by fishing gear (see **Section 4.3.5.4**). Unfortunately, there were no shipwreck targets identified during the deepwater multibeam survey conducted during this cruise and no ROV dives possible in search of the *San Demetrio*.

4.3.5 Site Analysis

4.3.5.1 Ostfriesland

The battleship *Ostfriesland* was sunk as part of the Billy Mitchell-Project B experiments on 21 July 1921. This site was identified during a multibeam survey in 2011 and subsequently investigated using the ROVs *Kraken 2* and *Jason II* in 2012 and 2013, respectively (NF-2012-ROV-23; RB-2013-J2-693; RB-2013-J2-696).

Ostfriesland lies in approximately 112 m of water, north of Norfolk Canyon (**Figure 4-6**)[291]. The hull is orientated in a northwest-southeast configuration, with the stern to the north. As she sunk, *Ostfriesland* turned turtle, went down by the stern, and now rests keel up on the seafloor supported by her six main gun turrets. The stern of the *Ostfriesland* took the brunt of the impact with the seafloor, cracking the back of the ship. The result is a complete athwartships break in the ship running along a bulkhead slightly forward of the stern. Site specifications and imagery of *Ostfriesland* are shown in **Figure 4-6**.

[291] "Bombing *Ostfriesland*," Box 170, Folder 6; GU-U.S. Air Operations-Bombing Tests, Naval Aircraft Operations Flight, Air Stations; RCONRL, RG 45; National Archives, College Park, MD.

Wreck Specifications:

Center: 37°10′ N; 74°35′ W (coordinates generalized)
Max water depth: 112 m (367 ft)
Min target water depth: 94 m (308 ft)
Target length: 167 m (547 ft)
Central target length: 114 m (374 ft)

Multibeam Imagery

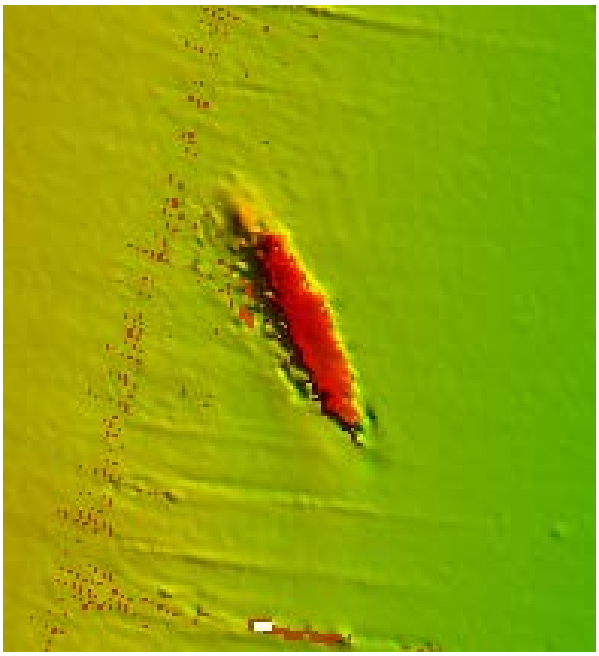

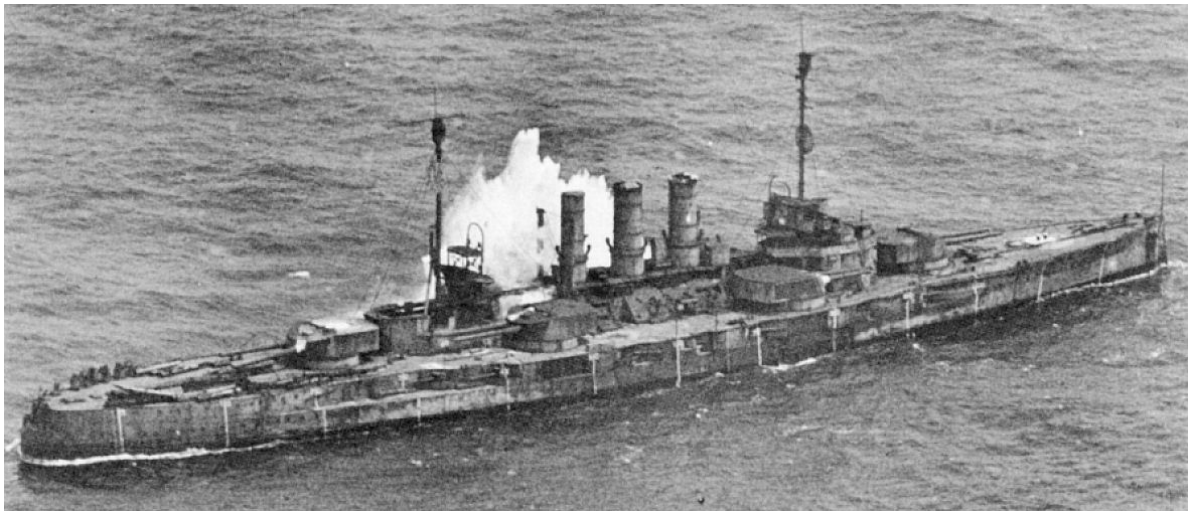

Figure 4-6. Site specifications and imagery for the SMS *Ostfriesland.*

4.3.5.1.1 The Lower Hull

The stern of *Ostfriesland* is relatively well preserved. It rests upside down on the fantail. The stern torpedo tube survives intact. The vessel's two rudders are still in place; the starboard rudder is orientated fore and aft; the port rudder is orientated a few degrees to port. The port rudder is impacted more heavily by fishing nets than the starboard rudder (**Figure 4-7**). Immediately forward of the rudders are the remains of the three propeller hubs, but the propellers themselves are missing. The port and starboard propeller hubs, shafts, and brackets are intact and *in situ*. The center propeller hub and shaft is broken and has collapsed. It lies lower down toward the seafloor orientated slightly to port (**Figure 4-7**).

Figure 4-7. The rudders of *Ostfriesland* and the remains of the central propeller shaft (center bottom).

Figure 4-8. Aft edge of athwartships crack in the hull of *Ostfriesland* showing trawl doors to the left.

The skeg and keel at the *Ostfriesland*'s stern are well preserved, as is the outside of the lower hull in the stern. Forward from the port propeller hub, the port shaft is damaged. The starboard shaft is better preserved. Slightly forward of the fantail and skeg there is a major break in the ship's keel separating the hull into two parts. The break consists of a crack in the hull, which runs along a bulkhead just aft of the engine room in the stern (**Figure 4-9**). The forward edge of the crack is relatively clean, but the aft edge is more complex. A secondary crack was found along the aft edge of the major break, which was created as a result of part of the hull dropping toward the seafloor. On the port side (western side) of the secondary crack are the remains of a set of trawl doors. The line that would have towed the trawl runs from the doors up and over the hull and is caught in the secondary crack (**Figure 4-8**).

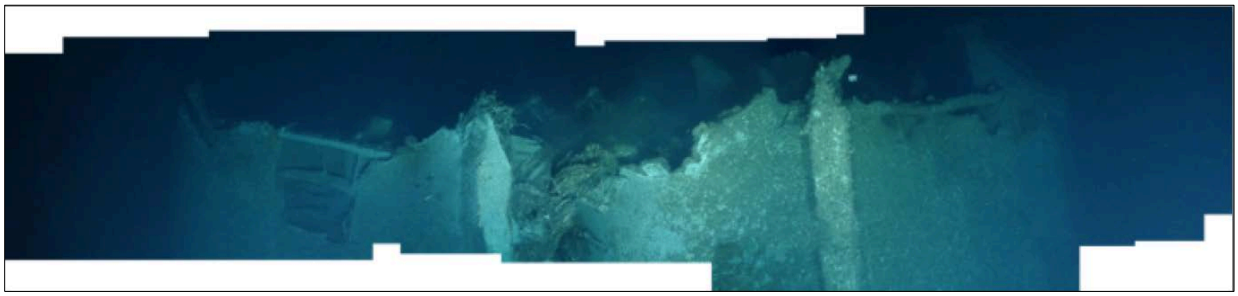

Figure 4-9. Forward edge of athwartships crack in the hull of *Ostfriesland.*

The midships section of the lower hull is largely intact. Forward of the crack, the lower hull is minimally impacted by fishing gear. The remains of the port and starboard bilge keels are readily apparent and well preserved as are through-hull fittings including the main strainers for salt intakes for the boilers. The strainer on the starboard side is missing, but the port strainer is still in place. The port and starboard, forward and aft side torpedo doors are all present (**Figure 4-10**)[292]. The armor belt is also largely intact, although it has started to separate from the lower hull in several places (**Figure 4-11**). Elsewhere along the run of the lower hull there are several relatively minor structural cracks.

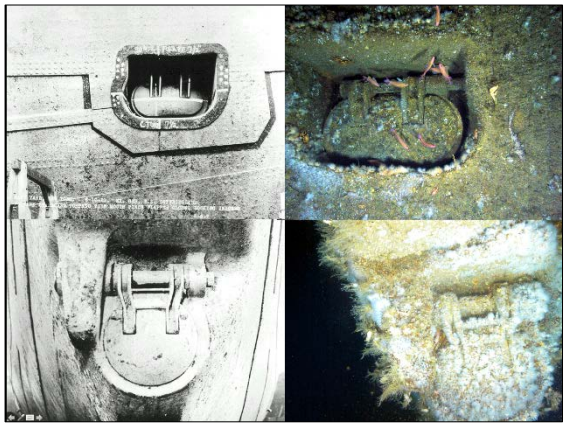

Figure 4-10. Historic images and on-site images of *Ostfriesland* port beam (upper images) and torpedo door in the bow (lower images).

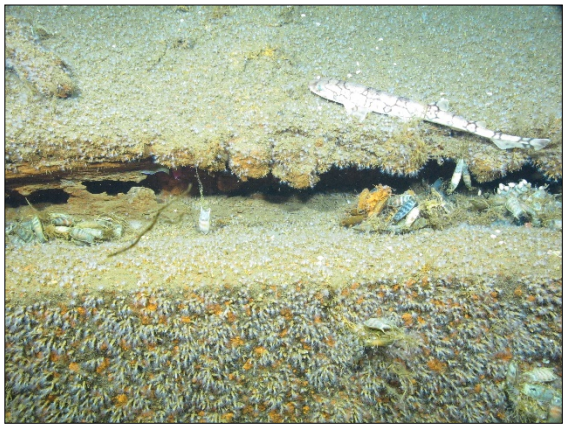

Figure 4-11. Upper edge of armor belt from *Ostfriesland*.

[292] "*Osfriesland*," Box 21, 19-A-9B; Album Prints of United States Ships, 1883-1941, Records of the Bureau of Ships, RG 19; National Archives, College Park, MD.

The forward section of the lower hull likewise is intact. The bow torpedo tube door is in place and in good condition. The prow of the vessel has suffered damage from fishing nets. A section of net is still attached, supported by fishing buoys. Adjacent to that is a section of fresh rust associated with a recent impact on the bow (**Figure 4-12**).

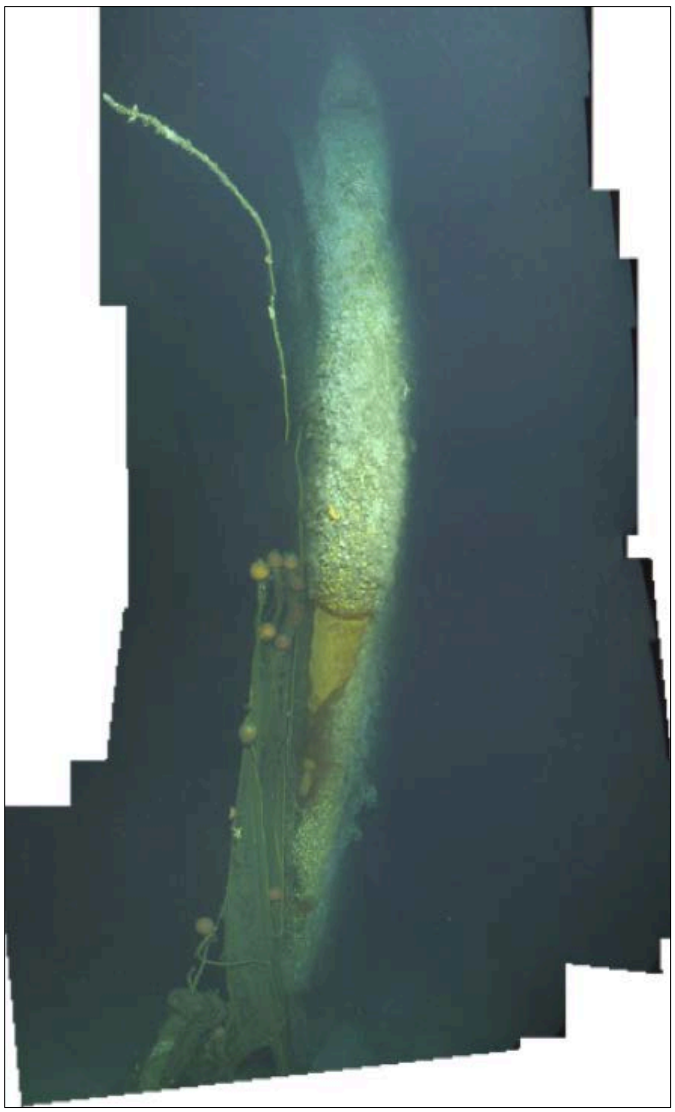

Figure 4-12. Inverted bow of the *Ostfriesland* showing net and impact damage on the prow and the forward torpedo tube door at the top of the image.

4.3.5.1.2 Guns and Superstructure

Observations of the guns and superstructure of *Ostfriesland* were difficult because the vessel rests on its six main gun turrets - keel up. The gun turrets, however, supported the hull sufficiently for some observations to be made of the remains between the main deck and the seafloor. Documentation and observations were facilitated by three additional factors: 1) a 2 m deep scour runs along the starboard side that allows some access; 2) there are several major breaches of the hull caused by bombing damage and site degradation, including a major rupture in the hull on the port side just aft of the bow; and 3) several features can be observed on the seafloor outside the hull.

The *Ostfriesland* preserves the full complement of weapons systems for a World War I German battleship—primary, secondary, and tertiary. Each of the 12 in gun turrets is visible by looking into a gap between the gun deck and seafloor on both sides of the vessel. In addition, each of the fourteen 5.9 in (15 cm) guns is in place and can be readily observed on the outside of the ship. All the torpedo doors (bow and stern; two on the starboard, and two on the port side) are present, observable, and intact. No evidence of anti-aircraft guns was found.

A considerable hole was found in the port side forward adjacent to the washrooms. A series of toilet bowls can be seen still attached to the iron sewage pipes (**Figure 4-13**). At least one urinal is present on the sand in this area (**Figure 4-14**), and the glass remains in many portholes (**Figure 4-15**). In addition, the remains of a mast of *Ostfriesland* are on the seafloor close to midships on the port side.

An anchor chain still runs out of one of the hawse pipes on the starboard side and runs a considerable distance off into the sand. There is no anchor chain running out of the port hawse pipe (**Figure 4-16**).

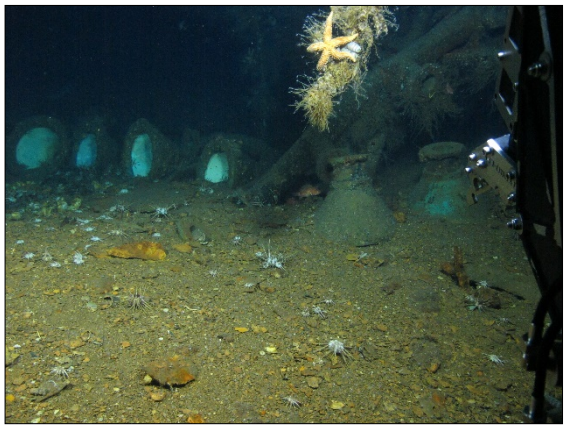

Figure 4-13. Latrines from *Ostfriesland*.

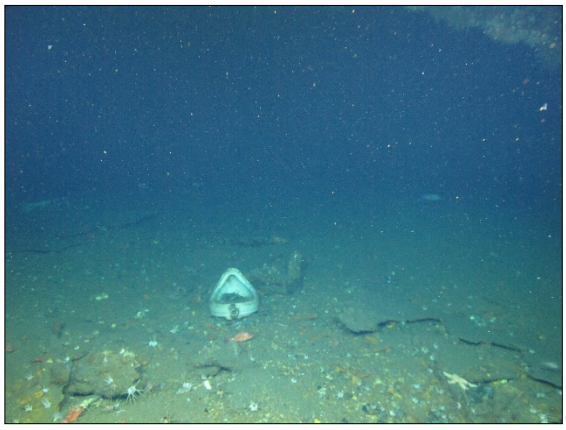

Figure 4-14. Urinal from *Ostfriesland*.

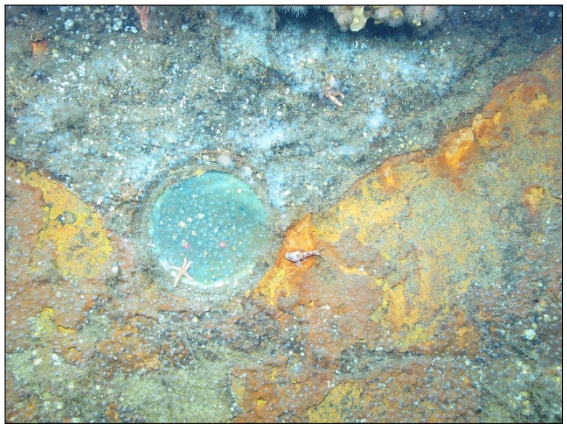

Figure 4-15. Port hole from *Ostfriesland*.

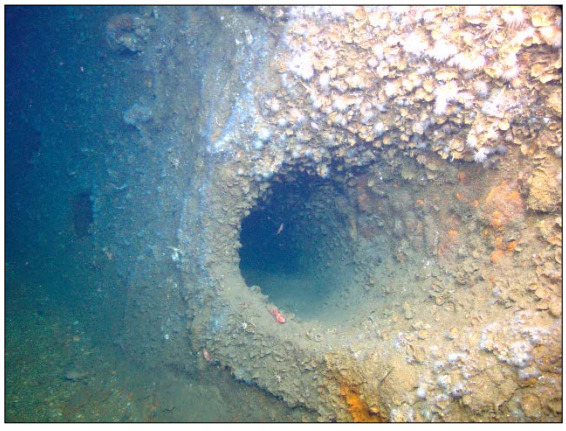

Figure 4-16. Port hawse pipe from *Ostfriesland*.

4.3.5.1.3 Anthropogenic Impacts

The lower hull of a World War I battleship was designed to withstand considerable impact. As with most wrecked battleships from this era, *Ostfriesland* turned turtle while sinking and came to rest on her gun turrets. The site and many of its inner features, therefore, are largely protected by the outer shell formed by the lower hull. Nevertheless, there is significant damage to the site. Some fishing gear and lines rest or are attached to the lower hull in several places. Fresh rust observed in the bow is most likely associated with the impact of fishing gear, but may be due to anchoring on the site. In addition, the major crack in the stern renders that part of the vessel vulnerable to further damage. The ship's rudders are exposed and have been impacted by fishing gear. In addition, a series of ruptures in the hull, most noticeably one in the port bow, has rendered some artifacts highly susceptible to looting, in particular those associated with the washrooms and latrines.

4.3.5.2 Frankfurt

The German cruiser *Frankfurt* was sunk as part of the Billy Mitchell-Project B experiments on 18 July 1921. The wreck was identified during a multibeam survey of the 2011 mapping cruise and was subsequently investigated using the ROVs *Kraken 2* and *Jason II* during the 2012 and 2013 sampling cruises respectively (NF-2012-ROV-24; RB-2013-J2-694). Site specifications and imagery of *Frankfurt* are shown in **Figure 4-17**[293].

The remains of *Frankfurt* lie in a northeast-southwest configuration with the stern to the north. A substantial scour is associated with the prevailing currents at the stern and along the port side. The bow of *Frankfurt* appears to have taken the brunt of the impact with the seafloor and is heavily damaged. This is indicated in the multibeam imagery and confirmed by on-site ROV investigations.

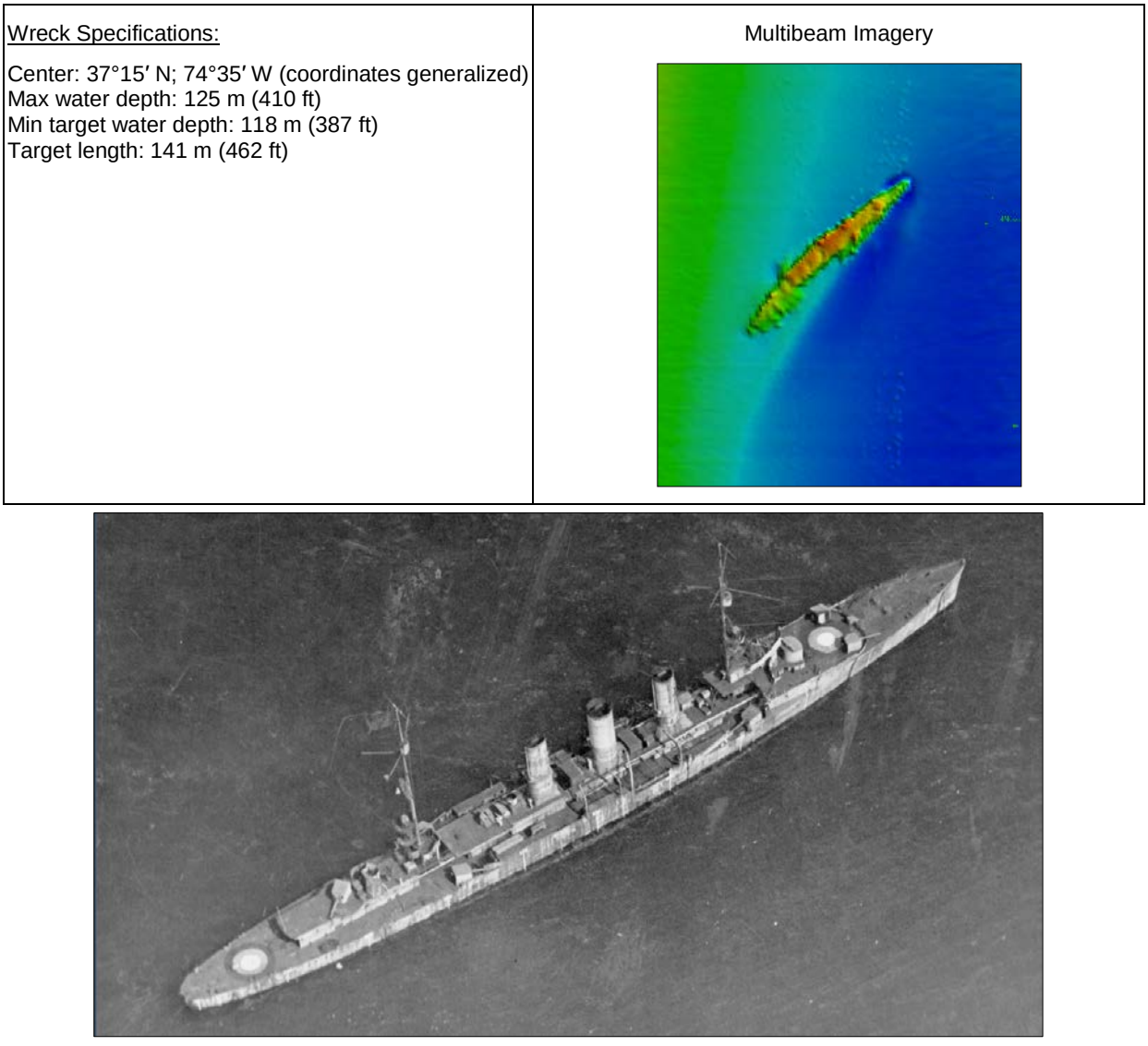

Figure 4-17. Site specifications and imagery for *Frankfurt.* Historic image shows *Frankfurt* just prior to her sinking.

[293] "The Ex-German Light Cruiser *Frankfurt*," Box 170, Folder 6; GU-U.S. Air Operations-Bombing Tests, Naval Aircraft Operations Flight, Air Stations; RCONRL, RG 45; National Archives, College Park, MD.

4.3.5.2.1 The Guns

Frankfurt's armament comprised eight 5.9 in (15 cm), two 3.46 in (8.8 cm) anti-aircraft guns, and four 20 in (50 cm) torpedo tubes. On-site investigations identified components of the main armament (the 5.9 in (15 cm) guns) and the torpedo tubes, but to date the remains of the anti-aircraft guns have been elusive. Historic imagery and footage indicate that these guns were present at the time of the vessel's sinking. The eight 5.9 in (15 cm) guns can be analyzed in terms of pairs: two in the bow (port and starboard guns), two just aft of the bridge (port and starboard guns), two aft of the three smoke stacks (port and starboard guns), and two in the stern (both on the centerline of the ship; one close to the fantail and the other slightly forward on a half deck). The observed configuration of these guns on the wreck of *Frankfurt* is as follows:

- The aftermost gun (i.e., on the fantail) was removed prior to sinking. The gun mount (pedestal) still survives and is *in situ*.
- The second stern gun on the centerline of the ship located on the half deck in the stern became displaced during the wrecking process and currently lies inside the wreck on the port side. The gun is resting on its starboard side with the muzzle pointing aft. The gun mount and part of the deck upon which the gun stood are still attached. The inside of the turret, including the breach of the gun and firing mechanisms, is clearly visible. During on-site investigations for the 2012 sampling cruise, the muzzle of this gun was resting on the remains of the half deck (**Figure 4-18**). During investigations for the 2013 sampling cruise, the muzzle was found to have fallen from the half deck and was resting farther down in the hull, still pointing aft. This indicates that processes of active site degradation were evident at the *Frankfurt*.

Figure 4-18. Muzzle of the 5.9 in (15 cm) gun toward the stern of *Frankfurt* with the turret in the background as observed during the 2012 sampling cruise.

- The port and starboard guns aft of the smoke stacks are the only pair of guns still in their original location. Each gun is resting on its mount, but in each case the surrounding superstructure is heavily degraded. Both guns are highly vulnerable to damage and collapse. At the time of sinking, the muzzles of both guns were likely pointing forward, but during the sinking process, the muzzles appear to have rotated somewhat and are currently facing close to aft.
- The port and starboard guns just aft of the bridge were both displaced as a result of the ship's sinking and subsequent site formation processes. The starboard gun has fallen down toward the bottom of the hull, with its muzzle pointed up in the water column. The aft face of the turret is orientated toward the seafloor, with the top and port side of the turret pointing forward toward the bow. The port gun is also displaced. It lies on its port side with the muzzle facing forward. Part of the gun's breach is visible, but the turret itself is partly covered by the remains of the foremast, which has collapsed and come to rest running athwartships. The gun mount is still attached to the turret.
- The impact of *Frankfurt*'s bow with the seafloor displaced the port and starboard guns in that part of the ship. The port gun lies on the seafloor toward the outer edge of the debris field. It lies on its port side, with its gun mount still attached and its muzzle pointing forward. The starboard gun appears to be missing and must have fallen clear of the wreck as she sank.

4.3.5.2.2 The Bow

The starboard bow of *Frankfurt* still has some integrity, but the port side comprises a debris field with material scattered both inside and outside the original configuration of the hull. The debris field includes the remains of a capstan with a set of bits immediately outboard. Running forward from the capstan is a chain that also intersects with a small section of hull plating and a hawse pipe (the chain runs through the hawse pipe). A small, disarticulated section of the ship's prow is close to the hawse pipe. The capstan and bits are covered with fishing net and immediately aft of them are the remains of the port side gun turret. The turret rests on its port side with the muzzle pointing forward. It is still connected to its mount, which has likewise fallen on its port side. Aft of the turret, also in the debris field, are the remains of the ship's conning tower that was originally located immediately aft of *Frankfurt*'s bow guns.

The starboard bow of *Frankfurt* has greater integrity and includes a section of outer hull plating that has fallen inwards. Toward the forward end of that plating, the steel plates of the outer hull have been concertinaed as a result of the bow's impact with the seafloor. Along the run of the intact starboard hull plating there are a number of features, including the remains of the starboard bow torpedo tube door.

4.3.5.2.3 The Bridge Section

The section of *Frankfurt* in the vicinity of the bridge is heavily damaged. On either side of the hull is a gun. The muzzle of the starboard gun points straight up into the water column and the muzzle of the port gun points toward the bow. In between are two sections of the foremast, one running athwartships on the port side. The other section of the mast comprises the lower portion of the mast *in situ*. On the starboard side close to the gun turret is what appears to be part of the crow's nest or possibly a section of the bridge. Fishing gear was seen in this area suspended in the water column by floats.

4.3.5.2.4 Midships

The midships section of *Frankfurt* comprises the remains of the steam plant, the locations of the triple smoke stacks, the remains of the mainmast, and two guns. The hull in this section is relatively intact and is supported by the boilers and machinery. The boilers are not visible, except through holes in the deck and outer hull. There are several major breaches of the hull. One is associated with the central smoke

stack that provides access to the inner hull, and a second is associated with bomb damage on the port side where the hull has been blasted outward. This latter section has its own debris field outboard to port. A smaller debris field also is on the port side. Sections of the outer hull on both the port and starboard side have collapsed inward. The result of these site formation processes is a complex matrix of outer hull plating, steam pipes, electrical wire, smoke stack debris, deck, and steel frames. In addition, the remains of at least three davits that would have supported the ship's boats are visible.

Toward the aft end of the amidships section are the remains of port and starboard guns still *in situ*, with their muzzles pointing aft (the starboard gun points aft and slightly inboard). Both guns still sit on their pedestals/gun mounts, but most of the deck and outer hull are badly degraded in this area. In between the guns are the remains of the mainmast, the lower portion of which is still *in situ*. In addition, part of a major athwartships bulkhead and a matrix of fishing net extends into the water column, supported by floats.

4.3.5.2.5 The Stern

The stern of *Frankfurt* is the best preserved section of the wreck and is almost intact (**Figure 4-19**). The superstructure, deck, fairlead, and wire rope brackets on the aft section are well preserved. A substantial scour is visible at the stern of *Frankfurt* on both sides of the hull rendering the rudder, prop shafts, propeller shaft brackets, and bearings all exposed. The propellers, however, are not present. Historical evidence suggests they were removed before the sinking. The stern of *Frankfurt* is relatively free from anthropogenic impacts, although some fishing net is present on port propeller hub and along several sections of the port and starboard side. The deck in the fantail is largely intact, although several plates are missing on the starboard side. Slightly forward of the fantail on the starboard side, the vessel is damaged, and part of the deck has fallen outboard. The port side is likewise damaged, and the outer hull plating is missing or has fallen off. The aftermost gun mount, located on the centerline of the ship in the fantail, is still present, but the turret itself is missing (the turret was removed before the sinking). Immediately forward of this gun mount is a substantial section of the half deck that supported the second gun turret at the stern of *Frankfurt*, again on the centerline of the vessel. This gun, however, has fallen to port and rests on its starboard side. The gun mount is still attached to the turret and the gun's muzzle is pointed toward the stern. Fresh rust was visible in this part of the hull in 2013, and the muzzle of the gun had slipped from the position it was in in 2012. A matrix of wire rope is visible on the starboard side of the half deck.

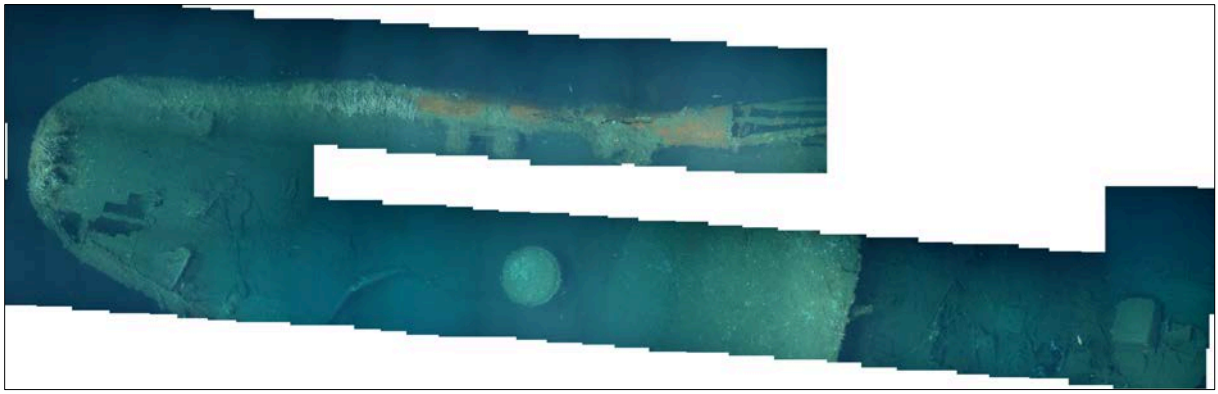

Figure 4-19. The stern of *Frankfurt* showing the fantail, fairlead, aftermost gun mount, and half deck.

Forward of the half deck, *Frankfurt* has suffered more extensive damage. This is likely a combination of bombing damage from the Project B experiments and site degradation. The sides of the ship have suffered greater damage in this area and the deck has collapsed to a greater extent than in the fantail. The remains of a water tank are visible along with a bathroom sink.

4.3.5.2.6 Anthropogenic Impacts

Frankfurt is both one of the best preserved ex-German warships associated with the Billy Mitchell-Project B experiments, but also the most vulnerable. The stern of the ship is almost entirely intact, yet there is evidence of ongoing collapse and active degradation. The wreck has suffered moderate impacts from fishing gear, most notably in the bow, just forward of the stern where net is suspended in the water column and the port propeller hub. *Frankfurt* requires immediate attention and further documentation and study.

4.3.5.3 G-102

The destroyer *G-102* was sunk as part of the Billy Mitchell-Project B air bombing experiments on 13 July 1921. The wreck was identified during a multibeam survey for the 2011 mapping cruise and was subsequently investigated using the ROVs *Kraken 2* and *Jason II* in 2012 and 2013, respectively (NF-2012-ROV-26; RB-2013-J2-692). Site specifications and imagery of the *G-102* are shown in **Figure 4-20**[294].

Wreck Specifications:

Center: 37°10′ N; 74°35′ W – coordinates generalized
Max water depth: 105 m (344 ft)
Min target water depth: 102 m (334 ft)
Target length: 301 m (462 ft)

Figure 4-20. Site specifications and imagery for the *G-102*. Historic image shows the *G-102* just prior to her sinking.

4.3.5.3.1 Hull and Machinery

The historic film footage of the bombing of the *G-102* (commissioned by General Mitchell) shows a series of explosions, one on the port bow, one on the port stern, and one close to midships on the starboard side. The film and contemporary documents suggest that a 300 lb bomb was then dropped and fell into the forward smokestack of the ship. Following a further series of explosions, the vessel sunk by the bow. The stern became vertical as the vessel went down.

The remains of the *G-102* are consistent with the video and written accounts of the vessel's loss. The hull sits on the seafloor in a north-south configuration. The ship's bow suffered considerable damage during the bombing action and then took the full force of the impact with the seafloor. As a result, the *G-102*'s bow is almost completely destroyed. Parts of the hawse pipes remain and there is a debris field associated with the bow, but the hull structure is generally disarticulated. Hull plating concertinaed at the bow is evidence of the severity of the impact of the ship with the seafloor. The *G-102*'s bridge became

[294] "Destroyer *G-102*," Box 170, Folder 6; GU-U.S. Air Operations-Bombing Tests, Naval Aircraft Operations Flight, Air Stations; RCONRL, RG 45; National Archives, College Park, MD.

dislodged during sinking and broke into multiple parts. The main section came to rest on its port side close to its original position. Inside the bridge, a series of windows from the parabolic windshield are visible along with the ship's telegraph, binnacle, and steering control system (**Figure 4-21**).

Figure 4-21. Bridge of the *G-102*.

Evidence of an implosion at the site is consistent with film footage and accounts of the sinking, including ductwork that appears to have been drawn in by a vacuum. Bomb damage also is evident, particularly aft of midships on the starboard side where the gunnel has been blown outward. Across the site, there is piping associated with the ship's steam, fuel, water, and sewage systems. A matrix of electrical cable also is visible. Parts of the deck and its associated features have collapsed downward and are present on the site.

Although plans and machinery specifications for early 20th century destroyers are rare, the archaeological evidence from the site of the *G-102* is revealing. Site investigations showed the presence of three 3-drum, oil-fired, water tube boilers, which produced steam that drove two high-pressure low-pressure (and perhaps cruising) steam turbines. The turbines turned two screw propellers. The boilers are arranged sequentially along the centerline of the ship. Three-drum boilers comprise two water drums at the base and a steam drum at the top in a pyramid arrangement. Along the sides of the boiler are water tubes with the oil-fired furnace in the middle. The first of the boilers on the *G-102* is located immediately aft of the remains of the bridge (**Figure 4-22**). The steam drum is in place, but its forward end has dropped down into the base of the furnace. The second boiler is immediately aft of the first and is the best preserved of the three. The steam drum is in place, although many water tubes on either side have become degraded. A space between the second and third boiler is occupied by part of the deck, which has collapsed downward into the lower hull. The third boiler is the most degraded; the steam drum became dislodged during the sinking process and came to rest on the port side the ship adjacent to boiler 1. The remains of one of the ship's telegraphs are present on the floor of one of the boiler rooms.

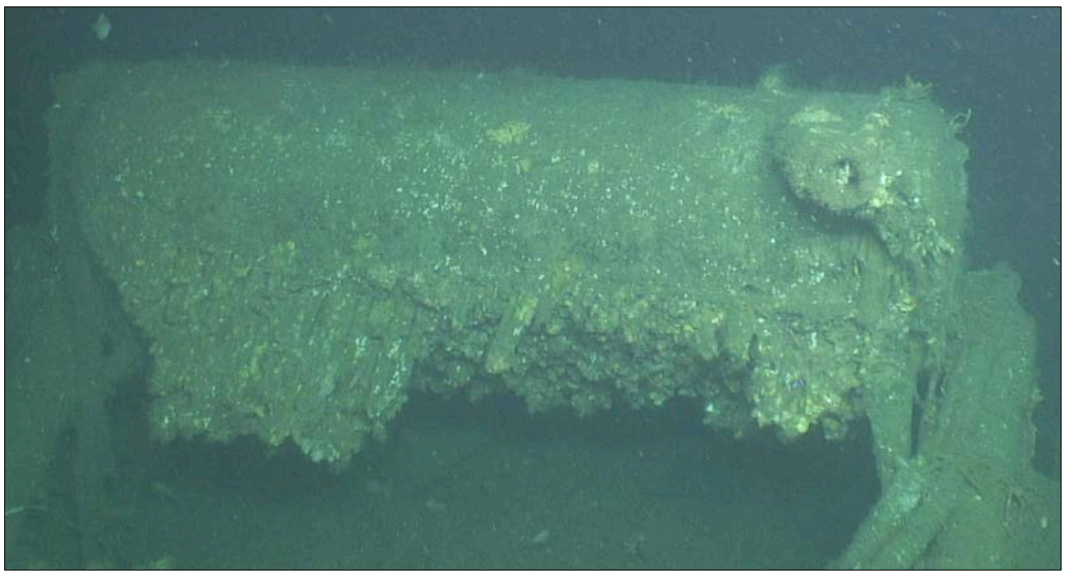

Figure 4-22. The remains of an oil-fired water tube boiler from the *G-102*.

The *G-102*'s steam turbines are arranged in staggered fashion with the starboard turbine farther forward in the ship than the port turbine. The turbines comprise small high-pressure and large low-pressure units with reduction gears in between. Inboard of each turbine, close to the centerline of the ship, is a condenser. Looking at the two turbines from toward the stern of the ship reveals that the port turbine high-pressure unit is farthest aft. Moving forward is the port low-pressure turbine and a condenser to its starboard on the centerline of the ship. Almost immediately adjacent to that condenser is the starboard high-pressure turbine and forward of that is the starboard low-pressure turbine. To port of the starboard low-pressure turbine is its condenser. Each turbine-condenser combination has an associated circulating pump.

The only intact part of the *G-102* is the ship's stern, which rests on the seafloor listing approximately 10° to 15° to port (**Figure 4-23**). The fantail is relatively intact (**Figure 4-24**). Although the propellers are missing, the propeller shafts are visible at various points along the run of the aftermost part of the ship. The propeller shaft bracket and bearing are present on the starboard side, but are not visible on the port side. This is, in part, due to the port list of the vessel's stern. Part of the propeller guard that sat outboard of the ship, however, is still present and visible on the port side. The propeller guard is missing on the starboard side (**Figure 4-25**).

Figure 4-23. Stern of the *G-102.*

SS

Figure 4-24. Fantail of the *G-102* showing fishing net on starboard side.

Figure 4-25. Starboard propeller hub, brace, and shaft of the *G-102*.

The deckhouse toward the stern of the ship is no longer present, and the ship's hull has collapsed from that point forward, but the provisioning and store rooms that sat underneath where the deckhouse stood are still extant. Forward on the starboard side of that feature is an open doorway with a ladder on the forward wall. On the port side the door is farther aft and, unlike the starboard side door opening, there is a hinged door still in place. The gun that would have been present on top of the deckhouse in the stern was not present when the vessel was sunk.

Slightly forward of the stern, the port side of the ship has collapsed inward and part of the decking sits on top of it. There is a set of bits and a sink bowl in this area along with a section of the port side with porthole windows still in place.

4.3.5.3.2 Anthropogenic Impacts

The remains of the *G-102* have been considerably damaged by site formation processes, including the bombing of the vessel, the ship's impact with the seafloor, natural degradation over time, and anthropogenic impacts from fishing gear and ground tackle (**Figure 4-26**). The damage from fishing gear is highly evident and severely detrimental to the archaeological integrity of the site (**Figure 4-27**). While the stern is generally intact, the starboard quarter is covered in fishing net. This includes two columns of net attached to floats that sit in the water column on the starboard stern. Moving forward on the starboard side, fishing gear has torn into the bulwark. There are also patches of fresh corrosion on the starboard side and elsewhere caused either by fishing gear or ground tackle from possible anchoring on the site.
A fishing trawl also has hit the port side of the vessel just forward of the stern pulling part of the hull inboard. An oval shaped trawl door is visible on the site just aft of the port turbine.

Figure 4-26. Bomb damage on the port side stern of the *G-102*.

Figure 4-27. Fishing gear damage to the *G-102.*

4.3.5.4 V-43

The destroyer *V-43* was sunk on 15 July 1921 by fire from surface ships as part of the Billy Mitchell-Project B experiments. The wreck was identified during a multibeam survey for the 2011 mapping cruise and was subsequently investigated using the ROVs *Kraken 2* and *Jason II* in 2012 and 2013 respectively (NF-2012-ROV-27 pt1; J2-695). Site specifications and imagery of the *V-43* are shown in **Figure 4-28**[295]. The identification of the site as *V-43* rather than the *S-132* was made largely through historical records. It is known that the *V-43* was anchored south of the *S-132*.

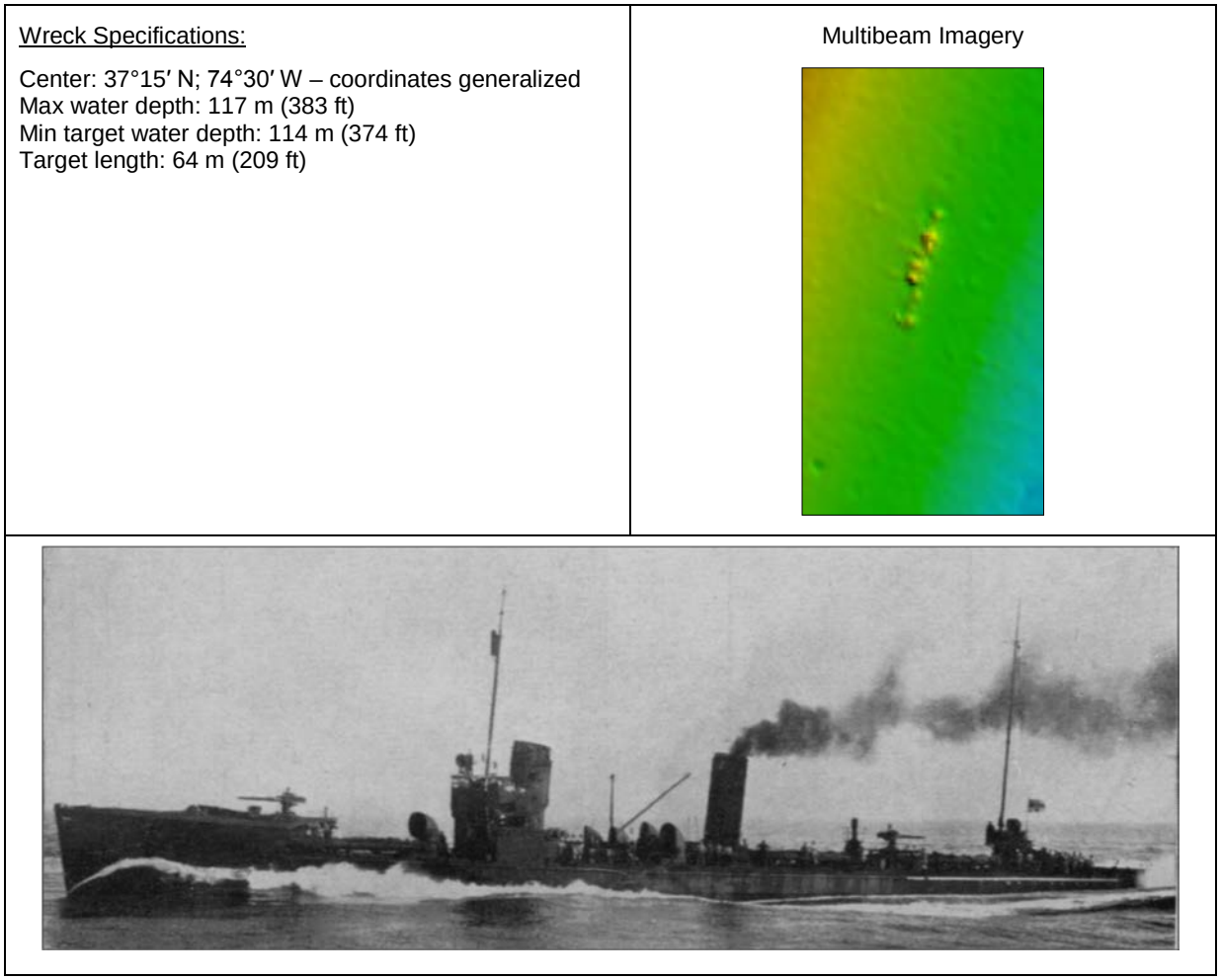

Figure 4-28. Site specifications and imagery for the *V-43.*

4.3.5.4.1 Hull and Machinery

Historic accounts of the sinking of the *V-43* indicate that U.S. Navy destroyers *Leary* and *Herbert* inflicted damage to the vessel's bridge and port side.[296] Subsequently, an attack from the battleship USS *Florida* resulted in ten hits from 5 in guns on the starboard side of the *V-43*. The ex-German warship then sank by the bow.

[295] "German Destroyer *V-43*," H.M. Le Fleming, *Warships or World War I* (London: I. Allan Ltd, 1962), 195.

[296] See **Section 4.2.3.9** for citations.

The remains of the *V-43* sit on the seafloor in water depth of approximately 64 m in a north-south configuration with the stern to the south. The ship's bow is badly degraded. There is some evidence of bits, hawse pipes, and chain, but the vessel's bow is generally disarticulated and covered with fishing net. There are no substantial intact elements of the ship's bridge. Along the run of the hull both the port and starboard bulwarks have collapsed downward or inward in multiple areas and the sides of the ship have been heavily impacted by fishing gear (**Figure 4-29**). While the bridge and sides of the ship are severely degraded, the machinery is well preserved, better preserved in fact than the machinery on the destroyer *G-102*.

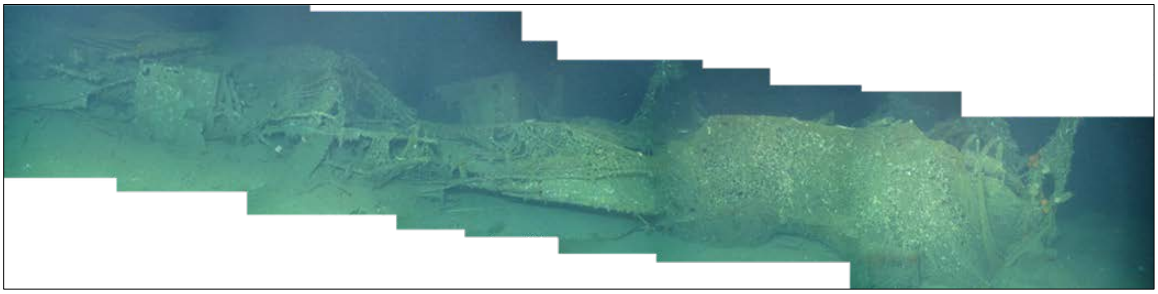

Figure 4-29. Photomosaic of the port side of the *V-43.*

The exact arrangement of the boilers, turbines, and condensers is difficult to discern from historical sources available in the United States, but the archaeological evidence is clear. Site investigations showed that the *V-43* was propelled by three 3-drum, oil-fired, water tube boilers, which produced steam that drove two high-pressure low-pressure combination steam turbines. Each turbine turned a screw propeller. The three-drum boilers comprise two water drums at the base and a steam drum at the top in a pyramid arrangement. Along the sides of the boiler are water tubes with the oil-fired furnace in the middle. The first of the boilers is located on the centerline of the ship immediately aft of the original location of the bridge. Although part of the outer casing of the boiler is missing, the boiler is well preserved with the furnace, water tubes, and drums still in place. Smoke from the boiler was ventilated via the forward of two smoke stacks. Aft of the first boiler are two more identical boilers sitting side-by-side (**Figure 4-30**). The uptakes from these boilers were trunked into the aftermost of the vessel's two smoke stacks. Aft of the second and third boilers are two high-pressure low-pressure combination geared steam turbines, one on the port side and one on the starboard side. Each of these turned a propeller shaft. Inboard of these shafts and just aft of the turbines were port and starboard condensers servicing their respective turbines. The pumps for the condensers were likely outboard of each unit.

Figure 4-30. Side-by-side boilers 2 and 3 of the *V-43*.

The *V-43*'s stern has been heavily impacted by fishing gear and is almost completely encased with net. Part of the ship's depth charge launching gear appears to be present. In addition, the port shaft, shaft bracket, and propeller bearing are visible through the fishing net. The propellers are not present and neither is evidence of the propeller guards. The port shaft can also be traced all the way from the bearing to the high-pressure port turbine (**Figure 4-31**). The lower part of the after deckhouse, which appears to have accommodated a washroom, storeroom, and workshop, is still mostly intact in the stern, although it has become dislodged and is rotated 90° to starboard (**Figure 4-32**). The glass in the portholes of the deckhouse is no longer present. A doorway allows for views inside that reveal piping. Close by, resting on the forward face of the condensers, are the remains of one of the ships gun mounts (**Figure 4-33**). No guns were fitted to the ship when she was sunk. Also present are what appear to be the partial remains of a mast. Two sinks near one of the boilers can be seen under fishing net.

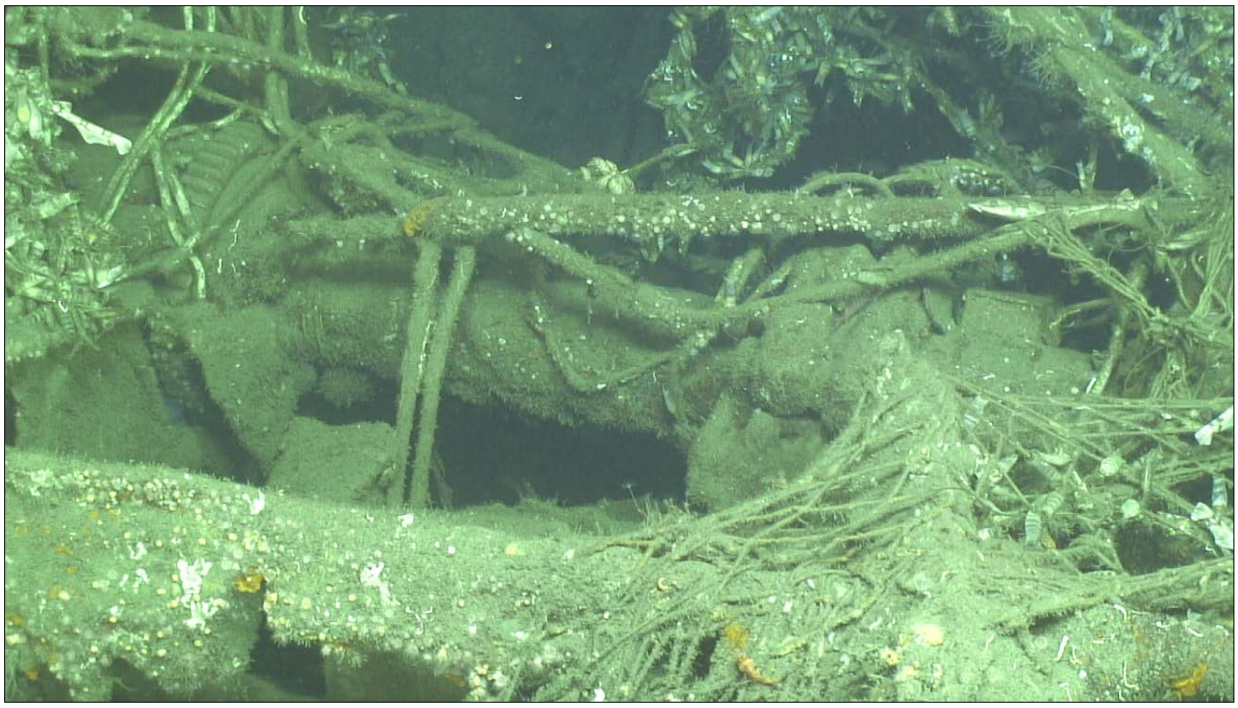

Figure 4-31. Port propeller shaft connection to turbine.

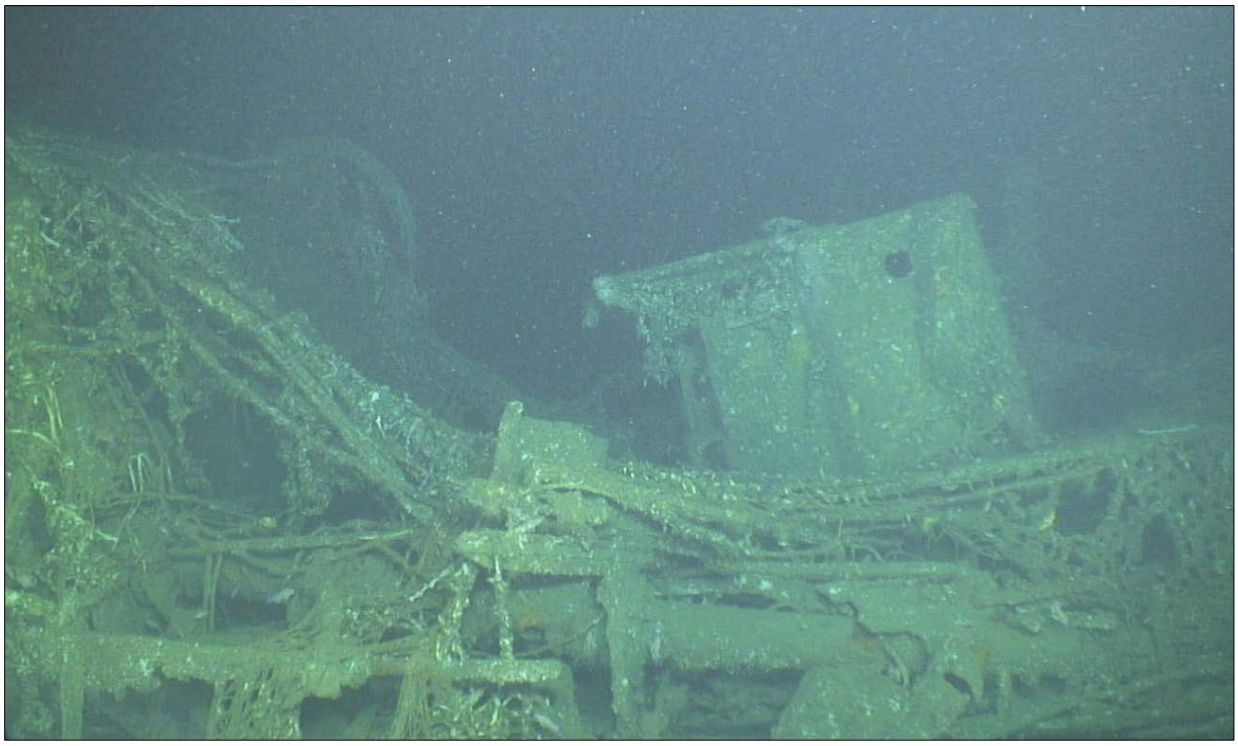

Figure 4-32. After deck house turned 90° to starboard and port propeller shaft in the foreground.

Figure 4-33. *V-43* condensers and gun mount resting on their forward edge.

4.3.5.4.2 Anthropogenic Impacts

The remains of the *V-43* have been considerably damaged by various site formation processes, including shell fire from surface ships; the ship's impact with the seafloor; natural degradation over time; and anthropogenic impacts from fishing gear, ground tackle, and possibly diver visitation. The *V-43* has suffered extensive damage from fishing nets. The stern is almost completely encased in fishing net as are many other parts of the wreck. Clumps of fishing net on the stern supported by floats extend into the water column (**Figure 4-34**). They also run off along the seafloor on the starboard side in the stern. The remains of the after deckhouse have some net damage, while the remains of the *V-43*'s bow are also heavily impacted. The internal machinery spaces have suffered less damage and the boilers, in particular, are well preserved. Portholes and glass has been removed from the aft deckhouse.

Figure 4-34. The stern of the *V-43* showing the impact of fishing net on the site.

4.3.5.5 S-132

The destroyer *S-132* was sunk on 15 July 1921 by fire from surface ships as part of the Billy Mitchell-Project B experiments. The wreck was identified during a multibeam survey for the 2011 mapping cruise and was subsequently investigated using the ROV *Kraken 2* in 2012. Site investigations of the *S-132* were cut short due to shortage of time and logistical difficulties experienced during the 2012 sampling cruise (NF-2012-ROV-27 pt.2). Site specifications and imagery of the *S-132* are shown in **Figure 4-35**[297]. The identification of the site as *S-132* rather than the *V-43* was made largely through historical records. It is known that the *S-132* was anchored north of the *V-43*.

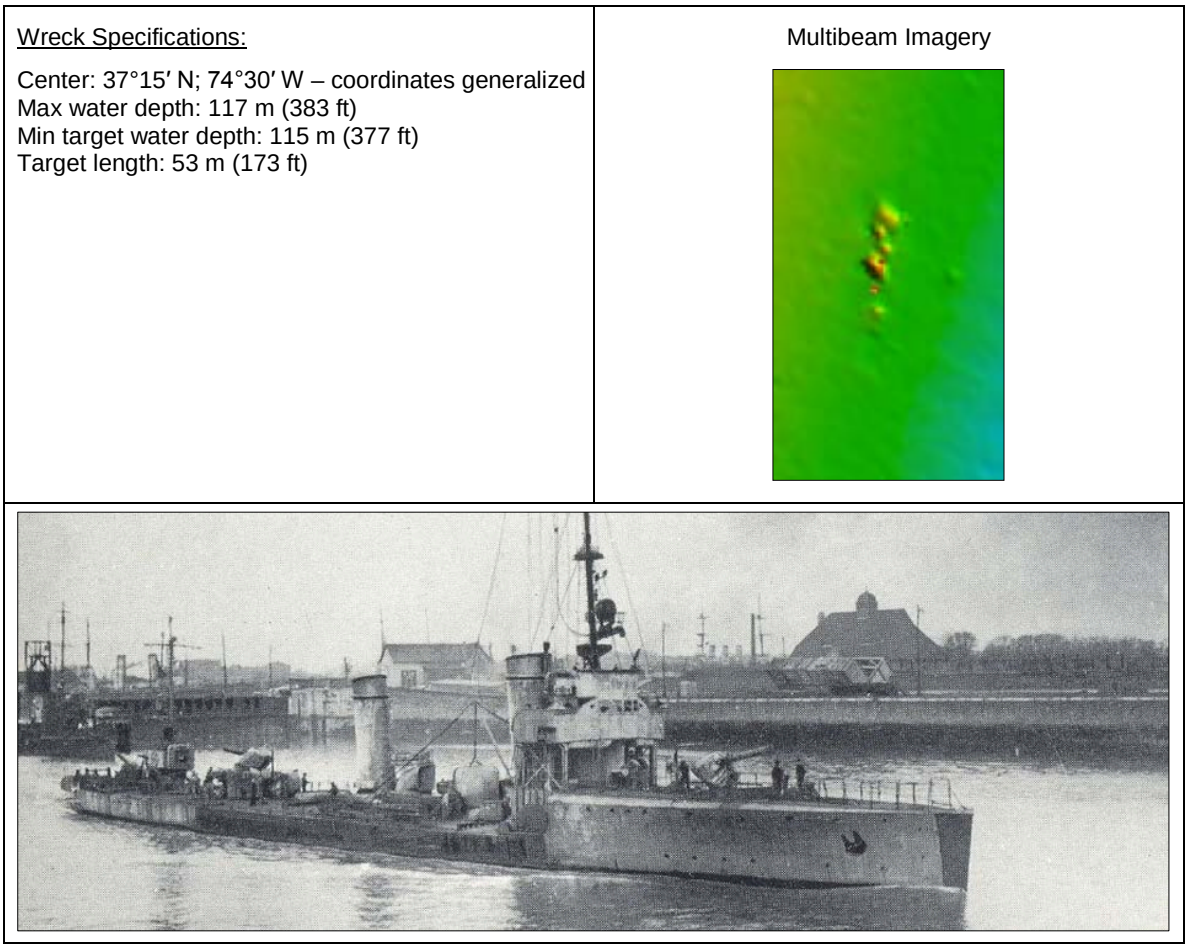

Figure 4-35. Site specifications and imagery for the *S-132*. Historic picture depicts the destroyer *S-139*, a vessel identical in design to the *S-132.*

4.3.5.5.1 Hull and Machinery

Historic accounts of the sinking of the *S-132* indicate that the U.S. Navy destroyers *Leary* and *Herbert* scored six hits on her starboard side including one on the bridge, another at the forward stack, a third close to the waterline of the fire room and engine room, and a fourth above the waterline aft.[298] After

[297] "*S-139* (Grosse Torpedoboot Mob 1916)," http://forum.ioh.pl/viewtopic.php?p=204783, Website accessed 9 September 2016.

[298] See **Section 4.2.3.9** for citations.

that, the battleship USS *Delaware* opened fire scoring 13 hits on the vessel's starboard side. The *S-132* rolled a little to starboard and sank by the stern.

The remains of the *S-132* sit on the seafloor in water depth of approximately 53 m in a north-south configuration with the stern to the north. The ship's bridge, stem, and stern are badly degraded, having suffered extensive damage from the original assault, subsequent sinking, and commercial fishing. In the bow, there is some debris associated with the ship's bridge. This debris extends some way into the water column, but it is covered in fishing net. Although the bow has collapsed and is disarticulated in the stem, some structure remains, particularly on the starboard side.

Unlike the other destroyers sunk as part of the Billy Mitchell-Project B experiments, the midships section of the *S-132* is relatively intact. A substantial portion of the ship's deck still survives *in situ*, including deck features, hatches, davit supports, and through deck fittings. The machinery, particularly the ship's boilers, has supported the central part of the ship and is still *in situ*. Openings in the deck for smoke stacks, ventilation flues, and hatches provide access points allowing inspection of the machinery and boiler spaces, but the exact configuration of the propulsion plant cannot be fully determined. It appears that the first boiler on the centerline of the ship is immediately aft of the bridge. An opening for the forward smoke stack immediately aft of that boiler and cracks in the deck above it shows that the unit is still intact. The boiler appears to be a three-drum, oil-fired, water tube unit like the ones present on the *V-43* and *G-102*.

Immediately aft of the opening for the smoke stack is a small round hatch in the deck, which provided airlock access. The hatch cover is missing. Inside the hull on the aftermost wall leading to that hatch is a ladder (**Figure 4-36**). The deck is fairly intact moving aft of the hatch, but approximately 20 ft toward the stern there is a second hatch and a second opening for a smoke stack. The hatch was accessed by a ladder, which is still *in situ* on the forward edge of the opening. The hatch cover is missing. The opening for the second smoke stack is similar to the first. While the intact deck surrounding this opening obscures full views of the machinery, it appears that two boilers sitting side-by-side occupy the space immediately aft of the opening for the second smoke stack. This configuration is similar to the boilers of the *V-43*. The condition and location of the boilers can be seen because the hull plating is missing on both the port and starboard sides of the ship. In addition, the absence or degradation of the outer hull plating allows for observation of internal machinery as well as the framing pattern (**Figure 4-37**).

The starboard side of the wreck aft of the bridge is less intact that than the port side. This is consistent with accounts of the sinking, which suggest that the vessel's starboard side took the brunt of the naval shelling. Several holes in the hull on both the port and starboard side reveal ballast bricks stacked between the frames, in many cases still *in situ* (**Figure 4-38**). One of these was recovered during investigations of the wreck in 2012. Some of the bricks are fashioned to lock into one another. The brick that was recovered has the initials KMS, representing Kaiserliche Marine (Schiffe)—German Imperial Navy Ship—stamped into it (**Figure 4-39**).

Figure 4-36. Forward hatch and stack opening on the *S-132*.

Figure 4-37. Port side frames on the *S-132.*

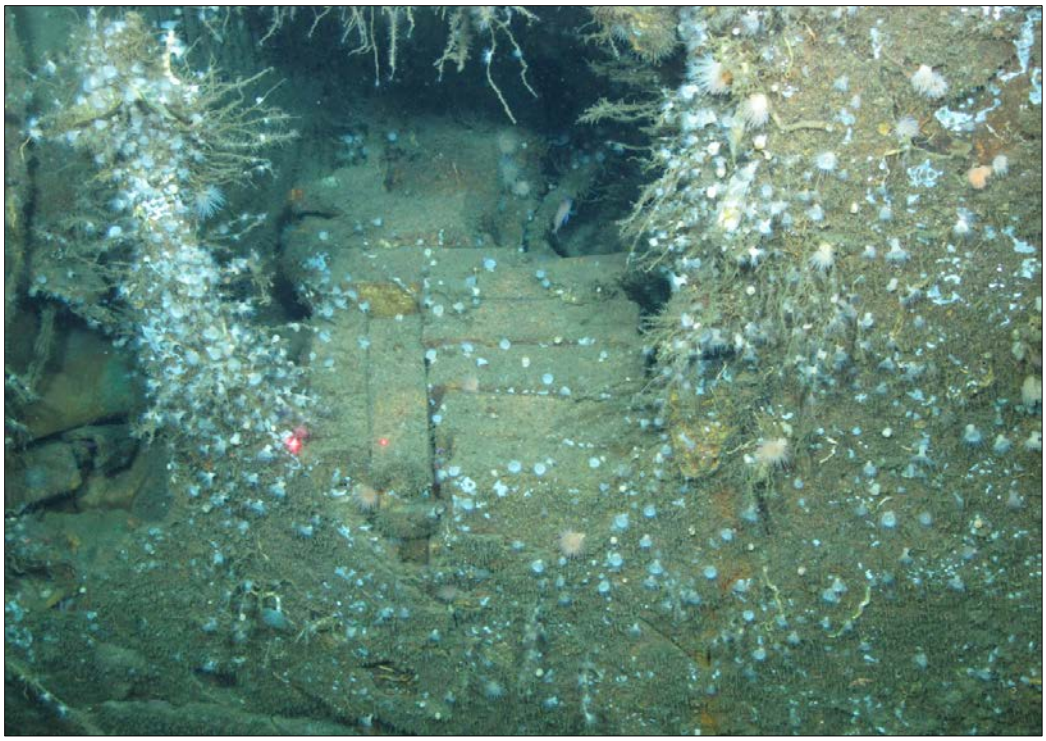

Figure 4-38. Breach in the hull on the port side port side of the *S-132* showing stacked ballast bricks.

Figure 4-39. Ballast brick recovered from the destroyer *S-132* during Leg 3 of the 2012 sampling cruise.

The stern of the *S-132* is mostly disarticulated. The remains of the ship's turbines and condensers are present, but determining their exact arrangement was not possible due to lack of time on the wreck in 2012 (two wrecks had to be investigated in one dive) and the presence of a dense mat of fishing net. It is clear, however, that the condensers are aft of the turbines and seem to be the same configuration and type as on the *V-43*, that is with the condensers side-by-side aft and slightly inboard of the turbines. The starboard turbine is more exposed than the port turbine (**Figure 4-40**). In general, the structure of the machinery and its arrangement on the *S-132* is similar to that of the *V-43*. Other features include part of a mast outside the hull in the stern on the port side, what appears to be part of a fuel oil gauge in the stern, a gun mount on the starboard side near the stern, and a matrix of piping and electrical cable.

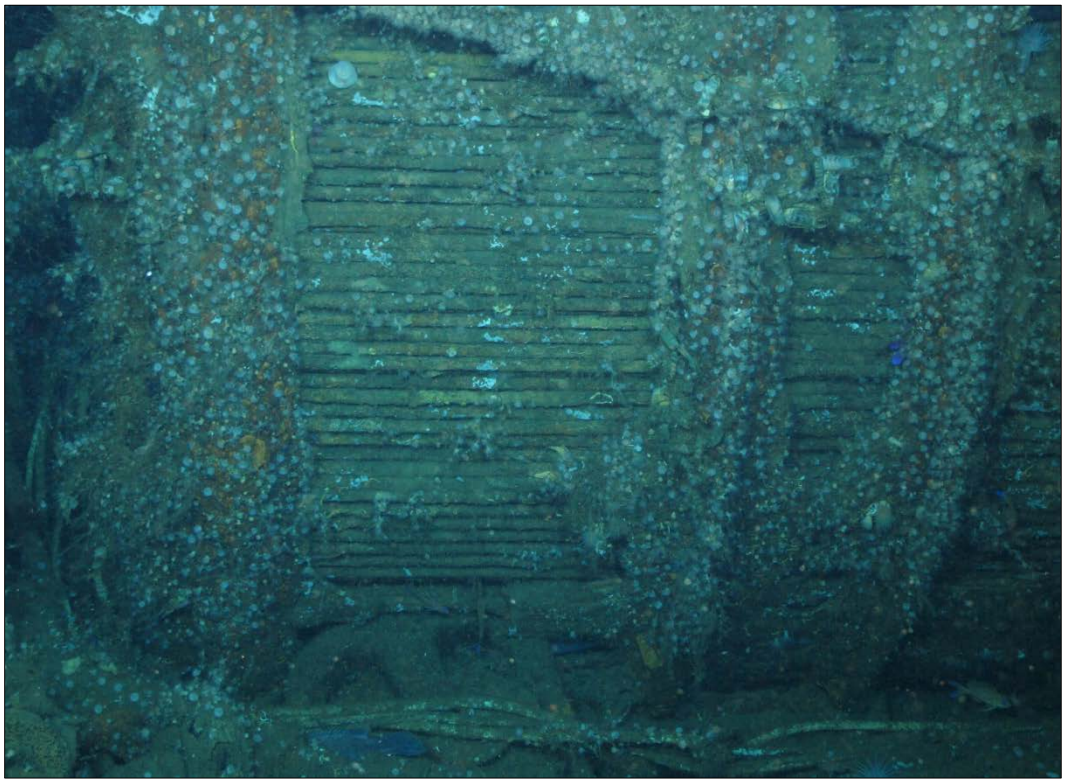

Figure 4-40. Starboard condenser on the *S-132*.

4.3.5.5.2 Anthropogenic Impacts

The remains of the *S-132* have been considerably damaged by various site formation processes, including shell fire from surface ships, the ship's impact with the seafloor, natural degradation over time, and impacts from fishing gear and ground tackle. Though the damage from fishing gear is substantial in the bow (including the bridge location) and the stern, the midships section of the ship has survived relatively well. The starboard side aft of the bridge has suffered more damage than the port side, but that pattern is reversed forward of the bridge where the starboard side is slightly better preserved than the port side. Nevertheless, substantial portions of the deck and sides of the ship are still in place. Some fishing gear midships has impacted the forward part of the surviving deck. Fresh corrosion in the area was caused by the impact of fishing gear or ground tackle on the hull. A thick blanket of fishing net and tackle is present in the stern. This is particularly evident on the port side where the net runs out from the wreck along the seafloor. A substantial column of fishing net supported by commercial fishing floats is on the starboard side around midships. Extensive recreational fishing is evident at the site, including line and a lighted lure that was still flashing when the vessel was investigated in 2012.

4.3.5.6 UB-148

The submarine *UB-148* was sunk on 22 June 1921 by fire from USS *Sicard* as part of the Billy Mitchell-Project B experiments. The University of Rhode Island identified the wreck in 2006 during a multibeam and side-scan sonar survey. The site was investigated using the ROV *Kraken 2* during the 2012 mapping cruise (NF-2012-ROV-22-UB-148 pt. 1). Site specifications and imagery of the *UB-148* are shown in **Figure 4-41**[299].

<u>Wreck Specifications:</u>

Center: 37°10′ N; 74°45′ W – coordinates generalized
Max water depth: 90 m (295 ft)
Min target water depth: 80 m (262 ft)
Target length: 45 m (147 ft)

Multibeam Imagery

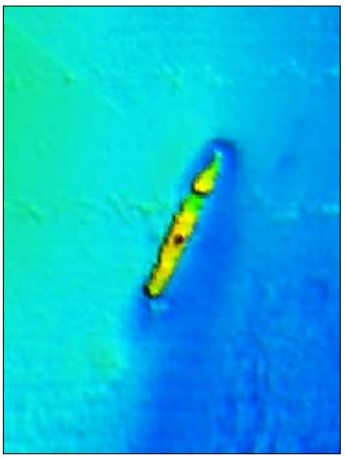

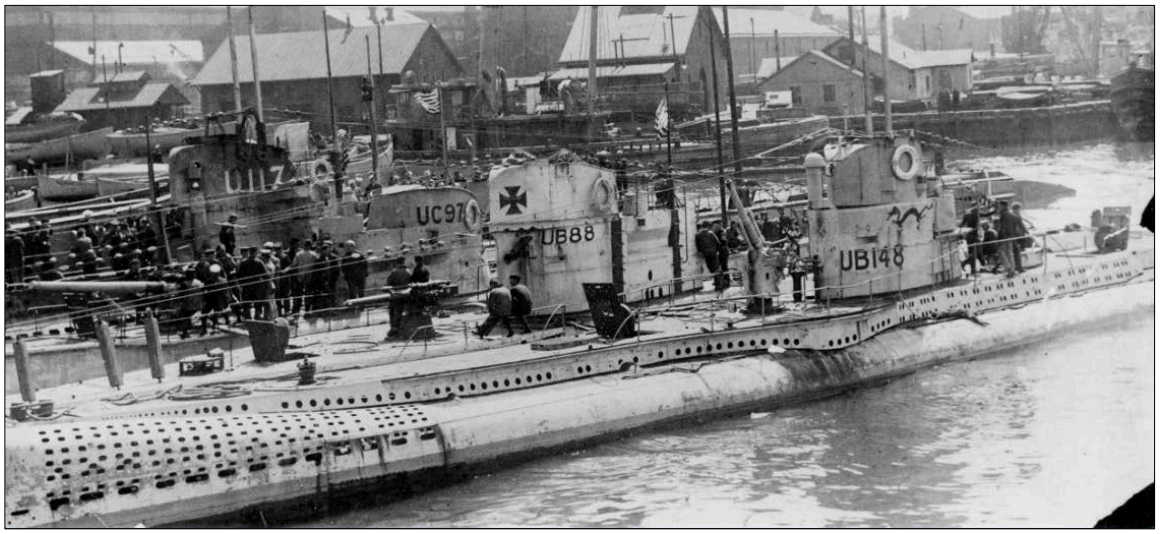

Figure 4-41. Site specifications and imagery for the *UB-148*. Historic image shows *UB-148* prior to her sinking.

[299] "U-*117*, *UC-97*, *UB-88* & *UB-148*," NavSource Online: Submarine Photo Archive, http://navsource.org/archives/08/500/0843206.jpg. Website accessed 9 September 2016.

4.3.5.6.1 Hull, Machinery, and Weapons

On-site documentation of the *UB-148* was extremely limited. The project team had the opportunity to visit the site on one occasion and was able to conduct only a brief overall reconnaissance of the wreck. Evidence suggest that the *UB-148* was sunk as a result of shell fire striking the ship just forward of the stern, but the vessel was also hit forward of the conning tower on the starboard side.

The remains of the *UB-148* sit on the seafloor in water depth of approximately 45 m in a north-northeast, south-southwest configuration, with the bow to the south. Multibeam data show a substantial scour on the port side of the ship and significant damage to the hull in a section midway between the conning tower and the stern. On-site investigations revealed that the outer hull is intact in some parts of the wreck and degraded in others. The outer hull is missing in several areas along the run of the hull, but the pressure hull is intact.

The bow of the *UB-148* is encased in commercial fishing net, part of which extends into the water column and is supported by a buoy. The remains of the forward torpedo tubes are present with the doors closed (**Figure 4-42**). Part of the wooden deck is also still present in the bow. There are also a series of high-pressure air flasks in the bow, some of which are displaced and lying in the sand on the port side while others are still in place on the hull.

Figure 4-42. Bow caps for torpedo tubes on the *UB-148*.

Just aft of the bow on the starboard and port sides, there is a section where the outer hull is missing, but the pressure hull is intact. The starboard side is more damaged than the port side in this regard. This area is significantly impacted by commercial fishing gear. The torpedo-loading hatch is located in this area as are the remains of the submarine's 10.5 cm (4.13 in) gun mount. These features are immediately forward of the conning tower.

As with all the submarines sunk during the Billy Mitchell-Project B experiments, the fairwater surrounding the conning tower is missing, but the periscope supports have survived. On the forward face of the conning tower is an unidentified fitting that might have been associated with navigation, steering, or high-pressure air (**Figure 4-43**). The conning tower hatch is present and is located just forward of the periscope mounts. The outer hull is intact on either side of the conning tower.

Aft of the conning tower the hull is fairly well preserved. A compressed air flask is visible just aft of it in the sand on the port side.

Midway between the conning tower and the stern, the hull of the *UB-148* is heavily damaged. In this section, both the outer hull and pressure hull are ruptured suggesting an explosion, perhaps from incoming shellfire. The exposed interior of the pressure hull reveals a complex matrix of electrical cable and piping.

The stern of the vessel is more intact. While the wooden deck is missing, sections of the pressure hull and outer hull are well preserved. Commercial fishing net is present at the stern, some of which is suspended in the water column by fishing floats. These impacts are particularly prevalent on the port side. A single round hole in the stern is part of the remains of the aft torpedo tube (**Figure 4-44**).

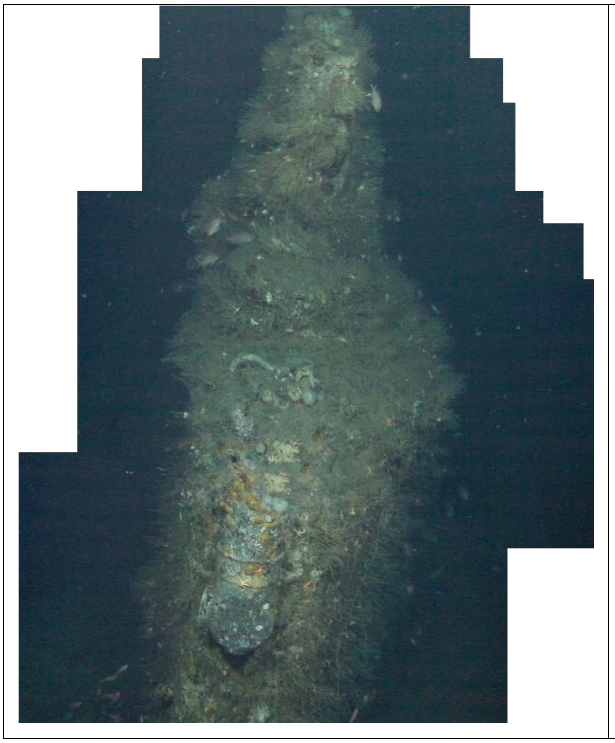

Figure 4-43. Forward face of the *UB-148* conning tower.

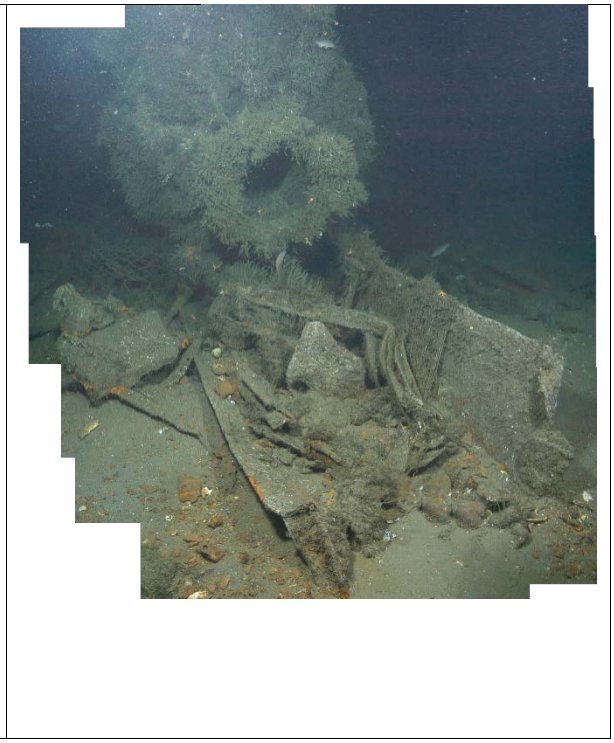

Figure 4-44. Remains of the stern torpedo tube on the *UB-148*.

4.3.5.6.2 Anthropogenic Impacts

The remains of the *UB-148* have been considerably damaged by various site formation processes, including shell fire from surface ships, the ship's impact with the seafloor, natural degradation over time, and impacts from fishing gear and ground tackle. The most substantial damage to the hull is in a section midway between the conning tower and the stern. The damage from shellfire striking this section of the vessel likely caused the submarine to sink. In this area, both the outer hull and pressure hull are ruptured. Damage from fishing gear is substantial particularly in the bow and the stern. In the latter area, some fishing net is suspended in the water column by fishing floats. Elsewhere the vessel is relatively well preserved. The conning tower is intact along with much of the pressure hull and sections of the outer hull. Even areas of the wooden deck still survive.

4.3.5.7 U-140 (Kapitanleutnant Weddigen)

The U-*140* was sunk on 22 June 1921 by fire from USS *Dickerson* as part of the Billy Mitchell-Project B experiments.[300] This site was identified during a multibeam and side-scan sonar survey in 2006. The University of Rhode Island obtained some poor-quality video footage of the site using a small ROV in 2008. The wreck was investigated using the ROV *Kraken 2* during the 2012 sampling cruise (NF-2012-ROV-22 pt.2). Site investigations of the U-*140* were cut short due to shortage of time and logistical difficulties experienced during this sampling cruise. As a result, site reconnaissance investigations were incomplete. Site specifications and imagery of the U-*140* are shown in **Figure 4-45**[301].

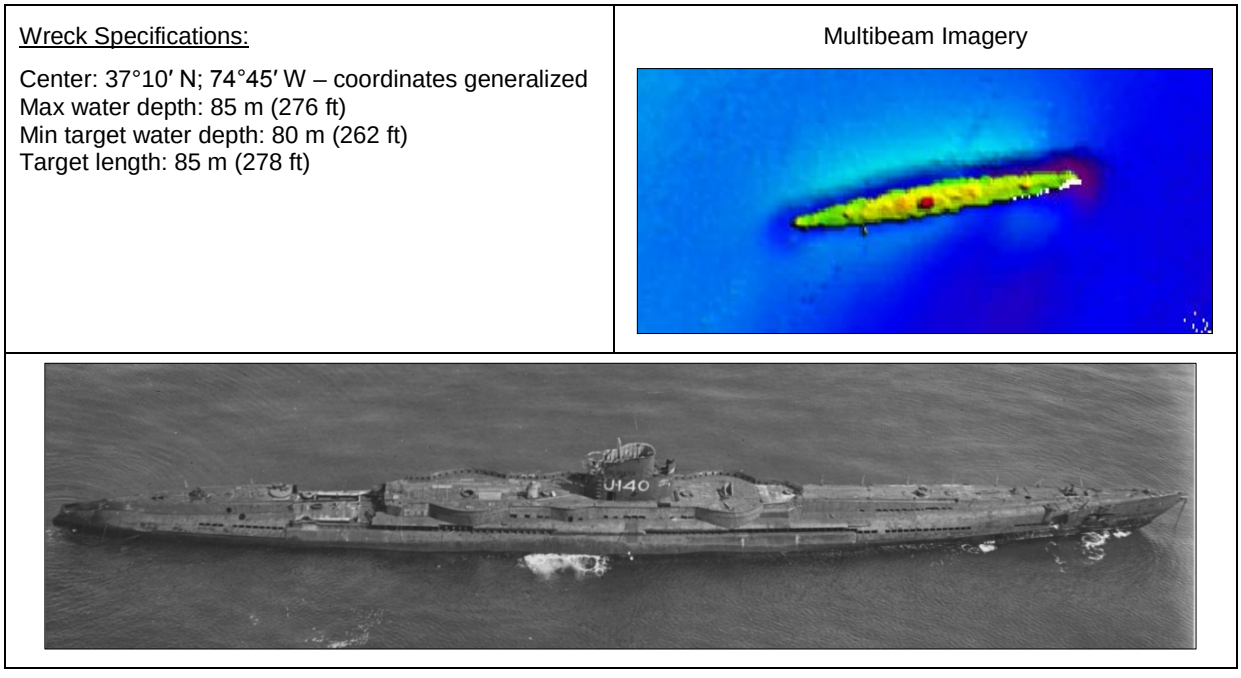

Figure 4-45. Site specifications and imagery for the U-*140*. Historic image shows U-*140* immediately prior to her sinking.

[300] See **Section 4.2.3.9** for citations.

[301] "U-*140*," www.hrnm.navy.mil/content/history/museums/nmusn/explore/photography/ships-us.html. Website accessed 9 September 2016.

4.3.5.7.1 Hull, Machinery, and Weapons

The remains of the U-*140* lie in water depth of approximately 85 m. The hull is orientated in an east-west direction with the stern to the east. Although otherwise fairly well intact, there is a sizeable entanglement of fishing net on the stern supported by floats. As indicated in the multibeam data and confirmed by on-site investigations, a substantial scour is visible around the stern, which has left the rudder and props exposed. The rudder, dive planes, and propellers are still in place (**Figure 4-46**). Fishing net as well as monofilament line is visible on the stern dive planes and rudder.

Figure 4-46. Starboard dive plane and propeller shaft of the U-*140* including damage from fishing gear.

Close to midships, the conning tower is well preserved, although the fairwater has degraded and is missing. It appears the periscopes were retracted at the time of the sinking or the supports are missing. Just aft of the conning tower there appears to be the remains of two air vents that serviced the engine room. Between the conning tower and the air vents, a hole in the hull penetrates through the deck and the pressure hull. This appears to be the result of shellfire by *Dickerson* and was certainly one of the causes of the U-*140*'s sinking. Just aft of the air vents is what appears to be the top of an ammunition locker and then aft of that the remains of the aft 5.9 in (15 cm) gun mount. A compressed air flask is next to the conning tower on the port side. Forward of the conning tower is an access hatch, and forward of that the remains of the vessel's forward (5.9 in [15 cm]) gun mount. No guns were in place at the time of the vessel's sinking.

Fresh corrosion damage is visible along the run of the hull, and sections of the outer hull are missing. In general, however, the pressure hull is mostly intact except for the major hull breach just aft of the conning tower.

The bow of the U-*140* is heavily impacted by fishing net, which obscured observing many features. On-site investigations, however, confirmed the presence of torpedo doors and tubes, compressed air flasks, and chain in the sand at the bow.

4.3.5.7.2 Anthropogenic Impacts

The remains of the U-*140* have been considerably damaged by various site formation processes, including shell fire from surface ships, the ship's impact with the seafloor, natural degradation over time, and impacts from fishing gear and ground tackle. There is considerable fishing net damage to the hull of the U-*140* in the bow as well as the stern.

4.3.5.8 U-117

The U-*117* was sunk as part of the Billy Mitchell-Project B experiments on 22 June 1921. This site was identified during a multibeam and side-scan sonar survey in 2006. The University of Rhode Island obtained some poor-quality video footage of the site using a small ROV in 2008. The wreck was investigated using the ROV *Kraken 2* during the 2012 sampling cruise (NF-2012-ROV-30). Site specifications and imagery for the U-*117* are shown in **Figure 4-47**[302].

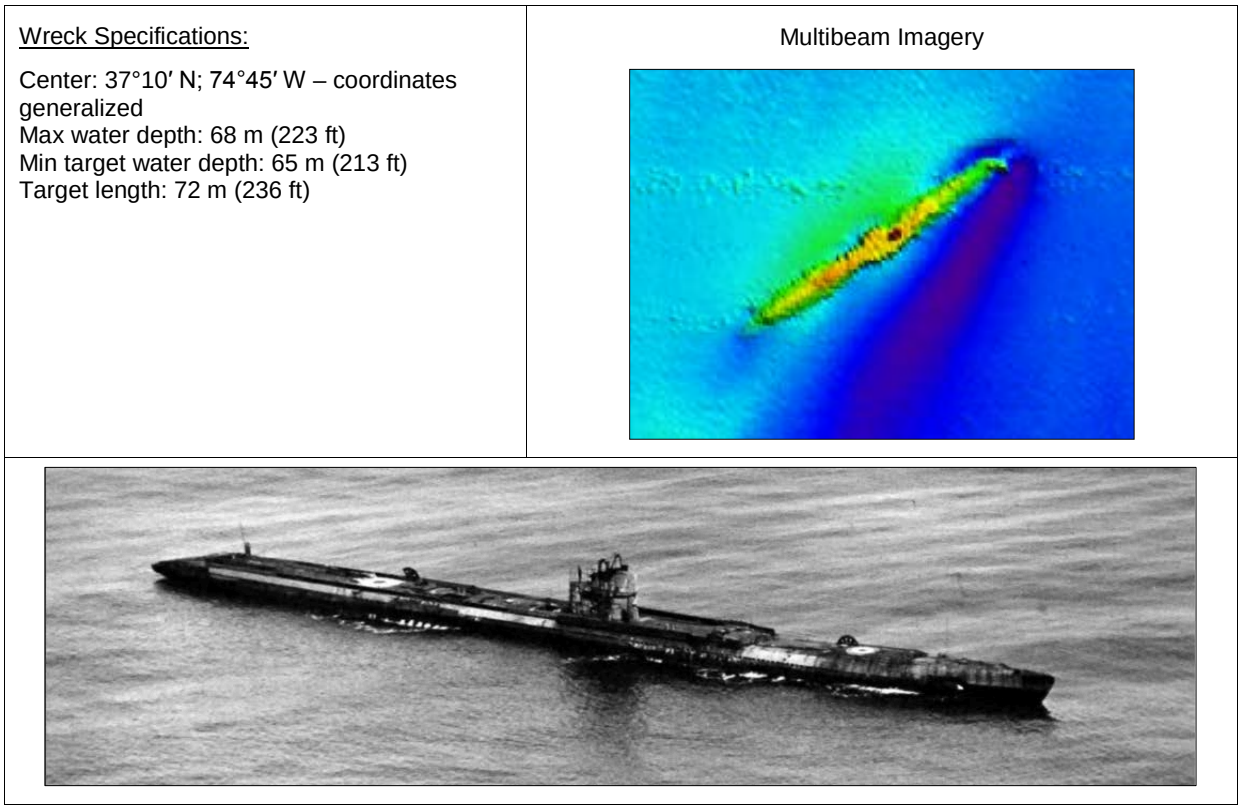

Figure 4-47. Site specifications and imagery for the U-*117*. Historic image shows U-*117* immediately prior to her sinking.

4.3.5.8.1 Hull, Machinery and Weapons

The U-*117* lies in approximately 68 m of water. The hull is orientated in a northeast-southwest configuration with the bow to the northeast. Multibeam survey data indicated that there was a substantial scour at the stern of the vessel that extended down the port side. This was confirmed by on-site investigations.

The stern of the U-*117* is partially buried and has little relief. As a result, it is relatively free of fishing gear. Nevertheless, this part of the wreck is heavily degraded and damaged. In the stern, the remains of the submarine's 39 in (100 cm) mine chutes are visible along with the storage racks for mines. This element of the wreck represents an important source of archaeological information that requires further documentation. The aft bulkhead of the pressure hull is exposed in the stern, as are the propeller shafts.

Moving forward from the stern, the pressure hull is intact as are many of the frames that supported the outer hull. Much of the outer hull plating, however, is missing or degraded. There is some fishing line supported by a float on the port side just forward of the stern that extends some distance into the water

[302] "U-*117*" http://477768.livejournal.com/3631407.html. Website accessed 9 September 2016.

column. Moving forward from the float and line, the pressure hull is still largely intact. The remains of a mine-loading hatch are well preserved and free from net. Immediately forward of the hatch, a small amount of decking has survived. The outer hull plating is missing in this area, but again the frames are still present. Forward of the loading hatch are the remains of the aft gun mount that supported the 3.46 in (8.8 cm) deck gun. This gun was not present when the vessel was sunk. Adjacent and slightly forward of the gun mount is a thick mat of fishing net on the starboard side.

Moving forward from the gun mount and outboard of the pressure hull are two sets of tanks, and forward of that what appears to be a ventilation intake for the engine room as well as a personnel access hatch located just aft of the conning tower (**Figure 4-48**).

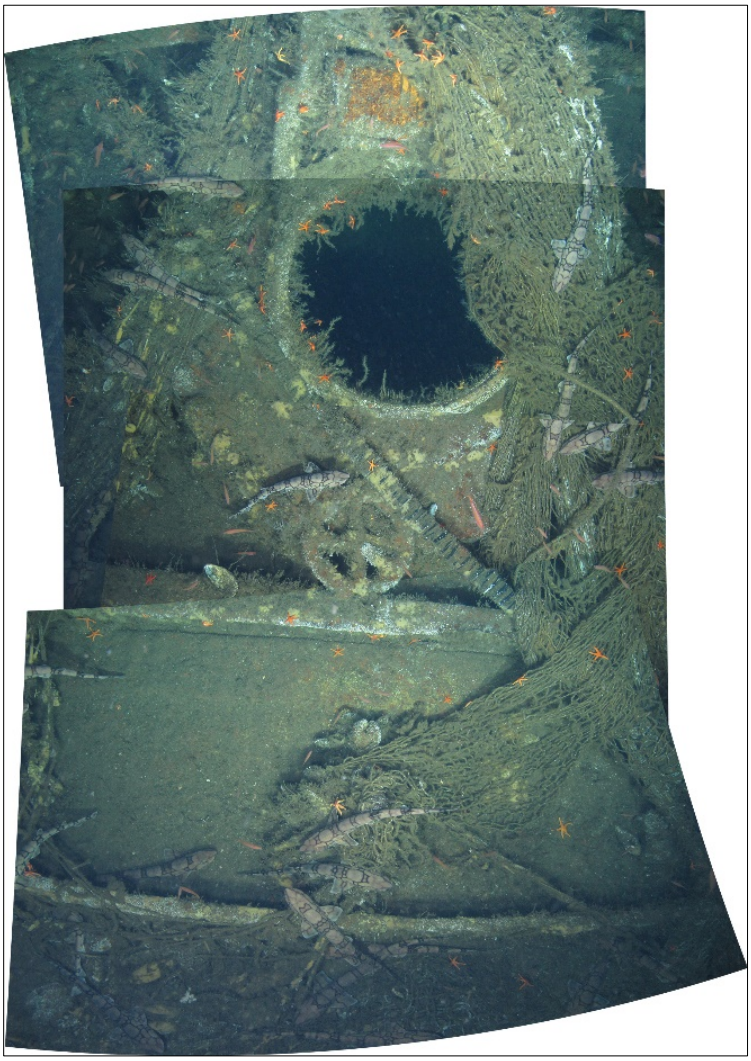

Figure 4-48. Possible ventilation intake aft of the conning tower on the U-*117.*

The conning tower has twin periscope mounts and an access hatch, which is forward of the periscope mounts. The port side of the conning tower has suffered some degree of impact damage. The outer hull is considerably damaged around midships on the starboard side and is most likely associated with the Billy Mitchell-Project B bombings.

Forward of the conning tower, the pressure hull is still intact. A set of bits is on the starboard side, and forward of that an access hatch, and then the remains of the submarine's 5.9 in (15 cm) gun mount,

which is a substantial structure with bolts still in pace. Outboard of the bits and gun mount are tanks and compressed air flasks, some of which are still *in situ*. Moving toward the bow, an access hatch and torpedo-loading hatch are visible. Also in this area are several compressed air flasks, both on the port and starboard side.

The bow of the U-*117* is the most heavily damaged part of the wreck. Damage was caused by a combination of bomb damage, impact with the seafloor, and extensive fishing gear. An extensive matrix of fishing net rests on the bow of the U-*117*, some of which is suspended in the water column by fishing floats. The archaeological remains in this area comprise a debris field. One of the most important components is a starboard upper torpedo tube complete with torpedo door-bow cap assemblage (**Figures 4-49** and **4-50**). Part of the anchor chain runs across the torpedo tube. In addition, there is another of the torpedo doors-bow cap in the sand near the torpedo tube. The upper port torpedo tube is not attached to the starboard one. It is presumably buried in the sand close by. The fishing net in the bow encases what may be a hawse pipe. Fresh corrosion is visible in the bow.

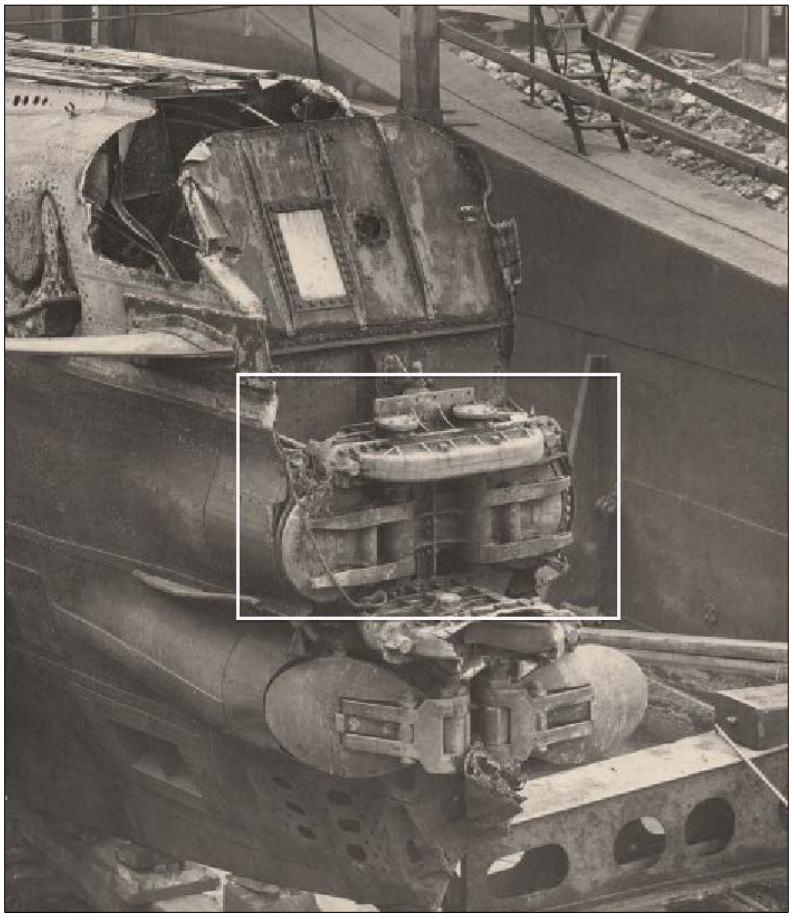

Figure 4-49. Bow caps and doors from the *UB-110.*[303]

[303] http://cdn.rsvlts.com/wp-content/uploads/2015/04/8770771018_a076686bf4_k.jpg Website accessed 9 September 2016.

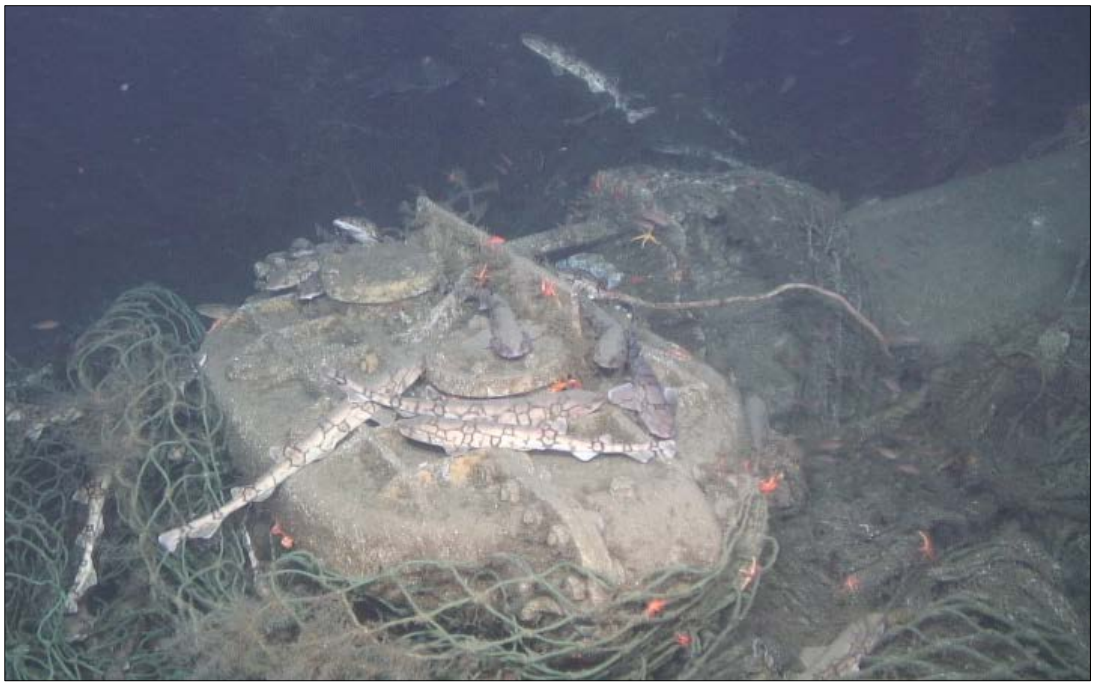

Figure 4-50. Torpedo tube and bow cap control mechanism on the U-*117.* (Compare with bow caps from the *UB-110* shown in **Figure 4-49**).

4.3.5.8.2 The remains of the U-*117* have been considerably damaged by various site formation processes including bomb damage from the Billy Mitchell-Project B experiments, the ship's impact with the seafloor, natural degradation over time, and impacts from fishing gear and ground tackle. Some fishing line is supported by a float on the port side forward of the stern that extends into the water column. In addition, a thick mat of fishing net is visible forward of the aft gun mount on the starboard side. While the pressure hull is generally intact, the outer hull is mostly degraded or missing. Some evidence of impact damage from fishing or ground tackle was seen on the port side of the conning tower. It appears that the most significant bomb damage to the U-*117* was on the starboard side around midships.

4.3.5.9 USS Washington (BB-47)

4.3.5.9.1 Hull

The USS *Washington*, a *Colorado*-class battleship, was never commissioned. The ship was used as a target and sunk by the U.S. Navy on 25 November 1924 in compliance with the terms of the Washington Treaty for the Limitations of Naval Armaments. She was 75.9% complete at the time. No guns had been installed. She was sunk by the battleships *New York* and *Texas*.[304] Site specifications and imagery of *Washington* are shown in **Figure 4-51**.

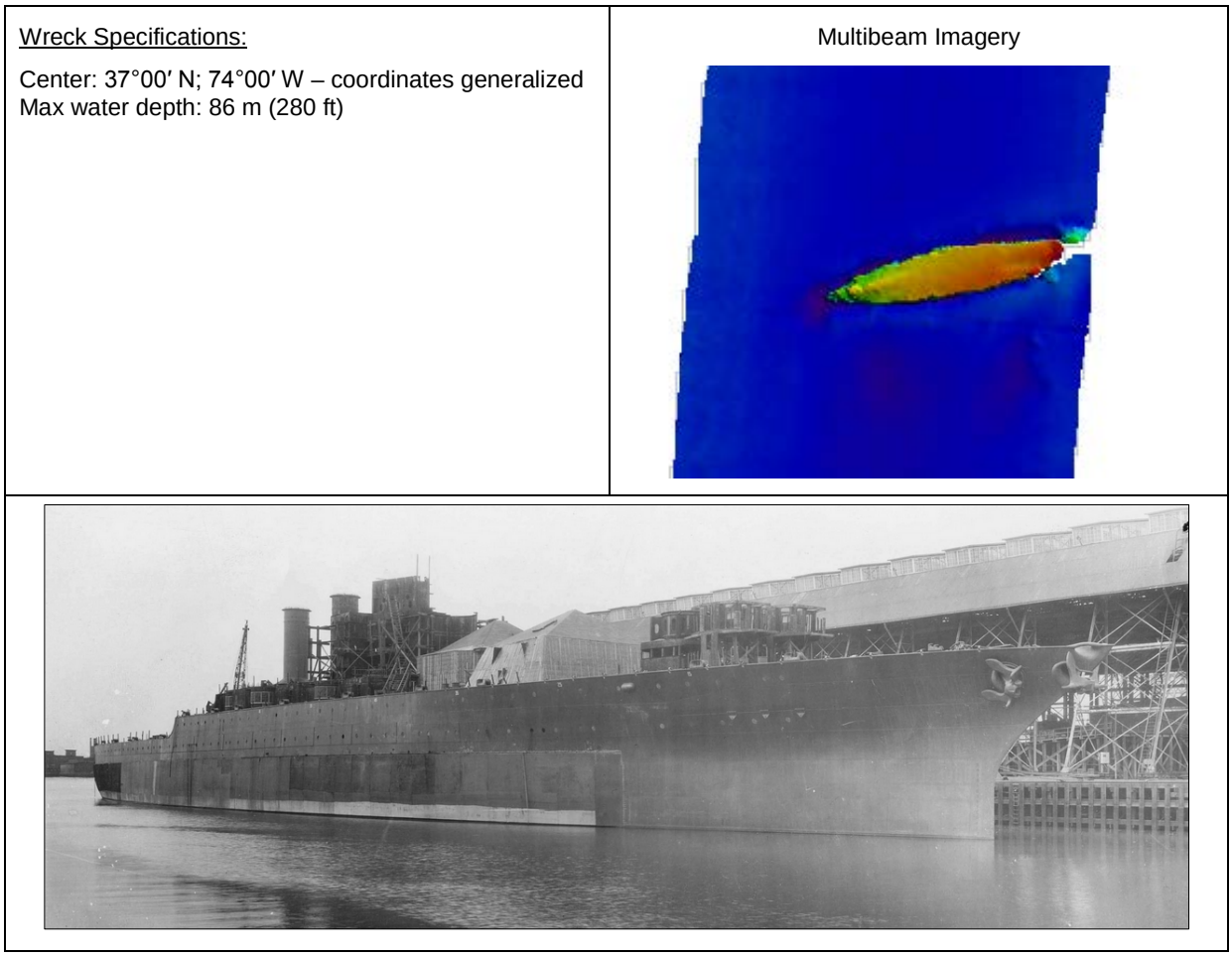

Figure 4-51. Site specifications and imagery for USS *Washington* (*BB-47*). Historic image shows *Washington* during construction.[305]

The wreck was identified during the 2011 mapping cruise at its location south of the head of Norfolk Canyon. *Washington* was briefly investigated during the 2012 sampling cruise (NF-2012-ROV-29).

[304] U.S. Department of the Navy, "The Battleships." Website accessed 9 September 2016 at: http://www.navy.mil/navydata/ships/battleships/bb-list.asp

[305] U.S. National Archives photo no. 19-lc-22D 48, from NARA, College Park

The wreck sits in water depth of approximately 86 m and is orientated in an east-west configuration with the stern to the west. Like many battleships, including *Ostfriesland*, she turned turtle while sinking and now sits on the seafloor keel up.

The stern of *Washington* is the best-preserved part of the wreck. The ship's rudder and fantail are intact. The rudder is turned slightly to port. *Washington*'s four propellers were removed prior to the vessel's sinking. On-site investigations also revealed that all four propeller shafts are missing. The starboard and port support brackets and bearings for the shafts are, however, in place (**Figure 4-52**). The vessel's single axial rudder is likewise complete, well preserved, and virtually free of fishing net.

Washington's lower hull is intact but has suffered considerable corrosion damage such that many steel plates are thin, damaged, corroded, or missing (**Figure 4-53**). The remains of the ship's bilge keels are present, but also are damaged. The lower hull of *Washington* has been more susceptible to rusting and degradation than the lower hull of *Ostfriesland*. This may be due to differences in steel construction quality and manufacturing.

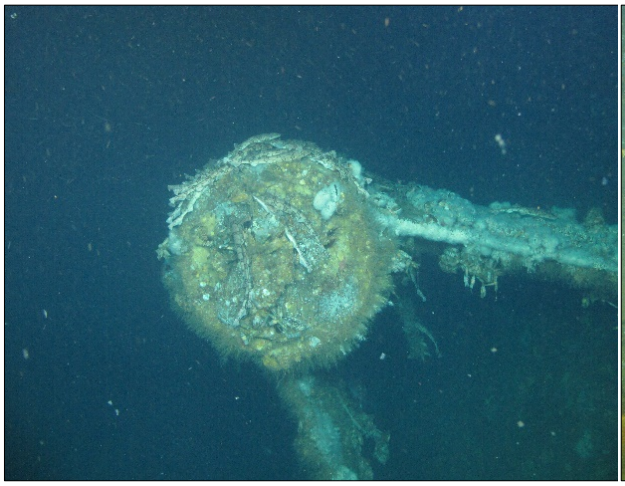

Figure 4-52. Aft propeller bearing on the starboard side of USS *Washington.*

Figure 4-53. Damage to the lower hull of USS *Washington.*

Scours are visible along the port and starboard sides of *Washington*, but the scour on the starboard side (i.e., the northern side) is more prevalent. Some parts of the starboard side of the hull and armor belt are fairly well preserved, but the steel plates in other parts have rusted through, exposing the frames and double-hull construction (**Figure 4-54**). In other areas, the steel plates have separated from one another. In an area on the starboard side forward of midships, the hull has been blown outward, likely caused by shellfire from *New York* and *Texas*. No portholes were fitted prior to the vessel sinking and are, therefore, not present on the site. On the port side, toward the bow and just outboard of the hull, there is a large, as yet unidentified, cylindrical object approximately 7 m in diameter that was likely on the deck of the ship when she sank. It is not part of a turret or smoke stack. *Washington* was never fitted out, so there are few, if any, removable artifacts.

Toward the bow, a substantial athwartships break in the hull appears to run along a watertight bulkhead. Forward of this break, *Washington* is shown to have suffered considerable damage and fragmentation; the bow comprises a field of debris that consists of several major structural components. This includes the prow of the ship that still supports the port and starboard hawse pipes. Chain can still be seen exiting the starboard hawse pipe (**Figure 4-55**). Other elements of the bow are broken and

disarticulated. Overall, it appears that the bow took the full impact of *Washington*'s contact with the seafloor.

Figure 4-54. Missing hull plating starboard side of USS *Washington.*

Figure 4-55. Starboard hawse pipe and chain of USS *Washington.*

4.3.5.9.2 Anthropogenic Impacts

The remains of *Washington* have suffered significantly less damage from fishing gear. This is most likely because a wreck site is marked on the navigation chart close to the actual location of the site. The vessel probably sunk by the bow resulting in significant damage to the forward end of the ship and helping to preserve the stern. Beyond the site formation processes associated with the original attack on the vessel and its subsequent sinking, the remains of *Washington* suffer from extensive corrosion and moderate structural collapse.

4.4 CONCLUSIONS AND RECOMMENDATIONS

The mid-Atlantic OCS intersects with some of the most historically significant waters in the United States. The area has a long and rich history connected with exploration, warfare, commerce, fishing, and recreation. It encompasses the historic approaches to Chesapeake Bay and Delaware Bay and, by extension, key mid-Atlantic ports such as Norfolk, Baltimore, Wilmington, and Philadelphia. Four centuries of intense maritime use have left a rich repository of cultural material on the seafloor on the edge of the shelf as well as in deeper waters off to the east. Although important archaeological sites may be associated with many aspects of the history of the OCS, three themes and time periods have particular significance: ships from early European exploration and settlement, the Billy Mitchell-Project B experiments, and ships from the Battle of the Atlantic. By far, the most significant theme represented in the study sites was from the Billy Mitchell-Project B fleet.

The archaeological resources identified in this study are significant and include sites that are potentially eligible for nomination to the National Register of Historic Places, possibly as a National Historic District. The Atlantic Deepwater Canyons study highlighted the national and international significance of historic and archaeological resources in the study area while at the same time identifying areas for further inquiry.

4.4.1 Project B—Nomination of the Billy Mitchell Fleet to the National Register of Historic Places

The central recommendation for this study is that the shipwrecks that comprise the Billy Mitchell-Project B fleet be nominated to the National Register of Historic Places as the Billy Mitchell-Project B Historic District. Project B was a series of military tests that took place off the coast of Virginia in June and July of 1921. When executed, this joint Navy-Army operation was considered the largest and most complicated naval arms test in the history of the United States. It was the first major U.S. test to include the underwater, surface, and aerial characteristic of modern naval warfare. The only such test to use former enemy warships as objects of study and as targets, Project B also included the first successful use of a remotely guided battleship as a test target. Historically significant as an innovative military test, Project-B is also important for its influence on the domestic civilian and military political landscape and the role of the United States as a leader in international Naval Arms Control. Project B is directly related to the calling of the Washington Conference of 1921 and the content and signing of the Washington (Five Power) Treaty of February 1921. Through the intervention of Army Brigadier General William "Billy" Mitchell, Project B became the center of a national debate over the efficacy and efficiency of military aircraft and battleships. Mitchell was the most famous and broadly influential military aviator in the United States during the 1920s and is considered the father of the modern United States Air Force. The climax of Project B—the sinking of the German dreadnought battleship *Ostfriesland* by Army bombers under Mitchell's direct command—became the high point of his military career and public influence. Mitchell's willfully disobeying of Project B testing protocols and directors during the operations contributed to his later heroic status as a visionary and maverick. Mitchell's final residence is already a National Historic Landmark, and the Billy Mitchell-Project B Historic District has an even stronger association with his career and influence in the history of American military aviation.

Beyond their connection with the tests, the Project B wrecks are significant in the history of warship design. Although German built, the vessels were commissioned into the United States Navy and became objects of studies that substantially influenced the design of U.S. submarines and battleships built during the interwar period. Two submarines, the U-*117* and U-*140*, engaged in major offensives along the coast of the United States and sank many ships in the late summer and early fall of 1918. The ships are significant for their association with Treaty of Versailles and use as public trophies in events such as the Victory Bond drive of 1920. No other World War I−1920s era underwater historic landscapes of comparable significance exist in U.S. waters. Indeed, the Billy Mitchell-Project B Historic District is an internationally significant historic cultural landscape. Each Project B site is potentially eligible for nomination to the National Register of Historic Places. As part of the Atlantic Deepwater Canyons study, a draft nomination has been completed for the district. The boundaries and associated geographic coordinates proposed for the Billy Mitchell-Project B Historic District are shown in **Figure 4-56**.

Geographic Coordinates for the Proposed Boundary:

Latitude (N)	Longitude (W)
37°17′30.0000″	74°32′30.0000″
37°12′15.0000″	74° 6′00.0000″
37°12′15.0000″	74°47′00.0000″
37°10′00.0000″	74°47′00.0000″
37°10′00.0000″	74°33′30.0000″
37°17′30.0000″	74°31′30.0000″

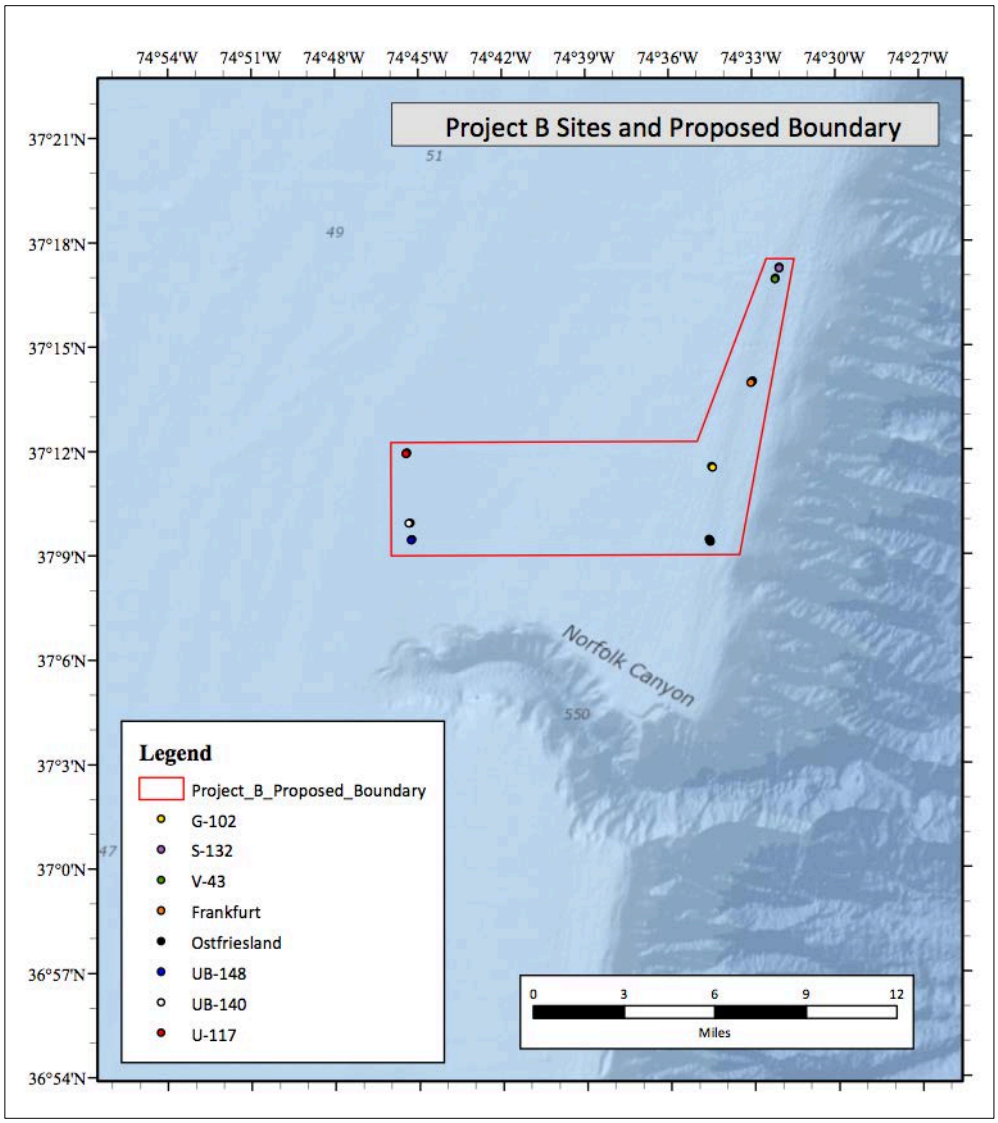

Figure 4-56. Proposed boundary of Billy Mitchell-Project B Historic District.

4.4.2 Charting the Wrecks

Public release of the geographic coordinates of the Billy Mitchell-Project B wrecks could be considered as an intermediate step toward protecting the sites. Although the agency has a well-grounded general policy of not releasing coordinates, the impacts from fishing gear have significantly damaged the sites, and it is possible that charting the wrecks would assist in reducing these kinds of impacts and thereby assist in preserving efforts for these nationally and internationally significant sites. The USS *Washington*, which is charted although not identified correctly in AWOIS, has suffered less damage from fishing gear. It appears that the marking of the wreck on nautical charts has helped protect the site. Preferable still, would be the creation of a National Register Historic District, as recommended, which would identify the area containing shipwrecks, which would help mitigate some of the unfortunate impacts on the sites from fishing gear.

4.4.3 Specific Recommendations for Individual Project B Shipwrecks

4.4.3.1 Ostfriesland

Although *Ostfriesland* has suffered a degree of damage from fishing gear and site visitation, the orientation and configuration of the hull has protected the site. There are areas of active corrosion on the site and the vessel will likely suffer some additional deterioration over the next decade. Since the site is occasionally visited by technical divers, some removable artifacts, particularly those associated with the washrooms, maybe at risk. BOEM should consider whether any artifacts should be recovered and conserved to mitigate that risk. In addition, it is recommended that a small ROV be used to penetrate under the inverted wreck and document the *Ostfriesland*'s main battery. Such a vehicle could also document and image the crack in the stern of the vessel.

4.4.3.2 Frankfurt

The *Frankfurt* is one of the best preserved ex-German warships associated with the Billy Mitchell-Project B experiments and also one of the most vulnerable. The stern of the vessel is the best preserved section of the wreck and is almost intact. The superstructure, deck, fairlead, and wire rope brackets on the aft section have all survived. Between visits to the site in 2012 and 2013, however, part of the stern collapsed. This was evidenced by a shift in the location of one of *Frankfurt*'s guns and deterioration on the ship's starboard side. *Frankfurt* requires immediate additional work and study. The stern of the vessel is one of the best preserved examples of a World War I era light cruiser and further study and documentation are urgent.

4.4.3.3 The Destroyers

Although the *G-102*, *V-43*, and *S-132* have suffered considerable damage from fishing gear, elements of each site still can yield important historical and archaeological information. The most significant additional data to be obtained relates to the machinery, particularly the boilers, condensers, and turbines. Representing significant 20th century technological innovation, these elements are well preserved on destroyers *G-102* and *V-43*. The machinery on the *S-132* is still inside the remaining hull structure.

4.4.3.4 The Submarines

The submarines from the Billy Mitchell-Project B fleet represent important elements of early 20th century German underwater technology. They also embody deep cultural and symbolic meaning regarding World War I and World War II attempts by western powers to control the Atlantic shipping lanes. Although few artifacts could be taken by visitors, the submarines rest in relatively shallow waters (65 to 80 m) and remain vulnerable to anthropogenic impacts.

On-site documentation of the *UB-148* during this study was extremely limited. The Atlantic Deepwater Canyons team visited the site only once and, even then, was able to conduct just a brief overall reconnaissance of the wreck. Further documentation of the wreck is recommended. Particular attention should be paid to the bow and the forward torpedo tubes. Likewise, further documentation of the U-*117* is desirable because the debris field likely extends beyond that which was documented for this study. The U-*140* also is worthy of further study, although the presence of fishing net in the water column at the bow and the stern limits the effectiveness of downward photography.

4.4.4 Other Sites Requiring Study

4.4.4.1 Ocean Venture

The freighter *Ocean Venture* was sunk in February 1942 by the U-*108*. A target believed to be the vessel was identified during multibeam survey operations of the 2012 sampling cruise. The team of the Atlantic Deepwater Canyons study intended to conduct ROV reconnaissance dives on the site in 2012 and 2013, but on both occasions technical difficulties precluded those dives. In 2012, the dive was prevented by an accident at the end of the cruise that resulted in the loss of the *Kraken 2* and a subsequent effort to recover the vehicle from the seafloor. In 2013, the site was deemed to be too shallow to safely operate the ROV *Jason II*. The *Ocean Venture* is a good example of a Battle of the Atlantic site off the east coast of the United States. A reconnaissance ROV dive is recommended to confirm that the multibeam target identified during the 2012 sampling cruise on the *Nancy Foster* is indeed the remains of the *Ocean Venture.* If conducted, that dive should also assess the vessel's archaeological integrity and condition.

4.4.4.2 Grumman Hellcat F6F

The project team attempted to locate and conduct ROV dives on the Grumman *Hellcat F6F* airplane reported to be in Baltimore Canyon. This was not possible in either 2012 or 2013. The location of the airplane is not fully understood, but locating the site and assessing its condition could be considered important. Such an investigation would also provide an important wreck for biological studies in Baltimore Canyon that could then be compared with Norfolk Canyon.

4.4.4.3 San Demetrio

In 1942, the British Merchant ship *San Demetrio* was sunk by the German submarine U-*404* while on route from Baltimore to Halifax, Nova Scotia, with a cargo of alcohol and motor spirits. Earlier in 1940, the vessel was attacked by the German warship *Admiral Scheer*. During that incident, the crew took to lifeboats. They later returned to the ship, put out the fires, and sailed her back across the Atlantic Ocean. The narrative attracted considerable public attention at the time and in 1943, a wartime film titled "San Demetrio London," staring Walter Fitzgerald and Robert Beatty, was made about the incident. The vessel is also the subject of a book titled "The Saga of the San Demetrio." The ship symbolizes the life and death struggle of merchant mariners and the U-boat war during the Battle of the Atlantic. We recommend that the search for *San Demetrio* be continued as part of the need to understand the preservation and disposition of cultural resources off the edge of the OCS. Hull-mounted multibeam, however, is not a suitable tool for such a search because water depths in the area approach 2,000 m and hull-mounted systems do not provide sufficient resolution to reliably identify the site. Instead, the survey should use a deep tow side-scan sonar or an AUV mounted with at least side-scan sonar and, preferably, also a multibeam bathymetry system.

4.4.4.4 Deepwater Shipwreck off North Carolina

In July 2015, a team of researchers under the direction Cindy Van Dover, director of the Duke University Marine Laboratory, was on board the RV *Atlantis* looking for moorings that had been deployed in 2012. Data from the side-scan sonar of the AUV *Sentry* indicated a target in deep water off the coast of North Carolina. Investigations using the human occupied vehicle (HOV) *Alvin* revealed what appeared to be a late 18th century shipwreck site containing wine bottles, brick, a navigational instrument, and anchor and chain. Although this discovery was too late to be considered during the Atlantic Deepwater Canyons study, studying the site would complement the current project and provide data about sites in deeper waters off the OCS. Site documentation and biological study at this site off North Carolina should be considered.[306]

4.4.4.5 Bow Mariner

The remains of the *Bow Mariner*, a tanker carrying ethanol, diesel, and fuel oil that caught fire on 28 February 2004 and sank midway between Baltimore and Washington canyons (37° 55'; 74° 15' – coordinates generalized), could be investigated. The NOAA ship *Thomas Jefferson* surveyed the shipwreck with multibeam in 2009.

4.4.4.6 USS Virginia and USS New Jersey

In 1923, the U.S. military, coaxed and cajoled by Brigadier General Billy Mitchell, extended its air power experiments. This time the targets were the old American battleships USS *New Jersey* and USS *Virginia*, which were sunk off Cape Lookout, North Carolina. The remains of these two battleships have been identified. They are directly tied to and associated with the Billy Mitchell-Project B wrecks and require archaeological monitoring and assessment. A project to document and image the remains of *Virginia* and *New Jersey* could be considered. However, given that ocean currents at these sites often approach or exceed 3 knots, the project design and equipment must be carefully considered.

4.4.5 Areas Requiring Additional Study

In designing the Atlantic Deepwater Canyons study, project archaeologists attempted to select sites that represented the spatial distribution of cultural resources in the area; were located in different water depths; and were in proximity to the three principal canyons. Unfortunately, logistical and technical (available equipment) limitations forced the archaeologists to focus on Norfolk Canyon. As a result, our knowledge of archaeological sites in the area is still skewed toward the shallow waters (<200 m) and toward the vicinity of Norfolk Canyon. Very few shipwrecks have been identified in water depths between 200 and 1,500 m or near Baltimore and Washington canyons. While this project generated significant archaeological information; financial, technical, and logistical limitations prevented the team from tackling the systemic biases in archaeological knowledge. Even after this study, archaeological data in the vicinities of Washington and Baltimore canyons and in deep water off the edge of the shelf remain limited. Further work that targets the deep water areas off the OCS and Washington and Baltimore canyons might be considered a priority. If such a project were funded, survey assets, platforms, systems, and vehicles would need to be carefully selected to provide high-resolution acoustic imaging (multibeam and side-scan sonar) of the seafloor. In addition, sufficient dedicated survey time would need to be provided. Only in this way will deep water archaeological sites off the OCS be fully identified and assessed.

---

[306] "Centuries-Old Shipwreck Discovered off North Carolina Coast," NC State News 17 July 2015. https://news.ncsu.edu/2015/07/shipwreck-2015/ Wyatt Massey, "Mystery shipwreck found off North Carolina coast" CNN 21 July 2015. http://edition.cnn.com/2015/07/20/us/shipwreck-discovered-north-carolina-feat/ Websites accessed 9 September 2016.

4.4.6 Paleoarchaeological Prospecting and Study

With very limited ROV time, archaeologists working on the Atlantic Deepwater Canyons study could devote only two dives to archaeological prospecting and paleoarchaeological landscape reconstruction. Reconnaissance dives during the project targeted areas that were thought to hold some potential for ancient sites of human habitation on the OCS. Unfortunately, these dives produced no definitive results. Although some cobble was identified during one dive, no artifacts were associated with it, and there was no sign of worked stone. If BOEM seeks to assess the potential for sites of human habitation on the OCS, a project should be designed dedicated to achieving that aim. Such a project would require substantial time and funding.

This page intentionally left blank

CHAPTER 5. PHYSICAL OCEANOGRAPHIC PROCESSES WITHIN MID-ATLANTIC BIGHT CANYONS

Andrew J. Davies, Craig M. Robertson, Furu Mienis, Gerard C.A. Duineveld, Nancy Prouty, Brendan Roark, Steve W. Ross, and Sandra D. Brooke

5.1 INTRODUCTION

Submarine canyons are dramatic and widespread topographic features crossing continental and island margins, connecting shelves to the deep ocean (De Leo et al. 2010). These connective features can be subject to enhanced organic matter flux and deposition through entrainment of coastal detrital export, dense shelf water cascade, and channeling of resuspended particulate material (De Leo et al. 2010). Canyon systems are characterized by unique complex patterns in hydrography and sediment transport and accumulation (Garcia et al. 2008), leading to the development of ecological drivers that can influence biodiversity, including the displacement of deepwater species to coastal zones, topographically induced upwelling, enhanced mixing via internal tides, and the focusing of tidal bores (Vetter and Dayton 1998, Cacchione et al. 2002). It is crucial to understand the physical regimes and ecological patterns within canyon systems (Levin et al. 2001), as uniqueness of ecosystems is an important factor in their conservation and management (Auster et al. 2011).

This chapter characterizes the hydrodynamics within two Mid-Atlantic Bight (MAB) canyons (Baltimore and Norfolk canyons). The MAB extends over 500 km of the continental shelf and slope from Cape Cod to Cape Hatteras and is characterized by a complex interplay of hydrography, including tidal forcing, wind events, rivers, and Gulf Stream interactions. Intense short-term variability in the MAB can be driven by the Gulf Stream, whereby lateral oscillations of the Gulf Stream can result in movement of substantial amounts of water, heat, and nutrients onto the shelf (Fitzgerald and Chamberlin 1981). Surface currents in the MAB generally flow to the southwest, but the complex topography of shelf break canyons interact with flow, particularly through tidal activity and internal waves (Keller and Shepard 1978). **Chapter 5** of the Atlantic Deepwater Canyons study focused on hydrodynamics and hydrography that are relevant to deepsea corals and other biota within canyons, concentrating on the long-term observation of water movement, sediments, temperatures, and salinity.

5.1.1 Mid-Atlantic Bight Canyons

Twenty-six major canyons have been recorded between Nova Scotia and Cape Hatteras (Shepard and Dill 1966). Over the last decade, the region has received intense scientific interest mainly due to the need to understand the processes governing continental shelf productivity combined with availability and technological advancement of high-resolution multibeam sonar, hydrographic survey equipment, and precision benthic sampling devices. The MAB region has been of particular prospecting interest to the oil and gas industries. To address the potential impacts of these industries, most of the early canyon studies were commissioned by Bureau of Ocean Energy Management (formerly Minerals Management Services, U.S. Department of the Interior). Obelcz et al. (2014) provided a detailed account of the morphological differences among MAB canyons. They highlighted that the morphology and orientation of canyon heads, steepness and density of sidewall gullies and the character of the continental shelf surrounding the canyon edges were all canyon specific (Obelcz et al. 2014), which should lead to substantial differences in the hydrography of each canyon.

This study focused on Baltimore and Norfolk canyons and the nearby slope. These canyons were chosen due to their large size and presence of heterogeneous hard bottom habitats that are important for the growth of cold-water coral species (Hecker et al. 1983; **Chapter 8**). These two canyons are approximately 75 km apart and cut 31 km (Baltimore Canyon) and 25 km (Norfolk Canyon) into the MAB shelf. The earliest geological study reported these two canyons as inactive in terms of sediment

transport, having sediment profiles rich in silt and clay (Keller and Shepard 1978). In contrast, canyons to the north of Hudson Canyon have profiles comprising higher proportions of sand and gravel (Hecker et al. 1983). However, more recent studies on MAB hydrography and geomorphology have shown that these canyons are actually highly dynamic transporters of sediments under specific hydrographic conditions (Forde 1981, Csanady et al. 1988, Csanady and Hamilton 1988, Gardner 1989a, Churchill and Cornillon 1991, Obelcz et al. 2014).

5.1.2 Baltimore Canyon

Baltimore Canyon lies 125 km southeast of the entrance to Delaware Bay and continues for a distance of 25 km between its head and 1,500 m depth (**Figure 5-1**). The width of the canyon is 3 km near the canyon's head, increasing to 8 km at the shelf break (at approximately 100 m water depth). The canyon axis curves southward at the upper reaches before turning eastward with increasing depth and lying in an east-west orientation at 3,000 m (Obelcz et al. 2014). The cross-section profile in the continental slope is V-shaped with a maximum relief of 700 m at the shelf break and becomes U-shaped in the lower canyon (1,000 m). Obelcz et al. (2014) noted the northern and southern sides of the canyon have steep near vertical walls starting approximately 8 km along the canyon axis, and the head of the canyon contains a series of large terraces and steps below the rim of the canyon between 110 and 130 m depth and traces laterally for several kilometers along the arch of the canyon rim. Where the canyon emerges onto the upper continental rise, topographic relief decreases to approximately 100 m, forming an indistinct fan valley on the abyssal plain (Gardner 1989b).

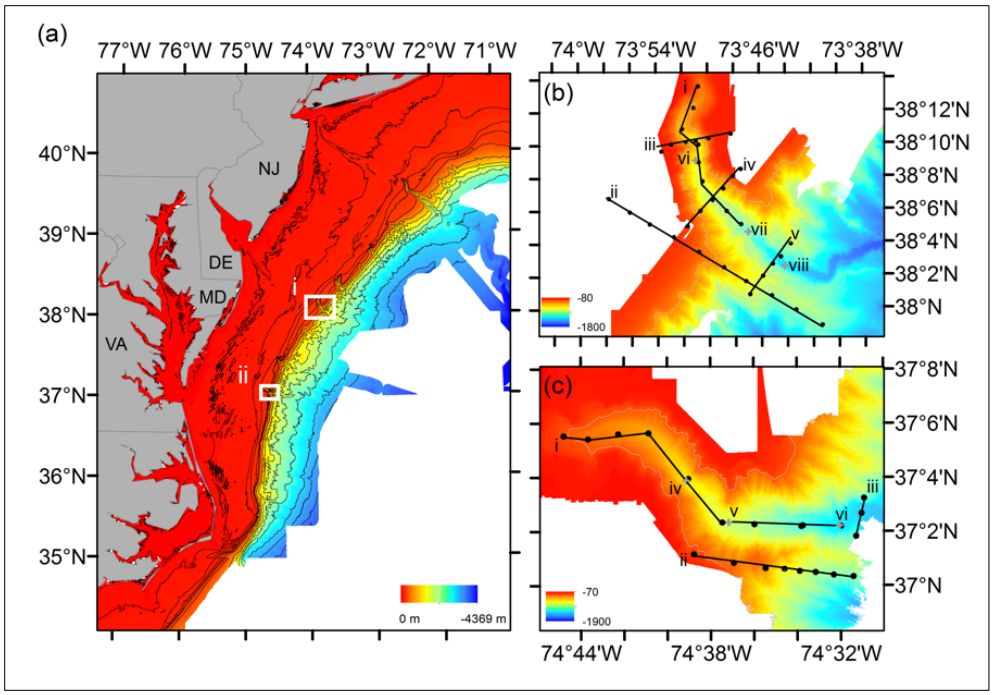

Figure 5-1. The sampling regime within the Mid-Atlantic Bight off the eastern United States. (a) Overview of the numerous canyons that intersect the shelf; location of Baltimore Canyon (i) and Norfolk Canyon (ii) are shown as inset frames. Subfigures (b) and (c) show the sampling design carried out during research cruises in 2011, 2012, and 2013. (b) In Baltimore Canyon, (i) canyon conductivity-temperature-depth (CTD) transect, (ii) slope CTD transect, (iii) upper canyon traverse CTD transect, (iv) mid-canyon traverse CTD transect, (v) lower canyon traverse CTD transect, (vi) shallow lander, (vii) mid-mooring, and (viii) deep lander. (c) In Norfolk, (i) canyon CTD transect, (ii) slope CTD transect, (iii) lower canyon traverse CTD transect, (iv) shallow benthic lander, (v) mid-mooring, and (vi) deep lander. Bathymetry is shown as the inset color scale bar.

Modern supply of material to Baltimore Canyon is from pelagic and reworked shelf sediments (Gardner 1989b). Gardner (1989a, 1989b) observed shelf break sediment resuspension in Baltimore Canyon coupled with subsequent advection by currents. Previous observation by Pierce (1976) showed detached turbid layers moving away from adjacent mid-slopes near Baltimore Canyon and cited low-density flows moving down canyons as a principal means of sediment transport. However, Gardner (1989a, 1989b) found little evidence of substantial resuspension along the slope and instead observed significant resuspension of sediment in the canyon between 200 and 600 m and sometimes down to 800 m. Resuspension occurred in the upper canyon, but there was no evidence of turbidity currents moving down the canyon axis to 1,000 or 1,500 m. According to Gardner (1989a, 1989b), resuspension was caused by tidal currents focused by the canyon axis in winter, early spring, and sometimes during other periods of the year. Furthermore, Gardner (1989a, 1989b) added that the portions of sediment that are resuspended in the upper canyon generally flow away from the canyon along density surfaces. Outside the canyon walls, currents dilute and diffuse the sediment over the adjacent slope or out into the open ocean.

The conclusions of Gardner (1989a, 1989b) point toward the focusing of tidal energy, along Baltimore Canyon axis in the form of internal waves, as the source of resuspension events and high concentrations of particles. Resuspension occurs primarily during flood and to a lesser extent during ebb flows and is most intense and episodic when the water is poorly stratified (i.e., during late winter and early spring [March–April]), though periodic events may occur at other times. Gardner (1989a, 1989b) described resuspension events as most intense between 275 and 600 m, which corresponded with the depth interval of 200 to 800 m where particle concentrations in the water column were highest. Very little resuspension was observed on the continental slope, along the canyon axis below 1,000 m or on the canyon walls. At 275 m, in the canyon axis net transport was down canyon, but at 600 m, transport was strongly up-canyon, implying that between the two depth sites, a zone of net convergence was present (Gardner 1989b).

5.1.3 Norfolk Canyon

Norfolk Canyon is the second most studied of the MAB canyons and is located 45 km south of Chesapeake Bay (Forde 1981). Norfolk Canyon is sigmoidal in shape and runs in a west-to-east orientation, perpendicular to the shelf (**Figure 5-1**). The broad axial bend (9 to 10 km) seaward of the canyon head coincides with a change from relatively smooth downward slope in the upper reaches of the thalweg to a more rugose profile in the lower reaches of the canyon (Obelcz et al. 2014). Various degrees of steep wall habitat are found in the lower reaches of Norfolk Canyon that run parallel to the axis of the canyon and are dissected by numerous tributaries. The rim morphology and subbottom stratigraphy are more distinct than in other MAB canyons, with the southern rim having a highly irregular morphology, showing short escarpments and steep indentations (Obelcz et al. 2014). The northeast wall of the canyon contains several notches, possibly areas where blocks of sediment have slumped from the steep canyon walls. Terrace-like modulations on both canyon walls at 300 m depth and several smaller terraces on the northeast wall between 100 and 200 m are reported (Forde 1981). Terraces such as these may have been cut during low sea stands or could be the result of other processes, which will be discussed in a later section; therefore, Norfolk Canyon is likely to have had a different source of sediments than Wilmington and Baltimore canyons (Forde 1981).

To date, very few published works on the hydrography of Norfolk Canyon exist. However, Hecker et al. (1983) noted that Norfolk Canyon is unique among MAB canyons in general and briefly reported unusually high current velocities and evidence of recent erosional activities, which are exceptions for most MAB canyons. The only directly measured current parameter in the canyon was by Shepard and Dill (1966), who reported periodic current velocities greater than 30 cm s^{-1} at 30 m above bottom in 573 m water depth, and they suggested that these current speeds in the upper reaches are important mechanisms for sediment displacement in Norfolk Canyon.

5.1.4 Water Masses of the Mid-Atlantic Bight Canyons

The oceanography of MAB waters is one of the best studied in the world (Robinson and Brink 2006), with the structure of the frontal boundary separating shelf, slope, and Gulf Stream water masses of the MAB being well reported (see detailed reviews in Bigelow 1933, Cresswell 1967, Beardsley and Winant 1979, Posmentier and Houghton 1981). Complex hydrographic structures of the MAB water column are the result of the interaction between major current circulation patterns (Csanady and Hamilton 1988), position of shelf-slope fronts (Voorhis et al. 1976, Houghton et al. 1986, Garvine et al. 1988), entrainment of shelf waters by Gulf Stream eddies (Churchill et al. 1989, Lillibridge et al. 1990), Gulf Stream meanders, water column stratification, and upwelling events (Houghton et al. 1982, Csanady and Hamilton 1988). In addition, sources of freshwater have a substantial effect on the oceanography of the region. Loder et al. (1998) reported three major sources of freshwater to the northeastern North American shelf: 1) Ocean transport of relatively fresh subpolar water onto the northern Labrador shelf, 2) Continental runoff, most significant in the St Lawrence River system and the Labrador and Mid-Atlantic Bight shelves, 3) the melting sea-ice on the Labrador and northeast Newfoundland shelves, and 4) the North Atlantic subpolar gyre and its multibranching western boundary current, the Labrador Current. **Table 5-1** shows the diagnostic temperature and salinity parameters for the major North West Atlantic oceanic water masses and MAB water masses extracted from the literature.

Table 5-1. Temperature and salinity signatures for major oceanic water masses and MAB water mass constituents.

Oceanic Source Water Mass	Depth (m)	MAB Component Water Mass	Diagnostic Signature		Reference
			Temperature (°C)	Salinity (pss)	
Shelf water	<200	Shelf surface water (including summer thermocline)	>25	30−32	Church et al. (1984)
			11−25	30−34.75	Church et al. (1984), Csanady and Hamilton (1988)
NACW or WNACW	<500	Shelf-slope front Warm slope water	2−18	34.9−36	Csanady and Hamilton (1988)
			7−20	35−36.7	Emery and Meincke (1986)
			>8	>34.8	Drinkwater et al. (1999)
			7−11	34.8−35.2	Horne (1978)
			>8−13	>34.8−35.6	Csanady and Hamilton (1988), Drinkwater et al. (1999)
LSW	>500−1,500	n/a	<8	<34.8	Drinkwater et al. (1999)
WASIW		Cold slope water	3−9	34−35.1	Emery and Meincke (1986)
			5−8	32.5−33	Church et al. (1984), Csanady and Hamilton (1988)
Gulf Stream	>500−1,500	Gulf Stream shallow	>23	>35	Rasmussen (2005), Csanady and Hamilton (1988)
			19.4	36.3	Churchill and Cornillon (1991)
		Gulf Stream deep	9−14	>35	Rasmussen (2005), Csanady and Hamilton (1988)
NADW	1,500−bottom	n/a	1.5−4	34.8−35	Emery and Meincke (1986)

LSW = Labrador Sea Water, WNACW = West North Atlantic Central Water, NACW = North Atlantic Central Water, WASIW = Western Atlantic Subarctic Intermediate Water, and NADW = North Atlantic Deep Water. pss = practical salinity scale. Depths are cited according to Emery and Meincke (1986). n/a = data not applicable.

In this chapter, the oceanography of Baltimore and Norfolk canyons is described from deployments of state-of-the-art benthic landers and moorings, and conductivity-temperature-depth (CTD) profiles and transects. The landers and moorings recorded multiple parameters for a period of almost a year and were designed to capture seasonal variation and provide the most comprehensive dataset of canyon conditions in the MAB. We hypothesize that the transport of material through canyons is accelerated by strong physical processes (such as tidal flows, internal waves) that impinge on abrupt topography. Given that

Baltimore and Norfolk canyons are substantially different in orientation, shape, and overall morphology. We hypothesize that although sedimentary patterns will be similar (both canyons are fed by the same shelf and water masses and lack direct river input into the canyons), differences were observed in current velocities, topographic steering of currents, and variations in temperature-salinity patterns, which may ultimately lead to differences in environmental drivers and benthic communities.

5.2 MATERIALS AND METHODS

5.2.1 CTD Data

Three research cruises collected CTD data using slightly different instruments to record water column environmental profiles and collect water samples (**Section 3.2.6**). The 2011 mapping cruise (NF-11-04) and the 2012 sampling cruise (NF-12-07) on the *Nancy Foster* used a Sea-Bird Electronics, Inc. (SBE) 911*plus* CTD with a rosette of twelve 5-L Niskin bottles. In addition to conductivity (Siemens m^{-1}), CTtemperature (°C), and depth (m), the CTD also measured turbidity (Seapoint, formazin turbidity units), dissolved oxygen (mL L^{-1}), altitude (m), and salinity (practical salinity scale, calculated). The 2013 sampling cruise (RB-13-03-HBH) on the *Ronald H Brown* used an SBE 9*plus* CTD with a rosette of twelve 10-L Niskin bottles. In addition to conductivity (Siemens m^{-1}), temperature (°C), and depth (m), the CTD instrument also measured turbidity (Seapoint, formazin turbidity units), dissolved oxygen (mL L^{-1}), altitude (m), pH, and fluorescence (relative units [RU]). CTD transects were taken down the axes of and across sections of both canyons, and during these casts, the CTD array was lowered from the surface to as close to the bottom as feasible (usually ~10 m above the seafloor). The transects were completed, where possible, within one section of a tidal cycle (**Figure 5-1**).

5.2.2 Benthic Landers and Moorings

Four benthic landers and two moorings were deployed during the 2012 sampling cruise on board the *Nancy Foster* (**Figures 5-1** and **5-2**; also see **Section 3.2.3**). The landers were large metal frame structures equipped with various recording instruments and placed on the seabed. Four deployments (one mooring in each canyon and two landers in Norfolk Canyon) were undertaken on 17 and 18 August 2012 followed by deployment of two landers in Baltimore Canyon on 5 and 6 September 2012 (see **Figure 5-1** for locations). The placement of these instruments followed a shallow (~600 m), mid (~1,000 m), and deep (~1,300 m) design with the depths consistent between the two canyons. The duration of the deployment was for approximately one full year (August 2012 to August 2013), except for the two landers in Baltimore Canyon that were recovered for at-sea servicing between 16 and 18 May 2013 to replace their acoustic release mechanisms.

In Baltimore Canyon, the benthic landers were of the University of North Carolina, Wilmington (UNCW) design (**Figure 5-2**) and consisted of an aluminum tripod frame approximately 2 m in height equipped with an acoustic release and several buoyancy spheres. The instrumentation load included a Sarl Technicap PPS 4/3 sediment trap programmed to rotate a sample bottle (250 mL) at 30-day intervals, delivering 12 samples during the one-year deployment. Temperature, salinity, turbidity, dissolved oxygen, and bottom currents were measured using an Aanderaa recording current meter (RCM) string logger. All RCM probes were mounted approximately 1.5 m off bottom with the exception of the current meter, which was approximately 2 m off the bottom (**Figure 5-2**). The shallow lander was initially deployed at a depth of 603 m (38°09'01.4400" N, 73°50'57.2400" W) and the deep lander at a depth of 1,318 m (37°02'32.5800" N, 73°44'09.1800" W) (**Figure 5-1**). Both landers were recovered and redeployed in roughly the same area between 16 and 18 May 2013. Final recovery occurred on the 24 August 2013. All sensors were logged on a 15 min interval.

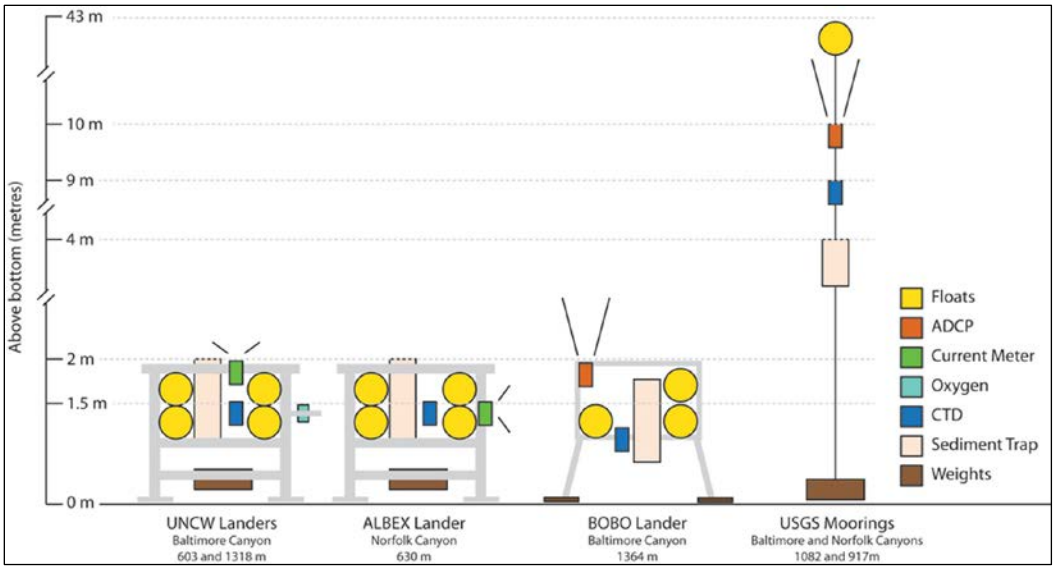

Figure 5-2. Schematic diagrams of the lander and mooring technology deployed in the MAB canyons, including instrumentation loading and placements. Some equipment not shown for clarity, such as acoustic releases and satellite beacons.

In Norfolk Canyon, two benthic landers of different designs from the Royal Netherlands Institute for Sea Research (NIOZ) were deployed. First, the shallow lander was of the ALBEX (Autonomous Lander for Biological Experiments) design, and consisted of an aluminum tripod frame approximately 2 m in height with a central acoustic release mechanism and several buoyancy spheres (**Figure 5-2**). The instrumentation on the ALBEX lander consisted of a Sarl Technicap PPS 4/3 sediment trap programmed to rotate a sample bottle (250 mL) at 30-day intervals. Currents were monitored using a Nortek Aquadopp current meter mounted approximately 1.5 m off the bottom, and temperature, salinity, and pressure were measured by an SBE MicroCAT CTD. Turbidity and fluorescence were measured using Wetlabs sensors at 1.5 m above bottom. This lander was initially deployed at a depth of 630 m (37°03'52.5600" N, 74°39'07.1400" W) (**Figure 5-1**). Attempts were made to recover the lander in August 2013; however, these failed, and the lander was assumed lost. Later, the ALBEX lander was discovered washed ashore in the Bahamas in January 2015 with instruments in a recoverable state; however, those data were not analyzed in this report.

Second, the BOBO (bottom boundary layer) lander was deployed in the deep station of Norfolk Canyon (**Figure 5-2**). This lander consisted of an aluminum tripod frame, 2 m in height, with a release weight attached to the central part of the lander (**Figure 5-2**). The instrumentation on the BOBO lander consisted of a Sarl Technicap PPS 4/3 sediment trap programmed to rotate a 250 mL sample bottle at 30-day intervals. Currents were monitored using an upward-looking 1200 kHz Teledyne RDI acoustic Doppler current profiler (ADCP) programmed with a bin distance of 0.5 m over 39 bins mounted at 2 m above bottom. In addition, an SBE conductivity temperature (CT) instrument was mounted at 1.5 m above bottom to monitor temperature and salinity. Turbidity and fluorescence was measured using Wetlabs sensors at 1.5 m above bottom, and a second turbidity sensor was also deployed (Seapoint) at 1.5 m above bottom. This deep lander was deployed at a depth of 1,364 m (37°03'52.5600" N, 74°32'01.2000" W) (**Figure 5-1**). All sensors were logged at a 15 min interval.

Two moorings of a U.S. Geological Survey (USGS) design (**Figure 5-2**) were placed at roughly midpoint between the two landers in each canyon (**Figure 5-1**). These systems consisted of a Honjo Parflux sediment trap with thirteen 500 mL bottles mounted 4 m above bottom. Temperature and salinity were measured using an SBE MicroCAT 37 mounted 9 m above bottom and an upward-looking 300 kHz ADCP at 10 m above bottom. The ADCP was programmed with a bin distance of 2 m over 54 bins.

The mooring in Baltimore Canyon was deployed at 1,082 m depth (37°04'39.4200" N, 73°46.957 W), and the mooring in Norfolk Canyon at a depth of 917 m (37°02'19.8000" N, 74°37'09.4800" W) (**Figure 5-1**). All sensors were logged at a 5 min interval.

5.2.3 Data Analyses

5.2.3.1 Water Masses

Water column profiles using the shipboard CTD systems (described above) were collected during 2011, 2012, and 2013 (**Tables 5-2** and **5-3**). In total, 15 complete CTD transects were collected from both canyons, of which seven transects (**Table 5-2**) were used for characterizing the water column. Some CTD transects were rejected for analysis, because they either covered too little distance or occurred over an extended period (thereby incurring artifacts associated with tidal cycles). In Baltimore Canyon, two main transects were collected: the first along the axis of the canyon and the second on the adjacent slope (**Table 5-2**). Three across-canyon transects (upper, middle, and lower canyon traverses) were used to investigate changes in the water column across the width of the canyon. Three transects were analyzed for Norfolk Canyon; these had similar starting and ending depths. However, the slope transect started at the halfway point of the canyon transect to enable the two transects to cover similar depth ranges (**Figure 5-1**, **Table 5-2**). Due to logistical constraints, only one transverse canyon transect located in the lower portions of Norfolk Canyon was collected.

Raw data were processed using the SBE Data Processing Software. Downcast data were averaged to 1 m bin size and visually checked to remove obvious outliers. Visualization of the water column for each transect was conducted using the Surfer 8 contouring and 3-D surface mapping package (Golden Software, LLC). The Inverse Distance to Power interpolation method was used to create grid-based contour maps of the water column along the transect length based on distance, depth, and water parameters of interest. Six parameters were used: temperature, salinity, fluorescence, turbidity, density (sigma theta), and oxygen to assess water column patterns. Transect bottom profiles were created from bathymetric data for each canyon in Esri's ArcMap 10.2 and were inserted as a post-map layer to visualize seabed topography for each contour map. Temperature-salinity diagrams were drawn in the program R using the "*oce*: Analysis of Oceanographic data" (Kelley and Richards 2015) and used to diagnose oceanographic water masses over the sampled areas.

Table 5-2. CTD station casts used to generate transect analyses in Baltimore and Norfolk canyons. Data from both **Tables 5-2** and **5-3** were used characterize water masses within the Mid-Atlantic Bight.

Canyon	Transect	Date	Station	Distance (km)	No. of Casts	Depth Range (m)
Baltimore	Canyon Axis	21 Aug 2012	NF12 036-044	18.5	9	251−1,032
	Slope	28 Aug 2012	NF12 096-105	27.9	10	105−1,068
	Upper Transverse	19 Aug 2012	NF12 013-018	8.1	6	104−586
	Middle Transverse	20 Aug 2012	NF12 022-027	8.8	6	123−854
	Lower Transverse	24 Aug 2012	NF12 057-061	7.4	5	914−1,257
Norfolk	Canyon Axis	3 May 2013	RB13 003-012	22	10	237−1,312
	Slope	13 May 2013	RB13 061-068	11.1	8	277–1,078
	Transverse	18 May 2013	NF12 001, NF12 003-004	2.6	3	1,067−1,384

Table 5-3. Individual CTD station casts used for water mass identification in Baltimore and Norfolk canyons. Data from both **Tables 5-2** and **5-3** were used characterize water masses within the Mid-Atlantic Bight.

Canyon Cruise	Transect	Date	Station	Latitude (N)	Longitude (W)	Depth (m)
Baltimore (NF-11-04)	Canyon Axis	9 June 2011	NF 2011-010	38°05′25.04″	73°47′41.64″	1,005
		9 June 2011	NF 2011-011	38°06′42.16″	73°49′32.88″	873
		9 June 2011	NF 2011-012	38°07′56.75″	73°51′01.08″	710
		9 June 2011	NF 2011-013	38°09′22.97″	73°50′43.44″	625
		9 June 2011	NF 2011-014	38°10′53.40″	73°51′59.40″	495
		9 June 2011	NF 2011-015	38°12′22.25″	73°50′47.04″	348
		9 June 2011	NF 2011-016	38°14′37.90″	73°50′07.08″	163
Norfolk (NF-11-04)	Canyon Axis	13 June 2011	NF 2011-024	37°02′31.60″	74°35′01.32″	1,001
		13 June 2011	NF 2011-025	37°02′21.62″	74°37′04.08″	751
		13 June 2011	NF 2011-026	37°03′39.17″	74°38′32.28″	528
		13 June 2011	NF 2011-027	37°04′47.24″	74°40′06.96″	492
		13 June 2011	NF 2011-028	37°05′19.32″	74°41′54.24″	295
		13 June 2011	NF 2011-029	37°05′36.31″	74°43′51.96″	268
		13 June 2011	NF 2011-030	37°06′10.55″	74°45′40.68″	106

5.2.3.2 Geostrophic Flow

A rough estimate of the geostrophic transport between shelf and slope water masses was determined by application of the geostrophic flow equation, sometimes referred to as the thermal wind equation (Simpson and Sharples 2012). The calculation is a simplification of the equations governing the horizontal component of velocity and can be used to calculate the horizontal velocity under geostrophic approximation. The geostrophic equation gives the following formula for the estimated velocity of canyon water masses across water column profiles, where g is gravity (9.81 m s^{-2}), ρ is the reference density (1,020 kg m^{-3}), f is the Coriolis force parameter for a latitude of 35°N (4.37×10^{-05}), $\Delta\rho$ is the difference in density between two water profiles (for each 1 m bin), and Δx is the distance between stations in the transect (across canyon southwest-to-northeast):

$$\frac{du}{dz} = \frac{g}{\rho f} \cdot \frac{\Delta\rho}{\Delta x}$$

In applying the geostrophic flow equation it is necessary to set a level at which the velocity is known (or assumed to be zero). In our calculations, the velocity was set to zero at the seabed. Differences in water density, for all profiles in each transect from surface to bottom, were calculated at 1 m depth intervals, to determine the horizontal velocity over the entire water column, assuming constant geostrophic flow. These data were used in Surfer 8 to create contour maps that show the direction of water flow within the canyon (negative = down canyon and positive = up canyon).

5.2.3.3 Benthic Landers and Moorings

Upon recovery of lander and mooring systems, data from each sensor were downloaded and formatted for subsequent error checking and archiving. The lengths of deployment were different for the UNCW and NIOZ/USGS systems. Two datasets were created for Baltimore Canyon, due to the UNCW systems being recovered in May 2013. The first was a deployment series of continuous data from August 2012 to May 2013, when data from the USGS mooring were down-sampled to match the time

interval of the UNCW systems. These data were used for time series analysis when missing records do not allow for calculation, such as spectral and tidal analysis. The second was a continuous dataset with a 2-day gap in May, and again the USGS mooring recording interval was down-sampled to match the time interval of the UNCW systems. These data were used mostly for visualization purposes. None of the Norfolk Canyon deployments were recovered for servicing; and as such, a single continuous dataset was created with the USGS mooring data down-sampled to match the lander recording interval.

Data analysis of the lander and mooring was mostly conducted within the statistical program R (R Core Team 2015), predominantly using the package "*oce*: Analysis of Oceanographic data" (Kelley and Richards 2015), with specific analyses described as follows. Tidal analysis was conducted using the MATLABtlab package *t_tide* (Pawlowicz et al. 2002), with power spectra calculated using the *spectrum* function within the core R package. Up and down canyon flow was calculated by rotating *uv* velocity components from current meters and ADCPs using the following equation, where *c* (constant of 90°) and θ (bearing of canyon to determine up/down motion) are in radians:

$$Canyon\ flow = v(\sin(c-\theta)) + u(\cos(c-\theta)$$

Under this calculation, negative values indicate an up-canyon flow, and positive values a down-canyon flow.

5.2.3.4 Surface Weather Data

Surface weather conditions that were related to episodic events recorded by the landers and moorings were obtained from the National Oceanic and Atmospheric Administration's National Ocean Service Center for Operational Oceanographic Products and Services (CO-OPS). In particular, data were obtained for realized and predicted tidal height, and wind speed and direction from Ocean City Inlet, Maryland.

5.3 RESULTS

5.3.1 Temperature-Salinity from CTD Profiles

The CTD profiles undertaken during the 2011, 2012, and 2013 cruises all demonstrate a typical inverted "V" shape (**Figure 5-3**). This pattern persists throughout the different months that these profiles were collected, but the shape and extent changes due to mixing and seasonal stratification of the water column (**Figures 5-3a**,**b**). For example, within Baltimore Canyon in June 2011, the tip of the inverted "V" was characterized by warmer (13.5 °C) and more saline (34.35) water (**Figure 5-3c**). In August-September 2012, the tip was characterized by colder (8.5 °C) and fresher (salinity of 33) water (**Figure 5-3a**). In contrast, temperature and salinity of the tip for the adjacent slope at Baltimore transect in 2012 was 10.7 °C and 33.7, respectively (**Figure 5-3a**). The "V" in Norfolk Canyon in 2011 was characterized by water temperatures of 9 °C and salinity of 33.1 and 7.7 °C, 33.6 in April–May 2013 (**Figures 5-3b** and **5-3d**). West North Atlantic Central Water (WNACW, **Table 5-1**) was evident on all transects including those conducted on the slopes and dominated the conditions in deeper parts (>200 m) of the MAB slope with salinities ranging from 35 to 35.6 and temperatures from 4 °C to 12 °C (**Figure 5-3**).

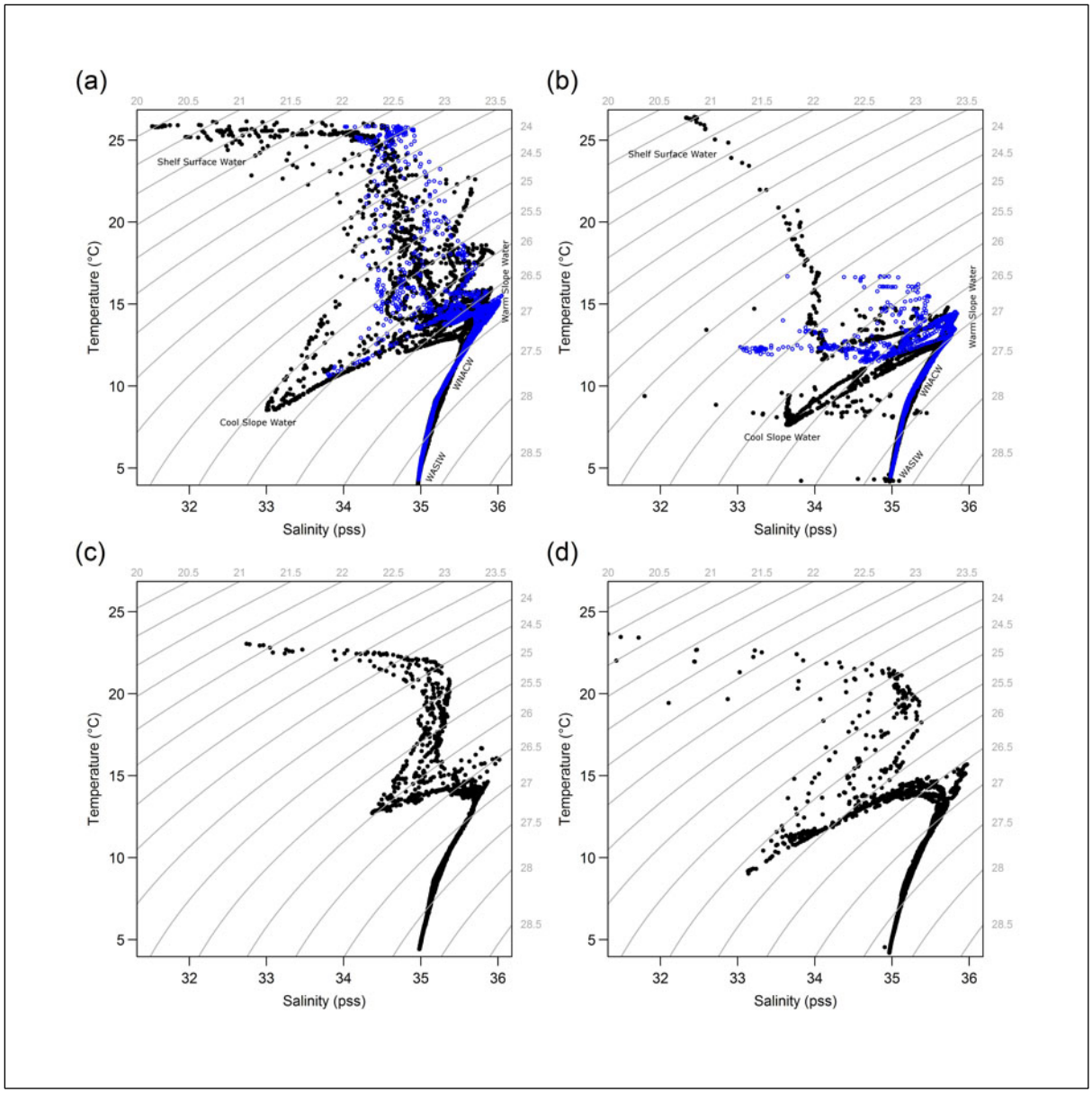

Figure 5-3. Temperature-salinity diagrams indicating major water masses observed in the MAB area. For (a) all Baltimore Canyon profiles from August–September 2012, (b) all Norfolk Canyon profiles from April–May 2013, (c) all Baltimore Canyon profiles from June 2011, and (d) all Norfolk Canyon profiles from June 2011. In (a) and (b), blue open circles represent data from slope transects. Gray values around the outside of the plot indicate density as sigma theta (kg m^{-3}). (pss = practical salinity scale; WASIW = Western Atlantic Subarctic Intermediate Water; WNACW = West North Atlantic Central Water.)

5.3.2 Temperature-Salinity from CTD Transects

In both canyons and slopes, WNACW with its diagnostic near vertical temperature-salinity signature occurred below the thermocline generally in deeper water, forming the lower limits of the shelf-slope front (**Figures 5-4** and **5-5**). A second cold water mass was evident below WNACW (temperature 4 °C to 5 °C, salinity ~35, **Figure 5-3**) and can be identified as Western Atlantic Subarctic Intermediate Water (WASIW) (**Table 5-1**, >500 m, 3 °C to 9 °C, salinities between 34 and 35.1). WASIW was observed (>700 m; 4 °C to 5 °C, salinity ≤35) in contact with the seabed and first appeared deep in the middle canyon transverse transect close to the bottom (**Figure 5-6**). WASIW was more prominent lower down canyon axes with increasing depth (**Figures 5-4** and **5-5**). In both canyons, WNACW and WASIW were found farther up-canyon due to the shelf incising nature of the canyons, but did not flow as far on the adjacent slope (**Figures 5-4** and **5-5**). On the adjacent slopes, WNACW and WASIW meet the shelf-slope frontal system at the shelf break (approximately 100 m).

Both canyons and corresponding slopes exhibited movement of the shelf-slope front and movement of WNACW and WASIW up the length of the canyon axis, although this was more pronounced in Baltimore Canyon (**Figures 5-4** and **5-5**). **Figure 5-4a** shows the progressive temperature-salinity plots for Baltimore Canyon overlain with a canyon axis topographic profile. A clear change in the water masses present along the length of the transect was apparent, and a different pattern was observed in the adjacent slope transect (**Figure 5-4b**). A thermocline was present at approximately 100 m (25 °C, salinities <34.7), particularly within the canyon (**Figure 5-4a**). Toward the head of the canyon, a strong presence of the shelf-slope front (**Figures 5-3a**,**b** and **5-4a**), characteristic of MAB water masses, was visible starting at 0 to 2.4 km along the transect (11 °C, salinity of 34; **Figure 5-4a**). This front occurred in the upper reaches of Baltimore Canyon, becoming weaker at the 7.7 km station, after which it was met by the near straight profile of WNACW (**Figure 5-4a**). WNACW was present along the axis of the canyon and was detected in the upper, mid, and low across-canyon transects (**Figure 5-6**). WASIW occurred below WNACW, occupying the deepest parts of the canyon (**Figure 5-6c**) and was also observed in the mid and upper transects (**Figures 5-6a**,**b**). Toward the upper edges of the canyon, WNACW was met again by the slope-shelf front (**Figure 5-6**). Interestingly, only at the 16.3 km station an additional water mass was observed at approximately 60 m depth and may be Gulf Stream water (**Figure 5-4a**, 9 °C to 14 °C, salinities >35).

The Norfolk Canyon plots show a different pattern compared with Baltimore Canyon in that the persistent WNACW did not reach the head of the canyon but was met by the shelf-slope front at 3.7 km along the transect (**Figure 5-5a**). The profile for the shallower parts of the transect (0 to 3.7 km) also differs from Baltimore in that there seems to be very little shelf surface water signature, only cold slope intrusion water (**Figure 5-5a**). These most likely reflect the time of year that sampling was undertaken and the dynamic nature of MAB water masses. The Norfolk Canyon axis also shows the presence of Labrador Sea Water (LSW; temperatures ~9 °C and salinity of 34.3) between the 5.9 and 13.8 km stations (**Figure 5-5**). These appear as a small cluster of points between the shelf-slope front and WNACW and were not present in any of the Baltimore transects.

The corresponding slope transects from each canyon area demonstrated similar patterns, although in Baltimore the deep WNACW and WASIW water masses only appeared along the deeper half of the transect (**Figures 5-4b** and **5-5b**; between stations 11.8 and 27.9 km). The shelf-ward side of the transect (0 to 2.8 km), again showed the presence of the cold slope inverted “V” and the warmer shelf waters, indicative of the shelf-slope front (**Figure 5-4b**). The appearance of WNACW occurred seaward from the 11.8 km station, which differed from the canyon axis (**Figure 5-4**). WNACW and WASIW can be clearly seen inshore on the Norfolk slope transect, meeting the shelf-slope front close to the start of the transect (**Figure 5-5b**; 2.8 km). The front occupies the whole water column and becomes weaker nearer the shelf break where WNACW and WASIW fill the majority of the water column (**Figure 5-5b**).

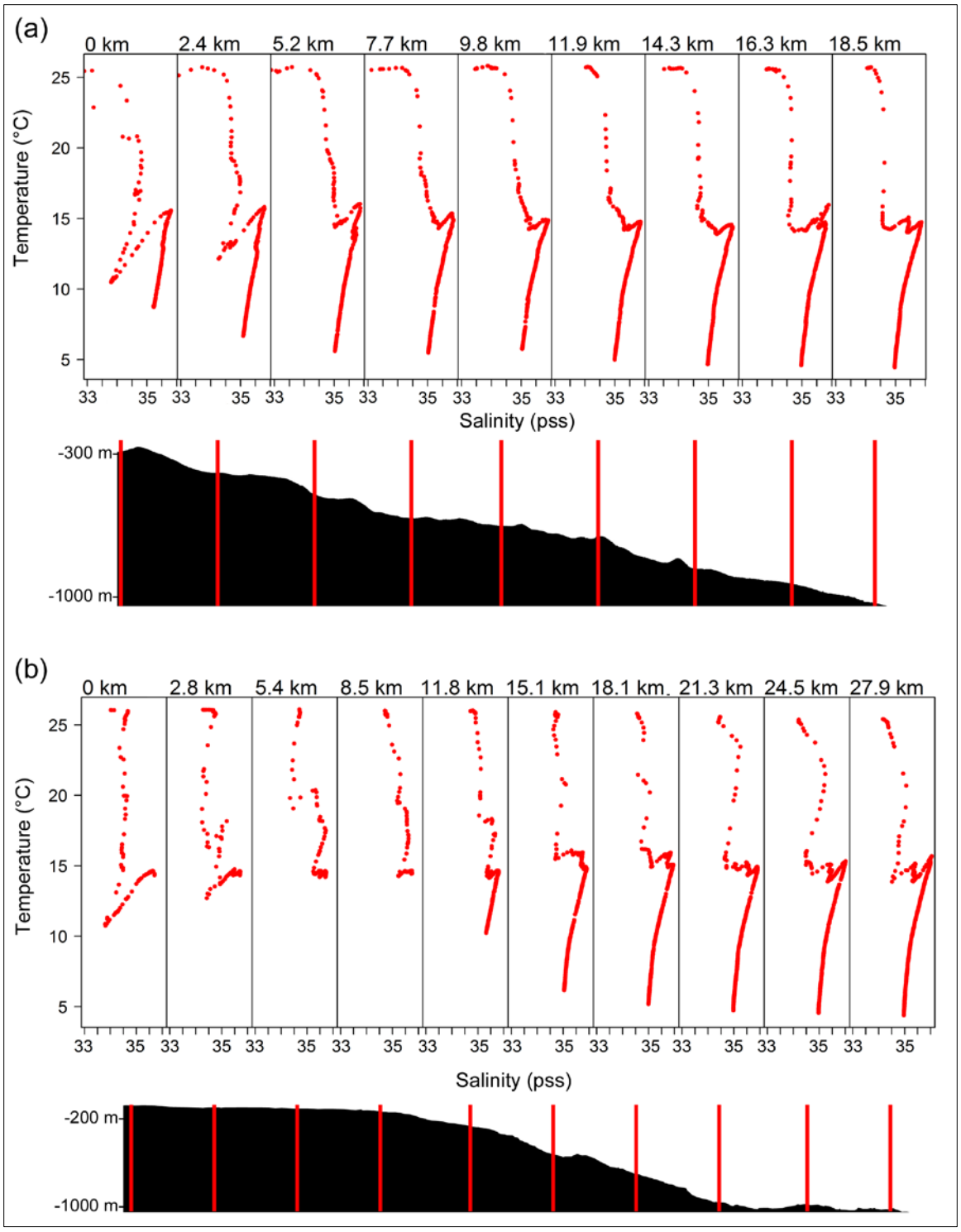

Figure 5-4. Temperature-salinity diagrams for the CTD transects along the axis of Baltimore Canyon. The corresponding location for each profile is shown on the topographic profile below within the (a) canyon transect and (b) adjacent slope transect. All CTD profiles were undertaken during August 2012.

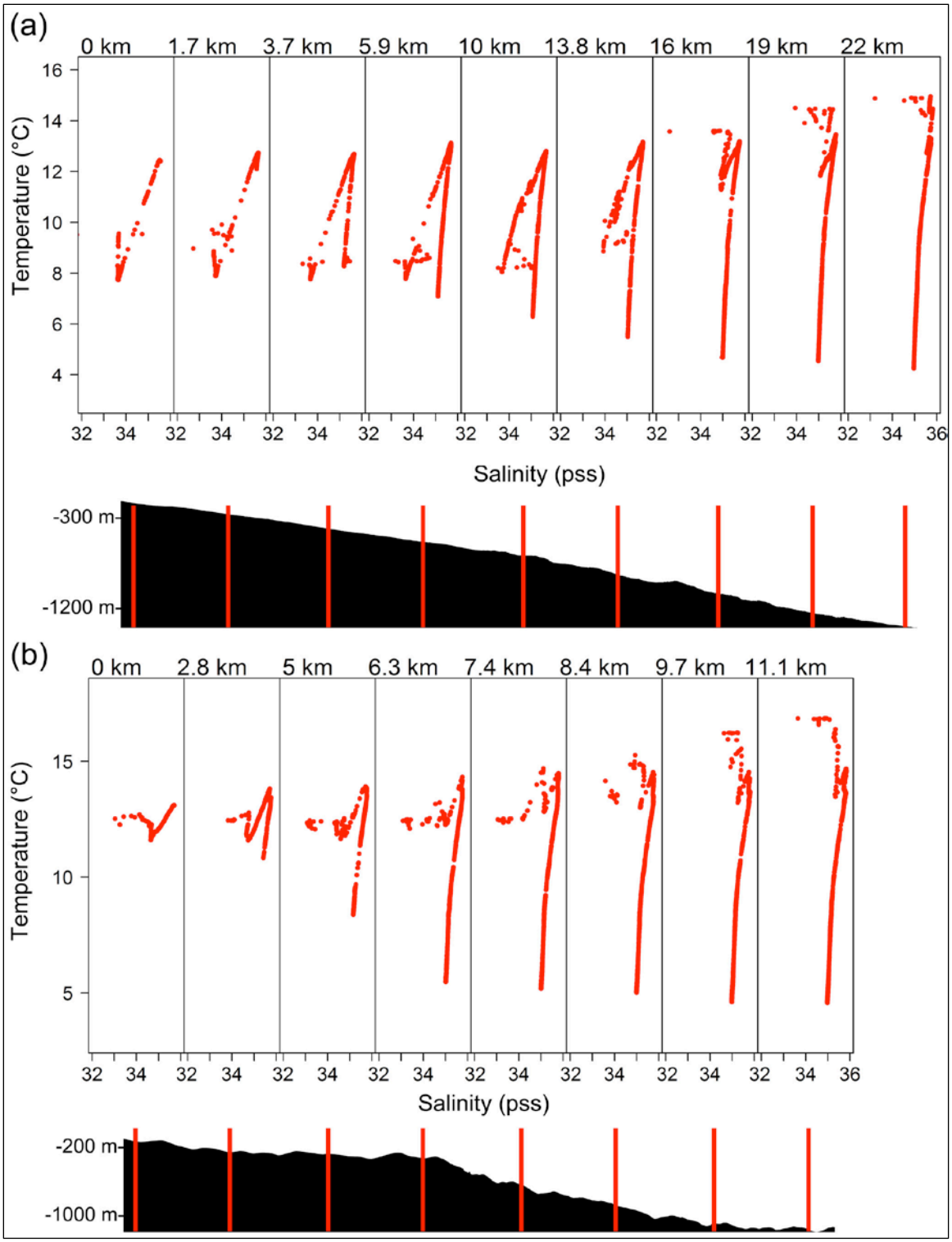

Figure 5-5. Temperature-salinity diagrams for the CTD transects along the axis of Norfolk Canyon. The corresponding location for each profile is shown on the topographic profile below within the (a) canyon transect and (b) adjacent slope transect. All CTD profiles were undertaken during May 2013.

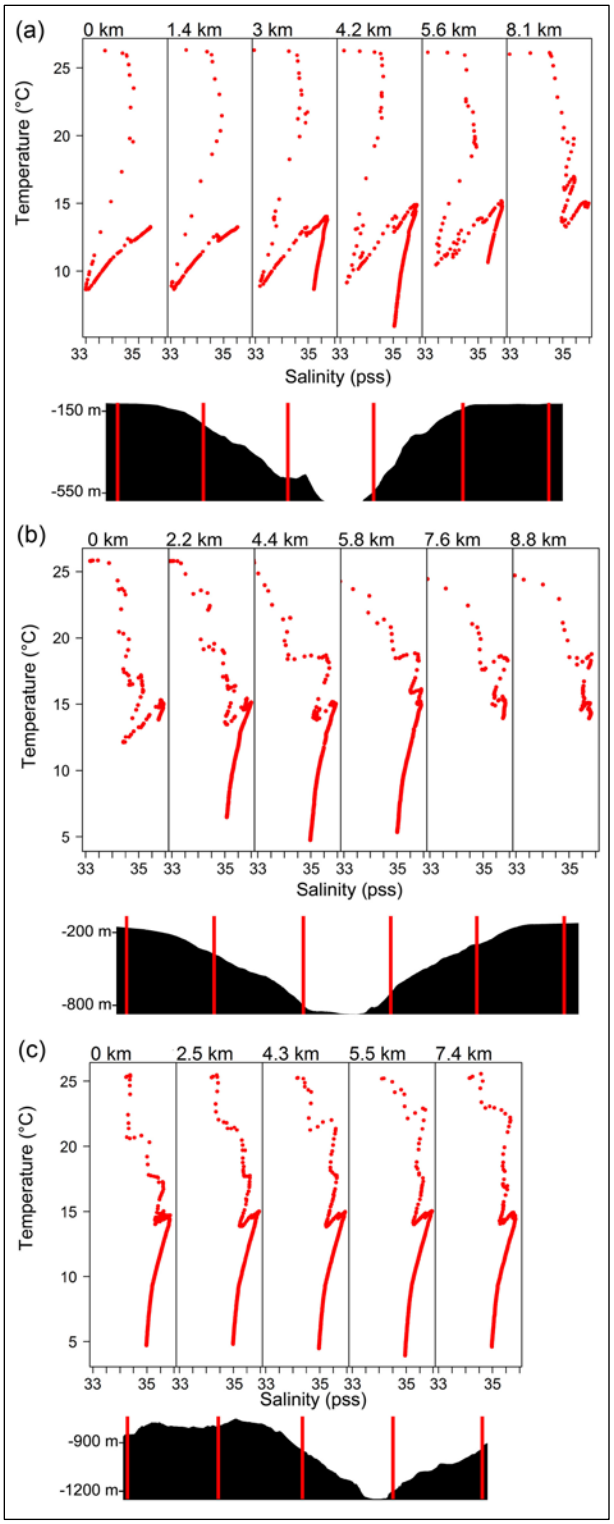

Figure 5-6. Temperature-salinity diagrams for the CTD transects across Baltimore Canyon. The corresponding location for each profile is shown on the topographic profile below; a) upper canyon cross-sectional transect, b) mid-canyon cross-sectional transect, and c) lower canyon cross-sectional transect. All CTD profiles were undertaken during August 2012.

5.3.3 Water Column Contour Mapping

CTD transects plotted as contoured maps suggested relatively stable conditions for most parameters within the two canyons and corresponding slopes (**Figures 5-7** to **5-11**). In Baltimore, the transect running through the central axis of the canyon demonstrated the presence of a large intermediate nepheloid layer (**Figure 5-7**) that was absent from the adjacent slope (**Figure 5-8**). This layer extended from the mouth of the canyon from 200 m to approximately 900 m and was recorded in both 2011 and 2012, suggesting a persistent feature. Toward the surface, in both the slope and canyon transects, an intrusion of highly saline water (~35.8) with a temperature between 14 °C and 15 °C was evident at approximately 100 to 250 m (**Figures 5-7** and **5-8**). This intrusion was clearly observed in the upper canyon CTD profile that traversed perpendicular across the canyon (**Figure 5-9**). In each transect, there was a low oxygen (minimum 3.1 mL L^{-1}) zone between 100 and 300 m, below which levels increased to 5.5 mL L^{-1}. Fluorescence in all transects showed high levels in surface waters, but no detectable amounts below 200 m (**Figures 5-7** and **5-8**).

The Norfolk Canyon CTD profile demonstrated conditions similar to those at Baltimore, particularly with respects to temperature and salinity below 200 m water depth (**Figure 5-10**). However, a more pronounced intrusion of saline water was observed at depths shallower than 200 m, which was under a cold (8 °C) and low salinity (minimum ~33.8) water (**Figure 5-10**). A similar pattern was observed on the slope transect running in parallel to the canyon (**Figure 5-11**). As in Baltimore, fluorescence was low below 200 m, with no detectable patterns. Also, oxygen concentrations decreased from the surface, to around 3.1 mL L^{-1} at 300 m and then increased in deeper waters to a high of 5.5 mL L^{-1} (**Figures 5-10** and **5-11**). The key difference between Norfolk and Baltimore was the absence of a large single nepheloid layer. Instead, what appear to be clouds of sediment were detected at various depths within the canyon. These clouds were observable at approximately 100 m intervals from 300 m depth and were absent from the slope (**Figures 5-10** and **5-11**).

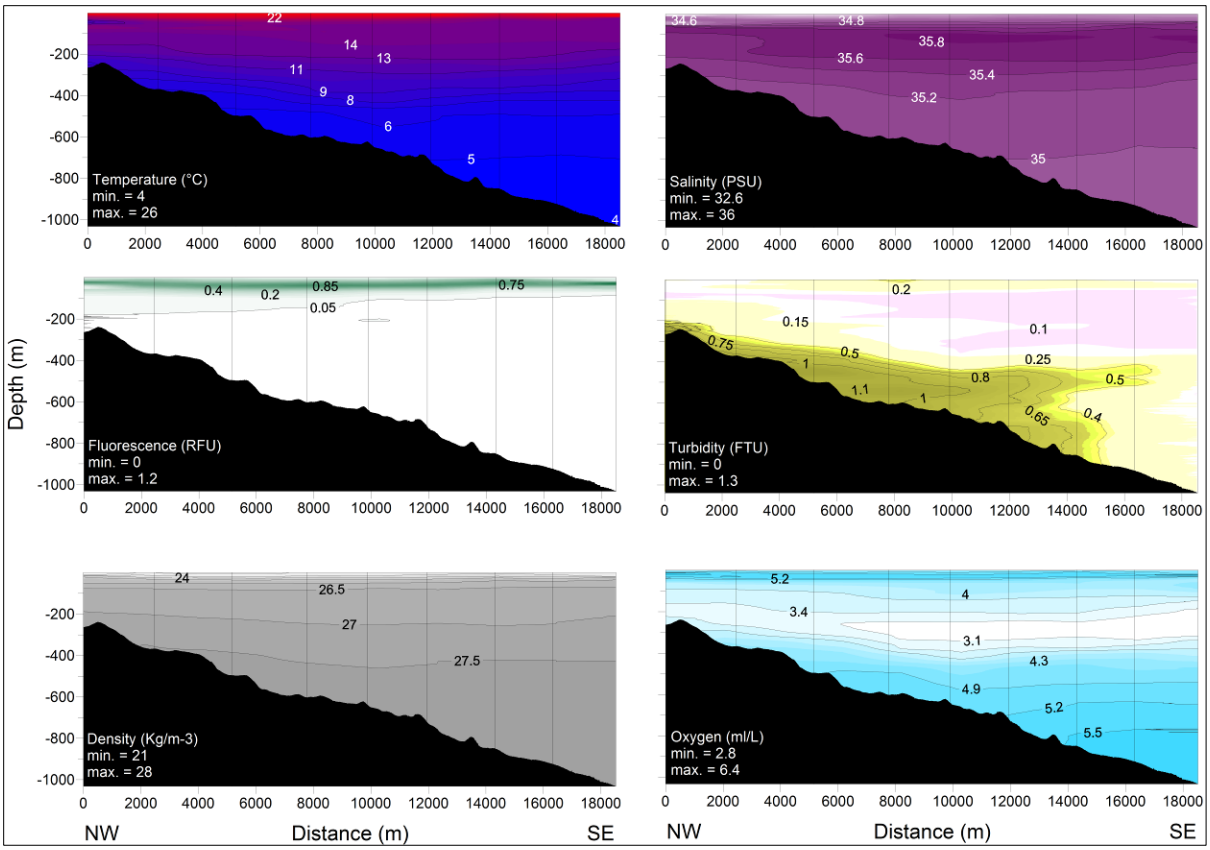

Figure 5-7. Water column characteristics derived from CTD profiling along the Baltimore Canyon axis transect. Six variables used to characterize the water column were temperature, salinity, fluorescence, turbidity, density, and oxygen. The range and units for each variable are shown as minimum and maximum. Dark lines show the position of CTD casts along the transect, including extreme margins in the plot (number of casts = 9).

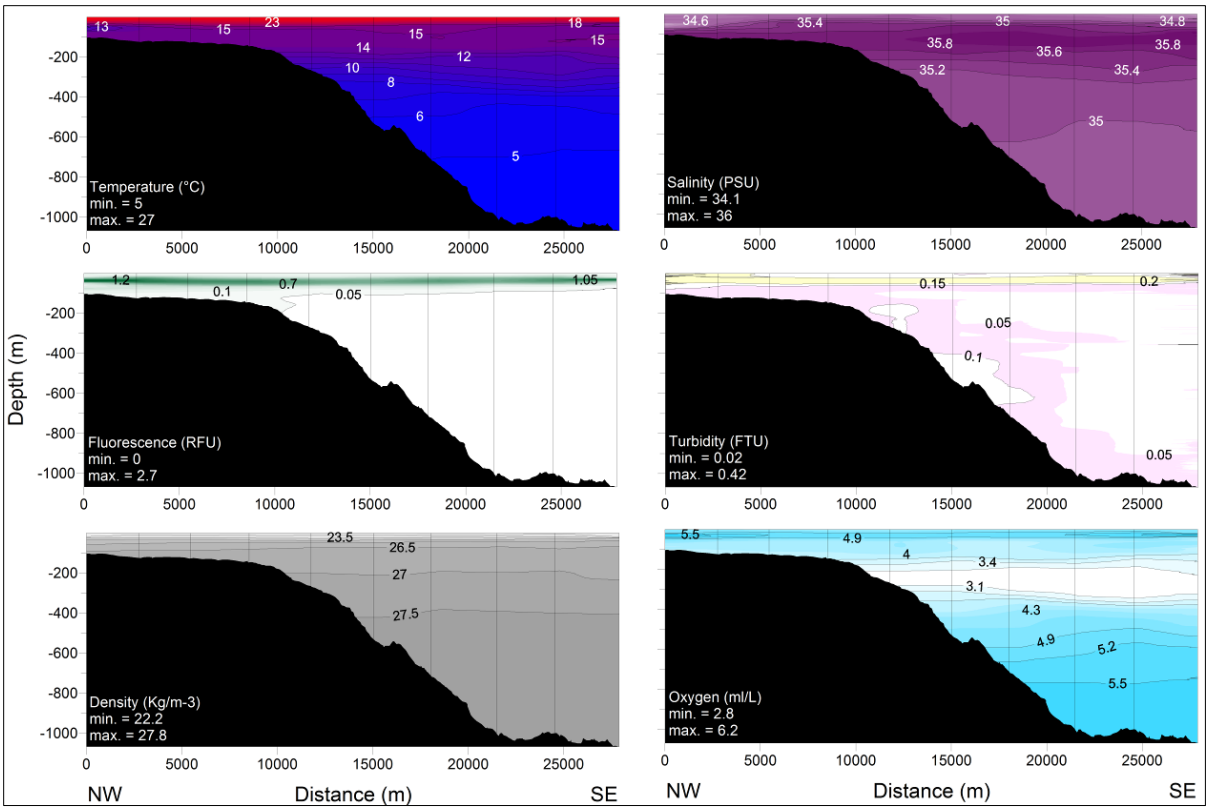

Figure 5-8 Water column characteristics derived from CTD profiling along the Baltimore Canyon open slope transect. Six variables used to characterize the water column were temperature, salinity, fluorescence, turbidity, density, and oxygen. The range and units for each variable are shown as minimum and maximum. Dark lines show the position of CTD casts along the transect, including extreme margins in the plot (number of casts = 10).

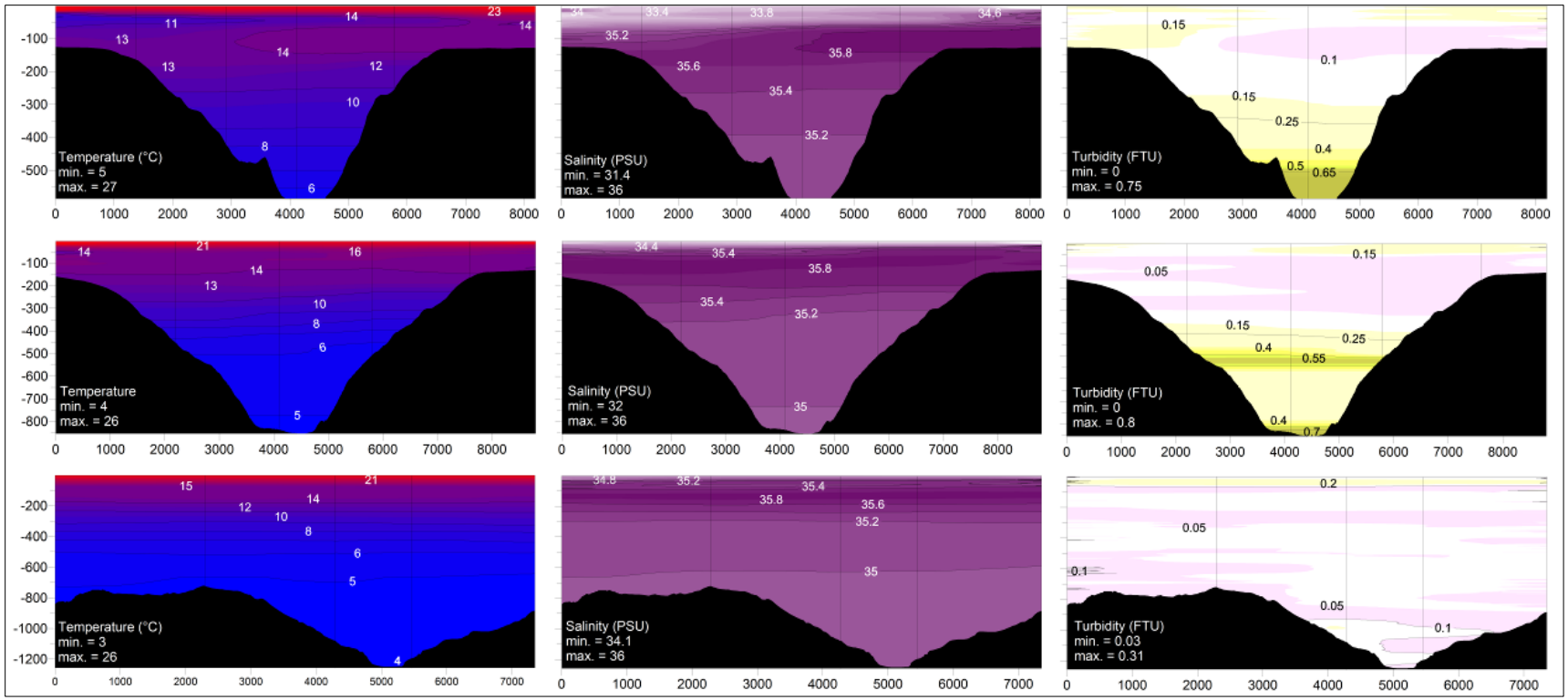

Figure 5-9 Cross canyon CTD profiles for temperature (first column), salinity (second column) and turbidity (third column) running perpendicular across Baltimore Canyon. From top row: upper canyon approximately 8 km from the initial mouth of the canyon, mid-canyon 15 km from the initial mouth of the canyon, and lower canyon 25 km from the initial mouth of the canyon. Dark lines show the position of CTD casts along the transect. Dark lines show the position of CTD casts along the transect, including extreme margins in the plot (number of casts = 6).

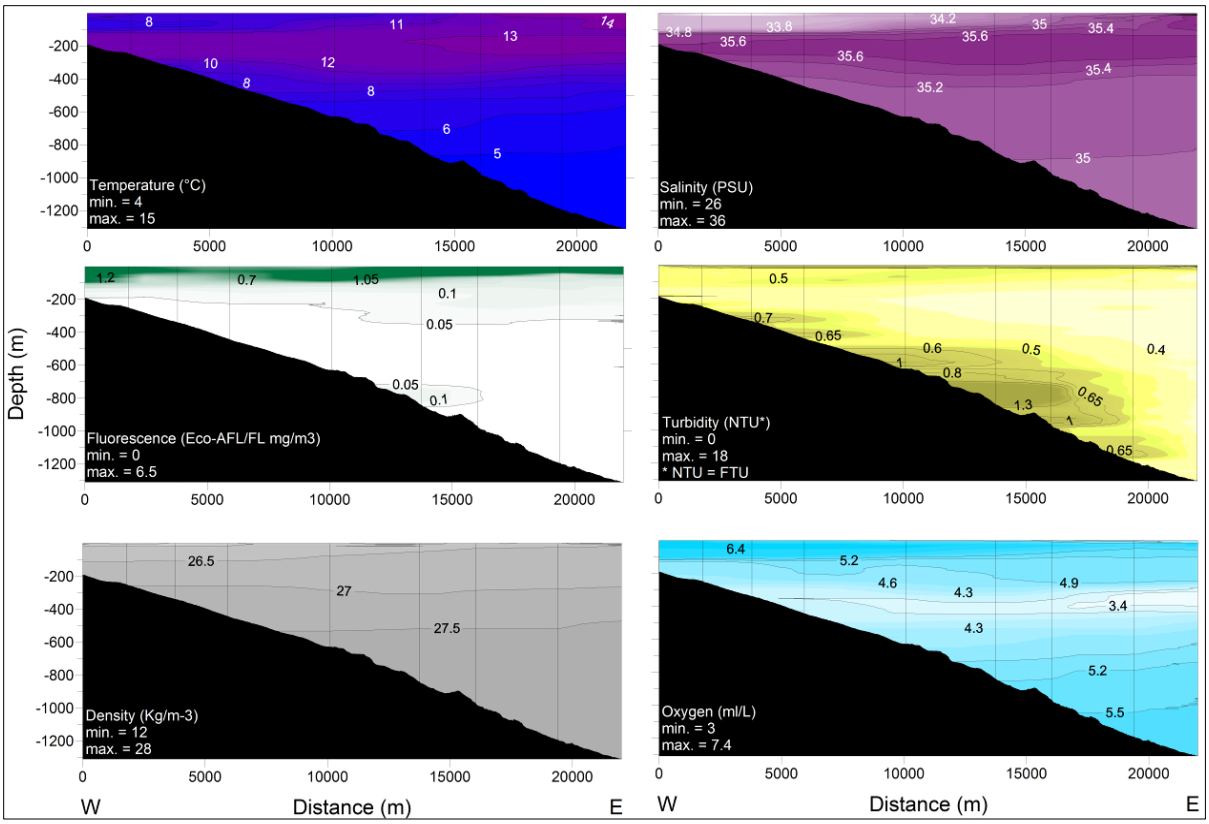

Figure 5-10. Water column characteristics derived from CTD profiling along the Norfolk Canyon axis transect. Six variables used to characterize the water column were temperature, salinity, fluorescence, turbidity, density, and oxygen. The range and units for each variable are shown as minimum and maximum. Dark lines show the position of CTD casts along the transect, including extreme margins in the plot (number of casts = 9).

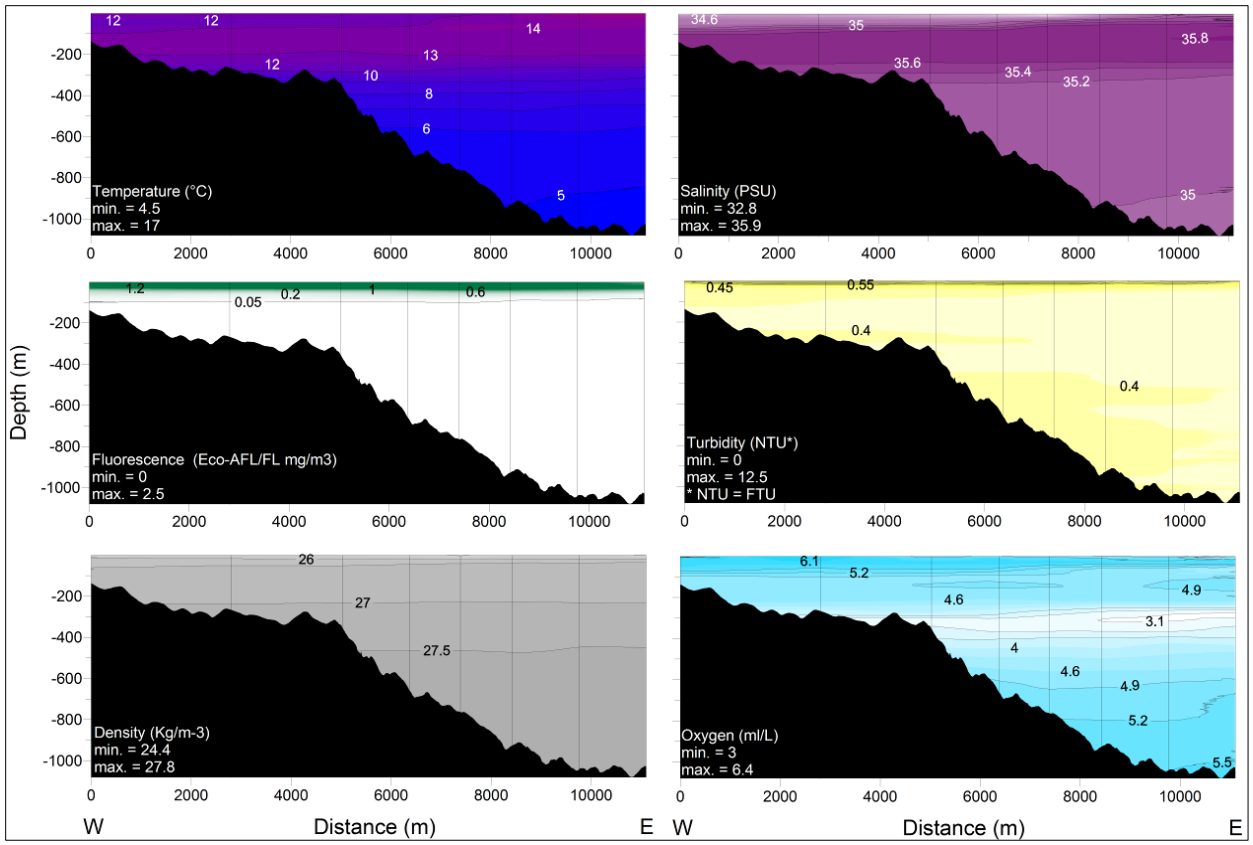

Figure 5-11. Water column characteristics derived from CTD profiling along the Norfolk Canyon open slope transect. Six variables used to characterize the water column were temperature, salinity, fluorescence, turbidity, density, and oxygen. The range and units for each variable are shown as minimum and maximum. Dark lines show the position of CTD casts along the transect, including extreme margins in the plot (number of casts = 8).

5.3.4 Geostrophic Flow

The three transverse canyon transects from Baltimore were used to calculate the horizontal component flow velocities up and down the canyon (**Figure 5-12**). The average and direction of flow and the proportion of flow, based on the geostrophic flow theory, are summarized in **Table 5-4**. The upper and middle transects show maximum down canyon current flow from -3.6 and -2.6 m s^{-1}, respectively. These fast current speeds are observed in surface waters (<200 m), with visible small pockets of up-canyon flow in the upper canyon surface waters (<50 m) on either side of the canyon axis (**Figures 5-12a**,**b**). The lower canyon transect (**Figure 5-12c**) captured a very different pattern to that calculated for the shallower reaches, whereby bottom water moved up-canyon, and there was an increase in the size of the shallow pockets of upward flowing water either side of the canyon axis. The upward flowing water mass can be identified as WASIW (temperatures <8 °C, salinities >34.8), the same signature observed in **Figure 5-4** that traveled up the entire length of the canyon. Interestingly, this upward flowing WASIW coincides with the water mass at the offshore protrusion of the nepheloid layer (**Figure 5-7**) and appears to be an interface between two water masses along the 27.5 kg m^3 isopycnal (~450 to 500 m). The upper parts of the nepheloid layer were entrained by overlying WNACW traveling offshore (i.e., down canyon), producing a seaward finger-like projection at approximately 400 m (**Figure 5-7**).

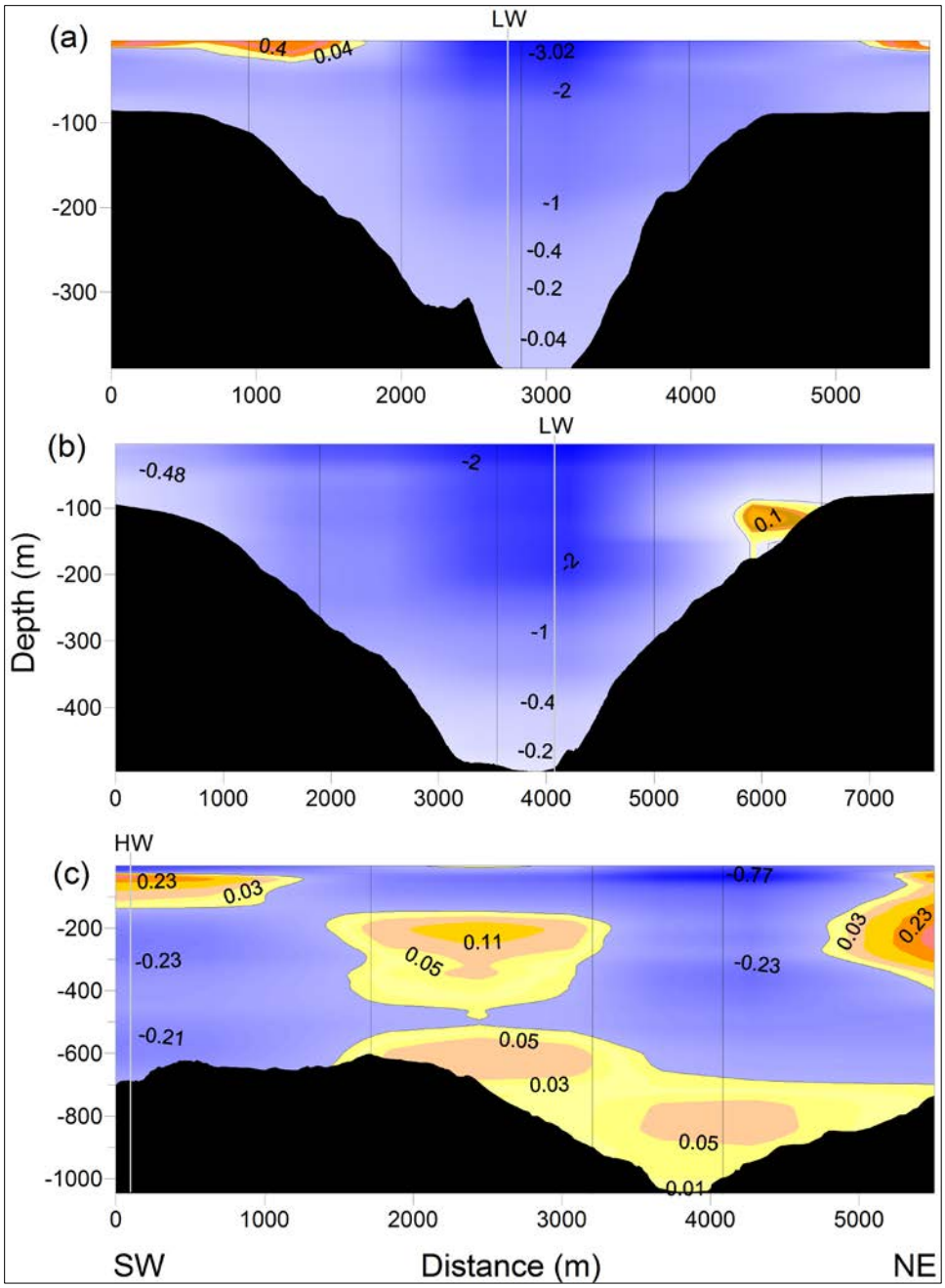

Figure 5-12. Contour maps for up-canyon and down-canyon flow velocities as calculated by the geostrophic flow equation, Baltimore Canyon transverse transects (a: upper, b: middle, and c: lower canyon). Blue denotes down-canyon water flow (negative values) and orange denotes up-canyon water flow (positive values). Gray lines show the tidal state (measured to nearest tidal buoy, Ocean City, Maryland) where LW = low water and HW = high water. Dark lines show the position of CTD casts along the transect, including extreme margins in the plot (number of casts = 6).

Table 5-4. Net up-down canyon current velocities (m sec^{-1}) as calculated by the thermal winds equation and the proportion (% flow) of the water column contributing to up- or down-canyon flow.

Canyon	Transect	Direction	Net Flow (m s^{-1})	Percent
Baltimore	Upper	Up-Down	-0.553	--
		Up	0	0
		Down	-0.553	100
	Mid	Up-Down	-0.843	--
		Up	0.112	10
		Down	-0.982	90
	Lower	Up-Down	-0.060	--
		Up	0.099	35
		Down	-0.182	65
Norfolk	Lower	Up-Down	-0.083	--
		Up	1.537	61
		Down	1.001	39

Despite having only one valid across canyon transect on which to investigate water flow up and down Norfolk Canyon, some interesting differences in velocity were observed. **Figure 5-13** shows a large layer of up-canyon flowing bottom water (max = 2.5 m s^{-1}) reaching from 350 to 1,000 m. This water mass can again be characterized as up-canyon flowing WASIW (temperatures <8 °C, salinities >34.8). Compared with the Baltimore deep canyon transect, the speed of the upward flow was more than an order magnitude higher in the deeper reaches of Norfolk (1.5 m s^{-1}) than in Baltimore (0.099 m s^{-1}) (**Table 5-4**).

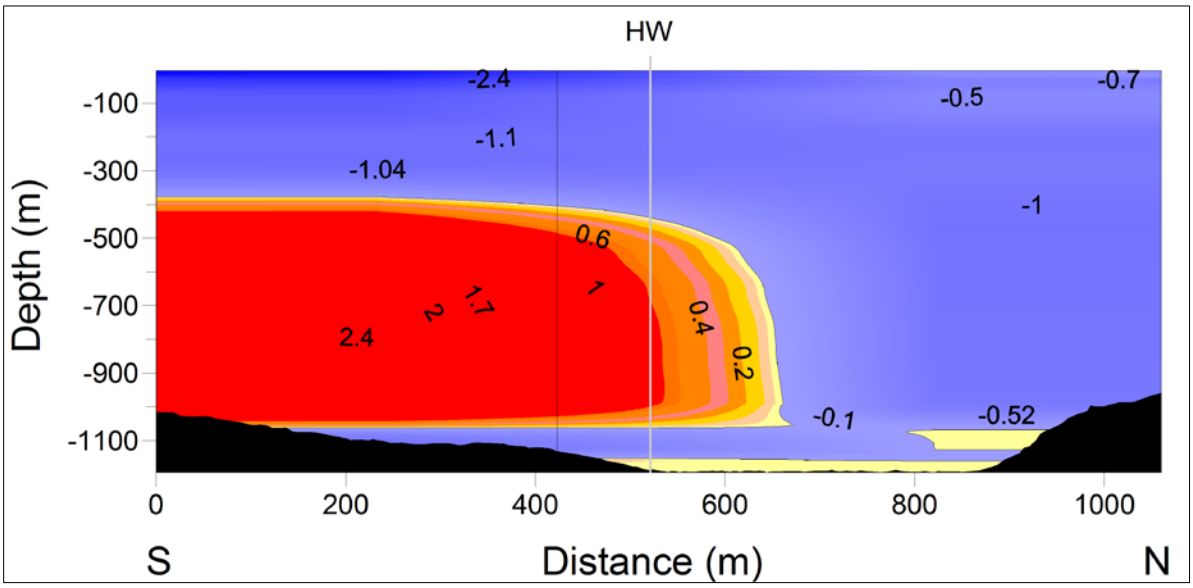

Figure 5-13. Contour maps for up-down canyon flow velocities as calculated by the geostrophic flow equation, lower Norfolk Canyon transverse transect, 23 km from the initial mouth of the canyon. Blue denotes down-canyon water flow (negative values) and orange denotes up-canyon water flow (positive values). Gray lines show the tidal state (measured to nearest tidal buoy, Ocean City, Maryland) where HW = high water. Dark lines show the position of CTD casts along the transect, including extreme margins in the plot (number of casts = 3).

5.3.5 Benthic Lander and Mooring Observations

5.3.5.1 Baltimore Canyon

The data from landers generally supported the CTD observations reported above and provided continuous time series of conditions near the seafloor. In Baltimore Canyon, the shallow station (**Figures 5-1** and **5-14**, 603 m water depth), demonstrated variable conditions in all parameters measured, with temperature fluctuating between 4.5 °C and 8.6 °C and a mean of 5.4 °C (standard deviation [SD] 0.47). Current intensities also varied greatly, with peak current velocity reaching 66.2 cm s^{-1} and a mean of 13.7 cm s^{-1} (SD 9.03). Dissolved oxygen concentration ranged between 4.65 and 7.4 mg L^{-1} with a mean of 6.6 mg L^{-1} (SD 0.3). Sigma theta calculated from salinity, temperature, and depth fell between 26.11 and 27.71 kg m^3 with a mean of 27.49 kg m^3 (SD 0.1). Turbidity varied throughout the measurement period, indicating intense and periodic sediment resuspension/transport events at this location. Peaks in turbidity appeared to correspond with temperature fluctuations (Spearman's rank correlation on 24-hour moving average data for first deployment, $r = 0.48$, $p < 0.001$), indicating sediments were transported from shallower and warmer waters. Warmer waters were also correlated with higher current speeds (Spearman's rank correlation on 24-hour moving average data for first deployment, $r = 0.49$, $p < 0.001$).

Toward the end of the time series, after the recovery for at-sea servicing (indicated on **Figure 5-14** by X and dotted vertical lines on each plot), all recorded variables demonstrated differences from the first part of the deployment. This possibly reflects three scenarios:

1. An alteration to the redeployment location in contrast with the first period (i.e., distance to large topographical features, such as canyon walls). Accurately plotting the position of a benthic lander is not possible without high-resolution multibeam and visual observations, which were not undertaken during these deployments.
2. Disruption to lander position after deployment, for example, a high-velocity flow event peaking at 63 cm s^{-1} caused the lander to tilt by 30° and returned to rest at a tilt of 8° (compared with previous 3°).
3. Potential sensor shift or malfunction (but this is highly unlikely).

The magnitude of all variables decreased, which was driven by season. Data from the early part of the first deployment had a similar signature, and conditions were increasingly variable between October and May. This change was substantial for many variables. For example, in the temperature series, the first deployment period had a standard deviation in temperature of 0.47 °C compared with the second period of 0.24 °C. Similar reductions in variability were present in salinity (standard deviation reduction of 0.03), current speed (1.43 cm s^{-1}), oxygen (0.13 mg L^{-1}), and turbidity (16.52 RU). Because the reason for the observed changes was not known, some subsequent analyses in this chapter were conducted using only the first deployment period to allow consistent comparison with landers and moorings in other locations that were not moved during the observation period.

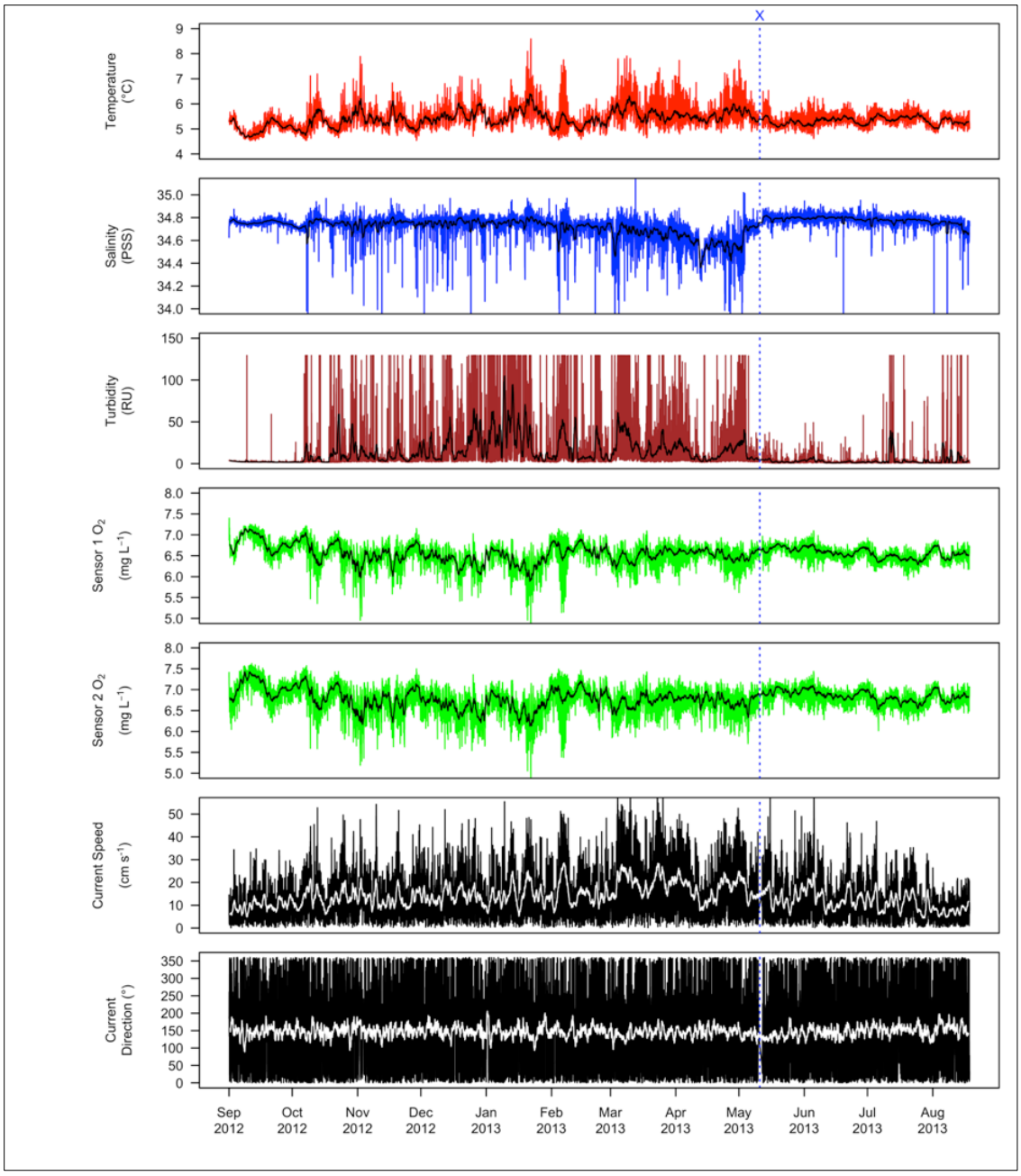

Figure 5-14. Oceanographic variables (indicated by y-axis titles) extracted from the shallow lander in Baltimore Canyon (depth: 603 m). Black or white lines represent a 24-hour moving average filter for each variable. All sensors recorded at 1.5 m above bottom except for currents at 2 m above bottom, which were recorded at a 15 min interval. The data gap between May and June, highlighted by X on the temperature plot and the dotted line through all series, was due to lander recovery and redeployment.

The mid-canyon area (1,082 m) was monitored using a mooring system with a limited sensor load that was mounted higher in the water column compared with the shallow and deep landers (**Figures 5-2** and **5-15**). This area of the Baltimore Canyon was characterized by temperatures that ranged from 4 °C to 5.1 °C with a mean of 4.5 °C (SD 0.16). Maximum current velocity was 42.3 cm s^{-1} and a mean of 8.7 cm s^{-1} (SD 5.6). Sigma theta calculated from salinity and pressure (depth constant due to no pressure

sensor) ranged from 27.55 to 27.9 kg m^3 with a mean of 27.7 kg m^3 (SD 0.02). This site demonstrated moderate positive linkage between current velocity and temperature (Spearman's rank correlation on 24 hour moving average data for first deployment, $r = 0.43$, $p < 0.001$). Although this mooring was not recovered for servicing in May 2013, there appeared to be similar suppression in variability, as for the shallow lander, observed in the latter part of the dataset for temperature (SD 0.07 °C) and current velocity (SD 1.56 cm s^{-1}), indicating that this change may be seasonally related.

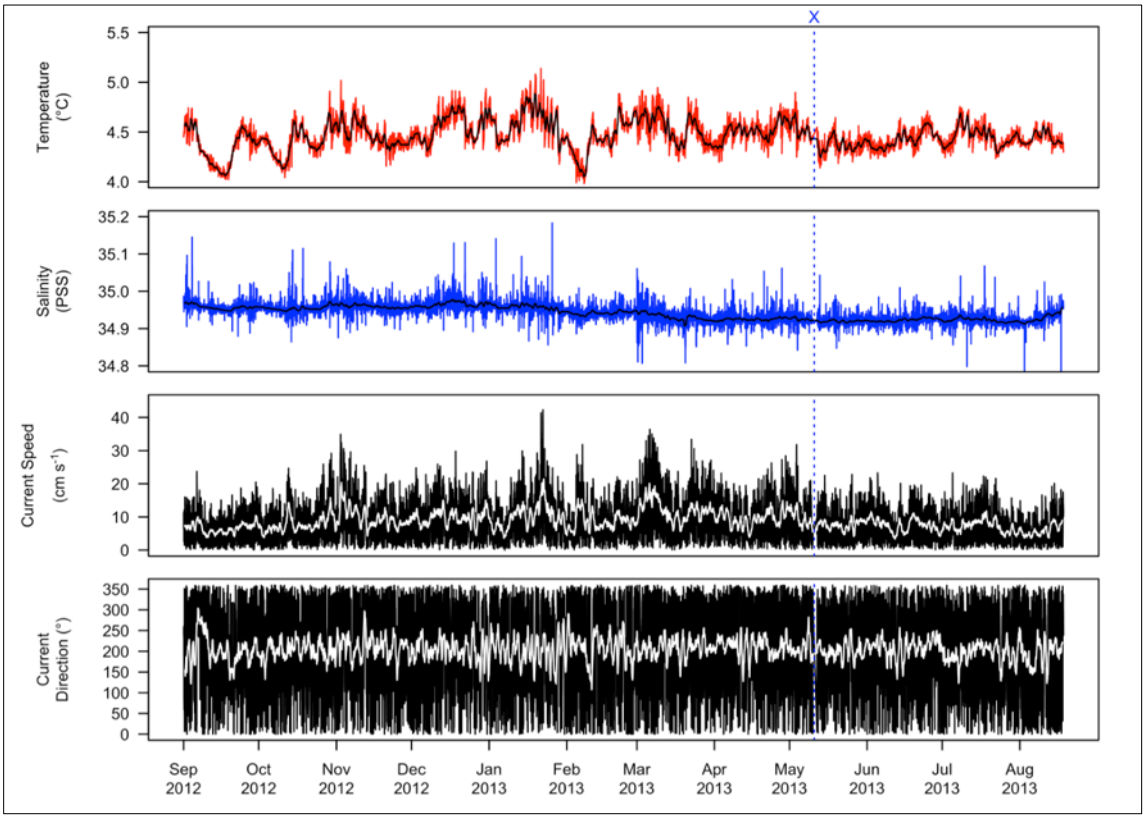

Figure 5-15. Oceanographic variables (indicated by y-axis titles) extracted from the mid-mooring in Baltimore Canyon (depth: 1,082 m). Black or white lines represent a 24-hour moving average filter for each variable. Sensor set differed from the other deployments in this canyon. Current data were obtained at 14.24 m above bottom, temperature and salinity at 9 m above bottom. Currents were recorded at a 15 min interval, temperature and salinity at a 5 min interval. For clarity, these data were resampled to a 15 min interval to match all sensors. The gap in data between May and June, highlighted by X on the temperature plot and the dotted line through all series, was due to lander recovery and redeployment and is repeated on the plot to allow direct comparison with other sites in the lander.

The deeper region of Baltimore Canyon was monitored using a lander of the same design as the shallow station, with a similar sensor load (**Figures 5-2** and **5-16**). Temperatures fluctuated between 3.8 °C and 4.74 °C with a mean of 4.2 °C (SD 0.16). Maximum current velocity was 29.2 cm s^{-1}, with a mean speed of 6.6 cm s^{-1} (SD 3.27). Dissolved oxygen concentration ranged from 6.8 to 7.4 mg L^{-1} with a mean of 7.12 mg L^{-1} (SD 0.09). Sigma theta calculated from salinity, temperature, and depth fell between 26.07 and 28.09 kg m^3, mean 27.99 kg m^3 (SD 0.03). At this site, peaks in turbidity were positively correlated with current velocity (Spearman's rank correlation on 24-hour moving average data for first deployment, $r = 0.62$, $p < 0.001$), and there was a strong relationship between current velocity and temperature (Spearman's rank correlation on 24-hour moving average data for first deployment, $r = 0.75$, $p < 0.001$). This indicates that warmer sediment-laden waters are transported to the deeper parts of the

canyon. There were no notable correlations between temperature and current direction, or turbidity and direction. As with the shallow station, this lander was also recovered for servicing, and again the time series appeared to show differences between the first and second deployments, with a marked shift in salinity and turbidity (**Figure 5-16**), standard deviation reduced by 0.08 °C for temperature, 0.68 cm s^{-1} in current velocity, and 0.05 mg L^{-1} in oxygen.

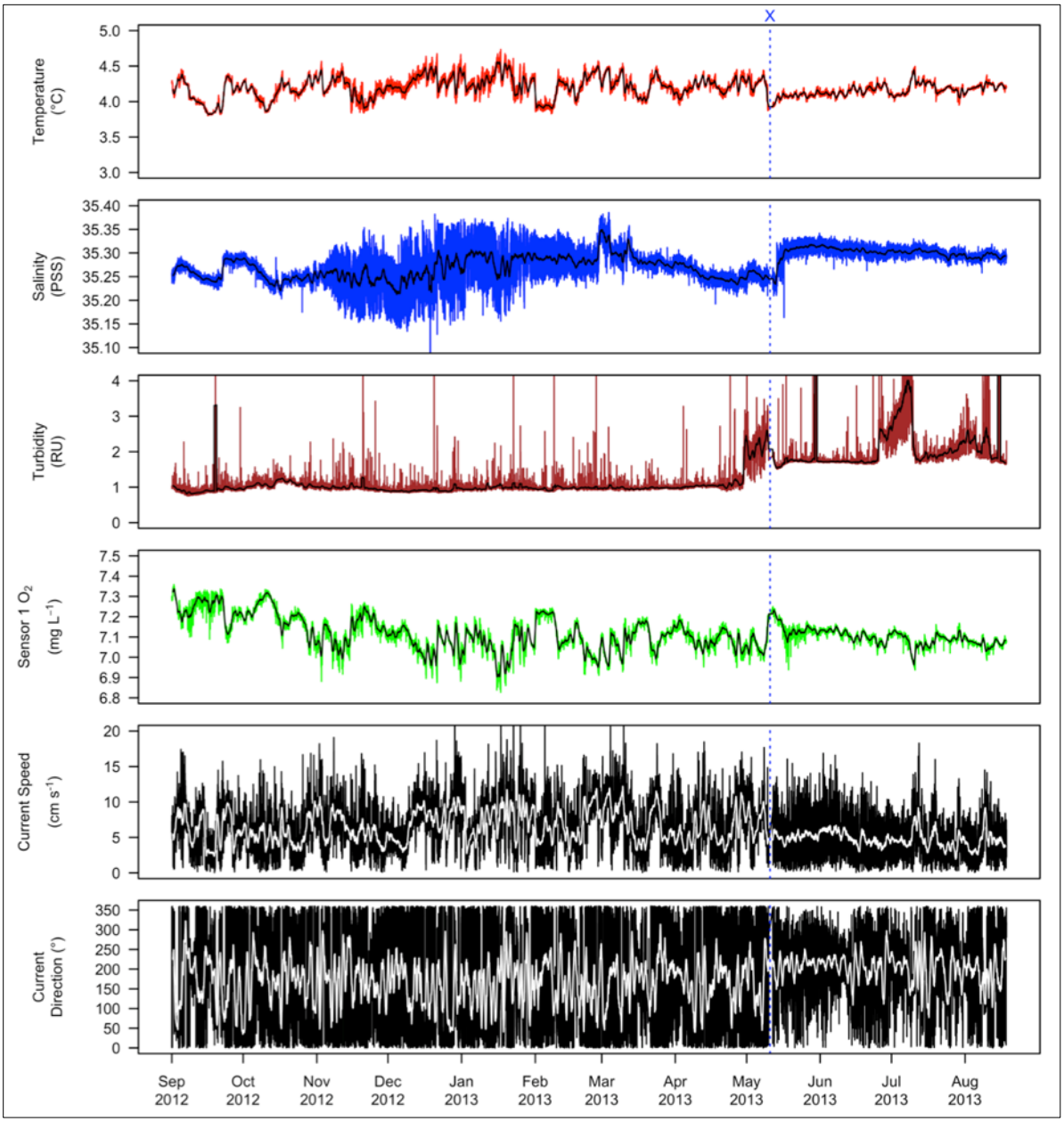

Figure 5-16. Oceanographic variables (indicated by y-axis titles) extracted from the deep lander in Baltimore Canyon (depth: 1,318 m). Black or white lines represent a 24-hour moving average filter for each variable. All sensors recorded at 1.5 m above bottom except for currents at 2 m above bottom, which were recorded at a 15 min interval. The data gap between May and June, highlighted by X on the temperature plot and the dotted lines through all series, was due to lander recovery and redeployment.

5.3.5.1.1 Variation Between Locations Within the Canyon

Direct comparison between stations in Baltimore Canyon was possible for current velocity, current direction, temperature, and salinity, but as the mid-mooring was not measuring at the same height above bottom, comparisons with this mooring should be taken with caution. Density kernels revealed substantial differences for all variables (**Figure 5-17**). The shallow lander appeared to be the most distinct, with a unimodal structure for salinity and a broad range of temperatures, with higher current speeds indicating that a relatively warm current swept the area, which appears to be dominated by a single water mass (**Figure 5-17**). The mid-mooring and deep lander displayed some similarities, with substantial overlap in temperatures and current velocity; however, the mid-canyon was warmer and had a greater incidence of current speeds above 15 cm s^{-1}. The salinity records from the mid-mooring showed a slight bimodal structure to the density kernel, indicating mixing, likely between two water masses (**Figure 5-17**). The deep lander was in the coldest and most saline water mass and had the weakest currents of all stations. This site also demonstrated slight bimodality in salinity. Current direction density kernels indicated substantial variability between locations in the canyon (**Figure 5-17**).

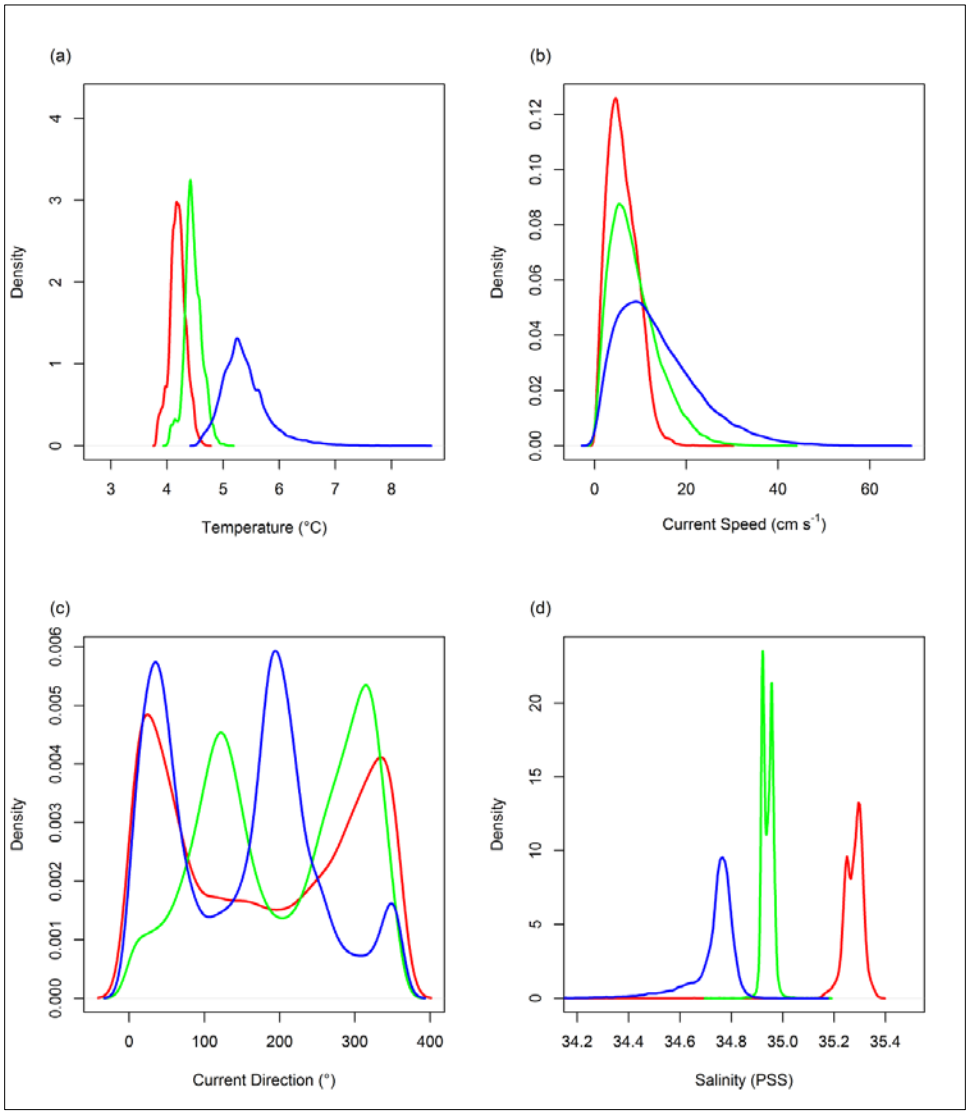

Figure 5-17. Density kernels of parameters (a) temperature, (b) current speed, (c) current direction, and (d) salinity from the deep (red), mid (green), and shallow (blue) stations in Baltimore Canyon.

Radial histogram plots show that at the shallow lander, flows were predominantly along a 45° and 200° axis, following the general residual flow on the shelf (**Figure 5-18**). This is reflected in progressive vector plots, whereby the shallow area experienced tidal flow, with general movement toward the northeast (**Figure 5-19**). Subsetting the full series into 60-day bins reveals strong tidal modulation of the flow as well as some disruption to the residual flow occurring between days 60−90 and 180−200 (**Figure 5-19**), which correspond to a residual flow that is pushed off the shelf and toward the open ocean. A marked shift in the residual flow direction was observed at the mid-mooring where a significant alignment with the orientation of the canyon occurred (**Figure 5-19**). However, this pattern was initially variable during the first 60 days of deployment, and some variation occurred during days 120 to 180 (**Figure 5-19e**). The deep lander had the most consistent residual flow that was identical in direction to the shallow station (**Figure 5-19**). However, transport was less tidally regulated than in the shallow station, demonstrating far greater movement to the northeast. Each of the 60 day bins for the deep station showed some tidal modulation, but it was much lower in magnitude than in the two shallower stations (**Figure 5-19**).

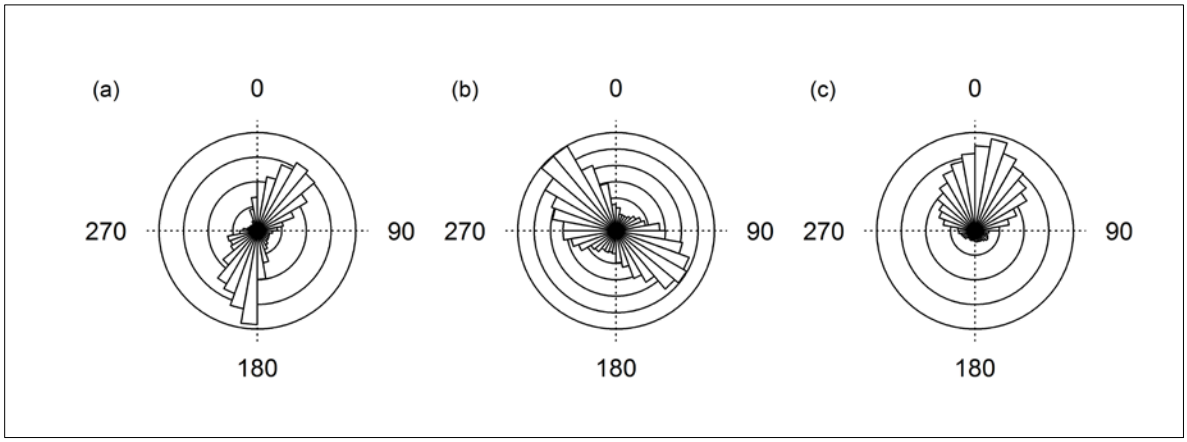

Figure 5-18 Radial histograms showing predominant flow direction from current meter data for (a) shallow lander, (b) mid-mooring, and (c) deep lander in Baltimore Canyon.

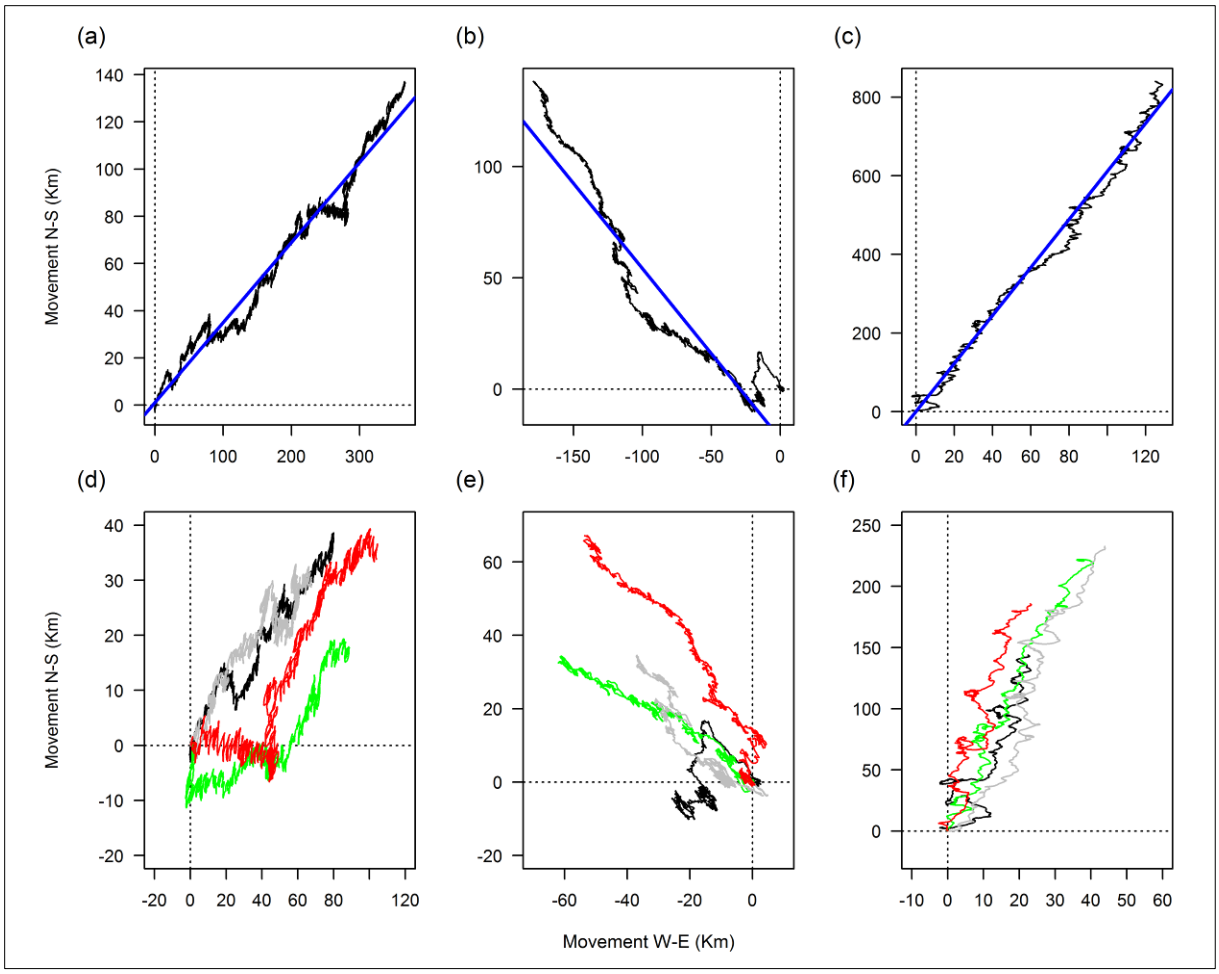

Figure 5-19. Progressive vectors for each station at Baltimore Canyon. The first row of plots shows vectors for the first part of the Baltimore Canyon deployments for (a) shallow lander, (b) mid-mooring, and (c) deep lander. Blue lines indicate the general direction of the residual flow. The second row of plots shows 60-day subsets of the overall time series. Black lines indicate the first 60 days, green 60 to 120 days, gray 120 to 180 days, and red 180 to 240 days for the (d) shallow lander, (e) mid-mooring, and (f) deep lander.

To assess whether canyon walls affected current direction, several bins of current speeds were extracted from the mid-mooring, which was equipped with an upward-looking ADCP. Current velocities were relatively homogenous throughout the measured bins, with a slight acceleration closer to the seabed (**Figure 5-20a**). Direction showed a more pronounced difference, where current directions at higher bins were more focused than those lower to the seafloor. The slight deviation in flow direction at the 14 m and 34 m bins relative to other bins likely indicate some alteration to direction by low-lying topography less than 34 m high, while the higher bins are more likely steered by the overall canyon topography (**Figure 5-20b**).

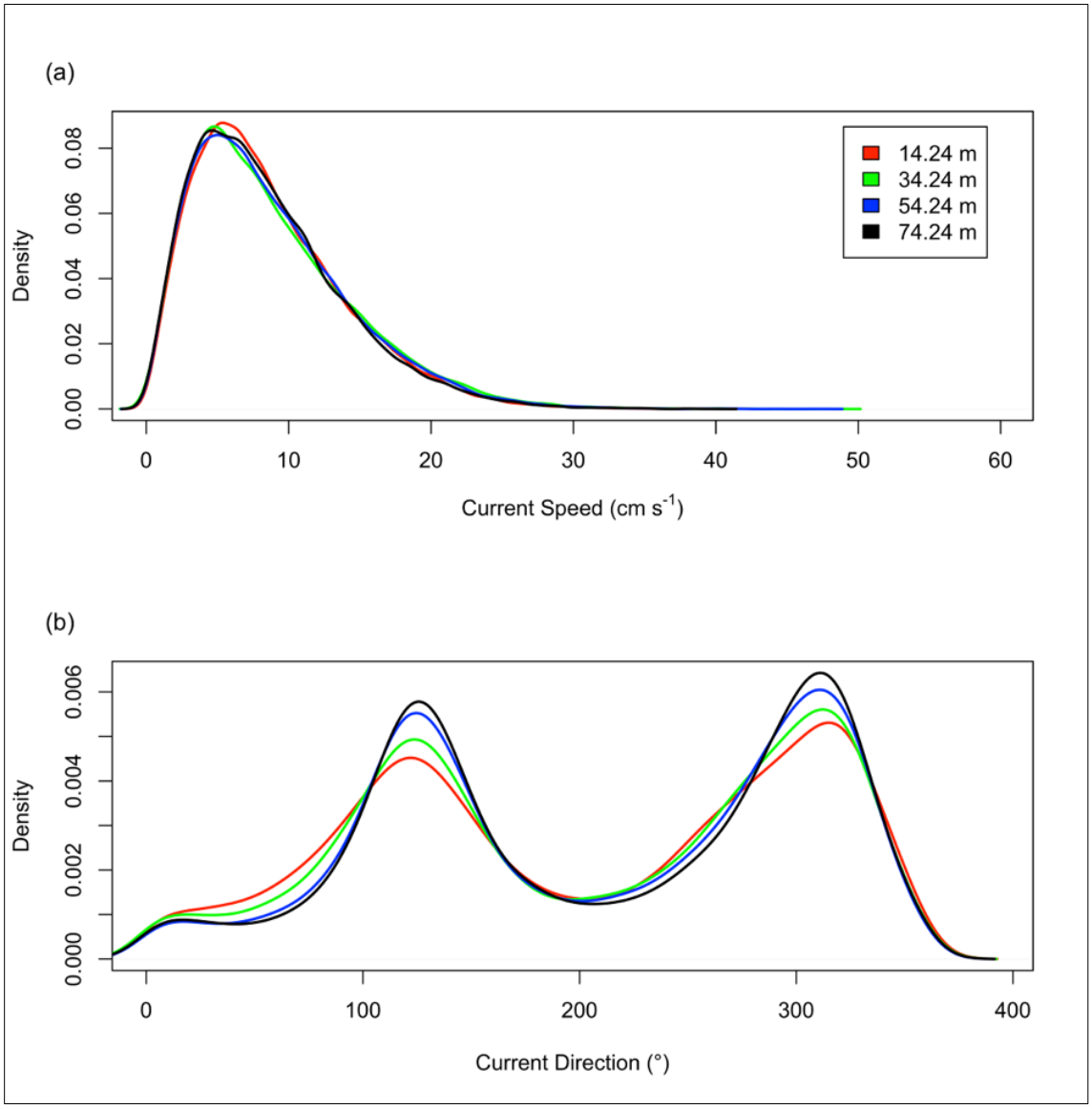

Figure 5-20. Density kernels for two parameters obtained from the mid-canyon ADCP. (a) current speed and (b) current direction from different water heights. Note data reliability at the 94.24 m and 114.24 m bins were poor and therefore were omitted from the plot.

The near-bottom flow direction corrected to reflect the flow along the canyon axis demonstrated that all stations in Baltimore Canyon had flow that was generally up-canyon (**Figure 5-21**). This was most pronounced in the deepest station where flow moved approximately 400 km up-canyon over the entire time series (**Figure 5-21a**). In the mid-canyon, the flow moved approximately 220 km up over the entire

time series (**Figure 5-21b**), and in the shallow station, the pattern included periods of both down- and up-canyon flow with the cumulative distance eventually reaching 71 km of up-canyon travel (**Figure 5-21c**).

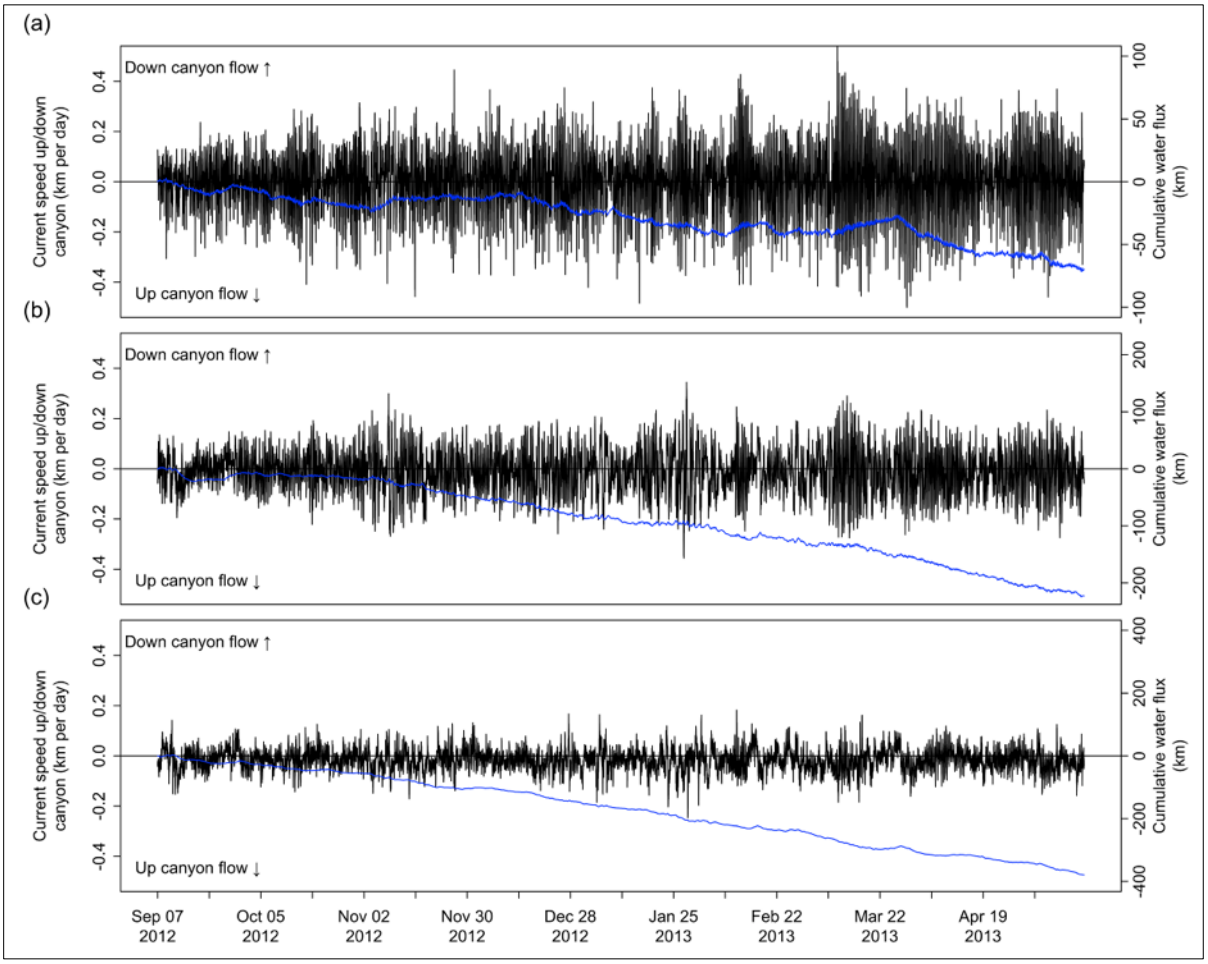

Figure 5-21. Flow velocity along the Baltimore Canyon axis corrected for the canyon axis orientation. (a) Shallow canyon (603 m) orientated at 170°, (b) mid-canyon (1,082 m) orientated at 120°, (c) deep canyon (1,318 m) orientated at 125°. Black line indicates flow velocity for each reading, blue line indicates cumulative flow across the time series. Negative values indicate that water movement is up-canyon (i.e., toward the shelf), and positive values indicate water moving down the Canyon (i.e., toward the abyssal plain).

5.3.5.1.2 Linkages Between Locations Within the Canyon

There were apparent links between lander stations with respect to variables that were measured concurrently. Temperature in Baltimore Canyon, for instance, was best correlated between the shallow and mid-stations at a lag of -1.01 days, indicating that the mid-station is leading the shallow station. In essence, up-canyon transport of water from the mid-station took 24.24 hours (or two M2 tidal cycles) to reach the shallow station (**Figure 5-22a**). Temperature transport from the deep to shallow lander station also detected up-canyon movement and took longer, at approximately -2.56 days or five tidal cycles (**Figure 5-22b**). However, the mid- to deep-station linkage demonstrated a different pattern whereby conditions at the mid-station strongly matched those at the deep station after approximately 5.76 hours. The broad range of high correlations that fit across several lags indicates that the linkage is stable with little variation (**Figure 5-22c**). The oxygen profile between shallow to deep demonstrated the strongest fit

at negative lags (with a maximum after -0.06 days or 1.44 hours), indicating some limited up-canyon flow from the deep to the shallow station (**Figure 5-22d**). Other variables such as turbidity and salinity showed little correspondence between stations (not shown in figure).

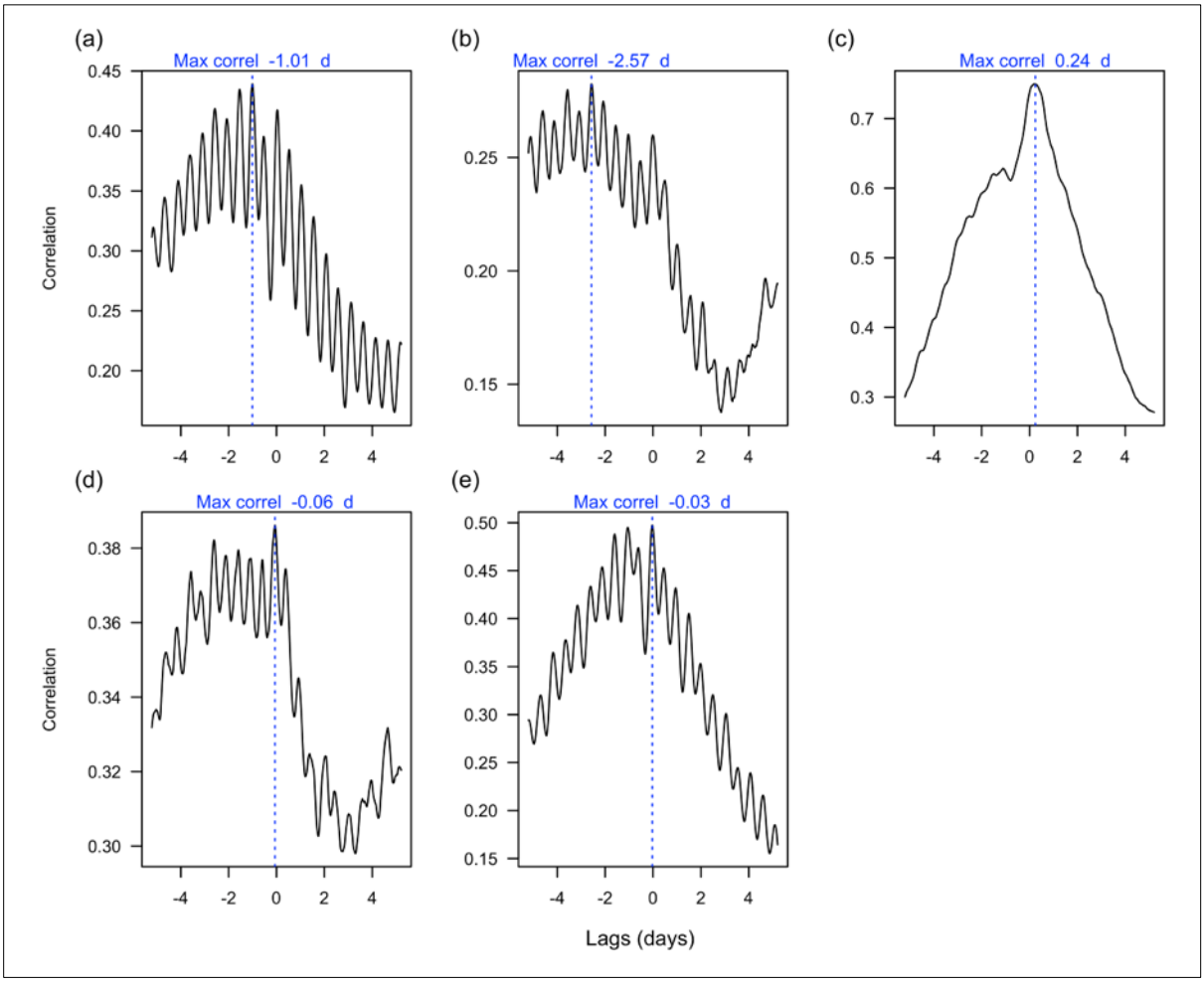

Figure 5-22. Cross-correlations to determine linkages between landers and moorings in Baltimore and Norfolk canyons. (a) Temperature in Baltimore Canyon, between shallow and mid-stations, (b) temperature in Baltimore Canyon, shallow to deep, (c) temperature in Baltimore Canyon, mid to deep, (d) oxygen concentration in Baltimore Canyon, shallow to deep, and (e) temperature in Norfolk Canyon, mid to deep. Where lag is negative, the second variable is compared with past conditions at first variable.

5.3.5.1.3 Tidal Influences Within the Canyon

There was clear evidence of a strong tidal influence within Baltimore Canyon that extended throughout in most major variables, including current velocity components and temperature. In particular, the semidiurnal lunar tidal constituent M2 was particularly pronounced in current speed data at all stations (**Figure 5-23**). In the shallow station, the M2 amplitude from harmonic tidal analysis was greatest at 9.155 $cm^2\ s^{-1}$, with the next strongest constituent being the S2 (the semidiurnal solar tidal constituent) with amplitude of 3.974 cm s^{-1}. The mid-canyon sensor detected the same relative pattern with decreased amplitude of 4.43 cm s^{-1} for M2 and 1.87 cm s^{-1} for S2. Finally, at the deepest station, the amplitude of the M2 constituent was 1.43 cm s^{-1} and 0.49 cm s^{-1} for S2. Temperature showed a similar pattern in the shallow and mid-canyon, with strong M2 modulated pattern; however, this signal was absent in the deep canyon, reflecting a more stable temperature regime at depth (**Figure 5-24**). Removing the high frequency

tidal constituents from the current speed sensors showed a fairly regular periodicity that appears to potentially fit a spring-neap tidal cycle (14.75 d). The pattern was most pronounced at the shallow lander and mid-mooring (**Figure 5-25**), especially during the latter parts of the observation period between January and May. The deepest station had a less convincing fit with the spring-neap cycle; however, there were some consistent patterns such as the bimodal peaks that occurred during the first half of November, the second half of December, mid-January, and the end of February to March.

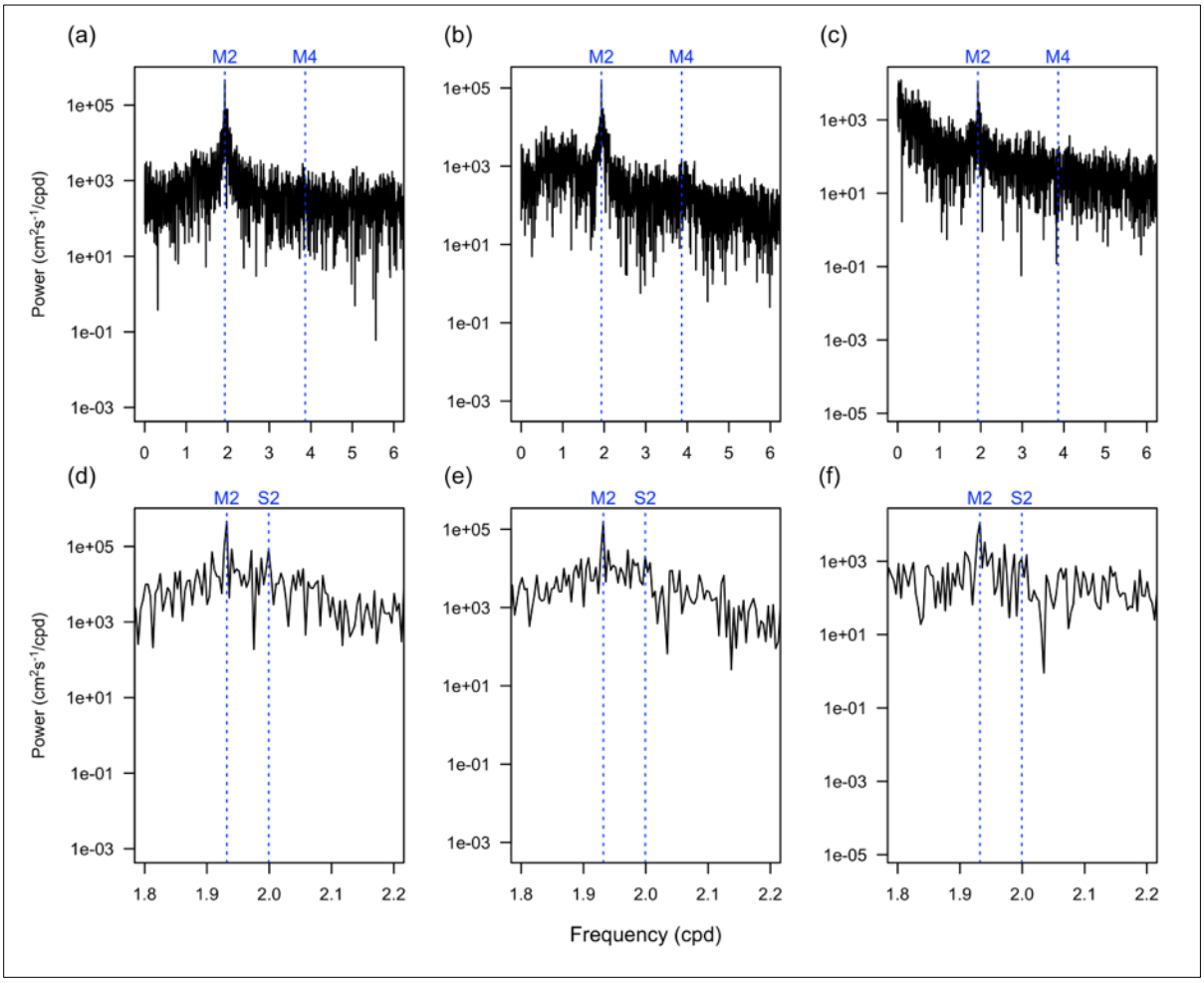

Figure 5-23. Power spectra of current velocity components u,v from Baltimore Canyon. X-axes are truncated on (d) through (f) to focus on the M2 and S2 tidal components. Shallow lander (a) and (d), mid-mooring (b) and (e), and deep lander (c) and (f). Frequency in counts per day (cpd). Time series used 1st series.

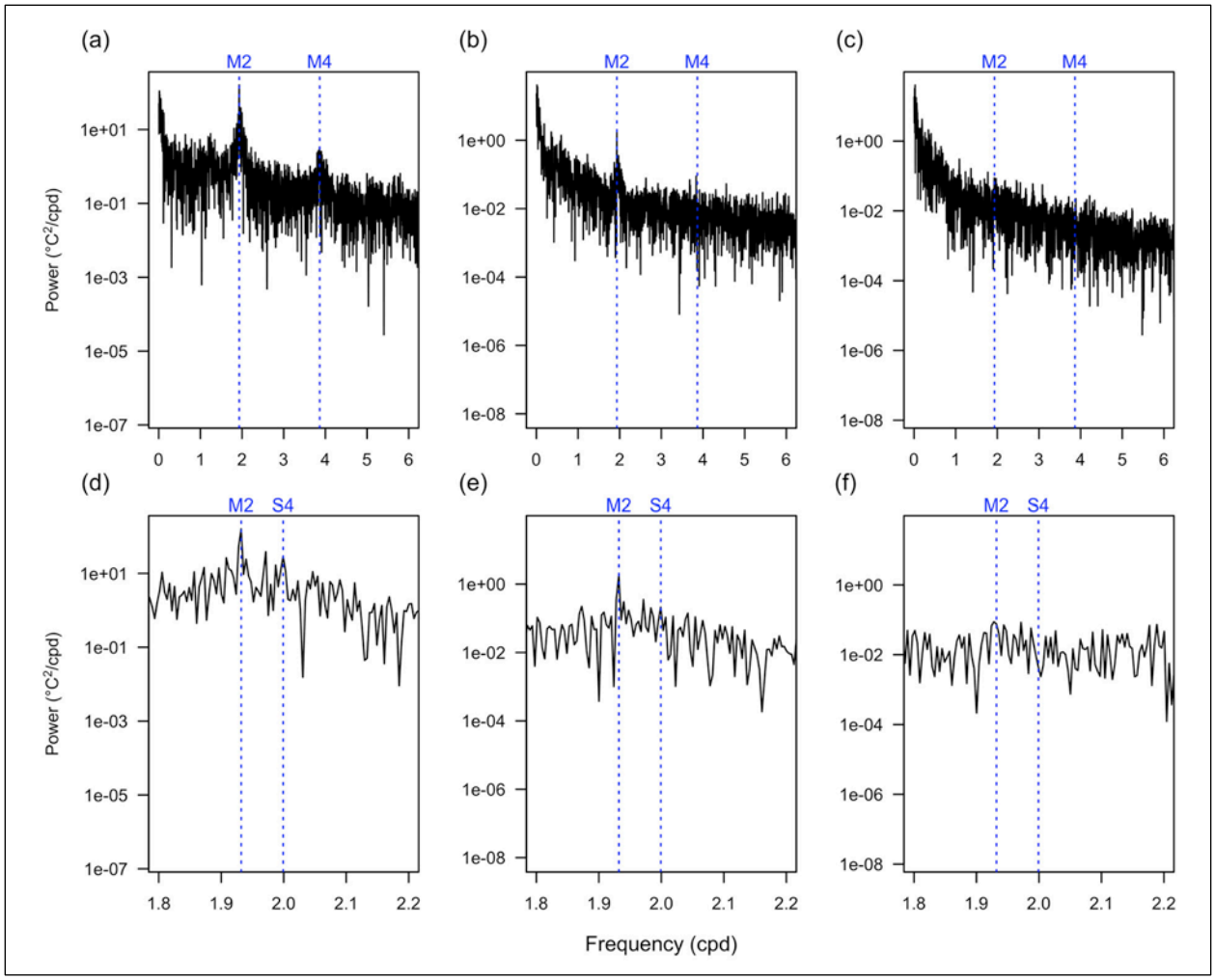

Figure 5-24. Power spectra of the temperature signal from Baltimore Canyon. X-axes are truncated on (d) through (f) to focus on the M2 and S2 tidal components. Shallow lander (a) and (d), mid-mooring (b) and (e), and deep lander (c) and (f). Frequency in counts per day (cpd). Time series used 1st series.

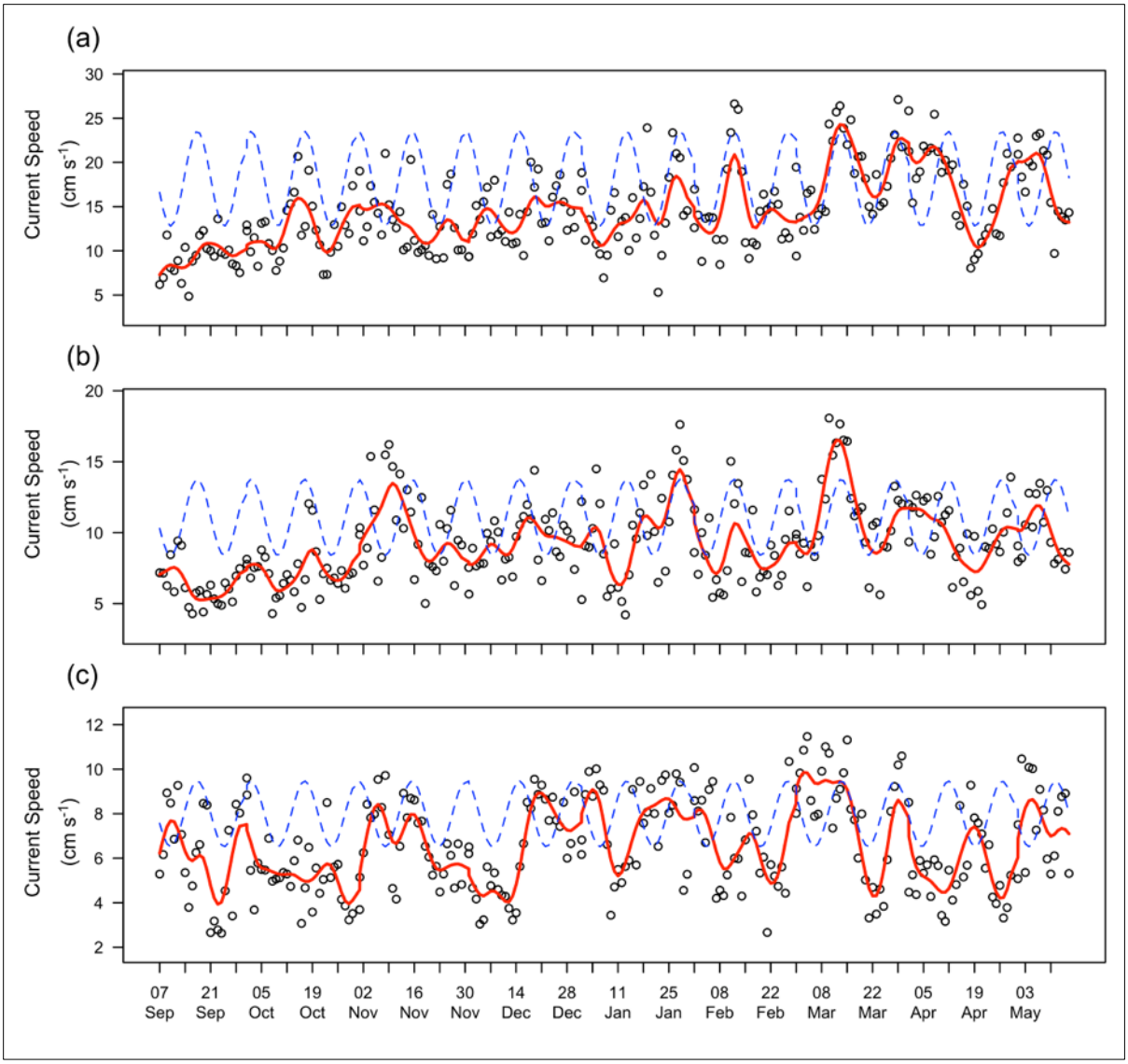

Figure 5-25. Low-pass filtered current speed to remove high frequency tidal signal (25-hour period) for Baltimore Canyon. From the (a) shallow lander, (b) mid-mooring, and (c) deep lander for continuously collated data from September to May. The red line in each plot is a cubic smoothing spline fitted to the 25-hour mean; the blue dashed line in each plot is a 14.75-day approximation of a spring-neap tidal cycle.

5.3.5.2 Norfolk Canyon

The data from the lander and mooring generally supported CTD observations and provided an uninterrupted time series of conditions near the seafloor. However, the ALBEX lander that was deployed within the shallow (630 m) part of Norfolk Canyon was lost and, therefore, no data were available for this area. The mid-station (**Figures 5-2** and **5-26**; 917 m water depth), demonstrated variable conditions in all parameters measured with no distinct events within the time series. However, between April and May 2013, the salinity sensor shifted markedly over a period of approximately 4 days (**Figure 5-27**). Initially the sensor averaged approximately 34.8 but decreased to 34.6, which persisted for 20 days before rising abruptly to a mean of 34.9. Preceding this, there was a period of low current velocities and suppression in the temperature signal, indicating an unknown disruption to the sensor. Therefore, caution should be taken when interpreting variables extracted from this mooring; the following values focus only on data

outside 10 April to 13 May 2013 period. The mid-canyon was characterized by temperature fluctuation between 3.96 °C and 6.1 °C with a mean of 4.84 °C (SD 0.26). Current intensities also varied greatly, with peak current velocity reaching 81.7 cm s^{-1} and a mean of 17.78 cm s^{-1} (SD 11.3). Sigma theta calculated from salinity, temperature, and depth fell between 27.33 and 27.9 kg m^3 with a mean of 27.6 kg m^3 (SD 0.06). The mid-canyon was typified by salinities between 34.56 and 35.24, mean 34.87 (SD 0.07). Warmer waters were weakly correlated with higher current speeds (Spearman's rank correlation on 24-hour moving average data for first deployment, $r = 0.3$, $p < 0.001$).

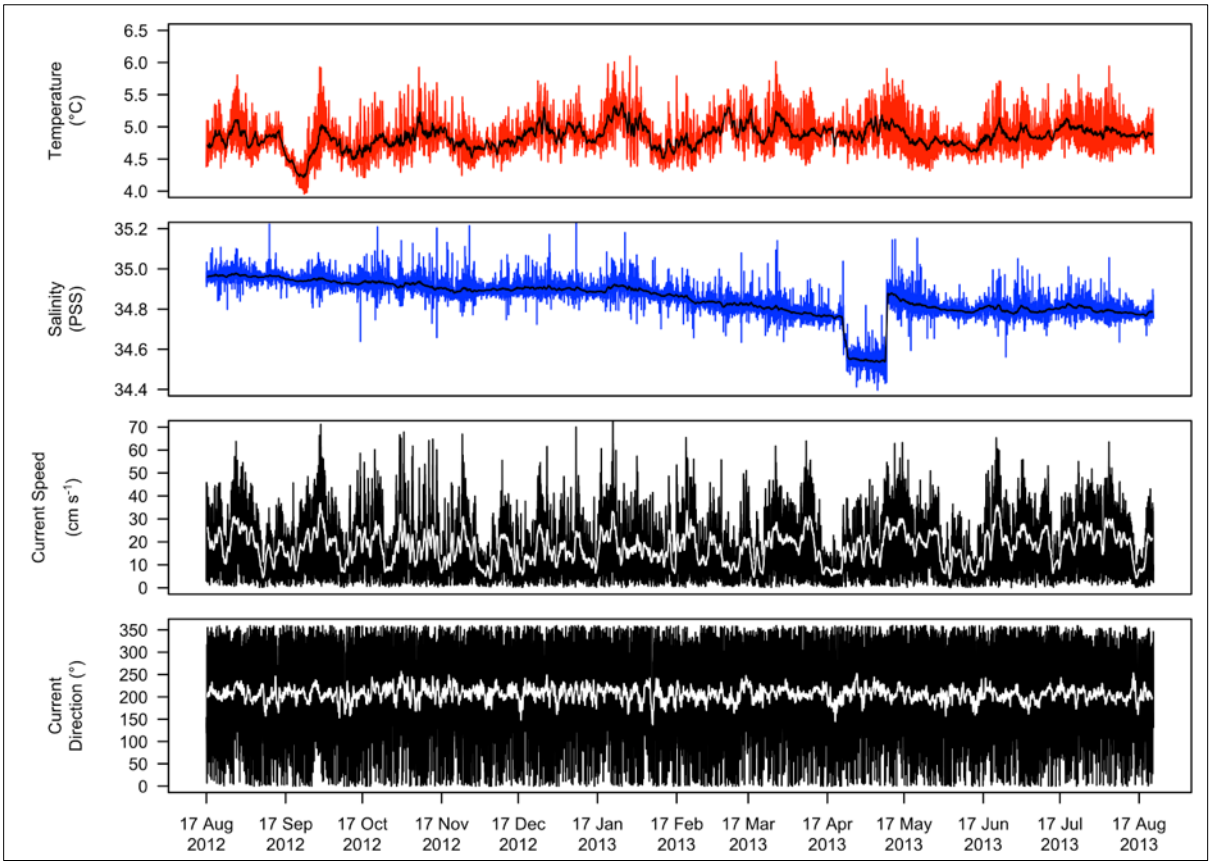

Figure 5-26. Oceanographic variables (indicated by y-axis titles) extracted from the mid-mooring in Norfolk Canyon (depth: 917 m). Black or white lines represent a 24-hour moving average filter for each variable. Sensor set differed from the other deployments in this canyon. Current data were obtained at 14.25 m above bottom, temperature and salinity at 9 m above bottom. Currents were recorded at a 15 min interval, temperature and salinity at a 5 min interval. For clarity, data were resampled to a 15 min interval to match all sensors.

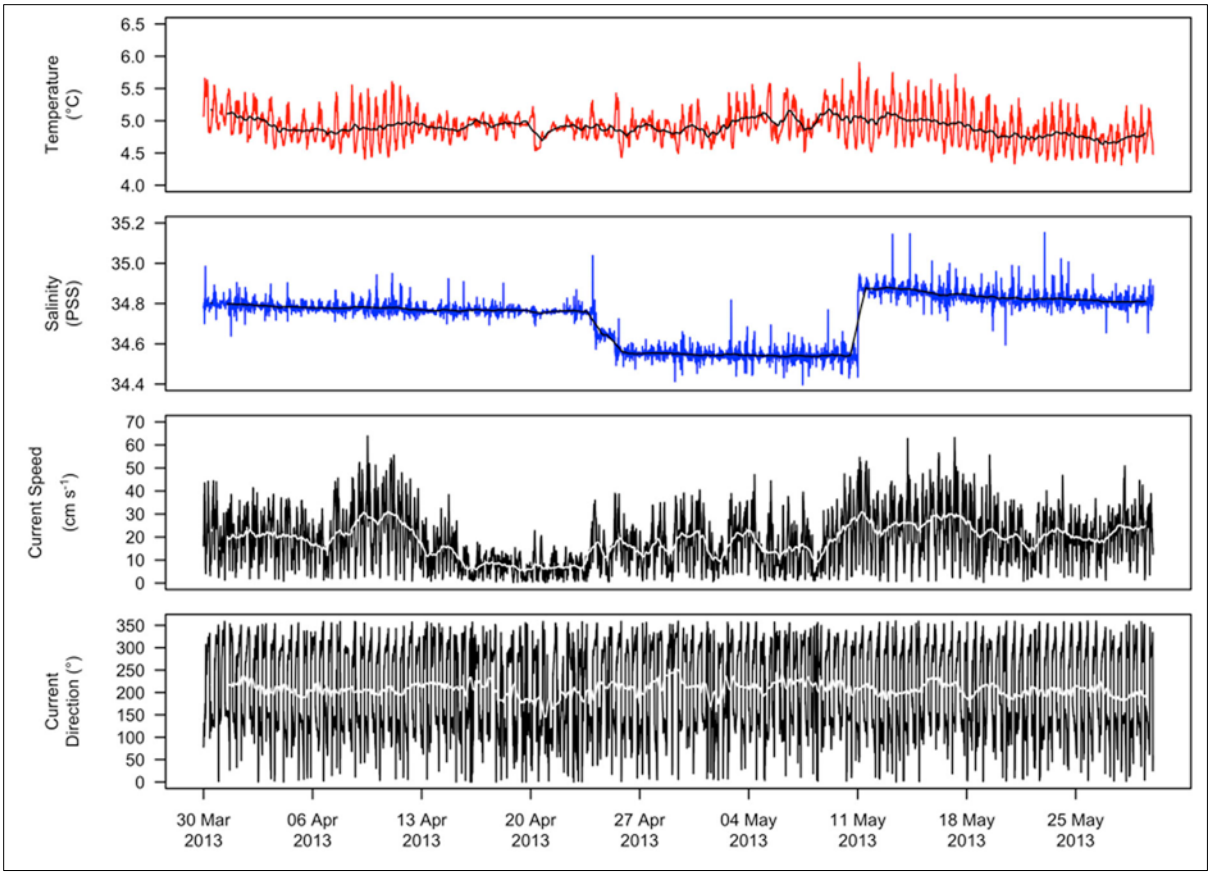

Figure 5-27. Subset of oceanographic variables (indicated by y-axis titles) extracted from the mid-mooring in Norfolk Canyon during a disruption to the salinity sensor. Black or white lines represent a 24-hour moving average filter for each variable. A full description of panels is provided in **Figure 5-26**.

The deeper region of Norfolk Canyon was monitored using a lander (**Figures 5-2** and **5-28**). This site had some obvious events that were distinguishable from the background time series in the temperature, turbidity, and fluorescence sensors (mid-October 2012, mid-December 2012, mid-January 2013, late February 2013, and early July 2013). Each event appears to have increased turbidity corresponding with increased fluorescence and current speeds. On some occasions, this also corresponded with reduced salinity and higher temperatures. During the deployment, turbidity was high, and both sensors eventually reached the maximum of their detectable ranges. However, other sensors still appeared to log credible data (**Figure 5-28**). In the deep canyon, temperatures fluctuated between 3.72 °C and 5.25 °C with a mean of 4.2 °C (SD 0.15). Maximum current velocity was 94 cm s^{-1} (on 10 March 2013) with a mean speed of 7.98 cm s^{-1} (SD 5.58). Fluorescence ranged between 0.12 and 14.25 RU with a mean of 0.24 RU (SD 0.34). Sigma theta calculated from salinity, temperature, and depth fell between 27.47 and 27.8 kg m^3, mean 27.71 kg m^3 (SD 0.04). Peaks in turbidity were weakly correlated with increased current velocity (Spearman's rank correlation on 24-hour moving average data for first deployment, $r = 0.37$, $p < 0.001$) and were intermediately correlated with fluorescence (Spearman's rank correlation on 24-hour moving average data for first deployment, $r = 0.57$, $p < 0.001$). There was a slightly stronger relationship between current velocity and temperature (Spearman's rank correlation on 24-hour moving average data for first deployment, $r = 0.38$, $p < 0.001$).

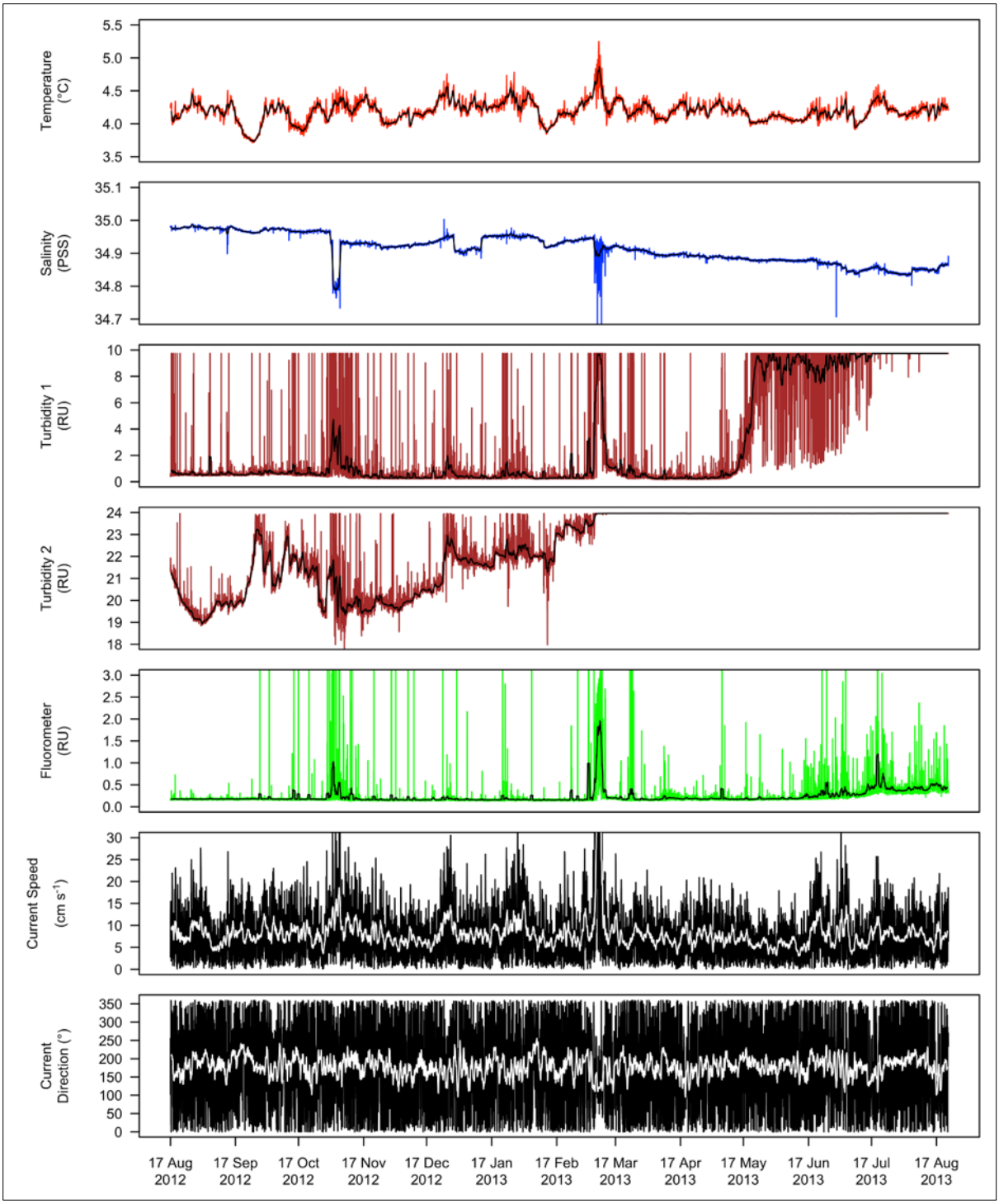

Figure 5-28. Oceanographic variables extracted from the deep lander in Norfolk Canyon (depth: 1,364 m). Black or white lines represent a 24-hour moving average filter for each variable. Sensor set differed from the other deployments in this canyon. Current data were obtained at 3.06 m above bottom; temperature, salinity, turbidity, and fluorescence at 2 m above bottom. Currents were recorded at a 15 min interval, temperature and salinity at a 5 min interval. For clarity, data were resampled to a 15 min interval to match all sensors.

5.3.5.2.1 Variation Between Locations Within the Canyon

Direct comparison between the mid and deep stations in Norfolk Canyon was possible for current velocity, current direction, temperature, and salinity; however, because the mid-mooring was not measuring at the same height above bottom and suffered from some sensor disruption, comparisons with this mooring should be taken with caution. Density kernels revealed substantial differences between all variables (**Figure 5-29**). The mid-mooring was generally warmer, with a broader range of current speeds and a bimodal salinity peak. The deep area of the canyon appears to have many peaks in salinity centered on a narrow range of salinities from 34.8 to 35, and no readings were greater than that level. Current direction in both areas of the canyon demonstrated a strong tidally driven bimodal pattern, with each area having fairly restricted flow orientation (**Figure 5-29c**).

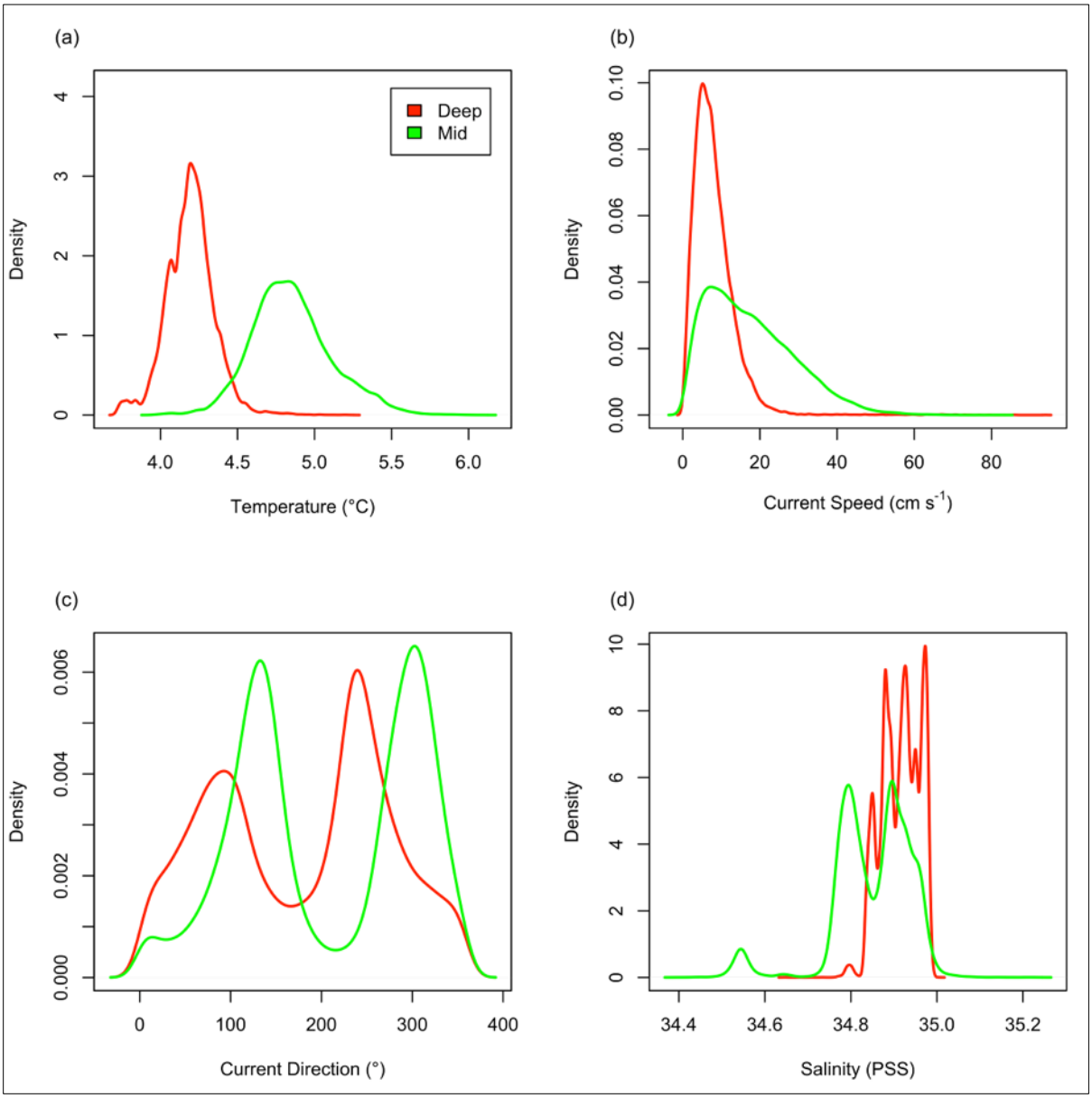

Figure 5-29. Density kernels of parameters (a) temperature, (b) current speed, (c) current direction, and (d) salinity from the deep (red) and mid (green) stations in Norfolk Canyon.

The canyon walls have a large influence on flow at the mid and deep stations in the canyon. Radial histogram plots show that the mid-canyon region had strongly bimodal flow along a 135° and 315° axis, following the dog-leg like shape of Norfolk Canyon (**Figure 5-30a**). The progressive vector diagram supports this and reveals the prevailing flow to be along a northwest axis, which is oriented up-canyon (**Figure 5-31a**). This up-canyon flow is tidally driven, but the pattern is disrupted by three episodic events where a northerly flow dominates. These three discrete events occurred between 6 September and 22 October 2012 (black series in **Figure 5-31c**), 26 December 2012 and 18 January 2013 (gray series in **Figure 5-31c**), and 11 and 26 April 2013 (blue series in **Figure 5.31c**). Closer investigation of the time series from the sensors during these events reveals a suppression in the regular temperature signal, but no clear deviation in current speed, flow direction, or salinity. The deep canyon station was markedly different, with a predominant flow direction toward the southwest (235°). There were also flow directions toward a 90° bearing, but this was less common than the southwesterly flow (**Figure 5-30b**). Progressive vector diagrams support the general flow direction, but revealed a single significant event where the flow direction veered 90°, matching the orientation of the canyon at that location and showed only slight tidal modulation (**Figure 5-31**). This event occurred between 23 February and 11 March 2013 (**Figure 5-31d**). For further analysis, see **Section 5.3.5.3**.

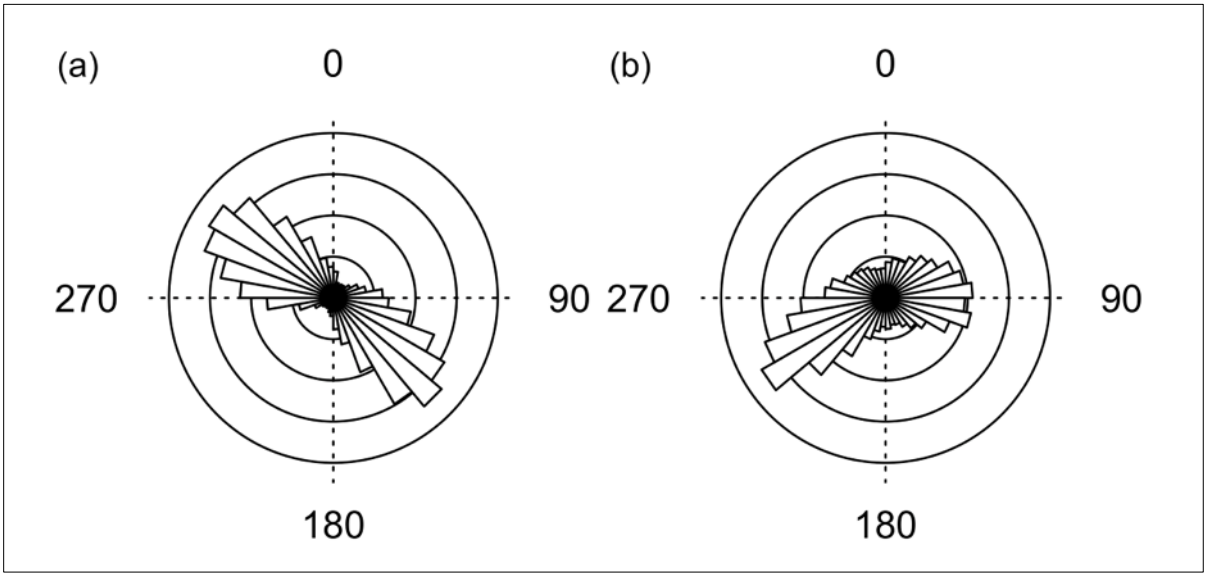

Figure 5-30. Radial histograms showing predominant flow direction from current meter data for (a) shallow lander, (b) mid-mooring, and (c) deep lander in Baltimore Canyon.

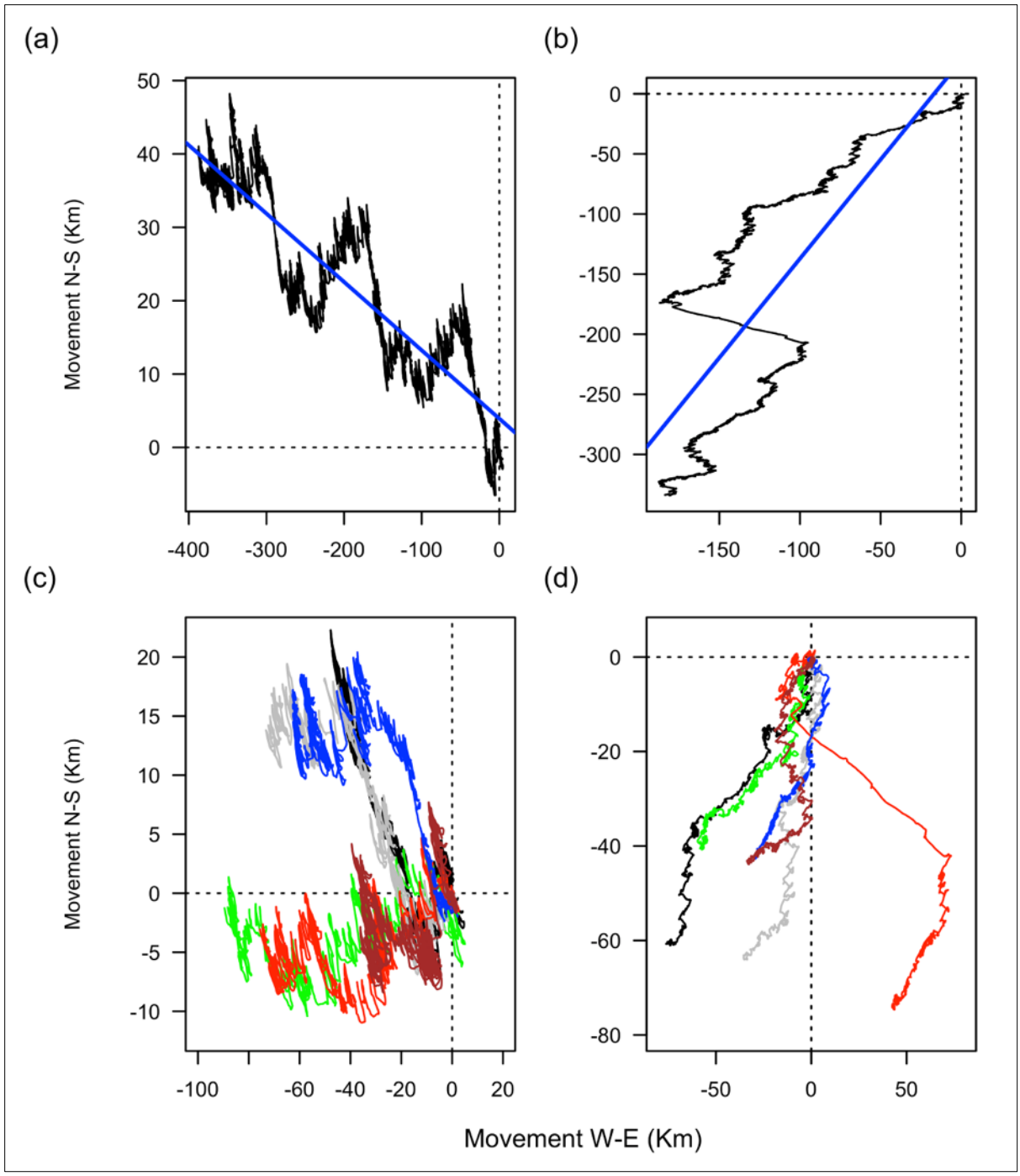

Figure 5-31. Progressive vectors for each station at Norfolk Canyon. The first row of plots shows vectors for the first period landers were deployed in Baltimore Canyon for (a) mid-mooring and (b) deep lander. Blue lines indicate the general direction of the residual flow. The second row of plots shows 60-day subsets of the overall time series, with black lines indicating the first 60 days, green 60 to 120 days, gray 120 to 180 days, red 180 to 240 days, blue 240 to 300 days, and brown 300 to 360 days for (c) mid-mooring and (d) deep lander.

To assess whether the canyon walls affected current direction, several bins of current speeds were extracted from the mid-mooring and the deep lander, both of which were equipped with an upward-looking ADCP, although at different frequencies. The mid-mooring bins started at 14.25 m above bottom and collected data to approximately 114.25 m above bottom (**Figure 5-32**), while the deep lander bins started at 3.06 m above bottom and scanned to approximately 18.06 m above bottom (**Figure 5-33**). The mid-mooring recorded bottom-intensified currents at 14.25 m, with generally slower speeds occurring higher in the water column (**Figure 5-32a**). The general directions of flow were relatively similar throughout the scanned range, with great differences at the 14.25 and 114.25 m bins (**Figure 5-32b**). The deep lander scanned over a smaller distance and recorded generally slower speeds near the seafloor, which increased in speed at 15.56 and 18.06 m above bottom (**Figure 5-33a**). The direction of flow was relatively similar at different heights above bottom, with the greatest differences being 18.06 m compared with other bins (**Figure 5-33b**).

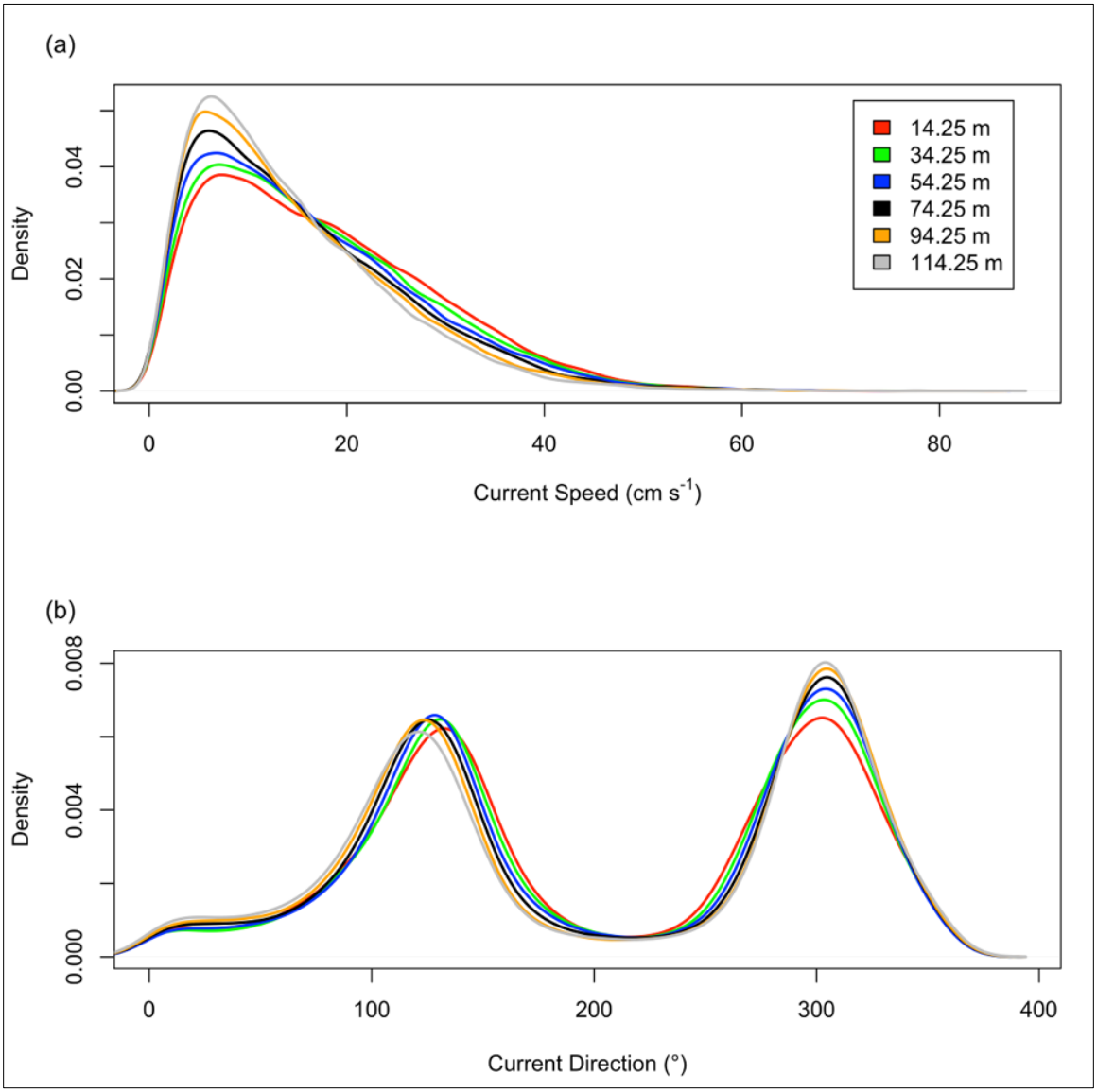

Figure 5-32. Density kernels for two parameters obtained from the mid-canyon ADCP in Norfolk Canyon (a) current speed and (b) current direction at different heights above bottom.

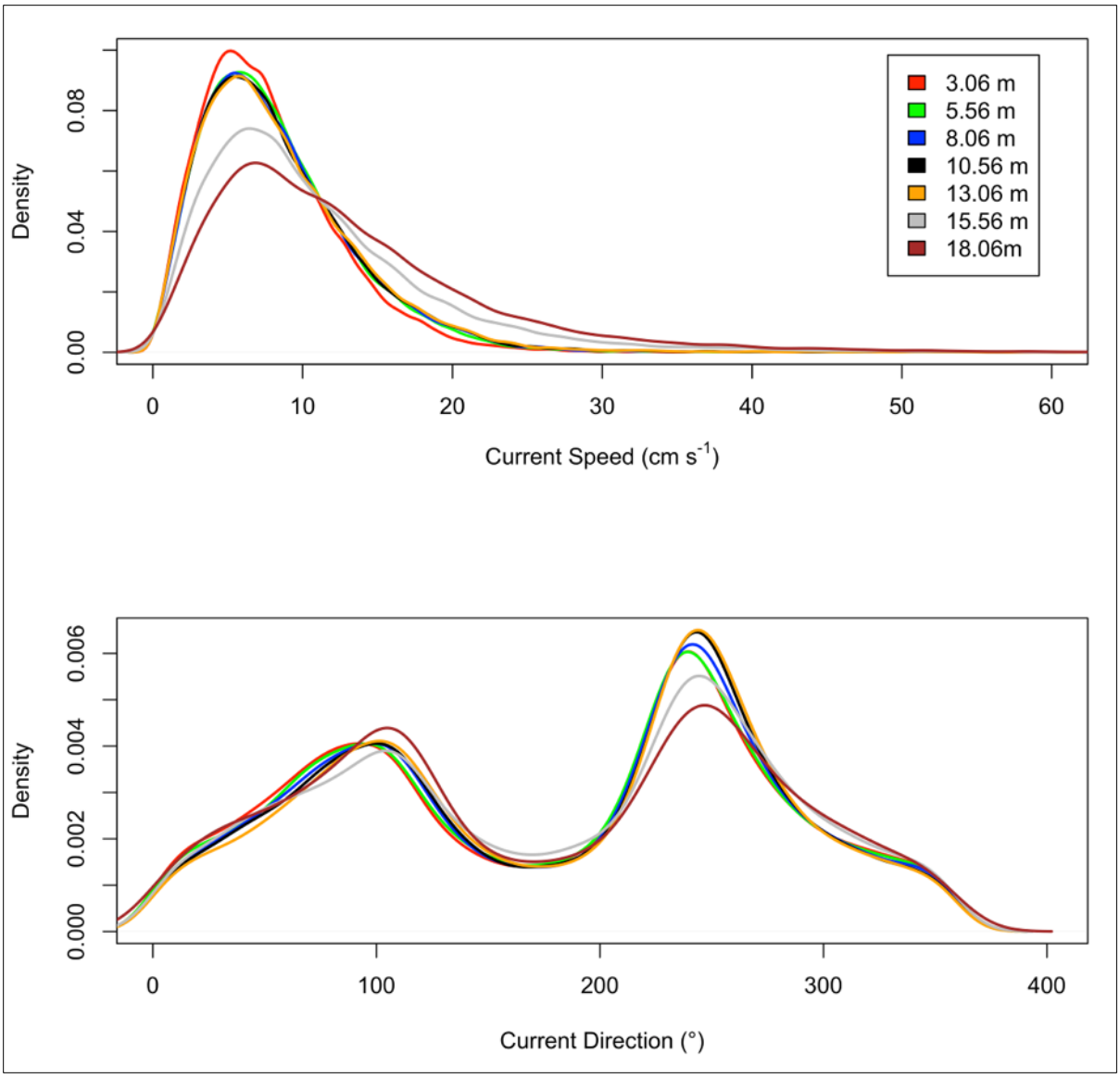

Figure 5-33. Density kernels for two parameters obtained from the deep canyon ADCP in Norfolk Canyon (a) current speed and (b) current direction at different heights above bottom.

The near-bottom flow direction, corrected to reflect the flow along the canyon axis, demonstrated that all stations in Norfolk Canyon had flow that was generally up-canyon (**Figure 5-34**). This was more pronounced in the mid-canyon station where flow moved approximately 380 km up-canyon over the entire time series (**Figure 5-34a**). In the deep canyon, the flow was characterized by general up-canyon movement throughout the series; however, the large episodic event in March dominated the time series (**Figure 5-34b**).

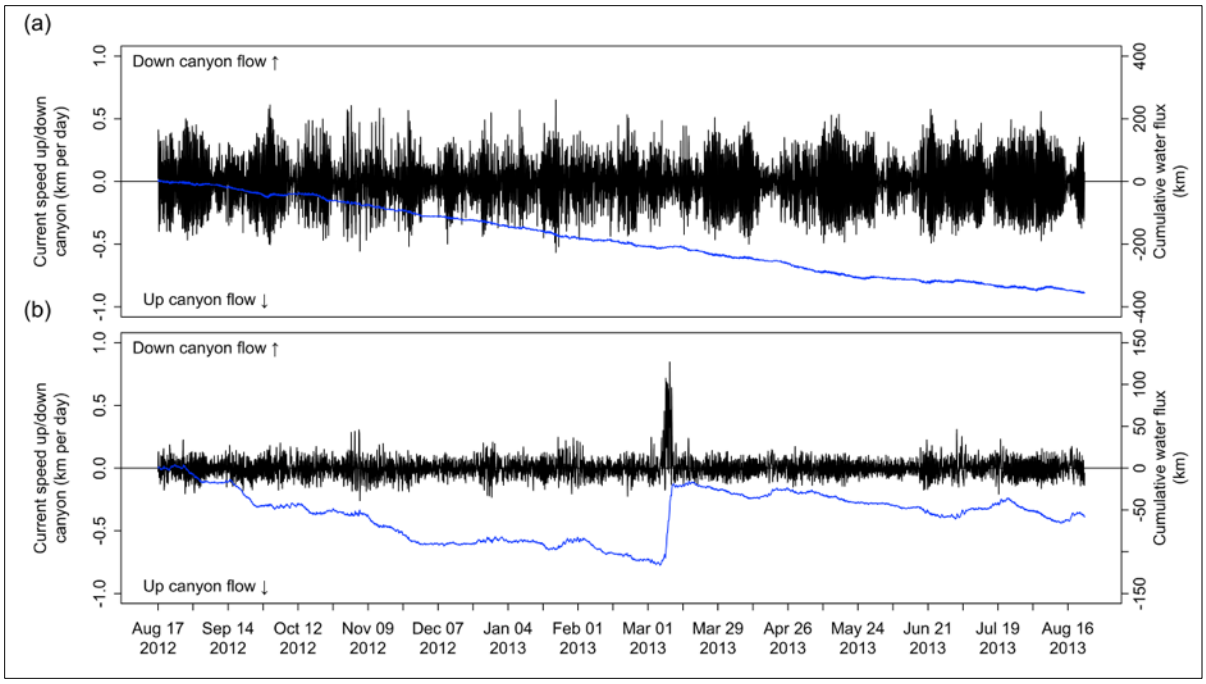

Figure 5-34. Flow velocity along the Norfolk Canyon axis for the canyon axis before the station. (a) mid-canyon (917 m), orientated at 120°; (b) deep canyon (1,364 m), orientated at 110°. Black line indicates flow velocity for each reading, blue line indicates cumulative flow across the time series. Negative values indicate that water movement is up-canyon (i.e., toward the shelf), and positive values indicate water moving down canyon (i.e., toward the abyssal plain).

5.3.5.2.2 Linkages Between Locations Within the Canyon

Due to the reduced sensor loads and the missing lander at the shallow part of Norfolk Canyon, only the temperature link between the mid and deep stations could be analyzed in detail. Similar to Baltimore Canyon (**Figure 5-22**), there was a link between the two parts of Norfolk Canyon (**Figure 5-22e**). The strongest intermediate correlations were observed in two batches, the first was at a lag of approximately 0.5 to 1.5 hours and the second at approximately 25 to 25.75 hours. This indicates that there was likely transport between the two sites, and the transport was likely tidally driven.

5.3.5.2.3 Tidal Influences Within the Canyon

There was also clear evidence of a strong tidal influence within Norfolk Canyon that was evident in most major variables, including current velocity components and temperature. The semidiurnal lunar constituent M2 was pronounced in current speed data at both stations (**Figure 5-35**). In the mid-station, the M2 amplitude from harmonic tidal analysis was greatest at 15.23 cm s^{-1}, with the next strongest constituent being the S2 with an amplitude of 3.04 cm s^{-1}. The M4 constituent was also observed with an amplitude of 1.94 cm s^{-1} (**Figure 5.35**). The deep station also exhibited strong amplitude in the M2 tide of 4.71 cm s^{-1}, and lower S2 at 0.84 cm s^{-1}. These tidal signals are stronger than those observed in Baltimore Canyon at similar depths. Both locations within Norfolk Canyon demonstrated a convincing fit to a spring-neap tidal cycle (14.75 days), especially at the start of the observations in August to September 2012 (**Figure 5-36**).

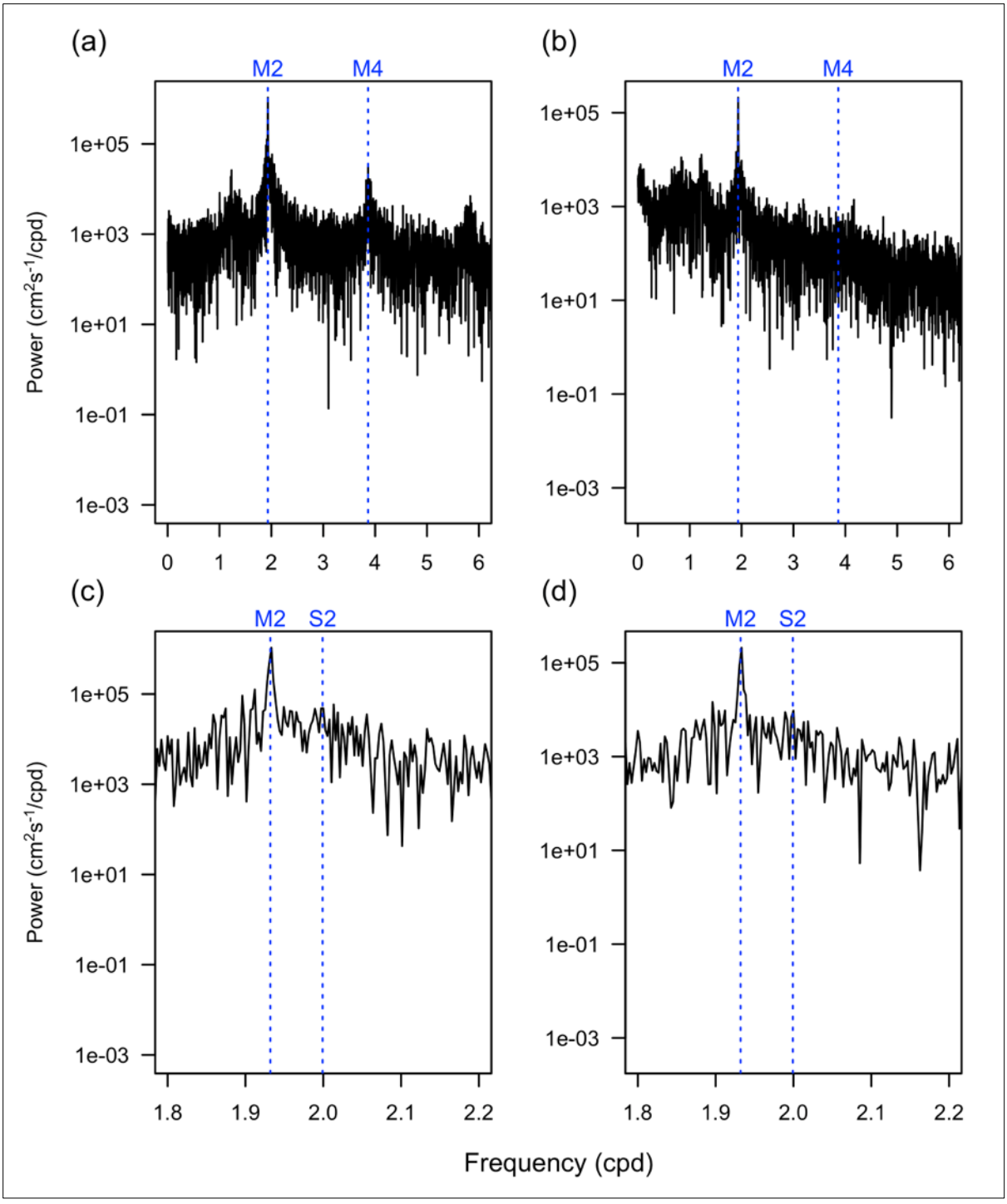

Figure 5-35. Power spectra of current velocity from Norfolk Canyon. The x-axes on (c) and (d) are truncated to focus on the M2 and S4 tidal components. Mid-mooring (a) and (c), deep lander (b) and (d). Frequency in counts per day (cpd).

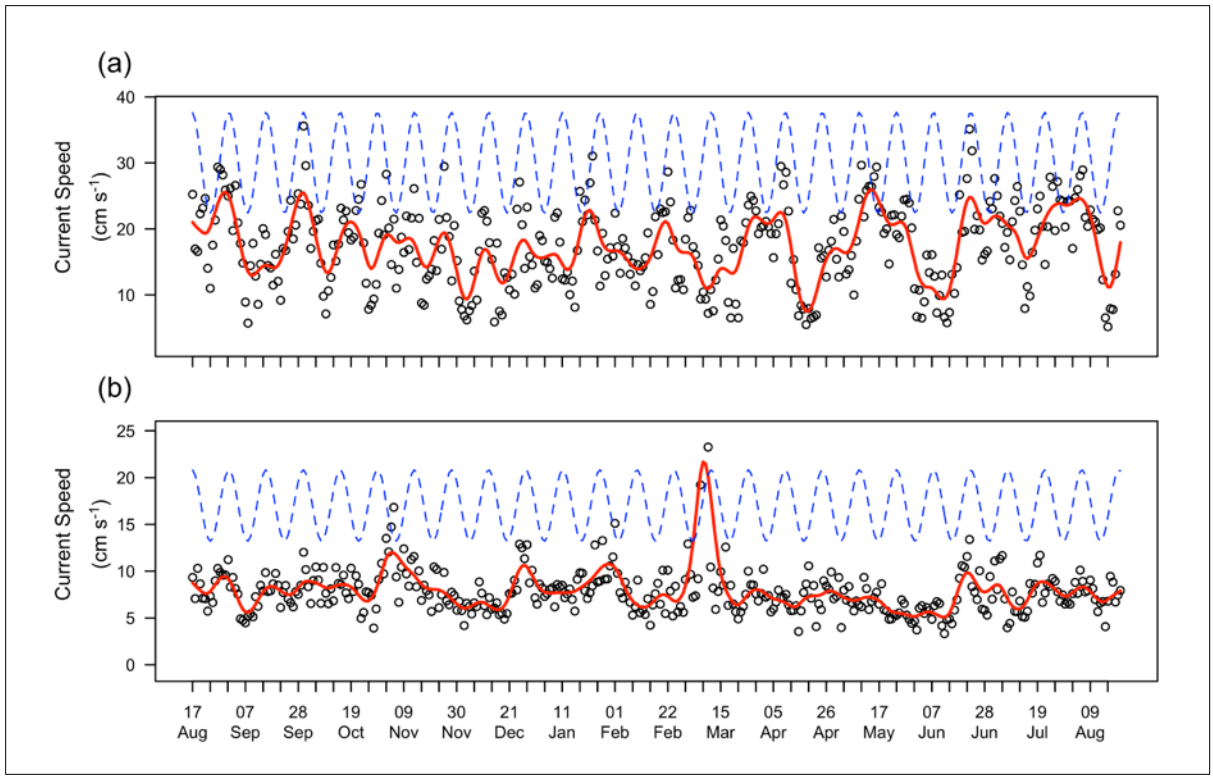

Figure 5-36. Low-pass filtered current speed to remove high frequency tidal signal (25-hour period) for Norfolk Canyon. From the (a) mid-mooring and (b) deep lander the full year time series. The red line in each plot is a cubic smoothing spline fitted to the 25-hour mean, the blue dashed line in each plot is a 14.75-day approximation of a spring-neap tidal cycle.

5.3.5.3 Episodic Events Within MAB Canyons

5.3.5.3.1 Turbidity Layer Within Baltimore Canyon

There was a noticeable sediment cloud within the Baltimore Canyon between 200 and 900 m (**Figure 5-7**). This sediment cloud was present in ship-based CTD casts in both 2011 and 2012 surveys and therefore can be assumed to be a fairly persistent feature within the canyon. The time series of data from the bottom landers and mooring support this, with high turbidity prevalent throughout the entire monitoring period at the shallow lander (**Figure 5-37a**). The intense backscatter was not as prevalent within the mid-canyon region, but waves of sediment occur periodically and appear to extend to approximately 50 m above bottom in the acoustic backscatter (**Figure 5-37b**). These waves are likely tidally driven, as they matched the M2 tidal frequency. The turbidity signal at the deep station was largely absent with limited evidence of suspended material, indicating that the sediment remains entrained within the upper 1,000 m of the canyon and does not make it to the deep station (**Figure 5-37c**).

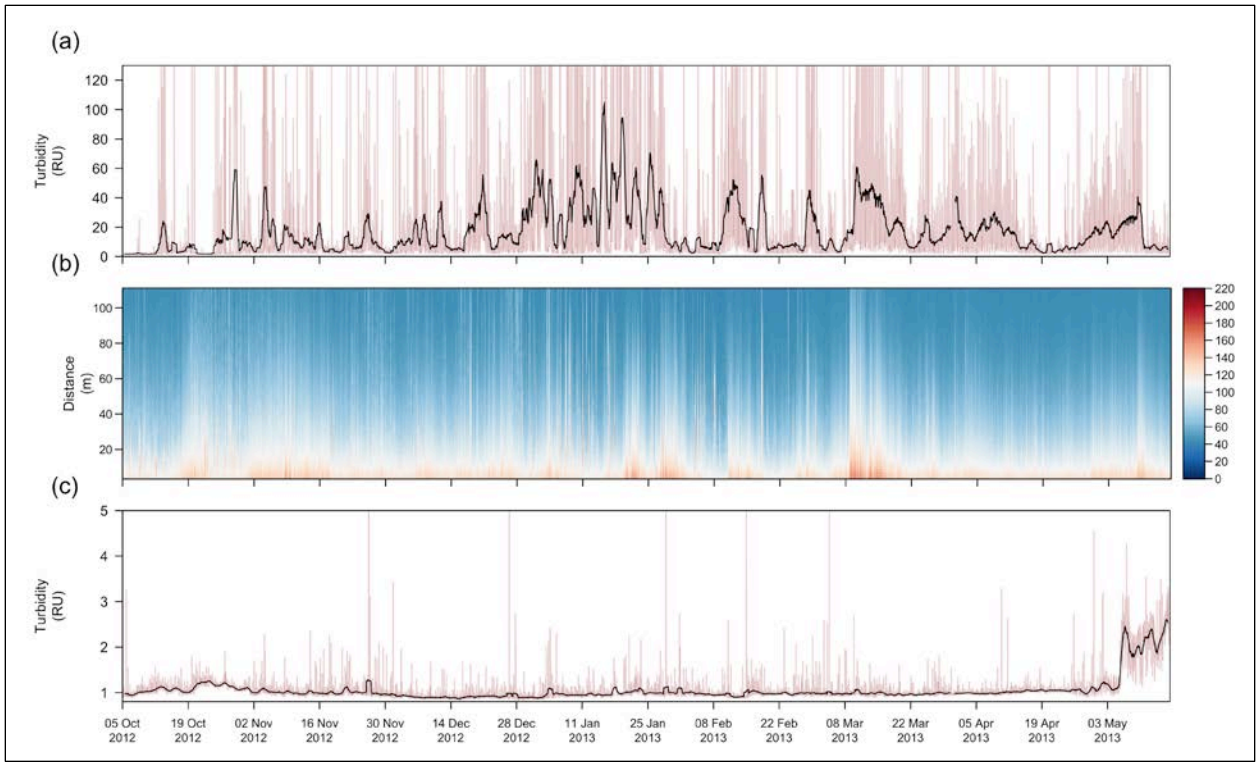

Figure 5-37. Turbidity data from Baltimore Canyon showing (a) optical backscatter from the shallow lander (603 m), (b) acoustic backscatter from upward-looking ADCP at the mid-mooring (1,082 m), and (c) optical backscatter from the deep lander station (1,318 m). Toward the end of the observation period, some fouling of the deep sensor may have occurred. Note the change in y-axis scale between the shallow lander (a) and the deep lander (c) due to different sensor settings.

The sediment cloud could be driven by the interaction between tidal motions up and down the canyon causing localized resuspension. Furthermore, this turbidity may be enhanced by a combination of critical slope angle and deeper water originating internal waves breaking within the resuspension depth zone. The deep and mid-stations both demonstrate consistent up-canyon water flow throughout the duration of the time series (**Figure 5-21**) while the shallow station, having a general up-canyon pattern, has periods of hiatus where flow was slack or down canyon (**Figure 5-21**). In this area, the turbidity signal was positively correlated with temperature and current speeds (Spearman's rank correlation on 24-hour moving average data for first deployment, $r = 0.48$, $p < 0.001$ and $r = 0.49$, $p < 0.001$, respectively), indicating that bottom waters from the head of the canyon are being mixed within the turbid layer by strong currents. Surface weather patterns did not appear to correspond with the turbidity signal at the shallow station, indicating that the suspension is likely caused by tidal driven oscillations, although the turbidity sensor output was too noisy to prove this.

5.3.5.3.2 Tidal Disruption Events in the Mid-Mooring at Norfolk Canyon

In the mid-station of Norfolk Canyon, the general pattern of tidal flow was disrupted by net up-canyon flow three times during the observation period (**Figures 5-31a** and **5-38**). These events corresponded with changing water masses on the surface, including when warmer water on the shelf is replaced by the colder shelf water or LSW from the north (**Figures 5-38a**,**b**) and vice versa (**Figure 5 38c**). During these periods, up-canyon flow dominates over the tidal signal. There was no clear link with these events and bottom temperatures or current velocity (with the exception of canyon flow being on average stronger up-canyon than down canyon).

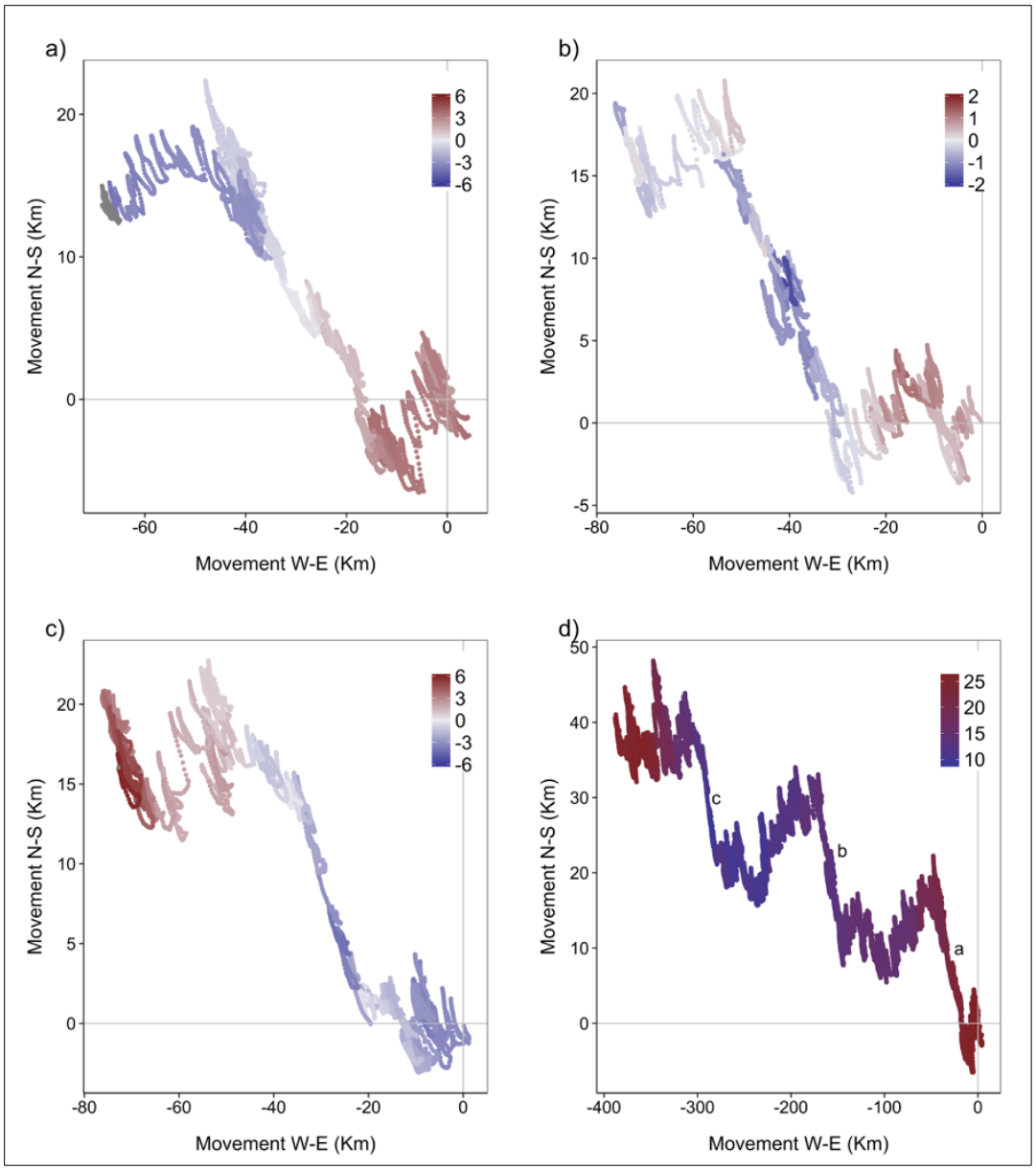

Figure 5-38. Progressive vector diagrams focused on particular periods where disruption to the normal tidal signal occurs at the mid-mooring within Norfolk Canyon (917 m). During these periods, a protracted upward canyon flow was observed. The plots are colored with daily sea surface temperature anomaly from above the station for each period (a, b, and c) and daily sea surface temperature above the station (d). (a) Event occurring between 17 August and 1 November 2012, b) event between 1 December 2012 and 1 February 2013, c) event between 1 April and 1 June 2013, and d) overview of entire time series labeled with subplot letter to illustrate event period.

5.3.5.3.3 Storm-Driven Events

Norfolk Canyon is generally a turbid environment, with areas of concentrated suspended sediment evident between 200 m and 1,200 m in CTD transects (**Figure 5-10**). Throughout the observational period from September 2012 to late August 2013, the mid-mooring detected high levels of acoustic backscatter near the seabed (**Figure 5-39**). These appeared related to tides over the M2 and M4 tidal cycles

(**Figure 5-39**). There were several periods where high incidences of turbidity were detected in the optical backscatter sensor and the acoustic backscatter from the upward-looking ADCP of the deep canyon lander (**Figures 5-28** and **5-39**). In particular, two significant events were clearly distinguishable where turbidity exceeded background levels for several days and corresponded with periods of elevated fluorescence (**Figure 5.39**). The first event was in late October to early November 2012 and coincided with Hurricane Sandy. The second event was in early to mid-March 2013 and coincided with a powerful nor'easter storm. The patterns from these two storms were less clear in mid and deep sensors deployed in Baltimore Canyon (**Figure 5-37**); some peaks were detected in the shallow lander optical turbidity sensor that match the storms (**Figure 5-37a**).

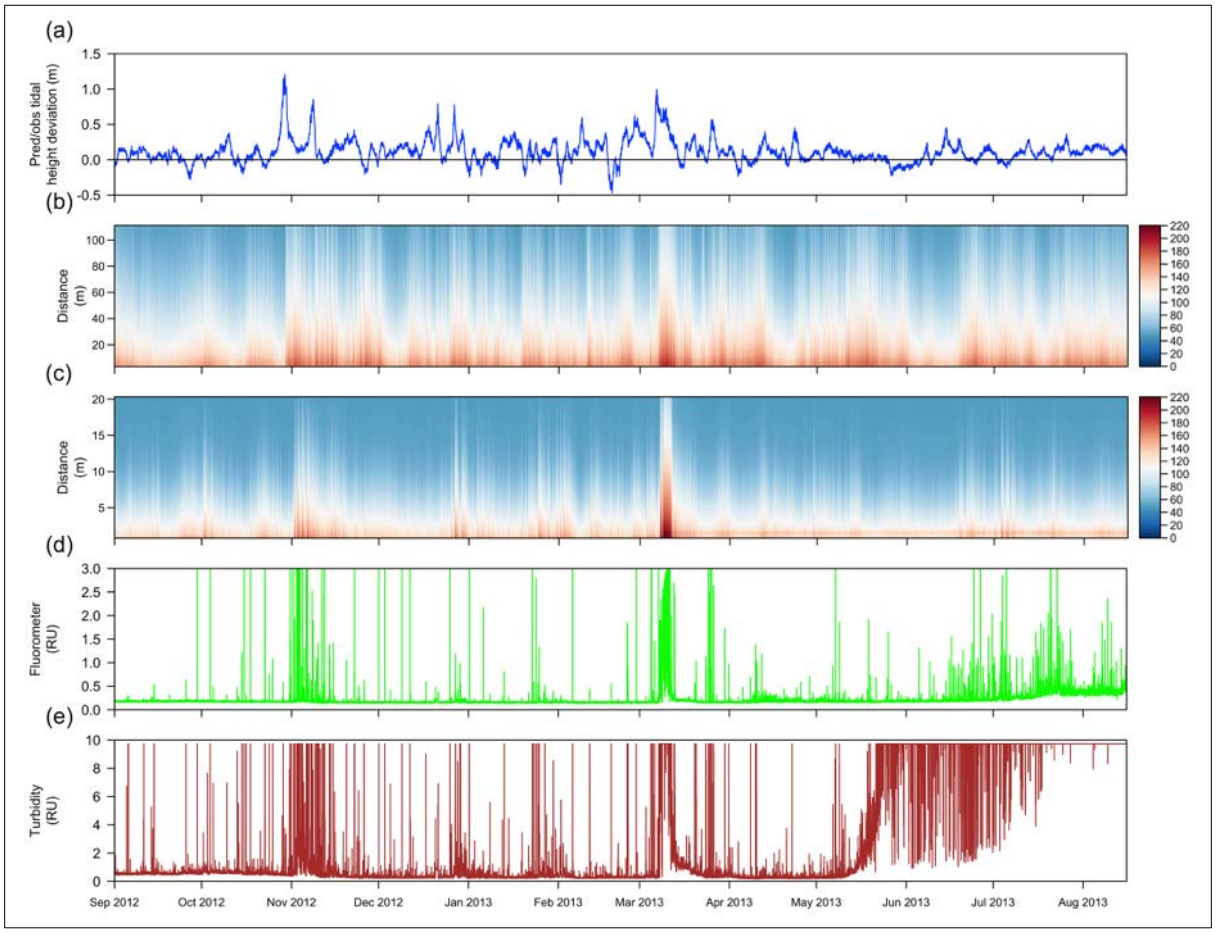

Figure 5-39. Suspended sediments within Norfolk Canyon for 1 year. a) Deviation between predicted and observed tidal height at Ocean City Inlet, Maryland (positive values indicate that observed tides were greater than predicted). b) Relative turbidity (beam averaged acoustic backscatter) from the upward-looking ADCP (mounted 10 m above bottom) at the mid-canyon (917 m). c) Relative turbidity from acoustic backscatter recorded from the upward-looking ADCP mounted 2 m above bottom at the deep canyon (1,364 m). d) Fluorescence from the deep sensor. e) Relative turbidity from the optical backscatter sensor at the deep canyon.

The first event in late October 2012 was notable for the prolonged high turbidity event detected in both optical and acoustic backscatter sensors (**Figure 5-40**). Starting at the mid-canyon on 30 October, the acoustic backscatter signal increased dramatically (**Figure 5.40b**). The high backscatter was recorded in the full detection range of the upward-looking ADCP (>130 m above bottom), and persisted until 16 November. The signal was clearly affected by the tide, giving the appearance of waves at both the

mid- and deep stations (**Figures 5-40b** and **5-40e**). During the event, conditions in the area changed, mean current velocity increased at both stations compared with the week prior to the event onset, with a mean increase of approximately 4 cm s^{-1} at both stations. Maximum observed velocity was also higher during the event with a peak at the mid-canyon of 67.8 cm s^{-1} compared with a maximum of 50.9 cm s^{-1} in the previous week, and the deep lander recording 33.9 cm s^{-1} compared with 20 cm s^{-1} in the previous week (**Figure 5-40g**). During the event, the mean intensity of the optical backscatter sensor increased by 2.6 times compared to the previous week and fluorescence almost doubled. During the event, the temperature signal increased slightly at the deep canyon, with an increase in maximum temperature of 0.16°C, and mean salinity decreased slightly. In the mid-canyon, maximum observed temperature increased by 0.5 °C, and salinity was similar to that observed in the previous week (**Figures 5-40d** and **5-40f**). In Baltimore Canyon, two peaks in suspended sediment concentration were detected by the optical turbidity sensor of the shallow lander (**Figure 5-37a**). However, there was no clear signal detected in the mid- or deep sensors (**Figures 5-37b**,**c**). This is likely due to the unique convergence zone in the middle of the canyon causing much of the transported sediment to pass over the mid-canyon area.

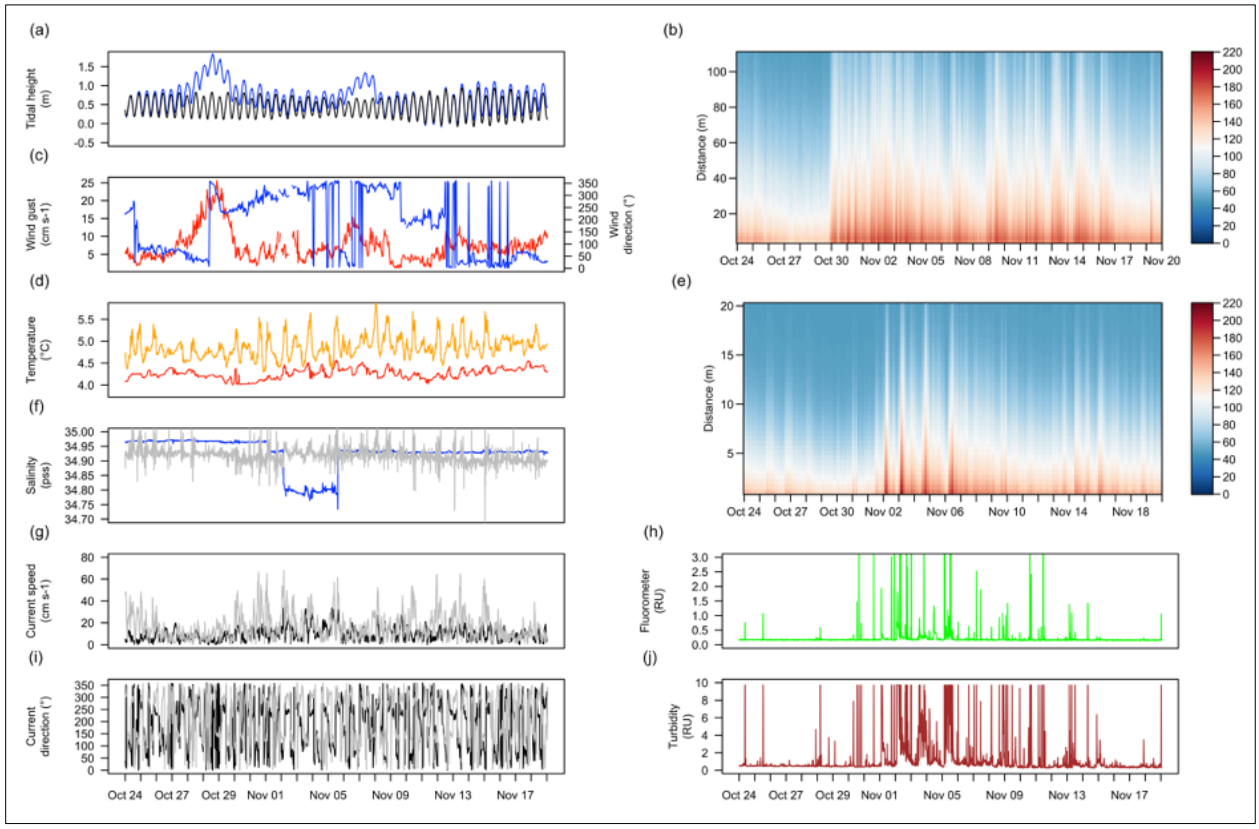

Figure 5-40. A turbidity event observed during October 2012 in the mid (917 m) and deep Norfolk Canyon (1,364 m). (a) Predicted (black line) and observed (blue line) tidal height from Ocean City Inlet, Maryland. (b) Relative turbidity (beam averaged acoustic backscatter) from the upward-looking ADCP (mounted 10 m above bottom) at the mid-canyon. (c) Wind gust speed and wind direction from Ocean City Inlet. (d) Temperature series from the mid (orange) and deep (red) sensors. (e) Relative turbidity from acoustic backscatter recorded from the upward-looking ADCP mounted 2 m above bottom at the deep canyon. (f) Salinity series from the mid (gray) and deep (blue) sensors. (g) Current speed from a single bin from the mid ADCP at 14.25 m above bottom (gray) and deep ADCP at 3.06 m above bottom (black). (h) Fluorescence from the deep sensor. (i) Current direction from the same single bins used in (g) at the mid (gray) and deep (black) ADCPs. (j) Relative turbidity from the optical backscatter sensor at the deep canyon.

The second recorded event in 2013 was more substantial in terms of both current speed and suspended sediment loading and occurred between 7 and 14 March primarily in Norfolk Canyon. This was detected primarily in the progressive vector diagram (**Figure 5-31d**), which demonstrated a significant deviation in flow direction perpendicular to the residual flow, and water flowed in a general down-canyon direction (**Figure 5-34**). During the period of this event, there was still evidence of previously observed tidal patterns at this site, as flow moved rapidly down-canyon but was periodically curtailed by the tide. At the deep site, the mean current speed increased by 13.2 cm s^{-1} over the period of the event, reaching a maximum speed of 94 cm s^{-1} (**Figure 5-41**). This pattern was not observed in the mid-canyon where mean speed was 7.69 cm s^{-1} lower during the event than during the previous week; maximum recorded velocity did increase from 45.8 to 55.7 cm s^{-1}. During the event, the maximum temperature increased by only 0.09 °C at the mid-station and 0.69 °C at the deep station (**Figure 5-41**). Salinity decreased at the deep station from a minimum of 34.94 during the previous week to 34.65 during the event. During the event, the mean intensity of the optical backscatter increased by 6.2 times compared with the previous week, and fluorescence almost tripled. In Baltimore Canyon, this period coincided with elevated suspended sediment levels in both the shallow and mid-canyon stations, but not the deep station (**Figure 5-37**). Speculatively, the intense nature of this event (as detected in Norfolk Canyon) was so great that it overrode the convergence zone effect, allowing sediment to travel through it and at least past the mid-mooring (**Figure 5-37b**). However, this momentum does not appear to have been maintained at the deep station, as no clear signal was observed (**Figure 5-37c**).

Comparing the onset of these events with coastal weather and tidal observations indicates that it appears to be triggered by a period of high winds that disrupted the predicted tidal pattern on the shelf (a shift of approximately 1 m in tidal height). This was driven by high wind speeds in excess of 20 m s^{-1} and a persistent northerly wind that lasted for several days (**Figures 5-40** and **5-41**). These winds triggered the passage of sediment-laden waters down the canyon and, presumably, onto the abyssal plain. The exact origin of the event and its passage through the canyon was less clear. The mid-canyon mooring did not detect an increase in mean current velocity, but peak speed was greater during the events (e.g., a recorded high of 55.7 cm s^{-1} on 7 March 2013, which occurred on a down canyon bearing). Several peaks in current speed were also evident in the mid-canyon mooring, and these speeds generally occurred when the flow direction at both stations was down canyon. It is likely that the source of the event was within the canyon, as the salinity series from the mid- and deep canyon overlapped when the flow direction recorded at both stations was similar. No freshening of the salinity sensor nor any increase in temperature was recorded in the mid-canyon, likely indicating that the movement consisted of WASIW water that extended up to the mouth of the canyon (**Figure 5-5**). Passage of the flow increased in speed with depth, culminating in speeds greater than 60 cm s^{-1} that lasted for several days, gathering even more suspended material in a sediment flow that extended at least 20 m into the water column at the deep mooring (**Figure 5-41**).

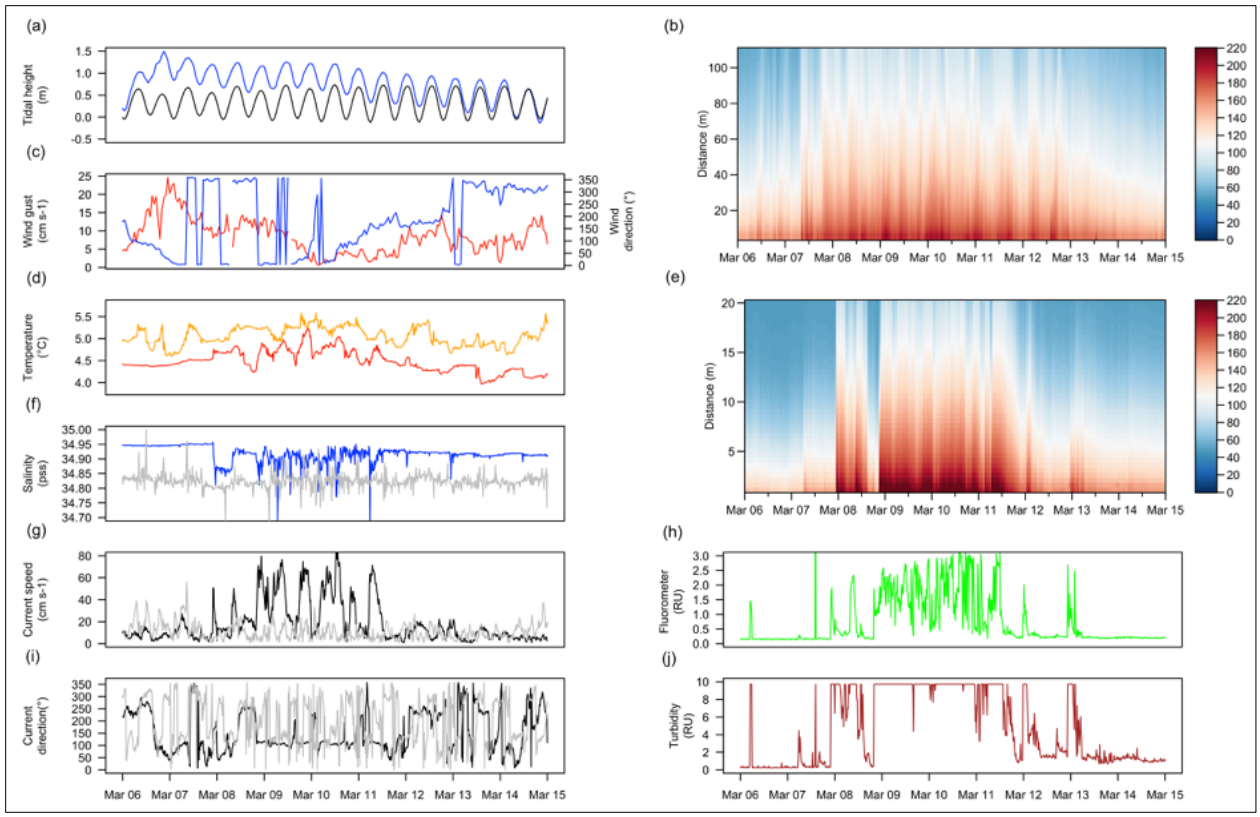

Figure 5-41. A turbidity event observed during March 2013 in the mid (917 m) and deep Norfolk Canyon (1,364 m). (a) Predicted (black line) and observed (blue line) tidal height from Ocean City Inlet, Maryland. (b) Relative turbidity (beam averaged acoustic backscatter) from the upward-looking ADCP (mounted 10 m above bottom) at the mid-canyon. (c) Wind gust speed and wind direction from Ocean City Inlet. (d) Temperature series from the mid (orange) and deep (red) sensors. (e) Relative turbidity from acoustic backscatter recorded from the upward-looking ADCP mounted 2 m above bottom at the deep canyon. (f) Salinity series from the mid (gray) and deep (blue) sensors. (g) Current speed from a single bin from the mid ADCP at 14.25 m above bottom (gray) and deep ADCP at 3.06 m above bottom (black). (h) Fluorescence from the deep sensor. (i) Current direction from the same single bins used in (g) at the mid (gray) and deep (black) ADCPs. (j) Relative turbidity from the optical backscatter sensor at the deep canyon.

5.4 DISCUSSION

Canyon systems often act as conduits for the transport of sediments and organic matter from continental margins to the abyssal plain (Canals et al. 2006, Palanques et al. 2006, Levin and Sibuet 2012, Puig et al. 2014). Despite a substantial body of work within many canyons around the world (Puig et al. 2014), the long temporal (12 months) and high frequency (5 to 15 min) measurements presented here are among the first for canyon studies. This chapter assessed the physical conditions within two MAB canyons, Baltimore and Norfolk, using state-of-the-art benthic moorings and landers deployed for a full year as well as intensive CTD profiling of the water column at periods during the project. Five of the six lander/mooring deployments were successfully recovered, and those data were analyzed for this report. These deployments revealed high current velocities, intense clouds of turbidity, and surface-driven stochastic events that persisted for several days, revealing the two MAB canyons to be highly dynamic ecosystems.

5.4.1 Canyon Water Masses

The MAB region has been surveyed intensely, particularly with respect to water mass characterization (Cacchione et al. 2002, Rasmussen 2005, Churchill and Gawarkiewicz 2014). However, the majority of these studies were not focused on the MAB canyons, although many authors acknowledged the influence of canyon topography on shelf exchange (Church et al. 1984, Churchill et al. 1993, Rasmussen 2005, Martin et al. 2006). Although the CTD profiling conducted in this study provided only a snapshot of the structure of the water column in the summer in Baltimore Canyon (August 2012) and early spring at Norfolk Canyon (May 2013), it was conducted throughout the area of the canyons and their adjacent slopes, extending from the upper reaches along the canyon axis to depths of approximately 1,300 m. Both canyons exhibited temperature-salinity profiles that substantially differed from their respective adjacent slopes. In both cases, the morphology of the canyons allowed deeper water masses to infiltrate the continental shelf by 5 to 11 km more than on the adjacent slope. In this study, there was no evidence of Gulf Stream meanders in any CTD profiles (except for a small signature detected in one station (16.3 km station [**Figure 5.4a**]), which agrees with paleoecology data (**Chapter 17**). Previous surveys were limited to the surface waters above 300 m and conducted over smaller areas (Hecker et al. 1983, Csanady and Hamilton 1988, Churchill et al. 1993, Churchill and Gawarkiewicz 2009, Churchill and Gawarkiewicz 2014).

This study, like others, recorded well-developed shelf-slope frontal signatures, typical of the MAB shelf break (Cacchione et al. 2002, Rasmussen 2005, Churchill and Gawarkiewicz 2014). The frontal system, the inverted "V" profile (**Figures 3–6**), was found along canyon and slope transects and was most prominent over the shelf break (approximately 100 m), generally becoming weaker with increasing distance offshore. Near-bottom temperature and salinity measurements show the presence of WNACW in the upper parts of the canyons comprising fully oceanic water (salinities between 35 and 35.8) with temperatures between 6 °C and 13 °C. Farther down the canyons, waters became markedly cooler, indicative of WASIW, with salinities of approximately 35 and temperatures between 4 °C and 10 °C. These conditions were within the extrapolated tolerance ranges of many cold-water coral species, including scleractinians such as *Lophelia pertusa* (Davies et al. 2008, Davies and Guinotte 2011) and solitary octocoral species such as *Paragorgia arborea* (Yesson et al. 2012). In addition, the water mass analyses detected no rapid or substantial changes in temperature or salinity that could disrupt coral physiology (Brooke et al. 2013). Instead, the canyons, in terms of these variables, appeared relatively stable during the observation periods.

5.4.2 Environmental Conditions Within the Canyons

The benthic landers and moorings revealed that shallow and middle areas in Baltimore Canyon experienced a strong semidiurnal tidal signature that did not extend to the deep lander. However, in Norfolk Canyon a semidiurnal influence was detected. Tidal influences have been detected in other submarine canyons, for example, M2 and S2 constituents have been observed in Monterey Canyon that declined in strength with depth (Xu and Noble 2009). The fact that a semidiurnal constituent was detected in deep Norfolk Canyon, is likely due to the shape of the canyon, straight, in contrast to the dog-leg morphology of Baltimore Canyon. Shallower and mid stations of the canyons were generally warmer, with higher current velocities across the entire series, while deeper areas had substantially slower mean current speeds and temperatures more than 1 °C cooler. However, these average temperatures were relatively low across all of the stations (approximately 4 °C to 6 °C), indicating that below the shallow lander in Baltimore (600 m water depth) and the mid-canyon lander in Norfolk (917 m), conditions were close to the edge of the tolerances of several coral taxa (Davies et al. 2008, Davies and Guinotte 2011). However, corals appear to thrive in this region even at low temperatures. Congruent studies within the canyon found substantial evidence of an abundant coral community within the canyon (**Chapter 8**; Brooke and Ross 2014), indicating that the cool temperatures within the canyons are unlikely to limit corals in this region.

Current velocities, in contrast, were less stable than temperatures. Norfolk Canyon harbored greater current speeds along the canyon axis, with maximum speeds reaching 81.7 and 94 cm s^{-1} at the middle and deep stations, respectively. These occurred as intense, often turbidity-laden currents and ranged in strength and duration during the year of observation at Norfolk Canyon. As the moorings and landers were placed along the canyon axis, it is not clear what the shape of the turbidity currents are, and how much they impinged on the canyon walls (and on fauna such as cold-water corals). Remotely operated vehicle (ROV) observations along the canyon walls noted very high turbidity on most dives in the 550 to 700 m depth range (**Chapter 8**). Also, upward-looking ADCP's placed at 917 m within Norfolk Canyon recorded the presence of elevated turbidity at 120 m above bottom, suggesting that these are substantial transportation events. These events, especially the most significant in terms of intensity, corresponded with strong surface storms, a common driver for turbidity currents within canyons around the world (Puig et al. 2014). Furthermore, the significant event that occurred in March 2013 corresponded with a substantial mass deposition event that lasted for more than a week. These flows are responsible for substantial sediment deposition and may have contributed to the loss of the upper canyon lander in Norfolk. Additionally, data from the sediment traps (**Chapter 6**) suggest substantial sedimentation events in Norfolk and Baltimore canyons that caused malfunctions in the sediment traps. Interestingly, these turbidity flows corresponded with increased levels of fluorescence, suggesting that an influx of fresh organic material from the shelf is delivered to the deeper areas of the canyon during these events.

In Baltimore Canyon, slower maximum current velocities of 66, 42.3, and 29.2 cm s^{-1} were recorded in the shallow, middle, and deep canyon stations, respectively, that were generally less extreme than current flow in Norfolk. Only one major turbidity current event was detectable during March 2013 among generally high turbidity within the canyon, mostly related to the presence of a strong turbidity layer observed in CTD data and a persistent record of optical and acoustic backscatter at the shallow and middle stations (a proxy for suspended sediment levels; see **Chapter 6** for sediment trap analysis). Many ROV dives within the canyon encountered high turbidity above approximately 600 m (**Chapter 8**). Turbidity layers are a consistent feature of many canyons around the world (Baltimore Canyon, Gardner 1989b; Gulf of Lions, Durrieu de Madron 1994; Nazaré, de Stigter et al. 2007; Whittard, Huvenne et al. 2011). In this study, both Baltimore and Norfolk canyons had clearly observable turbidity layers; however, the two canyons exhibited markedly different turbidity structures.

The turbidity layer in Baltimore Canyon was confined along isopycnals to waters below the thermocline (approximately 300 m) and extended 15 km along the axis of the canyon to approximately 800 m water depth. The seaward upper finger-like projection is identical to that described by Gardner (1989b) for Baltimore Canyon, indicating that this feature is highly stable over many decades and seasons. The mechanism creating this was observed by Hecker et al. (1983) and explained by Gardner (1989a, 1989b) as the presence of a convergence zone, driven under certain circumstances by tidal bores and the focusing of internal wave energy. During this process, water flows up-canyon to meet down canyon flowing water, forming a convergence zone in the middle of the canyon where the turbidity layer ends. From the CTD data collected in this study, the convergence zone likely occurs at the meeting point of the shelf-slope front and WNACW with deeper WASIW, probably located at or at least related to the conspicuous northeast bend in orientation within the canyon (**Figure 5-1**). The implications of this turbidity layer are that in areas shallower than 800 m, resuspended sediment may settle onto hard substrate adjacent to the canyon axis and could interfere with colonization of hard substrates by sessile fauna such as corals. In addition, clear patterns of organic matter distribution and particle sizes can be seen within the canyon axis above and below the convergence zone, likely leading to differences in benthic infauna (**Chapters 6** and **9**).

The turbidity layers in Norfolk Canyon were located deeper on the axis and observed as smaller separate layers between 400 and 1,100 m water depth. The mechanism that drives these sediment clouds was not as clear as in Baltimore Canyon, with no water mass convergence zone observed. Instead, these turbidity layers may indicate multiple locations of disturbance, potentially a result of separate

resuspension events caused by the tidal movement of water up and down canyon. It is possible that canyon morphology also plays a role, given that Norfolk Canyon has a different orientation than Baltimore Canyon and has faster current speeds, which may reduce the strength of the intrusion of tidal bore water. In contrast with Baltimore, which had clear areas of resuspension and deposition, the sediment profiles in Norfolk Canyon consisted of larger particles and were more homogenous throughout the canyon (**Chapter 6**). Although sediment accumulation rates were highest at approximately 1,100 m water depth, enhanced deposition was not reflected in enhanced concentrations of organic matter, which were overall high along the Norfolk Canyon axis (likely driven by recurrent turbidity flows). The distinct turbidity layers and resuspension and deposition zones are all important in driving differences in the benthic infaunal community structure in both canyons (**Chapter 9**), as observed in previous studies (Vetter and Dayton 1998, Sorbe 1999, Ingels et al. 2009, De Leo et al. 2010, Rex and Etter 2010).

5.4.3 Up or Down Water Movement

Geostrophic flow calculations allowed for an approximation of the up or down canyon flow through upper middle and lower locations in Baltimore Canyon. Unfortunately, only one (lower) across-canyon transect was conducted in Norfolk Canyon, which limited inter-canyon comparison. Baltimore Canyon exhibited down canyon current flow in the upper and middle regions of the canyon, decreasing in velocity from surface to bed (600 to 850 m). In the deeper areas of the canyon, bottom water, comprising 35% of the water column, traveled up-canyon. This water was consistent with cold WASIW traveling up-canyon. The near-seabed observations and geostrophic flow calculations from the landers and moorings all showed up-canyon water movement, diminishing in strength from deep to shallow areas, which has been shown in previous canyon studies on both side of the Atlantic (Shepard and Dill 1966, Gardner 1989a, Amaro et al. 2015).

Several possible reasons could explain why the CTD data contradicts the persistent up-canyon flow. First, the CTD data are a single point in time observation and may have insufficient temporal resolution to detect net upward current flow. Furthermore, it is possible that the CTD profiling captured a brief down-canyon current, perhaps an excursion from the normal predominant up-canyon flow. Second, the observed net up-canyon flowing waters could have been present only near the seabed (current meters were 2 m above bottom and CTD data were limited to approximately 10 m above bottom). Norfolk Canyon also had similar up-canyon current flow, although current velocities were ten times higher than in Baltimore Canyon. The upward flowing bottom water in Norfolk Canyon represented 61% of the water column reaching from 400 m to the seafloor (~1,200 m). The benthic landers and moorings also indicated up-canyon water motion; however, the movement was stronger in the mid-canyon area than in the deeper area of the canyon.

These data agree with the view that tidally-driven, cold bore-like water moves up-canyon (Gardner 1989a, 1989b). Studies in other canyons found that net flow can be up-canyon, for example, in the Whittard Canyon (Amaro et al. 2015). In Baltimore Canyon, the net residual flow is stronger on the up-canyon orientation leading to this pronounced upward flow and has been observed to occur up to 600 m water depth (Hunkins 1988). Although net water movement in Baltimore and Norfolk canyons is up-canyon, sediment transport and reworking is driven largely by substantial episodic turbidity flows in Norfolk Canyon, which eject sediment through the deepest parts of the canyon, while Baltimore Canyon tends to transport material via advection from the turbidity cloud (Gardner 1989b).

5.4.4 Conclusions

This chapter characterized the hydrodynamic drivers influencing Baltimore and Norfolk canyons and assessed the overall oceanographic factors likely to affect canyon-dwelling biota. Our interpretation of the conditions within Norfolk Canyon was somewhat hindered by the loss of the ALBEX lander (630 m). It was originally speculated that the ALBEX lander was lost due to burial by an episodic turbidity event that might have occurred in the canyon or due to a failure of its acoustic release. The lander resurfaced in the

Bahamas and was subsequently recovered. Any usable data retrieved from the lander were not available for inclusion in this report. However, our observations significantly enhance the understanding of MAB canyon oceanographic regimes because of increased instrumentation, higher recording resolution, and longer deployment duration. Generally, our findings show that both canyons are strikingly different, which was unexpected because of their proximity to each other. Differences between the two canyons are seen across many other disciplines incorporated in the overall study (i.e., geological studies, benthic invertebrate communities, and benthic infaunal communities; **Chapters 6**, **8**, and **9**, respectively). The relationship between these water mass movements over tidal cycles seems pivotal to the hydrodynamics and sediment regimes and thus the physical stresses exerted on the benthos in both canyons.

The conditions within the two canyons demonstrate environments that are typified by regular disturbance, such as those generated from tides and significant stochastic disturbance driven by surface weather patterns. Many of our observations, particularly those that are temporally persistent, have been reported in earlier canyon studies within the MAB area (e.g., Gardner 1989a, 1989b), implying that many of the observed processes are persistent on time scales of decades. The unique oceanographic regimes specific to each canyon control the distribution and extent of turbidity layers found in these two MAB canyons. These mechanisms are likely the most important contributors to the differences seen between Baltimore and Norfolk canyons. Understanding these processes is crucial for quantifying the extent to which the processes influence unique canyon habitats and fauna.

5.5 LITERATURE CITED

Amaro T, de Stigter H, Lavaleye M, Duineveld G. 2015. Organic matter enrichment in the Whittard Channel; its origin and possible effects on benthic megafauna. Deep-Sea Research Part I-Oceanographic Research Papers. 102:90–100.

Auster PJ, Gjerde K, Heupel E, Watling L, Grehan A, Rogers AD. 2011. Definition and detection of vulnerable marine ecosystems on the high seas: problems with the “move-on” rule. ICES Journal of Marine Science. 68:254–264.

Beardsley RC, Winant CD. 1979. On the mean circulation in the Mid-Atlantic Bight. Journal of Physical Oceanography. 9:612–619.

Bigelow HB. 1933. Studies of the waters on the continental shelf, Cape Cod to Chesapeake Bay. I. The cycle of temperature. Massachusetts Institute of Technology and Woods Hole Oceanographic Institution. 135 p.

Brooke S, Ross SW. 2014. First observations of the cold-water coral *Lophelia pertusa* in mid-Atlantic canyons of the USA. Deep-Sea Research Part II: Topical Studies in Oceanography. 104:245–251.

Brooke S, Ross SW, Bane JM, Seim HE, Young CM. 2013. Temperature tolerance of the deep-sea coral *Lophelia pertusa* from the southeastern United States. Deep-Sea Research Part II: Topical Studies in Oceanography. 92:240–248.

Cacchione DA, Pratson LF, Ogston AS. 2002. The shaping of continental slopes by internal tides. Science. 296:724–727.

Canals M, Puig P, Durrieu de Madron X, Heussner S, Palanques A, Fabres J. 2006. Flushing submarine canyons. Nature. 444:354–357.

Church TM, Mooers CNK, Voorhis AD. 1984. Exchange processes over a Middle Atlantic Bight shelfbreak canyon. Estuarine Coastal and Shelf Science. 19:393–411.

Churchill JH, Cornillon PC. 1991. Water discharged from the Gulf Stream north of Cape Hatteras. Journal of Geophysical Research. 96:22227–22243.

Churchill JH, Gawarkiewicz G. 2009. Shelfbreak frontal eddies over the continental slope north of Cape Hatteras. Journal of Geophysical Research-Oceans. 114:C02017.

Churchill JH, Gawarkiewicz GG. 2014. Shelf water and chlorophyll export from the Hatteras slope and outer shelf. Journal of Geophysical Research-Oceans. 119:4291–4304.

Churchill JH, Cornillon PC, Hamilton P. 1989. Velocity and hydrographic structure of subsurface shelf water at the Gulf Stream's edge. Journal of Geophysical Research-Oceans. 94:10791–10800.

Churchill JH, Levine ER, Connors DN, Cornillon PC. 1993. Mixing of shelf, slope and Gulf-Stream water over the continental slope of the Middle Atlantic Bight. Deep-Sea Research Part I: Oceanographic Research Papers. 40:1063–1085.

Colman S, Halka J. 1990. Ancient channels of the Susquehanna River beneath Chesapeake Bay and the Delmarva Peninsula. Geological Society of America Bulletin. 102:1268–1279.

Cresswell GM. 1967. Quasi-synoptic monthly hydrography of the transition region between coastal and slope water south or Cape Cod, Massachusetts. Report No. 67-35. Woods Hole Oceanographic Institution.

Csanady GT, Hamilton P. 1988. Circulation of slopewater. Continental Shelf Research. 8:565–624.

Csanady GT, Churchill JH, Butman B. 1988. Near-bottom currents over the continental slope in the Mid-Atlantic Bight. Continental Shelf Research. 8:653–671.

Davies A, Guinotte J. 2011. Global habitat suitability for framework-forming cold-water corals. PLoS ONE. 6(4):e18483.

Davies AJ, Wisshak M, Orr JC, Roberts JM. 2008. Predicting suitable habitat for the cold-water reef framework-forming coral *Lophelia pertusa* (Scleractinia). Deep-Sea Research Part I-Oceanographic Research Papers. 55:1048–1062.

De Leo FC, Smith CR, Rowden AA, Bowden DA, Clark MR. 2010. Submarine canyons: hotspots of benthic biomass and productivity in the deep sea. Proceedings of the Royal Society B: Biological Sciences. 277:2783–2792.

de Stigter HC, Boer W, de Jesus Mendes PA, Jesus CC, Thomsen L, van den Bergh GD, van Weering TCE. 2007. Recent sediment transport and deposition in the Nazaré Canyon, Portuguese continental margin. Marine Geology. 246:144–164.

Drinkwater KF, Mountain DB, Herman A. 1999. Variability in the slope water properties off eastern North America and their effects on the adjacent shelves. 1999 ICES Annual Science Conference, Theme Session O: 08 Global Change Aspects.

Durrieu de Madron XD. 1994. Hydrography and nepheloid structures in the Grand-Rhône Canyon. Continental Shelf Research. 14:457–477.

Emery WJ, Meincke J. 1986. Global water masses: summary and review. Oceanologica Acta. 9:383–391.

Fitzgerald JL, Chamberlin JL. 1981. Anticyclonic warm core Gulf Stream eddies off the northeastern United States in 1979. Annales Biologiques (Copenhagen). 36:44–51.

Forde E. 1981. Evolution of Veatch, Washington, and Norfolk Submarine Canyons: inferences from strata and morphology. Marine Geology. 39:197–214.

Garcia R, Van Oevelen D, Soetaert K, Thomsen L, De Stigter HC, Epping E. 2008. Deposition rates, mixing intensity and organic content in two contrasting submarine canyons. Progress in Oceanography. 76:192–215.

Gardner WD. 1989a. Periodic resuspension in Baltimore Canyon by focusing of intemal waves. Journal of Geophysical Research 94:18,185–194.

Gardner WD. 1989b. Baltimore Canyon as a modern conduit of sediment to the deep sea. Deep-Sea Research Part A: Oceanographic Research Papers. 36:323–358.

Garvine RW, Wong KC, Gawarkiewicz GG, Mccarthy RK, Houghton RW, Aikman F. 1988. The morphology of shelfbreak eddies. Journal of Geophysical Research-Oceans. 93:15593–15607.

Hecker B, Logan DT, Gandarillas FE, Gibson PR. 1983. Canyon and slope processes study, vol. III: biological processes. Report for the U.S. Department of the Interior, Minerals Management Service, under contract no. 14-12-0001-29178. Palisades (NY): Lamont-Doherty Geological Observatory. 212 p.

Hickey BM. 1997. The response of a steep-sided, narrow canyon to time-variable wind forcing. Journal of Physical Oceanography. 27:697–726.

Horne EPW. 1978. Interleaving at the subsurface front in the slope water off Nova Scotia. Journal of Geophysical Research. 83:3659–3671.

Houghton RW, Schlitz R, Beardsley RC, Butman B, Chamberlin JL. 1982 The Middle Atlantic Bight cold pool−evolution of the temperature structure during summer 1979. Journal of Physical Oceanography. 12:1019–1029.

Houghton RW, Olson DB, Celone PJ. 1986. Observation of an anticyclonic eddy near the continental shelf break south of New England. Journal of Physical Oceanography. 16:60–71.

Hunkins K. 1988. Mean and tidal currents in Baltimore Canyon. Journal of Geophysical Research-Oceans. 93:6917–6929.

Huvenne VAI, Tyler PA, Masson DG, Fisher EH, Hauton C, Hühnerbach V, Le Bas TP, Wolff GA. 2011. A picture on the wall: innovative mapping reveals cold-water coral refuge in submarine canyon. PLoS ONE. 6:e28755.

Ingels J, Kiriakoulakis K, Wolff GA, Vanreusel A. 2009. Nematode diversity and its relation to the quantity and quality of sedimentary organic matter in the deep Nazare Canyon, Western Iberian Margin. Deep-Sea Research Part I: Oceanographic Research Papers. 56:1521–1539.

Keller G, Shepard FP. 1978. Currents and sedimentary processes in submarine canyons off the northeastern United States. In: Stanley DJ, Kelling G, editors. Sedimentation in submarine canyons, fans and tenches. Stroudsberg (PA): Dowden, Hutchinson and Ross Inc. p. 15–32.

Kelley D, Richards C. 2015. oce: Analysis of Oceanographic Data. R package version 0.9-17. [accessed 2016 Apr 14]. http://CRAN.R-project.org/package=oce.

Levin LA, Sibuet M. 2012. Understanding continental margin biodiversity: a new imperative. Annual Review of Marine Science. 4:79–112. doi:10.1146/annurev-marine-120709-142714.

Levin LA, Etter RJ, Rex MA, Gooday AJ, Smith CR, Pineda J, Stuart CT, Hessler RR, Pawson D. 2001. Environmental influences on regional deep-sea species diversity. Annual Reviews in Ecology, Evolution and Systematics. 32:51–93.

Lillibridge JL, Hitchcock G, Rossby T, Lessard E, Mork M, Golmen L. 1990. Entrainment and mixing of shelf slope waters in the near-surface Gulf Stream. Journal of Geophysical Research-Oceans. 95(C8):13065–13087.

Loder JW, Petrie B, Gawarkiewicz GG. 1998. The coastal ocean off northeastern North America: a large-scale view. In: Robinson AR, Brink K, editors. The sea, volume 11: the global coastal ocean-regional studies and syntheses (Chapter 5). John Wiley & Sons. p. 105–133.

Martin J, Palanques A, Puig P. 2006. Composition and variability of downward particulate matter fluxes in the Palamos submarine canyon (NW Mediterranean). Journal of Marine Systems. 60:75–97.

Obelcz J, Brothers D, Chaytor J, ten Brink U, Ross SW, Brooke S. 2014. Geomorphic characterization of four shelf-sourced submarine canyons along the U.S. Mid-Atlantic continental margin. Deep-Sea Research Part II: Topical Studies in Oceanography. 104:106–119.

Palanques A, Durrieu de Madron X, Puig P, Fabres J, Guillén J, Calafat A, Canals M, Heussner S, Bonnin J. 2006. Suspended sediment fluxes and transport processes in the Gulf of Lions submarine canyons. The role of storms and dense water cascading. Marine Geology. 234:43–61.

Pawlowicz R, Beardsley B, Lentz S. 2002. Classical tidal harmonic analysis including error estimates in MATLAB using T_TIDE. Computers and Geosciences. 28:929–937.

Pierce JW. 1976. Suspended sediment transport at the shelf break and over the outer margin. In: Stanley DJ, Swift DJP, editors, Marine sediment transport and environmental management. New York (NY): Wiley. p. 437–458.

Posmentier ES, Houghton RW. 1981. Springtime evolution of the New England shelf break front. Journal of Geophysical Research-Oceans. 86:4253–4259. doi:10.1029/JC086iC05p04253.

Puig P, Palanques A, Martin J. 2014. Contemporary sediment-transport processes in submarine canyons. Annual Review of Marine Science. 6:53–77.

Rasmussen LL. 2005. Slope water, Gulf Stream, and seasonal influences on southern Mid-Atlantic Bight circulation during the fall-winter transition. Journal of Geophysical Research. 110:C02009.

R Core Team. 2015. R: a language and environment for statistical computing. R Foundation for Statistical Computing, Vienna, Austria. [accessed 2016 Apr 14]. http://www.R-project.org/.

Rex MA, Etter RJ. 2010. Deep-sea biodiversity: pattern and scale. Cambridge (MA): Harvard University Press. 368 p.

Robinson AR, Brink K. 2006. The sea, volume 14A: the global coastal ocean: interdisciplinary regional studies and syntheses. Cambridge (MA): Harvard University Press. 840 p.

Shepard FP, Dill RF. 1966. Submarine canyons and other sea valleys. Chicago (IL): Rand McNally. 381 p.

Simpson JH, Sharples J. 2012. Introduction to the physical and biological oceanography of shelf seas. Cambridge (UK): Cambridge University Press. 448 p.

Sorbe JC. 1999. Deep-sea macrofaunal assemblages within the benthic boundary layer of the Cap-Ferret Canyon (Bay of Biscay, NE Atlantic). Deep-Sea Research Part II: Topical Studies in Oceanography. 46:2309–2329.

Vetter EW, Dayton PK. 1998. Macrofaunal communities within and adjacent to a detritus-rich submarine canyon system. Deep-Sea Research Part II: Topical Studies in Oceanography. 45:25–54.

Voorhis AD, Webb DC, Millard RC. 1976. Current structure and mixing in the shelf/slope water front south of New England. Journal of Geophysical Research. 81:3695–3708.

Xu JP, Noble MA. 2009. Currents in Monterey Submarine Canyon. Journal of Geophysical Research. 114:C03004.

Yesson C, Taylor ML, Tittensor DP, Davies AJ, Guinotte J, Baco A, Black J, Hall-Spencer JM, Rogers AD. 2012. Global habitat suitability of cold-water octocorals. Journal of Biogeography. 39:1278–1292.

This page intentionally left blank

CHAPTER 6. GEOLOGICAL STUDIES

Furu Mienis, Gerard C.A. Duineveld, Brendan Roark, Amanda Demopoulos, Nancy Prouty, Pamela Campbell-Swarzenski, Michael Rhode, Sandra D. Brooke, and *Steve W. Ross*

6.1 INTRODUCTION

Vast areas of the slope bordering the world's continents have been incised by submarine canyons (see Harris and Whiteway 2011 for an overview), which are particularly numerous along active margins with high river-derived sediment export. The evolution of submarine canyons is generally considered to be driven by two different processes: 1) slumping, slope failure, and other mass wasting events; and 2) erosive turbidity flows derived from fluvial shelf and upper slope sources (Harris and Whiteway 2011, Brothers et al. 2013). Depending on local geography, topography, and hydrography, canyons may act as conduits for sediment and associated compounds from the continental shelf all the way down into the deep sea (Canals et al. 2006, Allen and Durrieu de Madron 2009). Most canyons are morphologically complex and have distinct sediment characteristics and spatially variable accumulation rates (Schmidt et al. 2001, de Stigter et al. 2007).

The differential sedimentation regime within canyons can influence the organic composition of sediments and the abundance of fauna thriving on these resources. Local deposition centers of sediment and organics may form hotspots for detritivorous bottom dwelling organisms as were found in the Portuguese Nazaré and New Zealand's Kaikoura canyons (Amaro et al. 2006, De Leo et al. 2010). Also, enhanced food availability from suspended nutrients passing through the canyon may support sessile suspension feeding organisms, including deepsea coral and sponge communities. These communities are often found on vertical cliffs and are associated with increased biodiversity and biological activity, which has been documented from the northeast Atlantic in Whittard Canyon and canyons in the northwest Mediterranean (Huvenne et al. 2011, Morris et al. 2013, Gori et al. 2013).

Currently, processes governing recent sediment transport and deposition in canyons, including mass fluxes of particles, organic matter, and anthropogenic substances, are still poorly known for most canyons (van Weering and Weaver 2007). Mass particle transport through canyons often has a periodic or episodic character with varying time scales. Episodic events over long time scales include earthquakes or slope failures inducing massive turbidity flows (Puig et al. 2014). On short to medium time scales, gravity flows have been documented, triggered by various events including storms, river floods, and trawling (Talling et al. 2013 and references therein). Severe storms have been found to trigger mass gravity flows in several canyons around the world either by wave action releasing sediment near the canyon head or by transport of shelf sediment toward the canyon (Puig et al. 2014). In order to capture the source and impact of these events, it is essential to deploy *in situ* equipment over appropriate time scales (Talling et al. 2013). This costly prerequisite explains the paucity of monitoring data from canyons in general including most of the large canyons in the Mid-Atlantic Bight (MAB) of the United States.

The MAB is incised by 13 major canyons of varying size, shape, and morphological complexity (**Figure 6-1**). Baltimore Canyon is one of the best studied canyons, which according to Gardner (1989a, 1989b), currently has a diminished sediment supply. Erosion and sedimentation are mainly related to off-shelf spill in canyon heads, failure of the steep canyon walls, and resuspension by bottom currents and internal waves (Gardner 1989a). The nearby Norfolk Canyon is situated in the same oceanographic setting as Baltimore Canyon—it is located at the same distance to the coast, it contains shelf-derived sediments, and it lacks river input (Obelcz et al. 2014). Bennet et al. (1985), however, characterized Norfolk Canyon as a conduit for the transport of fine-grained sediment with high organic carbon content. In addition, areas containing high suspended particulate concentrations were found within the canyon.

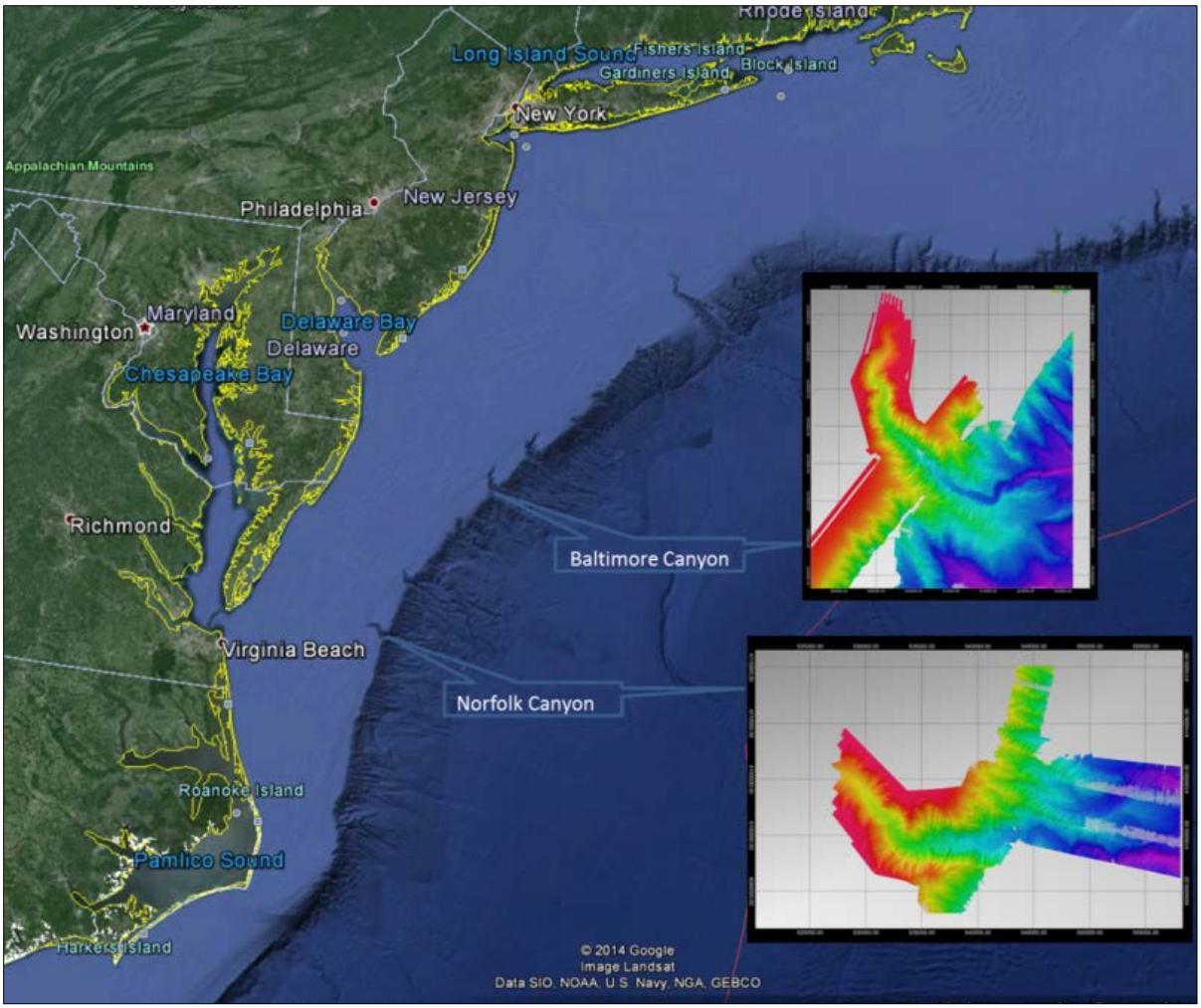

Figure 6-1. Mid-Atlantic Bight and positions of Baltimore and Norfolk canyons. Insets show bathymetric (multibeam) maps of the two canyons.

The difference in sedimentology between these two MAB canyons may have important repercussions for the local fauna. In several canyons around the world, sediment grain-size and organic fraction, in combination with topography and depth, represent important variables that generally correlate well with the distribution of metazoan fauna (Valentine et al. 1980, Ingels et al. 2011, LeDuc et al. 2013, Kenchington et al. 2014). In general, sediment composition (e.g., grain size, organic fraction) is an important determinant of soft sediment benthic community structure on small (meter) to medium (kilometer) scales. On larger scales, hydrodynamic conditions, physicochemical properties of the water column, and particulate organic carbon flux are becoming more important (Wei et al. 2010, Reiss et al. 2011, Dutertre et al. 2013).

In response to progressing exploration for mineral resources into the deep water of the MAB, the U.S. Bureau of Ocean Energy Management (BOEM) initiated a multidisciplinary project on two of the largest canyons in the MAB (i.e., Norfolk and Baltimore canyons) (**Figure 6-1**). This project covered a range of topics varying from (micro) biology to sedimentology (see **Chapter 1**, Introduction, and **Chapter 19**, Synthesis). One of the primary objectives of this project was to describe and understand the distribution of (vulnerable) ecosystems in the MAB canyons, which included a comprehensive study examining the sediment fauna, sedimentological characteristics, and water column properties of Baltimore and Norfolk canyons. In the present study, we compare sediments and sedimentation in the two canyons in

the context of hydrographical observations obtained from shipboard conductivity-temperature-depth (CTD) casts during three cruises and during a one-year deployment of current and turbidity meters and sediment traps (**Chapter 5**).

Two hypotheses were formulated at the start of the study. First, canyons incising the MAB shelf, including Norfolk and Baltimore, capture sediment and organic carbon. This transport ultimately enriches the canyon floor sediment, resulting in higher concentration and quality of carbon than the adjacent slope. Second, given Baltimore and Norfolk canyons have a very different morphology and orientation from each other, and previous reports indicated differences in sediment grain size and transport properties (Bennett et al. 1985), the canyons have different sedimentation patterns and accumulation rates, which most likely explain the differing faunal communities between the two canyons.

6.2 METHODS

The samples and data for this study were collected in 2012 and 2013 during three of the four project cruises (see **Chapter 3** for cruise descriptions, schedules, and a list of samples collected).

- The 2012 sampling cruise (NF-12-07) on the National Oceanic and Atmospheric Administration (NOAA) ship *Nancy Foster* consisted of three legs. During Leg 1 (15−31 August 2012), benthic landers and moorings with sediment traps were deployed in the two canyons, followed by CTD profiling of the water column in Baltimore Canyon and box core and monocore sampling of sediments in the canyon and on the adjacent shelf. During Leg 3 (17 September to 2 October 2012) a limited number of box core samples were collected in Norfolk Canyon.
- During the 2013 sampling cruise (May 2013), the majority of box core and monocore sediment samples and water column profiles from Norfolk Canyon were collected during a cruise on the NOAA ship *Ronald H Brown*.
- During the 2013 instrument retrieval cruise (August 2013), the benthic landers and moorings were retrieved and additional CTD casts were conducted in both canyons using the NOAA ship *Nancy Foster*.

6.2.1 Box Core Samples

Box core samples were collected to study sedimentology, benthic biodiversity (fauna) (**Chapter 8**), and microbiology (**Chapter 12**). The box corer was designed by the Royal Netherlands Institute for Sea Research (NIOZ) with a cylindrical core tube (30 cm diameter, 55 cm height) and a trip valve to prevent flushing of the sample during ascent (**Figure 6-2A**). The box corer was lowered vertically on a steel wire until the core tube penetrated into the sediment. At this point, the tension on the wire slackened, which released the trip valve, closing off the top of the core. During recovery, the spade was pulled underneath the box corer, thereby sealing the sample inside the core tube.

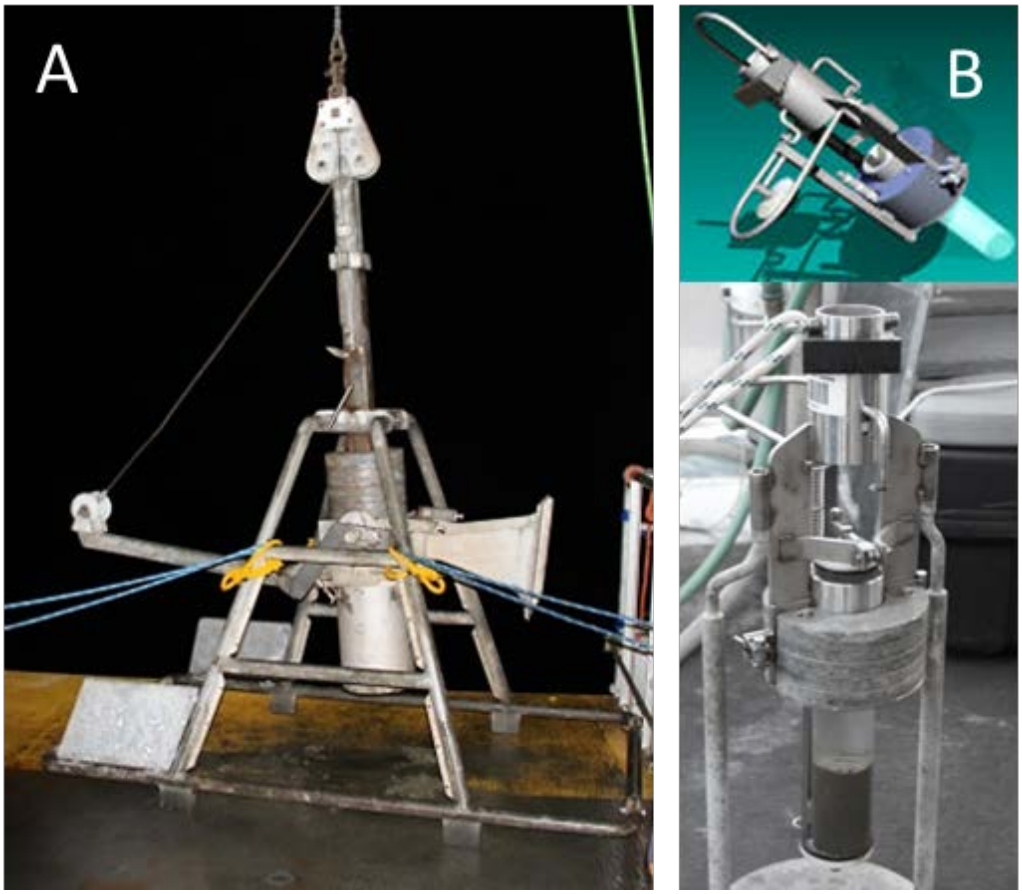

Figure 6-2. Box corer and monocorer designed by the Royal Netherlands Institute for Sea Research (NIOZ). (A) box corer shown with circular 30 cm core tube and trip valve inside (not visible); (B) monocorer, which is a single tube version of the multi corer that was suspended beneath the CTD/rosette sampler frame. After penetration and pulling the corer from the sediment, the tube is closed by an arm that is released by the impact on the seafloor.

Box core samples were collected in Baltimore and Norfolk canyons on transects along the canyon axis and on the adjacent open slope (**Figures 6-3** and **6-4**). The sampling scheme was designed in order to characterize sedimentary characteristics in the different depth zones of the upper and middle parts of the canyon. These areas within the canyons are assumed the most active parts in terms of particle transport and deposition. Transects on the open slope enabled differentiation between canyon-derived effects and general slope processes operating on a regional scale. It was hypothesized that in response to gradients in sediment composition in the upper and middle canyon, there will be a corresponding zonation pattern in metazoan and microbial benthic communities. Sampling for sedimentology was therefore combined with faunal sampling (**Chapter 8**).

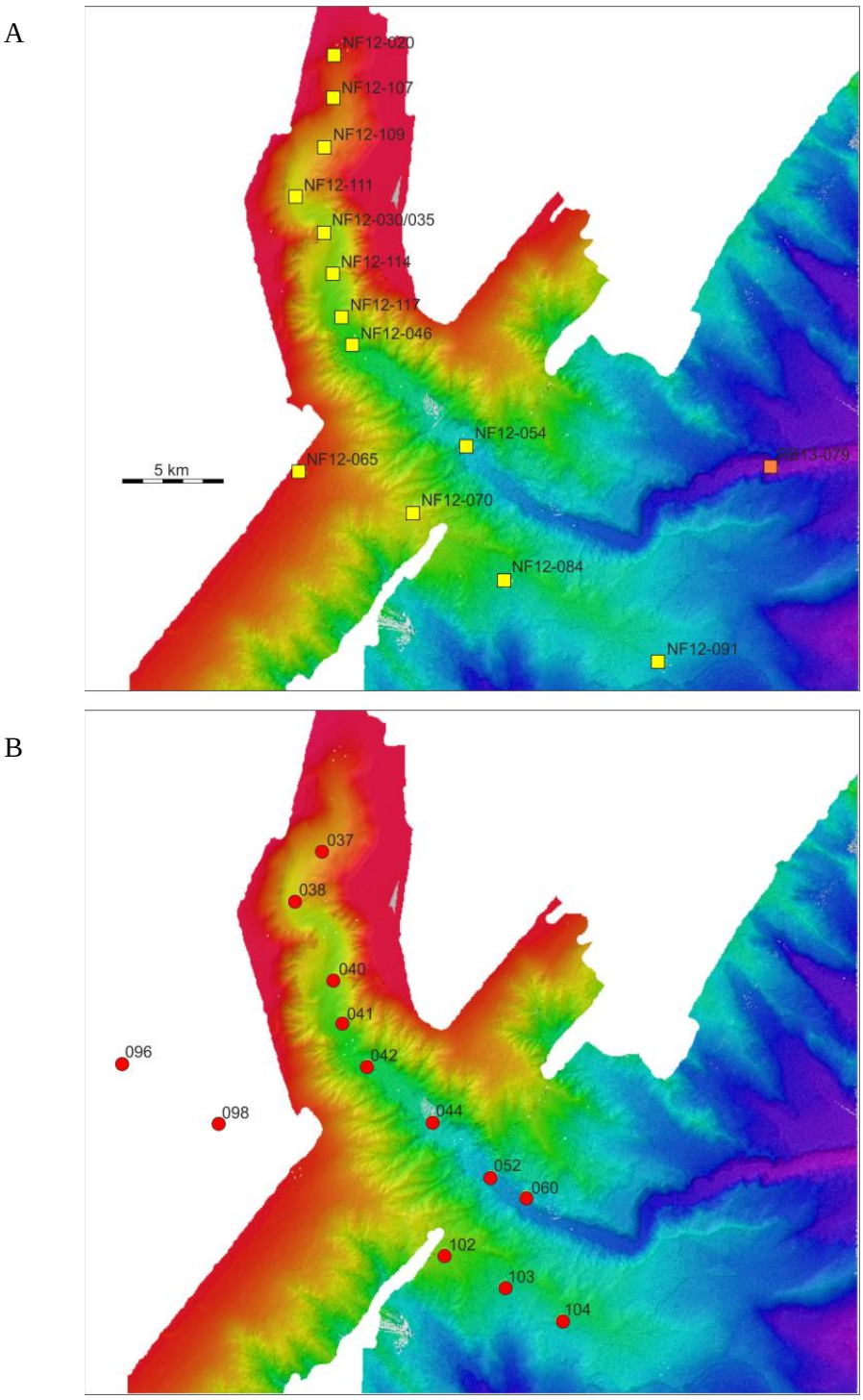

Figure 6-3. Baltimore Canyon sediment sampling locations. (A) Box core samples collected during the 2012 sampling cruise on the *Nancy Foster* (NF) and the 2013 sampling cruise on the *Ronald H Brown* (RB). (B) Monocore samples collected on the 2012 sampling cruise.

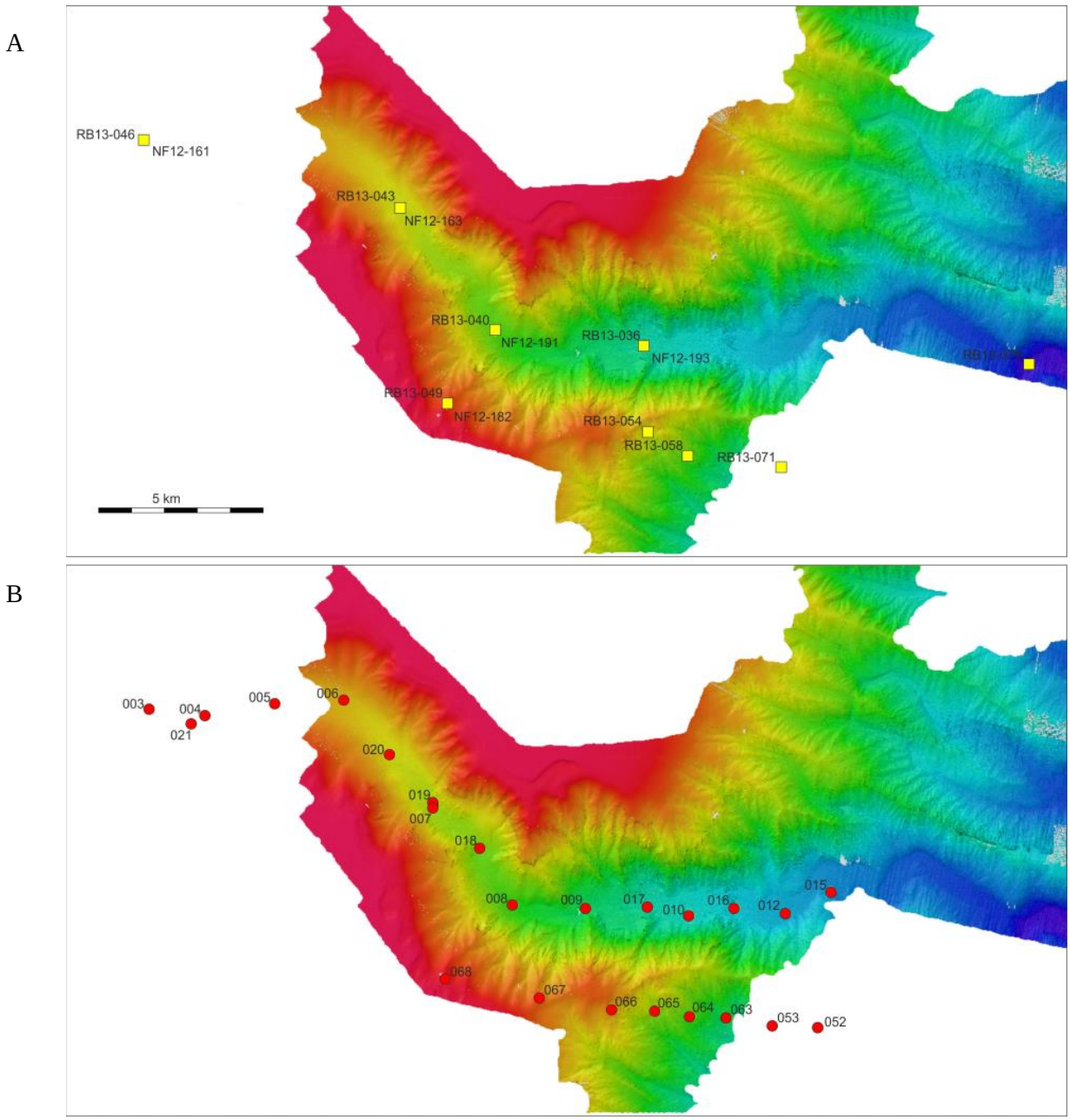

Figure 6-4. Norfolk Canyon sediment sampling locations. (A) Box core samples collected during the 2012 sampling cruise on the *Nancy Foster* (NF) and the 2013 sampling cruise on the *Ronald H Brown* (RB). (B) Monocore samples collected on the 2013 sampling cruise.

Once on deck, subcores for sedimentological analysis were extracted from the box corer by inserting a PVC liner. In addition, sediment cores for analyses of organic carbon, nitrogen, stable isotopes, and phytopigments were collected by inserting an acrylic subcore in a box core sample (see **Section 6.2.2** for detailed description of analysis). Subcores for sedimentology were sealed and transported to NIOZ, the Netherlands. Before opening the box cores, X-ray images were made (Faxitron 43855F cabinet X-ray system) to study the internal sedimentary structure. Cores were split into two crescent parts using a NIOZ-designed core cutter, which splits the PVC liner longitudinally, and then the sediment was cut with a wire. Immediately following splitting, both core halves were photographed using a camera from the Avaatech X-Ray fluorescence (XRF) core scanner, which creates a high-resolution digital color image (Richter at al. 2006). The subcore with the highest quality was kept as a reference core and stored at 4 °C. A sedimentological description was made of the reference core half, and the core was scanned with the Avaatech XRF core scanner in order to determine down-core changes in the present elements of the surface sediment layer. XRF measurements are a fast and nondestructive way to determine the chemical composition of the sediment. Calcium/iron (Ca/Fe) and calcium/titanium (Ca/Ti) ratios were used in this study as indication for changes in the amount of terrestrial material present in the sediment.

The other core half was entirely used for grain size analysis and lead-210 (^{210}Pb) measurements, which were used to determine sediment accumulation rates. The top 3 cm of the core was cut in 0.5 cm slices, while the rest of the core was cut in 1 cm slices. In addition, a needle-less syringe was used to collect a fixed volume of sample every 5 cm, used to calculate the dry bulk density and porosity of the sediment. All samples were weighed and freeze dried. When dry, samples were weighed again. The sediment slices were used for grain size measurements (bulk fraction) using a Beckman Coulter LS 12,320 grain size analyzer, which uses laser diffraction and light scattering to determine the particle size (0 to 2,000 µm). The sediment slices were also homogenized, and samples were taken for ^{210}Pb measurements to determine accumulation rates. All samples were prepared in digitubes and 1 mL of polonium-209 (^{209}Po) tracer solution was added together with 10 mL of hydrochloric acid (HCl). Via leaching, ^{209}Po causes spontaneous deposition of ^{210}Pb from the sediment on silver discs. In order to prevent iron deposits, ascorbic acid was added. After leaching silver discs were cleaned with ethanol and dried, then analyzed with the Canberra Alpha Analyst. In order to calculate the actual accumulation rates (ω), the supported ^{210}Pb value and initial activity were fitted in a one-dimensional two-layer diffusion model in which mixing occurs only in the surface mixed layer. Here we assume that there is a constant ^{210}Pb flux and sedimentation rate (de Stigter et al. 2007). ^{210}Pb profiles are plotted on a cumulative mass scale to avoid sediment compaction effects. In sandy cores, the sand fraction was removed by wet sieving over a 63 µm sieve to reduce particle size-related variation of ^{210}Pb.

6.2.2 Monocore Samples

The monocorer (**Figure 6-2B**) is a single tube version of a multi corer that was suspended underneath the CTD/rosette sampler frame. The monocore collections facilitated high-resolution sampling in and outside the canyon at each CTD station (**Figure 6-3B** and **6-4B**). Cores retrieved with the monocorer, as well as subcores taken with the box corer, were used for analyses of organic carbon (C_{org}), nitrogen (N), stable isotopes, and phytopigments.

Cores were sliced on board into 1 cm slices, which were immediately frozen. Samples were shipped frozen to NIOZ in the Netherlands for further analyses. At NIOZ, all samples were freeze dried and homogenized. Phytopigments were analyzed in surface slices (0 to 1 cm) of sediment samples. Pigments were extracted from freeze-dried sediment by adding 95% methanol to 0.5 g sediment. This mixture was cooled in ice and sonicated during seven bursts of 12 s with an interval of 30 s. The mixture was subsequently centrifuged at 5,000 revolutions per minute (rpm) for 8 minutes, and the supernatant was filtered over a 0.2 µm polytetrafluoroethylene (PTFE) membrane; 50 µL of the filtrate was then injected in the high-performance liquid chromatography (HPLC) instrument. The HPLC is a Waters Instrument Acquity UPLC H-Class system consisting of a quaternary solvent manager, column manager set at 25 °C,

and sample manager coupled to a eλ photodiode-array and fluorescence detector. The column used was a Grace Allsphere ODS-2, 3-µm (analytical). Phytopigments were identified and quantified using a library based on pigment standards (DHI, Denmark). From the results of the pigment analysis, intact chlorophyll-*a* concentrations were taken as a proxy for fresh phytodetritus biomass.

Organic carbon and nitrogen content were measured on a Thermo Organic Elemental Analyser Flash 2000 and stable carbon and nitrogen isotopes were measured on a Thermo Delta V Advantage Isotope Ratio MS. Prior to analysis, samples for measurements of C_{org} were acidified with HCl to remove all inorganic carbon. Standards used for C and N were acetaniline and ureum, respectively.

Molecular composition of the surface sediment (0 to 0.5 and 0 to 1 cm) from the sediment cores were analyzed by gas chromatography-mass spectrometry (GC-MS) at the U.S. Geological Survey (USGS) Pacific Coastal Marine Science Centers Organic Geochemistry laboratory in Menlo Park and Santa Cruz, California. Samples were extracted with a solvent system consisting of a hexane/acetone (1:1) mixture followed by a second extraction in dichloromethane/methanol (2:1) mixture. Compounds (*n*-alkanes (F1), polycyclic aromatic hydrocarbons (PAHs) (F2), and sterols/ketones (F3)) were identified by retention time of known standards in addition to mass spectral confirmation. Lipid biomarkers (sterol and *n*-alkane) concentrations (µg g^{-1}) are reported normalized to organic content of dry sediment. Major organic matter sources to the sterol and *n*-alkane molecular signatures were investigated by calculating relative proportions of marine, terrestrial higher plants, and anthropogenic/petroleum contributions. Relative contributions from natural (autochthonous versus allochthonous) and anthropogenic organic matter sources were calculated following designations from Pisani et al. (2013). Terrestrial organic matter composition of sediments was quantified using concentrations of odd-numbered *n*-alkanes in the C_2 to C_{31} range as well as the sterols campesterol, stigmasterol, and β-sitosterol. Marine components were determined using concentrations of the sterols cholesterol and brassicasterol as well as odd- and even-numbered *n*-alkanes in the C_{15} to C_{19} range. The anthropogenic components were determined using the sterol composition of coprostanol, epicoprostanol, and 5-β-coprostanone and the isoprenoid hydrocarbons pristane and phytane.

Radiocarbon (^{14}C) ages were determined at the National Ocean Sciences Accelerator Mass Spectrometry (NOSAMS) facility. Approximately 50 mg of acidified (1.2N HCl) sediment was converted to CO_2 and graphitized for accelerator mass spectrometry (AMS) (Vogel et al. 1987). Radiocarbon ages were calculated using the Libby half-life of 5,568 years. The $D^{14}C$ values (i.e., radiocarbon values without age correction) were age corrected to account for decay that took place between collection (or death) and the time of measurement using the following equation:

$$\Delta^{14}C = (Fm*\text{age correction})-1)*1{,}000$$

where age correction is defined as exp(1950-year of measurement)/8267) (Stuiver and Polach 1977). Radiocarbon results are reported as $\Delta^{14}C$ (‰) and conventional radiocarbon age after applying a $\Delta^{13}C$ correction (Stuiver and Polach 1977).

Neodymium isotopes ($^{143}Nd/^{144}Nd$) were determined at the Woods Hole Oceanographic Institution (WHOI) NEPTUNE multicollector inductively coupled-mass spectrometry (ICP-MS) (Hart and Blusztajn 2006; Escrig et al. 2012). The internal precision is 5 to 10 µg g^{-1} (2σ); external precision, after adjusting 0.511847 for the La Jolla Nd standards, was estimated to be 15 to 25 µg g^{-1} (2σ). In brief, following sequential leaching methods of Bayon et al. (2002), carbonates were removed with 10% acetic acid, and iron-manganese (Fe-Mn) oxides were removed by 1 M hydrochloride in 25% acetic acid. Neodymium was isolated using a single-stage column method consisting of a lanthanide-specific cation exchange resin (Scher and Delany 2010). All results were correct against the JNdi-1 standard ($^{143}Nd/^{144}Nd = 0.512104$). $^{143}Nd/^{144}Nd$ ratios were converted to εNd using a value of 0.512636 for chondritic uniform reservoir.

6.2.3 Sediment Traps on Benthic Landers and Moorings

During the 2012 sampling cruise, four benthic landers (NIOZ, University of North Carolina, Wilmington [UNCW]) and two moorings (USGS) were deployed for 1 year in Baltimore and Norfolk canyons. The sampling design enabled the examination of canyon characteristics, including the movement of particulate material up and down canyon, propagation of internal waves, water parameter variability, and particle fluxes. One lander was placed near the head and the mouth of each canyon, and the mooring was placed within the middle of the canyon between each lander site (**Figure 6-5**; **Chapter 5**). During Leg 1 of the 2012 sampling cruise, the NIOZ Bottom Boundary Layer (BOBO) lander was deployed near the mouth of Norfolk Canyon on 17 August 2012 in approximately 1,364 m depth. The NIOZ Autonomous Lander for Biological Experiments (ALBEX) lander and the USGS mooring were also deployed the same day at the head of Norfolk Canyon (about 630 m depth) and near the central region of Norfolk Canyon (about 917 m depth), respectively. A USGS mooring was deployed near the center of Baltimore Canyon on 18 August in a water depth of approximately 1,082 m. The two UNCW landers were deployed in Baltimore Canyon during Leg 2 of the 2012 sampling cruise, one at the mouth of the canyon (1,318 m depth) on 5 September 2012 and one near the head of the canyon (603 m depth) on 6 September. Because of concerns about the UNCW lander acoustic release configurations, these two landers were retrieved, serviced, and returned (16 and 17 May 2013) to the same deployment sites during the 2013 sampling cruise.

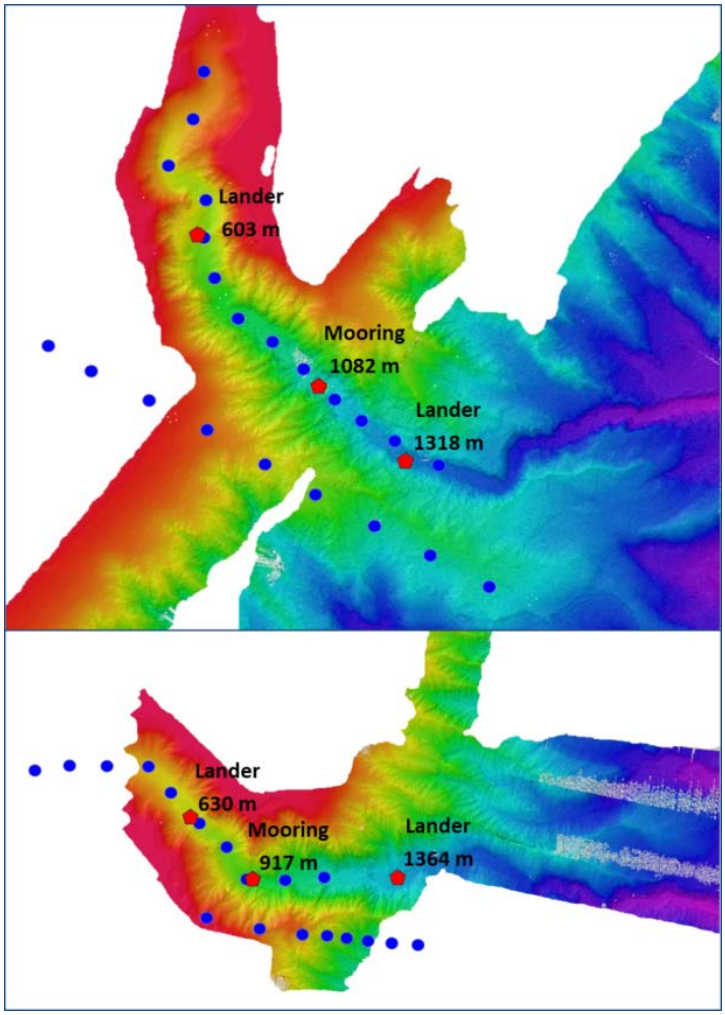

Figure 6-5. Position of moorings, landers, and CTD stations in Baltimore Canyon (top) and Norfolk Canyon (bottom).

Each of the four landers held a Technicap PPS4/3 sediment trap (aperture of 0.05 m^2 mounted about 2 m above bottom) programmed to rotate a sample bottle (250 mL) at 30-day intervals, delivering 12 samples during the one-year deployment. The two USGS moorings were equipped with a Honjo Parflux sediment trap with 13 (500 mL) bottles programmed to rotate on a 30-day interval mounted at 4 m above bottom.

Sediment trap bottles were filled with a pH buffered solution of mercuric chloride ($HgCl_2$) in seawater. Unfortunately, a large event that moved massive amounts of sediment down the Norfolk Canyon and upper part of the Baltimore Canyon clogged the funnels of all sediment traps completely in December 2012, which meant that only two or three samples could be retrieved and analyzed from each series. The only sediment trap that showed an almost complete sampling series was retrieved from the UNCW lander that was deployed at the Baltimore Canyon deep lander site.

Sediment trap samples were split with a rotor splitter in five equal splits. Two splits were rinsed thoroughly to remove sea salt and mercury chloride after which they were frozen, freeze dried, and weighed to calculate mass fluxes. These samples were analyzed for ^{210}Pb, organic carbon, nitrogen, phytopigments, stable isotopes, trace metals, biomarkers and ^{14}C (see **Sections 6.2.1** and **6.2.2** for detailed method descriptions).

Trace element concentrations for sediment trap samples were determined by ICP-MS at the USGS Mass Spectrometry Facilities in Denver, Colorado. 50 to 100 mg of sediment was digested using a 4-acid procedure ($HF + HCl + HNO_3 + HClO_4$), taken to dryness, and residue dissolved in 5 to 20 mL of 5% to 13% HNO_3 with a dilution factor of 10^3 to 10^4 (Briggs and Meier 2002).

6.2.4 CTD/Niskin Samples

Vertical profiles were made of the water column properties using a CTD-rosette deployed inside and outside Baltimore and Norfolk canyons to establish if both canyons act as conduits for suspended and dissolved material (**Figure 6-5**; **Chapter 5**). For this purpose, transects of CTD stations were planned that would reveal the optimal contrast between the canyon and adjacent slope. The CTD system used on the 2012 sampling cruise consisted of a Sea-Bird Electronics Inc. (SBE) 911*plus* CTD profiler attached to a rosette containing twelve 5 L Niskin bottles. The 2013 sampling cruise on the *Ronald H Brown* used an SBE 9*plus* CTD with a rosette of twelve 10 L Niskin bottles. Water samples were collected from selected depths along the profiles for measurement of aragonite saturation state, nutrient concentrations, trace metals, and particulate organic matter (POM).

Bottom water samples collected with the CTD profiler were filtered over combusted preweighed glass fiber filters (GFFs). At each station, 10 L of bottom water were filtered and filters were immediately frozen after filtration. Filters were freeze dried and weighed to calculate the amount of suspended particulate matter in the water column. Filters were analyzed for phytopigment concentrations and organic carbon content.

Seawater samples were collected in Baltimore Canyon at a shallow site (NF-2012-138), mid-depth site (NF-2012-128), deep site (NF-2012-130), and mid-depth shelf site (NF-2012-149). Seawater samples also were collected at a mid-depth site in Norfolk Canyon (NF-2012-158). Seawater was collected directly from the Niskin bottle rosette using acid-cleaned Teflon coated tubing attached to a polypropylene filter holder that was preloaded with an acid-cleaned polysulfone filter and attached to a vacuum pump. Filters were acid cleaned by placing in a 1 L low-density polyethylene bottle and soaking in trace metal grade HCl. Water from two 5 L Niskin bottles were collected per given sample water depth for replicates. Water column particulate matter for trace element measurements was collected by filtering approximately 5 L of seawater on acid-cleaned 0.45 µm polysulfone filters (47 mm). The filter holders with preloaded filters were double bagged in polyethylene zip-lock bags and kept frozen for transport back to the laboratory. Trace element concentrations of the suspended particulate matter were determined by ICP-MS at the USGS Mass Spectrometry Facilities in Denver, Colorado by digesting the filters following procedures

outlined in Planquette and Sherrell (2012). Data included a blank correction, as determined from digesting procedural filter blanks, and are reported in µg g^{-1} and are corrected for the weight of the sample and the filter.

6.3 RESULTS

6.3.1 Box Core Samples

6.3.1.1 Baltimore Canyon

During Leg 1 of the 2012 sampling cruise (14 August to 2 September) targeting Baltimore Canyon, four to five replicate box core samples were collected at nine stations along the canyon axis and at four stations along the open slope (**Figure 6-3A**). Subsamples were taken for sedimentological analysis, including X-ray imaging, grain size, ^{210}Pb profiles, and XRF. An overview of the line scan images from each subcore combined with the respective X-ray image is presented in **Figure 6-6**. Measurements of porosity, grain size (mean and median), XRF results (ratio Ca/Ti, Ca/Fe), and sediment accumulation rates are summarized in **Table 6-1**.

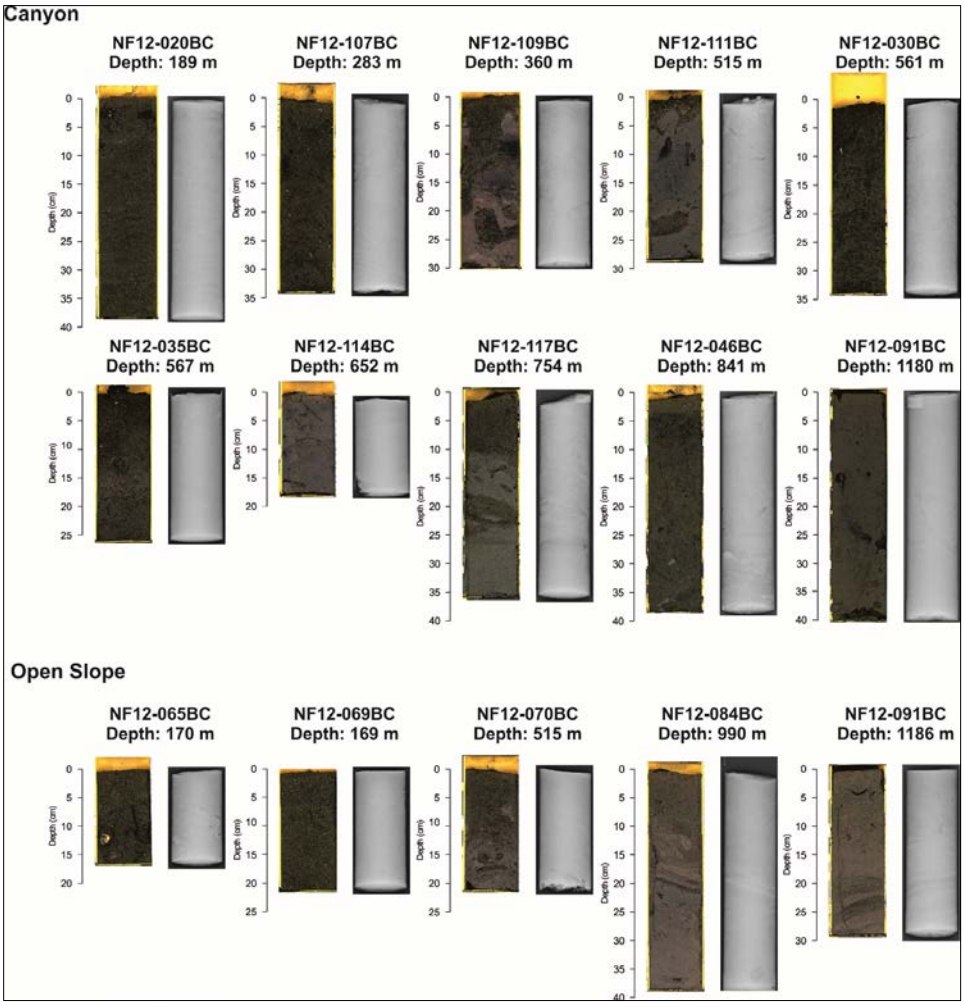

Figure 6-6. Line scan and X-ray images of the subcores taken in Baltimore Canyon and along the adjacent slope. Clay pebbles or a clay layer were observed in most of the cores (360 to 754 m water depth) taken along the canyon axis, indicating the presence of a paleo-sediment surface.

Table 6-1. Summary of sedimentological features of sediment cores collected in Baltimore Canyon.

Station	Water Depth (m)	Porosity (Avg.)	Grain Size Mean			Grain Size Median			Ca/Ti			Ca/Fe			ω ($g\ cm^{-2}\ y^{-1}$)
			Low	High	Avg.	Low	High	Avg.	Low	High	Avg.	Low	High	Avg.	
Baltimore Canyon															
NF2012-020	198	0.55	31	64	51	36	109	75	9.9	26.4	19.5	1.6	2.8	2.2	0.05
NF2012-107	283	0.41	65	149	104	82	199	155	5.0	15.9	8.2	0.5	2.2	1.1	0.04
NF2012-109	360	0.49	7	126	45	8	180	60	0.8	7.9	2.8	0.1	1.0	0.3	0.15
NF2012-111	517	0.58	9	121	36	9	252	57	2.6	5.2	3.3	0.2	0.4	0.3	0.12
NF2012-030	561	0.41	53	581	211	30	700	286	1.2	8.5	7.1	0.1	0.8	0.6	0.05
NF2012-035	567	0.32	136	570	351	348	696	517	1.8	16.1	5.4	0.1	0.8	0.4	0.10
NF2012-114	652	0.50	8	17	10	8	14	11	1.9	2.5	2.3	0.2	0.3	0.2	0.03
NF2012-117	754	0.57	11	93	41	12	152	58	5.0	8.5	6.3	0.5	1.0	0.7	0.10
NF2012-046	841	0.68	12	35	23	13	136	22	4.9	10.7	7.0	0.4	1.2	0.7	0.21
NF2012-054	1,180	0.78	14	18	16	14	17	15	5.3	7.5	6.5	0.4	0.7	0.5	0.24
Open Slope															
NF2012-069	169	0.42	112	267	183	196	359	270	15.1	39.3	22.7	1.7	3.1	2.2	0.24
NF2012-070	515	0.45	19	103	59	19	130	84	2.0	7.5	5.3	0.2	0.9	0.6	0.03
NF2012-084	990	0.56	8	29	17	8	40	19	1.1	8.2	3.1	0.1	0.8	0.3	0.06
NF2012-091	1,186	0.65	8	23	15	8	21	13	2.2	11.9	7.0	0.2	1.1	0.7	0.04

ω = sediment accumulation rate; Ca/Fe = ration of calcium/iron; Ca/Ti = ratio of calcium/titanium; $g\ cm^{-2}\ y^{-1}$ = grams per cm^2 per year.

Sediment in the upper canyon (200 to 300 m water depth) was characterized by homogenous sand with shell fragments and signs of bioturbation. Mean grain size varied between 51 and 104 µm and showed a clear bimodal distribution with a main mode that ranged from 127.6 to 203.5 µm (**Figure 6-7**). Ca/Ti and Ca/Fe were relatively high throughout the cores collected in this part of the canyon (**Table 6-1**). Within the middle part of the Baltimore Canyon (360 to 754 m water depth) all cores contained a sandy layer a few centimeters thick on top of a compacted red/grey clay layer. The clay layer was characterized by a low porosity and low Ca/Fe and Ca/Ti ratios. In the middle part of the canyon, grain size distributions become significantly more variable. Multimodal distributions were the most common, occurring in subcores NF2012-109BC, NF2012-111BC, NF2012-114BC, and partly in NF2012-117BC (**Figure 6-7**). The main mode ranged from 185.3 to 223.4 µm. Station NF2012-30/35BC (560 m water depth) showed a different sedimentology, consisting of very coarse sand, small pebbles, and shell fragments at the sediment surface. Grain size became finer down core, with mean grain size at this depth still being coarse compared with other sediment cores, varying between 211 and 351 µm. From ≥800 m water depth, sediments became more homogenous and finer. The deepest core collected at 1,180 m water depth consisted of silty clay with an olive black color. After retrieval, a strong sulfidic smell was noted from the sediments, possibly indicating high organic matter content.

^{210}Pb activity in sediments collected along the Baltimore Canyon axis was highly variable, ranging from 73.7 to 1,758.9 mBq g^{-1} at the sediment surface, to a steady background level of approximately 20 mBq g^{-1} deeper within the cores (**Figure 6-8**). In the middle part of the canyon, ^{210}Pb values reached background levels at the depth of the compacted clay layer, indicating an older age for this sediment layer. In most subcores, the vertical profile was interrupted by the presence of a surface mixed layer and/or subsurface ^{210}Pb maxima caused by bioturbation. The sediment accumulation rates calculated from the ^{210}Pb profiles were low to moderate, ranging from 0.030 to 0.24 g cm^{-2} y^{-1}. These rates varied throughout the entire canyon, indicating a heterogeneous sedimentation pattern. The highest accumulation rates were found at water depths between 360 and 517 m (0.12 to 0.15 g cm^{-2} y^{-1}) and at the deepest stations (water depths between 840 and 1,180 m, 0.21 to 0.24 g cm^{-2} y^{-1}) of the canyon. Accumulation rates were low between 561 and 754 m water depth.

The shallowest core taken on the adjacent open slope consisted of homogeneous sand with shell fragments and pebbles. Sand dominated the top of cores taken in deeper parts along the slope (>515 m) and showed the presence of clay layers and lenses down core (**Figure 6-6**). This clay layer was similar to the clay layer observed in cores collected from mid-canyon (360 to 754 m water depth). Mean grain size at the shallowest station was 183 µm. Average grain size along the open slope decreased with depth, ranging from 15 to 183 µm (**Table 6-1**). Throughout the shelf and open slope nearly all the grain size distributions showed a bimodal distribution with one distinct peak that was significantly higher (**Figure 6-7**). Within the upper part of the shelf (169 to 170 m water depth), the primary mode of the bimodal distribution ranged from 269.2 to 356.1 µm. Within the middle part of the shelf and open slope (515 m water depth), the grain size distribution showed a unimodal distribution, but became more irregular at grain sizes <60 µm and >120 µm. The clear main mode ranged from 105.9 to 127.7 µm. On the open slope, Ca/Ti and Ca/Fe ratios were highest at the shallowest and deepest stations and lowest near the middle part of the transect. Total ^{210}Pb activity was less variable and lower than within the canyon. The sediment accumulation rates ranged from 0.025 to 0.24 g cm^{-2} y^{-1}, with highest rates found at shallow depth (169 to 170 m) (**Figure 6-9**).

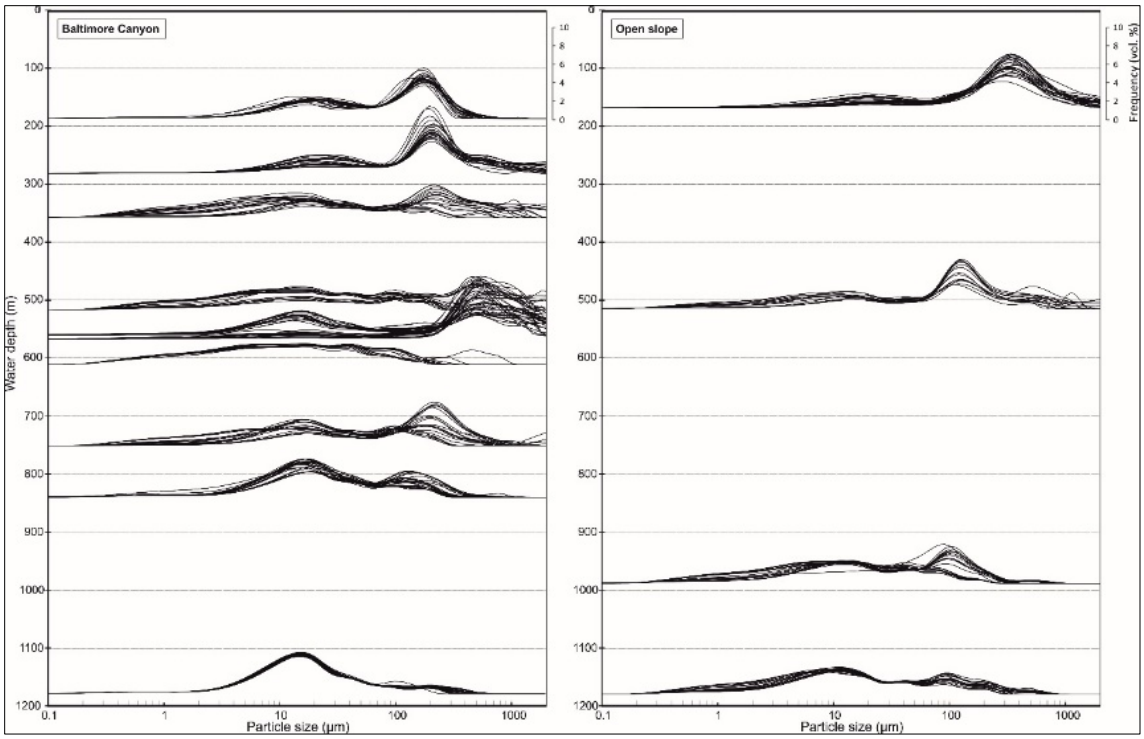

Figure 6-7. Down-core grain size distributions of cores taken in the Baltimore Canyon and on the adjacent open slope. Two distinct zones were observed in the Baltimore Canyon showing coarse sand in the upper part and fine sediment in the lower part of the canyon.

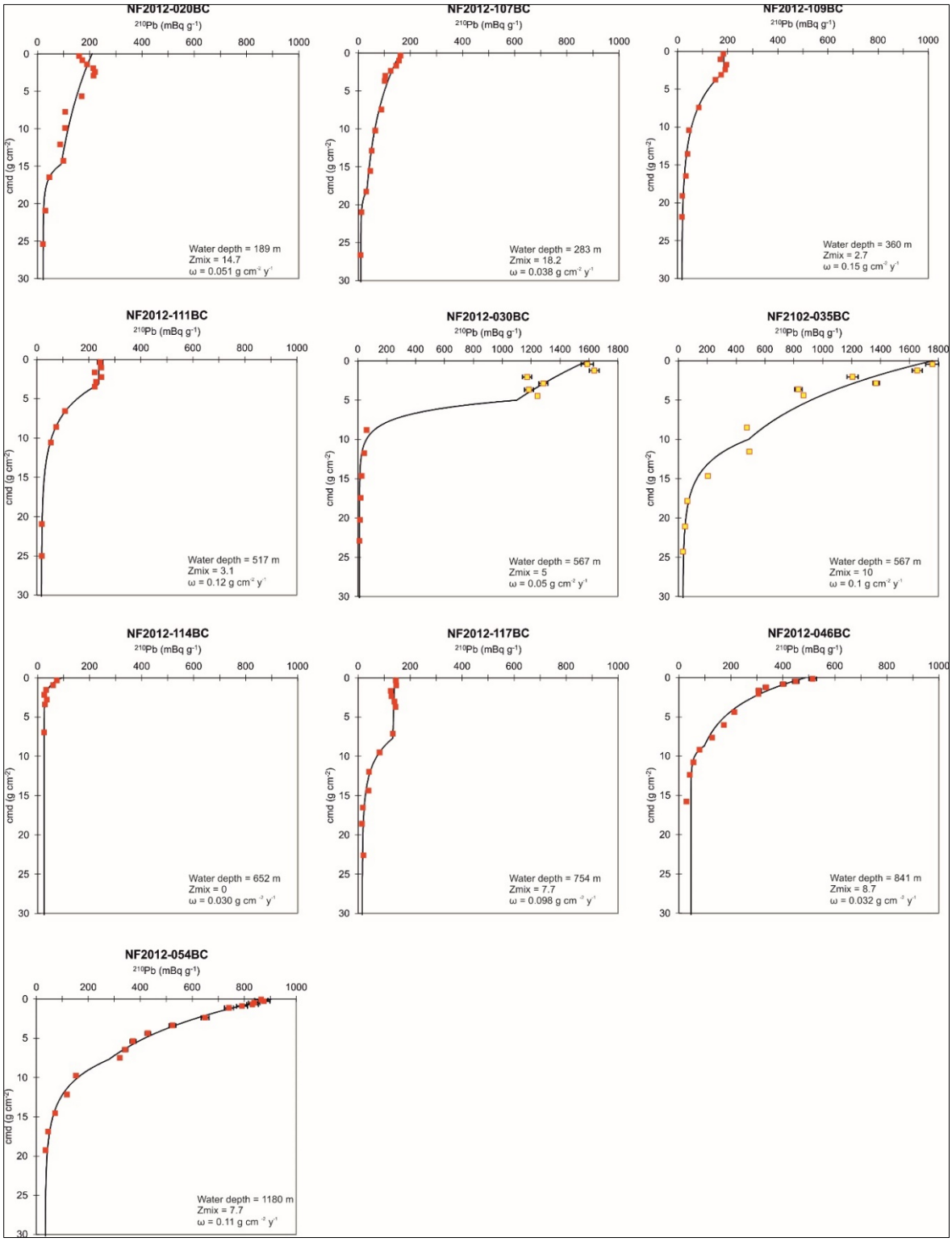

Figure 6-8. Profiles showing the total ^{210}Pb activity (mBq g^{-1}) versus cumulative mass depth (cmd, g cm^{-2}) of subcores taken along the axis of the Baltimore Canyon. Sediment accumulation rates (ω) along the Baltimore Canyon axis. Zmix (g cm^{-2}) is the depth at which biological mixing occurs. Yellow symbols indicate samples that have been fractionated before measurements.

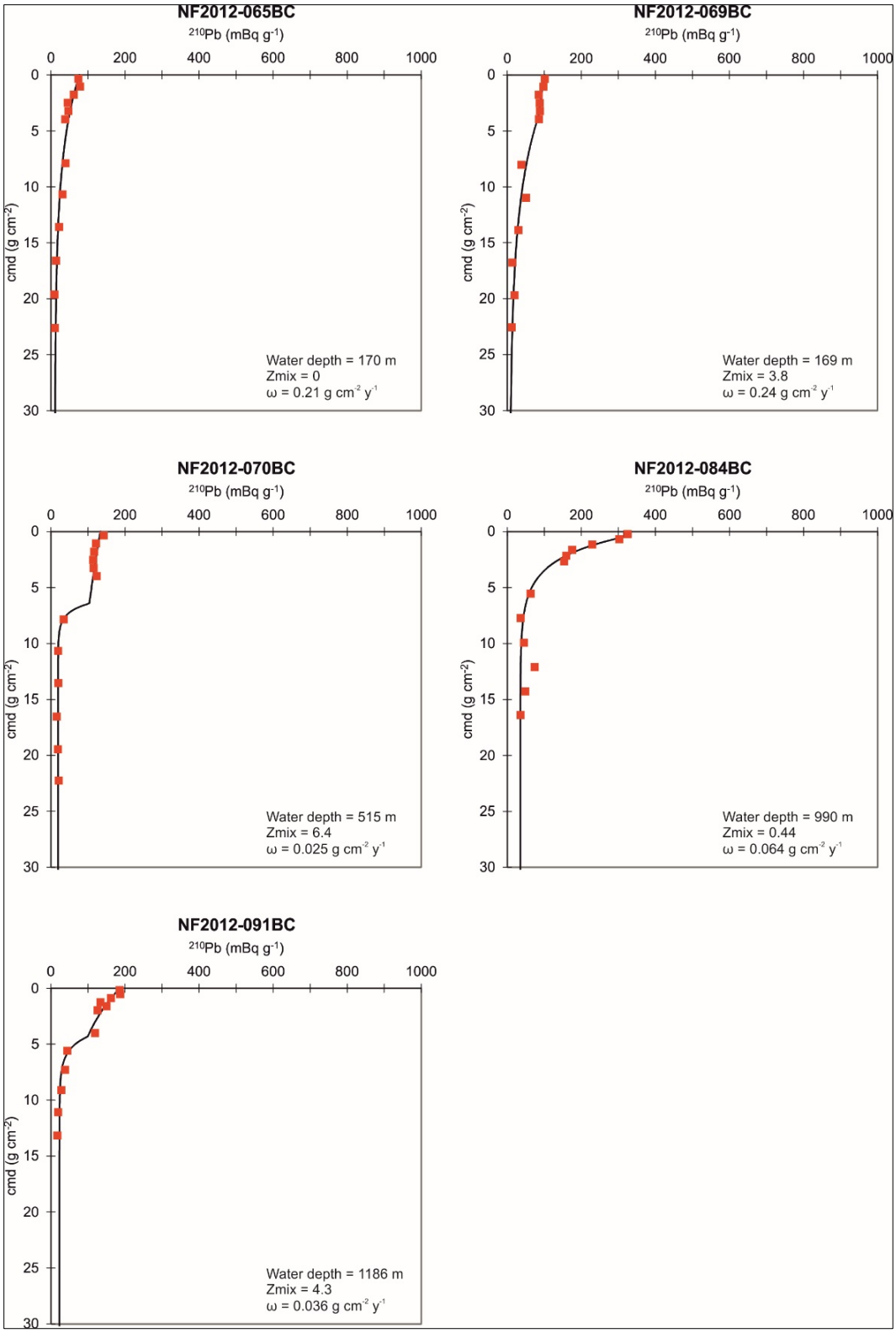

Figure 6-9. Profiles showing the total ^{210}Pb activity (mBq g^{-1}) versus cumulative mass depth (cmd, g cm^{2}) of subcores taken on the adjacent open slope of the Baltimore Canyon. Sediment accumulation rates (ω) along the open slope. Zmix (g cm^{-2}) is the depth at which biological mixing occurs.

6.3.1.2 Norfolk Canyon

During Leg 3 of the 2012 sampling cruise, two to three replicate box core samples were taken at five stations along the Norfolk Canyon axis and at two stations on the adjacent open slope. The Norfolk Canyon was resampled during the 2013 sampling cruise, in particular on the deeper part of the slope and one location on the canyon axis. The 2013 samples were analyzed for fauna and chemical parameters (**Section 6.3.2.2**). At five stations sampled during the 2012 cruise (four canyon, one slope), one box core was subsampled for X-ray imaging, analyses of grain size, sediment accumulation using ^{210}Pb profiles, and XRF. An overview of the line scan images from each subcore combined with the respective X-ray image is presented in **Figure 6-10**. Measurements of grain size, XRF results (ratio Ca/Ti, Ca/Fe), and sediment accumulation rates are summarized in **Table 6-2**.

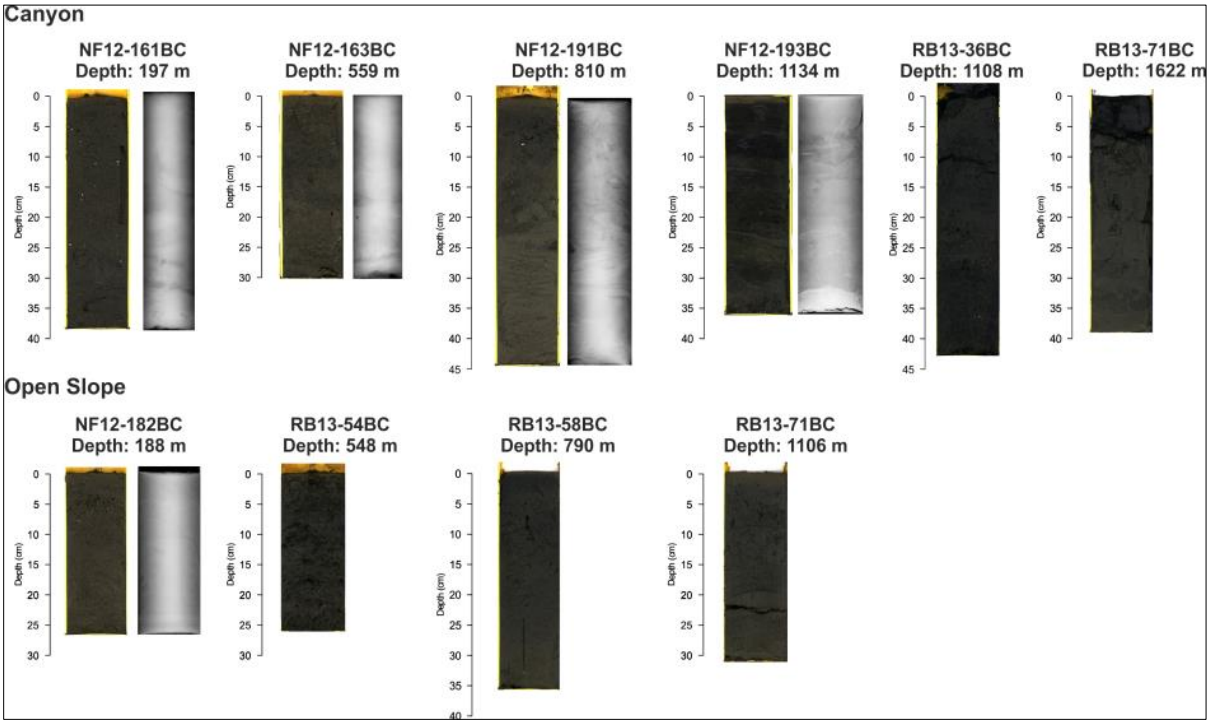

Figure 6-10. An overview showing the line scan and X-ray images of subcores taken in the Norfolk Canyon and on the adjacent open slope.

Table 6-2. Summary of sedimentological features of sediment cores collected in Norfolk Canyon.

Sample Number	Depth (m)	Porosity (Avg.)	Grain Size Mean			Grain Size Median			Ca/Ti			Ca/Fe			ω ($g\ cm^{-2}\ y^{-1}$)
			Low	High	Avg.	Low	High	Avg.	Low	High	Avg.	Low	High	Avg.	
Norfolk Canyon															
NF2012-161	196	0.65	32	51	43	30	63	45	5.8	10.6	8.9	0.4	1.4	1.0	0.55
NF2012-163	559	0.58	27	74	49	23	124	63	5.6	10.4	7.9	0.5	1.2	0.9	0.19
NF2012-191	810	0.65	49	102	36	62	148	120	7.6	12.5	10.2	0.7	1.8	1.1	0.22
NF2012-193	1,134	0.81	16	384	47	18	622	66	5.9	13.0	7.3	0.4	1.2	0.6	0.13
RB2013-036	1,108	0.60	17	189	33	19	298	42	4.8	21.4	7.5	0.2	1.5	0.6	0.66
RB2013-078	1,622	0.62	12	26	18	14	32	20	6.9	8.8	7.7	0.4	0.8	0.6	0.18
Open Slope															
NF2012-182	188	0.48	49	102	75	62	148	66	8.0	18.2	12.5	1.21	1.94	1.6	0.2
RB2013-056	548	0.31	27	47	36	23	60	35	6.1	11.5	8.4	0.5	0.9	0.8	0.13
RB2013-059	790	0.59	14	28	16	15	21	17	6.4	8.4	7.9	0.4	1.5	0.7	0.14
RB2013-073	1,106	0.54	13	18	14	14	20	16	7.5	8.8	8.2	0.7	0.8	0.7	0.16

ω = sediment accumulation rate; Ca/Fe = ration of calcium/iron; Ca/Ti = ratio of calcium/titanium; g cm^{-2} y^{-1} = grams per cm^2 per year.

Unlike cores taken from the Baltimore Canyon, which contained a distinct clay layer, sediment cores taken along the Norfolk Canyon axis showed a more homogeneous down-core sediment distribution. All cores contained shell fragments and evidence of bioturbation. The cores consisted of sandy silty clay, and down core, no changes in porosity were observed. The grain size distribution indicated decreasing proportions of sand and increasing proportions of clay with depth in the canyon (**Figure 6-11**). Mean grain size varied between 18 and 49 µm. Cores (RB13-036, NF12-191, and 193 collected at 1,135, 810, and 1,108 m, respectively) contained two distinct layers. The upper part of the cores consisted of sandy silty clay, while below 25 cm a coarse sand layer was observed. This sand layer was characterized by increased porosity and Ca/Fe and Ca/Ti ratios, which were highest at shallow water depths. ^{210}Pb activity measured in canyon sediments was highly variable ranging from 196 to 729 mBq g^{-1} at the sediment surface and decreasing to a steady background level of 15 mBq g^{-1} at greater core depth. In some cores, the background value was not reached, indicating excess ^{210}Pb activity beyond the length of the cores (**Figure 6-12**). Most cores showed either the presence of a bioturbated surface layer or ^{210}Pb subsurface maxima caused by large burrowers. The sediment accumulation rates ranged from 0.18 to 0.66 g cm^{-2} y^{-1}, with the highest rate present at 196 m (NF12-161) and 1,108 m (RB13-036). In general, sediment accumulation rates were higher in Norfolk Canyon than in Baltimore Canyon.

The shallowest core taken on the adjacent open slope consisted of sandy silty clay. Cores taken at greater depth consisted of silty clay (**Figure 6-11**). All cores showed the presence of shell fragments, and core RB13-056 even contained a piece of *Lophelia pertusa* at 24 cm core depth. Down core, no changes in porosity were observed. Average grain size and porosity decreased with water depth, and the same trend was observed in the Ca/Fe and Ca/Ti ratios (**Table 6-2**). Highest values were found at the shallowest station (188 m water depth) as was also observed in the Norfolk Canyon. ^{210}Pb activity in open slope sediments ranged from 108 to 668 mBq g^{-1} in the surface layer. The shallowest cores showed the presence of a bioturbated surface layer in the upper 5 cm (cumulative mass depth [cmd]). Sediment accumulation rates varied between 13 and 22 g cm^{-2} y^{-1} (**Figure 6-13**). The highest accumulation rate was found at station NF12-182 at 188 m water depth. In general, accumulation rates were lower compared with samples collected along the canyon axis. However, accumulation rates on the adjacent shelf of the Norfolk Canyon were up to three times higher than accumulation rates found along the Baltimore adjacent open slope.

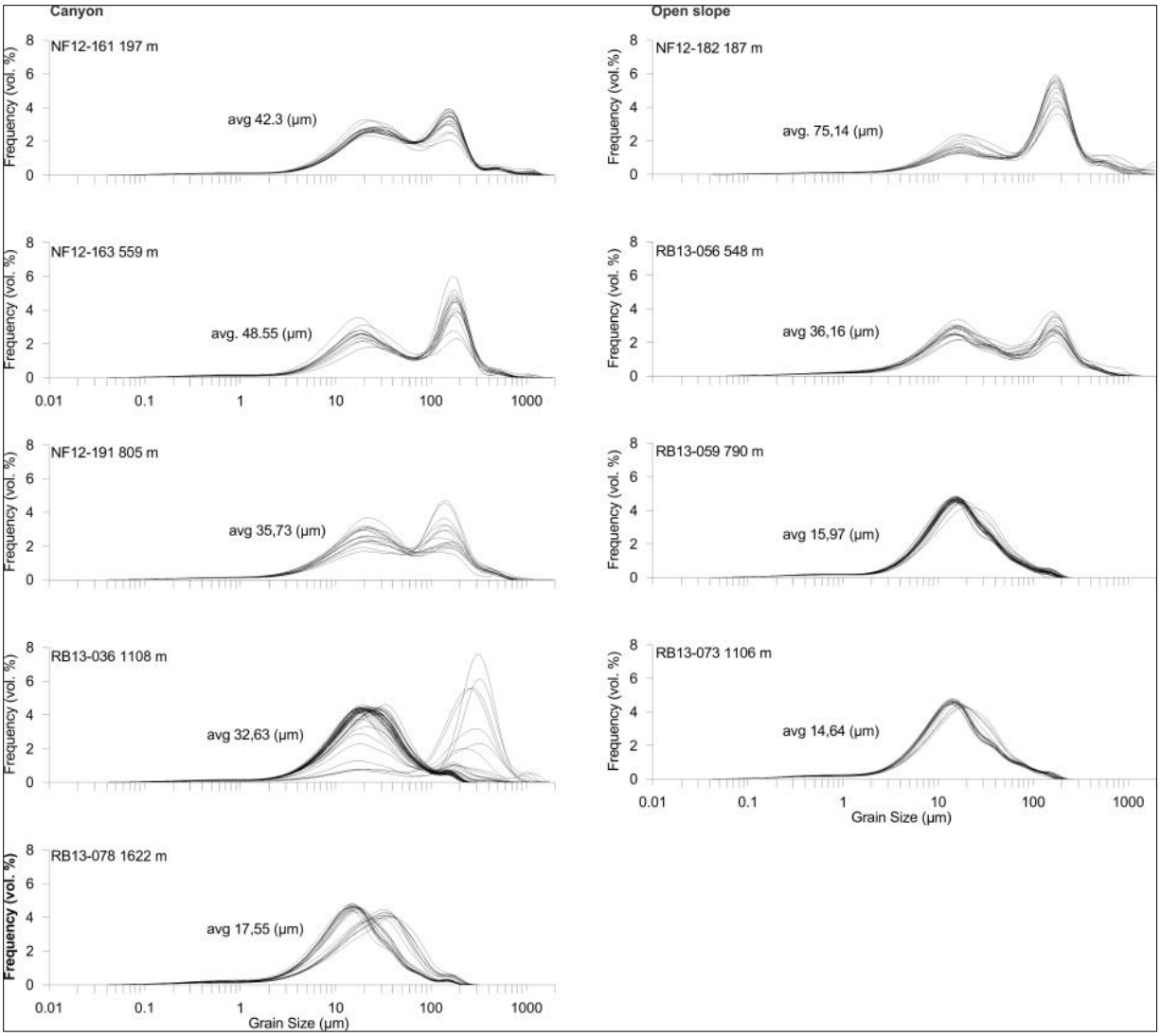

Figure 6-11. Down-core variability in grain size distribution in Norfolk Canyon (left) and on the adjacent open slope (right). Core RB13-036 showed the presence of a coarse grained sandy layer, which is likely related to a turbidite.

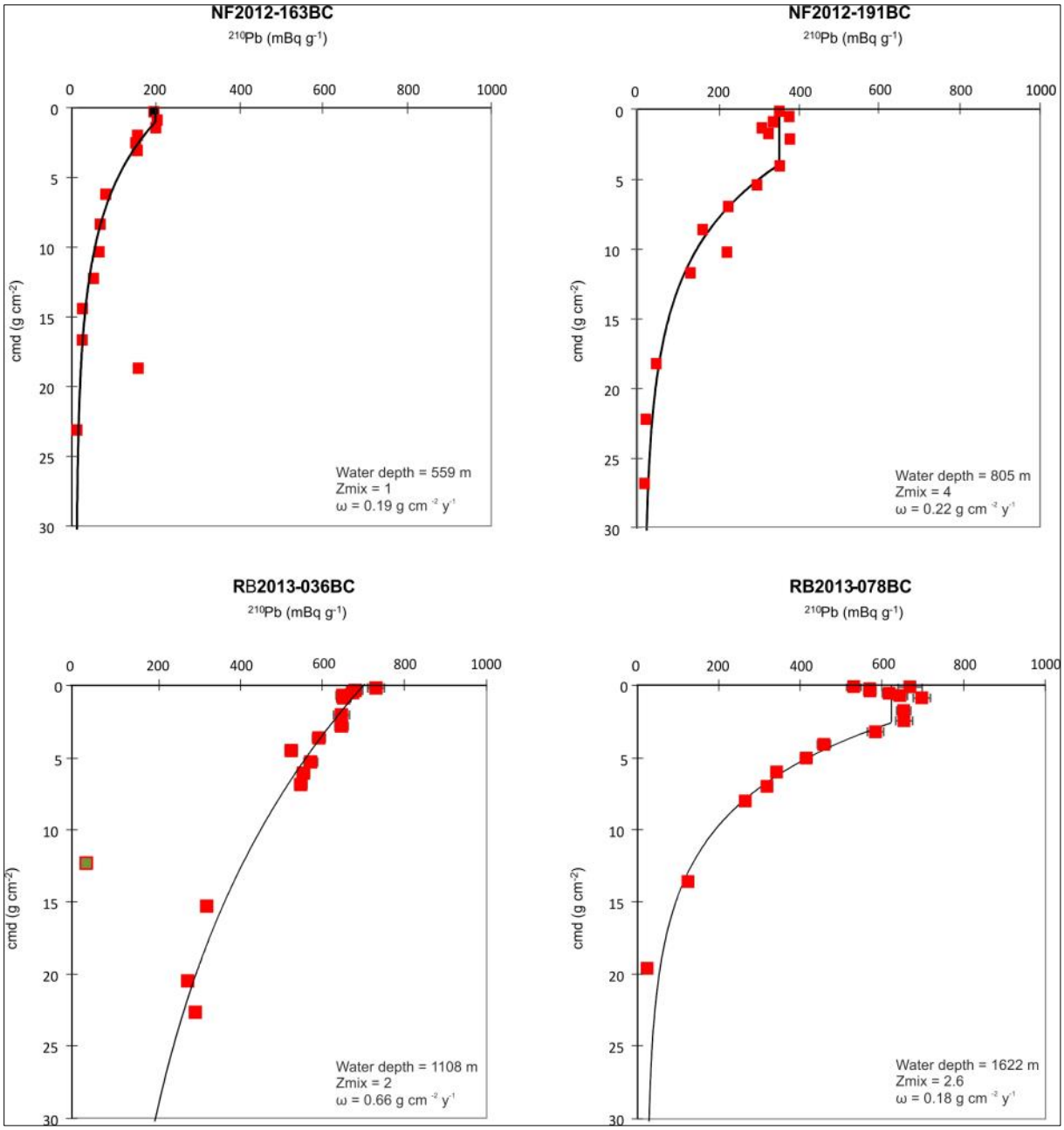

Figure 6-12. Profiles showing the total ^{210}Pb activity (mBq g^{-1}) versus cumulative mass depth (cmd, g cm^{-2}) of subcores taken along the axis of the Norfolk Canyon. Sediment accumulation rates (ω). Zmix (g cm^{-2}) is the depth at which biological mixing occurs.

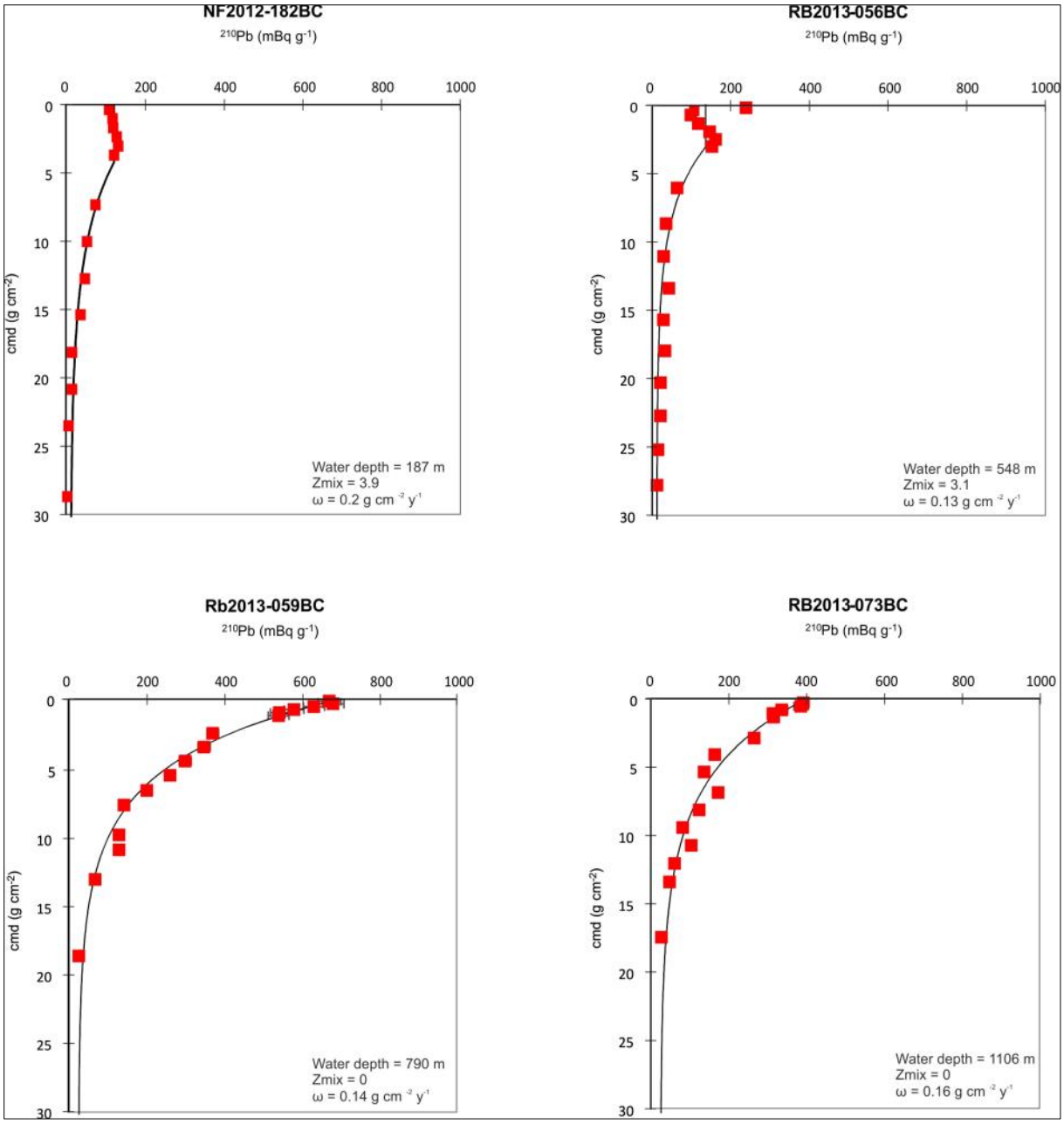

Figure 6-13. Profiles showing the total ^{210}Pb activity (mBq g^{-1}) versus cumulative mass depth (cmd, g cm^{-2}) of subcores taken on the adjacent open slope of the Norfolk Canyon. Sediment accumulation rates (ω). Zmix (g cm^{-2}) is the depth at which biological mixing occurs.

6.3.2 Surface Sediments

The 0 to 1 cm surface slice of sediment cores collected with the monocorer or as subcores from box core samples were used to analyze concentrations of C_{org}, N, bulk stable isotopes of C and N, phytopigments, and the molecular composition of organic matter in the two canyons.

6.3.2.1 Baltimore Canyon

Concentrations of C_{org}, N, and chlorophyll-*a* in Baltimore Canyon and adjacent slope are plotted in **Figure 6-14** and summarized in **Table 6-3**. Percent C_{org} in the surface sediment inside Baltimore Canyon varied between 0.76% and 3.48%. At mid-canyon depth (841 m, NF2012-046), a break was visible with low values (<1%) up canyon and higher values down canyon (>1%). The $\delta^{13}C$ values were all in a narrow range (-21.8% to -23.9%) and indicative of a marine origin (**Figure 6-15**). Organic carbon in the upper part of the canyon (shallower than 841 m) was slightly more depleted in ^{13}C (i.e., lower $\delta^{13}C$) than in the deeper part. Percent total N in the surface sediment in the upper canyon was very low (<0.1%). Higher concentrations of N (>0.3%) were measured in the deeper part of the canyon (**Figure 6-14**). Sediment ^{15}N was slightly more depleted in the deeper part, similar to ^{13}C, perhaps suggesting more fresh organic matter (**Figure 6-15**). Percent calcium carbonate ($CaCO_3$) also showed a mid-canyon break at 841 m depth, with high values in the deeper part (**Table 6-3**). Like C_{org} and N, chlorophyll-*a* concentrations showed a separation between low values in the upper part of the canyon (<841 m water depth) and higher values in the deeper part.

Percent C_{org} and total N on the adjacent slope were low and in the range of the upper canyon (<1%) except for some of the deeper cores (**Figure 6-14**). Also the chlorophyll-*a* concentrations on the slope were low overall and in the range of values found in the upper canyon. Summarizing, two distinct zones were observed in Baltimore Canyon with the deeper part being more enriched in organic matter (**Figure 6-14**; **Table 6-3**).

Radiocarbon ages of Baltimore Canyon and adjacent slope surface sediment samples varied from 9,730 to 1,440 years before present (YBP), representing a $\delta^{14}C$ range of -704.55‰ to -170.15‰ (**Table 6-4**). The oldest age was found in the mid-depth canyon sample at NF-2012-114 (652 m water depth), with no relationship between sediment ^{14}C age and canyon depth. In comparison, the oldest ^{14}C age on the slope transect was at the deepest site, 3,180 YBP at 1,186 m. Neodymium isotope values from surface sediments collected in Baltimore Canyon and adjacent slope were between 0.5120 and 0.5121, equivalent to a εNd range of -9.694 to -11.567 (**Table 6-5**). There was no statistical difference (Student *t*-test; $P \geq 0.05$) between canyon and slope Nd isotope values. The average Nd isotope values from both the slope and canyon (0.51208) were consistent with Nd isotope values from Hudson River sediments (0.51206; Goldstein et al. 1984).

The total concentrations of *n*-alkanes for surface sediment samples from Baltimore Canyon and the adjacent slope represent a resolved *n*-alkane range from C_{14} to C_{32} as well as detectible amounts of the isoprenoid hydrocarbons pristane (pr) and phytane (ph) (**Table 6-6**). Total *n*-alkanes concentration (439 μg g^{-1}) was enriched at the mid-canyon site (652 m) and was dominated by the high molecular weight *n*-alkanes (*n*-C_{27} and *n*-C_{29}) as well as elevated pristane concentrations. In comparison, the deep (1,180 m) and shallow (283 m) Baltimore Canyon sites yielded total *n*-alkane concentrations between 9 and 13 μg g^{-1}, respectively, and were instead dominated by *n*-C_{19} and *n*-C_{20} at the shallow site and *n*-C_{19} and *n*-C_{27} at the deep site. The *n*-alkane composition of the slope samples was dominated by the low molecular weight *n*-alkanes (i.e., *n*-C_{19} and *n*-C_{20}) with a resolved *n*-alkane range from C_{14} to C_{25}. The isoprenoid hydrocarbons pristane and phytane were absent from the slope surface sediment sample (**Table 6-6**). The total *n*-alkane concentration was depleted at the deep site (1,186 m; 5 μg g^{-1}) and enriched at the mid-canyon site (990 m; 95 μg g^{-1}).

The average total sterol concentration in the surface sediments of Baltimore Canyon was 8 μg g^{-1} (SD 3). The dominant sterol in the canyon surface sediments varied from campesterol at the shallow site, cholestanol at the mid-canyon site, and β-sitosterol at the deep site (**Table 6-7**). The sterol cholesterol was only dominant at the mid-slope site (515 m water depth) whereas campesterol dominated the shallow slope site (170 m water depth). Total sterol concentrations in the slope sediments ranged from 11 to 25 μg g^{-1}. Sterols concentrations were below detection limit in the two deeper slope sites (990 and 1,186 m water depths).

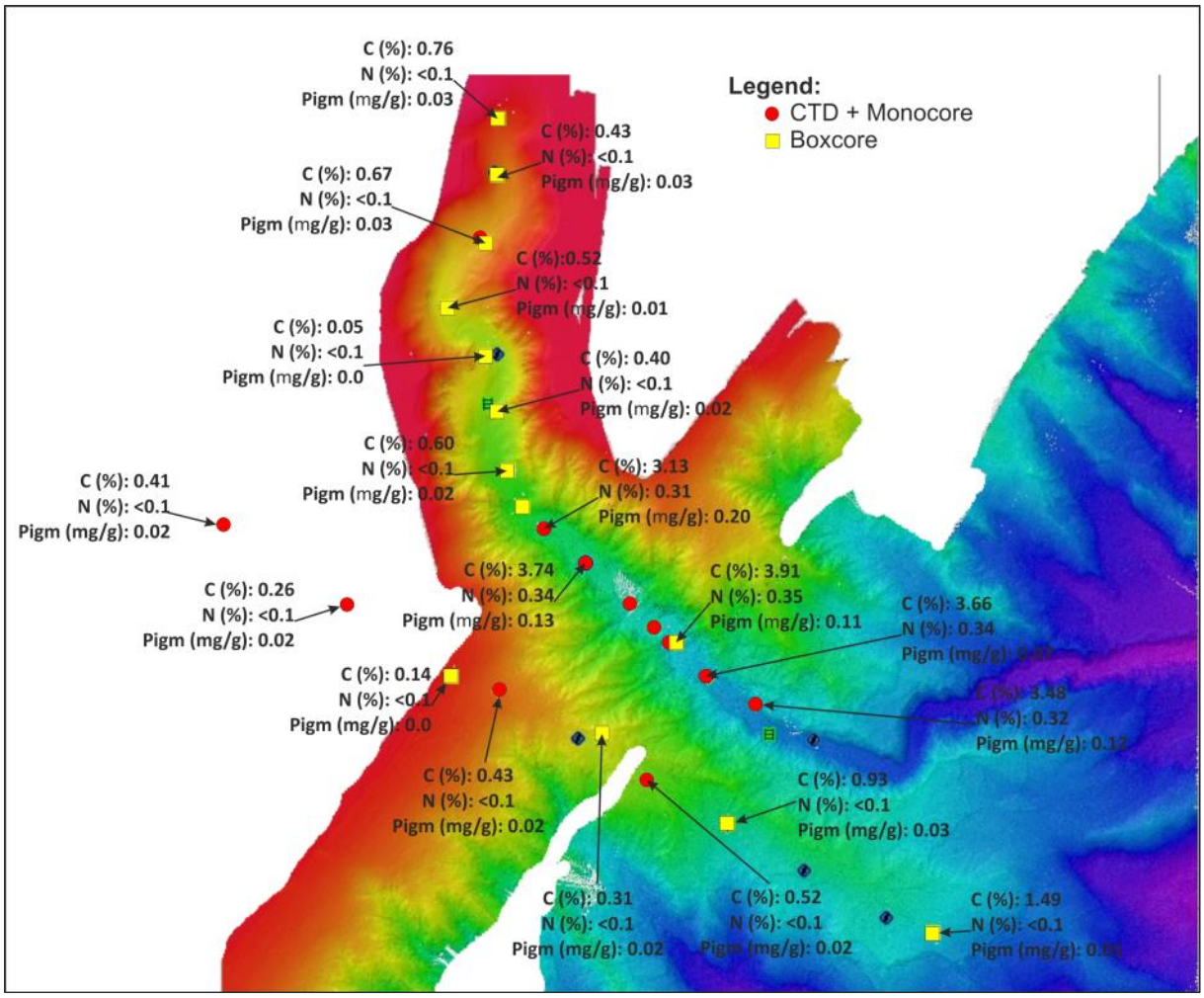

Figure 6-14. Concentrations of organic carbon (C), nitrogen (N), and chlorophyll-*a* in the surface sediments (0 to 1 cm) of Baltimore Canyon and the adjacent slope. Note the two distinctive zones in the canyon axis transect with relatively low concentrations in the upper part and higher concentrations in the lower part.

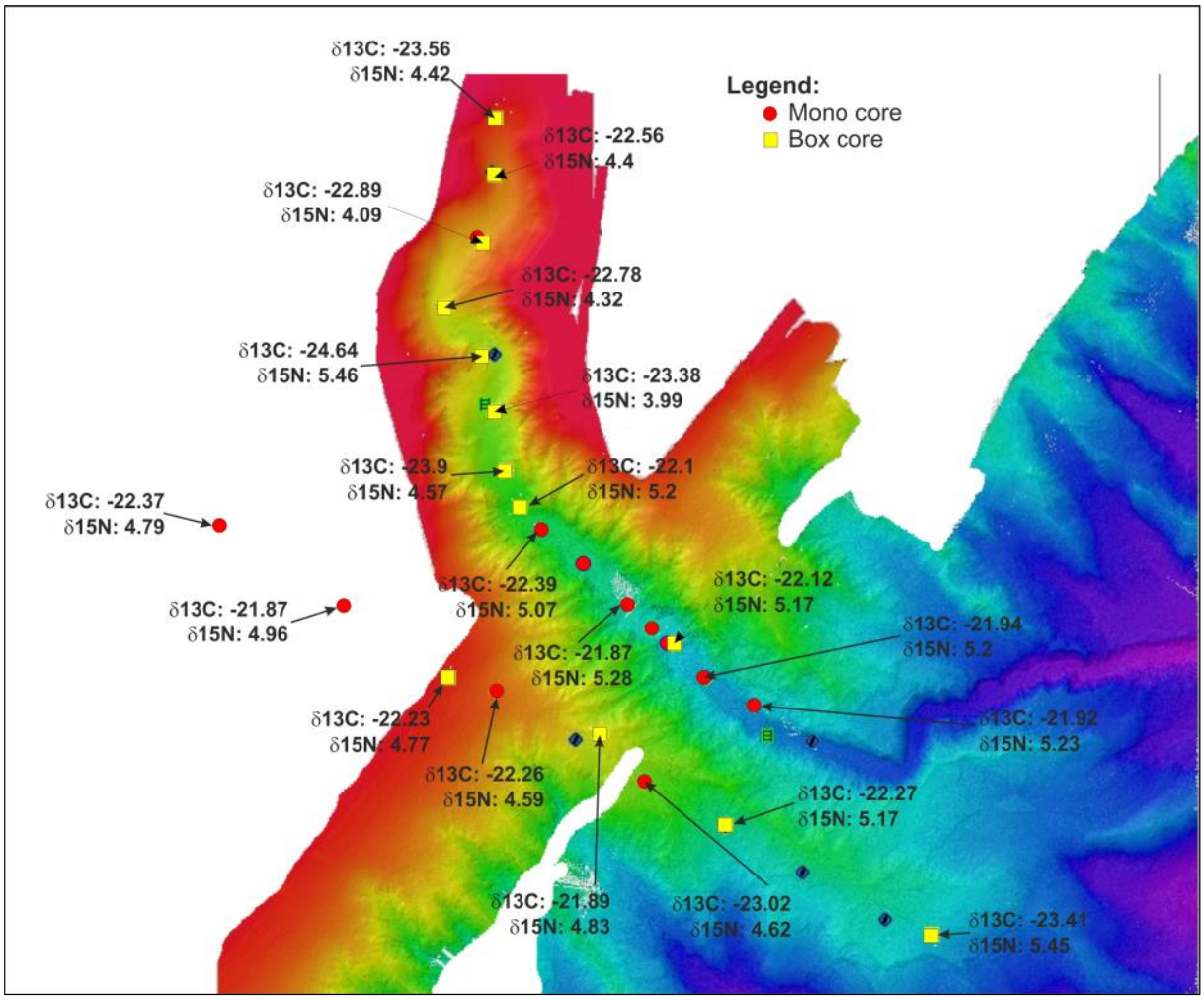

Figure 6-15. Carbon and nitrogen isotope ratios of surface sediments (0 to 1 cm) of Baltimore Canyon and the adjacent slope.

Table 6-3. Summary of organic carbon (C_{org},), nitrogen, calcium carbonate ($CaCO_3$), stable isotopes of C and N; and phytopigments in surface sediment samples from Baltimore and Norfolk canyons.

Station	Sample Type	Depth (m)	Date	Latitude (N)	Longitude (W)	N (%)	δ15N	Corg (%)	δ13C	C/N	CaCO3 (%)	Pigments (mg g-1)
Baltimore Canyon												
NF2012-020	BC	198	19 Aug 2012	38°14′35.46″	73°50′36.72″	<0.1	4.4	0.76	-23.7	--*	15.3	0.03
NF2012-107	BC	283	28 Aug 2012	38°13′28.92″	73°50′40.26″	<0.1	4.4	0.43	-22.6	--*	11.2	0.03
NF2012-037	MC	363	21 Aug 2012	38°12′13.26″	73°51′03.48″	<0.1	4.1	0.67	-22.9	--*	8.2	0.03
NF2012-038	MC	514	21 Aug 2012	38°10′56.34″	73°51′58.26″	<0.1	4.3	0.52	-22.7	--*	7.8	0.01
NF2012-030	BC	561	20 Aug 2012	38°09′57.96″	73°51′00.66″	<0.1	5.5	0.05	-24.6	--*	3.5	0.02
NF2012-040	MC	644	22 Aug 2012	38°08′51.78″	73°50′42.60″	<0.1	4.0	0.40	-23.4	--*	7.5	0.02
NF2012-041	MC	730	22 Aug 2012	38°07′44.76″	73°50′26.40″	<0.1	4.6	0.60	-23.9	--*	9.6	0.02
NF2012-046	BC	841	22 Aug 2012	38°07′01.92″	73°50′07.14″	0.15	5.2	1.55	-22.1	10.1	19.7	0.08
NF2012-042	MC	867	22 Aug 2012	38°06′35.94″	73°49′39.00″	0.31	5.1	3.13	-22.4	10.0	25.2	0.2
NF2012-044	MC	1,068	22 Aug 2012	38°05′07.08″	73°47′29.82″	0.34	5.3	3.74	-21.9	10.9	27.0	0.13
NF2012-053	BC	1,120	23 Aug 2012	38°04′15.24″	73°46′41.82″	0.35	5.2	3.91	-22.1	11.2	28.6	0.1
NF2012-052	MC	1,209	23 Aug 2012	38°03′39.96″	73°45′36.66″	0.34	5.2	3.66	-21.9	10.9	27.1	0.07
NF2012-060	MC	1,278	24 Aug 2012	38°03′07.20″	73°44′38.88″	0.32	5.2	3.48	-21.9	10.9	31.2	0.12
Baltimore Slope												
NF2012-096	MC	113	27 Aug 2012	38°06′44.28″	73°57′39.84″	<0.1	4.8	0.41	-22.4	--*	10.1	0.02
NF2012-098	MC	125	27 Aug 2012	38°05′09.96″	73°54′34.80″	<0.1	5.0	0.26	-21.9	--*	9.3	0.02
NF2012-065	BC	170	25 Aug 2012	38°03′45.00″	73°51′56.10″	<0.1	4.8	0.14	-22.2	--*	9.5	0
NF2012-100	MC	262	27 Aug 2012	38°03′27.00″	73°50′48.72″	<0.1	4.6	0.43	-22.3	--*	13.1	0.02
NF2012-070	BC	515	25 Aug 2012	38°02′36.60″	73°48′12.48″	<0.1	4.8	0.31	-21.9	--*	9.2	0.02
NF2012-102	MC	692	28 Aug 2012	38°01′39.00″	73°47′09.96″	<0.1	4.6	0.52	-23.0	--*	9.8	0.02
NF2012-084	BC	990	26 Aug 2012	38°00′50.04″	73°45′12.24″	0.10	5.2	1.15	-22.2	11.4	16.2	0.03
NF2012-103	MC	1,000	28 Aug 2012	38°00′46.08″	73°45′10.44″	<0.1	--b	0.71	-22.4	--*	14.4	0.04
NF2012-091	BC	1,186	27 Aug 2012	37°58′38.64″	73°40′09.78″	<0.1	5.5	1.49	-23.4	--*	24.0	0.01
Norfolk Canyon												
RB-2013-003	MC	190	3 May 2013	37°05′31.50″	74°44′47.76″	0.23	5.59	1.52	-22.3	6.6	20.8	1.5
RB-2013-046	BC	195	4 May 2013	37°05′41.10″	74°44′47.70″	0.27	5.86	2.40	-21.7	8.8	26.0	2.9
RB-2013-021	MC	212	5 May 2013	37°05′16.56″	74°43′55.92″	0.55	5.87	5.34	-21.3	9.8	36.4	7.6
RB-2013-005	MC	341	6 May 2013	37°05′36.18″	74°42′15.48″	0.53	5.70	4.58	-21.5	8.7	34.9	5.6
RB-2013-006	MC	440	7 May 2013	37°05′38.16″	74°40′51.96″	0.53	5.67	5.14	-21.6	9.7	35.2	4
RB-2013-020	MC	537	8 May 2013	37°04′46.32″	74°39′54.36″	0.57	5.62	5.54	-21.5	9.7	31.5	4.4

Table 6-3. (Continued).

Station	Sample Type	Depth (m)	Date	Latitude (N)	Longitude (W)	N (%)	δ15N	Corg (%)	δ13C	C/N	CaCO3 (%)	Pigments (mg g-1)
RB-2013-043	BC	559	9 May 2013	37°04′33.48″	74°39′38.28″	0.51	5.72	5.50	-21.6	10.9	37.2	4.7
RB-2013-019	MC	629	10 May 2013	37°03′58.92″	74°39′04.68″	0.51	5.63	5.52	-21.5	10.8	36.7	2.5
RB-2013-011	MC	777	22 May 2013	37°02′13.08″	74°26′15.72″	0.43	5.67	4.28	-21.7	9.9	26.2	2.5
RB-2013-040	BC	805	11 May 2013	37°02′33.84″	74°37′45.00″	0.41	5.85	3.77	-21.6	9.3	36.5	2.9
RB-2013-008	MC	855	12 May 2013	37°02′20.28″	74°37′27.84″	0.50	5.54	5.16	-21.6	10.3	30.6	3.2
RB-2013-077	BC	1,108	13 May 2013	37°02′19.50″	74°34′46.68″	0.54	5.32	5.26	-21.7	9.8	31.6	1.6
RB-2013-038	BC	1,110	14 May 2013	37°02′19.08″	74°34′47.52″	0.54	5.78	5.50	-21.7	10.2	41.5	3.1
RB-2013-017	MC	1,113	15 May 2013	37°02′17.58″	74°34′44.76″	0.51	5.56	5.58	-21.8	11.0	37.3	3.6
RB-2013-010	MC	1,184	16 May 2013	37°02′09.60″	74°33′54.36″	0.51	5.49	5.45	-21.7	10.6	32.5	3.7
RB-2013-016	MC	1,255	17 May 2013	37°02′16.20″	74°32′58.92″	0.55	5.61	5.60	-21.6	10.3	36.2	6.4
RB-2013-034	MC	1,614	18 May 2013	36°51′48.90″	74°29′23.64″	0.22	6.12	2.34	-21.8	10.8	34.9	n/a
RB-2013-031	MC	1,616	19 May 2013	36°51′46.74″	74°29′24.72″	0.25	5.67	2.69	-21.7	10.9	32.8	n/a
RB-2013-082	BC	1,619	20 May 2013	37°02′00.36″	74°27′01.14″	0.58	5.34	5.86	-21.7	10.1	33.0	n/a
RB-2013-078	BC	1,622	21 May 2013	37°02′00.48″	74°27′01.38″	0.59	5.48	5.64	-21.7	9.6	33.3	n/a
Norfolk Slope												
RB-2013-068	MC	131	23 May 2013	37°01′09.12″	74°38′49.20″	0.08	4.69	0.57	-23.8	7.1	15.4	0.9
RB-2013-049	BC	187	24 May 2013	37°01′23.04″	74°38′44.76″	0.19	5.36	1.25	-21.8	6.5	22.4	0.1
RB-2013-067	MC	307	25 May 2013	37°00′50.16″	74°36′55.80″	0.06	4.00	0.52	-23.5	7.9	11.1	0
RB-2013-054	BC	549	26 May 2013	37°00′56.88″	74°34′41.52″	0.11	4.86	0.88	-22.2	8.4	20.6	0.1
RB-2013-065	MC	681	27 May 2013	37°00′37.02″	74°34′35.04″	0.38	5.37	4.24	-21.8	11.0	31.2	1.6
RB-2013-059	BC	790	28 May 2013	37°00′32.52″	74°33′53.22″	0.40	5.30	4.46	-22.0	11.1	31.8	n/a
RB-2013-064	MC	800	29 May 2013	37°00′32.10″	74°33′53.28″	0.40	5.71	3.45	-21.8	8.7	29.9	0.8
RB-2013-069	BC	804	30 May 2013	37°00′32.46″	74°33′53.88″	0.39	5.37	3.86	-21.8	9.9	28.2	0.5
RB-2013-053	MC	1,107	31 May 2013	37°00′21.96″	74°32′12.84″	0.36	5.32	4.12	-21.9	11.3	42.1	0.2
RB-2013-071	BC	1,118	1 June 2013	37°00′20.76″	74°32′01.44″	0.33	5.45	3.46	-21.9	10.4	31.9	n/a

* C/N not calculated due to low N content of sample (<0.1%).

BC = box core; C = carbon; $CaCO_3$ = calcium carbonate; C_{org} = organic carbon; MC = monocore; N = nitrogen; $\delta^{13}C$ and $\delta^{15}N$ are stable isotope ratios for C and N, respectively; n/a = samples not analyzed.

Table 6-4. Radiocarbon results from surface sediment and sediment trap samples collected in Baltimore Canyon.

Station	Lab ID	Sample Type	Depth (m)	Latitude (N)	Longitude (W)	F Modern	Fm Err	Age YBP	Age Err (Years)	$\Delta^{14}C$ (‰)
NF-2012-107	126881	Surface sediment (0−0.5 cm) canyon	283	38°13.484′	73°50.671′	0.7801	0.0024	1,990	25	-225.69
NF-2012-114	126882	Surface sediment (0−0.5 cm) canyon	652	38°08.888′	73°50.742′	0.2977	0.0018	9,730	50	-704.55
NF-2012-054	126880	Surface sediment (0−0.5 cm) canyon	1,180	38°04.344′	73°46.397′	0.8361	0.0018	1,440	15	-170.15
NF-2012-065	126883	Surface sediment (0−0.5 cm) slope	170	38°03.750′	73°51.935′	0.7140	0.0027	2,710	30	-291.33
NF-2012-070	126884	Surface sediment (0−0.5 cm) slope	515	38°02.611′	73°48.208′	0.7146	0.0024	2,700	25	-290.73
NF-2012-084	126885	Surface sediment (0−0.5 cm) slope	990	38°00.833′	73°45.204′	0.7457	0.0020	2,360	20	-259.89
NF-2012-091	126886	Surface sediment (0−0.5 cm) slope	1,186	37°58.643′	73°40.163′	0.6728	0.0018	3,180	20	-332.21
NF-2012-131-1	126887	Sediment trap	1,318	38°02.543′	73°44.153′	0.8526	0.0020	1,280	20	-153.75
NF-2012-131-2	126888	Sediment trap	1,318	38°02.543′	73°44.153′	0.8719	0.0018	1,100	15	-134.65
NF-2012-131-3	126889	Sediment trap	1,318	38°02.543′	73°44.153′	0.8850	0.0019	980	15	-121.57
NF-2012-131-4	126890	Sediment trap	1,318	38°02.543′	73°44.153′	0.8744	0.0018	1,080	15	-132.12
NF-2012-131-5	126891	Sediment trap	1,318	38°02.543′	73°44.153′	0.8713	0.0020	1,110	20	-135.2
NF-2012-131-6	126892	Sediment trap	1,318	38°02.543′	73°44.153′	0.8805	0.0028	1,020	25	-126.07
NF-2012-131-7	126893	Sediment trap	1,318	38°02.543′	73°44.153′	0.8754	0.0019	1,070	15	-131.13
NF-2012-131-9	126894	Sediment trap	1,318	38°02.543′	73°44.153′	0.8703	0.0019	1,120	15	-136.23
NF-2012-131-10	126895	Sediment trap	1,318	38°02.543′	73°44.153′	0.8758	0.0018	1,070	15	-130.77
NF-2012-131-11	126896	Sediment trap	1,318	38°02.543′	73°44.153′	0.8689	0.0024	1,130	20	-137.55

$\Delta^{14}C = = \left[\frac{\left({}^{14}C / {}^{12}C \right)_{spl}}{\left({}^{14}C / {}^{12}C \right)_{std}} - 1 \right] * 1000$; Fm Err = fraction modern error; F Modern = fraction modern; YBP = years before present.

Table 6-5. Neodymium isotope ($^{143}Nd/^{144}Nd$) results for surface sediment (0 to 1 cm) samples from Baltimore Canyon.

Station	Sample Type	Depth (m)	Latitude (N)	Longitude (W)	143Nd/144Nd	εNd
NF-2012-107	Surface sediment (0−0.5 cm) canyon	283	38°13′29.04″	73°50′40.26″	0.512067	-11.0995
NF-2012-114	Surface sediment (0−0.5 cm) canyon	652	38°08′53.28″	73°50′44.52″	0.512043	-11.5677
NF-2012-054	Surface sediment (0−0.5 cm) canyon	1,180	38°04′20.64″	73°46′23.82″	0.512064	-11.1580
NF-2012-065	Surface sediment (0−0.5 cm) slope	170	38°03′45.00″	73°51′56.10″	0.512139	-9.6950
NF-2012-070	Surface sediment (0−0.5 cm) slope	515	38°02′36.66″	73°48′12.48″	0.512074	-10.9629
NF-2012-084	Surface sediment (0−0.5 cm) slope	990	38°00′49.98″	73°45′12.24″	0.512125	-9.9681
NF-2012-091	Surface sediment (0−0.5 cm) slope	1,186	37°58′38.58″	73°40′09.78″	0.512062	-11.1970

Table 6-6. *n*-alkane concentrations (µg g^{-1}) in surface sediment (0 to 1 cm) samples from Baltimore and Norfolk canyons. The first three Baltimore stations are situated in the canyon and the subsequent four stations on the adjacent slope (**Table 6-4**). The Norfolk stations are all situated in the canyon.

Station	*n*-C_{14}	*n*-C_{15}	*n*-C_{16}	*n*-C_{17}	pr	*n*-C_{18}	ph	*n*-C_{19}	*n*-C_{20}	*n*-C_{21}	*n*-C_{22}	*n*-C_{23}	*n*-C_{24}	*n*-C_{25}	*n*-C_{26}	*n*-C_{27}	*n*-C_{28}	*n*-C_{29}	*n*-C_{30}	*n*-C_{31}	*n*-C_{32}
Baltimore Canyon																					
NF-2012-107[C]	0.49	1.59	0.81	0.78	0.25	1.20	0.44	1.59	1.54	1.32	n/d	0.71	n/d	n/d	n/d	0.61	n/d	0.39	n/d	n/d	n/d
NF-2012-114[C]	1.96	0.00	3.02	2.65	1.39	2.43	n/d	6.84	4.99	4.79	5.62	13.22	19.32	38.55	44.79	68.61	51.06	71.75	34.55	49.19	14.37
NF-2012-054[C]	0.12	0.38	0.30	0.43	0.26	0.38	0.32	1.13	0.58	0.63	0.36	0.35	n/d	0.66	0.48	1.08	n/d	0.98	n/d	0.31	n/d
NF-2012-065[S]	7.38	7.89	4.95	3.90	0.00	4.35	n/d	5.41	5.35	n/d	n/d	n/d	n/d	4.05	n/d	n/d	n/d	n/d	n/d	n/d	n/d
NF-2012-070[S]	0.00	2.37	2.16	n/d	n/d	2.13	n/d	3.59	3.46	2.67	1.74	n/d	2.41	2.76	n/d	n/d	n/d	n/d	n/d	n/d	n/d
NF-2012-084[S]	0.00	n/d	13.27	n/d	n/d	18.81	n/d	32.49	30.48	n/d	n/d	n/d	n/d	n/d	n/d	n/d	n/d	n/d	n/d	n/d	n/d
NF-2012-091[S]	0.34	n/d	1.19	n/d	n/d	1.10	n/d	1.88	n/d	n/d	n/d	n/d	n/d	n/d	n/d	n/d	n/d	n/d	n/d	n/d	n/d
Norfolk Canyon																					
NF-2012-193[C]	0.01	0.08	0.04	0.10	0.03	0.05	0.07	0.11	0.00	0.06	0.04	0.05	n/d	0.04	n/d	0.08	n/d	0.12	n/d	0.11	n/d
NF-2012-161[C]	0.01	0.39	0.26	0.27	0.16	0.25	0.46	0.64	0.22	0.37	0.10	0.22	n/d	0.19	n/d	0.52	n/d	0.65	n/d	0.64	n/d
NF-2012-191[C]	0.06	0.30	0.18	0.23	0.09	0.24	0.05	0.41	0.16	0.13	0.09	0.14	n/d	0.19	n/d	0.53	n/d	0.71	n/d	0.61	n/d
NF-2012-163[C]	0.03	0.23	0.11	0.11	0.04	0.11	0.03	0.24	0.12	0.15	0.09	0.10	n/d	0.12	0.03	0.26	n/d	0.22	n/d	0.27	n/d

[C] = stations situated in the canyon; n/d = below detection limit; [S] = stations situated on the adjacent slope.

Table 6-7. Sterol concentrations (µg g^{-1}) in surface sediment (0 to 1 cm) samples from Baltimore and Norfolk canyons. The first three Baltimore stations are situated in the canyon and the subsequent two stations on the adjacent slope (**Table 6-4**). The Norfolk stations are all situated in the canyon.

Station	coprostanol	epicoprostanol	5-B-coprotanaone	22-dehydrocholesterol	cholesterol	cholestanol	brassicasterol	campesterol	stigmasterol	B-sitosterol	stigmastanol
Baltimore Canyon											
NF-2012-107[C]	n/d	n/d	n/d	n/d	1.61	0.89	1.21	2.61	0.89	1.00	0.64
NF-2012-114[C]	n/d	0.24	n/d	n/d	1.47	2.98	1.00	2.42	1.21	1.24	0.00
NF-2012-054[C]	n/d	n/d	n/d	n/d	0.94	0.49	0.87	0.78	0.08	1.26	0.35
NF-2012-065[S]	n/d	n/d	n/d	n/d	2.60	0.87	n/d	13.10	4.39	1.50	2.13
NF-2012-070[S]	n/d	n/d	n/d	n/d	2.38	1.21	1.31	2.08	1.36	1.18	1.42
Norfolk Canyon											
NF-2012-193[C]	0.21	n/d	0.69	0.40	2.34	1.35	1.76	0.44	1.60	2.17	0.87
NF-2012-161[C]	0.16	n/d	0.30	0.27	0.97	0.99	0.86	0.27	1.09	1.31	1.39
NF-2012-191[C]	0.08	n/d	0.22	0.17	0.94	0.67	0.69	n/d	0.73	0.90	0.81
NF-2012-163[C]	0.04	n/d	0.11	0.05	0.48	0.35	0.32	0.06	0.36	0.43	0.47

[C] = stations situated in the canyon; n/d = below detection limit; [S] = stations situated on the adjacent slope.

6.3.2.2 Norfolk Canyon

Percent C_{org} in the surface sediment inside Norfolk Canyon fell within a narrow range (3.77% to 5.75%), except for outliers at the two shallowest (<200 m) and two deepest stations (>1,600 m) (**Table 6-3**; **Figure 6-16**). The $\delta^{13}C$ values were also in a narrow range (-21.3‰ to -21.8‰), without a clear depth-related pattern (**Figure 6-17**). This pattern is mirrored by percent total N. C/N ratios in the canyon were also in a narrow range (8.8 to 10.8), increasing with depth. Except for two shallowest stations (<200 m), percent carbonate was relatively homogeneous throughout the canyon. Chlorophyll-*a* concentrations in the canyon were invariably high and without a distinct relation with depth.

Samples taken on the upper slope between 131 and 549 m had C_{org} and total N values that were approximately 5 to 10 times lower than samples from the deeper slope sediments where values were close, albeit slightly lower, than those found inside the canyon (**Figure 6-16**). Similar to C and N concentrations, percent carbonate was lower in the upper slope samples, but otherwise percentages were comparable to those found inside the canyon. Chlorophyll-*a* concentrations were overall much lower in the slope than in the canyon sediments.

In summary, Norfolk Canyon was relatively enriched compared with the adjacent slope (and Baltimore Canyon) and lacked a clear zonation with depth. Such a zonation seems present on the adjacent slope where the deeper stations are relatively more enriched (**Figure 6-16**).

The total concentration of *n*-alkanes in surface sediment samples from Norfolk Canyon represent a resolved *n*-alkane range from C_{14} to C_{32} as well as detectible amounts of the isoprenoid hydrocarbons pristane (pr) and phytane (ph) (**Table 6-6**). The dominant *n*-alkanes were *n*-$C_{19,}$ *n*-$C_{27,}$ *n*-$C_{29,}$ and *n*-$C_{31.}$ Total *n*-alkane concentrations ranged from 1 to 12 µg g^{-1} with an enrichment at the mid-canyon site (572 m) whereas the deep canyon site (1,135 m) was depleted. Total sterol concentrations from surface sediments in Norfolk Canyon ranged from 3 to 12 µg g^{-1}. The two dominant sterols were cholesterol and β-sitosterol (**Table 6-7**). No slope sediments from adjacent to Norfolk Canyon were analyzed.

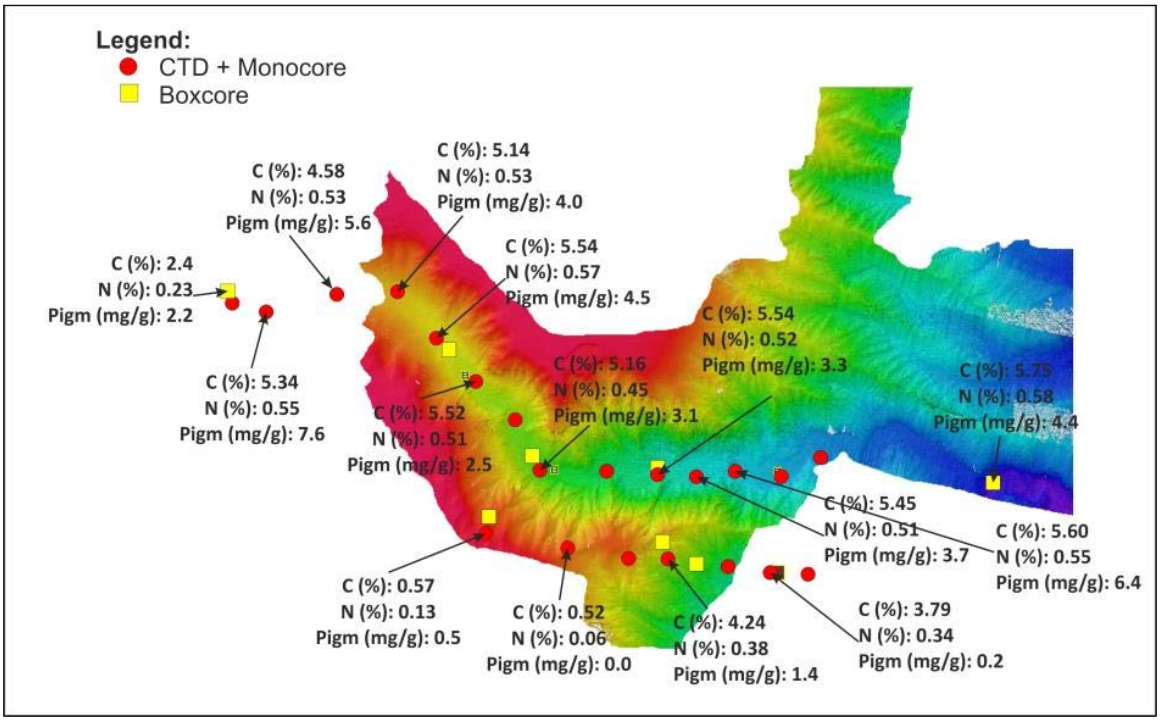

Figure 6-16. Concentrations of organic carbon (C), nitrogen (N), and chlorophyll-*a* in surface sediments (0 to 1 cm) of Norfolk Canyon and the adjacent slope.

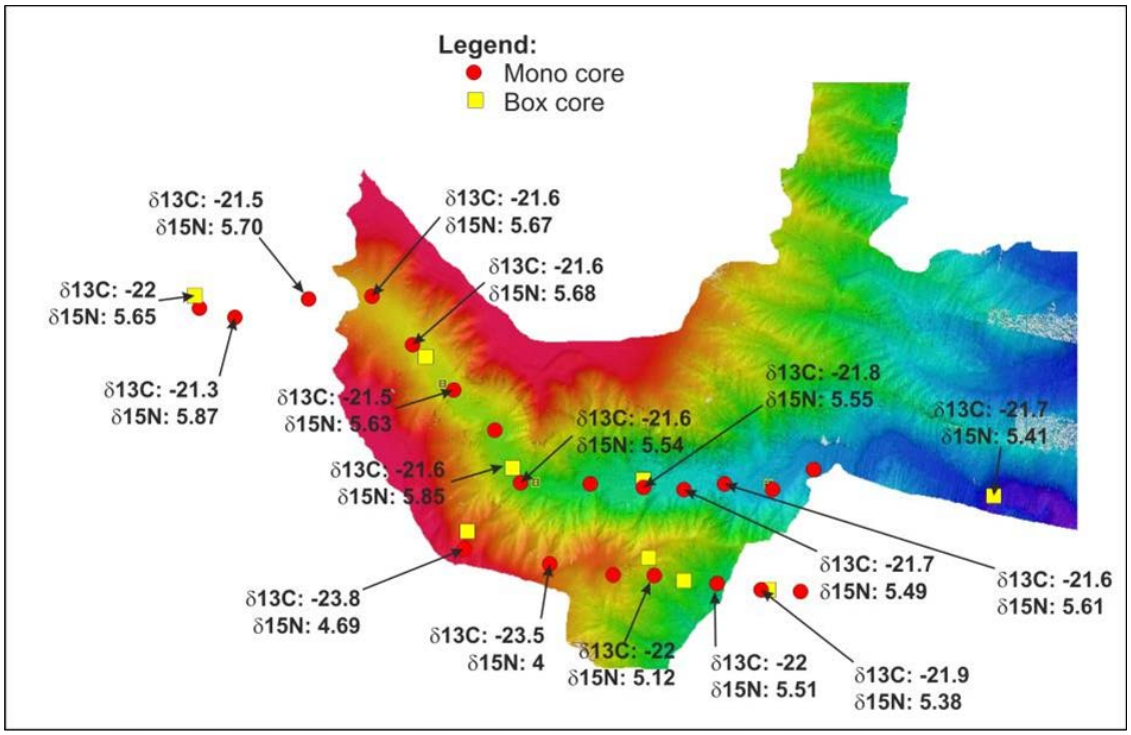

Figure 6-17. Carbon and nitrogen isotopes of surface sediments (0 to 1 cm) of Norfolk Canyon and the adjacent open slope.

6.3.3 Sediment Trap Samples

Each of the moored instruments carried a sediment trap programmed to collect settling particles near the seafloor over a 30-day interval. However, only the UNCW lander deployed at the Baltimore Canyon deep lander site (approximately 1,318 m water depth) yielded a complete series of samples. In all other cases, the sample series was compromised by mass flux events that filled up the traps completely, leaving only a few samples intact.

The results of the UNCW trap are shown in **Figure 6-18** and **Table 6-8**. The mass fluxes in the trap at 1,318 m depth in Baltimore Canyon were in a narrow range during the first 7 months (4.7 to 9 g m^{-2} d^{-1}) and somewhat lower during the last 3 months. There were two periods of relatively elevated mass flux, September−October 2012 and January−February 2013. The value in September−October 2012 was distinctly higher than in the preceding and following periods and possibly indicates a resuspension event (**Chapter 5**). Percent C_{org} and total N did not vary significantly between periods and patterns of C, N fluxes therefore closely resembled those of mass flux (**Figure 6-18**). Likewise, ^{210}Pb activity in the trap material showed little variation over time and fluxes therefore displayed a similar temporal pattern as the mass flux. Higher mass fluxes corresponded to low ^{210}Pb values, indicating transport of relatively aged material during periods of increased mass flux. Chlorophyll-*a* concentrations showed more variability between successive samples. Peak chlorophyll-*a* flux occurred in May−June 2013 with a secondary peak documented in October−November 2012. The chlorophyll-*a*/phaeopigment ratio was also highest in May−June 2013, indicating a supply of relatively fresh phytodetritus.

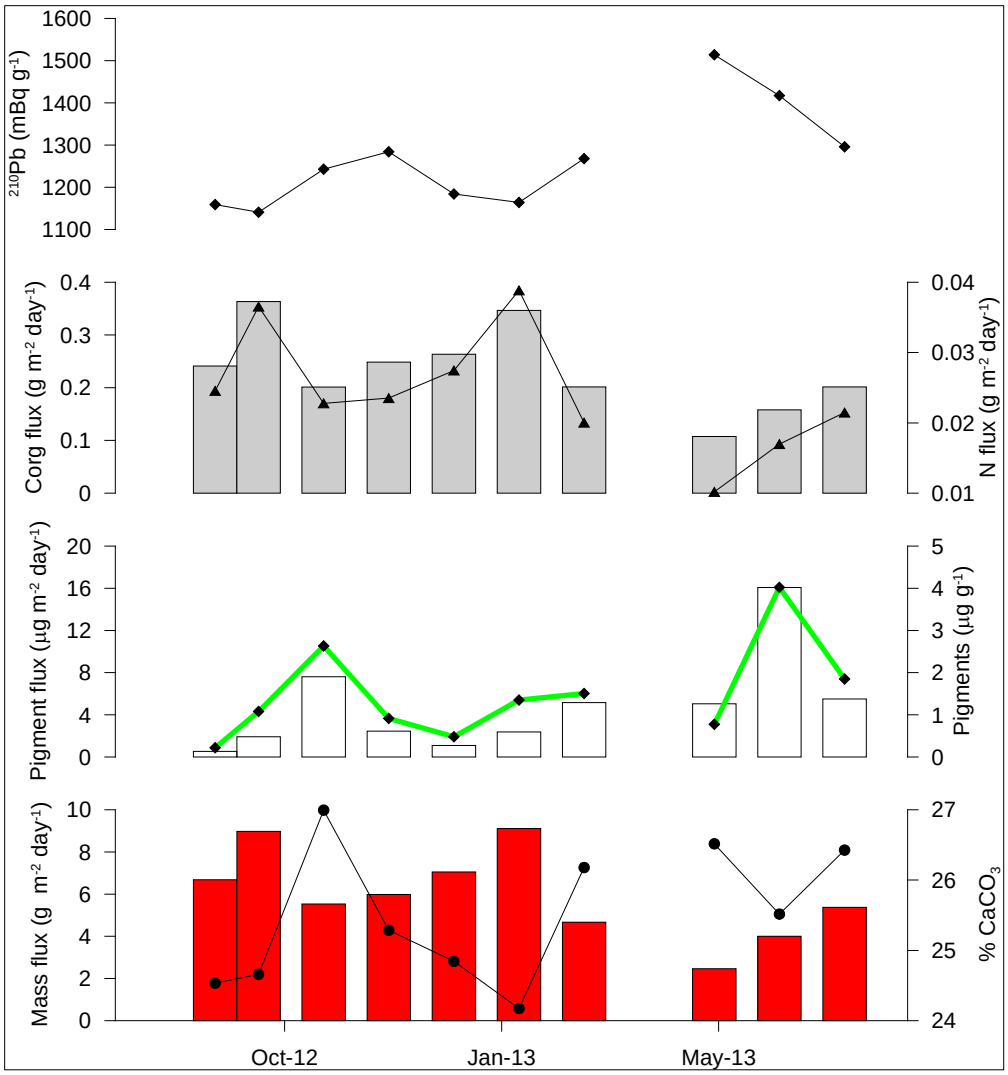

Figure 6-18. Mass flux (g m^{-2} $d^{-1)}$, calcium carbonate ($CaCO_3$) content (%), pigment flux (µg m^{-2} d^{-1}), pigment content (µg g^{-1}), C_{org} and N flux (g m^{-2} d^{-1}), and ^{210}Pb (mBq g^{-1}) values of sediment trap samples collected at the Baltimore Canyon deep lander site. Samples were taken at a monthly resolution, except the first sample, which was collected over a period of 20 days.

Table 6-8. Summary of fluxes, percentages of nitrogen and organic carbon (C_{org}), stable C and N isotope ratios, ^{210}Pb, and chlorophyll-*a* measured in sediment trap samples.

Sample ID	Date	Canyon	Instrument	Depth (m)	Mass Flux (g m^{-2} d^{-1})	N (%)	$\delta^{15}N$	C_{org} (%)	$\delta^{13}C$	C/N	^{210}Pb (mBq g^{-1})	Chl-*a* (µg m^{-2} d^{-1})
NF-2012-132-1	7 Sept 2012	Baltimore	UNCW lander	603	16.5	0.39	4.9	3.73	-22.6	9.5	890	n/a
NF-2012-132-2	26 Sept 2012				52.2	0.38	4.9	3.70	-22.2	9.7	713	n/a
NF-2012-012-1	27 Aug 2012		USGS mooring	1,082	4.5	0.42	4.6	3.85	-22.2	9.1	1,107	n/a
NF-2012-012-2	26 Sept 2012				3.9	0.36	4.9	3.21	-22.1	8.9	1,115	n/a
NF-2012-131-1	06 Sept 2012		UNCW lander	1,318	6.7	0.37	5.0	3.61	-22.4	9.8	1,159	0.9
NF-2012-131-2	26 Sept 2012				9.0	0.41	5.0	4.05	-22.5	9.9	1,141	4.3
NF-2012-131-3	26 Oct 2012				5.5	0.41	4.9	3.64	-22.0	8.8	1,243	10.5
NF-2012-131-4	25 Nov 2012				6.0	0.39	4.9	4.15	-22.0	10.6	1,284	3.7
NF-2012-131-5	25 Dec 2012				7.1	0.39	5.0	3.74	-22.2	9.6	1,184	1.9
NF-2012-131-6	24 Jan 2013				9.1	0.43	5.0	3.81	-22.1	8.9	1,164	5.4
NF-2012-131-7	23 Feb 2013				4.7	0.43	4.8	4.32	-22.3	10.1	1,268	6.0
NF-2012-131-9	24 April 2013				2.5	0.41	4.6	4.36	-22.2	10.5	1,514	3.1
NF-2012-131-10	24 May 2013				4.0	0.42	4.3	3.95	-22.8	9.3	1,417	16.1
NF-2012-131-11	23 June 2013				5.4	0.40	4.8	3.75	-22.4	9.4	1,296	7.4
NF-2012-003-1	27 Aug 2012	Norfolk	BOBO lander	1,364	7.3	0.48	5.0	4.65	-22.3	9.7	1,028	n/a
NF-2012-003-2	26 Sept 2012				14.2	0.50	5.1	4.59	-22.1	9.1	995	n/a
NF-2012-003-3	26 Oct 2012				39.6	0.56	4.9	5.16	-22.3	9.2	776	n/a

$\delta^{13}C$ = carbon Isotope; $\delta^{15}N$ = nitrogen isotope; BOBO = Bottom Boundary Layer (lander); C/N = carbon/nitrogen ratio; n/a = samples not analyzed; UNCW = University of North Carolina, Wilmington (lander); USGS = U.S. Geological Survey (mooring).

Radiocarbon ages of sediment trap material recovered from the Baltimore Canyon deep lander site ranged between 980 (SD 15) and 1,280 (SD 20) ^{14}C YBP with an average age of 1,096 ^{14}C YBP (SD 18) (**Table 6-4**). The most negative δ^{14}C value (-153.75‰) occurred in the first month of the deployment (September 2012), with little variability in δ^{14}C observed throughout the remaining part of the year. The total concentration of *n*-alkanes for sediment trap samples from Baltimore Canyon deep lander site represents a resolved *n*-alkane range from C_{14} to C_{33} as well as detectible amounts of the isoprenoid hydrocarbons pristane (pr) and phytane (ph) (**Table 6-9**). Total *n*-alkane concentrations ranged from <1 to 12 µg g^{-1}, with October 2012 yielding elevated *n*-alkane concentrations. Overall, the *n*-alkane composition was dominated by *n*-C_{29}, except in March 2013 when *n*-C_{24} was anomalously elevated. Phytane was detected in the samples from September−November of 2012, but was absent from the following months. The sediment trap sample from June 2012 contained enriched pristane relative to the other months, but overall both pristane and phytane concentrations were <1 µg g^{-1} (**Table 6-9**). Overall, the dominant sterol was cholesterol, with total sterol concentrations ranging from 1 to 30 µg g^{-1}. Enrichment was observed in sediment trap material from November 2012 where cholesterol contributed 30% of the total sterol concentration (**Table 6-10**).

A suite of trace elements was measured from the sediment trap samples collected at the Baltimore Canyon deep lander site (**Table 6-11**). Iron (Fe) and aluminum (Al) dominated the trace element composition of the sediment traps, with average monthly Fe and Al concentrations of 56 330 and 32 780 µg g^{-1}, respectively, and showed little variability throughout the deployment period. After Fe and Al, barium (Ba), phosphorous (P), strontium (Sr), and manganese (Mn) contributed to the elemental composition. Variability, evaluated as percent contribution of standard deviation to total elemental concentration, was greatest for cadmium (Cd) and molybdenum (Mo) at 4% and 3%, respectively. Peak values for Cd and Mo occurred in May and June, with a smaller enrichment in November (**Figure 6-19**). These months are also characterized by enrichment in total sterol concentration.

Table 6-9. Sediment trap *n*-alkane concentrations (µg g^{-1}) from the Baltimore Canyon deep lander site.

Sample ID	*n*-C_{14}	*n*-C_{15}	*n*-C_{16}	*n*-C_{17}	pr	*n*-C_{18}	ph	*n*-C_{19}	*n*-C_{20}	*n*-C_{21}	*n*-C_{22}	*n*-C_{23}	*n*-C_{24}	*n*-C_{25}	*n*-C_{26}	*n*-C_{27}	*n*-C_{28}	*n*-C_{29}	*n*-C_{30}	*n*-C_{31}	*n*-C_{32}
NF-2012-131-1	n/d	n/d	0.10	n/d	0.09	0.27	0.12	n/d	0.14	0.10	0.16	0.15	0.43	0.36	0.38	0.69	0.46	0.57	0.19	0.19	n/d
NF-2012-131-2	n/d	0.04	0.03	n/d	n/d	0.08	0.03	n/d	0.04	0.03	n/d	0.06	0.50	0.30	0.70	1.56	1.94	2.55	1.75	1.32	0.53
NF-2012-131-3	n/d	0.02	0.05	0.03	0.03	0.02	0.07	n/d	0.06	0.04	0.07	0.08	0.07	0.13	0.09	0.15	0.06	0.10	n/d	n/d	n/d
NF-2012-131-4	n/d	0.02	n/d	0.01	0.01	0.02	n/d	0.03	n/d	0.19	n/d	n/d	n/d	n/d	n/d	n/d	n/d	n/d	n/d	n/d	n/d
NF-2012-131-5	0.07	0.08	0.06	n/d	n/d	0.05	n/d	n/d	0.04	0.05	n/d	0.07	0.07	0.11	0.06	0.17	n/d	0.20	n/d	n/d	n/d
NF-2012-131-6	n/d	0.08	0.07	0.04	0.04	0.08	n/d	0.05	0.07	0.06	0.05	0.09	0.07	0.13	0.07	0.18	0.05	0.22	n/d	0.07	n/d
NF-2012-131-7	0.02	0.06	0.06	0.02	0.03	0.05	n/d	0.03	0.04	0.03	0.05	0.05	3.67	0.08	0.03	0.09	n/d	0.09	n/d	0.04	n/d
NF-2012-131-9	0.02	0.12	0.10	0.04	0.06	0.07	n/d	0.03	0.08	0.06	0.04	0.05	0.04	0.07	0.01	0.06	0.01	0.07	n/d	n/d	n/d
NF-2012-131-10	0.01	0.01	n/d	n/d	0.19	n/d	n/d	0.06	n/d	0.14	0.02	0.21	0.07	0.24	0.00	0.27	n/d	0.37	n/d	0.19	n/d
NF-2012-131-11	n/d	n/d	n/d	0.03	0.03	0.02	n/d	0.02	0.01	0.02	0.02	0.06	n/d	0.09	0.02	0.10	0.01	0.10	n/d	0.05	0.01

n/d = below detection limit.

Table 6-10. Sediment trap sterol concentrations (µg g^{-1}) from the Baltimore Canyon deep lander site.

Sample ID	coprostanol	epicoprostanol	5-B-coprotanaone	22-dehydrocholesterol	cholesterol	cholestanol	brassicasterol	campesterol	stigmasterol	B-sitosterol	stigmastanol
NF-2012-131-1	n/d	n/d	0.72	1.27	3.80	1.21	2.31	0.42	1.10	1.74	1.13
NF-2012-131-2	n/d	0.41	0.87	n/d	0.81	n/d	n/d	0.25	0.27	0.83	n/d
NF-2012-131-3	n/d	n/d	n/d	3.85	9.02	n/d	6.75	3.61	2.85	3.51	0.89
NF-2012-131-4	n/d	n/d	0.34	0.62	2.30	0.57	0.90	0.33	0.71	1.09	0.29
NF-2012-131-5	n/d	n/d	0.63	0.67	2.17	0.92	1.10	0.54	1.02	1.31	0.36
NF-2012-131-6	n/d	0.22	0.37	3.19	1.81	1.28	1.52	0.91	1.21	1.75	1.12
NF-2012-131-7	0.12	0.23	n/d	n/d	0.37	2.36	n/d	0.57	0.27	0.32	0.58
NF-2012-131-9	n/d	n/d	0.11	n/d	0.16	0.12	n/d	0.11	0.27	0.20	0.35
NF-2012-131-10	0.13	0.18	0.21	0.94	5.44	8.37	1.44	0.35	1.18	1.52	1.58
NF-2012-131-11	n/d	n/d	0.05	n/d	0.28	0.60	0.08	0.10	0.08	0.09	0.07

n/d = below detection limit.

Table 6-11. Sediment trap trace element concentrations (μg g^{-1}) from the Baltimore Canyon deep lander site.

Sample ID	Al	P	V	Cr	Mn	Fe	Cu	Zn	Sr	Mo	Cd	Cs	Ba	La	Tl	Pb	Th	U
NF-2012-131-1	58 200	837	92.9	69.6	538	33 600	29.7	91.4	279	0.66	0.12	4.5	449	31.3	0.51	25.9	9.31	2.05
NF-2012-131-2	56 800	870	92	69.4	530	32 700	27.5	85.7	283	0.88	0.14	4.5	415	31.3	0.5	28	9.15	2.16
NF-2012-131-3	55 200	886	89.3	66.9	476	31 900	28.3	85	298	1.1	0.15	4.4	418	30.4	0.5	26.8	8.84	2.07
NF-2012-131-4	57 300	841	91.6	69.4	648	32 900	28.5	85.4	298	0.79	0.13	4.5	428	32.3	0.51	28.9	9.38	2.18
NF-2012-131-5	57 000	834	91.1	68.3	696	32 800	27.9	84.6	285	0.85	0.1	4.5	424	33.4	0.51	28.6	9.65	2.13
NF-2012-131-6	54 200	872	85.2	67.5	568	31 700	25	82.8	266	0.91	0.11	4.3	386	31.6	0.48	28	9.23	2.04
NF-2012-131-7	56 200	943	91.6	73.6	501	33 100	29.1	88.9	287	0.96	0.14	4.7	422	32.8	0.5	28.4	9.25	2.16
NF-2012-131-9	55 800	948	90.7	68.2	465	32 900	30.7	89.7	318	1.4	0.23	4.7	475	32.6	0.52	29.4	9.44	2.26
NF-2012-131-10	56 800	859	91.4	69.1	440	33 600	30.3	86	306	1.8	0.34	4.8	469	33.5	0.53	28.9	9.3	2.18
NF-2012-131-11	55 800	877	90.9	67.4	405	32 600	30	82.5	290	0.88	0.2	4.7	466	32.4	0.5	27.1	8.81	2.04

Al = aluminum; Ba = barium; Cd = cadmium; Cr = chromium; Cs = cesium; Cu = copper; Fe = iron; La = lanthanum; Mn = manganese; Mo = molybdenum; P = phosphorus; Pb = lead; Sr = strontium; Th = thorium; Tl = thallium; U = uranium; V = vanadium; Zn = zinc.

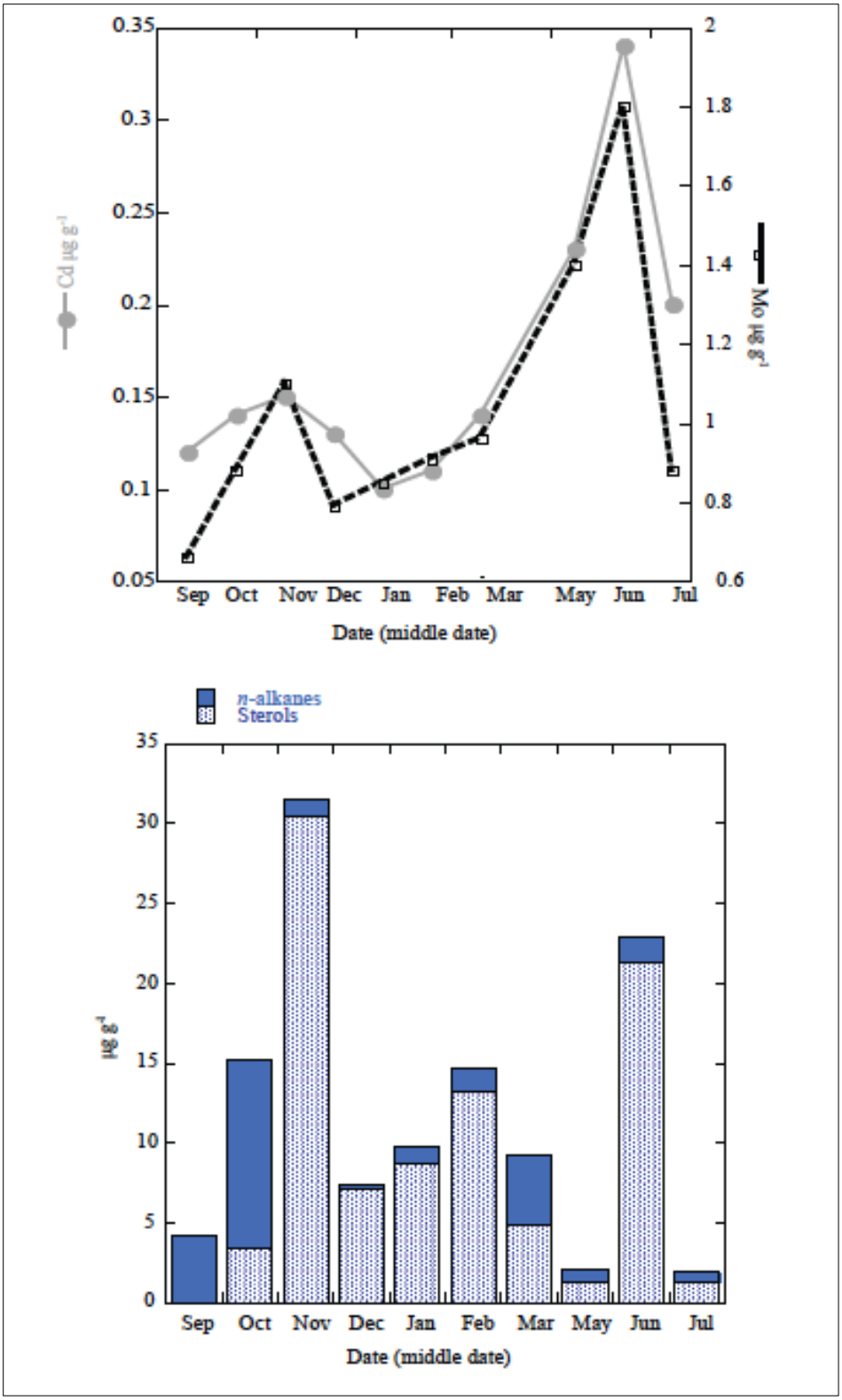

Figure 6-19. Monthly composition of trace elements cadmium (Cd) and molybdenum (Mo) from the Baltimore Canyon deep lander site showing enrichment in June and a secondary peak in November. The months of June and November are also characterized by elevated sterol concentrations.

6.3.4 CTD/Niskin Samples

During Leg 1 of the 2012 sampling cruise, bottom water samples were collected and analyzed for carbon and nitrogen at four stations along the axis of Baltimore Canyon covering a depth range from 366 to 1,270 m. A comparable set of four samples from corresponding depths in Norfolk Canyon were collected during the 2013 sampling cruise. The results of the analysis are shown in **Table 6-12**. Despite the small number of observations, there is a distinct difference between the two sample sets, i.e., percent C_{org} and total N in bottom water samples from Norfolk Canyon were higher than those taken in Baltimore Canyon. C/N ratios were much higher in Baltimore Canyon. Stable N isotope ratios ($\delta^{15}N$) were variable and did not show a clear difference between canyons. However, the sediment ^{13}C values in Baltimore Canyon were more depleted than those in Norfolk Canyon. The C/N ratios and $\delta^{13}C$ point to older and refractory suspended organic matter in Baltimore Canyon.

Trace element composition and variability of Al, Nd, Fe, and lanthanum (La) with water depth and site are shown in **Figure 6-20**. Error bars reflect standard deviation based on replicates for a given water depth. Particulate (>0.45 μm) element concentrations were enriched at the shallow station in Baltimore Canyon (NF-2012-138), in the subsurface (~100 m), and at the bottom (~600 m) in the mid-canyon stations in Baltimore (NF-2012-128) as well as Norfolk Canyon (NF-2012-158). In comparison, trace element profiles at the Baltimore Canyon deep station (NF-2012-130) and slope station (NF-2012-149) do not exhibit elevated trace metal particulate concentration at 600 m. Instead, trace element composition for the Baltimore Canyon slope site was consistently low whereas the deep site showed slight enrichment near the bottom (~1,200 m) (**Table 6-13**). Both the subsurface and ~600 m trace element enrichments coincide with elevated turbidity. The 2-D profile for Fe, based on extrapolated trace element profile data, also shows a subsurface enrichment extending down canyon to approximately 8 km away from the head of the canyon. Whereas the turbidity data show the nepheloid layer detaching from the canyon wall, the 2-D profile indicates continuous trace element enrichment along the canyon floor down to almost 1,200 m.

Table 6-12. Concentrations of organic carbon (C_{org}), nitrogen (N), and stable carbon ($\delta^{13}C$) and nitrogen ($\delta^{15}N$) isotope ratios in near-bottom suspended particulate matter samples collected in Baltimore and Norfolk canyons.

Canyon	Station	Depth (m)	Date	Latitude (N)	Longitude (W)	N (%)	δ15N	C_{org} (%)	δ13C	C/N
Baltimore	NF12-037	363	21 Aug 2012	38°12′13.08″	73°51′03.48″	0.17	6.6	2.4	-21.7	14.2
	NF12-016	591	19 Aug 2012	38°10′12.84″	73°50′55.80″	0.13	2.7	1.5	-22.2	11.0
	NF12-044	1,041	22 Aug 2012	38°05′07.14″	73°47′29.82″	0.22	5.7	3.4	-24.2	15.5
	NF12-060	1,270	24 Aug 2012	38°03′07.32″	73°44′27.96″	0.07	6.5	1.3	-25.9	18.9
Norfolk	RB13-005	337	03 May 2013	37°05′36.12″	74°42′15.84″	0.52	4.9	5.4	-21.1	10.3
	RB13-007	606	03 May 2013	37°03′56.88″	74°39′01.80″	0.84	6.7	8.2	-21.1	9.7
	RB13-009	974	03 May 2013	37°02′15.96″	74°35′58.20″	0.65	5.1	6.2	-19.9	9.5
	RB13-016	1,249	04 May 2013	37°02′16.14″	74°32′56.76″	0.57	5.9	5.2	-19.6	9.2

Table 6-13. Trace element concentrations (μg g^{-1}) in suspended particulate matter filtered (>0.45 μm) at discrete water column depths in Baltimore and Norfolk canyons.

Canyon	Station	Site	Depth (m)	Neodymium (Nd)		Lanthanum (La)		Aluminum (Al)		Iron (Fe)	
				Mean	SD (σ)	Mean	SD (σ)	Mean	SD (σ)	Mean	SD (σ)
Baltimore	NF-2012-138	Upper canyon	10	0.004	0.003	0.011	0.005	1.000	n/a	2.700	1.697
	NF-2012-138	Upper canyon	20	0.004	n/a	0.009	n/a	2.000	n/a	0.920	n/a
	NF-2012-138	Upper canyon	50	0.051	0.019	0.089	0.061	16.500	2.121	42.600	4.525
	NF-2012-138	Upper canyon	100	0.068	0.023	0.078	0.034	45.000	15.556	73.500	22.769
	NF-2012-138	Upper canyon	150	0.012	0.003	0.017	0.001	9.000	4.243	13.900	5.233
	NF-2012-138	Upper canyon	250	0.025	0.028	0.029	0.033	19.500	20.506	28.560	31.311
	NF-2012-128	Mid-canyon	10	0.001	0.000	0.005	0.002	1.500	0.707	2.000	0.707
	NF-2012-128	Mid-canyon	50	0.007	0.000	0.008	0.000	4.000	1.414	6.625	2.157
	NF-2012-128	Mid-canyon	100	0.004	0.001	0.005	0.002	3.000	1.414	5.540	2.744
	NF-2012-128	Mid-canyon	150	0.018	0.009	0.029	0.019	6.800	1.131	9.385	1.294
	NF-2012-128	Mid-canyon	300	0.020	0.007	0.020	0.008	15.000	5.657	22.000	8.768
	NF-2012-128	Mid-canyon	644	0.050	0.021	0.053	0.020	43.500	17.678	67.900	28.001
	NF-2012-130	Lower canyon	10	0.001	0.001	0.004	0.004	1.500	0.707	4.855	4.603
	NF-2012-130	Lower canyon	50	0.005	0.003	0.008	0.005	2.500	2.121	3.455	2.906
	NF-2012-130	Lower canyon	100	0.003	0.000	0.004	0.001	3.000	1.414	5.805	4.533
	NF-2012-130	Lower canyon	200	0.005	0.003	0.004	0.004	3.500	2.121	4.715	3.981
	NF-2012-130	Lower canyon	600	0.008	0.001	0.008	0.002	6.700	0.990	9.845	1.068

Table 6-13. (Continued).

Canyon	Station	Site	Depth (m)	Neodymium (Nd)		Lanthanum (La)		Aluminum (Al)		Iron (Fe)	
				Mean	SD (σ)	Mean	SD (σ)	Mean	SD (σ)	Mean	SD (σ)
Baltimore (Cont'd.)	NF-2012-130	Lower canyon	1,140	0.042	0.005	0.044	0.006	36.500	2.121	52.250	5.162
	NF-2012-149	Slope	10	0.004	0.001	0.007	0.000	2.000	n/a	2.450	0.071
	NF-2012-149	Slope	50	0.006	0.002	0.008	0.002	2.500	0.707	4.380	1.245
	NF-2012-149	Slope	100	0.003	n/a	0.003	n/a	2.000	n/a	2.400	0.283
	NF-2012-149	Slope	150	0.004	0.001	0.003	0.001	3.000	n/a	3.300	0.141
	NF-2012-149	Slope	350	0.006	0.002	0.006	0.002	4.500	2.121	5.705	2.553
	NF-2012-149	Slope	678	0.014	0.002	0.015	0.004	12.500	3.536	16.450	3.889
Norfolk	NF-2012-158	Mid-canyon	150	0.010	0.002	0.012	0.003	6.750	1.061	10.305	2.539
	NF-2012-158	Mid-canyon	300	0.041	0.007	0.043	0.008	35.500	6.364	51.400	7.354
	NF-2012-158	Mid-canyon	621	0.107	0.020	0.113	0.021	95.200	13.859	143.500	21.920

n/a = replicate not available.

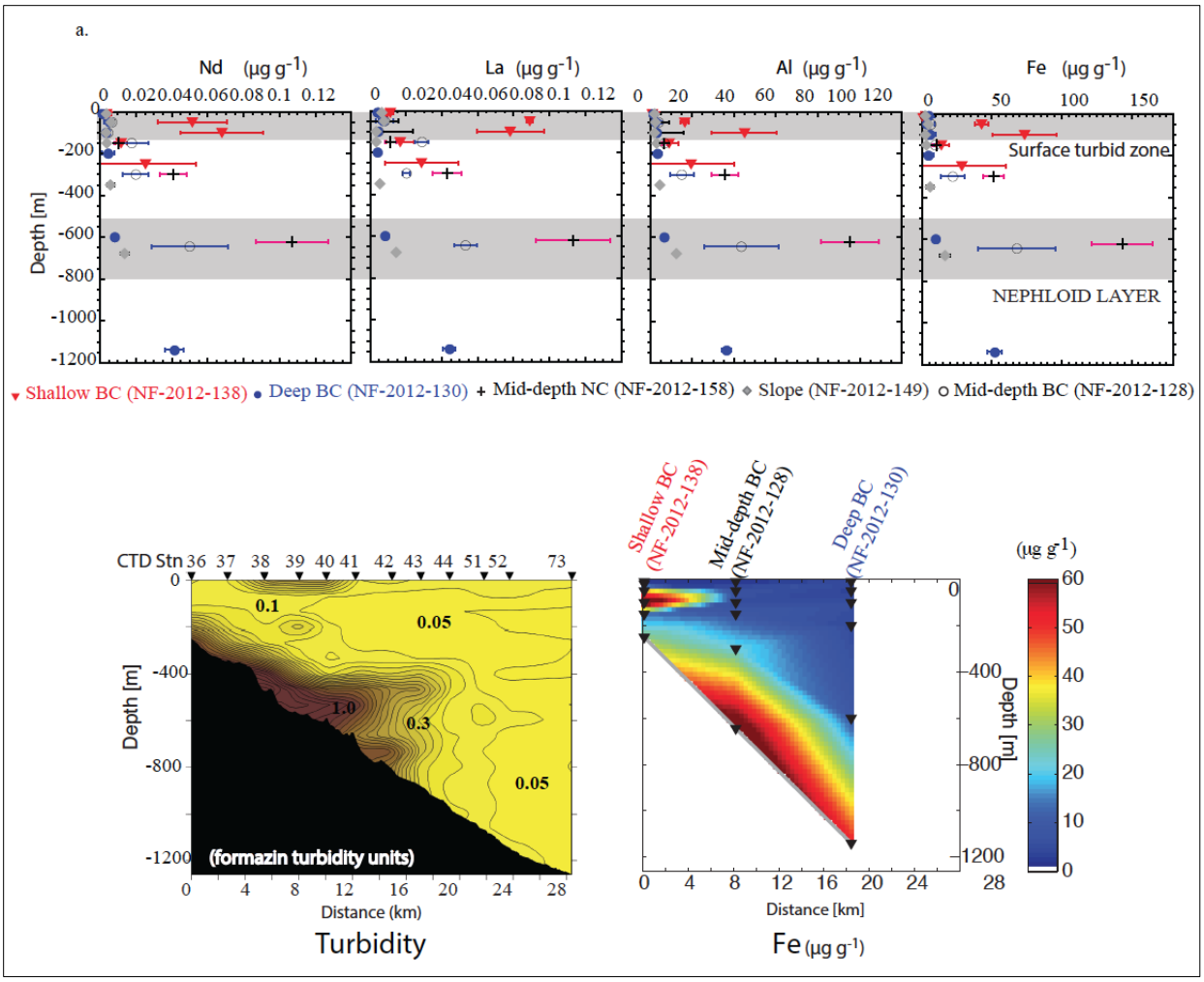

Figure 6-20. Particulate matter trace element concentrations (µg g^{-1}; neodymium [Nd], lanthanium [La], aluminum [Al], and iron [Fe]) from collecting and filtering (>0.45 µm) water at discrete depths at three stations in Baltimore Canyon (BC) and adjacent slope and one station in Norfolk Canyon (NC). The extrapolated Fe concentration illustrates a 2-D profile compared with the turbidity profile from Baltimore Canyon.

6.4 DISCUSSION

The U.S. Mid-Atlantic continental margin contains approximately 30 to 40 shelf-sourced canyons (Harris and Whiteway 2011). Besides Baltimore and Norfolk canyons, there are two other major canyons in this part of the MAB: Wilmington Canyon and Washington Canyon. All canyons incise the same continental shelf and slope, have their heads at approximately 60 nautical miles (nmi) from shore, and have no connection with a major river system. They also share the fact that they are nonbranched (Obelcz et al. 2014). According to the subdivision of submarine canyons suggested by Harris and Whiteway (2011), these characteristics classify them as shelf-sourced or Type 2 canyons. Both Baltimore and Norfolk canyons have broad meandering axes with a comparable axial profile gradient over the upper 15 km (Obelcz et al. 2014). One of the main objectives of this project was to describe and understand the distribution of (vulnerable) ecosystems in the MAB canyons. This distribution is likely linked to sedimentology and the availability of food within the canyon system. We hypothesized that 1) canyons incising the MAB shelf capture sediment and organic carbon, enriching canyon floor sediment, resulting in higher concentration and quality of carbon than the adjacent slope, and 2) given Baltimore and Norfolk

canyons have a different morphology and orientation, the canyons have different sedimentation patterns and accumulation rates, which correspond to differing faunal communities.

A study by Gardner (1989a, 1989b) in Baltimore Canyon showed significant turbidity and resuspension in the upper canyon associated with internal tides traveling up canyon. Turbidity was much lower over the deeper part of Baltimore Canyon axis (~1,000 m) in Gardner's (1989a, 1989b) study. The transition between turbid and clear water consisted of interleaving plumes, which were advected away from the canyon on density interfaces. Net transport of water was down canyon in the upper axis and up canyon in the lower part of the axis, implying a convergence. As a result, Baltimore Canyon has a very distinctive division in the water column along its axis. Consequences of this division for the sediment composition or benthic fauna have not been reported in these earlier studies. Also, comparable data on currents, particle distribution, and fauna in Norfolk Canyon are lacking. Hence, these topics were a part of the Atlantic Deepwater Canyons study.

6.4.1 Surface Sediment and Distinctive Zones

Analysis of the box cores taken along the Baltimore Canyon axis revealed a clear heterogeneity in sediment composition. Based on the parameters analyzed in the cores (i.e., porosity, grain size, Ca/Ti and Ca/Fe, and sedimentation), the axis can be divided into two zones: an upper Zone I with mixed sediment and low porosity and a Zone II located in the deeper part of the canyon (841 to 1,180 m) containing fine, silty sediment with a homogenous composition and high porosity. The cores from the middle part of the canyon (360 to 754 m) were characterized by a sandy top layer, overlaying a compacted clay layer, associated with low Ca/Ti and Ca/Fe ratios and low ^{210}Pb activity. These results indicate that the clay is significantly older and represents an eroded and reworked paleo surface with a different elemental composition than the overlying sandy sediment. The presence of this clay layer together with the evidence of reworking could explain the irregular ^{210}Pb activity profiles that were present in the middle part of the canyon. At a water depth of ~560 m in Zone I of Baltimore Canyon (NF2012-30BC), the most recent layer of sediment shows a marked depletion in fine material (coarse sand), which could point to local winnowing of the surface layer (**Table 6-1**). At a distance of 2 km down canyon from this station, the surface sediment had an anomalously old ^{14}C age (9,730 ^{14}C YBP (SD 50) at NF-2012-114 **(Table 6-4**), which may be related to winnowing in this part of the canyon. This region is also marked by elevated high molecular weight *n*-alkanes, particularly *n*-C_{27} and *n*-C_{29} (**Figure 6-21**) indicative of organic input from riverine transported terrestrial source (Eglinton and Hamilton 1967), and the sterol cholestanol. Enhanced resuspension at this depth is also consistent with the elevated near-bed turbidity values that were observed on CTD casts near this depth and elevated lithogenic material in the suspended particulate matter, particularly in comparison with the slope profile (**Chapter 5**). According to Gardner (1989a), currents have opposite directions in the upper and lower part of Baltimore Canyon (i.e., down canyon versus up-canyon, respectively). This gives rise to a convergence zone mid-canyon. The enhanced turbidity values and winnowed sediment that were observed at approximately 560 m in this study could point to the presence of such a convergence zone. Cores from the lower part (Zone II) of the canyon are characterized by high porosity, high ^{210}Pb activity (unknown ^{210}Pbsupp activity) and high accumulation rates, suggesting that this area is a deposition zone within the canyon. The deposition zone is associated with the tail end of the turbidity cloud that was observed in the water column (**Chapter 5**). Thus, fine resuspended sediments from Zone I are most likely deposited in the deeper part of the canyon (Zone II). In the SEEP-I and II studies (Walsh et al. 1988, Biscaye et al. 1988), the exchange of organic matter between shelf and slope of the MAB was examined. Biscaye and Anderson (1994) suggested that MAB canyons channel sediment from the shelf to the slope and serve as a reservoir, providing shelf-derived particles to the mid-slope depocenter. These shelf-sourced sediments represent a belt of fine sediment with elevated concentrations of organic carbon at a water depth of approximately 1,000 m along the entire MAB. During the SEEP studies, measurements were only made across the open slope. We have shown that the same holds for the MAB canyons, which also show the presence of a depocenter between 840 and 1,100 m water depth, showing enriched values of organic matter and pigments and higher accumulation

rates. Canyons therefore act as conduits and/or storage for labile organic matter. Anderson et al. (1994) showed that half of the carbon in the mid-slope depocenter is aged and refractory and is presumably supplied by lateral transport. Results from this study indicate an average radiocarbon age of slope surface sediment from Baltimore Canyon of 2,738 ^{14}C YBP (SD 25). Labile carbon, according to Biscaye and Anderson (1994), is virtually mineralized in less than 1 year.

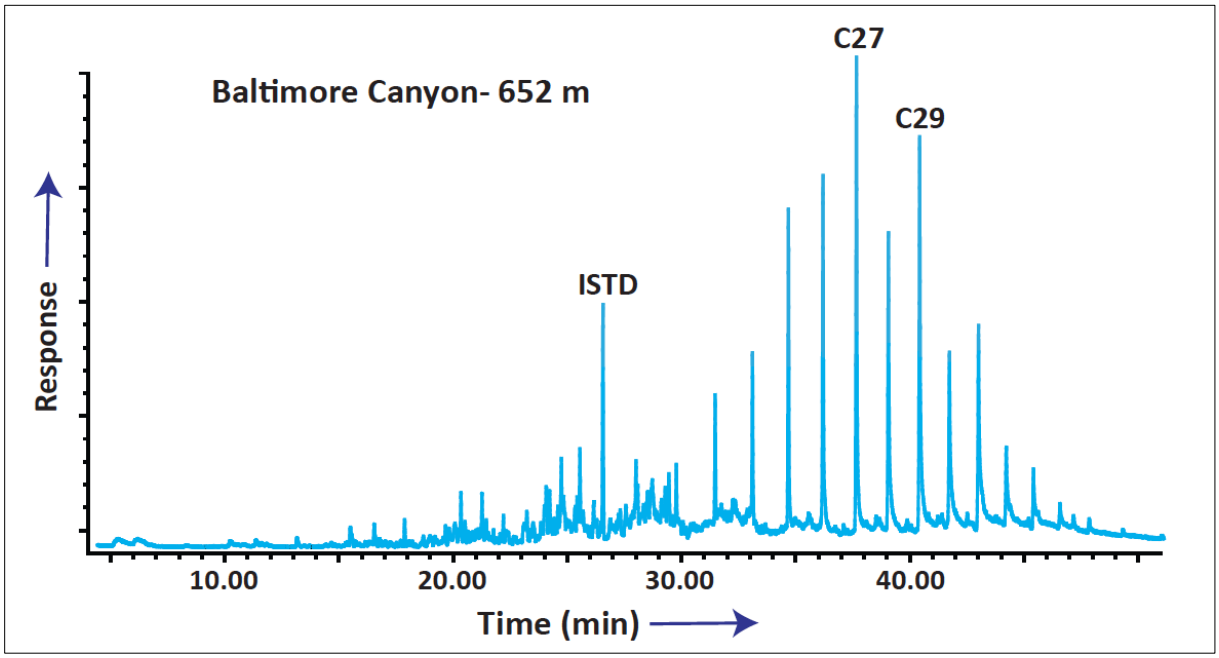

Figure 6-21. Chromatogram of *n*-alkane from a surface sediment sample collected in Baltimore Canyon at 652 m depth illustrating enrichment of the high molecular weight *n*-alkanes C_{27} and C_{27}. (Note: ISTD refers to an internal standard.)

The sediment composition on the open slope does not show a similar heterogeneity as the Baltimore Canyon, but instead is characterized by an increase in finer sediment and porosity with depth. Furthermore, concentrations of lithogenic material in suspended particulate matter on the open slope were low compared with concentration within the canyon at a comparable depth (~600 m). The upper part of the open slope (169 to 170 m water depth) consists of homogenous medium sand and is characterized by a high amount of reworking and low ^{210}Pb activity. The high accumulations rates calculated for the upper part of the open slope are presumably not reliable because either an inappropriate model was used or strong mixing with shelf sediment occurred throughout the entire subcore. The middle and bottom parts of the open slope (515 to 1,186 m water depth) consist of clayey sand. Accumulation rates are low and similar to that of areas within the canyon that experience little sedimentation. In addition, ^{14}C ages of surface sediments on the slope are aged relative to those at comparable depths in the canyon.

A similar zonation was not observed in Norfolk Canyon. All cores taken along the canyon axis showed a homogeneous distribution of sandy sediment, and grain size decreased with increasing depth. Accumulation rates in the upper and middle canyon were high compared with Baltimore Canyon. In Norfolk Canyon, sedimentation patterns are also likely steered by the hydrodynamic conditions. Turbidity profiles along the canyon axis do not show a large and delimited turbidity cloud as was observed in Baltimore Canyon, instead there were several bottom and intermediate nepheloid layers between 400 and 1,100 m water depth (**Chapter 5**). The presence of multiple nepheloid layers likely indicates resuspension of sediment at different depths, resulting in a uniform drape of sediment along the canyon axis. In Norfolk Canyon, sediment accumulation rates were highest around 1,100 m water depth, which could be related to the depocenter as described by Biscaye and Anderson (1994). However, enhanced deposition was not

reflected in enhanced concentrations of organic matter, which were overall high along the Norfolk Canyon axis.

6.4.2 Sediment Cores and Organic Carbon Transport

According to the C, N, and phytopigment data (**Figure 6-14**), Baltimore Canyon contains two distinctive zones, consistent with the zones indicated from the sediment texture and accumulation rate data described above. The sediments in the upper and middle part (189 to 754 m water depth) of the canyon axis have similar characteristics (low concentrations of C, N, and pigments), just as the shallow shelf station. By contrast, the deeper part of the canyon (841 to 1,180 m water depth) shows a clear and significant enrichment in all parameters (C, N, and pigments). The coincidence of fine surface sediments with higher C and N at the deeper canyon stations is consistent with increased surface area and sorption to fine particles (Mayer 1994). Low C and N content in the upper and middle part would accordingly suggest that the rate of transport of the fine-grained sediment within the upper and middle part (189 to 754 m water depth) of the canyon is relatively fast and does not allow for prolonged or intermediate deposition and mineralization. The difference in chlorophyll concentrations between upper and lower Baltimore Canyon cannot be directly coupled to grain size, but rather points to differential removal of fine phytodetritus (and silt) in the upper canyon. The upper canyon (~280 m) is characterized by marine-derived sources of organic matter whereas at approximately 1,180 m the marine component composition is reduced (**Figure 6-22**). This is most likely related to the lower canyon being an accumulation area of silt associated with carbon of predominantly terrestrial origin. Currently, Baltimore Canyon does not physically connect with a major river system. However, the average Nd isotope values from both the Baltimore slope and canyon suggest connectivity with adjacent watersheds, particularly the Hudson River, where southward currents have the potential to advect Hudson River discharges to the south toward Baltimore Canyon. This connectivity helps explain the terrestrial-derived organic matter signature in both the surface sediment and sediment trap samples (**Figures 6-22** and **6-24**). Likewise, the aged radiocarbon dates reflect organic carbon that was photosynthetically fixed thousands of years ago, as previously documented in riverine carbon exported from the Hudson River Watershed (Raymond and Bauer 2001).

Sediments along the slope adjacent to Baltimore Canyon show no enrichment in N or pigments with increasing depth as was found along the Baltimore Canyon axis. Only percent C_{org} was elevated at the deepest slope stations (**Table 6-3**). This locally high carbon content is most likely explained by "old" refractory carbon supplied to mid-slope sediments at water depths of approximately 1,000 m in the MAB (Anderson et al. 1994), consistent with relatively older ^{14}C age (3,180 YBP).

The distribution of C, N, and chlorophyll in surface sediments in Norfolk Canyon was markedly different from Baltimore Canyon. Concentrations of all three compound classes were up to 5 to 10 times higher than values observed in the Baltimore Canyon and showed a more homogeneous distribution along the canyon axis. Further, the biomarker data captured a smooth trend from terrestrial-dominated to marine-dominated organic matter in the Norfolk Canyon surface sediment transects (**Figure 6-23**). The higher levels of organics, particularly enhanced phytopigment concentrations, present throughout Norfolk Canyon compared with Baltimore Canyon might be explained by the spring bloom on the northeastern U.S. continental shelf, as the samples were collected just after this event. While the inner and middle shelf has a maximum chlorophyll concentration in fall and winter, the shelf break/slope waters have a spring maximum (Ryan et al. 1999, Xu et al. 2011). Hence the latter bloom could have fueled the canyon and slope in May with fresh organics (e.g., phytodetritus). The elevated pigment flux corresponds with increased biomarker concentrations (especially sterols), indicating greater primary production as the sterols are tracers of marine-derived organic matter. Cd and Mo increase during this period as well, in concert with ^{210}Pb, suggesting increased scavenging during the blooms as a result of enhanced surface production.

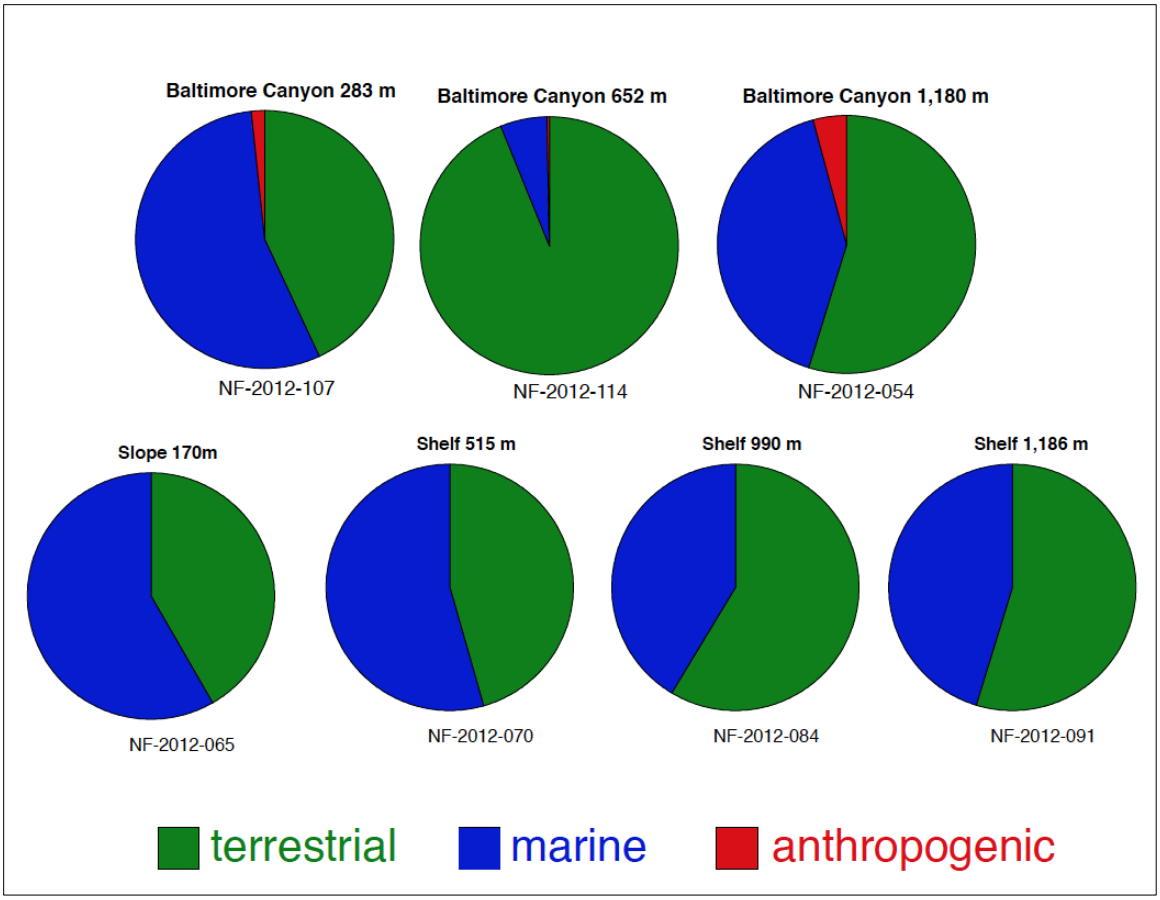

Figure 6-22. Relative proportions of marine, terrestrial higher plants, and anthropogenic/ petroleum contributions to surface sediments from Baltimore Canyon and adjacent slope. Terrestrial organic matter components of sediments were quantified using concentrations of odd numbered *n*-alkanes in the C_{21} to C_{31} range as well as the sterols campesterol, stigmasterol, and β-sitosterol. Marine components were determined using the sterols cholesterol and brassicasterol concentrations as well as odd and even numbered *n*-alkanes in the C_{15} to C_{19} range. The anthropogenic components were determined using the sterol composition of coprostanol, epicoprostanol, and 5-β-coprostanone and the isoprenoid hydrocarbons pristane and phytane.

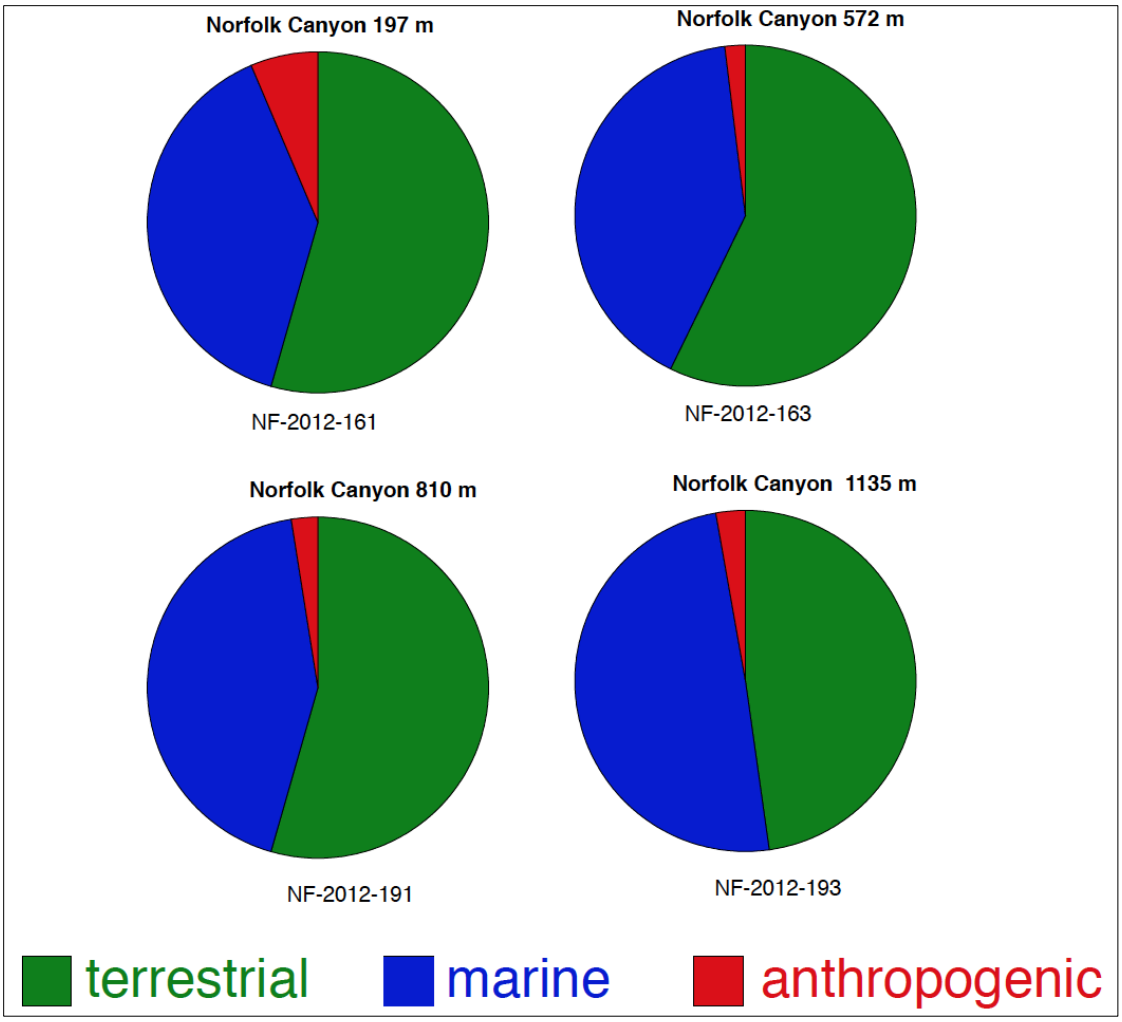

Figure 6-23. Relative proportions of marine, terrestrial higher plants, and anthropogenic/petroleum contributions to surface sediments from Norfolk Canyon. Terrestrial organic matter components in sediments were quantified using concentrations of odd numbered *n*-alkanes in the C_{21} to C_{31} range as well as the sterols campesterol, stigmasterol, and β-sitosterol. Marine components were determined using the sterols cholesterol and brassicasterol concentrations as well as odd and even numbered *n*-alkanes in the C_{15} to C_{19} range. The anthropogenic components were determined using the sterol composition of coprostanol, epicoprostanol, and 5-β-coprostanone and the isoprenoid hydrocarbons pristane and phytane.

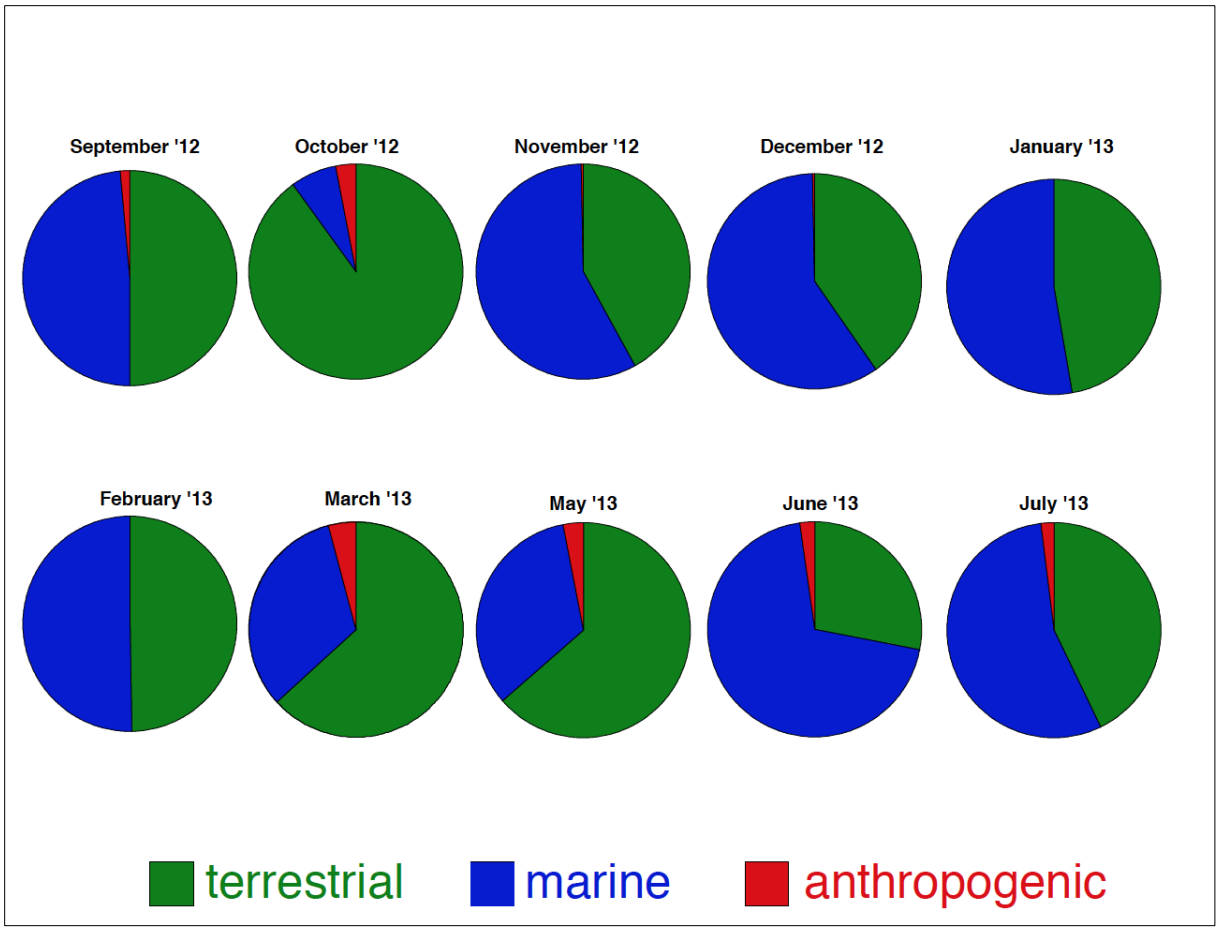

Figure 6-24. Relative proportions of marine, terrestrial higher plants, and anthropogenic/petroleum contributions to monthly sediment trap samples from Baltimore Canyon deep lander site (1,318 m water depth). Terrestrial organic matter composition of sediments was quantified using concentrations of odd numbered *n*-alkanes in the C_{21} to C_{31} range as well as the sterols campesterol, stigmasterol, and β-sitosterol. Marine components were determined using the sterols cholesterol and brassicasterol concentrations as well as odd and even numbered *n*-alkanes in the C_{15} to C_{19} range. The anthropogenic components were determined using the sterol composition of coprostanol, epicoprostanol, and 5-β-coprostanone and the isoprenoid hydrocarbons pristane and phytane.

The slope sediment next to Norfolk Canyon indeed had higher concentrations of pigments (>10 fold) than the Baltimore slope sampled during the preceding September. Concentrations of C on the slope showed a typical increase toward the 1,000 m isobath in accordance with the mid-slope depocenter (Anderson et al. 1994). However, in contrast to Baltimore slope where N content was low throughout the slope, the N content on the Norfolk slope measurably increased from 680 m depth onwards. Interestingly, Milliman (1994) noted a difference between the (normalized) N content of slope sediment south versus north of Norfolk Canyon with higher values to the south down to Cape Fear. Milliman (1994) explains these higher N values by the narrowing shelf in combination with the local confluence of major currents. The current dataset showing high C and N concentrations throughout Norfolk Canyon points to the canyon being an intermediary source of the elevated organic N (and C), which is laterally transported along the margin with the southward Virginia Current.

In summary, the geochemistry of surface sediment and sediment trap samples supports the hypothesis that the two canyons serve as conduits for transport of shelf sediment and associated refractory, organic

matter to the deep sea. In addition, the absence of anthropogenic-sourced organic matter in the slope compared with canyon sediment (**Figure 6-22**) provides evidence that canyons could also channel contaminants. In spite of the fact that the two canyons share certain features such as the same slope, distance from the coast, and absence of direct river input, they are distinctly different with respect to sedimentology and organic matter composition and distribution along their axis.

6.5 LITERATURE CITED

Allen SE, Durrieu de Madron X. 2009. A review of the role of submarine canyons in deep-ocean exchange with the shelf. Ocean Science. 5:607–620.

Amaro T, Billett DSM, Gooday AJ, Pattenden A, de Stigter H, Weaver PPE. 2006. Deep-sea canyon fauna on the Portuguese margin. Geophysical Research Abstracts. 8:10953.

Anderson RF, Gilbert T, Kemp PF, Trumbore S, Biscaye PE. 1994. Carbon budget for the mid-slope depocenter of the Middle Atlantic Bight. Deep-Sea Research Part II: Topical Studies in Oceanography. 41:669–703.

Bayon G, German CR, Boella RM, Milton JA, Taylor RN, Nesbitt RW. 2002. An improved method for extracting marine sediment fractions and its application to Sr and Nd isotopic analysis. Chemical Geology. 187:179–199.

Bennett RH, Lehman L, Hulbert MH, Harvey GR, Bush SA, Forde EB, Crews P, Sawyer WB. 1985. Interrelationships of organic carbon and submarine sediment geotechnical properties. Marine Geotechnology. 6:61–98.

Biscaye PE, Anderson RF. 1994. Fluxes of particulate matter on the slope of the southern Middle Atlantic Bight: SEEP-II. Deep-Sea Research II: Topical Studies in Oceanography. 41:459–509.

Biscaye PE, Flagg CN, Falkowski PG. 1988. The shelf edge exchange processes experiment, SEEP-II: an introduction to hypotheses, results and conclusions. Deep-Sea Research Part II: Topical Studies in Oceanography. 41:231–252.

Briggs PH, Meier AL. 2002. The determination of forty-two elements in geological materials by inductively coupled plasma–mass spectrometry. US Geological Survey Open File Report 02-223-I.

Brothers DS, ten Brink US, Andrews BD, Chaytor JD, Twichell DC. 2013. Geomorphic process fingerprints in submarine canyons. Marine Geology. 337:53–66.

Canals M, Puig P, de Madron XD, Heussner S, Palanques A, Fabres J. 2006. Flushing submarine canyons. Nature. 444:354–357.

De Leo FC, Smith CR, Rowden AA, Bowden DA, Clark MR. 2010. Submarine canyons: hotspots of benthic biomass and productivity in the deep sea. Proceedings of the Royal Society B-Biological Sciences. 277:2783–2792. doi:10.1098/rspb.2010.0462.

de Stigter HC, Boer W, de Jesus Mendes PA, Jesus CC, Thomsen L, van den Bergh GD, van Weering TCE. 2007. Recent sediment transport and deposition in the Nazaré Canyon, Portuguese continental margin. Marine Geology. 246:144–164.

Dutertre M, Hamon D, Chevalier C, Ehrhold A. 2013. The use of the relationships between environmental factors and benthic macrofaunal distribution in the establishment of a baseline for coastal management. ICES Journal of Marine Science. 70:294–308.

Eglinton G, Hamilton RJ. 1967. Leaf epicuticular waxes. Science. 156:1322–1335.

Escrig S, Bézos A, Langmuir CH, Michael PJ, Arculus R. 2012. Characterizing the effect of mantle source, subduction input and melting in the Fonualei Spreading Center, Lau Basin: constraints on the origin of the boninitic signature of the back-arc lavas. Geochemistry, Geophysics, Geosystems. 13:Q10008.

Gardner WD. 1989a. Baltimore Canyon as a modern conduit of sediment to the deep sea. Deep-Sea Research Part A Oceanographic Research Papers. 36(3):323–358. doi:10.1016/0198-0149(89)90041-1.

Gardner WD. 1989b. Periodic resuspension in Baltimore Canyon by focusing of internal waves. Journal of Geophysical Research−Oceans. 94*(*C12*)*:18185–18194. doi*:*10.1029/JC094iC12p18185.

Goldstein SL, O'Nions RK, Hamilton PJ. 1984. A Sm-Nd study of atmospheric dusts and particulate from major river systems. Earth and Planetary Science Letters. 70(2):221–236. [accessed Apr 19]. http://dx.doi.org/10.1016/0012-821X(84)90007-4.

Gori A, Orejas C, Madurell T, Bramanti L, Martins M, Quintanilla E, Marti-Puig P, Lo Iacono C, Puig P, Requena S, Greenacre M, Gili JM. 2013. Bathymetrical distribution and size structure of cold-water coral populations in the Cap de Creus and Lacaze-Duthiers canyons, northwestern Mediterranean. Biogeosciences. 10(3):2049–2060. doi:10.5194/bg-10-2049-2013.

Harris PT, Whiteway T. 2011. Global distribution of large submarine canyons: Geomorphic differences between active and passive continental margins. Marine Geology. 285:69–86.

Hart SR, Blusztajn J. 2006. Age and geochemistry of the mafic sills, ODP site 1276, Newfoundland margin. Chemical Geology. 235:222–237.

Huvenne VAI, Tyler PA, Masson DG, Fisher EH, Hauton C, Hűhnerbach V, Le Bas TP, Wolff GA. 2011. A picture on the wall: innovative mapping reveals cold-water coral refuge in submarine canyon. PLoS ONE 6. doi:10.1371/journal.pone.0028755.

Ingels J, Tchesunov AV, Vanreusel A. 2011. Meiofauna in the Gollum Channels and the Whittard Canyon, Celtic Margin−how local environmental conditions shape nematode structure and function. PLoS ONE. 6(5): e20094. doi:10.1371/journal.pone.0020094.

Kenchington EL, Cogswell AT, MacIsaac KG, Beazley L, Law BA, Kenchington TJ. 2014. Limited depth zonation among bathyal epibenthic megafauna of the Gully submarine canyon, northwest Atlantic. Deep Sea Research Part II – Topical Studies in Oceanography Special Issue. 104:67–82.

Leduc D, Rowden AA, Nodder SD, Berkenbusch K, Probert PK, Hadfield MG. 2013. Unusually high food availability in Kaikoura Canyon linked to distinct deep-sea nematode community. Deep-Sea Research Part II – Topical Studies in Oceanography Special Issue. 104:310–318.

Mayer LM. 1994. Surface area control of organic carbon accumulation in continental shelf sediments. Geochimica et Cosmochimica Acta. 58(4):1271–1284. [accessed 2016 Apr 19]. http://dx.doi.org/10.1016/0016-7037(94)90381-6.

Milliman JD. 1994. Organic matter content in U.S. Atlantic continental slope sediments: decoupling the grain-size factor. Deep-Sea Research Part II – Topical Studies in Oceanography. 41:797–808.

Morris KJ, Tyler PA, Masson DG, Huvenne VIA, Rogers AD. 2013. Distribution of cold-water corals in the Whittard Canyon, NE Atlantic Ocean. Deep-Sea Research Part II – Topical Studies in Oceanography. 92:136–144.

Obelcz J, Brothers D, Chaytor J, ten Brink U, Ross SW, Brooke S. 2014. Geomorphic characterization of four shelf-sourced submarine canyons along the US Mid-Atlantic continental margin. Deep-Sea Research Part II – Topical Studies in Oceanography Special Issue. 104:106–119.

Pisani O, Oros DR, Oyo-Ita OE, Ekpo BO, Jaffé R, Simoneit BRT. 2013. Biomarkers in surface sediments from the Cross River and estuary system, SE Nigeria: assessment of organic matter sources of natural and anthropogenic origins. Applied Geochemistry. 31:239–250.

Planquette H, Sherrell RM. 2012. Sampling for particulate trace element determination using water sampling bottles: methodology and comparison to *in situ* pumps. Limnology and Oceanography: Methods. 10:367–388.

Puig P, Palanques A, Martin J. 2014. Contemporary sediment-transport processes in submarine canyons. Annual Review of Marine Science. 6:53–77.

Raymond PA, Bauer JE. 2001. Riverine export of aged terrestrial organic matter to the North Atlantic Ocean. Nature. 409:497–500.

Reiss H, Cunze S, König K, Neumann H, Kröncke I. 2011. Species distribution modelling of marine benthos: a North Sea case study. Marine Ecology Progress Series. 442:71–86.

Richter TO, van der Gaast S, Koster B, Vaars A, Gieles R, de Stigter HC, De Haas H, van Weering TCE. 2006. The Avaatech XRF core scanner: technical description and applications to NE Atlantic sediments. Geological Society, London, Special Publications. 267:39–50.

Ryan JP, Yoder JA, Cornillon PC. 1999. Enhanced chlorophyll at the shelfbreak of the Mid-Atlantic Bight and Georges Bank during the spring transition. Limnology and Oceanography. 44:1–11.

Scher HD, Delaney ML. 2010. Breaking the glass ceiling for high resolution Nd isotope records in early Cenozoic paleoceanography. Chemical Geology. 269:329–338.

Schmidt S, de Stigter HC, van Weering TCE. 2001. Enhanced short-term sediment deposition within the Nazaré Canyon, North-East Atlantic. Marine Geology. 173:55–67.

Stuiver M, Polach HA. 1977. Discussion reporting of 14C data. Radiocarbon. 19:355–363.

Talling PJ, Paull CK, Piper DJW. 2013. How are subaqueous sediment density flows triggered, what is their internal structure and how does it evolve? Direct observations from monitoring of active flows. Earth Science Reviews. 125:244–287.

Valentine PC, Uzmann JR, Cooper RA. 1980. Geology and biology of oceanographer submarine canyon. Marine Geology. 38:283–312.

van Weering CE., Weaver PPE. 2007. Canyon Processes, an introduction. Marine Geology 246:65-68.

Vogel JS, Southon JE, Nelson DE. 1987. Catalyst and binder effects in the use of filamentous graphite for AMS. Nuclear Instruments and Methods in Physics Research Section B: Beam Interactions with Materials and Atoms. 29:50–56.

Walsh JJ, Biscaye PE, Csanady GT. 1988. The 1983–1984 shelf edge exchange processes. SEEP-I experiment – hypotheses and highlights. Continental Shelf Research. 8:435–456.

Wei CL, Rowe GT, Hubbard GF, Scheltema AH, Wilson GDF, Petrescu I, Foster JM, Wicksten MK, Chen M, Davenport R, Soliman Y, Wang YN. 2010. Bathymetric zonation of deep-sea macrofauna in relation to export of surface phytoplankton production. Marine Ecology Progress Series. 399:1–14.

Xu Y, Chant R, Gong D, Castelao R, Glenn S, Schofield O. 2011. Seasonal variability of chlorophyll-*a* in the Mid-Atlantic Bight. Continental Shelf Research. 31:1640–1650.

This page intentionally left blank

CHAPTER 7. PREDICTIVE HABITAT MODELING

Andrew J. Davies, Craig M. Robertson, Michael Rhode, Maya Wolff, Steve W. Ross, and Sandra D. Brooke

7.1 INTRODUCTION

Continental slopes are generally characterized as inclined seabed, and in many regions they display heterogeneous landscapes with a wide range of features (Levin and Dayton 2009). These features include canyons, which act as conduits for sediment and organic matter transport from the shelf to the deep sea. Submarine canyons are locally dramatic, widespread topographic features with steep walls extending up to 200 miles long and 3 miles deep, connecting shelf-margins to deep ocean basins (De Leo et al. 2010). Their importance has continued to emerge over the last two decades as research effort has increased, but understanding the physical parameters within the canyon system has been identified as a key area of research (Levin et al. 2001). Physical parameters are important drivers that will yield insight into habitat variability and ecological patterns and fundamental functioning of canyon systems. Canyons are considered as potential hotspots and refugia of biodiversity where dynamic physical processes characterized by complex patterns of hydrology, sediment transport, and accumulation are all acknowledged as important ecological drivers in the deep ocean (Levin et al. 2001, Garcia et al. 2008, De Leo et al. 2010).

7.1.1 Corals in Canyons

The awareness of deepsea corals (also called cold-water corals) and their ecological significance has grown rapidly over the last two decades and can be attributed to the ever-increasing pressures on deepwater resources (Levin et al. 2001, Glover and Smith 2003, Davies et al. 2007). Deepsea corals, belonging to the phylum Cnidaria, are azooxanthellate and generally found in waters more than 200 m deep. The most studied major taxonomic group within the phylum is Scleractinia (hard corals). Some species can form large biogenic structures and Octocorallia (soft corals), which are generally solitary non-reef forming, but many do form structures. The term reef often is used to describe a submerged structure rising from the surrounding seafloor that forms a hazard to shipping (Wood, 1999). However, as most records of deepsea coral species originate from deep waters, the term reef often is applied to structures formed by deepsea coral frameworks that alter sediment deposition, provide complex structural habitat, and are subject to the processes of growth and (bio)erosion (Rogers, 1999; Roberts et al., 2006).

Canyons have been suggested to act as natural refugia for deepsea corals and other marine life (Stiles et al. 2007, Menot et al. 2010) due to the heterogeneous terrain, restricting access. Of all studied physical factors, suitable seabed substrate, water temperature, and salinity are obvious requirements that must be met to enable the colonization and growth of deepsea corals (Freiwald et al. 2004, Freiwald and Roberts 2005, Roberts et al. 2009). Most deepsea coral species require exposed hard substrate for larval settlement and growth (Wilson 1979), and since many corals are long-lived, the areas that they inhabit must be stable over long time periods. The best known of these deepsea corals is *Lophelia pertusa*, the main reef-forming scleractinian coral known to date. Considerable effort has been made in defining the environmental drivers that control *L. pertusa* distribution. Although these parameters are relatively well known, especially when compared with other deepsea coral species, the processes governing reproduction, larval dispersal, recruitment, and settlement are still not completely understood (Davies et al. 2008, Davies and Guinotte 2011).

In general, deepsea coral ecosystems commonly occur from water depths of approximately 200 m to depths where cold deepwater masses with temperature regimes of <4 °C prevail (Freiwald et al. 2004). The majority of reefs formed by scleractinian deepsea corals are found at water depths between 200 and 400 m (down to 800 m in some parts of the northeast Atlantic Ocean) in regions that contain hard

substrate, temperatures between 4 °C and 12 °C and oceanic salinities of approximately 35 (Dullo et al. 2008, Davies and Guinotte 2011). Recently, studies in the northeast Atlantic have established a positive relationship between strong near-bottom currents, often generated by internal waves, and the presence of deepsea corals (Davies et al. 2009). Coral growth is driven by tidal variability, benthic boundary resuspension, hydraulic jumps, and turbidity events that enhance the delivery of organic matter to deepsea corals from surface waters or enriched shelf areas (White et al. 2005, Davies et al. 2009). Although the habitat requirements of reef-forming scleractinians are well described, other equally important coral taxa are far less well studied. Octocorals are also found throughout much of the ocean (Yesson et al. 2012) and, like *L. pertusa*, have defined tolerances for temperature, salinity, and other environmental variables that make them candidates for species distribution modeling.

7.1.2 Mid-Atlantic Bight Canyons

Submarine canyons are a major feature along the northeast United States continental shelf and slope extending from Cape Hatteras to as far north as Atlantic Canada. The MAB region contains a high diversity of unique habitats within a relatively small area, some recognized as rich coral habitats (Hecker et al. 1980, Hecker 1990). Undoubtedly, these productive deepsea coral ecosystems are important areas for the diversity of the MAB region, but very little was known about the coral communities prior to this study (**Chapter 2**). The MAB can generally be described as a gently sloping, sandy and relatively flat continental shelf (a seaward slope of 0.16° to 0.33°) that extends from southern New England to Cape Hatteras, North Carolina (Kelling and Stanley 1970). It is fairly homogenous, but with exceptions at the shelf break (including canyons), the Hudson Shelf Valley, and areas of glacially rafted hard bottom (Packer et al. 2007). The main topographic features within the MAB are the Hudson Shelf Valley and Canyon and several other major canyons including the Norfolk and Baltimore canyons, which are the focus of this study (Hecker et al. 1980, Packer et al. 2007, Bachman et al. 2012).

Rich communities of sessile benthic suspension feeders have been observed on the steep walls of canyons in the MAB region (Hecker et al. 1980). Hard rocky substrate with suitable current conditions for deepsea coral community development are limited and patchy within the MAB canyons, with the majority of benthic habitat being soft sediment or compacted clays that are unsuitable for many coral species. This produces discontinuous distributions of many species throughout the canyons. However, given limited study in the area, the distribution of deepsea corals is not well known along the slope and canyons of the MAB (Hecker et al. 1980, Watling and Auster 2005, Packer et al. 2007). Until recently (2014), focused deepsea coral studies were rare in the region, which contrasts with the adjacent northeast U.S. (Packer et al. 2007) and southeast U.S. (Ross and Nizinski 2007) regions. Available information indicates that the MAB canyon corals are dominated by octocorals, solitary Scleractinia, and anemones (Cairns 1981, Packer et al. 2007) rather than the large concentrations of reef-forming scleractinian corals that dominate coral communities within the southeast U.S. and Gulf of Mexico (Brooke and Schroeder 2007, Ross and Nizinski 2007).

7.1.3 Baltimore Canyon – Environmental Setting and Coral Observations

Baltimore Canyon is positioned on the continental shelf, 125 km southeast of the entrance to Delaware Bay (**Figure 7-1)**. One of the larger submarine canyons along the east coast of the United States, this canyon has a typical V-shaped cross-section, cutting 17 km into the continental shelf. The width of the canyon is 3 km near the head increasing to 8 km wide at the shelf break (**Figure 7-1a**, Gardner 1989). No existing channel is evident from the canyon head across the shelf to Delaware Bay. The canyon axis curves southward at its head before turning eastward with increasing depth, until it is oriented due east-west at 3,000 m (Hecker et al. 1983). At approximately 1,500 m, the canyon turns into a leveed system as it merges with the upper continental rise without a distinct fan formation (Gardner 1989, Obelcz et al. 2014). The canyon extends 25 km between its head and 1,500 m depth as it merges onto the abyssal plain.

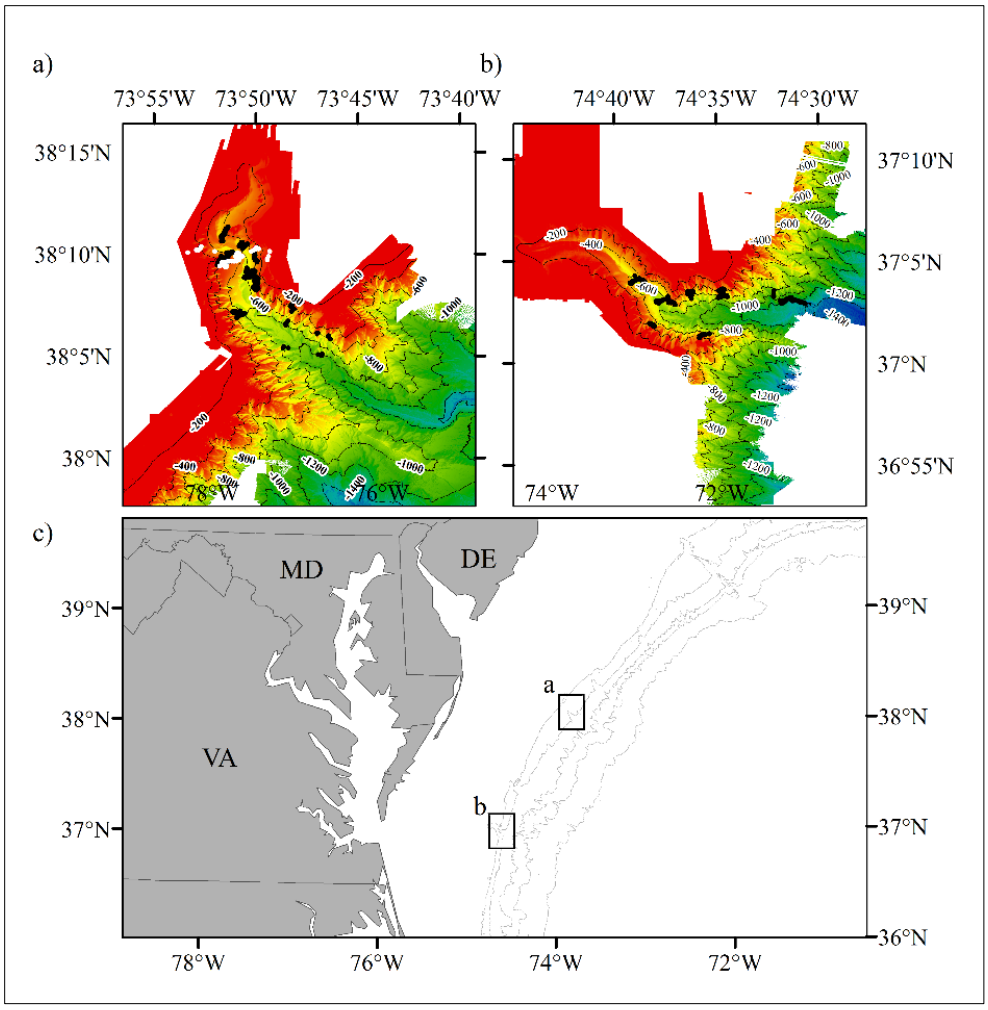

Figure 7-1. Canyons of interest and extent of analyses. a) Baltimore Canyon, b) Norfolk Canyon (both with 200 m contours), and c) overview with bathymetric contours at 100, 600, 1,600, 2,000, and 2,500 m. Black points in both panels represent modern coral observations and white points in panel a) represent historical coral observations from the 1980s and 1990s.

In contrast to the MAB region, Baltimore Canyon has now been relatively well surveyed for corals through several recent studies (including this study and other National Oceanic and Atmospheric Administration [NOAA] explorations). Corals are locally abundant in Baltimore Canyon, which is known as an important coral area (Bachman et al. 2012). Historical accounts of coral and substrate distribution in the canyon have been documented from several studies conducted in the early 1980s on the functioning of MAB canyons (Hecker et al. 1980, Hecker et al. 1983, Hecker 1990, Bachman et al. 2012). Some of the historical identifications have now been renamed or the identifications changed (**Chapter 2**). Hecker et al. (1983) reported that the coral population of Baltimore Canyon tended to be less abundant and diverse than in canyons farther north, although both hard and soft coral species were reported at most depths.

Because many of the coral species are restricted to hard substrates, it was suggested that this finding largely reflects the fact that Baltimore Canyon generally exhibits limited exposed hard substrate. One particular note by Hecker et al. (1983) was that the dominant coral species in Baltimore Canyon was a small unidentified white sea pen, a major component of the shallow water faunal assemblage that occurs on soft sediment in water depths ranging from 100 to 300 m. Highest abundances were reported from 200 to 300 m and they occurred in dense patches on the east wall of the canyon. At depths below 400 m,

where the canyon axis constricts and bends, outcrops and talus blocks are exposed. On exposed substrate, several coral species that only grow on hard substrates were observed by Hecker et al. (1980), including *Paragorgia arborea, Acanthogorgia armata, Primnoa resedaeformis, Acanthogorgia grandiflora,* and the soft corals *Capnella florida* (accepted name: *Duva florida*) and *Anthomastus agassizii* (Hecker et al. 1980, Hecker et al. 1983).

Most MAB octocoral species fall under the order Alcyonacea, characterized as mostly erect large colony-forming species apart from some stoloniferous or encrusting forms (Cairns et al. 2012). Skeletal elements are variable and may comprise sparse to abundant calcareous spines called sclerites, scattered throughout the colony or, in the case of many gorgonians, they may be constructed of scleroprotein, which provides the colony structure and rigidity (Cairns et al. 2012). The scleractinian hard corals recorded in the region mostly belong to the family *Caryophyllidae.* Most are solitary genera such as *Dasmosmilia, Desmophyllum,* and *Flabellum,* although colonial genera have recently been reported. The solitary stony coral *Dasmosmilia lymani* occurred in dense localized patches near the head of Baltimore Canyon, but it was absent from many other areas in the canyon (Hecker et al. 1983). Other stony corals previously found included *Flabellum* sp. and *Desmophyllum dianthus,* with other types of corals recorded in low abundances (*Eunephthya florida* accepted as *Duva florida; Acanthogorgia armata; Paragorgia arborea;* and *Primnoa resedaeformis*) (Hecker et al. 1983). The 2012 and 2013 sampling cruises conducted during the Atlantic Deepwater Canyons study successfully documented the first records of *L. pertusa* in Baltimore Canyon (Brooke and Ross 2014).

7.1.4 Norfolk Canyon – Environmental Setting and Coral Observations

Norfolk Canyon is one of the major canyons in the MAB region and is located 45 km south of Chesapeake Bay, Maryland and 130 km south of Baltimore Canyon (Forde 1981). Norfolk Canyon has a sigmoidal shape running in a west-to-east orientation cutting 23 km into the shelf (**Figure 7-1b**). Like other canyons, a broad axial bend (9 to 10 km) seaward of the canyon head, coincides with a change from relatively smooth downward slope in the upper reaches of the canyon axis, to a more rugose axial profile in the lower reaches of the canyon (Obelcz et al. 2014). The canyon morphology has been attributed to episodic erosive and depositional forces and fluvial sources such as the Susquehana River-Chesapeake Bay drainage system (Forde 1981, Colman and Halka 1990), although the palaeo-shelf channel is poorly established (Knebel and Spiker 1977). Various degrees of steep wall habitat are found in the lower reaches, parallel to the axis of the canyon, and are dissected by numerous tributaries (**Figure 7-1b**). The rim morphology and subbottom stratigraphy in Norfolk Canyon are more distinct than in other MAB canyons, showing short escarpments and steep indentations (Obelcz et al. 2014).

Norfolk Canyon is the second most studied of the MAB canyons, and much of the early biological information comes from geological submersible dives conducted in the late 1970s and early 1980s (Hecker et al. 1983, Rhoads and Hecker 1994). These early reports explored the northeast wall of the canyon and reported massive sandstone cliffs with large numbers of octocorals such as *E. florida (D. floria)* and *P. arborea*, anemones, ophiuroids, crinoids, and a variety of other taxa. The cliffs were also inhabited by the gorgonian *A. armata*. The deeper parts of Norfolk Canyon were explored during the 1978 ALVIN dives (Malahoff et al. 1982), but the only outcrops inhabited by corals were on the north wall between 1,050 and 1,198 m. Mudstone outcrops in this region supported numerous *A. armata* and *D. cristigalli (D. dianthus)* as well as a few individuals of an unidentified coral. Soft substrate deeper in the canyon supported sea pens (*Pennatula* sp.) and the small octocoral *Anthomastus grandifloris*. As in Baltimore Canyon, research cruises conducted during the Atlantic Deepwater Canyons study also documented the first records of live *Lophelia pertusa* in Norfolk Canyon (Brooke and Ross 2014).

7.1.5 Habitat Suitability Modeling

Identifying areas of suitable habitat for organisms in areas that are fundamentally understudied is difficult, but is becoming increasingly important from a conservation and management perspective

(Ardron et al. 2008). Given that the deep ocean is one of the most poorly studied areas on earth with the total area surveyed by scientists estimated at <0.01% (van den Hove and Moreau 2007), it is important that a full array of tools be used. One tool that is increasingly being adopted in the deep sea is habitat suitability modeling (Davies et al. 2008, Guinan et al. 2009a, Davies and Guinotte 2011, Yesson et al. 2012). Contingent on the target species and available data, relatively simple mathematical models can be used at a variety of different scales to identify areas that may contain suitable habitat for deepsea species. The scale of these mathematical models can range from local (Guinan et al. 2009a) to regional (Leverette and Metaxas 2005, Davies et al. 2008, Howell et al. 2011) and global (Tittensor et al. 2009, Davies and Guinotte 2011, Yesson et al. 2012).

The major driver for the proliferation of modeling efforts in the deep ocean has been the development of presence-only approaches. Early studies used Ecological Niche Factor Analysis (ENFA) (Hirzel et al. 2002), with newer studies adopting higher performance approaches such as Maxent (Phillips et al. 2006). In principle, all habitat suitability models take a similar approach, where they combine spatial data on the environment with some knowledge of where an organism has been recorded to calculate a niche. The models extrapolate the niche by estimating a complete response curve to the partial distribution. This estimate can then be applied to the input environmental data to predict how suitable a location is which may not contain a species observation (Vierod et al. 2014). Given that this type of modeling is an emerging field, especially for the deep sea, it is widely accepted that the models may differ from the reality in the field (see critiques in Davies et al. 2008, Davies and Guinotte 2011, Vierod et al. 2014). One of the major shifts occurring in habitat suitability modeling is a move toward exploiting high-quality datasets, including those derived from multibeam echo-sounder data (e.g., Rengstorf et al. 2012, Ross and Howell 2013). Although these data require significant financial investment to collect and interpret, it is often the best available data that can be attained for deepsea habitats. When supplemented with other high-quality data such as from underwater vehicles and accurately positioned cameras, significant benefits can be achieved from fitting models based on multibeam data (Rengstorf et al. 2012). However, before it can be used in habitat suitability models, multibeam data (depth and the intensity of signal return), needs to be converted into descriptor variables that bear some reflection of the geophysical or hydrodynamic variability in an area (Wilson et al. 2007).

The ocean floor is highly variable, with features extending over a wide range of spatial scales from the very small (tens of meters, such as banks or small highs) to the very large (hundreds of kilometers, such as seamounts, canyons, or shelves). These features can be extracted from bathymetry and used to provide descriptor variables that can assist in understanding species linkages within their surrounding environment (e.g., Henry et al. 2010). When extracted from multibeam bathymetry, terrain variables can represent the seafloor at very high resolutions, sometimes at meter or even submeter accuracy. Given this, it is no surprise that these terrain variables are increasingly being used by studies modeling species distributions (Wilson et al. 2007, Dolan et al. 2008, Guinan et al. 2009a, Guinan et al. 2009b, Rengstorf et al. 2012). Studies generally extract similar sets of variables, ranging from slope calculations to complex feature extraction such as bathymetric position indices, which aim to describe features that are above or below a given area (Wright et al. 2005).

In this study, we focused on the Baltimore and Norfolk canyons, areas for which high-resolution multibeam bathymetry was collected in advance of the observational data collected during the Atlantic Deepwater Canyon study. As a real-world preliminary test, we aimed to build initial habitat suitability models for deepsea corals based on high-resolution multibeam data and historical observations that were taken several decades ago. This was to test the hypothesis that historical observation data could provide insight into modern day coral distribution and may assist in the design of future observation surveys. Subsequently, we conducted visual surveys of the two canyons using remotely operated vehicles (ROVs) equipped with high-resolution cameras and accurate spatial positioning systems, and we used observations from these surveys to construct modern day habitat suitability models for each canyon.

7.2 METHODOLOGY

7.2.1 Multibeam Bathymetry

Multibeam bathymetry for the Baltimore and Norfolk canyons on the eastern shelf break of the United States was collected during the 2011 mapping cruise with the NOAA ship *Nancy Foster* (**Chapter 3** for survey details). The multibeam system consisted of a hull-mounted 95 kHz Simrad EM1002 with 111 beams per ping over a maximum coverage sector of 150° (equidistant beam spacing). Survey speed was approximately 6 to 10 knots. Raw data were tidally and sound velocity corrected and post-processed using version 7 of CARIS HIPS and SIPS to produce bathymetry at 10 m resolution on the x and y axes, and binned to 1 m on the z axis for both canyons. Multibeam was projected into a universal transverse Mercator (UTM) coordinate system (Zone 18 North) with all analysis conducted within this projected space in ArcGIS 10.

7.2.2 Terrain Variables

Multiple terrain attributes were extracted from the multibeam data for each canyon (**Table 7-1**) following several techniques and algorithms described in Wilson et al. (2007). Before the terrain variables were calculated, the multibeam bathymetry was initially smoothed by taking the mean of a 3 × 3 cell moving window centered around each individual pixel for some analyses to produce more spatially coherent terrain variability variables. Aspect, defined as the direction of maximum slope, was calculated from smoothed bathymetry with the DEM Tools 4-cell method built into DEM Tools version 2.1.375 (Jenness 2012) and was converted to continuous radians following Wilson et al. (2007). The bathymetric position index (BPI) is an approach to determine topographical features based on their relative position within a neighborhood. BPI can be calculated over fine or broad scales to capture smaller or larger terrain features, respectively. Positive values indicate relief such as peaks and crests; negative values indicate troughs or depressions. BPI was calculated from smoothed bathymetry using annulus settings of 1 and 25 (scale factor of 250) for the broad scale and 1 and 5 (scale factor 50) for the fine scale (Wright et al. 2005).

Curvature describes terrain features and may provide an indication of how water would interact with the terrain. All curvature variables were calculated using DEM Tools (4-cell approach) and smoothed bathymetry (Jenness 2012). Profile curvature describes how concave features (positive values) could cause flow deceleration as it flows over a point, and convex features (negative values) indicate areas where flow could accelerate (Jenness 2012). Positive plan and tangential curvatures describe convex features that might cause water flow to diverge around a point, and negative values describe areas where flow would converge (Jenness 2012). Slope was calculated with the DEM Tools 4-cell method. Slope is defined as the gradient in the direction of the maximum slope and is expressed in degrees and percent. Several slope derivatives also were calculated. Slope variability, calculated from the difference between the minimum and maximum slope within a 10-cell circular radius in ArcGIS version 10, provided a measure of relative relief (Ruszkiczay-Rüdiger et al. 2009).

Standard deviation of slope and elevation were derived following Grohmann et al. (2011); these variables highlight areas with large changes in both variables. Standard deviation of slope was found to be particularly sensitive to sudden changes in slope (Grohmann et al. 2011). Values were calculated using a 10 × 10 cell-moving window. Rugosity, terrain ruggedness index (TRI), roughness, and vector ruggedness measure (VRM) all generally describe the variability of the seafloor relief (Wilson et al. 2007). Rugosity is defined as the ratio of the surface area to the planar area across a neighborhood of a central pixel (Jenness 2012). TRM is defined as the mean difference between a central pixel and its surrounding cells and roughness which is the largest intercell difference of a central pixel and its surrounding cell (Wilson et al. 2007). VRM was adapted from a method first proposed by Hobson (1972) and may represent terrain ruggedness better than current ruggedness indices, such as TRI, by reducing the

influence of slope (Sappington et al. 2007). Two moving windows were used with 3 × 3 cells and 21 × 21 cells to capture variability at different spatial scales. Examples of terrain variables that were generated are shown in **Figures 7-2** and **7-3** for Baltimore and Norfolk canyons, respectively

Table 7-1. Geophysical and environmental variables created from multibeam and other environmental data for Baltimore and Norfolk canyons. "−" indicates no unit or a dimensionless value. * indicates layer upscaled as per Davies and Guinotte (2011).

Variable Name	Unit	Name	Reference
Bathymetry Variables			
Bathymetry	m	depth	Vol II: Appendix A
Bathymetry smoothed	m	depth3x3_fm	Derived
Standard deviation of elevation	−	stdev_elev	Grohmann et al. (2011)
Terrain Variables – Orientation			
Aspect	Degree	aspect	Jenness (2012)
Aspect – eastness	−	aspect_e	Wilson et al. (2007)
Aspect – northness	−	aspect_n	Wilson et al. (2007)
Terrain Variables – Curvature			
Curvature – profile	−	prof_curv	Jenness (2012)
Curvature – plan	−	plan_curv	Jenness (2012)
Curvature – tangential	−	tang_curv	Jenness (2012)
Terrain Variables – Slope			
Slope	Degrees	slope	Jenness (2012)
Slope in percent	Percent	slope_perc	Jenness (2012)
Slope variability	−	slopevar	Ruszkiczay-Rüdiger et al. (2009)
Standard deviation of slope	−	stdev_slope	Grohmann et al. (2011)
Terrain Variables – Topographic Position			
Bathymetric position index − broad	−	bpi_broad	Wright et al. (2005)
Bathymetric position index − fine	−	bpi_fine	Wright et al. (2005)
Topographic position index	−	tpi	Wilson et al. (2007)
Terrain Variables – Variability			
Roughness	−	roughness	Wilson et al. (2007)
Rugosity	−	rugosity	Jenness (2012)
Terrain ruggedness index	−	tri	Wilson et al. (2007)
Terrain ruggedness index − Riley	−	tri_riley	Riley et al. (1999)
Vector ruggedness measure	−	vrm_3x3	Sappington et al. (2007)
	−	vrm_21x21	Sappington et al. (2007)
Carbonate Chemistry Variables			
Omega aragonite*	Ω_{ARAG}	arag_stein	Steinacher et al. (2009)
Omega aragonite*	Ω_{ARAG}	arag_orr	Orr et al. (2005)
Omega calcite*	Ω_{CALC}	calc_stein	Steinacher et al. (2009)
Omega calcite*	Ω_{CALC}	calc_orr	Orr et al. (2005)
Chemical Variables			
Nitrate*	μmol L^{-1}	nit	Garcia et al. (2006b)
Phosphate*	μmol L^{-1}	phos	Garcia et al. (2006b)
Salinity*	pss	sal	Boyer et al. (2005)
Silicate*	μmoL L^{-1}	sil	Garcia et al. (2006b)
Oxygen Variables			
Apparent oxygen utilization*	mol O_2 m^{-3}	aoxu	Garcia et al. (2006b)
Dissolved oxygen*	mL L^{-1}	diso2	Garcia et al.,(2006a)
Percent oxygen saturation*	% O_2^S	pos	Garcia et al. (2006b)
Other Variables			
Temperature*	°C	temp	Boyer et al. (2005)

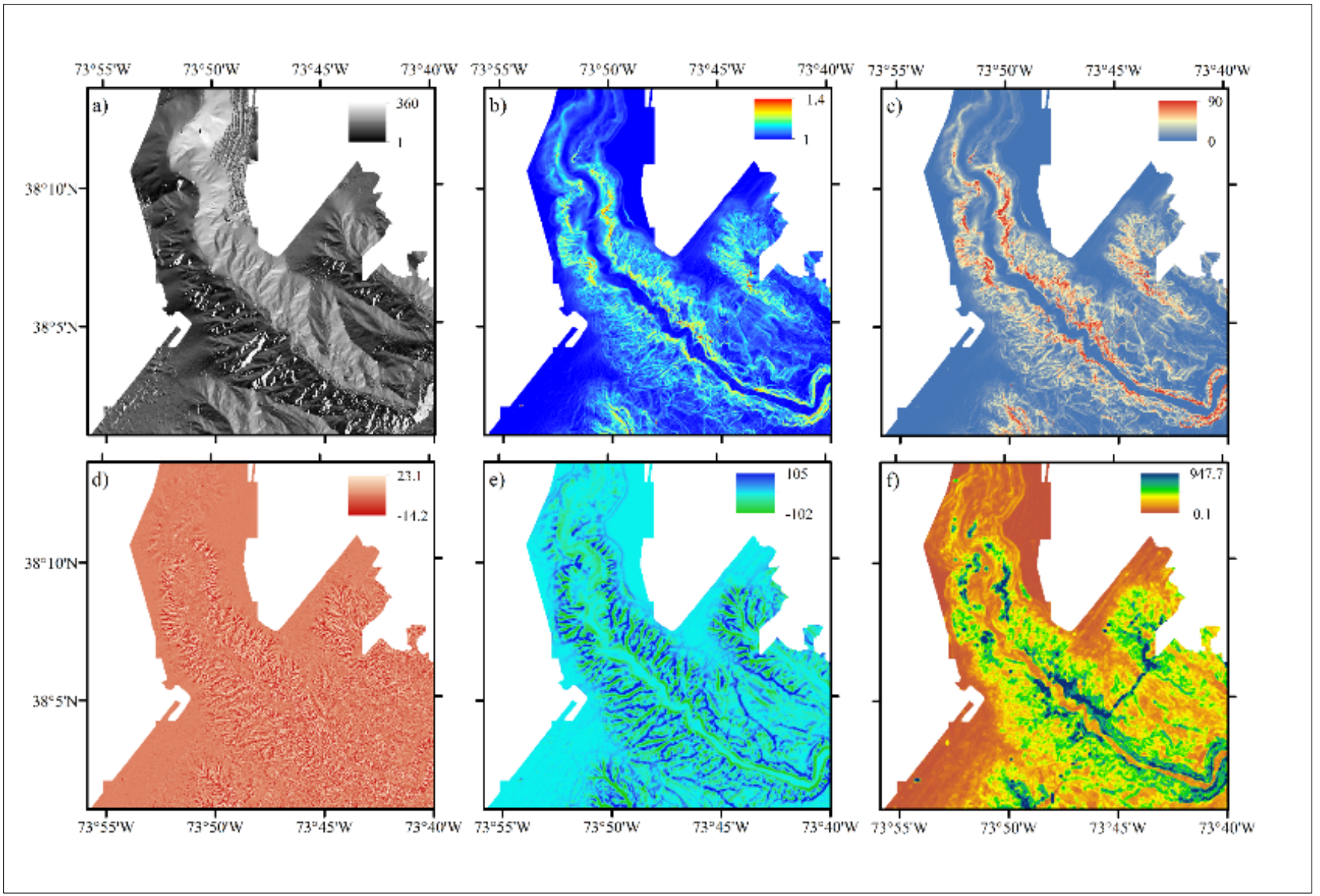

Figure 7-2. Terrain variables generated from multibeam bathymetry from Baltimore Canyon. a) aspect, b) rugosity, c) slope, d) tangential curvature, e) bathymetric position index – broad, f) slope variability. See **Table 7-1** for further details on each variable.

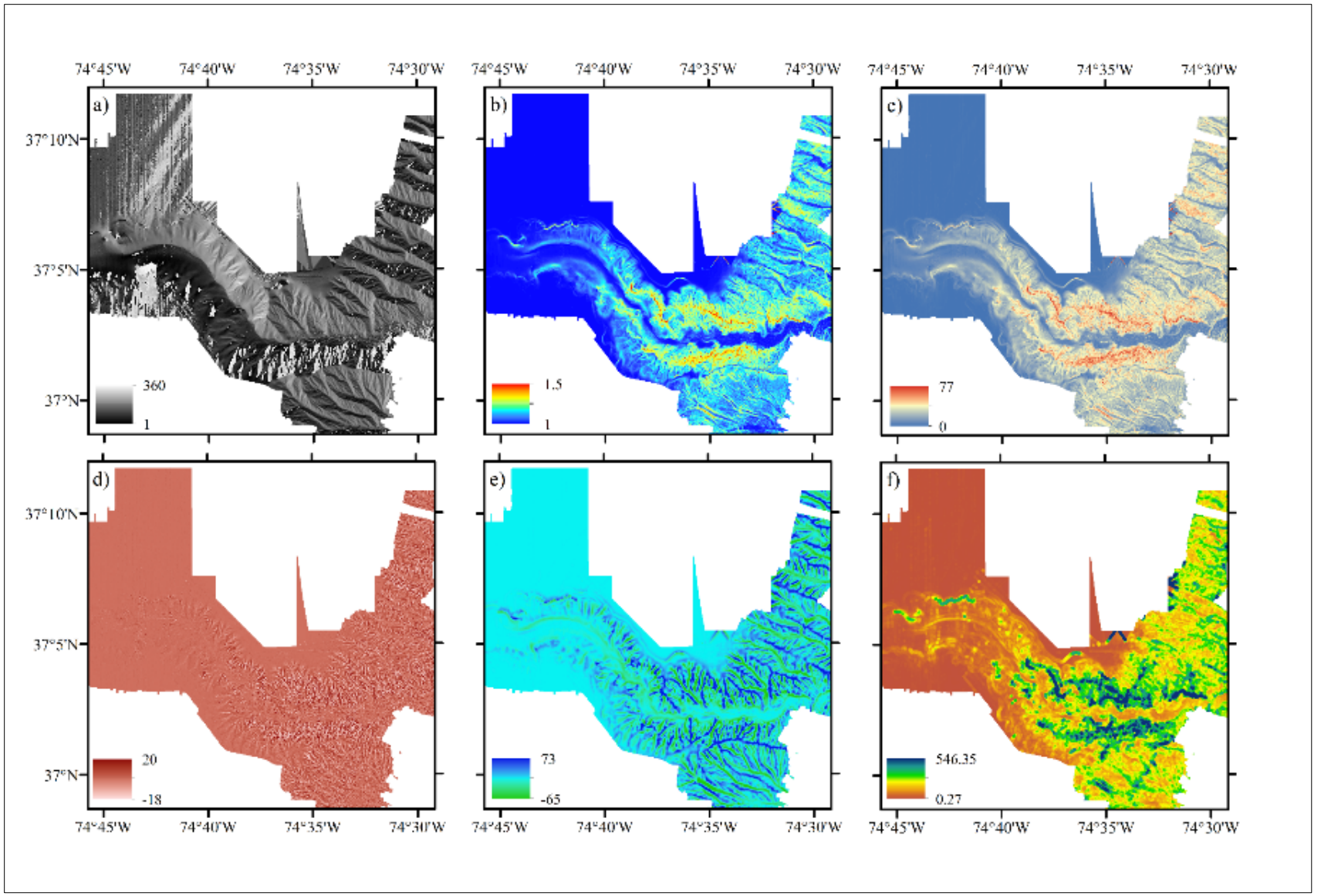

Figure 7-3 Terrain variables generated from multibeam bathymetry from Norfolk Canyon. a) aspect, b) rugosity, c) slope, d) tangential curvature, e) bathymetric position index – broad, f) slope variability. See **Table 7-1** for further details on each variable.

7.2.3 Environmental Variables

The variable up-scaling approach presented by Davies and Guinotte (2011) was used to create environmental variables (**Table 7-1**). This approach takes gridded layers of varying initial spatial scales (i.e., 0.25 ° for temperature and salinity; 1 ° for all other gridded variables) of an environmental variable and drapes them over bathymetry to provide an indication of conditions near the seabed; it has been proven to work well over global and regional scales (Davies and Guinotte 2011, Guinotte and Davies 2014). In this report, these environmental layers must be considered as representing general conditions in the MAB region because the highly variable topography of the canyon will not yield a good prediction of environmental variables at such a small spatial scale. Limited profiles of the water column were collected with a Sea-Bird Electronics, Inc. SBE 911*plus* conductivity-temperature-depth profiler in Baltimore and Norfolk canyons (bottom reading was at approximately 15 m above bottom). Data were collected for turbidity (Seapoint, formazin turbidity units), dissolved oxygen (mg L^{-1}), depth (m), conductivity (Siemens m^{-1}), temperature (°C), salinity, and pH (see **Chapter 5** and **Vol II: Appendix A**). These casts were compared using Pearson correlation with the modeled layers to determine their relative accuracy for certain areas of the seafloor (**Figure 7-4**). Local data such as those from benthic landers, moorings, and CTD casts (**Chapters 5** and **6**) are not suitable for use in such a geospatial model because the data are not continuous throughout the canyon.

7.2.4 Variable Groupings

Each terrain and environmental variable was assigned to one of several broad variable groups (**Table 7-1**). These groups were designed to identify and segregate variables that were likely to be highly correlated as they were created using similar calculations or were built upon data of similar origin (Yesson et al. 2012). These groupings included the following environmental variables:

- **Bathymetry** variables created from the multibeam data or derived explicitly from it, such as standard deviation of elevation;
- **Orientation** terrain variables focused on aspect calculations;
- **Curvature** terrain variables that explain how water would behave when traveling over an elevation surface;
- **Slope** terrain variables, including slope-derived variables such as slope variability and standard deviation of slope;
- **Topographic position** terrain variables that explain the location of features relative to surroundings;
- **Variability** terrain variables that show how rugose terrain is within given areas;
- **Carbonate chemistry** variables extracted from global models including those for aragonite and calcite (Orr et al. 2005, Steinacher et al. 2009);
- **Chemical** variables that included nutrient and salinity datasets from World Ocean Atlas;
- **Oxygen** variables, focusing on oxygen measurements from World Ocean Atlas; and
- **Temperature**, which was retained in a group of its own due to its high importance for marine organisms.

Each variable within a variable grouping was assessed for correlation with other variables using 10,000 randomly spaced points throughout the model extent; the correlation matrices (using Pearson correlation) are shown in **Figures 7-5** and **7-6** for Baltimore and Norfolk canyons, respectively. Most variables were independent of each other (Pearson correlation <0.75), allowing their use in models without causing inflation in variable importance (Vierod et al. 2014).

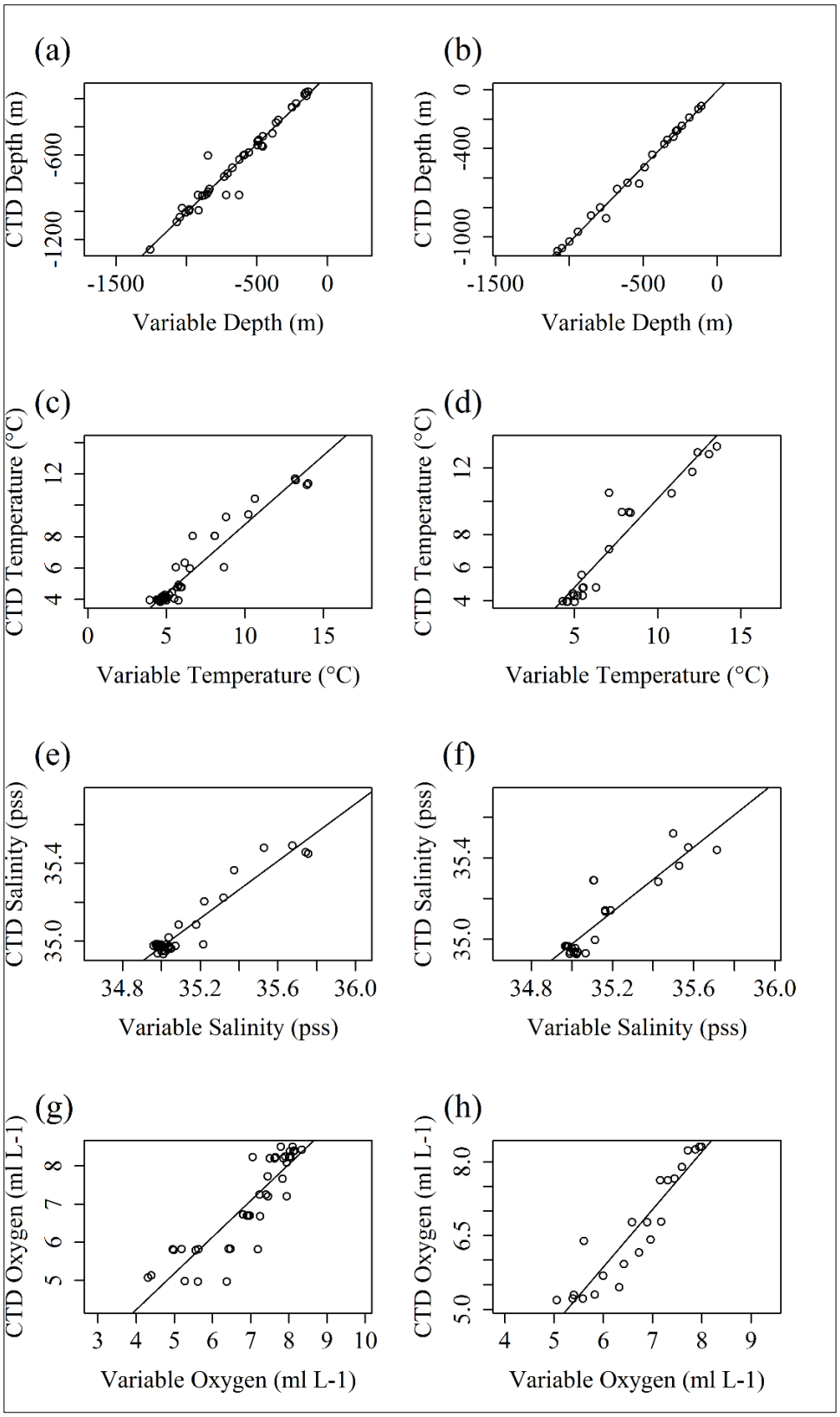

Figure 7-4. Environmental variable performance compared with independent CTD data. a) depth (*n* = 17), b) temperature (*n* = 17), c) dissolved oxygen (*n* = 12), and d) salinity (*n* = 17).

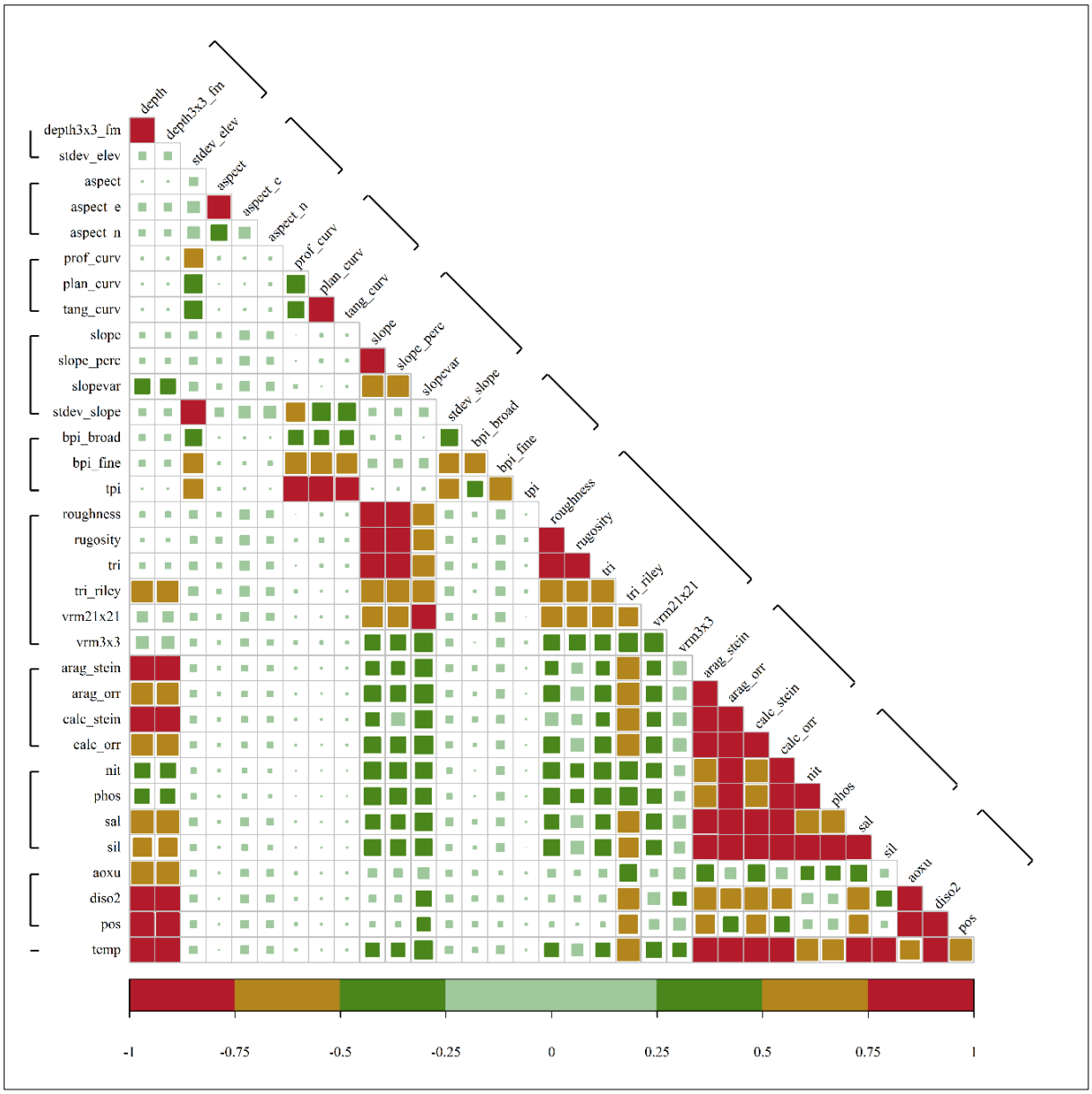

Figure 7-5. Correlations between variables for Baltimore Canyon (based on 10,000 randomly placed points). The matrix indicates global correlations between variables. The legend at the base of the plot shows the correlation strength; lower correlations are shown by a smaller square for clarity. Values in red (correlation >0.75) indicate the cut off whereby variables were considered co-linear.

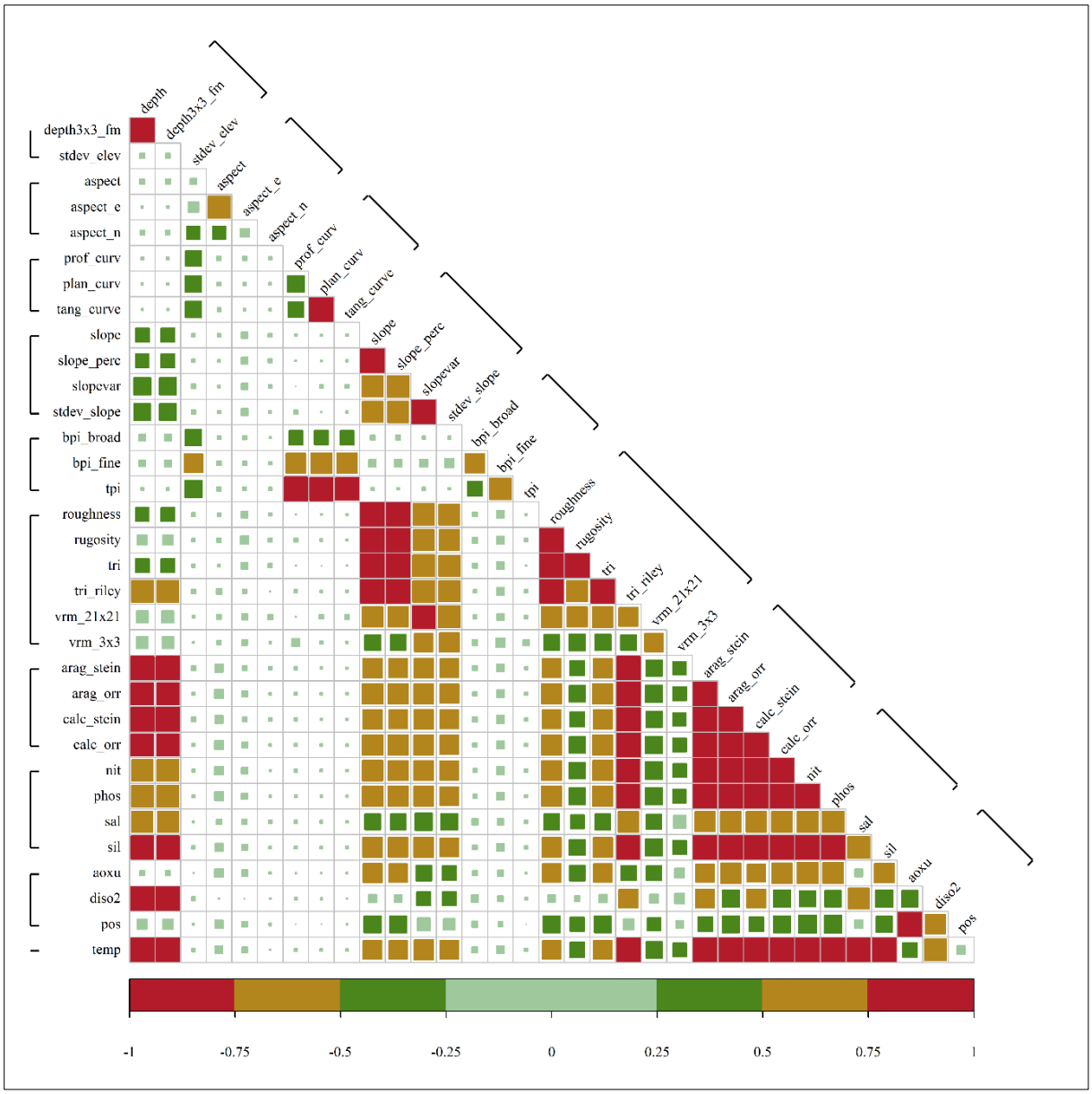

Figure 7-6. Correlations between variables for Norfolk Canyon (based on 10,000 randomly placed points). The matrix indicates global correlations between variables. The legend at the base of the plot shows the correlation strength; lower correlations are shown by a smaller square for clarity. Values in red (correlation >0.75) indicate the cut off whereby variables were considered co-linear.

7.2.5 Historical Observation Data

Historical submersible dives were conducted in the 1980s and 1990s using the submersible *Johnson Sea Link* in Baltimore Canyon (Hecker et al. 1983). The historical dives were analyzed for habitat and benthic fauna as a precursor to the 2012 and 2013 sampling cruises for this study (**Chapter 2**). In total, 58 positive position fixes of the submarine were recovered from the archive material (five dives in total: 1,084, 1,085, 1,087, 1,089, and 1,090) (**Figure 7-1a**). The habitat at these positions was described using the Southeastern United States Deep-Sea Corals (SEADESC) Initiative classification scheme (Partyka et al. 2007) in addition to some canyon-specific habitat types (**Chapter 2**). To maximize available data for historical modeling, broad groups from SEADESC were used to create 45 fauna records and 28 hard ground records, with categories including "Rock/ledges with attached fauna," "Pavement with attached fauna," and "Consolidated sediment with attached fauna." It was not possible to fully determine the exact level of positioning error within this historical dataset due to the low accuracy of the submersible navigation equipment, conversion errors from Loran C (used during the dives) to geographic information system (GPS), and the general lack of position fixes reported in the video. Therefore, each location point was converted with a 50 m radius buffer, which was selected to encapsulate, to some extent, the unknown positioning error from the historical data. The mean of raster cells that fell within the buffer was calculated (~70 to 80) for each terrain and environmental variable (**Table 7-1**).

7.2.6 Modern Observation Data

Modern observations of Baltimore and Norfolk canyons were taken with ROVs during the 2012 and 2013 sampling cruises (**Figure 7-1**; see **Chapter 3** for ROV dive locations). The 2012 observations were collected using the University of Connecticut's *Kraken 2*, a Max Rover class science-configured vehicle capable of operating to 1,000 m (although most dives were shallower than 800 m). Position was continuously recorded using an ORE Trackpoint II ultrashort baseline (USBL) tracking system combined with a Winfrog integrated navigation system. Visual data was mostly collected using a Kongsberg OE14-502 high definition (HD) video camera. Two parallel lasers mounted 10 cm apart were turned on most of the time when using the video camera. Multiple dives were undertaken, usually with different objectives, but most dives emphasized bottom transecting, collecting and photographing specimens on or near the bottom. During each ROV dive, audio annotations of dive activities were made directly on video, and these were used to extract the locations of coral features in conjunction with positioning data from the USBL. Observations during the 2013 sampling cruise were collected using the Woods Hole Oceanographic Institution's *Jason II*, capable of diving to depths of 6,500 m. The ROV navigation system was a Sonardyne Ranger USBL that recorded position of the vehicle every few seconds and allowed the pilots and scientists to observe the ROV track in near real-time. Visual information was collected from an Insite Mini-ZeusHD video camera with two parallel lasers mounted 10 cm apart. ROV protocol was similar to the 2012 dives, with an emphasis on bottom transecting.

From the modern observations, 9 taxonomic groups for Baltimore Canyon and 11 for Norfolk Canyon had sufficient observations for analysis. Some species had only limited numbers of observations within the canyons and therefore were not used. Individual observations used in each model were first filtered to remove spatial duplicates (records that fell within the same grid cell) to eliminate spatial bias that can inflate the importance of certain variables (Vierod et al. 2014). In Baltimore Canyon, these duplicates included the octocorals *Anthothela grandiflora* (*n* = 76), *Paragorgia arborea* (*n* = 342), *Paramuricea grandis* (*n* = 28), and *Primnoa resedaeformis* (*n* = 149) as well as the scleractinian species *Desmosphyllum dianthus* (*n* = 7). Hard substrate (*n* = 1,230), groups of all octocorals (*n* = 377) and scleractinian coral (*n* = 21) observations were also modeled. In Norfolk Canyon, the octocorals *Acanthogorgia aspera* (*n* = 92), the genus *Anthomastus* (*n* = 9), *Anthothela grandiflora* (*n* = 90), *Paragorgia arborea* (*n* = 282), and *Primnoa resedaeformis* (*n* = 89) and the scleractinians *Desmophyllum dianthus* (*n* = 84), *Lophelia pertusa* (*n* = 27), and *Solenosmilia variabilis* (*n* = 17) were modeled. As in

Baltimore Canyon, groupings of hard substrate (n = 539), octocorals (n = 424), and scleractinians (n = 109) were modeled.

7.2.7 Species Distribution Models

Historical and modern data were used in the presence-only modeling approach Maxent. This approach assumes that the best way to determine an unknown distribution is to maximize entropy based on constraints derived from environmental variables (Phillips et al. 2006). Maxent generally outperforms other presence-only approaches such as Ecological Niche Factor Analysis and has become widely used in mapping within data-poor environments (Elith et al. 2006, Tittensor et al. 2009, Vierod et al. 2014). The algorithm is supplied within a user-friendly Java software package (Maxent version 3.3.3k). The default model parameters were used as they have performed well in other studies (a convergent threshold of 1 to 5, maximum iteration value of 500, and a regularisation multiplier of 1; Phillips and Dudík 2008).

Two sets of models were run for each species:

1. Initial variable selection with all variables following Yesson et al. (2012), whereby all variables were assessed for explanatory power on their own, and in models run with all variables minus one to assess for variables that contain significant information not present in other variables (variable that decreased the gain the most when omitted).
2. The highest scoring variable within each variable group was selected for specific model runs; groups that did not have a variable scoring >0.7 area under curve (AUC) were omitted from the run. Variables that decreased the gain the most were retained even if they were not the highest scoring variable in a variable group (however, on rare occasions where covariation was high between these variables [Pearson correlation >0.75], the decreased gain variable was retained and the highest scoring variable omitted). This mechanism attempted to reduce the number of covariates used in the models, a complication that hinders many predictive modeling efforts, especially when variables are based on similar input data such as terrain variables from multibeam or derived variables developed using models, i.e., carbonate chemistry parameters (Davies and Guinotte 2011).

To assess the contribution and, therefore, the importance of each variable in the model, a jack-knifing procedure was used. This approach compares the contribution of each variable (when absent from the model) with a second model that included the variable. To assess the overall model performance, a threshold-independent procedure was used that included a receiver operating characteristic (ROC) curve with AUC for the test localities. Usually, this is run on a single model using a random selection of locations as a test dataset; however, recently cross-validation metrics have been used (Tittensor et al. 2009) and are now included within Maxent. To calculate the AUC for each model, the presence data was randomly partitioned into 10 datasets, each containing 90% training (used to build a model) and 10% test (used to validate the model) records, and the mean AUC was taken from the 10 model runs. With presence-only data, Phillips et al. (2006) define the AUC statistic as the probability that a presence site is ranked above a random background site. In this situation, AUC scores of 0.5 indicate that the discrimination of the model is no better than random and the maximum AUC value is 1. The final habitat suitability maps were produced by applying the calculated models to all cells in the study region, using a logistic link function to yield a habitat suitability index between 0 and 1 (Phillips and Dudík 2008).

7.3 RESULTS

7.3.1 Generation of Terrain and Environmental Variables

Twenty-one terrain variables were extracted from the multibeam bathymetry for each canyon, and they clearly show variation in topographic complexity and terrain (see **Table 7-1** for generated variables, **Figures 7-2** and **7-3**). From these variables, most of the heterogeneous substrate was found on the walls of both canyons. In Baltimore Canyon, heterogeneous terrain was found throughout the depth profile of the canyon, with particular concentration in the mid and deeper areas. In Norfolk Canyon, deeper areas of the canyon held concentrations of heterogeneous seafloor. In all variables, the presence of the canyon thalweg was obvious, appearing as a flat homogenous area running down the middle of each canyon. Due to the paucity of video data transitioning across multiple canyon features and the relatively coarse bathymetry (10 m^2) in relation to visual observations, no truthing of terrain features was conducted in this study.

In addition to terrain variables, several environmental datasets including chemical variables, carbonate chemistry, oxygen, and temperature were also collected (**Table 7-1**). The fit of several of these environmental variables was assessed with CTD casts taken in the area during the 2011 mapping cruise. In total, there were four variables assessed, including the sounding depth (Pearson correlation, $r = 0.99$, $n = 17$), temperature (Pearson correlation, $r = 0.99$, $n = 17$), salinity (Pearson correlation, $r = 0.99$, $n = 17$), and dissolved oxygen (Pearson correlation, $r = 0.93$, $n = 12$) (**Figure 7-4**). All variables showed close correlations with the CTD data, except for dissolved oxygen, which had a nonlinear relationship between the environmental variable and the observed data. This was likely an artifact of the 1° input data used in the variable creation process. Hence, models based on this variable must be treated with some caution.

7.3.2 Environmental Requirements

In Baltimore Canyon, most octocorals were found in the shallower reaches that were sampled, between 300 and 600 m (**Figure 7-7**). *Paramuricea grandis,* in particular, was found within a narrow depth range between 350 and 450 m. In contrast, *Paragorgia arborea* and *Primnoa resedaeformis* had a broader range, extending down to 600 m (there were, however, some outlying observations of *P. arborea* at 800 m, the maximum dive depth). In the model variable selection process, depth was among the most important for all octocoral genera, with AUC scores >0.945. The most important terrain variables were different for each genus, but most consistent were slope and variability of slope as well as rugosity and vector ruggedness measure (21 × 21 cell window). These indicate that most octocorals were found on heterogeneous terrain, in areas with intermediate slopes (**Table 7-2**). With respect to variability of slope variable, most species demonstrated a unimodal fit (*Anthothela grandiflora, P. arborea,* and *P. resedaeformis*). However, *P. grandis* had a bimodal distribution, possibly an artifact of the low number of observations, but this species was found on both flat and sloping habitats. For the coarse continuous environmental variables, calcite was important for all species except *P. resedaeformis,* which scored marginally higher for the aragonite (calcite and aragonite variables were very closely correlated and likely contained similar data). In chemical variables, phosphate scored highest for *Anthothela grandiflora, P. arborea,* and *P. grandis*. However, silicate was most important for *P. resedaeformis*. These variables did not appear to discriminate well for octocorals with fairly consistent ranges. Oxygen variables were also important for all species, scoring AUC values >0.91; however, the exact variable was different among species. *Anthothela grandiflora* and *P. arborea* scored highest for the variable apparent oxygen utilization, *P. grandis* with percent oxygen saturation, and *P. resedaeformis* with dissolved oxygen. As with chemical variables, the response for oxygen variables was fairly consistent across variables, with dissolved oxygen concentrations ranging between 3 and 5 mg L^{-1} for all octocoral genera. Temperature was also important with AUC >0.934 for all genera and showed broad temperature responses for *Anthothela grandiflora, P. arborea,* and *P. resedaeformis* (5 °C to 8 °C). The limited

number of *P. grandis* records appeared restricted to warmer waters (~8 °C), indicative of the shallower areas where this coral was found. The limited numbers of observations of both scleractinian coral species make any interpretation of their habitat requirement within the canyon difficult. The seven observations of *Desmophyllum* occurred in the deeper reaches of the canyon (~700 m), within colder waters (4 °C) that had a higher level of oxygen (5 mg L^{-1}) (**Figure 7-7**).

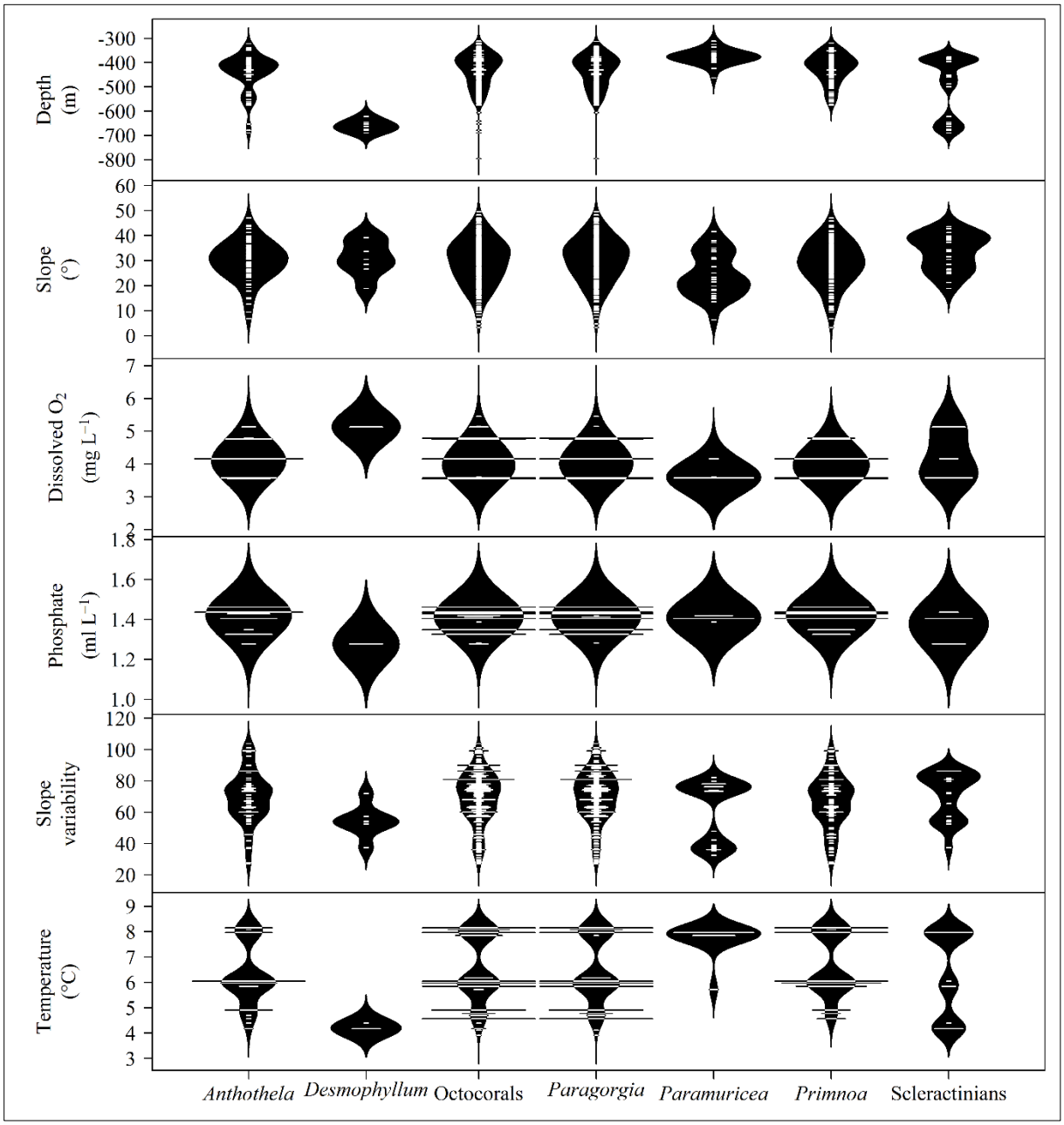

Figure 7-7. Beanplots of species environmental requirements from Baltimore Canyon. The black 'beans' represent frequency distribution profiles; wider sections indicate higher sample density; and white horizontal bars show frequency distribution relative to the overall sample number for each bean (Kampstra 2008).

Table 7-2. Variable selection for each species or group in Baltimore Canyon using test area under curve (AUC) values from a Maxent model based on a single variable. Values in bold indicate highest scoring per group and were used in the final model. Underlined values indicate the variable that decreased the model gain the most when omitted from a model with all other variables; in situations where this was not the highest scoring variable in a group, this variable was used instead of the highest scoring variable, providing the value was >0.7.

Variable	*Anthothela grandiflora*	*Desmophyllum dianthus*	Hard Substrate	Octocorals	*Paragorgia arborea*	*Paramuricea grandis*	*Primnoa resedaeformis*	Scleractinians
Bathymetry Variables								
depth	**0.953**	0.653	**0.899**	**0.943**	**0.948**	**0.974**	**0.945**	**0.911**
depth 3 × 3_fm	0.954	0.654	0.899	0.944	0.948	0.974	0.946	0.91
stdev_elev	0.516	0.64	0.521	0.587	0.595	0.525	0.54	0.5
Terrain Variables – Orientation								
aspect	0.795	0.532	0.728	0.838	0.851	0.913	0.758	0.594
aspect_e	**0.719**	0.655	**0.702**	**0.813**	**0.829**	**0.916**	**0.728**	0.426
aspect_n	0.668	0.5	0.599	0.626	0.642	0.722	0.619	0.525
Terrain Variables – Curvature								
prof_curv	**0.843**	**0.864**	0.692	0.749	0.778	0.645	0.707	**0.832**
plan_curv	0.809	0.67	0.694	**0.788**	**0.778**	0.651	0.708	0.659
tang_curv	0.746	0.801	0.685	0.771	0.75	**0.744**	**0.712**	0.55
Terrain Variables – Slope								
slope	**0.974**	**0.974**	**0.876**	**0.95**	0.928	**0.935**	**0.954**	**0.982**
slope_perc	0.974	0.974	0.876	0.95	0.928	0.935	0.954	0.982
slopevar	0.956	0.919	0.847	0.936	**0.933**	0.906	0.941	0.965
stdev_slope	0.953	0.943	0.805	0.912	0.908	0.919	0.887	0.946
Terrain Variables – Topographic Position								
bpi_broad	0.71	0.246	**0.76**	0.793	**0.814**	**0.966**	**0.79**	0.566
bpi_fine	0.798	0.418	0.684	0.752	0.771	0.822	0.76	0.651
tpi	**0.855**	0.628	0.677	**0.797**	0.77	0.778	0.746	**0.831**
Terrain Variables – Variability								
roughness	0.975	**0.982**	0.874	0.953	0.931	0.934	0.953	0.983
rugosity	**0.975**	0.974	**0.878**	**0.952**	0.932	0.935	0.955	0.982
tri	0.975	0.972	0.878	0.952	0.931	0.938	**0.956**	0.982
tri_riley	0.793	0.885	0.643	0.768	0.745	0.613	0.735	0.848
vrm_3 × 3	0.902	0.812	0.716	0.863	0.856	0.816	0.828	0.862
vrm_21 × 21	0.928	0.978	0.844	0.92	**0.933**	**0.973**	0.912	**0.991**

Table 7-2. (Continued).

Variable	*Anthothela grandiflora*	*Desmophyllum dianthus*	Hard Substrate	Octocorals	*Paragorgia arborea*	*Paramuricea grandis*	*Primnoa resedaeformis*	Scleractinians
Carbonate Chemistry Variables								
arag_stein	0.934	0.381	0.937	0.968	0.972	0.979	**0.957**	0.872
arag_orr	0.737	0.857	0.898	0.928	0.936	0.93	0.894	**0.894**
calc_stein	**0.935**	0.373	0.935	**0.97**	**0.975**	**0.981**	0.956	0.873
calc_orr	0.771	**0.881**	0.911	0.94	0.943	0.948	0.929	0.906
Chemical Variables								
nit	0.941	0.845	0.934	0.971	0.973	0.983	0.961	**0.906**
phos	**0.948**	0.807	0.936	0.97	**0.975**	**0.987**	0.966	0.89
sal	0.693	**0.947**	0.924	0.964	0.977	0.893	0.969	0.473
sil	0.942	0.813	0.933	**0.971**	0.969	0.982	**0.972**	0.894
Oxygen Variables								
aoxu	**0.917**	**0.749**	0.93	0.965	**0.973**	0.981	0.965	0.864
diso2	0.888	0.67	0.935	**0.966**	0.971	0.971	**0.971**	**0.878**
pos	0.915	0.735	0.93	0.966	0.973	**0.984**	0.948	0.846
Other Variables								
temp	**0.934**	0.361	0.936	**0.971**	**0.976**	**0.986**	**0.963**	**0.893**

In Norfolk Canyon, most observed coral species were found in the shallow reaches, between 300 and 400 m, while the genus *Anthomastus* and the species *S. variabilis* were found deeper between 1,100 and 1,400 m. *A. aspera and D. dianthus,* with bimodal distributions, were found in both shallow and deep sampled areas (**Figure 7-8**). Similar to Baltimore Canyon, depth was important in the model variable selection process, with AUC score ranging between a low of 0.761 and a high of 0.982. However, the most important variables for many species were those that incorporated slope or a metric of variability such as rugosity (**Table 7-3**). The two broad depth groupings led to species-level differences in the environmental requirements for many variables. Deeper dwelling species were found in areas with higher levels of dissolved oxygen (~6 mg L^{-1}), while shallower species had levels of ~3.5 mg L^{-1}). Shallower species were mostly found in areas with phosphate concentrations between 1.25 and 1.3 mL L^{-1} and species that occupied deeper areas with phosphate concentrations between 1.16-1.18 mL L^{-1}. Temperature also reflected these two depth clusters, with shallower species found in warmer waters of approximately 8 °C and deeper species at approximately 4°C (**Figure 7-8**). All coral species were found in areas with some degree of slope, mostly between 20° and 50°, with some high levels of slope variability **Figure 7-8**). Variable selection showed that the shallower species, such as *Anthothela grandiflora*, *L. pertusa*, *P. arborea*, and *Primnoa resedaeformis*, scored AUC >0.9 for many environmental variables (oxygen, nutrients, carbonate chemistry, and temperature) (**Table 7-3**).

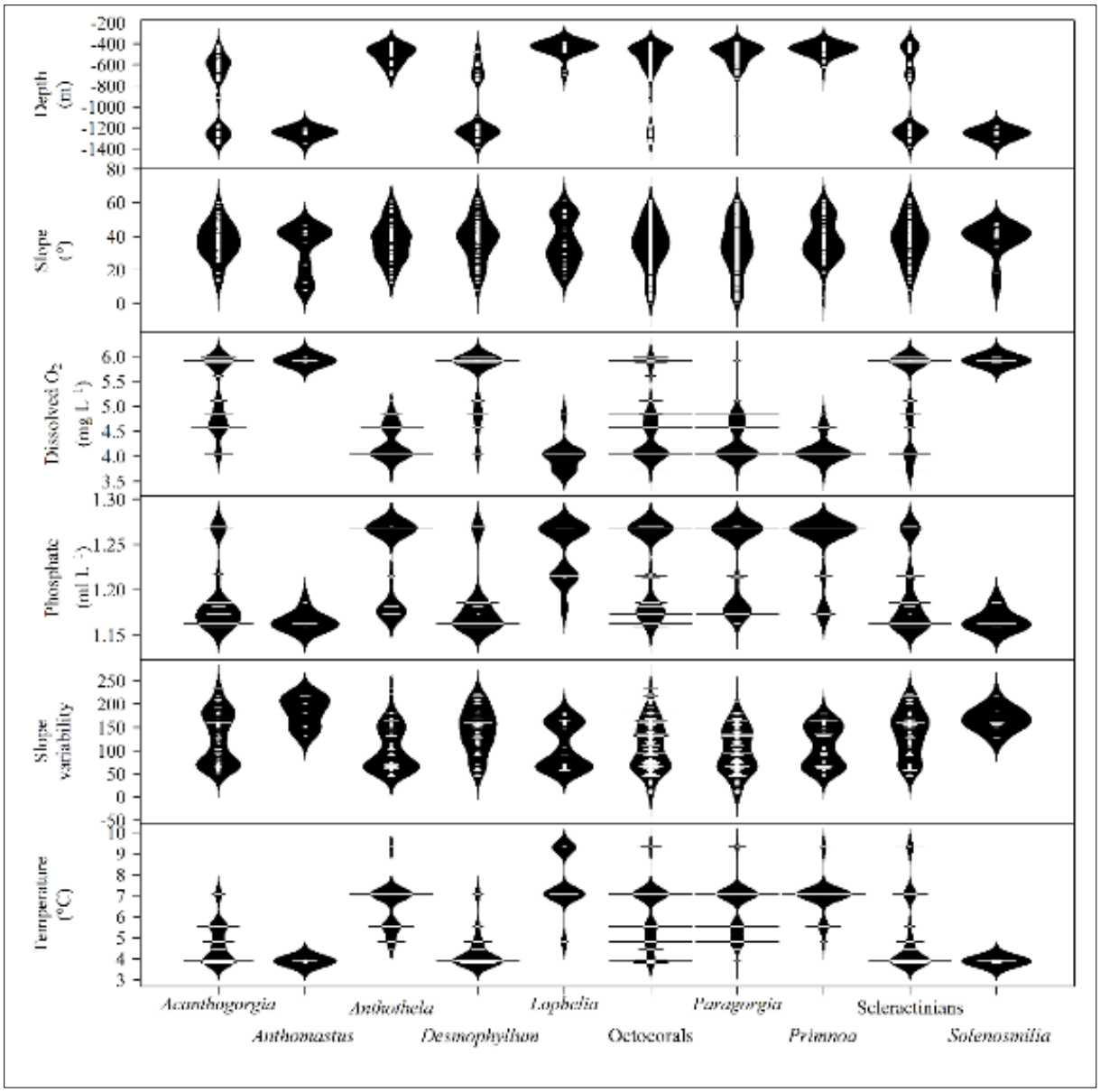

Figure 7-8. Beanplots of species environmental requirements from Norfolk Canyon. The black 'beans' represent frequency distribution profiles; wider sections indicate higher sample density; and white horizontal bars show frequency distribution relative to the overall sample number for each bean (Kampstra 2008).

Table 7-3. Variable selection for each species or group in Norfolk Canyon using test area under curve (AUC) from a Maxent model based on a single variable. Values in bold indicate highest scoring per group and were used in the final model. Underlined values indicate the variable that decreased the model gain the most when omitted from a model with all other variables; in situations where this was not the highest scoring variable in a group, this variable was used instead of the highest scoring variable, providing the value was >0.7.

Variable	*Acanthogorgia aspera*	*Anthomastus*	*Anthothela grandiflora*	*Desmophyllum dianthus*	Hard Substrate	*Lophelia pertusa*	Octocorals	*Paragorgia arborea*	*Primnoa resedaeformis*	Scleractinians	*Solenosmilia variabilis*
Bathymetry Variables											
depth	**0.889**	**0.761**	**0.959**	**0.914**	**0.898**	**0.982**	**0.926**	**0.957**	**0.978**	**0.899**	**0.968**
depth3x3_fm	0.89	0.762	0.96	0.915	0.897	0.982	0.927	0.958	0.978	0.9	0.966
stdev_elev	0.592	0.5	0.559	0.565	0.542	0.507	0.538	0.531	0.451	0.558	0.751
Terrain Variables – Orientation											
aspect	0.797	0.688	0.606	0.828	0.73	0.56	0.718	0.64	0.761	0.826	0.894
aspect_e	0.712	0.673	0.629	0.725	0.68	0.488	**0.703**	0.65	**0.739**	0.725	0.791
aspect_n	**0.772**	**0.798**	0.617	**0.817**	0.667	0.62	0.603	0.551	0.688	**0.832**	**0.83**
Terrain Variables – Curvature											
prof_curv	**0.879**	0.003	**0.839**	**0.897**	**0.843**	**0.874**	**0.809**	**0.803**	0.807	**0.888**	0.656
plan_curv	0.84	0.123	0.836	0.848	0.815	0.568	0.776	0.76	**0.808**	0.823	0.746
tang_curve	0.795	0.465	0.834	0.801	0.767	0.593	0.755	0.742	0.806	0.783	**0.797**
Terrain Variables – Slope											
slope	0.966	0.799	**0.957**	0.966	0.931	0.965	0.9	0.909	**0.966**	0.97	0.957
slope_perc	0.966	0.799	0.957	0.966	0.931	0.965	0.9	0.911	0.966	0.97	0.957
slopevar	0.973	**0.997**	0.947	0.991	**0.946**	**0.969**	**0.929**	**0.943**	0.96	0.981	**0.997**
stdev_slope	**0.975**	0.996	0.933	**0.99**	0.934	0.911	0.905	0.931	0.935	**0.986**	0.996
Terrain Variables – Topographic Position											
bpi_broad	0.807	**0.932**	0.733	0.715	0.751	**0.794**	**0.783**	0.755	0.763	0.692	0.774
bpi_fine	0.842	0.5	0.802	0.667	0.794	0.775	0.772	0.761	0.811	0.811	**0.852**
tpi	**0.876**	0.006	**0.827**	**0.901**	**0.809**	0.692	0.777	**0.767**	**0.826**	**0.829**	0.639
Terrain Variables – Variability											
roughness	0.963	0.829	0.961	0.973	**0.939**	0.957	**0.908**	**0.917**	**0.973**	0.969	0.969
rugosity	**0.966**	0.841	**0.961**	**0.975**	0.938	0.963	0.906	0.909	0.971	**0.973**	0.978
tri	0.964	0.801	0.959	0.972	0.934	**0.964**	0.904	0.906	0.967	0.972	0.967
tri_riley	0.923	0.902	0.826	0.971	0.85	0.743	0.794	0.77	0.794	0.935	**0.984**
vrm_3x3	0.924	**0.988**	0.849	0.909	0.88	0.853	0.818	0.849	0.872	0.927	0.964
vrm_21x21	0.943	0.938	0.943	0.95	0.917	0.892	0.888	0.894	0.878	0.952	0.933
Carbonate Chemistry Variables											
arag_stein	0.859	0.741	0.96	0.86	0.907	**0.973**	0.942	**0.965**	0.975	0.852	0.722
arag_orr	0.761	0.585	0.848	**0.902**	0.87	0.853	0.926	0.946	0.888	0.844	0.598
calc_stein	**0.865**	**0.757**	**0.954**	0.862	0.903	0.971	**0.938**	0.96	**0.979**	0.857	**0.73**
calc_orr	0.845	0.655	0.825	0.895	0.895	0.853	0.929	0.948	0.891	**0.883**	0.643

Table 7-3. (Continued).

Variable	*Acanthogorgia aspera*	*Anthomastus*	*Anthothela grandiflora*	*Desmophyllum dianthus*	Hard Substrate	*Lophelia pertusa*	Octocorals	*Paragorgia arborea*	*Primnoa resedaeformis*	Scleractinians	*Solenosmilia variabilis*
Chemical Variables											
nit	0.706	0.526	**0.942**	0.833	0.874	0.947	0.919	**0.964**	**0.979**	0.63	**0.751**
phos	**0.83**	0.549	0.939	0.847	0.911	0.926	0.929	0.957	0.904	**0.837**	0.75
sal	0.703	0.595	0.768	0.635	0.924	**0.962**	**0.939**	0.948	0.874	0.749	0.585
sil	0.789	0.515	0.964	**0.858**	0.916	0.959	0.939	0.96	0.956	0.752	0.74
Oxygen Variables											
aoxu	0.691	0.542	**0.941**	0.804	0.901	0.96	0.92	0.956	**0.955**	0.746	**0.764**
diso2	**0.712**	**0.705**	0.893	**0.841**	0.906	**0.975**	0.916	0.953	0.943	**0.782**	0.716
pos	0.675	0.576	0.94	0.804	0.906	0.961	**0.921**	**0.957**	0.952	0.74	0.568
Other Variables											
temp	**0.822**	**0.735**	**0.962**	**0.88**	0.926	**0.974**	**0.941**	**0.968**	**0.974**	**0.835**	**0.728**

7.3.3 Modern Observation Model Predictions

The *a priori* variable selection procedure identified several key variables likely to influence or describe the distribution of coral species within Baltimore and Norfolk canyons that were used to model species distributions (**Tables 7-2** and **7-3**). For Baltimore Canyon, all models constructed with more than 14 records produced AUC values >0.938 that were significantly greater than that of a random prediction (0.5; Wilcoxon rank-sum test, $p < 0.01$) (**Figure 7-9** and **Appendix 7-A**, **Figures 7-A1** through **7-A8**[1]). The *a priori* variable selection process identified between 6 (hard substrate and *D. dianthus* only) and 11 variables that were likely to influence the position of coral species in the canyon. All models had high levels of training gain, indicating that the validation observations were in areas that were substantially different from background conditions (**Table 7-4**).

For Norfolk Canyon, all models constructed with more than 17 records produced AUC values >0.976 that were significantly greater than that of a random prediction (0.5; Wilcoxon rank-sum test, $p < 0.01$) (**Figure 7-10** and **Figures 7-A9** through **7-A19**). The *a priori* variable selection process for Norfolk Canyon identified between 5 (hard substrate only) and 10 variables that were likely to influence the position of coral species. All models had high levels of training gain, indicating that the validation observations were in areas that were substantially different from background conditions (**Table 7-5**). These two parameters (AUC and training gain) indicate strong performance of the models and the produced predictions fit the test data well. However, due to the low number of input points, caution must be taken when interpreting the predictions because the spatial distribution of the input points was low compared to the geographic extent of the canyon, and the general number of locality points was limited.

[1] Note: All subsequent references to figures preceded by "7-A" refer to figures in Appendix 7-A.

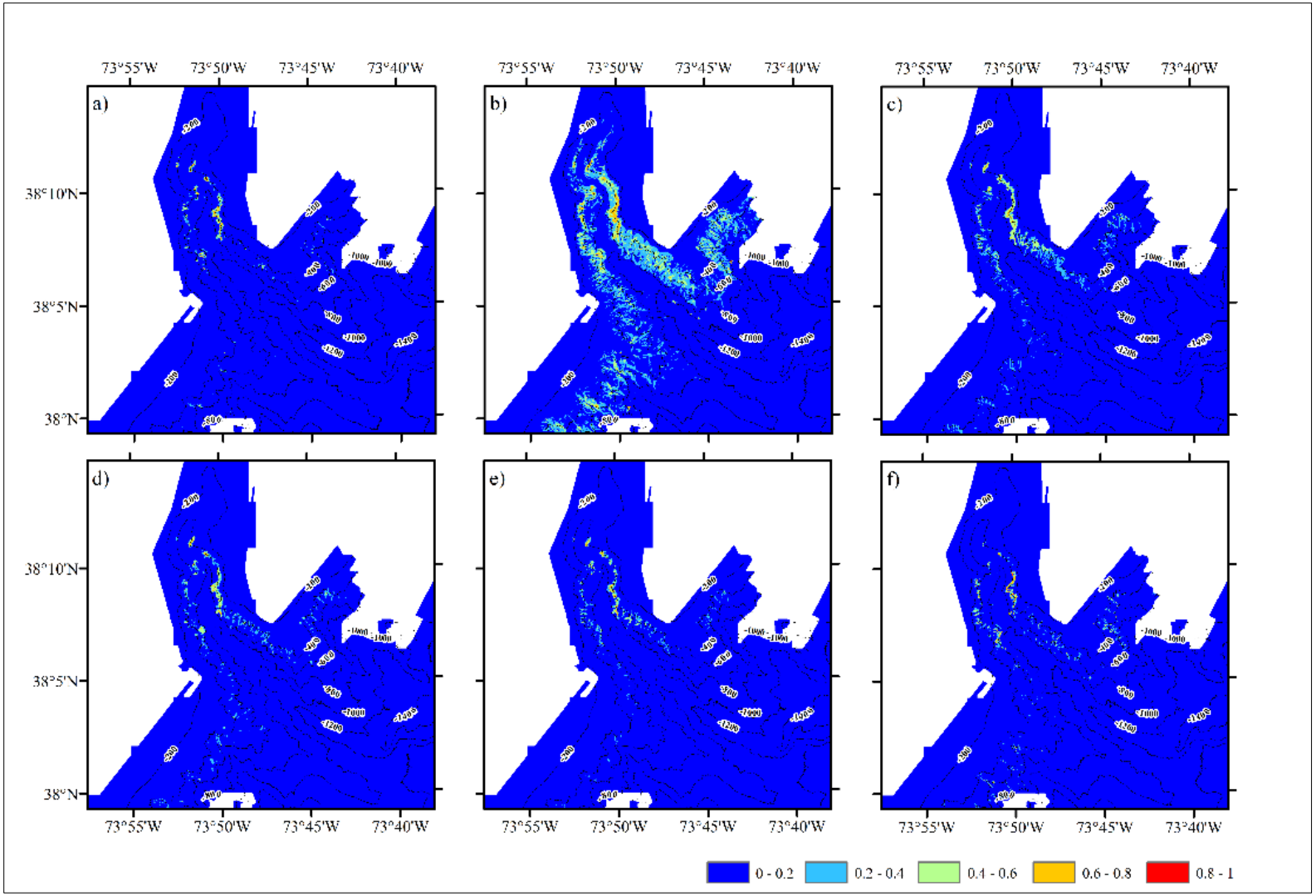

Figure 7-9. Predictive modeled outputs for specific groups and species from Baltimore Canyon. a) *Anthothela*, b) hard substrate, c) octocorals, d) *Paragorgia*, e) *Primnoa*, and f) scleractinians. See **Table 7-4** for validation statistics. Habitat suitability values presented in the legend range from blue (low habitat suitability) to red (high habitat suitability).

Table 7-4. Model evaluation statistics (means, values in parentheses are standard deviation) for the final Maxent models in Baltimore Canyon for each species or group based on previously selected variables. Certain variables (arag_stein, aspect_n, bpi_fine, tri, tri_riley and vrm_3×3) were not used by any model and are omitted from this table. "−" indicates that this variable was not used in the individual species model.

Variable	*Anthothela grandiflora*	*Desmophyllum dianthus*	Hard Substrate	Octocorals	*Paragorgia arborea*	*Paramuricea grandis*	*Primnoa resedaeformis*	Scleractinians
n Train (Test)	68.4 (7.6)	6 (1)	1,107 (123)	339.3 (37.7)	307.8 (34.2)	25.2 (2.8)	134.1 (14.9)	18.9 (2.1)
Training gain (SD)	3.984 (0.046)	4.34 (0.189)	4.34 (0.189)	2.918 (0.011)	3.098 (0.013)	4.873 (0.051)	3.709 (0.019)	4.337 (0.064)
Test AUC (SD)	0.992 (0.006)	0.998 (0.003)	0.938 (0.004)	0.98 (0.003)	0.982 (0.004)	0.997 (0.002)	0.991 (0.003)	0.996 (0.002)
aoxu	1.517 (0.04)	0.128 (0)	−	−	2.104 (0.01)	−	2.238 (0.019)	−
arag_orr	−	−	−	−	−	−	−	0.586 (0.041)
aspect_e	0.394 (0.034)	−	0.243 (0.007)	0.665 (0.011)	0.698 (0.02)	1.045 (0.096)	0.563 (0.037)	−
bpi_broad	−	−	0.48 (0.01)	−	0.703 (0.022)	2.806 (0.184)	0.91 (0.053)	−
calc_orr	−	0.934 (0)	−	−	−	−	−	−
calc_stein	1.667 (0.035)	−	−	2.098 (0.012)	2.166 (0.016)	2.3 (0.043)	2.136 (0.019)	−
depth	1.998 (0.041)	−	1.262 (0.003)	1.89 (0.01)	1.977 (0.009)	2.483 (0.038)	2.133 (0.02)	1.452 (0.046)
diso2	−	−	−	1.916 (0.011)	−	−	−	1.506 (0.065)
nit	−	−	−	−	−	−	−	1.404 (0.057)
phos	2.157 (0.065)	−	−	−	2.234 (0.011)	2.93 (0.028)	2.281 (0.014)	−
plan_curv	−	−	−	0.639 (0.022)	0.662 (0.015)	−	1.953 (0.037)	−
pos	−	−	−	−	−	3.379 (0.09)	−	−
prof_curv	0.288 (0.024)	0.19 (0.08)	−	−	−	−	−	0.325 (0.06)
roughness	−	1.809 (0.16)	−	−	−	−	−	−
rugosity	2.264 (0.055)	−	1.054 (0.009)	1.802 (0.01)	−	−	−	−
sal	−	0.448 (0.047)	−	−	−	−	−	−
sil	−	−	−	2.15 (0.016)	−	−	−	−
slope	2.248 (0.057)	1.839 (0.213)	1.03 (0.008)	1.776 (0.01)	−	1.291 (0.081)	−	2.896 (0.106)
slopevar	1.885 (0.069)	−	0.857 (0.008)	−	1.794 (0.017)	−	0.65 (0.029)	−
tang_curv	−	−	−	−	−	0.403 (0.051)	−	−
temp	1.8 (0.045)	−	−	2.109 (0.012)	2.216 (0.011)	2.731 (0.064)	2.358 (0.019)	1.156 (0.042)
tpi	−	−	−	0.57 (0.024)	−	−	−	0.85 (0.109)
vrm_21x21	−	−	−	1.537 (0.011)	1.549 (0.017)	3.115 (0.122)	1.984 (0.038)	2.648 (0.077)

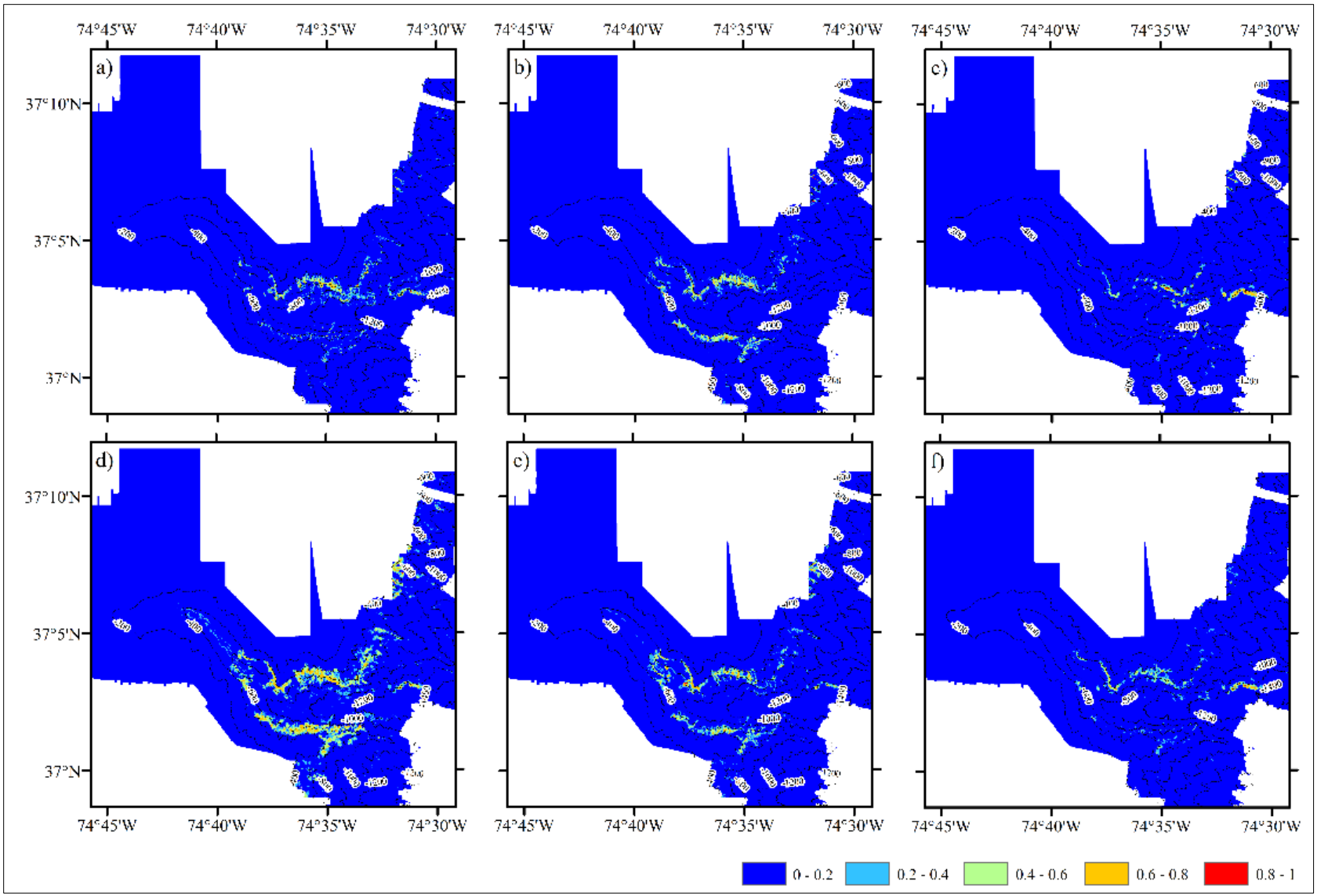

Figure 7-10. Predictive modeled outputs for specific groups and species from Norfolk Canyon. a) *Acanthogorgia*, b) *Anthothela*, c) *Desmophyllum*, d) hard substrate, e) octocorals, and f) scleractinians. See **Table 7-5** for validation statistics. Habitat suitability values presented in the legend range from blue (low habitat suitability) to red (high habitat suitability).

Table 7-5. Model evaluation statistics (means, values in parentheses are standard deviation) for the final Maxent models in Norfolk Canyon for each species or group based on previously selected variables (Variable vrm_21 × 21 was not used by any model and is omitted from this table). "−" indicates that this variable was not used in the individual species model.

Variable	*Acanthogorgia aspera*	*Anthomastus*	*Anthothela grandiflora*	*Desmophyllum dianthus*	Hard Substrate	*Lophelia pertusa*	Octocorals	*Paragorgia arborea*	*Primnoa resedaeformis*	Scleractinians	*Solenosmilia variabilis*
n Train (Test)	82.8 (9.2)	8 (1)	81 (9)	75.6 (8.4)	485.1 (53.9)	24.3 (2.7)	381.6 (42.4)	253.8 (28.2)	80.1 (8.9)	98.1 (10.9)	15.3 (1.7)
Training gain (SD)	3.446 (0.029)	5.309 (0.144)	3.526 (0.042)	3.597 (0.038)	3.597 (0.038)	4.13 (0.102)	2.569 (0.008)	2.917 (0.019)	3.913 (0.045)	3.483 (0.023)	5.665 (0.023)
Test AUC (SD)	0.989 (0.005)	0.999 (0.001)	0.99 (0.005)	0.987 (0.006)	0.965 (0.005)	0.996 (0.006)	0.976 (0.003)	0.979 (0.011)	0.989 (0.009)	0.988 (0.007)	0.999 (0.001)
aoxu	−	−	1.935 (0.046)	−	−	−	−	−	2.354 (0.019)	−	0.567 (0.012)
arag_orr	−	−	−	0.7 (0.017)	−	−	−	−	−	−	−
arag_stein	−	−	−	−	−	1.867 (0.043)	−	2.12 (0.02)	−	−	−
aspect_e	−	−	−	−	−	−	0.245 (0.012)	−	0.311 (0.048)	−	−
aspect_n	0.346 (0.02)	0.983 (0.049)	−	0.584 (0.034)	−	−	−	−	−	0.375 (0.029)	1.165 (0.022)
bpi_broad	−	0.14 (0.165)	−	−	−	0.535 (0.091)	0.473 (0.008)	−	−	−	−
bpi_fine	−	−	−	−	−	−	−	−	−	−	0.584 (0.12)
calc_orr	−	−	−	−	−	−	−	−	−	0.776 (0.018)	−
calc_stein	0.876 (0.018)	0.539 (0.025)	1.925 (0.05)	−	−	−	1.441 (0.016)	−	2.357 (0.045)	−	1.221 (0.041)
depth	0.932 (0.026)	0.386 (0.006)	2.061 (0.031)	0.985 (0.039)	1.244 (0.006)	2.168 (0.061)	1.523 (0.012)	2.028 (0.014)	2.574 (0.019)	1.075 (0.022)	1.494 (0.046)
diso2	0.495 (0.034)	0.64 (0.007)	−	0.582 (0.047)	−	1.542 (0.072)	−	−	−	0.895 (0.048)	−
nit	−	−	1.924 (0.061)	−	−	−	−	2.075 (0.023)	2.461 (0.022)	−	0.711 (0.021)
phos	0.875 (0.034)	−	−	−	−	−	−	−	−	1.066 (0.047)	−
plan_curv	−	−	−	−	−	−	−	−	0.741 (0.053)	−	−
pos	−	−	−	−	−	−	1.415 (0.018)	2.051 (0.025)	−	−	−
prof_curv	0.787 (0.06)	−	0.782 (0.036)	0.821 (0.037)	0.601 (0.014)	0.497 (0.061)	0.622 (0.021)	0.506 (0.019)	−	0.99 (0.041)	−
roughness	−	−	−	−	1.521 (0.017)	−	1.699 (0.024)	1.658 (0.026)	2.637 (0.059)	−	−
rugosity	2.555 (0.065)	−	2.496 (0.086)	2.586 (0.077)	−	−	−	−	−	2.506 (0.06)	−
sal	−	−	−	−	−	0.282 (0.046)	1.369 (0.019)	−	−	−	−
sil	−	−	−	0.435 (0.028)	−	−	−	−	−	−	−
slope	−	−	2.478 (0.087)	−	−	−	−	−	−	−	−
slopevar	2.619 (0.047)	3.213 (0.123)	2.095 (0.054)	3.045 (0.053)	1.678 (0.015)	2.251 (0.058)	1.738 (0.025)	1.685 (0.02)	2.445 (0.065)	2.837 (0.05)	4.4 (0.052)
tang_curv	−	−	−	−	−	−	−	−	−	−	0.022 (0.011)
temp	1.03 (0.037)	0.61 (0.005)	2.26 (0.043)	0.754 (0.025)	−	2.017 (0.057)	1.676 (0.018)	2.257 (0.023)	2.677 (0.017)	1.315 (0.064)	1.041 (0.032)
tpi	0.6 (0.051)	−	0.804 (0.045)	0.824 (0.048)	0.566 (0.016)	−	−	0.526 (0.021)	0.83 (0.06)	0.916 (0.045)	−
tri	−	−	−	−	−	2.43 (0.105)	−	−	−	−	−
tri_riley	−	−	−	−	−	−	−	−	−	−	3.695 (0.161)
vrm_3x3	−	0.619 (0.098)	−	−	−	1.555 (0.083)	−	−	−	−	−

Anthothela grandiflora was predicted in the mid reaches of Baltimore Canyon and was particularly constricted on the eastern flank (**Figure 7-9a**). Terrain variables had the highest training gain for this species, demonstrating they were found in sloping topography that was rugose but had relatively low gain for easterly aspect and profile curvature (**Table 7-4**). *Paragorgia arborea* and *Primnoa resedaeformis* were similarly distributed in the mid reaches and extended into some potentially deeper areas in the canyon, but the suitability was relatively low in deeper water. *P. arborea* had higher training gains for environmental variables than for terrain variables, potentially indicating a stronger link with fundamental variables that could affect physiology than with environmental variables that explain how water moves across a surface. *P. resedaeformis* was similar to *P. arborea* with higher training gains for environmental variables than for terrain variables. Gains for oxygen utilization, phosphate, and temperature were particularly high for *P. resedaeformis* (**Table 7-4**). The prediction for *Paramuricea grandis* was constrained to the eastern flank of the canyon, mostly between 200 and 600 m (**Figure 7-A6**). This species demonstrated strong training gains for both terrain (vector ruggedness measure and bathymetric position index) and environmental variables (percent oxygen saturation and temperature) (**Table 7-4**). The low number of observations for *D. dianthus* made any prediction or niche description problematic; tentatively, suitable habitat for *D. dianthus* was predicted mostly in deeper parts of the canyon, with some hotspots on highly sloping topography on both flanks (Figure 7-A2). Training gains for this species were low, with the highest gains being for roughness and slope (**Table 7-4**). This species had highest gain for phosphate, followed by slope variability and percent oxygen saturation, indicating some fundamental links but some reliance on slope for the provision of altered water flow (**Table 7-4**). The hard substrate model had the highest number of observations (n = 1,230) and was constructed using terrain variables only. The model predicted hard substrate throughout the canyon, but it was more frequent on the eastern flank; in the deeper areas, suitability decreased (**Figure 7-9b**). Training gains for this group were lower than those for coral species and were highest for depth, rugosity, and slope (**Table 7-4**).

Two areas in Norfolk Canyon were predicted to be suitable for *A. aspera*: the northern flank in mid depths between 400 and 600 m and a deeper area at approximately 1,200 m. Suitable habitat was less common on the southern flank of the canyon (**Figure 7-10a**). The training gain for *A. aspera* was strongest for two terrain variables (slope variability and rugosity), while gains were <1 for environmental variables (except for temperature) (**Table 7-5**). Suitable habitat for *Anthothela grandiflora* was found between depths of 400 and 600 m on both the northern and southern flanks of the canyon (**Figure 7-10b**). Training gain was high for both terrain and environmental variables except for profile curvature (**Table 7-5**). The abundance of observed *D. dianthus* was greater in Norfolk than in Baltimore Canyon, with an area at 600 m showing highly suitable habitat, and a further cluster of suitable habitat at approximately 1,200 m depth on the northern flank (**Figure 7-10c**). Terrain variables had the highest training gain for this species, with rugosity and slope variability having greater gains than environmental variables (**Table 7-5**). Norfolk Canyon *L. pertusa* strongly followed the 400 m depth contour, and suitable habitat was mostly predicted on the northern flank, with only limited prediction on the southern flank (**Figure 7-A11**). Training gain for *L. pertusa* in Norfolk Canyon was highest for terrain ruggedness index, slope variability, depth, and temperature, but it was low for salinity, perhaps indicating the lack of importance of this variable over small spatial scales (**Table 7-5**). Suitable habitat for *Paragorgia arborea* was mostly restricted between 400 and 600 m on both flanks of the canyon, with some suitable areas within the canyon mouth (**Figure 7-A16**). Training gain was high for most environmental variables, with the highest being for temperature, followed by percent oxygen saturation, aragonite, and depth. However, training gains for terrain variables were lower (**Table 7-5**). *Primnoa resedaeformis* was found between 400 and 600 m, but had a constrained distribution of suitable habitat limited mostly to the flanks of the canyon (**Figure 7-A17**). Training gain for *P. resedaeformis* was high in both environmental and terrain variables (temperature, roughness, and slope variability) (**Table 7-5**). The genera *Anthomastus* and species *S. variabilis* were infrequently observed hence results from models must be interpreted with caution. The distribution of *Anthomastus* was constrained between 400 and 600 m on both flanks of the canyon and training gain was high for slope variability; other variables were low (**Figure 7-A10**;

Table 7-5). Suitable habitat for *S. variabilis* was predicted between 1,200 and 1,400 m within the deeper areas of the canyon only (**Figure 7-A19**). Training gain was high for slope variability, followed by terrain ruggedness index and depth (**Table 7-5**). The distribution of hard ground was predicted to be mostly between 400 and 800 m, largely on the flanks of the canyon (**Figure 7-10d**). Training gains for hard ground were highest for slope variability, roughness, and depth (**Table 7-5**).

The predictions for records grouped into "octocorals" and "scleractinians" within each canyon demonstrated a generally broader distribution for octocorals (**Figures 7-9c** and **7-10e**) that largely encompassed the predicted suitable habitat for scleractinians (**Figures 7-9f** and **7-10f**). In Baltimore Canyon, both groups were predominantly found on the eastern flank, with a lesser extent of habitat on the western flank **(Figures 7-9c**,**f**). In Norfolk Canyon, both groups were predicted to have suitable habitat on the northern flank of the canyon, while octocorals were also predicted to have suitable habitat on the southern flank. The area of suitable habitat on the northern flank at 1,200 m depth was more pronounced for scleractinians than for octocorals (**Figures 7-10e**,**f**).

7.3.4 Historic Observation Model Predictions

The *a priori* variable selection process for the historic observations identified 10 key variables that were likely to influence or describe the distribution of fauna (9 variables) and hard ground (5 variables) in Baltimore Canyon (**Table 7-6**). For the faunal prediction, the model performed well, with an AUC of 0.927 and a training gain of 1.86. The distribution of these records was most strongly explained by silicate, calcite, depth, and temperature (**Table 7-6**). High suitability for fauna was predicted to be concentrated at the mouth of the canyon between 400 and 600 m, with limited suitable habitat predicted on the flanks, as observed in the modern prediction (**Figure 7-11b** and **Figure 7-A20**). The historic hard substrate model also performed well using the test procedure with an AUC of 0.956 and a training gain of 1.95. This prediction also followed a similar pattern to that of fauna, with extensive areas of hard substrate predicted in the mid reaches of the canyon between 400 and 600 m (**Figure 7-11c** and **Figure 7-A21**). Using the limited subset of terrain variables, the hard ground prediction was mostly explained by depth, with low training gain for terrain ruggedness index, slope variability, standard deviation of elevation, and tangential curvature (**Table 7-6**).

Table 7-6. Variable selection and model evaluation statistics for the historical fauna and hard grounds in Baltimore Canyon. Variable selection was using test area under curve (AUC) values from a Maxent model based on a single variable. Values in bold indicate highest scoring per group and were used in the final model. Underlined values indicate the variable that decreased the model gain the most when omitted from a model with all other variables; in situations where this was not the highest scoring variable in a group, this variable was used instead of the highest scoring variable providing it was >0.7.

Variable	Fauna AUC	Hard Substrate AUC	Fauna Gain	Hard Gain
n Train (Test)	–	–	40.5 (4.5)	25.2 (2.8)
Training gain (SD)	–	–	1.86 (0.08)	1.95 (0.062)
Test AUC (SD)	–	–	0.927 (0.05)	0.956 (0.026)
Bathymetry Variables				
depth	**0.903**	**0.95**	1.055 (0.031)	1.33 (0.046)
depth3x3_fm	0.902	0.95	–	–
stdev_elev	0.751	0.681	–	0.307 (0.028)
Terrain Variables – Orientation				
aspect	0.762	0.647	–	–
aspect_e	**0.818**	0.661	0.49 (0.043)	–
aspect_n	0.764	0.616	–	–

Table 7-6. (Continued).

Variable	Fauna AUC	Hard Substrate AUC	Fauna Gain	Hard Gain
Terrain Variables − Curvature				
prof_curv	**0.795**	0.594	0.046 (0.006)	−
plan_curv	0.738	0.5	−	−
tang_curv	0.757	**0.71**	−	0.013 (0.001)
Terrain Variables − Slope				
slope	0.629	0.678	−	−
slope_perc	0.628	0.677	−	−
slopevar	0.643	**0.776**	−	0.234 (0.037)
stdev_slope	**0.749**	0.718	0.212 (0.039)	−
Terrain Variables – Topographic Position				
bpi_broad	0.66	0.68	−	−
bpi_fine	0.526	0.542	−	−
tpi	**0.82**	0.563	0.055 (0.006)	−
Terrain Variables – Variability				
roughness	0.65	0.607	−	−
rugosity	0.624	0.667	−	−
tri	0.621	0.677	−	−
tri_riley	**0.836**	**0.848**	0.536 (0.042)	0.641 (0.06)
vrm_3x3	0.815	0.764	−	−
vrm_21x21	0.747	0.737	−	−
Carbonate Chemistry Variables				
arag_stein	0.922	−	−	−
arag_orr	0.501	−	−	−
calc_stein	**0.923**	−	1.075 (0.028)	−
calc_orr	0.514	−	−	−
Chemical Variables				
nit	0.884	−	−	−
phos	0.896	−	−	−
sal	0.711	−	−	−
sil	**0.906**	−	0.959 (0.07)	−
Oxygen Variables				
aoxu	**0.875**	−	0.894 (0.046)	−
diso2	0.834	−	−	−
pos	0.85	−	−	−
Other Variables				
temp	**0.903**	−	0.973 (0.045)	−

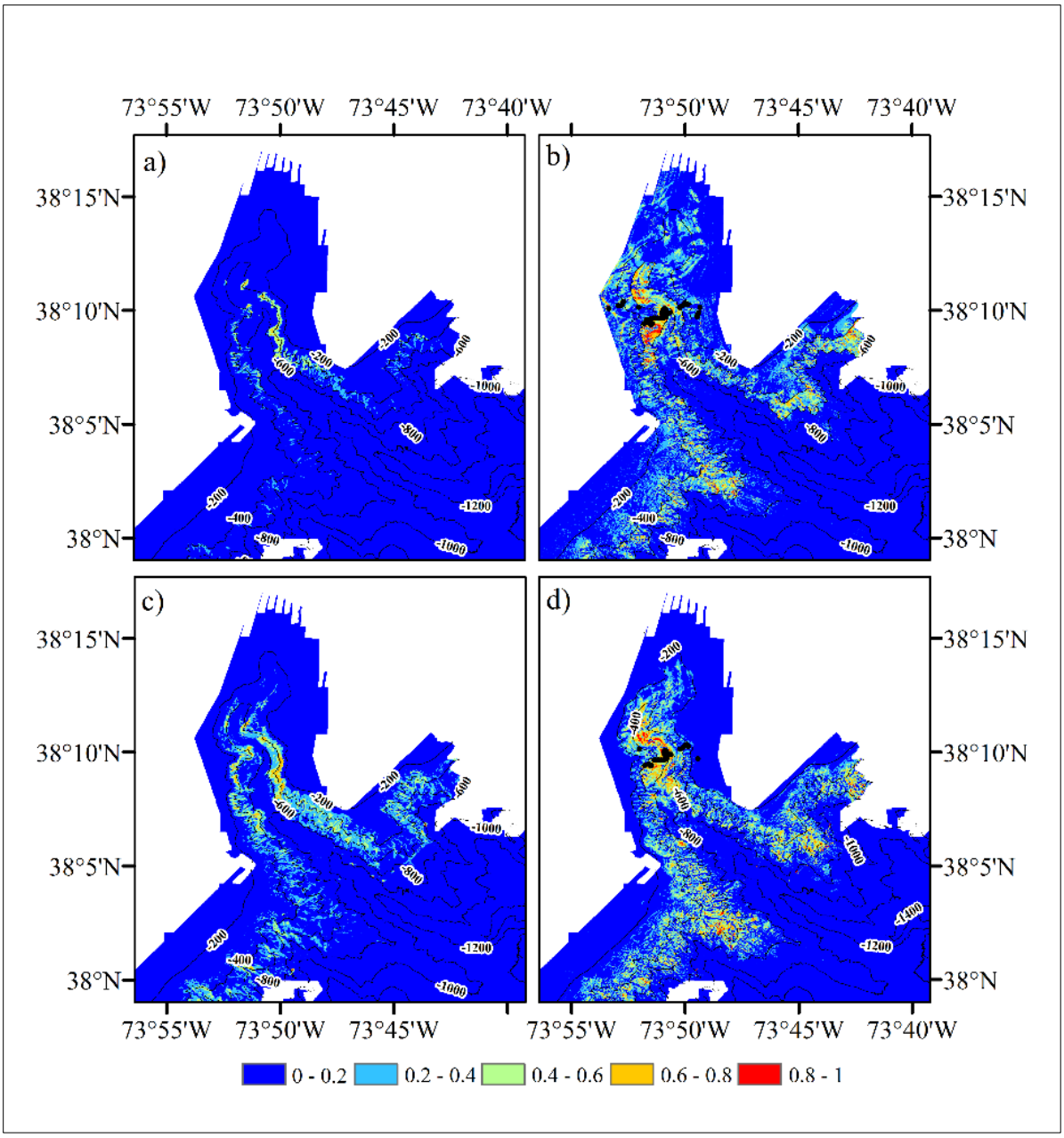

Figure 7-11. Historic versus modern predictions. For a) modern octocoral prediction, b) historic faunal model, c) modern hard ground prediction, d) historic hard ground prediction. Black dots on historic predictions (b and d) denote locations of historic observations. Habitat suitability values presented in the legend range from blue (low habitat suitability) to red (high habitat suitability). See **Tables 7-4** and **7-6** for validation statistics.

7.3.5 Comparing Historic Against Modern Predictions

The correspondence of the historic prediction with modern predictions for both hard grounds and fauna were low when comparing 10,000 randomly points placed throughout the canyon (**Figure 7-11**). Points were retained only when habitat suitability values for both historic and modern predictions were >0.1 (Pearson Correlation: Hard grounds: df = 913, r = -0.10, p = 0.002; Fauna: df = 172, r = -0.02, p - 0.761). However, comparing the model performance at the location of historic presences against the modern models produced acceptable AUC scores of 0.759 (0.02 SE) for fauna and 0.860 (0.02 SE) for hard grounds. Vice versa, at the location of modern presences, the modern model performance against the historic models was also acceptable with AUC scores of 0.790 (0.006 SE) for fauna and 0.820 (0.004 SE) for hard grounds.

Data compatible with most GISs are available for all modeled outputs as GeoTIFF format.

7.4 DISCUSSION

Most habitat suitability modeling studies in the deep sea have focused on broad-scale models (Davies et al. 2008, Tittensor et al. 2009, Davies and Guinotte 2011), but recently there has been increasing effort toward local-scale modeling (Guinan et al. 2009a, Guinan et al. 2009b). However, these local-scale approaches have so far required substantial survey effort prior to the generation of models (e.g., significant multibeam and visual camera surveys). In this chapter, we attempted to first model the distribution of fauna and hard grounds within a canyon using only recently collected multibeam data, coupled with archived visual information from *Johnson Sea-Link* dives conducted in the 1980s (Hecker et al. 1980; Hecker et al. 1983) as part of an exploratory effort to assist future cruise planning in Baltimore Canyon. We then modeled the distribution of fauna and hard grounds using the same multibeam data along with modern observations made during the 2012 and 2013 sampling cruises, including ROV video surveys coupled with highly accurate spatial positioning systems for Baltimore and Norfolk canyons.

7.4.1 Describing Habitats Using Terrain Variables

In this study, 21 terrain variables were generated from multibeam data (**Table 7-1**). These variables were designed to explain how variable topography was and in some situations, may have strong correspondence to, areas that could be subject to altered current speeds or could be clear of sediment, factors that are of ecological relevance (Wilson et al. 2007, Dunn and Halpin 2009, Ismail et al. 2015). Terrain variables have now become widely used, as previous studies have found strong synergies with species such as deepsea corals and sloping or variable topography in both empirical observation data (Genin et al. 1986, Jensen and Frederiksen 1992, Davies et al. 2009) and habitat suitability models (Guinan et al. 2009b, Rengstorf et al. 2012). This has held true in Baltimore and Norfolk canyons whereby slope variability (a measure of relative relief, Ruszkiczay-Rüdiger et al. 2009), slope (calculated by the 4-Cell Method, Jenness 2012) and rugosity/roughness (Wilson et al. 2007, Jenness 2012) were consistent contributors to models for most species. Terrain variables are especially valuable, as they can be generated from elevation data, such as multibeam, without placing any equipment in the water. This provides the potential for detailed prediction with relatively little effort compared with previous habitat mapping approaches. Given that multibeam allows for survey of the seafloor at resolutions that are beginning to rival those of terrestrial topographical surveys (Brown et al. 2011), there is great potential for its use in marine habitat suitability modeling, providing that some visual evidence of species distribution is available that matches the spatial scale of the data.

7.4.2 Predictions Using Historic Data

The biggest challenge with the historic modeling component of this study was the lack of high-quality observations of the seafloor, a common problem for many deepsea modeling studies (Davies et al. 2008).

Historical data were obtained from digitized video from *Johnson Sea-Link* dives undertaken in the canyon during the 1980s. However, these archived videos often did not have high-quality spatial fixes and the audio narrative was often sporadic in terms of describing locations or times that could be used to cross-reference with spatial fixes. Usable data were scarce and the lack of visual resolution in the old tapes made specific faunal identification difficult. We used SEADESC criteria, a scheme widely used to create a generic classification schema for coral habitat (Ross and Nizinski 2007). However, given the generality of the classification scheme, only two very broad criteria could be extracted for this study. Classes that contained a description of attached fauna were grouped into a "faunal" model irrespective of the organism observed, and any mention of hard substrate clear of sediment was grouped into "hard grounds." Although these models are coarse and of limited utility in determining suitable habitat at high taxonomic resolutions, they provided some indication of areas of the canyons that are likely to harbor sessile marine species and bare rock that could potentially be colonized by these species.

Based on the historic faunal model, most of the suitable habitat was predicted to occur in the shallower parts of the canyon (**Figure 7-11**). However, this likely reflects several factors. The first is the limited geographical and depth extent of the visual observations, which were clustered in the shallower parts of the canyon (**Figure 7-1a**) and did not extend below 1,000 m due to the depth limits of the submersible used in the survey. The survey essentially captured only a small part of the fauna at the site, and many records are unlikely to match those that were found deeper. A second factor is that the historic survey traversed the canyon head and spent time in areas of limited slope and hard substrate; hence, the majority of coral location points are likely to represent the white sea pen species reported extensively by Hecker et al. (1983). The third factor is that due to the limited depth range, the predictions were extrapolated widely beyond the bounds of the survey; because the niche of the observations was not fully captured, it lends to the development of predictions that remain relatively constrained within a certain depth range. This effect is amplified in deepsea models where changes in depth often lead to very large changes in other variables, especially temperature and salinity, that can be relevant for some species (Davies et al. 2008).

7.4.3 Predictions Using Modern Data

The modern model generally performed better than the historic models for Baltimore and Norfolk canyons. Modern predictions were based on a greater quantity of presence observations that were collated from surveys conducted throughout a larger area in each canyon (**Figure 7-1**, **Tables 7-4** and **7-5**). In addition, these models used observations that were obtained from accurate ROV positioning systems that allowed each observation to have a position fix, and the surveys used high-definition cameras with good lighting, allowing for detailed descriptions of the underlying geology and identification of species that were present.

The presence dataset consisted of data for nine distinct genera or species, five of which were sufficiently abundant for valid modeling (>17 occurrences). Even very limited observation data can be used by the Maxent algorithm, which demonstrates the utility of the approach for speculative modeling efforts (Pearson et al. 2007). However, the species niche is unlikely to be well represented with limited numbers of presences over small areas, and Maxent often over-predicts suitable habitat when using small presence datasets compared with other methods, so care must be taken in interpretation (Papeş and Gaubert 2007, Pearson et al. 2007).

In Baltimore Canyon, the modern model predictions consistently showed the eastern flank of the canyon to contain the majority of the suitable habitat for most species. The eastern flank contained the most rugose terrain (**Figure 7-2**), especially within the depth window of 400 to 600 m where most deepsea coral species are likely to be found (Davies and Guinotte 2011, Yesson et al. 2012). In Norfolk Canyon, there was a similar weighting of suitable habitat on the northern flank of the canyon for most species, and the northern flank also appeared to contain more rugose and sloping terrain than the southern flank. It is possible that large-scale oceanographic patterns may be interacting with the topography of the

canyon in any of the following ways: drive the development of more rugose terrain, clear mobile sediments from the area, or promote water mass characteristics that would support coral growth (Csanady et al. 1988, Csanady and Hamilton 1988, Rasmussen 2005, Dullo et al. 2008).

There have been several predictive modeling studies within this region of the Atlantic Ocean for deepsea corals. These studies, predominantly at global and regional scales, have been built using different species observations and environmental variables (Davies and Guinotte 2011, Yesson et al. 2012, Kinlan et al. 2013). In all cases, these models heavily over-predicted suitable habitat for a variety of coral groups within the Baltimore and Norfolk canyons (**Figures 7-12** and **7-13**). In contrast, the models discussed in this chapter were spatially focused into these canyons using the best available continuous environmental data in the form of high-resolution multibeam (10 m cell size). This results in spatially constrained predictions that are more likely to accurately predict where corals are likely to be found. Previous studies have shown that the integration of multibeam data into predictive modeling studies can yield a substantial enhancement in model skill (Howell et al. 2011, Rengstorf et al. 2013). This occurs mostly through capturing finer scale spatial heterogeneity in the underlying substrate or the ability to extract areas of hard grounds that are essential for most species of coral modeled in this study (Dunn and Halpin 2009, Rengstorf et al. 2013, Robert et al. 2014).

The finest scale existing model for the northeastern Atlantic Ocean is that of Kinlan et al. (2013). However, direct comparison of the modern scleractinian model with the Kinlan et al. (2013) scleractinian model for the area was not possible, as their observation data were based largely on scleractinians found in soft bottom habitats (Kinlan et al. 2013). Essentially, Kinlan et al. (2013) deemed that much of the canyon was suitable for scleractinian corals, with particular high suitability on the canyon axis through 1,400 m (**Figure 7-12e**). The historic model presented here demonstrated a similar pattern in the shallower reaches of the canyon (**Figure 7-11**), but predicted no suitable habitat on the canyon axis deeper than 600 m. The Alcyonacea model in Kinlan et al. (2013) bore a greater resemblance to the modern models discussed in this chapter, with highly suitable habitat predicted on the flanks of the canyon mostly between 400 and 1,000 m in Baltimore Canyon and 400 to 600 m in Norfolk Canyon (**Figures 12b** and **13b**). Comparison with the modern octocoral models for both canyons demonstrate some mismatches. In Baltimore Canyon, suitable habitat was found to strongly follow the 400 m contour and did not extend as deep as in Kinlan et al. (2013) (**Figures 7-12a**,**b**). In Norfolk Canyon, Kinlan et al. (2013) predicted a large area of suitable habitat where the modern octocoral model from this chapter did not (between 400 and 600 m) (**Figures 7-13a**,**b**). Direct comparisons between models such as these are problematic because they were constructed using substantially different species and environmental data.

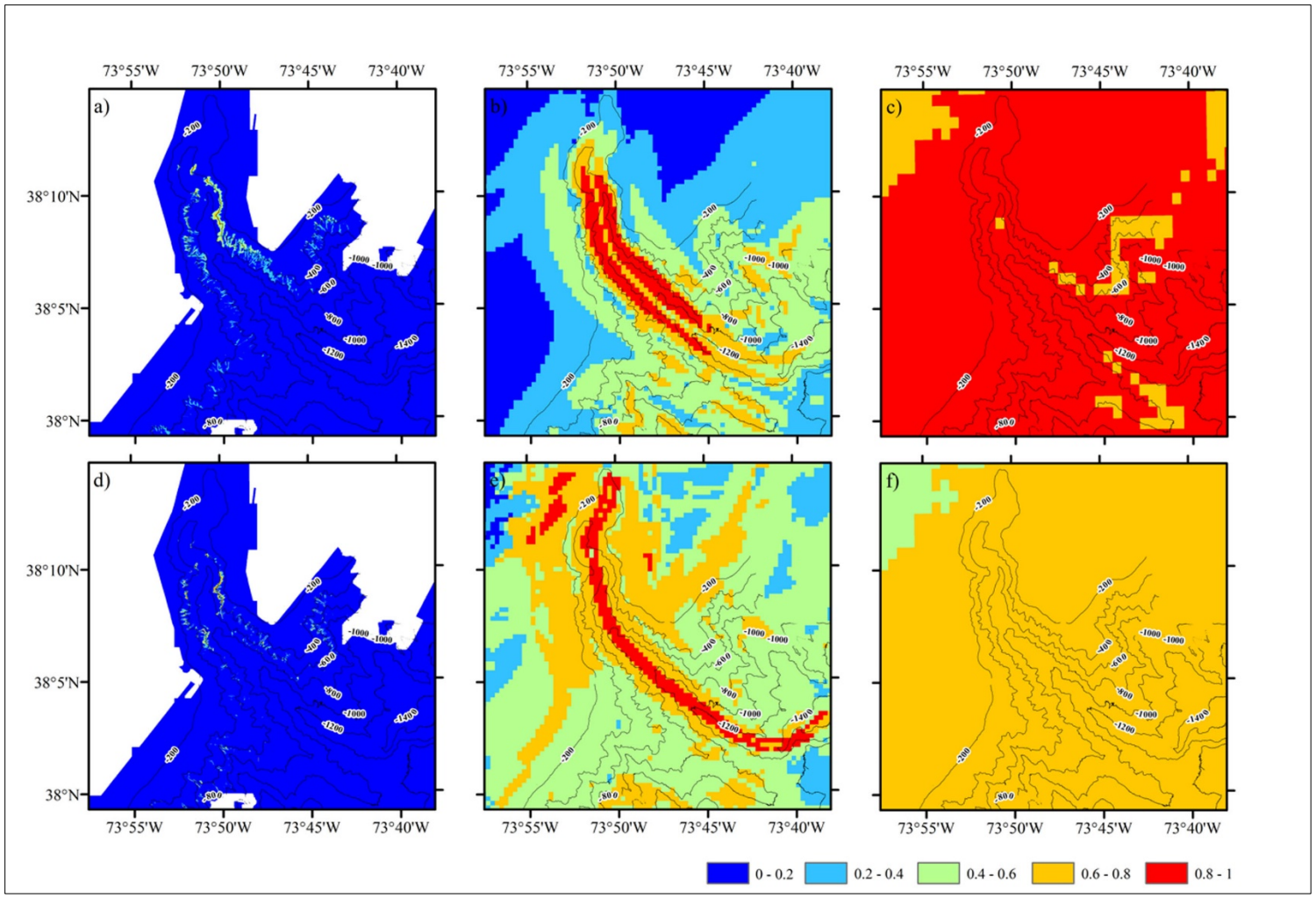

Figure 7-12. Predictive model comparisons for Baltimore Canyon at different cell resolutions. Octocorals a) from this chapter (10 m cell resolution), b) Alcyonacea from Kinlan et al. (2013) (370 m resolution), c) Alcyonacea from Yesson et al. (2012) (1,000 m resolution), scleractinians d) from this chapter (10 m resolution), e) scleractinians from Kinlan et al. (2013) (370 m resolution), and f) scleractinians from Davies and Guinotte (2011) (1,000 m resolution). Habitat suitability values presented in the legend range from blue (low habitat suitability) to red (high habitat suitability).

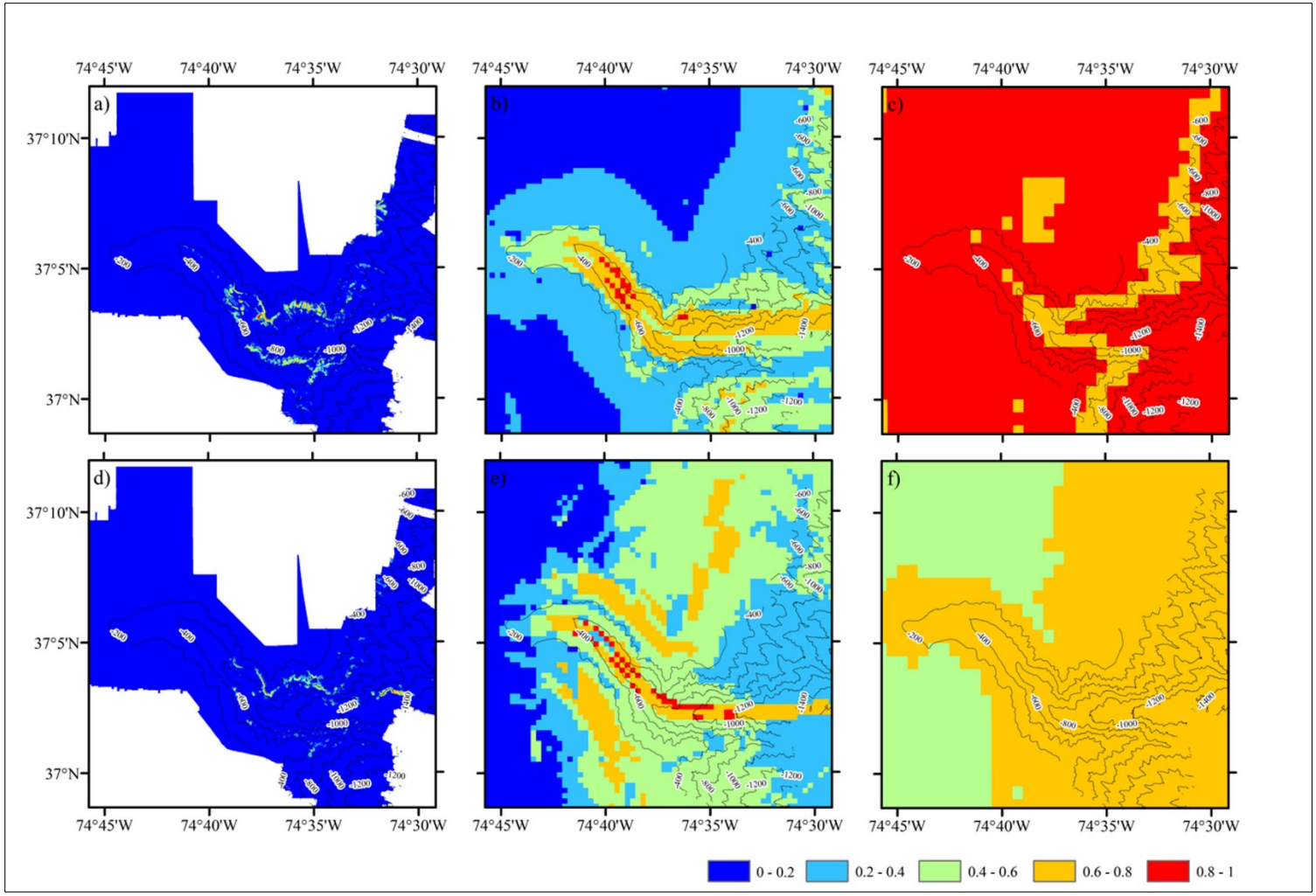

Figure 7-13. Predictive model comparisons for Norfolk Canyon at different cell resolutions. Octocorals a) from this chapter (10 m cell resolution), b) Alcyonacea from Kinlan et al. (2013) (370 m resolution), c) Alcyonacea from Yesson et al. (2012) (1,000 m resolution), scleractinians d) from this chapter (10 m resolution), e) scleractinians from Kinlan et al. (2013) (370 m resolution), and f) scleractinians from Davies and Guinotte (2011) (1,000 m resolution). Habitat suitability values presented in the legend range from blue (low habitat suitability) to red (high habitat suitability).

7.4.4 Historic Data-Driven Models to Inform Our Surveys and Cruise Planning

AUC scores for modern presence points compared with the historic habitat suitability models showed the historic models were better than random at predicting potential distribution of modern day fauna and hard grounds and as such should have value as an exploratory planning tool. However, the high AUC scores are misleading because the historic models for Baltimore Canyon demonstrated little visual correspondence with modern models and over-predicted suitable habitat for both fauna and hard grounds. The AUC statistic has been used in most presence-only modeling studies in the deep ocean (Vierod et al. 2014), but its use has been criticized (Jiménez-Valverde 2012). Although the historic models show statistical correspondence, the actual real-world relevance and utility may be very different.

In this exploratory analysis, the historic fauna data were spatially limited and focused on different habitats than those targeted in the modern survey (**Section 7.4.2**). Therefore, if surveys targeted toward specific components of the fauna were planned based on the historic fauna model, time would have been wasted in surveying the wrong areas of the canyon. The historic hard ground model was a slightly better fit than the historic faunal model to the modern observations based on AUC, and would not be affected by taxonomic issues. However, it still bore only limited correspondence to the modern data. Although our data are not promising in the use of historic data as a potential tool for exploratory mapping, several recommendations can be made:

1. This approach will work only if there is a sufficient abundance of observations that are spread throughout the area to be modeled to capture a wide breadth of a target niche.
2. Historic data need geospatial fixes and some metric of error, which were lacking in this case. This was the major obstacle in our inability to build a large observation dataset. While historic observations with position fixes on the order of kilometers are fine for broad-scale models, they are incompatible with high-resolution local-scale modeling as attempted here.
3. The act of developing a model early, before cruise planning started, generated a series of terrain and environmental variables that were valuable in discussions. These data were then used once modern observations arrived in order to build the modern models.

7.5 CONCLUSIONS

This study assessed whether historic location data could be mined from previous visual information to construct historic habitat suitability models using environmental variables derived from multibeam and modern oceanographic data. The study also built modern models from high-quality observations from ROV video footage. There was limited correspondence between the historic model and the modern models, and it is easy to discard the historic models as useless. However, there were benefits of conducting an exercise in advance of undertaking new sampling cruises, in that we generated terrain variables that led to cruise planning discussions and drove the creation of a coherent sampling design. The historic modeling exercise led to the collation of modern models that demonstrate what appear to be coherent predictions of a diverse set of fauna within the canyons that are far more constrained than those developed previously in this region (Davies and Guinotte 2011, Yesson et al. 2012, Kinlan et al. 2013). It is clear that high-quality visual observations with accurate position fixes produce better predictions of both fauna and substrate at resolutions that are useful in cruise planning, management, and conservation.

7.6 LITERATURE CITED

Ardron J, Gjerde K, Pullen S, Tilot V. 2008. Marine spatial planning in the high seas. Marine Policy. 32:832–839.

Bachman M, Clifford N, Packer D, Stevenson D, Auster P, Valentine P, Ford K. 2012. Essential fish habitat (EFH) omnibus amendment. Deep-sea corals of the northeast region: species, habitats and proposed coral zones and vulnerability to fishing impacts. Draft: 03/28/12. New England Fisheries Management Council. 97 pp.

Boyer TP, Levitus S, Garcia HE, Locamini RA, Stephens C, Antonov JI. 2005. Objective analyses of annual, seasonal, and monthly temperature and salinity for the World Ocean on a 0.25° grid. International Journal of Climatology. 25:931–945.

Brooke S, Ross SW. 2014. First observations of the cold-water coral *Lophelia pertusa* in mid-Atlantic canyons of the USA. Deep-Sea Research Part II: Topical Studies in Oceanography. 104:245–251.

Brooke S, Schroeder WW. 2007. State of deep coral ecosystems in the Gulf of Mexico region: Texas to the Florida Straits. In: Lumsden SE, Hourigan TF, Bruckner AW, Dorr G, editors. The state of deep coral ecosystems of the United States. Silver Spring (MD): NOAA Technical Memorandum CRCP-3. p. 271–306.

Brown CJ, Smith SJ, Lawton P, Anderson JT. 2011. Benthic habitat mapping: a review of progress towards improved understanding of the spatial ecology of the seafloor using acoustic techniques. Estuarine, Coastal and Shelf Science. 92:502–520.

Cairns SD. 1981. Marine flora and fauna of the northeastern United States: Scleractinia. U.S. Dept. of Commerce, National Oceanic and Atmospheric Administration, National Marine Fisheries Service, Scientific Publications Office.

Cairns S, Gershwin L, Brook F. 2012. Phylum Cnidaria: corals, medusae, hydroids, myxozoans. In: Gordon DPE, editor. New Zealand inventory of biodiversity: kingdoms Bacteria, Protozoa, Chromista, Plantae, Fungi Volume 3. Christchurch (NZ): Canterbury University Press. p. 59–101.

Colman S, Halka J. 1990. Ancient channels of the Susquehanna River beneath Chesapeake Bay and the Delmarva Peninsula. Geological Society of America Bulletin. 102:1268–1279.

Csanady GT, Hamilton P. 1988. Circulation of slopewater. Continental Shelf Research. 8:565–624.

Csanady G, Churchill J, Butman B. 1988. Near-bottom currents over the continental slope in the Mid-Atlantic Bight. Continental Shelf Research. 8:653–671.

Davies AJ, Guinotte JM. 2011. Global habitat suitability for framework-forming cold-water corals. PLoS ONE. 6:e18483.

Davies AJ, Roberts JM, Hall-Spencer J. 2007. Preserving deep-sea natural heritage: emerging issues in offshore conservation and management. Biological Conservation. 138:299–312.

Davies AJ, Wisshak M, Orr JC, Roberts JM. 2008. Predicting suitable habitat for the cold-water reef framework-forming coral *Lophelia pertusa* (Scleractinia). Deep-Sea Research Part I. 55:1048–1062.

Davies AJ, Duineveld GCA, Lavaleye MSS, Bergman MJN, Van Haren H, Roberts JM. 2009. Downwelling and deep-water bottom currents as food supply mechanisms to the cold-water coral *Lophelia pertusa* (Scleractinia) at the Mingulay Reef Complex. Limnological Oceanography. 54:620–629.

De Leo FC, Smith CR, Rowden AA, Bowden DA, Clark MR. 2010. Submarine canyons: hotspots of benthic biomass and productivity in the deep sea. Proceedings of the Royal Society B: Biological Sciences. 277:2783–2792.

Dolan MFJ, Grehan AJ, Guinan JC, Brown C. 2008. Modelling the local distribution of cold-water corals in relation to bathymetric variables: adding spatial context to deep-sea video data. Deep-Sea Research Part I-Oceanographic Research Papers. 55:1564–1579.

Dullo WC, Flögel S, Rüggeberg A. 2008. Cold-water coral growth in relation to the hydrography of the Celtic and Nordic European continental margin. Marine Ecology Progress Series. 371:165–176.

Dunn DC, Halpin PN. 2009. Rugosity-based regional modeling of hard-bottom habitat. Marine Ecology Progress Series. 377:1–11.

Elith J, Graham CH, Anderson RP, Dudík M, Ferrier S, Guisan A, Hijmans RJ, Huettmann F, Leathwick JR, Lehmann A, et al. 2006. Novel methods improve prediction of species distributions from occurrence data. Ecography. 29:129–151.

Forde E. 1981. Evolution of Veatch, Washington, and Norfolk submarine canyons: inferences from strata and morphology. Marine Geology. 39:197–214.

Freiwald A, Roberts JM. 2005. Cold-water corals and ecosystems. Berlin Heidelberg: Springer-Verlag. 1209 p.

Freiwald A, Fosså JH, Grehan A, Koslow T, Roberts JM. 2004. Cold-water coral reefs. Cambridge (UK): UNEP-WCMC.

Garcia HE, Locarnini RA, Boyer TP, Antonov JI. 2006a. World ocean atlas 2005, volume 3: dissolved oxygen, apparent oxygen utilization, and oxygen saturation. Levitus S, editor. Washington (DC): U.S. Government Printing Office. NOAA Atlas NESDIS 63. 342 p.

Garcia HE, Locarnini RA, Boyer TP, Antonov JI. 2006b. World ocean atlas 2005, volume 4: nutrients (phosphate, nitrate, silicate). Levitus S, editor. Washington (DC): U.S. Government Printing Office. NOAA Atlas NESDIS 64. 396 p.

Garcia R, Van Oevelen D, Soetaert K, Thomsen L, De Stigter HC, Epping E. 2008. Deposition rates, mixing intensity and organic content in two contrasting submarine canyons. Progress in Oceanography. 76:192–215.

Gardner WD. 1989. Baltimore Canyon as a modern conduit of sediment to the deep sea. Deep-Sea Research Part A: Oceanographic Research Papers. 36:323–358.

Genin A, Dayton PK, Lonsdale PF, Speiss FN. 1986. Corals on seamount peaks provide evidence of current acceleration over deep-sea topography. Nature. 322:59–61.

Glover AG, Smith CR. 2003. The deep-sea floor ecosystem: current status and prospects of anthropogenic change by the year 2025. Environmental Conservation. 30:219–241.

Grohmann CH, Smith MJ, Riccomini C. 2011. Multiscale analysis of topographic surface roughness in the Midland Valley, Scotland. IEEE Transactions on Geoscience and Remote Sensing. 49(4):1200-1213.

Guinan J, Brown C, Dolan M, Grehan A. 2009a. Ecological niche modelling of the distribution of cold-water coral habitat using underwater remote sensing data. Ecological Informatics. 4(2):83–92.

Guinan J, Grehan AJ, Dolan MFJ, Brown C. 2009b. Quantifying relationships between video observations of cold-water coral cover and seafloor features in Rockall Trough, west of Ireland. Marine Ecology Progress Series Marine Ecology Progress Series. 375:125–138.

Guinotte JM, Davies AJ. 2014. Predicted deep-sea coral habitat suitability for the US west coast. PLoS ONE. 9(4): e93918.

Hecker B. 1990. Variation in megafaunal assemblages on the continental margin south of New England. Deep-Sea Research Part A: Oceanographic Research Papers. 37:37–57.

Hecker B, Blechschmidt G, Gibson P. 1980. Epifaunal zonation and community structure in three mid- and north Atlantic canyons. Final report for the canyon assessment study in the Mid-and North Atlantic Areas of the U.S. Outer Continental Shelf. Prepared for the U.S. Department of Interior, Bureau of Land Management under contract BLM AA5 51-CT8-49. Palisades (NY): Lamont-Doherty Geological Observatory.

Hecker B, Logan DT, Gandarillas FE, Gibson PR. 1983. Canyon and slope processes study, vol. III: biological processes. Report for the U.S. Department of the Interior, Minerals Management Service, under contract no. 14-12-0001-29178. Palisades (NY): Lamont-Doherty Geological Observatory. 212 p. [accessed 2016 June 1]. http://invertebrates.si.edu/boem/reports/CASPS_vol3.pdf.

Henry LA, Davies AJ, Roberts JM. 2010. Beta diversity of cold-water coral reef communities off western Scotland. Coral Reefs. 29:427–436.

Hirzel AH, Hausser J, Chessel D, Perrin N. 2002. Ecological-niche factor analysis: how to compute habitat-suitability maps without absence data? Ecology. 83:2027–2036.

Hobson RD. 1972. Surface roughness in topography: quantitative approach. In: Chorley RJ, editor. Spatial analysis in geomorphology. New York (NY): Harper and Row. p. 221-245.

Howell KL, Holt RD, Pulido Endrino I, Stewart H. 2011. When the species is also a habitat: comparing the predictively modelled distributions of *Lophelia pertusa* and the reef habitat it forms. Biological Conservation. 144:2656–2665.

Ismail K, Huvenne VAI, Masson DG. 2015. Objective automated classification technique for marine landscape mapping in submarine canyons. Marine Geology. 362:17–32.

Jenness J. 2012. DEM surface tools. Jenness Enterprises. [accessed 2016 May 23]. http://www.jennessent.com/arcgis/surface_area.htm.

Jensen A, Frederiksen R. 1992. The fauna associated with the bank-forming deep-water coral *Lophelia pertusa* (Scleractinaria) on the Faroe Shelf. Sarsia. 77:53–69.

Jiménez-Valverde A. 2012. Insights into the area under the receiver operating characteristic curve (AUC) as a discrimination measure in species distribution modelling. Global Ecology and Biogeography. 21:498–507.

Kampstra P. 2008. Beanplot: A boxplot alternative for visual comparison of distributions. Journal of Statistical Software. 28:Code Snippet 1.

Kelling G, Stanley DJ. 1970. Morphology and structure of Wilmington and Baltimore submarine canyons, eastern United States. The Journal of Geology. 78(6):637–660.

Kinlan B, Poti M, Drohan A, Packer D, Nizinski M, Dorfman D, Caldow C. 2013. Digital data: predictive models of deep-sea coral habitat suitability in the U.S. northeast Atlantic and mid-Atlantic regions. Downloadable digital data package. Department of Commerce (DOC), National Oceanic and Atmospheric Administration (NOAA), National Ocean Service (NOS), National Centers for Coastal Ocean Science (NCCOS), Center for Coastal Monitoring and Assessment (CCMA), Biogeography Branch, and NOAA National Marine Fisheries Service (NMFS), Northeast Fisheries Science Center (NEFSC). Released and accessed August 2013. http://coastalscience.noaa.gov/projects/detail?key=35.

Knebel H, Spiker E. 1977. Thickness and age of surficial sand sheet, Baltimore Canyon trough area. American Association of Petroleum Geologists Bulletin. 61:861–871.

Leverette TL, Metaxas A. 2005. Predicting habitat for two species of deep-water coral on the Canadian Atlantic continental shelf and slope. In: Freiwald A, Roberts JM (eds.), Cold-water corals and ecosystems. Berlin Heidelberg (Germany): Springer-Verlag. p. 467–479.

Levin LA, Dayton PK. 2009. Ecological theory and continental margins: where shallow meets deep. Trends in Ecological Evolution. 24:606–617.

Levin LA, Etter RJ, Rex MA, Gooday AJ, Smith CR, Pineda J, Stuart CT, Hessler RR, Pawson D. 2001. Environmental influences on regional deep-sea species diversity. Annual Review of Ecology, Evolution, and Systematics. 32:51–93.

Malahoff A, Embley R, Fornari D. 1982. Geomorphology of Norfolk and Washington Canyons and the surrounding continental slope and upper rise as observed with DSRV *Alvin*. In: Scrutton RA, Talwani M, editors. The ocean floor. New York (NY): John Wiley and Sons. p. 97–111.

Menot L, Sibuet M, Carney RS, Levin LA, Rowe GT, Billett DSM, Poore G, Kitazato H, Vanreusel A, Galéron J, et al. 2010. New perceptions of continental margin biodiversity life in the world's oceans. Hoboken (NJ): Wiley-Blackwell. p. 79–102.

Obelcz J, Brothers D, Chaytor J, Brink Ut, Ross SW, Brooke S. 2014. Geomorphic characterization of four shelf-sourced submarine canyons along the U.S. Mid-Atlantic continental margin. Deep-Sea Research Part II: Topical Studies in Oceanography. 104:106–119.

Orr JC, Fabry VJ, Aumont O, Bopp L, Doney SC, Feely RA, Gnanadesikan A, Gruber N, Ishida A, Joos F, et al. 2005. Anthropogenic ocean acidification over the twenty-first century and its impact on calcifying organisms. Nature. 437:681–686.

Packer D, Boelke D, Guida V, McGee LA. 2007. State of deep coral ecosystems in the northeastern US region: Maine to Cape Hatteras. In: Lumsden SE, Hourigan TF, Bruckner AW, Dorr G, editors. The state of deep coral ecosystems of the United States. Silver Spring (MD): NOAA Technical Memorandum CRCP-3. p. 195–232.

Papeş M, Gaubert P. 2007. Modelling ecological niches from low numbers of occurrences: assessment of the conservation status of poorly known viverrids (Mammalia, Carnivora) across two continents. Diversity and Distributions. 13:890–902.

Partyka ML, Ross SW, Quattrini AM, Sedberry GR, Birdsong TW, Potter J. 2007. Southeastern United States Deep-Sea Corals (SEADESC) initiative: a collaborative effort to characterize areas of habitat-forming deep-sea corals. Silver Spring (MD): NOAA Technical Memorandum OER 1. 176 p.

Pearson RG, Raxworthy CJ, Nakamura M, Peterson AT. 2007. Predicting species distributions from small numbers of occurrence records: a test case using cryptic geckos in Madagascar. Journal of Biogeography. 34(1):102–117.

Phillips SJ, Anderson RP, Schapire RE. 2006. Maximum entropy modeling of species geographic distributions. Ecological Modelling. 190:231–259.

Phillips SJ, Dudík M. 2008. Modeling of species distributions with Maxent: new extensions and a comprehensive evaluation. Ecography. 31:161–175.

Rasmussen LL. 2005. Slope water, Gulf Stream, and seasonal influences on southern Mid-Atlantic Bight circulation during the fall-winter transition. Journal of Geophysical Research. 110:C02009.

Rengstorf A, Yesson C, Brown C, Grehan A. 2012. Towards high-resolution habitat suitability modelling of vulnerable marine ecosystems in the deep-sea: resolving terrain attribute dependencies. Marine Geodesy. 35:343–361.

Rengstorf AM, Yesson C, Brown C, Grehan AJ. 2013. High-resolution habitat suitability modelling can improve conservation of vulnerable marine ecosystems in the deep sea. Journal of Biogeography. 40(9):1702–1714.

Rhoads DC, Hecker B. 1994. Processes on the continental slope off North Carolina with special reference to the Cape Hatteras region. Deep-Sea Research Part II: Topical Studies in Oceanography. 41:965–980.

Riley SJ, DeGloria SD, Elliot R. 1999. A terrain ruggedness index that quantifies topographic heterogeneity. Intermountain Journal of Sciences. 5:23–27.

Robert K, Jones DOB, Tyler PA, Van Rooij D, Huvenne VAI. 2014. Finding the hotspots within a biodiversity hotspot: fine-scale biological predictions within a submarine canyon using high-resolution acoustic mapping techniques. Marine Ecology. 36(4):1256–1276.

Roberts JM, Wheeler AJ, Freiwald A. 2006. Reefs of the deep: the biology and geology of cold-water coral ecosystems. Science. 213(5773):543–547.

Roberts JM, Wheeler AJ, Freiwald A, Cairns S. 2009. Cold-water corals: the biology and geology of deep-sea coral habitats. Cambridge (UK): Cambridge University Press. 334 p.

Rogers AD. 1999. The biology of *Lophelia pertusa* (Linnaeus 1758) and other deep-water reef-forming corals and impacts from human activities. International Review of Hydrobiology. 84(4):315–406.

Ross SW, Nizinski MS. 2007. State of deep coral ecosystems in the U.S. Southeast Region: Cape Hatteras to southeastern Florida. In: Lumsden SE, Hourigan TF, Bruckner AW, Dorr G, editors. The state of deep coral ecosystems of the United States. Silver Spring (MD): NOAA Technical Memorandum. p. 233–270.

Ross RE, Howell KL. 2013. Use of predictive habitat modelling to assess the distribution and extent of the current protection of 'listed' deep-sea habitats. Diversity and Distribution. 19:433–445.

Ruszkiczay-Rüdiger Z, Fodor L, Horváth E, Telbisz T. 2009. Discrimination of fluvial, eolian and neotectonic features in a low hilly landscape: a DEM-based morphotectonic analysis in the Central Pannonian Basin, Hungary. Geomorphology. 104:203–217.

Sappington JM, Longshore KM, Thomson DB. 2007. Quantifiying landscape ruggedness for animal habitat analysis: a case study using bighorn sheep in the Mojave Desert. Journal of Wildlife Management. 71:1419–1426.

Steinacher M, Joos F, Frölicher TL, Plattner G-K, Doney SC. 2009. Imminent ocean acidification projected with the NCAR global coupled carbon cycle-climate model. Biogeosciences. 6:515–533.

Stiles M, Ylitalo-Ward H, Faure P, Hirshfield M. 2007. There's no place like home: deep seafloor ecosystems of New England and the mid-Atlantic. Oceana. [accessed 2016 May 23]. http://oceana.org/sites/default/files/reports/NewEnglandTrawlReport_low1.pdf.

Tittensor DP, Baco AR, Brewin PE, Clark MR, Consalvey M, Hall-Spencer J, Rowden A, Schlacher T, Stocks K, Rogers AD. 2009. Predicting global habitat suitability for stony corals on seamounts. Journal of Biogeography. 36:1111–1128.

van den Hove S, Moreau V. 2007. Ecosystems and biodiversity in deep waters and high seas: a scoping report on their socio-economy, management and governance. United Nations Environment Programme-World Conservation Monitoring Centre. Cambridge (UK): UNEP-WCMC. 84 p.

Vierod ADT, Guinotte JM, Davies AJ. 2014. Predicting the distribution of vulnerable marine ecosystems in the deep sea using presence-background models. Deep-Sea Research Part II: Topical Studies in Oceanography. 99:6–18.

Watling L, Auster P. 2005. Distribution of deep-water Alcyonacea off the northeast coast of the United States. In: Freiwald A, Roberts JM, editors. Cold-water corals and ecosystems. Berlin Heidelberg (Germany): Springer-Verlag. p. 279–296.

White M, Mohn C, de Stigter H, Mottram G. 2005. Deep-water coral development as a function of hydrodynamics and surface productivity around the submarine banks of the Rockall Trough, NE Atlantic. In: Freiwald A, Roberts JM, editors. Cold-water corals and ecosystems. Berlin Heidelberg (Germany): Springer-Verlag. p. 503–514.

Wilson JB. 1979. “Patch” development of the deep-water coral *Lophelia pertusa* (L.) on Rockall Bank. Journal of the Marine Biological Association of the United Kingdom. 59:165–177.

Wilson MFJ, O’Connell B, Brown C, Guinan JC, Grehan AJ. 2007. Multiscale terrain analysis of multibeam bathymetry data for habitat mapping on the continental slope. Marine Geodesy. 30:3–35.

Wood, R. 1999. Reef Evolution. Oxford (UK): Oxford University Press.

Wright DJ, Lundblad ER, Larkin EM, Rinehart RW, Murphy J, Cary-Kothera L, Draganov K. 2005. ArcGIS Benthic Terrain Modeler. Corvallis (OR): Oregon State University, Davey Jones Locker Seafloor Mapping/Marine GIS Laboratory, and NOAA Coastal Services Center.

Yesson C, Taylor ML, Tittensor DP, Davies AJ, Guinotte J, Baco A, Black J, Hall-Spencer JM, Rogers AD. 2012. Global habitat suitability of cold-water octocorals. Journal of Biogeography. 39:1278-1292.

Appendix 7-A

Maxent Prediction Models for Baltimore and Norfolk Canyons

(Data Archive in ZIP Format of GIS-Compatible Files of Appendix 7-A, Figures 7-A1 to 7-A21 available in GeoTIFF Format)

This page intentionally left blank

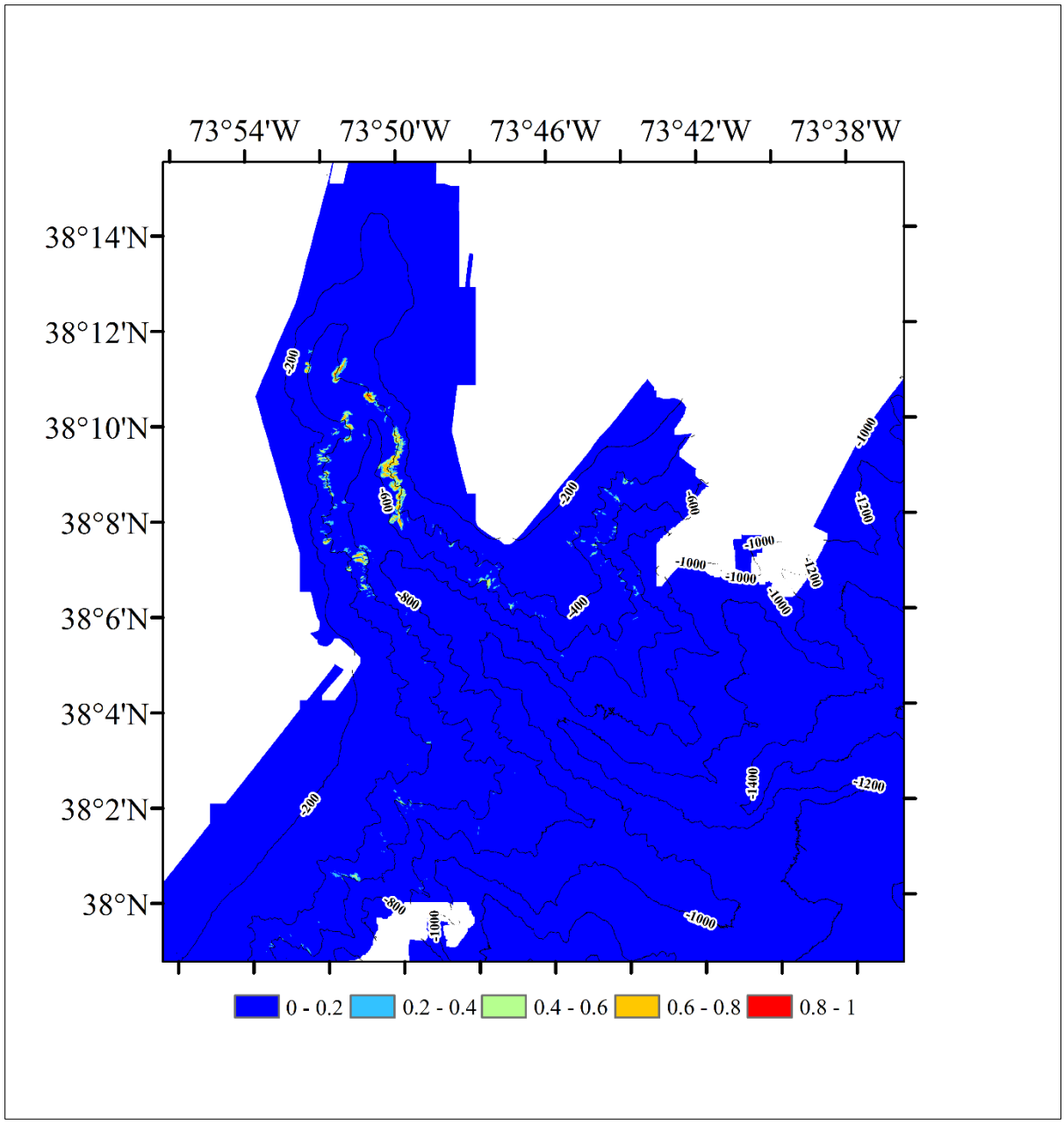

Figure 7-A1. The final *Anthothela* Maxent prediction for Baltimore Canyon. (See **Table 7-A1** for evaluation statistics.).

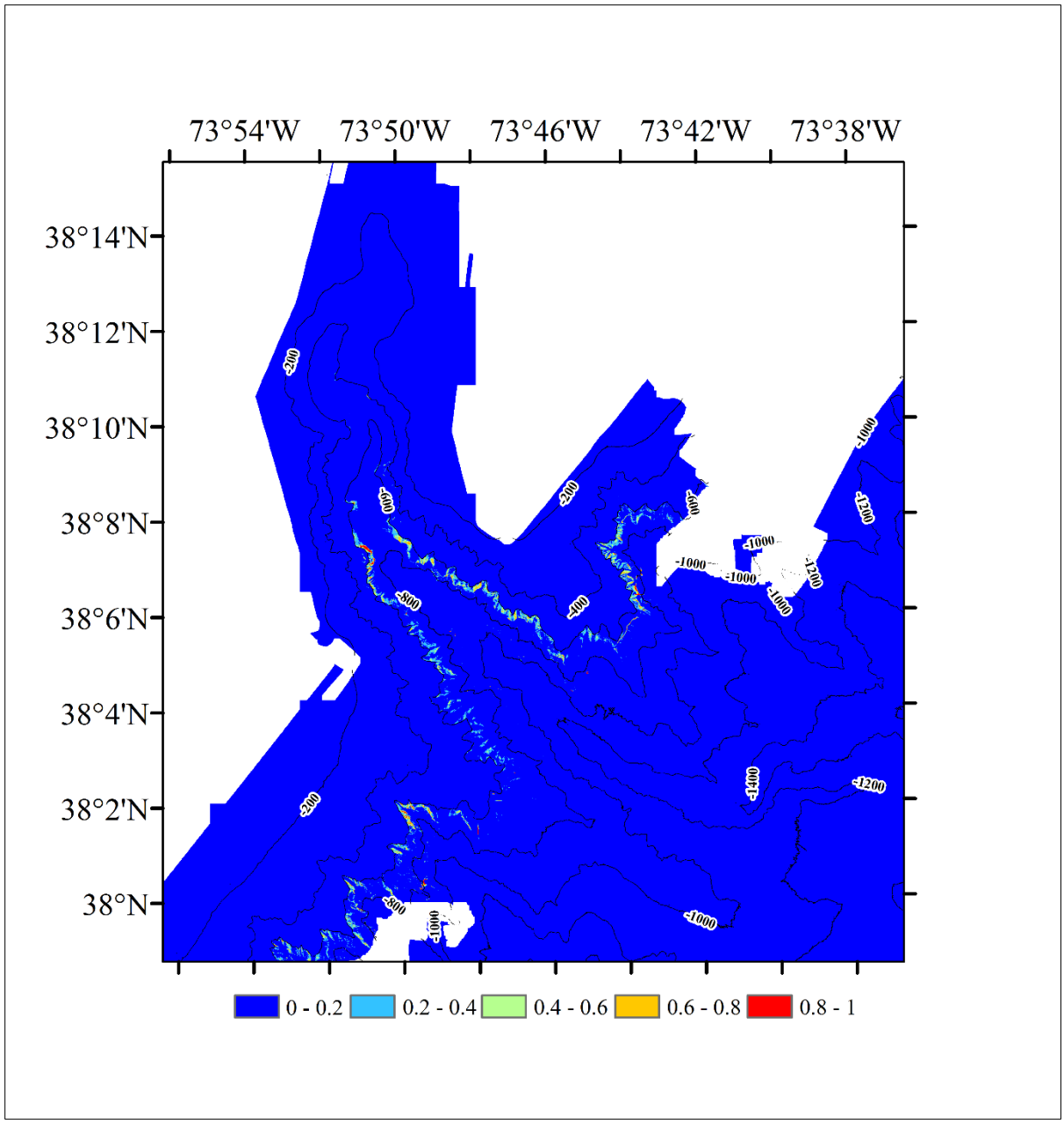

Figure 7-A2. The final *Desmophyllum* Maxent prediction for Baltimore Canyon. (See **Table 7-A1** for evaluation statistics.)

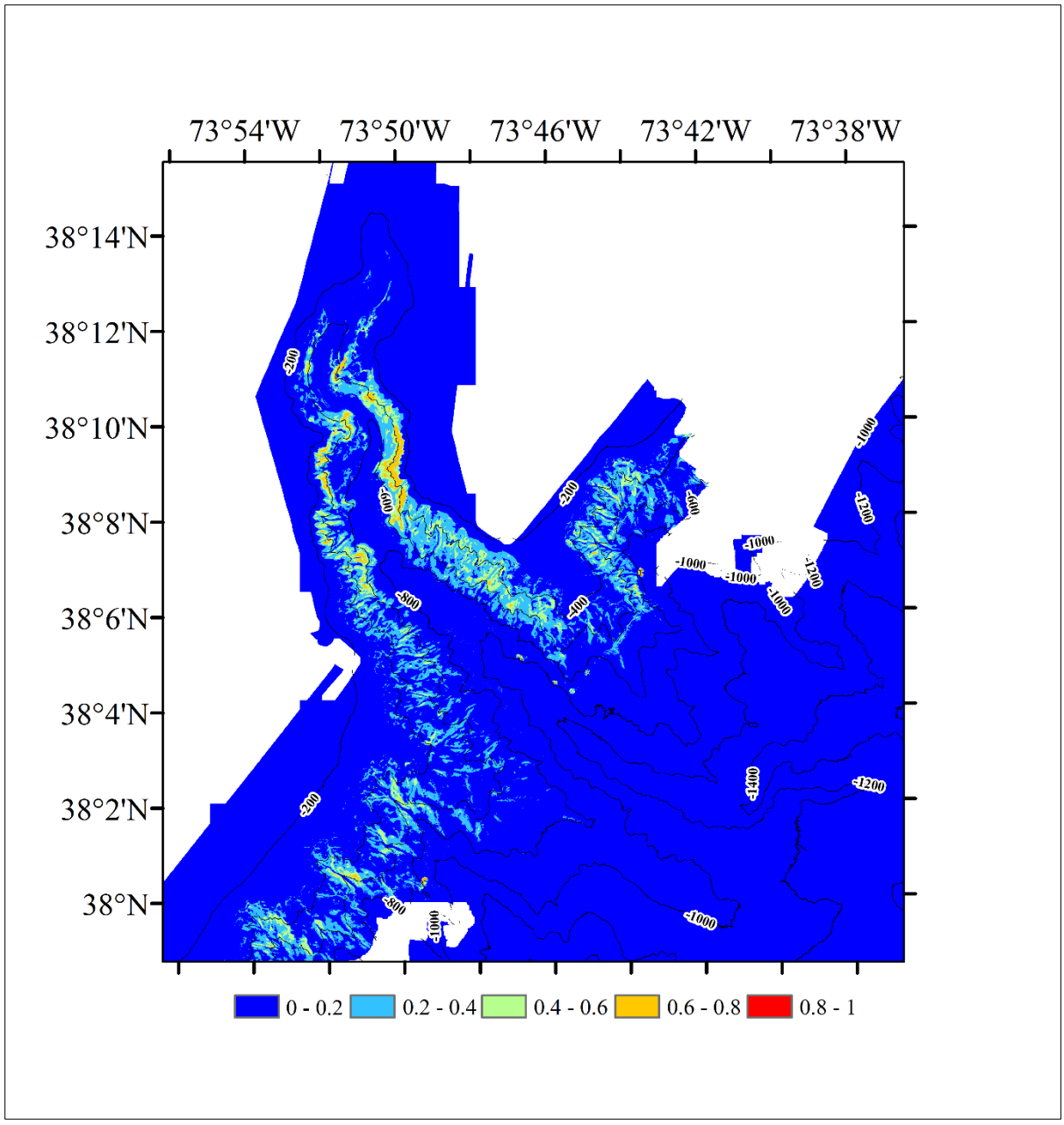

Figure 7-A3. The final hard substrate Maxent prediction for Baltimore Canyon. (See **Table 7-A1** for evaluation statistics.)

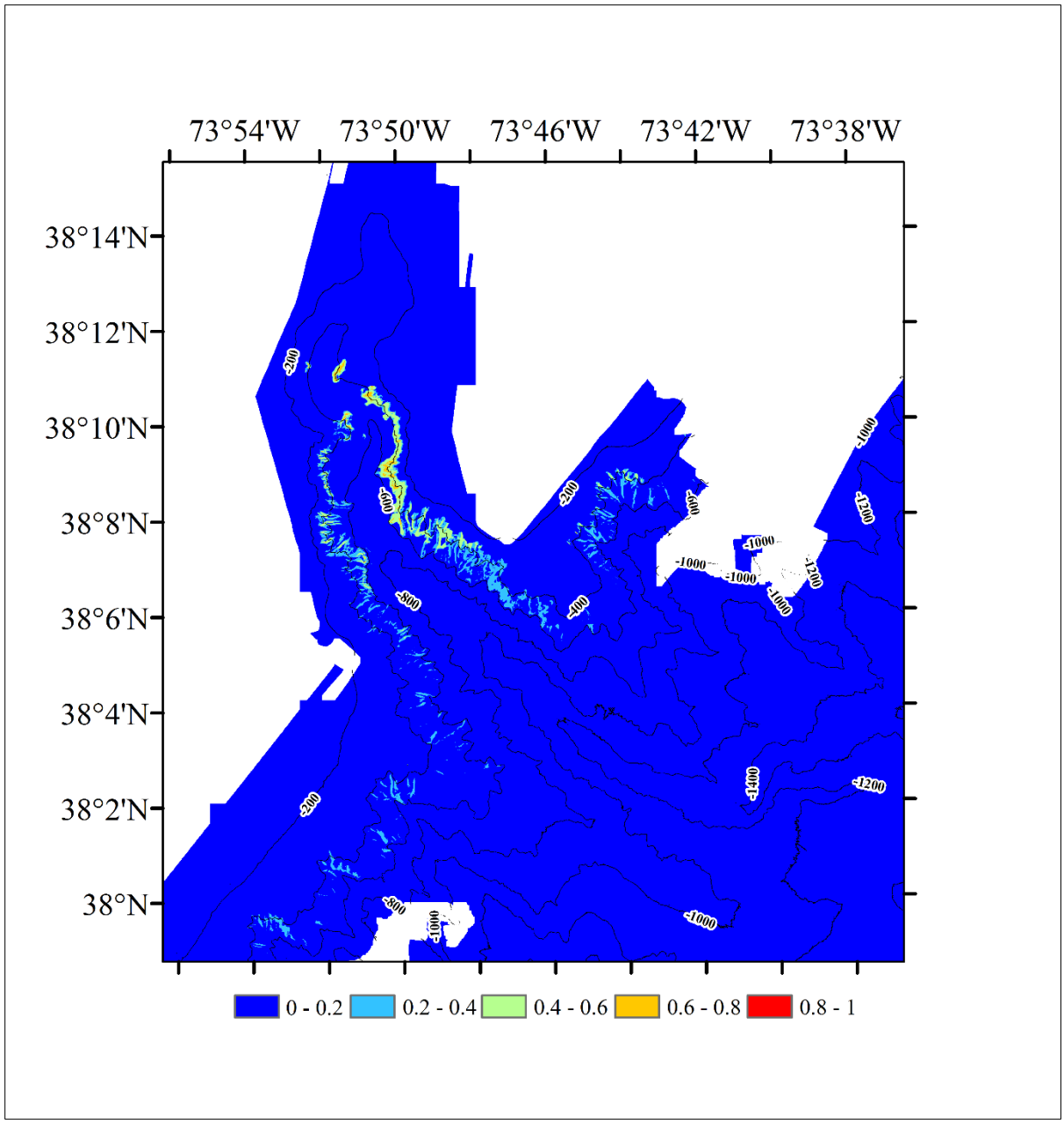

Figure 7-A4. The final octocoral group Maxent prediction for Baltimore Canyon. (See **Table 7-A1** for evaluation statistics.)

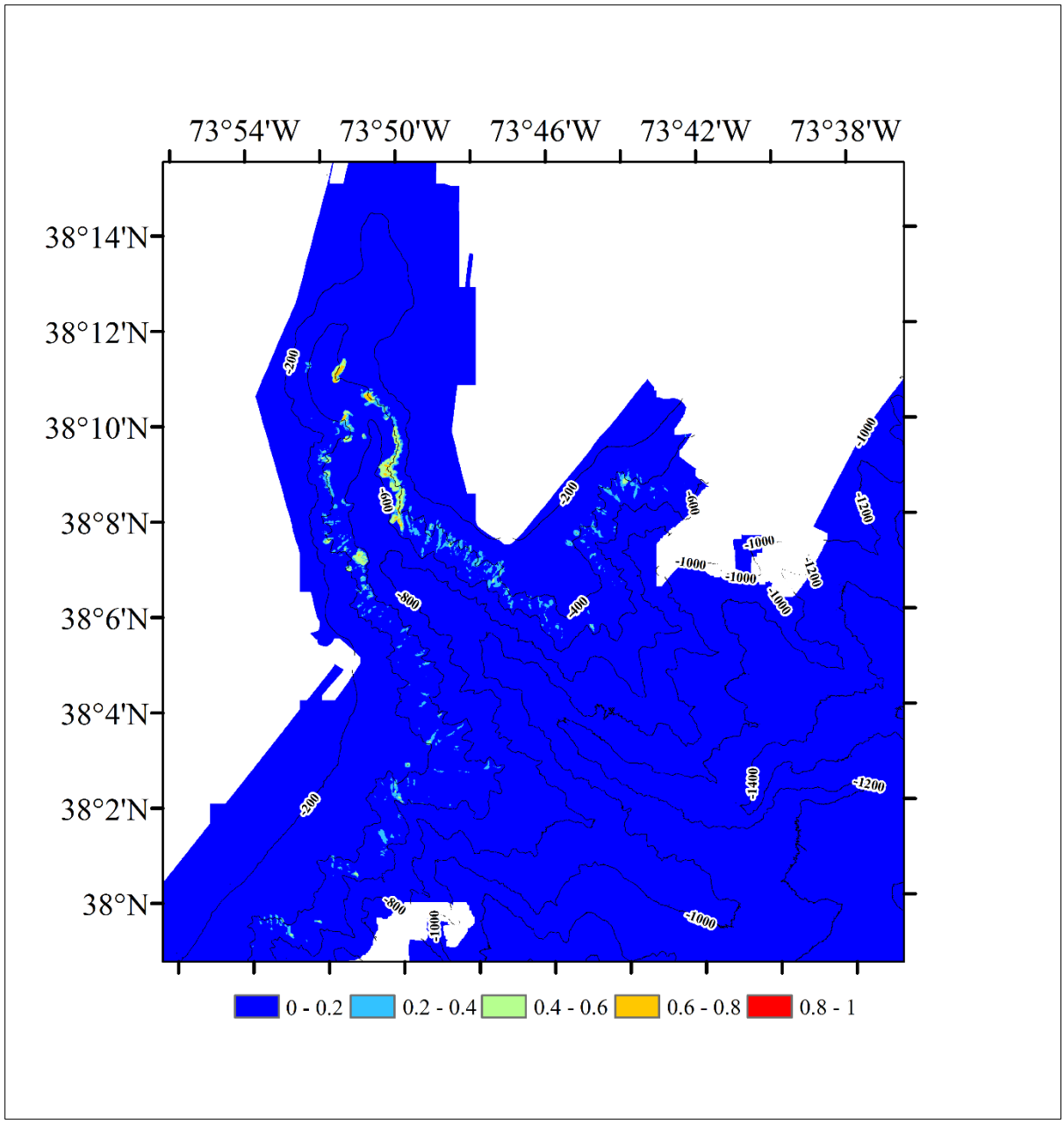

Figure 7-A5**.** The final *Paragorgia* Maxent prediction for Baltimore Canyon. (See **Table 7-A1** for evaluation statistics.)

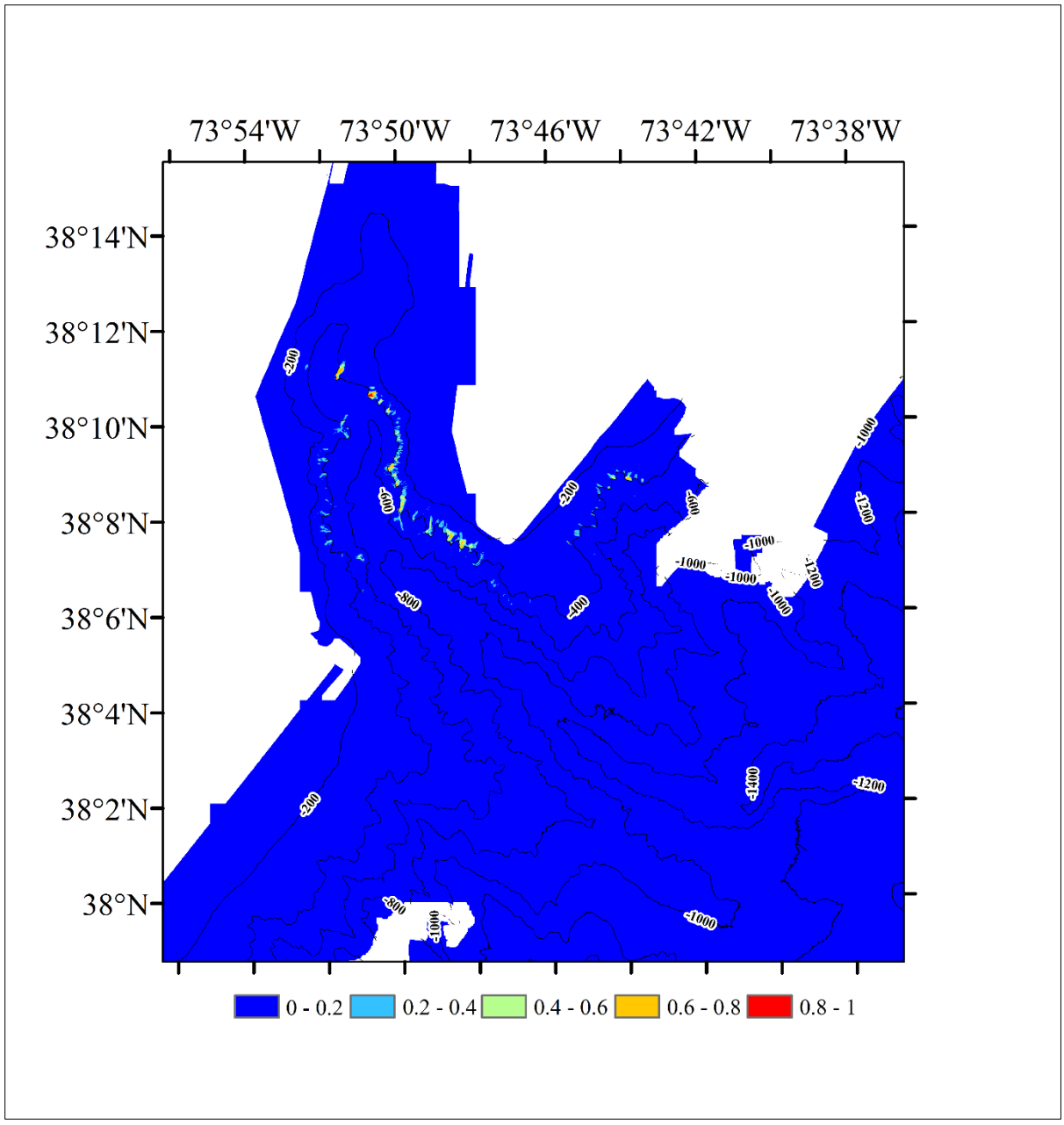

Figure 7-A6. The final *Paramuricea* Maxent prediction for Baltimore Canyon. (See **Table 7-A1** for evaluation statistics.)

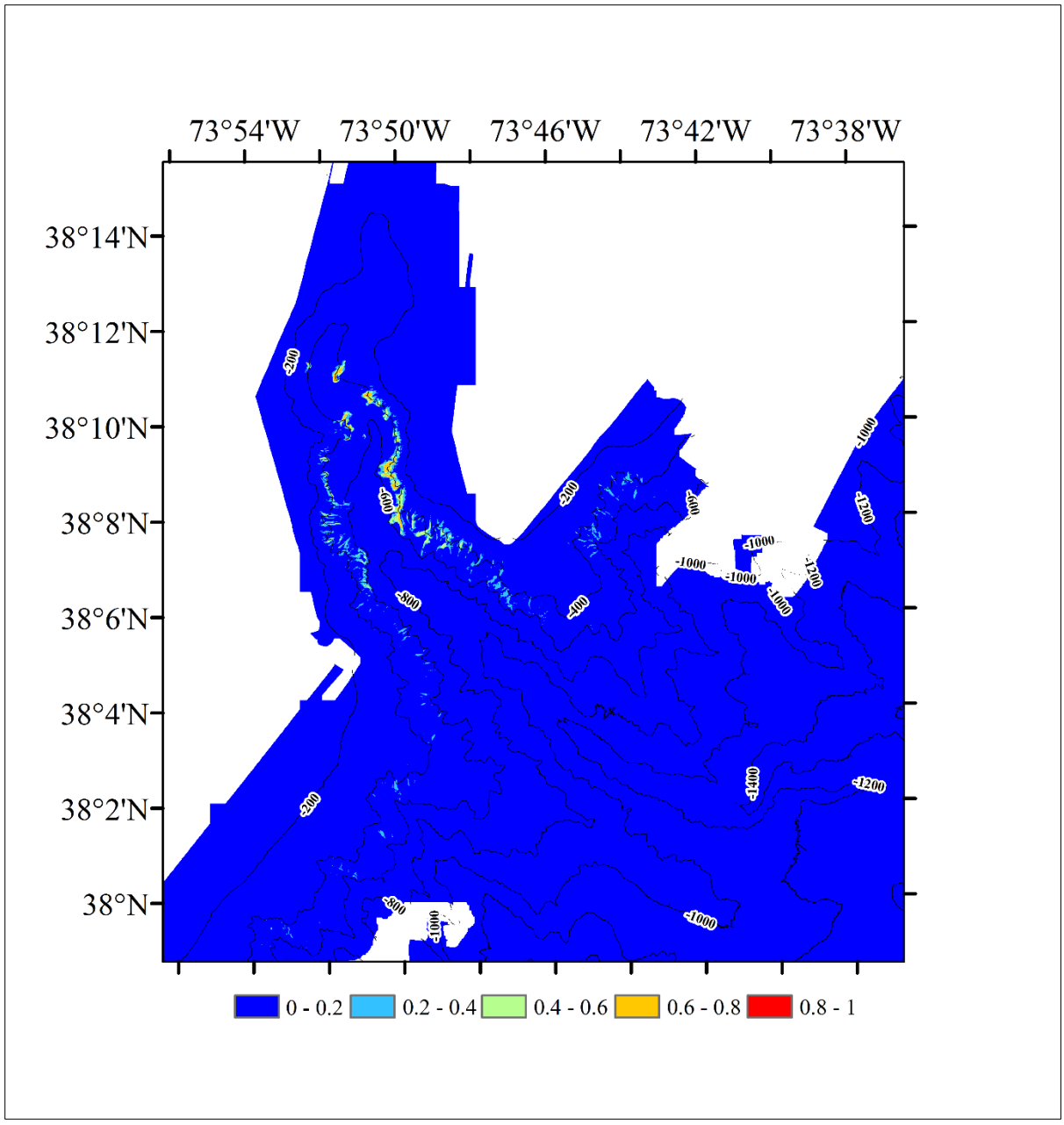

Figure 7-A7. The final *Primnoa* Maxent prediction for Baltimore Canyon. (See **Table 7-A1** for evaluation statistics.)

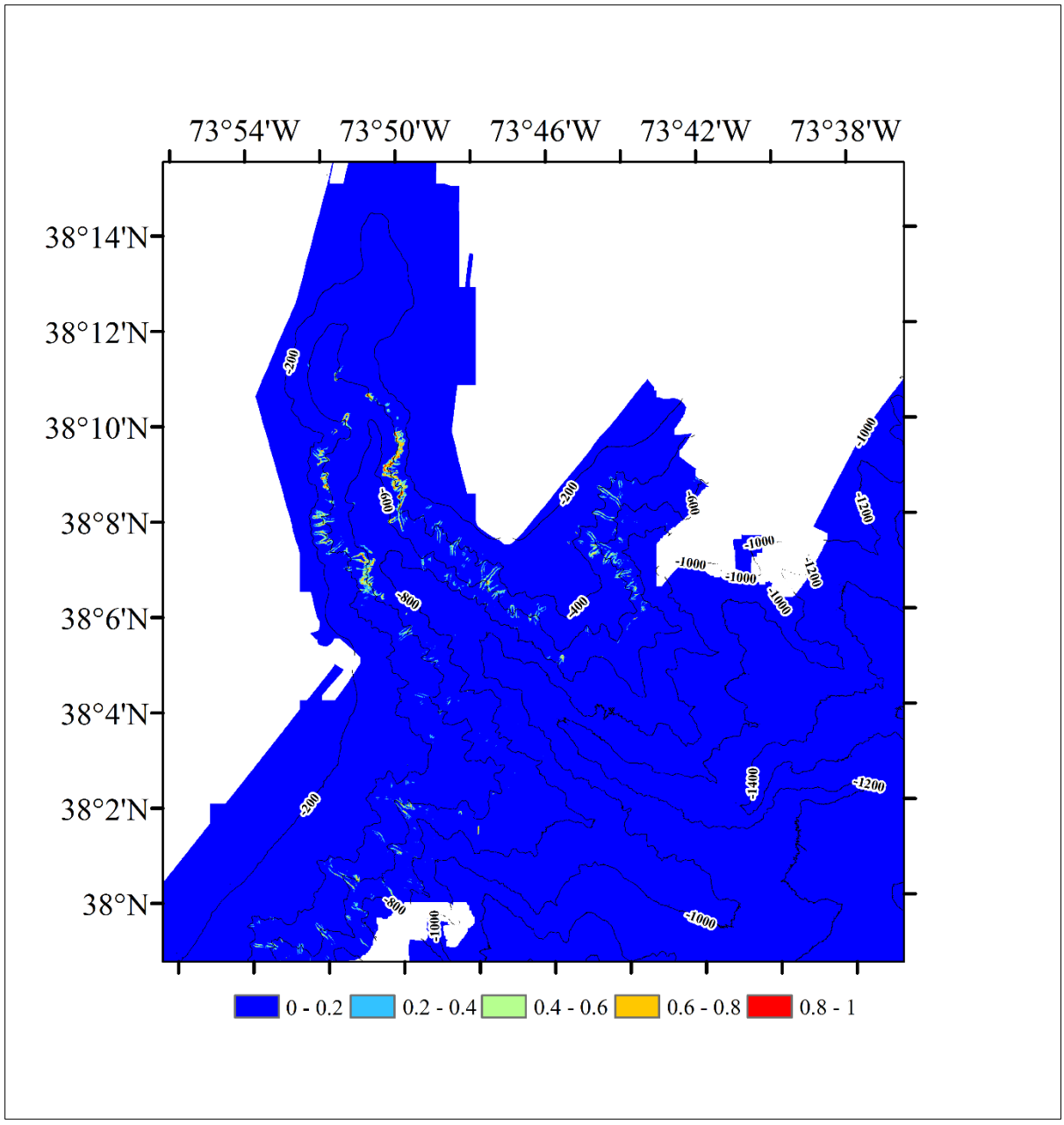

Figure 7-A8. The final scleractininan group Maxent prediction for Baltimore Canyon. (See **Table 7-A1** for evaluation statistics.)

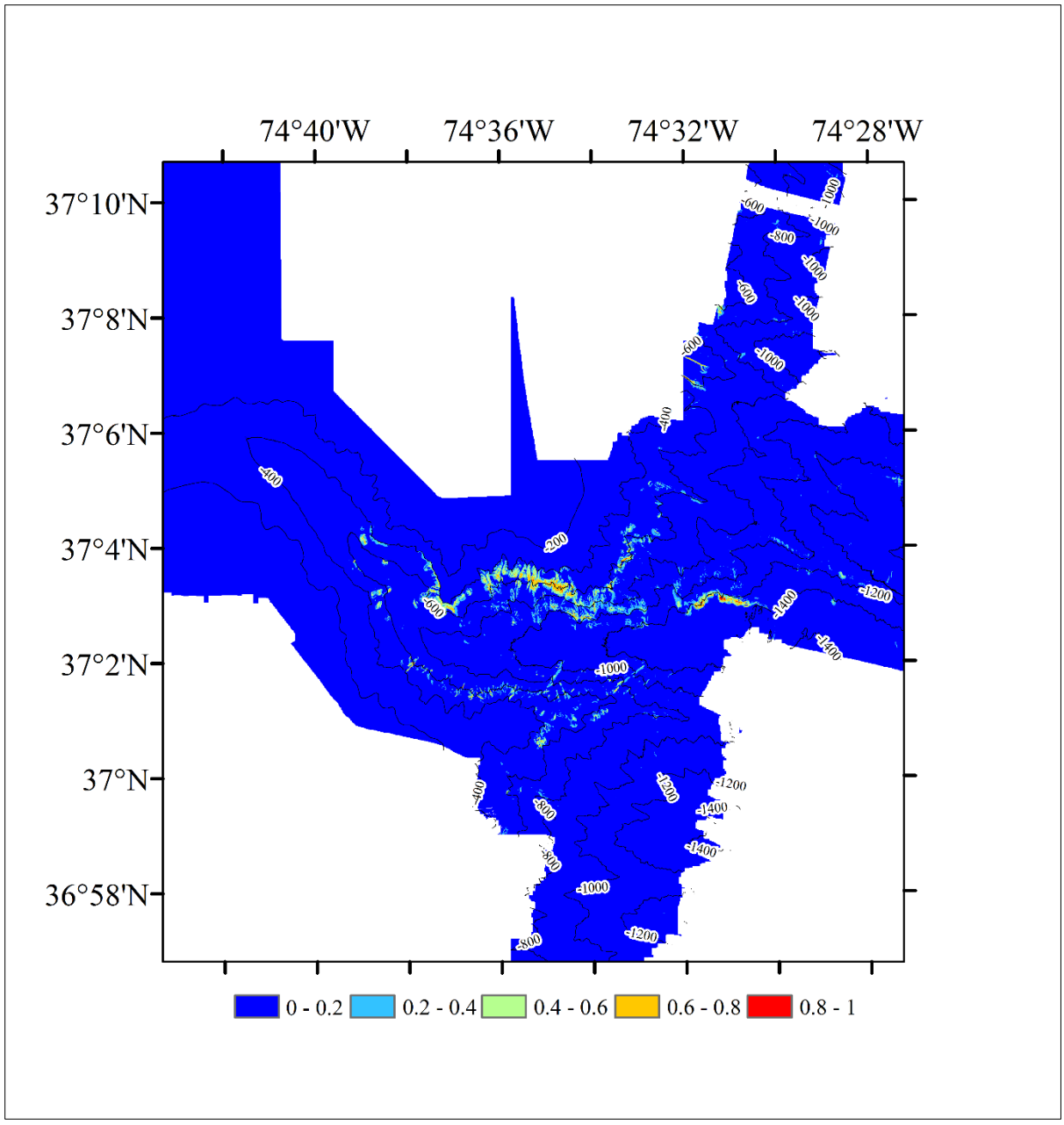

Figure 7-A9. The final *Acanthogorgia* Maxent prediction for Norfolk Canyon. (See **Table 7-A2** for evaluation statistics.)

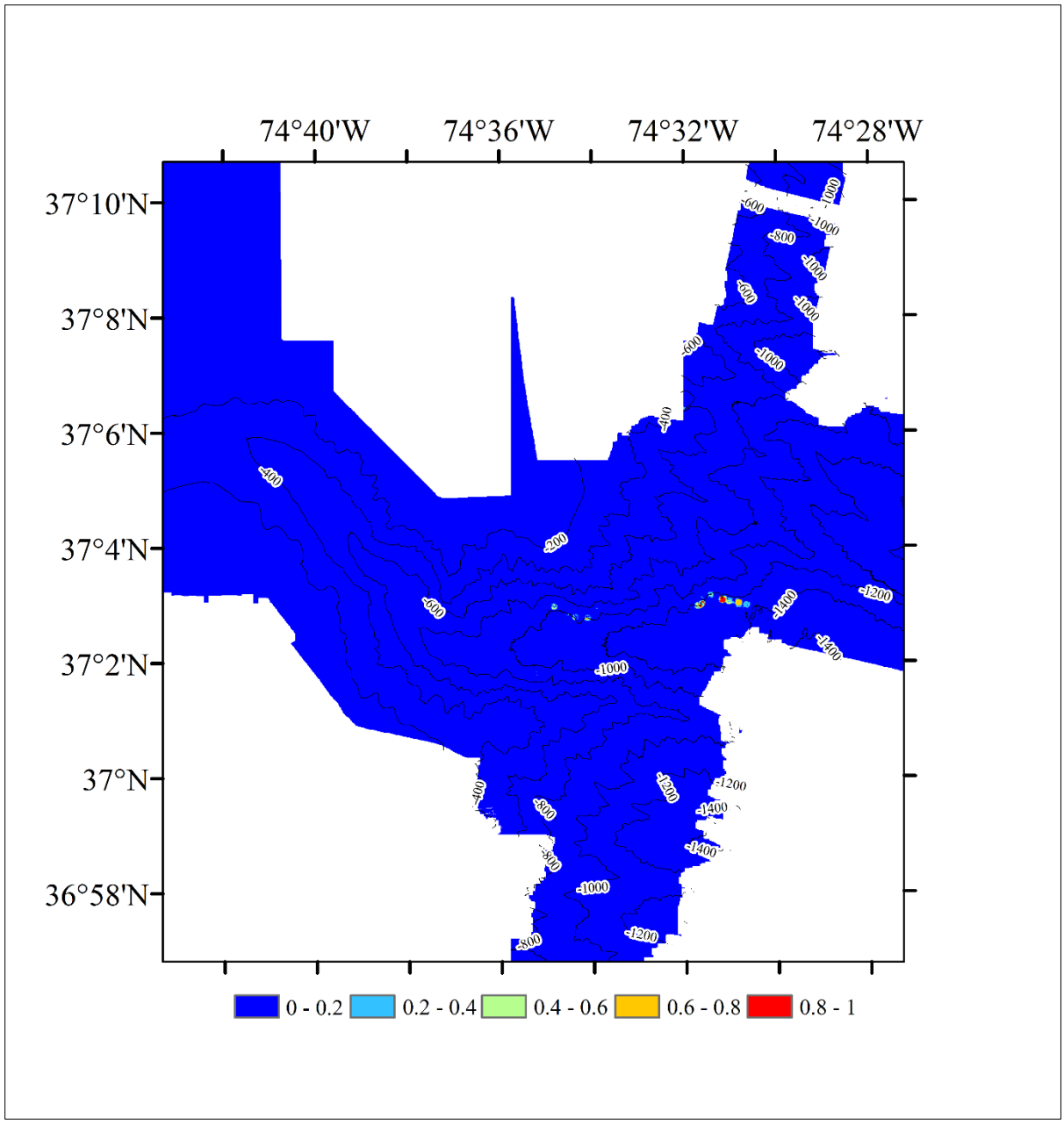

Figure 7-A10. The final *Anthomastus* Maxent prediction for Norfolk Canyon. (See **Table 7-A2** for evaluation statistics.)

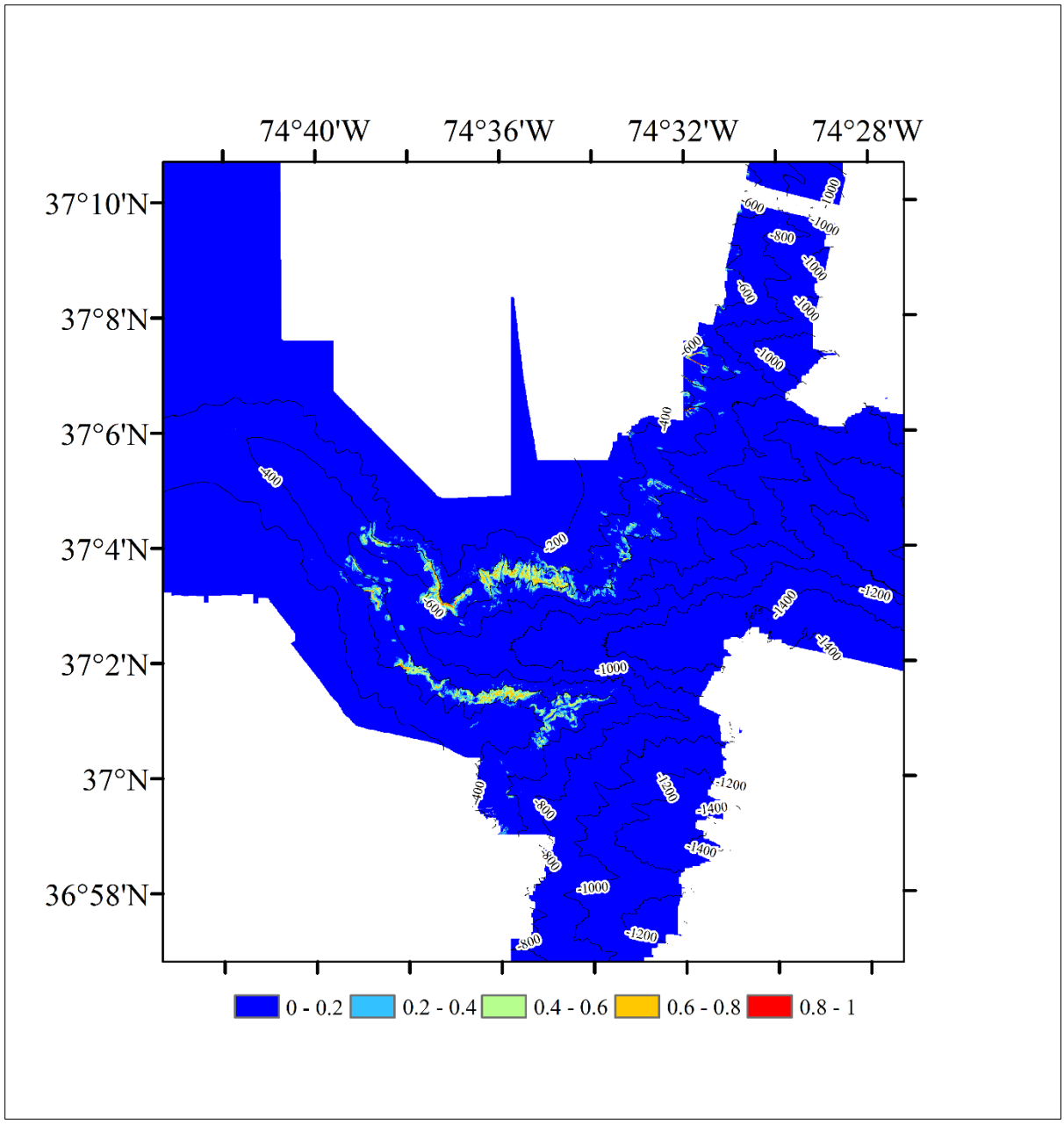

Figure 7-A11. The final *Anthothela* Maxent prediction for Norfolk Canyon. (See **Table 7-A2** for evaluation statistics.)

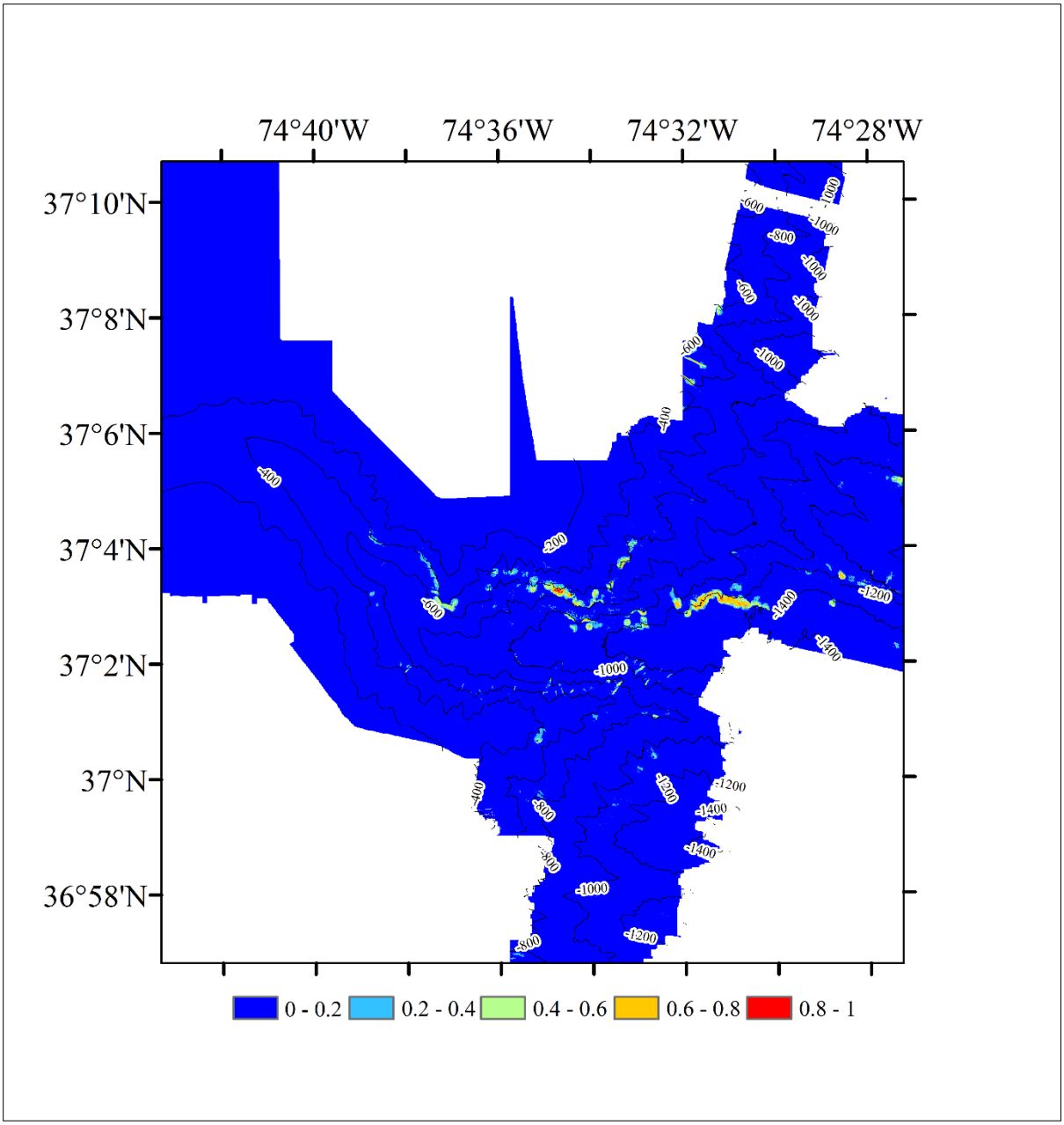

Figure 7-A12. The final *Desmophyllum* Maxent prediction for Norfolk Canyon. (See **Table 7-A2** for evaluation statistics.)

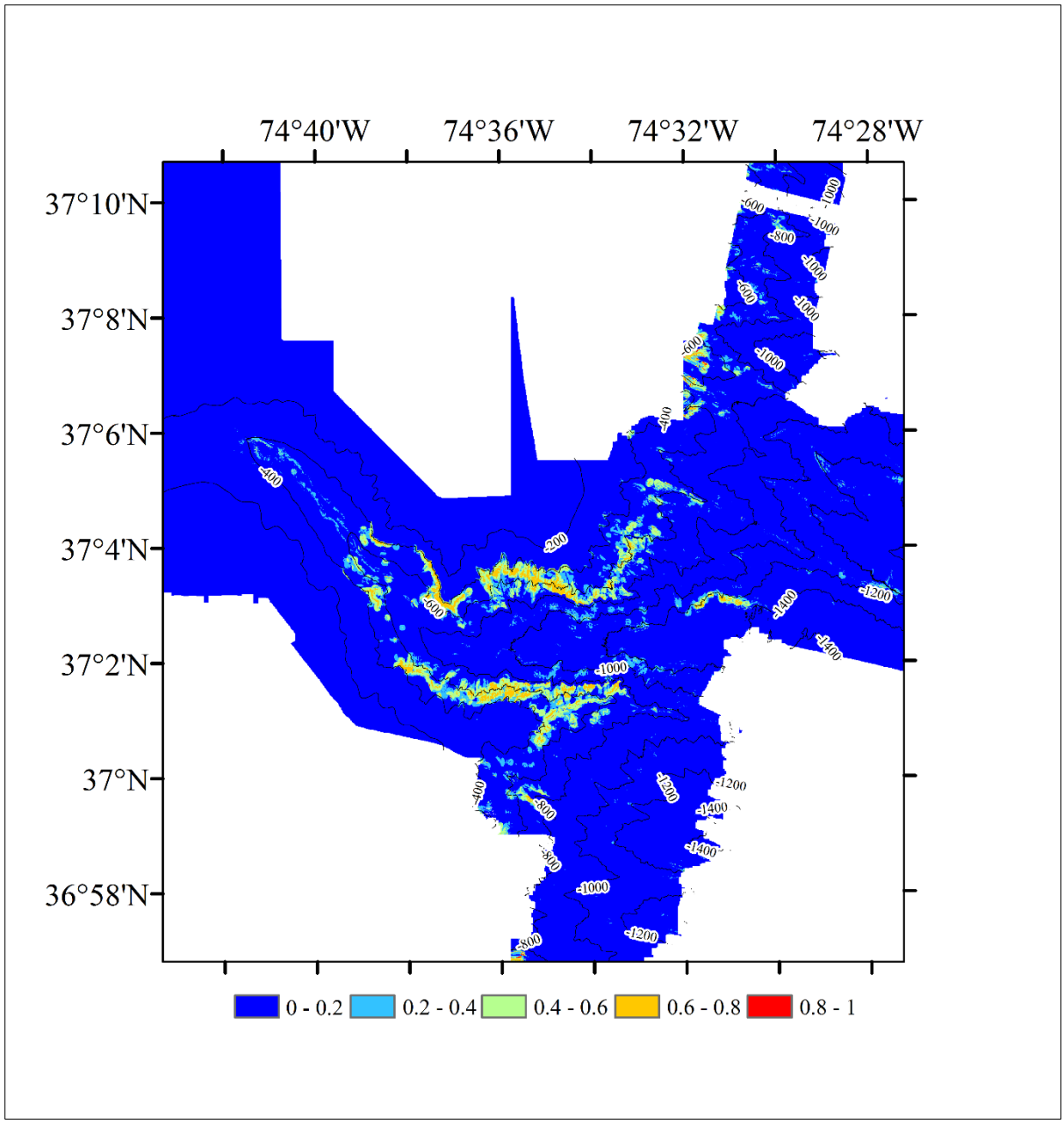

Figure 7-A13. The final hard substrate Maxent prediction for Norfolk Canyon. (See **Table 7-A2** for evaluation statistics.)

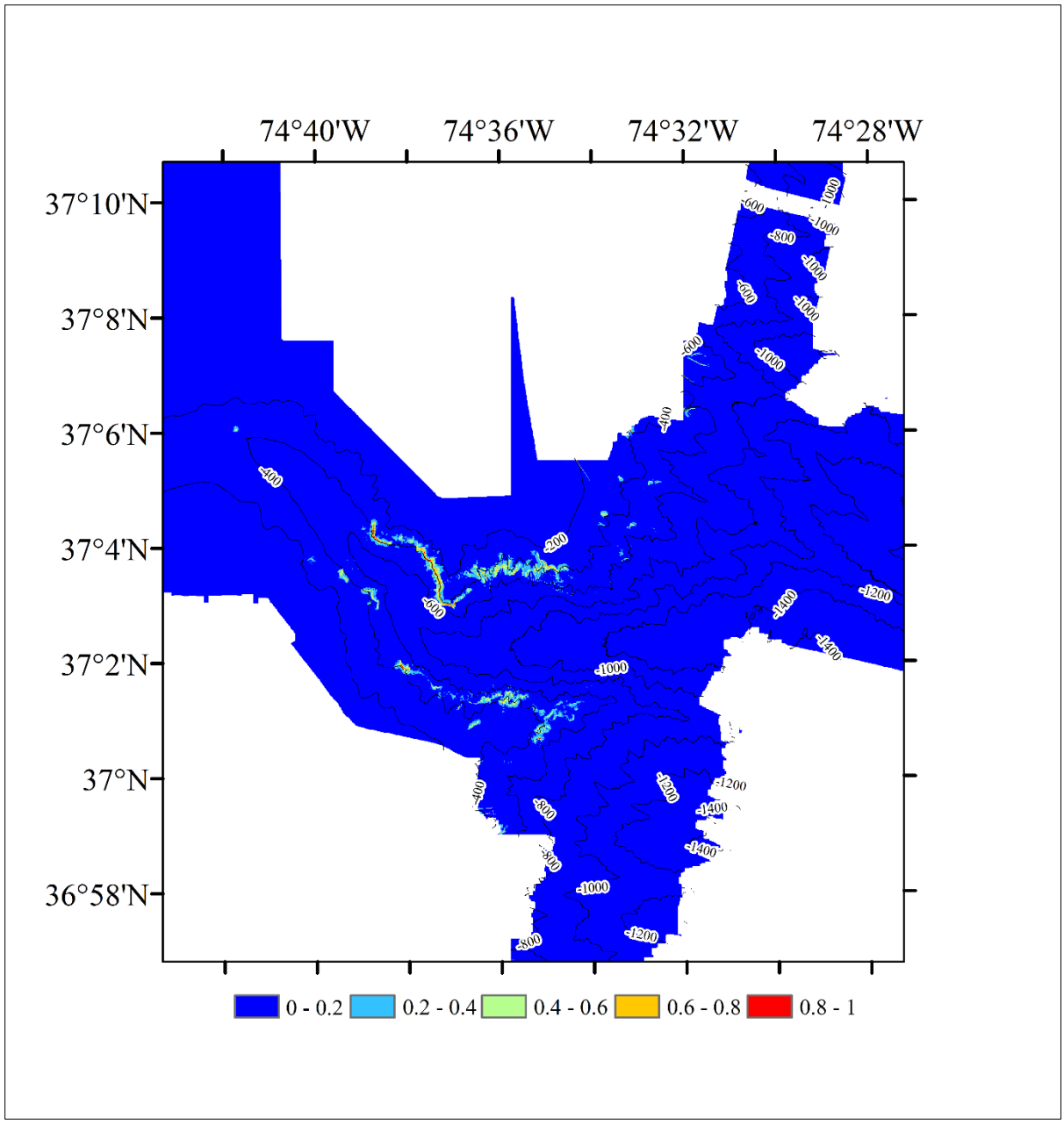

Figure 7-A14. The final *Lophelia* Maxent prediction for Norfolk Canyon. (See **Table 7-A2** for evaluation statistics.)

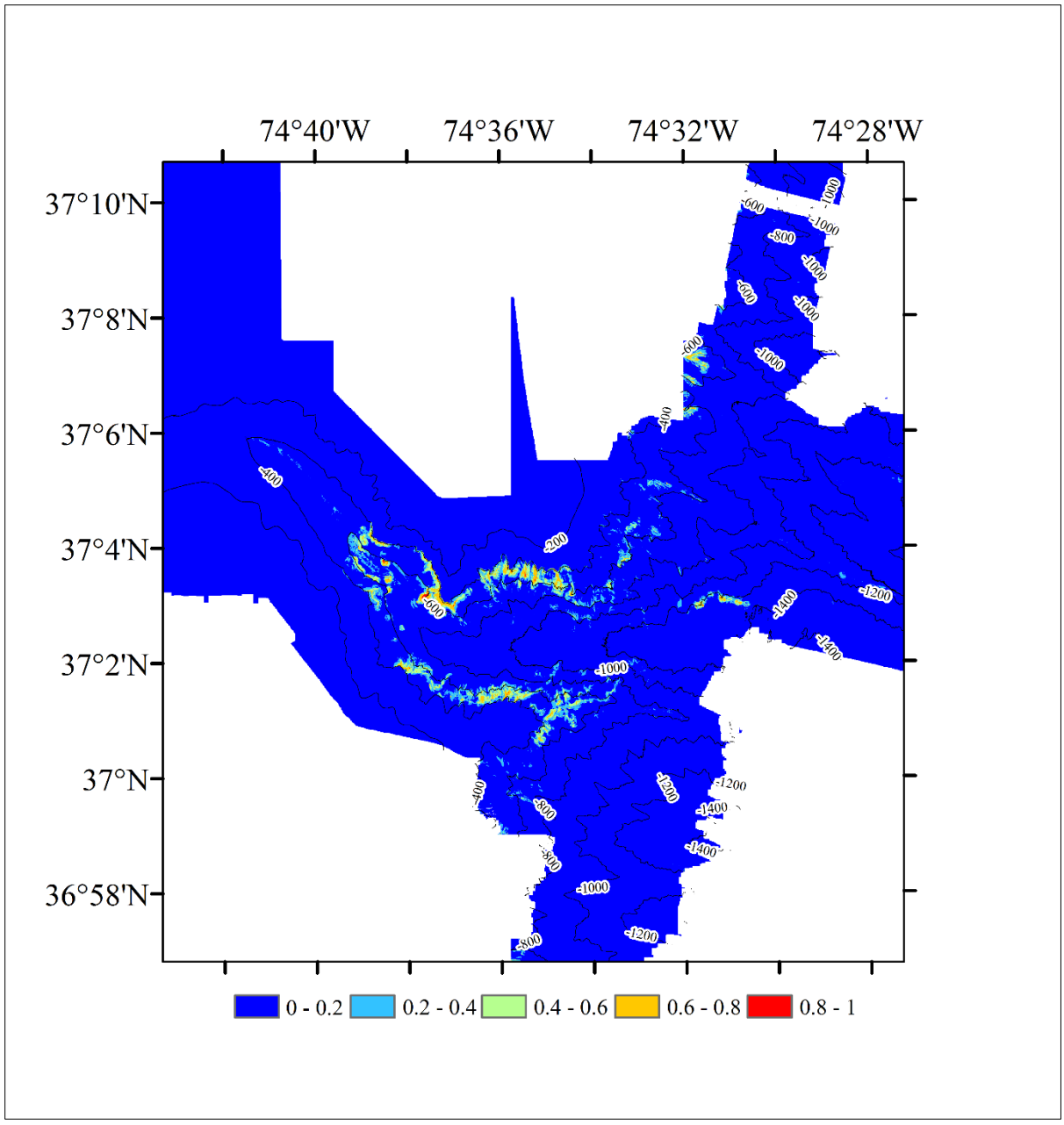

Figure 7-A15. The final octocoral group Maxent prediction for Norfolk Canyon. (See **Table 7-A2** for evaluation statistics.)

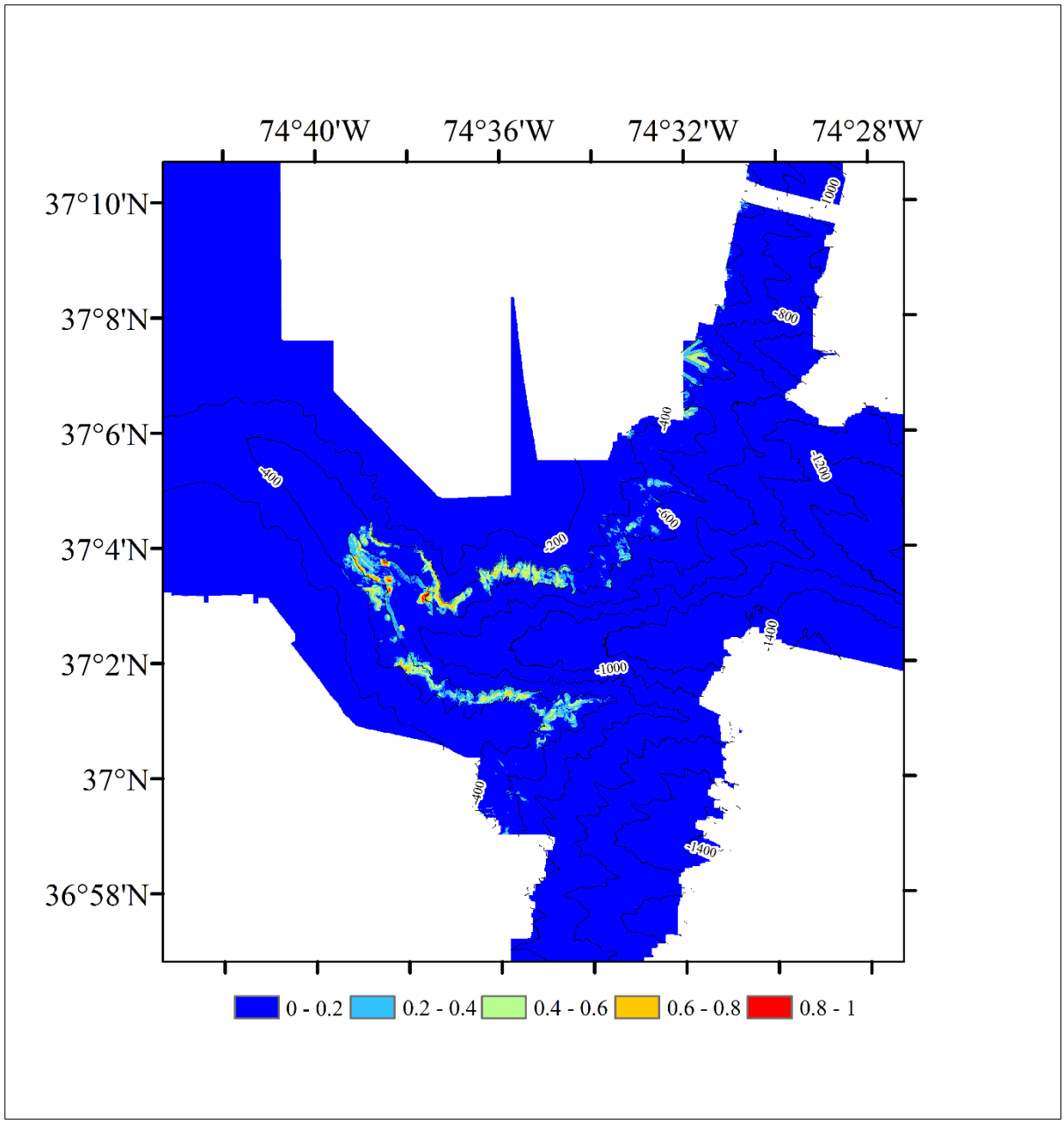

Figure 7-A16. The final *Paragorgia* Maxent prediction for Norfolk Canyon. (See **Table 7-A2** for evaluation statistics.)

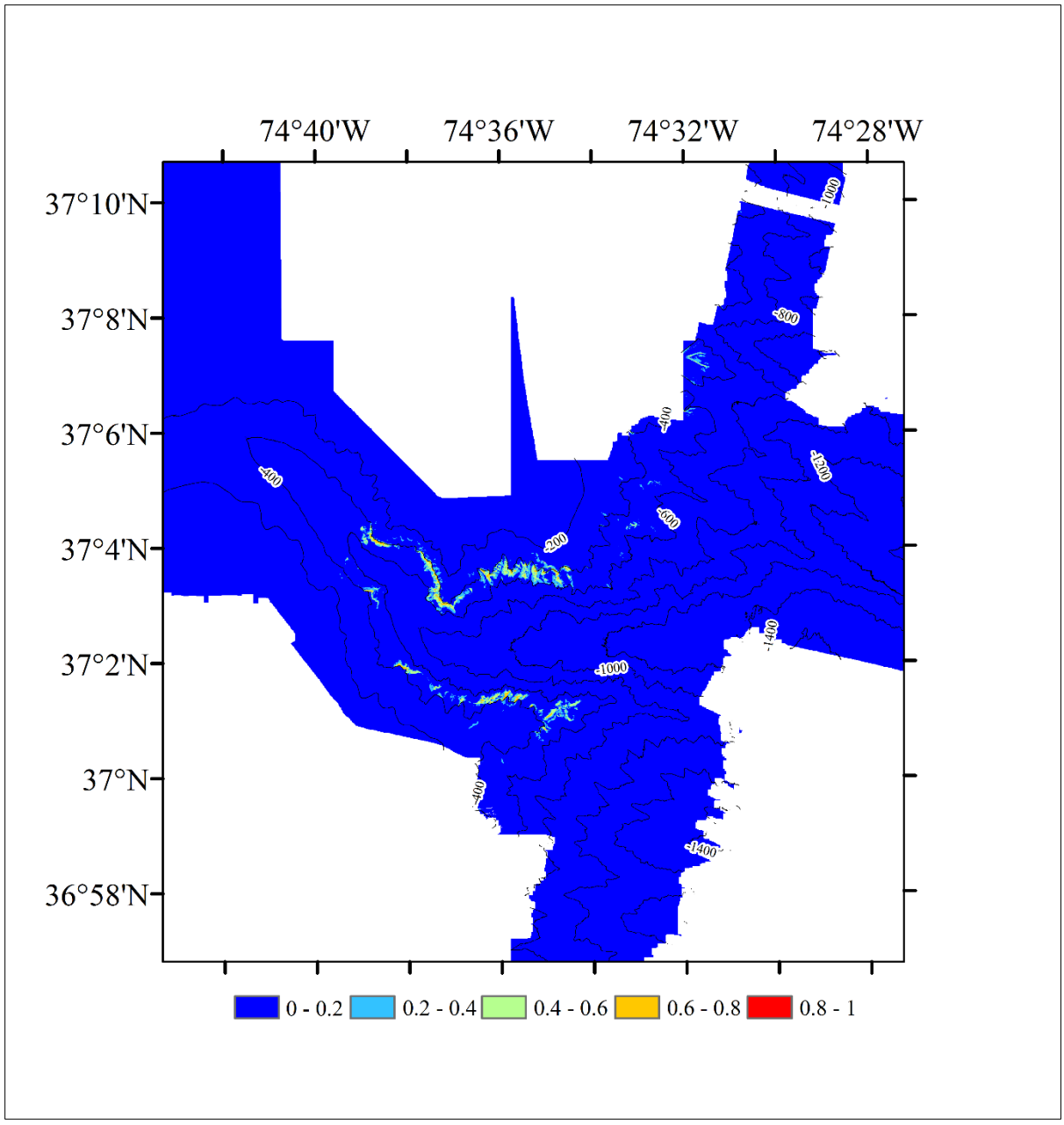

Figure 7-A17. The final *Primnoa* Maxent prediction for Norfolk Canyon. (See **Table 7-A2** for evaluation statistics.)

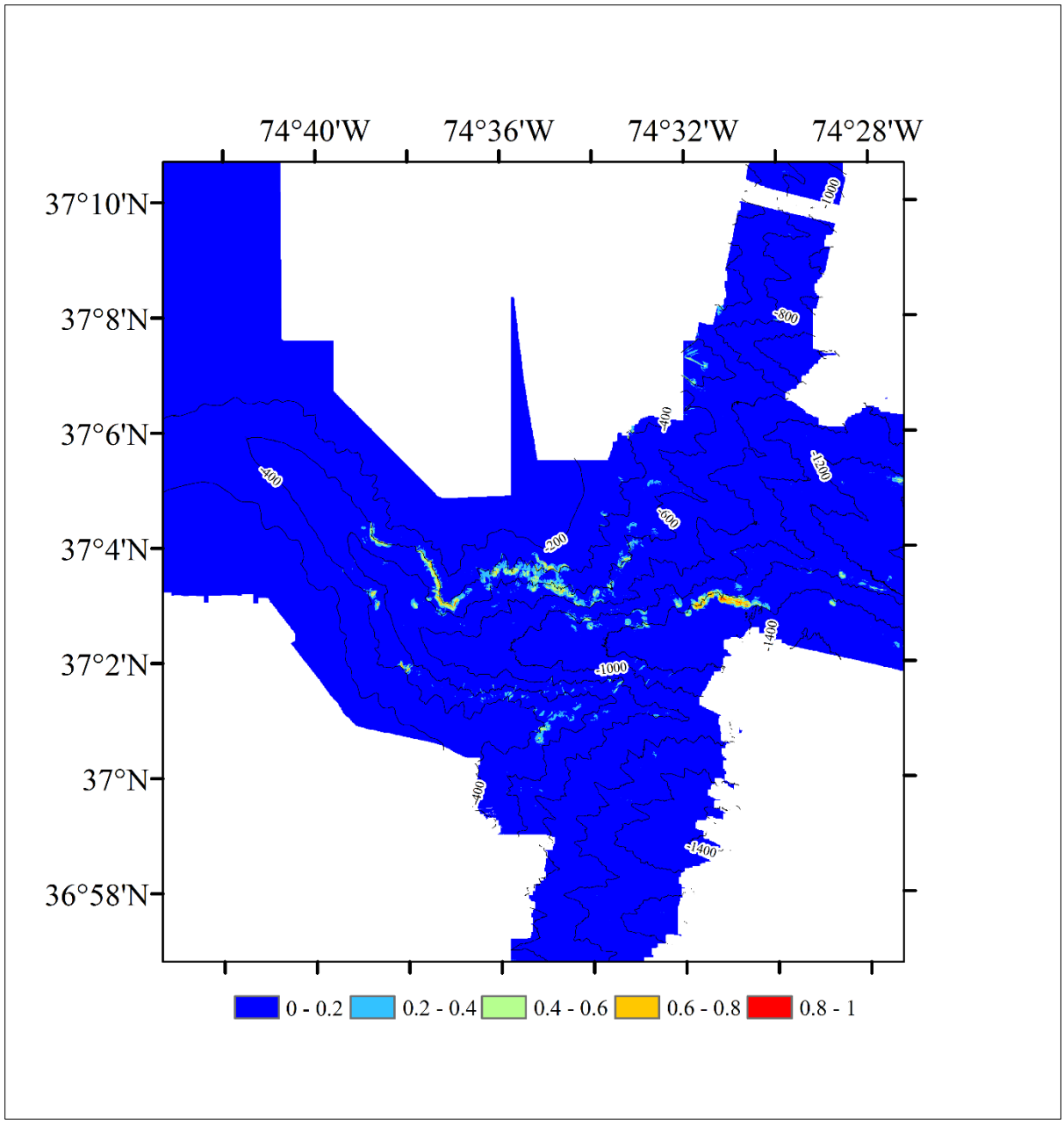

Figure 7-A18. The final scleractinian group Maxent prediction for Norfolk Canyon. (See **Table 7-A2** for evaluation statistics.)

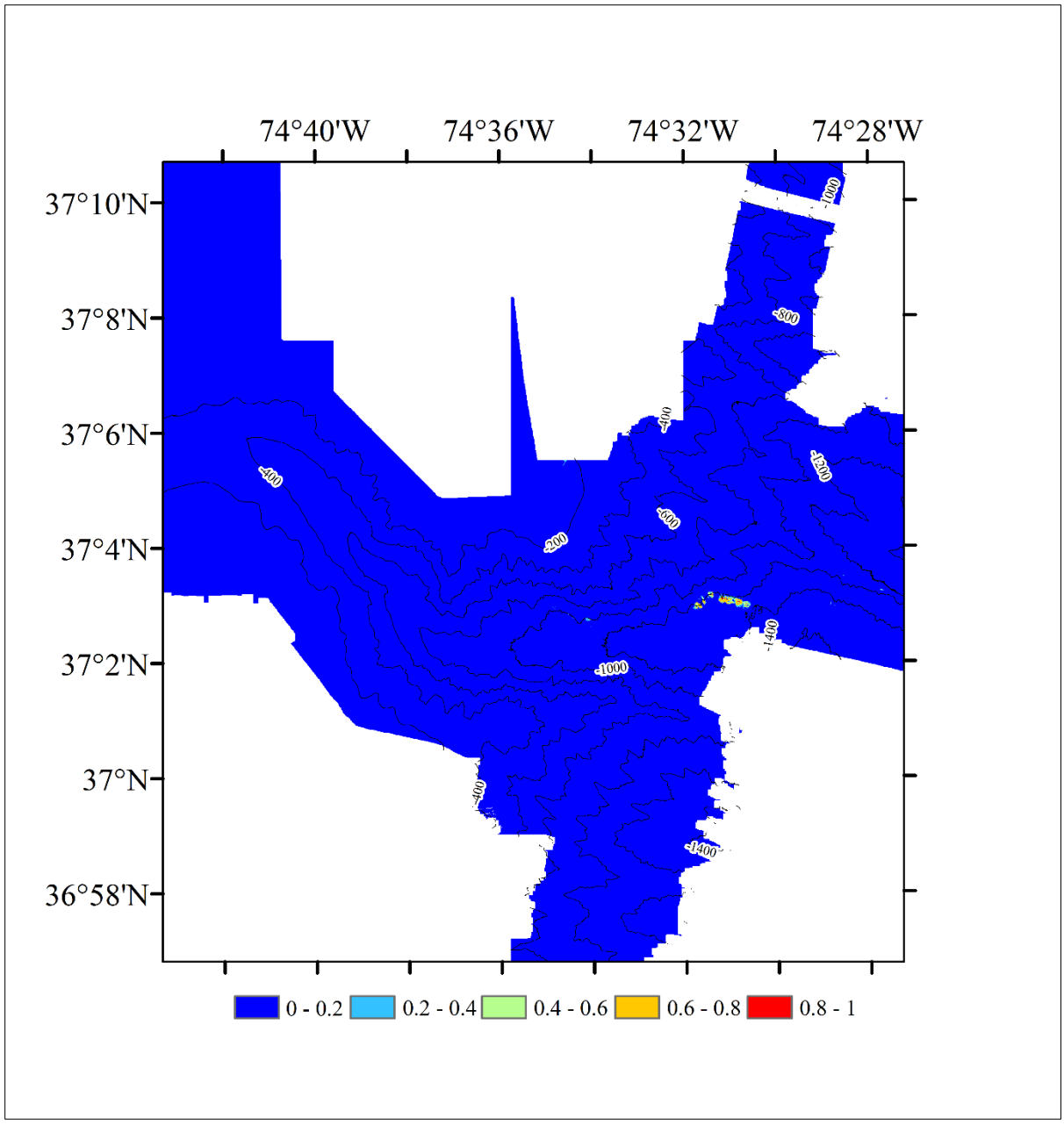

Figure 7-A19. The final *Solenosmilia* Maxent prediction for Norfolk Canyon. (See **Table 7-A2** for evaluation statistics.)

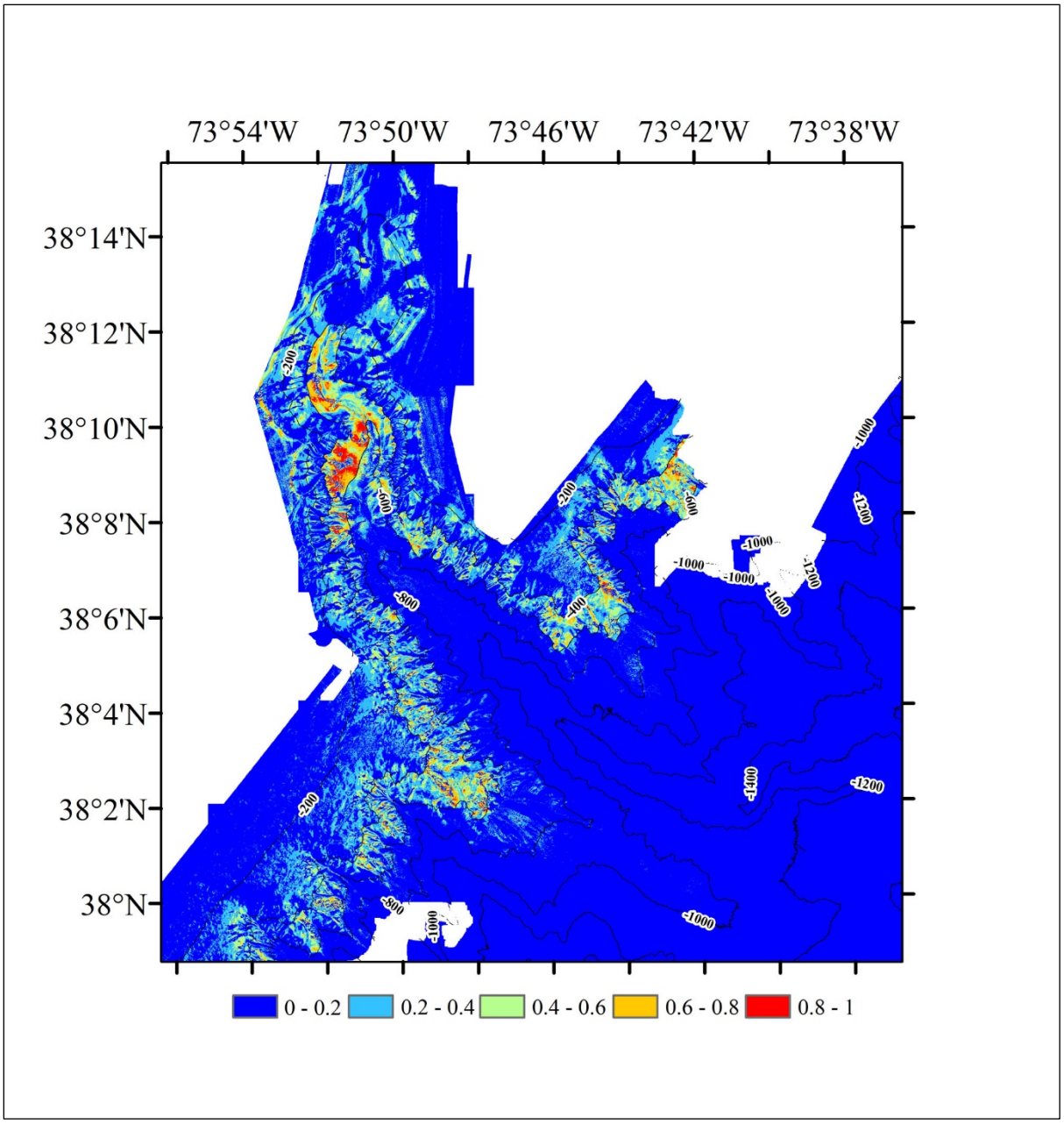

Figure 7-A20. The final historic faunal Maxent prediction for Baltimore Canyon. (See **Table 7-A3** for evaluation statistics.)

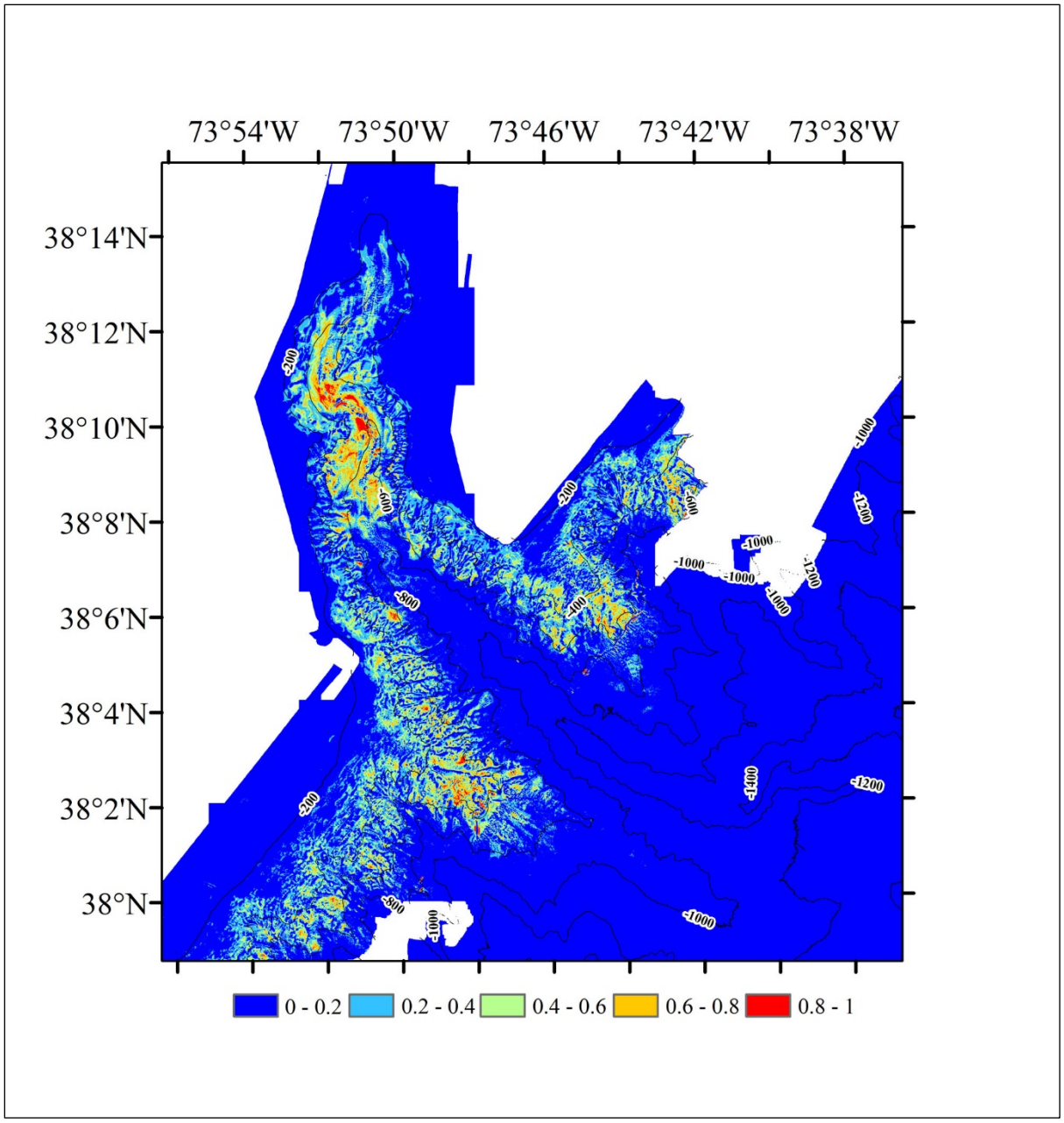

Figure 7-A21. The final historic hard ground Maxent prediction for Baltimore Canyon. (See **Table 7-A3** for evaluation statistics.)

Table 7-A1. Model evaluation statistics (means, values in parentheses are standard deviation) for the final Maxent models in Baltimore Canyon for each species or group based on previously selected variables. Certain variables (arag_stein, aspect_n, bpi_fine, tri, tri_riley and vrm_3×3) were not used by any model and are omitted from this table. "−" indicates that this variable was not used in the individual species model. (**Table 7-A1** was duplicated from **Table 7-4** for reader convenience.)

Variable	*Anthothela grandiflora*	*Desmophyllum dianthus*	Hard Substrate	Octocorals	*Paragorgia arborea*	*Paramuricea grandis*	*Primnoa resedaeformis*	Scleractinians
n Train (Test)	68.4 (7.6)	6 (1)	1,107 (123)	339.3 (37.7)	307.8 (34.2)	25.2 (2.8)	134.1 (14.9)	18.9 (2.1)
Training gain (SD)	3.984 (0.046)	4.34 (0.189)	4.34 (0.189)	2.918 (0.011)	3.098 (0.013)	4.873 (0.051)	3.709 (0.019)	4.337 (0.064)
Test AUC (SD)	0.992 (0.006)	0.998 (0.003)	0.938 (0.004)	0.98 (0.003)	0.982 (0.004)	0.997 (0.002)	0.991 (0.003)	0.996 (0.002)
aoxu	1.517 (0.04)	0.128 (0)	−	−	2.104 (0.01)	−	2.238 (0.019)	−
arag_orr	−	−	−	−	−	−	−	0.586 (0.041)
aspect_e	0.394 (0.034)	−	0.243 (0.007)	0.665 (0.011)	0.698 (0.02)	1.045 (0.096)	0.563 (0.037)	−
bpi_broad	−	−	0.48 (0.01)	−	0.703 (0.022)	2.806 (0.184)	0.91 (0.053)	−
calc_orr	−	0.934 (0)	−	−	−	−	−	−
calc_stein	1.667 (0.035)	−	−	2.098 (0.012)	2.166 (0.016)	2.3 (0.043)	2.136 (0.019)	−
depth	1.998 (0.041)	−	1.262 (0.003)	1.89 (0.01)	1.977 (0.009)	2.483 (0.038)	2.133 (0.02)	1.452 (0.046)
diso2	−	−	−	1.916 (0.011)	−	−	−	1.506 (0.065)
nit	−	−	−	−	−	−	−	1.404 (0.057)
phos	2.157 (0.065)	−	−	−	2.234 (0.011)	2.93 (0.028)	2.281 (0.014)	−
plan_curv	−	−	−	0.639 (0.022)	0.662 (0.015)	−	1.953 (0.037)	−
pos	−	−	−	−	−	3.379 (0.09)	−	−
prof_curv	0.288 (0.024)	0.19 (0.08)	−	−	−	−	−	0.325 (0.06)
roughness	−	1.809 (0.16)	−	−	−	−	−	−
rugosity	2.264 (0.055)	−	1.054 (0.009)	1.802 (0.01)	−	−	−	−
sal	−	0.448 (0.047)	−	−	−	−	−	−
sil	−	−	−	2.15 (0.016)	−	−	−	−
slope	2.248 (0.057)	1.839 (0.213)	1.03 (0.008)	1.776 (0.01)	−	1.291 (0.081)	−	2.896 (0.106)
slopevar	1.885 (0.069)	−	0.857 (0.008)	−	1.794 (0.017)	−	0.65 (0.029)	−
tang_curv	−	−	−	−	−	0.403 (0.051)	−	−
temp	1.8 (0.045)	−	−	2.109 (0.012)	2.216 (0.011)	2.731 (0.064)	2.358 (0.019)	1.156 (0.042)
tpi	−	−	−	0.57 (0.024)	−	−	−	0.85 (0.109)
vrm_21x21	−	−	−	1.537 (0.011)	1.549 (0.017)	3.115 (0.122)	1.984 (0.038)	2.648 (0.077)

Table 7-A2. Model evaluation statistics (means, values in parentheses are standard deviation) for the final Maxent models in Norfolk Canyon for each species or group based on previously selected variables (Variable vrm_21 × 21 was not used by any model and is omitted from this table). "−" indicates that this variable was not used in the individual species model. (**Table 7-A2** was duplicated from **Table 7-5** for reader convenience.)

Variable	*Acanthogorgia aspera*	*Anthomastus*	*Anthothela grandiflora*	*Desmophyllum dianthus*	Hard Substrate	*Lophelia pertusa*	Octocorals	*Paragorgia arborea*	*Primnoa resedaeformis*	Scleractinians	*Solenosmilia variabilis*
n Train (Test)	82.8 (9.2)	8 (1)	81 (9)	75.6 (8.4)	485.1 (53.9)	24.3 (2.7)	381.6 (42.4)	253.8 (28.2)	80.1 (8.9)	98.1 (10.9)	15.3 (1.7)
Training gain (SD)	3.446 (0.029)	5.309 (0.144)	3.526 (0.042)	3.597 (0.038)	3.597 (0.038)	4.13 (0.102)	2.569 (0.008)	2.917 (0.019)	3.913 (0.045)	3.483 (0.023)	5.665 (0.023)
Test AUC (SD)	0.989 (0.005)	0.999 (0.001)	0.99 (0.005)	0.987 (0.006)	0.965 (0.005)	0.996 (0.006)	0.976 (0.003)	0.979 (0.011)	0.989 (0.009)	0.988 (0.007)	0.999 (0.001)
aoxu	−	−	1.935 (0.046)	−	−	−	−	−	2.354 (0.019)	−	0.567 (0.012)
arag_orr	−	−	−	0.7 (0.017)	−	−	−	−	−	−	−
arag_stein	−	−	−	−	−	1.867 (0.043)	−	2.12 (0.02)	−	−	−
aspect_e	−	−	−	−	−	−	0.245 (0.012)	−	0.311 (0.048)	−	−
aspect_n	0.346 (0.02)	0.983 (0.049)	−	0.584 (0.034)	−	−	−	−	−	0.375 (0.029)	1.165 (0.022)
bpi_broad	−	0.14 (0.165)	−	−	−	0.535 (0.091)	0.473 (0.008)	−	−	−	−
bpi_fine	−	−	−	−	−	−	−	−	−	−	0.584 (0.12)
calc_orr	−	−	−	−	−	−	−	−	−	0.776 (0.018)	−
calc_stein	0.876 (0.018)	0.539 (0.025)	1.925 (0.05)	−	−	−	1.441 (0.016)	−	2.357 (0.045)	−	1.221 (0.041)
depth	0.932 (0.026)	0.386 (0.006)	2.061 (0.031)	0.985 (0.039)	1.244 (0.006)	2.168 (0.061)	1.523 (0.012)	2.028 (0.014)	2.574 (0.019)	1.075 (0.022)	1.494 (0.046)
diso2	0.495 (0.034)	0.64 (0.007)	−	0.582 (0.047)	−	1.542 (0.072)	−	−	−	0.895 (0.048)	−
nit	−	−	1.924 (0.061)	−	−	−	−	2.075 (0.023)	2.461 (0.022)	−	0.711 (0.021)
phos	0.875 (0.034)	−	−	−	−	−	−	−	−	1.066 (0.047)	−
plan_curv	−	−	−	−	−	−	−	−	0.741 (0.053)	−	−
pos	−	−	−	−	−	−	1.415 (0.018)	2.051 (0.025)	−	−	−
prof_curv	0.787 (0.06)	−	0.782 (0.036)	0.821 (0.037)	0.601 (0.014)	0.497 (0.061)	0.622 (0.021)	0.506 (0.019)	−	0.99 (0.041)	−
roughness	−	−	−	−	1.521 (0.017)	−	1.699 (0.024)	1.658 (0.026)	2.637 (0.059)	−	−
rugosity	2.555 (0.065)	−	2.496 (0.086)	2.586 (0.077)	−	−	−	−	−	2.506 (0.06)	−
sal	−	−	−	−	−	0.282 (0.046)	1.369 (0.019)	−	−	−	−
sil	−	−	−	0.435 (0.028)	−	−	−	−	−	−	−
slope	−	−	2.478 (0.087)	−	−	−	−	−	−	−	−
slopevar	2.619 (0.047)	3.213 (0.123)	2.095 (0.054)	3.045 (0.053)	1.678 (0.015)	2.251 (0.058)	1.738 (0.025)	1.685 (0.02)	2.445 (0.065)	2.837 (0.05)	4.4 (0.052)
tang_curv	−	−	−	−	−	−	−	−	−	−	0.022 (0.011)
temp	1.03 (0.037)	0.61 (0.005)	2.26 (0.043)	0.754 (0.025)	−	2.017 (0.057)	1.676 (0.018)	2.257 (0.023)	2.677 (0.017)	1.315 (0.064)	1.041 (0.032)
tpi	0.6 (0.051)	−	0.804 (0.045)	0.824 (0.048)	0.566 (0.016)	−	−	0.526 (0.021)	0.83 (0.06)	0.916 (0.045)	−
tri	−	−	−	−	−	2.43 (0.105)	−	−	−	−	−
tri_riley	−	−	−	−	−	−	−	−	−	−	3.695 (0.161)
vrm_3x3	−	0.619 (0.098)	−	−	−	1.555 (0.083)	−	−	−	−	−

Table 7-A3. Variable selection and model evaluation statistics for the historical fauna and hard grounds in Baltimore Canyon. Variable selection was using test area under curve (AUC) values from a Maxent model based on a single variable. Values in bold indicate highest scoring per group and were used in the final model. Underlined values indicate the variable that decreased the model gain the most when omitted from a model with all other variables; in situations where this was not the highest scoring variable in a group, this variable was used instead of the highest scoring variable providing it was >0.7. (**Table 7-A3** was duplicated from **Table 7-6** for reader convenience.)

Variable	Fauna AUC	Hard Substrate AUC	Fauna Gain	Hard Gain
n Train (Test)	–	–	40.5 (4.5)	25.2 (2.8)
Training gain (SD)	–	–	1.86 (0.08)	1.95 (0.062)
Test AUC (SD)	–	–	0.927 (0.05)	0.956 (0.026)
Bathymetry Variables				
depth	**0.903**	**0.95**	1.055 (0.031)	1.33 (0.046)
depth3x3_fm	0.902	0.95	–	–
stdev_elev	0.751	0.681	–	0.307 (0.028)
Terrain Variables − Orientation				
aspect	0.762	0.647	–	–
aspect_e	**0.818**	0.661	0.49 (0.043)	–
aspect_n	0.764	0.616	–	–
Terrain Variables − Curvature				
prof_curv	**0.795**	0.594	0.046 (0.006)	–
plan_curv	0.738	0.5	–	–
tang_curv	0.757	**0.71**	–	0.013 (0.001)
Terrain Variables − Slope				
slope	0.629	0.678	–	–
slope_perc	0.628	0.677	–	–
slopevar	0.643	**0.776**	–	0.234 (0.037)
stdev_slope	**0.749**	0.718	0.212 (0.039)	–
Terrain Variables – Topographic Position				
bpi_broad	0.66	0.68	–	–
bpi_fine	0.526	0.542	–	–
tpi	**0.82**	0.563	0.055 (0.006)	–
Terrain Variables – Variability				
roughness	0.65	0.607	–	–
rugosity	0.624	0.667	–	–
tri	0.621	0.677	–	–
tri_riley	**0.836**	**0.848**	0.536 (0.042)	0.641 (0.06)
vrm_3x3	0.815	0.764	–	–
vrm_21x21	0.747	0.737	–	–
Carbonate Chemistry Variables				
arag_stein	0.922	–	–	–
arag_orr	0.501	–	–	–
calc_stein	**0.923**	–	1.075 (0.028)	–
calc_orr	0.514	–	–	–

Table 7-A3. (Continued).

Variable	Fauna AUC	Hard Substrate AUC	Fauna Gain	Hard Gain
Chemical Variables				
nit	0.884	–	–	–
phos	0.896	–	–	–
sal	0.711	–	–	–
sil	**0.906**	–	0.959 (0.07)	–
Oxygen Variables				
aoxu	**0.875**	–	0.894 (0.046)	–
diso2	0.834	–	–	–
pos	0.85	–	–	–
Other Variables				
temp	**0.903**	–	0.973 (0.045)	–

This page intentionally left blank

CHAPTER 8. BENTHIC INVERTEBRATE COMMUNITIES

Sandra D. Brooke, Maya Wolf-Watts, Austin. D. Heil, Kirstin Meyer, Katharine Coykendall, Michael Rhode, Craig M. Young, and Steve W. Ross

8.1 INTRODUCTION

The complex interplay of physical and geological factors in canyon systems contributes to the observed patchiness in faunal assemblages (McClain and Barry 2010). Exposed hard substrates are common in some canyons and are generally found on the upper rims where currents are elevated, and sometimes in the axis where boulders have been carried by turbidity flows (Stanley and Fenner 1973, Hecker et al. 1980, Malahoff et al. 1982). Hard substrates may also occur on outcrops along canyon walls where currents keep substrate clear of sediment. Hard substrates often support dense communities of sessile suspension and filter feeders such as cnidarians and sponges, which provide habitat for other faunal assemblages. Extensive holes and tunnels occur in various locations and depths in most Mid-Atlantic Bight (MAB) canyons (Cacchione et al. 1978, Hecker et al. 1980, Malahoff et al. 1982) and are inhabited by several mobile species (Grimes et al. 1986). These excavations appear to be created primarily by red crabs (*Chaceon quinquedens*) and tilefish (*Lopholatilus chamaeloenticeps*) (Malahoff et al. 1982, Grimes et al. 1986). In soft sediments, burrowing animals maintain sediment aeration, increasing habitat suitability for other infauna. Fauna include occasional dense aggregations of sessile benthic megafauna such as pennatulid octocorals and burrowing cerianthid anemones (Mann 1982, Shepard et al. 1986, Wilson 1991) as well as abundant mobile fauna (Rowe 1972). The mobile invertebrate fauna of the western Atlantic canyons is dominated by echinoderms (sea cucumbers, sea urchins, brittle stars, and sea stars), many of which feed on organic material deposited in the sediment (Rowe 1972). The distribution of sessile hard bottom fauna along the slope of the northeastern United States has not been extensively studied (Hecker et al. 1980, 1983; Watling and Auster 2005, Packer et al. 2007). However, available information indicates that the dominant cnidarian taxa in the mid-Atlantic canyons are octocorals, solitary scleractinia, and anemones (Cairns 1981, Packer et al. 2007) rather than the reef-forming stony corals (*Lophelia pertusa*, *Enallopsammia profunda*) that dominate the southeastern United States or Gulf of Mexico (Brooke and Schroeder 2007, Ross and Nizinski 2007).

The National Oceanic and Atmospheric Administration (NOAA) ship *Okeanos Explorer* conducted multibeam surveys with water column backscatter between September 2011 and August 2013. During these surveys, several sites of gas bubble emissions were identified. More than 570 gas plumes were identified at water depths ranging from 50 to 1,700 m between North Carolina and New England. Four of these sites were surveyed in 2013, revealing large methane seeps with dense associated chemosynthetic fauna (Quattrini et al. 2015). Before these discoveries, only 3 methane seeps (also known as cold seeps) were known from the east coast of the United States: 2 in the Blake Ridge area (Van Dover et al. 2003, Brothers et al. 2013) and another putative site off the southern flank of Baltimore Canyon that was observed by Hecker during towed camera surveys in 1982 (Hecker et al. 1983). The Blake Ridge chemosynthetic fauna was dominated by beds of the large mussel *Bathymodiolus heckerae* and the small clam *Vesicomya* cf. *venusta*, and the relative importance of methanotrophy was slightly greater than thiotrophy (~60% vs. 40%). Gas hydrates were also observed at these sites, which were located at >2,000 m depth on the Blake Ridge Diapir. Chemosynthetic ecosystems (in addition to deepwater corals) are defined as “high-density deepwater (>300 m) benthic communities” by the Bureau of Ocean Energy Management (BOEM) and are protected from direct damage by energy industry activities through a Notice to Lessees and Operators (2009-G40) issued by BOEM to holders of federal mineral leases. The Baltimore seep site was therefore targeted for exploration in 2012 as part of the 2012 sampling cruise for the Atlantic Deepwater Canyons study. Two large bubble plumes were identified near the mouth of Norfolk Canyon during the NOAA 2013 multibeam surveys (Skarke et al., 2014); this site also was explored during 2013 Sampling Cruise (Vol. II, Appendix A).

Identification of species through morphological features has historically been the only available method to classify organisms. In recent years, genetic analysis has supplemented and sometimes supplanted the traditional approaches to taxonomic classification. DNA barcoding has become an increasingly popular, and oftentimes controversial, method that seeks to unite species identification. DNA barcoding uses a short standard, unique genetic sequence (i.e., barcode) to aid in taxonomic identification, uncover cryptic diversity, and quantify and standardize levels of intra- and interspecific genetic diversity when considering species delineations (Savolainen et al. 2005). The mitochondrial cytochrome oxidase subunit 1 (mtCOI) gene has been the barcode gold standard because of its ubiquity and level of polymorphism in the animal kingdom. A wealth of DNA barcoding studies has been performed and are underway, as evidenced by The Barcode of Life Data System (BOLD) database (Ratnasingham and Hebert 2007), which contains 4.4 million barcode sequences from over 247,000 formally described species as of 8 October 2015. In the Atlantic Deepwater Canyons study, mtCOI barcodes are provided for urchin and mussel samples collected from the mid-Atlantic canyons (MAC) to add to the genetic resources available for deepsea species from the western Atlantic Ocean, put the species into phylogenetic context, and quantify intraspecific genetic diversity, where possible.

In addition to natural habitats, the MAB includes many shipwrecks and other artificial substrate. This chapter discusses approaches used to identify and document the distribution of different habitat types encountered in the canyons and describes sessile and mobile invertebrate fauna associated with each type of habitat, for both natural and artificial substrate. Most shipwrecks studied (the Billy Mitchell-Project B fleet, **Chapter 4**) were sunk within a month of each other; therefore, comparisons of their associated biological communities are not confounded by length of time on the seafloor. Community differences may be influenced by physical or biological factors such as currents, availability of particulate food, larval dispersal and settlement, or competition. Data on invertebrate megafaunal distribution from both natural and artificial substrate will be examined in the context of habitat type, environmental variables, and, where available, reproductive biology and larval lifespan, to provide insight into the mechanisms that drive the observed distributions.

8.2 METHODS

8.2.1 Habitat Characterization

8.2.1.1 Natural Substrate

During the 2012 sampling cruise, 20 dives were conducted during Leg 1 and Leg 2 using the remotely operated vehicle (ROV) *Kraken 2*. Eighteen dives were made in Baltimore Canyon and two in Norfolk Canyon. Fifteen of the Baltimore Canyon dives targeted coral and hard bottom habitats (covering a depth ranging from 234 to 1,001 m), and the remaining three dives focused on the methane seep area (412 to 434 m). During the 2013 sampling cruise, 13 dives were conducted using the ROV *Jason II*, three of which were methane seep dives (two in Norfolk Canyon, 1,421 to 1,612 m; one in Baltimore Canyon, 353 to 441 m) and one was a coral-targeted dive in Baltimore Canyon (288 to 388 m). The remaining nine dives focused on coral and hard bottom habitats in Norfolk Canyon and covered a depth ranging from 320 to 1,390 m (see project cruise reports in Volume II Appendices A, B, and C and **Chapter 3** for details of the cruises).

The ROV navigation files (which recorded latitude, longitude, and depth) and the dive videos were synchronized via their time codes so that position and depth data could be assigned to observations on the video. ROV navigation time was recorded in Greenwich Mean Time (GMT) and was translated into Eastern Standard Time (EST) for the habitat and faunal analysis because EST was more biologically relevant and allowed for ease of comparison with other data. The video data were “cleaned” by removing all unusable video footage and sections where the ROV was stationary (usually for sampling). The remainder of the video was categorized into one of six geological habitat types (**Table 8-1**; **Figure 8-1**).

These habitats were modified from those used in the historical data analysis (**Chapter 2**) because some were not relevant, and others did not precisely capture the habitats observed in the canyons. In addition to the habitat descriptions, video data were further classified according to percent cover (<25%, 25% to 75%, >75%) of structure-forming cnidarians (SFC) and category of SFC (large corals, large anemones/cup corals, and mixed). The habitat type and SFC categories are described in **Table 8-1**. The habitat analysis generated georeferenced habitat types and percent cover of SFC, which were used to create maps of dive tracks with habitat and SFC superimposed on bathymetry.

Processing video of the cold seeps discovered in 2012 (Baltimore Canyon) and 2013 (Norfolk Canyon) was performed in the same manner as for the general canyons dives, but the geological habitat types were different, as were the percent cover categories. The cold-seep habitats were either soft sediment or mixed soft sediment and hard substrate with different percentages (0%, <25%, 25% to 75%, >75%) of dead mussels (**Figure 8-2**). In addition, there were four categories (0%, <25%, 25% to 75%, >75%) of live mussel cover (**Table 8-2**).

Table 8-1. Habitat characterization codes used for coral-targeted dives.

Habitat Type	
S	Soft sediment with no hard substrate visible. Slope may be flat to steep.
SR	Soft sediment with small pieces of rock or emergent hard substrate (EHS). < 50% cover of hard substrate. Slope may be flat to steep.
R	Isolated rock, rubble, EHS. > 50% cover of hard substrate. Slope may be flat to steep.
PB	Large areas of EHS or consolidated sediment that forms hard pavement. >50% cover of hard substrate. Slope may be flat to steep.
B	Large boulder of rock or consolidated sediment. Slope may be flat to steep.
W	Walls and steep slopes (rock or consolidated sediment), steep profile.
Categories of Structure-Forming Cnidarians (SFC)	
1	0
2	<25% cover
3	25% to 75% cover
4	>75% cover
TC	Large corals: *Paragorgia, Primnoa, Anthothela, Paramuricea, Lophelia, Solenosmilia*
LA	Large anemones and small corals: Cerianthids, *Actinoscyphia, Bolocera,* cup corals
M	Mix of TC and LA

Table 8-2. Habitat characterization codes used for seep-targeted dives.

Habitat Type	
S	Soft sediment, no mussels.
SDM1	Soft sediment with <25% dead mussel shells.
SDM2	Soft sediment with 25–75% dead mussel shells.
SDM3	Soft sediment with >75% dead mussel shells.
MS	Mixed soft sediment and hard substrate, no mussels.
MSDM1	Mixed soft sediment and hard substrate with <25% dead mussel shells.
MSDM2	Mixed soft sediment and hard substrate with 25–75% dead mussel shells.
MSDM3	Mixed soft sediment and hard substrate >75% dead mussel shells.
Categories of Live Mussel Cover	
LM0	0
LM1	<25% cover
LM2	25% to 75% cover
LM3	>75% cover

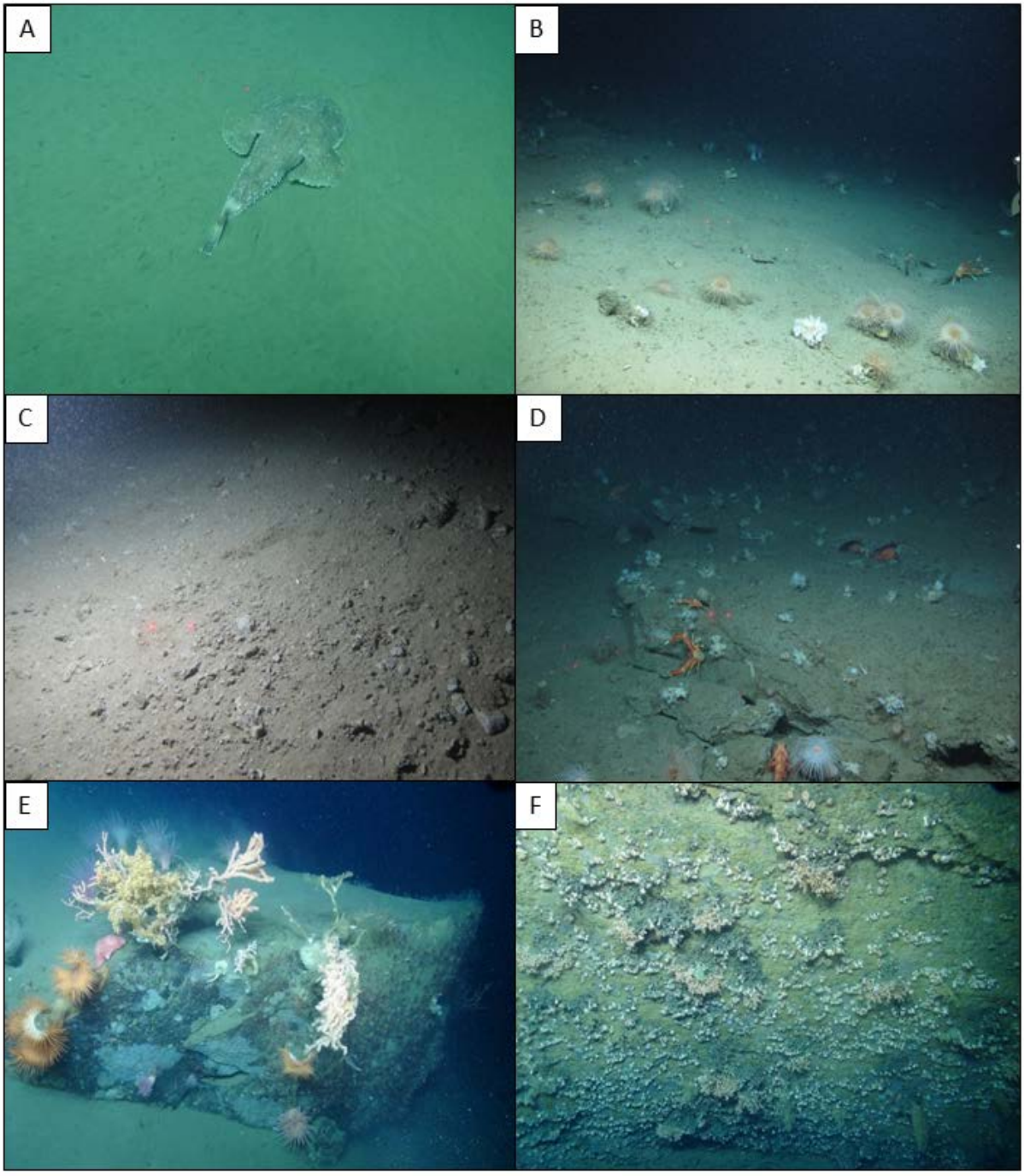

Figure 8-1. Examples of different canyon habitat types: A) S: soft sediment with no hard substrate visible, B) SR: soft sediment with small pieces of rock or emergent hard substrate C) R: isolated rock, rubble >50% cover of hard substrate, D) PB: large areas of hard substrate >50% cover, E) B: large boulder of rock or consolidated sediment, and F) W: walls and steep slopes.

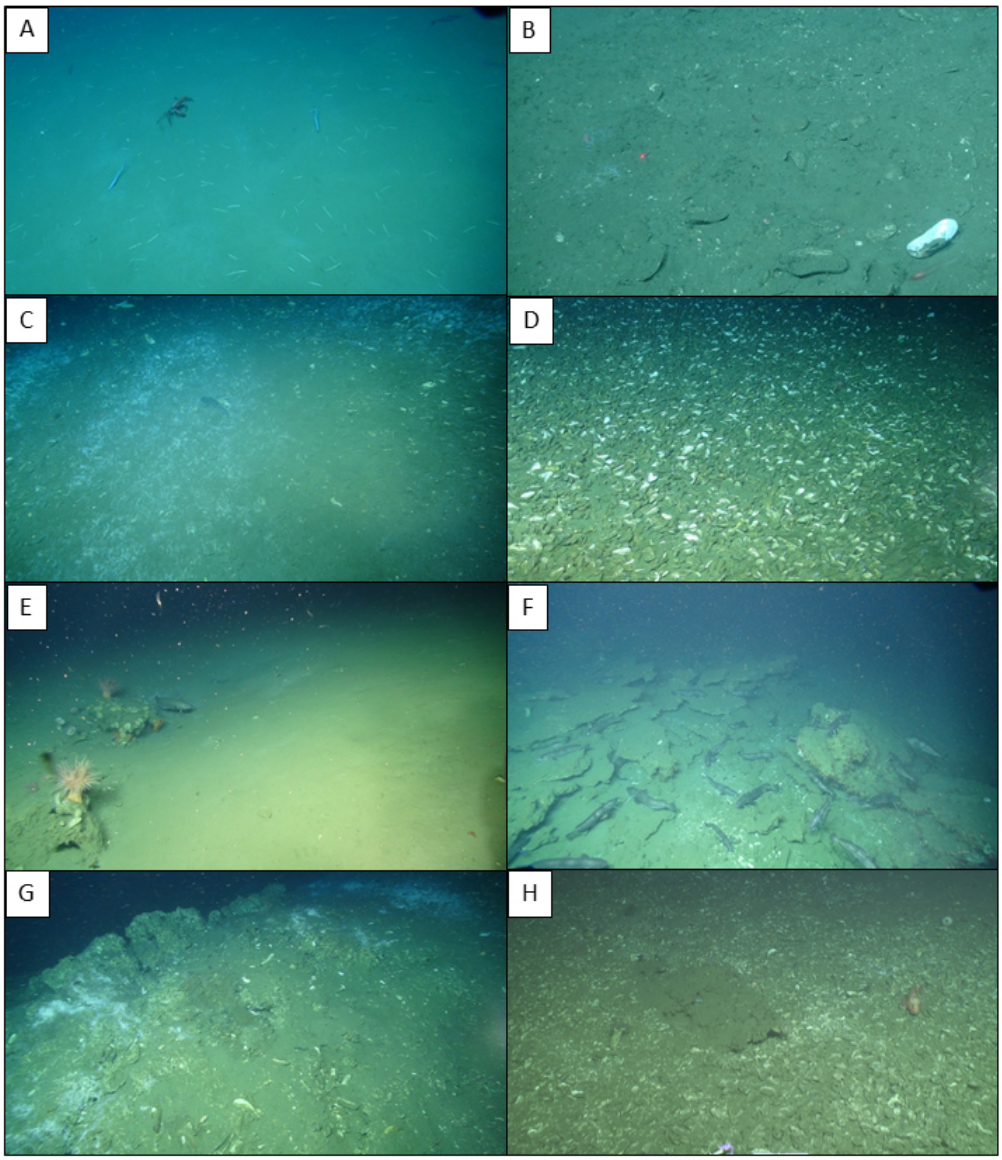

Figure 8-2. Cold-seep habitat types: A) S: soft sediment with no mussels, B) SDM1: soft sediment with <25% dead mussel shells, C) SDM2: soft sediment with 25% to 75% dead mussel shells, D) SDM3: soft sediment with >75% dead mussel shells, E) MS: mixed soft sediment and hard substrate, no mussels, F) MSDM1: mixed soft sediment and hard substrate with <25% dead mussel shells, G) MSDM2: mixed soft sediment and hard substrate with 25% to 75% dead mussel shells, and H) MSDM3: mixed soft sediment and hard substrate >75% dead mussel shells.

8.2.1.2 Artificial Substrate

Video recorded by *Kraken 2* and *Jason II* ROVs of eight shipwrecks during the 2012 and 2013 sampling cruises was analyzed to describe the invertebrate megafaunal communities present on shipwrecks (**Table 8-3**). Video was converted into still images by taking frame grabs. In 2012, the archaeology ROV dives did not conduct dedicated transects for biological objectives; therefore, videos were recorded with no consistent speed or distance from the shipwrecks, and the ROV's lasers remained off for most of each dive. To analyze the 2012 ROV videos, frame grabs were obtained from each video whenever the surface of the shipwreck came into clear view. Frame grabs that were too far away or close

to the shipwreck, such that the invertebrate megafauna could not be clearly discerned, were excluded from analysis. Thirty eligible frame grabs were then randomly subselected from each shipwreck and analyzed. In 2013, a subset of the shipwrecks was revisited with the *Jason II* ROV and a portion of each ROV dive was allocated for biological objectives (a total of four transects was recorded from three shipwrecks). Nonoverlapping frame grabs were obtained from the ROV video, and 40 frame grabs were randomly subselected from each transect. The adequate number of frame grabs was determined by the rarefaction curves. In 2012, 30 frames were required for the species accumulation curves to reach the asymptote, but in 2013, 40 frames were required.

Table 8-3. Shipwrecks surveyed to document history and biology during the 2012 and 2013 sampling cruises for the Atlantic Deepwater Canyons study.

Shipwreck Number	Survey Date	ROV Dive Number	ROV	Shipwreck Type	Max. Height Above Seafloor (m)
W1	22 Sept 2012	ROV-2012-NF-22	*Kraken 2*	Submarine	No data
W2	23 Sept 2012	ROV-2012-NF-23	*Kraken 2*	Battleship	18
W3	24 Sept 2012	ROV-2012-NF-24	*Kraken 2*	Cruiser	7
W4	26 Sept 2012	ROV-2012-NF-26	*Kraken 2*	Destroyer	3
W5-1	26 Sept 2012	ROV-2012-NF-27	*Kraken 2*	Destroyer	3
W5-2	26 Sept 2012	ROV-2012-NF-27	*Kraken 2*	Destroyer	2
W6	27 Sept 2012	ROV-2012-NF-29	*Kraken 2*	Battleship	No data
W7	28 Sept 2012	ROV-2012-NF-30	*Kraken 2*	Submarine	3
W4	20 May 2013	ROV-2013-J2-692	*Jason II*	Destroyer	3
W2	21 May 2013	ROV-2013-J2-693	*Jason II*	Battleship	18
W5-1	23 May 2013	ROV-2013-J2-695	*Jason II*	Destroyer	3

Two hundred random points were overlain on each image, and the percentage of points belonging to the same plane was calculated. One hundred minus this number was interpreted as an estimate of shipwreck surface complexity. The points that intersected a net or other lost fishing gear were also counted, and the approximate percent cover of fishing gear was calculated. Frame grabs were categorized according to whether they showed the top, middle, or bottom of the respective shipwrecks. “Bottom” was defined as a frame grab in which the seafloor was visible or was known to be directly adjacent to the seafloor based on video context. “Top” was defined similarly for frame grabs in which the water column above the shipwreck was visible or was known to be located at the top of the shipwreck based on video context; all other frame grabs were defined as “middle.” In addition, frame grabs were categorized according to whether they featured a vertical, horizontal, slanted, or complex surface; the underside of the shipwreck; or a structure that protruded from the shipwreck (referred to as a “pillar”). Frame grabs also were classified by which side of the shipwreck they originated from north versus south and east versus west.

8.2.1.3 Physical Environment

Data for physical variables around the habitats of interest were collected with a Sea-Bird Electronics, Inc. SBE 19*plus* data logger, which was attached to the ROV and collected high-frequency data on depth (m), dissolved oxygen (mL L^{-1}), temperature (^{o}C), salinity, pH, and turbidity (formazin turbidity unit [FTU]) throughout each dive. Two Niskin type water collection bottles were mounted on the ROV to collect near-bottom water samples from each dive. Water samples were analyzed for nutrients and carbonate chemistry including dissolved organic carbon (µmol kg^{-1}), total alkalinity (µmol kg^{-1}), pCO_2 (µatm), CO_2 (µmol kg^{-1}), HCO_3 (µmol kg^{-1}), CO_3^{2-} (µmol kg^{-1}), calcite, and saturation state of aragonite (Ω_{Arag}) and calcite ($\Omega_{Calcite}$). Carbon chemistry data may influence the distribution of octocorals and stony corals and therefore are potentially important factors to correlate with species observations.

8.2.2 Community Association

8.2.2.1 Natural Substrate

Spreadsheets containing the habitat data were used as templates for community data (presence and abundance of invertebrate megafauna). To generate high-resolution information with uniform-sized replicates, each habitat category was split into 1 min intervals. Any segments of habitat type of <1 min were discarded because these would introduce error into the statistical analysis. All corals and large anemones were counted for each time interval. The number of observations for each species, location, depth range, habitat type, and environmental conditions is presented in **Table 8-4**. Fewer large invertebrates were found on soft sediments than on hard substrate, and identification to species was problematic for most taxa therefore only general observations on distribution were possible. Red crabs were the dominant mobile invertebrate and were easily identified so these were counted during the video analysis; in addition, gravid females and mating pairs were noted.

Video from the seeps was split into 30-s intervals because the Baltimore seep habitats were very patchy, and smaller time intervals resulted in fewer discarded video segments. In addition to the habitat types and live mussel categories, other fauna were recorded and counted during the community assessment. This was not done for the canyon dives in coral habitats because most fauna could not be identified to a level that would be meaningful for community analysis.

These data were analyzed using multivariate nonparametric statistics (Primer-E V6 software; Clarke and Gorley 2006) to detect significant differences among the communities; the influence of dominant species on community structure; and the degree of association among habitat type, invertebrate assemblages, and environmental conditions.

8.2.2.2 Artificial Substrate

Percent cover of sessile invertebrates was estimated by overlaying 200 random points on each video frame grab, and the number of points meeting each sessile invertebrate taxon was counted. Where species could not be identified, “morphotypes” were used in the place of taxonomic names. For example, three encrusting taxa could not be identified therefore they were described as pink, white, or yellow encrusting taxon. These were probably either sponges or colonial tunicates, but this could not be verified without a physical sample. The different morphotype designations were used consistently throughout the analysis of the wreck fauna. Mobile invertebrates were also recorded from each frame grab by simple count. Voucher specimens of the most common species were collected in 2012 using the ROV *Kraken 2* and were identified by consulting relevant literature and taxonomic experts.

Primer V6 was used to calculate multivariate statistics based on log(x+1)-transformed data in a Bray-Curtis similarity matrix. Invertebrate communities that appeared on shipwrecks were analyzed for size and orientation of each shipwreck, the type of ship, the complexity of shipwreck surfaces, and the amount of fishing gear present.

8.2.3 Invertebrate Species Inventory

Representatives of invertebrate species collected with ROVs or otter trawls were preserved in 10% formalin or 95% ethanol and were identified to the highest taxonomic resolution possible. Most species were identified morphologically; however, a selection of species was preserved for genetic analysis (DNA barcoding), for comparison with morphological taxonomy, and to potentially identify cryptic species in these little known environments.

Table 8-4. Number of observations, depth range, habitat type, and environmental conditions associated with corals in Baltimore and Norfolk canyons.

Species/Taxa	No. of Observations	Depth (m)	Habitat Types	Temp. (°C)	DO (mL L^{-1})	pH	Turbidity
Baltimore Canyon							
Desmophyllum dianthus	174	660–672	B, W	4.96–5.17	5.19–5.27	8.07–8.09	52.57–62.56
Lophelia pertusa	5	374–381	W	6.88–7.78	2.86–2.95	8.04–8.05	55.37–55.62
Solenosmilia variabilis	0	—	—	—	—	—	—
Antipathidae	0	—	—	—	—	—	—
Parazoanthidae	169	334–448	R, PB, B, W	5.69–9.88	2.46–4.90	8.00–8.07	22.51–90.14
Acanthogorgia aspera	0	—	—	—	—	—	—
Anthothela grandiflora	571	320–672	PB, B, W	5.02–9.91	1.76–5.30	7.94–8.09	22.51–110.90
Duva florida	1,078	288–396	R, PB, B, W	5.80–11.16	2.24–4.84	8.00–8.10	14.57–90.67
Keratoisis cf grayi	3	428–447	W	6.73–7.27	4.11–4.43	7.96–8.03	27.47
Paragorgia arborea	5,697	331–793	R, PB, B, W	4.86–10.26	1.99–5.08	7.96–8.10	22.51–227.97
Paramuricea placomus	281	306–559	SR, R, W	6.37–9.51	3.73–4.91	8.03–8.08	52.87–144.81
Norfolk Canyon							
Desmophyllum dianthus	34,314	417–1,390	R, PB, B, W	4.10–8.63	2.95–5.32	8.06–8.15	3.85–192.15
Lophelia pertusa	19	386–424	W	6.39–8.49	2.60–2.83	7.97–8.11	14.42–65.39
Solenosmilia variabilis	306	1,264–1,388	PB, B, W	4.10–4.29	2.13–4.41	8.11–8.12	3.85–11.10
Antipathidae	9	956–1,339	SR, B, W	4.15	4.11	8.11	174.14
Parazoanthidae	531	384–1,326	SR, R, PB, B, W	4.12–10.51	2.10–4.45	8.05–8.13	9.08–291.56
Acanthogorgia aspera	1,340	422–1,341	SR, R, PB, B, W	4.10–6.67	2.55–5.30	8.05–8.12	3.85–192.15
Anthothela grandiflora	1,709	385–714	R, B, W	4.96–9.09	2.07–5.09	8.04–8.15	11.14–192.15
Duva florida	3,370	416–522	R, B, W	5.22–8.65	2.11–5.09	8.06–8.11	18.92–291.56
Keratoisis cf grayi	9	421–1,223	SR, R, B, W	4.10–7.51	n/a	n/a	n/a
Paragorgia arborea	2,166	383–716	SR, R, PB, B, W	4.94–11.41	2.07–5.32	8.04–8.15	10.38–219.23
Paramuricea placomus	256	421–460	PB, W	6.65–6.87	2.38–3.54	8.09–8.11	16.18–45.47
Primnoa resedaeformis	1,641	387–683	R, B, W	4.94–10.91	2.06–4.66	8.04–8.15	12.7–192.15

B = large boulder of rock or consolidated sediment (slope may be flat to steep); PB = large areas of EHS or consolidated sediment that forms hard pavement, >50% cover of hard substrate (slope may be flat to steep); R = Isolated rock, rubble, EHS, > 50% cover of hard substrate (slope may be flat to steep); SR = soft sediment with small pieces of rock or EHS, <50% cover of hard substrate (slope may be flat to steep; W = walls and steep slopes (rock or consolidated sediment), steep profile. n/a = data not available; "—" indicates no data.

8.2.3.1 DNA Barcoding

Two Echinoderm families (Echinidae and Cidaridae) and one Mollusca family (Mytilidae) were selected for bar coding. The Echinidae (*n* = 21, 1,311 to 1,613 m) and the Mytilidae were collected from Baltimore (*n* = 43; 362 to 507 m) and Norfolk (*n* = 55; 1,487 to 1,612 m) seeps using an ROV, and the Cidaridae (*n* = 5; 160 to 165 m) were collected with an otter trawl from the shelf near the head of Norfolk Canyon. Sampling location and sample numbers for each taxon are listed in **Table 8-5**.

Table 8-5. Sampling information of urchins and mussels collected from Baltimore and Norfolk canyons. A range of depths from the entire ROV dive or otter trawl was reported when the depth of the sample was unknown.

Genus	Sample No.	Date	Dive/Trawl No.	Site/Canyon	Depth (m)
Gracilechinus	MAC287	8 May 2013	J2-682	Norfolk seep	1,570
Gracilechinus	MAC312	8 May 2013	J2-682	Norfolk seep	1,570
Gracilechinus	MAC315-17	8 May 2013	J2-682	Norfolk seep	1,548
Gracilechinus	MAC342-345	9 May 2013	J2-683	Norfolk seep	1,476
Gracilechinus	MAC353-358	9 May 2013	J2-683	Norfolk seep	1,481
Gracilechinus	MAC370-372	9 May 2013	J2-683	Norfolk seep	1,487
Gracilechinus	MAC378-379	9 May 2013	J2-683	Norfolk seep	1,487
Gracilechinus	MAC415-416	11 May 2013	J2-685	Norfolk canyon	1,311
Cidaris	MAC209-213	4 May 2013	RB-023	Norfolk canyon	160−165
"Bathymodiolus"	MAC537	16 May 2013	J2-689	Baltimore seep	362
"Bathymodiolus"	MAC539-544	16 May 2013	J2-689	Baltimore seep	364
"Bathymodiolus"	MAC545-555	16 May 2013	J2-689	Baltimore seep	400
"Bathymodiolus"	MAC557	16 May 2013	J2-689	Baltimore seep	401
"Bathymodiolus"	MAC561	16 May 2013	J2-689	Baltimore seep	401
"Bathymodiolus"	MAC300-304	27 Aug 2012	NF-08	Baltimore seep	430
"Bathymodiolus"	MACM101-109	27 Aug 2012	NF-08	Baltimore seep	430
"Bathymodiolus"	MACm32-36	7 Sept 2012	NF-14	Baltimore seep	407−507
"Bathymodiolus"	MACm39	7 Sept 2012	NF-14	Baltimore seep	407−507
"Bathymodiolus"	MACm44-46	7 Sept 2012	NF-14	Baltimore seep	407−507
"Bathymodiolus"	MAC283-286	8 May 2013	J2-682	Norfolk seep	1,570
"Bathymodiolus"	MAC288-299	8 May 2013	J2-682	Norfolk seep	1,570
"Bathymodiolus"	MAC306	8 May 2013	J2-682	Norfolk seep	1,570
"Bathymodiolus"	MAC310	8 May 2013	J2-682	Norfolk seep	1,570
"Bathymodiolus"	MAC311	8 May 2013	J2-682	Norfolk seep	1,587
"Bathymodiolus"	MAC313	8 May 2013	J2-682	Norfolk seep	1,570
"Bathymodiolus"	MAC314	8 May 2013	J2-682	Norfolk seep	1,548
"Bathymodiolus"	MAC320-321	8 May 2013	J2-682	Norfolk seep	1,594
"Bathymodiolus"	MAC322-323	8 May 2013	J2-682	Norfolk seep	1,535
"Bathymodiolus"	MAC326-327	8 May 2013	J2-682	Norfolk seep	1,612
"Bathymodiolus"	MAC338-341	9 May 2013	J2-683	Norfolk seep	1,487
"Bathymodiolus"	MAC343	9 May 2013	J2-683	Norfolk seep	1,457−1,485
"Bathymodiolus"	MAC346-352	9 May 2013	J2-683	Norfolk seep	1,457−1,485
"Bathymodiolus"	MAC359-369	9 May 2013	J2-683	Norfolk seep	1,476−1,487
"Bathymodiolus"	MAC373-377	9 May 2013	J2-683	Norfolk seep	1,487

Recently, Thubalt et al. (2013) used the new genus reassignment, *Gigantidas mauritanicus* and *Gigantidas childressi*, recognized by The Paris Museum of Natural History, though some public database records are conflicting on the validity of this designation. In the Atlantic Deepwater Canyons study, *Bathymodiolus* is used for consistency, and although we recognize the uncertainty, the genus will be used without quotation marks.

Tissue (mostly gonad) was taken from the urchins and adductor or mantle tissue was taken from the mussels. All tissue was preserved in 95% molecular grade ethanol. Genomic DNA was extracted via the Gentra Puregene Tissue protocol (Qiagen). The final elution volumes of DNA in water were 60 to 100 µL.

A portion of the mitochondrial cytochrome oxidase gene (mtCOI) was amplified from mussels using the Folmer primers, HCO2198 and LCO1490 (Folmer et al. 1994). Fifty microliter PCRs were performed according to Won et al. (2003) using 1 µL DNA template. For urchin samples, the Folmer primers were modified as follows:

urchLCO1490 5'- TTTCTACTAAYCACAAGGACATYGG -3'; and
urchHCO2198 5'- TANRCYTCNGGGTGDCCRAARARYCA -3'.

The following PCR recipe was then used: 1× PCR GoTaq Flexi buffer (Promega), 2 mM $MgCl_2$, 0.2 mM dNTPs (Thermofisher), 0.2 µM of each primer, 5× of bovine serum albumin, and four 1.25 units of GoTaq Flexi *Taq* polymerase in a final volume of 50 µL. PCRs were amplified under the following conditions: 94 ºC for 3 min, then 35 cycles of 94 ºC for 1 min, 50 ºC for 1 min, and 72 ºC for 1 min, then 72 ºC for 7 min, and a final hold at 10 ºC. Five microliters of PCRs from all taxa were electrophoresed on a 1.5% agarose gel to check for single-copy, successful amplification. If more than one band was visible, the remaining PCR was loaded onto a 1% agarose gel, and the larger band was excised from the gel and purified using the QiaQuick gel extraction protocol (Qiagen). PCRs with single bands were purified with QiaQuick PCR purification protocol (Qiagen). Cleaned products were cycle-sequenced in both the forward and reverse direction using the following protocol: 1µL purified PCR as template, 1 µL BigDye Terminator v3.1 Ready Reaction Mix (Thermofisher), 1 µL of 5-µM primer, 2 µL of 5× Sequencing buffer (Thermofisher), and 5 µL molecular grade water for a final volume of 10 µL. Cycle sequencing was performed on a Bio-Rad or Eppendorff thermal cyclers under the following conditions: 95 ºC for 3 min, then 29 cycles of 95 ºC for 20 s, 50 ºC for 20 s, and 60 ºC for 4 min, with final extension of 60 ºC for 5 min. Cycle sequencing products were purified using AGENCOURT CLEANSEQ beads (Beckman Coulter) according to the manufacturer's protocol. Final products were resuspended in 25 to 30 µL molecular grade water. A total of 25 µL of purified product was loaded onto an ABI 3130xl DNA sequencer (Thermofisher). DNA sequences were edited using Sequencher 5.2.2 (Genecodes). After aligning sequences from both the forward and reverse directions, regions with ambiguous bases were omitted from subsequent analyses. The National Center for Biotechnology Information (NCBI) GenBank nucleotide database (Benson et al. 2013) was queried with mtCOI consensus sequences from each individual. DNA sequences were aligned and translated into amino acids using the invertebrate mtDNA translation table in MEGA6.06 (Tamura et al. 2013) to ensure no stop codons were present. Also in MEGA6.06, the best fit evolutionary model was predicted and used to construct a maximum likelihood phylogenetic tree for each taxon. Statistical significance of branch locations was tested with 500 bootstrap replications. Clades with <50% bootstrap support were collapsed into unresolved polytomies. Bootstrap values >50% were reported.

Mitochondrial COI sequences from *Gracilechinus* and *Echinus* urchins available in the GenBank database were included in the *Gracilechinus* phylogenetic analysis. An initial *Cidaris* phylogenetic analysis was constructed with MAC sequences trimmed to 469 nucleotides and all overlapping mtCOI sequences available from the order Cidaroida mined from both the NCBI GenBank and BOLD databases (Ratnasingham and Hebert 2007). This included individuals from the following Cidaroida genera: *Acanthocidaris, Aprorocidaris, Cidaris, Ctenocidaris, Eucidaris, Goniocidaris, Histocidaris, Notocidaris,*

Phalacrocidaris, *Rhynchocidaris*, *Stereocidaris*, and *Stylocidaris*. *Echinus esculentus* was used as an outgroup. The subsequent phylogeny reported in the results consists of a subset of taxa closely related to MAC samples as construed from the larger tree. Taxa from the Atlantic Ocean also were included in the second, smaller phylogeny (**Table 8-5**). A sequence from *Strongylocentrotus purpuratus* was used as an outgroup.

A subset of *Bathymodiolus childressi*, *B. mauritanicus*, and *B. aff. childressi* sequences available in the GenBank database were included in the mussel phylogenetic analysis and haplotype network (**Table 8-6**). *Tamu fisheri* was chosen as an outgroup. Genetic diversity indices were estimated with DnaSP 5.10 (Librado and Rozas 2009). A haplotype network for MAC mussels was drawn with Network 4.6.1.3 (Fluxus Technology Ltd.) using a median-joining method coupled with a maximum-parsimony heuristic algorithm (Bandelt et al. 1999).

Table 8-6. Taxa included in phylogenetic analyses. NCBI GenBank database accession numbers or BOLD database IDs (with *) of sequences included in the maximum likelihood trees (**Figures 8-23 A**,**B**, **8-24B**) and haplotype network (**Figure 8-24 A**).

Taxon	No. of Ind.*	GenBank/BOLD	Location	Figure
Echinus esculentus	5	KF642987-89; KF500005-6[1]	Pacific	8-23A
Echinus melo	1	KF642990[1]	Pacific	8-23A
Gracilechinus affinis	1	KF500007[1]	Northeast Atlantic	8-23A
Gracilechinus alexandri	2	KF500008, 014[1]	North Atlantic	8-23A
Gracilechinus atlanticus	1	KF500009[1]	Southeast, central Atlantic	8-23A
Gracilechinus elegans	3	KJ29122-24[1]	North Atlantic	8-23A
Gracilechinus elegans	1	KF500010[1]	North Atlantic	8-23A
Gracilechinus euryporus	1	KF642986[1]	Pacific	8-23A
Gracilechinus lucidus group A	2	KF500011, KF642992[1]	Pacific	8-23A
Gracilechinus lucidus group B	2	KF500012, KF642991[1]	Pacific	8-23A
Gracilechinus multidentatus	5	EU869927-31[1]	Pacific	8-23A
Gracilechinus stenoporus	1	KF500013[1]	Southeast, central Atlantic	8-23A
Strongylocentrotus purpuratus	1	HM5s42410[2]	Outgroup	8-23A
Cidaris abyssicola	1	KC626153[3]	Gulf of Mexico, Yucatan	8-23B
Cidaris cidaris	1	JN091894[4]	North Atlantic	8-23B
Cidaroida	7	MIWAE149-13, 155-13, 157-13, 158-13* MIWAE168-13−170-13*	Gulf of Guinea	8-23B
Cidaroidea group A	5	MIWAE150-13−153-13, 190-13*	Cape Verde Islands	8-23B
Echinus esculentus	1	KF500006[1]	Outgroup	8-23B
Eucidaris tribuloides tribuloides	4	KC626169-171,173[3]	Gulf of Mexico, Yucatan	8-23B
Histocidaris australiae	2	NZECA618-09-619-09*	New Zealand	8-23B
Histocidaris sp	4	NZECA608-10-611-10*	New Zealand	8-23B
Stylocidaris affinis	1	JN091903[4]	North Atlantic	8-23B
Stylocidaris lineata	1	JN091904[4]	North Atlantic	8-23B
"*Bathymodiolus*" *childressi*	99	EU288175[5]; KM024170-219, 221–268[6]	Northern Gulf of Mexico	8-24A
	22	EU288175[5]; KM024171, 183−184, 186, 188 KM024191, 203, 206−207, 218−219, 221, 224 KM024245, 248, 253, 255, 257, 263, 267−268[6]	Northern Gulf of Mexico	8-24B
"*Bathymodiolus*" *mauritanicus*	10	AY649801[7]; FJ890502[8] EU288159, 161−164, 168, 170, 172[5]	Barbados, Gulf of Cadiz	8-24A
	3	AY649801[7]; EU288163, 168[5]	Barbados, Gulf of Cadiz	8-24B
"*Bathymodiolus*" *aff. childressi*	16	DQ513425-440[9]	Barbados	8-24A
	6	DQ513425−426, 428, 435−436, 438[9]	Barbados	8-24B

Table 8-6. (Continued).

Taxon	No. of Ind.*	GenBank/BOLD	Location	Figure
Bathymodiolus sp. A	1	EF051242[10]	Nigerian seep	8-24B
Bathymodiolus azoricus	4	FJ766851, 876, 883, 935[11]	Northern Gulf of Mexico	8-24B
Bathymodiolus boomerang	2	DQ513448-449[9]	Northern Gulf of Mexico	8-24B
Bathymodiolus aff. boomerang	2	DQ513442, 450[9]	West Africa	8-24B
Bathymodiolus brooksi	4	AY649798[7]; KM024112, 136, 139[6]	Northern Gulf of Mexico	8-24B
Bathymodiolus heckerae	3	DQ513441[9]; KM024287, 301[6]	Northern Gulf of Mexico	8-24B
Bathymodiolus puteoserpentis	3	AY649796[7]; FJ766950[11]; JQ844853[12]	Mid-Atlantic Ridge	8-24B
Tamu fisheri	1	AY649803[7];	Outgroup	8-24B

[1] Minin et al. 2015.
[2] Corstorphine, unpubl.
[3] Bribiesca-Contreras et al. 2013.
[4] Brosseau et al. 2012.
[5] Genio et al. 2008.
[6] Faure et al. 2015.
[7] Jones et al. 2006.
[8] Lorion et al. 2010.
[9] Olu-Le Roy et al. 2007.
[10] Cordes et al. 2007).
[11] Faure et al. 2009.
[12] van der Heijden et al. 2012.
* No. of ind. = number of individuals per taxon used in the indicated analysis.
BOLD database = Barcode of Life Data System (Ratnasingham and Hebert 2007).
National Center for Biotechnology Information (NCBI) GenBank nucleotide database (Benson et al. 2013).

8.3 RESULTS

8.3.1 Habitat Characterization

8.3.1.1 Natural Substrate

Video from the ROV dives was used only when the vehicle was in transect configuration (**Section 3.2**) with lasers on and adequate visibility. Applying these criteria generated 2 542 min (~42.4 h) of usable video for habitat and community analysis of Baltimore Canyon. During the 2012 sampling cruise, two coral-targeted dives were conducted in Norfolk Canyon and an additional nine dives during the 2013 sampling cruise. Usable video from these dives amounted to 2 198 minutes (~36.6 h). Four dives targeted the Baltimore seep (three in 2012 and one in 2013) and two dives (both in 2013) targeted the Norfolk seeps. These videos provided 660 min (11 h) of usable video at Baltimore seep and 298 min (~5 h) at Norfolk seep. For each dive, a habitat map was constructed and overlaid on local bathymetry; the habitat maps (and associated coral locations along the dive track) for coral-targeted dives in Baltimore and Norfolk canyons were then compiled in chronological order (**Appendix 8-A)**. Each page represents a single dive with the habitat map in the top panel and coral locations along the dive track in the lower panel. The habitat tracks represent locations where the ROV video quality was sufficiently good to allow identification of benthic fauna. Where video quality was poor, there is no habitat data resulting in gaps along the dive track.

Habitat maps for Baltimore seep dives (ROV-2012-NF-07, 08, and 14 and ROV-2013-RB-689) and Norfolk seep dives (ROV-2013-RB-682, 683) are presented in chronological order (**Appendix 8-B**). The active methane release area (as indicated by bacterial mats or live mussel cover) of the Baltimore seep (360 to 430 m depth) has a patchy distribution and several areas had variable quantities of dead mussel shells or authigenic carbonate with no live mussels, which may indicate ephemeral or very low seepage. Authigenic carbonate occurred in isolated patches, occasionally with live mussels attached; however, structures were mostly exposed rock. The Norfolk seep site was much deeper than the Baltimore seep (1,485 to 1,600 m) and showed very active methane seepage along two well-defined ridge features (Skarke et al. 2014), which supported almost continuous very dense coverage of live mussels. Vigorous bubble plumes were visible along both ridges, and at several locations, the topography was very rugged due to the precipitation of massive authigenic carbonate structures. Gas (methane) hydrates were observed at several locations in both Norfolk seeps, but were absent from the Baltimore seep, which is shallower than the depth at which gas hydrates are stable in this region (Skarke et al. 2014).

8.3.1.2 Artificial Substrate

The average complexity of shipwreck surfaces varied by wreck, as did the amount of fishing gear attached to the wreck **(Figure 8-3**). Shipwrecks exhibited different orientations on the seafloor, with the major axes of shipwrecks W1, W3, W5 1, W6, and W7 oriented primarily northeast-southwest. Wrecks W2 and W4 were oriented primarily northwest-southeast, while shipwreck W5-2 was oriented primarily north-south (**Figure 8-4**). The maximum height off the seafloor varied by wreck (**Table 8-3**).

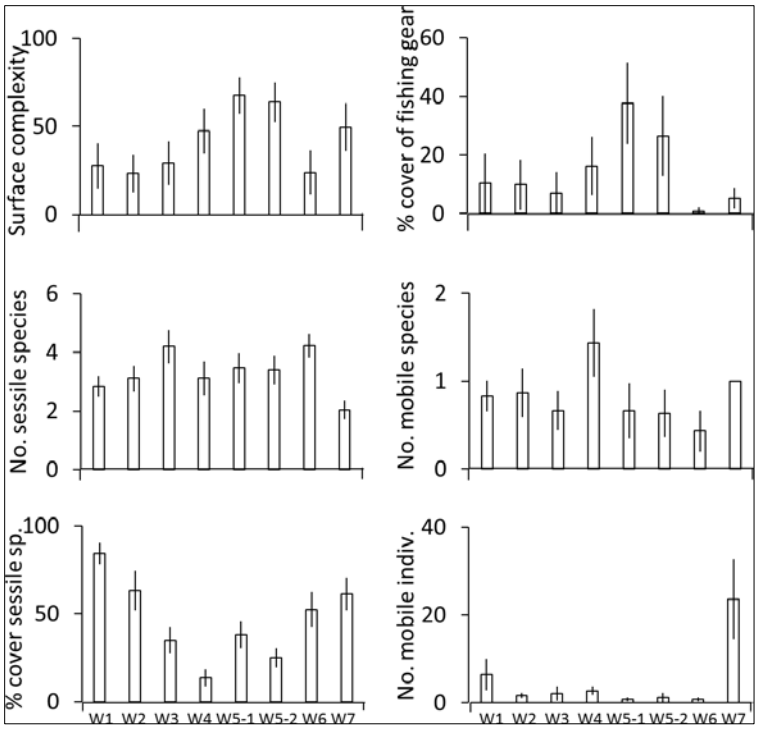

Figure 8-3. Average surface complexity, percent cover of fishing gear, abundance, and species richness of sessile and mobile invertebrates (see Y-axis labels) at eight shipwrecks off the east coast of the United States. Shipwreck numbers as per **Table 8-10**. Error bars represent 95% confidence intervals.

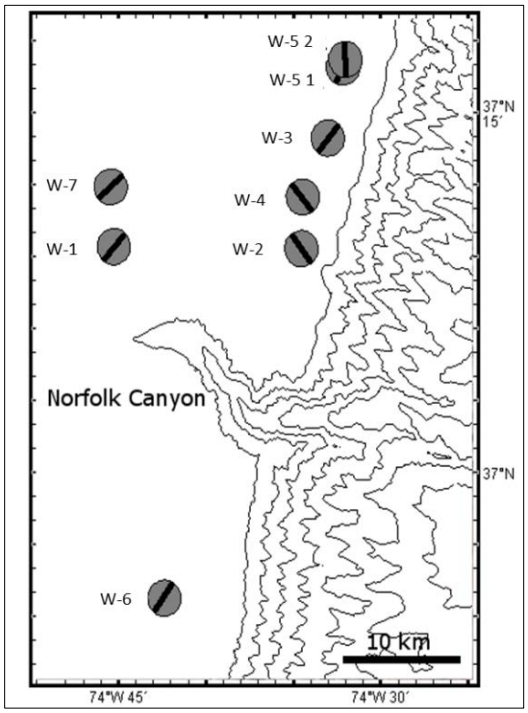

Figure 8-4. Map of shipwreck sites. Black lines indicate orientation of the major axis of each shipwreck.

8.3.1.3 Physical Environment

Table 8-7 shows the average (standard deviation [SD]) and range of the environmental data collected during all ROV dives conducted over natural habitats. These data reflect only near-bottom conditions throughout the dives, and depth data are provided for reference. Each variable shows depth-related trends; temperature and salinity decrease and density increases with depth similarly for both canyons (**Figures 8-5 A**,**B**,**C**). The relationship between depth and each variable is nonlinear; beyond approximately 600 m depth, the curves flatten and there is less change with increasing depth. Oxygen and pH generally increased with depth (**Figures 8-5 D**,**E**), but average oxygen levels were generally lower in Norfolk Canyon than in Baltimore Canyon at comparable depths. Turbidity varied for both canyons with no distinct trends at mid depths, but it was consistently lower at depths >1,000 m (**Figure 8-5 F**). Carbonate chemistry data analyzed from water samples collected with Niskin bottles attached to the ROV are shown in **Table 8-8**. These samples were taken from near-bottom near corals or cold seeps. Aragonite saturation state value ranged from 1.15 to 1.57, with an average value of 1.41 (SD 0.07). Samples collected from coral habitats were in the same depth range as samples collected from cold seeps. Water samples collected during some conductivity-temperature-depth (CTD) casts were analyzed for carbonate chemistry. These samples were combined with the ROV near-bottom data to generate depth-integrated Ω_{Arag} (**Figure 8-6**). Between 100 and 200 m depth, Ω_{Arag} declined rapidly from approximately 2.4 to 1.6, it then declined more slowly with depth to a minimum of approximately 1.2. No substantial differences were apparent between canyons and between canyon and seep habitats at comparable depths, although data were insufficient for statistical analysis.

Environmental data collected during ROV dives on artificial substrates are shown in **Table 8-9**. Three sites were not analyzed for biological communities (NF-ROV-21, 25, 28), but are included to present all data collected. Dive depths at the shipwreck sites were considerably less than dive depths at the canyons, and the environmental conditions reflected these shallower, warmer conditions. The wrecks did not show the high turbidity values associated with the canyons, which generally have a more active hydrodynamic regime than the shelf.

Table 8-7. Average, standard deviation (SD), and range of environmental data collected during ROV dives over natural habitats. Water column data have been removed; therefore, only near-bottom environmental conditions are shown.

Dive No. (canyon)	Depth (m)			Temp (°C)			Salinity			Oxygen (mL L^{-1})			pH			Density			Turbidity		
	Avg.	SD	Range	Avg.	SD	Range	Avg.	SD	Range	Avg.	SD	Range	Avg.	SD	Range	Avg.	SD	Range	Avg.	SD	Range
NF-01 (BC)	531.2	58.1	436–617	6.0	0.4	5.5–7.3	35.0	<0.1	35.0–35.1	4.8	0.2	4.1–5.1	8.0	<0.1	7.97–7.99	27.6	<0.1	27.5–27.6	—	—	—
NF-02 (BC)	348.7	65.5	270–524	8.8	1.4	5.7–11.2	35.2	0.1	35.0–35.4	3.5	0.6	3.0–4.9	8.0	<0.1	7.94–8.00	27.3	0.1	27.1–27.6	—	—	—
NF-03 (BC)	530.5	118.4	175–776	6.3	1.3	4.9–13.5	35.0	0.1	35.0–35.8	4.6	0.7	2.9–5.4	8.0	<0.1	7.96–8.08	27.6	0.1	26.9–27.7	—	—	—
NF-04 (BC)	712.5	157.7	479–976	5.1	0.5	4.5–6.4	35.0	<0.1	34.9–35.0	5.2	0.3	4.3–5.7	8.0	<0.1	8.01–8.03	27.7	<0.1	27.5–27.7	—	—	—
NF-05 (BC)	464.7	36.3	414–526	6.7	0.7	5.8–7.9	35.1	<0.1	35.0–35.1	4.5	0.4	3.7–5.0	8.0	<0.1	7.98–8.03	27.5	0.1	27.4–27.6	—	—	—
NF-06 (BC)	394.7	49.2	278–518	8.1	1.0	6.1–10.6	35.0	0.1	34.9–35.3	2.5	0.8	1.7–4.7	8.0	<0.1	7.97–8.00	27.3	0.1	27.1–27.6	—	—	—
NF-07* (BC)	415.4	9.7	400–439	7.3	0.1	7.2–7.6	35.1	<0.1	35.0–35.1	3.8	<0.1	3.7–3.9	8.0	<0.1	7.95–7.97	27.4	<0.1	27.4–27.5	—	—	—
NF-08* (BC)	414.1	9.9	404–439	7.3	0.1	7.2–7.4	35.1	<0.1	35.0–35.1	3.9	<0.1	3.9–3.8	8.0	<0.1	7.95–7.96	27.4	<0.1	27.4–27.5	—	—	—
NF-09 (BC)	426.0	73.7	315–560	7.6	0.6	5.9–8.9	35.1	<0.1	35.0–35.2	3.9	0.3	3.4–4.8	—	—	—	—	—	—	—	—	—
NF-10 (BC)	413.8	73.5	322–562	8.0	0.7	6.4–9.5	35.2	<0.1	35.1–35.3	3.9	0.3	3.3–4.6	8.0	<0.1	7.98–8.01	27.4	0.1	27.2–27.6	—	—	—
NF-11 (BC)	718.2	150.8	448–966	5.0	0.4	4.6–6.2	35.0	<0.1	35.0–35.1	5.3	0.3	4.6–5.6	8.0	<0.1	8.02–8.05	27.7	<0.1	27.6–27.7	—	—	—
NF-12 (NC)	588.9	45.6	497–633	5.4	0.5	5.1–6.9	35.0	<0.1	35.0–35.1	5.0	0.3	4.3–5.3	8.0	<0.1	7.99–8.02	27.6	<0.1	27.5–27.7	—	—	—
NF-13 (BC)	348.4	48.3	282–470	8.3	0.8	6.7–9.7	35.2	0.1	35.1–35.3	3.6	0.3	3.2–4.4	8.0	<0.1	7.99–8.03	27.4	0.1	27.2–27.5	—	—	—
NF-14* (BC)	404.2	35.1	352–497	7.0	0.4	6.1–7.9	35.1	<0.1	35.0–35.1	4.0	0.3	3.5–4.6	8.0	<0.1	8.01–8.06	27.5	<0.1	27.4–27.6	—	—	—
NF-15 (BC)	402.9	84.6	275–563	7.3	1.0	5.6–9.2	35.1	0.1	35.0–35.2	4.1	0.5	3.2–5.0	8.0	<0.1	7.99–8.07	27.5	0.1	27.3–27.6	57.7	25.4	37.8–227.9
NF-16 (BC)	413.5	61.8	334–538	6.8	1.1	5.6–8.6	35.1	0.1	35.0–35.2	4.4	0.6	3.5–5.0	8.0	<0.1	8.00–8.09	27.5	0.1	27.3–27.6	62.6	10.6	42.7–109.2
NF-17 (BC)	672.3	70.4	560–793	5.1	0.2	4.9–5.7	35.0	<0.0	34.9–35.01	5.2	0.1	4.9–5.4	8.1	<0.0	8.05–8.10	27.7	<0.1	27.6–27.7	75.0	86.9	45.9–150.1

Table 8-7. (Continued).

Dive No. (canyon)	Depth (m)			Temp (°C)			Salinity			Oxygen (mL L^{-1})			pH			Density			Turbidity		
	Avg.	SD	Range	Avg.	SD	Range	Avg.	SD	Range	Avg.	SD	Range	Avg.	SD	Range	Avg.	SD	Range	Avg.	SD	Range
NF-18 (BC)	560.1	77.5	433–729	5.3	0.4	4.7–6.0	35.0	<0.0	35.0–35.0	5.1	0.2	4.7–5.5	8.1	<0.0	8.0–8.1	27.6	<0.0	27.6–27.7	69.8	15.1	53.4–143.0
NF-19 (BC)	426.5	92.0	299–596	6.5	1.2	4.9–9.4	35.1	0.1	35.0–35.3	4.5	0.6	3.3–5.4	8.1	<0.0	8.0–8.1	27.5	0.1	27.3–27.7	64.7	15.5	46.8–144.8
NF-20 (NC)	582.2	120.5	378–747	5.5	0.6	4.9–7.3	35.0	<0.0	35.0–35.1	5.0	0.4	3.9–5.3	8.1	<0.0	8.0–8.1	27.6	0.1	27.5–27.7	82.2	26.5	47.8–182.3
RB-679 (NC)	734.3	34.7	683–768	6.2	0.3	5.6–6.5	35.1	<0.0	35.0–35.1	4.5	0.1	4.4–4.9	8.1	<0.0	8.1–8.2	27.6	<0.0	27.5–27.6	123.7	61.3	66.2–264.6
RB-680 (NC)	534.5	64.6	422–629	6.7	0.9	5.8–8.1	35.1	<0.0	35.0–35.2	3.2	0.4	1.9–4.1	8.1	<0.0	8.1–8.1	27.5	0.1	27.3–27.6	26.3	19.0	12.6–219.9
RB-681 (NC)	440.8	26.7	413–612	7.5	0.5	5.7–8.5	35.1	<0.0	34.9–35.3	2.8	0.3	2.2–4.2	8.1	<0.0	8.1–8.1	27.4	0.1	27.2–27.6	35.3	21.1	12.4–163.3
RB-682* (NC)	1,571.0	29.8	1,521–1,610	4.0	0.0	3.9–4.0	35.0	<0.0	34.9–35.0	4.4	0.4	3.4–5.2	8.1	<0.0	8.1–8.1	27.8	<0.0	27.7–27.8	7.5	11.2	2.4–81.7
RB-683* (NC)	1,493.4	31.7	1,432–1,564	4.0	0.1	3.9–4.1	35.0	<0.0	35.0–34.9	4.6	0.4	3.4–5.2	8.1	<0.0	8.1–8.1	27.8	<0.0	27.7–27.8	6.7	10.9	2.2–105.8
RB-684 (NC)	419.0	19.5	383–497	8.3	1.6	6.0–11.4	35.2	0.1	34.9–35.5	3.0	0.5	2.2–4.1	8.1	<0.0	8.1–8.1	27.4	0.2	27.0–27.6	77.0	63.2	12.7–291.6
RB-685 (NC)	1,341.4	40.1	1,257–1,398	4.2	0.1	4.1–4.3	35.0	<0.0	34.9–35.0	4.1	0.5	2.9–5.1	8.1	<0.0	8.0–8.1	27.7	<0.0	27.7–27.8	11.5	16.3	3.5–174.1
RB-686 (NC)	491.7	47.7	400–618	6.8	0.5	5.5–7.8	35.1	<0.0	35.0–35.1	3.0	0.4	2.1–4.4	8.1	<0.0	8.0–8.1	27.5	0.1	27.4–27.6	34.9	22.0	10.4–123.5
RB-687 (NC)	539.7	98.9	385–714	6.3	0.9	5.3–8.2	35.1	<0.0	34.9–35.2	3.3	0.5	2.1–4.7	8.1	<0.0	8.0–8.1	27.5	0.1	27.3–27.7	21.2	9.4	9.9–90.9
RB-688 (NC)	—	—	—	—	—	—	—	—	—	—	—	—	—	<0.0	—	—	—	—	—	—	—
RB-689* (BC)	390.1	24.1	356–437	8.8	0.5	7.3–9.4	35.2	<0.0	35.0–35.3	2.6	0.3	1.7–3.5	8.0	<0.0	7.9–8.0	27.3	0.1	27.2–27.6	14.9	10.0	7.6–68.7
RB-690 (BC)	353.8	20.9	288–388	9.7	0.9	8.3–12.1	35.3	0.1	35.1–35.6	2.8	0.3	2.0–3.5	8.1	<0.0	8.0–8.1	27.2	0.1	27.0–27.5	30.8	12.2	8.7–11.1
RB-691 (NC)	421.8	7.3	406–449	8.3	0.2	7.6–8.7	35.2	<0.0	35.1–35.3	2.6	0.2	2.1–3.1	8.0	<0.0	8.0–8.1	27.4	<0.0	27.3–27.5	33.9	12.8	21.1–111.9

Cells with "—" indicate no data (either instrument was not turned on or the sensor malfunctioned).
* Denotes a cold-seep dive.

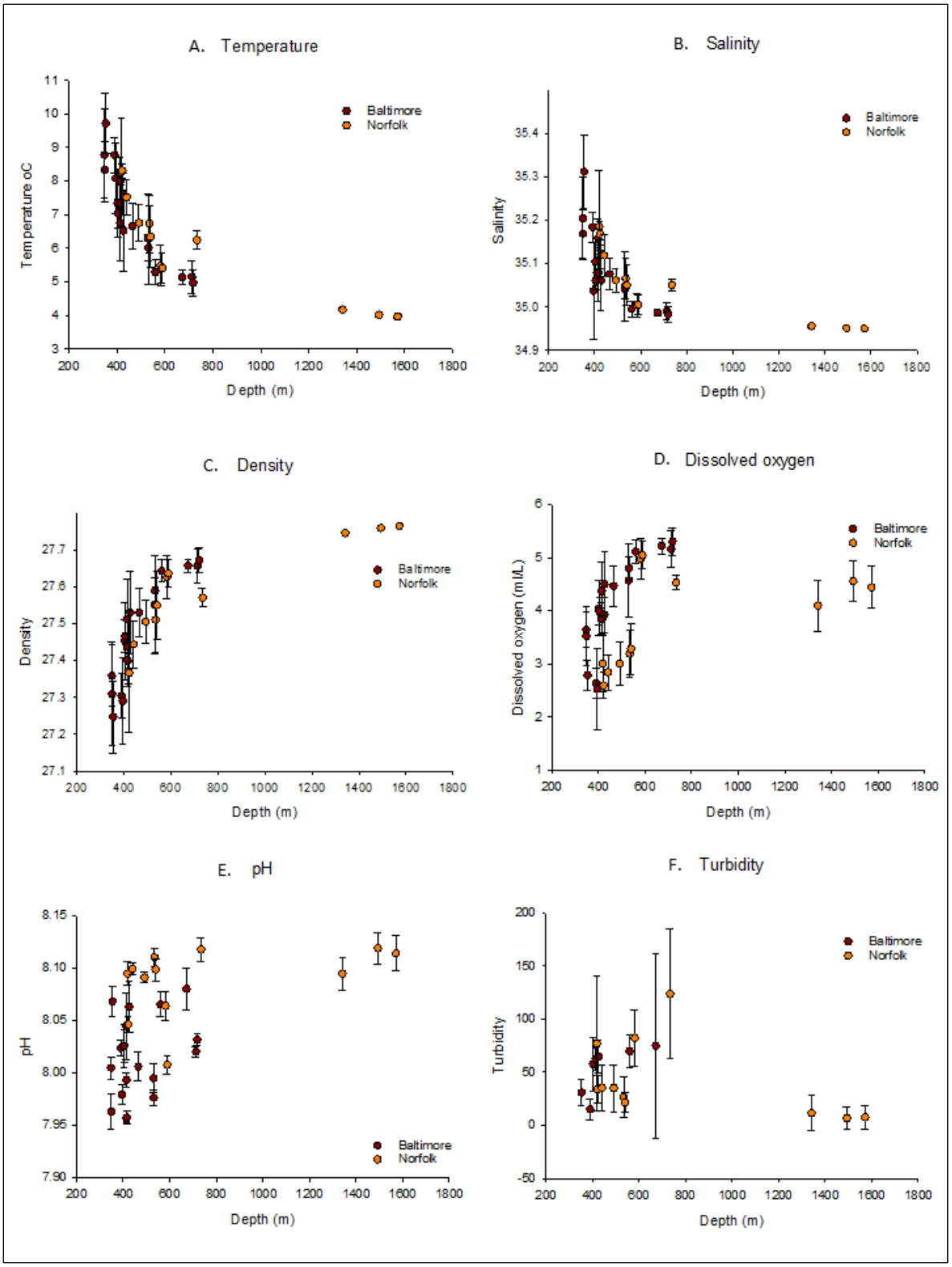

Figure 8-5. Environmental data collected during ROV dives for: A) temperature, B) salinity, C) density, D) dissolved oxygen, E) pH, and F) turbidity. Water column data have been removed.

Table 8-8. Carbonate chemistry of bottom samples collected with Niskin bottles attached to the ROVs. Samples analyzed by NOAA Pacific Marine Environmental Laboratory, Washington.

Site Name	Depth (m)	DIC ($\mu mol\ kg^{-1}$)	TA ($\mu mol\ kg^{-1}$)	pH	pCO_2 (μatm)	CO_2 ($\mu mol\ kg^{-1}$)	HCO_3^- ($\mu mol\ kg^{-1}$)	CO_3^{2-} ($\mu mol\ kg^{-1}$)	$\Omega_{Calcite}$	Ω_{Arag}
Baltimore Canyon	278	2,195.8	2,334.3	7.90	556.97	23.77	2,063.39	108.61	2.45	1.57
Baltimore Canyon	307	2,198.0	2,324.9	7.90	553.41	25.05	2,071.90	101.05	2.27	1.45
Baltimore Canyon	321	2,189.0	2,329.2	7.93	507.59	22.98	2,057.46	108.58	2.43	1.55
Baltimore Canyon	384	2,187.8	2,318.4	7.94	495.45	23.84	2,061.85	102.07	2.26	1.44
Baltimore Canyon	384	2,194.0	2,322.2	7.92	516.60	24.42	2,068.50	101.08	2.24	1.42
Baltimore Canyon	438	2,175.2	2,311.7	7.97	454.10	22.57	2,047.91	104.73	2.29	1.46
Baltimore Canyon	439	2,181.9	2,314.0	7.95	475.85	23.37	2,056.06	102.47	2.24	1.43
Baltimore Canyon	466	2,185.6	2,321.4	7.96	465.00	22.90	2,058.17	104.58	2.28	1.45
Baltimore Canyon	492	2,182.2	2,317.4	7.95	466.74	22.93	2,055.17	104.12	2.26	1.44
Baltimore Canyon	513	2,189.4	2,320.5	7.91	518.24	24.02	2,062.74	102.61	2.22	1.42
Baltimore Canyon	517	2,182.7	2,315.4	7.95	464.42	23.17	2,057.01	102.49	2.21	1.41
Baltimore Canyon	523	2,186.3	2,316.9	7.95	469.32	23.49	2,061.48	101.30	2.18	1.39
Baltimore Canyon	559	2,190.6	2,323.4	7.94	482.23	23.45	2,064.25	102.92	2.20	1.40
Baltimore Canyon	946	2,188.7	2,317.8	7.95	442.74	23.28	2,066.24	99.13	1.96	1.25
Baltimore Canyon	970	2,165.3	2,312.0	8.00	388.55	20.55	2,036.07	108.66	2.14	1.37
Norfolk Canyon	381	2,192.5	2,317.5	7.92	516.32	24.77	2,068.73	98.99	2.19	1.40
Norfolk Canyon	381	2,208.5	2,323.2	7.89	556.74	26.71	2,088.22	93.55	2.07	1.32
Norfolk Canyon	393	2,190.6	2,314.8	7.92	524.91	24.95	2,067.16	98.49	2.18	1.39
Norfolk Canyon	419	2,190.1	2,318.4	7.91	537.47	24.59	2,064.30	101.21	2.23	1.42
Norfolk Canyon	514	2,186.4	2,318.7	7.94	478.52	23.41	2,060.37	102.58	2.21	1.41
Norfolk Canyon	631	2,179.7	2,312.8	7.97	440.32	22.79	2,054.94	101.97	2.15	1.37
Norfolk Canyon	741	2,177.4	2,314.9	7.97	433.65	22.18	2,050.80	104.41	2.15	1.37
Baltimore Seep	398	2,192.2	2,319.4	7.91	536.72	24.74	2,066.88	100.58	2.22	1.42
Baltimore Seep	411	2,191.3	2,320.0	7.93	500.97	24.14	2,066.10	101.02	2.22	1.42
Baltimore Seep	422	2,196.0	2,316.6	7.90	537.88	25.57	2,073.81	96.61	2.12	1.35
Norfolk Seep	1,387	2,168.7	2,307.7	7.98	399.55	21.42	2,044.03	103.25	1.87	1.20
Norfolk Seep	1,480	2,165.3	2,304.4	7.97	396.97	21.31	2,040.96	103.03	1.83	1.18
Norfolk Seep	1,601	2,173.9	2,312.4	7.97	397.19	21.45	2,049.86	102.58	1.78	1.15

DIC = dissolved inorganic carbon; TA = total alkalinity.

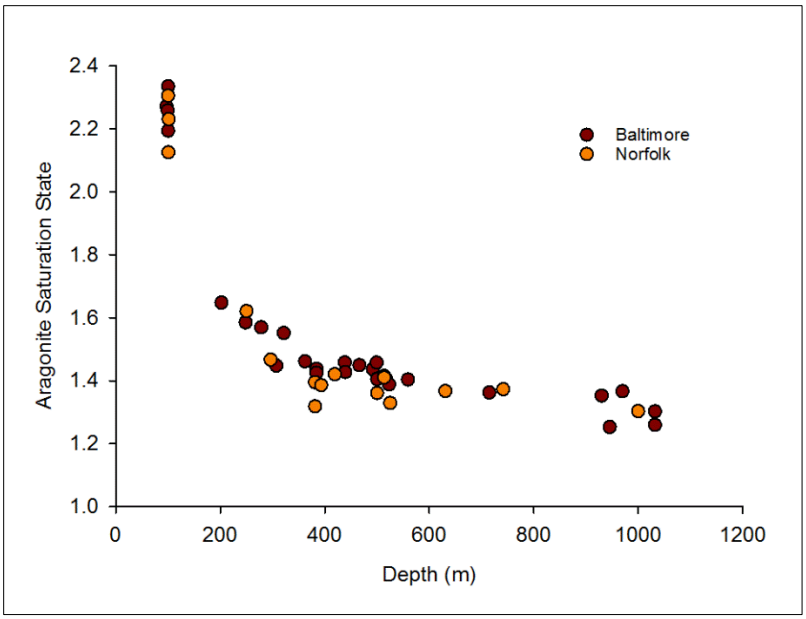

Figure 8-6. Aragonite saturation state data for Baltimore and Norfolk canyons, compiled from water samples collected during ROV dives and CTD casts.

Table 8-9. Average, standard deviation (SD), and range of environmental data collected during ROV dives over artificial substrate. Water column data have been removed; therefore, only near-bottom environmental conditions are shown.

Dive No. (wreck)	Depth (m)			Temp (°C)			Salinity			Oxygen (ml/L)			pH			Density			Turbidity		
	Avg.	SD	Range	Avg.	SD	Range	Avg.	SD	Range	Avg.	SD	Range	Avg.	SD	Range	Avg.	SD	Range	Avg.	SD	Range
NF-21	42.4	0.1	30.0–43.4	14.1	4.4	12.0–25.0	33.2	0.1	33.1–34.5	4.5	0.1	4.5–6.1	8.1	<0.1	8.0–8.3	25.1	<0.1	24.7–25.5	61.2	17.9	52.0–199.9
NF-22 (W-1)	75.8	4.5	50.0–81.0	12.7	2.6	11.2–23.4	34.2	0.3	33.5–35.0	4.2	0.2	4.1–6.1	8.1	<0.1	8.1–8.3	25.9	0.1	25.6–26.4	55.9	23.0	43.3–200.0
NF-23 (W-2)	—	—	—	—	—	—	—	—	—	—	—	—	—	—	—	—	—	—	—	—	—
NF-24 (W-3)	120.6	2.9	110.0–27.1	15.1	2.2	14.3–22.7	35.7	0.1	35.5–35.8	3.9	0.2	3.8–6.6	8.1	<0.1	8.1–8.3	26.6	0.1	26.5–26.8	42.9	8.9	37.1–100.0
NF-25	551.5	12.9	530.0–577.7	7.5	3.8	5.8–22.9	35.1	0.2	35.0–35.9	4.8	0.2	4.5–6.2	8.1	<0.1	8.1–8.3	27.6	<0.1	27.5–27.8	88.9	42.1	45.8–200.0
NF-26 (W-4)	102.0	1.4	95.0–105.1	15.6	2.7	14.5–23.1	35.8	<0.1	35.8–35.8	4.0	0.3	4.0–6.3	8.2	<0.1	8.1–8.3	26.7	<0.1	26.6–26.7	37.9	3.4	35.4–55.0
NF-27 (W5-1,2)	114.9	1.8	111.0–117.9	14.7	2.1	14.0–23.0	35.7	<0.1	35.8–35.9	3.8	0.4	3.6–6.2	8.1	<0.1	8.1–8.3	6.7	<0.1	26.7–26.8	46.3	1.3	44.6–50.0
NF-28	114.8	5.1	107.0–126.0	15.9	3.2	14.3–23.1	35.7	<0.1	35.7–35.8	4.0	0.3	3.9–6.3	8.2	<0.1	8.1–8.3	26.7	<0.1	26.6–26.7	70.4	32.3	48.7–200.0
NF-29 (W-6)	81.8	2.5	75.0–85.8	15.3	2.8	14.2–23.9	35.7	0.1	35.4–35.7	3.9	0.3	3.8–6.4	8.1	<0.1	8.1–8.3	26.7	<0.1	26.5–26.7	51.1	9.0	44.8–84.0
NF-30 (W-7)	—	—	—	—	—	—	—	—	—	—	—	—	—	—	—	—	—	—	—	—	—
J-692 (W-4)	99.9	1.6	96.0–102.1	13.2	0.4	13.1–15.1	33.4	0.6	32.5–34.6	3.3	1.0	2.2–6.2	25.2	0.6	24.5–26.4	8.2	<0.1	8.1–8.3	19.7	6.2	15.4–45.1
J-693 (W-2)	100.1	1.3	94.0–108.6	13.3	<0.1	13.4–15.1	29.8	<0.1	29.8–32.5	1.7	<0.1	1.7–5.7	22.3	<0.1	22.3–24.5	8.2	<0.1	8.2–8.3	11.8	5.4	7.8–34.6
33J-694 (W-3)	115.9	2.7	107.5–123.9	13.4	0.4	13.4–16.4	35.4	1.3	35.9–35.7	3.2	0.6	2.7–6.1	26.6	1.0	26.8–26.9	7.7	0.9	8.2–8.3	14.2	3.5	10.3–33.6
J-695 (W5-1)	—	—	—	—	—	—	—	—	—	—	—	—	—	—	—	—	—	—	—	—	—
J-696 (W-2)	97.9	3.7	93.4–111.9	15.2	2.2	13.5–21.7	35.7	<0.1	35.7–35.8	5.2	0.6	4.7–6.9	26.9	<0.1	26.9–27.2	8.2	<0.1	8.2–8.7	12.6	6.7	9.1–40.9

Cells with "—" indicate no data (instrument was either not turned on or the sensor malfunctioned).

8.3.2 Community-Habitat Associations

8.3.2.1 Natural Substrate

8.3.2.1.1 Canyons Habitats

The diversity of corals was relatively low in both canyons with locally high abundance for some species; however, diversity of other sessile hard substrate fauna was high, particularly anemones and sponges. Octocoral species that were observed in both canyons include the gorgonians *Paragorgia arborea* (**Figure 8-7 A**), *Primnoa resedaeformis* (**Figure 8-7 B**), *Anthothela grandiflora*[1] (**Figure 8-7 C**), *Paramuricea placomus* (**Figure 8-7 E**), and the soft corals *Anthomastus* sp. (**Figure 8-7 H**) and *Duva florida* (**Figure 8-7 I**). The small yellow gorgonian *Acanthogorgia aspera* (**Figure 8-7 D**) was common in Norfolk Canyon, but was not observed in Baltimore Canyon. Isidid octocorals ("bamboo corals") (**Figure 8-7 F**) were observed infrequently in the canyon habitats, but some pennatulid octocorals ("sea pens") and large numbers of the bamboo coral *Acanella arbuscula* (**Figure 8-7G**) were brought up in five deep trawls (1,576 to 1,694 m) near the mouth of Norfolk Canyon. Hexacoral taxa observed in both canyons included scleractinian corals (stony corals) *Lophelia pertusa* (**Figure 8-8A**) and the cup corals *Desmophyllum dianthus* and *Javania* sp. (**Figures 8-8 C**,**D**), the yellow zoanthid (Parazoanthidae) (**Figure 8-8 G**), and large anemones (**Figure 8-8 H-J**). The scleractinian corals *Solenosmilia variabilis* and *Flabellum alabastrum* (**Figure 8-8 B**,**E**), and antipatharians ("black corals") including *Telopathes magna* (**Figure 8-8 F**) were found only in the deeper areas of Norfolk Canyon (>956 m). None of these species were documented in Baltimore Canyon, but some shallow-water cup corals (*Dasmosmilia lymani*) were trawled from near the head of the canyon at a depth of approximately 270 m. The overall distribution of these species within each canyon is presented in **Figures 8-9 A**,**B** and **8-10 A**,**B**.

Visual comparisons of the habitat maps and the coral locations shown in **Appendix 8-A** indicate that both octocorals and hexacorals (a cnidarian subclass that includes all stony corals, anemones, and zoanthids) are found predominantly on walls and steep slopes and on large boulders of rock or consolidated sediment. However, the habitat map of Dive 3 (ROV-2012-NF-03) shows an almost continuous track of soft sediment with low levels of faunal cover, and several colonies of the gorgonian *Paramuricea placomus* were observed toward the northern end of the dive track. This species was seen on flat ledges with thick sediment cover rather than on walls or overhanging ledges, which were more typical for other gorgonians (**Table 8-4**). Conversely, Dive 17 (ROV-2012-NF-17) found large amounts of steep wall but very few corals. Some habitat maps indicate high SFC cover, but no octocorals or stony corals. These areas are dominated by large anemones, such as *Bolocera tuediae*, *Actinioscyphia* sp., or Cerianthidae (tube-dwelling anemones), which were classified as SFC because they are large and often abundant. Areas dominated by large anemones occurred frequently in both Baltimore Canyon (ROV-2012-NF-02, 13, 15, 16) and Norfolk Canyon (ROV-2013-RB-686, 688, 691). The common octocorals, including the gorgonians *P. arborea*, *P. resedaeformis*, *A. grandiflora*, and *A. aspera*, the bamboo coral *Keratoisis* sp. (**Table 8-4**), and the zoanthid Parazoanthidae (which grows over gorgonian colonies) were all found in similar habitats and environments (**Table 8-4**). Some species of stony corals *S. variabilis* and *L. pertusa* were found under conditions that are more restricted.

[1] Cryptic species and possibly a cryptic genus have been identified for this coral (**Chapter 13**). Because it is not possible to visually distinguish between these taxa, *A. grandiflora* will be used to represent this taxonomic complex.

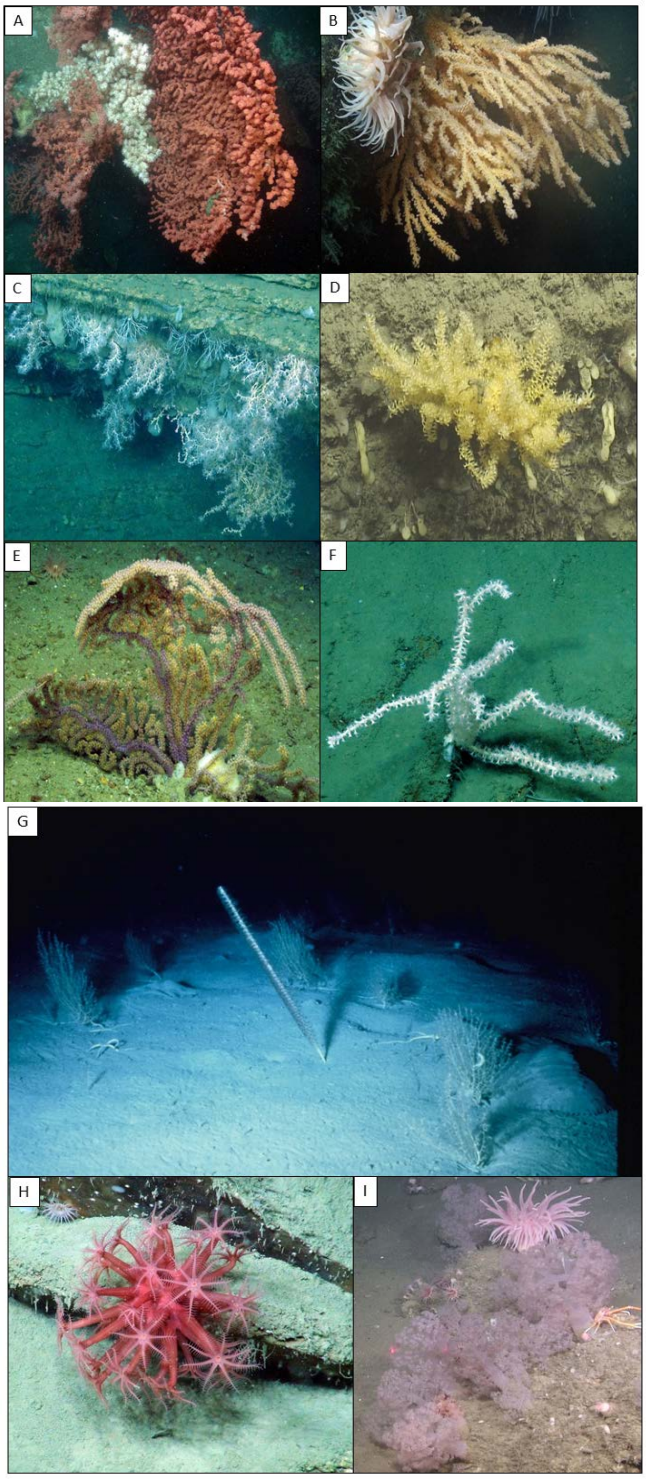

Figure 8-7. Octocorals observed in Baltimore and Norfolk canyons: A) *Paragorgia arborea*, B) *Primnoa resedaeformis*, C) *Anthothela grandiflora*, D) *Acanthogorgia aspera*, E) *Paramuricea placomus*, F) *Keratoisis cf grayi*, G) bamboo coral *Acanella arbuscula* and sea pen *Funiculina quadrangularis*, H) *Anthomastus* sp., and I) soft coral *Duva florida.*

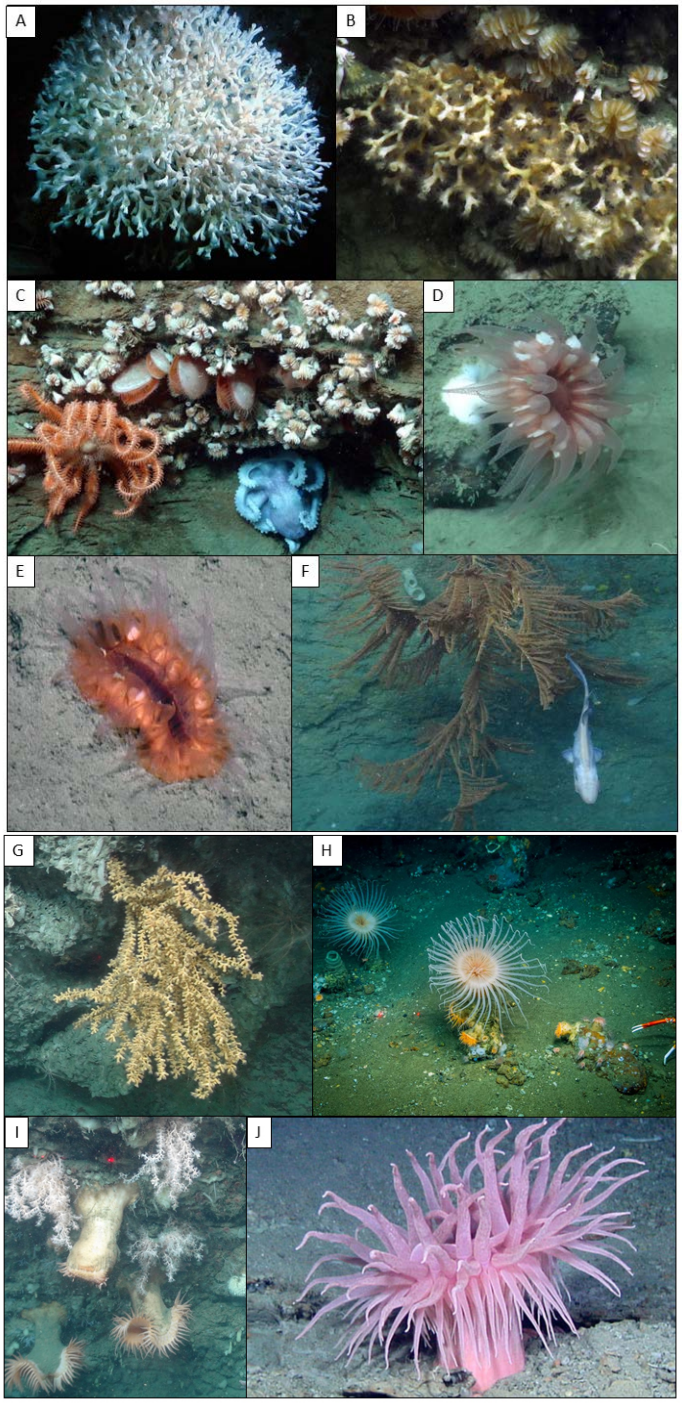

Figure 8-8. Hexacorals observed in Baltimore and Norfolk canyons. A) *Lophelia pertusa*, B) *Solenosmilia variabilis*, C) *Desmophyllum dianthus*, D) *Javania* cf *cailleti*, E) *Flabellum alabastrum*, F) *Telopathes magna*, G) Zoanthids (*Parazoanthus* sp.) overgrowing dead octocoral skeleton, H) Cerianthid anemones, I) *Actinoschyphia* sp., and J) *Bolocera tuediae.*

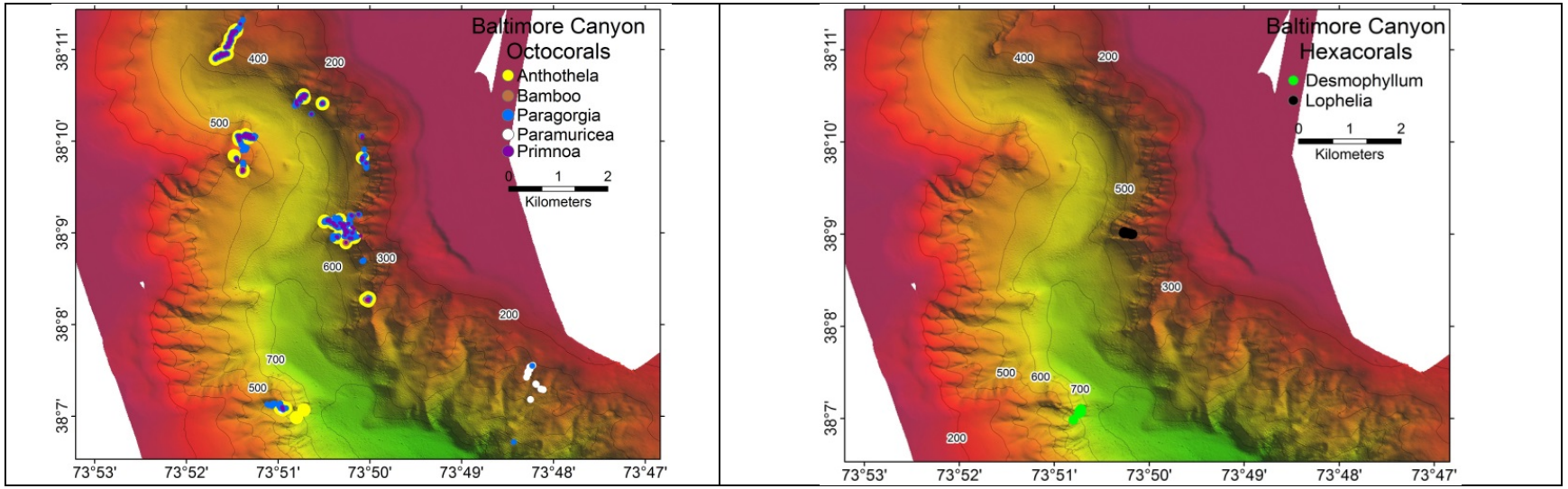

Figure 8-9. Distribution of: A) octocorals and B) hexacorals observed during ROV dives in Baltimore Canyon.

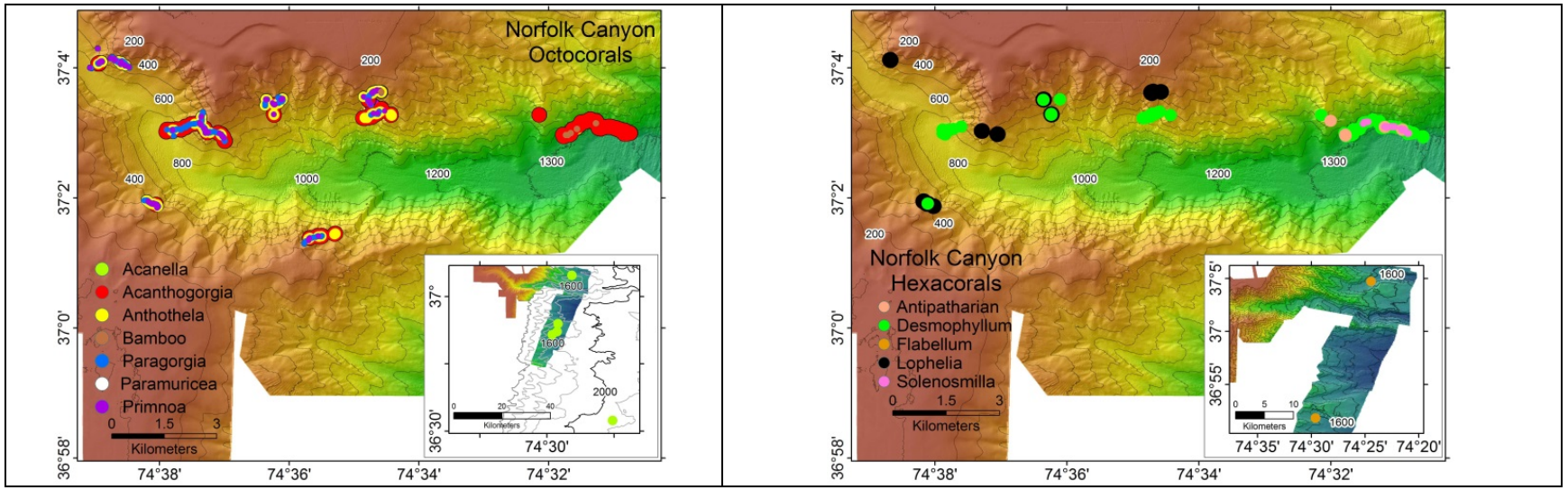

Figure 8-10. Distribution of: A) octocorals and B) hexacorals observed during ROV dives in Norfolk Canyon.

The number of observations per hour of ROV transect time was calculated for each octocoral and hexacoral taxa (except the very rare) documented during video analysis of each canyon (**Figures 8-11** and **8-12**). The most common species overall was the cup coral *Desmophyllum dianthus* with >34 000 records; however, most (>30,000) were from one long deep wall in Norfolk Canyon. A steep wall on the western flank of Baltimore Canyon also had several clusters of this cup coral, but *D. dianthus* were generally observed in groups of one to three. Of the gorgonians, *P. arborea* was the most common in both canyons, although they were observed more often in Baltimore than in Norfolk Canyon. These colonies also were the largest of the corals observed, often reaching more than 2 m in height and width. The soft coral *Duva florida* was locally abundant in both canyons, but it was not frequently observed, although the habitats where they were found were similar to habitats of other gorgonians (**Table 8-4**).

Coral distributions were compared using multivariate statistics to determine any significant differences between canyons, depths, and habitat types and to identify potential environmental drivers for the observed distributions. Octocoral and hexacoral data were treated separately because combining the data introduced too many missing data cells. For the same reason, the very rare species also were removed. Included in the analyses were octocorals *Paragorgia arborea, Primnoa resedaeformis, Paramuricea placomus, Anthothela grandiflora, Acanthogorgia aspera,* and *Duva florida* and hexacorals *Lophelia pertusa, Desmophyllum dianthus, Solenosmilia variabilis,* Antipathidae, and Parazonathidae. Before the analysis, data were fourth-root transformed to reduce the dominance of very abundant species. Bray-Curtis resemblance matrices were created and multidimensional scaling (MDS) plots were generated for octocorals and hexacorals by canyon (**Figures 8-13 A**,**B**), by depth (**Figures 8-14 A**,**B**), and by habitat type (**Figures 8-15 A**,**B**). An analysis of similarity (ANOSIM) was applied to the resemblance matrix for both taxonomic groups for each factor compared. Octocorals showed significant differences in distribution by canyon ($R = 0.09$, $p < 0.001$), by depth ($R = 0.38$, $p < 0.001$), and by habitat type ($R = 0.10$, $p < 0.001$). Hexacorals showed significant differences in distribution by canyon ($R = 0.1$, $p < 0.001$) and depth ($R = 0.69$, $p < 0.001$), but no significant differences by habitat type ($R = -0.01$, $p = 0.92$).

The environmental data (depth, temperature, DO, pH, turbidity) were square root transformed and normalized. The correlation between depth and temperature was high (92.3%), but it did not exceed the 95% correlation limit for exclusion of a variable and was therefore included in further analyses. The BEST routine (Primer V6) was used to generate correlations between environmental data and coral abundance by comparing resemblance matrices. For the octocorals, depth and temperature combined showed the greatest correlation with coral distribution ($\rho = 0.462$) with pH as the next most highly correlated variable ($\rho = 0.434$), followed by turbidity ($\rho = 0.401$) and oxygen ($\rho = 0.397$), all in combination with temperature and/or depth. For the hexacorals, depth and temperature showed the greatest correlations both separately (depth $\rho = 0.669$, temperature $\rho = 0.648$) and together ($\rho = 0.669$). The next most highly correlated variable was pH ($\rho = 0.642$), followed by turbidity ($\rho = 0.593$) and oxygen ($\rho = 0.585$), all in combination with temperature and/or depth. Principal component analysis (PCA) on octocoral environmental data resulted in the highest coefficients for temperature and depth in PC1 (0.520, 0.599), followed by pH (0.523) and turbidity (0.312); oxygen was the highest (0.727) in PC2. Together, PC1 and PC2 accounted for 82.8% of the variation. A PCA for hexacoral environmental data showed the same trends with highest coefficients for temperature and depth in PC1 (0.525, 0.560), followed by pH (0.502) and turbidity (0.396). As with the octocorals, oxygen was the highest (0.863) in PC2. Together, PC1 and PC2 accounted for 84.5% of the variation. The PCA graphs for octocorals and hexacorals (**Figures 8-16 A**,**B**) show a clear distinction by canyon. To determine whether the relationship among environmental variables and coral abundance is statistically significant, the RELATE routine (Primer V6) was applied to the matched coral and environmental resemblance matrices using a Spearman Rank correlation. The results showed a statistically significant relationship among environmental variables and octocoral abundance ($\rho = 0.388$, $p = 0.001$) and hexacoral abundance ($\rho = 0.537$, $p = 0.001$).

Red crabs (*Chaceon quinquedens*) were much more commonly observed in Baltimore Canyon than in Norfolk Canyon (**Figures 8-17 A-D**) and were most abundant at depths between 400 and 800 m. The deepest observation was in Norfolk Canyon at 1,500 m, but only several isolated individuals were seen at these depths. The shallower sites, however, often showed large numbers of individuals (up to 72 in one area). Red crabs were abundant at the Baltimore seep and were seen feeding on the mussels; however, only two observations of red crabs were seen at Norfolk seep (1,480 and 1,550 m), most likely because of the much greater depth. Observations of red crabs from our study declined rapidly beyond approximately 800 m, although they have been documented as deep as 1,800 m (Wigley et al. 1975). Red crabs were frequently observed as mating pairs in both years and both canyons, but gravid females (except for one observation) were seen only in 2012 (**Figure 8-17 C**).

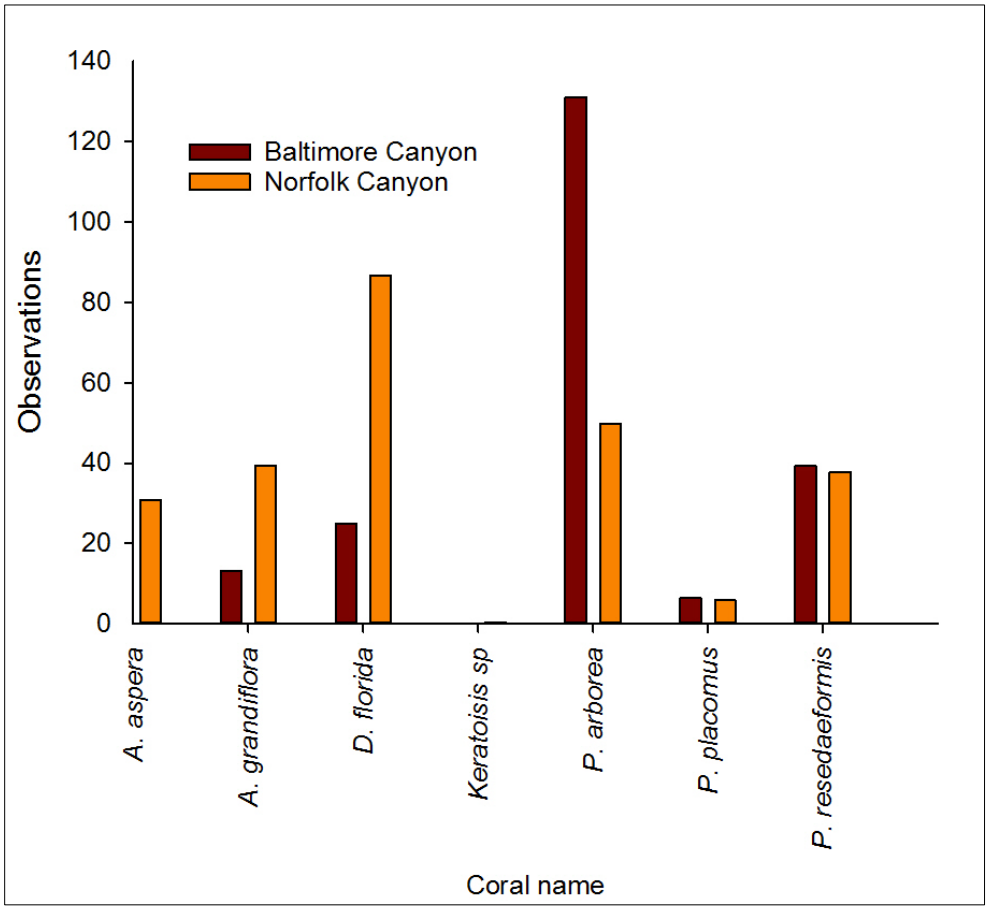

Figure 8-11. Number of octocoral observations per hour of ROV transects in Baltimore and Norfolk canyons

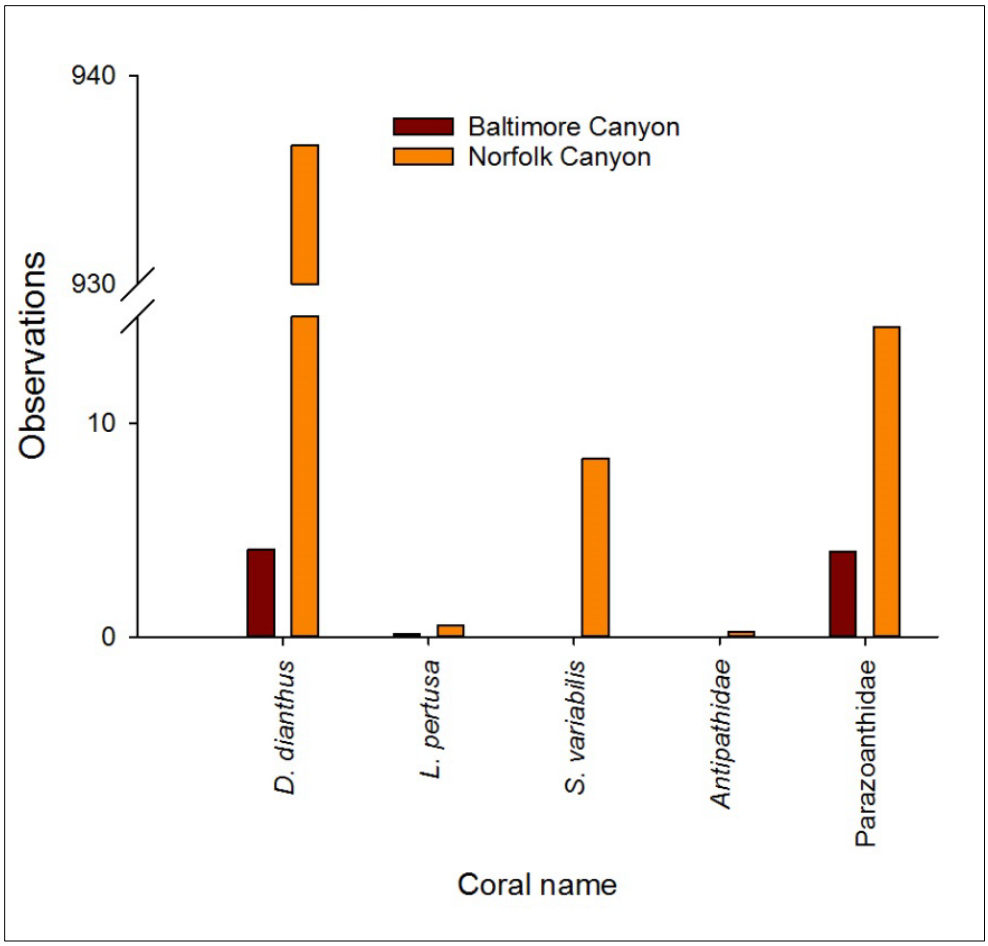

Figure 8-12. Number of hexacoral observations per hour of ROV transects in Baltimore and Norfolk canyons

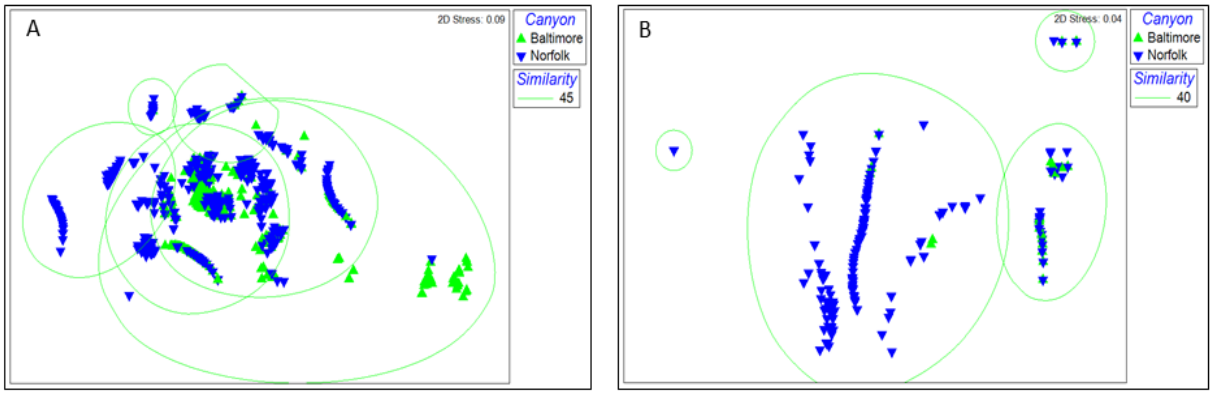

Figure 8-13. Multidimensional scaling plots for: A) octocorals and B) hexacorals by canyon.

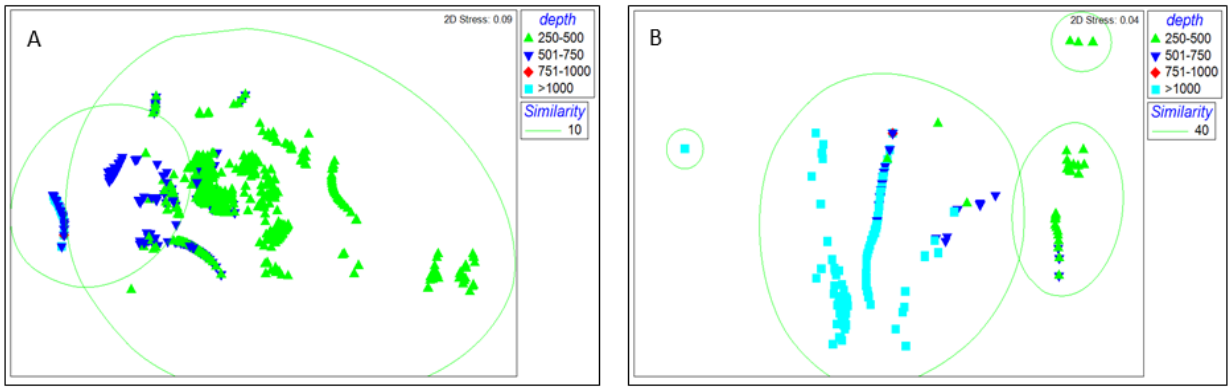

Figure 8-14. Multidimensional plots for: A) octocorals and B) hexacorals by depth.

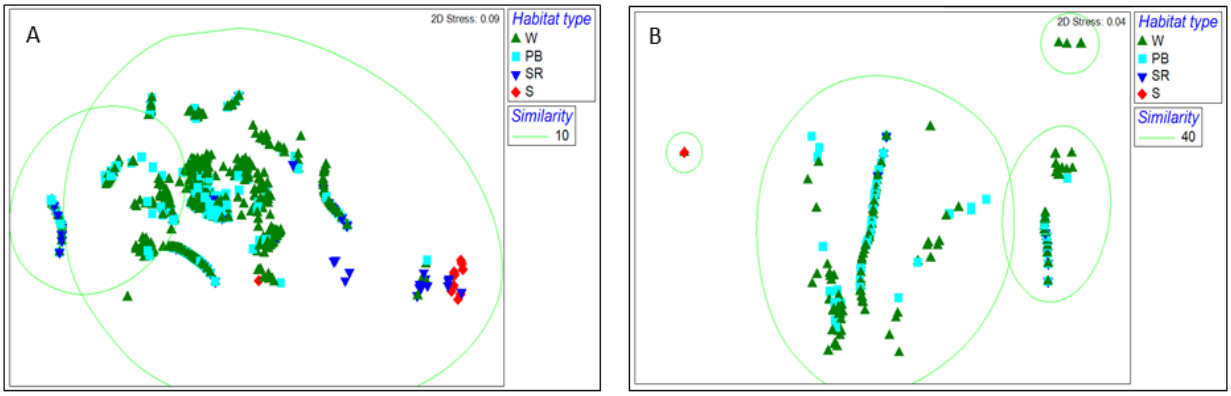

Figure 8-15. Multidimensional plots for: A) octocorals and B) hexacorals by habitat type. PB = large areas of emergent hard substrate (EHS) or consolidated sediment that forms hard pavement, >50% cover of hard substrate (slope may be flat to steep); S = soft sediment with no hard substrate visible (slope may be flat to steep); SR = soft sediment with small pieces of rock or EHS, <50% cover of hard substrate (slope may be flat to steep); W = walls and steep slopes (rock or consolidated sediment), steep profile.

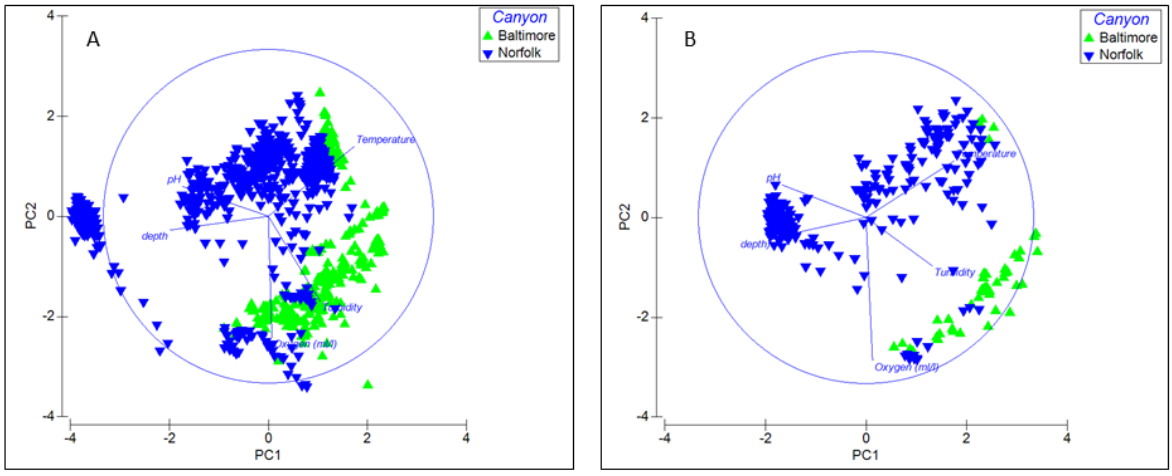

Figure 8-16. Principal component analysis (PCA) plots of environmental variables for: A) octocorals and B) hexacorals by canyon.

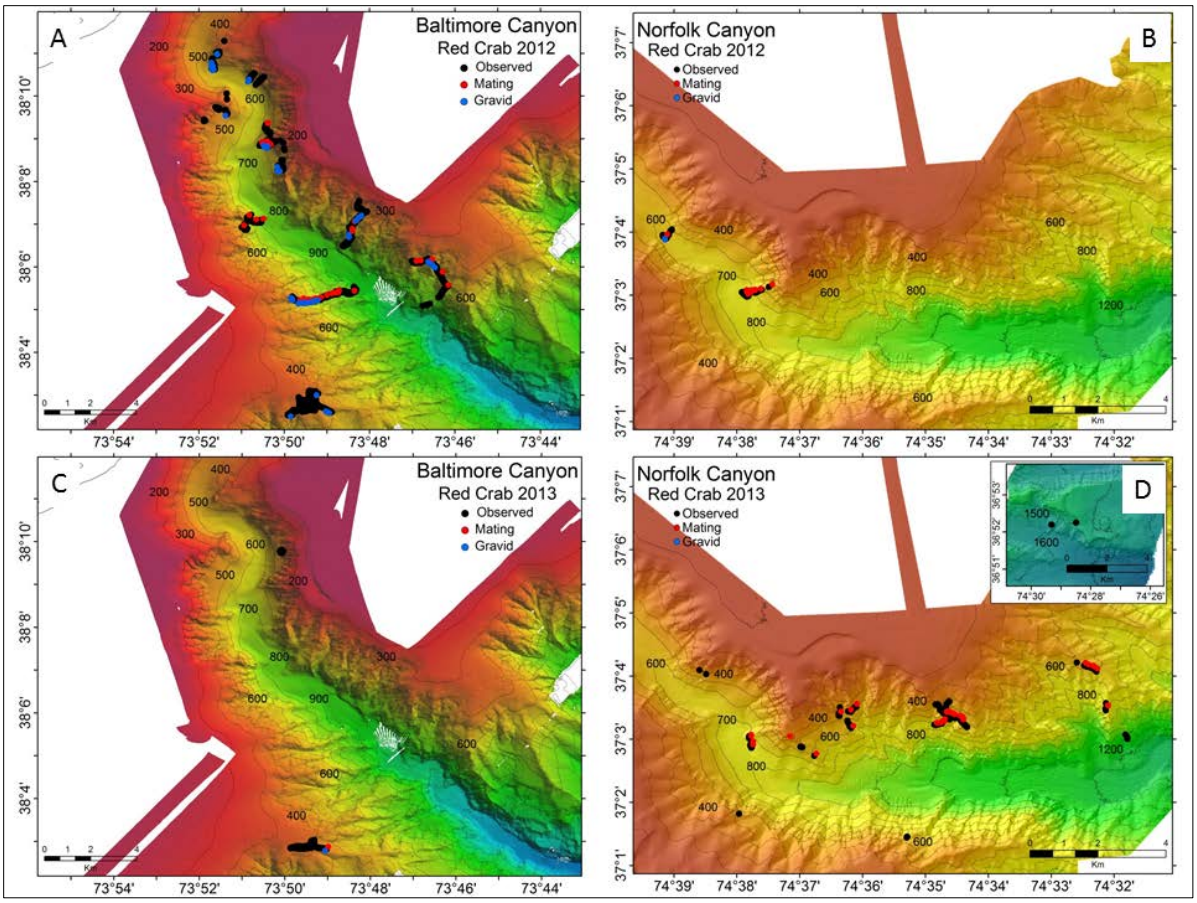

Figure 8-17. Distribution of individual, mating, and gravid red crabs (*Chaceon quinquedens*) observed in Baltimore and Norfolk canyons during the 2012 and 2013 sampling cruises.

8.3.2.1.2 Cold-Seep Habitats

Cold seeps near Baltimore and Norfolk canyons were dominated by the chemosynthetic mussel *Bathymodiolus childressi*, which hosts symbiotic bacteria that metabolize methane as an energy source (Childress et al. 1986). Collections from the Baltimore seep in 2012 confirmed the first record of this species in the western Atlantic margin (Coykendall, **Section 8.3.3.1.3**), and specimens collected in 2013 from the Norfolk seep also were identified as *B. childressi* (Coykendall, **Section 8.3.3.1.3**). The seeps were very different from each other in the distribution and cover of live mussels, which are a biological indicator of seepage activity (**Figures 8-18** and **8-19**; **Appendix 8-B**).

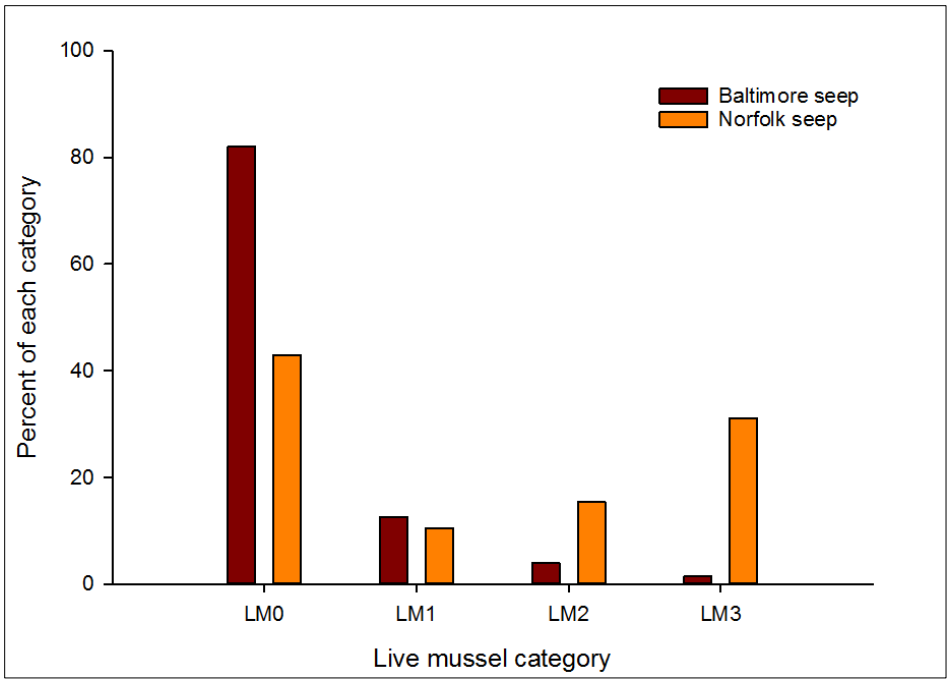

Figure 8-18. Differences in categories of live mussel cover observed during ROV dives at Baltimore and Norfolk seeps.

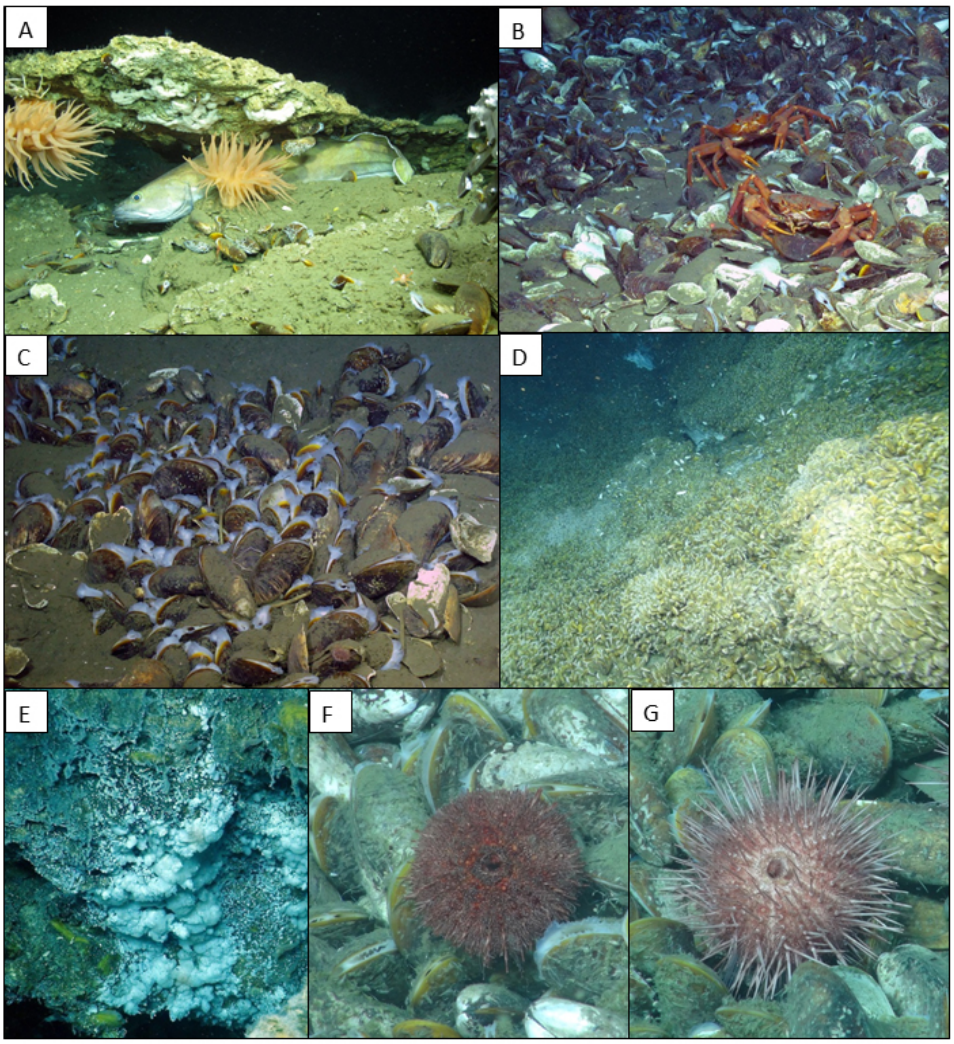

Figure 8-19. Images of A) sponges and anemones on authigenic carbonate at Baltimore seep, B) red crabs eating seep mussels at Baltimore seep, C) live mussel patch at Baltimore seep, D) live mussels covering authigenic carbonate structures at Norfolk seep, E) methane hydrate at Norfolk seep, F) *Echinus wallisi,* and G) *Gracilechinus alexandri* at Norfolk seep.

Baltimore seep (390 to 430 m) has a patchy distribution with some areas completely covered in live mussels and other areas with only dead shells, bacterial mats, authigenic carbonate, or a mixture of these features. On the periphery of the seep and among dead mussel shells, dense patches of quill worms (*Hyalinoecia* sp.) were observed in higher concentrations than in other areas of soft sediment in Baltimore Canyon. Other fauna frequently observed at Baltimore seep were different species of crabs and anemones in addition to a hemispherical demosponge (*Polymastia* sp.) that frequently colonized authigenic carbonate. The most common crabs were red crabs (*Chaceon quinquedens*). Other decapods included the "Jonah crab" *Cancer borealis*, the spider crab *Rochinia crassa*, the galatheid crabs *Eumunida picta* and *Munida* sp. and the hermit crab *Pagurus* sp. The most common anemones associated with the seeps were large pink *Bolocera tuediae* and the "Venus flytrap anemone" *Actinoscyphia* sp., which was observed on exposed authigenic carbonate. Patches of Cerianthidae (tube-dwelling anemones) also were observed during seep dives, mostly outside the active seepage area. The only species that were found in greater numbers in high live mussel areas (i.e., active seepage areas) compared with low live mussel areas were

C. quinquedens, which were observed feeding on live mussels and *C. borealis*. Apart from *B. childressi*, none of the fauna associated with Baltimore seep were chemosynthetic or seep endemics; however, considering the relatively limited sampling at this seep, the presence of other endemic species cannot be excluded.

The Norfolk seep (1,485 to 1,600 m) invertebrate communities were different from Baltimore with only *Actinoscyphia* sp. in common and at very low numbers at the Norfolk seep. The most common invertebrate associates were the brittle star *Ophiomusium lymani* and *Chiridota heheva*, a seep-endemic holothurian (**Figure 8-19**) observed in large numbers intertwined with live mussels. Other common associated fauna were dark red, pink/red[2], and white spiny urchins (*Echinus wallisi, Gracilechinus alexandri*, and *G. affinis*, respectively [**Section 8.3.3.1.2**]) that were living among the mussel beds.

The Baltimore and Norfolk seeps had completely different associated communities (the only species in common were *B. childressi* and *Actinoscyphia* sp.); therefore, the two seep communities were not statistically compared. For each seep area, data from all ROV dives were combined and the factors driving community structure were investigated using Primer V6 software. Habitat types (**Table 8-2**) were reduced from eight to four: sediment (S), mixed hard and soft substrate (MS), sediment with dead mussel shells (SDM) and mixed substrate with dead mussels (MSDM). Substrate type and live mussel cover (**Table 8-2**) were used as factors in the MDS plots and statistical analyses.

For the Baltimore seep, species abundance data were fourth-root transformed, but the quill worm abundance still dominated the abundance data therefore a presence/absence transform was applied to reduce the effect of their numerical dominance in the community. A Bray-Curtis resemblance matrix was generated and MDS plots were made showing community structure distribution by substrate (**Figure 8-20 A**) and by live mussel cover (**Figure 8-20 B**). A two-way ANOSIM was used to test for differences between habitat types and levels of live mussel cover. There was an overall significant difference ($R = 0.125$, $p = 0.001$) between substrate groups (across all mussel cover categories). Pairwise tests between groups were all significantly different apart from mixed substrate versus MSDM ($R = 0.07$, $p = 0.91$). There was also an overall significant difference ($R = 0.226$, $p = 0.001$) between categories of live mussel cover across all substrate groups. Pairwise tests showed that all groups were significantly different from each other, but the greatest differences were between no live mussels and very high cover ($R = 0.493$, $p = 0.001$).

For Norfolk seep, a fourth-root transform was applied to all species before the Bray-Curtis resemblance matrix and MDS plots were generated to show community structure relationships by substrate (**Figure 8-21 A**) and live mussel cover (**Figure 8-21 B**). A two-way ANOSIM was used to test for differences between habitat types and levels of live mussel cover. There was no significant difference ($R = -0.047$, $p = 0.989$) between habitat types (across all mussel cover categories), particularly between MSDM and soft SDM ($R = -0.094$, $p = 0.999$). There was, however, a significant difference between live mussel categories across all habitat types ($R = 0.273$, $p = 0.001$). Pairwise comparisons showed significant differences between all categories except LM1 and LM2 ($R = -0.026$, $p = 0.814$). As with Baltimore seep, the greatest differences were between no live mussels and highest live mussel cover ($R = 0.516$, $p = 0.001$).

[2] The color of *G. alexandri* was categorized as 'red' in the Echinoid bar-coding section. No *E. wallisi* were sequenced.

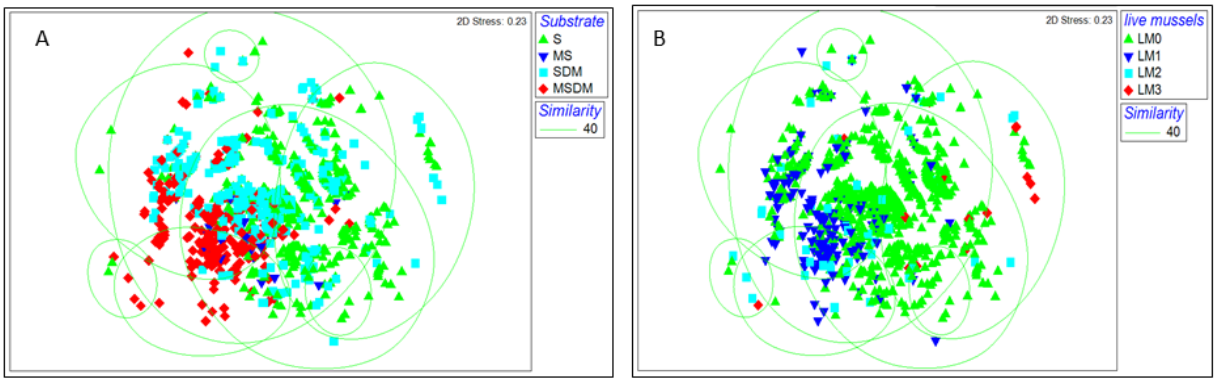

Figure 8-20. Multidimensional scaling plots for Baltimore seep community structure by: A) substrate and B) live mussel cover.

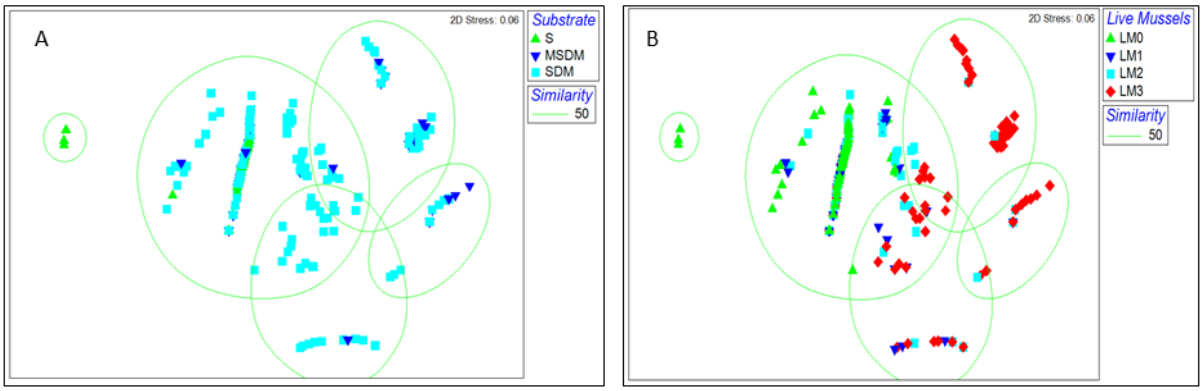

Figure 8-21. Multidimensional scaling plots for Norfolk seep community structure by: A) substrate and B) live mussel cover.

8.3.2.2 Artificial Substrate

Species accumulation curves indicate that an asymptote was reached or nearly reached for each shipwreck in each year, indicating that most species present on the wrecks were effectively sampled (**Figure 8-22**). A total of 35 morphotypes were observed on the eight shipwrecks. Of these morphotypes, 21 were identified at least to genus. A species list of invertebrate fauna present at each shipwreck is listed in **Table 8-10**. One morphotype, called the "brown tube complex," consisted of proteinaceous tubes, most likely constructed by a polychaete, with multiple species living as epibionts on them, including at least two hydroids, two bryozoans, one gammarid amphipod, one pycnogonid, one ophiuroid echinoderm, one errant polychaete, and one serpulid polychaete, all living on or around one another. Because it was impossible to visually differentiate among the many species in ROV video, brown tube complex was treated as one morphotype for the purposes of this analysis.

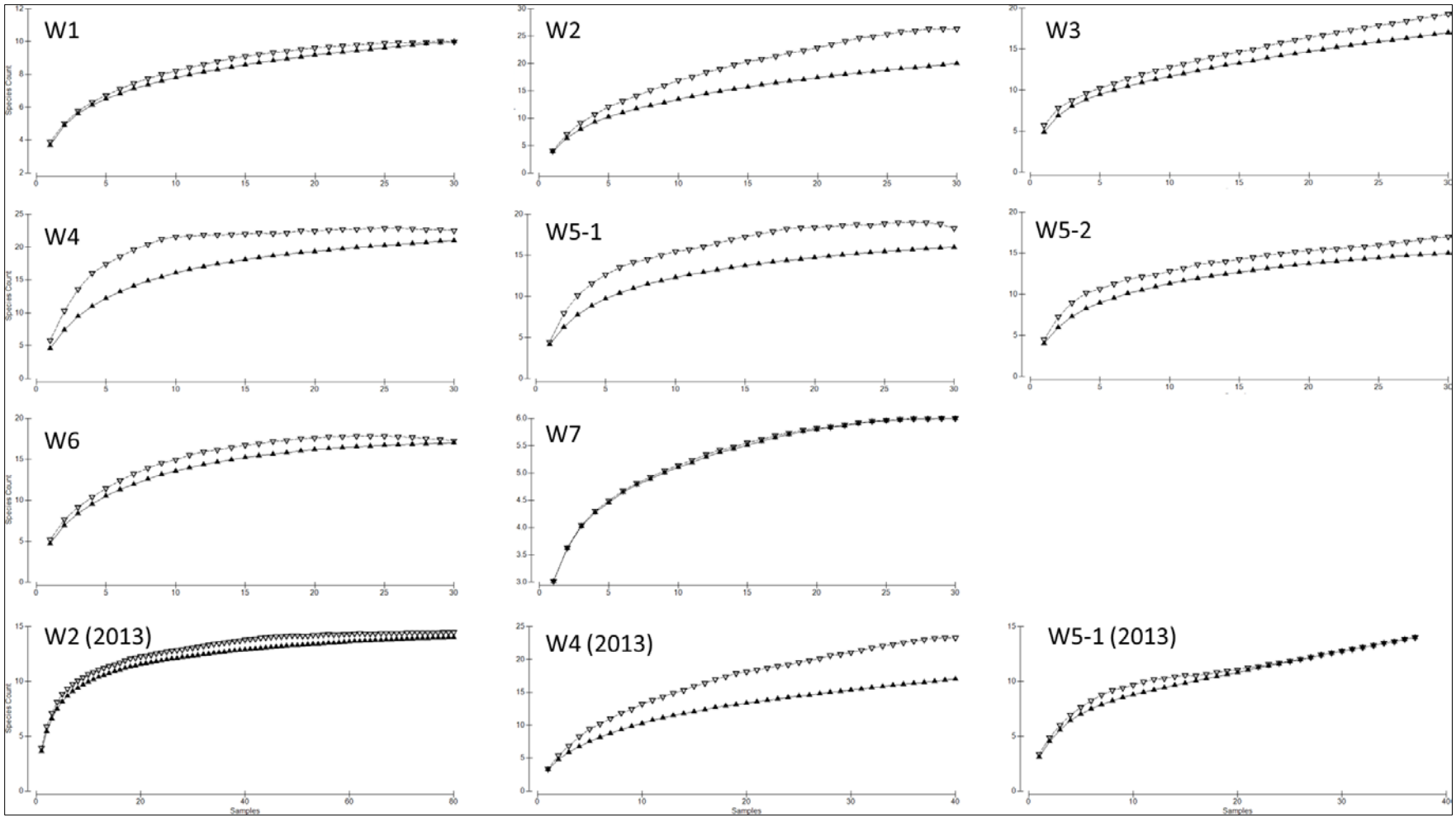

Figure 8-22. Permutated species-accumulation curves for each shipwreck. The x axis represents number of samples and the Y axis the species count for each wreck. Black triangles indicate observed species; white triangles indicate the Chao1 index. Graphs in the bottom row are for shipwrecks sampled in 2013.

Table 8-10. Taxa present at each shipwreck. A "•" indicates presence; D indicates a dominant species on that wreck.

Taxa or Morphotype	Shipwreck Number							
	W1	W2	W3	W4	W5-1	W5-2	W6	W7
White encrusting taxon	•	•	•	•	•	•	•	•
Yellow encrusting taxon	•	•	•	D	•	•	D	D
Pink encrusting taxon							•	
Metridium senile	D						•	
Hormathiidae	•	D	•	•	•	•	•	
Halcurias pilatus			•		•	•		
Small white anemone		•	D		D	D	•	
Giant purple anemone				•				
White zoanthids	•	D	•	•	•	•	D	•
Smaller zoanthid		D					•	
Brown tube complex	D	•		D	•		•	D
Plumularia setacea	•			•			•	•
Corynidae		D	•		•	•	•	
Pine hydroid			•	•		•		
Paracyathus pulchellus	•	•	•	•	•		•	
Crassostrea virginica		•	•	•	•			
Diodora tanneri		•	•	•	•			
Red shrimp						D		
Rochinia crassa		•	•	•	D	•	•	
Euchirograpsus americanus		x		•				
Cancer borealis				•				
Paguristes lymani		•			•	•		
Munida sp.		•		•				
Serpulid polychaete		•	•	•	•	•	•	
Henricia oculata	D						D	D
Henricia sp.				•				
Sclerasterias tanneri		D	D	•	•	D	•	
Sclerasterias sp.				•			•	
Coronaster briareus	•	•	•	•	•			
Odontaster hispidus		•	•	•	•	•		
Ophiocomina sp.			•	•				
Stylocidaris lineata		•		D		•		
Stylocidaris affinis		•	•	D		•		
Coelopleurus floridanis		•						

A different set of species was found to be dominant on each wreck. Dominant species were defined as those species whose total abundance was at least one order of magnitude greater than that of other, rarer species present on the wreck. Some dominant species followed geographical patterns; for example, “small white anemone” is a dominant species on wrecks W3, W5-1, and W5-2, which are all located in the northeast corner of the study area, but “yellow encrusting sponge” is dominant on wrecks W4, W6, and W7, which are widely separated across the study area (**Table 8-10**, **Figure 8-4**).

Patterns in the distribution and diversity of fauna within a single shipwreck were complex, varied, and often not significant. The abundance and richness of sessile and mobile invertebrate faunas, on the top, middle, and bottom of each wreck, varied by wreck, with a different pattern apparent on each one. In most cases, the differences between abundance and richness on different parts of the wreck were not significant (**Figure 8-23**). The only wreck that showed significant multivariate differences among the top, middle, and bottom of the wreck was W5-1 (ANOSIM, $R = 0.414$, $p = 0.002$). No statistical relationships were found between invertebrate richness or abundance and the complexity of shipwreck surfaces when analyzed within a single wreck. In addition, no significant relationships were found between invertebrate richness or abundance and the percent cover of fishing gear when analyzed within each wreck. No consistent patterns in species richness or faunal abundance were found between different surfaces (vertical, horizontal, slanted, complex, underside, or pillar). However, ANOSIM revealed significant differences between surfaces for five of the eight shipwrecks (W3, $R = 0.573$, $p = 0.001$; W4, $R = 0.258$, $p = 0.001$; W5-2, $R = 0.269$, $p = 0.024$; W6, $R = 0.336$, $p = 0.019$; W7, $R = 0.258$, $p = 0.021$). Multivariate differences between the north-south or east-west sides of a single wreck were significant for only wreck W1 (two-way crossed ANOSIM, north-south, $R = 0.338$, $p = 0.044$; east-west, $R = 0.398$, $p = 0.020$).

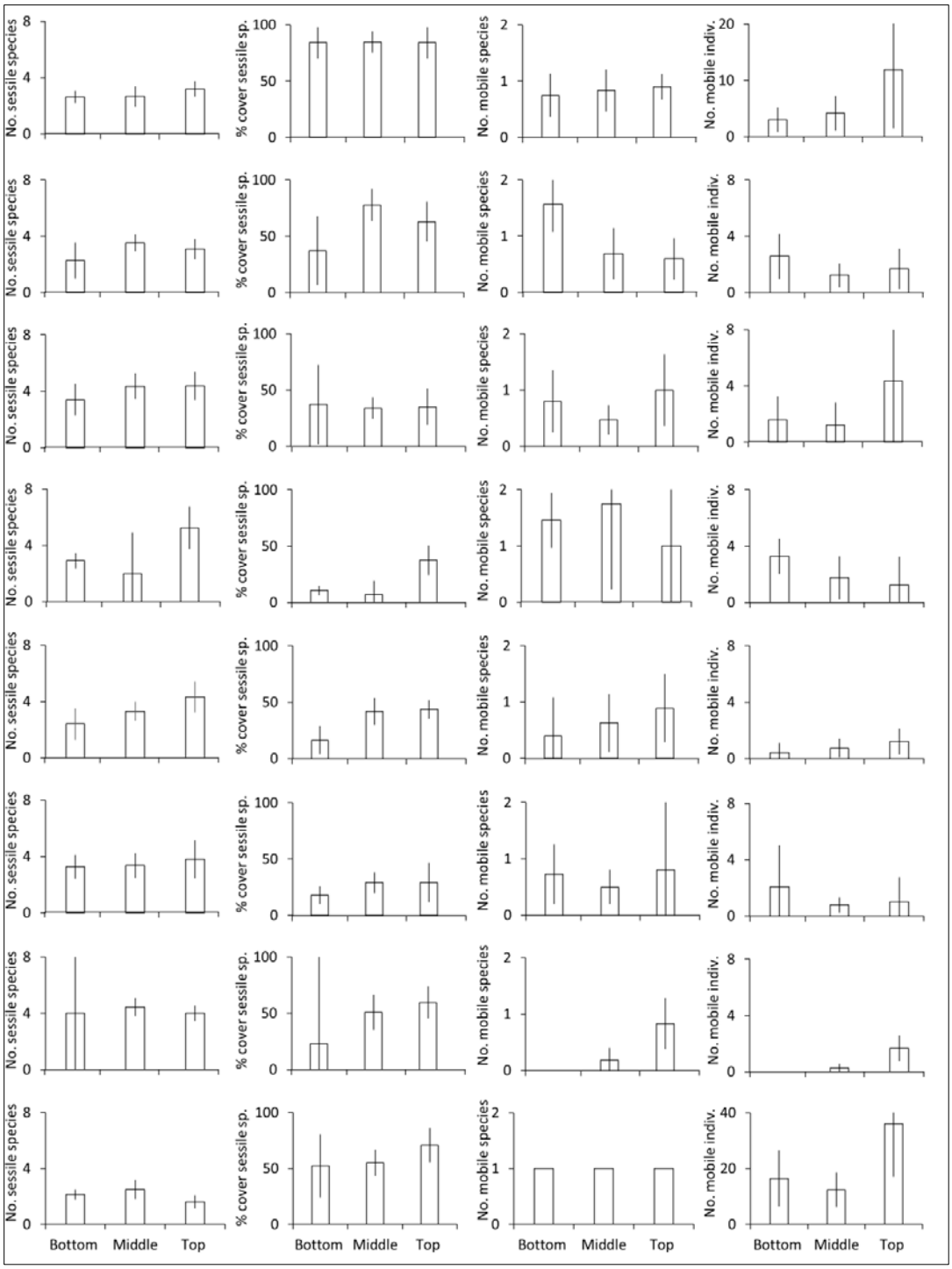

Figure 8-23. Average abundance and species richness (see Y-axis labels) of sessile and mobile fauna at the bottom, middle, and top of eight shipwrecks off the east coast of the United States. Wreck numbers from top to bottom: W1, W2, W3, W4, W5-1, W5-2, W6, and W7. "Bottom" indicates frame grabs where the seafloor was visible or known to be directly adjacent to the seafloor; "Top" indicates frame grabs where the water column above the shipwreck was visible or known to be located at the top of the shipwreck; all other frame grabs were defined as "Middle." Error bars indicate 95% confidence intervals.

8.3.3 Invertebrate Species Inventory

Approximately 3,500 invertebrate specimens were identified from collections made during the Atlantic Deepwater Canyons study, either from targeted or incidental sampling with the ROV or by trawling. The majority of specimens were identified by taxonomic experts, but when this was not possible, specimens were identified to the highest taxonomic resolution possible without expert opinion. The most common phyla collected in Baltimore Canyon were Arthropoda (*n* = 1,007), Cnidaria (*n* = 315), Echinodermata (*n* = 165), Annelida (*n* = 150), and Mollusca (*n* = 145). Norfolk Canyon collections were similar; the largest collection was the Cnidara (*n* = 471) followed by Arthropoda (*n* = 416), Echinodermata *(n* = 369), Mollusca (*n* = 303), and Annelida (*n* = 80). The taxa are presented in **Appendix 8-C**, and a database with specimen images will be archived at CSA Ocean Sciences Inc. in Stuart, Florida.

8.3.3.1 DNA Barcoding

8.3.3.1.1 Spiny Urchins

A 565 nucleotide fragment was amplified from 21 spiny urchins with GenBank accession numbers MG137216-36. Two groups were evident in the sequencing results that correlated with color morph: white, *N* = 12 and red, *N* = 9. A single white individual, MAC415, grouped more closely with the red individuals and therefore it was included in the red group when estimating sequence diversity statistics. The consensus sequence for both groups was compared to the public NCBI GenBank nucleotide database using the search algorithm blastn. The white group consensus sequence matched with 100% identity (*E*-value 0.0, 99% query coverage) to *Gracilechinus affinis* (KF500007). Close matches (identity of 99%) occurred with several other *Gracilechinus* species as well. The red group consensus sequence matched with 100% identity (*E*-value 0.0, 99% query coverage) to *Gracilechinus alexandri* (KF500008, KF500014) and a single *Gracilechinus elegans* (KF500010) sequence. When considering all 21 samples, there were a total of 34 polymorphic sites and 10 unique haplotypes. The average number of pairwise nucleotide differences between sequences was 14.2. Within the white group, four mutations resulted in four unique haplotypes within 12 sequences. The average number of pairwise nucleotide differences between sequences was 0.8. Within the red group, six total mutations resulted in six unique haplotypes within nine sequences with an average number of pairwise nucleotide of 1.9. When comparing the two groups, 24 fixed nucleotide differences were found between them. Furthermore, mutations found in each group (white = 4, red = 6) were unique to those groups (mutations are not shared between the groups). The average number of pairwise nucleotide differences between populations was 26.5.

Figure 8-24 A shows the maximum likelihood phylogeny results for the mid-Atlantic canyons *Gracilechinus* samples, which form two separate clades. The white color morphs, *N* = 12, cluster with six other *Gracilechinus* species. *G. affinis*, a western Atlantic species, has 100% sequence identity with the MAC white color morphs. However, other eastern and central Atlantic species, *G. atlanticus* and *G. stenoporus* as well as representatives of Pacific species *G. lucidus, G. multidentatus,* and *G. euryporus* (recently assigned to *Gracilechinus* from *Echinus*) (Pawson et al. 2015) also share the clade, and the relationships within this group cannot be resolved with statistical significance. The MAC red color morphs, *N* = 9, form a separate clade that includes two *G. alexandri* individuals and a single *G. elegans* sequence (KF500010), found in the NCBI GenBank database, but not included in the study published by Minin et al. (2015). Because this sequence does not group with the other *G. elegans* included in the analysis, which were basal to the white-morph clade, it is assumed that KF500010 was misidentified.

A single representative of the genus *Echinus*, *E. wallisi,* is known from the western Atlantic. A single specimen was collected from the Norfolk seep and was identified morphologically but was not included in the samples that were sequenced and no genetic information for the species is in the NCBI GenBank nucleotide database (Benson et al. 2013). Therefore, only *Gracilechinus* sequences could be used for phylogenetic analysis in this study.

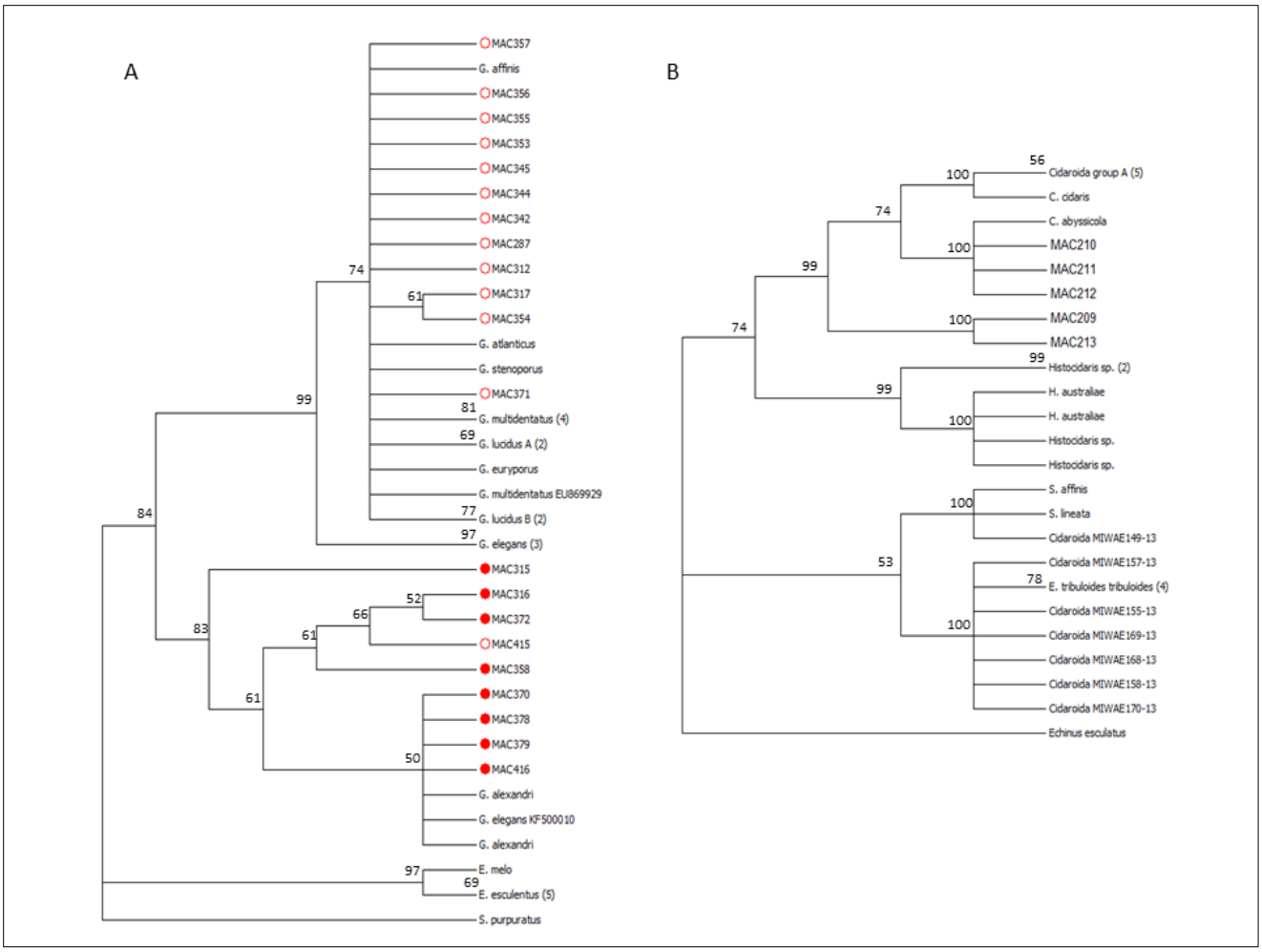

Figure 8-24. Maximum likelihood phylogenetic trees based on partial mtCOI sequence data. Bootstrap probability values reported for each node. Number of sequences per species, if more than one, inside parentheses after name. A) *Gracilechinus* echinoid urchins. Color of circles indicates color morph of sample. B) cidaroid urchins.

8.3.3.1.2 Pencil Urchins

A 662 base pair fragment was amplified from all 5 cidaroid samples with GenBank accession numbers MF996377-81. Two groups were evident in the sequencing results: MAC210, MAC211, MAC212 (Group 1), and MAC209, MAC213 (Group 2). The consensus sequence for both groups was compared with the public GenBank nucleotide database using the search algorithm blastn. For both Group 1 and Group 2, the best match was *Cidaris abyssicola*, although Group 1 was a closer match (100% identity, *E*-value 0.0, 70% query coverage) compared with Group 2 (96% identity, *E*-value 0.0, 100% query coverage). These sequences contained two unique haplotypes, with a total of 18 mutations, and an average number of nucleotide differences of 13.2. All five sequences were translated into 220 amino acids using the invertebrate mitochondrial code in MEGA6.06, with no amino acid changes among individuals. Each group has a single, unique haplotype with an average number of nucleotide differences of 18.

The maximum likelihood phylogeny results for cidaroid samples are shown in **Figure 8-24 B**. Three MAC individuals (Group 1) fell within a clade including *C. abyssicola* with 100% bootstrap support. The next closest clade to the MAC/*C. abyssicola* clade contains five unclassified Cidaroida individuals from the same project in the BOLD database (Ratnasingham and Hebert 2007) and collected from the Cape Verde Islands off West Africa, which are sister to *C. cidaris*. MAC Group 2 was strongly supported as the outgroup to the clade containing the Group 1 samples. The next closest group consists of *Histocidaris* sp., all collected from New Zealand. Other Atlantic Cidaroida, including unclassified individuals from the Gulf of Guinea, *Stylocidaris* sp. from the North Atlantic, and *Eucidaris t. tribuloides* from the Gulf of Mexico form a separate, more distantly related clade. Our barcoding efforts suggest that samples of the MAC pencil urchin contain two different taxa: Group 1 that is synonymous with or closely related to *C. abyssicola* and Group 2 that is ancestral to the MAC/*C. abyssicola* and West African samples. Group 2 does not associate with *C. cidaris*. Based solely on mtCOI barcoding data, it is possible that MAC Group 2 represents either *C. blakei* or *C. rugosa*. However, because MAC Group 2 samples fall outside of the clades containing known *Cidaris* species, it also is possible that Group 2 belongs to another closely related genus lacking representatives in public genetic databases.

8.3.3.1.3 Seep Mussels

A 657 base pair fragment of mtCOI was amplified and sequenced in 97 mussels from Baltimore and Norfolk seeps. The consensus sequence from all individuals was used to search the GenBank database with the search algorithm blastn. The closest matches, with 100% identity, were sequences from two *Bathymodiolus childressi* individuals with GenBank accession numbers EU288175 (*E*-value 0.0, query cover 75%) and KM024172 (*E*-value 0.0, query coverage 73%). The next closest matches, with 99% identity, were approximately 40 other sequences from additional *B. childressi* individuals. When all 97 sequences were translated to amino acid sequences using the Drosophila mitochondrial code in DnaSP, 218 amino acids result with no amino acid changes between individuals. Several *B. mauritanicus* individuals were also highly similar (98% identity, *E*-value 0.0, query coverage 71% to 75%).

Ninety-nine *Bathymodiolus childressi* from the Gulf of Mexico, 10 *B.mauritanicus*, and 16 *B. aff. childressi* mined from GenBank were included in haplotype diversity analyses (**Figures 8-25 A**; **Table 8-6**) along with MAC samples. A graphical representation of mtCOI sequence diversity within and between species of *Bathymodiolus* is shown in **Figure 8-25 A**. The haplotype network contains 71 total unique mtCOI haplotypes from 216 individuals. Four large clusters were evident in the network. All *B. mauritanicus* (green and yellow) and *B. aff. childressi* (red) haplotypes grouped together. This cluster contained a single individual sampled in Baltimore Canyon, MACM34, which was two mutational steps away from *B. aff. childressi* (DQ513428) from the Barbados Accretionary Prism, Orenoque A site and 15 mutational steps away from the closest MAC sample. Individuals from MAC and the Gulf of Mexico (GOM) formed the remaining three large clusters. All clusters contain a frequent haplotype and include

individuals from each population: GOM, Baltimore, and Norfolk. Each cluster is closely related to the others with common haplotypes separated by one to three mutational steps. Less common haplotypes were separated by no more than three steps. These results indicate that MAC mussels were not genetically differentiated by canyon, nor were they significantly different from GOM *B. childressi*. One exception involved a single individual captured from Baltimore Canyon that appeared more closely related to *B. mauritanicus/B. aff. childressi* sampled from West Africa, the Gulf of Cadiz, and the Barbados Accretionary Prism. Moreover, *B. childressi* exhibit high levels of genetic diversity at the mtCOI locus.

Sequences were trimmed to 437 nucleotides so that all sequences were the same length for analyses in DnaSP. Diversity indices and summary statistics for several groups are reported in **Table 8-11**. The sequences were grouped as follows: Baltimore Canyon mussels (*N* = 42); Norfolk Canyon mussels (*N* = 48); all MAC mussels (*N* = 90); Gulf of Mexico (GOM) *B. childressi* (*N* = 99); all *B. childressi* mussels (*N* = 189); and *B. mauritanicus*, which also includes *B. aff. childressi* individuals and a single MAC individual, based on the haplotype network (*N* = 27); (**Figure 8-25 A**). The number of polymorphic sites, mutations, and haplotype diversity between all groups was very similar. Moreover, average number of nucleotide differences within groups (2.03 to 2.25) were similar to between-group comparisons (2.04 to 2.19), except for *"B." childressi* versus *B. mauritanicus* (12.3). Baltimore and Norfolk populations share the fewest number of mutations (five), which was less than the six shared mutations between the two species *B. childressi* and *B. mauritanicus*. Pooling Baltimore and Norfolk samples (MAC group), the MAC and GOM groups shared 15 mutations.

The maximum likelihood, phylogenetic analysis resulted in all MAC mussels, except for MACM34, forming a clade with all GOM *B. childressi* individuals with 91% bootstrap support (**Figure 8-25B**). This clade falls within a larger clade containing all *B. mauritanicus* and *B. aff. childressi* individuals, and MACM34 with 98% bootstrap support. The *B. childressi*, *B. mauritanicus*, and MAC mussel clade is separate from the remaining clades. *B. brooksi* from the GOM is the most ancestral species of this separate clade, though with low bootstrap support. A clade including an undescribed species of *Bathymodiolus* from the coast of Niger, *B. aff. boomerang* from the Congo-Angola margin, *B. boomerang* from the Barbados Accretionary Prism, and *B. heckerae* from the GOM and Blake Ridge off the coast of South Carolina had bootstrap support of 96%, but some internal relationships are less supported. In this analysis, *B. heckerae* and *B. boomerang* from Barbados are paraphyletic but distinct from *B. aff boomerang* and the Niger species.

Table 8-11. Summary statistics of genetic diversity within the mtCOI gene of chemosynthetic mussels computed in DnaSP version 5.10.01.

Population	N	S	H	Hd	k	η
All	216	60	71	0.89	4.38	67
GOM	99	38	39	0.87	2.19	40
Baltimore	42	15	16	0.85	2.03	17
Norfolk	48	17	19	0.85	2.09	18
MAC	90	27	31	0.85	2.05	30
"B".childressi	189	49	58	0.86	2.15	55
"B".mauritanicus	27	17	13	0.9	2.25	17
"*B." chi* vs. *"B." mau*	216	60	71	0.892	12.31	6
Baltimore vs. Norfolk	90	27	31	0.85	2.04	5
Baltimore vs. GOM	141	43	45	0.86	2.13	11
Norfolk vs. GOM	147	39	52	0.87	2.19	9
GOM vs. MAC	189	49	58	0.86	2.16	15

GOM = "*B". childressi* from GOM in the GenBank nucleotide database (Benson et al. 2013); MAC = mid-Atlantic canyons and includes Baltimore and Norfolk populations; "*B*." *childressi* includes MAC and GOM.
N = sample size; S = number of polymorphic sites; H = the number of unique haplotypes; Hd = haplotype diversity; k = the average number of pairwise nucleotide differences between sequences within populations (rows 1−6) and between populations (rows 7–11); η = number of mutations within populations (rows 1−6) or number of shared mutations between populations (rows 7−11). n/a = not applicable.

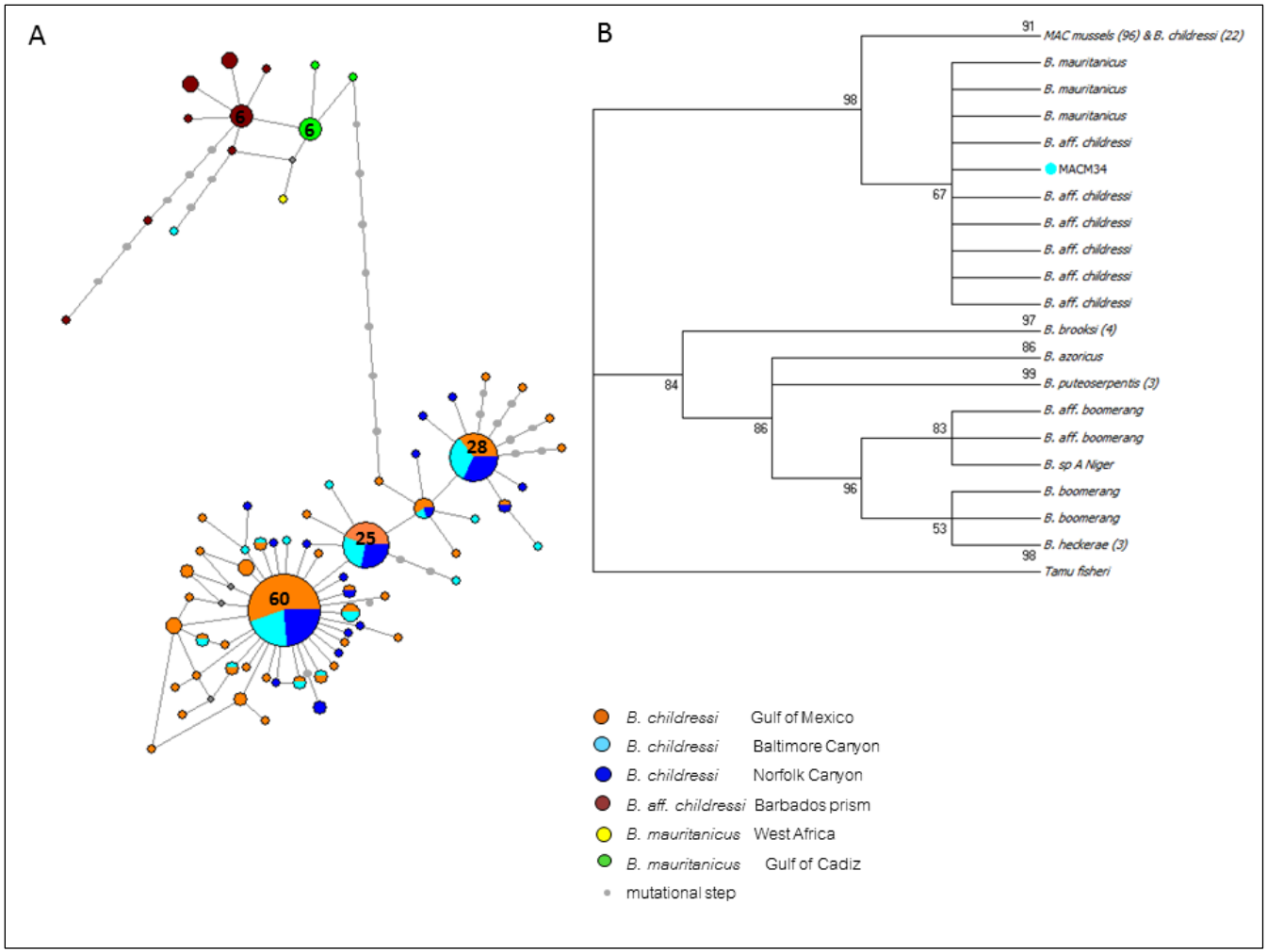

Figure 8-25. A. Haplotype network depicting mtCOI diversity within "*Bathymodiolus" childressi* from the mid-Atlantic canyons and closely related species. Size of circles is proportional to the number of individuals that share the haplotype and numbers >5 are shown. Inferred mutational steps linking haplotypes are shown if >1. "*B." childressi* from the Gulf of Mexico, "*B." aff. childressi*, and "*B." mauritanicus* were taken from GenBank and accession numbers (see **Table 8.6**).
B. Maximum likelihood trees of MAC mussels drawn in Mega6.06. Bootstrap values (out of 500) >50% are reported. **Table 8.6** lists the genus, species, and sampling locations (when available) of individuals from this study and mined from GenBank. Number of individuals represented at terminal nodes in parentheses if >1.

8.4 DISCUSSION

8.4.1 Natural Substrate − Canyons Habitats

Before the Atlantic Deepwater Canyons study was conducted, only 462 records existed for deepsea corals in the Mid-Atlantic Bight (MAB) region (MAFMC 2015), and these were primarily soft-sediment species such as the bamboo coral *Acanella arbuscula*, the cup corals *Flabellum alabastrum* and *Dasmosmilia lymani*, and sea pens (Pennatulacea) that were trawled from the shelf and slope. Earlier studies of deepsea corals within the canyons were few (**Chapter 2**), but some large gorgonians had been reported (Hecker et al. 1980, 1983) for Baltimore and Norfolk canyons. Data from this project increased the number of coral observations for the two canyons by several orders of magnitude over historical records and included new observations of *Lophelia pertusa* for the MAB (Brooke and Ross 2014) and new records of *Solenosmilia variabilis* for Norfolk and Baltimore canyons. These findings illustrate the level of new information that was derived from relatively few dives in these poorly studied habitats.

Statistical analyses of coral abundance and distribution show differences between canyons and water depths, but only octocorals show differences within habitat type. Hexacorals were most frequently observed on walls, boulders, or other areas with little or no sediment, which may be interpreted as a lower tolerance to sediment load than octocoral species. The distributions of both taxa are most highly correlated with temperature or depth followed by pH, turbidity, and oxygen. Temperature has long been recognized as a primary driver of deepsea coral distributions (Roberts et al. 2009) so this is not a surprising outcome.

The second most significant factor was pH, which is unexpected because the differences in pH seemed too small to statistically correlate strongly with coral distribution; however, pH correlated positively with temperature, which may have increased its importance in the analysis. High turbidity and sediment load can clog feeding structures of corals, which is why they are generally not found in high sediment environments. Both canyons have periodically high turbidity levels, but Baltimore Canyon has a persistent nepheloid layer between 400 and 800 m depth (**Chapter 6**) where many common corals occur. Notable differences between the canyons include the very high abundance of the gorgonian octocoral *Paragorgia arborea*, in Baltimore Canyon, which shows they can tolerate the turbidity and may even benefit from it nutritionally (**Chapter 16**). The higher abundance of stony corals in Norfolk Canyon, particularly *L. pertusa* (Brooke and Ross 2014), which occurs in the same depth zone as the common octocorals, may be due to the more uniform lower turbidity levels. The environmental data used for these analyses were collected during the ROV dives and do not necessarily reflect long-term conditions; however, the dives occurred over a 2 to 4 week period in two different years and covered a wide depth range; therefore, the data were considered useful for distributional analysis.

The most abundant and widely distributed of the gorgonians was *P. arborea*; colonies, which were often very large (>2 m tall/wide) and found in a wide range of habitats exhibiting a number of different phenotypes (white, pink, and red color morphs; robust and delicate branches). These differences were not genetically defined because all *Paragorgia* phenotypes collected were verified as *P. arborea* using mitochondrial gene sequencing (**Chapter 13**). Color and branching structure variation also occurs in other species of deepsea corals; *L. pertusa* colonies often have orange pigmentation in their tissues (although this is rare in the western Atlantic, and all colonies observed during the Atlantic Deepwater Canyons study were white) and may have heavily calcified (forma *brachycephala*) or fragile (forma *gracilis*) branching patterns (Brooke and Schroeder 2007). Coral pigments are created by different forms of carotenoids, which are derived from diet (Elde et al. 2012) and can also be vertically transmitted through the eggs of pigmented colonies (Larsson et al. 2014). The purpose of these pigments has not been resolved definitively, but possibilities include antioxidant and antibiotic properties (Shnit-Orland et al. 2008, Elde et al. 2012). Bacterial communities associated with orange *L. pertusa* colonies were different from white colonies, suggesting selection of bacterial communities by the coral through expression of

different metabolites (Neulinger et al. 2008). The authors speculated that the sulfur-oxidizing bacteria associated with white colonies may provide nutritional benefits in habitats where less food is available. In the eastern Atlantic, different colored colonies of *L. pertusa* are frequently found adjacent to each other in high food environments such as fjords, but offshore reefs where food is more limited *L. pertusa* are dominated by white colonies (Neulinger et al. 2008). Heavily calcified *L. pertusa* colonies are usually found in different habitats from the fragile forms, probably because of selection by environmental variables (Brooke and Schroeder 2007). In the MAB canyons; however, different phenotypes of *P. arborea* were observed together with no clear distribution structure; therefore, the selective benefits/costs of the different phenotypes are unclear but warrant further study. Other common octocoral species that usually co-occurred were *Primnoa resedaeformis* and *Anthothela grandiflora* whose habitat associations and ranges of depth and environmental conditions were similar.

Some species of octocorals were observed infrequently, but were locally highly abundant; these include the gorgonian *Paramuricea placomus* and the soft coral *Duva florida.* Most coral species were found on steep terrain with little or no sediment accumulation, but *P. placomus* was an exception. A single patch comprising approximately 250 individuals was observed once in each canyon and on both occasions, the colonies were primarily distributed along the top of a flat rocky ledge with a sand veneer. The sediment layer was sufficiently thick in some places that the underlying hard substrate was invisible. Corals cannot usually tolerate high sediment environments because particles can clog feeding and respiration apparatus. Exceptions include *L. pertusa,* which has a moderately high tolerance to sediment load (Brooke et al. 2009), but corals must produce mucus to remove particles, and this is an energetically expensive process that cannot be sustained over long periods. The *P. placomus* colonies can evidently tolerate chronic suspended sediment or episodic high sediment deposition, which may enable them to exploit habitats that other species cannot. Flat sandy/rocky terraces were frequently observed in both canyons, but the very limited number of *P. placomus* observations implies the presence of a controlling factor (e.g., current speed, food, larval delivery) beyond habitat availability. The soft coral *D. florida* occurred in few locations but in extremely high numbers; they were observed in habitats similar to other octocorals (i.e., rocky boulders or walls). As in the case of *P. placomus*, the distribution of *D. florida* appears to be driven by factors other than habitat.

The hexacorals were generally less abundant than the octocorals in Baltimore and Norflok canyons with two exceptions: a yellow zoanthid, *Parazoanthus*[3] sp. that grows over dead (and possibly live) octocorals and the cup coral *Desmophyllum dianthus*. *Parazoanthus* sp. had often completely overgrown the "host" octocoral skeleton and was observed growing on partially live colonies. Zoanthids were also observed on *A. grandiflora, P. placomus,* and *P. resedaeformis* (but not *P. arborea*) and were considerably more abundant in Norfolk Canyon than in Baltimore Canyon. The abundance of *P. placomus* and *P. resedaeformis* was comparable between the two canyons; however, more *A. grandiflora* was seen in Norfolk Canyon. The distribution of *Parazoanthus* sp. may therefore be determined, to some extent, by the distribution of the host species as well as the environmental tolerances of the zoanthid. The extremely high numbers of *D. dianthus* in Norfolk Canyon were observed during a single ROV dive (J2-685). A series of deep (~1,200 m) walls were heavily colonized by thousands of small *D. dianthus* as well as the colonial stony coral *Solenosmilia variabilis* and a new species of file shell (*Acesta cryptadelphe,* Gagnon et al. 2015). This extreme abundance was observed only on the deep walls of Norfolk Canyon where the individuals were small with fragile skeletons. In shallower habitats, this species occurred as large heavily calcified single specimens or in small clusters and were generally uncommon. The deposition of organic material (food) and Ω_{Arag} decreases with increasing depth (Feely et al. 2004), making it more difficult to produce calcified skeletons (Fabry 2008). At the deep Norfolk Canyon sites, Ω_{Arag} is approximately1.2, but in shallower areas, Ω_{Arag} is approximately 1.5, which

[3] Yellow zonathids overgrowing *P. placomus* were identified using sequence data as *Corallizoanthus* (**Chapter 13**); however, zoanthids collected from other octocorals were identified morphologically by J. Reimer as *Parazoanthus*. This taxon is currently being revised. Reimer's identification will be used in our analysis, but this genus may belong to *Corallizoanthus.*

may explain the observed differences in size and skeletal structure. Extremely high abundances have been observed elsewhere for this species (~1,500 individuals m^{-2} in the Chilean fjords, Forsterra and Haussermann 2003), and in waters with low Ω_{Arag} (Fillinger and Richter 2013). This species is gonochoristic with large numbers of small eggs (**Chapter 11**), which indicates a broadcast spawning strategy with dispersive larvae. It is possible that the availability of large areas of good habitat (steep wall with little sedimentation) in Norfolk Canyon enabled high recruitment, but growth rates were reduced by low food and Ω_{Arag}. The reverse conditions exist in shallower areas, potentially creating the different observed distributions and size structures in this species.

The deep coral reefs in the South Atlantic Bight and GOM are constructed by the stony corals *Lophelia pertusa* and *Enallopsammia profunda,* which can create large bioherms of consolidated coral rubble with live coral on the flanks and peaks. These deep reefs are highly diverse with gorgonians, antipatharians, sponges, and other mobile and sessile invertebrates (Brooke and Schroeder 2007, Ross and Nizinski 2007). The deepsea corals that colonize the numerous seamounts and canyons of the northeastern United States are primarily octocorals with some species of black corals and stony corals, but the overall coral species diversity is low (Packer et al. 2007). The western Atlantic Ocean is divided into 2 biogeographic provinces: the Warm Temperate Carolinian Province south of Cape Hatteras, North Carolina, and the Western Atlantic Boreal Region that extends from Cape Hatteras north to Labrador, Canada. There has, however, been some disagreement over the geographic extent of the boreal region because many fauna from the MAB belong to the southern Carolinian province; however, a recent realignment of marine biogeographic provinces (Briggs and Bowen 2012) places the MAB in the northern boreal region. Their study was based on fishes, but deepsea coral fauna from the canyons also more closely resembles those of the northeastern United States than those in the South Atlantic Bight. The three most frequently observed species of octocorals in the MAB also are common in the northeastern United States but are either absent (*P. resedaeformis, A. grandiflora*) or very rare (*P. arborea*) in the South Atlantic Bight and GOM (Brooke and Schroeder 2007, Ross and Nizinski 2007). Other species such as *L. pertusa, S. variabilis,* and *D. dianthus* are broadly distributed and are found throughout the North Atlantic. One exception is the gorgonian *Acanthogorgia aspera,* which was frequently observed in Norfolk Canyon. This species has not been documented north of Cape Hatteras before the Atlantic Deepwater Canyons study (Watling and Auster 2005, **Chapter 13**) and is therefore more allied to the Carolinian province; the congener *A. armata* occurs in the northern boreal province.

Although the Atlantic Deepwater Canyons study greatly increased our understanding of the corals and associated communities of MAB canyons, these observations were limited by time and technical capability. There are undoubtedly more coral species, and wider distributions of observed species, than were encountered during this study.

Observations of red crabs during our study were similar to those from other studies in that they were most abundant at mid-depth ranges (400 to 800 m). Earlier work reported that gravid females were usually found <400 m depth (Kelly et al. 1982), whereas our study observed egg-bearing crabs as deep as 600 m. This could be a regional variation or due to some other factor; however, there are insufficient data to explain these differences. The eggs are carried on the female's abdomens for approximately 9 months before they are released as planktonic larvae. Although spawning synchrony within red crab populations is not apparent, several authors have suggested increased larval release between January and June (Wigley et al. 1975, Haefner 1978, Erdman et al. 1991). This timing may account for the large number of gravid females observed during our September cruise, but many fewer during the May cruise. There is very little recent (past decade) literature on the biology and ecology of this species; however, like most deepsea species it is slow growing and long-lived and therefore it probably cannot sustain high fishing pressure. The red crab fishery for the western North Atlantic is currently relatively small, and although some fishing occurs in the canyons, the rugged topography is avoided by the fishers. Red crabs were most frequently observed over bare sediment, but they also inhabit hard substrate areas, which may provide a refuge from fishing pressure.

8.4.2 Natural Substrate – Cold-Seep Habitats

The Atlantic Deepwater Canyons study includes the first detailed description of two chemosynthetic seeps in the MAB. The Baltimore seep was observed by Hecker during a series of camera tows in and around Baltimore Canyon, but it was not described beyond an observation of mussel beds (Hecker et al. 1983). This was the first observation of potential chemosynthetic communities in the MAB region, and there have been no further investigations in the area until the 2012 sampling cruise. The Norfolk seep was discovered during the 2013 sampling cruise when the ROV *Jason II* was deployed to ground truth two bubble plumes observed during the NOAA Ship *Okeanos Explorer* multibeam mapping cruise in 2013. Subsequent NOAA cruises documented several other cold seeps along the MAB, all at depths >1,000 m (Skarke et al. 2014). The widespread seepage that was discovered along the western Atlantic margin is possibly the result of gas hydrate disassociation. Gas hydrates were observed in the deeper Norfolk seep, but the Baltimore seep is too shallow (high temperature, low pressure) to support intact gas hydrates. These shallow seeps may be the result of stranded hydrate deposits, which are dissociating and releasing the methane that supports seep communities (Skarke et al. 2014). The closest seeps to the MAB sites are the Blake Ridge and Cape Fear methane seeps off South Carolina. These seeps are deeper (2,155 and 2,600 m, respectively) than either Baltimore or Norfolk seeps and have a different community composition (van Dover et al. 2003, Brothers et al. 2013). The MAB seep communities have only one chemosynthetic species (the seep mussel), but the Blake Ridge seeps have both methanotrophic (*Bathymodiolus heckerae*) and thiotrophic (*Vesicomyia* cf *venusta*) fauna, as do the cold seeps in the northern GOM (Cordes et al. 2007).

The chemosynthetic mussels collected at both seeps were identified as *Bathymodiolus childressi*, which is the seep mussel commonly found in the northern GOM methane seeps. This is the first record of *B. childressi* on the eastern continental margin of North America and was from the Atlantic Deepwater Canyons study; this record was published in Arellano et al. (2014). Larvae of *B. childressi* occur in the euphotic surface waters and may disperse for up to 1 year (Arellano et al. 2014), and larval dispersal simulations (Young et al. 2012) support the GOM as a potential origin for the *B. childressi* at the MAB seeps. The closely related species, *B. mauritanicus*, exhibits an amphi-Atlantic distribution (Olu et al. 2010, Cordes et al. 2007, Olu-Le Roy et al. 2007; Genio et al. 2008), which suggests similar long-range dispersal capabilities in closely related con-specifics (Arellano et al. 2014). A single *B. mauritanicus* sampled from Baltimore Canyon expands the known amphi-Atlantic distribution of this species and raises the possibility of a viable yet undiscovered population on the western Atlantic margin. Alternatively, dispersal of *B. mauritanicus* may have occurred from known populations along the Atlantic Equatorial Belt, which leads to two alternative hypotheses for future studies: dispersal and settlement of *B. mauritanicus* are rare in the northwestern Atlantic, or dispersal and settlement are common, but environmental or ecological factors prevent a population from establishing. Co-occurrence of other *Bathymodiolus* species within a single patch is common from sites in the GOM (Faure et al. 2015); however, competition cannot be ruled out as a mechanism that limits the population viability of *B. mauritanicus*.

The Blake Ridge seep was dominated by *Bathymodiolus heckerae* (Van Dover et al. 2003), a species also known from the West Florida Escarpment seep (3,288 m) and other deep seep sites in the GOM (Faure et al. 2015). However, Van Dover et al. (2003) cautioned that more sampling must be done to conclude that Blake Ridge harbors only a single mussel species. Further exploration of the MAB seeps would lend insight into the dispersal capabilities and distributions of different species of chemosynthetic mussels.

The seep mussels were the only endemic species found at the Baltimore seep; however, there were unusually high numbers of two *Hyalinoecia* species (*H. artifex* and *H. tubicola*), commonly known as quill worms, around and within this seep that were not observed in such abundance elsewhere. These polychaete worms (family Onuphidae) are common in deepsea soft-sediment habitats. They secrete transparent tubes and are mobile scavengers, which often aggregate in areas of high food (Budaeva 2012).

Isotopic studies (**Chapter 16**) support the scavenging feeding behavior of quill worms, but show no indication that the worms are consuming depleted (seep) carbon sources. Although the worms are not feeding on bacterial mats or other direct seep food sources, their high abundance is presumably related to increased food supply generated by seep-associated fauna. Most species associated with Baltimore seep were more common in areas with low live mussel cover (i.e., away from active seepage). Exceptions were the red crab (*Chaceon quinquedens*), which was observed feeding on the live mussels, and the Jonah crab (*Cancer borealis*), which was not observed feeding on mussels, but is probably capable of doing so. Sessile benthic species such as sponges (*Polymastia* sp.), anemones (*Bolocera tuediae*), and the octocoral *P. arborea* (on one occasion), colonized exposed authigenic carbonate, some together with active methane bubbles and live mussels. These species have very thin tissue with no protection from ambient environmental conditions; however, methane does not appear to inhibit their survival, allowing them to take advantage of the hard substrate produced by methanotrophic bacteria. Corals also co-occur with active seepage in the northern GOM where live *L. pertusa* colonies were observed adjacent to a bacterial mat and active bubble plumes (Brooke, pers. obs.). The statistical differences between communities with mixed hard and soft substrate and those with only soft sediment are driven by the sessile benthic fauna on the exposed authigenic carbonate.

The Norfolk seep site was composed of two ridges perpendicular to each other and approximately 800 m in length. Unlike Baltimore seep, which was flat with occasional carbonate boulders, the Norfolk seep was extremely rugged with massive carbonate features usually covered in live mussels. Bubble plumes were common and appeared continuous; gas hydrates were frequently observed and many areas were thickly colonized with white bacterial mats and filaments. Another obvious difference between the seeps was the extremely high numbers of small live mussels, which dominated the mussel populations in some locations. The Norfolk seep therefore appeared to be much more geologically and biologically dynamic than the Baltimore seep. Statistical analysis showed no significant difference among habitat types (unlike Baltimore seep); this outcome was driven by the small numbers of habitat S (soft sediment, no mussel shells) and the absence of MSDM. Most authigenic carbonate was covered in live mussels or (rarely) exposed with no fauna.

Echinoderms are usually not common at vent or seep sites; however, some exceptions include urchins, ophiuroids, and holothurians (Smirnov et al. 2000). The apodid holothurian *Chiridota heheva*, endemic to cold seeps and wood structures at bathyal/abyssal depths (Pawson and Vance 2004), was observed in high numbers entwined among the live mussels at Norfolk seep. This species was originally described from Georgia, Florida, and Puerto Rico. These observations in the MAB are therefore a northern range extension for this species. Sea cucumbers are deposit feeders, ingesting sediment and extracting organic material. The order Apodida does not have tube feet and are usually sedentary burrow-dwellers that ingest sand adjacent to their burrows rather than the more mobile holothurians that occur on open sediment. The feeding behavior of *C. heheva* is not known, but in many places the mussels were coated in a thick layer of sediment or bacterial filaments that the holothurians may have been grazing. *C. heheva* also were observed among mussel beds adjacent to patches of bare sediment. These sedentary holothurians may be exploiting the localized abundant food supply associated with the methane seep. Other echinoderms also observed at the Norfolk seep included a white ophiuroid (*Ophiomusium lymani*) and three species of urchin (*Echinus wallisi, Gracilechinus alexandri,* and *G. affinis*). The apparently rare *E. wallisi*, which ranges from Cape Cod to Georgia in 460 to 1,885 m depth, is the only member of *Echinus* currently known from the western Atlantic Ocean (Pawson et al. 2015). The other two species, however, also have been documented from seep areas in the northern GOM and represent taxonomic links between the MAB and GOM deepsea fauna. Members of the shrimp family Alvinocaridae are almost exclusively associated with chemosynthetic environments. *Alvinocaris markensis* was collected from the Norfolk seeps, but was originally described from the Mid-Atlantic Ridge hydrothermal vents (Williams 1988). An unidentified species of *Alvinocaris* also was documented from the Blake Ridge, but this seep fauna are different from the MAB seeps; therefore, the Alvinocarid shrimp possibly is a different species. If so, the closest *A. markensis* to the Norfolk seeps is >3,000 km away.

8.4.3 Artificial Substrate

Patterns of abundance and species richness within each shipwreck were varied and complex. The wrecks themselves formed diverse and heterogeneous habitats with different sizes, states of destruction, and extents of fishing gear. Large nets often were observed entangled with structures on the shipwreck, and the nets were sometimes heavily colonized. For example, on wreck W7, fishing nets and their attached floats formed semisolid pillars extending above the wreck, which were covered in brown tube complex and the asteroid *Henricia oculata*. In other cases, fishing nets were heavily settled by encrusting sponges.

Different dominant species were found on each shipwreck, because elsewhere in the study area and especially in the adjacent canyons, hard substrate species exist in patches. In the case of the shipwrecks, one wreck may constitute a "patch" that is dominated by a small number of species. Wreck W1 in particular featured high dominance by the brown tube complex on the northwest side while the southeast side of the wreck was dominated by "brown anemone." The brown anemone may be a member of the genus *Metridium*, which are capable of reproducing by asexual fission. Just a few individuals of this genus that recruited by chance to the shipwreck may be capable of reproducing and dominating the entire side of the shipwreck. The mechanisms by which brown tube complex may have assembled are less clear. Although many epifauna on the proteinaceous tubes may reproduce asexually, it is unclear how the tubes themselves came to cover such large areas on wrecks W1, W4, and W7 at such high densities. Nevertheless, the tube complex formed a complex habitat on the wrecks, which serve as an important shelter and substrate for a variety of fauna.

Shipwrecks constitute anthropogenic hard substrate habitats in areas that would otherwise feature primarily or exclusively soft sediments. As such, they may play an important role by increasing habitat heterogeneity and benthic community diversity and function. The presence of hard substrate enables colonization by sessile suspension feeders that would otherwise be excluded from these areas. Larvae that arrive at the shipwrecks, far away from any other hard substrate habitat, may have delayed metamorphosis and been in the water column for a long time; therefore, shipwrecks may provide a "rescue effect" by providing habitat for wayward larvae that have been carried away from their natural substrate (Marshall and Keough 2003). The shipwrecks investigated in the Atlantic Deepwater Canyons study have great historical significance as well as biological significance by providing hard substrate habitats for a variety of invertebrate fauna.

8.4.4 Invertebrate Species Inventory

The most common phyla collected in both canyons were the Cnidaria and Arthropoda followed by the Echinodermata, Mollusca, and Annelida. The cnidarians were targeted for collections to fulfill the various project objectives. The abundances of cnidarians in the collected samples therefore did not necessarily represent true community structure. The arthropods were a large and abundant group that included crabs (Anomuran and Braychuran), shrimps, euphausids, and amphipods. Many arthropod samples were collected opportunistically because members of this phylum are common coral-associates, particularly shrimps and galatheid crabs. A significant number of red crabs that were taken in the trawls are not included in this count as they were identified, measured, and discarded. Representatives of the Echinodermata included urchins, brittle stars, and sea stars, all moderately common, especially brittle stars, which can occur in large monospecific patches. Because Echinoderms are abundant and easy to collect, they were often targets for sampling. The Mollusca are primarily represented by the seep mussels, which were collected for a number of different objectives, but others included a new species of file shell (*Acesta* cf *cryptadelphe*) (Gagnon et al. 2015) and some gastropods. Sponges were extremely diverse and abundant but were not often targets for collection because they can be difficult to identify. Sponges are a diverse and important phylum that deserves considerably more attention; however, the decision to collect and process the specimens was balanced against the challenges of identifying them,

particularly the Hexactinellidae (glass sponges). The same is true of the anemones, which also are a large, ecologically important and diverse group that is taxonomically problematic.

8.4.4.1 Urchins

Within the urchin family Echinidae, two extant genera occur in the northwest Atlantic, *Gracilechinus* and *Echinus*. The four known *Gracilechinus* species are *G. affinis*, *G. gracilis*, *G. tylodes*, and *G. alexandri*. In a previous survey of the northern GOM, Pawson et al. (2015) noted a paucity of echinoderms associated with cold-seep habitats. Exceptions in their study included *Gracilechinus alexandri* urchins that were associated with chemosynthetic mussels (*Bathymodiolus* sp.). Nineteen out of 21 *Gracilechinus* samples we analyzed were collected from the Norfolk seep where *Bathymodiolus* mussels were the dominant megafauna. However, we observed two species, one red and one white, of *G. affinis* whose 11 representatives were all white, and *G. alexandri*, which contained eight red and one white color morphs. Both species co-occurred at the Norfolk seep but were not present in the Baltimore Canyon seep. The depth range of both species mostly overlaps with each other and overlaps with the depth of the Baltimore Canyon seep (Pawson et al. 2015), indicating that the lack of urchins at Baltimore Canyon seep is not due to depth limitations. The two individuals collected from outside the Norfolk seep site within Norfolk Canyon fell in the *G. alexandri* clade, which contained all red color morphs. Of the two collected outside the seep site, one was the single white *G. alexandri*. Another species of urchin, *Echinus wallisi*, the single representative of *Echinus* in the western Atlantic, was collected from the Norfolk seep and was identified morphologically but was not included in the samples that were sequenced. In general, little genetic data are available in public databases from species in the Echinidae family. Future endeavors to add to the genetic resources from Echinidae species may elucidate currently problematic classifications of species within this family (Pawson et al. 2015, Minin et al. 2015).

A phylogenetic analysis using morphological characters from extant and fossil taxa support the order Cidaroida as a robust clade and a primitive sister group to all other echinoids (Kroh and Smith 2010). However, classification within Cidaroida based on morphology and molecular phylogenetic studies is scarce (Brosseau et al. 2012). Seven extant *Cidaris* species and subspecies are known from the Atlantic: *C. abyssicola, C. blakei, C. cidaris, C. c. cidaris, C. c. meridionalis, C. nuda,* and *C. rugosa*. Three of these, *C. abyssicola, C. blakei*, and *C. rugosa*, are known from the western Atlantic Ocean or the Gulf of Mexico. Brosseau et al. (2012) constructed a maximum likelihood tree from 17 genera of Cidaroida. The authors targeted a fragment of the mtCOI gene not commonly used in DNA barcoding studies and nonoverlapping with data used in this study, making comparisons difficult. Although many sampled genera overlap, few species do. As a result, species associations seen in their phylogeny are not congruent with this study. The most notable difference is that the authors found *Histocidaris* to be the most ancestral genus within Cidaroidea, and *C. cidaris* shared a clade with *Stereocidaris microtuberculata* and *Goniocidaris* spp., whereas in this study, *Histocidaris* spp. are the most closely related to *Cidaris* spp. Notably, most internal branches (Brosseau et al. 2012) have <50% bootstrap support. In our results, *Goniocidaris* is polyphyletic with respect to many other Cidaroida taxa including *Stereocidaris*, and both genera are distant from *Cidaris* representatives. The incongruences illustrate the need for standardization of taxa and gene fragments used across studies.

8.4.4.2 Mussels

The bivalve family Mytilidae contains the genus *Bathymodiolus*, a diverse group of deepsea mussels found in chemosynthetic habitats. As more populations are discovered, phylogenetic studies are performed to understand the evolutionary origins of the group and evolution of habitat utilization (i.e., hydrothermal vent, methane seep, wood, or whale fall) (Miyazaki et al. 2004, Jones and Vrijenhoek 2006, Jones et al. 2006, Kyuno et al. 2009, Lorion et al. 2010, Thubaut et al. 2013). Several studies indicate the complexity of the relationships within the subfamily Bathymodiolinae, especially within the genus *Bathymodiolus*. Previous studies that included *Bathymodiolus childressi* (first described by

Gustafson et al. (1998) and closely related taxa have shown a paraphyletic relationship among several species of *Bathymodiolus* and species from the genus *Gigantidas* (Jones and Vrijenhoek 2006; Kyuno et al. 2009; Thubaut et al. 2013), leading some authors to use the nomenclature "Bathymodiolus" to indicate the uncertainty of genus designation in this clade. Morphological identification of species within Bathymodiolinae often is problematic (Faure et al. 2015), which illustrates the utility of genetic tools to identify newly discovered populations. Our results showed that the seeps near Baltimore and Norfolk canyons were dominated by a single species, *Bathymodiolus childressi*, which is the first record of this species outside the Gulf of Mexico. A single individual was collected from the Baltimore Canyon seep site whose closest relative is *B. mauritanicus*, a species known from west Africa (Cosel 2002, Jones et al. 2006, Cordes et al. 2007, Olu-Le Roy et al. 2007), Barbados (Cordes et al. 2007, Olu-Le Roy et al. 2007), and the Gulf of Cadiz (Genio et al. 2008). This also is the first report of *B. childressi* and *B. mauritanicus* co-occurring at the same seep site. The most geographically proximate biological seep community to the mid-Atlantic seep sites known to date, Blake Ridge off the coast of South Carolina, harbors a single species of mussel as well, *B. heckerae* (Van Dover et al. 2003). However, both mid-Atlantic seeps occur at shallower depths than the known depth distribution of *B. heckerae* (Cordes et al. 2007). On the other hand, *B. childressi* larvae from the GOM have been projected to reach the mid-Atlantic based on ocean circulation and Lagrangian larval transport models (Young et al. 2012). Additionally, *B. childressi* larvae have been recovered in plankton tows (Arellano et al. 2014) and their larvae can survive up to a year in the water column, demonstrating a great potential for dispersal (Arellano et al. 2009). This suggests that depth may play a more important role in the biogeographic patterns of seep species of *Bathymodiolus* in the Atlantic than distance from other populations. However, further exploration of the U.S. Atlantic seaboard is necessary to draw conclusions concerning the geographic range and dispersal capabilities of *Bathymodiolus*.

8.5 SUMMARY

The Atlantic Deepwater Canyons study has substantially increased our understanding of invertebrate fauna, particularly the structure-forming corals in the canyons and two recently discovered cold seeps, as well as the ecological value of artificial substrates. As expected, the distribution of invertebrates in the canyons are influenced by habitat type and environmental conditions, and the complexity of the physical and biotic conditions has generated a high diversity of fauna that does not occur on the shelf. The distribution of many species is patchy, or they are found only in certain habitat types or depth ranges whereas other species are found in a wide range of habitats. Although the canyons are protected from fishing impacts, largely by their rugged topography, there was a significant amount of fishing gear (traps, lines, nets) observed in both natural and artificial habitats. In June 2015, the Mid Atlantic Fisheries Management Council (MAFMC) proposed to create a Coral Habitat Area of Particular Concern to protect an area of approximately 98 420 km2 of vulnerable canyon and slope habitats to bottom-tending fishing gear. This project and others (funded by NOAA's Deep Sea Coral Research and Technology Program and NOAA's Ocean Exploration and Research Program) provided data to assist MAFMC in generating boundaries for the protected areas. Considerable outreach efforts have brought the deep-sea corals of the mid-Atlantic canyons to the attention of the public, which responded in support of the MAFMC protection efforts of deep-sea corals in the region. The MAFMC proposal is currently under consideration at the Department of Commerce, and it is expected to be implemented to preserve these fragile and valuable resources.

8.6 LITERATURE CITED

Arellano SM, Van Gaest AL, Johnson SB, Vrijenhoek RC, Young CM. 2009. Spawning, Development, and the Duration of Larval Life in a Deep-Sea Cold-Seep Mussel. Biological Bulletin. 216 (2):149-162.

Arellano SM, Van Gaest AL, Johnson SB, Vrijenhoek RC, Young CM. 2014. Larvae from deep-sea methane seeps disperse in surface waters. Proceeding of the Royal Society B Biological Sciences 281(1786). doi:Artn 20133276.

Bandelt HJ, Forster P, Rohl A. 1999. Median-joining networks for inferring intraspecific phylogenies. Molecular Biology and Evolution. 16(1):37–48.

Benson DA, Cavanaugh M, Karsch-Mizrachi I, Lipman DJ, Savers EW. 2013. Genbank nucleic acids research (database issue) D36–42. doi:10.1093/nar/gks1195. https://www.ncbi.nlm.nih.gov/genbank.

Briggs JC, Bowen BW. 2012. A realignment of marine biogeographic provinces with particular reference to fish distributions. Journal of Biogeography. 39:12–30.

Brooke S, Schroeder WW. 2007. Chapter 7: State of deep coral ecosystems in the Gulf of Mexico region: Texas to the Florida Straits. In: Lumsden SE, Hourigan TF, Bruckner AW, editors. The state of deep coral ecosystems of the United States. Silver Spring (MD): National Oceanic and Atmospheric Administration. NOAA Technical Memorandum NOS-CRCP-3. p. 271–306.

Brooke S, Ross SW. 2014. First observations of the cold-water coral *Lophelia pertusa* off the mid-Atlantic coast of the United States. Deep-Sea Research II. 104:241–251.

Brooke S, Holmes M, Young CM. 2009. Effects of sediment on two morphotypes of *Lophelia pertusa* from the Gulf of Mexico. Marine Ecology Progress Series. 390:137–144.

Brosseau O, Murienne J, Pichon D, Vidal N, Eleaume M, Ameziane N. 2012. Phylogeny of Cidaroida (Echinodermata: Echinoidea) based on mitochondrial and nuclear markers. Organisms Diversity and Evolution. 12(2):155–165.

Brothers DS, ten Brink US, Andrews, BD, Chaytor JD. 2013. Geomorphic characterization of the U.S. Atlantic continental margin. Marine Geology. 338:46–63.

Budaeva N. 2012. *Leptoecia midatlantica*, a new species of the deep-sea quill-worms (Polychaeta: Onuphidae: Hyalinoeciinae) from the Mid-Atlantic Ridge. Zootaxa. 3176:45–60.

Cacchione DA, Rowe GT, Malahoff A. 1978. Submersible investigation of outer Hudson submarine canyon, pp. 42–50. In: Stanley D, Kelling JG, editors. Sedimentation in submarine canyons, fans, and trenches. Stroudsburg (PA): Dowdon, Hutchings and Ross, Inc.

Cairns SD. 1981. Marine flora and fauna of the northeastern United States: Scleractinia. NOAA Technical Report NMFS Circ. 438:1–14.

Childress JJ, Fisher CR, Brooks JM, Kennicutt II MC, Bidigare R, Anderson A. 1986. A methanotrophic marine molluscan symbiosis: mussels fueled by gas. Science. 233:1306–1308.

Clarke KR, Gorley RN. 2006. Primer v6: User manual/Tutorial. Primer-E. Plymouth, UK.

Cordes EE, Carney SL, Hourdez S, Carney RS, Brooks JM, Fisher CR. 2007. Cold seeps of the deep Gulf of Mexico: community structure and biogeographic comparisons to Atlantic equatorial belt seep communities. Deep-Sea Research I. 54(4):637–653.

Cosel, R. von. 2002. A new species of bathymodioline mussel (mollusca, Bivalvia, Mytilidae) from Mauritania (West Africa), with comments on the genus *Bathymodiolus* Kenk and Wilson, 1985. Zoosystema. 24(2): 259-271.

Elde AC, Pettersen R, Bruheim P, Järnegren J, Johnsen G. 2012. Pigmentation and spectral absorbance signatures in deep-water corals from the Trondheimsfjord, Norway. Marine Drugs. 10:1400–1411.

Erdman RB, Blake NJ, Lockhart FD, Lindberg WJ, Perry HM, Waller RS. 1991. Comparative reproduction of the deep-sea crabs *Chaceon fenneri* and *C. quinquedens* (Brachyura: Geryonidae) from the northeast Gulf of Mexico. Invertebrate Reproduction and Development. 19:175–184.

Fabry VJ. 2008. Ocean science – Marine calcifiers in a high-CO_2 ocean. Science. 320:102–1022.

Faure B, Schaeffer SW, Fisher CR. 2015. Species distribution and population connectivity of deep-sea mussels at hydrocarbon seeps in the Gulf of Mexico. PLoS ONE 10(4). doi:ARTN e0118460 10.1371/journal.pone.0118460.

Feely RA, Sabine CL, Lee K, Berelson W, Kleypas J, Fabry VJ, Millero FJ. 2004. Impact of anthropogenic CO_2 on the $CaCO_3$ system in the oceans. Science. 305:362–366.

Fillinger L, Richter C. 2013. Vertical and horizontal distribution of *Desmophyllum dianthus* on Comau Fjord, Chile: a cold water coral thriving at low pH. PeerJ. doi:10.7717/peerj.194.

Folmer O, Black M, Hoeh W, Lutz R, Vrijenhoek R. 1994. DNA primers for amplification of mitochondrial cytochrome c oxidase subunit I from diverse metazoan invertebrates. Molecular Marine Biology and Biotechnology. 3(5):294–299.

Forsterra G, Haussermann V. 2003. First report on large scleractinian (Cnidaria: Anthozoa) accumulations in cold-temperate shallow water of south Chilean fjords. Zoologische Verhandelingen Leiden. 345:117–128.

Gagnon JM, Kenchington E, Port A, Anstey LJ, Murillo FJ. 2015. Morphological and genetic variation in North Atlantic giant file clams, *Acesta* spp. (Bivalvia: Limidae), with description of a new cryptic species in the northwest Atlantic. Zootaxa. 4007(2):151–180.

Genio L, Johnson SB, Vrijenhoek RC, Cunha MR, Tyler PA, Kiel S, Little CTS. 2008. New record of "*Bathymodiolus" mauritanicus* Cosel 2002 from the Gulf of Cadiz (NE Atlantic) mud volcanoes. Journal of Shellfish Research. 27(1):53–61.

Grimes CB, Able KW, Jones RS. 1986. Tilefish, *Lopholatilus chamaeleonticeps*, habitat, behavior and community structure in Mid-Atlantic and southern New England waters. Environmental Biology of Fishes. 15:273–292.

Gustafson RG, Turner RD, Lutz RA, Vrijenhoek RC. 1998. A new genus and five new species of mussels (Bivalvia, Mytilidae) from deep-sea sulfide/hydrocarbon seeps in the Gulf of Mexico. Malacologia. 40(1–2):63–112.

Haefner PA Jr. 1978. Seasonal aspects of the biology, distribution and relative abundance of the deep-sea red crab *Geryon quinquedens* Smith, in the vicinity of the Norfolk Canyon, Western North Atlantic. Proceedings of the National Shellfish Association. 68:49–62.

Hecker B, Blechschmidt G, Gibson P. 1980. Epifaunal zonation and community structure in three mid- and north Atlantic canyons. Final report for the canyon assessment study in the Mid-and North Atlantic Areas of the U.S. Outer Continental Shelf. Prepared for the U.S. Department of Interior, Bureau of Land Management under contract BLM AA5 51-CT8-49. Palisades (NY): Lamont-Doherty Geological Observatory.

Hecker B, Logan DT, Gandarillas FE, Gibson PR. 1983. Canyon and slope processes study, vol. III: biological processes. Report for the U.S. Department of the Interior, Minerals Management Service, under contract no. 14-12-0001-29178. Palisades (NY): Lamont-Doherty Geological Observatory. 212 p. [accessed 2016 June 1]. http://invertebrates.si.edu/boem/reports/CASPS_vol3.pdf.

Jones WJ, Vrijenhoek RC. 2006. Evolutionary relationships within the "*Bathymodiolus" childressi* group. Cahiers De Biologie Marine. 47(4):403–407.

Jones,WJ, Won YJ, Maas PAY, Smith PJ, Lutz RA, Vrijenhoek RC. 2006. Evolution of habitat use by deep-sea mussels. Marine Biology. 148(4):841–851.

Kelly P, Sulkin SD, Van Heukelem WF. 1982. A dispersal model for larvae of the deep sea red crab *Geryon quinquedens* based on behavioral regulation of vertical migration in the hatching stage. Marine Biology. 72:35–43.

Kroh A, Smith AB. 2010. The phylogeny and classification of post Palaeozoic echinoids. Journal of Systematic Palaeontology. 8:147–212.

Kyuno A, Shintaku M, Fujita Y, Matsumoto H, Utsumi M, Watanabe H, Fujiwara Y, Miyazaki JI. 2009. Dispersal and differentiation of deep-sea mussels of the genus *Bathymodiolus* (Mytilidae, Bathymodiolinae). Journal of Marine Biology. doi:10.1155/2009/625672.

Larsson AI, Järnegren J, Strömberg SM, Dahl MP, Lundälv T, Brooke S. 2014. Embryogenesis and larval biology of the cold-water coral *Lophelia pertusa.* PLoS ONE. 9(7):e102222.

Librado P, Rozas J. 2009. DnaSP v5: a software for comprehensive analysis of DNA polymorphism data. Bioinformatics. 25(11):1451–1452. doi:10.1093/bioinformatics/btp187.

Lorion J, Buge B, Cruaud C, Samadi S. 2010. New insights into diversity and evolution of deep-sea Mytilidae (Mollusca: Bivalvia). Molecular Phylogenetics and Evolution. 57(1):71–83.

Malahoff A, Embley RW, Fornari DJ. 1982. Geomorphology of Norfolk and Washington canyons and the surrounding continental slope and upper rise as observed from DSRV *Alvin*. p. 97–111. In: Scrutton RA, Talwani M, editors. The ocean floor. New York (NY): John Wiley and Sons.

Mann KH. 1982. Ecology of coastal waters. Berkeley (CA): University of California Press.

Marshall DJ, Keough M. 2003. Variation in the dispersal potential of non-feeding invertebrate larvae: the desperate larva hypothesis and larval size. Marine Ecology Progress Series. 255:145–153.

McClain CR, Barry JP. 2010. Habitat heterogeneity, disturbance, and productivity work in concert to regulate biodiversity in deep submarine canyons. Ecology. 91(4):964–976.

Mid-Atlantic Fishery Management Council. 2015. Deep sea corals amendment to the Atlantic mackerel, squid and butterfish fishery management plan. Public Information Document, January 2015. 95 p.

Minin KV, Petrov NB, Vladychenskaya IP. 2015. Sea urchins of the genus *Gracilechinus* (Fell and Pawson, 1966) from the Pacific Ocean: morphology and evolutionary history. Marine Biology Research. 11(3):253–268.

Miyazaki JI, Shintaku M, Kyuno A, Fujiwara Y, Hashimoto J, Iwasaki H. 2004. Phylogenetic relationships of deep-sea mussels of the genus *Bathymodiolus* (Bivalvia: Mytilidae). Marine Biology. 144(3):527–535.

Neulinger SC, Järnegren J, Ludvigsen M, Lochte K, Dullo WC. 2008. Phenotype-specific bacterial communities in the cold-water coral *Lophelia pertusa* (Scleractinia) and their implications for the coral's nutrition, health, and distribution. Applied and Environmental Microbiology. 74(23):7272–7285.

Olu-Le Roy K, von Cosel R, Hourdez S, Carney SL, Jollivet D. 2007. Amphi-Atlantic cold-seep Bathymodiolus species complexes across the equatorial belt. Deep-Sea Research I. 54(11):1890–1911.

Olu K, Cordes EE, Fisher CR, Brooks JM, Sibuet M, Desbruyeres D. 2010. Biogeography and potential exchanges among the Atlantic equatorial belt cold-seep faunas. PLoS ONE 5(8). doi:ARTN e11967.

Packer DB, Boelke D, Guida V, McGee LA. 2007. Chapter 5: State of deep coral ecosystems in the northeastern region: Maine to Cape Hatteras. In: Lumsden, SE, Hourigan TF, Bruckner AW, editors. The state of deep coral ecosystems of the United States. Silver Spring (MD): National Oceanic and Atmospheric Administration. NOAA Technical Memorandum NOS-CRCP-3. p. 195–232.

Pawson DL, Vance DJ. 2004. *Chiridota heheva*, new species from western Atlantic deep-sea cold seeps and anthropogenic habitats (Echinodermata: Holothuroidea: Apodida). Zootaxa. 534:1–12.

Pawson DL, Nizinski MS, Ames CL, Pawson DJ. 2015. Deep-sea echinoids and holothurians (Echinodermata) near cold seeps and coral communities in the northern Gulf of Mexico. Bulletin of Marine Science. 91(2):167–204.

Quattrini AM, Nizinski MS, Chaytor JD, Demopoulos AW, Roark EB, France SC, Moore JA, Heyl T, Auster PJ, Kinlan B, Ruppel C, Elliott KP, Kennedy BRC, Lobecker E, Skarke A, Shank TM. 2015. Exploration of the canyon incised continental margin of the northeastern United States reveals dynamic habitats and diverse communities. PLoS One. 10 (10): e0139904.

Ratnasingham S, Hebert PDN. 2007. BOLD: The barcode of life data system. Molecular Ecology Notes. 7(3):355–364. doi:10.1111/j.1471-8286.2006.01678.x.

Roberts JM, Wheeler AW, Freiwald A, Cairns S. 2009. Cold-water corals: the biology and geology of deep-sea habitats. Cambridge (UK): Cambridge University Press. 334 p.

Ross SW, Nizinski MS. 2007. Chapter 6: State of deep coral ecosystems in the US southeast region: Cape Hatteras to southeastern Florida. In: Lumsden SE, Hourigan TF, Bruckner AW, editors. The state of deep coral ecosystems of the United States. Silver Spring (MD): National Oceanic and Atmospheric Administration. NOAA Technical Memorandum NOS-CRCP-3. p. 233–270.

Rowe GT. 1972. The exploration of submarine canyons and their benthic faunal assemblages. Proceeding of the Royal Society of Edinburgh. B 73(17):159–169.

Savolainen V, Cowan RS, Vogler AP, Roderick GK. 2005. Theme issue 'DNA barcoding of life'. Philosophical Transactions of the Royal Society. B 360(1462).

Shepard AN, Theroux RB, Cooper RA, Uzmann JR. 1986. Ecology of *Ceriantharia* (Coelenterata, Anthozoa) of the northwest Atlantic from Cape Hatteras to Nova Scotia. Fishery Bulletin. 84:625–646.

Shnit-Orland M, Kushmaro A. 2008. Coral mucus bacteria as a source for antibacterial activity. In: Riegl BM, Dodge RE, editors. 11th International Coral Reef Symposium Proceedings. Fort Lauderdale (FL); 2008 July 7–11. p. 256–259.

Skarke A, Ruppel C, Kodis M, Brothers D, Lobecker E. 2014. Widespread methane leakage from the sea floor on the northern US Atlantic margin. Nature Geoscience. 7(9):657–661.

Smirnov AV, Gebruk AV, Gulkin SV, Shank T. 2000. A new species of holothurian (Echinodermata: Holothuroidea) from hydrothermal vent habitats. Journal of Marine Biology Association of the UK. 80:321–328.

Stanley DJ, Fenner P. 1973. Underwater television survey of the Atlantic outer continental margin near Wilmington Canyon. Washington (DC): Smithsonian Institution Press. 54 p.

Tamura K, Stecher G, Peterson D, Filipski A, Kumar S. 2013. MEGA6: Molecular Evolutionary Genetics Analysis Version 6.0. Molecular Biology and Evolution. 30(12):2725–2729.

Thubaut J, Puillandre N, Faure B, Cruaud C, Samadi S. 2013. The contrasted evolutionary fates of deep-sea chemosynthetic mussels (Bivalvia, Bathymodiolinae). Ecology and Evolution. 3(14):4748–4766.

Van Dover CL, Aharon P, Bernhard JM, Caylor E, Doerries M, Flickinger W, Gilhooly W, Goffredi SK, Knick KE, Macko SA, et al. 2003. Blake Ridge methane seeps: characterization of a soft-sediment, chemosynthetically based ecosystem. Deep-Sea Research I. 50(2):281–300.

Watling L, Auster PJ. 2005. Distribution of deep-water Alcyonacea off the northeast coast of the United States. In: Freiwald A, Roberts JM, editors. Cold-water corals and ecosystems. Berlin Heidelberg (Germany): Springer-Verlag. p. 259–276.

Wigley RL, Theroux RB, Murray HE. 1975. Deep-sea red crab, *Geryon quinquedens*, survey off northeastern United States. Marine Fisheries Review. 37(8):1–21.

Williams AB. 1988. New marine decapod crustaceans from waters influenced by hydrothermal discharge, brine, and hydrocarbon seepage. Fisheries Bulletin 86:263–287.

Wilson WHJ. 1991. Competition and predation in marine soft-sediment communities. Annual Review of Ecology, Evolution, and Systematics 21:221–241.

Won Y, Young CM, Lutz RA, Vrijenhoek RC. 2003. Dispersal barriers and isolation among deep-sea mussel populations (Mytilidae: Bathymodiolus) from eastern Pacific hydrothermal vents. Molecular Ecology 12(1):169–184.

Young CM, He R, Emlet RB, Li Y, Qian H, Arellano SM, Van Gaest A, Bennett KC, Wolf M, Smart TI, Rice ME. 2012. Dispersal of deep sea larvae from the intra-American seas: simulations of trajectories using ocean models. International Society for Computational Biology. doi:10.1093/icb/ics090 1–14.

This page intentionally left blank

Appendix 8-A

Habitat Maps (and Associated Coral Locations) for Coral-Targeted Dives in Baltimore and Norfolk Canyons

This page intentionally left blank

Baltimore Canyon Coral-Targeted Dives

2012 Sampling Cruise

NOAA Ship *Nancy Foster* and ROV *Kraken 2*

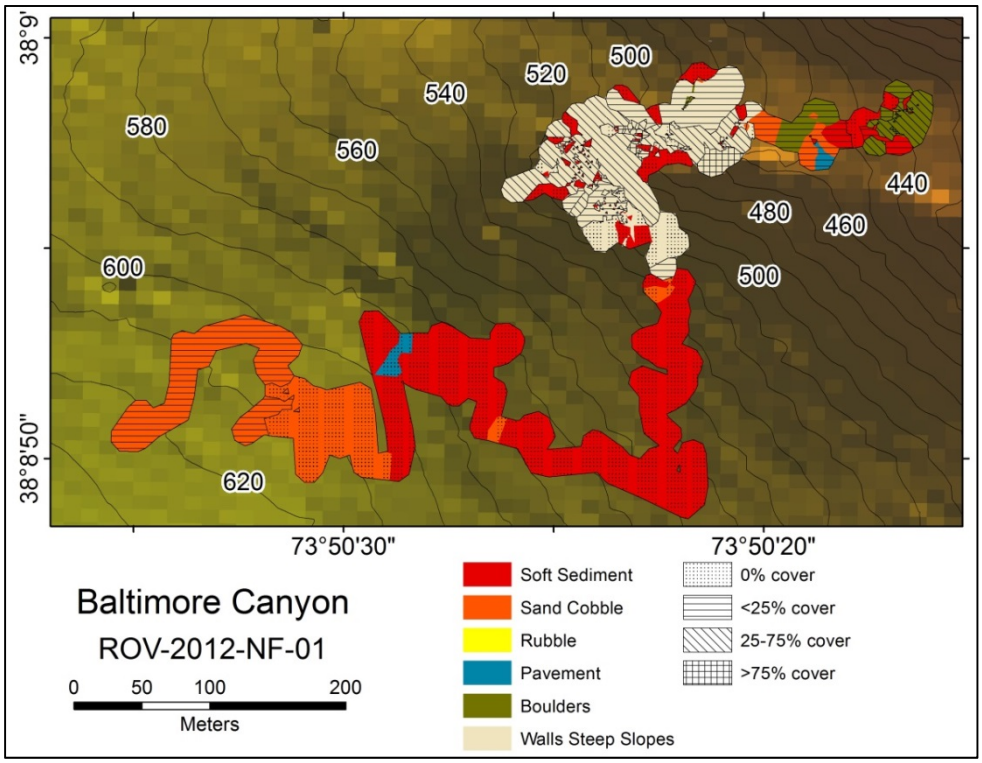

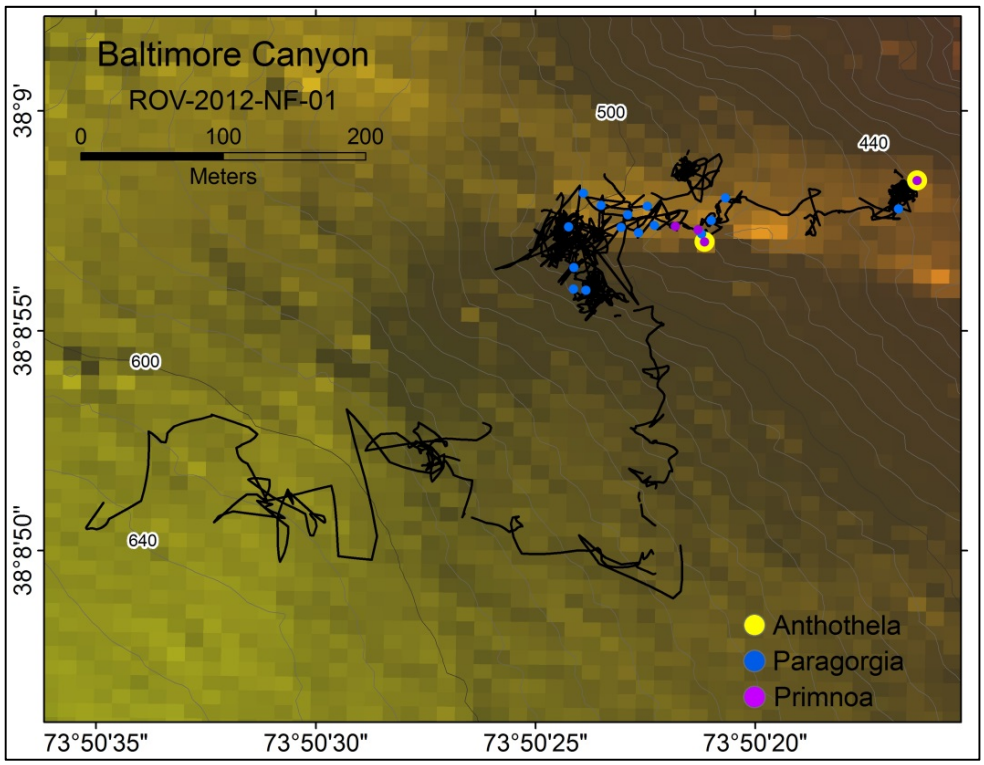

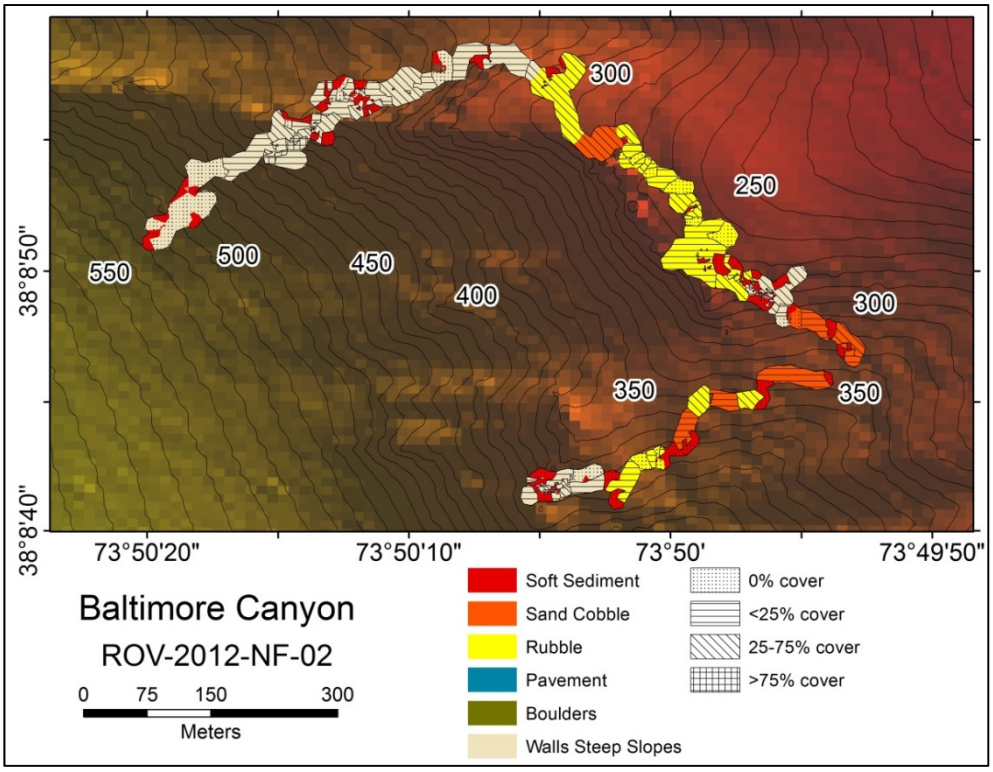
300
250
500
550
450
400
300
350
350
38°8'50"
38°8'40"
73°50'20"
73°50'10"
73°50'
73°49'50"
Baltimore Canyon
ROV-2012-NF-02
0 75 150 300
Meters
Soft Sediment
Sand Cobble
Rubble
Pavement
Boulders
Walls Steep Slopes
0% cover
<25% cover
25-75% cover
>75% cover

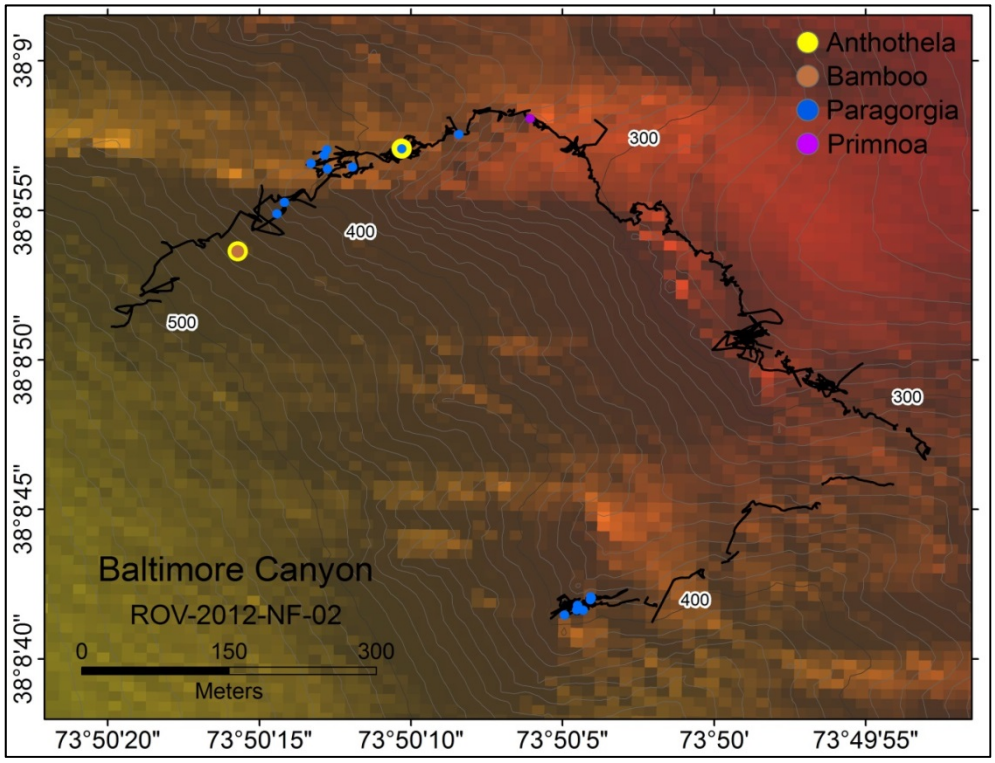
Anthothela
Bamboo
Paragorgia
Primnoa
300
400
500
300
400
38°9'
38°8'55"
38°8'50"
38°8'45"
38°8'40"
Baltimore Canyon
ROV-2012-NF-02
0 150 300
Meters
73°50'20"
73°50'15"
73°50'10"
73°50'5"
73°50'
73°49'55"

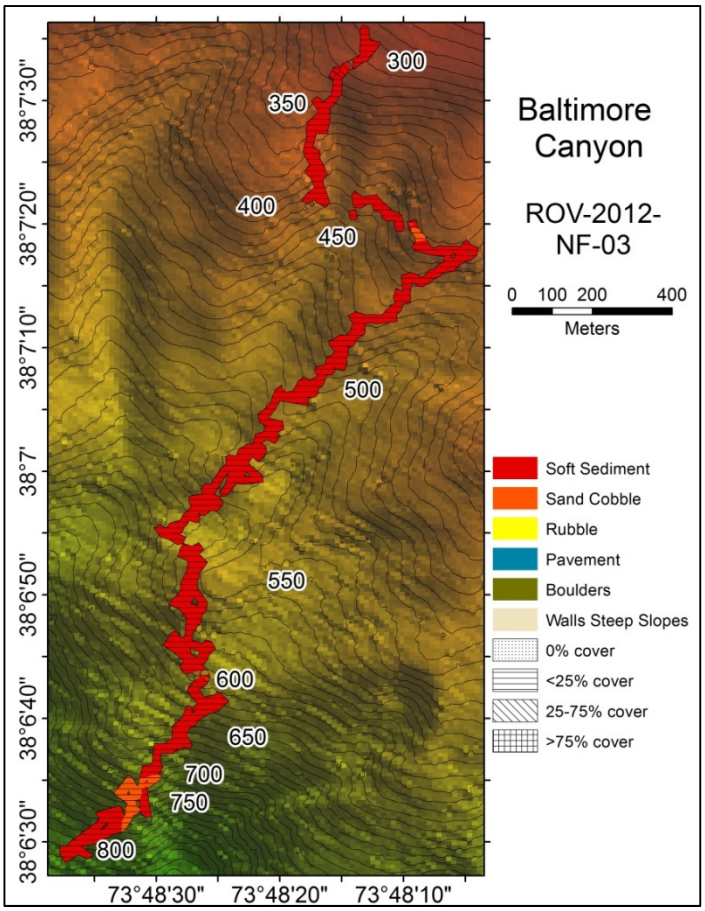
Baltimore Canyon
ROV-2012-NF-03
0 100 200 400
Meters
Soft Sediment
Sand Cobble
Rubble
Pavement
Boulders
Walls Steep Slopes
0% cover
<25% cover
25-75% cover
>75% cover
300
350
400
450
500
550
600
650
700
750
800
38°7'30"
38°7'20"
38°7'10"
38°7'
38°6'50"
38°6'40"
38°6'30"
73°48'30"
73°48'20"
73°48'10"

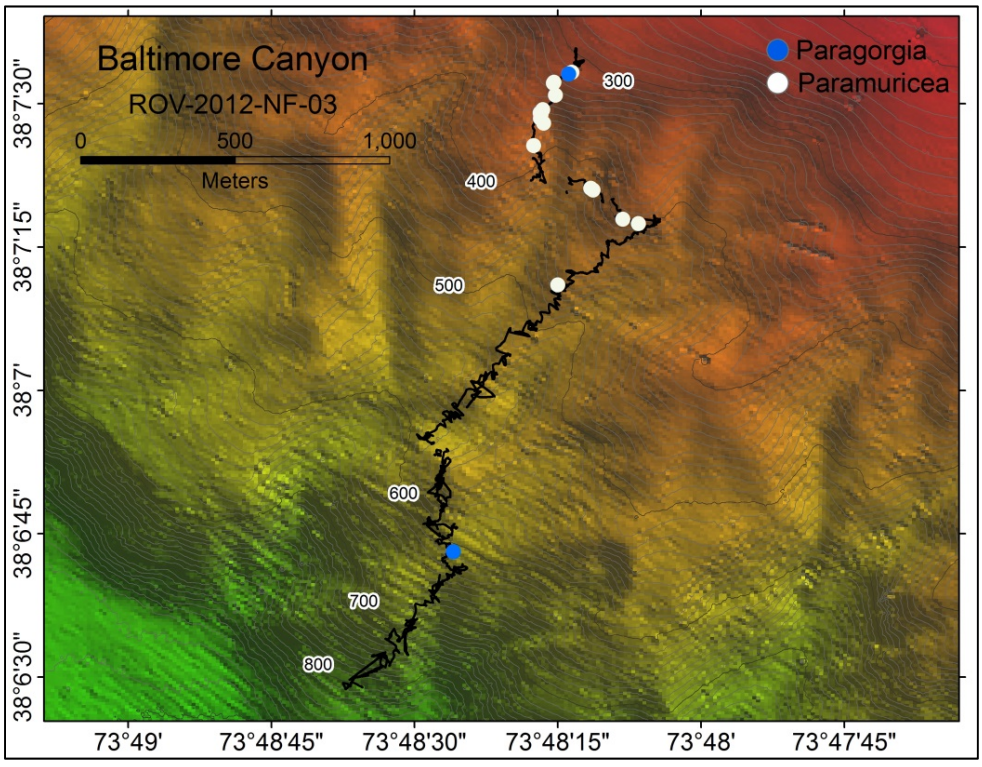
Baltimore Canyon
ROV-2012-NF-03
0 500 1,000
Meters
Paragorgia
Paramuricea
300
400
500
600
700
800
38°7'30"
38°7'15"
38°7'
38°6'45"
38°6'30"
73°49'
73°48'45"
73°48'30"
73°48'15"
73°48'
73°47'45"

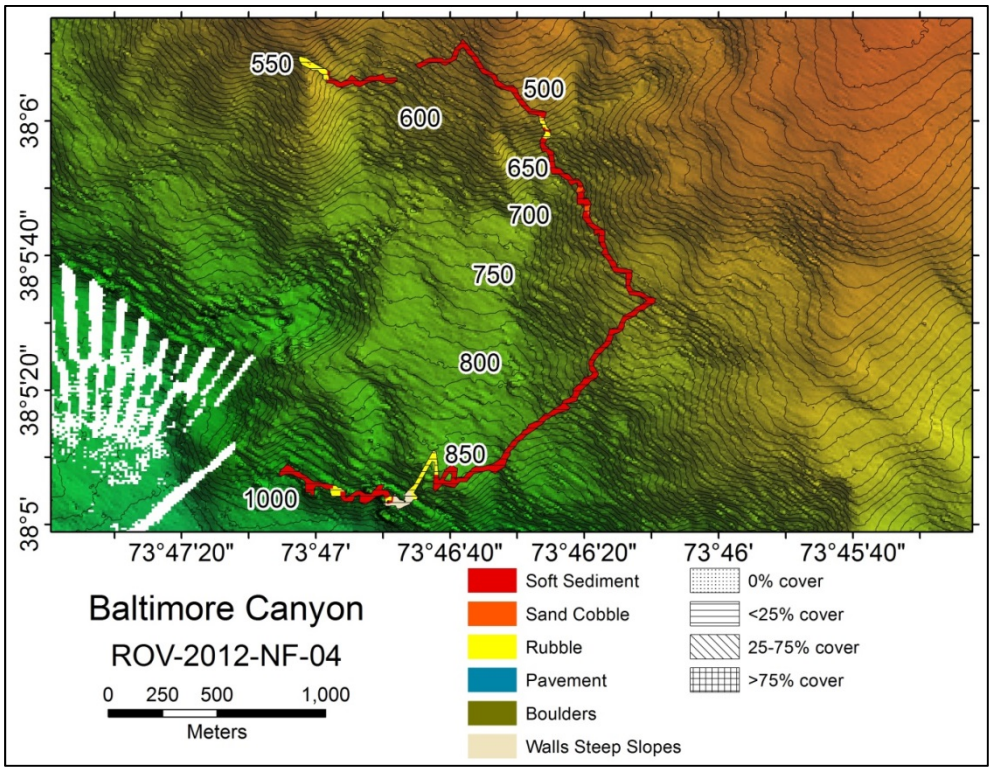

No corals were observed during this dive

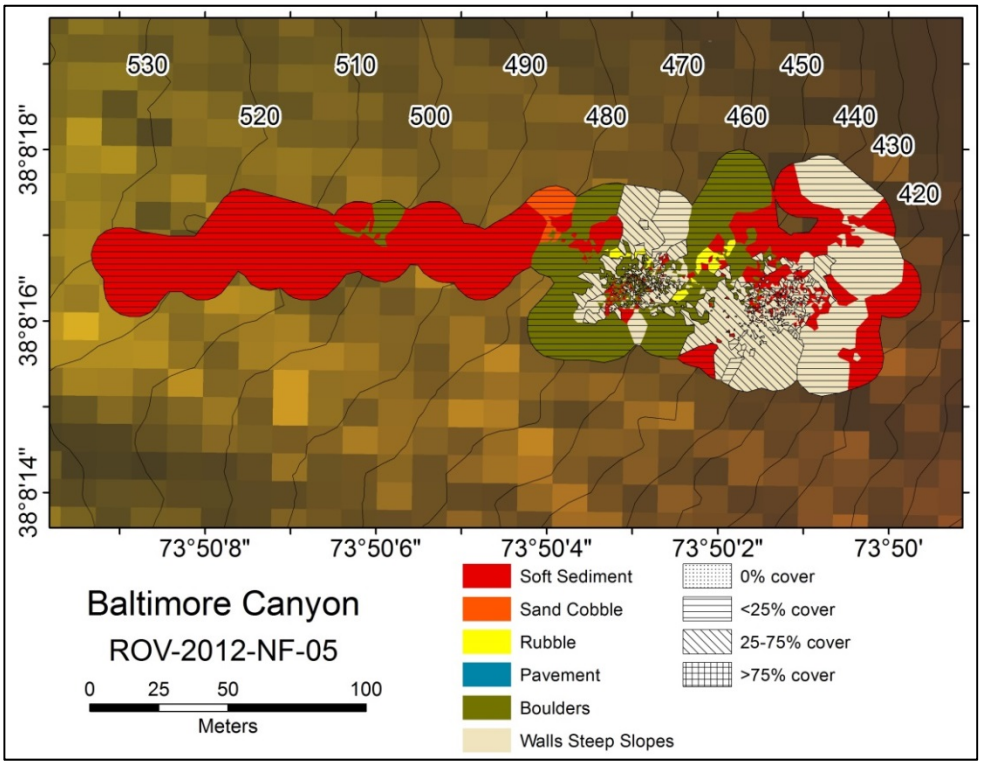
530
510
490
470
450
520
500
480
460
440
430
420
38°8'18"
38°8'16"
38°8'14"
73°50'8"
73°50'6"
73°50'4"
73°50'2"
73°50'
Baltimore Canyon
ROV-2012-NF-05
0 25 50 100
Meters
Soft Sediment
Sand Cobble
Rubble
Pavement
Boulders
Walls Steep Slopes
0% cover
<25% cover
25-75% cover
>75% cover

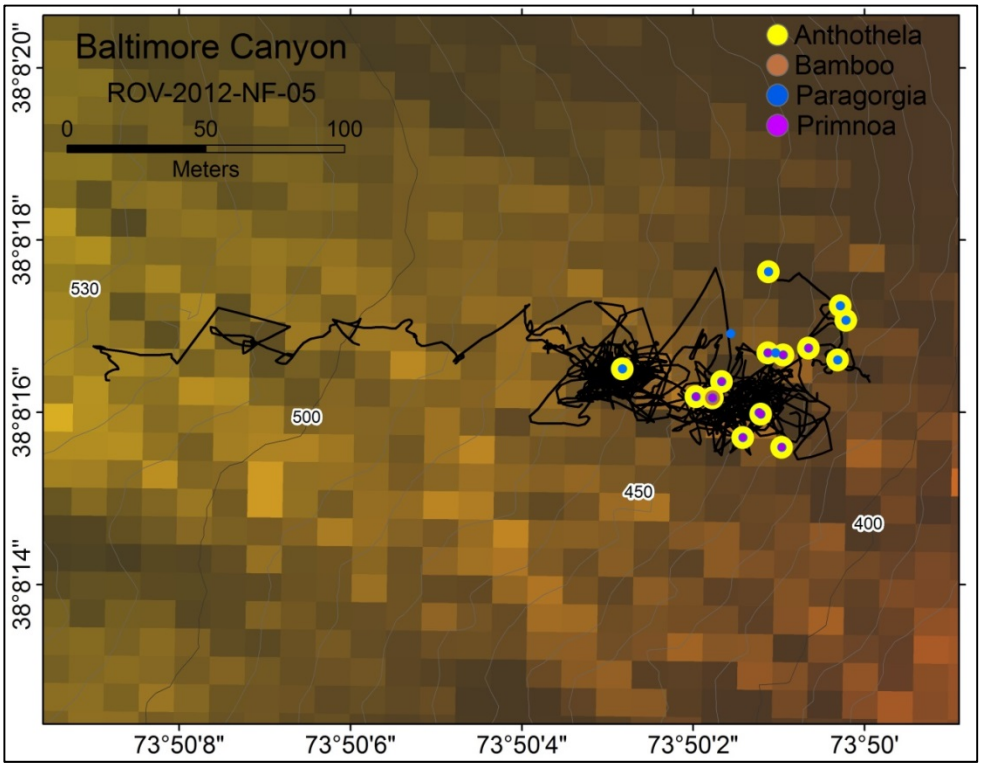
Baltimore Canyon
ROV-2012-NF-05
0 50 100
Meters
Anthothela
Bamboo
Paragorgia
Primnoa
530
500
450
400
38°8'20"
38°8'18"
38°8'16"
38°8'14"
73°50'8"
73°50'6"
73°50'4"
73°50'2"
73°50'

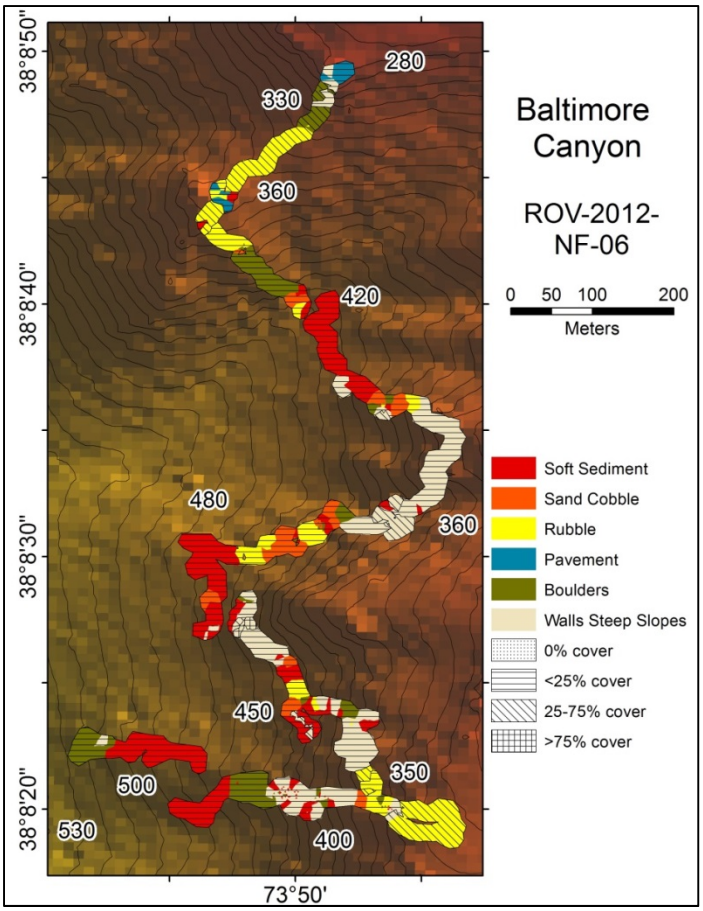
Baltimore Canyon
ROV-2012-NF-06
0 50 100 200
Meters
Soft Sediment
Sand Cobble
Rubble
Pavement
Boulders
Walls Steep Slopes
0% cover
<25% cover
25-75% cover
>75% cover
280
330
360
420
480
360
450
500
350
530
400
38°8'50"
38°8'40"
38°8'30"
38°8'20"
73°50'

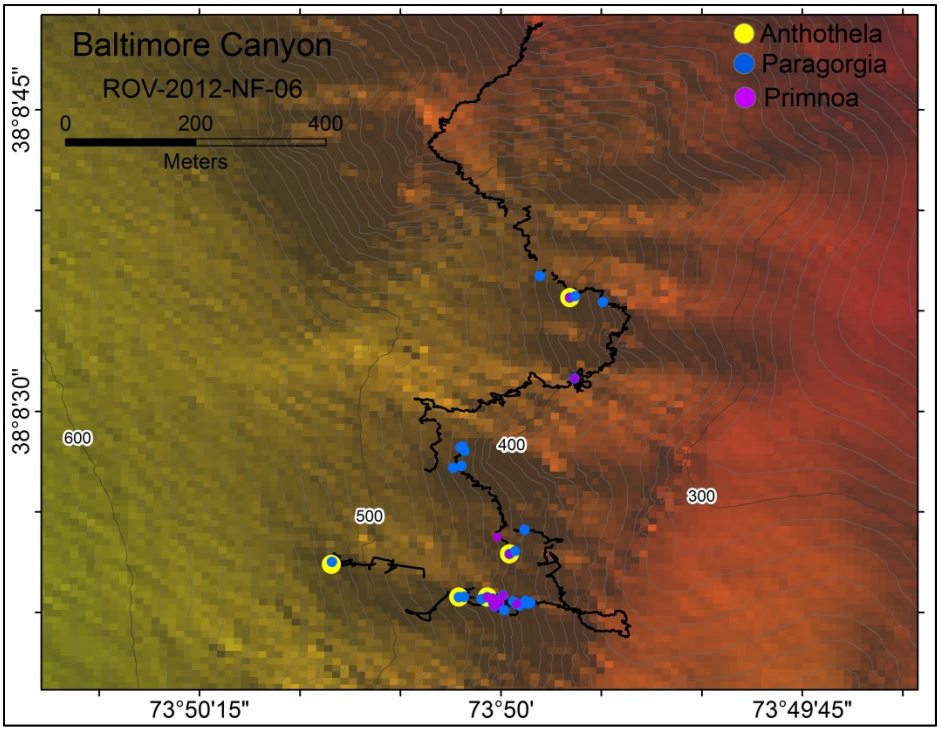
Baltimore Canyon
ROV-2012-NF-06
0 200 400
Meters
Anthothela
Paragorgia
Primnoa
600
400
300
500
38°8'45"
38°8'30"
73°50'15"
73°50'
73°49'45"

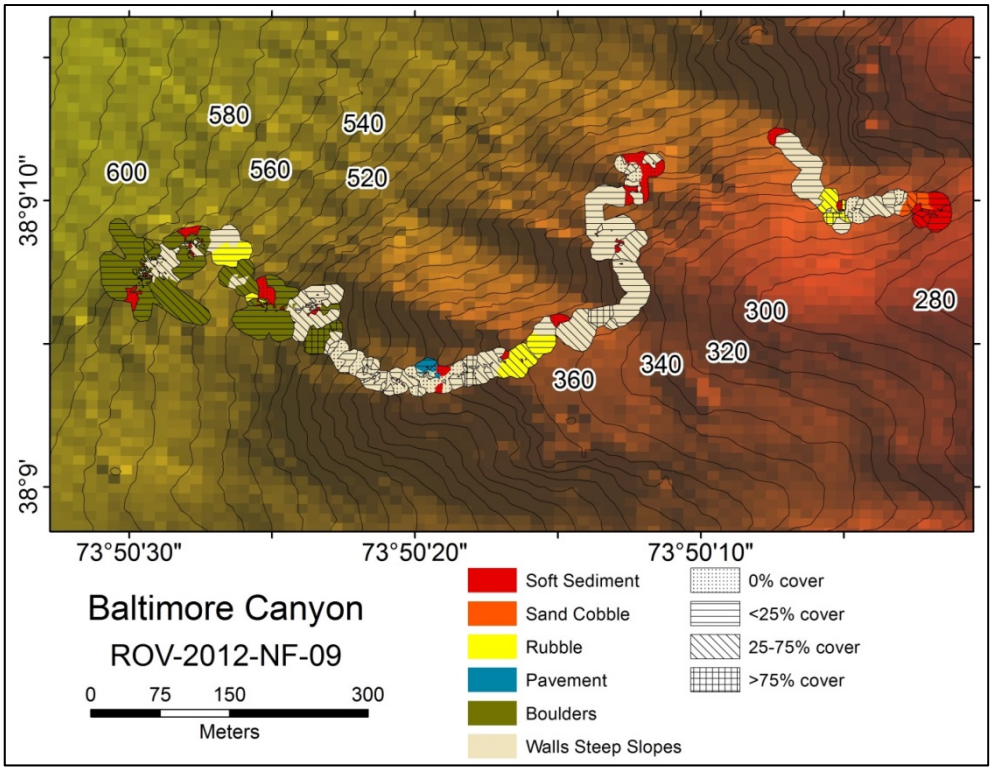
580
540
600
560
520
300
280
320
340
360
38°9'10"
38°9'
73°50'30"
73°50'20"
73°50'10"
Baltimore Canyon
ROV-2012-NF-09
0 75 150 300
Meters
Soft Sediment
Sand Cobble
Rubble
Pavement
Boulders
Walls Steep Slopes
0% cover
<25% cover
25-75% cover
>75% cover

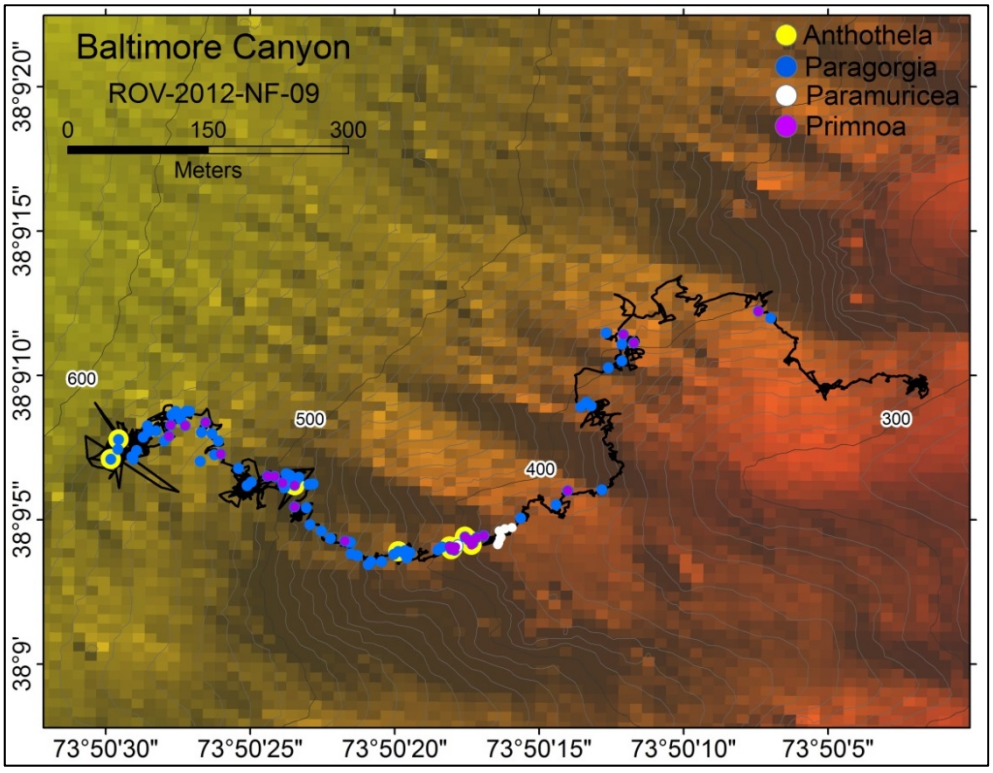
Baltimore Canyon
ROV-2012-NF-09
0 150 300
Meters
Anthothela
Paragorgia
Paramuricea
Primnoa
600
500
400
300
38°9'20"
38°9'15"
38°9'10"
38°9'5"
38°9'
73°50'30"
73°50'25"
73°50'20"
73°50'15"
73°50'10"
73°50'5"

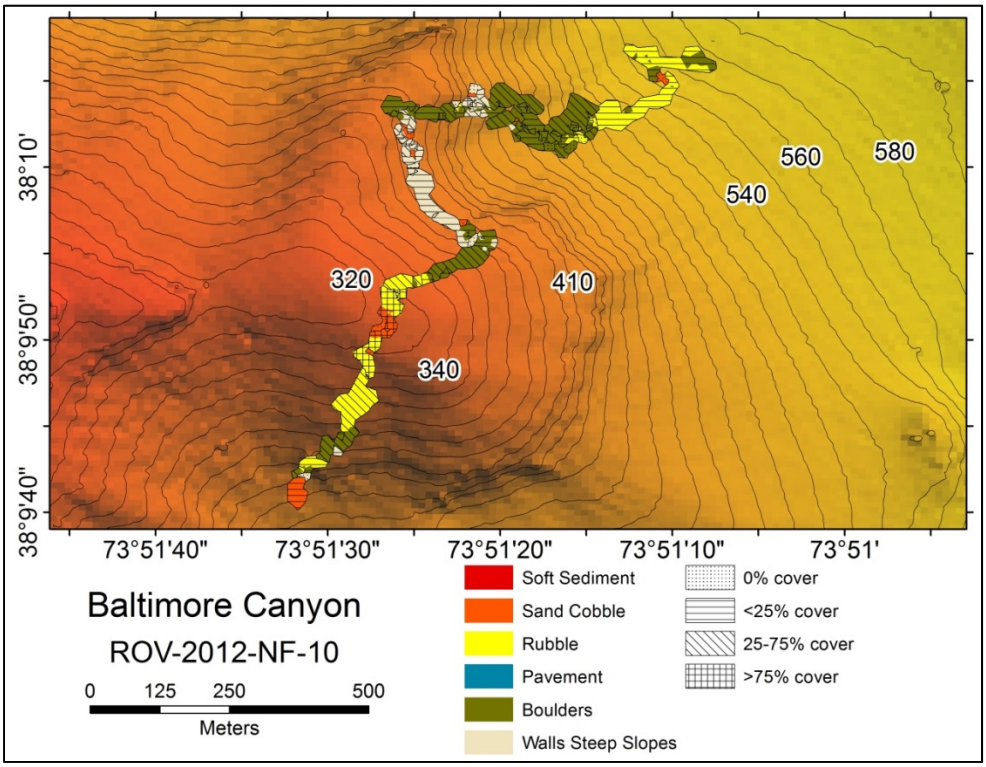
38°10'
38°9'50"
38°9'40"
73°51'40"
73°51'30"
73°51'20"
73°51'10"
73°51'
320
340
410
540
560
580
Baltimore Canyon
ROV-2012-NF-10
0 125 250 500
Meters
Soft Sediment
Sand Cobble
Rubble
Pavement
Boulders
Walls Steep Slopes
0% cover
<25% cover
25-75% cover
>75% cover

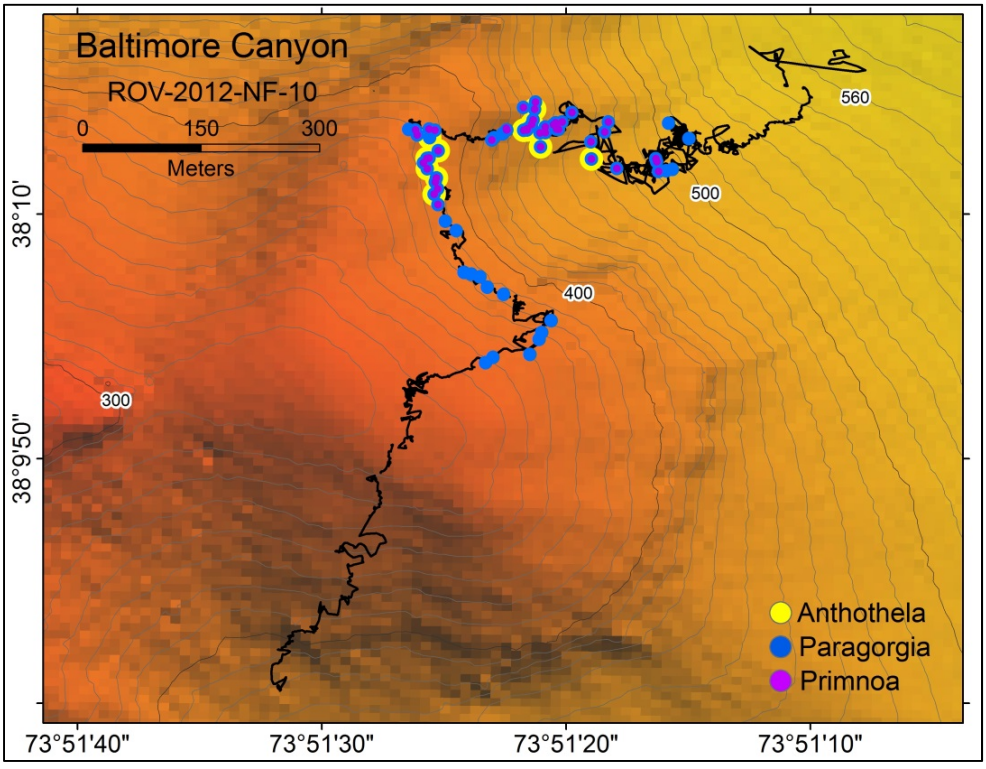
Baltimore Canyon
ROV-2012-NF-10
0 150 300
Meters
38°10'
38°9'50"
73°51'40"
73°51'30"
73°51'20"
73°51'10"
300
400
500
560
Anthothela
Paragorgia
Primnoa

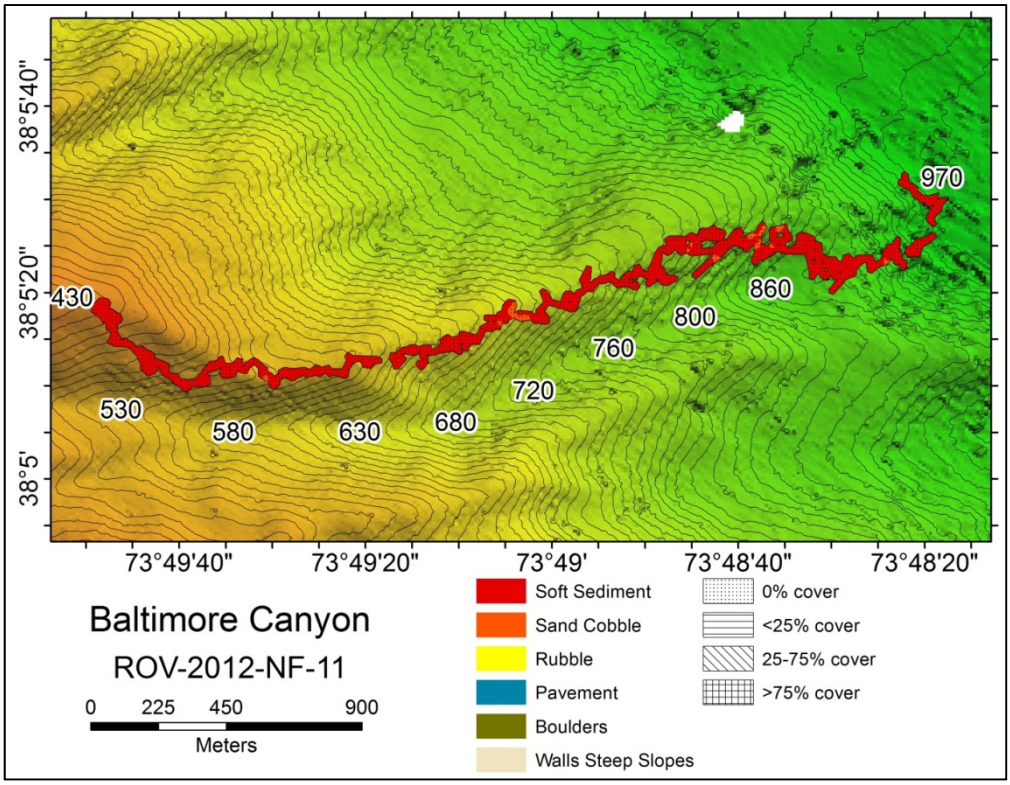

No corals were observed during this dive

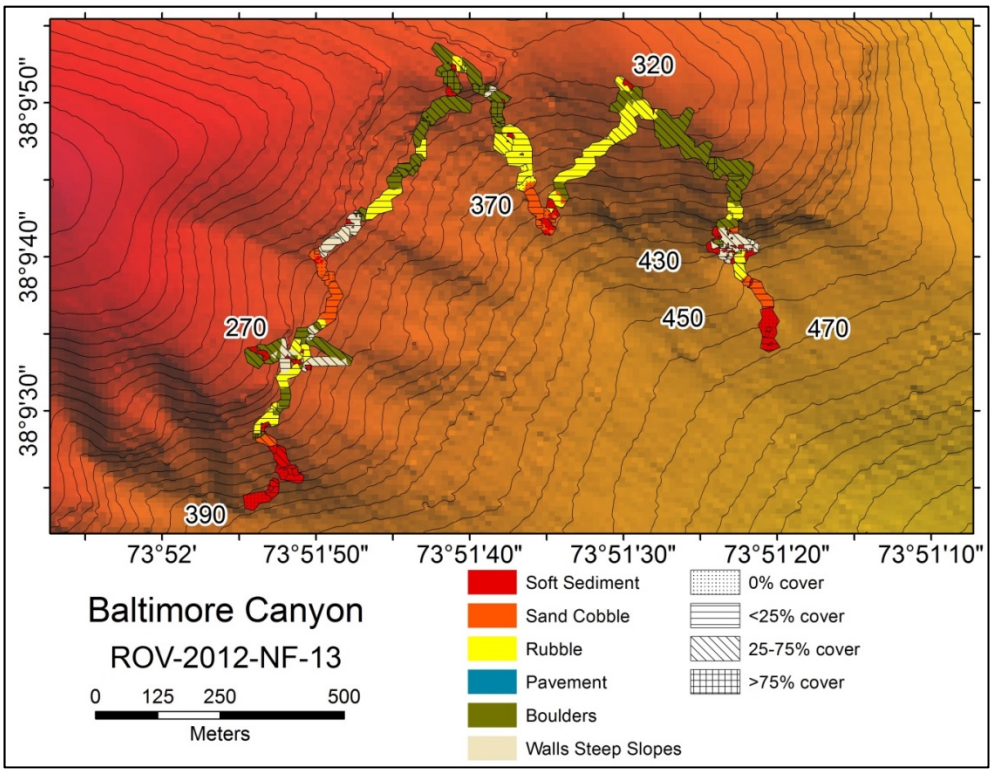
320
370
430
450
470
270
390
38°9'50"
38°9'40"
38°9'30"
73°52'
73°51'50"
73°51'40"
73°51'30"
73°51'20"
73°51'10"
Baltimore Canyon
ROV-2012-NF-13
0 125 250 500
Meters
Soft Sediment
Sand Cobble
Rubble
Pavement
Boulders
Walls Steep Slopes
0% cover
<25% cover
25-75% cover
>75% cover

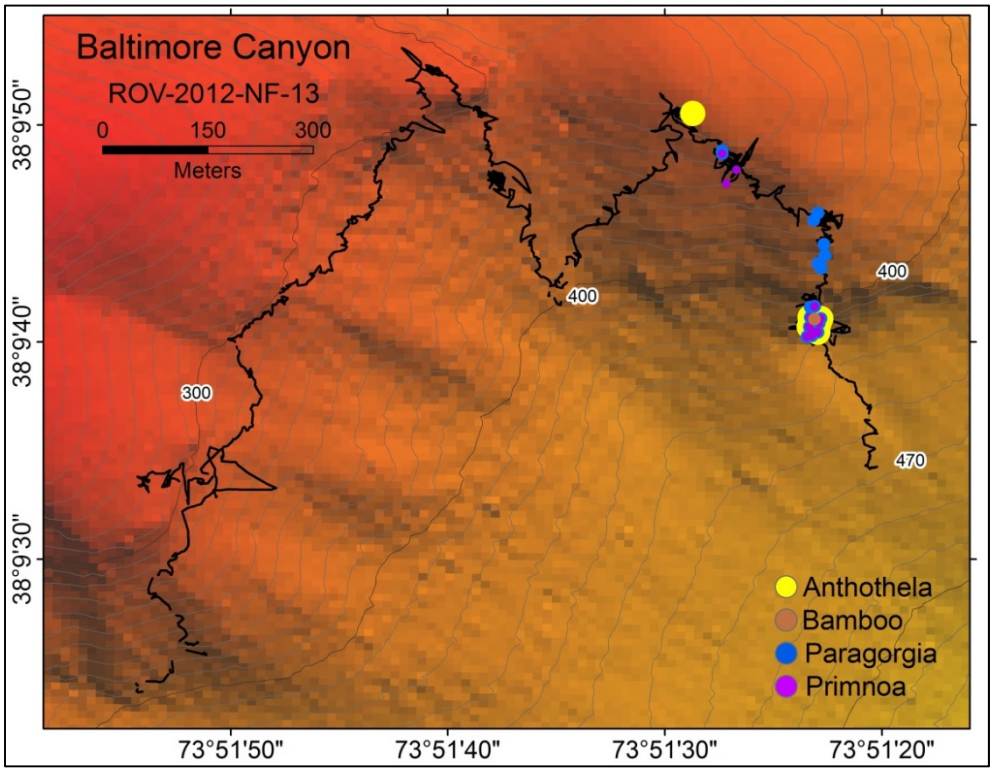
Baltimore Canyon
ROV-2012-NF-13
0 150 300
Meters
400
400
300
470
38°9'50"
38°9'40"
38°9'30"
73°51'50"
73°51'40"
73°51'30"
73°51'20"
Anthothela
Bamboo
Paragorgia
Primnoa

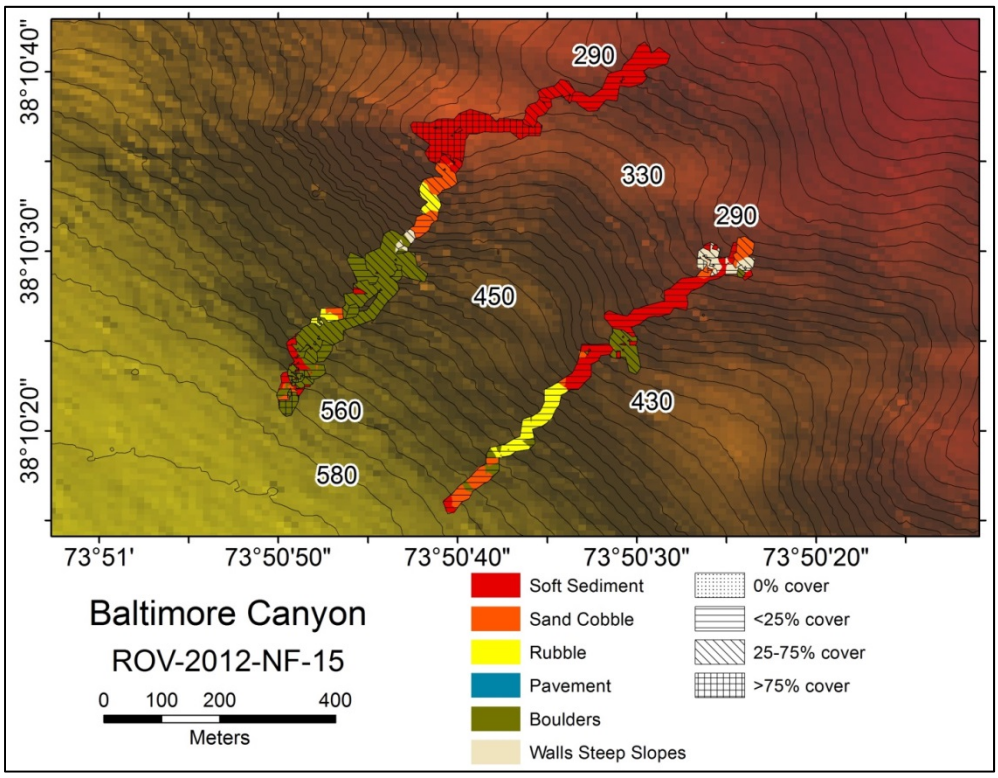
290
330
290
450
430
560
580
38°10'40"
38°10'30"
38°10'20"
73°51'
73°50'50"
73°50'40"
73°50'30"
73°50'20"
Baltimore Canyon
ROV-2012-NF-15
0 100 200 400
Meters
Soft Sediment
Sand Cobble
Rubble
Pavement
Boulders
Walls Steep Slopes
0% cover
<25% cover
25-75% cover
>75% cover

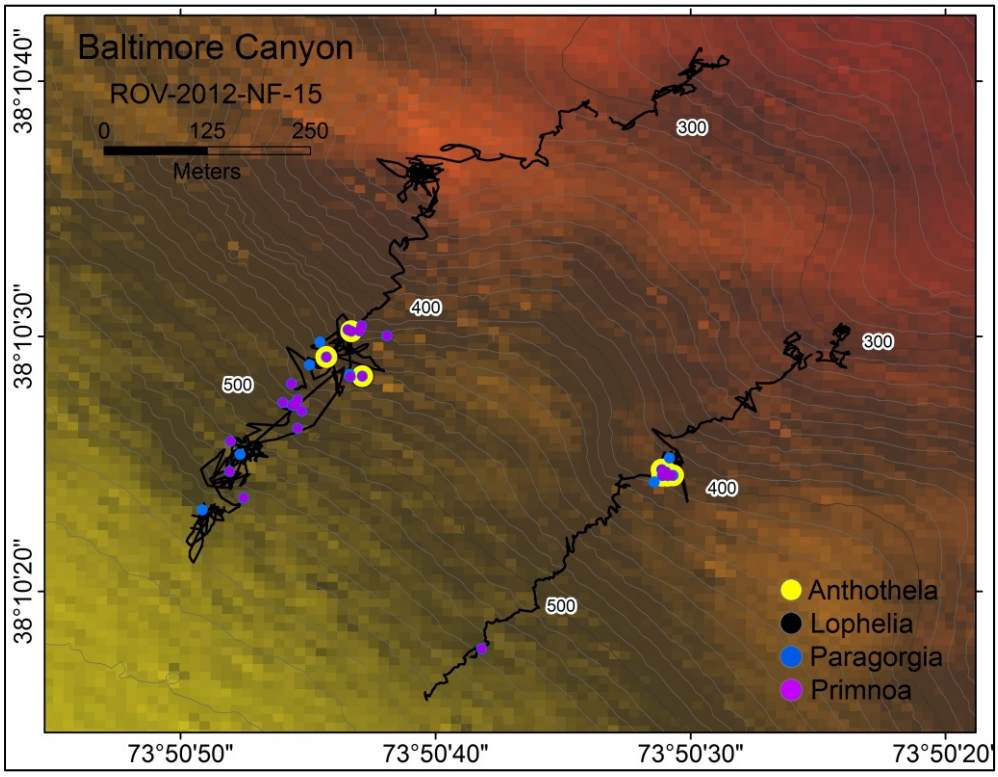
Baltimore Canyon
ROV-2012-NF-15
0 125 250
Meters
300
400
500
300
400
500
38°10'40"
38°10'30"
38°10'20"
73°50'50"
73°50'40"
73°50'30"
73°50'20"
Anthothela
Lophelia
Paragorgia
Primnoa

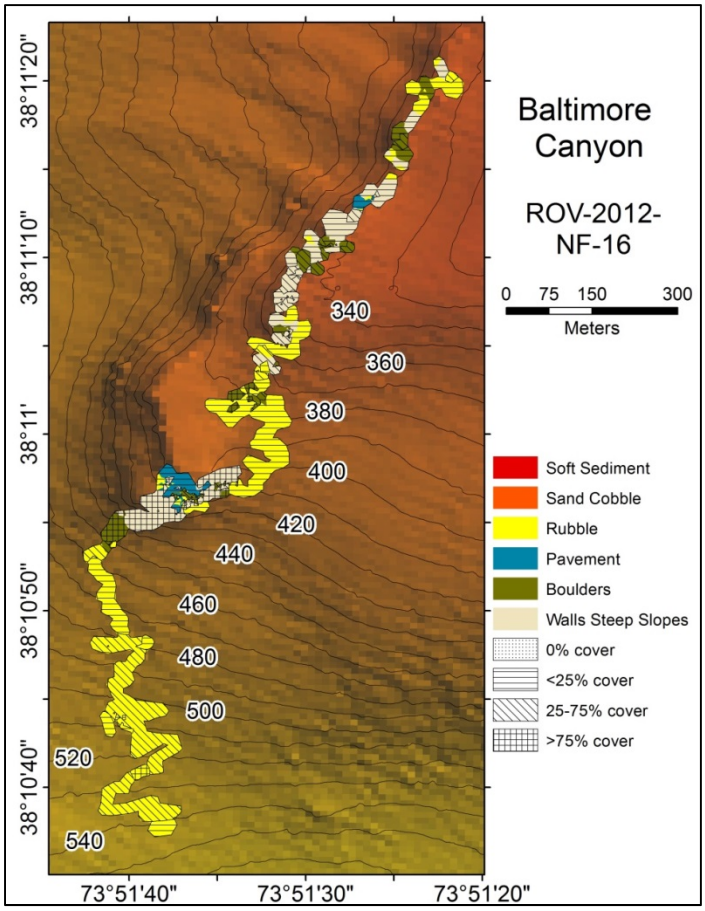
Baltimore Canyon
ROV-2012-NF-16
0 75 150 300
Meters
340
360
380
400
420
440
460
480
500
520
540
Soft Sediment
Sand Cobble
Rubble
Pavement
Boulders
Walls Steep Slopes
0% cover
<25% cover
25-75% cover
>75% cover
38°11'20"
38°11'10"
38°11'
38°10'50"
38°10'40"
73°51'40"
73°51'30"
73°51'20"

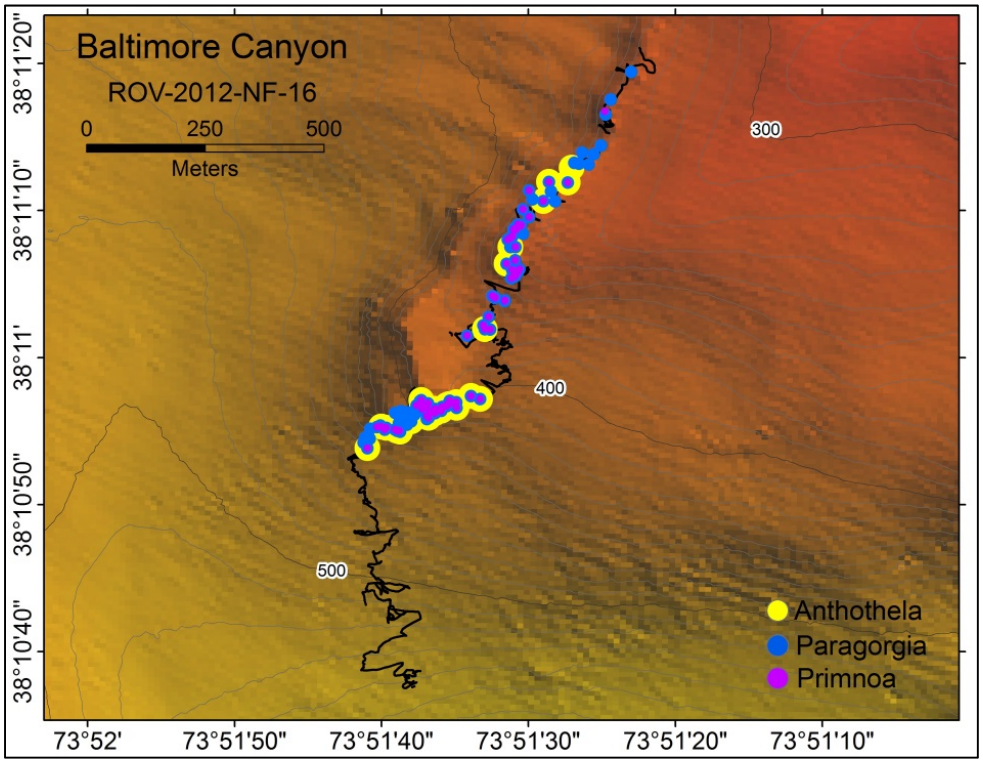
Baltimore Canyon
ROV-2012-NF-16
0 250 500
Meters
300
400
500
Anthothela
Paragorgia
Primnoa
38°11'20"
38°11'10"
38°11'
38°10'50"
38°10'40"
73°52'
73°51'50"
73°51'40"
73°51'30"
73°51'20"
73°51'10"

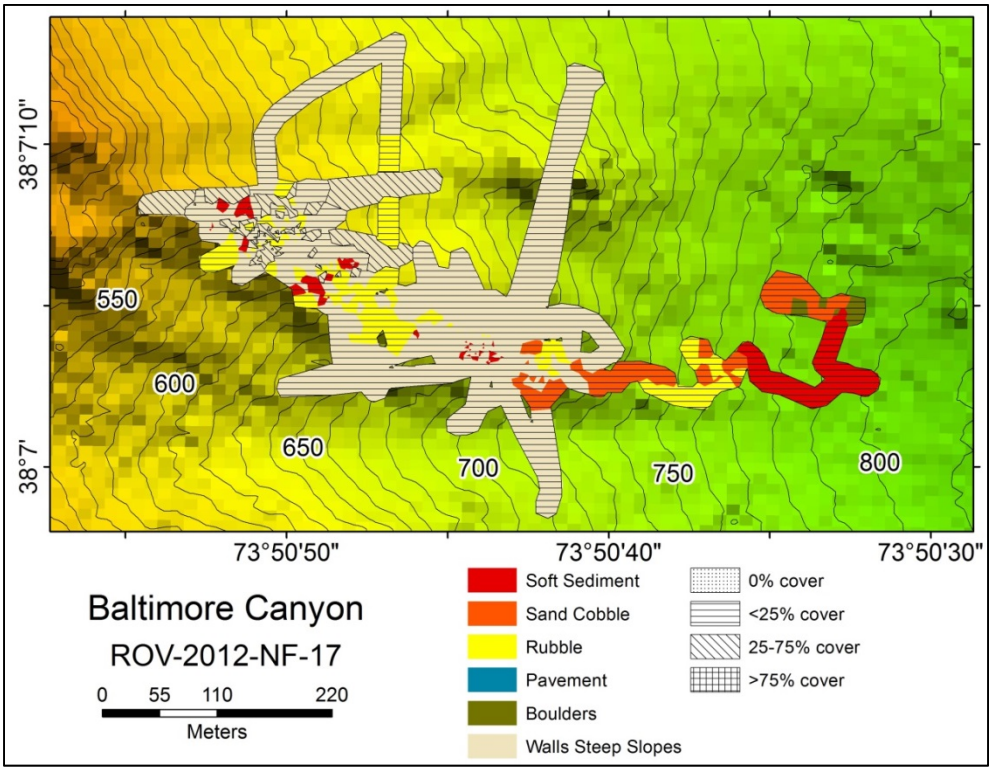
38°7'10"
38°7'
550
600
650
700
750
800
73°50'50"
73°50'40"
73°50'30"
Baltimore Canyon
ROV-2012-NF-17
0 55 110 220
Meters
Soft Sediment
Sand Cobble
Rubble
Pavement
Boulders
Walls Steep Slopes
0% cover
<25% cover
25-75% cover
>75% cover

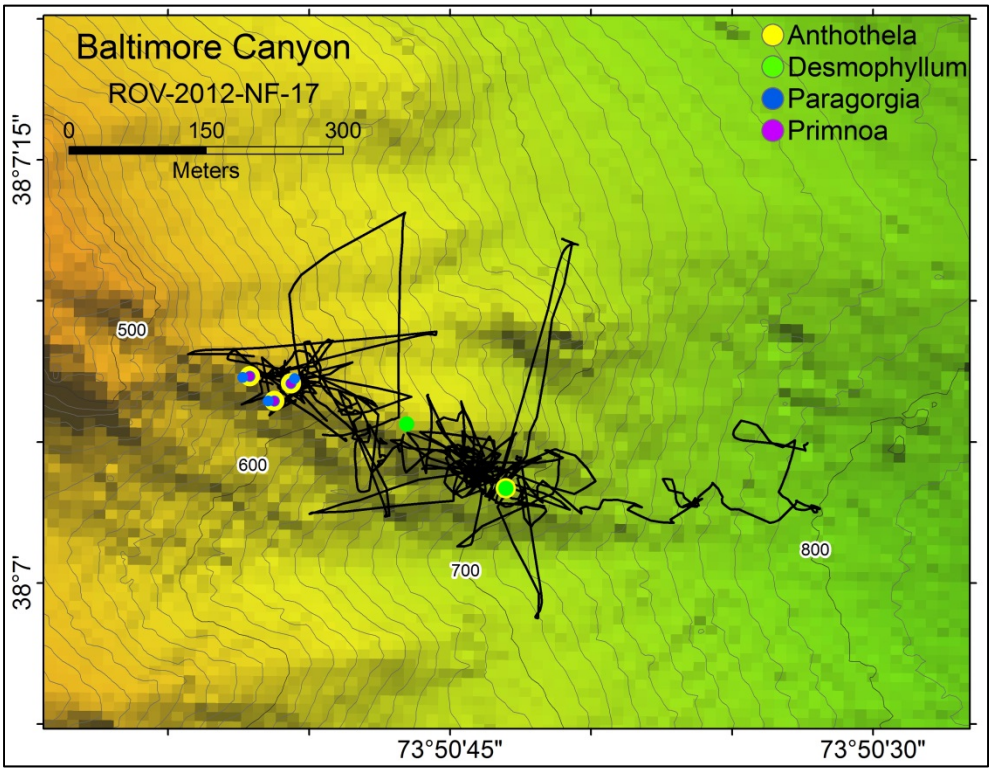
Baltimore Canyon
ROV-2012-NF-17
0 150 300
Meters
Anthothela
Desmophyllum
Paragorgia
Primnoa
38°7'15"
38°7'
500
600
700
800
73°50'45"
73°50'30"

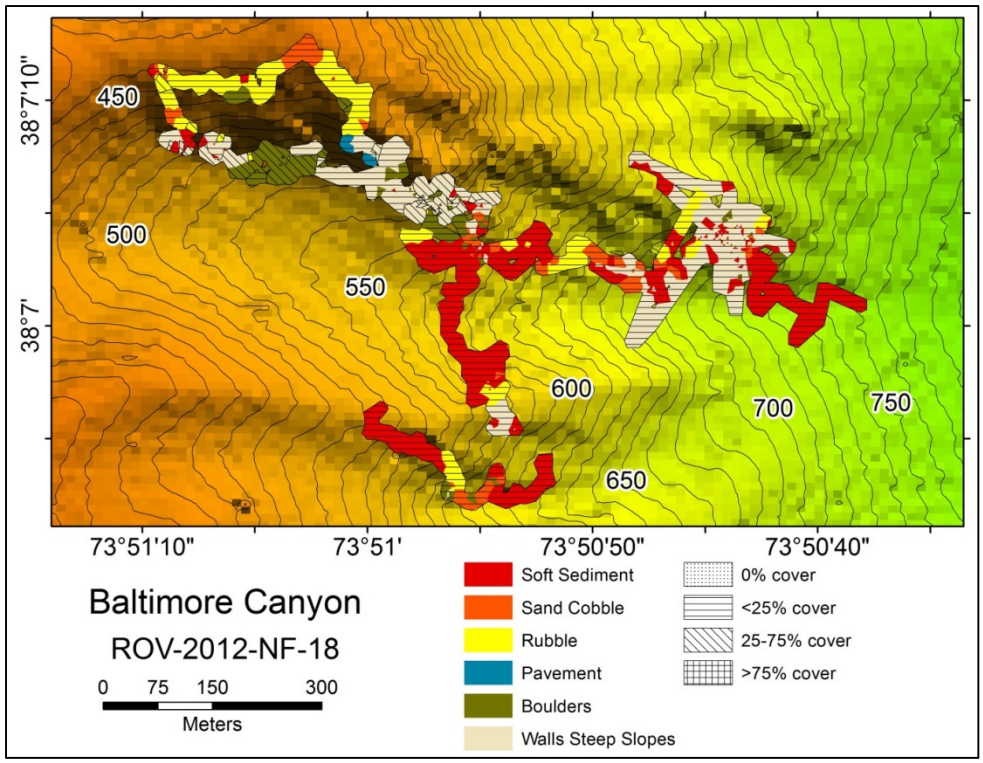
38°7'10"
38°7'
450
500
550
600
650
700
750
73°51'10"
73°51'
73°50'50"
73°50'40"
Baltimore Canyon
ROV-2012-NF-18
0 75 150 300
Meters
Soft Sediment
Sand Cobble
Rubble
Pavement
Boulders
Walls Steep Slopes
0% cover
<25% cover
25-75% cover
>75% cover

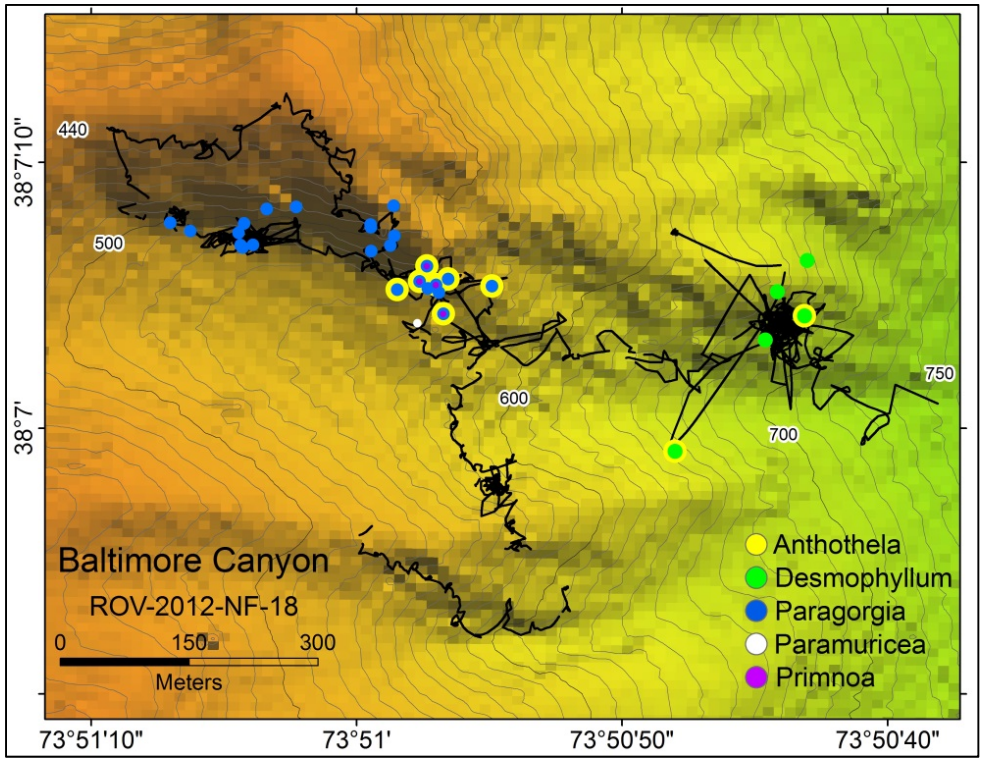
38°7'10"
38°7'
440
500
600
700
750
73°51'10"
73°51'
73°50'50"
73°50'40"
Baltimore Canyon
ROV-2012-NF-18
0 150 300
Meters
Anthothela
Desmophyllum
Paragorgia
Paramuricea
Primnoa

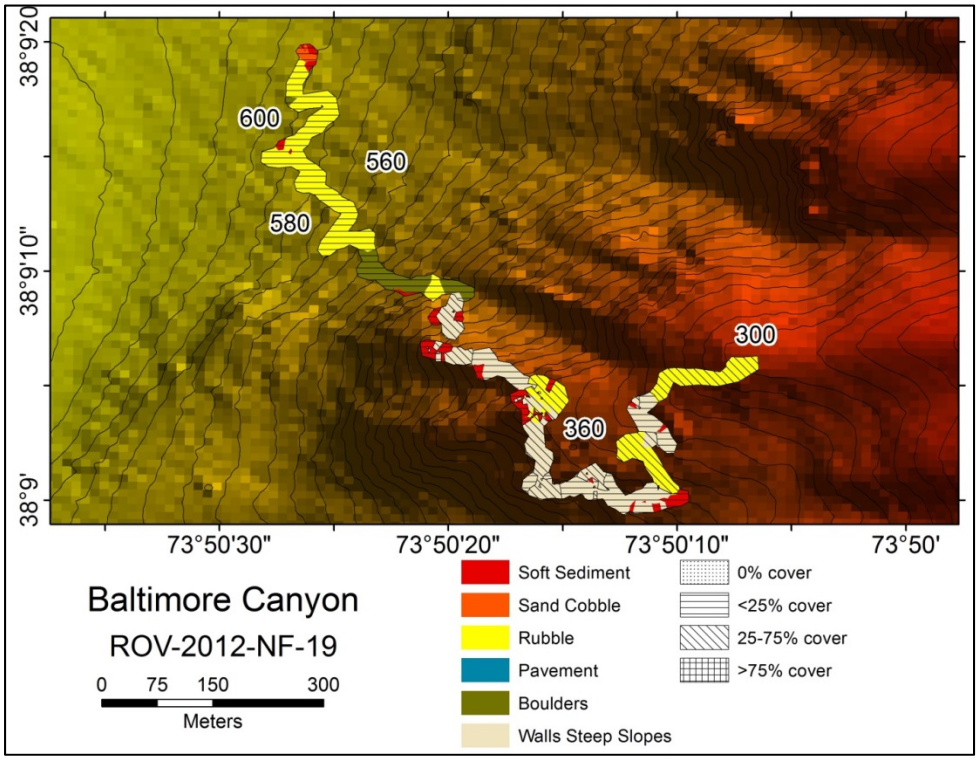
38°9'20"
38°9'10"
38°9'
600
560
580
300
360
73°50'30"
73°50'20"
73°50'10"
73°50'
Baltimore Canyon
ROV-2012-NF-19
0 75 150 300
Meters
Soft Sediment
Sand Cobble
Rubble
Pavement
Boulders
Walls Steep Slopes
0% cover
<25% cover
25-75% cover
>75% cover

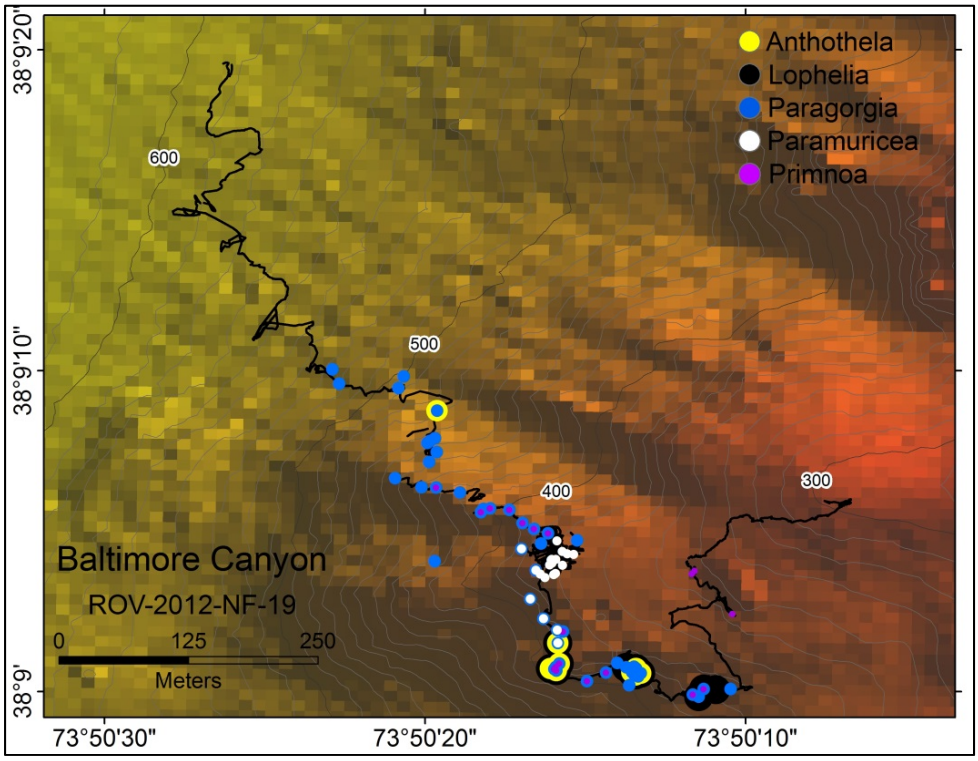
38°9'20"
38°9'10"
38°9'
600
500
400
300
73°50'30"
73°50'20"
73°50'10"
Anthothela
Lophelia
Paragorgia
Paramuricea
Primnoa
Baltimore Canyon
ROV-2012-NF-19
0 125 250
Meters

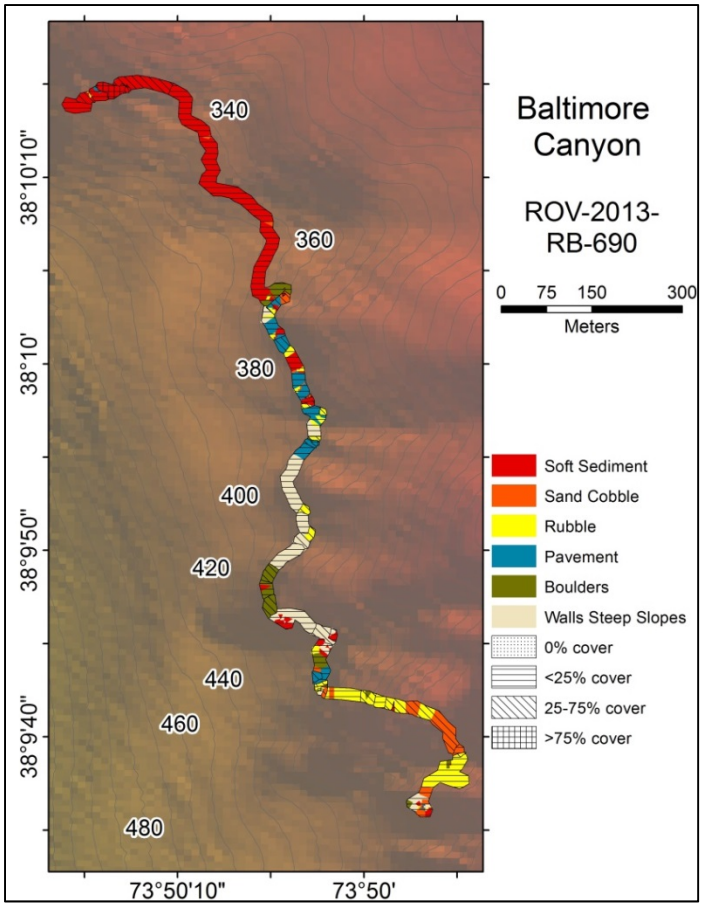

2013 Sampling Cruise: NOAA Ship *Ronald H. Brown* and ROV *Jason II*

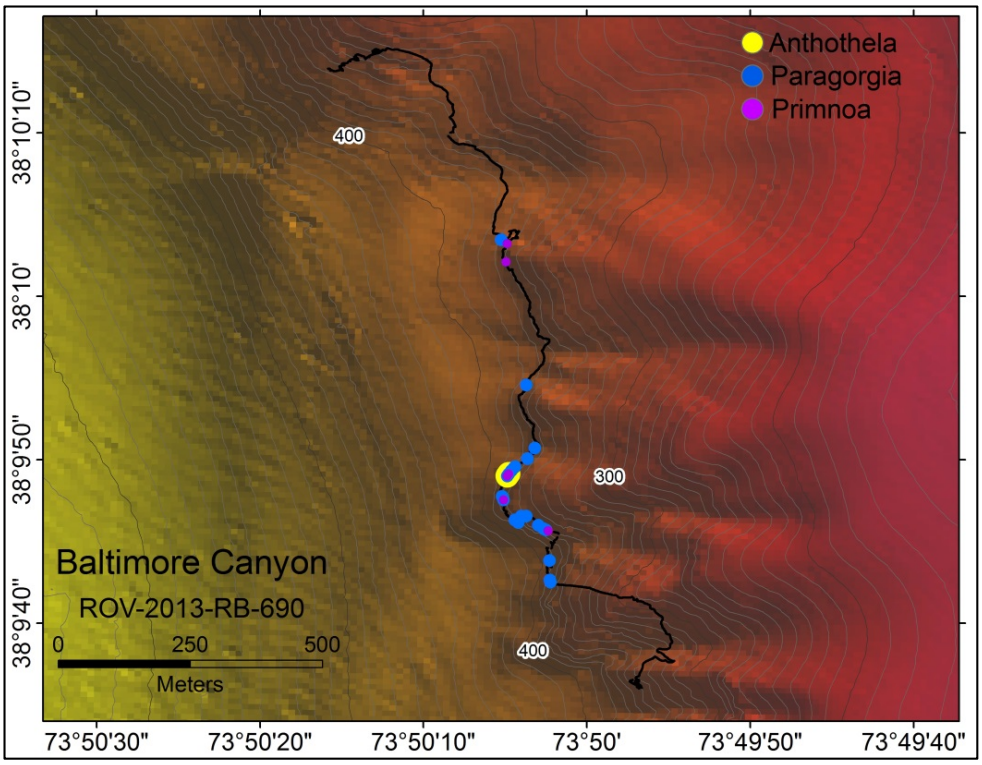

Norfolk Canyon Coral-Targeted Dives

2012 Sampling Cruise

NOAA Ship *Nancy Foster* and ROV *Kraken 2*

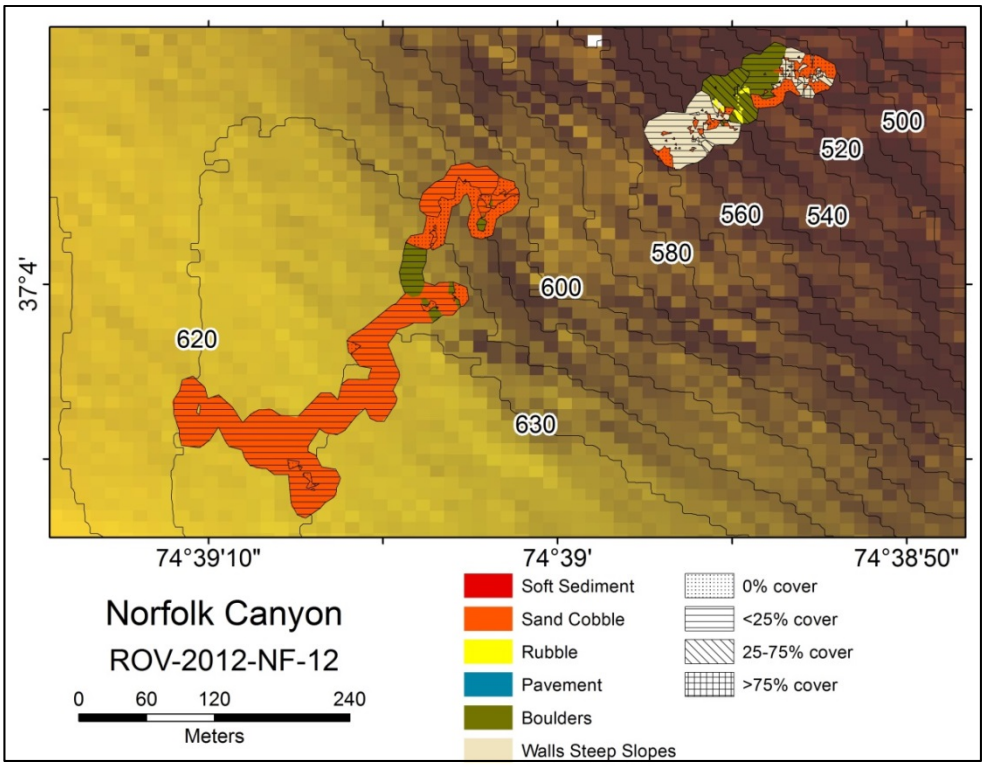

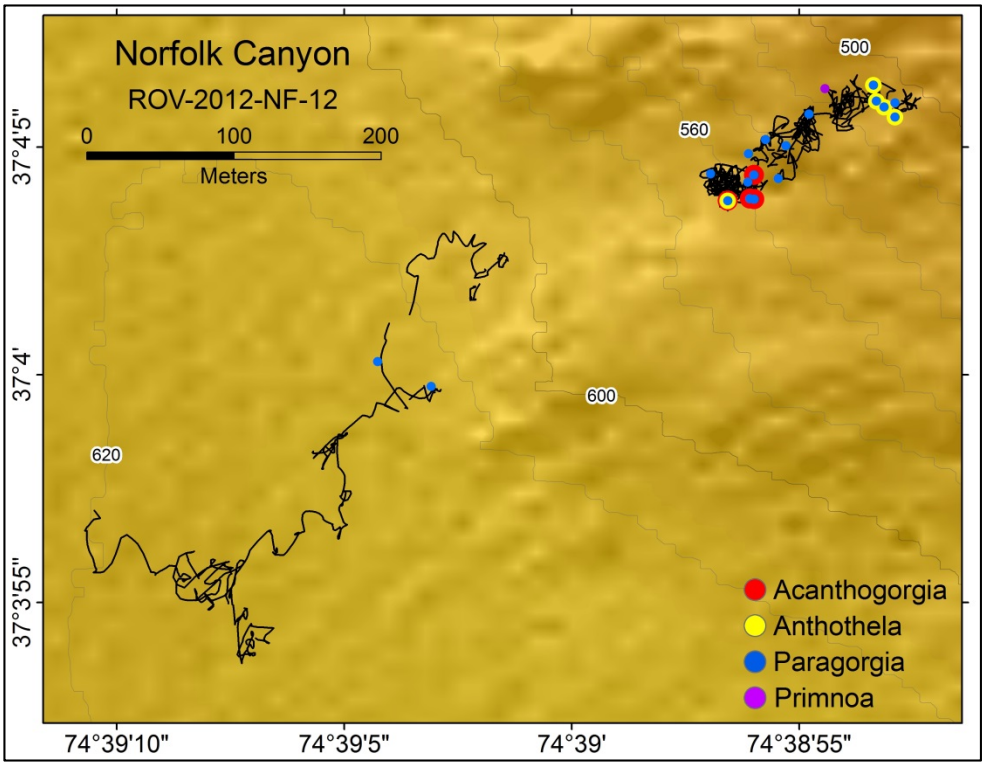

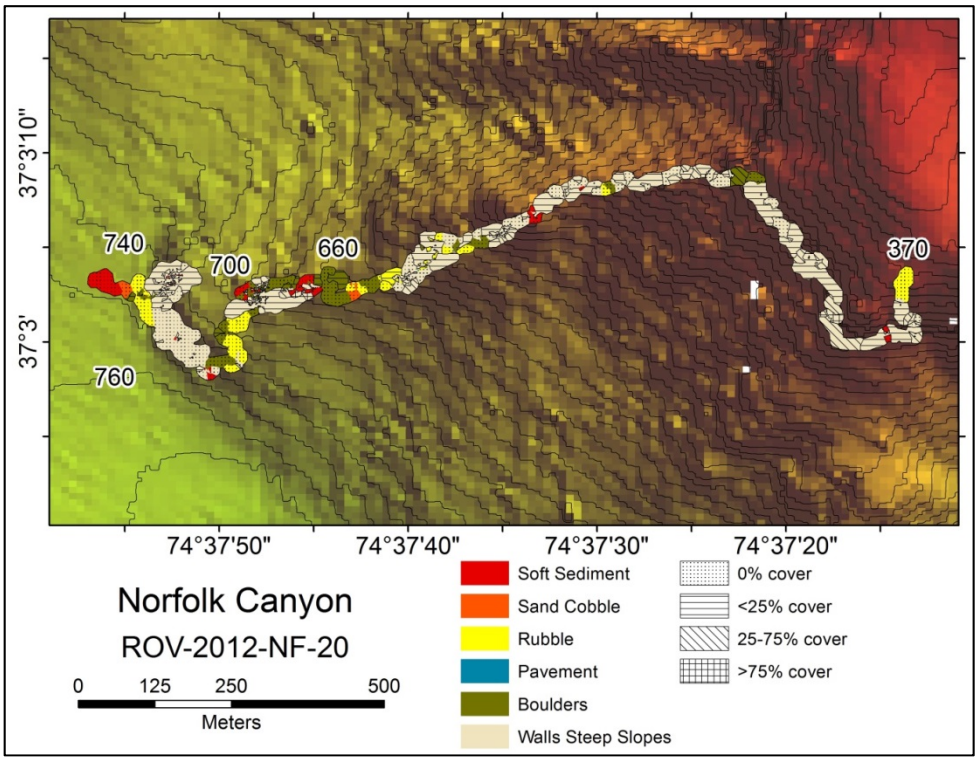
37°3'10"
37°3'
740
700
660
370
760
74°37'50"
74°37'40"
74°37'30"
74°37'20"
Norfolk Canyon
ROV-2012-NF-20
0 125 250 500
Meters
Soft Sediment
Sand Cobble
Rubble
Pavement
Boulders
Walls Steep Slopes
0% cover
<25% cover
25-75% cover
>75% cover

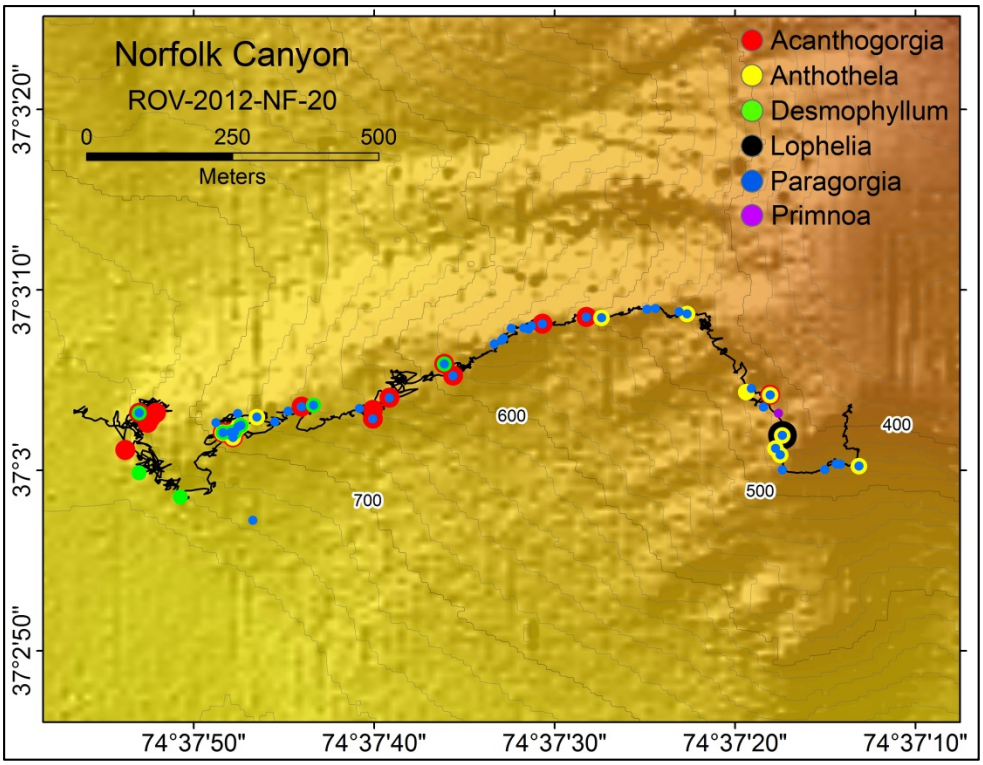
Norfolk Canyon
ROV-2012-NF-20
0 250 500
Meters
Acanthogorgia
Anthothela
Desmophyllum
Lophelia
Paragorgia
Primnoa
37°3'20"
37°3'10"
37°3'
37°2'50"
600
400
700
500
74°37'50"
74°37'40"
74°37'30"
74°37'20"
74°37'10"

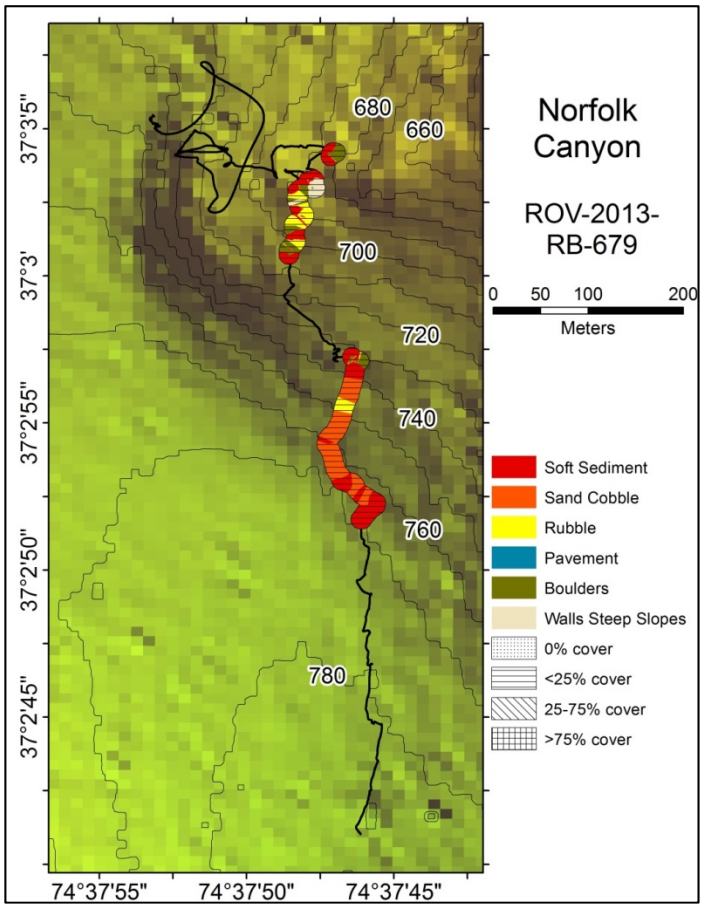

2013 Sampling Cruise: NOAA Ship *Ronald H. Brown* and ROV *Jason II*

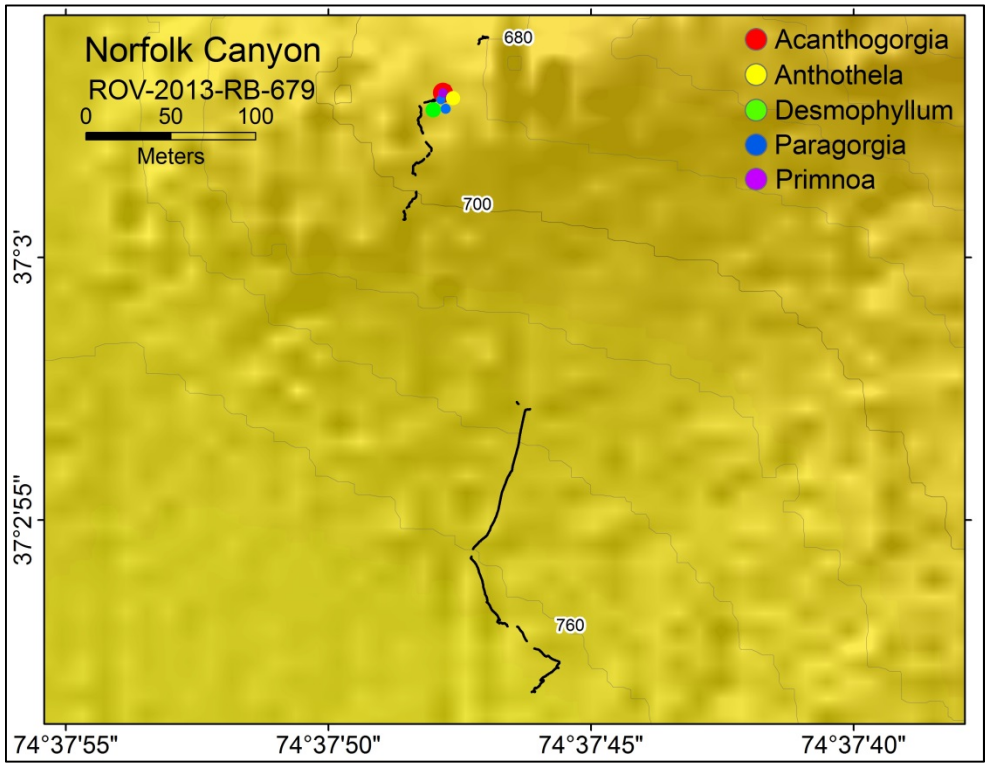

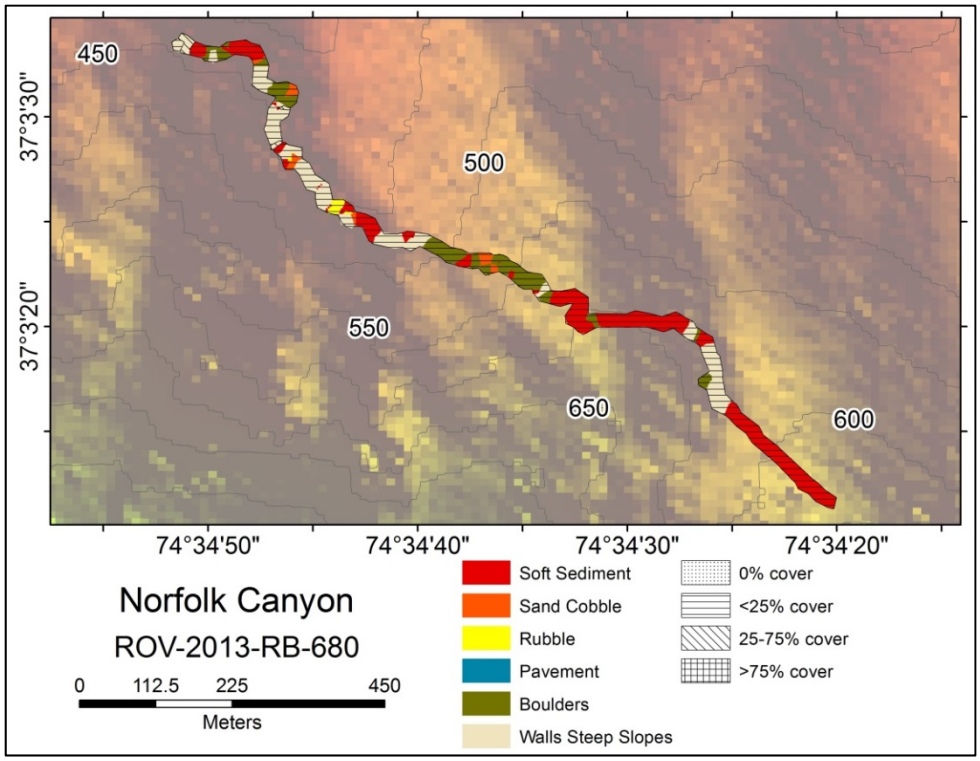
450
500
550
650
600
37°3'30"
37°3'20"
74°34'50"
74°34'40"
74°34'30"
74°34'20"
Norfolk Canyon
ROV-2013-RB-680
0 112.5 225 450
Meters
Soft Sediment
Sand Cobble
Rubble
Pavement
Boulders
Walls Steep Slopes
0% cover
<25% cover
25-75% cover
>75% cover

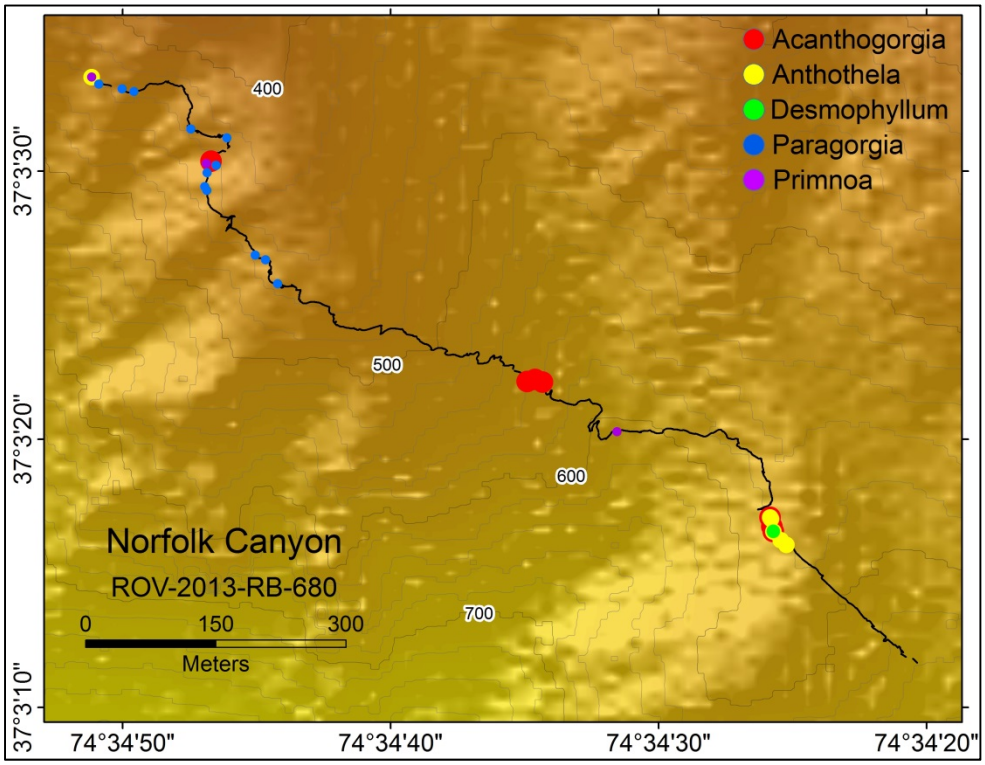
Acanthogorgia
Anthothela
Desmophyllum
Paragorgia
Primnoa
400
500
600
700
37°3'30"
37°3'20"
37°3'10"
74°34'50"
74°34'40"
74°34'30"
74°34'20"
Norfolk Canyon
ROV-2013-RB-680
0 150 300
Meters

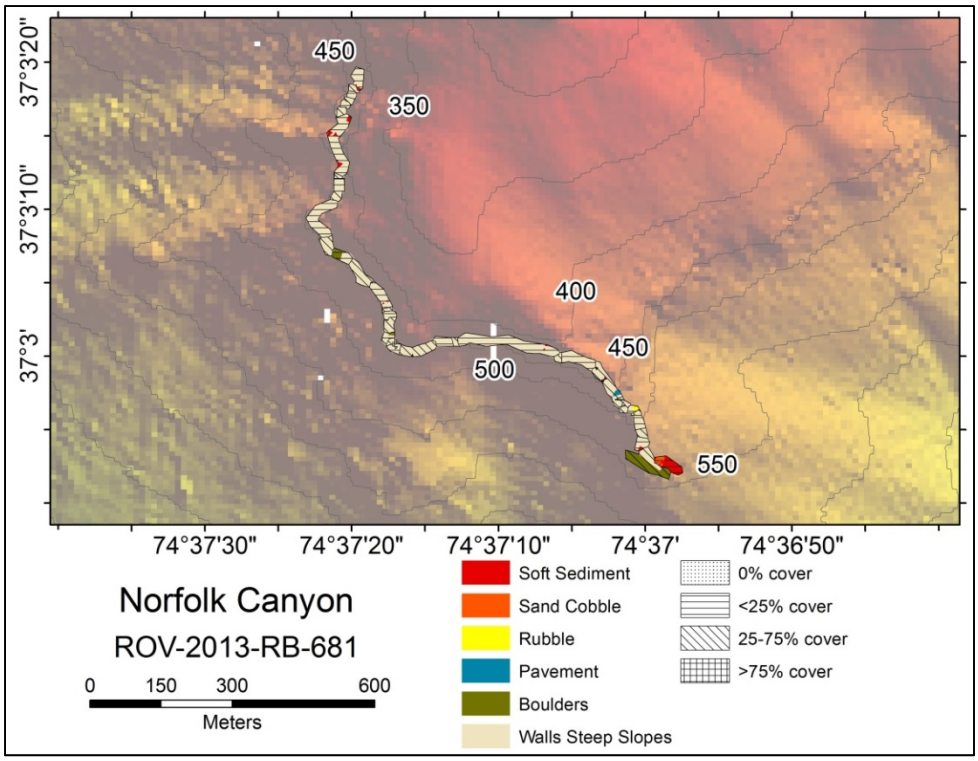
450
350
400
450
500
550
37°3'20"
37°3'10"
37°3'
74°37'30"
74°37'20"
74°37'10"
74°37'
74°36'50"
Norfolk Canyon
ROV-2013-RB-681
0 150 300 600
Meters
Soft Sediment
Sand Cobble
Rubble
Pavement
Boulders
Walls Steep Slopes
0% cover
<25% cover
25-75% cover
>75% cover

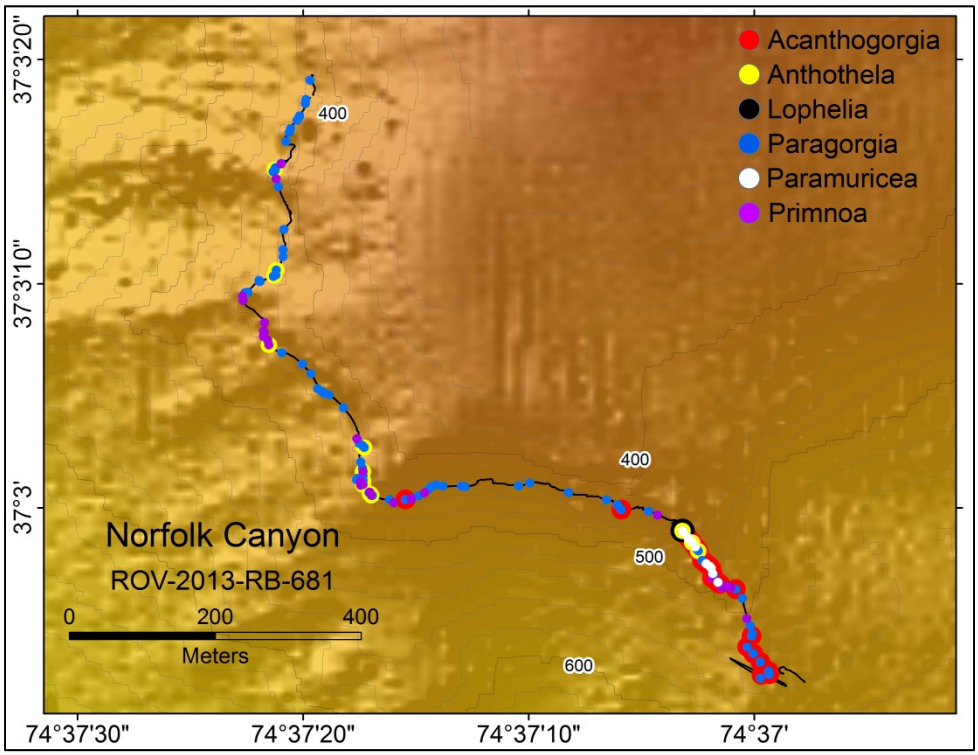
Acanthogorgia
Anthothela
Lophelia
Paragorgia
Paramuricea
Primnoa
400
400
500
600
37°3'20"
37°3'10"
37°3'
74°37'30"
74°37'20"
74°37'10"
74°37'
Norfolk Canyon
ROV-2013-RB-681
0 200 400
Meters

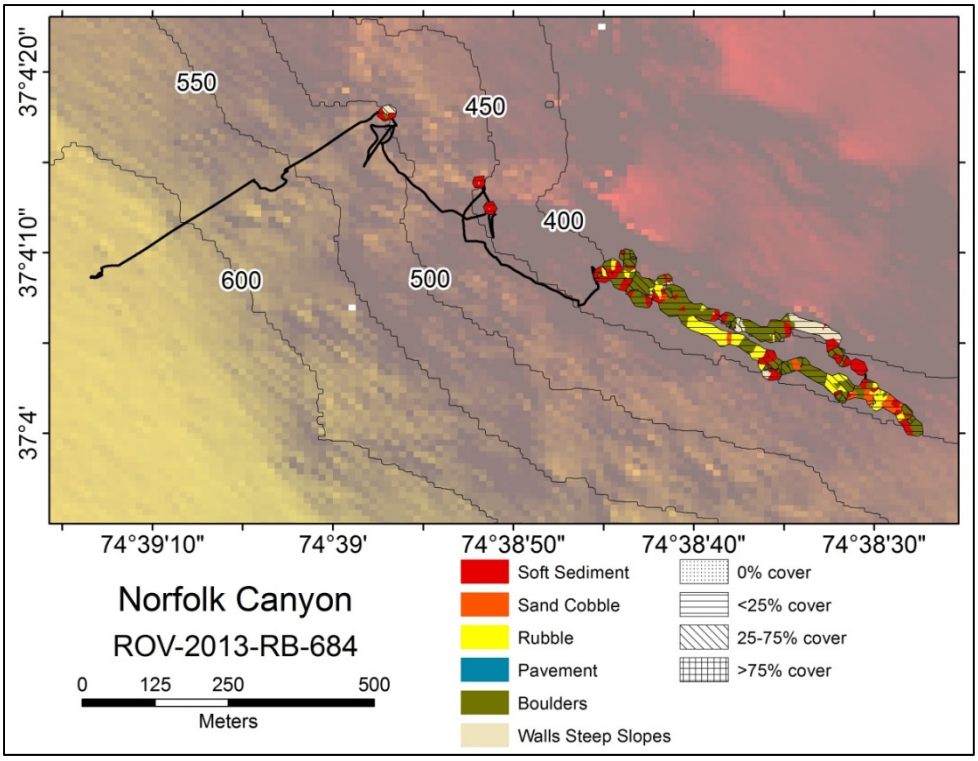
37°4'20"
37°4'10"
37°4'
550
450
400
600
500
74°39'10"
74°39'
74°38'50"
74°38'40"
74°38'30"
Norfolk Canyon
ROV-2013-RB-684
0 125 250 500
Meters
Soft Sediment
Sand Cobble
Rubble
Pavement
Boulders
Walls Steep Slopes
0% cover
<25% cover
25-75% cover
>75% cover

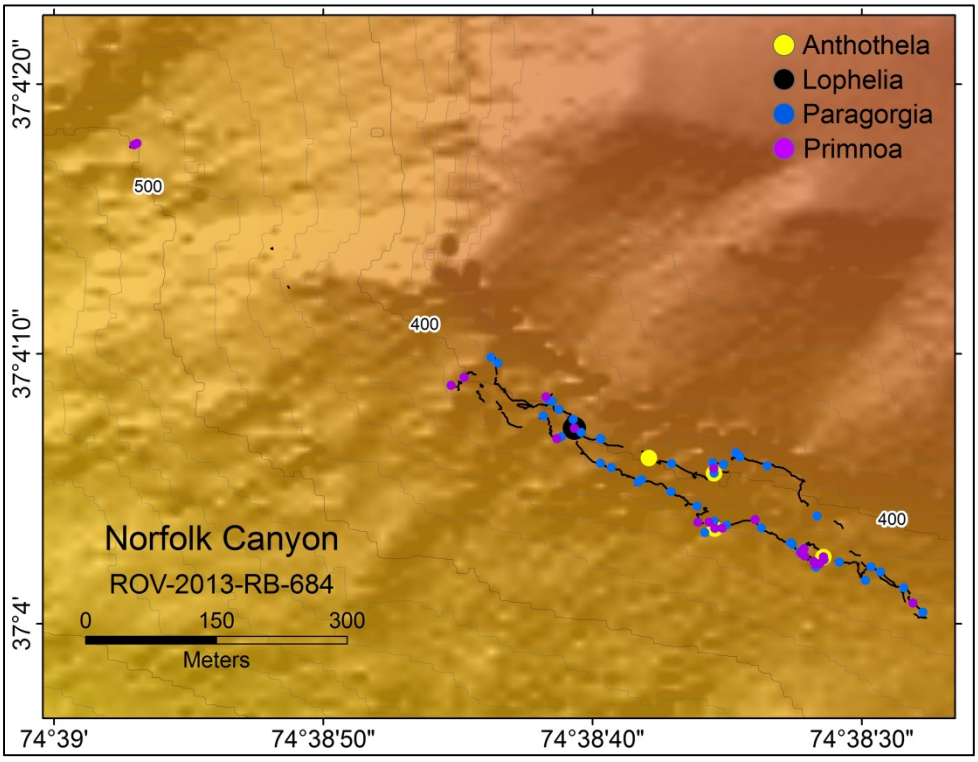
37°4'20"
37°4'10"
37°4'
500
400
400
Anthothela
Lophelia
Paragorgia
Primnoa
Norfolk Canyon
ROV-2013-RB-684
0 150 300
Meters
74°39'
74°38'50"
74°38'40"
74°38'30"

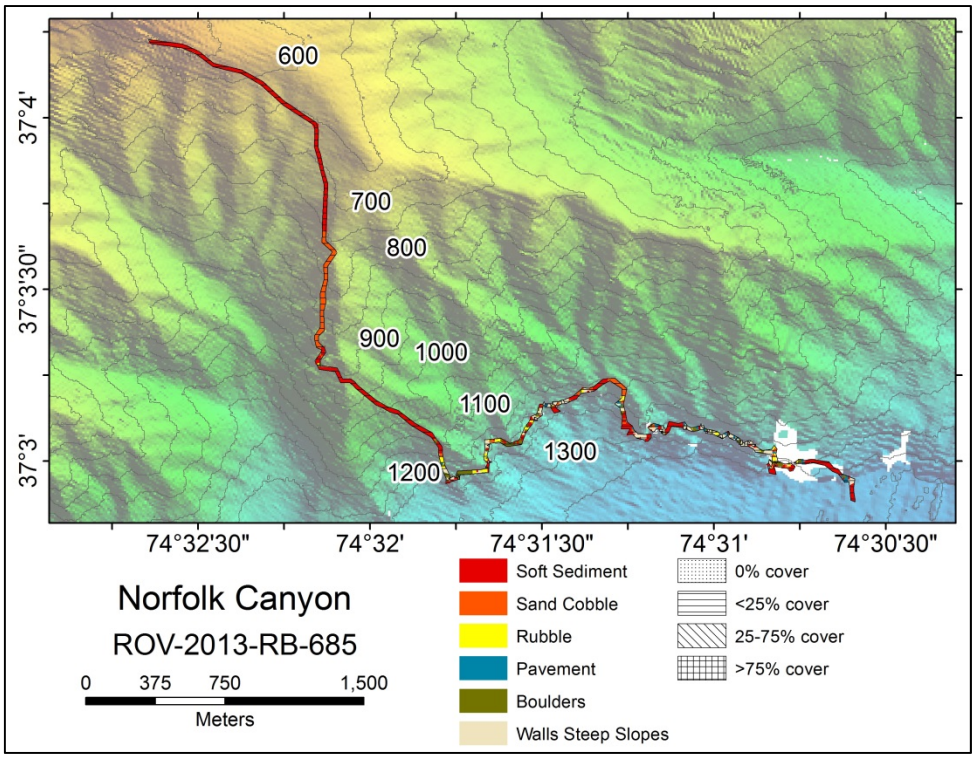
600
700
800
900
1000
1100
1200
1300
37°4'
37°3'30"
37°3'
74°32'30"
74°32'
74°31'30"
74°31'
74°30'30"
Norfolk Canyon
ROV-2013-RB-685
0 375 750 1,500
Meters
Soft Sediment
Sand Cobble
Rubble
Pavement
Boulders
Walls Steep Slopes
0% cover
<25% cover
25-75% cover
>75% cover

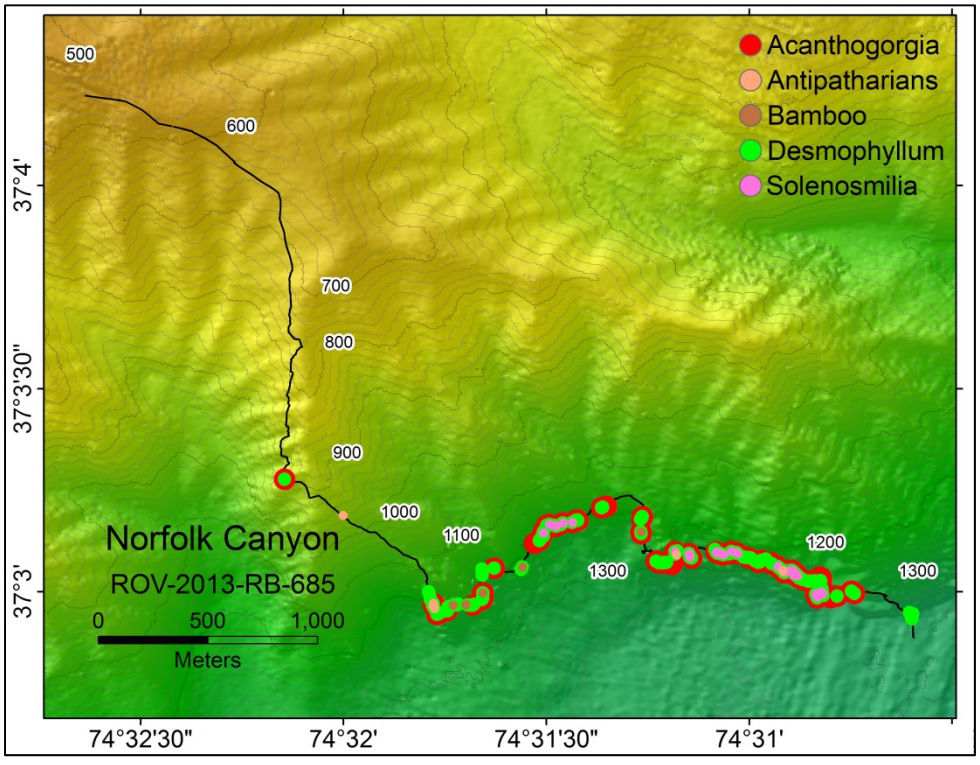
500
600
700
800
900
1000
1100
1200
1300
1300
37°4'
37°3'30"
37°3'
74°32'30"
74°32'
74°31'30"
74°31'
Norfolk Canyon
ROV-2013-RB-685
0 500 1,000
Meters
Acanthogorgia
Antipatharians
Bamboo
Desmophyllum
Solenosmilia

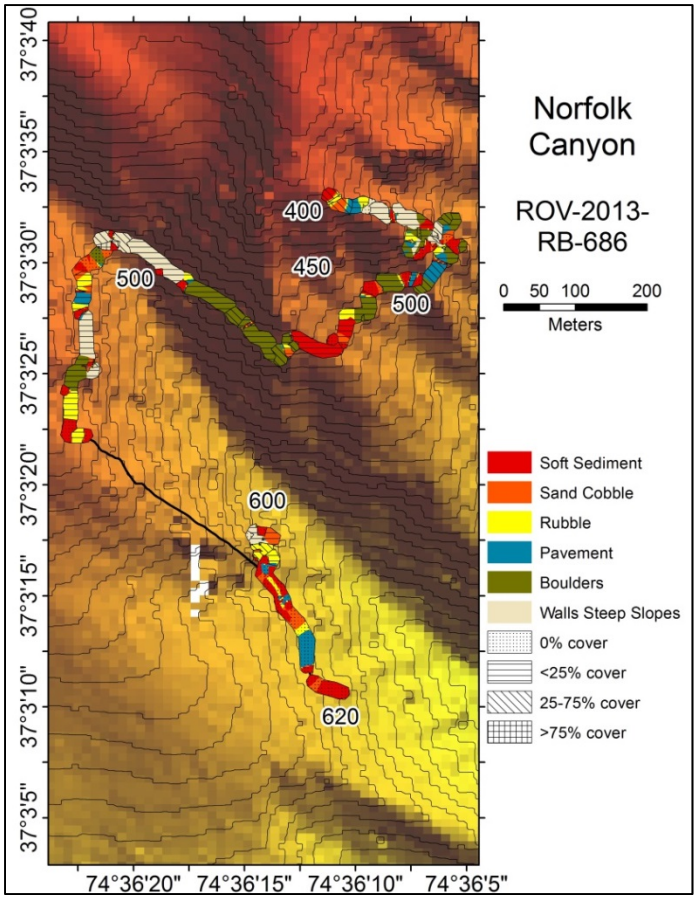
Norfolk
Canyon
ROV-2013-
RB-686
0 50 100 200
Meters
Soft Sediment
Sand Cobble
Rubble
Pavement
Boulders
Walls Steep Slopes
0% cover
<25% cover
25-75% cover
>75% cover
400
450
500
500
600
620
37°3'40"
37°3'35"
37°3'30"
37°3'25"
37°3'20"
37°3'15"
37°3'10"
37°3'5"
74°36'20"
74°36'15"
74°36'10"
74°36'5"

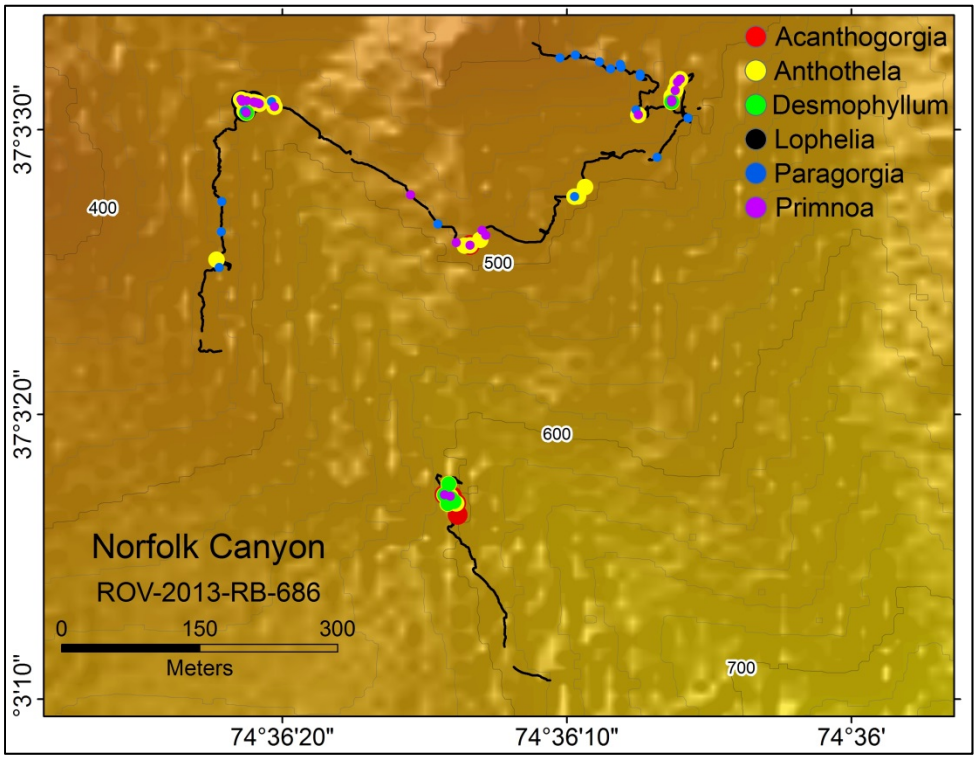
Acanthogorgia
Anthothela
Desmophyllum
Lophelia
Paragorgia
Primnoa
400
500
600
700
Norfolk Canyon
ROV-2013-RB-686
0 150 300
Meters
37°3'30"
37°3'20"
°3'10"
74°36'20"
74°36'10"
74°36'

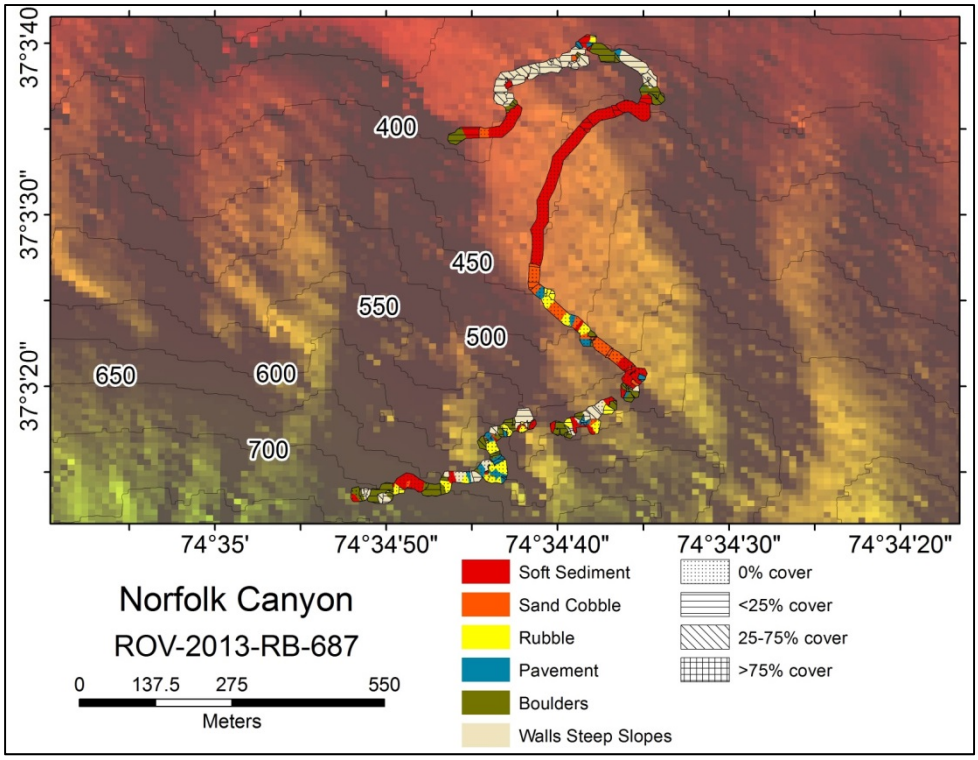
37°3'40"
37°3'30"
37°3'20"
400
450
550
500
650
600
700
74°35'
74°34'50"
74°34'40"
74°34'30"
74°34'20"
Norfolk Canyon
ROV-2013-RB-687
0 137.5 275 550
Meters
Soft Sediment
Sand Cobble
Rubble
Pavement
Boulders
Walls Steep Slopes
0% cover
<25% cover
25-75% cover
>75% cover

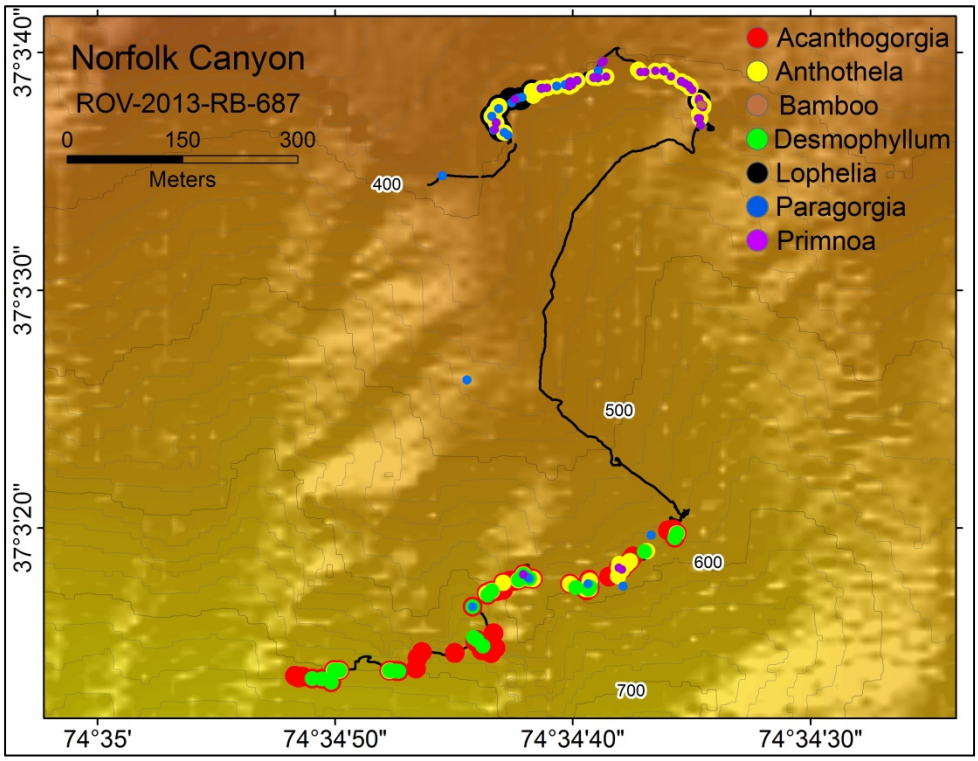
Norfolk Canyon
ROV-2013-RB-687
0 150 300
Meters
Acanthogorgia
Anthothela
Bamboo
Desmophyllum
Lophelia
Paragorgia
Primnoa
37°3'40"
37°3'30"
37°3'20"
400
500
600
700
74°35'
74°34'50"
74°34'40"
74°34'30"

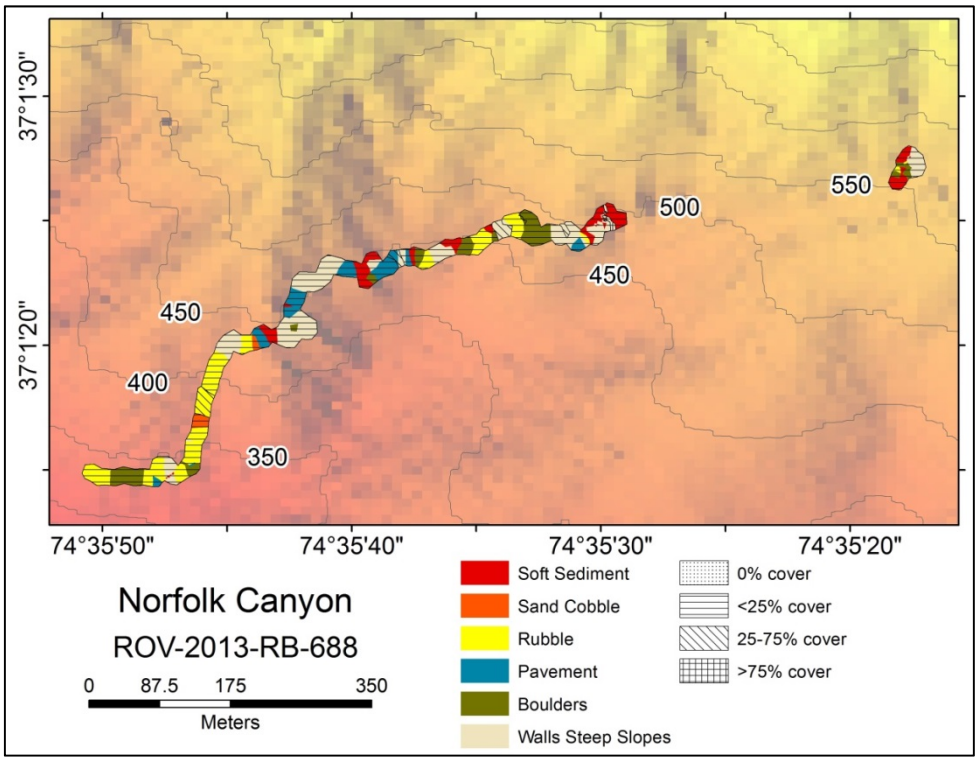
37°1'30"
37°1'20"
74°35'50"
74°35'40"
74°35'30"
74°35'20"
550
500
450
450
400
350
Norfolk Canyon
ROV-2013-RB-688
0 87.5 175 350
Meters
Soft Sediment
Sand Cobble
Rubble
Pavement
Boulders
Walls Steep Slopes
0% cover
<25% cover
25-75% cover
>75% cover

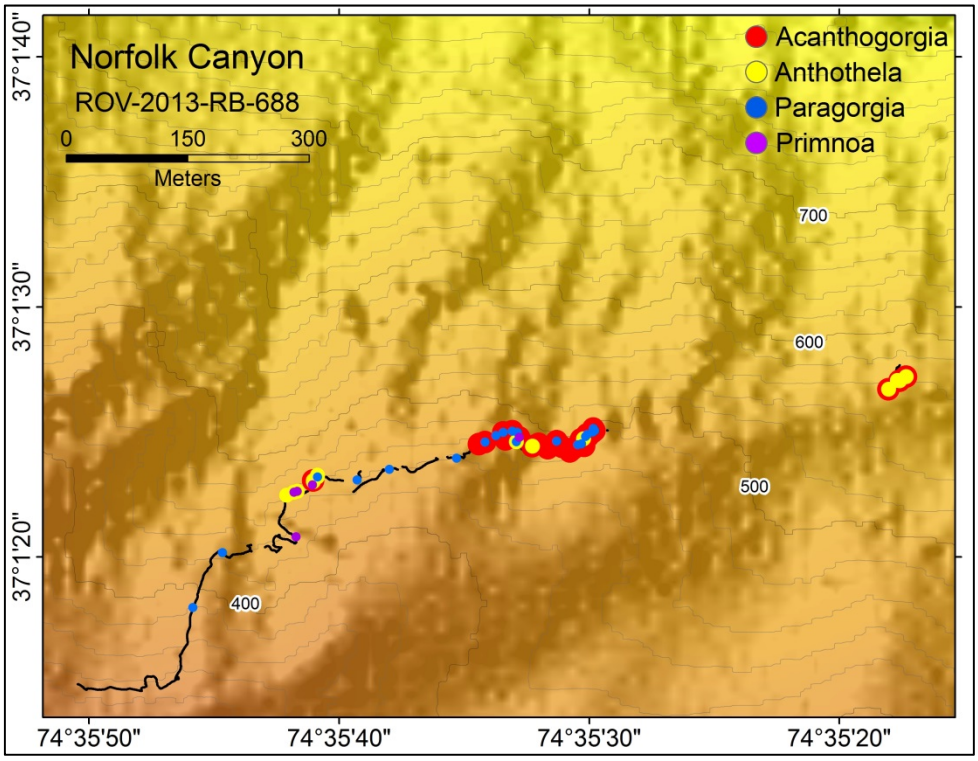
37°1'40"
37°1'30"
37°1'20"
74°35'50"
74°35'40"
74°35'30"
74°35'20"
Norfolk Canyon
ROV-2013-RB-688
0 150 300
Meters
Acanthogorgia
Anthothela
Paragorgia
Primnoa
700
600
500
400

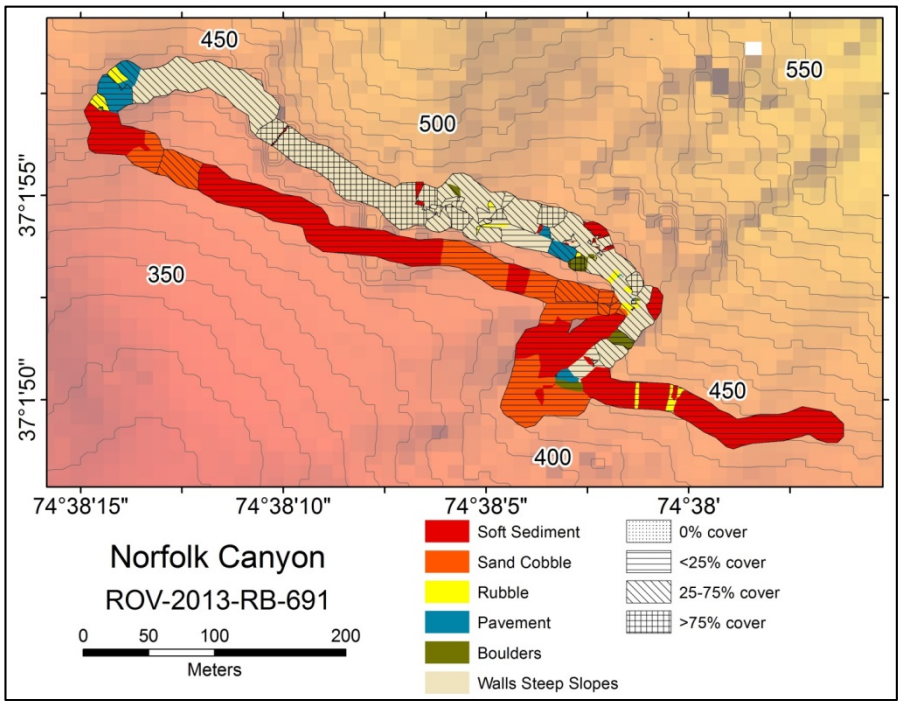
450
550
500
350
450
400
37°1'55"
37°1'50"
74°38'15"
74°38'10"
74°38'5"
74°38'
Norfolk Canyon
ROV-2013-RB-691
0 50 100 200
Meters
Soft Sediment
Sand Cobble
Rubble
Pavement
Boulders
Walls Steep Slopes
0% cover
<25% cover
25-75% cover
>75% cover

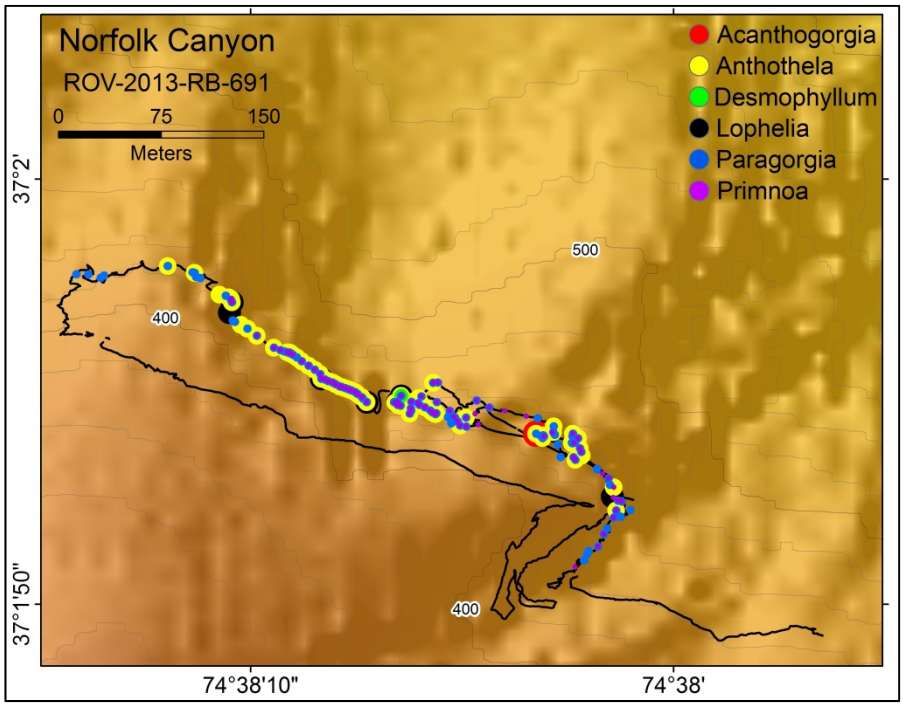
Norfolk Canyon
ROV-2013-RB-691
0 75 150
Meters
Acanthogorgia
Anthothela
Desmophyllum
Lophelia
Paragorgia
Primnoa
500
400
400
37°2'
37°1'50"
74°38'10"
74°38'

Page intentionally left blank

Appendix 8-B

Habitat Maps for Baltimore and Norfolk Canyon Seep Dives

This page intentionally left blank

Baltimore Canyon Seep-Targeted Dives

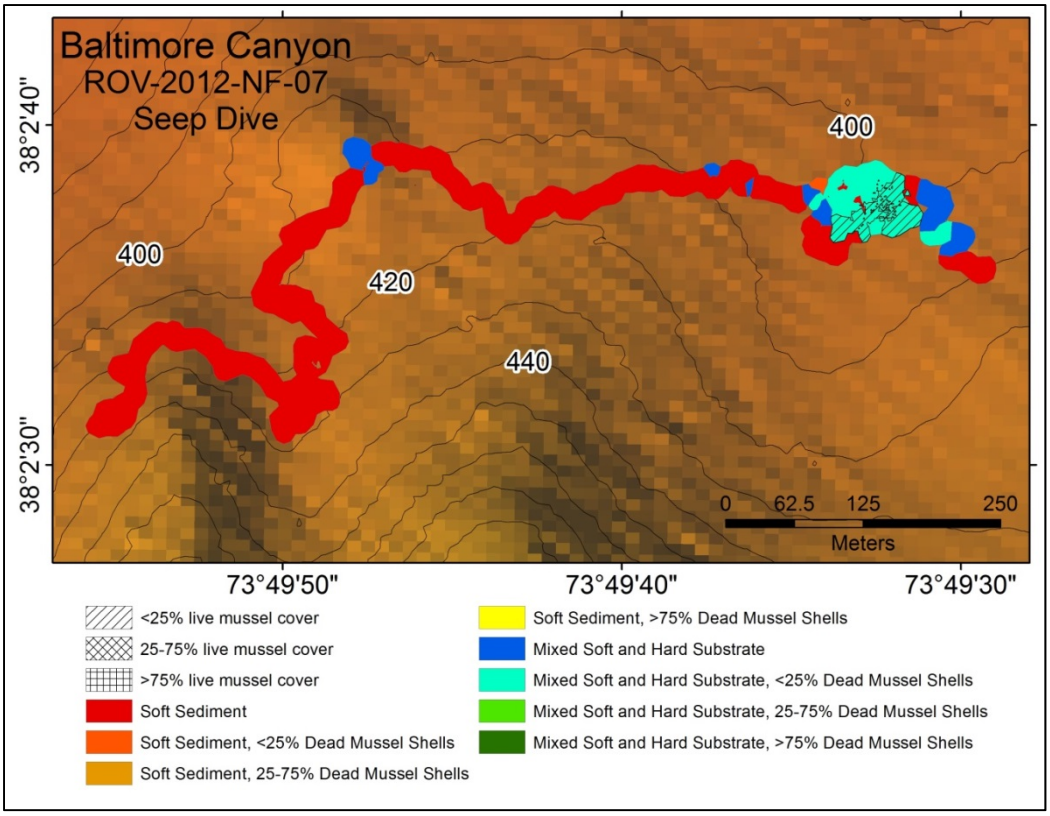

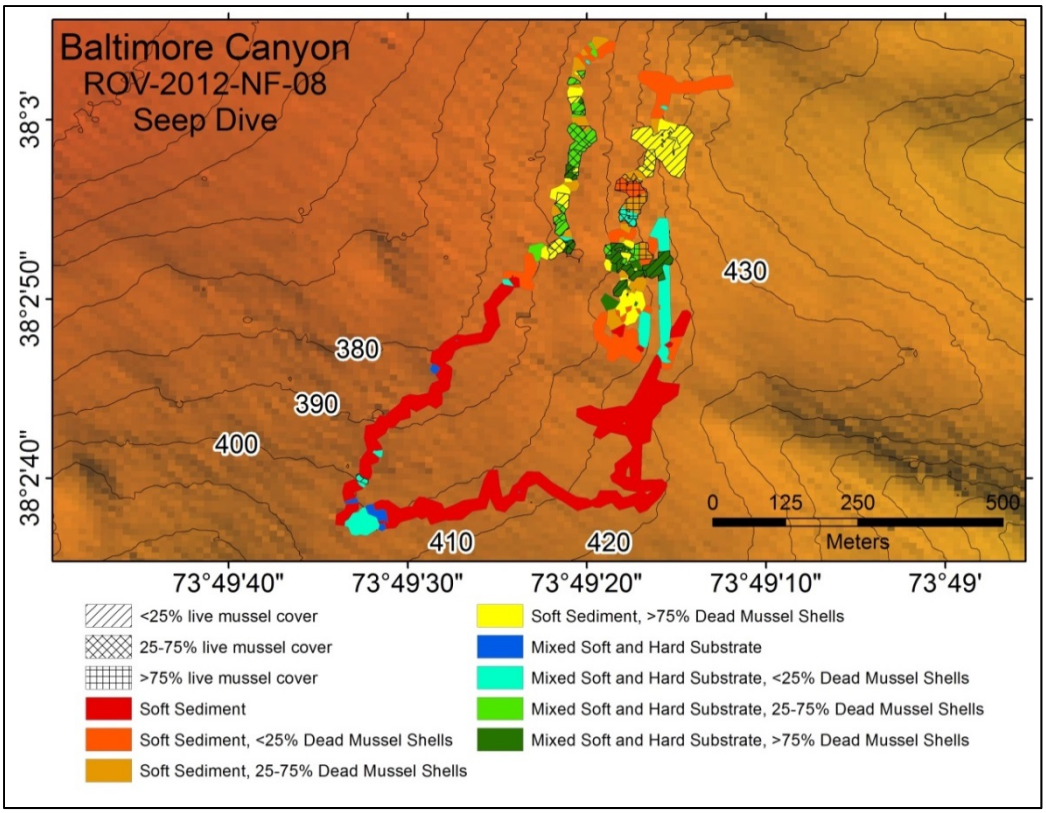

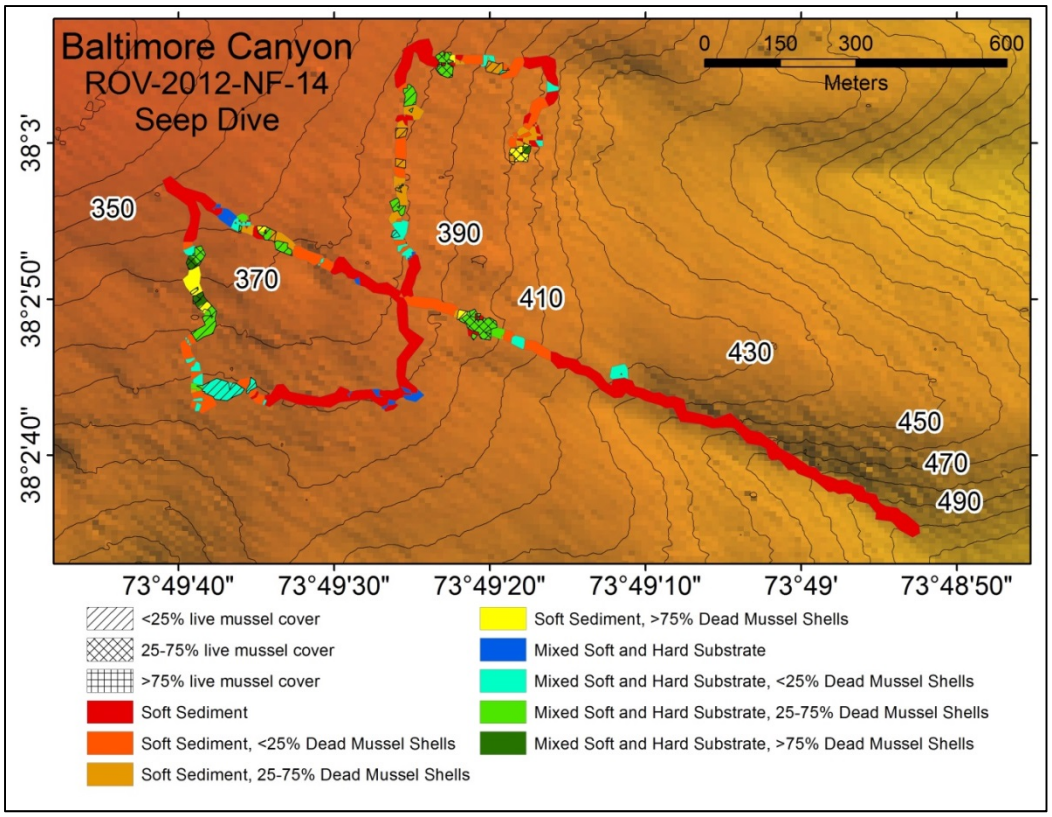
Baltimore Canyon
ROV-2012-NF-14
Seep Dive
0 150 300 600
Meters
350
370
390
410
430
450
470
490
38°3'
38°2'50"
38°2'40"
73°49'40"
73°49'30"
73°49'20"
73°49'10"
73°49'
73°48'50"
<25% live mussel cover
25-75% live mussel cover
>75% live mussel cover
Soft Sediment
Soft Sediment, <25% Dead Mussel Shells
Soft Sediment, 25-75% Dead Mussel Shells
Soft Sediment, >75% Dead Mussel Shells
Mixed Soft and Hard Substrate
Mixed Soft and Hard Substrate, <25% Dead Mussel Shells
Mixed Soft and Hard Substrate, 25-75% Dead Mussel Shells
Mixed Soft and Hard Substrate, >75% Dead Mussel Shells

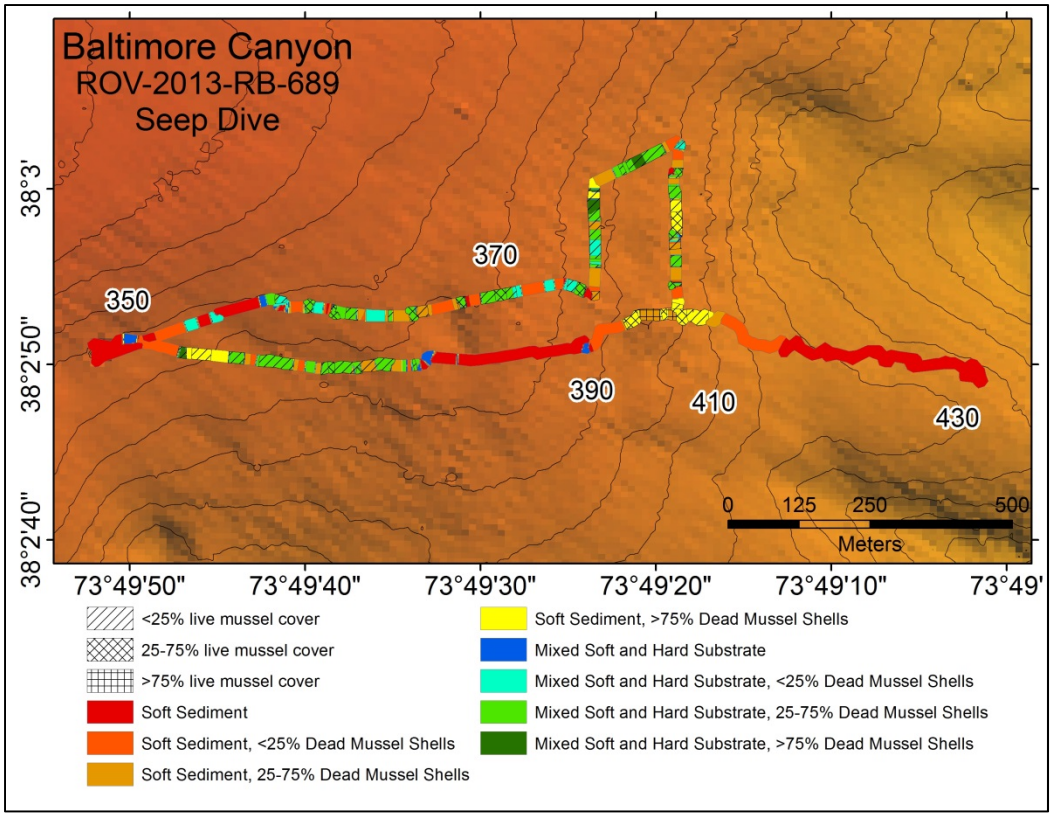
Baltimore Canyon
ROV-2013-RB-689
Seep Dive
350
370
390
410
430
0 125 250 500
Meters
38°3'
38°2'50"
38°2'40"
73°49'50"
73°49'40"
73°49'30"
73°49'20"
73°49'10"
73°49'
<25% live mussel cover
25-75% live mussel cover
>75% live mussel cover
Soft Sediment
Soft Sediment, <25% Dead Mussel Shells
Soft Sediment, 25-75% Dead Mussel Shells
Soft Sediment, >75% Dead Mussel Shells
Mixed Soft and Hard Substrate
Mixed Soft and Hard Substrate, <25% Dead Mussel Shells
Mixed Soft and Hard Substrate, 25-75% Dead Mussel Shells
Mixed Soft and Hard Substrate, >75% Dead Mussel Shells

Norfolk Canyon Seep-Targeted Dives

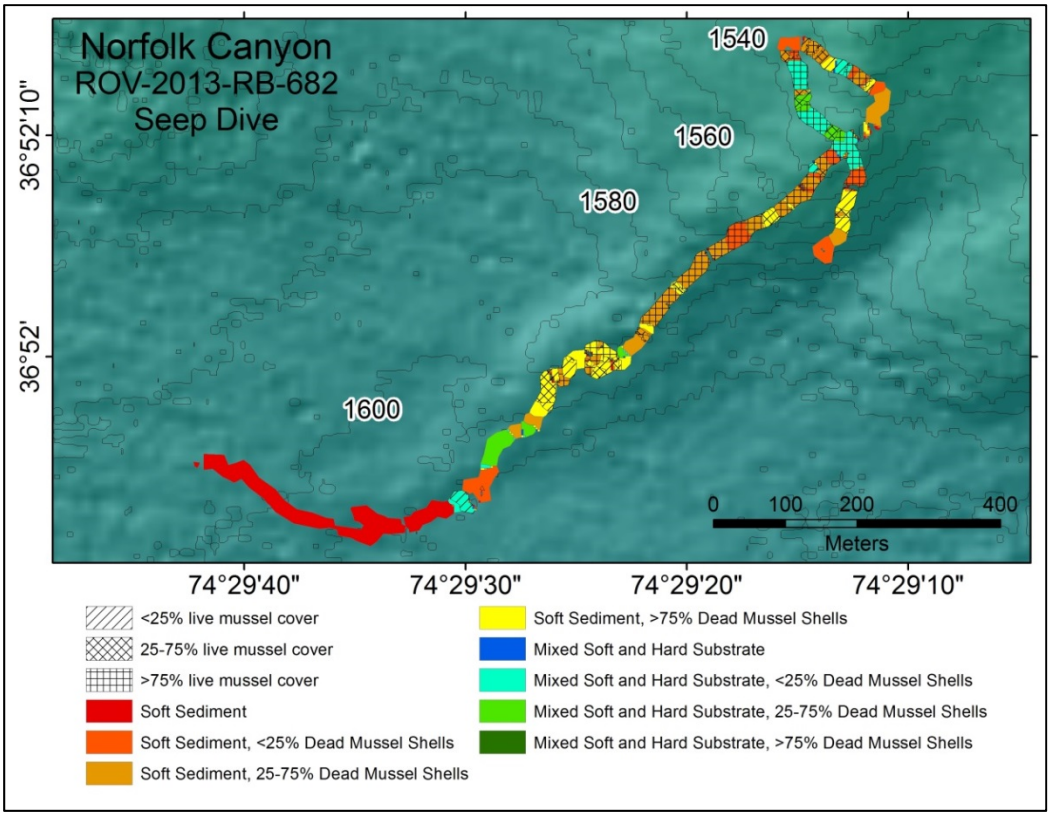

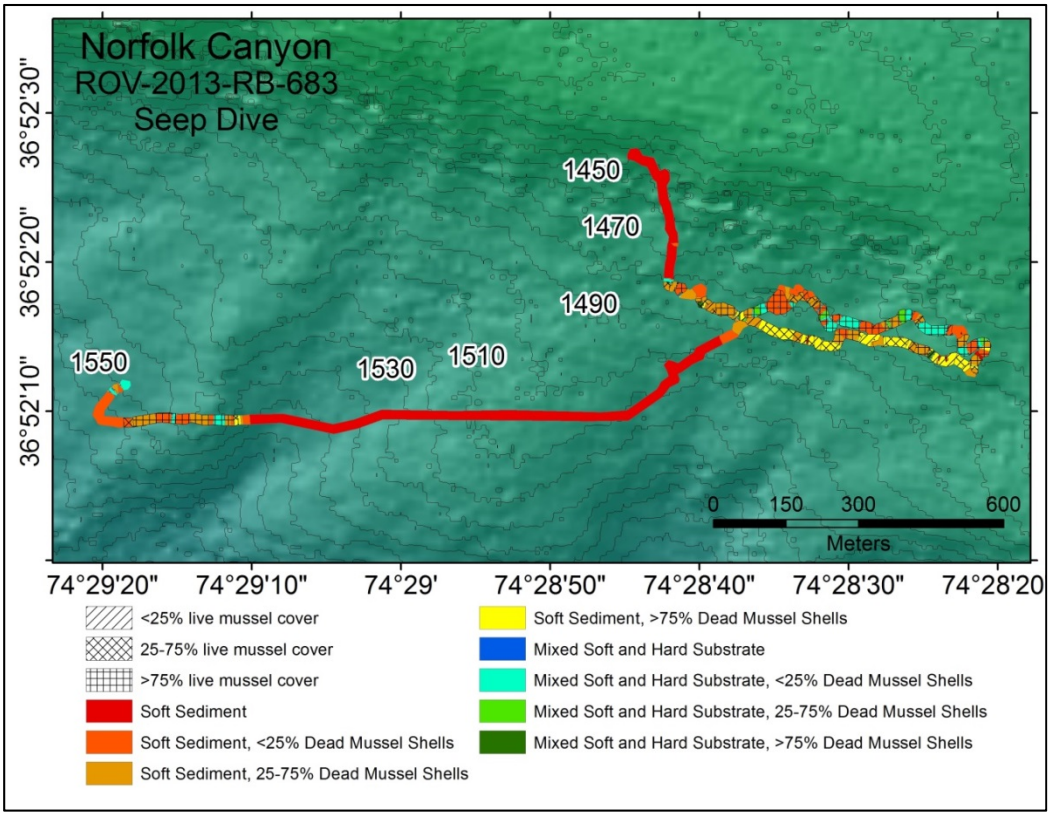

This page intentionally left blank

Appendix 8-C

Inventory of Invertebrate Taxa

This page intentionally left blank

Table 8-C. Inventory of invertebrate taxa.

Phylum	Class	Order	Family	Genus Species
Porifera	Demospongiae	Poecilosclerida	Cladorhizidae	Unidentified
			Coelosphaeridae	*Lissodendoryx* sp.
			Mycalidae	*Mycale* sp.
		Polymastiida	Polymastiidae	*Polymastia* sp.
		Suberitida	Halichondriidae	*Ciocalapata* sp.
				Topsentia sp.
				Demosponge
	Hexactinellida	Lyssacinosida	Rossellidae	*Vazella pourtalesi*
Cnidaria	Anthozoa	Antipatharia	Antipathidae	*Telopathes magna*
			Cladopathidae	*Sibopathes* sp.
		Scleractinia	Caryophylliidae	*Desmophyllum dianthus*
				Lophelia pertusa
				Solenosmilia variabilis
				Dasmosmilia lymani
				Paracyathus pulchellus
				Paracyathus stearnsii
			Flabellidae	*Flabellum alabastrum*
		Pennatulacea	Pennatulacea	*Pennatula aculeata*
			Virgulariidae	*Stylatula elegans*
			Anthoptilidae	*Anthoptilum cf grandiflorum*
			Funiculinidae	*Funiculina quadrangularis*
			Umbellulidae	*Umbellula cf. lindahli*
		Actiniaria	Actiniidae	*Bolocera tunediae*
			Actinoscyphiidae	*Actinoscyphia* sp.
			Halcuriidae	*Halcurias* sp.
			Hormathiidae	Unidentified
			Unidentified	*Actiniaria* sp. 1
				Actiniaria sp. 2
				Actiniaria sp. 3
				Actiniaria sp. 4
				Actiniaria sp. 5
		Corallimorpharia	Unidentified	Unidentified
		Alcyonacea	Acanthogorgiidae	*Acanthogorgia armata*
			Alcyoniidae	*Anthomastus* sp.
			Anthothelidae	*Anthothela grandiflora*
			Isididae	*Acanella arbuscula*
				Keratoisis grayi
			Neptheidae	*Duva florida*
			Paragorgiidae	*Paragorgia arborea*
			Plexauridae	*Paramuricea placomus*
			Primnoidae	*Primnoa resedaeformis*
		Zoantharia	Epizoanthidae	*Parazoanthus* sp. 1
				Parazoanthus sp. 2

Table 8-C. (Continued).

Phylum	Class	Order	Family	Genus Species
Cnidaria	Hydrozoa	Anthoathecata	Eudendridae	*Eudendrium* sp.
		Leptothcata	Tiarannidae	*Modeeria rotunda*
			Haleciidae	*Halecium* sp.
				Halecium delicatulum
				Halecium sessile
			Lafoedae	*Lafoea dumosa*
				Zygophylax crassitheca
			Sertulariidae	*Sertularia tenera*
Arthropoda	Malacostraca	Euphausiacea	Euphausiidae	*Euphausia distinguenda*
				Euphausia spinifera
				Meganyctiphanes norvegica
				Stylocheiron elongatum
				Thysanopoda pectinata
				Thysanoessa macrura
				Meganyctiphanes norvegica
				Euphausia gibboides
				Euphausia spinifera
				Meganyctiphanes norvegica
				Nyctiphanes couchii
			Bentheuphausiidae	*Bentheuphausia amblyops*
		Decapoda	Aristeidae	*Aristeus antillensis*
			Penaeidae	*Metapenaeopsis goodei*
				Parapenaeus politus
				Parapenaeus sp.
				Trachypenaeus constrictus
				Trachypenaeus sp.
				Penaeus setiferus
				Penaeus sp
				Xiphopenaeus kroyeri
				Xiphopenaeus sp.
			Sicyoniidae	*Sicyonia* sp.
			Solenoceridae	*Hymenopenaeus laevis*
				Mesopenaeus tropicalis
				Pleoticus muelleri
				Pleoticus robustus
				Hadropenaeus affinis
				Hymenopenaeus debilis
			Sergestidae	*Acetes americanus carolinae*
				Eusergestes arcticus
				Eusergestes arcticus
			Pasiphaeidae	*Leptochela (Leptochela) bermudensis*
				Parapasiphae sulcatifrons
				Pasiphaea multidentata
				Pasiphaea sp.
			Bresiliidae	Unidentified
			Nematocarcinidae	*Nematocarcinus cursor*

Table 8-C. (Continued).

Phylum	Class	Order	Family	Genus Species
Arthropoda	Malacostraca	Decapoda	Palaemonidae	*Brachycarpus biunguiculatus*
				Periclimenes iridescens
			Alpheidae	*Alpheus* sp.
			Hippolytidae	*Hippolyte obliquimanus*
				Spirontocaris liljeborgii
			Processidae	*Processa guyanae*
				Processa hemphilli
				Processa profunda
			Pandalidae	*Plesionika holthuisi*
				Dichelopandalus leptocerus
				Dichelopandalus sp.
				Heterocarpus ensifer
				Pandalus borealis
				Pandalus montagui
				Pandalus propinqvus
				Plesionika holthuisi
				Heterocarpus ensifer
			Crangonidae	*Philocheras gorei*
				Pontophilus brevirostris
				Pontophilus norvegicus
				Sabinea hystrix
			Nephropidae	*Homarus americanus*
			Polychelidae	*Stereomastis nana*
			Galatheidea	*Galathea rostrata*
				Galathea rostrata
			Diogenidae	*Paguristes cf. moorei*
				Paguristes lymani
				Paguristes moorei
				Paguristes sp.
			Paguridae	*Tomopaguropsis problematica*
			Homolidae	*Homola barbata*
			Latreilliidae	*Latreillia elegans*
			Leucosiidae	*Ebalia* sp.
				Iliacantha subglobosa
			Epialtidae	*Rochinia crassa*
				Rochinia sp.
				Rochinia tanneri
			Inachoididae	*Euprognatha rastellifera*
				Batrachonotus fragosus
				Collodes robustus
				Euprognatha rastellifera
				Euprognatha rastellifera
				Arachnopsis filipes
			Parthenopidae	*Spinolambrus pourtalesii*
			Cancridae	*Cancer borealis*
				Cancer plebejus

Table 8-C. (Continued).

Phylum	Class	Order	Family	Genus Species
Arthropoda	Malacostraca	Decapoda	Geryonidae	*Chaceon quinquedens*
			Palicidae	*Palicus faxoni*
				Palicus sicus
			Plagusiidae	*Euchirograpsus americanus*
			Acanthephyridae	*Acanthephyra eximia*
			Alvinocarididae	*Alvinocaris markensis*
			Eumunididae	*Eumunida picta*
				Eumunida cf. picta
				Eumunida sp.
			Munididae	*Munida* sp.
				Munida iris
				Munida longipes
				Munida pusilla
				Munida sp.
				Munida valida
			Munidopsidae	*Munidopsis* sp.
			Polybidae	*Bathynectes maravigna*
			Unidentified	*Heterocarpus cf. ensifer*
		Amphipoda	Unciolidae	*Unciola* sp.
			Phrosinidae	*Phrosina cf semilunata*
			Lestrigonidae	*Hyperietta cf. luzoni*
			Hyperiidae	*Themisto abyssorum*
				Themisto sp.
		Pycnogonida	Pantopoda	Unknown
		Maxillopodia	Pedunculata	Unknown
Mollusca	Gastropoda	Archaeogastropoda	Fissurellidae	*Diodora tanneri*
		Neogastropoda	Buccinidae	*Colus* sp.
				Colus stimpsoni
			Turridae	*Turridae*
	Cephalopoda	Sepioidea	Sepiolidae	*Rossia megaptera*
				Semirossia tenera
		Oegopsida	Brachioteuthidae	*Brachioteuthis beani*
			Enoploteuthidae	*Abralia veranyi*
			Ommastrephidae	*Illex illecebrosus*
			Mastigoteuthidae	*Magnoteuthis magna*
		Octopoda	Bathypolypodidae	*Bathypolypus bairdii*
	Bivalvia	Nuculoida	Yoldiidae	*Yoldiella* sp.
			Malletiidae	*Malletia* sp.
		Mytiloida	Mytilidae	*Bathymodiolus childressi*
		Limoida	Limidae	*Acesta cryptadelphe*
		Veneroida	Semelidae	*Abra profundorum*
		Anomalodesmata	Verticordiidae	*Verticordia* sp.
	Scaphopoda	Dentaliida	Dentaliidae	*Scaphopoda* − cf. *Dentalium* sp.

Table 8-C. (Continued).

Phylum	Class	Order	Family	Genus Species
Annelida	Polychaeta	Phyllodocida	Nephtyidae	Unidentified
			Aphroditidae	*Aphrodita aculeata*
			Polynoidae	*Eunoe cf. nodosa*
				Eunoe sp.
				Eunoe sp. 2
			Aplacophora	*Solenogastres* sp.
			Sigalionidae	Unidentified
			Glyceridae	Unidentified
		Eunicida	Eunicidae	*Eunice pennata*
				Eunice sp.
				Eunice sp. 2
			Onuphidae	*Hyalinoecia artifex*
				Hyalinoecia tubicola
				Onuphidae
				Onuphis sp.
		Terebellida	Flabelligeridae	Unidentified
			Sternaspidae	*Sternaspis* sp.
			Terebellidae	Unidentified
		Spionida	Spionidae	Unidentified
Sipuncula			Rossellidae	*Stegopoma plicatile*
				tubulariid sp.
			Sipunculidae	*Sipunculus norvegicus*
				Sipuncula sp.
Echinodermata	Crinoidea	Comatulida	Antedonidae	*Leptometra celtica*
	Asteroidea	Paxillosida	Astropectinidae	*Persephonaster echinulatus*
				Plutonaster agassizi agassizi
				Astropecten alligator
				Astropecten americanus
				Astropecten sp.
			Porcellanasteridae	*Porcellanaster ceruleus*
		Valvatida	Odontasteridae	*Odontaster hispidus*
				Odontaster robustus
			Poraniidae	*Porania cf. pulvillus*
				Porania pulvillus insignis
				Porania pulvillus pulvillus
				Poraniomorpha hispida
			Solasteridae	*Solaster cf. earlli*
		Spinulosida	Echinasteridae	*Henricia oculata*
				Henricia sp.
				Henricia antillarum
		Forcipulatida	Asteriidae	*Coronaster briareus*
				Stephanasterias sp.
				Leptasterias polaris
				Sclerasterias contorta
				Sclerasterias tanneri
				Sclerasterias contorta

Table 8-C. (Continued).

Phylum	Class	Order	Family	Genus Species
Echinodermata	Asteroidea	Forcipulatida	Asteriidae	*Stephanasterias albula*
Echinodermata	Ophiuroidea	Ophiurida	Amphiuridae	*Amphipholis* sp.
				Amphipholis squamata
				Amphiura otteri
				Amphiura sp.
			Ophiacanthidae	*Ophiacantha* sp.
			Ophiactidae	*Ophiactis* sp.
				Ophiopholis aculeata
				Ophiopholis sp.
				Ophiura robusta
				Ophiura sarsii
			Ophiocomidae	*Ophiocomina* sp.
			Ophiomyxidae	*Ophiomyxa* sp.
				Ophiophrixus sp.
			Ophiolepididae	*Ophiomusium cf lymani*
		Euryalida	Asteronychidae	*Asteronyx loveni*
			Gorgonocephalidae	*Gorgonocephalus* sp.
	Echinoidea	Cidaroida	Cidaridae	*Cidaris abyssicola*
				Stylocidaris affinis
				Cidaris sp.
				Stylocidaris lineata
			Histocidaridae	*Histocidaris sharreri*
		Echinothurioida	Echinothuriidae	*Hygrosoma petersii*
			Phormosomatidae	*Phormosoma placenta*
		Arbacioida	Arbaciidae	*Coelopleurus floridanus*
		Clypeasteroida	Echinarachniidae	*Echinarachnius parma*
		Camarodonta	Echinidae	*Echinus wallisi*
				Gracilechinus affinis
				Echinus tylodes
				Gracilechinus affinis
				Gracilechinus alexandri
	Holothuroidea	Aspidochirotida	Synallactidae	*Paelopatides* sp.
			Mesothuriidae	*Zygothuria lactea*
		Apodida	Chirodotidae	*Chiridota heheva*
Cephalorhyncha	Priapulida	Unidentified	Unidentified	Unidentified
Chordata	Thaliacea	Pyrosomatida	Pyrosomatidae	*Pyrosoma* sp.

CHAPTER 9. BENTHIC INFAUNAL COMMUNITIES OF BALTIMORE AND NORFOLK CANYONS

Craig Melville Robertson, Jill R. Bourque, and Amanda W.J. Demopoulos

9.1 INTRODUCTION

The imperative for finding, cataloging, and understanding continental margin diversity derives from the many key functions, goods and services provided by margin ecosystems and by an increasingly deleterious human footprint on our continental slopes (Levin and Dayton 2009). Progress in seafloor mapping technology and direct observation has revealed unexpected heterogeneity, with a mosaic of habitats and ecosystems linked to geomorphological, geochemical, and hydrographic features that are capable of influencing biotic diversity (Levin and Sibuet 2012).

Submarine canyons are dramatic and widespread topographic features crossing continental and island margins in oceans, connecting shelf-margins to deep ocean basins (Harris and Whiteway 2011). Their importance as biodiversity hotspots has continued to emerge over the last two decades as research efforts have increased. Understanding the physical parameters within a canyon system is a primary factor for understanding habitat variability and ecological patterns within the confines of canyon systems (Levin et al. 2001). Margin sediments exhibit ubiquitous depth zonation (Carney et al. 2005), with a diverse suite of species that occupy restricted bathymetric ranges along any given section of the margin. Major shifts in composition among taxa are observed at the shelf-slope transition zone (canyons <500 m), along the upper slope (1,000 m), and at the lower slope transition zone (<3,000 m) (Gibson et al. 2005).

In the deep sea, macrofaunal assemblages are generally limited by the availability of allochthonous organic material (Rowe et al. 1982, Billet et al. 1983, Rex et al. 2005, Smith et al. 2008) where macrofaunal densities usually decline with depth and distance from the shore (Rowe et al. 1982, Houston and Haedrich 1984, Rex et al. 2005). However, canyon fauna can experience enhanced food supply through the resuspension and deposition of organic-rich sediments, delivered by increased current velocities within the confines of the canyon (Rowe 1971, Shepard et al. 1974). As a result, canyons are often reported as sustaining enhanced abundances and biomass compared with nearby open slope habitats at similar depths (Vetter and Dayton 1998, Duineveld et al. 2001, De Leo et al. 2010) as well as enhancing regional (γ) and local (α) biodiversity (Hecker et al. 1983, Vetter and Dayton 1998, De Leo et al. 2010, Vetter et al. 2010). Furthermore, enhanced habitat heterogeneity can also be a major structuring agent of ecological assemblages, promoting beta (β) diversity (McClain and Barry 2010) in canyon environments.

Canyon systems have often been described as biodiversity hotspots, especially at mid-slope depths (Levin and Sibuet 2012) where physical processes, characterized by complex patterns in hydrography, promote topographically induced upwelling, enhanced mixing via internal tides, and the focusing of tidal bores (Vetter and Dayton 1998, Cacchione et al. 2002). Additionally, sediment transport and accumulation (García et al. 2008) represent important influential ecological drivers. Factors such as substrata heterogeneity (Levin and Sibuet 2012) and concentration of organic matter (De Leo et al. 2010) have been suggested to explain higher faunal diversity, abundance, and benthic productivity found in canyon systems compared with surrounding areas. Bathymetric patterns of species diversity have been attributed to changes in sediment characteristics (Etter and Grassle 1992), productivity, currents, oxygen, disturbance, and the interplay of biotic effects with depth and latitude (Levin et al. 2001, Carney et al. 2005).

Recent studies report on the uniqueness of canyon benthic communities and habitats and the view that no two canyons are alike (Cunha et al. 2011). Certain submarine canyons may maintain

characteristic and unique faunas, but more often canyon macrofaunal assemblages show high dominance and locally reduced biodiversity (Rowe 1971, Gage 1997, Curdia et al. 2004, Cunha et al. 2011), especially in areas of high organic enrichment (Vetter and Dayton 1998, 1999). Macrofaunal assemblages in deeper reaches of canyons, approaching the lower continental rise, tend to be similar to those found at abyssal plains. However, the low taxonomic resolution and differences in the level of taxa identification available from published studies hinder comparisons among studies as well as a full assessment of biodiversity and endemism (Gage et al. 1995, Escobar Briones et al. 2008).

It is likely that canyon communities are distinct, although much of the work on biological complexity of these communities remains unknown (Weaver et al. 2004) and understanding the drivers shaping benthic community structure and habitats has only just begun. Although the dynamics of environmental processes such as current flow, sediment transport, and flux have been partly determined in several large canyon systems around the world (Puig et al. 2014), their influence and interaction with the benthos has, for most studies, remained undefined. With this insight, the future of canyon research is likely to include the myriad of physical environmental factors working in synergy to create the unique canyon environmental settings, habitats, and communities. In improving our knowledge of the environmental influences on canyon communities, there is a need to define these processes and, in particular, to quantify the net fluxes of nutrients and carbon, as well as heat and salt (Allen and Durrieu de Madron 2009), in order to build a holistic ecological assessment of wider continental margin carbon flow to abyssal habitats.

9.1.1 Study Area and Previous Work

The Mid-Atlantic Bight (MAB) shelf is known for atypically high organic inputs resulting from enhanced surface productivity (Schaff et al. 1992, DeMaster et al. 1994, Rex and Etter 2010). The interplay of continental shelf and slope topography with circulation patterns of the South Atlantic Bight, slope bottom, and the Gulf Stream near Cape Hatteras, clearly promotes high productivity and allows the southern MAB to be a region for modern carbon export to the neighboring shelf and slope (Schaff et al. 1992, Csanady and Hamilton 1988, Yoder et al. 1985). Some of the highest macrofaunal abundances and biomass values were recorded at the bathyal habitats of the southern MAB continental shelf (Grassle and Maciolek 1992, Blake and Grassle 1994, Blake and Hilbig 1994), but comparable data from submarine canyons in the region are lacking. However, a previous study by Rowe et al. (1982) in the largest canyon in the western Atlantic, Hudson Canyon, showed that benthic macrofauna communities are generally more diverse and have greater abundance at the head of the canyon than in nearby slope areas. Similar results were reported for northern MAB canyon megafaunal and epifaunal populations (Hecker and Blechschmidt 1979) and macrofauna from Scripps and La Jolla canyons in the northeast Pacific (Vetter and Dayton 1998), thus demonstrating how canyons can enhance regional (γ) and local (α) biodiversity (Vetter et al. 2010).

This study focused on Baltimore and Norfolk canyons along the MAB (**Figure 2-1**), lying south of Hudson Canyon. These canyons were chosen due to their large size and rugged steep hard substrate habitats, which are prerequisites for vulnerable and sensitive deepsea corals. Previous geological studies have reported these two canyons as inactive in terms of sediment transport and with sediment profiles rich in silt and clay (Keller and Shepard 1978). However, more recent studies on MAB hydrography and geomorphology have shown Baltimore and Norfolk canyons to be unique continental features that are highly dynamic transporters of sediments under specific hydrographic conditions (Forde et al. 1981, Csanady et al. 1988, Csanady and Hamilton 1988, Gardner 1989, Churchill and Cornillon 1991, Obelcz et al. 2014).

Some previous work has occurred for deepsea meiofaunal communities in the western Atlantic, and there have been no previous canyon-specific studies in the mid-Atlantic region. Meiofaunal studies have been conducted to both the north and south of Baltimore Canyon, including offshore Martha's Vineyard, Massachusetts (Wigley and McIntyre 1964), the Nova Scotian Rise (Thistle et al.

1985, Aller and Aller 1986), offshore Cape Hatteras, North Carolina (Aller and Aller 2002, Coull et al. 1977, Tietjen 1971), and at Blake Ridge, North Carolina (Robinson et al. 2004). Although some studies sampled single deep locations (Thistle et al. 1985, Aller and Aller 1986, Robinson et al. 2004), those conducted offshore Martha's Vineyard (Wigley and McIntyre 1964) and Cape Hatteras (Aller and Aller 2002, Coull et al. 1977, Tietjen 1971) sampled across a depth gradient (40 to 567 m), providing some insight into the effect of depth on meiofaunal communities. In both areas, meiofaunal abundance and biomass generally decreased with increasing depth, corresponding with an increase in mud content (Wigley and McIntyre 1964, Aller and Aller 2002, Coull et al. 1977, Tietjen 1971). Because no previous canyon work exists near our study site, meiofaunal community comparisons are limited to previous work conducted in the western Iberian Margin (Garcia et al. 2007, Bianchelli et al. 2010, Ingels et al. 2011a) and Whittard Canyon (Ingels et al. 2011b). In all the studies, canyon meiofaunal communities differed from adjacent slope habitats; however, differences in density and diversity varied among canyons.

9.1.2 Chemosynthetic Habitats

In addition to soft sediment and hard substrate habitats, submarine canyons on the western Atlantic margin are located near areas of hydrocarbon seepage (cold seeps) from the seafloor, giving rise to chemosynthetic communities. Although originally thought to be unusual on the western U.S. Atlantic margin, increasing numbers of seep areas have been documented since 2011 (**Chapter 1**, Skarke et al. 2014). Prior to 2011, only two chemosynthetic seep areas were known from this region, the Blake Ridge Diapir (Paull et al. 1995, Van Dover et al. 2003) and the Cape Fear Diapir (Brothers et al. 2013), both in deep water (2,100 to 2,600 m) off South Carolina. During this study, two recently discovered shallower chemosynthetic seeps were examined near Baltimore Canyon (366 to 402 m) and Norfolk Canyon (1,457 to 1,602 m).

Cold seeps occur worldwide where methane is forced upward through the sediment by pressure gradients (Levin 2005). Anaerobic oxidation of methane and sulfate reduction results in the formation of carbonates and often high concentrations of hydrogen sulfide in sediments, which is toxic to most fauna. The flow of seep products through sediments results in recognizable biogenic habitats, including mussel and clam beds, microbial mats, tube worm aggregations (Bernardino et al. 2012); some fauna depend on chemoautotrophic endosymbiotic bacteria for nutrition (Kochevar et al. 1992). In addition, the chemosynthetic organisms (e.g., mussels, tubeworms, clams) act as ecosystem engineers (Jones et al. 1996) by creating three-dimensional habitat for diverse communities (Van Dover and Trask 2000, Bergquist et al. 2003, Ross et al. 2015).

Sediment biota associated with seep communities, including microbial mats and clam beds, have been studied in many locations worldwide (Levin 2005); however, sediments associated with mussel habitats have only been examined at a few locations, including the Blake Ridge Diapir (Robinson et al. 2004) and the Gulf of Guinea (Menot et al. 2010). Densities of macrofauna in seep sediments are commonly higher than in background nonseep sediments, while density differences among seep habitat types have been variable (Bernardino et al. 2012). At the Blake Ridge Diapir, sediment communities adjacent to mussels contained higher macrofaunal densities than microbial mat sediments, although macrofaunal densities were low for all sampled habitats (0 to 6,400 individuals m^{-2}; Robinson et al. 2004).

Infaunal community composition and diversity associated with different seep habitats are also known to be distinct (Levin 2005, Menot et al. 2010, Bernardino et al. 2012), both from one another and from background nonseep sediments. Microbial mat habitats often exhibit low diversity and high dominance of a few tolerant taxa compared with other seep and nonseep habitats due to high sediment sulfide concentrations (Sahling et al. 2002, Levin et al. 2003). However, low sulfide concentrations in clam beds on the California slope were found to increase macrofaunal diversity by supporting populations of both ambient and sulfophilic taxa (Levin et al. 2003). At Blake Ridge,

mussel-associated habitats had higher diversity than microbial mats and nonseep sediments (Robinson et al. 2004). Dorvilleid polychaetes, often particularly abundant in microbial mat habitats (Levin et al. 2003, Sahling et al. 2002, Robinson et al. 2004), are common in seep habitats (Levin 2005). Other characteristic seep fauna include the polychaete families Siboglinidae, Capitellidae, and Ampharetidae as well as oligochaetes and thyasirid bivalves (Dando et al. 1991, Levin et al. 2000, 2003). At Blake Ridge, mussel sediment communities were more similar to nonseep communities than to microbial mat communities, suggesting that mussels help maintain low concentrations of methane and sulfide, facilitating communities more similar to nonseep sediments (Robinson et al. 2004). Communities at seep clam beds in the Gulf of Guinea were similar to mussel sediments (Menot et al. 2010), suggesting similar community function and sediment geochemical parameters of sediments occupied by chemosynthetic bivalves. The occurrence of endemic species in seep habitats may be a function of depth (Levin 2005), with many species occupying seep sediments comprising the regionally available taxa pool (Levin et al. 2005). In addition, depth patterns have been observed among seep sites, with upper bathyal depths (200 to 1,500 m) different from deeper depths (Bernardino et al. 2012). Given the 1,000 m depth difference between the Baltimore Canyon and Norfolk Canyon seep sites, we expect to find community assemblage differences between sites as well as among microbial mat, mussel, and nonseep sediments.

9.1.3 Hard Substrate Habitats

In addition to the soft sediment habitats that dominate canyon environments, hard substrates often occur in multiple forms in the canyon environment, including along canyon walls, as boulders previously deposited by turbidity flows or glaciers, and along the upper rims of the canyon. Hard substrates are characterized by exposed rock or consolidated mud and steep slopes with elevated current conditions that minimize sedimentation. The presence of hard substrates increases the substrate heterogeneity present in canyon systems. Rich and diverse coral and invertebrate communities often colonize hard substrates (Huvenne et al. 2011, Brooke et al.; **Chapter 8**), sustained by suitable current conditions for food delivery, with soft sediment habitats at their base. The sedimentary areas adjacent to hard substrates may act as deposition zones and contain high amounts of organic matter that fall down the steep slopes (McClain and Barry 2010). Sediment communities adjacent to hard substrate coral habitats are known to differ from background soft sediments in the deep sea (Demopoulos et al. 2014), and we investigated this relationship within canyon systems.

Habitat heterogeneity at multiple spatial scales within a system is a major factor in structuring faunal assemblages and promoting higher diversity (McClain and Barry 2010). Hard substrates within submarine canyons have been studied primarily in the context of the presence of deepsea corals (also called cold-water corals) (Mortensen et al. 2005, Orejas et al. 2009, Baker et al. 2012) due to their status as critical and sensitive species and habitats. However, little research has been conducted on the adjacent sediment macrofaunal communities (McClain and Barry 2010). In Monterey submarine canyons, McClain and Barry (2010) found variable relationships of macrofaunal density, diversity, and species richness in relation to proximity to cliff faces, while all locations exhibited high species turnover at distances <30 m from cliff faces. In addition, sediments adjacent to cliff faces had increased mass flux of carbon estimated from sediment traps, with higher sediment grain size and lower percent organic carbon compared with sediments located farther from the cliff face (McClain and Barry 2010). Further evidence of increased megafaunal activity (e.g., bioturbation) in near-cliff sediments suggests that sediment macrofauna residing adjacent to hard substrates are experiencing high levels of disturbance, resulting in distinct communities (McClain and Barry 2010) that increase the overall biodiversity of submarine canyon systems.

9.1.4 Objectives

The primary goal of this study was to explore and assess benthic infaunal communities occurring in and adjacent to submarine canyons in the MAB, specifically targeting Baltimore and Norfolk canyons, and their relationships to environmental drivers, such as biogeochemical, sedimentological, and depth gradients. Our study examined habitats within the canyon axis, adjacent slope, canyon hard substrates, and nearby seeps. The following test objectives were addressed:

1. Canyon macrofaunal and meiofaunal community assemblages, including density, diversity, and community composition, differ from those found on adjacent slopes at similar depths.
2. Canyon axis and slope macro- and meio-infaunal communities are structured by environmental gradients, including depth, sediment transport, and food availability.
3. Sediment macrofaunal communities differ among seep (i.e., mussel beds and microbial mats) and nonseep (background soft sediment) habitats.
4. Macrofaunal community assemblages associated with hard substrate habitats, including density, diversity, and community composition, exhibit depth-related patterns within a canyon and differ from nonhard substrate, canyon sediment communities.

9.2 METHODS

9.2.1 Field Sampling

9.2.1.1 Box Core Samples

Sediment samples were collected during the August 2012 sampling cruise and the May 2013 sampling cruise (**Tables 9-1** and **9-2** sampling summary). Samples were collected along two transects tracing the thalweg of both canyons and the adjacent slopes. Transects covered similar depth ranges from the continental shelf at approximately 200 m to the continental rise at approximately 1,200 m water depth (**Figure 9-1** and **9-2**). In each canyon and adjacent slope four major sampling stations were chosen that formed a canyon and adjacent slope transect, respectively. Each station comprised five replicate box core samples at Baltimore sites (**Figure 9-1**) and four replicates at Norfolk sites (**Figure 9-2**). Additional box core samples were collected at intermediate depths between the main stations in Baltimore Canyon (**Figure 9-1**).

Sediment cores were collected using a box corer designed by the Royal Netherlands Institute for Sea Research (NIOZ) with a core diameter of 30 cm (0.07 m^2) and height of 55 cm. The box corer was equipped with a trip valve to prevent flushing of the sample during ascent (**Figure 9-3**). Samples were quality controlled once on board by assessing the level of sediment disturbance on the sediment surface to ensure the vertical distribution of sediment layers associated infauna were intact. Samples that showed signs of leakage, over penetration, or sediment slumping were discarded. Overlying water was drained over a 300 μm sieve to retain suspended fauna and was added to the bulk sample during washing. Box core samples were first subcored with push cores (6.35-cm diameter polycarbonate tubes) and monocores (6-cm diameter polycarbonate tubes) for additional faunal, sediment grain size, and geochemical analyses. The subcores were inserted 15 cm into the box core sediment, extracted, and processed. The remaining sediment, down to a depth of 15 cm, defined as "bulk," was removed from the box corer for the bulk macrofaunal diversity and community analysis. The material was placed in a 20-L bucket and rehydrated with filtered surface seawater. The sediment was slowly turned over by hand in the bucket and then poured in stages over a 20-cm sieve of 300 μm. The sample was washed through the sieve using a gentle stream of water, taking care not to damage the infauna.

Washed material was then placed into sample bottles and covered with seawater. Bulk box core samples were fixed in 10% buffered formalin, sealed, recorded, and stored for transportation to the Bangor University Laboratory. A total of 57 replicate samples were processed: 24 box core samples from Baltimore Canyon (**Table 9-1**) and 33 from Norfolk Canyon (**Table 9-2**).

Table 9-1. Geographic coordinates, station locations, and analyses of sediment samples collected during the 2012 sampling cruise in Baltimore Canyon.

Station	Date	Latitude (N)	Longitude (W)	Depth (m)	Analysis	Location Designation
NF-2012-019	5	38°14′35.59"	73°50′36.96″	189	BC, MF, ME, SC	Canyon 180 m
NF-2012-021	19 Aug 2012	38°14′35.41″	73°50′36.74″	189	MF, ME	Canyon 180 m
NF-2012-028	20 Aug 2012	38°14′34.15″	73°50′36.60″	191	BC, MF, ME	Canyon 180 m
NF-2012-029	20 Aug 2012	38°14′34.19″	73°50′36.67″	191	BC, MF	Canyon 180 m
NF-2012-032	21 Aug 2012	38°09′58.25″	73°51′00.36″	563	BC, MF, ME, SC	Canyon 550 m
NF-2012-033	21 Aug 2012	38°09′58.25″	73°51′00.25″	564	MF, ME	Canyon 550 m
NF-2012-034	21 Aug 2012	38°09′58.39″	73°51′00.00″	565	BC, MF, ME	Canyon 550 m
NF-2012-035	21 Aug 2012	38°09′58.57″	73°50′59.93″	567	BC, MF	Canyon 550 m
NF-2012-045	22 Aug 2012	38°07′01.20″	73°50′08.88″	840	BC, MF, ME, SC	Canyon 900 m
NF-2012-047	22 Aug 2012	38°07′02.64″	73°50′05.28″	848	BC, MF, ME	Canyon 900 m
NF-2012-049	23 Aug 2012	38°07′03.00″	73°50′04.20″	844	BC, MF, ME	Canyon 900 m
NF-2012-050	23 Aug 2012	38°07′03.07″	73°50′04.31″	844	MF	Canyon 900 m
NF-2012-055	23 Aug 2012	38°04′20.64″	73°46′23.52″	1,179	BC, MF, ME, SC	Canyon 1,180 m
NF-2012-056	23 Aug 2012	38°04′20.64″	73°46′23.52″	1,179	BC, MF, ME	Canyon 1,180 m
NF-2012-062	24 Aug 2012	38°04′19.56″	73°46′23.88″	1,180	BC, MF, ME	Canyon 1,180 m
NF-2012-063	24 Aug 2012	38°04′19.81″	73°46′24.13″	1,180	MF	Canyon 1,180 m
NF-2012-064	24 Aug 2012	38°03′45.00″	73°51′56.16″	168	BC, MF, ME, SC	Slope 180 m
NF-2012-066	25 Aug 2012	38°03′45.00″	73°51′56.16″	170	BC, MF, ME	Slope 180 m
NF-2012-067	25 Aug 2012	38°03′45.00″	73°51′56.16″	168	BC, MF, ME	Slope 180 m
NF-2012-069	25 Aug 2012	38°03′45.29″	73°51′56.23″	169	MF	Slope 180 m
NF-2012-071	25 Aug 2012	38°02′36.53″	73°48′12.38″	513	MF, ME, SC	Slope 550 m
NF-2012-072	25 Aug 2012	38°02′36.60″	73°48′12.24″	514	BC, MF, ME	Slope 550 m
NF-2012-076	25 Aug 2012	38°02′36.60″	73°48′12.24″	510	BC, MF, ME	Slope 550 m
NF-2012-088	26 Aug 2012	38°02′36.96″	73°48′11.52″	502	BC, MF	Slope 550 m
NF-2012-082	26 Aug 2012	38°00′49.68″	73°45′12.60″	990	BC, MF, ME, SC	Slope 900 m
NF-2012-085	26 Aug 2012	38°00′50.04″	73°45′12.24″	991	BC, MF, ME	Slope 900 m
NF-2012-087	26 Aug 2012	38°00′50.04″	73°45′12.24″	991	BC, MF, ME	Slope 900 m
NF-2012-089	26 Aug 2012	38°00′40.39″	73°45′15.59″	1,030	MF	Slope 900 m
NF-2012-090	27 Aug 2012	37°58′38.64″	73°40′09.84″	1,185	BC, MF, ME, SC	Slope 1,180 m
NF-2012-092	27 Aug 2012	37°58′38.64″	73°40′09.84″	1,187	BC, MF, ME	Slope 1,180 m
NF-2012-093	27 Aug 2012	37°58′38.64″	73°40′09.84″	1,186	BC, MF, ME	Slope 1,180 m

Table 9-1. (Continued).

Station	Date	Latitude (N)	Longitude (W)	Depth (m)	Analysis	Location Designation
NF-2012-095	27 Aug 2012	37°58′38.71″	73°40′09.84″	1,186	MF	Slope 1,180 m
NF-2012-106*	28 Aug 2012	38°13′29.21″	73°50′40.20″	280	MF	Canyon 280 m
NF-2012-108*	28 Aug 2012	38°12′10.73″	73°50′57.91″	360	MF	Canyon 360 m
NF-2012-110*	29 Aug 2012	38°10′55.20″	73°51′55.87″	518	MF	Canyon 518 m
NF-2012-112*	29 Aug. 2012	38°08′53.16″	73°50′44.95″	652	MF	Canyon 652 m
NF-2012-117*	29 Aug 2012	38°07′44.47″	73°50′28.32″	754	MF	Canyon 754 m
NF-2012-118*	29 Aug 2012	38°04′20.75″	73°52′46.56″	139	MF	Slope 139 m

* Not included in main analysis.
BC = bulk box core processed for macrofauna; MF = subsampled push core processed for macrofaunal analysis; ME = subsampled push core processed for meiofaunal analysis; SC = core processed for sediment geochemistry.

Table 9-2. Geographic coordinates, station locations, and analyses of sediment samples collected during the 2012 and 2013 sampling cruises in Norfolk Canyon.

Station	Date	Latitude (N)	Longitude (W)	Depth (m)	Analysis	Location Designation
NF-2012-159	19 Sept 2012	37°05′39.73″	74°44′50.03″	196	BC, MF	Canyon 190 m
RB-2013-046	11 May 2013	37°05′41.10″	74°44′47.69″	195	BC, MF, SC	Canyon 190 m
RB-2013-047	11 May 2013	37°05′41.21″	74°44′47.65″	195	BC, MF	Canyon 190 m
RB-2013-048	11 May 2013	37°05′41.21″	74°44′47.65″	195	BC, MF	Canyon 190 m
NF-2012-162	19 Sept. 2012	37°04′33.53″	74°39′40.32″	573	BC, MF	Canyon 550 m
RB-2013-043	11 May 2013	37°04′33.49″	74°39′38.27″	559	BC, MF, SC	Canyon 550 m
RB-2013-044	11 May 2013	37°04′33.49″	74°39′38.09″	557	BC, MF	Canyon 550 m
RB-2013-045	11 May 2013	37°04′33.42″	74°39′38.09″	558	BC, MF	Canyon 550 m
NF-2012-164	20 Sept 2012	37°02′34.37″	74°37′45.23″	819	BC, MF	Canyon 800 m
RB-2013-040	10 May 2013	37°02′33.83″	74°37′45.01″	805	BC, MF, SC	Canyon 800 m
RB-2013-041	10 May 2013	37°02′33.90″	74°37′45.12″	803	BC, MF	Canyon 800 m
RB-2013-042	10 May 2013	37°02′34.08″	74°37′45.30″	804	BC, MF	Canyon 800 m
NF-2012-192	28 Sept 2012	37°02′19.32″	74°34′47.57″	1,133	BC, MF	Canyon 1,110 m
RB-2013-038	10 May 2013	37°02′19.07″	74°34′47.50″	1,110	BC, MF, SC	Canyon 1,110 m
RB-2013-039	10 May 2013	37°02′19.25″	74°34′47.82″	1,110	BC, MF	Canyon 1,110 m
RB-2013-077	15 May 2013	37°02′19.50″	74°34′46.70″	1,108	BC, MF	Canyon 1,110 m
NF-2012-181	24 Sep. 2012	37°01′24.24″	74°38′42.79″	188	BC, MF	Slope 190 m
RB-2013-049	11 May 2013	37°01′23.05″	74°38′44.77″	187	BC, MF, SC	Slope 190 m
RB-2013-050	11 May 2013	37°01′28.02″	74°38′50.24″	187	BC, MF	Slope 190 m

Table 9-2. (Continued).

Station	Date	Latitude (N)	Longitude (W)	Depth (m)	Analysis	Location Designation
RB-2013-051	11 May 2013	37°01′26.94″	74°38′45.38″	187	BC, MF	Slope 190 m
NF-2012-183	24 Sept 2012	37°00′56.23″	74°34′43.00″	550	BC, MF	Slope 550 m
RB-2013-054	12 May 2013	37°00′56.88″	74°34′41.52″	549	BC, MF, SC	Slope 550 m
RB-2013-055	12 May 2013	37°00′56.88″	74°34′41.34″	549	BC, MF	Slope 550 m
RB-2013-056	12 May 2013	37°00′56.88″	74°34′41.41″	548	BC	Slope 550 m
RB-2013-059	13 May 2013	37°00′32.51″	74°33′53.21″	790	BC	Slope 800 m
RB-2013-060	12 May 2013	37°00′32.58″	74°33′52.99″	790	BC, MF	Slope 800 m
RB-2013-069	14 May 2013	37°00′32.47″	74°33′53.86″	804	BC, MF, SC	Slope 800 m
RB-2013-070	14 May 2013	37°00′32.22″	74°33′53.86″	805	BC, MF	Slope 800 m
RB-2013-071	14 May 2013	37°00′20.77″	74°32′01.43″	1,118	BC, MF	Slope 1,110 m
RB-2013-073	15 May 2013	37°00′20.77″	74°32′01.32″	1,105	BC, MF, SC	Slope 1,110 m
RB-2013-075	15 May 2013	37°00′21.17″	74°32′01.14″	1,103	BC, MF	Slope 1,110 m
RB-2013-076	15 May 2013	37°00′20.88″	74°32′00.89″	1,100	BC, MF	Slope 1,110 m

BC = bulk box core processed for macrofauna; MF = subsampled push core processed for macrofaunal analysis; SC = core processed for sediment geochemistry.

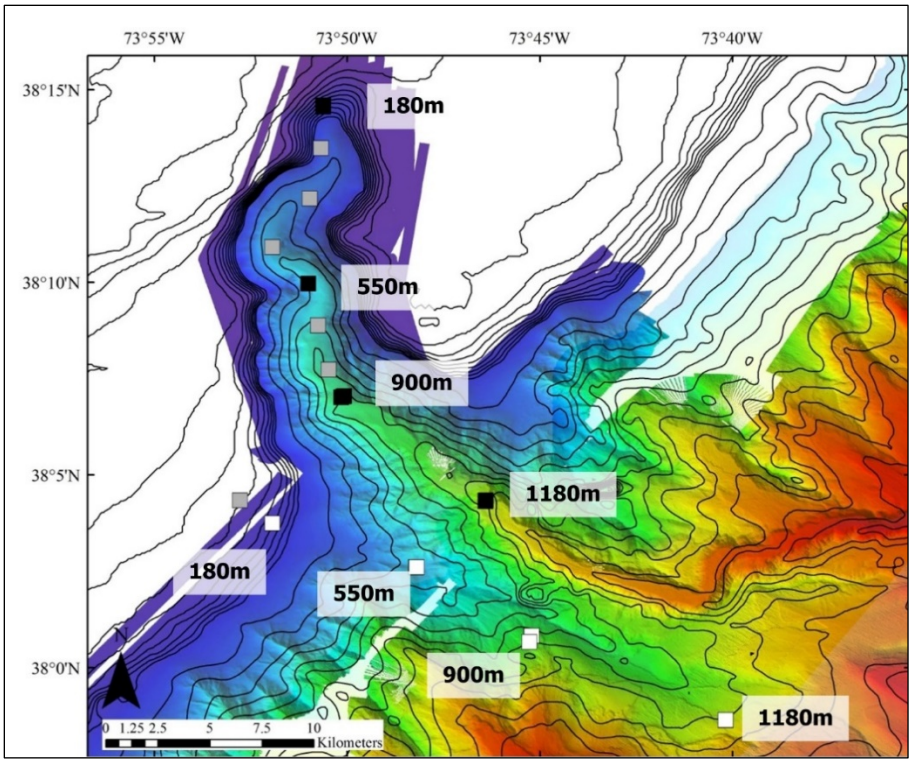

Figure 9-1. Box core sampling locations in Baltimore Canyon with depths indicated for locations included in the main analysis. ■ = Canyon axis transect; ■ = other depths sampled but not included in main analysis; □ = slope transect. Base map data from NOAA.

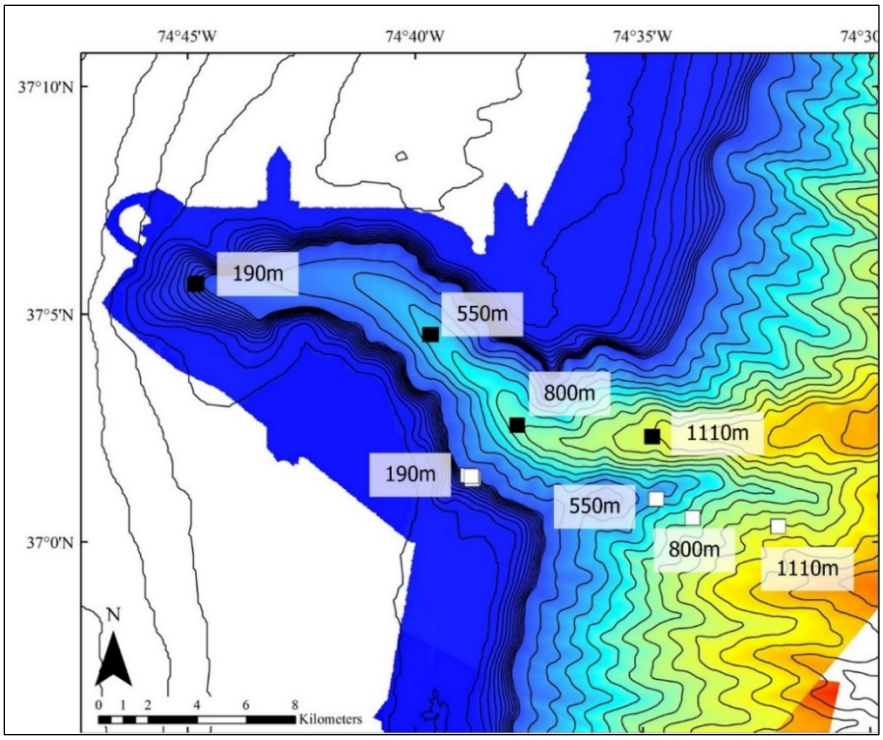

Figure 9-2. Box core sampling locations in Norfolk Canyon with depths indicated for locations included in the main analysis. ■ = Canyon axis transect; □ = slope transect. Base map data from NOAA.

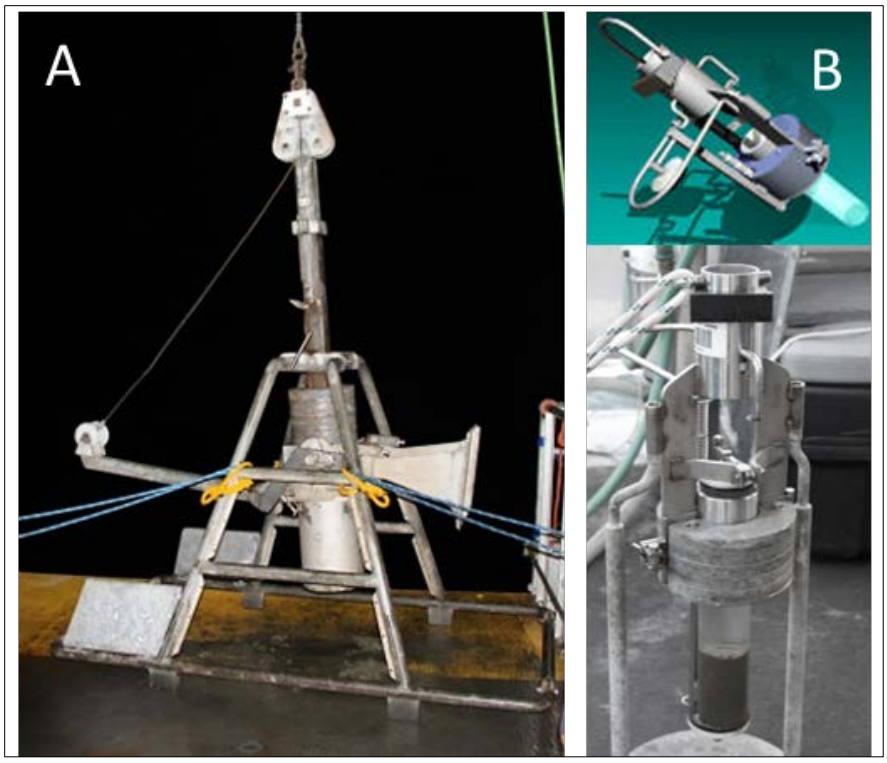

Figure 9-3. Box corer with circular 30-cm core tube and trip valve inside (not visible) (a) and monocorer, which is single tube version of the multicorer (b). After penetration and pulling the corer from the sediment, the tube is closed by an arm, which is released by the impact on the seafloor. The box corer was designed by the Royal Netherlands Institute for Sea Research (NIOZ).

9.2.1.2 Push Core Samples

Push core samples collected during the study were extruded and sectioned into 0 to 2, 2 to 5, and 5 to 10 cm slices for either faunal or sediment geochemistry analysis. Sediment sections used for infaunal community assessment were preserved whole in a 10% buffered formalin solution until they were returned to the laboratory. Sediment geochemistry core sections were frozen until returned to the laboratory.

9.2.1.3 Chemosynthetic Habitats

Soft sediments in microbial mats, adjacent to mussel beds, and corresponding background soft sediments were sampled at the Baltimore Canyon seep (BCS) site in 2012 using the *Kraken 2* remotely operated vehicle (ROV) and in 2013 using the *Jason II* ROV (**Figure 9-4**). Soft sediments located within and adjacent to chemosynthetic habitats were sampled at the Norfolk Canyon seep (NCS) site in 2013 using the *Jason II* ROV (**Table 9-3**, **Figure 9-5**). Additional background soft sediments were collected at comparable depths along the main axis of Norfolk Canyon using a NIOZ box corer subsampled with push corers (**Table 9-3**).

Table 9-3. Station location for chemosynthetic habitat cores collected near Baltimore and Norfolk canyons during the 2012 and 2013 sampling cruises.

Canyon	Station	Date	Core	Habitat	Depth (m)	Latitude (N)	Longitude (W)	Analysis
Baltimore	ROV-2013-RB-689	16 May 2013	RB13-D689-PC01	Microbial mat	366	38°02′52.76″	73°49′44.94″	MF
Baltimore	ROV-2013-RB-689	16 May 2013	RB13-D689-PC02	Microbial mat	366	38°02′52.76″	73°49′44.94″	MF
Baltimore	ROV-2013-RB-689	16 May 2013	RB13-D689-PC03	Mussel	372	38°02′53.52″	73°49′31.22″	MF
Baltimore	ROV-2013-RB-689	16 May 2013	RB13-D689-PC04	Mussel	372	38°02′53.52″	73°49′31.22″	MF
Baltimore	ROV-2013-RB-689	16 May 2013	RB13-D689-PC05	Microbial mat	402	38°02′59.82″	73°49′18.88″	MF
Baltimore	ROV-2013-RB-689	16 May 2013	RB13-D689-PC07	Mussel	400	38°02′54.53″	73°49′18.95″	MF
Baltimore	ROV-2013-RB-689	16 May 2013	RB13-D689-PC08	Mussel	400	38°02′54.53″	73°49′18.95″	MF
Baltimore	ROV-2012-NF-11	30 Aug 2012	NF12-D11-1	Background	446	38°05′30.16″	73°48′18.68″	MF
Baltimore	ROV-2012-NF-11	30 Aug 2012	NF12-D11-2	Background	446	38°05′30.16″	73°48′18.68″	MF
Baltimore	ROV-2012-NF-11	30 Aug 2012	NF12-D11-3	Background	446	38°05′30.16″	73°48′18.68″	MF
Baltimore	ROV-2012-NF-08	27 Aug 2012	NF12-D08-1	Microbial mat	412	38°02′37.28″	73°49′32.45″	MF
Baltimore	ROV-2012-NF-08	27 Aug 2012	NF12-D08-2	Background	412	38°02′37.28″	73°49′32.45″	MF
Norfolk	ROV-2013-RB-682	8 May 2013	RB13-D682-PC03	Microbial mat	1,602	36°51′57.02″	74°29′26.99″	SC
Norfolk	ROV-2013-RB-682	8 May 2013	RB13-D682-PC02	Microbial mat	1,602	36°51′57.02″	74°29′26.99″	MF
Norfolk	ROV-2013-RB-682	8 May 2013	RB13-D682-PC06	Microbial mat	1,590	36°51′59.90″	74°29′24.94″	SC
Norfolk	ROV-2013-RB-682	8 May 2013	RB13-D682-PC09	Microbial mat	1,590	36°51′59.90″	74°29′24.94″	MF
Norfolk	ROV-2013-RB-683	9 May 2013	RB13-D683-PC01	Microbial mat	1,487	36°52′17.04″	74°28′39.29″	MF
Norfolk	ROV-2013-RB-683	9 May 2013	RB13-D683-PC02	Microbial mat	1,487	36°52′17.04″	74°28′39.25″	SC
Norfolk	ROV-2013-RB-683	9 May 2013	RB13-D683-PC08	Microbial mat	1,457	36°52′15.13″	74°28′22.44″	SC
Norfolk	ROV-2013-RB-683	9 May 2013	RB13-D683-PC09	Microbial mat	1,457	36°52′15.31″	74°28′22.48″	MF
Norfolk	ROV-2013-RB-683	9 May 2013	RB13-D683-PC07	Microbial mat	1,467	36°52′16.43″	74°28′26.26″	MF
Norfolk	ROV-2013-RB-682	8 May 2013	RB13-D682-PC08	Mussel	1,576	36°52′04.30″	74°29′19.36″	MF
Norfolk	ROV-2013-RB-682	8 May 2013	RB13-D682-PC05	Mussel	1,576	36°52′04.30″	74°29′19.36″	SC
Norfolk	ROV-2013-RB-682	8 May 2013	RB13-D682-PC07	Mussel	1,565	36°52′05.77″	74°29′17.59″	MF
Norfolk	ROV-2013-RB-682	8 May 2013	RB13-D682-PC04	Mussel	1,585	36°52′01.60″	74°29′21.70″	SC
Norfolk	ROV-2013-RB-682	8 May 2013	RB13-D682-PC01	Mussel	1,585	36°52′01.60″	74°29′17.59″	MF
Norfolk	ROV-2013-RB-683	9 May 2013	RB13-D683-PC05	Mussel	1,482	36°52′17.00″	74°28′34.79″	MF
Norfolk	ROV-2013-RB-683	9 May 2013	RB13-D683-PC04	Mussel	1,482	36°52′17.08″	74°28′34.82″	SC
Norfolk	ROV-2013-RB-683	9 May 2013	RB13-D683-PC03	Mussel	1,487	36°52′18.05″	74°28′41.27″	MF
Norfolk	RB-2013-078	15 May 2013	RB13-078-PC06	Background	1,622	37°02′00.49″	74°27′01.40″	MF
Norfolk	RB-2013-082	18 May 2013	RB13-082-PC06	Background	1,619	37°02′00.35″	74°27′01.15″	MF
Norfolk	RB-2013-083	18 May 2013	RB13-083-PC02	Background	1,620	37°02′00.35″	74°27′01.08″	MF
Norfolk	RB-2013-083	18 May 2013	RB13-083-PC01	Background	1,620	37°02′00.35″	74°27′01.08″	SC

MF = core processed for faunal analysis; SC = core processed for sediment geochemistry.

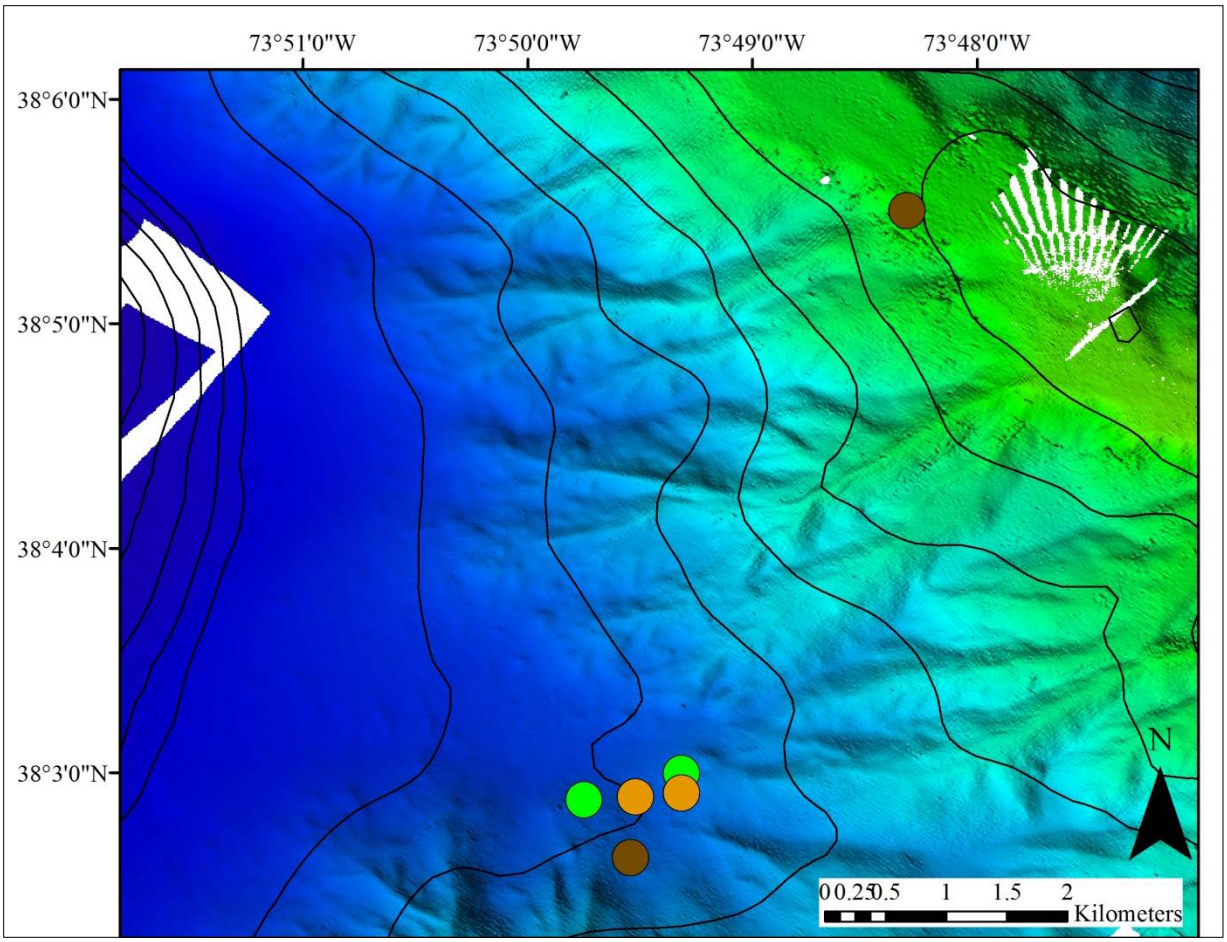

Figure 9-4. Sampling locations of chemosynthetic seep and background habitats at Baltimore Canyon. ● = Microbial mats; ● = mussel beds; ● = background soft sediments. Base map data from NOAA.

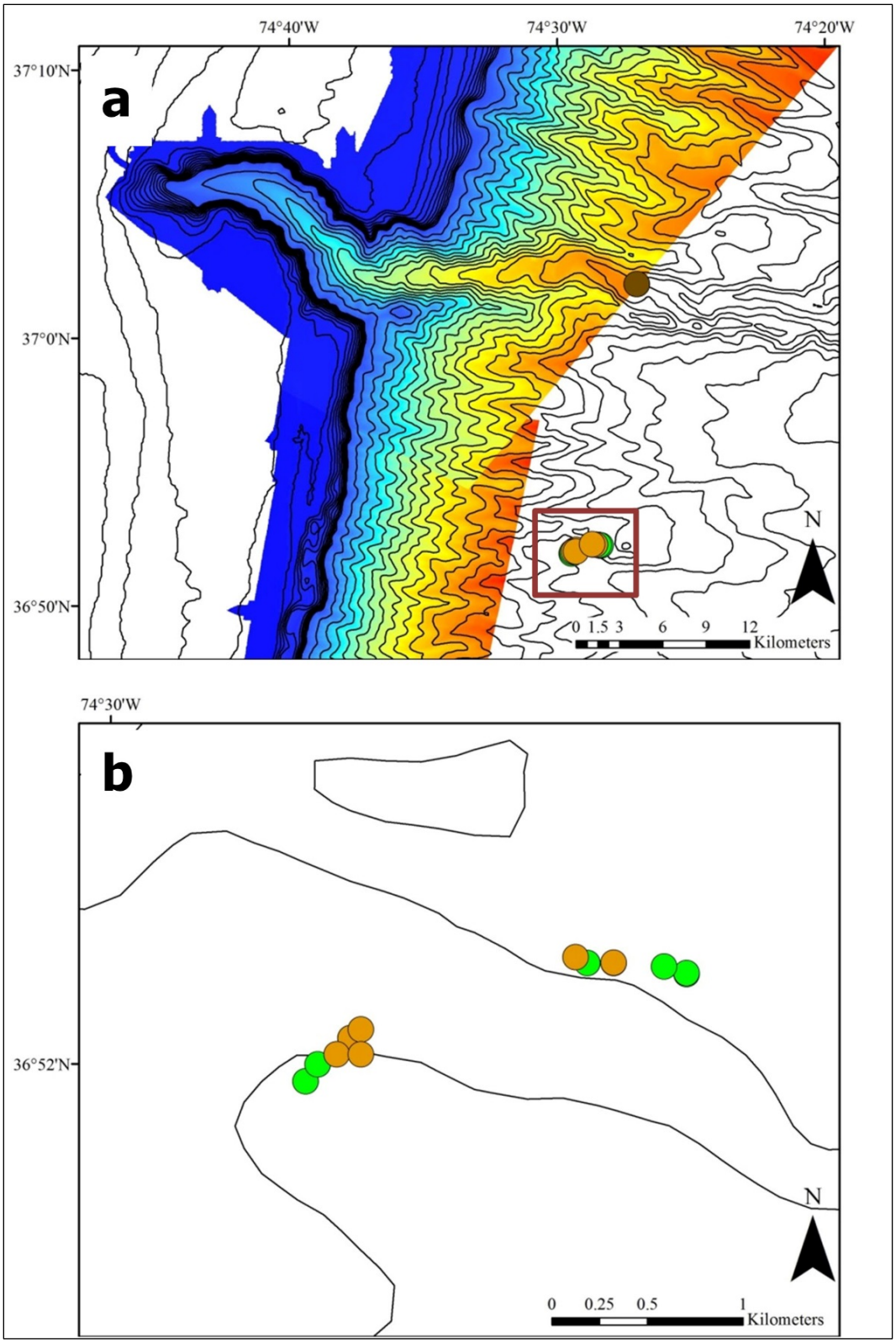

Figure 9-5. a) Sampling locations of seep and background habitats at Norfolk Canyon, b) detailed map of seep habitat sampling at Norfolk Canyon seep. ● = Microbial mats; ● = mussel beds; ● = background soft sediments. Base map data from NOAA.

9.2.1.4 Hard Substrate Habitats

Soft sediments near hard substrate habitats were sampled from Norfolk Canyon during the 2013 sampling cruise using the ROV *Jason II* (**Figure 9-6**). A total of 24 push cores were collected adjacent (~1 m) to hard substrate habitats (**Table 9-4**) at depths ranging from 400 to 1,342 m. Thirteen cores were processed for macrofauna and 11 cores were processed for sediment geochemistry (**Section 9.2.1.2** and **Chapter 6**).

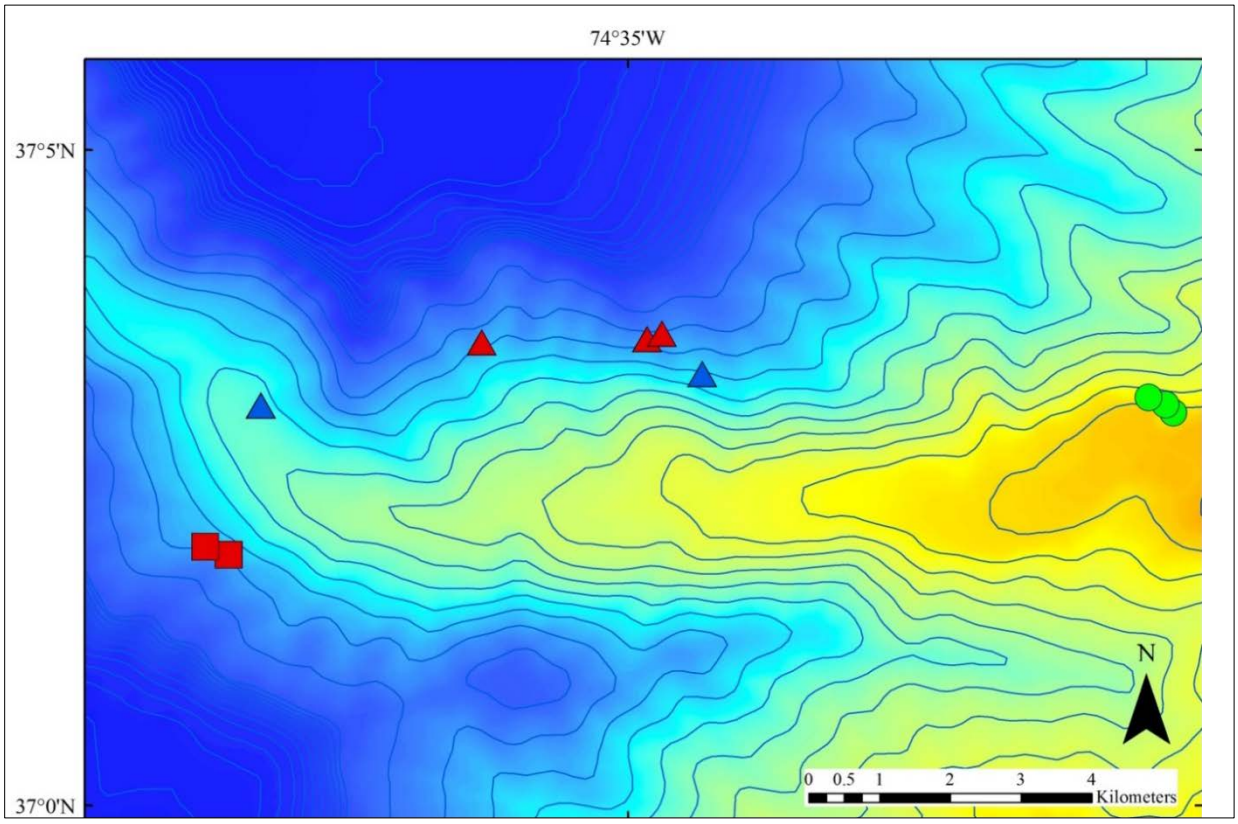

Figure 9-6. Sampling locations of sediments adjacent to hard substrates in Norfolk Canyon. ■ = 400−500 m South; ▲= 400−500 m North; ▲= 500−700 m North; ● = 1,200−1,400 m North. Base map data from NOAA.

Table 9-4. Station locations for push core samples collected from hard bottom habitat in Norfolk Canyon during the 2013 sampling cruise.

Station	Date	Core	Depth (m)	Latitude (N)	Longitude (W)	Analysis
ROV-2013-RB-679	2 May 2013	RB13-D679-PC02	688	37°03'03.20"	74°37′47.96"	MF
ROV-2013-RB-679	2 May 2013	RB13-D679-PC03	688	37°03'03.13"	74°37'47.91"	MF
ROV-2013-RB-679	2 May 2013	RB13-D679-PC09	688	37°03'03.21"	74°37'47.96"	SC
ROV-2013-RB-680	5 May 2013	RB13-D680-PC02	443	37°03'33.42"	74°34'51.36"	SC
ROV-2013-RB-680	5 May 2013	RB13-D680-PC07	443	37°03'33.49"	74°34'51.25"	MF
ROV-2013-RB-680	5 May 2013	RB13-D680-PC09	585	37°03'17.58"	74°34'25.95"	SC
ROV-2013-RB-680	5 May 2013	RB13-D680-PC03	585	37°03'17.56"	74°34'25.98"	MF
ROV-2013-RB-680	5 May 2013	RB13-D680-PC06	585	37°03'17.58"	74°34'25.95"	MF
ROV-2013-RB-685	11 May 2013	RB13-D685-PC02	1,342	37°03'00.00"	74°30'50.40"	MF
ROV-2013-RB-685	11 May 2013	RB13-D685-PC03	1,342	37°02'59.00"	74°30'50.04"	SC

Table 9-4. (Continued).

Station	Date	Core	Depth (m)	Latitude (N)	Longitude (W)	Analysis
ROV-2013-RB-685	11 May 2013	RB13-D685-PC05	1,273	37°03'02.89"	74°30'53.45"	MF
ROV-2013-RB-685	11 May 2013	RB13-D685-PC06	1,273	37°03'03.60"	74°30'54.00"	SC
ROV-2013-RB-685	11 May 2013	RB13-D685-PC08	1,252	37°03'05.80"	74°31'02.71"	MF
ROV-2013-RB-685	11 May 2013	RB13-D685-PC09	1,252	37°03'05.76"	74°31'02.59"	SC
ROV-2013-RB-686	13 May 2013	RB13-D686-PC01	482	37°03'32.39"	74°36'07.19"	SC
ROV-2013-RB-686	13 May 2013	RB13-D686-PC02	482	37°03'31.05"	74°36'06.31"	MF
ROV-2013-RB-687	14 May 2013	RB13-D687-PC02	400	37°03'37.39"	74°34'43.36"	SC
ROV-2013-RB-687	14 May 2013	RB13-D687-PC01	400	37°03'36.00"	74°34'44.41"	MF
ROV-2013-RB-691	18 May 2013	RB13-D691-PC01	451	37°01'53.79"	74°38'02.28"	SC
ROV-2013-RB-691	18 May 2013	RB13-D691-PC02	451	37°01'53.78"	74°38'02.28"	MF
ROV-2013-RB-691	18 May 2013	RB13-D691-PC03	419	37°01'57.75"	74°38'13.26"	SC
ROV-2013-RB-691	18 May 2013	RB13-D691-PC06	419	37°01'57.76"	74°38'13.26"	MF
ROV-2013-RB-691	18 May 2013	RB13-D691-PC04	450	37°01'53.83"	74°38'03.02"	SC
ROV-2013-RB-691	18 May 2013	RB13-D691-PC05	450	37°01'53.83"	74°38'02.99"	MF

MF = core processed for faunal analysis; SC = core processed for sediment geochemistry.

9.2.2 Laboratory Methods

9.2.2.1 Macrofauna – Box Core Samples

Bulk infaunal samples were shipped to the School of Ocean Sciences at Bangor University, Wales, UK, where they were cataloged and stored. Each sample was stained with rose bengal prior to sieving. Sediment samples were rinsed over 1 mm, 500 µm, and 300 µm sieves using freshwater under a fume hood. Infauna was separated from the sediment, identified to the lowest practical taxonomic level, and enumerated under stereo and compound microscopy. Putative species lists were used for those genera for which little to no literature was available. In some cases, particularly genera of Polychaeta, specimen staining with methylene blue and methyl green histological preparations was used to highlight external features to aid identification. Specimens were stored in 70% industrial methylated spirits. Macrofaunal data from box core samples collected only from Baltimore Canyon were included for analyses.

9.2.2.2 Macrofauna – Push Core Samples

Formalin-preserved sediment fractions were transported to the benthic ecology laboratory at the U.S. Geological Survey Wetland and Aquatic Research Center in Gainesville, Florida. Samples were stained with rose bengal and washed through a 300-µm mesh sieve to retain the macrofauna portion. Macrofauna were sorted with a dissecting microscope and identified to the lowest practical taxonomic level, including family level for polychaetes, oligochaetes, peracarid crustaceans, and mollusks and stored in 70% ethanol. Macrofaunal data from push core samples were used for all analyses of vertical distribution of sediment fauna from both canyons and all analyses in Norfolk Canyon, hard substrate habitats, and seep habitats. Because not all push cores penetrated to 10 cm depth for seep samples, analyses were conducted on only the 0–2 and 2–5 cm fractions.

9.2.2.3 Sediment Geochemistry – Push Core Samples

Frozen preserved sediment fractions were transported to the benthic ecology laboratory at the U.S. Geological Survey. Subsamples of geochemistry cores were analyzed for the stable carbon and nitrogen isotopes, and percent carbon and nitrogen. Sediment samples were homogenized prior to drying and acidified with 1.0 N phosphoric acid before weighing into tin boats. Sediments were analyzed for

stable carbon and nitrogen isotope composition referenced to Vienna PeeDee Belemnite and atmospheric nitrogen gas, respectively. Analyses were conducted at Washington State University using a Costech (Valencia, U.S.) elemental analyzer interfaced with a GV Instruments (Manchester, UK) Isoprime isotope ratio mass spectrometer. Isotope ratios were expressed in standard delta notation, $\delta^{13}C$ and $\delta^{15}N$, as per mil (‰). Grain size analysis was performed on sections of the sediment geochemistry cores using the Folk method (Folk 1968). Sediment geochemistry data from push cores were used for analysis with Baltimore Canyon meiofauna. Sediment geochemical parameters from box core samples processed by NIOZ (**Chapter 6**) were used for macrofaunal comparisons.

9.2.2.4 Meiofauna – Push Core Samples

Meiofaunal communities were assessed from three replicates of the push cores collected and processed for macrofauna from Baltimore Canyon and slope environments. Sediment from the 0- to 2-cm push core fraction was sieved over a 45 μm mesh and extracted using the Ludox centrifugation technique (Burgess 2001). Extracted animals were then sorted with a dissecting microscope and identified to order level or higher. A random subsample of 220 nematodes was collected from each analyzed sample. Extracted nematodes were dehydrated into glycerine and mounted on slides, with approximately 10 nematodes per slide. Nematodes were identified to genera level under a compound microscope with a 100× oil immersion lens. Nematode feeding groups were assigned according to Wieser (1953).

9.2.3 Data Analysis

Abundance of individuals and univariate measures of biodiversity were analyzed using one-way or two-way analysis of variance (ANOVA) followed by post-hoc analysis using Tukey's honestly significant difference (HSD) test for multiple comparisons. All data were tested for normality and heteroscedasticity using Shapiro-Wilk and Levene's tests (Zar 1999) and $\log_e$-transformed when necessary. If transformation did not achieve normality, a nonparametric Kruskal-Wallis test or Student–NewmanKeuls (SNK) test was used on univariate measures. Depth relationships with abundance and diversity measures were tested using Spearman's rank correlation. A significance level of $p < 0.05$ was used in all tests. Univariate statistics were computed with the program R (R Development Core Team 2011). Diversity was examined using the total number of taxa present in each core (Sp), Margalef's species richness index (d), the Shannon-Wiener diversity index ($H'\log_e$), Pielou's evenness (J'), rarefaction analysis, and Fisher's α based on untransformed abundance data using DIVERSE in PRIMER Statistical Software Version 6 (Clarke and Gorley 2006).

Community structure was assessed by examining the overall contribution of higher level taxa, including Polychaeta, Oligochaeta, Crustacea, Mollusca, and other taxa. Other taxa included Halacaridae, Anthozoa, Hydrozoa, Holothuroidea, Ophiuroidea, Nemertea, Enteropneusta, Chaetognatha, Sipuncula, Echiura, and Platyhelminthes. Multivariate analysis of community structure was performed on square-root transformed abundance data using Bray-Curtis similarities in PRIMER Version 6 (Clarke and Gorley 2006). Communities were examined using one-way or two-way analysis of similarity (ANOSIM). Similarity of percentages (SIMPER) was used to identify the taxa responsible for discriminating between communities, and to assess the variability of the communities. Variability among Bray-Curtis similarities was also assessed using multivariate dispersion (MVDISP). Average multivariate dispersion values (MVDISP) calculate the relative distance between replicate samples and hence quantifies the variability of community assemblage in multivariate space, based on Bray-Curtis similarity matrices across canyon and slope habitats and along the depth gradient.

To further address the relationship of the environmental variables to the multivariate community data, distance-based linear modeling (DistLM) and distance-based redundancy analysis (dbRDA) in conjunction with principal coordinates ordination (PCO) were performed using the PERMANOVA+ add on package to PRIMER 6 (Anderson et al. 2008). DistLM performs nominal tests of each variable's explanatory power on community structure and builds a multivariate statistical model of explanatory

power of a suite of variables when considered together. Variables included were depth, grain size characteristics (percent sand, mud), stable isotopic composition ($\delta^{13}C$ and $\delta^{15}N$), chlorophyll *a* concentration, and organic carbon and nitrogen content. Replicate depths of faunal densities were averaged prior to analysis in PERMANOVA.

9.3 RESULTS

9.3.1 Benthic Macrofauna

9.3.1.1 Baltimore Canyon

9.3.1.1.1 Canyon and Slope Habitats

Station locations, geographic position, associated depth, and analysis type for the Baltimore Canyon sampling campaign are shown in **Table 9-1**. Baltimore Canyon community analysis was based on three replicate bulk box core samples along each transect; 24 samples in total were analyzed along both canyon and slope habitats. Overall, 1.455 m^2 of seabed sediment surface area was analyzed (**Table 9-5**). These samples yielded 15,017 individuals, representing 484 taxa across canyon and slope transects. Of the total taxa, 174 (36%) were singleton taxa and 97 (20%) were doubleton taxa. Singleton taxa and doubleton taxa are the proportions of taxa that occur once or twice in the entire dataset. The canyon yielded 9,754 individuals from 326 taxa and 5,263 individuals from 347 taxa were collected from the adjacent slope habitats. Of the total number of taxa recorded in both habitats, 157 taxa (32.4%) were found only in the canyon habitats compared with 132 taxa (27.3%) found only in the adjacent slope habitats.

Table 9-5. Macrofaunal abundance, number of taxa, associated depths, and sampled area for bulk box core samples collected in Baltimore Canyon and adjacent slope.

Station No.	Depth (m)	Area (m^2)	Abundance	
			No. of Individuals	No. of Taxa
Canyon				
NF-2012-019	189	0.061	1,341	95
NF-2012-028	191	0.061	1,587	73
NF-2012-029	191	0.061	1,394	99
NF-2012-032	563	0.061	259	65
NF-2012-034	565	0.061	189	60
NF-2012-035	567	0.052	152	47
NF-2012-045	840	0.061	1,005	48
NF-2012-047	847	0.061	1,248	54
NF-2012-049	844	0.061	1,198	57
NF-2012-055	1,179	0.059	389	60
NF-2012-056	1,179	0.059	557	91
NF-2012-062	1,180	0.061	435	82
Mean			812.83	69.25
Slope				
NF-2012-064	168	0.061	471	84
NF-2012-066	170	0.061	966	96
NF-2012-067	168	0.061	903	93
NF-2012-072	514	0.061	667	101
NF-2012-076	510	0.061	234	50
NF-2012-088	502	0.061	297	49
NF-2012-082	990	0.061	439	90
NF-2012-085	991	0.061	291	78
NF-2012-087	991	0.061	295	78

Table 9-5. (Continued).

Station No.	Depth (m)	Area (m^2)	Abundance	
			No. of Individuals	No. of Taxa
NF-2012-090	1,185	0.061	170	63
NF-2012-092	1,187	0.061	288	54
NF-2012-093	1,186	0.061	242	60
Mean			438.58	74.66
Summary				
Total		1.455	15,017	484
Canyon				326
Slope				357

Sample depths, surface area, and abundances for each of the bulk box core samples from Baltimore Canyon are presented in **Table 9-5**. Significant differences (**Figure 9-7**) were found between the density in the canyon axis and the adjacent slope habitats (two-way ANOVA, $F = 37.98$, $p = <0.001$), among depths (two-way ANOVA, $F = 37.66$, $p = <0.001$) and for the habitat and depth interaction (two-way ANOVA, $F = 13.40$, $p = <0.001$). Highest infaunal abundances in both habitats were found at 180 m depth stations (Canyon: 23,617 individuals m^{-2}, SE 1,000; Slope: 12,786 individuals m^{-2}, SE 2,082) and abundances generally decreased with depth (**Figure 9-7**). Most strikingly, Baltimore Canyon densities displayed a bimodal distribution created by a sharp decline at 550 m and an increase at 900 m canyon stations. Macrofaunal densities at all depths inside the canyon were significantly different from each other. In contrast to the canyon axis, the slope habitat showed a gradual decrease in densities with increased depth, although only densities at 180 m were significantly higher than those at the deeper slope stations (SNK, 550 m, $p = <0.05$; 900 m, $p = <0.01$; 1,180 m, $p = <0.01$). Canyon macrofaunal densities at 180 and 900 m were significantly higher than at corresponding depths on the slope, based on pairwise tests (SNK, **Figure 9-7**).

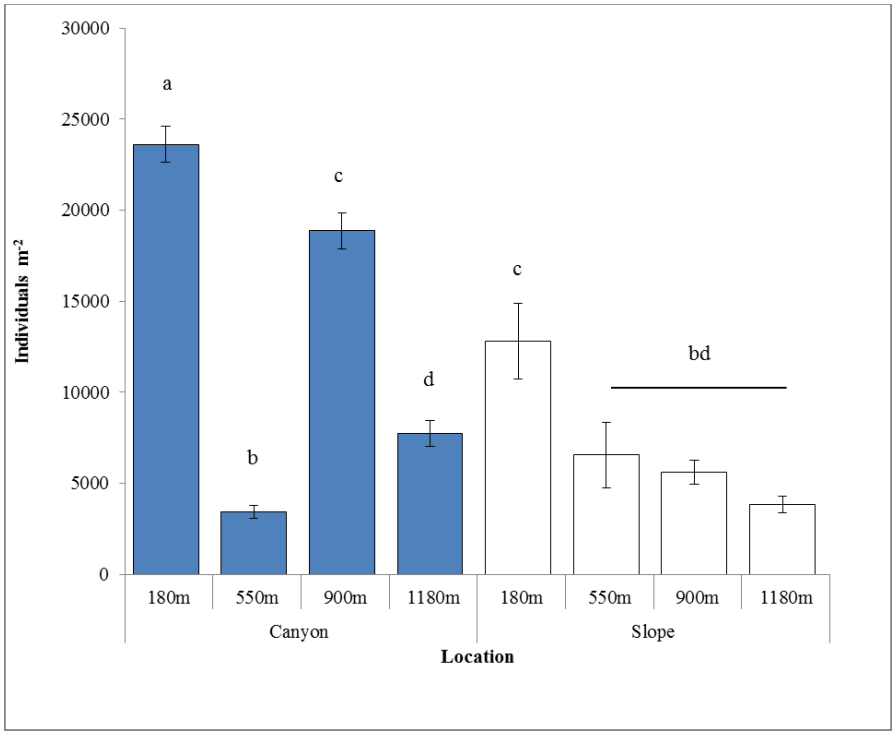

Figure 9-7. Mean macrofaunal density by depth for Baltimore Canyon and slope transects. Letters indicate statistical groupings ($p < 0.05$). Error bars represent standard error.

No significant differences in the number of taxa were found between canyon and slope habitats (Kruskall-Wallis, df = 1, $p = 0.488$); however, significant differences were found between depth groups (Kruskall-Wallis, df = 3, $p = 0.046$). For canyon stations, the number of taxa at 180 m was significantly higher than at all other depths (Kruskall-Wallis, $p = <0.05$). The shallowest slope stations (180 m) had the highest mean number of taxa (89.6) of the two habitats, whereas the lowest (53.3) number of taxa was found at middle canyon stations (900 m). Both canyon and slope transects showed differing patterns in diversity as measured by the Shannon-Wiener diversity index ($H'\log_e$, **Table 9-6**). Canyon habitats followed a similar pattern as the density data, namely a bimodal distribution with increasing depth, which was not evident across slope depths (**Figure 9-7**). Significant differences in diversity were found between canyon and slope habitats (two-way ANOVA, $F = 15.70$, $p = 0.001$) and among depths (two-way ANOVA, $F = 4.81$, $p = 0.014$), with a significant interaction of habitat and depth (two-way ANOVA, $F = 16.46$, $p < 0.001$). Overall, the canyon stations showed a decrease in diversity at mid-canyon stations (900 m) followed by a sharp increase at the deepest sampled stations (1,180 m). Conversely, diversity of the slope habitats remained the same across depths, with a slight increase at 900 m. Pairwise tests (SNK) of macrofauna diversity (H') revealed 900 m stations as driving the main differences between canyon and adjacent slope habitats (SNK, $p <0.01$). Although diversity was lowest at mid-canyon depths (900 m, 2.47), the highest diversity (3.89) was found at the same depths on the adjacent slope. Within the canyon, diversity at 900 m was also the lowest of all other depths (SNK, 180 m, $p < 0.05$; 550 m, $p < 0.05$; 1,180 m, $p < 0.05$). Using family level rarefaction (**Figure 9-8**), slope habitat diversity appeared to exceed canyon diversity, indicated by the steeper initial curve compared with canyon habitats. Of the two curves, slope habitats were further from approaching an asymptote, suggesting inadequate sampling of slope habitats. More sampling would be needed to fully assess the diversity on the slope adjacent to Baltimore Canyon.

Table 9-6. Average macrofaunal diversity indices from bulk box core samples collected in Baltimore Canyon and slopes. Values in parentheses represent one standard error.

Habitat/Location	*N*	*d*	*J'*	$H'(\log_e)$	Fisher's α	N1	MVDISP
Canyon 180 m	3	9.34 (0.58)	0.77 (0.01)	3.53 (0.08)	12.55 (0.89)	34.43 (2.50)	0.347
Canyon 550 m	3	7.12 (0.52)	0.88 (0.00)	3.59 (0.07)	10.13 (0.82)	36.57 (2.57)	1.52
Canyon 900 m	3	5.65 (0.10)	0.62 (0.02)	2.52 (0.11)	7.19 (0.13)	12.64 (1.26)	0.24
Canyon 1,180 m	3	8.70 (0.83)	0.84 (0.01)	3.66 (0.11)	12.25 (1.30)	39.42 (4.16)	0.907
Slope 180 m	3	10.00 (0.15)	0.79 (0.01)	3.62 (0.03)	14.04 (0.13)	37.26 (1.03)	0.827
Slope 550 m	3	7.52 (1.39)	0.84 (0.01)	3.49 (0.19)	10.54 (2.12)	33.96 (7.21)	1.387
Slope 900 m	3	9.61 (0.31)	0.88 (0.01)	3.91 (0.02)	14.01 (0.43)	50.05 (1.18)	1.467
Slope 1,180 m	3	7.26 (0.34)	0.89 (0.00)	3.65 (0.05)	10.33 (0.65)	38.44 (1.81)	1.307

d = Margalef's species richness; *J'* = Pielou's evenness; $H'(\log_e)$ = Shannon-Wiener diversity index; N1 = Hill's index; MVDISP = multivariate dispersion.

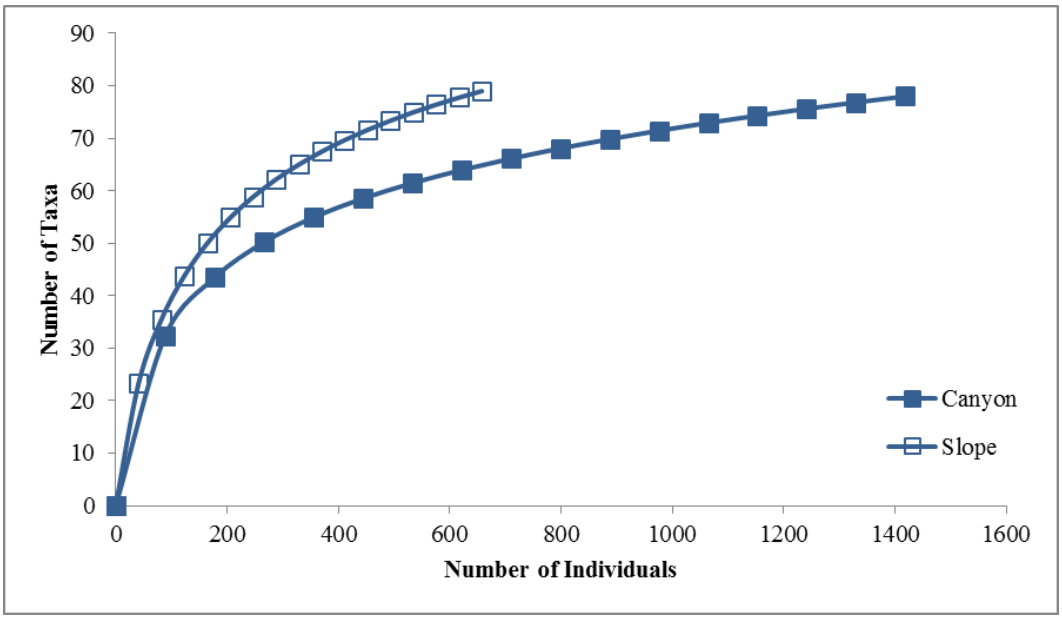

Figure 9-8. Coleman rarefaction of macrofaunal communities in Baltimore Canyon and slope habitats.

Vertical distributions down to 10-cm sediment depth (**Figure 9-9**) revealed that >50% of infauna were located in the uppermost 2 cm of sediment, closest to the sediment-water interface across both canyon and slope habitats. However, differences in vertical distributions did occur. Vertical distributions of infauna were more variable in canyon than in slope habitats across all depths. For example, at 900 m within the canyon, 85% of the infaunal density was located in the upper 2 cm of sediment, indicating that the community comprises mostly surface-dwelling species as opposed to deeper burrowing species. All the canyon and slope stations exhibited the following down core vertical distribution pattern: 0 to 2 cm was the highest, followed by 2 to 5 cm and 5 to 10 cm. Canyon station at 900 m was notably different, where 0 to 2 cm represented the highest proportion (85%).

Overall community composition varied with depth in both canyon and slope habitats (**Figure 9-10**). Across the entire Baltimore Canyon study area, the majority of infauna were Polychaeta (46%) followed by Mollusca (31%) and Crustacea (12%). At 900 m canyon stations, large proportions of Mollusca (74%), namely bivalves (Yoldiellinae and Thyasiridae), were recorded, which contributed greatly to differences between canyon and slope habitats. Canyon stations showed higher proportions of Mollusca (36%) across depth groups compared with the slope (27%). Additionally, slope habitats showed higher proportions of Crustacea and Oligochaeta (17% and 8%, respectively) than canyon habitats (8% and 4%).

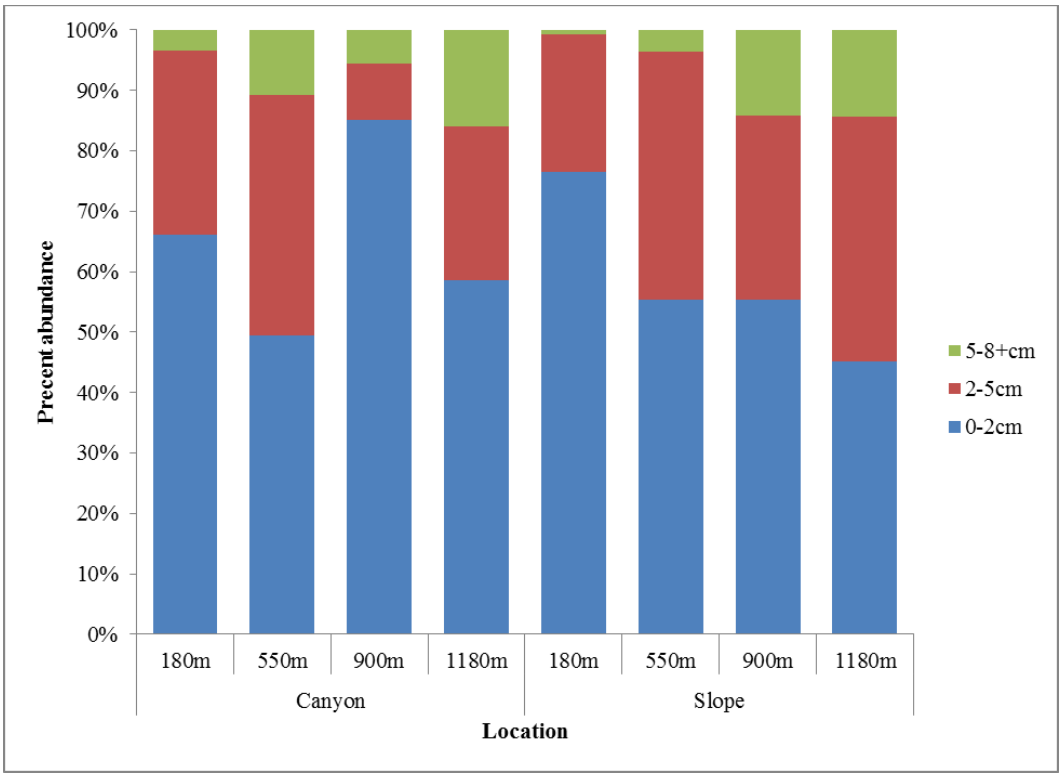

Figure 9-9. Percent abundance of individuals within each vertical sediment fraction for Baltimore Canyon and slope habitats sampled with push corers.

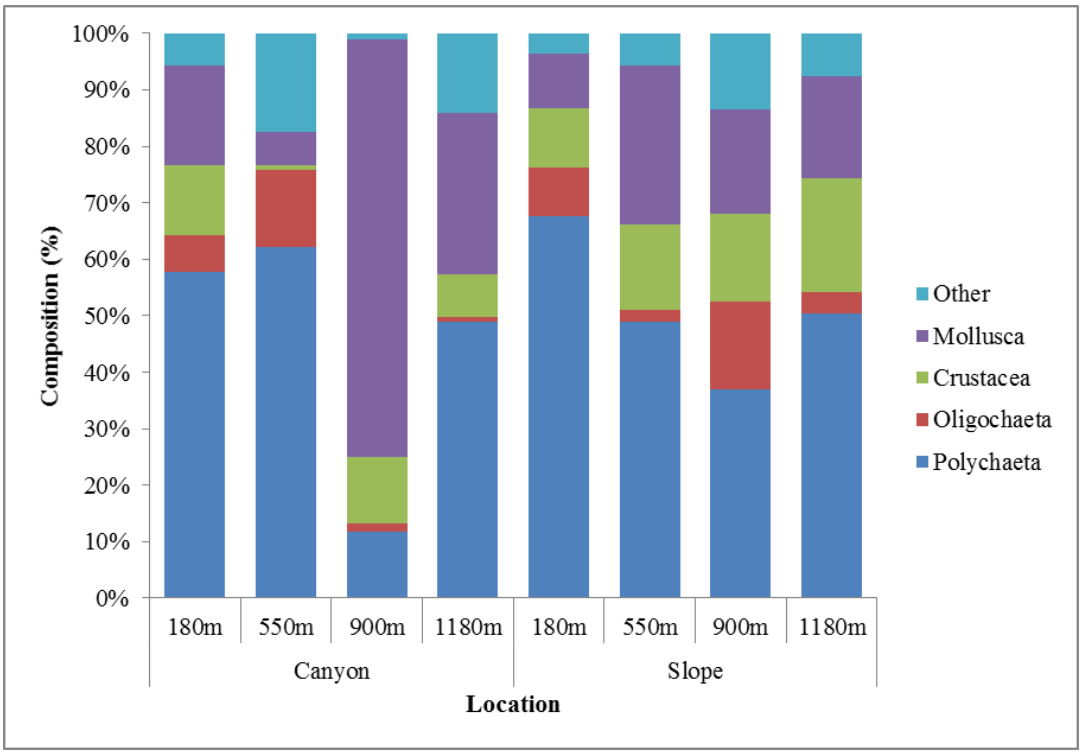

Figure 9-10. Percent composition of macrofaunal communities based on higher taxonomic groups for Baltimore Canyon and slope habitats.

Community assemblages (**Figure 9-11**) were significantly different between canyon and slope habitats (two-way ANOSIM, $R = 0.997$, $p = 0.001$) and among depths (two-way ANOSIM, $R = 1$, $p = 0.002$). Among depth groups, all pairwise combinations were significantly different (all depths; $R = 1$, $p = 0.01$). Cluster analysis (**Figure 9-12**) indicated clear grouping of replicates by habitat and along the depth gradient. Interestingly, canyon stations were divided into two groups at opposite ends of the dendrogram (**Figure 9-12**), indicating strongly dissimilar community assemblages between upper (180 and 550 m) and lower (900 and 1,180 m) canyon stations. All slope assemblages, except those at 180 m, grouped together across the depth gradient. Increased multivariate dispersion (MVDISP, **Table 9-6**) values can be regarded as a symptom of a community stressor (Clarke and Warwick 1993) in multidimensional space. Overall, slope habitats had higher average dispersion values compared with canyon community assemblages. All canyon MVDISP values were <1 except for the 550 m location. Values <1 can indicate a more homogenous and less variable community structure. However, at 550 m MVDISP = 1.52, the highest for the entire study. This result indicates higher than normal community variability or degree of assemblage fragmentation possibly resulting from disturbance at these stations. Slope dispersion values were lowest at 180 m (0.827) and higher at the deeper slope depths, indicating an increasing degree of community variability with increased depth.

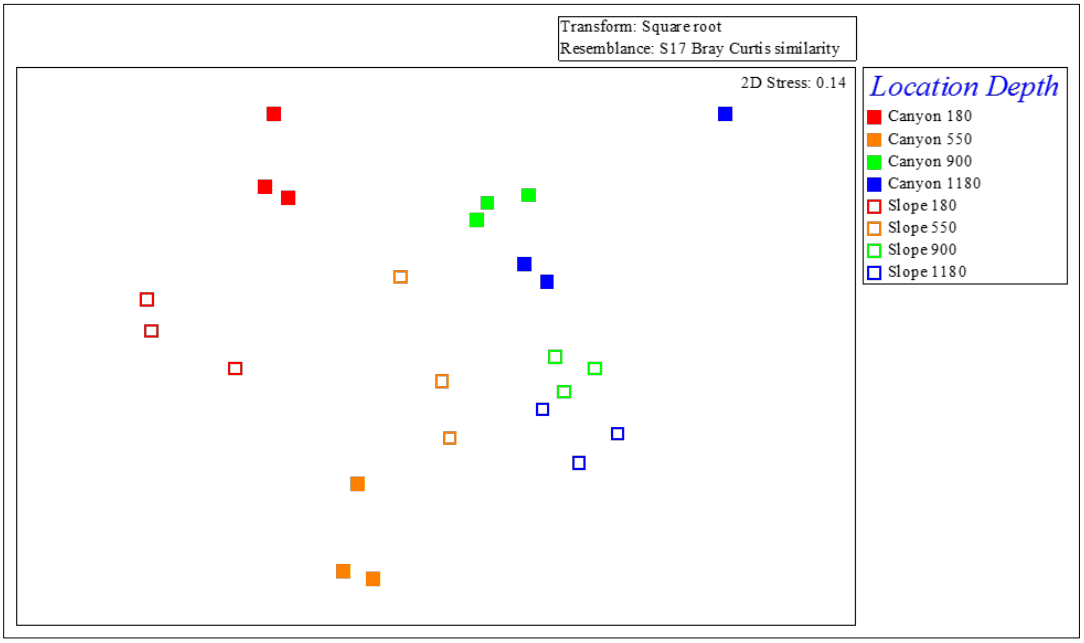

Figure 9-11. Nonmetric multidimensional scaling of Baltimore Canyon and slope benthic community assemblages based on Bray-Curtis similarities of square-root transformed abundance data.

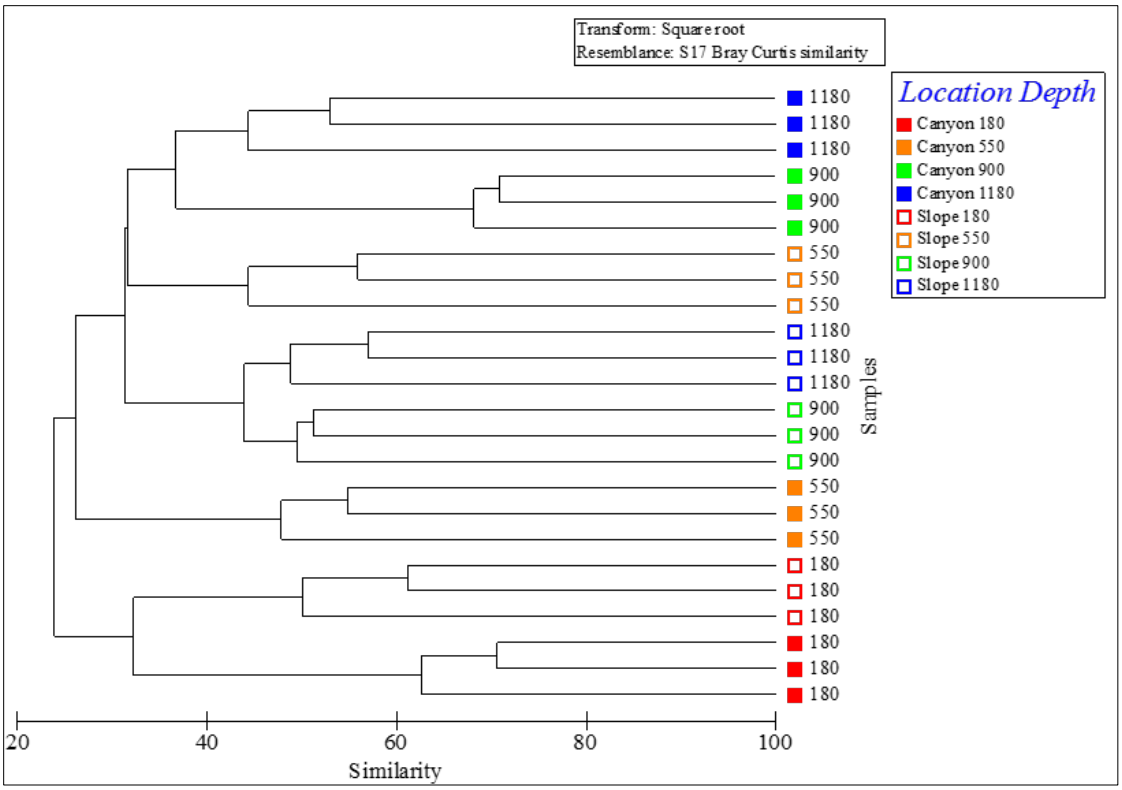

Figure 9-12. Cluster analysis dendrogram for Baltimore Canyon and slope benthic infaunal community assemblages based on Bray-Curtis similarities of square-root transformed abundance data.

SIMPER analysis revealed that canyon and slope community assemblages (family level) were very dissimilar (69.89%, **Table 9-7**). Across depth groups, Baltimore Canyon communities were more similar (56.29%) than slope communities (42.34%). Thirteen families contributed to 40% of the overall observed community patterns. Among the highest contributors were two bivalve families, Thyasiridae (5.96%) and Yoldiidae (5.52%), followed by the polychaete families Cossuridae (4.5%) and Dorvilleidae (2.85%). At the species level (putative or otherwise), SIMPER analysis (**Table 9-8**) showed high levels of dissimilarity between canyon and slope habitats. Average dissimilarity using species level data was higher (78%) than at family level, although similarity within habitats was similar to family level data (canyon = 54% and slope = 45% similarity). Taxa contributing to 40% of the explained assemblages at species level were from 26 families and of these the highest contributing taxa were again from Thyasiridae, Yoldiidae, and Cossuridae taxa.

PCO explained 47.2% of the differences between community assemblages on two axes (PCO1 and PCO2, **Figure 9-13**). Environmental parameters overlaid as vectors revealed that PCO1 was largely a function of increasing depth (Pearson correlation, 0.97) and grain size (clay = -0.84 and sand = 0.73, **Chapter 6**). PCO2 was negatively associated with sediment enrichment processes ($\delta^{13}C$ = -0.51, $\delta^{15}N$ = -0.49, and chlorophyll *a* = -0.45). Additionally, the percentage of silt (not shown in **Figure 9-13**) had a high negative correlation with PCO2 (-0.61). Deeper canyon communities (900 and 1,180 m) were distinct from deeper slope communities by the influence of higher sediment organic enrichment. Canyon and slope communities at 550 m were strongly separated by sedimentary $\delta^{15}N$ enrichment. All of the environmental parameters, excluding percent carbon, were identified using DistLM as the best model explaining the observed variability in community structure (**Table 9-9**, 63%, DistLM, AICc = 183.23). The Akaike information criterion with correction for small sample sizes (AICc) is a statistical measure of relative statistical model quality for a given set of data.

Table 9-7. Similarity of percentages (SIMPER) for benthic infaunal assemblages (family level) in Baltimore Canyon and adjacent slope habitats. Only taxa contributing to 40% to community dissimilarity are shown. Mean abundances are square-root transformed.

Groups: Canyon vs. Slope Average dissimilarity = 69.89%	Canyon	Slope		
Average similarity (%)	56.29	42.34		
Taxa	Mean Abundance (Individuals m^{-2})		Contribution (%)	Cumulative (%)
Thyasiridae	41.11	17.51	5.96	5.96
Yoldiidae	35.27	12.03	5.52	11.48
Cossuridae	37.4	3.79	4.5	15.98
Dorvilleidae	33.51	16.75	2.85	18.83
Paraonidae	28.15	40.9	2.85	21.68
Typhlotanaidae	14	15.28	2.77	24.45
Scaphopoda	19.34	5.36	2.73	27.18
Tubificidae	26.92	26.59	2.42	29.59
Cirratulidae	26.67	25.49	2.33	31.92
Maldanidae	16.89	13.66	2.18	34.1
Sipuncula	20.52	12.38	2.05	36.15
Nemertean	14.55	8.05	1.96	38.11
Spionidae	16.76	9.16	1.93	40.04

Table 9-8. Similarity of percentages (SIMPER) for benthic infaunal assemblages (species level) in Baltimore Canyon and adjacent slope habitats. Only taxa contributing to 40% of community dissimilarity are shown. Mean abundances are square-root transformed.

Groups: Canyon vs. Slope Average dissimilarity = 77.61	Canyon	Slope		
Average similarity	53.90	44.11		
Taxa	Mean Abundance (individuals m^{-2})		Contribution (%)	Cumulative (%)
Mendicula ferruginosa/Adontorhina spp.	20.09	8.02	2.64	2.64
Yoldiella nana	27.61	5.98	2.45	5.09
Cossura longocirrata	30.67	7.64	2.35	7.44
Thyasira sp1	8.55	13.38	1.85	9.30
Dentaliidae spp.	14.77	7.71	1.40	10.69
Ennucula sp1	6.52	4.23	1.30	11.99
Chaetodermatidae sp1	14.20	2.40	1.15	13.14
Pelecypoda spp.	8.10	6.76	1.14	14.28
Tubificidae sp1	13.51	10.08	1.03	15.31
Lucinoma foliosa	14.11	0.34	1.01	16.32
Galathowenia oculata	13.95	5.19	1.00	17.32
Aricidea suecica	0.00	9.29	1.00	18.33
Prionospio cirrifera	8.56	2.80	0.98	19.30
Alvania jeffreysi	5.95	3.76	0.95	20.25
Paraonis reductus	3.98	5.64	0.94	21.19
Yoldiella spp.	5.04	4.91	0.93	22.12
Tharyx spp. cf *acutus*	7.17	5.42	0.91	23.03

Table 9-8. (Continued).

Taxa	Mean Abundance (individuals m^{-2})		Contribution (%)	Cumulative (%)
Tubificidea sp2	4.64	6.71	0.90	23.93
Aphelochaeta sp1	10.86	2.73	0.86	24.79
Macrostylis / Nannoniscidae	7.94	10.57	0.86	25.65
Aphelochaeta sp2	2.61	8.44	0.84	26.49
Aricidea simplex	2.17	13.47	0.84	27.33
Abyssoninoe abyssorum	5.40	1.74	0.80	28.13
Ceratocephale loveni	6.93	0.34	0.79	28.92
Aricidea sp3 cf *catherinae*	4.84	12.15	0.79	29.71
Euclymene spp.	5.35	3.74	0.78	30.49
Meiodorvillea sp A	10.87	6.16	0.78	31.27
Glycera capitata	8.18	4.87	0.71	31.98
Enchytraeidae *Grania/Randidrilus* sp	1.50	5.15	0.65	32.63
Capitellidae sp6	5.34	0.00	0.65	33.28
Thyasira sp4 near *T. obsoleta/croulinensis*	7.01	1.06	0.65	33.93
Harpinia laevis/proquina	6.16	0.00	0.63	34.56
Mendicula ferruginosa/pygmaea	2.81	5.95	0.62	35.18
Ilyarachna sp1	0.67	5.67	0.62	35.80
Harpinia pectinata	5.47	1.15	0.61	36.41
Tanaidacea sp1 indet	1.58	5.59	0.61	37.03
Owenidae spp.	3.82	3.76	0.60	37.63
Levinsenia gracilis	5.28	2.47	0.60	38.23
Ophelina chaetifera cylindricaudata	4.60	2.04	0.59	38.82
Polycirrus sp1 cf *haematodes*	3.33	1.26	0.56	39.39
Lumbrineris cingulata/sp. C	4.43	5.97	0.56	39.94

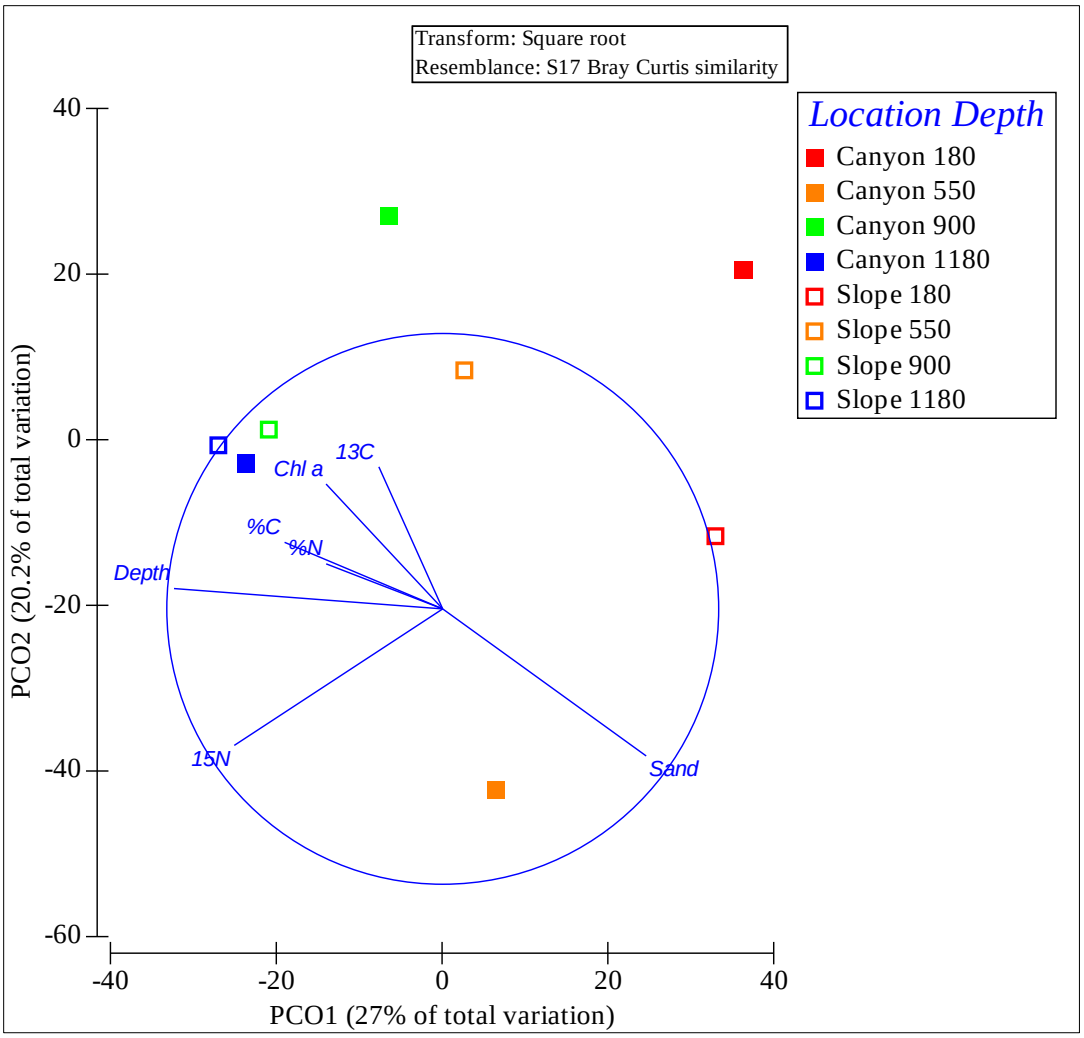

Figure 9-13. Principal coordinates ordination for Baltimore Canyon and slope benthic community assemblages, including environmental parameter vectors. Environmental parameters included sediment grain size (Sand), surface sediment chlorophyll *a* (Chl *a*), percent organic carbon (%C), percent total nitrogen (%N), $\delta^{13}C$ (13C), $\delta^{15}N$ (15N), and depth.

Table 9-9. Results from the distance-based linear modeling (DistLM) of environmental variables with community composition in Baltimore Canyon and slope environments.

Variable	SS(trace)	Pseudo-*F*	*P*	Prop.
Depth	10,077.0	4.705	0.001	0.176
$\delta^{13}C$	5,502.3	2.342	0.003	0.096
Percent carbon	6,848.4	2.992	0.002	0.120
$\delta^{15}N$	8,695.6	3.944	0.001	0.152
Percent nitrogen	6,479.5	2.810	0.002	0.113
Sand content	8,965.7	4.089	0.001	0.157
Chlorophyll *a*	7,717.8	3.431	0.001	0.135
AICc	R^2	RSS	Selections	
183.23	0.63827	20,691	All variables, excluding percent carbon	
183.23	0.63821	20,695	All variables, excluding $\delta^{13}C$	
183.24	0.63811	20,700	All variables, excluding $\delta^{15}N$	

Table 9-9. (Continued).

AICc	R^2	RSS	Selections
183.26	0.63781	20,717	All variables, excluding sand content
183.26	0.63779	20,718	All variables, excluding percent nitrogen
183.26	0.57096	24,541	All variables, excluding percent carbon, $\delta^{15}N$
183.31	0.63695	20,766	All variables, excluding chlorophyll *a*
183.37	0.63615	20,812	All variables, excluding depth
183.41	0.69907	17,213	All variables
183.47	0.56717	24,758	All variable, excluding $\delta^{13}C$, $\delta^{15}N$
Total SS(trace)	–	57,200	–

AICc = Akaike information criterion, corrected; Prop. = proportion of variance explained by each variable; Pseudo-*F* = pseudo-*F* statistic; R^2 = proportion of explained variation attributable to each variable; SS = sum of squares; RSS = residual sum of squares.

9.3.1.1.2 Chemosynthetic Habitats

A total of 1,608 macrofaunal individuals were collected from microbial mats, mussels, and background soft sediment habitats at BCS, encompassing 63 taxa. Taxa included 25 Polychaete families, 15 Crustacea families, and 16 Mollusca families.

Macrofaunal density differed among BCS habitats (**Figure 9-14**; one-way ANOVA, $F = 7.58$, df = 2,9, $p = 0.011$), with the highest densities recorded in bacterial mats (83,649 individuals m^{-2}, SE 28,466), followed by mussel habitats (27,646 individuals m^{-2}, SE 4,464) and background soft sediments (**Figure 9-14**; 15,719 individuals m^{-2}, SE 1,582). Density was significantly greater in bacterial mats compared with background soft sediments (Tukey's HSD, $p = 0.009$). Higher proportions of macrofaunal individuals occurred in the upper 2 cm of bacterial mat sediments (**Figure 9-15**; 79%) compared with mussel sediments (76%) and soft sediments (76%).

Diversity also differed among BCS habitats (**Table 9-10**). Shannon-Wiener diversity index ($H'\log_e$) was significantly lower in bacterial mat sediments than in both mussel and background sediments (one-way ANOVA, $F = 159.21$, df = 2,9, $p < 0.0001$). Comparable diversity results were obtained using rarefaction (**Figure 9-16**) where bacterial mat sediments had the lowest diversity, while mussels and background sediments were similar. Except for microbial mat communities, which approached an asymptote, background and mussel communities were under-sampled. All habitats combined (not shown) approach an asymptote, suggesting adequate regional sampling of taxa.

Table 9-10. Macrofaunal diversity at Baltimore Canyon seep habitats. Values in parentheses represent one standard error.

Habitat	*N*	*d*	*J'*	$H'(\log_e)$	Fisher's α	N1	MVDISP
Mat	4	1.20 (0.14)	0.49 (0.06)	0.96 (0.11)	1.52 (0.18)	2.67 (0.28)	1.21
Mussel	4	5.74 (0.35)	0.87 (0.03)	2.82 (0.07)	13.52 (1.45)	16.95 (1.18)	1.00
Background	4	5.08 (0.22)	0.92 (0.02)	2.80 (0.07)	14.04 (1.42)	16.57 (1.18)	0.79

d = Margalef's species richness; *J'* = Pielou's evenness; $H'(\log_e)$ = Shannon-Wiener diversity index; N1 = Hill's index; MVDISP = multivariate dispersion.

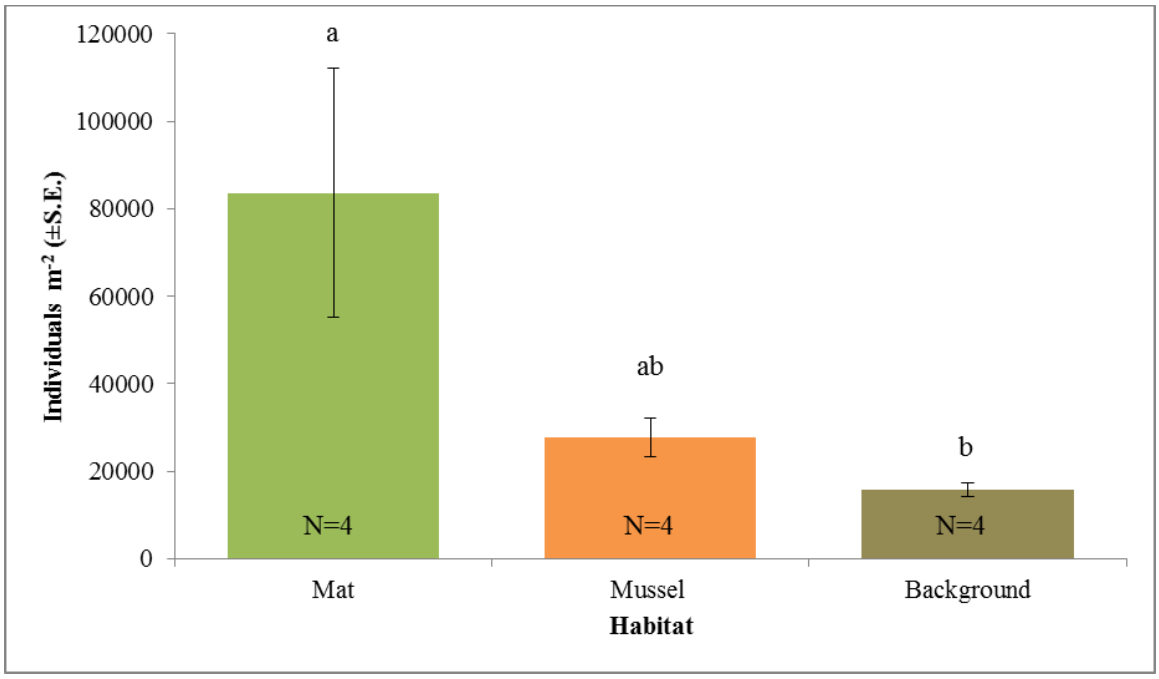

Figure 9-14. Mean macrofaunal density at Baltimore Canyon seep habitats. Letters indicate statistical groupings based on Tukey's HSD. Error bars represent standard error.

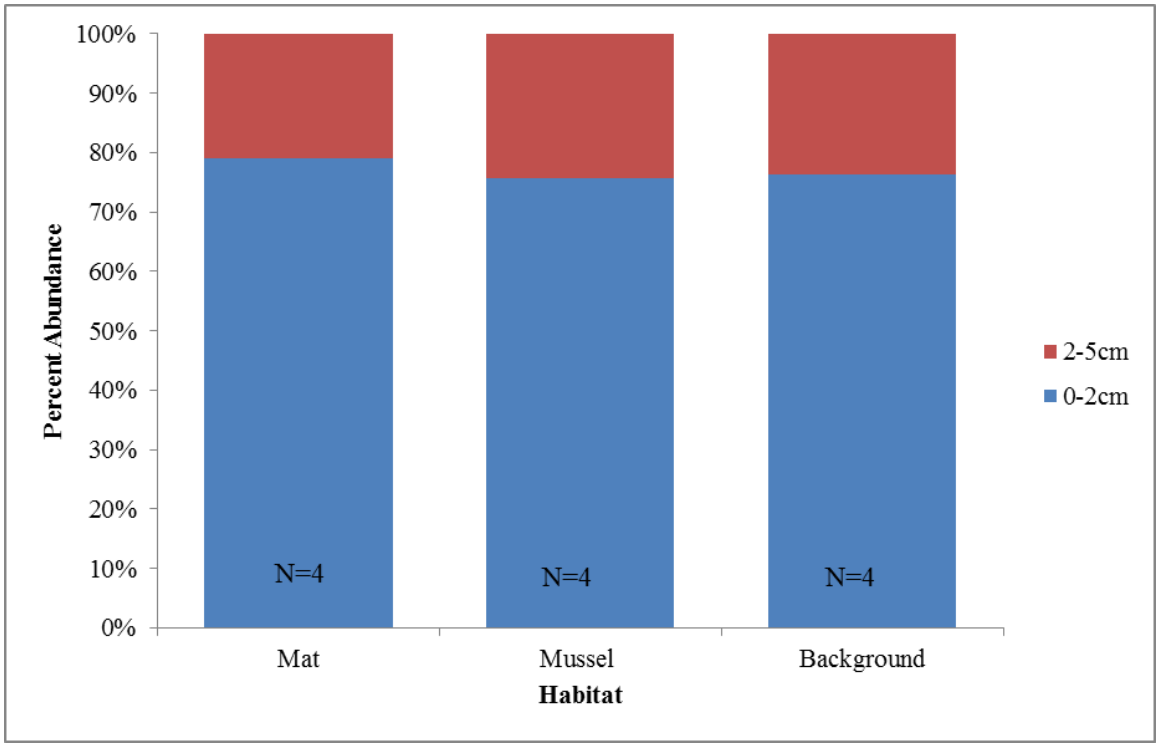

Figure 9-15. Percent abundance of macrofauna within each vertical sediment fraction for Baltimore Canyon seep habitats.

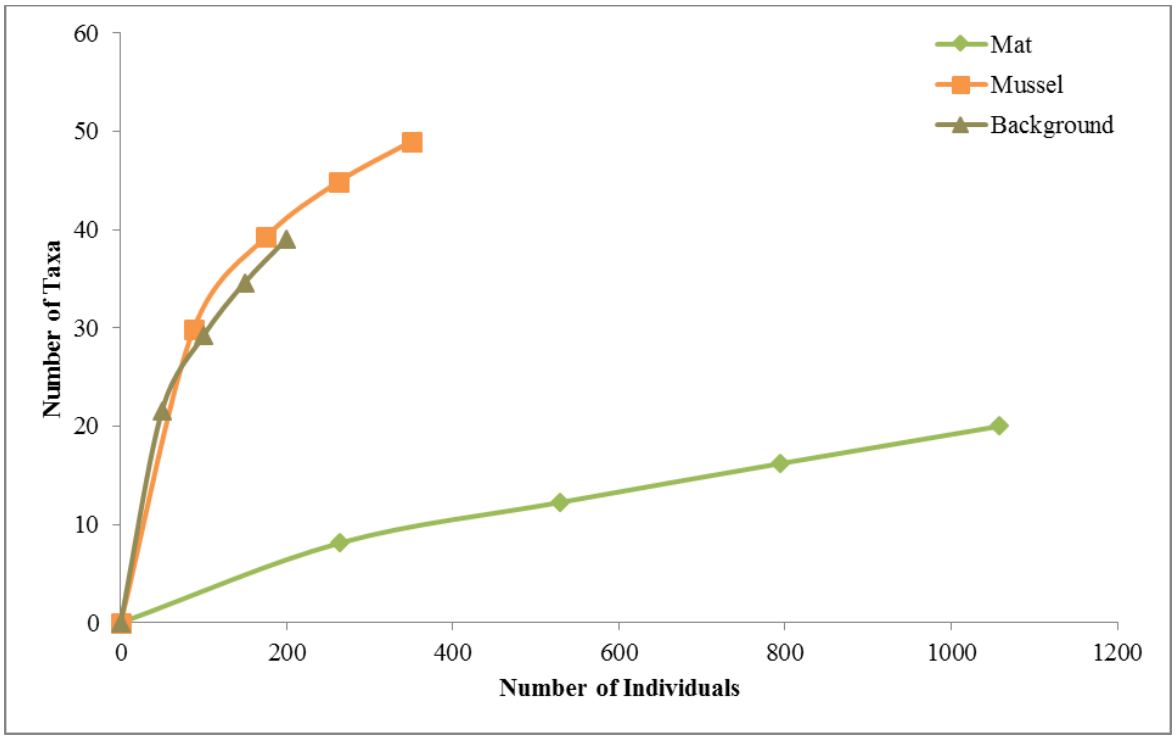

Figure 9-16. Coleman rarefaction of macrofaunal communities at Baltimore Canyon seep habitats.

Bacterial mat and mussel habitats contained different macrofaunal communities than background soft sediments (**Figure 9-17**). Both bacterial mat and mussel habitats had a higher proportion of oligochaetes (31% and 13%, respectively) compared with background sediments (2%), while background soft sediments had higher proportions of mollusks (18%) and other taxa (12%). Mussel habitats had the highest proportion of crustaceans (23%) while bacterial mat sediments contained <1%. Community structure was significantly different among all three habitat types (**Figure 9-18**, one-way ANOSIM, $R = 0.78$, $p = 0.01$). Bacterial mat communities were distinct from both mussel and background habitats ($R = 1$, $p = 0.029$) due to high densities of Capitellidae (Polychaeta), Dorvilleidae (Polychaeta), and Tubificidae (Oligochaeta), contributing to the dissimilarity with mussel habitats (33%) and with background habitats (42%). Mussel habitats also differed from background soft sediment habitats ($R = 0.51$, $p = 0.029$) with increased densities of Tubificidae (Oligochaeta), Leptocheliidae (Tanaidacea), and Typhlotanaidae (Tanaidacea), but low densities of Opheliidae (Polychaeta) and Yoldiidae (Bivalvia) contributing 23% of the dissimilarity.

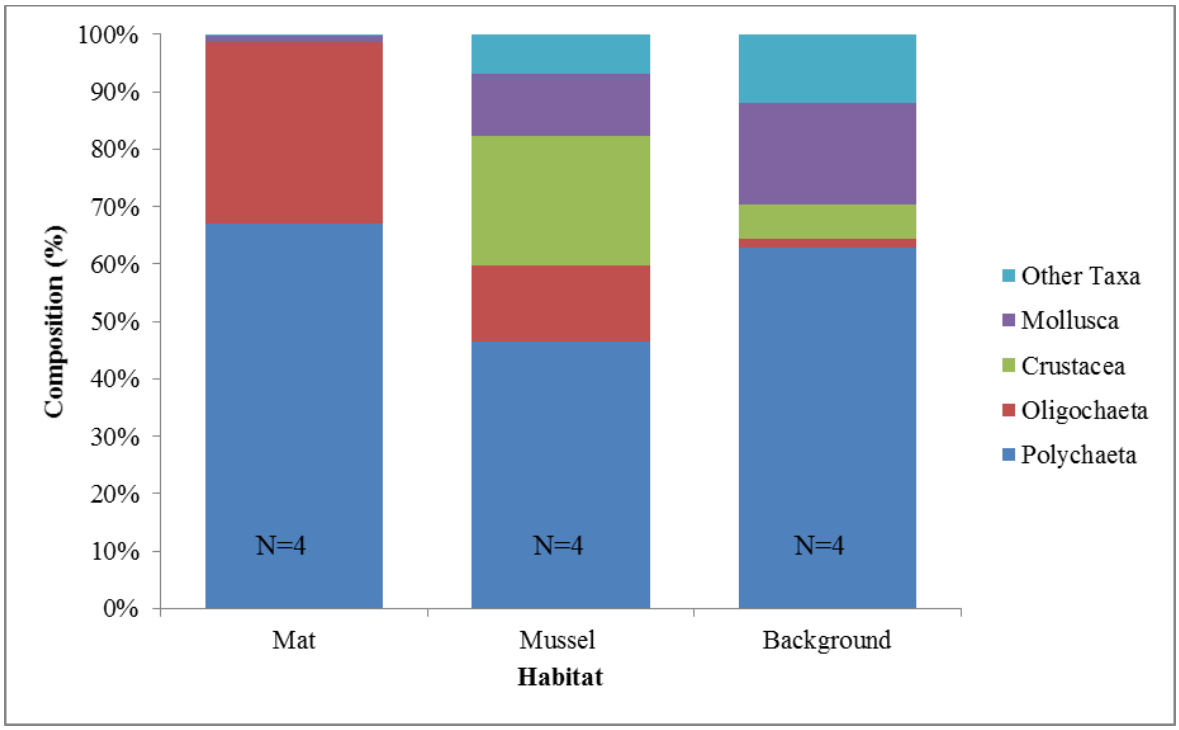

Figure 9-17. Major taxonomic composition of Baltimore Canyon seep communities.

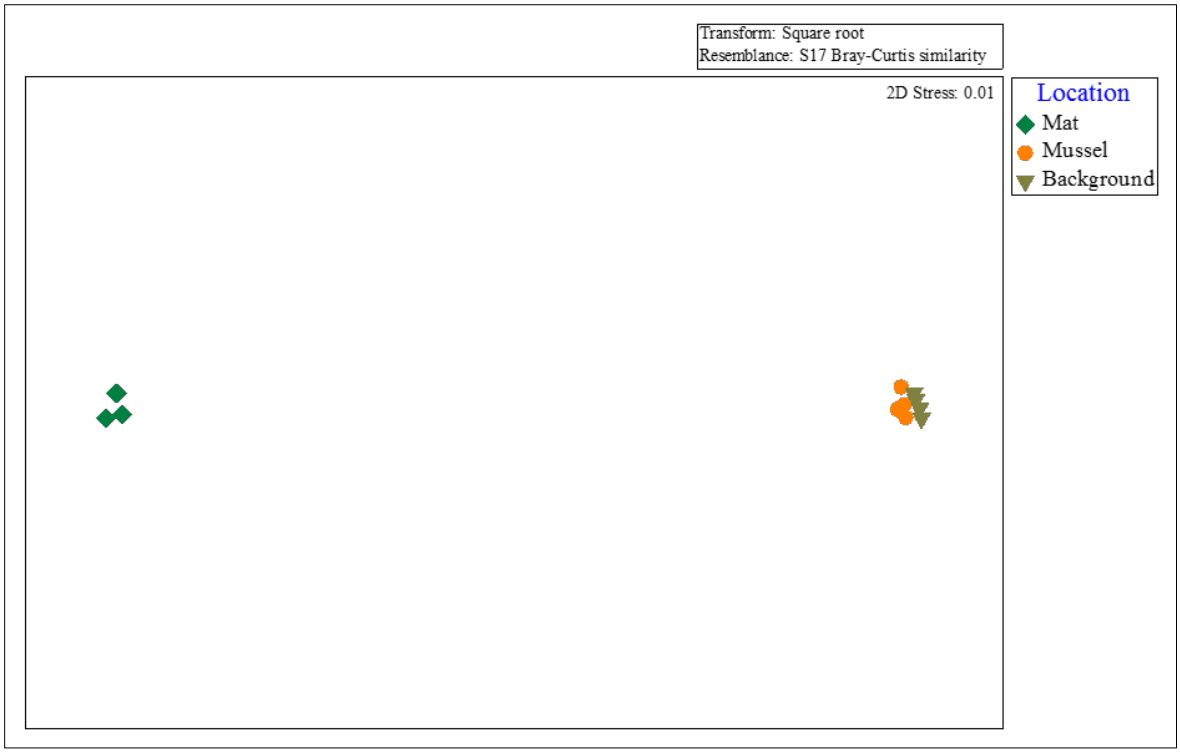

Figure 9-18. Nonmetric multidimensional scaling of box core samples collected near Baltimore Canyon seep habitats based on Bray-Curtis similarities of square-root transformed abundance data.

Although we have no direct measurements of sediment geochemistry for BCS, visual observations of the sediment cores processed provided insight into the chemical environment experienced by fauna living in the sediment. Cores collected in microbial mat sediments **(Figures 9-19** and **9-20a**) were all dark gray, indicative of a reducing environment, and had a distinct smell of hydrogen sulfide. Microbial mats were all white. Cores collected near mussels (**Figure 9-21**) differed from the microbial mat sediments, with a medium brown layer extending 4 to 10 cm down core, indicating oxygenation within the sediments, and they lacked any smell. Cores collected in background soft sediments, including one collected within a meter of a microbial mat core (**Figure 9-20b**), were similar to the mussel cores containing an oxygenated surface layer.

Figure 9-19. Push core collected in white microbial mat sediments at the Baltimore Canyon seep.

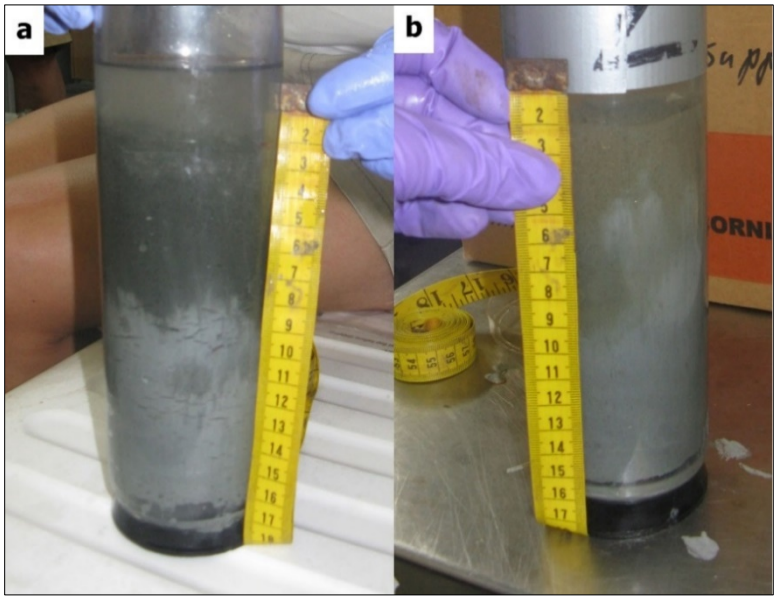

Figure 9-20. Push cores collected at station ROV-2012-NF-08 (a) in microbial mat and (b) <1 m away in background soft sediments.

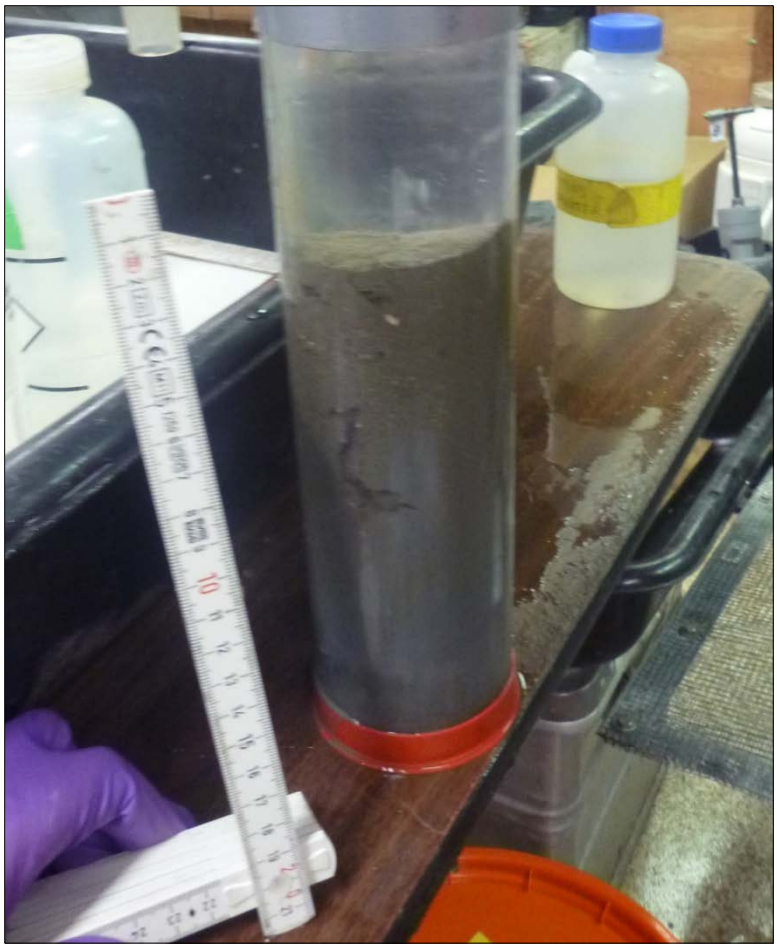

Figure 9-21. Push core collected adjacent to mussels (<1 m) at the Baltimore Canyon seep.

9.3.1.2 Norfolk Canyon

9.3.1.2.1 Canyon and Slope Habitats

A total of 2,596 individuals were collected from push cores in Norfolk Canyon (**Table 9-11**), including 1,648 individuals from canyon habitats and 948 individuals from the slope environment. Eighty-nine taxa were collected from all locations, including 58 taxa from canyon habitats and 76 taxa from slope habitats. Of all taxa recovered from Norfolk sampling sites, fewer taxa (13) were unique to canyon habitats compared with slope habitats (31 taxa). Canyon habitats had higher percentages of singleton taxa (29%) than adjacent slope areas (21%). Macrofaunal abundance patterns differed between canyon and slope habitats in Norfolk Canyon (**Figure 9-22**). Within the canyon axis, macrofaunal density exhibited a bimodal pattern similar to Baltimore Canyon, with high abundances at shallow (190 m) and deeper (800 m) stations (SNK, p = <0.05), but low densities at mid-canyon (550 m) and deepest (1,110 m) locations (SNK, p <0.05). In contrast, on the adjacent slope, macrofaunal density decreased with depth (Spearman correlation, $\rho = -0.743$, $p = 0.0024$), with the highest abundance at the shallow (190 m) location (SNK, $p < 0.05$) and lower abundances at deepest stations (SNK, $p < 0.05$).

Table 9-11. Macrofaunal abundance, number of taxa, associated depths and sampled area from push core samples collected in Norfolk Canyon and adjacent slope.

Station No.	Depth (m)	Area (m^2)	Abundance	
			No. of Individuals	No. of Taxa
Canyon				
RB-2013-046	195	0.003	318	30
RB-2013-047	195	0.003	179	26
RB-2013-048	195	0.003	24	12
NF-2012-159	196	0.003	94	12
RB-2013-043	559	0.003	35	17
RB-2013-044	557	0.003	45	21
RB-2013-045	558	0.003	56	20
NF-2012-162	573	0.003	78	17
RB-2013-040	805	0.003	105	22
RB-2013-041	803	0.003	258	14
RB-2013-042	804	0.003	176	18
NF-2012-164	819	0.003	89	13
RB-2013-038	1,110	0.003	17	10
RB-2013-039	1,110	0.003	67	15
RB-2013-077	1,108	0.003	42	17
NF-2012-192	1,133	0.003	65	14
Mean			103.14	17.38
Slope				
NF-2012-181	188	0.003	60	17
RB-2013-049	187	0.003	161	37
RB-2013-050	187	0.003	137	31
RB-2013-051	187	0.003	155	33
NF-2012-183	550	0.003	57	17
RB-2013-054	549	0.003	86	21
RB-2013-055	549	0.003	74	18
RB-2013-060	790	0.003	7	5
RB-2013-069	804	0.003	20	11
RB-2013-070	805	0.003	61	27
RB-2013-071	1,118	0.003	39	22
RB-2013-073	1,105	0.003	31	19
RB-2013-075	1,103	0.003	34	20
RB-2013-076	1,100	0.003	26	18
Mean			67.76	21.14
Summary				
Total		0.095	2,596	89
Canyon			1,648	58
Slope			948	76

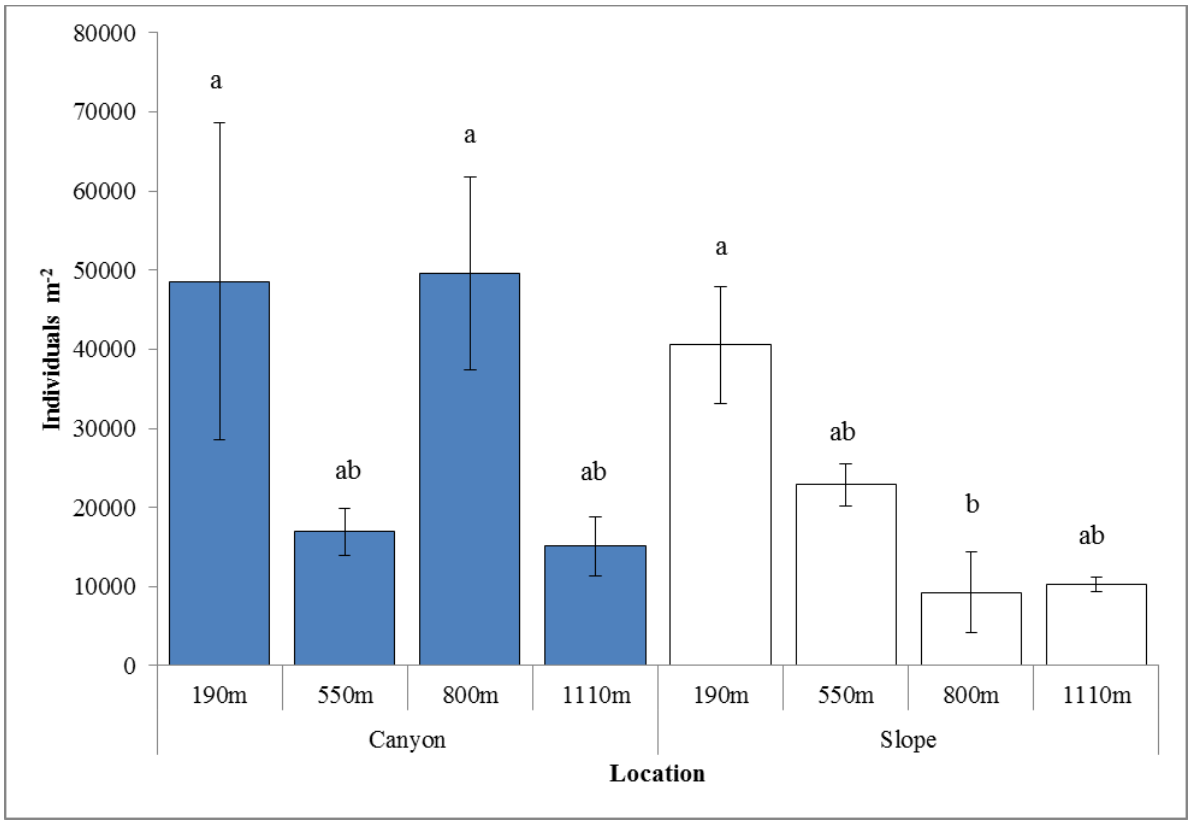

Figure 9-22. Mean macrofaunal density by depth for Norfolk Canyon and slope transects. Letters indicate statistical grouping ($p < 0.05$). Error bars represent standard error.

In general, vertical distributions (**Figure 9-23**) of infauna across habitats and depths sampled at Norfolk Canyon differed from Baltimore Canyon. More than 50% of the macrofauna was concentrated in the upper 0 to 2 cm for all depths except 190 m in the canyon and 550 and 800 m on the slope. Canyon stations at 190 and 800 m had elevated abundances of infauna species penetrating deeper into the sediment layers (2 to 10 cm) than canyon stations at 550 and 1,110 m. These differences, as in Baltimore Canyon, are likely related to the large sediment grain sizes and potentially higher current speeds within the canyon, which allow for greater penetration on the sediment oxic layer. On slope habitats, similar increases in infaunal utilization of deeper sediments is evident only at shelf stations (180 m).

Community composition varied between canyon and slope environments in Norfolk Canyon (**Figure 9-24**). Within Norfolk Canyon, the proportion of Polychaeta reflected the pattern of macrofaunal density, with high proportions at shallow (71%, 190 m) and deeper (67%, 800 m) depths but lower proportions at mid (37%, 550 m) and deep (41%, 1,110 m) depths, with a corresponding increase in Mollusca (35% to 40%). In contrast, slope habitats had high proportions of polychaetes at shallow (74%, 190 m) and mid (81%, 550 m) depths, but low proportions at deeper depths (43% at 800 m, 54% at 1,110 m) with corresponding increases in other taxa (20% to 30%).

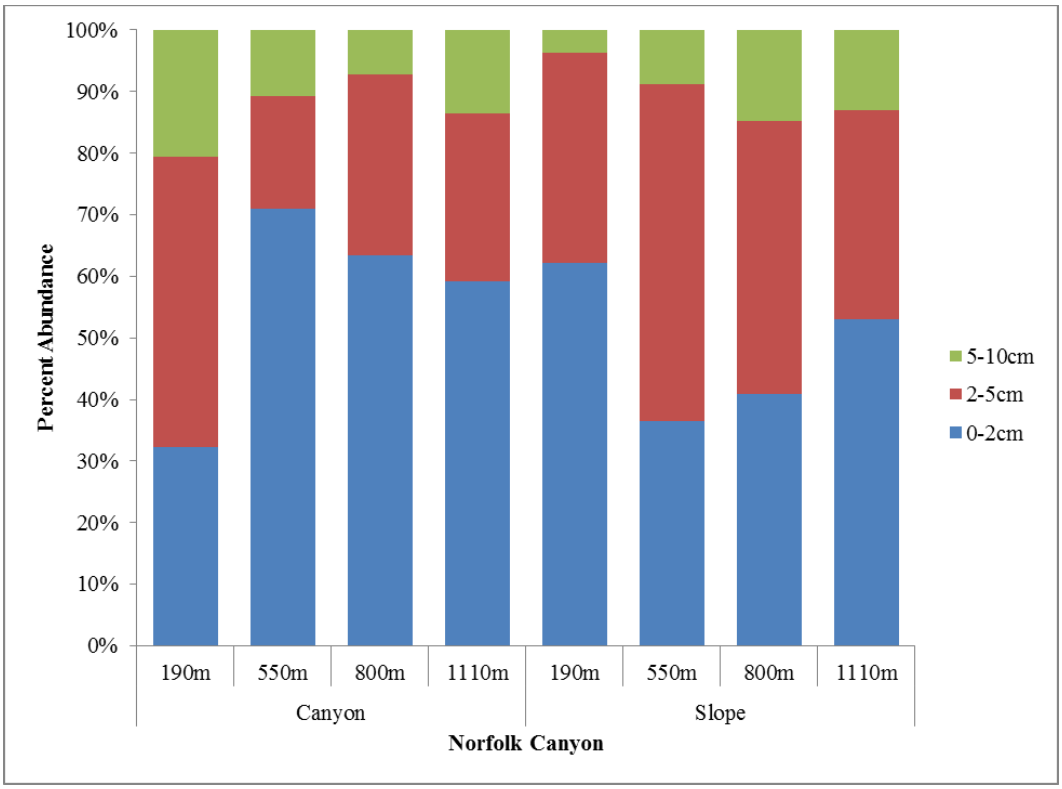

Figure 9-23. Percent abundance of individuals within each vertical sediment fraction for Norfolk Canyon and slope habitats.

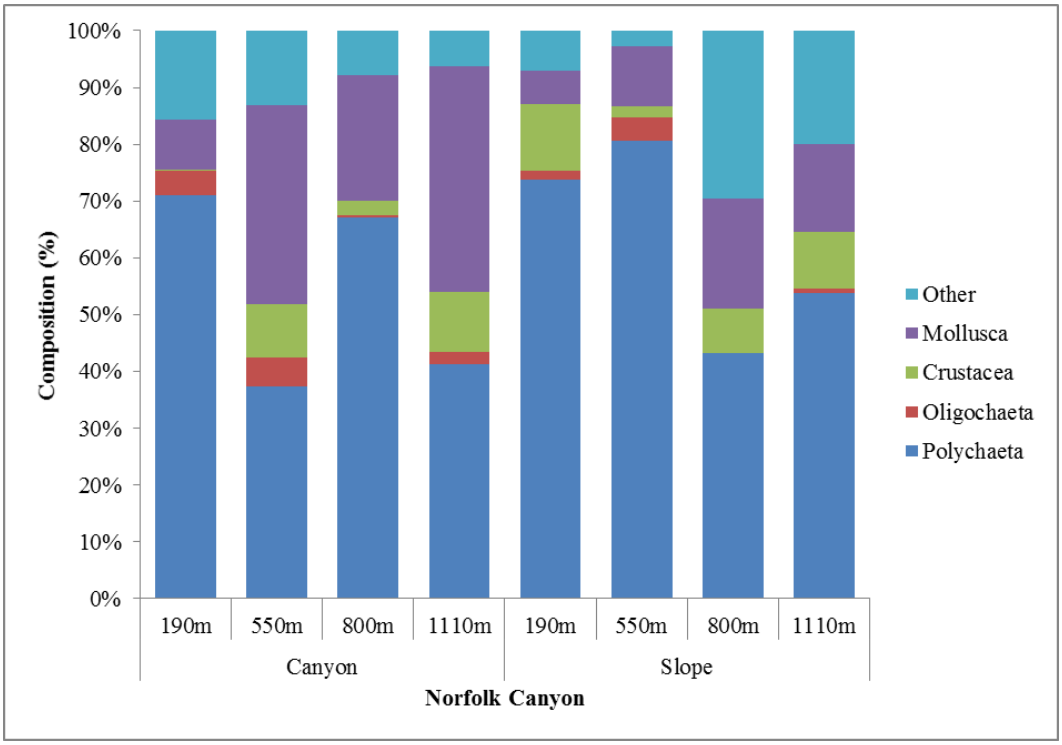

Figure 9-24. Major taxonomic composition of Norfolk Canyon and slope communities.

Overall, diversity between canyon and slope habitats (*H′*, **Table 9-12**) was significantly different (two-way ANOVA, $F = 4.66$, $p = 0.042$), as well as along the depth gradient (two-way ANOVA, $F = 3.44$, $p = 0.034$) and with the habitat and depth interaction (two-way ANOVA, $F = 3.15$, $p = 0.045$). Diversity was higher at the slope 190 m stations compared with the same depth within the canyon (pairwise tests SNK, $p = <0.05$). Among canyon depths, diversity was highest at 550 m and lowest at 800 m. In pairwise comparisons within canyon, Shannon-Wiener diversity index was higher at 550 m than at deeper stations 800 m (SNK, $p = <0.01$) and 1,110 m (SNK, $p = <0.05$), while 1,110 m had higher diversity than 800 m (SNK, $p < 0.05$). Rarefaction curves showed differences in the initial ascent of taxa accumulation, and slope habitats remained the steeper of the two, mirroring the same pattern as Baltimore slope habitats (**Figure 9-25**). Similarly, the Norfolk slope curve showed flattening out at approximately 70 taxa compared with the canyon habitats approaching the asymptotic value at >50 taxa. The analysis implies that slope habitats were more diverse than canyon habitats and require more sampling to fully assess total infaunal biodiversity.

Table 9-12. Macrofaunal diversity from push cores at Norfolk Canyon and slope habitats. Values in parentheses represent one standard error.

Habitat	*N*	*d*		*J′*		*H′*(log$_e$)		Fisher's α		N1		MVDISP
Canyon 190 m	4	3.86	(0.64)	0.73	(0.02)	2.10	(0.13)	7.00	(1.12)	8.40	(1.09)	1.22
Canyon 550 m	4	4.54	(0.33)	0.90	(0.02)	2.62	(0.09)	11.55	(1.83)	13.90	(1.13)	0.78
Canyon 800 m	4	3.16	(0.48)	0.59	(0.12)	1.67	(0.37)	5.13	(1.16)	6.47	(2.31)	0.95
Canyon 1110 m	4	3.42	(0.30)	0.87	(0.04)	2.27	(0.12)	7.93	(1.45)	9.84	(1.11)	1.30
Slope 190 m	4	5.86	(0.68)	0.81	(0.03)	2.73	(0.22)	12.07	(1.50)	16.29	(2.87)	0.67
Slope 550 m	3	4.06	(0.10)	0.73	(0.03)	2.12	(0.05)	7.99	(0.21)	8.34	(0.40)	0.40
Slope 800 m	3	3.91	(1.26)	0.92	(0.04)	2.19	(0.36)	12.13	(3.27)	10.13	(3.34)	1.77
Slope 1110 m	4	5.32	(0.14)	0.94	(0.00)	2.80	(0.03)	21.35	(1.68)	16.40	(0.59)	0.99

d = Margalef's species richness; *J′* = Pielou's evenness; *H′*(log$_e$) = Shannon-Wiener diversity index; N1 = Hill's index; MVDISP = multivariate dispersion.

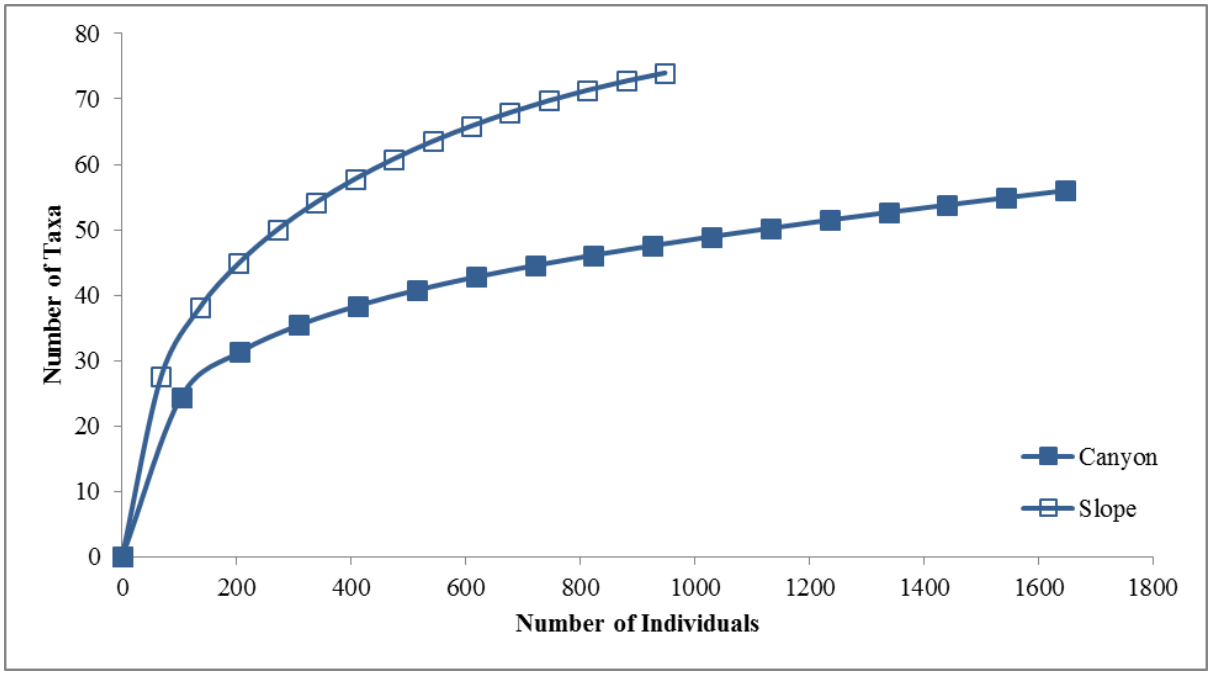

Figure 9-25. Coleman rarefaction of macrofaunal communities in Norfolk Canyon and slope habitats.

Community structure was significantly different between canyon and slope habitats and among depths (**Figure 9-26**, two-way ANOSIM$_{habitats}$, $R = 0.74$, $p = 0.0001$; two-way ANOSIM$_{depth}$, $R = 0.60$, $p = 0.0001$). Pairwise tests revealed significant community assemblage differences between canyon and slope habitats at all four depth groups (180, 550, 800, and 1,110 m, $p < 0.014$). Cluster analysis of community assemblages showed that most replicates grouped by depth with some exceptions (**Figure 9-27**). Canyon stations had weaker grouping among replicates than slope habitats, although shallow depths (550 and 800 m) showed stronger groupings, as reflected in the multivariate dispersion values. Highest community dissimilarity based on MVDISP was present at 800 m slope stations, 190 m and 1,110 m canyon stations (**Table 9-12**).

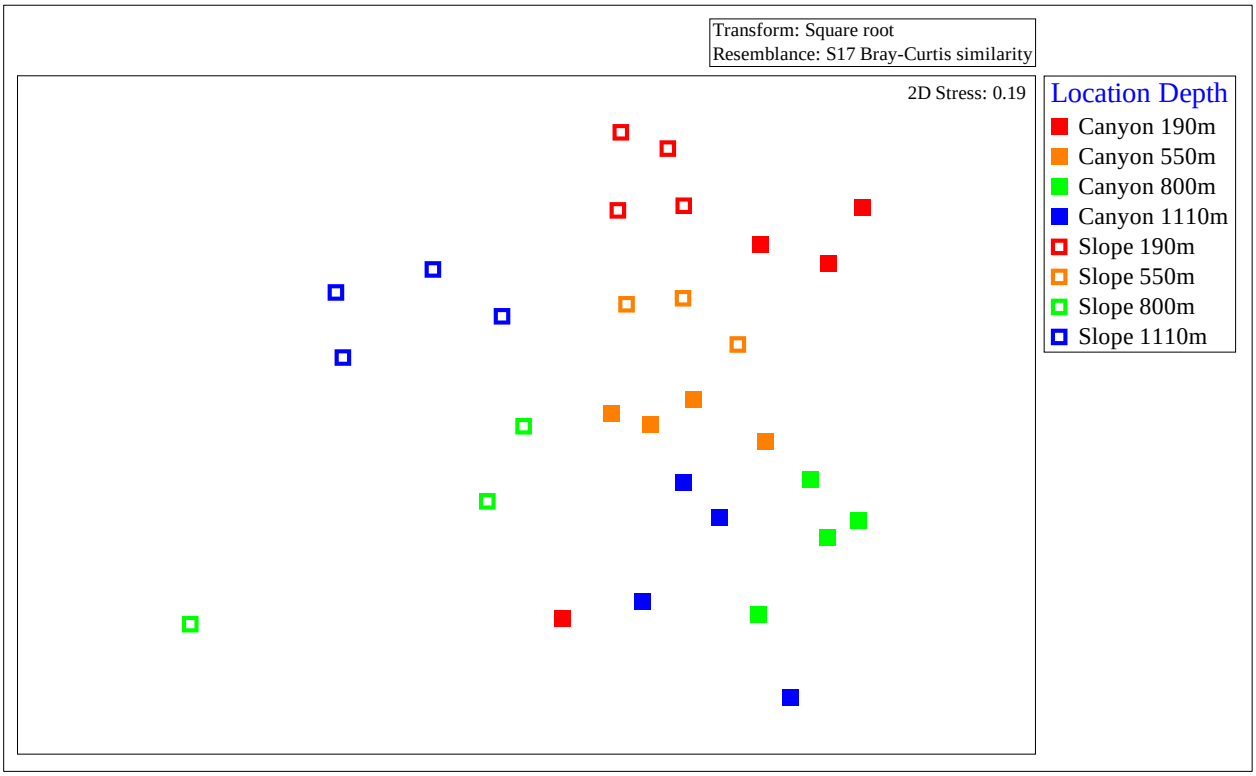

Figure 9-26. Nonmetric multidimensional scaling of cores collected in Norfolk Canyon and adjacent slope habitats based on Bray-Curtis similarities of square-root transformed abundance data.

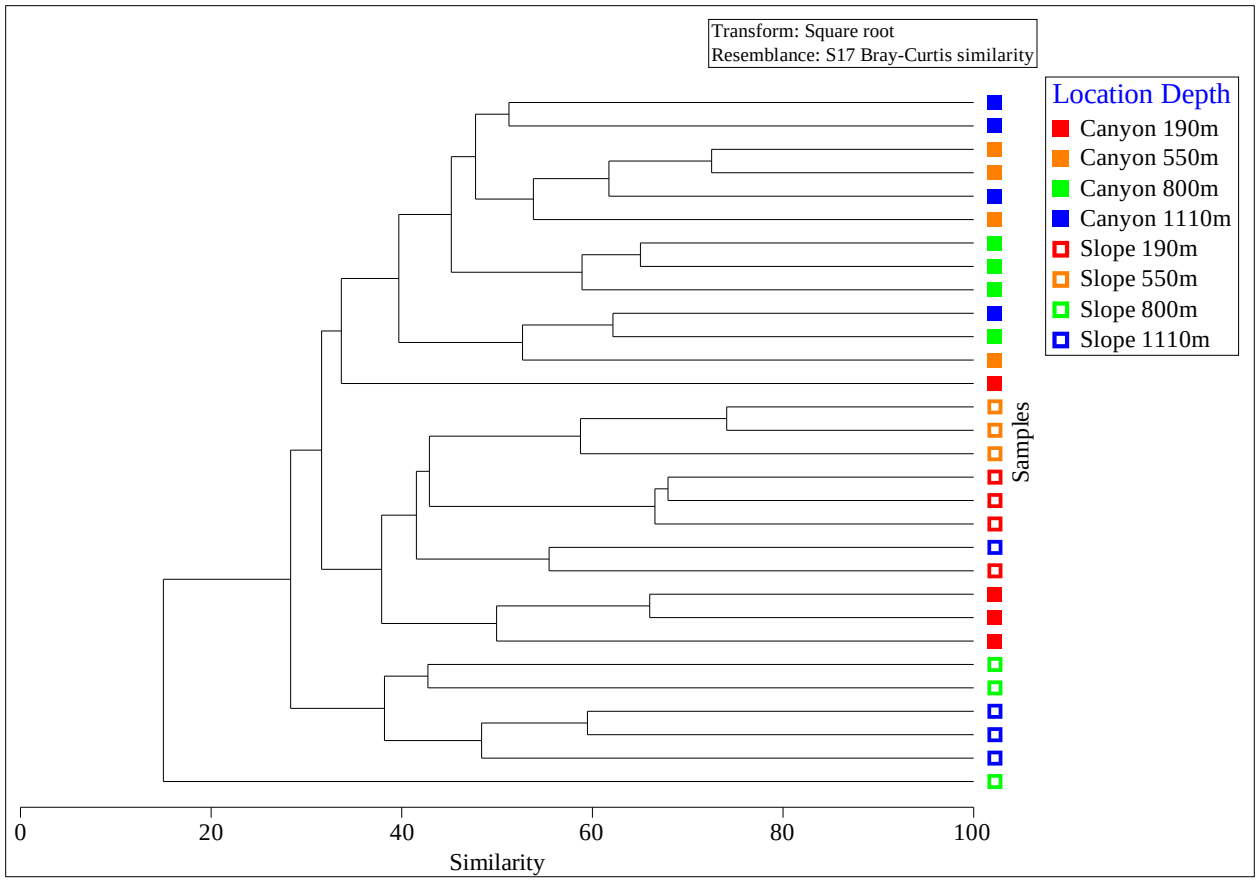

Figure 9-27. Cluster analysis dendrogram for Norfolk Canyon and slope benthic infaunal community assemblages based on Bray-Curtis similarities of square-root transformed abundance data.

Community dispersion values were among the lowest at all slope stations, except at 800 m (1.77). Furthermore, nonmetric multidimensional scaling of community assemblages (**Figure 9-26**) reflected MVDISP results, where community assemblages present in both canyon and slope habitats were separated along the depth gradient, with the greatest separation occurring at 800 m (slope), and 190 and 1,110 m (canyon). Macrofaunal community structure was assessed via SIMPER analysis to identify which taxa were the most important contributors to infaunal assemblages. Family level assemblages between canyon and slope habitats were 71% dissimilar (**Table 9-13**). Community assemblages on the adjacent slope wereless similar (35.4%) than canyon habitats (40.1%). Ten families constituted 42% of the observed community variation across both habitats. Among the highest contributions to overall community patterns were the the bivalve family Yoldiidae (5.57%), followed by polychaete family Capitellidae (5.49%), Paraonidae polychaetes (5.21), and Cirratulidae (4.82%).

Table 9-13. Similarity of percentages (SIMPER) for benthic infaunal assemblages in Norfolk Canyon and adjacent slope habitats. Only taxa contributing to >2% to community dissimilarity are shown. Mean abundances are square-root transformed.

Groups: Canyon vs. Slope Average dissimilarity = 70.63	Canyon	Slope		
Average similarity	40.13	35.42		
Taxa	Mean abundance (Individuals m^{-2})		Contribution (%)	Cumulative (%)
Yoldiidae	2922.59	157.98	5.57	5.57
Capitellidae	7227.49	541.64	5.49	11.06
Paraonidae	2547.39	3475.51	5.21	16.27
Cirratulidae	177.73	3024.15	4.82	21.09
Cossuridae	5410.74	609.34	4.56	25.65
Scaphopoda indet	1856.24	361.09	4.03	29.68
Hydrozoa	1244.08	586.77	3.2	32.88
Lumbrineridae	612.16	1354.10	3.08	35.96
Nerillidae	947.87	90.27	2.95	38.91
Tubificidae	868.88	406.23	2.8	41.71
Ampharetidae	473.93	789.89	2.49	44.19
Nereididae	0.00	496.50	2.38	46.58
Phoxocephalidae	710.90	225.68	2.36	48.93
Sipuncula	592.42	203.11	2.22	51.15
Dorvilleidae	19.75	1038.14	2.19	53.34
Spionidae	572.67	541.64	2.16	55.51
Nemertea	217.22	519.07	2.11	57.62
Nephtyidae	572.67	45.14	2.09	59.71
Turbellaria	375.20	473.93	2.08	61.79
Ophiuroidea	1066.35	22.57	2.01	63.8

In order to assess potential drivers of community differences between canyon and slope habitats and across depths, PCO of the macrofaunal communities was examined by incorporating sediment biogeochemistry. The first two PCO axes (**Figure 9-28**) explained 56.4% of the total infaunal community variability. PCO1 axis was negatively correlated with sediment grain size (-0.56) and positively correlated with all other variables (0.49-0.71). The PCO2 axis was positively correlated with organic enrichment parameter chlorophyll *a* (0.35), sand (0.64), and stable nitrogen isotopes (0.41) but negatively correlated with depth (-0.59), percent carbon and nitrogen (-0.33), and the C:N ratio (-0.36). Sediment chlorophyll *a* concentration and stable isotopic composition provided the greatest separation between canyon and slope habitats. Depth was the only environmental parameter to individually significantly influence community infaunal assemblages across all habitats, explaining 24.2% of the variation in macrofaunal communities (DistLM, $p = 0.024$, **Table 9-14**). Although not significant, all the other environmental parameters individually explained 16.6-22.5% of the community variation (DistLM, $p > 0.06$, **Table 9-14**). Depth was selected as the best model for explaining the observed community patterns (24.2%, DistLM, AICc = 61.59); however, each individual environmental variable fell within one unit of the lowest AICc value (61.8-62.4, **Table 9-14**).

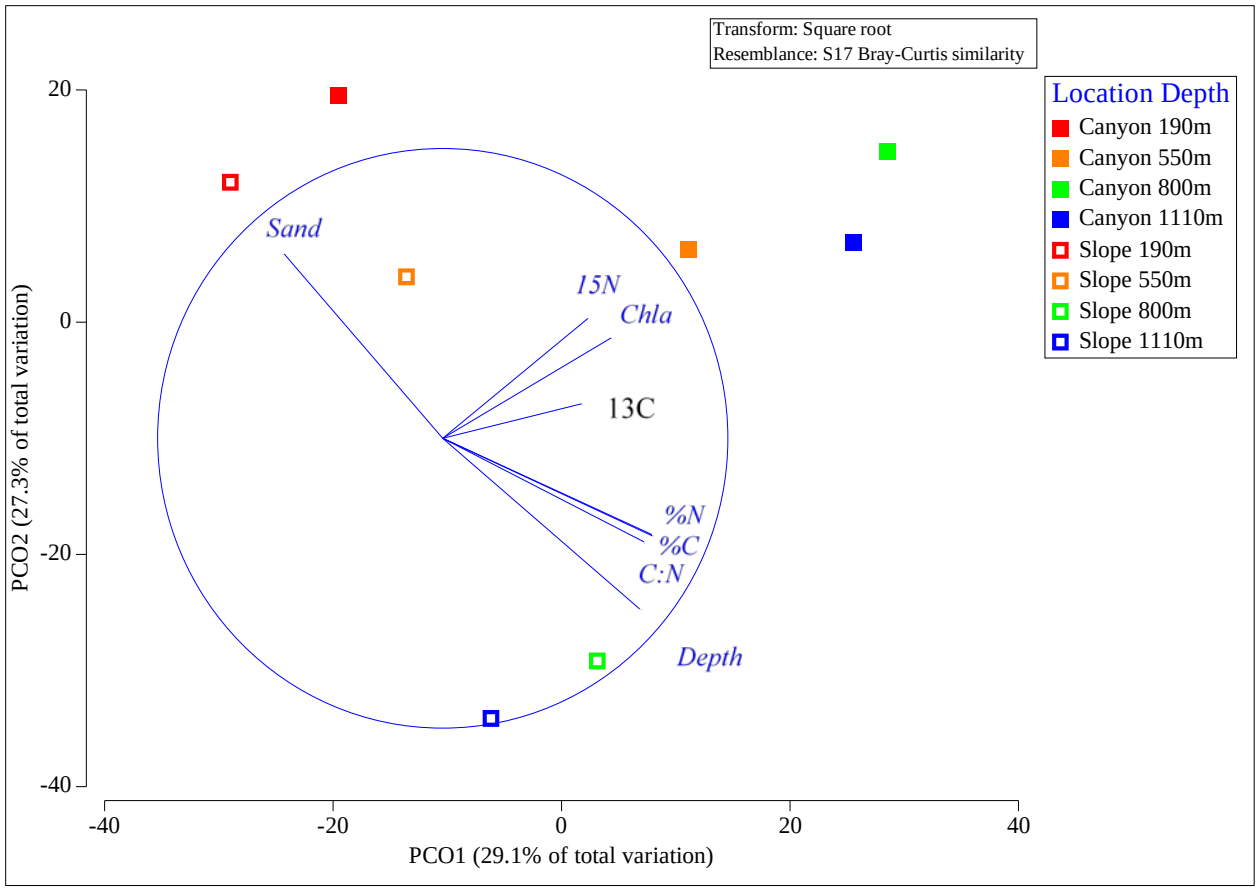

Figure 9-28. Principal coordinates ordination for Norfolk Canyon and slope benthic community assemblages, including environmental parameter vectors. Environmental parameters included sediment grain size, surface sediment chlorophyll *a*, percent organic carbon, percent total nitrogen, $\delta^{13}C$, $\delta^{15}N$, and depth.

Table 9-14. Results from the distance-based linear modeling (DistLM) of environmental variables with community composition in Norfolk Canyon and slope environments.

Variable	SS(trace)	Pseudo-*F*	*P*	Prop.
Depth	2,541.00	1.923	0.0244	0.24271
$\delta^{13}C$	1,735.90	1.1926	0.2871	0.16581
Percent carbon	2,284.60	1.6748	0.0842	0.21822
$\delta^{15}N$	2,043	1.4549	0.1466	0.19516
Percent nitrogen	2,308.00	1.6968	0.0713	0.22046
Sand content	2,353.70	1.7402	0.0634	0.22482
C:N	2,232.20	1.626	0.081	0.21322
Chlorophyll *a*	1,922.20	1.3494	0.204	0.1836
AICc	R^2	RSS	Selections	
61.59	0.24271	7,928	Depth	
61.777	0.22482	8,116	Sand	
61.822	0.22046	8,161	Percent nitrogen	
61.845	0.21822	8,185	Percent carbon	

Table 9-14. (Continued).

Variable	SS(trace)	Pseudo-*F*	*P*	Prop.
61.896	0.21322	8,237	C:N	
62.077	0.19516	8,426	$\delta^{15}N$	
62.191	0.1836	8,547	Chlorophyll *a*	
62.364	0.16581	8,733	$\delta^{13}C$	
64.753	0.44159	5,846	$\delta^{15}N$, Sand	
64.821	0.43678	5,897	Depth, $\delta^{15}N$	
Total SS(trace)	–	10,469	–	

AICc = Akaike information criterion, corrected; Prop. = proportion of variance explained by each variable;
Pseudo-*F* = pseudo-*F* statistic; R^2 = proportion of explained variation attributable to each variable; SS = sum of squares.

9.3.1.2.2 Chemosynthetic Habitats

A total of 1,001 macrofaunal individuals were collected from microbial mats, mussels, and background soft sediment habitats at NCS, encompassing 55 taxa. Taxa included 29 Polychaete families, 12 Crustacea families, and 9 Mollusca families.

Macrofaunal density patterns among habitat types at NCS were similar to those observed at BCS. Macrofaunal density differed among NCS habitats (one-way ANOVA, $F = 10.87$, df = 2,10, $p = 0.003$), with the highest densities recorded in bacterial mats (**Figure 9-29**; 47,962 individuals m^{-2}, SE 13,547), followed by mussel habitats (**Figure 9-29**; 10,427 individuals m^{-2}, SE 1,558) and background soft sediments (**Figure 9-29**; 8,110 individuals m^{-2}, SE 380). Density was significantly greater in bacterial mats compared with mussel sediments (Tukey's HSD, $p = 0.007$) and background soft sediments (Tukey's HSD, $p = 0.007$). Higher proportions of macrofaunal individuals were found in the upper 2 cm in bacterial mat sediments (**Figure 9-30**, 84%) compared with mussel sediments (66%) and soft sediments (55%).

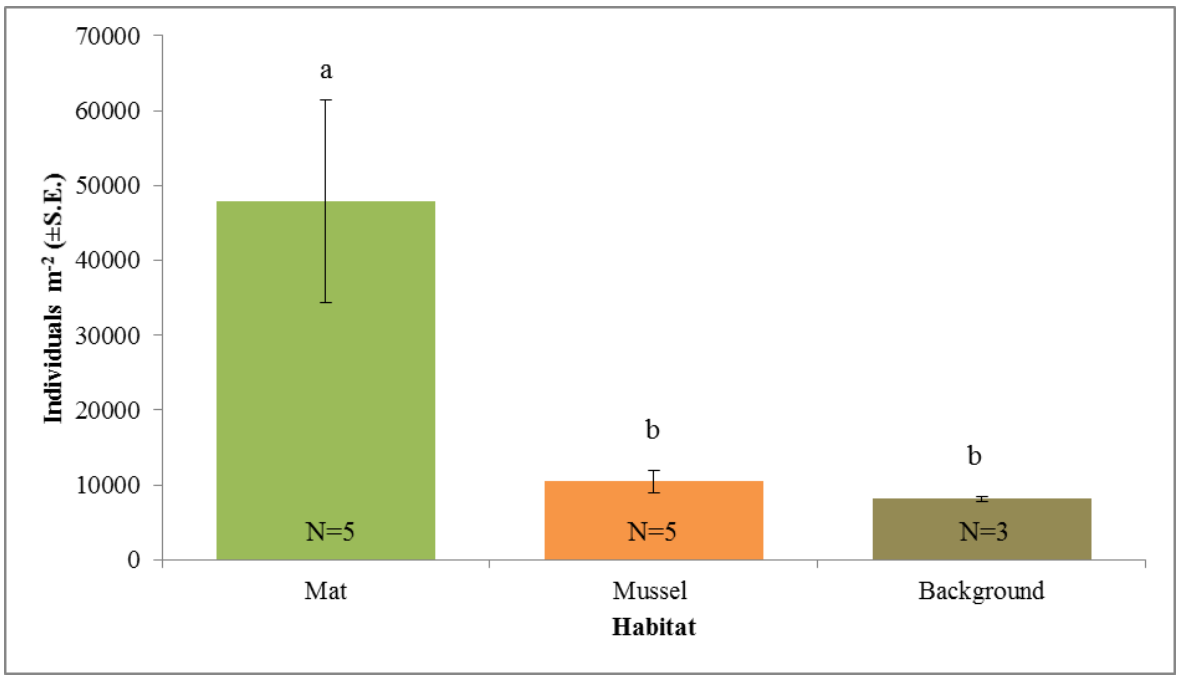

Figure 9-29. Mean macrofaunal density at Norfolk Canyon seep habitats. Letters represent statistical groupings based on Tukey's HSD. Error bars represent standard error.

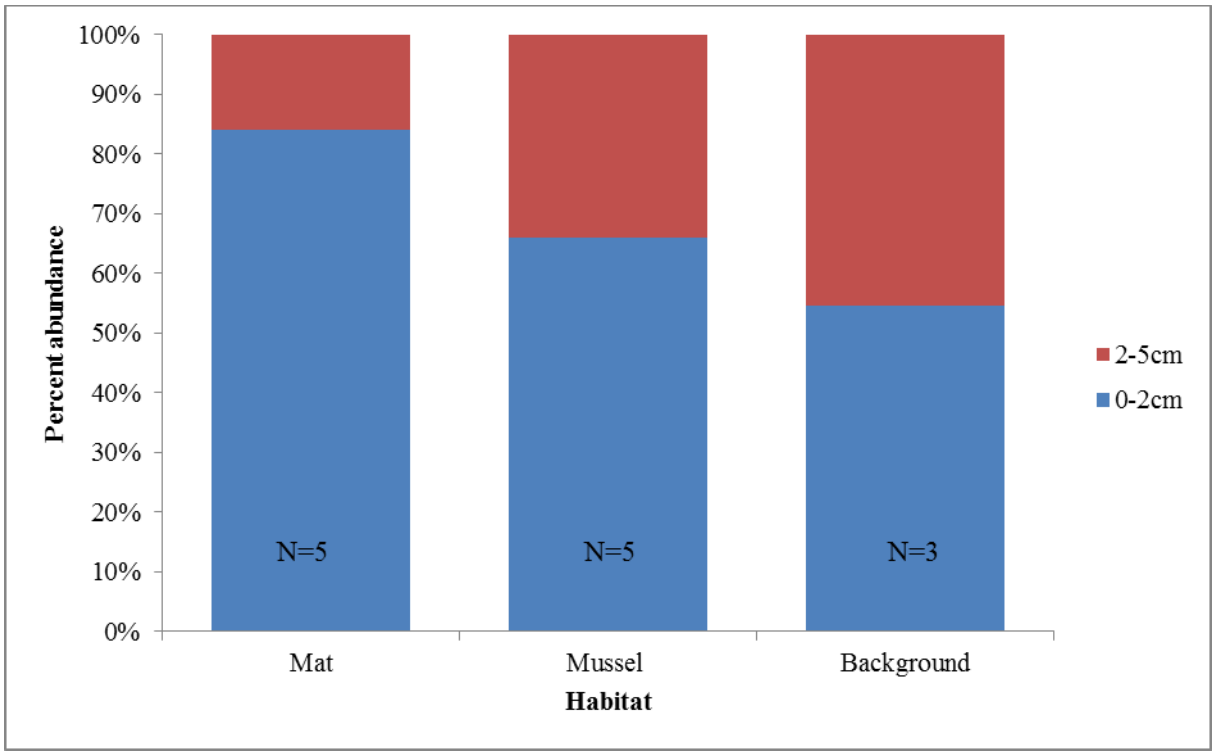

Figure 9-30. Percent abundance of individuals within each vertical sediment fraction for Norfolk Canyon seep habitats.

There was no difference in diversity among NCS seep habitats (**Table 9-15**). Shannon-Wiener diversity index ($H'\log_e$) was similar among bacterial mat, mussel, and background sediments (one-way ANOVA, $F = 1.11$, df = 2,10, $p = 0.37$), with the lowest diversity observed in mussel habitats and the highest in background soft sediments. However, evenness was lowest in microbial mat habitats and highest in background soft sediments. Rarefaction of habitats at NCS obtained similar results as univariate diversity measures (**Figure 9-31**). Background and mussel communities were under-sampled, but rarefaction approached an asymptote for microbial mat communities, suggesting adequate sampling. Rarefaction of all habitats at NCS combined (not shown) reaches an asymptote, suggesting adequate regional sampling of taxa.

Table 9-15. Macrofaunal diversity at Norfolk Canyon seep habitats. Values in parentheses represent one standard error.

Habitat	*N*	*d*	*J'*	$H'(\log_e)$	Fisher's α	N1	MVDISP
Mat	5	3.30 (0.54)	0.70 (0.07)	1.96 (0.26)	6.22 (1.62)	8.02 (1.91)	1.37
Mussel	5	2.65 (0.27)	0.85 (0.03)	1.95 (0.12)	5.43 (0.91)	7.22 (0.90)	0.69
Background	3	3.83 (0.61)	0.92 (0.03)	2.37 (0.19)	13.93 (6.03)	11.15 (2.27)	0.81

d = Margalef's species richness; *J'* = Pielou's evenness; $H'(\log_e)$ = Shannon-Wiener diversity index; N1 = Hill's index; MVDISP = multivariate dispersion.

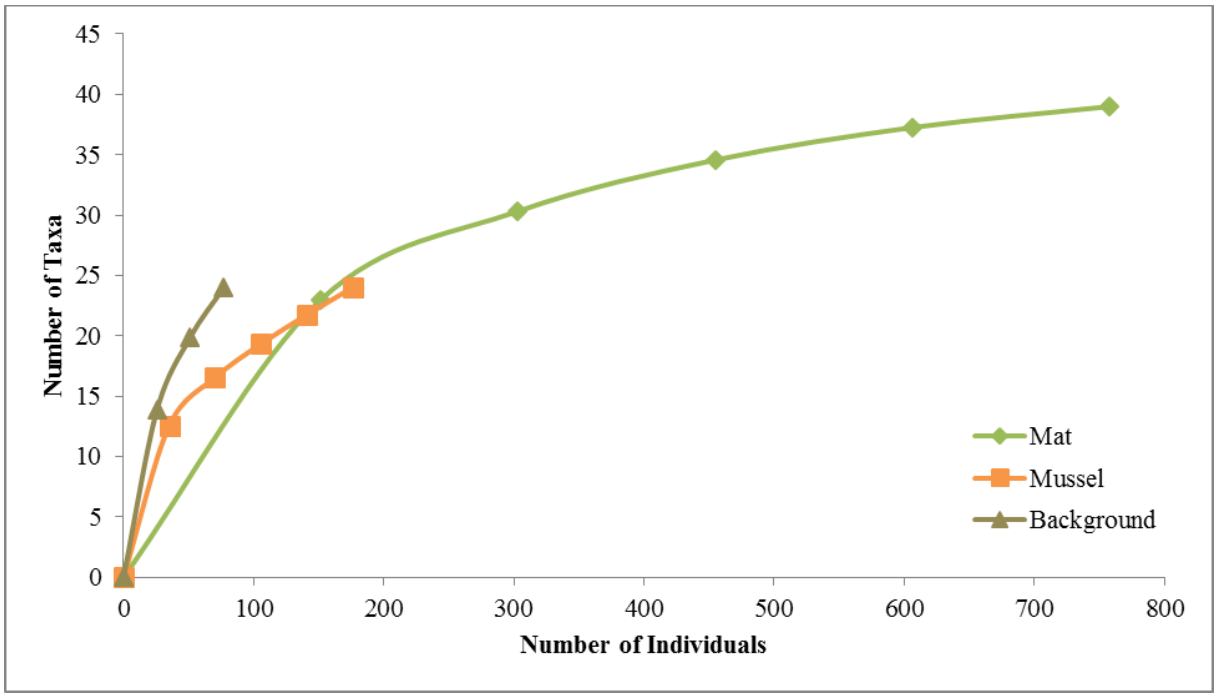

Figure 9-31. Coleman rarefaction of macrofaunal communities at Norfolk Canyon seep habitats.

Bacterial mat and mussel habitats contained different macrofaunal communities than background soft sediments (**Figure 9-32**). Both bacterial mat and background habitats were dominated by polychaetes (77% and 73%, respectively) while mussel habitats were dominated by crustaceans (50%). Background sediments contained higher proportions of mollusks (13%) compared with bacterial mats (4%) and mussels (3%). Community structure was significantly different among all three habitat types (**Figure 9-33**; one-way ANOSIM, $R = 0.76$, $p = 0.02$). Bacterial mats differed from both mussel ($R = 0.77$, $p = 0.008$) and background habitats ($R = 0.53$, $p = 0.036$) by high densities of Capitellidae (Polychaeta), Dorvilleidae (Polychaeta), and Spionidae (Polychaeta) contributing 26% of the dissimilarity with mussel habitats and 27% dissimilarity with background habitats. Mussel habitats also differed from background soft sediment habitats ($R = 1$, $p = 0.018$), with higher densities of Oedicerotidae (Amphipoda) and Spionidae (Polychaeta), and lower densities of Cossuridae (Polychaeta) and Paraonidae (Polychaeta) than in background sediments, contributing 31% of the dissimilarity.

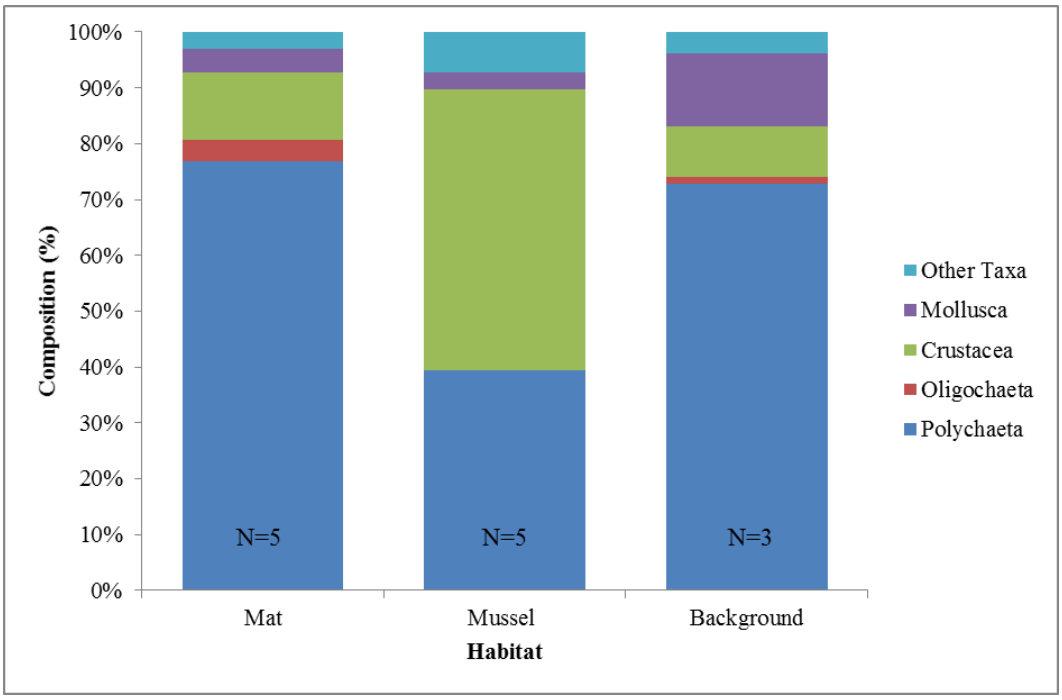

Figure 9-32. Major taxonomic composition of Norfolk Canyon seep communities.

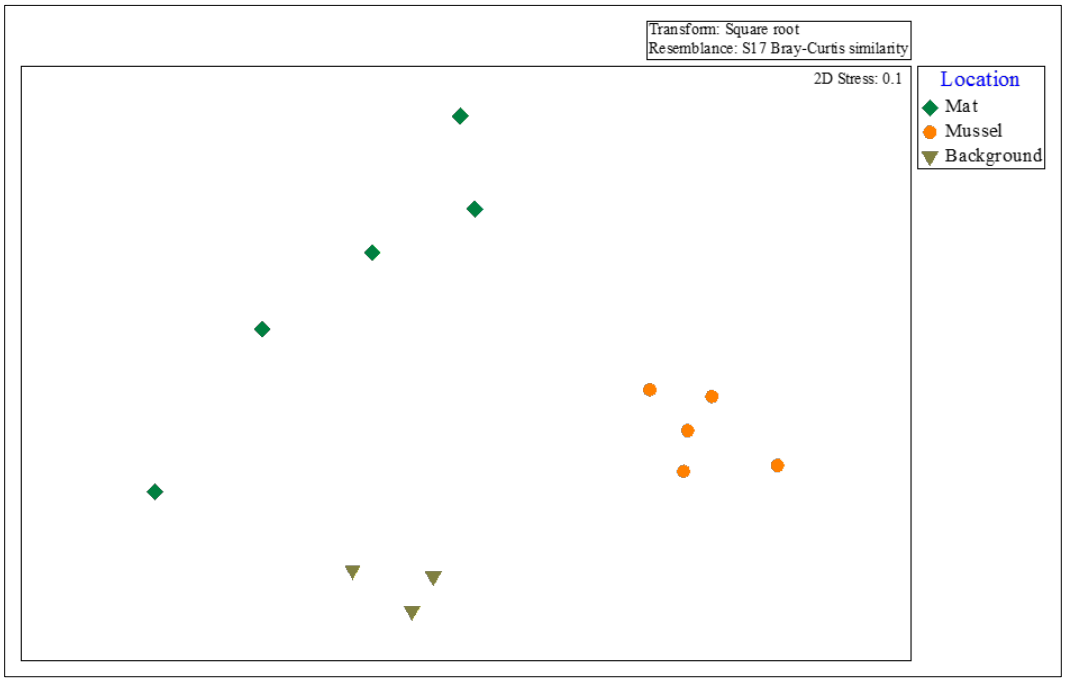

Figure 9-33. Nonmetric multidimensional scaling of cores collected near Norfolk Canyon seep habitats based on Bray-Curtis similarities of square-root transformed abundance data.

Visual observations of sediment cores collected at NCS provided insight into the sediment geochemistry. The surface colors of microbial mats collected were either yellow (**Figure 9-34**) or white. The surface layer (1−7 cm) of all but two of the microbial mat cores had a surface layer (1−7 cm) of brown sediment indicative of oxygen penetration. All of the cores collected near mussels also had a surficial oxygenated layer, ranging from 5 to 8 cm in thickness (**Figure 9-35**). Only one microbial mat

core had a slight sulfidic smell. In contrast, background soft sediment sediment cores (**Figure 9-36**) were characterized by a uniform medium or dark brown color that extended down core to at least 10 cm.

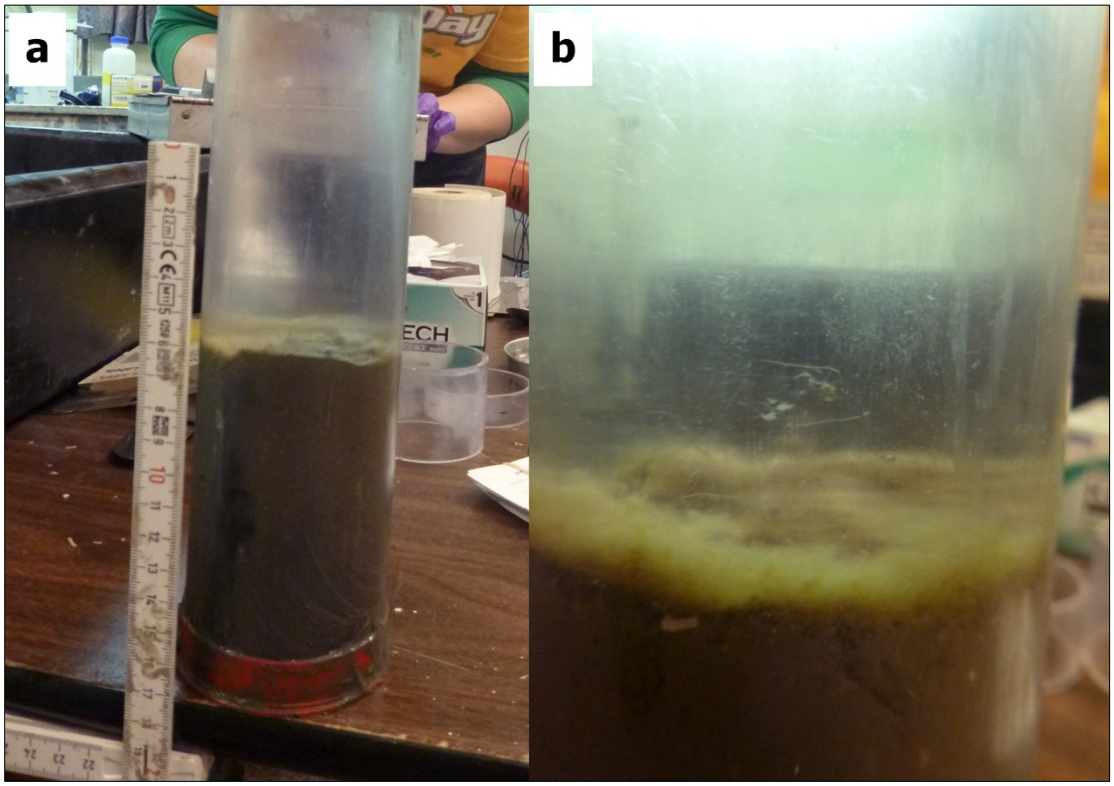

Figure 9-34. a) Push core collected in yellow microbial mat at the Norfolk Canyon seep and b) close-up of yellow microbial mat.

Figure 9-35. Push core collected near mussels at the Norfolk Canyon seep.

Figure 9-36. Push core subsampled from box core of background soft sediments near Norfolk Canyon seep.

9.3.1.2.3 Hard Substrate Habitats

A total of 653 macrofaunal individuals were collected from cores taken near hard substrate habitats in Norfolk Canyon. Individuals encompassed 64 taxa, including 31 Polychaete families, 9 Crustacea families, and 14 Mollusca families.

Macrofaunal density was similar among hard substrate habitats regardless of depth regime or side of the canyon (**Figure 9-37**, one-way ANOVA, $F = 1.32$, df = 3, 9, $p = 0.33$). There was no linear relationship between macrofaunal density and depth for hard substrate habitats (Spearman correlation, $\rho = 0.121$, $p = 0.69$). The proportion of taxa found in the uppermost sediment fraction (0−2 cm, **Figure 9-38**) increased with water depth. Sediments collected from the south side of the canyon exhibited a more even vertical distribution of fauna for each fraction compared with sediments from the north side of the canyon.

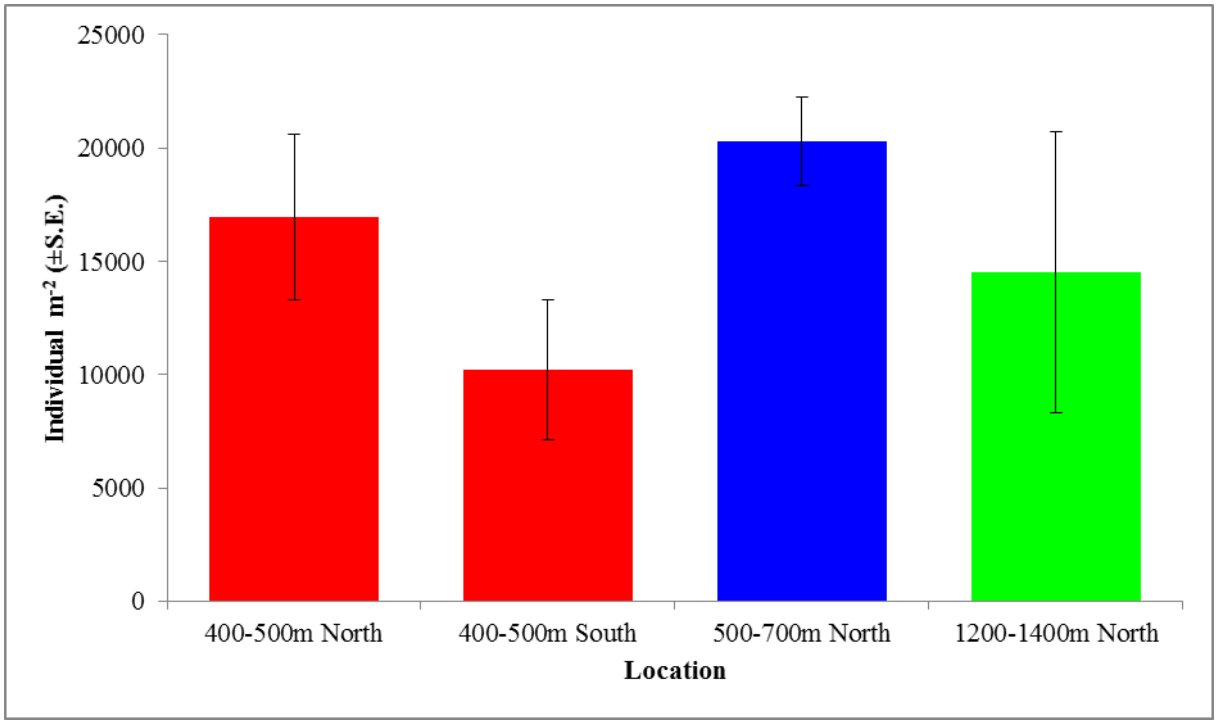

Figure 9-37. Mean macrofaunal density at hard substrate habitats. Error bars represent standard error.

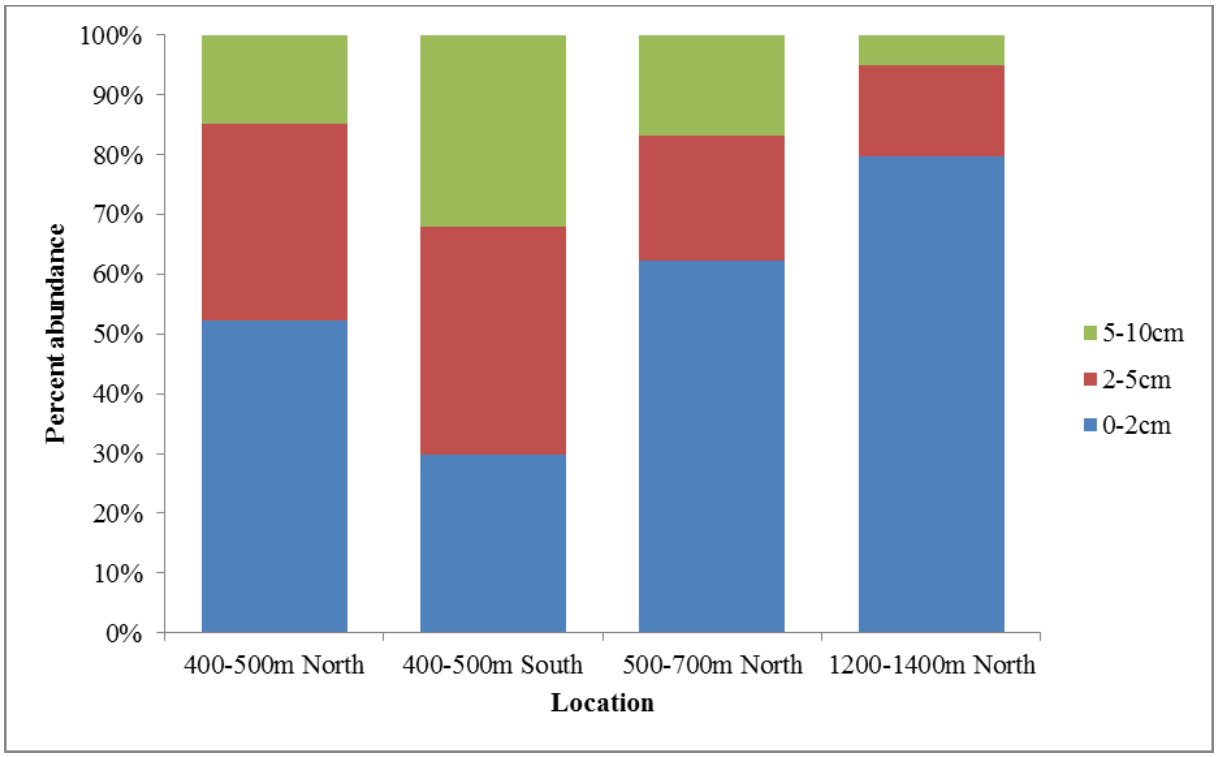

Figure 9-38. Percent abundance of individuals within each vertical sediment fraction for hard substrate habitats.

There was a difference in diversity among hard substrate habitats, potentially related to spatial location within Norfolk Canyon (**Table 9-16**). Shannon-Wiener diversity index ($H'\log_e$) was similar among depth regimes on the north side of the canyon (North) (Tukey's HSD, $p > 0.4$), but was significantly lower on the south side of the canyon (South) compared with similar depths on the north side (Tukey's HSD, $p = 0.018$). Similar diversity results were obtained using rarefaction (**Figure 9-39**) with the lowest diversity occurring at locations on the south side of the canyon. Under sampling was evident within each depth range, with none of the rarefaction lines approaching an asymptote. However, all depth locations combined reached an asymptote, suggesting adequate sampling of the total hard substrate communities within the canyon.

Table 9-16. Macrofaunal diversity at hard bottom habitat locations. Values in parentheses represent one standard error.

Habitat	*N*	*d*	*J'*	*H'*($\log_e$)	Fisher's α	N1	MVDISP
400–500 m North	3	5.53 (0.58)	0.90 (0.02)	2.79 (0.07)	15.61 (1.57)	16.35 (1.20)	0.75
400–500 m South	3	2.71 (0.36)	0.83 (0.06)	1.91 (0.17)	6.21 (1.64)	6.96 (1.10)	1.42
500–700 m North	4	4.54 (0.80)	0.86 (0.02)	2.55 (0.20)	10.45 (2.94)	13.66 (2.66)	0.81
1,200–1,400 m North	3	4.63 (0.62)	0.90 (0.04)	2.55 (0.06)	13.48 (1.84)	12.81 (0.81)	1.21

d = Margalef's species richness; *J'* = Pielou's evenness; *H'*($\log_e$) = Shannon-Wiener diversity index; N1 = Hill's index; MVDISP = multivariate dispersion.

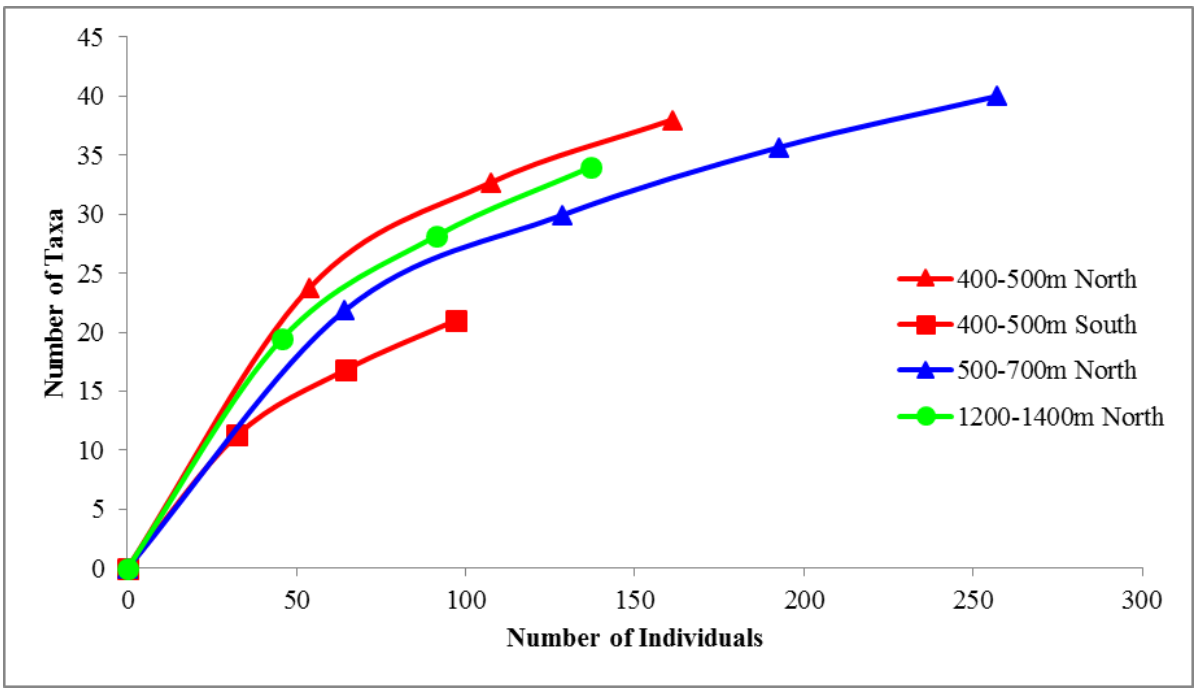

Figure 9-39. Coleman rarefaction of macrofaunal communities at hard substrate habitats.

Macrofaunal communities varied among hard substrate habitats (**Figure 9-40**). Dominance of polychaetes decreased with depth, consistent with patterns observed at similar depths along the canyon axis (**Figure 9-24**), ranging from 56% to 63% at 400 to 500 m depths to 43% at 1,200 to 1,400 m depths. The decreased dominance of polychaetes corresponded to increased proportions of mollusks, which ranged from 2% to 17% at 400–500 m depths up to 40% at 1,200–1,400 m depths. A large proportion of oligochaetes were present at the 400–500 m South location (28%), four times greater than at any other location. Community structure was significantly different among hard substrate habitats (**Figure 9-41**, one-way ANOSIM, $R = 0.54$, $p = 0.001$); however, the low number of replicates per depth range only allowed for pairwise comparisons with 500–700 m North locations. Community structure at 500-700 m North was significantly different from both 400-500 m South ($R = 0.593$, $p = 0.029$) and 1,200–1,400 m North ($R = 0.63$, $p = 0.029$), but was more similar to 400–500 m North ($R = 0.352$, $p = 0.086$). The highest multivariate variability was observed at 400–500 m South, followed by 1,200-1,400 m North (**Table 9-16**, MVDISP).

Macrofaunal densities near hard substrates were similar to densities observed in the canyon axis at the closest comparable depths (550 and 1,110 m, **Section 9.3.1.2.1**). Densities in the 400–500 m and 500-700 m depth ranges (**Figure 9-37**) were similar to those observed at 550 m within the axis, while those collected at 1,200–1,400 m were similar to those collected at 1,110 m (**Figure 9-22**). However, diversity differed among hard substrate and canyon axis communities. Shannon diversity (H') of communities collected on the south side of the canyon (**Table 9-16**) were similar to those observed at 550 m in the canyon axis (**Table 9-12**), while all other hard substrate locations had higher diversity than comparable depths (550 and 1,110 m). In addition, rarefaction of all hard substrate samples exhibited higher diversity than for all samples collected in the canyon axis (**Figure 9-42**), suggesting that hard substrate communities significantly contribute to regional biodiversity.

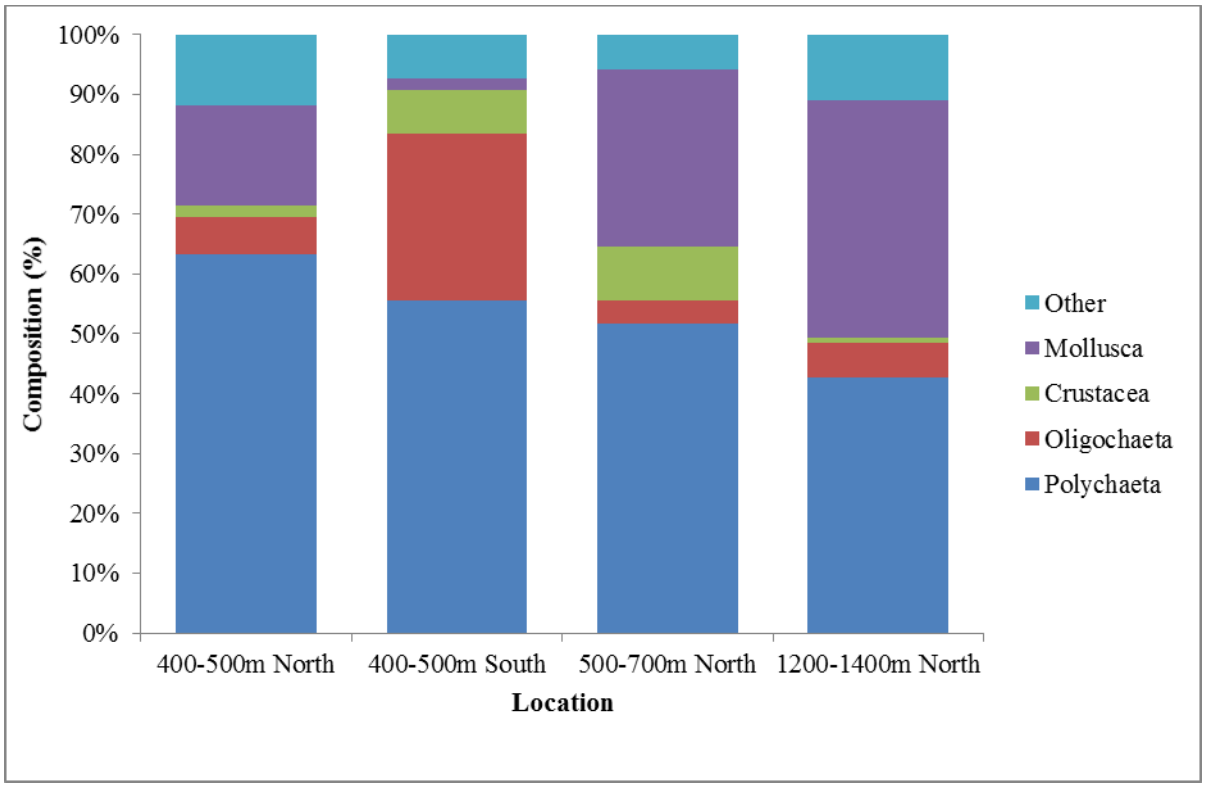

Figure 9-40. Major taxonomic composition of hard substrate macrofaunal communities.

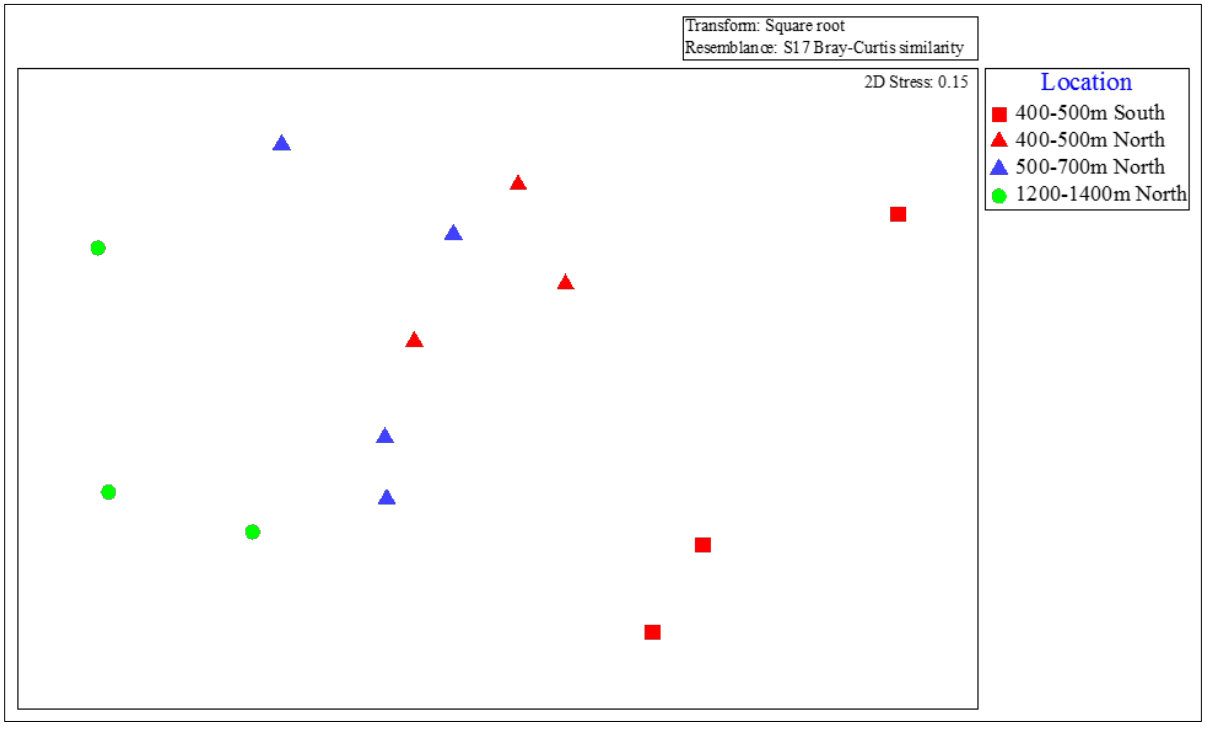

Figure 9-41. Nonmetric multidimensional scaling of cores collected near hard substrate habitats based on Bray-Curtis similarities of square-root transformed abundance data.

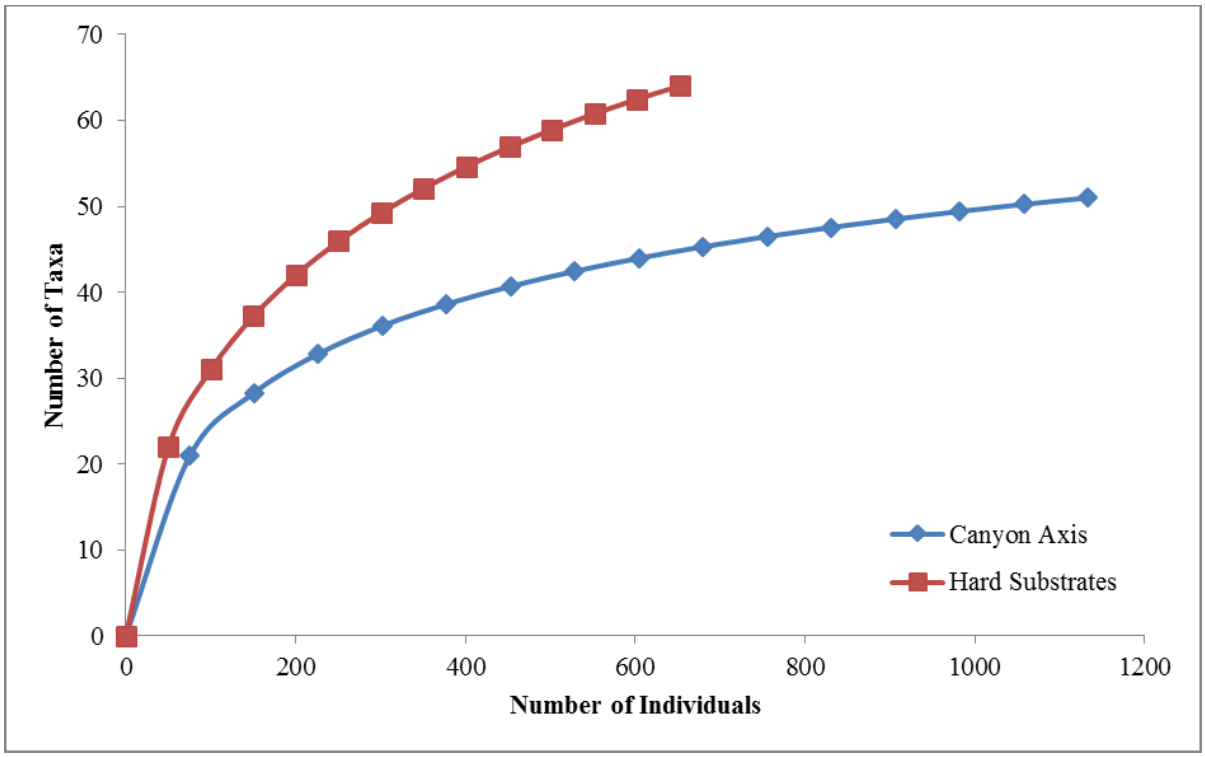

Figure 9-42. Coleman rarefaction of macrofaunal communities in all hard substrate habitats and all depths within the axis of Norfolk Canyon.

9.3.2 Benthic Meiofauna

9.3.2.1 Baltimore Canyon

9.3.2.1.1 Canyon and Slope Habitats

Patterns in meiofaunal density differed between canyon axis and slope locations (**Figure 9-43**). In the canyon axis, the lowest meiofaunal densities occurred at 550 m (Tukey's HSD, $p < 0.002$), similar to macrofaunal densities at the same depth (**Figure 9-7**), and exhibited no overall pattern in densities with depth (Spearman correlation, $\rho = -0.07$, $p = 0.8$). In contrast, meiofaunal density in slope locations increased with depth (Spearman correlation, $\rho = 0.8$, $p = 0.002$), opposite of what occurred in the macrofauna. Pairwise comparison of canyon and slope meiofaunal densities at individual depths revealed that densities in slope habitats at 180 m were significantly lower than canyon stations at 180 m (Kruskal Wallis $\chi^2 = 3.85$, $p = 0.049$).

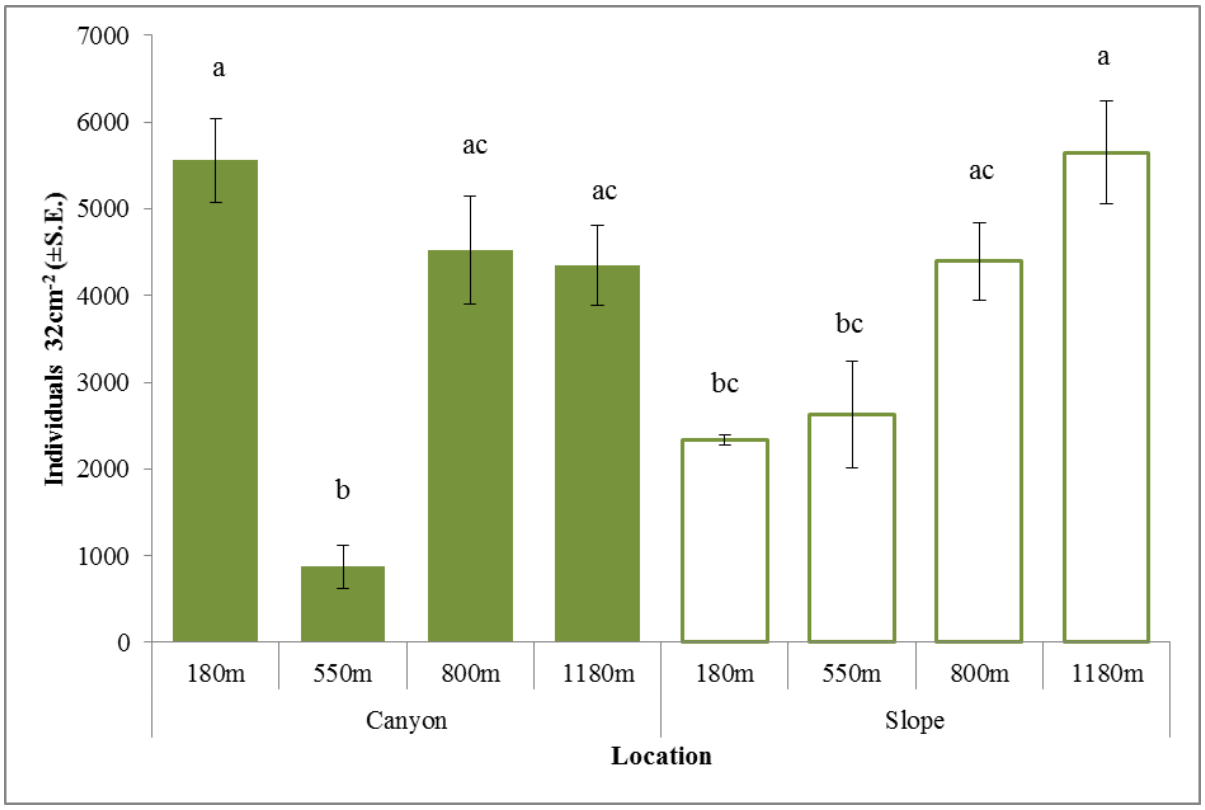

Figure 9-43. Mean meiofaunal density in surface sediments (0 to 2 cm) in Baltimore Canyon axis and slope locations. Letters indicate statistical grouping ($p < 0.05$). Error bars represent standard error.

Overall meiofaunal diversity varied among canyon axis and slope locations. In the canyon, Shannon diversity (**Table 9-17**) increased with depth (Spearman correlation, $\rho = 0.7$, $p = 0.01$). For slope locations, diversity was the highest at the shallow station (180 m) but exhibited no relationship with depth (Spearman correlation, $\rho = -0.3$, $p = 0.4$). Pairwise comparisons of canyon and slope meiofaunal diversity found significantly higher Shannon diversity in 180 m slope habitats (ANOVA, $F = 85.9$, $p < 0.01$) but lower diversity at 900 m slope habitats (ANOVA, $F = 8.4$, $p = 0.04$). Overall community composition also differed among canyon axis and slope locations. Nematodes dominated all sediments (**Figure 9-44**), comprising >75% of the community at all locations. In the canyon axis, dominance of nematodes decreased with depth, replaced by increasing proportions of arthropods. The proportion of mollusks was highest at the 800 m canyon axis location, similar to results documented for macrofaunal communities. In slope locations, the 550 m depth location had the highest dominance of nematodes (95%) while the shallowest station (180 m) had the lowest proportion (75%) of nematodes.

There was a significant difference in meiofaunal community assemblages between canyon and slope habitats (**Figure 9-45**; two-way ANOSIM $R = 0.58$, $p = 0.007$) and among depths (two-way ANOSIM $R = 0.64$, $p = 0.001$). The highest multivariate variability (MVDISP, **Table 9-17**) occurred at the 550 m stations. The carbon to nitrogen ratio (47%), sand content (35%), and percent organic carbon (35%) individually explained a significant portion of the variation (**Figure 9-46**, **Table 9-18**, DistLM, $p < 0.05$) in meiofaunal communities. The C:N ratio, however, provided the "best" explanation for structuring meiofaunal communities (DistLM, AICc = 42.4).

Table 9-17. Meiofaunal diversity at hard bottom habitat locations. Values in parentheses represent one standard error.

Location	*N*	*d*	*J′*	*H′*($\log_e$)	Fisher's α	N1	N:C	EG(51)	Overall MVDISP	Nematode MVDISP
Canyon 180 m	3	1.16 (0.07)	0.20 (0.48)	0.48 (0.01)	1.32 (0.08)	1.62 (0.02)	18.84 (0.81)	25.47 (2.06)	0.64	0.8
Canyon 550 m	3	1.26 (0.10)	0.23 (0.52)	0.52 (0.06)	1.51 (0.14)	1.71 (0.21)	10.68 (4.91)	25.09 (1.01)	1.60	1.787
Canyon 900 m	3	1.19 (0.24)	0.37 (0.86)	0.86 (0.06)	1.36 (0.28)	2.36 (0.16)	5.91 (0.95)	20.63 (0.85)	1.07	0.693
Canyon 1,180 m	3	1.20 (0.14)	0.32 (0.75)	0.75 (0.00)	1.37 (0.17)	2.13 (0.09)	4.41 (0.54)	25.28 (0.90)	0.75	0.293
Slope 180 m	3	1.33 (0.04)	0.36 (0.86)	0.86 (0.02)	1.55 (0.05)	2.38 (0.09)	5.17 (0.65)	25.18 (1.49)	0.29	1.307
Slope 550 m	3	0.84 (0.22)	0.10 (0.22)	0.22 (0.05)	0.97 (0.24)	1.27 (0.17)	146.8 (110)	27.08 (3.27)	1.71	1.6
Slope 900 m	3	1.43 (0.09)	0.21 (0.52)	0.52 (0.04)	1.65 (0.11)	1.70 (0.15)	10.31 (4.13)	22.26 (0.74)	1.47	0.987
Slope 1,180 m	3	1.39 (0.06)	0.24 (0.62)	0.62 (0.01)	1.59 (0.07)	1.86 (0.07)	6.17 (0.72)	22.90 (0.20)	0.48	0.533

d = Margalef's species richness; *J′* = Pielou's evenness; *H′*($\log_e$) = Shannon-Wiener diversity index; N1 = Hill's index; N:C= Nematode to copepod ratio;
EG(51) = nematode diversity as the expected genera in 51 individuals; Overall MVDISP = multivariate dispersion of total meiofaunal community; Nematode MVDISP = multivariate dispersion of nematode community.

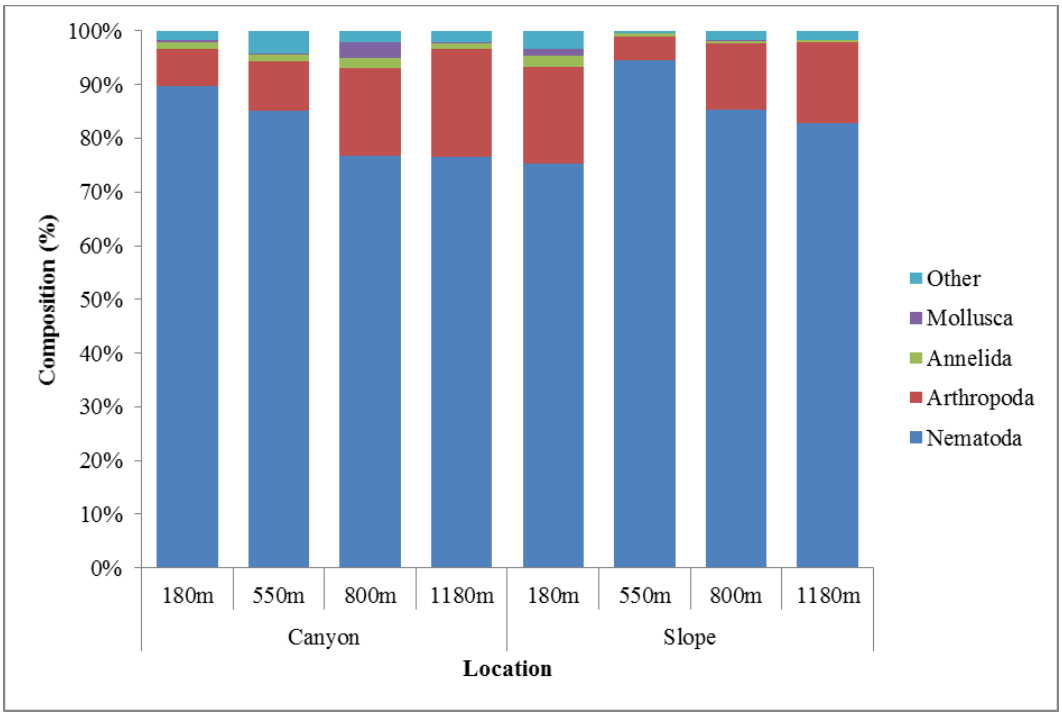

Figure 9-44. Overall meiofaunal taxonomic composition in surface sediments (0 to 2 cm) in Baltimore Canyon axis and slope locations.

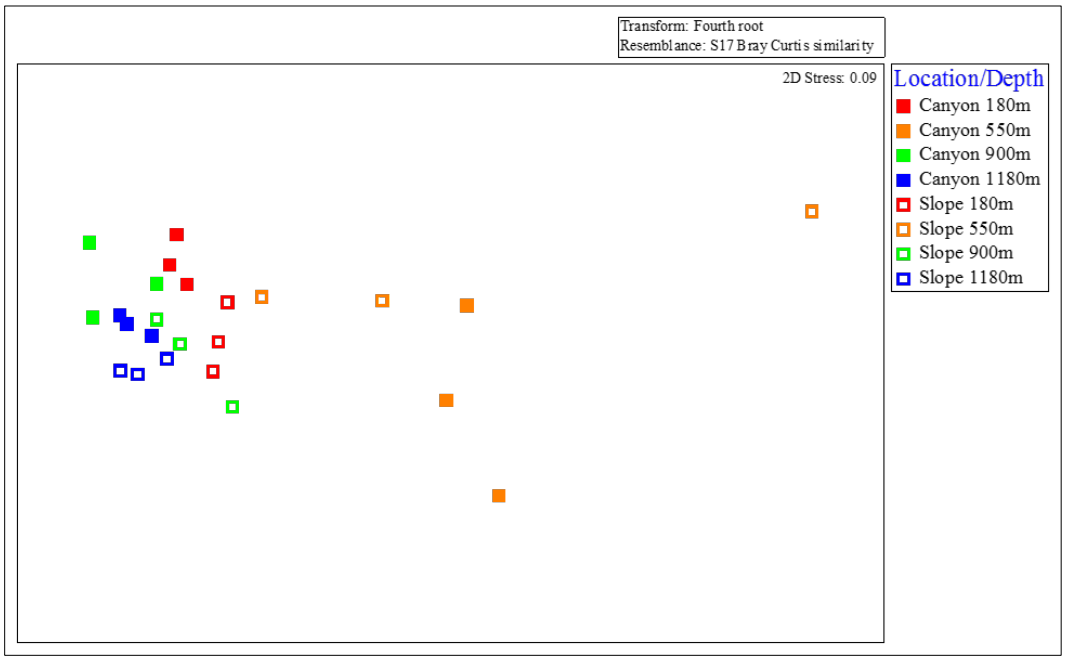

Figure 9-45. Nonmetric multidimensional scaling of Baltimore Canyon and slope meiofaunal community assemblages in surface (0 to 2 cm) sediments based on Bray-Curtis similarities of fourth-root transformed abundance data.

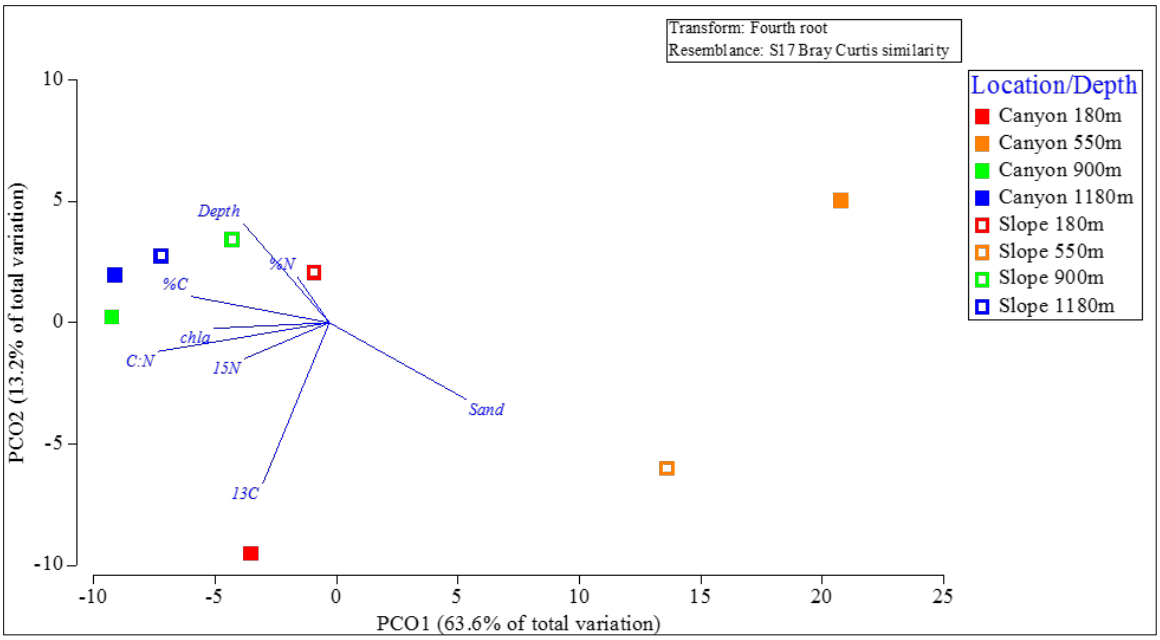

Figure 9-46. Principal coordinates ordination of Baltimore Canyon and slope meiofaunal communities, including environmental parameter vectors. Environmental parameters included sediment grain size, surface sediment chlorophyll *a*, percent organic carbon, percent total nitrogen, $\delta^{13}C$, $\delta^{15}N$, and depth.

Table 9-18. Results from the distance-based linear modeling (DistLM) of environmental variables with overall meiofauna community in Baltimore Canyon and slope environments.

Variable	SS(trace)	Pseudo-*F*	*P*	Prop.
Chlorophyll *a*	361.0	2.156	0.078	0.264
$\delta^{13}C$	217.7	1.138	0.293	0.159
Percent carbon	481.9	3.273	0.047	0.353
$\delta^{15}N$	189.3	0.966	0.377	0.139
Percent nitrogen	144.2	0.709	0.548	0.106
Depth	274.4	1.509	0.218	0.201
Sand content	473.5	3.185	0.045	0.347
C:N	643.97	5.356	0.0044	0.472
AICc	R^2	RSS	Selections	
42.414	0.47166	721.370	C:N	
44.035	0.35297	883.410	Percent carbon	
44.111	0.34678	891.870	Sand content	
45.061	0.26438	1,004.400	Chlorophyll *a*	
45.593	0.60959	533.040	Percent carbon, percent nitrogen	
45.723	0.20096	1,091.000	Depth	
45.925	0.59306	555.610	$\delta^{13}C$, C:N	
46	0.58924	560.830	Sand content, C:N	
46.28	0.15946	1,147.600	$\delta^{13}C$	
46.237	0.57689	577.690	Depth, C:N	
Total SS(trace)	–	1,365.300	–	

AICc = Akaike information criterion, corrected; Prop. = proportion of variance explained by each variable; Pseudo-*F* = pseudo-*F* statistic; R^2 = proportion of explained variation attributable to each variable; SS = sum of squares; RSS = residual sum of squares.

Nematode communities exhibited similar patterns between canyon and slope locations. There was no relationship between nematode genera diversity (EG51) and depth in either canyon (Spearman correlation, $\rho = -0.11$, $p = 0.7$) or slope (Spearman correlation, $\rho = -0.37$, $p = 0.2$) habitats (**Table 9-17**). Although lowest genera diversity occurred at 900 m depths in both canyon and slope habitats, there was no significant difference in diversity among depths in either the canyon (one-way ANOVA, $F = 3.17$, df = 3,8, $p = 0.084$) or slope (Kruskal Wallis, $\chi^2 = 1.97$, $p = 0.57$) habitats. Nematode feeding group composition (**Figure 9-47**) differed between canyon and slope habitats. In slope habitats, selective deposit feeders increased in proportion with increasing depth, while the proportion of epistrate feeders decreased with depth. However, both 550 m canyon and slope locations contained the highest proportion of predators and scavengers (**Figure 9-47**).

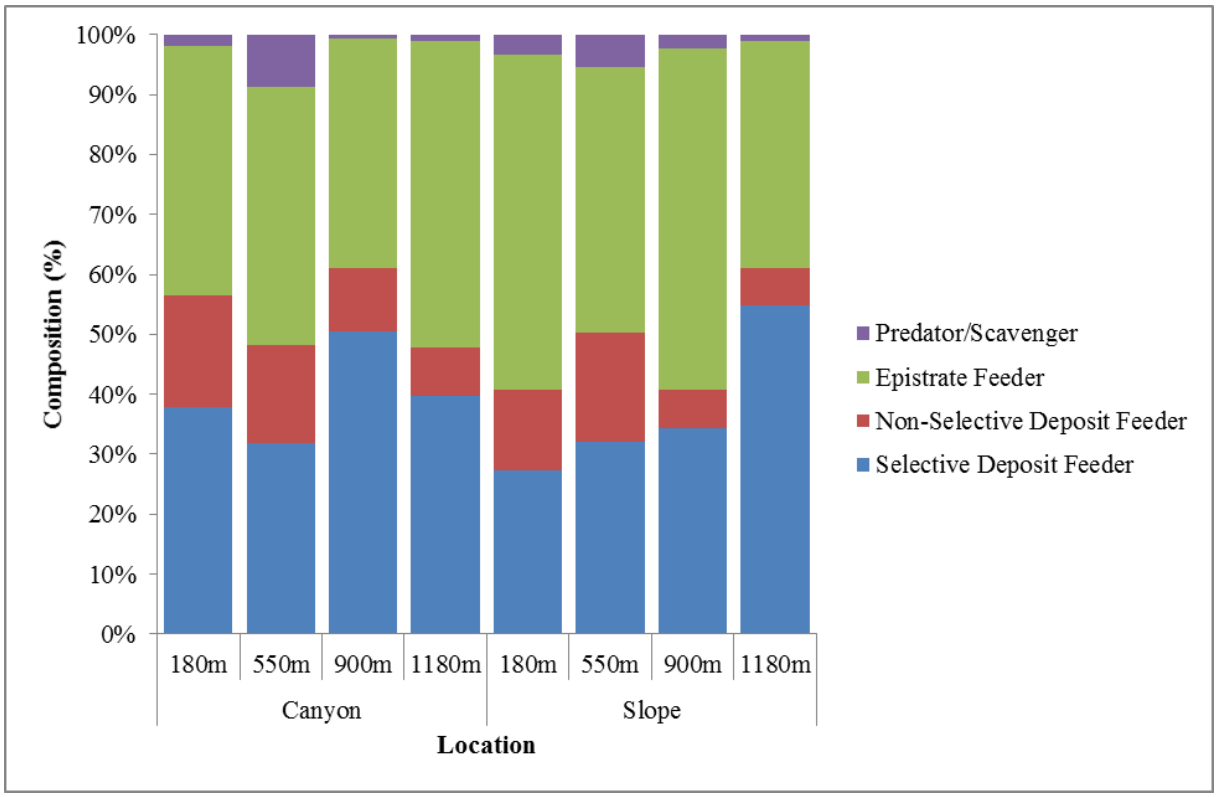

Figure 9-47. Nematode feeding group composition at Baltimore Canyon axis and slope locations.

Nematode genera composition differed between canyon and slope communities (**Figure 9-48**; two way ANOSIM, $R = 0.824$, $p = 0.001$) and among depths (two-way ANOSIM, $R = 0.722$, $p = 0.001$). Depth was the only environmental variable tested that individually explained a significant portion of the variation in nematode communities (DistLM, 20.7%, **Table 9-19**, **Figure 9-49**). Depth additionally provided the "best" explanatory variable combination for structuring nematode communities; however, all the individual variables were within one unit of the AICc value for depth (62.051 to 62.833, **Table 9-19**). The best two-variable combination was depth and the C:N ratio, which explained 36.9% of the variation in nematode communities.

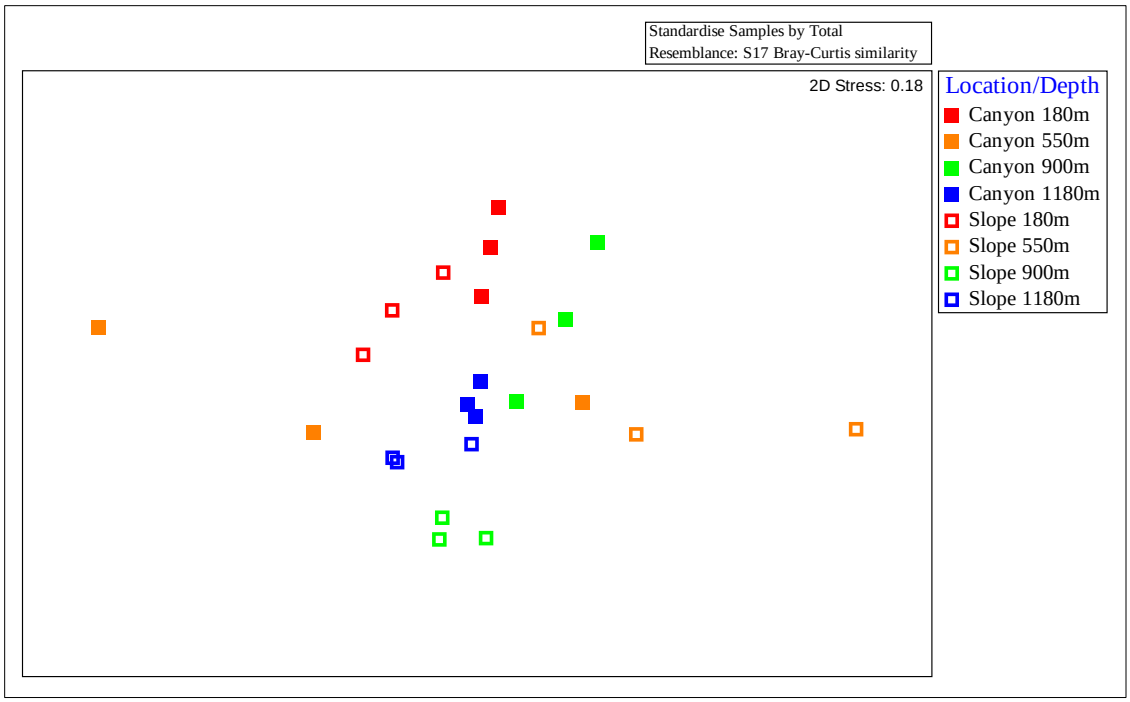

Figure 9-48. Nonmetric multidimensional scaling of Baltimore Canyon and slope nematode community assemblages in surface (0 to 2 cm) sediments based on Bray-Curtis similarities of square-root transformed standardized nematode genera data.

Table 9-19. Results from the distance-based linear modeling (DistLM) of environmental variables with nematode community in Baltimore Canyon and slope environments.

Variable	SS(trace)	Pseudo-*F*	*P*	Prop.
Chlorophyll *a*	1,258.6	0.815	0.748	0.120
$\delta^{13}C$	1,469.3	0.974	0.562	0.140
Percent carbon	1,813.7	1.250	0.159	0.172
$\delta^{15}N$	1,404.1	0.924	0.599	0.133
Percent nitrogen	1,704.1	1.160	0.278	0.162
Depth	2,176.7	1.565	0.038	0.207
Sand content	2,121.9	1.516	0.051	0.202
C:N	1,744.3	1.193	0.2014	0.166
AICc	R^2	RSS	Selections	
61.998	0.20691	8,343.500	Depth	
62.051	0.2017	8,398.300	Sand content	
62.339	0.1724	8,706.500	Percent carbon	
62.403	0.1658	8,775.900	C:N	
62.439	0.16198	8,816.100	Percent nitrogen	
62.649	0.13967	9,050.900	$\delta^{13}C$	
62.707	0.13346	9,116.100	$\delta^{15}N$	
62.833	0.11964	9,261.600	Chlorophyll *a*	
65.772	0.36875	6,640.900	Depth, C:N	
65.835	0.36383	6,692.700	Sand content, C:N	
Total SS(trace)	–	10,520.000	–	

AICc = Akaike information criterion, corrected; Prop. = proportion of variance explained by each variable; Pseudo-*F* = pseudo-*F* statistic; R^2 = proportion of explained variation attributable to each variable; SS = sum of squares; RSS = residual sum of squares.

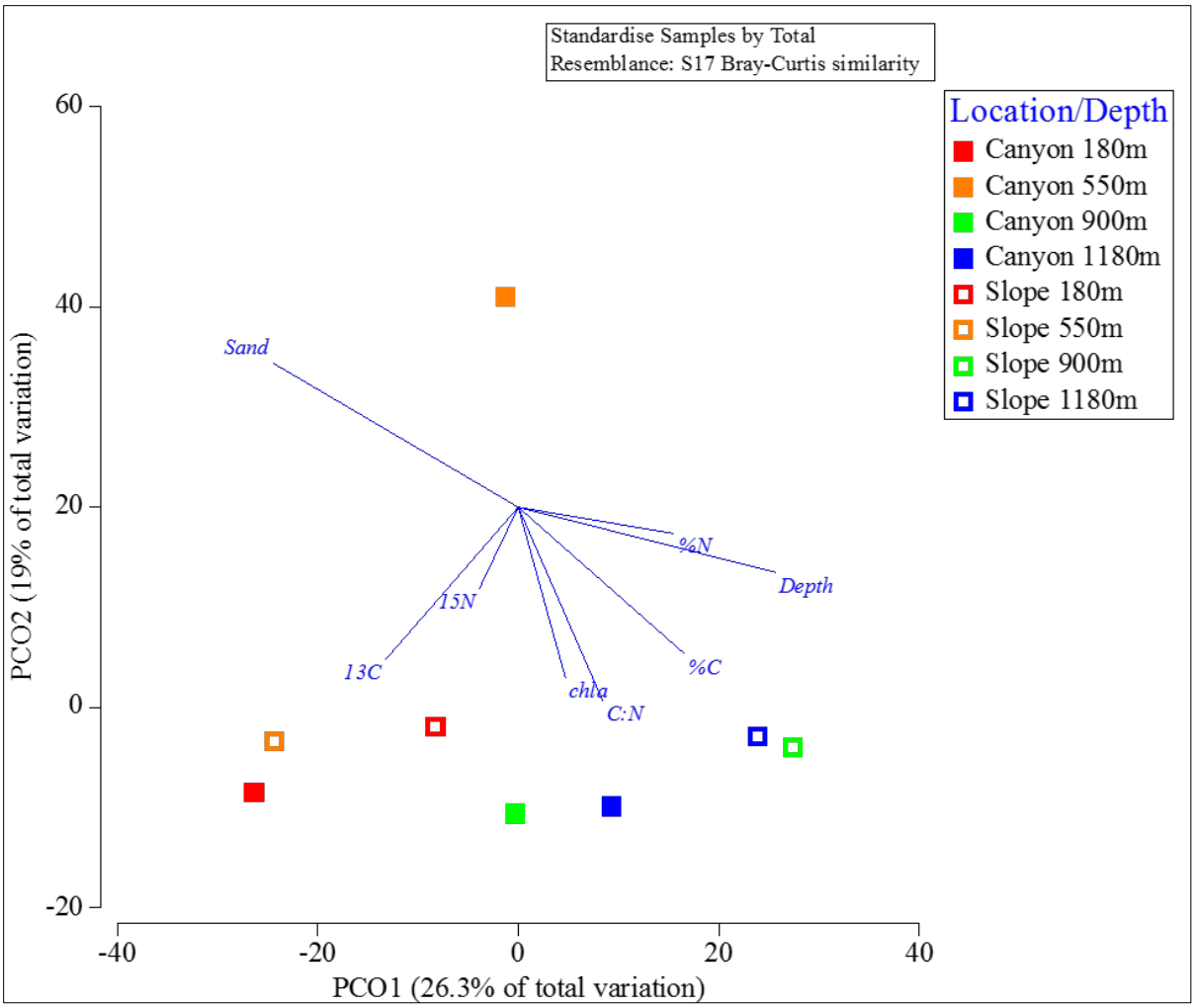

Figure 9-49. Principal coordinates ordination of Baltimore Canyon and slope nematode communities including environmental parameter vectors. Environmental parameters included sediment grain size, surface sediment chlorophyll *a*, percent organic carbon, percent total nitrogen, $\delta^{13}C$, $\delta^{15}N$, and depth.

9.4 DISCUSSION

9.4.1 Canyon Ecosystem Ecology

For this discussion, the macrofauna community trends were considered in the context of the physical environments that shape them. The synergy between canyon and slope geology and sediment dynamics (**Chapter 6**) and oceanographic regimes (**Chapter 5**) creates specific ecological conditions that structure the faunal patterns observed in each canyon. Although the Atlantic Deepwater Canyons study incorporated a multidisciplinary approach to holistically assess benthic community dynamics, only a few of the possible physical pressures that influence these communities were measured. It would therefore not be correct to assume the exact causative drivers that shape the communities, but instead provide an insight into the dynamics of canyon ecosystems, functioning and infaunal distributions.

At both Baltimore and Norfolk study sites, differences were found in the benthic infaunal communities within canyon and slope habitats. Given the proximity of these two canyons to one another (~60 km apart), this finding is surprising. Most community metrics differed significantly between

canyons and slopes and across the depth gradients, supporting the view that canyon systems harbor different communities compared with open slope habitats. Furthermore, data from this study suggest that MAB canyons have highly variable habitats and it is likely that no two canyons in the region are alike. Specific environmental controls were identified as important structuring variables influencing communities found in each of the habitat types.

The relationships among tidally driven water movement, suspended sediment load in the nepheloid layer, and the deposition of sediments are pivotal to understanding and interpreting the benthic community patterns in MAB canyons. These physical processes govern the distribution of currents, sediments, and organic enrichment and are important in explaining differences in faunal communities (**Chapters 4** and **5**). The formation of a hydrographic convergence zone between two water masses at ~800 m, the influence of current speeds on sediment grain size distributions in each zone, and the role of the convergence zone in the maintenance of suspended sediment loading and sediment organic enrichment all represent important environmental drivers that influence soft sediment infaunal communities. Furthermore, geochemical characteristics of habitats used in the analysis are a reflection of physical environmental pressures. Assessing faunal structure and functional roles alongside the environmental gradients in both canyon and slope habitats provides insight into the ecosystem ecology of MAB canyon biomes.

9.4.1.1 Baltimore and Norfolk Canyon Macrofauna

Differences in Baltimore Canyon and slope benthic communities mirror differences documented in the environment (**Chapters 5** and **6**). Baltimore and Norfolk slope macrofaunal densities exhibited steady decreases with increasing depth, consistent with previous studies conducted in other deepsea sediment environments (Levin and Gooday 2003, Rex and Etter 2010). However, in canyon habitats, there was a striking bimodal distribution in both macrofaunal and meiofaunal densities. The highest canyon macrofaunal abundances were recorded at the shallowest stations nearest the shelf, and canyon abundances were almost double that of slope habitats. In Baltimore Canyon, the bimodal distribution in macrofaunal densities (**Figure 9-7**) corresponded with changes in sediment characteristics and organic loading.

Similarly, the suppressed diversity observed at the 900 m canyon station coincided with the shift to finer sediments, organically enriched surface sediments, and slower current speeds, all of which were associated with a well-defined deposition center in the lower reaches of Baltimore Canyon (Zone II as described in **Chapter 6**). The decrease in diversity also corresponded with increased infaunal densities and increased dominance of *Yoldiella* and *Thyasira* bivalve species at 900 m, most likely a consequence of the sediment organic enrichment gradient in Zone II. At deeper canyon communities (1,180 m), deposit-feeding polychaete species, namely *Capitella, Cossura, and Tharyx* species, were among the highest abundances found and are known indicators of organically enriched sediments.

In contrast, shallower stations (550 m) were characterized by sandy sediments left behind because of swift currents winnowing away finer organic-rich sediments. The persistent nepheloid layer arising from this depth zone is indicative of local resuspension, probably associated with the mid-canyon convergence zone in Baltimore Canyon (Gardner 1989, **Chapter 5**). Incorporation of organic matter is reduced by winnowing of organic-rich materials by increased current speeds (Bouma 1965, Vetter and Dayton 1998). Important community assemblage contributors at this depth were surface deposit-feeding mobile polychaete species *Prionospio* sp. and *Nereimyra* sp. and deposit-feeding sessile *Polycirrus* sp. These data suggest that this section in Baltimore Canyon, due to these specific cumulative environmental drivers, including rapid currents and low organic matter content, is a somewhat stressful habitat. High average dispersion value, low densities, and higher species dominance (low evenness *J'*) at mid-canyon stations are consistent with frequent disturbance and community fragmentation caused by the persistent flushing and bi-directional movement of canyon water flows associated with the canyon water mass convergence zone (Zone I, **Chapters 5** and **6**). Similar trends are apparent on the adjacent slope habitat

with decreasing densities and relatively even diversity, as expected from reduced delivery of organic material with increased distance from coastlines, generally reflecting a more quiescent, less disturbed environment. Lower macrofaunal densities and sediment organic concentrations, however, coincide with increasing dispersion values and, in a somewhat contradicting manner, may indicate that mid and lower depth slope habitats endure degrees of environmental pressure that probably differ from canyon habitats.

Vertical distribution within the sediments showed relatively even distributions of resident infauna, especially at slope habitats. Interestingly, resident infauna at 550 m canyon stations showed deeper penetration of the sediment that is likely related to the higher porosity and larger grain size, which allows greater penetration of the oxic layers in the sediment. In contrast, at the 900 m stations, most infauna occurred in the upper layers of the sediment, with less fauna residing in deeper layers and this likely indicates a shallowing of the redox layer as a result of higher sediment enrichment and presumably less oxygen. Furthermore, key community members driving differences between canyon and slope were two dominant bivalve families, Thyasiridae and Yoldiidae. Thyasirid bivalves are known to contain chemoautotrophic endosymbionts, and their high abundance suggests sufficient concentrations of hydrogen sulfide in the sediments (supported by field work observations) to sustain endosymbiotic production (Dando et al. 1991). In addition, Thyasirid genera are burrowing species favoring organic-rich muds and silts. Yoldiidae are also thought to be associated with fine enriched sediments and are a common deepwater species. These two families occurred in high numbers at 900 m canyon stations (36%), presumably benefiting from the undisturbed enriched sediments in the deposition center (Zone II, **Chapter 6**).

Multivariate analyses defined the differences between canyon and slope community assemblages and the environmental variables potentially driving these differences. Nonmetric multidimensional scaling showed clear separation in the community structure of canyon and slope habitats, with increased magnitude of separation and variability along the depth gradient, which can be interpreted as a "canyon effect" on the infaunal community assemblages. Although shallow shelf stations from both habitats were most similar, these similarities declined and community variability increased with depth. An important strength in this study was the simultaneous measurement of physical parameters, sediments, and biogeochemistry, providing valuable explanatory insight of observed patterns in the soft sediment communities. Ordination analyses and distance-based linear models alluded to the importance of sediment grain sizes and enrichment processes in structuring community assemblages for complex deepsea systems, and although these results are encouraging, the models only explain small portions of the variability in the dataset (**Figure 9-13**), leaving a large proportion of community trends unexplained (53%).

This study has resolved the influence of these biogeochemical parameters and can allude to hydrographic pressures acting on the communities. However, the limiting factor has been the ability to directly relate current speeds and tidally driven water movement to both canyon and slope macrofaunal assemblages, due to: 1) the temporal and spatial scale differences between benthic samples and *in situ* canyon oceanographic measurements and 2) the high costs associated with additional deployments of landers and moorings on adjacent slope habitats. Future research fully quantifying the tidally driven hydrography, sediment transport and bed shear stress, along with concomitant measurements of sediment biogeochemistry would be required to further explain canyon-specific ecological patterns. Additionally, the quality and temporal variability of fresh and refractory organic matter reaching these habitats are relatively unknown and would add valuable insight. The influence of seabed topography should not be discounted as a potential variable driving community patterns, and analysis is currently underway to add terrain variables to ordination analyses for both canyons and slopes in order to help estimate their role in structuring infaunal benthos.

In general, macrofaunal densities from Norfolk Canyon and slope habitats followed the same patterns as for Baltimore Canyon habitats. Densities declined along the same depth range as in Baltimore Canyon, potentially a result of similar physical pressures working on communities at the mid-canyon stations

(550 to 900 m). Diversity of slope macrofauna followed a similar pattern to the density data with lower diversity occurring at mid-slope depths, in contrast to the even diversity observed at Baltimore slope habitats. Differences in diversity indices between Norfolk and Baltimore slope habitats indicate some degree of environmental pressures structuring benthic communities and are reflected in high average dispersion values that occurred at deeper Norfolk slope depths.

Interestingly, the density, diversity, and community patterns (**Figures 9-13** and **9-28**) in Norfolk Canyon appear to be very similar to Baltimore Canyon despite the two canyons exhibiting very different sediment profiles, organic enrichment distributions, and hydrographic regimes (**Chapters 5** and **6**). No data were found in Norfolk Canyon to support the presence of a mid-canyon deposition or winnowing. The differences in organic matter distribution between Norfolk and Baltimore canyons may be a function of temporal variability in surface primary production as these two canyons were sampled during different seasons. Norfolk was sampled in a more productive season (May 2013) and, therefore, was perhaps inundated with organic matter deposited during the spring bloom, which would have obscured previous patterns in the organic matter source. This highlights the need for temporally coherent datasets across seasonal patterns. Without such data, temporal changes in environmental and ecological patterns cannot be fully assessed. Nevertheless, our data suggest that infaunal assemblages may show a more sensitive response to canyon processes than snapshot organic matter concentrations.

Generally, sediments in Norfolk Canyon were more homogeneous than in Baltimore Canyon, and they were organically enriched compared with the adjacent slope (and Baltimore Canyon). Sediment chlorophyll *a* concentration in Norfolk Canyon was higher than Baltimore Canyon and did not change significantly with depth. Furthermore, Norfolk Canyon habitats lacked the clear resuspension and deposition zones with depth observed in Baltimore, although sediment enrichment data suggest that the slope stations are more enriched than the canyon habitat and may indicate some deposition zone outside the canyon (**Chapter 6**). This could explain the high diversity at lower slope stations. However, enhanced deposition was not reflected in enhanced concentrations of organic matter, which were overall high along the Norfolk Canyon axis. Sediments on the adjacent slope were composed of increasingly finer sediments and higher porosity with increasing depth. Vertical distributions of infauna showed higher proportions of the community residing in the upper 0 to 5 cm of the sediment, most likely a function of faster current speeds and the deepening of the sediment oxic layer. The proportions of the primary phyla at canyon stations differed between both canyons. Although both canyons exhibited the same overall pattern in macrofaunal densities and diversity, Norfolk had differing proportions of phyla across depth gradients. Most noticeable were the equal proportions of bivalve Mollusca and Polychaeta associated with low abundances at 550 m and the reduced proportions of Mollusca at 800 m compared with Baltimore. Additionally, at deeper slope habitats near Baltimore, large proportions of Crustacea were present, which contrasts with the much lower densities of these taxa near Norfolk at similar depths. Overall, no interpretable pattern seems to be evident and is an example of the difficulty in decoupling biological and environmental data. What is evident, however, is that two similar canyons and slopes harbor different infaunal community structures, despite their proximity.

Community similarity analyses were similar in both canyons, although the spread in community data from Norfolk indicates there is more variability in these environments. The variability, however, may be an artifact of differing sample sizes (box core and push core samples) in each canyon and further efforts are underway to include Norfolk box cores, combine box core and push core datasets, and strengthen our results. Ordination analyses revealed similar influences associated with organic enrichment, sediment grain sizes, and depth. Community differences between the two canyon systems are likely related to sediment regimes and the interaction of hydrography and topography delivering specific influences to the canyon communities. The high (68%) dissimilarity between the two Baltimore Canyon habitats was associated with chlorophyll *a* and percent nitrogen and carbon, driving the separation of the macrofaunal communities between canyon and slope habitats along the depth gradient. Specific polychaete families, Capitellidae, Cirratulidae, and Cossuridae, were identified as important members of the community

responsible for this high dissimilarity. These families are associated with organic enrichment and disturbance, especially for Capitellidae (Pearson and Rosenberg, 1978, Tsutsumi et al. 1990). Unlike in Baltimore Canyon, only one bivalve family (Yoldiidae) was an important community member, based on SIMPER analysis, and the family Thyasiridae was relatively less important. These intercanyon differences may be explained by the differing sediment profiles and current regimes between canyons. Norfolk canyon had twice the current speed of Baltimore Canyon (**Chapter 5**) and sediments were composed of a more homogenous, larger grain size sediment drape, facilitating deeper oxygen penetration and potentially lowering sulfide concentrations, which may explain the lack of Thyasiridae found in Norfolk Canyon.

9.4.1.2 Regional Macrofauna Comparisons

Macrofaunal densities in Baltimore and Norfolk canyons were within the range previously reported for the continental margin off the northeast United States (Blake et al. 1987, Maciolek et al. 1987, Blake and Grassle 1994, Blake and Hilbig 1994), although direct comparisons may be hindered as many studies were not specifically canyon-focused. Abundances reported for the Cape Hatteras continental shelf and margin were slightly higher than those reported here (40,000 to 100,000 individuals m^{-2}; Blake et al. 1994, Blake and Grassle 1994, Aller et al. 2002). Macrofaunal densities at comparable depths in Hudson Canyon (200 to 1,500 m) (1,880 to 9,280 individuals m^{-2}; Rowe et al. 1982) were lower than in this study. Overall, diversity (H') was two-thirds to one-half less (2.43 to 3.46) than H' estimates from noncanyon shelf studies in the western Atlantic ($H' = 6.6$, Grassle and Maciolek 1992), although slope habitats showed higher than expected diversity compared with canyon habitats, in concurrence with the above referenced studies. The differences in diversity estimates between Baltimore and Norfolk canyons were not assessed due to the differing taxonomic resolution. Baltimore Canyon infauna were identified to species level and Norfolk Canyon infauna were identified to family level. Previous Hudson Canyon studies (Rowe et al. 1982) reported canyon diversity estimate ranges ($H' = 3.2$ to 3.99) similar to those found in Baltimore Canyon ($H' = 2.47$ to 3.89) in this study.

Although there are extensive benthic studies (Blake et al. 1987, Maciolek et al. 1987, Blake and Grassle 1994, Blake and Hilbig 1994) examining the macrofaunal abundance and diversity along the U.S. east coast continental margin and rise, across spatial and temporal scales, the Atlantic Deepwater Canyons study represents the first canyon-specific macroinfaunal work for the MAB. Few canyon-specific studies exist for the northwest Atlantic Ocean, although these earlier continental margin studies provide context for general comparisons between MAB canyons and the wider continental margin biodiversity. Additionally, much of the previous benthic macrofaunal research was situated off Cape Hatteras and the margin ecosystems associated with the departure of the Gulf Stream and its heightened productivity from the narrow continental shelf in the region. Comparisons with these studies may therefore not be very meaningful given the stark contrasts between MAB canyon habitats and the high habitat heterogeneity of the MAB shelf and continental rise.

Most studies report considerable variation in macrofaunal densities on the shelf, especially between shelf break depths and the continental slope (500 to <1,200 m). Grassle and Maciolek (1992), Blake and Grassle (1994) and Blake and Hilbig (1994) examined macrofauna from an area slightly south of the MAB shelf across similar depth gradients. High macrofaunal abundances (maximum 89,000 individuals m^{-2}, Blake and Grassle 1994) were reported for the open slope habitats compared with maximum mean of 23,600 individuals m^{-2} (Baltimore Canyon) and 50,000 individuals m^{-2} (Norfolk Canyon), in this study. The study by Grassle and Maciolek (1992) focused on deeper slope and upper rise depths (1,500 to 2,000 m) and together with others (Blake and Maciolek 1994, Blake and Hilbig 1994, Blake and Grassle 1994) represent some of the most comprehensive estimates of abundances and diversity for deepwater slope soft sediment communities.

Results from the ASCAR programme, which was situated slightly farther south than the present study (off Cape Hatteras), yielded very high abundances (highest 89,556 individuals m^{-2} at 530 m, Blake and Hilbig 1994) and diversity (1,202 species) along the continental margin. The stations at 800 m depth off Charleston, South Carolina, were located in one of the most diverse benthic habitats yet encountered in the marine environment (Blake and Grassle, 1994). A total of 436 species were recorded and the highest diversity measurement encountered at any station in the three ACSAR regions ($H' = 6.93$) was more than twice the diversity found in our study. Grassle and Maciolek (1992) combined ACSAR regional datasets to include samples from the Carolinas in the south to the Canadian border in the north (1,500 to 2,200 m), representing an additional 321 box core samples, to assess species numbers present on the northwest Atlantic continental habitats. Taking these samples into account, 1,597 species of benthic invertebrates have been identified from the northwest and mid-Atlantic continental slope. Given that species accumulation curves and rarefaction plots were steep in the relatively homogeneous mid-Atlantic, it is likely that heterogeneous environments, such as those found off the Carolinas, would yield even higher species projections.

These studies (Grassle and Maciolek 1992, Blake and Grassle 1994, Blake and Hilbig 1994) recognized that the U.S. north and mid-Atlantic upper slope has the most diverse communities on the U.S. continental margin and suggested these similarly high diversities across depth contours are probably the result of a greater diversity of sediment types found in the region. These sediment types are influenced by the Gulf Stream and the western boundary undercurrent. Our study found an average of 76 families at Baltimore and Norfolk slope habitats, considerably less than in previous studies (171 families, Grassle and Maciolek, 1992), although our limited sampling effort must be taken into account when comparing estimates of diversity and abundance. However, our study approaches similar numbers of taxa (484) to the above studies at Baltimore sites with a maximum 23,600 individuals m^{-2} at shelf depths and maximum of 50,000 individuals m^{-2} at Norfolk sites. Similarly, Blake and Hilbig (1994) found a mean abundance of macrofauna of 46,255 individuals m^{-2} and reported 280 species from 16 box core samples representing 1.44 m^2 of surface area.

9.4.1.3 Baltimore Canyon Meiofauna

Meiofaunal communities in Baltimore Canyon reflected the environmental conditions observed. The canyon environment is structured by a shift in dynamic conditions, with a resuspension zone at depths shallower than 800 m, characterized by increased grain size, high turbidity, and low food availability. A deposition zone occurs at depths >800 m, characterized by low turbidity, high sedimentation, and high food availability. We observed the greatest change in meiofaunal communities around the transition between the two zones, at 550 and 900 m, with increased variability in the communities. In contrast, the adjacent slope is characterized by low turbidity and food availability at all depths, and there was high variability in meiofaunal communities at the 550 m depth. The high variation at 550 m on the slope may be due in part to moderate sediment resuspension in the area, indicated by the presence of higher turbidity in overlying waters, or from increased habitat heterogeneity since the depth is located in an area of increased slope. Similar changes in meiofaunal communities have been observed along the shelf-slope transition zone offshore Cape Hatteras (Tietjen 1971), coinciding with a change in sediment type from sand to silty sand.

Meiofaunal densities observed in this study were generally higher than those found offshore Cape Hatteras by Tietjen (1971) and Coull et al. (1977), but similar to those reported by Aller and Aller (2002) at comparable depths. The low meiofaunal densities within the canyon at 550 m were similar to all three studies at comparable depths (Tietjen 1971, Coull et al. 1977, Aller and Aller 2002). Meiofaunal densities were also higher than those reported off Martha's Vineyard, Massachusetts (Wigley and McIntyre, 1964); however, their study used a sieve mesh size of 74 µm while our study used the more commonly accepted smaller 45-µm sieve. Thus, meiofaunal densities were expected to be higher in our study due to the sieve size difference. For canyon-specific environments, meiofaunal densities observed

in Baltimore Canyon are similar to those reported for the Whittard Canyon in the northeast Atlantic at similar depths (700 to 100 m, Ingels et al. 2011b), suggesting similarities in meiofaunal population dynamics between canyon systems.

Individual results in this study varied based on the taxonomic level applied, with order level or higher assessed for overall meiofaunal communities and genera level assessed for nematode communities. Since all communities were dominated by nematodes, a decrease in overall meiofaunal diversity highlights the reduction of the rarer taxa, including kinorhynchs, mollusks, tardigrades, peracarid crustaceans, and sipunculids. The increase in overall diversity with depth observed in this study is opposite to diversity patterns observed offshore Cape Hatteras (Tietjen 1971, Coull et al. 1977) where the occurrence of rare taxa decreased with depth. However, the diversity of nematode genera did not change with depth, suggesting that the sediment environment supports similar numbers of genera. Yet the composition of these genera changed with depth, highlighting the importance of taxonomic turnover along a depth gradient for regional biodiversity. Although assessed at the species level, Tietjen (1976) found decreasing nematode diversity with increasing depth. A reduction in overall diversity was most apparent at the 550 m depth habitats, characterized by low food availability and large grain size, suggesting highly dynamic areas. Slight reductions in nematode diversity were observed at the 900 m depth habitat, associated with high sediment organic content and deposition, suggesting a negative response to organic enrichment as seen in other nematode communities (Schratzberger and Warwick 1998, Gambi et al. 2003, Ingels et al. 2009).

The feeding ecology of nematode assemblages present in canyon and slope habitats provides insight into the functional ecology in Baltimore Canyon. Increased proportions of nonselective deposit feeders and predators occurred at shallow (190 m) and mid-canyon (550 m) depths, corresponding with increased sand content, which is consistent with low food availability in the resuspension zone. In contrast, the deeper stations (900 and 1,180 m) located in the deposition zone had higher proportions of selective deposit feeders, corresponding with increased mud and organic content. The smaller buccal cavity in selective deposit feeders (Wieser 1953) suggests a preference for habitats with smaller grain size sediments (e.g., mud), representing material that can be easily ingested. Similar results were observed offshore Cape Hatteras, North Carolina (Tietjen 1971), and in Nazaré Canyon offshore northwest Portugal (Garcia et al. 2007) where nematode feeding groups were related to grain size and food availability. The use of DistLM on multivariate meiofaunal communities has been applied to other canyon systems (Ingels et al. 2011b) and provides insight into how the entire community is responding to the physical environment, as opposed to individual univariate measures (e.g., density, diversity). In both the canyon and slope habitats, meiofaunal abundance increased with the C:N ratio, and both habitats had low C:N (i.e., food quality) and abundance at the 550 m depth. The C:N ratio, a proxy for food quality, can be an indicator of food freshness, with high values indicative of carbon-rich material. Combined with depth, these two environmental parameters provide the best explanation of the variation in meiofaunal and nematode communities among all sampling locations.

Although this study provides a foundation for meiofaunal studies in western Atlantic submarine canyons, the collection scheme only allowed for sampling at a single point in time, limiting our understanding of temporal variability in these communities. Canyons are known to experience episodic events, which can involve temporary increases in sedimentation and/or food availability through transport from cascading events (Canals et al. 2006) or seasonal productivity in surface waters, both of which are known to affect benthic biomass and biodiversity (Soltwedel 2000, Garcia et al. 2007). Although we have addressed some aspects of spatial scale on meiofaunal communities (e.g., station replicates, depth), we are unable to evaluate how temporal variability in food supply and current regime (Glover et al. 2010, Ingels and Vanreusel 2013, Ramalho et al. 2014) may be regulating Baltimore Canyon communities. Given that food availability is the primary structuring agent responsible for meiofaunal communities, we expect factors that affect the deposition of phytodetritus will subsequently have an effect on benthic communities. Due to the temporal fluxes of organic carbon, nitrogen, and pigments observed in sediment

traps deployed in Baltimore Canyon (**Figure 6-18**), we would predict meiofaunal community changes to occur on similar time scales (<1 month) given the short generation time and high turnover potential of meiofaunal communities (Heip et al. 1985). In addition, large-scale disturbance events (e.g., storms) have the capability to produce long-term changes, with interannual differences documented in meiofaunal communities in Nazaré Canyon that lasted multiple years (Ramalho et al. 2014). Future research examining canyon meiofaunal communities and their environment over time will enhance understanding of their sensitivity and response to disturbance over long and short time scales.

Like other submarine canyons around the world, meiofaunal communities in Baltimore Canyon are structured by the physical environment, which is a complex interaction of bathymetric gradients, sediment transport, and food availability. This is the first study of meiofauna in any western Atlantic submarine canyon, and it provides baseline information on density, diversity, and community composition in the MAB. This information is important for understanding meiofaunal community dynamics and how they relate to environmental patterns and also for understanding patterns in macrofaunal and megafaunal communities since meiofaunal communities are responsible for a significant amount of sediment remineralization and support significant trophic pathways (Leguerrier et al. 2003), providing an important role in overall carbon turnover.

9.4.2 Chemosynthetic Systems Ecology

9.4.2.1 Baltimore Canyon Seeps

Density differences among habitat types, similar to those observed at BCS, have been recorded at other seep sites, with macrofaunal abundances in seep habitats commonly higher than in background soft sediments (Levin and Mendoza 2007). However, differences in macrofaunal densities among seep habitats (i.e., microbial mats, clam beds, mussel beds) have been variable (Bernardino et al. 2012). Microbial mat sediments near Costa Rica had macrofaunal densities two times higher than in clam beds (400 to 1,796 m, Bernardino et al. 2012) while those on the Pacific margin (252 to 770 m) had higher densities in clam beds (Levin et al. 2010, Levin et al. 2003, Levin et al. 2006). The high densities observed in microbial mat habitats at BCS differ from the pattern observed at the closest regional seep habitats at Blake Ridge where mussel bed habitats contained higher macrofaunal densities than microbial mats (Robinson et al. 2004), although only two cores were collected near mussel habitats.

Macrofaunal densities in microbial mat sediments in this study (83,649 individuals m^{-2} [SE 28,466], with a maximum of 138,073 individuals m^{-2}) were the second highest recorded for any seep environment. The highest densities recorded were from microbial mats in the Gulf of Mexico (Green Canyon: 700 m, 277,100 individuals m^{-2}). High densities of macrofauna also have been recorded in frenulate fields on the Norwegian margin (Håkon Mosby, 1,256 m, 67,741 individuals m^{-2} [SE 14,743]; Bernardino et al. 2012), microbial mats on the northern California margin (525 m, 62,160 individuals m^{-2}; Levin et al. 2006), and an ampharetid bed in New Zealand (1,057 m, 56,728 individuals m^{-2} [SE 4,784], up to 84,000 individuals m^{-2}; Thurber 2010). Macrofaunal densities in microbial mat and mussel sediments at BCS were at least four times greater than microbial mat and mussel sediments collected at the nearest previously known seep located 802 km to the southeast at Blake Ridge (2,150 m, microbial mats: 1,600 to 2,400 individuals m^{-2}; mussels: 3,600 to 6,400 individuals m^{-2}; Robinson et al. 2004). Given the BCS site is shallower than all these locations and as a result may experience higher concentrations of exported organic matter compared with deeper seeps, we would expect higher densities at the shallower seep. In addition, macrofaunal densities in microbial mats were higher than all other nearby sampled locations (Baltimore Canyon and slope, **Section 9.3.1.1.1**) and were closest in density to shallower (190 m) canyon habitats. Seep sediments at BCS therefore represent an area of unusually high standing stock of infaunal benthos in the mid-Atlantic region, likely a result of the additional food source provided by the seeps in an otherwise food-limited habitat.

Differences in community assemblages and diversity among habitat types have been documented at multiple seep sites worldwide (Bernardino et al. 2012). Low diversity in microbial mat habitats is a general pattern observed at other seeps; for example, microbial mat habitats in Pacific margin seeps had lower diversity than in nearby clam beds (Levin et al. 2010, Bernardino et al. 2012). Microbial mat sediments were dominated by the annelid families Capitellidae, Dorvilleidae, and Tubificidae commonly found in seeps and other organic-enriched environments. Dorvilleids are often a dominant polychaete family in seep communities (Levin 2005), and capitellids are considered opportunistic taxa, highly tolerant to environmental stress. In contrast, sediments adjacent to mussels contained high proportions of crustaceans, particularly amphipods and tanaids. Amphipods are known to be sensitive to organic enrichment and increased hydrocarbon concentrations, and their distribution at BCS may also be reflecting this intolerance to the high methane emissions likely present at microbial mat habitats, which while unmeasured, we expect varying high fluxes over small spatial scales (Sassen et al. 1994, Levin et al. 2003). In addition, the presence of tolerant taxa in microbial mats may indicate high sediment sulfide concentrations that are toxic to many fauna. Higher diversities within mussel and background sediments and higher similarity between habitats (51%) compared with microbial mats (14% to 20%) suggest that these habitats may be more stable and less stressful.

Specific geochemical properties of seep sediments, albeit unmeasured in this study, are likely structuring infaunal communities. Sediments supporting microbial mats are known to sustain high rates of methane emissions, high concentrations of sulfide, and low oxygen penetration (Levin et al. 2003, Bernardino et al. 2012). Although the sediment chemical environment was not quantified, the low oxygen penetration was inferred from the microbial mat cores, consistent with what has been reported in the literature. In contrast, mollusk-dominated habitats (e.g., clam beds) often have lower methane emission rates and lower sulfide concentrations near the sediment surface (Sahling et al. 2002, Boetius and Suess 2004, Levin 2005). Given the similarity of faunal communities between clam bed and mussel bed habitats in previous studies (Menot et al. 2010), we expect similar sediment chemistry in mussel sediments. Animals occupying sediments below microbial mats must be tolerant to high concentrations of sulfide, while those near mussel habitats do not require a high tolerance. The faunal composition, as discussed above, likely reflects these different environmental tolerances.

There are potential limitations to the comparisons made between BCS habitats and background soft sediments. First, all of the background sediments were collected in August 2012, while all but one core of seep sediments were collected in May 2013. Seasonality in surface productivity and hydrodynamic regimes, as well as disturbance events, promotes shifts in community assemblages. However, there was no observed difference in the abundance of taxa in the upper 2 cm of sediments, which might have been expected if there had been an organic enrichment event during this period. Second, three of the four background cores were collected within the axis of Baltimore Canyon, while the seep was located on the adjacent slope. The closest sampled slope location was at 550 m, while the ones used in the analysis from the canyon axis were at 446 m. However, the background core collected near microbial mat habitats (NF12-D08-2, **Table 9-3**) was more similar to the background cores collected within the canyon axis (48% to 65%) than to the mat cores collected 1 m away (16%), suggesting that the inclusion of this sample as a background soft sediment core was appropriate.

9.4.2.2 Norfolk Canyon Seeps

Seep habitats at NCS exhibited patterns in macrofaunal abundance among habitat types that were similar to those observed at BCS, with increased density within microbial mat sediments compared with mussel-associated sediment and background soft sediments. In addition, macrofaunal density in microbial mats was also high at NCS in this study (47,962 individuals m^{-2}, SE 13,547) compared with microbial mat habitats at similar depths in other locations (Bernardino et al. 2012). However, the magnitude of the difference in macrofaunal abundance between habitat pairs was higher at NCS; macrofaunal densities in microbial mat sediments were 4.6 times greater than those in mussel-associated sediments, while at BCS,

microbial mat communities were only three times greater than mussels. The greater difference in densities is likely a result of the greater depth location of NCS habitats. For background soft sediments, faunal communities are typically structured by food availability, where the export of phytodetritus from coastal regions and from surface waters (Rex and Etter 2010) results in decreasing faunal densities with depth where food availability becomes more limited. However, the presence of additional food sources at seeps provides a localized increase in food availability and the capability of supporting highly dense infaunal assemblages. At shallow depths where nonseep food resources are less limited, the additional input of seep production may not be as critical to infauna. Greater differences between seep and nonseep sediment communities have been observed at deeper seeps (Levin 2005), suggesting the greater importance of the additional nutrition source provided by the seep.

The higher proportion of taxa found in the upper 2 cm of sediments in microbial mats versus deeper sediments is a response of taxa to the sediment geochemical environment that surrounds them. Low oxygen and potentially high sulfide restricts the fauna to the surface sediments in microbial mats, while increased oxygen penetration may allow more individuals to survive in deeper sediments at mussel and background sediments. The ability of organisms to survive deeper in the sediment also provides a mechanism to transfer organic material to the subsurface through bioturbation, potentially enhancing food availability in deeper sediments. Similar sediment-depth patterns were reported for mussel-associated sediments sampled in the Gulf of Guinea (Menot et al. 2010) where higher proportions of macrofaunal densities were present subsurface (1 to 5 cm) and suggested to be related to food availability.

There are potential limitations to the comparisons made between NCS habitats and background soft sediments. First, is the difference in methodology used to collect seep cores and background cores, specifically push core versus box core samples. Box corers are known to be susceptible to bow wave effects and allow disturbance to surface layers. Bow wave effects were minimized by reducing the speed of descent of the box corer as it approached the seafloor. Additionally, the NIOZ box corer completely seals upon triggering, preventing the loss of surface sediment layers. The subcoring with push core tubes provides direct sample-size effort comparisons for our study. The second difference is the distance away from the seep location and the location of the box core collections. Box core samples were collected at similar depths; however, the collection location was 18 to 19 km from the seep habitats and was also located at the base of the canyon channel, while the seep habitats were located on the adjacent slope. Canyon and slope communities differ at comparable depths (190 to 1,110 m) at Norfolk Canyon (**Section 9.4.1.2**), suggesting that slope communities at 1,600 m would also differ from those observed in the canyon axis. Given the higher similarity between mussel and background communities at BCS, we would expect nearby soft sediments at NCS to be more similar to the mussel community assemblages.

Like chemosynthetic communities at BCS, community assemblages of sediment macrofauna at NCS are likely driven by the underlying sediment geochemistry associated with microbial mat and mussel habitats. Increased variability was observed in microbial mat communities at NCS compared with mussel communities, while individual samples collected in each habitat had a similar spatial variation (0.1 to 1.7 km, ~100 m in depth); thus, neither distance nor depth accounts for the increased variation. Community variation in microbial mats suggests the geochemical parameters near mussel beds are more consistent across spatial scales than in microbial mats at NCS. Varying fluxes of seepage over small and large spatial scales have been reported on the Pacific margin and Gulf of Mexico seeps (Sassen et al. 1994, Levin et al. 2003), particularly within microbial mat habitats (Sassen et al. 1994). The high variability in microbial mat communities suggests variation in seepage among sampling locations, which is likely to yield high variability in the fauna. Further analysis of sediment geochemistry from microbial mat and mussel habitats will provide specific evidence of the environmental parameters structuring macrofaunal communities.

9.4.3 Hard Substrate Habitat Ecology

A lack of depth-related pattern in macrofaunal densities from hard substrate sediments in Norfolk Canyon was also observed in communities in the canyon axis, suggesting some canyon-specific processes may be influencing both habitats. Canyon axis community patterns were influenced by sediment grain size and organic nitrogen content, resulting in changes in macrofaunal density with sediment transport and food availability. Although hard substrate densities from 400 to 700 m (**Figure 9-37**) were similar to the 550 m canyon axis densities (**Figure 9-22**), we did not see evidence of the increase in macrofaunal densities seen at 800 m in the canyon axis, suggesting some level of decoupling. Other factors may be affecting the fauna adjacent to canyon walls, and decoupling of depth and density patterns may be due to "edge effects" in hydrodynamic flow, by which different amounts of material are deposited from down-canyon currents as well as deposition from cliff faces that may alter the flux of nutrients delivered to sediments. In Monterey Canyon, McClain and Barry (2010) observed an overall decrease in macrofaunal density with depth from 595 m to 1,010 m and 2,500 m in cliff-adjacent sediments; however, their inclusion of only those three depths may have enhanced the density differences among their sites.

Although no patterns were observed for density and diversity among sampling locations on the north side of Norfolk Canyon, a depth-related continuum was observed in community assemblages. Despite the lack of statistical power, the multivariate results suggest that 400 to 500 m communities also differ from those found at 1,200 to 1,400 m, providing a depth separation for <700 m and >1,200 m. One potential explanation for similar communities across a wide depth range (300 m) is the spatial separation of individual sampling locations. Although the depths varied, some samples collected at 400 to 500 m and 500 to 700 m were located closer to each other (0.7 km) than to other samples in the same depth range (2 to 5 km, **Figure 9-6**). Assuming similar environmental parameters are present, physical proximity can promote similar communities due to dispersal constraints of taxa and may even reflect source and sink populations down slope.

The greatest difference among sediment hard substrate communities occurred between those collected on the north side of Norfolk Canyon versus the south side of the canyon, which may be an indicator of the varying hydrodynamic conditions occurring on the north side versus the south side of the canyon. Anticyclonic circulation has been observed in Baltimore Canyon (Hunkins 1988) and other submarine canyons (Durrieu de Madron 1994, She and Klinck 2000), and analogous to river environments, current speeds and sediment deposition differ between inner and outer bends, all suggesting differential hydrodynamic regimes on individual sides of a submarine canyon. High current velocities have been reported from Norfolk Canyon (Hecker et al. 1983, **Chapter 5**). In addition, lander and mooring deployments in this study in Norfolk Canyon indicated that canyon walls have a large influence on flow at mid- and deep-canyon depths (**Chapter 5**). The only comparable dataset is from Monterey Canyon (McClain and Barry 2010) where an entire transect sampled macrofauna from one side of the canyon to the other. McClain and Barry (2010) observed similar reductions in diversity adjacent to cliff faces but no differences in abundance on both sides of the canyon. However, given the increasing evidence that no two canyons are alike (Cunha et al. 2011), comparisons between Monterey Canyon and Norfolk Canyon are limited. However, overall comparisons between north and south sides of the canyon axis are limited due to the limited sampling effort on the south side of the canyon; further sampling would be required to fully assess for differences in biological and environmental parameters.

For communities located on the north side of the canyon, there was no difference in macrofaunal diversity among locations, but diversity was higher than in communities observed at similar depths in the canyon axis (**Tables 9-13** and **9-9**). McClain and Barry (2010) observed declining diversity with depth of cliff faces where the shallowest cliffs sampled (595 m) had the highest diversity whereas macrofauna collected from deeper cliff faces (1,010 and 2,500 m) had the lowest diversity. However, the sampling locations studied by McClain and Barry (2010) were all located in different areas of Monterey Canyon, with only the deep station located along the main canyon axis. Thus, we would expect varying hydrodynamic regimes among stations as opposed to the relatively consistent flow patterns present in the

main axis of Norfolk Canyon. Although the canyon axis communities exhibited patterns that reflected the primary environmental factors within the canyon (e.g., sediment transport, food availability), no similar pattern was observed in hard substrate communities; however, the inclusion of sediment geochemical data in future analyses will help elucidate the relationship of these parameters in hard substrate sediments.

Sediment communities adjacent to hard substrates contribute significantly to the regional biodiversity present in Norfolk Canyon. Despite the slightly lower sampling effort for hard substrate habitats (13 cores) versus the canyon axis (16 cores), a higher number of taxa were encountered in sediments adjacent to hard substrate habitats, and many taxa differed between the two habitats. These results further suggest the presence of different environmental conditions adjacent to hard substrates, given that individual taxa preferentially occupy areas with a specific range of sediment biogeochemical parameters. Although previous studies have focused on the epi-megafaunal communities (e.g., deepsea corals) associated with hard substrates, our results highlight that the scale of influence from these habitats extends some distance away from the hard substrates. The influence of hard substrate habitats on adjacent sediments presented here is consistent with results found for deepsea coral habitats (Demopoulos et al. 2014) where sediment communities up to 1,000 m away differed from other regional soft sediment communities.

9.5 LITERATURE CITED

Allen SE, Durrieu de Madron X. 2009. A review of the role of submarine canyons in deep-ocean exchange with the shelf. Ocean Science Discussions. 5:607–620.

Aller JY, Aller RC. 1986. Evidence for localized enhancement of biological associated with tube and burrow structures in deep-sea sediments at the HEEBLE site, western North Atlantic. Deep-Sea Research Part A: Oceanographic Research Papers. 33:755–790.

Aller JY, Aller RC, Green MA. 2002. Benthic faunal assemblages and carbon supply along the continental shelf/shelf break-slope off Cape Hatteras, North Carolina. Deep-Sea Research Part II: Topical Studies in Oceanography. 49:4599–5625.

Anderson M, Gorley RN, Clarke KR. 2008. PERMANOVA+ for PRIMER: Guide to software and statistical methods. Plymouth (UK): PRIMER-E Ltd.

Baker KD, Wareham VE, Snelgrove PVR, Haedrich RL, Fifield DA, Edinger EN, Gilkinson KD. 2012. Distributional patterns of deep-sea coral assemblages in three submarine canyons off Newfoundland, Canada. Marine Ecology Progress Series. 445:235–249.

Bergquist DC, Ward T, Cordes EE, McNelis T, Howlett S, Kosoff R, Hourdez S, Carney R, Fisher CR. 2003. Community structure of vestimentiferan-generated habitat islands from Gulf of Mexico cold seeps. Journal of Experimental Marine Biology and Ecology. 289:197–222.

Bernardino AF, Levin LA, Thurber AR, Smith CR. 2012. Comparative composition, diversity and trophic ecology of sediment macrofauna at vents, seeps and organic falls. PLoS ONE 7.

Bianchelli S, Gambi C, Zeppilli D, Danovaro R. 2010. Metazoan meiofauna in deep-sea canyons and adjacent open slopes: a large-scale comparison with focus on the rare taxa. Deep-Sea Research Part 1: Oceanographic Research Papers. 57:420–433.

Billet DSM, Lampitt RS, Rice AL, Mantoura RFC. 1983. Seasonal sedimentation of phytoplankton to the deep-sea benthos. Nature. 302:520–522.

Blake JA, Grassle JF. 1994. Benthic community structure on the U.S. South Atlantic slope off the Carolinas: spatial heterogeneity in a current-dominated system. Deep-Sea Research Part II: Topical Studies in Oceanography. 41:835–874.

Blake JA, Hilbig B. 1994. Dense infaunal assemblages on the continental slope off Cape Hatteras, North Carolina. Deep-Sea Research Part II: Topical Studies in Oceanography. 41:875–899.

Blake JA, Hecker B, Grassle JF, Brown B, Wade M, Boehm PD, Baptiste E, Hilbig B, Maciolek N, Petrecca R, Ruff RE, Starczak V, Watling L. 1987. Study of biological processes on the US South Atlantic slope and rise, Phase 2. Final Report for the U.S. Department of the Interior Minerals Management Service under Interagency Agreement No. 14-12-0001-30064. Battelle New England Marine Research Laboratory.

Boetius A, Suess E. 2004. Hydrate Ridge: a natural laboratory for the study of microbial life fueled by methane from near-surface gas hydrates. Chemical Geology. 205:291–310.

Bouma AH. 1965. Sedimentary characteristics of samples collected from some submarine canyons. Marine Geology. 3:291–320.

Brothers LL, Van Dover CL, German CR, Kaiser CL, Yoerger DR, Ruppel CD, Lobecker E, Skarke AD, Wagner JKS. 2013. Evidence for extensive methane venting on the southeastern U.S. Atlantic margin. Geology. 41:807–810.

Burgess R. 2001. An improved protocol for separating meiofauna from sediments using colloidal silica sols. Marine Ecology Progress Series. 214:161–165.

Cacchione DA, Pratson LF, Ogston AS. 2002. The shaping of continental slopes by internal tides. Science. 296:724–727.

Canals M, Puig P, de Madron XD, Heussner S, Palanques A, Fabres J. 2006. Flushing submarine canyons. Nature. 444:354–357.

Carney R, Gibson R, Atkinson R, Gordon J. 2005. Zonation of deep biota on continental margins. Oceanography and Marine Biology Annual Review. 43:211.

Churchill JH, Cornillon PC. 1991. Gulf Stream water on the shelf and upper slope north of Cape Hatteras. Continental Shelf Research. 11:409–431.

Clarke KR, Gorley RN. 2006. PRIMER v6: User Manual/Tutorial. Plymouth (UK): PRIMER-E.

Coull BC, Ellison RL, Fleeger JW, Higgins RP, Hope WD, Hummon WD, Rieger RM, Sterrer WE, Thiel H, Tietjen JH. 1977. Quantitative estimates of the meiofauna from the deep sea off North Carolina, USA. Marine Biology. 39:233–240.

Csanady GT, Hamilton P. 1988. Circulation of slopewater. Continental Shelf Research. 8:565–624.

Csanady GT, Churchill JH, Butman B. 1988. Near-bottom currents over the continental slope in the Mid-Atlantic Bight. Continental Shelf Research. 8:653–671.

Cunha MR, Paterson GLJ, Amaro T, Blackbird S, de Stigter HC, Ferreira C, Glover A, Hilario A, Kiriakoulakis K, Neal L, et al. 2011. Biodiversity of macrofaunal assemblages from three Portuguese submarine canyons (NE Atlantic). Deep-Sea Research Part II: Topical Studies in Oceanography. 58:2433–2447.

Curdia J, Carvalho S, Ravara A, Gage JD, Rodrigues AM, Quintino V. 2004. Deep macrobenthic communities from Nazare Submarine Canyon (NW Portugal). Scientia Marina. 68:171–180.

Dando PR, Austen MC, Burke RA, Kendall MA, Kennicutt MC, Judd AC, Moore DC, O'Hara SCM, Schmaljohann R, Southward AJ. 1991. Ecology of a North Sea pockmark with an active methane seep. Marine Ecology Progress Series. 70:49–63.

De Leo FC, Smith CR, Rowden AA, Bowden DA, Clark MR. 2010. Submarine canyons: hotspots of benthic biomass and productivity in the deep sea. Proceedings of the Royal Society of London: Series B, Biological Sciences. 277:2783–2792.

DeMaster DJ, Pope RH, Levin LA, Blair NE. 1994. Biological mixing intensity and rates of organic carbon accumulation in North Carolina slope sediments. Deep-Sea Research Part II: Topical Studies in Oceanography. 41:735–753.

Demopoulos AWJ, Bourque JR, Frometa J. 2014. Biodiversity and community composition of sediment macrofauna associated with deep-sea *Lophelia pertusa* habitats in the Gulf of Mexico. Deep-Sea Research Part 1: Oceanographic Research Papers. 93:91–103.

Duineveld G, Lavaleye M, Berghuis E, de Wilde P. 2001. Activity and composition of the benthic fauna in the Whittard Canyon and the adjacent continental slope (NE Atlantic). Oceanologica Acta. 24:69–83.

Durrieu de Madron X. 1994. Hydrography and nepheloid structures in the Grand-Rhône canyon. Continental Shelf Research. 14:457–477.

Escobar Briones E, Estrada Santillán EL, Legendre P. 2008. Macrofaunal density and biomass in the Campeche Canyon, Southwestern Gulf of Mexico. Deep-Sea Research Part II: Topical Studies in Oceanography. 55:2679–2685.

Etter RJ, Grassle JF. 1992. Patterns of species diversity in the deep sea as a function of sediment particle size diversity. Nature. 360:576–578.

Folk RL. 1968. Petrology of sediment rocks. Austin (TX): Hemphill Publishing Company.

Forde EB, Stanley DJ, Sawyer WB, Slagle KJ. 1981. Sediment transport in Washington and Norfolk submarine canyons. Applied Ocean Research. 3:59–62.

Gage JD. 1997. High benthic species diversity in deep-sea sediments: the importance of hydrodynamics. In: Ormond RFG, Gage JD, Angel MV, editors. Marine biodiversity: patterns and processes. Cambridge (UK): Cambridge University Press.

Gage JD, Lamont PA, Tyler PA. 1995. Deep-sea macrobenthic communities at contrasting sites off Portugal, preliminary results: introduction and diversity comparisons. Internationale Revue der gesamten Hydrobiologie und Hydrographie. 80:235–250.

Gambi C, Vanreusel A, Danovaro R. 2003. Biodiversity of nematode assemblages from deep-sea sediments of the Atacama slope and trench (South Pacific Ocean). Deep-Sea Research Part 1: Oceanographic Research Papers. 50:103–117.

Garcia R, Koho KA, De Stigter HC, Epping E, Koning E, Thomsen L. 2007. Distribution of meiobenthos in the Nazare Canyon and adjacent slope (western Iberian Margin) in relation to sedimentary composition. Marine Ecology Progress Series. 340:207–220.

García R, van Oevelen D, Soetaert K, Thomsen L, De Stigter HC, Epping E. 2008. Deposition rates, mixing intensity and organic content in two contrasting submarine canyons. Progress in Oceanography. 76:192–215.

Gardner WD. 1989. Baltimore Canyon as a modern conduit of sediment to the deep sea. Deep-Sea Research Part A: Oceanographic Research Papers. 36:323–358.

Gibson RN, Atkinson RJA, Gordon JDM. 2005. Zonation of deep biota on continental margins. Oceanography and Marine Biology Annual Review. 43:211–278.

Glover AG, Gooday AJ, Bailey DM, Billett DSM, Chevaldonné P, Colaco A, Copley J, Cuvelier D, Desbruyeres D, Kalogeropoulou V. 2010. Temporal change in deep-sea benthic ecosystems: a review of the evidence from recent time-series studies. Advances in Marine Biology. (58):1–95.

Grassle JF, Maciolek NJ. 1992. Deep-sea species richness: regional and local diversity estimates from quantitative bottom samples. The American Naturalist. 139:313–341.

Harris, PT, Whiteway T. 2011. Global distribution of large submarine canyons: geomorphic differences between active and passive continental margins. Marine Geology. 285:69–86.

Hecker B, Blechschmidt G. 1979. Final historical coral report for the canyon assessment study in the Mid- and North Atlantic areas of the U.S. Outer Continental Shelf. Prepared for the US Department of the Interior, Bureau of Land Management. Palisades (NY): Lamont-Doherty Geological Observatory.

Hecker B, Logan DT, Gandarillas FE, Gibson PR. 1983. Canyon and Slope Processes Study, Vol. III: Biological Processes. Prepared for the US Department of the Interior, Minerals Management Service. Palisades (NY): Lamont-Doherty Geological Observatory. [accessed 2016 June 1]; 212 p. http://invertebrates.si.edu/boem/reports/CASPS_vol3.pdf.

Heip C, Vincx M, Vranken G. 1985. The ecology of marine nematodes. Oceanography and Marine Biology Annual Review. 23:399–489.

Houston KA, Haedrich RL. 1984. Abundance and biomass of macrobenthos in the vicinity of Carson Submarine Canyon, northwest Atlantic Ocean. Marine Biology. 82:301–305.

Hunkins K. 1988. Mean and tidal currents in Baltimore Canyon. Journal of Geophysical Research: Oceans. 93:6917–6929.

Huvenne VAI, Tyler PA, Masson DG, Fisher EH, Hauton C, Hühnerbach V, Le Bas TP, Wolff GA. 2011. A picture on the wall: innovative mapping reveals cold-water coral refuge in submarine canyon. PLoS ONE. 6:e28755.

Ingels J, Vanreusel A. 2013. The importance of different spatial scales in determining structural and functional characteristics of deep-sea infauna communities. Biogeosciences, 10:4547–4563.

Ingels J, Kiriakoulakis K, Wolff GA, Vanreusel A. 2009. Nematode diversity and its relation to the quantity and quality of sedimentary organic matter in the deep Nazaré Canyon, western Iberian Margin. Deep-Sea Research Part 1: Oceanographic Research Papers. 56:1521–1539.

Ingels J, Billett DSM, Kiriakoulakis K, Wolff GA, Vanreusel A. 2011a. Structural and functional diversity of Nematoda in relation with environmental variables in the Setubal and Cascais canyons, western Iberian Margin. Deep-Sea Research Part II: Topical Studies in Oceanography. 58:2354–2368.

Ingels J, Tchesunov AV, Vanreusel A. 2011b. Meiofauna in the Gollum Channels and the Whittard Canyon, Celtic Margin-how local environmental conditions shape nematode structure and function. PLoS ONE 6.

Jones CG, Lawton JH, Shachak M. 1996. Organisms as ecosystem engineers. In: Samson FB, Knopf FK, editors. Ecosystem management. New York (NY): Springer. doi:10.1007/978-1-4612-4018-1_14. p. 130–147.

Keller GH, Shepard FP. 1978. Currents and sedimentary processes in submarine canyons off the northeast United States. Sedimentation in submarine canyons, fans, and trenches. Stroudsburg (PA): Dowden, Hutchinson and Ross.

Kochevar RE, Childress JJ, Fisher CR, Minnich E. 1992. The methane mussel: roles of symbiont and host in the metabolic utilization of methane. Marine Biology. 112:389–401.

Leguerrier D, Niquil N, Boileau N, Rzeznik J, Sauriau P-G, Le Moine O, Bacher C. 2003. Numerical analysis of the food web of an intertidal mudflat ecosystem on the Atlantic coast of France. Marine Ecology Progress Series. 246:17–37.

Levin LA. 2005. Ecology of cold seep sediments: Interactions of fauna with flow, chemistry and microbes. Oceanography and Marine Biology Annual Review. 43:1–46.

Levin L, Gooday AJ. 2003. The deep Atlantic Ocean. In: Tyler PA, editor. Ecosystems of the world volume 28: ecosystems of the deep ocean, book 28. Amsterdam (NL): Elsevier.

Levin LA, Mendoza GF. 2007. Community structure and nutrition of deep methane-seep macrobenthos from the North Pacific (Aleutian) margin and the Gulf of Mexico (Florida Escarpment). Marine Ecology. 28:131–151.

Levin LA, Dayton PK. 2009. Ecological theory and continental margins: where shallow meets deep. Trends in Ecology & Evolution. 24:606–617.

Levin LA, Sibuet M. 2012. Understanding continental margin biodiversity: a new imperative. Annual Review of Marine Science. 4:79.

Levin LA, James DW, Martin CM, Rathburn AE, Harris LH, Michener RH. 2000. Do methane seeps support distinct macrofaunal assemblages? Observations on community structure and nutrition from the northern California slope and shelf. Marine Ecology Progress Series. 208:21–39.

Levin L, Etter RJ, Rex MA, Gooday AJ, Smith CR, Pineda J, Stuart CT, Hessler RR, Pawson D. 2001. Environmental influences on regional deep-sea species diversity. Annual Review of Ecology, Evolution, and Systematics. 32:51–93.

Levin LA, Ziebis W, Mendoza GF, Growney VA, Tryon MD, Brown KM, Mahn C, Gieskes J, Rathburn AE. 2003. Spatial heterogeneity of macrofauna at northern California methane seeps: influence of sulfide concentration and fluid flow. Marine Ecology Progress Series. 265:123–139.

Levin LA, Ziebis W, Mendoza GF, Growney-Cannon V, Walther S. 2006. Recruitment response of methane-seep macrofauna to sulfide-rich sediments: an *in situ* experiment. Journal of Experimental Marine Biology and Ecology. 330:132–150.

Levin LA, Mendoza GF, Gonzalez JP, Thurber AR, Cordes EE. 2010. Diversity of bathyal macrofauna on the northeastern Pacific margin: the influence of methane seeps and oxygen minimum zones. Marine Ecology. 31:94–110.

Maciolek N, Grassle JF, Hecker B, Boehm PD, Brown B, Dade B, Steinhauer WG, Baptiste E, Ruff RE, Petrecca R. 1987. Study of the biological processes on the U.S. mid-Atlantic slope and rise: volume 2. Final Report prepared for the US Department of the Interior, Minerals Management Service.

McClain CR, Barry JP. 2010. Habitat heterogeneity, disturbance, and productivity work in concert to regulate biodiversity in deep submarine canyons. Ecology. 91:964–976.

Menot L, Galéron J, Olu K, Caprais JC, Crassous P, Khripounoff A, Sibuet M. 2010. Spatial heterogeneity of macrofaunal communities in and near a giant pockmark area in the deep Gulf of Guinea. Marine Ecology. 31:78–93.

Mortensen PB, Buhl-Mortensen L, Freiwald A, Roberts JM. 2005. Deep-water corals and their habitats in The Gully, a submarine canyon off Atlantic Canada. In: Freiwald A, Roberts JM, editors. Cold-water corals and ecosystems. Berlin Heidelberg: Springer-Verlag.

Obelcz J, Brothers D, Chaytor J, Brink Ut, Ross SW, Brooke S. 2014. Geomorphic characterization of four shelf-sourced submarine canyons along the U.S. Mid-Atlantic continental margin. Deep-Sea Research Part II: Topical Studies in Oceanography. 104:106–119.

Orejas C, Gori A, Iacono CL, Puig P, Gili JM, Dale MRT. 2009. Cold-water corals in the Cap de Creus canyon, northwestern Mediterranean: spatial distribution, density and anthropogenic impact. Marine Ecology Progress Series. 397:37–51.

Paull CK, Ussler W, Borowski WS, Spiess FN. 1995. Methane-rich plumes on the Carolina continental rise: associations with gas hydrates. Geology. 23:89–92.

Pearson TH, Rosenburg R. 1978. Macrobenthic succession in relation to organic enrichment and pollution of the marine environment. Oceanography and Marine Biology Annual Review. 16:229–311.

Puig P, Palanques A, Martín J. 2014. Contemporary sediment-transport processes in submarine canyons. Annual Review of Marine Science. 6:53–77.

Ramalho SP, Adão H, Kiriakoulakis K, Wolff GA, Vanreusel A, Ingels J. 2014. Temporal and spatial variation in the Nazaré Canyon (western Iberian margin): Inter-annual and canyon heterogeneity effects on meiofauna biomass and diversity. Deep-Sea Research Part 1 Oceanographic Research Papers 83:102–114.

R Development Core Team. 2011. R: a language an environment for statistical computing. Vienna (AU): R Foundation for Statistical Computing.

Rex MA, Etter RJ. 2010. Deep-sea biodiversity: pattern and scale. Harvard (MA): Harvard University Press.

Rex MA, McClain CR, Johnson NA, Etter RJ, Allen JA, Bouchet P, Warén A. 2005. A source sink hypothesis for abyssal biodiversity. The American Naturalist. 165:163–178.

Robinson CA, Bernhard JM, Levin LA, Mendoza GF, Blanks JK. 2004. Surficial hydrocarbon seep infauna from the Blake Ridge (Atlantic Ocean, 2150 m) and the Gulf of Mexico (690–2240 m). Marine Ecology. 25:313–336.

Ross SW, Rhode M, Quattrini AM. 2015. Demersal fish distribution and habitat use within and near Baltimore and Norfolk Canyons, U.S. middle Atlantic slope. Deep-Sea Research Part 1: Oceanographic Research Papers. 103:137–154.

Rowe GT. 1971. Observations on bottom currents and epibenthic populations in Hatteras Submarine Canyon. Deep-Sea Research and Oceanographic Abstracts. 18:569–576.

Rowe GT, Polloni PT, Haedrich RL. 1982. The deep-sea macrobenthos on the continental margin of the northwest Atlantic Ocean. Deep-Sea Research Part A: Oceanographic Research Papers. 29:257–278. doi:10.1016/0198-0149(82)90113-3.

Sahling H, Rickert D, Lee RW, Linke P, Suess E. 2002. Macrofaunal community structure and sulfide flux gas hydrate deposits from the Cascadia convergent margin, NE Pacific. Marine Ecology Progress Series. 231:121–138.

Sassen R, MacDonald IR, Requejo AG, Guinasso NL, Kennicutt M, Sweet ST, Brooks JM. 1994. Organic geochemistry of sediments from chemosynthetic communities, Gulf of Mexico slope. Geo-Marine Letters. 14:110–119.

Schaff TR, Levin L, Blair N, DeMaster D, Pope R, Boehme S. 1992. Spatial heterogeneity of benthos on the Carolina continental slope: large (100 km)-scale variation. Marine Ecology Progress Series. 88:143–160.

Schratzberger M, Warwick RM. 1998. Effects of the intensity and frequency of organic enrichment on two estuarine nematode communities. Marine Ecology Progress Series. 164:83–94.

She J, Klinck JM. 2000. Flow near submarine canyons driven by constant winds. Journal of Geophysical Research: Oceans. 105:28671–28694.

Shepard FP, Marshall NF, McLoughlin PA. 1974. Currents in submarine canyons. Deep-Sea Research and Oceanographic Abstracts. 21:691–706.

Skarke A, Ruppel C, Kodis M, Brothers D, Lobecker E. 2014. Widespread methane leakage from the sea floor on the northern US Atlantic margin. Nature Geoscience. 7:657–661.

Smith CR, De Leo FC, Bernardino AF, Sweetman AK, Arbizu PM. 2008. Abyssal food limitation, ecosystem structure and climate change. Trends in Ecology & Evolution. 23:518–528.

Soltwedel T. 2000. Metazoan meiobenthos along continental margins: a review. Progress in Oceanography. 46:59–84.

Thistle D, Yingst JY, Fauchald K. 1985. A deep-sea benthic community exposed to strong near-bottom currents on the Scotian Rise (western Atlantic). Marine Geology. 66:91–112.

Thurber AR. 2010. Microbe-metazoan interactions at Pacific Ocean methane seeps [Ph.D. Dissertation]. San Diego (CA): University of California San Diego.

Tietjen JH. 1971. Ecology and distribution of deep-sea meiobenthos off North Carolina. Deep-Sea Research and Oceanographic Abstracts. 18:941–957.

Tietjen JH. 1976. Distribution and species diversity of deep-sea nematodes off North Carolina. Deep-Sea Research and Oceanographic Abstracts. 23:755–768.

Tsutsumi H, Fukunaga S, Fujita N, Sumida M. 1990. Relationship between growth of *Capitella* sp. and organic enrichment of the sediment. Marine Ecology Progress Series. 63:157–162.

Van Dover CL, Trask JL. 2000. Diversity at deep-sea hydrothermal vent and intertidal mussel beds. Marine Ecology Progress Series. 195:169–178.

Van Dover CL, Aharon P, Bernhard JM, Caylor E, Doerries M, Flickinger W, Gilhooly W, Goffredi SK, Knick KE, Macko SA, et al. 2003. Blake Ridge methane seeps: characterization of a soft-sediment, chemosynthetically based ecosystem. Deep-Sea Research Part 1: Oceanographic Research Papers. 50:281–300.

Vetter EW, Dayton PK. 1998. Macrofaunal communities within and adjacent to a detritus-rich submarine canyon system. Deep-Sea Research Part II: Topical Studies in Oceanography. 45:25–54.

Vetter EW, Dayton PK. 1999. Organic enrichment by macrophyte detritus, and abundance patterns of megafaunal populations in submarine canyons. Marine Ecology Progress Series. 186:137–148.

Vetter EW, Smith CR, De Leo FC. 2010. Hawaiian hotspots: enhanced megafaunal abundance and diversity in submarine canyons on the oceanic islands of Hawaii. Marine Ecology. 31:183–199.

Warwick RM, Clarke KR. 1993. Increased variability as a symptom of stress in marine communities. Journal of Experimental Marine Biology and Ecology. 172:215–226.

Weaver P, Billett DSM, Boetius A, Danovaro R, Freiwald A, Sibuet M. 2004. Hotspot ecosystem research on Europe’s deep-ocean margins. Oceanography. 17:132–143.

Wieser W. 1953. The relationship between oral cavity shape, eating habits and occurrence in wild marine nematodes: an environmentally-morphological study. Arkiv för Zoologi. 2:439–484.

Wigley RL, McIntyre AD. 1964. Some quantitative comparisons of offshore meiobenthos and macrobenthos south of Martha's Vineyard. Limnology and Oceanography. 9:485–493.

Yoder JA, Atkinson LP, Bishop S, Blanton JO, Lee TN, Pietrafesa LJ. 1985. Phytoplankton dynamics within Gulf Stream intrusions on the southeastern United States continental shelf during summer 1981. Continental Shelf Research. 4:611–635.

Zar JH. 1999. Biostatistical analysis. Upper Saddle River (NJ): Prentice Hall.

CHAPTER 10. A MOLECULAR PERSPECTIVE ON ANOMURAN BIODIVERSITY

Katharine Coykendall, Cheryl Morrison, and Martha Nizinski

10.1 INTRODUCTION

A crucial first step in characterizing newly explored habitats and ascertaining the health of an ecosystem for future management decisions is surveying biodiversity at the species and population levels. Within submarine canyons, deepsea corals (also called cold-water corals) and other large sessile invertebrates act as foundation species and ecosystem engineers within these deepsea communities. Many species observed in association with foundational species (i.e., associates) play important and complex roles within deepsea ecosystems. Crustaceans belonging to the infraorder Anomura (e.g., squat lobsters, hermit crabs) are commonly observed in association with foundation species comprising most deepsea ecosystems. Anomurans contribute to nutrient cycling, both within and between biological assemblages, by functioning as grazers, prey, predators, and scavengers (Lovrich and Thiel 2011). Previous studies that examine species diversity of anomurans in the Atlantic Ocean have focused on the northeastern Atlantic Ocean fauna (Macpherson and Segonzac 2005, Matzen da Silva et al. 2011, Garcia-Merchan et al. 2012). Thus, the species diversity of anomurans in the northwestern Atlantic Ocean is likely higher than previously reported.

Genetic data provide the means to measure biological diversity at its most basic level. These data may aid in species identifications or identification of species complexes (e.g., cryptic species) when taxonomic/morphological knowledge is lacking or unresolved (Radulovici et al. 2009). DNA sequence data of the cytochrome *c* oxidase subunit I gene, also known as COI barcoding, is an important tool to efficiently catalog biodiversity. COI barcoding uncovers genetic diversity within a taxon and often can be used to assign individuals to a species (Hebert et al. 2003, Stoeckle 2003). Additionally, COI data are used to address regional and local diversity as well as patterns of speciation. Within Crustacea (Costa et al. 2007) and Decapoda (Matzen da Silva et al. 2011), COI barcoding has been used to assign individuals to species with some success.

In this chapter, we assess the biodiversity of anomurans in two mid-Atlantic canyons and examine the genetic diversity within species of anomurans observed in these canyons. Specifically, are populations of anomurans that occur in canyon habitats genetically similar to those of conspecifics outside of canyons? Alternatively, do canyon populations differ from conspecific slope or neighboring canyon populations, suggesting limited dispersal and gene flow? Additionally, are species assemblages of anomurans observed in these mid-Atlantic canyons similar to those assemblages reported from the continental shelf and slope of the Northwest Atlantic Ocean and Gulf of Mexico? Or, alternatively, are these canyon assemblages unique and possibly composed of endemic species?

To address these questions, we collected squat lobsters (superfamilies Galatheoidea and Chirostyloidea) and hermit crabs (superfamily Paguroidea) in Norfolk and Baltimore canyons. COI gene sequence information were analyzed to identify anomuran taxa and intraspecific diversity when possible.

10.2 METHODS

10.2.1 Sample Collection

General site and sample information for all anomurans collected for this project are presented in **Tables 10-1** and **10-2**, respectively. Crabs were collected by remotely operated vehicle (2012, *Kraken 2*, University of Connecticut; 2013, *Jason II*, Woods Hole Oceanographic Institution) or otter trawl. Once on board the research vessel, individuals were preserved in 95% to 100% ethanol.

Table 10-1. Dive and collection site information for anomurans sampled in the Atlantic Deepwater Canyons study area. Latitude and longitude coordinates are recorded in degrees and minutes. For dives conducted during the 2012 sampling cruise using the remotely operated vehicle (ROV) *Kraken 2*, geographic coordinates were recorded from the on-bottom location. For dives conducted during the 2013 sampling cruise using the ROV *Jason II*, coordinates from the first sampled anomuran are recorded. For otter trawl samples, coordinates were recorded from the beginning of the trawl.

Dive Number	Latitude	Longitude	Method	Date	Canyon
NF-2012-02	38°05′13.2000″	073°30′02.5200″	K2	19 Aug 2012	Baltimore
NF-2012-03	38°04′28.9200"	073°28′55.2000″	K2	21 Aug 2012	Baltimore
NF-2012-05	38°04′58.0800"	073°30′05.7600″	K2	23 Aug 2012	Baltimore
NF-2012-06	38°05′01.3200"	073°30′05.0400″	K2	24 Aug 2012	Baltimore
NF-2012-07	38°01′33.2400"	073°29′41.2800″	K2	26 Aug 2012	Baltimore
NF-2012-09	38°05′28.6800"	073°30′17.6400″	K2	28 Aug 2012	Baltimore
NF-2012-13	38°05′44.5200"	073°30′48.2400″	K2	6 Sept 2012	Baltimore
NF-2012-18	38°04′12.7200"	073°30′26.6400″	K2	11 Sept 2012	Baltimore
NF-2012-19	38°05′35.5200"	073°30′15.8400″	K2	12 May 2012	Baltimore
J2-689	38°02′49.9200"	073°49′35.4000″	J2	16 May 2013	Baltimore, seep
J2-690	38°10′14.5200"	073°50′13.9200″	J2	17 May 2013	Baltimore
RB-13-023	37°03′01.4400"	074°20′40.2000″	OT	4 May 2013	Norfolk
RB-13-025	37°03′18.7200"	074°20′42.3600″	OT	4 May 2013	Norfolk
RB-13-026	37°03′09.3600"	074°20′33.3600″	OT	4 May 2013	Norfolk
J2-680	37°03′25.5600"	074°34′44.0400″	J2	5 May 2013	Norfolk
RB-13-029	37°02′35.5200"	074°15′02.1600″	OT	7 May 2013	Norfolk
RB-13-030	36°32′22.5600"	074°16′30.7200″	OT	7 May 2013	Norfolk
J2-684	37°04′05.5200"	074°38′36.2400″	J2	10 May 2013	Norfolk
J2-685	37°02′56.7600"	074°30′36.3600″	J2	11 May 2013	Norfolk
J2-686	37°03′29.1600"	074°36′08.6400″	J2	13 May 2013	Norfolk
J2-687	37°03′37.8000"	074°34′42.9600″	J2	14 May 2013	Norfolk
J2-688	37°01′24.6000"	074°35′34.0800″	J2	15 May 2013	Norfolk

J2 = *Jason II* ROV; K2 = *Kraken 2* ROV; OT = otter trawl; ROV = remotely operated vehicle.

Table 10-2. Information on samples of anomurans from which genetic information was collected.

Sample Number	Superfamily	Taxon	Dive Number	Canyon	Depth (m)
MAC-13-412	Chirostyloidea	*Eumunida picta*	J2-684	Norfolk	411
MAC-13-414	Chirostyloidea	*Eumunida picta*	J2-684	Norfolk	411
MAC-13-489	Chirostyloidea	*Eumunida picta*	J2-686	Norfolk	486
MAC-13-523	Chirostyloidea	*Eumunida picta*	J2-687	Norfolk	390
MAC-13-526	Chirostyloidea	*Eumunida picta*	J2-687	Norfolk	390
MAC-13-536	Chirostyloidea	*Eumunida picta*	J2-688	Norfolk	453
MAC-13-563	Chirostyloidea	*Eumunida picta*	J2-689	Baltimore	388
MAC-13-564	Chirostyloidea	*Eumunida picta*	J2-689	Baltimore	388
MAC-13-565	Chirostyloidea	*Eumunida picta*	J2-689	Baltimore	388
MAC-13-566	Chirostyloidea	*Eumunida picta*	J2-689	Baltimore	388
MAC-13-570	Chirostyloidea	*Eumunida picta*	J2-690	Baltimore	361
MAC-13-571	Chirostyloidea	*Eumunida picta*	J2-690	Baltimore	338
MAC-13-572	Chirostyloidea	*Eumunida picta*	J2-690	Baltimore	361
MAC-13-573	Chirostyloidea	*Eumunida picta*	J2-690	Baltimore	361
MAC-13-575	Chirostyloidea	*Eumunida picta*	J2-690	Baltimore	339
MAC-13-576	Chirostyloidea	*Eumunida picta*	J2-690	Baltimore	365
MAC-13-577	Chirostyloidea	*Eumunida picta*	J2-690	Baltimore	339
MAC-12-025	Chirostyloidea	*Eumunida picta*	NF-2012-02	Baltimore	401
MAC-12-038	Chirostyloidea	*Eumunida picta*	NF-2012-05	Baltimore	445
MAC-12-039	Chirostyloidea	*Eumunida picta*	NF-2012-05	Baltimore	445
MAC-12-050	Chirostyloidea	*Eumunida picta*	NF-2012-07	Baltimore; seep	410
MAC-12-051	Chirostyloidea	*Eumunida picta*	NF-2012-07	Baltimore; seep	411
MAC-12-067	Chirostyloidea	*Eumunida picta*	NF-2012-09	Baltimore	376
MAC-12-068	Chirostyloidea	*Eumunida picta*	NF-2012-09	Baltimore	382
MAC-12-069	Chirostyloidea	*Eumunida picta*	NF-2012-09	Baltimore	398
MAC-12-071	Chirostyloidea	*Eumunida picta*	NF-2012-09	Baltimore	403
MAC-12-143	Chirostyloidea	*Eumunida picta*	NF-2012-13	Baltimore	409
MAC-12-144	Chirostyloidea	*Eumunida picta*	NF-2012-13	Baltimore	409
MAC-12-192	Chirostyloidea	*Eumunida picta*	NF-2012-18	Baltimore	527
MAC-12-084	Chirostyloidea	*Eumunida picta*	NF-2012-19	Baltimore	377
MAC-12-085	Chirostyloidea	*Eumunida picta*	NF-2012-19	Baltimore	377
MAC-12-086	Chirostyloidea	*Eumunida picta*	NF-2012-19	Baltimore	381
MAC-12-026	Galatheioidea	*Munida iris*	NF-2012-03	Baltimore	375
MAC-12-027	Galatheioidea	*Munida iris*	NF-2012-03	Baltimore	379
MAC-12-028	Galatheioidea	*Munida iris*	NF-2012-03	Baltimore	377
MAC-12-029	Galatheioidea	*Munida iris*	NF-2012-03	Baltimore	379
MAC-13-207A	Galatheioidea	*Munida iris*	RB-13-023	Norfolk	163
MAC-13-207B	Galatheioidea	*Munida iris*	RB-13-023	Norfolk	163
MAC-13-207C	Galatheioidea	*Munida iris*	RB-13-023	Norfolk	163
MAC-13-207D	Galatheioidea	*Munida iris*	RB-13-023	Norfolk	163
MAC-13-207E	Galatheioidea	*Munida iris*	RB-13-023	Norfolk	163
MAC-13-207F	Galatheioidea	*Munida iris*	RB-13-023	Norfolk	163
MAC-13-207G	Galatheioidea	*Munida iris*	RB-13-023	Norfolk	163

Table 10-2. (Continued).

Sample Number	Superfamily	Taxon	Dive Number	Canyon	Depth (m)
MAC-13-207H	Galatheioidea	*Munida iris*	RB-13-023	Norfolk	163
MAC-13-207I	Galatheioidea	*Munida iris*	RB-13-023	Norfolk	163
MAC-13-207J	Galatheioidea	*Munida iris*	RB-13-023	Norfolk	163
MAC-13-207K	Galatheioidea	*Munida iris*	RB-13-023	Norfolk	163
MAC-13-207L	Galatheioidea	*Munida iris*	RB-13-023	Norfolk	163
MAC-13-207M	Galatheioidea	*Munida iris*	RB-13-023	Norfolk	163
MAC-13-207N	Galatheioidea	*Munida iris*	RB-13-023	Norfolk	163
MAC-13-207O	Galatheioidea	*Munida iris*	RB-13-023	Norfolk	163
MAC-13-207P	Galatheioidea	*Munida iris*	RB-13-023	Norfolk	163
MAC-13-207Q	Galatheioidea	*Munida iris*	RB-13-023	Norfolk	163
MAC-13-207R	Galatheioidea	*Munida iris*	RB-13-023	Norfolk	163
MAC-13-207S	Galatheioidea	*Munida iris*	RB-13-023	Norfolk	163
MAC-13-207T	Galatheioidea	*Munida iris*	RB-13-023	Norfolk	163
MAC-13-207U	Galatheioidea	*Munida iris*	RB-13-023	Norfolk	163
MAC-13-207V	Galatheioidea	*Munida iris*	RB-13-023	Norfolk	163
MAC-13-603	Galatheioidea	*Munida iris*	RB-13-025	Norfolk	183
MAC-13-608	Galatheioidea	*Munida iris*	RB-13-025	Norfolk	183
MAC-13-609	Galatheioidea	*Munida iris*	RB-13-025	Norfolk	183
MAC-13-610	Galatheioidea	*Munida iris*	RB-13-025	Norfolk	183
MAC-13-612	Galatheioidea	*Munida iris*	RB-13-025	Norfolk	183
MAC-13-602	Galatheioidea	*Munida iris*	RB-13-026	Norfolk	263
MAC-13-604	Galatheioidea	*Munida iris*	RB-13-026	Norfolk	263
MAC-13-605	Galatheioidea	*Munida iris*	RB-13-026	Norfolk	263
MAC-13-606	Galatheioidea	*Munida iris*	RB-13-026	Norfolk	263
MAC-13-607	Galatheioidea	*Munida iris*	RB-13-026	Norfolk	263
MAC-13-217	Galatheioidea	*Munida valida*	J2-680	Norfolk	458
MAC-13-465	Galatheioidea	*Munida valida*	J2-686	Norfolk	489
MAC-12-045	Galatheioidea	*Munida valida*	NF-2012-06	Baltimore	441
MAC-13-280	Galatheioidea	*Munidopsis curvirostra*	RB-13-029	Norfolk	1603
MAC-13-281	Galatheioidea	*Munidopsis curvirostra*	RB-13-029	Norfolk	1603
MAC-13-277	Galatheioidea	*Munidopsis curvirostra*	RB-13-030	Norfolk	1682
MAC-13-428	Galatheioidea	*Munidopsis* sp.	J2-685	Norfolk	1388
MAC-13-429	Galatheioidea	*Munidopsis* sp.	J2-685	Norfolk	1388
MAC-13-430	Galatheioidea	*Munidopsis* sp.	J2-685	Norfolk	1388
MAC-13-403	Paguroidea	*Pagurus* sp.	J2-684	Norfolk	403
MAC-13-404	Paguroidea	*Pagurus* sp.	J2-684	Norfolk	403
MAC-13-463	Paguroidea	*Pagurus* sp.	J2-684	Norfolk	405
MAC-13-558	Paguroidea	*Pagurus* sp.	J2-689	Baltimore	374
MAC-13-559	Paguroidea	*Pagurus* sp.	J2-689	Baltimore	374
MAC-13-560	Paguroidea	*Pagurus* sp.	J2-689	Baltimore	374

10.2.2 DNA Extraction, Amplification, Sequencing

DNA was extracted from eggs or tissue from legs or abdomen using either Qiagen's Puregene Tissue kit or a DNeasy kit. A fragment of the mitochondrial COI gene was amplified using the forward primer LCO1490 (Folmer et al. 1994) and the reverse primer COI-H (Machordom and Macpherson 2004). Polymerase chain reactions (PCRs) were performed with the following concentrations of reagents: 1X GoTaq Flexi PCR buffer (Promega), 2 mM of $MgCl_2$ (Promega), 10 mM of GeneAmp dNTPs (Life Technologies), 5 µM of each primer, 0 to 0.4 mg mL^{-1} BSA (New England Biolabs), 0.1 unit of GoTaq Flexi (Promega), 2 to 20 ng of DNA, and laboratory grade water to adjust volume to 25 µL. PCR reactions were performed on BioRad or Eppendorff thermalcyclers under the following conditions: initial denaturation of 94 ºC for 3 min, then 29 to 34 cycles of 94 ºC for 1 min, 50 ºC to 56 ºC for 1 min, 72 ºC for 1 min, and a final extension step of 72 ºC for 7min. PCR products were electrophoresed on a 1.5% agarose gel at 95 V for 30 min to ensure single-band amplification. PCR products were purified using Qiaquick PCR purification spin columns (Qiagen) according to manufacturer's protocol. The purified products were resuspended in 30 to 40 µL of laboratory grade water. Cycle sequencing for subsequent Sanger sequencing reactions were performed using 1 µL of purified PCR as template, 1 µL BigDye® Terminator v3.1 Ready Reaction Mix (Applied Biosystems), 1 µL of 5 µM primer, 2 µL of 5X Sequencing buffer (Applied Biosystems), and 5 µL of molecular grade water for a final volume of 10 µL.

Products were sequenced in both forward and reverse directions to assure accuracy. Cycle sequencing was performed on a BioRad or Eppendorff thermal cycler under the following conditions: 95 ºC for 3 min, then 29 cycles of 95 ºC for 20 s, 50 ºC for 20 s, and 60 ºC for 4 min with final extension of 60 ºC for 5 min. Cycle sequencing products were purified using AGENCOURT® CLEANSEQ® beads (Beckman Coulter) according to the manufacturer's protocol. Final products were resuspended in 25 to 30 µL of molecular grade water. Twenty-five microliters of purified product were loaded onto an ABI 3130xl DNA sequencer (Applied Biosystems).

10.2.3 Mitochondrial DNA Sequence Analysis

DNA sequences were edited using Sequencher 5.2.2 (Genecodes). After aligning sequences from both the forward and reverse directions, regions with ambiguous bases were omitted from subsequent analyses. The National Center for Biotechnology Information (NCBI) GenBank nucleotide database (Benson et al. 2013) was queried with COI consensus sequences from each individual. DNA sequences were aligned and translated into amino acids using the invertebrate mtDNA translation table in MEGA6.06 (Tamura et al. 2013) to ensure no stop codons were present. To quantify genetic distance between species, uncorrected *p*-distances were calculated. The best-fit evolutionary model (MEGA6.06) was used to construct a maximum likelihood phylogenetic tree for each group of anomurans using 500 bootstraps to determine significance. At every nucleotide site included in the analysis, 10% (at most) could be missing (90% cutoff per site). COI sequences representing various anomuran taxa available in GenBank were included in phylogenetic analyses (**Table 10-3**) as well as *Munida microphthalma*, reported in Morrison and Nizinski (2010). Bootstrap percentages greater than 50 were reported. Uncorrected *p*-distances were computed against a subset of species from each phylogeny. Genetic diversity indices were estimated using DnaSP 5.10 (Librado and Rozas 2009). The *Drosophila* mitochondrial translation table was applied to all datasets. DNA sequences of *Eumunida picta* individuals from Cape Lookout, North Carolina (CLO), and Viosca Knoll (VK826), Gulf of Mexico (Coykendall et al. [in revision]), including a putative *Eumunida* cryptic species, were included in some analyses to compare diversity and differentiation within and between populations. COI sequences from closely related species reported in GenBank (Benson et al. 2013) were used to estimate intraspecific genetic diversity for comparison. Haplotype networks were drawn (Network 4.6.1.3; Fluxus Technology Ltd.) using a median-joining method coupled with a maximum-parsimony heuristic algorithm (Bandelt et al. 1999).

Table 10-3. GenBank accession numbers (GAS) of sequences used in phylogenies and interspecific genetic diversity comparisons.

Genus	Species	GAS	Genus	Species	GAS
Munida	*M. acantha*	AY350926,928	*Munidopsis*	*M. albatrossae*	DQ677692
	M. alonsoi	AY350930,933		*M. antonii*	DQ677677–678
	M. armilla	AY350937–938		*M. aries*	DQ677691
	M. caeli	EU418000,002		*M. bracteosa*	DQ677684
	M. clinata	AY350940,942		*M. cascadia*	DQ677694
	M. compressa	AY350943–944		*M. comarge*	JN166772
	M. congesta	AY350945		*M. crenatirostris*	JN166778, 780
	M. delicata	EU418001		*M. curvirostra*	FJ581768–770
	M. distiza	AY350947,949		*M. cylindrophthalma*	JN166784
	M. eclepsis	AY350951,953		*M. dasypus*	JN166774, 776
	M. gordoae	AY350954,956		*M. exuta*	DQ677690
	M. gracilis	KJ544249–250		*M. kensleyi*	JN166775
	M. gregaria	AY700163,165		*M. kensmithi*	DQ677706, 709
	M. guttata	AY350960–961		*M. lauensis*	EF157850, 852
	M. intermedia	JN564830–831		*M. longimanus*	JN166770
		JQ348884		*M. polymorpha*	DQ860146
	M. lailai	EU418012		*M. quadrata*	DQ882093
	M. leagora	AY350963,967		*M. recta*	DQ677696–697
	M. lenticularis	AY350972		*M. scotti*	DQ677703,705
	M. leptosyne	AY350973		*M. segonzaci*	DQ677683
	M. leviantennata	AY350974		*M. sp B*	EF157849
	M. mendagnai	EU417998–799		*M. sp D*	JN166763
	M. militaris	AY350975		*M. tiburon*	DQ677673
	M. notata	AY350976,979		*M. trifida*	JN166764–765
	M. ofella	AY350980		*M. vrijenhoeki*	DQ677675
	M. ommata	AY350982,984	*Pagurus*	*P. acadianus*	FJ581812,815
	M. pagesi	AY350985		*P. alatus*	JN107574, JQ306240
	M. parca	EU418010–011		*P. arcuatus*	FJ581816
	M. proto	AY350986		*P. bernhardus*	JN107578
	M. psamathe	AY350987–988		*P. brachiomastus*	KC347543, 555
	M. psylla	AY350992		*P. cuanensis*	JN107584–585
	M. quadrispina	DQ882090,092		*P. excavatus*	JN107586,JQ30621
	M. rhodonia	AF283885–886		*P. forbesii*	KF962980–981
	M. rogeri	AY350993		*P. granosimanus*	GU442255, 292
	M. rosula	AY350994		*P. hirsutiusculus*	GU442398–412
	M. rubrodigitalis	AF283887		*P. longicarpus*	FJ581820, KP254774
	M. rufiantennulata	AY350995		*P. minutus*	JX502977–978
	M. rugosa	JQ306225		*P. ochotensis*	KC347559, 561
	M. rutllanti	JQ305920,6226		*P. pectinatus*	KC347557–558
	M. sp. B	AY351028–029		*P. pollicaris*	AF483160, 171
	M. sp. A	AY351024–026		*P. prideaux*	JQ306026,257
	M. sp. C	AY351027		*P. proximus*	KC347562–563

Table 10-3. (Continued).

Genus	Species	GAS	Genus	Species	GAS
Munida	*M. spilota*	AY350996–997	*Pagurus*	*P. pseudosculptimanus*	KF962982–983
(Cont'd.)	*M. spinosa*	AY700177, KF051391	(Cont'd.)	*P. pubescens*	JN107599, JQ305957
	M. stia	AY351000–001		*P. samuelis*	GU443010, 060
	M. subrugosa	AY700172,174		*P. similis*	HM180751
	M. taenia	AY351002,006		*P.* sp A	JQ348885
	M. thoe	AY351012,DQ011203		*P. venturensis*	GU442190–191
	M. tiresias	AY351014			
	M. tuberculata	AY351015			
	M. tyche	AY351016–017			
	M. zebra	AY351022,DQ011206			

10.3 RESULTS

10.3.1 Superfamily Galatheoidea

Individuals from two genera, *Munida* and *Munidopsis*, representing Families Munididae and Munidopsidae, respectively, were examined. Phylogenetic relationships of species, including western Atlantic taxa and their congeners, are illustrated for the first time. However, comparisons of inter-canyon genetic differentiation are limited due to small sample sizes.

10.3.1.1 Munida

Two species, *Munida iris* and *M. valida* (**Figure 10-1A**, **B**), were collected from Baltimore and Norfolk canyons. Fifty-four putative species, including *M. valida* and *M. iris* from this study, eight additional species that occur in the Atlantic Ocean, and *M. microphthalma* from the Gulf of Mexico (Morrison and Nizinski 2010), were included in the analysis.

Munida iris occurs throughout the eastern and western North Atlantic Ocean (Baba et al. 2008). This species was numerically dominant ($N = 36$) in our collections and occurred at the shallowest sampled depths (163 to 263 m). Most individuals were collected by otter trawl near Norfolk Canyon; four individuals were collected by ROV in Baltimore Canyon. All mid-Atlantic canyon (MAC) samples identified as *M. iris* form a monophyletic clade (**Figure 10-1C**). The closest relative, *M. rutllanti* (97% sequence identity with *M. iris*), has a wide geographic distribution, ranging from the western coast of Africa and southern European coast to the Mediterranean and Ionian seas and the Gulf of Mexico (Baba et al. 2008). These sister species and three additional species form a larger clade. *Munida subrugosa* and *M. gregaria*, two taxa reported from southern South America, form a paraphyletic clade and possibly represent a single species (this study and Perez-Barros et al. 2008). These taxa are most closely related to *Munida quadrispina*, a northeastern Pacific species (Baba et al. 2008). Although many relationships remain unresolved between deeper branches, the *M. iris/M. rutllanti* clade has 100% support; *M. iris/M. rutllanti* clade and sister species *M. quadrispina* and *M. subrugosa/gregaria* has 75% support.

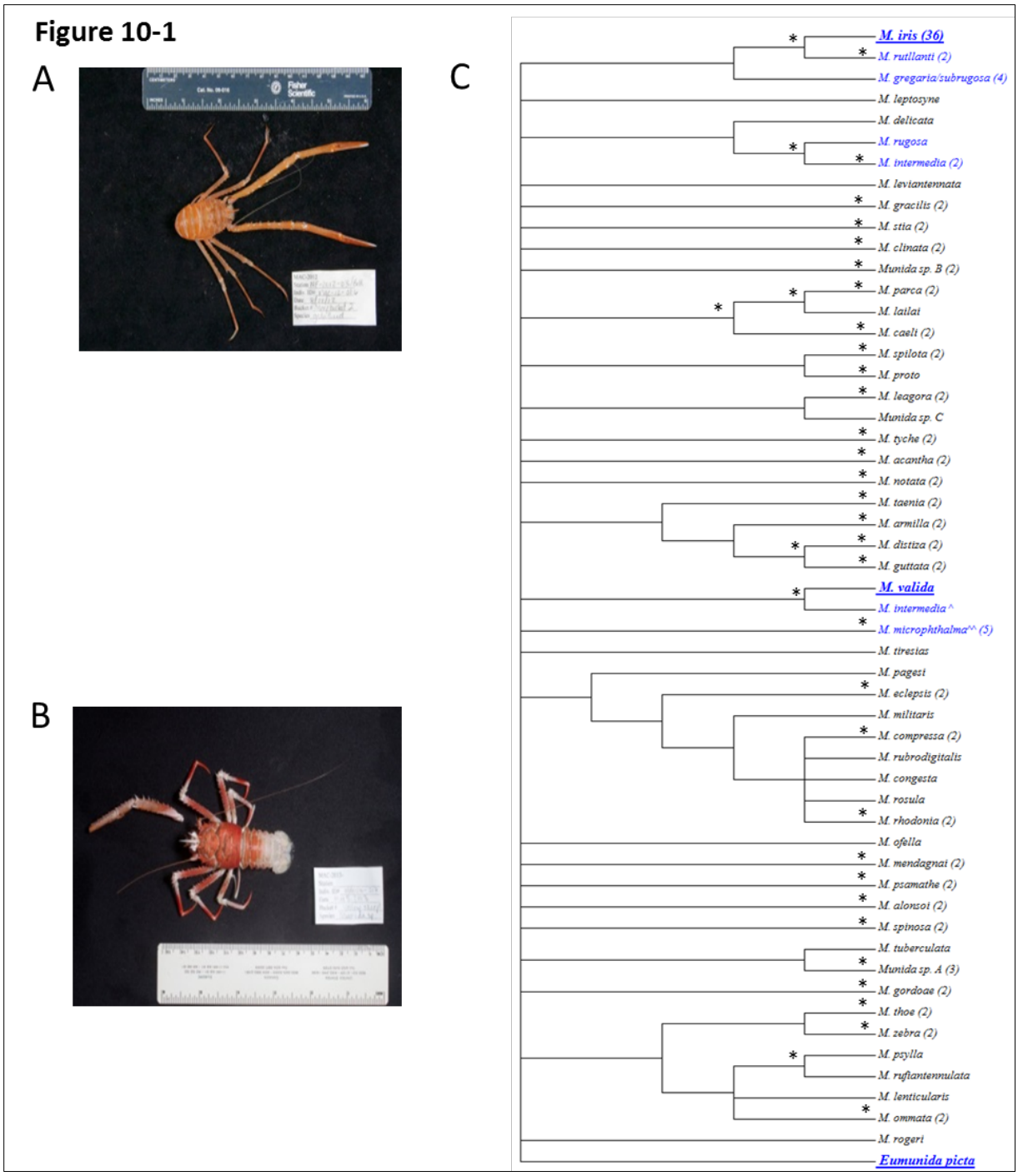

Figure 10-1. A) *Munida iris*; B) *Munida valida*; C) maximum likelihood phylogeny of COI sequences from *Munida* species, using GTR +G +I model of evolution, estimated in MEGA 6.06. Taxa in blue are found in the Atlantic Ocean. Branches with less than 50% bootstrap support were collapsed into a polytomy. Taxa in bold and underlined were collected in Baltimore and Norfolk canyons during the Atlantic Deepwater Canyons study. GenBank accession numbers of taxa not collected in this study are listed in **Table 10-3**. Sample sizes >1 are in parentheses after the taxon name. **M. intermedia* (JQ348884) likely misidentified. **Represents taxa reported by Morrison and Nizinski (2010). *Bootstrap support >95%.

Haplotype diversity, *Hd*, for *M. iris* was high (95%). Notably, when compared with a subset of other species of *Munida*, *M. iris* had the highest number of mutations resulting in an amino acid change (*nSyn* = 2) and the highest average number of pairwise sequence differences within *Munida* (*k* = 5.7) (**Table 10-4**). A haplotype network (**Figure 10-2**), including the 36 MAC *M. iris* COI sequences, illustrates little reticulation (i.e., homoplasy, back mutation, or recombination). However, many haplotypes shown in **Figure 10-2** are inferred, not sampled. Of the 22 COI haplotypes recovered from the 36 *M. iris* samples, three haplotypes were shared between Baltimore and Norfolk canyon samples. If populations from the two canyons were distinct, haplotypes would be segregated by canyon.

Fixed genetic differences between Atlantic species ranged from 6 (*M. iris* vs *M. rutllanti*) to 73 (*M. iris* vs *M. intermedia*). Genetic divergence between *M. iris* and its other clade neighbors (see above) ranged from 2% to 12% (**Table 10-5**). Comparisons of genetic divergence within a subset of *Munida* species revealed *M. iris* was most divergent from *M. ommata* and *M. leagora* (18%). These species occur in the Pacific Ocean.

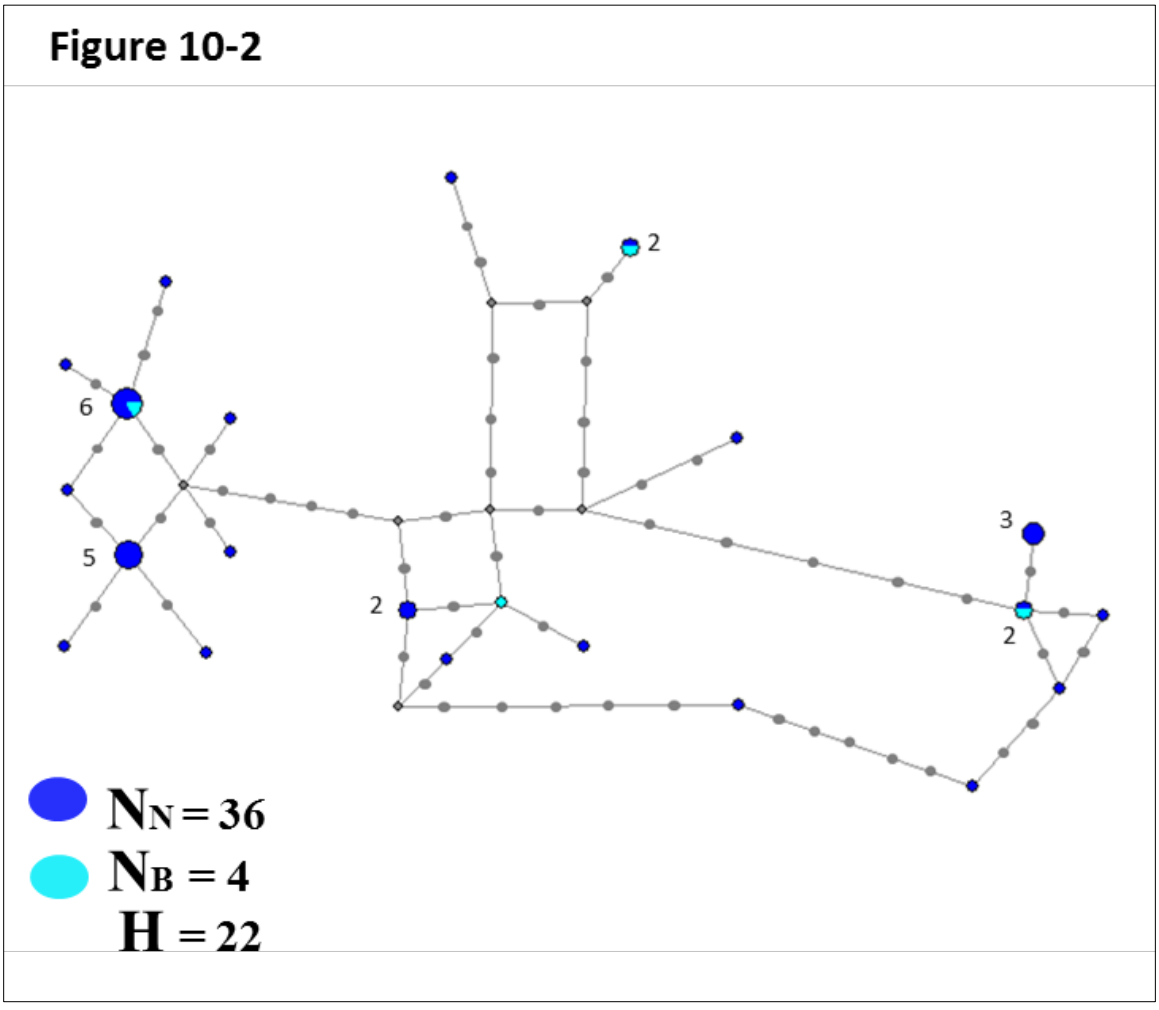

Figure 10-2. *Munida iris* haplotype network drawn in Network 4.6.1.3. Circles represent unique haplotypes and are proportional to the number of individuals sharing that haplotype. Number of individuals sharing the same haplotype, if >1, are shown next to circles in figure. N_N = number of samples from Norfolk Canyon; N_B = number of samples from Baltimore Canyon; *H* = number of unique haplotypes. Gray dots represent transitional, inferred haplotypes.

Table 10-4. Genetic diversity indices within species of anomurans. All analyses were performed in DnaSP 5.10. For *Eumunida picta*, populations from Cape Lookout (CLO); Viosca Knoll 826 (VK826); and the mid-Atlantic canyons (MAC, this study) were analyzed. *N* = number of sequences; *bp* = number of base pairs of the COI gene that were used in the analyses; *aa* = number of amino acids upon translation using the *Drosophila* translation table; *H* = number of total, unique haplotypes in the data; H_d = haplotype diversity; *S* = number of variable sites; *η* = number of mutations; Singletons = number of mutations occurring once in the dataset; *Syn* = number of synonymous changes; *nSyn* = number of nonsynonymous changes; *k* = number of pairwise differences between sequences; St. L = St. Lawrence, Canada; M/L = Manus/Lau Basin.

Taxon	Sampling Location	*N*	*bp*	*aa*	*H*	H_d	*S*	*η*	Singletons	*Syn*	*nSyn*	*k*
Munida iris	**MAC**	**36**	**576**	**191**	**22**	**0.95**	**25**	**26**	**9**	**24**	**2**	**5.7**
Munida intermedia	NE Atlantic	24	548	182	24	1.00	22	22	11	22	0	3.5
Munida gregaria	SW Pacific	96	618	206	29	0.61	28	29	17	29	0	1.0
Munida thoe	SW Pacific	34	543	180	33	1.00	33	39	18	39	0	4.4
Munida gracilis	New Zealand	52	525	175	36	0.96	47	51	33	48	0	3.6
M. curvirostra	**MAC and St.L**	**6**	**441**	**146**	**1**	**0**	**0**	**0**	**0**	**0**	**0**	**0**
M. lauensis	M/L Pacific	116	441	146	5	0.07	4	4	4	3	1	0.07
Eumunida picta	**MAC**	**32**	**541**	**180**	**24**	**0.98**	**29**	**29**	**13**	**28**	**1**	**4.3**
Eumunida picta	CLO	28	566	188	22	0.98	28	28	12	26	2	4.9
Eumunida picta	VK826	28	563	187	20	0.96	39	40	26	40	0	5.3
Eumunida picta	Total	88	541	180	58	0.97	56	58	26	55	3	4.7
Eumunida annulosa	SW Pacific	93	562	186	59	0.99	79	93	14	86	6	13.3
Eumunida sternomaculata	SW Pacific	40	553	183	27	0.95	19	23	7	22	1	2.9
***Pagurus* sp.**	***MAC***	***6***	***526***	***175***	***5***	***0.93***	***13***	***13***	***11***	***13***	***0***	***4.8***
Pagurus pubescens	N Atlantic	15	570	189	12	0.97	30	32	16	32	0	7.8
Pagurus longicarpus	NW Atlantic	57	580	192	32	0.94	48	52	21	52	0	9.4
Pagurus prideaux	NE Atlantic	27	591	196	16	0.84	24	24	18	23	1	2.4
Pagurus brachiomastus	NW Pacific	26	577	192	24	0.99	66	73	23	63	4	12.6
Pagurus granosimanus	NE Pacific	48	486	161	44	1.00	48	50	28	49	1	4.8
Pagurus samuelis	NE Pacific	60	563	187	33	0.96	34	34	19	33	1	3.4
Pagurus hirsutiusculus	N Pacific	43	580	193	5	0.50	5	5	2	5	0	0.9

Table 10-5. Genetic distances (uncorrected *p*-distances) between select *Munida* species. GAS = GenBank accession numbers, ID = Sample ID; entries in bold are from this study (MAC) or Morrison and Nizinski (2010). *M. intermedia** = divergent sequence from other *M. intermedia.*

Species	GAS/ID	1	2	3	4	5	6	7	8	9	10	11	12	13	14
1. M. asprosoma	JF727303														
2. M. gregaria	AY700165	0.16													
3. M. guttata	AY350961	0.15	0.16												
4. M. intermedia	JN564831	0.17	0.18	0.19											
*5. M. intermedia**	JQ348884	0.13	0.16	0.17	0.18										
6. M. iris	**MAC612**	0.16	0.12	0.17	0.17	0.16									
7. M. leagora	AY350967	0.16	0.17	0.10	0.19	0.18	0.18								
8. M. microphthalma	**CH07_42_1**	0.14	0.15	0.16	0.17	0.13	0.16	0.15							
9. M. ommata	AY350984	0.13	0.18	0.14	0.19	0.15	0.18	0.14	0.15						
10. M. parca	EU418011	0.16	0.17	0.14	0.18	0.17	0.17	0.15	0.16	0.15					
11. M. rugosa	JQ306225	0.18	0.16	0.17	0.10	0.18	0.16	0.17	0.16	0.16	0.17				
12. M. rutllanti	JQ306226	0.16	0.12	0.18	0.18	0.16	0.02	0.18	0.16	0.18	0.17	0.17			
13. M. subrugosa	AY700174	0.16	0.01	0.17	0.18	0.16	0.11	0.17	0.15	0.18	0.17	0.16	0.12		
14. M. valida	**MAC217**	0.15	0.18	0.16	0.20	0.09	0.16	0.16	0.15	0.15	0.18	0.17	0.17	0.18	
15. M. zebra	DQ011206	0.14	0.17	0.14	0.19	0.16	0.17	0.15	0.15	0.10	0.14	0.17	0.17	0.17	0.16

Three individuals of *M. valida* were collected: two from Norfolk Canyon (458 to 489 m) and one from Baltimore Canyon (441 m). Unambiguous sequences of the COI gene were obtained for only one of the three individuals (MAC217) collected in Norfolk Canyon. The quality of sequence data from the other two individuals was marginal. Thus, a fragment of an alternative gene, nuclear gene 28S, was sequenced for all three individuals to verify the identity of the two individuals with marginal COI sequence data. The 28S sequences of the two individuals in question were identical to that of MAC217 (data not shown), indicating that these three individuals were *M. valida*. A query of GenBank suggested *M. intermedia* is the closest relative (JQ348884; 92% sequence identity; 98% query coverage; *E*-value = 0.0), submitted by Matzen da Silva et al. (2011). However, this result was based on only one sequence. Aligning this sequence (JQ348884) to other sequences identified as *Munida intermedia* (JN564830–53) results in a mere 82% sequence identity. Thus, JQ348884 (indicated with "*" was considered to be misidentified and was excluded from any analyses involving *M. intermedia*. Phylogenetic analysis supports this hypothesis. JQ348884 grouped with *M. valida* with 99% bootstrap support, whereas other *M. intermedia* individuals clustered with *M. rugosa* and *M. delicata* elsewhere in the tree (**Figure 10-1C**). Based on GenBank blast results, the next closest relative to *M. valida*, was *M. rosula* (87% sequence identity; 100% query coverage; *E*-value = 2e-164), a species reported from the southwest Pacific (Baba et al. 2008). However, according to the maximum likelihood phylogenetic results, *M. rosula* belongs in an unresolved clade with six other species. This clade has 85% bootstrap support and does not include *M. valida*. Fixed differences were not computed due to the small sample size of *M. valida*. *M. valida* and its closest relative, *M. intermedia*^ (JQ348884), were 9% divergent; differences between *M. valida* and other Atlantic species of *Munida* ranged from 15% to 20%. The 20% difference, occurring between *M. valida* and *M. intermedia*, was the largest observed in the phylogeny of *Munida* species.

10.3.1.2 Munidopsis

Six individuals of *Munidopsis* were identified from the material collected in Norfolk and Baltimore canyons. *Munidopsis curvirostra* (*N* = 3) (**Figure 10-3A**) was collected at the deepest sampling locations (1,603 to 1,682 m). All three specimens shared a single haplotype; *M. curvirostra* collected from the Gulf of St. Lawrence, Canada, (GenBank accession number FJ581768) was a 100% match to these specimens. Phylogenetic analysis (**Figure 10-3B**) included 23 described and 2 undescribed species from GenBank, 4 described and 2 undescribed species from a previous study of chemosynthetic communities in the Gulf of Mexico (Morrison and Nizinski 2010), and 1 described and 1 undescribed species from this study. Of these, 21 species occur in the Atlantic Ocean.

In general, the phylogenetic analysis of the genus *Munidopsis* contained more resolved relationships than did the analysis for the genus *Munida* (**Figure 10-3B**). Based on the phylogeny, the closest relatives to *M. curvirostra* are the sister species *M. crenatirostris* and *M. cylindrophthalma* (94% bootstrap support) reported from the southwestern Pacific and the Indian and western Pacific oceans, respectively (Baba et al. 2008). These three species are included in a larger clade (50% bootstrap support), which includes *M. penescabra* from the Gulf of Mexico (Morrison and Nizinski 2010) and *M. polymorpha*, an anchialine-cave dwelling, shallow-water species endemic to the Canary Islands (Cabezas et al. 2012). Genetic distances between *M. curvirostra* and other species (**Table 10-6**) within the larger clade ranged from 11% (vs. *M. cylindrophthalma*) to 18% (vs. *M. penescabra*). *Munidopsis trifida* was most divergent from *M. curvirostra* with 20% difference.

The three additional individuals of *Munidopsis* collected from the canyons may represent a species new to science. Morphological analyses suggest it may be related to *M. serricornis*, a species previously thought to be cosmopolitan, but now restricted to the Atlantic Ocean (Ahyong 2014). No genetic resources of *M. serricornis* are available in public databases. Unambiguous, identical sequences of the COI gene were obtained for two of the three individuals (MAC428 and MAC429). Based on sequence identity, *M. trifida* (84%), reported throughout the Pacific and Indian oceans (Baba et al. 2008), and *M. comarge* (87%), occurring off western Australia and New Zealand (Taylor et al. 2010), are the closest

relatives to the MAC samples (99% bootstrap support; **Figure 10-3B**). Both *M. trifida* and *M. comarge* belong to the *M. serricornis* species complex (Ahyong 2014), further suggesting that these MAC individuals may be part of that species group. Genetic divergence between MAC428 and 429 and their closest relatives ranged from 11% to 13%; divergences between MAC428 and 429 and species across the phylogeny were larger, ranging from 19% to 23% (**Table 10-6**).

Overall, the range of genetic distances between species of *Munidopsis* was larger than the range observed in species of *Munida*. Moreover, many genetic distance values in the Munidopsis analysis were greater than 20%.

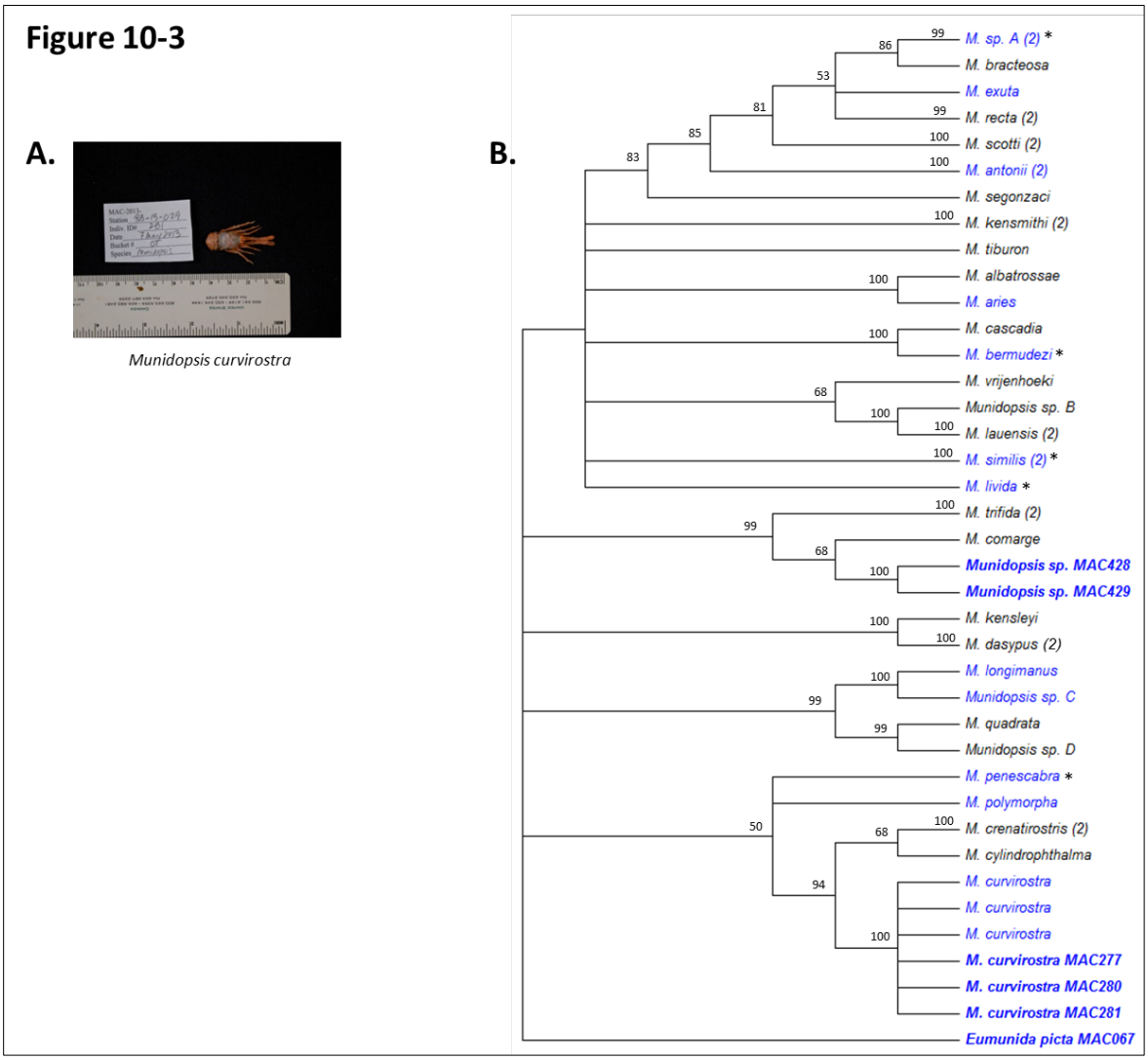

Figure 10-3. A) *Munidopsis curvirostra*; B) maximum likelihood phylogeny of COI sequences from *Munidopsis* species. Taxa in blue are found in the Atlantic Ocean. Branches with less than 50% bootstrap support were collapsed into a polytomy. Taxa in bold were collected in Baltimore and Norfolk canyons during the Atlantic Deepwater Canyons study. GenBank accession numbers of taxa not collected in this study are listed in **Table 10-3**. Sample sizes >1 are in parentheses after the taxon name. *Represents taxa included in Morrison and Nizinski (2010).

Table 10-6. Genetic distances (uncorrected *p*-distances) between select *Munidopsis* species. GAS = GenBank accession numbers, ID = Sample ID; entries in bold are from this study (MAC) or Morrison and Nizinski (2010).

Species	GAS/ID	1	2	3	4	5	6	7	8	9	10	11	12	13	14	15	16	17	18	19	20	21
1. *Munidopsis* sp. A	**AD4195-01_AC818**																					
2. M. exuta	DQ677690	0.02																				
3. M. antonii	DQ677677	0.04	0.02																			
4. M. aries	DQ677691	0.11	0.11	0.12																		
5. M. bermudezi	**J2-282-01**	0.11	0.11	0.11	0.11																	
6. M. similis	**J2-270_AT340**	0.10	0.11	0.10	0.13	0.12																
7. M. livida	**J2-282-02**	0.11	0.11	0.10	0.13	0.12	0.12															
8. Munidopsis sp.	**MAC428**	0.21	0.21	0.23	0.21	0.20	0.21	0.20														
9. M. longimanus	JN166770	0.23	0.24	0.23	0.21	0.21	0.22	0.20	0.23													
10. Munidopsis sp. C	**AD4174-01_GC600**	0.22	0.23	0.23	0.22	0.21	0.21	0.21	0.23	0.03												
11. M. penescabra	**CH-07-226-01**	0.21	0.21	0.21	0.22	0.21	0.21	0.21	0.21	0.21	0.20											
12. M. polymorpha	DQ860146	0.21	0.21	0.21	0.22	0.22	0.20	0.20	0.19	0.17	0.17	0.15										
13. M. cylindrophthalma	JN166784	0.20	0.21	0.21	0.21	0.22	0.20	0.19	0.19	0.18	0.17	0.17	0.16									
14. M. curvirostra	**MAC280**	0.21	0.21	0.21	0.21	0.21	0.19	0.21	0.20	0.19	0.19	0.18	0.14	0.11								
15. M. kensmithi	DQ677709	0.11	0.11	0.11	0.11	0.11	0.12	0.13	0.22	0.20	0.21	0.21	0.19	0.20	0.20							
16. M. scotti	DQ677703	0.03	0.03	0.03	0.11	0.12	0.11	0.11	0.21	0.23	0.22	0.22	0.22	0.21	0.22	0.11						
17. M. recta	DQ677696	0.02	0.02	0.02	0.12	0.11	0.10	0.10	0.21	0.23	0.23	0.20	0.21	0.20	0.21	0.11	0.03					
18. M. comarge	JN166772	0.19	0.19	0.20	0.20	0.19	0.18	0.20	0.11	0.20	0.20	0.19	0.17	0.18	0.19	0.19	0.19	0.20				
19. M. dasypus	JN166774	0.20	0.21	0.20	0.21	0.21	0.19	0.21	0.20	0.21	0.21	0.20	0.17	0.18	0.19	0.19	0.21	0.21	0.18			
20. M. lauensis	EF157850	0.13	0.13	0.12	0.14	0.12	0.14	0.15	0.22	0.25	0.24	0.22	0.23	0.21	0.22	0.12	0.12	0.12	0.20	0.22		
21. M. quadrata	DQ882093	0.21	0.22	0.22	0.20	0.21	0.21	0.19	0.21	0.13	0.13	0.22	0.18	0.18	0.21	0.22	0.21	0.21	0.20	0.21	0.23	
22. M. trifida	JN166764	0.20	0.20	0.20	0.20	0.21	0.20	0.21	0.13	0.20	0.20	0.19	0.18	0.21	0.20	0.20	0.20	0.19	0.11	0.20	0.20	0.19

10.3.2 Chirostyloidea

A single species of chirostylid was collected in Norfolk and Baltimore canyons. *Eumunida picta* (family Eumunididae, **Figure 10-4A**), collected at 339 to 527 m depth, was the second most abundant species in our collection of anomurans (*N* = 32). Over half of the *E. picta* collected in both Baltimore (*N* = 26) and Norfolk canyons (*N* = 6) were small and assumed to be juveniles. Of the larger, presumed mature individuals, at least two were gravid. Twenty-four of the 32 *E. picta* sampled from the two canyons had unique COI haplotypes. This high haplotype diversity value (98%; **Table 10-4**) is comparable to diversity levels reported for populations of *E. picta* collected previously off Cape Lookout, North Carolina (CLO) and at Viosca Knoll (VK826), Gulf of Mexico (Coykendall et al. 2017). Twenty nine mutations were observed among MAC *E. picta* COI sequences. The majority of these were synonymous mutations (i.e., do not result in an amino acid change); one mutation was nonsynonymous (results in an amino acid change). Haplotype diversities within populations of *E. picta* from MAC, CLO, and VK826 were high (0.96 to 0.98; **Table 10-4**). Similarly, other species of *Eumunida* such as *E. annulosa* and *E. sternomaculata*, both from the southwestern Pacific Ocean (Baba et al. 2008), had high haplotype diversities (0.99 and 0.95, respectively; **Table 10-4**). Numbers of pairwise nucleotide differences between sequences within populations of *E. picta* ranged from 4.3 to 5.3, which is comparable to pairwise differences observed in other species of *Eumunida* (2.9 to 13.3; **Table 10-4**). However, the presence of cryptic diversity likely inflates the value for *E. annulosa* (13.3; Puillandre et al. 2011).

No fixed mutational differences were observed between the MAC population of *E. picta* and those populations from CLO and VK826, located 307 km south and approximately 2,500 km southwest from the MAC, respectively. Between-group mean genetic distances were 1% for all three comparisons. In a previous study, genetic data suggested a separate lineage closely related to *E. picta* (i.e, Clade II), occurring in the western Atlantic Ocean (Coykendall et al. [in revision]). The number of fixed mutational differences between MAC and Clade II was eight; between CLO and Clade II, five; and between VK826 and Clade II, zero. Genetic divergence was estimated between MAC *E. picta* and the following: *E. picta* Clade II, *E. annulosa* and *E. sternomaculata*, and the southeastern Atlantic species *E. squamifera* (Baba et al. 2008). *E. picta* and *E. annulosa* showed the greatest divergence (10%); number of fixed differences between these species was nine. *Eumunida picta* and *E. sternomaculata* exhibited a 9% divergence and twice as many fixed differences (*N* = 18). Divergence between *E. picta* and *E. squamifera* was slightly lower (7%) than divergences from each of the Pacific species. *Eumunida picta* and *E. picta* Clade II exhibited the least divergence (3%). However, this value is higher than divergence values reported for other closely related species comparisons (i.e., *Munida iris* vs. *M. rutllanti*, **Table 10-5**; *Munidopsis recta* vs. several species, **Table 10-6**).

A haplotype network (**Figure 10-4B**) constructed from sequences obtained from MAC individuals of *E. picta* and samples previously collected from CLO and the Gulf of Mexico revealed a complex pattern of relationships as well as high genetic diversity within and between sampling sites included in the analysis. No geographic structuring was revealed among individuals; haplotypes were shared between canyons and other sampling localities. No haplotypes from either canyon grouped with Clade II haplotypes (**Figure 10-4B**). The most common haplotype (*N* = 16) was shared between canyons, CLO, and VK826. These results lend support to the hypothesis of the presence of one geographic population of *E. picta* extending from Viosca Knoll, Gulf of Mexico to the MAC. Given that no Clade II COI haplotypes were present in individuals collected in the canyons, Cape Lookout appears to be the northernmost boundary of this cryptic clade.

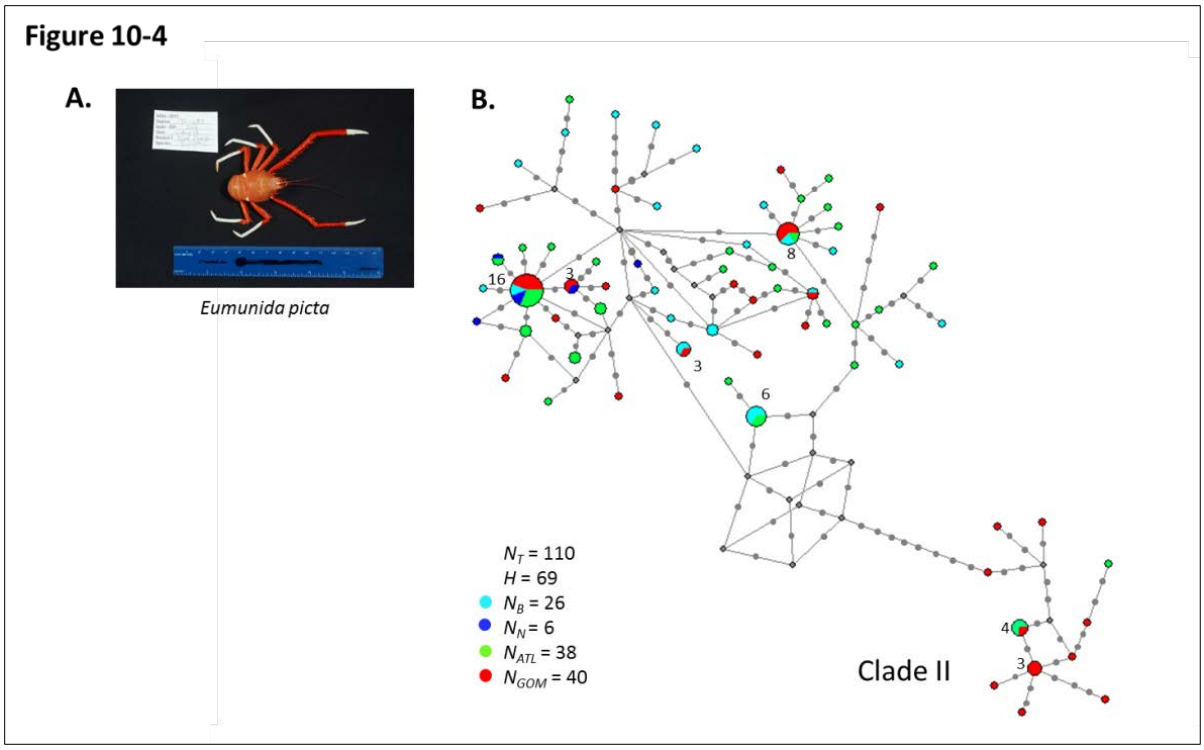

Figure 10-4. A) *Eumunida picta*; B) Haplotype network drawn in Network 4.6.1.3. Circles represent unique haplotypes and are proportional to the number of individuals sharing that haplotype. Number of individuals sharing the same haplotype, if >2, are shown next to circles in figure. N_T = total number of samples; N_{CLO} = number of samples from Cape Lookout, North Carolina; N_{VK826} = number of samples from Viosca Knoll 826, Gulf of Mexico; N_N = number of samples from Norfolk Canyon; N_B = number of samples from Baltimore Canyon; H = number of unique haplotypes. Gray dots represent transitional, inferred haplotypes. A putative cryptic species uncovered in Coykendall et al. 2017, denoted as Clade II.

10.3.3 Paguroidea

Six left-handed hermit crabs were sampled; three from a seep habitat in Baltimore Canyon (374 m) and three from Norfolk Canyon (403 m). The three specimens from Baltimore Canyon possessed black or dark grey egg masses. The closest relatives to the canyon individuals, based on a GenBank query, were *Pagurus pseudosculptimanus* and *P. alatus* (88% sequence identity, *E*-value = 0.0), both from the northeast Atlantic Ocean. Variance of pairwise differences between sequences obtained from species of *Pagurus* was similar to those reported for *Eumunida* spp. (k = 0.92 to 12.56 vs. 2.9 to 13.3, respectively), and larger than those reported for *Munida* spp. (1.00 to 5.70) (**Table 10-4**). The six MAC hermit crabs had an H_d value of 0.93 and an intermediate value of k = 4.8, indicating that many unique, moderately divergent haplotypes are represented. Of 13 polymorphic sites observed across 526 base pairs, 11 were singletons and all were synonymous changes. The three hermit crabs collected in Baltimore Canyon had six polymorphic sites; the three Norfolk Canyon hermit crabs had 13 polymorphic sites. However, low sample sizes preclude drawing any definitive conclusions on intraspecific diversity.

Genetic divergence between the two canyons was relatively small with an average number of nucleotide differences of 4.9 (**Table 10-4**). No fixed differences between sampling sites were observed. The maximum likelihood phylogeny comprised two major clades (**Figure 10-5**). The MAC hermit crabs formed a monophyletic clade with 100% bootstrap support and were contained within the clade that included 10 Atlantic species. The MAC individuals of *Pagurus* were ancestral to the internal clade, which

contained six *Pagurus* spp. from the northeastern Atlantic Ocean (78% bootstrap support). MAC hermit crabs showed a higher affinity to these northeastern Atlantic species than they did to the northwestern Atlantic species *P. longicarpus* and *P. pollicaris*. In fact, of the species included in the genetic distance analysis (**Table 10-7**), the most divergent species from the MAC hermit crabs (as represented by MAC403) was *P. pollicaris* (20%). *Pagurus alatus* and *P. pseudosculptimanus*, both from the Mediterranean Sea, were the least genetically distant from MAC403 (12%). *Pagurus longicarpus* and *P. pollicaris* formed the most ancestral branch of this 10-species clade (60% bootstrap support; **Figure 10-5**). The second major clade in the phylogeny (91% bootstrap support) contained 13 species and included species from both the Atlantic and Pacific oceans. Within this clade, some sister species relationships were highly significant (e.g., *P. acadianus* and *P. bernhardus*, 98% bootstrap support), but many relationships among these species of *Pagurus* remain unresolved.

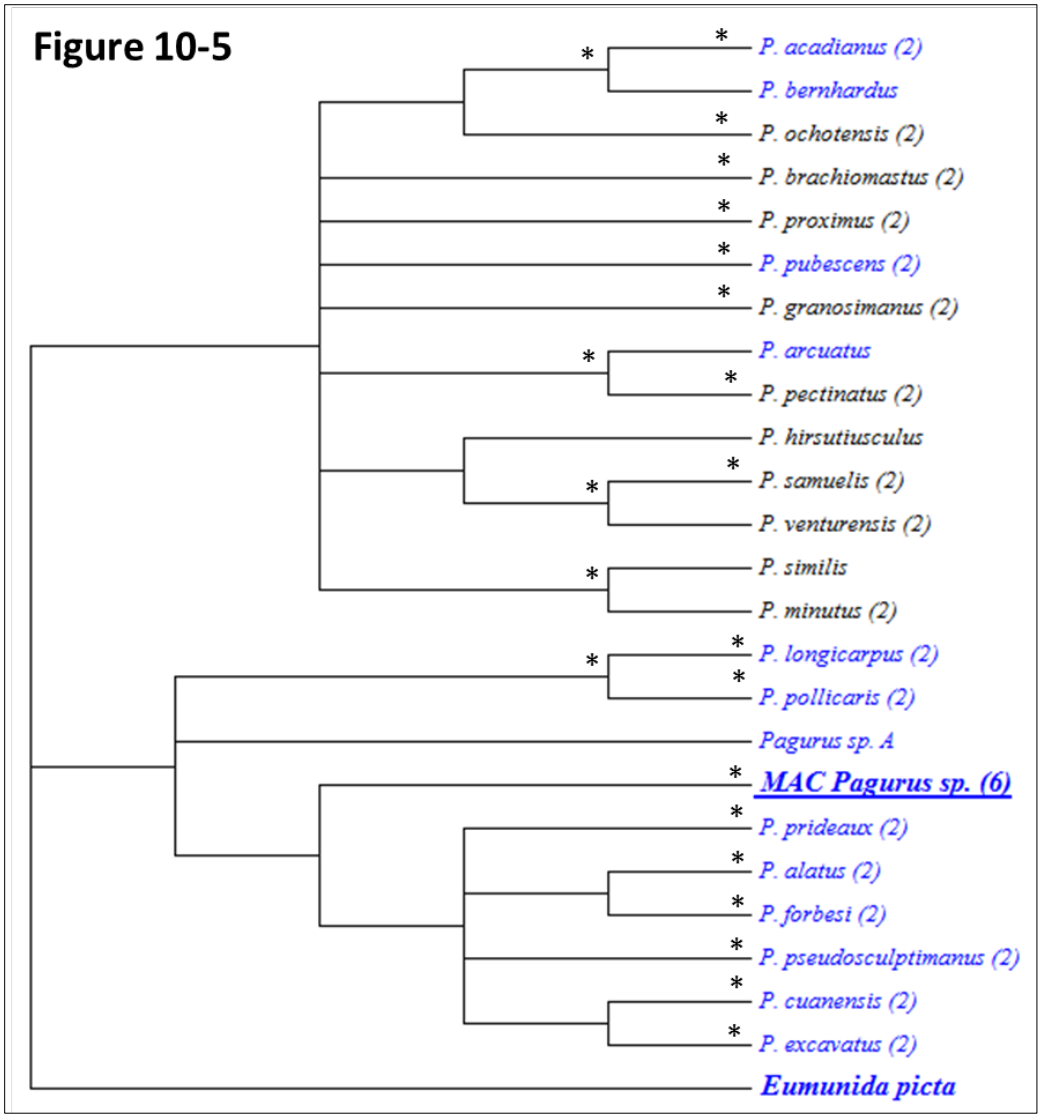

Figure 10-5. Maximum likelihood phylogeny of COI sequences from *Pagarus* species. Taxa in blue are found in the Atlantic Ocean. Branches with <50% bootstrap support were collapsed into a polytomy. Taxa in bold and underlined were collected in Baltimore and Norfolk Canyons during the Atlantic Deepwater Canyons study. GenBank accession numbers of taxa not collected in this study are listed in **Table 10-3**. Sample sizes >1 are in parentheses after the taxon name. *Bootstrap support ≥95%.

Table 10-7. Genetic distances (uncorrected *p*-distances) between select *Pagurus* species. GAS = GenBank accession numbers, ID = Sample ID; entries in bold are from this study (MAC).

Species	GAS/ID	1	2	3	4	5	6	7	8	9	10	11	12	13	14	15	16
1. P. acadianus	FJ581812																
2. P. alatus	JN107574	0.16															
3. P. arcuatus	FJ581816	0.13	0.16														
4. P. bernhardus	JN107578	0.07	0.15	0.13													
5. P. cuanensis	JN107584	0.16	0.13	0.17	0.15												
6. P. excavates	JN107586	0.17	0.13	0.20	0.18	0.12											
7. P. forbesii	KF962980	0.16	0.10	0.18	0.15	0.12	0.16										
8. P. granosimanus	GU442255	0.15	0.17	0.12	0.14	0.19	0.20	0.18									
9. P. longicarpus	FJ581820	0.17	0.15	0.17	0.16	0.17	0.19	0.15	0.18								
10. P. ochotensis	KC347559	0.10	0.16	0.15	0.10	0.18	0.18	0.17	0.14	0.17							
11. P. pollicaris	AF483160	0.20	0.19	0.18	0.21	0.18	0.20	0.19	0.19	0.16	0.21						
12. P. prideaux	JQ306026	0.16	0.13	0.18	0.15	0.14	0.14	0.13	0.19	0.16	0.18	0.20					
13. P. pseudosculptimanus	KF962982	0.17	0.10	0.18	0.15	0.11	0.12	0.10	0.17	0.16	0.17	0.19	0.12				
14. P. pubescens	JN107599	0.11	0.15	0.12	0.12	0.17	0.19	0.18	0.15	0.17	0.14	0.20	0.19	0.17			
15. P. similis	HM180751	0.14	0.14	0.14	0.13	0.16	0.17	0.16	0.14	0.18	0.15	0.20	0.16	0.14	0.13		
16. Pagurus sp.	**MAC403**	0.15	0.12	0.15	0.15	0.14	0.14	0.13	0.18	0.17	0.16	0.20	0.14	0.12	0.15	0.16	
17. P. venturensis	GU442190	0.14	0.15	0.12	0.12	0.16	0.18	0.17	0.14	0.16	0.14	0.19	0.16	0.15	0.13	0.12	0.16

10.4 DISCUSSION

10.4.1 Galatheoidea

Results from the 2012 and 2013 sampling cruises to Baltimore and Norfolk canyons included collections of individuals from three anomuran superfamilies: Galatheoidea, Chirostyloidea, and Paguroidea. Within Galatheoidea, samples included taxa from two families: Munididae and Munidopsidae. *Munida iris,* a widely distributed species found throughout the western North Atlantic, was the second most abundant species represented in our collections. High abundance of this species is not surprising; *M. iris* accounted for greater than 90% of squat lobsters previously collected by trawl (N = 280 collections) in the Mid-Atlantic Bight (MAB; near Norfolk and Toms canyons; Wenner 1982). In this study, high levels of haplotype diversity (H_d) were observed in *M. iris* and its congeners, suggesting that genetic diversity is high in *Munida* spp. *Munida iris* also displayed the largest intraspecific genetic divergence (k = 5.7) for species of *Munida* with available COI sequence data (**Table 10-4**). Haplotypes did not segregate by canyon, suggesting that a single species is represented in the populations sampled. Because only four individuals were collected from Baltimore Canyon, additional samples from this canyon are needed to make a more definitive conclusion regarding divergence between canyons populations. The closest known relative of *M. iris* is *M. rutllanti*, a species that occurs in the Mediterranean Sea. In fact, *M. iris* and *M. rutllanti* were previously considered subspecies of *M. iris*, but were recently elevated to species level (Baba et al. 2008)**.** Although genetic evidence suggests the divergence between these species was recent, this close relationship is supported by our phylogenetic analysis in which these species form a well-supported monophyletic clade (**Figure 10-1C**).

Although *Munida. valida, M. longipes* (since reclassified as *Agononida longipes,* Baba and de Saint Laurent 1996), *M. forceps*, and *M. microphthalma* also were collected during previous trawl surveys in the MAB (Wenner 1982), the present collections from Norfolk and Baltimore canyons yielded just three individuals of *M. valida*. Known to occur from New England to Curaçao and throughout the Gulf of Mexico (Williams 1984, Felder et al. 2009), *M. valida* was reported to be common along the Hatteras continental slope at depths of 400 to 900 m, but were rare or absent in Hatteras Canyon (Rowe 1971). Few individuals of *M. valida* were observed in this study, thus suggesting either inefficient sampling methods or potentially unsuitable habitat for this species. In Baltimore and Norfolk canyons, a nepheloid layer, present at depths corresponding to the depth distribution reported for *M. valida*, made sampling difficult (**Chapter 5**). While the presence of dense, suspended sediment hinders observation and sampling, the nepheloid layer may prevent species like *M. valida* from successfully colonizing canyon habitat.

Based on sequence identity, our single genetic sample of *M. valida* appeared most closely related to an individual, presumably misidentified as *M. intermedia* (GenBank accession: JQ348884), collected in the Gulf of Cadiz (Matzen da Silva et al. 2011) and *M. rosula*, collected from New Caledonia (Machordom and Macpherson 2004). The distributions of genetic distances between Atlantic and Pacific species included in our analyses and *M. valida* completely overlap. Pacific Ocean species are not necessarily more divergent from the species of *Munida* we collected than congeneric Atlantic species. Therefore, mechanisms that drive genetic divergence within *Munida* do not act at the ocean basin level.

Our phylogenetic tree of the genus *Munida* (**Figure 10-1C**) includes more Atlantic species than any other phylogenetic study of *Munida* to date. These results illustrate that more recent evolutionary relationships have high support, but deeper and likely older relationships remain unresolved. The high levels of polymorphism in COI in *Munida* are indicative of a fast mutation rate, which makes COI a suitable marker for delineating closely related species. Yet back mutations (where a nucleotide mutates, then reverts to a previous state) accumulate, which obscures more distant relationships. Adding additional genetic information from genes with slower mutation rates would elucidate relationships at internal nodes

(Avise 1994, Chu et al. 2009). Previous phylogenetic studies of *Munida* that considered COI and 16S (i.e., gene with slower mutation rate) data as well as combined maximum likelihood with Bayesian results (Machordom and Macpherson 2004, Cabezas et al. 2011) are concordant with our predominant patterns of relationships. However, relationships between these species remain poorly resolved. More extensive sampling in general (Bracken-Grissom et al. 2013), including more species from the Atlantic Ocean and Mediterranean Sea in particular (Cabezas et al. 2011), and adding genetic information from slower evolving genes (Chu et al. 2009) would help resolve ambiguities in the phylogenetic resolution of *Munida*.

Munidopsis is the most speciose genus within the family Munidopsidae (Ahyong et al. 2013), with 71 species reported from the Atlantic Ocean (Baba et al., 2008). However, we collected only two species, both from Norfolk Canyon, across all dives between 2012 and 2013. In previous MAB trawl surveys, four species within the family Munidopsidae were collected: *M. curvirostra*, *M. similis*, *M. aries* (listed as *M. sundi*), and *Galacantha rostrata* (listed as *M. rostrata*) (Wenner 1982). Our three individuals of *M. curvirostra* were genetically identical to each other and to three specimens from the Gulf of St. Lawrence, Canada, indicating high gene flow in this species across the Northwest Atlantic Ocean. The other three individuals of *Munidopsis* are likely members of a new species and share identical haplotypes. Both species in our dataset lack intraspecific diversity at the COI locus, but sample sizes are too low to draw definitive conclusions. Low intraspecific genetic diversity has been observed in other species of *Munidopsis*. Although in general, population genetic data for species of *Munidopsis* are sparse. However, Thaler et al. (2014) and Jones and Macpherson (2007) estimated intraspecific and interspecific genetic diversity in species occurring at Pacific hydrothermal vent habitats and other Pacific Ocean sites. Similar to our results, both studies revealed very small (typically <1%) haplotype diversities based on COI sequences, even for species with large geographic ranges. For example, the haplotype diversity of *M. lauensis* is an order of magnitude lower than all other anomuran species (**Table 10-4**). Given that Thaler et al. (2014) observed five unique haplotypes in 116 individuals, and assuming the genetic diversity levels are similar to those of the Atlantic species we collected, our sample size would have to exceed 24 individuals before another unique haplotype is observed.

Our data display a wide range of genetic divergences between species of *Munidopsis*. Levels of genetic divergence overlap when comparisons are examined between species within an ocean basin and between species occurring in different ocean basins. Thus, closest relatives do not necessarily inhabit the same ocean basin. This pattern is similar to that observed in species of *Munida*. However, levels of divergence observed in *Munidopsis* were greater than values observed in *Munida*. Jones and Macpherson (2007) also observed a wide range of interspecific divergences in species of *Munidopisis* from the Pacific Ocean. In their species comparisons, lower values (i.e., closest relative) did not necessarily correspond to the most morphologically similar species pair. Conversely, some species exhibited low genetic differentiation, yet differed greatly morphologically. Therefore, species of *Munidopsis* have moderate to high levels of genetic divergence, however, these differences do not necessarily correspond to differences in geographic separation or similarities in morphology.

10.4.2 Chirostyloidea

By combining our current collections and population genetics data for *Eumunida picta* from the southeastern United States and the Gulf of Mexico (Coykendall et al. [in revision]), we gain a more comprehensive assessment of intraspecific diversity and biogeographic patterns for this species. *Eumunida picta* was the second most abundant species of anomuran collected during this study. Previous examination of genetic diversity of *E. picta* associated with *Lophelia pertusa* habitats off the southeastern United States and in the Gulf of Mexico revealed a putative cryptic species (Clade II; Coykendall et al., in review). This cryptic species, known from the Gulf of Mexico to Cape Lookout, North Carolina, appears to be rare (13% of individuals; Coykendall et al. [in revision]). No individuals of *E. picta* collected in this study are members of Clade II. This finding suggests that Cape Lookout may represent the northern limit

of distribution for this putative species. However, due to the rarity of Clade II individuals, further sampling is required to determine if members of Clade II are present in the western Atlantic canyons. COI haplotypes of *E. picta* did not group by sampling site (**Figure 10-4B**). Moreover, no fixed DNA differences in pairwise comparisons were observed between VK826, CLO, and MAC populations. Thus, it appears that high levels of gene flow are occurring between populations from the Gulf of Mexico, the Atlantic continental slope, and the MACs.

10.4.3 Paguroidea

The six hermit crabs collected, three from each canyon, are likely the same species based on sequence identity. Overall, intraspecific diversity is high within *Pagurus* spp. and MAC hermit crabs are similar to its congeners. The wide range of diversity values within species is exemplified in haplotype diversities ranging from 0.5 to 1.0 and average number of pairwise differences between 0.9 and 12.6 (**Table 10-4**). Similar to *Munida* and *Eumunida*, *Pagurus* species exhibit high levels of intraspecific diversity. Results of our phylogenetic analysis place MAC individuals within a single clade that is basal to a larger monophyletic clade that includes six Atlantic species of *Pagurus* (**Figure 10-5**). Previous studies of hermit crab taxonomy have emphasized the great morphological variation that makes classification difficult for this group (Lemaitre 1986, McLaughlin et al. 2007). Biogeographic patterns in some hermit crab species suggest limited connectivity among ocean basins. For example, two continental shelf species, *P. longicarpus* and *P. pollicaris*, occurring in the western Atlantic from Canada to the Gulf of Mexico, exhibited genetic structuring across their geographic range, indicating a barrier to gene flow (i.e., limited connectivity) between the Gulf of Mexico and the Atlantic Ocean (Young et al. 2002).

When contrasting our phylogenetic analysis with the Bayesian topology constructed by Muñoz et al. (2014), relationships between species of *Pagurus* differ. The most striking difference is the discord in the placement of *P. pubescens* and *P. bernhardus*. Their results support *P. alatus* and *P. forbesii* as sister taxa with 100% posterior probability and place *P. pubescens* and *P. bernhardus* as the most recent ancestors of *P. alatus* and *P. forbesii* with 74% posterior probability. In contrast, our phylogenetic analysis suggests that *P. bernhardus* and *P. pubescens* are not sister taxa; these species were placed in an entirely different, distantly related clade (**Figure 10-5**). Our phylogenetic analysis does suggest *P. forbesii* and *P. alatus* are sister species. However, this hypothesis has only marginal support (54%). Although the Bayesian phylogeny from Muñoz et al. (2014) exhibits high posterior probabilities for the association between *P. pubescens* and *P. bernardus* and seemingly higher support for *P. forbesii* and *P. alatus* (54% bootstrap vs. 74% posterior probability), their analysis included only eastern North Atlantic representatives of the genus *Pagurus*. Our phylogeny contains all eight species from their study as well as four additional known species from the Atlantic, one undescribed Atlantic species, 10 Pacific species, and the MAC species. According to our analysis, the two closest relatives to *P. bernhardus*, *P. acadianus*, and *P. ochotensis* were omitted from the Muñoz et al. study. Furthermore, previous studies using simulated data have shown that posterior probabilities inferred with Bayesian analyses can overestimate the robustness of phylogenetic associations (Cummings et al. 2003, Erixon et al. 2003). Our analysis still contains several unresolved relationships deeper within the phylogeny. However, these relationships may be resolved by including more genetic or morphological data.

10.4.4 Genetic Barcoding in Anomurans

COI barcoding can improve our understanding of biodiversity (Radulovici et al. 2009). Several recent studies exemplify the utility of COI barcoding in describing anomuran diversity. For example, Puillandre et al. (2011) and Matzen da Silva et al. (2011) used Kimura-2 Parameter genetic distance measure of the COI gene to infer species boundaries within sampled squat lobster taxa. In some instances, small K2P distances revealed close relationships between separate taxa, thus suggesting that diversity is overestimated (Puillandre et al. 2011). Conversely, a bimodal distribution of K2P distances may indicate the presence of a putative cryptic species (e.g., *Eumunida annulosa*; Puillandre et al. 2011). However, the

polymorphism that COI exhibits in most anomurans, except for *Munidopsis* spp., suggests this gene may not be the most useful in resolving older relationships within phylogenies. Additional mtDNA gene information, such as that obtained from the ribosomal16S gene and more slowly evolving nuclear genes used for intergenic and interfamilial analyses (Lefebure et al. 2006), often provides resolution of internal polytomies. For example, Bracken-Grissom et al. (2013) investigated two mitochondrial genes other than COI, three nuclear genes, and morphological data for 19 of 20 extant families to construct an anomuran phylogeny. In their comprehensive analysis, six of seven superfamilies were monophyletic. However, when only molecular data are examined, *Munidopsis*, *Munida*, *Eumunida*, and *Pagurus* were either paraphyletic or polyphyletic, and *Paguroidea* contained members of *Lithodoidea*. Incorporating morphological data resolved some of the generic relationships to monophyletic clades, but the families *Paguridae* and *Munididae* were still paraphyletic. Another phylogenetic study focusing on *Munidopsidae* used both COI and 16S to examine relationships within the family. In this analysis, two additional galatheoid genera were contained within *Munidopsis*, suggesting the genus is paraphyletic (Ahyong et al. 2011b). Clearly, deeper sampling within these families, coupled with more comprehensive genetic data analysis, is necessary to resolve evolutionary relationships within this diverse group (Bracken-Grissom et al. 2013).

Although our results included representatives from speciose groups of squat lobsters and hermit crabs, phylogenetic results are limited because of a paucity of comparative genetic information for most species, especially those from the Northwest Atlantic Ocean. Continuing to build comprehensive reference libraries of voucher specimens with DNA sequence information will allow for more accurate assessments of marine biodiversity (Radulovici et al. 2009), especially from the underrepresented deep sea.

10.5 CONCLUSIONS

Our findings examine the diversity of anomurans collected in two MACs from an evolutionary perspective. One species of *Munidopsis* is likely new to science and has affinities with the *M. serricornis* complex. The single species of *Pagurus* collected from Baltimore and Norfolk canyons is more closely affiliated with northeastern Atlantic species than northwestern Atlantic species (*P. pollicaris*, *P. longicarpus*, and *P. acadianus*). We have incorporated two western North Atlantic species of galatheoids into a phylogenetic context for the first time (*Munida iris* and *Munida valida*). Our phylogenetic analysis of *Munidopsis* is the most comprehensive analysis to date and includes more species from the northwestern Atlantic than previously published works. The western Atlantic exhibits the highest level of squat lobster species endemism of the eight biogeographic ocean provinces (Schnabel et al. 2011), yet this region is often the least represented in phylogenetic studies of squat lobsters. Phylogenetic studies that exclude Atlantic samples are missing crucial information.

Our results suggest that intraspecific genetic diversity is high in species of *Pagurus*, *Eumunida*, and *Munida*. This suggests that evolutionary or ecological forces are influencing processes similarly in genera from three different superfamilies of Anomura. In contrast, species of *Munidopsis* exhibited very low genetic diversity within species and moderate to large interspecific diversity. Widespread gene flow is evidenced in identical, shared haplotypes between *M. curvirostra* from Norfolk Canyon and Gulf of St. Lawrence, Canada.

Comparisons between slope and canyon populations and between ocean basins were only possible for *E. picta*. Results from these analyses suggest that individuals from Baltimore Canyon are part of the same genetic population as individuals from the continental slope of the southeastern United States and the Gulf of Mexico. Whereas divergence between populations of *E. picta* is low, *Munida iris* exhibited a weak signal of divergence (**Figure 10-2**). Collections of *M. iris* were almost exclusively from a single sampling site, so the divergence observed cannot be explained by geographic distance or inter-canyon effects. Equal numbers of hermit crabs were collected from each canyon, though sample sizes were low

(N = 3 per canyon). Nevertheless, intraspecific diversity and interspecific divergence measures were similar to the high levels observed for *Munida*, *Eumunida*, and other species of *Pagurus*.

Sampling of anomurans for this study was biased toward species encountered in relation to the main project objectives. In particular, those species found near or on other invertebrate species, especially deepsea corals, were targeted for collection. Trawling also was conducted in habitats adjacent to coral and seep sites. Thus, those species that occur on soft substrates off the main axis of the canyons were not collected. Additionally, our results do not take into account specimens observed but not sampled. Noticeably absent from our data are samples from water depths between 490 and 1,390 m and below 1,680 m. Sampling in these intermediate depths by ROV proved difficult due to the presence of a nepheloid layer (**Chapter 5**). The increased amount of suspended sediment and turbidity and decreased visibility made ROV collections very difficult. Therefore, our results should be viewed as a lower limit of the diversity present in this ecosystem. Considering the vast network of submarine canyons that span the outer continental shelf and continental slope of the Northwest Atlantic Ocean, the abundance and diversity of anomurans, and the general lack of genetic information available for northwestern Atlantic species, future biodiversity surveys should highlight the collection, identification, and genetic analysis of anomurans.

10.6 LITERATURE CITED

Ahyong ST. 2014. Deep-sea squat lobsters of the *Munidopsis serricornis* complex in the Indo-West Pacific, with descriptions of six new species (Crustacea: Decapoda: Munidopsidae). Records of the Australian Museum. 66(3):197–216. doi:10.3853/j.2201-4349.66.2014.1630.

Ahyong ST, Schnabel KE, Macpherson E. 2011a. Phylogeny and fossil record of marine squat lobsters, pp. 73–104. In: Poore GCB, Ahyong ST, Taylor J, editors. The biology of squat lobsters. Boca Raton (FL): CRC Press.

Ahyong ST, Andreakis N, Taylor J. 2011b. Mitochondrial phylogeny of the deep-sea squat lobsters, Munidopsidae (Galatheoidea). Zoologischer Anzeiger−A Journal of Comparative Zoology. 250(4):367–377. doi:http://dx.doi.org/10.1016/j.jcz.2011.06.005.

Ahyong ST, Taylor J, Mccallum AW. 2013. New species and new records of deepwater munidid squat lobsters from north-western Australia: Onconida, Bathymunida, Crosnierita, Plesionida and Torbenella. Zootaxa. 3734(1):23–37.

Avise JC. 1994. Molecular markers, natural history, and evolution. New York (NY): Chapman and Hall.

Baba K, de Saint Laurent M. 1996. Crustacea Decapoda: Revision of the genus Bathymunida Balss, 1914, and description of six new related genera (Galatheidae). In: Crosnier A, editor. Résultats des Campagnes MUSORSTOM, volume 15. Paris (France): Mémoires du Muséum National d' Histoire Naturelle. 168:433–502.

Baba K, Macpherson E, Poore GCB, Ahyong ST, Bermudez A, Cabezas P, Lin CW, Nizinski M, Rodrigues C, Schnabel KE. 2008. Catalogue of squat lobsters of the world (Crustacea: Decapoda: Anomura−families Chirostylidae, Galatheidae and Kiwaidae). Zootaxa. (1905):1–220.

Bandelt HJ, Forster P, Rohl A. 1999. Median-joining networks for inferring intraspecific phylogenies. Molecular Biology and Evolution. 16(1):37–48.

Benson DA, Cavanaugh M, Karsch-Mizrachi I, Lipman DJ, Savers EW. 2013. GenBank nucleic acids research (database issue) D36–42. doi:10.1093/nar/gks1195.

Bracken-Grissom HD, Cannon ME, Cabezas P, Feldmann RM, Schweitzer CE, Ahyong ST, Felder DL, Lemaitre R, Crandall KA. 2013. A comprehensive and integrative reconstruction of evolutionary history for Anomura (Crustacea: Decapoda). BMC Evolutionary Biology. 13:128. doi:Artn 12810.1186/1471-2148-13-128.

Cabezas P, Lin CW, Chan TY. 2011. Two new species of the deep-sea squat lobster genus *Munida* Leach, 1820 (Crustacea: Decapoda: Munididae) from Taiwan: morphological and molecular evidence. Zootaxa. (3036):26–38.

Cabezas P, Alda F, Macpherson E, Machordom A. 2012. Genetic characterization of the endangered and endemic anchialine squat lobster *Munidopsis polymorpha* from Lanzarote (Canary Islands): management implications. ICES Journal of Marine Science. 69(6):1030–1037. doi:10.1093/icesjms/fss062.

Chu KH, Tsang LM, Ma KY, Chan TY, Ng PKL. 2009. Decapod phylogeny: what can protein coding genes tell us? In: Martin JW, Crandall KA, Felder DL, editors. Decapod Crustacean phylogenetics. Crustacean issues, vol 18. Boca Raton (FL): CRC Press.

Costa FO, deWaard JR, Boutillier J, Ratnasingham S, Dooh RT, Hajibabaei M, Hebert PDN. 2007. Biological identifications through DNA barcodes: the case of the Crustacea. Canadian Journal of Fisheries and Aquatic Sciences. 64(2):272–295. doi:10.1139/F07-008.

Coykendall DK, Morrison CL, Nizinski MS. 2017. Genetic diversity within *Eumunida picta*, a squat lobster associated with *Lophelia pertusa* reefs in the western Atlantic Ocean. In: Demopoulos AWJ, Ross SW, Kellogg CA, Morrison CL, Nizinski M, Prouty NG, Galkiewicz JP, Gray MA, Springmann MJ, Coykendall DK, et al. Deepwater program: *Lophelia* II continuing ecological research on deep-sea corals and deep reef habitats in the Gulf of Mexico: U.S. Geological Survey Open-File Report. In revision.

Cummings MP, Handley SA, Myers DS, Reed DL, Rokas A, Winka K. 2003. Comparing bootstrap and posterior probability values in the four-taxon case. Systematic Biology. 52(4):477–487. doi:10.1080/10635150390218213.

Erixon P, Svennblad B, Britton T, Oxelman B. 2003. Reliability of Bayesian posterior probabilities and bootstrap frequencies in phylogenetics. Systematic Biology. 52(5):665–673. doi:10.1080/10635150390235485.

Felder DL, Alvarez F, Goy JW, Lemaitre R. 2009. Decapoda (Crustacea) of the Gulf of Mexico, with comments on the Amphionidacea, vol 1. Gulf of Mexico origin, waters, and biota, volume 1, biodiversity. College Station (TX): Texas A&M University Press.

Folmer O, Black M, Hoeh W, Lutz R, Vrijenhoek R. 1994. DNA primers for amplification of mitochondrial cytochrome c oxidase subunit I from diverse metazoan invertebrates. Molecular Marine Biology and Biotechnology. 3(5):294–299.

Garcia-Merchan VH, Robainas-Barcia A, Abello P, Macpherson P, Palero F, Garcia-Rodriguez M, de Sola LG, Pascual M. 2012. Phylogeographic patterns of decapod crustaceans at the Atlantic-Mediterranean transition. Molecular Phylogenetics and Evolution. 62 (2):664–672. doi:10.1016/j.ympev.2011.11.009.

Hebert PDN, Cywinska A, Ball SL, DeWaard JR. 2003. Biological identifications through DNA barcodes. Proceedings of the Royal Society B-Biological Sciences. 270(1512):313–321. doi:10.1098/rspb.2002.2218.

Jones WJ, Macpherson E. 2007. Molecular phylogeny of the east pacific squat lobsters of the genus *Munidopsis* (Decapoda: Galatheidae) with the descriptions of seven new species. Journal of Crustacean Biology. 27(4):477–501.

Lefebure T, Douady CJ, Gouy M, Gibert J. 2006. Relationship between morphological taxonomy and molecular divergence within Crustacea: proposal of a molecular threshold to help species delimitation. Molecular Phylogenetics and Evolution. 40(2):435–447. doi:10.1016/j.ympev.2006.03.014.

Lemaitre R. 1986. Western atlantic species of the *Parapagurus Pilosimanus* complex (Anomura: Paguroidea: Parapaguridae): Description of a new species and morphological variations. Journal of Crustacean Biology. 6(3):525–542. doi:10.1163/193724086X00370.

Librado P, Rozas J. 2009. DnaSP v5: a software for comprehensive analysis of DNA polymorphism data. Bioinformatics. 25(11):1451–1452. doi:10.1093/bioinformatics/btp187.

Lovrich GA, Thiel M. 2011. Ecology, physiology, feeding and trophic role of squat lobsters. In: Poore GCB, Ahyong ST, Taylor J, editors. The biology of squat lobsters. Boca Raton (FL): CRC Press.

Machordom A, Macpherson E. 2004. Rapid radiation and cryptic speciation in squat lobsters of the genus *Munida* (Crustacea, Decapoda) and related genera in the South West Pacific: molecular and morphological evidence. Molecular Phylogenetics and Evolution. 33(2):259–279. doi:10.1016/j.ympev.2004.06.001.

Macpherson E, Segonzac M. 2005. Species of the genus *Munidopsis* (Crustacea, Decapoda, Galatheidae) from the deep Atlantic Ocean, including cold-seep and hydrothermal vent areas. Zootaxa. (1095):3–60.

Matzen da Silva JM, Creer S, dos Santos A, Costa AC, Cunha MR, Costa FO, Carvalho GR. 2011. Systematic and evolutionary insights derived from mtDNA COI barcode diversity in the Decapoda (Crustacea: Malacostraca). PLoS ONE. 6(5): e19449. doi:10.1371/journal.pone.0019449.

McLaughlin PA, Lemaitre R, Sorhannus U. 2007. Hermit crab phylogeny: a reappraisal and its “fall-out.” Journal of Crustacean Biology. 27(1):97–115. doi:10.1651/S-2675.1.

Morrison CL, Nizinski MS. 2010. Phylogeographic affinities of squat lobsters (Decaopoda: Galatheidae) from lower continental slope cold seep habitats in the northern Gulf of Mexico. In: Ross SW, Demopoulos AWJ, Kellogg CA, Morrison CL, Nizinski MS, Ames CL, Casazza TL, Gualtieri D, Kovacs K, McClain J, Quattrini AM, Roa Varón A, Thaler A, editors. Deepwater program: studies of Gulf of Mexico lower continental slope communities related to chemosynthetic and hard substrate habitats. U.S. Geological Survey Open-File Report 2012-1032. St. Petersburg (FL): U.S. Department of the Interior, U.S. Geological Survey. 301 p.

Muñoz JEG, Cuesta JA, Raso JEG. 2014. Taxonomic study of the *Pagurus forbesii* "complex" (Crustacea: Decapoda: Paguridae). Description of *Pagurus pseudosculptimanus* sp. nov from Alboran Sea (Southern Spain, Western Mediterranean Sea). Zootaxa. 3753(1):25–46.

Perez-Barros P, D'Amato ME, Guzman NV, Lovrich GA. 2008. Taxonomic status of two South American sympatric squat lobsters, *Munida gregaria* and *Munida subrugosa* (Crustacea: Decapoda: Galatheidae), challenged by DNA sequence information. Biological Journal of the Linnean Society. 94(2):421–434. doi:10.1111/j.1095-8312.2008.00987.x.

Puillandre N, Macpherson E, Lambourdière J, Cruaud C, Boisselier-Dubayle MC, Samadi S. 2011. Barcoding type specimens helps to identify synonyms and an unnamed new species in *Eumunida* Smith, 1883 (Decapoda: Eumunididae). Invertebrate Systematics (formerly Invertebrate Taxonomy). 25(4):322–333.

Radulovici AE, Sainte-Marie B, Dufresne F. 2009. DNA barcoding of marine crustaceans from the Estuary and Gulf of St Lawrence: a regional-scale approach. Molecular Ecology Resources. 9:181-187. doi:10.1111/j.1755-0998.2009.02643.x.

Rowe GT. 1971. Observations on bottom currents and epibenthic populations in Hatteras submarine canyon. Deep-Sea Research and Oceanographic Abstracts. 18(6):569–581. doi:10.1016/0011-7471(71)90123-9.

Schnabel KE, Cabezas P, McCallum A, Macpherson E, Ahyong ST, Baba K. 2011. Worldwide distribution patterns of squat lobsters. In: Poore GCB, Ahyong ST, Taylor J, editors. The biology of squat lobsters. Boca Raton (FL): CRC Press. p. 149–182

Stoeckle M. 2003. Taxonomy, DNA, and the bar code of life. Bioscience. 53(9):796–797. doi:10.1641/0006-3568(2003)053[0796:Tdatbc]2.0.Co;2.

Tamura K, Stecher G, Peterson D, Filipski A, Kumar S. 2013. MEGA6: Molecular evolutionary genetics analysis version 6.0. Molecular Biology and Evolution. 30(12):2725–2729. doi:10.1093/molbev/mst197.

Taylor J, Ahyong ST, Andreakis N. 2010. New records and new species of the munidopsine squat lobsters (Decapoda: Anomura: Galatheidae: Munidopsinae) from Australia. Zootaxa. 2642:1–18.

Thaler AD, Plouviez S, Saleu W, Alei F, Jacobson A, Boyle EA, Schultz TF, Carlsson J, Van Dover CL. 2014. Comparative population structure of two deep-sea hydrothermal-vent-associated decapods (*Chorocaris* sp. 2 and *Munidopsis lauensis*) from southwestern Pacific back-arc basins. PLoS ONE. 9(7). doi:ARTN e10134510.1371/journal.pone.0101345.

Wenner EL. 1982. Notes on the distribution and biology of Galatheidae and Chirostylidae (Decapoda: Anomura) from the Middle Atlantic Bight. Journal of Crustacean Biology. 2(3):360–377.

Williams A. 1984. Shrimps, lobsters, and the crabs of the Atlantic coast of the eastern United States, Maine to Florida. Washington (DC): Smithsonian Institution Press.

Young AM, Torres C, Mack JE, Cunningham CW. 2002. Morphological and genetic evidence for vicariance and refugium in Atlantic and Gulf of Mexico populations of the hermit crab *Pagurus longicarpus*. Marine Biology. 140(5):1059–1066.

CHAPTER 11. INVERTEBRATE REPRODUCTIVE BIOLOGY

Sandra D. Brooke and Anthony S. Sogluizzo

11.1 INTRODUCTION

Some of the processes that drive seasonal reproduction of invertebrates in shallow water (diurnal and lunar cycles) are attenuated or absent in the deep sea. Environmental signals, such as subtle changes in temperature, currents (e.g., upwelling), or tidal signals, may influence reproductive cycles, but timing of reproduction in deepsea benthic organisms is probably driven by the seasonal influx of particulate organic carbon (Tyler et al. 1993, Witte 1996) derived from surface blooms of phytoplankton and zooplankton. Monthly samples collected over several years are required to accurately describe the gametogenic cycle of a species; however, in the deep sea, expense and logistical constraints often preclude such sampling. Gametogenic cycles can be derived from sporadic sampling over several years, providing different time periods are covered. It is possible that organisms within similar taxonomic and trophic groups with similar reproductive strategies will use the same environmental factors as reproductive cues, in which case, fauna with the same reproductive strategies (broadcast spawning or brooding) from the same depth and location should all have similar reproductive cycles. If the reproductive cycles vary across taxa, we can conclude that different species use different cues or food sources, and/or that reproduction is genetically predetermined by internal rhythms. Some species may exhibit continuous reproduction, as in many chemosynthetic species that have a continuous food supply and stable environment (Tyler and Young 1999). If canyons have a consistent high-quality food supply, we may expect to find more species that have continuous reproduction, and higher fecundity, within the canyon influence compared with species found outside the canyons.

Research on deepsea corals has proliferated over the past 15 years, focusing primarily on structure-forming species such as *Lophelia pertusa*. Despite this increase in effort, information on the reproductive biology of *L. pertusa* was not published until quite recently (Waller and Tyler 2005, Brooke and Jarnegren 2013). Using samples collected from the northeast Atlantic, these authors reported a seasonal reproductive cycle with one cohort per year, culminating in a protracted spawning period of several weeks beginning in late January. Waller and Tyler (2005) also reported information on gametogenic cycles of *Madrepora oculata,* suggesting two cohorts per year. In contrast to structure-forming colonial species, which appear to be uniformly gonochoric (separate sexes) broadcast spawners, deepsea (also called cold-water) solitary scleractinian corals such as *Flabellum* sp. (Waller and Tyler 2011, Mercier et al. 2011), *Caryophyllia* sp. (Waller et al. 2005), and *Fungiacyathus* sp. (Waller et al. 2002; Flint et al. 2007) have various reproductive strategies. These reproductive strategies include hermaphroditism (simultaneous and sequential), gonochorism, brooding, and broadcast spawning.

The octocorals (subclass Alcyonaria) comprise three suborders (Alcyonacea, Pennatulacea and Helioporacea), of which the Alcyonacea is the largest and most diverse. The sea pens are all broadcast spawners, which suggests that this strategy may be phylogenetically constrained (Watling et al. 2011). The majority of the octocoral samples collected from the canyons were members of the Alcyonacea, mostly gorgonians with a small number of true soft corals. Despite their widespread distribution and often high abundance, there has been very little research on reproductive biology of deepsea octocorals, but the limited published material shows some putative trends or consistencies among the taxa studied. The soft corals (suborder Alcyoniina) studied to date are gonochoric brooders with either continuous (Cordes et al. 2001, Sun et al. 2010) or seasonal gametogenesis (Mercier and Hamel 2011). Reproductive traits of Antarctic gorgonians described in the older literature (Brito et al. 1997, Versluys 1906) suggest that gonochorism and brooding are common features of deepsea octocorals. Some gorgonians, however, (e.g., members of the Primnoidae and Isididae) are broadcast spawners that release gametes to be fertilized in the water column (Beazley and Kenchington 2012, Mercier and Hamel 2011, Orejas et al.

2002). Broadcast-spawning species generally either reproduce periodically (Orejas et al. 2002, Mercier and Hamel 2011) or annually (Mercier and Hamel 2011).

The distribution of some deepsea corals covers a wide range of latitudes and crosses ocean basins. These include the abundant structure-forming species *L. pertusa, Desmophyllum dianthus, Primnoa resedeformis,* and *Paragorgia arborea,* all of which were found during our study. Differences in reproductive period and/or fecundity within a species may differ across latitudes (Orejas et al. 2007, Brooke unpublished data). The samples from the Atlantic Deepwater Canyons study were compared with published information on conspecifics or congeners from different regions to try to identify factors that drive the timing of reproduction in deepsea coral taxa.

The overall goals of this study component were to provide information on the reproductive biology (strategy and timing) of dominant deepwater benthic fauna, particularly habitat-forming corals, in Baltimore and Norfolk canyons. Environmental data from other study components, such as benthic landers, conductivity-temperature-depth (CTD) casts and remotely operated vehicle (ROV) dives will be used to provide context for the observed reproductive cycles. The objectives of this study on invertebrate reproductive biology were to:

- Add to the existing database on reproductive timing of L. pertusa from the North Atlantic.
- Assess reproductive status of other scleractinians (*Solenosmilia variabilis, Flabellum* sp., *Desmophyllum dianthus*, and *Dasmosmilia lymani*) and gorgonians (*Paragorgia arborea, Primnoa resedeformis, Anthothela grandiflora, Acanthogorgia aspera,* and *Paramuricea placomus*). Other dominant taxa such as echinoderms (sea urchins) and seep mussels (*Bathymodiolus childressi*) were sampled to establish overall trends in reproductive cycles of canyon fauna and to determine whether reproductive strategies and cycles are synchronous across taxa.
- Examine relationships between gamete development and seasonal changes in physical conditions.

Reproductive cycles cannot be fully described with only two field seasons; however, since little is known about reproduction of cnidarians and other invertebrates in the canyons of the Mid-Atlantic Bight (MAB), any information collected will be valuable. For some of the species, there is information available on conspecifics from different regions. In such cases, comparisons will be made between these and new data generated by this study to identify regional differences within species and help elucidate the factors influencing timing of reproduction in deepsea species.

11.2 METHODS

11.2.1 Corals

Samples of corals were collected during the September 2012 and May 2013 sampling cruises (see **Chapter 3** for cruise schedules, vessels, and equipment). Most of the samples were collected using an ROV; the exceptions were the cup corals *D. lymani* and *Flabellum alabastrum* and the sea urchins *Hygrosoma petersii* and *Cidaris abyssicola,* which were collected using the otter trawl. Details of coral collections are shown in **Table 11-1**. Where possible, approximately30 samples per species, location, and time period were processed for histological examination. Each sample comprised several small branches (colonial corals) or several individuals (solitary corals), which were placed in 10% fully buffered formalin. Samples remained in formalin for the duration of the cruise, but were transferred into 70% ethanol in the laboratory. Prior to histological processing, the calcified skeleton of each sample was dissolved in 10% hydrochloric acid for 2 to 12 hours depending on the degree of calcification. The large

solitary corals were cut into halves or quarters using a diamond band saw prior to decalcification. After decalcification, polyps were rinsed in distilled water then dehydrated through a series of ethanol concentrations (70%, 80%, 95%, and 100%). The tissues were then cleared overnight using toluene or Histoclear and embedded in paraffin wax, then sliced into 8-µm sections using a microtome. The sections were mounted onto microscope slides, dried for 12 hours, and stained using Mayer's Haematoxylin (which stains DNA dark blue) and Eosin B (which stains cytoplasmic proteins bright red). After staining, the sections were mounted and left to dry. Sequential images of all the sections were taken using an Optronics digital camera attached to an Olympus BX50 compound microscope. For each female fragment, 50 oocytes were measured from 3 to 5 polyps (occasionally more polyps were needed to meet the required number of oocytes). Only those oocytes with visible nucleoli were measured. This ensured that the same egg was not measured more than once, as the nucleolus is so small (approximately 9-µm diameter) that it only appears in one 8-µm slice. The oocyte area was measured and recorded using Digimizer image analysis software. Oocyte "feret" diameter was calculated using the following formula, which estimates the diameter of a hypothetical circle with the same area as the object measured.

$$\text{Feret diameter} = \frac{\sqrt{4 \times \text{area}}}{\pi}$$

Table 11-1. Number of each species of coral processed from the 2012 and 2013 sampling cruises for the Atlantic Deepwater Canyons study.

Species	Collection date	Location	Depth (m)	No. of Samples
Scleractinia				
Dasmosmilia lymani	7 Sept. 2012	Baltimore Canyon	214–271	21
Desmophylum dianthus	10–11 Sept. 2012	Baltimore Canyon	680–690	15
	11–18 May 2013	Norfolk Canyon	478–578 1,334–1,390	12 5
Flabellum alabastrum	6–7 May 2013	Norfolk Canyon	1,614–1,670	22
Lophelia pertusa	12 Sept. 2012	Baltimore Canyon	389	4
	6–18 May 2013	Norfolk Canyon	387–581	18
Solenosmilia variablilis	11–12 May 2013	Norfolk Canyon	1,209–1,326	10
Gorgonacea				
Acanthogorgia aspera	5–15 May 2013	Norfolk Canyon	460–1,336	26
Anthothela grandiflora	28 Aug. to 13 Sept. 2012	Baltimore Canyon	400–638	14
	5–15 May 2013	Norfolk Canyon	404–631	10
Paragorgia arborea	18 Aug. to 13 Sept. 2012	Baltimore Canyon	450–737	29
	2–18 May 2013	Norfolk Canyon	382–719	33
Paramuricea placomus	28 Aug. to 12 Sept. 2012	Baltimore Canyon	375–382	13
Primnoa resedaeformis	18 Aug. to 13 Sept. 2012	Baltimore Canyon	450–560	14
	5–18 May 2013	Norfolk Canyon	400–573	14

Oocytes from each female (individual or colony) within a species and sampling period were split into different size categories to generate a size-frequency distribution. The frequencies were changed to percentages and an average and standard deviation was calculated for each size class. Oocyte diameters and size-frequency distributions were used to infer the timing and periodicity of female gametogenic cycles. Oocyte sizes vary by species so size alone is not a valid indicator of maturity. The developmental stage of each female was assessed using criteria described in Waller and Tyler (2005) as follows:

- Stage I: Oogonia are visible in the mesenterial lamellae;
- Stage II: Pre-vitellogenic oocytes are small with thin wall and basophilic cytoplasm;
- Stage III: Early vitellogenic oocytes with a small amount of cytoplasm;

- Stage IV: Late vitellogenic oocytes with granulated cytoplasm and thick cortical periphery; and
- Stage V: Post spawning, with some remaining eggs. Where there is sufficient data, oocyte diameter will be compared between sampling months and years using a student's *t*-test.

Male reproductive maturity was documented qualitatively by developmental stage, as size of spermatocysts can vary greatly within a single developmental stage, unlike oocytes, which increase in size as they develop. Male gametogenic cycles were documented by stages as follows:

- Stage I (early spermatogenesis): Spermatocysts are lined with spermatocytes but lumens are empty;
- Stage II (maturation phase): Thick layer of spermatocytes with some spermatozoa present, but with mostly empty lumens;
- Stage III (mature): Spermatocyst lumens are filled with spermatozoa; and
- Stage IV (post spawn): Spermatocysts are empty of spermatozoa, except occasional remnants of spawning (Waller and Tyler 2005, Brooke and Jarnegren 2013).

11.2.2 Other Species

Other species processed for reproduction included dominant seep fauna such as the seep mussel and various species of echinoderms from hard and soft substrate. Many were collected using the bottom trawl and were therefore usually species living on soft substrate. Some species were collected in high numbers, however, up to ~30 per time period and location were processed for reproduction (**Table 11-2**). Specimens were fixed in formalin on board the ship and transferred to 70% ethanol in the laboratory. The processing was similar to that described for corals except decalcification was not necessary because the gonad material could be dissected from the skeleton or shell prior to processing.

Table 11-2. Number of "other" (noncoral) species processed for histology from the 2012 and 2013 sampling cruises for the Atlantic Deepwater Canyons study.

Species	Collection date	Location	Depth (m)	No. of Samples
Echinodermata				
Gracilechinus affinis	8−9 May 2013	Norfolk Canyon	1,481−1,585	8
Echinus wallisi	8−9 May 2013	Norfolk Canyon	1,487−1,547	13
Hygrosoma petersii	6 May 2013	Norfolk Canyon	1,614	6
Cidaris abyssicola	4 May 2013	Norfolk Canyon	160	5
Mollusca				
Bathymodiolus childressi	26−27 Aug. to 7 Sept. 2012	Baltimore Canyon	400−430	31
Bathymodiolus childressi	16 May 2013	Baltimore Canyon	365−400	14
Bathymodiolus childressi	8−9 May 2013	Norfolk Canyon	1,475−1,565	29

11.3 RESULTS

11.3.1 Corals

11.3.1.1 Dasmosmilia lymani

Dasmosmilia lymani is a small solitary coral that lives on soft sediment and was sampled during one otter trawl in September 2012 (**Table 11-1**). Of the 21 individuals processed, only one of the samples was female and the remainder had no gametogenic material. The average oocyte diameter of the single female

was 56.66 µm (SD = 8.81) (**Figure 11-1**). The size-frequency distribution of oocytes in the single female sample (**Figure 11-2**) shows a dominance (41.4%) of oocytes in the 50- to 59.9-µm size range, with the smaller (40 to 49.9 µm) and larger (60 to 69.9 µm) categories representing 22.0% and 27.4% of the oocytes, respectively. Oocytes were primarily late-stage vitellogenic oocytes (**Figure 11-3**), some with a granular cortical layer, which means the individual was potentially ready to spawn. There were no indications of brooding or hermaphroditism in this species, which implies a gonochoric broadcast-spawning strategy; however, this cannot be determined with certainty from a single sample.

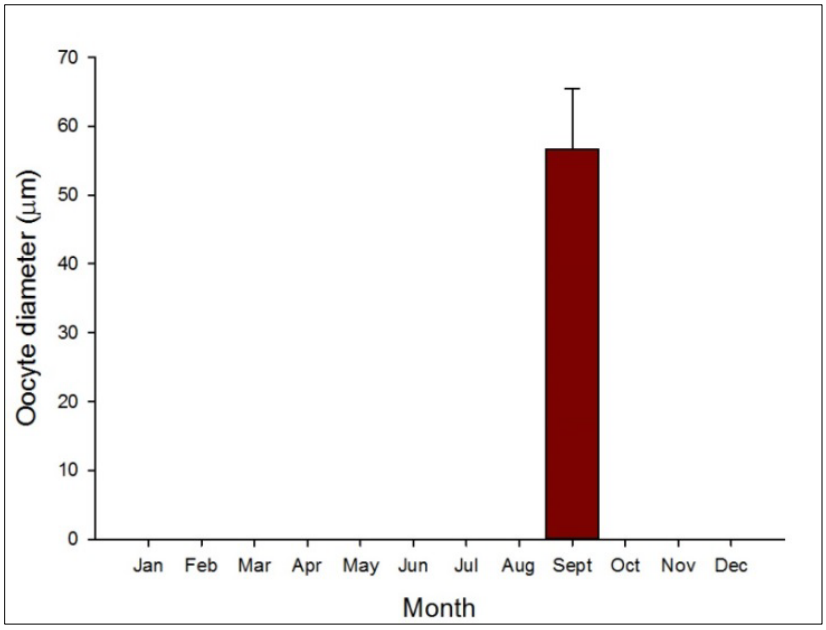

Figure 11-1. *Dasmosmilia lymani* average oocyte diameter for a single female specimen collected in September 2012.

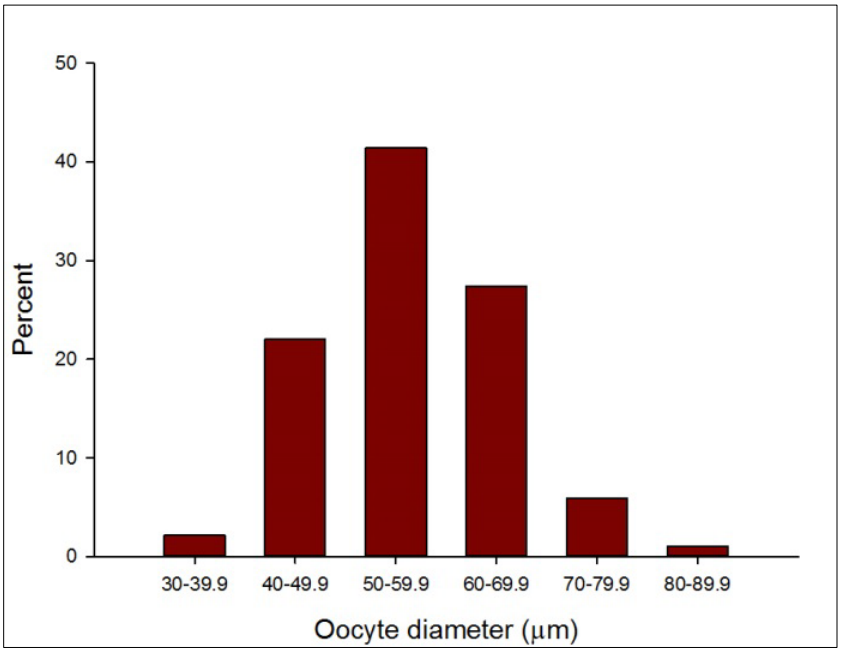

Figure 11-2. *Dasmosmilia lymani* oocyte size-frequency distribution. The x-axis shows the oocyte size category and the y-axis shows the percentage of total eggs within each size category.

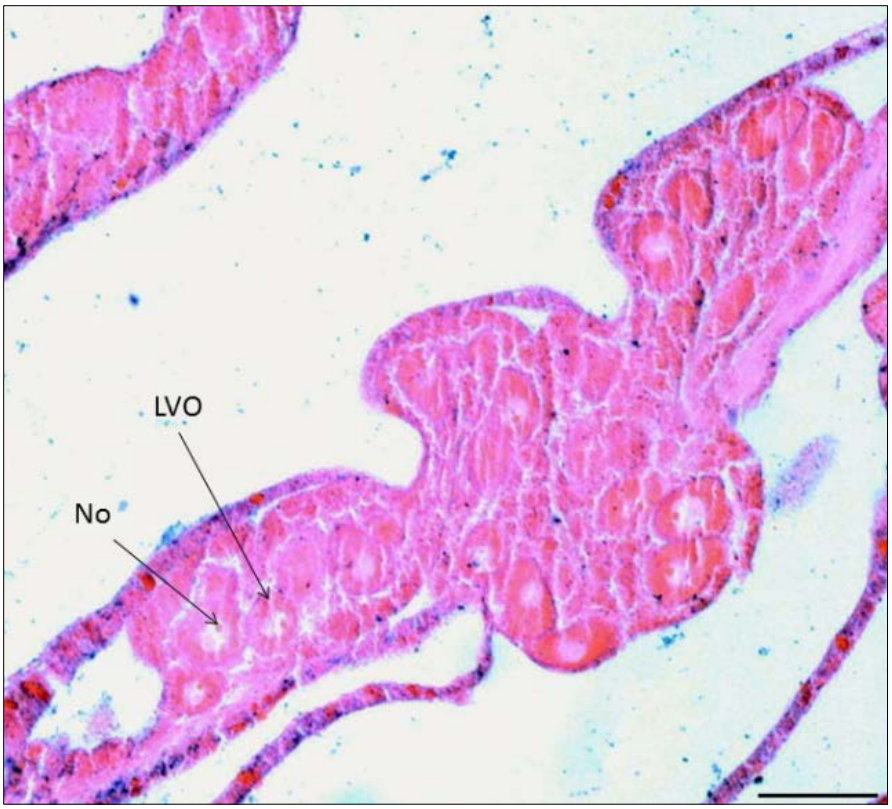

Figure 11-3. *Dasmosmilia lymani* female from September 2012 sampling cruise. *LVO* = late vitellogenic oocytes; No = nucleolus. Scale bar represents 100 µm.

11.3.1.2 Desmophyllum dianthus

In May 2013, samples of the cup coral *D. dianthus* were collected from two depth ranges (**Table 11-1**); however, there were no oocyte data from the deep site as the only sample that contained gametes was a male with Stage II spermatocysts. Of the 15 samples processed from September 2012, 3 were female, 10 were male, and 2 had no gametes. The 17 samples from May 2013 comprised 4 females, 4 males, and 9 with no gametes. Female samples from September 2012 showed an average oocyte diameter of 96.3 µm (SD 2.98) whereas those collected in May 2013 were smaller with an average oocyte diameter of 60.2 µm (SD 3.96) (**Figure 11-4**). The average oocyte diameters for each sampling period were compared using a *t*-test and were significantly different ($t = -14.6$, $p < 0.001$) from each other. The size-frequency distributions (**Figure 11-5**) showed different dominant size categories between the sampling months, as expected from their different average oocyte diameters. In September, 33% of oocytes fell into the 90- to 99.9-µm size category, and in May, 38.3% fell into the 50- to 59.9-µm category. However, the shapes of the distributions were similar, indicating a steady increase in oocyte size from May to September. The 2012 males were Stage III, and those from 2013 were less mature at Stage II, which coincided with the development of the females **(Figure 11-6**, **A–D**). There were no indications of hermaphroditism or brooding in the samples so *D. dianthus* appears to be a gonochoric broadcast-spawning species. These combined data indicate a single annual gametogenic cycle with culmination in a (possibly protracted) spawning event in late fall.

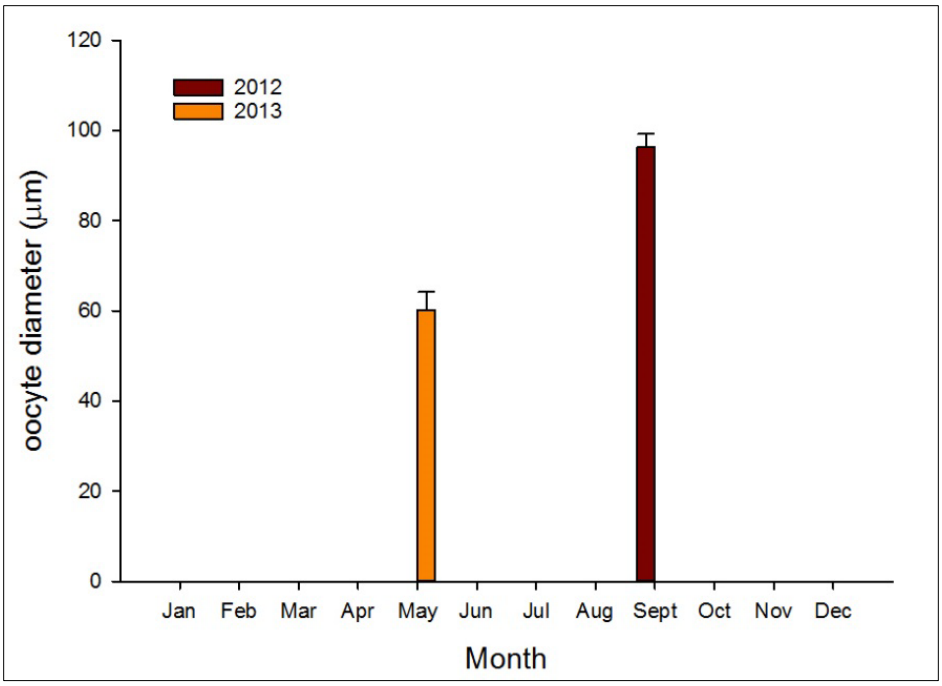

Figure 11-4. *Desmophyllum dianthus* oocyte size-frequency distribution for September 2012 and May 2013 samples. The x-axis shows the oocyte size category and the y-axis shows the percentage of total eggs within each size category.

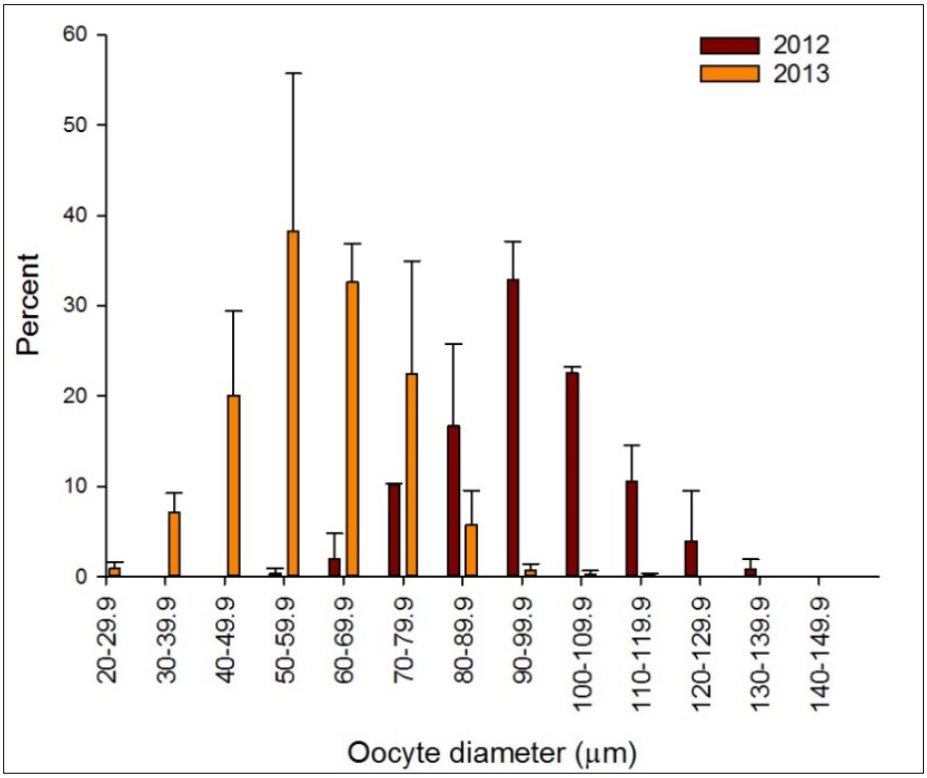

Figure 11-5. *Desmophyllum dianthus* average oocyte diameter for females collected in September 2012 and May 2013.

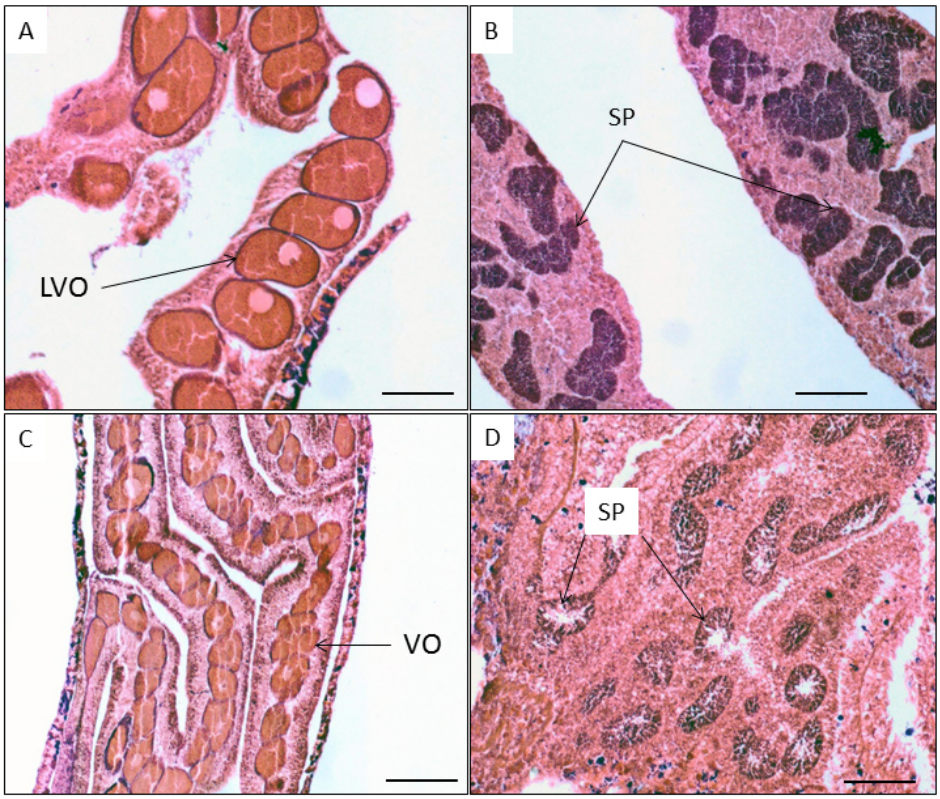

Figure 11-6. *Desmophyllum dianthus* A) late vitellogenic oocytes from female collected in September 2012, B) Stage III spermatocytes from male collected September 2012, C) vitellogenic oocytes from female collected in May 2013, D) Stage II spermatocysts from male collected May 2013. *LVO* = late vitellogenic oocytes, *VO* = vitellogenic oocytes, SP = spermatocysts. Scale bar represents 100 µm.

11.3.1.3 Flabellum alabastrum

Collections of the cup coral *F. alabastrum*, a solitary soft-sediment species, were made using an otter trawl in May 2013 (**Table 11-1**). Of the 22 specimens processed, 8 were female, 11 were male, and 3 had no gametes. This species had large oocytes with an average diameter of 306.5 µm (SD 212.1) (**Figure 11-7**). The oocyte diameters and size-frequency distributions show oocytes within a wide range of size classes with high variation within each size category, but there are indications of separate cohorts (**Figure 11-8**). Some extremely large mature oocytes (900 to 999.9 µm) were noted, but none of the earliest stages (oogonia). Males had Stage II and Stage III spermatocysts within the same individual, but no Stage I spermatocysts were observed, which concurs with patterns observed in the females (**Figure 11-9**). There were no indications of hermaphroditism or brooding in any of the samples so this species appears to be a gonochoric broadcast spawner with a continuous rather than annual reproductive cycle.

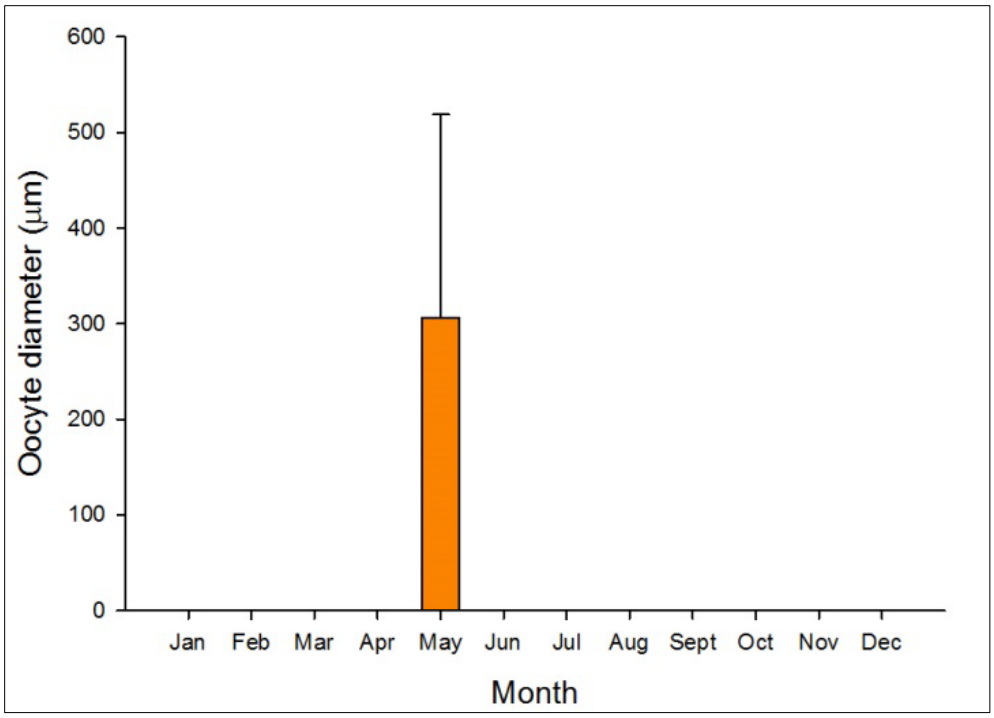

Figure 11-7. *Flabellum alabastrum* average oocyte diameter for females collected in May 2013.

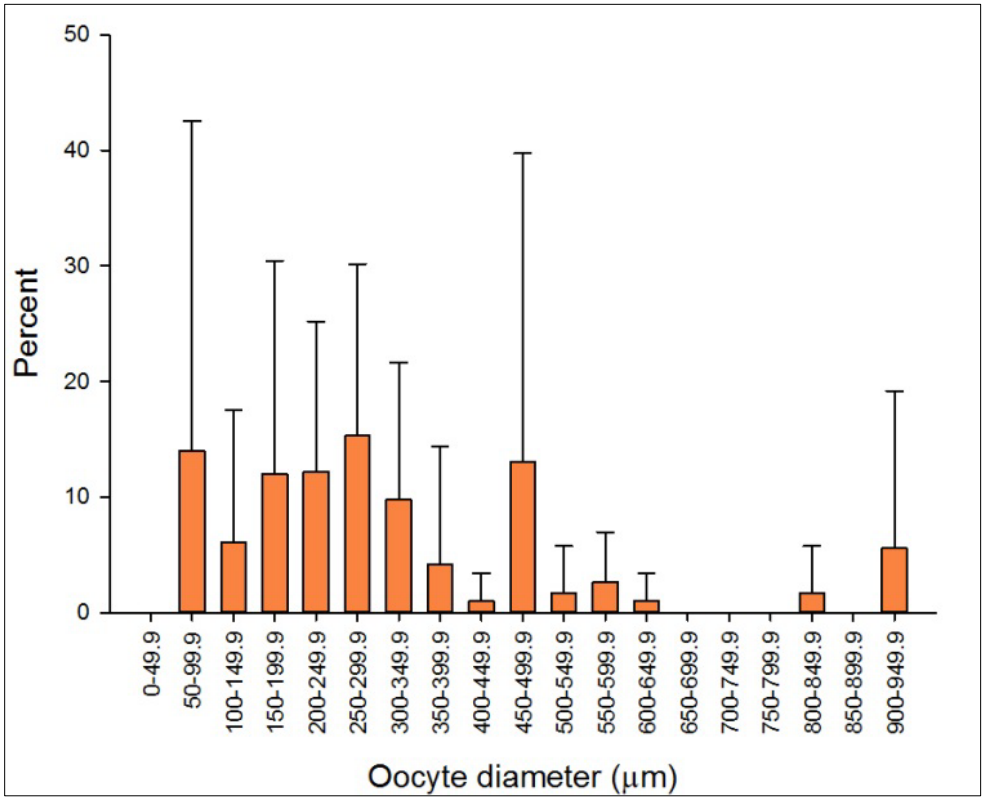

Figure 11-8. *Flabellum alabastrum* oocyte size-frequency distribution for May 2013 samples. The x-axis shows the oocyte size category and the y-axis shows the percentage of total eggs within each size category.

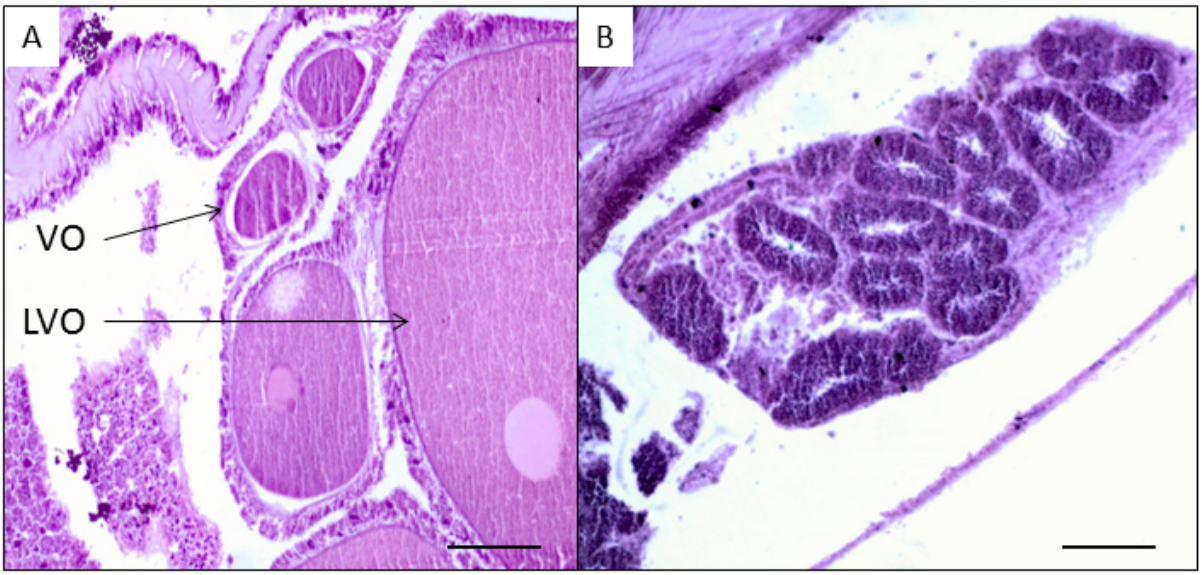

Figure 11-9. *Flabellum alabastrum* A) female showing a range of developmental stages, B) male showing Stage II spermatocysts. *VO* = vitellogenic oocytes; *LVO* = late vitellogenic oocytes. Scale bar represents 100 µm.

11.3.1.4 Lophelia pertusa

Samples of *L. pertusa* were collected in September 2012 and May 2013 (**Table 11-1**). Only 4 samples were collected in 2012; of these, 3 were females and 1 had no reproductive material. In 2013, 18 samples were collected resulting in 9 females, 3 males, and 6 that had no gametes. The 2012 females had an average oocyte diameter of 73.2 µm (SD 1.33) and the 2013 females' average was 38.0 µm (SD = 2.84) (**Figure 11-10**). The average oocyte diameters for each sampling period were compared using a *t*-test and were significantly different from each other ($t = -17.14$, $p < 0.001$). The oocyte size-frequency graph (**Figure 11-11**) shows a distinct distribution for each year. In 2012, the dominant (43%) oocyte size category was 70 to 79.0 µm and in 2013, the dominant category (56%) was 30 to 39.9 µm. These distinct developmental cohorts indicate a single annual reproductive cycle, culminating in a spawning period that is probably protracted, as the cohorts are not tightly clustered around the dominant size class. The oocytes observed in the September 2012 females are late vitellogenic but are not fully developed and ready to spawn. There were no males collected to compare stages so it is not possible to determine the precise spawning period from these data. The 2013 samples show early vitellogenic oocytes and Stage II spermatocysts (**Figure 11-12**). This species is a gonochoric broadcast spawner, and there were no indications of hermaphroditism or brooding in these samples.

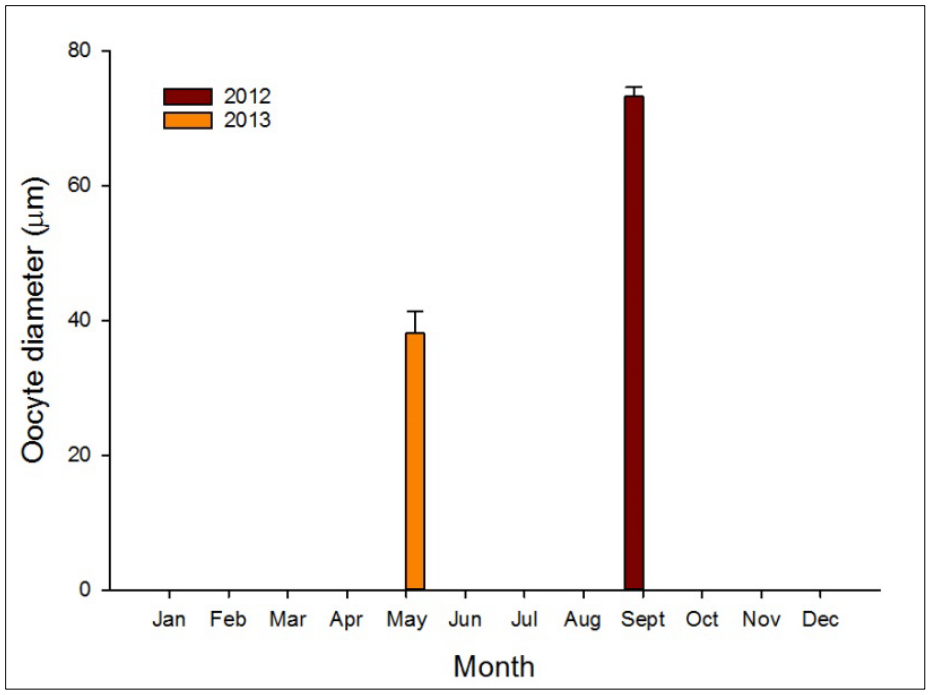

Figure 11-10. *Lophelia pertusa* average oocyte diameter for females collected in September 2012 and May 2013.

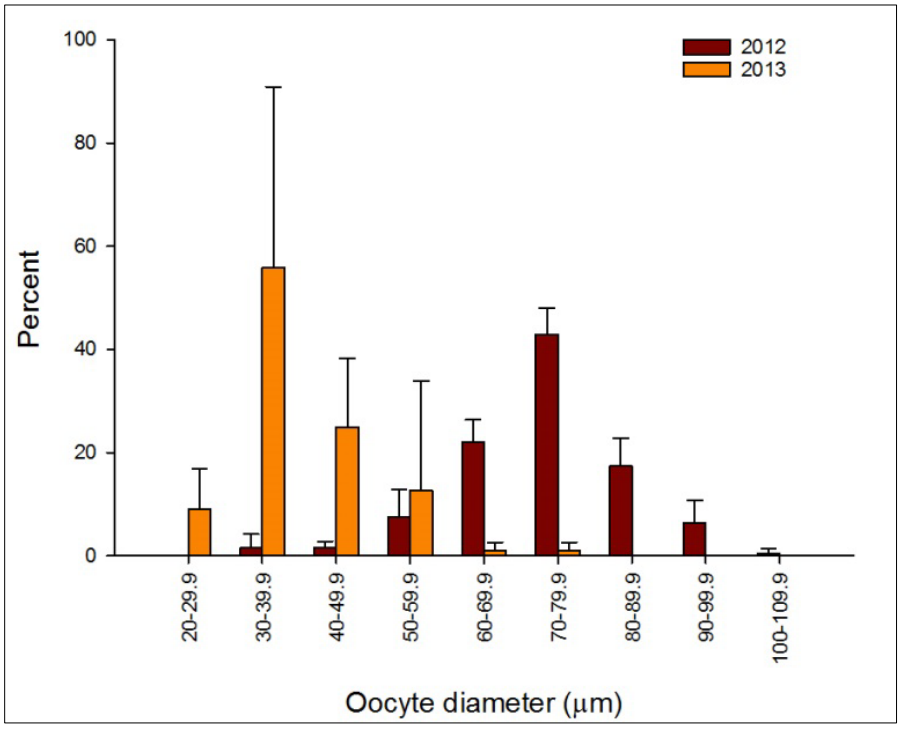

Figure 11-11. *Lophelia pertusa* oocyte size-frequency distribution for September 2012 and May 2013 samples. The x-axis shows the oocyte size category and the y-axis shows the percentage of total eggs within each size category.

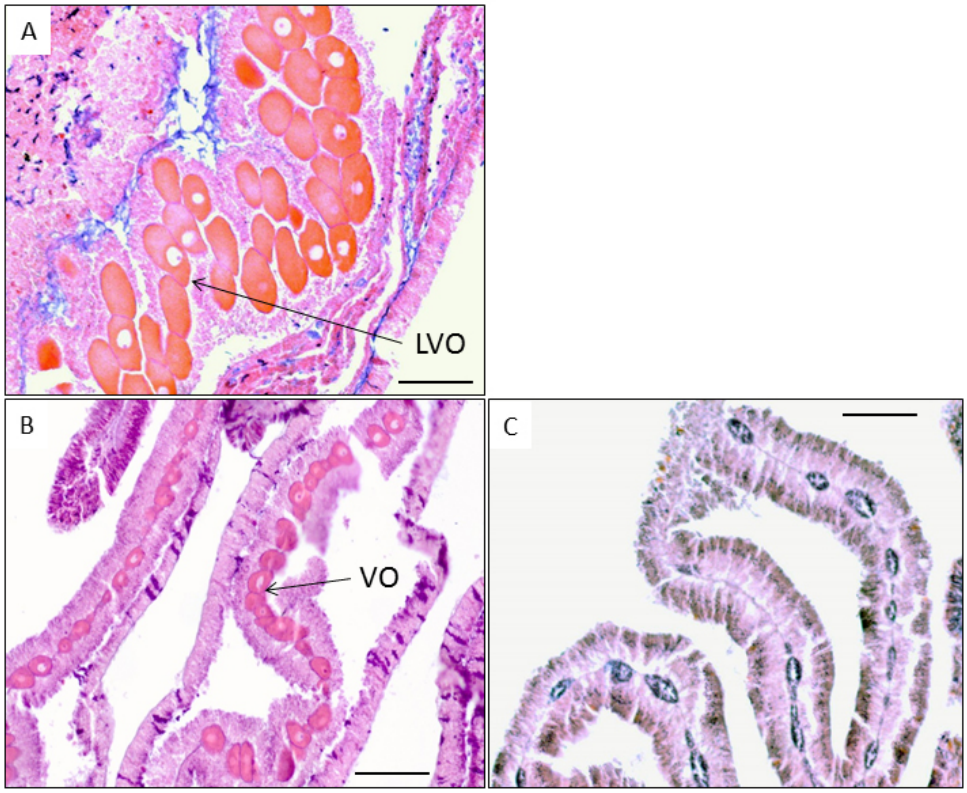

Figure 11-12. *Lophelia pertusa* A) female collected September 2012 showing late vitellogenic oocytes, B) female collected May 2013 showing vitellogenic oocytes, C) male collected May 2013 with Stage II spermatocysts. *VO* = vitellogenic oocytes; *LVO* = late vitellogenic oocytes. Scale bar represents 100 µm.

11.3.1.5 Solenosmilia variabilis

Samples of *S. variabilis* were collected only in May 2013 (**Table 11-1**). Of the 10 samples processed, 7 were female and the remainder had no gametes. The average oocyte diameter was 55 µm (SD 12.4) (**Figure 11-13**) and the size-frequency distribution shows the dominant (28%) size class to be 60 to 69.9 µm (**Figure 11-14**). This distribution spanned a broad range of size categories (120 to 109.9 µm), but showed only a single cohort. Some of the oocytes were late vitellogenic stage, but most were vitellogenic but immature (**Figure 11-15**). Since there were no male samples to compare developmental stage, it is not possible to determine the spawning period from these data. There were no indications of hermaphroditism or brooding and these data indicate that *S. variabilis* is a gonochoric broadcast-spawning species with a single (annual) reproductive cycle.

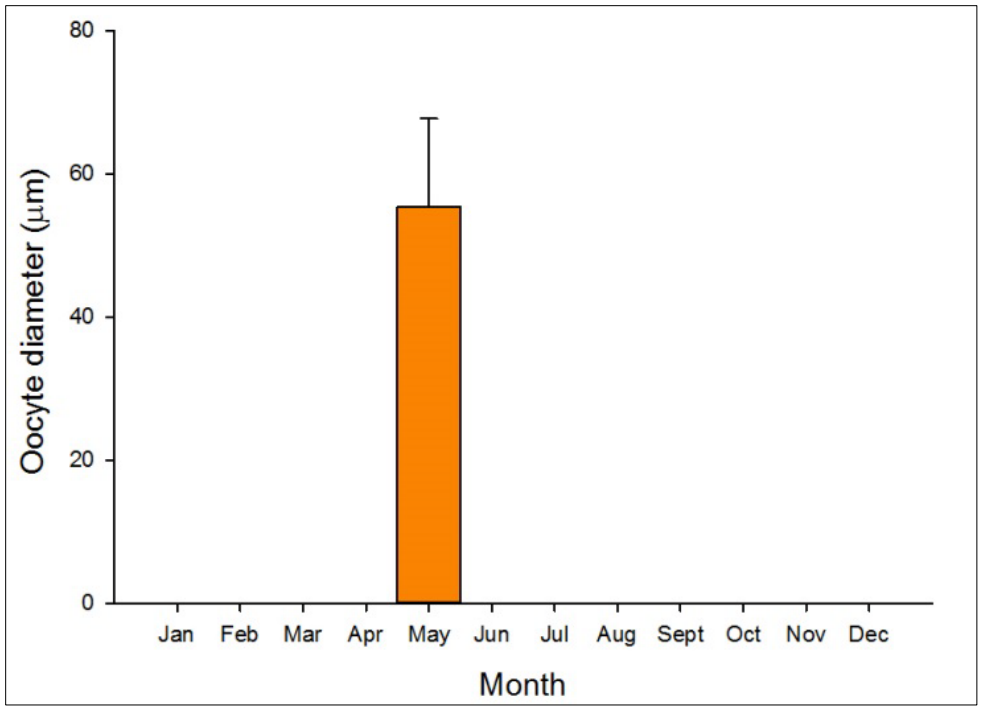

Figure 11-13. *Solensmilia variabilis* average oocyte diameter for females collected in May 2013.

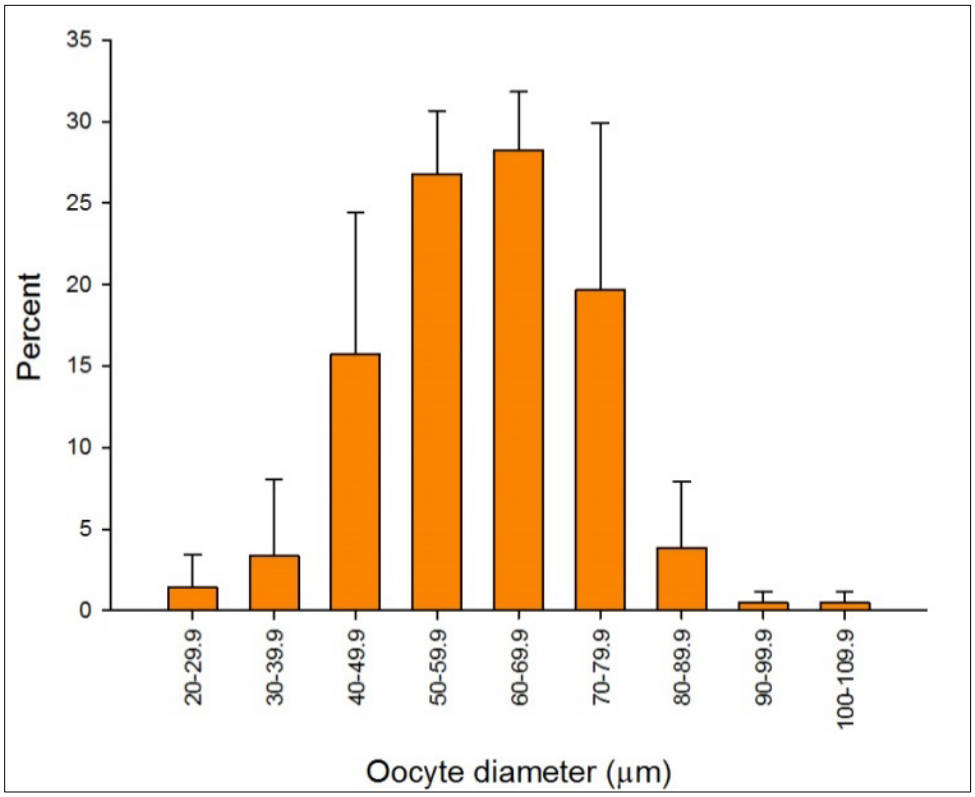

Figure 11-14. *Solensmilia variabilis* oocyte size-frequency distribution for May 2013 samples. The x-axis shows the oocyte size category and the y-axis shows the percentage of total eggs within each size category.

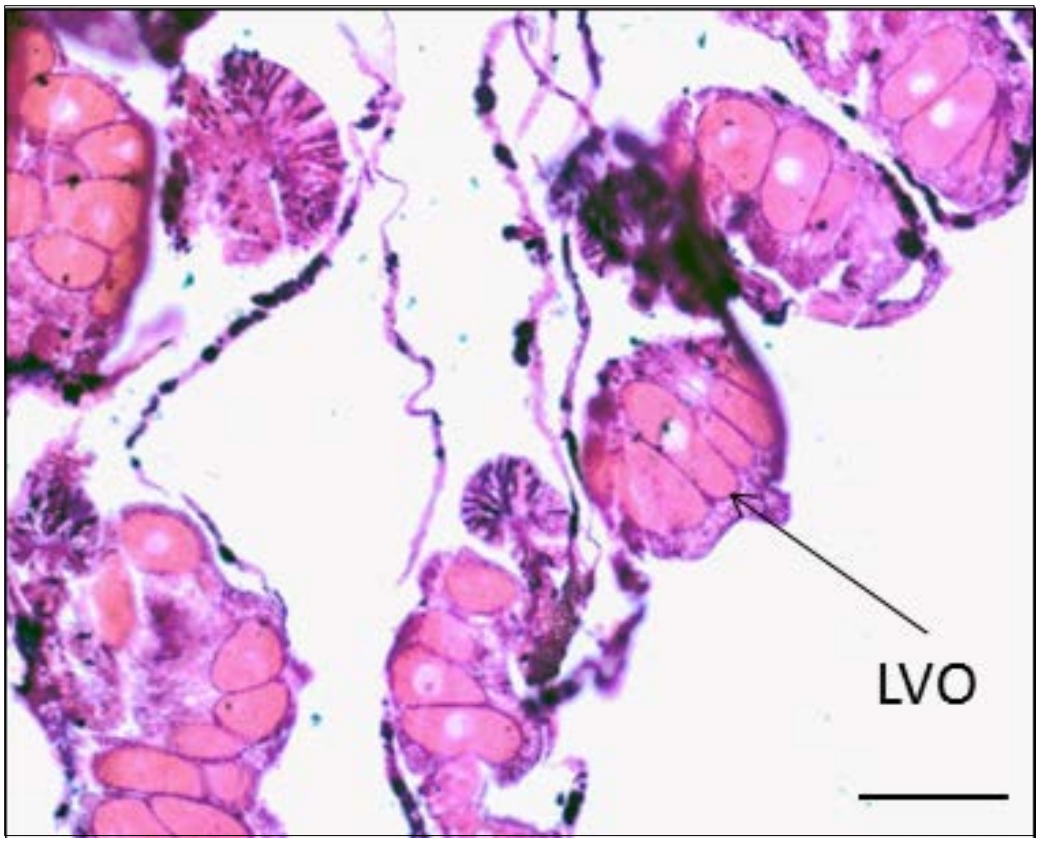

Figure 11-15. *Solensmilia variabilis* female. *VO* = vitellogenic oocytes; *LVO* = late vitellogenic oocytes. Scale bar represents 100 µm.

11.3.1.6 Acanthogorgia aspera

Samples of *A. aspera* were collected only in May 2013 (**Table 11-1**). Of the 26 samples processed, 9 were female, 2 were male, and the remainder contained no gametes. The mean oocyte diameter was 108 µm (SD 15.3) (**Figure 11-16**). The size-frequency distribution shows oocytes in a wide range of size categories from 30 to 219.9 µm. There are some indications of different cohorts, especially in the smaller size classes but this becomes less distinct as the oocytes mature (**Figure 11-17**). This pattern is also apparent within each individual female, but the populations were not tightly synchronized, as evidenced by the high variance within each size class. The males had Stage I and Stage III spermatocysts, which provide evidence for multiple cohorts rather than continuous developmental cycles; however, with so few males, interpretation of the data should be made with caution (**Figure 11-18**). There was no evidence of hermaphroditism or brooding, so the available data indicate that this species is a gonochoric broadcast spawner.

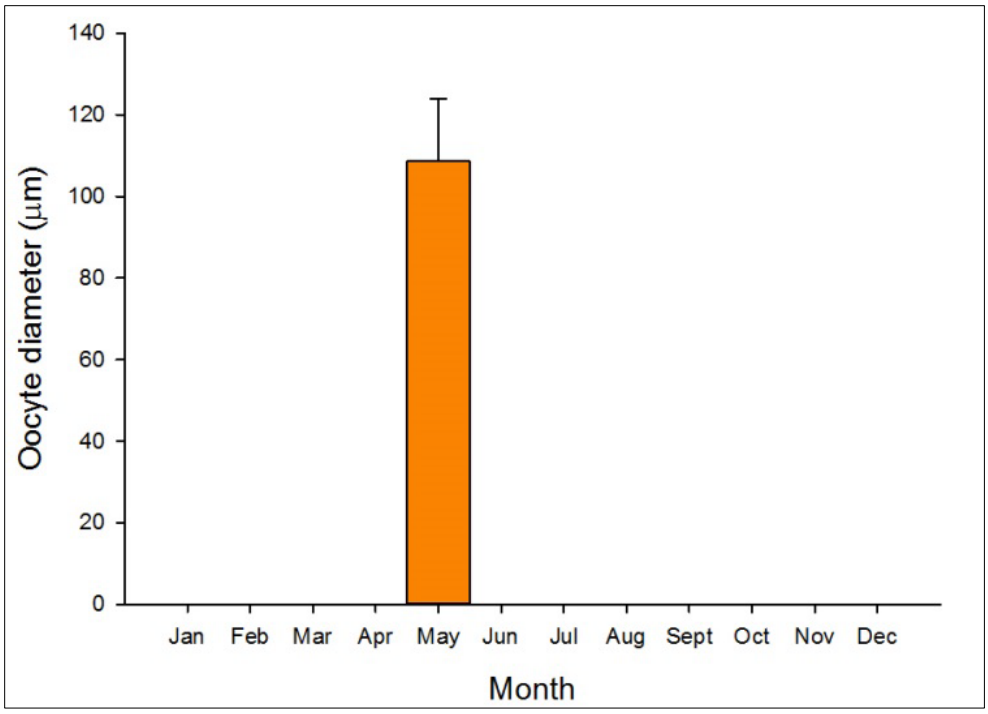

Figure 11-16. *Acanthogorgia aspera* average oocyte diameter for females collected in May 2013.

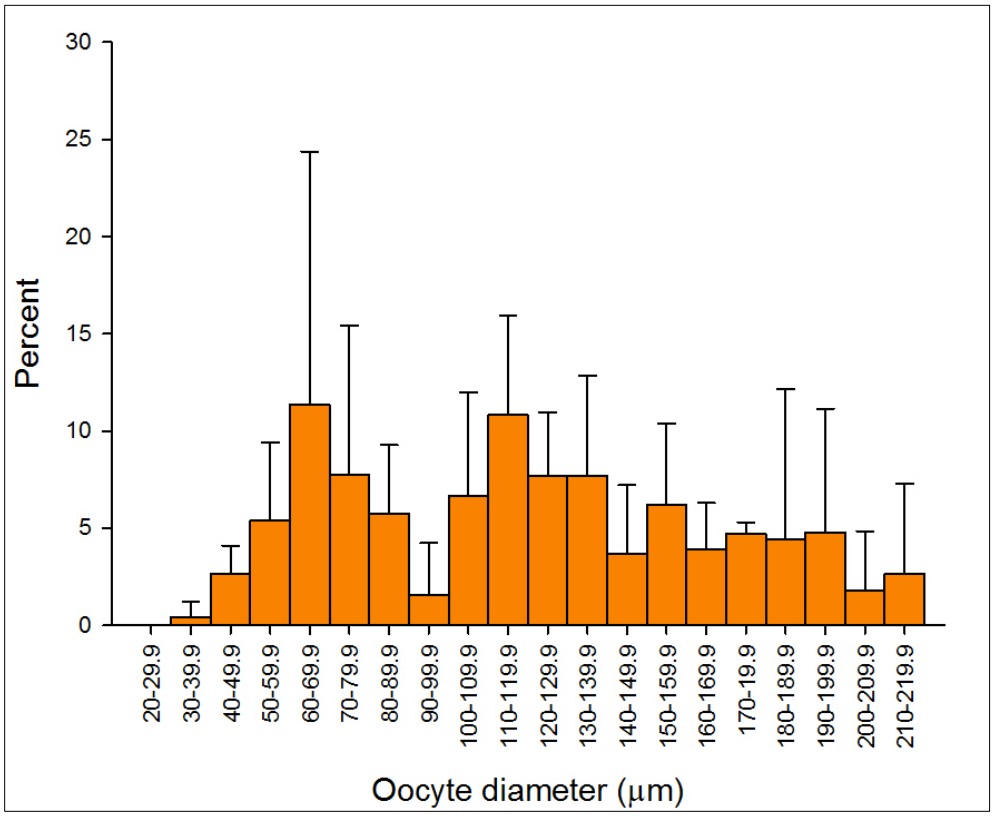

Figure 11-17. *Acanthogorgia aspera* oocyte size-frequency distribution for May 2013 samples. The x-axis shows the oocyte size category and the y-axis shows the percentage of total eggs within each size category.

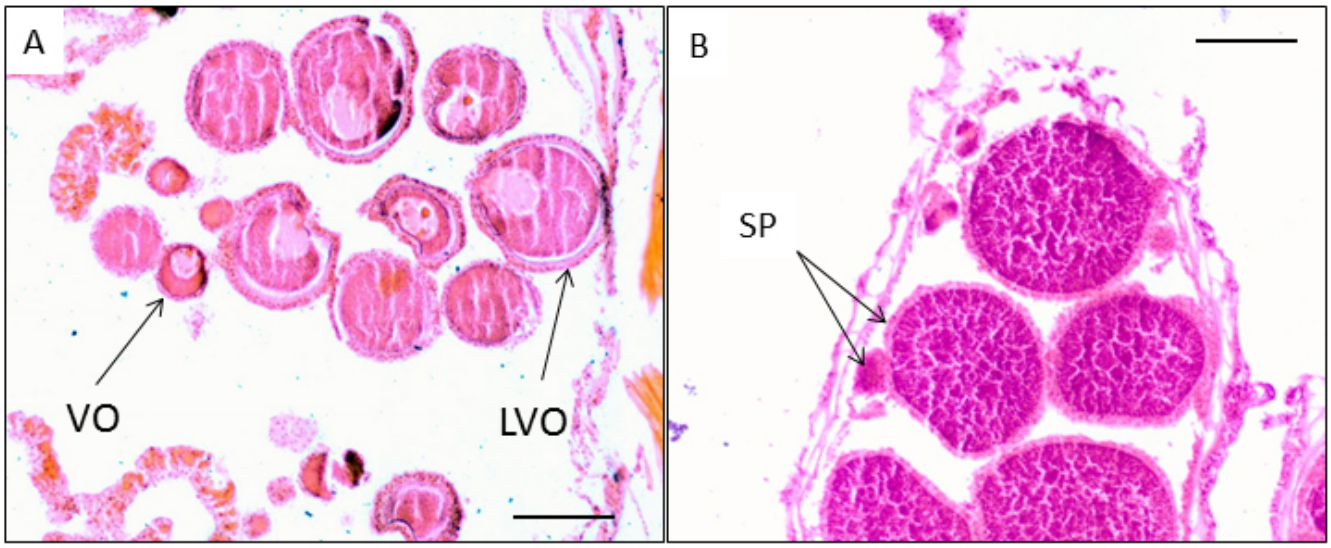

Figure 11-18. *Acanthogorgia aspera* A) female showing a range of oocyte developmental stages, B) male showing Stage I and Stage III spermatocysts. *VO* = vitellogenic oocytes, *LVO* = late vitellogenic oocytes; *SP* = spermatocysts. Scale bar represents 100 µm.

11.3.1.7 Anthothela grandiflora

Samples of *A. grandiflora* were collected in September 2012 and May 2013 (**Table 11-1**). Of the 14 samples processed from 2012, 3 were female, 8 were male, and the remainder had no gametes. The 10 samples from 2013 contained 5 females, 3 males, and 2 with no gametes. The average oocyte diameter for the females collected in 2012 was 213.5 µm (SD 37.4), and was 68.8 µm (SD 31.6) for the 2013 samples (**Figure 11-19**). The average oocyte diameters for each sampling period were compared using a *t*-test and were significantly different from each other ($t = -6.61$, $p < 0.001$). The size-frequency distribution shows clear cohorts within each year; both years show a similar distribution for the smaller size classes, but the second cohort in September 2012 has larger oocytes (140 to 269.9 µm) than those from May 2013 (110 to 219.9 µm) (**Figure 11-20**). The different size classes can be seen clearly in the histological sections where mature oocytes with a granular envelope occur in the same sample as smaller immature oocytes (**Figure 11-21A**). The males also show multiple stages of spermatocysts within the same individual (**Figure 11-21B**), which supports evidence from the female samples for multiple cohorts within the population and within individuals. There were no indications of hermaphroditism or brooding in these samples, so this species appears to be a gonochoric broadcast spawner with periodic spawning events.

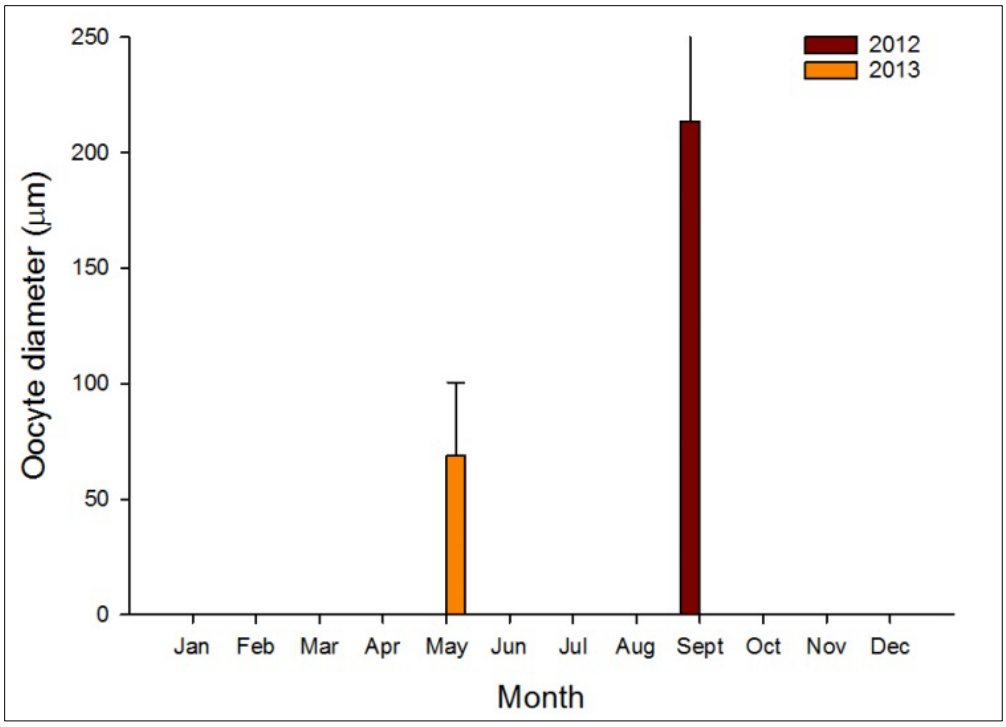

Figure 11-19. *Anthothela grandiflora* average oocyte diameter for females collected in September 2012 and May 2013.

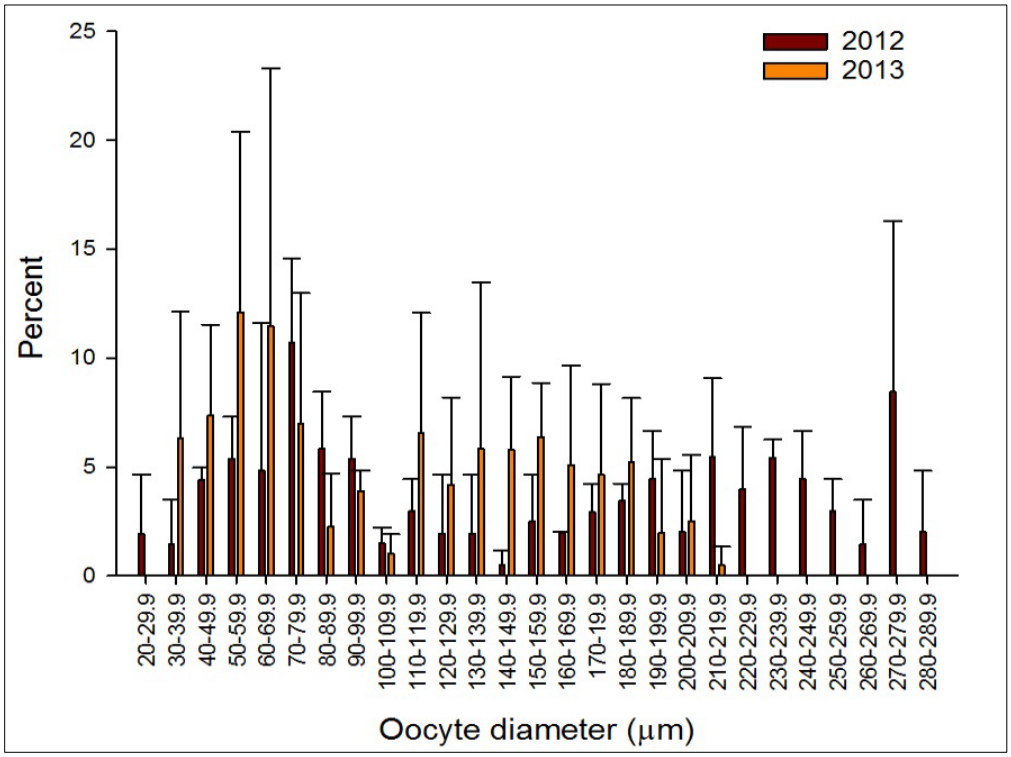

Figure 11-20. *Anthothela grandiflora* oocyte size-frequency distribution for September 2012 and May 2013 samples. The x-axis shows the oocyte size category and the y-axis shows the percentage of total eggs within each size category.

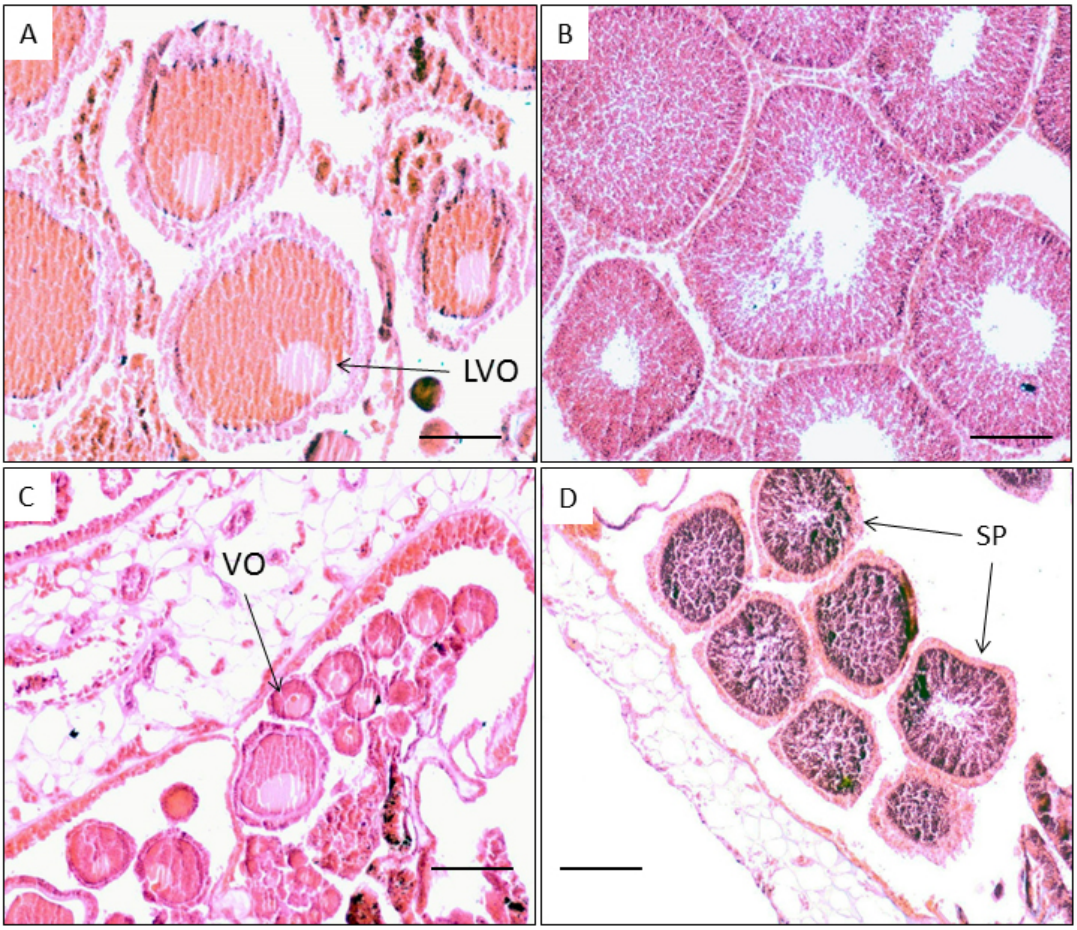

Figure 11-21. *Anthothela grandiflora* A) female showing mature late vitellogenic oocytes, B) male with Stage II and Stage III spermatocysts, C) female with small vitellogenic oocytes, D) male with Stage II and Stage III spermatocysts. *VO* = vitellogenic oocytes, *LVO* = late vitellogenic oocytes; *SP* = spermatocysts. Scale bar represents 100 µm.

11.3.1.8 Paragorgia arborea

Samples of *P. arborea* were collected in September 2012 and May 2013 (**Table 11-1**). Of the 29 samples processed from 2012, 15 were female, 10 were male, and 4 had no gametes. The 33 samples from 2013 contained 10 females, 7 males, and 16 with no gametes. The average oocyte diameter for the females collected in 2012 was 103.9 µm (SD 15.6), and was 79.8 µm (SD 25.6) for the 2013 samples (**Figure 11-22**). The average oocyte diameters for each sampling period were compared using a *t*-test and were not significantly different from each other (t = -1.92, p = 0.09). The size-frequency distribution is heavily skewed towards the smaller size classes (~20 to 150 µm), with much smaller numbers of larger eggs (~150 to 450 µm) (**Figure 11-23**). Males from both years had primarily Stage I and Stage II with some Stage III spermatocysts, which concurs with the developmental pattern of the females (**Figure 11-24**). There were no indications of hermaphroditism or brooding in these samples, so this species appears to release eggs, probably with continuous small spawning events, rather than brooding internally.

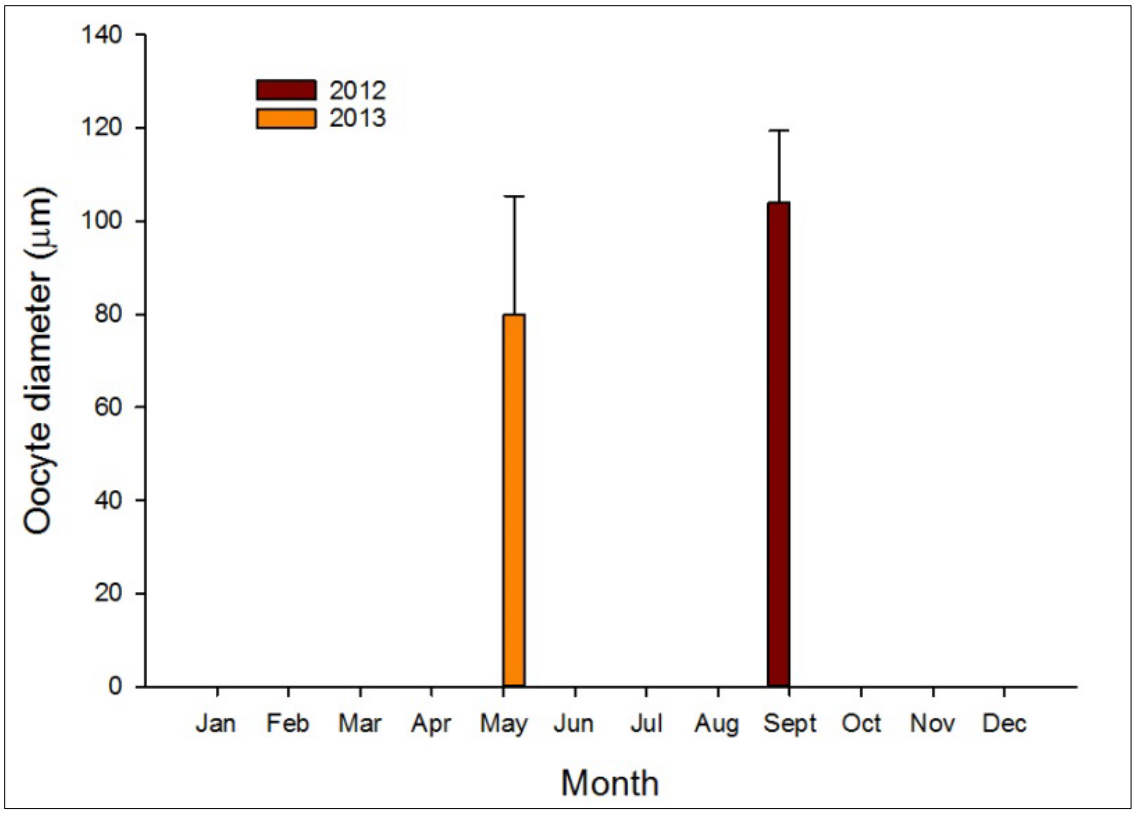

Figure 11-22. *Paragorgia arborea* average oocyte diameter for females collected in September 2012 and May 2013.

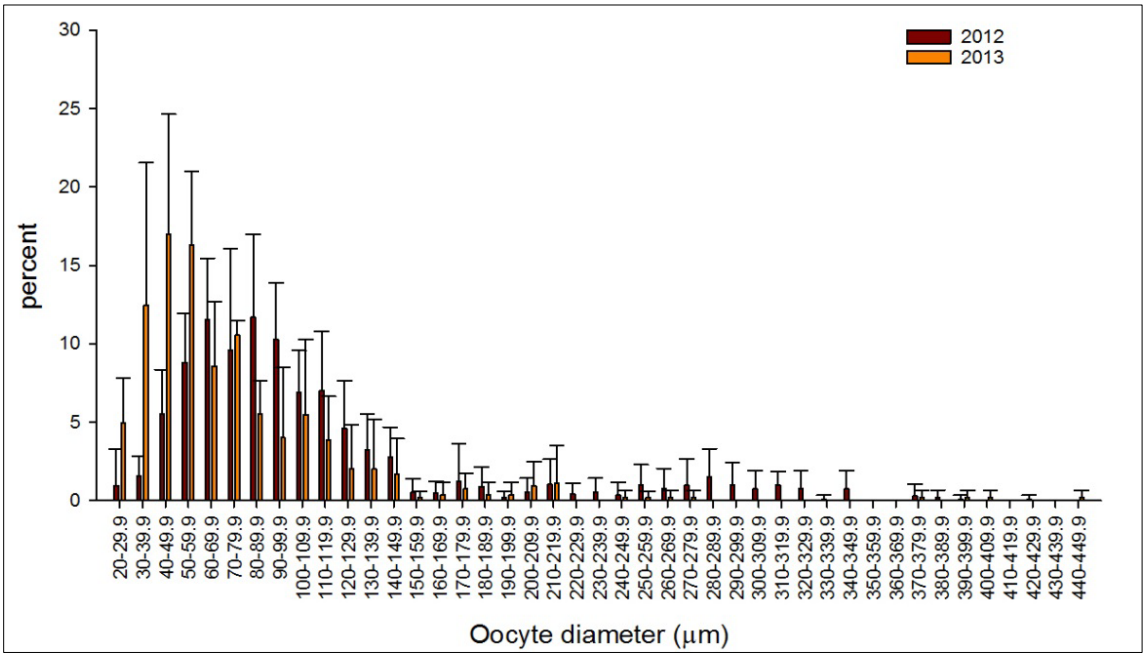

Figure 11-23. *Paragorgia arborea* oocyte size-frequency distribution for September 2012 and May 2013 samples. The x-axis shows the oocyte size category and the y-axis shows the percentage of total eggs within each size category.

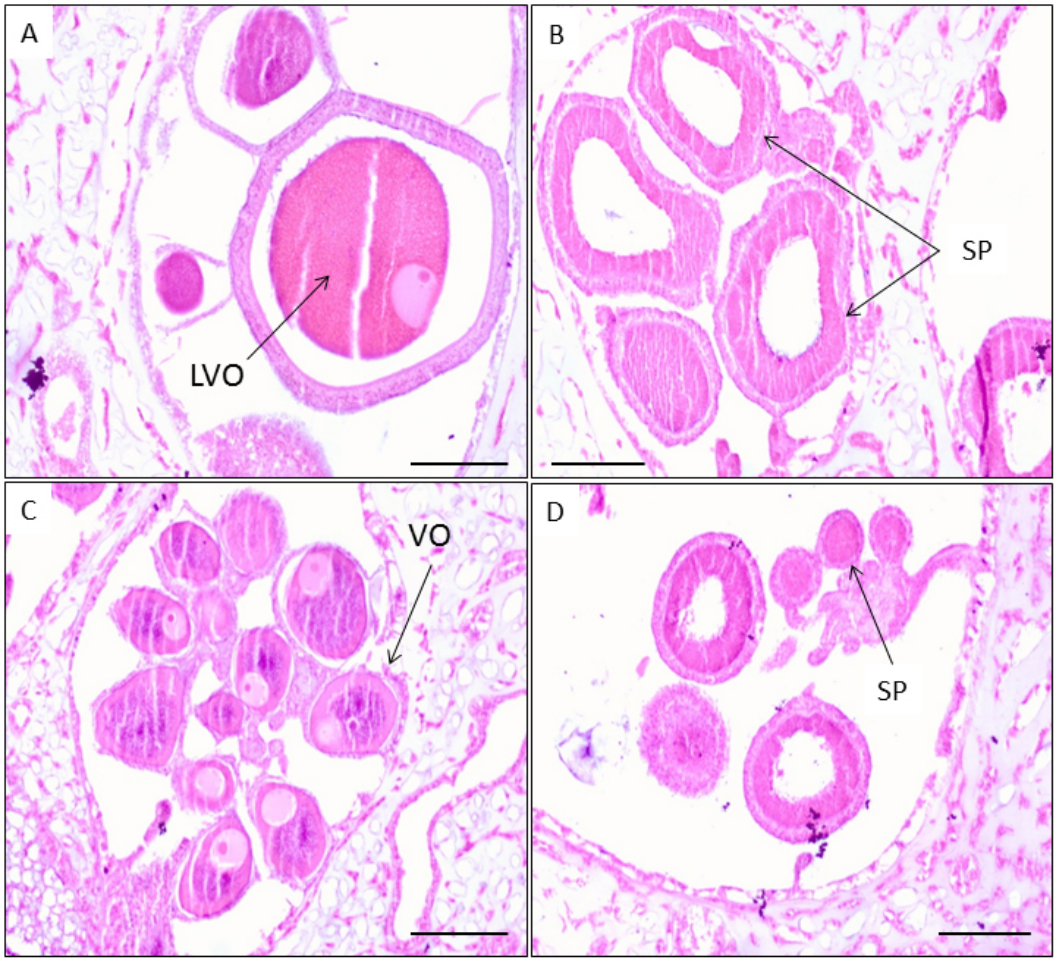

Figure 11-24. *Paragorgia arborea* A) female showing large mature and smaller immature oocytes, B) male showing large Stage II spermatocysts, C) small vitellogenic and pre-vitellogenic oocytes, D) Stage I and Stage II spermatocysts. *VO* = vitellogenic oocytes; *LVO* = late vitellogenic oocytes; *SP* = spermatocysts. Scale bar represents 100 µm.

11.3.1.9 Paramuricea placomus

Samples of *P. placomus* were collected only in September 2012 (**Table 11-1**). Of the 12 individuals processed, 7 were male and the remaining 5 had no gametes. Spermatozoa were predominantly late Stage III with spermatozoa, but Stage I spermatocysts were also present (**Figure 11-25**). A single sample had only Stage I spermatocysts and intermediate stages were absent from all individuals. Neither oocytes nor embryos were observed in any of the samples. With so few samples of one gender and time period, it is not possible to determine the reproductive strategy of this species; however, the data indicate that *P. placomus* is gonochoric and when the samples were collected in September, the population was at the end of one cycle and beginning another.

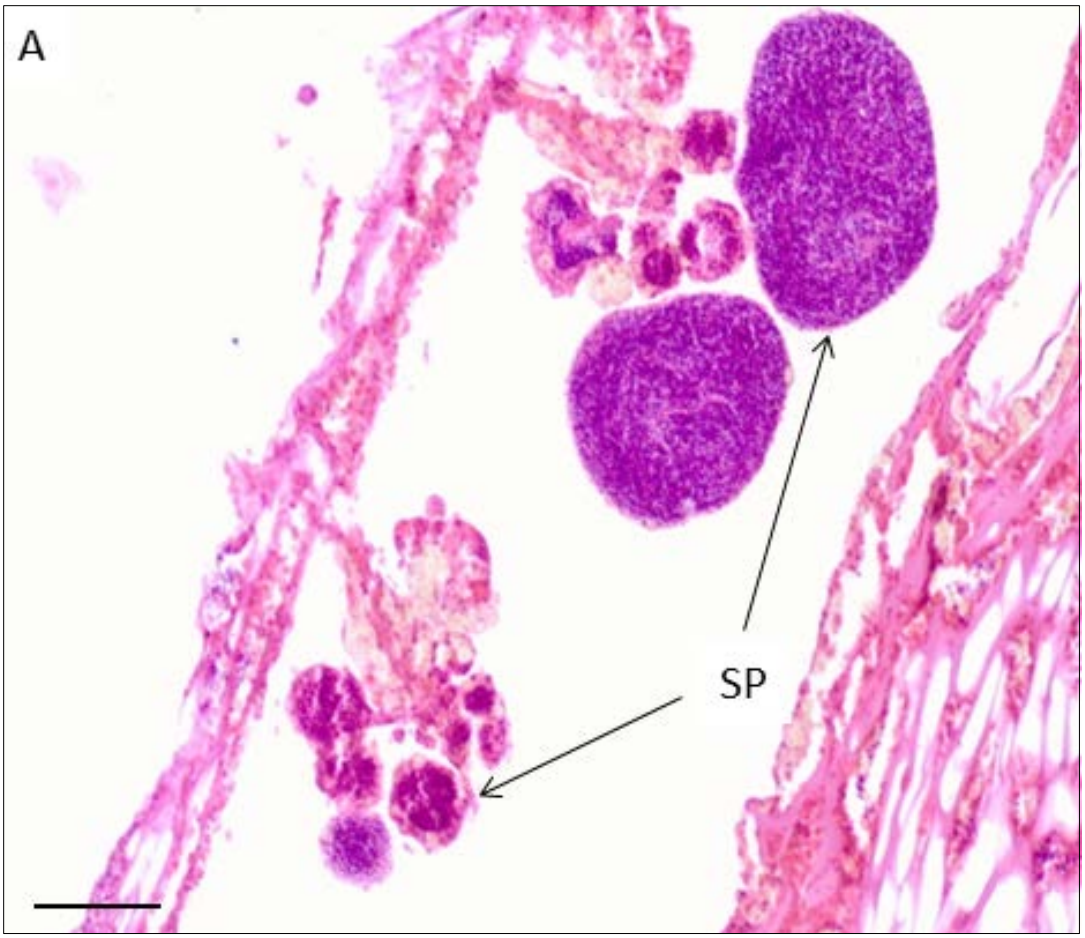

Figure 11-25. *Paramuricea placomus* male. *SP* = spermatocysts. Scale bar represents100 µm.

11.3.1.10 Primnoa resedaeformis

Samples of *P. resedaeformis* were collected in September 2012 and May 2013 (**Table 11-1**). Of the 14 samples processed from 2012, 5 were female, 7 were male, and 2 had no gametes. The 14 samples from 2013 contained 2 females, 4 males, and 8 with no gametes. The average oocyte diameter for the females collected in 2012 was 337.2 µm (SD 196.8), and was 128.7 µm (SD 12.3) for the 2013 samples (**Figure 11-26**). The average oocyte diameters for each sampling period were compared using a *t*-test and were not significantly different from each other ($t = 1.14$, $p = 0.23$). The size-frequency distribution shows some differences between years. In 2012 there were no clear cohorts and all size classes were represented but in 2013 there was an apparent cohort, but with high variance between individuals (**Figure 11-27**). Female samples from 2012 comprised one individual that had only small oocytes (<150 µm) whereas the other samples had a range of size classes, up to 577 µm (**Figure 11-28**). In 2013, the smaller size classes were dominant with few oocytes >250 µm. The male samples contained all stages in both years. This species is probably a broadcast spawner because there were no indications of hermaphroditism or brooding in the samples. There was no clear seasonality to the reproductive cycle, but there were some indications of separate cohorts, therefore, periodic cycles are possible. More data are needed to determine timing of gametogenesis in this species.

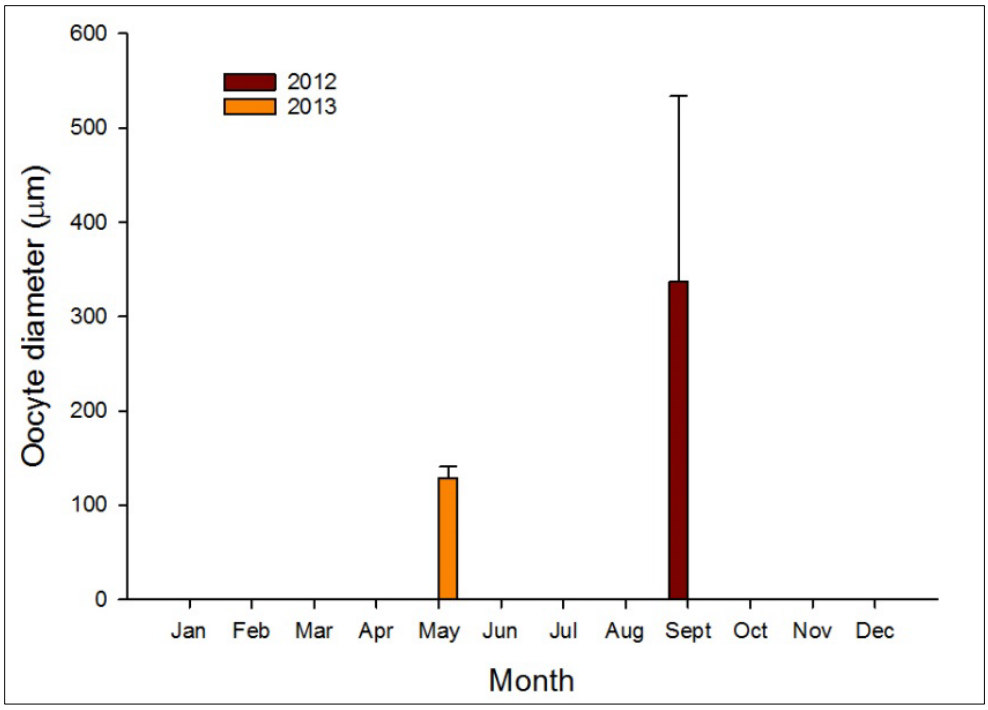

Figure 11-26. *Primnoa resedaeformis* average oocyte diameter for females collected in September 2012 and May 2013.

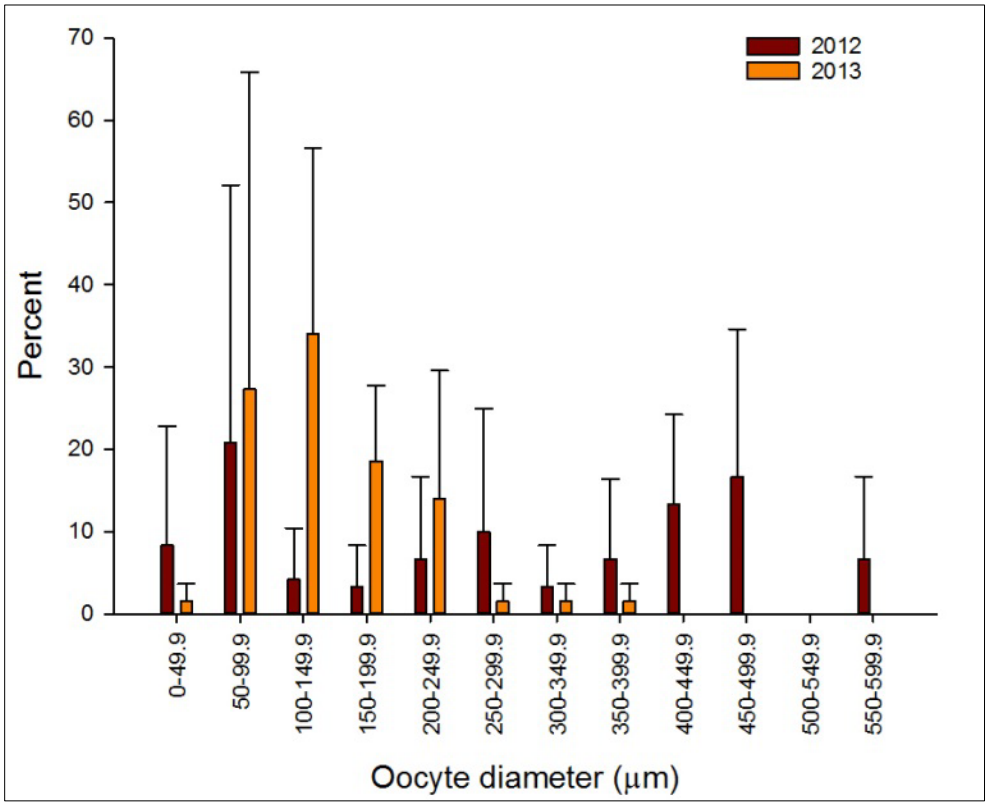

Figure 11-27. *Primnoa resedaeformis* oocyte size-frequency distribution for September 2012 and May 2013 samples. The x-axis shows the oocyte size category and the y-axis shows the percentage of total eggs within each size category.

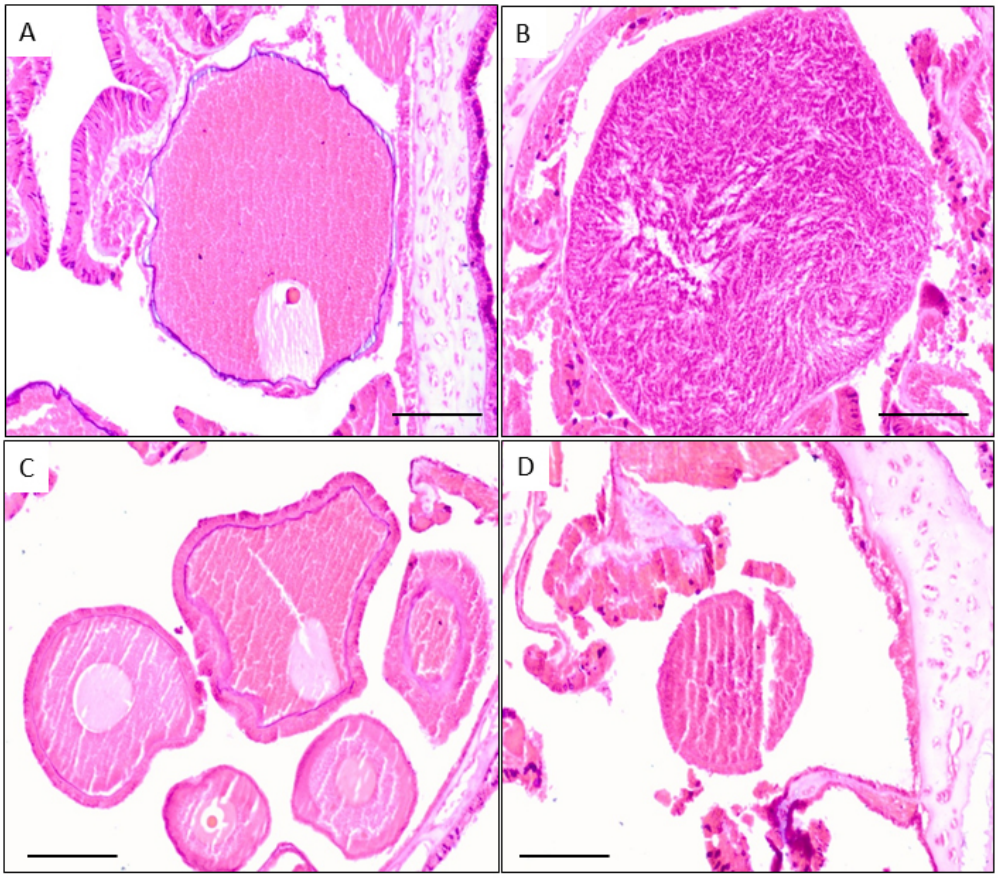

Figure 11-28. *Primnoa resedaeformis* A) female sample from 2012 showing large late vitellogenic oocyte, B) male sample from 2012 with late Stage III spermatocyst, C) female sample from 2013 showing vitellogenic oocytes of different developmental stages, D) male from 2013 showing Stage II and Stage III spermatocyst. Scale bar represents100 µm.

11.3.2 Other Species

11.3.2.1 Seep Urchins

Samples of two species of sea urchins, *Gracilechinus affinis* and *Echinus wallisi* (family Echinidae), were collected from the Norfolk Canyon seep in May 2013 (**Table 11-2**). Eight *G. affinis* were processed; of these, 4 were female, 3 were male, and 1 had no gametes. Thirteen *E. wallisi* were collected, resulting in 5 females, 4 males, and 4 without gametes. The oocytes for both species were small with an average diameter of 32.9 µm (SD 3.9) for *G. affinis* and 32.8 µm (SD 3.9) for *E. wallisi* (**Figure 11-29**). A *t*-test showed no significant difference between the average oocyte diameter of the two species ($t = 0.718$, $p = 0.50$). The size-frequency distribution shows that the dominant size classes are 20 to 29.9 and 30 to 39.9 µm for both species, with occasional large oocytes (**Figure 11-30**). A Mann Whitney Rank Sum Test found no significant difference between the size-frequency distributions from the different species ($U = 40.0$, $p = 0.19$). The female gonads from both species contained oogonia and pre-vitellogenic oocytes, and male gonads from both species contained immature spermatocytes (**Figure 11-31**). These data are insufficient to determine reproductive patterns, but the available evidence suggests synchronized development within the individuals and species, and that both species are developing on a similar schedule.

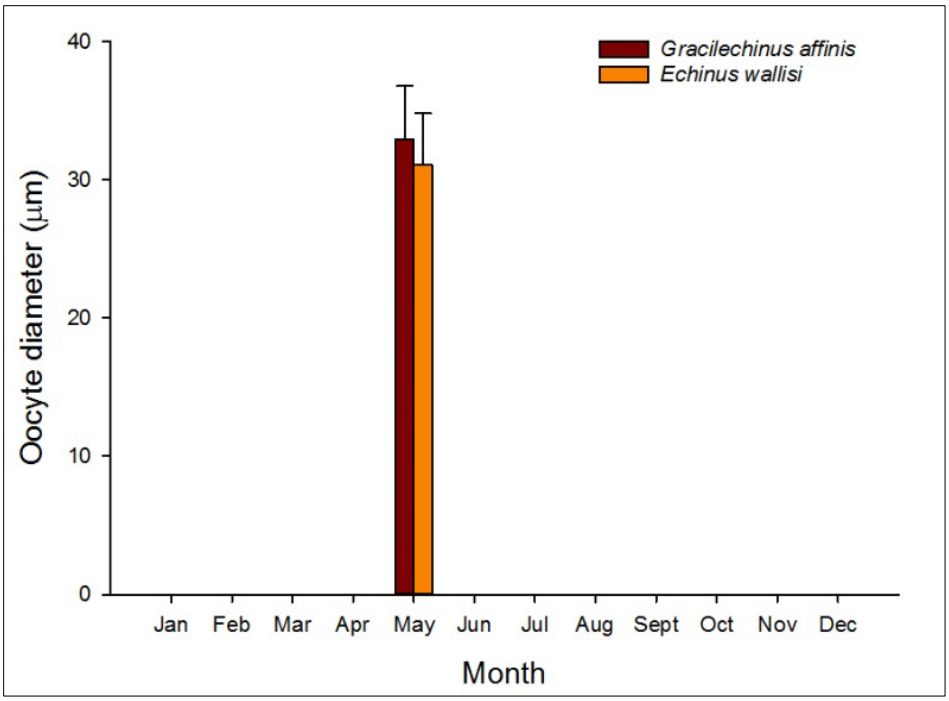

Figure 11-29. Average oocyte diameters of *Gracilechinus affinis* and *Echinus wallisi* females collected in May 2013 from Norfolk Canyon seep.

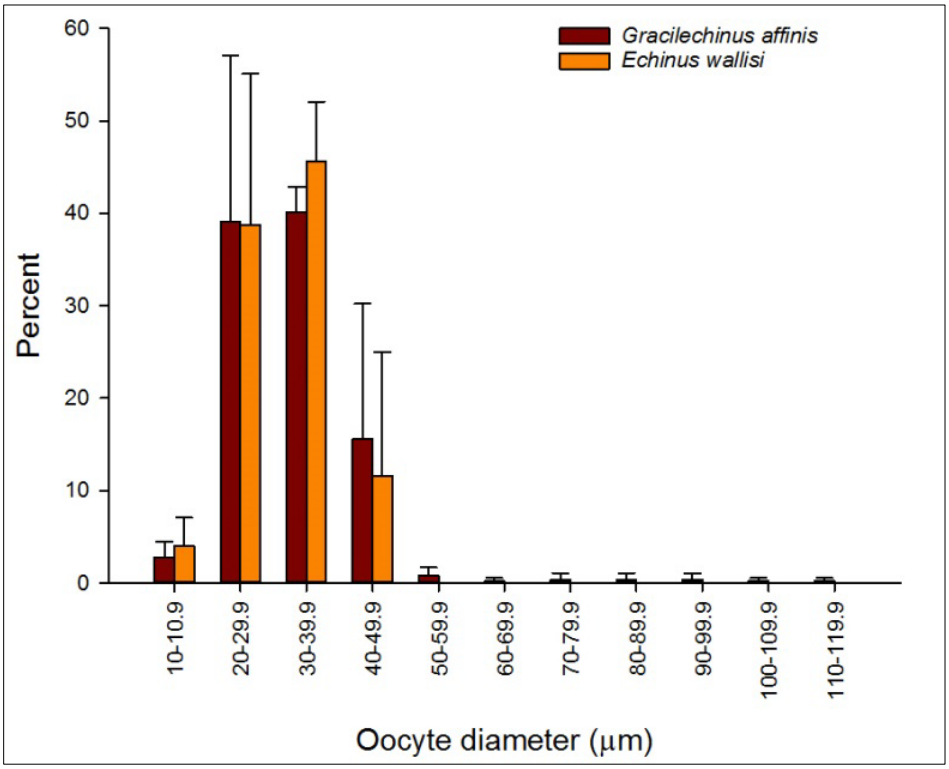

Figure 11-30. Oocyte size-frequency distribution for *Gracilechinus affinis* and *Echinus wallisi* females collected May 2013 from Norfolk Canyon seep. The x-axis shows the oocyte size category and the y-axis shows the percentage of total eggs within each size category.

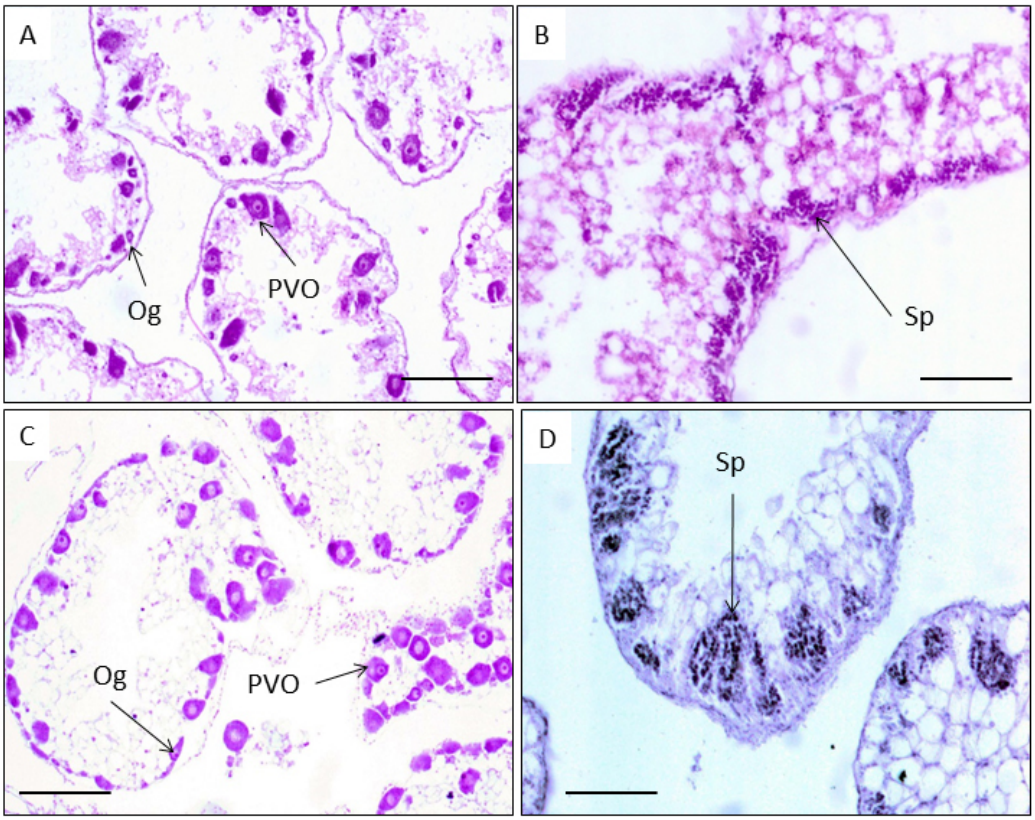

Figure 11-31. Sea urchins from Norfolk Canyon seep. A) female *Gracilechinus affinis* gonads showing oogonia and small pre-vitellogenic oocytes, B) male G. *affinis* gonads showing Stage I spermatocytes, C) female *Echinus wallisi* with oogonia and pre-vitellogenic oocytes, D) male E. *wallisi* gonads showing Stage I spermatocytes. *Og* = oogonia; *PVO* = pre-vitellogenic oocytes; *Sp* = spermatocytes. Scale bar represents 100 µm.

11.3.2.2 Hygrosoma petersii

Samples of the sea urchin *Hygrosoma petersii* were collected in May 2013 using an otter trawl (**Table 11-2**). Of the 6 samples processed, 2 were female, 2 were male, and the remaining 2 had no gametes. The average oocyte diameter was 61.1 µm (SD 36.0) (**Figure 11-32**). The large variance in the average oocyte diameter is explained by the size-frequency distribution, which shows dominance of the 20- to 59.9-µm size classes, but also has relatively high numbers of larger oocytes (**Figure 11-33**). The images of female gonads show a range of oocyte size classes, with the pre-vitellogenic to early vitellogenic stages dominating with occasional larger vitellogenic oocytes and developing oogonia on the periphery of the gonad (**Figure 11-34A**). The males also reflected this range of developmental stages with mature spermatozoa and primarily spermatocytes within the same individual (**Figure 11-34B**). With this limited data, it is difficult to determine the timing of reproductive cycles. The dominance of the smaller size classes may be interpreted as a single cohort, but the significant number of larger oocytes indicates that continuous reproduction is a more likely strategy. There was no evidence of hermaphroditism or brooding in the samples, therefore, this is likely a gonochoric broadcast-spawning species.

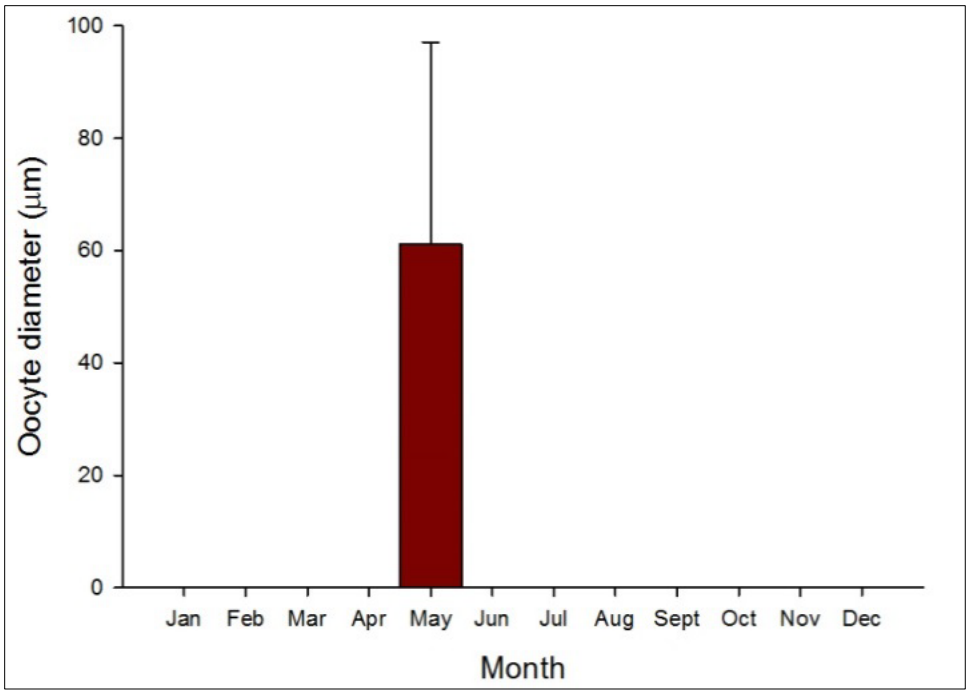

Figure 11-32. Average oocyte diameters of *Hygrosoma petersii* females collected in May 2013 from Norfolk Canyon.

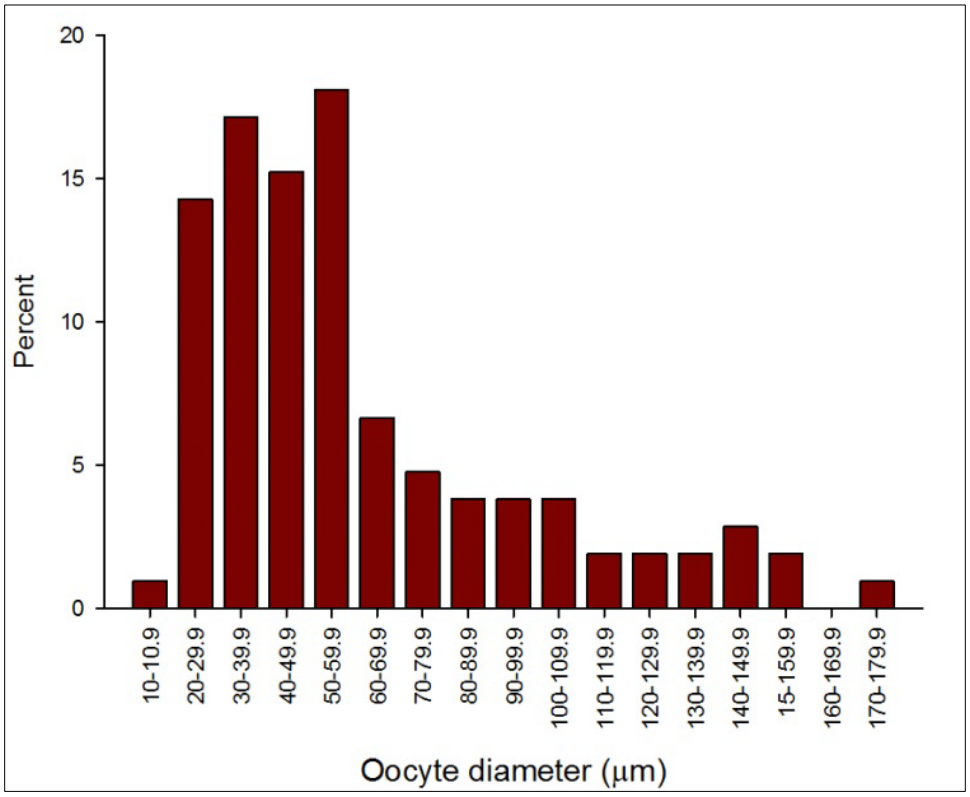

Figure 11-33. Oocyte size-frequency distribution for *Hygrosoma petersii* females collected May 2013 from Norfolk Canyon. The x-axis shows the oocyte size category and the y-axis shows the percentage of total eggs within each size category.

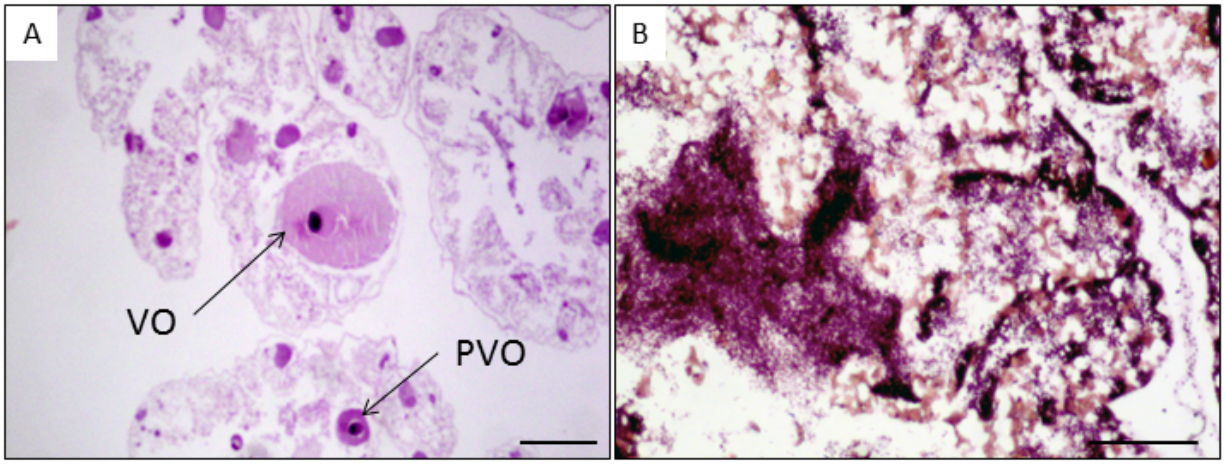

Figure 11-34. *Hygrosoma petersii* A) female gonads from May 2013 showing pre-vitellogenic and vitellogenic oocytes and small oogonia, B) male gonad showing mature sperm in the center and spermatogonia on the periphery of the gonad. *VO* = vitellogenic oocytes; *PVO* = pre-vitellogenic oocytes. Scale bar represents 100 µm.

11.3.2.3 Cidaris abyssicola

Samples of the pencil urchin *Cidaris abyssicola*, a soft-sediment species, were collected from the head of Norfolk Canyon in 2013 using an otter trawl (**Table 11-2**). Of the 5 samples processed, only 1 was female and the others had no gametes. The average oocyte diameter was 50.3 µm (SD 15.6) for the single female (**Figure 11-35**). The size-frequency distribution shows a clear single cohort with the dominant (29%) category being 30 to 39.9 µm (**Figure 11-36**). The oocytes span a wide range of size categories (10 to 99.9 µm), indicating that gametogenesis is not tightly synchronized within the individual, and several different development stages were present simultaneously (**Figure 11-37**). With only one sample and no male samples, determining the reproductive periodicity is not possible, but this species is clearly a gonochoric broadcast spawner.

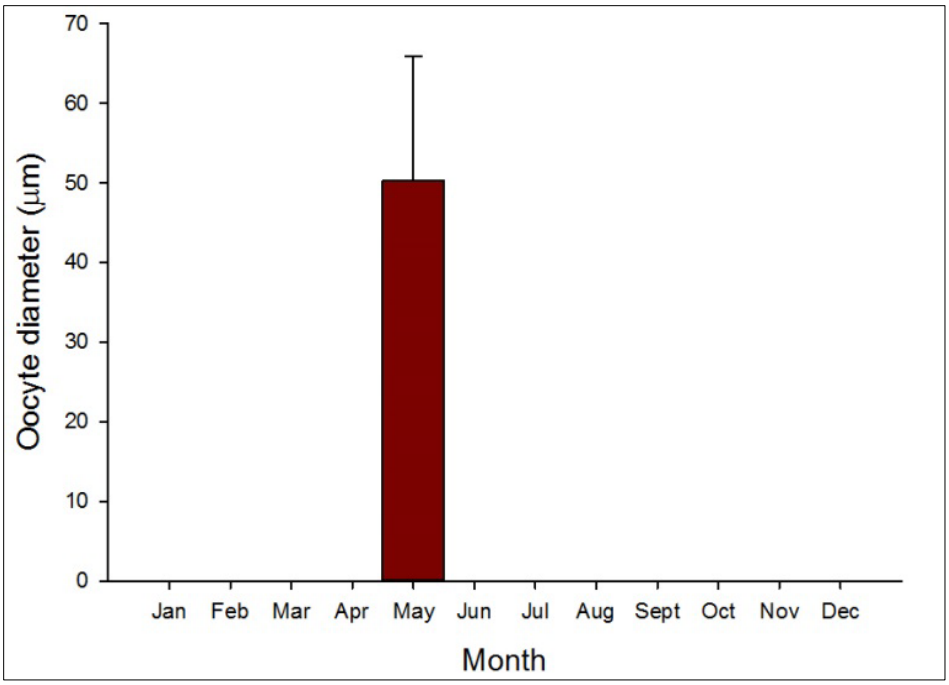

Figure 11-35. Average oocyte diameters of *Cidaris abyssicola* females collected in May 2013 from Norfolk Canyon.

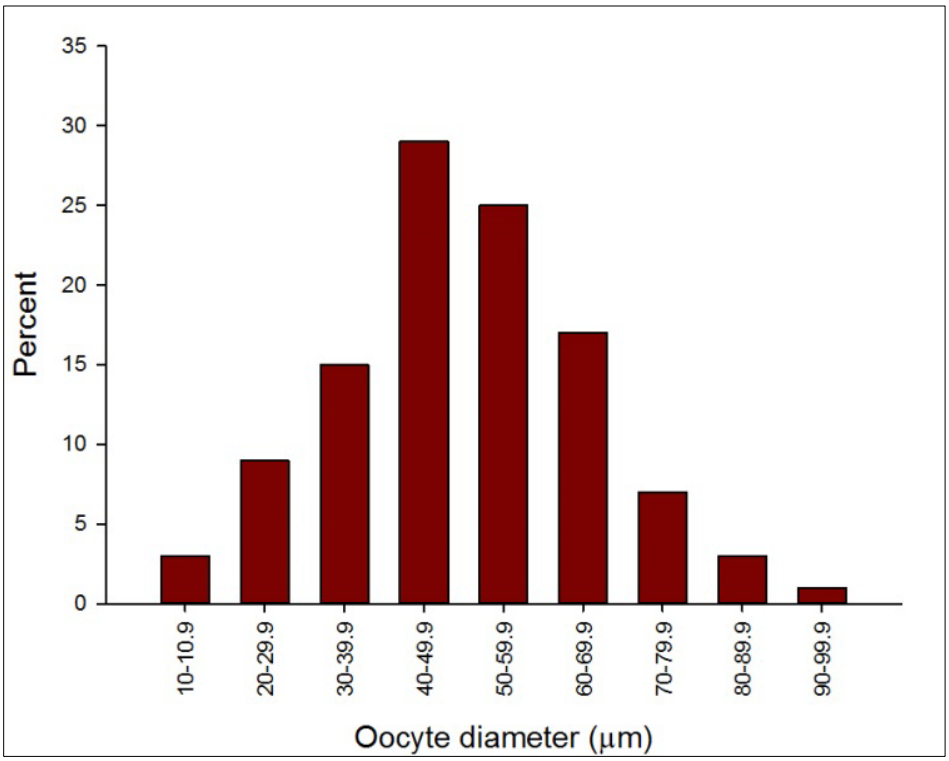

Figure 11-36. Oocyte size-frequency distribution for *Cidaris abyssicola* females collected May 2013 from Norfolk Canyon. The x-axis shows the oocyte size category and the y-axis shows the percentage of total eggs within each size category.

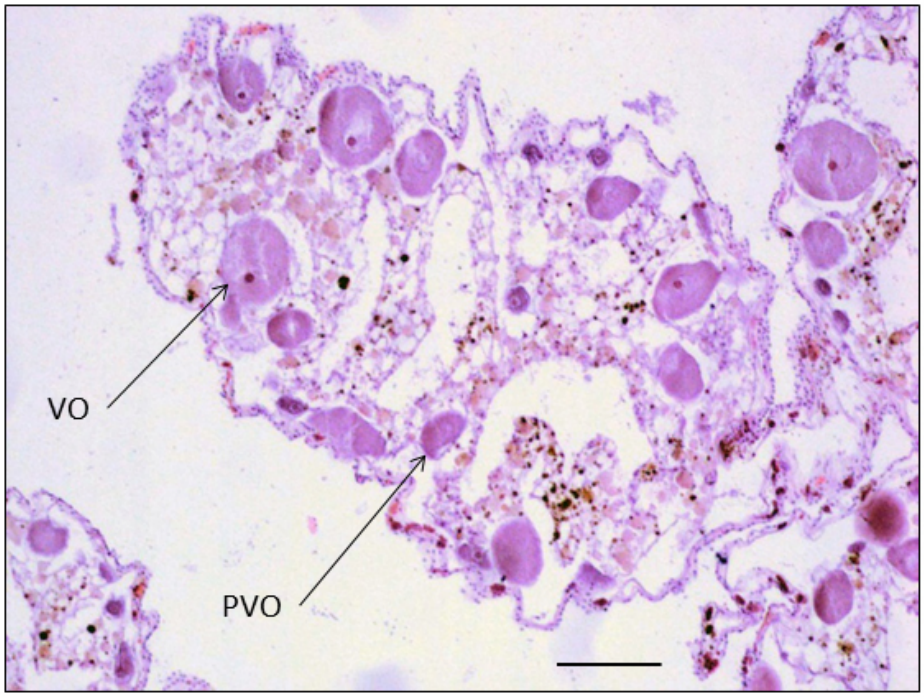

Figure 11-37. *Cidaris abyssicola* female showing small pre-vitellogenic and vitellogenic oocytes. *VO* = vitellogenic oocytes; *PVO* = pre-vitellogenic oocytes. Scale bar represents 100 µm.

11.3.2.4 Bathymodiolus childressi

Samples of the mussel *Bathymodiolus childressi* were collected from the Baltimore Canyon seep in September 2012 and from both Baltimore and Norfolk canyon seeps in May 2013 (**Table 11-2**). Thirty-one samples were processed from Baltimore Canyon seep in September 2012, of which 7 were females, 9 were males, and 15 had no gametes. The 29 samples from Baltimore Canyon seep included 9 females, 11 males, and 9 without gametes. Of the 14 samples processed from Norfolk Canyon seep in May 2013, 7 were female, 3 were male, and 4 had no gametes. Average oocyte diameter for Baltimore Canyon seep females was 34.9 µm (SD 2.26) in 2012 and 35.6 µm (SD 2.8) in 2013. Norfolk Canyon seep females from 2013 had an average oocyte diameter of 38.4 µm (SD 4.5) (**Figure 11-38**). A one-way ANOVA showed no statistically significant differences among all sampling times and locations ($F = 2.31$, $p = 0.13$). The size-frequency distribution was similar for all sampling dates and locations, with a dominant size class of 30 to 39.9 µm for all females (**Figure 11-39**). Both female and male samples from all sampling periods contained a range of developmental stages, with the majority being late-stage gametes (**Figure 11-40**). This species is a gonochoric broadcast spawner that appears to have no seasonal developmental cycle. The data indicate that they reproduce continuously, probably spawning small batches periodically throughout the year.

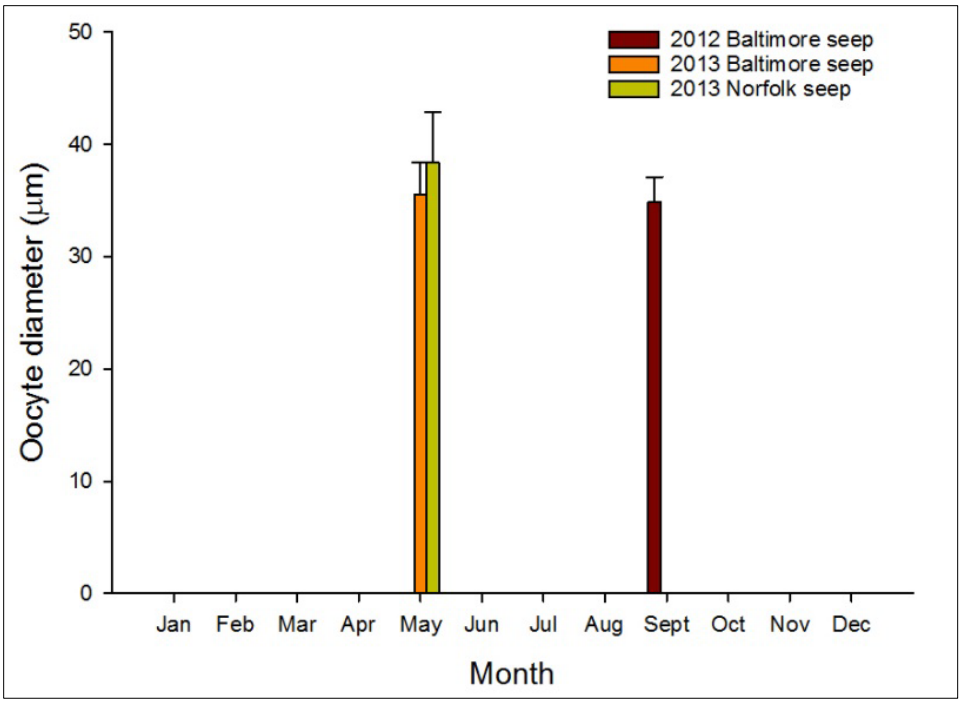

Figure 11-38. Average oocyte diameters of *Bathymodiolus childressi* females collected in August and September 2012 from Baltimore Canyon seep, and May 2013 from Baltimore and Norfolk Canyon seeps.

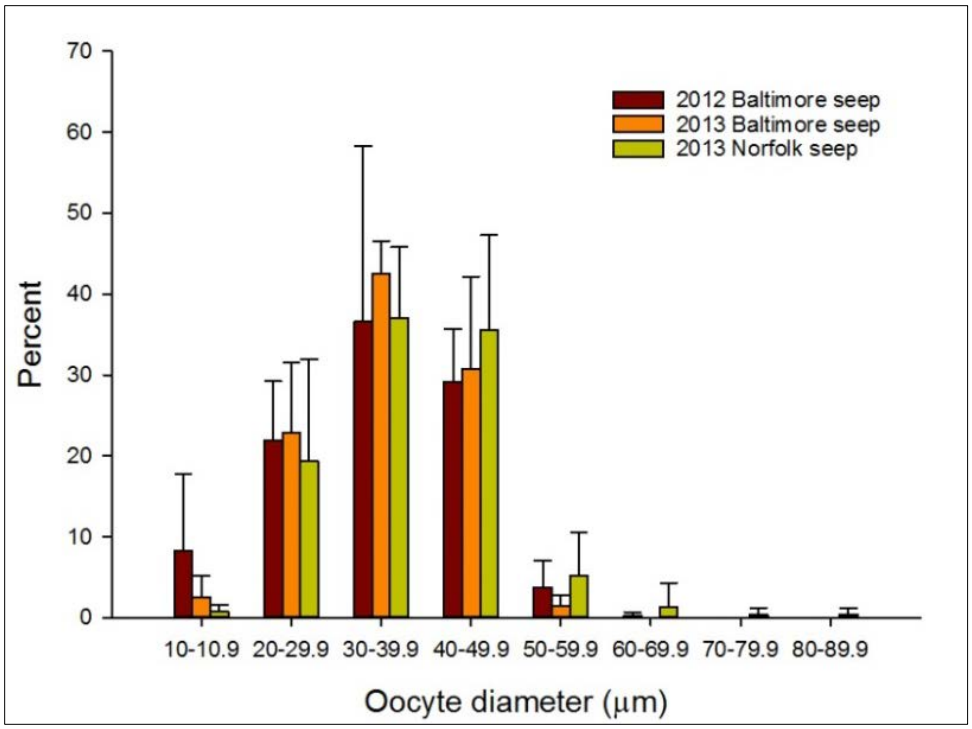

Figure 11-39. Oocyte size-frequency distribution for *Bathymodiolus childressi* females collected in August and September 2012 from Baltimore Canyon seep and May 2013 from Baltimore and Norfolk Canyon seeps. The x-axis shows the oocyte size category and the y-axis shows the percentage of total eggs within each size category.

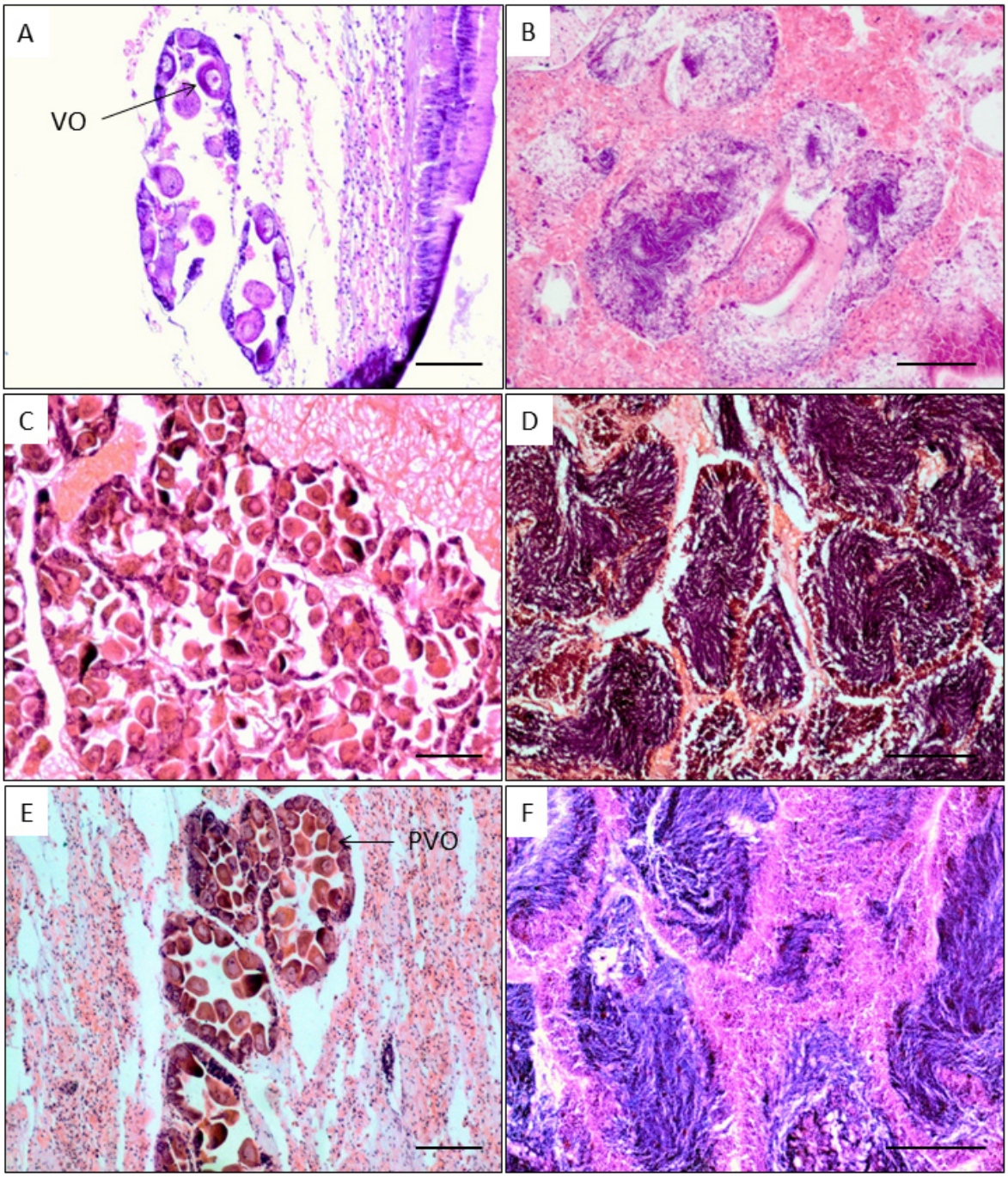

Figure 11-40. *Bathymodiolus childressi* A) female from August 2012 Baltimore Canyon seep showing vitellogenic oocytes, B) male from August 2012 Baltimore Canyon seep showing spermatozoa, C) female from May 2013 Baltimore Canyon seep showing vitellogenic oocytes, D) male from May 2013 Baltimore Canyon seep showing spermatozoa, E) female from May 2013 Norfolk Canyon seep showing pre-vitellogenic and vitellogenic oocytes, F) male from May 2013, Norfolk seep showing spermatozoa. *PVO* = pre-vitellogenic oocytes; *VO* = vitellogenic oocytes. Scale bar represents 100 µm.

11.4 DISCUSSION

11.4.1 Corals

Over the past two decades, the level of exploration and research that has focused on deepsea corals has increased tremendously; however, there are still gaps in our understanding of basic coral biology, including reproduction and early life histories. Monthly samples of replicate individuals collected over multiple years are ideal for adequate description of the reproductive periodicity of a species. With a few exceptions such as fjords or steep nearshore habitats, deepwater species live far offshore and can only be accessed during periods of clement weather. Consequently, much of the existing information on reproductive processes of deepsea corals comes from limited samples, time periods, and locations. Despite these limitations, some interesting trends in the reproductive biology of deepsea corals have become apparent. Corals as a group can have a wide range of reproductive strategies, including gonochorism, hermaphroditism, broadcast spawning, and brooding. Gonochorism has been proposed as a more primitive trait than hermaphroditism (Goffredo et al. 2002), but with a greater potential for dispersal and maintaining genetic diversity over a broad area (Szmant 1986). Most shallow coral species are hermaphroditic (Harrison 2011), but the majority of deepsea corals are gonochoric broadcast spawners, and hermaphroditism and brooding are rare (Roberts et al. 2009). The exceptions to this generalization are the soft corals (Neptheidae and Alcyoniidae) which are all brooders (Watling et al. 2011).

The species in this study showed no evidence of hermaphroditism or brooding and therefore fit the general pattern observed for most other deepsea coral species. Some species brood externally, but given the extensive handling of the samples prior to processing, it is likely that any external planulae would have been dislodged. Most species in this study also showed evidence of seasonality or periodicity in their developmental cycles. This trait is common in shallow gonochoric broadcast-spawning corals (Harrison 2011), some of which have a very high level of synchrony within a population. This synchronized development increases the probability of male and female gametes being released simultaneously into the water column, thereby increasing fertilization rates (Oliver and Babcock 1992, Levitan et al. 2004). Reproductive cycles and the factors that influence them are well studied in shallow water and include seasonal changes in water temperature, day length, wind and current patterns, day length, and lunar cycles (Harrison 2011, and references therein). Some of these factors are not relevant to deepsea corals living in areas where light cannot penetrate, but changes in temperature and lunar/tidal cycles are detectable in the deep sea and may influence reproduction (Roberts et al. 2005, Dodds et al. 2007, Gori et al. 2007, Mercier et al. 2011). Seasonal changes in food availability may be an important factor in driving deepsea coral reproduction (Burgess and Babcock 2005, Waller and Tyler 2005). Reproduction is energetically costly, particularly the production of lipid-rich eggs, and seasonal food pulses may promote various aspects of reproductive biology such as onset of gametogenesis, larval release, and settlement (Tyler et al. 1982, Orejas et al. 2002). Collecting relevant biotic and abiotic data from the deep sea on time scales sufficient to make meaningful correlations is extremely challenging, and conducting manipulative experiments to determine causation is even more so; therefore, the drivers of reproduction in deepsea fauna remain largely conjectural.

The solitary coral *Dasmosmilia lymani* (family Caryophyllidae) was an atypical species for this study as it lives in soft sediment and in relatively shallow water. This species has been reported from the North Atlantic, Pacific, and Antarctic oceans at depths of 37 to 366 m (Cairns 1979, 1995) and occurs in patches on the western Atlantic margin (Hecker and Blechschmidt 1980, Pierdomenico et al. 2015). This species appears to be gonochoric as only eggs were observed and it had a single cohort of egg sizes, which implies periodic or seasonal reproduction, at least within the individual. The eggs of *D. lymani* were quite small (~60 µm) for mature vitellogenic eggs, so this species may produce small planktotrophic larvae. There are however, no published studies on the reproduction of this species with which to compare our findings, and interpretation of such limited data should be made with caution.

Another soft-sediment solitary coral, *Flabellum alabastrum* (family Flabellidae), was collected in May 2013 from a deep area (~1,600 m) off Norfolk Canyon. The reproductive strategy in this species was also gonochoric broadcast spawning, but unlike *D. lymani*, the eggs within and among individuals were composed of a range of developmental stages, indicating continuous reproduction. The eggs of this species were very large (>1,000 µm) and probably give rise to lecithotrophic larvae (Waller 2005). The findings of this study concur with other published information on *F. alabastrum* from the Porcupine Sea Bight in the northeast Atlantic Ocean (Waller 2003), but ours is the first study on the reproduction of this species in the western Atlantic Ocean.

The large "cockscomb" cup coral *Desmophyllum dianthus* (family Caryophyllide) is a cosmopolitan species that is found in small clusters (or occasionally in very large numbers) on hard substrates at depths as shallow as 8 m in the Patagonian fjords to 2,460 m (Cairns 1994, 1995). There have been several studies on the biology and paleoecology of this species (Lazier et al. 1999, Adkins et al. 2004, Thresher et al. 2011), but nothing has been published to date on the reproductive biology. Information from this study indicates that *D. dianthus* is a gonochoric broadcast-spawning species that has an annual reproductive cycle. Males from the September sample were not fully mature, but were in an advanced stage of development and some of the oocytes had a granular cortical layer, indicating advanced maturity; therefore, we estimate a spawning period of late fall for the canyons populations. Samples collected from approximately 1,300 m were much smaller than those from shallower depths. Apart from one male (which was at the same developmental stage as the shallower samples collected in May 2013), the deep samples had no reproductive material. This could have been a consequence of food limitation at depth, or the population may have been too young to be reproductively active. A study of the demography of *D. dianthus* from the Tasman Sea concluded that recruitment events occurred approximately every 20 years (Thresher et al. 2011). The authors suggested this was caused by either very infrequent reproduction (due to limited food resources) or rare successful recruitment events. The data from our study show a relatively high reproductive output on an annual schedule, but the occurrence of *D. dianthus* in the canyons was generally rare (**Chapter 8**) so it is plausible that the distribution of this species is limited by recruitment rather than low reproductive potential.

The cosmopolitan reef-building scleractinian *Lophelia pertusa* (family Caryophyllidae) is the most well-studied deepsea coral species. The reproductive and larval biology have been described from the northeast Atlantic populations (Waller and Tyler 2005, Brooke and Jarnegren 2013, Larsson et al. 2014), which have an annual gametogenic cycle culminating in a protracted spawning period from late January to mid-March, peaking in February. The average oocyte diameter of the mid-Atlantic populations was larger than for the Norway populations for the same time period. Comparing the relative sizes and oocyte growth, the estimated peak spawning period for *L. pertusa* in the mid-Atlantic canyons is in December. Spawning periods for this species from elsewhere in the western Atlantic Ocean show regional differences; peak spawning in the Gulf of Mexico occurs in October (CSA International, Inc. 2007) and is estimated to be November in the southeastern United States (Demopoulos et al. [date unknown]). The reasons for these differences are not known, but they may be related to environmental factors such as temperature (although temperature does not vary on the same schedule as the reproductive cycles), or biotic factors such as food supply, which is driven by regional organic material deposition and zooplankton dynamics.

The female *Solenosmilia variabilis* (family Caryophyllidae) samples from May 2013 had a relatively small average oocyte diameter and a few larger more mature eggs; unfortunately, there were no male samples to more accurately assess developmental stage. Samples of this species were collected during a single cruise in April from seamounts off New Zealand and both males and females were reproductively mature (Burgess and Babcock 2005). The average oocyte diameter of those samples was 148 µm (SD = 14), which was considerably larger than the females in our study. The growth rate of *S. variablis* oocytes is not known and cannot be determined without at least two sampling times from the same

location. The available evidence suggests that gametes from the mid-Atlantic canyons populations would continue to develop as a cohort culminating in a spawning period, probably in the winter or early spring.

All scleractinian species in this study are gonochoric broadcast spawners and, with the exception of *F. alabastrum*, all appear to have annual (or periodic) reproductive cycles. From the species that were sampled in both years, all were more mature in September than in May and therefore seem to be following a similar annual cycle.

The gorgonian *Acanthogorgia aspera* (family Acanthogorgiidae) does not occur farther north than Norfolk Canyon but its congener *A. armata* occurs in more northern regions (Watling and Auster 2005). The reason for this species' distribution is not clear as both species are found under similar environmental conditions. The data from this study indicate that *A. aspera* has multiple cohorts of oocytes probably resulting in periodic spawning although there is no published information on this species or congeners with which to compare the information from our study. The largest eggs documented for *A. aspera* were approximately 220 µm, which most likely results in lecithotrophic larvae, which have generally shorter lifespans than planktotrophic larvae and theoretically a more limited dispersal potential.

The gorgonian *Anthothela grandiflora* (family Anthothelidae) is abundant on hard substrates in Baltimore and Norfolk canyons. It frequently colonizes other dead octocoral skeletons and sometimes seems to be overgrowing live coral. It is found throughout the North Atlantic from 50 to 1,150 m (Watling and Auster 2005), but there is very little information available on the reproduction or any other aspects of the biology of this species. Genetic analysis (**Chapter 13**) showed that most of the samples collected were *A. grandiflora,* but an undescribed species and a putative different genus "*Lateothela*" *grandiflora* were also identified. These cannot be distinguished morphologically, therefore, all *Anthothela* species were considered *A. grandiflora* for this reproductive analysis. As with the scleractinians, samples of this species collected in September 2012 had a larger oocyte diameter than those collected in May 2013. The size-frequency curves revealed multiple cohorts for each sampling period, with small oocytes present in both samples, but the second cohort of the September samples had larger and more mature oocytes than the samples collected in May. Development of the male gametes matched the females; most of the spermatocysts were Stage II (May) or Stage II-III (September) with a low number of early Stage I. This pattern implies a continuous production of gametes, with a periodic maturation and spawning of a subset of oocytes. This strategy may allow a more rapid turnover of gametes and possibly more frequent release than those species that do not initiate gametogenesis until after they have spawned the previous cohort. The largest eggs of this species were approximately 300 µm, implying production of lecithotrophic larvae.

The most common gorgonian species observed in the canyons was *Paragorgia arborea* (family Paragorgiidae); unlike the species discussed so far, *P. arborea* skeletons are thick and fibrous, overlaid with a layer of tissue approximately 2 mm thick. The gametes occur at the base of the feeding polyps and in pockets near the surface of the coenenchyme. The average oocyte diameters from the different sampling dates are not different from each other and the size-frequency distribution is dominated by smaller size classes with what appears to be a continuous development of larger eggs (~400 to 450 µm). Unlike several of the other species studied, there is no apparent periodicity in the reproduction of this species. Broadcast spawners usually have synchronous reproduction within populations, releasing large numbers of gametes into the water column simultaneously to increase fertilization success. Among brooders, spawning synchrony may not be as important because eggs are retained either inside the polyps or on the colony surface until fertilization occurs (Coma et al. 1995a, Dahan and Benayahu 1997). Babcock (1990) suggests that brooding may be a strategy, which compensates for low fecundity by enhancing survival of larvae by providing a refuge from predation. The gamete distribution data strongly indicate that *P. arborea* should be a brooding species, rather than a broadcast spawner, but no embryos or planulae were observed in the female colonies. The egg size is also rather small for an internal brooding species, which usually have large oocytes (>600 µm, Orejas et al. 2002); however, surface brooders may attain fertilization with relatively small oocytes (300 to 580 µm), as they are exposed to large volumes of

water (and potentially sperm) flowing past the colony (Gutierrez-Rodriguez and Lasker 2004). A study of recruitment dynamics of *P. arborea* off eastern Canada (Lacharité and Metaxas 2013) concluded that *P. arborea* is most likely a brooder, and this study concurs with their findings, although there is no direct proof from the histological analysis.

Samples of the gorgonian *Paramuricea placomus* (family Paramuricidae) were collected only during September 2012, and all samples processed were either male or had no gametes. The gametes in the spermatocysts either were late-stage spermatozoa or Stage I spermatogonia. This distribution suggests the end of one cohort and the beginning of another, but does not provide any information on reproductive periodicity or strategy, although the presences of just sperm suggest this species is gonochoric. Reproduction of *P. placomus* has not been documented, but there are several studies on the reproductive biology of a shallow Mediterranean congener *Paramuricea clavata* (Coma et al. 1995a, 1995b). This species was also found to be gonochoric and had a seasonal reproductive cycle that lasted 12 to 18 months. Eggs and sperm were spawned over a period of 2 months during the summer and embryos were brooded externally in a mucous layer associated with the female colonies for approximately 1 week, after which they settled close to the parent colonies. After most of the females were spent, almost 80% of the males still had ripe spermatocysts. One can speculate that the population of *P. placomus* in Baltimore Canyon was at the end of the spawning cycle, which would explain why there were no female gametes observed, but the males may have retained ripe sperm, like their shallow congeners. The shallow *P. clavata*, however, showed no overlapping reproductive cycles in the males as did *P. placomus*. This species was observed twice during the research cruises for this project (once in each canyon) and on both occasions, the colonies were in a moderate but dense patch on top of an exposed ledge. If *P. placomus* has the same short larval dispersal as the shallow *P. clavata*, this would explain the high-density patches observed in the canyon.

One of the most abundant gorgonians in both canyons was *Primnoa resedaeformis* (family Primnoidae). This species occurs throughout the North Atlantic in deep shelf to bathyal depths (Costello et al. 2001). Like many other species in this study, *P. resedaeformis* is a gonochoric broadcast-spawning species, with a larger average oocyte diameter in September than in May when the population was dominated by small size classes; however, the population variance was so high that the differences were not significant. Data from other time periods are needed to determine whether any seasonal signal exists. At the level of the individuals, the oocytes fell into grouped size classes so there seems to be some periodicity within each colony. Releasing gametes into the water column is a risk, which is counteracted in many broadcast-spawning species by tight synchrony of large numbers of gametes (reviewed by Giese and Kanatani 1987). Small, asynchronous release of gametes for external fertilization does not seem a successful reproductive strategy unless this species is brooding externally or has some other mechanism to facilitate fertilization. A study of *P. resedaeformis* from eastern Canada also showed no apparent periodicity or population synchrony for this species (Mercier and Hamel 2011); however, a four-year field study from the same region showed high recruitment of *P. resedaeformis* onto settlement blocks, indicating high reproductive success (Lacharité and Metaxas 2013).

11.4.2 Other Species

Sea urchins in the family Echinidae are gonochoric broadcast spawners that have five gonads positioned below the upper surface of the test. Each gonad has a single duct leading to the gonopore, through which gametes are released. Initial gamete development occurs on the germinal epithelium (outer edge) of the gonad and as development progresses the gonad fills with gametes. There is a great deal more information available for deepsea echinoderms than for deepsea corals because echinoderms generally live on soft sediment and can therefore be sampled using trawls rather than the sophisticated underwater vehicles required to collect hard substrate fauna. The most comprehensive studies of deepsea echinoderms, including *Echinus affinis* (now *Gracilechinus affinis*), were conducted on the Rockall Trough area in the northeastern Atlantic Ocean (Tyler and Gage 1984a). Samples of *E. affinis* had annual

spawning events, but gametogenic cycles were approximately 14 months in duration, with one cycle beginning 2 months prior to the end of the previous cycle. These samples spawned in January and February, releasing eggs of 100 to 120 µm in diameter. Congeners (*E. alexandri* and *E. acutus*, now both *Gracilechinus*) from the northeastern Atlantic slope had very similar reproductive cycles to *E. affinis* (Tyler and Gage 1984a). The two seep urchins in this study, *G. affinis* and *E. wallisi*, showed the same reproductive patterns, with average oocyte diameters of approximately 30 to 35 µm in May. The size-frequency distributions for both species show tightly grouped oocyte size classes, which indicate synchronous reproductive cycles (both within and between species). The oocyte diameters from this study indicate that these species are on a similar schedule to those studied from the Rockall Trough. The authors postulated that larval development is probably planktotrophic, with settlement occurring in April and May. The larval period coincided with sinking of organic matter from surface primary production, which might provide a suitable larval food source, and that organic matter deposited on the seafloor in late spring/summer could provide energy for vitellogenesis (Tyler and Gage 1984a). This pattern of phytodetrital deposition is similar to that found during our study (**Chapter 6**), so we can tentatively conclude that reproductive cycles of conspecifics in the western and eastern North Atlantic are similar and probably driven by the same seasonal fluctuations in food availability.

The soft-bodied urchin *Hygrosoma petersii* (family Echinothuriidae) is a cosmopolitan species that lives at slope to abyssal depths (200 to 3,700 m) (Felder and Camp 2009). This species has a different reproductive strategy than the spiny urchins discussed previously. The average oocyte diameter was larger for *H. petersii* and the size-frequency distribution indicated continuous reproduction rather than seasonal, with a peak in the 20- to 60-µm size classes and fewer smaller eggs. A study of five species of echinothuroid urchins from the Rockall Trough in the northeastern Atlantic Ocean (Tyler and Gage 1984b) also showed continuous reproduction, but all the species studied (including *H. petersii*) had much larger egg sizes (up to 1,500 µm). By comparison, the oocyte sizes found in our study were small, with a maximum of <200 µm), but the single female sample that was processed does not necessarily represent an entire population; this particular female may have recently released the largest of her oocytes, leaving the less mature to develop further.

The pencil urchin *Cidaris abyssicola* is found in the western Atlantic Ocean, including the Gulf of Mexico and the Caribbean in depths of 13 to 800 m (Felder and Camp 2009). The single female of this species had a range of oocyte size classes from 10 to 90 µm, but the distribution indicates a single cohort rather than a continuous production of oocytes. With only one female and no males it is not possible to determine timing of reproductive cycles. A study of congener *Cidaris cidaris* from the Rockall Trough showed no indications of seasonality, but the authors acknowledged that there were too few samples to identify seasonal cycles (Tyler and Gage 1984b).

Mussels of the genus *Bathymodiolus* are one of the most speciose and widely distributed genera from cold seeps and hydrothermal vents (Tyler et al. 2007). Bathymodiolids have symbiotic chemoautotrophic bacteria in their tissues, which provide energy to the host mussel. These bacteria may be thiotrophic or methanotropic (using sulphide or methane respectively), but *Bathymodiolus childressi* can also filter feed on particles in the water column (Pile and Young 1999). Reproduction of *B. childressi* from cold seeps in the Gulf of Mexico was studied over a period of 9 years, during which samples were obtained for 5 years (1995, 1997, 2002, 2003, and 2004) and 9 months (Tyler et al. 2007). This study found strong developmental synchrony between males and females, which began gametogenesis in November, followed by oocyte growth and proliferation of spermatozoa from February to September, with spawning occurring from October to February. This study also found some differences in the timing of gametogenesis among different sites. These seasonal reproductive cycles and site-specific differences were not observed in the samples collected from the mid-Atlantic seeps; there was no significant difference between samples collected from Baltimore seep in September versus May, or from Baltimore versus Norfolk Canyon seeps from May 2013. The Tyler et al. (2007) study showed an average oocyte diameter of approximately 22 µm in May, whereas our study showed an average of approximately 37 µm.

Their September samples showed an average oocyte diameter of approximately 35 µm, which was similar to the samples from the mid-Atlantic seeps and was the maximum average oocyte size observed the Gulf of Mexico. The data from the mid-Atlantic seeps show synchronized cohorts among individuals and different populations, which indicate a single annual reproductive cycle as observed in the Gulf of Mexico. However, the observation of an equally mature and synchronized population from several months earlier in the year rather confounds this conclusion and indicates that more work needs to be done to elucidate reproductive cycles at these seeps.

11.5 SUMMARY

Ten species of corals were collected during the September 2012 and May 2013 sampling cruises in Baltimore and Norfolk canyons, although not all species were collected in both years or from both canyons. Samples also came from a broad depth range and from different parts of the canyons. All of these differences can introduce confounding variability. However, the data from this study, while far from ideal, has provided information on reproductive biology of 5 scleractinian and 5 gorgonian species from a region where no information previously existed. This is also the first information published on 4 of the 10 coral species studied, some of which are common, widespread species. This illustrates that despite the tremendous research effort that has focused on deepsea corals in recent years, there are still major information gaps on the basic biology of these species. Where comparisons could be made for the coral species, our new data supported previous findings.

Unlike deepsea corals, echinoderms have been well studied for many years, even at depth. These animals are usually found on soft sediment and are readily obtained in large numbers using dredges and trawls. With the exception of *C. abyssicola*, other studies provided comparative information and our findings generally concurred with past research. The apparent absence of a seasonal signal in the seep mussels warrants further research, which may reveal a flexible reproductive strategy in this species.

The majority of the species in this study showed some seasonality in their reproductive cycles. While reproductive strategy is taxonomically constrained, several environmental and biotic factors may influence the timing of reproduction in deepsea environments, the most likely being temperature and food. Temperature was recorded at three depths for one year during this study, and the data revealed a great deal of variation, but no clear seasonal signal in either canyon (**Chapter 5**). Food supply in the deep sea is related to timing of plankton blooms, which peak in the spring and fall in the North Atlantic (**Chapter 6**). The spring/summer flux of organic material was suggested as an energetic driver of vitellogenesis in deepsea echinoids, and this also fits the developmental cycles of the canyons' corals (for those species with seasonal cycles), which advance further in September than in May. Further research is needed before these observations can be rigorously tested.

11.6 LITERATURE CITED

Adkins JF, Henderson GM, Wang S-L, O'Shea S, Mokadem F. 2004. Growth rates of the deep-sea scleractinia *Desmophyllum cristagalli* and *Enallopsammia rostrata*. Earth and Planetary Science Letters. 227:481–490.

Babcock R. 1990. Reproduction and development of the blue coral *Heliopora coerulea* (Alcyonaria: Coenothecalia). Marine Biology. 104:475–481.

Beazley LI, Kenchington EL. 2012. Reproductive biology of the deep-water coral *Acanella arbuscula* (Phylum Cnidaria: Class Anthozoa: Order Alcyonacea), northwest Atlantic. Deep-Sea Research II. 68:92–104.

Brito TAS, Tyler PA, Clarke A. 1997. Reproductive biology of the Antarctic octocoral *Thouarella variabilis (*Wright and Studer, 1889). In: den Hartog JC, van Ofwegen LP, van der Spoel S, editors. Proceedings of the 6th international conference on coelenterate biology. Leiden (Netherlands): Nationaal Naturhistorisch Museum. p. 63–69.

Brooke S, Jarnegren J. 2013. Reproductive periodicity of the deep-water scleractinian coral, *Lophelia pertusa* from the Trondheim Fjord, Norway. Marine Biology. 160:139–153.

Burgess SN, Babcock RC. 2005. Reproductive ecology of three reef-forming deep-sea corals in the New Zealand region. In: Freiwald A, Roberts JM, editors. Cold water corals and ecosystems. Berlin Heidelberg: Springer-Verlag. p. 701–713.

Cairns SD. 1979. The deep-water Scleractinia of the Caribbean and adjacent waters. Studies on the Fauna of Curacao. 57(180):341 p.

Cairns, SD. 1994. Scleractinia of the temperate North Pacific. Smithsonian Contributions to Zoology. 557.

Cairns SD. 1995. The marine fauna of New Zealand: Scleractinia (Cnidaria: Anthozoa). New Zealand Oceanographic Institute Memoir. 103:210.

Coma R, Zabala M, Gili JM. 1995a. Reproduction and cycle of gonadal development in the Mediterranean gorgonian *Paramuricea clavata*. Marine Ecology Progress Series. 117:173–183.

Coma R, Zabala M, Gili JM. 1995b. Sexual reproductive effort in the Mediterranean gorgonian *Paramuricea clavata*. Marine Ecology Progress Series. 117:185–192.

Cordes EE, Nybakken JW, VanDykhuizen G. 2001. Reproduction and growth of *Anthomastus ritteri* (Octocorallia: Alcyonacea) from Monterey Bay, California, USA. Marine Biology. 138:491–501.

Costello MJ, Emblow CS, White RJ, editors. 2001. European register of marine species: a check-list of the marine species in Europe and a bibliography of guides to their identification. Collection Patrimoines Naturels. 50:104–105.

CSA International, Inc. 2007. Characterization of northern Gulf of Mexico deepwater hard-bottom communities with emphasis on *Lophelia* coral. U.S. Department of the Interior, Minerals Management Service, Gulf of Mexico OCS Region, New Orleans, LA. OCS Study MMS 2007-044. 169 p. + app.

Dahan M, Benayahu Y. 1997. Reproduction of *Dendronephthya hemprichi* (Cnidaria: Octocorallia): year-round spawning in an azooxanthellate soft coral. Marine Biology. 129:573–579.

Dodds LA, Roberts JM, Taylor AC, Marumbini F. 2007. Metabolic tolerance of the cold-water coral *Lophelia pertusa* (Scleractinia) to temperature and dissolved oxygen change. Journal of Experimental Marine Biology and Ecology. 349:205–214.

Demopoulos AWJ, Ross SW, Kellogg CA, Morrison CL, Nizinski M, Prouty NG, Galkiewicz JP, Gray MA, Springmann MJ, Coykendall DK, et al. [date unknown]. Deepwater program: Lophelia II continuing ecological research on deep-sea corals and deep reef habitats in the Gulf of Mexico: U.S. Geological Survey Open-File Report. In revision.

Felder DL, Camp DK, editors. 2009. Gulf of Mexico–origins, waters, and biota. Volume 1, Biodiversity. College Station (TX): Texas A&M Press. 1374 p.

Flint H, Waller R, Tyler P. 2007. Reproductive ecology of *Fungiacyathus marenzelleri* from 4100 m depth in the Northeast Pacific Ocean. Marine Biology. 151:843–849.

Giese AC, Kanatani H. 1987. Maturation and spawning. In: Geise AC, Pearse JS, Pearse VB, editors. Reproduction of marine invertebrates vol. 9. General aspects: seeking unity in diversity. Pacific Grove (CA): The Boxwood Press; Palo Alto (CA): Blackwell Scientific Publications. p. 251–239

Goffredo S, Arnone S, Zaccanti F. 2002. Sexual reproduction in the Mediterranean solitary coral *Balanophyllia europaea* (Scleractinia, Dendrophylliidae). Marine Ecology Progress Series. 229:83–94.

Gori A, Linares C, Rossi S, Coma R, Gilli JM. 2007. Spatial variability in reproductive cycle of the gorgonians *Paramuricea clavata* and *Eunicella singularis* (Anthozoa Octocorallia) in the western Mediterranean Sea. Marine Biology. 151:1571–1584.

Gutierrez-Rodriguez C, Lasker HR. 2004. Reproductive biology, development, and planula behavior in the Caribbean gorgonian *Pseudopterogorgia elisabethae*. Invertebrate Biology. 123(1):54–67.

Harrison P. 2011. Sexual reproduction of scleractinian corals. In: Dubinsky Z, Stambler N, editors. Coral reefs: an ecosystem in transition. Dordrecht Heidelberg London New York: Springer. p. 59–85.

Hecker B, Blechschmidt G, Gibson P. 1980. Epifaunal zonation and community structure in three mid- and north Atlantic canyons. Final report for the canyon assessment study in the Mid-and North Atlantic Areas of the U.S. Outer Continental Shelf. Prepared for the U.S. Department of Interior, Bureau of Land Management under contract BLM AA5 51-CT8-49. Palisades (NY): Lamont-Doherty Geological Observatory.

Lacharité M, Metaxas A. 2013. Early life history of deep-water gorgonian corals may limit their abundance. PLoS ONE. 8(6): e65394. doi:10.1371/journal.pone.0065394.

Larsson AI, Järnegren J, Strömberg SM, Dahl MP, Lundälv T, Brooke S. 2014. Embryogenesis and larval biology of the cold-water coral *Lophelia pertusa.* PLoS ONE. 9 (7): e102222.

Lazier AV, Smith JE, Risk MJ, Schwarcz HP. 1999. The skeletal structure of *Desmophyllum cristagalli*: The use of deep-water corals in sclerochronology. Lethaia. 32:119–13.

Levitan DR, Fukami H, Jara , Kline D, McGovern TM, McGhee KE, Swanson CA, Knowlton N. 2004. Mechanisms of reproductive isolation among sympatric broadcast spawning corals of the *Montastraea annularis* species complex. Evolution. 58:308–323.

Mercier A, Hamel JF. 2011. Contrasting reproductive strategies in three deep-sea octocorals from eastern Canada: *Primnoa resedaeformis*, *Keratoisis ornata*, and *Anthomastus grandifloras*. Coral Reefs. 30:337–350.

Mercier A, Sun Z, Baillon S, Hamel JF. 2011. Lunar rhythms in the deep sea: evidence from the reproductive periodicity of several marine invertebrates. Journal of Biological Rhythms. 26(1):82–86.

Oliver J K, Babcock RC. 1992. Aspects of the fertilization ecology of broadcast spawning corals: Sperm dilution effects and *in situ* measurements of fertilization. The Biological Bulletin. 183:409–417.

Orejas C, Lopez-Gonzalez PJ, Gili JM, Teixido N, Gutt J, Arntz WE. 2002. Distribution and reproductive ecology of the Antarctic octocorals *Ainigmaptilon antarcticum* in the Weddell Sea. Marine Ecology Progress Series. 231:101–114.

Orejas C, Gili JM, López-González PJ, Hasemann C, Arntz WE. 2007. Reproductive patterns of four Antarctic octocorals in the Weddell Sea: an inter-specific, shape, and latitudinal comparison. Marine Biology. 150:551–563.

Pierdomenico M, Guida VG, Macelloni L, Chiocci FL, Rona PA, Scranton MI, Asper V, Diercks A. 2015. Sedimentary facies, geomorphic features and habitat distribution at the Hudson Canyon head from AUV multibeam data. Deep-Sea Research II. 121:112–125.

Pile AJ, Young CM. 1999. Plankton availability and retention efficiencies by cold-seep symbiotic mussels. Limnology and Oceanography. 44:1833–1839.

Roberts JM, Peppe OC, Dodds LA. 2005. Monitoring environmental variability around cold water coral reefs: the use of a benthic photolander and the potential of seafloor observatories. In: Freiwald A, Roberts JM, editors. Cold water corals and ecoystems. Berlin Heidelberg: Springer-Verlag. p. 715–729.

Roberts JM, Wheeler AW, Freiwald A, Cairns S, editors. 2009. Cold-water corals: the biology and geology of deep-sea habitats. Cambridge (UK): Cambridge University Press. 334 p.

Sun Z, Hamel JF, Mercier A. 2010. Planulation periodicity, settlement preferences and growth of two deep-sea octocorals from the northwest Atlantic. Marine Ecology Progress Series. 410:71–87.

Szmant AM. 1986. Reproductive ecology of Caribbean reef corals. Coral Reefs. 5:43–54.

Thresher RE, Adkins J, Thiagarajan N. 2011. Modal analysis of the deep-water solitary scleractinian *Desmophyllum dianthus* on SW Pacific seamounts: Inferred recruitment periodicity. Coral Reefs. doi:10.1007/s00338-011-0806-7.

Tyler PA, Gage JD. 1984a. Seasonal reproduction of *Echinus affinis* (Echinodermata: Echinoidea) in the Rockall trough, northeast Atlantic Ocean. Deep Sea Research Part 1. Oceanographic Research Papers. 31(4):387–402.

Tyler PA, Gage JD. 1984b. The reproductive biology of echinothurid and cidarid sea urchins from the deep sea (Rockall Trough, North East Atlantic Ocean). Marine Biology. 80:63–74.

Tyler PA, Young CM. 1999. Reproduction and dispersal at vents and cold seeps. Journal of the Marine Biological Association of the United Kingdom. 79:193–208.

Tyler PA, Grant A, Pain SL, Gage JD. 1982. Is annual reproduction in deep sea echinoderms as response to their environment? Nature. 300:747–750.

Tyler PA, Campos-Creasy LS, Giles LS. 1993. Environmental control of quasi-continuous and seasonal reproduction in deep-sea benthic invertebrates; preliminary observations,. In: Young CM, Eckelbarger KJ, editors. Reproduction, larval biology and recruitment of the deep-sea benthos. p. 158–178.

Tyler PA, Young CM, Dolan E, Arellano SM, Brooke SD, Baker M. 2007. Gametogenic periodicity in the chemosynthetic cold-seep mussel *"Bathymodiolus" childressi*. Marine Biology. 150:829–840.

Versluys J. 1906. Die Gorgoniden der Siboga-Expedition. II. Die Primnoidae. Siboga-Expeditie. 13a:1-87.

Waller RG. 2003. The reproductive ecology of deep water scleractinians [PhD thesis]. School of Ocean and Earth Science, Southampton Oceanography Center. 351 p.

Waller RG. 2005. Deep-water Scleractinia (Cnidaria: Anthozoa) current knowledge of reproductive processes. In: Friewald A, Roberts JM, editors. Cold water corals and ecosystems. Berlin Heidelberg: Springer-Verlag. p. 691–700.

Waller RG, Tyler PA. 2005. The reproductive biology of two deep-water, reef-building scleractinians from the NE Atlantic Ocean. Coral Reefs. 24(3):514–522.

Waller RG, Tyler PA. 2011. Reproductive patterns in two deep-water solitary corals from the north-east Atlantic: *Flabellum alabastrum* and *F. angulare* (Cnidaria: Anthozoa: Scleractinia). Journal of the Marine Biological Association of the United Kingdom. 91(3):669–675.

Waller RG, Tyler PA, Gage JD. 2002. The reproductive ecology of the deep-sea scleractinian coral *Fungiacyathus marenzelleri* (Vaughan, 1906) in the northeast Atlantic Ocean. Coral Reefs. 21:325–331.

Waller RG, Tyler PA, Gage JD. 2005. Sexual reproduction in three hermaphroditic deep-sea Caryophyllia species (Anthozoa: Scleractinia) from the NE Atlantic Ocean. Coral Reefs. 24:594–602.

Watling L, Auster P. 2005. Distribution of the deep water Alcyonacea off the northeast coast of the United States. In: Friewald A, Roberts JM, editors. Cold water corals and ecosystems. Berlin Heidelberg: Springer-Verlag. p. 259–264.

Watling L, France SC, Pante E, Simpson A. 2011. Biology of deep-water octocorals. Advances in Marine Biology. 60:41–123.

Witte U. 1996. Seasonal reproduction in deep-sea sponges triggered by vertical flux. Marine Biology. 124:571–581.

This page intentionally left blank

CHAPTER 12. CANYONS MICROBIOLOGY STUDIES

Christina A. Kellogg and Stephanie N. Lawler

12.1 INTRODUCTION

Off the eastern coast of the United States, several deep canyons cut through the continental shelf, acting like funnels to move sediment from the shelf out to the deep seafloor. Exposed rock outcrops and ledges along the walls of these canyons provide important habitat for deepsea corals and sponges. Although a few scientific expeditions have visited these canyons in the 1970s (Hecker and Blechschmidt 1979, Hecker et al. 1980), their purpose was mainly to map the contours and capture photographs of the bottom using manned submersibles and towed cameras. Our knowledge of the biodiversity in these complex ecosystems is limited; we know little about the macrofauna (e.g., fishes, crabs, sponges, and deepsea corals) and even less about the microbiota.

The research described in this report was conducted from 2011 to 2015 as part of the Bureau of Ocean Energy Management (BOEM) study, entitled "Atlantic Deepwater Canyons" study. This work used molecular and microbiological techniques to examine the microbial ecology and diversity associated with Baltimore and Norfolk canyons. Specifically, this work focused on the microbial ecology of four species of octocorals (*Acanthogorgia aspera*, *Anthothela grandiflora*, *Paramuricea placomus,* and *Primnoa resedaeformis*), the microbial diversity in sediments within and outside the canyons, and a settling plate experiment designed to characterize microbial biofilm formation on a variety of hard substrates.

12.2 CORAL MICROBIAL ECOLOGY

12.2.1 Introduction

Coral microbial ecology encompasses the relationships and interactions within the coral-associated microbial community as well as between that community, the coral host, and the surrounding environment. Microbial associates have been shown to be key players in coral biology, serving functions like cycling nutrients (Kimes et al. 2010, Raina et al. 2009, Shashar et al. 1994) and producing antimicrobial compounds to keep unwanted microbes from infecting the coral (Ritchie 2006, Zhang et al. 2013). There is evidence that many corals maintain conserved bacterial communities, distinct from the water column, sediments, and nearby corals of other species (e.g., Frias-Lopez et al. 2002, Kellogg et al. 2009, Neulinger et al. 2008, Rohwer et al. 2002). Tropical corals have been most intensively studied over the past 15 years (reviewed in Mouchka et al. 2010, Thompson et al. 2015). However, deepsea coral (also called cold-water corals) ecosystems are equally important microbial landscapes.

Research addressing the bacterial communities associated with deepsea corals has been limited due to the expense and difficulty of obtaining uncontaminated samples. While there has been significant focus over the past decade on the microbial associates of the deepsea coral *Lophelia pertusa* (Galkiewicz et al. 2011, Galkiewicz et al. 2012, Hansson et al. 2009, Kellogg 2008, Kellogg et al. 2009, Kellogg et al. 2017, Neulinger et al. 2008, Neulinger et al. 2009, Schöttner et al. 2009, van Bleijswijk et al. 2015, Yakimov et al. 2006), few other deepsea scleractinians (Hansson et al. 2009, Meisterzheim et al. 2016) and octocorals (Gray et al. 2011, Penn et al. 2006) have been studied.

No corals from the mid-Atlantic canyons have been previously sampled to describe their microbial communities. Characterizing the bacterial communities associated with deepsea corals in these canyons will increase our knowledge of the biodiversity in these ecosystems and provide critical baseline microbiomes for future studies in the event of natural or anthropogenic changes (e.g., coral disease outbreaks, oil spills, or climate change).

12.2.2 Methods

12.2.2.1 Field Sampling Methods

Coral samples were collected in Baltimore and Norfolk canyons by remotely operated vehicle (ROV) during the 2012 and 2013 sampling cruises; see **Chapter 3** for cruise details. Coral species, collection location, depth, water temperature, and salinity are listed in **Table 12-1**.

Small pieces of each coral colony (~5 to 15 cm) were removed using the ROV's manipulator arm and placed into individual polyvinyl chloride (PVC) quivers that had been washed, ethanol sterilized, filled with freshwater, and sealed with a rubber stopper while the ROV was on deck. The freshwater was evacuated at depth when the quiver was opened to receive the coral sample, so that only seawater local to the coral samples was entrained during collection. Each coral sample was placed in a separate quiver and sealed at depth to prevent microbial contamination from other corals or different water masses during ascent. Upon recovery of the ROV, the samples were removed from the quivers using ethanol-sterilized forceps, trimmed if necessary with ethanol-sterilized shears, and placed into individual sterile, 50 mL tubes. The tubes were filled with RNA*later* solution to preserve the samples, placed at 4 ºC overnight to allow the fixative to infiltrate the samples, and then transferred to -20 ºC until ready for processing. If sufficient biomass remained, specimen photos were taken of the samples, and pieces were shared with the coral genetics efforts (**Table 12-2**; **Chapters 13** and **14**).

During the 2013 sampling cruise, bacteria were also cultured from coral samples that had sufficient biomass remaining after pieces were preserved for molecular analysis. Using sterile technique, one to three polyps were removed from each coral and placed into a sterile aluminum weigh boat. One milliliter sterile 1× phosphate-buffered saline (PBS) was added, and the coral tissue was macerated to produce a slurry. This slurry was spread-plated onto agar plates containing Jensen I3 medium (Jensen and Fenical 1995) and incubated at 4°C to best simulate *in situ* temperatures. Jensen I3 medium was chosen because of its ability to culture Gram-positive bacteria from marine environments, while most marine agars culture predominantly Gram-negative bacteria.

12.2.2.2 Laboratory Methods

Nucleic acid (DNA) was extracted from the coral samples following the protocol described in Sunagawa et al. (2010). Small clippings of coral tissue (one to four polyps per sample) were taken from each octocoral using sterile forceps and shears and then placed into the bead tube supplied with the MO BIO PowerPlant DNA extraction kit. The protocol was modified by increasing the incubation period with proteinase K from 60 to 90 minutes. Extracted DNA was quantified using the PicoGreen DNA quantification kit, and quality confirmed by PCR amplification of the 16S rRNA gene, using either primers Eco8F (Edwards et al. 1989) and 1492R (Stackebrandt and Liesack 1993), or 63F (Marchesi et al. 1998) and 1542R (Pantos et al. 2003). Unamplified DNA extracted from the coral samples was sequenced by 454 pyrosequencing using GS FLX Titanium chemistry (Selah Genomics, Greenville, South Carolina) and primers targeting the V4 to V5 variable region of the 16S rRNA gene (Claesson et al. 2010) following Roche 454's standard protocol for amplicons (454 Life Sciences Corp 2011).

Bacterial culture plates from the cruise were evaluated, and distinct individual bacterial colonies were restreaked to purity on fresh agar plates. Isolates were inoculated into 5 mL liquid Jensen I3 medium and grown at 4 °C in a shaking incubator until the medium became turbid. The tubes were centrifuged at 500 × *g* to pellet the bacterial cells. Bacterial DNA was extracted using the Qiagen DNeasy kit following the manufacturer's protocol for Gram-positive bacteria and sent out for Sanger sequencing of the 16S rRNA gene.

Table 12-1. Deepsea coral samples collected for microbiology and corresponding environmental data.

Sample ID	Date	Collection Time	Dive No.	Quiver No.	Coral	Depth (m)	Latitude (N)	Longitude (W)	Temp (°C)	Salinity
Baltimore Canyon										
ROV-2012-NF-01-Q6	18 Aug 2012	17:25	01	06	*Primnoa resedaeformis*	450	38°08′58.24″	73°50′16.62″	6.2	35.1
ROV-2012-NF-01-Q7	18 Aug 2012	17:34	01	07	Anthothelidae	451	38°08′58.01″	73°50′16.42″	6.4	35.1
ROV-2012-NF-02-Q6	18 Aug 2012	13:17	02	06	*Primnoa resedaeformis*	383	38°08′56.72″	73°50′10.41″	9.0	35.2
ROV-2012-NF-02-Q7	19 Aug 2012	18:24	02	07	Anthothelidae	401	38°08′41.82″	73°50′04.14″	6.8	35.1
ROV-2012-NF-05-Q6	23 Aug 2012	13:53	05	06	*Primnoa resedaeformis*	443	38°08′16.15″	73°50′01.26″	7.4	35.1
ROV-2012-NF-05-Q7	23 Aug 2012	14:08	05	07	*Primnoa resedaeformis*	443	38°08′16.00″	73°50′00.95″	7.4	35.1
ROV-2012-NF-06-Q6	24 Aug 2012	12:12	06	06	*Primnoa resedaeformis*	430	38°08′20.82″	73°50′00.08″	7.5	35.0
ROV-2012-NF-06-Q7	24 Aug 2012	11:54	06	07	*Primnoa resedaeformis*	431	38°08′20.69″	73°50′00.17″	7.5	34.9
ROV-2012-NF-09-Q6	28 Aug 2012	13:07	09	06	*Primnoa resedaeformis*	506	38°09′06.30″	73°50′23.67″	7.3	35.1
ROV-2012-NF-09-Q7	28 Aug 2012	13:28	09	07	*Primnoa resedaeformis*	494	38°09′05.10″	73°50′23.35″	7.3	35.1
ROV-2012-NF-10-Q6	29 Aug 2012	12:30	10	06	*Primnoa resedaeformis*	500	38°09′59.11″	73°51′20.88″	7.6	35.1
ROV-2012-NF-10-Q7	29 Aug 2012	12:07	10	07	*Primnoa resedaeformis*	508	38°10′02.46″	73°51′16.21″	7.6	35.1
ROV-2012-NF-13-Q6	6 Sept 2012	10:22	13	06	*Anthothela grandiflora*	434	38°09′41.35″	73°51′23.27″	7.1	35.1
ROV-2012-NF-13-Q7	6 Sept 2012	10:08	13	07	*Anthothela grandiflora*	432	38°09′39.85″	73°51′22.19″	7.5	35.1
ROV-2012-NF-15-Q6	8 Sept 2012	10:22	15	06	*Anthothela grandiflora*	416	38°10′24.64″	73°50′31.07″	7.2	35.1
ROV-2012-NF-15-Q7	8 Sept 2012	14:38	15	07	*Anthothela grandiflora*	457	38°10′30.44″	73°50′42.45″	6.8	35.1
ROV-2012-NF-16-Q6	9 Sept 2012	1:01	16	06	Anthothelidae	435	38°10′55.06″	73°51′39.01″	5.7	35.0
ROV-2012-NF-16-Q7	9 Sept 2012	11:57	16	07	*Anthothela grandiflora*	436	38°10′55.15″	73°51′39.93″	6.3	35.0
ROV-2012-NF-17-Q6	10 Sept 2012	14:18	17	06	*Anthothela grandiflora*	575	38°07′07.80″	73°50′50.70″	5.7	35.0
ROV-2012-NF-17-Q7	10 Sept 2012	14:02	17	07	*Anthothela grandiflora*	575	38°07′05.56″	73°50′51.68″	5.7	35.0
ROV-2012-NF-18-Q6	11 Sept 2012	13:06	18	06	*Anthothela* sp.	524	38°07′05.37″	73°50′56.51″	5.5	35.0
ROV-2012-NF-18-Q7	11 Sept 2012	11:21	18	07	*Anthothela grandiflora*	679	38°07′04.52″	73°50′43.67″	5.1	35.0
ROV-2012-NF-19-Q1	12 Sept 2012	11:29	19	01	*Paramuricea placomus*	379	38°09′04.90″	73°50′16.80″	6.0	35.0
ROV-2012-NF-19-Q2	12 Sept 2012	11:12	19	02	*Paramuricea placomus*	381	38°09′05.04″	73°50′15.80″	5.8	35.0
ROV-2012-NF-19-Q5	12 Sept 2012	11:00	19	05	*Paramuricea placomus*	381	38°09′04.63″	73°50′15.81″	5.8	35.0
ROV-2012-NF-19-Q6	12 Sept 2012	10:49	19	06	*Paramuricea placomus*	382	38°09′10.61″	73°50′15.81″	6.0	35.0
ROV-2012-NF-19-Q7	12 Sept 2012	10:38	19	07	*Paramuricea placomus*	382	38°09′04.74″	73°50′15.92″	5.9	35.0

Table 12-1. (Continued).

Sample ID	Date	Collection Time	Dive No.	Quiver No.	Coral	Depth (m)	Latitude (N)	Longitude (W)	Temp (°C)	Salinity
Norfolk Canyon										
ROV-2012-NF-12-Q6	5 Sept 2012	12:31	12	06	*Primnoa resedaeformis*	535	37°04′06.10″	74°38′53.78″	6.2	35.0
ROV-2012-NF-12-Q7	5 Sept 2012	12:55	12	07	*Primnoa resedaeformis*	523	37°04′02.54″	74°38′56.19″	6.6	35.1
ROV-2012-NF-20-Q1	13 Sept 2012	17:00	20	01	*Primnoa resedaeformis*	434	37°03′08.12″	74°37′21.45″	6.3	35.0
ROV-2013-RB-681-Q1	6 May 2013	12:59	681	01	*Acanthogorgia aspera*	513	37°02′54.17″	74°37′00.28″	6.5	35.1
ROV-2013-RB-681-Q2	6 May 2013	13:27	681	02	*Acanthogorgia aspera*	512	37°02′54.33″	74°37′00.23″	6.5	35.1
ROV-2013-RB-681-Q3	6 May 2013	13:22	681	03	*Acanthogorgia aspera*	512	37°02′54.32″	74°37′00.26″	6.5	35.1
ROV-2013-RB-684-Q1	10 May 2013	10:42	684	01	*Primnoa resedaeformis*	411	37°04′07.01″	74°38′40.66″	10.8	35.5
ROV-2013-RB-684-Q2	10 May 2013	12:08	684	02	*Primnoa resedaeformis*	441	37°04′03.64″	74°38′35.61″	9.0	35.2
ROV-2013-RB-684-Q3	10 May 2013	12:00	684	03	*Primnoa resedaeformis*	441	37°04′03.67″	74°38′35.61″	9.0	35.3
ROV-2013-RB-684-Q4	10 May 2013	7:34	684	04	*Primnoa resedaeformis*	498	37°04′17.76″	74°38′57.02″	6.3	35.1
ROV-2013-RB-684-Q5	10 May 2013	7:40	684	05	*Primnoa resedaeformis*	498	37°04′17.75″	74°38′57.09″	6.3	35.1
ROV-2013-RB-685-Q2	11 May 2013	21:25	685	02	*Acanthogorgia aspera*	1,328	37°02′59.42″	74°30′49.58″	4.1	35.0
ROV-2013-RB-685-Q3	11 May 2013	18:09	685	03	*Acanthogorgia aspera*	1,336	37°02′59.61″	74°30′48.83″	4.2	35.0
ROV-2013-RB-685-Q4	11 May 2013	17:20	685	04	*Acanthogorgia aspera*	1,312	37°03′00.08″	74°30′44.85″	4.1	35.0
ROV-2013-RB-685-Q5	11 May 2013	17:04	685	05	*Acanthogorgia aspera*	1,311	37°02′59.64″	74°30′44.43″	4.2	35.0
ROV-2013-RB-686-Q2	13 May 2013	9:27	686	02	*Lateothela grandiflora*	480	37°03′30.91″	74°36′21.07″	6.6	35.1
ROV-2013-RB-686-Q3	13 May 2013	11:23	686	03	*Primnoa resedaeformis*	479	37°03′30.98″	74°36′20.81″	6.6	35.1
ROV-2013-RB-686-Q4	13 May 2013	6:51	686	04	*Anthothela grandiflora*	581	37°03′16.88″	74°36′14.17″	5.9	35.0
ROV-2013-RB-686-Q5	13 May 2013	6:54	686	05	*Anthothela* sp.	581	37°03′16.92″	74°36′14.18″	5.9	35.0
ROV-2013-RB-687-Q2	14 May 2013	8:03	687	02	*Primnoa resedaeformis*	576	37°03′17.86″	74°34′41.80″	5.5	35.0
ROV-2013-RB-687-Q3	14 May 2013	8:27	687	03	*Anthothela* sp.	594	37°03′17.57″	74°34′40.03″	5.6	35.0
ROV-2013-RB-687-Q4	14 May 2013	6:11	687	04	Anthothelidae	704	37°03′14.07″	74°34′50.04″	5.3	35.0
ROV-2013-RB-687-Q5	14 May 2013	7:14	687	05	*Anthothela grandiflora*	606	37°03′17.31″	74°34′43.60″	5.7	35.0
ROV-2013-RB-688-Q1	15 May 2013	7:51	688	01	*Anthothela grandiflora*	559	37°01′27.47″	74°35′17.39″	5.8	34.9
ROV-2013-RB-688-Q2	15 May 2013	10:03	688	02	*Anthothela* sp.	474	37°01′24.34″	74°35′32.69″	6.5	35.0
ROV-2013-RB-688-Q3	15 May 2013	10:24	688	03	*Lateothela grandiflora*	474	37°01′24.74″	74°35′32.80″	6.4	35.0
ROV-2013-RB-688-Q4	15 May 2013	7:32	688	04	*Anthothela* sp.	557	37°01′27.12″	74°35′17.35″	5.8	34.9
ROV-2013-RB-688-Q5	15 May 2013	7:39	688	05	*Anthothela grandiflora*	560	37°01′27.29″	74°35′17.52″	5.8	34.9

Table 12-2. Deepsea coral samples collected for microbiology and corresponding genetic ID for shared samples. Samples that did not have sufficient biomass to share do not have a genetic ID.

Sample ID	Coral	Genetic ID†
ROV-2012-NF-01-Q6	*Primnoa resedaeformis*	MAC-12-CM-014
ROV-2012-NF-01-Q7	Anthothelidae	MAC-12-CM-011
ROV-2012-NF-02-Q6	*Primnoa resedaeformis*	MAC-12-CM-019
ROV-2012-NF-02-Q7	Anthothelidae	–
ROV-2012-NF-05-Q6	*Primnoa resedaeformis*	MAC-12-CM-034
ROV-2012-NF-05-Q7	*Primnoa resedaeformis*	MAC-12-CM-037
ROV-2012-NF-06-Q6	*Primnoa resedaeformis*	MAC-12-CM-044
ROV-2012-NF-06-Q7	*Primnoa resedaeformis*	MAC-12-CM-043
ROV-2012-NF-09-Q6	*Primnoa resedaeformis*	MAC-12-CM-062
ROV-2012-NF-09-Q7	*Primnoa resedaeformis*	MAC-12-CM-063
ROV-2012-NF-10-Q6	*Primnoa resedaeformis*	MAC-12-CM-077
ROV-2012-NF-10-Q7	*Primnoa resedaeformis*	MAC-12-CM-076
ROV-2012-NF-13-Q6	*Anthothela grandiflora*	BLT 1201-5
ROV-2012-NF-13-Q7	*Anthothela grandiflora*	BLT 1201-4
ROV-2012-NF-15-Q6	*Anthothela grandiflora*	BLT 1401-4
ROV-2012-NF-15-Q7	*Anthothela grandiflora*	BLT 1407-1
ROV-2012-NF-16-Q6	Anthothelidae	–
ROV-2012-NF-16-Q7	*Anthothela grandiflora*	BLT 1501-1
ROV-2012-NF-17-Q6	*Anthothela grandiflora*	BLT 1601-2
ROV-2012-NF-17-Q7	*Anthothela grandiflora*	BLT 1601-4
ROV-2012-NF-18-Q6	*Anthothela* sp.	BLT 1702-1
ROV-2012-NF-18-Q7	*Anthothela grandiflora*	BLT 1701-1
ROV-2012-NF-19-Q1	*Paramuricea placomus*	BLT 1801-5
ROV-2012-NF-19-Q2	*Paramuricea placomus*	BLT 1801-4
ROV-2012-NF-19-Q5	*Paramuricea placomus*	BLT 1801-3
ROV-2012-NF-19-Q6	*Paramuricea placomus*	BLT 1801-2
ROV-2012-NF-19-Q7	*Paramuricea placomus*	BLT 1801-1
ROV-2012-NF-12-Q6	*Primnoa resedaeformis*	MAC-12-CM-129
ROV-2012-NF-12-Q7	*Primnoa resedaeformis*	MAC-12-CM-128
ROV-2012-NF-20-Q1	*Primnoa resedaeformis*	MAC-12-CM-095
ROV-2013-RB-681-Q1	*Acanthogorgia aspera*	–
ROV-2013-RB-681-Q2	*Acanthogorgia aspera*	NFK12011
ROV-2013-RB-681-Q3	*Acanthogorgia aspera*	NFK12021
ROV-2013-RB-684-Q1	*Primnoa resedaeformis*	NFK13011/MAC-13-405
ROV-2013-RB-684-Q2	*Primnoa resedaeformis*	NFK13021/MAC-13-406
ROV-2013-RB-684-Q3	*Primnoa resedaeformis*	NFK13022/MAC-13-407
ROV-2013-RB-684-Q4	*Primnoa resedaeformis*	NFK13031/MAC-13-408
ROV-2013-RB-684-Q5	*Primnoa resedaeformis*	NFK13041/MAC-13-409
ROV-2013-RB-685-Q2	*Acanthogorgia aspera*	NFK1405
ROV-2013-RB-685-Q3	*Acanthogorgia aspera*	NFK1404
ROV-2013-RB-685-Q4	*Acanthogorgia aspera*	NFK1402
ROV-2013-RB-685-Q5	*Acanthogorgia aspera*	NFK1403
ROV-2013-RB-686-Q2	*Lateothela grandiflora*	NFK1502
ROV-2013-RB-686-Q3	*Primnoa resedaeformis*	NFK1504/MAC-13-482

Table 12-2. (Continued).

Sample ID	Coral	Genetic ID†
ROV-2013-RB-686-Q4	*Anthothela grandiflora*	NFK1508
ROV-2013-RB-686-Q5	*Anthothela* sp.	NFK1510
ROV-2013-RB-687-Q2	*Primnoa resedaeformis*	–
ROV-2013-RB-687-Q3	*Anthothela* sp.	NFK1601
ROV-2013-RB-687-Q4	Anthothelidae	–
ROV-2013-RB-687-Q5	*Anthothela grandiflora*	NFK1602
ROV-2013-RB-688-Q1	*Anthothela grandiflora*	NFK1704
ROV-2013-RB-688-Q2	*Anthothela* sp.	NFK1705
ROV-2013-RB-688-Q3	*Lateothela grandiflora*	NFK1707
ROV-2013-RB-688-Q4	*Anthothela* sp.	NFK1708
ROV-2013-RB-688-Q5	*Anthothela grandiflora*	NFK1709

†Genetic IDs beginning with "MAC" are from the Morrison laboratory (see **Chapter 14**); those beginning with "BLT" or "NFK" are from the France laboratory (see **Chapter 13**).

12.2.2.3 Bioinformatic Analysis

The software QIIME 1.9 (Caporaso et al. 2010a, Caporaso et al. 2010b) was used to process and analyze the sequence data. A fully commented, step-by-step workflow describing the analysis and all the scripts used is available on Github [https://github.com/chriskellogg]. The libraries were split and the following quality parameters enforced: length between 200 and 700 base pairs (bp), quality score of 25 with a 50-bp running quality window, 1 primer mismatch allowed, and a maximum homopolymer run of 6 (Kunin et al. 2010). The data were then denoised to reduce sequencing errors (Kunin et al. 2010, Quince et al. 2009). A relatively new open-reference method of picking operational taxonomic units (OTUs) was used (Rideout et al. 2014) that combined closed OTU picking against a reference database (Greengenes release 13_8; [DeSantis et al. 2006]) with a *de novo* method for any remaining OTUs to maximize classification of novel sequences. We used the usearch61 OTU-picking method (Edgar 2010) in this script since it incorporates chimera checking. Alignments were performed using PyNAST (version 1.2.2) (Caporaso et al. 2010b, Caporaso et al. 2010b), and taxonomy was assigned with uclust (Edgar 2010). Absolute singletons (OTUs that only occur once in a given dataset) were removed from the OTU table as a default in this method. Any sequences that classified as nonbacterial (i.e., archaeal, eukaryotic, chloroplast, or mitochondrial) were removed in a post OTU-picking filtering step. The sequence libraries were rarefied to the number of sequences in the lowest abundance sample of that particular coral prior to running alpha and beta diversity statistics. Alpha diversity metrics included Chao1 richness (Chao 1984), Shannon index (Shannon 1948), and Simpson's evenness (Simpson 1949). Beta diversity was examined using weighted and unweighted unit fraction (Unifrac) (Lozupone and Knight 2005).

12.2.3 Results

During Legs 1 and 2 (15 August to 14 September) of the 2012 sampling cruise aboard the R/V *Nancy Foster*, a total of 20 dives were completed using the *Kraken 2* ROV; 15 of those dives collected coral samples for microbiology (**Table 12-1**). On Leg 1 (30 April to 19 May) of the 2013 sampling cruise aboard the R/V *Ronald H. Brown*, a total of 13 dives were completed using the *Jason II* ROV; coral samples for microbiology were collected during 6 of these dives (**Table 12-1**).

12.2.3.1 Acanthogorgia aspera

Acanthogorgia species were not observed in Baltimore Canyon during collection dives. Samples from seven individual colonies of *A. aspera* were collected from Norfolk Canyon during the 2013 sampling cruise. The collections occurred at two depth horizons: three samples from 512 to 513 m, and four samples from 1,311 to 1,336 m (**Table 12-1**). Bacterial DNA from five colonies was submitted for 454 sequencing. Unfortunately, two samples did not sequence well, and the preliminary analysis of the remaining three samples produced conflicting results: each sample's bacterial community looked completely different from the others. This was unexpected and unlike all the other corals examined in this study. It is suspected that there may have been a problem with the extractions or sequencing.

Of the 69 bacterial isolates cultured from corals in Norfolk Canyon, 31 were from *A. aspera* (**Table 12-3**). All were 98% to 100% similar to previously described bacteria, with the majority being *Pseudoalteromona*s species, followed by *Shewanella*, *Colwellia*, *Alteromonas*, *Moritella*, *Halomonas*, and *Pseudomonas*.

12.2.3.2 Anthothela grandiflora

This work on Anthothelidae was published in Frontiers in Microbiology in March 2016 (Lawler et al. 2016). In total, samples from 23 individual colonies of coral visually identified as *A. grandiflora* were collected: 12 from Baltimore Canyon and 11 from Norfolk Canyon. Genetic analysis by Rachel Clostio and Scott France (**Chapter 13**) later clarified that 12 were in fact *A. grandiflora*, 5 were a new *Anthothela* species, and 2 were a new genus, recently described under the name *Lateothela grandiflora* (Moore et al. 2017, referred to as '*Alcyonium grandiflorum*' in Lawler et al. 2016) (**Table 12-1**). There was insufficient material from four of the samples to conduct genetic testing, and so those have been labeled "Anthothelidae" in the tables since we cannot be sure of the host genotype.

A total of 1 308 658 raw reads were generated from the 23 coral samples. After removal of low-quality reads, 889 914 sequences remained to be denoised. After denoising, samples that contained less than 10 000 sequences (ROV-2012-NF-02-Q7, ROV-2013-RB-686-Q2, ROV-2013-RB-687-Q3, and ROV-2013-RB-688-Q2) were removed prior to OTU selection to maximize the sequence data available. Furthermore, Anthothelidae corals with no confirmed genetic identification were also removed at this stage (ROV-2012-NF-01-Q7, ROV-2012-NF-02-Q7, ROV-2012-NF-16-Q6, and ROV-2013-RB-687-Q4), leaving 16 samples for full bioinformatic analysis (**Table 12-4**).

Examining the bacterial sequences associated with the Anthothelidae corals at the phylum level (**Figure 12-1**) reveals that *Lateothela grandiflora* (RB.688Q3) has a very different bacterial community compared to the other samples. While dominated by Proteobacteria, it also has a mixture of Planctomycetes, Bacterioidetes, Actinobacteria, and Acidobacteria that are largely absent from the other *Anthothela* samples. This view of the bacterial communities also shows that the *Anthothela* sp. samples (**Figure 12-1**; NF.18Q6, RB.686Q5, and RB.688Q4) are indistinguishable from the *A. grandiflora* samples. This was confirmed by analysis of similarities (ANOSIM), which showed no significant difference between the two species (ANOSIM: $R = 0.03$, $P = 0.27$). Both have bacterial communities dominated by Proteobacteria and Spirochaetes with small amounts of Firmicutes. Further, **Figure 12-1** shows that there are no bacterial community differences based on canyon of origin (ANOSIM: $R = -0.02$, $P = 0.45$).

Table 12-3. Bacterial isolates from corals collected in Norfolk Canyon in 2013.

Coral	Bacterial Isolate	Top GenBank[1] Match	Sequence Accession No.	Identities		Total Sequence Length
				Sequence Length	Match (%)	
Acanthogorgia aspera	681-Q2-BW1	*Pseudoalteromonas* sp. AECF-28	JQ618847.1	202/205	99	205
A. aspera	681-Q2-BW2	Uncultured bacterium clone ST11C8	JQ436109.1	348/350	99	350
A. aspera	681-Q2-BW3	Uncultured bacterium clone MF-Apr-96 (*Colwellia*)	HQ225237.1	507/513	99	513
A. aspera	681-Q2-BW4	*Pseudoalteromonas* sp. SBS2-1	KF220481.1	515/515	100	515
A. aspera	681-Q2-BW5	*Shewanella hanedai*	AB681737.1	601/602	99	602
A. aspera	681-Q2-BW6	*Alteromonas* sp. 114Z-2	JX310120.1	633/634	99	634
A. aspera	681-Q3-BB1	*Pseudoalteromonas* sp. SBS2-1	KF22048.1	586/586	100	586
A. aspera	681-Q3-BP1	Uncultured bacterium clone MF-Apr-96 (*Colwellia*)	HQ225237.1	646/647	99	649
A. aspera	681-Q3-BP2	*Pseudoalteromonas tetraodonis* strain XH147	KC179000.1	526/527	99	526
A. aspera	681-Q3-BP3	Uncultured *Colwellia* sp. clone OTU_C6_SP2_103	JF928746.1	688/692	99	692
A. aspera	681-Q3-BW1	*Pseudoalteromonas* sp. 2SHT	KC884676.1	577/579	99	592
A. aspera	681-Q3-BW2	*Pseudoalteromonas* sp. QD254Down-2	KC689813.1	442/442	100	442
A. aspera	681-Q3-BW4	*Pseudoalteromonas* sp. 2A	JN848335.1	668/669	99	668
A. aspera	681-Q3-BW5	Uncultured *Moritella* sp.	AB819648.1	91/93	98	93
A. aspera	685-Q2-BW1	*Pseudomonas xanthomarina* isolate ANS-34Co	HG008728.1	684/684	100	684
A. aspera	685-Q2-BW2	*Pseudoalteromonas* sp. SBS2-1	KF220481.1	744/744	100	744
A. aspera	685-Q2-BW3	*Halomonas meridiana* strain SK256-29	JX429832.1	682/682	100	682
A. aspera	685-Q2-BW5	*Pseudoalteromonas paragorgicola* strain N224	KF193897.1	488/491	99	491
A. aspera	685-Q3-BW1	Uncultured *Alteromonas* sp. clone Klon5-MesoVII	KC899212.1	675/675	100	675
A. aspera	685-Q3-BW6	*Pseudoalteromonas* sp. SBS2-1	KF220481.1	670/670	100	670
A. aspera	685-Q4-BW1	*Pseudoalteromonas paragorgicola* strain N224 16S	KF193897.1	653/653	100	653
A. aspera	685-Q4-BW4	*Pseudoalteromonas* sp. enrichment culture clone IC1-62	HQ448939.1	529/532	99	532
A. aspera	685-Q4-BW5	*Pseudoalteromonas* sp. SEM6	AB274762.1	462/462	100	462
A. aspera	686-Q2-BW1	*Shewanella* sp. Cv8a	EU278329.1	603/604	99	606
A. aspera	686-Q2-BW2	*Pseudoalteromonas* sp. SBS2-1	KF220481.1	533/535	99	535
A. aspera	686-Q2-BW3	*Shewanella* sp. Cv8a	EU278329.1	594/595	99	595
A. aspera	686-Q2-BW4	*Shewanella* sp. N14	FN433072.1	516/517	99	517
A. aspera	686-Q2-BW6	*Pseudoalteromonas paragorgicola* strain N224	KF193897.1	516/516	100	516
A. aspera	686-Q4-BW1	*Moritella abyssi* strain: CT08	AB554718.1	529/531	99	531
A. aspera	686-Q4-BW5	*Pseudoalteromonas paragorgicola* strain N224	KF193897.1	591/592	99	592

Table 12-3. (Continued).

Coral	Bacterial Isolate	Top GenBank[1] Match	Sequence Accession No.	Identities		Total Sequence Length
				Sequence Length	Match (%)	
A. aspera	686-Q4-BW6	*Pseudoalteromonas espejiana* strain XH123	KC178899.1	697/697	100	697
Anthothela sp.	686-Q5-BB2	Uncultured bacterium clone MF-Apr-96 (*Colwellia*)	HQ225237.1	146/147	99	147
Anthothela sp.	686-Q5-BB3	Uncultured bacterium clone MF-Apr-96 (*Colwellia*)	HQ225237.1	606/607	99	607
Anthothela sp.	686-Q5-BP3	*Pseudoalteromonas* sp. 2SHT	KC884676.1	340/342	99	342
Anthothela sp.	686-Q5-BW1	Uncultured bacterium clone MF-Apr-96 (*Colwellia*)	HQ225237.1	478/486	99	486
Anthothela sp.	686-Q5-BW2	Uncultured bacterium clone MF-Apr-96 (*Colwellia*)	HQ225237.1	580/581	99	581
Anthothela sp.	686-Q5-BW6	Uncultured *Vibrio* sp. clone leech333_A12	JX024158.1	583/583	100	583
Anthothela sp.	687-Q3-BP1	*Pseudoalteromonas* sp. NBRC 107703	AB682654.1	627/627	100	627
Anthothela sp.	687-Q3-BW1	Uncultured bacterium clone A84	AY373421.1	569/570	99	570
Anthothela sp.	687-Q3-BW2	*Pseudoalteromonas* sp. SBS2-1	KF220481.1	512/513	99	513
Anthothelidae	687-Q4-BB1	*Pseudoalteromonas* sp. 2A	JN848335.1	515/519	99	519
Anthothelidae	687-Q4-BW1	Uncultured bacterium clone G13T5.7_D5 (*Colwellia*)	JN621598.1	541/545	99	545
Anthothelidae	687-Q4-BW2	*Lophelia*-associated bacterial clone 4873K4-B28	HQ640796.1	525/532	99	537
Anthothelidae	687-Q4-BW4	Uncultured bacterium clone G13T5.7_D5 (*Colwellia*)	JN621598.1	482/495	97	495
Primnoa resedaeformis	684-Q1-BW2	Uncultured *Colwellia* sp. OTU_C5_SP2_99	JF928743.1	632/637	99	637
P. resedaeformis	684-Q1-BW3	Uncultured bacterium clone HglApr145 (*Pseudoalteromonas*)	JX015631.1	566/566	100	566
P. resedaeformis	684-Q1-BW5	*Pseudoalteromona*s sp. C1	KF170314.1	711/711	100	711
P. resedaeformis	684-Q1-BW6	Uncultured *Psychrobacter* sp. clone MLN5.9mbsf_c55	JQ349458.1	693/694	99	694
P. resedaeformis	684-Q2-BP1	Uncultured *Colwellia* sp. clone OTU_C5_SP2_99	JF928743.1	635/639	99	638
P. resedaeformis	684-Q2-BP2	Uncultured bacterium clone MF-Apr-96 (*Colwellia*)	HQ225237.1	763/764	99	766
P. resedaeformis	684-Q2-BW1	Bacterial isolate 6203-C4 (*Shewanell*a)	HM173292.1	575/575	100	575
P. resedaeformis	684-Q2-BW2	Slope strain DIII4*	AF254106.1	551/552	99	552
P. resedaeformis	684-Q2-BW3	*Pseudoalteromonas* sp. AECF-16	JQ618830.1	587/589	99	589
P. resedaeformis	684-Q2-BW4	*Shewanella hanedai* strain: NBRC 102223	AB681737.1	609/609	100	609
P. resedaeformis	684-Q2-BW5	Uncultured bacterium clone SW-Apr-27 (*Colwellia*)	HQ203921.1	423/432	98	431
P. resedaeformis	684-Q2-BW6	Slope strain DIII4* 16S	AF254106.1	550/551	99	551
P. resedaeformis	684-Q2-BY1	*Photobacterium kishitanii* strain S-27	JF412253.1	646/646	100	646
P. resedaeformis	684-Q3-BP1	*Pseudoalteromonas* sp. SBS2-1	KF220481.1	576/579	99	579
P. resedaeformis	684-Q3-BW1	Uncultured bacterium clone HglApr145 (*Pseudoalteromonas*)	JX015631.1	842/847	99	847
P. resedaeformis	684-Q3-BW2	*Pseudoalteromonas* sp. 2A	JN848335.1	749/750	99	749
P. resedaeformis	684-Q3-BW3	Uncultured bacterium clone HglApr145 (*Pseudoalteromonas*)	JX015631.1	802/807	99	807

Table 12-3. (Continued).

Coral	Bacterial Isolate	Top GenBank[1] Match	Sequence Accession No.	Identities		Total Sequence Length
				Sequence Length	Match (%)	
P. resedaeformis	684-Q3-BW4	*Pseudoalteromonas* sp. NBRC 107703	AB682654.1	715/715	100	715
P. resedaeformis	684-Q3-BW5	*Shewanella hanedai* strain: NBRC 102223	AB681737.1	600/601	99	601
P. resedaeformis	684-Q3-BW6	*Shewanella hanedai* strain: NBRC 102223	AB681737.1	652/653	99	653
P. resedaeformis	684-Q5-BP1	Uncultured bacterium clone HglApr145 (*Pseudoalteromonas*)	JX015631.1	734/734	100	734
P. resedaeformis	684-Q5-BW1	*Shewanella hanedai* strain: NBRC 102223	AB681737.1	551/553	99	553
P. resedaeformis	684-Q5-BW3	*Moritella* sp. JAM-GA22	AB526345.1	568/575	99	575
P. resedaeformis	684-Q5-BW5	Uncultured bacterium clone A84 (*Colwellia*)	AY373421.1	603/604	99	604
P. resedaeformis	684-Q5-BW5	*Shewanella hanedai* strain: NBRC 102223	AB681737.1	635/635	100	635

[1] The National Center for Biotechnology Information (NCBI) GenBank nucleotide database (Benson et al. 2013).

Table 12-4. Final sequence numbers and alpha diversity metrics for Anthothelid corals.

Coral	Canyon	Sample ID	Number of Reads[1]	OTU	Chao1 Richness	Shannon Index	Simpson Evenness
Anthothela grandiflora	Baltimore	ROV-2012-NF-13-Q6	29,474	43	62.13	1.53	0.048
Anthothela grandiflora	Baltimore	ROV-2012-NF-13-Q7	26,064	49	119.00	2.16	0.074
Anthothela grandiflora	Baltimore	ROV-2012-NF-15-Q6	19,005	40	97.75	1.59	0.064
Anthothela grandiflora	Baltimore	ROV-2012-NF-15-Q7	24,553	45	69.00	1.88	0.064
Anthothela grandiflora	Baltimore	ROV-2012-NF-16-Q7	25,060	42	105.33	1.61	0.052
Anthothela grandiflora	Baltimore	ROV-2012-NF-17-Q6	26,819	49	109.00	1.29	0.034
Anthothela grandiflora	Baltimore	ROV-2012-NF-17-Q7	10,333	56	83.27	2.48	0.079
Anthothela grandiflora	Baltimore	ROV-2012-NF-18-Q7	11,969	95	209.83	2.51	0.044
Anthothela grandiflora	Baltimore	ROV-2013-RB-686-Q4	24,843	30	56.00	1.60	0.089
Anthothela grandiflora	Norfolk	ROV-2013-RB-687-Q5	14,269	66	109.50	2.52	0.062
Anthothela grandiflora	Norfolk	ROV-2013-RB-688-Q1	14,289	80	113.21	1.61	0.022
Anthothela grandiflora	Norfolk	ROV-2013-RB-688-Q5	298,193	77	110.00	1.90	0.029
Anthothela sp.	Baltimore	ROV-2012-NF-18-Q6	13,039	49	87.00	2.68	0.105
Anthothela sp.	Norfolk	ROV-2013-RB-686-Q5	32,479	67	101.50	2.38	0.057
Anthothela sp.	Norfolk	ROV-2013-RB-688-Q4	254,947	215	446.92	3.09	0.028
Lateothela grandiflora	Norfolk	ROV-2013-RB-688-Q3	13,216	423	457.44	5.54	0.018

[1] All samples were rarefied to 10,333 sequences before diversity indices were calculated. OTU = operational taxonomic unit.

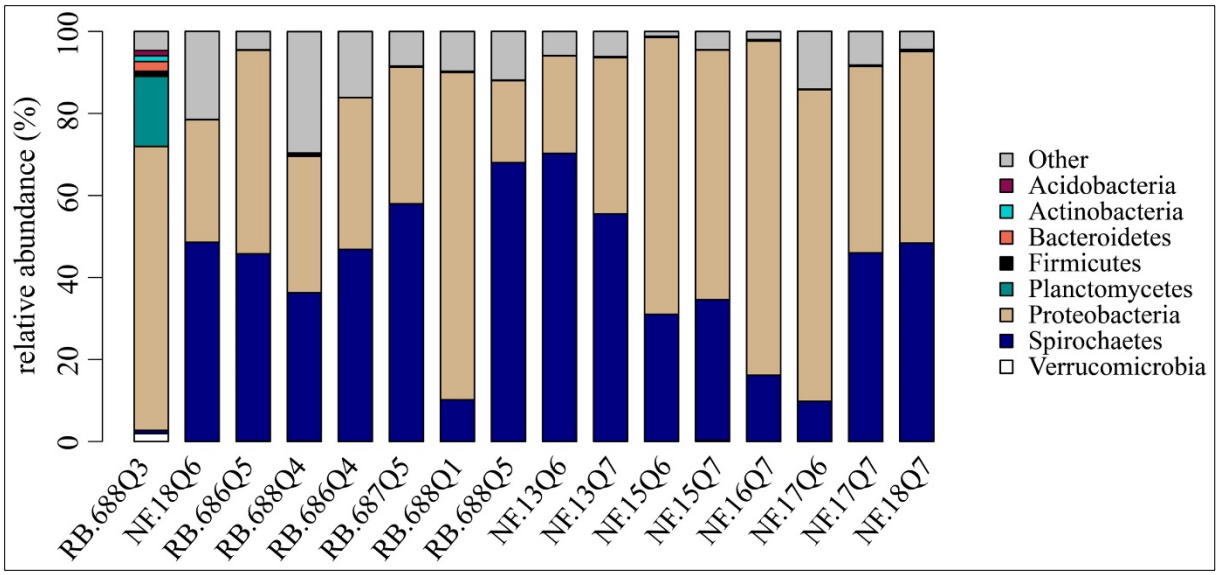

Figure 12-1. Relative abundance of bacterial phyla in Anthothelidae corals. Phyla present at ≥1% relative abundance in at least one sample. All remaining taxa are summarized as "Other." Samples collected from Baltimore Canyon begin with the letters "NF" and those from Norfolk Canyon with "RB."

Due to the phylum-level conservation of bacterial-community diversity within the genus *Anthothela*, the 15 *Anthothela* spp. samples were evaluated to assess if there were specific OTUs held in common (i.e., a core microbiome [Shade and Handelsman 2012]). At the most stringent requirement (presence in 100% of the samples), a single *Spirochaeta* sp. was identified. When the requirement was relaxed to taxa present in 90% of the samples, four conserved taxa were observed: unclassified bacteria from orders Oceanospirillales, Kiloniellales, and Campylobacterales, plus the previously identified genus *Spirochaeta*.

Anthothelidae bacterial community data have been archived online in a USGS data release (Kellogg and Lawler 2015) and in the National Center for Biotechnology Information (NCBI)'s Sequence Read Archive under Bioproject number PRJNA296835.

Bacterial isolates were cultured from *Anthothela* sp. and unclassified Anthothelidae samples (**Table 12-3**). The isolates were mainly *Colwellia* and *Pseudoalteromonas*, but there was also one *Vibrio*, and one match to a sequence previously derived from *L. pertusa* (Kellogg et al. 2009).

12.2.3.3 Paramuricea placomus

This work on *P. placomus* was published in PeerJ in September 2016 (Kellogg et al. 2016). Five samples of *P. placomus* were collected from a single flat plateau in Baltimore Canyon on 12 September 2012 (**Table 12-1**). Samples ROV-2012-NF-19-Q2, ROV-2012-NF-19-Q5, ROV-2012-NF-19-Q6 and ROV-2012-NF-19-Q7 were all within 1 m of each other and were collected without repositioning the ROV. The ROV was then moved a short distance away (2 to 3 m) to collect ROV-2012-NF-19-Q1. The final specimen, ROV-2012-NF-19-Q1, was a larger colony, with a dark purple stalk and mainly yellow polyps, in contrast to the other four specimens, which had much paler lavender stalks and more variegated polyps.

A total of 18 999 raw reads were generated from the five coral samples. Two of the samples (ROV-2012-NF-19-Q6 and ROV-2012-NF-19-Q7) sequenced poorly, with just over 400 sequences each, so they were removed prior to OTU selection to maximize the sequence data available (**Table 12-5**).

Table 12-5. Final sequence numbers and alpha diversity metrics for *Paramuricea placomus*.

Coral	Canyon	Sample ID	Number of Reads[1]	OTU	Chao1 Richness	Shannon Index	Simpson Evenness
P. placomus	Baltimore	ROV-2012-NF-19-Q1	4 300	105	107.80	3.98	0.057
P. placomus	Baltimore	ROV-2012-NF-19-Q2	7 268	107	117.91	3.58	0.047
P. placomus	Baltimore	ROV-2012-NF-19-Q5	5 635	168	170.36	4.57	0.031

[1] All samples were rarefied to 4300 sequences before diversity indices were calculated.
OTU = operational taxonomic unit.

Examining the bacterial sequences associated with *P. placomus* at the phylum level (**Figure 12-2**) reveals relatively consistent bacterial communities, dominated by Proteobacteria with varying amounts of Planctomycetes, Firmicutes, Actinobacteria, and Tenericutes. However, a closer examination at the family level reveals interesting differences between sample ROV-2012-NF-19-Q1 and samples ROV-2012-NF-19-Q2 and ROV-2012-NF-19-Q5 (**Figure 12-3**). Similarity percentages (SIMPER) analysis (Clarke 1993) showed the average dissimilarity between ROV-2012-NF-19-Q1 and ROV-2012-NF-19-Q2 or ROV-2012-NF-19-Q5 was 50.63 to 51.03, and the bacterial groups responsible for more than 5% of that dissimilarity were Legionellales (11.9%), Vibrionaceae (7.1% to 9.4%), and Mycoplasmataceae (7.7% to 9.0%). The average dissimilarity between samples ROV-2012-NF-19-Q2 and ROV-2012-NF-19-Q5 was 44.04 and was driven by Xanthomonadaceae (7.5%) and Bacillaceae (6.8%). All three *P. placomus* samples showed higher relative abundance of gammaproteobacterial families (**Figure 12-3**; shades of pink/purple) compared to alphaproteobacterial families (**Figure 12-3**; shades of blue).

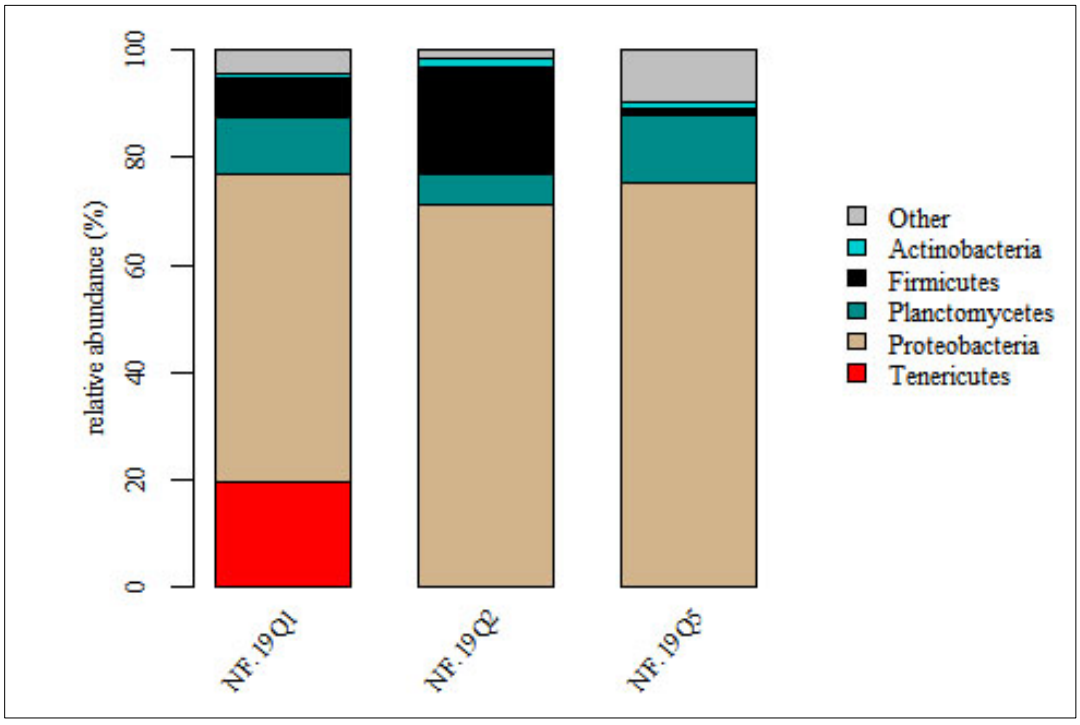

Figure 12-2. Relative abundance of bacterial phyla in *Paramuricea placomus*. Phyla present at ≥1% relative abundance of the total taxa are shown. All remaining taxa are summarized as "Other."

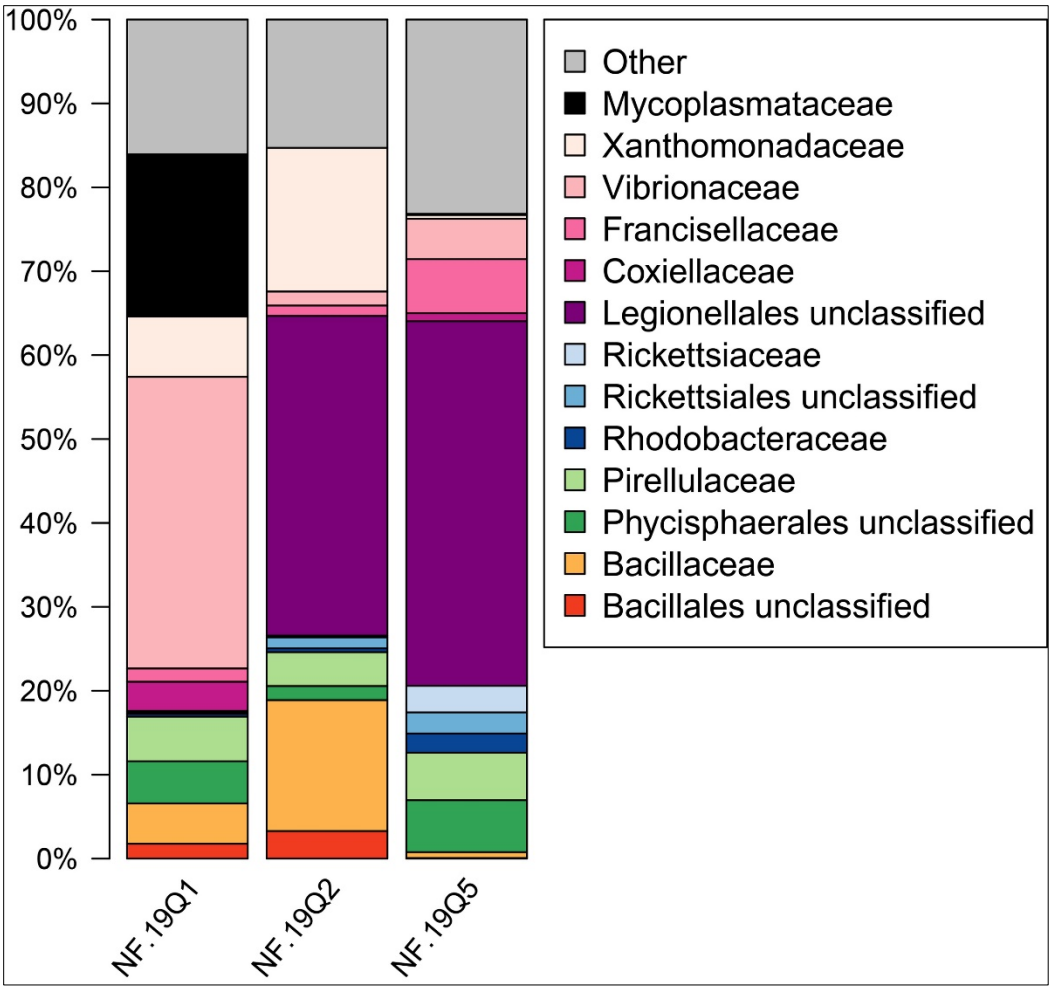

Figure 12-3. Relative abundance of lower taxonomic groups in *Paramuricea placomus*. Families (or the nearest identifiable phylogenetic level) that represent ≥1% relative abundance of the total taxa are shown. All remaining taxa are summarized as "Other." Tenericutes are black. Gammaproteobacterial groups are in shades of pink–purple and alphaproteobacterial groups are in shades of blue. Planctomycetes are in shades of green. Firmicutes are in shades of orange.

Sequences shared by all three samples were examined to identify the core bacterial taxa of *P. placomus* (characterized to the lowest possible taxon, down to genus, **Table 12-6**). Given the small sample size for this coral, we have opted for the most conservative approach; requiring the OTU to be present in 100% of the samples. For each sample, the relative abundance of each taxon is shown in relation to the total taxa (**Table 12-6**). For samples ROV-2012-NF-19-Q5 and ROV-2012-NF-19-Q2, the core taxa make up 75% to nearly 90% of the total community, suggesting a strong species-specific bacterial community. The core taxa constitute 68% of sample ROV-2012-NF-19-Q1, despite its visibly different appearance at the family level (**Figure 12-3**).

Paramuricea placomus bacterial community data have been archived online both in a USGS data release (Kellogg 2015) and in NCBI's Sequence Read Archive under Bioproject number PRJNA297333.

Table 12-6. Core bacterial taxa shared by all three *Paramuricea placomus* samples and their relative abundance in each sample as a percentage of the total taxa. Core bacterial taxa are identified to the lowest practical taxonomic level.

Core Taxa					NF12.19Q1	NF12.19Q2	NF12.19Q5
Phylum	Class	Order	Family	Genus			
Actinobacteria	Actinobacteria	Actinomycetales	Microbacteriaceae	*Curtobacterium*	<0.1	0.1	0.1
Actinobacteria	Actinobacteria	Actinomycetales	Propionibacteriaceae	*Propionibacterium*	0.3	0.6	0.9
Bacteroidetes	Flavobacteriia	Flavobacteriales	Flavobacteriaceae	–	1.0	<0.1	0.2
Firmicutes	Bacilli	Bacillales	–	–	1.8	3.3	0.1
Firmicutes	Bacilli	Bacillales	Alicyclobacillaceae	*Alicyclobacillus*	0.4	0.1	<0.1
Firmicutes	Bacilli	Bacillales	Bacillaceae	*Bacillus*	4.8	15.6	0.7
Planctomycetes	Phycisphaerae	Phycisphaerales	–	–	5.0	1.7	6.2
Planctomycetes	Planctomycetia	Pirellulales	Pirellulaceae	–	5.3	4.0	5.7
Proteobacteria	Alphaproteobacteria	Rhizobiales	Bradyrhizobiaceae	*Bradyrhizobium*	0.9	0.4	<0.1
Proteobacteria	Alphaproteobacteria	Rhizobiales	Phyllobacteriaceae	–	0.6	0.1	<0.1
Proteobacteria	Alphaproteobacteria	Rhodobacterales	Rhodobacteraceae	–	0.3	0.4	2.0
Proteobacteria	Alphaproteobacteria	Rhodospirillales	Rhodospirillaceae	*Magnetospirillum*	0.2	0.3	0.1
Proteobacteria	Betaproteobacteria	Burkholderiales	Alcaligenaceae	–	<0.1	0.2	0.1
Proteobacteria	Betaproteobacteria	Burkholderiales	Comamonadaceae	–	0.3	1.3	0.7
Proteobacteria	Deltaproteobacteria	NB1-j	JTB38	–	0.7	0.2	0.9
Proteobacteria	Epsilonproteobacteria	Campylobacterales	–	–	0.3	0.6	0.8
Proteobacteria	Gammaproteobacteria	Alteromonadales	–	–	0.2	1.7	0.5
Proteobacteria	Gammaproteobacteria	Alteromonadales	OM60	–	0.3	<0.1	0.2
Proteobacteria	Gammaproteobacteria	Enterobacteriales	Enterobacteriaceae	–	0.3	0.5	0.2
Proteobacteria	Gammaproteobacteria	Legionellales	–	–	0.1	38.1	43.5
Proteobacteria	Gammaproteobacteria	Legionellales	Francisellaceae	–	1.6	1.2	6.4
Proteobacteria	Gammaproteobacteria	Pseudomonadales	Moraxellaceae	*Acinetobacter*	0.4	0.5	0.2
Proteobacteria	Gammaproteobacteria	Pseudomonadales	Pseudomonadaceae	*Pseudomonas*	1.3	<0.1	0.7
Proteobacteria	Gammaproteobacteria	Vibrionales	Vibrionaceae	–	34.3	0.7	1.3
Proteobacteria	Gammaproteobacteria	Vibrionales	Vibrionaceae	*Enterovibrio*	0.1	0.9	3.3
Proteobacteria	Gammaproteobacteria	Vibrionales	Vibrionaceae	*Photobacterium*	0.4	<0.1	0.2
Proteobacteria	Gammaproteobacteria	Xanthomonadales	Xanthomonadaceae	–	0.3	0.1	0.2
Proteobacteria	Gammaproteobacteria	Xanthomonadales	Xanthomonadaceae	*Lysobacter*	6.9	17.0	0.1
				Total	68.1	89.6	75.3

12.2.3.4 *Primnoa resedaeformis*

Samples from 20 individual colonies of *Pr. resedaeformis* were collected for microbiology: 10 from Baltimore Canyon and 10 from Norfolk Canyon (**Table 12-1**). Two separate sequencing runs were done to accommodate these samples, but unfortunately, the sequencing run for the Norfolk samples (44 379 raw sequences) did not perform as well as the run for the Baltimore samples (162 006 raw sequences). One Baltimore sample, ROV-2012-NF-10-Q7 did not yield any sequences. Five samples, ROV-2012-NF-12-Q6, ROV-2012-NF-12-Q7, ROV-2012-NF-20-Q1, ROV-2013-RB-684-Q2, and ROV-2013-RB-686-Q3 had less than 2 500 sequences and were removed prior to OTU selection to maximize the sequence data available. This left 14 samples for bioinformatics analysis (**Table 12-7**).

Examining the bacterial sequences associated with *Pr. resedaeformis* at the phylum level (**Figure 12-4**) revealed relatively consistent bacterial communities, dominated by Proteobacteria, with varying amounts of Planctomycetes, Firmicutes, Actinobacteria and Tenericutes, but distinguishable from the community seen in *P. placomus* (**Figure 12-2**) by the additional presence of Bacterioidetes and Verrucomicrobia. Further, **Figure 12-4** clearly shows that there are not bacterial community differences based on canyon of origin (ANOSIM: R = -0.007, P = 0.46).

Primnoa resedaeformis bacterial community data have been archived online both in a USGS data release (Kellogg and Goldsmith 2017) and in the NCBI's Sequence Read Archive under Bioproject number PRJNA348705.

Twenty-five bacterial isolates were cultured from *Pr. resedaeformis* samples (**Table 12-3**). The isolates were dominated by *Pseudoalteromonas*, *Colwellia*, and *Shewanella* species. One of the *Shewanella* sp. was a 100% match to a bacterial sequence previously obtained from a gorgonian coral (*Plumarella superba*) in the Aleutian Islands (Gray et al. 2011). There was also one isolate each of *Photobacterium*, *Psychrobacter*, and *Moritella*.

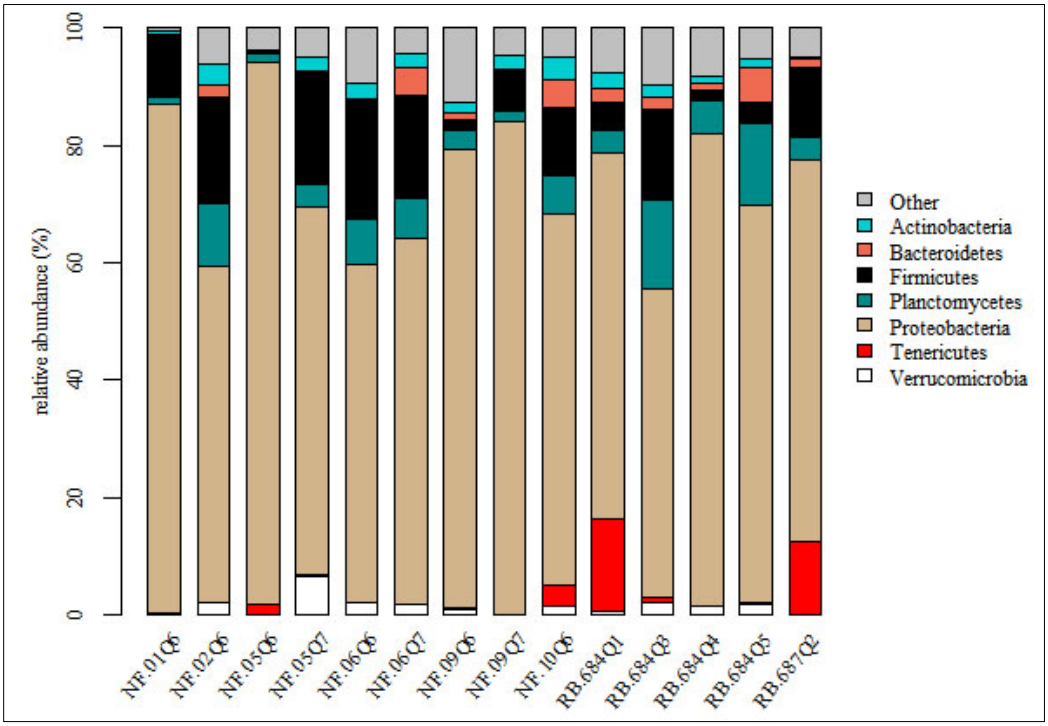

Figure 12-4. Relative abundance of bacterial phyla in *Primnoa resedaeformis*. Phyla present at ≥1% relative abundance of the total taxa are shown. All remaining taxa are summarized as "Other."

Table 12-7. Final sequence numbers and alpha diversity metrics for *Primnoa resedaeformis*.

Coral	Canyon	Sample ID	Number of Reads*	OTU	Chao1 Richness	Shannon Index	Simpson Evenness
P. resedaeformis	Baltimore	ROV-2012-NF-01-06	22,448	84	115.50	1.92	0.022
P. resedaeformis	Baltimore	ROV-2012-NF-02-Q6	17,031	314	414.56	5.68	0.040
P. resedaeformis	Baltimore	ROV-2012-NF-05-Q6	23,285	66	91.00	1.36	0.022
P. resedaeformis	Baltimore	ROV-2012-NF-05-Q7	11,425	207	273.50	4.58	0.035
P. resedaeformis	Baltimore	ROV-2012-NF-06-Q6	7,546	219	265.5	5.21	0.052
P. resedaeformis	Baltimore	ROV-2012-NF-06-Q7	14,653	297	402.22	5.22	0.037
P. resedaeformis	Baltimore	ROV-2012-NF-09-Q6	6,773	235	300.28	5.23	0.043
P. resedaeformis	Baltimore	ROV-2012-NF-09-Q7	5,024	115	128.13	4.37	0.064
P. resedaeformis	Baltimore	ROV-2012-NF-10-Q6	4,261	168	233.81	5.28	0.116
P. resedaeformis	Norfolk	ROV-2013-RB-684-Q1	2,561	178	233.62	4.75	0.061
P. resedaeformis	Norfolk	ROV-2013-RB-684-Q3	3,176	273	318.02	6.12	0.054
P. resedaeformis	Norfolk	ROV-2013-RB-684-Q4	4,753	183	232.88	5.01	0.054
P. resedaeformis	Norfolk	ROV-2013-RB-684-Q5	5,820	241	289.37	5.21	0.026
P. resedaeformis	Norfolk	ROV-2013-RB-687-Q2	2,557	159	246.14	4.78	0.072

* All samples were rarefied to 2,557 sequences before diversity indices were calculated. OTU = operational taxonomic unit.

12.2.4 Discussion

Relatively little is known about deepsea coral microbiomes in comparison to those of tropical corals. Prior to this study, no microbial assessment had been completed on any species of gorgonian coral present in these canyons. It was unknown if the environmental isolation and/or different nutrient and sediment regimes of these canyons would impact the diversity of the coral's bacterial community. It has been shown in *L. pertusa*, a deepsea scleractinian coral, that some portion of its bacterial community varies based on location/environmental parameters (Neulinger et al. 2008, Schöttner et al. 2012).

In most of the marine environment, Proteobacteria dominate the bacterial diversity. This is true for many tropical coral species (Bourne and Munn 2005, Frias-Lopez et al. 2002, Mouchka et al. 2010) as well as deepsea corals, both scleractinians and octocorals (Galkiewicz et al. 2011, Hansson et al. 2009, Neulinger et al. 2008, Penn et al. 2006, van Bleijswijk et al. 2015). In this study, similar trends were observed, both in 16S rRNA amplicon data (**Figures 12-1** through **12-4**) and cultured bacterial isolates (**Table 12-3**).

12.2.4.1 Acanthogorgia aspera

The *A. aspera* samples were of particular interest due to the two depth horizons that were sampled (~500 m versus ~1,300 m). No differences in bacterial diversity are obvious from the cultured isolates, regardless of host depth (**Table 12-3**). However, culture-based diversity data are limited compared with those derived from 16S rRNA amplicon sequencing (Rohwer et al. 2001). Unfortunately, the samples did not sequence consistently or deeply enough to allow amplicon analysis.

12.2.4.2 Anthothela grandiflora

The bacterial diversity in *Anthothela* samples (both *A. grandiflora* and *Anthothela* sp.) was distinctly different from that present in the new genus *Lateothela grandiflora* (**Figure 12-1**). The main driver of this difference was the presence of Spirochaetes, which dominated more than half of the *Anthothela* spp. samples. Functional characteristics displayed by this group include nitrogen and carbon fixation (Baker et al. 2015, Kimes et al. 2010, Lilburn et al. 2001). Members of the phylum Spirochaetes are commonly found in association with invertebrates, including species of termites (Breznak 2002), oligochaete worms (Blazejak et al. 2005), sponges (Taylor et al. 2005), and tropical corals (Casas et al. 2004, Closek et al. 2014, Kimes et al. 2010). Previous studies using clone libraries have observed Spirochaetes in association with some deepsea corals (Gray et al. 2011, Kellogg et al. 2009, Penn et al. 2006); however, they have only recently been identified by pyrosequencing as a dominant member of the bacterial microbiome in corals (Lawler et al. 2016, van de Water et al. 2016).

Previous studies have addressed the importance of nitrogen cycling in photosynthetic corals, suggesting the influence of fungi, cyanobacteria, and/or dinoflagellate symbionts on the biochemical processes (Lesser et al. 2004, Lesser et al. 2007, Pernice et al. 2012, Shashar et al. 1994, Wegley et al. 2007). While it is evident that nitrogen availability is one of the driving factors in the proliferation and health of tropical coral hosts, little is known about its influence in deepsea coral holobionts. The core bacterial groups (*Spirochaeta*, Oceanospirillales, Kiloniellales, and Campylobacterales) observed in *Anthothela* spp. samples are theoretically capable of performing an almost complete nitrogen cycle (**Figure 12-5**). *Spirochaeta* are recognized for their role in nitrogen fixation (Lilburn et al. 2001), during which nitrogen gas (N_2) is converted to readily available organic compounds. Several members of the order Campylobacterales have been recognized for their contributions through nitrate ammonification (Tiedje 1988). This is the process by which nitrate is converted to ammonium, thereby recycling nitrogen back into the system. Members of the order Oceanospirillalles contribute through the reduction of nitrate to nitrite (Kurahashi and Yokota 2007). Lastly, members of the order Kiloniellales show great potential in the processing of molecular nitrogen through denitrification, in which nitrates are reduced back to nitrogen gas for utilization by nitrogen-fixing bacteria (Imhoff and Wiese 2014). Further investigations,

such as specifically targeting genes of the nitrogen cycle or metagenomics, are needed to more concretely describe the roles of these core bacteria.

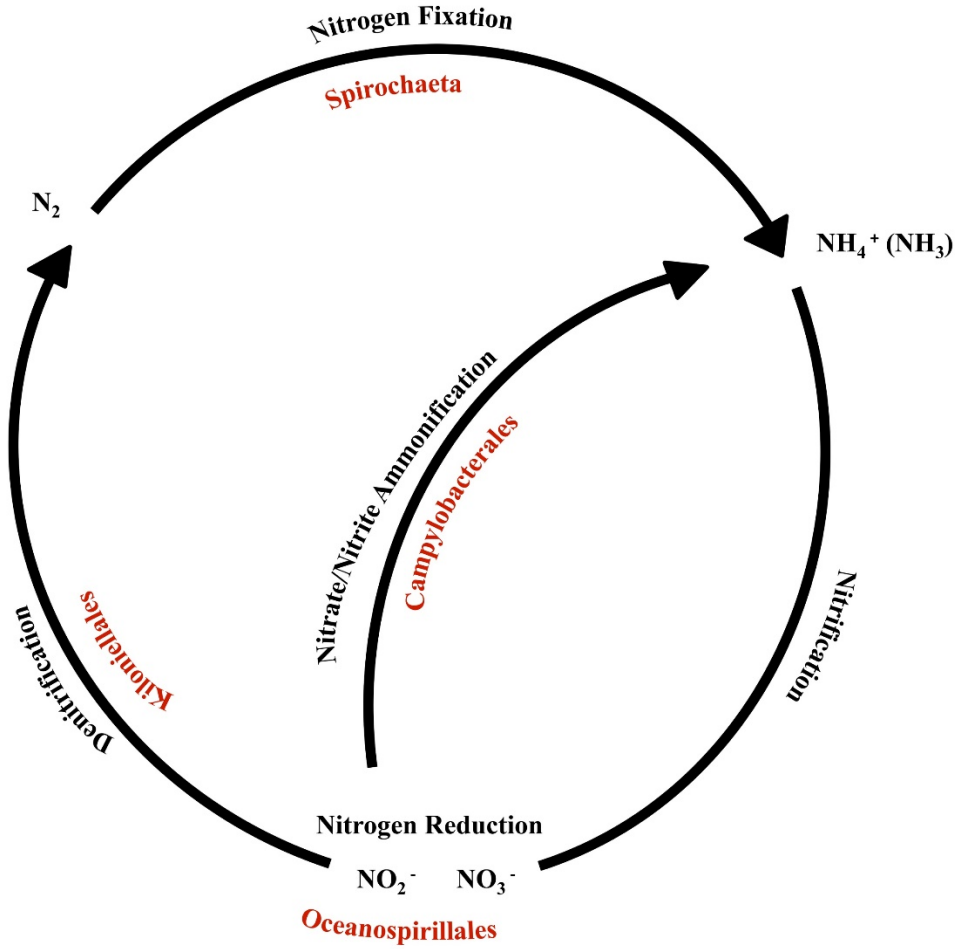

Figure 12-5. *Anthothela* spp. core bacterial groups and their potential contributions to the nitrogen cycle. This diagram illustrates the bacterial groups present in the *Anthothela* core and their previously recognized roles within the nitrogen cycle. (Adapted from: Wegley et al. 2007).

12.2.4.3 Paramuricea placomus

While similar at the phylum level (**Figure 12-2**), when examined at the family level, pronounced differences were observed between sample ROV-2012-NF-19-Q1 and samples Q2 and Q5; most notably reductions in unclassified Legionellales and alphaproteobacterial groups, and increases in Vibrionaceae and Mycoplasmataceae (**Figure 12-3**). *Mycoplasma* sp. sequences were previously found associated with other deepsea corals, including *L. pertusa* (Kellogg et al. 2009, Neulinger et al. 2008, Neulinger et al. 2009) and octocorals, including a bamboo coral (order Alcyonacea, family Isididae) (Penn et al. 2006), *Cryogorgia koolsae* (Gray et al. 2011), and *Plumarella superba* (Gray et al. 2011). Sequences within the family Mycoplasmataceae were also present in some samples of *Pr. resedaeformis* examined in this study.

All *P. placomus* at the collection site were variegated in color (purple/yellow); however, sample ROV-2012-NF-19-Q1 had a much darker purple stalk and yellow polyps, while the remaining samples had paler stalks and a mixture of purple and yellow polyps. An intriguing possible explanation for the pattern seen in **Figure 12-3** is that different color variants of *P. placomus* support different bacterial

communities, as has been found with different color morphs of corals *L. pertusa* (Neulinger et al. 2008) and *Montipora capitata* (Shore-Maggio et al. 2015). More replicates of each color variant are required to confirm this hypothesis.

The bacterial community of a temperate sister-species, *P. clavata*, is dominated almost exclusively by a single bacterial genus, *Endozoicomonas* (La Rivière et al. 2013, Vezzulli et al. 2013). We did not detect this genus or its family (Hahellaceae) in any of our *P. placomus* samples, and even the order Oceanospirillales to which it belongs only averaged 0.2% relative abundance. The genus *Endozoicomonas* has been found to dominate other species of temperate corals in the Mediterranean (Bayer et al. 2013a, Bayer et al. 2013b), and a recent study has suggested a coadaptation between clades of bacteria within the family Hahellaceae and several temperate gorgonian species (La Rivière et al. 2015). *Endozoicomonas* also was detected in several healthy tropical corals (Apprill et al. 2013, Bourne and Munn 2005, Correa et al. 2013, Duque-Alarcón et al. 2012, Kvennefors et al. 2010, Morrow et al. 2012, Sunagawa et al. 2010, Sunagawa et al. 2009), suggesting an important functional role that remains to be discovered. A few *Endozoicomonas* (or Hahellaceae) sequences have been detected in bacterial communities associated with *L. pertusa* (Kellogg et al. 2009, van Bleijswijk et al. 2015) and with *Anthothela* spp., indicating that this group's absence in *P. placomus* was not driven by a cold-temperature or other depth-related limitation. This raises the question of whether the absence of this bacterial group in *P. placomus* is driven by biogeography (due to the isolated nature of this particular coral population) or whether this could be a diagnostic feature of this species' microbiome.

12.2.4.4 Primnoa resedaeformis

Genetic analysis of *P. resedaeformis* has shown clearly distinguishable populations that occupy Baltimore and Norfolk canyons (**Chapter 14**, Section 14.3.2.2). However, there was no significant difference in the coral-associated bacterial communities between the two canyons.

Evaluation of the presence of a core microbiome in *P. resedaeformis* is ongoing, as is a comparison against samples from a sister-species, *P. pacifica*. Both are complicated by the fact that the Norfolk Canyon samples have such low sequence reads compared with Baltimore Canyon samples. Either read depth (and therefore much information) must be sacrificed through rarefaction to compare all samples at the same level or Norfolk samples may be dropped to preserve the greater sequencing depth (and information) in the Baltimore samples. The completion of this work is outside the timeline of this report; analyses should be available at a later date for publication as a journal article.

12.3 SEDIMENT MICROBIAL COMMUNITIES

12.3.1 Introduction

Even soft, featureless seafloor environments host a thriving community if you look closely enough. The objective of this study was to examine the microbial diversity, both prokaryotic and eukaryotic, of deepsea sediments. The experimental design was to take replicate box cores at a series of depths inside the valley of each canyon and then to take "control" box cores at similar depths outside the canyon on the continental slope. These samples will allow comparisons within and between canyons as well as generating baseline microbial diversity data for submarine canyons. The intention is also to look for correlations among environmental parameters (e.g., grain size, sediment chemistry; **Chapter 6**), infaunal taxa (**Chapter 9**), and the patterns of microbial taxa.

12.3.2 Methods

12.3.2.1 Field Sampling Methods

During the 2012 sampling cruise, 16 box cores were collected inside Baltimore Canyon: 4 at 190 m, 4 at 560 m, 4 at 840 m, and 4 at 1,180 m. Corresponding samples were then collected on the slope outside Baltimore Canyon: 4 at 170 m, 4 at 500 m, 4 at 1,000 m, and 4 at 1,180 m, for a total of 32 box cores. In 2013, 9 box cores were collected inside Norfolk Canyon: 2 at 190 m, 3 at 560 m, 3 at 800 m, and one at 1,110 m. At corresponding depths outside Norfolk Canyon, 13 box cores were collected: 3 at 190 m, 3 at 550 m, 3 at 800 m, and 4 at 1,110 m, for a total of 22 box cores.

For each box core that was collected, a dedicated subcore of sediment was taken for microbiology (**Table 12-8**). Simultaneously, replicate subcores were taken from the same box core and processed for geology/geochemistry (**Chapter 6**) and infauna (**Chapter 9**). A temperature probe was inserted into the sediment to approximately 3 cm deep as soon as the box core was on deck and clear to approach, but likely the samples (especially the deeper ones) have warmed during the retrieval (**Table 12-8**). Pore water salinity was also recorded when possible. Seawater on top of each core was gently removed using a 60 cc syringe. A sterilized long-handled spatula was used to collect sediment samples from the top 3 to 5 cm of each subcore. Aliquots of sediment (1.25 mL scoop) were put into sterile 5 mL cryovials with sterile-filtered seawater and flash-frozen in liquid nitrogen for bacterial direct counts. Smaller aliquots (0.62 mL scoop) of sediment were transferred to sterile 15 mL tubes, to which were added 4 mL sterile-filtered seawater and 450 μL 40% paraformaldehyde to preserve the samples for FISH. The samples for FISH were stored for 18 to 24 hours at 4 °C, then washed three times with sterile-filtered seawater, centrifuged at 10 000 × *g* for 5 minutes between washes to pellet the sediment, and then stored in 70% ethanol–30% sterile-filtered seawater at -20 °C. A second sterile 15 mL scoop was filled with sediment and directly frozen at -20 °C for DNA extraction/sequencing.

12.3.2.2 Laboratory Methods

Many cryovials ruptured or exploded in the liquid nitrogen dewar after the 2012 sampling cruise, so the direct enumeration of bacterial cells could not be completed. Knowing that there was nothing to compare against (and considering the difficulty of bringing liquid nitrogen to sea), no samples were collected for direct counts during 2013. The samples for FISH were transferred to the -20 °C in the laboratory and remain in storage pending results from the sequencing that would direct their usage.

In April 2014, frozen sediment samples were thawed for extraction following the protocol used by the Earth Microbiome Project (EMP 2016). When available, samples from three box cores per depth were extracted, for a total of 45 samples being processed. Duplicate extractions were done for each sample (total = 90) using the MOBIO PowerSoil DNA Isolation Kit (Lot no. PS14A22) with the additional incubations prescribed by the EMP protocol. The duplicate extractions were combined at the end of the protocol, resulting in 100 μL per sample. The samples were transferred to two 96-well plates and sent to Argonne National Lab for Illumina sequencing following the EMP protocol.

12.3.2.3 Bioinformatic Analysis

Analysis is in progress for the 16S rRNA (prokaryotic) and 18S rRNA (eukaryotic) sequences from the sediment samples. The completion of these analyses is outside the timeline of this report; analyses should be available at a later date for publication as a journal article.

Table 12-8. Sediment samples and corresponding environmental data. ND = not determined.

Sample ID	Date	Collection Time	Site	Depth (m)	Latitude (N)	Longitude (W)	Temp (°C)	Salinity
NF-2012-019-C	19 Aug 2012	21:35	Baltimore Canyon	189	38°14′35.58″	73°50′36.72″	ND	36.0
NF-2012-021-F	19 Aug 2012	23:19	Baltimore Canyon	189	38°14′35.40″	73°50′36.72″	ND	ND
NF-2012-028-C	20 Aug 2012	20:34	Baltimore Canyon	191	38°14′53.40″	73°50′36.60″	13.2	37.0
NF-2012-029-F	20 Aug 2012	21:12	Baltimore Canyon	191	38°14′34.20″	73°50′36.66″	14.3	37.0
NF-2012-032-I	21 Aug 2012	00:31	Baltimore Canyon	563	38°09′58.26″	73°51′00.36″	12.2	ND
NF-2012-033-L	21 Aug 2012	01:26	Baltimore Canyon	564	38°09′58.26″	73°51′00.24″	12.9	ND
NF-2012-034-O	21 Aug 2012	02:23	Baltimore Canyon	565	38°09′58.38″	73°51′00.00″	13.2	ND
NF-2012-035-C	21 Aug 2012	03:35	Baltimore Canyon	567	38°09′58.56″	73°50′59.94″	14.7	ND
NF-2012-045-C	22 Aug 2012	20:57	Baltimore Canyon	840	38°07′01.32″	73°50′09.00″	9.8	37.0
NF-2012-047-F	22 Aug 2012	23:06	Baltimore Canyon	848	38°07′02.70″	73°50′05.28″	10.0	36.0
NF-2012-049-I	23 Aug 2012	01:01	Baltimore Canyon	844	38°07′03.06″	73°50′04.32″	9.0	36.0
NF-2012-050-L	23 Aug 2012	02:01	Baltimore Canyon	844	38°07′03.06″	73°50′04.32″	10.6	36.0
NF-2012-055-C	23 Aug 2012	21:44	Baltimore Canyon	1,179	38°04′20.76″	73°46′23.64″	6.5	36.0
NF-2012-056-F	23 Aug 2012	22:52	Baltimore Canyon	1,179	38°04′20.76″	73°46′23.52″	6.0	36.0
NF-2012-062-C	24 Aug 2012	20:57	Baltimore Canyon	1,180	38°04′19.56″	73°46′24.00″	7.0	36.0
NF-2012-063-F	24 Aug 2012	22:03	Baltimore Canyon	1,180	38°04′19.80″	73°46′24.12″	6.5	36.0
NF-2012-064-I	24 Aug 2012	23:49	Off Baltimore	168	38°03′45.00″	73°51′56.04″	14.3	36.0
NF-2012-066-L	25 Aug 2012	00:37	Off Baltimore	170	38°03′45.00″	73°51′56.04″	14.8	36.0
NF-2012-067-O	25 Aug 2012	01:06	Off Baltimore	168	38°03′44.40″	73°51′56.22″	13.8	36.0
NF-2012-069-C	25 Aug 2012	01:48	Off Baltimore	169	38°03′45.30″	73°52′07.02″	13.9	36.0
NF-2012-071-C	25 Aug 2012	04:36	Off Baltimore	513	38°02′36.54″	73°48′12.36″	11.5	36.0
NF-2012-072-F	25 Aug 2012	05:11	Off Baltimore	514	38°02′36.48″	73°48′12.36″	10.3	36.0
NF-2012-076-C	25 Aug 2012	20:59	Off Baltimore	510	38°02′36.48″	73°48′12.30″	10.5	36.0
NF-2012-082-F	26 Aug 2012	02:03	Off Baltimore	990	38°00′49.80″	73°45′12.49″	6.5	36.0
NF-2012-085-I	26 Aug 2012	04:40	Off Baltimore	991	38°00′49.92″	73°45′12.24″	8.1	36.0
NF-2012-087-L	26 Aug 2012	06:22	Off Baltimore	991	38°00′49.92″	73°45′12.24″	8.4	36.0
NF-2012-088-C	26 Aug 2012	21:03	Off Baltimore	502	38°02′36.96″	73°48′11.53″	9.6	36.0
NF-2012-089-F	26 Aug 2012	22:46	Off Baltimore	1,030	38°00′40.38″	73°45′15.60″	8.1	36.0
NF-2012-090-I	27 Aug 2012	01:06	Off Baltimore	1,185	37°58′38.58″	73°40′09.78″	6.1	36.0
NF-2012-092-L	27 Aug 2012	03:04	Off Baltimore	1,187	37°58′38.52″	73°40′09.78″	5.3	36.0
NF-2012-093-O	27 Aug 2012	04:03	Off Baltimore	1,186	37°58′38.52″	73°40′09.78″	5.8	36.0

Table 12-8. (Continued).

Sample ID	Date	Collection Time	Site	Depth (m)	Latitude (N)	Longitude (W)	Temp (°C)	Salinity
NF-2012-095-C	27 Aug 2012	06:02	Off Baltimore	1,186	37°58' 38.70″	73°40' 09.84″	8.5	36.0
RB-2013-38 D	10 May 2013	01:23	Norfolk Canyon	1,110	37°02' 19.08″	74°34' 47.52″	15.0	33.0
RB-2013-40-1	10 May 2013	21:00	Norfolk Canyon	805	37°02' 33.84″	74°37' 45.00″	14.0	16.4
RB-2013-41-3	10 May 2013	22:08	Norfolk Canyon	803	37°02' 33.90″	74°37' 45.12″	14.0	34.2
RB-2013-42-5	10 May 2013	23:09	Norfolk Canyon	804	37°02' 34.08″	74°37' 45.30″	14.0	34.3
RB-2013-43-7	11 May 2013	12:49	Norfolk Canyon	559	37°04' 33.48″	74°39' 38.28″	14.2	26.2
RB-2013-44-9	11 May 2013	01:37	Norfolk Canyon	557	37°04' 33.48″	74°39' 38.10″	13.2	29.5
RB-2013-45-11	11 May 2013	02:27	Norfolk Canyon	558	37°04' 33.42″	74°39' 38.10″	13.5	34.0
RB-2013-46-13	11 May 2013	03:54	Norfolk Canyon	195	37°05' 41.10″	74°44' 47.70″	10.5	27.0
RB-2013-48-7	11 May 2013	04:48	Norfolk Canyon	195	37°05' 41.22″	74°44' 47.64″	11.1	32.2
RB-2013-49-9	11 May 2013	06:05	Off Norfolk	187	37°01' 23.04″	74°38' 44.76″	ND	ND
RB-2013-50-15	11 May 2013	06:29	Off Norfolk	187	37°01' 28.02″	74°38' 50.22″	12.0	33.6
RB-2013-51-17	11 May 2013	06:55	Off Norfolk	187	37°01' 26.94″	74°38' 45.36″	12.0	29.1
RB-2013-54-1	12 May 2013	20:05	Off Norfolk	549	37°00' 56.88″	74°34' 41.52″	13.3	34.3
RB-2013-55-3	12 May 2013	20:51	Off Norfolk	549	37°00' 56.89″	74°34' 41.34″	13.3	34.3
RB-2013-56-b	12 May 2013	21:40	Off Norfolk	548	37°00' 56.88″	74°34' 41.40″	ND	ND
RB-2013-60-5	13 May 2013	02:39	Off Norfolk	790	37°00' 32.58″	74°33' 52.98″	12.3	34.0
RB-2013-69-1	14 May 2013	20:45	Off Norfolk	804	37°00' 32.46″	74°33' 53.88″	17.0	35.2
RB-2013-70-d	14 May 2013	21:43	Off Norfolk	805	37°00' 32.22″	74°33' 53.88″	17.0	35.3
RB-2013-71-d	14 May 2013	23:12	Off Norfolk	1,118	37°00' 20.76″	74°32' 01.44″	19.0	35.4
RB-2013-73-d	15 May 2013	01:47	Off Norfolk	1,105	37°00' 20.76″	74°32' 01.44″	20.2	35.5
RB-2013-75-1	15 May 2013	15:35	Off Norfolk	1,103	37°00' 21.18″	74°32' 01.14″	14.3	34.4
RB-2013-76-1	15 May 2013	16:56	Off Norfolk	1,100	37°00' 20.88″	74°32' 00.90″	14.0	34.1

12.4 MICROBIAL BIOFILMS ON ARTIFICIAL SUBSTRATA (SETTLING PLATE ARRAYS)

12.4.1 Introduction

All underwater surfaces are rapidly covered in biofilms of living things, starting with microbes. The mixed community of bacteria in a particular biofilm can determine what marine invertebrates, such as corals, sponges, echinoderms, molluscs, barnacles, and worms, will chose to settle and grow in that location (reviewed by Wieczorek and Todd 1998). In this way, the microbes orchestrate understudied effects on the benthic community structure at the ecosystem level, making them the original ecosystem architects.

One of the objectives of this project was to deploy settling plate arrays using different materials to examine the composition of naturally forming biofilms at different depths in both Baltimore and Norfolk canyons, using benthic landers (**Chapter 3**, **Section 3.2.6**). The intention was to leave the experiments in place on the seafloor for approximately 1 year.

12.4.2 Methods

12.4.2.1 Field Sampling Methods

Each settling plate array was constructed of 13 cm × 13 cm plates of calcium carbonate (coral limestone), sandstone, and stainless steel, threaded on a central nylon rod and separated by PVC spacers (**Figure 12-6**). The stainless steel plates were 0.5 cm thick and the stone plates were approximately 1.0 cm thick. Due to concern about oxidation interactions between the stainless steel plate and the frames of the benthic landers, the steel plates were always placed in the middle of each array. Four arrays were attached to each of the four benthic landers (16 arrays, 48 plates) using large cable ties; half had calcium carbonate plates at the top and half had sandstone plates at the top.

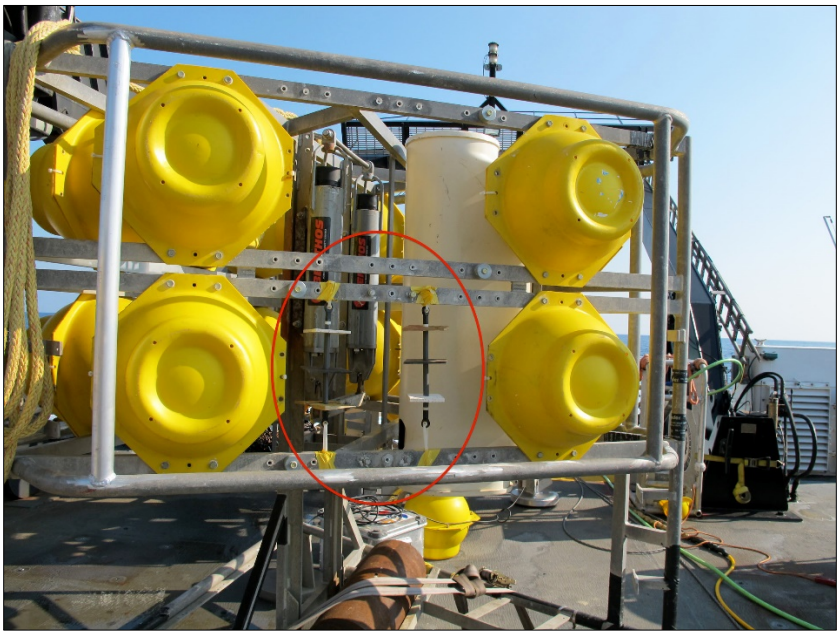

Figure 12-6. Settling plate arrays mounted on a benthic lander. A red circle highlights the two arrays mounted on the facing side of the lander. The left array has a calcium carbonate plate on top, steel in the middle, and sandstone at the bottom. The right array has sandstone on top, steel in the middle, and calcium carbonate at the bottom.

Four arrays were mounted on the Royal Netherlands Institute for Sea Research (NIOZ) BOBO lander at a height of 41 cm (16 in.) above the bottom of the lander. The BOBO lander was launched on 17 August 2012 at the mouth of Norfolk Canyon (latitude 37°02′13.0200″, longitude 074°32′01.1760″, depth 1,364 m). This lander was retrieved and the settling plate arrays recovered on 23 August 2013.

Four arrays were mounted on the NIOZ Albex lander at a height of 109 cm (43 in.) above the bottom of the lander. The Albex lander was launched on 17 August 2012 at the head of Norfolk Canyon (latitude 37°03′52.5600″, longitude 074°39′07.1640″, depth 600 m). This lander was unable to be recovered during the 2013 sampling cruise, but came ashore in the Bahamas months later. The infrastructure was recovered, but the settling plate experiment was not.

Four arrays were mounted on each of two University of North Carolina–Wilmington (UNCW) landers at a height of 91 cm (36 in.) above the bottom of the lander for deployment in Baltimore Canyon. One lander was launched on 5 September 2012 at the mouth of Baltimore Canyon (latitude 38°02′32.6998″, longitude 073°44′04.9798″, depth 1,340 m). The other lander was launched on 6 September 2012 at the head of Baltimore Canyon (latitude 38°09′00.3636″, longitude 073°50′52.4976″, depth 617 m). These landers were retrieved on 16 May 2013 (mouth) and 17 May 2013 (head) after spending 8 months on the seafloor. The lander at the head of Baltimore Canyon had been inundated by sediment; however, all settling plate arrays were recovered.

When landers were successfully retrieved, the settling plate arrays were removed, and each plate was placed in a pre-sized seal-a-meal bag and covered in RNA*later* preservative. Air was pressed out of the bags, and then they were heat-sealed. The plates were stored at 4°C overnight to allow the preservative to penetrate the biofilm and then transferred to -20°C storage until returned to the laboratory.

12.4.2.2 Laboratory Methods

Plates were removed from their bags using sterile technique and placed into sterile stainless steel pans. Biofilms were airbrushed off each plate using ~60 mL sterile 1× PBS and then passed through a sterile 500-micron stainless steel screen to remove hydroids. The microbe-containing liquid was split into two sterile 50 mL tubes (roughly 30 mL per tube) and centrifuged at 500 rpm (46 × *g*, Beckman JLA 10.500 rotor) for 30 minutes to pellet any sediment or larger particulates. The supernatant was decanted into fresh tubes and then centrifuged at 15 000 × *g* for 30 min to pellet the microorganisms. DNA was then extracted from each microbial pellet using the Qiagen DNeasy kit, following the manufacturer's protocol for Gram-positive bacteria.

Unamplified DNA extracted from the biofilm samples was sequenced by 454 pyrosequencing using GS FLX Titanium chemistry (Selah Genomics, Greenville, South Carolina) and primers targeting the V4-V5 variable region of the 16S rRNA gene (Claesson et al. 2010) following Roche 454 Life Sciences Corp's standard protocol for amplicons (454 Life Sciences Corp 2011).

12.4.2.3 Bioinformatic Analysis

A preliminary analysis was run but was later found to contain errors. The biofilm sequences are being reanalyzed using the same workflow for 454 pyrosequencing datasets described above for corals in **Section 12.2.2.3**.

12.4.3 Results

Due to the loss of the samples from the Albex lander at the head of Norfolk Canyon, there is not a complete dataset from Norfolk Canyon. As such, it was decided not to process the settling plates from the mouth of Norfolk Canyon. Those plates have been offered (still frozen in preservative) to Leila Hamdan, Principal Investigator for SCHEMA: Shipwreck Corrosion, Hydrocarbon Exposure, Microbiology and Archaeology, a BOEM-funded project in the Gulf of Mexico that is also using settling plates to examine

microbial biofilm formation. That project is using Illumina sequencing rather than 454, and adding these plates to their pipeline would give them a geographic outgroup to compare against the Gulf of Mexico.

We received 16S rRNA amplicon data from the sequencing vendor, and raw numbers of sequences for each settling plate can be found in **Table 12-9**. Reanalysis of these sequences is ongoing. Completion of these analyses is outside the timeline of this report; analyses should be available at a later date for publication as a journal article.

12.5 CONCLUSIONS

Using16S rRNA amplicon sequencing, the coral genera *Anthothela*, *Paramuricea*, and *Primnoa* were shown to all have distinct bacterial communities (**Figures 12-1**, **12-2**, and **12-4**). *Anthothela grandiflora* and *Anthothela* sp. were indistinguishable based on bacterial community diversity, indicating that bacterial communities may be conserved at the genus level in this coral family. Proteobacteria were a major component for all corals. *Anthothela* spp. were distinguished by the co-dominance of Spirochaetes, which were minor or absent in the other two corals examined. Both *P. placomus* and *Pr. resedaeformis* had similar communities at the phylum level, including Plantomycetes, Firmicutes, Actinobacteria, and Tenericutes, but were distinguished by larger relative abundance of Bacteriodetes and Verrucomicrobia in *Pr. resedaeformis*. Unlike many temperate and tropical corals, which have been found to be dominated by *Endozoicomonas* ribotypes, these deepsea coral microbiomes had few (*Anthothela* spp.) or none (*P. placomus* and *Pr. resedaeformis*).

For the two coral species that were sampled from both Baltimore and Norfolk canyons (*A. grandiflora* and *Pr. resedaeformis*), there was no evidence of bacterial community structuring by environmental factors (e.g., temperature, salinity, and depth). The main observed driver of bacterial community composition was the coral host genus.

The culture medium used to isolate bacteria from these corals (Jensen I3) appears biased toward the growth of *Pseudoalteromonas*, *Shewanella*, and *Colwellia* species. Two of the isolates were identified as 99% to 100% similar to bacterial sequences previously obtained from other deepsea coral species.

Analyses are ongoing for the 16S and 18S rRNA amplicon surveys in the canyons sediments and the settling plate biofilm experiment.

Any use of trade, firm, or product names in this report is for descriptive purposes only and does not imply endorsement by the U.S. Government.

12.6 LITERATURE CITED

454 Life Sciences Corp. 2011. 454 sequencing system guidelines for Amplicon Experimental Design. Branford (CT):454 Life Sciences Corp. 46 p. [accessed 2016 April 6]. http://my454.com/downloads/my454/applications-info/454SequencingSystem_GuidelinesforAmpliconExperimentalDesign_July2011.pdf.

Apprill A, Hughen K, Mincer T. 2013. Major similarities in the bacterial communities associated with lesioned and healthy Fungiidae corals. Environmental Microbiology. 15:2063–2072.

Baker BJ, Lazar CS, Teske AP, Dick GJ. 2015. Genomic resolution of linkages in carbon, nitrogen, and sulfur cycling among widespread estuary sediment bacteria. Microbiome. 3:14.

Bayer T, Arif C, Ferrier-Pagès C, Zoccola D, Aranda M, Voolstra CR. 2013a. Bacteria of the genus *Endozoicomonas* dominate the microbiome of the Mediterranean gorgonian coral *Eunicella cavolini*. Marine Ecology Progress Series. 479:75–84.

Bayer T, Neave MJ, Alsheikh-Hussain A, Aranda M, Yum LK, Mincer T, Hughen K, Apprill A, Voolstra CR. 2013b. The microbiome of the Red Sea coral Stylophora pistillata is dominated by tissue-associated *Endozoicomonas* bacteria. Applied and Environmental Microbiology. 79:4759-4762.

Benson DA, Cavanaugh M, Karsch-Mizrachi I, Lipman DJ, Savers EW. 2013. GenBank nucleic acids research (database issue) D36–42. doi:10.1093/nar/gks1195.

Blazejak A, Erséus C, Amann R, Dubilier N. 2005. Coexistence of bacterial sulfide oxidizers, sulfate reducers, and spirochetes in a gutless worm (Oligochaeta) from the Peru margin. Applied and Environmental Microbiology. 71:1553–1561.

Bourne DG, Munn CB. 2005. Diversity of bacteria associated with the coral *Pocillopora damicornis* from the Great Barrier Reef. Environmental Microbiology. 7:1162–1174.

Breznak JA. 2002. Phylogenetic diversity and physiology of termite gut Spirochetes. Integrative and Comparative Biology. 42:313–318.

Caporaso JG, Kuczynski J, Stombaugh J, Bittinger K, Bushman FD, Costello EK, Fierer N, Gonzalez Peña A, Goodrich JK, Gordon JI, Huttley GA, Kelley ST, Knights D, Koenig JE, Ley RE, Lozupone CA, McDonald D, Muegge BD, Pirrung M, Reeder J, Sevinsky JR, Turnbaugh PJ, Walters WA, Widmann J, Yatsunenko T, Zaneveld J, Knight R. 2010a. QIIME allows analysis of high-throughput community sequencing data. Nature Methods. 7:335–336.

Caporaso JG, Bittinger K, Bushman FD, DeSantis TZ, Andersen GL, Knight R. 2010b. PyNAST: a flexible tool for aligning sequences to a template alignment. Bioinformatics. 26:266–267.

Casas V, Kline DI, Wegley L, Yu Y, Breitbart M, Rohwer F. 2004. Widespread association of a *Rickettsiales*-like bacterium with reef-building corals. Environmental Microbiology. 6:1137–1148.

Chao A. 1984. Nonparametric estimation of the number of classes in a population. Scandinavian Journal of Statistics. 11:265–270.

Claesson MJ, Wang Q, O'Sullivan O, Greene-Diniz R, Cole JR, Ross RP, O'Toole PW. 2010. Comparison of two next-generation sequencing technologies for resolving highly complex microbiota composition using tandem variable 16S rRNA gene regions. Nucleic Acids Research. 38:e200.

Clarke KR. 1993. Non-parametric multivariate analyses of changes in community structure. Australian Journal of Ecology. 18:117–143.

Closek CJ, Sunagawa S, DeSalvo MK, Piceno YM, DeSantis TZ, Brodie EL, Weber M, Voolstra CR, Andersen GL, Medina M. 2014. Coral transcriptome and bacterial community profiles reveal distinct Yellow Band Disease states in *Orbicella faveolata*. The ISME Journal. 8:2411–2422.

Correa H, Haltli B, Duque C, Kerr R. 2013. Bacterial communities of the gorgonian octocoral *Pseudopterogorgia elisabethae*. Microbial Ecology. 66:972–985.

DeSantis TZ, Hugenholtz P, Larsen N, Rojas M, Brodie EL, Keller K, Huber T, Dalevi D, Hu P, Andersen GL. 2006. Greengenes, a chimera-checked 16S rRNA gene database and workbench compatible with ARB. Applied and Environmental Microbiology. 72:5069–5072.

Duque-Alarcón A, Santiago-Vázquez LZ, Kerr RG. 2012. A microbial community analysis of the octocoral *Eunicea fusca*. Electronic Journal of Biotechnology. 15(5):1–9.

[EMP] Earth Microbiome Project. 2016. DNA extraction protocol. [updated 2016 Feb 16; accessed 2016 Apr 19]. http://www.earthmicrobiome.org/emp-standard-protocols/dna-extraction-protocol/.

Edgar RC. 2010. Search and clustering orders of magnitude faster than BLAST. Bioinformatics. 26:2460-2461.

Edwards U, Rogall T, Blocker H, Emde M, Bottger EC. 1989. Isolation and direct complete nucleotide determination of entire genes: characterization of a gene coding for 16S ribosomal RNA. Nucleic Acids Research. 17:7843–7853.

Frias-Lopez J, Zerkle AL, Bonheyo GT, Fouke BW. 2002. Partitioning of bacterial communities between seawater and healthy, black band diseased, and dead coral surfaces. Applied and Environmental Microbiology. 68:2214–2228.

Galkiewicz JP, Pratte ZA, Gray MA, Kellogg CA. 2011. Characterization of culturable bacteria isolated from the cold-water coral *Lophelia pertusa*. FEMS Microbiology Ecology. 77:333–346.

Galkiewicz JP, Stellick SH, Gray MA, Kellogg CA. 2012. Cultured fungal associates from the deep-sea coral *Lophelia pertusa*. Deep-Sea Research Part I–Oceanographic Research Papers. 67:12–20.

Gray MA, Stone RP, McLaughlin MR, Kellogg CA. 2011. Microbial consortia of gorgonian corals from the Aleutian islands. FEMS Microbiology Ecology. 76:109–120.

Hansson L, Agis M, Maier C, Weinbauer MG. 2009. Community composition of bacteria associated with cold-water coral *Madrepora oculata*: within and between colony variability. Marine Ecology Progress Series. 397:89–102.

Hecker B, Blechschmidt G. 1979. Final historical coral report for the canyon assessment study in the Mid- and North-Atlantic areas of the U.S. Outer Continental Shelf. Manuscript report prepared for U.S. Department of Interior, Bureau of Land Mangement. Palisades (NY): Lamont-Doherty Geological Observatory.

Hecker B, Blechschmidt G, Gibson P. 1980. Epifaunal zonation and community structure in three mid- and north Atlantic canyons. Final report for the canyon assessment study in the Mid-and North Atlantic Areas of the U.S. Outer Continental Shelf. Prepared for the U.S. Department of Interior, Bureau of Land Management under contract BLM AA5 51-CT8-49. Palisades (NY): Lamont-Doherty Geological Observatory.

Imhoff JF, Wiese J. 2014. The Order Kiloniellales. In: Rosenberg E, DeLong EF, Lory S, Stackebrandt E, Thompson CC, editors. The prokaryotes. Berlin (Germany): Springer. p. 301–306.

Jensen PR, Fenical W. 1995. The relative abundance and seawater requirements of Gram-positive bacteria in near-shore tropical marine samples. Microbial Ecology. 29:249–257.

Kellogg CA. 2008. Microbial ecology of *Lophelia pertusa* in the northern Gulf of Mexico. Reston (VA): U.S. Geological Survey. Open-File Report 2008-1148, OCS Study MMS 2008-015.

Kellogg CA. 2015. Cold-water coral microbiomes (*Paramuricea placomus*) from Baltimore Canyon: raw and processed data. U.S. Geological Survey data release. St. Petersburg (FL): U.S. Geological Survey. [updated 2016 Apr 16; accessed 2016 Jun 1]. http://dx.doi.org/10.5066/F7HQ3WZZ.

Kellogg CA, Lawler SN. 2015. Cold-water coral microbiomes (*Anthothela* spp.) from Baltimore and Norfolk Canyons: raw and processed data. U.S. Geologial Survey data release. St. Petersburg (FL): U.S. Geological Survey. [updated 2016 Apr 21; accessed 2016 Jun 1]. http://dx.doi.org/10.5066/F7CZ356K.

Kellogg CA, Goldsmith DB. 2017. Cold-water coral microbiomes (*Primnoa* spp.) from Gulf of Alaska, Baltimore Canyon, and Norfolk Canyon: raw data: U.S. Geological Survey data release. St. Petersburg (FL): U.S. Geological Survey. [updated 2017 Jan 12; accessed 2017 Aug 9]. http://dx.doi.org/10.5066/F7P55KMJ.

Kellogg CA, Lisle JT, Galkiewicz JP. 2009. Culture-independent characterization of bacterial communities associated with the cold-water coral *Lophelia pertusa* in the northeastern Gulf of Mexico. Applied and Environmental Microbiology. 75:2294–2303.

Kellogg CA, Ross SW, Brooke SD. 2016. Bacterial community diversity of the deep-sea octocoral *Paramuricea placomus*. PeerJ. 4:e2529.

Kellogg CA, Goldsmith DB, Gray MA. 2017. Biogeographic comparison of *Lophelia*-associated bacterial communities in the western Atlantic reveals conserved core microbiome. Frontiers in Microbiology. 8:796.

Kimes NE, Van Nostrand JD, Weil E, Zhou J, Morris PJ. 2010. Microbial functional structure of *Montastraea faveolata*, an important Caribbean reef-building coral, differs between healthy and yellow-band diseased colonies. Environmental Microbiology. 12:541–556.

Kunin V, Engelbrektson A, Ochman H, Hugenholtz P. 2010. Wrinkles in the rare biosphere: pyrosequencing errors can lead to artificial inflation of diversity estimates. Environmental Microbiology. 12:118–123.

Kurahashi M, Yokota A. 2007. *Endozoicomonas elysicola* gen. nov., sp. nov., a ɣ-proteobacterium isolated from the sea slug *Elysia ornata* Systematic and Applied Microbiology. 30:202–206.

Kvennefors ECE, Sampayo E, Ridgway T, Barnes AC, Hoegh-Guldberg O. 2010. Bacterial communities of two ubiquitous Great Barrier Reef corals reveals both site- and species-specificity of common bacterial associates. PLoS ONE. 5:e10401.

La Rivière M, Roumagnac M, Garrabou J, Bally M. 2013. Transient shifts in bacterial communities associated with the temperate gorgonian *Paramuricea clavata* in the northwestern Mediterranean Sea. PLoS ONE. 8:e57385.

La Rivière M, Garrabou J, Bally M. 2015. Evidence for host specificity among dominant bacterial symbionts in temperate gorgonian corals. Coral Reefs. 34:1087–1098.

Lawler, SN, Kellogg CA, France SC, Clostio RW, Brooke SD, Ross, SW. 2016. Coral-associated bacterial diversity is conserved across two deep-sea *Anthothela* species. Frontiers in Microbiology. 7:458.

Lesser MP, Mazel CH, Gorbunov MY, Falkowski PG. 2004. Discovery of symbiotic nitrogen-fixing cyanobacteria in corals. Science. 305:997–1000.

Lesser MP, Falcón LI, Rodríguez-Román A, Enríquez S, Hoegh-Guldberg O, Iglesias-Prieto R. 2007. Nitrogen fixation by symbiotic cyanobacteria provides a source of nitrogen for the scleractinian coral *Montastraea cavernosa*. Marine Ecology Progress Series. 346:143–152.

Lilburn TG, Kim KS, Ostrom NE, Byzek KR, Leadbetter JR, Breznak JA. 2001. Nitrogen fixation by symbiotic and free-living Spirochetes. Science. 292:2495–2498.

Lozupone C, Knight R. 2005. UniFrac: a new phylogenetic method for comparing microbial communities. Applied and Environmental Microbiology. 71:8228–8235.

Marchesi JR, Sato T, Weightman AJ, Martin TA, Fry JC, Hiom SJ, Wade WG. 1998. Design and evaluation of useful bacterium-specific PCR primers that amplify genes coding for bacterial 16S rRNA. Applied and Environmental Microbiology. 64:795–799.

Meistertzheim A-L, Lartaud F, Arnaud-Haond S, Kalenitchenko D, Bessalam M, Le Bris N, Galand PE. 2016. Patterns of bacteria-host associations suggest different ecological strategies between two reef building cold-water coral species. Deep-Sea Research Part I-Oceanographic Research Papers. 114:12–22.

Moore KM, Alderslade P, Miller KJ. 2017. A taxonomic revision of *Anthothela* (Octocorallia: Scleraxonia: Anthothelidae) and related genera, with the addition of new taxa, using morphological and molecular data. Zootaxa. [accessed 2017 Aug 21]. http://dx.doi.org/10.11646/zootaxa.4304.1.1

Morrow KM, Moss AG, Chadwick NE, Liles MR. 2012. Bacterial associates of two Caribbean coral species reveal species-specific distribution and geographic variability. Applied and Environmental Microbiology. 78:6438–6449.

Mouchka ME, Hewson I, Harvell CD. 2010. Coral-associated bacterial assemblages: current knowledge and the potential for climate-driven impacts. Integrative and Comparative Biology. 50:662–674.

Neulinger SC, Järnegren J, Ludvigsen M, Lochte K, Dullo W-C. 2008. Phenotype-specific bacterial communities in the cold-water coral *Lophelia pertusa* (Scleractinia) and their implications for the coral's nutrition, health, and distribution. Applied and Environmental Microbiology. 74:7272–7285.

Neulinger SC, Gärtner A, Järnegren J, Ludvigsen M, Lochte K, Dullo W-C. 2009. Tissue-associated "*Candidatus* Mycoplasma corallicola" and filamentous bacteria on the cold-water coral *Lophelia pertusa* (Scleractinia). Applied and Environmental Microbiology. 75:1437–1444.

Pantos O, Cooney RP, Le Tissier MDA, Barer MR, O'Donnell AG, Bythell JC. 2003. The bacterial ecology of a plague-like disease affecting the Caribbean coral *Montastrea annularis*. Environmental Microbiology. 5:370–382.

Penn K, Wu D, Eisen JA, Ward N. 2006. Characterization of bacterial communities associated with deep-sea corals on Gulf of Alaska seamounts. Applied and Environmental Microbiology. 72:1680-1683.

Pernice M, Meibom A, Van Den Heuvel A, Kopp C, Domart-Coulon I, Hoegh-Guldberg O, Dove S. 2012. A single-cell view of ammonium assimilation in coral-dinoflagellate symbiosis. The ISME Journal. 6:1314–1324.

Quince C, Lanzén A, Curtis TP, Davenport RJ, Hall N, Head IM, Read LF, Sloan WT. 2009. Accurate determination of microbial diversity from 454 pyrosequencing data. Nature Methods. 6:639–641.

Raina J-B, Tapiolas D, Willis BL, Bourne DG. 2009. Coral-associated bacteria and their role in the biogeochemical cycling of sulfur. Applied and Environmental Microbiology. 75:3492–3501.

Rideout JR, He Y, Navas-Molina JA, Walters WA, Ursell LK, Gibbons SM, Chase J, McDonald D, Gonzalez A, Robbins-Pianka A, Clemente JC, Gilbert JA, Huse SM, Zhou HW, Knight R, Caporaso JG. 2014. Subsampled open-reference clustering creates consistent, comprehensive OTU definitions and scales to billions of sequences. PeerJ. 2: e545.

Ritchie KB. 2006. Regulation of microbial populations by coral surface mucus and mucus-associated bacteria. Marine Ecology Progress Series. 322:1–14.

Rohwer F, Breitbart M, Jara J, Azam F, Knowlton N. 2001. Diversity of bacteria associated with the Caribbean coral *Montastraea franksi*. Coral Reefs. 20:85–91.

Rohwer F, Seguritan V, Azam F, Knowlton N. 2002. Diversity and distribution of coral-associated bacteria. Marine Ecology Progress Series. 243:1–10.

Schöttner S, Hoffmann F, Wild C, Rapp HT, Boetius A, Ramette A. 2009. Inter- and intra-habitat bacterial diversity associated with cold-water corals. The ISME Journal. 3:756–759.

Schöttner S, Wild C, Hoffmann F, Boetius A, Ramette A. 2012. Spatial scales of bacterial diversity in cold-water coral reef ecosystems. PLoS ONE. 7:e32093.

Shade A, Handelsman J. 2012. Beyond the Venn diagram: the hunt for a core microbiome. Environmental Microbiology. 14:4–12.

Shannon C. 1948. A mathematical theory of communication. Bell System Technical Journal. 27:379–423.

Shashar N, Cohen Y, Loya Y, Sar N. 1994. Nitrogen fixation (acetylene reduction) in stony corals: evidence for coral-bacteria interactions. Marine Ecology Progress Series. 111:259–264.

Shore-Maggio A, Runyun CM, Ushijima B, Aeby GS, Callahan SM. 2015. Differences in bacterial community structure in two color morphs of the Hawaiian reef coral, *Montipora capitata*. Applied and Environmental Microbiology. 81:7312–7318.

Simpson E. 1949. Measurement of diversity. Nature. 163:688.

Stackebrandt E, Liesack W. 1993. Nucleic acids and classification. In: Goodfellow M, O'Donnell AG, editors. Handbook of new bacterial systematics. London (UK): Academic Press. p. 152–189.

Sunagawa S, DeSantis TZ, Piceno YM, Brodie EL, DeSalvo MK, Voolstra CR, Weil E, Andersen GL, Medina M. 2009. Bacterial diversity and white plague disease-associated community changes in the Caribbean coral *Montastraea faveolata*. The ISME Journal. 3:512–521.

Sunagawa S, Woodley CM, Medina M. 2010. Threatened corals provide underexplored microbial habitats. PLoS ONE. 5: e9554.

Taylor MW, Schupp PJ, de Nys R, Kjelleberg S, Steinberg PD. 2005. Biogeography of bacteria associated with the marine sponge *Cymbastela concentrica*. Environmental Microbiology. 7:419–433.

Thompson JR, Rivera HE, Closek CJ, Medina M. 2015. Microbes in the coral holobiont: partners through evolution, development, and ecological interactions. Frontiers in Cellular and Infection Microbiology. 4:1–20.

Tiedje JM. 1988. Ecology of denitrification and dissimilatory nitrate reduction to ammonium. Biology of Anaerobic Microorganisms. 717:179–244.

van Bleijswijk JDL, Whalen C, Duineveld GCA, Lavaleye MSS, Witte HJ, Mienis F. 2015. Microbial assemblages on a cold-water coral mound at the SE Rockall Bank (NE Atlantic): interactions with hydrography and topography. Biogeosciences Discussions. 12:1509–1542.

van de Water JAJM, Melkonian R, Junca H, Voolstra CR, Reynaud S, Allemand D, Ferrier-Pagès C. 2016. Spirochaetes dominate the microbial community associated with the red coral *Corallium rubrum* on a broad geographic scale. Scientific Reports. 6:27277.

Vezzulli L, Pezzati E, Huete-Stauffer C, Pruzzo C, Cerrano C. 2013. 16SrDNA pyrosequencing of the Mediterranean gorgonian *Paramuricea clavata* reveals a link among alterations in bacterial holobiont members, anthropogenic influence and disease outbreaks. PLoS ONE. 8:e67745.

Wegley L, Edwards R, Rodriguez-Brito B, Liu H, Rohwer F. 2007. Metagenomic analysis of the microbial community associated with the coral *Porites astreoides*. Environmental Microbiology. 9:2707–2719.

Wieczorek SK, Todd CD. 1998. Inhibition and facilitation of settlement of epifaunal marine invertebrate larvae by microbial biofilm cues. Biofouling. 12:81–118.

Yakimov MM, Cappello S, Crisafi E, Trusi A, Savini A, Corselli C, Scarfi S, Giuliano L. 2006. Phylogenetic survey of metabolically active microbial communities associated with the deep-sea coral *Lophelia pertusa* from the Apulian plateau, Central Mediterranean Sea. Deep-Sea Research Part I. 53(1):62–75.

Zhang X-Y, He F, Wang G-H, Bao J, Xu X-Y, Qi S-H. 2013. Diversity and antibacterial activity of culturable actinobacteria isolated from five species of the South China Sea gorgonian corals. World Journal of Microbiology and Biotechnology. 29(6):1107–16.

This page intentionally left blank

CHAPTER 13. CORAL TAXONOMY AND CONNECTIVITY

Rachel W. Clostio and Scott C. France

13.1 INTRODUCTION

The distribution of deepsea corals is not well known along the slope of the northeastern United States (Hecker et al. 1980, Watling and Auster 2005, Packer et al. 2007). There have been even fewer studies directly targeting deepsea corals in canyons of the Mid-Atlantic Bight (MAB) (Hecker et al. 1980, 1983, Quattrini et al. 2015). Available information indicates that the MAB canyons are dominated by octocorals (Alcyonacea), solitary stony corals (Scleractinia), and anemones (Actiniaria) (Cairns 1981, Packer et al. 2007) rather than the large concentrations of reef-forming stony corals (*Lophelia pertusa, Enallopsammia profunda*) that dominate the southeastern United States and Gulf of Mexico (Brooke and Schroeder 2007, Ross and Nizinski 2007, Brooke and Ross 2014). Deepsea coral data for the northeastern United States show that a higher diversity of these corals have beenss found along the slope, particularly in canyons (Hecker et al. 1980), with a lower diversity along the continental shelf and abyssal plain (Packer et al. 2007).

Submarine canyons represent areas with enhanced currents, high organic input, and exposed hard substrates (steep walls, emergent hard bottom, talus fields). Because these conditions are important for many species of deepsea corals, the canyon environment is expected to support more diverse coral communities than the noncanyon slope. These rough bottoms are typically avoided when trawling and images from camera sled tows and submersible dives provide most of the information on species occurrences, distribution of habitat type, and associated faunal assemblages in the MAB canyons. However, it is notoriously difficult to accurately identify octocorals from image data alone (Quattrini et al. 2015). Most of what is known about deepsea corals in Norfolk and Baltimore canyons is from ALVIN submersible dives conducted in 1978 (Norfolk), *Johnson Sea-Link* submersible dives in Baltimore and Norfolk canyons in 1981 (Hecker et al. 1983), and photographs from camera sled tows conducted in 1980 (Norfolk and Baltimore, Hecker et al. 1980). Previous studies off the northeastern United States have found that some octocoral species such as *Acanthogorgia armata* and *Anthothela grandiflora* are closely associated with hard substrates often found along canyon walls. Octocoral species such as the sea pen *Pennatula* sp. and the bamboo coral *Acanella arbuscula* have adapted to anchor in soft sediments and are associated with the soft bottom of the slope. Other species, such as *Paragorgia arborea, Primnoa resedaeformis*, and *Paramuricea* sp., can be found in both canyons and on the slope. Some studies have found few differences in species composition between canyons and the adjacent slope areas (Haedrich et al. 1975). However, Hecker et al. (1980) found that corals were both denser and more diverse within most canyons compared with the nearby slope habitats. During these studies, species identification was often limited by the quality of images and cryptic morphology, which makes it likely that our current understanding of species associated with canyons is inaccurate. To date, it has not been possible to examine population connectivity between canyons and the adjacent slope, or among canyons, because adequate samples have been lacking.

Some deepsea features (e.g., seamounts) may support a high number of endemic species or genetically isolated populations where genetic isolation is maintained by hydrographic phenomena, distance from suitable habitats, or by life history strategies (Shank 2010). Given their close proximity to each other, the active hydrography of the MAB slope, and the abundance of broadcast-spawning taxa, high levels of endemism or population isolation are not expected in the MAB canyons. Even within canyons, deepsea corals have a naturally patchy distribution due to larval supply, recruitment, and post-settlement survival. These patches are typically composed of closely related colonies (Costantini et al. 2007, Mokhtar-Jamaï et al. 2013). This local-patchiness could result from recruitment of larvae from

distinct parental colonies or clonal propagation from a local source (Liu et al. 2005). Identification of the mode of origin of dense stands of deepsea corals within canyons is critical to conservation management.

The Atlantic Deepwater Canyons Study is one of the first in the MAB area that included identification of species based on images, collection of specimens for morphological identification, and the sequencing of barcoding genes (*mtMutS, cox1*) for genetic identification. Following identification, current genetic tools provide the opportunity to examine connectivity between canyon and slope habitats and measure individual relatedness within patches. Therefore, the following hypotheses will be addressed:

1. that species richness of MAB submarine canyons does not differ from open slope communities at similar depths;
2. that populations of octocoral species found in the canyons and the open continental slope are not genetically isolated, and
3. that isolated patches of octocorals are the result of local recruitment versus clonal propagation.

13.2 METHODS

13.2.1 Octocorals

13.2.1.1 Sampling

Specimens were collected either by remotely operated vehicles (ROVs) (*Kraken 2* during the 2012 sampling cruise and *Jason II* during the 2013 sampling cruise) or otter trawl. *In situ* images were taken of all samples collected by ROV. Fragments from all specimens to be used in genetic analyses were stored on board the ship in 5 mL vials, 15 mL Falcon tubes, 50 mL Falcon tubes, or Whirl-Pak bags (Nasco, Fort Atkinson, Wisconson) and preserved with 95% ethanol. See **Chapter 3** for additional sampling details.

Additional specimens of the genus *Paramuricea*, collected from octocoral gardens in the deep Gulf of Maine (Auster et al. 2013), approximately 770 km north of Baltimore Canyon, were included in the analyses as comparative material. These specimens were collected in 2003 and 2013 aboard the R/V *Connecticut* and the F/V *Langley*, respectively.

13.2.1.2 Taxonomic Identification

Specimens were identified to the lowest taxonomic level possible by S.C. France using primary taxonomic literature and starting from genus-level keys provided in Bayer (1981) and Williams (1995).

13.2.1.3 DNA Extraction

Total genomic DNA was extracted from Octocorallia species using either a single-chloroform-only extraction method (Berntson et al. 2001, France 2007) or the Eppendorf EpMotion 5075 (Eppendorf, Hamburg, Germany) and the Macherey-Nagel NucleoSpin 96 Tissue Kit (Macherey-Nagel Inc., U.S.). DNA was then quantified for all samples using the NanoDrop Lite Spectrophotometer (Thermo Scientific, U.S.). Samples used for genomics were also quantified using the VersaFluor fluorometer (Bio-Rad, U.S.).

13.2.1.4 Amplification and Sequencing of Gene Regions

To identify octocorals using genetic barcodes, the mismatch repair gene homolog (*mtMutS*) was amplified using polymerase chain reaction (PCR) for all specimens collected by ROVs and at least two specimens of each species collected by trawl. Because various mitochondrial gene arrangements are known among octocorals (e.g., Brockman and McFadden 2012), primer combinations varied by species (**Table 13-1**). Additionally, *cox1*, which typically shows lower diversity than *mtMutS* for octocorals

(McFadden et al. 2011), was amplified for a subset of each species to further confirm species identifications (**Table 13-1**).

Table 13-1. Primer combinations used to amplify msh1 and IGR+cox1 region for each species, including the original primer reference.

Forward Primer	Reverse Primer	Genus	Reference
msh1			
ND42599f	MUT3458r	*Paramuricea, Anthothela, Acanthogorgia*	France and Hoover 2002, Sánchez et al. 2003
ND42599f	MutChry3458R	*Primnoa*, Pennatulacea (order)	France and Hoover 2002, Pante et al. 2012
CO3Bam5657f	MUT3458r	*Acanella, Keratoisis*	Brugler and France 2008, Sánchez et al. 2003
cytb1279f	MUT3458r	*Paragorgia*	Thoma 2013, Sánchez et al. 2003
IGR + cox1			
ND6P5371R	CO1LA8363r	*Paragorgia, Acanella, Keratoisis*	Thoma 2013, Brugler and France 2008
COII8068xF	COIoctR	*Primnoa*, Pennatulacea (order)	McFadden et al. 2011, France and Hoover 2002
COII8068xF	COI8492	*Paramuricea, Anthothela, Acanthogorgia*	McFadden et al. 2011, Smith et al. 2004

PCR amplifications used GoTaq polymerase (Promega) and included 5 µL of 5X GoTaq Green buffer, 2 mM $MgCl_2$, 0.4 µM dNTPs mix, 0.24 µM of each primer, 5 µg of bovine serum albumin (BSA, Sigma), and 1 U of GoTaq polymerase. The PCR conditions for *mtMutS* were as follows: 95 °C for 2 min, 35 cycles of 95 °C for 20 s, 50 °C for 30 s, 72 °C for 50 s, and a final step of 72 °C for 5 min. The PCR conditions for *cox1* were 94 °C for 3 min, 30 cycles of 94 °C for 20 s, 46 °C for 30 s, 72 °C for 60 s, and a final step of 72 °C for 2 min for all species except *Paragorgia*, which required an annealing temperature of 55 °C.

All amplified products were sent to Beckman Coulter Genomics (Beckman Coulter, Inc., Maryland) for Sanger sequencing. Sequence traces were edited at University of Louisiana at Lafayette using Sequencher version 4.6 (Gene Codes Corp., U.S.). Each sequence was then queried against the the National Center for Biotechnology Information (NCBI) GenBank nucleotide database (Benson et al. 2013) using the BLASTn algorithm (NCBI). For Pennatulacea specimens, additional sequences were acquired from GenBank and alignments of DNA sequences were accomplished using Clustal W (Thompson et al. 1994) in the program BioEdit (Hall 1999). Aligned sequence datasets were then analyzed using the maximum likelihood method in RAxML 7.2.8 through the CIPRES web portal (Stamatakis et al. 2008).

13.2.1.5 Restriction-Site Associated DNA (RAD)

Single nucleotide polymorphisms (SNPs) were isolated and used to examine genetic diversity of octocorals from Baltimore and Norfolk canyons. Genomic DNA from colonies of *Paragorgia arborea*, *Primnoa resedaeformis*, and *Anthothela grandiflora* collected from both canyons were sent to Georgia Genomics Facility (University of Georgia, Athens, Georgia) to generate restriction-site associated DNA (RAD) sequences using a modified version of double digest RAD protocol (Peterson et al. 2012, Graham et al. 2015). Genomic DNA from *Paramuricea placomus* specimens collected from Baltimore Canyon for clonality studies were prepared the same way, as well as additional *P. placomus* samples from the Gulf of Maine for comparison.

Genomic DNA for each individual was double digested with two restriction enzymes (*XbaI* and *EcoR1*). Adapters with individual barcodes were then ligated to the ends of restriction fragments and fragments 500bp to 600bp were isolated. PCR was then used to amplify only fragments containing

restriction cut sites at the ends. Fragments were then paired-end sequenced on an Illumina MiSeq, HiSeq or NextGen using either PE75 (*Paramuricea*) or PE150 chemistry (Illumina, Inc., U.S.).

Raw sequence reads were processed *de novo* using STACKS 1.17 (Catchen et al. 2011). CutAdapt (Martin 2011) was used to remove contaminating i7 and i5 adapter sequences. The process radtags program from the STACKS pipeline (Hohenlohe et al. 2013) was used to discard reads with a Phred quality score below 10 or reads missing the restriction cut site. All remaining reads were then trimmed to the same length. Only the forward reads (R1) were subsequently analyzed by individual in ustacks to avoid any possible linkage with SNPs obtained from corresponding R2 reads. The bounded model was used with an error rate range of 0 to 0.15, as recommended by previous studies (Catchen et al. 2013, Hohenlohe et al. 2010). An exploratory analysis of the RAD data was conducted by varying the STACKS parameters *–m* (2, 4, 6) in ustacks and *–n* (1, 3) in cstacks as suggested by Mastretta-Yanes et al. (2015). The final optimum set of parameters minimized missing data, reduced the possibility of SNP error, and minimized the genetic dissimilarity among individuals sampled from the same site.

13.2.1.6 Analysis of Population Structure and Clonality

GENEPOP 4.3 (Raymond and Rousset 1995) was used to detect deviations from Hardy-Weinberg equilibrium (HWE) and linkage disequilibrium (LD) among pairs of loci. GenAlEx 6.5 (Peakall and Smouse 2012) was used to calculate F_{ST} between sampling sites with 9,999 permutations of the data. BAYESCAN 2.1 (Foll and Gaggiotti 2008) was used to identify loci that might be under selection.

The program STRUCTURE v2.3.4 (Pritchard et al. 2000) was used to assign individuals to population clusters, employing the correlated allele frequency and the admixture ancestry models. Values of K from 1 to 5 were considered and the optimum K value was determined by the highest mean likelihood value using the STRUCTURE HARVESTER webserver (Earl and von-Holdt 2012). For each value of K, 20 independent analyses were run for 100,000 generations after a burn-in of 50,000 MCMC generations. To determine cluster membership coefficients, the program CLUMPP (Jakobsson and Rosenberg 2007) was used to permute across all 20 runs of the optimal K value using the GREEDY algorithm. Final results were displayed using Distruct 1.1 (Rosenberg 2004).

The R packages Adegenet (Jombart 2008) and Poppr (Kamvar et al. 2014) were used to conduct principal component analyses (PCA) and examine multilocus genotypes for clonality, respectively. For PCA analyses, missing data were replaced by the mean allele frequencies of the entire data set. Adegenet was also used to calculate the proportion of shared alleles among *Paramuricea* colonies sampled from Baltimore Canyon.

13.2.2 Other Species

13.2.2.1 Amplification and Sequencing of Gene Regions

In addition to octocorals, DNA from specimens of the subclass Hexacorallia (order Zoantharia, $n = 13$; Actiniaria, $n = 15$; Antipatharia, $n = 2$) was also extracted using the aforementioned protocols. A nuclear internal transcribed spacer (ITS) region was amplified and sequenced for Zoantharia following the protocol of Swain (2010). For Actiniaria (sea anemones), the ribosomal ITS1-*5.8S*-ITS2 region was amplified and sequenced using the primers 18SUniv.fw and 28SAct.rev, as described in the methods of Stoletzki and Schierwater (2005). Two antipatharian (black corals) specimens were amplified and sequenced at three gene regions (*trnW, cox3-cox1, nad5-nad1*) using previously published primers (Thoma et al. 2009). All sequencing was carried out as previously described for Octocorallia specimens.

13.2.2.2 Taxonomic Identification

All generated zoanthid sequences were sent to T. Swain (Northwestern University, Evanston, Illinois) and all actiniarian sequences were sent to M. Daly (Ohio State University, Columbus, Ohio) for

comparison to their research databases of sequences from these taxa. In addition, images of sea anemones collected by ROV were sent to D. Fautin (University of Kansas, Lawrence, Kansas) for review. Antipatharian sequences were compared with the NCBI GenBank nucleotide database using BLASTn.

13.3 RESULTS

13.3.1 Octocorals

13.3.1.1 Species Diversity

A total of 523 colonies belonging to the subclass Octocorallia Haeckel, 1866, were sampled during the 2012 and 2013 cruises. The majority of these samples were collected within the canyons by an ROV (373), with the remaining samples (150) collected using otter trawls. A total of 225 samples (164 ROV, 61 trawl) were collected on the 2012 sampling cruise using the *Kraken 2* ROV (University of Connecticut), and another 298 samples (209 ROV, 89 trawl) were collected during the 2013 sampling cruise using the ROV *Jason II* (WHOI). Octocorals sampled within the canyons were collected between 321 m to 1,362 m (**Figure 13-1**). Trawl samples were collected at depths ranging from 388 to 1,712 m.

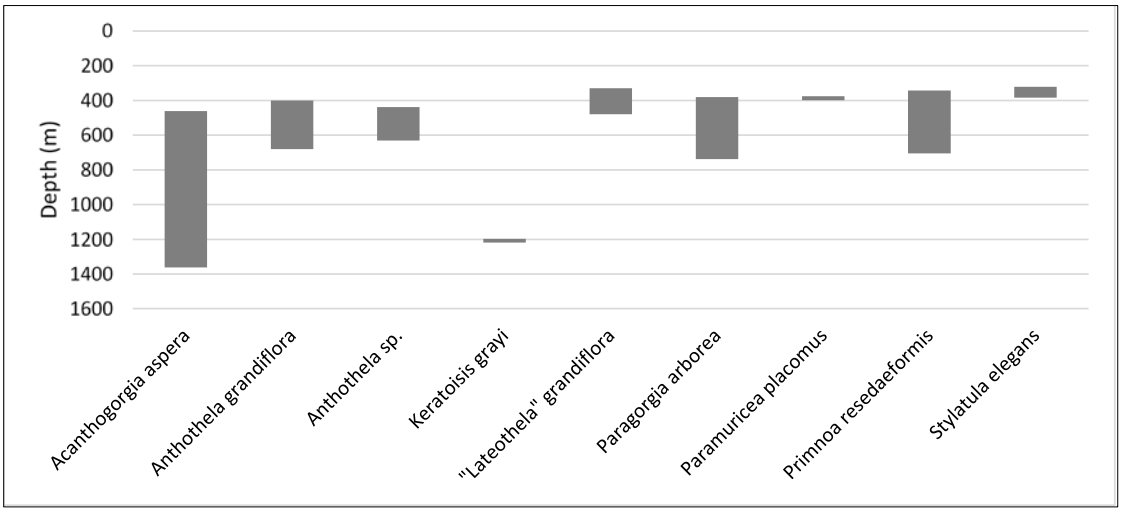

Figure 13-1. The collection depth (m) for all octocoral species sampled by ROV during 2012 and 2013 cruises.

Among the samples collected were 14 genera from 12 families of Octocorallia (Acanthogorgiidae Gray, 1859: *Acanthogorgia* Gray, 1857; Anthothelidae Broch, 1916: *Anthothela* Verrill, 1879, *Lateothela* Moore et al. 2017; Paragorgiidae Kükenthal, 1916: *Paragorgia* Milne Edwards, 1857; Primnoidae Milne Edwards, 1857: *Primnoa* Lamouroux, 1812; Plexauridae Gray, 1859: *Paramuricea* Kölliker, 1865; Isididae Lamouroux, 1812: *Acanella* Gray, 1870, *Keratoisis* Wright, 1869; Pennatulidae Ehrenberg, 1834: *Pennatula* Linnaeus, 1758; Virgulariidae Verrill, 1868: *Stylatula* Verrill, 1864; Anthoptilidae Kölliker, 1880: *Anthoptilum* Kölliker, 1880; Funiculinidae Gray, 1870: *Funiculina* Lamarck, 1816; Umbellulidae Kölliker, 1880: *Umbellula* Gray, 1870; Nephtheidae Gray, 1862: *Duva* Koren and Danielsseen, 1883). The dominant ocotocoral species collected within the canyons were *Paragorgia arborea* (Linnaeus 1758) and *Primnoa resedaeformis* (Gunnerus 1763). The species *Pennatula aculeata* (Danielssen 1860) and *Acanella arbuscula* (Johnson 1862) were the most numerous octocorals collected from the slope adjacent to Norfolk Canyon (**Table 13-2**).

Table 13-2. Octocorals collected by ROV dives during the 2012 and 2013 sampling cruises in Baltimore and Norfolk canyons.

Taxa	Species	Baltimore Canyon	Norfolk Canyon
Order Alcyonacea			
Suborder Alcyoniidea			
Nephtheidae	*Duva florida* (Rathke 1806)		X
Suborder Scleraxonia			
Paragorgiidae	*Paragorgia arborea (*Linné 1758)	X	X
Anthothelidae	*Anthothela grandiflora (*Sars 1856)	X	X
	Anthothela sp.	X	X
	Lateothela grandiflora (Tixier-Durivault and d'Hondt 1974)	X	X
Suborder Calcaxonia			
Primnoidae	*Primnoa resedaeformis* (Gunnerus 1763)	X	X
Isididae	*Keratoisis grayi* (Wright 1869)		X
	Acanella arbuscula (Johnson 1862)		
Suborder Holaxonia			
Plexauridae	*Paramuricea placomus* (Linné 1758)	X	
Acanthogorgiidae	*Acanthogorgia aspera* (Pourtalés 1867)		X
Order Pennatulacea			
Suborder Sessiliflorae			
Anthoptilidae	*Anthoptilum grandiflorum* (Verrill 1897)		
Funiculinidae	*Funiculina quadrangularis* (Pallas 1766)		
Umbellulidae	*Umbellula cf. lindahli* Kölliker 1875		
Suborder Subsessiliflorae			
Pennatulidae	*Pennatula aculeata* Danielssen 1860		
Virgulariidae	*Stylatula elegans* (Danielssen 1860)	X	

In Baltimore Canyon, 151 colonies were collected over the course of 20 ROV dives with a total of 4,469 min of bottom time (**Table 13-3**). The depth of collections ranged from 321 to 681 m. The most frequently collected species in Baltimore Canyon were *Paragorgia arborea* and *Primnoa resedaeformis*. Other species collected included *Paramuricea placomus*, *Anthothela grandiflora, Anthothela* sp., *Lateothela grandiflora*, and *Stylatula elegans*. *Paramuricea placomus* were collected only from Baltimore Canyon.

A total of 222 colonies were sampled from Norfolk Canyon over 13 ROV dives, for a total dive time of 8,599 min (**Table 13-3**). The depth range of collections was from 382 to 1,362 m. As in Baltimore Canyon, *Paragorgia arborea* and *Primnoa resedaeformis* were the most frequently collected octocorals. Other octocorals collected in Norfolk Canyon included *Anthothela grandiflora, Anthothela* sp., *Lateothela grandiflora*, *Acanthogorgia aspera*, *Keratoisis grayi*, *Stylatula elegans,* and a true soft coral *Duva florida* (previously *Capnella florida* Rathke, 1806 and *Gersemia florida* Rathke, 1806). *Keratoisis grayi* were sampled only in Norfolk Canyon, and from deeper than 1,200 m, a depth range not sampled by ROV in Baltimore Canyon. *Paramuricea* was not collected from Norfolk Canyon during the cruises but was observed later while studying ROV video (**Chapter 8**, **Section 8.3.2.1.1**). Octocorals also were collected from six trawl tows conducted in and adjacent to Norfolk Canyon at depths ranging from 388 to 1,712 m (**Table 13-4**). The most numerous species of octocoral collected from the slope were *Acanella* spp., followed by *Pennatula aculeata*. Two species of *Acanella* were collected, *A. arbuscula* and *A. scarletae* (Heestand Saucier et al. 2017). The latter is a new species described from these collections and is so far known only from Norfolk Canyon. Other species collected only from trawls included the sea pens *Umbellula cf. lindahli, Funiculina quadrangularis*, and *Anthoptilum cf. grandiflorum.*

Table 13-3. Number of each octocoral species collected by ROV dives during the 2012 and 2013 sampling cruises.

Dive	Canyon	*Acanthogorgia*	*Anthothela*	*Lateothela*	*Paragorgia*	*Paramuricea*	*Primnoa*	*Stylatula*	*Keratoisis*	*Duva*
ROV-2012-NF-01	Baltimore	–	1	–	12	–	2	–	–	–
ROV-2012-NF-02	Baltimore	–	–	2	5	–	1	–	–	–
ROV-2012-NF-03	Baltimore	–	–	–	–	–	–	–	–	–
ROV-2012-NF-04	Baltimore	–	–	–	–	–	–	–	–	–
ROV-2012-NF-05	Baltimore	–	1	–	6	–	2	–	–	–
ROV-2012-NF-06	Baltimore	–	–	–	4	–	3	–	–	–
ROV-2012-NF-07	Baltimore	–	–	–	2	–	–	–	–	–
ROV-2012-NF-08	Baltimore	–	–	–	1	–	–	–	–	–
ROV-2012-NF-09	Baltimore	–	1	–	9	5	6	–	–	–
ROV-2012-NF-10	Baltimore	–	–	–	5	–	6	–	–	–
ROV-2012-NF-11	Baltimore	–	–	–	–	–	–	–	–	–
ROV-2012-NF-12	Norfolk	2	–	–	2	–	5	–	–	–
ROV-2012-NF-13	Baltimore	–	3	1	5	–	5	–	–	–
ROV-2012-NF-14	Baltimore	–	–	–	2	–	–	–	–	–
ROV-2012-NF-15	Baltimore	–	2	–	6	–	5	–	–	–
ROV-2012-NF-16	Baltimore	–	1	2	1	–	3	–	–	–
ROV-2012-NF-17	Baltimore	–	3	–	1	–	–	–	–	–
ROV-2012-NF-18	Baltimore	–	5	–	4	–	–	–	–	–
ROV-2012-NF-19	Baltimore	–	–	–	–	16	–	–	–	–
ROV-2012-NF-20	Norfolk	1	2	–	6	–	3	–	–	–
ROV-2012-NF-25	Norfolk	1	–	–	–	–	–	–	–	–
ROV-2013-RB-679	Norfolk	–	–	–	1	–	–	–	–	–
ROV-2013-RB-680	Norfolk	6	3	–	8	–	4	–	–	–
ROV-2013-RB-681	Norfolk	10	2	–	12	–	7	–	–	–
ROV-2013-RB-682	Norfolk	–	–	–	–	–	–	–	–	–
ROV-2013-RB-683	Norfolk	–	–	–	–	–	–	–	–	–
ROV-2013-RB-684	Norfolk	–	3	1	12	–	16	–	–	–
ROV-2013-RB-685	Norfolk	15	–	–	–	–	–	–	2	
ROV-2013-RB-686	Norfolk	1	12	1	8	–	7	–	–	–
ROV-2013-RB-687	Norfolk	7	24	2	12	–	4	–	–	–
ROV-2013-RB-688	Norfolk	–	–	–	–	–	–	–	–	–
ROV-2013-RB-689	Baltimore	–	–	–	–	–	–	–	–	–
ROV-2013-RB-690	Baltimore	–	–	–	–	–	3	6	–	–
ROV-2013-RB-691	Norfolk	–	–	–	6	–	7	1	–	6
	Total	43	63	9	130	21	89	9	2	6

Table 13-4. Number of genetic samples obtained from octocoral species collected by otter trawls during the 2012 and 2013 sampling cruises.

Trawl	Canyon	*Acanella arbuscula*	*Acanella scarletae*	*Anthoptilum*	*Funiculina*	*Paragorgia*	*Pennatula*	*Primnoa*	*Umbellula*
NF-2012-167*	Norfolk	–	–	–	–	5	–	2	–
NF-2012-176*	Norfolk	–	–	–	–	1	11	–	–
NF-2012-179	Norfolk	–	–	–	–	–	1	3	–
NF-2012-188	Norfolk	–	–	–	–	–	38	–	–
RB-13-001	Norfolk	–	–	–	–	–	14	–	–
RB-13-028	Norfolk	3	1	2	–	–	–	–	4
RB-13-029	Norfolk	–	–	–	–	–	–	–	1
RB-13-030	Norfolk	22	20	1	1	–	–	–	2
RB-13-032	Norfolk	3	1	–	1	–	–	–	–
RB-13-033	Norfolk	–	1	2	–	–	–	–	–
	Total	28	23	5	2	6	64	5	7

* Located within Norfolk Canyon.

Three species of *Anthothela* were discovered that each had distinct *mtMutS* and *cox1* sequences. *Anthothela grandiflora* was the most commonly collected Anthothelidae in both canyons (*n* = 15 Baltimore, *n* = 23 Norfolk). Another species of *Anthothela* was also found in both canyons (*n* = 2 Baltimore, *n* = 22 Norfolk). This undescribed species differed from *A. grandiflora* by only a single base pair at *mtMutS* and at *cox1*. Colonies of *Anthothela* with this same sequence haplotype have also been found off the western coast of Australia. A third species, identified while at sea as belonging to *Anthothela*, turned out to belong to the newly described genus *Lateothela grandiflora*, which differs from *A. grandiflora* by 5% (p-distance) at *mtMutS* and 2% at *cox1*. It was collected from both canyons (*n* = 5 Baltimore, *n* = 4 Norfolk) and is now known to be relatively common along the coasts of Norway, Iceland, Brazil, Gulf of Mexico, and likely elsewhere in the Atlantic (Moore et al. 2017).

A total of 54 specimens of the bushy bamboo coral *Acanella* was collected from otter trawls (**Table 13-4**) conducted adjacent to Norfolk Canyon. Sequencing of *mtMutS* and *cox1* for 51 specimens revealed two haplotypes. One haplotype is associated with colonies identified as *Acanella arbuscula*; this species is common in the North Atlantic and distributed worldwide. The second haplotype, observed from 21 colonies, differs from *A. arbuscula* haplotype by 1 bp at *mtMutS* and is a new species *A. scarletae*, so far known only from these collections (Heestand Saucier et al. 2017). Other bamboo corals collected included *Keratoisis*. Two bamboo coral colonies were sampled using the ROV *Jason II* in 2013, both identified as *Keratoisis grayi* (**Table 13-3**). Each colony had a unique *mtMutS* haplotype. The haplotype associated with NFK1406 has previously been found in specimens collected from the Bahamas and off the coast of Newfoundland, while the other haplotype (from NFK1414) is associated with *Keratoisis* found on the New England Seamounts, off the coast of Newfoundland, and in Baffin Bay.

The majority of sea pens (Pennatulacea) were collected from trawls, except for nine *Stylatula elegans* colonies sampled during three ROV dives (**Table 13-3**). The most numerous sea pen collected was *Pennatula aculeata*, which was collected from four otter trawls, all sampled from depths shallower than 500 m (**Table 13-4**). Most of the *P. aculeata* specimens had the same haplotype; however, there were six specimens that had a short tandem repeat within the *mtMutS* gene that has not been previously reported (**Table 13-5**). The seven *Umbellula* specimens that were recovered came from three trawls, all sampling at depths >1,600 m (**Table 13-4**). Based on previous collections from the MAB and the depth range sampled, it is most likely that these specimens are *Umbellula lindahli*. Two samples identified as *Funiculina* were also collected from trawls (**Table 13-4**). These samples had *mtMutS* sequences that were a 100% match to sequences in the NCBI GenBank nucleotide database identified as *Funiculina quadrangularis* by Gary C. Williams (California Academy of Sciences, San Francisco, California; **Figure 13-2**). Based on available published data, this is the first report and collection of *F. quadrangularis* in the MAB. Finally, 12 specimens collected from the trawls were identified as *Anthoptilum grandiflorum*, which has been previously reported from the canyon slopes. When compared to published *Anthoptilum grandiflorum cox1* sequences (not able to obtain *mtMutS* sequences for this species), these specimens show 0.5% difference (**Figure 13-3**). This leaves open the possibility that these specimens are a different species of *Anthoptilum*.

Table 13-5. Number of short tandem repeats (CCCAAACAG) found in six *Pennatula aculeata mtMutS* sequences.

Specimen ID	Number of Repeats
TR16941	5
TR16925	8
TR16913	7
TR16926	6
TR16911	5
TR1764	5

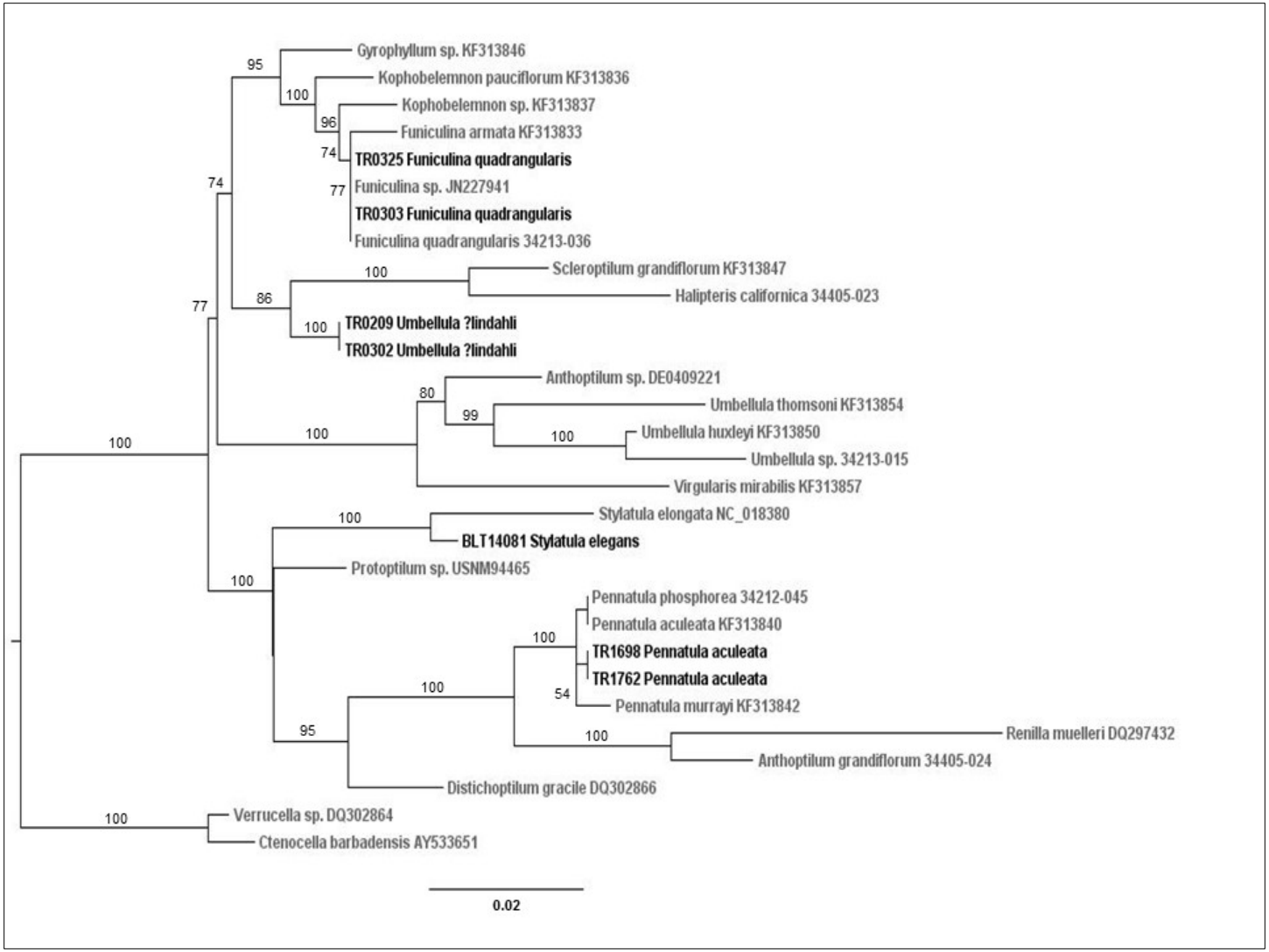

Figure 13-2. Phylogeny of Pennatulacea based on *mtMutS* sequence data, including four species that were collected during the 2012 and 2013 sampling cruises (highlighted in boldface). Maximum likelihood analysis conducted using RAxML with 1,000 bootstraps. Only branches with >50% bootstrap support are shown. The scale bar indicates the number of substitutions per site. Sequences of species indicated in gray were retrieved from the NCBI Genbank nucleotide database.

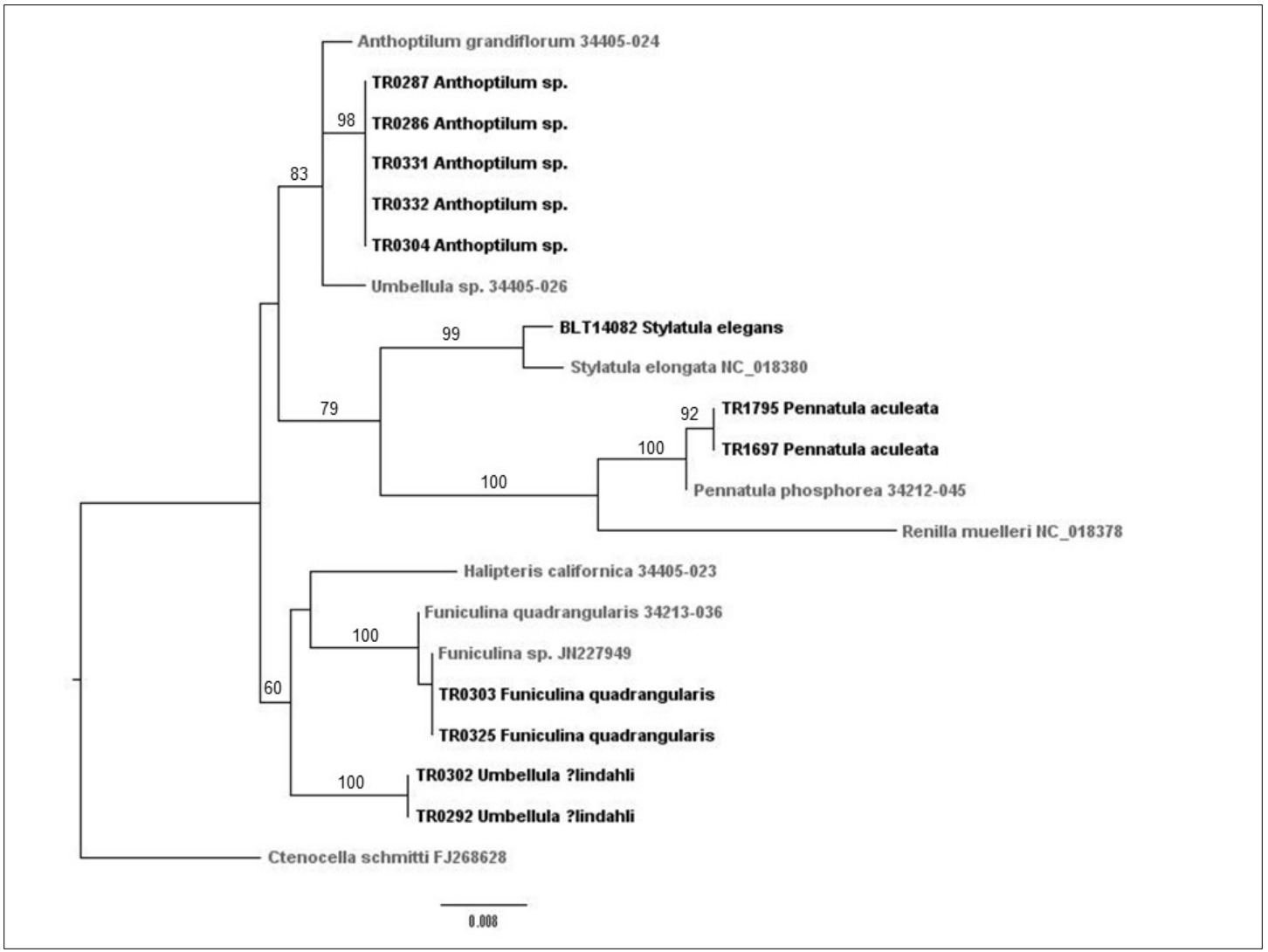

Figure 13-3. Phylogeny of Pennatulacea based on *cox1* sequence data, including five species were collected during the 2012 and 2013 sampling cruises (highlighted in boldface). Maximum likelihood analysis conducted using RAxML with 1,000 bootstraps. Only branches with >50% bootstrap support are shown. The scale bar indicates the number of substitutions per site. Sequences of species indicated in gray were retrieved from the NCBI GenBank nucleotide database.

13.3.1.2 Population Connectivity

13.3.1.2.1 Anthothela, Paragorgia, and Primnoa

Analyses of population structure between Baltimore Canyon and Norfolk Canyon revealed only low genetic differentiation among colonies of the three octocoral species examined: *Paragorgia arborea*, *Primnoa resedaeformis* and *Anthothela grandiflora*. The SNPs data obtained come from fewer specimens than were collected from the canyons, particularly for *Pr. resedaeformis*, because tissues of some samples apparently did not preserve well and had highly degraded DNA, which was a problem for generating the RAD sequences. After removing samples that failed to produce any sequence data, had a minimal number of sample reads, or a high proportion of missing data, the final samples sizes for *A. grandiflora*, *Pr. resedaeformis* and *Pa. arborea*, were $n = 35$, $n = 29$ and $n = 128$, respectively. Graphical representations of the genetic differentiation based on the SNPs data are shown in plots of the first two PCA axes in **Figures 13-4** to **13-6**. Although there is some separation of colonies from the two canyons, particularly for *Pr. resedaeformis*, most of the points form overlapping clusters. The patterns revealed in these plots are reflected in F_{ST} values, which are statistically different from zero (i.e., panmixia) but indicate only weak genetic differentiation: *A. grandiflora* ($F_{ST} = 0.023$, $p = 0.009$), *Pr. resedaeformis* ($F_{ST} = 0.085$, $p = 0.0001$) and *Pa. arborea* ($F_{ST} = 0.011$, $p = 0.005$). The trawled *Pa. arborea* specimens from Norfolk Canyon were analyzed separately and showed equally weak genetic differentiation from Baltimore Canyon colonies ($F_{ST} = 0.009$) and, as expected, virtually no differentiation from ROV-collected colonies in Norfolk Canyon ($F_{ST} = 0.0001$). These results are supported by STRUCTURE analyses, which showed that a single population cluster (K = 1) had the highest log likelihood value for *A. grandiflora* and *Pr. resedaeformis*. When testing the parameter value K = 2, membership coefficients showed that most colonies displayed mixed membership to both clusters (**Figures 13-7** and **13-8**). However, for *Pa. arborea*, the most likely K value was K = 3 (**Figure 13-9**), corresponding to each canyon population and a third cluster comprised of two divergent colonies from Baltimore Canyon (BLT1012, BLT1013). No spatial data were recorded for these two individuals but it is possible based on the ROV track line that they were collected farther west, away from other specimens collected during the same dive. These could therefore be from an isolated group of recruits that are the result of a long distance dispersal event. Despite the apparent division into K = 3 clusters, many *Pa. arborea* colonies from one canyon were assigned to the other canyon (**Figure 13-9**), suggesting genetic exchange between the canyons.

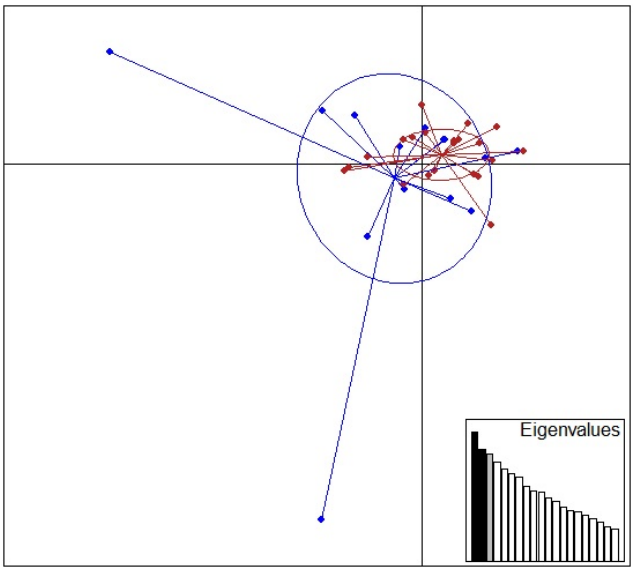

Figure 13-4. Principal component analysis of *Anthothela grandiflora* colonies collected from Baltimore Canyon (blue) and Norfolk Canyon (red).

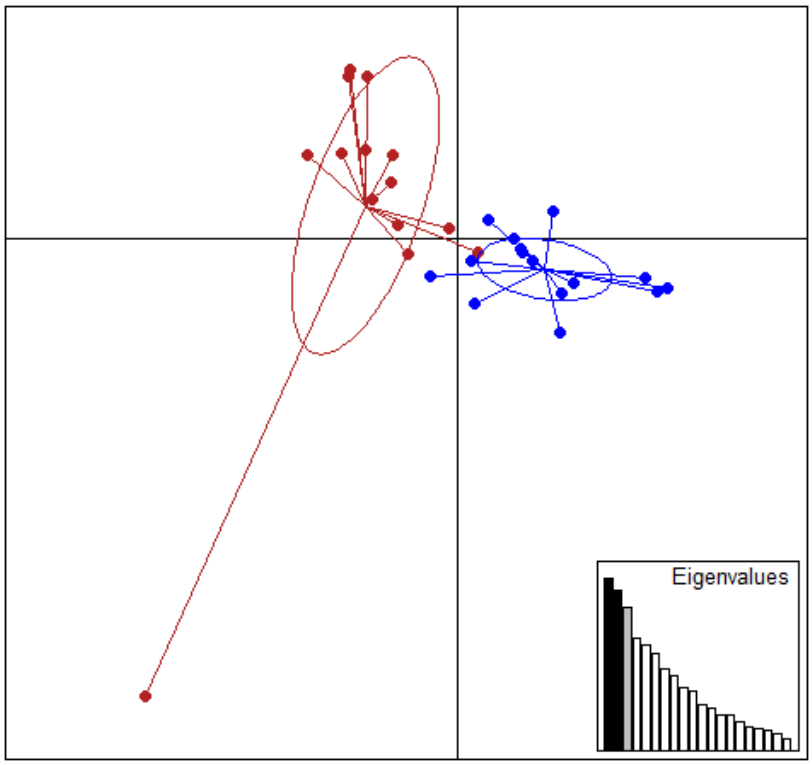

Figure 13-5. Principal component analysis of *Primnoa resedaeformis* colonies collected from Baltimore Canyon (blue) and Norfolk Canyon (red).

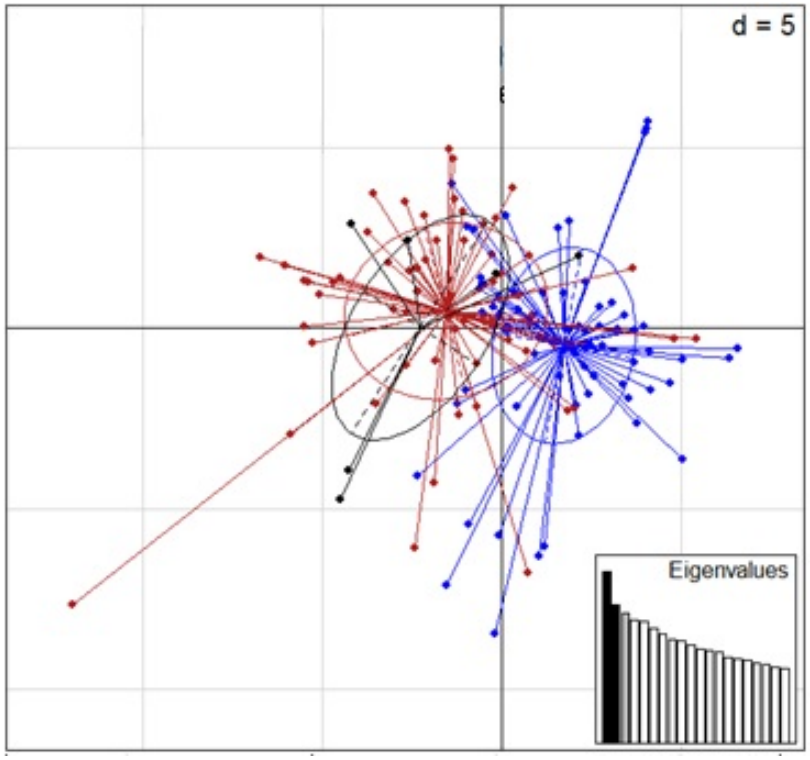

Figure 13-6. Principal component analysis for *Paragorgia arborea* specimens collected from Baltimore Canyon (blue), Norfolk Canyon (red), and otter trawls (black).

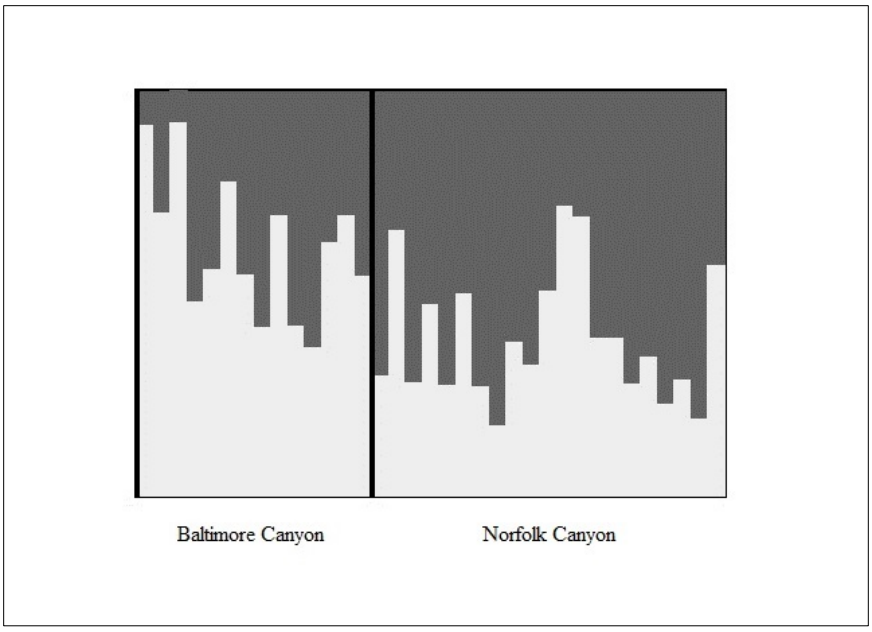

Figure 13-7. Membership coefficients for K = 2 analysis in STRUCTURE for *Anthothela grandiflora* colonies sampled from Baltimore Canyon and Norfolk Canyon. Each line segment represents a single colony and each color represents the individual's estimated membership coefficients in the K clusters (y-axis).

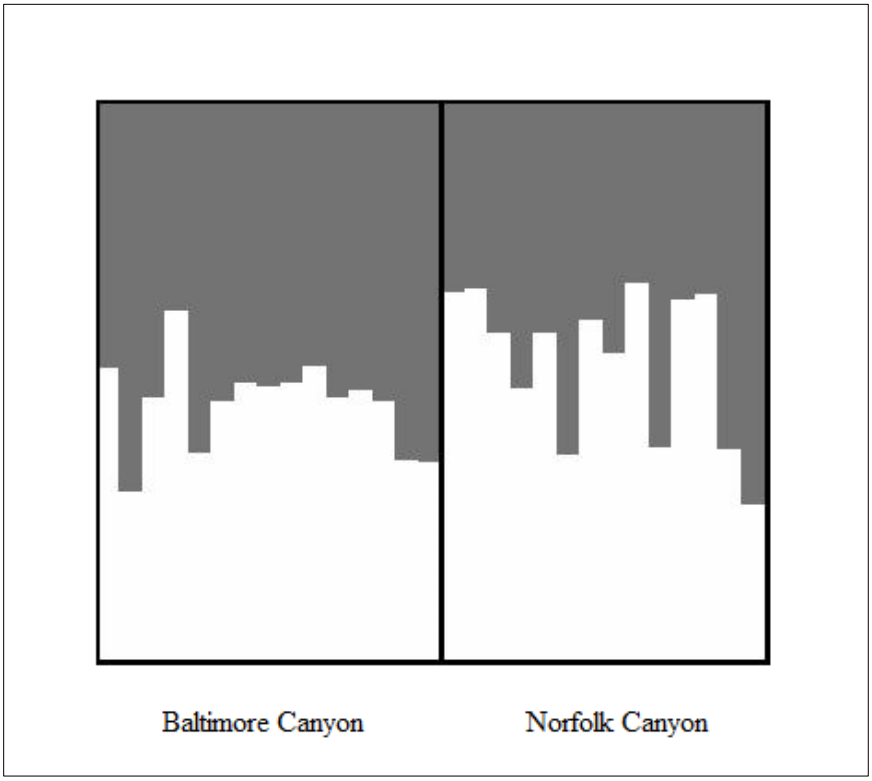

Figure 13-8. Membership coefficients for K = 2 analysis in STRUCTURE for *Primnoa resedaeformis* colonies sampled from Baltimore Canyon and Norfolk Canyon. Each line segment represents a single colony and each color represents the individual's estimated membership coefficients in the K clusters (y-axis).

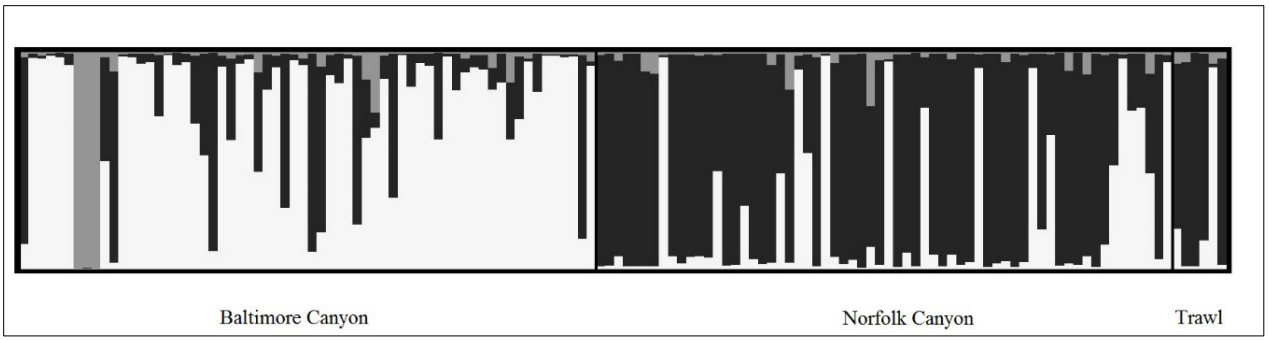

Figure 13-9. Membership coefficients for K = 3 analysis in STRUCTURE for *Paragorgia arborea* colonies collected from Baltimore Canyon and Norfolk Canyon, and specimens collected from otter trawls conducted adjacent to Norfolk Canyon. Each line segment represents a single colony and each color represents the individual's estimated membership coefficients in the K clusters (y-axis).

13.3.1.2.2 Paramuricea

RAD sequence reads were successfully obtained from 30 individuals (*n* = 18 Baltimore Canyon, *n* = 12 Gulf of Maine) and were used in STACKS analyses. The mean number of reads obtained per an individual was 1 646 735 (SD 732 540, *n* = 30), and individual values ranged from 136 806 to 3 614 820 reads. One Gulf of Maine sample was dropped from further analyses due to a low number of reads (92% fewer reads than the mean). The average guanine-cytosine (GC) nucleotide content for reads was ~36%, which is within the appropriate range for invertebrates (Saccone and Pesole 2005). On average, 51 657 (SD 21 298, *n* = 29) reads were removed due to low quality. Only the read 1 sequences for each individual were used for the final analysis, leaving a mean number of 823 572 (SD 332 705, *n* = 29) reads per individual.

After varying the *–m* and *–n* parameters of ustacks and cstacks, respectively, and examining PCA analyses to determine which combination of parameters minimized genetic dissimilarity between individuals from the same sampling site, *–m* 4 and *–n* 3 were the parameters chosen for the optimized data set (all PCA analyses showed the same general pattern of genetic diversity among individuals, **Figure 13-10**). Using the optimized data set a mean of 602,561 (SD 108 432, *n* = 29) SNPs were identified per individual with an average allele depth of 37.40 (SD 7.89, *n* = 29). Only loci present in all individuals that had a minor allele frequency >0.03 were retained. This resulted in a final data set that included 129 loci present in individuals from both sampling sites. An additional dataset was created to examine clonality among Baltimore Canyon colonies that resulted in 162 loci. No loci were found to be under selection using BayeScan.

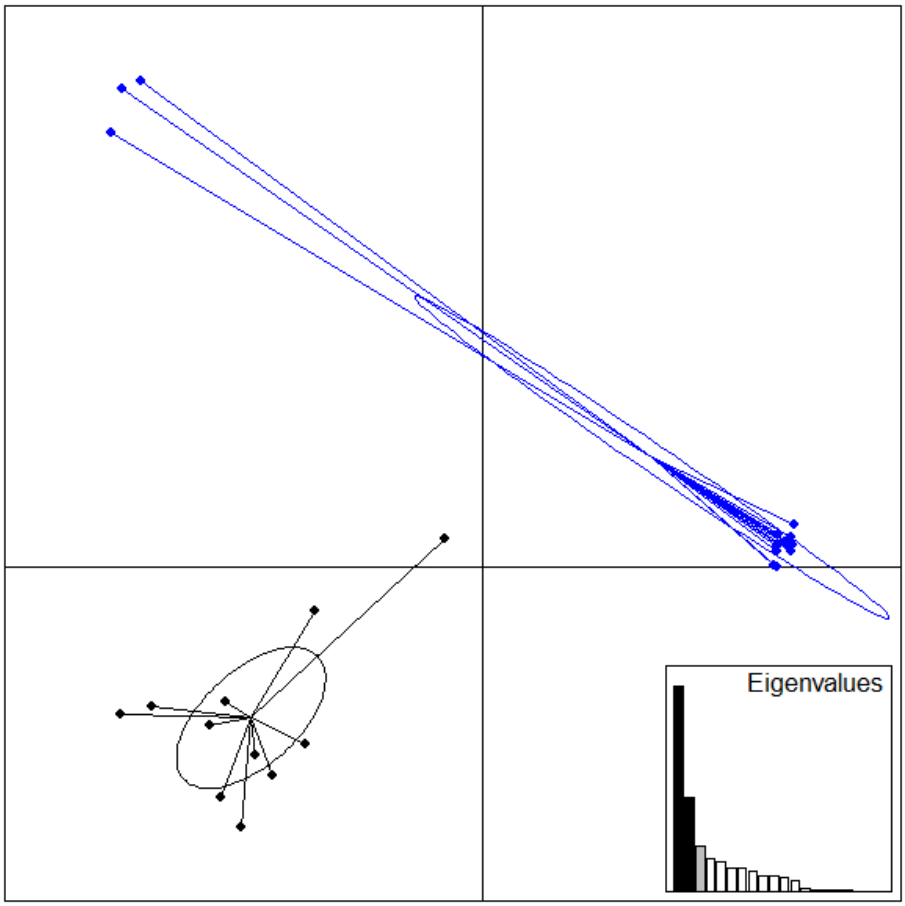

Figure 13-10. Principal component analysis of *Paramuricea placomus* from Baltimore Canyon (blue) and the Gulf of Maine (black).

There was strong genetic differentiation between samples from Baltimore Canyon and the Gulf of Maine (F_{ST} = 0.17). The value of K with the highest mean likelihood was K = 2, although K = 3 was also biologically meaningful (**Figure 13-11**). All individuals sampled from the Gulf of Maine created one cluster, and most individuals sampled from Baltimore Canyon clustered together. Two individuals sampled from Baltimore Canyon showed strong membership to the Gulf of Maine; based on these results it is likely those two individuals were contaminated and were removed from further analyses. Three individuals showed approximately 40% membership to the Gulf of Maine based on the STRUCTURE analysis. However, the PCA analysis showed these same three individuals clustered together away from all other samples. It is possible that these three individuals have partial membership to another population that was not sampled.

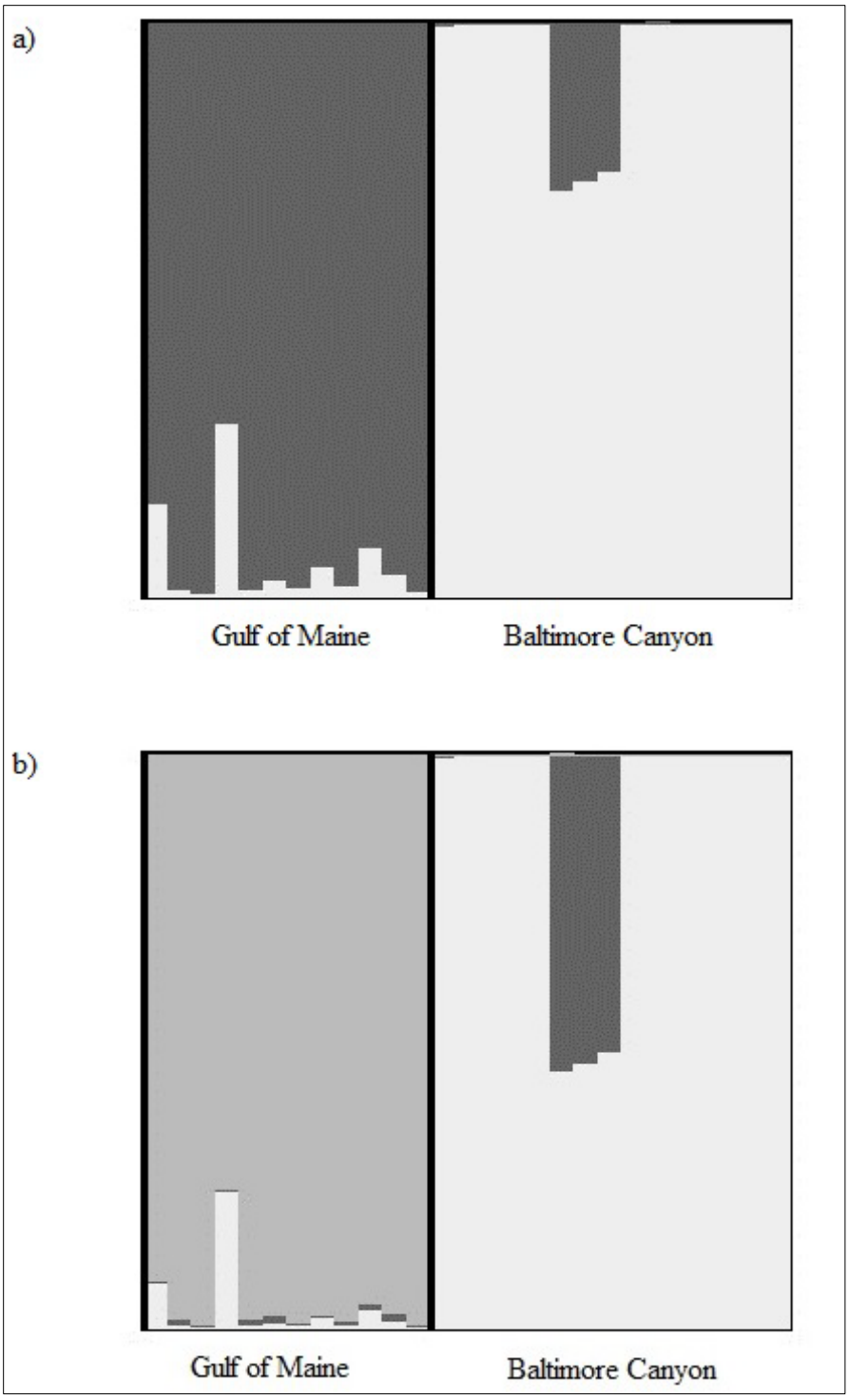

Figure 13-11. Membership coefficients for a) K = 2 analysis and b) K = 3 analysis in STRUCTURE for *Paramuricea placomus* sampled from Baltimore Canyon and the Gulf of Maine. Each line segment represents a single colony and each color represents the individual's estimated membership coefficients in the K clusters (y-axis).

13.3.1.3 Clonality

Clonality among *Paramuricea placomus* colonies collected in a small area of Baltimore Canyon was estimated; each colony had a unique multilocus genotype (n = 15). There was a clear break in the proportion of shared alleles among the colonies. The majority of individuals (12) showed values between 0.97 and 0.99. However, three individuals had values between 0.41 and 0.43 when compared to the other Baltimore Canyon *Paramuricea*. The same three individuals were genetically similar to each other (~0.98). These results suggest two recruitment events occurred at the site, and possibly with subsequent propagation from the initial recruits. Inbreeding coefficients for all individuals were high (F > 0.49, **Figure 13-12**).

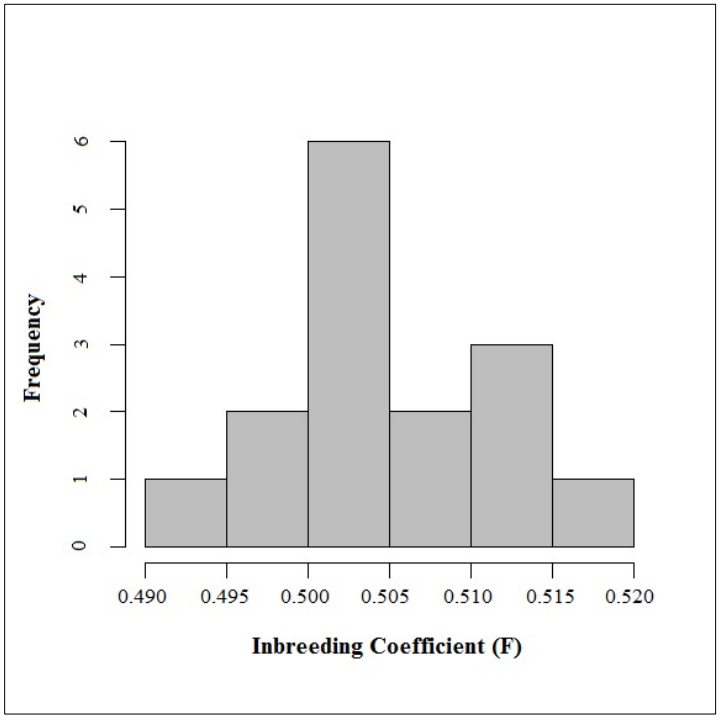

Figure 13-12. Inbreeding coefficients (*F*) for 15 *Paramuricea placomus* colonies sampled from Baltimore Canyon (162 loci).

13.3.2 Other Species

13.3.2.1 Species Diversity

In addition to the focal subclass Octocorallia, a few other anthozoans, from the subclass Hexacorallia, were collected and examined. Two colonies of black coral (Antipatharia: Schizopathidae) were sampled from Norfolk Canyon and both were identified as *Telopathes magna* (**Chapter 8**, **Figure 8-8 F**). This species has also been found off the continental slope of Nova Scotia and on several of the New England and Corner Rise Seamounts (Thoma et al. 2009, Macisaac et al. 2013). Three different species of Zoanthidea were identified using DNA sequence data. One zoanthid, recovered only in trawls, was identified as a Crustacea-symbiotic *Epizoanthus* sp. that is closely related to *Epizoanthus arenaceus*, *Epizoanthus ramosus* and *Epizoanthus balanorum*. The second zoanthid, collected from Norfolk Canyon, was identified as a Demospongiae-symbiotic *Parazoanthus* sp., closely related to *Parazoanthus anguicomus* and *Parazoanthus axinellae*. *Parazoanthus* in this group have previously been collected from shallow tropical and temperate waters (TD Swain, pers. comm.) but not the deep sea. The third zoanthid was collected in Baltimore Canyon and was found overgrowing a *Paramuricea* colony. This specimen was identified as an Alcyonacea-symbiotic *Corallizoanthus* known to occur in the deep sea.

Several sea anemone (Actiniaria) specimens were collected from both otter trawls and ROV dives. A total of eight specimens were selected to represent the diversity collected and were sequenced across an ITS region between nuclear ribosomal genes 5.8S and 28S. DNA sequences indicated all eight individuals belonged to the suborder Nynantheae Carlgren, 1899, infraorder Thenaria Carlgren, 1899, which includes all actiniarians with a defined and adherent base (Daly et al. 2008). Two specimens collected by ROV (NFK1808, NFK6021) belonged to the superfamily Actinioidea Rafinesque, 1815 (~ Endomyaria Stephenson, 1921). The ITS sequences for these two individuals clustered with *Bolocera* Gosse, 1860 and *Liponema* Hertwig, 1888, both of which are known deepsea taxa. All of the remaining specimens sequenced belonged to the superfamily Metridiodea Carlgren, 1983 (~Acontiaria Stephenson, 1935). Four of these metridiodean specimens clustered within the Cuticuata clade (Rodríguez et al. 2014). Trawled specimen TR1682 clustered with *Chondrophellia* and *Paraphelliactis* (Rodríguez et al. 2014), and TR17913 clustered with *Kadosactis* and some other deepsea actiniarians although this node has weak support within the Cuticuata clade. Two ROV-collected samples (NFK5021, NFK7011) clustered with *Amphianthus, Actinoscyphia* and *Nemanthus*. Two other ROV-collected metridiodean specimens clustered within the Acuticulata clade (Rodríguez et al. 2014). NFK7053 appears to be a new lineage within Acuticulata and clustered outside of a large clade that included the families Sagartiidea Grosse, 1858 and Metridiidae Carlgren, 1893, and NFK3011 appears to belong to the genus *Metridium*.

13.4 DISCUSSION

13.4.1 Octocorals

Most octocorals collected in Baltimore Canyon and Norfolk canyons have been previously reported for the MAB region. However, new species with cryptic morphology were also discovered using DNA sequence data. Previously recorded species in the MAB included *Paragorgia arborea, Primnoa resedaeformis, Anthothela grandiflora*, *Acanella arbuscula, Keratoisis grayi*, *Duva florida* (previously *Capnella florida*), *Pennatula aculeata*, *Umbellula lindahli*, and *Stylatula elegans* (Hecker et al. 1980, Watling and Auster 2005, Packer et al. 2007). A new species of *Acanella* (*A. scarletae*) and a new genus (*Lateothela*) closely related to *Anthothela* were discovered in the canyons as well as new distribution occurrences for *Acanthogorgia aspera* (Norfolk Canyon only), *Funiculina quadrangularis* (Norfolk Canyon only), and *Paramuricea placomus* (Baltimore Canyon only).

It was hypothesized that species richness within the MAB canyons would not differ from open slope habitats sampled by otter trawl. In the Atlantic Deepwater Canyons Study, species richness was similar between the two habitats but species composition differed. Octocoral species that require hard substrate were more commonly collected within the canyons, while species that prefer soft sediment were trawled from the slope. Hecker et al. (1980) found that Baltimore Canyon had a lower number of octocoral species compared to other canyons in the MAB. In this study, the number of octocoral species collected and identified in Baltimore Canyon (7) and Norfolk Canyon (7) was the same (excluding *Duva florida,* which was sampled on the final ROV dive). In both canyons, *Paragorgia arborea* and *Primnoa resedaeformis* were the most frequently observed (**Chapter 8**) and collected octocorals. Only two octocoral species present in Norfolk Canyon were not observed in Baltimore Canyon: *Acanthogorgia aspera* and *Keratoisis grayi*. Colonies of the genus *Acanthogorgia* (unidentified) have been previously observed in Baltimore Canyon from camera tows (Hecker et al. 1980) but were not collected by us during this study. *Paramuricea placomus* was the only species collected from Baltimore Canyon that was not also found in Norfolk Canyon. However, during post-cruise video analysis *Paramuricea* colonies were observed in Norfolk Canyon (**Chapter 8**, **Section 8.3.2.1.1**). *Paramuricea* has been reported from several western North Atlantic canyons north of the MAB (Breeze et al. 1997, Hecker et al. 1980, Quattrini et al. 2015).

The minor differences in species occurrence noted here could be attributed to either differences in the available habitat or differences in sampling effort with depth. Earlier studies in the MAB noted that

Baltimore Canyon appeared to be a less active canyon with fewer exposed outcrops, while Norfolk Canyon appeared more active (Hecker et al. 1980, Bennett et al. 1985, Gardner 1985). More recently, Obelcz et al. (2014) found that Baltimore Canyon had equal roughness on both the north and south walls, while Norfolk Canyon's northern wall was steeper and rougher than the southern wall. In our study, a greater number of ROV dives in Norfolk Canyon were conducted on the northern wall. Obelcz et al. (2014) also suggested that these two canyons have had different sediment sources, and that the geomorphology of Baltimore Canyon indicates that it is subject to frequent discharges of fine-grain sediment, which may limit the accessibility of hard substrates. Nonetheless, in both canyons features that were likely to support coral communities, such as escarpments and steep ridges, were preferentially targeted and explored, so these canyon-scale differences in geomorphology may not be a factor in the minor differences in species occurrence observed. Collection depth influenced the species differences between canyons. The deepest collections in Baltimore Canyon occurred at 681 m but in Norfolk Canyon extended down to 1,362 m. This should not have limited the collection of *Acanthogorgia*, which were sampled from a depth range also sampled in Baltimore Canyon, but *Keratoisis* was found only at depths >1,000 m in Norfolk Canyon (**Table 13-2**).

Octocoral species diversity has previously been noted to be higher within the MAB canyons than on the adjacent slopes (Hecker et al. 1980). However, Hecker et al. (1980) also stated that the fauna of Baltimore Canyon closely resembled that of the slope in that both had low species richness and abundance. In the current study the number of octocoral species collected within the canyons (9) was not substantially larger that the number collected on the adjacent slope (8); however, the species assemblage was markedly different. On the slope adjacent to Norfolk Canyon most of octocorals collected belonged to the order Pennatulacea, species that are adapted to living in soft sediments. *Pennatula aculeata* was the dominant octocoral collected from trawls between 380 m and 500 m depth; at depths >1,500 m the sea pens *Anthoptilum grandiflorum*, *Funiculina quadrangularis*, and *Umbellula lindahli* were collected, although in smaller numbers. Non-pennatulacean octocorals collected by trawl on the slope included the bamboo coral *Acanella arbuscula.* These colonies can modify their holdfasts to grow as root-like structures on soft sediment and are well known from continental slopes.

The occurrence of *Acanthogorgia aspera* in Norfolk Canyon is the furthest north in the Atlantic Ocean that this species has been reported. *Acanthogorgia aspera* has previously been found in the Gulf of Mexico and in the North Atlantic from Cape Hatteras to the Florida Straits (Watling and Auster 2005, Brooke and Schroeder 2007). *Acanthogorgia armata* has been previously recorded in the MAB but was not found among our collections in Baltimore Canyon or Norfolk Canyon based on morphological and molecular identification (Watling and Auster 2005, Packer et al. 2007). *Funiculina quadrangularis* has also been reported in the Gulf of Mexico as well as many other places worldwide, but this is the first documented occurrence in the MAB region (Brooke and Schroeder 2007, Greathead et al. 2007, Wareham and Edinger 2007). *Funiculina armata* has been reported in the MAB but was not collected during this study (World Register of Marine Species [WoRMS], van Ofwegen 2015). The fact that these two new occurrences are within the range of closely related sister species suggests that some of the previous records for *A. armata* and *F. armata* may not have been verified using both morphology and genetics. In the western Atlantic, *Paramuricea placomus* is known to occur in the Gulf of Maine, Oceanographer Canyon, and off Georgia, Florida and Cuba (Ross and Nizinski 2007). This is the first verified occurrence of *P. placomus* in Baltimore Canyon, although it appears to be rare. During camera tows conducted in 1980 colonies of *Paramuricea* were not observed in Baltimore Canyon (Hecker et al. 1980) and in the current study *Paramuricea* were found at only a single site in each of the two canyons assessed. The single population sampled in Baltimore Canyon appeared to have been negatively impacted by a fishing line that was observed adjacent to a cluster of colonies, including touching the bases of some. On one side of the line there were no colonies observed, giving the impression that the line may have scraped over the bottom dislodging sessile fauna. Of the remaining *Paramuricea* sampled within this patch, genetic diversity among colonies was low (see clonality discussion below).

Octocorals collected from Baltimore and Norfolk canyons were initially thought to be additional samples of the common canyon inhabitant *Anthothela grandiflora*. Genetic analyses revealed that these were a species in a different genus, the newly described *Lateothela grandiflora* (Moore et al. 2017). *L. grandiflora* were collected in far fewer numbers than *A. grandiflora* (n = 9 vs. 63), and because these taxa were not recognized as different on ROV video *in situ*, it suggests *Lateothela* is less abundant than *A. grandiflora* in the canyons. In addition to the genetic differences, these two species also have very different bacterial communities associated with them (**Chapter 12**).

It was also hypothesized that populations of common structure-forming octocorals would not be isolated from slope populations. However, this hypothesis was not testable because species composition between canyon populations and slope populations was different. High levels of connectivity were observed between populations from Baltimore Canyon and Norfolk Canyon for *Anthothela grandiflora, Primnoa resedaeformis* and *Paragorgia arborea*. This was expected given the close proximity of the two canyons (~70 km) and based on the results from a previous study in the North Atlantic (Thoma et al. 2009). Genetic differentiation (as measured by F_{ST}) between canyon populations of *P. resedaeformis* was slightly higher than seen in *P. arborea* and *A. grandiflora*; these results are similar to those found using microsatellites (**Chapter 14**, **Section 14.3**). Similar patterns of low F_{ST} have been observed using microsatellite loci in other deepsea coral species (Baco and Shank 2005). However, strong genetic differentiation was observed between *Paramuricea placomus* colonies sampled from Baltimore Canyon and the Gulf of Maine, which suggests that geographic distance does influence variation between populations even for widely distributed, long-lived species with low mutation rates. A significant genetic differentiation was also observed between Baltimore Canyon and the Gulf of Maine for *P. resedaeformis* using microsatellite loci (**Chapter 14**).

The study tested the hypothesis that isolated patches of *Paramuricea* were the result of local recruitment rather than clonal propagation. Within the cluster of *Paramuricea placomus* colonies sampled in Baltimore Canyon two groups were identifed. Individual relatedness among colonies within each group was high, but was much lower between the groups. A recent RADseq study on the sea anemone *Nematostella vectinsis* found a distinct difference in pairwise genotypic similarities between potential clones (99.0% to 99.9%) and nonpotential clones (61.2% to 86.5%, Reitzel et al. 2013). Although no pairs of individuals with genetic similarities as high as 99.9% were found, which would suggest evidence of clonal propagation, the high values suggest that each group is composed of closely related siblings. An explanation for this pattern could be that there were at least two independent recruitment events bringing settling larvae to this area from different parents. Once these recruits grew to mature size their offspring larvae settled nearby, thus creating a patch of two groups, each the offspring of a different parental colony. If this scenario is correct, it implies local recruitment is an important process. If instead there were many larval recruits arriving from different parent colonies, more low genetic similarity values would have been observed in pairwise comparisons; that is, there would be more genetic variation across colonies and fewer directly related individuals. Furthermore, the high fixation index observed ($F > 0.49$) is typically only seen in self-fertilizing plants (Hartl and Clark 2007). Studies on reproductive success and individual relatedness in *Paramuricea clavata*, a shallow-water species, have found that asexual reproduction is negligible but larval dispersal is limited, leading to a strong level of self-recruitment and a high proportion of half-sib relationships (Mokhtar-Jamaï et al. 2013). *P. clavata* is a surface brooder with distinct male and female colonies. Little is known about the reproductive strategy of deepsea *Paramuricea*. In the Atlantic Deepwater Canyons Study, however, many *Paramuricea placomus* colonies were observed to be hermaphroditic (**Chapter 11**, **Section 11.3.1**). These colonies therefore have the potential to self-fertilize at the colony level (although mechanisms are usually present to prevent self-fertilization, so it is more likely they are brooders with short-lived planulae, although no direct evidence for this was found [S. Brooke, pers. Comm.]). The high genetic similarity between individuals could also be due to an overall low genetic variability in octocorals (McFadden et al. 2010). Although low variability has been shown for mitochondrial genes, there are too few data available to conclude if this will affect nuclear genes as well. Finally, it must be noted that the group comprised of three colonies also showed

unique bacterial communities (**Chapter 12**, **Section 12.2.3.3**). A question remains as to why there are concordant patterns between coral and bacterial genetic signals. Possibilities include that larvae travel with bacteria and so bacterial communities reflect differences in the coral parent colonies; that bacteria respond to coral cues governed by genetics; or that the two genetic signals actually come from the same source, i.e. both methods have independently sampled the same source of DNA, either microbial or octocoral. The latter seems less likely based on the GC nucleotide content (34% to 38%) of the RAD loci used for our analyses, which were within a range typical of anthozoans (Saccone and Pesole 2005). In bacteria the mean GC content can range widely (25% to 67%) across species but for most of the genomes that have been sequenced GC content is >38%.

13.4.2 Other Species

The opportunity to sample octocorals and other sessile anthozoan cnidarians in these canyons for genetic analyses is impacted by the depth range and geomorphology targeted and the sampling assets deployed. Trawls, which during this project were conducted on flatter floors of the canyon and on the slope adjacent to the canyon, were dominated by sea pens (Anthozoa, Octocorallia, Pennatulacea) and sea anemones (Anthozoa, Hexacorallia, Actiniaria) rather than the gorgonians that were most often observed on more rugged habitats using the ROV. Actiniarians were abundant in many areas in the canyons traversed during ROV transects, but largely were not a target of collections, and thus species richness and relationship to slope species is unknown.

Two specimens of the black coral *Telopathes magna* were collected from Norfolk Canyon. This is the first report of this species in Norfolk Canyon; however, it has recently been documented in other Atlantic canyons farther north (Quattrini et al. 2015).

13.5 CONCLUSIONS

This study set out to test three hypotheses. The results indicate that:

- Octocoral species richness was similar between the two MAB submarine canyons and open slope communities, but species composition differed, a function of the availability of hard substrate in the canyons versus soft sediments of the outer continental slope. In comparison to earlier studies in the area, it is obvious that the method of sampling (camera tows vs ROV collection vs trawling) as well as depth of sampling has an influence on the species identified. Differences in the depth range sampled in the two canyons accounts for some differences in species composition, e.g. the bamboo coral *Keratoisis*, and genetic analyses allowed for identification of taxa previously unreported from the MAB canyons as well as discovery of new species.
- Populations of the octocorals *Anthothela grandiflora*, *Primnoa resedaeformis* and *Paragorgia arborea* show high levels of genetic connectivity between Baltimore Canyon and Norfolk Canyon.
- A cluster of *Paramuricea placomus* colonies in Baltimore Canyon appeared to comprise two groups of closely related siblings, suggesting local recruitment is an important process and no evidence for clonal propagation.

This study is one of few to have collected deepsea corals in sufficient numbers to enable examination of population genetic structure among canyons and clonality for an isolated patch of colonies. The information from this study will be an important contribution to future studies on deepsea corals in the MAB region.

13.6 LITERATURE CITED

Auster PJ, Kilgour M, Packer D, Waller R, Auscavitch S, Watling L. 2013. Octocoral gardens in the Gulf of Maine (NW Atlantic). Biodiversity. 14:193–194. doi:10.1080/14888386.2013.850446.

Baco AR, Shank TM. 2005. Population genetic structure of the Hawaiian precious coral *Corallium lauuense* (Octocorallia: Corallidae) using microsatellites. In: Freiwald A, Roberts JM, editors. Cold-water corals and ecosystems. Berlin Heidelberg (Germany): Springer-Verlag. p. 663–678.

Bayer FM. 1981. Key to the genera of Octocorallia exclusive of Pennatulacea (Coelenterata: Anthozoa), with diagnoses of new taxa. Proceedings of the Biological Society of Washington. 94:902–947.

Bennett RH, Lehman L, Hulbert MH, Harvey GR, Bush SA, Forde EB, Crews P, Sawyer WB. 1985. Interrelationship of organic carbon and submarine sediment geotechnical properties. Marine Geotechnology. 6:61–98.

Benson DA, Cavanaugh M, Karsch-Mizrachi I, Lipman DJ, Savers EW. 2013. GenBank. Nucleic Acids Research 41(Database Issue): D36-42. doi:10.1093/nar/gks1195. www.ncbi.nlm.nih.gov/genbank.

Berntson EA, Bayer FM, McArthur AG, France SC. 2001. Phylogenetic relationships within the Octocorallia (Cnidaria: Anthozoa) based on nuclear 18S rRNA sequences. Marine Biology. 138:235-246.

Breeze H, Butler M, Davis DS. 1997. Distribution and status of deep sea corals off Nova Scotia. Halifax (Nova Scotia): Ecology Action Centre.

Brockman SA, McFadden CS. 2012. The mitochondrial genome of *Paraminabea aldersladei* (Cnidaria: Anthozoa: Octocorallia) supports intramolecular recombination as the primary mechanism of gene rearrangement in octocoral mitochondrial genomes. Genome Biology Evolution. 4:994–1006. doi:10.1093/gbe/evs074.

Brooke S, Ross SW. 2014. First observations of the cold-water coral *Lophelia pertusa* off the mid-Atlantic coast of the United States. Deep-Sea Research II. 104:241–251.

Brooke S, Schroeder WW. 2007. State of deep coral ecosystems in the Gulf of Mexico region: Texas to the Florida Straits. In: Lumsden SE, Hourigan TF, Bruckner AW, Dorr G, editors. The state of deep coral ecosystems of the United States. NOAA Technical Memo CRCP-3. Silver Spring (MD): National Oceanic and Atmospheric Administration. p. 271–306.

Brugler MR, France SC. 2008. The mitochondrial genome of a deep-sea bamboo coral (Cnidaria, Anthozoa, Octocorallia, Isididae): genome structure and putative origins of replication are not conserved among octocorals. Journal of Molecular Evolution. 67:125–136.

Cairns SD. 1981. Marine flora and fauna of the northeastern United States: Scleractinia. NOAA Technical Report, NMFS Circular. US Department of Commerce. 438:1–14.

Catchen JM, Amores A, Hohenlohe P, Cresko W, Postlethwait JH. 2011. Stacks: building and genotyping loci *de novo* from short-read sequences. G3: Genes, Genomes, Genetics. 1:171–181.

Catchen JM, Hohenlohe PA, Bassham S, Amores A, Cresko WA. 2013. Stacks: an analysis tool set for population genomics. Molecular Ecology. 22:3124–3140.

Costantini F, Fauvelot C, Abbiati M. 2007. Fine-scale genetic structuring in *Corallium rubrum*: evidence of inbreeding and limited effective larval dispersal. Marine Ecology Progress Series. 340:109–119.

Daly M, Chaudhuir A, Gusmão L, Rodríguez E. 2008. Phylogenetic relationship among sea anemones (Cnidaria: Anthozoa: Actiniaria). Molecular Phylogenetics and Evolution. 48:292–301.

Earl DA, vonHoldt BM. 2012. STRUCTURE HARVESTER: a website and program for visualizing STRUCTURE output and implementing the Evanno method. Conservation Genetics Resources. 4:359–361.

Foll M, Gaggiotti O. 2008. A genome-scan method to identify selected loci appropriate for both dominant and codominant markers: a Bayesian perspective. Genetics. 180:977–993.

France SC, Hoover LL. 2002. DNA sequences of the mitochondrial *COI* gene have low levels of divergence among deep-sea octocorals (Cnidaria: Anthozoa). Hydrobiologica. 471:149–155.

France SC. 2007. Genetic analysis of bamboo corals (Cnidaria: Octocorallia: Isididae): does lack of colony branching distinguish *Lepidisis* from *Keratoisis*? Bulletin of Marine Science. 81:323–333.

Gardner. 1985. Balitmore Canyon as a modern conduit of sediment to the deep sea. Deep-Sea Research A. 36:323–358.

Grahman CF, Glenn TC, McArthur AG, Boreham, DR, Kieran T, Lance S, Manzon RG, Martino, Pierson T, Rodgers, Wilson JY, Somers CM. 2015. Impacts of degraded DNA on restriction enzyme associated DNA sequencing (RADseq). Molecular Ecological Research. 15(6):1304–1315. doi:10.1111/1755-09910.12404.

Greathead CF, Donnan DW, Mair JM, Saunders GR. 2007. The sea pens *Virgularia mirabilis, Pennatula phosphorea* and *Funiculina quadrangularis:* distribution and conservation issues in Scottish waters. Journal of Marine Biology. 87:1095–1103.

Haedrich RL, Rowe GT and Polloni PT. 1975. Zonation and faunal composition of epibenthic populations on the continental slope south of New England. Journal of Marine Research. 33:191–212.

Hall TA. 1999. BioEdit: a user-friendly biological sequence alignment editor and analysis program for Windows 95/98/NT. Nucleic Acids Symposium Series. 41:95–98.

Hartl DL, Clark AG. 2007. The principles of population genetics, 4th ed. Sunderland (MA): Sinauer Associates, Inc. 545 p.

Hecker B, Blechschmidt G, Gibson P. 1980. Epifaunal zonation and community structure in three mid- and north Atlantic canyons. Final report for the canyon assessment study in the Mid-and North Atlantic Areas of the U.S. Outer Continental Shelf. Prepared for the U.S. Department of Interior, Bureau of Land Management under contract BLM AA5 51-CT8-49. Palisades (NY): Lamont-Doherty Geological Observatory.

Hecker B, Logan DT, Gandarillas FE, Gibson PR. 1983. Canyon and slope processes study, vol. III: biological processes. Report for the U.S. Department of the Interior, Minerals Management Service, under contract no. 14-12-0001-29178. Palisades (NY): Lamont-Doherty Geological Observatory. 212 p. [accessed 2016 June 1]. http://invertebrates.si.edu/boem/reports/CASPS_vol3.pdf.

Heestand Saucier E, Sajjadi A, France SC. 2017. A taxonomic review of the genus *Acanella* (Cnidaria: Octocorallia: Isididae) in the North Atlantic Ocean, with descriptions of two new species. Zootaxa. 4323:359–390.

Hohenlohe PA, Bassham S, Etter PD, Stiffler N, Johnson EA, Cresko WA. 2010. Population genomics of parallel adaption in threespine stickleback using sequenced RAD tags. PLoS Genetics. 6:e1000862. doi:10.1371/journal.pgen.1000862.

Jakobsson M, Rosenberg NA. 2007. CLUMPP: a cluster matching and permutation program for dealing with label switching and multimodality in analysis of population structure. Bioinformatics. 23:1801-1806.

Jombart T. 2008. Adegenet: an R package for the multivariate analysis of genetic markers. Bioinformatics. 24:1403–1405.

Kamvar ZN, Tabima JF, Grünwald NJ. 2014. Poppr: an R package for genetic analysis of populations with clonal, partially clonal, and/or sexual reproduction. Peer J. 2:e281.

Liu SYV, Yu HT, Fan TY, Dai CF. 2005. Genotyping the clonal structure of a gorgonian coral *Junceella juncea* (Anthozoa: Octocorallia), using microsatellite loci. Coral Reefs. 24:352–358.

Macisaac KG, Best M, Brugler MR, Kenchington ELR, Anstey LJ, Jordan T. 2013. *Telopathes magna* gen. nov., spec. nov. (Cnidaria: Anthozoa: Antipatharia: Schizopathidae) from deep waters off Atlantic Canada and the first molecular phylogeny of the deep-sea family Schizopathidae. Zootaxa. 3700:237–258.

Martin M. 2011. Cutadapt removes adapter sequences from high-throughput sequencing reads. EMBnet.journal. 17:10–12. doi:http://dx.doi.org/10.14806/ej.17.1.200.

Mastretta-Yanes A, Arrigo N, Alvarez N, Jorgenen TH, Pinero D, Emerson BC. 2015. Restriction site-associated DNA sequencing, genotyping error estimation and *de novo* assembly optimization for population genetic inference. Molecular Ecology. 15:28–41.

McFadden CS, Sánchez JA, France SC. 2010. Molecular phylogenetic insights into the evolution of Octocorallia: a review. Integrated Comparative Biology. 50(3):389–410. doi:10.1093/icb/icq056.

McFadden CS, Benayahu Y, Pante E, Thoma JN, Nevarez PA, France SC. 2011. Limitations of mitochondrial gene barcoding in Octocorallia. Moecular Ecology Resources. 11(1):19–31.

Mokhtar-Jamaï K, Coma R, Wang J, Zuberer F, Féral JP, Aurelle D. 2013. Role of evolutionary and ecological factors in the reproductive success and the spatial genetic structure of the temperate gorgonian *Paramuricea clavata.* Ecology and Evolution. 3:1765–1779.

Moore KM, Alderslade P, Miller KJ. 2017. A taxonomic revision of *Anthothela* (Octocorallia: Scleraxonia: Anthothelidae) and related genera, with the addition of new taxa, using morphological and molecular data. Zootaxa. 4304: 1-212.

Obelcz J, Brothers D, Chaytor J, Brink U, Ross SW, Brooke S. 2014. Geomorphic characterization of four shelf-sourced submarine canyons along the U.S. Mid-Atlantic continental margin. Deep-Sea Research II. 104:106–119.

Packer DB, Boelke D, Guida V,McGee LA. 2007. State of deep coral ecosystems in the northeastern US region: Maine to Cape Hatteras. In: Lumsden SE, Hourigan TF, Bruckner AW, Dorr G, editors. The state of deep coral ecosystems of the United States. NOAA Technical Memo CRCP-3. Silver Spring (MD): National Oceanic and Atmospheric Administration. p. 195–232.

Pante E, France SC, Couloux A, McFadden CS, Samadi S, Watling L. 2012. Origin and in-situ diversification of Chrysogorgiid octocorals. PLoS ONE. 7:e38357. doi:10.1371/journal.pone.0038357.

Peakall R, Smouse PE. 2012. GenAlEx 6.5: a genetic analysis in Excel. Population genetic software for teaching and research – an update. Bioinformatics. 28:2537–2539.

Peterson BK, Weber JN, Kay EH, Fisher HS, Hoekstra HE. 2012. Double digest RADseq: an inexpensive method for *de novo* SNP discovery and genotyping model and non-model species. PLoS ONE. 7:e32253. doi:10.1371/journal.pone.0037135.

Pritchard JK, Stephens M, Donnelly P. 2000. Inference of population structure using multilocus genotype data. Genetics. 155:945–959.

Quattrini A, Nizinski M, Chaytor J, Demopoulos A, Roark B, France S, Moore J, Heyl T, Auster P, Kinlan B, Ruppel C, Elliott K, Kennedy B, Lobecker E, Skarke A, Shank T. 2015. Exploration of the canyon-incised continental margin of the Northeastern Unites States reveal dynamic habitats and diverse communities. PLoS ONE. 10:e0139904. doi:10.1371/journal.pone.0139904.

Raymond M, Rousset F. 1995. GENEPOP version 1.2: population genetics software for exact tests and ecumenicism. Journal of Heredity. 86:248–249.

Reitzel AM, Herrera S, Layden MJ, Martindale MQ, Shank TM. 2013. Going where traditional markers have not one before: utility of and promise for RAD sequencing in marine invertebrate phylogeography and population genetics. Molecular Ecology. 22:2953–2970.

Rodríguez E, Barbeitos MS, Brugler MR, Crowley LM, Grajales A, Gusmão L, Häussermann V, Reft A, Daly M. 2014. Hidden among sea anemones: the first comprehensive phylogenetic reconstruction of the order Actiniaria (Cnidaria: Anthozoa: Hexacorallia) reveals a novel group of Hexacorals. PLoS ONE. 9: e96998. doi:10.1371/journal.pone.0096998.

Rosenberg NA. 2004. DISTRUCT: a program for the graphical display of population structure. Molecular Ecology Notes. 4:137–138.

Ross SW, Nizinski MS. 2007. State of deep coral ecosystems in the U.S. Southeast Region: Cape Hatteras to southeastern Florida. In: Lumsden SE, Hourigan TF, Bruckner AW, Dorr G, editors. The state of deep coral ecosystems of the United States. NOAA Technical Memo, CRCP-3. Silver Spring (MD): National Oceanic and Atmospheric Administration. p. 233–270.

Saccone C, Pesole G. 2005. Handbook of comparative genomics: principles and methodology. Hoboken (NJ): John Wiley & Sons, Inc. p. 20–26.

Sánchez JA, McFadden CS, France SC, Lasker HR. 2003. Molecular phylogenetic analyses of shallow-water Caribbean octocorals. Marine Biology. 142:975–987.

Shank T. 2010. Seamounts: deep ocean laboratories of faunal connectivity, evolution, and endemism. Oceanography. 23:108–122.

Smith PJ, McVeagh SM, Mingoia JT, France SC. 2004. Mitochondrial DNA sequence variation in deep-sea bamboo coral (Keratoisidine) species in the southwest and northwest Pacific Ocean. Marine Biology. 144:253–261.

Stamatakis A, Hoover P, Rougemont J. 2008. A rapid bootstrap algorithm for the RAxML web servers. Systematic Biology. 57:758–771.

Stoletzki N, Schierwater B. 2005. Genetic and color morph differentiation in the Caribbean sea anemone *Condylactis gigantean*. Marine Biology. 147:747–754.

Swain TD. 2010. Evolutionary transitions in symbioses: dramatic reductions in bathymetric and geographic ranges of Zoanthidea coincide with loss of symbioses with invertebrates. Molecular Ecology. 19:2587–2598.

Thoma JN, Pante E, Brugler MR, France SC. 2009. Deep-sea octocorals and antipatharians show no evidence of seamount-scale endemism in the NW Atlantic. Marine Ecology Progressive Series. 397:25–35.

Thoma JN. 2013. Molecular and morphological diversity of sea fans with emphasis on deep-sea octocorals of the order Alcyoncea Lamouroux, 1812 [PhD dissertation]. Lafayette (LA): University of Louisiana at Lafayette.

Thompson JD, Higgins DG, Gibson TJ. 1994. CLUSTAL W: improving the sensitivity of progressive multiple sequence alignment through sequence weighting, position-specific gap penalties and weight matrix choice. Nucleic Acids Research. 22:4673–4680.

Wareham V, Edinger EN. 2007. Distribution of deep-sea corals in the Newfoundland and Labrador region, Northwest Atlantic Ocean. Bulletin of Marine Science. 81:289–313.

Watling L, Auster PJ. 2005. Distribution of deep-water Alcyonacea off the Northeast coast of the United States. In: Freiwald A, Roberts JM, editors. Cold-water corals and ecosystems. Berlin Heidelberg (Germany): Springer-Verlag. p. 259–276.

Williams GC. 1995. Living genera of sea pens (Coelenterata: Octocorallia: Pennatulacea): illustrated key and synopses. Zoological Journal of the Linnean Society. 113:93–140.

van Ofwegen, L. 2015. Funiculina armata. World Register of Marine Species (WoRMS). http://marinespecies.org/aphia.php?p=taxdetails&id=286621 on 2015-07-27.

This page intentionally left blank

CHAPTER 14. SCLERACTINIAN CORAL BIODIVERSITY AND PATTERNS OF INTER-CANYON CONNECTIVITY AMONG FOUR CORAL SPECIES

Cheryl L. Morrison, D. Katharine Coykendall, Marcus J. Springmann, Kelsey M. Shroades, Lakyn R. Sanders, Rhian G. Waller, Steve W. Ross, and Sandra D. Brooke

14.1 INTRODUCTION

14.1.1 Canyons and Cold-Water Coral Biodiversity

Submarine canyons are common features along continental and island margins worldwide that connect continental shelves to deep ocean basins (Shepard and Dill 1966, Harris and Whiteway 2011). A suite of characteristics make canyons unique and important ecologically relative to nearby continental slope habitats. Canyons are complex topographic, geologic, and oceanographic features that create dynamic environments with enhanced flux of organic matter and nutrient transport (Vetter and Dayton 1999, Puig et al. 2014). Highly variable currents created by internal waves and tides, dense shelf water cascading (de Stigter et al. 2007), and turbidity currents may either flush canyons or redistribute sediments and organic matter (Canals et al. 2006, Masson et al. 2010). These characteristics likely enhance productivity by increasing food availability and quality, thus allowing canyons to play important roles in the feeding and reproduction of benthic species distributed along continental margins (Vetter et al. 2010, Morris et al. 2013). As such, submarine canyons are known to be major sources of habitat heterogeneity (McClain and Barry 2010) and may be biomass hotspots where biodiversity is higher than surrounding slope habitats (Vetter and Dayton 1998, Tyler et al. 2009, De Leo et al. 2010, Vetter et al. 2010). In fact, both canyons and seamounts have been termed "keystone structures," which may be thought of as benthic islands of enhanced food availability and habitat diversity relative to neighboring deepsea habitats (Vetter et al. 2010). Habitat characterization of several canyons off the northeastern U.S. coast found that both depth and broad-scale habitat features shape species richness and composition (Quattrini et al. 2015a). For decapod crustaceans and fishes, species richness decreased with depth, but not for corals. Researchers noted a turnover of species at moderate to lower slope depths, coincident with boundaries between water masses (Quattrini et al. 2015a). Canyons may also form natural refuges for faunal communities that are sensitive to anthropogenic disturbance such as cold-water corals (Orejas et al. 2009, De Mol et al. 2010, Huvenne et al. 2011, Baker et al. 2012, Gori et al. 2013, Morris et al. 2013, Brooke and Ross 2014, Ross et al. 2015). The steep, rugged topography found in canyons may create hard substrate for coral settlement, and strong currents remove sediment and deliver food to suspension-feeding organisms such as corals. Corals are often recognized as important foundation species of deepsea habitats, since the physical structure they create may be inhabited either by epifaunal communities (Buhl-Mortensen and Mortensen 2004, Buhl-Mortensen and Mortensen 2005, Etnoyer and Morgan 2005) or by fishes (Ross and Quattrini 2007, Ross et al. 2015). Despite the potential for canyon communities to play a critical role as larval sources for the recolonization of damaged sites elsewhere (Vetter et al. 2010, Del Leo et al. 2010), little is known about the scale of dispersal among canyons or between canyons and habitats occurring on nearby continental margins.

14.1.2 Measuring Dispersal in the Sea via Genetic Connectivity

Identifying the scale of larval dispersal among habitats has been a challenge in marine ecology for decades (Grantham et al. 2003, Kinlan and Gaines 2003, Hixon 2011). Knowledge of the degree to which populations are connected through larval dispersal can guide effective management efforts (Cowen et al. 2006, Cowen et al. 2007, Botsford et al. 2009). Population genetics is often used to describe connectivity by comparing allele frequencies among spatially discrete subpopulations. Higher similarity suggests that

gene flow is occurring over time, whereas significant differences in allele frequencies may signify persistent barriers to larval exchange.

The majority of studies of marine connectivity focus on shallow-water environments, particularly tropical reef fishes (see Hixon 2011 for review). Shallow marine habitats were once considered open systems with ample exchange of larvae over large distances, but multiple studies have challenged this paradigm, and it is now accepted that local recruitment and small-scale population structure are common despite the lack of obvious physical barriers (Levin 2006, Cowan and Sponagule 2009). In other words, even though marine larvae may have the potential for long-distance dispersal, they often settle locally due to a combination of factors such as oceanographic conditions, larval behavior, and increasing mortality that is associated with extended time in the water column (Cowen et al. 2000, Strathman et al. 2002, Levin 2006).

Both biological and physical processes influence larval dispersal (Cowen and Sponagule 2009). Biological attributes such as timing of reproduction, larval lifespan, behavior (i.e., swimming versus passive movement in currents), buoyancy, and feeding behavior may influence dispersal distances (Young et al. 2012). Additionally, successful settlement and post-settlement survival and growth are all necessary for successful recruitment into a population. It is also known that, in general, larval mortality is high, and for some marine organisms, pelagic larval duration (PLD) is positively correlated with dispersal distance (Bohonak 1999, Shanks et al. 2003, Selkoe and Toonen 2011, Young et al. 2012). Following expectations for a short PLD, several coral species with brooded larvae exhibited higher levels of genetic structuring than spawning species with longer PLDs (Hellberg 1996, Ayre and Hughes 2000, Whitaker 2004, Underwood et al. 2009). However, many broadcast spawning corals exhibited evidence of limited dispersal between reefs or regions (Ayre and Hughes 2004, Baums et al. 2005, Underwood et al. 2007, Miller and Ayre 2008, Underwood et al. 2009). For shallow-water corals, in general, genetic data have suggested that most recruitment is local, yet occasional long-distance dispersal can occur across tens to hundreds of kilometers (Ayre and Hughes 2000, Miller and Ayre 2008, Gorospe and Karl 2013).

Ecosystems within the deep sea often occur over large geographic scales, yet are spatially fragmented across the entire range with stretches of unsuitable habitat separating habitat patches (e.g., cold-water coral reefs, methane seeps, hydrothermal vents). Although less is known about patterns of connectivity in the deep sea, recent studies have suggested common themes. First, similar to shallow populations along coastlines, including many coral species along the Great Barrier Reef (Ayre and Hughes 2004), larval exchange among populations that are close in proximity may be more likely than among distant populations. Therefore, the stepping-stone model of gene flow (Kimura and Weiss 1964) may be appropriate for many deepsea populations, particularly those arranged linearly along continental margins (LeGoff-Vitry et al. 2004a, Morrison et al. 2011), mid-oceanic ridge axes (Coykendall et al. 2011, reviewed by Vrijenhoek 2010), or linear arrays of seamounts (Samadi et al. 2006, Thoma et al. 2009, Smith et al. 2004). We have also learned that stretches of open ocean may interrupt a linear array of reefs (Ayre and Hughes 2004) or vent populations (Vrijenhoek 2010) and create an effective barrier to dispersal, decreasing connectivity abruptly and creating regionally isolated populations. For example, the deepsea scleractinian coral species *Desmophyllum dianthus* as well as two antipatharian species, *Antipathes robillardi* and *Stichopathes variabilis*, exhibited genetic subdivision across large ocean expanses in the South Pacific Ocean (Miller et al. 2010). Additionally, regionally restricted populations were detected using genetic data in both *Lophelia pertusa* (Morrison et al. 2011) and *Paragorgia arborea* (Herrera et al. 2012). Concordance among regional connectivity patterns of these co-distributed species indicates that physical forces (e.g., prevailing currents, eddies, upwelling) may restrict larval dispersal among regions. However, no genetic subdivision was detected for two other coral species (*Solenosmilia variablis, Madrepora oculata*) using the same mitochondrial and nuclear gene regions (Miller et al. 2010). Conversely, using microsatellites instead of mitochondrial DNA, Becheler et al. (2015, in press) identified distinct genetic populations of *Madrepora oculata* among canyons in the Bay of Biscay (eastern North Atlantic Ocean), yet co-occurring *Lophelia pertusa* were panmictic. Clearly, no

generalized connectivity pattern applies to all coral species. Regional differentiation of deepsea fauna that inhabit continental slope habitats may not be limited to benthic organisms such as corals. Even mobile species, such as fishes (e.g., *Helicolenus dactylopterus*; Aboim et al. 2005), squid (Shaw et al. 1999), scavenging isopods (France and Kocher 1996), and red crabs (Weinberg et al. 2003), exhibit regional structuring (Rogers 2002). Suggested mechanisms that may prevent panmixia of continental slope species include physical barriers such as continents, large expanses of deep water and deepwater sills (Cowart et al. 2013), structuring of the water column (density layers), currents that intersect features (Marsh et al. 2000), rugged topography (canyons and seamounts), oxygen minimum zones (Rogers 2002), and depth (Zardus et al. 2006, Rex and Etter 2010, Miller et al. 2011, Constantini et al. 2011, Baco and Cairns 2012, Quattrini et al. 2015b). In addition, species-specific life history strategies, especially related to spawning, may also act to limit exchange of individuals between populations (Rogers 2002, Rosser 2015).

14.1.3 Cold-Water Corals in the Mid-Atlantic Bight Canyons

The U.S. Atlantic margin is incised with 30 to 40 shelf-sourced submarine canyons (Andrews et al. 2013, Quattrini et al. 2015a). Thirteen of these canyons occur in the Mid-Atlantic Bight (MAB) from Cape Hatteras to Cape Cod. Two of the larger canyons in the MAB region, Baltimore and Norfolk canyons (**Figures 14-1** to **14-4**), occur approximately 130 km apart and were studied in detail as part of the Atlantic Deepwater Canyons study, a multiyear, multidisciplinary project. These passive margin canyons are shelf-sourced and are similar in size, yet geophysical surveys that compared fine-scale morphology among the canyons found differences in the morphology and orientation of canyon heads, steepness and density of sidewall gullies (Obelcz et al. 2014). Baltimore Canyon has a more linear shape and there was evidence of recent small-scale sediment transport. In contrast, Norfolk Canyon had a convex axial thalweg profile and sediment infilling at the canyon head.

Prior to the current study, Baltimore and Norfolk canyons had been moderately explored for corals, mostly using trawls over soft bottom (Hecker et al. 1980, Bachman et al. 2012). The following coral species had been documented in both canyons: the scleractinian (stony) solitary corals *Desmophyllum dianthus* and *Flabellum alabastrum* and the octocorals *Anthomastus grandifloras*, *Paragorgia arborea*, *Primnoa resedaeformis*, and *Acanthogorgia armata* (Hecker et al. 1980, 1983; Bachman et al. 2012.). Several coral species were known only from Baltimore Canyon: the scleractinian coral *Dasmosmilia lymani* and the octocorals *Anthomastus agassizii*, *Capnella florida* (now *Duva florida)*, *Acanella arbuscula*, and *Anthothela grandiflora* (Hecker et al. 1980, 1983; Bachman et al. 2012). One octocoral species, *Gersemia fructicosa*, was known only from Norfolk Canyon (Hecker et al. 1980, Bachman et al. 2012). During the present study, observations of both octocorals and scleractinian corals indicated that most were found on walls and steep slopes and on large boulders of rock or consolidated sediment (**Chapter 8**). Additionally, the presence of *Lophelia pertusa* was confirmed in both canyons (Brooke and Ross 2014) along with a *Javania* species and the octocorals *Paramuricea placomus, Anthomastus* sp., and *Duva florida* (**Chapter 8**). The Isisidid (bamboo) octocorals *Keratoisis grayi* and *Acanella arbuscula* were collected by remotely operated vehicle (ROV) and trawl, respectively, from Norfolk Canyon (**Chapter 13**). In deeper waters of Norfolk Canyon (>956 m), the scleractinian coral *Solenosmilia variabilis* and the antipatharian coral *Telopathes magna* were observed on canyon walls, and the octocoral *Acanella arbuscula* was trawled over soft sediment (**Chapter 8**). The most frequently collected species in the canyons were *Primnoa resedaeformis* and *Paragorgia arborea*, and the most numerous octocorals collected during this project from the continental slope adjacent to Norfolk Canyon were *Acanella arbuscula* and *Pennatula aculeate* (**Chapter 13**).

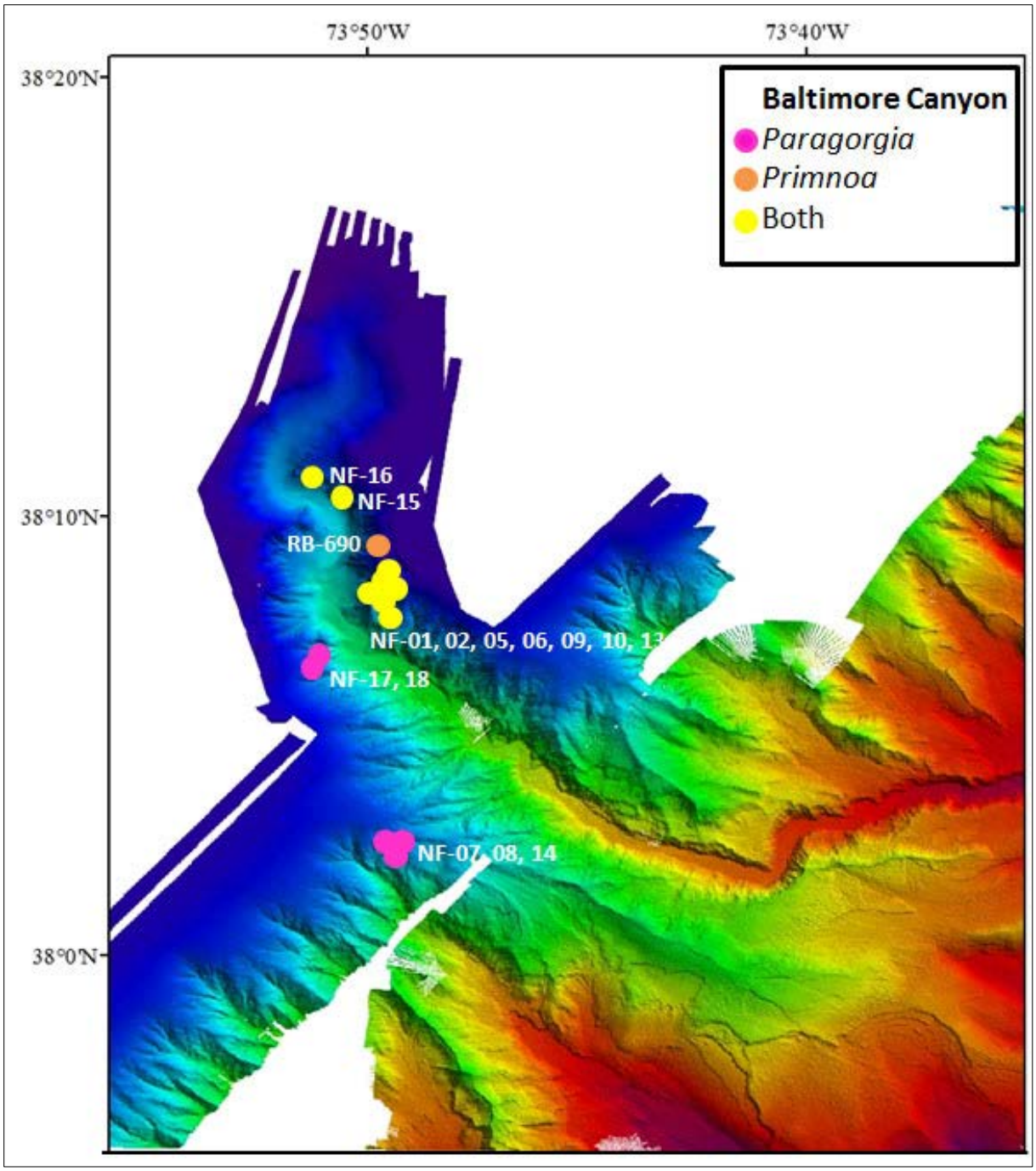

Figure 14-1. Multibeam image of Baltimore Canyon showing dive locations where the octocorals *Paragorgia arborea* and *Primnoa resedaeformis* were collected for genetic analysis.

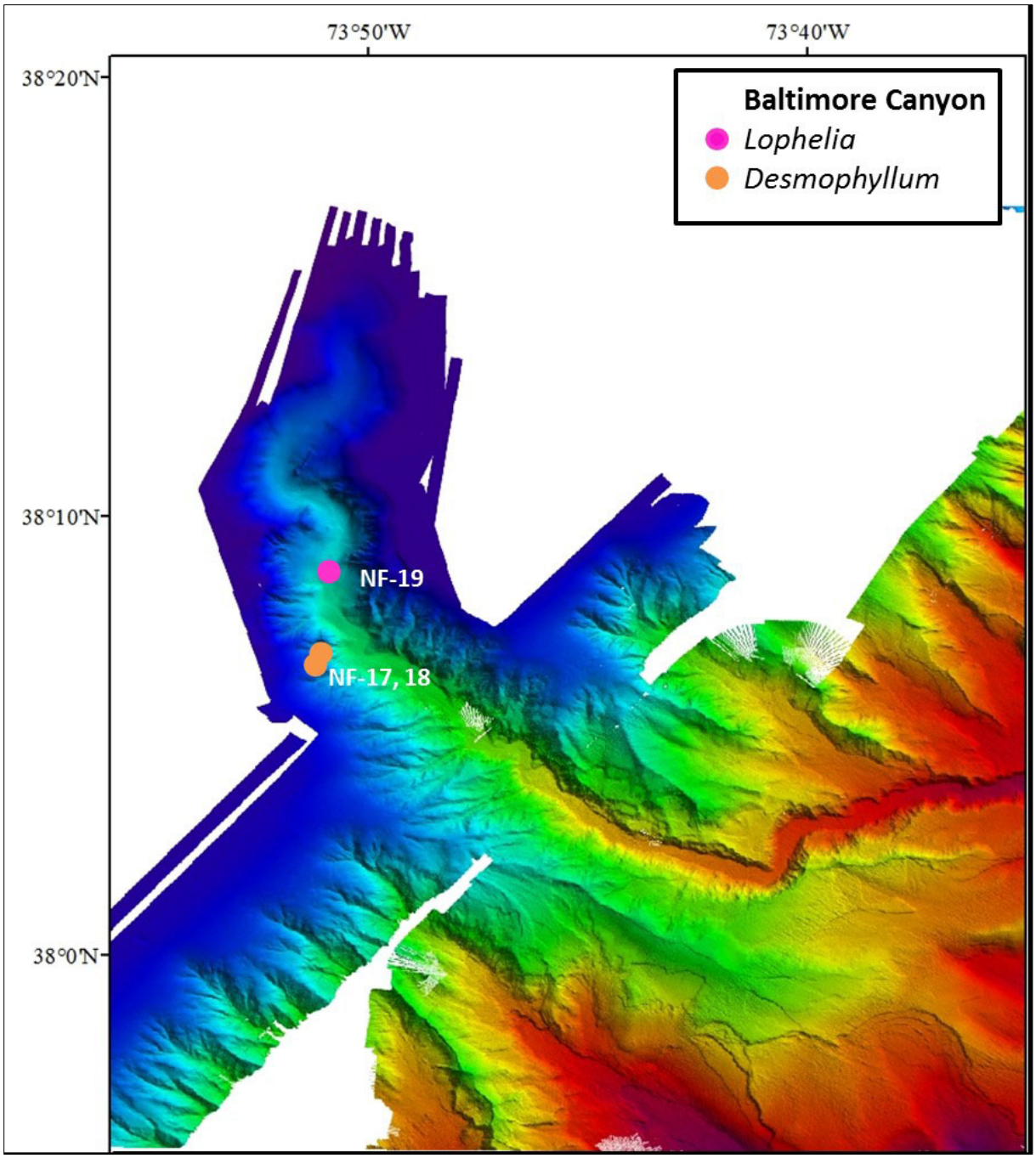

Figure 14-2. Multibeam image of Baltimore Canyon showing dive locations where the scleractinian corals *Lophelia pertusa* and *Desmophyllum dianthus* were collected for genetic analysis.

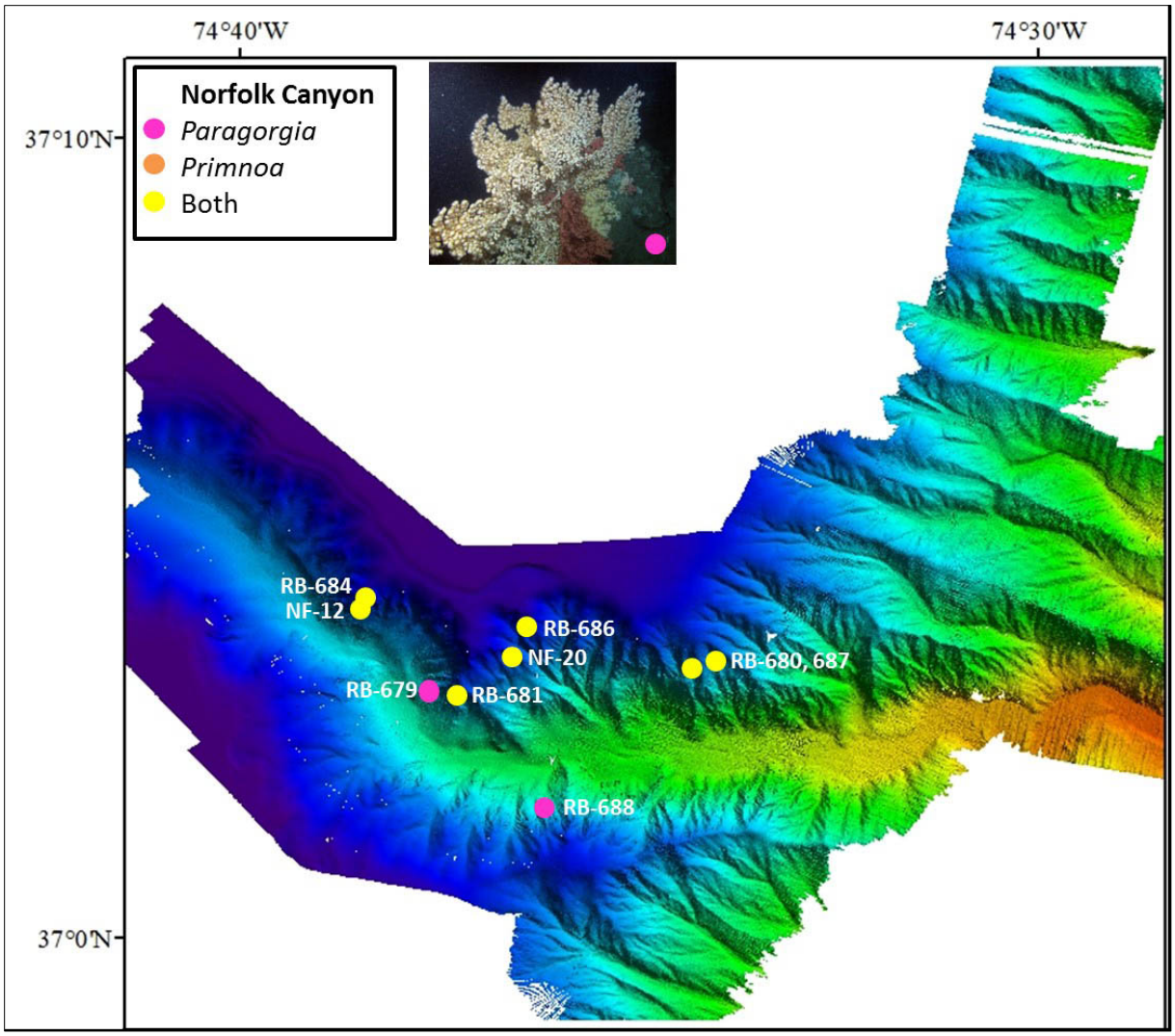

Figure 14-3. Multibeam image of Norfolk Canyon showing dive locations where the octocorals *Paragorgia arborea* and *Primnoa resedaeformis* were collected for genetic analysis.

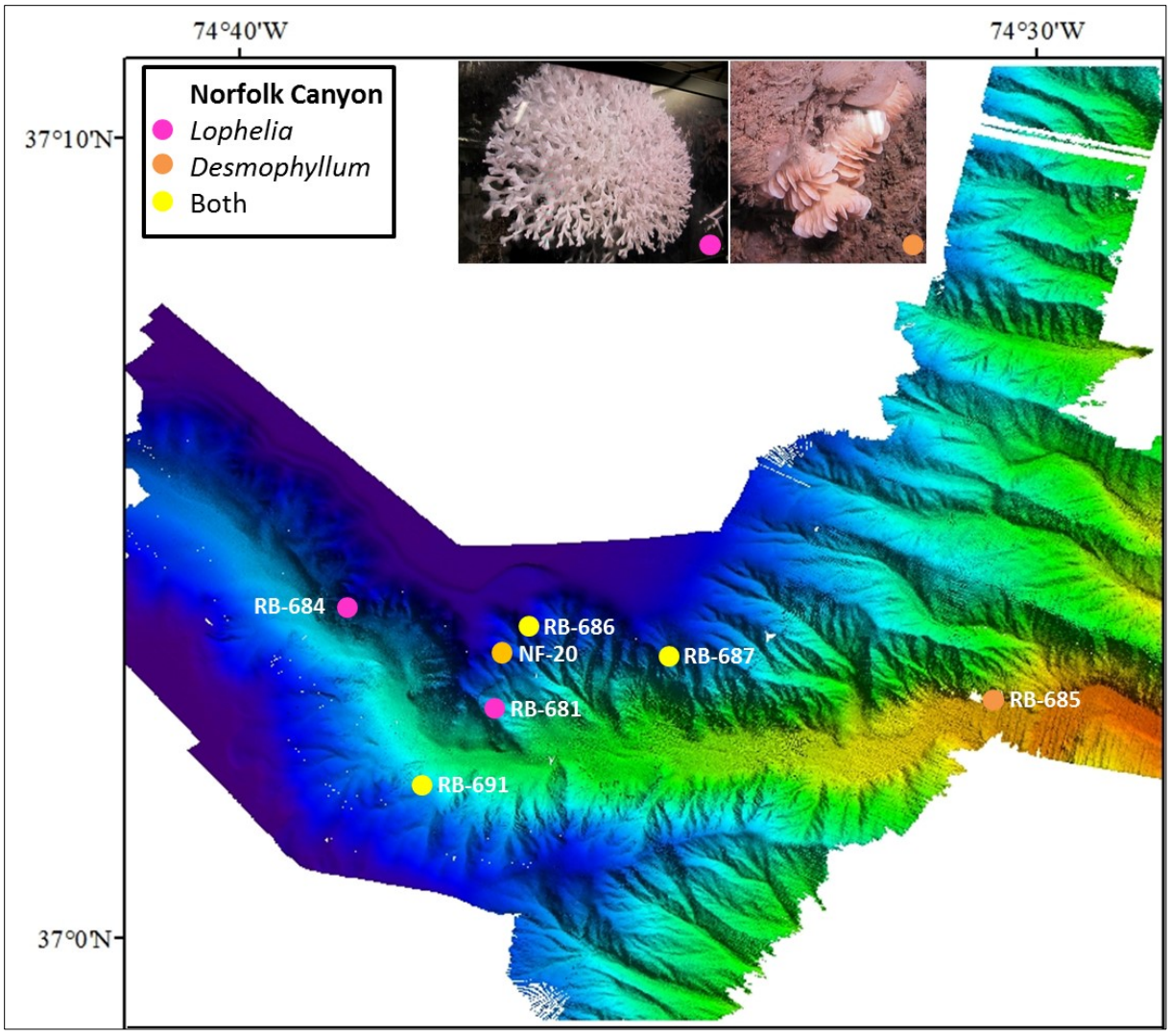

Figure 14-4. Multibeam image of Norfolk Canyon showing dive locations where the scleractinian corals *Lophelia pertusa* and *Desmophyllum dianthus* were collected for genetic analysis.

14.1.4 Study Objectives

The overall goal of the Atlantic Deepwater Canyons study was to improve our understanding of the benthic communities, including corals that reside in and around canyons in the MAB region. In this study, genetic techniques were used to:

1. Examine biodiversity of scleractinian corals using informative mitochondrial DNA markers and appropriate phylogenetic analyses; and
2. Estimate population genetic structure of abundant deepsea coral species using species-specific microsatellite markers.

Here we report on phylogenetic assessments of scleractinian coral species (*Flabellum* species collected from soft substrate via trawl and four species belonging to the family Caryophylliidae collected from canyon walls) as well as estimates of population genetic structuring among two habitat-forming gorgonian coral species (*Primnoa resedaeformis* and *Paragorgia arborea*) and two scleractinian coral species (*Lophelia pertusa* and *Desmophyllum dianthus*) that occur in Norfolk and Baltimore canyons.

14.2 METHODS

14.2.1 Sample Collection

High quality observations of these coral habitats and precision collections were afforded by the use of ROVs. ROV dives were conducted during the 2012 and 2013 sampling cruises. The National Oceanic and Atmospheric Administration (NOAA) ship *Nancy Foster* was used in 2012 (17 August to 14 September) along with the *Kraken 2* ROV (University of Connecticut), and Baltimore Canyon was emphasized. In 2013, Norfolk Canyon was emphasized, using the NOAA ship *Ronald H. Brown* and the *Jason II* ROV (Woods Hole Oceanographic Institution) for observations and sampling (30 April to 27 May). A total of 34 ROV dives were accomplished during the cruises, allowing for extensive observations of canyon habitats and coral fauna (see **Chapter 3** for cruise and sampling details).

Obtaining adequate numbers of georeferenced samples for population genetic analyses of deepsea taxa can be challenging and time consuming (Hilário et al. 2015; Becheler et al. 2015, in press). In order to maximize the numbers of georeferenced samples that could be obtained on each ROV dive, we used modified PVC quivers and rubber stoppers that could hold discrete samples. Seven quivers were fastened to the outside of the biobox of the *Kraken 2* ROV during the 2012 sampling cruise (**Figure 14-1**). Discrete samples could also be held in the eight suction buckets and/or the biobox, which was divided into three sections for most *Kraken 2* dives during the 2012 sampling cruise. A rotating quiver carousel that held 18 quivers (designed by Kevin Joy, University of Connecticut) was mounted to the deck of the *Jason II* ROV during the 2013 sampling cruise (**Figure 14-2**). Rubber stoppers that were a size smaller than the top stoppers allowed each quiver to be divided into two sections where two discrete samples could be held. To further maximize sampling capacity, multiple coral types were occasionally placed together in a quiver, since they could be distinguished by type upon ROV retrieval. During all ROV dives, when sampling occurred, time, depth, bottom location, and coral quiver number were recorded. Once the ROV was recovered, samples were moved to a cold room and processed gradually. Samples were given a unique identification number, and the collection container was recorded. Deck photographs were taken of representative samples. Tissue samples were removed with sterile forceps and placed on Flinders Technical Associates (FTA) cards and in 2 mL Eppendorf tubes filled with 95% ethanol for DNA preservation.

Four species of stony corals (Scleractinia, family: Caryophylliidae) were collected from the MAB canyons: *Lophelia pertusa*, *Solenosmilia variabilis*, *Desmophyllum dianthus*, and *Dasmosmilia lymani*. Several coral species were moderately abundant in both canyons, including the octocorals *Primnoa resedaeformis* and *Paragorgia arborea*, and the solitary scleractinian coral *Desmophyllum dianthus*. The ROV dives also provided the first observations of the structure-forming scleractinian coral *Lophelia pertusa* in the MAB (Brooke and Ross 2014). *Lophelia pertusa* was present, but rare, in both Baltimore and Norfolk canyons (Brooke and Ross 2014).

Four coral species were targeted within each canyon in order to allow estimation of connectivity among canyons (*P. resedaeformis*, *P. arborea*, and *D. dianthus*), or between canyons and continental slope populations (*L. pertusa*) via population genetic analyses based upon microsatellite genotyping. Coral collections in Baltimore Canyon resulted in 35 *P. resedaeformis*, and 64 *P. arborea* octocoral samples (**Figure 14-3**), plus three *L. pertusa*, and 31 *D. dianthus* scleractinian coral samples (**Figure 14-4**; **Table 14-1**). Sampling in Norfolk Canyon resulted in 69 *P. arborea* and 56 *P. resedaeformis* octocoral samples (**Figure 14-5**), plus 15 *L. pertusa* and 61 *D. dianthus* scleractinian samples (**Figure 14-6**; **Table 14-1**). Most of the coral samples were obtained at intermediate depth ranges in the canyons (300−800 m). One *Jason II* ROV dive in Norfolk Canyon (RB-685; **Figure 14-4**) allowed sampling of *D. dianthus* at deeper depths (1,250−1,390 m). Several individuals of the colonial scleractinian coral *Solenosmilia variabilis* were collected from similar depths on dive RB-685 as well. Trawl samples produced 56 individuals of *Flabellum alabastrum* (Norfolk Canyon, depth ~1,600 m) and

two *Caryophyllia* sp. or *Dasmosmilia lymani* cup corals (depth ~162 m) for genetic analysis (**Table 14-1**). In total, 224 octocoral and 177 scleractinian coral samples were preserved for genetic analysis (**Table 14-1**). Previous sampling of *L. pertusa* reefs (Morrison et al. 2011) allowed for estimates of connectivity between MAB canyon samples and populations from the Gulf of Mexico and North Atlantic Ocean (**Table 14-2**). Cape Canaveral samples of *L. pertusa* included in the 14 locus analysis were obtained during a research cruise on the R/V *Seward Johnson* using the *Johnson Sea Link* submersible (5–17 August 2009; S. Ross, Chief Scientist). Comparative *P. resedaeformis* samples were obtained on a research cruise using the R/V *Connecticut* and the ROV *Kraken 2* (University of Connecticut) from two sites in the Gulf of Maine: western Jordan Basin (43°19.75’ N, 67°47.76’ W) and Outer Schoodic Ridge (44°09.84’ N, 67°36.80’ W).

A 

B 

Figure 14-5. A. White coral sampling quivers being secured on the deck of the *Kraken 2* ROV during the 2012 sampling cruise. B. *Primnoa resedaeformis* sample in the *Kraken 2* ROV manipulator before placement into a coral quiver.

A. 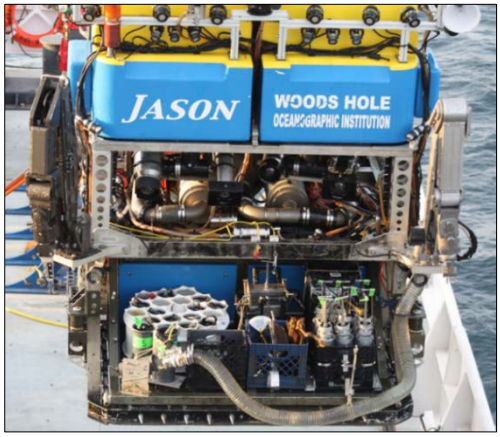

B. 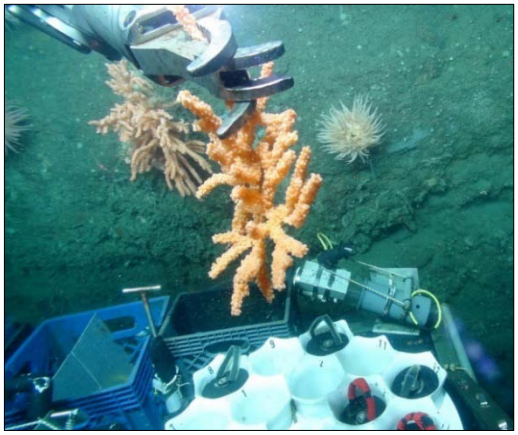

Figure 14-6. A. The *Jason II* ROV back on deck of the R/V *Ronald H. Brown* after a dive. ROV deck loaded with sampling gear, including carousel of coral quivers (white, left side of deck). B. *Jason II* ROV manipulator taking a sample of *Primnoa resedaeformis* and placing it in the coral quiver carousel.

Table 14-1. Collection information for octocoral and scleractinian coral samples from Baltimore and Norfolk canyons.

Canyon	Station	Gear	Date	Depth Range	*Primnoa*	*Paragorgia*	*Lophelia*	*Desmophyllum*	Other
Baltimore	ROV-2012-NF-01	ROV	18 Aug. 2012	450–634	2	12	0	0	0
	ROV-2012-NF-02	ROV	19 Aug. 2012	402–530	1	5	0	0	0
	ROV-2012-NF-05	ROV	23 Aug. 2012	400–540	2	6	0	0	0
	ROV-2012-NF-06	ROV	24 Aug. 2012	234–530	3	4	0	0	0
	ROV-2012-NF-07	ROV	26 Aug. 2012	412–444	0	2	0	0	0
	ROV-2012-NF-08	ROV	27 Aug. 2012	412–454	0	1	0	0	0
	ROV-2012-NF-09	ROV	28 Aug. 2012	313–574	6	9	0	0	0
	ROV-2012-NF-10	ROV	29 Aug. 2010	425–574	6	5	0	0	0
	ROV-2012-NF-13	ROV	6 Sept. 2012	404–478	4	6	0	0	0
	ROV-2012-NF-14	ROV	7 Sept. 2012	407–507	0	2	0	0	0
	ROV-2012-NF-15	ROV	8 Sept. 2012	276–577	5	6	0	0	0
	ROV-2012-NF-16	ROV	9 Sept. 2012	343–551	3	1	0	0	0
	ROV-2012-NF-17	ROV	10 Sept. 2012	569–830	0	1	0	21	0
	ROV-2012-NF-18	ROV	11 Sept. 2012	521–748	0	4	0	10	0
	ROV-2012-NF-19	ROV	12 Sept. 2012	302–608	0	0	3	0	0
	ROV-2013-RB-690	ROV	17 May 2013	288–388	3	0	0	0	0
Total					35	64	3	31	0
Norfolk	ROV-2012-NF-12	ROV	4 Sept. 2012	512–638	5	2	0	0	0
	ROV-2012-NF-20	ROV	13 Sept. 2012	385–766	3	6	1	9	0
	ROV-2013-RB-679	ROV	2 May 2013	676–789	0	1	0	0	0
	ROV-2013-RB-680	ROV	5 May 2013	441–640	4	8	0	0	0
	ROV-2013-RB-681	ROV	6 May 2013	421–616	9	12	1	0	0
	ROV-2013-RB-684	ROV	10 May 2013	320–611	16	12	1	0	0
	ROV-2013-RB-685	ROV	11 May 2013	539–1,390	0	0	0	28	10 (*Soleno*.)
	ROV-2013-RB-686	ROV	13 May 2013	394–607	7	8	2	10	0
	ROV-2013-RB-687	ROV	14 May 2012	386–710	3	6	7	12	0
	ROV-2013-RB-688	ROV	15 May 2013	326–557	0	8	0	0	0
	ROV-2013-RB-691	ROV	18 May 2013	444–520	9	6	5	1	0
	RB-2013-023	OT	4 May 2013	160–165	0	0	17	0	2 (cup corals)
	RB-2013-028	OT	5 May 2013	1,614–1,643	0	0	0	0	7 (*Flabellum*)
	RB-2013-029	OT	7 May 2013	1,576–1,629	0	0	0	0	17 (*Flabellum*)
	RB-2013-030	OT	7 May 2013	1,670–1,694	0	0	0	0	2 (*Flabellum*)
	RB-2013-035	OT	9 May 2013	1,608–1,674	0	0	0	0	10 (*Flabellum*)
Total					56	69	17	60	66
Species Total					91	133	20	91	66

Table 14-2. Regional *Lophelia pertusa* sampling localities, location and average sampling depth, sample size (N), and mean allelic patterns per locality estimated from eight microsatellite loci.

Locality	Latitude °N	Longitude °W	Avg. Depth (m)	N	N_A	H_O	H_E	F_{IS}
Gulf of Mexico								
Garden Banks (GB)	27°25′12″	-93°35′59.9″	527	19	13.00	0.685	0.804	0.149
Green Canyon (GC)	27°36′0″	-91°49′47.9″	527	12	9.75	0.620	0.814	0.254
Mississippi Canyon (MC) 751	28°11′24″	-89°47′59.9″	441	25	13.50	0.707	0.816	0.141
Tanker *Gulf Oil* (GO)	28°9′36″	-89°45′0″	533	9	8.00	0.729	0.752	0.019
Tanker *Gulfpenn* (GP)	28°26′24″	-89°19′11.9″	540	16	12.38	0.692	0.820	0.158
Viosca Knoll (VK) 862	29°6′35.9″	-88°23′24″	317	17	11.63	0.684	0.806	0.154
VK906	29°4′12″	-88°22′47.9″	380	64	17.50	0.605	0.840	0.288
VK826	29°8′59.9″	-88°1′11.9″	455	135	25.00	0.690	0.836	0.184
West Florida Slope (WFS)	26°10′47.9″	-84°42′35.9″	468	51	18.63	0.669	0.823	0.197
North Atlantic Ocean								
Miami Terrace (MTR)	*26°6′0″*	*-79°50′24″*	*287*	*15*	11.75	0.675	0.800	0.169
Cape Canaveral (CCN)	*28°17′23.9″*	*-79°36′35.9″*	*737*	*24*	15.13	0.684	0.790	0.134
Jacksonville (JAX)	*30°31′11.9″*	*-79°39′35.9″*	*591*	*24*	16.00	0.699	0.806	0.138
Savannah (SAV)	*31°44′23.9″*	*-79°12′0″*	*511*	*16*	13.25	0.707	0.831	0.149
Stetson Banks (SAV)	*32°15′35.9″*	*-77°28′48″*	*589*	*38*	22.00	0.703	0.843	0.177
Cape Fear (CFR)	*33°34′12″*	*-76°27′35.9″*	*394*	*20*	16.63	0.766	0.865	0.108
Cape Lookout (CLO)	*34°12′36″*	*-75°52′47.9″*	*398*	*58*	24.50	0.669	0.841	0.178
Norfolk Canyon (NC)	*37°03′53″*	*-74°37′29.9″*	*390*	*14*	12.13	0.651	0.850	-0.005
Baltimore Canyon (BC)	*38°09′01″*	*-73°50′22.4″*	*417*	*3*	3.63	0.625	0.646	0.236
Manning Seamount (MAN)	*38°13′11.9″*	*-60°31′12″*	*1,418*	*6*	4.63	0.363	0.569	0.454
Rehoboth Seamount (REH)	*37°28′11.9″*	*-59°57′0″*	*1,679*	*7*	5.50	0.526	0.610	0.118
Rockall Bank (RB)	*55°30′0″*	*-15°48′0″*	*562*	*9*	7.63	0.701	0.704	0.027
Mingulay (MNG)	*56°48′36″*	*-7 25′47.9″*	*153*	*6*	7.25	0.633	0.717	0.132
Sula Ridge (SULA)	*64°5′59.9″*	*8°5′59.9″*	*295*	*6*	4.63	0.583	0.592	-0.008
Trondheim Fjord (TRD)	*63°16′48″*	*9°33′0″*	*140*	*14*	10.5	0.592	0.720	0.188
Nordleska (NRD)	*63°36′35.9″*	*9°23′24″*	*160*	*10*	7.25	0.638	0.693	0.092
			Mean	25.29	12.87	0.654	0.769	0.155

N is sample size; N_A is the mean number of alleles per locus; *H*o and H_E are observed and expected heterozygosity; F_{IS} is the inbreeding coefficient of an individual relative to the subpopulation.

14.2.2 Molecular Methods

14.2.2.1 DNA Extractions

Total DNA was isolated from preserved coral tissue and/or FTA cards using the tissue protocol from the PureGene DNA extraction kit (Gentra Systems Inc., Minneapolis, Minnesota). DNA concentrations were determined by fluorescence assay (Labarca and Paigen 1980) and integrity of the DNA was visualized on 1% agarose gels (Sambrook et al. 1989).

14.2.2.2 DNA Sequencing

For coral phylogeny, DNA sequences were obtained for the 16S mitochondrial DNA (mtDNA) gene region, allowing for comparisons with large numbers of scleractinian coral sequences from previous work (see below). We used polymerase chain reaction (PCR) primers designed by Le Goff-Vitry et al. (2004b) to amplify the 16S mtDNA gene region: 16S LP16SF: TTGACCGGTATGAATGGTGT, and LP16SR: TCCCCAGGGTAACTTTTATC.

PCRs were performed with the following concentrations of reagents: 1× GoTaq Flexi PCR buffer (Promega), 2 mM of $MgCl_2$ (Promega), 10 mM of GeneAmp dNTPs (Life Technologies), 0.5 µM of each primer, 5× BSA (New England Biolabs), 0.04 unit of GoTaq Flexi (Promega), 2 µL of DNA (2.0 to 50 ng μL^{-1}), and laboratory grade water to adjust volume to 25 µL. Negative controls (no DNA template) were run with each PCR reaction. PCR reactions were performed on BioRad or Eppendorff thermalcyclers under the following conditions: initial denaturation of 94 ºC for 5 min, then 34 cycles of 94 ºC for 30 s, 50 ºC to 55 ºC for 30 s, 72 ºC for 1 min, and a final extension step of 72 ºC for 10 min. PCR products were electrophoresed on a 1.5% agarose gel at 95V for 30 min to ensure single band amplification. PCR products were either purified directly or excised from the agarose gel and purified using Qiaquick PCR purification spin columns (Qiagen) according to manufacturer's protocol. The purified products were re-suspended in 30 to 40 µL of laboratory grade water. Cycle sequencing for subsequent Sanger sequencing reactions were performed using 1 µL of purified PCR as template, 1 µL BigDye® Terminator v3.1 Ready Reaction Mix (Applied Biosystems), 1 µL of 5 µM primer, 2 µL of 5 × Sequencing buffer (Applied Biosystems), and 5 µL of molecular grade water for a final volume of 10 µL. Products were sequenced in both forward and reverse directions to assure accuracy. Cycle sequencing was performed on a BioRad or Eppendorff thermal cycler under the following conditions: 95 ºC for 3 min, then 29 cycles of 95 ºC for 20 s, 5 ºC for 20 s, and 60 ºC for 4 min with final extension of 60 ºC for 5 min. Cycle sequencing products were purified using AGENCOURT® CLEANSEQ® beads (Beckman Coulter) according to the manufacturer's protocol. Final products were re-suspended in 25 to 30 µL molecular grade water. Twenty-five microliters of purified products were loaded onto an ABI 3130xl DNA sequencer (Applied Biosystems).

DNA sequences were edited in Sequencher 5.2.2 (GeneCodes). After manually trimming low-quality regions at the beginning and end of the sequence reads, forward and reverse sequences for each individual were aligned and edited, and a consensus sequence was used in further analyses.

14.2.2.3 Microsatellite Genotyping

Nine microsatellite loci were developed from two Baltimore Canyon *Paragorgia arborea* samples (Coykendall and Morrison 2015) that were shotgun sequenced using a 454 GS Junior (Roche) next-generation sequencer. Loci were amplified singly via PCR following conditions in Coykendall and Morrison (2015), with a final reaction volume of 15 µL.

Next-generation sequencing was also used to develop microsatellite loci for *Primnoa resedaeformis* and its sister taxon, *P. pacifica* (Morrison et al. 2015). Nine of these loci amplified successfully and were polymorphic in our canyons samples: Prim014, Prim022, Prim026, Prim060, Prim068, Prim069,

Prim074, Prim094, and Prim096. Loci were amplified singly via PCR following conditions in Morrison et al. 2015, with a final reaction volume of 20 µL.

PCR conditions for amplification of eight microsatellite loci designed for *L. pertusa* (LpeA5, LpeC44, LpeC52, LpeC61, LpeC142, LpeC151, LpeD3, LpeD5) followed Morrison et al. (2008a). Five additional microsatellite markers designed from next-generation sequencing data were used for several *L. pertusa* populations (including canyon samples) from Gulf of Mexico [Garden Banks (GB); Green Canyon (GC); Mississippi Canyon 751 (MC751); Tanker *Gulf Oil* (GO); Tanker *Gulfpenn* (GP); Viosca Knoll 862, 906, and 826 (VK862, VK906, VK826); and West Florida Slope (WFS)]; and the northwestern Atlantic Ocean [Miami Terrace (MTR); Cape Canaveral (CCN); and Cape Lookout (CLO)]. These loci were: LpeG20, LpeG50, LpeG54, LpeG62, and LpeG63 (see Hennige et al. 2014). All *L. pertusa* PCR amplifications were carried out in 20 µL reactions.

Since a close genetic relationship has been estimated between *L. pertusa* and *Desmophyllum dianthus* (Morrison et al. 2008b, Addamo et al. 2012), the *L. pertusa* microsatellite markers were also tested on *D. dianthus*. Nine of the *L. pertusa* markers amplified and were polymorphic in *D. dianthus*: LpeA5, LpeC44, LpeC52, LpeC61, LpeC142, LpeD3, LpeG20, LpeG54, LpeG33. Amplification conditions for *D. dianthus* matched those in Morrison et al. (2008a).

For all coral genotyping, fluorescent DNA fragments were analyzed using an ABI 3130xl Genetic Analyzer (Applied Biosystems) with GeneScan-500 LIZ internal size standard. GeneMapper v.5.0 fragment analysis software (Applied Biosystems) was used to score, bin, and output allelic data.

14.2.3 Analyses

14.2.3.1 Phylogenetic Analyses

DNA sequences were edited using Sequencher 5.2.2 (Genecodes). After aligning sequences from both the forward and reverse directions, regions with ambiguous bases were omitted from subsequent analyses. The National Center for Biotechnology Information (NCBI) GenBank nucleotide database (Benson et al. 2013) was queried with consensus sequences from each individual. Sequences were combined with Caryophylliidae 16S sequences found in GenBank (**Appendix 14-A**, **Table 14-A1**) and initially aligned using the AliBee multiple alignment tool in GeneBee (Brodsky et al. 1992, Brodsky et al. 1995). Sequence alignments were further adjusted by eye in MEGA6.06 (Tamura 2013) and trimmed to 414 nucleotides. The best fit evolutionary model selection was performed treating gaps or missing data as partial deletions with a site coverage cutoff of 75%. The best fit model with the lowest Bayesian Information Criterion (BIC) score was used to construct a maximum likelihood phylogenetic tree with 500 bootstrap replications to determine the significance of branch positions. *Madrepora oculata* (RB09GM45) (family: Oculinidae) collected from the Gulf of Mexico was used as the outgroup. Bootstrap percentages >50% were reported.

14.2.3.2 Population Genetic Analyses

Individuals missing data at more than three loci were removed from further analysis. Individuals with identical multilocus genotypes (MLGs) were identified using the program GenAlEx v. 6.5b4 (Peakall and Smouse 2006, 2012). Unique MLGs were used in subsequent analyses. The unbiased probability of identity (P_{ID}; Kendall and Stewart 1977) that two unrelated individuals share the same MLG by chance was calculated for increasing locus combinations using GenAlEx.

Loci were tested for fit to statistical assumptions of population genetic analyses. Observed and expected heterozygosities under Hardy-Weinberg equilibrium (HWE), and fixation indices per locus and locality were calculated using GenAlEx. Exact tests for HWE and linkage disequilibrium were performed using Genepop on the Web (Raymond and Rousset 1995). To assess levels of inbreeding, Weir and Cockerham's (Weir and Cockerham 1984) estimators f and F, analogous to Wright's inbreeding

coefficients F_{IS} and F_{IT} (Wright 1951), respectively, were calculated for each locality and tested for statistical significance by 1,000 permutations with FSTAT ver. 2.9.3.2 (Goudet 1995). The estimators f and F depend on population size and history, but not on sampling scheme (Weir and Cockerham 1984). Because observed allelic diversity can be proportional to sample size (Leberg 2002), the allelic richness (number of alleles per locality) and private allelic richness (expected number of unique alleles in a sample rarified to smallest sample size) were calculated by rarefaction in HP-RARE (Kalinowski 2005). Sequential Bonferroni adjustments for multiple tests (Rice 1989) were used on these and other multiple tests.

For each microsatellite dataset, loci were searched to identify those potentially under selection using LOSITAN (Antao et al. 2008), which implements F_{ST}-outlier tests. Simulations were run under infinite alleles and stepwise mutation models using default settings (50 000 replications).

Several techniques were used to describe genetic relationships between populations as estimated from microsatellite data. First, for species with data for more than two canyons, population genetic differentiation among localities was examined through pairwise F_{ST} allele frequency-based estimates (Weir and Cockerham1984). Significance of F_{ST} values was tested using 999 pairwise population permutations in GenAlEx. Another distance-based procedure, analysis of molecular variance (AMOVA; Excoffier et al. 1992) was used to partition genetic variation among populations (all species) and regions (*P. resedaeformis, L. pertusa*), using 999 permutations in GenAlEx. When significant genetic structuring was (Mantel 1967) detected by AMOVA and numbers of sampled populations were adequate (N > 3), partial Mantel tests were performed using the Isolation by Distance Web Service (IBDWS) v. 3.23 (Jensen et al. 2005) to assess whether the association between linearized genetic distance (F_{ST}) and geographic distance was statistically significant (Wright 1943) through calculation of the slope and intercept of the relationship using reduced major axis regression. The Mantel tests were repeated with log-transformed genetic and geographic distance matrices. For *D. dianthus* sampled at two different depth ranges in Norfolk Canyon, an indicator matrix was included to assess the effects of depth on genetic distance. Principal coordinates analysis (PCoA), a multivariate technique that plots the major patterns in multivariate datasets such as multiple loci and multiple populations, was also used for species with more than two populations sampled (*P. resedaeformis, L. pertusa*). Because numbers of individuals differed between samples, Nei's unbiased genetic distances were calculated and PCoA was computed from these distance matrices in GenAlEx.

Next, an allele frequency model-based Bayesian clustering approach (Pritchard et al. 2000) was implemented in STRUCTURE v. 2.3.4 (Hubisz et al. 2009). This method infers the number of genetic clusters (K) from MLG data by minimizing HWE and linkage disequilibrium among loci within groups and assigning individuals (probabilistically) to each cluster. Because models utilizing collection location information as priors are useful for small datasets and weak structuring (Hubisz et al. 2009), locality designations were included as priors. Settings for all runs also included an admixture model (i.e., individuals may have mixed ancestry), correlated allele frequencies (Falush et al. 2003), and 200 000 MCMC iterations after a burn-in of 50 000 iterations. Ten independent chains were run to test each value of K. The optimum number of clusters was determined by evaluating the values of K as the highest mean likelihood of the probability of the number of clusters given the data observed, ln Pr(X|K) (Pritchard et al. 2000), and ΔK (Evanno et al. 2005). This information was compiled and graphed using STRUCTURE Harvester v.0.56.1 (Earl and vonHoldt 2012). Each cluster identified in the initial STRUCTURE run was analyzed separately using the same settings to identify potential within-cluster structure since detection of fine-scale structuring can be limited with large datasets (Jakobsson et al. 2008).

14.3 RESULTS

14.3.1 Phylogenetic Analyses

14.3.1.1 Flabellum

Mitochondrial 16S sequence data were obtained for three *Flabellum alabastrum* samples taken from three different otter trawls in Norfolk Canyon at depths ranging from 1,602 to 1,682 m (MAC 276, 278, and 334; **Figure 14-7**; GenBank accession numbers MG241536-MG241538; Table 14.A1). These sequences were aligned with 25 *Flabellum* 16S mtDNA sequences available in GenBank, representing 13 species from the family: Flabellidae. Most of these GenBank sequences were from species that inhabit the South Pacific Ocean (Australia and New Caldonia; Stolarski et al. 2011) or Japan (Ikeno et al. 2010). There was only one species from the Atlantic Ocean available in GenBank for *F. angulare* (LeGoff-Vitry et al. 2004b). *Enallopsammia rostrata*, a species also belonging to the Complex clade of corals but in a different family (Dendrophyliidae), was used as an outgroup. The final alignment was 422 base pairs in length. The HKY nucleotide substitution model was chosen as the best fit for the data and was used in creating a maximum likelihood estimate of phylogeny for *Flabellum* species.

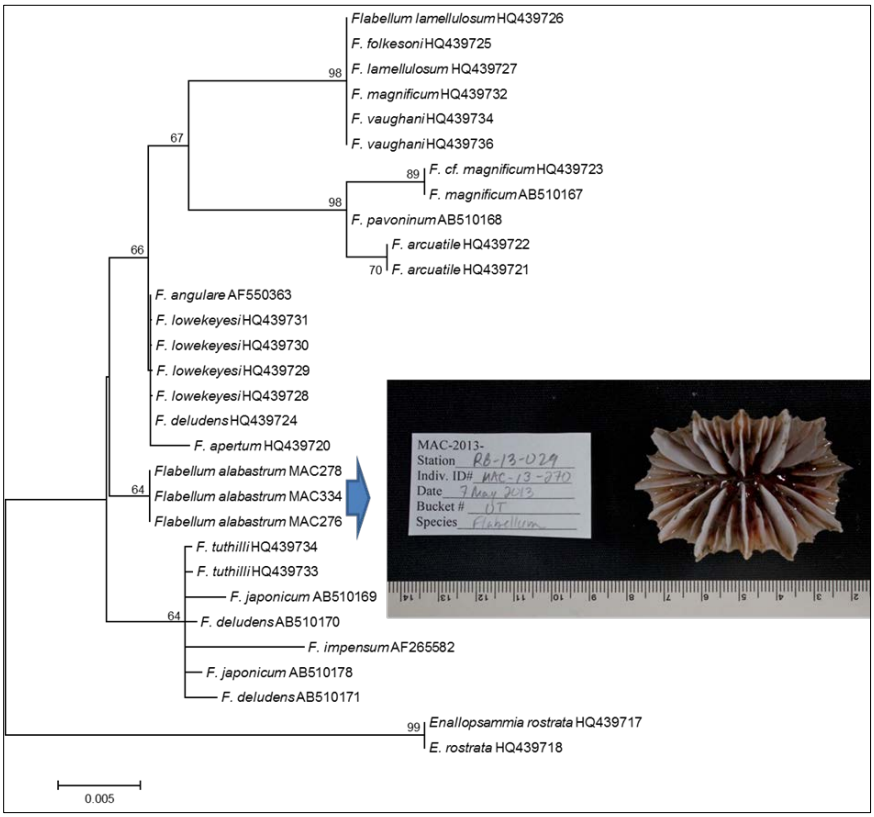

Figure 14-7. The evolutionary history among *Flabellum* species was inferred by using the maximum likelihood method based on the Hasegawa-Kishino-Yano model (Hasegawa et al. 1985). The tree with the highest log likelihood (-795.5530) is shown. The percentage of trees in which the associated taxa clustered together is shown next to the branches. Initial tree(s) for the heuristic search were obtained automatically by applying Neighbor-Join and BioNJ algorithms to a matrix of pairwise distances estimated using the maximum composite likelihood approach and then selecting the topology with superior log likelihood value. The tree is drawn to scale, with branch lengths measured in the number of substitutions per site. The analysis involved 30 nucleotide sequences. A total of 428 positions were in the final dataset. Evolutionary analyses were conducted in MEGA6 (Tamura et al. 2013).

The most distinctive clades in the *Flabellum* phylogeny contained species from Australia (*F. lamellulosum, F. folkensi, F. magnificum, and F. vaughani*) and Japan/New Caldonia (*F. cf. magnificum, F. pavonium,* and *F. arcuatile*) (**Figure 14-7**; top, with bootstrap support values of 98). The three *F. alabastrum* from Norfolk Canyon formed a unique clade, yet relationships of the Norfolk Canyon samples and two other clades were not highly supported by bootstrap analysis (**Figure 14-7**; middle, bootstrap values ~65%). *Flabellum angulare*, the only other species from the Atlantic available for phylogenetic analysis, fell into a different clade than the *F. alabastrum* individuals from Norfolk Canyon.

14.3.1.2 Caryophylliids

Phylogenetic relationships among the four Caryophylliidae species collected in the MAB canyons (GenBank accession numbers MG241539-MG241564; Table 14.A1) in addition to sequences from related taxa available in GenBank (Romano and Cairns 2000, LeGoff-Vitry et al. 2004b, Miller et al. 2010, Kitahara et al. 2010, Addamo et al. 2012, Benson et al. 2013, Zeng et al. 2014) are presented in **Figure 14-8**. For each Caryophyllidae species, mtDNA 16S sequences had identical haplotypes with their conspecifics in our collections, including *Lophelia pertusa* from the MAB canyons, Miami Terrace, and the Gulf of Mexico areas. One large clade that was not supported by bootstrap analysis included all *L. pertusa* and *Desmophyllum dianthus* MAB canyons samples, and most other sequences from these taxa that were available in GenBank. The sequences for each of these taxa were intermingled and not differentiated from each other. Also included in this clade was a sequence for *Caryophyllia smithii* (JQ611358; from the Ionian Sea; Addamo et al. 2012) that grouped with a *D. dianthus* sequence (JQ611357; Addamo et al. 2012). Another sequence for *C. smithii* (JQ611349; Strait of Gibraltar; Addamo et al. 2012) matched the sequence of *Dasmosmilia lymani* produced for this study (**Figure 14-8**). Sequences from MAB canyons *Solenosmilia variabilis* matched others for this taxon in GenBank. *Solenosmila variabilis* formed a clade with all other *Caryophyllia* species included in the analysis, plus *Dasmosmilia lymani* and *Cristopatrochus rugosus* (50% bootstrap support, **Figure 14-8**). The *Solenosmila* sequences included from GenBank were from the South Pacific Ocean (Miller et al. 2010, Zeng et al. 2014) and were invariant from the MAB canyons *S. variabilis* sequences. Relationships among the *Caryophyllia* species and *S. variabilis* were unresolved; however, affinities among some of the *Caryophyllia* species were apparent (e.g., *C. calveri, C. scobinosa, C. unicristata, C. transversalis, C. grandis*; **Figure 14-8**). One *D. dianthus* sequence (GQ868690; Stolarksi et al. 2011) grouped with *Christopatrochus rugosus* (AF265600; Romano and Cairns 2000) and *Caryophyllia versicolorata* (HQ439689; Stolarski et al. 2011). The four sequences included for *Dasmosmilia lymani* did not group together, but instead grouped with other *Caryophyllia* species. Our MAB canyons *D. lymani* sequences were identical to *C. smithii* (JQ611349; Addamo et al. 2012) and these sequences formed a clade (**Figure 14-8**). Two of the *D. lymani* sequences formed a clade with *C. atlantica* (HQ439766-67; Stolarski et al. 2011), and the other *D. lymani* sequence grouped with *C. transversalis* (FJ788125) and *C. grandis* (FJ788118; Kitahara et al. 2010). The basal taxon for this large clade was *C. ralphae*, which was also basal to a clade containing *Caryophyllia* species and *Dasmosmilia lymani* in the analysis of Stolarski et al. (2011).

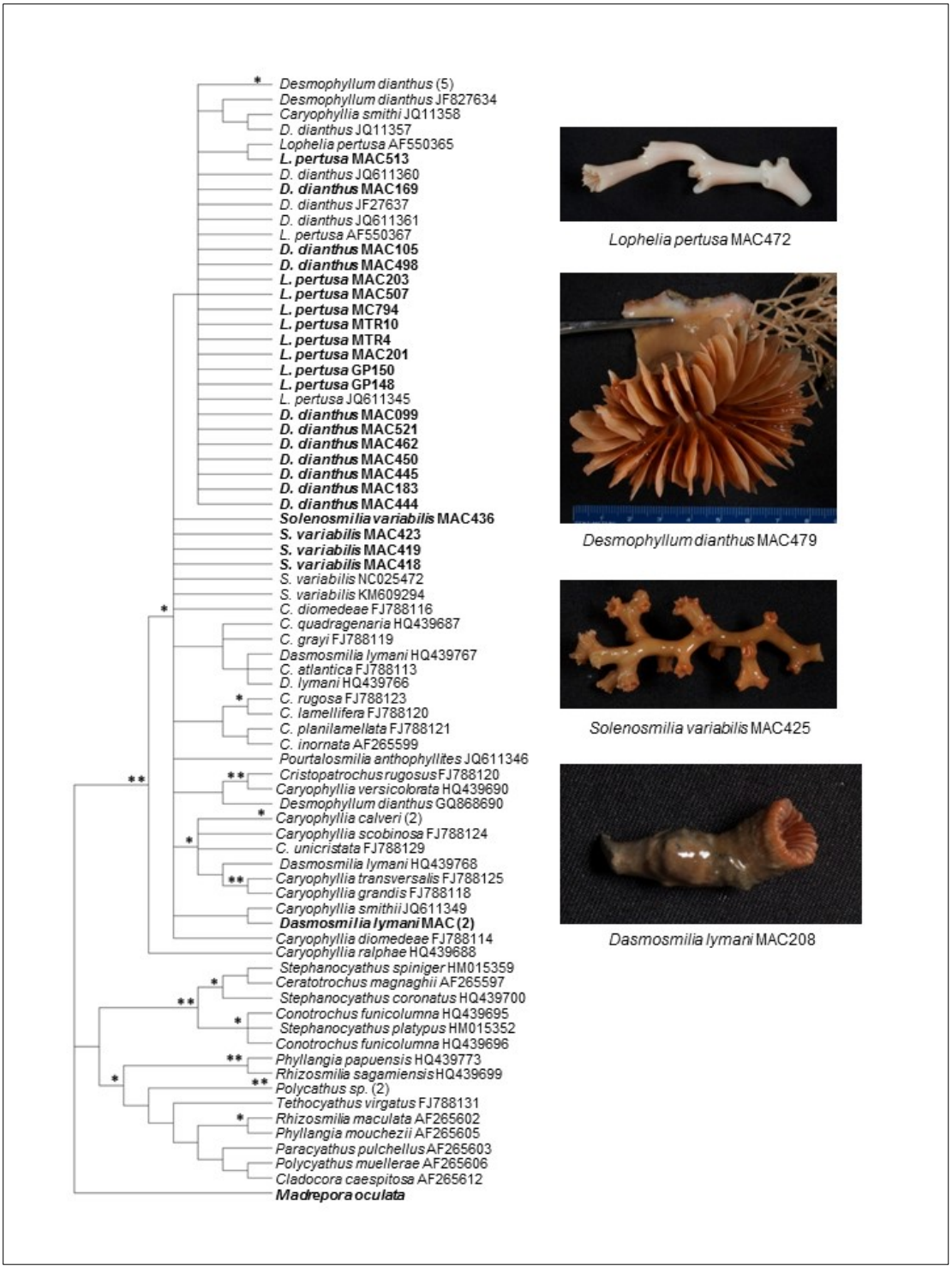

Figure 14-8. Maximum likelihood phylogenetic tree of scleractinian coral species (family: Caroyphylliidae) constructed from mitochondrial 16S DNA sequences in MEGA6.06. Samples from the Mid-Atlantic Bight canyons are in bold. *= Bootstrap support (out of 500) >50%, **= Bootstrap support >90%. GenBank accession numbers are given after species names for sequences obtained from the National Center for Biotechnology Information GenBank nucleotide database (Benson et al. 2013). Number of individuals, if >1, are in parentheses after the taxon name.

14.3.2 Population Genetic Analyses

14.3.2.1 Genetic Differentiation Within Paragorgia arborea

The microsatellite dataset generated for *P. arborea* included 124 individuals (60 from Baltimore Canyon, 64 from Norfolk Canyon) genotyped at eight loci. Eight of the 132 original samples were excluded from further analysis due to missing data at three or more loci. Each of the 124 individuals in the final dataset had a unique MLG. The P_{ID} for this set of loci was 3.3×10^{-05}. Measures of genetic diversity for *P. arborea* were higher in the Baltimore Canyon samples compared with Norfolk Canyon samples (**Table 14-3**). Numbers of alleles per locus and rarified allelic richness averaged 4.75 and 4.64, respectively (**Table 14-3**). Private allelic richness was more than twice as high for the Baltimore Canyon *P. arborea* samples (**Table 14-3**). Average heterozygosities ranged from 0.468 in Norfolk Canyon to 0.501 in Baltimore Canyon. The Baltimore Canyon *P. arborea* population had a slightly negative fixation index, indicating heterozygote excess, whereas the Norfolk Canyon had a positive *F* value, indicating a heterozygote deficit (F_{IS}, **Table 14-3**). Departures from HWE were not significant when tested at all locus and population combinations (**Appendix 14-A**, **Table 14-A2**). Linkage disequilibrium was not detected in any of the 56 pairwise comparisons (not shown). None of the loci appeared to be under selection in the F_{ST}-outlier test (not shown).

No genetic structuring was detected between canyon populations of *P. arborea* in an AMOVA-based estimate ($F_{ST} = 0.005$, $P < 0.086$; **Table 14-4**). Similarly, only one cluster was detected among *P. arborea* canyon individuals using the Bayesian software STRUCTURE (**Figure 14-9 A–D**).

Table 14-3. *Paragorgia arborea* sampling localities, average sampling depth, sample size (*N*), and mean allelic patterns per locality based on eight microsatellite loci.

Locality	Avg. Depth (m)	*N*	N_A	*A*r	*A*p	H_O	H_E	*f*
Baltimore Canyon	472	60	5.00	4.86	0.77	0.501	0.492	-0.008
Norfolk Canyon	482	64	4.50	4.41	0.32	0.468	0.480	0.032
Mean	477	124*	4.75	4.64	0.55	0.485	0.486	0.012

N is the number of unique multilocus genotypes (*with total instead of mean in last row); N_A is the mean number of alleles per locus; *A*r and *A*p are allelic and private allelic richness, respectively, with rarefaction for a corresponding sample size of 92 alleles; *H*o and *H*e are observed and expected heterozygosity; *f*, Weir and Cockerham (1984) estimator of F_{IS} inbreeding coefficient, is given in the last column, with no significant deviations from panmixia after false discovery rate of 0.05.

Table 14-4. Results from analysis of molecular variance partitioning genetic variance among and within Baltimore and Norfolk Canyon populations of *Paragorgia arborea*.

Variation	df	Est. Var.	F_{ST}	*P*
Among populations	1	0.010	–	–
Within populations	246	1.960	–	–
Total	247	1.970	0.005	0.086

df = degrees of freedom; Est. Var., estimated variance; FST, genetic differentiation among populations; P = probability value (not significant at >0.05).

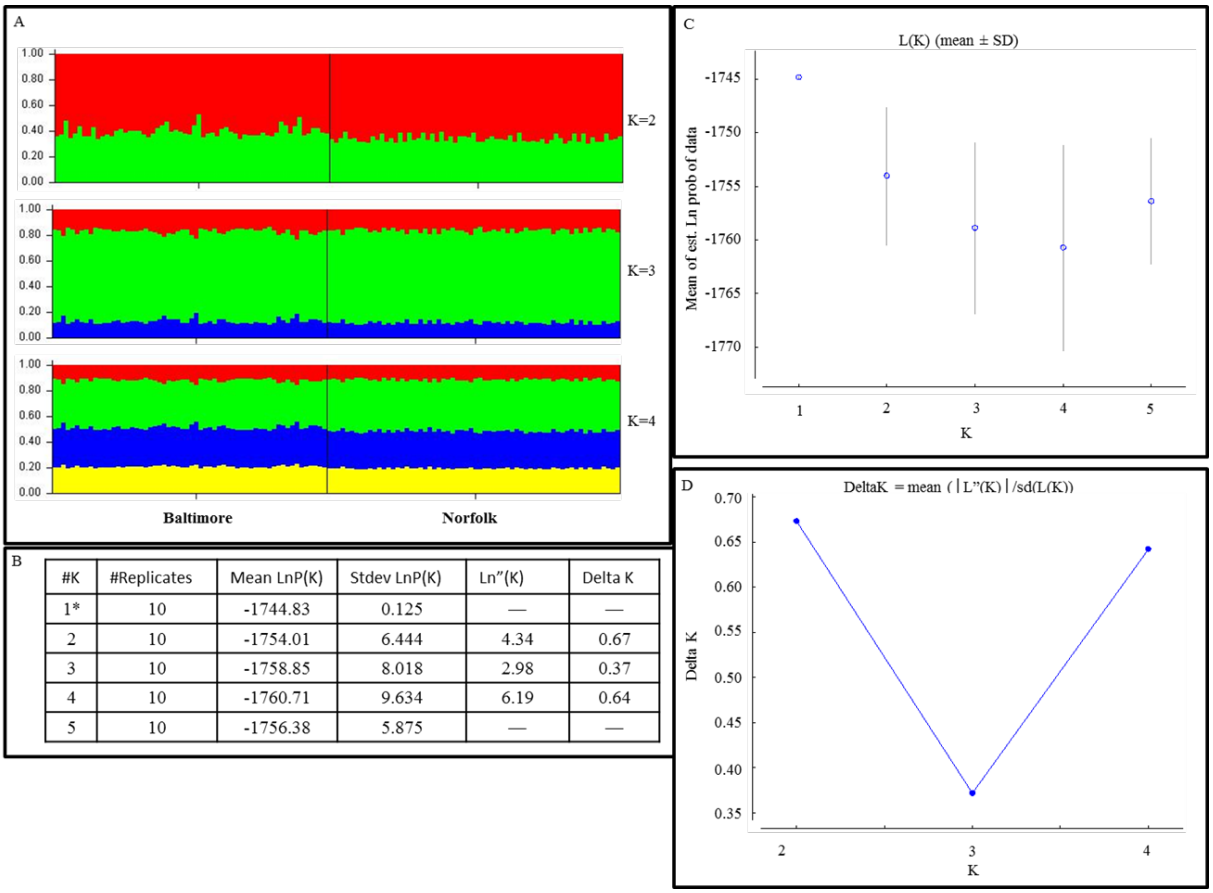

B

#K	#Replicates	Mean LnP(K)	Stdev LnP(K)	Ln''(K)	Delta K
1*	10	-1744.83	0.125	—	—
2	10	-1754.01	6.444	4.34	0.67
3	10	-1758.85	8.018	2.98	0.37
4	10	-1760.71	9.634	6.19	0.64
5	10	-1756.38	5.875	—	—

Figure 14-9. A. Bayesian clustering of *Paragorgia arborea* individuals from the Mid-Atlantic Bight canyons based upon multilocus genotypes at eight microsatellite loci. Within bar plots, each individual is represented by a vertical bar partitioned into sections with lengths proportional to estimated probability of membership into K clusters. B. Mean statistics for each of K clusters, estimated using STRUCTURE Harvester (Earl and vonHoldt 2012). C. Mean estimated log probability of the data for each of the K clusters. D. Delta K plot, based on the rate of change in the log probability of the data (Evanno method, Evanno et al. 2005). No significant genetic structuring was detected in the dataset; the most likely number of clusters is K = 1.

14.3.2.2 Genetic Differentiation Within Primnoa resedaeformis

The *Primnoa resedaeformis* microsatellite dataset included 102 individuals from Baltimore and Norfolk canyons, plus representative samples from western Jordan Basin and Outer Schoodic Ridge in the Gulf of Maine (**Table 14-5**). The P_{ID} using this set of loci was 8.1×10^{-5}. The mean number of alleles per locus ranged from 2.89 (Outer Schoodic Ridge) to 4.22 (Baltimore Canyon; N_A, **Table 14-5**). Rarified allelic richness ranged from 2.9 in the Baltimore Canyon population to 3.22 in the Schoodic Ridge population, and averaged 3.01. Private allelic richness was lowest in the Jordan Basin population (0.01) and highest in the Norfolk Canyon population (0.61; A_p, **Table 14-5**). Observed heterozygosities ranged from 0.391 in Baltimore Canyon to 0.441 in Outer Schoodic Ridge and averaged 0.427. Heterozygote deficits were detected at certain loci in Schoodic (*Prim*60 and *Prim*74) and Jordan (*Prim*69) populations, but no loci were out of Hardy-Weinberg equilibrium across all *P. resedaeformis* populations (H_O, **Table 14-4**; **Appendix 14-A**, **Table 14-A3**). Linkage disequilibrium was not significant among pairs of loci ($\alpha = 0.05$, $P < 0.000446$; not shown). None of the loci appeared to be under selection based on the F_{ST}-outlier test (not shown).

Table 14-5. *Primnoa resedaeformis* sampling localities, average sampling depth, sample size (N), and mean allelic patterns per locality based on eight microsatellite loci.

Locality	Avg. Depth (m)	*N*	N_A	*A*r	*A*p	H_O	H_E	*f*
Baltimore Canyon	438	32	4.22	2.90	0.59	0.391	0.402	0.003
Norfolk Canyon	462	42	4.00	2.98	0.61	0.438	0.450	0.011
Western Jordan Basin	218	15	3.11	2.92	0.01	0.437	0.440	0.042
Outer Schoodic Ridge	179	13	2.89	3.22	0.51	0.441	0.489	0.140
Mean	324	102*	3.56	3.01	0.43	0.427	0.438	0.032

N is the number of unique multilocus genotypes (*with total numbers of individuals instead of mean, last row); N_A is the mean number of alleles per locus; *A*r and *A*p are allelic and private allelic richness, respectively, with rarefaction for a corresponding sample size of 24 alleles; H_O and H_E are observed and expected heterozygosity; *f*, Weir and Cockerham (1984) estimator of F_{IS} inbreeding coefficient (given in the last column) with no significant deviations from panmixia after false discovery rate of 0.05.

Pairwise estimates of F_{ST}'s were high for all comparisons, ranging from 0.033 (between Schoodic and Jordan sites) to 0.331 (between Norfolk and Schoodic; **Table 14-6**), and were all significantly different from zero. The highest pairwise F_{ST} values were between the Baltimore and Norfolk canyons *P. resedaeformis* populations and the Schoodic Ridge population (F_{ST} = 0.312 and 0.331, respectively, **Table 14-6**). The F_{ST} estimate between canyons for *P. resedaeformis* was the highest out of any of the coral species compared in this study (F_{ST} = 0.117, **Table 14-6**).

Table 14-6. Estimates of F_{ST} (below diagonal) and numbers of migrants per generation (*N*m, above diagonal) between populations of *Primnoa resedaeformis* based upon analysis of molecular variance using eight microsatellite loci.

Population	Baltimore	Norfolk	Schoodic	Jordan
Baltimore		0.001	0.001	0.001
Norfolk	0.117		0.001	0.001
Schoodic	0.312	0.331		0.026
Jordan	0.241	0.278	0.033	

When variance in allele frequencies was examined in an AMOVA framework, significant structuring was detected among *P. resedaeformis* populations, with approximately 20% to 23% of variance attributed to among populations or regional population clusters (**Table 14-7**). Variance was maximized when populations were grouped by two regions comprising the two canyons and two Gulf of Maine populations (23% variance among regions, F_{ST} = 0.298, **Table 14-7**). A positive correlation between genetic (PhiPT) and geographic distances was detected in a Mantel test (**Figure 14-10**), suggesting that a stepping stone model of gene flow may be appropriate for *P. resedaeformis.* In a PCoA, each of the sampled *P. resedaeformis* populations appeared unique, as each fell in a different quadrant of the PCoA plot, with more separation between canyons than Gulf of Maine populations (**Figure 14-11**).

Table 14-7. Results from analysis of molecular variance among Baltimore and Norfolk canyons and regional groupings including Gulf of Maine (GoM) for *Primnoa resedaeformis populations.*

	Variation	df	Est. Var.	Percent	F_{ST}	*P*
4 populations	Among populations	3	0.502	22	–	–
	Within populations	200	1.748	78	–	–
	Total	203	2.250	100	0.223	0.001*
2 clusters	Among regions	1	0.561	23	–	–
Canyons	Among populations	2	10.805	7	–	–
GoM	Within populations	200	1.748	70	–	–
	Total	203	2.488	100	0.298	0.001*

Table 14-7. (Continued).

	Variation	df	Est. Var.	Percent	F_{ST}	*P*
3 clusters	Among regions	2	0.454	20	–	–
Baltimore	Among populations	1	0.072	3	–	–
Norfolk	Within populations	200	1.748	77	–	–
GoM	Total	203	2.274	100	0.232	0.001*

df = degrees of freedom; SS = sum of squares; Est. Var. = estimated variance; Percent = percent of total variance; F_{ST} = genetic differentiation among populations; *P* = probability value (* significant at <0.05).

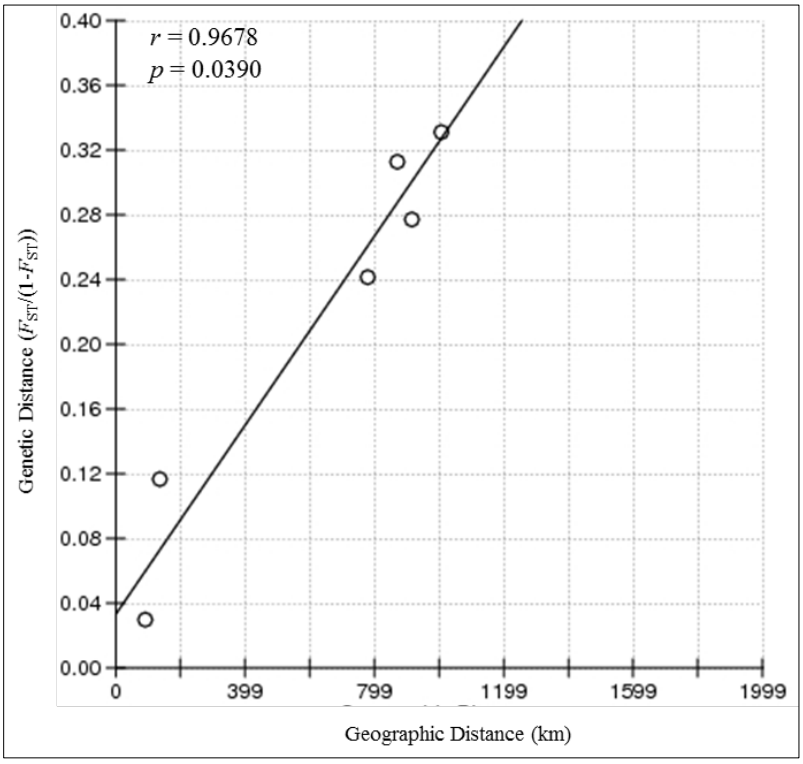

Figure 14-10. Scatterplots of genetic distance (pairwise PhiPT, nine microsatellite loci) with respect to geographical distance for *Primnoa resedaeformis* populations.

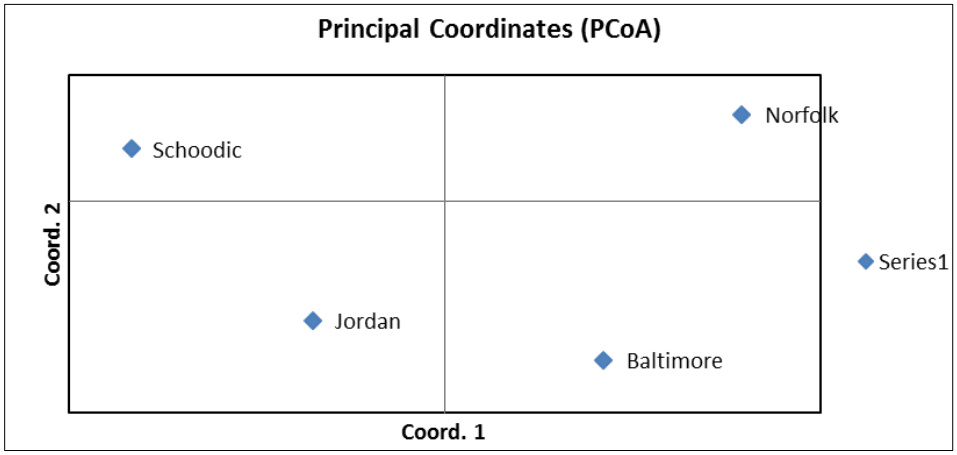

Figure 14-11. Results of principal coordinates analysis based upon Nei's unbiased genetic distances between populations of *Primnoa resedaeformis*.

Bayesian clustering detected two or three clusters of genetically similar individuals in the *P. resedaeformis* dataset (**Figure 14-12 A–D**). Plots of log likelihoods suggested three clusters were optimal (**Figure 14-11 C**), and the two canyons populations were separated in bar plots for K = 3 (**Figure 14-11A**). However, two clusters were optimal by the Evanno method **(Figure 14-12 D)**, representing canyons and Gulf of Maine populations, respectively. When a second STRUCTURE analysis was performed including only the canyons *P. resedaeformis* individuals, two canyon-specific clusters were recovered **(Figure 14-13 A–D)**.

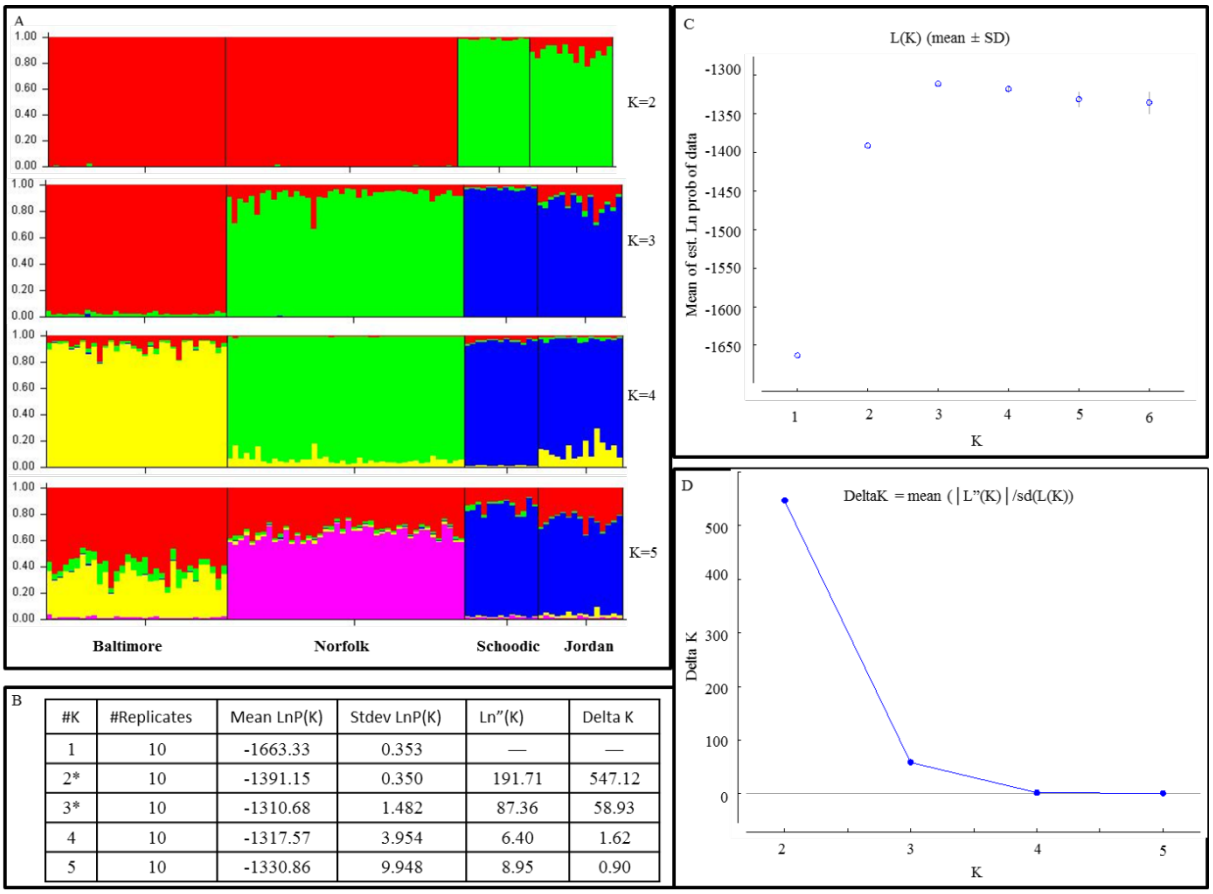

B

#K	#Replicates	Mean LnP(K)	Stdev LnP(K)	Ln"(K)	Delta K
1	10	-1663.33	0.353	—	—
2*	10	-1391.15	0.350	191.71	547.12
3*	10	-1310.68	1.482	87.36	58.93
4	10	-1317.57	3.954	6.40	1.62
5	10	-1330.86	9.948	8.95	0.90

Figure 14-12. A. Bayesian clustering of *Primnoa resedaeformis* individuals from the Mid-Atlantic Bight canyons and the Gulf of Maine (Schoodic and Jordan) based upon multilocus genotypes at eight microsatellite loci. Within bar plots, each individual is represented by a vertical bar partitioned into sections with lengths proportional to estimated probability of membership into K clusters. B. Mean statistics for each of K clusters, estimated using STRUCTURE Harvester (Earl and vonHoldt 2012). C. Mean estimated log probability of the data for each of the K clusters. D. Delta K plot, based on the rate of change in the log probability of the data (Evanno method, Evanno et al. 2005). Significant genetic structuring was detected in the dataset; the most likely number of clusters is either K = 2 or K = 3.

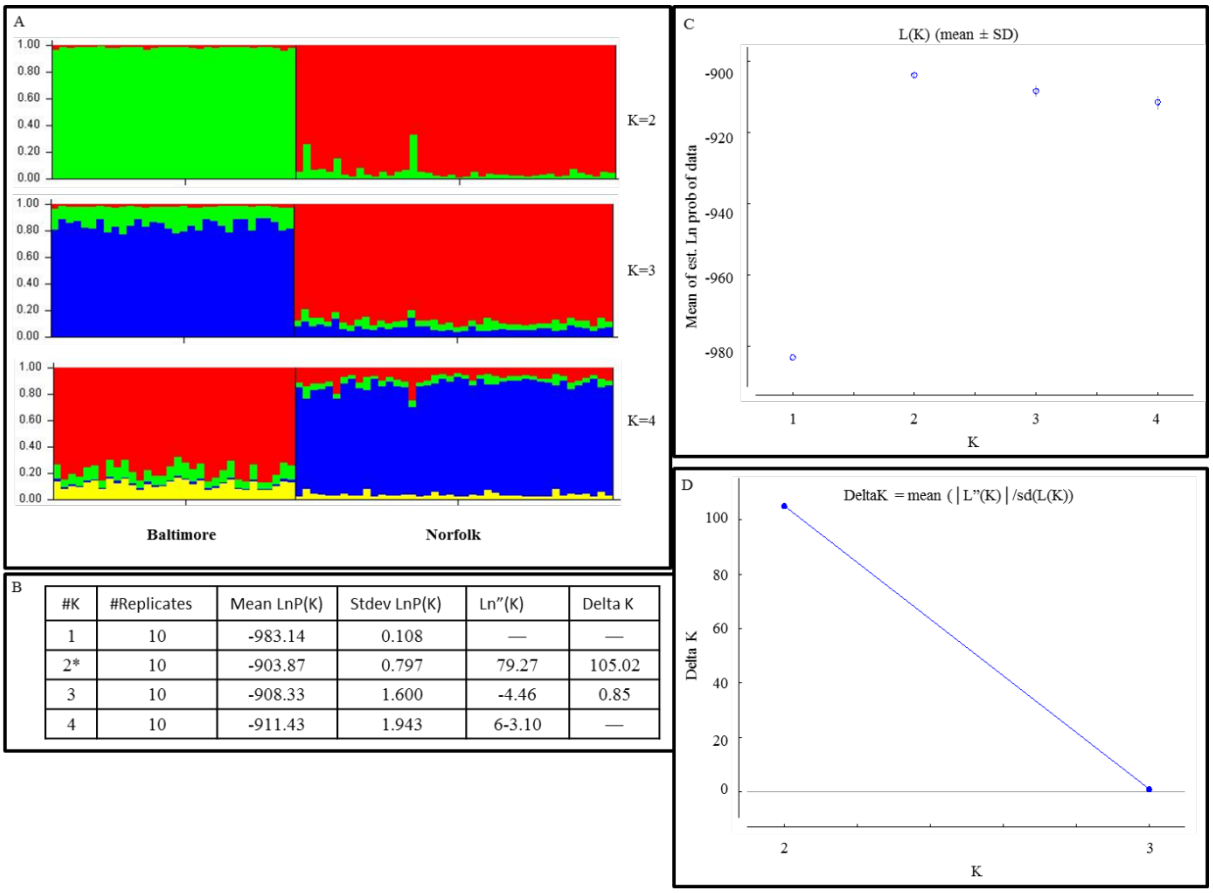

B

#K	#Replicates	Mean LnP(K)	Stdev LnP(K)	Ln"(K)	Delta K
1	10	-983.14	0.108	—	—
2*	10	-903.87	0.797	79.27	105.02
3	10	-908.33	1.600	-4.46	0.85
4	10	-911.43	1.943	6-3.10	—

Figure 14-13. A. Bayesian clustering of *Primnoa resedaeformis* individuals from the Mid-Atlantic Bight canyons based upon multilocus genotypes at eight microsatellite loci. Within bar plots, each individual is represented by a vertical bar partitioned into sections with lengths proportional to estimated probability of membership into K clusters. B. Mean statistics for each of K clusters, estimated using STRUCTURE Harvester (Earl and vonHoldt 2012). C. Mean estimated log probability of the data for each of the K clusters. D. Delta K plot, based on the rate of change in the log probability of the data (Evanno method, Evanno et al. 2005). Significant genetic structuring was detected in the dataset; the most likely number of clusters was K = 2.

14.3.2.3 Genetic Differentiation Within Desmophyllum dianthus

The *D. dianthus* microsatellite dataset included 80 individuals genotyped at nine loci (**Table 14-8**; **Appendix 14-A**, **Table 14-A4**). The P_{ID} using this set of loci was 1.7×10^{-14}. The mean number of alleles per locus ranged from 14.22 (Norfolk Canyon deep) to 16.11 (Baltimore Canyon; **Table 14-8**). Rarified allelic and private allelic richness were similar for the *D. dianthus* populations, averaging 13.68 and 3.55, respectively (Ar, Ap; **Table 14-8**). Observed heterozygosities ranged from 0.497 (Norfolk Canyon deep) to 0.585 in (Baltimore Canyon), and heterozygote deficits were detected in each population (F_{IS}; **Table 14-8**; **Appendix 14-A**, **Table 14-A4**). Three loci had significant heterozygote deficits across populations (LpeC44, LpeC61 and LpeG33; **Appendix 14-A**, **Table 14-A4**). Two loci were outliers in the F_{ST}-outlier test for selection (LpeC44 and LpeG20). Analyses were run with and without these loci in order to determine the potential impact selection may have on results.

Table 14-8. *Desmophyllum dianthus* sampling localities, average sampling depth, sample size (*N*), and mean allelic patterns per locality based on nine microsatellite loci.

Locality	Avg. Depth (m)	*N*	N_A	*A*r	*A*p	H_O	H_E	*f*
Baltimore Canyon	687	31	16.11	13.92	3.15	0.585	0.748	0.214*
Norfolk Canyon shallow	630	23	14.33	13.78	3.83	0.498	0.753	0.374*
Norfolk Canyon deep	1,320	26	14.22	13.35	3.68	0.497	0.742	0.265*
Mean	879	80*	14.89	13.68	3.55	0.526	0.748	0.284*

N is number of unique multilocus genotypes (*with total numbers of individuals instead of mean, last row); N_A is the mean number of alleles per locus; *A*r and *A*p are allelic and private allelic richness, respectively, with rarefaction for a corresponding sample size of 24 alleles; H_O and *H*e are observed and expected heterozygosity, respectively; *f*, Weir and Cockerham (1984) estimator of F_{IS} inbreeding coefficient (given in the last column), *significant deviations from panmixia after false discovery rate of 0.05.

Pairwise estimates of F_{ST} were low for all comparisons, yet differences between the Baltimore Canyon and the Norfolk shallow population, as well as the Norfolk shallow and deep populations, were significant, but did not remain so following Bonferroni correction (**Table 14-9**). The Baltimore Canyon population was slightly less differentiated from the Norfolk deep population than the Norfolk shallow population. When variance in allele frequencies was compared among *D. dianthus* populations in an AMOVA framework (**Table 14-10**), a higher and significant F_{ST} estimate resulted when the Norfolk Canyon samples were separated out by collection depths ("3 populations," **Table 14-10**). Bayesian clustering of *D. dianthus* individuals suggested that only one cluster exists in the dataset (**Figure 14-14**). Results did not vary when seven loci were used, removing those potentially under selection (not shown).

Table 14-9. Estimates of pairwise F_{ST} (below diagonal) between populations of *Desmophyllum dianthus* based on analysis of molecular variance using nine microsatellite loci. None of the pairwise F_{ST} values were significant after sequential Bonferroni correction ($P \leq 0.017$).

Population	Baltimore	Norfolk Shallow	Norfolk Deep
Baltimore		0.024	0.270
Norfolk Shallow	0.007		0.031
Norfolk Deep	0.002	0.007	

Table 14-10. Results from analysis of molecular variance among canyons of *Desmophyllum dianthus* populations.

	Variation	df	Est. Var.	Percent	F_{ST}	*P*
2 populations	Among populations	1	0.009	0	–	–
Baltimore	Within populations	158	3.439	100	–	–
Norfolk	Total	159	3.447	100	0.003	0.104
3 populations						
Baltimore	Among populations	2	0.017	0	–	–
Norfolk Deep	Within populations	157	3.431	100	–	–
Norfolk Shallow	Total	159	3.448	100	0.005	0.021*

df = degrees of freedom; Est. Var., estimated variance; Percent, percent of total variance; F_{ST}, genetic differentiation among populations; *P* = probability value (* significant at <0.05).

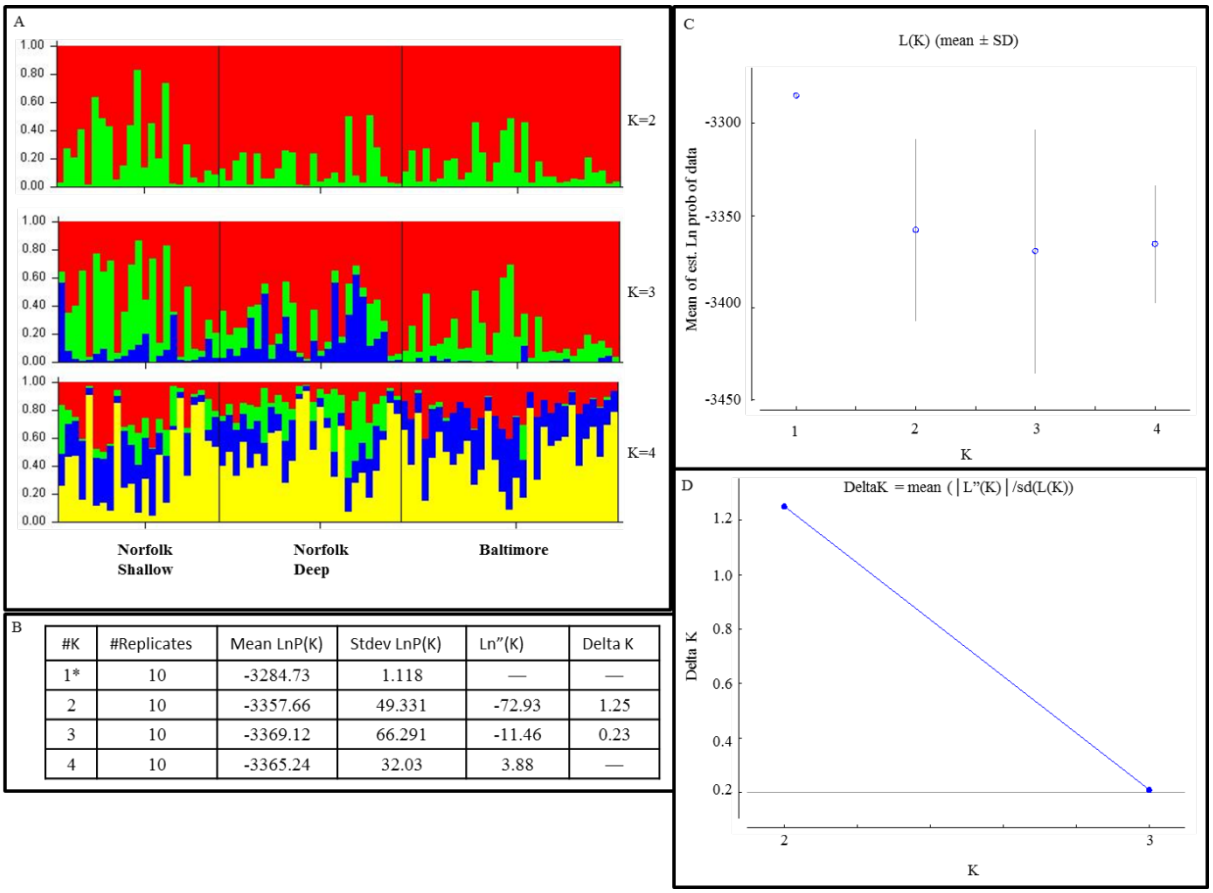

B

#K	#Replicates	Mean LnP(K)	Stdev LnP(K)	Ln"(K)	Delta K
1*	10	-3284.73	1.118	—	—
2	10	-3357.66	49.331	-72.93	1.25
3	10	-3369.12	66.291	-11.46	0.23
4	10	-3365.24	32.03	3.88	—

Figure 14-14. A. Bayesian clustering of *Desmophyllum dianthus* individuals from the Mid-Atlantic Bight canyons based on multilocus genotypes at eight microsatellite loci. Within bar plots, each individual is represented by a vertical bar partitioned into sections with lengths proportional to estimated probability of membership into K clusters. B. Mean statistics for each of K clusters, estimated using STRUCTURE Harvester (Earl and vonHoldt, 2012). C. Mean estimated log probability of the data for each of the K clusters. D. Delta K plot, based on the rate of change in the log probability of the data (Evanno method, Evanno et al., 2005). Significant genetic structuring was detected in the dataset; the most likely number of clusters was K = 2.

14.3.2.4 Genetic Differentiation Within Lophelia pertusa

Two microsatellite datasets were analyzed for *L. pertusa*. The first dataset provides the widest geographic context for *L. pertusa* connectivity by expanding the analysis presented in Lunden et al. (2014) to include MAB canyon populations. This dataset included eight microsatellite loci MLGs for 617 individuals representing 25 *L. pertusa* populations from the Gulf of Mexico and the northwestern and northeastern Atlantic Ocean. The second dataset included 383 *L. pertusa* individuals from the Gulf of Mexico and northwestern Atlantic populations that were genotyped at 14 loci (**Appendix 14-A**, **Table 14-A5**). Use of additional loci improved the ability to detect unique genetic individuals, as the probability of identity went from 6.7×10^{-8} using eight loci to 5.2×10^{-17} using 14 loci. Several of the loci were outliers based upon the F_{ST}-outlier test (LpeG20, LpeG54, LpeA5, LpeG50, and LpeG63). Analyses were run with and without these loci, but results remained the same, so results from the larger dataset are shown.

Based on the *L. pertusa* dataset using 14 microsatellite loci, average numbers of alleles per population ranged from 7.21 in Miami Terrace to 17.86 in VK826 (**Table 14-11**). Rarified allelic richness ranged

from 6.91 in Miami Terrace to 7.62 in the MAB canyons (**Table 14-12**). The Cape Lookout population had the highest rarified average private allelic richness (*A*p = 1.04; **Table 14-11**), and the MAB canyons population had the second highest (*A*p = 0.78), whereas the *Gulf Oil* and VK826 had the lowest (*A*p = 0.27). Observed heterozygosities ranged from 0.575 (Miami Terrace, H_O, **Table 14-12**) to 7.34 (*Gulf Oil*). As previously detected in *L. pertusa* (LeGoff-Vitry et al. 2004a, Morrison et al. 2011, Dahl et al. 2012), heterozygote deficits were apparent in most populations, with the exception of the *Gulf Oil* population (H_O; **Table 14-12**), plus the *Gulfpenn*, VK862, Miami Terrace, and Baltimore Canyon populations did not have any loci that were out of HWE (**Appendix 14-A**, **Table 14-A5**). Loci with heterozygote deficits varied with population, and no loci were out of equilibrium across all populations (**Appendix 14 A**, Table 14-A5). Estimates of levels of inbreeding from *F*-statistics ranged from 0.071in the *Gulf Oil* population to 0.268 in the Miami Terrace population, with the MAB canyons population having the second highest value (0.249; F_{IS}; **Table 14-12**).

Pairwise estimates of F_{ST} among *L. pertusa* populations revealed that the Gulf of Mexico VK862 population was undifferentiated from several others in the gulf (*Gulfpenn*, VK826, West Florida Slope; **Table 14-12**). The *Gulf Oil L. pertusa* population significantly differentiated from the Garden Banks and VK826 populations. The majority of pairwise comparisons between Gulf of Mexico and northwestern Atlantic *L. pertusa* populations were significant. However, the MAB canyons populations were not significantly differentiated from the *Gulfpenn*, VK862, VK906 and West Florida Slope populations (**Table 14-13**).

Table 14-11. *Lophelia pertusa* sampling localities, location and average sampling depth, number of samples genotyped (*N*), and mean allelic patterns per locality based on 14 microsatellite loci.

Locality	Avg. Depth (m)	*N*	N_A	*A*r	*A*p	H_O	H_E	*f*
Garden Banks	527	19	10.86	7.34	0.42	0.683	0.774	0.139*
Mississippi Canyon 751	441	24	11.57	7.36	0.24	0.683	0.767	0.130*
Tanker *Gulf Oil*	533	9	7.29	6.98	0.27	0.734	0.743	0.071
Tanker *Gulfpenn*	540	10	8.14	7.34	0.37	0.640	0.775	0.221*
Viosca Knoll 862	317	17	10.36	7.38	0.30	0.675	0.768	0.151*
Viosca Knoll 906	380	60	14.43	7.33	0.25	0.623	0.788	0.216*
Viosca Knoll 826	455	121	17.86	7.39	0.27	0.654	0.794	0.180*
West Florida Slope	468	47	14.00	7.34	0.29	0.644	0.778	0.185*
Miami Terrace	327	9	7.21	6.91	0.74	0.575	0.737	0.268*
Cape Canaveral	659	28	12.36	7.38	0.69	0.597	0.778	0.245*
Cape Lookout	392	22	12.36	7.61	1.04	0.642	0.778	0.198*
Norfolk Canyon	417	14	9.93	7.62*	0.78*	0.615	0.783	0.249*
Baltimore Canyon	390	3	3.57	n/a	n/a	0.631	0.618	n/a
Mean	403	383*	10.76	7.33	0.47	0.646	0.760	0.253

N is the number of unique multilocus genotypes (*with total numbers of individuals instead of mean, last row); N_A is the mean number of alleles per locus; *A*r and *A*p are allelic and private allelic richness, respectively, averaged over loci with rarefaction for a corresponding sample size of 16 alleles and canyon samples grouped together due to low sample size in Baltimore Canyon; H_o and *H*e are observed and expected heterozygosity, respectively; *f*, Weir and Cockerham (1984) estimator of F_{IS} inbreeding coefficient (given in the last column), *significant deviations from panmixia after false discovery rate of 0.05. n/a = not applicable; due to low sample size for Baltimore Canyon, these samples were included with Norfolk Canyon.

Table 14-12. Estimates of pairwise F_{ST} (below diagonal) between populations of *Lophelia pertusa* based upon analysis of molecular variance using 15 microsatellite loci. Bold values indicate pairwise F_{ST} values that were significant after sequential Bonferroni correction ($P \leq 0.001$).

Population	GB	MC751	GO	GP	VK862	VK906	VK826	WFS	MTR	CCN	CLO	MAC
GB		0.004	0.001	0.021	0.177	0.013	0.036	0.015	0.001	0.001	0.001	0.001
MC751	0.013		0.052	0.076	0.392	0.054	0.009	0.202	0.001	0.001	0.001	0.001
GO	**0.028**	0.012		0.019	0.005	0.002	0.001	0.011	0.001	0.001	0.001	0.001
GP	0.014	0.009	0.023		0.456	0.167	0.222	0.094	0.005	0.001	0.001	0.144
VK862	0.004	0.001	0.021	0.000		0.092	0.417	0.455	0.001	0.001	0.001	0.010
VK906	0.007	0.004	0.020	0.005	0.004		0.153	0.002	0.001	0.001	0.001	0.023
VK826	0.005	0.006	**0.021**	0.003	0.000	0.001		0.077	0.001	0.001	0.001	0.001
WFS	0.007	0.002	0.014	0.006	0.000	0.003	0.002		0.001	0.001	0.001	0.003
MTR	**0.041**	**0.033**	**0.063**	0.028	**0.031**	**0.036**	**0.032**	**0.036**		0.001	0.002	0.001
CCN	**0.040**	**0.032**	**0.052**	**0.032**	**0.025**	**0.038**	**0.032**	**0.033**	0.**031**		0.001	0.001
CLO	**0.050**	**0.039**	**0.060**	**0.036**	**0.040**	**0.047**	**0.039**	**0.042**	0.016	**0.020**		0.001
MAC	**0.019**	**0.021**	**0.032**	0.007	0.011	0.007	**0.009**	0.012	**0.033**	**0.031**	**0.041**	

GB = Garden Banks; GO = *Gulf Oil*; GP = *Gulfpenn*; VK = Viosca Knoll; WFS = West Florida slope; MTR = Miami Terrace; CCN = Cape Canaveral; CLO = Cape Lookout; MAC = Mid-Atlantic Bight canyons.

Table 14-13. Results from analysis of molecular variance among canyons and regional groupings of *Lophelia pertusa* populations.

	Variation	df	Est. Var.	Percent	F_{ST}	*P*
12 populations	Among populations	11	0.089	2	–	–
	Within populations	754	5.564	98	–	–
	Total	765	5.652	100	0.016	0.001*
2 regions	Among regions	1	0.103	2	–	–
GoM	Among populations	10	0.050	1	–	–
NW Atlantic	Within populations	754	5.564	97	–	–
	Total	765	5.716	100	0.027	0.001*
3 regions	Among regions	2	0.131	2	–	–
GoM	Among populations	10	0.037	1	–	–
SEUS	Within populations	753	5.564	97	–	–
Canyons	Total	765	5.732	100	0.029	0.001*

df = degrees of freedom; Est. Var. = estimated variance; Percent = percent of total variance; F_{ST} = genetic differentiation among populations; *P* = probability value (* significant at <0.05). GoM = Gulf of Mexico; SEUS = southeastern U.S.

When variance in allele frequencies was examined in an AMOVA framework, genetic structuring was detected, with approximately 2% of variance attributed to that among populations or regions, which was significantly different from zero in each case ($P < 0.001$, **Table 14-13**). Without considering regional structuring, the overall F_{ST} was 0.016, ('12 populations,' **Table 14-13**). Variance was maximized when populations were grouped regionally, as the overall F_{ST} estimate increased when populations were assigned to Gulf of Mexico vs. Atlantic regions '2 regions,' $F_{ST} = 0.027$, **Table 14-13**), or Gulf, southeastern United States (SEUS), and Canyons populations ('3 regions,' $F_{ST} = 0.029$, **Table 14-13**). A significant correlation between genetic and geographic distance was evident when Gulf of Mexico and Atlantic populations were compared (**Figure 14-15A**). However, a negative correlation between genetic and geographic distance was evident when only northwestern Atlantic *L. pertusa* populations were included in a Mantel test (**Figure 14-15 B**). In a PCoA based upon Nei's unbiased genetic distances from 14 microsatellite loci and 12 *L. pertusa* populations, the MAB canyons populations (MAC) clustered with the Gulf of Mexico populations, while the other northwest Atlantic populations were separated from each

other as well as from the Gulf of Mexico populations (**Figure 14-16**). The *Gulf Oil* population was an outlier from the other Gulf of Mexico populations (**Table 14-16**).

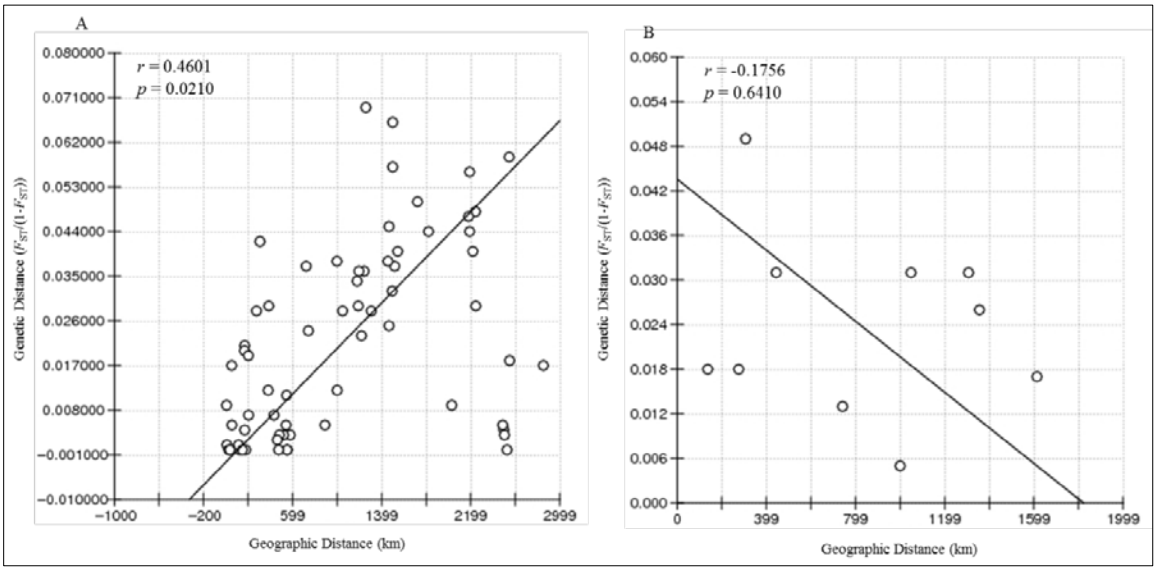

Figure 14-15. Scatterplots of pairwise, linearized genetic distance (14 microsatellite loci) with respect to geographical distance for *Lophelia pertusa (*A) Gulf of Mexico and Atlantic populations (B) northwestern Atlantic populations.

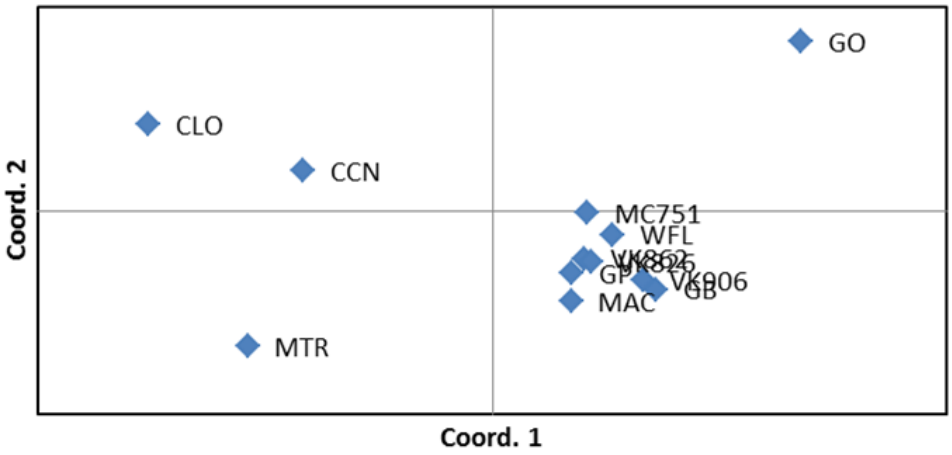

Figure 14-16. Principal components analysis of Nei's unbiased genetic distances from 12 Lophelia populations using 14 microsatellite loci. Sample site abbreviations were: Garden Banks (GB), Mississippi Canyon 751 (MC751), Tanker *Gulf Oil* (GO), Tanker *Gulfpenn* (GP), Viosca Knoll 862, 906, and 826 (VK862, VK906, VK826), West Florida Slope (WFS), Miami Terrace (MTR), Cape Canaveral (CCN), Cape Lookout (CLO), and MAB canyons (MAC).

Regional structuring was evident between among Gulf of Mexico, SEUS, and northern Atlantic Ocean populations, as three clusters of *L. pertusa* populations were detected among the 25 populations included in the STRUCTURE analysis of 8 loci (**Figure 14-17**). This regional structuring among *L. pertusa* populations matched previous analyses using eight or nine microsatellite loci and many of the same *L. pertusa* populations (Morrison et al. 2011, Lunden et al. 2014). In the present analysis, the MAB canyons populations appeared admixed, with individuals being assigned to both the Gulf of Mexico and SEUS *L. pertusa* populations (**Figure 14-17**). A similar pattern of admixture in assignments to Gulf of Mexico and SEUS clusters was evident when 14 loci and 12 populations were tested (**Figure 14-18**). In this analysis, between two and four clusters were recovered based upon the mean estimated log likelihood probabilities (**Figure 14-18C**), and two clusters were recovered as the most likely explanation of the data by the Evanno method (**Figure 14-18D**). As seen in the analysis with eight loci, *L. pertusa* individuals from the canyons populations were mixed in assignment between the Gulf of Mexico and SEUS clusters (**Figure 14-18A**). At increasing values of K (e.g., K = 3 and K = 4, **Figure 14-18A**), the Miami Terrace and Cape Lookout *L. pertusa* populations form a cluster, and the canyons individuals were admixed between the Cape Canaveral population and the Gulf of Mexico. This is surprising given the closer proximity of Cape Lookout relative to Cape Canaveral *L. pertusa* populations (approximately 307 and 1,000 km from Norfolk Canyon, respectively). Examining structuring for the MAB canyons and SEUS *L. pertusa* individuals only, a total of four genetic clusters resulted, and genetic affinities between the Miami Terrace and Cape Lookout populations, as well as Cape Canaveral and Canyons populations, are supported through individual assignments (**Figure 14-19**). At higher values of K (e.g., K = 3, 4, and 5; **Figure 14-19**A, individuals from the Cape Canaveral population were especially admixed, with a fraction of individuals assigned to the MTR/CLO cluster, the Canyons cluster, and an additional unique cluster that did not appear elsewhere.

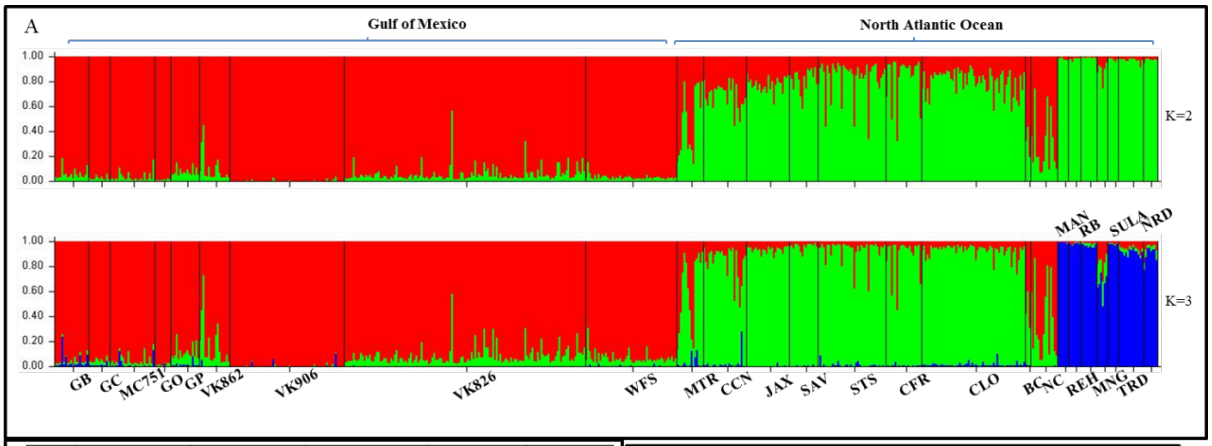

B

#K	#Replicates	Mean LnP(K)	Stdev LnP(K)	Ln''(K)	Delta K
1	10	-26002.06	1.106	—	—
2	10	-25172.87	56.048	406.57	7.254
3*	10	-24750.25	11.018	470.79	42.728
4	10	-24798.42	168.830	114.53	0.678
5	10	-24961.12	342.456	142.07	0.414

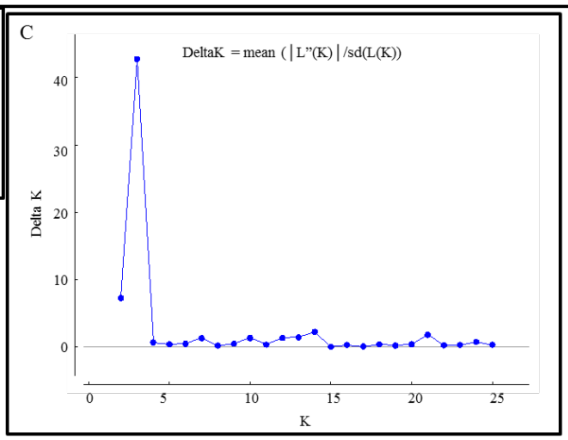

Figure 14-17. A. Bayesian clustering of 617 Lophelia pertusa individuals from the Mid-Atlantic Bight canyons based upon multilocus genotypes at eight microsatellite loci. Within bar plots, each individual is represented by a vertical bar partitioned into sections with lengths proportional to estimated probability of membership into K clusters. B. Mean statistics for each of K clusters, estimated using STRUCTURE Harvester (Earl and vonHoldt, 2012). C. Delta K plot based on the rate of change in the log probability of the data (Evanno method, Evanno et al., 2005). Significant genetic structuring was detected in the dataset; the most likely number of clusters was K = 3. Sample site abbreviations were: Garden Banks (GB), Green Canyon (GC), Mississippi Canyon 751 (MC751), Gulf Oil (GO), Gulfpenn (GP), Viosca Knoll 862, 906 and 826 (VK862, VK906, VK826), West Florida Slope (WFS), Miami Terrace (MTR), Cape Canaveral (CCN), Jacksonville (JAX), Savannah (SAV), Stetson Banks (STS), Cape Fear (CFR), Cape Lookout (CLO), Baltimore Canyon (BC), Norfolk Canyon (NC), Manning Seamount (MAN), Rehoboth Seamount (REH), Rockall Banks (RB), Mingulay (MNG), Sula Ridge (SULA), Nordleska (NRD), and Trondheim Fjord (TRD).

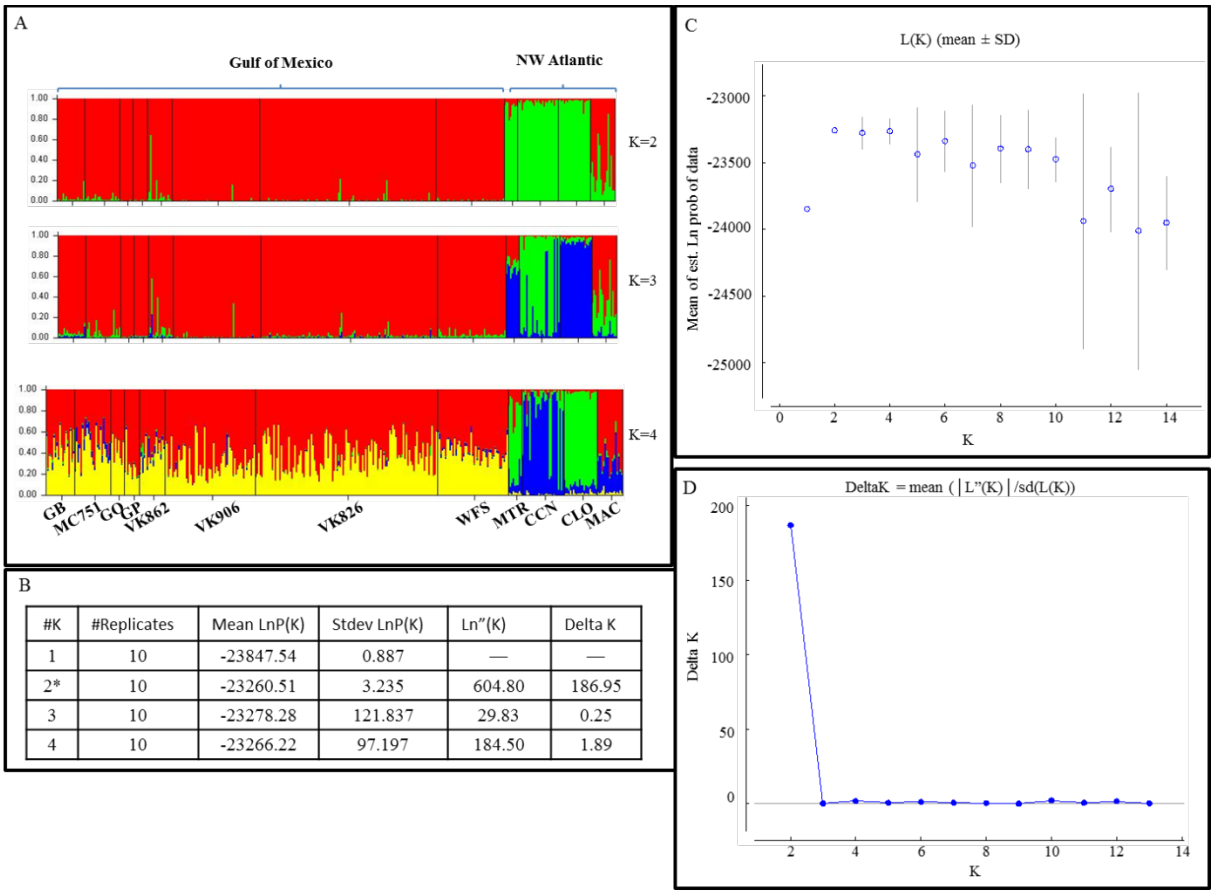

B

#K	#Replicates	Mean LnP(K)	Stdev LnP(K)	Ln"(K)	Delta K
1	10	-23847.54	0.887	—	—
2*	10	-23260.51	3.235	604.80	186.95
3	10	-23278.28	121.837	29.83	0.25
4	10	-23266.22	97.197	184.50	1.89

Figure 14-18. A. Bayesian clustering of 383 *Lopehlia pertusa* individuals from the Mid-Atlantic Bight canyons based upon multilocus genotypes at 14 microsatellite loci. Within bar plots, each individual is represented by a vertical bar partitioned into sections with lengths proportional to estimated probability of membership into K clusters. B. Mean statistics for each of K clusters, estimated using STRUCTURE Harvester (Earl and vonHoldt, 2012). C. Mean estimated log probability of the data for each of the K clusters. D. Estimated Delta K plot based on the rate of change in the log probability of the data (Evanno method, Evanno et al., 2005). Significant genetic structuring was detected in the dataset; the most likely number of clusters was K = 2. Sample site abbreviations were: Garden Banks (GB), Mississippi Canyon 751 (MC751), Gulf Oil (GO), *Gulfpenn* (GP), Viosca Knoll 862, 906 and 826 (VK862, VK906, VK826), West Florida Slope (WFS), Miami Terrace (MTR), Cape Canaveral (CCN), Cape Lookout (CLO), and MAB canyons (MAC).

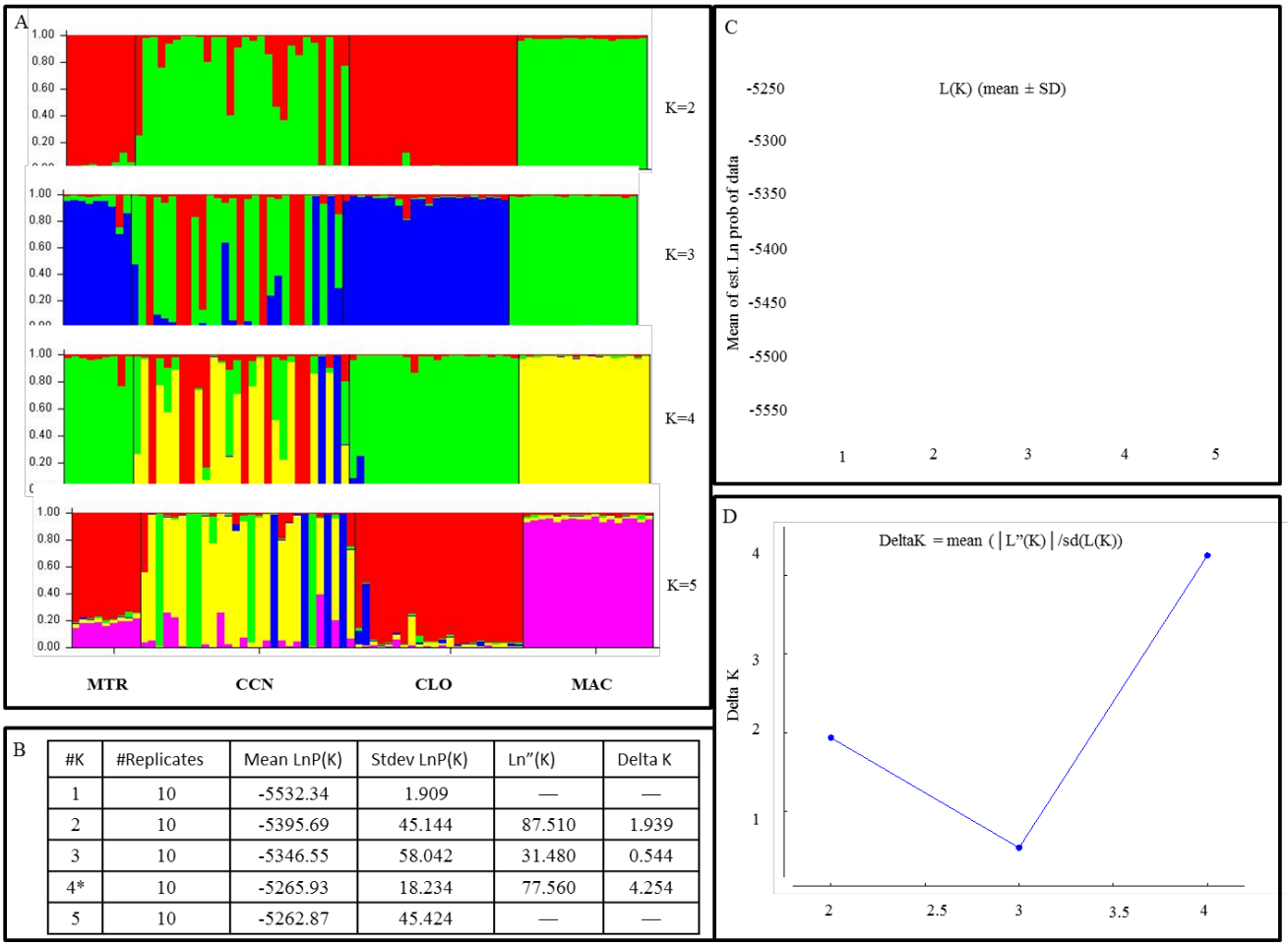

B

#K	#Replicates	Mean LnP(K)	Stdev LnP(K)	Ln"(K)	Delta K
1	10	-5532.34	1.909	—	—
2	10	-5395.69	45.144	87.510	1.939
3	10	-5346.55	58.042	31.480	0.544
4*	10	-5265.93	18.234	77.560	4.254
5	10	-5262.87	45.424	—	—

Figure 14-19. A. Bayesian clustering of *Lophelia pertusa* individuals from the Mid-Atlantic Bight (MAB) canyons based on multilocus genotypes at 14 microsatellite loci. Within bar plots, each individual is represented by a vertical bar partitioned into sections with lengths proportional to estimated probability of membership into K clusters. B. Mean statistics for each of K clusters, estimated using STRUCTURE Harvester (Earl and vonHoldt, 2012). C. Mean estimated log probability of the data for each of the K clusters. D. Estimated Delta K plot, based on the rate of change in the log probability of the data (Evanno method, Evanno et al., 2005). Significant genetic structuring was detected in the dataset; the most likely number of clusters was K = 2. Sampling locations are labeled: Miami Terrace (MTR), Cape Canaveral (CCN), Cape Lookout (CLO), and MAB canyons (MAC).

14.4 DISCUSSION

Comprehensive sampling of corals from two MAB canyons allowed for an analysis of phylogenetic affinities of five scleractinian coral species present in canyons as well as analysis of connectivity among canyons for four coral taxa. These collections and analyses expand knowledge regarding patterns of diversity in both scleractinian corals and octocorals in the MAB canyons. Through comparisons of genetic connectivity between different species within the same habitat, we gain insight into effective dispersal of several abundant coral species. Assessment of patterns of connectivity among deepsea corals in canyon habitats will expand our understanding of the functioning of and potential sensitivities to disturbance of these ecosystems. Habitat fragmentation may escalate with increasing resource exploitation (Hilário et al. 2015), therefore increasing the urgency for studies of connectivity.

14.4.1 MAB Coral Biodiversity

Although scleractinian corals are not highly diverse in the western North Atlantic Ocean, we were able to shed light on the evolutionary history of several species that occur in the MAB canyons.

The genus *Flabellum* originated approximately 77.5 million years ago (mya) (Stolarski et al. 2011). The solitary coral *Flabellum alabastrum*, collected in Norfolk Canyon, is common on the continental slope and on seamounts in the North Atlantic Ocean from Georgia to Davis Strait at depths between 357 and 2,000 m (Cairns and Hoeksema 2015). It inhabits a wide depth range in canyons off Newfoundland (400−2,500 m; Baker et al. 2012). This is the first phylogenetic analysis of *F. alabastrum*, and sequences were unique relative to other *Flabellum* sequences available for comparison. Relationships among the *Flabellum* species included in our phylogenetic analysis were not well supported (**Figure 14-17**). The addition of sequence data from other gene regions may be necessary to resolve historical relationships more accurately.

The genus *Caryophyllia* originated approximately 160 mya (Stolarski et al. 2011), and is the most diverse genus of azooxanthellate Scleractinia, with 66 recent species and 195 fossil taxa (Kitahara et al. 2010). Our phylogenetic analysis included 16 species of *Caryophyllia*, plus two genera that are similar in morphology: *Crispatotrochus* and *Dasmosmilia* (Kitahara et al. 2010), and other species belonging to the family Caryophylliidae. A close relationship between *Desmophyllum dianthus* and *L. pertusa* was reported previously (Morrison et al. 2008b, Addamo et al. 2012), and this affinity was supported by our mtDNA 16S phylogenetic analysis (**Figure 14-8**). Even though some of the sequences in GenBank included in this analysis represented samples collected far from the MAB canyons (e.g., the South Pacific Ocean), sequences from both of these taxa were intermingled in our phylogenetic tree. These results do not suggest that the MAB canyons populations are differentiated from each other or from populations elsewhere for these widely distributed species. Similarly, canyons *S. variabilis* were not differentiated from those collected in the South Pacific Ocean. Sequences from MAB canyons *Dasmosmilia lymani* grouped with *C. smithii*, not with other sequences representing this taxon. In the Stolarksi et al. (2011) analysis, three *D. lymani* sequences fell into two clades that match their placement in our analysis (**Figure 14-8**). Combined results suggest *Dasmosmilia lymani* likely needs further taxonomic investigation. This analysis also supports the findings of Kitahara et al. (2010) showing that *Caryophyllia* species formed a natural grouping including *Dasmosmilia lymani* and *Cristopatrochus rugosus*.

For both phylogenetic analyses presented here, relationships among taxa were not well resolved using the mtDNA 16S gene. Unlike most other animals surveyed where protein-coding or ribosomal mitochondrial DNA (mtDNA) genes are commonly used to describe patterns of variation within species, anthozoan mtDNA evolves slowly and, as a result, little variation within species exists (Romano and Palumbi 1997, van Oppen et al. 1999, Shearer et al. 2002, Fukami and Knowlton 2005). The entire mtDNA genomes of two *S. variabilis* individuals from New Zealand differed by only five bases (0.03%; Zeng et al. 2014), and mtDNA genomes from two *L. pertusa* individuals differed by one substitution (Flot et al. 2013). Sequence identity between mtDNA genomes of *S. variabilis* and *L. pertusa* was 97.5%

(Zeng et al. 2014). Therefore, more variable markers, such as microsatellites (Quattrini et al. 2015b) or other nuclear markers (e.g., SNPs, Herrera et al. 2015), may be necessary to resolve some of the close relationships within the Flabellidae and the Caryophylliidae.

14.4.2 Connectivity Among MAB Canyon Coral Populations

Shared patterns of species diversity and genetic structuring across unrelated but co-distributed species may indicate that oceanographic features affect connectivity of many species in similar ways (Cunningham and Collins 1998, Cho and Shank 2010). On the other hand, contrasting patterns of population structure observed among species within the same habitat may indicate that different life histories are driving resultant dispersal patterns (i.e., lecithotrophic vs. planktotrophic larvae).

In four of the cold-water coral species examined in Baltimore and Norfolk canyons, both connectivity and isolation were observed. Canyons populations of three cold-water coral species examined, *P. arborea*, *D. dianthus,* and *L. pertusa*, were not genetically differentiated, suggesting at least some ongoing larval dispersal between canyons. Connectivity between canyons populations of *P. arborea* was somewhat expected, given the broad-scale regional structuring found in the global analysis of *P. arborea* biodiversity by Herrera et al. (2012). In their analyses, *P. arborea* populations from the northwestern Atlantic shared haplotypes, and high connectivity among populations was estimated in this area as well as within other Pacific regions (e.g., western, eastern, and southern Pacific). Despite the use of different markers (microsatellites vs. DNA sequence data) and fewer populations sampled (present study), our results agree with the conclusion of Herrera et al. (2012) that gene flow is adequate to maintain cohesiveness among *P. arborea* populations in the western North Atlantic Ocean.

This is the first population genetic study of *Primnoa resedaeformis*. Generally, *P. resedaeformis* has a smaller geographic distribution than *P. arborea* and is commonly found only in the North Atlantic Ocean. In contrast to the high connectivity estimated for *P. arborea*, MAB canyons populations of *P. resedaeformis* were genetically distinct, suggesting that gene flow is limited between Norfolk and Baltimore canyons for this species. The contrasting patterns of connectivity between *P. arborea* and *P. resedaeformis* is surprising given these species often co-occur in both canyons. Given the similar diversity indices and P_{ID} values in the microsatellite datasets (*P. arborea* = 3.3×10^{-5}, *P. resedaeformis* = 8.1×10^{-5}), it is unlikely that differences in resolution in the species-specific microsatellite loci used in this study account for the contrasting patterns of connectivity observed. Selection acting on certain markers could inflate estimates of differentiation, yet none was detected in our analyses.

Early life history traits, such as timing of reproduction, reproductive output and fertilization success, larval type, behavior and planktonic duration, and successful recruitment, all influence connectivity (Underwood and Fairweather 1989, Young et al. 2012, Rosser 2015). Information regarding reproductive characteristics for the two octocorals studied is limited, but has been improved by this study (**Chapter 11**). Although it has been suggested that *P. arborea* may brood larvae (Lacharité and Metaxas 2013), no embryos were observed in the MAB canyons sampled (**Chapter 11**). Eggs in *P. arborea* were large, suggesting lecithotrophic (nonfeeding) larvae, which are usually short lived. However, the continuous gametogenic cycles noted in MAB canyon *P. arborea* may provide opportunity for encountering current regimes that facilitate dispersal, despite relatively short larval duration (**Chapter 11**). Given the large size of reproductive colonies (up to 3 m; Broch 1912, Verrill 1922, Tendal 1992) that consist of hundreds of polyps, fecundity is likely high. Reproductive characteristics in *P. resedaeformis* include broadcast spawning and nonfeeding larvae (Mercier and Hamel 2011). Although the gametogenic cycle of *P. resedaeformis* was reported as continuous oogenesis and overlapping oocyte cohorts and likely spans more than a year (Mercier and Hamel 2011), data from the MAB canyons suggest a limited spawing period and short larval duration, (**Chapter 11**). Given fewer opportunities to encounter varied current regimes relative to *P. arborea*, larvae of *P. resedaeformis* may be more likely to be retained within canyons as waters generally move along canyon axes (**Chapter 11**). A Pacific Ocean sister taxon *P. pacifica* has long gamete development times and spawns gametes into the water column

where they are fertilized externally, followed by the development of nonfeeding larvae (Waller et al. 2014). Larval recruitment in *P. pacifica* may be highly sporadic (Waller et al. 2014). Although we do not know actual larval durations for either species, the fact that they both have nonfeeding larvae suggests that larval durations may be comparable.

Colony morphology and shape may allow species to exploit different microhabitats, even in close proximity. It was noted that differences in colony size and morphology of these two octocoral species in Atlantic Canada may influence the food sources and the immediate waters that surround (Mortensen and Buhl-Mortensen 2005). By studying video records, it was noted that *P. resedaeformis*, a smaller (maximum 1 m tall; Broch 1912, Madsen 1944) and more bushy species, inhabited the near-bottom environment where they experience turbulent currents whereas *P. arborea* developed large planar colonies (up to 3 m) that reached above turbulent bottom waters and faced perpendicular to the uni- or bidirectional, fast-flowing currents (Mortensen and Buhl-Mortensen 2005). If a similar scenario holds true in the MAB canyons, turbulent currents experienced by *P. resedaeformis* may entrain larvae and greatly decrease dispersal distance. Conversely, *P. arborea* larvae may be transported much farther in the swift currents they are able to reach due to larger colony size and planar growth form.

Post-recruitment survival may differ between the species as well. *Paragorgia arborea* was the most abundant and widely distributed species of gorgonians in the study area (**Chapter 8**), *Paragorgia arborea* also colonized more diverse habitat types than *P. resedaeformis* in both canyons (**Chapter 8**) . The higher abundances of *P. arborea* observed in Baltimore Canyon, where a more persistant nephloid layer was present, suggest that this species may be more tolerant to increased turbidity (**Chapter 8**). Additionally, stable isotope analysis suggests that *P. arborea* may derive some nutritional value from high turbidity (**Chapter 16**). Post-settlement mortality was high for *P. resedaeformis* on settlement plates off Atlantic Canada (Lacharité and Metaxas 2013). Although depth ranges did not differ for these species in the MAB canyons, generally, *P. arborea* has a larger depth distribution than *P. resedaeformis* (Mortensen and Buhl-Mortensen 2004, Wareham and Edinger 2007, Tong et al. 2012, Watanabe et al. 2009, Edinger et al. 2011). A 4-year study in the Gulf of Maine suggested that larval recruitment was high for *P. resedaeformis* at intermediate depths (500−650 m, similar to the depths sampled in the MAB canyons), yet the species was absent at greater depths (750−800 m), possibly due to a lack of suitable substrate (Lacharité and Metaxas 2013). Similarly, a negative relationship between the presence of *P. resedaeformis* and depth was observed off Nova Scotia, but a positive relationship with depth was observed for *P. arborea* (Watanabe et al. 2009). It was suggested that factors that change with depth, such as temperature or fishing pressure, may affect these two species differently (Watanabe et al. 2009). It would be informative to know whether the larvae of *P. resedaeformis* and *P. arborea* differ in their tolerance to factors that change with depth.

The use of a different marker type (SNPs) and fewer samples genotyped provided higher estimates of connectivity among Baltimore and Norfolk canyons for *P. resedaeformis* (**Chapter 13**). A STRUCTURE analysis suggested that only one genetic grouping existed in the *P. resedaeformis* samples from both MAB canyons (**Chapter 13**; **Figure 13-8**). However, a principal component analysis (PCA) showed slight separation between the two canyons, suggesting some divergence among canyons (**Chapter 13**; **Figure 13-5**). A pairwise estimate of F_{ST} between the MAB canyon *P. resedaeformis* populations was substantially lower using SNPs (F_{ST} = 0.06; **Chapter 13**) than microsatellites (F_{ST} = 0.117; **Table 14-6**).

These marker types (SNPs and microsatellites) may vary in mutation rates, which could lead to different estimates of connectivity. It has been demonstrated that the ability to detect departures from panmixia in marine species is more powerful when high mutation rate markers, such as microsatellites, are used (Waples and Gaggiotti 2006). Further, large numbers of loci (>20) and adequate sample sizes (e.g., 50 samples per population) increase the power of connectivity analyses (Waples and Gaggiotti 2006). Although our study had fewer loci (9) and samples (average 35 per population) than are ideal, the use of high mutation rate markers allowed detection of a departure from panmixia for *P. resedaeformis*. The number of loci and individuals included in the SNP study (**Chapter 13**) is not stated, and mutation

rates for these newly developed SNP loci are unknown. SNP typing additional individuals, and adding more distant populations such as the Gulf of Maine, may allow for a more equivalent comparison of connectivity patterns generated by these different molecular markers. In contrast, both studies supported high connectivity for MAB canyons *Paragorgia arborea* populations (F_{ST} = 0.01 with SNPs [**Chapter 13**] vs. F_{ST} = 0.005 with microsatellites, **Table 14-4**).

Desmophyllum dianthus typically occurs in high abundance on outcrops (Packer et al. 2007, Baker et al. 2012), and the species may be considered an indicator of vertical cliff-like structures (Baker et al. 2012). Shared haplotypes among Pacific populations separated by thousands of kilometers suggests high dispersal ability in this species (Addamo et al. 2012). Our results support this hypothesis, given low F_{ST} values between canyon populations (**Table 14-9**). Sampling additional populations would allow for more robust conclusions regarding connectivity of *D. dianthus* in the northwest Atlantic.

Sampling *D. dianthus* populations from both shallow and deep sites in the MAB canyons allowed an initial examination of the possible effects of depth on population connectivity. Limited vertical larval dispersal has been suggested based upon genetic data for the cosmopolitan species *D. dianthus* in the Pacific waters off Australia and New Zealand where stratification of deep water masses may entrain larvae and prevent mixing among depth strata (Miller et al. 2011). The depth-differentiation hypothesis (Rex and Etter 2010) suggests that divergent selection across environmental gradients may cause population differentiation, leading to new and/or cryptic deepsea species. Depth-related divergence has been identified in molluscs (Chase et al. 1998, Etter et al. 1999, Goffredi et al. 2003, Etter et al. 2005, Zardus et al. 2006, Jennings et al. 2013, Etter and Bower 2015), polychaetes (Lundsten et al. 2010, Schüller 2011, Cowart et al. 2014), amphipods (France and Kocher 1996), primnoid octocorals (Baco and Cairns 2012), and the red coral *Corallium rubrum* (Constantini et al. 2011). Isolation by depth was confirmed in an octocoral species, *Callogorgia delta*, using microsatellite data (Quattrini et al. 2015b). Clearly, environmental factors associated with depth may create important abiotic gradients that may influence population structuring in the deep sea (Quattrini et al. 2015b).

In our study, minimal genetic differentiation occurred between shallow (630−687 m) and deep (1,320 m) *D. dianthus* populations (F_{ST} = 0.007; **Table 14-9**), yet this value was significant and of the same magnitude observed among canyons (**Table 14-9**). In an AMOVA framework, F_{ST} increased and became significant when the deep *D. dianthus* population was treated as a third population (**Table 14-10**). Unfortunately, an isolation-by-depth Mantel test could not be performed due to the low power this analysis would have with only three data points. The shallow *D. dianthus* observed in both MAB canyons were rarer and had more robust skeletons than those found in large numbers on deeper canyon walls (**Chapter 8**). Overall, the genetic data presented here is suggestive that depth may be as important as distance in isolating MAB canyons *D. dianthus*, but additional sampling is required before conclusions can be drawn. Isolation by depth may be stronger above and below 1,400 m, where a transition in fish fauna in the MAB canyons has been observed (Ross et al. 2015). This depth likely marks the transition from Western Atlantic Subarctic Intermediate Waters (WASIW) that dominate at mid-canyon depths (500−1,500 m), and North Atlantic Deep Water (NADW) that dominates below 1,500 m (**Chapter 5**).

Taken together, the comparisons of connectivity among MAB canyons populations of four coral species highlight the complexities of determining evolutionarily significant connectivity among marine species. For each species, an interplay between life history traits and oceanographic features shape the scale of connectivity. Therefore, unique patterns of connectivity are likely and may not be predictable based on knowledge of basic larval types or durations, as has been suggested previously (Patarnello et al. 2007, Galarza et al. 2009, Mokhtar-Jamaï et al. 2011, Sivasundar and Palumbi 2010). Disentangling species-specific effects from environmental effects will continue to be a challenge (Kelly et al. 2010).

14.4.3 Connectivity Among Canyon and Other Continental Slope Cold-Water Coral Populations

For *P. resedaeformis*, an isolation by distance (IBD) pattern suggests that a stepping-stone model of gene flow may explain the observed genetic variation. Two additional populations from the Gulf of Maine were quite distinct genetically from Norfolk and Baltimore canyons populations, with values of F_{ST} that were much higher than the other corals compared in this study (0.278–0.331; **Table 14-6**). The high level of differentiation among all *P. resedaeformis* populations, and the IBD pattern, are suggestive of short effective larval dispersal in this species. In other octocoral species, such as *Paramuricea clavata* (Mokhtar-Jamaï et al. 2011) and *Corallium rubrum* (Ledoux et al. 2010), an IBD pattern has been observed among Mediterranean Sea populations. Oceanographic barriers to dispersal created by hydrodynamic processes likely contribute to the IBD patterns observed in *P. clavata* (Mokhtar-Jamaï et al. 2011). The detection of an IBD pattern may make estimating dispersal distances biologically meaningful (Rousset 1997, Palumbi 2003).

On a regional scale, MAB canyons populations of *L. pertusa* appeared distinct from other populations on the continental slope in the western Atlantic. In fact, no matter which set of microsatellite loci were used or which type of analysis performed, the canyons *L. pertusa* populations appeared quite differentiated from the population in closest geographic proximity (Cape Lookout, 307 km away; **Table 14-12**; **Figures 14-18** and **14-19**). Instead, the MAB canyons *L. pertusa* populations appeared admixed between Gulf of Mexico and Atlantic *L. pertusa*, yet at least some individuals had greater genetic affinities with Gulf of Mexico populations (**Table 14-12**; **Figures 14-17** and **14-18**). Out of three northwest Atlantic *L. pertusa* populations genotyped at 14 loci, the canyons shared some genetic affinity with Cape Canaveral, a population that also looked admixed in some analyses (**Figure 14-19**). There are several possible explanations for this pattern.

Despite close geographic proximity, Cape Lookout and the MAB canyons occur in different marine biogeographic provinces that are defined by faunal similarities and endemism (Briggs and Bowen 2012). Biogeographic provinces defined by similarities of deepwater Scleractinia places the MAB canyons in a cold-temperate province that extends from Cape Hatteras to the Gulf of Maine, whereas Cape Lookout belongs to the warm temperate SEUS province (Cairns and Chapman 2001). Similarly, benthic organisms found in the MAB canyons have greater faunal affinities with the boreal province defined by shallow-water fishes (Briggs and Bowen, 2012), which coincides with the cold-temperate province defined by corals (**Chapter 8**). Regional genetic structuring in *L. pertusa* has also been concordant with coral-defined biogeographic provinces (Morrison et al. 2011). The concordance with deepwater scleractinian provinces suggests that oceanographic processes may influence coral larvae in a similar manner, restricting gene flow between provinces.

The ages of the populations likely differ substantially, which may affect genetic signatures. *Lophelia pertusa* south of Cape Hatteras often form bioherms that may have been in place for up to 7 million years (Matos et al. 2015). In contrast, given the sizes of *L. pertusa* colonies observed in the MAB canyons, it was estimated that they range in age from 20 to 400 years (Brooke and Ross 2014). The potential longevity of genetic individuals at bioherms may have altered the genetic signature of these populations relative to the younger individuals found in the MAB canyons.

The *L. pertusa* colonies observed during this project occurred in depths between 379 and 479 m (Brooke and Ross 2014) where North Atlantic Central Water and/or West North Atlantic Central Water occurs in both MAB canyons (**Chapter 5**). Conditions within the MAB canyons suggest highly dynamic environments, with high current velocities, intense turbidity clouds, and surface-driven stochastic events (**Chapter 5**). Although there was no evidence of Gulf Stream meanders in the canyons during this study (**Chapter 5**), onshore intrusions of Gulf Stream ring waters occasionally move onshore and may facilitate the migration of marine species to the MAB (Zhang and Gawarkiewicz 2015). Given the rarity of *L. pertusa* in the MAB canyons and the various sizes encountered (suggestive of numerous recruitment

events; Brooke and Ross 2014), occasional long-distance dispersal events may be possible, delivering *L. pertusa* larvae from either the Gulf of Mexico or bioherms off the SEUS via the Gulf Stream. Such onshore intrusions likely influence long-distance dispersal of several fishes, such as bluefish (Hare and Cowan 1996) and American eel, from the Sargasso Sea (Rypina et al. 2014). A close genetic connection was also found between "*Bathymodiolus*" *childressi* cold-seep mussels found near the canyons and Gulf of Mexico populations (**Chapter 8**), suggesting that long-distance dispersal between the Gulf of Mexico and the MAB also occurs in seep mussels. Recently, as predicted by Young et al. (2012), larvae of *"B." childressi* have been found in the euphotic zone where currents move faster than those at benthic cold-seep sites (Arellano et al. 2014). It was suggested that these larvae may live up to a year, making long-distance dispersal a possibility (Young et al. 2012, Arellano et al. 2014). The life span of *L. pertusa* larvae was estimated to be approximately 3 weeks (Larsson et al. 2014, Brooke and Ross 2014), considerably less than *"B." childressi*. Eggs and embryos of *L. pertusa* are negative or neutrally buoyant, but larvae are capable of swimming (Larsson et al. 2014). Whether their behavior or tolerance to warmer temperatures allows them to reach faster flows higher in the water column is unknown.

Gaps in sampling *L. pertusa* may explain the apparent gulf-like signature of the MAB canyons samples. There may be additional, unsampled *L. pertusa* populations in the western Atlantic that would be a closer larval source, yet have more gulf-like genetic characteristics (e.g., off the Bahamas or the Caribbean). Sampling of additional canyons *L. pertusa* populations as well as other potential source populations (e.g., Caribbean) would help refine estimates of larval sources.

14.4.4 Conservation Implications

This research establishes baselines for continued genetic monitoring of several abundant canyon coral species. Genetic diversity was high in canyons populations, thus providing the potential for adaptive evolution should environmental conditions change. Three of the four species examined, *P. arborea*, *D. dianthus* and *L. pertusa*, were not genetically differentiated, suggesting at least some ongoing larval dispersal between Norfolk and Baltimore canyons. In the event of habitat destruction, populations of these species may recover, given enough time and restoration of suitable conditions. However, for *P. resedaeformis*, limited effective dispersal implies that recovery of populations will mainly rely on self-recruitment, and habitat destruction could mean permanent removal of the species. In other words, one conservation strategy may not be ideal for all canyons coral species, and both local and regional protective measures may be necessary.

14.4.5 Future Considerations

Although the scleractinian corals are not highly diverse in the northwest Atlantic, there are still many instances where molecular data do not match morphological identifications, especially within the Caryophylliidae. Continuing to develop new marker types, and to pair molecular and morphological identifications whenever possible, should provide the most robust species lists and may also shed light on accurate evolutionary relationships.

While this research provides the first look at patterns of connectivity among several abundant coral species inhabiting the MAB canyons, comparative material from other canyons and/or continental slope populations would greatly enhance the robustness of results. This research verifies the utility to multispecies examination of genetic connectivity to guide conservation efforts. Combining estimates of genetic connectivity with modeling of biophysical circulation will likely lead to an increased understanding of the scales and patterns of connectivity among deepsea corals inhabiting canyons along the east coast of the United States (e.g., derived oceanographic distances, White et al. 2010). Reproductive periodicity, larval type, and behaviors are fundamental processes that need further investigation (Hilário et al. 2015).

Metadata, as well as raw microsatellite datasets associated with this project, have been archived online in a USGS data release (Morrison et al., 2017).

"Any use of trade, firm, or product names is for descriptive purposes only and does not imply endorsement by the U. S. Government."

14.5 LITERATURE CITED

Aboim MA, Menezes GM, Schlitt T, Rogers AD. 2005. Genetic structure and history of populations of the deep-sea fish *Helicolenus dactylopterus* (Delaroche, 1809) inferred from mtDNA sequence analysis. Molecular Ecology. 14(5):1343–1354.

Addamo AM, Reimer JD, Taviani M, Freiwald A, Machordom A. 2012. *Desmophyllum dianthus* (Esper, 1794) in the scleractinian phylogeny and its intraspecific diversity. PLoS ONE. 7(11):e50215.

Andrews BD, Chaytor JD, ten Brink US, Brothers DS, Gardner JV. 2013. Bathymetric terrain model of the Atlantic margin for marine geological investigations. U.S. Geological Survey Open-File Report 2012-1266.

Antao T, Lopes A, Lopes RJ, Beja-Pereira, Luikart AG. 2008. LOSITAN: a workbench to detect molecular adaptation based on a F_{ST}-outlier method. BMC Bioinformatics. 9:323.

Arellano SM, Van Gaest AL, Johnson SB, Vrijenhoek RC, Young CM. 2014. Larvae from deep-sea methane seeps disperse in surface waters. Proceedings of the Royal Society of London. Series B, Biological Sciences. 281:20133276

Ayre DJ, Hughes TP. 2000. Genotypic diversity and gene flow in brooding and spawning corals along the Great Barrier Reef, Australia. Evolution. 54(5):1590–1605.

Ayre DJ, Hughes TP. 2004. Climate change, genotypic diversity and gene flow in reef-building corals. Ecology Letters. 7(4):273.

Bachman M, Clifford N, Packer D, Stevenson D, Auster P, Valentine P, Ford K. 2012. Essential fish habitat (EFH) omnibus amendment. Deep-sea corals of the northeast region: species, habitats, and proposed coral zones and vulnerability to fishing impacts. Draft: 03/28/12. New England Fisheries Management Council. 97 p.

Baco AR, Cairns SD. 2012. Comparing molecular variation to morphological species designations in the deep-sea coral *Narella* reveals new insights into seamount coral ranges. PLoS ONE. 7(9):e45555.

Baker KD, Wareham VE, Snelgrove PVR, Haedrich RL, Fifield DA, Edinger EN, Gilkinson KD. 2012. Distributional patterns of deep-sea coral assemblages in three submarine canyons off Newfoundland, Canada. Marine Ecology Progress Series. 445:235–249.

Baums IB, Miller MW, Hellberg ME. 2005. Regionally isolated populations of an imperiled Caribbean coral, *Acropora palmata*. Molecular Ecology. 14:1377–1390.

Becheler R, Cassone AL, Noël P, Mouchel O, Morrison CL, Arnaud-Haond S. 2015. Low incidence of clonality in cold water corals revealed through a standardized protocol adapted to deep sea sampling. Deep Sea Research Part II Topical Studies in Oceanography. doi:10.1016/j.dsr2.2015.11.013. In press.

Benson DA, Cavanaugh M, Karsch-Mizrachi I, Lipman DJ, Savers EW. 2013. GenBank Nucleic Acids Research (Database Issue) D36-42. doi:10.1093/nar/gks1195.

Bohonak AJ. 1999. Dispersal, gene flow, and population structure. Quarterly Review of Biology. 74(1):21–45.

Botsford LW, White JW, Coffroth MA, Paris CB, Planes S, Shearer TL, Thorrold SR, Jones GP. 2009. Connectivity and resilience of coral reef metapopulations in marine protected areas: matching empirical efforts to predictive needs. Coral Reefs. 28:327–337.

Briggs JC, Bowen BW. 2012. A realignment of marine biogeographic provinces with particular reference to fish distributions. Journal of Biogeography. 39:12–30.

Broch H. 1912. Die Alcyonarien des Trondhjemsfjordes II. Gorgonacea. Kgl Norske Vidensk Selskabs Skrifter. 1912(2):1–48.

Brodsky LI, Vasiliev AV, Kalaidzidis YL, Osipov YS, Tatuzov RL, Feranchuk SI. 1992. GeneBee: the program package for biopolymer structure analysis. Dimacs. 8:127–139.

Brodsky LI, Ivanov VV, Kalaidzidis YL, Leontovich AM, Nikolaev VK, Feranchuk SI, Drachev VA. 1995. GeneBee-NET: Internet-based server for analyzing biopolymers structure. Biochemistry. 60(8):923–928.

Brooke S, Ross SW. 2014. First observations of the cold-water coral *Lophelia pertusa* in mid-Atlantic canyons of the USA. Deep-Sea Research Part II. 104:245–251.

Buhl-Mortensen L, Mortensen PB. 2004. Crustaceans associated with the deepwater gorgonian corals *Paragorgia arborea* (L., 1758) and *Primnoa resedaeformis* (Gunn., 1763). Journal of Natural History. 38:1233–1247.

Buhl-Mortensen L, Mortensen PB. 2005. Distribution and diversity of species associated with deep-sea gorgonian corals off Atlantic Canada. In: Freiwald A, Roberts JM, editors. Cold-water corals and ecosystems. Berlin Heidelberg (Germany): Springer-Verlag. p. 849–879.

Cairns SD, Chapman RE. 2001. Biogeographic affinities of the North Atlantic deep-water Scleractinia. In: Willison JHM, Jall J, Gass SE, editors. Proceedings of the first international symposium on deep-sea corals. Halifax (NS): Ecology Action Center. p. 30–57.

Cairns S, Hoeksema B. 2015. *Flabellum* (*Ulocyathus*) *alabastrum*. World Register of Marine Species [Internet]. [updated 2010 Aug 25; accessed 2016 Apr 22]. http://www.marinespecies.org/aphia.php?p=taxdetails&id=135194.

Canals M, Puig P, de Madron D, Heussner S, Palanques A, Fabres J. 2006. Flushing submarine canyons. Nature. 444:354–357.

Chase MR, Etter RJ, Rex MA, Quattro JM. 1998. Bathymetric patterns of genetic variation in a deep-sea protobranch bivalve, *Deminucula atacellana*. Marine Biology. 131:301–308.

Cho W, Shank TM. 2010. Incongruent patterns of genetic connectivity among four ophiuroid species with differing coral host specificity on North Atlantic seamounts. Marine Ecology 31. [Suppl 1]: 121–143.

Constantini F, Rossi S, Pintus E, Cerrano C, Gili JM, Abbiati M. 2011. Low connectivity and declining genetic variability along a depth gradient in *Corallium rubrum* populations. Coral Reefs. 30:991-1003.

Cowart DA, Huang C, Arnaud-Haond S, Carney SL, Fisher CR, Schaeffer SW. 2013. Restriction to large-scale gene flow vs. regional panmixia among cold seep *Escarpia* spp. (Polychaeta, Siboglinidae). Molecular Ecology. 22:4147–4162.

Cowart DA, Halanych KM, Schaeffer SW, Fisher CR. 2014. Depth-dependent gene flow in Gulf of Mexico cold seep *Lamellibrachia* tubeworms (Annelida: Siboglinidae). Hydrobiologia. 736(1):139-154.

Cowen RK, Sponaugle S. 2009. Larval dispersal and marine population connectivity. Annual Review of Marine Science. 1:443–466.

Cowen RK, Lwiza KM, Sponaugle S, Paris CB, Olson DB. 2000. Connectivity of marine populations: open or closed? Science. 287:857–9.

Cowen RK, Paris CB, Srinivasan A. 2006. Scaling of connectivity in marine populations. Science. 311:522–527.

Cowen RK, Gawarkiewicz G, Pineda J, Thorrold SR, Werner FE. 2007. Population connectivity in marine systems: an overview. Oceanography. 20(3):14–21.

Coykendall DK, Johnson SB, Karl SA, Lutz RA, Vrijenhoek RC. 2011. Genetic diversity and demographic instability in *Riftia pachyptila* tubeworms from eastern Pacific hydrothermal vents. BMC Evolutionary Biology. 11:96.

Coykendall, DK, Morrison CL. 2015. Nine microsatellite loci developed from the octocoral, *Paragorgia arborea*. Conservation Genetics Resources. 7(3):771–772.

(CSA) CSA Ocean Sciences Inc. Ross S, Brooke S, Baird E, Coykendall E, Davies A, Demopoulos A, FranceS, Kellogg C, Mather R, Mienis F, Morrison C, Prouty N, Roark B, Robertson C. 2017. Exploration and Research of Mid-Atlantic Deepwater Hard Bottom Habitats and Shipwrecks with Emphasis on Canyons and Coral Communities: Atlantic Deepwater Canyons Study. Draft Report. Sterling (VA): U.S. Dept. of the Interior, Bureau of Ocean Energy Management, Atlantic OCS Region. OCS Study BOEM 2017-xxx. 1,000 p. + apps.

Cunningham CW, Collins T. 1998. Beyond area relationships: extinction and recolonization in marine molecular biogeography. In: DeSalle R, Schierwater B, editors. Molecular approaches to ecology and evolution. Basel (Switzerland): Birkhauser-Verlag. p. 297–322.

Dahl MP, Pereya RT, Lundälv T, André C. 2012. Fine-scale spatial genetic structure and clonal distribution of cold-water coral *Lophelia pertusa*. Coral Reefs. 31:1135–1148.

De Leo FC, Smith CR, Rowden AA, Bowden,DA, Clark MR. 2010. Submarine canyons: hotspots of benthic biomass and productivity in the deep sea. Proceedings of the Royal Society of London. Series B, Biological Sciences. 277:2783–2792.

De Mol L, Van Rooij D, Pirlet H, Greinert J, Frank N, Quemmerais F, Henriet JP. 2010. Cold-water coral habitats in the Penmarc'h and Guilvinec Canyons, Bay of Biscay: deep-water versus shallow-water settings. Marine Geology. 282(1-2):40–52.

de Stigter HC, Boer W, Mendes PA, Jesus CC, Thomsen L, van den Bergh GD, van Weering TCE. 2007. Recent sediment transport and deposition in the Nazare Canyon, Portuguese continental margin. Marine Geology. 246:144–164.

Earl DA, vonHoldt BM. 2012. STRUCTURE HARVESTER: a website and program for visualizing STRUCTURE output and implementing the Evanno method. Conservation Genetics Resources. 4(2):359–361. doi:10.1007/s12686-011-9548-7. [accessed 2016 Apr 26]. http://taylor0.biology.ucla.edu/struct_harvest.

Edinger EN, Sherwood OA, Piper DJW, Wareham VE, Baker KD, Gilkinson KD, Scott DB. 2011. Geological features supporting deep-sea coral habitat in Atlantic Canada. Continental Shelf Research. 31:S69–S84.

Etnoyer P, Morgan LE. 2005. Habitat-forming deep-sea corals in the Northeast Pacific Ocean. In: Freiwald A, Roberts JM, editors. Cold-water corals and ecosystems. Berlin Heidelberg (Germany): Springer-Verlag. p. 331–343.

Etter RJ, Bower AS. 2015. Dispersal and population connectivity in the deep North Atlantic estimated from physical transport processes. Deep-Sea Research Part I. 104:159–172.

Etter RJ, Rex MA, Chase MC, Quattro JM. 1999. A genetic dimension to deep-sea biodiversity. Deep-Sea Research Part I. 46:1095–1099.

Etter RJ, Rex MA, Chase MC, Quattro JM. 2005. Population differentiation decreases with depth in deep-sea bivalves. Evolution. 59(7):1479–1491.

Evanno G, Regnaut S, Goudet J. 2005. Detecting the number of clusters of individuals using the software STRUCTURE: a simulation study. Molecular Ecology. 14:2611–2620.

Excoffier L, Smouse P, Quattro J. 1992. Analysis of molecular variance inferred from metric distances among DNA haplotypes: application to human mitochondrial DNA restriction data. Genetics. 131: 479–491.

Falush D, Stephens M, Pritchard JK. 2003. Inference of population structure using multilocus genotype data: linked loci and correlated allele frequencies: Genetics. 164:1567–1587.

Flot JF, Dahl M, André C. 2013. *Lophelia pertusa* corals from the Ionian and Barents seas share identical nuclear ITS2 and near-identical mitochondrial genome sequences. BMC Research Notes. 6:144.

France SC, Kocher TD. 1996. Geographic and bathymetric patterns of mitochondrial 16S rRNA sequence divergence among deep-sea amphipods, *Eurythenes gryllus*. Marine Biology. 126:633–643.

Fukami H, Knowlton N. 2005. Analysis of complete mitochondrial DNA sequences of three members of the *Montastraea annularis* coral species complex (Cnidaria, Anthozoa, Scleractinia). Coral Reefs. 24:410–417.

Galarza JA, Carreras-Carbonell J, Macpherson E, Pascual M, Roques S, Turner GF, Rico C. 2009. The influence of oceanographic fronts and early-life-history traits on connectivity among littoral fish species. Proceedings of the National Academy of Sciences of the United States of America. 106:1473–1478.

Goffredi SK, Hurtado LA, Hallam S, Vrijenhoek RC. 2003. Evolutionary relationships of deep-sea vent and cold seep clams (Mollusca: Vesicomyidae) of the 'pacifica/lepta' species complex. Marine Biology. 142:311–320.

Gori A, Orejas C, Madurell T, Bramanti L, Martins M, Quintanilla E, Marti-Puig P, Lo Iacono C, Puig P, Requena S, Greenacre M, Gili JM. 2013. Bathymetrical distribution and size structure of cold-water coral populations in the Cap de Creus and Lacaze-Duthiers canyons, northwestern Mediterranean. Biogeosciences. 10:2049–2060.

Gorospe KD, Karl SA. 2013. Genetic relatedness does not retain spatial pattern across multiple spatial scales: dispersal and colonization in the coral, *Pocillopora damicornis*. Molecular Ecology. 22:3721-3736.

Goudet J. 1995. FSTAT (Version 1.2): a computer program to calculate F-statistics. Journal of Heredity. 86:485–486.

Grantham BA, Eckert GL, Shanks AL. 2003. Dispersal potential of marine invertebrates in diverse habitats. Ecological Applications. 13:S108–S116.

Hare JA, Cowen RK. 1996. Transport mechanisms of larval and pelagic juvenile bluefish (*Pomatomus saltatrix*) from South Atlantic Bight spawning grounds to Middle Atlantic Bight nursery habitats. Limnology and Oceanography. 41(6):1264–1280.

Harris PT, Whiteway T. 2011. Global distribution of large submarine canyons: geomorphic differences between active and passive continental margins. Marine Geology. 285:69–86. doi:10.1016/j.margeo.2011.05.008.

Hasegawa M, Kishino H, Yano T. 1985. Dating the human-ape split by a molecular clock of mitochondrial DNA. Journal of Molecular Evolution. 22:160–174.

Hecker B, Blechschmidt G, Gibson P. 1980. Epifaunal zonation and community structure in three mid- and north Atlantic canyons. Final report for the canyon assessment study in the Mid-and North Atlantic Areas of the U.S. Outer Continental Shelf. Prepared for the U.S. Department of Interior, Bureau of Land Management under contract BLM AA5 51-CT8-49. Palisades (NY): Lamont-Doherty Geological Observatory.

Hecker B, Logan DT, Gandarillas FE, Gibson PR. 1983. Canyon and slope processes study, vol. III: biological processes. Report for the U.S. Department of the Interior, Minerals Management Service, under contract no. 14-12-0001-29178. Palisades (NY): Lamont-Doherty Geological Observatory. 212 p. [accessed 2016 June 1]. http://invertebrates.si.edu/boem/reports/CASPS_vol3.pdf.

Hellberg ME. 1996. Dependence of gene flow on geographic distance in two solitary corals with different larval dispersal. Evolution. 50(3):1167–1175.

Hennige SJ, Morrison CL, Form AU, Büscher J, Kamenos NA, Roberts JM. 2014. Self-recognition in corals facilitates deep-sea habitat engineering. Scientific Reports. 4:6782. DOI:10.1038/srep06782.

Herrera S, Shank TM, Sanchez J. 2012. Spatial and temporal patterns of genetic variation in the widespread antitropical deep-sea coral *Paragorgia arborea*. Molecular Ecology. 21(24):6053–6067.

Herrera S, Shank TM. 2015. RAD sequencing enables unprecedented phylogenetic resolution and objective species delimination in recalcitrant divergent taxa. bioRxiv. http://dx.doi.org/10.1101/019745.

Hilário A, Metaxas A, Gaudron SM, Howell KL, Mercier A, Mestre NC, Ross RE, Thurnherr AM, Young C. 2015. Estimating dispersal distance in the deep sea: challenges and applications to marine reserves. Frontiers in Marine Science. 2:6.

Hixon MA. 2011. 60 years of coral reef fish ecology: past, present, future. Bulletin of Marine Science. 87(4):727–765.

Hubisz MJ, Falush D, Stephens M, Pritchard JK. 2009. Inferring weak population structure with the assistance of sample group information. Molecular Ecology Resources. 9(5):1322–1332.

Huvenne VAI, Tyler PA, Masson DG, Fisher EH, Hauton C, Hühnerbach V, Le Bas TP, Wolff GA. 2011. A picture on the wall: innovative mapping reveals cold-water coral refuge in submarine canyons. PLoS ONE. 6:e28755.

Ikeno T, Tokuda Y, Ezaki Y, Goto SG, Numata H. 2010. Influence of different substrates on the evolution of morphology and life-history traits of azoosanthellate solitary corals (Sclaractinia: Flabellidae). Biological Journal of the Linnean Society of London. 101:184–192.

Jakobsson M, Scholz SW, Scheet P, Gibbs JR,VanLiere JM, Fung HC, Szpiech ZA, Degnan JH, Wang K, Guerreiro R, et al. 2008. Genotype, haplotype and copy-number variation in world-wide human populations. Nature. 451:998–1003.

Jennings RM, Etter RJ, Ficarra L. 2013. Population differentiation and species formation in the deep sea: the potential role of environmental gradients and depth. PLoS ONE. 8(10):e77594.

Jensen JL, Bohonak AJ, Kelley ST. 2005. Isolation by distance, web service. BMC Genetics. 6:13. doi:10.1186/1471-2156-6-13. [assessed 2016 Apr 28]. http://bmcgenet.biomedcentral.com/articles/10.1186/1471-2156-6-13.

Kalinowski ST. 2005. HP_RARE 1.0: a computer program for performing rarefaction on measures of allelic richness. Molecular Ecology Notes. 5: 187–189.

Kelly RP, Oliver TA, Sivasundar A, Palumbi SR. 2010. A method for detecting population genetic structure in diverse, high gene-flow species. Journal of Heredity. 101(4):423–436.

Kendall M, Stewart A. 1977. The advanced theory of statistics, vol. 1. New York (NY): Macmillan.

Kimura M, Weiss GH. 1964. The stepping stone model of population structure and the decrease of genetic correlation with distance. Genetics. 49(4):561–576.

Kinlan BP, Gaines SD. 2003. Propagule dispersal in marine and terrestrial environments: a community perspective. Ecology. 84:2007–2020.

Kitahara MV, Cairns SD, Miller DJ. 2010. Monophyletic origin of *Caryophyllia* (Scleractinia, Caryophylliidae), with descriptions of six new species. Systematics and Biodiversity. 8(1): 91–118.

Labarca C, Paigen K. 1980. A simple, rapid, and sensitive DNA assay procedure. Analytical Biochemistry. 102:344–352.

Lacharité M, Metaxas A. 2013. Early life history of deep-water gorgonian corals may limit their abundance. PLoS ONE. 8(6):e65394.

Larsson AI, Järnegren J, Strömberg SM, Dahl MP, Lundälv T, Brooke S. 2014. Embryogenesis and larval biology of the cold-water coral *Lophelia pertusa.* PLoS ONE. 9(7):e102222.

Leberg PL. 2002. Estimating allelic richness: effects of sample size and bottlenecks. Molecular Ecology. 11:2445–2449.

Ledoux JB, Mokhtar-Jamaï K, Roby C, Féral JP, Garrabou J, Aurelle D. 2010. Genetic survey of shallow populations of the Mediterranean red coral (*Corallium rubrum* Linnaeus, 1758): new insights into evolutionary processes shaping nuclear diversity and implications for conservation. Molecular Ecology. 19:675–690.

LeGoff-Vitry MC, Pybus OG, Rogers AD. 2004a. Genetic structure of the deep-sea coral *Lophelia pertusa* in the northeast Atlantic revealed by microsatellites and internal transcribed spacer sequences. Molecular Ecology. 13:537–549.

Le Goff-Vitry MC, Rogers AD, Baglow D. 2004b. A deep-sea slant on the molecular phylogeny of the Scleractinia. Molecular Phylogenetics Evolution. 30:167–177.

Levin L. 2006. Recent progress in understanding larval dispersal: new directions and digressions. Integrative and Comparative Biology. 46(3):282–297.

Lin MF, Luzon KS, Licuanan WY, Ablan-Lagman MC, Chen CA. 2011. Seventy-four universal primers for characterizing the complete mitochondrial genomes of scleractinian corals (Cnidaria: Anthozoa). Zoological Studies. 50(4):513–524.

Lunden JJ, McNicholl CG, Sears CR, Morrison CL, Cordes EE. 2014. Acute survivorship of the deep-sea coral *Lophelia pertusa* from the Gulf of Mexico under acidification, warming, and deoxygenation. Frontiers in Marine Science. 1(78):1–12.

Lundsten L, Schlining KL, Frasier K, Johnson SB, Kuhnz LA, Harvey JBJ, Clague G, Vrijenhoek RC. 2010. Time-series analysis of six whale-fall communities in Monterey Canyon, California, USA. Deep-Sea Research Part I. 57(12):1573–1584.

Madsen FJ. 1944. Octocorallia (Stolonifera–Telestacea–Xeniidae–Alcyonacea–Gorgonacea). The Danish Ingolf-Expedition. 5(13). Copenhagen: Bianco Luno A/S.

Mantel N. 1967. The detection of disease clustering and a generalized regression approach. Cancer Research. 27:209–220.

Marsh AG, Mullineaux LS, Young CM, Manahan DT. 2000. Larval dispersal potential of the tubeworm, *Riftia pachyptila* at deep-sea hydrothermal vents. Nature. 411:77–80.

Masson DG, Huvenne VAI, de Stigter HC, Wolff GA, Kiriakoulakis K, Arzola RG, Blackbird S. 2010. Efficient burial of carbon in a submarine canyon. Geology. 38(9):831–834.

Matos L, Mienis F, Wienberg C, Frank N, Kwiatkowski C, Groeneveld J, Thil F, Abrantes F, Cunha MR, Hebbeln D. 2015. Interglacial occurrence of cold-water corals off Cape Lookout (NW Atlantic): first evidence of the Gulf Stream influence. Deep-Sea Research Part I. 105:158–170.

McClain CR, Barry JP. 2010. Habitat heterogeneity, disturbance, and productivity work in concert to regulate biodiversity in deep submarine canyons. Ecology. 91(4):964–976.

Mercier AA, Hammel JF. 2011. Contrasting reproductive strategies in three deep-sea octocorals from eastern Canada: *Primnoa resedaeformis, Keratoisis ornata,* and *Anthomastus grandifloras*. Coral Reefs. 30:337–350.

Miller K, Ayre D. 2008. Population structure is not a simple function of reproductive mode and larval type: insights from tropical corals. Journal of Animal Ecology. 77(4):713–724.

Miller K, Williams AA, Rowden AA, Knowles C, Dunshea G. 2010. Conflicting estimates of connectivity among deep-sea coral populations. Marine Ecology. 31(Suppl. 1):144–157.

Miller KJ, Rowden AA, Williams A, Haussermann V. 2011. Out of their depth? Isolated deep populations of the cosmopolitan coral *Desmophyllum dianthus* may be highly vulnerable to environmental change. PLoS ONE. 6(5):e19004.

Mokhtar-Jamaï K, Pascual M, Ledoux JB, Coma R, Féral JP, Garrabou J, Aurelle D. 2011. From global to local genetic structuring in the red gorgonian *Paramuricea clavata*: the interplay between oceanographic conditions and limited larval dispersal. Molecular Ecology. 20:3291–3305.

Morris KJ, Tyler PA, Masson DG, Huvenne VIA, Rogers AD. 2013. Distribution of cold-water corals in the Whittard Canyon, NE Atlantic Ocean. Deep-Sea Research Part II. 92:136–144.

Morrison CL, Eackles MS, Johnson RL, King TL. 2008a. Characterization of 13 microsatellite loci for the deep-sea coral, *Lophelia pertusa* (Linnaeus 1758), from the western North Atlantic Ocean and Gulf of Mexico. Molecular Ecology Resources. 8:1037–1039.

Morrison CL, Johnson RL, King TL, Ross SW, Nizinski MS. 2008b. Molecular assessment of deep-sea Scleractinian coral biodiversity and population structure of *Lophelia pertusa* in the Gulf of Mexico. In: Sulak KJ, Randall MT, Luke KE, Norem AD, Miller JM, editors. Characterization of northern Gulf of Mexico deepwater hard bottom communities with emphasis on *Lophelia* Coral-*Lophelia* reef megafaunal community structure, biotopes, genetics, microbial ecology, and geology. USGS Open File Report 2008-1148, Chapter 4. Reston (VA): US Department of the Interior, US Geological Survey.

Morrison CL, Ross SW, Nizinski MS, Brooke S, Waller RG, Johnson RL, King TL. 2011. Genetic discontinuity among regional populations of *Lophelia pertusa* in the North Atlantic Ocean. Conservation Genetics. 12(3):713–729.

Morrison CL, Springmann MJ, Shroades KM, Stone RP. 2015. Development of twelve microsatellite loci in the red tree corals *Primnoa resedaeformis* and *Primnoa pacifica*. Conservation Genetics Resources. 7:763–765.

Morrison CL, Coykendall DK, Sanders LR. 2017. Microsatellite genotypes for four cold-water coral species (*Lophelia pertusa*, *Desmophyllum dianthus*, *Paragorgia arborea*, *Primnoa resedaeformis*) from Baltimore and Norfolk Canyons used to assess patterns of connectivity. USGS data release, https://doi.org/10.5066/F7827T74.

Mortensen PB, Buhl-Mortensen L. 2004. Distribution of deepwater gorgonian corals in relation to benthic habitat features in the Northeast Channel (Atlantic Canada). Marine Biology. 144:1223–1238.

Mortensen PB, Buhl-Mortensen L. 2005. Morphology and growth of the deepwater gorgonians *Primnoa resedaeformis* and *Paragorgia arborea*. Marine Biology. 147:775–788.

Obelcz J, Brothers D, Chaytor J, ten Brink U, Ross SW, Brooke S. 2014. Geomorphic characterization of four shelf-sourced submarine canyons along the US Mid-Atlantic continental margin. Deep-Sea Research Part II. 104:106–119.

Orejas C, Gori A, Lo Iacono C, Puig P, Gili JM, Dale MRT. 2009. Cold-water corals in the Cap de Creus Canyon, northwestern Mediterranean: spatial distribution, density and anthropogenic impact. Marine Ecology Progress Series. 397:37–51.

Packer D, Boelke D, Guida V, McGee L-A. 2007. State of deep coral ecosystems in the Northeastern US region: Maine to Cape Hatteras. In: Lumsden SE, Hourigan TF, Bruckner A, Dorr G, editors The state of deep coral ecosystems of the United States. Silver Spring (MD): National Oceanic and Atmospheric Administration.

Palumbi SR. 2003. Population genetics, demographic connectivity, and the design of marine reserves. Ecological Applications. 13(1):S146–S158.

Patarnello T, Volckaert FAM, Castilho R. 2007. Pillars of Hercules: is the Atlantic-Mediterranean transition a phylogeographic break? Molecular Ecology. 16:4426–4444.

Peakall R, Smouse PE. 2006. GENALEX 6: genetic analysis in Excel. Population genetic software for teaching and research. Molecular Ecology Notes. 6:288–295.

Peakall R, Smouse PE. 2012. GenAlEx 6.5: Genetic analysis in Excel. Population genetic software for teaching and research – an update. Bioinformatics. 28(19):2537–2539.

Pritchard JK, Stephens M, Donnelly P. 2000. Inference of population structure using multilocus genotype data. Genetics. 155:945–959.

Puig P, Palanques A, Martín J. 2014. Contemporary sediment-transport processes in submarine canyons. Annual Review of Marine Science. 6:5.1–5.25.

Quattrini AM, Nizinski MS, Chaytor JD, Demopoulos AWJ, Roark EB, France SC, Moore JA, Heyl T, Auster PJ, Kinlan B, et al. 2015a. Exploration of the canyon-incised continental margin of the northeastern United States reveals dynamic habitats and diverse communities. PLoS ONE. 10(10):e0139904.

Quattrini AM, Baums IB, Shank TM, Morrison CL, Cordes EE. 2015b. Testing the depth-differentiation hypothesis in a deepwater octocoral. Proceedings of the Royal Society of London. Series B, Biological Sciences. 282: 20150008.

Raymond M, Rousset F. 1995. GENEPOP (Version 1.2): population genetics software for exact tests and ecumenicism. Journal of Heredity. 86(3):248–249.

Rex MA, Etter RJ. 2010. Deep-sea Biodiversity: pattern and scale. Cambridge (MA): Harvard University Press.

Rice WR. 1989. Analyzing tables of statistical tests. Evolution. 43(1):223–225.

Rogers AD. 2002. Molecular ecology and evolution of slope species. In: Wefer G, Billet D, Hebbeln D, Jorgensen BB, Schluter M, Van Weering T, editors. Ocean Margin Systems. Berlin (Heidelberg): Springer-Verlag. p. 323–337.

Romano SL, Palumbi SR. 1997. Molecular evolution of a portion of the 16S ribosomal gene region in scleractinian corals. Journal of Molecular Evolution. 45:397–411.

Romano SL, Cairns SD. 2000. Molecular phylogenetic hypotheses for the evolution of scleractinian corals. Bulletin of Marine Science. 67(3):1043–1068.

Ross SW, Quattrini AM. 2007. The fish fauna associated with deep coral banks off the southeastern United States. Deep-Sea Research Part I. 54(6):975–1007.

Ross SW, Rhode M, Quattrini AM. 2015. Demersal fish distribution and habitat use within and near Baltimore and Norfolk Canyons, U.S. middle Atlantic slope. Deep-Sea Research Part I. 103:137–154.

Rosser NL. 2015. Asynchronous spawning in sympatric populations of a hard coral reveals cryptic species and ancient genetic lineages. Molecular Ecology. 24:5006–5019.

Rousset F. 1997. Genetic differentiation and estimation of gene flow from F-statistics under isolation by distance. Genetics. 145:1219–1228.

Rypina II, Llopiz JK, Pratt LJ, Lozier MS. 2014. Dispersal pathways of American eel larvae from the Sargasso Sea. Limnology and Oceanography. 59(5):1704–1714.

Samadi S, Bottan L, Macpherson E, Richer de Forges B, Boisselier MC. 2006. Seamount endemism questioned by geographic distribution and population genetic structure of marine invertebrates. Marine Biology. 149:1463–1475.

Sambrook J, Fritsch EF, Maniatis T. 1989. Molecular cloning: a laboratory manual. 2nd ed. Cold Spring Harbor (NY): Cold Spring Harbor Laboratory Press.

Schüller M. 2011. Evidence for a role of bathymetry and emergence in speciation in the genus *Glycera* (Glyceridae, Polychaeta) from the deep eastern Weddell Sea. Polar Biology. 34(4):549–564.

Selkoe KA, Toonen RJ. 2011. Marine connectivity: a new look at pelagic larval duration and genetic metrics of dispersal. Marine Ecology Progress Series. 436: 291–305.

Shanks AL, Grantham BA, Carr MH. 2003. Propagule dispersal and the size and spacing of marine reserves. Ecological Applications. 13:S159–69.

Shaw PW, Pierce GJ, Boyle PR. 1999. Subtle population structuring within a highly vagile marine invertebrate, the veined squid *Loligo forbesi*, demonstrated with microsatellite DNA markers. Molecular Ecology. 8(3):407–417.

Shearer TL, van Oppen MJH, Romano SL, Worheide G. 2002. Slow mitochondrial DNA sequence evolution in the Anthozoa (Cnidaria). Molecular Ecology. 11:2475–2487.

Shepard FP, Dill RF. 1966. Submarine canyons and other sea valleys. Chicago (IL): Rand McNally & Co. 381 p.

Sivasundar A, Palumbi SR. 2010. Life history, ecology and biogeography of strong genetic breaks among 15 species of Pacific rockfish, Sebastes. Marine Biology. 157:1433–1452.

Smith PJ, McVeagh SM, Mingoia JT, France SC. 2004. Mitochondrial DNA sequence variation in deep-sea bamboo coral (Keratoisidinae) species in the southwest and northwest Pacific Ocean. Marine Biology. 144:253–261.

Stolarski J, Kitahara MV, Miller DJ, Cairns SD, Marrocchi Y, Mazur M, Meibom A. 2011. The ancient evolutionary origins of Scleractinia revealed by azooxanthellate corals. BMC Evolutionary Biology. 11(1):316.

Strathmann RR, Hughes TP, Kuris AM, Lindeman KC, Morgan SG, Pandolfi JM, Warner RR. 2002. Evolution of local recruitment and its consequences for marine populations. Bulletin of Marine Science. 70:S377–396.

Tamura K, Stecher G, Peterson D, Filipski A, Kumar S. 2013. MEGA6: Molecular evolutionary genetics analysis version 6.0. Molecular Biology and Evolution. 30:2725–2729.

Tendal OS. 1992. The North Atlantic distribution of the octocoral *Paragorgia arborea* (L., 1758) (Cnidaria, Anthozoa). Sarsia. 77:213–217.

Thoma JN, Pante E, Brugler MR, France SC. 2009. Deep-sea octocorals and antipatharians show no evidence of seamount-scale endemism in the NW Atlantic. Marine Ecology Progress Series. 397:25-35.

Tong R, Purser A, Unnithan V, Guinan J. 2012. Multivariate statistical analysis of distribution of deep-water gorgonian corals in relation to seabed topography on the Norwegian Margin. PLoS ONE. 7:e43534.

Tyler P, Amaro T, Arzola R, Cunha MR, de Stiger H, Gooday A, Huvenne V, Ingels J, Kiriakoulakis K, Lastras G, et al. 2009. Europe's Grand Canyon: Nazaré submarine canyon. Oceanography. 22:48–57.

Underwood AJ, Fairweather PG. 1989. Supply-side ecology and benthic marine assemblages. Trends in Ecological Evolution. 4:16–20.

Underwood JN, Smith LD, van Oppen MJH, Gilmour JP. 2007. Multiple scales of genetic connectivity in a brooding coral on isolated reefs following catastrophic bleaching. Molecular Ecology. 16(4):771-784.

Underwood JN, Smith LD, van Oppen MJH, Gilmour JP. 2009. Ecologically relevant dispersal of corals on isolated reefs: implications for managing resilience. Ecology Applications. 19(1):18–29.

van Oppen MJH, Willis BL, Miller DJ. 1999. Atypically low rate of cytochrome b evolution in the scleractinian coral genus *Acropora*. Proceedings of the Royal Society of London. Series B, Biological Sciences. 266:179–183.

Verrill AE. 1922. The Alcyonaria of the Canadian Arctic Expedition, 1913–1918, with a revision of some other Canadian genera and species. Report of the Canadian Arctic Expedition 1913–18, vol. VIII. Molluscs, Echinoderms, Coelenterates, etc. Part G: *Alcyonaria* and *Actinaria*. Ackland, Ottawa.

Vetter EW, Dayton PK. 1998. Macrofaunal communities within and adjacent to a detritus-rich submarine canyon system. Deep-Sea Research Part II. 45(1-3):25–54.

Vetter EW, Dayton PK. 1999. Organic enrichment of macrophyte detritus, and abundance patterns of megafaunal populations in submarine canyons. Marine Ecology Progress Series. 186:137–148.

Vetter EW, Smith CR, De Leo FC. 2010. Hawaiian hotspots: enhanced megafaunal abundance and diversity in submarine canyons on the oceanic islands of Hawaii. Marine Ecology. 31:183–199.

Vrijenhoek RC. 2010. Genetic diversity and connectivity of deep-sea hydrothermal vent metapopulations. Molecular Ecology. 19(20):4391–4411.

Waller RG, Stone RP, Johnstone J, Mondragon J. 2014. Sexual reproduction and seasonality of the Alaskan Red Tree Coral, *Primnoa pacifica*. PLoS ONE. 9:e90893.

Waples RN, Gaggiotti O. 2006. What is a population? An empirical evaluation of some genetic methods for identifying the number of gene pools and their degree of connectivity. Molecular Ecology. 15:1419–1439.

Wareham VE, Edinger EN. 2007. Distribution of deep-sea corals in the Newfoundland and Labrador region, Northwest Atlantic Ocean. Bulletin of Marine Science. 81:289–312.

Watanabe S, Metaxas A, Sameoto J, Lawton P. 2009. Patterns in abundance and size of two deep-water gorgonian octocorals, in relation to depth and substrate features off Nova Scotia. Deep-Sea Research Part I. 56:2235-2248.

Weinberg JR, Dahlgren TG, Trowbridge N, Halanych K. 2003. Genetic differences within and between species of deep-sea crabs (*Chaceon*) from the North Atlantic Ocean. The Biological Bulletin. 204:318–326.

Weir BS, Cockerham CC. 1984. Estimating F-Statistics for the analysis of population structure. Evolution. 38(6):1358–1370.

Whitaker K. 2004. Non-random mating and population genetic subdivision of two broadcasting corals at Ningaloo Reef, Western Australia. Marine Biology. 144:593–603.

White C, Selkoe KA, Watson J, Siegel DA, Zacherl DC, Toonen RJ. 2010. Ocean currents help explain population genetic structure. Proceedings of the Royal Society of London. Series B, Biological Sciences. 277:1685–1694.

Wright S. 1943. Isolation by distance. Genetics. 28:114–138.

Wright S. 1951. The genetical structure of populations. Annals of Eugenics. 15:323–354.

Young CM, He R, Emlet RB, Li Y, Qian H, Arellano SM, Van Gaest A, Bennett KC, Wolf M, Smart TI, Rice ME. 2012. Dispersal of deep-sea larvae from the Intra-American Seas: simulations of trajectories using ocean models. Integrative and Comparative Biology. 52(4):483–496.

Zardus JD, Etter RJ, Chase MC, Rex MA, Boyle EE. 2006. Bathymetric and geographic population structure in the pan-Atlantic deep-sea bivalve *Deminucula atacellana* (Schenck, 1939). Molecular Ecology. 15(3):639–651.

Zeng C, Tracey DM, Clark MR, Rowden AA, Thomas LJ, Gardner JPA. 2014. The complete mitochondrial genome of the deep-sea stony coral *Solenosmilia variabilis* (Scleractinia, Caryophyliidae) and its inter-individual variation. Mitochondrial DNA. doi:10.3109/19401736.2014.971306.

Zhang WG, Gawarkiewicz GG. 2015. Dynamics of the direct intrusion of Gulf Stream ring water onto the Mid-Atlantic Bight shelf. Geophysical Research Letters. 42:7687–7695.

This page intentionally left blank

Appendix 14-A

Supplemental Tables for Patterns of Inter-Canyon Connectivity Among Four Coral Species

This page intentionally left blank

Table 14-A1. Mitochondrial 16S DNA sequences included in phylogenetic analyses.

Genus	Species	GenBank* ID	Reference	MAC ID
Caryophyllia	*atlantica*	FJ788113	Kitahara et al. 2010	–
	calveri	JQ611347-348	Addamo et al. 2012	–
	diomedeae	FJ788114 - 16	Kitahara et al. 2010	–
	grandis	FJ788117 - 18	Kitahara et al. 2010	–
	grayi	FJ788119	Kitahara et al. 2010	–
	inornata	AF265599	Romano and Cairns, 2007	–
	lamellifera	FJ788120	Kitahara et al. 2010	–
	planilamellata	FJ788121-22	Kitahara et al. 2010	–
	quadragenaria	HQ439687	Stolarski et al. 2011	–
	ralphae	HQ439688	Stolarski et al. 2011	–
	rugosa	FJ788123	Kitahara et al. 2010	–
	scobinosa	FJ788124	Kitahara et al. 2010	–
	smithii	JQ611349-50, -58	Addamo et al. 2012	–
	transversalis	FJ788125-26	Kitahara et al. 2010	–
	unicristata	FJ788127-29	Kitahara et al. 2010	–
	versicolorata	HQ439689-90	Stolarski et al. 2011	–
Ceratotrochus	*magnaghii*	AF265597	Romano and Cairns, 2007	–
Cladocora	*caespitosa*	AF265612	Romano and Cairns, 2007	–
Cladocora	*caespitosa*	JQ611352	Addamo et al. 2012	–
Conotrochus	*funicolumna*	HQ439695-96	Stolarski et al. 2011	–
Dasmosmilia	*lymani*	HQ439766-68	Stolarski et al. 2011	–
	lymani	FJ788130	Kitahara et al. 2010	–
	lymani	MG241564	CSA et al. 2017 (this study)	MAC208
	lymani	MG241563	CSA et al. 2017 (this study)	MAC216
Desmophyllum	*dianthus*	GQ868690, -94	Stolarksi et al. 2011	–
	dianthus	JF827631-34	Miller et al. 2011	–
	dianthus	JF827637-38	Miller et al. 2011	–
	dianthus	JQ611357	Addamo et al. 2012	–
	dianthus	JQ611360-61	Addamo et al. 2012	–
	dianthus	MG241562	CSA et al. 2017 (this study)	MAC105
	dianthus	MG241561	CSA et al. 2017 (this study)	MAC169
	dianthus	MG241560	CSA et al. 2017 (this study)	MAC183
	dianthus	MG241559	CSA et al. 2017 (this study)	MAC444
	dianthus	MG241558	CSA et al. 2017 (this study)	MAC445
	dianthus	MG241557	CSA et al. 2017 (this study)	MAC450
	dianthus	MG241556	CSA et al. 2017 (this study)	MAC462
	dianthus	MG241555	CSA et al. 2017 (this study)	MAC521
	dianthus	MG241554	CSA et al. 2017 (this study)	MAC099
Enallopsammia	*rostrata*	HQ439717-18	Stolarski et al. 2011	–
Flabellum	*alabastrum*	MG241538	CSA et al. 2017 (this study)	MAC276
	alabastrum	MG241536	CSA et al. 2017 (this study)	MAC278
	alabastrum	MG241537	CSA et al. 2017 (this study)	MAC334
	angulare	AF550363	LeGoff-Vitry et al. 2004b	–
	apertum	HQ439720	Stolarski et al. 2011	–
	arcuatile	HQ439721-22	Stolarski et al. 2011	–

Table 14-A1. (Continued).

Genus	Species	GenBank* ID	Reference	MAC ID
Flabellum	*deludens*	HQ439724	Stolarski et al. 2011	–
	deludens	AB51069, 71	Ikeno et al. 2010	–
	folkesoni	HQ439725	Stolarski et al. 2011	–
	impensum	AF265582	Romano and Cairns, 2007	–
	japonicum	AB510169, 78	Ikeno et al. 2010	–
	lamellulosum	HQ439726-27	Stolarski et al. 2011	–
	lowekeyesi	HQ439728-31	Stolarski et al. 2011	–
	magnificum	HQ439732	Stolarski et al. 2011	–
	magnificum	AB510167	Ikeno et al. 2010	–
	cf. magnificum	HQ439723	Stolarski et al. 2011	–
	pavoninum	AB510168	Ikeno et al. 2010	–
	tuthilli	HQ439733-34	Stolarski et al. 2011	–
	vaughani	HQ439734, 36	Stolarski et al. 2011	–
Lophelia	*pertusa*	AF550365	LeGoff-Vitry et al. 2004b	–
	pertusa	JQ611345	Addamo et al. 2012	–
	pertusa	MG241553	CSA et al. 2017 (this study)	GP148
	pertusa	MG241552	CSA et al. 2017 (this study)	GP150
	pertusa	MG241551	CSA et al. 2017 (this study)	MAC201
	pertusa	MG241549	CSA et al. 2017 (this study)	MAC203
	pertusa	MG241550	CSA et al. 2017 (this study)	MAC498
	pertusa	MG241548	CSA et al. 2017 (this study)	MAC507
	pertusa	MG241547	CSA et al. 2017 (this study)	MAC513
	pertusa	MG241546	CSA et al. 2017 (this study)	MC794
	pertusa	MG241545	CSA et al. 2017 (this study)	MTR010
	pertusa	MG241544	CSA et al. 2017 (this study)	MTR004
Madrepora	*oculata*	MG241543	CSA et al. 2017 (this study)	RB09GM045
Paracyathus	*pulchellus*	AF265603	Romano and Cairns, 2007	–
Phyllangia	*mouchezii*	AF265605	Romano and Cairns, 2007	–
	papuensis	HQ439773	Stolarski et al. 2011	–
Polycyathus	*muellerae*	AF265606	Romano and Cairns, 2007	–
	species	JF825140	Lin et al. 2011	–
Pourtalosmilia	*anthophyllites*	JQ611346	Addamo et al. 2012	–
Rhizosmilia	*maculata*	AF265602	Romano and Cairns, 2007	–
	sagamiensis	HQ439699	Stolarski et al. 2011	–
Solenosmilia	*variabilis*	HM015348-49	Miller et al. 2010	–
	variabilis	KM609293-94	Zeng et al. 2014	–
Solenosmilia	*variabilis*	MG241542	CSA et al. 2017 (this study)	MAC418
	variabilis	MG241541	CSA et al. 2017 (this study)	MAC419
	variabilis	MG241540	CSA et al. 2017 (this study)	MAC423
	variabilis	MG241539	CSA et al. 2017 (this study)	MAC436
Stephanocyathus	*coronatus*	HQ439700-01	Stolarski et al. 2011	–
	platypus	HM015352	Miller et al. 2010	–
	spiniger	HM015359	Miller et al. 2010	–
Tethocyathus	*virgatus*	FJ788131	Kitahara et al. 2010	–
	virgatus	HQ439702	Stolarski et al. 2011	–

* The National Center for Biotechnology Information (NCBI) GenBank nucleotide database (Benson et al. 2013).

Table 14-A2. Genetic diversity and differentiation in four *Paragorgia arborea* sampling localities, characterized using eight microsatellite loci.

Locality	Locus	N	N_A	*Ne*	I	H_O	H_E	F
Baltimore Canyon	Parb028	60	4	2.05	0.85	0.550	0.512	-0.075
	Parb042	60	5	2.80	1.27	0.650	0.643	-0.012
	Parb021	59	3	2.04	0.84	0.576	0.509	-0.132
	Parb022	58	3	2.23	0.89	0.552	0.552	0.001
	Parb078	60	4	1.16	0.32	0.150	0.141	-0.065
	Parb043	59	6	1.40	0.62	0.254	0.285	0.107
	Parb006	56	2	1.85	0.65	0.429	0.459	0.067
	Parb055	46	13	5.97	2.11	0.848	0.832	-0.018
Norfolk Canyon	Parb028	64	4	2.21	0.93	0.484	0.548	0.115
	Parb042	60	5	3.05	1.28	0.683	0.672	-0.017
	Parb021	63	3	2.01	0.81	0.460	0.503	0.086
	Parb022	63	3	2.26	0.89	0.492	0.557	0.117
	Parb078	62	3	1.29	0.41	0.242	0.227	-0.067
	Parb043	59	5	1.33	0.57	0.237	0.247	0.040
	Parb006	56	2	1.48	0.51	0.375	0.326	-0.149
	Parb055	53	11	4.15	1.84	0.774	0.759	-0.019
Mean		59	4.75	2.33	0.93	0.485	0.486	-0.001

For each locality and locus, the following are given: number of individuals genotyped (N), number of observed alleles (N_A), number of effective alleles (*Ne*), Shannon's Information Index (I), proportion of observed (H_O) and expected (H_E) heterozygotes, and fixation index (F).

Table 14-A3. Genetic diversity and differentiation in four *Primnoa resedaeformis* sampling localities, characterized using eight microsatellite loci.

Locality	Locus	N	N_A	*N*e	I	H_O	H_E	F
Baltimore Canyon	Prim069	32	4	1.88	0.80	0.438	0.468	0.066
	Prim060	32	3	1.89	0.72	0.469	0.471	0.005
	Prim068	32	3	1.62	0.62	0.375	0.382	0.019
	Prim074	32	6	2.21	1.13	0.438	0.548	0.201
	Prim014	32	3	1.17	0.31	0.156	0.146	-0.070
	Prim096	32	4	1.25	0.43	0.188	0.200	0.063
	Prim094	32	3	1.53	0.58	0.438	0.348	-0.257
	Prim026	32	6	2.08	0.93	0.625	0.520	-0.202
Norfolk Canyon	Prim069	40	4	1.30	0.51	0.250	0.228	-0.094
	Prim060	41	5	2.33	1.03	0.561	0.570	0.016
	Prim068	39	3	1.26	0.40	0.231	0.207	-0.116
	Prim074	40	4	3.13	1.18	0.675	0.680	0.008
	Prim014	42	3	1.55	0.58	0.310	0.355	0.128
	Prim096	40	4	1.73	0.70	0.575	0.423	-0.359
	Prim094	41	4	1.80	0.80	0.390	0.444	0.121
	Prim026	41	4	2.45	1.01	0.512	0.592	0.134
Jordan Basin	Prim069	12	2	1.80	0.64	0.333	0.444	0.250
	Prim060	13	3	1.27	0.43	0.077	0.210	0.634
	Prim068	13	4	3.07	1.22	0.692	0.675	-0.026
	Prim074	12	5	3.84	1.48	**0.500**	0.740	0.324
	Prim014	13	3	1.59	0.64	0.462	0.370	-0.248
	Prim096	13	3	1.91	0.77	0.692	0.476	-0.453
	Prim094	13	3	2.36	0.97	0.462	0.577	0.200
	Prim026	13	3	1.73	0.74	0.308	0.423	0.273
Schoodic Ridge	Prim069	15	3	2.27	0.89	0.267	0.560	0.524
	Prim060	14	3	1.24	0.41	0.214	0.196	-0.091
	Prim068	15	3	2.83	1.07	0.600	0.647	0.072
	Prim074	15	6	3.38	1.41	0.667	0.704	0.054
	Prim014	14	2	1.24	0.34	0.214	0.191	-0.120
	Prim096	15	2	1.38	0.45	0.333	0.278	-0.200
	Prim094	15	3	2.66	1.04	0.800	0.624	-0.281
	Prim026	15	2	1.47	0.50	0.400	0.320	-0.250
Mean		25	3.35	1.98	0.77	0.427	0.438	0.010

For each locality and locus, the following are given: number of individuals genotyped (N), number of observed alleles (N_A), number of effective alleles (*N*e), Shannon's Information Index (I), proportion of observed (H_O) and expected (H_E) heterozygotes (bolded number represents significant deviation from Hardy-Weinberg equilibrium after sequential Bonferroni corrections [$\alpha = 0.05$, $P < 0.00156$]), and fixation index (F).

Table 14-A4. Genetic diversity and differentiation in three *Desmophyllum dianthus* sampling localities, characterized using nine microsatellite loci.

Locality	Locus	N	N_A	*Ne*	I	H_O	H_E	F
Baltimore Canyon	LpeC44	27	30	25.58	3.32	**0.333**	0.961	0.653
	LpeA5	29	8	4.06	1.67	0.759	0.754	-0.006
	LpeC61	31	10	4.77	1.84	**0.323**	0.790	0.592
	LpeC52	30	4	1.19	0.37	0.100	0.157	0.362
	LpeD3	30	27	19.36	3.12	0.933	0.948	0.016
	LpeC142	31	26	17.32	3.03	0.935	0.942	0.007
	LpeG20	30	20	10.84	2.67	0.933	0.908	-0.028
	LpeG54	30	9	1.95	1.12	0.600	0.487	-0.231
	LpeG33	29	11	4.74	1.82	**0.345**	0.789	0.563
Norfolk Canyon D	LpeC44	21	20	15.75	2.86	**0.333**	0.937	0.644
	LpeA5	24	10	5.70	1.94	0.875	0.825	-0.061
	LpeC61	25	12	5.61	2.04	**0.240**	0.822	0.708
	LpeC52	25	3	1.08	0.19	0.080	0.078	-0.031
	LpeD3	26	27	18.03	3.13	**0.577**	0.945	0.389
	LpeC142	26	21	13.66	2.81	**0.577**	0.927	0.377
	LpeG20	26	19	10.65	2.67	0.923	0.906	-0.019
	LpeG54	23	6	1.85	0.97	0.565	0.460	-0.228
	LpeG33	23	10	4.64	1.81	**0.304**	0.776	0.608
Norfolk Canyon S	LpeC44	22	18	12.91	2.71	**0.273**	0.923	0.704
	LpeA5	23	7	4.10	1.59	0.652	0.756	0.138
	LpeC61	22	8	4.10	1.63	**0.364**	0.756	0.519
	LpeC52	23	7	1.53	0.83	**0.087**	0.346	0.749
	LpeD3	23	25	17.63	3.04	0.826	0.943	0.124
	LpeC142	23	27	17.93	3.11	0.696	0.944	0.263
	LpeG20	23	21	9.71	2.67	1.000	0.897	-0.115
	LpeG54	23	6	1.66	0.90	0.261	0.406	0.358
	LpeG33	23	10	5.16	1.95	**0.304**	0.806	0.623

For each locality and locus, the following are given: number of individuals genotyped (*N*), number of observed alleles (N_A), number of effective alleles (*Ne*), Shannon's Information Index (I), proportion of observed (H_O) and expected (H_E) heterozygotes (numbers in bold represent significant deviations from Hardy-Weinberg equilibrium after sequential Bonferroni corrections ($\alpha = 0.05$, $P < 0.00185$), and fixation index (F).

Table 14-A5. Genetic diversity and differentiation in 13 *Lophelia pertusa* sampling localities characterized using 14 microsatellite loci.

Locality	Locus	N	N_A	H_O	H_E	F
Garden Banks	LpeA5	19	8	0.842	0.726	-0.160
	LpeC44	18	17	0.611	0.883	0.308
	LpeC52	19	12	0.842	0.783	-0.076
	LpeC61	19	24	0.947	0.934	-0.015
	LpeC142	18	15	1.000	0.887	-0.127
	LpeC151	17	8	**0.176**	0.761	0.768
	LpeD5	19	10	0.474	0.828	0.428
	LpeG20	19	10	0.947	0.845	-0.121
	LpeG33	19	11	0.842	0.886	0.050
	Lpeg43	19	4	**0.105**	0.240	0.561
	LpeG50	19	17	1.000	0.916	-0.092
	LpeG54	17	8	0.706	0.798	0.115
	LpeG63	18	4	0.389	0.653	0.404
	LpeG62	19	4	0.684	0.693	0.012
MC751	LpeA5	23	7	0.609	0.753	0.192
	LpeC44	24	21	0.792	0.931	0.149
	LpeC52	24	12	0.750	0.775	0.032
	LpeC61	24	24	1.000	0.939	-0.065
	LpeC142	24	13	0.875	0.881	0.007
	LpeC151	24	6	0.625	0.678	0.078
	LpeD5	24	10	**0.500**	0.768	0.349
	LpeG20	24	16	1.000	0.916	-0.092
	LpeG33	23	12	0.783	0.885	0.115
	LpeG43	23	2	0.087	0.083	-0.045
	LpeG50	24	19	0.917	0.930	0.014
	LpeG54	24	9	0.667	0.850	0.216
	LpeG63	24	6	**0.375**	0.694	0.460
	LpeG62	24	5	0.583	0.650	0.103
Gulf Oil	LpeA5	9	7	0.889	0.790	-0.125
	LpeC44	8	11	0.750	0.891	0.158
	LpeC52	8	8	0.750	0.758	0.010
	LpeC61	9	13	0.889	0.877	-0.014
	LpeC142	9	9	1.000	0.827	-0.209
	LpeC151	9	5	0.556	0.747	0.256
	LpeD5	9	7	0.556	0.747	0.256
	LpeG20	9	5	0.778	0.728	-0.068
	LpeG33	9	9	0.889	0.840	-0.059
	LpeG43	9	3	0.444	0.500	0.111
	LpeG50	9	11	1.000	0.883	-0.133
	LpeG54	9	8	0.889	0.840	-0.059
	LpeG63	9	2	0.333	0.401	0.169
	LpeG62	9	4	0.556	0.574	0.032

Table 14-A5 (Continued).

Locality	Locus	N	N_A	H_O	H_E	F
Gulfpenn	LpeA5	10	3	0.900	0.645	-0.395
	LpeC44	9	12	0.444	0.901	0.507
	LpeC52	10	8	0.600	0.745	0.195
	LpeC61	10	16	1.000	0.930	-0.075
	LpeC142	10	12	0.900	0.900	0.000
	LpeC151	10	6	0.300	0.745	0.597
	LpeD5	10	7	0.500	0.695	0.281
	LpeG20	10	10	0.800	0.860	0.070
	LpeG33	10	10	0.800	0.855	0.064
	LpeG43	9	3	0.111	0.475	0.766
	LpeG50	10	11	0.900	0.885	-0.017
	LpeG54	10	7	0.700	0.785	0.108
	LpeG63	10	5	0.200	0.760	0.737
	LpeG62	10	4	0.800	0.675	-0.185
VK862	LpeA5	16	8	0.750	0.736	-0.019
	LpeC44	15	16	0.667	0.924	0.279
	LpeC52	17	10	0.588	0.798	0.262
	LpeC61	17	18	0.941	0.908	-0.036
	LpeC142	17	15	0.824	0.898	0.083
	LpeC151	16	5	0.375	0.695	0.461
	LpeD5	16	6	0.625	0.668	0.064
	LpeG20	17	14	1.000	0.884	-0.131
	LpeG33	17	15	1.000	0.900	-0.112
	LpeG43	13	4	0.231	0.213	-0.083
	LpeG50	17	17	0.941	0.920	-0.023
	LpeG54	16	8	0.625	0.822	0.240
	LpeG63	17	5	0.412	0.704	0.415
	LpeG62	17	4	0.471	0.685	0.313
VK906	LpeA5	60	9	0.783	0.779	-0.005
	LpeC44	58	31	0.741	0.934	0.206
	LpeC52	59	12	**0.254**	0.862	0.705
	LpeC61	60	32	0.950	0.949	-0.001
	LpeC142	60	18	0.883	0.907	0.026
	LpeC151	59	8	**0.475**	0.721	0.342
	LpeD5	58	12	**0.466**	0.805	0.422
	LpeG20	57	18	0.895	0.900	0.006
	LpeG33	56	16	0.875	0.906	0.034
	LpeG43	59	3	0.136	0.238	0.431
	LpeG50	60	22	0.900	0.930	0.032
	LpeG54	54	10	**0.463**	0.752	0.384
	LpeG63	57	7	**0.368**	0.666	0.447
	LpeG62	58	4	**0.534**	0.683	0.218

Table 14-A5 (Continued).

Locality	Locus	N	N_A	H_O	H_E	F
VK826	LpeA5	117	9	0.838	0.769	-0.090
	LpeC44	115	37	**0.791**	0.952	0.165
	LpeC52	119	16	**0.538**	0.823	0.346
	LpeC61	119	41	0.958	0.954	-0.004
	LpeC142	121	25	0.835	0.913	0.086
	LpeC151	119	11	**0.445**	0.719	0.380
	LpeD5	114	17	**0.404**	0.747	0.460
	LpeG20	118	23	0.805	0.912	0.117
	LpeG33	118	18	0.839	0.913	0.081
	LpeG43	115	5	**0.252**	0.378	0.332
	LpeG50	120	26	0.925	0.936	0.012
	LpeG54	117	10	**0.504**	0.758	0.335
	LpeG63	115	8	**0.417**	0.686	0.391
	LpeG62	117	4	0.598	0.668	0.104
West Florida Slope	LpeA5	45	8	0.689	0.748	0.079
	LpeC44	46	25	**0.696**	0.929	0.251
	LpeC52	47	13	0.702	0.843	0.167
	LpeC61	47	32	0.894	0.945	0.055
	LpeC142	47	19	0.936	0.913	-0.026
	LpeC151	47	9	0.511	0.713	0.284
	LpeD5	44	9	**0.364**	0.658	0.447
	LpeG20	40	17	0.850	0.902	0.058
	LpeG33	43	14	0.814	0.886	0.081
	LpeG43	46	3	0.130	0.196	0.334
	LpeG50	47	23	0.894	0.930	0.039
	LpeG54	47	11	**0.723**	0.848	0.147
	LpeG63	47	8	**0.319**	0.716	0.554
	LpeG62	47	5	**0.489**	0.672	0.272
Miami Terrace	LpeA5	9	5	0.556	0.741	0.250
	LpeC44	9	11	0.778	0.877	0.113
	LpeC52	9	7	0.778	0.741	-0.050
	LpeC61	9	14	1.000	0.901	-0.110
	LpeC142	9	7	0.889	0.827	-0.075
	LpeC151	9	5	0.333	0.623	0.465
	LpeD5	8	8	0.500	0.789	0.366
	LpeG20	7	4	0.286	0.653	0.563
	LpeG33	8	8	0.375	0.828	0.547
	LpeG43	9	2	0.000	0.346	1.000
	LpeG50	9	13	0.889	0.907	0.020
	LpeG54	8	5	0.250	0.688	0.636
	LpeG63	9	7	0.889	0.815	-0.091
	LpeG62	9	3	0.444	0.512	0.133

Table 14-A5 (Continued).

Locality	Locus	N	N_A	H_O	H_E	F
Cape Canaveral	LpeA5	28	9	0.964	0.820	-0.176
	LpeC44	24	22	**0.667**	0.913	0.270
	LpeC52	28	13	0.857	0.747	-0.147
	LpeC61	28	21	**0.714**	0.938	0.239
	LpeC142	27	14	0.815	0.875	0.069
	LpeC151	26	8	**0.385**	0.763	0.496
	LpeD5	28	12	0.536	0.722	0.258
	LpeG20	28	14	0.607	0.844	0.281
	LpeG33	28	19	0.714	0.927	0.230
	LpeG43	27	5	**0.296**	0.482	0.385
	LpeG50	28	16	0.821	0.888	0.075
	LpeG54	27	8	**0.370**	0.722	0.487
	LpeG63	28	8	**0.250**	0.714	0.650
	LpeG62	28	4	**0.357**	0.539	0.337
Cape Lookout	LpeA5	22	9	0.773	0.824	0.063
	LpeC44	20	19	0.700	0.933	0.249
	LpeC52	22	13	0.682	0.721	0.054
	LpeC61	22	21	0.818	0.920	0.111
	LpeC142	22	21	0.909	0.925	0.017
	LpeC151	22	8	**0.409**	0.746	0.452
	LpeD5	21	13	**0.476**	0.675	0.294
	LpeG20	20	7	**0.300**	0.680	0.559
	LpeG33	21	14	0.714	0.885	0.193
	LpeG43	22	5	**0.182**	0.598	0.696
	LpeG50	22	21	0.955	0.926	-0.031
	LpeG54	20	7	0.850	0.783	-0.086
	LpeG63	22	5	0.636	0.727	0.125
	LpeG62	22	4	0.500	0.465	-0.076
Baltimore Canyon	LpeA5	3	3	1.000	0.611	-0.636
	LpeC44	3	5	0.667	0.778	0.143
	LpeC52	3	5	0.667	0.778	0.143
	LpeC61	3	4	0.333	0.722	0.538
	LpeC142	3	3	0.667	0.611	-0.091
	LpeC151	3	4	0.667	0.667	0.000
	LpeD5	2	2	0.500	0.375	-0.333
	LpeG20	3	6	1.000	0.833	-0.200
	LpeG33	3	4	0.667	0.667	0.000
	LpeG43	3	2	0.333	0.278	-0.200
	LpeG50	3	5	1.000	0.778	-0.286
	LpeG54	3	2	0.000	0.444	1.000
	LpeG63	1	3	1.000	0.500	-1.000
	LpeG62	15	4	0.333	0.611	0.455

Table 14-A5 (Continued).

Locality	Locus	N	N_A	H_O	H_E	F
Norfolk Canyon	LpeA5	14	7	0.857	0.781	-0.098
	LpeC44	14	20	0.857	0.934	0.082
	LpeC52	12	12	0.750	0.851	0.118
	LpeC61	14	21	0.643	0.918	0.300
	LpeC142	13	12	0.769	0.867	0.113
	LpeC151	14	10	0.571	0.768	0.256
	LpeD5	14	6	0.357	0.747	0.522
	LpeG20	14	16	0.643	0.888	0.276
	LpeG33	14	14	0.786	0.901	0.127
	LpeG43	12	3	0.167	0.486	0.657
	LpeG50	14	16	0.929	0.903	-0.028
	LpeG54	14	6	0.500	0.676	0.260
	LpeG63	14	7	**0.286**	0.671	0.574
	LpeG62	12	4	0.500	0.573	0.127
	Mean	29	11	0.646	0.760	0.162

For each locality and locus, the following are given: number of individuals genotyped (N), number of effective alleles (N_A), Shannon's Information Index (I), proportion of observed (H_O) and expected (H_E) heterozygotes (numbers in bold represent significant deviations from Hardy-Weinberg equilibrium after sequential Bonferroni corrections [$\alpha = 0.05$, $P < 0.000275$]), and fixation index (F).

CHAPTER 15. FISH COMMUNITIES AND DIETS[1]

Steve W. Ross, Mike Rhode, and Ashley Horton

15.1 FISHES ASSOCIATED WITH DEEPWATER CANYONS

15.1.1 Introduction and Background

The deeper (>200 m) slope fish fauna is composed of species that are widely distributed either along the United States and Canadian east coasts or even throughout the broader North Atlantic Ocean. Although estuarine and shelf fishes are well studied, deepsea fishes of the region are much less well documented, and data tend to be clumped around a few selected study sites, including some canyons, and are largely based on trawl sampling (Markle and Musick 1974, Musick et al. 1992, Sulak and Ross 1996). The most comprehensive treatment of deepsea fishes of the mid-Atlantic was the unpublished study of Musick (1979), and some data from that study were also included in a larger scale fish community treatment by Sulak (1982). Moore et al. (2003) provided an annotated checklist of the deepsea fishes of the northern part of the mid-Atlantic to the Scotian slope. Canyon and other rough bottom areas of the mid-Atlantic were rarely sampled, but selected canyons were the subject of some studies involving direct observation methods (submersible, tow camera) (Lamont-Doherty Geological Observatory 1983, Grimes et al. 1987, Sulak and Ross 1996).

Many submarine canyons provide substantial complex habitat structures, including hard substrate attachment sites for sessile organisms. Biological excavations provide additional habitat heterogeneity, and these can be extensive in mid-Atlantic canyons (Malahoff et al. 1982, Grimes et al. 1986). Habitats provided by sessile fauna (such as deepsea corals) and other nonliving, reef-like substrate (rocks, cliffs) have a complex and geographically variable influence on the structure of benthic and midwater communities (Roberts et al. 2009, Young 2009, Quattrini et al. 2012). Some fishes have specific habitat requirements; however, the degree of habitat fidelity is often unclear, especially for deepsea fauna. Certain fishes are strongly or uniquely associated with deep reef habitats (including shipwrecks) off the southeastern United States and in the Gulf of Mexico (Ross 2007, Ross and Quattrini 2007, 2009; Sulak et al. 2007). In contrast, deep reefs of the northeastern and northwestern North Atlantic supported higher abundances of fishes than surrounding soft bottoms, but the species were the same as the overall slope background fauna (Costello et al. 2005, Auster 2005, Kutti et al. 2014). Certain fish and invertebrate species were so specific to Mid-Atlantic Bight (MAB) canyons that they might be “canyon indicator species” (Lamont-Doherty Geological Observatory 1983), but this requires confirmation, and in general deepsea fish habitat specificity remains poorly known with a few exceptions. Cusk (*Brosme brosme*) from this region are known to occur most frequently on complex habitats, including cold-water corals, and appear to have high site fidelity (Collette and Klein-MacPhee 2002, Hare et al. 2012). Likewise, chain dogfish (*Scyliorhinus retifer*) in the MAB are most common on complex, high profile substrate (Able and Flescher 1991).

Substrate heterogeneity (Rowe 1971, Vetter et al. 2010) and concentration of organic matter (Keller and Shepard 1978, De Leo et al. 2010) are the two factors often used to explain increased faunal diversity and abundance and higher productivity in canyons than in surrounding areas (De Leo et al. 2010). Faunal depth zonation patterns are related to decreasing food availability with depth (Carney 2005); however, canyons may have atypical depth zonation patterns because they concentrate organic materials and funnel

[1] The canyons fish community and habitat association information of Section 15.1 was published in a modified version as Ross et al. (2015a). The fish diet data of Section 15.2 are part of a Master's Thesis at University of North Carolina−Wilmington (Horton 2015). The shelf community and habitat association components of Section 15.3 were published in a modified version as Ross et al. (2016).

them down-slope. Analyses of fish assemblages found in each habitat will determine the influence of large-scale features (e.g., canyons) and smaller scale features (e.g., shipwrecks, seeps, or corals/rocks) on community structure and function. The slope and shelf of the MAB have a lower percentage of natural hard substrate compared with other regions (Steimle and Zetlin 2000). Thus, habitat may be limiting for fauna requiring hard substrate, and canyon reef-like habitats probably represent significant habitat resources in this region.

Submarine canyons are a dominant feature of the outer shelf and continental slope of the U.S. mid-Atlantic (Brothers et al. 2013). Our study focused on two of the larger canyons: Baltimore Canyon and Norfolk Canyon (**Figure 15-1**). Obelcz et al. (2014) reviewed the geology of these similar sized, shelf-sourced canyons and indicated that substantial sediments had been and, to a lesser extent, still are being transported through the canyons. Each canyon exhibited a series of terraces starting near the canyon rims, and in general the most rugged terrain was near the heads of the canyons and on the north walls (Obelcz et al. 2014, S.W. Ross pers. obs.). Hard substrate in these canyons was represented by scattered rocks, boulders, tallus fields and ridges, and walls of consolidated mud (Tucholke 1987, pers. obs.). Deepsea corals (mostly octocorals) are common on most hard substrate in and near the canyons, especially shallower than 1,000 m (Hecker and Blechschmidt 1980; also see **Chapter 8**), and contributed substantially to habitat complexity.

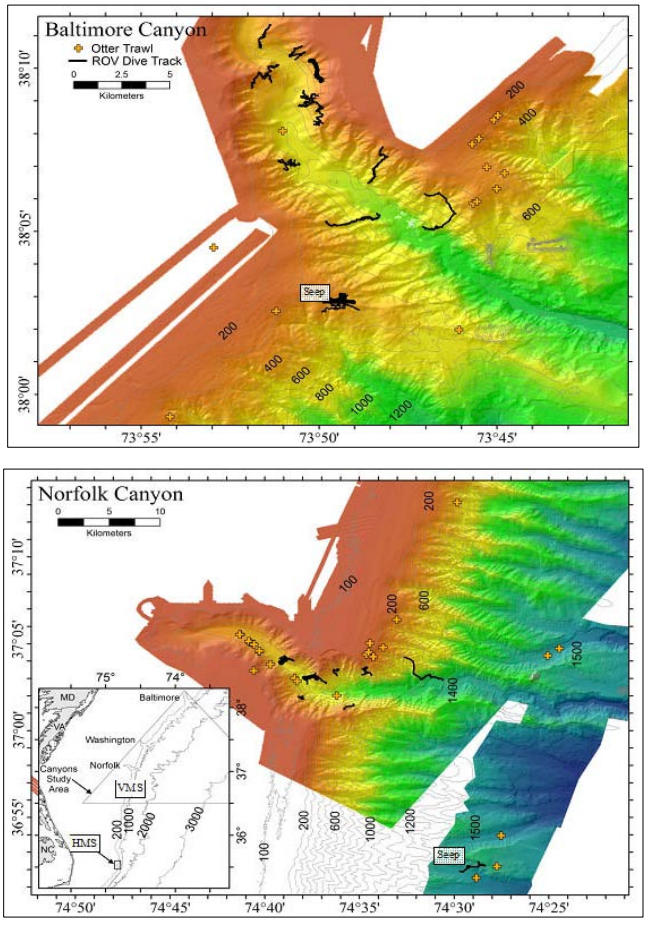

Figure 15-1. Bathymetric maps (depth in meters) derived from multibeam sonar of Baltimore and Norfolk canyons showing remotely operated vehicle (black lines) and trawl (crosses, starting locations) stations from the 2012 and 2013 sampling cruises. Inset shows the mid continental slope off Cape Hatteras (HMS) and Virginia Middle Slope (VMS) sites sampled by Sulak and Ross (1996). Two methane seeps south of each canyon are labeled.

Although not formally documented, a methane seep chemosynthetic community was suspected in the vicinity of Baltimore Canyon (B. Hecker, pers. comm.). This seep and another deeper seep near Norfolk Canyon (**Figure 15-1**) were located, and habitats and associated fishes were surveyed in both seep areas. See Skarke et al. (2014) for descriptions of newly discovered seeps in this region.

15.1.2 Methods

15.1.2.1 Field Sampling Methods

15.1.2.1.1 ROV Operations

Remotely operated vehicle (ROV) dives were conducted during the 2012 and 2013 sampling cruises for the Atlantic Deepwater Canyons Study (**Chapter 3**). The ROV position was continuously recorded using an ultra-short baseline tracking system. Color-shaded bathymetric geotiff maps (obtained from the 2011 mapping cruise) facilitated ROV navigation and video/biological sampling. Two parallel lasers mounted 10 cm apart were turned on most of the time when using the video cameras. High definition video was recorded to a hard drive during the dive, and copies of the dive video were made after each dive. Video was supplemented by digital still photography obtained opportunistically during dives. Fish sampling was accomplished by suction samplers connected to sampling buckets. A Sea-Bird Electronics, Inc. (SBE) 911*plus* conductivity-temperature-depth (CTD) instrument was attached to the ROV to record environmental data during each dive (see **Section 3.2.6** for details on CTD instrument).

Most ROV dives were during daylight and were scheduled for a 12-hour working day, but weather and gear logistics sometimes dictated shorter dives, and on some occasions dives were made during nighttime and for durations longer than 12 hours. ROV dives typically followed a similar pattern, emphasizing bottom transecting, collecting, and photographing specimens on or near the bottom. Position data were time-synchronized with all imagery and samples. ROV instruments recorded all times as Universal Transverse Mercator (UTM); however, because local time was used in the eventual analyses, local time was recorded on analog station sheets and on the audio.

A lead scientist directed each dive and made audio annotations of dive activities. All dives began at the deepest targeted location and worked upslope. During the descents, observations of distributions and behaviors of midwater fauna were recorded. Specimens were collected opportunistically throughout a dive. Standardized video transects were taken whenever the ROV moved from one location to another. During transects, the video camera was moved to a predetermined pan/tilt position, set on wide angle, and the ROV ran at slow speed close to the bottom. Transects were of variable lengths; some were short as frequent sampling interrupted the transects, and some were longer, covering wide ranges of habitats. Video transects were taken on every dive because these were the primary means of habitat and faunal characterization, but the number of transects varied per dive. Except when the ROV was in the water column, video recording and digital still photography were conducted throughout each dive. Every collection was documented with video. Fishes collected by ROV were preserved at sea in 10% formalin seawater solution.

15.1.2.1.2 Trawling

Bottom trawling was conducted off the stern using the ship's main winch deploying a 4.9 m head rope otter trawl (38.1 mm mesh). Upon reaching bottom, the trawl was towed for 30 min at a ground speed of 2 knots, usually against the surface current, then retrieved. This operation was repeated as many times as possible during the night watches. Multibeam sonar bathymetry maps were used to identify bottoms and depths that could be trawled. An attempt was made to sample as wide a depth range as possible in and around Baltimore and Norfolk canyons.

After each trawl, fishes were sorted from the catch and preserved in 10% formalin seawater solution. The gut cavities of larger specimens were injected with formalin to ensure preservation of stomach contents. Selected specimens were photographed at sea.

15.1.2.2 Laboratory Methods

15.1.2.2.1 Habitat Definitions

A main objective was to determine whether fishes were associated with general habitats. Because this study emphasized deepsea corals, these, as well as sponges, were noted as a habitat defining characteristic when they were abundant. Most "hard" substrate in Norfolk and Baltimore canyons was represented by consolidated sediments and were not true rocks (those being rare). To determine large-scale habitat use patterns in canyon areas, video and multibeam sonar data were used to develop five general habitat classifications (**Figure 15-2**):

- SS − Soft substrate sand/mud bottom: relatively flat with few structuring characteristics aside from burrows, depressions, and animal tracks.
- SSB − Steeply sloping mostly sand/mud bottom, often displaying burrows and mud clumps or small mud ledges with relief <0.5 m.
- GRR − Gravel, rocks, rubble fields; various sized rocks or gravel or consolidated mud "rocks" and usually <1 m in vertical profile, often with sand/mud channels among the hard substrate.
- WRR − Canyon walls, rocks, and ridges; the most rugged habitat usually with vertical walls (overall vertical profile >1 m) of consolidated mud with numerous cracks, burrows, overhangs, and crevices. Terraces often separated a series of walls and were included in this category.
- SDM25 − Soft substrate, <25% dead mussel shells; sandy seep area habitat, profile <0.2 m.
- SDM25-75 − Soft substrate, 25% to 75% dead mussel shells: seep area habitat, profile <0.2 m, moderate amount of sand visible.
- SDM75 − Soft substrate, >75% dead mussel shells; seep area habitat, profile <0.2 m, small amount of sand visible.
- MHS − Mixed hard-soft: seep habitat composed of authigenic carbonate rocks surrounded by sand, profile <1 m, no dead mussels present.
- MHS25 − Mixed hard-soft, <25% dead mussel shells; seep habitat composed of authigenic carbonate rocks surrounded by sand and dead mussel shells, profile <1 m.
- MHS25-75 − Mixed hard-soft, 25% to 75% dead mussel shells (see MHS25).
- MHS75 − Mixed hard-soft, >75% dead mussel shells (see MHS25).

For categories GRR, WRR and MHS through MHS75, two additional habitat attributes were assigned: abundant corals/sponges (approximately >30% cover) or few to no corals/sponges (approximately <30% cover). Additional habitat attributes were attached to seep categories SDM25 through MHS75 as follows: <25% live mussel cover, approximately 25% to 75% live mussel cover, >75% live mussel cover. Gas bubbling and bacterial mats were also noted during analysis of the videos.

For all canyon and seep habitats, additional habitat metrics included bottom depth and environmental data recorded by the CTD mounted on the ROV.

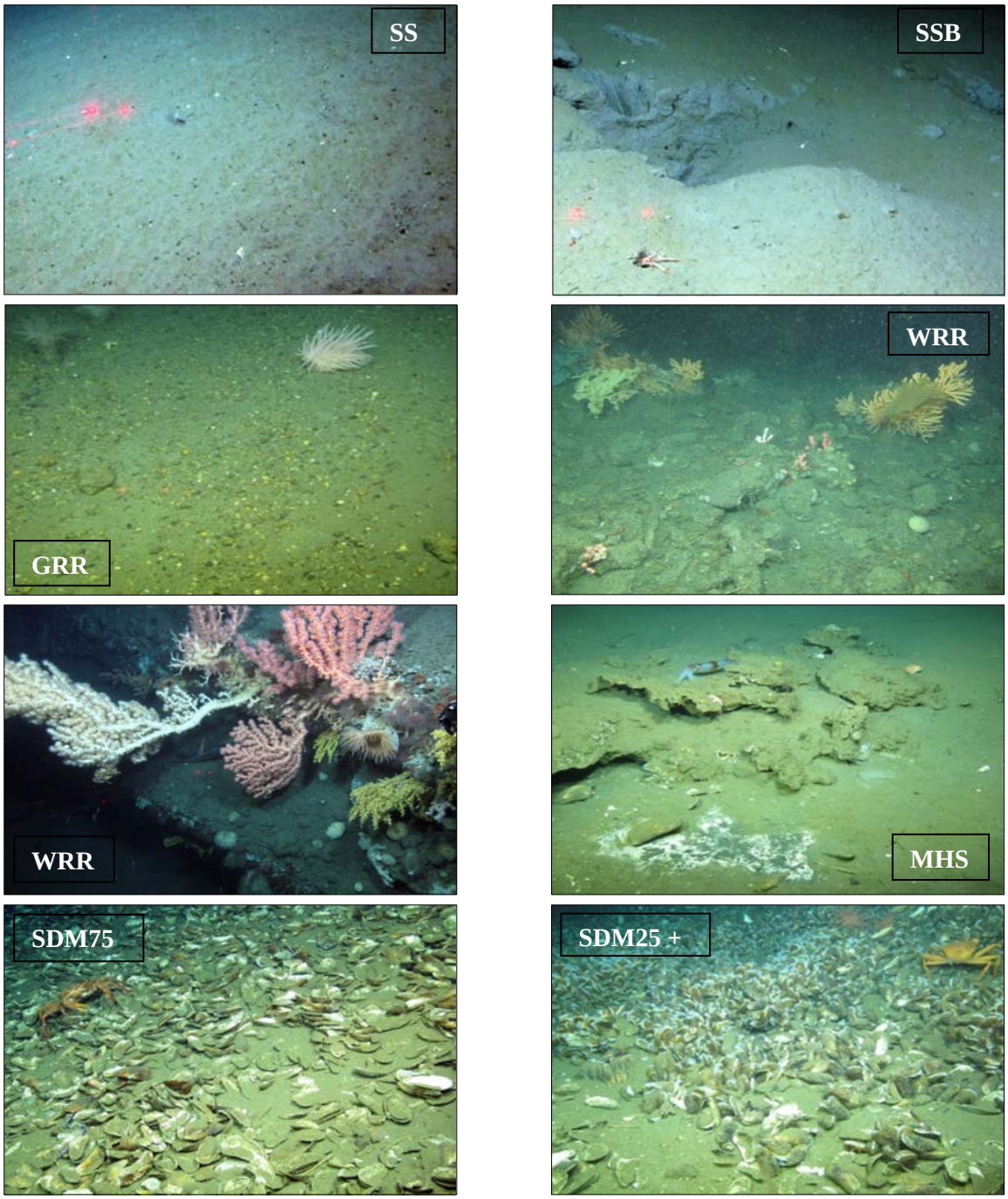

Figure 15-2. Photographs of benthic habitats taken *in situ* in and around Baltimore and Norfolk canyons. See Methods for more detailed habitat definitions. Red laser dots are 10 cm apart. SS = soft substrate sand/mud; SSB = steeply sloping sand/mud, some structure; GRR = gravel, rocks, rubble; WRR = walls, rocks, ridges, high profile (note extensive attached octocorals); MHS = mixed carbonate rocks, seeps, and sand (note white bacterial mat in foreground); SDM75 = sand bottom with >75% dead mussel cover; SDM25 (sand bottom with <25% dead mussels) ≥75% live mussel cover. Note *Chaceon quinquedens* (red crab) in bottom panels. Examples of all seep habitats are not provided (see Methods).

15.1.2.2.2 Video Analysis for Community and Habitat Association

Because direct observation methods are preferred for documenting fauna in complex habitats (see reviews in Ross and Quattrini 2007, 2009), ROV video camera recordings were the main data used to describe the fish communities and associated habitats on and around Baltimore and Norfolk canyons. Dive videos were viewed multiple times for habitat classifications and to document benthic fishes to the lowest possible taxa at the time of observation. ROV dive tracks were initially processed to conservatively remove erroneous tracking data (location points) as described by Partyka et al. (2007) and Quattrini et al. (2012). Video analysis to determine fish community structure and habitat associations was accomplished similar to that described in Ross and Quattrini (2007).

Video segments were designated when the ROV stopped or started movement, the video quality changed, or when the habitat changed. Depth from the ROV-mounted Sea-Bird data logger was recorded for every time segment. Unusable video (out of focus, too far off bottom, video malfunction, sediment clouds) was removed from the dataset.

The only data used in analyzing habitat associations and community patterns were of fishes observed during the transects. These data were supplemented as needed by the video recorded while the ROV was stationary or video was zoomed in. Species composition and relative abundances were compared among the habitat types. To compare abundances of all species within a particular habitat, relative (%) abundances were calculated (number of individuals per species per habitat/total # individuals observed per habitat x 100) using transect video data.

Species composition and relative abundances were compared within each habitat and among the habitat types using fish counts from the transect video. To compare abundances of all species within a habitat, relative (%) abundances were calculated as follows:

$$\left(\frac{\text{Number of individuals per taxa per habitat}}{\text{Total number of individuals observed per habitat}}\right) \times 100$$

Across-habitat comparisons were accomplished for all fishes identified to at least genus with overall abundances >5 individuals. That abundance level allows for the possibility of each taxa to occur in any of the five major habitat types (note for this purpose all seep habitats, SDM25-MHS75, combined = MHS). The relative (%) abundance of each species by habitat was calculated as follows:

$$\left(\frac{\text{Number of individuals in a particular habitat}}{\text{Total number of individuals of the same species from all 5 habitats}}\right) \times 100$$

Multivariate analyses, conducted in PRIMER 6 + PERMANOVA (Clarke and Warwick 2001, Clarke and Gorley 2006, Anderson et al. 2008), were used to determine differences in benthic fish assemblages among habitat types and depth zones. Sample units were the numbers of each species per habitat category per dive; samples with no species present were removed from the dataset. Typically, midwater fishes also were removed. Because transect times were variable, abundances of species were standardized per sample by dividing the number of individuals per species by the total number of fishes per sample. Standardized abundances were fourth-root transformed to down weight the common species relative to the rare species. Similarities between samples were calculated using a Bray-Curtis similarity coefficient. Based on the resulting matrix, a nonmetric multidimensional scaling ordination (MDS) plot and a dendrogram with group average linking were created. A SIMPROF test was used to determine if any samples clustered together according to depth. One-way analysis of similarities (ANOSIM) and post-hoc multiple comparison tests were then used to determine whether there were significant differences among fish assemblages in different habitats within depth zones. SIMPER analysis was used to determine which species contributed to the dissimilarities among habitat types. DistLM marginal tests also were used to determine the extent to which habitats and depth explained a proportion of the variation in assemblage structure. Habitats were coded as nominal, binominal categories and grouped as an indicator “Habitat” for this analysis (following Anderson et al. 2008).

Video data were supplemented by otter trawl catches, which added some species not observed in the video and helped confirm identifications of others. Most trawl tows were assumed to be on soft substrate, although on occasion some gear was damaged indicating rough bottom. Descriptive data (numbers, sizes, depths) are provided for the fishes collected by trawl.

15.1.2.2.3 Specimen Treatment

Fishes were rinsed in water and stored until analysis in 50% isopropyl alcohol. All specimens were sorted, identified to the lowest possible taxa, counted, and measured to the nearest millimeter standard length (SL) or total length (TL), depending on species. Problematic specimens were sent to experts for identification as needed. The life history stage of fishes was also recorded based on the condition of gonads. A fish was classified as juvenile when either no gonads or immature gonads were documented.

15.1.3 Results

15.1.3.1 Community Structure and Habitat Associations

All collections and observations combined yielded a total of at least 123 fish species. The combined ROV and trawl methods yielded a total of 118 fish species from on or near bottom. Four species were observed only in the water column: one large *Manta birostris* accompanied by two *Naucrates ductor* (pilot fish) and two *Remora* sp. observed at 379 m over the shallow methane seep and one *Sphyrna lewini* observed at 438 m in Baltimore Canyon. The flyingfish *Hirundichthys rondeletti* (242 mm), a surface species, was collected on deck.

ROV Data

Twenty-one of the total 34 ROV dives were conducted in and near Baltimore Canyon over a depth range of 234 to 1,001 m, resulting in 144.3 h of bottom observations (**Tables 3-5** and **3-6**; **Figure 15-1**). Thirteen dives were made in and near Norfolk Canyon covering a depth range of 326 to 1,612 m, yielding 150.9 h of observations **(Tables 3-5** and **3-6**; **Figure 15-1**). A relatively shallow (380 to 430 m) methane seep area near the mouth of Baltimore Canyon was visited during five ROV dives, and two dives were made on a deeper (1,455−1,610 m) seep southeast of Norfolk Canyon (**Figure 15-1**).

Despite the large vertical and horizontal distances covered during most ROV dives, bottom salinity exhibited little variability, with means from 35.0 to 35.3 and an overall range varying by less than one unit (34.6−35.9) (**Table 15-1**). Bottom temperatures were more variable by depth within and between dives (means = 4.0−9.6 °C), and as expected, the lowest temperatures (3.9−4.1 °C) and least variability were in the deepest dives (generally >1,000 m). The highest bottom temperatures (10.7−12.1 °C) and higher variability were in the shallower (usually <350 m) parts of the canyons (**Table 15-1**). Although ROV dives were in two different years and seasons (fall and spring), large-scale temporal variability in bottom temperature was not evident or, if present, it was overshadowed by depth-related patterns. Mean bottom dissolved oxygen values ranged from 2.5 to 5.2 mL L^{-1} (**Table 15-1**) and often varied by 1 to 2 mL L^{-1} during dives, mostly related to changes in depth.

At least 84 unique fish taxa in 52 families were identified from ROV transect video across all benthic habitats from Norfolk and Baltimore canyons (**Table 15-2**). Despite some environmental differences between Norfolk and Baltimore canyons (F. Mienis et al., unpubl. data; **Chapters 5** and **6**), we interpret the small differences in fish assemblages between the two canyon areas as insignificant and most likely due to different temporal and spatial sampling efforts between the two canyons. Thus, data from the canyons were merged, and further analyses emphasized depth and habitat effects. Each of the five general habitats exhibited a fairly diverse fish assemblage with species richness ranging from 37 to 57 species (**Table 15-2**, note all seep habitats, SDM25-MHS75, combined). The lowest numbers

of species in SSB (n = 37) and MHS (seep, n = 38) could be partially due to less video observation time in these habitats. Consolidating the two soft substrate habitats (SS and SSB) and the three more complex, reef-like habitats (GRR, WRR, and MHS) yielded a total of 62 fish species in each broader category.

Table 15-1. Bottom or near-bottom environmental data recorded during ROV dives for the 2012 and 2013 sampling cruises in and near Norfolk and Baltimore canyons. Data are means, ranges, and standard error of the means in parentheses during the bottom time portion of the dives. See **Tables 3-5** and **3-6** for dive dates, bottom time durations, and depth ranges.

Dive No.	Temperature (°C)	Salinity	Dissolved Oxygen (mL L^{-1})
ROV-2012-NF-01	6.3, 5.4−7.3 (0.00)	35.1, 35.0−35.2 (0.00)	4.6, 4.1−5.6 (0.00)
ROV-2012-NF-02	8.7, 5.7−11.3 (0.01)	35.2, 35.0−35.5 (0.00)	3.5, 3.0−5.0 (0.00)
ROV-2012-NF-03	6.8, 4.7−9.6 (0.01)	35.1, 35.0−35.3 (0.00)	4.3, 3.0−5.6 (0.00)
ROV-2012-NF-04	5.2, 4.5−6.4 (0.00)	35.1, 35.0−35.1 (0.00)	5.2, 4.3−5.8 (0.00)
ROV-2012-NF-05	7.0, 5.7−8.6 (0.01)	35.1, 35.0−35.2 (0.00)	4.3, 3.4−5.0 (0.00)
ROV-2012-NF-06[1]	7.8, 6.1−10.7 (0.01)	35.0, 34.7−35.3 (0.00)	–[1]
ROV-2012-NF-07	7.3, 7.2−7.7 (0.00)	35.1, 35.1−35.1 (0.00)	3.9, 3.7−3.9 (0.00)
ROV-2012-NF-08	7.3, 6.9-7.9 (0.00)	35.1, 35.0−35.2 (0.00)	3.9, 3.6−4.1 (0.00)
ROV-2012-NF-09	7.5, 5.8−9.2 (0.00)	35.1, 35.0−35.3 (0.00)	4.0, 3.3−4.9 (0.00)
ROV-2012-NF-10	7.9, 6.3-9.5 (0.00)	35.2, 34.9−35.5 (0.00)	3.9, 3.3−4.7 (0.00)
ROV-2012-NF-11	5.1, 4.6−6.2 (0.00)	35.0, 34.9−35.1 (0.00)	5.2, 4.5−6.3 (0.00)
ROV-2012-NF-12	5.5, 5.1−6.9 (0.00)	35.1, 35.0−35.1 (0.00)	5.0, 4.3−5.3 (0.00)
ROV-2012-NF-13	8.0, 6.6−9.7 (0.00)	35.1, 35.0−35.3 (0.00)	3.8, 3.2−4.4 (0.00)
ROV-2012-NF-14	7.2, 6.1−8.0 (0.00)	35.1, 35.0−35.2 (0.00)	3.9, 3.5−4.6 (0.00)
ROV-2012-NF-15	7.4, 5.6−9.3 (0.01)	35.1, 35.0−35.3 (0.00)	4.1, 3.2−5.0 (0.00)
ROV-2012-NF-16	6.8, 5.6−8.7 (0.01)	35.1, 34.9−35.3 (0.00)	4.4, 3.4−5.0 (0.00)
ROV-2012-NF-17	5.3, 4.8−5.8 (0.01)	35.0 35.0−35.1 (0.00)	5.1, 4.8−5.4 (0.00)
ROV-2012-NF-18	5.3, 4.7−6.0 (0.00)	35.0, 35.0−35.1 (0.00)	5.1, 4.7−5.6 (0.00)
ROV-2012-NF-19	7.0, 4.9−10.3 (0.01)	35.1, 35.0−35.4 (0.00)	4.3, 3.1−5.4 (0.00)
ROV-2012-NF-20	5.4, 4.9−7.3 (0.00)	35.0, 35.0−35.2 (0.00)	5.0, 3.9−5.3 (0.00)
ROV-2012-NF-25	5.9, 5.2−6.6 (0.00)	35.0, 34.9−35.1 (0.00)	4.7, 4.3−5.2 (0.00)
ROV-2013-RB-679	5.8, 4.8−6.6 (0.00)	35.0, 34.8−35.1 (0.00)	4.8, 4.4−5.3 (0.00)
ROV-2013-RB-680	7.0, 5.8−8.2 ±0.00	35.1, 34.8−35.4 (0.00)	3.1, 1.9−4.7 (0.00)
ROV-2013-RB-681	7.2, 5.6−8.7 (0.00)	35.1, 34.9−35.5 (0.00)	2.9, 1.8-4.8 (0.00)
ROV-2013-RB-682	4.0, 3.9−4.0 (0.00)	35.0, 34.9−35.0 (0.00)	4.3, 3.2−5.5 (0.00)
ROV-2013-RB-683	4.0, 3.9−4.1 (0.00)	35.0, 34.9−35.0 (0.00)	4.5, 3.3-5.3 (0.00)
ROV-2013-RB-684	8.2, 5.0−11.5 (0.00)	35.2, 34.6−35.9 (0.00)	2.9, 1.7−4.8 (0.00)
ROV-2013-RB-685[2]	4.3, 4.1−5.5 (0.00)	35.0, 34.9−35.0 (0.00)	4.0, 3.0−5.2 (0.00)
ROV-2013-RB-686	6.8, 5.5−7.9 (0.00)	35.1, 34.8−35.7 (0.00)	3.0, 1.9−4.5 (0.00)
ROV-2013-RB-687	6.6, 5.2−8.2 (0.00)	35.1, 34.8−35.4 (0.00)	3.1, 1.9−4.8 (0.00)
ROV-2013-RB-688[3]	6.9, 5.8−9.5 (0.01)	35.0, 34.8−35.3 (0.00)	–[3]
ROV-2013-RB-689	8.8, 7.3−9.4 (0.00)	35.2, 34.8−35.7 (0.00)	2.5, 1.6−3.6 (0.00)
ROV-2013-RB-690	9.6, 8.3−12.1 (0.00)	35.3, 35.1−35.6 (0.00)	2.8, 2.0−3.7 (0.00)
ROV-2013-RB-691	8.2, 6.5−8.7 (0.00)	35.2, 34.9−35.7 (0.00)	2.6, 1.8−4.0 (0.00)

[1] *Arctozenus risso* clogged the intake tube to the CTD DO pump.
[2] CTD shut off 2 hours before the end of the dive.
[3] Main CTD was not turned on; *Jason II* CTD used, no DO.

Table 15-2. Percent relative abundance of fishes observed during 2012 and 2013 ROV transects in and near Norfolk and Baltimore canyons within five general habitat types. The mixed hard/soft (MHS) habitat includes all seep habitats (see Methods for habitat definitions). Number of transect hours in each habitat and depth ranges (m) are below habitat type.

Taxa (numbers of individuals, length range in mm)	SS 45.71 h (267−1,606)	SSB 12.39 h (274−1,352)	GRR 24.12 h (273−1,354)	WRR 30.08 h (284−1,383)	MHS 14.34 h (356−1,608)
Myxinidae					
Myxine glutinosa (1, 355)	0.24	−	−	−	−
Scyliorhinidae					
Apristurus manis	−	0.09	0.10	0.10	−
Apristurus sp.	−	−	−	−	0.05
Scyliorhinus retifer (2, 349−398)	0.11	0.19	0.26	0.14	−
Etmopteridae					
Centroscyllium fabricii	−	−	−	0.02	−
Centrophoridae	−	−	−	−	−
Centrophorus granulosus	−	−	−	0.04	−
Torpedinidae					
Torpedo nobiliana	0.01	−	−	−	−
Rajidae					
Leucoraja cf. *garmani*	0.01	−	−	−	−
Rajidae (unidentified)	0.39	0.43	0.51	0.12	0.44
Chimaeridae					
Hydrolagus affinis	0.03	−	−	−	0.60
Rhinochimaeridae					
Harriotta raleighana	−	−	−	0.02	−
Halosauridae					
Aldrovandia sp.	0.65	0.28	0.03	0.08	1.04
Halosauridae (unidentified)	0.05	−	−	−	0.05
Notacanthidae					
Notacanthus chemnitzii	0.05	−	−	−	−
Anguilliformes (unidentified)	0.26	0.14	0.03	−	−
Anguillidae					
Anguilla rostrata	0.01	−	0.05	0.02	−
Synaphobranchidae					
Dysommina rugose (13, 156−308)	−	−	0.15	0.43	11.59
Synaphobranchus spp.	22.65	48.06	20.01	43.50	1.20
Synaphobranchidae (unidentified)	0.13	−	−	−	−
Ophichthidae					
Ophichthus cruentifer (1, 211)	0.13	0.05	−	0.04	−
Congridae					
Conger oceanicus	−	−	0.05	0.04	−
Nemichthyidae					
Nemichthys scolopaceus	0.11	−	−	−	−
Nemichthyidae (unidentified)	0.09	−	−	−	−
Nettastomatidae					
Nettenchelys sp.	−	−	−	0.04	−
Nettastomatidae (unidentified)	0.01	0.05	−	−	−

Table 15-2. (Continued).

Taxa (numbers of individuals, length range in mm)	SS 45.71 h (267−1,606)	SSB 12.39 h (274−1,352)	GRR 24.12 h (273−1,354)	WRR 30.08 h (284−1,383)	MHS 14.34 h (356−1,608)
Alepocephalidae (unidentified)	−	0.05	−	−	−
Gonostomatidae					
Cyclothone microdon (2, 50−55)	0.03	−	−	−	−
Stomiidae					
Stomias boa ferox	−	−	0.05	0.06	−
Stomias sp.	0.03	−	−	−	−
Stomiidae (unidentified)	0.04	−	−	0.02	−
Chlorophthalmidae					
Chlorophthalmus agassizi	2.92	0.52	0.05	−	2.08
Ipnopidae					
Bathypterois viridensis	0.20	−	−	−	−
Bathysauridae					
Bathysaurus sp.	0.04	−	−	−	−
Paralepididae					
Arctozenus risso (20, 97−234)	1.81	3.80	3.16	3.82	0.82
Paralepididae (unidentified)	0.01	−	−	−	−
Myctophidae					
Ceratoscopelus maderensis (5, 53−60)	0.40	−	2.78	−	−
Ceratoscopelus sp.	0.24	−	−	−	−
Myctophidae (unidentified) (3, 51)	9.58	0.09	−	−	9.79
Gadiformes (unidentified)	0.07	0.09	0.13	0.14	−
Macrouridae					
Coelorinchus sp.	0.26	0.19	−	−	0.98
Coryphaenoides rupestris	1.80	2.28	0.90	0.47	0.05
Coryphaenoides sp.	0.04	−	−	−	−
Macrourus sp.	−	0.05	0.03	−	−
Nezumia aequalis	0.04	−	−	−	0.05
Nezumia cf. *atlantica*	−	−	−	−	0.05
Nezumia bairdii	6.72	3.89	1.67	0.78	0.60
Nezumia longebarbata	−	−	−	0.06	0.05
Nezumia sclerorhynchus	0.07	−	0.54	0.41	0.05
Nezumia sp.	6.75	3.32	2.11	1.19	0.98
Macrouridae (unidentified)	0.72	1.04	0.08	0.06	0.11
Moridae					
Antimora rostrata	0.08	0.05	−	−	0.77
Gadella cf. *imberbis*	0.01	−	−	−	−
Laemonema barbatula	1.77	5.12	15.35	13.34	8.97
Laemonema sp.	0.03	−	−	−	−
Physiculus fulvus	0.01	−	−	−	−
Physiculus cf. *karrerae*	−	−	−	0.12	−
Gadidae (unidentified)	0.01	−	0.05	−	−
Lotidae					
Brosme brosme	−	−	1.13	2.35	2.24
Enchelyopus cf. *cimbrius*	0.03	−	−	−	−

Table 15-2. (Continued).

Taxa (numbers of individuals, length range in mm)	SS 45.71 h (267−1,606)	SSB 12.39 h (274−1,352)	GRR 24.12 h (273−1,354)	WRR 30.08 h (284−1,383)	MHS 14.34 h (356−1,608)
Gaidropsarus ensis	−	−	−	0.06	1.75
Phycidae					
Phycis chesteri	10.03	6.31	4.35	1.94	14.11
Urophycis chuss	0.09	0.19	0.51	0.57	2.62
Urophycis regia	0.04	−	−	−	0.87
Urophycis tenuis	−	−	−	0.31	−
Urophycis sp.	−	−	−	0.08	−
Phycidae (unidentified)	−	−	−	0.10	−
Merlucciidae					
Merluccius albidus (1, 157)	1.96	0.95	0.15	0.12	2.41
Ophidiiformes (unidentified)	0.26	1.09	0.18	0.33	1.31
Ophidiidae					
Benthocometes robustus (18, 56-112)	−	−	0.36	1.37	−
Dicrolene intronigra	1.30	2.28	0.10	0.33	3.28
Luciobrotula corethromycter	−	−	−	−	0.55
Ophidiidae (unidentified)	−	−	−	0.02	0.05
Brotulidae (unidentified)	−	−	−	0.02	0.38
Bythitidae					
Bythites cf. *fuscus* (2, 99−147)	−	−	−	−	−
Diplacanthopoma brachysoma (1,172)	−	−	0.13	−	−
Bythitidae (unidentified)	0.05	−	0.03	0.02	0.05
Lophiidae					
Lophius americanus (1, 254)	1.42	0.57	2.93	0.84	4.54
Chaunacidae					
Chaunax suttkusi	−	−	−	0.02	−
Ogcocephalidae					
Dibranchus atlanticus	0.07	−	0.03	0.04	−
Trachichthyidae					
Hoplostethus mediterraneus	−	−	−	2.96	−
Hoplostethus sp.	0.66	0.19	1.65	5.23	0.16
Berycidae					
Beryx sp.	−	−	−	0.02	−
Oreosomatidae					
Neocyttus helgae	−	−	−	0.14	−
Scorpaenidae					
Helicolenus dactylopterus	3.77	9.63	24.87	11.01	2.02
Trachyscorpia cristulata (1, 64)	0.03	−	−	−	0.11
Scorpaenidae (unidentified)	0.04	−	0.08	0.04	−
Peristediidae					
Peristedion miniatum	0.07	0.05	−	−	−
Peristedion sp.	0.15	0.19	0.05	−	−
Psychrolutidae					
Cottunculus thomsonii	−	0.05	0.03	0.06	−
Acropomatidae					

Table 15-2. (Continued).

Taxa (numbers of individuals, length range in mm)	SS 45.71 h (267−1,606)	SSB 12.39 h (274−1,352)	GRR 24.12 h (273−1,354)	WRR 30.08 h (284−1,383)	MHS 14.34 h (356−1,608)
Synagrops sp. A	0.09	−	−	−	−
Polyprionidae					
Polyprion americanus	−	−	−	0.02	−
Serranidae					
Anthias woodsi	−	−	0.03	−	−
Anthias sp.	−	0.05	0.08	0.08	−
Epigonidae (unidentified)	1.44	0.14	0.31	0.47	7.55
Zoarcidae					
Lycenchelys paxillus (1, 239)	0.01	−	−	−	0.11
Lycenchelys verrillii	2.58	1.47	0.23	0.04	0.38
Lycodes atlanticus	0.07	−	−	−	0.77
Lycodes terraenovae (1, 226)	0.05	−	−	−	−
Lycodes sp.	0.86	0.38	0.05	0.08	2.73
Melanostigma atlanticum	0.54	0.85	0.98	0.16	−
Zoarcidae (unidentified)	0.19	0.24	−	0.02	0.05
Gempylidae					
Gempylus serpens	0.01	−	−	−	−
Centrolophidae					
Hyperoglyphe perciformis	−	−	−	0.08	−
Paralichthyidae					
Citharichthys arctifrons (1, 85)	0.04	−	−	−	−
Paralichthyidae (unidentified)	0.22	−	−	−	−
Bothidae					
Monolene sp.	0.01	−	−	−	−
Pleuronectiformes (unidentified)	0.01	−	−	−	−
Pleuronectidae					
Glyptocephalus cynoglossus	14.05	4.84	0.33	0.14	0.05
Cynoglossidae					
Symphurus nebulosus (12, 37-74)	0.20	−	0.69	−	9.08
Symphurus sp.	0.51	0.05	11.73	5.66	1.59
Unidentified fishes	0.50	0.14	0.10	0.04	0.87

Relatively few fish species numerically dominated each of the major habitats (**Table 15-2**). In each habitat, 9 to 14 species comprised 82% to 90% of the fish abundance (**Table 15-2**). Five of the common taxa (*Synaphobranchus* spp., *Arctozenus risso*, *Laemonema barbatulum*, *Phycis chesteri*, *Helicolenus dactylopterus*) were abundant across all habitats, although abundances of *L. barbatulum* and *H. dactylopterus* were skewed toward the more rugged habitats. All fishes that occurred in only one or two habitats were uncommon (<0.9% abundance). If most or all *Hoplostethus* sp. (**Table 15-2**) were *H. mediterraneus*, which seems likely, then none of the more common taxa (>1.3% abundance) were unique to a single habitat (**Table 15-2**). However, *Dysommina rugosa, Benthocometes robustus*, and *B. brosme* were unique to the combined three complex habitats.

Multivariate analysis based on 68 fish species and 234 video samples indicated the strong influence of depth in assemblage structure. Depth explained a significant amount (19%) of the variation in assemblage structure (DistLM marginal test, $P = 0.001$), and the cluster analysis indicated that two

groups that were 95% dissimilar from each other corresponded to two depth zones, <1,400 m and >1,400 m (SIMPROF, $P < 0.05$) (**Figure 15-3**). Although two fish assemblages occurred deeper than and shallower than 1,400 m, a gradual faunal transition appeared between approximately 800 to 1,200 m. SIMPER analysis revealed that the species most influencing the deeper group separation were *Lycodes* sp., *Dicrolene introniger*, *Gaidropsaurus ensis*, *Hydrolagus affinis*, *Antimora rostrata*, and *Aldrovandia* sp., while the shallower group was most controlled by *Laemonema* sp., *P. chesteri*, *Nezumia bairdii*, *B. brosme*, and *H. dactylopterus*. Overall depth ranges and weighted mean depths of occurrence of the most common species clearly illustrated distinct shallow and deep groupings, each group displaying a relatively small depth range (**Figure 15-4**). A third group included species that had wide depth ranges overlapping the two extreme groups.

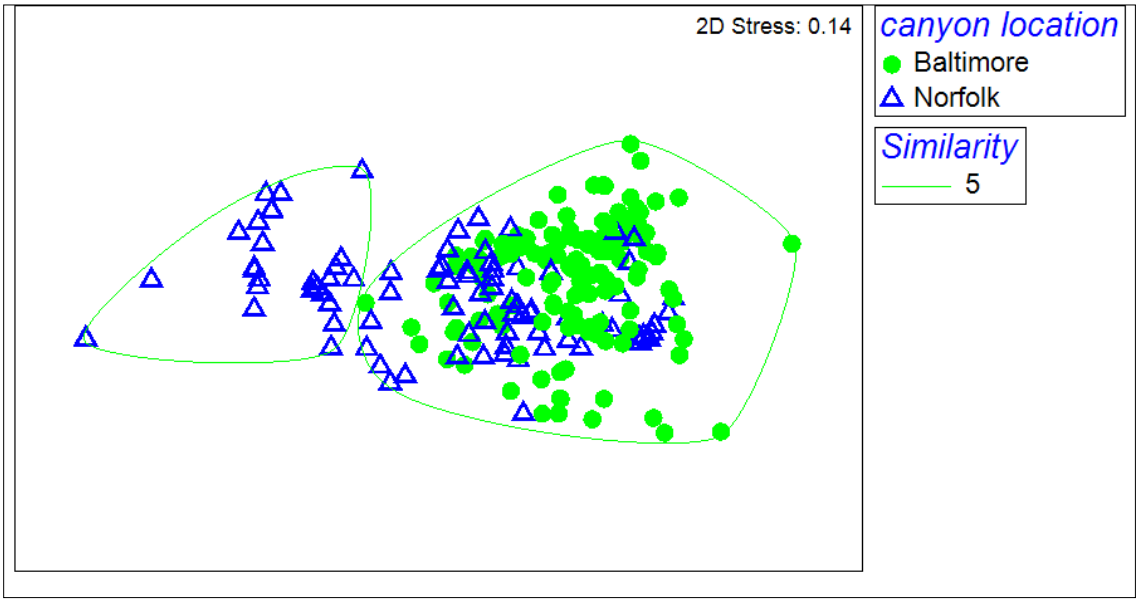

Figure 15-3. Multidimensional scaling (MDS) ordination based on the Bray-Curtis similarity matrix calculated from 234 samples and 68 fish species (standardized, fourth-root transformed) illustrating depth-related patterns in fish assemblages for the Norfolk and Baltimore canyon areas. From right to left samples are generally shallower to deeper.

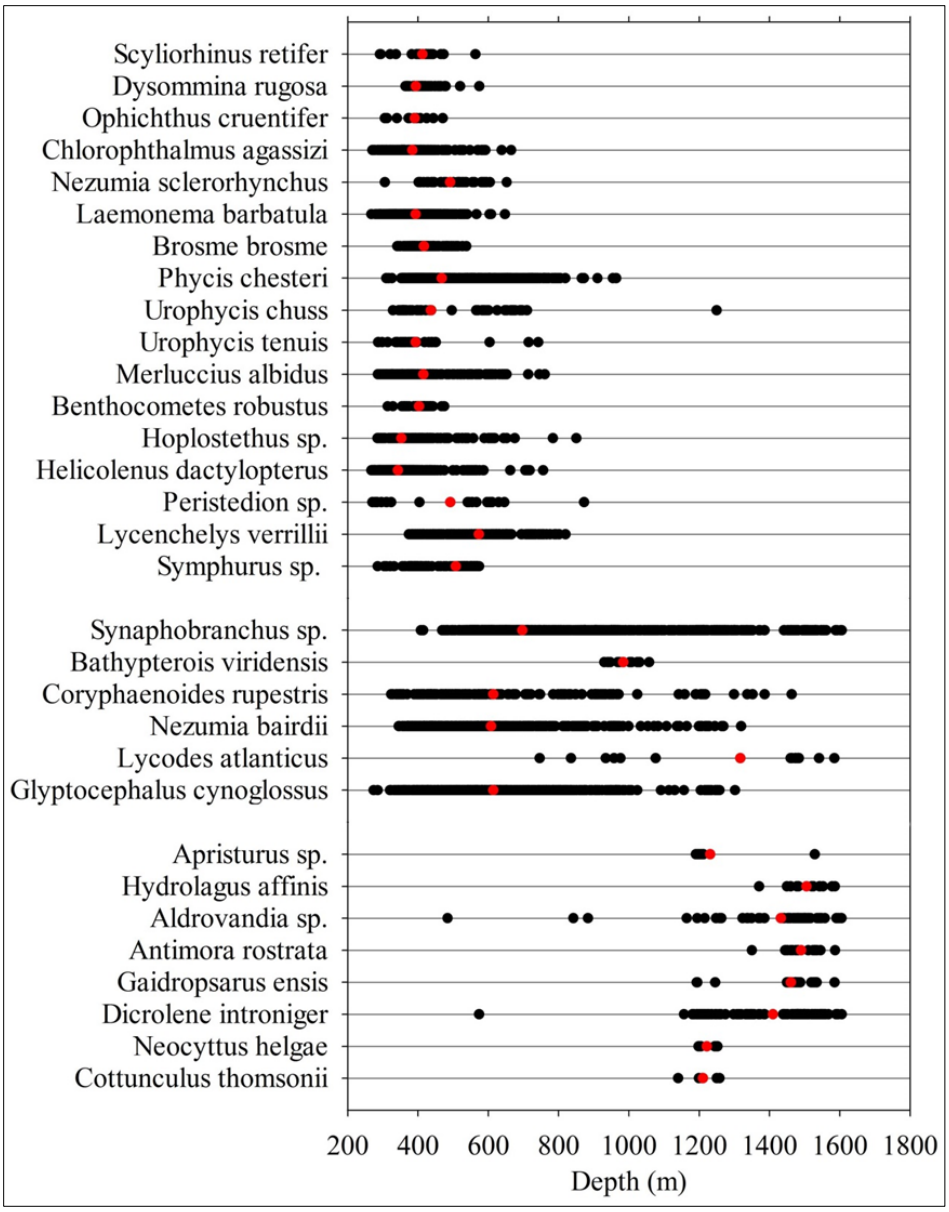

Figure 15-4. Depth ranges (black circles) and mean depths of occurrence weighted by abundance (red circles) of the dominant fishes collected in Norfolk and Baltimore canyons.

Multivariate analysis was also used to examine fish assemblage structure among habitats. Habitat explained a significant portion of the variation (17%, DistLM marginal test, $P = 0.001$) in assemblage structure. Because the deep (>1,400 m) fish group was related only to seep habitats, it is presented with analysis of seep communities. Fifty-three species of fishes and 196 video segments shallower than 1,400 m were used in MDS clustering of fishes across the 11 habitat categories (**Figure 15-5**). Although groupings are less clear than for depth zonation, a significant difference was noted in assemblages across these habitats (ANOSIM, global $R = 0.20$, $P = 0.001$). Pairwise comparisons indicated that fishes associated with sand (least complex habitat) were significantly different from all other habitats ($R = 0.12–0.62$, $P < 0.05$). Fishes influencing the soft bottom grouping (SIMPER) were *P. chesteri*, *N. bairdii*, *Glyptocephalus cynoglossus*, *Lophius americanus*, and *Merluccius albidus*. After sand, the next least complex habitat was sloping soft bottom with some structure, and the fish assemblage associated with SSB habitat was not significantly different from those on the next two least complex

habitats (SDM25 and SDM25-75), but was significantly different from all other habitats (R = 0.08−0.31, P < 0.05). Fish groups associated with the two complex habitats within the canyons (WRR and GRR) were not different from each other (R = 0.02, P > 0.05), but fish groups in WRR and GRR were different from approximately half of the seep habitats, especially those incorporating carbonate rocks. Fishes that distinguish the two canyon, reef-like habitats (SIMPER) were *Laemonema* spp., *Hoplostethus* spp., *B. brosme*, and *Benthocometes robustus*. Removing the two soft bottom habitats (SS, SSB), which lacked structure-forming corals, we examined whether coverage of corals and sponges on the more complex habitats influenced fish assemblages. Assemblage structure was not different among the complex habitats regardless of coral and sponge presence (ANOSIM, global R = 0.03, P = 0.06).

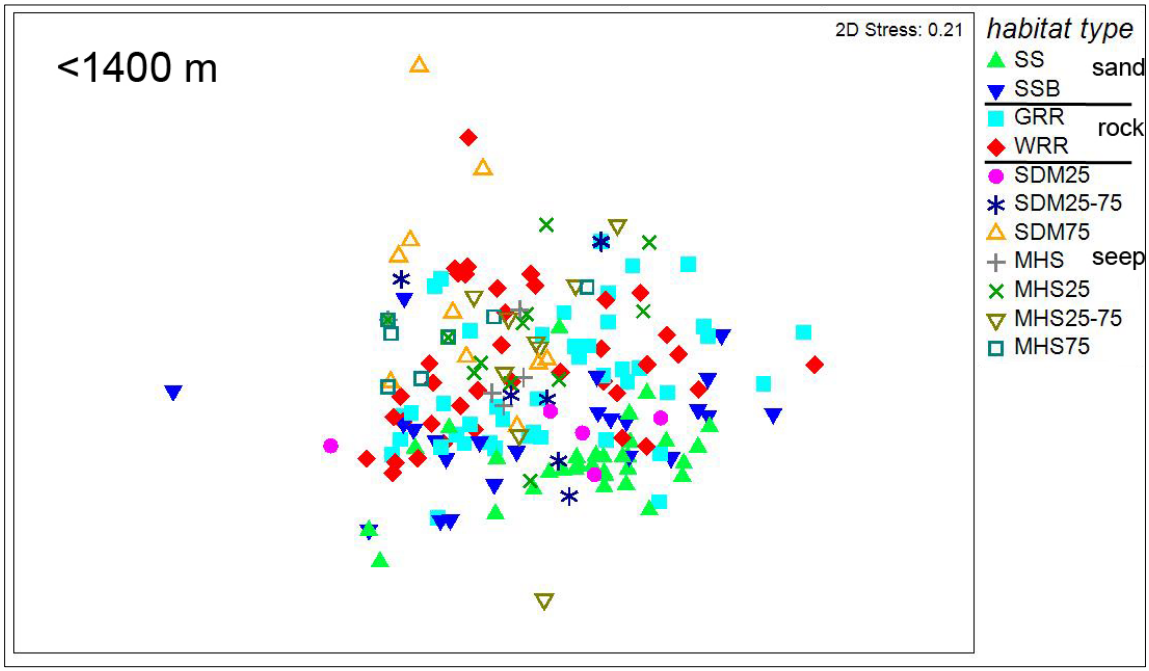

Figure 15-5. Multidimensional scaling (MDS) ordination based on the Bray-Curtis similarity matrix calculated from 196 samples and 53 fish species (standardized, fourth-root transformed) illustrating habitat use patterns shallower than 1,400 m in the Norfolk and Baltimore canyon areas.

Fish assemblages in the Baltimore and Norfolk canyon seep areas were examined in more detail (habitats SSB, GRR, and WRR omitted). Fish assemblages in the deep (>1,400 m) seep area were similar across habitats except that SDM25 and SDM25-75 were different from the most complex seep habitat (MHS75) (R = 0.45 and 0.51, P < 0.05). Removing the soft bottom habitat, the percentage of live mussels on the deep seep areas did not influence fish assemblage structure. More fish assemblage differences were noted across habitats at the shallow (<500 m) seep compared with the deep seep. The sand habitat assemblage was significantly different (R = 0.38−0.72, P < 0.05) from four of the most complex seep habitats (SDM75, MHS, MHS25, MHS75). Most (62%) pairwise comparisons of seep habitats (SDM25-MHS75) were not different from each other. Sand with >75% dead mussel cover (SDM75) was different from all other shallow seep habitats (R = 0.22−0.41, P < 0.05). Removing the sand habitat to examine the influence of live mussel cover yielded different results from the deeper seep comparisons. Habitats with 0% to 10% live mussel cover were generally different from those with >10% live mussels. In the shallow seep area, fishes characteristic (SIMPER) of the sand assemblage were *Symphurus nebulosus*, *N. bairdii*, *G. cynoglossus*, and *L. americanus*. *Laemonema* spp.,

L. americanus, *B. brosme*, and *D. rugose*. These fishes most influenced the assemblage structure of the more complex shallow seep habitats.

Relative abundances within a species across the five general habitats also revealed habitat specificity (**Figure 15-6**). Several commonly observed fishes (e.g., *G. ensis, D. rugosa, S. nebulosus, U. chuss, U. tenuis, L. americanus, B. brosme, L. barbatula, H. dactylopterus, Hoplostethus* sp., *B. robustus*) exhibited strong association with the three more complex habitats (MHS, WRR, GRR), while others (e.g., *D. introniger, M. albidus, L. verrillii, N. bairdii, C. coryphaenoides, Peristedion* sp.) were mostly observed on soft substrate (SS, SSB) (**Figure 15-6**). Relatively few species were well spread across all habitats (e.g., *P. chesteri, S. retifer, Synaphobranchus* spp.).

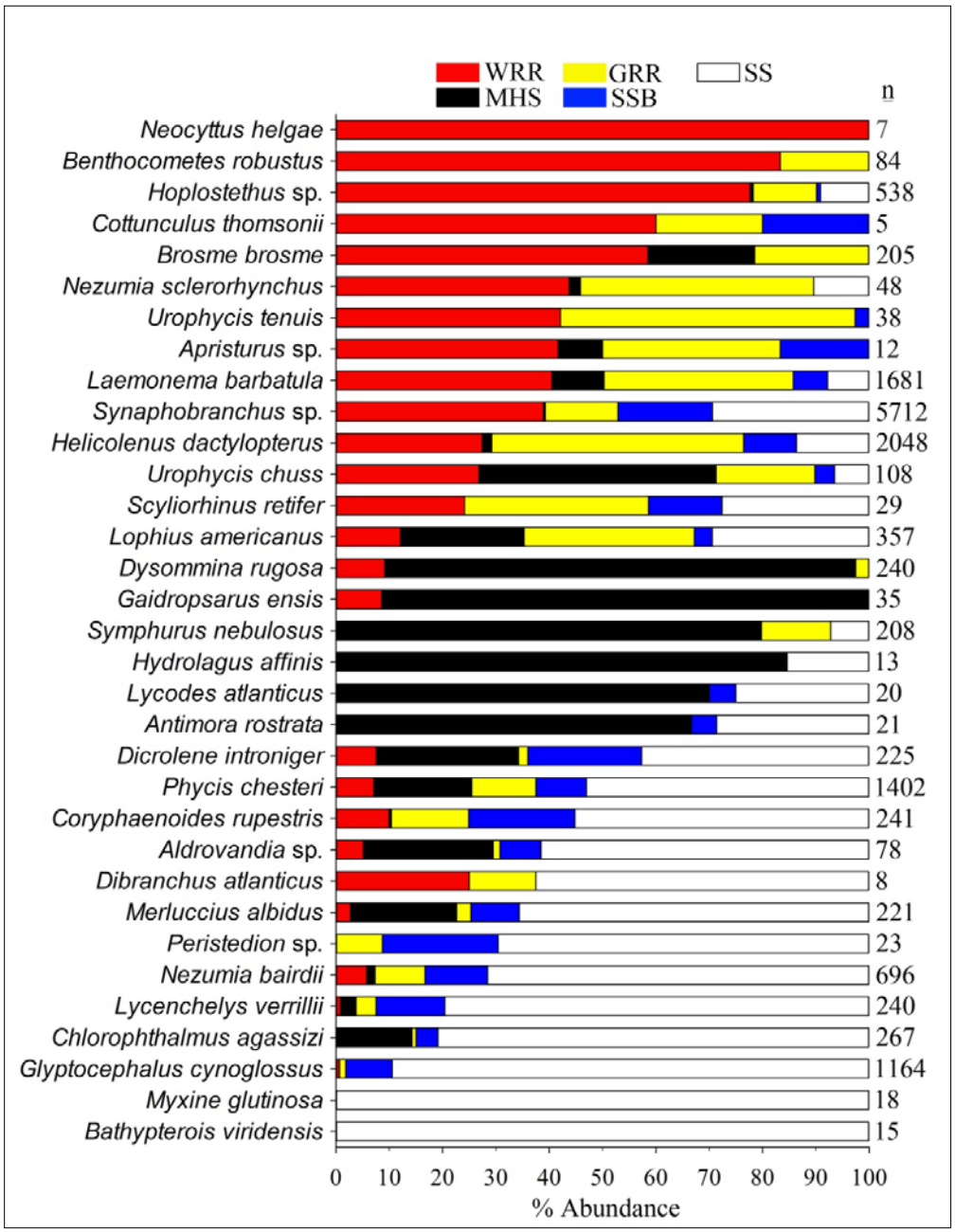

Figure 15-6. Within species relative (%) abundance across the five major habitat types (all seep habitats consolidated under MHS). *n* = number of individuals observed during transects.

Otter Trawl Data

Catches from 40 otter trawl tows over a depth range of 103 to 1,712 m supplemented the ROV video data (**Tables 3-5** and **3-6**, **Figure 15-1**). Fourteen trawls were in the vicinity of Baltimore Canyon, while 26 tows were in and near Norfolk Canyon. Because of the rugged nature of the canyon walls and thalwegs, most trawling occurred along the edges of canyons (**Figure 15-1**).

Seventy-eight fish species were identified from bottom trawl samples (**Table 15-3**). Although habitat cannot be precisely determined for the trawl stations, most trawls appeared to be on soft substrate based on multibeam sonar data, the catches, and ROV observations. Trawling added 34 benthic and midwater fish species and 7 families (Argentinidae, Sternoptychidae, Phosichthyidae, Melamphaidae, Sebastidae, Cryptacanthodidae, and Percophidae) not identified during ROV dives (**Table 15-2**).

Benthic fish families that contained the highest species richness (≥3 species) were Rajidae, Macrouridae, Moridae, Phycidae, Ophidiidae, Peristediidae, Zoarcidae and Cynoglossidae. The most abundant species (comprising 86% of total) collected by trawl were *Myxine glutinosa* (15.7%), *Synaphobranchus* spp. (3.6%), *Coelorinchus caelorhincus* (1.7%), *N. bairdii* (23.2%), *P. chesteri* (3.2%), *Urophycis regia* (2.1%), *H. mediterraneus* (13.3%), *H. dactylopterus* (7.7%), *Lycenchelys verrillii* (2.7%), *Citharichthys arctifrons* (5.7%), and *G. cynoglossus* (7.1%).

Table 15-3. Fishes collected by otter trawl during the 2012 and 2013 sampling cruises in and near Norfolk and Baltimore canyons. Number (Num) of fishes followed by length (mm). Depth ranges are in meters. No trawls were conducted in Baltimore Canyon in 2013.

Taxa	Norfolk Canyon				Baltimore Canyon	
	2012		2013		2012	
	Num (size)	Depth	Num (size)	Depth	Num (size)	Depth
Myxinidae						
Myxine glutinosa	159 (115–430)	389–580	328 (140–550)	255–392	57 (190–390)	214–406
Scyliorhinidae						
Apristurus sp.	–	–	–	–	1 (107)	700–800
Scyliorhinus retifer	5 (404–440)	400–510	2 (282–430)	255–388	2 (182–194)	136–140
Etmopteridae						
Centroscyllium fabricii	–	–	1 (590)	1,614–1,643	–	–
Etmopterus gracilispinis	1 (147)	402–480	–	–	–	–
Rajidae						
Amblyraja radiata	–	–	–	–	–	–
Leucoraja garmani	–	–	–	–	1 (364)	136–140
Leucoraja sp.	–	–	3 (72–77)	175–187	–	–
Malacoraja cf. senta	–	–	3 (380–440)	382–388	–	–
Rajella sp.	–	–	1 (90)	1,636–1,712	–	–
Halosauridae						
Aldrovandia affinis	–	–	1 (478)	1,504–1,550	–	–
Notacanthidae						
Notacanthus chemnitzii	1 (147)	460–500	–	–	2 (156–201)	360–800
Synaphobranchidae						
Synaphobranchus affinis	20 (143–211)	450–580	–	–	4 (183–310)	700–800
Synaphobranchus kaupii	62 (146–355)	450–580	10 (347–555)	1,576–1,643	29 (99–403)	700–800
Ophichthidae						
Ophichthus cruentifer	6 (254–333)	402–510	2 (291–342)	286–392	2 (286–312)	290–300
Congridae						
Conger oceanicus	–	–	1 (258)	180–185	–	–
Nemichthyidae						
Nemichthys curvirostris	4 (493–696)	389–580	–	–	4 (414–898)	360–540
Nemichthys scolopaceus	1 (754)	450–580	1 (610)	382–388	2	412–422
Nettastomatidae						
Nettastomatidae1	1	395–400	–	–	–	–
Argentinidae						
Argentina striata	–	–	–	–	1 (152)	214–300
Alepocephalidae						
Alepocephalus agassizii	–	–	10 (158–385)	1,504–1,712	–	–

Table 15-3. (Continued).

Taxa	Norfolk Canyon				Baltimore Canyon	
	2012		2013		2012	
	Num (size)	Depth	Num (size)	Depth	Num (size)	Depth
Sternoptychidae						
Argyropelecus aculeatus	–	–	1 (38)	1,576–1,629	1 (75)	–
Maurolicus weitzmani	1 (49)	103–120	3 (36–38)	160–187	27 (41–55)	136–300
Polyipnus asteroides	–	–	–	–	2 (37–56)	250–570
Phosichthyidae						
Polymetme thaeocoryla	–	–	3 (96–115)	286–340	18 (48–145)	214–420
Stomiidae						
Chauliodus sloani	2 (99)	400–580	–	–	–	–
Stomias affinis	–	–	1 (147)	1,614–1,643	–	–
Stomias boa ferox	–	–	–	–	2 (133–224)	360–422
Chlorophthalmidae						
Chlorophthalmus agassizi	–	–	13 (56–125)	160–340	12 (81–126)	300–570
Parasudis truculenta	–	–	–	–	3 (235–267)	400–540
Ipnopidae						
Bathypterois viridensis	1 (149)	450–580	–	–	–	–
Myctophidae						
Diaphus sp.	1 (46)	460–500	–	–	1 (60)	278–282
Myctophum affine	1 (56)	460–500	–	–	–	–
Myctophidae	5 (42–55)	405–510	20 (27–64)	175–1,643	15 (41–64)	136–800
Macrouridae						
Cetonurus cf. *globiceps*	–	–	1 (635)	1,670–1,694	–	–
Coelorinchus caelorhincus	9 (167–236)	400–580	20 (110–230)	286–1,046	28 (43–242)	214–800
Hymenogadus gracilis	–	–	–	–	2 (89)	360–380
Malacocephalus occidentalis	–	–	–	–	4 (126–219)	290–380
Nezumia aequalis	21 (100–150)	400–580	1 (122)	382–388	–	–
Nezumia bairdii	310 (47–251)	395–580	419 (39–310)	286–1,643	73 (65–305)	400–800
Nezumia sclerorhynchus	6 (63–176)	400–580	–	–	6 (72–117)	405–800
Nezumia sp.	–	–			–	–
Macrouridae	–	–	1	1,614–1,643	–	–
Moridae						
Antimora rostrata	–	–	12 (230–450)	1,504–1,694	–	–
Laemonema barbatula	–	–	1 (180)	376–392	–	–
Physiculus karrerae	1 (156)	400–423	–	–	–	–
Lotidae						
Enchelyopus cimbrius	19 (55–203)	395–510	9 (132–212)	286–392	3 (185–213)	300–422

Table 15-3. (Continued).

Taxa	Norfolk Canyon				Baltimore Canyon	
	2012		2013		2012	
	Num (size)	Depth	Num (size)	Depth	Num (size)	Depth
Phycidae						
Phycis chesteri	39 (72–299)	395–580	51 (46–376)	255–1,046	21 (66–383)	400–800
Urophycis chuss	1 (258)	403–408	8 (208–270)	175–1,046	4 (199–255)	214–380
Urophycis regia	23 (159–247)	103–400	21 (38–320)	160–392	27 (171–320)	136–300
Merlucciidae						
Merluccius albidus	8 (180–309)	395–510	1 (302)	255–270	16 (235–381)	214–570
Merluccius bilinearis	–	–	2 (274–281)	175–187	–	–
Ophidiidae						
Dicrolene intronigra	–	–	6 (210–248)	1,576–1,712	–	–
Lepophidium profundorum	1 (205)	103–120	12 (182–235)	180–340	5 (117–190)	136–300
Monomitopus agassizii	–	–	1 (194)	1,614–1,643	–	–
Ophidiidae1	1	400–423	–	–	–	–
Bythitidae						
Diplacanthopoma brachysoma	1 (161)	460–500	–	–	–	–
Lophiidae						
Lophius americanus	2 (117–492)	400–423	1 (318)	304–330	15 (280–532)	400–800
Chaunacidae						
Chaunax suttkusi	–	–	–	–	1 (192)	405–420
Ogcocephalidae						
Dibranchus atlanticus	4 (69–103)	400–500	–	–	4 (127–186)	300–570
Melamphaidae						
Poromitra magalops	–	–	1 (80)	1,614–1,643	–	–
Trachichthyidae						
Hoplostethus mediterraneus	458 (27–109)	395–580	1 (62)	376–392	2 (109–125)	400–540
Sebastidae						
Sebastes fasciatus	1 (448)	460–500	–	–	–	–
Scorpaenidae						
Helicolenus dactylopterus	3 (58–160)	405–510	123 (30–225)	160–340	139 (38–292)	214–570
Peristediidae						
Peristedion ecuadorense	1 (148)	460–500	–	–	–	–
Peristedion miniatum	1 (168)	460–500	–	–	2 (182)	278–300
Peristedion truncatum	–	–	–	–	1 (197)	214–300
Acropomatidae						
Synagrops bellus	2 (64–69)	395–400	–	–	–	–
Synagrops spinosus	1 (134)	103–120	–	–	–	–
Synagrops sp.	–	–	–	–	1 (83)	360–380

Table 15-3. (Continued).

Taxa	Norfolk Canyon				Baltimore Canyon	
	2012		2013		2012	
	Num (size)	Depth	Num (size)	Depth	Num (size)	Depth
Zoarcidae						
Lycenchelys verrillii	89 (65−163)	389−580	2 (129−137)	376−392	2 (131−143)	700−800
Lycodes esmarkii	3 (165−244)	450−580	−	−	−	−
Lycodes terraenovae	−	−	−	−	10 (150−275)	700−800
Melanostigma atlanticum	14 (93−135)	389−580	1 (105)	382−388	2 (96−125)	700−800
Cryptacanthodidae						
Cryptacanthodes maculatus	1 (153)	400−423	−	−	−	−
Percophidae						
Bembrops gobioides	−	−	−	−	1 (164)	300−360
Paralichthyidae						
Citharichthys arctifrons	18 (32−183)	103−480	1 (155)	286−340	177 (41−127)	136−420
Hippoglossina oblonga	2 (195−199)	103−120	1 (245)	175−187	7 (210−323)	136−380
Bothidae						
Monolene sessilicauda	−	−	1 (155)	287−340	2 (40−124)	278−380
Pleuronectidae						
Glyptocephalus cynoglossus	150 (43−313)	395−580	30 (151−340)	286−1,046	66 (86−354)	300−800
Cynoglossidae						
Symphurus billykrietei	−	−	16 (43−118)	286−392	12 (52−105)	136−420
Symphurus nebulosus	−	−	−	−	1 (85)	405−420
Symphurus stigmosus	−	−	−	−	1 (123)	400−481
Grand Total	1,485		1,148		821	

[1] Specimen damaged.

New Distributional and Noteworthy Records

One juvenile *Apristurus* sp. (too small for species identification) was collected by trawl near Baltimore Canyon in depths of 700 to 800 m. During ROV dive RB-685 in the mouth of Norfolk Canyon, at least 12 *Apristurus manis* (mostly adults) were observed usually near rugged canyon walls in depths of 1,191 to 1,212 m (**Figure 15-7A**). Known from both sides of the North Atlantic, in the western North Atlantic this catshark was reported from the Nova Scotia area, Block and Veatch canyons, and Bear Seamount (Markle et al. 1988, Kiraly et al. 2003, Moore et al. 2003), at depths of 600 to 1,900 m. Our records document a new southern range limit for this species. *Apristurus* sp. was also observed in a canyon area near Cape Hatteras, North Carolina (Sulak and Ross 1996), indicating penetration even farther south.

Dysommina rugosa was frequently observed (**Figure 15-7B**) always on deep reef habitats in both canyons and on the shallow seep over a depth ranging from 364 to 574 m. Thirteen specimens were collected (156−308 mm TL). This wide-ranging eel occurs in the western and east-central Pacific and Indian oceans and in the western Atlantic from Brazil, the Caribbean, Gulf of Mexico, and from Florida to off Cape Lookout, North Carolina (McEachran and Fechhelm 1998, Melo 2007, Ross and Quattrini 2009). These represent the first records of this species in the mid-Atlantic north of central North Carolina. Its cryptic behavior and association with rugged habitats (Ross and Quattrini 2007, Ross et al. 2015b) have prevented its distribution and abundance from being accurately reported.

One *Cetonurus* cf. *globiceps* (635 mm TL) was collected by trawl near the deep seep off Norfolk Canyon in 2013 (1,670−1,694 m), representing a significant northward extension of its range. This macrourid is known from the eastern Atlantic, western Pacific, and Indian oceans. In the western Atlantic Ocean, it was previously collected only from the Gulf of Mexico and eastern Caribbean in depths of 860 to 1,875 m (Iwamoto 1966, McEachran and Fechhelm 1998).

Although reported to occur on both sides of the Atlantic as well as the Pacific and Indian oceans (McMillan and Iwamoto 2014), the range of *Hymenogadus gracilis* in the western Atlantic seemed restricted to the northern Bahamas/Straits of Florida to the eastern Caribbean and Lesser Antilles (Marshall and Iwanoto 1973). However, one specimen of this species was trawled from near Norfolk Canyon (Middleton and Musick 1986). We collected two specimens of *H. gracilis* (both 89 mm TL) by trawl near Baltimore Canyon in depths of 360 to 380 m, which represent a slight northward range extension from Norfolk Canyon. This species appears to be uncommon in the region.

One *Nezumia* cf. *atlantica* was observed and photographed (**Figure 15-7C**, visual identification confirmed by T. Iwamoto, pers. comm.) on the deep seep at 1,462 m during dive RB-683. This rattail was previously known from the Gulf of Mexico through the eastern Caribbean to northern Brazil in depths of 366 to 1,097 m (Cohen et al. 1990). This record is both a new depth maximum as well as a significant northward extension.

Nezumia longibarbata is poorly known from scattered locations in the North Atlantic (Madeira, Hudson Canyon, off New Jersey, Gulf of Mexico) with a reported depth range of 1,466 to 2,346 m (Moore et al. 2003). This species is listed without comment as being trawled near Norfolk Canyon (Musick 1979) or elsewhere in the region (1,408−2,920 m, Sulak 1982). One specimen was observed during dive RB-683 (**Figure 15-7D**, photo identification confirmed by T. Iwamoto, pers. comm.) swimming over mussel beds at 1,457 m at the deep seep south of Norfolk Canyon. An additional four specimens were sighted in Norfolk Canyon (1,181−1,247 m) during dive RB-685, all on rugged canyon walls with coral cover. Besides confirming the occurrence of this species at new locations, these represent its shallowest records to date.

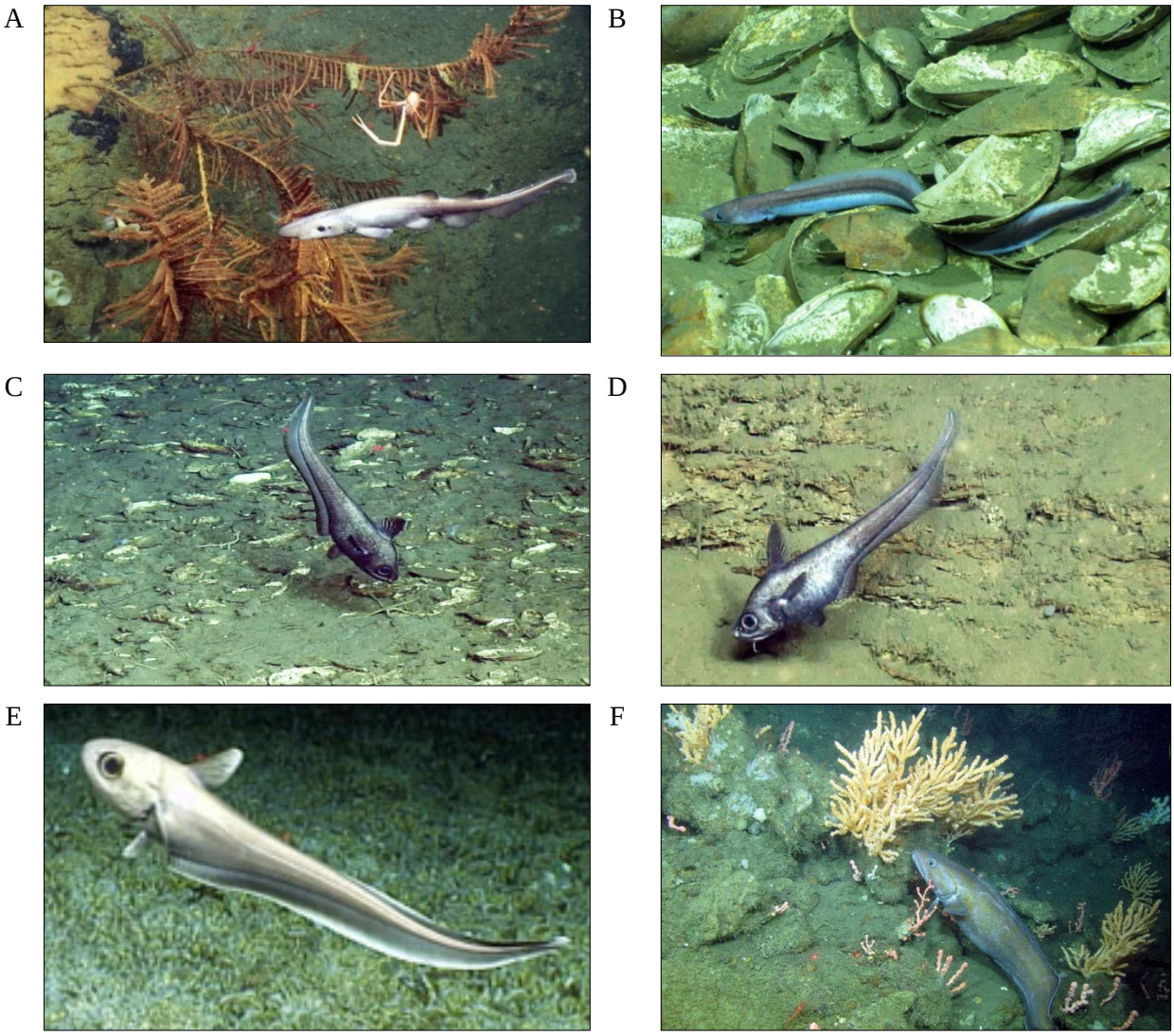

Figure 15-7. Photographs or video frame grabs of selected fishes encountered *in situ* from Baltimore and Norfolk canyons in 2012 and 2013. A) *Apristurus manis* swimming along a vertical wall in front of an antipatharian coral in Norfolk Canyon (1,200 m), 11 May 2013. Scaling laser dots indicate this fish is at least 50 cm long. B) *Dysommina rugosa* laying among dead *Bathymodiolus* sp. mussel shells at the seep site near Baltimore Canyon (431 m), 27 August 2012. C) *Nezumia* cf *atlantica* hovering over dead mussel shells and brittle stars at the deep seep site near Norfolk Canyon (1,462 m), 9 May 2013. Lasers indicate this specimen is about 32 cm long. D) *Nezumia longibarbata* at the base of a mud wall (1,247 m), 11 May 2013. Total length estimated by lasers to be about 27 cm. E) *Coryphaenoides rupestris* swimming over live *Bathymodiolus* sp. mussels at the deep seep site near Norfolk Canyon (1,467 m), 9 May 2013. Total length estimated by lasers to be at least 45 cm. F) *Brosme brosme* about 60 cm long moving over a rugged, coral covered wall in Baltimore Canyon (508 m), 29 August 2012.

Trawl collection of a *Physiculus karrerae* specimen (156 mm SL) in 400 to 423 m near Norfolk Canyon in 2012 helped confirm the ROV video observations of this species on canyon walls and rocky habitat (324−383 m). It was previously known from scattered locations in the Atlantic, but no farther north than Cape Lookout, North Carolina, in the western Atlantic where it was closely associated with deepsea coral reefs (Ross and Quattrini 2007).

Considering how frequently *B. brosme* was observed (341−537 m) in both canyons (**Table 15-2**, **Figure 15-7F**), it is odd that the few records south of New Jersey to Baltimore Canyon are unverified (Moore et al. 2003). Data herein confirm the new southern limit of its distribution to be at least Norfolk Canyon, where 128 individuals were observed. It ranges as far north as Greenland (Møller et al. 2010). As elsewhere (Collette and Klein-MacPhee 2002), all *B. brosme* observed in the Atlantic Deepwater Canyons Study occurred on or within rugged, hard bottom or canyon walls often associated with large tree corals. This behavior and habitat association likely has led to the lack of records in some areas.

Two *Bythites fuscus* (145 and 99 mm TL) were collected from Norfolk Canyon during dives RB-686 and 687. They were sitting on soft bottom in areas of dense corals in 488 and 432 m, respectively. Another one was observed at 477 m from dive 686 on the canyon wall, also in an area of dense corals. One tentatively identified as *B. fuscus* was on a rock at 1,224 m (dive 685). This species was considered rare, known from only four specimens, all occurring in the Labrador Sea (north of 61° N) in 530 to 675 m (Møller et al. 2010), thus, these records from Norfolk Canyon are the farthest south as well as the shallowest and deepest yet known. This species has probably escaped detection due to cryptic behavior and living in hard to sample habitats.

Neocyttus helgae was only recently reported from the western North Atlantic on the New England Seamounts and Lydonia Canyon (Moore et al. 2008). Baker et al. (2012) also observed this species on complex habitats off the Grand Banks, Canada. It also was observed on complex habitat off Ireland (Söffker et al. 2011). Seven large individuals were observed on dive RB-685 in Norfolk Canyon (1,198−1,252 m) and were always seen swimming along rugged, high profile canyon walls. These, plus other recent NOAA ROV observations of this fish in western North Atlantic canyons and the New England Seamounts, indicate it is fairly common on reef-like habitats in the western North Atlantic.

Peristedion ecuadorense has been reported from Virginia into the north-central Gulf of Mexico and from Honduras to northern Brazil and rarely the Lesser Antilles, 324 to 910 m (Miller and Richards 2002); however, the source and validity of the Virginia record are unclear. We collected one *P. ecudorense* (148 mm TL) by trawl near Norfolk Canyon in depths of 460 to 500 m, thus substantiating its occurrence north of North Carolina (Ross and Quattrini 2007). Some of the *Peristedion* sp. observed with the ROVs (**Table 15-2**) could have been this species, but video was inadequate for accurate identification.

The *Symphurus stigmosus* (123 mm TL) collected by trawl near Baltimore Canyon (400−481 m), represents a large extension of its range from off south Florida as well as a new depth record, previously 373 m (Munroe 1998).

Behavioral and Other Observations

Direct observation methods allow behaviors and other attributes to be assessed, albeit brief, that are otherwise unattainable in the deep sea and complex habitats (Ross and Quattrini 2007). Unnatural behavior resulting from ROV presence (noise, lights) was generally not obvious in this study except that some feeding events may have been facilitated by the lights attracting prey. We present some observations related to the canyons and prominent fishes.

Nezumia bairdii were frequently observed with isopod parasites on the back behind the first dorsal fin. The parasites appeared to be *Sycenus infelix*, also described by Ross et al. (2001) on the same fish species in this region. As in Gartner et al. (2008), dense aggregations of typically midwater fauna were often observed in the bottom water layer (bottom to a few meters above bottom). These mostly included squids (*Illex* sp.), myctophids, nettastomatids, and paralepedids. Various octocorals (particularly *Paragorgia arborea*) served as spawning substrate for some fishes. As reported for other catshark species (Etnoyer and Warrenchuk 2007), unidentified (but not *Scyliorhinus retifer*) uniform brown colored shark egg cases were frequently observed entangled in octocorals, especially *Paragorgia arborea*. Living eggs of another unidentified bony fish were collected and observed in octocorals.

Abundant benthic food resources of likely value to the fishes were observed on most dives in the canyons and seeps. Particularly notable were dense swarms of euphausids and amphipods that appeared to be resident in the sediments. Predation events witnessed were: brittle stars, anemones and hydroids captured midwater fishes, *Illex* sp. and *B. brosme* ate *Arctozenus rissoi*, red crab (*Chaceon quinquidens*) ate *Melanostigma atlanticum*, and *Synaphobranchus* sp. consumed unidentified shrimps. See **Section 15.2** on fish feeding habits.

Impacts from anthropogenic activity were observed in both canyons but less so in the two seeps, which are technically outside the canyons proper. Trash, especially plastics, was common and often entangled in corals. Lost fishing gear, including traps, various lines, and nets, was frequently observed, especially in the heads of canyons. Some ghost traps contained fishes. A *Centrophorus granulosus* was observed swimming along a canyon wall with a hook in its mouth. Although the proximate cause of disease cannot be determined, anthropogenic impact cannot be ruled out. Lesions on the body and head were observed on a *B. brosme* (RB-681) and a *C. granulosus* (RB-688).

15.1.4 Discussion

Fish fauna along the slope off the mid-Atlantic coast of the United States (>200 m, Cape Hatteras to Cape Cod) is composed of warm-temperate, cold-temperate, and boreal taxa that are widely distributed in the western North Atlantic Ocean or even throughout the broader North Atlantic. The slope ichthyofauna in this region exhibits latitudinal variability, with the warm to cool temperate fauna being replaced by colder water species going from south-to-north. Markel and Musick (1974) indicated that the fish fauna was different north and south of approximately 38°30′N (near Wilmington Canyon). Norfolk and Baltimore canyon areas usually exhibited greater affinity in fish species composition and abundance patterns (this study) with the area from Cape Hatteras to the above latitude, sharing 87% of the benthic and benthopelagic fishes trawled in that area (549−1,280 m, Markle and Musick 1974) and sharing 74% of the ichthyofauna observed by submersible in the Hatteras Middle Slope canyon area (326−800 m, ~180 km south of Norfolk Canyon, Sulak and Ross 1996). Despite a generally high affinity with the southern mid-Atlantic, the fish assemblages of the two canyons had a 67% (Markle and Musick 1974) and 96% (Haedrich et al. 1975) overlap with fishes trawled from 38°30′N to Cape Cod. In contrast, compared with the two canyons, the overlap in fish species composition north of Cape Cod declined to 38% of those observed by ROV in the Gulf of Maine (Auster 2005), 46% of those trawled off Nova Scotia (Markle et al. 1988), and off Newfoundland was 42% of those trawled (Snelgrove and Haedrich 1985) and 46% of those observed by ROV (Baker et al. 2012). The low overlap (46%) in species composition between our study and Musick (1979) was largely due to the latter's extensive sampling in deeper water and including stations north of 38°30′N. Much farther south of the two canyons, the fishes on and near deep reefs off the southeastern United States (366−783 m, Cape Lookout to Cape Canaveral; Ross and Quattrini 2007) shared 48% of species within the two canyons. Although these comparisons illuminate general zoogeographic patterns and suggest that many species have wide distributions, differences in sampling efforts and methods, as well as the possibility of fluctuating boundaries due to climate change, limit the accuracy of determining faunal boundaries. Nye et al. (2009) attributed a shift northward and deeper in many northeastern U.S. fish stocks (including species in this study) to warming water temperatures, and Møller et al. (2010) speculated that some fishes were moving north as far as Greenland in response to rising water temperatures. If true and persistent, major changes to regional zoogeography and fisheries will be likely.

Much of the northeastern United States and Canadian shelf and slope have been well sampled for fishes. Even so, the intense two-year surveys of the Norfolk and Baltimore canyons documented more fish species than previous studies along the east coast of the United States in similar depths, but other studies employed lower sampling efforts, mostly relied on trawling, and avoided rugged habitats. The relatively high species richness coupled with new range data for 12 species suggest that the canyon and seep habitats of the region require additional investigation, also suggested by Ross and Quattrini (2007)

for deep reefs. Although habitat was uncertain for some species, eight newly recorded species occupied complex habitats, again indicating that more sampling appropriate to the habitat (i.e., direct observation) is needed. Such additional sampling should be conducted across all habitats using the same standardized methods to avoid comparison issues resulting from different methods. Unfortunately, there are no data resulting from direct observation methods covering similar depths and habitats as this study in these or other canyons or the open slope of the mid-Atlantic.

The effect of canyons on faunal distribution and abundance appears to be variable, although most studies indicated that canyons supported different faunal structures (species composition, abundance) than neighboring slopes. Fish or invertebrate assemblages within canyons were different compared with those on the open slopes nearby (Rowe 1971, 1972, Vetter and Dayton 1998, 1999, De Leo et al. 2010, Kelly et al. 2010, Vetter et al. 2010), but such differences were sometimes restricted to certain depth zones. Other studies failed to detect differences in faunal composition between canyon and neighboring slope environments (Haedrich et al. 1975, Hecker et al. 1983, Houston and Haedrich 1984, King et al. 2008). The reasons for inconsistent results may be related to different organic inputs (Rowe et al. 1982, van Oevelen et al. 2011), different environmental conditions (De Leo et al. 2012), sediment type and dynamics (Cunha et al. 2011), physical oceanography (Kämpf 2007), and variability in methods and fauna examined. Aside from the fishes newly reported to the region (**Section 15.1.3.1**) whose distributional status is unclear, none of the fishes observed or collected here were unique to Norfolk or Baltimore canyons; however, some appear to be unique to certain habitats most common in the canyons. Fishes observed from the submersible on the flat, soft substrate slope approximately 35 km south of Norfolk Canyon exhibited a 93% overlap in species composition within the two canyons and similar abundance ranks of the dominant fishes (Sulak and Ross 1996). This also indicated a lack of difference in faunal composition between the canyons and the mid-Atlantic slope in general. On a larger scale these canyons may not significantly impact species composition, but at smaller scales they may influence spatial and abundance patterns by providing complex habitats and enhanced feeding conditions not common elsewhere. For example, *C. rupestris* (Snelgrove and Haedrich 1985, Baker et al. 2012) and several invertebrate taxa (Rowe 1971, Haedrich et al. 1975) have been called regional "canyon indicator species" because they are more frequent within canyons. Similarly, *B. brosme* could be considered a canyon indicator for the mid-Atlantic, but its frequency in canyons is more likely due to rugged habitat than a canyon effect because they were also common on rugged habitats outside the canyons.

Depth zonation of demersal deepsea fauna is common on continental margins (Carney 2005), but zonal definitions and boundaries vary due to differences in methods and data interpretations, low sampling effort, and the different faunal groups examined. The two completely different fish assemblages apparent from Norfolk and Baltimore canyons deeper and shallower than 1,400 m closely match two depth zones with a 1,500 m boundary reported for the overall North Atlantic slope fish fauna (Koslow 1993) and for fishes trawled off Newfoundland (Snelgrove and Haedrich 1985). More than two fish community depth zones were often noted along the western North Atlantic slope, but a zone boundary near 1,400 m was a common feature (Haedrich et al. 1975, Musick 1979, 1980, Valentine et al. 1980, Baker et al. 2012) as it is in other oceans (Gage and Tyler 1999, Carney 2005). The great differences in fish composition and abundance shallower and deeper than 1,400 m overshadowed the impact of habitats on community organization. Although some canyon habitats were missing or limited in the deepest areas examined, seeps and soft substrate occurred in both depth zones. Despite habitats that appeared to be structurally similar, the fauna was still different above and below 1,400 m. Because both seep areas were technically outside the canyons proper, the depth zonation does not appear to be a canyon effect either. Mean bottom temperatures (4.0−4.3 °C) were less variable and often 2−3 °C colder during the deepest dives, and the 4 °C isotherm often denotes a deepsea faunal boundary (Gage and Tyler 1999). Although temperature may influence slope fish distributions, continuous, long-term data are more relevant to biological function than the shorter duration data recorded during ROV dives or CTD casts. Such long-term data are needed to clarify environmental roles in depth structuring and

the impact of climate change. Reduction of apparent depth zones was attributed to higher regional productivity, which likely motivated fishes to move through wide depth ranges for feeding (Merrett and Marshall 1980, Snelgrove and Haedrich 1985). Shallower than 1,000 m, Norfolk Canyon and many areas of Baltimore Canyon exhibited much higher sediment organic carbon concentrations than the surrounding slope (Demopoulos et al., unpubl. data), which could influence the simplification of fish depth zones in the area. However, it is not clear that differences in trophic structure explain the two depth zone patterns revealed here because both zones appeared to have high available food resources (high sediment organic carbon, abundant potential invertebrate prey). See **Chapters 8**, **9**, and **16** for more information related to canyon food resources.

Although fish habitat association data continue to be lacking in the deep sea (especially ≥1,000 m), emerging evidence suggests that fish associations with complex habitat on the mid to upper slope (approximately <1,000 m) can range from seemingly obligate (Ross and Quattrini 2007, Quattrini et al. 2012) to more opportunistic (this study, Auster 2005, Costello et al. 2005, Baker et al. 2012, Kutti et al. 2014) to highly variable or not detectable (Biber et al. 2014). Degree of associations may vary by region; however, in most areas of the slope there is an affinity for complex habitats, as reported here, which may be expressed as different species composition or abundance patterns or both. The increasing rarity of complex habitat (seamounts excluded) and the decline of food quantity and quality with increasing depth argue against strong habitat association in deep environments where flexibility and opportunism might be advantageous (Ross and Quattrini 2007). The lack of distinct fish and habitat association below 1,400 m (this study), deeper than 800 m (Baker et al. 2012), and at 2,836 and 3,775 m (Auster et al. 1995) supports that argument. Ross and Quattrini (2007) cautioned that more direct observations are needed, especially below mid-slope depths.

Shallower than 1,400 m, habitat association patterns exhibited by many fishes of Norfolk and Baltimore canyons appeared to grade from least to most complex with increasing degrees of difference. Fishes associated with the two sand/mud categories were different from other canyon and most seep habitats, driven by species generally associated with soft substrate (Sulak and Ross 1996, Collette and Klein-MacPhee 2002). More variability was seen in fish assemblages associated with the complex canyon and seep habitats; however, certain taxa (*Laemonema* spp., *Hoplostethus* spp., *B. brosme, Benthocometes robustus, Dysommina rugosa,* and *Lophius americanus*) regularly characterized the reef-like habitats, as noted elsewhere (Collette and Klein-MacPhee 2002, Ross and Quattrini 2007). Although corals and sponges did not statistically influence fish assemblages in Norfolk and Baltimore canyons, their substantial contributions to habitat structure should not be ignored. Corals and sponges provide relief, rugosity, and overall enhanced complexity (Miller et al. 2012, Buhl-Mortensen et al. 2010). Even so, a clear cause and effect relationship between coral presence and fish assemblages remains elusive (Auster 2007, Baker et al. 2012, Biber 2014). Slope fishes are commonly reported to be more abundant around reefs with corals (Costello et al. 2005, Purser et al. 2013), but the functional linkage to corals is unclear.

In contrast to the interpretation by Baker et al. (2012) of the southeastern U.S. deep reef results (Ross and Quattrini 2007), we found that reef structure (including corals but not always dominated by corals) had a great impact on fish assemblages, with several species occurring only on deep reefs. That study did not explicitly test for effects of corals, and we note that dead coral framework supported about the same communities as living coral. The important factor for deepsea fish and habitat associations seems to be the level of complexity of the habitat, to which corals contribute. Some common fishes in these canyons were only seen on complex habitats and were often more abundant in the presence of corals (e.g., *B. brosme, D. rugosa, B. robustus*), but there was enough variability that coral and sponge presence alone did not support unique assemblages. One caveat to this is that octocorals seem to be a preferred substratum for egg laying in some fishes (catsharks, unknown teleost) (this study, Henry et al. 2013), and sea pens were reported to host larval *Sebastes* spp. (Baillon et al. 2012). Data on deepsea

communities is temporally limited (Auster 2007), especially from direct observation methods, and use patterns that may vary with seasons (as in reproduction) can be missed.

15.1.5 Summary

Norfolk and Baltimore canyons did not harbor unique fish communities; however, their distinctive geology (cliffs and walls, boulders) and oceanography (strong currents, high particulate loads) facilitated the development of complex habitats, which in turn influenced fish assemblage patterns. Thus, on a large scale (kilometers) the canyon effect is indirect, while on a smaller scale (10s to 100s of meters) canyon and shallow seep habitats had a direct impact on fish patterns of abundance and distribution.

Although lost fishing gear (trawls, traps, lines) was frequently observed, and habitat damage can result from this gear (this study, Miller et al. 2012, Fabri et al. 2014), the rugged canyons are generally difficult to fish with benthic trawls or long lines. Canyons likely serve as refugia from trawling (Valentine et al. 1980) and other anthropogenic disturbance (Huvenne et al. 2011), as perhaps illustrated by our observations of *B. brosme* (cusk). This fish has declined so drastically in the western North Atlantic that Canada listed it as threatened and the United States is evaluating it (Hare et al. 2012). Although trawl data may overestimate the cusk decline, there are generally not enough data on this species to accurately assess the stock in the western North Atlantic (occurred only in 6% of trawls in a 40-year survey, Hare et al. 2012). Given the cusk's proclivity for complex habitat and high site fidelity (Collette and Klein-MacPhee 2002), direct observations should yield better information on the status of this species. We collected no cusk by trawl, but it was a dominant species (mostly large adults) observed on rugged habitats in both canyons (weighted mean depth of occurrence = 416.5 m), with as many as 55 observed in one dive in Norfolk Canyon. Considering its abundance at the southern end of its known range and lack of observations outside the two canyons and rugged habitats, it appears that canyons and associated habitats provide refuge for this species. These canyons and surroundings have been recommended for protection by the Middle Atlantic Fishery Management Council (currently under review by U.S. Department of Commerce). This seems appropriate given the abundance of vulnerable habitats (corals, seeps), observations of anthropogenic impact, and the high fish species richness associated with Norfolk and Baltimore canyons.

15.2 Diets of Dominant Demersal Fishes in and around Norfolk and Baltimore Canyons

15.2.1 Introduction and Background

Diets of major fish species on the shelf of the northeastern United States have been fairly well described (see review in Smith and Link 2010), but trophodynamics of deepwater species remain poorly known. Various studies have addressed some aspects of deepwater trophodynamics (mostly for fishes) in the MAB (Sedberry and Musick 1978, Langton and Bowman 1980, Crabtree et al. 1991, Link and Alameida 2000), but these have not used a whole ecosystem approach, and most have not focused on specific habitats. Methratta and Link (2012) identified feeding hotspots for a few MAB fish species and attempted to correlate that with several habitat metrics. The overall goal of this study component is to characterize food webs within major large-scale biotopes (canyons and intercanyons) and to examine the trophic effects associated with smaller scale habitats (corals, hard bottom, soft substrate, and seeps). The fish diet data presented here are complemented by a broad scale analysis of food webs within and around Baltimore and Norfolk canyons based on stable isotope analyses (**Chapter 16**).

Canyons can concentrate organic matter and exhibit a net transport of organic matter and nutrients down-slope (Keller and Shepard 1978, Bennett et al. 1985, De Leo et al. 2010). Canyons also appear to support faunal communities different from surrounding areas, hypothetically due to trophic enrichment

(Rowe 1971, Rowe et al. 1982, De Leo et al. 2010, Vetter et al. 2010). Swarms of macrourid fishes have been observed in some mid-Atlantic canyons (B. Hecker, unpubl. photograph), and these may have congregated for feeding as observed elsewhere (Vetter and Dayton 1999). Benthic-pelagic coupling via the migrating midwater fauna may facilitate energy transfer between surface and bottom environments (Graf 1989, Gartner et al. 2008, Colaço et al. 2013), and canyons may trap or concentrate the migrating mesopelagic community (Greene et al. 1988, Macquart-Moulin and Patriti 1996). In addition, galatheoid squat lobsters and benthic fishes have been observed eating midwater animals (Hudson and Wigham 2003, S.W. Ross pers. obs.). Cold seeps and associated chemosynthetic communities exist near Baltimore and Norfolk canyons, and these may have a trophic impact on the fishes associated with them.

15.2.2 Methods

See **Section 15.1.2** for details of the study areas and ROV and trawling methods.

15.2.2.1 Diet Analysis

Stomach contents of 14 dominant species (*Dysommina rugosa, Synaphobranchus kaupii, Coelorinchus caelorhincus, Nezumia bairdii, Enchelyopus cimbrius, Phycis chesteri, Urophycis regia, Merluccius albidus, Benthocometes robustus, Lophius americanus, Helicolenus dactylopterus, Lycenchelys verrillii, Citharichthys arctifrons,* and *Glyptocephalus cynoglossus*) were assessed following methods of Ross and Moser (1995). Fish specimens were subsampled from each site to include all sizes and depths sampled, and the stomachs were removed for gut content analysis (GCA). Stomach fullness was estimated using a scale of 0% (empty), ≤5% (nearly empty), 25%, 50%, 75%, or 100% (full).

Percent frequency of prey occurrence and percent volume of prey are dietary importance indicators (Hyslop 1980). Thus, stomach contents were quantified using the following indices: abundance of prey species, percent volume of prey, and the percent frequency of occurrence of prey. Any material present in the mouth or esophagus was excluded from analyses. Stomach contents were placed on a Petri dish and identified to the lowest possible taxa. Similar prey species were then piled together on a grid of 1 mm squares and flattened to a uniform height, which was measured. The height multiplied by the number of squares occupied by the food item yielded volume in cubic millimeters. The sum of all prey volumes equaled the total volume of food in the stomach, and the volume of each prey item was converted to a percentage of the total prey volume (%V). The frequency of occurrence for a prey item equaled the number of times a prey item occurred in the fish species examined divided by the total number of stomachs with food analyzed for that species.

Although food items were identified to the lowest taxa possible, combining food items into larger taxonomic categories facilitated analyses and presentation. Food items found during GCA were grouped into 18 general food categories: Amphipoda, Annelida, Chaetognatha, Copepoda, Crustacea, Cumacea, Decapoda, Echinodermata, Euphausiacea, Fish, Foraminifera, Insecta, Isopoda, Mollusca, Mysida, Sipuncula, Tanaidacea, and Other. The food category Crustacea consisted of crustaceans other than amphipods, copepods, cumacids, decapods, euphausiids, isopods, mysids, ostracods, and tanaidacids. The food category Other consisted of unidentifiable organic and inorganic material as well as various other types of unidentifiable material. If food items were not present, stomach contents were described as “empty.” Everted stomachs were eliminated from GCA as were some stomachs that were missing due to poor specimen preservation. The percentage of empty stomachs was reported separately.

15.2.3 Results

Of the 14 species selected for stomach analysis, 2,050 total individuals were collected (**Table 15-4**) from in and around Norfolk and Baltimore canyons (**Figures 15-8** and **15-9**, **Table 15-5**). Stomachs were dissected from a random subsample of 1,284 of these fishes (**Table 15-6**). Fishes with stomachs

everted or missing totaled 125 (9.7%). A total of 1,158 (90.2%) stomachs were used for GCA, of which 245 (19.1%) were empty. The remaining 914 (71.2%) stomachs were used for percent volume and percent frequency calculations. Combining all fish species, Crustacea (16.2%), Euphausiacea (15.2%), fishes (14.8%), Decapoda (12.5%), organic material (11.9%), Annelida (10.4%), Mollusca (6.9%), Amphipoda (5.7%), and inorganic material (2.0%) made up 95.7% of the total food volume.

The following section describes food habits by species, in phylogenic order, and pertains only to the stomachs used for GCA. When describing the percent volume and frequency of prey consumed within each species, we first note the contributions from the 18 general food categories and then if available, the contributions of major items that were identified to lower taxonomic categories. Note the difference between the words *categories* and *items*.

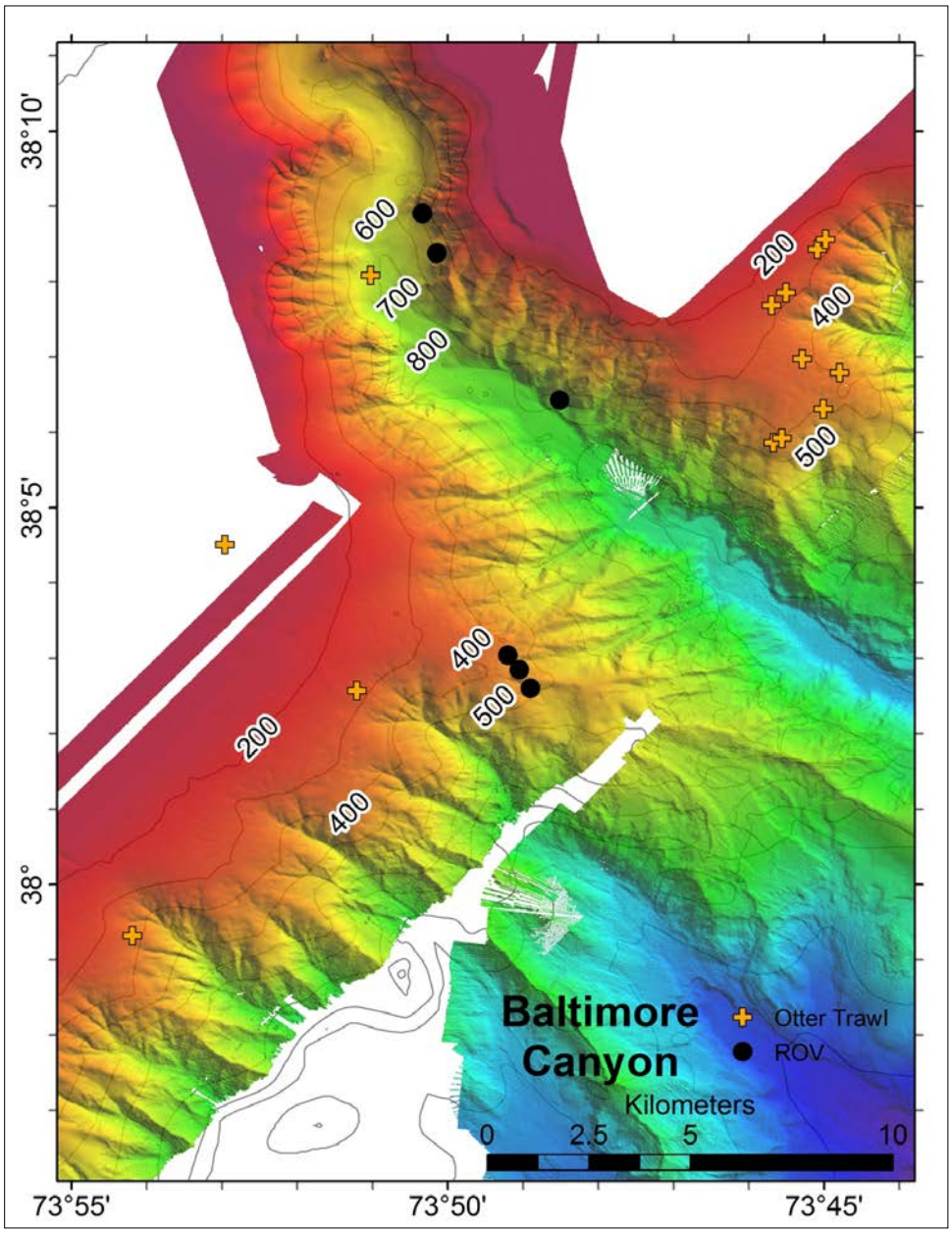

Figure 15-8. Stations in and around Baltimore Canyon where selected fish species were collected during the Atlantic Deepwater Canyons Study.

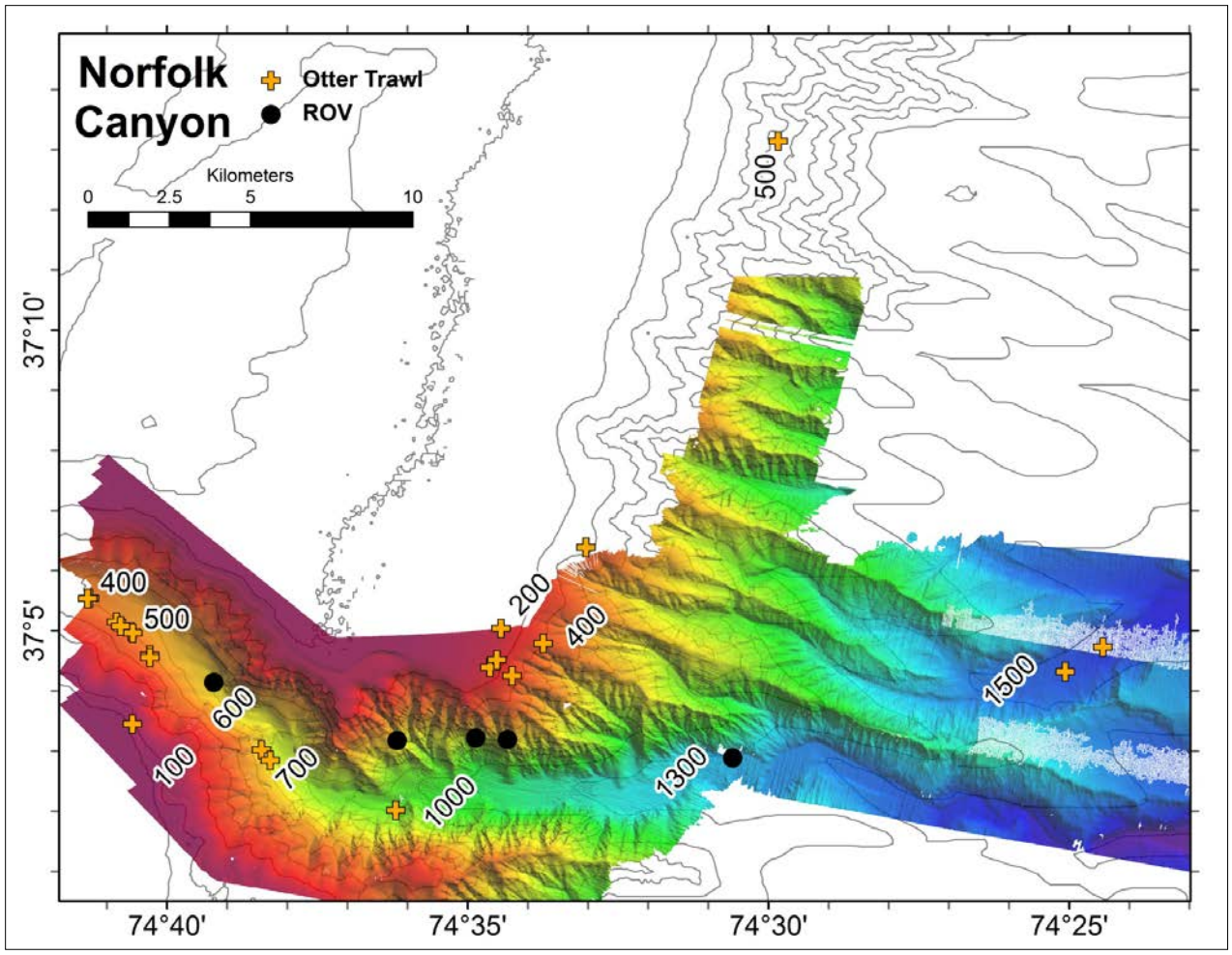

Figure 15-9. Stations in and around Norfolk Canyon where selected fish species were collected during the Atlantic Deepwater Canyons Study.

Table 15-4. Fish species selected for stomach analyses that were collected during the 2012 and 2013 sampling cruises for the Atlantic Deepwater Canyons Study. Number of fishes followed by length (mm). Depth ranges are in meters.

Species	2012 Sampling Cruise				2013 Sampling Cruise			
Scientific Name	OT Depth	No. Fishes (length)	ROV Depth	No. Fishes (length)	OT Depth	No. Fishes (length)	ROV Depth	No. Fishes (length)
Dysommina rugosa	–	–	413–430	2 (214–231)	–	–	397–489	11 (156–308)
Synaphobranchus kaupii	450–800	91 (99–403)	–	–	1,576–1,643	10 (347–555)	–	–
Coelorinchus caelorhincus	214–800	37 (43–242)	–	–	287–1,046	20 (110–230)	–	–
Nezumia bairdii	400–800	383 (47–305)	–	–	287–1,643	419 (39–310)	–	–
Enchelyopus cimbrius	300–510	22 (50–192)	–	–	287–392	9 (120–194)	–	–
Phycis chesteri	400–800	60 (59–334)	–	–	255–1,046	51 (41–340)	–	–
Urophycis regia	103–400	50 (140–274)	–	–	160–392	21 (33–284)	–	–
Merluccius albidus	214–570	24 (165–349)	374	1 (157)	255–270	1 (271)	–	–
Benthocometes robustus	–	–	389–409	3 (98–112)	–	–	393–1,388	15 (56–108)
Lophius americanus	400–800	17 (92–435)	571	1 (254)	304–330	1 (292)	–	–
Helicolenus dactylopterus	214–570	142 (31–242)	–	–	160–340	123 (24–190)	–	–
Lycenchelys verrillii	389–800	91 (65–163)	–	–	376–392	2 (125–133)	–	–
Citharichthys arctifrons	103–480	195 (27–146)	313	1 (85)	287–340	1 (139)	–	–
Glyptocephalus cynoglossus	300–800	216 (65–291)	–	–	287–1,046	30 (127–291)	–	–
Total		1,328	–	8	–	688	–	26

OT= otter trawl, ROV = *Jason II* and *Kraken 2* remotely operated vehicle. ROV depth range and location data are only for the period when the ROV was on the bottom.

Table 15-5. Stations where selected fish species were collected in the vicinity of Baltimore and Norfolk canyons during the 2012 and 2013 sampling cruises.

Station No.	Canyon	Date	Gear	Sample Time (min)	Start		End		Depth Range (m)
					Latitude (N)	Longitude (W)	Latitude (N)	Longitude (W)	
ROV-2012-NF-02	Baltimore	19 Aug 2012	ROV	451	38°08′54.06″	73°50′19.98″	38°08′41.34″	73°50′01.86″	402–530
ROV-2012-NF-03	Baltimore	21 Aug 2012	ROV	542	38°06′25.38″	73°48′30.60″	38°07′36.06″	73°48′11.28″	303–827
ROV-2012-NF-06	Baltimore	24 Aug 2012	ROV	571	38°08′22.62″	73°50′08.64″	38°08′49.20″	73°49′58.14″	234–530
ROV-2012-NF-08	Baltimore	27 Aug 2012	ROV	552	38°03′02.22″	73°49′12.00″	38°03′04.08″	73°49′18.78″	412–454
NF-2012-133	Baltimore	6 Sept 2012	OT: 3.5 m	30	38°04′30.48″	73°52′57.60″	38°03′29.76″	73°54′00.30″	136–140
NF-2012-134	Baltimore	7 Sept 2012	OT: 3.5 m	30	38°02′33.78″	73°51′12.24″	38°01′29.40″	73°52′01.26″	278–282
NF-2012-135	Baltimore	7 Sept 2012	OT: 3.5 m	30	37°59′19.08″	73°54′11.16″	37°58′11.58″	73°55′07.74″	360–380
NF-2012-139	Baltimore	7 Sept 2012	OT: 3.5 m	30	38°08′25.44″	73°45′05.10″	38°09′23.10″	73°44′36.24″	214–300

Table 15-5. (Continued).

Station No.	Canyon	Date	Gear	Sample Time (min)	Start		End		Depth Range (m)
					Latitude (N)	Longitude (W)	Latitude (N)	Longitude (W)	
ROV-2012-NF-14	Baltimore	7 Sept 2012	ROV	574	38°02′36.12″	73°48′53.94″	38°02′57.06″	73°49′19.56″	407–507
NF-2012-140	Baltimore	8 Sept 2012	OT: 3.5 m	30	38°07′50.82″	73°45′30.18″	38°08′57.54″	73°44′46.20″	290–300
NF-2012-141	Baltimore	8 Sept 2012	OT: 3.5 m	30	38°08′33.30″	73°44′58.68″	38°07′38.88″	73°45′42.06″	300–300
NF-2012-142	Baltimore	8 Sept 2012	OT: 3.5 m	30	38°06′58.26″	73°45′17.28″	38°08′10.68″	73°45′09.84″	300–360
NF-2012-143	Baltimore	9 Sept 2012	OT: 3.5 m	30	38°05′51.36″	73°45′40.26″	38°06′32.64″	73°44′40.08″	405–420
NF-2012-144	Baltimore	9 Sept 2012	OT: 3.5 m	30	38°06′47.28″	73°44′47.34″	38°05′46.02″	73°45′21.30″	400–540
NF-2012-145	Baltimore	10 Sept 2012	OT: 3.5 m	30	38°06′18.30″	73°45′00.42″	38°07′24.30″	73°44′54.18″	418–570
NF-2012-146	Baltimore	10 Sept 2012	OT: 3.5 m	30	38°05′55.08″	73°45′33.48″	38°06′59.34″	73°44′48.60″	412–422
NF-2012-147	Baltimore	10 Sept 2012	OT: 3.5 m	30	38°07′40.86″	73°45′41.64″	38°06′46.56″	73°46′48.84″	250–300
NF-2012-150*	Baltimore	12 Sept 2012	OT: 3.5 m	*					*
NF-2012-151	Baltimore	12 Sept 2012	OT: 3.5 m	30	38°08′04.80″	73°51′01.20″	38°07′22.14″	73°50′35.46″	700–800
NF-2012-167	Norfolk	20 Sept 2012	OT: 3.5 m	30	37°03′01.38″	74°38′25.56″	37°01′57.60″	74°38′08.46″	450–580
NF-2012-168*	Norfolk	21 Sept 2012	OT: 3.5 m	*	37°02′51.00″	74°38′16.92″			*
NF-2012-175	Norfolk	22 Sept 2012	OT: 3.5 m	30	37°05′32.58″	74°41′17.16″	37°05′03.84″	74°40′09.90″	405–510
NF-2012-176	Norfolk	22 Sept 2012	OT: 3.5 m	30	37°04′35.76″	74°40′16.98″	37°05′21.96″	74°41′00.00″	400–423
NF-2012-177	Norfolk	23 Sept 2012	OT: 3.5 m	30	37°05′08.94″	74°40′50.28″	37°04′03.06″	74°39′50.76″	389–402
NF-2012-179	Norfolk	23 Sept 2012	OT: 3.5 m	30	37°04′59.28″	74°40′35.64″	37°03′46.56″	74°39′39.24″	395–400
NF-2012-186	Norfolk	24 Sept 2012	OT: 3.5 m	30	37°03′27.12″	74°40′34.44″	37°02′18.84″	74°39′53.94″	103–120
NF-2012-187	Norfolk	24 Sept 2012	OT: 3.5 m	30	37°04′57.84″	74°40′34.08″	37°04′09.36″	74°39′41.46″	402–480
NF-2012-188	Norfolk	25 Sept 2012	OT: 3.5 m	30	37°05′32.34″	74°41′19.08″	37°04′45.54″	74°40′22.32″	403–408
NF-2012-189	Norfolk	26 Sept 2012	OT: 3.5 m	30	37°13′08.70″	74°29′50.28″	37°12′12.24″	74°30′08.40″	460–500
RB-2013-001	Norfolk	3 May 2013	OT: 3.5 m	30	37°05′04.86″	74°40′46.20″	37°05′42.66″	74°41′39.60″	382–388
RB-2013-002*	Norfolk	3 May 2013	OT: 3.5 m	30	37°04′33.36″	74°40′17.04″	37°05′18.18″	74°41′08.88″	376–392
RB-2013-013	Norfolk	4 May 2013	OT: 3.5 m	30	37°02′01.14″	74°36′11.76″	37°02′12.72″	74°35′15.96″	931–1,046
RB-2013-023	Norfolk	4 May 2013	OT: 3.5 m	30	37°05′02.46″	74°34′26.70″	37°05′56.94″	74°34′07.86″	160–165
RB-2013-024	Norfolk	4 May 2013	OT: 3.5 m	30	37°04′23.58″	74°34′37.92″	37°05′18.12″	74°34′09.78″	175–187
RB-2013-025	Norfolk	4 May 2013	OT: 3.5 m	30	37°04′31.26″	74°34′30.84″	37°05′36.84″	74°34′05.70″	180–185
RB-2013-026	Norfolk	5 May 2013	OT: 3.5 m	30	37°04′15.36″	74°34′15.72″	37°05′13.38″	74°33′44.10″	255–270
RB-2013-027	Norfolk	5 May 2013	OT: 3.5 m	30	37°04′47.46″	74°33′44.64″	37°05′52.32″	74°33′22.74″	304–330
RB-2013-028	Norfolk	5 May 2013	OT: 3.5 m	30	37°04′44.04″	74°24′26.40″	37°05′24.36″	74°23′39.60″	1,614–1,643
ROV-2013-RB-680	Norfolk	5 May 2013	ROV	515	37°03′11.64″	74°34′20.22″	37°03′33.42″	74°34′51.36″	441–640

Table 15-5. (Continued).

Station No.	Canyon	Date	Gear	Sample Time (min)	Start		End		Depth Range (m)
					Latitude (N)	Longitude (W)	Latitude (N)	Longitude (W)	
RB-2013-029	Norfolk	7 May 2013	OT: 3.5 m	30	37°04′19.32″	74°25′03.84″	37°05′00.66″	74°24′10.86″	1,576−1,629
ROV-2013-RB-684	Norfolk	10 May 2013	ROV	768	37°04′08.64″	74°39′13.20″	37°04′09.90″	74°38′43.80″	382−610
ROV-2013-RB-685	Norfolk	11 May 2013	ROV	1,650	37°02′53.28″	74°30′35.58″	37°04′13.26″	74°32′38.16″	541−1,388
ROV-2013-RB-686	Norfolk	13 May 2013	ROV	737	37°03′10.62″	74°36′10.38″	37°03′33.06″	74°36′11.22″	394−622
ROV-2013-RB-687	Norfolk	14 May 2013	ROV	773	37°03′13.32″	74°34′52.08″	37°03′34.44″	74°34′46.08″	397−711
ROV-2013-RB-689	Baltimore	16 May 2013	ROV	542	38°02′50.82″	73°49′02.64″	38°02′52.98″	73°49′18.90″	399−443
RB-2013-086	Norfolk	21 May 2013	OT: 3.5 m	30	37°06′23.28″	74°33′01.92″	37°05′29.16″	74°33′25.02″	287−340

OT = otter trawl, ROV = *Jason II* and *Kraken 2* remotely operated vehicles. ROV depth range and location data are only for the period when the ROV was on the bottom. * = poor quality or gear issue.

Table 15-6. Summary of gut content analysis for 14 selected fish species.

Species	No. of Individuals Collected	Stomachs Dissected	Stomachs with Food	Stomachs Empty	Stomachs Everted or Missing
Scientific Name					
Dysommina rugosa	13	13	4	9	0
Synaphobranchus kaupii	101	101	58	43	0
Coelorinchus caelorhincus	57	57	54	0	3
Nezumia bairdii	802	170	145	1	24
Enchelyopus cimbrius	31	28	19	0	9
Phycis chesteri	111	111	45	7	59
Urophycis regia	71	71	69	1	1
Merluccius albidus	26	26	9	6	11
Benthocometes robustus	18	17	10	7	0
Lophius americanus	19	19	9	10	0
Helicolenus dactylopterus	265	265	199	66	0
Lycenchelys verrillii	93	93	75	13	5
Citharichthys arctifrons	197	192	105	82	5
Glyptocephalus cynoglossus	246	121	113	0	8
Total	2,050	1,284	914	245	125

15.2.3.1 Species Diets

Dysommina rugosa

Stomachs were dissected from 13 individuals (**Table 15-6**), 157−305 mm TL, collected by ROV from five different stations. Four stomachs contained food and nine were empty. The mean percent fullness of all analyzed stomachs was 19.2% (**Figure 15-10A**). Two food items, *Sergestes arcticus* and *Thysanopoda pectinata*, were identified to species. Seven food categories were represented, and Decapoda, Euphausiacea, and Isopoda were the dominant food categories by volume (66.7%, 19.5%, and 7.2%, respectively) (**Figure 15-10B**). *Sergestes arcticus*, *Thysanopoda pectinata*, and unidentified Isopoda were the dominant food items consumed, contributing 60.0%, 12.8%, and 7.2%, respectively, to the overall volume. Of the 18 general food categories, Amphipoda, Decapoda, and Euphausiacea were the most frequent categories (75%, 50%, and 50%, respectively) (**Figure 15-10C**) in stomachs of *D. rugosa*. Of items identified to lower taxonomic levels, the most frequently ingested items were Hyperiidean amphipods and *S. arcticus* (50% and 50%, respectively).

Some females contained large egg masses and nematodes were found in some body cavities.

Synaphobranchus kaupii

Stomachs were dissected from 101 individuals (**Table 15-6**), 100−548 mm TL, collected by otter trawl from seven different stations. Fifty-eight stomachs contained food and 43 were empty. The mean percent fullness of all analyzed stomachs was 18.4% (**Figure 15-11A**). One item (*Thysanopoda* sp.) was identified to genus, and three crustacean families (Hyperiidae, Penaeidae, and Euphausiidae) were identified. Seven food categories were represented, and Fish and Decapoda were the dominant food categories by volume (30.0% and 23.0%, respectively) (**Figure 15-11B**). Unidentified fish remains, decapod shrimp, and crustacean parts were the dominant food items consumed by volume (30.0%, 18.0%, and 16.3%, respectively). Other and Crustacea were the most frequently found categories (67.2% and 29.3%, respectively) (**Figure 15-11C**). The most frequently ingested items were unidentified eye and organic material (43.1% and 34.5%, respectively). Unidentified eye lenses were found in 43.1% of the stomachs. These lenses had no flesh attached and were very small, usually a few millimeters in diameter or smaller. It was impossible to identify the animal that the lenses belonged to, but they are most likely Fish or Mollusca remains as both categories were present in the stomachs.

Most notable for this species was the presence of material in the mouths of the fish. This was most often unidentified organic material, but on occasion it was identified as euphausiid and crustacean parts, and once a lens was recorded. The species has a long stomach and food was usually found in the anterior portion of the stomach. This along with the regularity of material being found in the mouths may indicate that the stomachs of this species will not evert but are prone to partial or perhaps full regurgitation when brought to the surface.

Some females contained large masses of eggs. Many *S. kaupii* contained nematodes within their body cavities.

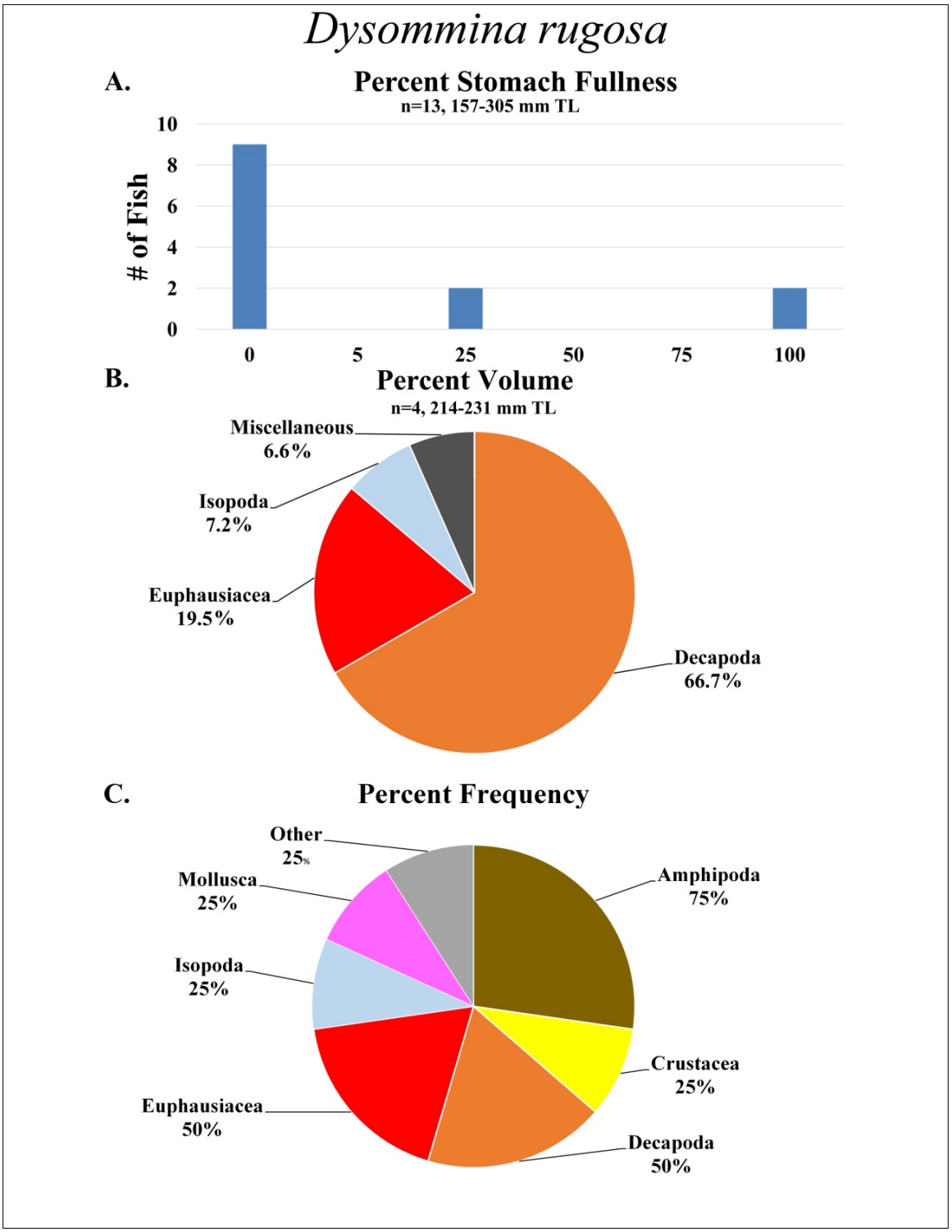

Figure 15-10. A) Percent stomach fullness for *Dysommina rugosa* collected from in and around Baltimore and Norfolk canyons. *n* = number of stomachs analyzed. B) Percent volume of food categories for stomachs that contained food. *n* = number of stomachs that contained food, size range given for individuals whose stomachs contained food. Miscellaneous includes Amphipoda (3.1%), Crustacea (2.5%), Other (1.0%), and Mollusca (<0.1%). C) Percent frequency of each food category present in an individual stomach.

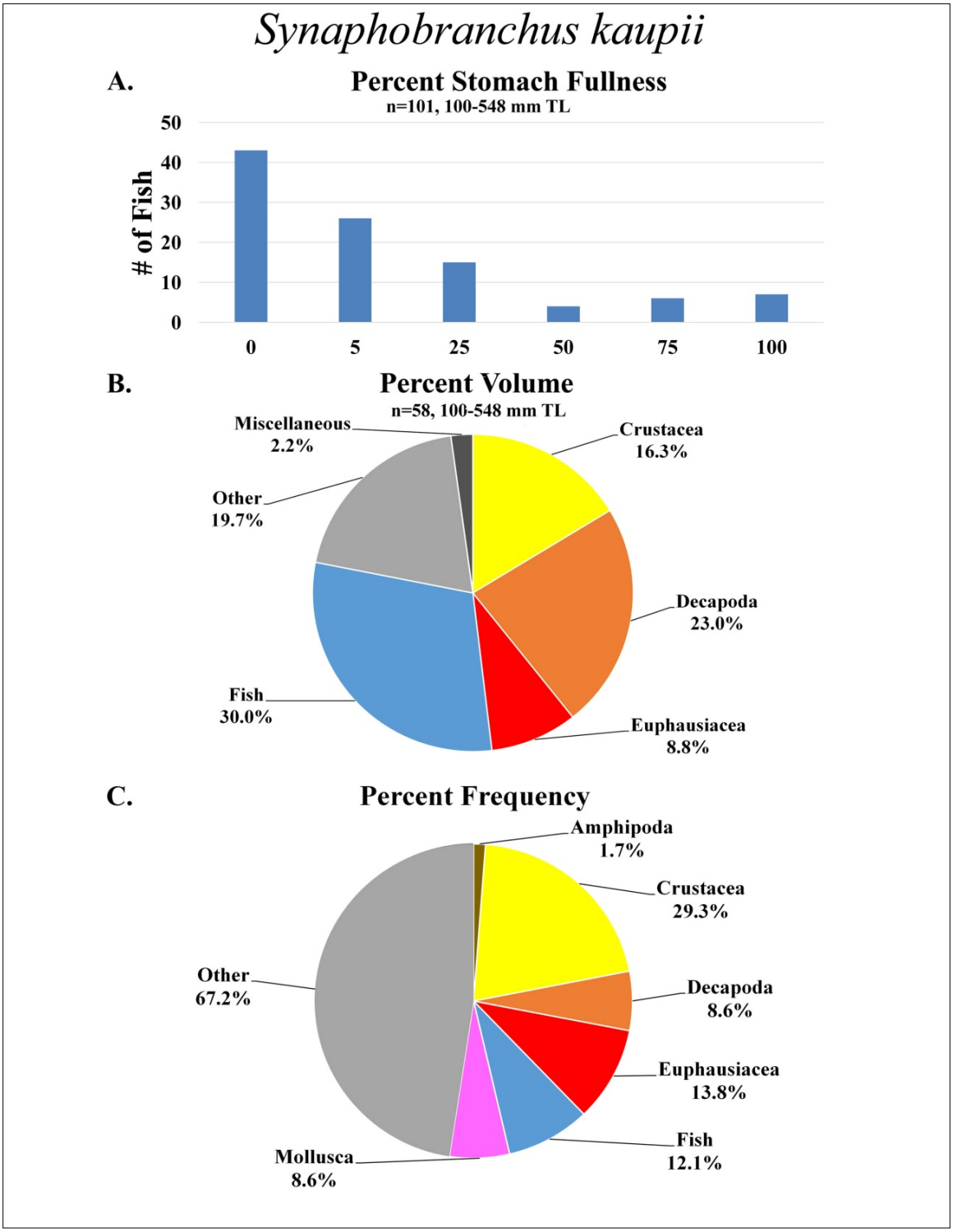

Figure 15-11. A) Percent stomach fullness for *Synaphobranchus kaupii* collected from in and around Baltimore and Norfolk canyons. *n* = number of stomachs analyzed. B) Percent volume of food categories for *S. kaupii* stomachs that contained food. *n* = number of stomachs containing food, size range given for individuals containing food. Miscellaneous includes Mollusca (2.0%) and Amphipoda (0.2%). C) Percent frequency of each food category present in an individual stomach.

Coelorinchus caelorhincus

Stomachs were dissected from 54 individuals (**Table 15-6**), 43−236 mm TL, collected by otter trawl from 17 different stations. All 54 stomachs contained food and had a mean percent fullness of 64.4% (**Figure 15-12A**). One euphausiid, *Thysanopoda pectinata*, was identified to species and two other items, *Eteone* sp. and *Thysanopoda* sp., were identified to genus. Eleven food categories were represented, and Euphausiacea and Other were the dominant categories by volume (36.4% and 22.5%, respectively) (**Figure 15-2B**). *Thysanopoda* sp., organic material, and unidentified crustacean parts were the dominant food items consumed, contributing 22.2%, 22.0%, and 13.0%, respectively, to the overall volume. Other, Annelida, and Amphipoda were the most frequently found categories (70.4%, 63.0%, and 51.9%, respectively) (**Figure 15-2C**). The most frequently ingested items were organic material and unidentified polychaete remains (66.7% and 53.7%, respectively). Nematodes were present in the body cavities of some fish.

Nezumia bairdii

Stomachs were dissected from 146 individuals (**Table 15-6**), 58−314 mm TL, collected by otter trawl from 21 different stations. All but one stomach contained food, and the mean percent fullness of all analyzed stomachs was 54.4% (**Figure 15-13A**). Two items, *Eteone* sp. and *Thysanopoda* sp., were identified to genus. Fourteen food categories were represented, and Annelida, Other, and Amphipoda were the dominant categories by volume (24.2%, 22.3%, and 14.3%, respectively) (**Figure 15-13B**). Organic material, unidentified polychaete remains, unidentified crustacean parts, and gammaridean amphipods were the dominant food items consumed, contributing 17.7%, 13.3%, 11.5%, and 7.7%, respectively, to the overall volume. The most frequently documented food categories following Other (51.4%) were Amphipoda, Annelida, and Crustacea (46.5%, 44.4%, and 42.4%, respectively) (**Figure 15-13C**). The most frequently ingested items were unidentified crustacean parts, unidentified polychaete remains, and organic material (42.4%, 38.2%, and 33.3%, respectively).

Nezumia bairdii specimens usually contained internal parasites (nematodes) within their body cavities. This species contained more parasites than any other species. Some specimens also had external parasites attached behind the first dorsal fin, as described by Ross et al. (2001).

Enchelyopus cimbrius

Stomachs were dissected from 19 individuals (**Table 15-6**), 48−192 mm SL, collected by otter trawl from 10 different stations. Every stomach contained food resulting in a mean percent fullness of 60% (**Figure 15-14A**). Two items, *Pseudeuphausia* sp. and *Elphidium* sp., were identified to genus. Eight food categories were represented, and Euphausiacea (34.9%) and Decapoda (17.3%) were the dominant categories by volume (**Figure 15-14B**). *Pseudeuphausia* sp., organic material, and gammaridean amphipods were the dominant food items consumed, contributing 29.1%, 16.9, and 14.1%, respectively, to the overall volume. Other was the most frequently found category (57.9%) (**Figure 15-14C**). The most frequently ingested items were organic material and gammaridean amphipods (47.4% and 31.6%, respectively).

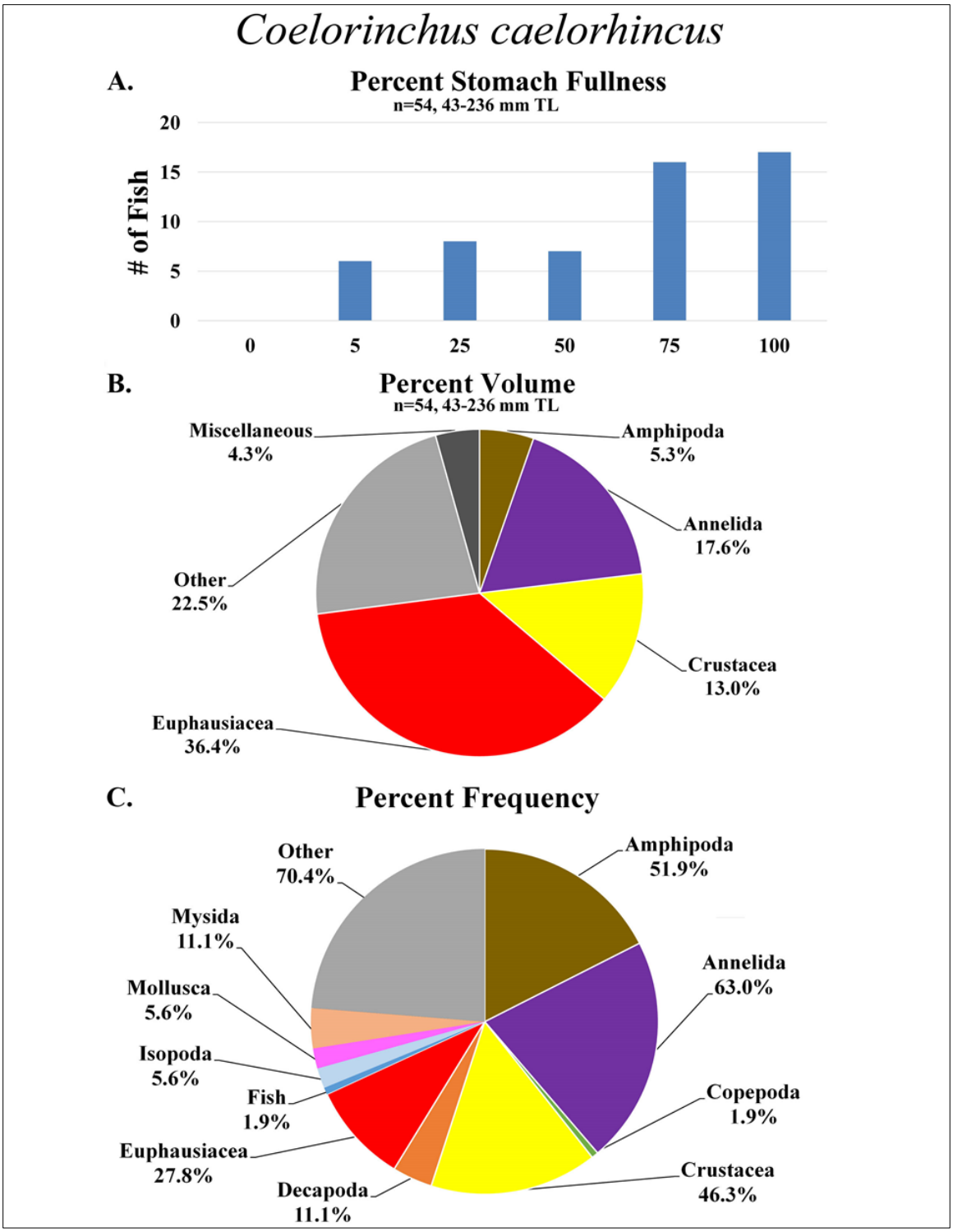

Figure 15-12. A) Percent stomach fullness for *Coelorinchus caelorhincus* collected from in and around Baltimore and Norfolk canyons. *n* = number of stomachs analyzed. B) Percent volume of food categories for *C. caelorhincus* stomachs that contained food. *n* = number of stomachs containing food, size range given for individuals containing food. Miscellaneous incudes Decapoda (3.1%), Mysida (0.5%), Isopoda (0.4%), Copepoda (0.1%), Fish (<0.1%), and Mollusca (<0.1%). C) Percent frequency of each food category present in an individual stomach.

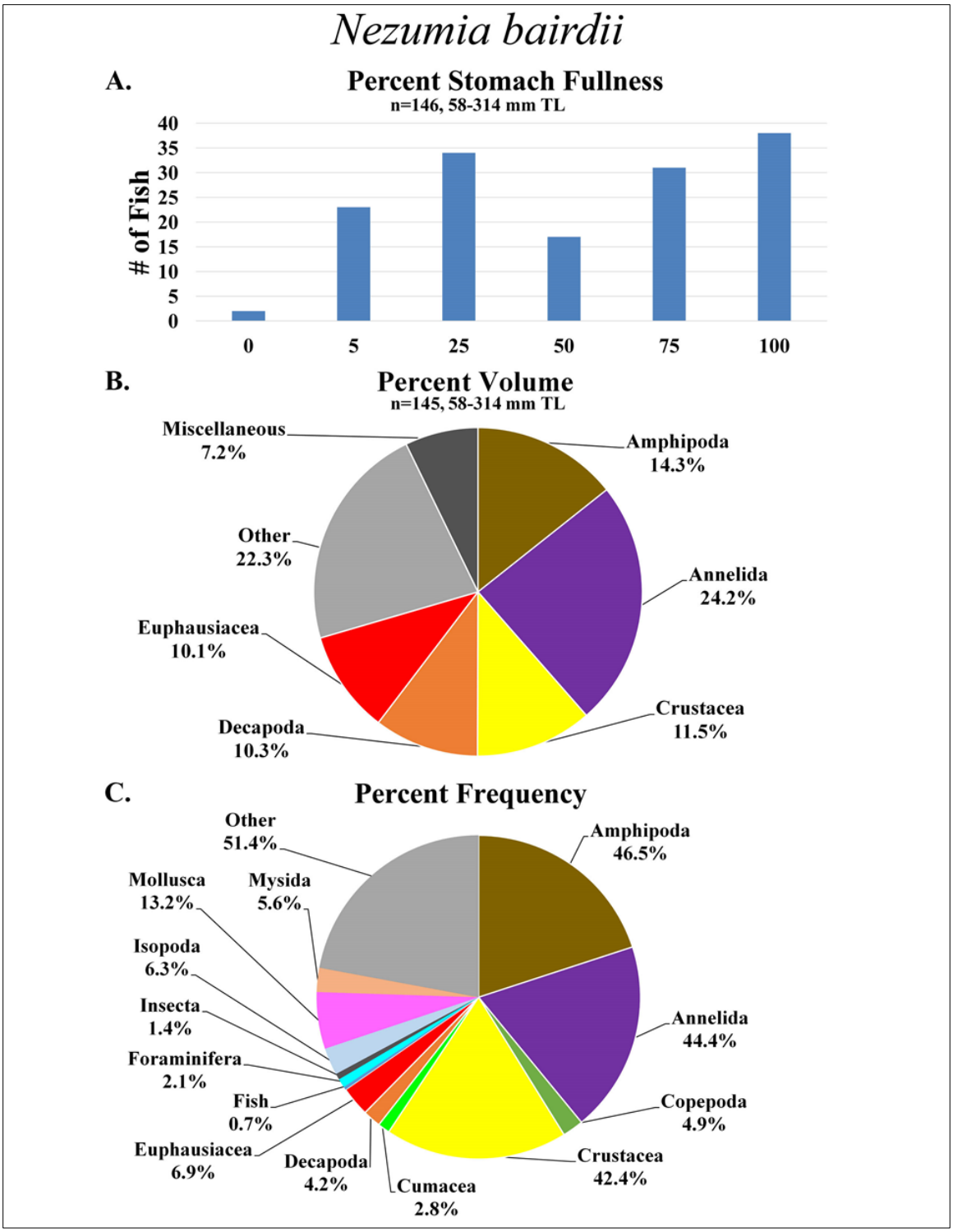

Figure 15-13. A) Percent stomach fullness for *Nezumia bairdii* collected from in and around Baltimore and Norfolk canyons. *n* = number of stomachs analyzed. B) Percent volume of food categories for *N. bairdii* stomachs that contained food. *n* = number of stomachs containing food, size range given for individuals containing food. Miscellaneous includes Mysida (3.1%), Mollusca (1.9%), Isopoda (0.7%), Insecta (0.6%), Copepoda (0.3%), Cumacea (0.3%), Fish (0.2), and Foraminifera (0.1%). C) Percent frequency of each food category present in an individual stomach.

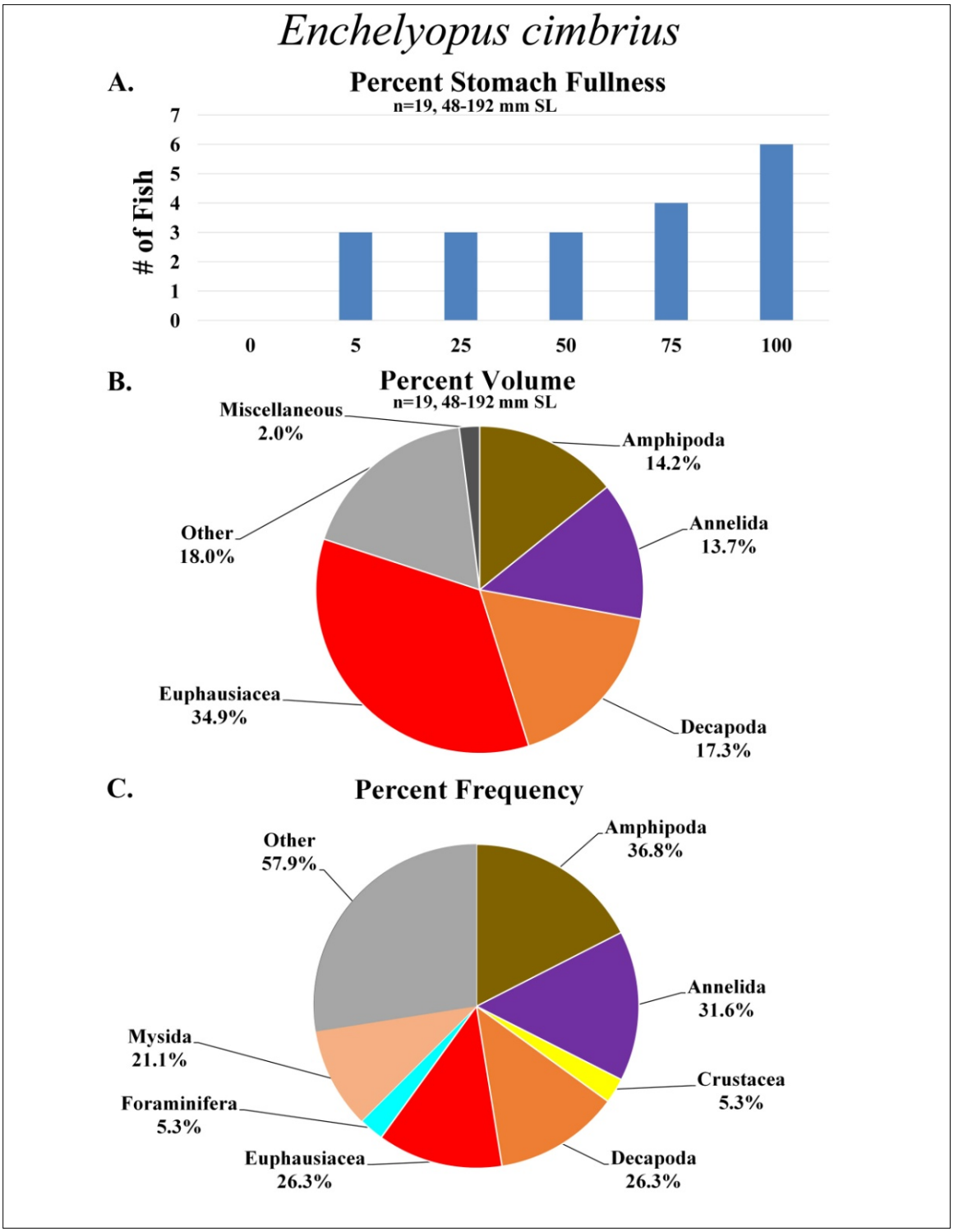

Figure 15-14. A) Percent stomach fullness for *Enchelyopus cimbrius* collected from in and around Baltimore and Norfolk canyons. *n* = number of stomachs analyzed. B) Perc*ent volume of food categories for E. cimbrius* stomachs that contained food. *n* = number of stomachs containing food, size range given for individuals containing food. Miscellaneous includes Mysida (1.7%), Crustacea (0.2%), and Foraminifera (0.1%). C) Percent frequency of each food category present in an individual stomach.

Phycis chesteri

Stomachs were dissected from 52 individuals (**Table 15-6**), 40−350 mm SL, collected by otter trawl from 13 different stations. Forty-five stomachs contained food, and the mean percent fullness of all analyzed stomachs was 48.5% (**Figure 15-15A**). A single item, *Helicolenus dactylopterus*, was identified to species. A total of seven food categories were represented, and Crustacea (38.9%) and Decapoda (16.8%) were the dominant categories by volume (**Figure 15-15B**). Unidentified crustacean parts and organic material were the dominant food items consumed, contributing 37.0% and 15.5%, respectively, to the overall volume. Other (42.2%) and Crustacea (33.3%) were the most frequently found categories (**Figure 15-15C**). Other than organic material (40.0%), unidentified crustacean parts, unidentified polychaete remains, and unidentified amphipods were the most frequently found food items (31.1%, 17.8%, and 11.1%, respectively).

Some specimens contained parasites (nematodes) within the body cavity.

Urophycis regia

Stomachs were dissected from 70 individuals (**Table 15-6**), 34−280 mm SL, collected by otter trawl from 10 different stations. Sixty-nine stomachs contained food items, and the mean percent fullness of all analyzed stomachs was 45.4% (**Figure 15-16A**). Several decapods (*Cancer irroratus, Euprognatha rastellifera, Munida iris, M. valida, Nematocarcinus cursor, and Sergestes arcticus*), euphausiids (*Tessarabrachion oculatum*), and fishes (*Glyptocephalus cynoglossus and Helicolenus dactylopterus*) were identified to species. Nine food categories were represented, and Mollusca, Fish, and Decapoda were the dominant food categories by volume (36.3%, 19.3%, and 14.6%, respectively) (**Figure 15-16B**). Unidentified cephalopods, *H. dactylopterus*, and *Euphausia* sp. were the dominant food items consumed, contributing 36.3%, 16.6%, and 11.7%, respectively, to the overall volume. Other, Amphipoda, and Decapoda were the most frequently found categories (62.3%, 46.4, and 36.2%, respectively) (**Figure 15-16C**). The most frequently ingested items were organic material, inorganic material, and ampeliscid amphipods (30.4%, 26.1%, and 26.1%, respectively). All Amphipoda prey were consumed by fish between 138 and 194 mm SL, and Decapoda and Euphausiacea were consumed by fish between 155 and 280 mm SL. All Fish and Mollusca prey items were found in stomachs of fish 155−280 mm SL, and only three of these were >250 mm.

Some stomachs of this species were abnormally thick and toughened whereas other stomachs contained holes. Nematodes were common in the body cavity of *U. regia*.

Merluccius albidus

Stomachs were dissected from 15 individuals (**Table 15-6**), 175−380 mm SL, collected by otter trawl and ROV from eight different stations. Nine stomachs contained food items, and the mean percent fullness of all analyzed stomachs was 36.7% (**Figure 15-17A**). One echinoderm, Ophioroidae, was identified to family, and the remaining food items were identified only to five different categories. Crustacea was the dominant food category by volume (64.6%) (**Figure 15-17B**), and the dominant food item contributing to the overall volume was unidentified crustacean parts (58.5%). Crustacea was also the most frequently found category (**Figure 15-17C**) and unidentified crustacean parts the most frequently ingested food items (88.9%).

Internal parasites were present, but were rare for *M. albidus*.

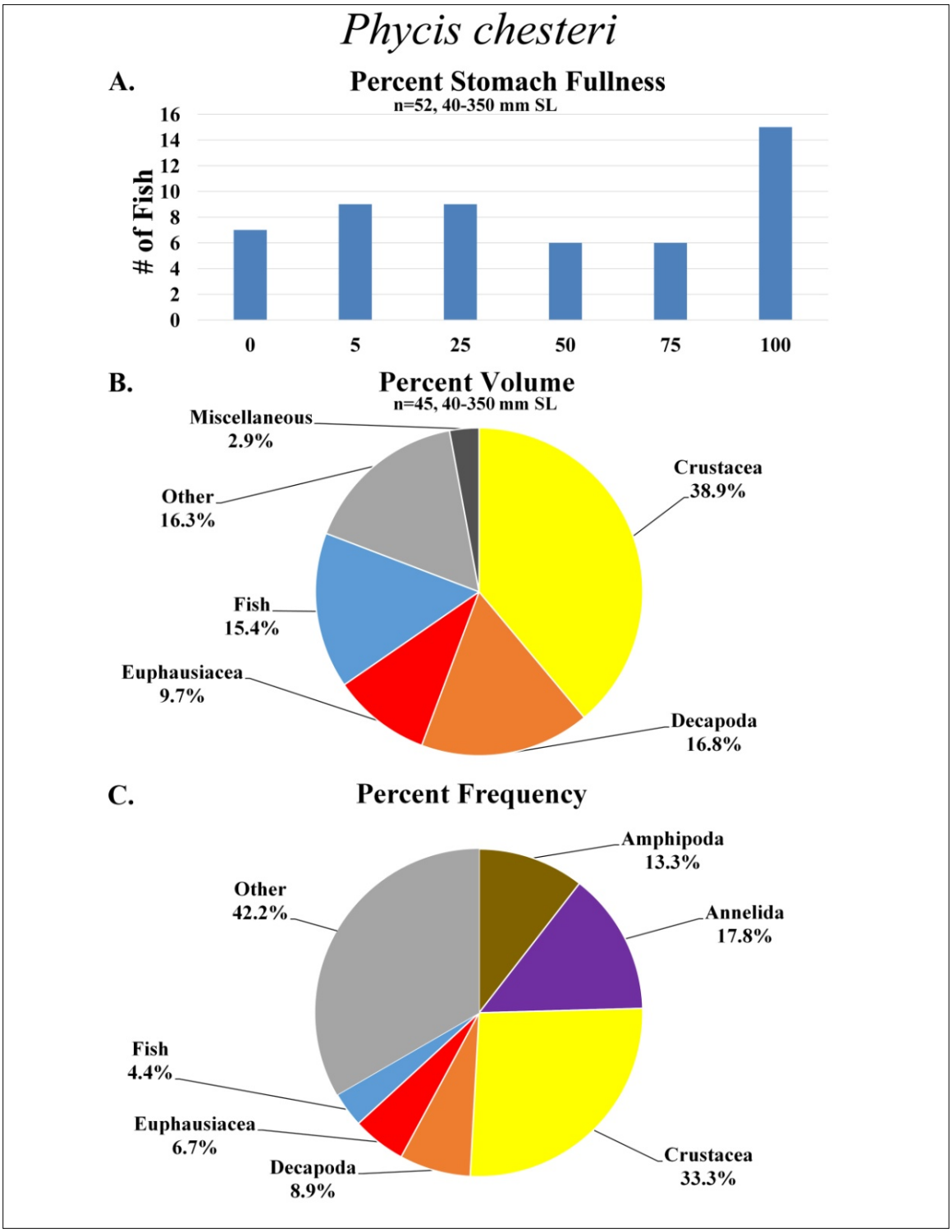

Figure 15-15. A) Percent stomach fullness for *Phycis chesteri* collected from in and around Baltimore and Norfolk canyons. *n* = number of stomachs analyzed. B) Percent volume of food categories for *P. chesteri* stomachs that contained food. *n* = number of stomachs containing food, size range given for individuals containing food. Miscellaneous includes Annelida (2.3%) and Amphipoda (0.6%). C) Percent frequency of each food category present in an individual stomach.

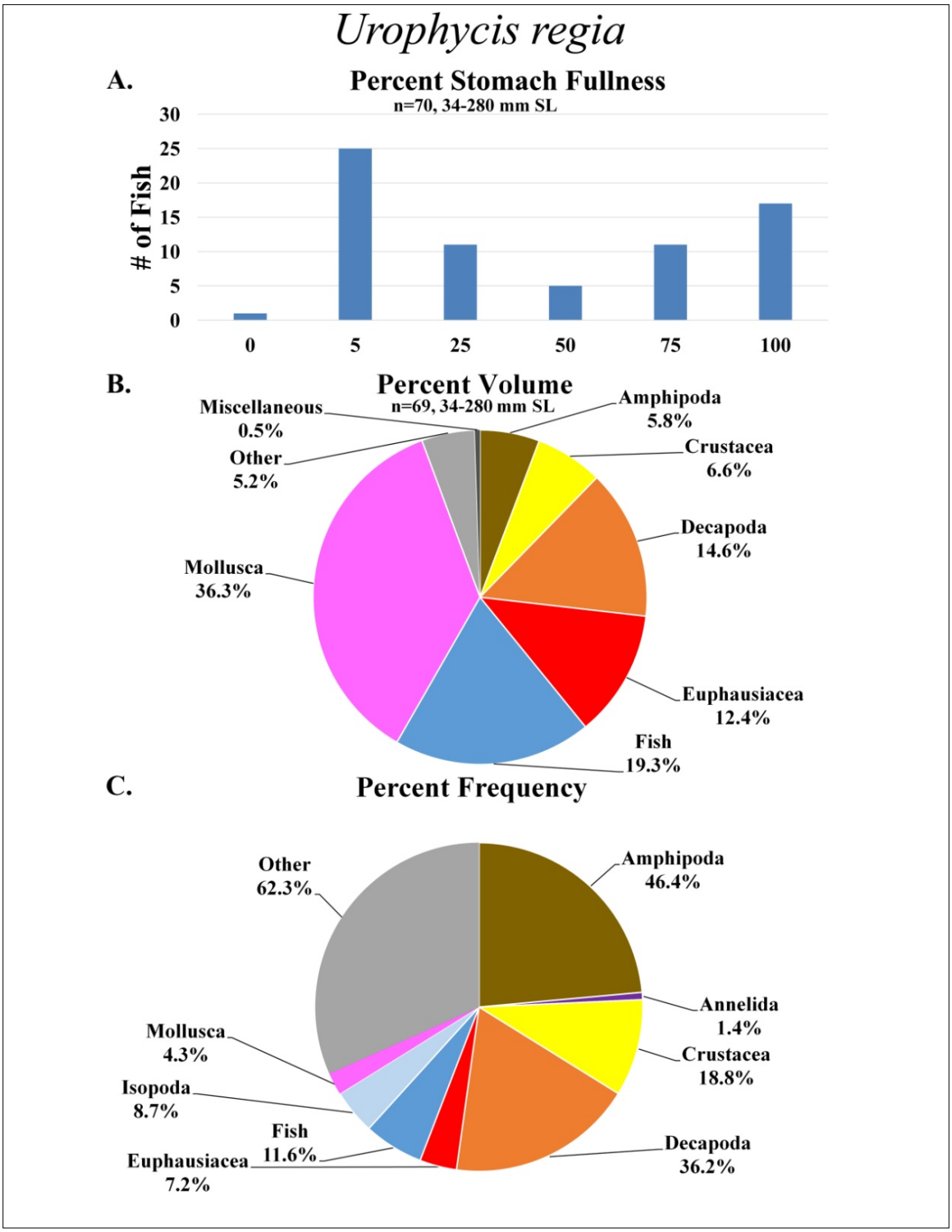

Figure 15-16. A) Percent stomach fullness for *Urophycis regia* collected from in and around Baltimore and Norfolk canyons. *n* = number of stomachs analyzed. B) Percent volume of food categories for *U. regia* stomachs that contained food. *n* = number of stomachs containing food, size range given for individuals containing food. Miscellaneous includes Isopoda (0.4%) and Annelida (<0.1%). C) Percent frequency of each food category present in an individual stomach.

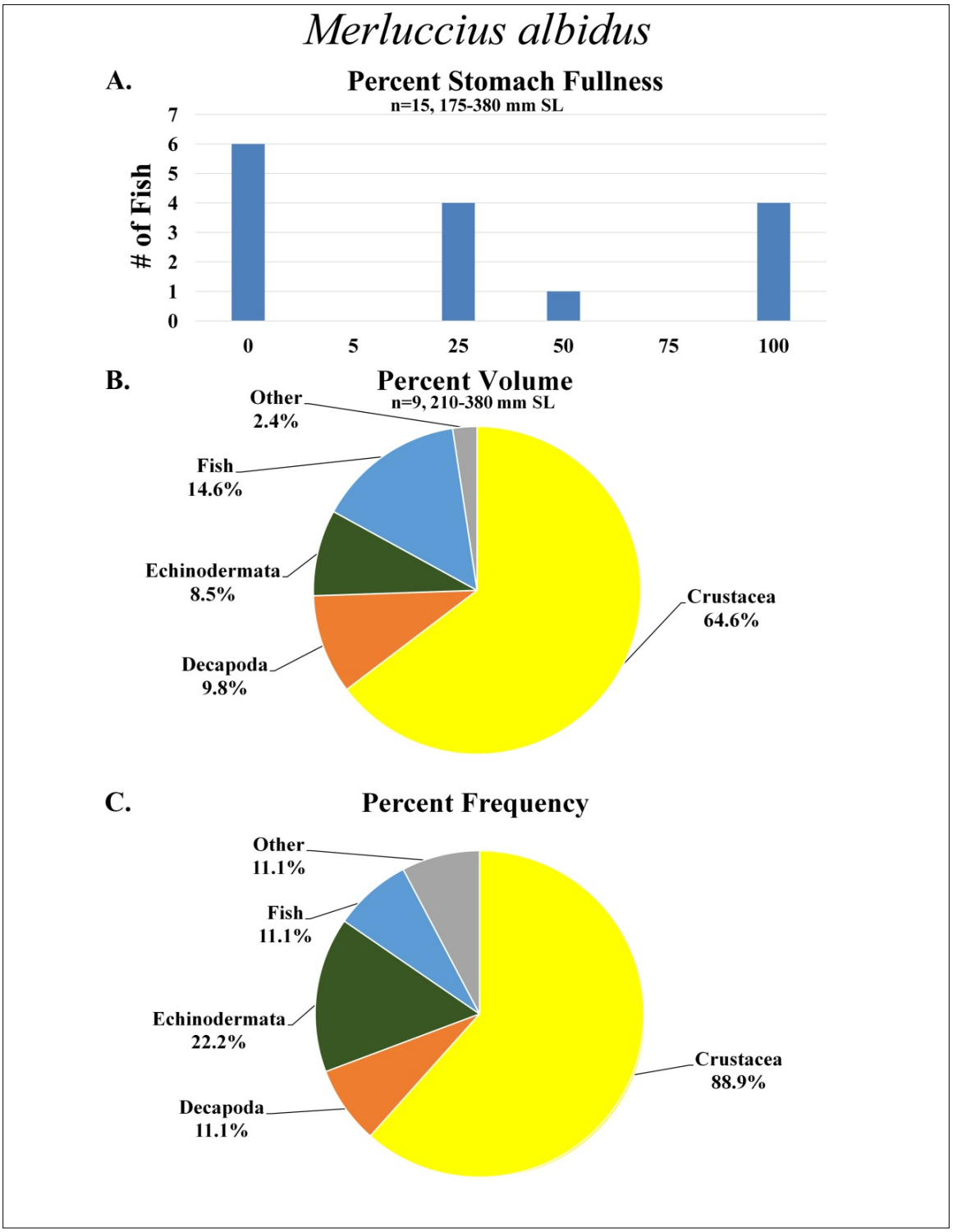

Figure 15-17. A) Percent stomach fullness for *Merluccius albidus* collected from in and around Baltimore and Norfolk canyons. *n* = number of stomachs analyzed. B) Percent volume of food categories for *M. albidus* stomachs that contained food. *n* = number of stomachs containing food, size range given for individuals containing food. C) Percent frequency of each food category present in an individual stomach.

Benthocometes robustus

Stomachs were dissected from 17 individuals (**Table 15-6**), 57−108 mm SL, collected by ROV from eight different stations. Ten fish stomachs contained food and seven were empty. The mean percent fullness of all analyzed stomachs was 22.9% (**Figure 15-18A**). One food item, *Nematobrachion sexspinosum*, was identified to species and one item, Euphausiidae, was identified to family. Six food categories were represented, and Euphausiacea, Crustacea, and Copepoda were the dominant food categories by volume (52.6%, 27.1%, and 14.3%, respectively) (**Figure 15-18B**). *Nematobrachion sexspinosum*, unidentified crustacean parts, and Euphausidae were the dominant food items consumed, contributing 32.1%, 27.1%, and 20.5%, respectively, to the overall volume. Crustacea, Copepoda, and Other were the most frequently consumed categories (80.0%, 60.0%, and 20.0%, respectively) (**Figure 15-18C**). The most frequently ingested items were unidentified crustacean parts (80%) and calanoid copepods (60%).

A few nematodes were found within the body cavities of *B. robustus*.

Lophius americanus

Stomachs were dissected from 19 individuals (**Table 15-6**), 95−438 mm SL, collected by otter trawl and ROV from nine different different stations. Nine fish stomachs contained food and 10 were empty. The mean percent fullness of all analyzed stomachs was 20.8% (**Figure 15-19A**). Three food items (*Dichelopandalus leptocerus*, *Sergestes arcticus*, and *Stylopandalus richardi*) were identified to species and one genus was identified (*Urophycis* sp.). Four food categories were represented, and Fish was the dominant food category by volume (89.0%) (**Figure 15-19B**). *Urophycis* sp. and unidentified fish remains were the dominant food items consumed, contributing 89.0% combined to the overall volume. Fish, Mollusca, and Other were the most frequently found categories (33.3%, 33.3%, 33.3%, respectively) (**Figure 15-19C**). The most frequently consumed food items were inorganic material (33.3%) and unidentified cephalopods (33.3%).

Nematodes were frequently found within the body cavity and intestines of these specimens. When stomachs were full of food, they were very full, as the stomachs stretched and expanded to fit prey items that were very large compared with the body size of the specimen.

Helicolenus dactylopterus

Stomachs were dissected from 265 individuals (**Table 15-6**), 24−250 mm SL, collected by otter trawl from 18 different stations. A total of 199 stomachs contained food items, and the mean percent fullness of all analyzed stomachs was 36.6% (**Figure 15-20A**). Several decapods (*Cancer irroratus, Munida iris, and M. valida*), euphausiids (*Meganyctiphanes norvegica, Nematobrachion boopis, Nematoscelis megalops,* and *Thysanopoda pectinata)*, and fish (*Helicolenus dactylopterus*) were identified to species. Thirteen food categories were represented, and Fish and Euphausiacea were the dominant food categories by volume (38.6% and 24.5%, respectively) (**Figure 15-20B**). Unidentified fish remains was the dominant food item consumed, contributing 31.4% to the overall volume. Other and Crustacea were the most frequently found categories (37.6% and 36.2%, respectively) (**Figure 15-20C**), whereas the most frequently ingested items were organic material and unidentified crustacean parts (27.6% and 36.2%, respectively).

An ectoparasite was recorded in one of the jars containing several specimens. Internal parasites (nematodes) were present in many specimens of this species. On occasion, stomachs were inflated but empty. Intestines were often observed to contain red colored digested material. Several specimens contained digested material inside the mouth.

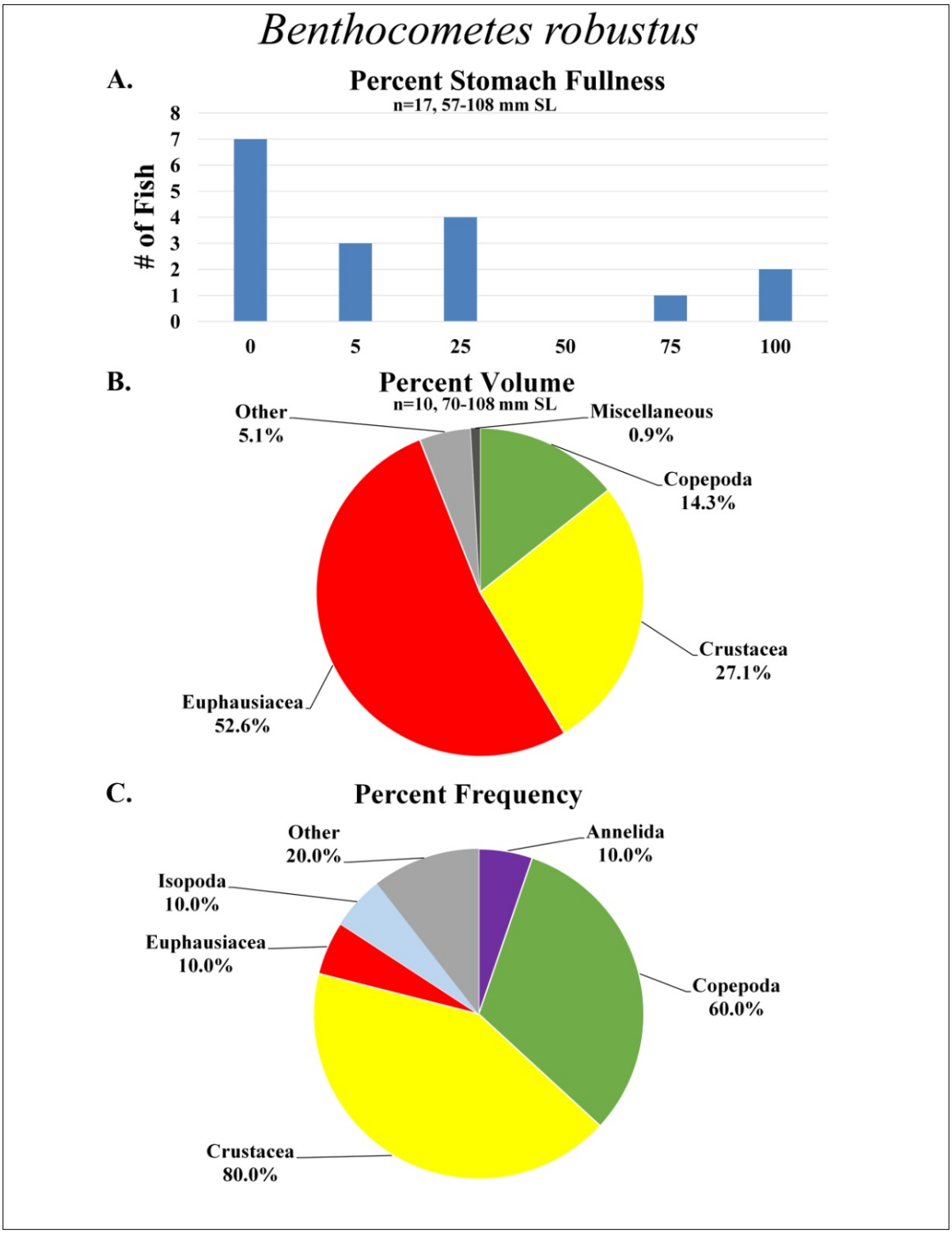

Figure 15-18. A) Percent stomach fullness for *Benthocometes robustus* collected from in and around Baltimore and Norfolk canyons. *n* = number of stomachs analyzed. B) Percent volume of food categories for *B. robustus* stomachs that contained food. *n* = number of stomachs containing food, size range given for individuals containing food. Miscellaneous includes Isopoda (0.9%). C) Percent frequency of each food category present in an individual stomach.

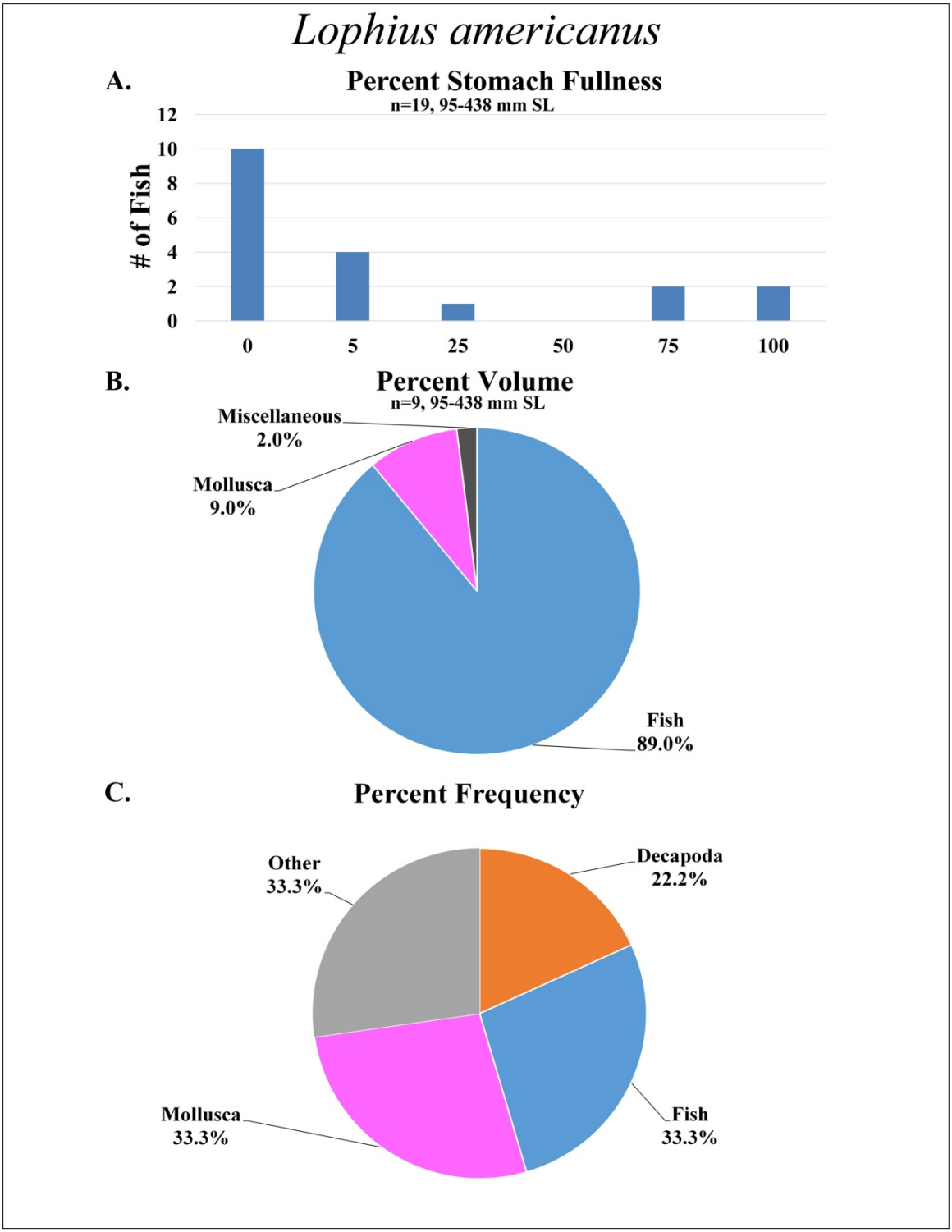

Figure 15-19. A) Percent stomach fullness for *Lophius americanus* collected from in and around Baltimore and Norfolk canyons. *n* = number of stomachs analyzed. B) Percent volume of food categories for *L. americanus* stomachs that contained food. *n* = number of stomachs containing food, size range given for individuals containing food. Miscellaneous includes Decapoda (1.8%) and Other (0.2%). C) Percent frequency of each food category present in an individual stomach.

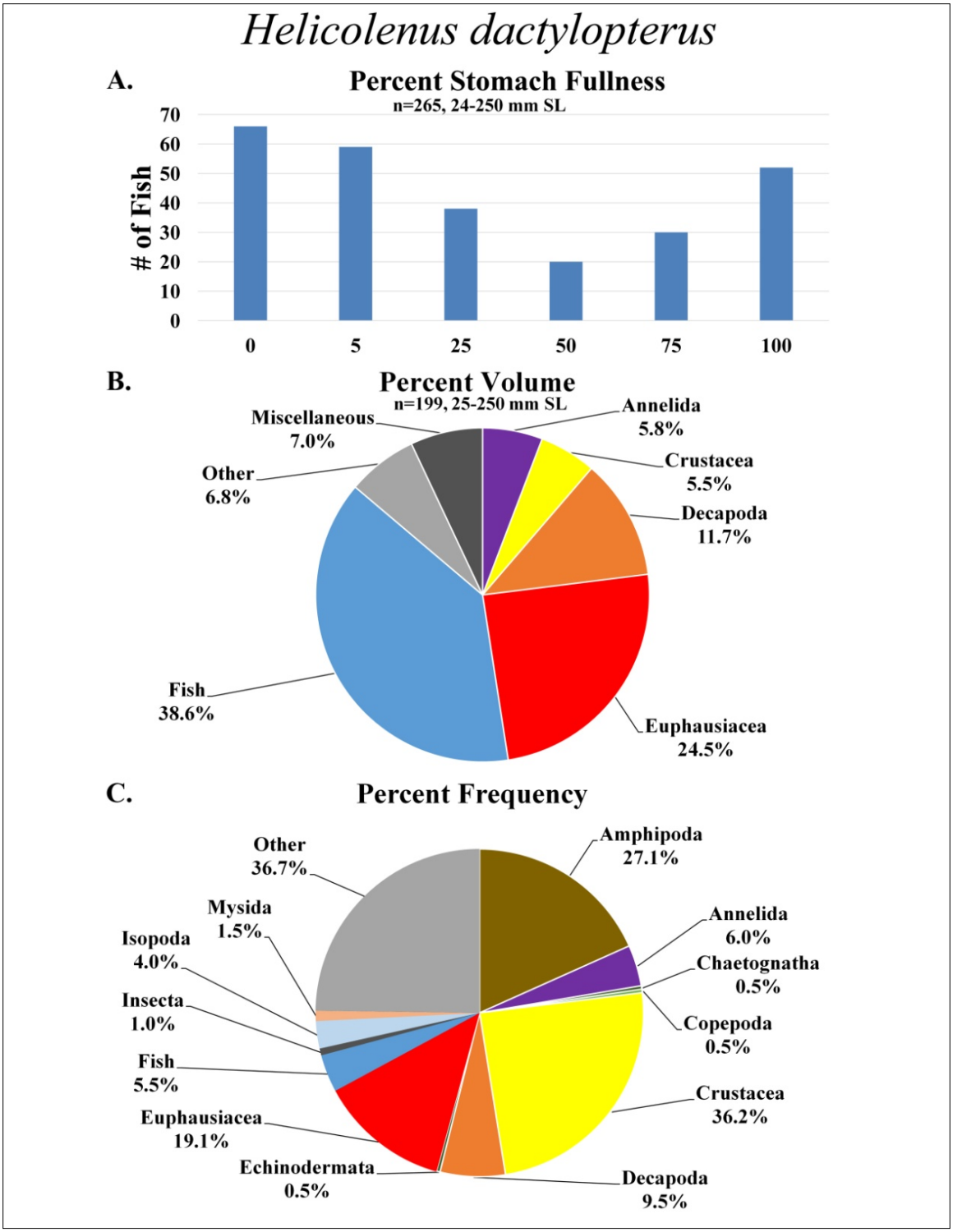

Figure 15-20. A) Percent stomach fullness for *Helicolenus dactylopterus* collected from in and around Baltimore and Norfolk canyons. *n* = number of stomachs analyzed. B) Percent volume of food categories for *H. dactylopterus* stomachs that contained food. *n* = number of stomachs containing food, size range given for individuals containing food. Miscellaneous includes Amphipoda (4.7%), Insecta (1.4%), Isopoda (0.4%), Echinodermata (0.2%), Chaetognatha (0.1%), Mysida (0.1%), and Copepoda (<0.1%). C) Percent frequency of each food category present in an individual stomach.

Lycenchelys verrillii

Stomachs were dissected from 88 individuals (**Table 15-6**), 62−160 mm SL, collected by otter trawl from 11 different stations. Seventy-five stomachs contained food items, and the mean percent fullness of all analyzed stomachs was 28.3% (**Figure 15-21A**). Two items, *Quinqueloculina laevigata* and *Retusa obtusa*, were identified to species. Seven food categories were represented, and Mollusca and Annelida were the dominant food categories by volume (37.3% and 24.0%, respectively) (**Figure 15-21B**). Unidentified bivalve, unidentified polychaete remains, and organic material were the dominant food items consumed (22.5%, 20.2%, and 17.8%, respectively). Other was the most frequently found category (56.0%) (**Figure 15-14C**). The most frequently ingested items were organic material and unidentified polychaete remains (44.4% and 27.6%, respectively).

Nematodes were sometimes found within body cavities. Digested material was sometimes found in the mouths of the specimens, possibly due to regurgitation.

Citharichthys arctifrons

Stomachs were dissected from 187 individuals (**Table 15-6**), 27−126 mm SL, collected by otter trawl and ROV from 14 different stations. One hundred five stomachs contained food items, and the mean percent fullness of all analyzed stomachs was 17.6% (**Figure 15-22A**). One item, Hyperidae, was identified to family. Eight food categories were represented, and Other and Crustacea were the dominant food categories by volume (30.0% and 28.0%, respectively) (**Figure 15-22B**). Unidentified crustacean parts, organic material, and inorganic material were the dominant food items consumed (28.0%, 19.3%, and 10.7%, respectively). Other and Crustacea were the most frequently found categories (56.2% and 50.5%, respectively) (**Figure 15-22C**), and the most frequently ingested items were unidentified crustacean parts (50.5%).

Three specimens appeared to have been bitten and were missing stomachs and intestines as a result. Two other specimens were bitten, but the stomachs and intestines remained intact.

Glyptocephalus cynoglossus

Stomachs were dissected from 113 individuals (**Table 15-6**), 74−295 mm SL, collected by otter trawl from 17 different stations. Every stomach contained food items, and the mean percent fullness of all analyzed stomachs was 40.2% (**Figure 15-23A**). One food item, *Lumbrineris fragilis*, was identified to species. Three other items (*Lumbrineris* sp., *Marphysa* sp., and *Thysanopoda* sp.) were identified to genus. Fifteen food categories were represented, and Annelida and Other were the dominant food categories by volume (46.7% and 30.3%, respectively) (**Figure 15-23B**). Organic material, *Marphysa* sp., unidentified polychaete remains, and unidentified bivalves were the dominant food items consumed (22.2%, 12.5%, 11.0%, and 9.7%, respectively). Annelida and Other were the most frequently found categories (83.2% and 82.3%, respectively) (**Figure 15-23C**). The most frequently ingested items were organic material and unidentified polychaete remains (71.7% and 56.6%, respectively).

Internal nematodes were recorded for this species. Sediment was frequently recorded within stomachs.

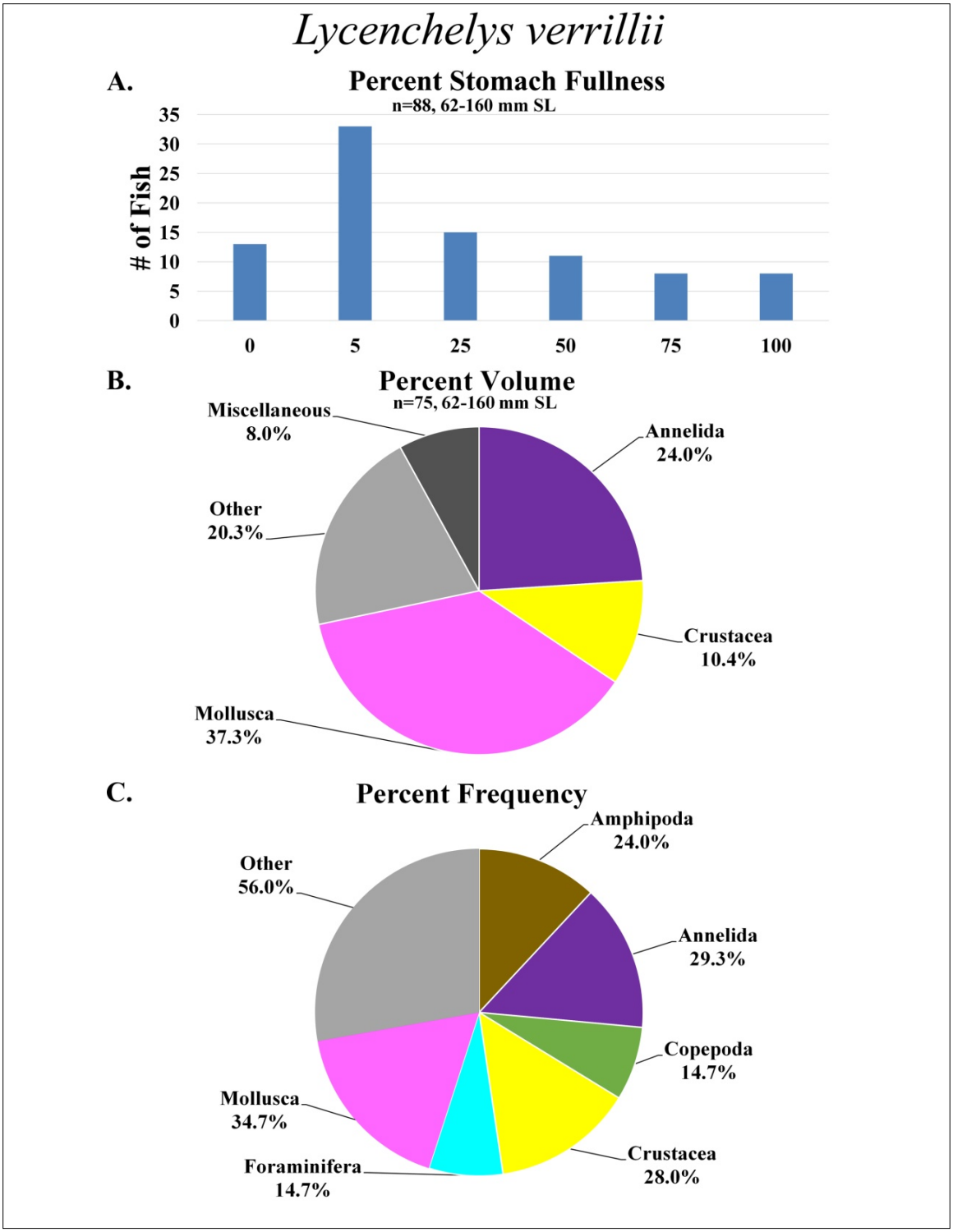

Figure 15-21. A) Percent stomach fullness for *Lycenchelys verrillii* collected from in and around Baltimore and Norfolk canyons. *n* = number of stomachs analyzed. B) Percent volume of food categories for *L. verillii* stomachs that contained food. *n* = number of stomachs containing food, size range given for individuals containing food. Miscellaneous includes Amphipoda (3.2%), Foraminifera (2.8%), and Copepoda (2.0%). C) Percent frequency of each food category present in an individual stomach.

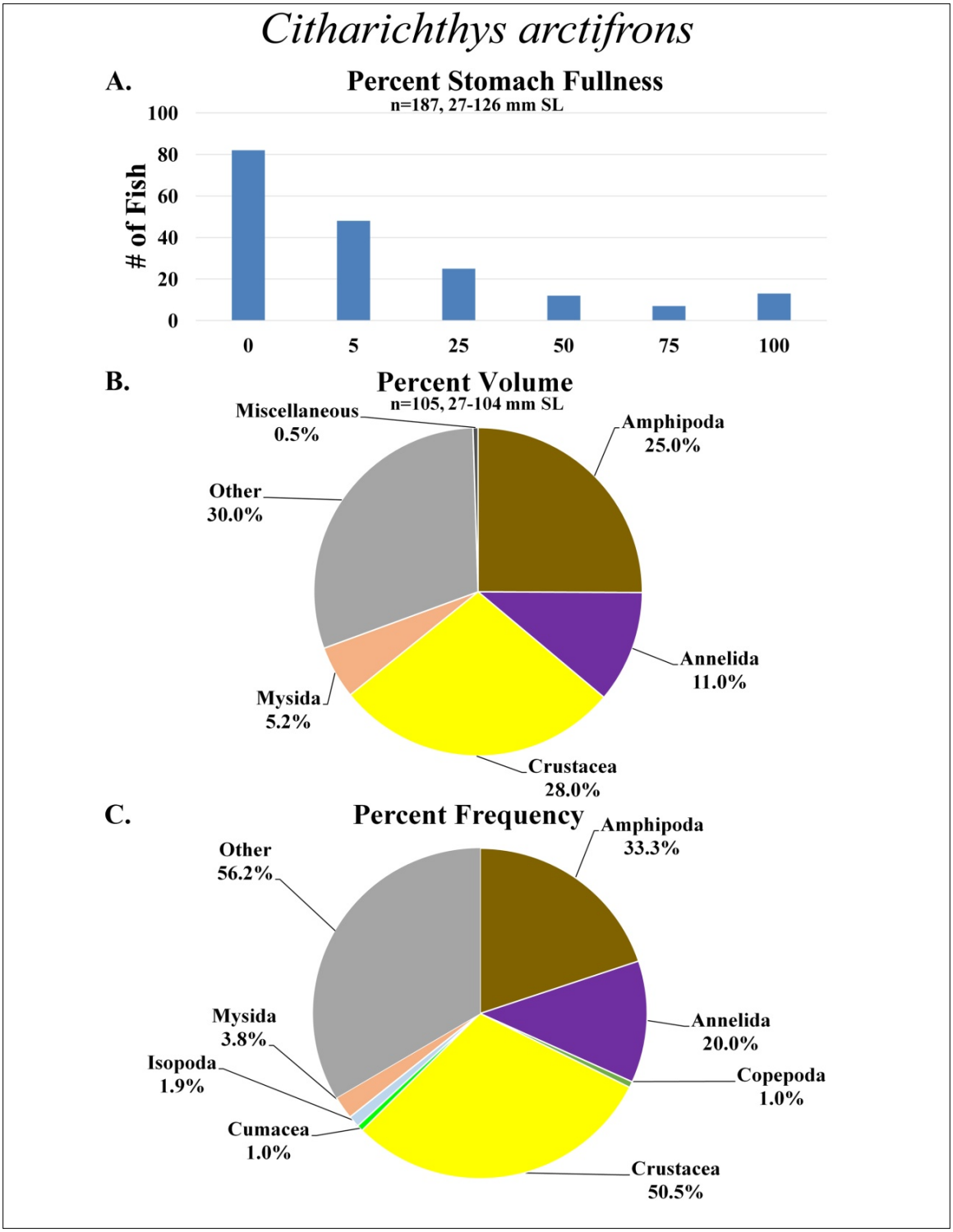

Figure 15-22. A) Percent stomach fullness for *Citharichthys arctifrons* collected from in and around Baltimore and Norfolk canyons. *n* = number of stomachs analyzed. B) Percent volume of food categories for *C. arctifrons* stomachs that contained food. *n* = number of stomachs containing food, size range given for individuals containing food. Miscellaneous includes Cumacea (0.2%), Isopoda (0.2%), and Copepoda (0.1%). C) Percent frequency of each food category present in an individual stomach.

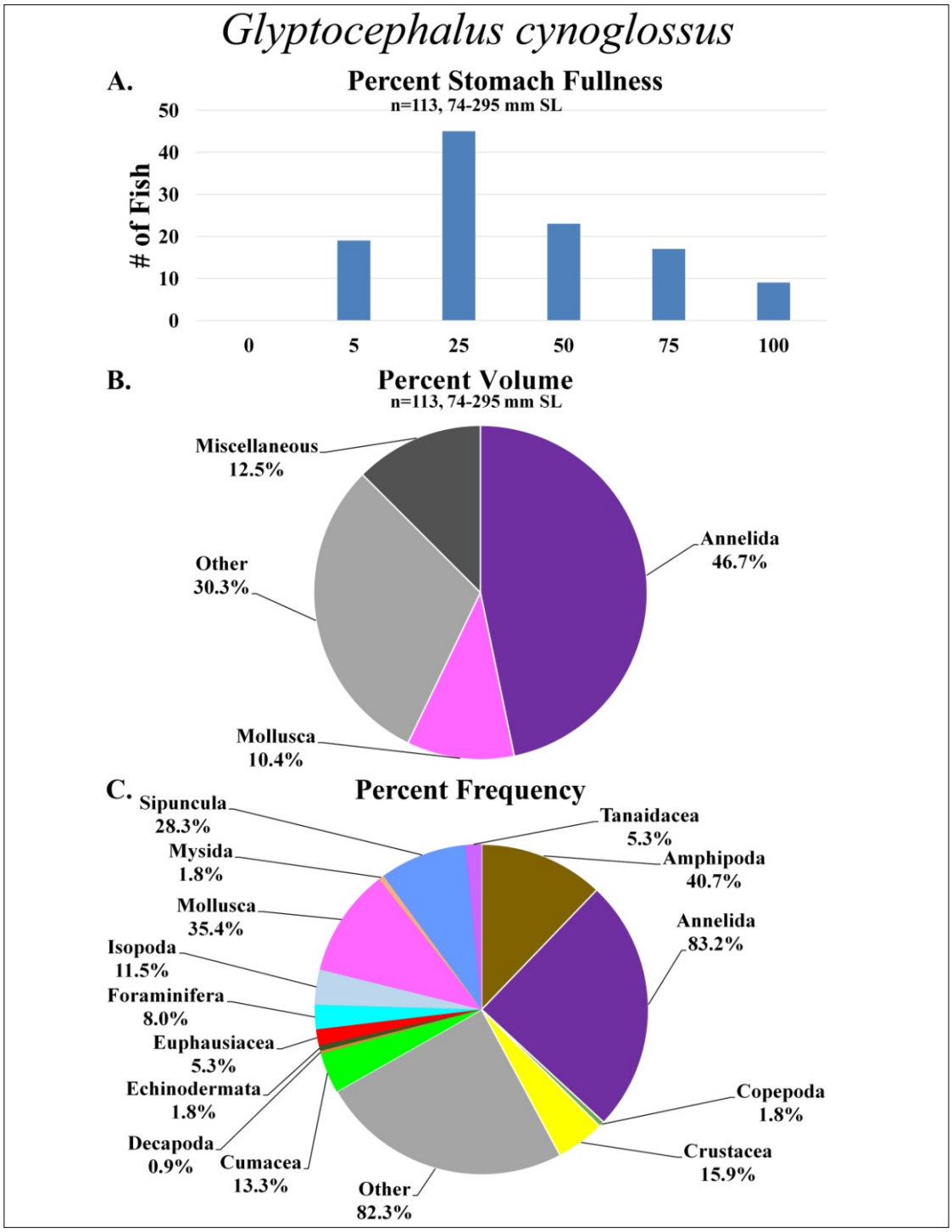

Figure 15-23. A) Percent stomach fullness for *Glyptocephalus cynoglossus* collected from in and around Baltimore and Norfolk canyons. *n* = number of stomachs analyzed. B) Percent volume of food categories for *G. cynoglossus* stomachs that contained food. *n* = number of stomachs containing food, size range given for individuals containing food. Miscellaneous includes Euphausiacea (4.4%), Amphipoda (3.0%), Crustacea (2.3%), Sipuncula (1.0%), Echinodermata (0.5%), Isopoda (0.4%), Cumacea (0.3%), Mysida (0.2%), Decapoda (0.1%), Foraminifera (0.1%), Tanaidacea (0.1%), and Copepoda (<0.1%). C) Percent frequency of each food category present in an individual stomach.

15.2.4 Discussion

Trophodynamic studies are crucial to understanding the health of the ocean's food webs and stability of marine ecosystems while also providing vital information for managing marine resources. To date, the most comprehensive trophic study in the mid-Atlantic region was conducted by Bowman et al. (2000) who used GCA to document the prey consumed by 178 fish species inhabiting the continental shelf of the northeastern United States. Smaller fishes (≤20 cm long) fed primarily on some combination of copepods, amphipods, mysids, polychaetes, chaetognaths, and small decopod shrimp, and larger fishes (>20 cm long) fed mostly on fishes, squid, decapod shrimp, and crabs (Bowman et al. 2000). Smith and Link (2010) analyzed the diets of 50 finfish inhabiting the northeast U.S. continental shelf ecosystem and reported that most fishes were generalist feeders with broad ranges of stomach contents. An ontogenetic shift was observed as larger fishes exhibited an increase in fish prey consumed (Smith and Link 2010). Another sizable study performed by Crabtree et al. (1991) compared the diets of 32 species of deepsea fishes from the western North Atlantic and the Bahamas. Overall, the fishes of the western North Atlantic were described as being more active foragers (Crabtree et al. 1991).

The current research on the feeding habits of the dominant species found in and around Baltimore and Norfolk canyons has added information to help understand the overall trophodynamics among these fish species and within these deepsea environments. Areas within and around Norfolk and Baltimore canyons appeared to have abundant food resources for bottom fishes. During most ROV dives, dense swarms of euphausiids and amphipods were observed in the sediments and near bottoms of the canyons (Ross et al. 2015a). More than half (52.5%) of the food volume consumed by all species combined was from the subphylum Crustacea, and of that euphausiids (15.2%) and amphipods (5.7%) were significant in several species. Also observed during ROV dives were *Synaphobranchus* sp. eating unidentified shrimps (dive NF-687) (Ross et al. 2015a). Decapoda, our catagory containing shrimp, made up 12.5% of the total overall volume found in our GCA. The following section discusses previously documented food habits by species (in phylogenetic order) and how they compared to this study's results.

15.2.4.1 Species Diets

Dysommina rugosa

Little is known of the biology of this eel species. Synaphobranchids in general are benthic eels often considered scavengers. *Dysommina rugosa* prefer complex habitats, like deep reefs (Ross and Quattrini 2007) and vents and seeps (Staudigel et al. 2006). Gut analysis from a Pacific vent site (Staudigel et al. 2006) shows that *D. rugosa* use these rugged areas as a habitat only, and the feeding that occurs is not on primary production (such as bacterial mats) but instead mostly on crustaceans. In the vicinity of hydrothermal vents, cutthroat eels have been documented feeding on shrimps and other invertebrates (Desbruyères et al. 2006).

Consistent with other studies (e.g., Ross et al. 2015a, 2015b), *D. rugosa* was often observed on the rugged deep reef habitats in both canyons and on the shallow seep. Collecting from these types of areas is challenging so all specimens were collected by ROV, limiting sample size. A common food item of *D. rugosa*, *Sergestes arcticus,* is an abundant constituent in the North Atlantic (Vestheim and Kaartvedt 2009) and is an extensive vertical migrator (Flock and Hopkins 1992). The rugged terrain is most likely a place for these decapods to take advantage of cover when not hunting for prey. Other prey consumed by *D. rugosa,* such as euphausiids, also make daily vertical migrations. The abundance of these types of items present in GCA suggests the eels in these canyons rely more on predation than a scavenging lifestyle. They also are an important link in the transfer of energy from shallow to deep sea.

Synaphobranchus kaupii

Described as a "large scavenging animal," *Synaphobranchus kaupii* may be one of the most active benthopelagic deepwater fishes (Bailey et al. 2005). Trenkel and Lorance (2011) noted that about half of the fish observed drift with the current, while the other half actively forage. With average swimming speeds of 0.15 m s^{-1}, this olfactory scavenger first detects carrion on the seafloor, and then must often swim, sometimes against a current, to the food source (Bailey et al. 2005).

The large number of stomachs found with little to no food may be a result of this fish's high metabolic activity (Bailey et al. 2005). The low mean fullness could also be a result of partial regurgitation of stomach contents when these fishes were brought to the surface. The most frequent item found in the stomachs was Other, more specifically organic material (34.5%). This could be a result of an increased metabolic system or the result of consuming decaying carrion. This may be why, despite a varied diet (we identified seven prey categories), all prey items were only partially recognizable.

Coelorinchus caelorhincus

With a large rostrum and an inferior positioned mouth, rattails are morphologically best suited for benthic feeding and scavenging. Macrourids are often attracted to baited camera arrays (Wilson and Smith 1984, Armstrong et al. 1992), indicating a tendency to scavenge for prey. The high occurrence of unidentified organic material (66.7%) in this study may be a result of *Coelorinchus caelorhincus* scavenging dead and decaying material off the bottom. Unidentifiable polycheate remains were also frequently ingested (53.7%) suggesting benthic feeding and possibly scavenging as items were too digested to identify.

Overall, most prey items were benthic organisms (copepods, amphipods, polychaetes, isopods, and mysids). However, a high volume (36.4%) of euphausiids found in the stomachs of larger *C. caelorhincus* is a bit unusual, and may indicate feeding movements off the bottom. Based on pelagic prey found in macrourid stomachs, Pearcy and Ambler (1974) suggested that in addition to scavenging, vertical migrations off bottom also occur. Based on the observations of dense euphausiid swarms observed in sediments and near bottoms of the canyons by Ross et al. (2015a) it seems more likely that these prey items were consumed through benthic feeding. The consumption by benthic predators of prey items that make large diel vertical migrations serves as an important link in the transfer of nutrients from food rich surface layers to food poor bottom layers.

Nezumia bairdii

Rattails have been reported to be predominantly benthic foragers feeding on infaunal and epifaunal polychaetes and epifaunal crustaceans, or mesopelagic foragers cosuming copepods and other crustaceans (Stevens and Dunn 2011). *Nezumia bairdii* feed as much on pelagic prey as they do benthic prey (Stevens and Dunn 2011). *N. bairdii* fed most frequently on crustaceans, such as hyperiid amphipods, euphausiids, and mysids, off the Flemish Cap (Rodríguez-Marín et al. 1994). In a study of 699 stomachs (Román et al. 2004), 87.3% contained food and 81.2% of the volume was crustaceans. Small bivalves, bottom shrimp, and polychaetes also played a minor role in diet composition (Rodríguez-Marín et al. 1994). Smaller *N. bairdii* fed primarilly on crustaceans, specifically gammaridean amphipods, copepods, and polychaetes, while larger *N. bairdii* consumed more decapods (Crabtree et al. 1991). Crabtree et al. (1991) found that *N. bairdii* consumed more decapods and teleosts with increasing size while also continuing to consume a variety of smaller benthic prey.

In our study, *N. bairdii* stomachs contained 14 different food categories, the second largest amount of all species examined. These fish exhibited a diverse diet, including polychaetes, amphipods, bivalves, gastropods, crustaceans, and even two insects, that was consistent with other studies, showing a high volume of benthic prey (Annelida 24.2%) as well as frequently occurring pelagic prey (e.g., copepods and mysids). Ontogenetic shifts in diet were less evident in our study. We saw amphipods and

polychaetes in a large portion of the stomachs regardless of size. However, decapods, found less frequently, were in the stomachs of only larger individuals (184−315 mm TL).

Enchelyopus cimbrius

Characterized as a grazer (Moyle and Cech 1988), *Enchelyopus cimbrius* has well-developed barbels with taste buds (Nagabhushanam 1965). Found primarily on the muddy substrate of the North Atlantic continental margin, this fish's diet consists of primarily polychaetes and shrimps (Langton and Bowman 1980) as well as bivalves, calanoid copepods, cumaceans, and decapods in the Gulf of Maine (Deree 1999).

As juveniles, this fish is less sedentary and feeds in the water column preferring planktonic prey (Moyle and Cech 1988), mostly planktonic copepods (Deree 1999). Smaller *E. cimbrius* (<70 mm SL) in our study fed primarily on gammaridean amphipods, mysids, and polychaetes. This appears to contradict other studies (Moyle and Cech 1988, Deree 1999); however, only three specimens in this size class were captured and analyzed. Older fish and adults are more sedentary and stay close to the substrate (Bigelow and Schroeder 1953). We found that in larger *E. cimbrus* the dominant categories by volume were Euphausiacea (34.9%) and Decapoda (17.3%). This is not surprising given the dense swarms of these prey types observed near the canyon bottoms (Ross et al. 2015a) and agrees with previous studies (Langton and Bowman 1980, Deree 1999), which suggested a diet relying on crustaceans.

In addition, unidentified organic material was present in almost half of the individuals studied (47.4%). Langton and Bowman (1980) describe polychaetes as a primary prey item for this species, but in our study, they comprised only 13.7% of the overall volume. It is possible the organic material present in the stomachs of individuals in this study was composed of heavily digested polychaetes or could have been material present in the polychaetes upon consumption. However, the high frequency of unidentified organic material is more likely a result of infaunal feeding behaviors of this species on benthic prey in muddy areas.

Phycis chesteri

Longfin hake feeding habits follow those of a typical benthopelagic predator and this fish was classified by Rodríguez-Marín (1995) as a low diversity feeder. Analysis of 347 stomachs from the northwest Atlantic found *Phycis chesteri* feeding almost exclusively on the decapod *Pandalus borealis* (Román et al. 2004). Rodríguez-Marín et al. (1994) reported a diet made up of copepods, amphipods, decapods, and mysids. Although several studies include the feeding habits of *P. chesteri*, comprehensive gut analysis of this species is sparse owing to the high regurgitation rate of specimens.

Of the 111 stomachs dissected, 59 (53.2%) were everted or missing. Although missing stomachs most likely decayed due to poor preservation, the everted stomachs were most likely due to the fish's closed gas bladder. In the stomachs containing food, 65.4% of the volume was made up of decapods and other crustaceans, agreeing with previous studies (Román et al. 2004, Rodríguez- Marín et al. 1994). The Other category (16.3%) was composed primarily of organic material, which could have been digested remains or benthic material consumed during predation. Two specimens (56 and 203 mm SL) had fish remains in their stomachs, the larger of which had an entire *Helicolenius dactylopterus*. The prey was slightly digested, ruling out the possibility of net feeding in the 30-minute tows. Juvenile *H. dactylopterus* often are pelagic, reinforcing the idea that while *P. chesteri* primarily feeds on benthic prey they do have a pelagic component to their diet.

Urophycis regia

Diet studies of *Urophycis regia* have shown that they consume pelagic invertebrates, such as euphausiids and other shrimps as well as fishes. Increasing amounts of pelagic fish prey are consumed with increasing *U. regia* size (Garrison and Link 2000). More specifically, spotted hake diets shift from

amphipods (at 10−100 mm sizes), to other crustaceans including amphipods, decapods, and euphausiids (≤250 mm), to primarily fish and squid (>250 mm) (Bowman and Michaels 1984). Langton and Bowman (1980) found that crustaceans (*Munida iris* and *M. valida*, amphipods, and *Cancer irroratus*) made up almost half (47.5%) the diet of their samples. They also found that fishes (gadids and flounder) formed a large portion (34.2%) of the spotted hake diet (Langton and Bowman 1980). Another prey item of significance was Mollusca, as squid and other unidentified cephalopoda made up 11.5% of the diets (Langton and Bowman 1980).

Consistent with the aforementioned studies, our results showed Mollusca (36.3%), Fish (19.3%), and Decapoda (14.6%) were the dominant food categories by volume. Three fish were found with Mollusca prey in their stomachs, two (164−174 mm SL) contained cephalopod tentacles and one (254 mm SL) contained an entire squid. This skewed the percent volume results, perhaps indicating that Mollusca played a more important role in the diets of these fish.

The crustaceans (*C. irroratus*, *Munida iris*, and *M. valida*) found in Langton and Bowman's (1980) study were all identified in our *U. regia* stomachs. We were not, however, able to discern the same ontogenetic shifts in diet. A larger sample size, containing additional larger individuals, would be needed for us to confirm this pattern.

Merluccius albidus

Garrison and Link (2000) found that *Merluccius albidus* preyed primarily on pelagic crustaceans and fishes. Juveniles in the Gulf of Mexico consumed mostly crustaceans whereas adults fed mostly on fishes and to a lesser extent shrimp and squid (Rohr and Gutherz 1977). Langton and Bowman (1980) showed that *M. albidus* relied heavily on fish prey, accounting for 93.4% of stomach contents, despite some relative difficulty identifying stomach contents (no fish could be identified further than family). Crustaceans made up a much smaller portion (5.5%) of the diets as did two pandalid shrimp and euphausiids (Langton and Bowman 1980).

Much like Langton and Bowman (1980), stomach contents in specimens from this study were difficult to identify, and only nine stomachs contained food. Although Fish was the second largest category by volume (14.6%), which corresponded to findings of other studys, remains were found in only one stomach. Crustacea was clearly the dominant food category by volume (64.6%) and frequency (88.9%). Although two items were identifiable as Malacostracian shrimp, the remaining items in this category were recognizable only as arthropods. Based on the level of prey identification, we could not determine if these crustaceans were pelagic.

Benthocometes robustus

Little is known of the feeding habits of *Benthocometes robustus*. The individuals from this study were collected by ROV and observed associated with the complex reef-like habitats within Baltimore and Norfolk canyons (Ross et al. 2015a). Ten stomachs contained food, and Euphausiacea, Crustacea, and Copepoda were the important food categories by volume (52.6%, 27.1%, and 14.3%, respectively). Only one stomach (from a 108 mm TL individual) contained euphausiid prey and comprised the entirety of the reported species volume. One of these prey items, *Nematobrachion sexspinosum*, has a broad distribution and has not been caught in large numbers (Brinton 1962). Only five have been caught in the North Atlantic in a known range of 28° to 29°N in the western Atlantic (Tattersall 1926, Leavitt 1938). Little is known about this prey item, but we do know they are vertical migrators.

Lophius americanus

Lophius americanus are opportunistic ambush predators whose diet consists mostly of a variety of fishes and squid (Armstrong et al. 1996, Bowman et al. 2000). *L. americanus* from off New Jersey fed mostly on fishes (*Urophycis chuss* and other unidentified teleost fishes) and on benthic invertebrates

like squid and red shrimp (Sedberry 1983). Cannibalism was observed, as smaller goosefish were an important prey item for larger individuals (Johnson et al. 2008, Armstrong et al. 1996). In a study of 699 *L. americanus* stomach contents in the MAB (Johnson et al. 2008), the four major taxonomic groups found were Cephalopda, Decapoda, Elasmobranchii, and Teleostei. Prey items by weight consisted primarily of fishes in the northern MAB and fishes and squid in the southern MAB. Although our sample size for this species is limited, five of the nine stomachs contained prey from the Fish and Mollusca categories. Two stomachs contained large physids, skewing the volumes to favor this prey item. Decapods were also found in two stomachs, which is consistent with Johnson et al. (2008).

A higher percentage of empty stomachs was observed in larger *L. americanus,* suggesting less frequent feeding (Armstrong et al. 1996) or regurgitation upon capture (Johnson et al. 2008). Although we did find a high rate of empty stomachs, which is typical of an opportunistic feeder, we cannot confirm that the rate was higher in larger fish. A larger sample size containing additional larger individuals would be needed to confirm this pattern.

Helicolenus dactylopterus

Helicolenus dactylopterus has a seasonally diverse diet consisting of benthic and benthopelagic prey (Neves et al. 2012). This may be correlated to different nutritional needs during spawning season. There are also ontogenetic shifts in diet (Consoli et al. 2010) as smaller individuals (<20 cm TL) consumed small crustaceans such as mysids and transitioned into a more specialized diet of shrimps and fishes as specimens grew larger (Neves et al. 2012). *H. dactylopterus* from the northwest Atlantic consumed mostly decapod crustaceans (Bowman et al. 2000).

Although decapods (Cancer irroratus, Munida iris, and M. valida) and euphausiids (*Meganyctiphanes norvegica*, *Nematobrachion boopis*, *Nematoscelis megalops*, and *Thysanopoda pectinata*) were the most identifiable prey, fishes contributed the most volume (38.6%) to the diets of *H. dactylopterus*. *H. dactylopterus* between 25 and 145 mm SL preyed predominantly on Amphipoda, Decapoda, Euphausiacea, Isopoda, Mysida, and Polychaeta. Larger fish between 173 and 250 mm SL consumed all the fish prey found in *H. dactylopterus* stomachs in this study. The Fish category was composed mostly of unidentifiable fish remains; however, *H. dactylopterus* also was identified, suggesting cannibalism. These findings are similar to those of previous studies stating that *H. dactylopterus* relies mostly on crustaceans and fish, and ontogenetic shifts in diet were evident.

Lycenchelys verrillii

In general, zoarcid fish are considered benthic, with a more sessile lifestyle in close contact with the bottom. Higgs et al. (2014) reported that at three large fish falls, most of the individuals making up the scavenging community were zoarcids. Feeding was not witnessed at the fall sites, as the zoarcid fish remained stationary until disturbed. Although this behavior of “roosting” by fish falls and baited traps is common in this family (Higgs et al. 2014), the main prey of eelpouts are typically benthic fauna such as crustaceans and amphipods (Houston and Haedrich 1986). Zoarcids could be attracted to the food falls to prey on scavenging invertebrates like amphipods. Crabtree et al. (1991) also documented *L. verrillii* as feeding heavily on bivalves and ophiuroids.

In our study Mollusca were the most dominant items consumed (22.5%) and consisted primarily of bivalves and gastropods. This category was followed closely by polycheate remains (20.2%). These data confirm that *L. verrilli* is a benthic feeder and rely heavily on bivalves as an important prey source, as noted by Crabtree et al. (1991). Inorganic and organic matter also made up 20.2% of their diet by volume and were found in 57% of the stomachs. This material could be a result of ingesting sediment while feeding on benthic organisms, or could be present in the organsims upon consumption by the fish.

Citharichthys arctifrons

Citharichthys arctifrons inhabiting the continental shelf of the northeastern United States fed almost exclusively on small benthic crustaceans, echinoderms, cnidarians, and polychaetes (Bowman et al. 2000, Link et al. 2002). Langton et al.(1981) reported that in fish collected in the mid-Atlantic, half (49.5%) the diet was made up of arthropods, primarily amphipods (16.3%) and euphausiids (14.1%). The annelid prey found in this region were primarily polycheates (Langton et al. 1981).

This study matches that of Bowman et al. (2000) and Link et al. (2002), showing that *C. arctifrons* relies heavily on crustaceans (28.0% by volume and 50.5% by frequency). Inorganic material composed a large portion (10.7%) of stomach contents, confirming that this species feeds in close contact with the benthos.

Glyptocephalus cynoglossus

Glyptocephalus cynoglossus are bottom feeders, which usually indicate a lower food diversity (Rodríguez-Marín 1995). Langton et al. (1981) reported 90% of prey in the mid-Atlantic fish collected were unidentified polychaetes, and 72.8% of the stomach contents in their northwest Atlantic study was composed of annelids. Similarly, Link et al. (2002) reported approximately 70% of the witch flounder stomachs they examined comprised polychaetes. Our results correspond to previous studies as Annelida was a dominant food category by volume (46.7%) as well as the most frequently ingested category (83.2%).

Although *G. cynoglossus* fed on polycheates regardless of fish size (Bowman and Michaels 1984), other components of their diet shift as they grow. The diet of individuals ≤300 mm primarily consists of euphausiids. As the fish get bigger, the diet changes to echinoderms (Bowman and Michaels 1984). Other documented prey include small benthic crustaceans, echinoderms, and cnidarians (Bowman et al. 2000). A study of 370 *G. cynoglossus* stomachs from the northwest Atlantic found polychaetes and crustaceans (Gammaridean amphipods) as main food sources and, to a minor extent, molluscs, echinoderms, and fishes (Román et al. 2004). In our study, this species had the highest diversity of prey items. We were unable to detect an ontogenetic shift in diet, primarily due to the lack of larger individuals. However, prey items such as echinoderms, euphausiids, and amphipods were found primarily in the larger individuals we collected.

A high volume and frequency of sediment was found in the stomachs of *G. cynoglossus* in this study. Common in certain taxa, the presence of sediment can indicate the ingestion of either sediment with infauna or prey that themselves are inundated with sediment at the time of ingestion (Gartner et al. 1997). Regardless, *G. cynoglossus* from our study sites seemed to be primarily benthic predators.

15.2.5 Summary

Submarine canyons in the middle-western North Atlantic Ocean provide diverse habitats and areas of enhanced productivity, and several of these canyons and surrounding slope habitats were recently proposed for protection by the Mid-Atlantic Fishery Management Council (under review by the U.S. Department of Commerce). Trophic studies and knowledge of fish feeding ecology are essential to understand the complex food webs and overall stability of these canyon systems to better manage these marine resources. Demersal fish fauna found within and around canyon systems aid energy transfer through food webs in deepsea ecosystems. These fishes consume benthic fauna, break down food parcels, and scatter organic matter over large areas, which serve as links to a wider trophic web (Reid et al. 2013). The Atlantic Deepwater Canyons Study has expanded information on the diet and feeding habit for these dominant demersal fishes as well as described diets of fishes from deeper locations than previously studied. Using GCA results along with stable isotope analysis data (**Chapter 16**) will help to provide a broad scale view of food webs within and around these canyons. Moving forward, more trophodynamic studies, widening geographic and depth ranges sampled, increasing the sample size of some fishes studied

here as well as focusing on additional species will better elucidate the importance of certain habitats and prey categories.

15.3 Fishes Associated with Shipwrecks and Natural Hardbottom on the Mid-Atlantic Bight Shelf

15.3.1 Introduction and Background

The mid-Atlantic (Cape Hatteras to Cape Cod) shelf and upper slope fish fauna is cool temperate with some input of fishes from colder and warmer regions to the north and south, respectively. The estuarine and shelf fishes are particularly well studied in this region (e.g., Grosslein and Azarovitz 1982, Colvocoresses and Musick 1984, Gabriel 1992, Murdy et al. 1997, Able and Fahay 1998) in large part due to decades of standardized government trawl surveys. Although these surveys and associated publications have well documented the open shelf and slope fish communities, they have generally avoided habitats that could not be trawled (i.e., canyon walls, rocky bottom, and shipwrecks).

The MAB shelf has a lower percentage of exposed natural hard substrate compared with other regions of U.S. Atlantic waters (Steimle and Zetlin 2000, SEAMAP-SA 2001). Thus, habitat may be limiting in the MAB for fauna requiring hard substrate, and introduced shipwrecks or other reef-like habitats probably represent significant habitat resources. Even so, there has been little treatment of the fishes associated with either natural or artificial hard bottom habitats in the MAB (Eklund 1988). Although direct observation techniques are preferred for assessing the fauna of rugged hard substrate (e.g., Caillet et al. 1999, Quattrini and Ross 2006, Ross and Quattrini 2007), these have not been widely used in the MAB. Two nearshore surveys in the MAB used direct observation to document fishes on various bottom types, including hard bottom, in depths ≤55 m (Auster et al. 1991, Diaz et al. 2003), but similar deeper water, middle to outer shelf assessments are lacking, aside from submersible surveys directed toward tilefish, *Lopholatilus chamaeleonticeps*, in depths of 117 to 268 m (Grimes et al. 1986). These studies noted that physical structure of the habitat correlated with fish distribution patterns, with higher profile, more complex habitats generally accumulating more fish species. Bioengineering by tilefish and red crabs (*Chaceon quinquedens*) in and near canyon heads also provided complex structured habitats for other outer shelf species.

Non-natural hard substrate (e.g., shipwrecks) aggregates fishes and invertebrates. The artificial reef effect of shipwrecks and other structures (drilling platforms, fish attracting devices) is well known, but is still surrounded by controversies (Stephan and Lindquist 1989, Christian et al. 1998, Perkol-Finkel et al. 2006). The use of artificial reefs and understanding their role in marine ecosystems are even more important considering the decline of natural reefs worldwide (Perkol-Finkel et al. 2006). It is unclear whether these structures actually increase populations of fishes as opposed to simply concentrating them; however, Arena et al. (2007) reported that vessel reefs off southeastern Florida supported significantly higher fish species richness and abundance than natural reefs, that the two habitats exhibited different community structures and trophic patterns, and suggested that vessel reefs enhanced local populations. The extent to which artificial reefs mimic natural reef functions requires further study, and artificial reefs may only approach the natural reef functions if their structures are similar (Perkol-Finkel et al. 2006).

As part of a larger survey of MAB submarine canyons and nearby features, historically important shipwrecks and other benthic habitats on the outer continental shelf near Norfolk Canyon were surveyed using ROVs during the 2012 and 2013 sampling cruises. During the Atlantic Deepwater Canyons Study, the degree to which fishes were associated with shipwrecks and the degree to which shipwrecks supported unique communities were investigated. Objectives of this section include the following:

1. The overall fish communities on artificial hard substrate (shipwrecks) and other habitats;
2. Species relative abundance; and

3. Behaviors and distributions on shipwreck and nonshipwreck open bottom for two seasons: fall 2012 and spring 2013.

15.3.2 Methods

Nine locations on the middle to outer continental shelf (42−126 m) of the southern MAB in the vicinity of Norfolk Canyon were surveyed using ROVs (**Table 15-7**, **Figure 15-24**). These sites were mapped with multibeam sonar during the 2011 mapping survey. The shallow NW-1 site was the only site that was entirely composed of flat, soft sediment habitat. Site NW-2 was dominated by a variety of hard, rough bottom, including boulders, rubble fields and walls of consolidated mud. The dominant habitat in seven study sites was composed of eight historically important shipwrecks, all sunk during the early 1920s (i.e., six were the *Billy Mitchell* fleet [Lee 1949]). The length and maximum height off bottom of the shipwrecks were W-1 (45 × 6 m), W-2 (167 × 18 m), W-3 (141 × 7 m), W-4 (301 × 3 m), W-5 (two wrecks ~685 m apart; 64 × 3 m and 53 × 2 m), W-6 (171 × 14 m), W-7 (72 × 3 m). The wrecks were surrounded by soft substrate (sand/gravel). All wrecks were covered to varying degrees with lost fishing gear (trawls).

15.3.2.1 Field Sampling Methods

ROV dives were conducted during Leg 2 of the 2012 sampling cruise using the *Kraken 2* ROV (University of Connecticut) deployed from the NOAA ship *Nancy Foster* (20−28 September 2012) and during Leg 3 of the 2012 sampling cruise using the ROV *Jason II* (Woods Hole Oceanographic Institute) deployed from the NOAA ship *Ronald H. Brown* (19−23 May 2013). The shallow soft bottom site (SS), natural hard bottom site (NHB), and wreck sites W-1, W-6, and W-7 were sampled with one ROV dive each, while the other wreck sites were sampled twice (W-3, W-4, and W-5) or three times (W-2) each, totaling 14 dives (**Table 15-7**). ROV position was continuously recorded using an ultrashort baseline tracking system, and navigation data were time-synchronized with all imagery and samples. An SBE 911*plus* CTD instrument was attached to the ROVs to record conductivity ($\mu S\ cm^{-1}$), temperature (°C), salinity, density ($\sigma\theta$, $kg\ m^{-3}$), dissolved oxygen (DO, $mL\ L^{-1}$), depth, and pH at a frequency of once per second during each dive. Only the temperature, salinity, and DO data recorded during dives while the ROVs were on or near bottom are presented.

ROVs accomplished video transects at slow speeds (<0.5 knots) across all habitat types with the vehicles as close to the seafloor as possible. During transects, color video cameras with scaling lasers (10 cm spacing) were positioned to record directly in front of the ROV and were set on wide angle (or near wide angle). The video camera recorded continuously throughout the dives (whether transecting or stationary), and digital still images were taken frequently to augment the video.

Table 15-7. Stations sampled by ROV during the 2012 (Kraken II) and 2013 (Jason II) sampling cruises in the vicinity of Norfolk Canyon.

Dive No.	Habitat Type	Date	Time	Total Time (min)	Start		End		Depth Range (m)
					Latitude (N)	Longitude (W)	Latitude (N)	Longitude (W)	
ROV-2012-NF-21	SS	20 Sept 2012	D	304	37°10′54.00″	74°56′14.40″	37°10′51.00″	74°56′15.60″	42−43
ROV-2012-NF-22	W-1	22 Sept 2012	D	622	37°09′24.00″	74°45′18.00″	n/a	n/a	81
ROV-2012-NF-23	W-2	23 Sept 2012	D	612	37°09′24.00″	74°34′36.00″	37°09′12.00″	74°34′24.00″	113
ROV-2012-NF-24	W-3	24 Sept 2012	D	519	37°13′54.00″	74°33′00.00″	37°14′00.00″	74°33′00.00″	124−126
ROV-2012-NF-26	W-4	26 Sept 2012	D	223	37°11′30.00″	74°34′24.00″	37°11′30.00″	74°34′24.00″	100−106
ROV-2012-NF-27	W-5	26 Sept 2012	D	363	37°16′54.00″	74°32′06.00″	37°17′12.00″	74°32′00.00″	118−119
ROV-2012-NF-28	NHB	27 Sept 2012	D	291	37°01′03.60″	74°39′15.60″	37°00′55.20″	74°39′38.40″	98−117
ROV-2012-NF-29	W-6	27 Sept 2012	D	251	36°54′48.00″	74°42′24.00″	36°54′48.00″	74°42′24.00″	84−85
ROV-2012-NF-30	W-7	28 Sept 2012	D	174	37°11′54.00″	74°45′24.00″	37°11′54.00″	74°45′24.00″	68−69
ROV-2013-RB-692	W-4	19 May 2013	N	295	37°11′30.00″	74°34′30.00″	37°11′30.00″	74°34′24.00″	91−105
ROV-2013-RB-693	W-2	20 May 2013	D	894	37°09′24.00″	74°34′24.00″	37°09′24.00″	74°34′42.00″	90−116
ROV-2013-RB-694	W-3	21 May 2013	D	861	37°13′54.00″	74°33′06.00″	37°14′00.00″	74°33′06.00″	101−126
ROV-2013-RB-695	W-5	22 May 2013	D	504	37°16′48.00″	74°32′06.00″	37°17′00.00″	74°32′12.00″	106−121
ROV-2013-RB-696	W-2	23 May 2013	D	197	37°09′24.00″	74°34′30.00″	37°09′24.00″	74°34′36.00″	90−114

Site Type: NHB = natural hard bottom site; SS= soft sediment bottom site; W = shipwreck site
NF = NOAA ship *Nancy Foster*; RB = NOAA ship *Ronald H. Brown*.
D = daytime 0800 to 2000 EDT; N = nighttime 2000 to 0800.
Total time and depth range are when ROV was on the bottom.

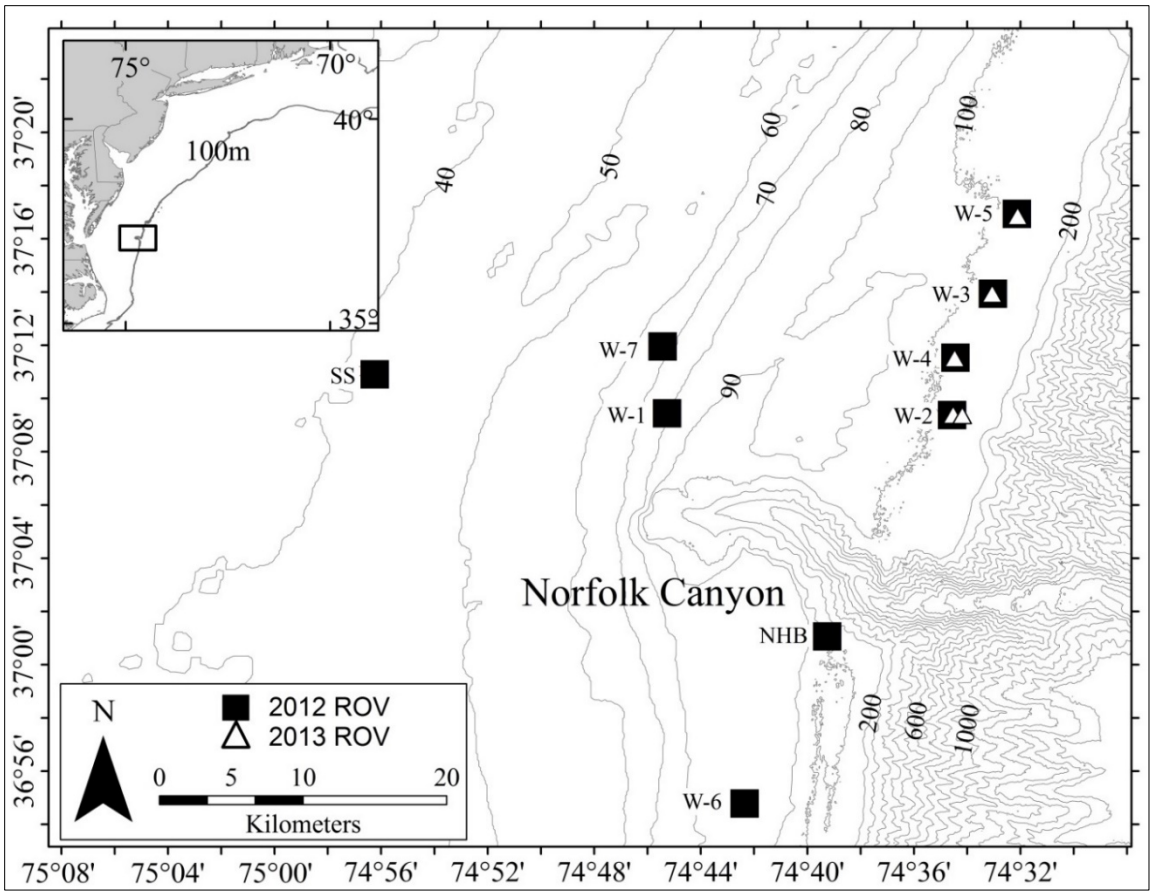

Figure 15-24. Shipwrecks (W-1 through W-7), natural hard bottom (NHB), and soft bottom (SS) sites surveyed for fish assemblages using ROV video during Leg 3 of the 2012 sampling cruise (20−28 September 2012) and Leg 2 of the 2013 sampling cruise (19−23 May 2013). Depth contours are in meters. Inset illustrates the Middle Atlantic Bight and study area (rectangle).

15.3.2.2 Laboratory Methods

15.3.2.2.1 Video Analysis

A main objective was to determine the degree to which fishes were associated with general habitats on a large scale; therefore, habitats were defined into the following two broad, relatively simple habitat classification types:

1. Soft substrate sand/mud bottom (SS) − relatively flat with few structuring features aside from gravel, burrows, depressions, and animal tracks; and
2. Artificial/shipwreck and natural hard bottom (AS/NHB) − included World War I era shipwrecks with substantial vertical profile and one site with natural hard bottom (consolidated mud, ledges, and boulders).

Additional habitat metrics included bottom depth and environmental data recorded by the CTD mounted on the ROV.

ROV video camera recordings, a preferred method for documenting fauna in complex habitats, were the main data used to describe the fish communities and associated habitats. ROV dive tracks were initially processed to conservatively remove erroneous tracking data (location points) as described by

Quattrini et al. (2012). Video analysis to determine fish community structure and habitat associations was accomplished similar to methods used by Ross and Quattrini (2007).

Dive videos were viewed multiple times for habitat classifications and to identify (to the lowest possible taxa) and count fishes by time of observation. Video segments were designated when the ROV stopped or started movement, the video quality changed, or when the habitat changed. Depth was recorded for every time segment, available from the ROV-mounted Sea-Bird data logger. Unusable video (out of focus, too far off bottom, video malfunction, sediment clouds) was removed from the dataset.

15.3.2.2.2 Community and Habitat Association Analysis

Species composition and relative abundances were compared within each habitat and between the two habitat types using fish counts from the wide-angle video. To compare abundances of all species within a habitat, relative (%) abundances were calculated (number of individuals per taxa per habitat/total number of individuals observed per habitat × 100). For between habitat comparisons, the analysis was restricted to benthic fishes identified to at least family level, with overall abundances ≥2. Occurrence of at least two individuals allowed for the possibility of a taxa occurring in both habitats during a dive. Relative (%) abundances by habitat were calculated for each taxa by dividing the number of individuals in a particular habitat by the total number of individuals of the same species from both habitats × 100.

Multivariate analyses were conducted in PRIMER 6 + PERMANOVA (Clarke and Warwick 2001, Clarke and Gorley 2006, Anderson et al. 2008) to determine differences in benthic fish assemblages between habitat types. Sample units were the numbers of each species per habitat (SS or AS/NHB) per dive; samples with no species present were removed from the dataset. Because transect times were variable, abundances of species were standardized per sample by dividing the number of individuals per species by the total number of fishes per sample. Standardized abundances were fourth-root transformed to down weight the abundant species relative to rare species. The Bray-Curtis similarity coefficient was used to calculate similarities between samples, and based on the resulting similarity matrix a nonmetric MDS plot and a dendrogram with group average linking were created. One-way ANOSIM and post-hoc multiple comparison tests were used to determine whether there were significant differences between fish assemblages in the two habitat types. SIMPER analysis was used to determine which species contributed to the dissimilarities among reef types.

15.3.3 Results

Fourteen ROV dives were completed on the nine study sites (42−126 m), nine dives in September 2012 and five in May 2013 (**Table 15-7**, **Figure 15-24**), resulting in a total of 84.4 h of video data on hard bottom habitat and 16.5 h on soft bottom. Soft bottom habitat was exclusively observed in the shallowest dive (**Table 15-7**, **Figure 15-24**); however, because only three unidentified skates were observed during this dive, it made little contribution to this study. Although shipwrecks and NHB were the foci of the remaining dives, soft bottom habitat surrounding the hard bottoms was also surveyed during those dives.

In September 2012, mean bottom temperatures varied by approximately 2.5 °C across the dives sites, with coldest temperatures (means = 11.9−13.0 °C), lowest salinities (means = 33.1−34.8), and highest DO (means = 4.0−4.5 mL L^{-1}) occurring at the shallower sites (42−81 m) (**Table 15-8**). Each of the five deeper sites (84−126 m) exhibited bottom temperatures (means = 14.2−14.5 °C), salinities (35.6−35.8), and DO (3.7−4.0 mL L^{-1}) similar to each other. In May 2013, the five deeper sites again showed little variation among sites, but were on average a degree colder than in 2012 (means = 13.2−13.4 °C). These sites showed more variations in salinity (means = 29.4−35.7) and DO (means = 2.4−4.7 mL L^{-1}) compared with 2012 data. It seems unlikely that these small differences were biologically significant to the fish communities.

Table 15-8. Bottom environmental data (means, ranges, and standard errors of the means in parenthesis) recorded by ROV-mounted Sea-Bird Electronics, Inc. data logger (one exception) during 2012 and 2013 sampling surveys of shipwrecks and sandy bottoms on the continental shelf near Norfolk Canyon.

Dive No.	Habitat Type	Temperature (°C)	Salinity	Dissolved Oxygen (mL L^{-1})
ROV-2012-NF-21-SS	Soft substrate	12.16, 11.95−12.29 (0.00072)	33.14, 33.16−33.17 (0.00009)	4.51, 4.45−4.55 (0.00016)
ROV-2012-NF-22-W1	Artificial/natural hard bottom	11.94, 10.73−14.61 (0.00294)	34.16, 32.92−34.94 (0.00147)	4.22, 4.08−5.54 (0.00050)
ROV-2012-NF-23-W2	Artificial/natural hard bottom	n/a*	n/a*	n/a*
ROV-2012-NF-24-W3	Artificial/natural hard bottom	14.31, 14.10−14.47 (0.00034)	35.65, 35.32−35.80 (0.00048)	3.88, 3.67−4.14 (0.00029)
ROV-2012-NF-26-W4	Artificial/natural hard bottom	14.47, 14.40−14.52 (0.00007)	35.78, 35.69−35.80 (0.00007)	3.98, 3.95−4.11 (0.00012)
ROV-2012-NF-27-W5	Artificial/natural hard bottom	14.15, 14.00−14.46 (0.00077)	35.75, 35.74−35.80 (0.00002)	3.69, 3.51−4.84 (0.00058)
ROV-2012-NF-28-NHB	Natural hard bottom	14.33, 14.22−14.39 (0.00015)	35.71, 35.50−35.77 (0.00036)	3.93, 3.83−4.06 (0.00035)
ROV-2012-NF-29-W6	Artificial/natural hard bottom	14.21, 13.86−14.30 (0.00091)	35.63, 35.12−35.72 (0.00131)	3.84, 3.67−4.85 (0.00038)
ROV-2012-NF-30-W7	Artificial/natural hard bottom	13.00, 12.53−13.41 (0.00127)	34.76, 34.45−35.09 (0.00080)	3.99, 3.87−4.78 (0.00042)
ROV-2013-RB-692-W4	Artificial/natural hard bottom	13.16, 13.09−13.32 (0.00047)	34.83, 32.20−35.72 (0.00854)	2.99, 1.81−4.22 (0.00420)
ROV-2013-RB-693-W2	Artificial/natural hard bottom	13.27, 13.18−13.50 (0.00029)	32.81, 29.66−33.14 (0.00325)	2.44, 1.38−4.31 (0.00178)
ROV-2013-RB-694-W3	Artificial/natural hard bottom	13.42, 12.90−13.49 (0.00037)	35.48, 32.64−35.94 (0.00270)	3.08, 2.09−4.46 (0.00208)
ROV-2013-RB-695-W5	Artificial/natural hard bottom	13.19, 13.10−13.45 (0.00037)	29.42, 26.38−35.18 (0.00095)	n/a*
ROV-2013-RB-696-W2	Artificial/natural hard bottom	13.32, 13.00−13.60 (0.00115)	35.69, 35.63−35.77 (0.00018)	4.71, 4.57−4.76 (0.00029)

*n/a = data taken from *Jason II* CTD, Sea-Bird not operating.

15.3.3.1 Community Structure and Habitat Associations

Thirty-six unique fish taxa, representing 25 families, were identified from the ROV video. Thirty-one of these occurred on the shipwrecks or NHB (14 species observed only on hard bottom), and 23 taxa occurred on the soft substrate (six occurred only on soft bottom) (**Table 15-9**). The lower number of species observed on the SS habitat was at least partly due to lower effort there (**Table 15-9**). Three taxa (*Carcharhinus* sp., *Seriola dumerili,* and *Mola mola*) that occurred over or near either habitat are actually considered more pelagic.

Table 15-9. Relative abundance (%) of fishes observed during ROV dives (2012 and 2013) on artificial (shipwrecks)/natural hard bottom (AS/NHB) and soft substrate (SS) habitats near Norfolk Canyon, Middle Atlantic Bight. Number of hours of observation (useable video) and depth ranges are under each habitat.

Taxa	AS/NHB 84.42 h, 63−126 m	SS 16.48 h, 40−126 m
Scyliorhinidae		
Scyliorhinus retifer, chain dogfish	30.158	56.489
Carcharhinidae		
Carcharhinus sp., requiem shark	0.002	−
Rajidae		
Leucoraja garmani, rosette skate	−	0.339
Rajidae (unidentified)	0.002	0.594
Ophichthidae		
Ophichthus cruentifer, margined snake eel	−	0.170
Congridae		
Conger oceanicus, conger eel	0.596	0.170
Gadiformes (unidentified), cods	0.002	0.085
Moridae		
Physiculus fulvus, metallic codling	0.094	−
Phycidae		
Phycis chesteri, longfin hake	0.002	−
Urophycis chuss, red hake	0.002	−
Urophycis regia, spotted hake	0.006	−
Urophycis sp.	0.083	0.085
Lophiidae		
Lophius americanus, goosefish	−	0.085
Trachichthyidae		
Gephyroberyx darwinii, big roughy	0.600	−
Centriscidae		
Macroramphosus scolopax, longspined snipefish	0.557	0.254
Scorpaenidae		
Scorpaena sp., scorpionfish	1.249	6.107
Triglidae		
Prionotus sp., searobin	0.004	0.085
Polyprionidae		
Polyprion americanus, wreckfish	0.004	−
Serranidae		
Anthias nicholsi, yellowfin bass	10.667	1.442
Anthias sp.	0.002	−
Baldwinella vivanus, red barbier	3.904	0.085
Centropristis striata , black sea bass	1.180	6.531
Hyporthodus nigritus, warsaw grouper	0.015	−
Hyporthodus niveatus, snowy grouper	0.058	0.085

Table 15-9. (Continued).

Taxa	AS/NHB 84.42 h, 63−126 m	SS 16.48 h, 40−126 m
Hyporthodus sp.	0.004	−
Pronotogrammus martinicensis, roughtongue bass	0.006	−
Anthiinae (unidentified)	44.606	1.442
Malacanthidae		
Caulolatilus microps, blueline tilefish	0.369	0.594
Caulolatilus sp.	−	0.339
Pomatomidae		
Pomatomus saltatrix, bluefish	0.137	1.781
Carangidae		
Seriola dumerili, greater amberjack	0.062	0.085
Sparidae		
Stenotomus chrysops, scup	0.009	0.509
Labridae		
Tautoga onitis, tautog	0.008	−
Tautogolabrus adspersus, cunner	0.729	0.254
Labridae (unidentified)	0.002	−
Caproidae		
Antigonia capros, deepbody boarfish	4.776	21.628
Paralichthyidae		
Paralichthys dentatus, summer flounder	0.002	0.085
Paralichthys oblongus, fourspot flounder	0.004	0.085
Bothidae (unidentified), lefteye flounders	−	0.254
Pleuronectidae		
Glyptocephalus cynoglossus, witch flounder	−	−
Hippoglossoides platessoides, American plaice	−	−
Cynoglossidae	−	−
Symphurus stigmosus, blotchfin tonguefish	−	0.085
Molidae		−
Mola mola, ocean sunfish	0.002	−
Unidentified fish	0.096	0.339

Fish assemblages on each habitat type were numerically dominated by relatively few species. On the AS/NHB substrate, seven taxa (*Scyliorhinus retifer, Scorpaena* sp., *Anthias nicholsi, Baldwinella vivanus, Centropristis striata, anthinine serranids, Antigonia capros*) comprised 96.5% of the community. Combined anthiinine serranids and *S. retifer* (**Figure 15-25A**,**B)** were each an order of magnitude (two orders of magnitude compared with most species) more abundant than any other taxa in any habitat. Most of the anthiniines observed were probably *B. vivanus*, but small, rapidly moving anthiniines can be difficult to identify *in situ*; some of these could have been *B. aureorubens, Hemanthias leptus*, or *Choranthias tenuis*. The smaller (~60−180 mm TL) Anthiinae occurred as dense aggregations whose members swam rapidly around hard bottom structures (**Figure 15-25A**), occasionally straying over nearby sandy bottom. Larger (usually ~130−200 mm TL) A. nicholsi were more solitary and often associated with the anthiniine schools (**Figure 15-25 A**,**B**). *Scyliorhinus retifer* were less abundant on the NHB than other habitats and occurred in massive numbers on the shipwrecks, often so densely packed that they lay on top of each other in layers several individuals thick (**Figure 15-25B**). Although many were observed laying on soft bottom, this was generally within tens of meters of the shipwrecks. Aggregations of *S. retifer* likely represent spawning-related activity because thousands of their egg cases were attached to the shipwrecks. Six of these taxa, excluding *B. vivanus*, comprised 93.6% of the fauna on SS bottom but often exhibited a lower percent contribution to SS habitat compared with the hard bottom.

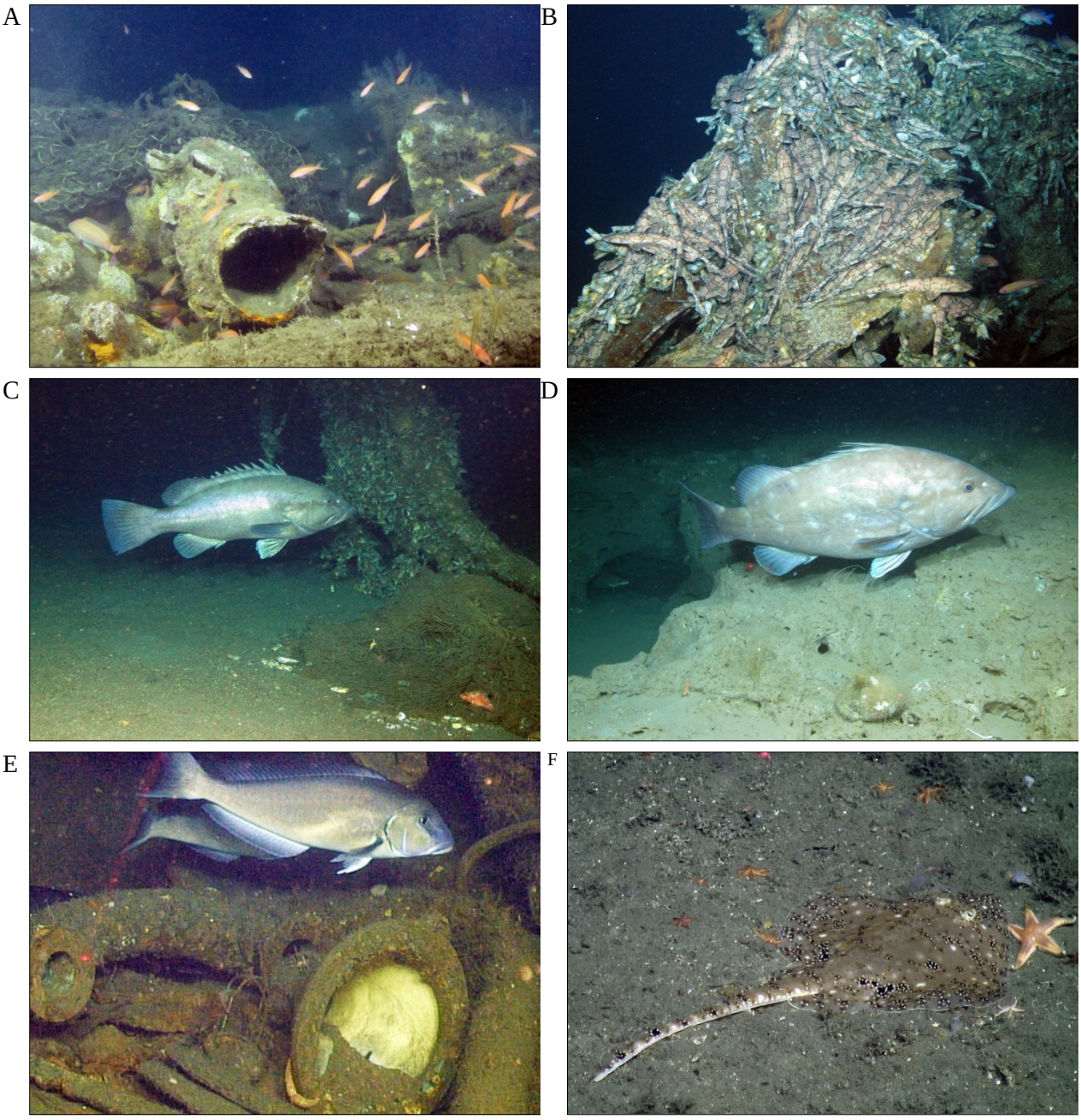

Figure 15-25. Photographs taken *in situ* of fishes and habitats surveyed with ROV in 2012 and 2013 near Norfolk Canyon: A) School of anthiine serranids and at least one yellowtail bass (*Anthias nicholsi*, mid-left) on shipwreck W-1, 81 m, 22 Sept 2012; B) dense aggregations of chain dogfish (*Scyliorhinus retifer*) laying on shipwreck structure (W-5, ~115 m, 26 Sept 2012) and four yellowfin bass (2 upper right, 2 lower right), red arrows indicate clusters of chain dogfish egg cases; C) warsaw grouper (*Hyporthodus nigritus*) and scorpionfish (*Scorpaena* sp., lower right lying on trawl net) on shipwreck W-5, 118 m, 26 Sept 2012; D) snowy grouper (*Hyporthodus niveatus*) on natural hard bottom site, ~110 m, 27 Sept 2013 (note scaling laser dots near anal fin indicate this fish is at least 150 cm long); E) two blueline tilefish (*Caulolatilus microps*) on shipwreck W-2, ~100 m, 20 May 2013; F) rosette skate (*Leucoraja garmaini*) on sandy habitat near shipwreck W-2,~100 m, 23 May 2013.

Species that were unique to either habitat occurred in low abundance (<1% of total within habitat). Because shelf communities are subjected to seasonal environmental variability and may exhibit seasonal distribution patterns, multivariate analysis was used (17 video samples and 29 species) to examine seasonal differences (fall 2012 versus spring 2013) in fish distributions at the nine sites. Season did not have a significant impact on fish assemblages (R = -0.024, P = 0.55). Likewise, no differences were noted in assemblage structure over the limited depth range examined (68−126 m, dive NF-21 excluded, R = 0.026, P = 0.40). The greatest distances between sites ≤50 km, and fish assemblages (excluding dive site NF-21) were not significantly (R = 0.13, P = 0.09) different in regard to distance from one another or distance from Norfolk Canyon. Thus, all data were combined for analysis of habitat influence.

Multivariate analysis using 26 video samples (excluding shallow dive NF-21) and 41 taxa indicated a significant difference (R = 0.499, P = 0.001) in fish assemblage structure between soft bottom and reef habitats (**Figure 15-26**). The natural hard bottom habitat grouped with the shipwreck hard bottom samples; the AS/NHB group was 60% dissimilar from the two soft bottom assemblages. Hard bottom video samples from the four deeper shipwrecks north of Norfolk Canyon (91−126 m, **Figure 15-24**) grouped closely together (**Figure 15-26**) even though samples represented two different years and seasons. The three hard bottom (shipwreck) samples from mid-shelf (68−85 m, **Figure 15-24**) were offset together in the overall AS/NHB group. The three mid-shelf sand bottom samples were also set apart from most other SS stations (**Figure 15-26**), suggesting at least some difference in communities along isobaths. Some deeper occurring fishes missing from those shallower three sites were *Physiculus fulvus, Gephyroberyx darwinii, Macroramphosus scolopax, Hyporthodus* spp., and *A. capros*, while two species common on the shallow sites, *Stenotomus chrysops* and *Tautoga onitis*, were not observed on the deeper sites. Fishes that most influenced the reef habitat group (SIMPER) were *S. retifer*, Anthiinae, *A. nicholsi, A. capros, Conger oceanicus, Scorpaena* sp., *B. vivanus, Tautogolabrus adspersus*, and *Caulolatilus microps*. All SS samples fell within the two soft bottom sample groups. Fishes that most influenced the SS groups were *S. retifer, Scorpaena* sp., *A. capros*, and *C. striata*.

Habitat preference was indicated by relative abundance patterns of most fishes. The AS/NHB reef habitats contained >90% of the abundance of each of 21 fish taxa (**Figure 15-27**), and far more individuals were observed in that habitat than in soft substrate habitat. Several species (e.g., *Prionotus* sp., *Paralichthys oblongus, P. dentatus*, and *S. chrysops*) frequently used both soft and hard bottom habitats, although several taxa (e.g., Bothidae, *Ophichthus cruentifer*, and *Leucoraja garmani*) were observed only on soft bottom (**Figures 15-26, 15-25F**).

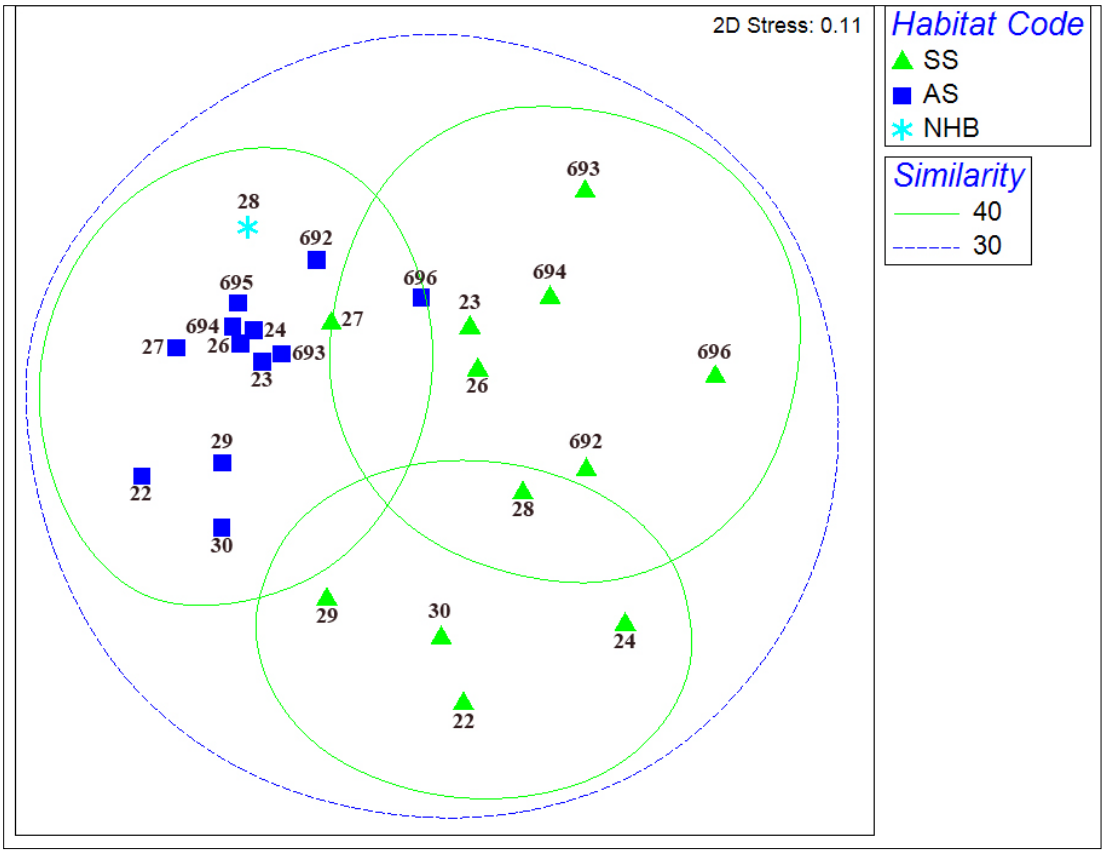

Figure 15-26. Multidimensional scaling (MDS) ordination of 26 video samples from artificial/shipwreck (AS), natural hard bottom (NHB), and soft sediment (SS) habitats based on the Bray-Curtis similarity matrix calculated from standardized, fourth-root transformed fish abundances (41 taxa). Numbers by symbols indicate dive numbers (see **Table 15-7**).

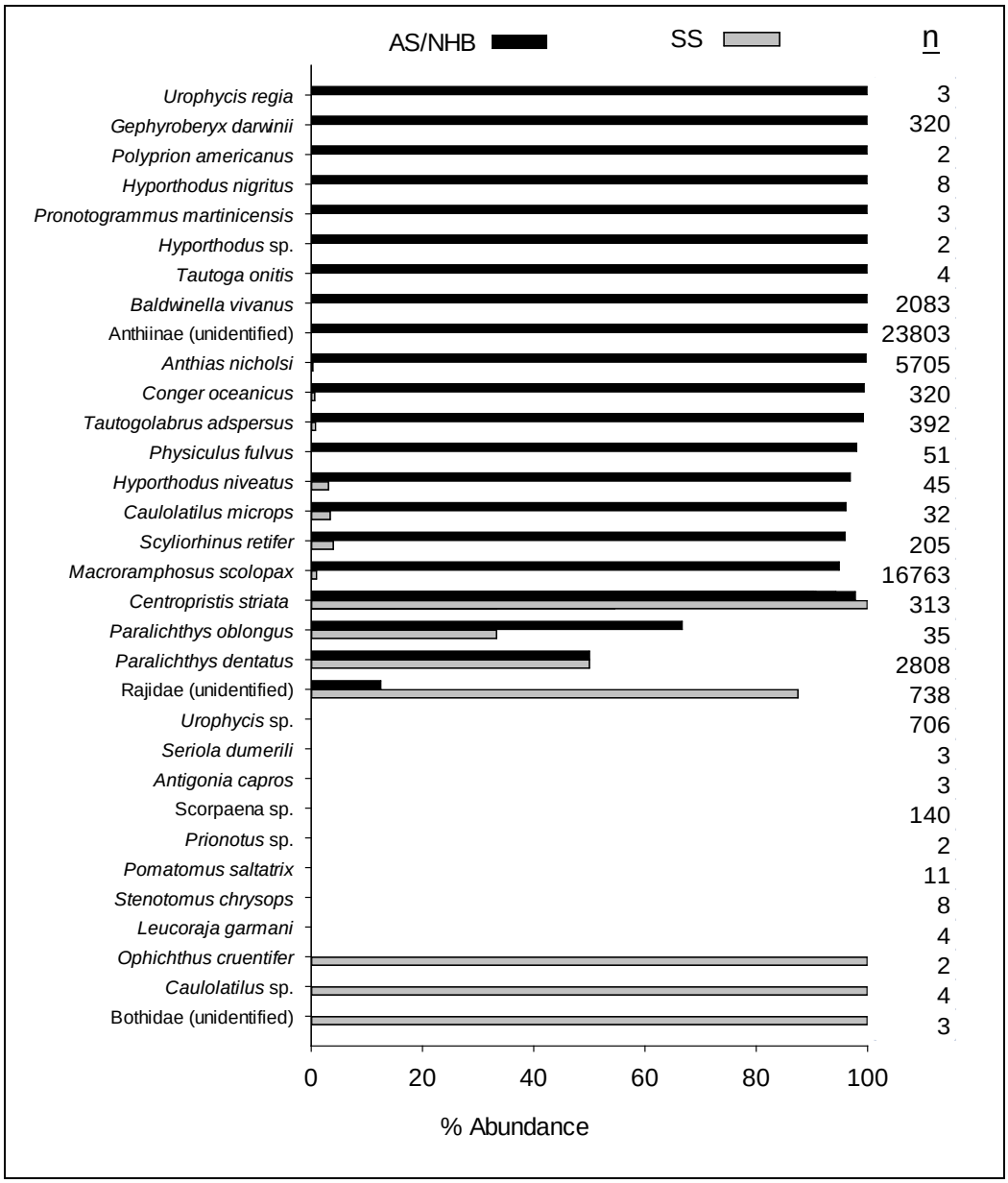

Figure 15-27. Within species relative (%) abundance across two habitat types (AS/NHB = artificial and natural hard bottom, SS = soft substrate) for benthic species including two or more individuals. n = number of individuals counted during video transects.

15.3.4 Discussion

Fishes occupying natural and artificial hard bottoms on the mid- to outer shelf of the MAB exhibited a different assemblage structure from the well-known (e.g., Murawski et al. 1983, Mahon et al. 1998) surrounding soft bottom ichthyofauna. Although the most abundant reef species were also counted on soft bottom, in most cases they were never far from the reef structure. The hard bottom habitats observed here were dominated by two groups whose species are generally considered to be reef associates: 1) a cool-temperate group (e.g., *S. retifer*, *C. striata*, *T. onitis*, *C. oceanicus*) having broad depth and latitudinal distributions as well as often broader habitat usage, and 2) a warm-temperate group (most Serranidae, *C. microps*, *A. capros*) with more restricted distributions and tighter association with reefs. The Serranidae (excluding *C. striata*) seem constrained to a relatively narrow depth range (~70 to at least

150 m) in the MAB, most likely related to the generally warmer (>10 °C) and less variable bottom water temperatures along the outer shelf of the southern MAB (Colvocoresses and Musick 1984). In contrast to most soft bottom associates, several abundant hard bottom species (**Figure 15-25A-E**; *A. nicholsi*, *B. vivanus*, *Hyporthodus* spp., *C. microps*) are further constrained by being at or near the northern limits of their adult ranges (Anderson and Heemstra 2012, Moore et al. 2003). Because many common hard bottom species (e.g., most Serranidae, *S. retifer*, and *A. capros*) likely have an obligate association with reef-like habitats (Able and Flescher 1991, Craig et al. 2011, Anderson and Heemstra 2012), the relatively limited hard bottom in the MAB (Steimle and Zetlin 2000) also would impact their distribution potential. Thus, the hard bottom fish community in the southern MAB, especially the warm-temperate component, is restricted by habitat availability, depth, and zoogeography; the latter two probably related to bottom temperature. Although this community appears to flourish, the limitations likely make it vulnerable to over fishing and habitat damage.

Results presented here differ substantially from other surveys of the MAB. Our ROV study sites overlapped with several areas of geographic fish assemblage groupings that were based on decades of bottom trawl surveys (Colvocoresses and Musick 1984, Mahon et al. 1998); however, most of the few species shared between this study and the two trawl-based studies were species that commonly occur on sandy bottoms (e.g., *L. americanus*, *Urophycis regia*, *P. oblongus*, *P. dentatus*). The most abundant taxa observed here (*S. retifer*, Anthiinae, *A. capros*) as well as others known to be reef associates (*Hyporthodus* spp., *Caulolatilus* spp., Labridae) were not reported in those trawl-based studies. The differences in species composition, largely resulting from sampling constraints imposed by trawls, emphasize the high degree of fish faunal separation between soft bottom and reef-like habitats in the MAB. Although Grimes et al. (1986) and Ross et al. (2015a) covered extensive complex habitats in the region using visual surveys, they reported only 2 (25% overlap) and 10n (12% overlap) fish species, respectively, in common with our observations. In those cases, the differences are due to both previous studies being conducted mostly deeper than and/or much farther north of this survey. Although also much farther north (~41° N), visual surveys over flat, mostly sand and shell bottom (55, 240, 712 m sites) yielded 37.5% fish species in common with this survey (Auster et al. 1995), most of which exhibit broad habitat affinity or affinity for soft bottom. In contrast, the MAB hard bottoms surveyed here shared 43% of the fish fauna with a deep (237−253 m) shipwreck off Cape Fear, North Carolina, assessed during one ROV dive (Quattrini and Ross 2006). Most of the reef associated fishes reported here were common on outer shelf hardgrounds throughout the southeastern United States (Grimes et al. 1982, Quattrini and Ross 2006), which also indicates a more warm-temperate affinity for the southern MAB reef fishes.

As with the mid- to outer shelf reefs examined here, the MAB inner shelf hard bottoms were dominated by relatively few, but different, fish species (*C. striata*, *Tautoga onitis*, *Tautogolabrus adspersus*). On the deeper shelf reefs (this study), these three species ranked in abundance below the top six species. However, the few shelf studies were conducted from much shallower (<35 m) waters (Briggs 1975, Feigenbaum et al. 1985, Eklund and Targett 1991), and two studies that heavily relied on trap data may have missed many small species. However, taxa like the Anthiinae, most common on deeper reefs (Anderson and Heemstra 2012), were probably not available to inshore reefs. Although regionally limited, hard bottom habitat and associated data are even rarer along the outer shelf (~100 m region, Steimle and Zetlin 2000). Despite the restricted scope of the deep shelf reefs, they support economically important fishes (groupers, tilefish, seabass) and high fish species richness, as do similar depth reefs south of Cape Hatteras (Parker and Ross 1986, Quattrini and Ross 2006).

Some degree of faunal stability along the MAB outer shelf is suggested by similarities between years/seasons for sites sampled both seasons. Although fish species may shift distributions by season in the MAB (Murawski et al. 1983), the relatively small (~2 °C) bottom temperature variation along the outer shelf (~100 m) resulted in consistent groupings of soft bottom species across seasons and years (Colvocoresses and Musick 1984). For the deeper shipwreck sites sampled during two seasons, we observed only a <1.5 °C mean bottom temperature difference between the two time periods. Although

more continuous and long-term environmental data are needed to capture more accurate means and especially variability, our results agreed with the much larger dataset from Colvocoresses and Musick (1984). Colton (1972) noted a series of warming and cooling trends on the shelf in the Gulf of Maine, but there was also little apparent change in distributions of four groundfish species correlated with this. Additionally, obligate reef fishes tend to be territorial, and if bottom temperatures remain within tolerances, a large component of the MAB outer shelf reef fish community (e.g., Anthiinae, *Hyporthodus* spp.) may display long-term temporal site fidelity.

Similar to other reports (Murawski et al. 1983, Nye et al. 2009, Møller et al. 2010), it is tempting to suggest that hard bottoms of the southern MAB are increasingly invaded by more warm-temperate species, possibly in response to rising ocean temperatures. North Carolina is the closest southern source where the species noted here are commonly encountered on extensive deeper hard bottoms (Grimes et al. 1982, Parker and Mays 1998, Quattrini and Ross 2006). Concrete evidence for historical distributional change is deficient due to a lack of appropriate sampling on deep reefs. Although Cape Henry, VA was listed with question as the northern limit of *C. microps* (Dooley 1978), our observations confirm its presence in the MAB (**Figure 15-27E**) and extend its range north of Norfolk Canyon. That species, plus *A. nicholsi*, had been reported from this region from the early 20th century (Firth 1933, 1937). *Hyporthodus niveatus* and *H. nigritus* (**Figure 15-27C**, **D**) were reported in New England waters as early as the late 19th century, but most of these were juveniles collected inshore and assumed to be strays (Smith 1971). Large adults (world tackle records) of *H. niveatus* were recently reported in the MAB recreational hook and line fishery (as was *C. microps*), but data presented here are the first descriptions of their relative abundance and adult habitat along the MAB outer shelf. Recent collections of *B. vivanus* near Wilmington Canyon represent the first records for the MAB (Moore et al. 2003), but this small, deep reef specific fish could have easily escaped detection. Similarly, our observations of three individuals of *Pronotogrammus martinicensis* in 92–96 m on the NHB represent a new northern range limit (from North Carolina, Anderson and Heemstra 2012), but this does not necessarily mean this species is newly arrived to the MAB. Although historical data are inadequate to evaluate change in long-term species composition patterns, this study, the first to examine outer shelf reef fishes of the region, should provide a baseline for future assessments.

15.4 LITERATURE CITED

Able KW, Fahay MP. 1998. First year in the life of estuarine fishes in the middle Atlantic Bight. New Brunswick (NJ): Rutgers University Press. 342 p.

Able KW, Flescher D. 1991. Distribution and habitat of chain dogfish, *Scyliorhinus retifer*, in the Mid-Atlantic Bight. Copeia. 1991:231–234.

Armstrong JD, Bagley PM, Priede IG. 1992. Photographic and acoustic tracking observations of the behaviour of the grenadier, *Coryphaenoides (Nematonurus) armatus*, the eel, *Synaphobranchus bathybius*, and other abyssal demersal fish in the North Atlantic Ocean. Marine Biology. 112:535-544.

Armstrong MP, Musick JA, Colvocoresses JA. 1996. Food and ontogenetic shifts in feeding of the goosefish, *Lophius americanus*. Northwest Atlantic Fishery Science. 18:99–103.

Anderson M, Gorley RN, Clark RK. 2008. Permanova+ for Primer: guide to software and statistical methods. Plymouth (UK): PRIMER-E.

Anderson WD Jr., Heemstra PC. 2012. Review of Atlantic and eastern Pacific anthiine fishes (Teleostei: Perciformes: Serranidae), with descriptions of two new genera. Transactions of the American Philosophical Society, Vol. 102, Part 2. Philadelphia (PA): American Philosophical Society. 173 p.

Arena PT, Jordan LKB, Spieler RE. 2007. Fish assemblages on sunken vessels and natural reefs in southeast Florida, USA. Hydrobiologia. 580:157–171.

Auster PJ. 2005. Are deep-water corals important habitats for fishes? In: Freiwald A, Roberts JM, editors. Cold-water corals and ecosystems. Berlin Heidelberg: Springer-Verlag. p. 747–760.

Auster PJ. 2007. Linking deep-water corals and fish populations. In: George RY, Cairns SD, editors. Conservation and adaptive management of seamount and deep-sea coral ecosystems. Miami (FL): University of Miami. p. 93–99.

Auster PJ, Malatesta RJ, LaRosa SC, Cooper RA, Stewart LL. 1991. Microhabitat utilization by the megafaunal assemblage at a low relief outer continental shelf site – Middle Atlantic Bight, USA. Journal of Northwest Atlantic Fisheries Science. 11:59–69.

Auster PJ, Malatesta RJ, LaRosa SC. 1995. Patterns of microhabitat utilization by mobile megafauna on the southern New England (USA) continental shelf and slope. Marine Ecology Progress Series. 127:77–85.

Bailey DM, Genard B, Collins MA, Rees JF, Unsworth SK, Battle EVJ, Bagley PM, Jamieson AJ, Priede IG. 2005. High swimming and metabolic activity in the deep-sea eel *Synaphobranchus kaupii* revealed by integrated in situ and in vitro measurements. Physiological and Biochemical Zoology. 78:(3)335–346.

Baillon S, Hamel JF, Wareham VE, Mercier A. 2012. Deep cold-water corals as nurseries for fish larvae. Frontiers in Ecology and the Environment. 10:351–356.

Baker KD, Haedrich RL, Snelgrove PVR, Wareham VE, Edinger EN, Gilkinson KD. 2012. Small-scale patterns of deep-sea fish distributions and assemblages of the Grand Banks, Newfoundland continental slope. Deep-Sea Research. I 65:171–188.

Bennett RH, Lehman L, Hulbert MH, Harvey GR, Bush SA, Forde EB, Crews P, Sawyer WB. 1985. Interrelationships of organic carbon and submarine sediment geotechnical properties. Marine Georesources and Geotechnology. 6:61–98.

Biber MF, Duineveld GCA, Lavaleye MSS, Davies AJ, Bergman MJN, van den Beld IMJ. 2014. Investigating the association of fish abundance and biomass with cold-water corals in the deep Northeast Atlantic Ocean using a generalized linear modeling approach. Deep-Sea Research II. 99:134–145.

Bigelow HB, Schroeder WC. 1953. Fishes of the Gulf of Maine. Fisheries Bulletin. 53:1–577.

Bowman RE, Michaels WL. 1984. Food of seventeen species of northwest Atlantic fish. National Oceanic and Atmospheric Administration (NOAA) Technical Memo NMFS-F/NEC 28. 183 p.

Bowman RE, Stillwill CE, Michaels ML, Grosslein MD. 2000. Food of northwest Atlantic fishes and two common species of squid. NOAA Technical Memo NMFS NE 155. 137 p.

Briggs PT. 1975. An evaluation of artificial reefs in New York's marine waters. NY Fish and Game Journal. 22:51–56.

Brinton, E. 1962. The distribution of Pacific euphausiids. Bulletin of the Scripps Institution of Oceanography, University of California. 8:51–270.

Brothers DS, ten Brink US, Andrews BD, Chaytor JD. 2013. Geomorphic characterization of the U.S. Atlantic continental margin. Marine Geology. 338:46–63.

Buhl-Mortensen L, Vanreusel A, Gooday AJ, Levin LA, Priede IG, Buhl-Mortensen P, Gheerardyn H, King NJ, Raes M. 2010. Biological structures as a source of habitat heterogeneity and biodiversity on the deep ocean margins. Marine Ecology. 31:21–50.

Cailliet GM, Andrews AH, Wakefield W, Moreno G, Rohdes KL. 1999. Fish faunal and habitat analyses using trawls, camera sleds and submersibles in benthic deep-sea habitats off central California. Oceanologica Acta. 22:579–592.

Carney RS. 2005. Zonation of deep biota on continental margins. Oceanography and Marine Biology: An Annual Review. 43:211–278.

Christian R, Steimle F, Stone R. 1998. Evolution of marine artificial reef development—a philosophical review of management strategies. Gulf of Mexico Science. 16:32–36.

Clarke KR, Gorley RN. 2006. PRIMER v6: user manual/tutorial. Plymouth (UK): PRIMER-E.

Clarke KR, Warwick RM. 2001. Change in Marine Communities: an approach to statistical analysis and interpretation. 2nd edition. Plymouth (UK): PRIMER-E.

Cohen DM, Inada T, Iwamoto T, Scialabba N. 1990. Gadiform fishes of the world (order Gadiformes). An annotated and illustrated catalogue of cods, hakes, grenadiers, and other Gadiform fishes known to date. FAO Fisheries Synopsis No. 125 Vol 10. Rome (Italy): Food and Agriculture Organization of the United Nations (FAO). 442 p.

Colaço A, Giacomello E, Porteiro F, Menzes GM. 2013. Trophodynamic studies on the Condor seamount (Azores, Protugal, North Atlantic). Deep-Sea Research II. 98:178–189.

Collette BB, Klein-MacPhee G. 2002. Fishes of the Gulf of Maine. Washington (DC): Smithsonian Institute Press. 768 p.

Colton JB Jr. 1972. Temperature trends and the distribution of groundfish in continental shelf waters, Nova Scotia to Long Island. Fishery Bulletin. 70:637–657.

Colvocoresses JA, Musick JA. 1984. Species associations and community composition of middle Atlantic Bight continental-shelf demersal fishes. Fishery Bulletin. 82:295–313.

Consoli P, Battaglia P, Castriota L, Esposito V, Romeo T, Andaloro F. 2010. Age, growth and feeding habits of the bluemouth rockfish, *Helicolenus dactylopterus dactylopterus* (Delaroche 1809) in the central Mediterranean (southern Tyrrhenian Sea). Applied Ichthyology. 26:583–591.

Costello MJ, McCrea M, Freiwald A, Lundalv T, Jonsson L, Brett BJ, van Weering TCE, de Haas H, Roberts JM, Allen D. 2005. Role of cold-water Lophelia pertusa coral reefs as fish habitat in the NE Atlantic. In: Freiwald A, Roberts JM, editors. Cold-water corals and ecosystems. Berlin (Germany): Springer-Verlag. p. 771–805.

Crabtree RE, Carter J, Musick JA. 1991. The comparative feeding ecology of temperate and tropical deep-sea fishes from the western North Atlantic. Deep-Sea Research. 38:1277–1298.

Craig MT, Sadovy de Mitcheson YJ, Heemstra PC. 2011. Groupers of the world: a field and market guide. Grahamstown (South Africa): NISC Ltd.

Cunha MR, Paterson GLJ, Amaro T, Blackbird S, de Stigter HC, Ferreira C, Glover A, Hilário A, Kiriakoulakis K, Neal L, Ravara A, Rodrigues CF, Tiago A, Billett DSM. 2011. Biodiversity of macrofaunal assemblages from three Portuguese submarine canyons (NE Atlantic). Deep-Sea Research II. 58:2433–2447.

De Leo FC, Smith CR, Rowden AA, Bowden DA, Clark MR. 2010. Submarine canyons: hotspots of benthic biomass and productivity in the deep sea. Proceeding of the Royal Society B. 277:2783–2792.

De Leo FC, Drazen JC, Vetter EW, Rowden AA, Smith CR. 2012. The effects of submarine canyons and the oxygen minimum zone on deep-sea fish assemblages off Hawaii. Deep-Sea Research I. 64:54–70.

Deree HL. 1999. Age and growth, dietary habits, and parasitism of the fourbeard rockling, *Enchelyopus cimbrius*, from the Gulf of Maine. Fisheries Bulletin. 97:39–52.

Desbruyères D, Segonzac M, Bright M, editors. 2006. Handbook of deep-sea hydrothermal vent fauna. 2nd edition (Denisia 18). Linz (Austria): Biologiezentrum der Oberösterreichische Landesmuseen. 544p.

Diaz RJ, Cutter GR Jr, Able KW. 2003. The importance of physical and biogenic structure to juvenile fishes on the shallow inner continental shelf. Estuaries. 26:12–20.

Dooley J.K. 1978. Systematics and biology of the tilefishes (Perciformes: Branchiostegidae and Malacanthidae), with descriptions of two new species. NOAA Technical Report NMFS Circular 411. 78 p.

Eklund AM. 1988. Fishes in habiting hard bottom reef areas in the Middle Atlantic Bight: Seasonality of species composition catch rates, and reproduction. MS thesis. University of Delaware. 98 pp.

Eklund AM, Target TE. 1991. Seasonality of fish catch rates and species composition from the hard bottom trap fishery in the Middle Atlantic Bight (US east coast). Fisheries Research. 12:1–22.

Etnoyer P, Warrenchuk J. 2007. A catshark nursery in a deep gorgonian field in the Mississippi Canyon, Gulf of Mexico. Bulletin of Marine Science. 81:553–559.

Fabri MC, Pedel, L, Beuck L, Galgani F, Hebbeln D, Freiwald A. 2014. Megafauna of vulnerable marine ecosystems in French Mediterranean submarine canyons: spatial distribution and anthropogenic impacts. Deep-Sea Research II. 104:184–207.

Feigenbaum D, Blair CH, Bell M, Martin JR, Kelly MG. 1985. Virginia's artificial reef study: description and results of year 1. Bulletin of Marine Science. 37:179–188.

Firth FE. 1933. *Anthias nicholsi*, a new fish taken off Virginia in the deep-water trawl fishery. Copeia. 1933:158–160.

Firth FE. 1937. Recent records extending the range of *Caulolatilus microps* north of Florida. Copeia. 1937:189.

Flock ME, Hopkins TL. 1992. Species composition, vertical distribution, and food-habits of the sergestid shrimp assemblage in the eastern Gulf of Mexico. Crustacean Biology. 12:210–223.

Gabriel WL. 1992. Persistence of demersal fish assemblages between Cape Hatteras and Nova Scotia, northwest Atlantic. Journal of the Northwest Atlantic Fisheries Science. 14:29–46.

Gage JD, Tyler PA. 1999. Deep-sea biology: a natural history of organisms at the deep-sea floor. Cambridge (UK): Cambridge University Press.

Garrison LP, Link JS. 2000. Diets of five hake species in the northeast United States continental shelf ecosystem. Marine Ecology Progress Series. 204:243–255.

Gartner JV Jr, Crabtree RE, Sulak KJ. 1997. Feeding at depth. In: Randall DJ, Farrell AP, editors. Deep-sea fishes. San Diego (CA): Academic Press. p 115–193.

Gartner JV Jr, Sulak KJ, Ross SW, Necaise AM. 2008. Persistent near-bottom aggregations of mesopelagic animals along the North Carolina and Virginia continental slopes. Marine Biology. 153:825–841.

Graf G. 1989. Benthic-pelagic coupling in a deep-sea community. Nature. 341:437–439.

Greene CH, Wiebe PH, Burczunski J, Youngbluth MJ. 1988. Acoustical detection of high-density krill demersal layers in the submarine canyons off Georges Bank. Science. 241:359–361.

Grimes CB, Manooch CS, Huntsman GR. 1982. Reef and rock outcropping fishes of the outer continental shelf of North Carolina and South Carolina, and ecological notes on the red porgy and vermilion snapper. Bulletin of Marine Science. 32:277–289.

Grimes CB, Able KW, Jones RS. 1986. Tilefish, *Lopholatilus chamaeleonticeps*, habitat, behavior and community structure in Mid-Atlantic and southern New England waters. Environmental Biology of Fishes. 15:273–292.

Grimes CB, Able KW, Jones RS, Twichell DC, Turner SC. 1987. Studies on tilefish fishery biology, ecology and bioerosion on the middle Atlantic and southern New England continental shelf. NOAA Symposium Series for Undersea Research. 2:49–69.

Grosslein MD, Azarovitz TR. 1982. Fish distribution (Mesa New York Bight Atlas Monograph No. 15). Albany (NY): New York Sea Grant Institute. 182 pp.

Haedrich RL, Rowe GT, Polloni PT. 1975. Zonation and faunal composition of epibenthic populations on the continental slope south of New England. Journal of Marine Research. 33:191–212.

Hare JA, Manderson JP, Nye JA, Alexander MA, Auster PJ, Borggaard DL, Capotondi AM, Damon-Randall KB, Heupel E. 2012. Cusk (*Brosme brosme*) and climate change: assessing the threat to a candidate marine fish species under the US Endangered Species Act. ICES Journal of Marine Science. 69:1753–1768.

Hecker B, Blechschmidt G. 1980. Final historical coral report for the canyon assessment study in the mid- and north Atlantic areas of the U.S. outer continental shelf. In: Hecker B, Blechschmidt G, Gibson P, editors. Epifaunal zonation and community structure in three mid- and north Atlantic canyons. Report by Lamont-Doherty Geological Observatory for the U.S. Department of Interior, Bureau of Land Management. Contract No. BLM AA5 51-CT8-49. p. A1–A114.

Hecker B, Logan DT, Gandarillas FE, Gibson PR. 1983. Megafaunal assemblages in Lydonia Canyon, Baltimore Canyon, and selected slope areas. In: Canyon and Slope Processes Study, Vol. III: Biological Processes. Report by Lamont-Doherty Geological Observatory for the U.S. Department of the Interior, Minerals Management Service. Contract no. 14-12-0001-29178. p. 1–210. [cited 1 June 2016]. Available from: http://invertebrates.si.edu/boem/reports/CASPS_vol3.pdf.

Henry LA, Navas JM, Hennige SJ, Wicks LC, Vad J, Roberts JM. 2013. Cold-water coral reef habitats benefit recreationally valuable sharks. Biological Conservation. 161:67–70.

Higgs ND, Gates AR, Jones DOB. 2014. Fish food in the deep sea: revisiting the role of large food-falls. PLoS ONE. 9(5): e96016.

Horton, A. 2015. Feeding habits of demersal fishes from Baltimore and Norfolk canyons and Hatteras middle slope [master's thesis]. Wilmington (NC): University of North Carolina-Wilmington.

Houston KA, Haedrich RL. 1984. Abundance and biomass of macrobenthos in the vicinity of Carson Submarine Canyon, northwest Atlantic Ocean. Marine Biology. 82:301–305.

Houston KA, Haedrich RL. 1986. Food habits and intestinal parasites of deep demersal fishes from the upper continental slope east of Newfoundland, northwest Atlantic Ocean. Marine Biology. 92:563-574.

Hudson IR, Wigham BD. 2003. In situ observations of predatory feeding behaviour of the galatheid squat lobster *Munida sarsi* using a remotely operated vehicle. Journal of the Marine Biology Association of the UK. 83:463–464.

Huvenne VAI, Tyler PA, Masson DG, Fisher EH, Hauton C, Hühnerbach V, Le Bas TP, Wolff GA. 2011. A picture on the wall: innovative mapping reveals cold-water coral refuge in submarine canyon. PLoS ONE 6:e28755.

Hyslop EJ. 1980. Stomach contents analysis—a review of methods and their application. Fish Biology. 17:411–429.

Iwamoto T. 1966. The macrourid fish *Cetonurus globiceps* in the Gulf of Mexico. Copeia. 1966:439–442.

Johnson AK, Richards RA, Cullen DW, Sutherland SJ. 2008. Growth, reproduction, and feeding of large monkfish, *Lophius americanus*. ICES Journal of Marine Science. 65:1306–1315.

Kämpf J. 2012. Lee effects of localized upwelling in a shelf-break canyon. Continental Shelf Research. 42:78–88.

Keller GH, Shepard FP. 1978. Currents and sedimentary processes in submarine canyons off the northeast United States, Chapter 2. In: Stanley DJ, Kelling G, editors. Sedimentation in submarine canyons, fans and trenches. Stroudsburg (PA): Dowden, Hutchinson and Ross, Inc. p. 15-32.

Kelly NE, Shea EK, Metaxas A, Haedrich RL, Auster PJ. 2010. Biodiversity of the deep-sea continental margin bordering the Gulf of Maine (NW Atlantic): relationships among sub-regions and to shelf systems. PLoS ONE. 5:e13832.

King NJ, Jamieson AJ, Bagley PM, Priede IG. 2008. Deep-sea scavenging demersal fish fauna of the Nazare Canyon system, Iberian coast, north-east Atlantic Ocean. Journal of Fish Biology. 72:1804-1814.

Kiraly SJ, Moore JA, Jasinski PH. 2003. Deepwater and other sharks of the U.S. Atlantic Ocean exclusive economic zone. Marine Fisheries Review. 65:1–63.

Koslow JA. 1993. Community structure in North Atlantic deep-sea fishes. Progress in Oceanography. 31:321–338.

Kutti T, Bergstad OA, Fosså JH, Helle K. 2014. Cold-water coral mounds and sponge-beds as habitats for demersal fish on the Norwegian shelf. Deep-Sea Research II. 99:122–133.

Lamont-Doherty Geological Observatory. 1983. Canyon and slope processes study, vols. I-III. Prepared for U.S. Department of the Interior, Minerals Management Service. Contract No. 14-12-0001-29178.

Langton RW, Bowman RE. 1980. Food of fifteen northwest Atlantic gadiform fishes. NOAA Technical Report NMFS SSRF-740. 23 p.

Langton RW, Bowman RE, US National Marine Fisheries Service. 1981. Food of eight northwest Atlantic pleuronectiform fishes. U.S. Department of Commerce, NOAA Technical Report NMFS SSRF No. 749.

Leavitt BB. 1938. The quantitative vertical distribution of macroplankton in the Atlantic Ocean Basin. Biology Bulletin. 74(3):376–394.

Lee J. 1949. The bombs heard round the world. Flying. 45:24–25, 68.

Link JS, Alameida FP. 2000. An overview and history of the food web dynamics program of the Northeast Fisheries Science Center, Woods Hole, Massachusetts. NOAA Technical Memo. NMFS-NE-159. 60 p.

Link JS, Bolles K, Milliken CJ. 2002. The feeding ecology of flatfish in the Northwest Atlantic. Northwest Atlantic Fishery Science. 30:1–17.

Macquart-Moulin C, Patrici G. 1996. Accumulation of migratory micronekton crustaceans over the upper slope and submarine canyons of the northwestern Mediterranean. Deep-Sea Research I. 43:579–601.

Mahon R, Brown SK, Zwanenburg KCT, Atkinson DB, Buja KR, Claflin L, Howell GD, Monaco ME, O'Boyle RN, Sinclair M. 1998. Assemblages and biogeography of demersal fishes of the east coast of North America. Canadian Journal Fisheries Aquatic Sciences. 55:1704–1738.

Malahoff A, Embley RW, Fornari DJ. 1982. Geomorphology of Norfolk and Washington Canyons and the surrounding continental slope and upper rise as observed from DSRV Alvin. In: Scrutton RA, Talwani M, editors. The ocean floor. New York (NY): John Wiley & Sons Ltd. p. 97–111.

Markle DF, Musick JA. 1974. Benthic-slope fishes found at 900 m depth along a transect in the western N. Atlantic Ocean. Marine Biology. 26:225–233.

Markle DF, Dadswell MJ, Halliday RG. 1988. Demersal fish and decapod crustacean fauna of the upper continental slope off Nova Scotia from LaHave to St. Pierre Banks. Canadian Journal of Zoology. 66:1952–1960.

Marshall NB, Iwamoto T. 1973. Family Macrouridae. In: Cohen DM, Marshall NB, Ebeling AW, Rosen DE, Iwamoto T, Sonoda P, McDowell SB, Weed WH III, Woods LP, edtors. Fishes of the western North Atlantic. Sears Foundation for Marine Research Number I, Part 6. New Haven (CT): Yale University. p. 496–662.

McEachran JD, Fechhelm JD. 1998. Fishes of the Gulf of Mexico. Vol. 1: Myxiniformes to Gasterosteiformes. Austin (TX): University of Texas Press.

McMillan P, Iwamoto T. 2014. Descriptions of four species of grenadier fishes of the genera *Hymenocephalus* and *Hymenogadus* (Teleostei, Gadiformes, Macrouridae) from the New Zealand region and Tasman Sea, including two new species of *Hymenocephalus*. Zootaxa. 3856:117–134.

Melo MRS. 2007. A new synaphobranchid eel (Anguilliformes: Synaphobranchidae) from Brazil, with comments on the species from the western South Atlantic. Copeia. 2007:315–323.

Merrett NR, Marshall NB. 1980. Observations on the ecology of deep-sea bottom-living fishes collected off northwest Africa 08°-27°N. Progress in Oceanography. 9:185–244.

Methratta ET, Link JS. 2012. Feeding hotspots for four northwest Atlantic groundfish species. ICES Journal of Marine Science. 69:1710–1721.

Middleton RW, Musick JA. 1986. The abundance and distribution of the family Macrouridae (Pisces: Gadiformes) in the Norfolk Canyon area. Fishery Bulletin. 84:35–62.

Miller GC, Richards WJ. 2002. Peristediidae. In: Carpenter KE, editor. The living marine resources of the western Central Atlantic. Vol. 2. Rome (Italy): FAO. p. 1278–1285.

Miller RJ, Hocevar J, Stone RP, Fedorov DV. 2012. Structure-forming corals and sponges and their use as fish habitat in Bering Sea submarine canyons. PLoS ONE. 7:e33885.

Møller PR, Nielsen JG, Knudsen SW, Poulsen JY, Sünksen K, Jørgensen OA. 2010. A checklist of the fish fauna of Greenland waters. Zootaxa. 2378:1–84.

Moore JA, Hartel KE, Craddock JE, Galbraith JK. 2003. An annotated list of deepwater fishes from off the New England region, with new area records. Northeastern Nature. 10:159–248.

Moore JA, Auster PJ, Calini D, Heinonen K, Barber K, Hecker B. 2008. False boarfish Neocytus helgae in the western North Atlantic. Bulletin of the Peabody Museum of Natural History. 49:31–41.

Moyle PB, Cech J. 1988. Fishes: an introduction to ichthyology. Englewood Cliffs (NJ): Prentice Hall.

Munroe TA. 1998. Systematic and ecology of tonguefishes of the genus *Symphurus* (Cynoglossidae: Pleuronectiformes) from the western North Atlantic Ocean. Fishery Bulletin. 96:1–182.

Murawski SA, Lange AM, Sissenwine MP, Mayo RK. 1983. Definition and analysis of multispecies otter-trawl fisheries off the northeast coast of the United States. Journal du Conseil/Conseil Permanent International pour l'Exploration de la Mer. 41:13–27.

Murdy EO, Birdsong RS, Musick JA. 1997. Fishes of Chesapeake Bay. Washington (DC): Smithsonian Institute Press. 324 p.

Musick JA. 1979. Community structure of fishes on the continental slope and rise off the middle Atlantic coast of the United States. Special Scientific Report No. 96. Virginia Institute of Marine Science.

Musick JA, Desfosse JC, Grogan ED. 1992. Fish assemblages at a deep-water sewage disposal site (DWD-106). Final Report to NOAA NMFS. 60 p.

Nagabhushanam AK. 1965. On the biology of the commoner gadoids in Manx waters. Journal of the Marine Biological Association of the United Kingdom. 45:615–657.

Neves A, Sequeira V, Paiva RB, Vieira AR, Gordo LS. 2012. Feeding habits of the bluemouth, *Helicolenus dactylopterus dactylopterus* (Delaroche, 1809) (Pisces: Sebastidae) in the Portuguese coast. Helgoland Marine Research. 66(2):189–197.

Nye JA, Link JS, Hare JA, Overholtz WJ. 2009. Changing spatial distribution of fish stocks in relation to climate and population size on the Northeast United States continental shelf. Marine Ecology Progress Series. 393:111–129.

Obelcz J, Brothers D, Chaytor J, ten Brink U, Ross SW, Brooke S. 2014. Geomorphic characterization of four shelf-sourced submarine canyons along the U.S Mid-Atlantic continental margin. Deep-Sea Research II. 104:106–119.

Parker RO Jr, Ross SW. 1986. Observing reef fishes from submersibles off North Carolina. NE Gulf Sci. 8:31–49.

Parker RO Jr, Mays RW. 1998. Southeastern U.S. deepwater reef fish assemblages, habitat characteristics, catches, and life history summaries. NOAA Technical Report NMFS 138. 41 p.

Partyka ML, Ross SW, Quattrini AM, Sedberry GR, Birdsong TW, Potter J. 2007. Southeastern United States deep sea corals (SEADESC) initiative: A collaborative effort to characterize areas of habitat-forming deep-sea corals. NOAA Technical Memorandum OAR OER 1. Silver Spring, MD. 176 p.

Pearcy WG, Ambler JW. 1974. Food habits of deep-sea macrourid fishes off the Oregon coast. Deep-Sea Research. 21(9):745.

Perkol-Finkel S, Shashar N, Benayahu Y. 2006. Can artificial reefs mimic natural reef communities? The roles of structural features and age. Marine Environmental Research. 61:121–135.

Purser A, Orejas C, Gori A, Tong R, Unnithan V, Thomsen L. 2013. Local variation in the distribution of benthic megafaunal species associated with cold-water coral reefs on the Norwegian margin. Continental Shelf Research. 54:37–51.

Quattrini AM, Ross SW. 2006. Fishes associated with North Carolina shelf-edge hardbottoms and initial assessment of a proposed marine protected area. Bulleting of Marine Science. 79:137–163.

Quattrini AM, Ross SW, Carlson MCT, Nizinski MS. 2012. Megafaunal-habitat associations at a deep-sea coral mound off North Carolina, USA. Marine Biology. 159:1079–1094.

Reid WDK, Sweeting CJ, Wigham BD, McGill RAR, Polunin NVC. 2013. High variability in spatial and temporal size-based trophodynamics of deep-sea fishes from the Mid-Atlantic Ridge elucidated by stable isotopes. Deep-Sea Research II. 98:412–420.

Roberts JM, Wheeler A, Freiwald A, Cairns S. 2009. Cold-water corals. Cambridge (UK): Cambridge University Press.

Rodríguez-Marín E, Punzón A, Paz J, Olaso J. 1994. Feeding of the most abundant fish species in Flemish Cap in summer 1993. NAFO Scientific Council Research Document No. 35, Serial No. N2403. 33 p.

Rodríguez-Marín E. 1995. Feeding relationships of demersal fish in Flemish Cap in summer 1993–1994. NAFO Scientific Council Research Document, No. 104, Serial No. N2627. 33 p.

Rohr BA, Gutherz EJ. 1977. Biology of offshore hake, *Merluccius albidus*, in the Gulf of Mexico. Fishery Bulletin. 75:147–158.

Román E, González C, Ceballos E. 2004. Food and feeding of most abundant fish species in Flemish Cap. NAFO Scientific Council Research Document. No. 58, Serial No. N5018.

Ross SW. 2007. Unique deep-water ecosystems off the southeastern United States. Oceanography. 20:130–139.

Ross SW, Moser ML. 1995. Life history of juvenile gag, *Mycteroperca microlepis*, in North Carolina estuaries. Bulletin of Marine Science. 56(1):222–237.

Ross SW, Quattrini AM. 2007. The fish fauna associated with deep coral banks off the southeastern United States. Deep-Sea Research I. 54:975–1007.

Ross SW, Quattrini AM. 2009. Deep-sea reef fish assemblage patterns on the Blake Plateau (western north Atlantic Ocean). Marine Ecology. 30:74–92.

Ross SW, Sulak KJ, Munroe TA. 2001. Association of *Sycenus infelix* (Crustacea: Isopoda: Aegidae) with benthopelagic rattail fishes *Nezumia* spp. (Macrouridae) along the western North Atlantic continental slope. Marine Biology. 138:595–601.

Ross SW, Rhode M, Quattrini AM. 2015a. Demersal fish distribution and habitat use within and near Baltimore and Norfolk canyons, U.S. middle Atlantic slope. Deep-Sea Research I. 103:137–154.

Ross SW, Brooke S, Quattrini AM, Rhode M, Watterson JC. 2015b. A deep‐sea community, including *Lophelia pertusa*, at unusually shallow depths in the western North Atlantic Ocean off northeastern Florida. Marine Biology. 162:635–648.

Ross SW, Rhode M, Viada S, Mather R. 2016. Fish species associated with shipwreck and natural hard-bottom habitats from the middle to outer continental shelf of the Middle Atlantic Bight near Norfolk Canyon. Fishery Bulletin. 114:45–57.

Rowe GT. 1971. Observations on bottom currents and epibenthic populations in Hatteras Submarine Canyon. Deep-Sea Research. 18:569–581.

Rowe GT. 1972. The exploration of submarine canyons and their benthic faunal assemblages. Proceedings of the Royal Society of Edinburgh (B). 73:159–169.

Rowe GT, Polloni PT, Haedrich RL. 1982. The deep-sea macrobenthos on the continental margin of the northwest Atlantic Ocean. Deep-Sea Research Part A. 29:257–278.

SEAMAP-SA. 2001. Distribution of bottom habitats on the continental shelf from North Carolina through the Florida Keys. Washington (DC): SEAMAP-SA Bottom Mapping Workgroup, Atlantic States Marine Fisheries Commission. 166 p.

Sedberry GR. 1983. Food habits and trophic relationships of a community of fishes on the outer continental shelf. NOAA Technical Report NMFS SSRF-773. 56 p.

Sedberry GR, Musick JA. 1978. Feeding strategies of some demersal fishes of the continental slope and rise off the Mid-Atlantic coast of the USA. Marine Biology. 44:357–375.

Skarke A, Ruppel C, Kodis M, Brothers D, Lobecker E. 2014. Widespread methane leakage from the sea floor on the northern US Atlantic margin. Nature Geosciences Letters. 7:657–661.

Smith CL. 1971. A revision of the American groupers: *Epinephelus* and allied genera. Bulletin of the American Museum of Natural History. 146:67-242.

Smith BE, Link JS. 2010. The trophic dynamics of 50 finfish and 2 squid species on the northeast US Continental Shelf. NOAA Technical Memo. NMFS-NE-216. 21 p.

Snelgrove PVR, Haedrich RL. 1985. Structure of the deep demersal fish fauna off Newfoundland. Marine Ecology Progress Series. 27:99–107.

Söffker M, Sloman KA, Hall-Spencer JM. 2011. In situ observations of fish associated with coral reefs off Ireland. Deep-Sea Research I. 58:818–825.

Staudigel H, Hart SR, Pile A, Bailey BE, Baker ET, Brooke S, Connelly DP, Haucke L, German CR, Hudson I, Jones D, Koppers AAP, Konter J, Lee R, Pietsch TW, Tebo BW, Templeton AS, Zierenberg R, Young CM. 2006. Vailulu`u Seamount, Samoa: life and death on an active submarine volcano. Proceedings of National Academy of Sciences U.S.A. 103:6448–6453.

Steimle FW, Zetlin C. 2000. Reef habitats in the Middle Atlantic Bight: abundance, distribution, associated biological communities, and fishery resource use. Marine Fisheries Review. 62:24–42.

Stephan DC, Lindquist DG. 1989. A comparative analysis of the fish assemblages associated with old and new shipwrecks and fish aggregating devices in Onslow Bay, North Carolina. Bulletin of Marine Science. 44:698–717.

Stevens DW, Dunn MR. 2011. Different food preferences in four sympatric deep-sea Macrourid fishes. Marine Biology. 158(1):59–72.

Sulak KJ. 1982. A comparative taxonomic and ecological analysis of temperate and tropical demersal deep-sea fish faunas in the western North Atlantic [PhD dissertation]. Miami (FL): University of Miami. 181 p.

Sulak KJ, Ross SW. 1996. Lilliputian bottom fish fauna of the Hatteras upper middle continental slope. Journal of Fisheries Biology. 49(Suppl. A):91–113.

Sulak KJ, Brooks RA, Luke KE, Norem AD, Randall M, Quaid AJ, Yeargin GE, Miller JM, Harden WM, Caruso JH, Ross SW. 2007. Demersal fishes associated with *Lophelia pertusa* coral and hard-substrate biotopes on the continental slope, northern Gulf of Mexico. In: George RY, Cairns SD, editors. Conservation and adaptive management of seamount and deep-sea coral ecosystems. Miami (FL): University of Miami. p. 65–92.

Tattersall WM. 1926. Crustaceans of the orders Euphausiacea and Mysidacea from the western Atlantic. Proceedings of the United States National Museum. 69(8):1–31.

Trenkel VM, Lorance P. 2011. Estimating *S. kaupii* densities: contribution of fish behavior to differences between bait experiments and visual strip transects. Deep-Sea Research Part I. 58:63–71.

Tucholke BE. 1987. Submarine geology. In: Milliman JD and Wright WR, editors. The marine environment of the US Atlantic continental slope and rise. Boston (MA): Jones and Bartlett. p. 56-113.

Valentine PC, Uzmann JR, Cooper RA. 1980. Geology and Biology of Oceanographer Submarine Canyon. Marine Geology. 38:283–312.

van Oevelen D, Soetaert K, Garcia R, de Stigter HC, Cunha MR, Pusceddu A, Danovaro R. 2011. Canyon conditions impact carbon flows in food webs of three sections of the Nazaré canyon. Deep-Sea Research II. 58:2461–2476.

Vestheim H, Kaartvedt S. 2009. Vertical migration, feeding and colouration in the mesopelagic shrimp *Sergestes arcticus*. Plankton Research. 31(11):1427–1435.

Vetter EW, Dayton PK. 1998. Macrofaunal communities within and adjacent to a detritus rich submarine canyon system. Deep-Sea Research II. 45:25–54.

Vetter EW, Dayton PK. 1999. Organic enrichment by macrophyte detritus, and abundance patterns of megafaunal populations in submarine canyons. Marine Ecology Progress Series. 186:137–148.

Vetter EW, Smith CR, De Leo FC. 2010. Hawaiian hotspots: enhanced megafauna abundance and diversity in submarine canyons on the oceanic islands of Hawaii. Marine Ecology. 31:183–199.

Wilson RR Jr, Smith KL Jr. 1984. Effect of near bottom current on detection of bait by the abyssal grenadier fishes *Coryphaenoides* spp., recorded in situ with a video camera on a free vehicle. Marine Biology. 84:83–91.

Young CM. 2009. Communities on deep-sea hard bottom. In: Wahl M, editor. Marine hard bottom communities. New York (NY): Springer. p. 39–60.

This page intentionally left blank

CHAPTER 16. FOOD-WEB STRUCTURE OF CANYON AND SLOPE-ASSOCIATED FAUNA REVEALED BY STABLE ISOTOPES

Amanda W.J. Demopoulos, Jennifer P. McClain-Counts, Steve W. Ross, Sandra Brooke, and Michael P. Rhode

16.1 INTRODUCTION

Food webs and associated trophic linkages among organisms are central themes in ecology that provide insight into the structure and function of ecosystems. In the deep sea, food webs rely on particulate flux raining from surface waters for energy (Klages et al. 2003), except for chemosynthetic communities, which rely on *in situ* production via chemosynthesis (Van Dover 2007). In general, the deep sea is a food limited environment because only a small percentage of organic carbon produced in surface waters settles to the seafloor (Gage and Tyler 1991, Klages et al. 2003, De La Rocha and Passow 2007). In contrast, relative to more quiescent slope environments, canyons can experience dynamic flow and turbulence. Internal tides can enhance turbulent mixing near the canyon seafloor leading to resuspension of sediments. Channeling of organic matter in deepsea canyons can enhance benthic productivity leading to high biodiversity (Vetter and Dayton 1998, 1999) and trophic complexity (Stefanescu et al. 1994, Cartes and Sorbe 1999). Thus, there may be a decoupling between the benthic-productivity relationships in canyon environments where food limitation may not be a driving factor influencing community structure. However, there have been only a few studies, often limited in depth range and spatial scale, that have examined the trophic pathways of deepsea canyons relative to adjacent slope environments (Duineveld et al. 2001, Fanelli et al. 2009, Cartes et al. 2010, Jeffreys et al. 2011).

Numerous canyons incise the U.S. Atlantic margin. Research examining Baltimore and Norfolk canyons has revealed distinctly different physical and geological environments. Baltimore Canyon was characterized by distinct resuspension (shallow depths) and deposition zones, whereas Norfolk Canyon exhibited continuous deposition along the length of the canyon axis (**Chapter 6**). Given these key differences in depositional environments and, consequently, the availability of food to the benthos, there may be corresponding differences in the canyon food webs. Examining food-web structure and food resource availability can help identify mechanistic drivers for diversity patterns (Rex 1977, Cartes and Carrasson 2004, Cartes et al. 2010).

Stable isotope analysis (SIA) is a useful method for discerning complex food webs, particularly in remote environments like the deep sea. Stable carbon isotopes ($\delta^{13}C$) closely reflect a consumer's food source (Fry and Sherr 1984, Peterson and Fry 1987), whereas stable nitrogen isotopes have been used to approximate trophic level because $\delta^{15}N$ values typically increase 2 to 5‰ with each trophic level (Minagawa and Wada 1984, Post 2002, McCutchan et al. 2003). Primary producers in a system exhibit distinct isotopic compositions due to the types of nutrients fixed and the associated photosynthetic or chemosynthetic pathways (Peterson and Fry 1987, Van Dover 2007). For example, SIA has been used to examine energy resources in reducing environments, including seep and vent fauna that contain symbionts, and for understanding trophic subsidies among heterotrophic fauna that reside in these environments (Paull et al. 1985, Kennicutt et al. 1988, Levin et al. 2000, Van Dover 2007). Photosynthetically derived material has a distinct $\delta^{13}C$ range (-25 to -15‰), whereas biogenic methane present at seeps is isotopically depleted in ^{13}C (<-50‰), resulting in low $\delta^{13}C$ values for fauna housing chemoautotrophic endosymbionts and heterotrophic fauna that consume seep-derived organic matter (e.g., free-living bacteria; Fry and Sherr 1984, Van Dover 2007, Thurber et al. 2010).

SIA has been used to complement traditional diet studies often plagued by unidentifiable material and empty stomachs (Boyle et al. 2012). Isotopes integrate over an extended period, whereas stomach content

analysis represents a short-term snapshot of a consumer's diet. SIA has been used to understand transfer of carbon through systems, including tracing its vertical transport from the sea surface to the seafloor, and back through diel vertical migrations, and lateral transport through the movement of demersal organisms among deepsea habitats (Trueman et al. 2014). In addition, SIA can help estimate food-chain length, trophic level, and changes in trophic level associated with growth at the species and community levels (France et al. 1998, Jennings et al. 2001, Al-Habsi et al. 2008). SIA can provide temporally and spatially integrated trophic estimates used to understand and define trophic linkages among species and communities (Davenport and Bax 2002, Harvey et al. 2002). The relationship between body size and trophic level based on SIA has been examined for demersal fish species to some extent (Jennings et al. 2002, Al-Habsi et al. 2008); however, there is still much to be learned regarding the trophic ecology of deepsea demersal fish communities.

The stable isotopic composition of sinking particles changes with depth due to preferential assimilation of the light isotopes during microbial metabolism (Mintenbeck et al. 2007); however, rapidly sinking particles may experience less fractionation than those sinking more slowly (Rau et al. 1991, Iken et al. 2001). Biological processing within the benthos can also result in increases in $\delta^{13}C$ and $\delta^{15}N$ values, leading to enriched isotope values up the food chain. Transport of carbon to the seafloor occurs through a number of different processes including vertical flux of phytodetritus produced in surface waters and through diel vertical migrators (DVM) including zooplankton, cephalopods, and fishes (Trueman et al. 2014). The dominant transport mechanism on the continental slope is passive deposition of particulate organic matter to the seafloor, leading to enriched isotopic composition due to the slow settlement process and ongoing microbial degradation (Mintenbeck et al. 2007). In contrast, within canyon environments, the rapid deposition of fresh organic matter to the seafloor can result in depleted ^{13}C and ^{15}N values relative to the older, more refractory, organic matter found on the slope environment. Therefore, different processes in the canyon and slope environments may lead to two dominant trophic pathways: 1) fresh phytoplanktonic production, ^{13}C depleted consumers or 2) decayed organic matter, ^{13}C enriched consumers.

The quality, quantity, and availability of organic matter utilized by deepsea benthos can influence the development of different trophic niches, which can be examined using SIA (Jeffreys et al. 2009, Jackson et al. 2011, Tecchio et al. 2013, Zapata-Hernández et al. 2014). Specific questions regarding trophic niches in the deep sea include:

- Are different species from same feeding group occupying distinct or overlapping trophic niches?
- Do canyon environments promote trophic diversity (e.g., several niches and large niche breadth), or trophic redundancy (e.g., species with overlapping trophic niches)?

The primary objective of this study was to assess deepsea food-web structure and trophic niches in Baltimore and Norfolk canyons and adjacent slopes along the mid-Atlantic margin using SIA and isotope niche width analysis. We hypothesized that the isotopic compositions of canyon versus slope fauna would be distinct, given differences in the physics and chemistry of the canyons and slopes and resulting quality and quantity of the organic matter available to the benthos. These differences should be evident across taxa and among and within feeding groups. We also used SIA to estimate trophic positions of invertebrates and fishes and to examine changes in trophic level with size for specific demersal fish species. Furthermore, comparisons were made between results from SIA for select fishes and stomach content analyses (**Chapter 15**) to characterize trophic relationships of fishes over time.

16.2 METHODS

16.2.1 Sample Collections

Sampling was conducted within and near two submarine canyons in the western Atlantic Ocean off the east coast of the United States (**Figure 16-1**). Additional details on the geomorphic characterization of each canyon were documented by Obelcz et al. (2014) and are presented in **Chapter 6**. Collections occurred during four research cruises in the late summer and early fall from 2011 to 2013 (**Appendix 16-A**, **Table 16-A1**). Multiple gear types, including otter trawls, NIOZ (Royal Netherlands Institute for Sea Research) box cores, ROV push cores, remotely operated vehicle (ROV) suction, and Niskin bottles were used to sample fauna, sediments, and seawater both inside and outside the canyons. Otter trawls (4.9 m head rope, 38.1 mm mesh), were deployed and towed for approximately 30 minutes at approximately 2 knots ground speed to sample benthic fauna. Sediment samples were collected using a NIOZ-designed box core with a cylindrical core (30 cm diameter, 50 cm height) deployed from the ship (**Chapter 3.2.4**). Smaller core tubes (31.65 cm^2 × 30 cm) were inserted into each core sample to collect sediments for analyses. Water samples were collected at various depths using Niskin bottles mounted on the vessel's conductivity-temperature-depth (CTD) rosette (**Chapter 3.2.6**). Collections were also conducted using the ROV *Kraken 2* (2012) and ROV *Jason II* (2013) (**Chapter 3.2.2**). Macrobenthic invertebrates were collected using either the suction systems or the manipulator arms on the ROVs, and sediments were collected using T-handle push cores (31.65 cm^2 × 30 cm) operated by the ROV manipulator arm. Additional water samples were collected using Niskin bottles attached to the ROV *Jason II*.

In 2012, four benthic landers, placed in the head and mouth of the canyons, and two moorings, placed in the middle of the canyons, were deployed for long-term geochemical and physical oceanographic data collection (**Chapter 3.2.3**). All data and gear were recovered in 2013. Fauna attached to the landers and moorings were removed and dissected for SIA using the methods described below.

Cores collected to analyze for sediment characteristics were sliced into fractions (0 to 2, 2 to 5 and 5 to 10 cm) and frozen for analyses at a later time. Vouchers for fishes and invertebrates were preserved in 10% seawater-formalin solution and later transferred into 50% isopropanol for storage. All fauna were sorted and identified to the lowest possible taxa (Brooke, Young, Davies, and Demopoulos laboratories for invertebrates and Ross laboratory for fishes).

Particulate organic material (POM) was collected to characterize the organic carbon baseline for isotopic analyses. POM was collected by filtering seawater (1 to 10 L) collected from Niskin bottles through a preweighed combusted glass microfiber filter (GFF).

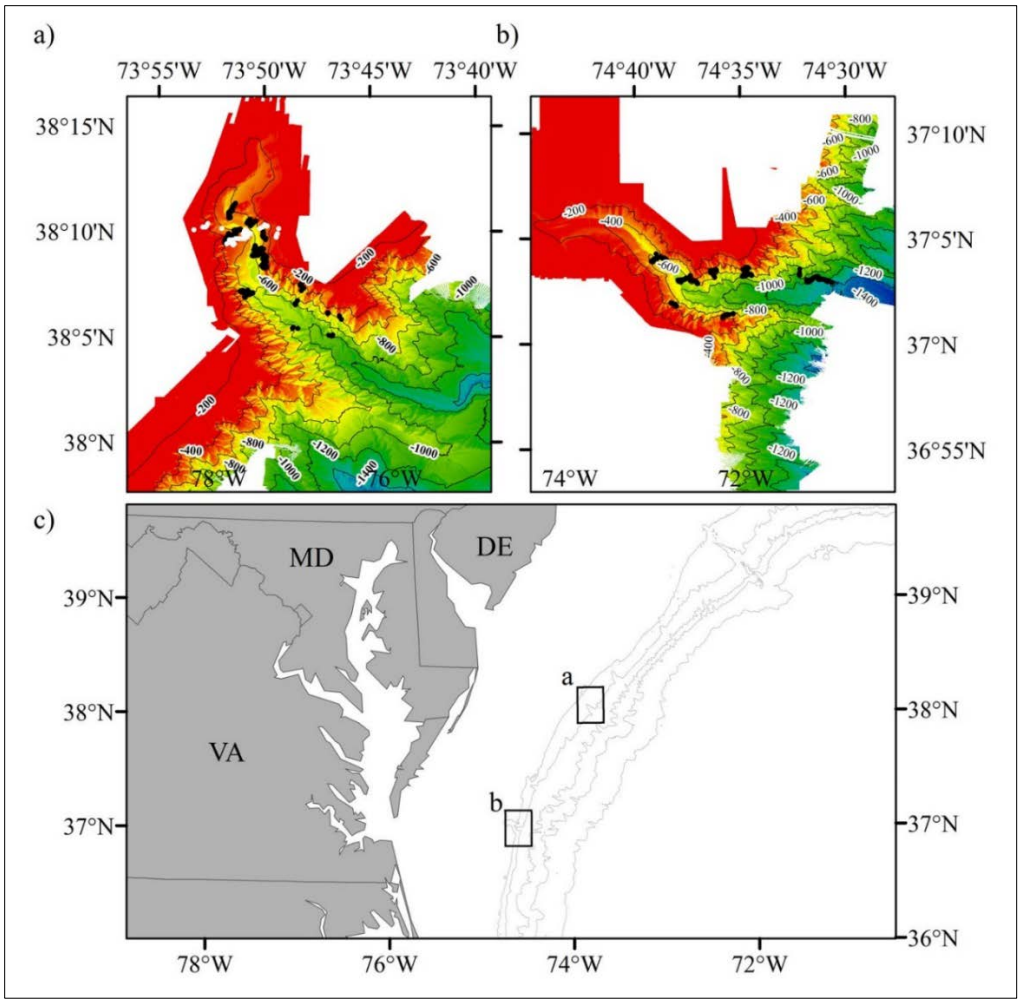

Figure 16-1. Canyons of interest and extent of analyses. a) Baltimore Canyon, b) Norfolk Canyon (both with 200 m contours), and c) overview with bathymetric contours at 100 m, 600 m, 1,600 m, 2,000 m, and 2,500 m. Black points in panels a) and b) represent modern coral observations and white points in panel a) represent historical coral observations from the 1980s and 1990s.

16.2.2 Isotope Sample Processing and Analysis

Dissections of fish and invertebrate tissues occurred prior to preservation. For consistency, tissue was removed from similar body regions based on taxa (e.g., muscle from the dorsal region of fishes, caudal tissue of shrimps; leg muscle for crabs; mantle, gill, and adductor muscle for molluscs; legs for brittle stars; gonads for urchins; and polyps for corals). Tissue samples were dried to a constant weight at 50 °C to 60 °C, ground to a fine powder and weighed into tin capsules. Invertebrate samples were acidified with 10% platinum chloride to remove inorganic carbon. POM filters were dried and treated with 1.0 N hydrochloric acid, then transferred into tin boats. Sediment samples were homogenized prior to drying and acidified with 1.0 N phosphoric acid before weighing into tin boats. Samples were analyzed for stable carbon and nitrogen isotope composition referenced to Vienna PeeDee Belemnite and atmospheric nitrogen gas, respectively. Analyses were conducted at Washington State University using a Costech (Valencia, California) elemental analyzer interfaced with a GV instruments (Manchester, UK) Isoprime isotope ratio mass spectrometer. Precision was verified using egg albumin calibrated against National Institute of Standards reference materials and reproducibility was monitored using organic

reference standards (Fry 2007). Isotope ratios were expressed in standard delta notation, $\delta^{13}C$ and $\delta^{15}N$, as parts per thousand (‰). Reported $\delta^{13}C$ values were taken from analyzed acidified samples and $\delta^{15}N$ values from nonacidified samples to avoid the potential artefact associated with acidification (Pinnegar and Polunin 1999).

16.2.3 Trophic Level Calculations

To approximate trophic level, we assumed trophic level fractionation of ^{15}N to be 3‰ (Wada et al. 1991, Post 2002, McCutchan et al. 2003) and that the primary consumers have a trophic level of 2. For trophic level (TR) calculations, $\delta^{15}N$ values from hydroids (class Hydrozoa) were used to represent the baseline primary consumer present in both canyon environments ($\delta^{15}N$ = 5.9‰ at Baltimore Canyon and 4.8‰ at Norfolk Canyon) based on the following calculation:

$$TR = (\delta^{15}N_{consumer}\text{-}\delta^{15}N_{hydroid}/3) + 2$$

Hydroids feed on suspended particulate organic matter (primary food source) and were ubiquitous in both canyon environments.

16.2.4 Fish Food Resource Calculations

We calculated ranges in isotope values for organisms expected to serve as food resources for fishes using the following approach. Using the ranges in fish isotope values (maximum and minimum values), "trophic shift boxes" were created in several $\delta^{13}C \times \delta^{15}N$ plots. Based on available literature for the fish species analyzed (**Section 16.4.2**), for these calculations, we assumed 1‰ fractionation in $\delta^{13}C$. For invertebrate consumers, we assumed 1.4‰ for $\delta^{15}N$ enrichment for the following fishes, *Citharichthys arctifrons*, *Coelorinchus caelorhincus*, *Enchelyopus cimbrius*, *Lycenchelys verrillii*, *Dibranchus atlanticus*, and *Dysommina rugosa*. For fish consumers, we assumed 3.3‰ for ^{15}N enrichment for the following fish species: *Nezumia bairdii*, *Merluccius albidus*, *Glyptocephalus cynoglossus*, *Helicolenus dactylopterus*, *Lophius americanus*, *Phycis chesteri*, *Urophycis regia*, and *Synaphobranchus kaupii*. These values were subtracted from the range in fish $\delta^{13}C$ and $\delta^{15}N$ values (France and Peters 1997, Post 2002, McCutchan et al. 2003). Potential food resources for the fishes were expected to fall within the trophic shift box.

16.2.5 Statistical Analysis

All data presented in tables and figures represent untransformed means (±1 SE) unless otherwise indicated.

For statistical comparisons of fauna between Baltimore and Norfolk canyons, between habitats (canyon and slope), and among feeding groups, data for multiple individuals of a single species were averaged from the canyon and slope habitats. To test for differences in stable isotopes among sites, habitats, depths, and feeding groups, we used species as replicates to avoid over-representation of the most abundant taxa. Because the isotope data often did not meet parametric assumptions, even after transformation, comparisons between Baltimore and Norfolk canyons and between canyon and slope environments were made using nonparametric Kruskal Wallis tests (Kruskal and Wallis 1952), with post-hoc paired comparisons using Mann-Whitney U test following Bonferroni correction for multiple comparisons. Between feeding groups, comparisons were made using *a priori* assignments based on literature review (e.g., Bergmann et al. 2009, Fanelli et al. 2011). Fish body size analysis relative to $\delta^{15}N$ was conducted for species that were examined for diet analysis in this study to identify ontogenetic shifts in trophic level and food sources with increased body size (standard or total length was used depending on the species).

Bayesian standard ellipse areas (SEA_B) were calculated to compare isotopic niche structure of fishes and invertebrates analyzed from the slope and canyon environments. SEA_B were estimated for the convex

hull encompassed by all species contained in the $\delta^{13}C/\delta^{15}N$ biplot space (Jackson et al. 2011) for each community-habitat combination. The SEA_B illustrates the total amount of niche space occupied by the population, and can be used to approximate the extent of the trophic diversity and utilized resources. In addition, the ellipses allow for estimation of the amount of trophic overlap between communities. The SEA_B were calculated using SIBER (Stable Isotope Bayesian Ellipses in R-Jackson et al. 2011) incorporated into the SIAR (Stable Isotope Analysis in R) statistical packages. SIAR and statistical analyses were performed using the R 2.14 software (R Development Core Team 2011) and SPSS 16.0 predictive analytics software (SPSS Inc. 2007).

16.3 RESULTS

16.3.1 Baltimore Canyon Food Web

A total of 995 samples, representing eight phyla, were analyzed for $\delta^{13}C$ and $\delta^{15}N$ isotope values. Stable isotope data indicated the main carbon source was derived from photosynthetic material (-22.9 to -15.5‰; **Table 16-A2**; **Figures 16-2a**,**b**,**c**). POM samples covered a broad range of nitrogen values (**Table 16-A2**), with average bottom POM enriched in ^{15}N compared with surface POM. Surface sediment analyzed from within the canyon and on the adjacent slope was enriched in ^{13}C but was depleted in ^{15}N compared with POM.

The food web encompassed approximately five trophic levels (**Figures 16-2a**,**b**,**c**). Several cnidarians and a few echinoderms occupied the lowest trophic levels (~2) followed by a mixture of echinoderms, cnidarians, and arthropods (mainly crustaceans), with fishes and an unidentified asteroid representing the highest order consumers (trophic levels 4−5) (**Figure 16-2a**).

Stable isotope results from Baltimore Canyon and nearby slope revealed that the fishes and invertebrates were composed of isotopically diverse feeding groups (**Table 16-A2**, **Figure 16-2a**,**b**,**c**). An unidentified asteroid and the Atlantic batfish *Dibranchus atlanticus*, an infaunal consumer, had the highest $\delta^{15}N$ values (14.1‰ and 13.9‰ [SE 0.3], respectively). Animals with the lowest $\delta^{15}N$ included the suspension feeder invertebrates Alcyonacea sp. 1 (2.7‰ [SE 0.9]) and Salpida (2.9‰, **Figure 16-2c**).

Several feeding groups occupied intermediate trophic levels including suspension feeders, with $\delta^{15}N$ values ranging from 2.7‰ (SE 0.9) (Alcyonacea sp.1) to 10‰ (the anemone *Halcurias* sp.), and the majority falling between 4 and 8‰ (**Figures 16-2a**,**c**). Corals had $\delta^{13}C$ values ranging from -22.6‰ (SE 0.2) (*Desmophyllum dianthus*) to -18.6‰ (SE 0.4) (*Dasmosmilia lymani*) and $\delta^{15}N$ values ranging from 2.7‰ (SE 0.9) (Alcyonacea sp. 1) to 7.3‰ (Alcyonacea sp. 2) (**Figure 16-3**).

Benthic consumers that feed on fishes and invertebrates residing at (e.g., infaunal or epifaunal) or near the benthos (suprabenthic) ranged in $\delta^{15}N$ from 5.4‰ (SE 0.4) for the asteroid *Persephonaster echinulatus* to 13.4‰ (SE 0.1) for the fish *Lophius americanus* (**Table 16-A2**). For suprabenthic feeders, the fish *Chaunax suttkusi* had the highest $\delta^{15}N$ values (12.4‰), whereas the crab *Rochinia crassa* had the lowest $\delta^{15}N$ values (6.8‰ [SE 1.0], **Table 16-A2**). $\delta^{13}C$ values for suprabenthic feeders ranged from -20.2 to -17.0‰ (SE 0.1) for the crab *Chaceon quinquedens* and unidentified macrourid fishes, (either *Nezumia bairdii* or *C. caelorhincus*), respectively.

Deposit feeders had $\delta^{15}N$ values ranging from 3.2‰ (SE 0.6) (the ophiuroid *Amphiura otteri*) to 11.2‰ (SE 0.5) (the annelid *Hyalinoecia* sp.) (**Figure 16-2c**). Epibenthic feeders *Unciola* sp. (Amphipoda) and *Agononida longipes* (Decapoda) had the lowest $\delta^{15}N$ of the epibenthic consumers, whereas the fishes *Lycodes terraenovae*, *Enchelyopus cimbrius*, and *Lycenchelys verrillii* had the highest $\delta^{15}N$ for this consumer group (12.5 to 12.7‰, **Table 16-A2**). $\delta^{15}N$ values for infaunal consumers ranged from 5.0‰ (SE 0.6) (the asteroid *Astropecten alligator*) to 13.9‰ (SE 0.3) (the fish *Dibranchus atlanticus*). Stable carbon isotope values for this group had a narrow range, from -17.7‰ (the eel *Notacanthus chemnitzii*) to -15.2‰ (SE 0.6) (*D. atlanticus*).

a)

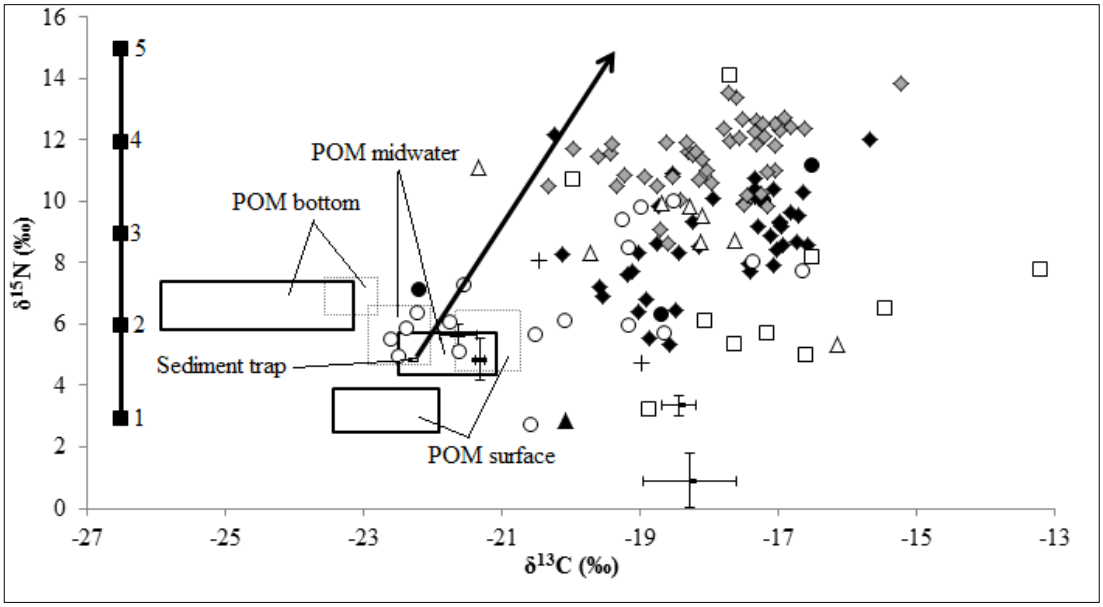

●	Annelida	♦	Chordata - Fish	○	Cnidaria	Δ	Mollusca	+	Porifera	X	Bryozoa	-	Plant
♦	Arthropoda	▲	Chordata - Invert	◊	Brachiopoda	□	Echinoderm	■	Sipuncula	–	Sediment		

b)

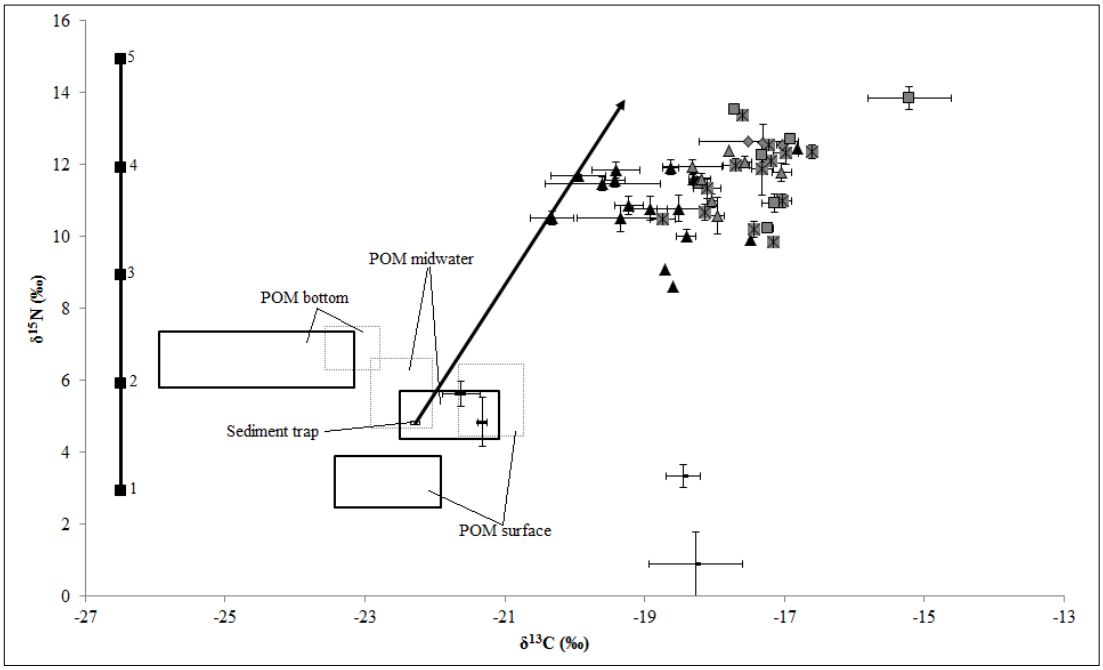

■	Infauna	X	Benthic	▲	Pelagics	○	Suspension	Δ	Unknown				
♦	Epibenthic	●	Scavenger	●	Omnivore	◊	Phytoplanktivore	-	Producer				
▲	Suprabenthic	♦	Microvore	■	Deposit	X	Unk. predator	–	Sediment				

c)

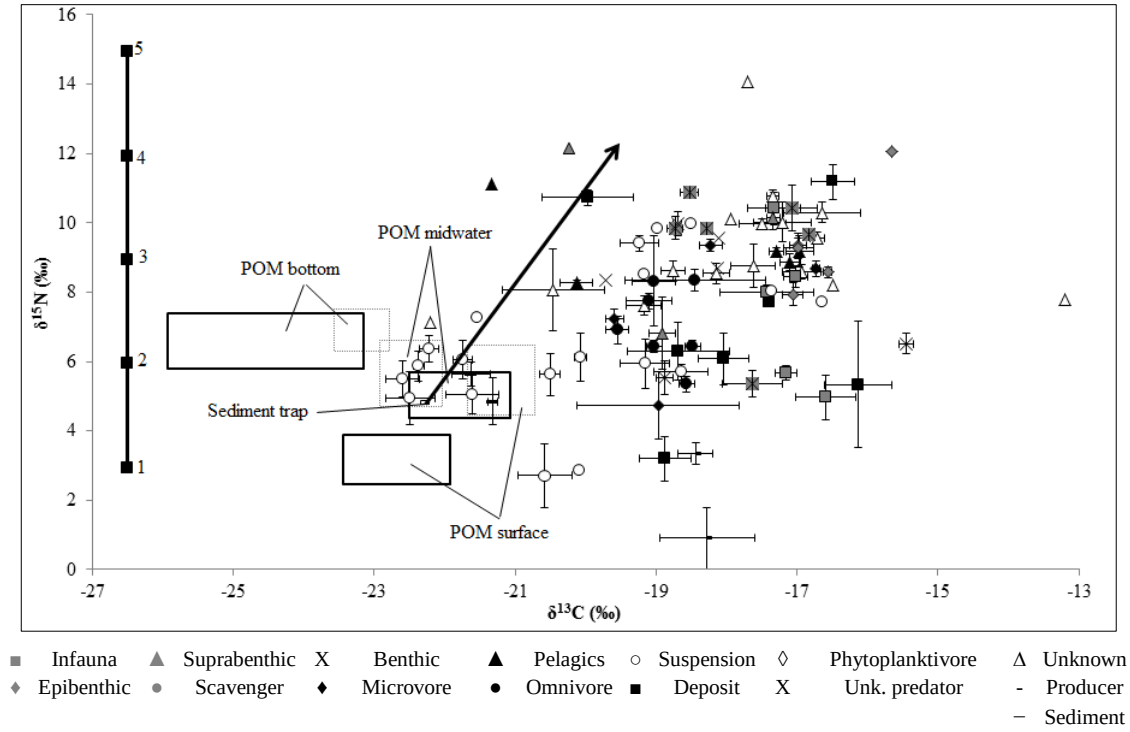

Figure 16-2. Average $\delta^{13}C$ vs. $\delta^{15}N$ (‰ ± SE) for primary producers, consumers, and surface sediments (0−2 cm) collected from nonseep habitats in Baltimore Canyon. a) Isotope data for all taxa with symbols representing taxonomic classification, b) isotope data for all fishes with symbols representing different feeding groups, c) isotope data for all invertebrates with symbols representing different feeding groups. Trophic level bar illustrates calculated trophic position (1−5) (see Methods). Boxes represent main potential carbon sources (average ‰ ± SE), solid lines represent samples collected out of the canyon, and dashed lines represent samples collected in the canyon. Arrow represents expected trophic shift for each trophic level (1‰ for $\delta^{13}C$ and 3‰ for $\delta^{15}N$), starting with average $\delta^{13}C$ and $\delta^{15}N$ for the sediment trap material.

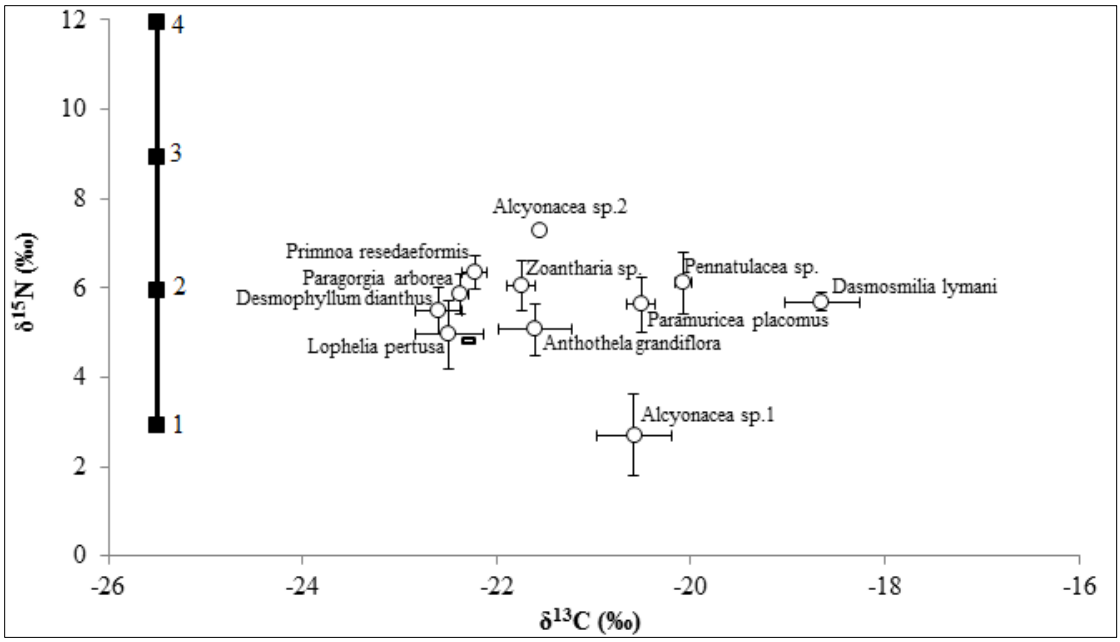

Figure 16-3. Average $\delta^{13}C$ vs. $\delta^{15}N$ (‰ ± SE) for corals collected from nonseep habitats in Baltimore Canyon. Trophic level bar illustrates calculated trophic position (1−4). Small rectangle represents sediment trap data (average ‰ ± SE).

Omnivores had $\delta^{15}N$ values ranging from 5.3‰ (SE 0.2) (the crab *Paguristes lymani*) to 8.3‰ (SE 0.3) (the euphausiid *Bentheuphausia amblyops*). Omnivores had intermediate $\delta^{13}C$ values compared with the other feeding groups and were primarily composed of crustaceans, and isotope values were consistent with serving as food for higher order invertebrate and fish consumers (see **Figure 16-2c** and the following subsections for more detailed diet analysis for fishes). Four taxa were characterized as microvores, consuming zooplankton that included cladorhizid sponges with the lowest $\delta^{15}N$ values (4.7‰ [SE 1.0]) and the pandalid shrimp *Atlantopandalus propinqvus* with the highest $\delta^{15}N$ values (9.3‰ [SE 0.2]). For pelagic consumers, the amphipod *Themisto* sp. had the lowest $\delta^{15}N$ values (8.3‰ [SE 0.1], TR 2.8), and the fish *Argentina striata* had the highest $\delta^{15}N$ of this feeding group (12.4‰, TR 4.2), indicating a wide isotopic range in the pelagic food resources available.

Several taxa could be classified only as unknown predators because of a lack of information on their feeding guild. These taxa included the seastar *Sclerasterias contorta* with the most enriched ^{13}C and depleted ^{15}N values of this feeding group. The squid *Brachioteuthis beani* had the highest $\delta^{15}N$ values (10‰ [SE 0.3]) of this group. Mesopelagic fishes occupied a wide range of trophic levels with $\delta^{15}N$ ranging from 8.6‰ (*Diaphus* sp.) to 11.7‰ (*Nemichthys scolopaceus*), with overlapping $\delta^{13}C$ values among *Stomias boa ferox*, *Polymetme thaeocoryla*, and *N. scolopaceus*.

16.3.2 Norfolk Canyon Food Web

A greater number of total samples, representing 11 phyla, were analyzed from Norfolk Canyon and nearby slope environments (N = 1,914 samples) than from Baltimore Canyon. Stable carbon isotope values indicated the main carbon source was derived from photosynthetic material (-24.2 to -12.6‰; **Table 16-A2**, **Figure 16-4a**,**b**,**c**). POM samples covered a broad range of nitrogen values, with average bottom POM enriched in nitrogen compared with surface and midwater POM.

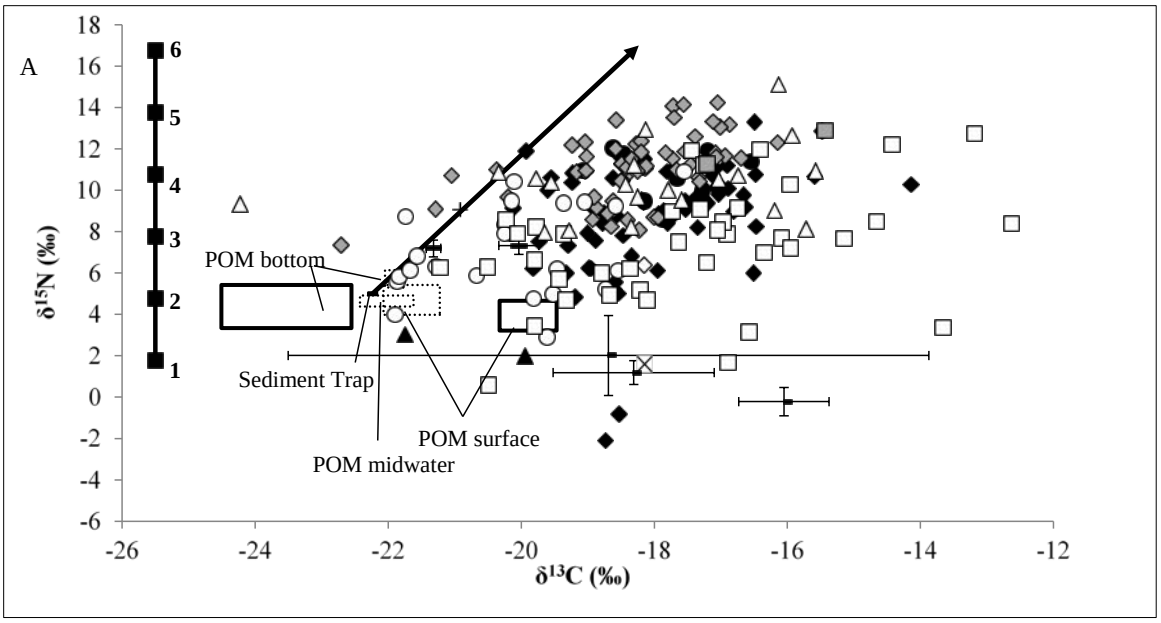

● Annelida ♦ Chordata - Fish ○ Cnidaria Δ Mollusca + Porifera X Bryozoa - Plant
♦ Arthropoda ▲ Chordata - Invert ◊ Brachiopoda □ Echinoderm ■ Sipuncula – Sediment

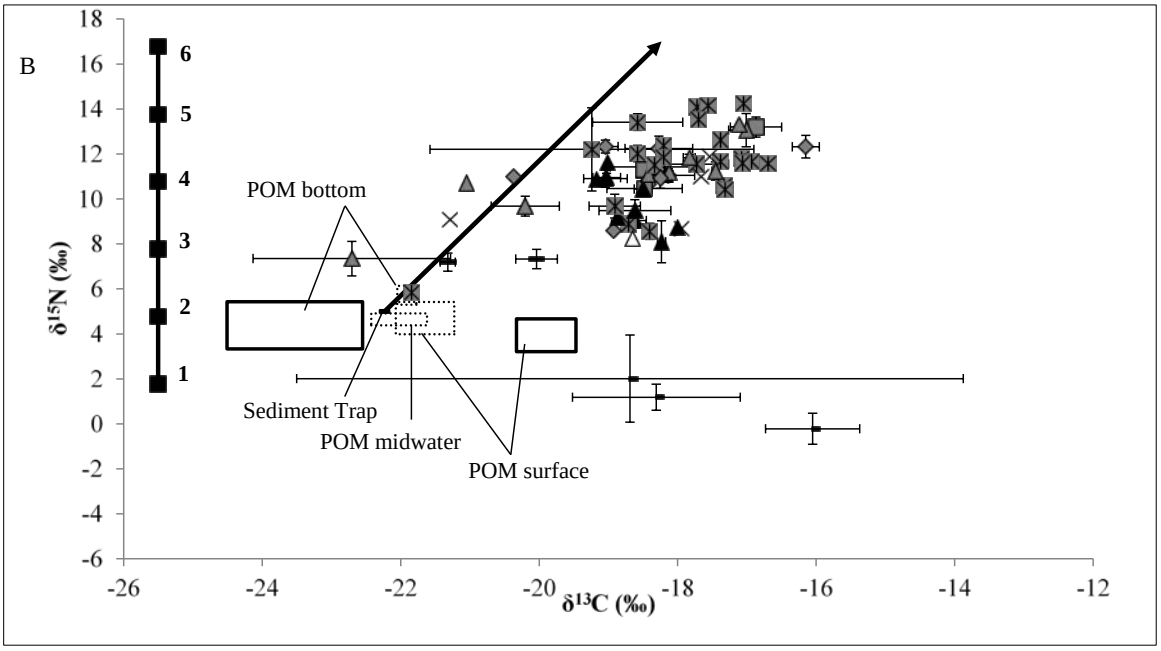

■ Infauna X Benthic ▲ Pelagics ○ Suspension Δ Unknown
♦ Epibenthic ● Scavenger ● Omnivore ◊ Phytoplanktivore - Producer
▲ Suprabenthic ♦ Microvore ■ Deposit X Unk. predator – Sediment

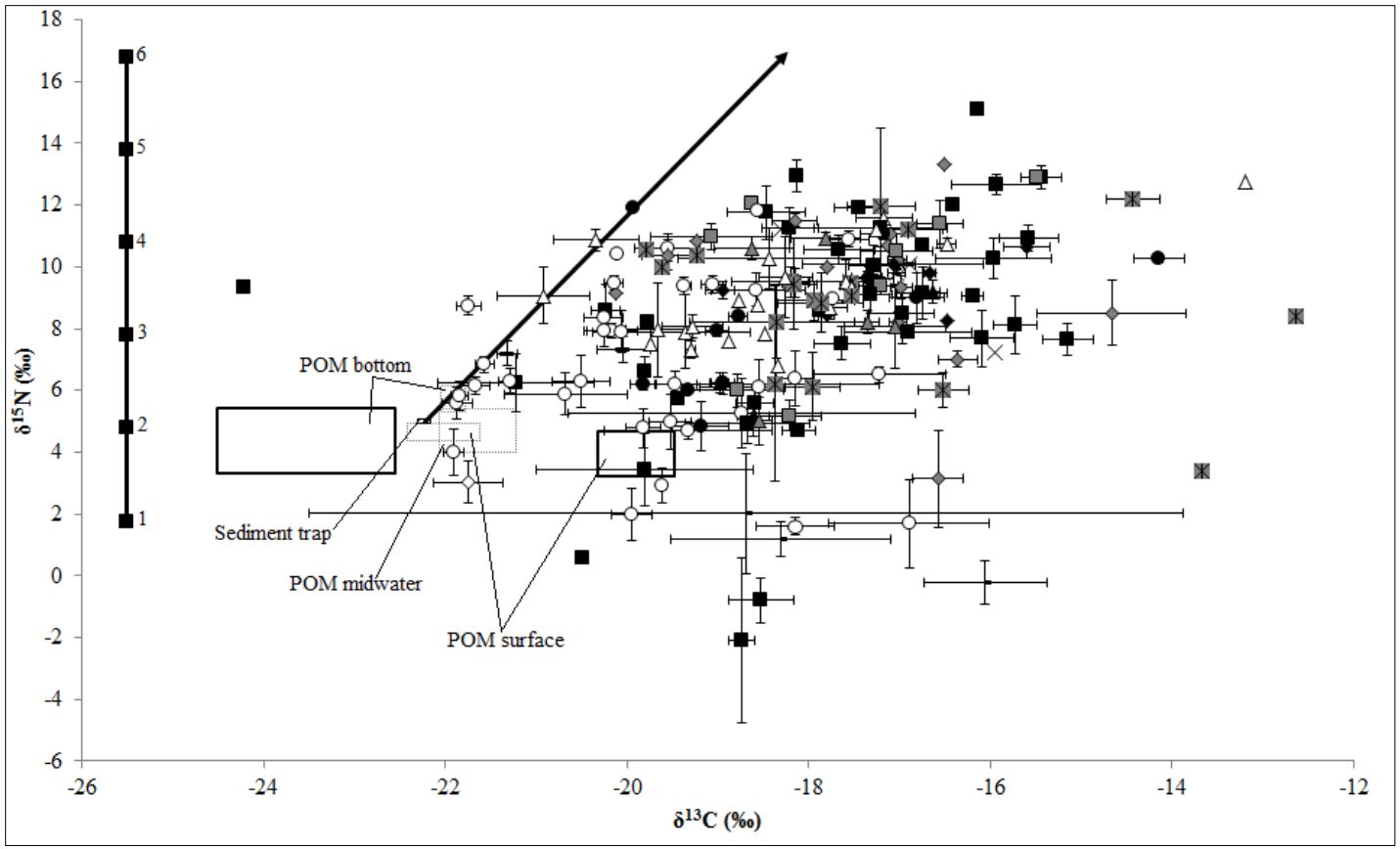

■ Infauna ▲ Suprabenthic X Benthic ▲ Pelagics ○ Suspension ◊ Phytoplanktivore Δ Unknown

♦ Epibenthic ● Scavenger ♦ Microvore ● Omnivore ■ Deposit X Unk. predator - Producer

− Sediment

Figure 16-4. Average $\delta^{13}C$ vs. $\delta^{15}N$ (‰ ± SE) for primary producers, consumers, and surface sediments (0−2 cm) collected from nonseep habitats in Norfolk Canyon. a) Isotope data for all taxa with symbols representing taxonomic classification, b) isotope data for all fishes with symbols representing different feeding groups, c) isotope data for all invertebrates with symbols representing different feeding groups. Trophic level bar illustrates calculated trophic position (1−6) (see Methods). Boxes represent main potential carbon sources (average ‰ ± SE), solid lines represent samples collected out of the canyon, and dashed lines represent samples collected in the canyon. Arrow represents expected trophic shift for each trophic level (1‰ for $\delta^{13}C$ and 3‰ for $\delta^{15}N$), starting with average $\delta^{13}C$ and $\delta^{15}N$ for the sediment trap material.

Norfolk Canyon and slope food web encompassed between five and six trophic levels (**Figure 16-4a**,**b**,**c**). Overall, more isotopic overlap in $\delta^{15}N$ values was found among all the taxa analyzed from Norfolk Canyon than from Baltimore Canyon. Fauna with the lowest $\delta^{13}C$ were the deposit feeders Aplacophora (-24.2‰), and the highest $\delta^{13}C$ value was measured in the benthic-feeding seastar *Odontaster* cf. *hispidus* (-12.6‰). Deposit feeders had the highest range in $\delta^{15}N$ values for all feeding groups, such as the decapod *Euprognatha rastellifera* (-2.1‰ [SE 2.7]) and the bivalve mollusc *Malletia* sp. (15.1‰).

Suspension feeders also exhibited a large range in $\delta^{15}N$ values from 1.6‰ (SE 0.3) (Bryozoan) to 11.8‰ (Scalpellidae) and $\delta^{13}C$ values (-21.9 to -16.9‰), which were consistent with the $\delta^{13}C$ range in their potential primary carbon source, POM. $\delta^{13}C$ values of specific suspension-feeding corals ranged from -21.9‰ (SE 0.1) (*Desmophyllum dianthus*, *Solenosmilia variabilis*) to -17.5‰ (SE 0.2) (*Umbellula* sp.), and $\delta^{15}N$ values from 2.9‰ (SE 0.6) (*Acanthogorgia sp.*) to 11.2‰ (*Sibopathes* sp., **Figure 16-5**).

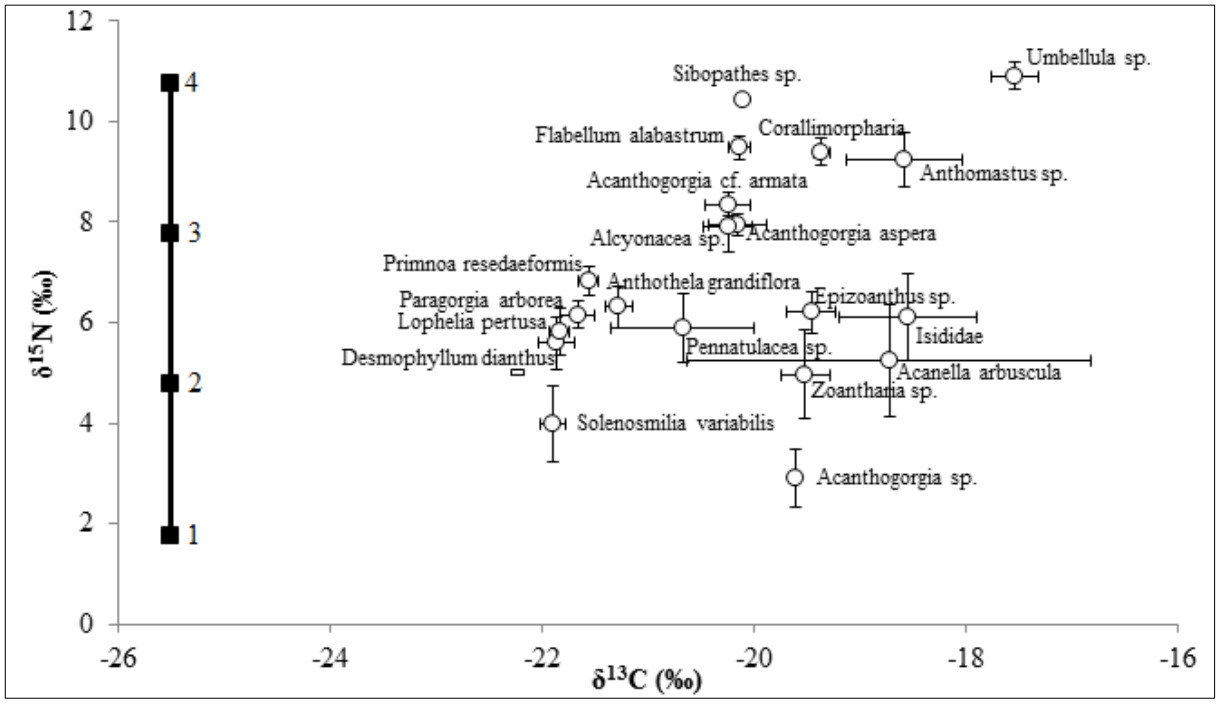

Figure 16-5. Average $\delta^{13}C$ vs. $\delta^{15}N$ (‰ ± SE) for corals collected from nonseep habitats in Norfolk Canyon. Trophic level bar illustrates calculated trophic position (1−4). Small rectangle represents sediment trap data (average ‰ ± SE).

Benthic consumers Nettastomatidae (eels) had the lowest $\delta^{13}C$ (-21.8‰) and $\delta^{15}N$ (5.8‰) values, whereas the asteroid *O. hispidus* had the highest $\delta^{13}C$ value (-12.6‰) and the fish *Aldrovandia affinis* had the highest $\delta^{15}N$ value (14.2‰). For suprabenthic feeders, the macrourid *Nezumia aequalis* was the most depleted in ^{13}C (-22.7‰ [SE 1.4]), whereas the ophiuroid *Asteronyx loveni* and the fish *Merluccius bilinearis* were the most enriched in ^{13}C (-17.0‰ [SE 0.6]). Suprabenthic feeders with the lowest $\delta^{15}N$ values were the crab *Rochinia tanneri* (5.0‰ [SE 0.8]), whereas the macrourid *Nezumia* sp. was the most enriched in ^{15}N (13.3‰).

Deposit-feeding Aplacophora had the lowest $\delta^{13}C$ values (-24.2‰), whereas the asteroid *Porcellanaster ceruleus* had the highest $\delta^{13}C$ values (-15.1‰ [SE 0.3]) of this feeding group. Epibenthic feeders had a large range in $\delta^{13}C$ and $\delta^{15}N$ values where the fish *Synagrops spinosus* had the lowest $\delta^{13}C$ value (-20.4‰) and the asteroid *Solaster earlli* had the highest $\delta^{13}C$ values (-14.7‰ [SE 0.8]). The asteroid *Stephanasterias albula* had the lowest $\delta^{15}N$ (3.1‰ [SE 1.6]), whereas the American lobster,

Homarus americanus, had the highest $\delta^{15}N$ (13.3‰). Infaunal feeders had a moderate range in $\delta^{13}C$ (from -19.1 to 15.5‰), with the polynoid polychaete and the crustacean *Sabinea hystrix* with the lowest and highest $\delta^{13}C$ values, respectively. The infaunal-feeding asteroid *Astropecten americanus* had the lowest $\delta^{15}N$ (5.2‰ [SE 0.5]) and the fish *Dibranchus atlanticus* had the highest $\delta^{15}N$ values (13.2‰ [SE 0.4]), similar to results from Baltimore Canyon.

For omnivores, copepods had the lowest $\delta^{13}C$ (-19.9‰) and highest $\delta^{15}N$ (11.9‰) values for this feeding group, whereas crustaceans had the highest $\delta^{13}C$ (-14.1‰ [SE 0.3]) (*Hippolyte obliquimanus*) and the lowest $\delta^{15}N$ (4.8‰ [SE 0.8]) values (*Majoidea* sp.). Microvores had the lowest $\delta^{13}C$ value (-18.9‰ [SE 0.1]) (the decapod *Pandalus montagui*) and the highest value for both $\delta^{13}C$ (-15.6‰ [SE 0.3]) and $\delta^{15}N$ (10.7‰ [SE 0.4]) (the penaeid shrimp *Trachypenaeus* sp.). Lastly, the pelagic consumer *Nemichthys scolopaceus* had the lowest $\delta^{13}C$ value (-19.2‰), whereas the shrimp *Processa profunda* had the highest $\delta^{13}C$ values (-16.6‰ [SE 0.1]). *Themisto abyssorum* had the lowest $\delta^{15}N$ (5.2‰ [SE 0.6]) and *Maurolicus weitzmani* had the highest $\delta^{15}N$ (11.6‰) values.

16.3.3 Fish Diet Analysis

Several fish species were selected for extensive diet analysis using stomach examination (**Chapter 15**), and results were compared with stable isotope values of these species collected from Baltimore and Norfolk canyons and slope environments to help understand the relationship between short- (stomach contents) and long-term assimilated diet information obtained from SIA (**Table 16-A3)**. Diet items estimated from stable isotope analyses (see methods section 16.2.4 for details on the methodology and associated assumptions) are presented for both Baltimore and Norfolk canyons combined, unless otherwise indicated.

Citharichthys arctifrons

Crustaceans were the dominant group identified as possible food resources for *C. arctifrons* collected from Baltimore and Norfolk canyons based on SIA (**Table 16-A3**). Specific crustacean food items inferred using SIA included brachyuran crabs (*Bathynectes maravigna, Cancer plebejus*), euphausiids (*Bentheuphausia amblyops, Nyctiphanes couchii*), the sergestid shrimp *Acetes americanus carolinae*, caridean shrimps (*Acanthephyra eximia, Atlantopandalus propinqvus, Dichelopandalus leptocerus*, *Dichelopandalus* sp., *Pandalus montagui, Processa guyanae*), penaeid shrimps (*Mesopenaeus tropicalis*, *Parapenaeus politus*, *Parapenaeus* sp.), unidentified shrimps (Shrimp sp. I, K, L, U), anomurans (*Agononida longipes*, *Eumunida* sp, *Munida iris*), and amphipods (e.g., *Unciola* sp.). Several species of molluscs (octopods, cephalopods [*Rossia megaptera* and *Semirossia tenera*], and gastropods), cnidarians (*Actiniaria* sp., *Actinoscyphia* sp., *Bolocera* sp., Hormathiidae, Corallimorpharia, and *Anthomastus* sp.), and polychaetes (*H. tubicola*) (**Table 16-A3**) also had isotope values consistent with serving as potential food sources. A significant relationship was documented between fish body length and $\delta^{15}N$, indicating this species changes its diet and feeds at higher trophic levels as it grows (**Figure 16-6)**.

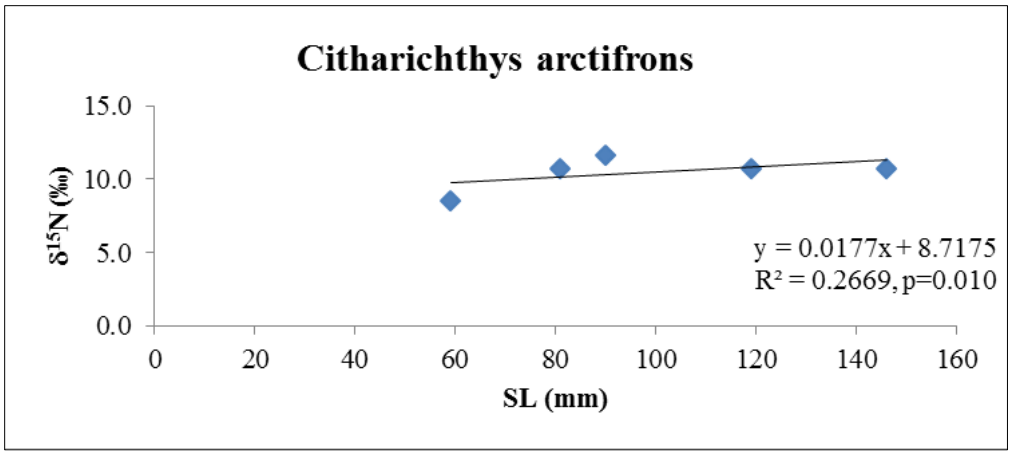

Figure 16-6. Relationship between fish standard length (SL) and $\delta^{15}N$ values from Norfolk Canyon and adjacent slope for *Citharichthys arctifrons*. Equation is given for the best fit line and R^2 value.

Glyptocephalus cynoglossus

Similar to *C. arctifrons*, crustaceans dominated the food items identified for *G. cynoglossus* based on SIA from both sites (**Table 16-A3**). Specific crustaceans included penaeids (*Hymenopenaeus debilis*, *P. politus*, *Parapenaeus* sp., *Penaeus* sp.), carideans (*A. eximia*, *Alpheus* sp., *A. propinqvus*, *Caridea* sp., *D. leptocerus*, *Dichelopandalus* sp., *Heterocarpus ensifer*, *Nematocarcinus cursor*, *P. montagui*, *Pasiphaea multidentata*, *Plesionika holthuisi*), brachyurans (*B. maravigna*, *Calappa* sp., *C. borealis*, *C. plebejus*, *Rochinia* cf. *tanneri*), sergestids (*A. americanus carolinae*), unidentified shrimps (Shrimp sp. A, I, L, M, S), euphausiids (*B. amblyops*, *Meganyctiphanes norvegica*), amphipods (*Unciola* sp., *Themisto* sp.), and isopods. Noncrustacean food resources identified through SIA included cnidarians (anemones, corals), echinoderms (asteroids, echinoids, ophiuroids, holothurians, crinoids), molluscs (bivalves, cephalopods, gastropods), polychaetes (Onuphidae, Terebellidae), and several fish species (18 species). Although a positive relationship was found between SL and $\delta^{15}N$, it was not significant (**Figure 16-7**).

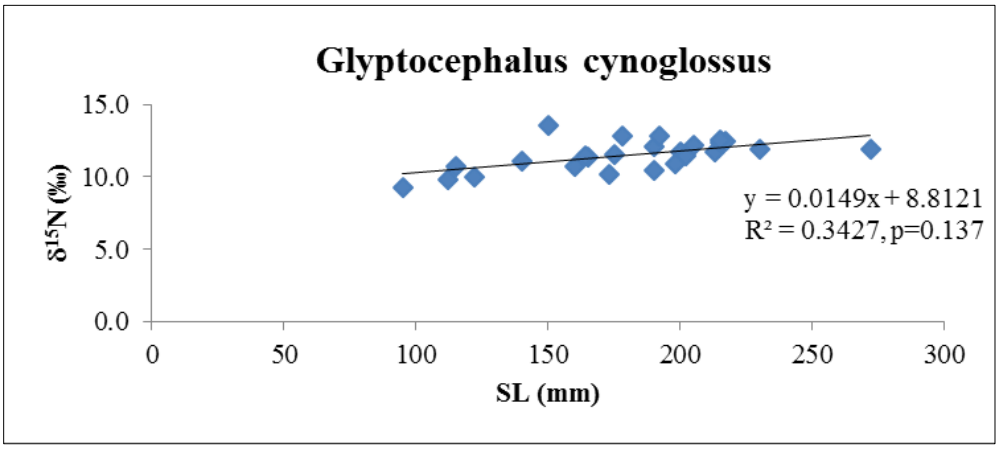

Figure 16-7. Relationship between fish standard length (SL) and $\delta^{15}N$ values from Norfolk Canyon and adjacent slope for *Glyptocephalus cynoglossus*. Equation is given for the best fit line and R^2 value.

Helicolenus dactylopterus

Several food items encompassing multiple taxa were identified by SIA for *H. dactylopterus*. Crustaceans dominated the diets of *H. dactylopterus*, encompassing 14 different taxa, including brachyuran crabs (*Brachyura* sp., *Latreillia elegans*, *R. crassa*, *Majoidea* sp., *R. tanneri*), carideans (*P. montagui*), anomurans (*Eumunida* sp., *Munidopsis* sp., *Paguristes moorei*), sergestids (*A. americanus carolinae)*, unidentified shrimps (Shrimp sp. I, R), euphausiids (Euphausiidae, *B. amblyops, M. norvegica, N. couchii, Thysanoessa macrura),* and amphipods *(T. abyssorum*, *Themisto* sp., *Unciola* sp.). Other possible food resources estimated by SIA included cnidarians *(*Hydrozoa, *Actiniaria* sp., *Bolocera* sp., *Epizoanthus* sp, *Zoantharia* sp., *Dasmosmilia lymani, Acanella arbuscula, Acanthogorgia aspera, Acanthogorgia* cf. *armata, Acanthogorgia* sp., *Alcyonacea* sp.*)*, seastars and brittlestars (*Astropecten alligator, Amphipholis* sp., *Gorgonocephalus* sp., *Ophiomusium lymani*, *Ophiopholis aculeata*, Ophiuroidea sp., *Ophiura sarsii*), urchins (*Gracilechinus alexandri*, *Histocidaris sharreri*), crinoids, and molluscs (the cephalopod *Bathyteuthis* sp.), gastropods, Nudibranchia*)*. The $\delta^{13}C$ values of fishes *Chauliodus sloani*, *Chlorophthalmus agassizi, Cryptacanthodes maculatus, Diaphus* sp., *M. atlanticum*, and *Polymetme thaeocoryla* were consistent with *H. dactylopterus*. Fish length and $\delta^{15}N$ values were positively correlated (**Figures 16-8** and **16-9)**, indicating that this species feeds at higher trophic levels as it grows.

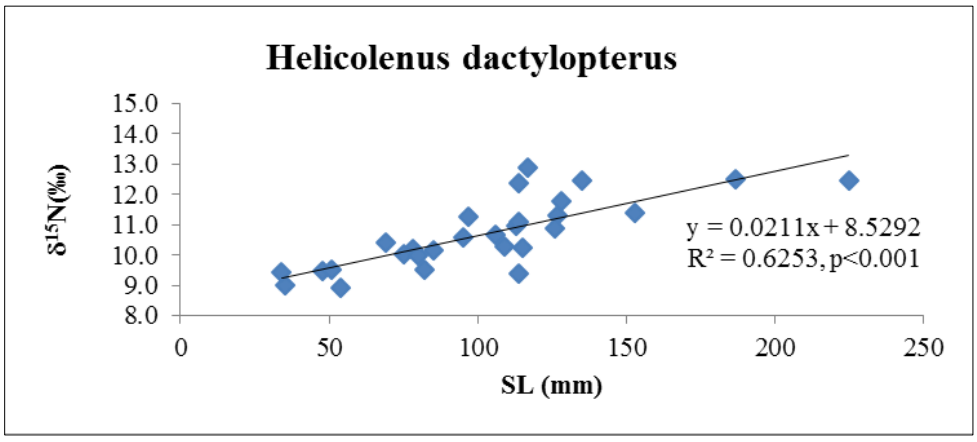

Figure 16-8. Relationship between fish standard length (SL) and $\delta^{15}N$ values from Baltimore Canyon and slope for *Helicolenus dactylopterus*. Equation is given for the best fit line and R^2 value.

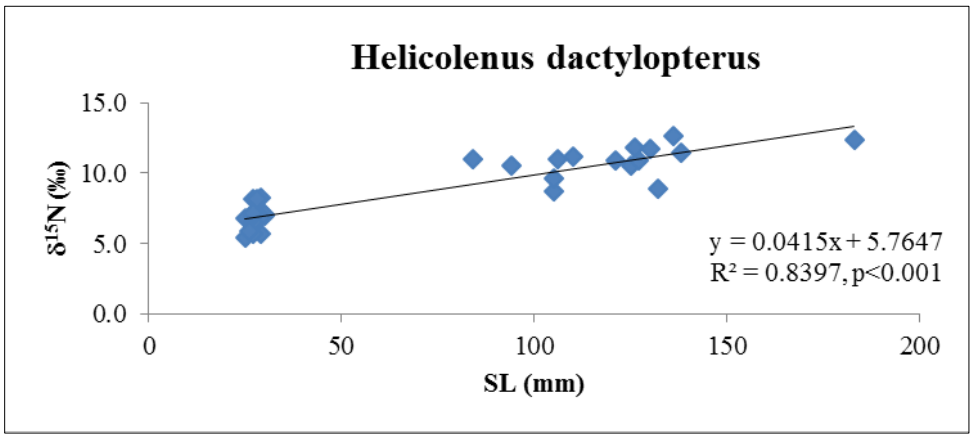

Figure 16-9. Relationship between fish standard length (SL) and $\delta^{15}N$ values from Norfolk Canyon and adjacent slope for *Helicolenus dactylopterus.* Equation is given for the best fit line and R^2 value.

Synaphobranchus kaupii

Shrimps (*A. americanus carolinae*, unidentified shrimp), euphausiids (*M. norvegica*, *N. couchii*), amphipods (*Themisto* sp.), isopods, cnidarians (Actiniaria, *Bolocera* sp., *A. aspera*, *A.*cf. *armata*, *Anthomastus* sp.), echinoderms (*Gorgonocephalus* sp., *G. alexandri*, *H. sharreri*), molluscs (*Bathyteuthis* sp., Naticidae, Nudibranchia), and fishes (*C. maculatus*, *H. dactylopterus*) were identified as potential food resources for *S. kaupii* based on SIA. Fish length was positively correlated with $\delta^{15}N$ values for fishes collected from Norfolk Canyon (**Figure 16-10**).

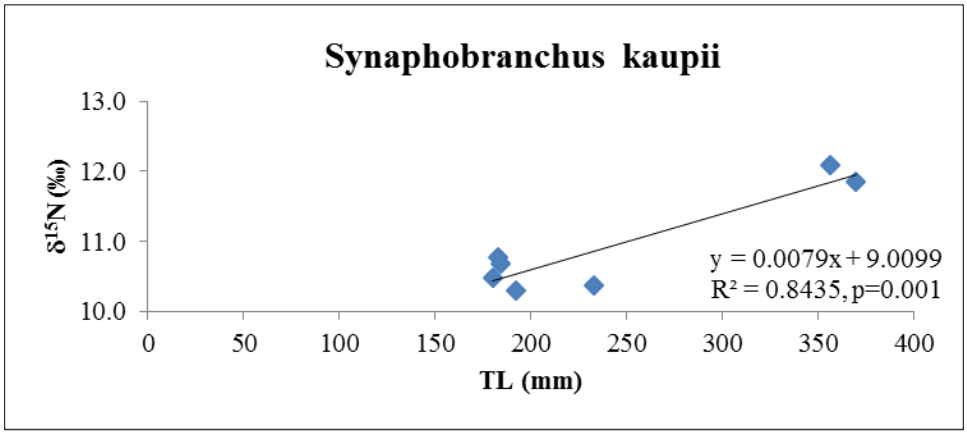

Figure 16-10. Relationship between fish total length (TL) and $\delta^{15}N$ values from Norfolk Canyon and adjacent slope for *Synaphobranchus kaupii*. Equation is given for the best fit line and R^2 value.

Dysommina rugosa

Dysommina rugosa was not collected from nonseep environments in Baltimore Canyon. However, several potential food resources for *D. rugosa* were identified from specimens collected at Norfolk Canyon, including Cirripedia, cephalopods (*Rossia* sp.), and octopods (*Bathypolypus bairdii*). Although the amphipods *Themisto* spp. had $\delta^{13}C$ values similar to *D. rugosa*, their $\delta^{15}N$ values placed them more than one trophic level below the fish $\delta^{15}N$. Fish length was positively correlated with $\delta^{15}N$ values at Baltimore Canyon seeps (**Figure 16-11**).

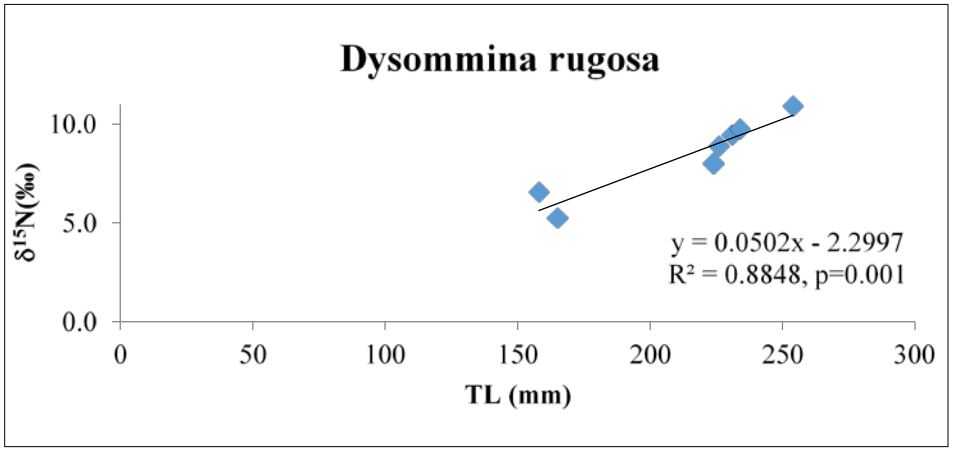

Figure 16-11. Relationship between fish total length (TL) and $\delta^{15}N$ values from Baltimore Canyon seep habitats for *Dysommina rugosa*. Equation is given for the best fit line and R^2 value.

Lophius americanus

Food items inferred from SIA for the goosefish, *L. americanus*, included brachyurans (*Calappa* sp., *C. plebejus, C. quinquedens*), carideans (*A. eximia, P. montagui*), sergestids (*A. americanus carolinae*), anomurans (*E. picta, Eumunida* sp. *Munidopsis* sp.), unidentified shrimps (Shrimp sp. A, I, R), euphausiids (*M. norvegica*), isopods, Cirripedia, cnidarians (Actiniaria sp. 1, *Actinoscyphia* sp., *Halcurias* sp., Corallimorpharia, *Flabellum alabastrum*, four octocorals), echinoderms (*Gorgonocephalu*s sp., Ophiuroidea sp., *G. alexandri, H. sharreri*), molluscs (*B. beani, R. megaptera, Rossia* sp., Naticidae, Nudibranchia), polychaetes (*H. tubicola*, Terebellidae), and fishes (22 species). Fish length was positively correlated with $\delta^{15}N$ values at Baltimore Canyon (**Figure 16-12**).

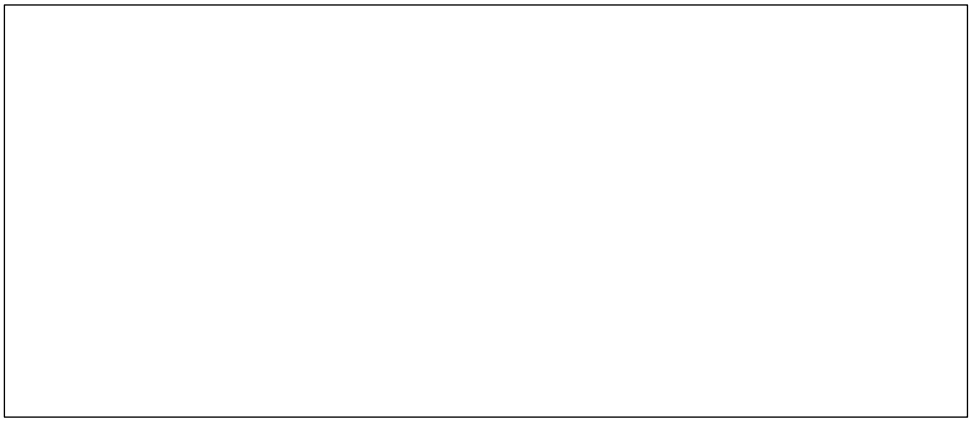

Figure 16-12. Relationship between fish standard length (SL) and $\delta^{15}N$ values from Baltimore Canyon and adjacent slope for *Lophius americanus*. Equation is given for the best fit line and R^2 value.

Dibranchus atlanticus

Only one item, American lobster, *Homarus americanus*, was identified as a possible food item for *D. atlanticus* collected from Baltimore Canyon. In contrast, a higher diversity of potential food resources for *D. atlanticus* from Norfolk Canyon was inferred from SIA, including brachyurans (*C. quinquedens, Chaceon* sp.), polychelids (*Stereomastis nana*), Cirripedia (Scalpellidae), octocorals (*Umbellula* sp.), echinoderms (*Ophiacantha* sp., *Echinus* sp.), cephalopods (*S.* cf. *tenera*), polychaetes (Eunicidae, Glyceridae, Onuphidae, *H. artifex, H. tubicola*), and sipunculids.

Lycenchelys verrillii

SIA identified only *E. picta* as a potential prey item for *L. verrillii* collected from Baltimore Canyon, whereas 30 different crustacea taxa were identified as food resources for specimens from Norfolk Canyon. Additional food resources estimated from SIA for specimens collected from Norfolk Canyon included cnidarians (Actiniaria, Corallimorpharia, *A.* cf. *armata*, *Anthomastus* sp., *Umbellula* sp.), echinoderms (Euryalina sp., *Ophiacantha* sp., *G. alexandri, H. sharreri, Phormosoma placenta*), molluscs (bivalves, *Rossia* sp., *S. tenera*, Turridae, Naticidae), polychaetes (*Hyalinoecia* sp., Onuphiidae, Polynoidae, Terebellidae), sipunculids, and pycnogonids.

Enchelyopus cimbrius

SIA revealed that decapods were a dominant food resource for *E. cimbrius*, including brachyurans (*C. plebejus*, *C. quinquedens*), carideans (*A. eximia*, *P. montagui*), and anomurans (*E. picta*, *Galathea rostrata*). Other noncrustacean prey items identified from SIA were cnidarians (Actiniaria, *Anthomastus* sp.), molluscs (*R. megaptera*, octopods), and polychaetes (*H. tubicola*). A significant relationship was documented between standard length and $\delta^{15}N$ (**Figure 16-13**), indicating that these fish feed at increased trophic levels as they grow.

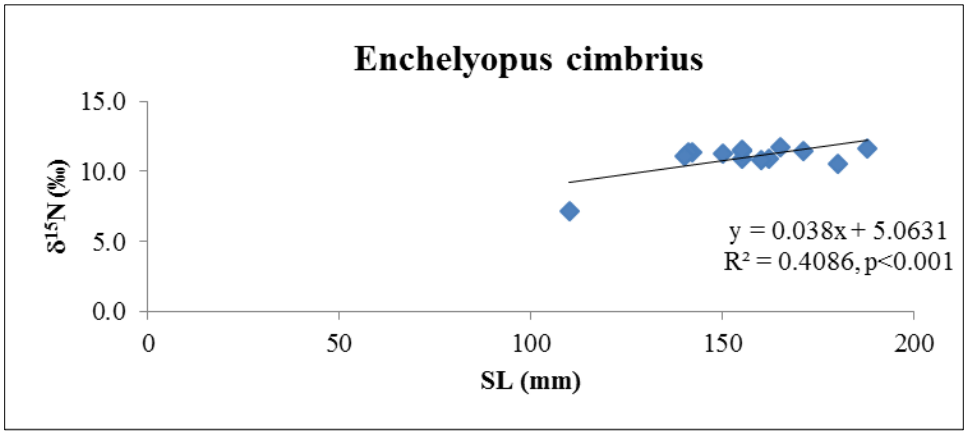

Figure 16-13. Relationship between fish standard length (SL) and $\delta^{15}N$ values from Norfolk Canyon and adjacent slope for *Enchelyopus cimbrius*. Equation is given for the best fit line and R^2 value.

Coelorinchus caelorhincus

Diets of *C. caelorhincus* primarily consisted of decapods including penaeids (*Aristeus antillensis*), brachyurans (*Calappa* sp., *C. plebejus*, *C. quinquedens*, *Chaceon* sp., *R.* cf. *tanneri*), carideans (*A. eximia*, *P. montagui*), sergestids (*A. americanus carolinae*), polychelids (*S. nana*), unidentified shrimp (Shrimp sp. B, C, S, T), and nondecapods, including euphausiids (*M. norvegica*) and isopods. Additional taxa identified as potential prey items included cnidarians (*Actiniaria* sp., *Anthomastus* sp.), molluscs (*R. megaptera*, *S.* cf. *tenera*, Naticidae, Nudibranchia), and polychaetes (*H. artifex*, *H. tubicola*, Polynoidae, Terebellidae).

Nezumia bairdii

The diets of *N. bairdii* were diverse, with 17 decapod taxa, 22 cnidarian taxa (anemones, corals), 14 echinoderm taxa, and 17 fishes identified as potential prey items based on SIA (**Table 16-A3**). Additional prey items may include euphausiids (Euphausiidae, *M. norvegica*, *N. couchii*, *T. macrura*), amphipods (*T. abyssorum*, *Unciola* sp.), molluscs (Aplacophora, *Bathyteuthis* sp., *S. tenera*, *B. bairdii*, Naticidae, Nudibranchia), and polychaetes (*H. tubicola*, Terebellidae). A significant positive correlation was documented between total length and $\delta^{15}N$ for *N. bairdii* at Norfolk Canyon (**Figure 16-14**), whereas a negative correlation was documented at Baltimore Canyon, although this relationship was not significant (**Figure 16-15**).

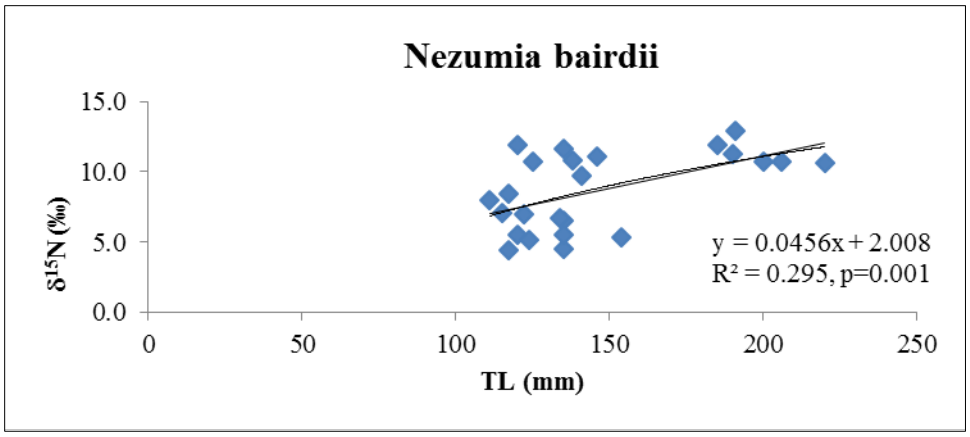

Figure 16-14. Relationship between fish total length (TL) and $\delta^{15}N$ values from Norfolk Canyon and adjacent slope for *Nezumia bairdii*. Equation is given for the best fit line and R^2 value.

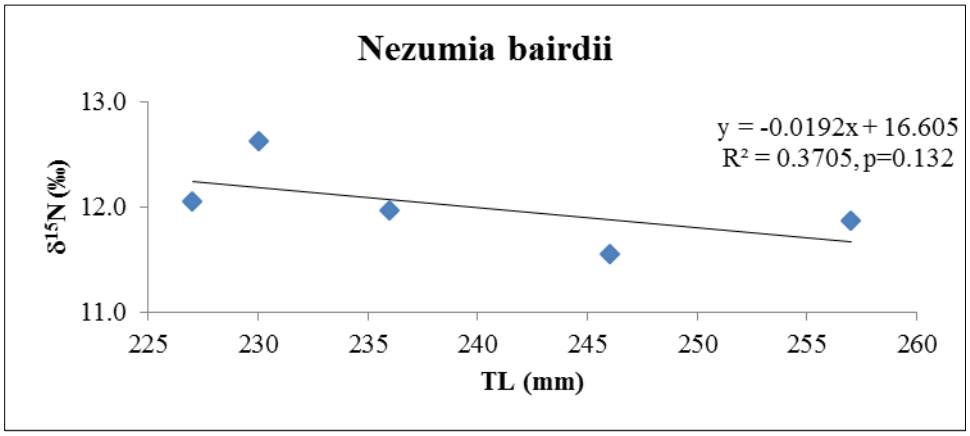

Figure 16-15. Relationship between fish total length (TL) and $\delta^{15}N$ values from Baltimore Canyon and adjacent slope for *Nezumia bairdii*. Equation is given for the best fit line and R^2 value.

Merluccius albidus

As with the other fishes examined, crustaceans were a dominant food source inferred from SIA. Specific taxa included brachyurans (*L. elegans*, *R. crassa*), sergestids (*A. americanus carolinae*), unidentified shrimp (Shrimp sp. I), euphausiids (*B. amblyops*, *M. norvegica*, *N. couchii*, *T. macrura*), and amphipods. Other taxa included cnidarians (Hydrozoa, *Bolocera* sp.), echinoderms (Ophiuroidea sp.), gastropods (Nudibranchia), polychaetes (Onuphiidae), and fishes (*P. thaeocoryla* and *Diaphus* sp.).

Phycis chesteri

Potential food items assimilated by *P. chesteri* based on stable isotope results included brachyurans (*R. crassa*, *Majoidea* sp., *R.* cf. *tanneri*), carideans (*P. montagui*), anomurans (*Eumunida* sp., *Munidopsis* sp., *P. moorei*), sergestids (*A. americanus carolinae*), unidentified shrimps (Shrimp sp. I, R), euphausiids (*M. norvegica, N. couchii, T. macrura*), amphipods (*Themisto* sp., *T. abyssorum*, *Unciola* sp.), isopods, cnidarians (11 taxa, anemones, corals), echinoderms (*A. alligator*, six ophiuroids, *G. alexandri, H. sharreri, S. lineata*), molluscs (Nudibranchia, *Bathyteuthis* sp.), and fishes (*C. sloani, C. agassizi*, *C. maculatus*, *Diaphus* sp., *M. atlanticum*, and *P. thaeocoryla*).

Urophycis regia

Crustaceans were identified as a dominant food resource, with taxa similar to *P. chesteri*: brachyurans (*Calappa* sp., *C. plebejus*, *R. crassa*, *R.* cf. *tanneri)*, carideans (*A. eximia*, *A. propinqvus*, Caridea, *P. montagui*, *P. multidentata*), sergestids (*A. americanus carolinae*), anomurans (*Eumunida* sp.), unidentified shrimps (Shrimp sp. A, I, M,), euphausiids (*B. amblyops*, *M. norvegica*, *N. couchii*, *T. macrura*), amphipods (*Themisto* sp.), isopods, cnidarians (Actiniaria sp., *Bolocera* sp., *Anthomastus* sp.), molluscs (*Bathyteuthis* sp., *B. beani*, bivalves, Naticidae, Nudibranchia), echinoderms (*Euryalin*a sp.), and fishes (11 fish species, including *H. dactylopterus*). Additionally, polychaetes (*H. tubicola*, Terebellidae) were also identified as potential prey items based on SIA. A significant positive correlation was documented between standard length and $\delta^{15}N$ for *U. regia* at Baltimore Canyon (**Figure 16-16**).

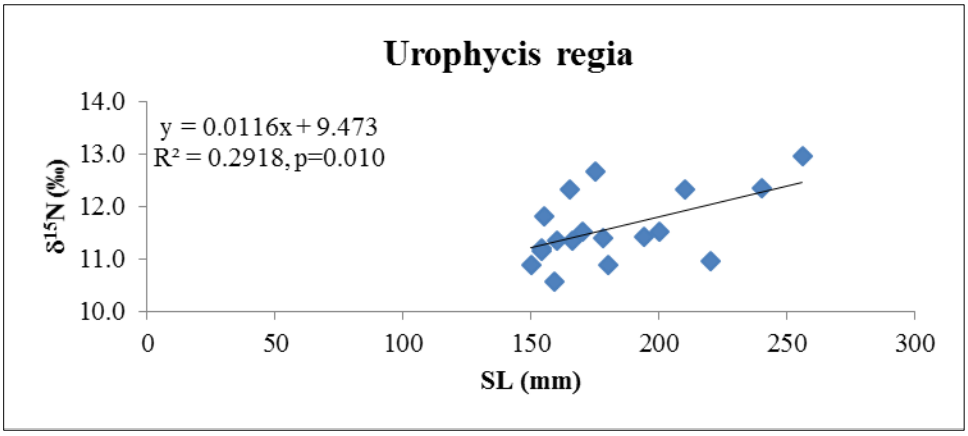

Figure 16-16. Relationship between fish standard length (SL) and $\delta^{15}N$ values from Baltimore Canyon and adjacent slope for *Urophycis regia*. Equation is given for the best fit line and R^2 value.

16.3.4 Chemosynthetic Communities

A total of 444 samples (277 from Baltimore Canyon seep and 167 from the Norfolk Canyon seep (**Table 16-A4**; **Figures 16-17a**,**b**), representing six phyla, were analyzed. Bottom water POM samples were depleted in ^{13}C and ^{15}N relative to bottom POM collected in the nonseep canyon stations (**Table 16-A3**). Stable isotope values of the fauna fell between two primary endmembers, phytoplankton ($\delta^{13}C$ > -25‰) and methane-derived carbon (<-40‰). Microbial mats sampled at Norfolk Canyon seeps were also depleted in ^{13}C (-29.4‰) relative to sediment organic matter.

The species collected at the seep sites near Baltimore Canyon that exhibited $\delta^{13}C$ values indicative of chemosynthetic production utilization (-75 to -28‰) were the mussel *Bathymodiolus childressi*, the eels *Dysommina rugosa* and *Symphurus nebulosus*, and the asteroid *Odontaster robustus* (**Figure 16-17a**). *Dysommina rugosa* and *S. nebulosus* had a wide range in isotope values; these fishes are known to be infaunal pickers, likely consuming sediment fauna depleted in ^{13}C. *Bathymodiolus childressi* house chemoautotrophic endosymbionts. Three different tissues (mantle, gill, and muscle) were processed from the *B. childressi*, with overlapping isotope values for both $\delta^{13}C$ and $\delta^{15}N$. However, gills were slightly depleted in ^{15}N relative to muscle, possibly due to limited fractionation of N in the gills compared with the muscle tissue, which is a function of the tissue-specific turnover time.

a)

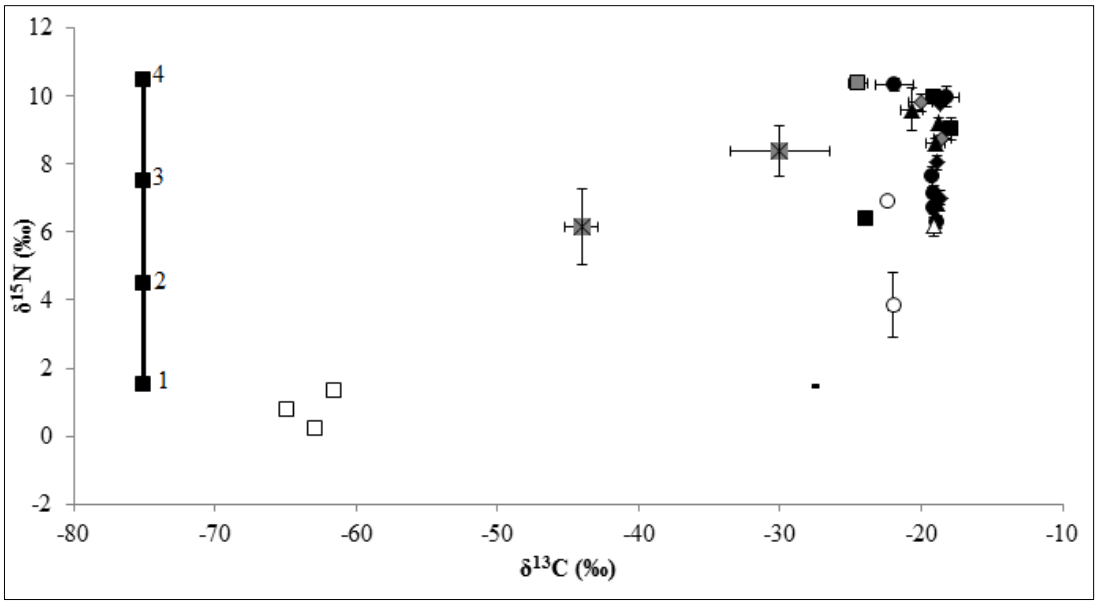

b)

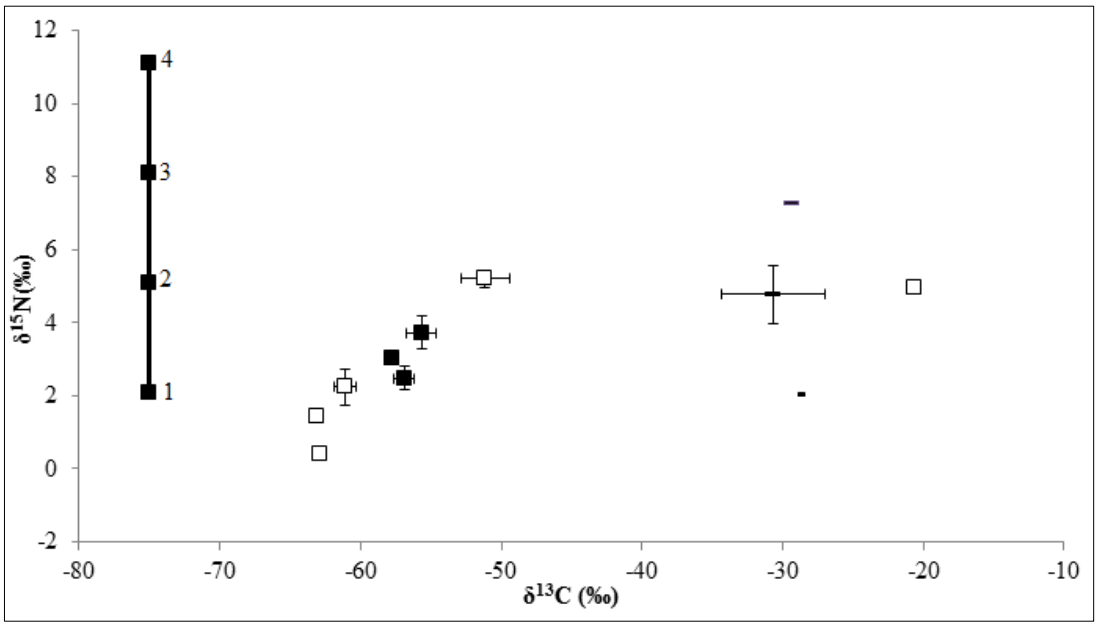

■ Infauna X Benthic ▲ Pelagics ○ Suspension
♦ Epibenthic ■ Deposit ● Omnivore Δ Unknown
● Scavenger ♦ Microvore □ Chemo - POM – Sediment-Microbial mat

Figure 16-17. Average $\delta^{13}C$ vs. $\delta^{15}N$ (‰ ± SE) for primary producers, consumers, and surface sediments (0−2 cm) collected from seep habitats in a) Baltimore and b) Norfolk canyons. Symbols represent feeding groups. Trophic level bar illustrates calculated trophic position (1−4) (see Methods).

Several other taxa collected in proximity to the Baltimore Canyon seeps were enriched in ^{13}C relative to *B. childressi, D. rugosa, S. nebulosus,* and *O. robustus,* including mobile species (mesopelagic fishes, several crustaceans), and sedentary coral, zoanthid, and anemone taxa (**Table 16-A4**; **Figure 16-17a**). Their $\delta^{13}C$ values were consistent with reliance on phytodetritus as a primary carbon source. This result indicates that the isotopic composition of available POM may vary spatially and temporally within the seep environments.

Although fewer taxa were collected and analyzed from the deeper seeps near Norfolk Canyon, all of them exhibited $\delta^{13}C$ values consistent with utilizing a chemosynthetic derived food source (**Table 16-A4**; **Figure 16-17b**). The *B. childressi* also had gill tissue depleted in ^{15}N relative to the muscle and mantle tissue, consistent with results from Baltimore Canyon seeps.

16.3.5 Among Habitat Feeding Group Comparisons and Isotope Niche Modeling

No significant differences were found in $\delta^{13}C$ or $\delta^{15}N$ values for all consumers analyzed between Baltimore and Norfolk canyons (Mann-Whitney U test [MWU], $\delta^{13}C$: 2,712 $p = 0.197$; $\delta^{15}N$: 2,851, $p = 0.408$). However, paired comparisons between coral species found in both canyons yielded significant differences for *Desmophyllum dianthus*, *Paragorgia arborea*, *Primnoa resedaeformis,* and Zoantharia; all were enriched in ^{13}C in Norfolk compared with Baltimore Canyon.

Overall tests between habitat (slope and canyon) isotopic differences were significant (Kruskal Wallis test [KW]: $\delta^{13}C$- $x^2 = 83.658$, $p < 0.001$; $\delta^{15}N$ - $x^2 = 36.252$, $p < 0.001$). All consumers from Baltimore Canyon were significantly depleted in ^{13}C and nominally depleted in ^{15}N relative to consumers found on the adjacent slope (MWU: $\delta^{13}C$, 1,168, $p < 0.001$; $\delta^{15}N$, 1,883, $p = 0.061$). Suspension feeders in the canyon were depleted in ^{13}C relative to the adjacent slope (MWU, 10, $p = 0.002$), whereas there was no significant difference in $\delta^{15}N$ (MWU, 46, $p = 0.856$). $\delta^{13}C$ values among coral species were significantly different (ANOVA, F7, 82 = 12.948, $p < 0.001$), with Alcyonacea spp., *Anthothela grandiflora*, and *Paramuricea placomus* enriched in ^{13}C relative to the other coral species.

Within Baltimore Canyon, significant differences were found among feeding groups (KW: $\delta^{13}C$: $x^2 = 27.411$, $p = 0.017$; $\delta^{15}N$, $x^2 = 25.117$, $p < 0.001$). Omnivores and bottom feeders (epibenthic and infaunal) were all enriched in ^{13}C and ^{15}N relative to suspension feeders. After pooling the bottom feeders (infaunal, epifaunal) into one benthic-feeding group, benthic feeders were significantly enriched in both ^{13}C and ^{15}N relative to suspension feeders (MWU: $\delta^{13}C$:13, $p < 0.001$; $\delta^{15}N$: 38, $p < 0.001$).

A significant positive linear correlation was found between depth and $\delta^{15}N$ for both canyon (Spearman's rank correlation coefficient, $p = 0.0025$, rho = 0.418) and slope (Spearman, $p = 0.007$, rho = 0.346) environments. However, there was no relationship between $\delta^{13}C$ and depth for either canyon ($p > 0.05$) or slope environments. Within the suspension feeder group, *Anthothela grandiflora* $\delta^{13}C$ values significantly decreased with depth (Pearson, $p = 0.027$, $R^2 = 0.59$); however, stable isotope data for the remaining coral species were not significantly related to depth.

Although there were significant differences between isotope values from Baltimore Canyon versus adjacent slope, there was a great deal of overlap in Bayesian standard ellipses (1.07‰^{2}) between fish communities found between these two zones (**Figure 16-18a**). In contrast, there was a greater separation and zero overlap between Bayesian standard ellipses calculated for invertebrate communities found in each zone, including the suspension feeders (**Figures 16-18b** and **16-19**).

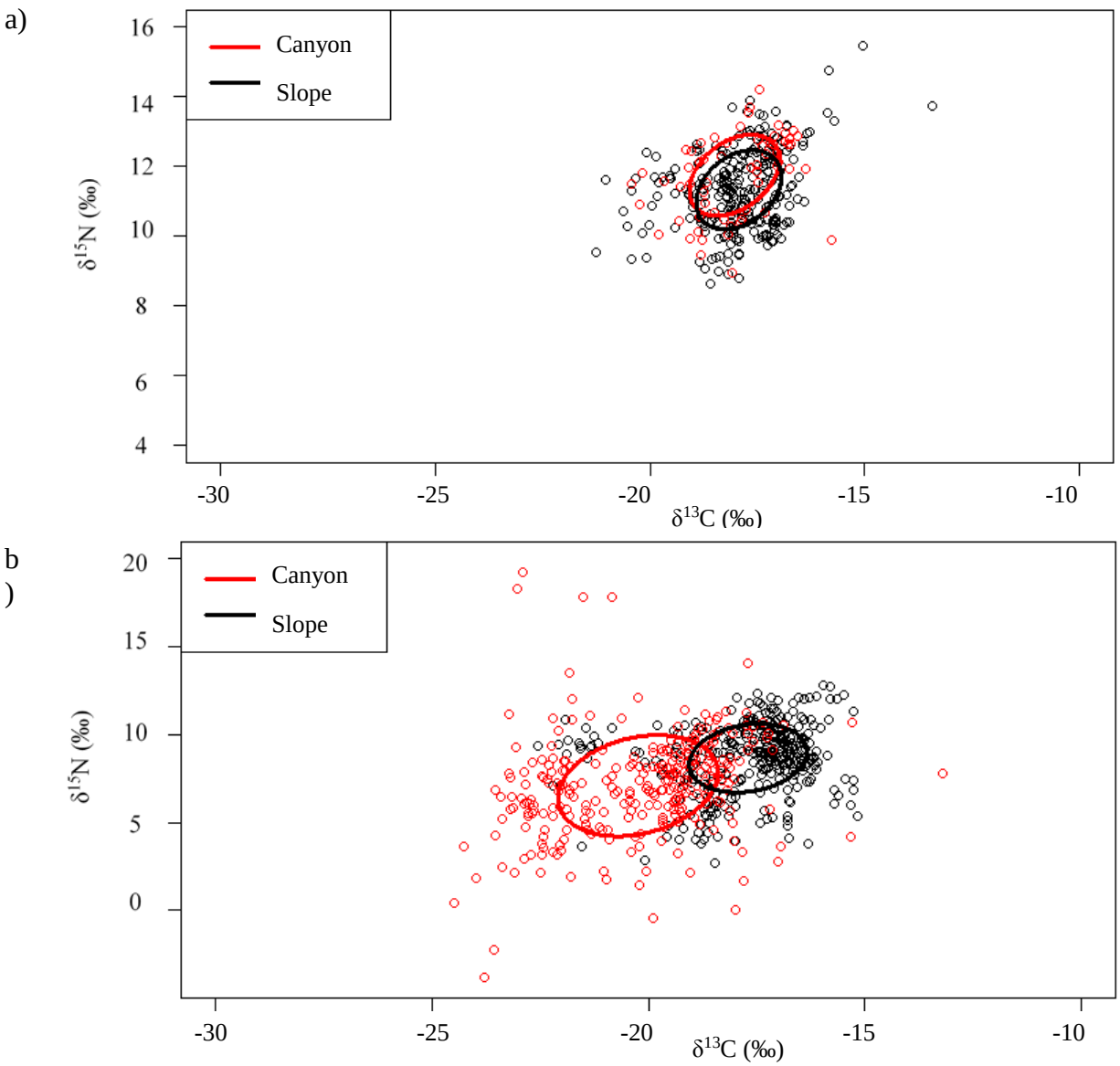

Figure 16-18. Stable isotope composition ($\delta^{13}C$ and $\delta^{15}N$, ‰) of Baltimore Canyon and slope a) fish communities and b) invertebrate communities. Bayesian standard ellipses represent the trophic niche and extent of communities. Ellipse area overlap in fish communities = 1.07‰^{2}; area of overlap in invertebrate communities = 0‰^{2}.

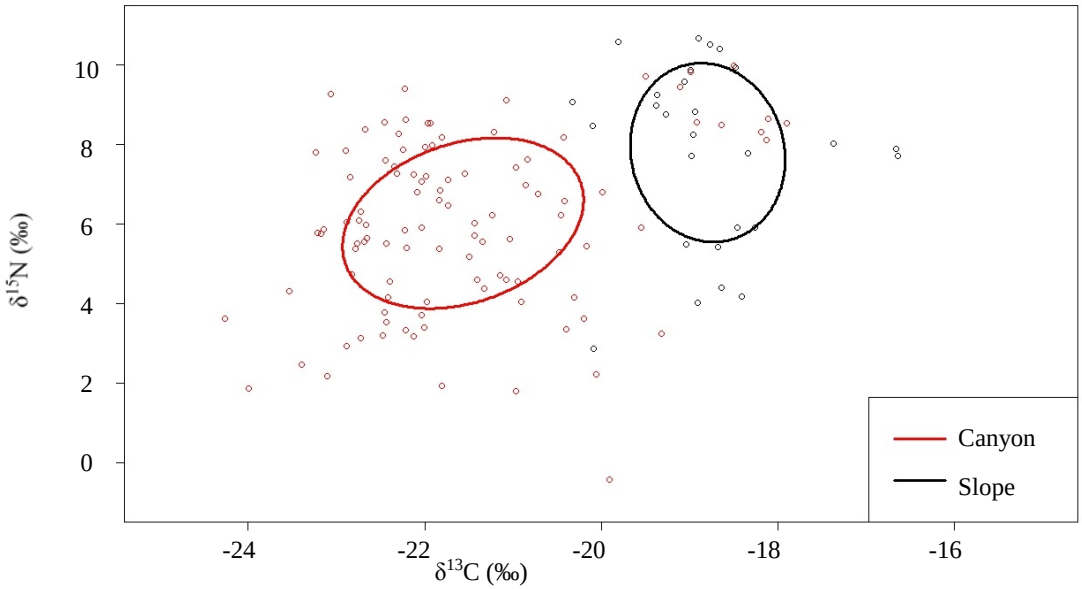

Figure 16-19. Stable isotope composition ($\delta^{13}C$ and $\delta^{15}N$, ‰) of suspension feeders collected in Baltimore Canyon and slope. Bayesian standard ellipses represent the trophic niche and extent of communities. Ellipse area overlap in suspension feeders from Baltimore Canyon and slope = 0‰^{2}.

For Norfolk Canyon, $\delta^{13}C$ values for consumers found within the canyon were significantly depleted relative to those found on the adjacent slope (MWU, 5,661, $p < 0.001$); however, $\delta^{15}N$ did not differ between canyon and slope (MWU, 8,141, $p = 0.860$). Feeding groups found within the canyon were isotopically distinct (KW, $\delta^{13}C$, $x^2 = 32.849$, $p < 0.001$; $\delta^{15}N$, $x^2 = 44.862$, $p < 0.001$) where bottom feeders were enriched in ^{13}C and ^{15}N relative to suspension feeders (**Figure 16-4c**), including epibenthic feeders ($\delta^{13}C$: 33, $p < 0.001$; $\delta^{15}N$: 18, $p < 0.001$), infaunal feeders ($\delta^{13}C$: 30, $p = 0.007$; $\delta^{15}N$: 370, $p = 0.020$), and omnivores ($\delta^{13}C$ 20, $p = 0.016$; $\delta^{15}N$: 25, $p = 0.037$). After grouping the bottom feeders (infaunal, epifaunal) into one benthic-feeding group, benthic feeders were significantly enriched in both ^{13}C and ^{15}N relative to suspension feeders (MWU: $\delta^{13}C$:307, $p < 0.001$, $\delta^{15}N$: 205, $p < 0.001$). There was a significant difference in the $\delta^{13}C$ and $\delta^{15}N$ values among suspension-feeding coral species (KW, $\delta^{13}C$: $x^2 = 148.43$, $p < 0.001$, $\delta^{15}N$: $x^2 = 104.45$, $p < 0.001$), and significant differences were present between several coral species pairs.

Similar to Baltimore Canyon, there was a positive linear correlation between $\delta^{15}N$ and depth in Norfolk Canyon ($p = 0.0032$, rho = 0.264), whereas $\delta^{13}C$ values significantly decreased with depth ($p = 0.013$, rho = -0.222). For the adjacent slope, $\delta^{13}C$ also decreased with depth ($p = 0.026$, rho = -0.193), but there was no relationship with $\delta^{15}N$ and depth. Several coral species had $\delta^{13}C$ isotope values that significantly increased with depth, including *Epizoanthus* sp. (Spearman, $p = 0.0075$, rho = 0.701), Pennatulacea sp. (Spearman, $p = 0.0082$, rho = 0.617), and *Umbellula* sp. (Spearman, $p = 0.046$, rho = 0.639). Stable nitrogen isotope values for *Acanthogorgia* spp. significantly increased with depth (Spearman, $p = 0.0431$, rho = 0.434).

There was some degree of overlap in Bayesian standard ellipses between fish communities (1.87‰^{2}) and invertebrate communities (3.24‰^{2}) found between the canyon and slope environments (**Figure 16-20a**,**b**). However, the greater degree of niche overlap in the Norfolk Canyon communities may be a consequence of the larger sample size compared with Baltimore Canyon. Suspension feeders between canyon and slope habitats had very little overlap (0.29‰^{2}) indicating that they utilize spatially discrete carbon sources within each habitat type (**Figure 16-21**).

a)

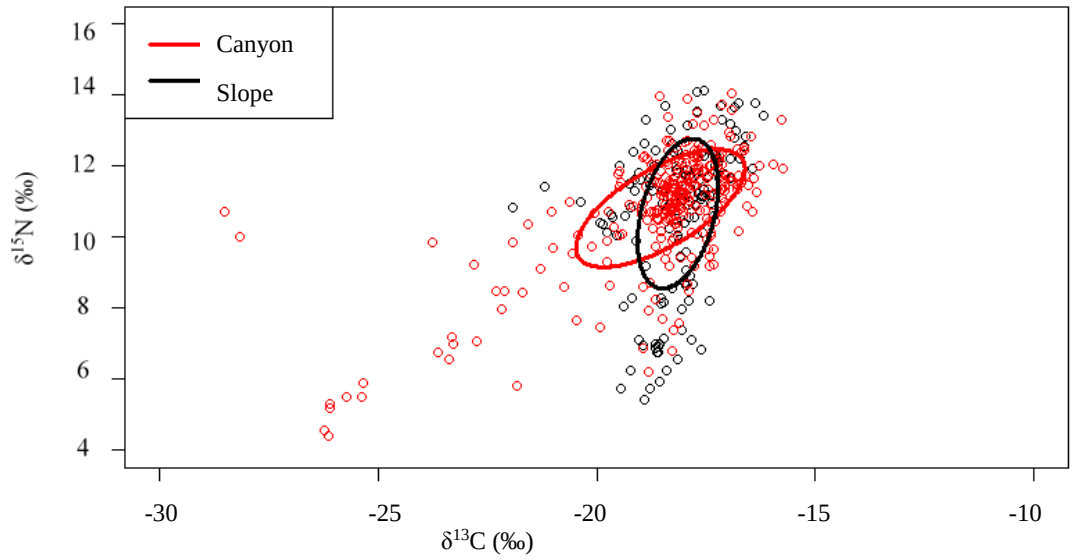

b)

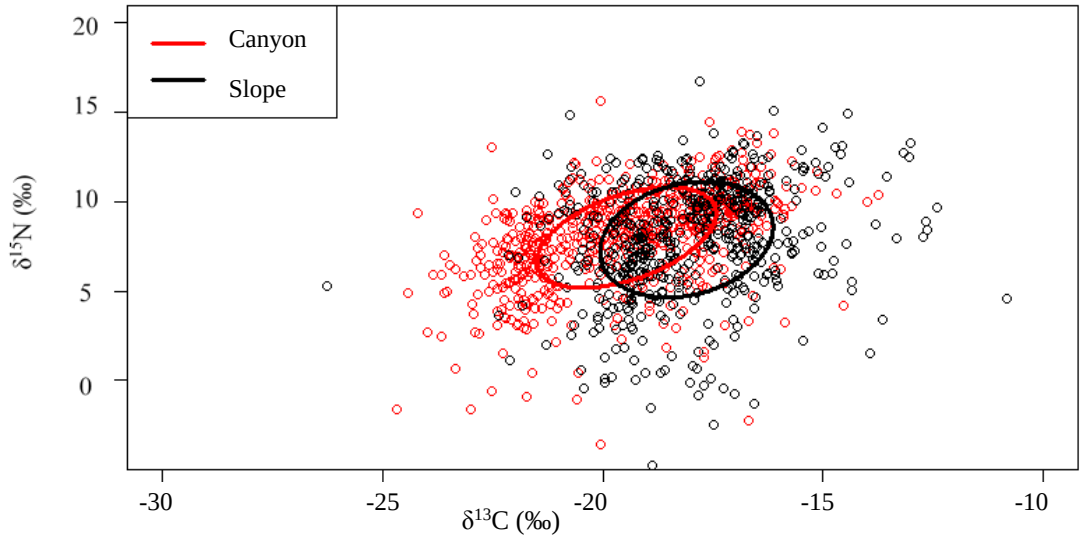

Figure 16-20. Stable isotope composition ($\delta^{13}C$ and $\delta^{15}N$, ‰) of Norfolk Canyon and slope a) fish communities and b) invertebrate communities. Bayesian standard ellipses represent the trophic niche and extent of communities. Ellipse area overlap in fish communities = 1.87‰^{2}; area overlap in invertebrate communities = 3.24‰^{2}.

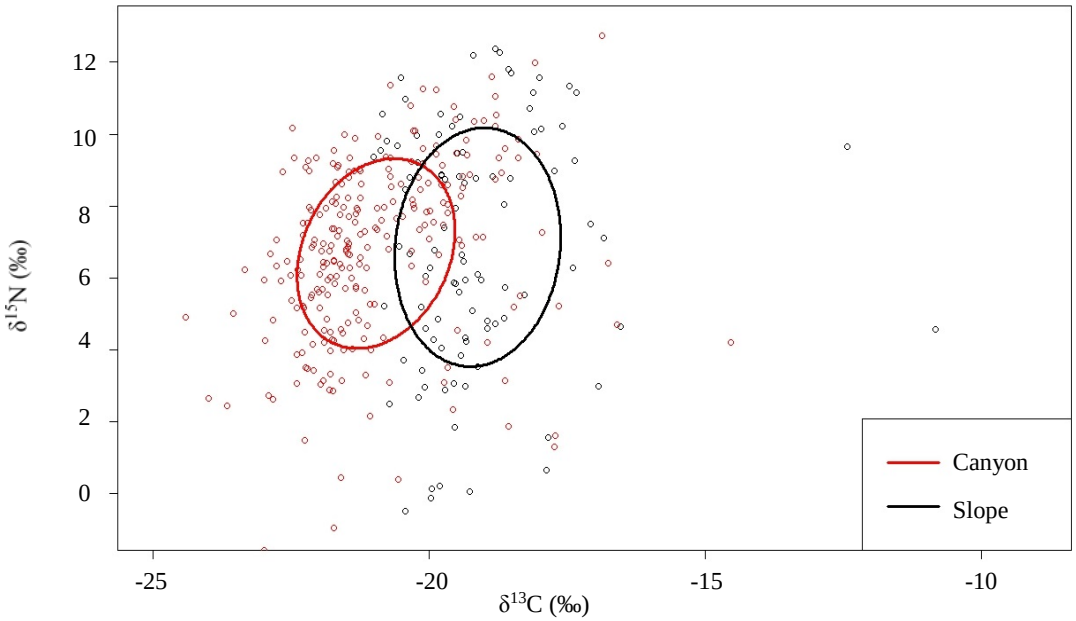

Figure 16-21. Stable isotope composition ($\delta^{13}C$ and $\delta^{15}N$, ‰) of suspension feeders collected in Norfolk Canyon and slope. Bayesian standard ellipses represent the trophic niche and extent of communities. Ellipse area overlap in suspension feeders from Norfolk Canyon and slope = 0.29‰^{2}.

16.4 DISCUSSION

Stable isotope analysis of canyon and slope communities revealed complex food webs and the quality and quantity of food available may be a major driver structuring the food webs in these deepsea ecosystems. Within the canyons, bottom POM was composed of relatively fresh organic matter, characterized by low $\delta^{13}C$ and $\delta^{15}N$ values, providing the baseline food source fueling diverse suspension-feeding communities. Other primary sources available on the seafloor included the macroalgae, *Sargassum*, which was enriched in ^{13}C relative to bottom POM. Although this was not an abundant carbon source, it could serve as a food source, albeit opportunistic, for deposit feeders that had enriched ^{13}C values, including various ophiuroids and *Colus stimpsoni*, which had particularly high $\delta^{13}C$ values.

16.4.1 Canyon and Slope Food Webs

16.4.1.1 Baltimore Canyon

Overall, the large spread and diversity of $\delta^{13}C$ values for consumer groups found in Baltimore Canyon and slope indicate that POM changes, both spatially and in quality, may be function of location within the canyon and adjacent slope. The wide range in $\delta^{15}N$ data indicates that the canyon and slope food webs in Baltimore Canyon are complex, supporting multiple trophic levels.

The highest order consumers based on $\delta^{15}N$ values were the infaunal consumer, *Dibranchus atlanticus*, and an unidentified Asteroidea. Asteroids demonstrate diverse feeding strategies, including deposit- and suspension-feeding, predation, and scavenging (Carey 1972, Sokolova 2000, Gale et al. 2013), representing several trophic levels (Iken et al. 2001, Bergmann et al. 2009), therefore, their high $\delta^{15}N$ values measured here are not unusual. However, the lack of species-level identification hinders more extensive diet analysis. Only four individuals of *D. atlanticus* were analyzed, so the general diet for this species should be estimated with care. This species is known to be an infaunal picker (Crabtree et al.

1991; see detailed diet analysis that follows), and infaunal benthos are plentiful in the canyon and slope sediments (**Chapter 9** and references therein). The high $\delta^{15}N$ values of this fish are not necessarily indicative of its being a top predator; rather, because all four individuals were collected on the adjacent slope where consumer isotope values were significantly higher than in the canyon, available food resources are isotopically enriched, leading to higher isotope values for the fish.

Isotopic separation among suspension feeders, illustrated in **Figure 16-2**C (all suspension feeders) and **Figure 16-3** (corals only), suggests that each suspension feeder may represent a distinct trophic niche. Niche specificity is a function of many factors, including species morphology and habitat specificity, and this strategy may help reduce interspecies competition in areas that are food poor or when resources are ephemeral (Iken et al. 2001, Sherwood et al. 2008). Although the canyon walls may not represent food poor environments, the deeper soft sediment thalweg and adjacent slope are relatively quiescent in comparison, limiting food to the benthos (Gage and Tyler 1991, Levin et al. 2001). Also, the spread in $\delta^{13}C$ values of suspension feeders indicates that there is some spatial variability in the isotopic composition of their food resource, with canyon suspension feeders depleted in ^{13}C relative to those found on the slope.

For suspension-feeding corals, stable isotope values varied among species, which may be related to differences in food selection, feeding habits, and habitat association (e.g., Sherwood et al. 2008, 2009). Several corals had $\delta^{13}C$ values similar to sediment trap material and were slightly enriched in ^{15}N (**Table 16-A2**; **Figure 16-3**), including scleractinians (*D. dianthus*, *L. pertusa*) and octocorals (*P. arborea*, *P. resedaeformis*), which is consistent with coral assimilation of fresh phytodetritus. The higher $\delta^{13}C$ and $\delta^{15}N$ values for the other coral species (e.g., *P. placomus, A. grandiflora,* Pennatulacea sp., *D. lymani*) relative to sediment trap material (**Figure 16-3**) may represent feeding on degraded POM that is ^{13}C and ^{15}N enriched (Sherwood et al. 2008) or consumption of zooplankton (Sherwood et al. 2009). The spread in the stable isotope data across coral taxa (**Figure 16-3**) may also be influenced by their habitat. For example, *P. arborea*, *P. resedaeformis, D. dianthus,* and *L. pertusa* reside on high-profile boulders and canyon walls (**Chapter 8**) where high currents transport fresh phytodetritus (Sherwood et al. 2008, Duineveld et al. 2012). In contrast, *P. placomus* were present in less steep terrain and in areas with sandy sediment covering the hard substrate (**Chapter 8**), corresponding to reduced current flow environments where organic matter can be reworked and recycled, leading to enriched stable isotope values (Ribes et al. 1999, Sherwood et al. 2008). Lastly, Pennatulacea sp. and *Dasmosmilia lymani* were trawled from areas of muddy sediment (**Chapter 8**) where their quiescent and deeper habitat leads to limited food supply (Gage and Tyler 1991, Levin et al. 2001). Their enriched $\delta^{13}C$ values relative to the other coral species suggest feeding on degraded organic material (Sherwood et al. 2008). Thus, feeding habits for the different coral species that reside within Baltimore Canyon are influenced by the substrate, and their diets, inferred from SIA, consequently vary in relation to the food availability and quality (Ribes et al. 1999, Coma et al. 2001, Sherwood et al. 2008).

In addition to corals, suspension-feeding anemones were enriched in ^{15}N (*Actinoscyphia* sp. and *Halcurias* sp.) and ^{13}C (Hormathiidae and Actiniaria), also a possible consequence of feeding on older, more reworked, and isotopically enriched organic material. *Actinoscyphia* sp., *Halcurias* sp., and unknown Actiniaria anemones were collected from within the resuspension zone (**Chapter 6**) of the canyon where organic material is reworked and degraded, leading to isotopic enrichment. Stable nitrogen isotope values can increase 3 to 5‰ as POM descends through the mesopelagic zone (Saino and Hattori 1987, Altabet 1988) as a result of microbial degradation releasing ^{15}N depleted compounds (Macko et al. 1986), leading to overall ^{15}N enrichment in consumers (Mintenbeck et al. 2007). *Actinoscyphia* sp. feeds on suspended detritus (Aldred et al. 1979) potentially isotopically enriched. These anemones are considered well adapted to trap detritus in weak, unidirectional currents (e.g., Mincks et al. 2008, Jeffreys et al. 2009) where food availability or quality may be low. The hormathiid anemones were collected on the adjacent slope where consumer isotope values were characteristically higher than canyon consumers overall (this study).

Deposit feeders present in the canyon and slope environments exhibited a wide range in stable isotope values, indicative of occupying large trophic niches (e.g., Mincks et al. 2008). These species tend to be omnivorous to limit competition for food (Gage and Tyler 1991, Jarre-Teichman et al. 1997, Fanelli et al. 2009). Although seasonality in food supply could influence the isotope pattern among these consumers and other feeding groups, the limited sediment trap data available from this study (**Chapter 6**; **Table 16-A2**) indicate that $\delta^{15}N$ values are consistent over time and across depths, ranging from 4.3 to 5.1‰.

16.4.1.2 Norfolk Canyon

As in Baltimore Canyon, the food web in Norfolk Canyon is complex and diverse where POM serves as the primary food source used among inhabitants. There is a greater spread in $\delta^{13}C$ and $\delta^{15}N$ values compared with Baltimore Canyon, which may be partly due to the greater number and diversity of samples collected. The large spread in $\delta^{13}C$ may also represent a continuum of feeding types from low $\delta^{13}C$ (pelagic) to high $\delta^{13}C$ (benthic feeders) (Sherwood et al. 2008, 2009). Overall, consumer groups occupied between five and six trophic levels. Deposit feeders had the largest range in $\delta^{15}N$ values, indicating high variability in their primary food source, possibly including sources derived by scavenging. It was not surprising that deposit feeders had higher $\delta^{15}N$ values relative to suspension feeders because these consumers more likely utilize organic matter that has been reworked and recycled over time (Lopez and Levinton 1987), leading to ^{15}N enrichment. Thus, isotopic differences among deposit feeders may indicate food consumption along a gradient in freshness, from fresh (low $\delta^{13}C/\delta^{15}N$) to degraded (high $\delta^{13}C/\delta^{15}N$, Jeffreys et al. 2009).

In contrast to Baltimore Canyon, corals from Norfolk Canyon represented a range of trophic levels and a large spread in carbon sources, which may be a consequence of spatial and temporal isotopic variability in the POM source or habitat association. In addition, some species of corals may be assimilating a mixture of food sources including fresh POM and small zooplankton (Kiriakoulakis et al. 2005, Sherwood et al. 2008, Duineveld et al. 2012). Although some suspension-feeding corals had $\delta^{13}C$ values consistent with POM bottom water, they were not enriched in ^{15}N relative to POM. Similar species of corals found in Baltimore Canyon, specifically *D. dianthus*, *L. pertusa*, *P. arborea*, *P. resedaeformis* and *S. variabilis*, occupied the same trophic niche in Norfolk Canyon. These animals were isotopically closest to the analyzed bottom water POM and sediment trap organic material, indicating that they select this material when fresh, leading to little isotopic fractionation in the coral tissue (Sherwood et al. 2008).

The isotopic continuum for coral species, from depleted to enriched ^{13}C and ^{15}N values, followed the same trend as Baltimore Canyon, with lower values associated with species residing on high-profile hard substrates (e.g., *L. pertusa*, *P. arborea*) and higher isotope values present in species residing in less dynamic, more quiescent sedimented environments (e.g., *F. alabastrum*, *Umbellula* sp.). Isotopic enrichment of *F. alabastrum* also may reflect feeding carnivorously on benthic infauna and demersal zooplankton (Sherwood et al. 2008). The antipatharian *Sibopathes* sp., had the second highest $\delta^{15}N$, which may represent consumption of degraded organic material or zooplankton (e.g., Sherwood et al. 2008); however, no zooplankton that were analyzed had isotope values consistent with $\delta^{13}C$ and $\delta^{15}N$ values of the *Sibopathes*. Although it is possible that food resources for this species were not sampled, their habitat association with lower energy environments (e.g., Sherwood et al. 2008) may also lead to isotopic enrichment in their food source. *Umbellula* sp. (sea pens) had the highest $\delta^{13}C$ and $\delta^{15}N$ values of the suspension feeders; all specimens analyzed were collected on the adjacent slope where the consumer isotope values were significantly higher than those within the canyon. Not surprising, *Umbellula* were found on soft substrates (**Chapter 8**) at depths (~1,500m) where organic matter experiences high isotope fractionation (e.g., Mintenbeck et al. 2007).

The infaunal pickers *Peristedion ecuadorense*, *P. miniatum*, and *Aldrovandia affinis* (Sedberry and Musick 1978) had the highest $\delta^{15}N$ values. All were enriched in ^{15}N relative to several taxa, including Brachyura crabs, *Umbellula* sp., Onuphidae worms, *Hyalinoecia* sp., *Munida* sp., *Cancer* sp.,

Ophiacantha sp., and Sipuncula worms. Based on stomach content analysis, diets for these fishes are composed of polychaetes, molluscs, small crustaceans, and brittle stars for *Aldrovandia* spp. Of these fish species, *A. affinis* has the highest diversity of food items (Sedberry and Musick 1978). Although the gape of these fishes is not large, the consistent capture of smaller, possibly juvenile specimens of crabs could be consumed and assimilated into tissue, as suggested by the stable isotope results.

16.4.2 Fish Diet Comparisons

Several fish species were selected for extensive diet analysis using results from examinations of stomach contents discussed in **Chapter 15.** These results were compared with stable isotope values of these species to help understand the relationship between short-term (stomach contents) and long-term assimilated diet information obtained from SIA. Although stomach analyses can provide species-specific details on prey consumed, the prevalence of unidentified fish and animal remains in stomachs reduces the ability to place fishes into distinct trophic guilds and can lead to higher estimates of diet overlap (Garrison and Link 2000a). SIA is an additional tool that is less time consuming than traditional stomach analysis, and can be used to help distinguish dietary differences based on assimilated prey and establish long-term feeding habits (Sherwood and Rose 2005). One caveat in using SIA to infer food resources for fishes is the assumption of trophic enrichment. The values assumed for trophic enrichment were based on statistical analysis of several species of freshwater and marine organisms (France and Peters 1997, Post 2002, McCutchan et al. 2003). However, very little data exist on trophic fractionation for deepsea species (Fanelli et al. 2009). Isotopic fractionation depends on multiple variables, including feeding strategies, metabolism, and the biochemical composition of the food resources (Vander Zanden and Rasmussen 2001, McCutchan et al. 2003, Fanelli et al. 2009). Our assumptions for trophic level fractionation were consistent with the few stable isotope studies of deepsea fishes (e.g., Boyle et al. 2012, Reid et al. 2013, Trueman et al. 2014).

From the results of this study, the stomach diet analysis of *Citharichthys arctifrons,* generally an infaunal picker (Link et al. 2002), indicated a selection of crustaceans as food resources that include hyperiid amphipods and euphausiids, and polychaetes. This is in agreement with results from other investigators (Langton and Bowman 1981, Link et al. 2002). SIA results were consistent with diets indicated from stomach content analysis, suggesting *C. arctifrons* consume similar prey over time (days to months). Certain potential prey items such as decapod crustaceans, inferred from SIA, seemed unlikely considering the small mouth gape of *C. arctifrons;* however, many decapods collected in trawls were small in size; some were possibly juvenile and could fit through the gape. Anemones also were identified as a food resource through stable isotopes (this study) and reported in the stomachs of these fishes (Link et al. 2002). Although several species of molluscs (cephalopods and gastropods) were identified as potential food based on SIA, cephalopods have not been previously reported as a food item for *C. arctifrons*. Larger Pleuronectiformes (e.g., *Paralichthys dentatus, P. oblongus*) have been documented to consume squids, including *Illex* and *Loligo* sp. (Link et al. 2002). However, given the smaller size of *C. arctifrons,* cephalopods would have to be small in size to be consumed. It is also possible that cephalopods may serve as a proxy for unsampled prey items that have similar isotopic compositions. Infaunal polychaetes dominated the diet of *C. arctifrons* (Link et al. 2002), but few polychaete specimens were sampled with the trawl. Polychaetes may utilize reworked organic matter that is ^{15}N enriched, (Fanelli et al. 2011) and may be isotopically similar to high trophic level predators like cephalopods. Given there is a significant relationship between fish body length and $\delta^{15}N$ values (**Figure 16-6**), *C. arctifrons* may consume isotopically enriched prey such as gadids, which were previously documented in stomachs (Link et al. 2002), with increasing size. Although ontogenetic diet shifts are unknown for *C. arctifrons,* its congener, *C. spilopterus,* increased piscivory with increasing size (Castillo-Rivera et al. 2000).

Stable isotope and stomach analyses also suggested similar diets for *Glyptocephalus cynoglossus,* consistent with this fish consuming similar food resources over both short (stomach contents) and long

(SIA) time scales. Diet, based on stomach content analysis in this study, was primarily composed of infaunal annelids, with larger size classes of fishes consuming euphausiids, amphipods, cnidarians, and echinoderms. This is in agreement with results found by other investigators (Langton and Bowman 1981, Bowmen and Michaels 1984, Bowman et al. 2000, Link et al. 2002, and Román et al. 2004). Although stomach analyses did not identify cnidarian and fish prey resources from the *G. cynoglossus* specimens examined in this study, several types of fishes (17 taxa), cnidarians (12 taxa), and echinoderms (16 taxa) were identified as possible food resources based on SIA, with representatives from these groups previously documented in stomachs (Maurer and Bowman 1975, Link et al. 2002, Román et al. 2004). The absence of annelid resources identified from the stable isotope analysis for Baltimore Canyon suggests that sampling may have missed these resources. In contrast, certain polychaetes (e.g., onuphids) from Norfolk Canyon had isotope values consistent with serving as food for *G. cynoglossus*. Stable isotope results indicate that these flatfishes feed at a slightly higher trophic level (Baltimore Canyon: 4.1, Norfolk Canyon: 4.3) than their related Pleuronectiformes (*C. arctifrons*, TR = 3.4), potentially consuming higher trophic level species. This pattern may be a result of the overall smaller size class of fish sampled for *C. arctifrons* (35 to 106 mm) compared with *G. cynoglossus* (79 to 264 mm). Additionally, the majority of *G. cynoglossus* analyzed for SIA were collected at depths >350 m, whereas most *C. arctifrons* were collected at depths <350 m. Stable nitrogen isotope values increased with depth, which may have resulted in the interspecific isotopic differences measured. The diversity in possible diet items identified through SIA is consistent with the different items found in the stomach contents in this study and may be a function of body size (**Figure 16-7**), food availability, and habitat use because changes in size and habitat have been suggested to influence diet shifts in fish communities (northeast United States continental shelf, Garrison and Link 2000a).

Stable isotope results for *H. dactylopterus* were consistent overall with the stomach analysis in this study, with crustaceans and fishes dominating their diets. This was also determined by other investigators (Neves et al. 2012). Specific crustaceans found in stomach contents in this study included *Cancer* sp., *M. iris, M. valida*, euphausiids (*M. norvegica, Nematobrachion boopis, Nematoscelis megalops, Thysanopoda pectinata*), and fish (e.g., *H. dactylopterus*). Although the euphausiid *M. norvegica* was identified as a possible food resource through both stable isotope and stomach analyses, different species of euphausiids (*B. amblyops, N. couchii, T. macrura*) and decapod crustaceans (Brachyura sp., *L. elegans*, *R. crassa, Eumunida* sp.) inferred from stable isotope data also were consistent with the broader taxonomic groups identified from the stomach contents. The cephalopod *Bathyteuthis* sp. was also identified as a possible food resource, consistent with stomach content analysis (Consoli et al. 2010). Although cnidarians (e.g., Actiniaria sp.1, *Bolocera* and corals) were identified by Neves et al. 2012 as a possible food item for *H. dactylopterus*, they were not recovered from stomachs during this study, which may be a consequence of their soft form making them difficult to identify from stomach contents (Gartner et al. 1997). Alternatively, *H. dactylopterus* may consume fish and crustacea that are isotopically similar to the cnidarians, yet were not captured in this study. Stomach contents from this study suggest that *H. dactlopterus* is a cannibal. However, stable isotope data from *H. dactylopterus* were not consistent with cannibalism, although other fish species (*Diaphus* sp. and *Polymetme thaeocoryla*) were identified as possible food resources. This may be a consequence of the overall smaller size class of *H. dactylopterus* collected and analyzed for SIA in this study and their possible selection of smaller food items. Diet composition of *H. dactylopterus* can be influenced by seasonal differences in food availability (Neves et al. 2012); however, similarities between prey identified with stable isotopes and stomach analyses suggest that decapods and fishes were routinely consumed and assimilated prey resources over time. From these study results, *Helicolenus dactylopterus* appears to feed at higher trophic levels as it grows (**Figure 16-8**), potentially selecting larger fishes and invertebrates, consistent with previous diet studies (Neves et al. 2012).

Synaphobranchus kaupii is generally considered a scavenger. Results from this study and previous studies (Houston and Haedrich 1986, Crabtree et al. 1991) found their diet is composed of fishes and crustaceans, including penaeid shrimps, euphausiids, and hyperiid amphipods. Stable isotope results from

Baltimore and Norfolk canyons, which generally agree with the literature, have also identified anemones and cephalopods as possible food resources for these fish. Anemones have not been documented in *S. kaupii* stomachs during this study nor by other investigators (Sedberry and Musick 1978). This may be a consequence of their soft form, which inhibits successful identification. The presence of mesopelagic fishes and cephalopods in the diet of *S. kaupii* may be a result of scavenging (Houston and Haedrich 1986), of opportunistically feeding on near bottom aggregations of mesopelagic fauna, or consumption of diel vertical migrators (Sedberry and Musick 1978, Gartner et al. 2008).

Stable isotope values for *D. rugosa* indicated several possible food items that agreed with existing diet studies, including this study where *D. rugosa* stomachs were dominated by crustaceans. However, stable isotope results did not identify euphausiids or isopods as potential prey, both important diet items found in the stomachs of this fish. Although *Themisto* spp. had $\delta^{13}C$ values similar to *D. rugosa*, their $\delta^{15}N$ values were lower than one trophic level below these fish. If this fish is feeding on a mixture of decapods and noncrustaceans, the integrated isotope value of the fish tissue could fall between these two sources (e.g., Demopoulos et al. 2007, 2008).

Diet items estimated through SIA were consistent with those obtained from stomachs of *L. americanus*, indicating that this fish consistently selects similar food resources over time. Food items for *L. americanus* discerned from stomach content analysis during this study included fishes (e.g., *Urophycis*) and decapod shrimps (*D. leptocerus*, *Sergestes arcticus*, and *S. richardi*). Noncrustacean prey may also play a role in the diets of *L.* americanus. Although cephalopods were documented in stomachs during this study and by other investigators (Maurer and Bowman 1975, Armstrong et al. 1996, Johnson et al. 2008), SIA also suggested cnidarians as potential prey. Considering the ambush predator style of *L. americanus* (Armstrong et al. 1996), cnidarians are not likely consumed; however, this source may be a proxy for isotopically and trophically similar prey items not sampled during this study.

Dibranchus atlanticus, an infaunal consumer (Scott and Scott 1988, Crabtree et al. 1991), was top level consumer based on SIA. Benthic fauna identified as potential prey in Norfolk Canyon using SIA was similar to fauna previously documented in stomachs. Potential prey items included cephalopods, various crustacea (amphipods, mysids, tanaids, euphausiids), polychaetes, bivalves, sea spiders, and echinoderms (brittle stars, starfish) (Scott and Scott 1988, Crabtree et al. 1991). Although isotope data from Baltimore Canyon suggested the American lobster *H. americanus* as a possible food source for this fish species, the mouth gape of *D. atlanticus* is too small to accommodate the size of the lobsters analyzed in this study. This fish species was collected on the adjacent slope, which contains fauna, including infaunal benthos, that are isotopically enriched relative to the canyon environment (**Figures 16-18a** and **16-20a**). Certain infauna may possibly be isotopically similar to *H. americanus*; however, no samples were collected to verify this. Similarly, SIA also suggested *Umbellula* sp. and sipunculids as prey items, which represent soft-bodied benthic fauna that are often difficult to identify in stomach analyses (Gartner et al. 1997). Sipunculids are present in the sediments (**Chapter 9**) and could serve as a food resource for this fish.

Diet items identified from the stomachs of epibenthic feeder *L. verrillii* during this study and by other investigators included crustaceans (amphipods), ophiuroids, bivalves, gastropods, polychaetes, and forams (Houston and Haedrich 1986, Crabtree et al. 1991). *Eumunida picta* was the only species identified as a food resource for *L. verrillii* from Baltimore Canyon based on SIA; however, fish sample size was very small (n = 2), limiting diet analysis from SIA. In contrast, a higher diversity of food items was identified from Norfolk Canyon, including several crustacean taxa, cnidarians (anemones and corals, *Umbellula* sp.), echinoderms (ophiuroids, echinoids), molluscs (bivalves, cephalopods, gastropods), and annelids (onuphids, polynoids, and terebellids). Thus, a variety of potential food items are available that could serve as resources to this fish, consistent with the diversity of food identified from stomach content analyses made during this study and by other investigators (Houston and Haedrich 1986, Crabtree et al. 1991).

Diets of *C. caelorhincus* inferred from stomach contents and stable isotope results were very similar, indicating some consistency in food selection over shorter (stomachs) and longer (SIA) time scales (**Table 16-A3**). From analyses conducted during this study and by other investigators, their stomachs contained various small crustaceans (amphipods, mysids, isopods, copepods), annelids (e.g., *Eteone* sp.), and euphausiids (e.g., *Thysanopoda pectinata* sp.) (Langton and Bowman 1980, Bowmen and Michaels 1984, Rodríguez-Marín 1994, Román et al. 2004). Although molluscs and polychaetes were not documented in stomachs of *C. caelorhincus* analyzed in this study, previous literature also identified molluscs (gastropods and cephalopods) and polychaetes as food items (Blaber and Bulman 1987, Madurell and Cartes 2006), consistent with our SIA results.

Stable isotope analysis during this study and previous investigations revealed that *E. cimbrius* may consume foods similar to those consumed by *C. caelorhincus* and were consistent with results from stomach content analysis suggesting a diet composed of crustaceans (amphipods, euphausiids, cumaceans, copepods, mysids, shrimps, isopods, *Pagurus* sp.), polychaetes, bivalves (*Mytilus edulis*), and forams (Keats and Steele 1990). However, only two individuals were sampled from Baltimore Canyon, which limits our understanding of the food resources utilized by this fish. For Norfolk Canyon, a larger diversity of food items was inferred from SIA for *E. cimbrius* because they were consistent with stomach content analysis during this study. Given the high proportion of unidentified material present in the stomach contents from this fish species, there are likely unidentified taxa important to their diet. A significant relationship was found between standard length and δ^{15}N values (**Figure 16-13**), indicating that *E. cimbrius* feeds at increased trophic levels as it grows. Previous literature noted increased consumption of annelids with size, with smaller specimens consuming crustaceans and larger specimens consuming mainly polychaetes (Keats and Steele 1990), and infaunal feeders were at the top of the trophic web in Norfolk Canyon based on stable isotopes.

For *Nezumia bairdii*, a diverse list of taxa was documented during this study and by previous investigations as prey items using both stable isotope and stomach analyses. *N. bairdii* diets consisted of copepods, euphausiids, amphipods, polychaetes, cnidarians (anemones), cephalopods, echinoderms, fishes, and larger decapod crustaceans, with a greater proportion of fishes as *N. bairdii* grows (Houston and Haedrich 1986, Rodriquez-Marin 1994). *N. bairdii* increased pelagic feeding with increasing size (Crabtree et al. 1991), supporting the ontogenetic diet shift documented with SIA (**Figure 16-14**). The presence of mesopelagic fishes in the diet of *N. bairdii* based on SIA is plausible considering that mesopelagic fishes often are common near the benthos (Gartner et al. 2008). Although it is uncertain if these macrourids were actively selecting and ingesting urchins, the stable isotope values for urchins could serve as a proxy for fish diet items that were unmeasured, including sediment macroinfauna.

The stomach contents of *Merluccius albidus* found during this study were difficult to identify overall, but contained crustaceans (pandalid shrimps, euphausiids) and adult fishes, similar to previous literature that identified pelagic crustaceans and fishes, shrimps, and squid in stomachs (Sedberry and Musick 1978, Langton and Bowman 1980, Garrison and Link 2000b). Isotopically, food items identified for *M. albidus* were consistent with results from stomach content analysis for the general taxa represented, suggesting consumption of similar prey resources over time. Differences in trophic level between canyons for this species (BC, TR = 3.7, NC, TR = 4.1) may be due to ontogenetic diet shifts because larger specimens of *M. albidus* increased piscivory with increasing size (Garrison and Link 2000b). Diets of smaller specimens (156 to 277 mm) analyzed from Norfolk Canyon may be isotopically influenced by decapods, whereas the larger specimens (224 to 361 mm) from Baltimore Canyon may have switched to a more piscivorous diet. For Norfolk Canyon, *M. albidus*, *E. cimbrius*, and *S. kaupii* had overlapping stable isotope values, indicating that these species also may have overlapping food resources, including those listed for *E. cimbrius*.

The similarity in diets found in the present study between the gadids *U. regia* and *P. chesteri* was previously reported based on stomach analyses (Sedberry and Musick 1978); however, these two fishes collected from Norfolk Canyon were isotopically distinct, suggesting selection and assimilation of

different food resources. Previous stomach analyses for *U. regia* reported *C. irroratus*, *Munida iris*, *M. valida*, euphausiids, amphipods, cephalopods, molluscs, and fishes with similar food resources also reported for *P. chesteri*. Those stomach analyses included decapods, amphipods, mysids, copepods, cephalopods, polychaetes, and fishes (*H. dactylopterus*, *Urophycis* sp.) (Maurer and Bowman 1975, Sedberry and Musick 1978, Garrison and Link 2000b).

Phycis chesteri and *U. regia* were isotopically indistinguishable in Baltimore Canyon and were potentially feeding on similar food resources over time. Most prey items inferred from SIA at Norfolk Canyon were similar for both species; however, trophic levels for *P. chesteri* (TR = 4.1) collected from Norfolk Canyon were lower than for *U. regia* (TR = 4.4). Interspecies differences in trophic levels may be due to size because smaller specimens of *P. chesteri* (SL = 50 to 300 mm) were analyzed compared with larger size *U. regia* (180 to 300 mm). This result may be due to differences in food selection or habitat use, given most of the *U. regia* was collected from outside of Norfolk Canyon. Additional taxa not observed in stomachs during this study but inferred from SIA included cnidarians (anemones and corals), echinoderms (ophiuroids), bivalves, and gastropods. Given the soft-bodied nature of anemones and corals, these taxa may have been missed in traditional stomach analysis. However, echinoderms have not been reported in stomach contents (Garrison and Link 2000b), but they may be isotopically similar to unmeasured food resources used by these fishes.

In general, fish stable isotope results complemented stomach analyses, and the overall the diet of fishes collected near Baltimore and Norfolk canyons were consistently dominated by the presence of Crustacea. However, the list of prey items documented from SIA and stomach analyses for several species was diverse and included multiple phyla. Predators may adapt a generalized feeding strategy in areas of low food availability (Sedberry and Musick 1978), which may be the case for fishes collected outside the canyons. Limited species-specific data were reported from stomach analyses, and diet identifications were primarily limited to higher classification or were unidentifiable material. The lack of more specific taxonomic data leads to increased estimates of diet overlap among species (Garrison and Link 2000a). However, stable isotope analyses provided another perspective on diets, shedding light on potential prey resources that may be missed in stomach analyses due to factors like digestion. Although not all taxa identified as potential prey are plausible, some of the SIA inferred prey resources may represent isotopically and trophically similar fauna that otherwise were not sampled. The insights from isotopic analyses may assist in determining how resources are partitioned among fish species (Reid et al. 2013, Trueman et al. 2014). Defining more distinct dietary preferences and resource partitioning among fishes may require incorporating temporal sampling and other variables (e.g., depth, location, and fish size) because these factors have been shown to influence the use of fish food resources off the coast of northeast United States (Garrison and Link 2000a).

16.4.3 Seeps

16.4.3.1 Isotopic Composition for the Known Symbiont Bearing Fauna

The mussel *Bathymodiolus childressi* harbors methanotrophic endosymbiotic bacteria, but also maintains a functional gut and can filter feed. Its reliance on these bacteria for nutrition is confirmed through the stable carbon isotope composition (**Table 16-A4**, $\delta^{13}C_{Gill}$ = -62.8‰ (SE 0.3) [Baltimore Canyon]; -62.9‰ (SE 0.3) [Norfolk Canyon]), consistent with what has been documented for *B. childressi* populations in the Gulf of Mexico (Brooks et al. 1987, MacAvoy et al. 2002). Because these mussels rely on a steady source of reduced compounds, their presence, abundance, and large range in size classes indicates that methane flux from the sediment is in continuous supply (e.g., Skarke et al. 2014). Continuous venting of putative methane gases was observed at Baltimore and Norfolk canyon seep locations. The long-term persistence of this supply over the lifetime of several mussel individuals is consistent with stable- and radio-isotope data obtained from muscle tissue and shells (**Chapter 17**; Prouty et al. 2016). Given these species can filter feed, additional sulfur isotope and molecular analysis of the gill

tissue coupled with mixing model calculations would be required to confirm mixotrophy (Kellermann et al. 2012) and to estimate the relative contribution of each nutritional resource.

16.4.3.2 Incorporation of Chemosynthetic Production into Heterotrophic Fauna

Bottom water POM was depleted in ^{13}C at both seep sites, possibly due to the contribution of isotopically-light, free-living bacteria present in the bottom water or resuspension of surface sediments. In addition, isotopically-light microbes ($\delta^{13}C$ = -29.4‰) were isolated from surface sediments at the Norfolk Canyon seep. Only a few taxa collected from the two seeps exhibited $\delta^{13}C$ values consistent with reliance on chemosynthetic production. From Baltimore Canyon, fauna utilizing seep production included the sea star *Odontaster robustus* and fishes *Dysommina rugosa* and *Symphurus nebulosus*. In addition, athough the average $\delta^{13}C$ value for the polychaete *Hyalinoecia* cf. *tubicola* indicates that these taxa rely on photosynthetically derived material, several individuals were isotopically light (-23.9 and -25.2‰), signifying potential utilization of seep-derived organic matter that is depleted in ^{13}C. However, most other taxa collected from the Baltimore Canyon seep environment, from primary consumers to higher order consumers, relied on photosynthetically derived organic matter, based on their $\delta^{13}C$ values. The deeper seep environment near Norfolk Canyon also hosted several heterotrophic invertebrate species that utilized chemosynthetic production, including the shrimps (*Alvinocaris markensis*) and urchins (*Echinus wallisi*, *Gracilechinus affinis*).

Overall, nutrition at these seeps is fueled by chemosynthetic bacteria, photosynthetically derived detritus, and suspended POM. Free-living chemoautotrophs on surfaces or in the water column can serve as food for deposit and suspension feeders (Demopoulos et al. 2010). Bacterial mats were extensive in certain areas observed on the ROV dives, and they may serve as a significant source of nutrients to the benthos (Levin and Mendoza 2007). The high diversity of isotopic compositions present at both sites indicates substantial trophic complexity that may result from high microbial diversity (Demopoulos et al. 2010). The presence of these seeps, and the variety of food resources available within, increase the overall trophic diversity for the canyon and slope environments examined during this study.

16.4.4 Food-Web Model for Canyons

Overall patterns in the $\delta^{13}C$ and $\delta^{15}N$ data indicate that the canyon and slope food webs are complex, utilizing various food resources with multiple trophic levels. Although stable isotope data of consumers were not different between Baltimore and Norfolk canyons, the isotopic distinctiveness between canyon and slope environments suggests that the primary food source, POM, undergoes different degradation pathways in these discrete systems (e.g., Macko et al. 1986, Fanelli et al. 2009). The slope and certain parts of the canyons may experience more episodic pulsed organic matter to the seafloor. Removal of isotopically-light lipids in POM during transport to the seafloor (or at the seafloor) can help explain the enrichment of ^{13}C POM (Mintenbeck et al. 2007). In addition, the range in consumer $\delta^{15}N$ values was high for both sites, consistent with a high diversity of food resources and consumers. Higher $\delta^{15}N$ values also are associated with higher water turbidity and nepheloid layer formation (Puig and Palanques 1998a, 1998b) via resuspension of the POM. Resuspended material consequently enriched in ^{13}C and ^{15}N can then become an important food source. Thus, substrate type and resuspension processes influence the food-web structure in these environments. As observed in this study, both canyons exhibited high turbidity and nepheloid layers at certain depths, which may substantially impact the canyon's trophic system (**Chapter 6**). Because of sampling limitations, it was not possible to test for seasonal patterns in the isotope data because most of the samples were collected in 2012 from Baltimore Canyon and environs and in 2013 from Norfolk Canyon. However, isotope data collected at any given time point integrate the assimilated diet over the previous several months (Lorrain et al. 2002).

SIA revealed distinct trophic niches based on analysis of different feeding groups, which may be associated with competition for food resources (Jeffreys et al. 2009). In terms of the overall trophic niche area, similar areas were calculated for fishes inhabiting the slopes versus within Baltimore Canyon, with

two-thirds overlap, indicating that fishes use similar resources in these two zones. For invertebrates, the niche area was two times greater in Baltimore Canyon than the adjacent slope, with no overlap (**Figure 16-18b**). This wider isotopic niche for canyon invertebrates, as approximated by larger SEA_B, indicates the presence of a broad group of taxa, with many serving as generalists (e.g., Tecchio et al. 2013, Zapata-Hernández et al. 2014), and the possible exploitation of both marine phytodetritus and terrestrially-derived organic matter. For Norfolk Canyon, the fish trophic niche area from the canyon was greater than from the slope. In contrast, the invertebrate trophic niche area was greater on the slope than in the canyon, possibly a consequence of the diversity of carbon resources available on the slope or greater sample size for SIA analysis. In addition, the narrower niche area in the canyon environment may result from a greater abundance of feeding specialists (e.g., Zapata-Hernández et al. 2014).

Statistical comparisons of the stable isotope data between slope and canyon environments suggest isotopic niche separation by feeding groups, particularly for suspension feeders. Suspension feeders (e.g., corals) had the most diverse stable isotope data (**Figures 16-3** and **16-5**), indicating they were undergoing vertical trophic niche expansion (cf. Fanelli et al. 2009, Jeffreys et al. 2009). Some suspension feeders utilize POM and capture invertebrate prey resources. Different sized particles can also influence the $\delta^{13}C$ values, indicating that the sizes of particles captured may differ among suspension feeders. Larger particles are enriched in heavy isotopes relative to the smaller particles (Rau et al. 1990, Gage and Tyler 1991, Tyler et al. 1995). Additionally, certain taxa exhibit biochemical responses to seasonal changes in quality of phytodetritus including some fauna collected in this study (*Actinoscyphia* sp., *Amphiura* sp., and *Hyalinoeci*a sp. [Jeffreys et al. 2009]). This suggests they may adapt their feeding strategy when food is limited. Higher order consumers, including benthic feeders, had stable isotope data that indicate separation among species with similar feeding strategies where the baseline food resource is consistent with carbon derived from photosynthetic material. Future analysis of the SEA_B by feeding groups to examine niche diversity and redundancy based on functional group will be valuable for resolving resource differentiation by feeding group.

Food-web length, which measures trophic linkages from primary producers to higher order consumers, is a major controlling factor in several ecological processes (Kondoh and Ninomiya 2009, Zapata-Hernández et al. 2014); it helps regulate biogeochemical processes and affects fisheries production. Although few studies have examined food-web length in the deep sea, in general, three trophic levels have been reported from different regions and depth zones (Fanelli et al. 2009, Gebruk et al. 2003, Iken et al. 2001, Zapata-Hernández et al. 2014). Although this study documented approximately five trophic levels, the average estimated trophic level was 3.1 for Baltimore Canyon and 3.4 for Norfolk Canyon and slope environments, close to estimates from other regions. This study represents the first assessment of the trophic structure using stable isotopes in Baltimore and Norfolk canyons and nearby slope environments; therefore, comparable datasets are lacking. Additional analysis of the stable isotope diversity, niche width modeling coupled with measures of canyon environmental parameters as proxies for habitat heterogeneity and complexity, will provide insights into mechanistic factors that help influence the trophic diversity and food webs in the mid-Atlantic canyon region.

16.5 LITERATURE CITED

Al-Habsi SH, Sweeting CJ, Polunin NVC, Graham NAJ. 2008. Delta N-15 and Delta C-13 elucidation of size-structured food webs in a Western Arabian Sea demersal trawl assemblage. Marine Ecology Progress Series. 353:55–63.

Aldred RG, Riemannzurneck K, Thiel H, Rice AL. 1979. Ecological observations on the deep-sea anemone *Actinoscyphia aurelia*. Oceanologica Acta. 2:389–395.

Altabet MA. 1988. Variations in nitrogen isotopic composition between sinking and suspended particles: implications for nitrogen cycling and particles transformation in the open ocean. Deep Sea Research. 35:535–554.

Armstrong MP, Musick JA, Colvocoresses JA. 1996. Food and ontogenetic shifts in feeding of the goosefish, *Lophius americanus*. Journal of Northwest Atlantic Fishery Science. 18:99–103.

Bergmann M, Dannheim J, Bauerfeind E, Klages M. 2009. Trophic relationships along a bathymetric gradient at the deep-sea observatory HAUSGARTEN. Deep Sea Research Part 1 Oceanographic Research Papers. 56:408–424.

Blaber SJM, Bulman CM. 1987. Diets of fishes of the upper continental slope of eastern Tasmania: content, calorific values, dietary overlap and trophic relationships. Marine Biology. 95:345–356.

Bowman RE, Michaels WL. 1984. Food of seventeen species of Northwest Atlantic fish. National Oceanic and Atmospheric Administration (NOAA) Technical Memorandum No. NMFS-F/NEC 28. 183 p.

Bowman RE, Stillwill CE, Michaels ML, Grosslein MD. 2000. Food of Northwest Atlantic fishes and two common species of squid. NOAA Tech Memo NMFS NE 155. 137 p.

Boyle MD, Ebert DA, Cailliet GM. 2012. Stable-isotope analysis of a deep-sea benthic-fish assemblage: evidence of an enriched benthic food web. Journal of Fish Biology. 80:1485–1507.

Brooks JM, Kennicutt M, Fisher CR, Macko SA, Cole K, Childress JJ, Vetter RD. 1987. Deep-sea hydrocarbon seep communities: evidence for energy and nutritional carbon sources. Science. 238:1138–1142.

Carey AG Jr. 1972. Food sources of sublittoral, bathyal and abyssal asteroids in the northeast Pacific Ocean. Ophelia. 10:35–47.

Cartes JE, Carrasson M. 2004. Influence of trophic variables on the depth-range distributions and zonation rates of deep-sea megafauna: the case of the Western Mediterranean assemblages. Deep Sea Research Part 1 Oceanographic Research Papers. 51:263–279.

Cartes JE, Sorbe JC. 1999. Estimating secondary production in bathyal suprabenthic peracarid crustaceans from the Catalan Sea slope (western Mediterranean; 391–1255 m). Journal of Experimental Marine Biology and Ecology. 239:195–210.

Cartes JE, Fanelli E, Papiol V, Maynou F. 2010. Trophic relationships at intrannual spatial and temporal scales of macro and megafauna around a submarine canyon off the Catalonian coast (western Mediterranean). Journal of Sea Research. 63:180–190.

Castillo-Rivera M, Kobelkowsky A, Chávez AM. 2000. Feeding biology of the flatfish *Citharichthys spilopterus* (Bothidae) in a tropical estuary of Mexico. Journal of Applied Ichthyology. 16:73–78.

Coma R, Ribes M, Gili JM, Hughs RN. 2001. The ultimate opportunists: consumers of seston. Marine Ecology Progress Series. 219:305–308.

Consoli P, Battaglia P, Castriota L, Esposito V, Romeo T, Andaloro F. 2010. Age, growth and feeding habits of the bluemouth rockfish, *Helicolenus dactylopterus dactylopterus* (Delaroche 1809) in the central Mediterranean (southern Tyrrhenian Sea). Journal of Applied Ichthyology. 26:583–591.

Crabtree RE, Carter J, Musick JA. 1991. The comparative feeding ecology of temperate and tropical deep sea fishes from the western North Atlantic. Deep-Sea Research. 38:1277–1298.

Davenport SR, Bax NJ. 2002. A trophic study of a marine ecosystem off southeastern Australia using stable isotopes of carbon and nitrogen. Canadian Joournal of Fisheries and Aquatic Sciences. 59:514-530.

De La Rocha CL, Passow U. 2007. Factors influencing the sinking of POC and the efficiency of the biological carbon pump. Deep-Sea Research Part II Topical Studies in Oceanography. 54:639–658.

Demopoulos AWJ, Fry B, Smith CR. 2007. Food web structure in exotic and native mangroves: a Hawaii-Puerto Rico comparison. Oecologia. 153:675–686.

Demopoulos AWJ, Cormier N, Ewel KC, Fry B. 2008. Use of multiple chemical tracers to define habitat use of Indo-Pacific mangrove crab *Scylla serrata* (Decapoda: Portunidae). Estuaries and Coasts. 31:371–381.

Demopoulos AWJ, Gualtieri D, Kovacs K. 2010. Food-web structure of seep sediment macrobenthos from the Gulf of Mexico. Deep‐Sea Research Part II Topical Studies in Oceanography. 57:1972-1981.

Deree HL. 1999. Age and growth, dietary habits, and parasitism of the fourbeard rockling, *Enchelyopus cimbrius*, from the Gulf of Maine. Fishery Bulletin. 97:39–52.

Duineveld G, Lavaleye M, Berghuis E, de Wilde P. 2001. Activity and composition of the benthic fauna in the Whittard Canyon and the adjacent continental slope (NE Atlantic). Oceanologica Acta. 24:69-83.

Duineveld GCA, Jeffreys RM, Lavaleye MSS, Davies AJ, Bergman MJN, Watmough T, Witbaard R. 2012. Spatial and tidal variation in food supply to shallow cold-water coral reefs of the Mingulay Reef complex (Outer Hebrides, Scotland). Marine Ecology Progress Series. 444:97–115.

Fanelli E, Cartes JE, Rumolo P, Sprovieri M. 2009. Food-web structure and trophodynamics of mesopelagic-suprabenthic bathyal macrofauna of the Algerian Basin based on stable isotopes of carbon and nitrogen. Deep Sea Research Part 1 Oceanographic Research Papers. 56:1504–1520.

Fanelli E, Papiol V, Cartes JE, Rumolo P, Brunet C, Sprovieri M. 2011. Food web structure of the epibenthic and infaunal invertebrates on the Catalan slope (NW Mediterranean): evidence from d13C and d15N analysis. Deep Sea Research Part 1 Oceanographic Research Papers. 58:98–109.

France RL, Peters RH. 1997. Ecosystem differences in trophic enrichment of ^{13}C in aquatic food webs. Canadian Journal of Fisheries and Aquatic Science. 54:1255–1258.

France R, Chandler M, Peters R. 1998. Mapping trophic continua of benthic foodwebs: body size-delta N-15 relationships. Marine Ecology Progress Series. 174:301–306.

Fry B. 2007. Coupled N, C and S stable isotope measurements using a dual-column gas chromatography system. Rapid Communications in Mass Spectrometry. 21:750–756.

Fry B, Sherr EB. 1984. $\delta^{13}C$ measurements as indicators of carbon flow in marine and freshwater ecosystems. Contributions in Marine Science. 27:13–47.

Gage JD, Tyler PA. 1991. Deep-sea biology: a natural history of organisms at the deep-sea floor. Cambridge (UK): Cambridge University Press. 524 p.

Gale KSP, Hamel JF, Mercier A. 2013. Trophic ecology of deep-sea Asteroidea (Echinodermata) from eastern Canada. Deep Sea Research I. 80:35–36.

Garrison LP, Link JS. 2000a. Dietary guild structure of the fish community in the northeast United States continental shelf ecosystem. Marine Ecology Progress Series. 202:231–240.

Garrison LP, Link JS. 2000b. Diets of five hake species in the northeast United States continental shelf ecosystem. Marine Ecology Progress Series. 2004:243–255.

Gartner JV Jr, Crabtree RE, Sulak KJ. 1997. Feeding at depth. In: Randall DJ and Farrell AP, editors. Deep-sea fishes. New York (NY): Academic Press. p. 115–193.

Gartner JV Jr, Sulak KJ, Ross SW, Necaise AM. 2008. Persistent near-bottom aggregations of mesopelagic animals along the North Carolina and Virginia continental slopes. Marine Biology. 153:825–841.

Gebruk AV, Krylova EM, Lein AY, Vinogradov GM, Anderson E, Pimenov NV, Cherkashev GA, Crane K. 2003. Methane seep community of the Hakon Mosby mud volcano (the Norwegian Sea): composition and trophic aspects. Sarsia. 88:394–403.

Harvey CJ, Hanson PC, Essington TE, Brown PB, Kitchell JF. 2002. Using bioenergetics models to predict stable isotope ratios in fishes. Canadian Journal of Fisheries and Aquatic Sciences. 59:115-124.

Horton, A. 2015. Feeding habits of demersal fishes from Baltimore and Norfolk canyons and Hatteras middle slope [master's thesis]. Wilmington (NC): University of North Carolina−Wilmington.

Houston KA, Haedrich RL. 1986. Food habits and intestinal parasites of deep demersal fishes from the upper continental slope east of Newfoundland, northwest Atlantic Ocean. Marine Biology. 92:563-574.

Iken K, Brey T, Wand U, Voigt J, Junghans P. 2001. Food web structure of the benthic community at the Porcupine Abyssal Plain (NE Atlantic): a stable isotope analysis. Progress in Oceanography. 50:383-405.

Jackson AL, Inger R, Parnell AC, Bearhop S. 2011. Comparing isotopic niche widths among and within communities: SIBER − stable isotope bayesian ellipse. Journal of Animal Ecology. 80:595–602.

Jarre-Teichman A, Brey T, Bathmann UV, Dahm C, Dieckmann GS, Gorny M, Klages M, Pages F, Plotz J, Schnack-Schiel SB, Stiller M, Arntz WE. 1997. Trophic flows in the benthic shelf community of the eastern Weddell Sea, Antarctica. In: Valencia J, Walton DWH, Battaglia B, editors. Antarctic communities: species, structure and survival. Cambridge (UK): Cambridge University Press. p. 118-134.

Jeffreys RM, Wolff GA, Murty SJ. 2009. The trophic ecology of key megafaunal species at the Pakistan Margin: evidence from stable isotopes and lipid biomarkers. Deep Sea Research Part 1 Oceanographic Research Papers. 56:1816–1833.

Jeffreys RM, Lavaleye MSS, Bergman MJN, Duineveld GCA, Witbaard R. 2011. Do abyssal scavengers use phytodetritus as a food resource? Video and biochemical evidence from the Atlantic and Mediterranean. Deep Sea Research Part 1 Oceanographic Research Papers. 58:415–428.

Jennings S, Pinnegar JK, Polunin NVC, Boon TW. 2001. Weak cross-species relationships between body size and trophic level belie powerful size-based trophic structuring in fish communities. Journal of Animal Ecology. 70:934–944.

Jennings S, Pinnegar JK, Polunin NVC, Warr KJ. 2002. Linking size-based and trophic analyses of benthic community structure. Marine Ecology Progress Series. 226:77–85.

Johnson AK, Richards RA, Cullen DW, Sutherland SJ. 2008. Growth, reproduction, and feeding of large monkfish, *Lophius americanus*. ICES Journal of Marine Science. 65:1306–1315.

Keats DW, Steele DH. 1990. The fourbeard rockling, *Enchelyopus cimbrius* (L.), in eastern Newfoundland. Journal of Fish Biology. 37:803–811.

Kellermann MY, Schubotz F, Elvert M, Lipp JS, Birgel D, Prieto-Mollar X, Dubilier N, Hinrichs KU. 2012. Symbiont-host relationships in chemosynthetic mussels: a comprehensive lipid biomarker study. Organic Geochemistry. 43:112–124.

Kennicutt M, Brooks JM, Bidigare R, Denoux GJ. 1988. Gulf of Mexico hydrocarbon seep communities-I. Regional distribution of hydrocarbon seepage and associated fauna. Deep Sea Research. 35:1639–1651.

Kiriakoulakis K, Fisher E, Wolff GA, Freiwald A, Grehan A, Roberts JM. 2005. Lipids and nitrogen isotopes of two deep-water corals from the North-East Atlantic: initial results and implications for their nutrition. In: Freiwald A, Roberts JM, editors. Cold-water corals and ecosystems. Berlin (Germany): Spring-Verlag. p. 715–729.

Klages M, Boetius A, Christensen JP, Deubel H, Piepenburg D, Schewe I, Soltwedel T. 2003. The benthos of Arctic Seas and its role for the carbon cycle at the seafloor. In: Stein R, Macdonald RW, editors. Heidelberg (Germany): Spring-Verlag. p. 139–167.

Kondoh M, Ninomiya K. 2009. Food-chain length and adaptive foraging. Proceedings of the Royal Society of London, Series B, Biological Sciences. 276:3113–3121.

Kruskal WH, Wallis WA. 1952. Use of ranks in one-criterion variance analysis. Journal of American Statistical Association. 47(260):583–621.

Langton RW, Bowman RE. 1980. Food of fifteen northwest Atlantic gadiform fishes. U.S. Department of Commerce, NOAA Tech Report NMFS SSRF-740. 23 p.

Langton RW, Bowman RE. 1981. Food of eight Northwest Atlantic pleuronectiform fishes. U.S. Department of Commerce, NOAA Tech Report NMFS SSRF-749. 16 p.

Levin LA, Mendoza GF. 2007. Community structure and nutrition of deep methane-seep macrobenthos from the North Pacific (Aleutian) Margin and the Gulf of Mexico (Florida Escarpment). Marine Ecology. 28:131–151.

Levin LA, James DW, Martin CM, Rathburn AE, Harris LH, Michener RH. 2000. Do methane seeps support distinct macrofaunal assemblages? Observations on community structure and nutrition from the northern California slope and shelf. Marine Ecology Progress Series 208:21–39.

Levin LA, Etter RJ, Rex MA, Gooday AJ, Smith CR, Pineda J, Stuart CT, Hessler RR, Pawson D. 2001. Environmental influences on regional deep-sea species diversity. Annual Review of Ecology and Systematics. 32:51–93.

Link JS, Bolles K, Milliken CG. 2002. The feeding ecology of flatfish in the Northwest Atlantic. Journal of Northwest Atlantic Fishery Science. 30:1–17.

Lorrain A, Paulet YM, Chauvaud L, Savove N, Donval A, Saout C. 2002. Differential d13C and d15N signatures among scallop tissues: implications for ecology and physiology. Journal of Experimental Marine Biology and Ecology. 275:47–61.

Lopez GR, Levinton JS. 1987. Ecology of deposit-feeding animals in marine sediments. The Quarterly Review of Biology. 62:235–260.

MacAvoy SE, Carney RS, Fisher CR, Macko SA. 2002. Use of chemosynthetic biomass by large, mobile, benthic predators in the Gulf of Mexico. Marine Ecology Progress Series. 225:65–78.

Macko SA, Fogel Estep ML, Engel MH, Hare PE. 1986. Kinetic fractionation of stable nitrogen isotopes during amino acid transamination. Geochimica et Cosmochimica Acta. 50:2143–2146.

Madurell T, Cartes JE. 2006. Trophic relationships and food consumption of slope dwelling macrourids from the bathyal Ionian Sea (eastern Mediterranean). Marine Biology. 148:1325–1338.

Maurer RO, Bowman RE. 1975. Food habits of marine fishes of the northwest Atlantic – Data Report. NMFS, Northeast Fisheries Center Laboratory Manual, 75-3.

McCutchan JH, Jr., Lewis WM, Jr., Kendall C, McGrath CC. 2003. Variation in trophic shift for stable isotope ratios of carbon, nitrogen, and sulfur. Oikos. 102:378–390.

Minagawa M, Wada E. 1984. Stepwise enrichment of ^{15}N along food chains: further evidence and the relation between $\delta^{15}N$ and animal age. Geochimica et Cosmochimica Acta. 48:1135–1140.

Mincks SL, Smith CR, Jeffreys RM, Sumida PYG. 2008. Trophic structure on the West Antarctic Peninsula shelf: detritivory and benthic inertia revealed by $\delta^{13}C$ and $\delta^{15}N$ analysis. Deep Sea Research II. 55:2502–2514.

Mintenbeck K, Jacob U, Knust R, Arntz WE, Brey T. 2007. Depth-dependence in stable isotope ratio delta N-15 of benthic POM consumers: the role of particle dynamics and organism trophic guild. Deep Sea Research Part 1 Oceanographic Research Papers. 54:1015–1023.

Neves A, Sequeira V, Paiva RB, Vieira AR, Gordo LS. 2012. Feeding habits of the bluemouth, *Helicolenus dactylopterus dactylopterus* (Delaroche, 1809) (Pisces: Sebastidae) in the Portuguese coast. Helgoland Marine Research. 66:189–197.

Obelcz J, Brothers D, Chaytor J, Brink Ut, Ross SW, Brooke S. 2014. Geomorphic characterization of four shelf-sourced submarine canyons along the U.S. Mid-Atlantic continental margin. Deep‐Sea Research Part II Topical Studies in Oceanography. 104:106–119.

Paull CK, Jull AJT, Toolin LJ, Linick T. 1985. Stable isotope evidence for chemosynthesis in an abyssal seep community. Nature. 317:709–711.

Peterson BJ, Fry B. 1987. Stable isotopes in ecosystem studies. Annual Review of Ecology and Systematics. 18:293–320.

Pinnegar JK, Polunin NVC. 1999. Differential fractionation of d13C and d15N among fish tissues: implications for the study of trophic interactions. Functional Ecology. 13:225–231.

Post DM. 2002. Using stable isotopes to estimate trophic position: models, methods, and assumptions. Ecology. 83:703–718.

Prouty NG, Sahy D, Ruppel CD, Roark EB, Condon D, Brokke S, Ross SW, Demopoulos AWJ. 2016. Insights into methan dynamics from analysis of authigenic carbonates and chemosynthetic mussels at newly-discovered Atlanic Margin seeps. Earth and Planetary Science Letters. 449:332–344. http://dx.doi.org/10.1016/j.epsl.2016.05.023.

Puig P, Palanques A. 1998a. Nepheloid structure and hydrographic control on the Barcelona continental margin, northwestern Mediterranean. Marine Geology. 149:39–54.

Puig P, Palanques A. 1998b. Temporal variability and composition of settling particle fluxes on the Barcelona continental margin (Northwestern Mediterranean). Journal of Marine Research. 56:639-654.

Rau GH, Teyssie JL, Rassoulzadegan F, Fowler SW. 1990. C-13/C-12 and N-15/N-14 variations among size-fractionated marine particles−implications for their origin and trophic relationships. Marine Ecology Progress Series. 59:33–38.

Rau GH, Sullivan CW, Gordon LI. 1991. Delta-C-13 and Delta-N-15 variations in Weddell Sea particulate organic-matter. Marine Chemistry. 35:355–369.

R Development Core Team. 2011. R: a language and environment for statistical computing. Vienna (Austria): The R Foundation for Statistical Computing. ISBN: 3-900051-07-0. [cited 29 July 2016]. Available from http://www.R-project.org/.

Reid WDK, Sweeting CJ, Wigham BD, McGill RAR, Polunin NVC. 2013. High variability in spatial and temporal size-based trophodynamics of deep-sea fishes from the Mid-Atlantic Ridge elucidated by stable isotopes. Deep Sea Research II. 98:412–420.

Rex M. 1977. Zonation in deep-sea gastropods: the importance of biological interactions to rates of zonation. European Marine Biology Symposium. 11:521–30.

Ribes M, Coma R, Gili JM. 1999. Heterogeneous feeding in benthic suspension feeders: the natural diet and grazing rate of temperate gorgonian *Paramuricea clavata* (Cnidaria: Octocorallia) over a year cycle. Marine Ecology Progress Series. 183:125–137.

Rohr BA, Gutherz EJ. 1977. Biology of offshore hake, *Merluccius albidus*, in the Gulf of Mexico. Fishery Bulletin. 75:147–158.

Rodríguez-Marín E, Punzón A, Paz J, Olaso J. 1994. Feeding of the most abundant fish species in Flemish Cap in summer 1993. NAFO Scientific Council Research Document, No. 35, Serial No. N2403. 33 p.

Román, E, González C, Ceballos E. 2004. Food and feeding of most abundant fish species in Flemish Cap. NAFO Scientific Council Research Document No. 58, Serial No. N5018.

Saino T, Hattori A. 1987. Geographical variation of the water column distribution of suspended particulate organic nitrogen and its ^{15}N natural abundance in the Pacific and its marginal seas. Deep Sea Research. 34:807–827.

Scott DM, Scott MG. 1988. Atlantic fishes of Canada. Canadian Bulletin of Fisheries and Aquatic Sciences 219. Toronto (Canada): University of Toronto Press. 731 p.

Sedberry GR. 1983. Food habits and trophic relationships of a community of fishes on the outer continental shelf. NOAA Tech Report NMFS SSRF-773. 56 p.

Sedberry GR, Musick JA. 1978. Feeding strategies of some demersal fishes of the continental slope and rise off the mid-Atlantic coast of the USA. Marine Biology. 44:357–375.

Sherwood GD, Rose GA. 2005. Stable isotope analysis of some representative fish and invertebrates of the Newfoundland and Labrador continental shelf food web. Estuarine, Coastal and Shelf Science. 63:537–549.

Sherwood OA, Jamieson RE, Edinger EN, Wareham VE. 2008. Stable C and N isotopic composition of cold-water corals from the Newfoundland and Labrador continental slope: examination of trophic, depth and spatial effects. Deep Sea Research Part 1 Oceanographic Research Papers. 55:1392–1402.

Sherwood OA, Thresher RE, Fallon SJ, Davies DM, Trull TW. 2009. Multi-century time-series of N-15 and C-14 in bamboo corals from deep Tasmanian seamounts: evidence for stable oceanographic conditions. Marine Ecology Progress Series. 397:209–218.

Skarke A, Ruppel C, Kodis M, Brothers D, Lobecker E. 2014. Widespread methane leakage from the sea floor on the northern US Atlantic margin. Nature Geoscience. 7:657–661.

Sokolova MN. 2000. Trophic structure of the deep-sea macrobenthos. Enfield (NH): Science Publishers.

SPSS Inc. 2007. Released 2007 for Windows, Version 16.0, Chicago, IL. [cited 16 August 2016]. Available from: http://www.ibm.com/analytics/us/en/technology/spss/spss.html#what-is-spss.

Stefanescu C, Morales-Nin, B., Massutí, E. 1994. Fish assemblages on the slope in the Catalan Sea (western Mediterranean): influence of a submarine canyon. Journal of Marine Biological Association of UK. 74:499–512.

Tecchio S, van Oevelen D, Soetaert K, Navarro J, Ramirez-Llodra E. 2013. Trophic dynamics of deep sea megabenthos are mediated by surface productivity. PLoS ONE 8(5). [accessed 12 April 2016]. Available from: http://dx.doi.org/10.1371/journal.pone.0063796.

Thurber AR, Kroeger K, Neira C, Wiklund H, Levin LA. 2010. Stable isotope signatures and methane use by New Zealand cold seep benthos. Marine Geology. 272:260–269.

Trueman CN, Johnston G, O'Hea B, MacKenzie KM. 2014. Trophic interactions of fish communities at midwater depths enhance long-term carbon storage and benthic production on continental slopes. Proceedings of the Royal Society Biological Sciences. 281(1787).

Tyler PA, Bronsdon SK, Young CM, Rice AL. 1995. Ecology and gametogenic biology of the genus Umbellula (Pennatulacea) in the North-Atlantic Ocean. International Review of Hydrobiology (*Internationale Revue der gesamten Hydrobiologie und Hydrographie*). 80:187–199.

Vander Zanden MJ, Rasmussen JB. 2001. Variation in $\delta^{15}N$ and $\delta^{13}C$ trophic fractionation: implications for aquatic food web studies. Limnology and Oceanography. 46:2061–2066.

Van Dover CL. 2007. Stable isotope studies in marine chemoautotrophically based ecosystems: an update. In: Michener R, Lajtha K, editors. Stable isotopes in ecology and environmental sciences, second edition. Blackwell Publishing. p. 202-237.

Vetter EW, Dayton PK. 1998. Macrofaunal communities within and adjacent to a detritus-rich submarine canyon system. Deep‐Sea Research Part II Topical Studies in Oceanography. 45:25–54.

Vetter EW, Dayton PK. 1999. Organic enrichment by macrophyte detritus, and abundance patterns of megafaunal populations in submarine canyons. Marine Ecology Progress Series. 186:137–148.

Wada E, Mizutani H, Minagawa M. 1991. The use of stable isotopes for food web analysis. Critical Reviews in Food Science and Nutrition. 30:361–371.

Zapata-Hernández G, Sellanes J, Thurber AR, Levin LA, Chazalon F, Linke P. 2014. New insights on the trophic ecology of bathyal communities from the methane seep area off Concepción, Chile (~36°S). Marine Ecology. 35:1–21.

Appendix 16-A

Supplemental Tables of Isotope Sampling Locations and Stable Isotope Study Results from Baltimore and Norfolk Canyons

This page intentionally left blank

Table 16-A1. Stations where isotope samples were collected near two mid-Atlantic canyons, Baltimore and Norfolk. OT = otter trawl, BC = box core, DN = dip net, ROV = Jason II and Kraken 2. ROV depth range and location are based on bottom time. *Indicates poor quality of data or gear issue.

Station	Date	Gear	Canyon	Start		End		Depth Range (m)
				Latitude (N)	Longitude (W)	Latitude (N)	Longitude (W)	
NF-2011-005	7 June 2011	CTD	Baltimore	38°10′39.72″	73°51′35.64″	38°10′39.72″	73°51′35.64″	195–459
NF-2011-N25	13 June 2011	CTD	Norfolk	37°02′21.12″	74°37′04.08″	37°02′18.96″	74°37′03.72″	199–750
NF-2012-024	20 Aug 2012	CTD	Baltimore	38°06′38.52″	73°49′40.08″	38°06′33.48″	73°49′30.72″	0–854
NF-2012-028	20 Aug 2012	BC	Baltimore	38°14′34.08″	73°50′36.60″	38°14′34.08″	73°50′36.60″	191–191
NF-2012-036	21 Aug 2012	CTD	Baltimore	38°13′31.80″	73°50′42.72″	38°13′31.80″	73°50′43.08″	0–250
NF-2012-078	25 Aug 2012	BC	Baltimore	38°02′36.24″	73°48′18.00″	38°02′36.24″	73°48′18.00″	510–510
NF-2012-097	27 Aug 2012	CTD	Baltimore	38°05′53.88″	73°56′04.20″	38°05′54.24″	73°56′03.48″	0–107
NF-2012-100	27 Aug 2012	CTD	Baltimore	38°03′27.00″	73°50′45.96″	38°03′28.80″	73°50′48.84″	0–252
NF-2012-102	28 Aug 2012	CTD	Baltimore	38°01′39.36″	73°47′09.60″	38°01′39.00″	73°47′09.96″	0–680
NF-2012-105	28 Aug 2012	CTD	Baltimore	37°58′56.64″	73°41′18.96″	37°58′56.28″	73°41′18.96″	0–1,066
NF-2012-131	5 Sept 2012	Lander	Baltimore	38°02′32.64″	73°44′04.92″	–	–	0–1,340
NF-2012-132	6 Sept 2012	Lander	Baltimore	38°09′00.36″	73°50′52.44″	–	–	0–617
NF-2012-133	6 Sept 2012	OT	Baltimore	38°04′30.36″	73°52′57.72″	38°03′29.88″	73°54′00.36″	136–140
NF-2012-134	7 Sept 2012	OT	Baltimore	38°02′33.72″	73°51′12.24″	38°01′29.28″	73°52′01.20″	278–282
NF-2012-135	7 Sept 2012	OT	Baltimore	37°59′18.96″	73°54′11.16″	37°58′11.64″	73°55′07.68″	360–380
NF-2012-139	7 Sept 2012	OT	Baltimore	38°08′25.44″	73°45′05.04″	38°09′23.04″	73°44′36.24″	214–300
NF-2012-140	8 Sept 2012	OT	Baltimore	38°07′50.88″	73°45′30.24″	38°08′57.48″	73°44′46.32″	290–300
NF-2012-141	8 Sept 2012	OT	Baltimore	38°08′33.36″	73°44′58.56″	38°07′39.00″	73°45′42.12″	300–300
NF-2012-142	8 Sept 2012	OT	Baltimore	38°06′58.32″	73°45′17.28″	38°08′10.68″	73°45′09.72″	300–360
NF-2012-143	9 Sept 2012	OT	Baltimore	38°05′51.36″	73°45′40.32″	38°06′32.76″	73°44′40.20″	405–420
NF-2012-144	9 Sept 2012	OT	Baltimore	38°06′47.16″	73°44′47.40″	38°05′45.96″	73°45′21.24″	400–540
NF-2012-145	10 Sept 2012	OT	Baltimore	38°06′18.36″	73°45′00.36″	38°07′24.24″	73°44′54.24″	418–570
NF-2012-146	10 Sept 2012	OT	Baltimore	38°05′54.96″	73°45′33.48″	38°06′59.40″	73°44′48.48″	412–422
NF-2012-147	10 Sept 2012	OT	Baltimore	38°07′40.80″	73°45′41.76″	38°06′46.44″	73°46′48.72″	250–300
NF-2012-148	11 Sept 2012	CTD	Baltimore	38°01′39.00″	73°47′11.40″	38°01′39.00″	73°47′11.40″	0–671
NF-2012-150*	12 Sept 2012	OT	Baltimore	38°01′59.16″	73°46′03.72″	–	–	0–700
NF-2012-151	12 Sept 2012	OT	Baltimore	38°08′04.92″	73°51′01.08″	38°07′22.08″	73°50′35.52″	700–800
NF-2012-154	13 Sept 2012	CTD	Norfolk	37°05′37.32″	74°42′13.32″	37°05′31.20″	74°42′17.28″	0–328
NF-2012-155	13 Sept 2012	CTD	Norfolk	37°05′36.24″	74°40′50.52″	37°05′26.88″	74°40′58.08″	0–428
NF-2012-156	13 Sept 2012	CTD	Norfolk	37°04′51.24″	74°40′03.00″	37°04′46.20″	74°40′05.52″	0–498
NF-2012-157	14 Sept 2012	CTD	Norfolk	37°03′59.04″	74°39′03.96″	37°03′59.04″	74°39′03.96″	0–621
NF-2012-167	20 Sept 2012	OT	Norfolk	37°03′01.44″	74°38′25.44″	37°01′57.72″	74°38′08.52″	450–580
NF-2012-168*	21 Sept 2012	OT	Norfolk	37°02′51.00″	74°38′16.80″	–	–	–
NF-2012-175	22 Sept 2012	OT	Norfolk	37°05′32.64″	74°41′17.16″	37°05′03.84″	74°40′09.84″	405–510
NF-2012-176	22 Sept 2012	OT	Norfolk	37°04′35.76″	74°40′17.04″	37°05′21.84″	74°40′59.88″	400–423
NF-2012-177	23 Sept 2012	OT	Norfolk	37°05′08.88″	74°40′50.16″	37°04′03.00″	74°39′50.76″	389–402
NF-2012-178	23 Sept 2012	OT	Norfolk	37°03′49.32″	74°39′41.76″	37°04′58.44″	74°40′37.20″	400–401
NF-2012-179	23 Sept 2012	OT	Norfolk	37°04′59.16″	74°40′35.76″	37°03′46.44″	74°39′39.24″	395–400
NF-2012-186	24 Sept 2012	OT	Norfolk	37°03′27.00″	74°40′34.32″	37°02′18.96″	74°39′54.00″	103–120
NF-2012-187	24 Sept 2012	OT	Norfolk	37°04′57.72″	74°40′33.96″	37°04′09.48″	74°39′41.40″	402–480
NF-2012-188	25 Sept 2012	OT	Norfolk	37°05′32.28″	74°41′18.96″	37°04′45.48″	74°40′22.44″	403–408
NF-2012-189	26 Sept 2012	OT	Norfolk	37°13′08.76″	74°29′50.28″	37°12′12.24″	74°30′08.28″	460–500

Table 16-A1. (Continued).

Station	Date	Gear	Canyon	Start		End		Depth Range (m)
				Latitude (N)	Longitude (W)	Latitude (N)	Longitude (W)	
NF-2013-001	23 Aug 2013	CTD	Norfolk	37°02′16.08″	74°35′54.60″	37°02′16.08″	74°35′54.60″	2–1,000
NF-2013-003	23 Aug 2013	CTD	Norfolk	37°03′16.92″	74°38′09.24″	37°03′16.92″	74°38′08.88″	0–711
NF-2013-004	23 Aug 2013	CTD	Norfolk	37°04′00.84″	74°39′06.12″	37°04′00.84″	74°39′06.12″	0–630
NF-2013-007	23 Aug 2013	CTD	Norfolk	37°02′10.32″	74°32′02.04″	37°02′10.32″	74°32′02.04″	0–1,004
NF-2013-008	23 Aug 2013	CTD	Baltimore	38°02′24.00″	73°44′03.48″	38°02′09.96″	73°44′02.76″	0–966
NF-2013-009	24 Aug 2013	CTD	Baltimore	38°04′36.84″	73°47′09.96″	38°04′24.60″	73°47′07.80″	0–966
NF-2013-010	24 Aug 2013	CTD	Baltimore	38°08′55.32″	73°50′47.40″	38°08′55.32″	73°50′47.40″	0–634
NF-2013-011	24 Aug 2013	CTD	Baltimore	38°02′56.40″	73°49′48.36″	38°02′56.40″	73°49′48.36″	0–335
NF-2013-015	24 Aug 2013	CTD	Baltimore	38°02′56.40″	73°49′07.68″	38°02′56.40″	73°49′07.68″	0–440
NF-2013-017	24 Aug 2013	CTD	Baltimore	38°02′56.04″	73°48′47.52″	38°02′56.04″	73°48′47.52″	0–508
NF-2013-018	24 Aug 2013	CTD	Baltimore	38°05′38.76″	73°48′19.80″	38°05′26.88″	73°48′22.32″	0–905
NF-2013-019	24 Aug 2013	CTD	Baltimore	38°06′21.60″	73°49′23.52″	38°06′21.60″	73°49′23.52″	0–896
NF-2013-020	25 Aug 2013	CTD	Baltimore	38°07′26.76″	73°50′16.08″	38°07′26.76″	73°50′16.08″	0–773
NF-2013-021	25 Aug 2013	CTD	Baltimore	38°08′48.84″	73°50′43.80″	38°08′48.84″	73°50′43.80″	0–632
RB-2013-001	3 May 2013	OT	Norfolk	37°05′04.92″	74°40′46.20″	37°05′42.72″	74°41′39.48″	382–388
RB-2013-002*	3 May 2013	OT	Norfolk	37°04′33.24″	74°40′17.04″	37°05′18.24″	74°41′08.88″	376–392
RB-2013-003	3 May 2013	CTD	Norfolk	37°05′31.56″	74°44′47.40″	37°05′31.56″	74°44′47.76″	0–188
RB-2013-004	3 May 2013	CTD	Norfolk	37°05′25.08″	74°43′39.72″	37°05′25.08″	74°43′40.08″	0–237
RB-2013-005	3 May 2013	CTD	Norfolk	37°05′36.24″	74°42′15.84″	37°05′36.24″	74°42′15.48″	0–337
RB-2013-006	3 May 2013	CTD	Norfolk	37°05′38.40″	74°40′51.96″	37°05′38.04″	74°40′51.96″	0–438
RB-2013-009	3 May 2013	CTD	Norfolk	37°02′16.08″	74°35′58.20″	37°02′16.80″	74°35′59.28″	0–974
RB-2013-010	3 May 2013	CTD	Norfolk	37°02′11.40″	74°33′48.60″	37°02′09.60″	74°33′54.36″	0–1,177
RB-2013-011	3 May 2013	CTD	Norfolk	37°02′13.20″	74°33′44.28″	37°02′11.76″	74°33′42.48″	0–252
RB-2013-013	4 May 2013	OT	Norfolk	37°02′00.96″	74°36′11.88″	37°02′12.84″	74°35′16.08″	931–1,046
RB-2013-015	4 May 2013	CTD	Norfolk	37°02′31.92″	74°31′01.20″	37°02′31.56″	74°31′01.20″	0–1,364
RB-2013-016	4 May 2013	CTD	Norfolk	37°02′31.56″	74°32′56.76″	37°02′16.08″	74°32′58.92″	0–1,249
RB-2013-017	4 May 2013	CTD	Norfolk	37°02′16.80″	74°34′42.24″	37°02′17.52″	74°34′44.76″	0–1,101
RB-2013-018	4 May 2013	CTD	Norfolk	37°03′13.68″	74°38′03.84″	37°03′15.48″	74°38′07.80″	0–726
RB-2013-020	4 May 2013	CTD	Norfolk	37°04′45.84″	74°39′52.92″	37°04′46.20″	74°39′54.36″	0–534
RB-2013-021	4 May 2013	CTD	Norfolk	37°05′23.28″	74°43′49.44″	37°05′16.44″	74°43′55.92″	0–208
RB-2013-022	4 May 2013	CTD	Norfolk	37°03′54.72″	74°38′54.60″	37°03′50.76″	74°38′57.48″	0–631
RB-2013-023	4 May 2013	OT	Norfolk	37°05′02.40″	74°34′26.76″	37°05′57.12″	74°34′08.04″	160–165
RB-2013-024	4 May 2013	OT	Norfolk	37°04′23.52″	74°34′37.92″	37°05′18.24″	74°34′09.84″	175–187
RB-2013-025	4 May 2013	OT	Norfolk	37°04′31.44″	74°34′30.72″	37°05′36.96″	74°34′05.88″	180–185
RB-2013-026	5 May 2013	OT	Norfolk	37°04′15.24″	74°34′15.60″	37°05′13.56″	74°33′44.28″	255–270
RB-2013-027	5 May 2013	OT	Norfolk	37°04′47.64″	74°33′44.64″	37°05′52.44″	74°33′22.68″	304–330
RB-2013-028	5 May 2013	OT	Norfolk	37°04′44.04″	74°24′26.28″	37°05′24.36″	74°23′39.48″	1,614–1,643
RB-2013-029	7 May 2013	OT	Norfolk	37°04′19.20″	74°25′03.72″	37°05′00.60″	74°24′10.80″	1,576–1,629
RB-2013-030*	7 May 2013	OT	Norfolk	36°53′57.48″	74°27′31.32″	36°54′05.40″	74°26′18.60″	1,670–1,694
RB-2013-031	7 May 2013	CTD	Norfolk	36°51′46.80″	74°29′24.72″	36°51′46.80″	74°29′24.72″	0–1,611
RB-2013-032*	7 May 2013	OT	Norfolk	36°52′11.28″	74°27′44.28″	36°51′51.48″	74°26′24.72″	1,504–1,550
RB-2013-033*	8 May 2013	OT	Norfolk	36°51′31.32″	74°28′49.08″	36°51′07.92″	74°27′37.08″	1,636–1,712
RB-2013-034	8 May 2013	CTD	Norfolk	36°51′47.52″	74°29′26.88″	36°51′48.96″	74°29′23.64″	0–1,611
RB-2013-035*	9 May 2013	OT	Norfolk	36°51′49.68″	74°29′37.32″	36°51′23.40″	74°28′33.96″	1,608–1,674
RB-2013-038	10 May 2013	BC	Norfolk	37°02′18.96″	74°34′47.64″	37°02′18.96″	74°34′47.64″	1,110
RB-2013-039	10 May 2013	BC	Norfolk	37°02′19.32″	74°34′48.00″	37°02′19.32″	74°34′48.00″	1,110

Table 16-A1. (Continued).

Station	Date	Gear	Canyon	Start		End		Depth Range (m)
				Latitude (N)	Longitude (W)	Latitude (N)	Longitude (W)	
RB-2013-040	10 May 2013	BC	Norfolk	37°02′33.72″	74°37′45.12″	37°02′33.72″	74°37′45.12″	805
RB-2013-041	10 May 2013	BC	Norfolk	37°02′34.08″	74°37′45.12″	37°02′34.08″	74°37′45.12″	803
RB-2013-042	10 May 2013	BC	Norfolk	37°02′34.08″	74°37′45.48″	37°02′34.08″	74°37′45.48″	804
RB-2013-043	11 May 2013	BC	Norfolk	37°04′33.60″	74°39′38.16″	37°04′33.60″	74°39′38.16″	559
RB-2013-044	11 May 2013	BC	Norfolk	37°04′33.60″	74°39′38.16″	37°04′33.60″	74°39′38.16″	557
RB-2013-045	11 May 2013	BC	Norfolk	37°04′33.60″	74°39′38.16″	37°04′33.60″	74°39′38.16″	558
RB-2013-046	11 May 2013	BC	Norfolk	37°05′41.28″	74°44′47.76″	37°05′41.28″	74°44′47.76″	195
RB-2013-048	11 May 2013	BC	Norfolk	37°05′41.28″	74°44′47.76″	37°05′41.28″	74°44′47.76″	195
RB-2013-049	11 May 2013	BC	Norfolk	37°01′23.16″	74°38′44.88″	37°01′23.16″	74°38′44.88″	187
RB-2013-052	11 May 2013	CTD	Norfolk	37°00′20.16″	74°31′18.48″	37°00′20.16″	74°31′18.48″	0–1,069
RB-2013-053	11 May 2013	CTD	Norfolk	37°00′21.96″	74°32′12.84″	37°00′21.96″	74°32′12.84″	0–1,092
RB-2013-054	12 May 2013	BC	Norfolk	37°00′56.88″	74°34′41.52″	37°00′56.88″	74°34′41.52″	549
RB-2013-055	12 May 2013	BC	Norfolk	37°00′56.88″	74°34′41.52″	37°00′56.88″	74°34′41.52″	548
RB-2013-056	12 May 2013	BC	Norfolk	37°00′56.88″	74°34′41.52″	37°00′56.88″	74°34′41.52″	548
RB-2013-063	13 May 2013	CTD	Norfolk	37°00′29.52″	74°33′09.36″	37°00′29.52″	74°33′09.72″	0–941
RB-2013-064	14 May 2013	CTD	Norfolk	37°00′32.04″	74°33′53.28″	37°00′32.04″	74°33′53.28″	0–791
RB-2013-065	14 May 2013	CTD	Norfolk	37°00′37.08″	74°34′35.04″	37°00′37.08″	74°34′35.04″	0–676
RB-2013-066	14 May 2013	CTD	Norfolk	37°00′38.88″	74°35′27.96″	37°00′38.88″	74°35′28.32″	0–356
RB-2013-067	14 May 2013	CTD	Norfolk	37°00′50.04″	74°36′55.80″	37°00′50.04″	74°36′55.80″	0–277
RB-2013-068	14 May 2013	CTD	Norfolk	37°01′09.48″	74°38′46.32″	37°01′09.12″	74°38′49.20″	0–126
RB-2013-069	14 May 2013	BC	Norfolk	37°00′32.40″	74°33′54.00″	37°00′32.40″	74°33′54.00″	804
RB-2013-073	15 May 2013	BC	Norfolk	37°00′20.88″	74°32′01.32″	37°00′20.88″	74°32′01.32″	1,105
RB-2013-079	16 May 2013	BC	Baltimore	38°03′41.04″	73°36′22.68″	38°03′41.04″	73°36′22.68″	1,608
RB-2013-083	18 May 2013	BC	Norfolk	37°02′00.24″	74°27′01.08″	37°02′00.24″	74°27′01.08″	1,620
RB-2013-084	19 May 2013	CTD	Norfolk	36°52′08.40″	74°29′38.04″	36°52′08.40″	74°29′38.04″	0–1,570
RB-2013-085	20 May 2013	CTD	Norfolk	37°02′15.00″	74°33′43.92″	37°02′15.36″	74°33′43.92″	0–1,180
RB-2013-086	21 May 2013	OT	Norfolk	37°06′23.40″	74°33′01.80″	37°05′29.04″	74°33′25.20″	287–340
RB-2013-087	21 May 2013	CTD	Norfolk	37°03′13.68″	74°38′04.92″	37°03′13.68″	74°38′04.92″	0–720
ROV-2012-NF-01	18 Aug 2012	ROV	Baltimore	38°08′49.56″	73°50′36.24″	38°08′56.76″	73°50′16.80″	450–634
ROV-2012-NF-02	19 Aug 2012	ROV	Baltimore	38°08′54.24″	73°50′20.04″	38°08′41.28″	73°50′02.04″	402–530
ROV-2012-NF-03	21 Aug 2012	ROV	Baltimore	38°06′25.56″	73°48′30.60″	38°07′36.12″	73°48′11.16″	303–827
ROV-2012-NF-04	22 Aug 2012	ROV	Baltimore	38°05′08.16″	73°47′03.84″	38°06′10.08″	73°47′02.04″	537–1,001
ROV-2012-NF-05	23 Aug 2012	ROV	Baltimore	38°08′16.44″	73°50′09.24″	38°08′14.64″	73°49′59.88″	400–540
ROV-2012-NF-06	24 Aug 2012	ROV	Baltimore	38°08′22.56″	73°50′08.52″	38°08′49.20″	73°49′58.08″	234–530
ROV-2012-NF-07	26 Aug 2012	ROV	Baltimore	38°02′31.56″	73°49′51.96″	38°02′35.52″	73°49′28.92″	412–444
ROV-2012-NF-08	27 Aug 2012	ROV	Baltimore	38°03′02.16″	73°49′12.00″	38°03′03.96″	73°49′18.84″	412–454
ROV-2012-NF-09	28 Aug 2012	ROV	Baltimore	38°09′07.92″	73°50′29.76″	38°09′10.44″	73°50′01.32″	313–574
ROV-2012-NF-10	29 Aug 2012	ROV	Baltimore	38°10′06.60″	73°51′08.64″	38°09′40.68″	73°51′31.68″	425–574
ROV-2012-NF-11	30 Aug 2012	ROV	Baltimore	38°05′35.16″	73°48′23.76″	38°05′18.60″	73°49′49.08″	446–938
ROV-2012-NF-12	4 Sept 2012	ROV	Norfolk	37°03′57.24″	74°39′10.80″	37°04′05.88″	74°38′52.80″	512–638
ROV-2012-NF-13	6Sept 2012	ROV	Baltimore	38°09′34.20″	73°51′20.52″	38°09′23.76″	73°51′54.36″	404–478
ROV-2012-NF-14	7 Sept 2012	ROV	Baltimore	38°02′36.24″	73°48′54.00″	38°02′57.12″	73°49′19.56″	407–507
ROV-2012-NF-16	9 Sept 2012	ROV	Baltimore	38°10′37.56″	73°51′39.96″	38°11′21.12″	73°51′22.68″	343–551
ROV-2012-NF-17	10 Sept 2012	ROV	Baltimore	38°07′01.20″	73°50′28.68″	38°07′06.96″	73°50′52.08″	569–830
ROV-2012-NF-18	11 Sept 2012	ROV	Baltimore	38°07′01.20″	73°50′44.16″	38°06′55.80″	73°51′00.00″	521–748
ROV-2012-NF-19	12 Sept 2012	ROV	Baltimore	38°09′19.08″	73°50′26.16″	38°09′02.88″	73°50′07.08″	302–608

Table 16-A1. (Continued).

Station	Date	Gear	Canyon	Start		End		Depth Range (m)
				Latitude (N)	Longitude (W)	Latitude (N)	Longitude (W)	
ROV-2012-NF-20	13 Sept 2012	ROV	Norfolk	37°03′03.60″	74°37′56.28″	37°03′02.16″	74°37′12.00″	385–766
ROV-2013-RB-679	2 May 2013	ROV	Norfolk	37°02′40.92″	74°37′46.20″	37°03′03.60″	74°37′47.28″	611–789
ROV-2013-RB-680	5 May 2013	ROV	Norfolk	37°03′11.52″	74°34′20.28″	37°03′33.48″	74°34′51.24″	423–642
ROV-2013-RB-681	6 May 2013	ROV	Norfolk	37°03′38.16″	74°34′53.76″	37°03′16.20″	74°37′19.92″	413–616
ROV-2013-RB-682	8 May 2013	ROV	Norfolk	36°51′51.48″	74°29′34.44″	36°51′51.48″	74°29′34.44″	1,520–1,612
ROV-2013-RB-683	9 May 2013	ROV	Norfolk	36°52′08.76″	74°29′18.60″	36°52′12.00″	74°29′18.24″	1,435–1,563
ROV-2013-RB-684	10 May 2013	ROV	Norfolk	37°04′08.76″	74°39′12.96″	37°04′09.84″	74°38′43.80″	322–610
ROV-2013-RB-685	11 May 2013	ROV	Norfolk	37°02′53.16″	74°30′35.28″	37°04′13.44″	74°32′38.04″	538–1,390
ROV-2013-RB-686	13 May 2013	ROV	Norfolk	37°03′10.80″	74°36′10.80″	37°03′33.12″	74°36′11.16″	391–620
ROV-2013-RB-687	14 May 2013	ROV	Norfolk	37°03′34.20″	74°36′06.84″	37°03′34.56″	74°34′46.20″	384–715
ROV-2013-RB-688	15 May 2013	ROV	Norfolk	37°01′27.48″	74°35′17.88″	37°01′15.24″	74°35′50.28″	323–561
ROV-2013-RB-689	16 May 2013	ROV	Baltimore	38°02′51.00″	73°49′02.64″	38°02′53.16″	73°49′18.84″	354–442
ROV-2013-RB-690	17 May 2013	ROV	Baltimore	38°10′13.80″	73°50′15.72″	38°09′38.88″	73°49′59.52″	289–464
ROV-2013-RB-691	18 May 2013	ROV	Norfolk	37°00′50.40″	74°40′40.80″	37°01′49.44″	74°37′56.28″	378–520
ROV-2013-RB-692	19 May 2013	ROV	Norfolk	37°11′30.48″	74°34′27.84″	37°11′30.12″	74°34′26.76″	103–105
ROV-2013-RB-693	20 May 2013	ROV	Norfolk	37°09′20.52″	74°34′25.68″	37°09′23.40″	74°34′40.08″	97–118
ROV-2013-RB-694	21 May 2013	ROV	Norfolk	37°13′55.20″	74°33′01.80″	37°13′59.52″	74°33′02.16″	118–127
ROV-2013-RB-695	22 May 2013	ROV	Norfolk	37°16′50.16″	74°32′06.72″	37°16′55.56″	74°32′04.92″	114–225

Table 16-A2. Stable isotope values ($\delta^{13}C$ and $\delta^{15}N$) for primary producers, surface sediments (0−2 cm), invertebrates and fishes collected from nonseep habitats in two mid-Atlantic canyons, Baltimore (BC) and Norfolk (NC). Where N is the number of specimens, average ‰ values (± SE) and ranges (min/max), C:N is the ratio of carbon to nitrogen, and TL is the calculated trophic level (see Methods). C:N data for POM calculated from actual amount of material analyzed, which was not available for all filters. The following n values represent number of samples used in C:N calculations for POM: *n* = 1 for BC POM in (bottom), *n* = 2 for BC POM in (surface), *n* = 3 for BC POM out (bottom), *n* = 1 for BC POM out (surface), *n* = 17 for NC POM in (bottom), *n* = 16 for NC POM in (midwater), *n* = 20 for NC POM in (surface), *n* = 7 for NC POM out (bottom), *n* = 8 for BC POM out (surface). (Blank cells indicate that no samples were analyzed for SIA; either species was not collected or no isotope sample was taken from the species.)

Taxa	Baltimore Canyon												Norfolk Canyon										
	N	$\delta^{13}C$			$\delta^{15}N$			C:N			TL		N	$\delta^{13}C$			$\delta^{15}N$			C:N			TL
Annelida																							
Annelida	1	-22.2	±	0.0	7.1	±	0.0	2.4	±	0.0	2.4												
Polychaeta	9	-17.2	±	0.4	10.0	±	0.6	4.4	±	0.2	3.4												
		-20.3	to	-16.3	7.5	to	12.1	3.7	to	5.6													
Eunicida																							
Eunicidae																							
Eunicidae													2	-17.2	±	0.4	11.9	±	2.6	4.0	±	0.1	4.4
														-17.6	to	-16.8	9.4	to	14.5	3.9	to	4.1	
Hyalinoecia artifiex													4	-18.5	±	0.4	11.8	±	0.9	5.5	±	0.4	4.3
														-19.2	to	-17.5	10.0	to	13.8	4.6	to	6.5	
Hyalinoecia cf. *tubicola*													13	-17.7	±	0.4	10.6	±	0.5	4.5	±	0.2	3.9
														-20.3	to	-15.7	8.3	to	13.8	3.5	to	5.5	
Hyalinoecia sp.	10	-16.5	±	0.3	11.2	±	0.5	4.3	±	0.3	3.8												
		-18.9	to	-15.5	8.3	to	12.8	3.9	to	6.9													
Hyalinoecia tubicola													40	-18.1	±	0.1	9.5	±	0.5	4.9	±	0.2	3.6
														-19.7	to	-16.2	1.4	to	13.7	2.8	to	7.6	
Onuphidae																							
Onuphidae	5	-18.7	±	0.7	6.3	±	0.8	3.6	±	0.3	2.1		5	-18.2	±	0.3	11.2	±	0.7	4.3	±	0.2	4.2
		-21.5	to	-17.6	3.6	to	8.5	2.5	to	4.2				-18.9	to	-17.1	8.7	to	12.2	3.8	to	5.0	
Onuphis sp.													5	-17.3	±	0.3	10.0	±	0.6	4.5	±	0.2	3.8
														-18.2	to	-16.6	8.2	to	11.9	4.3	to	5.1	
Phyllodocida																							
Aphroditidae													5	-16.6	±	0.3	11.4	±	0.8	4.2	±	0.1	4.2
														-17.4	to	-15.8	9.3	to	13.7	3.7	to	4.5	
Glyceridae													1	-18.6			12.0			4.3			4.4
Polynoidae													6	-19.1	±	0.7	11.0	±	0.4	3.8	±	0.6	4.1
														-22.2	to	-17.9	9.7	to	12.4	1.0	to	4.7	
Canalipalpata																							
Terebellidae													1	-17.9			8.6			4.7			3.3

Table 16-A2. (Continued).

Taxa	Baltimore Canyon												Norfolk Canyon										
	N	$\delta^{13}C$			$\delta^{15}N$			C:N			TL		N	$\delta^{13}C$			$\delta^{15}N$			C:N			TL
Arthropoda																							
Amphipoda																							
Amphipoda	26	-19.0	±	0.1	6.4	±	0.2	4.5	±	0.1	2.2		16	-19.8	±	0.1	6.2	±	0.2	4.9	±	0.1	2.5
		-19.9	to	-18.0	4.0	to	7.6	4.0	to	5.1				-20.9	to	-18.9	4.5	to	7.2	4.0	to	5.9	
Aoridae																							
Unciola sp.	1	-17.4			7.7			4.3			2.6		5	-18.6	±	0.2	5.6	±	0.6	4.4	±	0.3	2.3
														-19.3	to	-18.2	3.7	to	7.2	3.4	to	4.9	
Hyperiidae																							
Themisto abyssorum													4	-18.6	±	0.2	5.2	±	0.6	5.0	±	0.2	2.1
														-19.0	to	-18.1	3.4	to	6.2	4.6	to	5.5	
Themisto sp.	2	-20.1	±	0.2	8.3	±	0.1	5.1	±	0.4	2.8		13	-19.0	±	0.1	6.2	±	0.3	5.3	±	0.1	2.5
		-20.4	to	-19.9	8.2	to	8.3	4.7	to	5.5				-19.5	to	-18.3	4.0	to	8.1	4.7	to	5.9	
Copepoda																							
Copepoda													1	-19.9			11.9			7.8			4.4
Cirripedia																							
Cirripedia − barnacle													7	-19.6	±	0.4	10.6	±	0.4	5.4	±	0.3	3.9
														-20.7	to	-17.8	9.1	to	12.7	4.4	to	7.1	
Scalpelliformes																							
Scalpellidae																							
cf. Scalpellidae													1	-18.6			11.8			2.7			4.3
Decapoda																							
Alpheidae																							
cf. *Alpheus* sp.													5	-17.5	±	0.1	9.3	±	0.4	4.5	±	0.2	3.5
														-17.7	to	-17.2	8.2	to	10.0	3.9	to	4.8	
Aristeidae																							
Aristeus antillensis	2	-17.3	±	0.4	10.4	±	0.5	3.8	±	0.1	3.5												
		-17.7	to	-17.0	10.0	to	10.9	3.7	to	3.9													
Calappidae																							
cf. *Calappa* sp.													10	-17.9	±	0.4	8.9	±	0.6	4.1	±	0.1	3.4
														-20.3	to	-16.0	5.4	to	11.0	3.6	to	4.6	
Cancridae																							
Cancer borealis													16	-18.0	±	0.3	6.1	±	1.1	3.6	±	0.2	2.4
														-21.0	to	-16.5	-0.8	to	11.5	2.0	to	4.5	
Cancer cf. plebejus													3	-18.2	±	0.3	9.4	±	1.5	4.2	±	0.1	3.6
														-18.7	to	-17.8	6.5	to	11.0	4.0	to	4.4	
Cancer plebejus	11	-17.1	±	0.4	10.4	±	0.7	3.6	±	0.2	3.5		1	-17.5	±	0.0	9.5	±	0.0	4.0	±	0.0	3.6
		-19.6	to	-15.3	4.2	to	12.2	3.0	to	5.0													
cf. *Cancer borealis*													3	-16.9	±	0.4	11.2	±	0.2	3.8	±	0.0	4.1
														-17.5	to	-16.2	10.9	to	11.5	3.7	to	3.9	

Table 16-A2. (Continued).

Taxa	Baltimore Canyon												Norfolk Canyon										
	N	$\delta^{13}C$			$\delta^{15}N$			C:N			TL		N	$\delta^{13}C$			$\delta^{15}N$			C:N			TL
cf. *Cancer plebejus*													6	-17.9	±	0.5	8.8	±	0.9	4.1	±	0.1	3.4
														-19.6	to	-16.4	5.9	to	11.4	3.9	to	4.3	
Chirostylidae																							
Eumunida picta	7	-18.5	±	0.1	10.9	±	0.2	4.3	±	0.1	3.7		3	-19.2	±	0.5	10.4	±	0.7	3.9	±	0.2	3.9
		-19.2	to	-18.2	10.1	to	11.4	4.1	to	4.6				-20.3	to	-18.5	9.0	to	11.2	3.6	to	4.1	
Eumunida sp.	5	-18.7	±	0.1	9.8	±	0.3	3.8	±	0.1	3.3		1	-19.6			10.0			3.5			3.7
		-19.1	to	-18.4	9.2	to	10.9	3.6	to	4.0													
Crangonidae																							
Sabinea hystrix													1	-15.5			12.9			3.4			4.7
Diogenidae																							
cf. *Paguristes lymani*	10	-18.6	±	0.1	5.3	±	0.2	4.6	±	0.1	1.8												
		-19.3	to	-18.0	4.0	to	6.6	3.9	to	5.4													
Paguristes lymani													4	-17.3	±	0.1	9.5	±	0.2	4.1	±	0.1	3.6
														-17.5	to	-17.0	9.1	to	9.9	3.8	to	4.3	
Paguristes moorei													1	-19.3			6.0			4.1			2.4
Paguristes sp.													4	-17.3	±	0.3	9.6	±	0.4	4.0	±	0.0	3.6
														-17.8	to	-16.6	9.0	to	10.7	4.0	to	4.1	
Paguroidea													2	-16.8	±	0.3	9.0	±	0.8	4.0	±	0.1	3.4
														-17.1	to	-16.5	8.2	to	9.8	3.9	to	4.1	
Galathea rostrata													1	-19.2			10.8			4.0			4.0
Galatheoidea													1	-17.1			10.7			3.7			4.0
Hippolytidae																							
Hippolyte obliquimanus													3	-14.1	±	0.3	10.3	±	0.1	2.3	±	0.0	3.8
														-14.7	to	-13.7	10.0	to	10.4	2.3	to	2.4	
Geryonidae																							
Chaceon quinquedens	1	-20.2			12.2			4.2			4.1		20	-18.6	±	0.4	10.6	±	0.4	4.0	±	0.1	3.9
														-23.7	to	-16.8	5.9	to	13.2	3.4	to	4.7	
cf. *Chaceon* sp.	19	-17.3	±	0.1	10.1	±	0.3	3.7	±	0.1	3.4		12	-17.8	±	0.4	10.9	±	0.2	3.8	±	0.2	4.0
		-18.3	to	-16.3	6.9	to	12.3	3.0	to	4.5				-21.2	to	-16.9	9.2	to	11.6	2.5	to	4.2	
Inachoididae																							
cf. *Euprognatha rastellifera*													2	-18.7	±	0.1	-2.1	±	2.7	2.4	±	0.0	-0.3
														-18.9	to	-18.6	-4.8	to	0.6	2.4	to	2.4	
Euprognatha rastellifera													4	-18.5	±	0.4	-0.8	±	0.7	2.7	±	0.3	0.1
														-19.0	to	-17.5	-2.5	to	0.4	2.1	to	3.5	
Latreilliidae																							
Latreillia elegans	5	-18.5	±	0.1	6.4	±	0.2	3.5	±	0.1	2.2												
		-18.7	to	-18.1	6.1	to	6.9	3.3	to	3.9													

Table 16-A2. (Continued).

Taxa	Baltimore Canyon												Norfolk Canyon										
	N	$\delta^{13}C$			$\delta^{15}N$			C:N			TL		N	$\delta^{13}C$			$\delta^{15}N$			C:N			TL
Munididae																							
Agononida longipes	5	-17.1	±	0.1	7.9	±	0.3	3.6	±	0.1	2.7												
		-17.4	to	-16.6	7.2	to	8.6	3.2	to	3.8													
Munida iris	10	-17.0	±	0.2	9.3	±	0.3	4.0	±	0.1	3.1		25	-17.0	±	0.1	8.2	±	0.3	3.1	±	0.1	3.1
		-17.8	to	-15.4	7.5	to	10.2	3.2	to	4.3				-18.0	to	-16.2	5.5	to	10.6	1.9	to	4.2	
Munida iris iris													4	-17.0	±	0.1	10.2	±	0.2	4.1	±	0.1	3.8
														-17.2	to	-16.8	9.9	to	10.7	4.0	to	4.2	
Munida sp.													1	-17.1			11.0			1.9			4.1
Munida valida	26	-16.6	±	0.1	8.6	±	0.2	3.7	±	0.1	2.9												
		-17.2	to	-16.1	6.9	to	10.3	3.0	to	4.2													
Munidopsidae																							
Munidopsis sp.													1	-20.1			9.2			4.4			3.5
Nematocarcinidae																							
Nematocarcinus cursor													1	-17.5			9.1			4.2			3.4
Nephropidae																							
Homarus americanus	1	-15.7			12.0			3.8			4.0		1	-16.5			13.3			2.9			4.8
Oplophoridae																							
Acanthephyra eximia													2	-18.2	±	0.6	9.5	±	0.5	3.4	±	0.1	3.6
														-18.8	to	-17.5	9.0	to	10.0	3.4	to	3.5	
Pandalidae																							
Atlantopandalus propinqvus	32	-18.2	±	0.2	9.3	±	0.2	3.9	±	0.0	3.1		10	-17.4	±	0.2	9.7	±	0.2	3.3	±	0.1	3.6
		-19.9	to	-16.6	7.9	to	11.3	3.4	to	4.4				-18.2	to	-16.8	9.0	to	10.6	2.8	to	3.9	
Dichelopandalus leptocerus	6	-17.0	±	0.2	9.2	±	0.5	3.6	±	0.1	3.1		49	-17.5	±	0.1	9.4	±	0.2	3.0	±	0.1	3.5
		-17.6	to	-16.2	7.5	to	10.5	3.4	to	3.8				-19.9	to	-15.7	4.2	to	12.4	1.8	to	4.7	
Dichelopandalus sp.	10	-17.3	±	0.1	9.2	±	0.1	3.9	±	0.0	3.1		8	-17.3	±	0.1	9.5	±	0.2	3.8	±	0.1	3.6
		-17.7	to	-16.8	8.8	to	9.8	3.8	to	4.0				-17.6	to	-16.7	8.1	to	10.0	3.6	to	4.2	
Heterocarpus ensifer													10	-17.4	±	0.1	8.2	±	0.4	2.9	±	0.2	3.1
														-18.0	to	-16.7	5.4	to	9.5	2.4	to	3.8	
Pandalus borealis	5	-16.7	±	0.1	8.7	±	0.2	3.6	±	0.0	2.9												
		-16.8	to	-16.6	8.0	to	9.4	3.5	to	3.7													
Pandalus montagui													5	-18.9	±	0.1	9.2	±	0.3	4.1	±	0.1	3.5
														-19.2	to	-18.5	8.3	to	10.0	3.7	to	4.2	
Plesionika holthuisi													2	-16.9	±	0.1	10.1	±	0.1	3.9	±	0.0	3.8
														-17.0	to	-16.8	10.0	to	10.2	3.9	to	3.9	
Pasiphaeidae																							
Pasiphaea multidentata													5	-17.8	±	0.1	8.4	±	0.2	3.6	±	0.0	3.2
														-18.1	to	-17.6	7.8	to	9.1	3.5	to	3.7	

Table 16-A2. (Continued).

Taxa	Baltimore Canyon												Norfolk Canyon										
	N	$\delta^{13}C$			$\delta^{15}N$			C:N			TL		N	$\delta^{13}C$			$\delta^{15}N$			C:N			TL
Penaeidae																							
Penaeidae													1	-16.5			8.3			2.8			3.2
Parapenaeus politus	5	-17.0	±	0.2	8.4	±	0.3	3.6	±	0.1	2.8		8	-17.2	±	0.2	9.4	±	0.3	3.6	±	0.1	3.5
		-17.4	to	-16.4	7.8	to	9.6	3.4	to	3.8				-18.0	to	-16.2	8.5	to	10.9	3.1	to	3.9	
Parapenaeus sp.	5	-17.4	±	0.7	8.0	±	0.2	3.8	±	0.1	2.7												
		-19.1	to	-16.1	7.5	to	8.7	3.6	to	4.0													
Penaeus sp.													9	-17.1	±	0.1	10.1	±	0.3	3.8	±	0.1	3.8
														-17.6	to	-16.7	9.2	to	11.8	3.6	to	4.1	
Trachypenaeus sp.													5	-15.6	±	0.3	10.7	±	0.4	2.6	±	0.2	4.0
														-16.5	to	-15.1	9.4	to	11.7	2.3	to	3.5	
Xiphopenaeus sp.													5	-16.7	±	0.1	9.8	±	0.1	2.9	±	0.0	3.7
														-16.8	to	-16.5	9.5	to	10.0	2.8	to	2.9	
Pisidae																							
Rochinia crassa	4	-18.9	±	0.2	6.8	±	1.0	4.9	±	0.6	2.3												
		-19.3	to	-18.5	4.0	to	9.0	3.1	to	6.2													
Rochinia tanneri													2	-18.5	±	0.1	5.0	±	0.8	4.5	±	0.0	2.1
														-18.7	to	-18.4	4.2	to	5.8	4.4	to	4.5	
cf. Rochinia tanneri													1	-18.8			8.9			3.5			3.4
Polychelidae																							
Stereomastis nana													14	-18.2	±	0.2	11.5	±	0.2	3.7	±	0.1	4.2
														-19.9	to	-16.3	10.1	to	12.6	3.0	to	4.5	
Portunidae																							
Bathynectes maravigna	6	-17.0	±	0.1	9.3	±	0.4	3.0	±	0.0	3.5		4	-17.7	±	0.2	11.0	±	0.2	4.5	±	0.0	4.1
		-17.4	to	-16.6	8.7	to	11.0	2.9	to	3.2				-18.1	to	-17.4	10.4	to	11.3	4.5	to	4.5	
Processidae																							
Processa guyanae	7	-17.1	±	0.1	8.9	±	0.2	3.8	±	0.0	3.0												
		-17.7	to	-16.4	7.8	to	9.8	3.6	to	3.9													
Processa profunda													10	-16.6	±	0.1	9.2	±	0.4	4.1	±	0.1	3.5
														-17.1	to	-16.2	6.9	to	10.6	3.8	to	4.3	
Sergestidae																							
Acetes americanus carolinae	5	-19.1	±	0.3	7.7	±	0.2	3.7	±	0.0	2.6		52	-18.8	±	0.1	8.4	±	0.1	3.4	±	0.1	3.2
		-19.8	to	-18.2	7.3	to	8.5	3.6	to	3.8				-20.1	to	-16.9	7.2	to	10.1	2.4	to	4.6	
Solenoceridae																							
Hymenopenaeus debilis													5	-17.0	±	0.1	9.8	±	0.1	3.7	±	0.0	3.7
														-17.3	to	-16.7	9.5	to	10.0	3.6	to	3.9	
Mesopenaeus tropicalis	1	-16.8			9.6			3.6			3.2		5	-16.5	±	0.3	6.0	±	0.6	3.7	±	0.0	2.4
														-17.2	to	-15.7	5.0	to	7.8	3.5	to	3.8	
Brachyura	10	-18.9	±	0.1	5.5	±	0.5	3.2	±	0.1	1.9												
		-19.6	to	-18.3	2.7	to	7.5	2.7	to	3.8													

Table 16-A2. (Continued).

Taxa	Baltimore Canyon											Norfolk Canyon										
	N	$\delta^{13}C$			$\delta^{15}N$			C:N			TL	N	$\delta^{13}C$			$\delta^{15}N$			C:N			TL
Caridea												1	-17.9			9.0			3.9			3.4
Majoidea												4	-19.2	±	0.3	4.8	±	0.8	5.0	±	0.4	2.0
													-19.9	to	-18.4	3.4	to	6.4	4.3	to	6.2	
Shrimp	25	-19.2	±	0.2	7.6	±	0.3	4.6	±	0.2	2.4	1	-18.9			7.6			3.8			2.9
		-21.4	to	-16.8	4.9	to	9.5	3.5	to	6.5												
Shrimp sp. A												1	-18.5			7.8			4.0			3.0
Shrimp sp. B	1	-17.9			10.1			3.6			3.4											
Shrimp sp. C	4	-16.6	±	0.5	10.3	±	0.3	3.9	±	0.1	3.5											
		-18.2	to	-15.8	9.5	to	10.9	3.6	to	4.2												
Shrimp sp. H												5	-16.5	±	0.1	10.8	±	0.2	3.8	±	0.1	4.0
													-16.7	to	-16.1	10.1	to	11.1	3.7	to	4.2	
Shrimp sp. I	17	-18.8	±	0.2	8.6	±	0.3	4.0	±	0.1	2.9	1	-19.7	±	0.0	7.5	±	0.0	3.9	±	0.0	2.9
		-20.2	to	-17.8	5.6	to	10.6	3.4	to	4.6			-19.7	to	-19.7	7.5	to	7.5	3.9	to	3.9	
Shrimp sp. K	3	-16.9	±	0.3	8.6	±	0.2	3.7	±	0.1	2.9											
		-17.4	to	-16.5	8.3	to	9.0	3.6	to	3.8												
Shrimp sp. L	5	-18.1	±	0.2	8.5	±	0.3	3.6	±	0.0	2.9	1	-18.3			6.8			3.3			2.7
		-18.6	to	-17.6	7.4	to	9.0	3.6	to	3.7												
Shrimp sp. M												5	-17.8	±	0.2	8.7	±	0.4	2.8	±	0.0	3.3
													-18.5	to	-17.4	7.6	to	9.8	2.6	to	2.8	
Shrimp sp. Q												6	-17.2	±	0.3	11.6	±	0.5	3.2	±	0.4	4.3
													-18.7	to	-16.6	10.2	to	12.8	2.4	to	4.1	
Shrimp sp. R												5	-19.3	±	0.1	7.3	±	0.3	3.9	±	0.1	2.9
													-19.5	to	-19.2	6.9	to	8.0	3.7	to	4.1	
Shrimp sp. S	3	-17.5	±	0.3	10.0	±	0.2	3.7	±	0.0	3.3											
		-18.2	to	-17.1	9.7	to	10.2	3.7	to	3.8												
Shrimp sp. T	20	-17.3	±	0.1	10.8	±	0.2	3.8	±	0.0	3.6											
		-18.1	to	-16.7	8.8	to	12.1	3.5	to	4.1												
Shrimp sp. U	19	-16.7	±	0.1	9.6	±	0.2	3.6	±	0.0	3.2											
		-17.5	to	-15.9	8.6	to	11.9	3.3	to	4.0												
Isopoda												1	-18.6	±	0.0	8.8	±	0.0	5.1	±	0.0	3.3
Euphausiacea																						
Bentheuphausiidae																						
Bentheuphausia amblyops	10	-18.4	±	0.1	8.3	±	0.3	4.0	±	0.1	2.8											
		-19.0	to	-17.9	7.2	to	10.2	3.7	to	4.3												
Euphausiidae																						
Euphausiidae												9	-18.9	±	0.1	6.2	±	0.3	4.3	±	0.2	2.5
													-19.5	to	-18.4	4.0	to	7.4	3.5	to	4.9	
cf. *Meganyctiphanes norvegica*	11	-19.6	±	0.2	6.9	±	0.4	4.6	±	0.1	2.3											
		-20.7	to	-18.9	5.0	to	8.4	3.9	to	5.4												

Table 16-A2. (Continued).

Taxa	Baltimore Canyon												Norfolk Canyon										
	N	$\delta^{13}C$			$\delta^{15}N$			C:N			TL		N	$\delta^{13}C$			$\delta^{15}N$			C:N			TL
Meganyctiphanes norvegica													24	-19.0	±	0.1	7.9	±	0.2	3.7	±	0.2	3.1
														-20.3	to	-17.6	5.4	to	9.4	2.3	to	5.3	
Nyctiphanes couchii	2	-19.0	±	0.3	8.3	±	1.3	4.0	±	0.2	2.8												
		-19.3	to	-18.7	7.0	to	9.6	3.8	to	4.1													
Thysanoessa macrura	16	-19.6	±	0.1	7.2	±	0.3	4.4	±	0.1	2.4												
		-20.2	to	-17.6	4.3	to	9.6	3.8	to	5.0													
Pycnogonida (c)																							
Pycnogonida													17	-17.2	±	0.3	11.0	±	0.2	4.3	±	0.1	4.1
														-18.8	to	-15.6	9.5	to	12.1	3.8	to	5.4	
Brachiopoda																							
Brachiopoda													2	-18.2	±	0.2	6.4	±	0.9	3.2	±	0.6	2.5
														-18.4	to	-18.0	5.5	to	7.3	2.6	to	3.7	
Bryozoa																							
Bryozoa													2	-18.1	±	0.4	1.6	±	0.3	1.7	±	0.3	0.9
														-18.6	to	-17.7	1.3	to	1.9	1.3	to	2.0	
Chordata − Invertebrates																							
Pyrosomatida																							
Pyrosomatidae																							
Pyrosoma sp.													4	-21.7	±	0.4	3.0	±	0.7	4.6	±	0.7	1.4
														-22.4	to	-20.7	1.2	to	4.2	2.9	to	6.1	
Salpida																							
Salpida	1	-20.1			2.9			4.6			1.0												
Salpidae																							
Salpa sp.													5	-19.9	±	0.2	2.0	±	0.8	2.8	±	0.2	1.1
														-20.5	to	-19.1	-0.1	to	3.7	2.0	to	3.2	
Chordata − Fishes																							
Myxiniformes																							
Myxinidae																							
Myxine glutinosa	11	-18.1	±	0.2	11.3	±	0.3	4.5	±	0.1	3.8		43	-18.2	±	0.1	11.9	±	0.2	4.6	±	0.1	4.4
		-19.1	to	-17.0	9.8	to	13.2	4.2	to	5.1				-20.4	to	-17.1	9.1	to	14.0	3.9	to	5.4	
Carcharhiniformes																							
Scyliorhinidae																							
Scyliorhinus retifer	2	-17.4	±	0.0	10.2	±	0.2	3.4	±	0.1	3.4		5	-17.1	±	0.1	11.6	±	0.2	3.3	±	0.1	4.3
		-17.5	to	-17.4	10.0	to	10.4	3.3	to	3.4				-17.3	to	-16.9	11.0	to	12.2	3.1	to	3.6	
Rajiformes																							
Rajidae																							
Amblyraja radiata													1	-17.1			11.8			3.5			4.3
Leucoraja garmani	1	-17.2			9.9			3.1			3.3												
Malacoraja sp. (senta)													14	-17.3	±	0.1	10.4	±	0.3	3.8	±	0.1	3.9

Table 16-A2. (Continued).

Taxa	Baltimore Canyon												Norfolk Canyon										
	N	$\delta^{13}C$			$\delta^{15}N$			C:N			TL		N	$\delta^{13}C$			$\delta^{15}N$			C:N			TL
														-17.8	to	-16.4	9.2	to	12.5	3.3	to	4.4	
Rajella sp.													1	-16.7			11.6			3.9			4.3
Squaliformes																							
Etmopteridae																							
Etmopterus gracilispinis													1	-21.1			10.7			6.8			4.0
Anguilliformes																							
Congridae																							
Conger oceanicus													1	-17.3			10.6			3.9			3.9
Nemichthyidae																							
Nemichthys curvirostris	2	-19.6	±	0.8	11.5	±	0.2	5.4	±	0.9	3.8		4	-18.5	±	0.1	10.4	±	0.2	4.0	±	0.4	3.9
		-20.4	to	-18.8	11.3	to	11.7	4.5	to	6.3				-18.8	to	-18.3	10.0	to	10.8	2.9	to	4.7	
Nemichthys scolopaceus	2	-20.0	±	0.4	11.7	±	0.0	5.4	±	0.4	3.9		1	-19.2			10.9			4.5			4.0
		-20.3	to	-19.6	11.7	to	11.7	5.0	to	5.8													
Nettastomatidae																							
Nettastomatidae													1	-21.8			5.8			4.1			2.4
Ophichthidae																							
Ophichthus cruentifer													6	-18.9	±	0.4	9.7	±	0.5	4.3	±	0.1	3.6
														-19.8	to	-17.5	7.4	to	11.2	4.1	to	4.8	
Synaphobranchidae																							
Dysommina rugosa													3	-18.6	±	0.1	12.0	±	0.4	5.1	±	0.3	4.4
														-18.8	to	-18.4	11.5	to	12.7	4.6	to	5.7	
Synaphobranchus affinis	4	-19.4	±	0.3	11.9	±	0.2	5.7	±	0.5	4.0												
		-20.4	to	-19.0	11.5	to	12.4	4.9	to	7.2													
Synaphobranchus kaupii	7	-18.6	±	0.1	11.9	±	0.2	4.6	±	0.1	4.0		14	-19.0	±	0.2	11.0	±	0.2	4.8	±	0.1	4.1
		-18.9	to	-18.1	11.3	to	12.6	4.2	to	4.9				-19.9	to	-17.3	10.1	to	12.1	3.9	to	5.5	
Argentiniformes																							
Alepocephalidae																							
Alepocephalus agassizii													6	-19.0	±	0.2	12.3	±	0.3	3.6	±	0.1	4.5
														-19.5	to	-18.4	11.6	to	13.3	3.5	to	3.8	
Argentinidae																							
Argentina striata	1	-16.8			12.4			3.8			4.2												
Aulopiformes																							
Chlorophthalmidae																							
Chlorophthalmus agassizi	9	-18.7	±	0.2	10.5	±	0.1	4.3	±	0.2	3.5		11	-18.7	±	0.2	8.9	±	0.3	4.0	±	0.2	3.4
		-19.8	to	-18.1	9.9	to	11.2	3.4	to	5.3				-19.9	to	-17.4	8.0	to	10.4	3.2	to	4.9	
Parasudis truculenta	3	-18.3	±	0.1	11.6	±	0.1	3.8	±	0.1	3.9												
		-18.4	to	-18.2	11.3	to	11.8	3.7	to	3.9													

Table 16-A2. (Continued).

Taxa	Baltimore Canyon												Norfolk Canyon										
	N	$\delta^{13}C$			$\delta^{15}N$			C:N			TL		N	$\delta^{13}C$			$\delta^{15}N$			C:N			TL
Ipnopidae																							
Bathypterois viridensis													1	-18.4			10.7			3.9			4.0
Paralepididae																							
Arctozenus risso	9	-18.4	±	0.1	10.0	±	0.2	4.2	±	0.1	3.4		3	-18.2	±	0.1	8.1	±	0.9	4.1	±	0.1	3.1
		-19.1	to	-17.9	8.9	to	10.7	3.8	to	4.6				-18.3	to	-18.1	6.8	to	9.9	3.9	to	4.3	
Paralepididae													1	-17.9			8.7			4.2			3.3
Gadiformes																							
Lotidae																							
Enchelyopus cimbrius	2	-17.3	±	0.0	12.6	±	0.5	3.6	±	0.3	4.2		15	-18.1	±	0.4	11.1	±	0.3	3.7	±	0.0	4.1
		-17.3	to	-17.3	12.1	to	13.1	3.3	to	3.9				-23.3	to	-16.9	7.2	to	12.3	3.5	to	3.9	
Macrouridae																							
Cetonurus globiceps cf.													1	-18.5			11.3			3.8			4.2
Coelorinchus caelorhincus	12	-17.0	±	0.2	12.3	±	0.3	4.0	±	0.1	4.1		22	-17.4	±	0.1	11.7	±	0.2	3.6	±	0.1	4.3
		-17.4	to	-15.0	11.2	to	15.4	3.8	to	4.7				-18.1	to	-16.9	9.2	to	12.8	3.0	to	4.0	
Macrouridae sp.													1	-17.7			11.0			4.0			4.1
Malacocephalus occidentalis	2	-18.0	±	0.1	10.6	±	0.5	3.9	±	0.0	3.6												
		-18.1	to	-17.9	10.1	to	11.1	3.9	to	4.0													
Nezumia aequalis													3	-22.7	±	1.4	7.4	±	0.8	3.5	±	0.3	2.9
														-25.4	to	-20.5	5.9	to	8.5	2.9	to	3.8	
Nezumia bairdii	16	-17.6	±	0.1	12.1	±	0.1	4.0	±	0.0	4.1		39	-20.2	±	0.5	9.7	±	0.4	3.6	±	0.1	3.6
		-18.9	to	-17.0	10.5	to	12.9	3.8	to	4.3				-26.2	to	-16.8	4.4	to	13.7	2.8	to	3.9	
N. bairdii/C. caelorhinchus	5	-17.0	±	0.1	11.8	±	0.2	3.0	±	0.0	4.0												
		-17.6	to	-16.7	11.1	to	12.4	3.0	to	3.1													
Nezumia sp.													1	-17.1			13.3			3.9			4.9
Merluccidae																							
Merluccius albidus	14	-18.0	±	0.1	11.0	±	0.2	3.8	±	0.1	3.7		9	-18.1	±	0.0	11.2	±	0.1	3.8	±	0.0	4.1
		-18.6	to	-17.5	9.3	to	12.4	3.3	to	4.1				-18.3	to	-18.0	10.8	to	11.5	3.7	to	4.0	
Merluccius bilinearis													2	-17.0	±	0.3	13.1	±	0.7	3.5	±	0.2	4.8
														-17.3	to	-16.8	12.3	to	13.8	3.3	to	3.7	
Moridae																							
Antimora rostrata													2	-18.3	±	0.5	12.2	±	0.6	3.9	±	0.0	4.5
														-18.8	to	-17.8	11.7	to	12.8	3.8	to	3.9	
Laemonema barbatulum													1	-17.4			12.6			3.7			4.6
Physiculus karrerae													1	-18.3			11.5			3.7			4.2
Phycidae																							
Phycis chesteri	21	-18.2	±	0.1	11.5	±	0.2	3.8	±	0.1	3.9		38	-18.4	±	0.1	11.1	±	0.2	3.7	±	0.1	4.1
		-19.1	to	-17.7	10.3	to	12.9	3.0	to	4.3				-19.3	to	-17.5	6.2	to	12.7	2.2	to	4.1	
Urophycis chuss	4	-18.3	±	0.4	11.9	±	0.2	3.9	±	0.0	4.0		4	-17.5	±	0.1	11.2	±	0.4	3.7	±	0.1	4.2
		-19.5	to	-17.6	11.6	to	12.4	3.8	to	4.0				-17.6	to	-17.4	10.1	to	12.0	3.6	to	3.9	

Table 16-A2. (Continued).

Taxa	Baltimore Canyon												Norfolk Canyon										
	N	$\delta^{13}C$			$\delta^{15}N$			C:N			TL		N	$\delta^{13}C$			$\delta^{15}N$			C:N			TL
Urophycis regia	18	-18.2	±	0.1	11.6	±	0.2	4.0	±	0.0	3.9		20	-17.8	±	0.1	11.8	±	0.2	3.8	±	0.0	4.4
		-19.1	to	-17.2	10.6	to	13.0	3.8	to	4.4				-18.3	to	-16.6	10.9	to	13.1	3.3	to	4.1	
Lophiiformes																							
Chaunacidae																							
Chaunax suttkusi	1	-17.8			12.4			3.9			4.1												
Lophiidae																							
Lophius americanus	16	-17.6	±	0.1	13.4	±	0.1	3.6	±	0.1	4.5		2	-19.2	±	2.3	12.2	±	1.8	3.8	±	0.0	4.5
		-18.1	to	-17.0	12.9	to	14.2	2.9	to	4.1				-21.6	to	-16.9	10.4	to	14.1	3.7	to	3.8	
Ogcocephalidae																							
Dibranchus atlanticus	4	-15.2	±	0.6	13.9	±	0.3	3.7	±	0.2	4.6		4	-16.9	±	0.4	13.2	±	0.4	3.9	±	0.0	4.8
		-15.9	to	-13.4	13.3	to	14.8	3.2	to	4.2				-17.8	to	-16.2	11.9	to	13.8	3.8	to	4.0	
Notacanthiformes																							
Halosauridae																							
Aldrovandia affinis													1	-17.0			14.2			3.6			5.2
Notacanthidae																							
Notacanthus chemnitzi	1	-17.7			13.5			4.2			4.5		1	-18.5			11.3			3.8			4.2
Beryciformes																							
Trachichthyidae																							
Hoplostethus mediterraneus	2	-18.5	±	0.3	10.8	±	0.4	3.9	±	0.2	3.6		25	-18.2	±	0.0	11.1	±	0.1	3.9	±	0.1	4.1
		-18.8	to	-18.2	10.4	to	11.1	3.7	to	4.2				-18.6	to	-17.8	10.2	to	11.7	2.9	to	4.4	
Myctophiformes																							
Myctophidae																							
Myctophidae	14	-19.2	±	0.2	10.9	±	0.2	4.8	±	0.1	3.6		4	-19.0	±	0.3	10.9	±	0.4	4.5	±	0.1	4.0
		-20.5	to	-17.9	9.3	to	12.4	4.1	to	5.4				-19.4	to	-18.1	9.9	to	11.5	4.3	to	4.8	
Diaphus sp.	1	-18.6			8.6			4.2			2.9		1	-18.9			9.2			4.3			3.5
Myctophum affine													1	-18.0			8.7			3.8			3.3
Ophidiiformes																							
Bythitidae																							
Diplacanthopoma brachysoma													1	-17.5			11.9			3.6			4.4
Ophidiidae																							
Dicrolene introniger													3	-18.6	±	0.7	13.4	±	0.4	3.8	±	0.1	4.9
														-19.7	to	-17.5	12.7	to	13.8	3.7	to	3.9	
Lepophidium profundorum	5	-17.0	±	0.1	11.0	±	0.2	3.8	±	0.0	3.7		1	-16.9			11.7			3.8			4.3
		-17.5	to	-16.7	10.3	to	11.5	3.7	to	4.0													
Ophidiidae													1	-21.3			9.1			4.0			3.4

Table 16-A2. (Continued).

Taxa	Baltimore Canyon												Norfolk Canyon										
	N	$\delta^{13}C$			$\delta^{15}N$			C:N			TL		N	$\delta^{13}C$			$\delta^{15}N$			C:N			TL
Stomiiformes																							
Phosichthyidae																							
Phosichthyidae sp.	4	-19.4	±	0.2	11.6	±	0.2	5.3	±	0.3	3.9												
		-19.7	to	-19.0	11.0	to	11.9	4.7	to	5.9													
Polymetme thaeocoryla	1	-18.7	±	0.0	9.1	±	0.0	4.4	±	0.0	3.1												
Sternoptychidae																							
Argyropelecus aculeatus	1	-17.5			9.9			4.1			3.3												
Maurolicus weitzmani	6	-18.9	±	0.2	10.8	±	0.3	4.9	±	0.3	3.6		1	-19.0			11.6			4.3			4.3
		-20.1	to	-18.4	9.4	to	11.6	4.4	to	6.5													
Polyipnus asteroides	2	-19.3	±	0.6	10.5	±	0.4	4.3	±	0.6	3.5												
		-20.0	to	-18.7	10.2	to	10.9	3.7	to	4.9													
Stomiidae																							
Chauliodus sloani													2	-18.6	±	0.2	9.0	±	0.3	4.0	±	0.0	3.4
														-18.8	to	-18.5	8.7	to	9.4	4.0	to	4.1	
Stomias boa ferox	2	-20.3	±	0.3	10.5	±	0.2	5.6	±	0.3	3.5												
		-20.6	to	-20.0	10.3	to	10.7	5.3	to	5.9													
Scorpaeniformes																							
Peristediidae																							
Peristedion ecuadorense													1	-17.7			14.1			3.8			5.1
Peristedion miniatum	2	-17.3	±	0.1	11.9	±	0.7	3.9	±	0.0	4.0		1	-17.6			14.2			3.8			5.1
		-17.5	to	-17.2	11.2	to	12.6	3.9	to	3.9													
Peristedion truncatum	1	-17.2			12.1			4.1			4.1												
Scorpaenidae																							
Helicolenus dactylopterus	28	-18.1	±	0.1	10.7	±	0.2	4.1	±	0.1	3.6		38	-18.4	±	0.1	8.6	±	0.4	3.8	±	0.1	3.3
		-19.0	to	-17.4	8.9	to	12.9	3.8	to	5.0				-19.5	to	-17.6	5.4	to	12.7	3.1	to	5.0	
Sebastidae																							
Sebastes fasciatus													1	-17.7			13.5			4.0			4.9
Pleuronectiformes																							
Bothidae																							
Monolene sessilicauda	1	-17.2			12.5			4.2			4.2												
Cynoglossidae																							
Symphurus billykrietei	4	-17.1	±	0.2	10.9	±	0.3	4.0	±	0.0	3.7												
		-17.6	to	-16.7	10.5	to	11.4	4.0	to	4.0													
Symphurus nebulosus	1	-17.3			12.3			4.0			4.1												
Symphurus stigmosus	1	-16.9			12.7			3.1			4.3												
Paralichthyidae																							
Citharichthys arctifrons	32	-17.2	±	0.1	10.2	±	0.1	3.9	±	0.0	3.4		8	-18.5	±	0.5	10.5	±	0.3	4.0	±	0.1	3.9
		-18.2	to	-15.8	8.8	to	11.2	3.6	to	4.1				-22.1	to	-17.2	8.5	to	11.6	3.8	to	4.7	
Hippoglossina oblonga	6	-17.7	±	0.2	12.0	±	0.2	3.9	±	0.0	4.0		2	-18.2	±	0.1	12.4	±	0.2	3.8	±	0.1	4.5

Table 16-A2. (Continued).

Taxa	Baltimore Canyon												Norfolk Canyon										
	N	$\delta^{13}C$			$\delta^{15}N$			C:N			TL		N	$\delta^{13}C$			$\delta^{15}N$			C:N			TL
		-18.3	to	-17.1	11.5	to	12.8	3.7	to	4.0				-18.3	to	-18.1	12.1	to	12.6	3.8	to	3.9	
Pleuronectidae																							
Glyptocephalus cynoglossus	15	-16.6	±	0.1	12.4	±	0.2	3.9	±	0.0	4.1		30	-17.7	±	0.5	11.6	±	0.2	3.9	±	0.0	4.3
		-17.0	to	-16.3	11.0	to	13.2	3.7	to	4.2				-28.5	to	-15.7	9.2	to	13.6	3.7	to	4.1	
Perciformes																							
Acropomatidae																							
Synagrops bellus													2	-18.3	±	0.0	10.9	±	0.5	4.0	±	0.0	4.1
														-18.3	to	-18.2	10.5	to	11.4	3.9	to	4.0	
Synagrops spinosus													1	-20.4			11.0			6.9			4.1
Cryptacanthodidae																							
Cryptacanthodes maculatus													1	-18.9			8.6			4.1			3.3
Zoarcidae																							
Lycenchelys verrillii	2	-17.5	±	0.7	12.7	±	0.0	3.9	±	0.1	4.2		21	-18.4	±	0.6	11.4	±	0.2	3.8	±	0.0	4.2
		-18.2	to	-16.8	12.6	to	12.7	3.9	to	4.0				-28.2	to	-16.0	9.6	to	13.2	3.5	to	4.2	
Lycodes esmarkii													3	-16.2	±	0.2	12.3	±	0.5	3.7	±	0.1	4.5
														-16.4	to	-15.8	11.7	to	13.3	3.5	to	3.8	
Lycodes terraenovae	11	-17.0	±	0.1	12.5	±	0.1	4.1	±	0.0	4.2												
		-17.5	to	-16.7	12.0	to	12.9	3.9	to	4.4													
Melanostigma atlanticum													7	-18.6	±	0.5	9.5	±	0.5	5.1	±	0.4	3.6
														-20.7	to	-16.5	7.9	to	11.5	2.8	to	6.2	
Unknown fish													1	-18.6			8.2			3.9			3.2
Cnidaria																							
Actiniaria																							
Actiniaria sp.	16	-19.2	±	0.3	9.4	±	0.2	4.5	±	0.1	3.2		56	-19.0	±	0.1	9.4	±	0.3	4.3	±	0.1	3.6
		-21.2	to	-16.7	7.7	to	10.7	3.3	to	5.1				-21.2	to	-16.5	3.8	to	12.7	3.2	to	5.8	
Actiniaria sp. 1													10	-21.7	±	0.2	8.7	±	0.7	5.6	±	0.2	3.3
														-22.9	to	-20.3	2.7	to	10.8	4.2	to	6.6	
Actiniaria sp. 3	1	-16.6			7.7			3.3			2.6												
Actinoscyphiidae																							
Actinoscyphia sp.	1	-19.0			9.8			3.7			3.3												
Actiniidae																							
Bolocera sp.	6	-19.2	±	0.2	8.5	±	0.2	4.5	±	0.2	2.9												
		-20.1	to	-18.3	7.8	to	9.0	4.0	to	5.2													
Halicuriidae																							
Halcurias sp.	1	-18.5			10.0			4.1			3.3												
Hormathiidae																							
Hormathiidae sp.	1	-17.4			8.0			3.4			2.7												

Table 16-A2. (Continued).

Taxa	Baltimore Canyon												Norfolk Canyon										
	N	$\delta^{13}C$			$\delta^{15}N$			C:N			TL		N	$\delta^{13}C$			$\delta^{15}N$			C:N			TL
Alcyonacea																							
Alcyonacea sp.													3	-20.3	±	0.2	7.9	±	0.5	5.4	±	0.2	3.0
														-20.7	to	-20.0	7.1	to	8.8	5.1	to	5.6	
Alcyonacea sp.1	2	-20.6	±	0.4	2.7	±	0.9	3.4	±	0.4	0.9												
		-21.0	to	-20.2	1.8	to	3.6	3.0	to	3.8													
Alcyonacea sp.2	1	-21.5			7.3			5.0			2.4												
Acanthogorgiidae																							
Acanthogorgia aspera													5	-20.2	±	0.3	7.9	±	0.2	3.9	±	0.3	3.1
														-21.2	to	-19.7	7.3	to	8.6	2.9	to	4.5	
Acanthogorgia cf. *armata*													15	-20.3	±	0.2	8.3	±	0.2	3.6	±	0.1	3.2
														-21.3	to	-18.7	6.9	to	9.9	2.2	to	4.2	
Acanthogorgia sp.													2	-19.6	±	0.0	2.9	±	0.6	2.4	±	0.1	1.4
														-19.7	to	-19.6	2.3	to	3.5	2.3	to	2.5	
Alcyoniidae																							
Anthomastus sp.													4	-18.6	±	0.5	9.2	±	0.5	4.6	±	0.3	3.5
														-19.9	to	-17.4	8.2	to	10.7	4.1	to	5.4	
Anthothelidae																							
Anthothela grandiflora	7	-21.6	±	0.4	5.1	±	0.6	4.4	±	0.3	1.7		27	-21.3	±	0.1	6.3	±	0.4	4.0	±	0.2	2.5
		-23.4	to	-20.5	2.5	to	7.0	3.6	to	5.4				-22.4	to	-19.7	0.4	to	9.3	2.2	to	5.9	
Isididae																							
Isididae													5	-18.5	±	0.7	6.1	±	0.9	5.3	±	0.2	2.4
														-19.9	to	-16.6	4.0	to	8.2	4.9	to	5.9	
Acanella arbuscula													4	-18.7	±	1.9	5.2	±	1.1	2.7	±	0.3	2.2
														-22.2	to	-13.3	3.2	to	8.5	1.7	to	3.3	
Paragorgiidae																							
Paragorgia arborea	22	-22.4	±	0.1	5.9	±	0.4	4.6	±	0.2	2.0		38	-21.7	±	0.2	6.2	±	0.3	4.2	±	0.1	2.5
		-23.2	to	-21.8	2.9	to	9.4	3.6	to	5.9				-23.0	to	-16.8	2.9	to	10.2	2.7	to	5.9	
Plexauridae																							
Paramuricea placomus	10	-20.5	±	0.1	5.6	±	0.6	3.9	±	0.2	1.9												
		-21.0	to	-19.5	2.2	to	8.2	2.8	to	5.1													
Primnoidae																							
Primnoa resedaeformis	18	-22.2	±	0.1	6.4	±	0.4	4.7	±	0.1	2.1		33	-21.6	±	0.1	6.8	±	0.3	4.3	±	0.1	2.7
		-23.2	to	-21.2	1.9	to	8.6	3.2	to	5.7				-22.7	to	-20.0	4.0	to	9.4	2.6	to	5.9	
Antipatharia																							
Cladopathidae																							
Sibopathes sp.													2	-20.1	±	0.0	10.4	±	0.8	4.4	±	0.1	3.9
														-20.1	to	-20.1	9.6	to	11.2	4.3	to	4.5	

Table 16-A2. (Continued).

Taxa	Baltimore Canyon												Norfolk Canyon										
	N	$\delta^{13}C$			$\delta^{15}N$			C:N			TL		N	$\delta^{13}C$			$\delta^{15}N$			C:N			TL
Corallimorpharia																							
Corallimorpharia													3	-19.4	±	0.1	9.4	±	0.3	5.2	±	0.2	3.5
														-19.5	to	-19.3	8.9	to	9.8	5.0	to	5.5	
Pennatulacea																							
Pennatulacea sp.	2	-20.1	±	0.1	6.1	±	0.7	3.5	±	0.6	2.1		17	-20.7	±	0.7	5.9	±	0.7	4.0	±	0.2	2.4
		-20.2	to	-20.0	5.4	to	6.8	2.9	to	4.2				-24.0	to	-16.5	2.4	to	11.9	2.0	to	5.3	
Umbellulidae																							
Umbellula sp.													10	-17.5	±	0.2	10.9	±	0.3	4.1	±	0.1	4.0
														-18.5	to	-16.3	8.9	to	11.9	3.4	to	4.6	
Scleractinia																							
Caryophylliidae																							
Dasmosmilia lymani	2	-18.6	±	0.4	5.7	±	0.2	2.7	±	0.5	1.9												
		-19.0	to	-18.3	5.5	to	5.9	2.2	to	3.2													
Desmophyllum dianthus	12	-22.6	±	0.2	5.5	±	0.5	3.9	±	0.2	1.9		27	-21.9	±	0.2	5.6	±	0.5	4.0	±	0.2	2.3
		-24.3	to	-21.1	3.3	to	8.5	3.2	to	4.9				-24.4	to	-19.5	-1.6	to	10.7	1.9	to	5.7	
Lophelia pertusa	8	-22.5	±	0.4	5.0	±	0.8	4.5	±	0.4	1.7		12	-21.8	±	0.1	5.8	±	0.5	4.4	±	0.3	2.4
		-24.0	to	-20.9	1.9	to	7.8	3.2	to	5.9				-22.4	to	-21.4	3.1	to	7.9	2.5	to	5.9	
Solenosmilia variabilis													7	-21.9	±	0.1	4.0	±	0.8	3.4	±	0.3	1.7
														-22.4	to	-21.6	0.5	to	5.9	2.4	to	4.3	
Flabellum alabastrum													27	-20.1	±	0.1	9.5	±	0.2	4.7	±	0.2	3.6
														-21.0	to	-19.2	6.7	to	11.6	1.7	to	5.9	
Zoantharia																							
Zoantharia sp.	6	-21.7	±	0.1	6.0	±	0.6	4.7	±	0.3	2.0		15	-19.5	±	0.2	5.0	±	0.9	2.9	±	0.4	2.1
		-22.0	to	-21.1	4.0	to	7.1	3.9	to	6.1				-20.9	to	-17.8	-0.5	to	10.1	1.1	to	5.6	
Epizoanthidae																							
Epizoanthus sp.													13	-19.5	±	0.2	6.2	±	0.4	3.6	±	0.1	2.5
														-20.8	to	-17.8	3.0	to	9.8	2.6	to	4.2	
Hydrozoa																							
Hydrozoa	15	-19.2	±	0.4	5.9	±	0.7	3.6	±	0.1	2.0		13	-19.8	±	0.2	4.8	±	0.6	3.8	±	0.2	2.0
		-23.1	to	-17.9	-0.4	to	9.3	2.7	to	4.1				-21.7	to	-19.0	-1.0	to	8.5	2.9	to	6.2	
Echinodermata																							
Asteroidea																							
Asteroidea	1	-17.7	±	0.0	14.1	±	0.0	3.0	±	0.0	4.7		1	-13.2			12.7			3.9			4.7
Asteriidae																							
Sclerasterias contorta	6	-15.5	±	0.1	6.5	±	0.3	3.4	±	0.1	2.2		8	-16.0	±	0.3	7.2	±	0.4	3.2	±	0.1	2.8
		-15.7	to	-15.2	5.3	to	7.4	3.0	to	3.9				-17.1	to	-14.5	5.3	to	8.6	2.8	to	3.6	
Stephanasterias albula													7	-16.6	±	0.3	3.1	±	1.6	1.7	±	0.2	1.5
														-17.7	to	-15.4	-1.3	to	8.5	1.1	to	2.4	

Table 16-A2. (Continued).

Taxa	Baltimore Canyon												Norfolk Canyon										
	N	$\delta^{13}C$			$\delta^{15}N$			C:N			TL		N	$\delta^{13}C$			$\delta^{15}N$			C:N			TL
Stephanasterias sp.													5	-16.4	±	0.2	7.0	±	0.3	3.0	±	0.1	2.7
														-16.9	to	-15.7	6.1	to	7.5	2.6	to	3.4	
Astropectinidae																							
Astropecten alligator	10	-17.2	±	0.2	5.7	±	0.2	2.7	±	0.2	1.9		12	-18.8	±	0.5	6.0	±	0.5	2.9	±	0.1	2.4
		-18.3	to	-16.7	4.8	to	6.7	1.8	to	3.7				-21.2	to	-15.9	3.3	to	9.6	2.4	to	3.8	
cf. *Astropecten alligator*	5	-16.6	±	0.4	5.0	±	0.6	3.6	±	0.1	1.7												
		-18.0	to	-15.3	3.8	to	7.0	3.3	to	3.9													
Astropecten americanus													19	-18.2	±	0.4	5.2	±	0.5	3.5	±	0.2	2.1
														-20.3	to	-13.9	-0.1	to	8.4	2.0	to	5.5	
Persephonaster echinulatus	2	-17.6	±	0.4	5.4	±	0.4	3.5	±	0.4	1.8												
		-18.1	to	-17.2	5.0	to	5.7	3.2	to	3.9													
Plutonaster agassizi agassizi													10	-14.4	±	0.3	12.2	±	0.2	4.1	±	0.1	4.5
														-15.7	to	-13.0	11.3	to	13.3	3.8	to	4.7	
Pocellanasteridae																							
cf. *Porcellanaster* sp.													5	-16.1	±	0.3	7.7	±	0.9	3.5	±	0.2	3.0
														-17.2	to	-15.3	4.4	to	9.9	3.1	to	4.3	
Porcellanaster ceruleus													15	-15.1	±	0.3	7.7	±	0.5	3.8	±	0.2	3.0
														-17.5	to	-12.7	4.5	to	12.1	2.5	to	5.1	
Poraniidae																							
Poraniidae	1	-13.2			7.8			4.6			2.6												
Echinasteridae																							
Henricia antillarum													5	-16.8	±	0.3	9.1	±	0.8	3.4	±	0.2	3.5
														-17.7	to	-16.1	5.9	to	10.4	2.5	to	3.9	
Odontasteridae																							
Odontaster cf. *hispidus*													1	-12.6			8.4			8.9			3.2
Odontaster hispidus													1	-13.7			3.4			1.5			1.5
Solasteridae																							
Solaster cf. *earlli*													4	-14.7	±	0.8	8.5	±	1.1	2.7	±	0.2	3.2
														-16.7	to	-12.7	6.0	to	11.1	2.3	to	3.1	
Crinoidea																							
Crinoidea sp.													3	-20.5	±	0.3	6.3	±	0.8	3.2	±	0.2	2.5
														-21.1	to	-20.1	4.7	to	7.5	2.8	to	3.4	
Echinoidea																							
Arbaciidae																							
Coelopleurus floridanus													8	-21.2	±	0.9	6.3	±	0.9	4.3	±	0.3	2.5
														-26.3	to	-18.4	2.0	to	9.9	2.6	to	5.4	

Table 16-A2. (Continued).

Taxa	Baltimore Canyon												Norfolk Canyon										
	N	$\delta^{13}C$			$\delta^{15}N$			C:N			TL		N	$\delta^{13}C$			$\delta^{15}N$			C:N			TL
Cidaridae																							
Cidaris sp.	4	-18.0	±	0.4	6.1	±	0.7	3.3	±	0.3	2.0		1	-20.5			0.6			5.0			0.6
		-18.8	to	-17.1	4.5	to	7.8	2.8	to	4.2													
Stylocidaris lineata													2	-19.8	±	0.0	6.6	±	0.4	5.6	±	0.3	2.6
														-19.8	to	-19.8	6.2	to	7.1	5.3	to	5.9	
Echinidae																							
cf. *Gracilechinus affinis*													1	-16.4			12.0			4.3			4.4
Gracilechinus alexandri													1	-19.8			8.2			4.4			3.2
Echinus sp.													5	-17.4	±	0.3	11.9	±	0.1	5.6	±	0.2	4.4
														-18.4	to	-16.7	11.7	to	12.5	5.1	to	6.5	
Echinus tylodes	2	-20.0	±	0.6	10.7	±	0.2	5.2	±	0.4	3.6												
		-20.6	to	-19.3	10.5	to	10.9	4.8	to	5.6													
Histocidaridae																							
Histocidaris sharreri													5	-20.2	±	0.2	8.6	±	0.8	6.1	±	0.1	3.3
														-20.6	to	-19.7	6.4	to	10.6	5.9	to	6.5	
Echinothuriidae																							
Hygrosoma petersii													2	-16.9	±	0.7	7.9	±	0.1	5.1	±	0.4	3.0
														-17.6	to	-16.2	7.8	to	8.0	4.7	to	5.5	
Phormosomatidae																							
Phormosoma placenta													5	-17.3	±	0.2	9.1	±	0.6	5.0	±	0.2	3.4
														-18.1	to	-16.7	7.7	to	10.5	4.4	to	5.5	
Clypeasteroida																							
Clypeasteroida													4	-16.9	±	0.9	1.7	±	1.4	3.1	±	0.2	1.0
														-18.6	to	-14.5	-2.3	to	4.2	2.6	to	3.6	
Holothuroidea																							
Holothuroidea													10	-17.0	±	0.4	8.5	±	1.0	3.8	±	0.4	3.2
														-19.6	to	-16.4	4.1	to	10.5	2.6	to	5.2	
Synallactidae																							
cf. *Zygothuria lactea*													6	-16.0	±	0.6	10.3	±	0.6	4.3	±	0.4	3.8
														-17.4	to	-13.8	7.9	to	11.6	2.8	to	5.4	
Zygothuria lactea													13	-17.6	±	0.3	7.5	±	0.5	3.5	±	0.2	2.9
														-19.6	to	-16.4	4.1	to	10.5	2.6	to	5.2	
Ophiuroidea																							
Ophiuroidea sp.	1	-16.5			8.2			4.1			2.8		4	-19.4	±	0.7	7.9	±	1.2	3.5	±	0.5	3.0
														-21.0	to	-17.5	5.1	to	10.4	2.9	to	4.9	
Euryalida																							
Euryalida													1	-17.7	±	0.0	9.0	±	0.0	2.6	±	0.0	3.4

Table 16-A2. (Continued).

Taxa	Baltimore Canyon												Norfolk Canyon										
	N	$\delta^{13}C$			$\delta^{15}N$			C:N			TL		N	$\delta^{13}C$			$\delta^{15}N$			C:N			TL
Asteronychidae																							
Asteronyx loveni													8	-17.0	±	0.6	8.1	±	1.4	3.6	±	0.5	3.1
														-18.2	to	-13.3	0.8	to	13.1	1.0	to	5.5	
Gorgonocephalidae																							
Gorgonocephalus sp.													8	-20.1	±	0.3	7.9	±	0.7	3.6	±	0.2	3.0
														-21.6	to	-18.9	4.2	to	9.9	2.9	to	4.4	
Ophiurida																							
Amphiuridae																							
Amphipholis sp.													4	-18.7	±	0.7	4.9	±	0.7	3.5	±	0.1	2.1
														-19.7	to	-16.7	3.3	to	6.4	3.2	to	3.7	
Amphipholis squamata													2	-18.1	±	0.2	4.7	±	0.2	2.6	±	0.0	2.0
														-18.3	to	-17.9	4.5	to	4.9	2.6	to	2.6	
Amphiura otteri	9	-18.9	±	0.4	3.2	±	0.6	2.8	±	0.2	1.1												
		-21.1	to	-17.8	0.0	to	6.2	1.9	to	4.4													
Ophiacanthidae																							
Ophiacantha sp.													1	-17.3			11.2			4.4			4.1
Ophiactidae																							
Ophiopholis aculeata													1	-19.4			5.7			2.5			2.3
Ophiolepididae																							
Ophiomusium cf. *lymani*													3	-19.3	±	0.9	4.7	±	0.3	3.1	±	0.3	2.0
														-20.8	to	-17.7	4.3	to	5.2	2.8	to	3.6	
Ophiomusium lymani													16	-17.2	±	0.7	6.5	±	0.9	4.4	±	0.3	2.6
														-20.8	to	-10.8	0.1	to	10.4	1.6	to	6.8	
Ophiomyxidae																							
Ophiophrixus sp.													2	-18.4	±	1.1	6.2	±	3.2	3.1	±	0.4	2.5
														-19.5	to	-17.2	3.1	to	9.4	2.7	to	3.5	
Ophiuridae																							
Ophiura sarsii													4	-19.8	±	1.2	3.4	±	1.2	3.3	±	0.1	1.6
														-23.4	to	-18.3	0.7	to	6.3	2.9	to	3.5	
Mollusca																							
Aplacophora																							
Aplacophora													1	-24.2			9.3			4.6			3.5
Bivalvia																							
Bivalvia													12	-17.6	±	0.4	9.5	±	0.7	3.8	±	0.3	3.6
														-20.1	to	-15.2	5.9	to	13.9	1.9	to	5.9	

Table 16-A2. (Continued).

Taxa	Baltimore Canyon												Norfolk Canyon										
	N	$\delta^{13}C$			$\delta^{15}N$			C:N			TL		N	$\delta^{13}C$			$\delta^{15}N$			C:N			TL
Venerida																							
Semelidae																							
Abra profundorum													3	-15.9	±	0.5	12.7	±	0.3	4.0	±	0.3	4.6
														-16.8	to	-15.1	12.3	to	13.3	3.6	to	4.5	
Nuculanoida																							
Malletiidae																							
Malletia sp.													1	-16.1			15.1			3.7			5.4
Yoldiidae																							
Yoldiella sp.													1	-16.7			10.7			4.0			4.0
Myoida																							
Verticordiidae																							
Verticordia sp.													2	-18.1	±	0.0	12.9	±	0.5	4.3	±	0.1	4.7
														-18.2	to	-18.1	12.4	to	13.5	4.2	to	4.5	
Cephalopoda																							
Cephalopoda													9	-18.4	±	0.3	10.3	±	0.6	4.4	±	0.2	3.8
														-19.9	to	-17.4	6.3	to	12.2	3.3	to	5.1	
Decapodiformes																							
Bathyteuthidae																							
Bathyteuthis sp.	1	-19.7			8.3			3.6			2.8												
Oegopsida																							
Brathioteuthidae																							
Brachioteuthis beanii	2	-18.7	±	0.1	10.0	±	0.3	4.4	±	0.3	3.3												
		-18.8	to	-18.6	9.6	to	10.3	4.1	to	4.7													
Ommastrephidae																							
Illex cf. *illecebrosus*	1	-21.3			11.1			4.7			3.7												
Sepiida																							
Sepiolidae																							
Sepiolidae													1	-17.8			10.0			4.4			3.7
cf. *Rossia* sp.													1	-19.8			10.6			4.5			3.9
cf. *Semirossia tenera*	1	-18.1			8.7			4.0			2.9												
Rossia megaptera	1	-18.3			9.8			4.2			3.3												
Semirossia cf. *tenera*													1	-18.3			11.2			4.7			4.2
Semirossia tenera	1	-18.1			9.6			4.1			3.2												
Octopoda																							
Octopoda													4	-18.3	±	0.3	9.7	±	1.3	4.4	±	0.2	3.6
														-18.8	to	-17.6	6.2	to	12.4	4.1	to	4.9	

Table 16-A2. (Continued).

Taxa	Baltimore Canyon												Norfolk Canyon										
	N	$\delta^{13}C$			$\delta^{15}N$			C:N			TL		N	$\delta^{13}C$			$\delta^{15}N$			C:N			TL
Bathypolypodidae																							
Bathypolypus bairdii													14	-19.6	±	0.3	10.4	±	0.5	4.6	±	0.0	3.9
														-20.8	to	-17.4	8.9	to	15.6	4.3	to	4.9	
Gastropoda																							
Gastropoda	6	-17.6	±	0.3	8.8	±	0.6	4.6	±	0.1	2.9		8	-19.7	±	0.4	8.0	±	1.5	3.8	±	0.3	3.1
		-18.5	to	-16.5	5.9	to	9.9	4.4	to	5.2				-20.7	to	-18.1	1.2	to	12.2	2.3	to	4.6	
Neogastropoda																							
Buccinidae																							
Colus sp.													5	-16.2	±	0.1	9.0	±	0.1	4.1	±	0.1	3.4
														-16.5	to	-15.9	8.7	to	9.3	3.9	to	4.2	
Colus stimpsoni	4	-16.1	±	0.5	5.3	±	1.8	3.2	±	0.2	1.8												
		-17.0	to	-15.3	2.7	to	10.7	2.8	to	3.9													
Turridae																							
Turridae													4	-17.0	±	0.4	10.5	±	0.6	4.4	±	0.2	3.9
														-18.1	to	-16.2	9.0	to	11.7	4.0	to	4.8	
Littorinimorpha																							
Naticidae													4	-18.3	±	1.0	8.2	±	1.2	5.1	±	0.2	3.2
														-19.5	to	-15.4	6.8	to	11.7	4.5	to	5.5	
Nudibranchia													13	-19.3	±	0.3	8.1	±	0.4	3.8	±	0.2	3.1
														-22.2	to	-17.4	6.1	to	10.1	1.4	to	4.5	
Scaphopoda																							
Scaphopoda													8	-15.7	±	0.2	8.1	±	0.9	3.8	±	0.1	3.1
														-16.6	to	-14.8	5.3	to	12.5	3.5	to	4.3	
Dentaliida																							
Dentaliidae																							
cf. *Dentalium* sp.													10	-15.6	±	0.3	10.9	±	0.4	4.1	±	0.1	4.1
														-16.8	to	-13.8	9.1	to	13.1	3.8	to	4.9	
Mollusca sp.													5	-20.3	±	0.5	10.9	±	0.4	5.0	±	0.2	4.0
														-21.4	to	-19.1	9.9	to	12.2	4.4	to	5.7	
Porifera																							
Porifera	3	-20.5	±	0.7	8.1	±	1.2	3.9	±	0.3	2.7		6	-20.9	±	0.5	9.1	±	0.9	3.6	±	0.5	3.4
		-21.9	to	-19.6	5.7	to	9.3	3.3	to	4.2				-22.5	to	-19.4	6.9	to	13.1	1.3	to	4.5	
Poecilosclerida																							
Cladorhizidae	2	-19.0	±	1.2	4.7	±	1.0	4.3	±	0.3	1.6												
		-20.1	to	-17.8	1.7	to	7.8	4.3	to	4.3													

Table 16-A2. (Continued).

Taxa	Baltimore Canyon												Norfolk Canyon										
	N	$\delta^{13}C$			$\delta^{15}N$			C:N			TL		N	$\delta^{13}C$			$\delta^{15}N$			C:N			TL
Sipuncula																							
Sipuncula													18	-17.2	±	0.7	11.3	±	0.6	3.8	±	0.1	4.2
														-21.3	to	-11.8	7.4	to	15.4	3.2	to	4.2	
Golfingiida																							
Sipunculidae																							
Sipunculus norvegicus													14	-15.4	±	0.2	12.9	±	0.4	3.6	±	0.1	4.7
														-17.1	to	-14.4	11.2	to	15.5	3.2	to	4.9	
Plants																							
Fucales																							
Facaceae																							
cf. *Fucus* sp. (out)	4	-18.4	±	0.2	3.3	±	0.3	26.7	±	1.9	1.1												
		-18.9	to	-17.8	2.6	to	4.0	21.3	to	30.3													
Sargassaceae																							
Sargassum sp. (in)													3	-18.3	±	1.2	1.2	±	0.6	24.2	±	7.0	0.8
														-20.2	to	-16.0	0.1	to	1.9	10.1	to	31.5	
Sargassum sp. (out)	5	-18.3	±	0.7	0.9	±	0.9	24.9	±	2.7	0.3		3	-16.1	±	0.7	-0.2	±	0.7	45.7	±	5.3	0.3
		-20.9	to	-17.1	-1.2	to	4.0	15.8	to	31.3				-17.4	to	-15.2	-1.3	to	1.1	39.9	to	56.4	
Other																							
Detritus (out)													3	-18.7	±	4.8	2.0	±	1.9	62.6	±	14.4	1.1
														-28.3	to	-13.7	-1.3	to	5.4	37.7	to	87.6	
POM surface (in)	5	-21.2	±	0.5	5.5	±	1.0	10.6	±	1.9	1.8		24	-22.0	±	0.4	4.6	±	0.3	7.6	±	0.3	2.0
		-22.2	to	-20.0	3.1	to	8.3	8.7	to	12.6				-24.8	to	-19.7	2.2	to	7.4	5.6	to	11.3	
POM surface (out)	3	-22.7	±	0.8	3.2	±	0.7	8.2	±	0.5	1.1		11	-19.9	±	0.4	3.9	±	0.7	10.4	±	0.2	1.7
		-23.4	to	-21.2	2.4	to	4.6	7.3	to	8.9				-22.7	to	-18.7	-0.2	to	7.6	9.7	to	11.9	
POM midwater (in)	4	-22.5	±	0.4	5.7	±	1.0				1.9		18	-21.6	±	0.4	4.7	±	0.7	5.5	±	0.2	2.0
		-23.6	to	-21.7	4.5	to	8.5							-24.3	to	-18.8	-2.6	to	9.7	4.3	to	7.8	
POM midwater (out)	3	-21.8	±	0.7	5.0	±	0.7				1.7												
		-22.8	to	-20.4	4.1	to	6.3																
POM bottom (in)	8	-23.2	±	0.4	6.9	±	0.6	7.6			2.3		21	-21.9	±	0.1	5.7	±	0.4	8.0	±	0.4	2.3
		-25.1	to	-22.1	3.1	to	8.8							-23.2	to	-20.9	0.2	to	9.3	3.7	to	10.7	
POM bottom (out)	6	-24.5	±	1.4	6.6	±	0.8	8.4	±	1.0	2.2		10	-23.5	±	1.0	4.4	±	1.0	12.3	±	3.3	1.9
		-31.4	to	-22.2	4.0	to	8.6	6.3	to	9.4				-28.1	to	-21.3	0.1	to	9.4	5.4	to	28.3	
Sediment 0−2 cm (in)	10	-21.6	±	0.3	5.6	±	0.3	6.8	±	0.7	1.9		22	-21.3	±	0.1	7.2	±	0.4	10.9	±	3.3	2.8
		-22.8	to	-19.7	3.5	to	7.5	3.7	to	9.2				-22.5	to	-20.3	4.3	to	12.8	0.4	to	79.1	
Sediment 0−2 cm (out)	5	-21.3	±	0.1	4.8	±	0.7	5.8	±	0.8	1.6		4	-20.0	±	0.3	7.3	±	0.4	8.5	±	0.3	2.9
		-21.6	to	-21.2	2.7	to	6.6	4.1	to	8.4				-20.5	to	-19.2	6.5	to	8.4	7.7	to	9.2	
Sediment trap (**Chap. 6**)	14	-22.3	±	0.1	4.8	±	0.1	9.6	±	0.2	1.6		3	-22.2	±	0.1	5.0	±	0.1	9.3	±	0.2	2.1
		-22.8	to	-22.0	4.3	to	5.0	8.8	to	10.6				-22.3	to	-22.1	4.9	to	5.1	9.1	to	9.7	

Table 16-A3. Comparison of stomach content (STO) and stable isotope dietary (SIA) analyses for fishes collected in Baltimore (BC) and Norfolk (NC) canyons during the Atlantic Deepwater Canyons Study. Numbers indicate the number of taxa or species within the major group identified through stable isotope or stomach analyses. The "x" designates the presence of major taxa from stomach content analysis that were not identified past major taxa. Stomach data, representing a combination of data from Baltimore and Norfolk canyons, were collected during this project. Dashes (–) indicate taxa not present in stomach contents, but stable isotope analysis suggested these taxa as prey sources. (* See footnotes for source information. Fish diet data are from [1] Horton 2015.)

Canyon	BC	NC	STO	BC	NC	STO	BC	NC	STO	BC	NC	STO	BC	NC	STO	BC	NC	STO	BC	NC	STO	Source*
Analyses	SIA			SIA			SIA			SIA			SIA			SIA			SIA			
Taxa	*C. arctifrons*			*G. cynoglossus*			*H. dactylopterus*			*S. kaupii*			*D. rugosa*			*L. americanus*			*D. atlanticus**			
Arthropoda	21	4	x	5	26	x	14	16	x	2	7	x	0	1	x	2	17	x	1	4		1, 4, 8, 12
Decapoda	17	4		5	23		7	10	x	0	5	x	0	0	x	2	14	x	1	3		1, 3, 4, 5, 6, 9, 16
Penaeoidea	3	0		1	3		0	0		0	0	1	0	0		0	0		0	0		1
Brachyura	1	1		0	5		3	3	1	0	0		0	0		0	4		0	2		1, 10
Caridea	4	2		1	10		0	1		0	0		0	0		0	2	2	0	0		1, 10
Sergestidae	1	0		0	1		1	1		0	1		0	0	1	0	1	1	0	0		1
Anomura	3	1		0	7		1	2	2	0	0		0	0		2	3		0	0		1, 10
Astacidea	0	0		0	0		0	0		0	0		0	0		0	0		1	0		–
Polychelida	0	0		0	0		0	0		0	0		0	0		0	0		0	1		–
Unidentified shrimp	5	0		2	6		2	3	1	0	4	1	0	0		0	4		0	0		1, 7, 10, 13, 15
Euphausiacea	2	0	1	1	2	2	5	2	5	1	1	2	0	0	1	0	1		0	0		1, 7, 10, 11, 14
Amphipoda	2	0	2	1	2	2	2	4	1	1	0	1	0	0	2	0	0		0	0		1, 3, 5, 8, 10, 11,14, 16
Cumacea																						6
Mysida									x													1, 13, 14, 16
Isopoda					1				x		1				x		1					1
Cirripedia														1			1			1		–
Copepoda																						1, 5, 6, 16
Pycnogonida																						–
Cnidaria	4	4		1	12	x	4	8		2	3		0	0		2	7		0	1		4
Hydrozoa							1	1														–
Hexacorallia	4	3		1	5		3	2		2	0		0	0		2	3		0	0		–
Octocorallia	0	1		0	8		0	5		0	3		0	0		0	4		0	1		–
Echinodermata	0	0	x	0	16	x	0	11		0	3		0	0		0	4		0	2		1, 3, 4, 5, 12, 16

Table 16-A3. (Continued).

Canyon	BC	NC	STO	BC	NC	STO	BC	NC	STO	BC	NC	STO	BC	NC	STO	BC	NC	STO	BC	NC	STO	Source*
Analyses	SIA			SIA			SIA			SIA			SIA			SIA			SIA			
Asteroidea	0	0		0	2		0	1		0	0		0	0		0	0		0	0		–
Ophiuroidea	0	0		0	6		0	6		0	1		0	0		0	2		0	1		1, 5
Echinoidea	0	0		0	6		0	3		0	2		0	0		0	2		0	1		–
Crinoidea	0	0		0	1		0	1		0	0		0	0		0	0		0	0		–
Holothuroidea	0	0		0	1		0	0		0	0		0	0		0	0		0	0		–
Mollusca	4	2		1	7	1	1	2		1	3		0	2		2	7	x	0	1		1, 16
Aplacophora																						–
Bivalvia					1	x																1, 5, 6, 14
Cephalopoda	3	2		0	3		1	0		1	0		0	2		2	4	1	0	1		1, 2, 4, 9, 10, 15
Gastropoda	1	0		1	3		0	2		0	3		0	0		0	3		0	0		1
Annelida	0	1	2	0	4	2	0	0	1	0	0		0	0		0	2		0	5		–
Polychaeta	0	1		0	4		0	0		0	0		0	0		0	2		0	5		1, 4, 5, 10, 11, 12
Unidentified annelid			x			x			x													1, 4, 11, 12
Chordata																						–
Salpa								1														–
Pyrosoma																						–
Fish	0	0		1	17	x	2	6	1	0	3	x	0	0		9	17	4	0	0		1, 2, 4, 5, 7, 9, 10, 13, 16, 17
Porifera					1					1							1					–
Brachiopoda					1																	–
Bryozoa																						–
Sipuncula																				1		–
Foraminifera																						1
Other			x			x			x													1
Taxa	*L. verrillii*			*E. cimbrius*			*C. caelorhincus*			*N. bairdii*			*M. albidus*			*P. chesteri*			*U. regia*			
Arthropoda	1	30	x	1	6	x	7	13	x	7	22	x	9	1	x	9	15	x	12	12	x	1, 4, 8, 12
Decapoda	1	29		1	6	x	7	11		5	17	x	5	0		5	9	x	7	10	x	1, 3, 4, 5, 6, 9, 16
Penaeoidea	0	3		0	0		1	0		0	0		0	0		0	0		0	0		1
Brachyura	0	5		0	2		2	5		0	4		2	0		1	2		1	3	1	1, 10
Caridea	0	9		0	2		0	2		1	3		0	0	1	0	1		1	4		1, 10
Sergestidae	0	1		0	0		0	1		1	1		1	0		1	1		1	1		1

Table 16-A3. (Continued).

Canyon	BC	NC	STO	BC	NC	STO	BC	NC	STO	BC	NC	STO	BC	NC	STO	BC	NC	STO	BC	NC	STO	Source*
Analyses	SIA			SIA			SIA			SIA			SIA			SIA			SIA			
Anomura	1	8		1	2		0	0		0	4		0	0		1	2		1	0	2	1, 10
Astacidea	0	0		0	0		0	0		0	0		0	0		0	0		0	0		–
Polychelida	0	1		0	0		0	1		0	0		0	0		0	0		0	0		–
Unidentified shrimp	0	2		0	0	1	4	2		3	5		2	0	1	2	3		3	2	1	1, 7, 10, 13, 15
Euphausiacea	0	0		0	0	2	0	1	2	2	2	2	4	1	1	3	2		4	1	1	1, 7, 10, 11, 14
Amphipoda	0	0	1	0	0	2	0	0	1	0	3	3	1	0		1	3	1	1	0	1	1, 3, 5, 8, 10, 11, 14, 16
Cumacea						x																6
Mysida									x			x						x				1, 13, 14, 16
Isopoda		1						1	x								1			1		1
Cirripedia																						–
Copepoda						x			x			x						x				1, 5, 6, 16
Pycnogonida		1																				–
Cnidaria	0	7		0	2		0	2		2	20		2	0		2	11		2	2		4
Hydrozoa											1		1				1					–
Hexacorallia	0	4		0	1		0	1		2	9		1	0		2	4		2	1		–
Octocorallia	0	3		0	1		0	1		0	10		0	0		0	6		0	1		–
Echinodermata	0	5	1	0	0		1	0		0	14		0	1	x	0	10		0	1		1, 3, 4, 5, 12, 16
Asteroidea	0	0		0	0		1	0		0	2		0	0		0	1		0	0		–
Ophiuroidea	0	2	1	0	0		0	0		0	8		0	1	1	0	6		0	1		1, 5
Echinoidea	0	3		0	0		0	0		0	4		0	0		0	3		0	0		–
Crinoidea	0	0		0	0		0	0		0	0		0	0		0	0		0	0		–
Holothuroidea	0	0		0	0		0	0		0	0		0	0		0	0		0	0		–
Mollusca	0	9	2	1	2	1	1	5		2	8	1	0	1	1	1	2	1	2	4	1	1, 16
Aplacophora											1											–
Bivalvia		1	x			x						x								1		1, 5, 6, 14
Cephalopoda	0	5		1	2		1	3		2	4		0	0	1	1	0	1	2	1	1	1, 2, 4, 9, 10, 15
Gastropoda	0	3	1	0	0		0	2		0	3		0	1		0	2		0	2		1
Annelida	0	7	1	0	2	1	3	5	2	0	3	2	1	0		0	0	1	0	2		–
Polychaeta	0	7		0	2		2	5		0	3		1	0		0	0		0	2		1, 4, 5, 10, 11, 12
Unidentified annelid			x			x	1		x			x						x				1, 4, 11, 12

Table 16-A3. (Continued).

Canyon	BC	NC	STO	BC	NC	STO	BC	NC	STO	BC	NC	STO	BC	NC	STO	BC	NC	STO	BC	NC	STO	Source*
Analyses	SIA			SIA			SIA			SIA			SIA			SIA			SIA			
Chordata																						–
Salpa											1											–
Pyrosoma											1											–
Fish	0	0		0	0		0	0		2	17	x	2	0	x	2	6	2	2	11	x	1, 2, 4, 5, 7, 9, 10, 13, 16, 17
Porifera											1					1			1			–
Brachiopoda											1											–
Bryozoa											1											–
Sipuncula		1																				–
Foraminifera			x			x																1
Other			x			x			x			x						x				1

* Stomach contents were not analyzed for *D. atlanticus**

[1] Horton 2015; [2] Armstrong et al. 1996; [3] Bowman and Michaels 1984; [4] Bowman et al. 2000; [5] Crabtree et al. 1991; [6] Deree 1999; [7] Garrison and Link 2000b; [8] Houston and Haedrick 1986; [9.] Johnson et al. 2008; [10] Langston and Bowman 1980; [11] Langston and Bowman 1981; [12] Link et al. 2002; [13] Neves et al. 2012; [14] Rodríguez-Marín et al. 1994; [15] Rohr and Gutherz 1977; [16] Román 2004; [17] Sedberry 1983.

Table 16-A4. Stable isotope values ($\delta^{13}C$ and $\delta^{15}N$) for primary producers, surface sediments (0−2 cm), invertebrates, and fishes collected from seep habitats in Baltimore and Norfolk canyons. Where N is the number of specimens, average ‰ values (± SE) and ranges (min/max), C:N is the ratio of carbon to nitrogen, and TL is the calculated trophic level (see Methods).

Taxa	Baltimore Canyon											Norfolk Canyon										
	N	$\delta^{13}C$			$\delta^{15}N$			C:N			TL	N	$\delta^{13}C$			$\delta^{15}N$			C:N			TL
Annelida																						
Onuphidae																						
Hyalinoecia artifex	11	-17.8	±	0.1	9.1	±	0.3	4.1	±	0.1	3.5											
		-18.2	to	-17.5	7.2	to	10.6	3.7	to	4.8												
Hyalinoecia tubicola	12	-19.2	±	0.5	10.0	±	0.2	4.4	±	0.1	3.8											
		-23.8	to	-17.2	9.2	to	11.2	4.0	to	5.4												
Arthropoda																						
Amphipoda																						
Amphipoda	10	-18.8	±	0.2	6.3	±	0.1	4.4	±	0.2	2.6											
		-19.7	to	-18.1	5.3	to	6.8	3.5	to	5.3												
Lestrigonidae																						
cf. *Hyperietta luzoni*	16	-18.7	±	0.1	7.0	±	0.2	4.6	±	0.1	2.8											
		-19.6	to	-17.6	6.0	to	8.8	4.2	to	5.1												
Hyperiidae																						
Themisto sp.	11	-18.9	±	0.2	6.9	±	0.4	4.4	±	0.2	2.8											
		-19.8	to	-17.5	3.8	to	8.1	2.5	to	5.0												
Decapoda																						
Alvinocarididae																						
Alvinocaris markensis												7	-51.2	±	1.7	5.2	±	0.2	3.7	±	0.1	2.1
													-60.4	to	-46.7	4.2	to	5.8	3.5	to	4.0	
cf. *Alvinocaris markensis*												1	-20.6			5.0			7.7			2.0
Chirostylidae																						
Eumunida picta	3	-20.0	±	0.8	9.8	±	0.2	4.2	±	0.1	3.8											
		-21.6	to	-18.8	9.4	to	10.2	4.0	to	4.3												

Table 16-A4. (Continued).

Taxa	Baltimore Canyon											Norfolk Canyon										
	N	$\delta^{13}C$			$\delta^{15}N$			C:N			TL	N	$\delta^{13}C$			$\delta^{15}N$			C:N			TL
Munididae																						
Munida valida	2	-18.5	±	0.6	8.7	±	0.1	4.0	±	0.3	3.4											
		-19.1	to	-17.9	8.7	to	8.8	3.7	to	4.2												
Diogenidae																						
Paguristes cf. *moorei*	3	-21.9	±	1.4	10.3	±	0.2	4.2	±	0.1	4.0											
		-23.5	to	-19.2	10.0	to	10.7	4.1	to	4.3												
Paguristes lymani	2	-18.2	±	0.8	10.0	±	0.3	4.1	±	0.0	3.8											
		-19.0	to	-17.4	9.7	to	10.3	4.0	to	4.1												
Pandalidae																						
Pandalus montagui	1	-18.6			9.8			3.6			3.8											
Shrimp sp.	9	-19.1	±	0.2	6.2	±	0.3	3.9	±	0.1	2.6											
		-19.8	to	-17.3	4.8	to	7.3	3.5	to	4.6												
Euphausiacea																						
Euphausiidae																						
Euphausiidae	4	-19.1	±	0.1	7.1	±	0.2	4.7	±	0.2	2.9											
		-19.3	to	-18.8	6.6	to	7.8	4.2	to	5.1												
Nyctiphanes couchii	4	-19.1	±	0.2	6.7	±	0.3	4.1	±	0.0	2.8											
		-19.6	to	-18.8	6.0	to	7.4	4.0	to	4.2												
cf. *Thysanoessa macrura*	10	-19.3	±	0.2	7.6	±	0.3	4.1	±	0.1	3.1											
		-20.5	to	-18.2	5.9	to	8.8	3.8	to	4.5												
Thysanoessa macrura	8	-18.9	±	0.1	8.0	±	0.2	4.1	±	0.1	3.2											
		-19.2	to	-18.5	7.0	to	8.9	3.8	to	4.3												
Chordata − Fish																						
Anguilliformes																						
Synaphobranchidae																						
Dysommina rugosa	7	-30.0	±	3.6	8.4	±	0.7	4.4	±	0.1	3.3											
		-48.1	to	-20.2	5.2	to	10.9	4.2	to	5.1												

Table 16-A4. (Continued).

Taxa	Baltimore Canyon											Norfolk Canyon										
	N	$\delta^{13}C$			$\delta^{15}N$			C:N			TL	N	$\delta^{13}C$			$\delta^{15}N$			C:N			TL
Aulopiformes																						
Paralepididae																						
Arctozenus risso	3	-19.0	±	0.7	8.6	±	0.2	4.6	±	0.2	3.4											
		-19.6	to	-18.3	8.3	to	8.9	4.2	to	4.8												
Myctophiformes																						
Myctophidae																						
Ceratoscopelus maderensis	3	-18.7	±	0.1	9.2	±	0.2	4.6	±	0.1	3.6											
		-18.9	to	-18.6	8.9	to	9.5	4.5	to	4.7												
Pleuronectiformes																						
Cynoglossidae																						
Symphurus nebulosus	4	-24.5	±	0.7	10.4	±	0.2	4.1	±	0.0	4.0											
		-25.5	to	-22.5	10.0	to	10.9	4.0	to	4.1												
Cnidaria																						
Alcyonacea																						
Paragogiidae																						
Paragorgia arborea	3	-22.0	±	0.4	3.8	±	1.0	4.2	±	0.3	1.8											
		-22.7	to	-21.5	1.9	to	4.9	3.6	to	4.6												
Zoantharia																						
Zoantharia sp.	1	-22.3			6.9			5.4			2.8											
Echinodermata																						
Ophiurida																						
Ophiuridae																						
Ophiopholis aculeata	1	-23.9			6.4			3.1			2.6											
Valvatida																						
Odontasteridae																						
Odontaster robustus	3	-44.0	±	1.2	6.2	±	1.1	2.6	±	0.3	2.6											
		-46.1	to	-42.0	4.0	to	7.7	2.1	to	3.0												
Echinoida																						
Echinidae																						
Echinus cf. *wallisi*												1	-57.8			3.0			5.6			1.3
Echinus wallisi												8	-56.9	±	0.7	2.5	±	0.3	5.3	±	0.2	1.1
													-59.8	to	-52.5	1.1	to	3.6	4.6	to	6.0	

Table 16-A4. (Continued).

Taxa	Baltimore Canyon											Norfolk Canyon									
	N	$\delta^{13}C$			$\delta^{15}N$			C:N			TL	N	$\delta^{13}C$			$\delta^{15}N$			C:N			TL
Gracilechinus affinis												11	-55.7	±	1.1	3.7	±	0.5	6.1	±	0.2	1.6
													-58.7	to	-47.1	1.7	to	6.8	5.0	to	7.7	
Mollusca																						
Mytiloida																						
Mytilidae																						
Bathymodiolus childressi (gill)	47	-62.8	±	0.3	0.2	±	0.2	5.1	±	0.1	0.6	61	-62.9	±	0.3	0.4	±	0.2	5.1	±	0.1	0.5
		-67.8	to	-59.0	-1.6	to	3.0	3.4	to	6.7			-71.2	to	-59.5	-2.2	to	3.5	4.2	to	6.3	
Bathymodiolus childressi (mantle)	46	-64.8	±	0.4	0.8	±	0.2	6.7	±	0.2	0.8	60	-63.1	±	0.4	1.5	±	0.2	6.0	±	0.2	0.8
		-73.6	to	-59.3	-1.6	to	6.3	4.1	to	9.4			-69.8	to	-54.4	-0.9	to	4.5	3.9	to	9.3	
Bathymodiolus childressi (muscle)	46	-61.5	±	0.3	1.3	±	0.2	4.0	±	0.1	1.0	11	-61.1	0.7	0.7	2.2	±	0.5	4.2	±	0.1	1.1
		-68.4	to	-58.5	-1.3	to	4.3	3.2	to	6.2			-65.6	to	-57.8	-0.1	to	4.5	3.6	to	4.9	
Oegopsida																						
Ommastrephidae																						
Illex cf. *illecebrosus*	2	-20.6	±	0.8	9.6	±	0.6	4.3	±	0.0	3.7											
		-21.4	to	-19.9	9.0	to	10.3	4.3	to	4.4												
Other																						
Microbial mat												1	-29.4			7.3			5.3			2.7
POM (bottom)	1	-27.7			1.5			16.1			1.0	1	-28.9			2.1			40.3			1.0
Sediment (0−2)												5	-30.7	±	3.7	4.8	±	0.8				
													-40.3	to	-24.0	2.8	to	6.7				

CHAPTER 17. PALEOECOLOGY: MID-ATLANTIC CANYON DEEPSEA CORALS AND CHEMOSYNTHETIC COMMUNITIES

E. Brendan Roark, Nancy G. Prouty, Steve W. Ross, Amanda W.J. Demopoulos, Mackenzie Schoemann, and Diana Sahy

17.1 INTRODUCTION

17.1.1 Deepsea Corals

Deepsea corals (DSCs) are a new and unique paleoceanographic and paleoclimate archive that can extend our observations of ocean dynamics and climate to periods well before the onset of instrumental records. Geochemical records derived from the skeletons of DSCs offer continuous, high-resolution archives of changes in ocean chemistry and ocean circulation that play a central role in the earth's climate systems on multiple temporal scales. Given that some species of DSCs grow in tree-like fashion depositing growth rings, decadally resolved and perhaps even annually resolved records are possible with high-resolution sampling techniques. In addition, determining the life spans and growth rates of DSCs is vital for assessing the vulnerability of these organisms to natural and anthropogenic disturbances and the time scales of their recovery. Such information is critical to the effective management and conservation efforts of a wide range of resources including fisheries and energy resources.

Accurate determination of the age, longevity, and growth rates of DSCs is required for biological and ecological assessments as well as for the development of highly resolved age models for paleoceanographic studies. Carbonate and proteinaceous DSCs can be age-dated using a variety of independent radiometric methods including lead-210 (^{210}Pb), lead-radium (Pb-Ra), radiocarbon (^{14}C), thorium-uranium (^{230}Th/^{238}U) and, in some cases, sclerochronology. Largely based on radiocarbon measurements, multiple carbonate DSC species such as bamboo corals, *Corallium* sp., primnoids, and Enalopsamina can live for tens to hundreds of years (Druffel et al. 1990; Roark et al. 2005, 2006; Tracey et al. 2007; Sherwood et al. 2005; Houlbreque et al. 2010). Proteinaceous DSCs *Gerardia* sp. and *Leiopathes* sp. have extremely long life spans of ~2,700 and ~4,200 years, respectively (Roark et al. 2009). The temporal resolution of DSC archives can be extended well into the Holocene (Roark et al. 2006, 2009) and back as far as the Last Glacial Maximum by sampling subfossil specimens (Adkins et al. 1998, Robinson et al. 2005).

Considerable progress has been made over the last 15 years in the development of proxies in DSCs that reflect past environments, yielding quantitative *in situ* records of local environmental conditions over the lifetime of a DSC. Some proxy approaches for measuring the radiocarbon concentration in seawater to reconstruct ocean ventilation rates have been used successfully (e.g., Adkins et al. 1998, Robinson et al. 2005, Komugabe et al. 2014) while other proxies such as δ^{18}O and magnesium/calcium (Mg/Ca), which are typically used as temperature proxies, appear to be overprinted by "vital" effects (Smith et al. 2002, Gagnon et al. 2007). Other proxies not overprinted by vital effects such as neodymium (Nd) have been used as a tracer of ocean circulation, (cf., review Robinson et al. 2014). In proteinaceous DSCs, it is clear that the stable isotopic composition of the skeleton can be used as historical recorders of surface water processes such as biological productivity and the isotopic composition of source nutrients (Roark et al. 2005, 2009; Sherwood et al. 2005; Sherwood and Edinger 2009; Guilderson et al. 2013; Sherwood et al. 2014; Prouty et al. 2014). Thus, DSC proxy records have the potential to address important questions such as the role of ocean circulation as well as nutrient and carbon cycling, which are particularly important in a changing climate system. However, even in cases where the proxies are relatively straightforward to interpret, they have not been fully exploited because there are only a few collections of coral archives, and even fewer DSC collections linked to extensive modern water column chemistry data required for proxy calibration and validation. Finally, some of the geochemical analytical techniques are

limited to a small number of laboratories, further limiting the development of large numbers of DSC records (cf., Robinson et al. 2014).

While there is great promise in the proxy work being done in DSCs to develop paleoceanographic and paleoclimate records (cf., Robinson et al. 2014), the one area where DSC research has moved beyond the range of potential promise is in reconstructing water mass histories and ventilation rates. By developing independent chronometers such as U-series dating and pairing those results with radiocarbon measurements, several studies have shown that it is possible to reconstruct ventilation histories in different oceans as far back as the Last Glacial Maximum (Adkins et al. 1998, Goldstein et al. 2001, Cao et al. 2007, Frank et al. 2004, Robinson et al. 2005). Marine radiocarbon chronologies paired with U-series ages are one of the most widely used dating methods for oceanographic DSC studies. Coupled radiocarbon and U-series dates from the DSC *Desmophyllum cristagalli,* have been used to reconstruct ventilation rates of North Atlantic deep water during the last deglaciation with good success (Adkins et al. 1998, Goldstein et al. 2001, Frank et al. 2004, Robinson et al. 2005, Cao et al. 2007). DSCs have relatively high uranium concentrations in their carbonate skeleton, allowing the U-series method to become one of the most widely used dating methods (Edwards et al. 1987, Bard et al. 1990, Adkins et al. 1998, Lomitschka and Mangini 1999, Cheng et al. 2000, Goldstein et al. 2001) to determine absolute calendar ages. The U-series method has precisely and accurately dated DSCs as young as 3 years old and as old as 60,000 years old (Edwards et al. 2003). Coupling the U-Th dates with the radiocarbon analyses in the cup coral, *Desmophyllum cristagalli,* provides a direct measurement of past seawater $\Delta^{14}C$ (van de Flierdt et al. 2010). Absolutely dating the DSCs provides fundamental information to improving our understanding of the longevity, growth pattern, and rates of growth of DSCs.

In the Atlantic Ocean, *Desmophyllum* sp. and *Primnoid* sp. are the two most common DSCs used in paleoceanographic reconstructions. *Desmophyllum dianthus* is the focus of our discussion because it was the predominant species collected in the Baltimore and Norfolk canyons that was suitable for geochemical analyses. *Desmophyllum dianthus,* a scleractinian, a zooxanthellate cup coral, with an aragonite skeleton is broadly distributed throughout the Atlantic Ocean and can be found attached to hard rock substrate on seamounts, continental shelves, and in deepsea canyons (Cairns 1994, Anagnostou et al. 2011). *D. dianthus* can be found in water depths ranging from 35 to 2,500 m (Cairns 1994) and have a high thermal tolerance ranging from 1 °C to 28 °C (Stanley and Cains 1988). Age determination of *D. dianthus* is possible by using radiocarbon dating and U-Th dating of the aragonite skeleton (Cheng et al. 2000, Robinson et al. 2005). Growth rates of *D. dianthus* range from 0.5 to 2 mm y^{-1} (Adkins et al. 2004). Their life span is approximately 100 years and their skeletons are relatively large, up to 10 cm (Cheng et al. 2000, Adkins et al. 2004).

Solution and laser ablation inductively coupled plasmas mass spectrometry (LA ICP-MS) has been used to determine trace element ratios in carbonate skeletons of *D. dianthus*. Element ratio proxies can be used to reconstruct seawater properties and understand multiple environmental parameters such as variations in temperature, pH, nutrients, and carbonate ion concentrations through time in DSCs including *D. dianthus* specifically (Adkins et al. 1998, Blamart et al. 2007, Montagna et al. 2006, Sinclair and Risk 2006, van der Flierdt et al. 2006, Anagnostou et al. 2011). LaVigne et al. (2011) found a strong linear relationship between barium/calcium (Ba/Ca) concentration in seawater and Ba/Ca in the calcitic skeleton of bamboo corals. Montagna et al. (2006) and Anagnostou et al. (2011) found a strong correlation between Ba/Ca in the aragonite skeleton of *D. dianthus* and Ba/Ca in seawater and developed a linear calibration equation correlating the skeletal measured Ba/Ca ratio to the Ba concentration of seawater. Other proxies that have been used to assess nutrient dynamics in *D. dianthus* include phosphorus to calcium (P/Ca) (Montagna et al. 2006) and uranium to calcium (U/Ca) ratios (Anagnostou et al. 2011). LA ICP-MS allows for high high-resolution sampling (tens of micrometers) and fast analyses with minimal sample destruction.

Atmospheric carbon dioxide (pCO_2) has varied during glacial and interglacial periods over the past 800,000 years (Luthi et al. 2008, Petit et al. 1999). Atmospheric pCO_2 concentrations are rapidly

increasing from the preindustrial levels of 280 parts per million (ppm) to approximately 400 ppm and levels continue to rise as measured in July 2014 (Tans and Keeling 2014, Rollion-Bard et al. 2011, Luthi et al. 2008). This sharp increase is mainly a result of anthropogenic activity such as burning of fossil fuels (Le Quéré et al. 2009). The ocean is a major carbon sink, absorbing natural and anthropogenic CO_2 from the atmosphere (Sabine et al. 2004, Canadell et al. 2007).

Increasing atmospheric CO_2 results in more CO_2 mixing into the ocean surface, decreasing the carbonate ion concentration in the water column and thereby decreasing the pH, which lowers the carbonate saturation state and prevents carbonate minerals from forming (Hönisch and Hemming 2005). This can have a negative impact on DSCs, which construct their skeletons by the biological precipitation of calcium carbonate from seawater (Manzello et al. 2008, Hennige et al. 2015). DSC communities provide structure to support diverse communities and provide an important habitat for many fish and invertebrate species (e.g., brittle stars, sea stars, sea cucumbers, and sea urchins). The long-term response to increasing pCO_2 by marine calcifying organisms susceptible to ocean acidification (Hoegh-Guldberg et al. 2007) is a major concern for the management and conservation of corals. The first critical aspect to understanding ocean acidification is understanding the aragonite and calcite saturation states.

Numerous studies show the correlation between calcification rates of shells and coral skeletons and aragonite saturation state (Langdon and Atkinson 2005, Guinotte et al. 2003). A decrease in the carbonate ion concentration [CO_3^{2-}] lowers the aragonite saturation state (Ω_{arag}), which is defined as:

$$\Omega_{arag} = \frac{[Ca^{2+}]*[CO_3^{2-}]}{K^1_{arag}} \text{ (Equation 17.1)}$$

K^1_{arag} is the solubility product of aragonite (Guinotte et al. 2006). A saturation state of $\Omega_{arag} > 1$ indicates supersaturation while $\Omega_{arag} < 1$ is undersaturated (Krief et al. 2010). For marine organisms with carbonate skeletons, undersaturation prevents adequate aragonite precipitation (Guinotte et al. 2006). As a result, marine calcifying organisms are found in regions of the ocean that are supersaturated with respect to calcite or aragonite. The depth at which calcite and aragonite skeletal material dissolves in the water column is referred to as the calcite compensation depth (CCD). Solubility of calcium carbonate in seawater increases with depth. At the lysocline, depth in the ocean which the rate of dissolution increases, seawater becomes significantly undersaturated with respect to the calcium carbonate ions (James 2005). Below the saturation horizon it less likely those marine calcifying organisms will be able to precipitate skeletons or shells, particularly DSCs living at intermediate water depths.

Currently, DSC paleo-proxy development has focused on utilizing boron isotopic signatures ($\delta^{11}B$) as a proxy to reconstruct paleo-pH (Hemming and Hanson 1992, Klochko et al. 2006, Rollion-Bard et al. 2011), providing records of pH variation at intermediate and deep water depths during regional and global climate change events. Aragonite skeletons are rich in boron, making DSC species like *D. dianthus* ideal archives for pH reconstruction. The boron concentration in the aragonite skeleton ranges from 70 to 100 ppm (Douville et al. 2010), compared to ~10 to 20 ppm for calcitic foraminifera (Rae et al. 2011), allowing for high-resolution analyses of $\delta^{11}B$ in small sample sizes (Anagnostou et al. 2012). In addition, *D. dianthus* has a growth rate of ~0.to 2 mm y^{-1}, can be precisely dated by radiocarbon dating paired with U-Th dating (Adkins et al. 1998, Frank et al. 2004, Robinson et al. 2005) and with ~100 year lifespans, makes an ideal paleoarchive for pH reconstructions.

The development of paleo-reconstructions of pH requires understanding how boron is incorporated into the *D. dianthus* skeleton. Dissolved boron in modern seawater exists as boric acid $B(OH)_3$ and as borate ion $B(OH)_4^-$, the tetrahedral boron complex. With the boron composition of seawater remaining constant in comparison to its residence time in seawater, ~14 million years (Lemarchand et al. 2000, Paris et al. 2010), the isotopic composition of each boron species is pH dependent. The following process describes fractionation of boron isotopes in an aqueous solution:

$^{10}B(OH)_3 + {}^{11}B(OH)_4^- \leftrightarrow {}^{11}B(OH)_3 + {}^{10}B(OH)_4^-$ (Equation 17.2)

Boron isotopes are incorporated into biogenic and inorganic marine carbonates based on the ambient seawater pH. If seawater pH is < 9.0 then boric acid is dominant and if pH is >9.0 then borate ion will be most abundant (Hemming and Hanson 1992). In tropical corals and foraminifera calcite there is a ~1‰ increase in $\delta^{11}B$ for every 0.1 pH increase (Hönisch and Hemming 2005, Hönisch et al. 2009). Measuring $\delta^{11}B$ in carbonates is primarily restricted to using thermal ionization mass spectrometer (TIMS); however, in this study we used a novel LA ICP-MS methodology to reconstruct seawater pH at the mid-Atlantic canyons. Previous LA ICP-MS work using DSCs is restricted to using B/Ca ratios in DSCs to reconstruct paleo-pH rather than using the $\delta^{11}B$ isotopic composition of coral skeletons as a paleo-proxy (Trotter et al. 2011).

The overall goals of this component of the Atlantic Deepwater Canyons study were to examine the paleo-ecology of DSCs by examining multiple geochemical proxies in both the proteinaceous and carbonate skeletons of DSCs. This study focused on developing a multiproxy approach to deciphering the roles of natural and anthropogenic changes in intermediate and deepwater processes in the mid-Atlantic region of the east coast of the United States. Specific objectives included the following:

1. Use radiocarbon or U-Th dating methods to determine the age and lifespan of *D. dianthus* and if possible reconstruct past changes in ocean circulation and ventilation rates;
2. Use trace elements measured by LA ICP-MS to reconstruct nutrient dynamics and carbonate ion concentrations in intermediate water;
3. Use water column samples to help calibrate and develop biogeochemical proxies in DSCs;
4. Determine the utility of using LA ICP-MS to measure $\delta^{11}B$ in DSCs;
5. Determine the applicability of currently accepted pH-$\delta^{11}B$ calibration equation at Baltimore and Norfolk canyons and compare *in situ* measured pH values against reconstructed pH values derived using pH-$\delta^{11}B$ calibration equation; and
6. Reconstruct changes in ocean pH using subfossil *D. dianthus*.

17.1.2 Chemosynthetic Communities

The distribution of widespread methane leakage from the seafloor of the northern U.S. Atlantic margin (Skarke et al. 2014) has important implications for the global carbon cycle (Boetius and Wenzhofer 2013), continental slope stability, and related hazards (Dugan and Flemings 2000, ten Brink et al. 2014), but also the geographic extent of chemosynthetic communities (Quattrini et al. 2015). Seeps have been documented from the southeastern U.S. margin, the Cape Fear Diapir (Brothers et al. 2013), and the Blake Ridge Diapir (Paull et al. 1995, Van Dover et al. 2003) at depths ranging from 2,155 to 2,600 m. A study conducted in the early 1980s in Baltimore Canyon photographed a dense community of mussels at approximately 400 m using a towed camera sled (B. Hecker, pers. comm.), but no further work was conducted in this area until recently. Surveys conducted between 2011 and 2013 gathered geophysical data along the U.S. Atlantic margin and identified more than 500 gas plumes at water depths ranging from 50 to 1,700 m between Cape Hatteras and Georges Bank (Skarke et al. 2014). Observations of the area from remotely operated vehicles (ROV) included bubble streams, bacterial mats, chemosynthetic communities, authigenic carbonates, deepsea corals, and gas hydrates. Methane emissions from seeps in this region could conservatively yield 15 to 90 × 10^6 g y^{-1} (Skarke et al. 2014).

South of Cape Hatteras, deepwater seeps are associated with the intrusion of salt diapirs; gas advection and gas hydrate dissociation are facilitated by the high thermal conductivity of the diapirs, which shifts the phase boundary of the gas hydrate and free gas system (Hornbach et al. 2005). North of Cape Hatteras, the origin and evolution of the methane seeps supporting chemosynthetic communities remains elusive, partly because no underlying salt diapirs have been documented in the region, and

because, until recently, no suitable biological or geological specimens have been recovered from seep sites along the northern U.S. Atlantic margin.

This section explores the geochemistry, mineralogy, and petrology of authigenic carbonates and bivalve shells recovered by ROVs from the seep sites in Norfolk and the Baltimore canyons with the aim of tracing the origin and flow pathways of gas and fluids at both sites. Carbonates are common at cold seeps (Han and Suess 1989, Greinert et al. 2001, Campbell et al. 2002), leaving a robust fingerprint of hydrocarbon seep activity including evidence of local and regional controls on the source and flux of carbon and the conditions under which they formed (Formolo et al. 2004, Campbell 2006, Naehr et al. 2007, Magalhães et al. 2012). Key information on the timing and duration of fluid venting can be obtained through accurate uranium (U)-series dating techniques (Teichert et al. 2003, Bayon et al. 2009). Isotopic composition of shells from chemosynthetic bivalves living close to venting fluids also represents an important archive of the nature and variability of the venting. Taken together, geochemical information derived from both authigenic carbonates and bivalve shells collected from seep sites along the U.S. mid-Atlantic margin expand our understanding of the origin and formation of widespread seepage.

17.2 METHODS

17.2.1 Seawater Analyses

A Sea-Bird Electronics, Inc. (SBE) 911 *plus* conductivity-temperature-depth (CTD) instrument with a rosette of twelve 10 L Niskin bottles was used to record water column environmental profiles and collect water samples. The CTD instrument measured turbidity (Seapoint probe, formazin turbidity units), dissolved oxygen (mL L^{-1}), depth (m), conductivity (Siemens m^{-1}), temperature (°C), pH, and fluorescence (see **Chapter 3** for additional details). The CTD casts were conducted down canyon transects (starting at the head) in Baltimore and Norfolk canyons at uniform standard water sampling depths. The locations, water depths, and sampling depths are listed in **Appendix 17-A**. Samples were collected and analyzed following standard methods in several laboratories as described below.

17.2.1.1 Radiocarbon Content of Seawater

The radiocarbon content of seawater ΣCO_2 was measured by extracting the inorganic carbon as CO_2 gas, converting the gas to graphite, and counting the number of ^{14}C atoms in the sample directly using an accelerator mass spectrometer (AMS) at the National Ocean Sciences AMS (NOSAMS) Facility. Seawater collected at discrete depths was subsampled into 500 mL Pyrex reagent bottles by placing Tygon tubing on the Niskin bottle and flushing with approximately 50 mL of water. Bottles were filled from the bottom and allowed to flush for twice their volume prior to poisoning with mercuric chloride and storage. Following standard protocols (e.g., Dickson and Goyet 1994), total dissolved inorganic carbon (DIC) was quantitatively stripped via acidification and purging with nitrogen. Aliquots of cryogenically purified CO_2 were analyzed for $\delta^{13}C$ (‰), and the remaining CO_2 was reduced to elemental carbon (graphite) in the presence of iron catalyst and a stoichiometric excess of hydrogen similar to the method described by Vogel et al. (1987). Graphite targets were measured at NOSAMS to determine the radiocarbon value. Results are reported as $\Delta^{14}C$ (‰) in accordance with conventions set forth by Stuiver and Polach (1977). Isotopic ^{14}C results are reported as fraction modern (FM), $\Delta^{14}C$, and conventional radiocarbon age (^{14}C years before present [B.P.]).

17.2.1.2 Seawater Trace Elements

Water column particulate matter for trace element measurements was collected by filtering ~5 L of seawater on acid-cleaned 0.45-µm polysulfone filters (47 mm) in Baltimore Canyon at a shallow site (NF-2012-138), mid-depth (NF-2012-128), deep site (NF-2012-130), and mid-depth shelf site (NF-2012-149). Samples were also collected at a mid-depth site in Norfolk Canyon (NF-2012-158).

Filters were acid cleaned by placing in a 1 L low-density polyethylene bottle and soaked in trace metal grade hydrochloric acid (HCl). Seawater was collected directly from the Niskin bottle rosette using acid-cleaned Teflon coated tubing attached to a polypropylene filter holder that was preloaded with an acid-cleaned polysulfone filter and attached to a vacuum pump. Water from two 5 L Niskin bottles were collected per given water depth for replicates. The filter holder with a preloaded filter was double bagged in polyethylene zip-lock bags and kept frozen for transport back to the laboratory. Trace element concentrations of the suspended particulate matter were determined by ICP-MS at the U.S. Geological Survey (USGS) Mass Spectrometry Facilities in Denver, Colorado, by digesting the filters following procedures outlined in Planquette and Sherrell (2012). Data, which included a blank correction as determined from digesting procedural filter blanks, were reported in $\mu g\ g^{-1}$ and are corrected for the weight of the sample plus the filter.

17.2.1.3 Seawater Nutrients

Dissolved nutrient seawater samples collected at each station were stored in acid-cleaned high-density polyethylene 20 mL scintillation vials, which were triple washed with extra filtrate before saving the final sample for analysis. Samples collected for the nutrient analysis were frozen immediately until analyzed at the Geochemical and Environmental Research Group at Texas A&M University, College Station. Nutrient samples were analyzed on an Astoria-Pacific auto-analyzer. The nitrate/nitrite/silicate methods are based on Armstrong et al. (1967); phosphate is based on Bernhardt and Wilhelms (1967); and ammonium is based on Harwood and Kuhn (1970). The dissolved inorganic nitrogen (DIN) concentrations were calculated as the sum of nitrite, nitrate, and ammonium concentrations. Analytical detection limits were 0.01 μM for phosphate, 0.003 μM for nitrite, 0.05 μM for nitrate and silicate, and 0.08 μM for ammonium.

17.2.1.4 Neodymium Concentration of Seawater

Neodymium (Nd) concentration of seawater (~100 mL) was carefully weighed and spiked with ~50−100 mg Nd-50 spike. Bottles were left overnight to equilibrate and acidified with 0.1 mL of concentrated HCl per 100 mL of seawater. After the samples were equilibrated, ~50 μL of $FeCl_3$ was added to the seawater for co-precipitation and ~135 μL of fresh NH_4OH to bring the sample to a pH of ~8.5. Samples were spun down in the centrifuge and then redissolved for solution ICP-MS. We measured the following isotopes: ^{145}Nd, ^{146}Nd, samarium (^{149}Sm), and ^{150}Nd. The 100 mL water samples typically contained ~100 to 300 pg of Nd. Blanks were measured with each batch of 10 samples, and the blank had Nd = 0.5 to 1 pM.

17.2.1.5 Seawater $\delta^{18}O$ and δD

Seawater samples were measured for $\delta^{18}O$ and δD using a Picarro L2120i cavity ringdown spectrometer at the Stable Isotope Geoscience Facility at Texas A&M University, College Station. Isotope values were calibrated to the Vienna Standard Mean Ocean Water (VSMOW) reference standard using internal reference standards JGULF and KONA. The $\delta^{18}O$ and δD values in VSMOW2 for JGULF are 1.22‰ and 5.8‰, respectively, and for Kona are -6.86‰ and -50.8‰, respectively. Average internal precision is ±0.12 $\delta^{18}O$ and ±0.36‰ δD, and an external precision replicate of the same sample is ±0.26‰ $\delta^{18}O$ and ±1.1‰ δD.

17.2.1.6 Total Alkalinity

Seawater samples for DIC were preserved at sea using saturated mercuric chloride ($HgCl_2$), 200 μL $HgCl_2$ were added to 500 mL sample bottles, and 100 μL $HgCl_2$ were added to 250 mL sample bottles. The total alkalinity was measured by the potentiometric titration method (Millero et al. 1993, Dickson and Goyet 1994, Ono et al. 1998). Certified reference materials were analyzed with both the DIC and total

alkalinity samples as an independent verification of instrument calibrations (Dickson et al. 2007). The DIC and total alkalinity measurements including multiple inorganic system parameters such as pH, pCO_2, fCO_2, saturation states for calcite and aragonite, and concentrations of biocarbonate ions (HCO_3^-), carbonate ion (CO_3^{2-}), and dissolved carbon dioxide (CO_2) was completed using program CO2SYS developed by Lewis and Wallace (1998) using the carbonate constants defined by Lueker et al. (2000) together with measured water temperature, pressure, salinity, and nutrient concentration.

17.2.2 Deepsea Coral Methods

17.2.2.1 Deepsea Coral Sampling and Cleaning

Deepsea corals were collected by ROVs from Baltimore and Norfolk canyons during the 2012 and 2013 sampling cruises (see **Chapter 3** for cruise details). More than 50 live and dead specimens of the cup coral, *D. dianthus,* were collected between 400 and 1,400 m in Baltimore and Norfolk canyons (**Figure 17-1**) (**Table 17-1**).

Figure 17-1. *Desmophyllum* sp. cup corals. Left panel shows a cluster of three cup corals collected alive and right panel shows approximately eight dead cup corals collected at the same depth.

Table 17-1. *Desmophyllum dianthus* specimen list, collection status, and sampling location at Baltimore and Norfolk canyons.

Coral ID	Location	Depth (m)	Latitude (N)	Longitude (W)	Status
RB-685-1	Norfolk (deep)	1,328	37°03'03.34"	74°31'39.24"	Dead
RB-685-2	Norfolk (deep)	1,206	37°03'10.48"	74°31'25.76"	Alive
RB-685-3	Norfolk (deep)	1,328	37°03'10.48"	74°31'25.76"	Dead
RB-685-4	Norfolk (deep)	1,249	37°03'06.35"	74°31'04.16"	Dead
RB-685-5	Norfolk (deep)	1,251	37°03'06.23"	74°31'04.08"	Dead
RB-685-6	Norfolk (deep)	1,251	37°03'06.23"	74°31'04.08"	Dead
RB-685-7A	Norfolk (deep)	1,326	37°03'00.75"	74°30'46.79"	Dead
RB-685-7B	Norfolk (deep)	1,326	37°03'00.75"	74°30'46.79"	Dead
RB-685-8A	Norfolk (deep)	1,251	37°03'06.23"	74°31'04.08"	Dead
RB-685-8B	Norfolk (deep)	1,251	37°03'06.23"	74°31'04.08"	Dead
RB-685-9	Norfolk (deep)	1,326	37°03'00.75"	74°30'46.79"	Dead
RB-686-1	Norfolk (deep)	478	37°03'31.05"	74°36'21.10"	Alive
RB-686-2	Norfolk (deep)	581	37°03'16.12"	74°36'12.65"	Alive
RB-686-3	Norfolk (deep)	584	37°03'16.26"	74°36'13.18"	Alive
RB-686-4	Norfolk (deep)	578	37°03'16.14"	74°36'12.85"	Alive

Table 17-1. (Continued).

Coral ID	Location	Depth (m)	Latitude (N)	Longitude (W)	Status
RB-686-6	Norfolk (deep)	578	37°03'16.14"	74°36'12.85"	Dead
RB-686-3/4A	Norfolk (deep)	578	37°03'16.14"	74°36'12.85"	Dead
RB-686-3/4B	Norfolk (deep)	578	37°03'16.14"	74°36'12.85"	Dead
RB-687-1	Norfolk (northern canyon wall)	581	37°03'18.01"	74°34'39.60"	Alive
RB-687-3	Norfolk (northern canyon wall)	569	37°03'19.40"	74°34'37.17"	Alive
RB-687-5	Norfolk (northern canyon wall)	711	37°03'14.22"	74°34'49.96"	Alive
RB-687-6	Norfolk (northern canyon wall)	571	37°03'19.76"	74°34'35.56"	Alive
NF-17-1	Baltimore Canyon	680	38°07'01.20"	73°50'28.74"	Alive
NF-17-4	Baltimore Canyon	690	38°07'01.20"	73°50'28.74"	Alive
NF-18-3	Baltimore Canyon	680	38°07'01.32"	73°50'26.28"	Alive
NF-20-1	Norfolk Canyon	719	37°03'03.48"	74°37'56.34"	Dead
NF-20-2	Norfolk Canyon	706	37°03'03.48"	74°37'56.34"	Dead
NF-20-3	Norfolk Canyon	706	37°03'03.48"	74°37'56.34"	Dead
NF-20-4	Norfolk Canyon	706	37°03'03.48"	74°37'56.34"	Dead
NF-20-5	Norfolk Canyon	706	37°03'03.48"	74°37'56.34"	Dead
NF-20-6	Norfolk Canyon	706	37°03'03.48"	74°37'56.34"	Dead
NF-20-7	Norfolk Canyon	706	37°03'03.48"	74°37'56.34"	Dead
NF-20-8	Norfolk Canyon	706	37°03'03.48"	74°37'56.34"	Dead
NF-20-9	Norfolk Canyon	706	37°03'03.48"	74°37'56.34"	Dead
NF-20-10	Norfolk Canyon	706	37°03'03.48"	74°37'56.34"	Dead
NF-20-11	Norfolk Canyon	706	37°03'03.48"	74°37'56.34"	Dead
NF-20-12	Norfolk Canyon	706	37°03'03.48"	74°37'56.34"	Dead
NF-20-13	Norfolk Canyon	706	37°03'03.48"	74°37'56.34"	Alive

Marine carbonate samples, including DSCs recovered from the seafloor, marine canyons, and continental shelves, are likely to be contaminated by detrital sediment, organic material, or iron manganese (FeMn) coatings and each contaminate phase can alter the geochemical composition of the aragonite skeleton of *D. dianthus* (van de Flierdt et al. 2010). FeMn crusts form on the skeleton after death containing digenetic iron and manganese oxides trapping a significant amount of detrital material within the septa of the cup corals (Cheng et al. 2000) (**Figure 17-2**). The modern *D. dianthus* specimen (on the left) does not show any visible contamination of the coral's skeleton and only has detrital material trapped between the septa. Subfossil DSCs that are contaminated will have elevated concentrations of Th, U, Fe, Mn, Ti, Nd, and aluminum (Al) due to the FeMn crusts, detrital material, and organic material contamination (Cheng et al. 2000, van de Flierdt et al. 2010, Crocket et al. 2014).

Fossil *D. dianthus* specimens underwent a physical and chemical cleaning process to remove geochemical contamination caused by FeMn coating and detrital material (Adkins et al. 2002). The cleaning procedure developed by Shen and Boyle (1988), Cheng et al. (2000), and modified by van de Flierdt et al. (2010) was used to remove any geochemical contamination to the skeleton (**Table 17-2**). Before cleaning sections of the cup corals, samples were cut along longitudinal transects into quarters to make the size of cup coral sections more manageable, and single petals were cut off for radiocarbon dating and laser ablation analyses. Chemical cleaning was carried out by repeating a series of oxidative and reductive cleaning steps, with a final leaching step to remove any possible trace metal contamination in the coral skeleton (Shen and Boyle 1988, van de Flierdt et al. 2010).

Figure 17-2. Modern *Desmophyllum dianthus* (left) clean aragonite skeleton and subfossil *D. dianthus* (right) showing visible FeMn coating and detrital material on the outside of the cup coral's skeleton and between the septa.

Table 17-2. Cleaning steps for removing contamination to deepsea coral aragonite (From: van de Flierdt et al. 2010).

Steps	Action	Comments
1	Scraping FeMn coasting	FeMn is scraped off the coral prior to cleaning.
2	Physical cleaning	Any visible FeMn coating is removed as much as possible using a Dremel tool.
3	Precleaning	Samples are exposed to a 1:1 mixture of 30% peroxide and 1 N sodium hydroxide for 15−20 min while ultrasonicated. Repeated until no FeMn coating is visible. To remove any further organic stains on the skeleton, samples are dipped in 1:1 mixture of 30% peroxide and 1% percholric acid for 30 s to 2 min. Corals are transferred to acid-washed centrifuge tubes.
4	Oxidative cleaning	Washed in methanol for 20 min in the ultrasonicator and dipped in 0.2% nitric acid. Oxidative step consist of a 1:1 mixture of 30% hydrogen peroxide and 1 N sodium hydroxide for 20 min in heated ultrasonicator.
5	Reductive cleaning	Apply a mixture of citric acid, ammonium hydroxide, and hydrazine to remove any trace metal contamination. Samples are cleaned by heating in 100/~1 of reducing cleaning solution (0.25 M citric acid in 16 M ammonia), made up to 1 M in hydrazine (N_2H_4) for 30 min with a few seconds of ultrasonication. Coral pieces are rinsed with three portions of distilled water and further cleaned by heating in two heated water baths by a final room temperature rinse. Transferred into clean centrifuge tubes.
6	Final cleaning	Final leach is performed in dilute 0.2% nitric acid for 1 min than sonicated in a 1:1 mixture of 30% hydrogen peroxide and 1 N sodium hydroxide for 20 min. Final rinsing in Milli-Q water.

17.2.2.2 Deepsea Coral Radiocarbon Dating

Radiocarbon dating of the modern and fossil cup coral samples was completed at the Radiocarbon Dating Laboratory at the Research School of Earth Sciences, Australian National University. DSC samples were milled in 1 to 2 mm increments starting from the outermost edge directly under the living coral polyp layer (**Figure 17-3**). Milled powders were split, and 7 to 9 mg aliquots were prepared for radiocarbon dating using standard methods for carbonate samples (e.g., Guilderson et al. 2003). Briefly, the aliquots were placed in individual vacutainers and evacuated to $\leq 1 \times 10^{-3}$ Torr with gentle heating. A 0.5 mL aliquot of 85% phosphoric acid was injected into the vacutainer after which the vacutainer was placed on a heating block at 90°C for 1 hour. The resulting CO_2 was cryogenically purified to remove water, and transferred into individual graphite reduction reactors. The CO_2 was reduced to graphite at 570°C in the presence of iron catalyst and a stoichiometric excess of hydrogen, using procedures similar to those described in Vogel et al. (1987). The graphite/iron samples produced were then pressed into aluminum target holders for subsequent AMS analyses. Results are reported as per Stuiver and Polach (1977) and include a background subtraction based on ^{14}C-free calcite, and the $\delta^{13}C$ from the corresponding stable isotope split. Radiocarbon concentration is given as percent modern carbon (pMC), $\Delta^{14}C$ (‰), and conventional radiocarbon ages.

Figure 17-3. Top section of the petal milled off for radiocarbon dating. Approximately 1 to 2 mm of material was removed along the black dashed line.

Modern and fossil *D. dianthus* radiocarbon ages were calibrated using the CALIB program (Stuiver and Reimer 1993, Version 7.1) and Marine Reservoir Correction Database (MARINE13) to correct for local variation in the marine reservoir age, ΔR (Reimer et al. 2013, Stuiver and Braziunas 1993). We determined the ΔR = 95 ^{14}C years (SD 65) by averaging stations around the mid-Atlantic Ocean (Broecker and Olson 1961, Tanaka et al. 1990, Weidman and Jones 1993, Druffel 1997, McNeely et al. 2006) and comparing our *in situ* DIC ^{14}C water values at Baltimore and Norfolk canyons (**Table 17-3**). The majority of the DIC values represent surface waters except those from the Druffel (1997) study. Our measured *in situ* radiocarbon seawater ages at the intermediate water depths where the DSCs were living average 95 ^{14}C years (SD 20), making the ΔR = 95 ^{14}C years (SD 65) the most representative ΔR value for our study site.

Table 17-3. Radiocarbon dating of *Desmophyllum dianthus* collected from Baltimore and Norfolk Canyons. (σ = standard deviation.)

Coral ID	Depth (m)	Canyon	Status	$\delta^{13}C$	Percent Modern Carbon	±	$\Delta^{14}C$	±	^{14}C Age	±	Cal Year B.P.	Min Age	Max Age	Standard Deviation (σ)	Age Range (σ)	Probability Distribution
RB-686-1	478	Norfolk	Alive	-5.38 (2.0)	98.20	0.32	-18.0	3.2	145	30	149	2	282	68.3 (1σ)	9–33	0.19
															74–99	0.15
															106–114	0.05
															136–151	0.11
															173–225	0.36
															254–274	0.15
														95.4 (2σ)	2–41	0.17
															60–153	0.35
															169–234	0.31
															239–282	0.17
RB-686-2	581	Norfolk	Alive	-13.73 (2.0)	99.08	0.28	-9.2	2.8	75	25	98	31	251	68.3 (1σ)	35–71	0.56
															117–132	0.18
															230–251	0.27
														95.4 (2σ)	31–138	0.75
RB-686-3	584	Norfolk	Alive	-12.51 (2)	99.57	0.27	-4.3	2.7	35	25	35	10	60	n/a	Modern	n/a
RB-686-4	578	Norfolk	Alive	-8.89 (2)	98.47	0.27	-15.3	2.7	125	25	119	11	271	68.3 (1σ)	21–37	0.13
															66–118	0.45
															125–144	0.13
															216–231	0.12
															243–266	0.18
														95.4 (2σ)	11–46	0.16
															56–149	0.50
															186–271	0.35

Table 17-3. (Continued).

Coral ID	Depth (m)	Canyon	Status	$\delta^{13}C$	Percent Modern Carbon	±	$\Delta^{14}C$	±	^{14}C Age	±	Cal Year B.P.	Min Age	Max Age	Standard Deviation (σ)	Age Range (σ)	Probability Distribution
RB-686-3/4A	578	Norfolk	Dead	-5.89 (2.0)	98.42	0.30	-15.8	3.0	130	25	126	10	273	68.3 (1σ)	14−36	0.17
															68−118	0.40
															131−146	0.12
															190−191	0.01
															213−231	0.13
															244−268	0.17
														95.4 (2σ)	10−44	0.16
															57−150	0.46
															174−178	0.01
															184−273	0.37
RB-686-3/4 B	578	Norfolk	Dead	-5.39 (2)	92.77	0.33	-72.3	3.3	605	30	139	0	261	68.3 (1σ)	0−236	0.20
														95.4 (2σ)	0−261	1.00
RB-686-6	578	Norfolk	Dead	-0.83 (2.0)	93.17	0.32	-68.3	3.2	570	30	110	0	244	68.3 (1σ)	0−146	0.96
															165–175	0.04
														95.4 (2σ)	0−244	1.00
RB-687-1	581	Norfolk	Alive	-14.19 (2.0)	99.39	0.28	-6.1	2.8	50	25	50	25	75	n/a	Modern	n/a
RB-687-3	569	Norfolk	Alive	-5.95 (2)	95.35	0.26	-46.5	2.6	380	25	457	320	504	68.3 (1σ)	334−349	0.21
															439−444	0.06
															453−498	0.73
														95.4 (2σ)	320−378	0.30
															427−504	0.70
RB-687-6	571	Norfolk	Alive	-5.68 (2)	97.12	0.28	-28.8	2.8	235	25	286	0	312	68.3 (1σ)	155−166	0.34
															284−302	0.66
														95.4 (2σ)	0−11	0.06
														n/a	150−186	0.35

Table 17-3. (Continued).

Coral ID	Depth (m)	Canyon	Status	$\delta^{13}C$	Percent Modern Carbon	±	$\Delta^{14}C$	±	^{14}C Age	±	Cal Year B.P.	Min Age	Max Age	Standard Deviation (σ)	Age Range (σ)	Probability Distribution
NF-20-1	719	Norfolk	Dead	-3.91 (2)	90.62	0.29	-93.8	2.9	790	30	347	280	485	68.3 (1σ)	280–414	1.00
														95.4 (2σ)	224–485	0.98
NF-20-2	706	Norfolk	Dead	-7.89 (2)	92.74	0.30	-72.6	3.0	605	30	139	0	261	68.3 (1σ)	0–1	0.01
															64–236	0.99
															620–645	0.40
														95.4 (2σ)	0–261	1.00
NF-20-3	706	Norfolk	Dead	-3.09 (2)	91.74	0.30	-82.6	3.0	690	30	223	0	339	68.3 (1σ)	130–302	1.00
														95.4 (2σ)	0–16	0.01
															52–399	0.98
NF-20-4	706	Norfolk	Dead	-7.85 (2)	92.93	0.28	-70.7	2.8	590	25	125	47	251	68.3 (1σ)	47–149	0.62
															162–194	0.17
														95.4 (2σ)	0–251	1.00
NF-20-5	706	Norfolk	Dead	-7.90 (2)	92.36	0.39	-76.4	3.9	640	35	170	0	293	68.3 (1σ)	92–265	1.00
														95.4 (2σ)	0–293	1.00
NF-20-6	706	Norfolk	Dead	-6.31 (2)	91.63	0.27	-83.7	2.7	700	25	238	59	411	68.3 (1σ)	136–308	1.00
														95.4 (2σ)	59–411	0.99
NF-20-7	706	Norfolk	Dead	-8.30 (2)	92.85	0.27	-71.5	2.7	595	25	130	0	253	68.3 (1σ)	54–150	0.59
															160–200	0.22
															205–226	0.12
														95.4 (2σ)	0–253	1.00
NF-20-8	706	Norfolk	Dead	-1.85 (2)	92.36	0.26	-76.4	2.6	640	25	170	0	285	68.3 (1σ)	98–264	1.00
														95.4 (2σ)	0–285	1.00

Table 17-3. (Continued).

Coral ID	Depth (m)	Canyon	Status	$\delta^{13}C$	Percent Modern Carbon	±	$\Delta^{14}C$	±	^{14}C Age	±	Cal Year B.P.	Min Age	Max Age	Standard Deviation (σ)	Age Range (σ)	Probability Distribution
NF-20-9	706	Norfolk	Dead	-6.77 (2)	92.39	0.30	-76.1	3.0	635	30	165	0	283	68.3 (1σ)	91−60	1.00
														95.4 (2σ)	0−283	1.00
NF-20-10	706	Norfolk	Dead	-8.40 (2.0)	98.70	0.30	-13.0	3.0	105	25	112	21	266	68.3 (1σ)	32−43	0.10
															58−83	0.23
															89−91	0.02
															97−108	0.11
															112−137	0.24
															224−256	0.31
														95.4 (2σ)	21−144	0.72
															216−266	0.28
NF-20-11	706	Norfolk	Dead	-8.36 (2)	93.05	0.25	-69.5	2.5	580	25	117	0	246	68.3 (1σ)	0−146	0.95
															165−175	0.05
														95.4 (2σ)	0−246	1.00
Nf-20-12	706	Norfolk	Dead	-5.11 (2.0)	92.03	0.32	-79.7	3.2	665	30	193	0	331	68.3 (1σ)	117–284	1.00
														95.4 (2σ)	0–331	1.00
NF-20-13	706	Norfolk	Alive	-8.25 (2)	96.40	0.29	-36.0	2.9	295	25	389	296	454	68.3 (1σ)	303−320	0.29
															379−427	0.71
														95.4 (2σ)	296−334	0.30
															350−438	0.69
															444−454	0.02
RB-687-5	711	Norfolk	Alive	-7.93 (2)	99.44	0.27	-5.6	2.7	45	25	45	20	70	n/a	Modern	n/a
RB-685-1	1,328	Norfolk	Dead	-4.12 (2)	93.82	0.29	-61.8	2.9	515	25	531	508	619	68.3 (1σ)	519−540	1.00
														95.4 (2σ)	508−553	0.98
															612−619	0.02
RB-685-2	1,206	Norfolk	Alive	-5.68 (2)	99.12	0.27	-8.8	2.7	70	25	70	95	45	n/a	Modern	n/a

Table 17-3. (Continued).

Coral ID	Depth (m)	Canyon	Status	$\delta^{13}C$	Percent Modern Carbon	±	$\Delta^{14}C$	±	^{14}C Age	±	Cal Year B.P.	Min Age	Max Age	Standard Deviation (σ)	Age Range (σ)	Probability Distribution
RB-685-3	1,328	Norfolk	Dead	-0.84 (2)	92.86	0.32	-71.4	3.2	595	30	130	0	255	68.3 (1σ) 0.224	54−150	0.59
															160−200	0.22
															205−226	0.11
														95.4 (2σ)	205−226	0.12
RB-685-4	1,249	Norfolk	Dead	-3.90 (2)	93.81	0.33	-61.9	3.3	515	30	532	506	624	68.3 (1σ)	517−542	1.00
														95.4 (2σ)	506−556	0.93
															607−624	0.07
RB-685-5	1,251	Norfolk	Dead	-7.47 (2.0)	96.82	0.30	-31.8	3.0	260	30	305	0	431	68.3 (1σ)	155−166	0.13
															284−316	0.72
															408−421	0.15
														95.4 (2σ)	0−7	0.01
															151−171	0.12
															280−331	0.57
															357−431	0.30
RB-685-6	1,251	Norfolk	Dead	-8.69 (2)	99.35	0.27	-6.5	2.7	50	25	50	25	75	n/a	Modern	n/a
RB-685-7A	1,326	Norfolk	Dead	-5.88 (2.0)	98.39	0.34	-16.1	3.4	130	30	129	9	275	68.3 (1σ)	14−37	0.17
															66−118	0.38
															125−146	0.13
															189−192	0.02
															213−231	0.13
															243−268	0.18
														95.4 (2σ)	9−45	0.16
															56−151	0.44
															173−275	0.40
RB-685-7B	1,326	Norfolk	Dead	-8.91 (2)	93.16	0.30	-68.4	3.0	570	30	110	0	244	68.3 (1σ)	0−146	0.96
															165−175	0.04
														95.4 (2σ)	0−244	1.00

Table 17-3. (Continued).

Coral ID	Depth (m)	Canyon	Status	$\delta^{13}C$	Percent Modern Carbon	±	$\Delta^{14}C$	±	^{14}C Age	±	Cal Year B.P.	Min Age	Max Age	Standard Deviation (σ)	Age Range (σ)	Probability Distribution
RB-685-8A	1,251	Norfolk	Dead	-5.78 (2)	91.56	0.30	-84.4	3.0	710	30	253	64	422	68.3 (1σ)	138−322	1.00
														95.4 (2σ)	64−422	0.99
RB-685-8B	1,251	Norfolk	Dead	-7.86 (2)	93.03	0.26	-69.7	2.6	580	25	117	0	246	68.3 (1σ)	0−146	0.95
															165−175	0.05
														95.4 (2σ)	0−246	1.00
RB-685-9	1,326	Norfolk	Dead	-4.76 (2)	91.74	0.25	-82.6	2.5	695	25	231	56	405	68.3 (1σ)	134−303	1.00
														95.4 (2σ)	56−405	0.99
NF-17-1	690	Baltimore	Alive	-10.62 (2)	99.46	0.28	-5.4	2.8	45	25	45	20.0	70	n/a	Modern	n/a
NF-17-4	690	Baltimore	Alive	-9.18 (2)	99.80	0.31	-12.0	3.1	95	30	110	20.0	255	68.3 (1σ)	32−74	0.374
															77−82	0.033
															98−107	0.067
															113−136	0.231
															224−255	0.295
														95.4 (2σ)	20−144	0.72
															215−267	0.28
NF-18-3	680	Baltimore	Alive	-6.62 (2)	98.42	0.32	-15.8	3.2	130	30	129	9.0	275	68.3 (1σ)	14−37	0.166
															66−118	0.384
															125−146	0.13
															189−192	0.017
															213−231	0.127
															243−268	0.177
														95.4 (2σ)	9–45	0.157
															56−151	0.444
															173−275	0.399

17.2.2.3 Trace Element Laser Ablation

Our sampling strategy was to ablate along a single growth axis, on a single petal, representing a single time period (1 to 3 years) for each elemental ratio (**Figure 17-4**). Each growth axis was determined by visual examination of the coral petals.

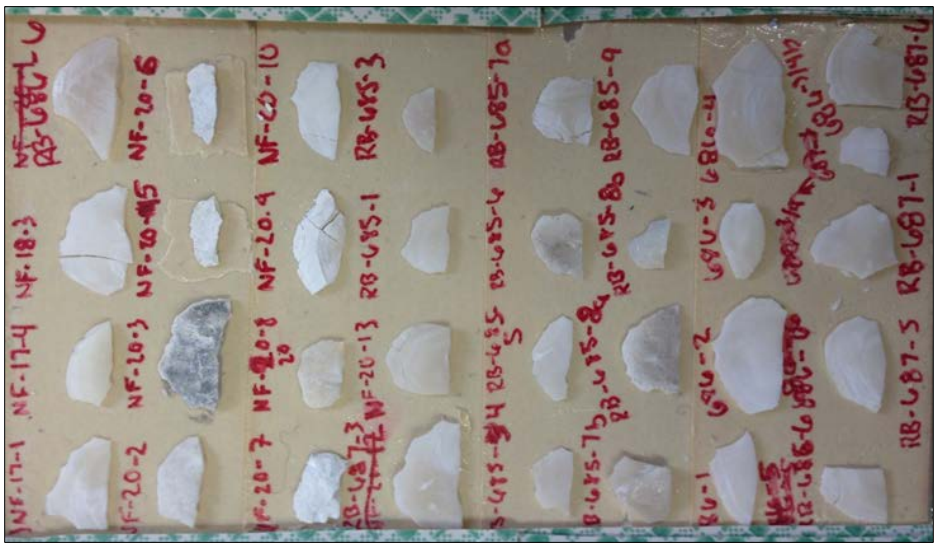

Figure 17-4. Thirty-three *Desmophyllum dianthus* petals removed from the top of the coral septa. Laser ablation ICP-MS measurements were done along growth bands representative of equal time as near as possible to the top edge of the sample representative of the most recent growth.

Laser ablation transects along the growth axis of eight *D. dianthus* septa were completed to reconstruct elemental variability across a constant growth horizon (**Figure 17-5**) and to construct time series. A growth rate of 1 mm y^{-1} was assumed for modern and fossil specimens based on an average growth rate from the current accepted growth rates for *D. dianthus*, which ranges from 0.5 to 2 mm y^{-1} (Adkins et al. 2004, Risk et al. 2002).

The LA ICP-MS methodology is based on protocols developed by Sinclair et al. (1998) and Fallon et al. (1999). Sample tracks were pre-ablated to remove any contamination on the surface of the cup corals. Contamination is typically restricted to the upper few microns of the DSC aragonite skeleton (Anagnostou et al. 2011), therefore, ~1 µm of material was removed by performing 10 pre-ablation scans (Günther et al. 2000, Hathorne et al. 2003). Samples were pre-ablated at 10 Hz with a spot size of 265 µm along the sampling track. The length of the ablated line sampled varied depending on the length of the cup corals petal or the length of the septum. Specimens were ablated in a sealed chamber with a pure helium (He) atmosphere (Eggins et al. 1998), with a movable mixing chamber that mixes the ablated material with argon (Ar) gas before injection into a Varian ICP-MS at Research School of Earth Sciences, Australian National University (ANU) in Canberra, Australia.

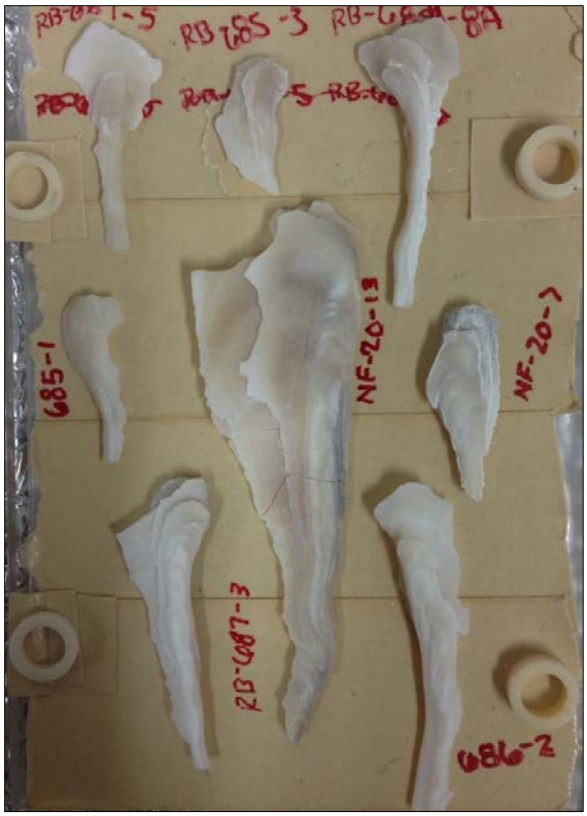

Figure 17-5. Eight modern and subfossil *Desmophyllum dianthus* septa used to reconstruct time series of trace element ratios. Laser ablation ICP-MS scans were made from the top of the septa down to the bottom representative of changes over the lifespan of the coral.

For each standard, we ablated a ~2 mm long line according to National Institute of Standards and Technology (NIST) 612 and ANU coral standards, which are used for drift correction and to calibrate elemental concentrations (Eggins and Shelley 2002, Hathorne et al. 2008, Anagnostou et al. 2011). NIST 612 glass standard is homogeneous for the following elements: beryllium (Be), Mg, Ca, strontium (Sr), Ba, REE (rare earth element), Th, U, zinc (Zn), Al, P, and Cl (Eggins and Shelley 2002). Most elements are within range for the NIST 612 standard of 34 to 40 μg g^{-1} (median = 37.7 μg g^{-1}) (Pearce et al. 1997). The ANU coral standard was used because it provided a matrix-matched standard for the *D. dianthus*, but it only has known concentration values for the following elements: B, Mg, Ca, Sr, Ba, and U. A sweep of elements including ^{31}P, ^{43}Ca, ^{25}Mg, ^{55}Mn, lithium (^{7}Li), ^{84}Sr, ^{138}Ba, ^{238}U, ^{146}Nd, ^{147}Sm, ^{66}Zn, and ^{11}B were measured and normalized to ^{43}Ca, the major constituent of the coral skeleton (Montagna et al. 2005). The element ^{43}Ca acts as an internal standard correcting for variations in ablation yield and for instrumental drift (Craig et al. 2000, Hathorne et al. 2003, Longerich et al. 1997) and was picked because it is measurable in NIST 612 and ANU coral standards. Concentrations for trace elements and trace metals are reported as μmol mol^{-1}. NIST 612 and ANU coral standards are closely matched matrix for the bulk composition and structure of the coral samples, correcting for any fractionation during the runs. ANU coral standard is considered to be a well-matched matrix to our unknown samples and homogeneous for elements B, Mg, Sr, Ba, and U. For the purposes of this study the NIST 612 standard will provide elemental ratios for P, and ANU coral standard will provide elemental ratios for Ba and U.

Trace element and trace metal signals in corals show a large amount of fine-scale variability that could represent various compositional features and heterogeneity within the coral skeleton. A moving average smoothing is applied to the data to remove this variability. The level of the moving average smoothing applied is dependent on the size of the spot and speed of the scan and is therefore subjective

based on each coral analysis. Our goal was to obtain a single mean elemental ratio representative of each coral measured. For our time series and single time span measurements, a 20-point smoothing was applied to the data because of the large spot size used and 10 to 20 s scan rate. We also compared the raw element ratio data against the 3-, 10-, and 20-point moving average smoothing for four of the coral petals to determine the variability within the different moving averages and the smoothing that was needed to calculate the elemental ratio mean for each specimen.

17.2.2.4 Laser Ablation Boron Isotopic Measurements

The laser ablation multicollector ICP-MS methodology is very similar to the trace element LA ICP-MS method. The only change was that ablated material with argon (Ar) gas was injected into a Thermo Finnigan Neptune ICP-MS at Research School of Earth Sciences, Australian National University. The background scans completed at the beginning and end of each run were used to calculate a background subtraction. The ANU in-house NEP standard, a modern day *Porites* coral and ANU in-house Davies Coral standard, were used because they are a close matrix match for *D. dianthus*. Standards were used to complete the drift correction by ablating the standard in between each unknown (Eggins and Shelley 2002, Hathorne et al. 2008, Anagnostou et al. 2011). Boron isotopic ratios are expressed in the conventional delta notation (δ) relative to the NEP and ANU in-house Davies Coral standard. Over course of the study, the LA ICP-MS analysis of the ANU Davies Coral standard $\delta^{11}B = 0.02‰$ relative to a reference value for this standard of 4.603. The NEP standard yielded a mean value of $\delta^{11}B = 0.1‰$ relative to a reference value for this standard of 4.590. Any outlier points were removed during the filtering of the datasets based on relatively large increases in the elemental signals from the adjacent coral material. Outliers commonly result from dust or other particulate contamination on the coral sample that enters the plasma. Instrument mass bias was corrected using a standard-sample-standard bracketing technique (Foster 2008, Wang et al. 2010). The average of the spots for each specimen is assumed to be representative of the bulk $\delta^{11}B$ within the top portion of the *D. dianthus* petal.

17.2.3 Chemosynthetic Communities Methods

17.2.3.1 Study Sites

A shallow (385 m) chemosynthetic community in Baltimore Canyon (38°03.086 N, 73°49.379 W) was sampled during a 2012 cruise (August 17 to September 14) aboard the NOAA ship *Nancy Foster* using the ROV *Kraken 2* from the University of Connecticut. The Baltimore Canyon site and a deeper (1,455 to 1,640 m) seep site in Norfolk Canyon (36°51.921 N, 74°29.574 W) were sampled during a 2013 cruise aboard the NOAA ship *Ronald H. Brown* using the ROV *Jason II* from the Woods Hole Oceanographic Institution. Active gas bubbling, dense colonies of chemosynthetic mussels, and bacterial mats were observed at both sites. Both seep communities were dominated by the deepsea mussels from the genus *Bathymodiolus* of which both live and dead specimens were sampled using the ROVs. Samples of biogenic carbonate were also taken from both seep sites.

17.2.3.2 X-Ray Diffraction

Sample mineralogy was determined microscopically in thin sections and by X-ray diffraction (XRD) using a Philips XRD with graphite monochromator at 40 kV and 45 mA. Step scans were run from 5° to 65° 2θ with 0.02° steps using CuKα radiation and a count time of 2 seconds per step following protocol described in (Hein et al. 2013). XRD digital scan data were analyzed with Philips X'Pert High Score software's search-and-match function to identify minerals (Cook et al. 1975). Mineral percentages were determined by multiplying unique peak intensities for each mineral in a sample by relative intensity factors. The products for all minerals in each sample were then summed to 100%. Carbonate content, reported as weight percent (wt%), was determined using a coulometer at the USGS Pacific Coastal and Marine Science Center, Santa Cruz, California.

17.2.3.3 Stable Isotopes

Stable carbon ($\delta^{13}C$) and oxygen ($\delta^{18}O$) isotopes were analyzed at the Stable Isotope Geosciences Facility at Texas A&M University. Authigenic carbonate samples were subsampled to isolate the cement and groundmass components. For the mussel shells, carbonate and periostracum (organic-rich outer layer) was collected along transects from the umbo to the ventral margin of an individual specimen at four discrete distances. Prior to analysis, the periostracum material was acidified to remove inorganic carbon. Data were generated from a Thermo Finnigan MAT 253 with a Kiel IV automated carbonate prep device and are reported in per mil (‰) relative to the international reference Vienna Pee Dee Belemnite (VPDB). Analytical uncertainties of ±0.04‰ for $\delta^{13}C$ and ±0.06‰ for $\delta^{18}O$ are reported based on the long-term daily measurements of the international carbonate standard, NBS-19. Sulfur isotopes ($\delta^{34}S$) were determined at the Washington State University Stable Isotope Core Laboratory. Mussel gill and seep sediment were combusted with an elemental analyzer (ECS 4010, Costech Analytical) coupled to a Thermo Finnigan Delta PlusXP continuous flow isotope ratio mass spectrometer (Brenna et al. 1997). Sulfur isotope ratios ($\delta^{34}S$) are reported in per mil (‰) relative to VCDT (Vienna Canon Diablo Troilite). Analytical accuracy (1σ) of $\delta^{34}S$ was determined by replicate analysis of the internal laboratory standard referenced to International Atomic Energy Agency (IAEA) standards, reported as 0.26‰ (n = 36), bovine internal standard at 0.47‰ (n = 18), and sample replicates 0.13‰ (n = 9).

17.2.3.4 Strontium Isotopes

Strontium isotope ($^{87}Sr/^{86}Sr$) compositions of the authigenic carbonates, mussel shells, and seawater samples were determined at the USGS facility at Menlo Park, California. Bottom water samples were filtered using 0.45 µm GFF. Authigenic carbonate samples were subsampled to isolate the cement and groundmass components, and mussel shell material was homogenized using an agate mortar and pestle. The mussel shell and authigenic components were digested in sealed Teflon vessels and leached to remove labile Sr. Strontium was separated from other ions using a cation exchange resin with HCl as the eluent. Purified Sr was converted to nitrate form, taken up in 30 µL of 0.15 M H_3PO_4 and loaded onto a Ta (tantalum) ribbon for mass spectrometric measurement. The isotopic composition was measured on a Finnigan MAT 261 multicollector mass spectrometer in static collection mode following methods described by Bullen et al. (1996). All reported values of $^{87}Sr/^{86}Sr$ were corrected for analytical fractionation to the standard $^{88}Sr/^{86}Sr$ ratio of 8.37521 (Steiger and Jäger 1977), and measurements are precise to ±0.00002 at the 95% confidence level.

17.2.3.5 Radiocarbon Analysis

Radiocarbon (^{14}C) analysis was performed on subsamples of authigenic carbonates and mussel shells collected from dead and live mussel specimens (**Appendix 17-B**). Samples were prepared for AMS radiocarbon (^{14}C) dating at the Keck Carbon Cycle AMS Laboratory at the University of California Irvine. Authigenic carbonate samples were subsampled to isolate the cement and groundmass components. Carbonate from the mussel shells was analyzed as a homogenized powder and as shell fragments. To test for potential contamination by secondary aragonite or calcite (Douka et al. 2010), duplicates were performed on samples treated with 10% HCl.

The carbonate samples were hydrolyzed to CO_2 in individual reaction chambers, evacuated, heated, and acidified with orthophosphoric acid at 90 °C. The resultant CO_2 was converted to graphite using an iron catalyst and the hydrogen reduction method (Vogel et al. 1987). Sample preparation backgrounds have been subtracted, based on measurements of ^{14}C-free calcite and oxalic acid I. All ^{14}C results were corrected for isotopic fractionation according to the conventions of Stuiver and Polach (1977) with $\delta^{13}C$ values measured on prepared graphite using the AMS spectrometer. Radiocarbon concentrations are given as $\Delta^{14}C$ and conventional radiocarbon age following Stuiver and Polach (1977).

17.2.3.6 U-Th Age Dating of Authigenic Carbonates

U-Th dating of authigenic carbonates was carried out at the NERC Isotope Geosciences Laboratory, British Geological Survey. Analytical protocols were aimed at ensuring (1) complete dissolution of the detrital material incorporated into the authigenic carbonates; and (2) oxidation of organic material liable to produce isobaric interferences during measurements of Th isotope ratios (Shen et al. 2002).

All evaporation steps took place in a closed EvapoClean device, in order to minimize cross-contamination and reduce fall-in blanks. Carbonate samples were dissolved in 8 M HNO_3, spiked with a mixed ^{229}Th-^{236}U tracer, left to equilibrate overnight, and dried. To ensure total dissolution of detrital mineral, samples were refluxed in a mixture of 11 M $HClO_4$: 29 M HF: 16 M HNO_3 (1:2:2.5), for 1 to 7 days using ~50 µL HF per mg of material. Following evaporation to dryness, samples went through two overnight oxidation steps in 2 mL 16 M HNO_3 and 0.2 mL 30% H_2O_2. The pre-concentration of U and Th was accomplished via Fe coprecipitation followed by the initial separation of U and Th on 0.6 mL columns using AG-1 × 8 anion exchange resin (Edwards et al. 1987). Thorium fractions were further purified using a second pass through AG-1 × 8 resin and were filtered using 0.22 µm syringe filters to remove resin particles. Both U and Th fractions were oxidised twice in 2 mL 16 M HNO_3 and 0.2 mL 30% H_2O_2, and dissolved in 1 mL 0.1 M HCl and 0.035 M HF. Prior to mass spectrometry, all samples were filtered to remove particles originating from the FEP beakers used for sample preparation.

Isotope ratio measurements were made on a Thermo Neptune Plus multicollector ICP-MS, with samples introduced via an Aridus II desolvating nebulizer. Uranium and thorium were measured separately, using an X skimmer cone coupled with normal and Jet sample cones, respectively. Measurements were made using static multicollector data collection protocols with ^{234}U and ^{230}Th measured on an axial secondary electron multiplier (SEM) and the remaining isotopes (^{233}U, ^{235}U, ^{236}U, ^{238}U and ^{229}Th and ^{232}Th) measured on Faraday cups equipped with 10^{11} Ω resistors. SEM/Faraday gain and exponential mass fractionation were monitored and corrected for via a sample-standard bracketing approach using CRM 112a U and mixed CRM 112a U + IRMM 3636 spike for U, and an in-house ^{229}Th-^{230}Th-^{232}Th reference solution calibrated against CRM 112a for Th. Hydride formation and tailing were monitored at the beginning of each analytical session, with measurements made at mass 237 and 239 while aspirating an unspiked CRM 112a solution, and were corrected off-line.

Uranium-thorium age calculations were performed using the decay constants of Cheng et al. (2013). Because the analysed samples consisted of mixtures of authigenic carbonate and detrital material, accurate interpretation of their U-Th age required a correction for the U and Th isotopic composition of the incorporated detritus. This correction was based on a theoretical detrital endmember composition assuming secular equilibrium in the ^{238}U decay chain (i.e., ($^{230}Th/^{238}U$) = ($^{234}U/^{238}U$) = 1), and a $^{232}Th/^{238}U$ activity ratio of 1.2 based on average values for the upper continental crust (Wedepohl 1995), with uncertainties arbitrarily set at ±50% (2σ).

17.3 RESULTS

17.3.1 Seawater Results

17.3.1.1 Nutrients

Nutrient depth profiles in both Baltimore and Norfolk canyons displayed surface water depletion and bottom-water enrichment in nitrate, phosphate, and dissolved silicate **(Figure 17-6**), with ammonia being the exception. Below the mixed layer, concentrations of nitrate, phosphate, and dissolved silicate were conservative and exhibited a homogenous distribution at depth. According to the results from the 2013 sampling cruise, the nutricline in Norfolk Canyon in the late spring was at approximately 400 m. This depth also marked the minimum O_2 concentration, coinciding with the nutrient maximum. The base of the thermocline in Norfolk Canyon was at 400 m as well. The shallower stations in Norfolk Canyon

displayed a slight enrichment in surface water phosphate and nitrate concentrations. There was a small enrichment in nutrient concentrations in bottom waters at the deep stations (RB-13-010 and RB-2013-011). The nutricline in Baltimore Canyon was defined from nutrient depth profiles collected during the 2012 sampling cruise in August. Maximum nutrient concentrations occurred at ~300 m, consistent with the thermocline depth in Baltimore Canyon. Dissolved O_2 concentrations were unavailable for comparison in Baltimore Canyon for the 2012 sampling period.

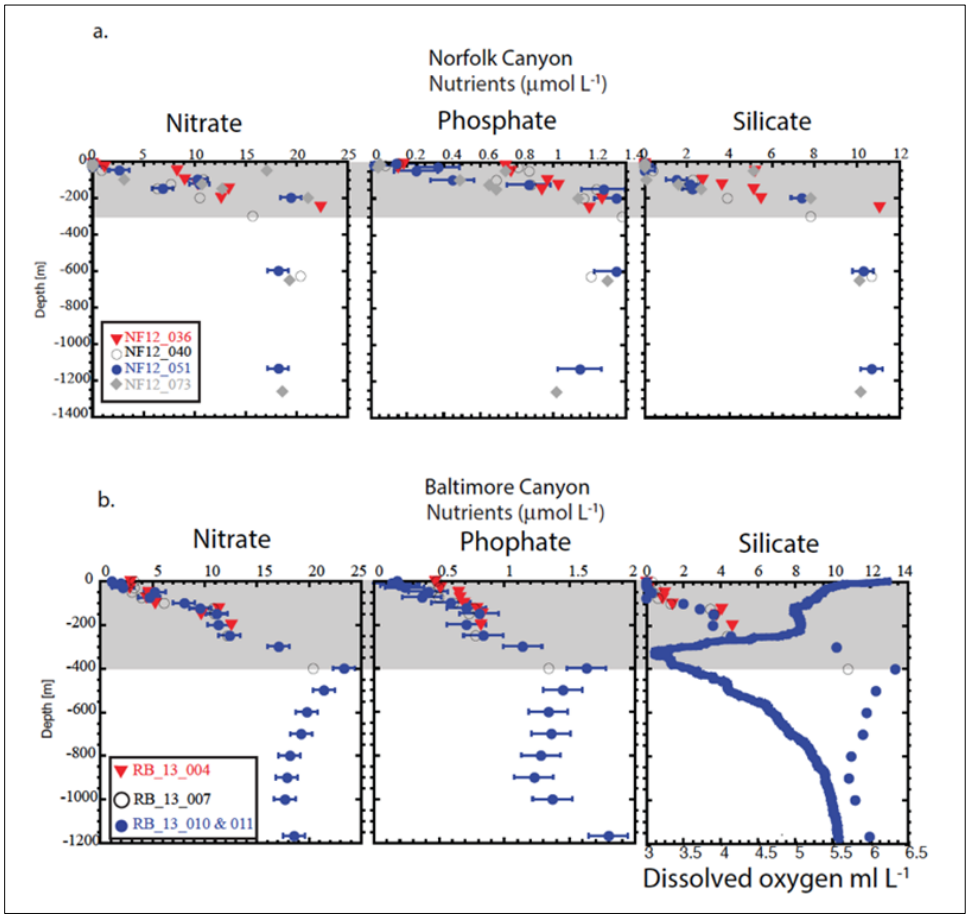

Figure 17-6. Nutrient vertical depth profiles from Norfolk (a) and Baltimore (b) canyons sampled along a down-canyon transect. Dissolved oxygen derived from the CTD sensor is shown for the Baltimore Canyon deep station (RB-13-010). Gray bar indicates depth of nutricline.

17.3.1.2 Radiocarbon ($\Delta^{14}C$)

Radiocarbon values of dissolved inorganic carbon (DIC ^{14}C) were enriched in the upper surface waters of Norfolk Canyon to a depth of ~300 m (**Figure 17-7**). Within the upper surface waters, the DIC ^{14}C signature was characterized by a range of $\Delta^{14}C$ values between 20‰ to 50‰. Below 300 m, DIC-$\Delta^{14}C$ values are progressively more depleted and display conservative behavior, consistently yielding a value of -20‰ at a depth of 400 m and below. Bottom water values of $\Delta^{14}C$-DIC at the deep stations were consistent with DIC-$\Delta^{14}C$ values at the seep sites (-24‰). The DIC-$\Delta^{14}C$ profile from the shallowest station, RB-13-004, displayed a slight depletion in the upper tens of meters with a $\Delta^{14}C$ peak value at ~125 m (47‰). DIC-$\delta^{13}C$ values followed a similar pattern but showed greater variability in the upper 300 m with maximum DIC-$\delta^{13}C$ values in the upper few meters (~1.2‰) (**Figure 17-7**), whereas DIC concentrations were inverse to DIC-$\delta^{13}C$ and followed a nutrient-like pattern with surface water depletion and a maximum DIC concentration of 2.14 µmol kg^{-1}at 300 m (**Figure 17-7**).

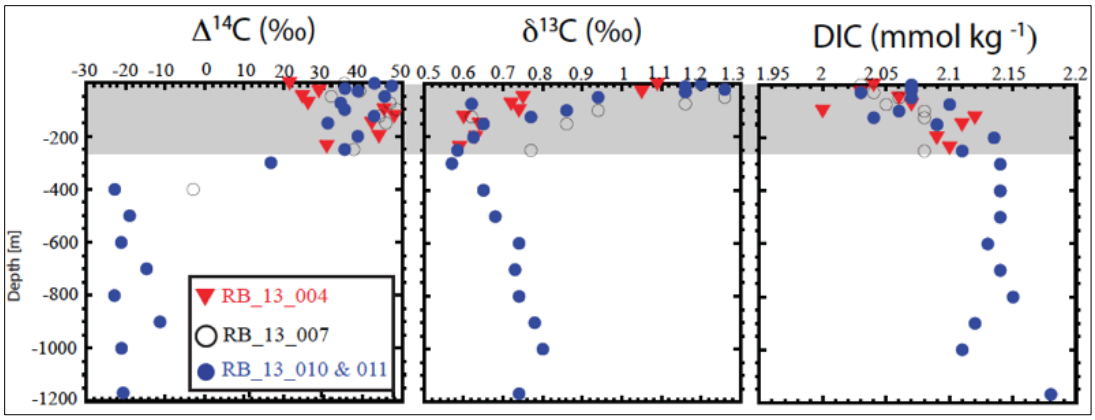

Figure 17-7. Dissolved inorganic carbon (DIC), DIC-radiocarbon ($\Delta^{14}C$), and DIC-stable carbon ($\delta^{13}C$) water depth profiles for Norfolk Canyon. Gray bar indicates depth of mixed layer.

17.3.1.3 Trace Metal Particulates

Particulate (>0.45 µm) trace element composition and variability for Al, neodymium (Nd), iron (Fe), and lanthanum (La) are shown in **Figure 17-8**. Error bars reflect standard deviation based on replicates for a given water depth. Particulate element concentrations were enriched at the shallow site in Baltimore Canyon (NF-2012-138) in the subsurface (~100 m) and at the bottom (~600 m) in the mid-canyon site in both the Baltimore (NF-2012-158) and Norfolk (NF-2012-128) canyons. In comparison, trace element profiles at the Baltimore Canyon deep site (NF-2012-130) and slope site (NF-2012-149) did not exhibit elevated trace metal particulate concentrations at 600 m. Instead, particulate trace element concentrations for the Baltimore Canyon slope site was consistently low, whereas the deep site profile showed slight enrichment near the bottom (~1,200 m) (**Table 17-4**). Enrichment observed at both the subsurface and ~600 m depths coincide with elevated turbidity levels. The two-dimensional (2-D) profile for Fe, based on extrapolated trace element profile data, also shows a subsurface enrichment extending down canyon to approximately 8 km from the head of the canyon. Whereas the turbidity data show the nepheloid layer detaching from the canyon wall, the 2-D profile indicates continuous trace element enrichment along the canyon floor down to almost 1,200 m.

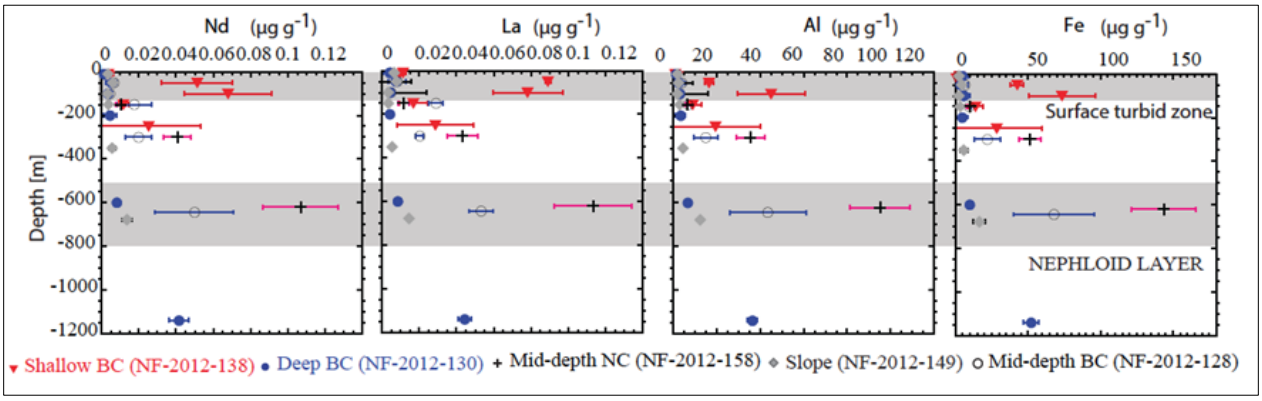

Figure 17-8. Trace element concentrations of particulate matter (µg g^{-1}; neodymium [Nd]; lanthanium [La]; aluminum [Al]; and iron [Fe]) measured from collecting and filtering (>0.45 µm) seawater at discrete depths at three stations in Baltimore Canyon (BC) and on the adjacent slope, and one station in Norfolk Canyon (NC). Extrapolated Fe concentration illustrating 2-D profile compared with turbidity profile from Baltimore Canyon. Gray bar indicates zones of enhanced turbidity.

Table 17-4. Trace element concentration (μg g^{-1}) of particulate matter filtered (>0.45 μm) at discrete water column depth. Values in parentheses indicate standard deviation (σ).

Station	Depth (m)	Nd (neodymium)	La (lanthanum)	Al (aluminum)	Fe (iron)
NF-2012-138	10	0.004 (0.003)	0.011 (0.005)	1.000 (n/a)	2.700 (1.697)
NF-2012-138	20	0.004 (n/a)	0.009 (n/a)	2.000 (n/a)	0.920 (n/a)
NF-2012-138	50	0.051 (0.019)	0.089 (0.06)1	16.500 (2.121)	42.600 (4.525)
NF-2012-138	100	0.068 (0.023)	0.078 (0.034)	45.000 (15.556)	73.500 (22.769)
NF-2012-138	150	0.012 (0.003)	0.017 (0.001)	9.000 (4.243)	13.900 (5.233)
NF-2012-138	250	0.025 (0.028)	0.029 (0.033)	19.500 (20.506)	28.560 (31.311)
NF-2012-128	10	0.001 (0.000)	0.005 (0.002)	1.500 (0.707)	2.000 (0.707)
NF-2012-128	50	0.007 (0.000)	0.008 (0.000)	4.000 (1.414)	6.625 (2.157)
NF-2012-128	100	0.004 (0.001)	0.005 (0.002)	3.000 (1.414)	5.540 (2.744)
NF-2012-128	150	0.018 (0.009)	0.029 (0.019)	6.800 (1.131)	9.385 (1.294)
NF-2012-128	300	0.020 (0.007)	0.020 (0.008)	15.000 (5.657)	22.000 (8.768)
NF-2012-128	644	0.050 (0.021)	0.053 (0.020)	43.500 (17.678)	67.900 (28.001)
NF-2012-130	10	0.001 (0.001)	0.004 (0.004)	1.500 (0.707)	4.855 (4.603)
NF-2012-130	50	0.005 (0.003)	0.008 (0.005)	2.500 (2.121)	3.455 (2.906)
NF-2012-130	100	0.003 (0.000)	0.004 (0.001)	3.000 (1.414)	5.805 (4.533))
NF-2012-130	200	0.005 (0.003)	0.004 (0.004)	3.500 (2.121)	4.715 (3.981)
NF-2012-130	600	0.008 (0.001)	0.008 (0.002)	6.700 (0.990)	9.845 (1.068)
NF-2012-130	1,140	0.042 (0.005)	0.044 (0.006)	36.500 (2.121)	52.250 (5.162)
NF-2012-149	10	0.004 (0.001)	0.007 (0.000)	2.000 (n/a)	2.450 (0.071)
NF-2012-149	50	0.006 (0.002)	0.008 (0.002)	2.500 (0.707)	4.380 (1.245)
NF-2012-149	100	0.003 (n/a)	0.003 (n/a)	2.000 (n/a)	2.400 (0.283)
NF-2012-149	150	0.004 (0.00)1	0.003 (0.00)1	3.000 (n/a)	3.300 (0.141)
NF-2012-149	350	0.006 (0.002)	0.006 (0.002)	4.500 (2.121)	5.705 (2.553)
NF-2012-149	678	0.014 (0.002)	0.015 (0.004)	12.500 (3.536)	16.450 (3.889)
NF-2012-158	150	0.010 (0.002)	0.012 (0.003)	6.750 (1.061)	10.305 (2.539)
NF-2012-158	300	0.041 (0.007)	0.043 (0.008)	35.500 (6.364)	51.400 (7.354)
NF-2012-158	621	0.107 (0.020)	0.113 (0.021)	95.200 (13.859)	143.500 (21.92)0

n/a = replicate not available.

17.3.2 Deepsea Coral Results

17.3.2.1 Laser Ablation ICP-MS Trace Elements

Mean element/Ca ratios were obtained by LA ICP-MS down the main growth axis of *D. dianthus* septa sections representing multiple years of growth. In addition, mean elemental/Ca ratios were obtained from along the top of a single septum representing a single time horizon (e.g., one point in time) when the coral last lived. Trace element variability (element/Ca) is reported for four of the single coral petal tops that were ablated, including *D. dianthus* specimens NF-17-1, NF-17-4, NF-20-10, and RB-686-6. These four specimens were selected based on the following criteria: 1) they were representative specimens from Baltimore and Norfolk canyons, 2) the radiocarbon age ranges of the *D. dianthus* specimens spanned different time periods, and 3) they were pristine samples representative of clean aragonite skeleton and petals that were not fractured along laser ablated sections. The four *D. dianthus* specimens were analyzed to determine the best moving average of the coral elemental ratio that is representative of the 1- to 3-year time domain represented by the spot size and scan pattern and that limits the higher frequency homogenous variability. Three-point, 10-point, and 20-point moving averages were applied to four of modern *D. dianthus* specimens; the average and standard deviations are reported in **Table 17-5**. The 20-point moving average removes the higher frequency variability that is unlikely to be representative of the 1- to 3-year time domain represented by the spot size and scanned track along a uniform growth band. (**Figures 17-9** through **17-12**). The higher frequency variability observed in the raw laser ablation tracks over a single growth band in the *D. dianthus* specimens is representative of the elemental homogeneity during the time period of the *D. dianthus* specimen's life.

Table 17-5. Element ratios from laser scan across the top portion of the septa from *D. dianthus* specimens representing the same time domain. The range for the average of the entire scan, raw values, and scan with a 3-, 10-, and 20-point moving averages are calculated. (Values in parentheses indicate standard deviation.)

Element Ratio (µmol mol-1)					
Specimen No.	Average	Raw	3-Point Smoothed	10-Point Smoothed	20-Point Smoothed
NF-17-1a					
P/Ca	73.98 (14.32)	24.48−164.34 (21.54)	36.23−134.31 (18.38)	44.47−113.02 (16.66)	53.46−101.28 (14.32)
Ba/Ca	8.45 (0.33)	7.08−10.29 (0.65)	7.30−9.38 (0.46)	7.77−9.36 (0.37)	7.95−9.05 (0.33)
U/Ca	2.08 (0.24)	1.28−3.03 (0.30)	1.38−2.87 (0.28)	1.57−2.66 (0.24)	1.68−2.54 (0.24)
NF-17-4b					
P/Ca	209.61 (39.74)	107.99–372.63 (47.43)	125.78−346.30 (43.32)	154.57−281.63 (38.71)	160.42−276.49 (39.74)
Ba/Ca	8.73 (0.35)	6.78–11.0 (0.74)	7.74−9.78 (0.44)	8.25−9.43 (0.35)	8.24−9.42 (0.35)
U/Ca	2.65 (0.23)	2.08−3.82 (0.30)	2.18–3.36 (0.27)	2.38−3.20 (0.25)	2.38−3.06 (0.23)
NF-20-10C					
P/Ca	67.53 (7.51)	23.19–113.82 (15.19)	34.66−88.45 (11.51)	50.82−79.94 (9.06)	51.15−77.59 (7.51)
Ba/Ca	7.57 (0.26)	6.07−10.01 (0.63)	6.57−8.91 (0.44)	7.12−8.67 (0.34)	7.21−8.05 (0.26)
U/Ca	1.18 (0.11)	0.07−1.70 (0.16)	0.82−1.61 (0.14)	0.90−1.46 (0.13)	0.92−1.38 (0.11)
RB-686-6d					
P/Ca	108.90 (22.39)	43.49−199.37 (32.34)	46.35−182.65 (30.99)	62.99−69.23 (27.29)	76.42−148.11 (22.39)
Ba/Ca	11.84 (0.88)	8.39−15.63 (1.38)	9.55−14.80 (1.15)	9.86−14.22 (1.03)	10.20−13.35 (0.88)
U/Ca	3.19 (0.12)	2.44−4.07 (0.27)	2.66−3.69 (0.21)	2.77−3.53 (0.16)	2.89−3.44 (0.12)

[a] Specimen NF-17-1 (Baltimore Canyon; depth 690 m; modern radiocarbon age of 45 ^{14}C y (SD 25))
[b] Specimen NF-17-4 (Baltimore Canyon; depth 690; radiocarbon age of 110 calibrated y B.P.)
[c] Specimen NF-20-10 (Norfolk Canyon; depth 706 m; radiocarbon age of 112 calibrated y B.P.)
[d] Specimen RB-686-6[1] is a subfossil of *Desmophyllum dianthus.* (Norfolk Canyon; depth 578 m; radiocarbon age of 600 calibrated y B.P.)

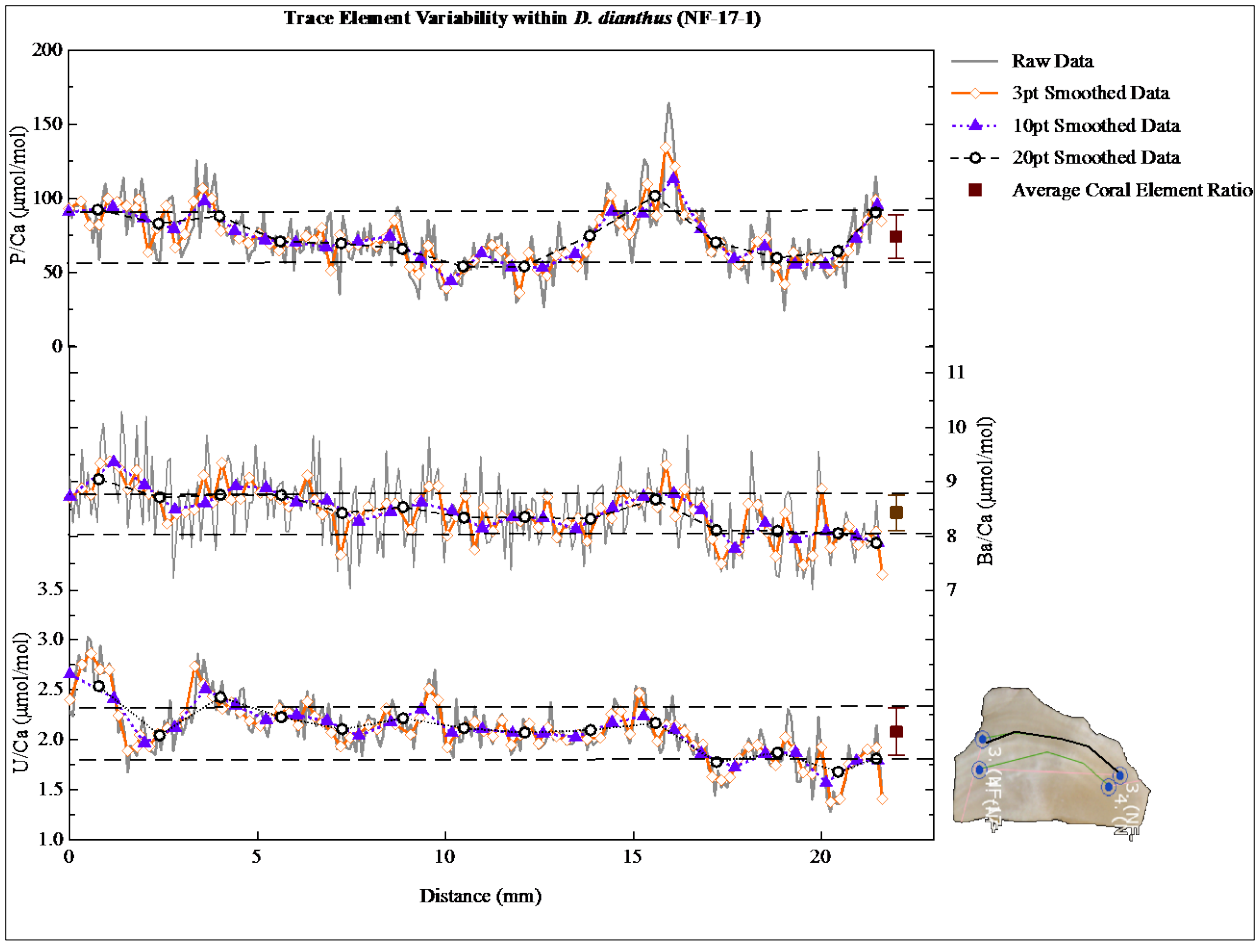

Figure 17-9. Laser ablation transect across top of a modern *Desmophyllum dianthus* septa measured on sample NF-17-1 to reconstruct the trace element variability along a single growth line equivalent to equal time. Raw data (gray line), 3-point smoothed data (red open diamond), 10-point smoothed data (purple closed triangle), 20-point smoothed data (black open circle), and the average elemental ratio for *D. dianthus* are plotted against distance. Sample NF-17-1 (radiocarbon age of 45 calibrated years B.P. (SD 25)) was collected from Baltimore Canyon at a depth of 690 m. Laser ablation tracks along the top of the septa are denoted in the image in the lower right corner.

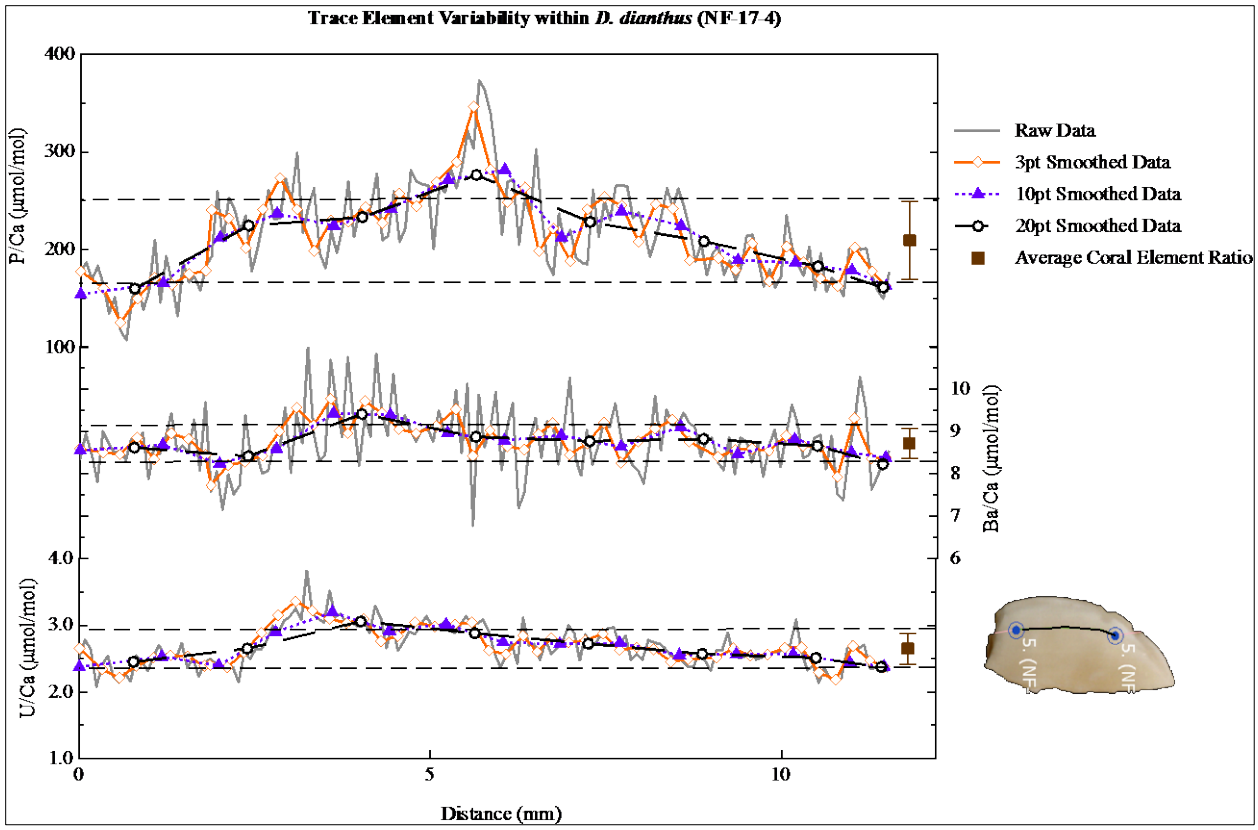

Figure 17-10. Laser ablation transect across top of a modern *Desmophyllum dianthus* septa measured on sample NF-17-4 to reconstruct the trace element variability along a single growth line equivalent to equal time. Raw data (gray line), 3-point smoothed data (red open diamond), 10-point smoothed data (purple closed triangle), 20-point smoothed data (black open circle), and the average elemental ratio for the *D. dianthus* are plotted against distance. Sample NF-17-4 (calibrated radiocarbon age of 110 cal. years B.P.) was collected in Baltimore Canyon at a depth of 690 m. Laser ablation tracks along the top of the septa are denoted in the image in the lower right corner.

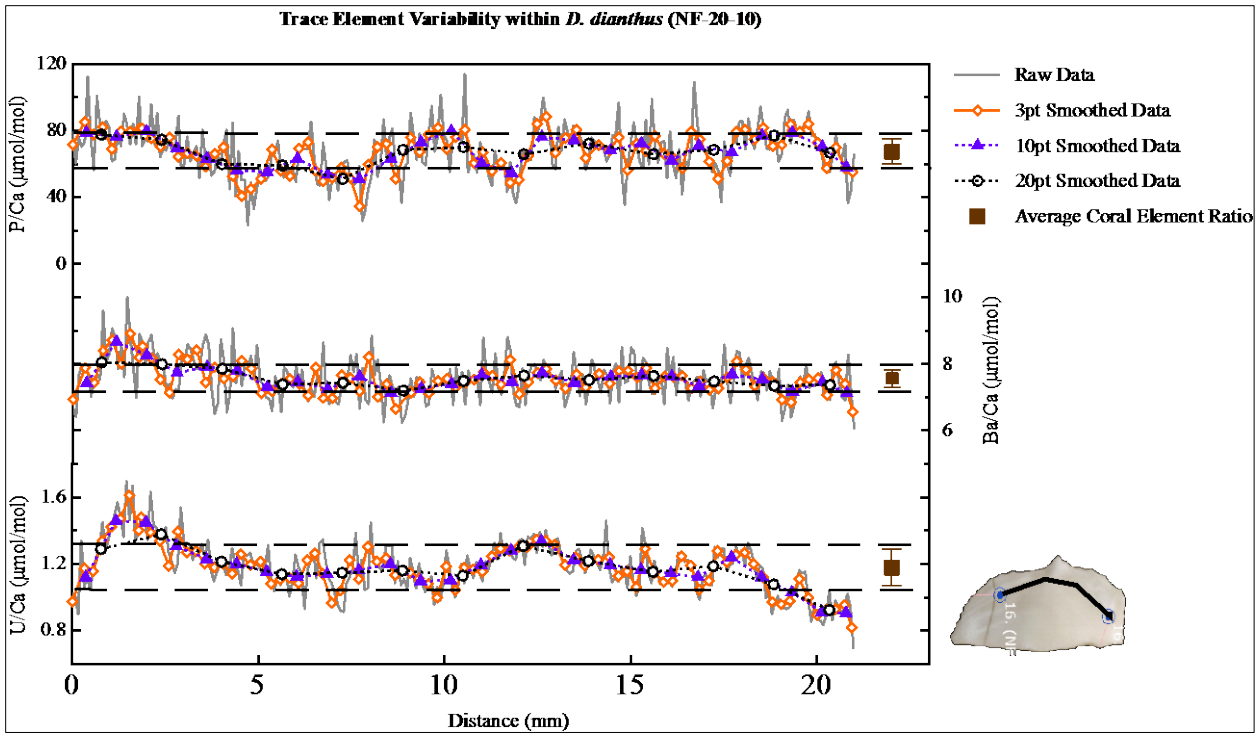

Figure 17-11. Laser ablation transect across top of a modern *Desmophyllum dianthus* septa measured on Sample NF-20-10 to reconstruct the trace element variability along a single growth line equivalent to equal time. Raw data (gray line), 3-point smoothed data (red open diamond), 10-point smoothed data (purple closed triangle), 20-point smoothed data (black open circle), and the average elemental ratio for the *D. dianthus* are plotted against distance. Sample NF-20-10 (radiocarbon age of 112 calibrated years B.P.) collected from Norfolk Canyon at a depth of 706 m. Laser ablation tracks along the top of the septa are denoted in the image in the lower right corner.

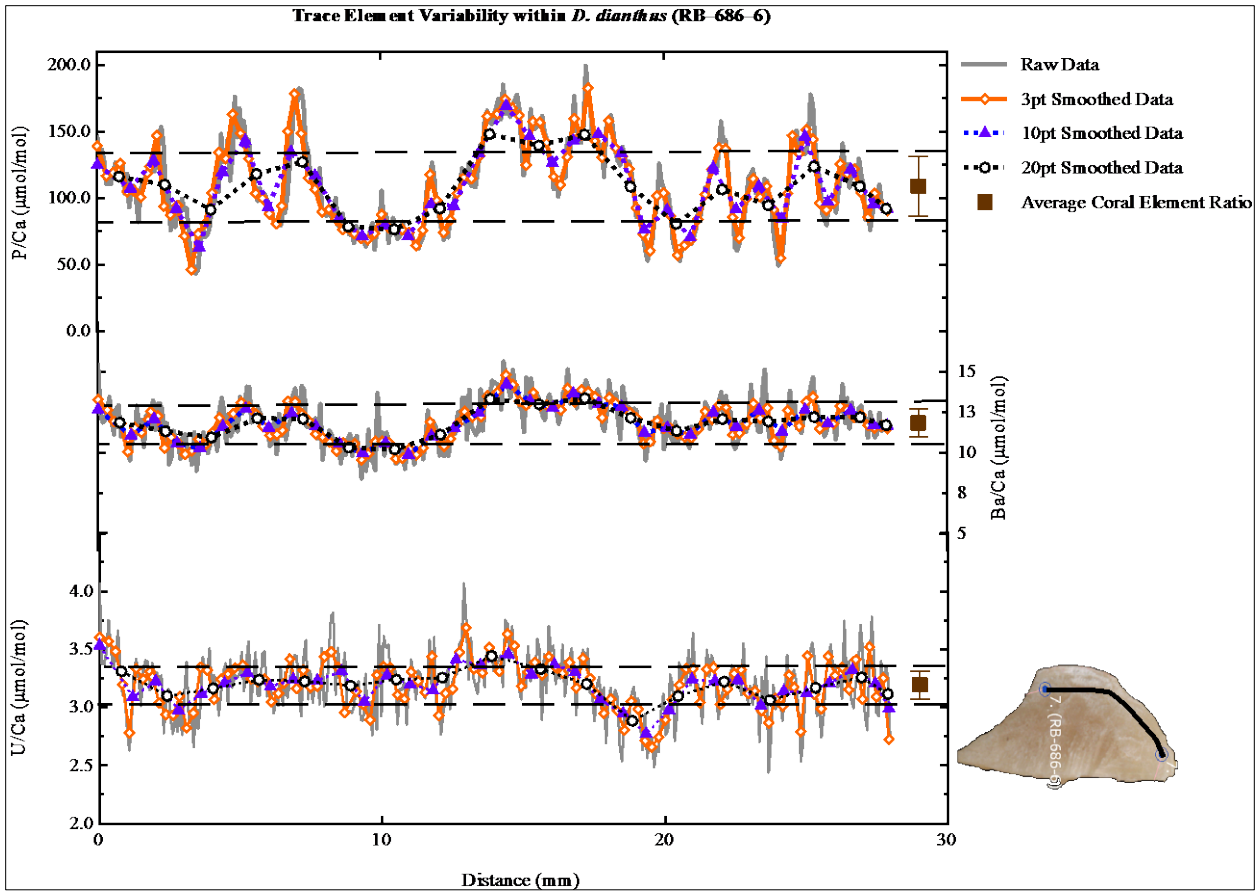

Figure 17-12. Laser ablation transect across top of a modern *Desmophyllum dianthus* measured on Sample RB-686-6 to reconstruct the trace element variability along a single growth line equivalent to equal time. Raw data (gray line), 3-point smoothed data (red open diamond), 10-point smoothed data (purple closed triangle), 20-point smoothed data (black open circle), and the average elemental ratio for the *D. dianthus* are plotted against distance. Sample RB-686-6 (radiocarbon age of 110 calibrated years B.P.) collected in Norfolk Canyon at a depth of 578 m. Laser ablation tracks along the top of the septa are denoted in the image in the lower right corner.

17.3.2.2 Laser Ablation Boron Isotopes

The boron isotope variation expressed as δ notation relative to the NEP and Davies Coral standards is as follows:

$$\delta^{11}B_{carbonate} = [(^{11}B/\ ^{10}B_{sample})/(^{11}B/\ ^{10}B_{standard}) - 1] \times 1{,}000 \quad \text{(Equation 17.3)}$$

Boron isotope compositions were normalized using the in-house NEP and Davies Coral standard using Equation 17.3. At Norfolk Canyon, modern *D. dianthus* living at intermediate water depths of 400 to 600 m had $\delta^{11}B = 24.75‰$. The subfossil *D. dianthus* collected at water depths between 400 and 600 m had $\delta^{11}B$ values ranging from 23.51‰ to 27.77‰. The three *D. dianthus* collected at Baltimore Canyon all had $\delta^{11}B = 23.51‰$ (**Figure 17-13**).

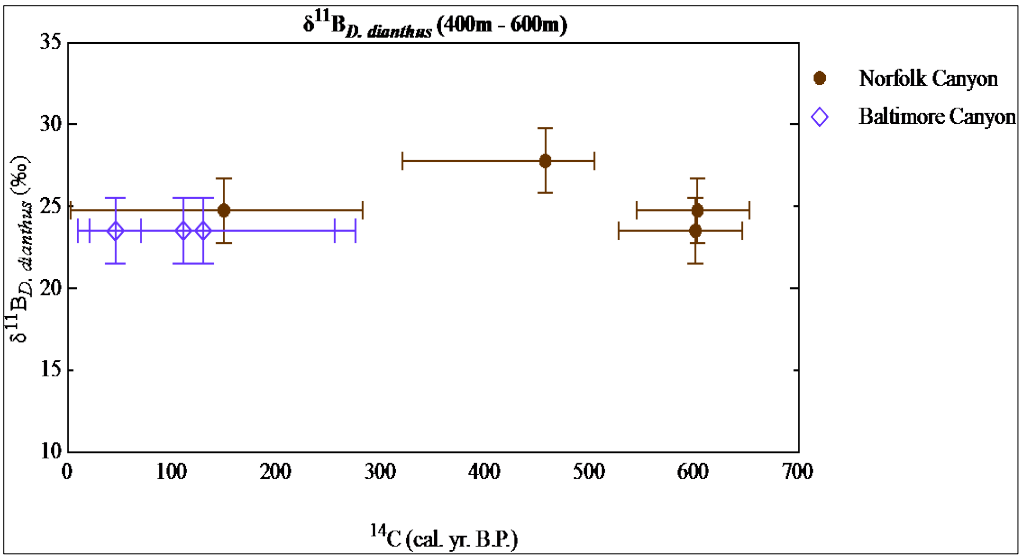

Figure 17-13. Measured $\delta^{11}B$ (‰) for *Desmophyllum dianthus* collected at intermediate depths (400 to 600 m) in Norfolk Canyon (brown closed circles) and Baltimore Canyon (purple open diamonds) plotted against calibrated radiocarbon age of the corals. Error bars on the x-axis represent the uncertainty of the radiocarbon ages, and on the y-axis, the uncertainty of the $\delta^{11}B$ measurements.

Modern *D. dianthus* collected from a depth range of 600 to 800 m in Norfolk Canyon had $\delta^{11}B$ = 23.51‰ while $\delta^{11}B$ of the subfossil *D. dianthus* specimens ranged from 23.51‰ to 29.62‰ (**Figure 17-14**). The modern *D. dianthus* collected from depths of 1,200 to 1,400 m in Norfolk Canyon had $\delta^{11}B$ = 23.46‰ while the subfossil *D. dianthus* $\delta^{11}B$ values ranged from 24.72‰ to 29.66‰ (**Figure 17-15**). The $\delta^{11}B$ values for each individual coral specimen are reported in **Table 17-6**. The relationship between the $\delta^{11}B$ isotopic composition of *D. dianthus* and ambient seawater pH (7.8 to 8.0) is shown in **Table 17-6** and **Figure 17-16**. There is a trend of decreasing $\delta^{11}B$ in *D. dianthus* skeleton with decreasing *in situ* pH. By applying Equation 17.4 (see Section 17.4.2.3.2 for discussion) to the measured $\delta^{11}B$, the $\delta^{11}B$ values are converted to pH_{sw}.

The relationship between the $\delta^{11}B$ isotopic composition of *D. dianthus* and ambient seawater pH (7.8 to 8.0) is shown in **Table 17-6** and **Figure 17-16**. There is a trend of decreasing $\delta^{11}B$ in *D. dianthus* skeleton with decreasing *in situ* pH. By applying Equation 17.4 to the measured $\delta^{11}B$ compositions, $\delta^{11}B$ values are translated to pH_{sw}. Modern *D. dianthus* $\delta^{11}B$ values (23.46‰ to 23.51‰) give seawater pH values of 8.4 when using Equation 17.4, compared with the *in situ* seawater pH = 7.9 (**Table 17-7**). There is an offset of ±0.5 between the *in situ* seawater pH and pH values derived from the pH-$\delta^{11}B$ calibration equation. The subfossil *D. dianthus* $\delta^{11}B$ values (23.51‰ to 29.66‰) when put into the pH- $\delta^{11}B$ calibration equation translate to a pH_{sw} range of 8.40 ± 0.02 to pH = 8.83 ± 0.02.

$$pH = pK_B - \log\left(\frac{\delta^{11}B_{sw} - \delta^{11}B_C}{\alpha_{B3-B4}\, x\, \delta^{11}B_C - \delta^{11}B_{sw} + 1{,}000\, x\, (\alpha_{B3-B4} - 1)}\right)$$ (Equation 17.4)

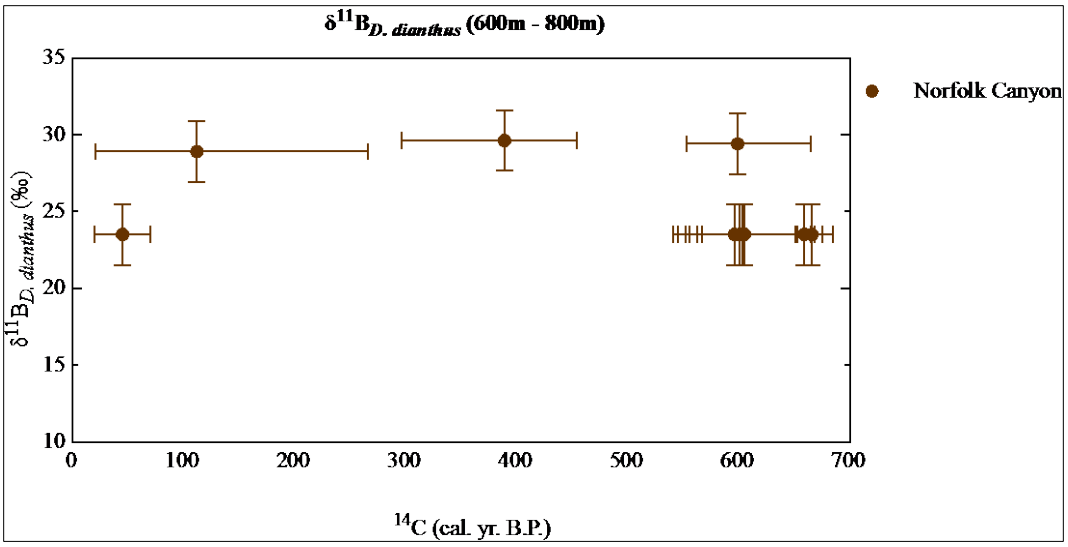

Figure 17-14. Measured $\delta^{11}B$ (‰) for *Desmophyllum dianthus* collected at intermediate depths (600 to 800 m) along Norfolk Canyon (brown closed circles) plotted against the calibrated radiocarbon age of the corals. Error bars on the x-axis represent the calibrated radiocarbon age range, and on the y-axis, the uncertainty of the $\delta^{11}B$ measurements.

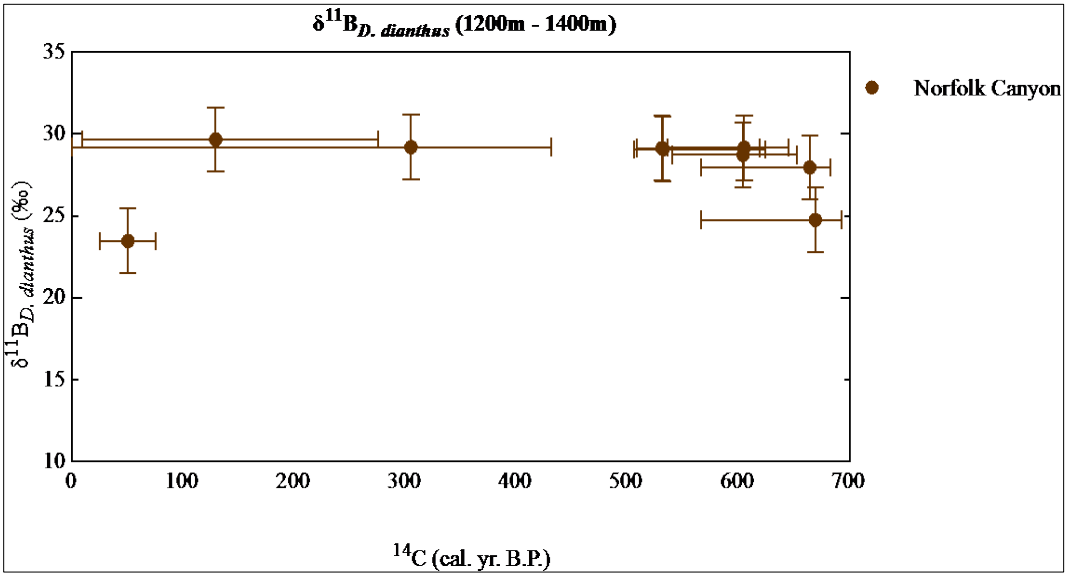

Figure 17-15. Measured $\delta^{11}B$ (‰) for *Desmophyllum dianthus* collected at deepwater depths (1,200 to 1,400 m) in Norfolk Canyon (brown closed circles) plotted against calibrated radiocarbon age of the corals. Error bars on the x-axis represent the uncertainty of the radiocarbon ages, and on the y-axis, the uncertainty of the $\delta^{11}B$ measurements.

Table 17-6. Boron isotopes, boron isotope composition of *Desmophyllum dianthus*, and paleo-pH reconstructed from *D. dianthus*.

Coral ID	Depth (m)	Canyon	Status	^{14}C Age	±	δ^{11}B Carb	STD (n = 2)	pH
RB-686-1	478	Norfolk	Alive	145	30	24.7481	1.98	8.51
RB-686-3/4b	578	Norfolk	Dead	605	30	24.7481	1.98	8.51
RB-686-6	578	Norfolk	Dead	570	30	23.5071	1.98	8.43
RB-687-3	569	Norfolk	Alive	380	25	27.7726	1.97	8.70
NF-20-2	706	Norfolk	Dead	605	30	23.5071	1.98	8.43
NF-20-3	706	Norfolk	Dead	690	30	23.5071	1.98	8.43
NF-20-5	706	Norfolk	Dead	640	35	23.5071	1.98	8.43
NF-20-6	706	Norfolk	Dead	700	25	23.5071	1.98	8.43
NF-20-7	706	Norfolk	Dead	595	25	23.5071	1.98	8.43
NF-20-8	706	Norfolk	Dead	640	25	23.5071	1.98	8.43
NF-20-9	706	Norfolk	Dead	635	30	29.4040	1.97	8.81
NF-20-10	706	Norfolk	Dead	105	25	28.8979	1.97	8.78
NF-20-13	706	Norfolk	Alive	295	25	29.6159	1.97	8.82
RB-687-5	711	Norfolk	Alive	45	25	23.5071	1.98	8.43
RB-685-1	1,328	Norfolk	Dead	515	25	29.1300	1.97	8.79
RB-685-3	1,328	Norfolk	Dead	595	30	28.7078	1.97	8.76
RB-685-4	1,249	Norfolk	Dead	515	30	29.0665	1.97	8.79
RB-685-5	1,251	Norfolk	Dead	260	30	29.1926	1.97	8.80
RB-685-6	1,251	Norfolk	Dead	50	25	23.4557	1.98	8.43
RB-685-7A	1,326	Norfolk	Dead	130	30	29.6577	1.97	8.83
RB-685-8A	1,251	Norfolk	Dead	710	30	24.7481	1.98	8.51
RB-685-8B	1,251	Norfolk	Dead	580	25	29.1503	1.97	8.79
RB-685-9	1,326	Norfolk	Dead	695	25	27.9446	1.97	8.71
NF-17-1 Line 1	690	Baltimore	Alive	45	25	23.5071	1.98	8.43
NF-17-1 Line 2	690	Baltimore	Alive	45	25	23.5071	1.98	8.43
NF-17-4	690	Baltimore	Alive	95	30	23.5071	1.98	8.43
NF-18-3	680	Baltimore	Alive	130	30	23.5071	1.98	8.43

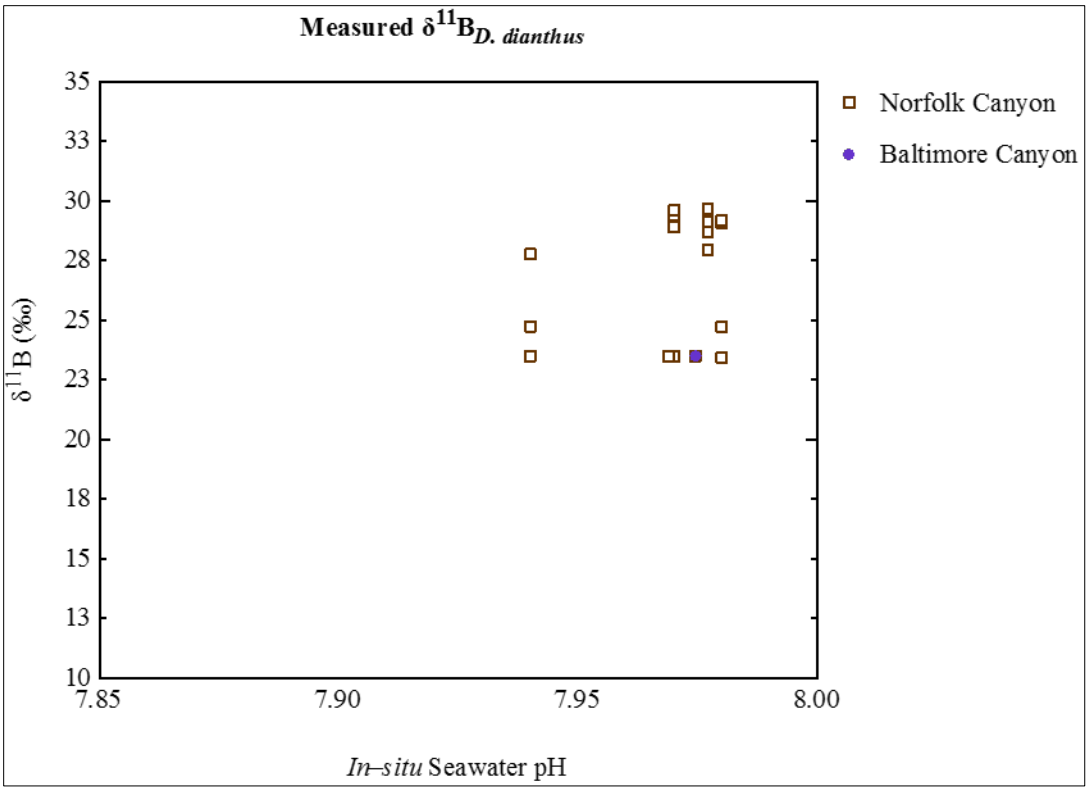

Figure 17-16. *Desmophyllum dianthus* $\delta^{11}B$ versus pH measurements made on water samples collected near to the depths at which the corals were collected. Specimens were collected in Norfolk Canyon (brown open squares) and Baltimore Canyon (purple closed circles).

Table 17-7. *In situ* pH and aragonite saturation state compared with $\delta^{11}B$ reconstructed pH at Baltimore and Norfolk canyons.

Coral ID	Depth (m)	Canyon	14C Age	±	Measured δ11B	±	Reconstructed pH	Salinity	Temp. (°C)	In Situ pH	Ωarag	TA (µmol kg-1)
RB-687-5	711	Norfolk	45	25	23.5071	0.02	8.43	35.00	5.42	7.97	1.37	2,314.89
RB-685-6	1,251	Norfolk	50	25	23.4557	0.02	8.43	34.97	4.32	7.98	1.30	2,308.21
NF-17-1 line 1	690	Baltimore	45	25	23.5071	0.02	8.43	34.99	4.91	7.97	1.36	2,310.30
NF-17-1 line 2	690	Baltimore	45	25	23.5071	0.02	8.43	34.99	4.91	7.97	1.36	2,310.30
NF-17-4	690	Baltimore	95	30	23.5071	0.02	8.43	34.99	4.91	7.97	1.36	2,310.30

$\Omega_{arag} = \Omega_{aragonit;}$ TA = total alkalinity.

17.3.3 Chemosynthetic Communities Results

17.3.3.1 X-Ray Diffraction and Petrography

Calcium carbonate ($CaCO_3$) dominates the authigenic carbonate samples (48% to 97%) but not the surrounding sediment (3% to 14%) (**Table 17-8**). Aragonite accounts for more than 60% of the groundmass and up to 99% of the carbonate cement (**Figure 17-17**), with secondary amounts (<15%) of low- and high-Mg calcite present, creating an aragonite-cemented intraclast breccia at both sites (**Figure 17-18**). The detrital fraction consists of poorly sorted accessory minerals such as quartz, feldspar, plagioclase, and pyroxene that form a matrix supported in a clay to silt-size sediment, consistent with grain size from the surrounding sediment. The clasts are subrounded to very angular, particularly in the

Baltimore Canyon specimen (**Figure 17-18**). Voids between intraclasts and bivalve shells are completely or partially filled with fibrous or bladed aragonite, showing multiple generations of mineral growth. Fractures intersect well-developed radiating crystals of aragonite in the Baltimore Canyon sample. Bioclasts were observed in both samples as intact shells, aragonite filled, or skeletal molds. The organic carbon (C_{org}) content of the authigenic carbonates was <0.4%, reflecting the dilution by the cement relative to the surrounding sediment (**Table 17-8**). The shell carbonate was dominated by aragonite and/or calcite with $CaCO_3$ ranging from 95% to 97% and C_{org} <0.1%.

Table 17-8. Mineralogy (dominant carbonate phase), stable isotope, percent calcium carbonate, and total organic carbon of authigenic carbonate cement and groundmass and sediment collected at the Baltimore and Norfolk Canyon seep sites. (Values in parentheses indicate standard deviation.)

Parameter	Sediment		Cement		Groundmass	
	Norfolk Canyon	Baltimore Canyon	Norfolk Canyon	Baltimore Canyon	Norfolk Canyon	Baltimore Canyon
Mineral	–	–	Aragonite	Aragonite	Aragonite	Aragonite
$\delta^{13}C$ (‰)	-31.9 (9.0)	-23.4 (3.0)	-47.3 (0.16)	-49.2 (0.21)	-44.3 (0.07)	-47.7 (0.92)
$CaCO_3$ (%)	13.9 (6.5)	3.3	97.2	85.1	72.5	47.6
C_{org} (%)	3.7 (1.4)	0.64 (0.14)	0.16	0.28	0.27	0.39
$\delta^{18}O$ (‰)	–	–	3.84 (0.07)	4.35 (0.06)	3.78 (0.03)	3.54 (0.04)

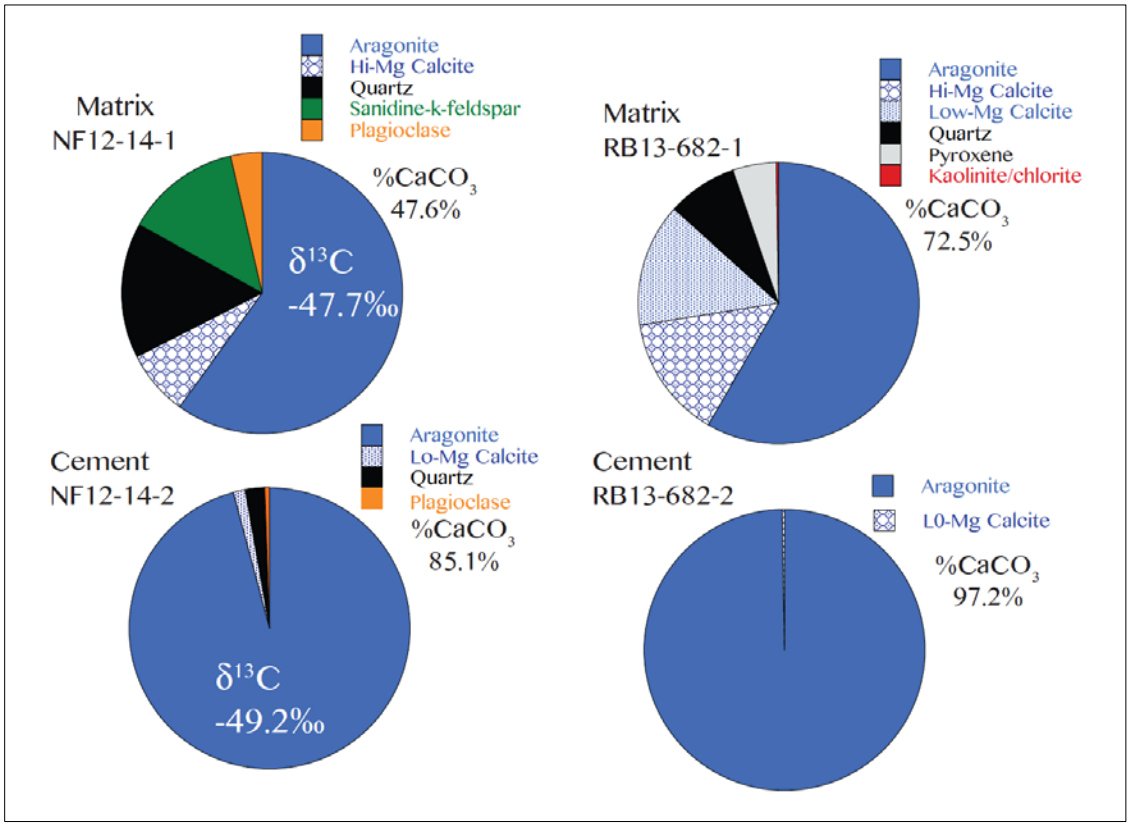

Figure 17-17. Mineralogic composition of authigenic carbonates from the cement and matrix portions for the authigenic samples collected from Baltimore Canyon seep site (NF-2012-14) and the Norfolk Canyon seep site (RB-2013-682) based on x-ray diffraction analysis. Stable carbon ($\delta^{13}C$) and percent CaCO3 are indicated on the respective components.

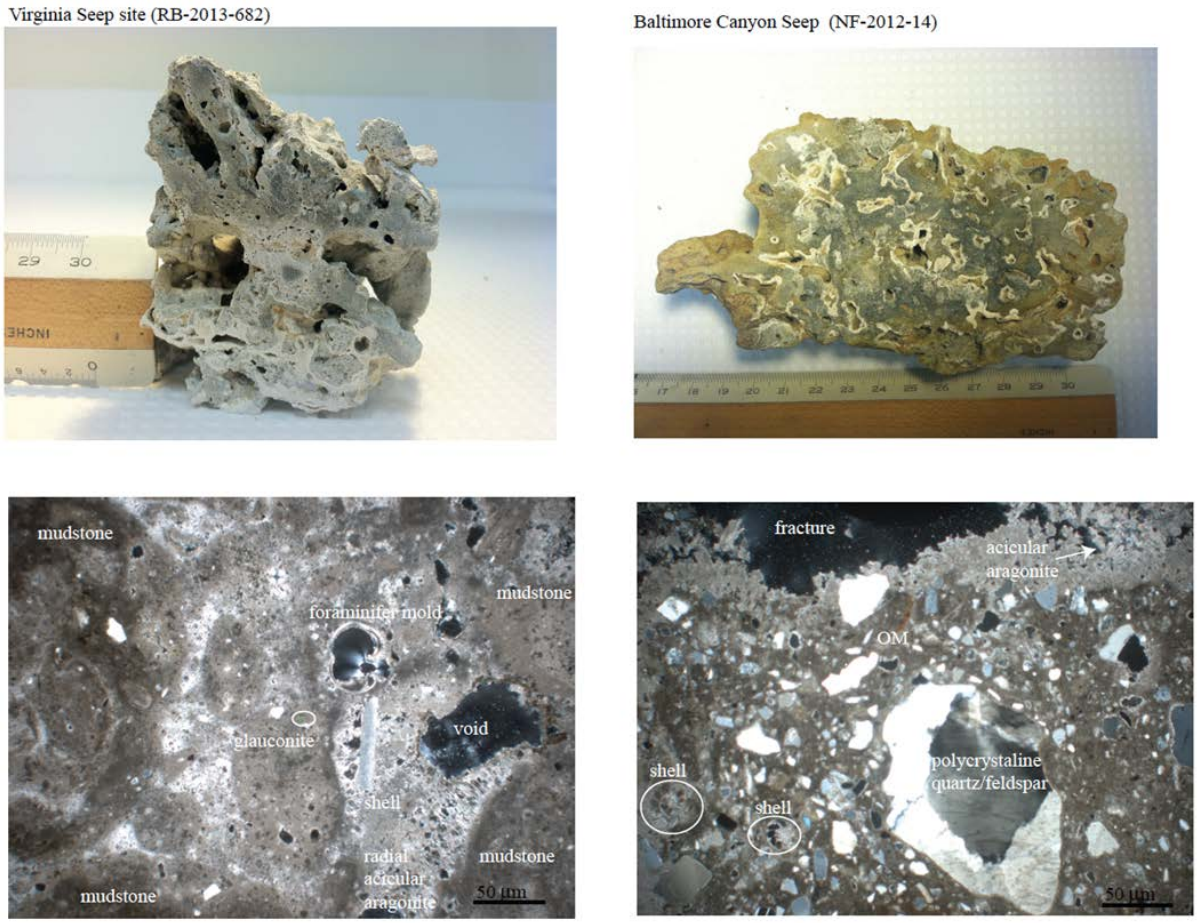

Figure 17-18. Photographic and petrographic thin section images (plane polarized light; 40×) of authigenic carbonates sampled at the Norfolk Canyon seep site (dive RB-2013-682) and Baltimore Canyon seep site (dive NF-2012-14). Infilling of voids by acicular aragonite, detrital grains, organic matter (OM), and bioclasts are noted in the matrix-supported clay to silt-size aragonite-dominated breccia.

17.3.3.2 Strontium Isotopes

The strontium isotope ($^{87}Sr/^{86}Sr$) compositions of the authigenic carbonates and mussel shells were investigated to constrain the fluid source and flow pathway for carbonate precipitation (Sample et al. 1993, Sample and Reid 1998). $^{87}Sr/^{86}Sr$ ratios for the authigenic carbonates, mussel shells, and water samples ranged from 0.70915 to 0.70924 (**Tables 17-9** and **17-10**). The average authigenic carbonate (n = 4) and mussel shell (n = 2) $^{87}Sr/^{86}Sr$ ratios at both sites were equivalent, 0.70920 (SD 3) × 10^{-5} and 0.70920 (SD 2) × 10^{-5}, respectively. In comparison, the average seawater (n = 6) $^{87}Sr/^{86}Sr$ ratio was 0.70917 (SD 2) × 10^{-5} but was not statistically different (Student's t-test; $P > 0.05$) from the authigenic carbonate and shell samples

Table 17-9. Isotope compositions, ages, and U-Th concentrations of bulk authigenic carbonates; conventional radiocarbon (^{14}C) age (years); corrected uranium-thorium derived age (years); initial $^{234}U/^{238}U$ ratio. Average and standard deviations (in parentheses) are reported except for ^{14}C age where age error is reported. Ranges of values are also reported as minimum and maximum values, and average ± 1 standard deviation. *Results for individual samples are presented in **Appendices 17-B** and **17-C**.

Parameter	Authigenic Carbonate	
	Norfolk Canyon	Baltimore Canyon
$\delta^{13}C$ (‰)	-45.51 (1.66) (*n* = 5)	-48.43 (1.02) (*n* = 4)
Min	-47.44	-49.33
Max	-44.23	-47.03
$\delta^{18}O$ (‰; *n* = 3)	3.80 (0.05) (*n* = 5)	3.95 (0.47) (*n* = 4)
Min	3.75	3.51
Max	3.89	4.39
$\Delta^{14}C$ (‰; *n* = 2)	-894 (11) (*n* = 4)	-878 (119) (*n* = 3)
Min	-908	-959
Max	-883	-740
^{14}C age (years)*	–	–
Min	17,200	10,770
Max	19,120	25,570
$^{87}Sr/^{86}Sr$	0.70919 (*n* = 2)	0.70921 (*n* = 2)
Min	0.70917	0.70918
Max	0.70920	0.70924
U-Th age (years)*	–	–
Min	1,810	14,880
Max	4,870	16,255
$^{234}U/^{238}U$	1.1468 (0.0013) (*n* = 5)	1.1486 (0.0005) (*n* = 5)
Min	1.1455	1.1480
Max	1.1482	1.1492
U (ppm)	3.6 (0.4) (*n* = 5)	4.3 (0.3) (*n* = 5)
Min	3.2	3.9
Max	4.2	4.6
Th (ppm)	0.19 (0.08) (*n* = 5)	0.37 (0.14) (*n* = 5)
Min	0.06	0.24
Max	0.27	0.59

17.3.3.3 Stable Carbon, Oxygen, and Sulfur Isotopes

At the Norfolk seep site, shells from both living and dead specimens yielded average $\delta^{13}C$ values of -2.59‰ (SD 1.68; *n* = 34) and -7.10‰ (SD 3.20; *n* = 16), respectively, and an average $\delta^{18}O$ value of 3.71‰ (SD 0.25; *n* = 34) and 3.82‰ (SD 0.39; *n* = 16), respectively (**Table 17-10**). No statistical difference (Student's *t*-test, $P > 0.05$) exists between shell $\delta^{18}O$ values of dead and living specimens; however, shells from living mussels were significantly enriched in ^{13}C relative to fossil specimens (Student's *t*-test, $P < 0.05$). Only shells from live mussel specimens were analyzed from the Baltimore Canyon seep site and yielded average shell $\delta^{18}O$ and $\delta^{13}C$ values of 2.57‰ (SD 0.28) and -6.84‰ (SD 1.97) (*n* = 30), respectively. At both sites, the shell $\delta^{13}C$ values were lighter relative to bottom water DIC $\delta^{13}C$ values (0.90‰ [SD 0.05]), but heavier relative to the regional methane $\delta^{13}C$ value (-68‰; Pohlman, pers. comm.). Baltimore Canyon shells were significantly heavier in $\delta^{13}C$ and $\delta^{18}O$, by ~4‰

and ~1‰, respectively, relative to shells from the Norfolk seep site. Shells also were enriched in ^{18}O relative to ambient seawater, where bottom water $\delta^{18}O$ values from the Norfolk and Baltimore canyon seep sites were 0.34‰ and 0.53‰, respectively.

Table 17-10. Geochemical composition of the *Bathymodiolus* shell carbonate and periostracum material and seawater for carbon, oxygen, and radiocarbon isotopes, radiocarbon (^{14}C) age (years); strontium isotope ratios for samples collected only at Norfolk. Average and standard deviations (in parentheses) are reported except for ^{14}C age where age error is reported. Ranges of values are also reported as minimum and maximum values.

Parameter	Mussel				Seawater	
	Carbonate Shell			Periostracum		
	Norfolk Canyon		Baltimore Canyon	Norfolk Canyon	Norfolk Canyon	Baltimore Canyon
	Live Specimen	Fossil Specimen				
$\delta^{13}C$ (‰)	-2.59 (1.68)	-7.10 (3.20)	-6.84 (1.97)	-56.99 (12.8)	0.90 (0.06)	–
Min	-6.53	-16.74	-10.91	-70.66	0.86	–
Max	0.19	-3.34	-3.39	-29.92	0.94	–
$\delta^{18}O$ (‰)	3.71 (0.25)	3.82 (0.39)	2.57 (0.28)	–	0.34 (0.1)	0.53 (0.1)
Min	3.11	3.46	2.06	–	–	–
Max	4.19	5.13	3.59	–	–	–
$\Delta^{14}C$ (‰)	-115 (3)	-160 (39)	-160 (52)	–	-24.17 (0.62)	–
Min	-117	-226	-220	–	-24.6	–
Max	-113	98	-129	–	-23.73	–
^{14}C age (years)	920 (20)	1,345 (20)	1,350 (20)	–	135 (7)	–
Min	905	765	1,045	–	130	–
Max	940	1,995	1,935	–	140	–
$^{87}Sr/^{86}Sr$	0.70920	–	–	–	0.70917	–
Min	0.70918	–	–	–	0.70915	–
Max	0.70921	–	–	–	0.70920	–

"–" indicates that either no samples were collected or analyses were not possible because of sample/specimen size limitations."

Shell isotopic variability over the lifespan of an individual specimen was calculated as the standard deviation (n = 8 to 12) stable isotope values from material collected along a transect from the umbo to the ventral margin. Variability ranged from 0.11‰ to 0.56‰ and 0.69‰ to 3.57‰ for shell $\delta^{18}O$ and $\delta^{13}C$ values, respectively. On average, lifespan $\delta^{18}O$ and $\delta^{13}C$ variability was 0.24‰ and 1.49‰, respectively. Lifespan variability represented <10% of the average shell $\delta^{18}O$ signature at both sites, but up to 42% of the average shell $\delta^{13}C$ signal at the Norfolk Canyon seep site and 21% at the Baltimore Canyon seep site. The mussel periostracum $\delta^{13}C$ signature from samples collected at the Norfolk seep site ranged from -70.66‰ to -29.92‰ (n = 40), with an average of -56.99‰ (SD 12.85) (**Table 17-10**). Mussel periostracum from the Baltimore Canyon seep site was not analyzed because sample preservation in ethyl alcohol precludes reliable $\delta^{13}C$ results.

The $\delta^{13}C$ signatures of the bulk authigenic carbonate from Baltimore and Norfolk canyon seep sites were -45.51‰ (SD 1.66; n = 5) and -48.43‰ (SD 1.02; n = 4), respectively (**Table 17-9**). However, compared with cement, the groundmass $\delta^{13}C$ values were heavier by 1‰ to 3‰ (**Table 17-8**). The bulk $\delta^{18}O$ values were similar between the sites, 3.80‰ (SD 0.05; n = 5) for Norfolk seep and 3.95‰ (SD 0.47; n = 4) for Baltimore Canyon seep with <1‰ difference between the groundmass and cement (**Table 17-8**). Authigenic carbonate $\delta^{18}O$ values were heavier (~3‰) relative to bottom water $\delta^{18}O$ values.

Sulfur ($\delta^{34}S$) isotopes were analyzed from *Bathymodiolis* gill tissues collected at each site. Gill $\delta^{34}S$ values ranged from -4.07‰ to 21.55‰ (**Table 17-11**), with no statistical difference between the sites

(Student's *t*-test, $P > 0.05$); however, the range of gill $\delta^{34}S$ values at Baltimore Canyon displayed a larger range compared with the Norfolk Canyon seep site, from -4.07‰ to 18.13‰ compared with 8.65‰ to 21.55‰. Periostracum $\delta^{34}S$ values from the Norfolk seep site were similar to gill $\delta^{34}S$ values, ranging from 8.82‰ to 22.65‰, averaging 16.63‰ (SD 4.01; $n = 28$). Overall, the gill and periostracum $\delta^{34}S$ values were heavier relative to typical hydrogen sulfide values (Michener and Schell 1994) and lighter relative to seawater sulfate (+20‰; Heyl et al. 2007). Seep sediment $\delta^{34}S$ values from the Norfolk seep site were heavier relative to hydrogen sulfide and lighter relative to seawater sulfate, with an average $\delta^{34}S$ value of 5.53‰ (SD 2.16; $n = 4$) at Norfolk and 2.42‰ (SD 3.62; $n = 5$) at Baltimore Canyon (**Table 17-11**).

Table 17-11. Sulfur isotope (per mil $\delta^{34}S$) for sediment samples and mussel gill and periostracum from *Bathymodiolus* specimens collected at Baltimore and Norfolk canyon seep sites. The average, standard deviation (in parentheses), and ranges of $\delta^{34}S$ values are reported.

Parameter	Gill		Periostracum		Sediment	
	Norfolk Seep	Baltimore Canyon	Norfolk Seep	Baltimore Canyon	Norfolk Seep	Baltimore Canyon
Average (±σ)	16.58 (3.37)	14.38 (5.15)	16.63 (4.01)	13.89 (1.24)	5.53 (2.16)	2.42 (3.62)
Range	8.65 to 21.55	-4.07 to 18.13	8.82 to 22.65	13.01 to 14.77	2.98 to 8.20	-2.62 to 6.30
n	23	20	28	2	4	5

17.3.3.4 Authigenic and Mussel Shells Radiocarbon

Authigenic carbonates were significantly depleted in ^{14}C, with $\Delta^{14}C$ values ranging from -960‰ to -740‰ with corresponding ^{14}C ages of 25,570 (SD 210) to 10,770 (SD 35) ^{14}C years (**Table 17-9**). The ^{14}C ages of mussel shells on the seabed were younger relative to the authigenic carbonate age (**Appendix 17-B**). The ^{14}C age of the mussel shells derived from living specimens varied from 905 (SD 20) to 1,935 (SD 20) ^{14}C years, and the average ^{14}C age of mussel shells derived from fossil specimens at the Norfolk seep site was 1,346 (SD 20) ^{14}C years (**Table 17-10**). There was no statistical difference (Student's *t*-test, $P > 0.05$) between fossil shell specimens that were pretreated with 10% HCl and those left untreated (**Appendix 17-B**), yielding an average ^{14}C age of 1,178 ^{14}C years and indicating that secondary aragonite and calcite are negligible.

17.3.3.5 U-Th Age Calculation

Authigenic carbonate cement samples contained 3.2 to 4.6 ppm U, and 0.06 to 0.59 ppm Th. The $^{230}Th/^{232}Th$ activity ratios were between 2.2 and 8.6, spanning a range similar to that of other occurrences of methane-related authigenic carbonates (Teichert et al. 2003, Bayon et al. 2009, Crémière et al. 2013, Feng et al. 2015). At each seep site, five U-Th ages were calculated from the carbonate cement of the authigenic carbonates (**Appendix 17-C**). The U-Th ages from Norfolk, corrected for initial ^{230}Th introduced by the incorporated detrital material, range from 1.81 (SD 0.81) to 4.87 kiloannum (ka) (SD 1.44). In comparison, the corrected U-Th ages of the Baltimore Canyon authigenic carbonate were older, ranging from 14.88 ka (SD 1.09) to 16.25 ka (SD 2.73)(**Table 17-9**) (Prouty et al. 2016).

17.4 DISCUSSION

17.4.1 Seawater Chemistry Discussion

The biolimiting nutrients, including nitrate, phosphate, and dissolved silicon, are depleted in the upper surface waters of Baltimore and Norfolk canyons. These results are consistent with the physical and biological processes responsible for their removal within the nutricline such as the growth of phytoplankton. Given the similarity between the individual depth profiles down canyon, the nutricline

appears to be homogenous along the length of each canyon with little spatial variability away from the head of the canyon. The consistent surface water depletions suggest little if any upwelling during the 2012 and 2013 sampling periods. This is captured in the 2-D profiles where the stratified structure in the nutrient data is consistent along the length of each canyon (**Figure 17-19**). In both canyons, the nutricline mimics the thermocline pattern. However, the nutrient profiles between the canyons differ slightly. The nutricline in Baltimore Canyon is approximately 100 m shallower relative to Norfolk Canyon. However, this may be a seasonal artifact where mixing at the end of the summer results in shoaling of the thermocline and a shallower mixed-layer depth. The overall pattern in both canyons, however, agrees with those derived from Ocean Data Viewer (latitude 38°23.24, longitude 73°49.36; Reimer et al. 2002) for vertical nitrate and phosphate profiles (**Figure 17-20**). The interaction between phytoplankton growth (i.e., nutrient uptake) is illustrated in the inverse relationship between the nutrient and O_2 profiles (**Figure 17-6**).

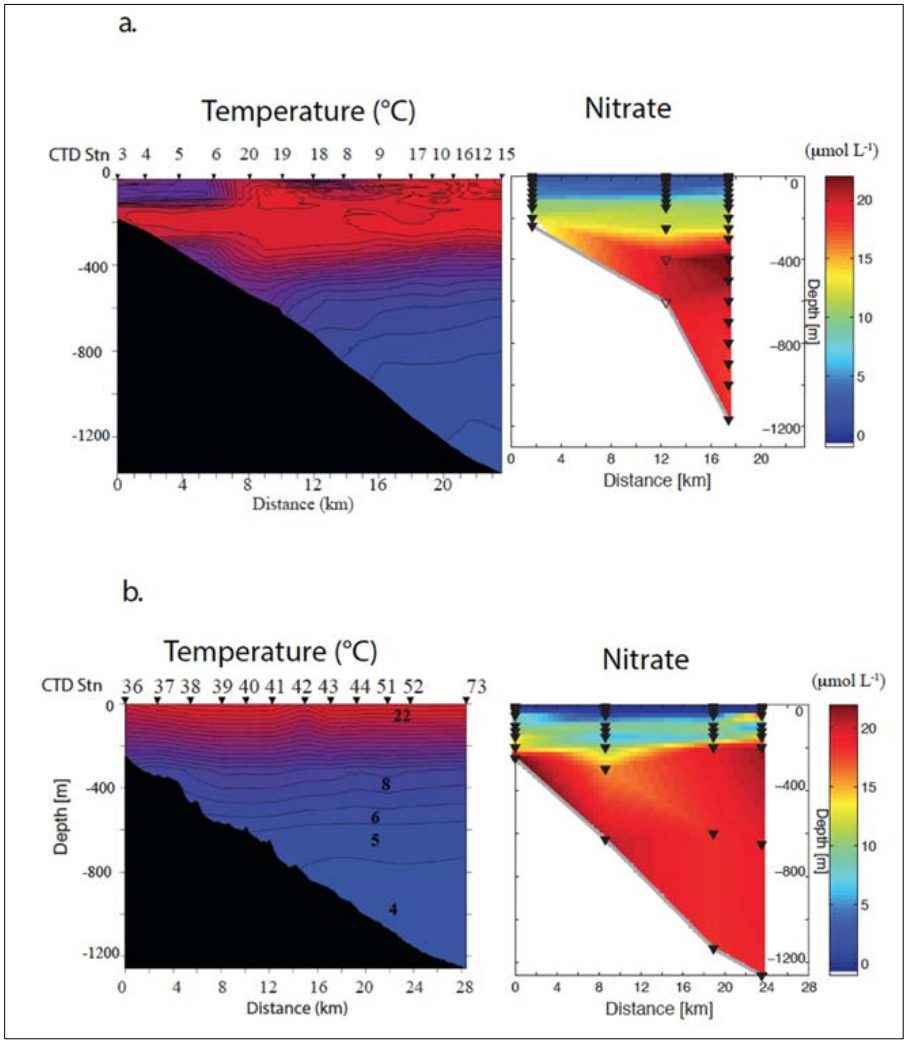

Figure 17-19. Extrapolated 2-D nutrient profile (nitrate [µmol L^{-1}]) compared with down-canyon temperature profile derived from CTD casts from (a) Norfolk Canyon and (b) Baltimore Canyon from three individual stations (black triangles).

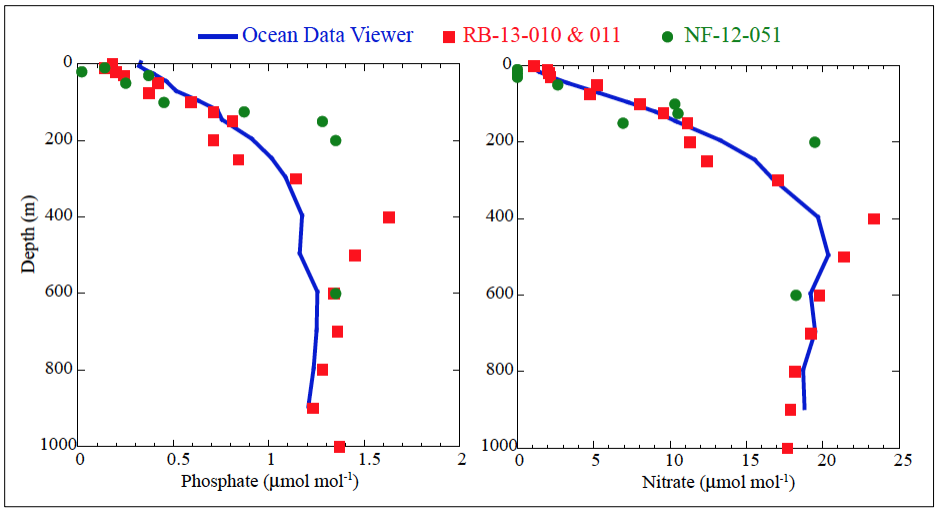

Figure 17-20. Comparison of nitrate and phosphate vertical profiles from Baltimore Canyon (NF-12-051) and Norfolk Canyon (RB-13-010 and RB-13-011) relative to those derived from Ocean Data Viewer (Schlitzer 2015) and World Ocean Atlas data.

The enriched $\Delta^{14}C$ signature of surface water DIC (>20‰) implies recent (i.e., decades) exchange with atmospheric CO_2. Despite depleted $\Delta^{14}C$-DIC values at depth, there is evidence of bomb-^{14}C[1] below the mixed-layer depth; $\Delta^{14}C$-DIC values are greater than -70‰ through the water column. According to the radiocarbon data, there is little if any evidence to support the intrusion of deep water into Norfolk Canyon nor is there evidence of upwelling within the canyon during the 2013 sampling period. In addition, the steep gradient in $\Delta^{14}C$-DIC at the base of the thermocline suggests little vertical exchange between surface and deeper waters, indicative of a highly stratified system. However, there is some indication of a freshwater influence with the temperature 2-D plots capturing a low temperature lens to a depth of 100 m near the head of the canyon (**Figure 17-20**). This area is also marked by lighter $\Delta^{14}C$ values in the surface (**Figure 17-21**), which are depleted by ~30‰ relative to the down-canyon surface samples. This difference may be indicative of freshwater input from the east bringing ^{14}C -depleted water (e.g., river water transported across the shelf) (Raymond and Bauer 2001). Phosphate is also enriched in this shallow, up-canyon cast as well (**Figure 17-6**). Results presented from Norfolk Canyon are consistent with those obtained from previous studies in the Mid-Atlantic Bight region (e.g., Bauer et al. 2001). Radiocarbon and nutrient data define two water masses in the canyons: an upper water mass forming the bottom of the thermocline and in exchange with the atmosphere, and a second mass forming the deeper zone, with the later characterized by depleted $\Delta^{14}C$-DIC values and enriched nutrient concentrations and little if any mixing within this deeper zone.

[1] Bomb-^{14}C refers to the addition of anthropogenic radiocarbon to the atmosphere and ocean surface as a result of thermonuclear weapons testing in the late 1950s and early 1960s.

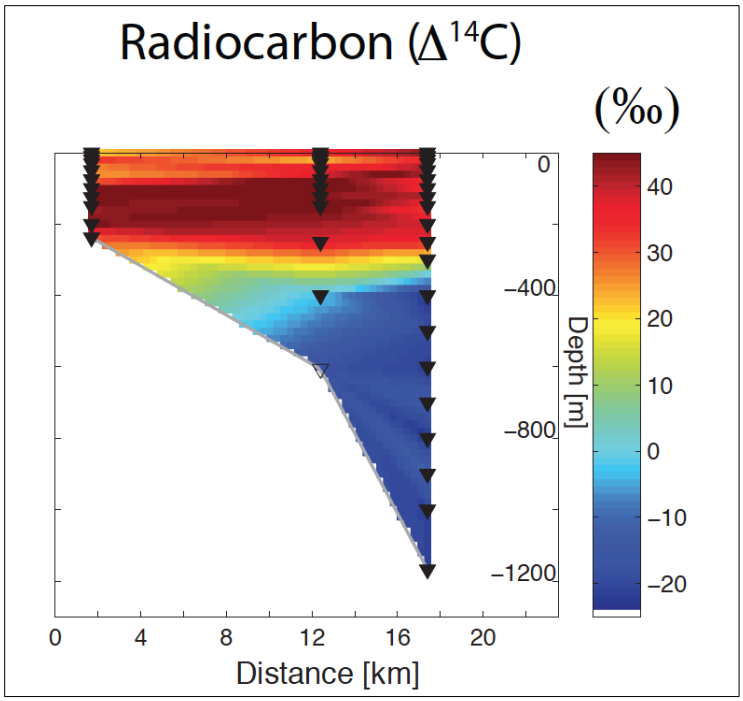

Figure 17-21. Extrapolated radiocarbon (Δ^{14}C-DIC) profile for Norfolk Canyon based on discrete water column data from three individual stations (black triangles).

In Baltimore Canyon, the CTD data captures a distinct turbidity zone between 400 and 800 m, and a second small turbid patch in the surface water near the canyon wall (8 km down canyon). The 400 to 800 m region contains a "nepheloid" layer (see **Chapter 5** for further discussion). Particulate (>0.45 µm) trace element concentrations show enrichment in the nepheloid layer in both canyons as well as elevated trace element concentrations from surface samples near the canyon wall. The 2-D profiles of the particulate trace metals capture the nepheloid layer and small surface enrichment (**Figure 17-22**). Whereas the turbidity data show the nepheloid layer detaching from the canyon wall (most likely as it encounters a high density water layer), the coarse CTD sampling for trace metals suggests the nepheloid layer continues downstream and at depth. Profiles conducted at deeper canyon depths were similar to the shelf profiles where bottom shear stresses are most likely not sufficient to suspend sediment. The distribution of dissolved nutrient and isotope data, as well as particle elemental composition in the water column, captures the interplay between the physical oceanography and the biological processes occurring within the canyons.

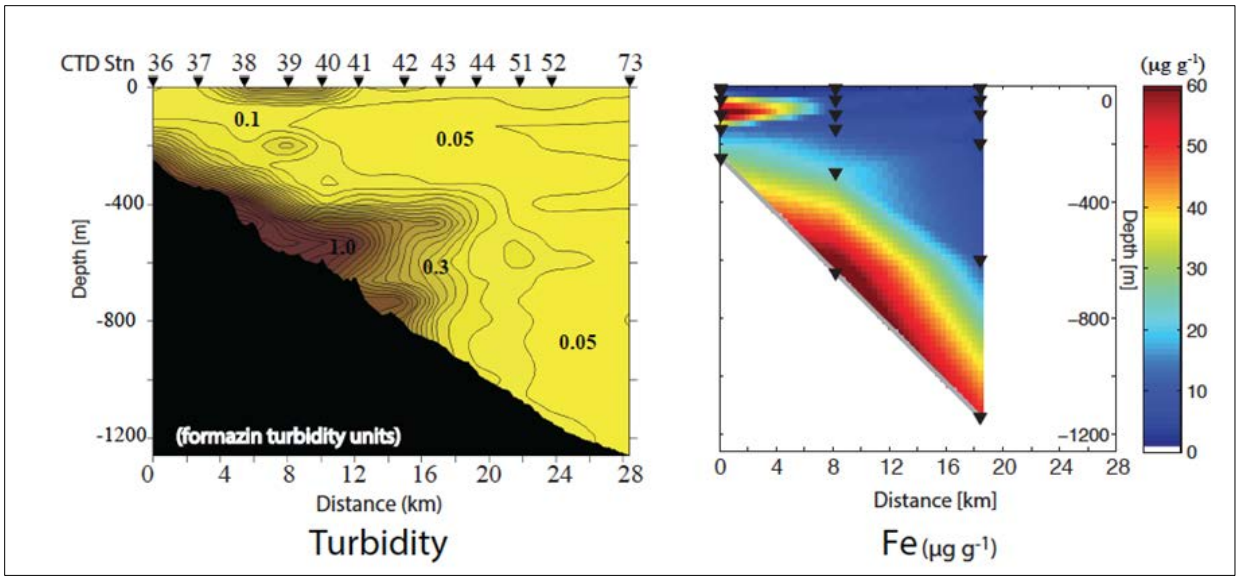

Figure 17-22. Baltimore Canyon turbidity (formazin turbitiy units) compared with extrapolated trace element (iron [Fe], µg g^{-1}) from three individual stations (black triangles).

17.4.2 Deepsea Coral Discussion

17.4.2.1 Radiocarbon Dating of Desmophyllum dianthus

The measured ^{14}C age can be converted to a calendar age using the CALIB program (Reimer et al. 2009; Stuiver and Reimer 1993, version 7.1) and by using Marine Reservoir Correction Database (MARINE13) to correct for regional variation in the marine reservoir age, ΔR (Reimer et al. 2013, Stuiver and Braziunas 1993). The ΔR is the difference between the modeled global surface ocean reservoir age (~400 ^{14}C years) and the regional surface ocean reservoir age (Stuiver et al. 1986). Bomb ^{14}C can be used to determine regional ΔR (Ingram and Southon 1996, Bondevik et al. 1999, Guilderson et al. 2005) and to establish age or validate skeleton chronologies in DSCs (Kerr et al. 2005, Roark et al. 2006). In this study, the radiocarbon dating method was used to date a large number of *D. dianthus* collected from Baltimore and Norfolk canyons to determine if there is any bomb carbon in the modern, living corals in order to calculate growth rates and life spans. All the radiocarbon ages are expressed as the median probability age (**Table 17-3**). Bomb carbon was not found in any of the modern *D. dianthus*, thus it was not possible to determine growth rates or life spans of individual corals using that method and radiocarbon age uncertainties preclude any meaningful lifespan determinations.

Ten modern and subfossil *D. dianthus* specimens collected between 400 and 600 m had radiocarbon ages of 10 to 60 cal. y B.P. for the modern live collected specimens while the subfossil specimens had radiocarbon ages of 545 to 653 cal. y B.P. (**Figure 17-23**) (refer to **Table 17-3** for uncertainties). *Desmophyllum dianthus* specimens collected in Norfolk and Baltimore canyons across a depth range of 600 to 800 m were radiocarbon dated (**Figure 17-24**). The *D. dianthus* specimens from Baltimore Canyon ranged in age from modern to 300 cal. y B.P., and the age of Norfolk Canyon specimens ranged from modern to 800 cal. y B.P. In Baltimore Canyon, the ages of the three *D. dianthus* specimens collected ranged from 20 to 275 cal. y B.P. At Norfolk Canyon, the age distribution ranged from 20 to 760 cal. y B.P. The difference in the age distribution between the two sites is likely due to the small number of samples (n = 3) collected in Baltimore Canyon compared with Norfolk Canyon (n = 14) where more specimens lead to a greater age distribution.

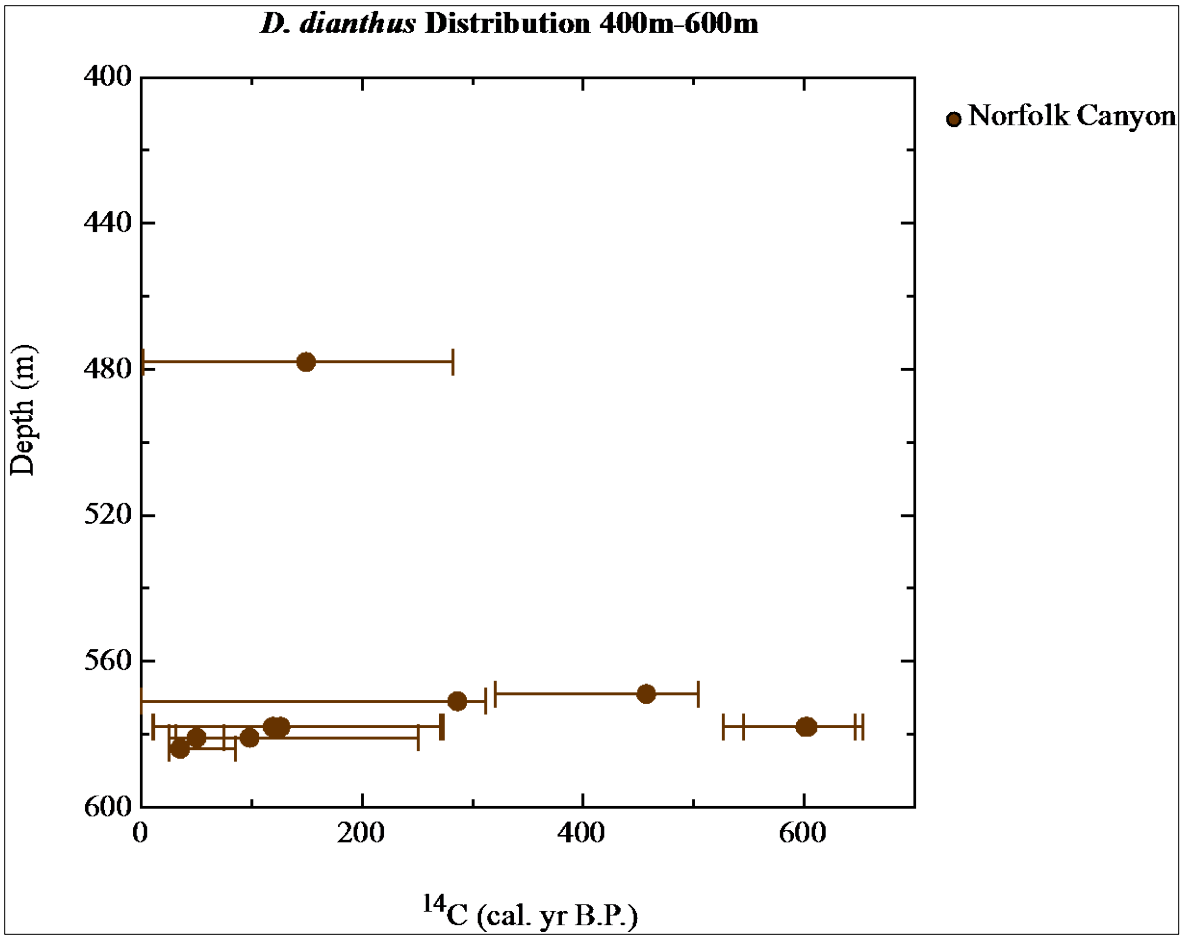

Figure 17-23. Calibrated radiocarbon ages (median probability age) of modern and subfossil *Desmophyllum dianthus* collected at intermediate depth ranges of 400 to 600 m in Norfolk Canyon (brown filled circles) showing the distribution of coral ages. Error bars for the corals are based on the calibrated minimum and maximum age of each specimen.

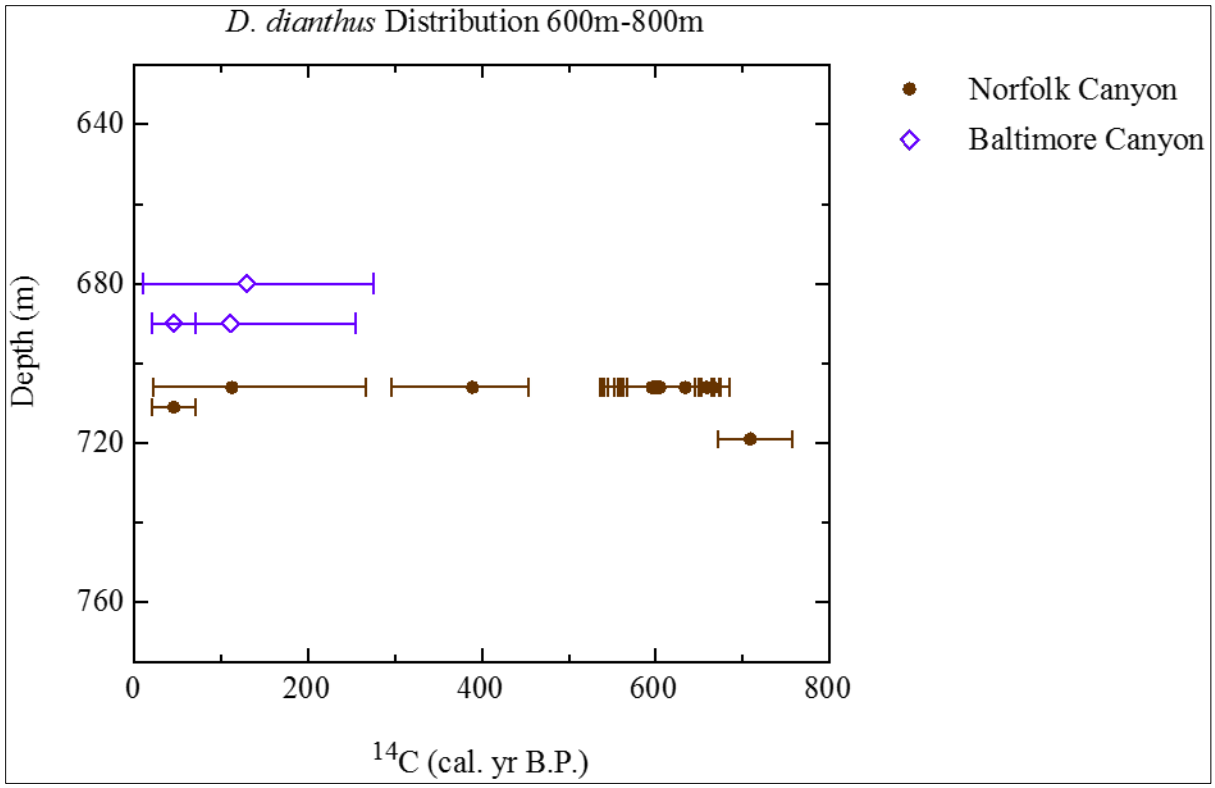

Figure 17-24. Calibrated radiocarbon ages (median probability age) of modern and subfossil *Desmophyllum dianthus* collected between 600 and 800 m in Norfolk Canyon (brown filled circles) and Baltimore Canyon (open purple triangles) showing the distribution of coral ages. Error bars for the corals are based on the calibrated minimum and maximum age of each specimen.

At Norfolk Canyon, 11 modern and subfossil *D. dianthus* specimens were collected at deepwater depths ranging from 1,200 to 1,400 m (**Figure 17-25**). The age distributions of these specimens ranged from 25 to 695 cal. y B.P. When comparing *D. dianthus* from the intermediate depth range with those from deeper water, two observations stand out: 1) there is a greater age range at the deeper depths; and 2) there are two distinct age groupings within the subfossil specimens, one group living from modern to ~300 years ago and the second group living from ~500 to ~700 years ago. None of the deepwater *D. dianthus* specimens from Norfolk Canyon were found to be living between ~300 to ~500 years ago.

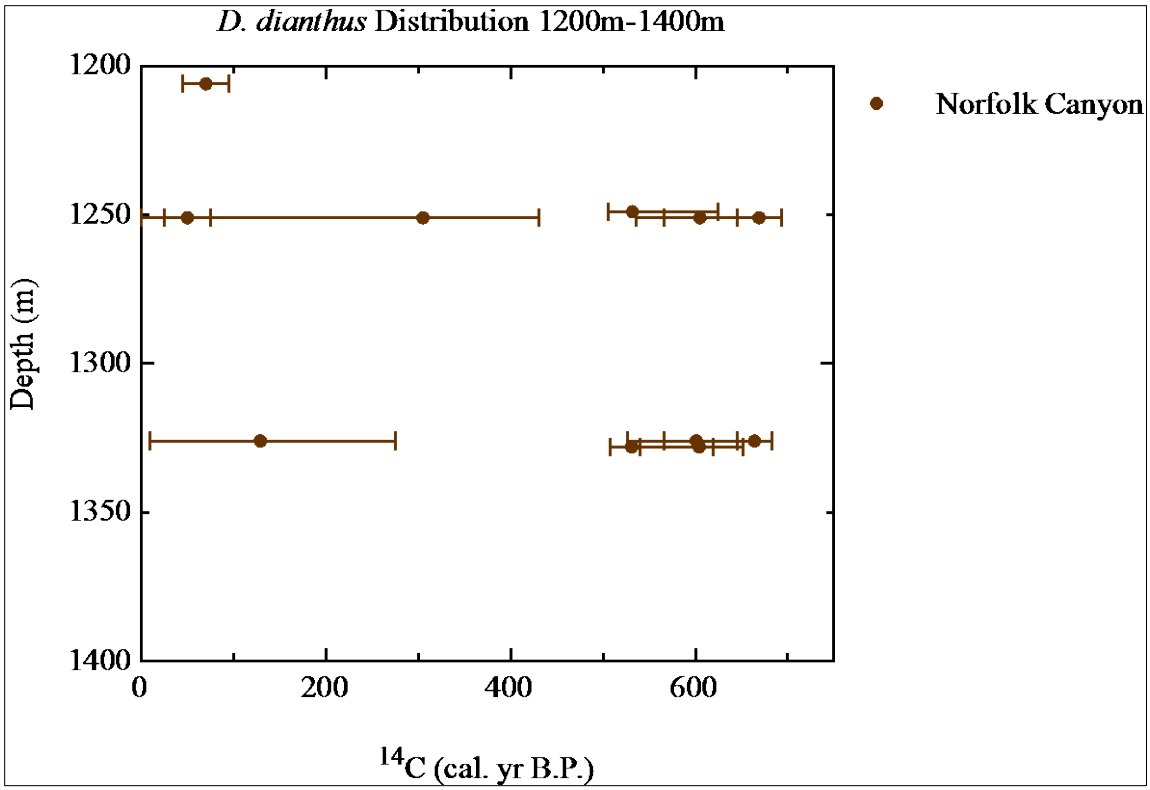

Figure 17-25. Calibrated radiocarbon ages (median probability age) of modern and subfossil *Desmophyllum dianthus* collected between 1,200 and 1,400 m in Norfolk Canyon (brown filled circles) showing the distribution of coral ages. Error bars for the corals are based on the calibrated minimum and maximum age of each specimen.

17.4.2.2 Laser Ablation ICP-MS Trace Elements

Elemental ratios have been explored as an independent means to determine seawater properties and reconstruct the variability of multiple environmental parameters including temperature, pH, nutrients, and carbonate ion system (Montagna et al. 2005). Paleo-proxies derived from the elemental ratios can be used to better determine how these parameters have varied through time at regional and global scales due to the recent efforts in developing methods for elemental and isotopic analyses using DSC skeletons (Adkins et al. 1998, Blamart et al. 2007, Gagnon et al. 2007, Montagna et al. 2006, Sinclair and Risk 2006, van der Flierdt et al. 2006, Anagnostou et al. 2011). *Desmophyllum dianthus* subfossil specimens from the mid-Atlantic canyons have great potential as recorders of intermediate and deepwater environmental variability in this region, especially when using the LA ICP-MS technique, which allows for high-resolution sampling on a scale down to the tens of micrometers on a single *D. dianthus* sample.

Paleo-proxy work has previously been successful using *D. dianthus* archives. This study expands on previously established proxies using a multiple proxy approach to reconstruct multiple environmental variables. Specifically, focusing on assessing nutrient dynamics and the carbonate system in Baltimore and Norfolk canyons back in time using barium to calcium (Ba/Ca) (Hart and Cohen 1996), phosphorus to calcium (P/Ca) (Montagna et al. 2006), and uranium to calcium (U/Ca) (Anagnostou et al. 2011).

17.4.2.2.1 P/Ca Nutrient Proxy

Phosphorus is a biolimiting macronutrient that plays a key role in biological productivity in surface waters (Montagna et al. 2005). Rapidly used by phytoplankton in the surface waters, phosphate is depleted in surface waters and rapidly exported as sinking biomass to the deep ocean (Montagna et al.

2006). In Baltimore Canyon, the measured phosphate concentrations in seawater ranged from 0.01 to 1.45 µmol L^{-1} (**Figure 17-26**) compared with Norfolk Canyon where seawater phosphate ranged from 0.14 to 2.06 µmol L^{-1} (**Figure 17-27**). The full oceanic seawater phosphate range is 0.5 to 3.0 µmol kg^{-1} (Anagnostou et al. 2011); thus, seawater phosphate measured at the canyons falls within the lower to middle part of the global range of seawater phosphate. In the North Atlantic, there is ongoing remineralization of organic particles in the deeper waters that creates variations in the phosphorus content at depth. The variations could be caused by changes in biological productivity and nutrient cycling of surface waters (Montagna et al. 2006).

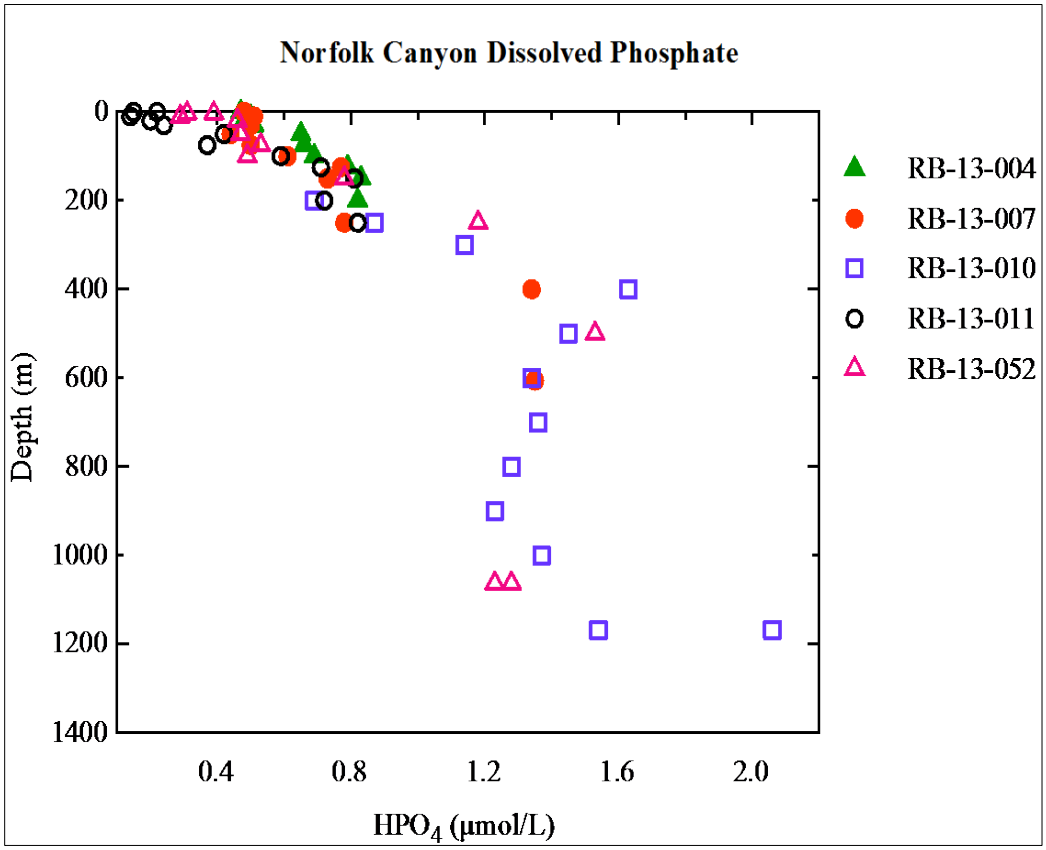

Figure 17-26. Dissolved phosphate concentrations (µmol L^{-1}) in seawater samples from Norfolk Canyon. Seawater samples were collected from five CTD casts during the 2013 sampling cruise in the summer (May). Location of the CTD casts are noted in **Appendix 17-A**.

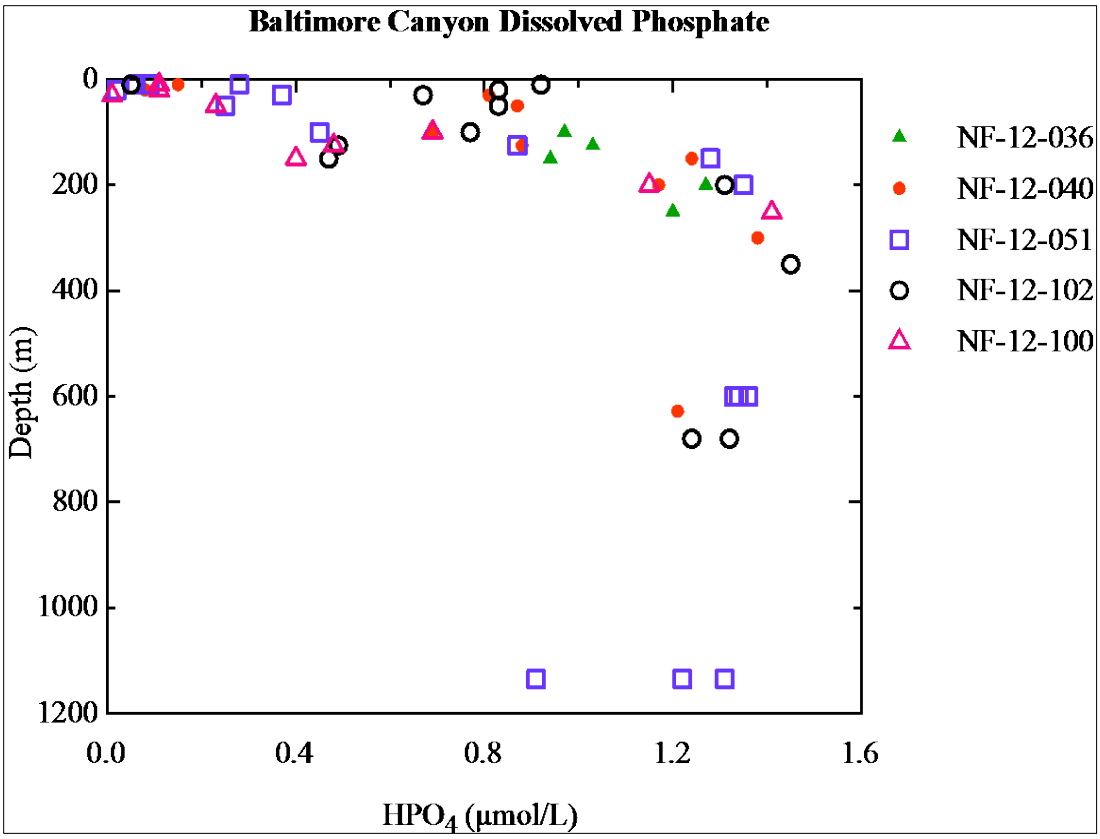

Figure 17-27. Dissolved phosphate concentrations (µmol L^{-1}) in seawater samples from Baltimore Canyon. Seawater samples were collected from five CTD casts during the 2012 sampling cruise in late summer (August). Location of the CTD casts are noted in **Appendix 17-A**.

In this study, the P/Ca ratios were measured along single growth lines from the top of the *D. dianthus* petal for 33 specimens (representing a single time horizon) and along a time-series transect down the growth axis (representing changes over the life span of the specimen) for eight *D. dianthus* using the LA ICP-MS technique (**Figure 17-4** and **17-5**). During laser ablation, uneven surfaces and regions of centers of calcification were avoided as previous research demonstrated anomalous ratios associated with these areas (Montagna et al. 2005).

Incorporation of P/Ca into the skeleton of *D. dianthus* is currently not well understood. Research focusing on using *in situ* seawater dissolved phosphate and P/Ca ratios measured in living corals from one region are necessary to help better understand the incorporation processes, an area where DSC research is currently lacking. Montagna et al. (2005) suggest that a considerable amount of phosphorous is stoichiometrically incorporated within the aragonite of *D. dianthus* skeleton during the crystal growth.

Application of the modern calibration equation published by Montagna et al. (2006) was used because of the strong correlation of seawater phosphate and P/Ca ratios ($r^2 = 0.99$, $P = 0.00001$):

$$\mathrm{DP}(\mu\mathrm{mol\ L^{-1}}) = 1.43(\pm 0.07) \times \mathrm{P/Ca\ (\mu mol/mol)} + 0.13(\pm 0.05) \quad \text{(Equation 17.5)}$$

Applying this calibration equation, the P/Ca (nutrient) ratios measured in the *D. dianthus* specimens yield dissolved seawater phosphate values of 0.24 to 1.70 µmol L^{-1}, which fall in line with seawater measured values of 0.1 to 2.5 µmol L^{-1}, demonstrating the utility of using P/Ca as a nutrient paleo-proxy. However, previous studies did not have ambient seawater measurements from the direct location of where the corals were collected to develop their calibration equations, which may explain some or all of the offset between the calculated and measured seawater phosphate values. Thus, a calibration equation

correlating *in situ* measured seawater phosphate with P/Ca ratios measured in the coral skeleton was generated using four modern *D. dianthus* and *in situ* seawater collected from Norfolk Canyon (0.14 to 2.06 µmol L^{-1}). One modern sample was excluded from our results because the coral was collected in Baltimore Canyon and was an outlier. The resulting calibration equation suggests that coral P/Ca is strongly correlated to dissolved seawater phosphate as evidenced by the regression of the measured P/Ca in corals against dissolved phosphate measurements in seawater (**Figure 17-28**) where the slope is 0.5 ± 0.1 (R^2 = 0.5) (n = 4).

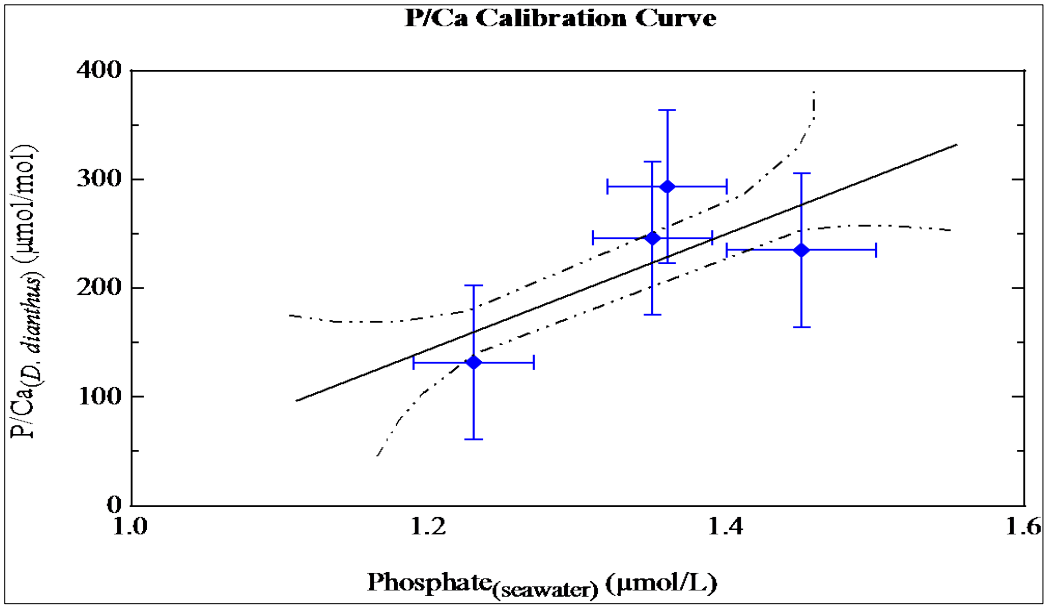

Figure 17-28. Calibration curve of measured P/Ca (µmol mol^{-1}) from four modern *Desmophyllum dianthus* versus dissolved seawater phosphate concentrations (µmol L^{-1}) collected from Norfolk Canyon. Uncertainties in the equation represent 1 standard deviation (SD). Error bars in the x-axis represent the standard deviation of the hydrographic data, and error bars in the y-axis represent 1 SD of the P/Ca measurement in the modern corals from Norfolk Canyon.

Comparison of our calibration to previously published calibration equations of Montagna et al. (2006) and Anagnostou et al. (2011) will help to determine the utility in using P/Ca to reconstruct past seawater phosphate. The Montagna et al. (2006) calibration equation for P/Ca has a slope of ~7 and the Anagnostou et al. (2011) equation a slope of ~0.6. The linear regression slope for our study was 0.5, very similar to the slope by Anagnostou et al. (2011). The variability in the P/Ca linear regression slopes is likely due to 1) sampling technique of ablating along calcification centers, 2) *in situ* seawater measurements and depth of the corals collected not being from the same depths, or 3) the small number of modern *D. dianthus* collected and analyzed from Norfolk Canyon. It is possible that a larger number of samples would provide less variation in the calibration equation. The variation between depth of coral collection and seawater collection ranges from approximately 80 m for corals collected in the 500 m depth range to 11 m for corals collected in the 700 m depth range, and to 83 m at 1,251 m. Discrepancies between the slopes, especially with respect to the equation published by Montagna et al. (2006), is likely due to differences in sampling approach. Montagna et al. (2006) ablated the outside thick layer of *D. dianthus*, which is more variable. Our sampling approach focused on ablating along a growth axis of the thick sections of the coral septa. Overall, the studies provide strong evidence for a direct relationship between ambient seawater dissolved phosphate and measured P/Ca in modern *D. dianthus.*

17.4.2.2.2 Ba/Ca Nutrient Proxy

Seawater barium reflects a nutrient-like distribution in the water column, mimicking silicates, and is likely a good proxy measurement to reconstruct upwelling and surface water primary productivity. Silicate and barium are similarly distributed in the water column and dissolved barium is removed from the surface waters and remineralized at depth as marine barite ($BaSO_4$) (Montagna et al. 2005). Barite is formed in microenvironments of decaying organic matter and siliceous plankton (Bishop 1998, LaVigne et al. 2011).

Ba/Ca incorporated into the skeleton of *D. dianthus* has been shown to be a proxy for trace refractory nutrients with little if any vital effects (LaVigne et al. 2011, Anagnostou et al. 2011, Hill et al. 2011, Sinclair et al. 2006). Anagoustou et al. (2011) determined the $D_{Ba} = 1.5 \pm 0.3$ for *D. dianthus* specimens that were globally distributed, suggesting Ba incorporation into aragonite skeleton is not influenced by changes in temperature, salinity, pressure or biological vital effects (Anagoustou et al. 2011, LaVigne et al. 2011).

Anagnostou et al. (2011) developed a modern calibration curve for Ba/Ca measured in *D. dianthus* collected from 18 globally distributed sites as follows:

$$\frac{Ba}{Ca}_{D.dianthus} (\mu mol/mol) = (0.104 \pm 0.024) \times Ba_{sw} + (2.415 \pm 1.536) \text{ (Equation 17.6)}$$

The linear regression slope is reported as 1.4 ± 0.3 ($R^2 = 0.6$), comparable to those from tropical corals and inorganic studies (Lea et al. 1989, Dietzel et al. 2004).

Due to a lack of ambient Ba/Ca seawater measurements completed during seawater collections we could not generate our own calibration equation, thus we applied previously published equations to our Ba/Ca ratios to reconstruct barium in seawater in Baltimore and Norfolk canyons. Application of the Anagnostou et al. (2011) calibration equation yields dissolved barium values of 58.72 to 106.73 nmol kg^{-1} (SD 5.74) and for subfossil samples yields dissolved barium of 52.85 to 122.48 nmol kg^{-1} (SD 15.74).

To further demonstrate the utility of these nutrient proxies, subfossil *D. dianthus* specimens were used to reconstruct the nutrient dynamics at Baltimore and Norfolk Canyons. Results from the subfossil *D. dianthus* samples living from ~300 to ~700 cal. y B.P. show a decrease in P/Ca ratios that is concurrent with a decrease Ba/Ca ratios (**Figure 17-29**). The decrease in P/Ca indicates less input from nutrient-rich intermediate and deep waters relative to the last 300 years. In comparison, P/Ca ratios from living specimens are almost double those from fossil specimens. The increase in seawater phosphate is likely due to greater influence of freshwater flux from river runoff into the mid-Atlantic canyons.

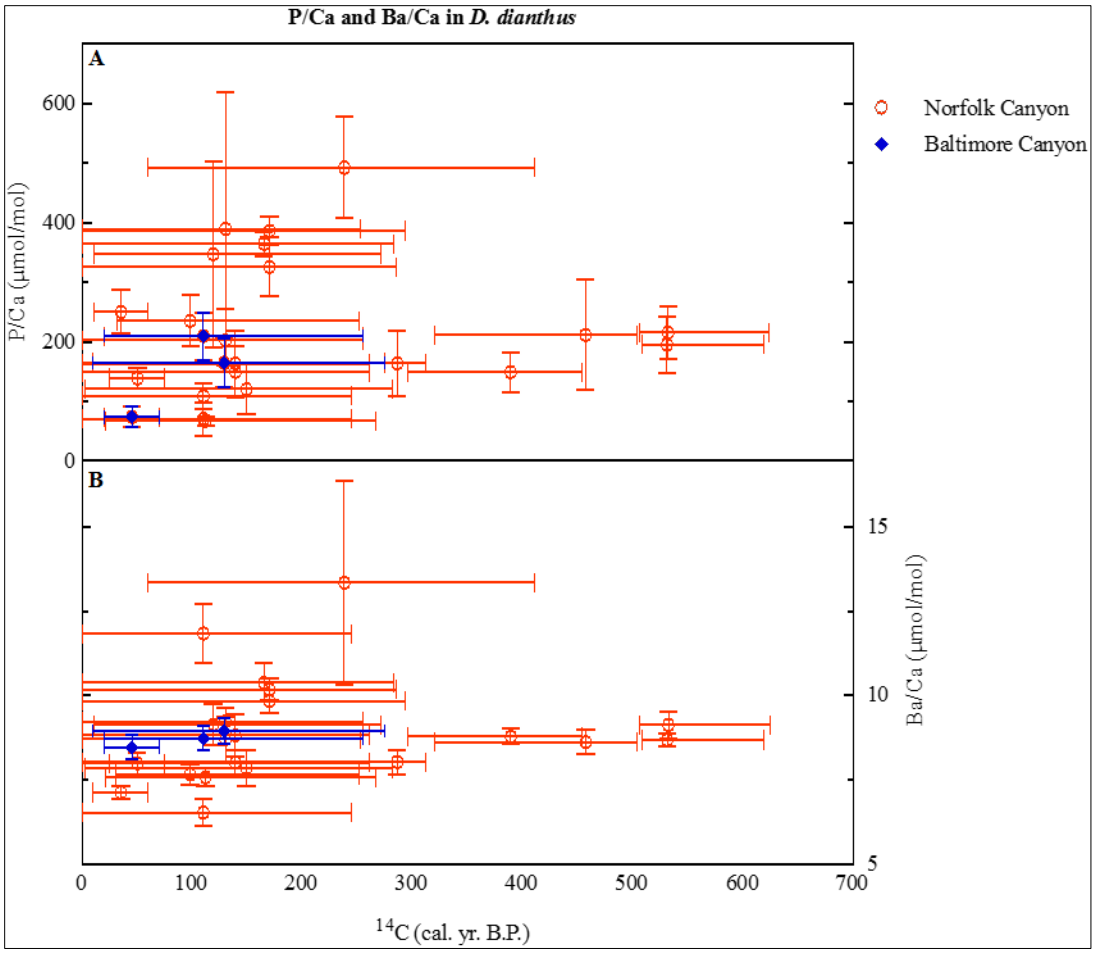

Figure 17-29. Measured mean elemental ratios of (A) P/Ca and (B) Ba/Ca (µmol mol^{-1}) versus the calibrated radiocarbon age of the modern and subfossil *Desmophyllum dianthus* specimens collected from Baltimore Canyon (blue filled triangles) and Norfolk Canyon (red open circles). Y-axis error bars represent the standard deviation (SD) of the P/Ca and Ba/Ca ratios and x-axis error bars represent the age range of the calibrated radiocarbon ages.

17.4.2.2.3 U/Ca Carbonate Ion Concentration Proxy

Growth and development of the skeletons of scleractinian corals in general, and *D. dianthus* specifically, are dependent on the concentration of carbonate ions available in seawater. Calcium carbonate saturation state, Ω, is the ratio of ion concentration ($[Ca^{2+}]x[CO^{2-}_3]$)/($[CaCO_3]$)(Marubini et al. 2003), and if there is an increase in carbonate ion concentrations in seawater, there is a greater opportunity for the coral's aragonite skeleton to form. There are multiple species of dissolved inorganic carbon in seawater; including bicarbonate and dissolved carbon dioxide, the proportions of which can depend on the pH of seawater (Marubini et al. 2003). The concentration of Ca^{2+} is conservative in seawater thus the concentration of CO^{2-}_3 directly influences the saturation state. Seawater chemistry of uranium is influenced by the carbonate ion forming complexes with the uranyl ion (UO_2^{2+}) (Langmuir 1978), thus allowing for U/Ca as a proxy measurement for past seawater carbonate ion concentrations.

Previous research published by Montagna et al. (2005) and Anagnostou et al. (2011) focused on the development of U/Ca (µmol mol^{-1}) ratios as a carbonate ion concentration proxy. Results from these studies show U/Ca is strongly correlated (R^2 = 0.6, n = 17) with ambient seawater carbonate ion concentration (µmol kg^{-1}) represented by the following equation:

$$\frac{U}{Ca_{coral}}\left(\frac{\mu mol}{mol}\right) = (-0.016 \pm 0.003)[CO_3^{2-}]\left(\frac{\mu mol}{kg}\right) + (3.2 \pm 0.3)$$ (Equation 17.7)

Spatial variability between the cup corals collected and the seawater measurements is one reason for scatter within the current calibration equations. In addition, variations within the U/Ca calibration equations could result from different sampling techniques such as ablating across centers of calcification.

The mean U/Ca ratios measured in this study for modern *D. dianthus* ranged from 1.37 to 3.20 µmol mol^{-1}, and for subfossil cup corals the range was 1.18 to 3.30 µmol mol^{-1}. Applying our measured U/Ca ratios to the current accepted U/Ca calibration equations yields carbonate ion concentrations in modern corals ranging from 38.96 to 83.32 µmol kg^{-1} and in subfossil corals ranges from 36.49 to 87.94 µmol kg^{-1}. The mean carbonate ion concentration for the modern corals is 63.31 ± 14.52 µmol kg^{-1} and in subfossil corals 60.74 ± 13.30 µmol kg^{-1}, suggesting 2.57 ± 1.82 µmol kg^{-1} higher carbonate ion concentration in the modern environment. However, this difference is within the uncertainty of measurements. The results from this study show U/Ca ratios have remained relatively constant from modern time through the last 700 years in the mid-Atlantic canyons, ranging from ~1.0 to ~4.0 µmol mol^{-1} (**Figure 17-30**).

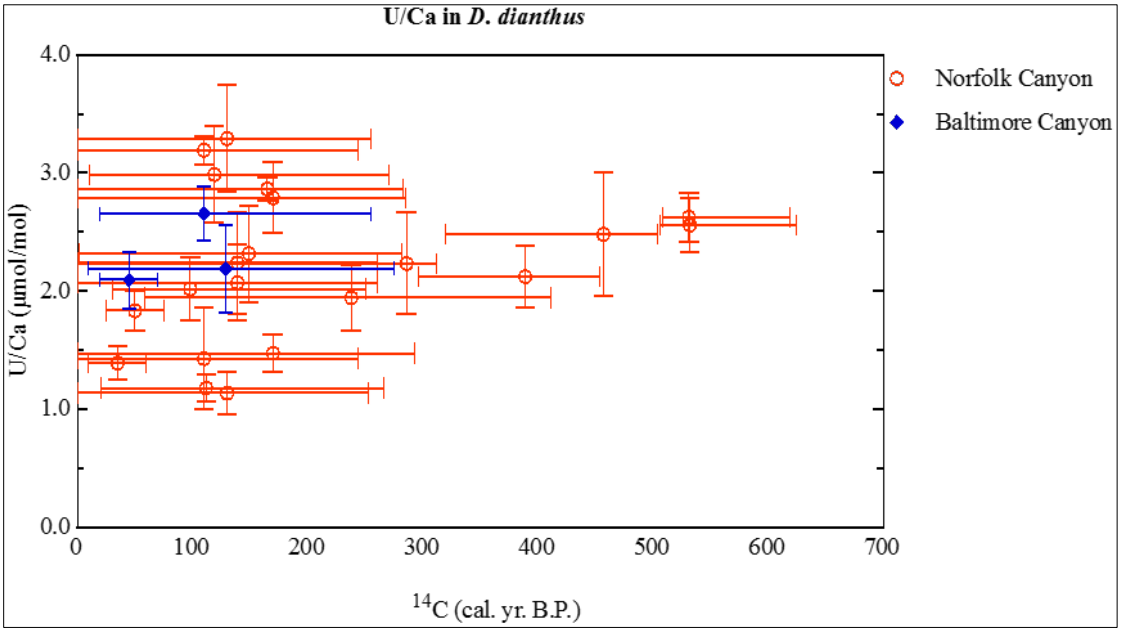

Figure 17-30. U/Ca ratios measured in *Desmophyllum dianthus* specimens collected in Baltimore Canyon (blue filled triangles) and Norfolk Canyon (red open circles) versus the calibrated radiocarbon age (year B.P.). Y-axis error bars represent the standard deviation (SD) of the U/Ca ratio and x-axis error bars represent age range of the calibrated radiocarbon ages.

17.4.2.2.4 Time Series Proxy Reconstruction

Two of the most recent climate change events include the Little Ice Age (LIA) (~1400 to 1900 AD) occurring just after the Medieval Warm Period (MWP) (~800 to 1300 AD) could be related to variations in North Atlantic thermohaline circulation. Variations in the high latitudes have been linked to centennial scale changes in the thermohaline circulation during the LIA and MWP (Keigwin 1996). However, these climate variations are outside the temporal coverage of the subfossil *D. dianthus* collected in this study, which spans the last ~700 years, during which no major climatic events occurred.

Previously published growth rates for *D. dianthus* ranged from 0.5 to 2 mm y^{-1} (Adkins et al. 2004, Risk et al. 2002) with lifespans of ~100 years (Adkins et al. 2004). A growth rate of 1.0 mm y^{-1} was used for the time-series reconstructions in this study in order to examine variability in nutrients and carbonate

ion systems over the past 700 years within Baltimore and Norfolk canyons. Mean coral elemental ratios (P/Ca, Ba/Ca, and U/Ca) are represented by the 20- point moving average smoothing discussed in Section 17.3.2.1.

The transect down the septa of specimen NF-20-7 represents approximately 14 years of growth with the specimen having a radiocarbon age of 255 cal. y B.P., thus this specimen represents a floating time period from ~1870 to 1884 (**Figure 17-31**). There are two major time periods of interest for the NF-20-7 nutrient (Ba/Ca and P/Ca) time-series reconstructions where there is a strong correlation in the variability of the nutrient proxies. From ~1870 to ~1872 AD, there was an increase in the nutrients to Norfolk Canyon, with Ba/Ca increasing ~1.4 µmol mol^{-1} and P/Ca increasing ~320 µmol mol^{-1}. From ~1879 to ~1881 AD, there was a decrease in Ba/Ca of ~1.4 µmol mol^{-1} and decrease in P/Ca of ~400 µmol mol^{-1}. The change in nutrient proxy ratios may reflect an increase in freshwater or riverine input into the region over that 3-year period. U/Ca ratios are consistent throughout the lifespan of the subfossil *D. dianthus*. The peak in 1874 AD could be due to 1) ablating across center of calcification, or 2) a real change in carbonate ion concentration over the 4-year period. Since we do not see the same changes in the Ba/Ca and P/Ca ratios, the observed U/Ca change is not an artifact of the region ablated, but likely represents an increase in the calcium carbonate ion concentration.

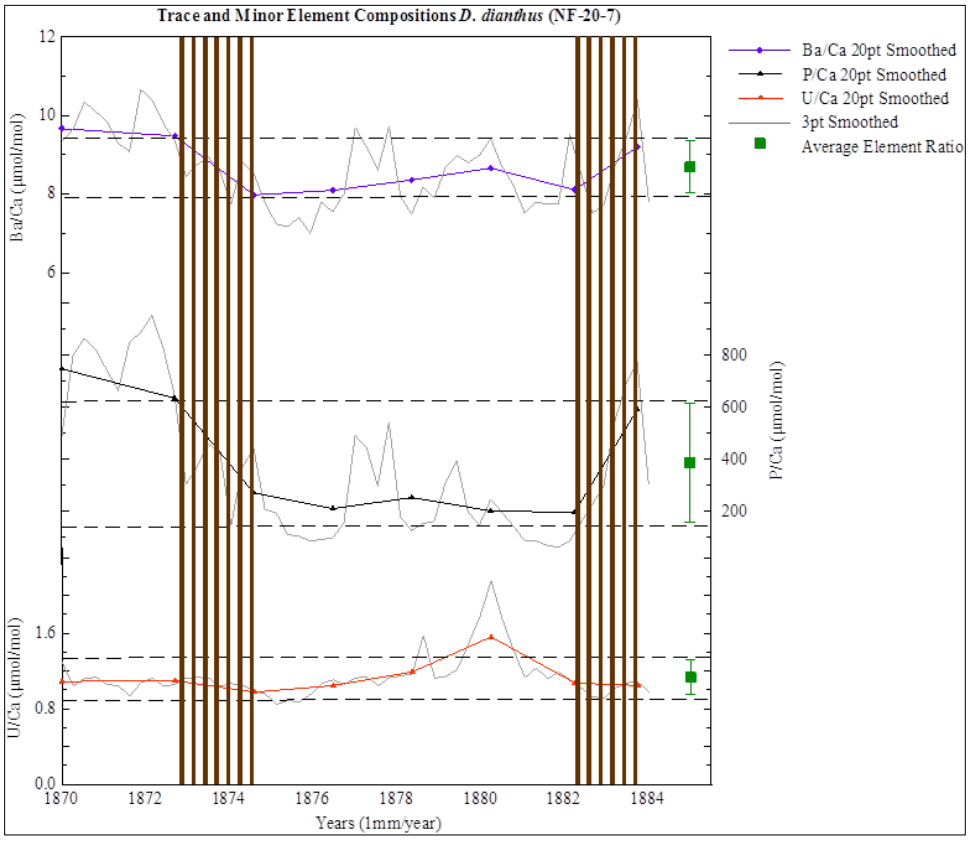

Figure 17-31. Laser ablation transect down the growth axis of *Desmophyllum dianthus* reconstructing trace element variability over a 14-year growth period (1884 to 1870) based on the radiocarbon calibrated age of 130 cal. y B.P. Age model assumes a growth rate of 1 mm y^{-1}. Date plotted as a 3-point smoothed data (gray line), 20-point smoothed data for each element, Ba/Ca (blue line), P/Ca (black line), U/Ca (red line), and the average elemental ratio (green filled square) for subfossil *D. dianthus.* Dotted line represents the uncertainty of the average elemental ratio for each transect.

Using subfossil specimen NF-20-13 collected in Norfolk Canyon, radiocarbon dated to be 455 cal. y B.P. with a transect of 40 mm down the septa results in a time series converting the period 1585 to 1625 AD (**Figure 17-32**). The area highlighted from 1603 to 1604 is an outlier due to ablating across a broken region of the *D. dianthus*. The Ba/Ca and P/Ca ratios spanning from ~1587 to ~ 1594 show a gradual increase in the two nutrient elemental ratios followed by a sharp decrease. This trend could be due to an increase in any of the following: 1) primary productivity in surface waters, 2) freshwater influence from the continental shelf, or 3) freshwater and nutrients in surface waters at Norfolk Canyon. The rest of the record shows little change, suggesting the time period represented was static with little variation in nutrient and carbonate ion concentrations.

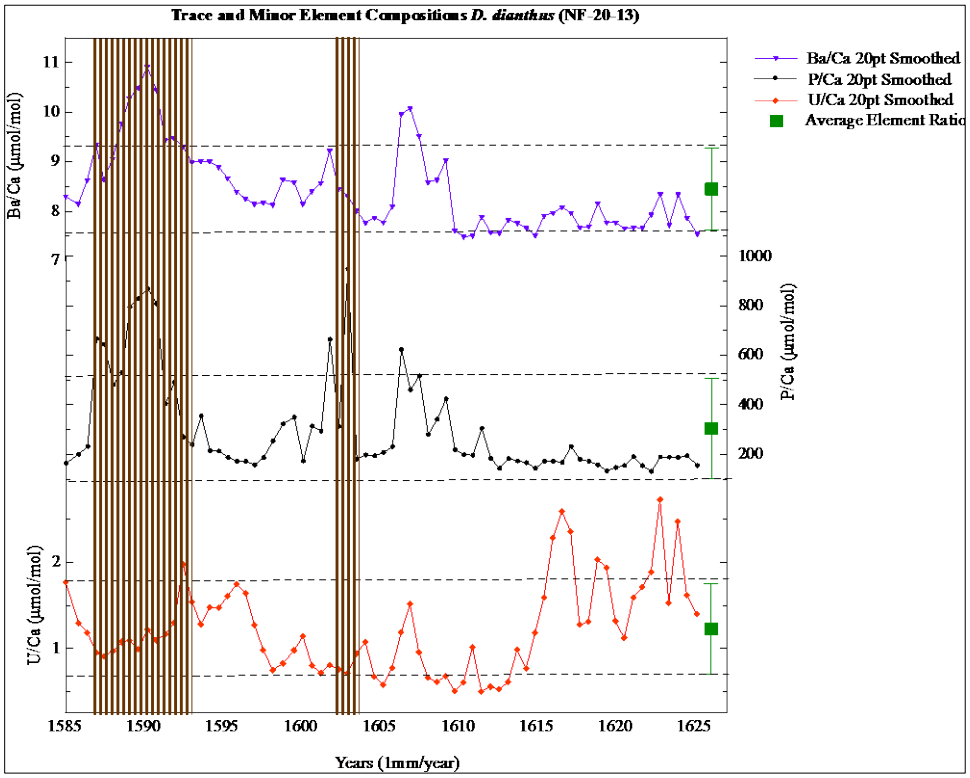

Figure 17-32. Laser ablation transect down the growth axis of *Desmophyllum dianthus* (specimen NF-20-13) collected from Norfolk Canyon reconstructing trace element variability over a 40-year period (~1585 to 1625) based on the radiocarbon calibrated age of 389 cal. y B.P. Age model assumes a growth rate of 1 mm y^{-1}. Date plotted is the 3-point smoothed data (gray line), 20-point smoothed data for each element, Ba/Ca (blue line), P/Ca (black line), U/Ca (red line), and the average elemental ratio (green filled square). The dotted line represents the uncertainty of the average elemental ratios for each transect.

17.4.2.2.5 Summary

In this study we applied novel LA ICP-MS methods to develop paleo-nutrient and pH proxies in solitary scleractinian cup corals, *D. dianthus* collected from Baltimore and Norfolk canyons in the mid-Atlantic Ocean. Twelve modern and 26 subfossil *D. dianthus* specimens were collected from water depths ranging from 400 to 1,400 m with an ambient seawater pH ranging from 7.89 to 8.00. Radiocarbon measurements indicate subfossil specimens span the last ~700 years. Modern seawater column chemistry (radiocarbon, nutrients, total alkalinity, and particulate trace elements) were measured to calibrate geochemical proxies in live collected specimens. This study focused on three paleo-proxies (P/Ca, Ba/Ca, and U/Ca) with application to nutrient dynamics and carbonate systems in the mid-Atlantic canyons.

In situ dissolved seawater phosphate measurements and P/Ca ratios from living corals were used to develop a calibration curve, yielding dissolved seawater phosphate values of 0.24 to 1.70 μmol L^{-1} derived from fossil coral specimens. In comparison, *in situ* seawater phosphate values for Baltimore Canyon ranged from 0.01 to 1.45 μmol L^{-1} and from 0.14 to2.06 μmol L^{-1} at Norfolk Canyon. Comparing the modern to past seawater phosphate measurements suggests little variability in seawater phosphorus concentrations in the mid-Atlantic canyons over the last 700 years.

Incorporation of barium into cup coral skeletons is not influenced by the biological processes of the coral, which supports the use of Ba/Ca as a reliable proxy to reconstruct variations in nutrient dynamics (LaVigne et al. 2011, Anagnostou et al. 2011, Hill et al. 2011, Sinclair et al. 2006). Due to the understanding of Ba/Ca as a paleo-proxy, we used previously published calibration equations to determine seawater barium distribution over the past 700 years in the mid-Atlantic canyons. Our results for Ba/Ca yield modern dissolved barium concentrations ranging from 58.72 to 106.73 nmol kg^{-1} (SD 15.74). The subfossil samples yield dissolved barium concentrations ranging from 52.85 to 122.48 nmol kg^{-1} (SD 15.74), suggesting there has been little change in the range of dissolved barium over the last ~700 years.

U/Ca is used as a carbonate ion concentration proxy, and previously published calibration equations were applied to measured U/Ca ratios in coral skeletons. The range of the calcium carbonate concentrations for the modern *D. dianthus* ranged from 38.96 to 83.32 μmol kg^{-1}. Applying the U/Ca ratios from the subfossil *D. dianthus* gave us calcium carbonate ranges from 36.49 to 87.94 μmol kg^{-1}. The calcium carbonate concentrations have remained relatively constant. Overall, comparing the modern results with the subfossil values suggest there has been little change in nutrient fluxes and the carbonate ion system in the mid-Atlantic canyon region over the last 700 years.

17.4.2.3 Laser Ablation Boron Isotopes

17.4.2.3.1 pH-δ^{11}B Proxy Calibration

Examining the boron isotope (δ^{11}B) pH technique requires some assumptions regarding the carbonate system. While the total DIC in seawater remains constant, a 0.2 pH increase translates to an atmospheric CO_2 concentration twice the present value (Pagani et al. 2005). Calculating pCO_2 from pH requires a robust measure of total alkalinity or DIC (Pearson and Palmer 2000), which is not available as part of these reconstructions. General principles of the boron isotopes as a proxy measurement for paleo-pH are based on boron existing as trigonal boric acid [$B(OH)_3$] and the tetrahedral borate ion [$B(OH)_4^-$] with isotope fractionation between the species in seawater. A key assumption for δ^{11}B proxy is that only the tetrahedral borate ion [$B(OH)_4^-$] species is incorporated into a coral's skeleton by biogenic calcifiers; the $\delta^{11}B_{carbonate}$ is assumed to be only of this borate species. This assumption is met by demonstrating that the borate ion is directly incorporated into the aragonite skeleton of the DSC while maintaining the tetrahedral coordination (Sen et al. 1994, Trotter et al. 2011).

The δ^{11}B value from subfossil *D. dianthus* specimens collected at intermediate water depths (400 to 800 m) varied from 23.51‰ to 29.62‰, whereas δ^{11}B values ranged from 23.46‰ to 29.66‰ from specimens collected at deepwater depths (1,200 to 1,400 m). Anagnostou et al. (2012) report a δ^{11}B range of 23.56‰ to 27.88‰ from globally distributed *D. dianthus* samples. DSC δ^{11}B values are found to be typically greater than what has been measured in tropical corals, suggesting a physiological cause of modification of the seawater pH in which corals grew. This modification would compensate for a range of seawater pH and saturation depth at which corals grow (Anagnostou et al. 2012).

If it is assumed the δ^{11}B in carbonates is representative of the $B(OH)_4^-$ component in seawater, the relationship between $\delta^{11}B_{D.\ dianthus}$ to pH values is expressed as (Zeebe and Wolf-Gladow 2001):

$$pH = pK_B - \log\left(\frac{\delta^{11}B_{sw} - \delta^{11}B_C}{\alpha_{B3-B4}\ x\ \delta^{11}B_C - \delta^{11}B_{sw} + 1{,}000\ x\ (\alpha_{B3-B4} - 1)}\right)$$ (Equation 17.8 [same as Equation 17.4])

The pK_B = 8.5682 (e.g., temperature of 25 °C and salinity of 40.7; Dickson 1990, Krief et al. 2010) is the dissociation constant between the $B(OH)_3$ and $B(OH)_4^-$ (i.e., with T = 8.5 °C and salinity of 35.7 practical salinity units [psu]) (Blamart et al. 2007). $\delta^{11}B_c$ is the boron isotopic composition of the carbonates; $\delta^{11}B_{sw}$ is the boron isotopic composition of the seawater (39.6‰; Foster et al. 2010, Spivack and Edmond 1986). The α_{B3-B4} is the fractionation factor between $B(OH)_3$ and $B(OH)_4^-$ based on Equation 17.2. There are several possible α_{B3-B4} values, ranging between ~1.0260 and ~1.0267 (Trotter et al. 2011). The theoretically derived value of 1.0194 calculated at 25 °C (Kakihana et al. 1977, Pagani et al. 2005, Klochko et al. 2006, Rollion-Bard and Erez 2010, Rollion-Bard et al. 2011, Trotter et al. 2011, Anagnostou et al. 2012) is typically used but is considered a lower extreme for marine carbonates (Hönisch et al. 2004). We used the recently experimentally measured value of 1.0272 (Klochko et al. 2006) determined by chemical equilibrium experiments using artificial seawater (Kakihana et al. 1997). Anagnostou et al. (2012) explores this relationship for *D. dianthus* with the following equation:

$$\Delta pH = -(0.75 \pm 0.12) \times pH_{sw} + (6.88 \pm 0.93) \text{ (1SE, } R^2 = 0.80) \text{ (Equation 17.9)}$$

The ΔpH is the difference between the calculated pH of the site of calcification and the ambient seawater pH (Anagnostou et al. 2012). Our ΔpH ranges from 0.13 to 0.48. Plotting our ΔpH versus the measured seawater pH values we get a slope of -2.4 with an R^2 = 0.04 (n = 27) (**Figure 17-33**). *D. dianthus* ΔpH values are higher compared with those from tropical corals (Trotter et al. 2012). This offset suggests that pH regulation is an important physiological process controlling calcification and that pH regulation is closely related to seawater saturation state (McCulloch et al. 2012). McCulloch et al. (2012) suggest that the pH regulation is an adaptive strategy for *D. dianthus* to help overcome environmental limitations of the deep ocean such as low calcite and aragonite saturation states found at deeper depths (McCulloch et al. 2012). The *D. dianthus* specimens in our study were collected at water depths (400 to 1,200 m) that are supersaturated with respect to the saturation states of aragonite and calcite.

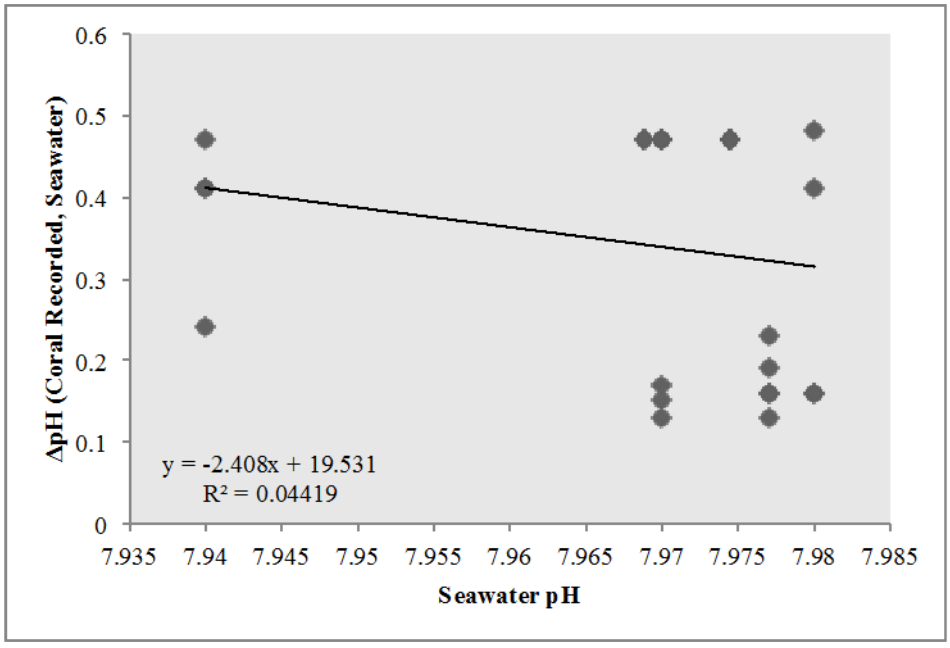

Figure 17-33. *Desmophyllum dianthus* reconstructed pH minus seawater pH (ΔpH) verses seawater pH, including linear regression line.

Seawater pH values can be calculated using the calibration relationships given by Equations 17.8 and 17.9. These equations are valid for the wide range of seawater pH values in which the corals grew (7.80 to 8.10). Comparing the *in situ* pH values with the pH-δ^{11}B derived values illustrates a scattering around the 1:1 line (**Figure 17-34**). The 0.5 offset between the *in situ* and derived pH values is a result of the $B(OH)_3$ and $B(OH)_4^-$ fractionation factor or a shift in the δ^{11}B within the coral's skeleton during its growth. Due to the offset seen within the modern seawater pH measurements, the reconstructed seawater pH measurements likely have a similar offset of 0.5 due to the environment of Baltimore and Norfolk Canyons has not significantly changed over the past 700 years.

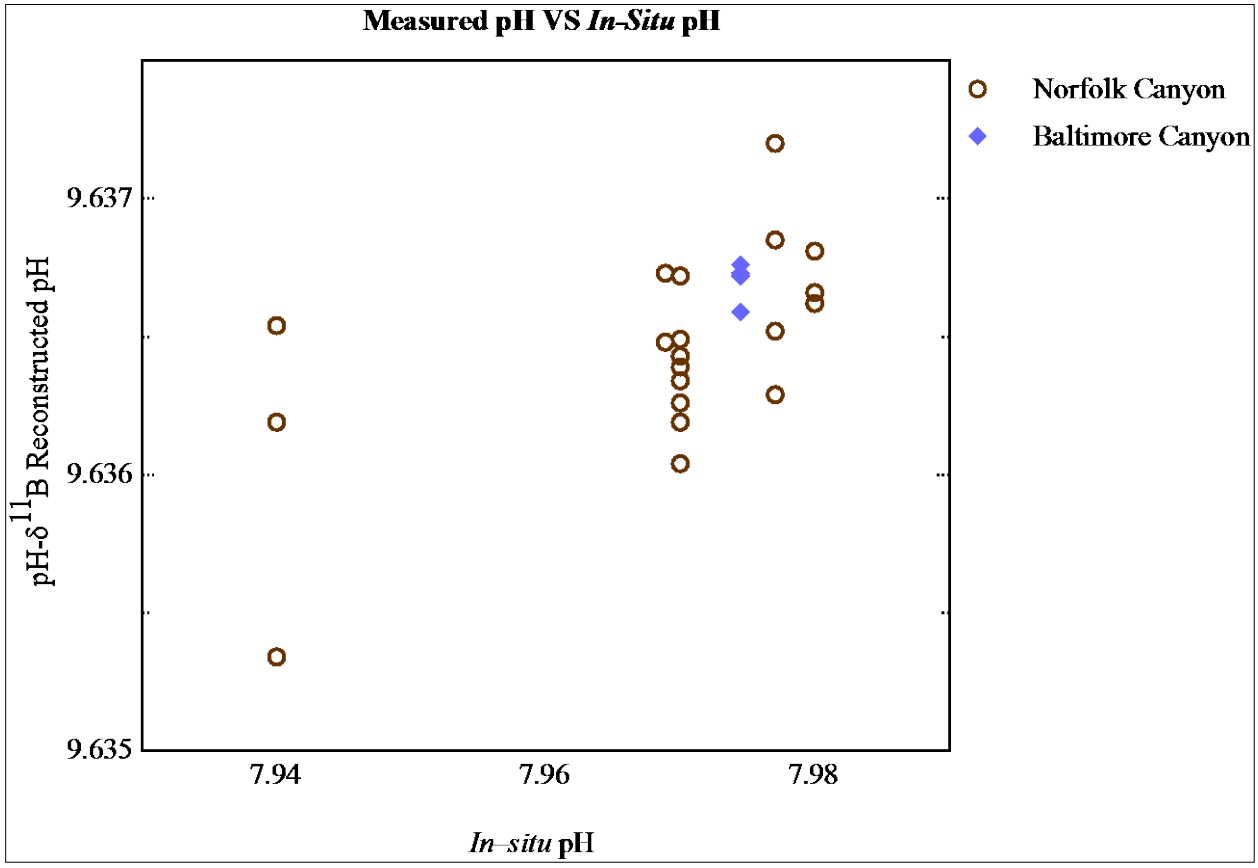

Figure 17-34. Measured pH values from water samples (*in situ*) plotted against pH-δ11B derived seawater pH values measured within the *D. dianthus* skeletons. Modern and fossil *D. dianthus* were in Norfolk Canyon (brown open circles) and Baltimore Canyon (purple filled triangles).

17.4.2.3.2 Paleo-pH Reconstructions

Temporal variations in boron isotopic composition of DSC skeletons provide a record of past seawater pH. Combined with *in situ* and instrumental data, these records can help determine the role of climate change and ocean acidification and their impact on coral calcification (D'Olivo et al. 2014). Using the δ^{11}B *D. dianthus* values with the pH-δ^{11}B calibration equation we can reconstruct seawater pH in the mid-Atlantic canyons region over the past 700 years (cal. y B.P.). The paleo-pH reconstruction is based on *D. dianthus* samples from three depth ranges: 400 to 600 m, 600 to 800 m, and 1,200 to 1,400 m (**Figure 17-35**). Reconstructed seawater pH across all three depths ranges from 8.4 to 8.9 and varies only slightly over the past 700 years. *D. dianthus* corals living during the last ~50 years (cal. y B.P.) have a consistent pH of 8.4, with a 0.2 to 0.3 pH increase occurring ~100 years ago, where pH values remain until ~550 years ago. From ~550 to 700 years, calculated pH values are much more variable, ranging

from 8.4 to 8.8. This variability is not significantly outside the uncertainties of the $\delta^{11}B$ measurements and calibration equations to be considered significant. Overall, the reconstructed seawater pH has remained relatively consistent during the past 700 years at Baltimore and Norfolk canyons. Results from this study demonstrate relatively constant seawater acidity levels consistent with a relatively static climate regime in the mid-Atlantic canyon regions over the last 700 years.

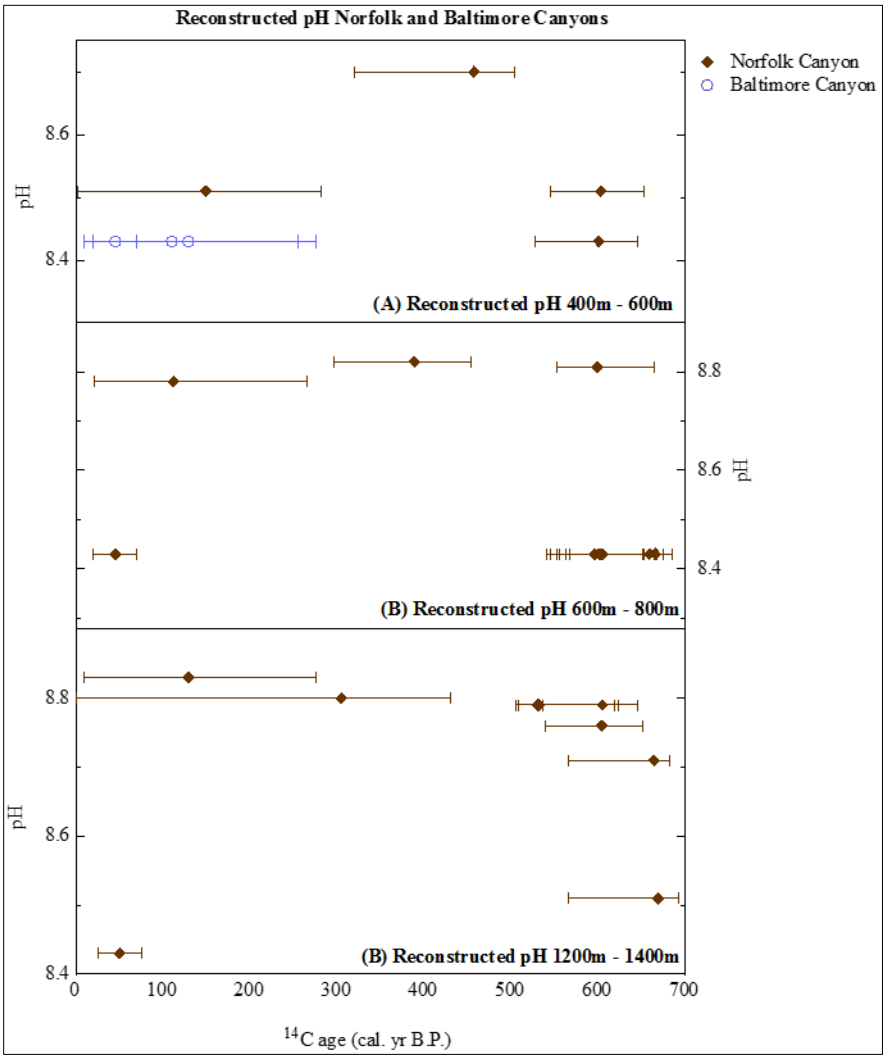

Figure 17-35. Reconstructed seawater pH based on $\delta^{11}B$ measurements from *Desmophyllum dianthus* specimens collected in Norfolk Canyon (brown closed diamonds) and Baltimore Canyon (purple open circles) verses calibrated radiocarbon ages spanning the last 700 years. Error bars on the x-axis represent the calibrated radiocarbon age range.

17.4.2.3.3 Summary

Boron isotope systematics for marine carbonates has been extensively studied for foraminifera and tropical corals (Hemming and Hanson 1992, Sanyal et al. 1995, Pearson and Palmer 2000, Hönisch and Hemming 2005, Yu and Elderfield 2007, Trotter et al. 2011), whereas only recently has the $\delta^{11}B$ proxy using cold-water corals been explored (McCulloch et al. 2012, Anagnostou et al. 2012). In this study, we focused on using the LA ICP-MS techniques to determine $\delta^{11}B$ variability in multiple *D. dianthus* specimens instead of TIMS methodology. LA ICP-MS methods have great promise for determining the isotopic composition of DSC skeletons, allowing many specimens to be sampled for high-resolution

datasets. Our results provide one of first empirical applications of pH-$\delta^{11}B$ calibration equation using *in situ* pH and *D. dianthus* $\delta^{11}B$ values to reconstruct seawater pH.

$\delta^{11}B$ values from five modern *D. dianthus* yield a range from 23.46‰ to 23.51‰, whereas the range from 22 subfossil *D. dianthus* was 23.46‰ to 29.67‰. These values are higher than $\delta^{11}B$ measured in tropical corals. These results from *D. dianthus* provide new constraints on the ocean carbonate system for the mid-Atlantic canyons over the last 700 years. Boron isotopes remain a powerful tool for reconstructing past seawater pH and also provide a valuable compliment to the carbonate ion concentration (U/Ca) proxy (Anagnostou et al. 2012). However, further investigation of the $\delta^{11}B$-pH equation is necessary in future $\delta^{11}B$ paleo-pH work. Application of the $\delta^{11}B$ proxy to other areas and different long-living DSC species such as *Corallium* will help determine ocean carbonate system response to rapid climate change events.

17.4.3 Chemosynthetic Communities Discussion

17.4.3.1 Authigenic Carbonate Formation

The aragonite-dominated authigenic carbonates form pavements and/or irregular blocky build-ups on the seafloor. The carbonates consist of bioclasts, organic matter, and angular clasts of terrigenous origin. While the contemporary Baltimore Canyon does not connect with a river system, rivers delivered a significant volume of sediment to the submarine canyons incising the shelf during Pleistocene sea-level lowstands (Kelling and Stanley 1970, Twichell et al. 1977, Forde et al. 1981). The fluvial influence on the canyons is observed in both the geomorphic features and grain size where coarse- to medium-grained, shelly terrigenous sands are observed adjacent to the canyon heads (Obelcz et al. 2014). The similarity between neodymium isotope ($^{143}Nd/^{144}Nd$) values from Baltimore Canyon surface sediment (0.51208; Prouty et al. 2015) and Hudson River sediment (0.51206; Goldstein and Jacobsen 1987) highlights the connectivity with proximal fluvial sources.

The authigenic carbonate texture results from *in situ* brecciation of weakly consolidated sediment, possibly triggered by seismic and venting-induced disturbances such as rapid sedimentation related to episodic and rapid release of trapped fluids or gases (Matsumoto 1990). Fractures cross cutting multiple generations of aragonite precipitate in the Baltimore Canyon authigenic carbonate (**Figure 17-18**) may signify past disturbance events. The dominance of aragonite over dolomite at both Baltimore and Norfolk Canyon seep sites suggests precipitation at or close to the seafloor where sufficiently high sulfate concentrations inhibit high-Mg calcite crystallization (Burton 1993, Savard et al. 1996, Bohrmann et al. 1998). This interpretation is consistent with carbonate $^{87}Sr/^{86}Sr$ and $^{234}U/^{238}U$ isotope results that indicate precipitation from seawater-derived fluids rather than deep-seated formation waters (Kraemer 1981, Naehr et al. 2007).

17.4.3.2 Anaerobic Oxidation of Methane

The main driver of authigenic carbonate precipitation at or near the sediment interface is anaerobic oxidation of methane (AOM) via sulfate reduction ($CH_4 + SO_4^{2-} \rightarrow HCO_3^- + HS^- + H_2O$). This reaction drives an increase in pore water alkalinity by the production of biocarbonate (HCO_3^-) and favors carbonate precipitation (Elvert and Suess 1999, Hinrichs et al. 1999, Thiel et al. 1999). Carbonate precipitation from methanogenesis can occur deeper in the sediment column (e.g., Greinert et al. 2001, Orphan et al. 2004, Gieskes et al. 2005) and is typically characterized by carbonate $\delta^{13}C$ values > -40‰ (Aharon et al. 1997). However, authigenic carbonate $\delta^{13}C$ values from Baltimore and Norfolk canyons are lighter (-45 to -48‰), in agreement with $\delta^{13}C$ values at cold seep sites where microbial AOM is the dominant driver of authigenic aragonite precipitation (Naehr et al. 2007). The authigenic carbonate $\delta^{13}C$ and $\delta^{18}O$ values are also consistent with Group I carbonates that typify carbonate precipitation of microbial origin in only a few centimeters below the sediment-water interface (Joseph et al. 2013).

In addition to AOM, sulfate reduction is also a dominant process that occurs in methane-rich sediments, resulting in sulfur fractionation in the pore water and sediment (Kemp and Thode 1968). Sulfate reduction may therefore help explain the light surface sediment $\delta^{34}S$ values (from -2.62 to 8.20‰) relative to seawater sulfate (+20‰; Heyl et al. 2007; **Table 17-11**). Production of hydrogen sulfide (H_2S) can then be used as a potential nutritional source for the surrounding chemosynthetic communities (e.g., Heyl et al. 2007). For example, Van Dover et al. (2003) reported that the mussel *Bathymodiolus heckerae* collected from Blake Ridge derives up to 25% of its organic sulfur from sulfide. Using a two end-member mixing model with a H_2S $\delta^{34}S$ value of -10‰ (Michener and Schell 1994) and average *Bathymodiolus* gill $\delta^{34}S$ values from each seep site, the reliance on H_2S as an energy source at Baltimore and Norfolk canyon seep sites was estimated at 16% and 14%, respectively. However, variable gill $\delta^{34}S$ values indicate uptake of up to 80% of H_2S (i.e., gill $\delta^{34}S$ value of -4.07‰ at the Baltimore Canyon seep site), suggesting that free-living or symbiotic thiotrophic bacteria may play a nutritional role at the base of the food web (Yamanaka et al. 2003). As an alternative to mussel tissue isotopic studies, the mussel shell periostracum derived from both living and dead specimens represents a valuable source of information about the seep environment. The similarity between the periostracum and mussel gill $\delta^{34}S$ values from Norfolk Canyon suggests a high degree of nutrient flow between the soft tissue, allowing for greater fidelity in using periostracum isotopic ratios in place of respirable tissues of living specimens (Delong and Thorp 2009). This is particularly essential when mussel tissue is not available, such as with archived specimens or those at quiescent vent sites.

17.4.3.3 Estimation of Fluid Composition and Age

The composition of the seeping fluids can also be characterized by the mussel shell $\delta^{13}C$ values, with differences between the living and dead specimens reflecting changes in the flux of methane in the past, or possibly a change in the composition of the seeping fluids (e.g., Becker et al. 2010). At both the Baltimore and Norfolk canyon seep sites, the shell carbonate and periostracum $\delta^{13}C$ values were lighter relative to bottom water DIC $\delta^{13}C$ values (**Table 17-10**). This difference suggests an additional carbon source for shell calcification and illustrates the decoupling between calcification and metabolic pathway (Aharon et al. 1997). The light periostracum $\delta^{13}C$ values (-57‰; **Table 17-10**) agree with previous work concluding that mussel shell periostracum originates from dietary sources and is an alternative to soft tissue for trophic studies (Geist et al. 2005). Assuming a regional methane $\delta^{13}C$ value of -68‰ (Pohlman person. comm.), the average percent contribution of methane to shell calcification was estimated at 11% at Baltimore Canyon and 5% at Norfolk Canyon. However, shell $\delta^{13}C$ values from dead specimens collected at Norfolk Canyon indicate a temporal shift in seepage activity and/or composition of seeping fluids. Specifically, a reduction in $\delta^{13}C$ values of up to 17‰ observed in the dead specimens is equivalent to a ~25% increase in methane contribution to shell calcification. Carbonate shell $\delta^{13}C$ variability also has the potential to record environmental changes, such as changes in fluid source, as well as fluid-venting activity over the lifespan of the mussels (e.g., Lietard and Pierre 2008). Although the precise chronology of the variability is unknown because of the difficulty in dating the specimens, estimates of ages of *B. brevior* and *B. thermophiles* range from 18 to more than 25 years (Schöne and Giere 2005). Therefore, lifespan $\delta^{13}C$ variability reported here may be related to changes in methane flow within several decades. The spatial distribution of living and dead mussels described in Ross et al. (2015) may also imply changing fluid composition or flux rates, as suggested by Hornbach et al. (2005) from ROV dives of the Blake Ridge Diapir.

The shell carbonate $\delta^{18}O$ isotopic signature at Norfolk overlaps with both *Bathymodiolus* and *Calyptogena* shell samples from other cold seeps (Lietard and Pierre 2008). In comparison, Baltimore Canyon shell $\delta^{18}O$ values are lighter, reflecting warmer water *in situ* temperatures (~9 °C) relative to the deeper, colder *in situ* temperatures (~4 °C) at Norfolk. Using bottom water $\delta^{18}O$ values from Baltimore and Norfolk canyons, the predicted carbonate $\delta^{18}O$ value (Epstein et al. 1953) precipitated at equilibrium

yields heavier carbonate $\delta^{18}O$ values relative to measured shell values from Baltimore and Norfolk by 0.68‰ and 0.42‰, respectively. Therefore, there is evidence of isotopic disequilibrium, indicating the influence of ^{18}O-poor water and/or warmer seeping fluids (e.g., Lietard and Pierre 2008). As a result, the predicted seawater temperatures, using an aragonite paleotemperature equation of Grossman and Ku (1986), are warmer by 1 °C to 3 °C compared with *in situ* temperatures.

The influence of methane is also captured in the light carbonate $\Delta^{14}C$ values and relatively old ^{14}C-derived ages of mussel shells from living specimens. Seawater samples collected near the Norfolk seep field yield an average $DI^{14}C$ value of -24.17‰ (SD 0.6), consistent with seawater $\Delta^{14}C$ values from below the mixed-layer depth in Norfolk Canyon (Roark et al. 2014). In contrast, the average mussel shell $\delta^{14}C$ value from living specimens from the Norfolk seep field is -115‰ (SD 3). Assuming a methane $\delta^{14}C$ signature of -880‰ (<0.12 pMC; Pohlman et al. 2009) and a DIC $\delta^{14}C$ signature of -24‰, ~10% of the carbon signature for shell calcification is derived from fossil carbon. As a result, the contribution from fossil carbon can yield a false ^{14}C carbonate age (e.g., Aharon et al. 1997).

Incorporation of fossil carbon can therefore result in discordance between the ^{14}C and U-Th-derived age of authigenic carbonate samples. The average $\delta^{14}C$ signatures of the authigenic carbonates are significantly depleted in ^{14}C, with values ranging from -894‰ to -878‰ and corresponding ^{14}C ages ranging from 17,985 to 19,350 ^{14}C years. In comparison, average U-Th ages from the Baltimore and Norfolk canyon seep sites were 1.8 to 4.9 ka and 14.9 to 16.3 ka, respectively. According to the U-Th ages, hydrocarbon seepage is believed to have initiated at the Baltimore Canyon seep field toward the end of the Pleistocene and more recently at the Norfolk seep site; however, the origin of seeps and gas expulsion geomorphic features (e.g., pockmarks and "gas blowouts") along the U.S. Atlantic margin remains uncertain (Hill et al. 2004, Newman et al. 2008, Brothers et al. 2014, Skarke et al. 2014).

17.4.3.4 Formation Model and Paleoenvironment

The occurrence of gas seeps and pockmarks associated with fluid expulsion at depths <500 m that are outside the methane hydrate stability field may have a microbial origin from either bacterial decay of organic matter or from gas hydrate dissociation with subsequent upslope migration (Skarke et al. 2014), or they may have a thermogenic origin at depth (Hill et al. 2004, Newman et al. 2008, Brothers et al. 2014). However, the geochemistry presented here precludes a thermogenic origin given carbonate $\delta^{13}C$ values < -40‰, consistent with the lack of evidence for thermogenic gas on this part of the margin. The Sr and U isotopes data also support a shallow-sourced fluid in equilibrium with seawater. This agrees with earlier work by Newman et al. (2008) that demonstrated the microbial origin of pore fluid DIC $\delta^{13}C$ values along the U.S. mid-Atlantic shelf break. Hill et al. (2004) argued that microbial gas flowing updip from dissociating gas hydrates is responsible for the distribution of gas blowouts in the region. However, there is no evidence in the discontinuous strata depicted in the seismic profiles to support channeling of gas updip to the Baltimore Canyon seeps (Ruppel 2015a et al.). Instead, overpressures within Pleistocene sediments, followed by vertical fluid and gas expulsion, is the preferred explanation (Brothers et al. 2014, Kluesner et al. 2015). This interpretation can be explained with the nonaquifer model of Dugan and Flemings (2002) where rapid sediment loading during Pleistocene sea-level lowstand created overpressure gradients, forcing fluids to migrate upward and outward toward the seafloor. The rapid release of trapped gases could also explain the brecciation and fractures observed in the Baltimore Canyon authigenic carbonate.

During the Pleistocene, significant volumes of sediment were delivered to the outer shelf, with much of it transported directly into shelf-sourced canyons and then offshore to deepsea fans (Shepard 1981, Poag 1992). The age of the Baltimore Canyon authigenic carbonate further supports a link between rapid loading of organic-rich sediment during the Pleistocene sea-level lowstand and subsequent fluid flow from overpressure. The presence of pockmarks adjacent to the Baltimore Canyon seep site (**Figure 17-36**), Brothers et al. 2014) is also indicative of fluid expulsion across the sediment-water

interface (Berndt 2005, Judd and Hovland 2007). As a result, slope instability in the region may be further linked to sedimentation rate and permeability rather than dissociation of gas hydrate, consistent with an assessment by ten Brink et al. (2014), which concluded that gas hydrate dissociation does not appear to contribute to the generation of landslides along the U.S. Atlantic margin. The ensuing Late Pleistocene to Holocene sea level rise increased hydrostatic pressure, which could move the seep field closer to the hydrate stability condition under isothermal conditions. However, dramatic bottom water warming between the presumed cold Late Pleistocene temperature and the ~9 °C observed in 2013 from *in situ* temperature measurements overwhelms the impact of increased pressure. The Baltimore Canyon seep field may, now or in the past, have emitted migrated methane that was released by gas hydrate dissociation at greater water depths; however *in situ* gas hydrate dissociation is ruled out as the source of methane emissions (Prouty et al. 2016).

Active venting at the Norfolk seep field at a depth of ~1,600 m is unique because it is well within the gas hydrate stability zone and there is no evidence of a salt diapir warming the overlying hydrate-bearing sediments. Therefore, methane leakage at this site requires a pathway for free gas to escape, such as faults, fractures, or chimneys below the seafloor (Berndt 2005, Judd and Hovland 2007). Skarke et al. (2014) describe flow pathways through fractured Eocene rock. This is consistent with recently collected high-resolution seismic profiles showing fractures channeling methane to the seafloor from hundreds of meters deep in the sediments at these deepwater sites (Ruppel et al. 2015b).

Despite the diverse local environmental factors that drive methane leakage at each seep site (i.e., a combination of trapping/release of gas, fault conduits, and leakage from sites of submarine landslides and tectonic induced erosion), there is evidence at both sites of upward flux of methane that is isotopically similar between the sites. This can occur when the intense methane fluxes move the sulfate-methane transition zone very close to the seafloor (Borowski et al. 1996). The shallow-sourced fluid maintains a distinct microbial “lineage,” most likely linked to long-term accumulation, compaction, and over-pressuring of organic-rich sediment. With continental slopes, canyons, and deepsea fans serving mainly as sinks for organic carbon (e.g., de Haas et al. 2002), the U.S. Atlantic margin could serve as a biomass hotspot to chemosynthetic communities supported by widespread methane leakage.

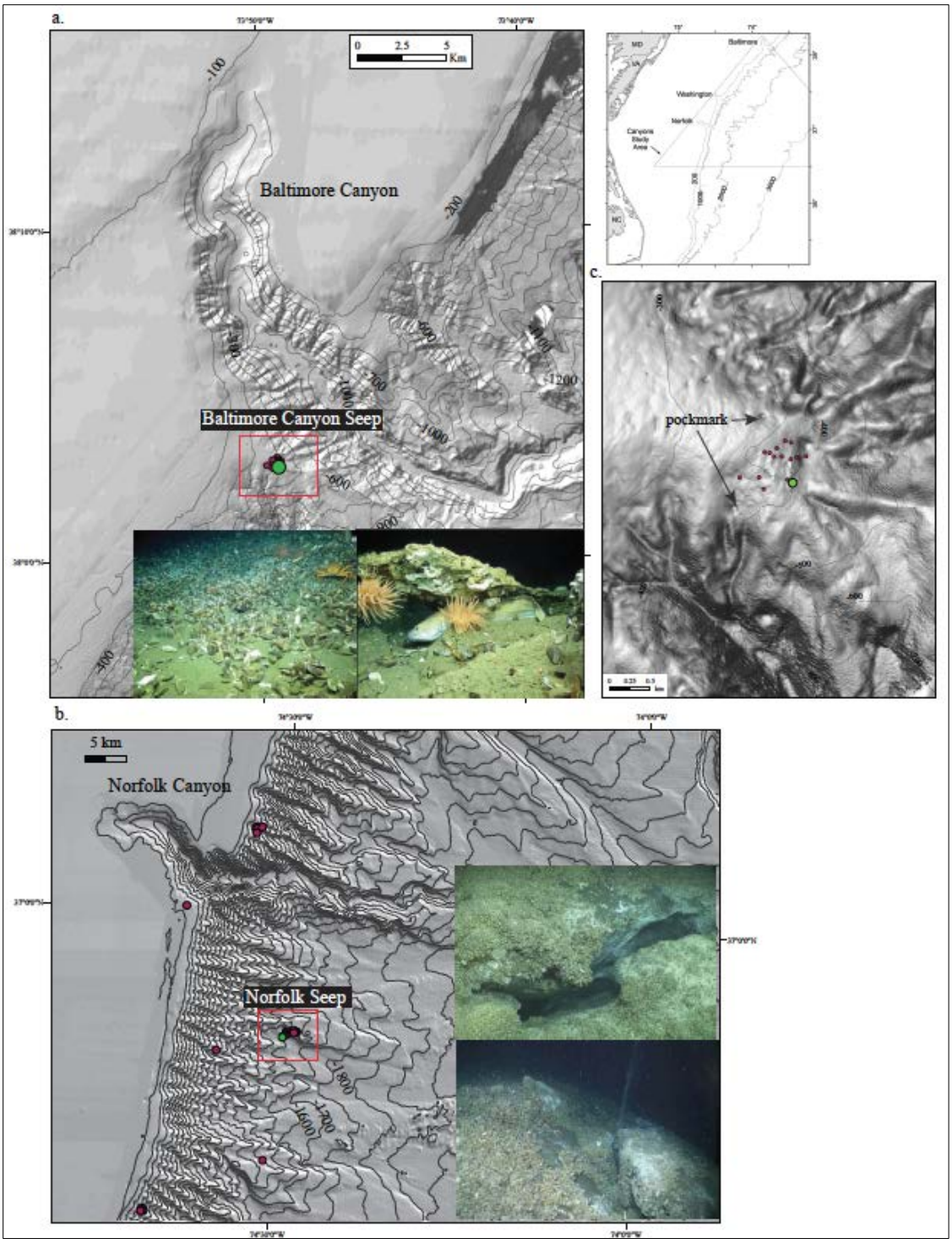

Figure 17-36. Shaded relief bathymetric maps (depth in meters) of (a) Baltimore Canyon and (b) Norfolk Canyon along the U.S. mid-Atlantic margin. The Baltimore and Norfolk canyon seep sites (red circles) from Skarke et al. (2014) and authigenic carbonate study sites (green circles). Enlarged map of Baltimore Canyon seep site (c) indicates presence of pockmarks within meters of the vents and authigenic carbonate sample site. *In situ* photos of benthic habitats in and around the respective seep sites are also shown.

17.4.3.5 Summary

The geochemistry, mineralogy, and petrology of authigenic carbonates and mussel shells collected from Baltimore and Norfolk Canyon seep sites along the mid-Atlantic continental margin provide new information on the history of methane venting and processes driving carbonate precipitation, as well as the origin and pathway of fluids. Taken together, the $^{234}U/^{238}U$, $^{87}Sr/^{86}Sr$, $\delta^{13}C$ and $\Delta^{14}C$ values support shallow precipitation of aragonite driven by AOM and at equilibrium with seawater. At Norfolk, comparison of shell $\delta^{13}C$ values from fossil and modern shells indicate a temporal shift in seepage activity and/or composition of seeping fluids. Comparison between shell $\delta^{13}C$ values of living and dead specimens from Norfolk suggests a ~25% increase in methane contribution. In addition, changes in shell $\delta^{13}C$ values during growth may be related to changes in methane flow throughout the organisms' lifespan (<25 years). The range of mussel gill and periostracum $\delta^{34}S$ values from both sites suggests an admixture of sulfur sources, hydrogen sulfide (H_2S), and seawater sulfate (SO_4), with the former sourced from sulfate reduction during AOM. Lighter mussel shell $\Delta^{14}C$ values highlight dilution of the ^{14}C pool with fossil carbon. As a result, authigenic carbonate ^{14}C- and U-Th-derived ages are discordant. According to U-Th ages, methane seepage is thought to have initiated at Baltimore Canyon seep field toward the end of the Pleistocene (~15 ka) and between ~2 to 5 ka at the Norfolk seep field (Prouty et al. 2016). Fluid flow from overpressure of sediment due to loading during the Pleistocene sea-level lowstand is the most likely mechanism to explain methane venting at Baltimore Canyon, whereas venting fluids at Norfolk, well within the gas hydrate stability zone, can be explained by flow through fractured Eocene strata (Skarke et al. 2014). There is little evidence in the carbonate geochemistry at either seep field to support deep-sourced fluid of thermogenic origin. The isotope and mineralogy of the carbonates indicate that microbial degradation of sedimentary organic matter is the common source of widespread methane that vents along the passive U.S. Atlantic margin. Results from this integrated approach provide critical clues for evaluating the ecological distribution of chemosynthetic communities and the formation processes driving the release of methane-rich fluids along passive margins and at cold-seep systems.

17.5 LITERATURE CITED

Adkins JF, Cheng H, Boyle EA, Druffel ERM, Edwards RL. 1998. Deep-sea coral evidence for rapid change in ventilation of the deep North Atlantic 15,400 years ago. Science. 280:725–728.

Adkins JA, Griffin S, Kashgarian M, Cheng H, Druffel ERM, Boyle EA, Edwards RL, Shen C. 2002. Radiocarbon dating of deepsea corals. Radiocarbon. 44(2).

Adkins JF, Henderson GM, Wang S-L, O'Shea S, Mokadem F. 2004. Growth rates of the deep-sea scleractinia *Desmophyllum cristagalli* and *Enallopsammia rostrata*. Earth and Planetary Science Letters. 227(3):481–490.

Aharon P, Schwarcz HP, Roberts HH. 1997. Radiometric dating of submarine hydrocarbon seeps in the Gulf of Mexico. Geological Society of America Bulletin. 109:568–579.

Anagnostou E, Sherrell RM, Gagnon A, LaVigne M, Field MP, McDonough WF. 2011. Seawater nutrient and carbonate ion concentrations recorded as P/Ca, Ba/ Ca, and U/Ca in the deep-sea coral *Desmophyllum dianthus*. Geochimica et Cosmochimica Acta. 75:2529–2543.

Anagnostou E, Huang K-F, You C-F, Sikes EL, Sherrell RM. 2012. Evaluation of boron isotope ratio as a pH proxy in the deep sea coral *Desmophyllum dianthus*: evidence of physiological pH adjustment. Earth and Planetary Science Letters. 349:251–260.

Armstrong FAJ, Stearns CR, Strickland JDH. 1967. The measurement of upwelling and subsequent biological processes by means of the Technicon AutoAnalyzer™ and associated equipment. Deep-Sea Research. 14(3):381–389.

Bard E, Harmelin B, Fairbanks RG. 1990. U–Th ages obtained by mass-spectrometry in corals from Barbados: sea level during the past 130000 years. Nature. 346(6283):456–458.

Bauer JE, Druffel ERM, Wolgast DM, Griffin S. 2001. Sources and cycling of dissolved and particulate organic radiocarbon in the northwest Atlantic continental margin. Global Biogeochemical Cycles. 15(3):615–636.

Bayon G, Henderson GM, Bohn M. 2009. U–Th stratigraphy of a cold seep carbonate crust. Chemical Geology. 260:47–56.

Becker EL, Lee RW, Macko SA, Faure BM, Fisher CR. 2010. Stable carbon and nitrogen isotope compositions of hydrocarbon-seep bivalves on the Gulf of Mexico lower continental slope. Deep-Sea Research Part II: Topical Studies in Oceanography. 57:1957–1964.

Berndt C. 2005. Focused fluid flow in passive continental margins. Philosophical Transcations of the Royal Society A. 363(1837):2855–2871. doi:10.1098/rsta.2005.1666.

Bernhardt H, Wilhelms A. 1967. The continuous determination of low level iron, soluble phosphate and total phosphate with the AutoAnalyzer ™. Technicon Symposia. 1:385–9.

Bishop JB. 1988. The barite-opal-organic carbon association in oceanic particulate matter. Nature. 332:341–343.

Blamart, D, Rollion-Bard C, Meibom A, Cuif J-P, Juillet-Leclerc A, Dauphin Y. 2007. Correlation of boron isotopic composition with ultrastructure in the deep-sea coral *Lophelia pertusa*: implications for biomineralization and paleo-pH. Geochemistry, Geophysics, Geosystems. 8(12): Q12001.

Boetius A, Wenzhofer F. 2013. Seafloor oxygen consumption fuelled by methane from cold seeps. Nature Geoscience. 6:725–734.

Bohrmann G, Greinert J, Suess E, Torres M. 1998. Authigenic carbonates from the Cascadia subduction zone and their relation to gas hydrate stability. Geology. 26:647–650.

Bondevik S, Birks HH, Gulliksen S, Mangerud J. 1999. Late Weichselian marine ^{14}C reservoir ages at the western coast of Norway. Quaternary Research. 52(1):104–114.

Borowski WS, Paull CK, Ussler W. 1996. Marine pore-water sulfate profiles indicate *in-situ* methane flux from underlying gas hydrate. Geology. 24:655–658.

Brenna JT, Corso TN, Tobias HJ, Caimi RJ. 1997. High-precision continuous-flow isotope ratio mass spectrometry. Mass Spectrometry Reviews. 16:227–258.

Broecker WS, Olson EA. 1961. Lamont radiocarbon measurements VIII: Radiocarbon. 3:176–204.

Brothers DS, Ruppel C, Kluesner JW, Brink US, Chaytor JD, Hill JC, Andrews BD, Flores C. 2014. Seabed fluid expulsion along the upper slope and outer shelf of the US Atlantic continental margin. Geophys Res Lett. 41:96–101.

Brothers LL, Van Dover CL, German CR, Kaiser CL, Yoerger DR, Ruppel CD, Lobecker E, Skarke AD, Wagner JKS. 2013. Evidence for extensive methane venting on the southeastern U.S. Atlantic margin. Geology. 41:807–810.

Bullen TD, Krabbenhoft DP, Kendall C. 1996. Kinetic and mineralogic controls on the evolution of groundwater chemistry and $^{87}Sr/^{86}Sr$ in a sandy silicate aquifer, northern Wisconsin, USA. Geochim Cosmochim Acta. 60:1807–1821.

Burton EA. 1993. Controls on marine carbonate cement mineralogy: review and reassessment. Chemical Geology. 105:163–179.

Cairns SD. 1994. Scleractinia of the temperate North Pacific. Smithsonian Contributions to Zoology. 557.

Canadell JG, Le Quéré C, Raupach MR, Field CB, Buitenhuis ET, Ciais P, Marland G. 2007. Contributions to accelerating atmospheric CO_2 growth from economic activity, carbon intensity, and efficiency of natural sinks. Proceedings of the National Academy of Sciences. 104(47):18866–18870.

Cao L, Fairbanks RG, Mortlock RA, Risk MJ. 2007. Radiocarbon reservoir age of high latitude North Atlantic surface water during the last deglacial. Quaternary Science Reviews. 26(5–6):732–742.

Campbell KA. 2006. Hydrocarbon seep and hydrothermal vent paleoenvironments and paleontology: past developments and future research directions. Palaeogeography, Palaeoclimatology, Palaeoecology. 232:362–407.

Campbell KA, Farmer JD, Des Marais D. 2002. Ancient hydrocarbon seeps from the Mesozoic convergent margin of California: carbonate geochemistry, fluids and paleoenvironments. Geofluids. 2:63–94.

Cheng H, Adkins J, Edwards RL Boyle EA. 2000. U–Th dating of deep-sea corals. Geochimica et Cosmochimica Acta. 64:2401–2416.

Cheng H, Edwards LR, Shen C-C, Polyak VJ, Asmerom Y, Woodhead J, Hellstrom J, Wang Y, Kong X, Spötl C, et al. 2013. Improvements in ^{230}Th dating, ^{230}Th and ^{234}U half-life values, and U–Th isotopic measurements by multi-collector inductively coupled plasma mass spectrometry. Earth and Planetary Science Letters. 371–372:82–91.

Cook HE, Johnson PD, Matti JC, Zemmels I. 1975. Methods of sample preparation and X-ray diffraction data analysis, X-ray mineralogy laboratory, deep sea drilling project, University of California, Riverside. In: Hayes DE, Frakes, LA, Barrett PJ, Burns DA, Chen Pei-Hsin, Ford AB, Kaneps AG, Kemp EM, McCollum DW, Piper DJW, et al., editors. Initial reports of the deep sea drilling project 28. Washington (DC): U.S. Government Printing Office. p. 99–1007.

Craig CA, Jarvis KE, Clarke LJ. 2000. An assessment of calibration strategies for the quantitative and semi-quantitative analysis of calcium carbonate matrices by laser ablation-inductively coupled plasma-mass spectrometry (LA-ICP-MS). Journal of Analytical Atomic Spectrometry. 15(8):1001–1008.

Crémière A, Bayon G, Ponzevera E, Pierre C. 2013. Paleo-environmental controls on cold seep carbonate authigenesis in the Sea of Marmara. Earth and Planetary Science Letters. 376:200–211.

Crocket KC, Lambelet M, van de Flierdt T, Rehkämper M, Robinson LF. 2014. Measurement of fossil deep-sea coral Nd isotopic compositions and concentrations by TIMS as NdO+, with evaluation of cleaning protocols. Chemical Geology. 374:128–140.

de Haas H, van Weering TCE, de Stigter H. 2002. Organic carbon in shelf seas: sinks or sources, processes and products. Continental Shelf Research. 22:691–717.

Delong MD, Thorp JH. 2009. Mollusc shell periostracum as an alternative to tissue in isotopic studies. Limnology and Oceanography Methods. 7:436–441.

Dickson AG. 1990. Thermodynamics of the dissociation of boric acid in synthetic 808 seawater from 273.15 to 318.15 K. Deep-Sea Research. 37:755–766.

Dickson AG, Goyet C. 1994. Handbook of methods for the analysis of the various parameters of the carbon dioxide system in sea water. Version 2 (No. ORNL/CDIAC-74). Oak Ridge (TN): Oak Ridge National Laboratory. doi:10.2172/10107773.

Dickson AG, Sabine CL, Christian JR. 2007. Guide to best practices for ocean CO_2 measurements. PICES Special Publication 3, IOCCP Report No. 8. Sydney (BC): North Pacific Marine Science Organization. 191 p.

Dietzel M, Gussone N, Eisenhauer A. 2004. Co-precipitation of Sr 2+ and Ba 2+ with aragonite by membrane diffusion of CO_2 between 10 and 50 C. Chemical Geology. 203(1):139–151.

D'Olivo JP, McCulloch MT, Eggins, SM, Trotter J. 2014. Coral records of reef-water pH across the central Great Barrier Reef, Australia: assessing the influence of river runoff on inshore reefs. Biogeosciences Discussions. 11(7):11443–11479.

Douka K, Hedges REM, Higham TFG. 2010. Improved AMS ^{14}C dating of shell carbonates using high-precision X-Ray Diffraction (XRD) and a novel density separation protocol (CarDS). Radiocarbon. 52:735–751.

Douville E, Paterne M, Cabioch G, Louvat P, Gaillardet J, Juillet-Leclerc A, Ayliffe LK. 2010. Abrupt sea surface pH change at the end of the Younger Dryas in the central sub-equatorial Pacific inferred from boron isotope abundance in corals (Porites). Biogeosciences. 7:2445–2459.

Druffel ER. 1997. Geochemistry of corals: proxies of past ocean chemistry, ocean circulation, and climate. Proceedings of the National Academy of Sciences. 94(16):8354–8361.

Druffel ERM, King LL, Belastock RA, Buesseler KO. 1990. Growth-rate of a deep-sea coral using Pb-210 and other isotopes. Geochimica et Cosmochimica Acta. 54 (5):1493–1500.

Dugan B, Flemings PB. 2000. Overpressure and fluid flow in the New Jersey continental slope: implications for slope failure and cold seeps. Science. 289:288–9.

Dugan B, Flemings PB. 2002. Fluid flow and stability of the US continental slope offshore New Jersey from the Pleistocene to the present. Geofluids. 2:137–146.

Edwards RL, Chen JH, Wasserburg GJ. 1987. ^{238}U-^{234}U-^{230}Th-^{232}Th systematics and the precise measurement of time over the past 500,000 years. Earth and Planetary Science Letters. 81:175–192.

Edwards RL, Gallup, Cheng H. 2003. Uranium-series dating of marine and lacustrine carbonates. Reviews in Mineralogy and Geochemistry. 52:363–405.

Eggins SM, Shelley JMG. 2002. Compositional heterogeneity in NIST SRM 610-617 glasses. Geostandards Newsletter. 26:269–286.

Eggins SM, Kinsley LPJ, Shelley JMG. 1998. Deposition and element fractionation processes during atmospheric pressure laser sampling for analysis by ICP–MS. Applied Surface Science. 127–129:278–286.

Elvert M, Suess E. 1999. Anaerobic methane oxidation associated with marine gas hydrates: superlight C-isotopes from saturated and unsaturated C20 and C25 irregular isoprenoids. Naturwissenschaften. 86:295–300.

Epstein S, Buchsbaum R, Lowenstam HA, Urey HC. 1953. Revised carbonate-water isotopic temperature scale. Bulletin of the Geological Society of America. 64:1315–1326.

Fallon SJ, McCulloch MT, van Woesik R, Sinclair DJ. 1999. Corals at their latitudinal limits: laser ablation trace element systematics in Porites from Shirigai Bay, Japan. Earth and Planetary Science Letters. 172:221–238.

Feng D, Cheng M, Kiel S, Qiu J-W, Yang Q, Zhou H, Peng Y, Chen D. 2015. Using Bathymodiolus tissue stable carbon, nitrogen and sulfur isotopes to infer biogeochemical process at a cold seep in the South China Sea. Deep-Sea Research Part I: Oceanographic Research Papers. 104:52–59.

Forde EB, Stanley DJ, Sawyer WB, Slagle KJ. 1981. Sediment transport in Washington and Norfolk submarine canyons. Applied Ocean Research. 3:59–62.

Formolo MJ, Lyons TW, Zhang C, Kelley C, Sassen R, Horita J, Cole DR. 2004. Quantifying carbon sources in the formation of authigenic carbonates at gas hydrate sites in the Gulf of Mexico. Chemical Geology. 205:253–264.

Foster GL. 2008. Seawater pH, pCO_2 and $[CO^{3}_{2-}]$ variations in the Caribbean Sea over the last 130 kyr: a boron isotope and B/Ca study of planktic foraminifera. Earth and Planetary Science Letters. 271:254–266.

Foster GL, Pogge von Strandmann PAE, Rae JWB. 2010. Boron and magnesium isotopic composition of seawater. Geochemistry, Geophysics, Geosystems. 11:Q08015.

Frank N, Paterne M, Ayliffe L, van Weering T, Henriet JP, Blamart D. 2004. Eastern North Atlantic deep-sea corals: tracing upper intermediate water delta ^{14}C during the Holocene. Earth and Planetary Science Letters. 219:297–309.

Gagnon AC, Adkins JF, Fernandez DP, Robinson LF. 2007. Sr/Ca and Mg/Ca vital effects correlated with skeletal architecture in a scleractinian deep-sea coral and the role of Rayleigh fractionation. Earth and Planetary Science Letters. 261:280–295.

Geist J, Auerswald K, Boom A. 2005. Stable carbon isotopes in freshwater mussel shells: environmental record or marker for metabolic activity? Geochimica et Cosmochimica Acta. 69:3545–3554.

Gieskes J, Mahn C, Day S, Martin JB, Greinert J, Rathburn T, McAdoo B. 2005. A study of the chemistry of pore fluids and authigenic carbonates in methane seep environments: Kodiak Trench, Hydrate Ridge, Monterey Bay, and Eel River Basin. Chemical Geology. 220:329–345.

Goldstein SJ, Jacobsen SB. 1987. The Nd and Sr isotopic systematics of river-water dissolved material: implications for the sources of Nd and Sr in seawater. Chemical Geology: Isotope Geoscience section. 66:245–272.

Goldstein SJ, Lea DW, Chakraborty S, Kashgarian M, Murrell MT. 2001. Uranium-series and radiocarbon geochronology of deep-sea corals: implications for Southern Ocean ventilation rates and the oceanic carbon cycle. Earth and Planetary Science Letters. 193(1):167–182.

Greinert J, Bohrmann G, Suess E. 2001. Gas hydrate-associated carbonates and methane-venting at Hydrate Ridge: classification, distribution, and origin of authigenic lithologies. In: Paull CK, Dillon WP, editors. Natural gas hydrates: occurrence, distribution, and detection. Geophysical Monograph Series 124. Washington (DC): American Geophysical Union. p. 99–113.

Grossman E, Ku TL. 1986. Oxygen and carbon isotope fractionation in biogenic aragonite: temperature effects. Isotope Geoscience. 59:59–74.

Guilderson TP, Southon JR, Brown TA. 2003. High-precision AMS ^{14}C results on TIRI/FIRI turbidite. Radiocarbon. 45(1):75–80.

Guilderson TP, Cole JE, Southon JR. 2005. Pre-bomb $\Delta^{14}C$ variability and the Suess effect in Cariaco Basin surface waters as recorded in hermatypic corals. Radiocarbon. 47(1):57–65.

Guilderson TP, McCarthy MD, Dunbar RB, Englebrecht A, Roark EB. 2013. Late Holocene variations in Pacific surface circulation and biogeochemistry inferred from proteinaceous deep-sea corals. Biogeosciences. 10(9):6019–6028.

Guinotte JM, Buddemeier RW, Kleypas JA. 2003. Future coral reef habitat marginality: temporal and spatial effects of climate change in the Pacific basin. Coral Reefs. 22(4):551–558.

Guinotte JM, Orr J, Cairns S, Freiwald A, Morgan L, George R. 2006. Will human-induced changes in seawater chemistry alter the distribution of deep-sea scleractinian corals? Frontiers in Ecology and the Environment. 4(3):141–146.

Günther D, Horn I, Hattendorf B. 2000. Recent trends and developments in laser ablation-ICP-mass spectrometry. Fresenius' Journal of Analytical Chemistry. 368(1):4–14.

Han MW, Suess E. 1989. Subduction-induced pore fluid venting and the formation of authigenic carbonates along the Cascadia continental margin: implications for the global Ca-cycle. Palaeogeography, Palaeoclimatology, Palaeoecology. 71:97–118.

Harwood JE, AL Kuhn. 1970. A colorimetric method for ammonia in natural waters. Water Research. 4:805–811.

Hart SR, Cohen AL. 1996. An ion probe study of annual cycles of Sr/Ca and other trace elements in corals. Geochimica et Cosmochimica Acta. 60:3075–3084.

Hathorne EC, Alard O, James RH, Rogers NW. 2003. Determination of intratest variability of trace elements in foraminifera by laser ablation inductively coupled plasma-mass spectrometry. Geochemistry, Geophysics, Geosystems. 4:8408.

Hathorne EC, James RH, Savage P, Alard O. 2008. Physical and chemical characteristics of particles produced by laser ablation of biogenic calcium carbonate. Journal of Analytical Atomic Spectrometry. 23(2):240–243.

Hein JR, Mizell K, Barnard PL. 2013. Sand sources and transport pathways for the San Francisco Bay coastal system, based on X-ray diffraction mineralogy. Marine Geology. 345:154–169.

Hemming NG, Hanson GN. 1992. Boron isotopic composition and concentration in modern marine carbonates. Geochimica et Cosmochimica Acta. 56:537–543.

Hennige SJ, Wicks LC, Kamenos NA, Perna G, Findlay HS, Roberts JM. 2015. Hidden impacts of ocean acidification to live and dead coral framework. In Proceeding of the Royal Society B. 282(1813):20150990.

Heyl TP, Gilhooly WP, Chambers RM, Gilchrist GW, Macko SA, Ruppel CD, Van Dover CL. 2007. Characteristics of vesicomyid clams and their environment at the Blake Ridge cold seep, South Carolina, USA. Marine Ecology Progressive Series. 339:169–184.

Hill JC, Driscoll NW, Weissel JK, Goff JA. 2004. Large-scale elongated gas blowouts along the US Atlantic margin. Journal of Geophysical Research: Solid Earth. 109(B9):2156–2202.

Hill TM, Spero HJ, Guilderson T, LaVigne M, Clague D, Macalello S, Jang N. 2011. Temperature and vital effect controls on bamboo coral (Isididae) isotope geochemistry: a test of the “lines method”. Geochemistry, Geophysics, Geosystems. 12(4).

Hinrichs KU, Hayes JM, Sylva SP, Brewer PG, DeLong EF. 1999. Methane-consuming archaebacteria in marine sediments. Nature. 398:802–805.

Hoegh-Guldberg O, Mumby PJ, Hooten AJ, Steneck SR, Greenfield P, Gomez E, Harvell CD, Sale PF, Edwards AJ, Caldeira K, et al. 2007. Coral reefs under rapid climate change and ocean acidification. Science. 318:1737–1742.

Hönisch B, Hemming NG, Grottoli AG, Amat A, Hanson GN, Bijma J. 2004. Assessing scleractinian corals as recorders for paleo-pH: empirical calibration and vital effects. Geochimica et Cosmochimica Acta. 68:3675–3685.

Hönisch B, Hemming NG. 2005. Surface ocean pH response to variations in pCO_2 through two full glacial cycles. Earth and Planetary Science Letters. 236:305–314.

Hönisch B, Hemming NG, Archer D, Siddall M, McManus JF. 2009. Atmospheric carbon dioxide concentration across the Mid-Pleistocene transition. Science. 324:1551–1554.

Hornbach MJ, Ruppel C, Saffer DM, Van Dover CL, Holbrook WS. 2005. Coupled geophysical constraints on heat flow and fluid flux at a salt diapir. Geophysical Research Letters. 32(24):L24802.

Houlbreque F, Roark EB, Guilderson TP, Dunbar RB, McCulloch M, Cuif JP, Meibom A. 2010. Uranium-series dating and growth characteristics of the deep-sea scleractinian coral: *Enallopsammia rostrata* from the Equatorial Pacific. Geochimica et Cosmochimica Acta. 74(8):2380-2395.

Ingram BL, Southon JR. 1996. Reservoir ages in eastern Pacific coastal and estuarine waters. Radiocarbon. 38(3):573–582.

James R. 2005. Marine biogeochemical cycles. 2nd ed. Oxford (UK): Butterworth-Heinemann. 130 p.

Joseph C, Campbell KA, Torres ME, Martin RA, Pohlman JW, Riedel M, Rose K. 2013. Methane-derived authigenic carbonates from modern and paleoseeps on the Cascadia margin: mechanisms of formation and diagenetic signals. Palaeogeography, Palaeoclimatology, Palaeoecology. 390:52–67.

Judd A, Hovland M. 2007. Seabed fluid flow: the impact on geology, biology and the marine environment. Cambridge (UK): Cambridge University Press.

Kakihana H, Kotaka M, Satoh S, Nomura M, Okamoto M. 1977. Fundamental studies on the ion-exchange separation of boron isotopes. Chemical Society of Japan B. 50:158–163.

Keigwin LD. 1996. The little ice age and medieval warm period in the Sargasso Sea. Science. 274(5292):1504.

Kelling G, Stanley DJ. 1970. Morphology and structure of Wilmington and Baltimore submarine canyons, eastern United States. The Journal of Geology. 78:637–660.

Kemp ALW, Thode HG. 1968. The mechanism of the bacterial reduction of sulphate and of sulphite from isotope fractionation studies. Geochimica et Cosmochimica Acta. 32:71–91.

Kerr LA, Andrews AH, Munk K, Coale KH, Frantz BR, Cailliet GM, Brown TA. 2005. Age validation of quillback rockfish (*Sebastes maliger*) using bomb radiocarbon. Fishery Bulletin. 103(1):97–107.

Klochko K, Kaufman AJ, Yoa W, Byrne RH, Tossell JA. 2006. Experimental measurement of boron isotope fractionation in seawater. Earth and Planetary Science Letters. 248:261–270.

Kluesner JW Ruppel CD, Brothers DS, Danforth WW, Edwards JH, and Hart PE. 2015. High-resolution seismic attribute analysis for the detection of methane hydrate and substrate fluid migration pathways along the central U.S. Atlantic margin. San Francisco (CA): American Geophysical Union (AGU) Fall Meeting.

Komugabe AF, Fallon SJ, Thresher RE, Eggins SM. 2014. Modern Tasman Sea surface reservoir ages from deep-sea black corals. Deep-Sea Research Part II: Topical Studies in Oceanography. 99:207-212.

Kraemer TF. 1981. ^{234}U and ^{238}U concentration in brine from geopressured aquifers of the northern Gulf of Mexico basin. Earth and Planetary Science Letters. 56:210–216.

Krief S, Hendy EJ, Fine M, Yam R, Meibom A, Foster GL, Shemesh A. 2010. Physiological and isotopic responses of scleractinian corals to ocean acidification. Geochimica et Cosmochimica Acta. 74:4988-5001.

Langdon C, Atkinson MJ. 2005. Effect of elevated pCO_2 on photosynthesis and calcification of corals and interactions with seasonal change in temperature/irradiance and nutrient enrichment. Journal of Geophysical Research: Oceans. 110(C9):1978–2012.

Langmuir D. 1978. Uranium mineral-solution equilibria. Geochimica et Cosmochimica Acta. 42:547-569.

LaVigne M, Hill TM, Spero HJ, Guilderson TP. 2011. Bamboo coral Ba/Ca: calibration of a new deep ocean refractory nutrient proxy. Earth and Planetary Science Letters. 312:506–515.

Lea DW, Shen GT, Boyle EA. 1989. Coralline barium records temporal variability in equatorial Pacific upwelling. Nature. 340:373–375.

Lemarchand D, Gaillardet J, Lewin E, Allegre CJ. 2000. The influence of rivers on marine boron isotopes and implications for reconstructing past ocean pH. Nature. 408(6815):951–954.

Le Quéré C, Raupach MR, Canadell JG, Marland G, Bopp L, Ciais P, Woodward FI. 2009. Trends in the sources and sinks of carbon dioxide. Nature Geoscience. 2:831–836.

Lewis E, Wallace, DWR. 1998. Program developed for CO_2 system calculations. ORNL/CDIAC-105. Oak Ridge (TN): Carbon Dioxide Information Analysis Center, Oak Ridge National Laboratory, U.S. Department of Energy.

Lietard C, Pierre C. 2008. High-resolution isotopic records ($\delta^{18}O$ and $\delta^{13}C$) and cathodoluminescence study of lucinid shells from methane seeps of the Eastern Mediterranean. Geo-Marine Letters. 28(4):195–203.

Lomitschka M, Mangini A. 1999. Precise U/Th dating of small and heavily coated samples of deep sea corals. Earth and Planetary Science Letters. 170:391–401.

Longerich HP, Jackson SE, Gunther D. 1997. Laser ablation inductively coupled plasma mass spectrometric transient signal data acquisition and analyte concentration calculation. Journal of Analytical Atomic Spectrometry. 12(3):391–391.

Lueker TJ, Dickson AG, Keeling CD. 2000. Ocean pCO_2 calculated from dissolved inorganic carbon, alkalinity, and equations for K1 and K2: validation based on laboratory measurements of CO_2 in gas and seawater at equilibrium. Marine Chemistry. 70:105–119.

Luthi D, Le Floch M, Bereiter B, Blunier T, Barnola J-M, Siegenthaler U, Raynaud D, Jouzel J, Fischer H, Kawamura K, Stocker TF. 2008. High-resolution carbon dioxide concentration record 650,000-800,000 years before present. Nature. 453:379.

Magalhães VH, Pinheiro LM, Ivanov MK, Kozlova E, Blinova V, Kolganova J, Vasconcelos C, McKenzie JA, Bernasconi SM, Kopf AJ, et al. 2012. Formation processes of methane-derived authigenic carbonates from the Gulf of Cadiz. Sediment Geology. (243–244):155–168.

Manzello DP, Kleypas JA, Budd DA, Eakin CM, Glynn PW, Langdon C. 2008. Poorly cemented coral reefs of the eastern tropical Pacific: Possible insights into reef development in a high-CO_2 world. Proceedings of the National Academy of Sciences. 105(30):10450–10455.

Marubini F, Ferrier–Pages C, Cuif JP. 2003. Suppression of skeletal growth in scleractinian corals by decreasing ambient carbonate-ion concentration: a cross-family comparison. Proceedings of the Royal Society of London B: Biological Sciences. 270(1511):179–184.

Matsumoto R. 1990. Vuggy carbonate crust formed by hydrocarbon seepage on the continental shelf of Baffin Island, northeast Canada. Geochemical Journal. 24:143–158.

McCulloch M, Falter J, Trotter J, Montagna P. 2012. Coral resilience to ocean acidification and global warming through pH up-regulation. Nature Climate Change. 2(8):623–627.

McNeely R, Dyke AS, Southon JR. 2006. Canadian marine reservoir ages, preliminary data assessment, Open File 5049. Geological Survey Canada. p. 3.

Michener RH, Schell DM. 1994. Stable isotope ratios as tracers in marine aquatic food webs. In: Lajtha K, Michener RH, editors. Stable isotopes in ecology and environmental science. Cambridge (MA): Blackwell Scientific Publications. p. 138–157.

Millero FJ, Zhang JZ, Lee K, Campbell DM. 1993. Titration alkalinity of seawater. Marine Chemistry. 44(2):153–165.

Montagna P, McCulloch M, Taviani M, Remia A, Rouse G. 2005. High-resolution trace and minor element compositions in deep-water scleractinian corals (*Desmophyllum dianthus*) from the Mediterranean Sea and the Great Australian Bight. In: Cold-water corals and ecosystems. Berlin Heidelberg (German): Springer-Verlag. p. 1109–1126.

Montagna P, McCulloch M, Taviani M, Mazzoli C, Vendrell B. 2006. Phosphorus in cold-water corals as a proxy for seawater nutrient chemistry. Science. 312(5781):1788–1791.

Naehr TH, Eichhubl P, Orphan VJ, Hovland M, Paull CK, Ussler W 3rd, Lorenson TD, Greene HG. 2007. Authigenic carbonate formation at hydrocarbon seeps in continental margin sediments: a comparative study. Deep Sea Research Part II: Topical Studies in Oceanography. 54:1268–1291.

Newman KR, Cormier M-H, Weissel JK, Driscoll NW, Kastner M, Solomon EA, Robertson G, Hill JC, Singh H, Camilli R. 2008. Active methane venting observed at giant pockmarks along the US mid-Atlantic shelf break. Earth and Planetary Science Letters. 267:341–352.

Obelcz J, Brothers D, Chaytor J, Brink Ut, Ross SW, Brooke S. 2014. Geomorphic characterization of four shelf-sourced submarine canyons along the U.S. Mid-Atlantic continental margin. Deep-Sea Research Part II: Topical Studies in Oceanography. 104:106–119.

Ono T, Watanabe S, Okuda K, Fukasawa M. 1998. Distribution of total carbonate and related properties in the North Pacific along 30°N. Journal of Geophysical Research Oceans. 1033(C13):30873–30883.

Orphan VJ, Ussler W, Naehr TH, House CH, Hinrichs KU, Paull CK. 2004. Geological, geochemical, and microbiological heterogeneity of the seafloor around methane vents in the Eel River Basin, offshore California. Chem Geol. 205:265–289.

Pagani M, Lemarchand D, Spivack A, Gaillardet J. 2005. A critical evaluation of the boron isotope-pH proxy: The accuracy of ancient ocean pH estimates. Geochimica et Cosmochimica Acta. 1:1953–961.

Paris G, Gaillardet J, Louvat P. 2010. Geological evolution of seawater boron isotopic composition recorded in evaporites. Geology. 38(11):1035–1038.

Paull CK, Ussler W, Borowski WS, Spiess FN. 1995. Methane-rich plumes on the Carolina continental rise: associations with gas hydrates. Geology. 23:89–92.

Pearce NJ, Perkins WT, Westgate JA, Gorton MP, Jackson SE, Neal CR, Chenery SP. 1997. A compilation of new and published major and trace element data for NIST SRM 610 and NIST SRM 612 glass reference materials. Geostandards Newsletter. 21(1):115–144.

Pearson PN, Palmer MR. 2000. Atmospheric carbon dioxide concentrations over the past 60 million years. Nature. 406(6797):695–699.

Petit JR, Jouzel J, Raynaud D, Barkov NI, Barnola JM, Basile I, Bender M, Chappellaz J, Davis M, Delaygue G, et al. 1999. Climate and atmospheric history of the past 420,000 years from the Vostok ice core, Antarctica. Nature. 399:429–436.

Planquette H, Sherrell RM. 2012. Sampling for particulate trace element determination using water sampling bottles: methodology and comparison to in situ pumps. Limnology and Oceanography: Methods. 10(5):367–388.

Poag CW. 1992. U.S. middle Atlantic continental rise: provenance, dispersal, and deposition of Jurassic to Quaternary sediments. In: Poag CW, Graciansky PC, editors. Geologic evolution of Atlantic continental rises. New York (NY):Van Nostrand Reinhold. p. 100–156.

Pohlman JW, Kaneko M, Heuer VB, Coffin RB, Whiticar M. 2009. Methane sources and production in the northern Cascadia margin gas hydrate system. Earth and Planetary Science Letters. 287:504–512.

Prouty NG, Roark EB, Koenig AE, Demopoulos AWJ, Batista BD, Kocar BD, Selby D, McCarthy MD, Mienis F, Ross SW. 2014. Deep-sea coral record of human impact on watershed quality in the Mississippi River Basin. Global Biogeochem Cycles. 28:29–43.

Prouty NG, Swarzenski P, Mienis F, Davies AJ, Demopoulos AWD, Condon D, Ross S, Brooke SS. 2015. Sources of organic matter to deep-sea corals living in submarine canyons of the Mid-Atlantic Bight region, U.S.A. 2015 Aquatic Sciences Meeting; 2015 Feb 22–27; Granada, Spain.

Prouty NG, Sahy D, Ruppel CD, Roark EB, Condon D, Brooke S, Ross SW, Demopoulos AWJ. 2016. Insights into methane dynamics from analysis of authigenic carbonates and chemosynthetic mussels at newly-discovered Atlantic margin seeps. Earth and Planetary Science Letters. 449:332–344. doi:10.1016/j.epsl.2016.05.023.

Quattrini AM, Nizinski MS, Chaytor JD, Demopoulos AWD, Roark EB, France SC, Moore JA, Heyl TP, Auster PJ, Kinlan B, et al. 2015. Exploration of the canyon-incised continental margin of the northeastern United States reveals dynamic habitats and diverse communities. PLoS ONE. 10(10):e0139904. doi:10.1371/journal.pone.0139904.

Rae JWB, Foster GL, Schmidt DN, Elliott T. 2011. Boron isotopes and B/Ca in benthic foraminifera: proxies for the deep ocean carbonate system. Earth and Planetary Science Letters. 302:403–413.

Raymond PA, Bauer JE. 2001. Riverine export of aged terrestrial organic matter to the North Atlantic Ocean. Nature. 409:497–500.

Reimer PJ, Baillie MG, Bard E, Bayliss A, Beck JW, Blackwell PG, Weyhenmeyer CE. 2009. IntCal09 and Marine09 radiocarbon age calibration curves, 0-50,000 years cal BP. Radiocarbon. 51(4):1111-1150.

Reimer PJ, Bard E, Bayliss A, Beck JW, Blackwell PG, Bronk RC, Buck CE, Cheng H, Edwards RL, Friedrich M, Grootes PM. 2013. IntCal13 and Marine13 radiocarbon age calibration curves 0-50,000 years cal BP. Radiocarbon. 55(4):1869–1887.

Risk MJ, Heikoop JM, Snow MG, Beukens R. 2002. Lifespans and growth patterns of two deep-sea corals: *Primnoa resedaeformis* and *Desmophyllum cristagalli*. Hydrobiology. 471: 125–131.

Roark EB, Guilderson TP, Flood-Page S, Dunbar RB, Ingram BL, Fallon SJ, McCulloch M. 2005. Radiocarbon-based ages and growth rates of bamboo corals from the Gulf of Alaska. Geophysical Research Letters. 32(4). doi:10.1029/2004GL021919.

Roark EB, Guilderson TP, Dunbar RB, Ingram BL. 2006. Radiocarbon-based ages and growth rates of Hawaiian deep-sea corals. Marine Ecology Progress Series. 327:1–14.

Roark EB, Guilderson TP, Dunbar RB, Fallon SJ, Mucclarone DA. 2009. Extreme longevity in proteinaceous deep-sea corals. Proceedings of the National Academy of Sciences. 106:5204–5208.

Roark EB, Prouty NG, Davies AJ, Demopoulos AWJ, Mieinis F. 2014. Using water column characteristics to better understand the cycling of dissolved and particulate matter in Norfolk and Baltimore Canyons. Ocean Sciences Meeting; 2014 Feb 23–28; Honolulu, HI.

Robinson LF, Adkins JF, Keigwin LD, Southon J, Fernandez DP, Wang SL, Scheirer DS. 2005. Radiocarbon variability in the western North Atlantic during the last deglaciation. Science. 310:1469-1473.

Robinson LF, Adkins JF, Frank N, Gagnon AC, Prouty NG, Roark EB, van de Flierdt T. 2014. The geochemistry of deep-sea coral skeletons: a review of vital effects and applications for palaeoceanography. Deep Sea Research Part II: Topical Studies in Oceanography. 99:184–198.

Rollion-Bard C, Erez J. 2010. Intra-shell boron isotope ratios in the symbiont-bearing benthic foraminiferan Amphistegina lobifera: implications for $\delta^{11}B$ vital effects and paleo-pH reconstructions. Geochimica et Cosmochimica Acta. 74:1530–1536.

Rollion-Bard C, Blamart D, Trebosc J, Tricot G, Mussi A, Cuif J-P. 2011. Boron isotopes as pH proxy: a new look at boron speciation in deep-sea corals using 11 B MAS NMR and EELS. Geochimica et Cosmochimica Acta. 75(4):1003–1012.

Ross SW, Rhode M, Quattrini AM. 2015. Demersal fish distribution and habitat use within and near Baltimore and Norfolk Canyons, U.S. middle Atlantic slope. Deep-Sea Research Part I: Oceanographic Research Papers. 103:137–154.

Ruppel, C, Kluesner, JW, Pohlman J, Brothers D, Colwell F, Krause S. and Treude T. 2015a. Methane hydrate dynamics on the U.S. Atlantic margin. DOE Fire-in-the-Ice. 15(2):10–13.

Ruppel C, Kluesner JW, Danforth W. 2015b. Imaging methane seeps and plumes on the U.S. Atlantic margin sound waves March June 2015. U.S. Geological Survey. [updated 2016 Dec 02; accessed 2015 March 20]. http://soundwaves.usgs.gov/2015/06/fieldwork3.html.

Sabine CL, Feely RA, Gruber N, Key RM, Lee K, Bullister JL, Rios AF. 2004. The oceanic sink for anthropogenic CO_2. Science. 305(5682):367–371.

Sample JC, Reid MR. 1998. Contrasting hydrogeologic regimes along strike-slip and thrust faults in the Oregon convergent margin: Evidence from the chemistry of syntectonic carbonate cements and veins. Bulletin of the Geological Society of America. 110:48–59.

Sample JC, Reid MR, Tobin HJ, Moore JC. 1993. Carbonate cements indicate channeled fluid flow along a zone of vertical faults at the deformation front of the Cascadia accretionary wedge (northwest U.S. coast). Geology. 21:507–510.

Sanyal A, Hemming NG, Hanson GN, Broecker WS. 1995. Evidence for a higher pH in the glacial ocean from boron isotopes in foraminifera. Nature. 373:234–236.

Savard M, Beauchamp B, Veizer J. 1996. Significance of aragonite cements around Cretaceous marine methane seeps. Journal of Sedimentary Research. 66:430–438.

Schlitzer R. 2015. Ocean data view. [accessed 2016 July 21]. odv.awi.de.

Schöne BR, Giere O. 2005. Growth increment and stable isotope variation in shells of the deep-sea hydrothermal vent bivalve mollusk Bathymodiolus brevior from the North Fiji Basin Pacific Ocean. Deep Sea Res I. 52:1896–1910.

Sen S, Stebbins JF, Hemming NG, Ghosh B. 1994. Coordination environments of B impurities in calcite and aragonite polymorphs: a ^{11}B MAS NMR study. American Mineralogist. 79:819–825.

Shen GT, Boyle EA. 1988. Determination of lead, cadmium and other trace metals in annually-banded corals. Chemical Geology. 67:47–62.

Shen C-C, Lawrence Edwards R, Cheng H, Dorale JA, Thomas RB, Bradley Moran S, Weinstein SE, Edmonds HN. 2002. Uranium and thorium isotopic and concentration measurements by magnetic sector inductively coupled plasma mass spectrometry. Chemical Geology. 185:165–178.

Shepard FP. 1981. Submarine canyons: multiple causes and long-time persistence. American Association of Petroleum Geologists Bulletin. 65:1062–1077.

Sherwood OA, Edinger EN. 2009. Ages and growth rates of some deep-sea gorgonian and antipatharian corals of Newfoundland and Labrador. Canadian Journal of Aquatic Science. 66:142–152.

Sherwood OA, Scott DB, Risk MJ, Guilderson TP. 2005. Radiocarbon evidence for annual growth rings in the deep-sea octocoral *Primnoa resedaeformis*. Ecology Progress Series. 301:129–134.

Sherwood OA, Guilderson TP, Batista FC, Schiff JT, McCarthy MD. 2014. Increasing subtropical North Pacific Ocean nitrogen fixation since the Little Ice Age. Nature. 505(7481):78–81.

Sinclair DJ, Risk MJ. 2006. A numerical model for trace-element coprecipitation in a physicochemical calcification system: application to coral biomineralization and trace element "vital effects." Geochimica et Cosmochimica Acta. 70:3855–3868.

Sinclair DJ, Kinsley LPJ, McCulloch MT. 1998. High resolution analysis of trace elements in corals by laser-ablation ICP-MS. Geochimica et Cosmochimica Acta. 62(11):1889–1901.

Skarke A, Ruppel C, Kodis M, Brothers D, Lobecker E. 2014. Widespread methane leakage from the sea floor on the northern US Atlantic margin. Nature Geoscience. 7:657–661.

Smith JE, Schwarcz HP, Risk MJ. 2002. Patterns of isotopic disequilibria in azooxanthellate coral skeletons. Hydrobiologia. 471:111–115.

Spivack AJ, Edmond JM. 1986. Boron isotope exchange between seawater and the oceanic crust. Geochimica et Cosmochimica Acta. 51(5):1033–1043.

Stanley Jr GD, Cairns SD. 1988. Constructional azooxanthellate coral communities: an overview with implications for the fossil record. Palaios. 233–242.

Steiger RH, Jager E. 1977. Subcommission on geochronology; convention on the use of decay constants in geo- and cosmochronology. Earth and Planetary Science Letters. 36:359–362.

Stuiver M, Polach HA. 1977. Discussion reporting of ^{14}C data. Radiocarbon. 19:355–363.

Stuiver M, Braziunas TF. 1993. Modeling atmospheric ^{14}C influences and ^{14}C ages of marine samples back to 10,000 BC. Radiocarbon. 35:137–189.

Stuiver M, Reimer PJ. 1993. Extended ^{14}C database and revised CALIB radiocarbon calibration program. Radiocarbon 35:215–230.

Stuiver M, Pearson GW, Braziunas T. 1986. Radiocarbon age calibration of marine samples back to 9000 cal yr BP. Radiocarbon. 28(2B):980–1021.

Tanaka N, Monaghan MC, Turekian KK. 1990. Radiocarbon balance of the Gulf of Maine, Long Island Sound and the Northern Middle Atlantic Bight: evidence for the extent of the Antartic Intermediate Water contribution. Journal of Marine Research. 48(1):75–87.

Tans P, Keeling R. 2014. ESRL Global Monitoring Division − Global Greenhouse Gas Reference Network. US Department of Commerce. [updated 2017 Aug 7; accessed 2015 Sept 05] http://www.esrl.noaa.gov/gmd/ccgg/trends/.

Teichert BMA, Eisenhauer A, Bohrmann G, Haase-Schramm A, Bock B, Linke P. 2003. U/Th systematics and ages of authigenic carbonates from Hydrate Ridge, Cascadia margin: recorders of fluid flow variations. Geochimica et Cosmochimica Acta. 67:3845–3857.

ten Brink US, Chaytor JD, Geist EL, Brothers DS, Andrews BD. 2014. Assessment of tsunami hazard to the U.S. Atlantic margin. Marine Geology. 353:31–54.

Thiel V, Peckmann J, Seifert R, Wehrung P, Reitner J, Michaelis W. 1999. Highly isotopically depleted isoprenoids: molecular markers for ancient methane venting. Geochimica et Cosmochimica Acta. 63:3959–3966.

Tracey DM, Neil H, Marriott P, Andrews AH, Cailliet GM, Sánchez JA. 2007. Age and growth of two genera of deep-sea bamboo corals (Family Isididae) in New Zealand waters. Bulletin of Marine Science. 81(3):393–408.

Trotter J, Montagna P, McCulloch M, Silenzi S, Reynaud S, Mortimer G, Martin S, Ferrier-Pagès C, Gattuso J-P, Rodolfo-Metalpa R. 2011. Quantifying the pH "vital effect"in the temperate zooxanthellate coral *Cladocora caespitosa*: validation of the boron seawater pH proxy. Earth and Planetary Science Letters. 303(3):163–173.

Twichell DC, Knebel HJ, Folger DW. 1977. Delaware River: evidence for its former extension to Wilmington submarine canyon. Science. 195:483–485.

van de Flierdt T, Robinson LF, Adkins JF, Hemming SR, Goldstein SL. 2006. Temporal stability of the neodymium isotope signature of the Holocene to Glacial North Atlantic. Paleoceanography. 21(4):PA4102. doi:10.1029/2006PA001340.

van de Flierdt T, Robinson LF, Adkins JF. 2010. Deep-sea coral aragonite as a recorder for the neodymium isotopic composition of seawater. Geochimica et Cosmochimica Acta. 74(21):6014–6032.

Van Dover CL, Aharon P, Bernhard JM, Caylor E, Doerries M, Flickinger W, Gilhooly W, Goffredi SK, Knick KE, Macko SA, et al. 2003. Blake Ridge methane seeps: characterization of a soft sediment, chemosynthetically based ecosystem. Deep Sea Research Part I: Oceanographic Research Papers. 50:281–300.

Vogel JS, Southon JR, Nelson DE. 1987. Catalyst and binder effects in the use of filamentous graphite for AMS. Nuclear Instruments & Methods in Physics Research Section B-Beam Interactions with Materials and Atoms. 29:50–56.

Wang BS, You CF, Huang KF, Wu SF, Aggarwal SK, Chung CH, Lin PY. 2010. Direct separation of boron from Na-and Ca-rich matrices by sublimation for stable isotope measurement by MC-ICP-MS. Talanta. 82(4):1378–1384.

Wedepohl KH. 1995. The composition of the continental crust. Geochimica et Cosmochimica Acta. 59:1217–1232.

Weidman CR, Jones GA. 1993. A shell-derived time history of bomb ^{14}C on Georges Bank and its Labrador Sea implications. Journal of Geophysical Research. 98(C8):14577–14588.

Yamanaka T, Mizota C, Fujiwara Y, Chiba H, Hashimoto J, Gamo T, Okudaira T. 2003. Sulphur isotopic composition of the deep-sea mussel *Bathymodiolus marisindicus* from currently active hydrothermal vents in the Indian Ocean. Journal of the Marine Biological Association of the UK. 83:841–848.

Yu J, Elderfield H. 2007. Benthic foraminiferal B/Ca ratios reflect deep water carbonate saturation state. Earth and Planetary Science Letters. 258:73–86.

Zeebe R, Wolf-Gladow DA. 2001. CO_2 in seawater: equilibrium, kinetics, isotopes. Elsevier Oceanography Series, vol. 65. Amsterdam (NL): Elsevier.

This page intentionally left blank

Appendix 17-A

Water Column Sampling Locations and Depths, and Results from Radiocarbon Analyses and U-Th Age Dating

This page intentionally left blank

Table 17-A1. Seawater samples CTD location and water depth at Baltimore and Norfolk canyons.

Station	CTD Site ID	Depth (m)	Latitude (N)	Longitude (W)	Niskin Bottle
RB-13-003	A	200	37°05′31.50″	74°44′47.46″	1
RB-13-003	A	200	37°05′31.50″	74°44′47.46″	2
RB-13-003	A	200	37°05′31.50″	74°44′47.46″	3
RB-13-003	A	200	37°05′31.50″	74°44′47.46″	4
RB-13-003	A	200	37°05′31.50″	74°44′47.46″	5
RB-13-003	A	0	37°05′31.50″	74°44′47.46″	6
RB-13-003	A	0	37°05′31.50″	74°44′47.46″	7
RB-13-003	A	0	37°05′31.50″	74°44′47.46″	8
RB-13-003	A	0	37°05′31.50″	74°44′47.46″	9
RB-13-003	A	0	37°05′31.50″	74°44′47.46″	10
RB-13-003	A	0	37°05′31.50″	74°44′47.46″	11
RB-13-003	A	0	37°05′31.50″	74°44′47.46″	12
RB-13-004	B	238	37°05′25.08″	74°43′39.84″	1
RB-13-004	B	238	37°05′25.08″	74°43′39.84″	2
RB-13-004	B	200	37°05′25.08″	74°43′39.84″	3
RB-13-004	B	150	37°05′25.08″	74°43′39.84″	4
RB-13-004	B	125	37°05′25.08″	74°43′39.84″	5
RB-13-004	B	100	37°05′25.08″	74°43′39.84″	6
RB-13-004	B	75	37°05′25.08″	74°43′39.84″	7
RB-13-004	B	50	37°05′25.08″	74°43′39.84″	8
RB-13-004	B	30	37°05′25.08″	74°43′39.84″	9
RB-13-004	B	20	37°05′25.08″	74°43′39.84″	10
RB-13-004	B	10	37°05′25.08″	74°43′39.84″	11
RB-13-004	B	0	37°05′25.08″	74°43′39.84″	12
RB-13-005	C	335	37°05′36.18″	74°42′15.54″	1
RB-13-005	C	335	37°05′36.18″	74°42′15.54″	2
RB-13-005	C	335	37°05′36.18″	74°42′15.54″	3
RB-13-005	C	335	37°05′36.18″	74°42′15.54″	4
RB-13-005	C	335	37°05′36.18″	74°42′15.54″	5
RB-13-005	C	335	37°05′36.18″	74°42′15.54″	6
RB-13-005	C	0	37°05′36.18″	74°42′15.54″	7
RB-13-005	C	0	37°05′36.18″	74°42′15.54″	8
RB-13-005	C	0	37°05′36.18″	74°42′15.54″	9
RB-13-005	C	0	37°05′36.18″	74°42′15.54″	10
RB-13-005	C	0	37°05′36.18″	74°42′15.54″	11
RB-13-005	C	0	37°05′36.18″	74°42′15.54″	12
RB-13-006	D	437	37°05′37.44″	74°40′52.38″	1
RB-13-006	D	437	37°05′37.44″	74°40′52.38″	2
RB-13-006	D	437	37°05′37.44″	74°40′52.38″	3
RB-13-006	D	437	37°05′37.44″	74°40′52.38″	4
RB-13-006	D	437	37°05′37.44″	74°40′52.38″	5
RB-13-006	D	437	37°05′37.44″	74°40′52.38″	6
RB-13-006	D	0	37°05′37.44″	74°40′52.38″	7
RB-13-006	D	0	37°05′37.44″	74°40′52.38″	8
RB-13-006	D	0	37°05′37.44″	74°40′52.38″	9

Table 17-A1. (Continued).

Station	CTD Site ID	Depth (m)	Latitude (N)	Longitude (W)	Niskin Bottle
RB-13-006	D	0	37°05′37.44″	74°40′52.38″	10
RB-13-006	D	0	37°05′37.44″	74°40′52.38″	11
RB-13-006	D	0	37°05′37.44″	74°40′52.38″	12
RB-13-007	F	606	37°03′57.12″	74°39′02.04″	1
RB-13-007	F	400	37°03′57.12″	74°39′02.04″	2
RB-13-007	F	250	37°03′57.12″	74°39′02.04″	3
RB-13-007	F	150	37°03′57.12″	74°39′02.04″	4
RB-13-007	F	125	37°03′57.12″	74°39′02.04″	5
RB-13-007	F	100	37°03′57.12″	74°39′02.04″	6
RB-13-007	F	75	37°03′57.12″	74°39′02.04″	7
RB-13-007	F	50	37°03′57.12″	74°39′02.04″	8
RB-13-007	F	30	37°03′57.12″	74°39′02.04″	9
RB-13-007	F	20	37°03′57.12″	74°39′02.04″	10
RB-13-007	F	10	37°03′57.12″	74°39′02.04″	11
RB-13-007	F	0	37°03′57.12″	74°39′02.04″	12
RB-13-008	H	838	37°02′20.10″	74°37′27.96″	1
RB-13-008	H	838	37°02′20.10″	74°37′27.96″	2
RB-13-008	H	838	37°02′20.10″	74°37′27.96″	3
RB-13-008	H	838	37°02′20.10″	74°37′27.96″	4
RB-13-008	H	838	37°02′20.10″	74°37′27.96″	5
RB-13-008	H	838	37°02′20.10″	74°37′27.96″	6
RB-13-008	H	0	37°02′20.10″	74°37′27.96″	7
RB-13-008	H	0	37°02′20.10″	74°37′27.96″	8
RB-13-008	H	0	37°02′20.10″	74°37′27.96″	9
RB-13-008	H	0	37°02′20.10″	74°37′27.96″	10
RB-13-008	H	0	37°02′20.10″	74°37′27.96″	11
RB-13-008	H	0	37°02′20.10″	74°37′27.96″	12
RB-13-009	J	838	37°02′16.08″	74°35′58.80″	1
RB-13-009	J	838	37°02′16.08″	74°35′58.80″	2
RB-13-009	J	838	37°02′16.08″	74°35′58.80″	3
RB-13-009	J	838	37°02′16.08″	74°35′58.80″	4
RB-13-009	J	838	37°02′16.08″	74°35′58.80″	5
RB-13-009	J	838	37°02′16.08″	74°35′58.80″	6
RB-13-009	J	0	37°02′16.08″	74°35′58.80″	7
RB-13-009	J	0	37°02′16.08″	74°35′58.80″	8
RB-13-009	J	0	37°02′16.08″	74°35′58.80″	9
RB-13-009	J	0	37°02′16.08″	74°35′58.80″	10
RB-13-009	J	0	37°02′16.08″	74°35′58.80″	11
RB-13-009	J	0	37°02′16.08″	74°35′58.80″	12
RB-13-010	L	1168	37°02′11.04″	74°33′48.00″	1
RB-13-010	L	1168	37°02′11.04″	74°33′48.00″	2
RB-13-010	L	1000	37°02′11.04″	74°33′48.00″	3
RB-13-010	L	900	37°02′11.04″	74°33′48.00″	4
RB-13-010	L	800	37°02′11.04″	74°33′48.00″	5
RB-13-010	L	700	37°02′11.04″	74°33′48.00″	6
RB-13-010	L	600	37°02′11.04″	74°33′48.00″	7

Table 17-A1. (Continued).

Station	CTD Site ID	Depth (m)	Latitude (N)	Longitude (W)	Niskin Bottle
RB-13-010	L	500	37°02′11.04″	74°33′48.00″	8
RB-13-010	L	400	37°02′11.04″	74°33′48.00″	9
RB-13-010	L	300	37°02′11.04″	74°33′48.00″	10
RB-13-010	L	250	37°02′11.04″	74°33′48.00″	11
RB-13-010	L	200	37°02′11.04″	74°33′48.00″	12
RB-13-011	L	250	37°02′11.04″	74°33′48.00″	1
RB-13-011	L	200	37°02′11.04″	74°33′48.00″	2
RB-13-011	L	150	37°02′11.04″	74°33′48.00″	3
RB-13-011	L	125	37°02′11.04″	74°33′48.00″	4
RB-13-011	L	100	37°02′11.04″	74°33′48.00″	5
RB-13-011	L	75	37°02′11.04″	74°33′48.00″	6
RB-13-011	L	50	37°02′11.04″	74°33′48.00″	7
RB-13-011	L	30	37°02′11.04″	74°33′48.00″	8
RB-13-011	L	20	37°02′11.04″	74°33′48.00″	9
RB-13-011	L	10	37°02′11.04″	74°33′48.00″	10
RB-13-011	L	0	37°02′11.04″	74°33′48.00″	11
RB-13-011	L	0	37°02′11.04″	74°33′48.00″	12
RB-13-012	N	1290	37°02′11.64″	74°31′57.30″	1
RB-13-012	N	1290	37°02′11.64″	74°31′57.30″	2
RB-13-012	N	1290	37°02′11.64″	74°31′57.30″	3
RB-13-012	N	1290	37°02′11.64″	74°31′57.30″	4
RB-13-012	N	1290	37°02′11.64″	74°31′57.30″	5
RB-13-012	N	1290	37°02′11.64″	74°31′57.30″	6
RB-13-012	N	0	37°02′11.64″	74°31′57.30″	7
RB-13-012	N	0	37°02′11.64″	74°31′57.30″	8
RB-13-012	N	0	37°02′11.64″	74°31′57.30″	9
RB-13-012	N	0	37°02′11.64″	74°31′57.30″	10
RB-13-012	N	0	37°02′11.64″	74°31′57.30″	11
RB-13-012	N	0	37°02′11.64″	74°31′57.30″	12
RB-13-015	O	1358	37°02′32.76″	74°31′02.16″	1
RB-13-015	O	1358	37°02′32.76″	74°31′02.16″	2
RB-13-015	O	1358	37°02′32.76″	74°31′02.16″	3
RB-13-015	O	1358	37°02′32.76″	74°31′02.16″	4
RB-13-015	O	1358	37°02′32.76″	74°31′02.16″	5
RB-13-015	O	1358	37°02′32.76″	74°31′02.16″	6
RB-13-015	O	0	37°02′32.76″	74°31′02.16″	7
RB-13-015	O	0	37°02′32.76″	74°31′02.16″	8
RB-13-015	O	0	37°02′32.76″	74°31′02.16″	9
RB-13-015	O	0	37°02′32.76″	74°31′02.16″	10
RB-13-015	O	0	37°02′32.76″	74°31′02.16″	11
RB-13-015	O	0	37°02′32.76″	74°31′02.16″	12
RB-13-016	M	1240	37°02′15.84″	74°32′55.92″	1
RB-13-016	M	1240	37°02′15.84″	74°32′55.92″	2
RB-13-016	M	1240	37°02′15.84″	74°32′55.92″	3
RB-13-016	M	1240	37°02′15.84″	74°32′55.92″	4
RB-13-016	M	1240	37°02′15.84″	74°32′55.92″	5

Table 17-A1. (Continued).

Station	CTD Site ID	Depth (m)	Latitude (N)	Longitude (W)	Niskin Bottle
RB-13-016	M	1240	37°02′15.84″	74°32′55.92″	6
RB-13-016	M	0	37°02′15.84″	74°32′55.92″	7
RB-13-016	M	0	37°02′15.84″	74°32′55.92″	8
RB-13-016	M	0	37°02′15.84″	74°32′55.92″	9
RB-13-016	M	0	37°02′15.84″	74°32′55.92″	10
RB-13-016	M	0	37°02′15.84″	74°32′55.92″	11
RB-13-016	M	0	37°02′15.84″	74°32′55.92″	12
RB-13-017	K	1097	37°02′16.20″	74°34′40.86″	1
RB-13-017	K	1097	37°02′16.20″	74°34′40.86″	2
RB-13-017	K	1097	37°02′16.20″	74°34′40.86″	3
RB-13-017	K	1097	37°02′16.20″	74°34′40.86″	4
RB-13-017	K	1097	37°02′16.20″	74°34′40.86″	5
RB-13-017	K	1097	37°02′16.20″	74°34′40.86″	6
RB-13-017	K	0	37°02′16.20″	74°34′40.86″	7
RB-13-017	K	0	37°02′16.20″	74°34′40.86″	8
RB-13-017	K	0	37°02′16.20″	74°34′40.86″	9
RB-13-017	K	0	37°02′16.20″	74°34′40.86″	10
RB-13-017	K	0	37°02′16.20″	74°34′40.86″	11
RB-13-017	K	0	37°02′16.20″	74°34′40.86″	12
RB-13-018	I	726	37°03′13.56″	74°38′03.72″	1
RB-13-018	I	726	37°03′13.56″	74°38′03.72″	2
RB-13-018	I	726	37°03′13.56″	74°38′03.72″	3
RB-13-018	I	726	37°03′13.56″	74°38′03.72″	4
RB-13-018	I	726	37°03′13.56″	74°38′03.72″	5
RB-13-018	I	726	37°03′13.56″	74°38′03.72″	6
RB-13-018	I	0	37°03′13.56″	74°38′03.72″	7
RB-13-018	I	0	37°03′13.56″	74°38′03.72″	8
RB-13-018	I	0	37°03′13.56″	74°38′03.72″	9
RB-13-018	I	0	37°03′13.56″	74°38′03.72″	10
RB-13-018	I	0	37°03′13.56″	74°38′03.72″	11
RB-13-018	I	0	37°03′13.56″	74°38′03.72″	12
RB-13-019	G	628	37°03′56.82″	74°38′58.98″	1
RB-13-019	G	628	37°03′56.82″	74°38′58.98″	2
RB-13-019	G	628	37°03′56.82″	74°38′58.98″	3
RB-13-019	G	628	37°03′56.82″	74°38′58.98″	4
RB-13-019	G	628	37°03′56.82″	74°38′58.98″	5
RB-13-019	G	628	37°03′56.82″	74°38′58.98″	6
RB-13-019	G	0	37°03′56.82″	74°38′58.98″	7
RB-13-019	G	0	37°03′56.82″	74°38′58.98″	8
RB-13-019	G	0	37°03′56.82″	74°38′58.98″	9
RB-13-019	G	0	37°03′56.82″	74°38′58.98″	10
RB-13-019	G	0	37°03′56.82″	74°38′58.98″	11
RB-13-019	G	0	37°03′56.82″	74°38′58.98″	12
RB-13-020	E	532	37°04′45.18″	74°39′51.42″	1
RB-13-020	E	532	37°04′45.18″	74°39′51.42″	2
RB-13-020	E	532	37°04′45.18″	74°39′51.42″	3

Table 17-A1. (Continued).

Station	CTD Site ID	Depth (m)	Latitude (N)	Longitude (W)	Niskin Bottle
RB-13-020	E	532	37°04′45.18″	74°39′51.42″	4
RB-13-020	E	532	37°04′45.18″	74°39′51.42″	5
RB-13-020	E	532	37°04′45.18″	74°39′51.42″	6
RB-13-020	E	0	37°04′45.18″	74°39′51.42″	7
RB-13-020	E	0	37°04′45.18″	74°39′51.42″	8
RB-13-020	E	0	37°04′45.18″	74°39′51.42″	9
RB-13-020	E	0	37°04′45.18″	74°39′51.42″	10
RB-13-020	E	0	37°04′45.18″	74°39′51.42″	11
RB-13-020	E	0	37°04′45.18″	74°39′51.42″	12
RB-13-021	B	247	37°05′28.32″	74°43′45.48″	1
RB-13-021	B	247	37°05′28.32″	74°43′45.48″	2
RB-13-021	B	247	37°05′28.32″	74°43′45.48″	3
RB-13-021	B	247	37°05′28.32″	74°43′45.48″	4
RB-13-021	B	247	37°05′28.32″	74°43′45.48″	5
RB-13-021	B	247	37°05′28.32″	74°43′45.48″	6
RB-13-021	B	0	37°05′28.32″	74°43′45.48″	7
RB-13-021	B	0	37°05′28.32″	74°43′45.48″	8
RB-13-021	B	0	37°05′28.32″	74°43′45.48″	9
RB-13-021	B	0	37°05′28.32″	74°43′45.48″	10
RB-13-021	B	0	37°05′28.32″	74°43′45.48″	11
RB-13-021	B	0	37°05′28.32″	74°43′45.48″	12
RB-13-022	F	633	37°03′54.66″	74°38′54.60″	1
RB-13-022	F	633	37°03′54.66″	74°38′54.60″	2
RB-13-022	F	300	37°03′54.66″	74°38′54.60″	3
RB-13-022	F	300	37°03′54.66″	74°38′54.60″	4
RB-13-022	F	150	37°03′54.66″	74°38′54.60″	5
RB-13-022	F	150	37°03′54.66″	74°38′54.60″	6
RB-13-022	F	100	37°03′54.66″	74°38′54.60″	7
RB-13-022	F	100	37°03′54.66″	74°38′54.60″	8
RB-13-022	F	50	37°03′54.66″	74°38′54.60″	9
RB-13-022	F	50	37°03′54.66″	74°38′54.60″	10
RB-13-022	F	10	37°03′54.66″	74°38′54.60″	11
RB-13-022	F	10	37°03′54.66″	74°38′54.60″	12
RB-13-ROV-681		426	37°03′01.61″	74°37′13.14″	
RB-13-031		1603	36°51′46.86″	74°29′24.90″	1
RB-13-031		1603	36°51′46.86″	74°29′24.90″	2
RB-13-031		1603	36°51′46.86″	74°29′24.90″	3
RB-13-031		1603	36°51′46.86″	74°29′24.90″	4
RB-13-031		1603	36°51′46.86″	74°29′24.90″	5
RB-13-031		1603	36°51′46.86″	74°29′24.90″	6
RB-13-031		5	36°51′46.86″	74°29′24.90″	7
RB-13-031		5	36°51′46.86″	74°29′24.90″	8
RB-13-031		5	36°51′46.86″	74°29′24.90″	9
RB-13-031		5	36°51′46.86″	74°29′24.90″	10
RB-13-031		5	36°51′46.86″	74°29′24.90″	11
RB-13-031		5	36°51′46.86″	74°29′24.90″	12

Table 17-A1. (Continued).

Station	CTD Site ID	Depth (m)	Latitude (N)	Longitude (W)	Niskin Bottle
RB-13-ROV-682	seep site	1602	36°51′56.87″	74°29′27.00″	ROV niskin
RB-13-034	seep site	1620	36°51′47.58″	74°29′27.00″	1
RB-13-034	seep site	1620	36°51′47.58″	74°29′27.00″	2
RB-13-034	seep site	1620	36°51′47.58″	74°29′27.00″	3
RB-13-034	seep site	1620	36°51′47.58″	74°29′27.00″	4
RB-13-034	seep site	1620	36°51′47.58″	74°29′27.00″	5
RB-13-034	seep site	1620	36°51′47.58″	74°29′27.00″	6
RB-13-034	seep site	3	36°51′47.58″	74°29′27.00″	7
RB-13-034	seep site	3	36°51′47.58″	74°29′27.00″	8
RB-13-034	seep site	3	36°51′47.58″	74°29′27.00″	9
RB-13-034	seep site	3	36°51′47.58″	74°29′27.00″	10
RB-13-034	seep site	3	36°51′47.58″	74°29′27.00″	11
RB-13-034	seep site	3	36°51′47.58″	74°29′27.00″	12
RB-13-ROV-683	seep site	1481	36°52′18.82″	74°28′37.34″	ROV niskin
RB-13-ROV-683	seep site	1481	36°52′18.82″	74°28′37.34″	ROV niskin
RB-13-052	Y	1063	37°00′20.28″	74°31′18.54″	1
RB-13-052	Y	1063	37°00′20.28″	74°31′18.54″	2
RB-13-052	Y	500	37°00′20.28″	74°31′18.54″	3
RB-13-052	Y	250	37°00′20.28″	74°31′18.54″	4
RB-13-052	Y	150	37°00′20.28″	74°31′18.54″	5
RB-13-052	Y	100	37°00′20.28″	74°31′18.54″	6
RB-13-052	Y	75	37°00′20.28″	74°31′18.54″	7
RB-13-052	Y	50	37°00′20.28″	74°31′18.54″	8
RB-13-052	Y	20	37°00′20.28″	74°31′18.54″	9
RB-13-052	Y	10	37°00′20.28″	74°31′18.54″	10
RB-13-052	Y	3	37°00′20.28″	74°31′18.54″	11
RB-13-052	Y	3	37°00′20.28″	74°31′18.54″	12
RB-13-053	X	1087	37°00′21.90″	74°32′13.08″	1
RB-13-053	X	1087	37°00′21.90″	74°32′13.08″	2
RB-13-053	X	1087	37°00′21.90″	74°32′13.08″	3
RB-13-053	X	1087	37°00′21.90″	74°32′13.08″	4
RB-13-053	X	1087	37°00′21.90″	74°32′13.08″	5
RB-13-053	X	1087	37°00′21.90″	74°32′13.08″	6
RB-13-053	X	3	37°00′21.90″	74°32′13.08″	7
RB-13-053	X	3	37°00′21.90″	74°32′13.08″	8
RB-13-053	X	3	37°00′21.90″	74°32′13.08″	9
RB-13-053	X	3	37°00′21.90″	74°32′13.08″	10
RB-13-053	X	3	37°00′21.90″	74°32′13.08″	11
RB-13-053	X	3	37°00′21.90″	74°32′13.08″	12
RB-13-ROV-685	Norfolk deep	1388	37°02′56.70″	74°30′35.92″	ROV Niskin
RB-13-063	W	940	37°00′29.40″	74°33′09.60″	1
RB-13-063	W	940	37°00′29.40″	74°33′09.60″	2
RB-13-063	W	940	37°00′29.40″	74°33′09.60″	3
RB-13-063	W	940	37°00′29.40″	74°33′09.60″	4
RB-13-063	W	940	37°00′29.40″	74°33′09.60″	5
RB-13-063	W	940	37°00′29.40″	74°33′09.60″	6

Table 17-A1. (Continued).

Station	CTD Site ID	Depth (m)	Latitude (N)	Longitude (W)	Niskin Bottle
RB-13-063	W	3	37°00′29.40″	74°33′09.60″	7
RB-13-063	W	3	37°00′29.40″	74°33′09.60″	8
RB-13-063	W	3	37°00′29.40″	74°33′09.60″	9
RB-13-063	W	3	37°00′29.40″	74°33′09.60″	10
RB-13-063	W	3	37°00′29.40″	74°33′09.60″	11
RB-13-063	W	3	37°00′29.40″	74°33′09.60″	12
RB-13-064	V	740	37°00′31.92″	74°33′53.34″	1
RB-13-064	V	740	37°00′31.92″	74°33′53.34″	2
RB-13-064	V	740	37°00′31.92″	74°33′53.34″	3
RB-13-064	V	740	37°00′31.92″	74°33′53.34″	4
RB-13-064	V	740	37°00′31.92″	74°33′53.34″	5
RB-13-064	V	740	37°00′31.92″	74°33′53.34″	6
RB-13-064	V	3	37°00′31.92″	74°33′53.34″	7
RB-13-064	V	3	37°00′31.92″	74°33′53.34″	8
RB-13-064	V	3	37°00′31.92″	74°33′53.34″	9
RB-13-064	V	3	37°00′31.92″	74°33′53.34″	10
RB-13-064	V	3	37°00′31.92″	74°33′53.34″	11
RB-13-064	V	3	37°00′31.92″	74°33′53.34″	12
RB-13-065	U	675	37°00′36.96″	74°34′35.04″	1
RB-13-065	U	675	37°00′36.96″	74°34′35.04″	2
RB-13-065	U	675	37°00′36.96″	74°34′35.04″	3
RB-13-065	U	675	37°00′36.96″	74°34′35.04″	4
RB-13-065	U	675	37°00′36.96″	74°34′35.04″	5
RB-13-065	U	675	37°00′36.96″	74°34′35.04″	6
RB-13-065	U	3	37°00′36.96″	74°34′35.04″	7
RB-13-065	U	3	37°00′36.96″	74°34′35.04″	8
RB-13-065	U	3	37°00′36.96″	74°34′35.04″	9
RB-13-065	U	3	37°00′36.96″	74°34′35.04″	10
RB-13-065	U	3	37°00′36.96″	74°34′35.04″	11
RB-13-065	U	3	37°00′36.96″	74°34′35.04″	12
RB-13-066	T	355	37°00′38.76″	74°35′28.20″	1
RB-13-066	T	355	37°00′38.76″	74°35′28.20″	2
RB-13-066	T	355	37°00′38.76″	74°35′28.20″	3
RB-13-066	T	355	37°00′38.76″	74°35′28.20″	4
RB-13-066	T	355	37°00′38.76″	74°35′28.20″	5
RB-13-066	T	355	37°00′38.76″	74°35′28.20″	6
RB-13-066	T	3	37°00′38.76″	74°35′28.20″	7
RB-13-066	T	3	37°00′38.76″	74°35′28.20″	8
RB-13-066	T	3	37°00′38.76″	74°35′28.20″	9
RB-13-066	T	3	37°00′38.76″	74°35′28.20″	10
RB-13-066	T	3	37°00′38.76″	74°35′28.20″	11
RB-13-066	T	3	37°00′38.76″	74°35′28.20″	12
RB-13-067	R	373	37°00′50.10″	74°36′55.68″	1
RB-13-067	R	373	37°00′50.10″	74°36′55.68″	2
RB-13-067	R	373	37°00′50.10″	74°36′55.68″	3
RB-13-067	R	373	37°00′50.10″	74°36′55.68″	4

Table 17-A1. (Continued).

Station	CTD Site ID	Depth (m)	Latitude (N)	Longitude (W)	Niskin Bottle
RB-13-067	R	373	37°00′50.10″	74°36′55.68″	5
RB-13-067	R	373	37°00′50.10″	74°36′55.68″	6
RB-13-067	R	373	37°00′50.10″	74°36′55.68″	7
RB-13-067	R	373	37°00′50.10″	74°36′55.68″	8
RB-13-067	R	373	37°00′50.10″	74°36′55.68″	9
RB-13-067	R	373	37°00′50.10″	74°36′55.68″	10
RB-13-067	R	373	37°00′50.10″	74°36′55.68″	11
RB-13-067	R	373	37°00′50.10″	74°36′55.68″	12
RB-13-068	P	125	37°01′09.48″	74°38′46.20″	1
RB-13-068	P	125	37°01′09.48″	74°38′46.20″	2
RB-13-068	P	125	37°01′09.48″	74°38′46.20″	3
RB-13-068	P	125	37°01′09.48″	74°38′46.20″	4
RB-13-068	P	125	37°01′09.48″	74°38′46.20″	5
RB-13-068	P	125	37°01′09.48″	74°38′46.20″	6
RB-13-068	P	125	37°01′09.48″	74°38′46.20″	7
RB-13-068	P	125	37°01′09.48″	74°38′46.20″	8
RB-13-068	P	125	37°01′09.48″	74°38′46.20″	9
RB-13-068	P	125	37°01′09.48″	74°38′46.20″	10
RB-13-068	P	125	37°01′09.48″	74°38′46.20″	11
RB-13-068	P	125	37°01′09.48″	74°38′46.20″	12
RB-13-ROV-687	Norfolk (mid)	393.65	37°03′37.99″	74°34′41.73″	Red Niskin
RB-13-ROV-687	Norfolk (mid)	393.65	37°03′37.99″	74°34′41.73″	Green Niskin
RB-13-ROV-689	Baltimore(seep)	400	38°02′38.50″	73°44′28.33″	Red Niskin
RB-13-ROV-689	Baltimore(seep)	400	38°02′38.50″	73°44′28.33″	Green Niskin
RB-13-ROV-691	Norfolk	421	37°01′55.26″	74°38′05.66″	Red Niskin
RB-13-084	Baltimore (seep)	1570	36°52′08.28″	74°29′38.04″	1
RB-13-084	Baltimore (seep)	1570	36°52′08.28″	74°29′38.04″	2
RB-13-084	Baltimore (seep)	1570	36°52′08.28″	74°29′38.04″	3
RB-13-084	Baltimore (seep)	1570	36°52′08.28″	74°29′38.04″	4
RB-13-084	Baltimore (seep)	1570	36°52′08.28″	74°29′38.04″	5
RB-13-084	Baltimore (seep)	1570	36°52′08.28″	74°29′38.04″	6
RB-13-084	Baltimore (seep)	3	36°52′08.28″	74°29′38.04″	7
RB-13-084	Baltimore (seep)	3	36°52′08.28″	74°29′38.04″	8
RB-13-084	Baltimore (seep)	3	36°52′08.28″	74°29′38.04″	9
RB-13-084	Baltimore (seep)	3	36°52′08.28″	74°29′38.04″	10
RB-13-084	Baltimore (seep)	3	36°52′08.28″	74°29′38.04″	11
RB-13-084	Baltimore (seep)	3	36°52′08.28″	74°29′38.04″	12
RB-13-085	L	1180	37°02′15.12″	74°33′43.98″	1
RB-13-085	L	1180	37°02′15.12″	74°33′43.98″	2
RB-13-085	L	600	37°02′15.12″	74°33′43.98″	3
RB-13-085	L	600	37°02′15.12″	74°33′43.98″	4
RB-13-085	L	200	37°02′15.12″	74°33′43.98″	5
RB-13-085	L	200	37°02′15.12″	74°33′43.98″	6
RB-13-085	L	100	37°02′15.12″	74°33′43.98″	7
RB-13-085	L	100	37°02′15.12″	74°33′43.98″	8
RB-13-085	L	50	37°02′15.12″	74°33′43.98″	9

Table 17-A1. (Continued).

Station	CTD Site ID	Depth (m)	Latitude (N)	Longitude (W)	Niskin Bottle
RB-13-085	L	50	37°02′15.12″	74°33′43.98″	10
RB-13-085	L	10	37°02′15.12″	74°33′43.98″	11
RB-13-085	L	10	37°02′15.12″	74°33′43.98″	12
RB-13-087	I	720	37°03′13.74″	74°38′04.88″	1
RB-13-087	I	720	37°03′13.74″	74°38′04.88″	2
RB-13-087	I	600	37°03′13.74″	74°38′04.88″	3
RB-13-087	I	600	37°03′13.74″	74°38′04.88″	4
RB-13-087	I	500	37°03′13.74″	74°38′04.88″	5
RB-13-087	I	500	37°03′13.74″	74°38′04.88″	6
RB-13-087	I	400	37°03′13.74″	74°38′04.88″	7
RB-13-087	I	400	37°03′13.74″	74°38′04.88″	8
RB-13-087	I	200	37°03′13.74″	74°38′04.88″	9
RB-13-087	I	200	37°03′13.74″	74°38′04.88″	10
RB-13-087	I	3	37°03′13.74″	74°38′04.88″	11
RB-13-087	I	3	37°03′13.74″	74°38′04.88″	12
RB-13-088	U	600	37°00′37.08″	74°34′43.44″	1
RB-13-088	U	600	37°00′37.08″	74°34′43.44″	2
RB-13-088	U	350	37°00′37.08″	74°34′43.44″	3
RB-13-088	U	350	37°00′37.08″	74°34′43.44″	4
RB-13-088	U	150	37°00′37.08″	74°34′43.44″	5
RB-13-088	U	150	37°00′37.08″	74°34′43.44″	6
RB-13-088	U	100	37°00′37.08″	74°34′43.44″	7
RB-13-088	U	100	37°00′37.08″	74°34′43.44″	8
RB-13-088	U	50	37°00′37.08″	74°34′43.44″	9
RB-13-088	U	50	37°00′37.08″	74°34′43.44″	10
RB-13-088	U	10	37°00′37.08″	74°34′43.44″	11
RB-13-088	U	10	37°00′37.08″	74°34′43.44″	12

Table 17-A2. Summary data results for radiocarbon analysis including ROV station number (Station no.), sample identification (Sample ID), laboratory identification number (Lab ID), sample type), fraction modern (Fm) relative to standard, fraction modern error, ^{14}C age, ^{14}C age error, $\Delta^{14}C$ value as defined in Stuiver and Polach (1977), and $\Delta^{14}C$ error. Fraction Modern (Fm) is a measurement of the deviation of the $^{14}C/^{12}C$ ratio of a sample from "Modern." Modern is defined as 95% of the radiocarbon concentration (in AD 1950) of NBS Oxalic Acid I normalized to $\delta^{13}C_{VPDB}$=-19 per mil (From: Olsson 1970). *Samples pretreated with 10% HCl.

Station No.	Sample ID	LAB ID	Sample type	Fm	±Fm Err	Age	Age Err	$\Delta^{14}C$ (‰)	$\pm\Delta^{14}C$ Err
RB-13-ROV-682	RB-13-682-1	149412	Authigenic carbonate-groundmass	0.1136	0.0010	17480	80	-887.3	1.0
RB-13-ROV-682	RB-13-682-2	149413	Authigenic carbonate -cement	0.1046	0.0010	18140	80	-896.2	1.0
RB-13-ROV-682	RB-13-682-3	149392	Authigenic carbonate -cement	0.1175	0.0010	17200	80	-883.4	1.0
RB-13-ROV-682	RB-13-682-4	149393	Authigenic carbonate -cement	0.0925	0.0010	19120	90	-908.2	1.0
RB-13-ROV-682	RB-13-682-5	149394	Shell in authigenic carbonate	0.6094	0.0013	3980	20	-395.3	1.3
RB-13-ROV-682	RB-13-682-6	149395	Shell in authigenic carbonate	0.6112	0.0013	3955	20	-393.5	1.3
NF-12-ROV-14	NF-12-14-1	149410	Authigenic carbonate-groundmass	0.0670	0.0010	21710	130	-933.5	1.0
NF-12-ROV-14	NF-12-14-2	149411	Authigenic carbonate -cement	0.0414	0.0010	25570	210	-958.9	1.0
NF-12-ROV-14	NF-12-14-3	149396	Authigenic carbonate -cement	0.2617	0.0011	10770	35	-740.3	1.1
RB-13-ROV-689	RB-13-ROV-689-M6	149398	Mussel shell (alive)	0.8782	0.0017	1045	20	-128.6	1.7
RB-13-ROV-689	RB-13-ROV-689-M6 (rep)	149399	Mussel shell (alive)	0.8747	0.0017	1075	20	-132.0	1.7
RB-13-ROV-689	RB-13-ROV-689-M10	149404	Mussel shell (alive)	0.7859	0.0015	1935	20	-220.2	1.5
RB-13-ROV-687	RB-13-ROV-687	149405	Mussel shell (dead)	0.8114	0.0016	1680	20	-194.9	1.6
RB-13-ROV-687	RB-13-ROV-687 (rep)	149415	Mussel shell (dead)	0.8078	0.0017	1715	20	-198.5	1.7
RB-13-ROV-683	RB-13-ROV-683-Q16A	149400	Mussel shell (dead)	0.7802	0.0015	1995	20	-225.8	1.5
RB-13-ROV-682	RB-13-ROV-682-MQ9	149401	Mussel shell (dead)	0.8558	0.0021	1250	20	-150.8	2.1
RB-13-ROV-682	RB-13-ROV-682- MQ8	149403	Mussel shell (dead)	0.9094	0.0017	765	15	-97.6	1.7
RB-13-ROV-682	RB-13-ROV-682	149414	Mussel shell (dead)	0.8667	0.0018	1150	20	-140.0	1.8
RB-13-ROV-682	RB-13-ROV-682	149402	Mussel shell (dead)	0.8632	0.0021	1180	20	-143.5	2.1
RB-13-ROV-682	RB-13-ROV-682 10% HCl*	149416	Mussel shell (dead)	0.8622	0.0018	1190	20	-144.5	1.8
RB-13-ROV-682	RB-13-ROV-682 10% HCl*	149417	Mussel shell (dead)	0.8624	0.0018	1190	20	-144.2	1.8
RB-13-ROV-683	RB-13-ROV-683-M3	149418	Mussel shell (alive)	0.8937	0.0017	905	20	-113.2	1.7
RB-13-ROV-683	RB-13-ROV-683-M17	149419	Mussel shell (alive)	0.8898	0.0018	940	20	-117.1	1.8

Table 17-A3. Summary of measured U-Th data for authigenic carbonate samples and activity ratios (AR) used for age calculation and U-Th ages.

Sample Name	U (ppm)	232Th (ppm)	Measured(a)						
			$^{230}Th/^{232}Th$ $AR_{(b)}$	$^{232}Th/^{238}U$ $AR_{(b)}$	2σ %	$^{230}Th/^{238}U$ $AR_{(b)}$	2 σ (%)	$^{234}U/^{238}U$ $AR_{(b)}$	2 σ (%)
RB-13-682 D	3.22	0.27	2.41	0.02766	0.06288501	0.06675	0.649856543	1.143	0.13
RB-13-682 E	3.39	0.26	2.78	0.02524	0.061234854	0.07007	0.458093007	1.143	0.12
RB-13-682 F	3.43	0.06	3.84	0.00623	0.06186828	0.02396	0.758787274	1.145	0.13
RB-13-682 G	4.21	0.21	2.22	0.01632	0.061512019	0.03621	0.556620436	1.143	0.11
RB-13-682 H	3.67	0.16	2.23	0.01435	0.061178697	0.03202	0.660834698	1.143	0.11
NF12-14 D	3.89	0.34	5.84	0.02899	0.060528967	0.16916	0.342541858	1.139	0.11
NF12-14 E	4.07	0.24	8.59	0.01941	0.063163377	0.16667	0.461304679	1.140	0.14
NF12-14 F	4.59	0.27	8.34	0.01916	0.061181627	0.15981	0.396534865	1.141	0.13
NF12-14 G	4.59	0.43	5.68	0.03103	0.063824742	0.17630	0.453872046	1.139	0.15
NF12-14 H	4.11	0.59	4.09	0.04681	0.049276856	0.19133	0.378463649	1.136	0.14

Sample Name	Corrected(a)								
	$^{230}Th/^{238}U$ $AR_{(b,c)}$	2s (%)	$^{234}U/^{238}U$ $AR_{(b,c)}$	2s %	Rho 08-48	Age (ka)		$^{234}U/^{238}U$ AR initial	2s
RB-13-682 D	0.04473	36.13	1.14639	1.04	0.271	4.34	1.6	1.148	0.01
RB-13-682 E	0.05009	29.26	1.14614	0.94	0.274	4.87	1.4	1.148	0.01
RB-13-682 F	0.01886	19.33	1.14541	0.26	0.226	1.81	0.4	1.146	0.00
RB-13-682 G	0.02292	41.85	1.14498	0.62	0.257	2.20	0.9	1.146	0.01
RB-13-682 H	0.02030	41.57	1.14472	0.54	0.254	1.95	0.8	1.146	0.01
NF12-14 D	0.14859	10.57	1.14294	1.06	0.337	15.1	1.7	1.149	0.01
NF12-14 E	0.15297	6.81	1.14186	0.71	0.335	15.6	1.1	1.148	0.01
NF12-14 F	0.14618	7.07	1.14281	0.70	0.331	14.9	1.1	1.149	0.01
NF12-14 G	0.15444	10.87	1.14229	1.13	0.340	15.8	1.8	1.149	0.01
NF12-14 H	0.15850	16.13	1.14132	1.72	0.346	16.3	2.7	1.148	0.02

(a) Activity calculated using λ230=9.17050E-6, λ234=2.82206E-6 (Cheng et al., 2013), λ232=4.93343E-11 (Holden et al., 1990), λ238=1.55125E-10 (Jaffrey et al., 1971),
(b) Activity ratios corrected for hydride formation, tailing, fractionation, SEM-Faraday yield, and tracer isotopic composition, and
(c) Corrected using a theoretical detrital composition of (232Th/238U) = 1.2 ± 0.6, (230Th/238U) = 1 ± 0.5 and (234U/238U) = 1 ± 0.5.

REFERENCES:

Cheng H, Edwards LR, Shen CC, Polyak VJ, Asmerom Y, Woodhead J, Hellstrom J, Wang Y, Kong X, Spötl C, Wang X, Calvin Alexander E Jr. 2013. Improvements in ^{230}Th dating, ^{230}Th and ^{234}U half-life values, and U–Th isotopic measurements by multi-collector inductively coupled plasma mass spectrometry. Earth and Planetary Science Letters. 371–372:82–91.

Holden NE. 1990. Total half-lives for selected nuclides. Pure and Applied Chemistry. 62(5):941–958

Jaffrey A, Flynn K, Glendenin L, Bentley W, Essling A. 1971. Precision measurement of half-lives and specific activities of ^{235}U and ^{238}U. Physical Review C. 4*(*5*)*:1889–1906. doi:10.1103/PhysRevC.4.1889.

Olsson IU. 1970. The use of oxalic acid as a standard. In: Olsson IU, editor. Radiocarbon variations and absolute chronology. Nobel Symposium, 12th Proc. New York (NY): John Wiley & Sons. p. 17.

CHAPTER 18. EDUCATION AND OUTREACH

Elizabeth Denton Baird and Art Howard

18.1 INTRODUCTION

Public outreach was an integral part of the Atlantic Deepwater Canyons study from its inception. Since 2001, the North Carolina Museum of Natural Sciences (NCMNS) has been collaborating with Dr. Steve Ross by providing education and outreach for deepwater exploration missions. The strength of this relationship led to an education and outreach plan for the "Deepwater Canyons: Pathways to the Abyss" project. These efforts consisted of two major components: web-based outreach and the completion of a high definition (HD) video production as well as the incorporation of educators into the research cruises when possible. These components allowed the mission to reach a variety of audiences throughout the entire project.

18.2 2011 MAPPING CRUISE

18.2.1 Web Presence

The 2011 mapping cruise (4–17 June 2011) aboard the National Oceanic and Atmospheric Administration (NOAA) ship *Nancy Foster* provided the starting point for the Deepwater Canyons: Pathways to the Abyss blog (NCMNS 2011). Designed by the webmaster at NCMNS, the blog includes four primary sections that could be updated for each cruise. "About the Mission" provides an overview of the current work, and "Meet the Team" introduces the science team through short biographies and photographs. "Home" is the section where the daily logs appear in chronological order. A section called "The Science," written by Sandra Brooke, Steve Ross, Rod Mather, and Jason Chator, is a broad overview of the project and helps link the individual cruises together. This site continues to remain active, providing excellent information on deepwater explorations. During the 2011 mapping cruise, Ross and Brooke wrote and posted the 13 blogs presented over the course of the mission. The site was most popular during the research cruises for its near real-time updates; however, it continues to be accessed long after the end of the project. In addition to the site hosted by NCMNS, both the NOAA Office of Ocean Exploration and Research (OER) and the U.S. Geological Survey (USGS) hosted sites about the project. For the 2011 mapping cruise, NOAA OER hosted a summary site. Ross, Brooke, and Mather provided a mission summary, mission plan, and slide show as well as an explanation of seafloor mapping (Ross et al. 2011). The USGS Diversity, Systematics, and Connectivity of Vulnerable Reef Ecosystems (DISCOVRE) Project website also covered the project (USGS 2013). The website links to four primary research themes: Benthic Ecology, Microbial Ecology, Paleoclimate, and Population Genetics. As papers on these topics are published, short abstracts are added to the site. The combination of multiple sites focused on this project strengthened the impact of the efforts.

18.2.2 Teacher at Sea

The timing of this cruise made it impossible to get a classroom teacher on board the ship; however, two students (Megan Prescott of the University of Washington, and Veronica Holton of the College of Charleston) participated. They worked the night shift and contributed to the creation of the 3D maps from the mission.

18.2.3 Video and Documentary

In order to maximize opportunities for having a videographer on board, initial planning and storyboarding for the documentary took place on shore during this cruise. Discussions of how to include

the variety of research objectives, collaborating agencies and diversity of footage took place. Images from the 2011 mapping cruise, including the 3D maps, were transferred to Art Howard (ARTWORK) for use in the final project.

18.3 2012 SAMPLING CRUISE

18.3.1 Web Presence

The Deepwater Canyons: Pathways to the Abyss website was updated to reflect the research focus of the 2012 sampling cruise (15 Aug.–3 Oct. 2012) aboard the NOAA ship *Nancy Foster*, including the use of the *Kraken 2* remotely operated vehicle (ROV) for exploration and sampling, and the updated "Meet the Team" section with biographies of the 15 science team members.

During Leg 1 of the cruise, 18 blogs were posted, including 4 that focused on the scientists on board (Steve Ross, Christina Kellogg, Katharine Coykendall, and Amanda Demopoulos). The goal of the four career-focused pieces was to help inspire the next generation of scientists. Other topics included a description of two benthic landers – Bottom Boundary Layer (BOBO) and Autonomous Lander for Biological Experiments (ALBEX) – an explanation of conductivity-temperature-depth (CTD) profilers and box cores, and an overview of ROV operations. The blog posts provided the foundation for, and are referenced in, later posts. The 2012 sampling cruise was also the first to document the cold-water seep site. Eighteen additional blogs were posted during Legs 2 and 3 of this mission, which included coverage of the "Billy Mitchell-Project B fleet" shipwreck sites.

During the mission, the science team members were also able to complete two live, interactive videoconferences into the Daily Planet Theater of the NCMNS—a three-story spherical space with seating for 65 people on the first floor as well as observation balconies on the second and third floors that can accommodate an additional 100 people. At least 50 people watched the programs from the different areas of the theater. Ross and Brooke participated in one broadcast, and students Esprit Saucier and Kirstin Meyer participated in the second. Both programs showcased the research, and Saucier and Meyer were able to show samples that had been recently collected.

In addition to the web presence hosted by NCMNS, NOAA OER provided daily coverage as a featured signature expedition on their website (NOAA 2012). Several members of the science team contributed background essays on the science objectives, deepwater habitats, lander technology, and science of canyons. Greg Boland from the Bureau of Ocean Energy Management (BOEM) presented an overview of the value of partnerships and this collaborative effort. Educational resources from NOAA were linked to the site, including multimedia missions and lessons tied to curriculum goals, such as "designing your own benthic lander" and "understanding chemosynthetic organisms." The daily blogs were managed by NOAA staff; however, they were primarily contributed by the science team.

18.3.2 Teacher at Sea

The length and timing of the cruise made it difficult for traditional classroom teacher participation. Dr. Eric Hanneman of the Educational Living Collection section of NCMNS joined the first segment of the cruise in the educator role. His background in aquarium science and his ability to communicate with the public made him a strong asset to the team. He assisted in all aspects of the work as well as managing the blog. Liz Baird (NCMNS) served as the educator during the second leg, working with the science team and, in addition to blogging, taking over some of the specimen photography. Megan Chesser, Teacher Education Specialist at NCMNS, joined the final leg of the mission to facilitate the live feed featuring the students and to continue the daily blog.

18.3.3 Video and Documentary

Work on the video and documentary continued during the 2012 sampling cruise. Howard joined the second leg of the cruise and captured the deployment of two of the landers as well as the ongoing CTD and benthic sampling operations. Howard provided the majority of the specimen photography in addition to many of the still shots used on the websites. All of the ROV footage was shared with Howard to use in the documentary. Howard also was asked to assist NOAA in the production of their new "OceanAge Career" series. He filmed science team members Steve Ross, Sandra Brooke, Jennifer McClain-Counts, Christina Kellogg, and Liz Baird as well as Lieutenant Commander Jablonski (the ship's captain). The final products of that effort can be seen via the NOAA OER website (NOAA 2015).

18.4 2013 SAMPLING CRUISE

18.4.1 Web Presence

The Deepwater Canyons: Pathways to the Abyss website was updated with information from the 2013 sampling cruise (30 April–27 May 2013) aboard the NOAA ship *Ronald H. Brown*. Over the course of the two legs of the cruise, 27 blogs were posted. The first leg focused on the biological communities of the canyons, and the second leg focused on the archaeological sites. A highlight of the cruise was the discovery of a vast, new chemosynthetic community off Norfolk Canyon at 1,600 m depth. The announcement was released collectively and appeared on numerous websites, including BOEM, the WordPress blog, NOAA Ocean Explorer, USGS, University of North Carolina-Wilmington, Florida State University, *Science Daily*, *Popular Science*, and *Discovery*. That announcement continues to record the highest number of hits on the WordPress site.

In addition to announcing the find via websites, there was a live, two-way interactive connection to the Daily Planet Theater at the NCMNS. Thanks to the cooperation of the ship's crew, who provided access to large portions of bandwidth from the internet connection, the audience in the theater could speak directly to the researchers at sea. It was a highlight to videoconference live from sea while exploring the newly discovered methane seep. The presentation was kicked off in Raleigh, North Carolina, by Howard showing some images from the 2012 expedition. Brooke, Roark, and Baird were then "interviewed" by Dr. Meg Lowman of the NCMNS. The crew for the Woods Hole Oceanographic Institution's *Jason II* ROV had previously allowed Baird to write a greeting to the audience at NCMNS inside the lid of the collection box, and during the broadcast they opened the box so that everyone at the NCMNS could see the greeting from the ocean floor (**Photo 18-1**).

This cruise was also covered by NOAA (2013) as a featured signature mission on its *Ocean Explorer* website. The website provided a wealth of background resources, including essays from Ross, Brooke, and Mather on the Science Objectives; the Archaeology of the Atlantic Canyons; the Hunt for Benthic Landers; and Deepwater Mid-Atlantic Canyons, Past, Present and Future. Daily logs were provided by the science team and NOAA staff. In addition to the linked NOAA education materials, the website includes a video clip with Ross and Brooke discussing the reasons we explore deepwater canyons.

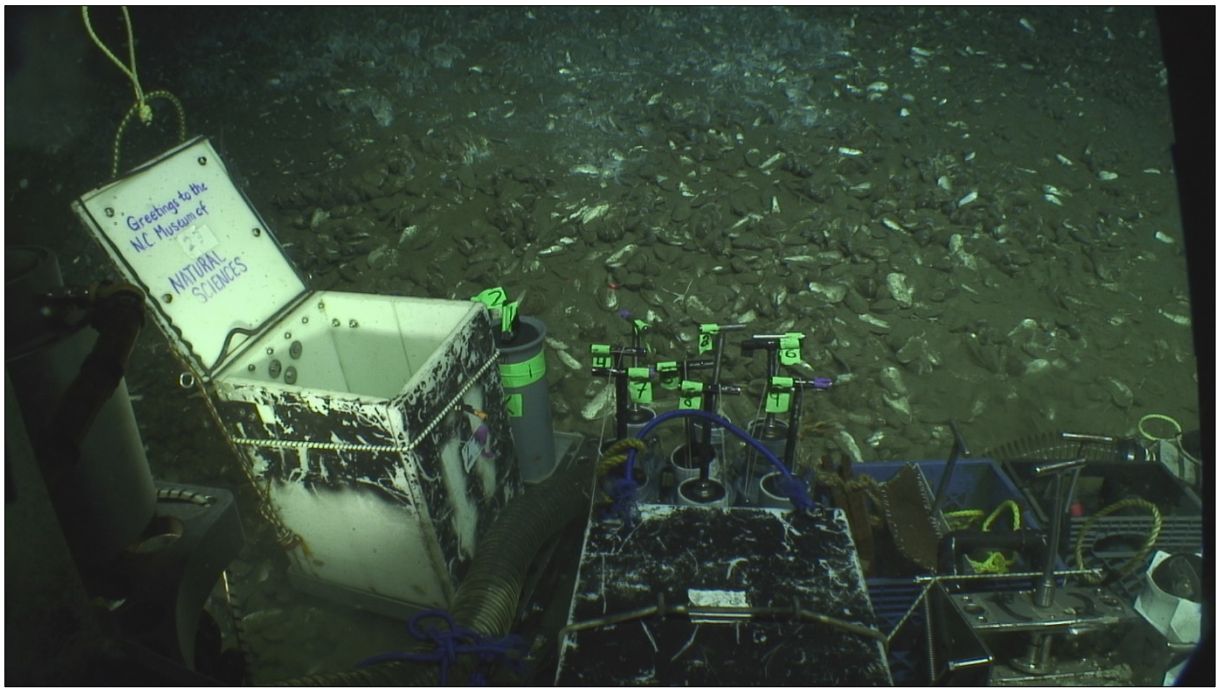

Photo 18-1. "Greetings to the NC Museum of Natural Sciences" from the methane seep site. Visitors in the Daily Planet Theater in Raleigh, North Carolina, were able to see live footage from the Jason II ROV during the 2013 sampling cruise aboard the NOAA ship Ronald H. Brown.

18.4.2 Teacher at Sea

The educator at sea role was filled by Baird during the first leg of the mission. In addition to writing the daily blogs and working as part of the science team on the ROV dives, Baird provided all of the still specimen photography. More than 3,000 images of specimens were taken during the first leg.
Walt Gurley, Co-Coordinator of the Visual World Investigate Lab at NCMNS, served as the educator on the second leg. He assisted with the night shift, wrote the daily blog, and was able to add historic footage of the bombing of the Billy Mitchell-Project B fleet to the site.

18.4.3 Video and Documentary

Work continued on the video and documentary. Howard joined the second leg of the mission in order to gather images related to the archaeological goals of the Deepwater Canyons: Pathways to the Abyss project. He provided the still specimen images for collections and gathered background information for the video.

18.5 2013 Instrument Retrieval Cruise

18.5.1 Web Presence

The 2013 instrument retrieval cruise (21–27 Aug. 2013) aboard the NOAA ship *Nancy Foster* was focused on the retrieval of benthic landers and moorings. Eleven blogs were posted during the cruise, including the successful recovery of one lander and the disappointment of having a "lost" lander, which was not recovered during the cruise, but was found later washed up on a beach in The Bahamas. Gabriela Hogue, Fish Collection Manager for the NCMNS, joined the mission and provided blogs about flying fish and wahoo and assisted the science team.

18.5.2 Teacher at Sea

Dacia Harris, a teacher at Asheville High School with part-time appointments at Shaw University in Raleigh and AB Technical Community College in Asheville, North Carolina, joined this mission as a teacher at sea. She assisted with writing blogs and with CTD operations. In addition, on board were three recent graduates from Cape Fear Community College: Colby Witt, Kelly Bryant, and Sarah Nall. The students worked the night shift, enhancing their knowledge and skills with CTDs and water filtration.

18.5.3 Video and Documentary

Howard completed the onboard filming for the video and documentary during this final lander retrieval cruise. He captured the joy of finding the lander as well as the dismay of losing one of them.

18.6 POST-CRUISE OUTREACH EDUCATION

The final editing and production of the HD video took place after the last cruise. Howard captured hundreds of hours of footage, including launch and recovery of ROVs and landers, deck and lab work, and science team meetings. For the production, he evaluated more than 36 terabytes of raw underwater video. In order to film the researchers in their home labs, Howard drove 3,600 miles, visiting scientists in six states. An unexpected addition to the video was the discovery of the lost lander in The Bahamas. Although Howard was not able to travel to The Bahamas, he was able to obtain an image of the lander to use in the final production. The initial draft of the video was ready for review in December 2014. Input was received from the entire science team before the final cut was made public.

The video, "Deepwater Canyons: Pathways to the Abyss," was released online by BOEM on 27 May 2015 (BOEM 2015). Collaborators released their own press announcements about the piece and showcased the work on their own websites. As of November 2015, it had been viewed online nearly 4,000 times. Other organizations have linked to the video, including OceanGate, Inc., a company that provides manned submersibles (OceanGate, Inc. 2015).

On 15 October 2015, NCMNS hosted a special evening presentation featuring the "Deepwater Canyons: Pathways to the Abyss" video. Dr. Elizabeth Shea from the Delaware Museum of Natural History was invited to speak on deepwater cephalopods; after her evening presentation, the audience moved to the Daily Planet Theater where the video was introduced by Baird. Ross, Howard, and Baird were on hand to answer questions after the viewing. More than 60 people attended the event. The production was shown daily at the American Geophysical Union Cinema during the AGU fall meeting 1-18 December 2015 in San Francisco, California.

The Deepwater Canyons: Pathways to the Abyss website continues to draw visitors. In summary, over the course of the project, 88 essays were posted on a wide variety of topics ranging from life at sea and descriptions of gear, to biographies of ship's crew and science team members. Since its creation in 2011, the site has received more than 51,000 views from approximately 17,000 viewers from 96 countries.

18.7 MEDIA ATTENTION AND AWARDS

The work of the Deepwater Canyons: Pathways to the Abyss team received media coverage in a variety of outlets throughout the project. The largest television station in North Carolina ran a piece just prior to the 2013 sampling cruise (WRAL 2013). In addition to airing that day, it was available online and linked to the WordPress site. North Carolina Sea Grant's *Coastwatch* magazine featured the project in its spring 2013 issue with an article explaining the project and highlighting Ross' work (Smith 2013). In 2014, Brooke was invited to give a presentation in Washington, DC at the National Geographic Museum. This event was hosted by the Pew Charitable Trusts and the Natural Resources Defense Council (NRDC) in support of protection of deepsea corals in the Atlantic canyons. In May 2015, Nancy Prouty was

featured in *Swimmer*, a magazine targeted toward master swimmers. The article, titled "Race to the Bottom" features Prouty (a master swimmer herself) and her work on deepwater corals (Howley 2015). The Virginia Coastal Zone Management Program featured a large article about the project in their magazine, *Virginia Coastal Zone Management* (Fall 2012–Winter 2013). In October 2015, Maryland Sea Grant College's *Chesapeake Quarterly* carried an article about the deepwater canyons exploration and highlighted how this project contributes to a deeper understanding of the diversity of life found in the canyons, which, in turn, informed policy decisions (Brainard 2015).

Photo 18-2. On behalf of the Deepwater Canyons: Pathways to the Abyss project, Greg Boland receives the Partners in Conservation Award from the Secretary of the Interior, Sally Jewell.

In January 2014, the Deepwater Canyons: Pathways to the Abyss project received one of the Department of the Interior's Partners in Conservation Awards (**Photo 18-2**). The announcement of this award follows:

> 1/16/2014
>
> WASHINGTON, D.C. – Secretary of the Interior Sally Jewell today presented the Department of the Interior's 2013 Partners in Conservation Awards to 20 public-private partnerships that have achieved exemplary conservation results through cooperation and community engagement. Together, the 20 award-winning partnerships include recipients representing more than 260 organizations and individuals from across the United States and the world.
>
> > *The Department of the Interior is proud to recognize the accomplishments of those who are innovating and collaborating in ways that address today's complex conservation and stewardship challenges," Secretary Jewell said at an awards ceremony at the Interior headquarters in Washington today. "These partnerships represent the gold standard for how Interior is doing business across the nation to power our future, strengthen tribal nations, conserve and enhance America's great outdoors and engage the next generation.*

> The Partners in Conservation Awards recognize outstanding examples of conservation legacies achieved when the Department of the Interior engages groups and individuals representing a wide range of backgrounds, ages and interests to work collaboratively to renew lands and resources.
>
> At the annual awards ceremony, the Department of the Interior celebrated conservation achievements that highlight cooperation among diverse federal, state, local and tribal governments; public and private entities; non-profit organizations; and individuals.
>
> Several awards also have bi-national or international partners.
>
> Welcoming senior leaders from the Government of Mexico, for example, Secretary Jewell was pleased to present an award to the "Minute 319 Bi-National Partnership" for implementation of the recent agreement between Mexico and the United States to cooperate on Colorado River water use and environmental issues. She also recognized the "Huron-Erie Corridor Initiative" for cooperation on the international boundary between Canada and the United States.
>
> The award winners also include innovative science research conservation partnerships such as the "Rigs to Reefs" and the "Ocean Renewable Energy Stewardship" programs, as well as landscape-level habitat restoration and conservation partnerships such as the Cienega Watershed in Arizona and Edwards Aquifer Initiative in Texas.
>
> Other partnerships prepare America's youth to be the next generation of environmental stewards for public lands through participation in corps, service learning, STEM and other educational and employment experiences. Examples of winning partnerships with a strong youth component include the Groundwork USA Network, Klamath Tribal Leadership Program, Center for Land Based Learning, Great Plains Nature Center and others.
>
> As an example of the scope and diversity of the 2013 winning partnerships, the "Minute 319 Bi-National Partnership" award recognizes agencies of the Mexico government, states in the Colorado River Basin, and water users and environmental organizations in both countries as well as partners from the Department of the Interior, Bureau of Reclamation, Fish and Wildlife Service and the U.S. Geological Survey (USGS). Likewise, the U.S.-Canada "Huron-Erie Corridor Initiative" brings together 34 federal, tribal, First Nation, state, provincial, local and nongovernmental groups.
>
> Diverse partners in "The Atlantic Canyons - Pathways to the Abyss" partnership include Interior's Bureau of Ocean Energy Management and USGS; the Commerce Department's National Oceanic and Atmospheric Administration; nine universities and colleges, the Woods Hole Oceanographic Institution; and four other private research organizations, museums, and institutes. They collaborate on the use of robotic underwater vehicles and other cutting-edge tools to discover and research deep-water coral habitats.

In November 2015, Ross and Brooke were notified that the Deepwater Canyons: Pathways to the Abyss project was the recipient of the National Oceanographic Partnership Program (NOPP) 2015 Excellence in Partnering Award. Ross was featured on WWAY, a Wilmington, North Carolina, television news station, with the announcement of this award (Morgan 2015). The award was presented in 2016 at the Ocean Sciences meeting, and the announcement read, in part:

> Atlantic Canyons: Pathways to the Abyss was voted to be the NOPP project that best exemplifies the program's partnership objectives by the Subcommittee on Ocean Science and Technology's Interagency Working Group on Ocean Partnerships (IWG-OP). You will soon receive a formal letter of recognition from the IWG-OP co-chairs.
>
> This award is meant to recognize the strong partnerships that have been built over time and their impact on the oceanographic community and was evaluated based on six characteristics:
>
> 1. Ocean sector diversity among partners;
>
> 2. Level of effort/involvement by partners;
>
> 3. Long-term commitment of partners beyond the NOPP-funding period;
>
> 4. The success of the partnership in meeting its project objectives;
>
> 5. Impact of the effort on ocean research and/or education; and

6. Distinguishing characteristics of the partnership that contributed to its success.

The education and outreach from this project captured the excitement of research at sea and highlighted the collaboration needed to succeed in science. The project's blog and video will remain available and accessible online and can provide a foundation for future work.

18.8 LITERATURE CITED

[BOEM] Bureau of Ocean Energy Management. 2015. **"**Pathways to the abyss" video is a virtual trip to the Atlantic Canyons: full spectrum of deep sea marine habitats revealed. [updated 2016 Apr 18; accessed 2016 Apr 18]. http://www.boem.gov/press05272015/.

Brainard J. 2015. The Grand Canyons off our coast. Chesapeake Quarterly. 14(3):4–11. College Park (MD): Maryland Sea Grant. [accessed 2016 Apr 18]. http://www.chesapeakequarterly.net/V14N3/index.html.

Howley EK. 2015. Race to the bottom. Swimmer. May–June 2015:31–34. Sarasota (FL): U.S. Masters Swimming, Inc. [accessed 2016 Apr 18]. http://www.usmsswimmer.com/201505/swimmercoralarticle.pdf.

Morgan M. 2015. UNCW professor receives prestigious award. Wilmington (NC): WWAYtv3. [updated 2015 Nov 18; accessed 2016 Apr 18]. http://www.wwaytv3.com/2015/11/18/uncw-professorstigious-award/.

[NOAA] National Oceanic and Atmospheric Administration. 2012. Deepwater Canyons 2012 expedition: mission logs. NOAA Office of Ocean Exploration and Research. [accessed 2016 Apr 18]. http://oceanexplorer.noaa.gov/explorations/12midatlantic/logs/logs.html.

NOAA. 2013. Deepwater Canyons 2013: pathways to the abyss. NOAA Office of Ocean Exploration and Research. [accessed 2016 Apr 18]. http://oceanexplorer.noaa.gov/explorations/13midatlantic/welcome.html.

NOAA. 2015. Ocean careers to inspire another generation of explorers. NOAA Office of Ocean Exploration and Research. [updated 2015 Dec 8; accessed 2016 Apr 18]. http://oceanexplorer.noaa.gov/edu/oceanage/welcome.html.

[NCMNS] North Carolina Museum of Natural Sciences. 2011. Deepwater Canyons: pathways to the abyss. [updated 2013 Aug 27; accessed 2016 Apr 18]. https://deepwatercanyons.wordpress.com/.

OceanGate, Inc. 2015. Scientists shed light on deep-water Atlantic Canyons. [accessed 2016 Apr 18]. http://www.oceangate.com/blog/2015-06-16-scientists-shed-light-atlantic-canyons.html.

Ross SW, Brooke S, Mather R. 2011. Deep-water Mid-Atlantic Canyons exploration 2011. NOAA Office of Ocean Exploration and Research. [accessed 2016 Apr 18]. http://oceanexplorer.noaa.gov/explorations/11midatlantic/welcome.html.

Smith P. 2013. Undersea exploration: charting new pathways to the abyss. Coastwatch. (2):10–16. Raleigh (NC): North Carolina Sea Grant. [accessed 2016 Apr 18]. https://ncseagrant.ncsu.edu/coastwatch/previous-issues/2013-2/spring-2013/undersea-exploration-charting-new-pathways-to-the-abyss/.

[USGS] US Geological Survey. 2013. DISCOVRE − Diversity, Systematics and Connectivity of Vulnerable Reef Ecosystems Project. [updated 2013 Apr 22; accessed 2016 Apr 18]. http://fl.biology.usgs.gov/DISCOVRE/index.html.

WRAL. 2013. Deep-sea exploration helps scientists keep oceans healthy. Raleigh (NC): WRAL.com. [accessed 2016 Apr 18]. http://www.wral.com/deep-sea-exploration-helps-scientists-keep-oceans-healthy/12381943/.

This page intentionally left blank

CHAPTER 19. SYNTHESIS

Sandra Brooke and Stephen Viada with contributions from the Atlantic Deepwater Canyons Investigators

19.1 INTRODUCTION

Interest in biologically productive and environmentally sensitive habitats such as submarine canyons has expanded in recent years within U.S. waters, with efforts funded by multiple U.S. federal agencies (Bureau of Ocean Energy Management [BOEM], National Oceanic and Atmospheric Administration [NOAA], and U.S. Geological Survey [USGS]). This increased attention tracks a worldwide expansion of submarine canyon research, as evidenced by the increase in canyon-related publications over the past decade (Ross et al. 2016a). Areas of interest are within BOEM's U.S. Atlantic Outer Continental Shelf (OCS) Region because of expanding energy industry activities. Recent studies conducted off the east coast of the United States have led to discoveries of new deepsea coral and methane-seep ecosystems as well as new information on the physical, chemical, and ecological functioning of canyon and outer shelf environments.

The Atlantic Deepwater Canyons study was a 5-year (2011–2016) comprehensive and multidisciplinary investigation, encompassing physical, biological, and archaeological studies that addressed numerous aspects of canyons and adjacent areas within the Mid-Atlantic Bight (MAB), which lies within the Mid-Atlantic Planning Area of the Atlantic OCS Region. During this study, scientists collected a vast amount of data, discovered new habitats (e.g., coral community habitats and two methane seeps), expanded the known ranges of several fishes and invertebrates (*Lophelia pertusa, Solenosmilia variabilis, Telopathes magna, Chiridota heheva,* and *Alvinocaris mauricola*), including a recently discovered bivalve (*Acesta cryptadelphe*), and visually surveyed 32 areas of natural substrate and 10 archaeological sites for the first time. Four research cruises provided the platform for mapping 6,404 km^2 of the deep MAB seafloor; completing 48 remotely operated vehicle (ROV) dives; deploying six long-term monitoring systems including two moorings and four benthic landers; collecting 106 box cores, 110 hydrographic profiles, and seawater casts; and conducting 32 otter trawls. The ROV dives collected 414 hours of video and concurrent environmental data as well as thousands of biological, chemical, and geological samples. These data were processed and analyzed by 13 principal investigators (not including post-doctorates, technicians, and students) at 12 different institutions and have already resulted in four openly available cruise reports submitted to NOAA's Office of Ocean Exploration, eight peer-reviewed publications in press or published, and more than 15 presentations at scientific symposia.

Education and outreach were also major components of this project and were managed by the North Carolina Museum of Natural Sciences (NCMNS). Prior to and during each research cruise, the museum hosted a website that posted information and daily blogs on cruise activities. NOAA's Office of Ocean Exploration Ocean Explorer website also posted mission summaries, daily logs, and images that documented cruise findings. USGS hosed a third website that also disseminated project and cruise information. In addition to this web presence, during both the 2012 and 2013 cruises, the NCMNS hosted a live interview via Skype from the ship to the museum auditorium. Several members of the science party gave video interviews for the NOAA Ocean Explorer Ocean Age web page. Students, teachers, and museum staff participated in the research cruises and the principal investigators have been interviewed for several news articles. Videographer Art Howard collected video and images during research cruises and also interviewed scientists at their home institutions to create a high-quality educational documentary called *Atlantic Canyons: Pathways to the Abyss*. This video is available via YouTube and has been watched by more than 6,000 viewers to date. It also has been shown many times in public and academic presentations. In addition to the scientific and educational achievements, this project received the

Department of the Interior 2013 Partners in Conservation Award and the National Ocean Partnership Program 2015 Excellence in Partnering award.

The results of the Atlantic Deepwater Canyons project show the value of integrated multidisciplinary studies. Incorporating physical and biological attributes of multiple canyons, seeps, open slopes, and shipwrecks over several years enabled our team to compile a comprehensive dataset that led to a broad understanding of these ecosystems. This chapter provides a synthesis of the data presented in the preceding chapters rather than simply summarizing the results. Elements of each separate chapter of the report can help interpret or explain the results from other research scientists. Although these links are recognized in the individual chapters, this synthesis attempts to bring the various elements together and present a holistic understanding of the canyon ecosystems.

19.2 Comparison of Historical and Modern Data

Past studies conducted in and around submarine canyon features of the MAB were reviewed in **Chapter 2**. These studies included submersible dives (*Johnson Sea-Link* [Harbor Branch Oceanographic Institution] and *Delta* [Delta Oceanics]) conducted between 1980 and 1993 in Baltimore, Hudson, Norfolk, Tom's, Wilmington, Lydonia, Lasse, Veatch, Atlantis, Hydrographer, Block, Munson, No Name, and Lindenkohl canyons and the Middle Grounds. Other data, collected using camera sleds (Hecker et al. 1980, 1983) were not analyzed during our project as the location precision was too low. The primary objectives of these surveys were to compare habitats among mid-Atlantic canyons (at depths ranging from 127 to 597 m), study tilefish behavior and habitats, and assess the impact of sewage discharges, primarily within soft sediment habitats. Data collected during submersible dives included video documentation along with station overviews, including site and dive metadata and a description of the biological and physical environment of the dive. Additional information such as maps of the dive site, images of different habitat types, and the submersible location were sometimes provided. Limited environmental data were available, and navigation data of the dives also were incomplete, which prevented continuous dive tracks from being created.

The earlier studies found notable differences among the canyons surveyed, although these differences were partly an artifact of the objectives of the different projects. Generally, the dominant habitat type observed in Wilmington, Tom's, and Hudson canyons and the Middle Grounds was soft sediment with occasional consolidated mud, whereas Baltimore and Norfolk canyons had a much greater representation of hard substrate habitats such as rocky ledges, rubble, and consolidated mud. Fauna assemblages in the different canyons reflected the dominant habitat type observed. For example, a greater representation of sessile benthic fauna, such as sponges and octocorals, was observed in Norfolk and Baltimore canyons (~45% of all fauna observed), whereas mobile or soft sediment fauna, such as crustaceans and echinoderms, dominated the other canyons and the Middle Grounds (~80% of observations). The more common fish species included tilefish (*Lopholatilus chamaeleonticeps*), blackbelly rosefish (*Helicolenus dactylopterus*), synaphobranchid eels (*Synaphobranchus* spp.), conger eels (Congridae), hake (Phycidae and Merlucciidae), skates (Rajidae), hagfish (Myxinidae), rattails (*Nezumia* spp.), and roughies (*Hoplostethus* spp.).

Technologies used in the Atlantic Deepwater Canyons study were more sophisticated than those used in earlier studies. One of the most useful tools we employed was multibeam sonar, which generates high-resolution bathymetric maps of the seafloor. These maps allow scientists to target specific habitat types and guide deployments of expensive underwater vehicles. Our ability to track and log vehicle location data has greatly improved since the earlier studies, which in combination with the bathymetric maps, allows us to pinpoint the location of observations, collections, and images. Previous studies used towed cameras (video and still cameras mounted on a weighted sled and towed by a support vessel) to collect habitat and community data. Cameras were operated using timers and intervalometers, and manual shutter releases (with weighted cables). Those cameras had no real-time feed and the location of the sled and cameras was approximated from the depth and estimated offset distance of the sled from the vessel.

Although habitat-fauna associations could be analyzed, distributional accuracy was low. Before the technology of digital imagery, images were captured on film and could be viewed only when developed back on shore. The scientists, therefore, had no ship-board ability to respond to any interesting habitats or observations, which we now can with modern digital imagery. During a study by Hecker et al. (1983), mussel beds (indicative of methane seepage) were discovered while reviewing images from their camera tows in Baltimore Canyon. Many modern camera sleds have real-time digital feed to the surface, so if Hecker and her colleagues had been using modern equipment, the Baltimore seep would probably have been explored more thoroughly and would have coincided with the discovery of cold seeps in the Gulf of Mexico (Paull et al. 1984), two decades or earlier than discovering the first North Atlantic seeps at the Blake Ridge (Van Dover et al. 2003).

Scientists collected data from several historical studies (**Chapter 2**) using submersibles, which were considered "state of the art" at the time. However, video and digital image resolution was much lower than the high-definition cameras used by most modern underwater vehicles, including the ROVs used during the present study. An additional challenge with historical video analysis was the deterioration in quality due to the age and storage conditions of the video and still films. Poor image quality made identifying fauna extremely difficult or impossible, so comparisons with modern data were challenging. Because the operators of these cruises recorded only discrete coordinates at variable time intervals (usually at the start and end of a dive, at sample collections and notable observations) continuous dive tracks were unavailable.

Navigation used during the early surveys was Loran-C, a system that used time delays in low-frequency radio signals transmitted by fixed land-based radio beacons to determine location that cannot be accurately translated into GPS coordinates. Today, vessel navigation relies on satellites (GPS), and continuous position keeping or tracking of underwater vehicles is maintained using ultra-short baseline (USBL), an underwater positioning system that uses vessel-mounted transceivers to detect the range and bearing to a target by means of acoustic signals. These advanced navigation systems allow all digital imagery, observations, and collections to be georeferenced together with depth records.

Sensors or dataloggers attached to underwater vehicles during dives have become standard equipment, which was not always the case with earlier studies. These environmental data also are linked through time stamps to the navigation and video data thereby providing a suite of variables for each observation, collection, etc. For the historical data analysis, dive logs contained only depth or other environmental information if recorded manually by the scientific observers. The *Johnson Sea-Link* (Harbor Branch Oceanographic Institution) submersible had a Sea-Bird conductivity-temperature-depth (CTD) instrument, but scientists did not routinely use these data and were not available for our analysis. Multiple environmental and biological data streams can now be analyzed using relatively new statistical approaches to determine community structure and identify relationships between species' distributions and habitats and environmental conditions.

Research submersibles used in earlier studies had ample sampling capacity and payload to collect and carry equipment, and much excellent research has been conducted using these vehicles. Contemporary deepsea research has trended toward using ROVs instead of submersibles, which is advantageous in many ways; however, ROVs also have limitations because of the risk of entangling the umbilical, especially in strong currents and complex topography.

Historical coral records generated from past studies, especially those of Hecker et al. (1980, 1983), were used to identify areas for the MAB canyon study and to generate preliminary predictive habitat models for the canyon's corals. This exercise showed that our recent data generated a much more refined and accurate predictive model than data that were extracted from previous studies (see **Chapter 5** for more details).

Education and outreach have played an increasingly important role in conserving deepsea resources; near real-time transmittal of high-quality images and global access to information through social media

has vastly expanded our ability to inform the public on ocean issues. Early studies did not appear to engage in public outreach (although outreach efforts may not have been reported) as project products were limited to reports and scientific publications. Federal agencies now require outreach components in their research grants, and the Atlantic Deepwater Canyons study had a considerable media presence for every research cruise. The advent of near real-time underwater footage has created a conduit for expanded public interest and engagement in deepsea conservation.

19.3 PHYSICAL DESCRIPTION OF THE STUDY AREA

19.3.1 Current and Sediment Regime

Baltimore and Norfolk canyons are relatively close together (75 km apart); both are large heterogeneous features located approximately 100 km offshore, and they incise deeply into the shelf (31 and 25 km for Baltimore and Norfolk, respectively). Both are non-branching shelf-sourced canyons (Harris and Whiteway 2011, Obelcz et al. 2014) that have no current connections to major river systems. Both canyons have a wide nonlinear axis, particularly Baltimore, which takes a "dog-leg" or distinct turn to the southeast (heading offshore) about mid-way along the axis. Despite large-scale similarities in these canyons, Obelcz et al. (2014) predicted that differences in morphology, orientation, steepness, and density of gullies and the type of adjacent continental shelf would lead to significant hydrographic differences between canyons. Our studies supported their predictions and demonstrated distinct differences in the physical attributes of the two canyons.

The upper slope waters in the region are dominated by Western North Atlantic Central Water (WNACW) with the cooler Western Atlantic Subarctic Intermediate Water (WASIW), which occurs deeper and farther offshore. Both canyons showed very different temperature-salinity profiles from their adjacent slope areas partly due to the intrusion of the deeper WASIW several kilometers farther up the canyons than on the shelf. The canyons both showed a distinction between the warmer upper- and mid-depths with higher current speeds than the cooler temperatures and slower currents in the deeper depths (>1,000 m). Both canyons showed semidiurnal tidal signals, which also have been detected in other submarine canyons; however, tidal influence and current regimes differed between the two canyons, probably due to differences in canyon morphology. Norfolk Canyon is relatively straight, allowing tidal signals to manifest throughout the canyon at all depths, but the angled shape of Baltimore Canyon probably dampened the tidal signals, which were weaker than for Norfolk Canyon at all depths (**Chapter 5**). This difference in shape also influenced the current regimes; Baltimore Canyon has a convergence zone (maintained by tidal bores and internal waves) at approximately 300 to 800 m depth where the WASIW travels up the canyon and meets the WNACW coming down canyon (Gardner 1989a). This convergence (likely related to the significant northeast bend in the canyon) causes a persistent scouring and sediment resuspension resulting in high turbidity levels. The seafloor within the convergence zone (primarily ~560 m depth) had a coarse sandy upper layer over a compacted clay layer, indicating long-term sediment winnowing by currents. The sandy layer had little fine material, which also indicated reworking or scouring under the convergence zone, and the sediments had lower organic content than outside the convergence area. Down canyon from this convergence zone (~1,000 m), sediments were finer and had higher accumulation rates and organic content. These deeper parts of the canyon are probably deposition centers for the resuspended sediment from the convergence zone as well as shelf-sourced, organically enriched fine sediment that occurs at 1,000-m depth throughout the MAB slope (Biscayne and Anderson 1994). The CTD profiling conducted during our study along the canyon axis showed a large turbidity cloud over the canyon floor at depths of 400 to 1,000 m, similar to earlier observations by Gardner (1989a). Consequences of this division inside Baltimore Canyon for the sediment composition or benthic fauna were not reported in the earlier studies.

Norfolk Canyon had higher current speeds along the canyon axis with no evidence of a convergence zone and a more consistent, but still high, turbidity distribution than Baltimore Canyon. Smaller separated

turbidity layers occurred over a wider depth range and were more uniformly deposited. Long-term measurements derived from our benthic landers and moorings showed that the most intense current-turbidity events in both canyons corresponded to strong surface storms, which were temporally sporadic and channeled fresh organic material from the shelf into the canyon axis. Accumulation rates and organic matter content for the mid and upper parts of Norfolk Canyon were higher than for Baltimore, with the highest deposition rates at approximately 1,100 m, which is similar to the rest of the MAB slope. Samples taken during different time periods (September 2012 vs. May 2013) showed a potential temporal signal in the input of organic matter, indicated by increased concentrations of phytodetrital material in Norfolk Canyon in May vs. Baltimore Canyon in September. This material could stimulate temporal patterns of growth and reproduction in the canyon and slope fauna. Observed temporal differences may be somewhat confounded by geographic differences in sediment nitrogen content, which is lower north of Norfolk Canyon than to the south (Milliman 1994) due to the geomorphology and hydrodynamics of the shelf.

Previous work (Biscaye and Anderson 1994) suggested that MAB canyons channel sediment from the shelf to the slope and provide shelf-sourced material to the mid-slope depths of the canyons. In addition, our study showed that percentages of organic material were consistently higher within both canyons than at similar depths on the slope, indicating trapping and accumulation of organic matter. Moreover, sediment organic carbon concentrations in Norfolk Canyon and on the adjacent slope were consistently higher than for Baltimore Canyon and slope, indicating some regional differences in organic material deposition, or possibly a temporal signal as the canyons were sampled during different time periods.

In summary, oceanographic and geological data collected during the Atlantic Deepwater Canyons study support the earlier geological studies (e.g., Gardner 1989a, 1989b) because significant differences in sedimentology, turbidity, and physical oceanography were discovered within and between the canyons; however, the biological consequences of the observed differences were not investigated prior to our research. Both canyons are highly dynamic systems, driven by a combination of tides and stochastic surface events (e.g., storms). The shape of Baltimore Canyon creates a convergence between two water masses, resulting in winnowing of the sediment at mid-depths, thereby creating high water-column turbidity and deposition in deeper parts of Baltimore Canyon. In Norfolk Canyon, a straighter channel allows for more consistent (but sometimes extreme) current flow, more widespread turbidity events and a more uniform deposition of sediment and organic material. Both canyons are depo-centers for organic material, including labile phytodetritus, sediments, and potentially anthropogenic contaminants. An increase in organic material deposition was observed in Norfolk Canyon in May 2013, probably as a response to the spring phytoplankton bloom. Although dynamic on small spatial and temporal scales, our studies of long-lived coral skeletons (**Chapter 17**) show that nutrient flux and carbonate chemistry of the canyons have been stable over long periods (at least 700 years), which is consistent with relatively stable climate over the MAB region over the same time period.

19.3.2 Methane Seepage

Until recently, the known presence of methane-seep communities along the U.S. western Atlantic margin was limited to two deep sites off the Blake Ridge, North Carolina (Van Dover et al. 2003, Brothers et al. 2013) and another putative site on the southern flank of Baltimore Canyon. During our 2012 sampling cruise, the existence of a methane community was verified at the Baltimore Canyon location, and subsequent surveys by NOAA and USGS discovered 570 gas expulsion sites (potential methane seeps) along the shelf and slope of the northeastern U.S. coast (Skarke et al. 2014). During our 2013 sampling cruise, two ROV dives were dedicated to ground truthing the bubble plumes observed during NOAA-USGS surveys, and we discovered the methane-seep field south of Norfolk Canyon at 1,455 to 1,610 m depth. Visual surveys from the NOAA ship *Okeanos* verified cold-seep communities at four additional sites along the MAB and northeastern U.S. coast, providing additional evidence for extensive methane communities in this region (Quattrini et al. 2015).

Gas expulsion may originate through thermogenic processes (production at high temperature and pressure) deep beneath the seafloor (Hill et al. 2004, Newman et al. 2008, Brothers et al. 2014) or biogenic processes (anaerobic microbial activity) near the seafloor surface (Skarke et al. 2014). A series of salt diapirs off South Carolina push upwards into the overlying sediments, creating venting pathways for gases. The high thermal conductivity of the salt diapirs destabilize the underlying methane hydrates and cause them to disassociate into methane gas, which is then released to the water column (Paull et al. 1995, Taylor et al. 2000). Like the MAB seeps, this methane is biogenic in origin and also supports chemosynthetic communities in two known areas, the Blake Ridge (2,155 m) and Cape Fear (2,600 m) diapirs (Brothers et al. 2013). Our study used carbon and U/Th isotopic analysis of authigenic carbonates collected from Baltimore and Norfolk seeps to determine the age and origin of the methane at each site (**Chapter 17**). Methane from both seeps has microbial origin, but the authigenic carbonates at the Baltimore seep are much older (~15 to 16 kilo annum [ka]) than at the Norfolk seep (~2 to 5 ka), and the mechanisms of seepage are different. The main driver of authigenic carbonate precipitation at both sites is anaerobic oxidation of methane (AOM) via sulfate reduction at or near the sediment interface (Prouty et al. 2016). The age of the authigenic carbonates and the occurrence of pockmarks at the Baltimore Canyon slope suggest a link between sediment deposition during Pleistocene low sea-levels and accumulation of pore fluid overpressure from sediment compaction, followed by the release of overpressure through subsequent venting. Fluid flow from this thick layer of sediments is the most likely mechanism to explain sustained methane venting at Baltimore Canyon, whereas venting fluids at the Norfolk seeps can be explained by methane flow through fractured bedrock (Skarke et al. 2014, Ruppel et al. 2015). The two MAB seeps investigated here are very different from each other; Baltimore seep is relatively shallow and has low relief with occasional authigenic carbonate boulders, whereas Norfolk seep was deep, extremely rugged, with large masses of carbonate, often with visible bubble plumes and exposed gas hydrates. Physically and geologically there are more similarities between the Blake Ridge and Norfolk seeps than between Norfolk and Baltimore, but the Blake Ridge biological communities are different from both MAB seeps for reasons that are not clear, but may be related to depth. The different depths, topography, origins, and venting activity of these seepage sites provide an interesting context for comparing the seep-associated communities.

19.4 Biological Communities in the Study Area

19.4.1 Hard Substrate Fauna

Prior to the initiation of this study, our knowledge of the distribution of hard substrates in the canyons was limited to the relatively few submersible dives or surface-operated camera drops conducted in the mid-Atlantic canyons. These studies identified some rocky habitats in the upper reaches of both Baltimore and Norfolk canyons, but did not explore the deeper parts of the canyons. Our study, although more extensive, was still limited in time and could not survey more than a small fraction of the canyons. In recent years, the availability of acoustic data in the form of high-resolution multibeam and side-scan sonar maps has greatly increased our ability to identify potential exposed hard substrate over large areas. These data were invaluable in identifying hard bottom habitat during this project; they facilitated our dive site selection and provided the foundation for our predictive habitat models (**Chapter 7**). The habitat models are discussed in greater detail later in this chapter, but essentially they predicted that the probable greatest areas of hard substrate would be at mid-depths along the northeastern and southwestern walls of the canyons, with more diffuse hard substrate predicted along the deeper walls primarily on the northern side. The predicted hard substrate in Norfolk Canyon was more evenly distributed along both walls and was more continuous than in Baltimore Canyon, and with slightly more predicted habitat for scleractinian (stony) corals. Since this study was focused on hard-bottom communities, most of the coral-targeted dive sites (i.e., non-seep sites) were conducted along the mid-depth walls of the canyons.

Octocorals were the dominant coral taxa in both canyons, inhabiting a range of different hard substrate types from walls and ledges to isolated boulders and rocks, and sea pens were common on soft sediment substrates. Their distribution spanned a wide range of depth and environmental conditions; they often occurred in high numbers or as large colonies. The dominant species was *Paragorgia arborea*, which was particularly abundant in Baltimore Canyon (>5,000 colonies observed) and often co-occurred with *Primnoa resedaeformis* and *Anthothela grandiflora*. The distribution of scleractinians was more limited, particularly within Baltimore Canyon. From our analysis, scleractinians seemed to have more rigorous habitat requirements than the octocorals because they were rarely found in locations other than steep walls or large boulders. The reasons for this apparent habitat limitation are not known but may be due to low sediment tolerance, the need for particular current regimes, or a particular substrate requirement that can only be found in such habitats. Such requirements may explain their scarcity in the mid-depths of Baltimore Canyon where the persistent nepheloid layer created high suspended sediment load. Conversely, *P. arborea* is very abundant within the nepheloid zone and can apparently tolerate such conditions. Trophic analysis (**Chapter 16**) indicates that *P. arborea* may even derive some nutritional benefit (organic enrichment) from the turbidity. In Norfolk Canyon, the turbidity was more uniform and current speeds were higher, and more scleractinians were observed than in Baltimore Canyon. Many stony coral observations were made along a deep steep wall near the mouth of the canyon. Since a comparable survey was not made in Baltimore, these observations cannot be used to compare the canyons; however, only five colonies of *Lophelia pertusa* were observed in Baltimore Canyon and 19 in Norfolk Canyon in comparable depths (with similar survey effort). The cup coral *Desmophyllum dianthus* was also more abundant at comparable depths in Norfolk than in Baltimore. These data suggest that the combination of physical and geological properties has a strong influence on driving the distributions of deepsea coral species in the canyons.

Other factors such as biogeographical boundaries, larval dispersal and recruitment, food preferences, etc., also influence the distribution of species but are more difficult to identify. During our study, the small yellow octocoral *Acanthogorgia aspera,* was observed only in Norfolk Canyon, despite the presence of apparently similar habitats in Baltimore Canyon and submersible observations by Hecker et al. (1980, 1983). More recent work (Watling and Auster 2005) indicated that Norfolk Canyon is the northernmost limit for the distribution of this species, but a congener, *A. armata,* has been documented from areas farther north. We did not observe either *Acanthogorgia* species in Baltimore Canyon, which is curious considering known records and earlier observations of this genus. Soft corals (Alcyonacea) were observed in both canyons, usually the small *Anthomastus* sp. that are sparsely distributed and do not provide significant habitat structure. In a few locations, mostly in Norfolk Canyon, the larger branching soft coral *Duva florida* occurred in localized but very abundant patches usually along the edge of ledges or pavements. Similarly, the gorgonian *Paramuricea placomus* occurred in large patches on the tops of terraces where sediment accumulation was significant. Neither of these habitat types was rare in either canyon, so something other than habitat availability must be driving the distribution of these octocorals. Data were insufficient to determine the reproductive strategies of either species, but *P. clavata* (a Mediterranean congener of *P. placomus*) is a brooding species, releasing well-developed larvae that settle close to the parent colonies, and neptheid soft corals are known to undergo fission, releasing daughter colonies that settle close to the adult. Both strategies would result in the observed large patches of *P. placomus* and *D. florida*; these are examples of species whose distributions are clearly defined by factors other than habitat or environmental conditions. Our study increased the range extension of the stony corals *Lophelia pertusa* and *Solenosmilia variabilis*, and also the black coral (Antipatharia) *Telopathes magna*. Black corals were recorded from only Norfolk Canyon where they were rare and observed at depths >900 m. The deeper parts of the Norfolk Canyon exhibited colder, more stable bottom temperatures and lacked the pervasive water-column turbidity that influenced the shallower communities. Since deep (>1000 m) surveys were not conducted in Baltimore Canyon, it is unknown whether the species found at the deep sites in Norfolk Canyon would also occur in Baltimore. Bamboo

corals (Isididae) also were uncommon on hard substrate in both canyons, but the soft sediment species *Acanella arbuscula* occurred in large patches on the deep slopes on the canyon flanks (**Section 19.3.2**).

Coral species richness was relatively low (<20 species of octocorals and hexacorals combined), although it is highly likely that more species remain to be discovered. One reason for low species richness may be the turbid conditions found in the canyons; corals generally do not thrive in habitats with high suspended sediments or high deposition rates. Particles can suffocate the small coral polyps and removing them expends energy. Corals that are abundant in the canyons are either tolerant of the environment or colonize particular habitat niches to avoid deleterious conditions (e.g., overhangs or steep walls with high current). The corals were a major component of the hard substrate communities, but the sponges and anemones appeared to be far more speciose. However, these are both problematic taxa to identify, and finding taxonomists that are willing and able to identify these taxa has proved difficult; consequently, we focused on those taxa that can be identified more easily.

The physical structure provided by the sessile communities supported an abundant and species-rich mobile community, which was dominated by echinoderms and crustaceans. Shrimps and squat lobsters were commonly observed on the coral colonies, as were ophiuroids and crinoids, whereas starfish and urchins were more usually observed on the nearby substrate. One of the dominant associates was the galatheoid *Eumunida picta*. A study of Anomuran genetic diversity (**Chapter 10**), showed that this species is in the same population as the southeastern US and Gulf of Mexico, indicating a significant level of connectivity among these regions. The complex habitats of the canyons also support abundant communities of small pelagic crustaceans; during ROV dives dense swarms of amphipods often obscured the camera view. Although this was exacerbated by the lights, it illustrates the high abundance of this potential food source in the canyons. The physical structure provided by the canyon geology and sessile communities also influences adjacent soft sediment habitats. In Norfolk Canyon, infaunal communities within 1 m of hard substrates exhibited similar densities but higher diversity than similar depths within the canyon axis (**Chapter 9**). The heterogeneous habitat and different hydrodynamic regimes that occur adjacent to hard substrates support an overall higher number of taxa, significantly contributing to the regional infaunal biodiversity.

The most obvious differences in the fish communities were related to depth zonation, regardless of the habitat occupied. Fish communities were not substantially different between the two canyons, but were significantly different above and below 1,400 m. Unlike shallower depths, those fishes deeper than 1,400 m did not exhibit significant affinity to particular habitats. Ross et al. (2016a, **Chapter 15**) suggested that the lack of strong habitat association with increasing depth may be related to the increasing uncertainty of resources, especially food. Even so, a few species (e.g., *Gaidropsarus ensis, Neocyttus helgae, Cottunculus thompsoni*) appeared to be more common on deep hard substrata compared with soft bottoms.

Of the 84 fish species identified from ROV video data, 62 occurred on or near complex hard substrata (**Chapter 15**; Ross et al. 2015). Above 1,400 m (in contrast to deeper waters), the hard bottom fish assemblage was significantly different from that of nearby soft bottoms. The fishes most associated with the canyon complex habitats were *Laemonema* spp., *Hoplostethus* spp., *Brosme brosme*, and *Benthocometes robustus*. Corals and sponges did not statistically influence fish community groupings but those organisms were important components of the complex habitat. The degree and nature of the influence of deepsea corals on fishes remain controversial (Auster 2007, Ross and Quattrini 2007, Biber 2014; **Chapter 15**); however, a few fish species (*B. brosme, D. rugosa, B. robustus*) in this study often were more abundant around corals. In addition, we observed that octocorals were used by a few species as egg-laying substrata (Ross et al. 2015). Unlike the sessile and sedentary invertebrates (corals and infauna), the fishes did not exhibit patterns that appeared to be associated with physical zonation of the canyons.

Trophic studies (**Chapter 16**) suggested different feeding guilds within hard substrate sessile-invertebrate fauna of the canyons. Stable isotope analyses of canyon and slope communities revealed complex food webs. Within the canyons, bottom particulate organic material (POM) was composed of relatively fresh organic matter, which was probably a major food source for the suspension-feeding communities. Several corals, including the scleractinians *D. dianthus* and *L. pertusa* and octocorals *P. arborea* and *P. resedaeformis,* had isotopic values that were consistent with fresh phytodetritus. Other hard substrate coral species (e.g., *P. placomus, A. grandiflora*) had carbon isotope values that were more indicative of degraded POM or zooplankton. The observed differences in food sources may be influenced by the habitat where the different species live; *P. arborea, P. resedaeformis, D. dianthus, S. variabilis,* and *L. pertusa* reside on high-profile boulders and canyon walls (**Chapter 8**) where high currents transport fresh phytodetritus (Sherwood et al. 2008, Duineveld et al. 2012). In contrast, *P. placomus* was present in less steep terrain, in areas where sandy sediment covered the hard substrate, corresponding to reduced current flow environments where organic matter can be reworked and recycled. Antipatharians were found only at depths greater than 1,000 m, and their stable isotope values were consistent with either zooplankton or reworked POM. These species were rare in the canyons and usually not found near other coral species. This taxon may be exploiting a food source that was insufficient to support the abundant populations of some other species. Where multiple species occur in high abundance in a particular habitat, the use of slightly different resource niches allows them to co-exist rather than outcompeting each other. Resource niches can include the exploitation of slightly different food sources; e.g., different sized polyps may capture different particle sizes, or different species may be able to exploit food of poor quality. The coral microbial community may contribute to niche partitioning if the bacteria contribute to the host energy needs (**Chapter 12**). Studies of the microbiomes of three deepsea coral species showed that each has a unique and species- or genus-specific microbial community, regardless of the location where they were collected. The microbiomes of two *Anthothela* species and *P. placomus* included bacterial species that were theoretically capable of complete or nearly complete nitrogen cycling, suggesting that bacterial associates contribute to nutritional cycles of the corals (**Chapter 12**; Lawler et al. 2016). Elucidating the structure and function of coral-associated microbial communities will help us understand how they contribute to deepsea coral ecology.

Studies of reproduction (**Chapter 11**) in five hard substrate coral species included three scleractinians (*L. pertusa, D. dianthus,* and *S. variabilis*) and five gorgonians (*A. grandiflora, A. aspera, P. placomus, P. arborea,* and *P. resedaeformis*). Of these, all were gonochoristic and most showed indications of either seasonal (*L. pertusa, D. dianthus, S. variabilis,* and *P. placomus*) or periodic (*A. grandiflora* and *A. aspera*) reproductive cycles; only one species had continuous gametogenesis (*P. arborea*). Data from one of the most common gorgonians, *P. resedaeformis,* were difficult to interpret and more time points are needed to understand whether this species has seasonal, periodic, or continuous reproductive cycles. A study of *P. resedaeformis* from eastern Canada showed no apparent periodicity or population synchrony (Mercier and Hamel 2011); however, a 4-year field study from the same region showed high recruitment onto settlement blocks, indicating good reproductive success (Lacharite and Metaxas 2013). Because only two time periods were sampled during the Atlantic Deepwater Canyons study, complete gametogenic cycles could not be described; however, for the seasonal species that were sampled in both years, all were more mature in September than in May and therefore seem to be following a similar pattern of seasonality. The limited data do not allow a thorough investigation of reproductive cycles, but seasonal influx of organic material and temperature have both been implicated as drivers of reproductive seasonality in deepsea species.

Reproductive strategy has potentially important consequences for population connectivity; the timing of gamete or larval release and planktonic duration influences the potential dispersal distance and direction. Species that broadcast spawn usually have small planktonic larvae that may feed in the water column. Little is known about larval duration for deepsea coral species; however, laboratory observations of the stony corals *Oculina varicosa* and *L. pertusa* indicate that their larvae are competent to settle after approximately 3 weeks (Brooke and Young 2005). Brooding species release well-developed larvae that

settle quickly after release and have a shorter potential dispersal distance. Egg size is often used as an indicator of larval lifespan; those >300 µm are generally nonfeeding (lecithotrophic) larvae that have short duration, and the smaller larvae may feed in the plankton and have longer lifespans. Of the coral species studied, all except *P. arborea* and *P. resedaeformis* (and possibly *A. aspera*) have maximum egg diameters indicative of dispersive larvae.

High levels of connectivity were observed between populations from Baltimore Canyon and Norfolk Canyon for the stony corals *L. pertusa* and *D. dianthus* and the octocorals *A. grandiflora* and *P. arborea* (**Chapters 13** and **14**). A study of population genetics in western Atlantic *P. arborea* populations supports our observation that this species has a widespread unstructured distribution with connectivity among populations (Herrera et al. 2012). The stony corals all have seasonal reproductive periods, but small eggs (long larval duration) and likely high dispersal potential, which would explain the unstructured populations. The octocorals *A. grandiflora* and *P. arborea* have large eggs, which implies short dispersal potential, and their gametogenic cycles are periodic (multiple) and continuous, respectively. A repeated or continuous reproductive strategy may provide more opportunities for encountering a current regime that facilitates dispersal, despite the short larval duration. In contrast to the high connectivity estimated for *P. arborea*, populations of *P. resedaeformis* were genetically distinct, suggesting that gene flow is limited between Norfolk and Baltimore canyons for this species. This is interesting as these two species both had large eggs, but gametogenic data indicate that *P. resedaeformis* has a seasonal reproductive cycle, whereas *P. arborea* reproduces continuously. The combination of limited spawning period and short larval duration may serve to retain larvae within the canyon as water masses move along the axis, creating population structure. A significant genetic differentiation also was observed between Baltimore Canyon and the Gulf of Maine for *P. resedaeformis* using microsatellite loci (**Chapter 14**). More data are needed to explore these preliminary observations, but even limited information is a useful foundation for testing hypotheses on the mechanisms of deepsea coral connectivity.

19.4.2 Soft Sediment Fauna

Soft sediment fauna of the MAB shelf and upper slope, mostly shallower than 300 m, have been extensively studied using trawls and dredges (Musick 1979, Theroux and Wigley 1998). While these techniques are useful for assessing species composition and broad-scale distributions, they do not provide information on fauna-habitat associations or small-scale patchiness, nor do they sample the sediment infauna or hard bottom fauna. This project used video analysis, trawls, and box corers to address some of these information gaps.

Soft sediment invertebrate megafauna observed during this project were generally sparser than those found on hard substrates, but sporadic patches of abundant sessile fauna were encountered. Canyon habitats were primarily surveyed with the ROV, whereas trawls were conducted primarily on the surrounding slope. While these data are not directly comparable, our observations and earlier work (Hecker et al. 1980, 1983; Mann 1982, Shepard et al. 1986) support the occurrence of sessile cnidarians such as large tube-dwelling anemones (order Ceriantharia), sea pens (order Pennatulacea), cup corals (*D. lymani* and *F. alabastrum*), and the bamboo corals *Acanella arbuscula and Acanella* sp. on canyon and slope soft bottom habitats. As with the hard substrate species, the sessile soft sediment fauna are found within species-specific depth ranges (**Chapter 8**). These species can occur individually or in large numbers, but their distribution is generally patchy rather than uniform (Hecker et al. 1983, Theroux and Wigley 1998; **Chapter 8**). The causes of these patchy distributions may be due to sporadic recruitment events or small-scale habitat or environmental conditions (McClain and Barry 2010, Levin and Sibuet 2012). Except for the cup corals, these sessile taxa provide habitat for several small sessile and mobile invertebrates thereby increasing the overall diversity of soft bottom communities. Sea pens can be found on soft sediment habitats throughout the world's oceans in shallow and deep waters, and are abundant along the eastern seaboard (Langton et al. 1990). The most abundant sea pens observed and collected during our study were *Pennatula aculeata* (382−388 m); the deeper areas were inhabited by other species

(e.g., *Funiculina quadrangularis*) and were infrequently encountered. Early studies of canyon benthic fauna of the western Atlantic documented deposit-feeding echinoderms as the dominant fauna (Rowe 1972) and noted that canyon fauna were generally more mobile than slope fauna, possibly as an adaptation to unstable canyon environments. The most common of the soft bottom invertebrates found in the MAB canyons and adjacent slope shallower than approximately 1,400 m also were mobile fauna, but decapod crustaceans were the most abundant followed by echinoderms and molluscs. The decapods were dominated by red crabs, which were the most abundant and widely distributed (400−1,200 m depth) species in both canyons (**Chapter 8**). Red crabs were observed mating and in gravid condition in both canyons, although no gravid females were encountered in Norfolk Canyon in 2013; the reason for this absence is unclear. As with the complex habitats (**Chapter 15**), 62 species of fishes were documented on soft bottoms from ROV video surveys. The fish compositions of soft bottom habitats (shallower than 1,400 m) were significantly different from all other more complex habitats (Ross et al. 2015). Species that most influenced the soft bottom statistical groupings were *Phycis chesteri*, *Nezumia bairdii*, *Glyptocephalus cynoglossus*, *Lophius americanus*, and *Merluccius albidus*. In addition, the cutthroat eels (*Synaphobranus* spp.) also were abundant over sandy bottoms.

Food resources in the canyons were generally composed of higher levels of labile organic material than on the slope (**Chapter 16**), resulting in depleted ^{15}N and ^{13}C stable isotope values for consumers in canyons and enriched values for those on the slope where organic material deposition is limited (Gage and Tyler 1992, Levin et al. 2001). This difference is evident in the stable carbon isotope data of suspension feeders on the soft sediment slopes (e.g., *Flabellum alabastrum*) versus the depleted values of suspension feeders on high-relief areas of the canyons (e.g., *L. pertusa*) (**Chapter 16**). In Baltimore Canyon, isotopic niche areas were similar for fishes that were sampled from the canyon and slope and there was substantial overlap, indicating fishes were using similar food resources in both habitats. The invertebrates, however, had no overlap in isotopic niche between canyon and slope. In Norfolk Canyon, the fish isotopic niche was broader in the canyon than on the slope, and for the invertebrates the reverse was true. These differences in trophic pattern among canyons and slopes may reflect the POM quality (e.g., freshness) and distribution within and between each canyon versus the adjacent slope (**Chapters 5** and **6**) and the species-specific responses to these differences.

Reproduction of MAB soft sediment fauna showed essentially two different strategies: seasonal broadcast spawning with small eggs and possibly planktotrophic larvae, and continuous or periodic spawning with large eggs and lecithotropic larvae. Timing of reproduction in deepsea species with noncontinuous cycles may be influenced by environmental factors, including the timing of food availability. Our data indicated increased deposition of phytodetrital material during May as a result of the spring phytoplankton bloom, and showed a persistent area of increased organic material at a depth of approximately 1,000 m on the shelf and slope. Examination of selected soft sediment fauna suggests that the majority of these species have annual reproductive cycles. Of the two cup corals and four species of echinoderms analyzed, only two species showed continuous reproduction (the cup coral *F. alabastrum* and the sea urchin *Hygrosoma petersi*). Two species that showed annual cycles were collected from >1,500 m (*Echinus wallisi* and *Gracilechinus affinis*) and two were <200 m (*Desmophyllum lymani* and *Cidaris abyssicola*). This variation among animals living in the same habitats results from a combination of species-specific constraints in reproductive strategy and environmental influences on those strategies. Additional samples are needed during different time periods to determine whether slope fauna reproduce on similar schedules as those in the canyons that have different environmental conditions and patterns of organic material deposition. Such information would help identify the factors that influence reproduction in these species, including whether conspecifics living in different conditions have similar cycles, or if environmental differences cause shifts in reproductive timing.

Distribution, diversity, and abundance of sediment infaunal communities showed differences with depth and between canyon and slope habitats, as expected considering other studies (Levin and Gooday 2003, Rex and Etter 2010), but also showed differences between canyons. For canyon habitats, the

highest abundances of infauna (macrofauna and meiofauna) occurred near the canyon heads, and both canyons showed bimodal distribution in faunal abundances, with a lower density at mid-depths. In Baltimore Canyon, the convergence zone coincides with the density minimum, whereas the mid-canyon density minimum in Norfolk Canyon cannot be accounted for by the same mechanism because no convergence was found in this canyon. Macrofauna that occupies slope habitats adjacent to both canyons showed decreased abundances with depth, but diversity patterns differed: Baltimore slope showed similar diversity with depth, but Norfolk slope had a bimodal pattern with reduced diversity at mid-depths (**Chapter 9**). The reasons for this were not clear, but may have been related to the temporal difference in sampling period. Sediment samples were taken from Baltimore in September, whereas collections from Norfolk occurred in May, which coincided with temporal deposition of phytodetrital material. This also would explain the consistently higher percentage values of organic carbon from Norfolk transects than those collected from Baltimore. At shallow depths (~180−190 m), slope communities were more similar to canyon communities, but these similarities decreased with depth, possibly as a result of differences in hydrodynamic regime and organic material deposition within and outside the canyons. Different macrofaunal communities were associated with each sediment type. Fine grained sediments had communities dominated by high abundances of bivalves and polychaete species that are known indicators of organic-rich sediments (**Chapter 9**). The sandy, scoured sediment under the Baltimore Canyon convergence zone showed lower overall faunal densities and a polychaete-dominated community that was more indicative of a stressful environment. While these analyses highlight the importance of sediment type and organic enrichment in structuring infaunal communities, they did not explain all of the observations, and localized hydrodynamics and seafloor topographic patterns may provide further insight into the distribution of communities. One limiting factor was the temporal and spatial separation of the hydrodynamic data and the geochemical-biological observations. Meiofaunal communities within Baltimore Canyon increased in diversity with depth. The greatest transition between community types occurred between the 550 and 900 m stations within the canyon. These depths correspond to the zones of resuspension versus deposition of organic material, respectively, within Baltimore Canyon; however, the same pattern was observed on the adjacent slope where the sediment and hydrodynamic regimes were different from the canyon. It is possible that the increasing steepness of the slope at these mid-depths caused a small sediment resuspension zone, leading to the overall low meiofaunal diversity but high nematode diversity. Meiofaunal communities are driven by a complex interaction of bathymetry, sediment dynamics, and food availability. Unlike macrofauna, meiofaunal communities can change rapidly in response to short temporal and spatial changes in the physical environment, and these small-scale habitat differences may be reflected by the observed communities. Given the short generation time and potential for rapid turnover of meiofaunal communities (Heip et al. 1985), differences in sampling time points and possible temporal changes in food availability will need to be factored into future comparisons of meiofauna between canyons.

19.4.3 Cold-Seep Fauna

Mussels collected from both seep sites were identified as *Bathymodiolus childressi* through molecular analysis (**Chapter 8**). Our samples from the Baltimore seep in 2012 were the first records of *B. childressi* from the western Atlantic margin and at the time, the closest known populations of this species were in the northern Gulf of Mexico (GoM). Since then, the Norfolk seep and three other sites have been documented along the western Atlantic (Skarke et al. 2014), but mussel identification has been verified only during our studies at Norfolk seep. Models of larval dispersal potential for *B. childressi* (Young et al. 2012) predict that, given the larval longevity and regional oceanographic conditions, it is theoretically possible for larvae spawned in the GoM to be transported to the eastern seaboard. Young et al. (2012) commented that it was surprising that this species had not been recorded at the Blake Ridge seeps. Our study confirmed the predicted presence of *B. childressi* in the MAB, but the reasons for its absence at the Blake Ridge seeps is unknown. The Blake Ridge seeps are both >2,000 m deep, so there is possibly a

depth-related distribution limitation; however, the dispersal model outputs also show *B. childressi* being carried beyond the North Carolina seeps and into the MAB region (Young et al. 2012).

Molecular analysis of gill tissue revealed only methanotrophic bacteria, with no indications of thiotrophy (S. Johnson et al. unpubl. data). Stable carbon isotopic analysis of mussel tissue indicates a chemosynthetic food source, but it did not distinguish between methanotrophy and thiotrophy (**Chapter 16**); analysis of sulfur isotopes, however, did indicate some reliance on thiotrophy, (**Chapter 17**). The Blake Ridge and Cape Fear sites off South Carolina have both methanotrophic (*Bathymodiolus heckerae*) and thiotrophic (*Vesicomyia* cf *venusta*) fauna (van Dover et al. 2003, Brothers et al. 2013) as do the cold seeps in the northern GoM (Cordes et al. 2007). The northern GoM populations of *B. childressi* also have a mixotrophic diet (Pile and Young 1999). Further work is needed to verify the presence of thiotrophic symbionts in the gills of MAB seep mussels and the extent to which their nutrition is partitioned into methanotrophy, thiotrophy, and also possibly external organic material (Pile and Young 1999).

Seep mussels from the northern GoM have seasonal reproductive cycles, with gametogenesis initiating in November–December, culminating in spawning that occurs during the following October to February (Tyler et al. 2007). Tyler et al. postulated that the mussel gametogenic cycles were timed to coincide with the early spring bloom that could provide food for the planktotrophic larvae. These seasonal reproductive cycles were not observed in the samples collected from the mid-Atlantic seeps (**Chapter 11**); there was no significant difference in oocyte sizes among samples collected from Baltimore seep in September vs. May, or from Baltimore vs. Norfolk seep in May 2013. Trophic data from our project were inconclusive with respect to external nutritional sources for MAB *B. childressi*, but because reproductive cycles at the MAB appear to be continuous, it seems that unlike the GoM, reproduction in the MAB is not driven by external food supply. The apparent absence of a seasonal signal in these seep mussels compared with those from the GoM warrants further research, which may reveal a flexible reproductive strategy in this species.

Significant differences were found between the depth, quantity of authigenic carbonate, and methane bubble plumes observed at the two MAB seeps. Differences also were observed in the abundance and distribution of chemosynthetic mussels. Live mussel cover at Baltimore seep was patchy and relatively low compared with Norfolk seep where the substrate was often completely covered with live mussels (**Chapter 8**). Although methane expulsion was not quantified, these observations imply much more active methane venting at Norfolk than Baltimore seep. Invertebrate megafaunal communities associated with the two seeps were very different from each other, with only two taxa in common (*B. childressi* and the large anemone *Actinoscyphia* sp.). Given the large depth difference (~1,200 m) between the two sites, it is likely that these differences were due to depth-temperature zonation, but some of the observed differences could also be due to their different topographic structure and degree of methane venting. Apart from the chemosynthetic mussels, there were no seep-endemic species documented at the Baltimore seep. In addition to the *B. childressi*, two seep-endemic species were collected from Norfolk seep; a very abundant holothurian (*Chiridota heheva*), which was also documented at the Blake Ridge seeps and the GoM (Pawson and Vance 2004), and the vent shrimp (*Alvinocaris markensis*), which has previously been documented only from the mid-Atlantic Ridge, but this also was probably the unidentified *Alvinocaris* sp. observed on the Blake Ridge (Van Dover et al. 2003). Both species have been previously found only in depths >2,000 m, therefore, it seems more likely that their absence from Baltimore seep is due to depth and temperature rather than seepage conditions (e.g., degree of gas expulsion).

Food web analysis of fauna collected from Baltimore seep showed only three species (besides *B. childressi*) with indications of chemosynthetic energy sources. These included two species of fish (*Dysommina rugosa* and *Symphurus nebulosus*) and a starfish (*Odontaster robustus*) (**Chapter 16**). The eel (*D. rugosa*) is an "infaunal picker" that may consume sediment fauna that are depleted in ^{13}C (indicative of chemosynthetic sources). The gut contents of these fishes showed a diet that comprised mostly crustaceans, but did not distinguish between infaunal and demersal taxa (**Chapter 15**). The

tonguefish (*S. nebulosus*) also was described as an infaunal picker. Interestingly, another species of tonguefish (*S. thermophilus*) is endemic to vent systems, feeding on crustaceans and polychaetes, and possibly also filamentous bacteria (Tyler 2005); however, *S. nebulosus* and *D. rugosa* were both found in habitats other than the Baltimore seep, therefore, they are clearly not seep endemics. The starfish (*O. robusta*) lives on soft sediment and is a deposit feeder, probably consuming isotopically depleted carbon from the seep sediments. Stable isotope data of other fauna collected from Baltimore seep indicated a photosynthetic food source. Taxa collected from the deeper seep near Norfolk Canyon all exhibited $\delta^{13}C$ values consistent with using chemosynthetically derived food; these included the shrimp *A. markensis* and urchins *Echinus wallisi* and *Gracilechinus affinis*. In summary, the seep food webs are complex with species-specific reliance on chemosynthetic and photosynthetic sources.

The red crab *Chaceon quinquedens* was common at the Baltimore seep and were observed apparently feeding on the mussels (**Chapter 8**); however, gravid and mating individuals were observed only on the periphery of the seep. Gravid females of the hydrothermal vent crab *Bythograea thermydron* is known to move away from the vents to protect their eggs (which are brooded externally) from the toxic vent chemicals (Perovich et al. 2003). This may also occur in nonchemosynthetic animals such as red crabs that feed at the seeps but whose embryos may be sensitive to methane. Red crabs were observed only twice at the Norfolk seep (which was beyond their usual depth range of <800 m). Other nonchemosynthetic species such as *Echinus wallisi* and *Gracilechinus affinis* from the Norfolk seep contained gametes (**Chapter 11**), which are therefore presumably tolerant of the chemical environment. Earlier work on *G. affinis* from soft bottom habitat the northeastern Atlantic shows a similar reproductive schedule to those in our study (**Chapter 11**). Tyler and Gage (1984) postulated that timing of reproductive cycles was driven by deposition of organic material in the late spring–summer. Our study also showed deposition of phytodetrital material in May (**Chapter 6**). There is, therefore, evidence that the reproductive cycles of these species at the Norfolk seep are driven (at least in part) by phytodetrital food influx, despite having access to a constant supply of seep-derived organic material. In contrast, the seep mussels collected during our study seem to have continuous reproductive cycles, which may be explained by the continuous methane flux; however, studies of other *B. childressi* populations show annual cycles, so more work is needed to understand the drivers of reproduction in this species.

Infaunal community composition and diversity associated with seep habitats are known to be distinct (Levin 2005, Menot et al. 2010, Bernardino et al. 2012), both from one another and from background nonseep sediments. Macrofaunal diversity is generally higher in seep habitats than ambient soft sediment, but differences among different seep habitats (microbial mats, mussel beds, etc.) are variable (Bernadino et al. 2012). The macrofaunal densities observed in seep-related sediments (i.e., under microbial mats and mussel beds) were higher at Baltimore and Norfolk seeps (**Chapter 9**) than those on the Blake Ridge (the closest studied seep sites ~ 800 km farther south), but were comparable to those in similar depth ranges elsewhere (Bernardino et al. 2012, Levin et al. 2006, Thurber 2010). Macrofaunal abundances at seep sites in our study were consistently higher than those at comparable depths on the slope, which supports the hypothesis that seeps are a source of energy at depths that are usually food-limited. Differences between slope and seep habitats have been hypothesized to increase with depth as food from surface productivity and shore-based sources decreases with depth (Levin 2005). This pattern was not supported by our data because the shallow Baltimore seep had a much greater difference between seep and slope habitats, particularly for microbial mat habitats, than the deep Norfolk seep.

Although we did not collect pore-water chemistry data, microbial mat environments are usually high in sulfides and methane; these sediments were inhabited by opportunistic taxa typically tolerant of environmental stress, such as some annelid species (Capitellidae, Dorvilleidae, and Tubificidae). Sediments adjacent to mussel beds and on the open slope had higher diversity with significantly different community structure. There were more crustaceans (mussel beds) and molluscs (open slope) in sediments outside the bacterial mats, suggesting that mats may be a more stressful environment. The observed

distribution of sediment fauna can be used as a proxy for sediment environmental conditions within the seep habitats, which vary over small and large spatial scales.

There were no seep-specific characteristics exhibited by the fishes associated with either seep, and no seep-endemic fishes were encountered (**Chapter 15**; Ross et al. 2015). As noted above, depth was a major factor that separated the fish fauna, and that largely explained the differences in fish assemblages between the two seeps. Shallower than 1,400 m, fishes occupying the complex seep habitats were significantly different from those on nearby soft bottoms. Although the degree of live mussel cover had no apparent influence on fish assemblages at the deep Norfolk seep, live mussel coverage did impact those at the shallow Baltimore seep (Ross et al. 2015). Fishes most characteristic of the shallow seep included *Laemonema* spp., *L. americanus*, *B. brosme*, and *D. rugosa* (Ross et al. 2015).

Overall, it appears that the differences in fauna (invertebrates and fishes) associated with Baltimore vs. Norfolk seep reflect depth-related changes in faunal abundance and diversity; in addition, some differences in community structure between the seeps also may be a function of their habitat complexity and geochemistry. It is clear that the physical and geological characteristics (aside from depth) of the two seeps were very different from each other, and these differences were strongly reflected in all the faunal groups studied.

19.5 ARCHAEOLOGICAL SETTING

All archaeological and associated biological studies were accomplished on the MAB shelf in depths less than 150 m in the vicinity of Norfolk Canyon. Eight 20th century shipwrecks (68−126 m) and two nonshipwreck sites were examined. The shallowest site, flat sandy bottom in 42 m, yielded little data and is not discussed further. The other nonshipwreck site was a natural hard bottom in 98 to 117 m. Although the focus of this project component was archaeological (and thus hard bottom), the sandy bottoms surrounding the wrecks also were surveyed for fish communities. The fishes and attached invertebrate communities were examined in detail on the shipwrecks.

The geology and physical oceanography of these sites are quite different from the deeper canyon and seep study sites. We observed more coarse sandy sediments, with occasional gravel, shell hash, and ripple marks at the outer shelf sites, indicative of bottom current influences. The seafloor of the outer shelf is generally uniform, with relatively little natural hard bottom (Steimle and Zetlin 2000). Oceanographic features of the outer shelf are controlled by a complex interplay of winds, climate, riverine input, tides, and Gulf Stream intrusions (Brooks 1996) and the primary water mass in this study area is referred to as the MAB shelf water (Churchill and Berger 1998). In contrast to the deeper study sites, the lower bottom salinities encountered at the shelf sites (Ross et al. 2016b) resulted from coastal water influx. Observed mean bottom temperatures were 4 °C to 8 °C warmer on the shelf than at the deeper sites, but dissolved oxygen levels were similar between the two depth zones (Ross et al. 2015b). The long-term transport of water along the outer shelf, including the inner Slope Sea, is to the southwest. Superimposed on this pattern are short-term variations resulting from storms, Gulf Stream effects, draughts/floods, and upwellings (Cook 1988).

19.5.1 Historical Shipwrecks

Although paleo-archaeological objectives were briefly considered, the primary focus of the archaeological studies was to locate and document shipwrecks that were sunk as the earliest demonstration of aerial warfare efficacy (**Chapter 4**). These ships, known as the "Billy Mitchell-Project B fleet," were sunk during the summer of 1921; their locations were poorly documented and their conditions were never investigated. Because of their historical significance and the presentation of new data from this project, these wrecks are being nominated to the National Register of Historic Places.

Of the 27 shipwrecks thought to occur in the study area (**Chapter 4**), eight were mapped with multibeam sonar and surveyed using ROVs. The multibeam maps also identified two other shipwrecks and sites of potential paleo-archaeological significance. The following eight shipwrecks were confirmed as part of the World War I-era warships sunk during the 1921 aerial bombing tests:

- German battleship *Ostfriesland* (94−112 m depth);
- German light cruiser *Frankfurt* (118−125 m depth);
- Torpedo boat destroyer *G-102* (102−105 m depth);
- Torpedo boat destroyer *S-132* (115−117 m depth);
- Torpedo boat destroyer *V-43* (114−117 m depth);
- German U-boat U-*117* (65−68 m depth);
- German U-boat U-*140* (80−85 m depth); and
- German U-boat *UB-148* (80−90 m depth).

An additional shipwreck, the USS *Washington*, also was identified during the Atlantic Deepwater Canyons study. *Washington* was used as a target and sunk by the U.S. Navy in 1924. She lies in 86 m depth. A multibeam sonar search was conducted in the area of the suspected location of the World War II wreck of the *San Demetrio*, but this wreck was not found. All Billy Mitchell-Project B wrecks that were surveyed exhibited damage from the aerial bombings or surface shelling. Otherwise, the wrecks were in generally good condition, but showed varying degrees of degradation. The large battleships, *Ostfriesland* and *Washington*, rested upside down on the seafloor, while the remaining wrecks were upright. All of the wrecks were entangled to varying degrees by lost fishing gear, mostly bottom trawls. This gear had apparently damaged some parts of the wrecks and recent rust indicated damage more recent than at the time of sinking. *Frankfurt* was the best preserved of the wrecks surveyed, but had some damage to the stern.

19.5.2 Fauna Associated with Shipwrecks

The eight shipwrecks examined in this study represent significant reef-like habitats in a region with relatively little hard substrate in shelf depths. A dive was made was made in 2012 (NF-ROV-28) in search of prehistoric human settlements, and some natural hard bottom was observed during this dive. The substrate comprised low-relief rubble with occasional small boulders. Dominant invertebrates were small white anemones, cidaroid urchins, and sponges. This dive was not analyzed for invertebrate fauna because the video was taken too high above the seafloor for sufficient taxonomic identification, and fauna were sparse and obviously different from the shipwreck invertebrate biota. Fishes associated with this site were documented and are reported in **Chapter 15** and by Ross et al. (2016b).

These shipwrecks are unusual features as they provide high-relief (2−18 m) complex habitat in an area that is dominated by low relief, primarily soft sediment habitat. In the MAB, these wrecks may provide species, especially those oriented toward complex habitats, with habitat that is naturally scarce or absent, thereby possibly increasing their abundance or distribution. As expected due to the depth and temperature differences, the fauna on these outer shelf sites were completely different from those observed in the deeper canyon and seep environments, with almost no overlap in species composition.

Invertebrates were abundant on all of the shipwrecks, although many could not be visually identified to genus or species, particularly anemones, zoanthids, and sponges. Thirty-four different taxa of benthic invertebrates were identified on or near the shipwrecks; of these 18 could be identified to genus or species. Invertebrate assemblages did not significantly differ with location on the wrecks, and wreck complexity did not appear to influence the invertebrate fauna. The abandoned fishing gear was often heavily colonized by invertebrates (e.g., asteroids and sponges) as was the wreck structure itself. Each wreck seemed to host different dominant invertebrates, which was unexpected given the wrecks' proximity to each other and their similar deployment time and depth ranges. Anemones, zoanthids,

hydroids, polychaetes (in a brown tube complex), a red shrimp, *Rochinia crassa*, *Henricia oculata*, *Sclerasterias tanneri*, *Stylocidaris lineata*, and *S. affinis* were variously dominant on different shipwrecks. Since the wrecks were all deployed at the same time, these differences were not due to temporal community succession, but may be related to vicarious recruitment events onto each wreck, followed by wreck-specific dominance of a species or suite of species. Ours is the first study of multiple shipwreck invertebrate communities at shelf-edge depths, and although limited in scope, it provides useful insights into the ecology of deep fouling communities (**Chapter 8**).

Fish assemblages on the shipwrecks were similar (33 species), but they were significantly different from the soft bottom fish community (25 species) (**Chapter 15**; Ross et al. 2016b). Hard bottom habitats were dominated by anthiine serranids, *Scyliorhinus retifer*, *Antigonia capros*, *Scorpaena* sp., and *Centropristis striata*. Season, depth, and location did not appear to influence the fish communities, suggesting a degree of stability in these ecosystems. The chain dogfish (*S. retifer*) occurred in massive numbers on the shipwrecks and used the wrecks as spawning substrates (Ross et al. 2016b). Since many fishes recorded on the shipwrecks are obligate reef species and are of subtropical affinity, the lack of reef habitat and cool bottom temperatures likely limit their distributions. Many fishes observed during the shelf surveys were uncommon to other trawl-based surveys (see Ross et al. 2016b), which illustrated the value of using visual methods to document the fauna of complex habitats.

19.6 PREDICTIVE HABITAT MODELING

Predictive habitat models have recently become popular tools that allow the distribution of deepsea corals to be predicted in unexplored or poorly known areas. These models use the habitat and environmental attributes of known coral locations; identify areas with similar attributes such as depth, terrain variables, and environmental conditions; and extrapolate coral distributions into those areas. Predicted distributions are assigned a probability rating based on the strength of similarity between the known and extrapolated distributions. The Atlantic Deepwater Canyons study conducted two predictive habitat modeling efforts (**Chapter 7**). The first model was produced using high-resolution bathymetry (generated during the 2011 mapping cruise) and data extracted from historical video analysis. The second model incorporated the same bathymetry and new high-resolution coral location and environmental data generated during the 2012 and 2013 cruises. The poor spatial and taxonomic resolution of the historical data posed a challenge for the modeling, which could use only broad categories such as “hard grounds” and “sessile fauna” to identify potential coral habitat. The historical data were also limited to <1,000 m depth, and many coral taxa were soft sediment species, which are not useful for identifying hard substrate habitat.

Limitations of the historical data resulted in a low-resolution model that over-predicted coral distribution and became less reliable at depths beyond the observed coral locations. Kinlan et al. (2013) also generated predictive habitat models for the MAB region using historical data and suffered similar problems of over-prediction of coral distributions, particularly for scleractinians because most historical records of stony corals are of soft sediment species captured in trawls. The broader depth range and accurate spatial, depth, and taxonomic data generated during our project enhanced the predictive accuracy of the models and refined the areas of likely coral habitat within the two canyons. As expected, the models generated using new data were superior to those using older records. Despite their limitations, however, in the absence of contemporary information, models using historical data are useful in understudied areas because they can broadly identify areas for further exploration.

Predictive habitat models must be assumed to over-predict suitable habitat to varying degrees in the deep ocean because they do not have access to all the variables that drive the distribution of each taxon. Biological factors such as recruitment rates, larval dispersal, small-scale habitat, or environmental preferences and food availability all influence coral distribution, but these factors cannot be measured practically on a broad scale. Environmental factors, however, can be measured more readily on both a short-term fine scale (through vehicle mounted instruments) and longer term scale by using moorings and

landers. Acquiring such data would increase the strength of correlations between coral observations and their habitat/environmental preferences. Improving the reliability of these potentially valuable management tools is a high priority because resource exploitation is moving farther offshore into areas that are poorly explored and have no regulations to protect vulnerable ecosystems.

19.7 MANAGEMENT AND CONSERVATION PERSPECTIVES

19.7.1 Natural Habitats

The overarching purpose of this study was to provide BOEM with information on the distribution of biological communities that may be sensitive to offshore energy industry activities, and to understand their ecological interactions and potential sensitivities to these human activities. A review of historical data revealed the presence of octocorals and some stony (scleractinian) corals in the upper reaches of both canyons; however, work completed during this project has revealed extensive communities of sessile hard-bottom invertebrates on the canyon walls over a wide depth range, and discovered several species of corals that had not been documented in the MAB. Multibeam surveys and predictive habitat models indicate that there are probably many more coral communities that have yet to be discovered. The two study canyons proved to have very different physical conditions (**Chapters 5**, **6**), and supported different coral assemblages (**Chapter 8**). Baltimore Canyon had an extremely turbid environment, and had very few stony corals and very high abundance of the octocoral *Paragorgia arborea*. Norfolk Canyon was less turbid and seemed to be more favorable for stony corals. Although correlation does not necessarily imply causation, it is reasonable to suppose that the persistently high suspended sediment levels limited stony corals. The turbidity in Baltimore Canyon is a natural phenomenon, but energy industry activities may create high sediment levels, which could potentially impact the more sediment-sensitive fauna such as stony corals. Sediment loading should be taken into consideration for management actions in sensitive habitats, not only spatially, but also temporally if appropriate. For example, when a vulnerable or valuable species is known to be spawning, there is precedent in some regions for curtailing activities that increase sediment load during that time-frame. The study of canyon invertebrate reproduction (**Chapter 11**) indicates that several broadcast-spawning species have similar gametogenic cycles. If further research confirms this trend, it may be plausible to protect the larval cohort of multiple species with a single management action.

An unexpected outcome of this project was the discovery of methane seeps (also known as cold seeps) and associated chemosynthetic communities near both canyons. Additional cold seeps and many more potential cold seeps were discovered by NOAA/USGS from 2011-2013. It is clear therefore that the MAB canyons and adjacent slope support widely distributed and extensive sensitive habitats that fall under the management mandate of BOEM.

Studies of genetic population structure show differences in regional connectivity among coral species, with some distributed uniformly across the canyons and others are more isolated, and indicates low connectivity, and therefore lower scope for recolonization after disturbance. It is currently unclear how MAB seep mussel populations are connected to others in the western Atlantic and elsewhere, but it is possible that the MAB mussel larvae originated in the Gulf of Mexico. Management and conservation strategies need to take population structure into account, as it affects species' vulnerability

The rugged topography of the canyon walls precludes most bottom-contact fishing gear, but during this study, lost lines and traps were often observed tangled in the rocky habitats and around corals. In 2016, NOAA fisheries created a large Deep Sea Coral Zone (~67,000 km^2) in the MAB to prevent damage to deep corals from fishing gear. This management area also encompasses the known cold seeps near Baltimore and Norfolk canyons. A number of species that are fished heavily on the shelf and slope were frequently observed in the canyons (Chapter 15), so in addition to protecting sensitive habitats, the

Deep Sea Coral Zone provides refuge areas that are a potential source of recruits to valuable fishery stocks.

19.7.2 Artificial Habitats

The shipwrecks in this study were usually severely enmeshed in fishing nets, indicating repeated interactions between the wrecks and bottom tending gear. These nets cause physical damage to the wrecks and created problems with historical assessment. One management option would be to create restricted access areas around the wrecks to prevent damage from fishing gear and divers in search of historical artefacts. Enforcement would be the greatest challenge with this approach, as it would serve to highlight the locations of the wrecks.

19.8 CHALLENGES AND LESSONS LEARNED

The following lists of some of the challenges faced during this project and the lessons learned during the course of this operationally difficult and intensive research effort.

- Weather limited operations, particularly since ROVs cannot be launched and recovered safely in moderate sea states.
- Technical difficulties with the ROV and associated gear caused loss or reduction of several dives.
- Underwater conditions (strong currents, low visibility, and derelict fishing gear) often limited ROV operations; a manned or other untethered vehicle might have performed better.
- Active fishing, including surface vessels and gear buoys, and lines limited operations due to potential gear conflicts.
- Problems arose with landers and moorings; a sediment storm caused loss of sediment data and destroyed live experiments. One lander and one mooring did not come to the surface on recall, but both were later recovered. The USGS mooring was recovered by the US Coast Guard (data used in this report) and the benthic lander washed ashore in the Bahamas. Because of ship scheduling, the moorings and landers were recovered on a separate cruise, without an ROV. In the future, recovery plans need to be incorporated into cruise planning.
- There were difficulties in obtaining invertebrate identifications, particularly anemones and sponges, which are numerically dominant and appear to be highly diverse. Coral diversity in the canyons seems to be low, but this does not appear to be reflected in other taxonomic groups. Include funding for expert identifications, plus genetic subsampling for bar-coding or a similar approach.
- Cryptic species are not always apparent during collections. Subsamples of each colony should be taken for genetic confirmation of taxonomic identification. It is critical for microbiome work to know the identity of the host. Ship time should be distributed evenly among study sites so that important data are captured during all cruises, particularly if cruises occur during different seasons. To extent possible, conduct cruises at times dictated by science needs, not by other scheduling issues. Lack of science input to scheduling in this project limited data interpretations.
- Communication among partners and collaborators is important during both the pre- and post-cruise activities to facilitate shared goals and deliverables.
- All permits, letters of permission, and other global study documents should be made available to all principal investigators in digital format from a central point of contact. These are often required in publications to confirm that samples were collected legally.

19.9 RECOMMENDATIONS FOR FUTURE STUDIES

- Assess future information needs for management and conservation purposes
- Incorporate more systematic biodiversity assessments for different canyon and cold-seep habitats.
- Address species richness of problematic dominant taxa such as anemones and sponges.
- Expand connectivity analysis for dominant species, including estimates of larval lifespan and larval dispersal models.
- Ground truth bubble plumes for cold seeps in the MAB and other areas and describe associated bacterial and faunal communities.
- Integrate water chemistry (methane and sulfides) into cold-seep studies and examine how this influences seep community age and structure.
- Conduct manipulative experiments (e.g., growth, survival) on dominant species using landers as a platform for experiments.
- Investigate the microbial role in nutrient cycling in deepsea coral species, especially nitrogen cycling.
- Investigate drivers of reproduction in canyon and slope species—expand studies on reproduction to address the timing of noncontinuous gametogenic cycles relative to environmental drivers. Compare timing of reproductive and environmental variables for conspecifics inside and outside the canyon.
- Increase temporal scope of studies to capture seasonal or periodic changes in canyon environments.
- Quantify tidally driven hydrography, sediment transport, and bed shear stress and correlate with simultaneous measurements of sediment biogeochemistry to further explain canyon-specific ecological patterns.
- Conduct amino acid compound-specific isotope analysis (CSIA), "fingerprinting" both marine organic material samples (water column and sediment) and faunal samples, which will enable interpretation of connections between planktonic and particulate food sources and transfer across multiple trophic levels.
- Use metagenomics to determine the dominant biogeochemical cycles in key habitats like coral gardens and seeps.
- Investigate nutritional sources (methanotrophy, thiotrophy, mixotrophy) for bathymodiolid seep mussels.

19.10 LITERATURE CITED

Auster PJ. 2007. Linking deep-water corals and fish populations. In: George RY, Cairns SD, editors. Conservation and adaptive management of seamount and deep-sea coral ecosystems. University of Miami. p. 93–99.

Bernardino AF, Levin LA, Thurber AR, Smith CR. 2012. Comparative composition, diversity and trophic ecology of sediment macrofauna at vents, seeps and organic falls. PLoS ONE 7.

Biber MF, Duineveld GCA, Lavaleye MSS, Davies AJ, Bergman MJN, van den Beld IMJ. 2014. Investigating the association of fish abundance and biomass with cold-water corals in the deep Northeast Atlantic Ocean using a generalized linear modeling approach. Deep-Sea Research II 99:134–145.

Biscaye PE, Anderson RF. 1994. Fluxes of particulate matter on the slope of the southern Middle Atlantic Bight: SEEP-II. Deep-Sea Research II: Topical Studies in Oceanography 41:459–509.

Brooke S, Young CM. 2005. Embryogenesis and larval biology of the ahermatypic scleractinian *Oculina varicose*. Marine Biology 146(4):665–675.

Brooks DA. 1996. Physical oceanography of the shelf and slope seas from Cape Hatteras to Georges Bank: a brief overview. Cambridge (MA): Blackwell Science.

Brothers DS, Ruppel C, Kluesner JW, Brink US, Chaytor JD, Hill JC, Andrews BD, Flores C. 2014. Seabed fluid expulsion along the upper slope and outer shelf of the US Atlantic continental margin. Geophysical Research Letters 41:96–101.

Brothers LL, Van Dover CL, German CR, Kaiser CL, Yoerger DR, Ruppel CD, Lobecker E, Skarke AD, Wagner JKS. 2013. Evidence for extensive methane venting on the southeastern U.S. Atlantic margin. Geology 41:807–810.

Churchill JH, Berger TJ. 1998. Transport of Middle Atlantic Bight shelf water to the Gulf Stream near Cape Hatteras. Journal of Geophysical Research 103(C13):30605–30621.

Cook SK. 1988. Physical oceanography of the Middle Atlantic Bight. In: Pacheco AL, editor. Characterization of the Middle Atlantic Water Management Unit of the Northeast Regional Action Plan. NOAA Tech. Memo. p. 1–49.

Cordes EE, Carney SL, Hourdez S, Carney RS, Brooks JM, Fisher CR. 2007. Cold seeps of the deep Gulf of Mexico: community structure and biogeographic comparisons to Atlantic equatorial belt seep communities. Deep-Sea Research Part I: Oceanographic Research Papers. 54(4):637–653. doi:10.1016/j.dsr.2007.01.001.

Duineveld GCA, Jeffreys RM, Lavaleye MSS, Davies AJ, Bergman MJN, Watmough T, Witbaard R. 2012. Spatial and tidal variation in food supply to shallow cold-water coral reefs of the Mingulay Reef complex (Outer Hebrides, Scotland). Marine Ecology Progress Series. 444:97–115.

Gage JD, Tyler PA. 1992. Deep-Sea Biology: a Natural History of Organisms at the Deep-Sea Floor. Cambridge University Press.

Gardner WD. 1989a. Baltimore Canyon as a modern conduit of sediment to the deep sea. Deep-Sea Research Part A. Oceanographic Research Papers 36:323-358. doi:10.1016/0198-0149(89)90041-1.

Gardner WD. 1989b. Periodic resuspension in Baltimore Canyon by focusing of internal waves. Journal of Geophysical Research. 94:18,185–194.

Harris PT, Whiteway T. 2011. Global distribution of large submarine canyons: geomorphic differences between active and passive continental margins. Marine Geology. 285:69–86.

Hecker B, Blechschmidt G, Gibson P. 1980. Epifaunal zonation and community structure in three mid- and north Atlantic canyons. Final report for the canyon assessment study in the Mid-and North Atlantic Areas of the U.S. Outer Continental Shelf. Prepared for the U.S. Department of Interior, Bureau of Land Management under contract BLM AA5 51-CT8-49. Palisades (NY): Lamont-Doherty Geological Observatory.

Hecker B, Logan DT, Gandarillas FE, Gibson PR. 1983. Canyon and slope processes study, vol. III: biological processes. Report for the U.S. Department of the Interior, Minerals Management Service, under contract no. 14-12-0001-29178. Palisades (NY): Lamont-Doherty Geological Observatory. 212 p. [accessed 2016 June 1]. http://invertebrates.si.edu/boem/reports/CASPS_vol3.pdf.

Heip C, Vincx M, Vranken G. 1985. The ecology of marine nematodes. Oceanography and Marine Biology Annual Review 23:399-489.

Herrera S, Shank TM, Sanchez J. 2012. Spatial and temporal patterns of genetic variation in the widespread antitropical deep-sea coral *Paragorgia arborea*. Molecular Ecology 21(24):6053-6067.

Hill JC, Driscoll NW, Weissel JK, Goff JA. 2004. Large-scale elongated gas blowouts along the US Atlantic margin. Journal of Geophysical Research: Solid Earth (1978–2012) 109.

Kinlan B, Poti M, Drohan A, Packer D, Nizinski M, Dorfman D, Caldow C. 2013. Digital data: Predictive models of deep-sea coral habitat suitability in the U.S. Northeast Atlantic and Mid-Atlantic regions. Downloadable digital data package. Department of Commerce (DOC), National Oceanic and Atmospheric Administration (NOAA), National Ocean Service (NOS), National Centers for Coastal Ocean Science (NCCOS), Center for Coastal Monitoring and Assessment (CCMA), Biogeography Branch and NOAA National Marine Fisheries Service (NMFS), Northeast Fisheries Science Center (NEFSC). http://coastalscience.noaa.gov/projects/detail?key=35.

Lacharite M, Metaxas A. 2013. Early Life History of deep-water gorgonian corals may limit their abundance. PLoS ONE 8(6): e65394. doi:10.1371/journal.pone.0065394.

Langton RW, Langton EW, Theroux RB, Uzmann JR. 1990. Distribution, behavior and abundance of sea pens, *Pennatula aculeata*, in the Gulf of Maine. Marine Biology 107:463–469.

Lawler SN, Kellogg CA, France SC, Clostio RW, Brooke SD, Ross SW. 2016. Coral-associated bacterial diversity is conserved across two deep sea *Anthothela* species. Frontiers in Microbiology. 7(458):1–18.

Levin LA. 2005. Ecology of cold seep sediments: interactions of fauna with flow, chemistry and microbes. Oceanography and Marine Biology Annual Review. 43:1–46.

Levin L, Gooday AJ. 2003. The deep Atlantic Ocean. In: Tyler PA editor. Ecosystems of the World Volume 28: Ecosystems of the Deep Ocean, Book 28. Amsterdam (NL): Elsevier.

Levin LA, Sibuet M. 2012. Understanding continental margin biodiversity: a new imperative. Annual Review of Marine Science 4:79-112. doi:10.1146/annurev-marine-120709–142714.

Levin L, Etter RJ, Rex MA, Gooday AJ, Smith CR, Pineda J, Stuart CT, Hessler RR, Pawson D. 2001. Environmental influences on regional deep-sea species diversity. Annual Review of Ecology, Evolution, and Systematics. 32:51–93.

Levin LA, Ziebis W, Mendoza GF, Growney-Cannon V, Walther S. 2006. Recruitment response of methane-seep macrofauna to sulfide-rich sediments: an *in situ* experiment. Journal of Experimental Marine Biology and Ecology 330:132-150.

Mann KH. 1982. Ecology of coastal waters. Berkeley (CA): University of California Press.

McClain CR, Barry JP. 2010. Habitat heterogeneity, disturbance, and productivity work in concert to regulate biodiversity in deep submarine canyons. Ecology. 91(4):964–976.

Menot L, Galéron J, Olu K, Caprais J-C, Crassous P, Khripounoff A, Sibuet M. 2010. Spatial heterogeneity of macrofaunal communities in and near a giant pockmark area in the deep Gulf of Guinea. Marine Ecology. 31:78–93.

Mercier A, Hamel JF. 2011. Contrasting reproductive strategies in three deep-sea octocorals from eastern Canada: *Primnoa resedaeformis*, *Keratoisis ornata*, and *Anthomastus grandifloras*. Coral Reefs. 30:337–350.

Milliman JD. 1994. Organic matter content in U.S. Atlantic continental slope sediments: Decoupling the grain-size factor. Deep Sea Research Part II: Topical Studies in Oceanography. 41:797–808.

Musick JA. 1979. Community structure of fishes on the continental slope and rise off the middle Atlantic coast of the United States. Spec. Sci. Rept. No. 96. Virginia Institute of Marine Science.

Newman KR, Cormier M-H, Weissel JK, Driscoll NW, Kastner M, Solomon EA, Robertson G, Hill JC, Singh H, Camilli R. 2008. Active methane venting observed at giant pockmarks along the U.S. mid-Atlantic shelf break. Earth and Planetary Science Letters. 267:341–352. doi:10.1016/j.epsl.2007.11.053.

Obelcz J, Brothers D, Chaytor J, Brink Ut, Ross SW, Brooke S. 2014. Geomorphic characterization of four shelf-sourced submarine canyons along the U.S. Mid-Atlantic continental margin. Deep-Sea Research Part II: Topical Studies in Oceanography. 104:106–119.

Paull CK, Hecker B, Commeau R, Freeman-Lynde RP, Neumann C, Corso WP, Golubic S, Hook JE, Sikes E, Curry J. 1984. Biological communities at the Florida Escarpment resemble hydrothermal vent taxa. Science (NY): 226:965–967.

Paull CK, Ussler W, Borowski WS, Spiess FN. 1995. Methane-rich plumes on the Carolina continental rise: associations with gas hydrates. Geology. 23:89–92.

Pawson DL, Vance DJ. 2004. *Chiridota heheva*, new species from western Atlantic deep-sea cold seeps and anthropogenic habitats (Echinodermata: Holothuroidea: Apodida). Zootaxa. 534:1–12.

Perovich G, Epifanio CE, Dittel AI, Tyler PA. 2003. Spatial and temporal patterns in development of eggs in the vent crab *Bythograea thermydron*. Marine Ecology Progress Series. 251:211–220.

Pile AJ, Young CM. 1999. Plankton availability and retention efficiencies by cold-seep symbiotic mussels. Limnology and Oceanography. 449:332–344.

Prouty NG, Sahy D, Ruppel CD, Roark EB, Condon D, Brooke S, Ross SW, Demopoulos AWJ. 2016. Insights into methane dynamics from analysis of authigenic carbonates and chemosynthetic mussels at newly discovered Atlantic Margin seeps. Earth and Planetary Science Letters 13856. doi:10.1016/j.epsl.2016.05.023.

Quattrini AM, Nizinski MS, Chaytor JD, Demopoulos AWD, Roark EB, France SC, Moore JA, Heyl TP, Auster PJ, Kinlan B, Ruppel C, Elliott KP, Kennedy BRC, Lobecker E, Skarke A, Shank T. 2015. Exploration of the canyon-incised continental margin of the northeastern United States reveals dynamic habitats and diverse communities. PLoS ONE 10(10): e0139904. doi:10.1371/journal.pone.0139904

Rex MA, Etter RJ. 2010. Deep-sea biodiversity: pattern and scale. Harvard University Press.

Ross SW, Quattrini AM. 2007. The fish fauna associated with deep coral banks off the southeastern United States. Deep-Sea Research I 54:975-1007.

Ross SW, Rhode M, Quattrini AM. 2015. Demersal fish distribution and habitat use within and near Baltimore and Norfolk canyons, U.S. middle Atlantic slope. Deep Sea Research Part I: Oceanographic Research Papers 103:137-154. doi:10.1016/j.dsr.2015.06.004.

Ross SW, Matos F, INCISE Working Group 2. 2016a. A bibliographic compilation of literature and related metadata concerning global submarine canyon research. [accessed 2016 July 8]. http://www.incisenet.org/working-groups/working-group-2.

Ross SW, Rhode M, Viada ST, Mather R. 2016b. Fish species associated with shipwreck and natural hard-bottom habitats from the middle to outer continental shelf of the Middle Atlantic Bight near Norfolk Canyon. Fishery Bulletin. 114:45–57.

Rowe GT. 1972. The exploration of submarine canyons and their benthic faunal assemblages. Proceedings of the Royal Society of Edinburgh Section B: Biological Sciences. 73(17):159–169.

Ruppel C, Kluesner JW, Danforth W. 2015. Imaging Methane Seeps and Plumes on the U.S. Atlantic Margin Sound Waves. U.S. Geological Survey.

Shepard AN, Theroux RB, Cooper RA, Uzmann JR. 1986. Ecology of *Ceriantharia* (Coelenterata, Anthozoa) of the northwest Atlantic from Cape Hatteras to Nova Scotia. Fisheries Bulletin. 84:625–-646.

Sherwood OA, Jamieson RE, Edinger EN and Wareham VE. 2008. Stable C and N isotopic composition of cold-water corals from the Newfoundland and Labrador continental slope: examination of trophic, depth and spatial effects. Deep Sea Res. Part I: Oceanographic Research Papers. 55:1392–1402.

Skarke A, Ruppel C, Kodis M, Brothers D, Lobecker E. 2014. Widespread methane leakage from the sea floor on the northern US Atlantic margin. Nature Geoscience. 7 (9):657–661.

Steimle FW, Zetlin C. 2000. Reef habitats in the Middle Atlantic Bight: abundance, distribution, associated biological communities, and fishery resource use. Marine Fisheries Review. 62(2):24-42. [accessed 2016 July 8]. http://spo.nwr.noaa.gov/mfr622/mfr6222.pdf.

Taylor MH, Dillon WP, Pecher IA. 2000. Trapping and migration of methane associated with the gas hydrate stability zone at the Blake Ridge Diapir: new insights from seismic data. Marine Geology. 164:79–89.

Theroux RB, Wigley RL. 1998. Quantitative composition and distribution of the macrobenthic invertebrate fauna of the continental shelf ecosystems of the northeastern United States. NOAA Technical Report NMFS-140. 240 p.

Thurber AR. 2010. Microbe-metazoan interactions at Pacific Ocean methane seeps. PhD dissertation, University of California San Diego, San Diego, CA.

Tyler J. 2005. Distribution, population characteristics and trophic ecology of a sulphophilic hydrothermal vent tonguefish (Pleuronectiformes: Cynoglossidae). Master's thesis, University of Victoria, Canada.

Tyler PA, Gage JD. 1984. Seasonal reproduction of *Echinus affinis* (Echinodermata: Echinoidea) in the Rockall trough, northeast Atlantic Ocean. Deep Sea Research Part I: Oceanographic Research Papers. 31(4):387–402.

Tyler PA, Young CM, Dolan E, Arellano SM, Brooke SD, Baker M. 2007. Gametogenic periodicity in the chemosynthetic cold-seep mussel "*Bathymodiolus" childressi*." Marine Biology. 150:829–840.

Van Dover CL, Aharon P, Bernhard JM, Caylor E, Doerries M, Flickinger W, Gilhooly W, Goffredi SK, Knick KE, Macko SA, Rapoport S, Raulfs EC, Ruppel C, Salerno JL, Seitz RD, Sen Gupta BK, Shank T, Turnipseed M, Vrijenhoek R. 2003. Blake Ridge methane seeps: characterization of a soft-sediment, chemosynthetically based ecosystem. Deep Sea Research Part I: Oceanographic Research Papers. 50(2):281–300.

Watling L, Auster P. 2005. Distribution of the deep water Alcyonacea off the northeast coast of the United States, pp. 259-264. In: Friewald A, Roberts JM, editors. Cold Water Corals and Ecosystems. Berlin Heidelberg: Springer-Verlag.

Young CM, He R, Emlet RB, Li Y, Qian H, Arellano SM, Van Gaest A, Bennett KC, Wolf M, Smart TI, Rice ME. 2012. Dispersal of deep sea larvae from the intra-American seas: simulations of trajectories using ocean models. International Society for Computational Biology. 52(4):483–496.

Department of the Interior (DOI)

The Department of the Interior protects and manages the Nation's natural resources and cultural heritage; provides scientific and other information about those resources; and honors the Nation's trust responsibilities or special commitments to American Indians, Alaska Natives, and affiliated island communities.

BOEM
Bureau of Ocean Energy Management

Bureau of Ocean Energy Management (BOEM)

The mission of the Bureau of Ocean Energy Management is to manage development of U.S. Outer Continental Shelf energy and mineral resources in an environmentally and economically responsible way.

BOEM Environmental Studies Program

The mission of the Environmental Studies Program is to provide the information needed to predict, assess, and manage impacts from offshore energy and marine mineral exploration, development, and production activities on human, marine, and coastal environments. The proposal, selection, research, review, collaboration, production, and dissemination of each of BOEM's Environmental Studies follows the DOI Code of Scientific and Scholarly Conduct, in support of a culture of scientific and professional integrity, as set out in the DOI Departmental Manual (305 DM 3).